Digitized by the Internet Archive
in 2026

https://archive.org/details/symposium-international-on-combustion_1959

SEVENTH SYMPOSIUM (INTERNATIONAL) ON COMBUSTION

BUTTERWORTHS PUBLICATIONS LTD.
88 KINGSWAY, LONDON, W.C.2

AFRICA: BUTTERWORTH & CO. (AFRICA) LTD.
DURBAN: 33/35 Beach Grove

AUSTRALIA: BUTTERWORTH & CO. (AUSTRALIA) LTD.
SYDNEY: 8 O'Connell Street
MELBOURNE: 430 Bourke Street
BRISBANE: 240 Queen Street

CANADA: BUTTERWORTH & CO. (CANADA) LTD.
TORONTO: 1367 Danforth Avenue

NEW ZEALAND: BUTTERWORTH & CO. (AUSTRALIA) LTD.
WELLINGTON: 49/51 Ballance Street
AUCKLAND: 35 High Street

U.S.A.

ACADEMIC PRESS INC., PUBLISHERS
111, FIFTH AVENUE
NEW YORK 3, NEW YORK

SEVENTH SYMPOSIUM

(INTERNATIONAL)

ON

COMBUSTION

At London and Oxford

28 August – 3 September, 1958

Published for

THE COMBUSTION INSTITUTE

LONDON

BUTTERWORTHS SCIENTIFIC PUBLICATIONS

1959

©
The Combustion Institute
1958
First Reprint 1971

All rights reserved

Brief quotations from this book for purposes of scientific discussion will be permitted

Set in Monotype Baskerville type
Made in Great Britain at the Pitman Press, Bath

PREFACE

At the invitation of the British Section of The Combustion Institute the Seventh Symposium (International) on Combustion was held in London and Oxford, 28 August to 3 September, 1958. The Institute of Fuel generously collaborated in the organization of the Symposium.

The inaugural meeting, 28 August, in the historic Lecture Room at the Royal Institution, where Rumford, Davy, Faraday, Dewar and other famous scientists had discoursed, evoked the shades of those audacious, inquiring minds. Texts of the addresses by Professor Sir Cyril Hinshelwood, Dr. Bernard Lewis, and Emeritus Professor Sir Alfred C. Egerton are printed in this volume. Mr. A. J. Nerad, Chairman of the Awards Subcommittee, announced that three awards had been established by The Combustion Institute to be conferred at each biennial symposium: The Alfred C. Egerton Medal (gold); The Bernard Lewis Medal (gold); The Silver Combustion Medal. Presentation of the first Alfred C. Egerton Medal was made to Sir Alfred by Professor A. R. J. P. Ubbelohde 'For his distinguished, continuing and encouraging contributions to the field of combustion.' Dr. Theodore von Kàrmàn presented the first Bernard Lewis Medal to Dr. Lewis 'For brilliant research in the field of combustion, particularly on minimum ignition energy.' The first Silver Combustion Medal was awarded by the President of The Combustion Institute to Professors Seiichiro Kumagai and Hiroshi Isoda 'For an outstanding paper presented at the Sixth Symposium on Combustion, 1956.' In the afternoon, tours were made to the combustion laboratories of the Imperial College of Science and Technology.

With the gracious permission of the Lord Mayor, the Sheriffs, and the Corporation of the City of London, a gala banquet was held in the evening amid the medieval splendour of the Guildhall. Speeches by Mr. T. C. Bailey, President-Elect of the Institute of Fuel, Dr. D. T. A. Townend, Emeritus Professor Sir Alfred C. Egerton, the Rt. Hon. Lord Brabazon of Tara, and Dr. Bernard Lewis, and the traditional 'Loving Cup Ceremony' lent emphasis to what Sir Alfred termed 'the brotherhood of science—friends in search of truth'.

On 29 August the Symposium was adjourned to Oxford. A special train, drawn by one of the new gas-turbine locomotives, was provided by British Railways to transport the participants to Oxford, where many were accommodated in various colleges of the University.

There were 18 technical sessions, each lasting about 100 minutes. Half the time was given to the presentation of certain of the papers that had been pre-printed; the second half was available for discussion of these papers and of others that had also been pre-printed. Many interesting discussions took place on the topics considered by the Symposium. The first two sessions were devoted to detonation and, in particular, the transition from flame propagation to detonation was discussed. These were followed by sessions on the spectroscopy and structure of flames in which modern methods of following the change of composition through a flame front were described. A considerable part of the Symposium was devoted to a consideration of the mechanism of combustion reactions. There were five sessions which came under this general heading, both hydrocarbons and other substances being considered. Other sessions were devoted to ionization in flames, the interaction of flames with surfaces, the mechanism of flame propagation, and turbulence in flames. In addition, one session dealt with ignition and limits of inflammability. For those with more practical and technical interests, there were two sessions on combustion in practical flowing systems, the first of which concentrated on model techniques. There were also sessions on special fuels and on instrumentation. An informal discussion on The Study of Combustion: Is it an Art or a Science? was presided over by Professor A. R. J. P. Ubbelohde one evening. Great credit is due to Dr. Linnett and the members of the Papers Subcommittee for having arranged such a stimulating and worthwhile programme.

Twenty countries were represented at the Symposium. There were 254 participants in attendance from Great Britain; 149 from the United States of America; 18 from Germany; 17 from France; 15 from Belgium; 14 from the Netherlands; 7 from Canada; 6 from the U.S.S.R.; 4 each from Japan, Spain and Sweden; 3 each from Italy and Switzerland; 2 each from Africa, Australia and Poland; and 1 each from Hungary, Liechtenstein, Norway and Yugoslavia.

The Institute's chartered flight, which left New York, 23 August, took 63 members to the Symposium. In addition, the U.S. Air Force and Navy provided passage on MATS planes for some 70 participants. The Institute gratefully acknowledges this service, as well as support for the Symposium by the U.S. Department of the Air Force through the Office of Scientific Research and Development Command, by the U.S. Department of the Army through the Office of Ordnance

Research, and by the U.S. Department of the Navy through the Office of Naval Research.

The U.K. Committee on Organization and the Hospitality Subcommittee provided a brilliant programme of entertainment which, in addition to the banquet, included a reception for overseas guests by Her Majesty's Government at Lancaster House, St. James's Palace, an evening of ballet at Covent Garden, a performance of *Hamlet* at Stratford-upon-Avon preceded by dinner and followed by supper in the Shakespeare Memorial Theatre Restaurant, an organ recital by Meredith Davies, F.R.C.O., in the Chapel of New College, Oxford, and a visit to Blenheim Palace, seat of the Duke of Marlborough and birthplace of Sir Winston Churchill.

The Honourable Lady Egerton and the members of her committee arranged a delightful series of events for the wives and other members of families of more than 120 participants. Small groups of ladies were entertained to tea in the homes of a number of Oxford hostesses, and excursions were made to the Cotswold Hills by coach and on the Thames River by steamer.

To the Finance Subcommittee and its Chairmen, Dr. J. S. Clarke and Mr. J. M. Campbell, and to the following who responded so generously in support of the Symposium, The Combustion Institute extends grateful appreciation:

U.S.A.

Aerojet-General Corporation
Air Reduction Company, Inc.
American Gas Association
Appalachian Electric Power Company
Atlantic Research Corporation
Bethlehem Steel Company
Boeing Airplane Company
Godfrey L. Cabot, Inc.
California Research Corporation
Canadian Industries Limited
Caterpillar Tractor Company
Cities Service Research and Development Company
Combustion Engineering, Inc.
Combustion and Explosives Research, Inc.
Continental Aviation & Engineering Corporation
Cummins Engine Company, Inc.
Curtiss-Wright Corporation
E. I. du Pont de Nemours & Company
Esso Research and Engineering Company
Ethyl Corporation
Experiment Incorporated
Fairchild Engine Division
Flame Research, Inc.
The Fluor Corporation, Ltd.
Ford Motor Company
The Garrett Corporation
General Dynamics Corporation
General Electric Company
  Aircraft Gas Turbine Division
  G. E. Research Laboratory
General Motors Corporation
  Allison Engine Division
  G. M. Research Laboratories
Gulf Research & Development Company
Hauck Manufacturing Company
Hercules Powder Company
Indiana & Michigan Electric Company
International Harvester Company
The M. W. Kellogg Company
Koppers Company, Inc.
Arthur D. Little, Inc.
The Lummus Company
Lycoming Division, A.V.C.O.
Marquardt Aircraft Company
National Airoil Burner Company, Inc.
National Northern Corporation
Office of Naval Research, U.S. Navy
Office of Ordnance Research, U.S. Army
Office of Scientific Research, U.S. Air Force
Ohio Power Company
Orenda Engines Limited, Canada
Owens-Corning Fiberglas Corporation
Phillips Petroleum Company
Pittsburgh Consolidation Coal Company
Pittsburgh Plate Glass Company
The Pure Oil Company
Richfield Oil Corporation
Shell Development Company
Socony Mobil Oil Company, Inc.
Solar Aircraft Company
Standard Oil Company (Indiana)
Standard Oil Company (Ohio)
Sun Oil Company
The Texas Company
Thompson Products, Inc.
Union Carbide Corporation
UnitedAircraft Corporation, Pratt & Whitney Division
United States Steel Corporation
Universal Oil Products Company
Westinghouse Aircraft Gas Turbine Division
Worthington Corporation

U.K.

Armstrong Siddeley Motors, Ltd.
Austin Motor Co., Ltd.
Babcock & Wilcox, Ltd.
Bristol Aeroplane Co., Ltd.
British Petroleum, Ltd.
Clayton Trust (Institution of Mechanical Engineers)
De Havilland Aircraft Co., Ltd.
Wm. Doxford & Sons, Ltd.

English Electric Co., Ltd.
Esso Petroleum Co., Ltd.
Imperial Chemical Industries, Ltd.
International Combustion, Ltd.
Institute of Fuel
Incandescent Heat, Ltd.
Joseph Lucas, Ltd.
Metropolitan Vickers Electrical Co., Ltd.
Midland Tar Distillers, Ltd.
Mobil Oil Co., Ltd.
C. & A. Parsons, Ltd.
Rolls-Royce, Ltd.
Shell Petroleum Co., Ltd.
United Steel Companies

The Combustion Institute expresses its sincere gratitude to the British Section, the Institute of Fuel, the Imperial College of Science and Technology, the City of London, and Oxford University for affording a uniquely memorable meeting. Special mention must be made of Messrs. R. W. Reynolds-Davies and D. W. Page, Miss Margaret Brown and Mrs. A. John, of the Institute of Fuel, Sir Alfred and Lady Egerton, Dr. and Mrs. J. W. Linnett, Mr. and Mrs. N. P. W. Moore, Drs. E. A. Watson and J. S. Clarke, Miss H. M. Smith, and all their associates whose indefatigable and selfless efforts resulted in an outstandingly successful Symposium.

THE COMBUSTION INSTITUTE

A non-profit professional society, incorporated in 1954, to promote the science and application of combustion and to disseminate knowledge in this field

Officers

President	Bernard Lewis
Vice President	Hoyt C. Hottel
Treasurer	Stewart Way
Assistant Treasurer	Bernard M. Sturgis
Secretary	Glenn C. Williams

Executive Office

Union Trust Building, Pittsburgh 19, Pennsylvania
Mrs. Helen G. Barnes, Executive Secretary

Board of Directors

Mr. J. L. Cooley	California Research Corporation
Professor Newman A. Hall	Yale University
Dr. Amos G. Horney	Office of Scientific Research, USAF
Professor H. C. Hottel	Massachusetts Institute of Technology
Dr. Bernard Lewis	Combustion and Explosives Research, Inc.
Mr. J. B. Macauley	Ethyl Corporation
Mr. A. J. Nerad	General Electric Company
Dr. Walter T. Olson	NASA Lewis Flight Propulsion Laboratory
Dr. Robert N. Pease	Princeton University
Dr. Edward H. Seymour	Reaction Motors, Inc.
Dr. B. M. Sturgis	E. I. du Pont de Nemours & Company, Inc.
Dr. W. J. Sweeney	Esso Research and Engineering Company
Dr. Stewart Way	Westinghouse Research Laboratories
Professor Glenn C. Williams	Massachusetts Institute of Technology
Dr. Lloyd L. Withrow	General Motors Research Laboratories

The Combustion Institute Committee

United States

Dr. David Altman (*Chairman*)	Aeronutronic Systems, Inc.
Mr. J. L. Cooley	California Research Corporation
Dr. Amos G. Horney	Office of Scientific Research, USAF
Dr. J. P. Longwell	Esso Research & Engineering Company
Dr. Walter T. Olson	NASA Lewis Flight Propulsion Laboratory
Professor Glenn C. Williams	Massachusetts Institute of Technology

Great Britain

Sir Alfred C. Egerton (*Chairman*)	Imperial College of Science and Technology, London
Dr. J. S. Clarke (*Secretary*)	Joseph Lucas Limited, Birmingham
Dr. J. W. Linnett	Queen's College, Oxford
Dr. Peter Lloyd	National Gas Turbine Establishment, Farnborough
Professor O. A. Saunders	Imperial College of Science and Technology, London

Australia

Mr. W. B. Kennedy	Department of Air, Melbourne

Belgium

Dr. Louis Deffet	Centre de Recherches pour l'Industrie des Produits Explosifs, Brussels

Canada	
Dr. J. S. Watson	National Research Council, Ottawa
France	
Professeur Paul Laffitte	Faculté des Sciences de l'Université de Paris
Germany	
Professor Dr. Wilhelm Jost	Institut für Physikalische Chemie der Universität, Göttingen
India	
Dr. M. S. Thacker	Council of Scientific and Industrial Research, New Delhi
Israel	
Dr. Abraham Hermoni	Ministry of Defence, Hakirya, Tel-Aviv
Italy	
Professor Cesare Codegone	Politechnico di Torino
Japan	
Professor Sakae Yagi	University of Tokyo
Netherlands	
Professor Dr. E. F. M. van der Held	Centraal Technische Institut, Delft
Spain	
Dr. Gregorio Millán	Instituto Nacional di Technica Aeronáutica, Madrid
Sweden	
Dr. C. H. Johansson	Nitroglycerin Aktiebolaget, Stockholm
Switzerland	
Professor K. Clusius	Physikalisch-Chemisches Institut der Universität, Zürich
Turkey	
Professor Dr. Hikmet Binark	Teknik Üniversitesi, Istanbul

1958 SYMPOSIUM SUBCOMMITTEES

U.K. Committee on Organization

Sir Alfred C. Egerton (*Chairman*)	Imperial College of Science and Technology, London
Mr. S. Bragg	Rolls-Royce Ltd., Derby
Dr. H. E. Crossley	(Representing the Institute of Fuel)
Dr. J. W. Linnett	Queen's College, Oxford
Dr. P. Lloyd	National Gas Turbine Establishment, Farnborough
Dr. A. C. Monkhouse	Institute of Fuel
Mr. N. P. W. Moore	Imperial College of Science and Technology, London
Professor O. A. Saunders	Imperial College of Science and Technology, London
Professor A. R. J. P. Ubbelohde	Imperial College of Science and Technology, London
Dr. J. S. Clarke (*Secretary*)	Joseph Lucas Ltd., Birmingham
Miss H. M. Smith (*Assistant Secretary*)	Joseph Lucas Ltd., Birmingham

Awards Subcommittee

Mr. A. J. Nerad (*Chairman*)	General Electric Company
Professor Newman A. Hall	Yale University
Dr. Amos G. Horney	Office of Scientific Research, USAF
Dr. Robert N. Pease	Princeton University
Dr. Edward H. Seymour	Reaction Motors, Inc.
Dr. D. G. Shepherd	Cornell University
Dr. Glenn C. Williams	Massachusetts Institute of Technology

Papers Subcommittee

Dr. J. W. Linnett (*Chairman*)	Queen's College, Oxford
Mr. S. Bragg	Rolls-Royce Ltd., Derby
Professor C. E. H. Bawn	University of Liverpool
Dr. J. H. Burgoyne	Imperial College of Science and Technology, London
Professor F. H. Garner	University of Birmingham
Dr. A. G. Gaydon	Imperial College of Science and Technology, London
Dr. P. Lloyd	National Gas Turbine Establishment, Farnborough
Professor R. G. W. Norrish	University of Cambridge
Dr. W. G. Parker	Royal Aircraft Establishment, Westcott
Professor M. W. Thring	University of Sheffield
Dr. D. T. A. Townend	British Coal Utilization Research Association, Leatherhead
Professor A. R. J. P. Ubbelohde	Imperial College of Science and Technology, London
Dr. H. P. Broida	National Bureau of Standards, U.S.A.
Dr. Marjorie W. Evans	Stanford Research Institute, U.S.A.
Mr. W. V. Hanzalek	Curtiss Wright Corporation, U.S.A.
Professor W. Jost	University of Göttingen, Germany
Professor P. Laffitte	University of Paris, France
Dr. Donald L. Mordell	McGill University, Canada
Dr. S. S. Penner	California Institute of Technology, U.S.A.
Dr. E. B. Rifkin	Ethyl Research Laboratories, U.S.A.
Dr. E. F. M. van der Held	Centraal Technische Institut, Holland
Dr. D. R. Warren	Aeronautical Research Laboratories, Australia

U.K. Finance Subcommittee

Dr. J. S. Clarke (*Chairman*)	Joseph Lucas Ltd., Birmingham
Sir Alfred C. Egerton	Imperial College of Science and Technology, London

Sir Harry Melville	Department of Scientific and Industrial Research, London
Mr. J. A. Oriel	Shell Ltd., London
Professor O. A. Saunders	Imperial College of Science and Technology, London
Dr. Llewellyn Smith	Rolls-Royce Ltd., Derby
Dr. E. A. Watson	Joseph Lucas Ltd., Birmingham

U.S. Finance Subcommittee

Mr. J. M. Campbell	General Motors Research Laboratories
Dr. D. P. Barnard	Standard Oil Company (Indiana)
Mr. W. G. Lovell	Ethyl Corporation
Mr. E. S. Nicholls	Socony Mobil Oil Company, Inc.
Mr. D. M. Sheldon	Shell Development Company
Dr. Blaine B. Wescott	Gulf Research and Development Company

Hospitality Subcommittee

Dr. J. W. Linnett (*Chairman*)
Professor O. A. Saunders (*Deputy Chairman*)
Mr. N. P. W. Moore (*Secretary*)
Mr. K. C. Hunt
Dr. C. J. Danby
Dr. D. T. A. Townend
Mr. W. V. Battcock
Dr. W. G. Parker

Ladies' Committee

Hon. Lady Egerton (*Chairman*)
Lady Bragg
Mrs. J. Brown
Mrs. C. J. Danby
Mrs. A. G. Gaydon
Mrs. A. S. Gordon
Mrs. J. W. Linnett
Mrs. A. C. Monkhouse
Mrs. N. P. W. Moore

CONTENTS

		Page
	Preface	v
	The Combustion Institute	ix
	1958 Symposium Subcommittees	xi
	List of Authors	xix
	Speeches at the Inaugural Meeting of the Symposium	
	Professor Sir Cyril Hinshelwood, *President of the Royal Society*	xxvii
	Dr. Bernard Lewis, *President of The Combustion Institute*	xxxi
	Emeritus Professor Sir Alfred Egerton	xxxvii
	Guildhall Banquet	xliii
	Introduction by Dr. J. W. Linnett, *Queen's College and Inorganic Chemistry Laboratory, Oxford University*	xlv

PART I—MECHANISM OF COMBUSTION REACTIONS

Paper No.		
1	Reactions of Hydrogen Atoms with Oxygen. *B. deB. Darwent and V. J. Krasnansky*	3
2	The Slow Reaction and Second Limit of the Hydrogen–Oxygen Reaction in Boric Acid Coated Vessels. *R. R. Baldwin and L. Mayor*	8
3	The Mercury Photosensitized Hydrogen–Oxygen Reaction at Low Oxygen Concentrations. *J. S. Watson*	17
4	Production of Hydrogen Peroxide in Reacting Mixtures of Hydrogen and Oxygen. *J. W. Linnett and C. P. Tootal*	23
5	The Rate and Mechanism of the Thermal Dissociation of Oxygen. *K. F. Herzfeld*	27
6	On some Reactions Occurring During the Explosion Induction Period. *V. V. Voevodsky*	34
7	Reactions of some Radicals and their Concentration in Flames. *V. N. Kondratiev*	41
8	Further Studies of Induction Periods in Mixtures of H_2, O_2 and NO_2. *P. G. Ashmore and B. P. Levitt*	45
9	Reactions of Atomic Oxygen and Atomic Nitrogen with Oxides of Nitrogen. *F. Kaufman and J. Kelso*	53
10	Effect of Oxygen on Thermal Decomposition of Nitric Oxide at High Temperatures. *F. Kaufman and L. J. Decker*	57
11	Recent Studies of the Oxidation and Decomposition Flames of Hydrazine. *P. Gray and J. C. Lee*	61
12	Mechanism Involved in the Photochemically Initiated Combustion of H_2S. *A. P. Zeelenberg*	68
13	First Limit Induction Time Studies of CS_2–O_2 Explosions. *F. R. Taylor and A. L. Myerson*	72
14	A Study of Vibrational Relaxation in Carbon Monoxide by Shock Waves and Infra-red Emission. *M. Windsor, N. Davidson and R. Taylor*	80
15	On the Perturbation of the Vibrational Equilibrium Distribution of Reactant Molecules by Chemical Reactions. *K. E. Shuler*	87

16 On the Analysis of Re-combination Reactions in an Expanding Gas Stream. *F. T. Smith* 93

17 Shock Tube Studies of Reaction Kinetics of Aliphatic Hydrocarbons. *H. S. Glick* 98

18 The Point of Attack in Hydrocarbon Oxidation—I. Propane. *R. Burt, C. F. Cullis, R. Larsen and G. J. Minkoff* 108

19 Products of Cool Flame Oxidation of Propane-2-^{13}C. *R. E. Ferguson and C. R. Yokley* 113

20 Some Problems of Elementary Reactions in Gas-Phase Slow Combustion. *Z. G. Szabó* 118

21 Rate Constants of Elementary Reactions in Hydrocarbon Oxidation—Low Temperature Oxidation of Lower Hydrocarbons. *J. H. Knox* 122

22 Rate Constants of Elementary Reactions in Hydrocarbon Oxidation—Competitive Oxidation of Lower Hydrocarbons. *J. H. Knox, R. F. Smith and A. F. Trotman-Dickenson* 126

23 Application of Radioactive Isotopes to Study the Mechanism of Some Oxidation Processes. *D. Gál, F. Dutka, L. Guczi and I. Kende* 128

24 Some Processes in Gaseous Slow Combustions. Formation of Carbon Monoxide and Carbon Dioxide. *G. Skirrow and C. F. H. Tipper* 134

25 On High-temperature Oxidation of Methane. *G. I. Kozlov* 142

26 A Mass Spectrometric Investigation of the Methane–Oxygen Reaction at Low Pressures. *D. J. Fabian and W. A. Bryce* 150

27 Kinetics and Mechanism of Methane Oxidation. *N. S. Enikolopyan* 157

28 Inhibition of Diethyl Ether–Oxygen Flames by Aliphatic Amines. *D. J. Waddington* 165

29 Stabilization by Aliphatic Amines of Free Radicals in Oxidation Systems. *C. F. Cullis and B. A. Khokhar* 171

30 Mechanism of Combustion Inhibition by Compounds Containing Halogen. *W. A. Rosser, H. Wise and J. Miller* 175

31 Effects of Surfaces on Combustion of Methane and Mode of Action of Anti-knocks Containing Metals. *D. E. Cheaney, D. A. Davies, A. Davis, D. E. Hoare, J. Protheroe and A. D. Walsh* 183

Discussion 188

PART II—SPECTROSCOPY OF FLAMES

32 Emission Spectra from Mixtures of Atomic Nitrogen and Organic Substances. *N. H. Kiess and H. P. Broida* 207

33 Spectrophotometric Studies of Laminar Flames—I. The Decay of Radical Radiation. *E. T. Child and K. Wohl* 215

34 Spectrophotometric Studies of Laminar Flames—II. The Flame Front. *R. Kushida and K. Wohl* 221

35 Emission and Absorption Spectra of Flat Flames. *G. N. Spokes* 229

36 Chemiluminescence and Radical Re-combination in Hydrogen Flames. *P. J. Padley and T. M. Sugden* 235

Discussion 243

PART III—IONIZATION IN FLAMES

37 Mass Spectrometry of the Ions Present in Hydrocarbon Flames. *P. F. Knewstubb and T. M. Sugden* 247

38 Ion Identification in Flames. *J. Deckers and A. van Tiggelen* 254

39 Comparative Study of Ionization in Acetylene–Oxygen and Acetylene–Nitrous Oxide Flames. *J. Poncelet, R. Berendsen and A. van Tiggelen* 256

40 Distribution of Ions in Low-pressure Flames. *T. Kinbara, J. Nakamura and H. Ikegami* 263

41 The Predominant Process of Electron Decay in the Mantle of an Acetylene–Air Flame. *H. Williams* 269

42 Ionization in Detonation Waves. *S. Basu and J. A. Fay* 277

Discussion 283

PART IV—STRUCTURE AND PROPAGATION OF FLAMES

43 Composition Traverses in Curved Laminar Flame Fronts. *G. H. Markstein* 289

44 Optical Flame Structure Studies: Some Conclusions concerning the Propagation of Flat Flames. *A. Levy and F. J. Weinberg* 296

45 Reactions of Simple Hydrocarbons in Flame Fronts—Microstructure of C_2 Hydrocarbon–Oxygen Flames. *R. M. Fristrom, W. H. Avery and C. Grunfelder* 304

46 Flame Structure Studies—IV. Pre-mixed Carbon Monoxide Combustion. *R. Friedman and R. G. Nugent* 311

47 Study of the Chemistry of Diffusion Flames. *A. S. Gordon, S. R. Smith and J. R. McNesby* 317

48 Mass Analysis of Flames and Flue Gases. *E. A. Bunt* 325

49 Deviation from the Kinetic Steady-state Approximation in a Free-radical Flame. *E. S. Campbell, J. O. Hirschfelder and L. M. Schalit* 332

50 An Action Principle for the Laminar Flame. *G. Rosen* 339

51 Excess Enthalpy and the Initiation and Stability of Combustion Waves. *G. von Elbe and B. Lewis* 342

52 Reaction Order in the Hydrogen–Bromine Flame from the Pressure Dependence of Quenching Diameter. *A. E. Potter, Jr., and E. Anagnostou* 347

53 Flame Propagation in Two-phase Mixtures. *I. N. Sundukov and A. S. Predvoditelev* 352

54 Generalized Flame Stability Diagram for the Prediction of Interchangeability of Gases. *D. W. van Krevelen and H. A. G. Chermin* 358

55 A Study of the Kinetics of Cyanogen Flames. *K. Scheller and W. E. McKnight* 369

56 Burning Velocity Measurements by the Constant-pressure Bomb Method. *W. A. Strauss and R. Edse* 377

57 High-temperature Oxidation and Burning of Carbon Monoxide. *G. K. Sobolev* 386

58 The Vertical Tube Reactor—A Tool for Study of Flame Processes. *K. G. Williams, J. E. Johnson and H. W. Carhart* 392

59 Experimental Temperature Gradients in Burning Drops. *A. R. Hall* 399

Discussion 407

PART V—IGNITION AND LIMITS OF INFLAMMABILITY

60 Some Factors Governing the Ignition Delay of a Gaseous Fuel. *R. E. Miller* 417

61 The Thermal Theory of Induction Periods and Ignition Delays. *P. Gray and M. J. Harper* 425

62 Ignition Delay of Propane in Air between 725–880°C under Isothermal Conditions. *C. J. Chang, A. L. Thompson and R. D. Winship* 431

63 Ignition Phenomena in Hydrogen–Air Mixtures. *H. E. Rose and T. Priede* 436

64 Ignition of Fuel–Air Mixtures by Hot Gases and its Relationship to Firedamp Explosions. *H. G. Wolfhard and M. Vanpée* 446

65 An Investigation of the Characteristics of Spark Discharges as Employed in Ignition Experiments. *H. E. Rose and T. Priede* 454

66 An Attempt at Measuring Homogeneous Ignition Temperatures. *J. A. Sage and F. J. Weinberg* 464

67 On some Consequences of the Thermal Theory of Ignition in a Fast Flow. *L. N. Khitrin* 470

68 Limits of Inflammability. *G. Dixon-Lewis and G. L. Isles* 475

69 Flame Temperatures of Limit Mixtures. *M. G. Zabetakis, S. Lambiris and G. S. Scott* 484

Discussion 488

PART VI—INTERACTION OF FLAMES AND SURFACES

70 The Quenching of Flame by Wire Gauzes. *K. N. Palmer* 497

71 Suppression of Explosion Waves in Gaseous Mixtures by Means of Fine Powders. *P. Laffitte and R. Bouchet* 504

72 Evaporation and Combustion of a Drop Contacting with a Hot Surface. *Z. Tamura and Y. Tanasawa* 509

73 New Aspects of Droplet Combustion. *H. Isoda and S. Kumagai* 523

74 Homogeneous–Heterogeneous Combustion of Carbon Monoxide in Narrow Tubes (Channels). *L. N. Khitrin and L. S. Solovyeva* 532

75 Combustion of a Gas Injected into a Hypersonic Boundary Layer. *G. W. Sutton* 539

76 Formation of Dispersed Carbon by Thermal Decomposition of Hydrocarbons. *P. A. Tesner* 546

77 Formation and Gasification of Carbon in an Atmosphere of Combustion Products. *E. F. M. van der Held* 554

78 Carbon Formation in Very Rich Hydrocarbon–Air Flames—I. Studies of Chemical Content, Temperature, Ionization and Particulate Matter. *J. M. Singer and J. Grumer* 559

Discussion 570

PART VII—TURBULENCE IN FLAMES

79 Flame Turbulence. *A. G. Prudnikov* 575

80 Calculation of Flame Velocity in Turbulent Stream. *E. S. Shetinkov* 583

81 Influence of Pressure on Rate of Flame Propagation in Turbulent Flow. *S. A. Goldenberg and V. S. Pelevin* 590

82 Theory of Rate of Spread of Confined Turbulent Pre-mixed Flames. *D. B. Spalding* 595

83 The Growth and Burn-out of Flame Surface in a Turbulent Stream. *B. Karlovitz* 604

84 Investigation of Pressure Effect on the Parameters of Turbulence and on Turbulent Burning. *V. A. Khramtsov* 609

85 Turbulent Flame Propagation by Large-scale Wrinkling of a Laminar Flame Front. *J. K. Richmond, J. Grumer and D. S. Burgess* 615

86 Turbulent Flame Blow-off Stability Effect of Auxiliary Gas Addition into Separation Zone. *F. Fetting, A. P. R. Choudhury, and R. H. Wilhelm* 621

Discussion 633

PART VIII—COMBUSTION IN PRACTICAL FLOWING SYSTEMS

87 Use of Aerodynamic Models in the Study of Industrial Furnaces, Particularly Open Hearth Furnaces. *A. Hogg, C. Holden and R. G. Siddall* 639

88 Simulation of Combustion Chamber Performance: Examination of the Predictions of an Analogue of a High Intensity Combustion Chamber. *D. G. Martin and J. D. Webb* 651

89 Simulation of Low Combustion Pressures by Water Injection. *A. H. Lefebvre and G. A. Halls* 654

90 A Non-acoustic Theory of Oscillations in Pressure-jet Oil-fired Combustion Chambers. *M. W. Thring* 659

91 Combustion Stability in a Spherical Combustor. *A. E. Clarke, A. J. Harrison and J. Odgers* 664

92 Stabilization of Flame in High Speed Flow by Pilot Flames. *W. P. Jensen and C. W. Shipman* 674

93 Theory of Flame Stabilization by a Bluff Body. *S. I. Cheng and A. A. Kovitz* 681

94 Studies of Exchange between Re-circulation Zone behind the Flame-holder and Outer Flow. *T. A. Bovina* 692

95 A Theoretical Analysis of Multi-stage Reaction Rate Controlled Systems. *J. W. Hardcastle* 697

96 Development of a Turbo-jet Altitude Windmill Re-light Correlation. *H. M. Brewster and A. Kush* 705

97 Determination of Rocket Motor Combustion Parameters by Means of a Diverging Reactor. *G. S. Gill, E. F. Eckel, F. A. Williams and S. S. Penner* 712

Discussion 725

PART IX—DETONATION AND ITS INITIATION

98 Detonability and Chemical Kinetics: Prediction of Limits of Detonability of Hydrogen. *F. E. Belles* 745

99 Limit and Spin Effects in Hydrogen–Oxygen Detonations. *W. E. Gordon, A. J. Mooradian and S. A. Harper* 752

100 Concerning Spin Detonation. *A. S. Predvoditelev* 760

101 Studies in Connection with Stabilized Gaseous Detonation Waves. *J. A. Nicholls, E. K. Dabora and R. L. Gealer* 766

102 On Automodelling Processes in Chemically Active Media. *A. S. Predvoditelev* 773

103 Theoretical Examination of Vibratory Movement of the Flame Front in Closed Vessels. *A. S. Predvoditelev* 779

104 Detonation Velocities in Liquid Fuel Vapours with Air or Oxygen at 100°C and Atmospheric Pressure. *R. P. Fraser* 783

105 The Generalized Hugoniot Adiabatic Curve. *Ya. K. Troshin* 789

106 On the Pre-detonation Period of Flame Propagation. *V. A. Popov* 799

107 On the Transition from Deflagration to Detonation. *S. R. Brinkley, Jr. and B. Lewis* 807

108 Some Observations on the Problem of Transition between Deflagration and Detonation. *G. K. Adams and D. C. Pack* 812

109 Deflagration to Detonation Transition. *M. A. Cook, D. H. Pack and W. A. Gey* 820

110 On the Development of Gaseous Detonation—Analysis of Wave Phenomena. *A. K. Oppenheim and R. A. Stern* 837

111 Formation of Detonation Wave during Combustion of Gas in Combustion Tube. *G. D. Salamandra, T. V. Bazhenova and I. M. Naboko* 851

112 The Formation and Structure of Gaseous Detonation Waves. *F. J. Martin and D. R. White* 856

113 Gas Ignition Behind the Shock Wave. *T. V. Bazhenova and R. I. Soloukhin* 866

Discussion 876

PART X—SPECIAL FUELS

114 Some Combustion Problems of High-energy Fuels for Aircraft. *W. T. Olson and P. C. Setze* 883

115 Flame Front Structures of Lean Diborane–Air and Diborane Hydrocarbon–Air Mixtures. *P. Breisacher, D. Dembrow and W. G. Berl* 894

116 A Study of Alkylsilane Flames. *M. Gerstein* 903

117 Spontaneous Ignition Properties of Metal Alkyls. *J. Marsel and L. Kramer* 906

118 The Combustion of Titanium and Zirconium. *P. L. Harrison* 913

Discussion 919

PART XI—INSTRUMENTATION IN COMBUSTION RESEARCH

119 The Continuous Flow Instrumental Analysis of Flame Gases. *F. H. Holderness and J. J. Macfarlane* 923

120 The Application of Gas Analysis to Combustion Chamber Development. *B. Toone and F. Arkless* 929

121 Application of Phase-discrimination Method of Detection to the Study of the Spectrum of the OH Radical in an Oxy-Acetylene Flame. *F. P. Dickey and J. M. Hoffman* 938

122 Measurements of Fluctuating Flame Temperature. *Masanaga Kunugi and Hiroshi Jinno* 942

123 Shock Tube Studies of Acetylene Decomposition. *W. J. Hooker* 949

124 Combustion of *n*-Heptane Spray in the Decomposition Products of Concentrated Hydrogen Peroxide. *J. D. Lewis and A. C. Merrington* 953

Discussion 958

LIST OF AUTHORS

Adams, G. K., Explosives Research and Development Establishment, Waltham Abbey, Essex, England 812
Anagnostou, E., Lewis Research Center, National Aeronautics and Space Administration, Cleveland, Ohio, U.S.A. 347
Arkless, F., Sinfin Combustion Laboratory, Rolls-Royce Ltd., Derby, England 929
Ashmore, P. G., Department of Physical Chemistry, University of Cambridge, England . 45
Avery, W. H., Applied Physics Laboratory, The Johns Hopkins University, Silver Spring, Maryland, U.S.A. 304
Baldwin, R. R., Department of Chemistry, The University, Hull, England 8
Basu, S., Department of Mechanical Engineering, Massachusetts Institute of Technology, Cambridge 39, Massachusetts, U.S.A. 277
Bazhenova, T. V., Institute of Energetics of the U.S.S.R. Academy of Sciences, Lenin Prospect 19, Moscow, U.S.S.R. 851, 866
Belles, F. E., Gas Dynamics Section, Lewis Research Center, National Aeronautics and Space Administration, Cleveland, Ohio, U.S.A. 745
Berendsen, R., University of Louvain, 98 rue de Namur, Louvain, Belgium 256
Berl, W. G., Applied Physics Laboratory, The Johns Hopkins University, Silver Spring, Maryland, U.S.A. 894
Bouchet, R., Laboratoire de Chimie Générale, Faculté des Sciences, Université de Paris, Paris, France 504
Bovina, T. A., Academy of Sciences, Moscow, U.S.S.R. 692
Breisacher, P., Applied Physics Laboratory, The Johns Hopkins University, Silver Spring, Maryland, U.S.A. 894
Brewster, H. M., Products Research Division, Esso Research and Engineering Company, Linden, New Jersey, U.S.A. 705
Brinkley, S. R., Jr., Combustion and Explosives Research, Inc., Oliver Building, Pittsburgh 22, Pennsylvania, U.S.A. 807
Broida, H. P., National Bureau of Standards, Washington 25, D.C., U.S.A. 207
Bryce, W. A., Chemistry Department, University of British Columbia, Vancouver 8, British Columbia, Canada 150
Bunt, E. A., Applied Physics Laboratory, The Johns Hopkins University, Silver Spring, Maryland, U.S.A. 325
Burgess, D. S., Branch of Physical Sciences, Division of Explosives Technology, Bureau of Mines, Pittsburgh 13, Pennsylvania, U.S.A. 615
Burt, R., Shell Research Laboratory, Thornton, Cheshire, England 108
Campbell, E. S., Department of Chemistry, New York University, New York 53, New York, U.S.A. 332
Carhart, H. W., Naval Research Laboratory, Washington 25, D.C., U.S.A. 392
Chang, C. J., Department of Mechanical Engineering, McGill University, Montreal 2, Canada 431
Cheaney, D. E., National Coal Board, Coal Research Establishment, Stoke Orchard, Cheltenham, England 183
Cheng, S. I., Aeronautical Engineering Department, Princeton University, Princeton, New Jersey, U.S.A. 681
Chermin, H. A. G., Staatsmijnen in Limburg, Central Laboratory, Geleen, Netherlands . 358
Child, E. T., The Texas Company, Beacon, New York, U.S.A. 215
Choudhury, A. P. R., 4/33 Fern Road, Ballygunge, Calcutta 19, India 621
Clarke, A. E., Joseph Lucas (Gas Turbine Equipment) Ltd., Hargher Clough, Burnley, Lancashire, England 664
Cook, M. A., Explosives Research Group, University of Utah, Salt Lake City, Utah, U.S.A. 820
Cullis, C. F., Chemistry Department, Imperial College, London, England 108, 171
Dabora, E. K., University of Michigan Research Institute, Ann Arbor, Michigan, U.S.A. . 766
Darwent, B. deB., Department of Chemistry, Catholic University of America, Washington 17, D.C., U.S.A. 3

DAVIDSON, N., Gates and Crellin Laboratories of Chemistry, California Institute of Technology, Pasadena, California, U.S.A. 80
DAVIES, D. A., Chemistry Department, Queen's College, University of St. Andrews, Dundee, Scotland 183
DAVIS, A., Chemistry Department, Queen's College, University of St. Andrews, Dundee, Scotland 183
DECKER, L. J., Physical Chemistry Section, Ballistic Research Laboratories, Aberdeen Proving Ground, Maryland, U.S.A. 57
DECKERS, J., School of Chemical Engineering, Princeton University, Princeton, New Jersey, U.S.A. 254
DEMBROW, D., Applied Physics Laboratory, The Johns Hopkins University, Silver Spring, Maryland, U.S.A. 894
DICKEY, F. P., Department of Physics and Astronomy, The Ohio State University, Columbus 10, Ohio, U.S.A. 938
DIXON-LEWIS, G., Houldsworth School of Applied Science, The University, Leeds 2, Yorkshire, England 475
DUTKA, F., Isotope Laboratory, Agreochemical Research Institute, Herman Otto u. 15, Budapest II, Hungary 128
ECKEL, E. F., Research, Rocketdyne, A Division of North American Aviation Inc., Canoga Park, California, U.S.A. 712
EDSE, R., Rocket Laboratory and the Department of Aeronautical Engineering, The Ohio State University, Columbus 10, Ohio, U.S.A. 377
ENIKOLOPYAN, N. S., Institute of Chemical Physics, Moscow V-133, Vorobyevskoye Chaussée 2, U.S.S.R. 157
FABIAN, D. J., Cerro de Pasco Corporation, La Oroya, Peru 150
FAY, J. A., Department of Mechanical Engineering, Massachusetts Institute of Technology, Cambridge 39, Massachusetts, U.S.A. 277
FERGUSON, R. E., Heat Division, National Bureau of Standards, Washington 25, D.C., U.S.A. 113
FETTING, F., Institute for Technical Chemistry, Technical High School, Hannover, Germany 621
FRASER, R. P., High Speed Fluid Kinetics Laboratory, Imperial College, London, England 783
FRIEDMAN, R., Kinetics and Combustion Division, Atlantic Research Corporation, Alexandria, Virginia, U.S.A. 311
FRISTROM, R. M., Applied Physics Laboratory, The Johns Hopkins University, Silver Spring, Maryland, U.S.A. 304
GÁL, D., Isotope Laboratory, Agreochemical Research Institute, Herman Otto u. 15, Budapest II, Hungary 128
GEALER, R. L., Ethyl Corporation, 1600 W. 8 Mile Road, Ferndale 20, Detroit, Michigan, U.S.A. 766
GERSTEIN, M., Propulsion Chemistry Division, Lewis Research Center, National Aeronautics and Space Administration, Cleveland, Ohio, U.S.A. 903
GEY, W. A., Naval Ordnance Test Station, China Lake, California, U.S.A. 820
GILL, G. S., Research, Rocketdyne, A Division of North American Aviation Inc., Canoga Park, California, U.S.A. 712
GLICK, H. S., Cornell Aeronautical Laboratory, Inc., Cornell University, Buffalo, New York, U.S.A. 98
GOLDENBERG, S. A., Institute of Energetics, Academy of Sciences, Lenin Prospect 19, Moscow, U.S.S.R. 590
GORDON, A. S., Office of Naval Research, U.S. Embassy, London, England 317
GORDON, W. E., Arthur D. Little, Inc., Cambridge, Massachusetts, U.S.A. 752
GRAY, P., School of Chemistry, Leeds University, Leeds 2, England 61, 425
GRUMER, J., Flame Research Section, Division of Explosives Technology, Bureau of Mines, Pittsburgh 13, Pennsylvania, U.S.A. 559, 615
GRUNFELDER, C., Applied Physics Laboratory, The Johns Hopkins University, Silver Spring, Maryland, U.S.A. 304
GUCZI, L., Isotope Laboratory, Agreochemical Research Institute, Herman Otto u. 15, Budapest II, Hungary 128
HALL, A. R., Ministry of Supply, Rocket Propulsion Establishment, Westcott, Aylesbury, Buckinghamshire, England 399

HALLS, G. A., Combustion Department, Rolls-Royce Ltd., Derby, England . . . 654
HARDCASTLE, J. W., Combustion Department, Armstrong Siddeley Motors Ltd., Coventry, England 697
HARPER, M. J., School of Chemistry, Leeds University, Leeds 2, England 425
HARPER, S. A., Radio Corporation of America, Lancaster, Pennsylvania, U.S.A. . . 752
HARRISON, A. J., Joseph Lucas (Gas Turbine Equipment) Ltd., Hargher Clough, Burnley, Lancashire, England 664
HARRISON, P. L., Laboratory for the Physics and Chemistry of Solids, Department of Physics, Cambridge University, Cambridge, England 913
HERZFELD, K. F., Physics Department, Catholic University of America, Washington, D.C., U.S.A. 27
HIRSCHFELDER, J. O., Chemistry Division, University of Wisconsin, Madison, Wisconsin, U.S.A. 332
HOARE, D. E., Chemistry Department, Queen's College, University of St. Andrews, Dundee, Scotland 183
HOFFMAN, J. M., Department of Physics and Astronomy, The Ohio State University, Columbus 10, Ohio, U.S.A. 938
HOGG, A., United Steel Companies Ltd., Research and Development Department, Swinden Laboratories, Moorgate, Rotherham, Yorkshire, England 639
HOLDEN, C., United Steel Companies Ltd., Research and Development Department, Swinden Laboratories, Moorgate, Rotherham, Yorkshire, England 639
HOLDERNESS, F. H., Ministry of Supply, National Gas Turbine Establishment, Pyestock, Farnborough, Hampshire, England 923
HOOKER, W. J., Chemistry Research Department, General Electric Research Laboratory, Schenectady, New York, U.S.A. 949
IKEGAMI, H., Institute of Physics, College of General Education, Komaba, Meguroku, Tokyo, Japan 263
ISLES, G. L., Houldsworth School of Applied Science, The University, Leeds 2, Yorkshire, England 475
ISODA, H., College of General Education, University of Tokyo, Meguroku, Tokyo, Japan . 523
JENSEN, W. P., Department of Chemical Engineering, Massachusetts Institute of Technology, Cambridge 39, Massachusetts, U.S.A. 674
JINNO, HIROSHI, Department of Industrial Chemistry, Kyoto University, Kyoto, Japan . 942
JOHNSON, J. E., Naval Research Laboratory, Washington 25, D.C., U.S.A. . . . 392
KARLOVITZ, B., Combustion and Explosives Research, Inc., Oliver Building, Pittsburgh 22, Pennsylvania, U.S.A. 604
KAUFMAN, F., Physical Chemistry Section, Ballistic Research Laboratories, Aberdeen Proving Ground, Maryland, U.S.A. 53, 57
KELSO, J. R., Physical Chemistry Section, Ballistic Research Laboratories, Aberdeen Proving Ground, Maryland, U.S.A. 53
KENDE, I., Isotope Laboratory, Agreochemical Research Institute, Herman Otto u. 15, Budapest II, Hungary 128
KHITRIN, L. N., Academy of Sciences, Lenin Prospect 19, Moscow, U.S.S.R. . . . 470, 532
KHOKHAR, B. A., Chemistry Department, Imperial College, London, England . . . 171
KHRAMTSOV, V. A., Moscow Physico-Technical Institute, Dolgoprudnaja, Moscow Region, U.S.S.R. 609
KIESS, N. H., National Bureau of Standards, Washington 25, D.C., U.S.A. 207
KINBARA, T., Institute of Physics, College of General Education, Komaba, Meguroku, Tokyo, Japan 263
KNEWSTUBB, P. F., Division of Applied Chemistry, National Research Council, Ottawa, Canada 247
KNOX, J. H., Department of Chemistry, Edinburgh University, Scotland 122, 126
KONDRATIEV, V. N., Academy of Sciences, Moscow, U.S.S.R. 41
KOVITZ, A. A., Mechanical Engineering Department, Northwestern University, Evanston, Illinois, U.S.A. 681
KOZLOV, G. I., Institute of Energetics, Academy of Sciences, Lenin Prospect 19, Moscow, U.S.S.R. 142
KRAMER, L., New York University, New York, U.S.A. 906
KRASNANSKY, V. J., National Bureau of Standards, Washington 25, D.C., U.S.A. . . 3

KUMAGAI, S., Department of Aeronautics, Faculty of Engineering, University of Tokyo, Bunkyo-ku, Tokyo, Japan 523
KUNUGI, MASANAGA, Department of Industrial Chemistry, Kyoto University, Kyoto, Japan . 942
KUSH, A., U.S. Naval Air Turbine Test Station, Trenton, New Jersey, U.S.A. 705
KUSHIDA, R., Marquardt Aircraft Company, Van Nuys, California, U.S.A. 221
LAFFITTE, P., Laboratoire de Chimie Générale, Faculté des Sciences, Université de Paris, Paris, France 504
LAMBIRIS, S., Branch of Gas Explosions, Division of Explosives Technology, U.S. Bureau of Mines, Pittsburgh 13, Pennsylvania, U.S.A. 484
LARSEN, R., Department of Chemical Engineering, Imperial College, London, England . 108
LEE, J. C., Department of Chemical Engineering, University College of Swansea, Singleton Park, Swansea, Glamorgan, Wales 61
LEFEBVRE, A. H., Combustion Department, Rolls-Royce Ltd., Derby, England . . . 654
LEVITT, B. P., Frick Chemical Laboratory, Princeton University, Princeton, New Jersey, U.S.A. 45
LEVY, A., Department of Chemical Engineering, Imperial College, London, England . . 296
LEWIS, B., Combustion and Explosives Research, Inc., Oliver Building, Pittsburgh 22, Pennsylvania, U.S.A. 342, 807
LEWIS, J. D., Ministry of Supply, Rocket Propulsion Establishment, Westcott, Aylesbury, Buckinghamshire, England 953
LINNETT, J. W., The Inorganic Chemistry Laboratory, Oxford, England 23
MACFARLANE, J. J., Ministry of Supply, National Gas Turbine Establishment, Pyestock, Farnborough, Hampshire, England 923
MCKNIGHT, W. E., Union Carbon and Carbide Corporation, Charleston, West Virginia, U.S.A. 369
MCNESBY, J. R., Department of Chemistry, Leeds University, Yorkshire, England . . 317
MARKSTEIN, G. H., Aerodynamic Research Department, Cornell Aeronautical Laboratory Inc., Buffalo 21, New York, U.S.A. 289
MARSEL, C. J., New York University, New York, U.S.A. 906
MARTIN, D. G. Department of Mechanical Engineering, Imperial College, London, England 651
MARTIN, F. J., General Electric Research Laboratory, Schenectady, New York, U.S.A. . 856
MAYOR, L., Bristol Aero-engines, Clifton, Bristol, England 8
MERRINGTON, A. C., Ministry of Supply, Rocket Propulsion Establishment, Westcott, Aylesbury, Buckinghamshire, England 953
MILLER, J., Ames Research Center, N.A.S.A., Sunnyvale, California, U.S.A. 175
MILLER, R. E., Department of Physical Chemistry, King's College, Newcastle upon Tyne, England 417
MINKOFF, G. J., Department of Chemical Engineering, Imperial College, London, England . 108
MOORADIAN, A. J., Atomic Energy of Canada Ltd., Chalk River, Ontario, Canada . . 752
MYERSON, A. L., Missile and Space Vehicle Department, General Electric Company, Philadelphia 24, Pennsylvania, U.S.A. 72
NABOKO, I. M., Institute of Energetics of the U.S.S.R. Academy of Sciences, Lenin Prospect 19, Moscow, U.S.S.R. 851
NAKAMURA, J., Institute of Physics, College of General Education, Komaba, Meguroku, Tokyo, Japan 263
NICHOLLS, J. A., Aeronautical Engineering Department, University of Michigan, Ann Arbor, Michigan, U.S.A. 766
NUGENT, R. G., Kinetics and Combustion Division, Atlantic Research Corporation, Alexandria, Virginia, U.S.A. 311
ODGERS, J., Joseph Lucas (Gas Turbine Equipment) Ltd., Hargher Clough, Burnley, Lancashire, England 664
OLSON, W. T., National Aeronautics and Space Administration, Lewis Research Center, Cleveland 35, Ohio, U.S.A. 883
OPPENHEIM, A. K., Division of Mechanical Engineering, University of California, Berkeley, California, U.S.A. 837
PACK, D. C., Department of Mathematics, Royal College of Science and Technology, Glasgow, Scotland 812
PACK, D. H., Explosives Research Group, University of Utah, Salt Lake City, Utah, U.S.A. 820

PADLEY, P. J., Department of Physical Chemistry, University Chemical Laboratory, Cambridge, England 235
PALMER, K. N., Department of Scientific and Industrial Research and Fire Offices' Committee Joint Fire Research Organization, Boreham Wood, Hertfordshire, England . . 497
PELEVIN, V. S., Institute of Energetics, Academy of Sciences, Lenin Prospect 19, Moscow, U.S.S.R. 590
PENNER, S. S., Division of Engineering, California Institute of Technology, Pasadena, California, U.S.A. 712
PONCELET, J., 51 rue Willem Kuhnen, Brussels, Belgium 256
POPOV, V. A., Institute of Energetics, Academy of Sciences, Lenin Prospect 19, Moscow, U.S.S.R. 799
POTTER, A. E., Jr., Reaction Kinetics Section, Lewis Research Center, National Aeronautics and Space Administration, Cleveland, Ohio, U.S.A. 347
PREDVODITELEV, A. S., Academy of Sciences, Lenin Prospect 19, Moscow, U.S.S.R. 352, 760, 773, 779
PRIEDE, T., Research Department, C.A.V. Ltd., Acton, London, England 436, 454
PROTHEROE, J., Chemistry Department, Queen's College, University of St. Andrews, Dundee, Scotland 183
PRUDNIKOV, A. G., Moscow Physico-Technical Institute, Dolgoprudnaja, Moscow Region, U.S.S.R. 575
RICHMOND, J. K., Division of Explosives Technology, Bureau of Mines, Pittsburgh 13, Pennsylvania, U.S.A. 615
ROSE, H. E., Mechanical Engineering Department, King's College, University of London, England 436, 454
ROSEN, G., Departments of Physics and Aeronautical Engineering, Princeton University, Princeton, New Jersey, U.S.A. 339
ROSSER, W. A., Jr., Chemistry Department, Stanford Research Institute, Menlo Park, California, U.S.A. 175
SAGE, J. A., Department of Chemical Engineering, Imperial College, London, England . 464
SALAMANDRA, G. D., Institute of Energetics of the U.S.S.R. Academy of Sciences, Lenin Prospect 19, Moscow, U.S.S.R. 851
SCHALIT, L. M., Department of Chemistry, New York University, New York 53, U.S.A. . 332
SCHELLER, K., Aeronautical Research Laboratory, Wright Air Development Center, Wright-Patterson Air Force Base, Ohio, U.S.A. 369
SCOTT, G. S., Branch of Gas Explosions, Division of Explosives Technology, U.S. Bureau of Mines, Pittsburgh 13, Pennsylvania, U.S.A. 484
SETZE, P. C., National Aeronautics and Space Administration, Lewis Research Center, Cleveland 35, Ohio, U.S.A. 883
SHETINKOV, E. S., Moscow Physico-Technical Institute, Dolgoprudnaja, Moscow Region, U.S.S.R. 583
SHIPMAN, C. W., Worcester Polytechnic Institute, Worcester, Massachusetts, U.S.A. . . 674
SHULER, K. E., National Bureau of Standards, Washington 25, D.C., U.S.A. 87
SIDDALL, R. G., Sheffield University, England 639
SINGER, J. M., Flame Research Section, Division of Explosives Technology, Bureau of Mines, Pittsburgh, Pennsylvania, U.S.A. 559
SKIRROW, G., Donnan Laboratories, Department of Inorganic and Physical Chemistry, Liverpool University, England 134
SMITH, F. T., Chemical Physics Department, Stanford Research Institute, Menlo Park, California, U.S.A. 93
SMITH, R. F., Department of Chemistry, Edinburgh University, Scotland 126
SMITH, S. R., Michelson Laboratory, U.S. N.O.T.S., China Lake, California, U.S.A. . . 317
SOBOLEV, G. K., Institute of Energetics, Academy of Sciences, Lenin Prospect 19, Moscow, U.S.S.R. 386
SOLOUKHIN, R. I., Institute of Energetics of the U.S.S.R. Academy of Sciences, Lenin Prospect 19, Moscow, U.S.S.R. 866
SOLOVYEVA, L. S., Institute of Energetics, Academy of Sciences, Lenin Prospect 19, Moscow, U.S.S.R. 532
SPALDING, D. B., Department of Mechanical Engineering, Imperial College, London, England 595
SPOKES, G. N., Department of Chemical Engineering, Imperial College, London, England . 229

STERN, R. A., Division of Mechanical Engineering, University of California, Berkeley, California, U.S.A. 837
STRAUSS, W. A., Rocket Laboratory and the Department of Aeronautical Engineering, The Ohio State University, Columbus 10, Ohio, U.S.A. 377
SUGDEN, T. M., Department of Physical Chemistry, University Chemical Laboratory, Cambridge, England 235, 247
SUNDUKOV, I. N., Institute of Energetics of the U.S.S.R. Academy of Sciences, Lenin Prospect 19, Moscow, U.S.S.R. 352
SUTTON, G. W., Aerosciences Laboratory, Missile and Space Vehicle Department, General Electric Company, Philadelphia, Pennsylvania, U.S.A. 539
SZABÓ, Z. G., Institute for Inorganic and Analytical Chemistry, University of Szeged, Szeged, Hungary 118
TAMURA, Z., Hitachi Research Laboratory, Hitachi, Ibaragi-Prefecture, Japan . . . 509
TANASAWA, Y., Department of Precision Engineering, Tohoku University, Sendai, Japan . 509
TAYLOR, F. R., Laboratories for Research and Development, The Franklin Institute, Philadelphia 3, Pennsylvania, U.S.A. 72
TAYLOR, R., Gates and Crellin Laboratories of Chemistry, California Institute of Technology, Pasadena, California, U.S.A. 80
TESNER, P. A., All Union Institute of Natural Gas, Moscow A-15, Poltavskaya 2/25, U.S.S.R. 546
THOMPSON, A. L., Gas Dynamics Laboratory, McGill University, Montreal 2, Canada . 431
THRING, M. W., Department of Fuel Technology and Chemical Engineering, Sheffield University, England 659
TIPPER, C. F. H., Donnan Laboratories, Department of Inorganic and Physical Chemistry, Liverpool University, England 134
TOONE, B., Sinfin Combustion Laboratory, Rolls-Royce Ltd., Derby, England . . . 929
TOOTAL, C. P., The Inorganic Chemistry Laboratory, Oxford, England 23
TROSHIN, YA. K., Institute of Chemical Physics, Academy of Sciences, Moscow, U.S.S.R. . 789
TROTMAN-DICKENSON, A. F., Department of Chemistry, Edinburgh University, Scotland . 126
VAN DER HELD, E. F. M., Central Technical Institute, Organization for Applied Scientific Research (T.N.O.), Netherlands 554
VAN KREVELEN, D. W., Staatsmijnen in Limburg, Central Laboratory, Geleen, Netherlands 358
VANPÉE, M., Division of Explosives Technology, Bureau of Mines, Pittsburgh, Pennsylvania, U.S.A. 446
VAN TIGGELEN, A., University of Louvain, 98 rue de Namur, Louvain, Belgium . . . 254, 256
VOEVODSKY, V. V., Institute for Chemical Physics, Moscow, U.S.S.R. 34
VON ELBE, G., Combustion and Explosives Research, Inc., Oliver Building, Pittsburgh 22, Pennsylvania, U.S.A. 342
WADDINGTON, D. J., Wellington College, Berkshire, England 165
WALSH, A. D., Chemistry Department, Queen's College, University of St. Andrews, Dundee, Scotland 183
WATSON, J. S., Division of Applied Chemistry, National Research Council, Ottawa, Ontario, Canada 17
WEBB, J. D., Department of Mechanical Engineering, Imperial College, London, England . 651
WEINBERG, F. J., Department of Chemical Engineering, Imperial College, London, England 296, 464
WHITE, D. R., General Electric Research Laboratory, Schenectady, New York, U.S.A. . 856
WILHELM, R. H., Department of Chemical Engineering, Princeton University, Princeton, New Jersey, U.S.A. 621
WILLIAMS, F. A., Harvard University, Cambridge 38, Massachusetts, U.S.A. . . . 712
WILLIAMS, H., Ministry of Supply, Rocket Propulsion Establishment, Westcott, Buckinghamshire, England 269
WILLIAMS, K. G., Naval Research Laboratory, Washington 25, D.C., U.S.A. . . . 392
WINDSOR, M. W., Physical Research Laboratory, Space Technology Laboratories, The Ramo-Wooldridge Corporation, Los Angeles 45, California, U.S.A. 80
WINSHIP, R. D., Department of Mechanical Engineering, McGill University, Montreal 2, Canada 431
WISE, H., Chemical Dynamics Section, Department of Chemical Physics, Stanford Research Institute, Menlo Park, California, U.S.A. 175
WOHL, K., Department of Chemical Engineering, University of Delaware, Newark, Delaware, U.S.A. 215, 221

Wolfhard, H. G., Division of Explosives Technology, Bureau of Mines, Pittsburgh, Pennsylvania, U.S.A. 446
Yokley, C. R., Heat Division, National Bureau of Standards, Washington 25, D.C., U.S.A. 113
Zabetakis, M. G., Branch of Gas Explosions, Division of Explosives Technology, U.S. Bureau of Mines, Pittsburgh 13, Pennsylvania, U.S.A. 484
Zeelenberg, A. P., Department of Physical Chemistry, Cambridge University, Cambridge, England 68

ADDRESS BY PROFESSOR SIR CYRIL HINSHELWOOD

[President of the Royal Society]

Flame and combustion have excited wonder from the earliest times, as is witnessed by the mythological stories of the bringing down of fire from heaven. In ordinary life fire is still one of the great marvels of the world, and the attribution to it of magical origins and properties is not surprising. The wonder has not been diminished by scientific investigation, though no doubt its character has changed. Nor has all the mystery been dispelled. Much is now understood about the processes of combustion and about the nature of flame, but the detailed analysis of these phenomena still offers great difficulties, and unsolved problems abound.

The subject is one of many facets. The propagation of flame presents first and foremost a problem in classical physics. Into an element of volume heat is conducted, or chemically active particles diffuse from a zone where rapid chemical change is already in progress. As a result of the temperature rise, or the presence of the active particles, fresh chemical action is stimulated. The temperature of the element rises or fresh active centres are produced in chain reactions. From the element heat is again conducted forward, or particles penetrate into another neighbouring one. A classical differential equation defines the balance of these various processes. The equation predicts the establishment, after a period of development, of a steady state in which flame is propagated forward with a definite velocity. If the gas itself is given a suitable streaming motion in the opposite direction the zone can be kept in one place and a stationary flame results. In its essence the problem is clear-cut, and in a very general form the equations are easily set up. At this point the difficulties begin.

In the first place, reaction velocity varies with temperature according to the Arrhenius equation and this gives the differential equation a form which makes it very hard to handle by ordinary methods. Secondly, the relation between rate of reaction and the concentrations of the components is usually quite complicated in real systems, even at a constant temperature. Both difficulties are increased by the fact that the actual mechanism of combustion may change between the temperature at which reaction first becomes appreciable and the maximum temperature reached in the flame. Added to all this is the fact that diffusion of energy and diffusion of material particles in general both play their parts in the phenomena actually observed and measured.

The tactics of investigation therefore must be to deal with one aspect at a time. When sufficient partial advances have been made it can only be hoped that modern computational methods may be called in to combine the results and give complete solutions applicable to individual systems.

The general mode of attack on the problem then comprises among others the following: study of simplified models for which the differential equation can be integrated (these usually involve an adjustable parameter): spectroscopic investigation of the entities occurring in flames under different conditions: detailed investigation of the kinetics of the combustion reaction itself as it takes place under isothermal conditions. Each of these aspects reveals much of interest.

Among the simplifying assumptions that have been made for the purpose of integrating the equations of flame propagation one set consists in idealizing the temperature dependence by using a suitable empirical modification of the Arrhenius law. In another (used by Zeldovich) it is assumed that the range between the ignition temperature, T_i, and the maximum, T_m, is so small compared with that between the initial temperature, T_o, and the ignition point that the heat used in further warming the gas in the actual reaction zone can be neglected. None of these procedures is quite satisfactory. Franze, Jost and Lesemann, on the other hand, treat the system involved in an ideal cold flame where the chemical change is propagated entirely by the diffusion of active particles. The idealization is less drastic than might appear at first sight because a steady concentration of atoms or radicals greatly exceeding the value corresponding to thermodynamic equilibrium itself represents one of the major characters of a greatly increased temperature. It is true that the effective chemical temperature is not expressed by the translational velocities of the molecules. But in the well known theory of explosion limits in a branching chain reaction it is generally possible to treat the system as if it were isothermal except in respect of the concentrations of particular active particles.

These ideas lead to two interesting fields of experimental investigation, the first consisting in experimental attempts to assess the relative importance in flame propagation of particle diffusion

and heat diffusion, and the second in the spectroscopic study of the non-equilibrium distributions of rotational or vibrational energy in reaction products. Very valuable information may come from studies of this kind, but the general lack of equilibrium between the various degrees of freedom of the system adds a further complication to any general theoretical treatment.

In the discussion of problems such as that of burning velocity or the formation in a gas mixture of successive cool flames, a rather over-simplified model is usually employed for the chemistry of the underlying reactions. Detailed study of the kinetics of oxidation reactions occurring at constant temperature reveals a wealth of detail and complexity. The rate of reaction is very seldom representable by a simple expression and indeed there are very few systems in which the oxidation mechanism itself does not present unsolved problems.

Of the universal occurrence of chain processes there is no doubt. Branching chains are frequent and explain the remarkable phenomena of upper and lower explosion limits where sometimes there is a rather abrupt transition from very slow reaction to inflammation. The slow development of chains with 'degenerate' branching is the basis of Semenov's well known theory of the induction period. The breaking of chains at a surface explains the very remarkable effects of vessel size on combustion rate and the surprisingly great influence that a chemically inert gas may have in accelerating combustion by impeding diffusion to the wall.

The kinetics of gaseous oxidation reactions have several highly characteristic and rather unusual features. One is the relation of the rate to the concentrations of the reacting substances. The rate usually increases fairly steeply with the concentration of the combustible substance, a fact which is easily enough understandable, but over wide ranges the rate is often independent of the oxygen concentration or may even decrease quite considerably with excess of oxygen. In some examples this phenomenon can be reasonably explained by a chain-terminating action of the oxygen. It is quite easy to imagine oxidized intermediates which propagate chains by alternate reaction with the combustible substance and with oxygen itself, but which may be destroyed if excess of the latter oxidizes them too far, perhaps even to carbon monoxide or carbon dioxide. No quite general explanation seems to have emerged, and it may be that a number of different mechanisms is involved. There is a similar absence of dependence on oxygen concentration in the oxidation of hydrazobenzene in solution, a reaction in which there is no evidence of chain mechanisms at all, and where the explanation simply appears to be that the rate determining step does not involve oxygen but depends upon an ionization of the substrate. A similar explanation cannot apply to the oxidation of gaseous hydrocarbons, which often takes place several hundred degrees below the temperature of the thermal decomposition.

Nevertheless, there seems to be little doubt that the peculiarities of the oxygen molecule are responsible for a good deal. O_2 is a bi-radical, which can yield R—O—O— and then R—O—O—R′. The single bond in the peroxide is weak, and splitting into two radicals R—O— and R′—O— readily occurs. Peroxides undoubtedly occur in the course of hydrocarbon combustion, and in some theories play a central part in the mechanism. In some cases the rate of reaction is proportional to the peroxide concentration. A radical $RCH_2.O$— derived from a paraffin could shed HCHO leaving R—, and copious production of formaldehyde is indeed often observed. The fission of R—O—O—R′ would give a branching chain, and the reaction rate would then be extremely sensitive to the stability of the peroxide. Very small modifications in it would cause large variations of velocity, and in fact one of the most remarkable characteristics of paraffin oxidations is their extraordinary sensitiveness to small structural changes in the hydrocarbon, especially to substitution by methyl groups.

Another school of thought places aldehydes in the central position of the active intermediates of hydrocarbon oxidation. It is quite true that additions of aldehyde may eliminate induction periods: it is also true that aldehydes themselves yield peroxides with great readiness, and sometimes the formation of peroxide can be shown to be accelerated by aldehyde addition. Causes and effects are, however, sometimes hard to disentangle and there remain plenty of chemical problems for solution.

Perhaps the two most interesting chemical phenomena connected with combustion reactions are, on the one hand, the anomalous temperature coefficient, and, on the other, the propagation of cool flames, the two being probably not unconnected with one another.

There are two theories of the cool flame, not, for reasons already indicated, sharply distinguishable. One is the thermal theory. If there is a homogeneous exothermic reaction $A \rightarrow X \rightarrow B$, where the temperature coefficient of the second step is greater than that of the first, rapid reaction can lead to self-heating which causes the concentration of X to drop. If X has an autocatalytic function, the reaction is quenched until the concentration of this intermediate has once again been built up. In the alternative theory, or perhaps one should say alternative form of theory, a somewhat similar cycle is maintained by the formation and consumption

of various intermediates in formally isothermal processes (Frank-Kamenetskii). Once again, it may be observed, in some cases (e.g. methyl ethyl ketone) there is a catastrophic drop in peroxide concentration when a cool flame passes. In other cases (e.g. diethyl ether) there is not. The role of the peroxides is therefore not always the same, nor indeed are the peroxides always of one and the same type.

The anomalous temperature coefficient occurs quite frequently. As the temperature rises the rate first increases, then falls, and then finally rises again. The intermediate zone where the rate falls with rising temperature is an almost unique phenomenon. It is probably associated with an alternative reaction destroying an intermediate which at lower temperatures acts as an effective autocatalyst, presumably by a chain-branching mechanism.

The situation generally, then, is that throughout the whole subject much pioneering work has been done, defining problems, revealing important phenomena, and hinting at or sketching out possible solutions. This is almost equally true of the hydrodynamic and thermal theories, of the identification of reaction sequences and of the formulation of reaction kinetics. The systematization of this work and the formulation of more precise theories is a formidable task but one which modern techniques offer every hope of fulfilling.

ADDRESS BY DR. BERNARD LEWIS

Remarks on Combustion Science

The renaissance in combustion research that we have witnessed during the past two decades has gained phenomenal momentum in the last eight or ten years. This year is, in fact, the tenth anniversary of the post-war symposia that have been organized by the Combustion Institute and its predecessor, the Standing Committee on Combustion.

The history of the development of science shows that science is evolutionary in character punctuated by brilliant notions or concepts and experimental discoveries. Many of the latter have been accidental. The evolutionary character of science results from the need to consider and give recognition to previous accomplishments. This is particularly true in a highly developed and complex field of inquiry such as combustion, the description of whose phenomena is dependent upon numerous scientific disciplines—chemistry, chemical kinetics, spectroscopy, thermochemistry, thermodynamics and fluid mechanics. Now more than ever the research worker in combustion approaches a new research effort only after he has fully acquainted himself with published results. He is thus motivated by past effort and, although it need not be so, this procedure generally places a restriction on his creativity, as it serves to promote objectivity which is but a step removed from empiricism. Now, the empirical approach to research is one that is imposed by circumstances on many of the workers in this complex field. None will deny that empiricism flourishes in direct proportion to ignorance of the physics and chemistry of the phenomena. It can and has been justified over and over again by the high degree of development of useful gadgets that have given man such spectacular sources of power. Empiricism can be too well justified. It feeds upon itself like a circular argument until today there are many who are convinced that it is less important to understand the phenomena than to produce an object or a useful correlation. As we have been told that the end justifies the means, perhaps there is strength in this utilitarian view. The great power of empiricism is its ability to produce a useful result in a relatively short time. On the other hand, the urge to obtain a quick solution to a problem places a severe limitation on creative scientific accomplishment. A classic example of the success of this method is the Edisonian experimental effort that attended search for additives to control engine knock. It culminated in the discovery of lead tetraethyl, but the vast experimental effort that was expended in this search for successful additives was of the nature of testing and it did not significantly contribute to the scientific understanding of fuels and fuel additives. To be sure, it was followed by an earnest and steady effort in fundamental research. Unhappily, the complexity of the subject is such that even today, after 35 years, it cannot be said that the physical chemist can rest on his laurels.

The availability of relatively large sums of money since the war for combustion research programmes to supplement development of combustion equipment produced a considerable research effort along purely scientific lines. This effort has not been adequate, and the employment of such funds for accomplishing set tasks has been greater than is good for the logical and healthy development of combustion science. Nevertheless, it cannot be denied that these sums have been responsible for creating a deep interest in combustion on the part of a large number of workers, many of whom are dedicating their professional careers to the subject. This in itself is an important achievement.

The research output of this corps of scientists and engineers all over the world is truly remarkable. It was for the purpose of categorizing the various subjects and bringing them together under one publication medium that the first in this series of symposia was organized in 1948. It was immediately apparent that it filled a long-felt need of the combustion research worker to have before him the sum total of latest thinking in his field of interest. Indeed, it is the purpose of the Combustion Institute to keep this important stimulus alive.

As one reviews the nearly 700 papers that have appeared in the four symposium volumes, the fifth volume soon to be issued, and in the Institute's new *Journal of Combustion and Flame*, one is impressed with the large amount of new phenomenological information and with the relative lack of new concepts. Perhaps this is to be expected anyway. New concepts which expand the horizon of science are hard to come by. We are, therefore, obliged to consider again and again what are the most fruitful avenues to the development of new concepts in our special field of science. Perhaps it is possible to obtain some clues as to methodology if we

consider a few concrete examples of the application of theoretical thought to experimental information.

The examples I wish to mention refer to the study of combustion wave propagation under laminar and turbulent conditions. They include the conceptual understanding and the interrelation of data on flame stabilization and quenching, minimum ignition energy, turbulent flame propagation and non-isotropic flame propagation. In the aggregate, they provide a fair understanding of the combustion wave in its complex totality.

There was a time when the behaviour of a flame, perched on the tip of a bunsen burner, was without known rules, and the arrest of flame by Davy's grid was an isolated observation unrelated to other flame properties—this, in spite of the earnest endeavour of those concerned with flames of this kind in practice to obtain correlations usable in practical problems introduced by changing fuels and changing demands. Yet nothing could be simpler than to visualize flash-back as being due to an excess of burning velocity occurring within the retarded boundary layer of a laminar stream, and from this to arrive at the concept of critical boundary velocity gradient for flash-back, the depth of penetration of quenching from a surface into the gas stream, and the quenching distance between plates and the quenching diameter of tubes. Nor did the experimental effort in verifying the quantitative relations of these measurable quantities involve the use of elaborate equipment. Yet it brought complete clarity in the connection that exists between Davy's grid and the annoying habit of a flame to flash-back into a burner tube. The concept of critical boundary velocity gradient permitted, by means of Poiseuille's equation, correlation of the limiting flow for stable flame with diameter of the burner tube. Furthermore, according to the concept of the flash-back mechanism, the boundary velocity gradient for flash-back is the ratio of burning velocity and depth of penetration of quenching, i.e.

$$g_F = \frac{S_u}{d_p} \qquad (1)$$

It thus became possible to calculate the depth of penetration from data on the critical boundary velocity gradient and the burning velocity. These calculated values of depth of penetration agreed well with quenching distances measured directly, thus completely verifying the initial concept. We have recently examined again another annoying habit of such burner flames. When the tube diameter exceeds the critical, the flame, on reducing the flow, tilts over to one side and partly penetrates into the burner tube before the critical velocity gradient for flash-back is reached. Consideration of the nature of the phenomenon suggested rather strongly that it is governed by the ratio of the pressure gradient in the combustion wave to the pressure gradient in the burner tube, and that at the threshold flow for flame tilt this ratio should have the same value for all burners and all mixtures. This is analogous to the critical value of the Reynolds number for the transition from laminar to turbulent flow. The dimensionless quantity concerned is readily found to be

$$\frac{RS_u^3[(\rho_u/\rho_b) - 1]}{2(\mu/\rho_u)^2 g}$$

where R is the tube diameter, S_u the burning velocity, ρ_u and ρ_b the densities of unburned and burned gases respectively, μ is the viscosity of the unburned gas and g is the boundary velocity gradient. The conclusion that this quantity should be constant at the threshold of flame tilt has stood the test satisfactorily for a wide range of flammable mixtures and burner tubes. The basic idea of flame stabilization when applied to the phenomenon of blow-off furnishes a ready correlation with all observable facts, such as effect of the nature of the ambient atmosphere on stability limits, and it permits a smooth extension of the generalized blow-off curves from the laminar to the turbulent flow range. These accomplishments together with simple experimental studies of flame structure, which have confirmed the expected relations between flow and flame shape, make it appear that the flame-and-flow problem posed by the burner flame has been essentially mastered.

Although in such flame-flow problems one is mainly concerned with the gross behaviour of a wave in a flow field, one also becomes cognizant of processes occurring inside the wave because of the effect of heat sinks on combustion waves, which produce quenching to a greater or lesser depth depending upon the nature of the flammable mixture. If a combustion wave is quenched by extracting heat from the gas, does not the reverse process, addition of heat, result in the formation of a combustion wave? The question seems trivial, but not so very long ago an electric spark, as a means of igniting flammable gas, was thought of not so much as a source of heat but as a source of high energy particles of all sorts, supposedly required to activate the chemical reaction; and the igniting property of the spark was believed to depend primarily upon voltage and oscillation characteristics of the discharge. Our own investigations immediately suggested a different picture. We found remarkably consistent and suggestive curves on merely plotting discharge energy *versus* mixture composition, taking care to separate the electrodes beyond the quenching distances, a precaution that previous investigators had not taken. On this basis the model of the incipient flame presented itself as a spherical combustion

wave of a minimal diameter. Having in mind the temperature profile of such wave, it seemed reasonable as a first assumption to neglect the transport of energy across the wave by the interdiffusion of reactants and products as against the transport of heat by conduction from the burned to the unburned gas. This suggestion introduced the concept of excess enthalpy because, as is readily shown by combustion wave theory, if diffusional transport of chemical enthalpy from the unburned gas is assumed to be negligible, the gas within the wave possesses a total enthalpy in excess of the ambient which, per unit area, is approximately given by

$$h = \frac{\lambda}{S_u}(T_b - T_u) \tag{2}$$

where λ is the coefficient of heat conductivity and T_b and T_u are the temperatures of burned and unburned gas, respectively. Our assumed flame would thus be visualized, in first approximation, as a small sphere of burned gas surrounded by a shell of burning gas of surface πd^2, where d is the diameter of the flame. The total excess enthalpy of the flame would then be

$$H = \pi d^2 h \tag{3}$$

It would be the function of the ignition source to furnish this amount of energy H within an initially very small volume and in a time that would be short compared to some characteristic time, say the time during which the wave progresses a distance comparable to its own width. The electric spark would seem to meet these conditions and the diameter d would seem to be determined merely by that separation of the electrodes above which the observed energy required for ignition does not change, and below which the energy required increases, i.e. the quenching distance.

How realistic is this view of spark ignition, and in particular the concept of the minimal flame consisting of a core of burned gas surrounded by a shell of reacting gas? To test this latter question, we make use of a length characteristic of the wave width. This length is the subtangent of the temperature curve through the wave at the point of steepest slope. We give it the symbol η_o and it is related to measurable quantities by the equation

$$\eta_o = \frac{\lambda}{C_p \rho_u S_u} \tag{4}$$

where C_p is the heat capacity. It is found that η_o never exceeds a value of about 1/20 of the flame diameter d measured by the above method, so that the wave width is indeed only a fraction of the minimum flame diameter or radius.

There is a further criterion which should be applied to the concept of the minimal flame capable of sustained growth. A few years ago, Karlovitz studied the problem of rupture of a combustion wave in a flow field. The experimental observation in this instance was made on a burner flame that had an annular pilot flame at its base and thus was prevented from blowing off even at very high gas velocities. Nevertheless, it was found that the flame ruptured at a distance well removed from the pilot above a critical gas velocity, leaving a short hollow flame attached to the rim through which the flammable mixture passed unignited. The problem was approached by Karlovitz on the basis of a simple concept which we may call flame-stretch. In brief, in divergent propagation of a combustion wave where the area of the wave increases, the area increment over a distance of propagation comparable to the wave width cannot be very large. This distance is again taken as η_o. Also, in divergent propagation the burning velocity increases so that the mass flow normal to the wave surface increases. This increase of mass flow over the distance η_o is the measure of flame stretch, and in the flow field under consideration it is represented by the dimensionless number

$$K = \frac{\eta_o}{U}\frac{dU}{dy} \tag{5}$$

Here U is the gas velocity at some given point of measurement in the flame surface and dU/dy is the gas velocity gradient parallel to this surface at the same point. K is the fractional increase of area of the wave as it propagates over a distance η_o. If K exceeds a critical value, the flame surface ruptures. From data on the flow field and combustion wave properties of the mixture used, Karlovitz found K at rupture to be about 2. Intuitively, this may be regarded as a reasonable value, as the wave could hardly be expected to withstand a stretch substantially larger than this over a propagation distance comparable to its wave width. It is believed that the resistance to stretch of a flame is different for different mixtures, flames of strong mixtures having a larger critical K number for rupture than flames of weaker mixtures. However, the data are not yet available for this differentiation.

On applying the concept of flame stretch to the minimal flame where the propagation is also divergent and the flow field is determined by the thermal expansion of the flame core, the expression for K is found to be

$$K = \frac{4\eta_o \rho_u/\rho_b}{d} \tag{6}$$

Taking as before $\eta_o/d \simeq 1/20$, and ρ_u/ρ_b between 5 and 8, K turns out to be of the order of 1 to 2. This value of K thus defines the condition that permits further growth of flame. At smaller values of d, K is larger and the flame vanishes. It

is in satisfactory agreement with the value of K found for the rupture criterion in the pilot-anchored burner flame. Thus, a common criterion has been brought to bear on two very different and seemingly unrelated flame-flow problems. It is expected that the K number will have other applications and will be fruitful in the elucidation and conceptual understanding of limits of flammability. It seems proper to refer to this number as the Karlovitz number.

Having established the reasonableness of the concept of minimal flame volume and its consistency with other flame data, we proceed now to compare experimental values of minimum ignition energies with values computed by means of the foregoing equations from data on burning velocities and minimal flame diameters. This comparison, carried out on mixtures of oxygen with hydrogen or various hydrocarbons with and without inert gas, leads to remarkably good agreement when the mixtures are low in diluent content of either inert gas or excess of either reactant. On the other hand, as the diluent content increases, the computed values are always found to increase above the experimental values, and if the mixture consists of air with a heavy hydrocarbon like propane and the fuel percentage is increased much beyond stoichiometric, the computed values exceed the experimental values by an order of magnitude. It is a well known fact that in mixtures typified by the latter, combustion waves propagate non-isotropically, i.e. they break up spontaneously into a cellular structure representing alternate areas of faster and slower propagation. It has been well established that this effect is due to stratification of the mixture by diffusion so that alternate regions of higher and lower oxygen concentration are formed. To make this process possible it is necessary that in the interdiffusion of the reactants and reaction products, the oxygen acquire a substantial concentration gradient in the unburned gas well ahead of the zone of chemical reaction. There exists a characteristic length D_{o_2}/S_u which characterizes the extent of the oxygen gradient, analogous to the characterization of the thermal gradient introduced earlier by the relation $\eta_o = (\lambda/C_p\rho_u S_u)$; D_{o_2} is the diffusion coefficient. It seems rather probable that in mixtures of this type the thermal gradient is less extended than the oxygen gradient so that one immediately obtains the relationship

$$D_{o_2} > \frac{\lambda}{C_p\rho_u} \tag{7}$$

Since in mixtures of this kind, that is very rich higher hydrocarbon–air mixtures, the diffusion of oxygen from the unburned to the burned side constitutes a counterflow of chemical enthalpy against the thermal gradient, this relation would signify, as can readily be demonstrated by combustion wave theory, that the combustion wave does not carry excess enthalpy but is deficient in enthalpy over that of the ambient. It follows that for such mixtures the theory, which is based on neglect of diffusional transport of enthalpy, fails completely in the sense that the computed value of minimum ignition energy far exceeds the experimental value. Here again we see the outline of a comprehensive understanding of diffusional phenomena comprising seemingly unrelated manifestations such as cellular flames and the non-concordance of computed and experimental minimum ignition energies. There is little doubt that this picture, as it appears to be emerging, will shed new light not only on the disputed question of excess enthalpy in flames and its consequences in ignition phenomena, but also on the problem of the nature of limits of flammability, in particular, whether absolute limits exist or whether they are the result of instability associated with flame-stretch and diffusional stratification.

We may note that equation 4 for η_o states that this characteristic length is inversely proportional to the burning velocity and the mixture density. It is an experimental fact for mixtures of, say, hydrocarbons, oxygen and nitrogen that the quenching distance at constant density is fairly accurately inversely proportional to the burning velocity; and for mixtures where the burning velocity does not change appreciably with pressure, the quenching distance is quite accurately inversely proportional to the density. One expects, *a priori*, that there should be an approximate proportionality between η_o and the quenching distance. Some years ago, we developed this relationship theoretically from considerations of heat loss from the flame to a solid surface by conduction. Now we see that the experimental behaviour of the quenching conforms to this deduction.

The studies just treated demonstrate that it is possible to develop new conceptional understandings from experimental observations and simple correlations wherever it is found that flame processes have some physical basis in common. In this approach no attempt is made to develop complete theories of the various phenomena; that is, no attempt is made to develop comprehensive sets of kinetic and fluid dynamic equations and to work out their solutions. I do not wish to underestimate the value of the continuing effort that is being directed toward the development of comprehensive theories of combustion wave phenomena, for even though the return may appear small at the moment, there is eventually a substantial gain in intuitive understanding which is indispensable when dealing with complex phenomena.

It is sometimes stated that the main problems of combustion science have been solved and that comparatively little remains to interest the scientist seeking new and exciting fields of endeavour. However, the quantities of interest in the phenomenological descriptions that I have discussed have not been evaluated in terms of molecular properties. Moreover, the comprehensive theories have not yet reached a state of sophistication where they can be conveniently and accurately employed for the treatment of experimental data. As long as these facts are so it would seem to me that combustion science must be regarded as still in its infancy and that the field, combining as it does radically different disciplines of chemistry, kinetics and fluid dynamics, will for a long time be a source of interesting and pleasurably challenging problems.

ADDRESS BY EMERITUS PROFESSOR SIR ALFRED EGERTON, F.R.S.

Sir Humphry Davy and The Royal Institution

Doubtless you guessed why it was chosen to hold the opening meeting here in the Royal Institution. Humphry Davy was the pioneer in the study of Combustion and Flame, and it was here that his work was done.

Most of you know quite as well as I do the story of this place and the story of Davy and how Faraday became his assistant, but, out of homage to those great men, should we not spend some of our time calling them to mind?

The Royal Institution was founded by Benjamin Thompson in 1799. Thompson was born at Woburn near Rumford, Mass., so when he was created a Count of the Holy Roman Empire he took the name Count Rumford. He belongs to the United States, to England, to Bavaria, to France; to the laws of radiation and conservation of energy; to oil lamps and to heating appliances, and a host of other affairs. Mr. Secretary—Colonel—Admiral—Philosopher Thompson—so Gibbon dubbed him. Although he approved of very little towards the end of his life, he would have approved wholeheartedly of our meeting here. That is just as well. I should indeed feel very nervous if the Count were suddenly to appear in angry mood, or Davy be disturbed and come up from the laboratory below, or Faraday bear down from over the clock courteously to inquire what business we had to be here!

How did Davy come to be associated with the Royal Institution? Dr. Garnett from Glasgow had been appointed Resident Director and Professor of Chemistry, but he wasn't happy in London; the Londoners were not happy about his Scotch accent, and he didn't get on with Rumford. So the Count looked around for a substitute to lecture. Dr. Hope of Edinburgh brought Davy to Rumford's attention. Davy, rather a wild lad from Cornwall, son of an improvident carver, had been an apothecary's apprentice in Penzance. His interest in chemical philosophy had won him repute and he was appointed to take charge of Dr. Beddoe's Pneumatic Institution in Bristol. There he had already made a name for himself in discovering the anaesthetic properties of nitrous oxide, and nearly killed himself by studying the effect of breathing carbon monoxide! He was still only 22 years of age when Rumford sent for him. Rumford apparently wondered whether the young man, though obviously clever and intrepid, might not be a little uncouth; however, he was appointed in April, 1801, as 'Assistant Lecturer in Chemistry'. He was to be allowed to lecture 'in the small lecture room'. He forthwith gave some lectures on 'Galvanic Phenomena' which received so much acclaim that Rumford announced 'let him command any arrangements which the Institution can afford'. On the very next day, he was promoted to lecture in 'the Great Theatre', where he held his audience spellbound; in fact it was Davy who brought renown to Rumford's creation—the Royal Institution.

Let us break off from Davy for a moment and take a look at the Institution. We are in number 21 Albemarle Street. It became the property of the Institution in the year of its foundation—1799. It was a brick Georgian house belonging then to a Mr. John Mellish. The main stairway is much as it was 160 years ago, when Mr. Mellish, returning from hunting with the Royal hounds and crossing Hounslow Heath, was shot and fatally injured by highwaymen. Sir Joseph Banks, Rumford, and the Managers of the newly formed Institution decided to acquire the property. Rumford set about reconstructing, along with his man Webster. 'The Great Theatre'—that is where we are—was built out from the north wall of the old house into what was once the garden. It was constructed, roof and all, with great imagination and its acoustics proved excellent. It seems to have been completed, too, with dispatch, for Dr. Garnett lectured in it and he left in May, 1801. (The small lecture room in which Davy was allowed to give his first lectures was probably down below where Mr. Webster used to demonstrate Rumford's stoves to artisans.) The great theatre remained through the century much as it was when first built. It was not until 1928 that it was reconstructed and brought into line with safety regulations. I can vouch that, in spite of renovation, the architect was able to retain the character and the general appearance of the old Theatre in which Davy, Faraday, Tyndall and Dewar lectured, for I had the good fortune to attend a series of lectures by Dewar here in 1904. (I heard as a schoolboy the Curies—Monsieur and Madame—lecture here in 1902 soon after the discovery of radium, and later saw Moissan distil a bar of gold in his electric

arc furnace: it was a memorable and spectacular experiment—the purple vapours of gold and the long green flames!) This lecture theatre is full of romance.

The façade of the Institution which appeared in the print on the cover of the Symposium pamphlet, and which is now undergoing repair, was erected in 1838. Various other changes in the old house took place from time to time.

The Royal Institution has maintained itself, conforming to the original proposals of Rumford, as a place where the progress and applications of science can be demonstrated. Through the genius of its professors, the Royal Institution has also been a unique centre of research. It still continues these traditions. Besides the well-known Friday Evening Discourses, Sir Lawrence Bragg, the present Director, has provided courses of lectures for senior classes of the schools in the Metropolitan area. This is a great contribution to science teaching, for some 12,000 to 15,000 boys and girls a year are now coming to hear lectures illustrated by historical demonstrations and up-to-date experimental equipment. Sir Lawrence continues research work also and the work done here on the constitution of the protein, myoglobin, along with Kendrew working in Cambridge, is in the van of modern research.

The following have been resident Professors of the Royal Institution:

Thomas Garnett
Thomas Young
Sir Humphry Davy
W. T. Brande
Michael Faraday
John Tyndall
Sir James Dewar
Sir William Bragg
Sir Henry Dale
Sir Eric Rideal
E. N. da C. Andrade
Sir Lawrence Bragg

Now to return to that young man Davy who brought renown to the Institution. What was he like? There is a copy in this building of the fine portrait by Thos. Lawrence which is in the possession of the Royal Society. One gets the impression from that painting that Davy was handsome and tall. He wasn't tall (at most 5 ft. 7 in.), but he was impressive and good-looking. The earlier portrait (at age 23) on the stairs here, by Howard, makes this evident. He won the hearts of London society, and it became 'the thing' for the intelligentsia of those days to attend his lectures. As a poet he commanded the respect and had the friendship of other writers of those days—Coleridge, Wordsworth, Maria Edgworth, Southey and later Walter Scott. He had great power of appeal. We owe to him, more perhaps than to anyone else, that sense of devotion which the pursuit of research into Nature's ways can inspire. He had faith in science in the cause of man. In spite of adulation, Davy never swerved from his devotion to science.

It was not long after Davy was appointed that his fame as a chemist became widespread. He received the Royal Society's Copley Medal in 1805, at the age of 27. His first Bakerian Lecture the following year brought him right to the fore as a chemical philosopher. In the next October he thrilled the scientific world by the isolation by electrolysis of potassium and sodium. As success followed success, the import of his work (all done here) was presented in a series of six Bakerian Lectures. He was appointed Secretary of the Royal Society in 1807, still continuing as Professor at the Royal Institution. In 1810 there was the brilliant paper on chlorine. Berzelius, one year younger than Davy, had been throughout these years his continental rival. Berzelius had to instruct his cook-assistant to speak no more of oxymuriatic acid, 'thou must call it chlorine, Anna, that is better!' Even Ampère in France was declaring Davy to be the greatest chemist of all time—they did not all there like to acknowledge it. Davy was scarcely 30 when he had reached the full height of this fame. Napoleon announced, soon after Davy's first Bakerian Lecture, that he would found a prize for the best experiment made in the course of each year in the galvanic field, and that he desired to give by way of encouragement the sum of 60,000 francs to the person who, by his experiments and discoveries, should 'advance the knowledge of electricity and galvanism as much as did Franklin and Volta'. Foreigners of all nations were admitted to the competition. The Committee of the Institut de France nominated Davy. This caused trouble because animosity existed between France and Great Britain at that time. Davy commented: 'Some people say I ought not to accept the prize and there have been foolish paragraphs in the papers to that effect, but, if the two countries or Governments are at war, the men of science are not. That would indeed be a civil war of the worst description. We should rather, through the instrumentality of men of science, soften the asperities of national hostility.' Davy never actually received the award. Had the tares of modern civilization already begun to choke the growth of Davy's ideals?

Not long after the isolation of potassium Davy became dangerously ill. The Royal Institution was besieged by anxious inquirers. He was held high in the public esteem. Cornish born, Davy was tough; he recovered. He soon caught up with those on the continent—Berzelius, Gay-Lussac and others who were busy electrolysing. Davy did not relish rivals: he had to be at the summit.

We pass on to the year 1812. I quote from the Minutes of the Managers of the Institution, 11 May, 1812. . . .

'Mr. Hatchett reported that Sir Humphry Davy, though he cannot pledge himself to deliver lectures, will be willing to accept the offices of Professor of Chemistry and Director of the Laboratory and Mineral Collection without salary.'

This minute really records the fact that Davy had fallen in love with a well-to-do widow, Mrs. Apreece, and had married this lady of society about whom Maria Edgworth wrote to a friend,

> Too many men have often seen
> their talents underrated,
> But Davy owns that his have been
> duly appreciated.

Lady Davy could hardly have appreciated the letter she received from him soon after marriage while working in Mr. Children's laboratory at Tonbridge, in which he made use of a 'compound more powerful than gunpowder destined perhaps at some time to change the nature of war. . . . An explosion took place which has done me no harm than that of preventing me working this day and which I should not mention at all except that you may hear some foolish exaggerated account of it.' It was nitrogen trichloride and he nearly lost the sight of an eye.

This is about the time Faraday steps into the picture.

Davy, though he would be continuing to work in the laboratory of the Royal Institution, was delivering his farewell lecture on 9 April, 1812. A youth of 20 was sitting in the gallery over the clock taking notes. Those notes and the notes of the other three lectures were written out by young Michael Faraday and bound by him. He was a bookseller and binder's apprentice. That is the quarto volume which he sent to Davy the following December asking for the favour of an interview, on the chance that he might be allowed 'to enter into the service of science'. Sir Humphry had no vacancy to offer, but he granted an interview and promised to arrange that books which the Institution needed to have bound should be delivered to him for that purpose. A little later, Davy's eye being troublesome again, Michael was allowed to help with some of his papers. Then, one day, the humble household in which Michael lived with his widowed mother was startled by the arrival of Sir Humphry Davy's coach, from which a footman alighted, and, knocking on the door, he left a note for young Faraday from Sir Humphry requesting him to call the next morning. Davy interviewed Faraday by the north window of the ante room. Fortunately, Mr. Payne, the laboratory assistant, had come to blows with Mr. Newman, the instrument maker, and Mr. Payne had to be dismissed from his post immediately. Faraday stepped into Mr. Payne's shoes, but not without the wise counsel given to him by Davy, and quoted by Faraday:

'At the same time that he thus gratified my desires as to scientific employment, he still advised me not to give up the prospects I had before me, telling me that Science was a harsh mistress; and, in a pecuniary point of view, but poorly rewarded those who devoted themselves to her service. He smiled at my notion of the superior moral feelings of philosophic men, and said he would leave me to the experience of a few years to set me right on that matter.'

As Professor Kendall recalls, 'Life at the Royal Institution was certainly full of excitements during the next few weeks, for the indomitable Davy had attacked with his voltaic battery various compounds of fluorine and would have isolated that element if it had not been so active chemically.' The fumes of hydrofluoric acid badly affected his nails and his eyes, so he turned once more for relaxation to nitrogen trichloride! On 9 April, Faraday wrote to his friend Abbott, 'I have escaped (not quite unhurt) from four different and strong explosions of the substance. . . . I was holding between my thumb and finger a small tube containing 7½ grains of it . . . the explosion was so rapid as to blow my hand open, tear off a part of one nail, and has made my fingers so sore that I cannot use them yet. On repeating the experiment this morning, the tube and a receiver were blown to pieces. I got a cut on my eyelid and Sir Humphry bruised his hand. The experiment was repeated again with a larger portion of the substance. It stood for a moment or two and then exploded with a fearful noise . . . Sir Humphry and I had masks on . . . Sir Humphry had his face cut in two places, and a violent blow on the forehead, struck through a considerable thickness of silk and leather. With this experiment he has for the present concluded.'

Such was Faraday's initiation in experimental chemistry under Davy.

The next episode was the travel with Lady Davy, Faraday and the portable chemical chest, fishing rods, etc., on the continent—almost a two-year journey of scientific inquiry to France, Italy, Sicily and back through Germany. The war against Napoleon was being fought, but Davy was given entry via Morlaix into the enemy country. They started off in October, 1813, and did not get back until April, 1815. Even so, their return was hurried, because the state of affairs was none too happy. Napoleon had escaped from Elba.

Davy was an incorrigible traveller—indeed his last book was entitled *Consolation in Travel, or the last days of a Philosopher*. Not so Faraday, who wrote to his mother when he got back from the big tour that he would never leave England again!

It was an awkward time for Faraday; the savants whom they met soon recognized the genius of Sir Humphry's valet-assistant. Much has been written about Davy's activities on that journey—some of it was related to the newly discovered element, iodine; some to such subjects as 'the colour used in painting by the ancients'. At Pistra-Mala, in the Apennines, Davy examined a column of fire produced by 'gaseous matter constantly disengaged from a schist stratum'. He got Faraday to collect some of the gas, returned to Florence and, in the laboratory of the Grand Duke, showed that the gas was 'marsh gas'. He said 'at some future period new sources of wealth may be opened to Tuscany from this invaluable mineral treasure'—a prophecy now fulfilled. This little investigation foreshadowed Davy's next achievement soon after he got home.

Faraday was soon busy getting things shipshape in the Royal Institution laboratory. Davy was not tidy.

In July, Davy accompanied by Lady Davy went to Scotland on a round of visits, and to shoot and probably to fish, as he had a passion for that sport. There had been some appalling mine accidents. 'A Society for the Prevention of Accidents in Coal Mines' had been formed. Mr. Buddle, a mine engineer, was convinced that 'they must look to scientific men for assistance to provide a cheap and effective remedy'. Their earlier approach to Davy had been delayed by his absence abroad, but now Dr. Gray (later Bishop of Bristol) made the approach and Davy's reply was: 'It will give me great satisfaction if my chemical knowledge can be any use in an inquiry so interesting to humanity, and I beg you will assure the Committee of my readiness to co-operate with them in any experiments or investigations on the subject. . . .' This reply was characteristic of him. He had great confidence in himself in solving such problems, and also he loved to feel that science was in the service of man. The problem and the stake were just such as appealed to him.

Towards the end of August he called at the Wallsend Colliery (near Newcastle), met Mr. Buddle, learnt about the problem and went off to shoot on the Yorkshire moors. Thinking probably accompanied his sport in the fresh air. When back in London, he received at the beginning of October the promised samples of firedamp and started his experiments. Less than a fortnight later, he wrote to Mr. Hodgson (the parson in the mining district): 'My experiments are going so successfully I hope in a few days to send you an account of them. I am going to be fortunate beyond my expectations'.

On 30 October he wrote to Dr. Gray describing his success and later sent details of four distinct models of the Safe lamp 'which depended on the principle that explosive mixtures of firedamp will not pass through small apertures or tubes'. Here are those actual lamps.

So the safety lamp was invented: it was based on a scientific inquiry into the manner in which heat can be conducted away from burning gases to such extent that the flame would be quenched. The speed of achievement was extraordinary.

We will not go into the rest of this story—you already know it well. There were great moments and moments of exasperation. Davy who, in spite of his warnings to Faraday, was an idealist, suffered in being drawn into the world of affairs, but throughout he held to his high principles. The lamp was a tremendous success: it made possible the development of the coal resources not only of England but elsewhere. England became rich. Neither Davy nor the Royal Institution financially profited, except in prestige. Davy was presented with some gold plate, which by his will he left to the Royal Society to be melted down to provide a medal. During the next two years (1815–1817) Davy was full out on the study of Combustion and Flame. Faraday was at his elbow. Is that perhaps why the work, although it had all Davy's dash, had a methodical character? I have always considered that the paper to the Royal Society in 1817 was a masterpiece and, in it, are the seeds of the whole subject in which the Combustion Institute interests itself. Bone commented 'there is no better model of logical experimental procedure, accurate reasoning, philosophical outlook, and fine literary expression'.

Davy examined the limits of combustion, experimented on the speed of flame travel, and the ignitability of mixtures, attempted determination of flame temperatures by rise of pressure during explosion, studied the effect of diluents, of inhibitors and of reduction of pressure on combustion. The quenching of flames, the minimum volume of flame for ignition, the production of carbon in flames, the abstraction of heat by surfaces, the catalytic effect of surfaces, slow flameless combustion, all these matters came within the range of his investigations.

There was romance and thrill in all that Davy did. His intrepid experiments on nitrous oxide and other gases, his instinct about the electrical character of the forces between substances, his spectacular isolation of the alkali metals; the demonstration of the elementary nature of chlorine; the discovery of Faraday, and Faraday's loyalty to his master; the travels all over Europe with his chemical chest; the rapidity with which he caught up with his rivals; the invention of the safety lamp; the birth of combustion as a specialized field of inquiry—all this was romantic. It is indeed romantic that the immense activity in

combustion evidenced by our fat Symposia volumes can be traced back along many paths leading to Davy and the fact that Faraday was then the new assistant in the laboratory.

I am not here to give an historical appreciation of Davy's work, but merely to recall to you his greatness and his importance in the development of combustion. Such a fierce flame shining bright and inspiring his contemporaries inevitably exhausted its energy supply. After the age of 45, he produced nothing of great consequence. After wandering around Europe for a year or two seeking to restore his health, the flame died away. Davy belonged to the world. His grave is in Geneva. The Royal Institution is his spiritual home and we pay homage to his memory.

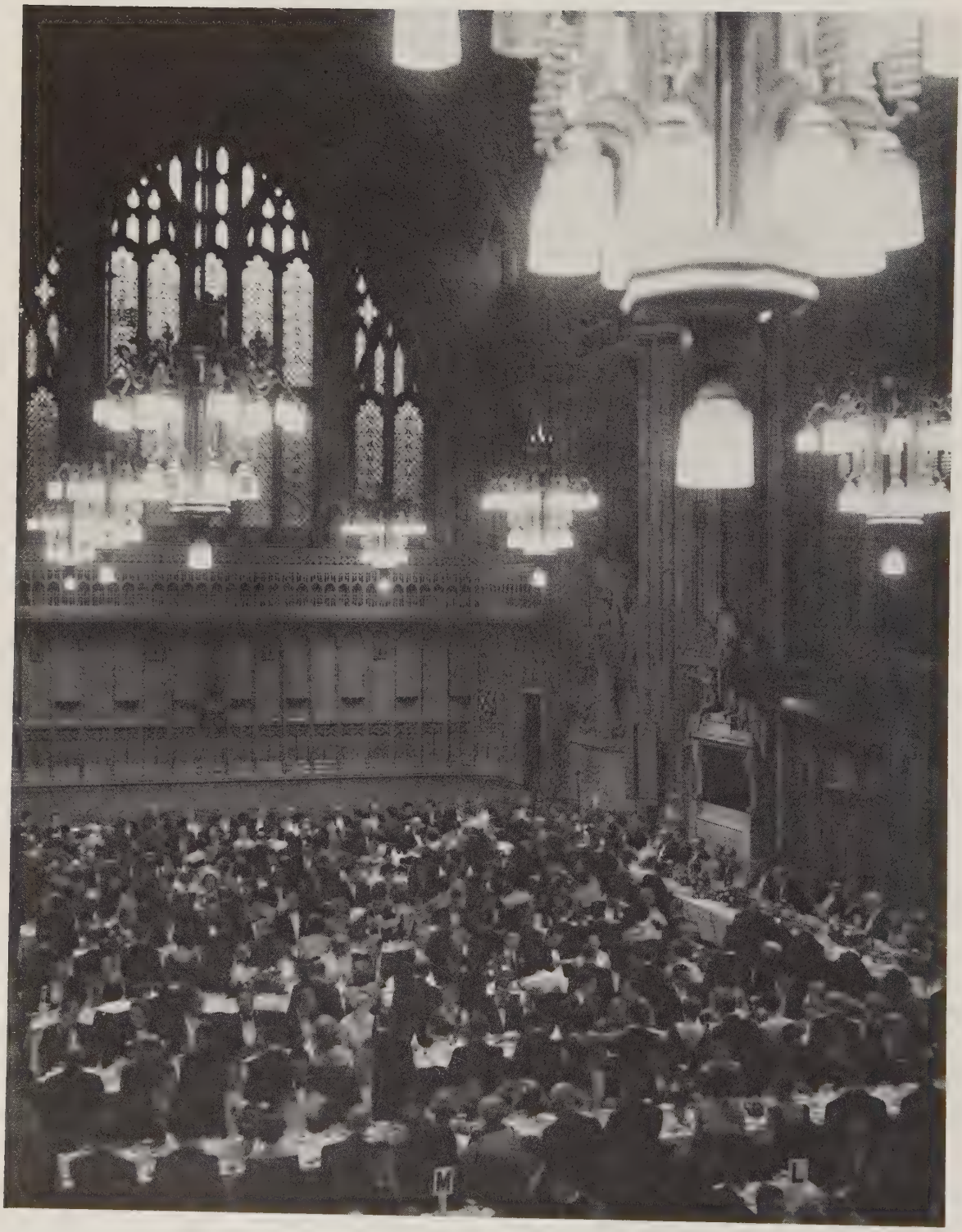

GUILDHALL BANQUET

On 28 August, the opening day of the Seventh Symposium (International) on Combustion, a banquet was held in the Guildhall by gracious permission of the Lord Mayor and the Corporation of the City of London. The guest of honour was the Rt. Hon. Lord Brabazon of Tara, G.B.E., M.C. The Guildhall, the seat of City government since the thirteenth century, now fully restored after grievous damage by fire, was the scene of great splendour. Gog and Magog, symbols of the City of London, their origin lost in the past history of the City, had been restored to their traditional places on each side of the gallery. Their reinstatement was at the express command of Sir Winston Churchill who had so often spoken from the high table of the Guildhall.

The delegates of the Symposium came with lively memories of the opening meeting in the historic lecture theatre of the Royal Institution. Those from abroad had attended a reception given by Her Majesty's Government at Lancaster House the previous evening, and many of them had also visited the ballet at the Royal Opera House, Covent Garden. Thus the Guildhall, bedecked with flowers as token of welcome, formed a fitting climax to the gathering of so many visitors sharing a common devotion to the subject of combustion.

Guests were received in the Art Gallery by Mr. T. C. Bailey, President-elect of the Institute of Fuel, supported by Emeritus Professor Sir Alfred Egerton, F.R.S., Chairman of the British Committee, and Dr. Bernard Lewis, President of the Combustion Institute. The organizing committee were gratified that Mr. T. C. Bailey had agreed to officiate as President of the Banquet: they were thus able to simultaneously honour the Institute of Fuel, at all times our devoted supporters, and Industry, without whose generosity the banquet, and perhaps the Symposium itself, could not have taken place.

At the high table, traditionally in the Guildhall stretching to the corners in the form of three sides of a rectangle, were representatives of 19 countries, of Government and Industrial Research, of the City of London, of the Civil Service, of the universities and the learned and professional societies. The Combustion Institute extended its hospitality to representatives of the many firms who had supported the efforts of the organizers.

The delegates were formally welcomed by Mr. T. C. Bailey who recalled the great traditions of the City of London, and of the Guildhall. Dr. D. T. A. Townend, C.B.E., a Freeman of the City of London, spoke warmly in praise of the ancient City Companies, always enlightened supporters of education and skill in craftsmanship, and ever willing to give their support to contemporary needs. Sir Alfred Egerton, for so many of us our Master, welcomed the guests of the Combustion Institute, in particular Lord Brabazon of Tara, who, we were reminded, held the first pilot's licence to be granted in the United Kingdom. Lord Brabazon regaled the company with his recollections of the great days of motoring and aviation, fields he had pioneered to the incalculable service of his country. With delight, Lord Brabazon reminded us that our work in the service of transport was not yet finished. Dr. Bernard Lewis spoke with pride of his family connections with London, and impressed on the company his faith in the future of the Combustion Institute. The untiring efforts of the Staff of the Institute of Fuel and the contribution of the British Committees of the Combustion Institute received his warm acknowledgement.

So the evening passed: the delegates rose in turn to the invitation of the President to drink a 'loving cup'—the ancient pledge of faith and friendship time-honoured in the City of London. With good company and lively conversation the banquet ended and we wandered out to the unexpected stillness of the City on a summer night.

We owe a debt to many men and organizations for their help and support. There was but one regret—at the last moment The Lord Mayor's locum tenens, Alderman Sir Noel Bowater, was prevented by illness from being with us to deliver the welcome of the City. Nevertheless the Guildhall had worked its magic and blessed our way to Oxford and to work.

N. P. W. Moore

INTRODUCTION

Dr. J. W. Linnett

The Seventh International Combustion Symposium was held in London and Oxford from 28 August to 3 September, 1958. It was different in a number of ways from its predecessors. For instance, it was the first to be held outside the United States of America. It was also the first at which pre-prints of accepted papers were supplied to participants. At the other four meetings since the war there have only been abstracts of the accepted papers in the hands of those attending the meeting; the papers themselves not appearing in print until the publication of the Symposium Volume. This change in the planning of the meeting merits some examination.

At recent Combustion Symposia about 100 to 130 of the papers submitted have been accepted. For the present one, roughly 200 were submitted —about the same number as were submitted for the 1956 Symposium. Some of the organizers of the 1958 Symposium felt, to begin with, that the number of papers considered at the meeting should be reduced below 100. The advantages of doing this are obvious: more detailed consideration and discussion of the papers accepted would be possible; parallel sessions could be avoided completely; a much less tight programme could be achieved. However, the high quality and large number of papers submitted made this impossible. In fact it was only possible to reduce the number down to what seemed to be the maximum manageable by excluding some very good papers which were not strictly on the topics to be dealt with. There seemed to be, in some cases, misunderstanding regarding the subjects announced in the first circular.

The result of the above was that, when the time came to plan the sessions, there were about 120 papers to be included in a meeting which was to be made up of 14 session periods each lasting about 100 minutes. Consequently, if there were no parallel sessions and this has much to commend it, there would only be 12 minutes available per paper for both presentation and discussion. Since it was decided, very early on, that the main aim must be to arrange that half the time was available for open discussion this meant that there were only six minutes left for the presentation of each paper. This calculation makes the unjustifiable assumption that there will be no wastage of time anywhere.

It was therefore decided that, in order to have plenty of time really available for open discussion of the papers, it was essential to pre-print them. In my opinion, which is confirmed by letters I have received, the meeting showed this to be an entirely correct decision. However, even with the advantage of pre-prints it was concluded that the schedule would still be too tight. Consequently it was decided to have four periods during which two sessions would take place at the same time. Because there were only four it was possible to choose the sessions so that the clashes were not too serious but inevitably there must have been some participants who, as a consequence, missed something they would have liked to have heard or to which they would have liked to have contributed.

It was also felt that if 50 minutes was allowed for discussion in each 100-minute session the quality and unity of the whole would be improved by asking a person knowledgeable in the field to open the discussion, and asking him to give some direction to it. Since there were to be pre-prints and since the main aim was to encourage open discussion as much as possible, it was decided that the time for the opener should be provided out of the first half of the session. In order to do this we came to the conclusion that, of the papers pre-printed, some would have to be taken as read, only about half being presented by their authors. This was the most difficult decision to make and, to reduce the chance of any paper being left out, the Openers of the Discussion were asked to make a particular point of bringing these unpresented papers into the discussion. In many cases this worked very well, but not in all.

Another feature which had been included in many of the earlier Symposia but which was omitted from this one was the group of eight or ten invited survey papers. This omission was made in order to create more time for free discussion. However, it is certain that a number of those attending must have felt that this was an unfortunate decision because many survey papers at previous Symposia have been most valuable. A good case can clearly be made for having them when many scientists interested in combustion are gathered together. It is a matter of weighing relative claims against the time available.

The long periods for discussion were most successful and I am not aware that there was any session when the discussion died prematurely. Those contributing to them were asked to write down what they had said and many did so with

the result that there are about 70 pages in this volume devoted to recording the discussion that took place. The individual statements sent in have hardly been altered but they have been brought into order by a number of editors who I would like to thank most sincerely. They were A. R. Ubbelohde, R. P. Fraser, N. P. W. Moore, D. B. Spalding, W. G. Parker, J. H. Burgoyne, F. Weinberg, S. L. Bragg, A. G. Gaydon, C. J. Danby, J. E. Dove, J. Cuthbert, A. Richmond and P. G. Dickens.

Only one Round Table was held on this occasion. It was under the accomplished chairmanship of Professor Ubbelohde and was concerned with the question as to whether combustion is an art or a science. Unfortunately the ordinary members on the floor did not respond sufficiently actively to the lead of the panel (Messrs. Bragg, Jost, Williams, Watson and Karlovitz). Perhaps the topic was somewhat too vague. In place of the other Round Table, Mr. Typaldos was invited to show a film that had been taken of combustion in a container that simulated a rocket chamber operating with liquid fuels. This film was a great success and was most instructive showing many interesting phenomena in a vivid and direct manner. An excellent running commentary was delivered by Mr. Typaldos while the film was being shown. After this a somewhat similar film which had been taken at Westcott was shown by Dr. Lewis. This was also most successful.

This introduction has considered so far the part of the meeting that was held in Oxford which might be described as the technical part. The opening session took place in London at the Royal Institution on 28 August, 1958. The opening address was given by Professor Sir Cyril Hinshelwood, President of the Royal Society, who surveyed the present position, dealing especially with the kinetics and mechanism of oxidation reactions. The second address was given by Dr. Bernard Lewis who dealt more with the state of our knowledge of flames, both laminar and turbulent, and of ignition phenomena. Thirdly, Sir Alfred Egerton gave an appreciation of Sir Humphry Davy and his great contributions to the field of combustion. This was a delightful combination of entertainment and instruction. All these three addresses are included in this volume. On the afternoon of the first day many participants visited the Imperial College of Science where arrangements had been made for them to see the work going on in combustion research, and also to see some of the laboratories. In the evening there was a memorable Banquet at the Guildhall.

A considerable proportion of the Oxford part of the meeting was devoted to the mechanism of oxidation processes, hydrocarbons and other substances being considered. One feature of this part of the meeting was the interest in making as direct observations as possible on individual reactions. In one of these sessions it was encouraging to note that contributions were made to one and the same discussion by a theoretical physicist, chemists and an engineer. It was perhaps less encouraging to find that the pure scientists could not answer the query of the engineer. Two sessions were devoted to 'combustion in practical flowing systems', one of them being concerned with models and the problem of scaling. There was one session on turbulence in flames which is also of interest to the practical combustion scientist. As regards flames there were sessions on their structure and propagation as well as on limits of inflammability and ignition. There have been sessions devoted to flame structure in all the recent symposia and it is clear that there has been steady progress in plotting the temperature through the flame, and now a most satisfactory start has been made in tracing changes in composition. Ionization in flames was given a session to itself and some very interesting papers were submitted on this rapidly developing subject. The transition from inflammation to detonation was considered in one session and produced some very good papers. It is clear that there is still a lot more to be said about this problem. There was a session devoted to instrumentation though papers that might have been included here appeared at all stages of the meeting. For instance there were papers dealing with mass spectrometers and the use of isotopes in other sessions. There is still great need for developing means of measuring temperature under the extreme conditions of a rocket motor, for example. Satisfactory sampling is also a great problem. Sessions were also held on Special Fuels, Spectroscopy and the Interaction of Flames and Surfaces.

Altogether the Symposium demonstrated, like its predecessors, the broad and active interest that exists in many aspects of combustion theory and practice. An abundance of good papers were submitted and the large attendance together with an invigorating discussion gave high hopes for the future both of combustion and the Institute.

PART I

MECHANISM OF COMBUSTION REACTIONS

I

REACTIONS OF HYDROGEN ATOMS WITH OXYGEN

B. DEB. DARWENT and V. J. KRASNANSKY

INTRODUCTION

There is much evidence[1] that the combination of H with O_2 occurs by a third order process. Since the third body is necessary only for removing the energy of the reaction, it should be possible to treat the combination as being composed of three separate processes:

$$H + O_2 \rightarrow HO_2^\star \quad (2)$$

$$HO_2^\star \rightarrow H + O_2 \quad (3)$$

$$HO_2^\star + M \rightarrow HO_2 + M \quad (4)$$

and, possibly, obtain information concerning the rates of the individual reactions.

Although there have been several, rather speculative, estimates of the rate constant for the third order combination, there have been very few attempts at measuring the rate constants of the individual reactions. Patrick and Robb[2] have estimated that about 10^3 collisions between H and O_2 are required before $HO_2^\star$ is formed and that the $HO_2^\star$ lives for at least 10^{-7} sec. On the other hand, mass-spectrometric measurements[3] indicate a life of about 5×10^{-12} sec. The experiments now reported were designed to measure those rate constants, or at least their ratios.

Theory of the method

The theory of the method is similar to that described by Darwent and Roberts[4] for measuring the rate constants of the reactions of H atoms with olefines. The method is based on the production of H atoms by the photolysis of some substance (HX):

$$HX + h\nu \rightarrow H + X \quad (0)$$

which is chosen so that the rate of the initial act is a function only of the absorbed intensity and independent of temperature and pressure. Furthermore, the H atom should be produced with energy corresponding to the thermal equilibrium value and, in the absence of any other substance, should disappear by only one process, e.g.:

$$H + HX \rightarrow H_2 + X \quad (1)$$

the rate constant and activation energy of which should be known accurately.

In the presence of oxygen, reactions 2, 3 and 4 are expected to occur. If those are the only processes in which H_2, H or $HO_2^\star$ are produced or removed, the fate of HO_2 being unimportant provided it does not produce or remove H_2, H or $HO_2^\star$, a steady state treatment yields the following identity:

$$\gamma = \phi/(1 - \phi) = (k_1/k_2)r(1 + k_3/(k_4 m)) \quad (A)$$

where r represents the ratio $[HX]/[O_2]$, and m the concentration of all substances that are capable of de-activating the $HO_2^\star$ in reaction 3. Thus, with constant r and t, γ should be a linear function of m^{-1}, the intercept being $(k_1/k_2)r$ and the slope $(k_1k_3/k_2k_4)r$.

If $HO_2^\star$ is long lived, so that $k_3 \approx 0$, γ will depend only on r and be independent of m at constant temperature. In this case the relationship may be simplified to:

$$1/\phi = 1 + k_2/(k_1 r) \quad (B)$$

so that ϕ^{-1} should be a linear function of r^{-1} with a positive intercept of unity.

In this investigation, H_2S was chosen as the source of H atoms since the quantum yield has been shown[5] to be close to unity and to be essentially independent of temperature, pressure and intensity. Also, experiments in which H_2S or D_2S were photolysed in the presence of a variety of hydrocarbons[4] showed that the H atom produced in the photolysis did not possess energy significantly in excess of the thermal equilibrium value. However, there is some doubt connected with the magnitude of the rate constant and activation energy of reaction 1 for H_2S since, although they are known for D_2S relative to those of the reaction:

$$D + H_2 \rightarrow HD + D$$

the activation energy of the latter reaction is still somewhat uncertain. In this respect HI or HBr would, possibly, have been preferable, but there is a strong indication[6] that the H atoms produced in the photolyses of those substances possess energy considerably in excess of the thermal value and experiments in these laboratories[7] have supported that conclusion.

EXPERIMENTAL

The H_2S and CO_2 were the purest commercial products available and were rendered free of air

by repeated condensation at — 196°C and distillation under high vacuum. The commercial oxygen was not sufficiently free of nitrogen for use in these experiments so that pure O_2 was obtained by gently heating potassium permanganate *in vacuo* and dried by passing it through a trap cooled in liquid nitrogen.

The light was obtained from a Hanovia type SH medium pressure quartz mercury arc and approximately collimated by a quartz lens. The incident intensity was varied by altering the diameter of a circular aperture in a stop placed between the lamp and the lens. The intensity of unreversed λ2,537 put out by another lamp of identical type was found to be entirely negligible.

The photolyses were carried out in a cylindrical quartz cell, 5 × 10 cm and about 200 cm^3 capacity, mounted axially in a cylindrical aluminium furnace, the ends of which were closed by a quartz plate and a transite stopper. The reaction system, of total volume approximately 800 cm^3, consisted of an all glass circulating pump[8] that displaced unidirectionally about 1 litre min^{-1} at the prevailing pressure, a trap and the reaction cell. It was connected, through traps, to a mercury manometer and to the storage, analytical and vacuum systems.

When the reaction mixture consisted only of H_2S, or H_2S and CO_2, the condensable gases were frozen out after the photolysis in the trap in the reaction system, and the uncondensable gas removed by a small mercury diffusion pump and measured in a combined Toepler pump and gas burette. When O_2 was present it was necessary to separate small amounts of H_2, of the order 10^{-2} mm Hg in the reaction system, from amounts of O_2, as great as 500 mm Hg. In those experiments the condensable gases were frozen out in the reaction system trap and the uncondensable gases admitted to a trap containing silica gel cooled to — 196°C. The silica gel trap was then isolated from the reaction system and the hydrogen, together with some oxygen, pumped into the gas burette. The oxygen in the resulting mixture was removed by slow admission to yellow phosphorus at 0°C and the hydrogen measured. The purity of the hydrogen was then determined by oxidation on copper oxide at 220°C or mass-spectrometrically. The method was tested with synthetic mixtures and shown to be as accurate as the measurement of the gas volumes.

Temperatures of 50, 93 and 150°C were used in these experiments. At the two lower temperatures the dark reaction between H_2S and O_2 was negligible. However, at 150°C there was a slow dark reaction that produced hydrogen. Accordingly, a correction of about 2 per cent was applied to those results and no results obtained above that temperature are included. No hydrogen was produced when the H_2S was frozen out before photolysis, indicating either that the reaction system was very free from mercury or that the gas was very dry.

Experiments in which 100 mm of H_2S was photolysed alone and mixed with 400 mm of CO_2 showed that the rate of formation of H_2 was not affected by the presence of CO_2. A similar conclusion had previously been reached[5] by photolysing H_2S in the presence of SF_6.

RESULTS

The results of a series of experiments in which a constant pressure of H_2S (5 mm Hg) was photolysed in the presence of varying pressures of O_2, at 150°C, are shown (*Figure 1*) as a plot of $1/\phi$ *versus* r^{-1}, in accordance with equation B. It is

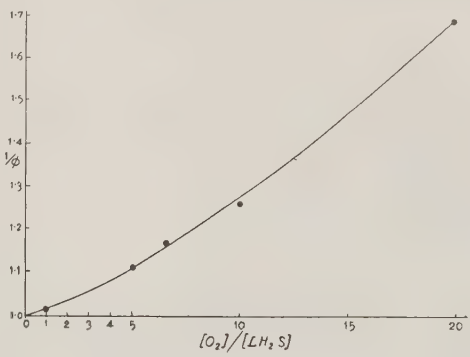

Figure 1. The effect of $[O_2]/[H_2S]$ *on* $1/\phi$ *at* 150°C *and constant pressure* (5 mm Hg) *of* H_2S

obvious that the relationship is not linear, although the intercept was unity, as required by that equation, and that the results deviate from theory in a manner that suggests strongly that deactivation of the HO_2^* is, in fact, necessary for the addition to be completed.

The necessity for that deactivation is shown more clearly by the results of a series of experiments, in which p_1 and p_2 (pressures of H_2S and O_2 respectively) were kept constant and the total pressure varied by the addition of CO_2. Those results, obtained at 150°C, are shown (*Figure 2*) as plots of γ *versus* $1/m$, in accordance with the requirements of equation A. The results represented by line *A*, obtained with 100 mm each of H_2S and O_2, obviously agree excellently with the theory. In other experiments the pressures of the reactants as well as the ratio of those pressures were altered and the results compared with those predicted from equation A on the basis of line *A*. The extent of the agreement is shown in *Figure 2* by the relationship between the experimental points and the theoretical lines *B* and *C*. The pressure of H_2S was varied from 100 mm to

5 mm Hg and the ratio r from 1·00 to 0·14; it is obvious that, even over such a wide variation, there is no serious or systematic deviation from the theoretical requirements.

The effect of temperature on the reaction is shown in *Figure 3*. Those results further support the proposed mechanism, since good agreement is obtained with equation A at all the temperatures.

The data obtained from *Figure 3* for the ratios of the rate constants are presented in Table 1. These data show that although the ratios k_1/k_2 and k_1k_3/k_2k_4 increase systematically with temperature, the increase being very nearly the same for both the ratios, k_3/k_4 is essentially independent of the temperature. For k_3/k_4 to be accurately independent of the temperature, the intercept at 93° would have to be decreased from 0·273 to 0·206; such a decrease is not inconsistent with the accuracy of the measurements. The line at 93° is less well defined than those at the two other temperatures since there are no experimental points at high pressures as there are at the other two temperatures. The slopes of all the lines in *Figure 3* are defined more precisely than the intercepts. In the Arrhenius plots of the intercepts (k_1/k_2) and the slopes (k_1k_3/k_2k_4), shown in *Figure 4*, the line joining the points for k_1/k_2 at 50 and 150°C is parallel to that for k_1k_3/k_2k_4 and the point for k_1/k_2 falls off the line. Since that point is admittedly less accurate than the others and only a small alteration in the value of the intercept would place it on this line, we have given no weight to the point for k_1/k_2 at 93°C.

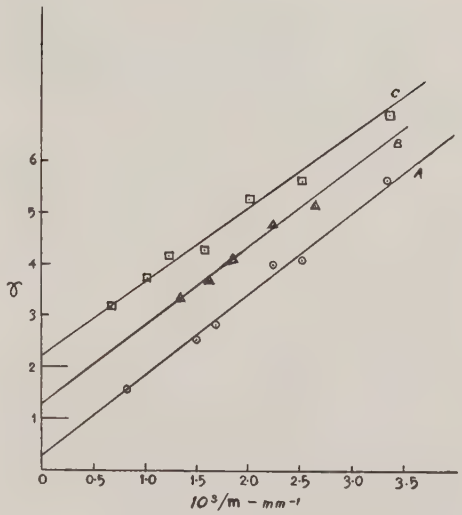

Figure 3. The effect of total pressure and temperature on γ

Line A—open circles: 50°C; H_2S = 100 mm; O_2 = 25 mm
Line B—triangles: 93°C; H_2S = 100 mm; O_2 = 50 mm
Line C—squares: 150°C; H_2S = 100 mm; O_2 = 100 mm

The abscissae of lines B and C have been displaced vertically by 1 and 2 units respectively

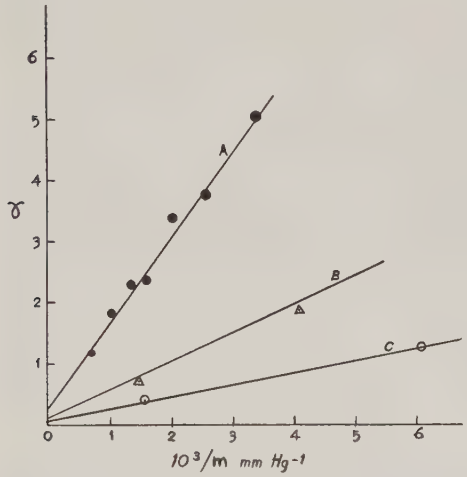

Figure 2. The effect of total pressure and $[H_2S]/[O_2]$ *on* γ *at* 150°C, *in the presence of varying amounts of* CO_2

Filled circles: H_2S = 100 mm; O_2 = 100 mm
Triangles: H_2S = 25 mm; O_2 = 75 mm
Open circles: H_2S = 5 mm; O_2 = 36 mm

A series of experiments at 50°C in which the total pressure was varied by increasing p_1 and p_2, maintaining the ratio constant in each series, gave results that differed markedly from those expected from the experiments in which p_1 and p_2 were kept constant and the total pressure varied by the addition of CO_2. Those results are compared in *Figure 5*. Line *C* was plotted from the same data used for line *A* of *Figure 3*, the ratio p_1/p_2 being 4·0. Lines *B* and *A* were obtained from experiments without CO_2, the ratios being 2·0 and 1·0 respectively. Although the slopes of the lines are very

TABLE 1

The Photolysis of H_2S in the Presence of O_2: Effect of Temperature on the Rate Constants

Temp. (°C)	r	*Intercept*	*Slope**	k_1/k_2	k_1k_3/k_2k_4*	k_3/k_4*
50	4·0	0·240	0·473	0·060	0·118	1·97
93	2·0	0·273	0·402	0·137	0·201	1·47
150	1·0	0·171	0·332	0·171	0·332	1·95

* Units—molecules $cm^{-3} \times 10^{-20}$.

close to $\frac{1}{2}$ and $\frac{1}{4}$ of that of line *A*, as required by equation A, the intercepts are very much greater than expected. The difference in the intercepts from the expected values has been ascribed to the occurrence of a reaction:

$$HO_2^{\star} + O_2 \rightarrow H + 2O_2 \qquad (5)$$

the evidence for which is discussed later in the paper.

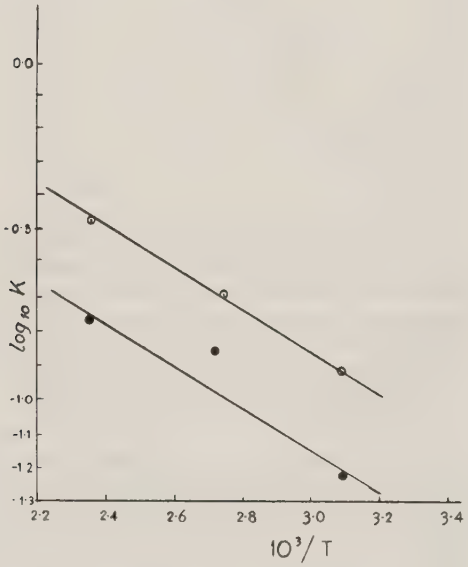

Figure 4. Effect of temperature on k_1/k_2 (filled circles) and k_1k_3/k_2k_4 (open circles)

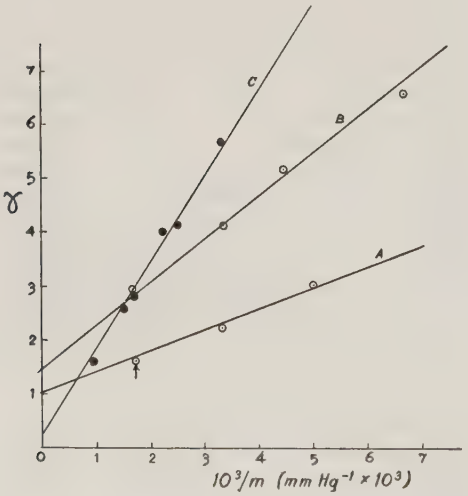

Figure 5. Effect of CO_2 on the reaction at 50°C

Line A: $CO_2 = 0$; $H_2S/O_2 = 1$
Line B: $CO_2 = 0$; $H_2S/O_2 = 2$
Line C: CO_2 *variable*; $H_2S = 100$; $O_2 = 25$ mm

Arrow indicates two coincident points one of which was obtained with intensity reduced sevenfold

DISCUSSION

Although the mechanism proposed is extremely plausible and the results, except those in the absence of CO_2, agree excellently with the requirements of the kinetics based on that mechanism, there are other reactions which are also plausible that, if they were important, could invalidate the conclusions drawn from the results. Accordingly, the possible occurrence of these other reactions will be discussed before an explanation of the differences observed in the absence of CO_2 is attempted.

The following reactions are all thermodynamically favourable:

$$HS + O_2 \rightarrow H + SO_2 \qquad (6)$$

$$HS + HO_2 \rightarrow H_2 + SO_2 \qquad (7)$$

$$H + HO_2 \rightarrow 2OH \qquad (8)$$

and, if they were important, the interpretation of the results would be uncertain since they represent additional sources of H and H_2 which were not included in equation A. If even one of the above reactions is included in the mechanism, an accurate rate equation can be obtained only if we include all of the other processes by which the radical in question can disappear. Such a procedure is extremely involved and does not provide rate equations that can be tested experimentally. Accordingly, the kinetics have been solved only for limiting cases, e.g. the effect of including reaction 6 has been examined under the assumptions (*a*) that reaction 6 represents the principal means of disappearance of HS and (*b*) that the HS radicals disappear principally by combination:

$$2HS \rightarrow H_2S + S \qquad (9)$$

Case (a)

$$k_6[O_2] \ll k_9[HS]$$

This gives the relationship

$$\phi = (k_1/k_2)r(2 + k_3/k_4m)$$

requiring ϕ to be a linear function of $1/m$ if r and the temperature are constant. The results show clearly that such a relationship is not obeyed experimentally.

Case (b)

$$k_6[O_2] \gg k_9[HS]$$

The relationship becomes:

$$\frac{1}{\phi} = \frac{k_9^{\frac{1}{2}}Ia^{\frac{1}{2}}}{k_9^{\frac{1}{2}}Ia^{\frac{1}{2}} + k_6p_2}\left[1 + \frac{k_2p_2}{k_1p_1} \cdot \frac{k_4m}{(k_3 + k_4m)}\right]$$

which is inconsistent with experiment. This may be shown by taking limiting values for the ratio $(k_9^{\frac{1}{2}}Ia^{\frac{1}{2}})/(k_6p_2)$. (1) If $k_9^{\frac{1}{2}}Ia^{\frac{1}{2}} \ll k_6p_2$, $1/\phi$ becomes proportional to $Ia^{\frac{1}{2}}$, which is contrary to experiment (see *Figure 5*). (2) If $k_9^{\frac{1}{2}}Ia^{\frac{1}{2}} \gg k_0p_2$ the above

equation becomes identical with equation A, which means, effectively, that reaction 6 is unimportant.

Similar treatments of reactions 7 and 8 also show that they cannot be important if the experimental results are valid. Hence the simple mechanism appears to be essentially correct, except for the discrepancy between the results obtained in the presence and absence of CO_2.

The discrepancy between the results in the presence and in the absence of CO_2 (*Figure 5*) shows that the simple mechanism is not completely adequate. The addition of the reaction

$$HO_2^{\star} + O_2 \rightarrow H + 2O_2 \qquad (5)$$

resolves the difficulty, since it leads to the relationship

$$\gamma = \frac{k_1}{k_2} r \left[1 + \frac{k_5 p_2}{k_4 m} + \frac{k_3}{k_4 m} \right] \qquad (C)$$

which is consistent with experiment. Thus, in the absence of CO_2 the term p_2/m becomes $1/(1 + r)$ and is constant in each series of experiments at constant r; hence the intercepts in the absence of CO_2 become $(k_1/k_2)r[1 + (k_5/k_4)(1 + r)^{-1}]$ and the slopes remain $(k_1/k_2)r(k_3/k_4)$. In the presence of CO_2 the intercepts remain $(k_1/k_2)r$ and the slopes become $(k_1/k_2)r(k_3 + k_5 p_2)/k_4$.

The values of the ratios of the rate constants were obtained from the data in *Figure 5*, as follows: The intercept and slope of line *C*, 0·24 and $1{\cdot}58 \times 10^3$ mm respectively, were assumed to be correct, since that line is well defined. Since r was 4·0, we get $k_1/k_2 = 0{\cdot}06$ from the intercept. Approximate values of 0·95 and 1·55 were obtained for the intercepts of lines *A* and *B*, for which the values of r were 1·0 and 2·0 respectively. These gave values of 30 and 36 for k_5/k_4. Taking the average value of 33 for k_5/k_4, we calculated corrected intercepts of 1·05 and 1·45 for lines *A* and *B* and drew the best lines based on those values of the intercepts. The slopes of those lines were $0{\cdot}37 \times 10^3$ and $0{\cdot}79 \times 10^3$ mm Hg respectively and, from those slopes, we calculate values of $6{\cdot}17 \times 10^3$ and $6{\cdot}60 \times 10^3$ mm for k_3/k_4. Using the average of these ($6{\cdot}38 \times 10^3$) we calculate the slope of line *C* to be $1{\cdot}56 \times 10^3$ whereas the experimental value is $1{\cdot}58 \times 10^3$ mm Hg. Thus the values of the ratios of the rate constants are mutually consistent.

In spite of the internal consistency of the data we do not consider that too much reliance should be placed on the value of k_5/k_4 quoted, since values ranging from 20 to less than one may be obtained from the same data by a different method of calculation.

Although oxygen was used in reaction 5 and in the subsequent calculations, H_2S or both O_2 and H_2S serve equally well from the point of view of the kinetics. However, there is a slight preference in favour of oxygen, since O_4 has been detected spectroscopically and may play a significant role as an intermediate in reaction 5.

Further information concerning the rate constants may be obtained from the data presented in *Figures 3* and *4* and in Table 1. Assuming the following cross-sections: $\sigma_H = 1{\cdot}06\,A$; $\sigma_{O_2} = 3{\cdot}61\,A$; $\sigma_{CO_2} = 4{\cdot}59\,A$; $\sigma_{HO_2} = 4{\cdot}67\,A$ we calculate the collision frequencies: $Z_1 = 1{\cdot}9 \times 10^{-9}$; $Z_2 = 5{\cdot}2 \times 10^{-10}$; $Z_4 = 4{\cdot}0 \times 10^{-10}$ sec^{-1} where the subscripts refer to the corresponding reaction, the concentrations being one molecule per cm^3.

Although the rate parameters for reaction 5 are not known, values of the P and E factors have been given[4] as 0·73 and 5·0 kcal mole^{-1} respectively for the similar process involving D atoms and D_2S. However, the value of E for that reaction is also rather uncertain, since it was based on that for the reaction

$$D + H_2 \rightarrow HD + H$$

which is itself uncertain, lying between 4·85 and 7·5 kcal mole^{-1}. Since the value of P_1 does not appear to be in serious doubt, we may calculate the value of P_2 from the experimental data; we find $P_2 = 0{\cdot}06(\pm\ 0{\cdot}01)$, which seems reasonable. Although even the lowest value suggested for E_1 requires E_2 to be about 2·0 kcal mole^{-1}, which does appear to be rather high, the collision yield for reaction 1 turns out to be $2{\cdot}4 \times 10^{-3}$ at 27°C, or about 400 collisions are necessary for the reaction to occur. This compares favourably with the estimate[2] of 10^3 collisions.

If we accept an average value of $1{\cdot}96 \times 10^{20}$ cm^3 molecule^{-1} for k_3/k_4 we may ascribe a maximum value of $1{\cdot}96 \times 10^{20} \times 4{\cdot}0 \times 10^{-10}$ sec^{-1} = 8×10^{10} sec^{-1} to k_3. This puts the minimum value of τ_3, the average life of $HO_2^{\star}$, at about $1{\cdot}1 \times 10^{-11}$ sec, which does seem rather long for the decomposition of a triatomic molecule. However, it is not inconsistent with previous estimates of 10^{-7} sec by Patrick and Robb[2] and 5×10^{-12} sec by Robertson[3].

This work received financial support from Project SQUID under Contract No. N6ori–105–Task 3.

REFERENCES

1 Lewis, B. and von Elbe, G. *Combustion, Flames and Explosions in Gases.* 1951. New York; Academic Press

2 Patrick, C. R. and Robb, J. C. *Disc. Faraday Soc.* 17 (1954) 98

3 Robertson, A. J. B. *Disc. Faraday Soc.* 17 (1954) 98

4 Darwent, B. deB. and Roberts, R. *Disc. Faraday Soc.* 14 (1953) 55

5 — — *Proc. Roy. Soc. A* 216 (1953) 344

6 Schwartz, H. A., Williams, R. R. and Hamill, W. H. *J. Amer. chem. Soc.* 74 (1952) 6007

7 Darwent, B. deB. and Krasnansky, V. J. Unpublished results

8 Watson, J. S. *Can. J. Tech.* 34 (1956) 373

2

THE SLOW REACTION AND SECOND LIMIT OF THE HYDROGEN–OXYGEN REACTION IN BORIC ACID COATED VESSELS

R. R. BALDWIN and L. MAYOR

INTRODUCTION

As pointed out by Sir C. N. Hinshelwood[1] in his 1946 Bakerian Lecture to the Royal Society, the hydrogen–oxygen reaction has provided one of the outstanding examples by which the principles of chain reactions have been illustrated. Moreover, with the recent interest in the relation between flame properties and chemical reaction velocity, considerable importance has attached to a detailed understanding of the H_2—O_2 system, since it is one of the few in which the main flame reactions are likely to be essentially those occurring also in the slow reaction. As a consequence of the considerable certainty as to certain aspects of its mechanism, its value as a tool in the study of other free radical reactions has also been demonstrated[2–4]. For all these reasons, therefore, a complete understanding of all aspects of this reaction is desirable.

The main reactions suggested in recent years are summarized below:

$$OH + H_2 = H_2O + H \quad (1)$$

$$H + O_2 = OH + O \quad (2)$$

$$O + H_2 = OH + H \quad (3)$$

$$H + O_2 + M = HO_2 + M \quad (4)$$

$$HO_2 \xrightarrow{\text{surface}} \tfrac{1}{2}H_2O_2 \quad (5)$$

$$HO_2 \xrightarrow{\text{surface}} \text{destruction} \quad (5a)$$

$$HO_2 + H_2O_2 = H_2O + O_2 + OH \quad (6)$$

$$H_2O_2 + M = 2OH + M \quad (7)$$

$$H_2O_2 = 2OH \quad (7a)$$

$$H + HO_2 = 2OH \quad (8)$$

$$HO_2 + H_2 = H_2O_2 + H \quad (11)$$

$$HO_2 + H_2 = H_2O + OH \quad (11a)$$

Reactions 1–4 with 5a provide the simplest interpretation of the second limit in salt coated vessels[1], which is then given by the expression $M = 2k_2/k_4$. Lewis and von Elbe[5,6] prefer reaction 5, the H_2O_2 then evaporating into the gas phase and being destroyed by reaction 6. Since a chain centre (OH) is thus regenerated from every three HO_2 radicals, the limit now becomes $3k_2/k_4$.

The slow reaction which develops at pressures significantly above the second limit in salt coated vessels is attributed to the reaction of HO_2 with H_2, in competition with the surface process 5 or 5a. By taking reactions 1–4, 5a and 11 or 11a, Hinshelwood and Willbourne[7] obtained a rate expression:

$$\frac{d[H_2O]}{dt} = \frac{An_0}{1 - \dfrac{2k_2}{k_4M} - \dfrac{k_{11}[H_2]}{k_{5a} + k_{11}[H_2]}} \quad (i)$$

where A, which lies between 1 and 2, is determined by the nature of the initiation process n_0 and other minor details of the scheme. Using the second and third limits to evaluate the variation of k_4 and k_{5a} with mixture composition, Hinshelwood and Willbourne were able to study the variation of n_0 with mixture composition. They found $n_0 \propto [H_2][M]$, and interpreted this as indicating a bimolecular dissociation of hydrogen as the initiation process. Lewis and von Elbe[8], however, estimate this dissociation to be too slow by a factor of 10^{13}, and prefer instead the bimolecular dissociation of H_2O_2, 7, formed in equilibrium concentration by reactions 6 and 11. A detailed analysis of possible reaction schemes, however, is hampered by the nature of expression i, which gives long chains only when the denominator is small and thus susceptible to small errors in the evaluation of k_4 and k_{5a} from second and third limit data.

In this period of temporary stagnation, the demonstration by Egerton and Warren[9] of quadratic branching in boric acid coated vessels was particularly opportune. They showed that in such vessels, the second limit is given by

$$M = C + B/[O_2]^{1/2} \quad (ii)$$

and interpreted this expression by a mechanism involving reactions 1–4, 5, 6, 7a and 8. While there seems little doubt that the quadratic branching reaction 8 is involved, the remaining mechanism is open to some criticism. In the first place, as pointed out by Warren[10], the fact that the constant C in expression ii agrees numerically with the second limit in salt coated vessels means that if reactions 5 and 6 occur in boric acid coated vessels, they must also occur in salt coated vessels.

It is not then obvious why quadratic branching is absent in salt coated vessels, and Warren assumes that the H_2O_2 formed by reaction 5 in salt coated vessels never escapes into the gas phase, and that reaction 6 occurs on the surface. The initiation reaction 7a, which plays an important part in determining the limits, is thus absent in salt coated vessels. A second difficulty is that it is necessary to assume a unimolecular first-order dissociation of H_2O_2, in conflict with evidence from the slow reaction, and from work presented in this paper. Dixon-Lewis, Linnett and Heath[11] overcome these objections by an ingenious modification of the Egerton–Warren scheme, but are forced to postulate another reaction, $HO_2 + H_2 \xrightarrow{\text{surface}} H_2O_2 + H$, for which no independent evidence is available. Moreover, their mechanism involves reaction 6, and convincing evidence for the absence of this reaction is given in this paper.

The present paper describes some observations on a reaction between H_2 and O_2 which was discovered accidentally during a study of the effect of withdrawal rate on the second limit in boric acid coated vessels[12]. In the freshly coated vessel at 500°C and 500 mm Hg pressure, the rate of reaction of a given H_2—O_2 mixture is quite small (*ca.* 2 mm Hg in 8 min). As the vessel is used, this rate increases quite slowly over a period of 10–14 days to a value of 6–8 mm in 8 min. Quite suddenly the rate then accelerates over a period of about one day, giving a pressure change of about 60 mm in 8 min. A preliminary examination of the kinetics of this reaction revealed quite unusual features, and a detailed study was undertaken in the hope that yet another method of attacking the problem of the H_2—O_2 mechanism had been found. Preliminary results have already been reported[13], and detailed accounts submitted for publication elsewhere[14]. In this paper, attention is mainly concentrated on a brief presentation of the main experimental features, and the relevant conclusions that can be drawn about the mechanism both of this slow reaction and the related second limit.

EXPERIMENTAL

The apparatus, purification procedures, and mixture compositions studied were essentially as described earlier[3,13]. Mixtures were prepared in the reaction vessel by separate admission to avoid passage through the explosive region. Second limits were determined by the withdrawal method, the mixing time being 15 sec both for fresh and aged boric acid coated vessels. Frequent tests were made to ensure that the withdrawal rates were sufficiently fast to avoid the depressed limits that may be obtained with slow rates[12]. Slow reactions were followed with a Bourdon gauge sensitive to within 0·05 mm Hg. Corrections for the dead volume between the reaction vessel and the gauge varied from about 10 per cent in the 51 mm vessel to about 100 per cent in the 15 mm diameter vessel.

As a check on reproducibility, the rate of a convenient mixture was determined at the beginning, in the middle and at the end of each day. Over a period of a month in one vessel, the maximum rate of this mixture only varied within ±4 per cent. Similar reproducibility was obtained for different vessels of the same diameter. This reproducibility did not seem disturbed if the vessel was left out of use evacuated, or filled with H_2, O_2 or water vapour, either at room temperature or at 500°C. The first run after such treatment usually gave a slightly longer induction period and a slightly lower maximum rate, but two or three trial runs restored both to the normal value[13]. The order of admission of gases was also shown[13] not to affect the rate. Tests showed that the rate of diffusion and condensation of water vapour into the cold part of the capillary entry tube was negligible, and that entry of fresh gases from the dead volume as the pressure in the reaction vessel decreased also had negligible effect[13].

RESULTS

Unless otherwise stated, all results refer to a 51 mm diameter vessel at 500°C.

Effect of oxygen mole fraction

Typical pressure–time curves are shown in *Figure 1* for a range of oxygen mole fractions (y) at 500 mm total pressure, the hydrogen mole fraction (x) being held constant at 0·28 by

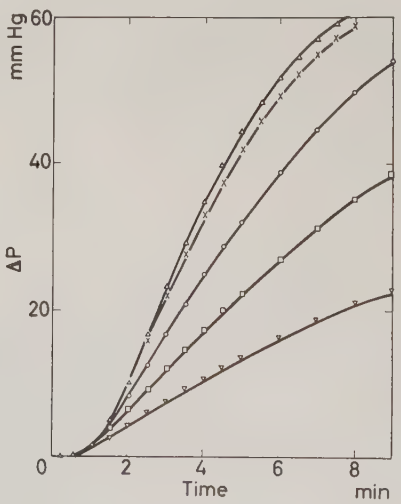

Figure 1. Pressure–time curves for varying oxygen mole fractions.
Total pressure 500 mm, $x = 0{\cdot}28$
$\triangle\ y = 0{\cdot}72$, $\times\ y = 0{\cdot}56$, $\odot\ y = 0{\cdot}28$,
$\boxdot\ y = 0{\cdot}14$, $\triangledown\ y = 0{\cdot}07$

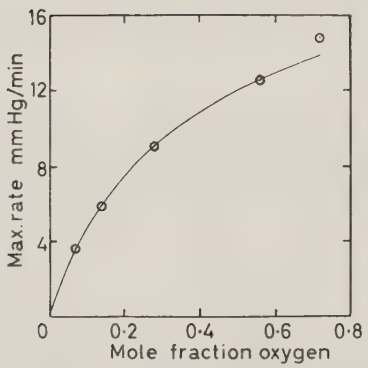

Figure 2. Variation of maximum rate with oxygen mole fraction.
Total pressure 500 mm, $x = 0{\cdot}28$
⊙ *experimental points* — *calculated curve from equation x*

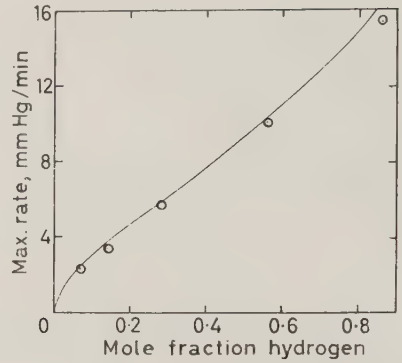

Figure 3. Variation of maximum rate with hydrogen mole fraction.
Total pressure 500 mm, $y = 0{\cdot}14$
⊙ *experimental points* — *calculated curve from equation x*

interchanging O_2 and N_2. *Figure 2* shows the variation of maximum rate $R(dP/dt)$ with oxygen mole fraction*. A plot of log R *versus* log y gives a reasonable line of gradient 0·60, but as shown later this indication of a straight chain reaction with self-termination is misleading, and is a consequence of the operation of two termination processes. The marked effect of O_2 contrasts with the reaction in porcelain[15] and salt coated vessels[6,7], where O_2 appears to have no greater effect than N_2.

Effect of hydrogen mole fraction

The effect of hydrogen mole fraction was investigated at constant oxygen mole fractions of 0·14 and 0·56 by interchanging H_2 and N_2, the results being shown in *Figures 3* and *4* respectively. In each case the points apparently lie on a straight line, but the fact that the straight line does not extrapolate through the origin indicates that the effect of H_2 is complex. The 'apparent order' of slightly less than unity with respect to H_2 contrasts with the values of 2–3 in porcelain[15], silica[16] and salt coated vessels[6,7].

Effect of total pressure

The variation of maximum rate with total pressure is shown in *Figure 5* for a 'standard' mixture

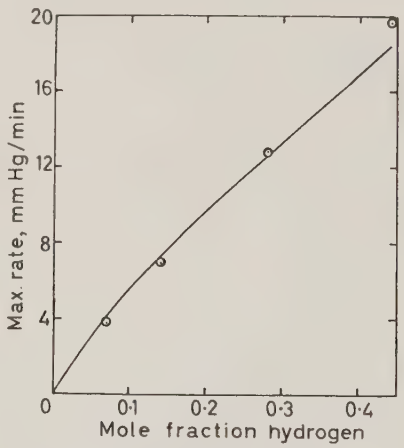

Figure 4. Variation of maximum rate with hydrogen mole fraction.
Total pressure 500 mm, $y = 0{\cdot}56$
⊙ *experimental points* — *calculated curve from equation x*

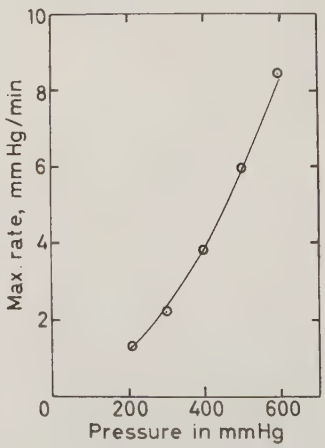

Figure 5. Variation of maximum rate with total pressure.
$x = 0{\cdot}28$, $y = 0{\cdot}14$
⊙ *experimental points* — *calculated curve from equation x*

* The autocatalytic nature of the reaction means that when the maximum rate is reached, the concentration of both reactants has changed (0–10 per cent) from the original values. It is convenient for presentation purposes to correct the experimental rates, using the known variation of rate with concentration of each reactant, for such consumption. Except in *Figure 6*, these corrected rates are used throughout this paper. The corrections are small (5–15 per cent); moreover, if the uncorrected rates and the actual concentrations at maximum rate are used, exactly the same conclusions about the mechanism and velocity constant ratios are obtained. In the case of the inert gas effects (*Figure 6*), it is more convenient to use the uncorrected rates, and to base the calculated curve on the composition at maximum rate.

of fixed composition ($x = 0{\cdot}28$, $y = 0{\cdot}14$). A plot of log R *versus* log P gives a reasonable straight line of gradient $1{\cdot}87 \pm 0{\cdot}07$. This low overall order provides a marked contrast to the high order reactions obtained with other surfaces[6,7,15,16].

Effect of inert gas

The effect of addition of N_2 was examined for the stoichiometric mixture and for two additional

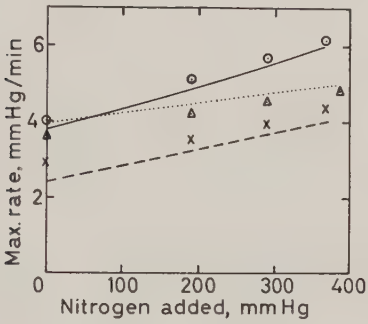

Figure 6. Effect of inert gas on maximum rate.
(Rates not corrected for consumption of reactants)
140 mm H_2 + 70 O_2 ⊙ *experimental* — *calculated*
180·5 mm H_2 + 29·5 O_2 × *experimental* --- *calculated*
59 mm H_2 + 151 O_2 △ *experimental* ··· *calculated*

mixtures, one containing a considerable excess of H_2, the other a considerable excess of O_2. In each case, increasing amounts of N_2 up to a maximum of about 400 mm were added to 210 mm of the H_2—O_2 mixture, the results being shown in *Figure 6*. For all mixtures, a significant increase in rate was obtained, the effect being least marked at low H_2/O_2 ratios. Though significant, this accelerating influence is substantially less than in salt coated vessels[6,7].

Effect of vessel diameter

The preceding observations were repeated in vessels of 36, 24 and 15 mm diameter, and in no case was any significant effect of vessel diameter obtained, the variation being quite random and within the limits obtained for different vessels of the same diameter. Typical results for the effect of varying oxygen mole fraction are shown in *Figure 7*. These observations provide a striking contrast to the marked diameter effect obtained with silica[17] and KCl coated vessels[6,7].

Effect of temperature

The variation of maximum rate with temperature was examined over the range 470–540°C using the standard mixture at a constant concentration corresponding to 500 mm and 500°C. The log $R - 1/T$ plot was closely linear over the whole range, the associated activation energy being $55{\cdot}8 \pm 0{\cdot}7$ kcal. This compares with values of at least 100 kcal quoted for salt coated vessels[18,19].

Induction periods

The induction period (defined either as the time for a given pressure change, or as the time to maximum rate) was little affected by oxygen mole fraction, total pressure, inert gas or vessel diameter, but decreased appreciably as the hydrogen mole fraction was increased, and more markedly as the temperature was increased.

MECHANISM OF THE SLOW REACTION

The preceding observations indicate the marked contrast between the kinetic features of this reaction in aged boric acid coated vessels, and those previously reported in Pyrex[6], silica[16], porcelain[15], Durabax[20] and salt coated vessels[6,7]. In elucidating the mechanism, the reason for the increase in rate as the surface ages must be considered. The simplest suggestion is that the aging process causes the surface to become very inefficient for the destruction of HO_2, so that the probability of reaction 11 or 11a increases. In this case, however, the kinetic features of the reaction should be essentially similar to those in salt coated vessels, except that one power of the dependence on total pressure would be removed by the absence of diffusion control on the surface destruction.

A number of points suggest that H_2O_2 plays an important part in the mechanism. The autocatalytic nature of the reaction in Pyrex vessels has been attributed by Lewis and von Elbe[8] to a poisoning effect of water vapour on the chain

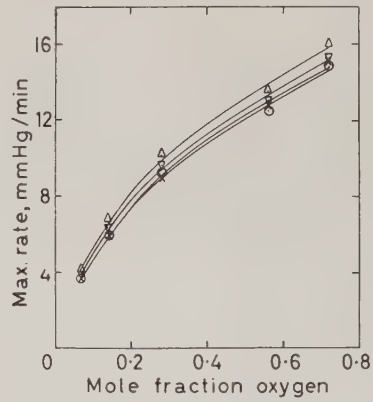

Figure 7. Effect of vessel diameter on maximum rate.
500 mm *pressure*, $x = 0{\cdot}28$
⊙ 51 mm *diameter* × 36 mm △ 24 mm ▽ 15 mm

termination properties of the surface. A similar explanation is implied by Chirkov[20] in discussing his observations in Durabax vessels. The absence of a diameter effect makes such an explanation extremely unlikely, and conclusive evidence against it is provided by the fact that addition of up to 22 mm of water vapour did not affect the maximum rate and caused only slight and irregular

changes in the induction period[13]. There is no alternative, therefore, but to attribute the induction period to the build-up of some relatively stable intermediate, and H_2O_2 appears the only possible agent.

A second piece of evidence for the importance of H_2O_2 in the mechanism comes from the accelerating influence of inert gas. Since there is no diameter effect, this influence of inert gas cannot be attributed to its role in preventing diffusion to the

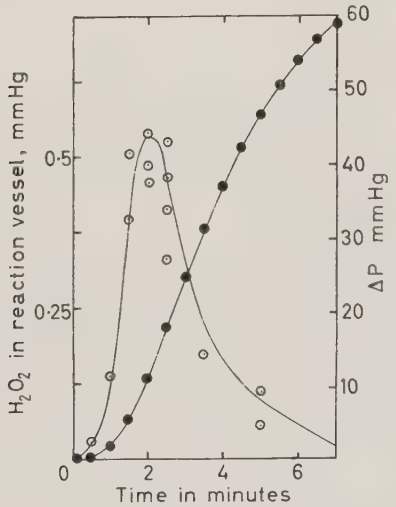

Figure 8. Detection of hydrogen peroxide in slow reaction.
500 mm *total pressure*, $x = 0{\cdot}28$, $y = 0{\cdot}72$
● *Pressure* ⊙ H_2O_2 (*different days*)

surface. Since increasing the concentration of inert gas reduces the rate of the branching reaction 2 relative to the non-branching reaction 4, it is difficult to see how acceleration by inert gas can be interpreted by its effect on reaction 4. The only reasonable alternative is an increase in the rate of dissociation of H_2O_2 by reaction 7. Even at this qualitative stage, therefore, evidence is provided that the dissociation of H_2O_2 occurs in bimolecular collisions.

To confirm that H_2O_2 is responsible for the autocatalytic nature of the reaction, a known sample of the reacting mixture was suddenly expanded, after a given time interval, into an evacuated trap cooled in liquid air. The H_2O_2 content of the trap was determined by colorimetric estimation with titanic sulphate, following essentially the procedure described by Egerton *et al.*[21]. A typical set of results is shown in *Figure 8*, and shows clearly the important part played by H_2O_2. The lack of precise reproducibility is attributed to decomposition of H_2O_2 vapour while passing through the connection to the sampling trap, this decomposition probably being accentuated by the grease on the tap of the sampling trap.

Since competition between reactions 11 and 5a would give the kinetic features of salt coated vessels, this H_2O_2 must be formed from HO_2 entirely by reaction 11, or entirely by the re-combination of HO_2 radicals either by the surface process 5 or the gas phase process 10.

$$2HO_2 = H_2O_2 + O_2 \qquad (10)$$

If reaction 11 predominates completely at the pressures used in the slow reaction studies, then 4 no longer leads to termination at the second limit, and the limits in aged vessels should be very much higher than in freshly coated or uncoated Pyrex vessels. Evidence given later shows that this is not the case. There seems little doubt, therefore, that the H_2O_2 is formed mainly by re-combination of HO_2 radicals either at the vessel surface or in the gas phase. In the former case, the function of aging is thus to ensure that all HO_2 radicals give rise to peroxide at the surface; in the latter case, it is probable that its function is to reduce the surface removal so that the gas phase concentration of HO_2 rises to a value at which the gas phase re-combination 10 predominates.

If H_2O_2 is to function as an active intermediate, dissociation by reaction 7 is inevitable. Competition between this dissociation and surface destruction of H_2O_2 can be ruled out by the absence of any diameter effect. If the peroxide always undergoes reaction 7, a straight chain is established by the reaction sequence

$$\overset{(4)}{\mathrm{H}} \rightarrow \overset{(5)\text{ or }(10)}{\mathrm{HO_2}} \rightarrow \overset{(7)}{\tfrac{1}{2}\mathrm{H_2O_2}} \rightarrow \overset{(1)}{\mathrm{OH}} \rightarrow \mathrm{H}$$

Branching by reactions 2 and 3 would thus cause the reaction to become explosive unless held in check by chain termination reactions. If 7 was the sole reaction of H_2O_2, k_7 would not enter into the kinetic expression. It is significant, however, that the overall activation energy of the reaction is close to the anticipated activation energy for reaction 7. A chain termination reaction between H_2O_2 and a chain centre thus seems inevitable. The mechanism is thus of the degenerate branching type described by Semenoff[22]; alternatively, H_2O_2 may be regarded as equivalent to two centres, where the reaction of H_2O_2 with a chain centre is a self-termination process, and the whole mechanism is of the branching, self-termination type.

The most likely reaction between a chain centre and H_2O_2 might appear to be reaction 6, used by a number of workers. A combination of reactions 1–4, 5, 6, and 7, however, gives the expression

$$\frac{\mathrm{d[H_2O]}}{\mathrm{d}t} = \frac{2k_2k_5k_7M'(k_4M + k_2)}{k_6(k_4M - 3k_2)(k_4M - k_2)} \qquad \text{(iii)}$$

This gives a diameter dependent reaction, effectively zero order with respect to H_2, O_2, and

total pressure. The diameter dependence introduced by k_5 can be eliminated by using reaction 10, but the remaining kinetic features are still entirely inconsistent with the experimental results. Conclusive evidence that reaction 6 does not occur is thus obtained.

If the kinetic expressions are worked out for the alternative termination reactions 14a and 15

$$H + H_2O_2 = H_2 + HO_2 \qquad (14a)$$

$$OH + H_2O_2 = H_2O + HO_2 \qquad (15)$$

the following expressions are obtained respectively

$$\frac{d[H_2O]}{dt} = \frac{2k_2k_7[O_2]M'(k_4M + k_2)}{k_{14a}(k_4M - k_2)} \qquad (iv)$$

$$\frac{d[H_2O]}{dt} = \frac{2k_1k_2k_7[H_2]M'(k_4M + k_2)}{k_{15}k_4M(k_4M - k_2)} \qquad (v)$$

In assessing the effect of hydrogen mole fraction in equations iv and v, the variation of the terms M and M' with mixture composition must be considered. Assuming the relative efficiencies of H_2, O_2 and N_2 are the same in reactions 4 and 7, and using the coefficients given[6] for O_2 and N_2 relative to H_2 as unity in reaction 4, then

$$M = mP, \qquad M' = m'P$$

where $$m = m' = x + 0{\cdot}35y + 0{\cdot}43z \qquad (vi)$$

and z is the mole fraction of nitrogen; k_4 is then the velocity constant when $M = H_2$.

The experimental features discussed previously appear to be intermediate between those indicated by expressions iv and v. Introducing both 14a and 15 into the reaction scheme gives a cubic equation for the stationary concentration of H_2O_2. By making assumptions which can later be justified, this equation can be solved to give a rate expression:

$$\frac{d[H_2O]}{dt} = \frac{2k_7[H_2O_2]M'(k_4M + k_2)}{(k_4M - k_2)} \qquad (vii)$$

where

$$[H_2O_2] = \frac{k_1[H_2]k_2[O_2]}{k_{15}k_4[O_2]M + k_{14a}k_1[H_2]} \qquad (viii)$$

Examination of expression vii shows that it will account qualitatively for the experimental results described earlier. In view of the remarkable reproducibility of the results, however, it is possible to carry out a precise quantitative analysis of a variety of possible mechanisms, and to draw the following detailed conclusions:

(*a*) *The dissociation of hydrogen peroxide*—The required order with respect to total pressure can only be obtained if the dissociation of H_2O_2 is written as the bimolecular collision process 7. Convincing support for the view of Lewis and von Elbe is thus obtained.

(*b*) *The reaction between* HO_2 *and* H—If the ratio $k_{15}k_4/k_{14a}k_1$ in equation viii is evaluated from the effect of oxygen mole fraction on the reaction rate, then equation vii predicts too small an effect of hydrogen, the rate at the highest mole fraction ($x = 0{\cdot}86$) being too low by a factor of nearly 100 per cent. While this discrepancy can be eliminated by a considerable reduction in the coefficients for O_2 and N_2 in equation vi for M', the opposing effects of M' in vii and M in viii then predict an inert gas effect which is far too small, and which, with one mixture composition, gives a rate independent of inert gas addition. The only alternative explanation is a contribution from reaction 11. At first sight this would appear unlikely, since if the ratio $k_{11}[H_2]/k_5$ is *ca.* unity at 500 mm pressure, a significant contribution from reaction 11 should occur at second limit pressures. The second limit determinations described later give little or no evidence for this. It is found, however, that the ratio $k_{11}[H_2]/k_5$ (or the equivalent term when the gas phase re-combination 10 is used) is multiplied by the factor k_4M/k_2 in the rate expression. Assuming that the second limit in KCl coated vessels is given by $2k_2/k_4$, and using the coefficients given in equation vi, then at 500°C, $k_2/k_4 = 18$, $M = 200$–400 (depending on mixture composition) at 500 mm pressure, and a relatively small contribution from $k_{11}[H_2]/k_5$ is magnified by a factor of 10–20 in the rate expression. Consequently, this reaction, while undetectable at the relatively low pressures at the second limit, may have a significant effect on the slow reaction.

(*c*) *The nature of reaction 11*—The reaction between HO_2 and H_2 can be written either as reaction 11 or 11a. Both these reactions have remarkably similar kinetic effects. In the former case it is the concentration of H_2O_2 that is affected in equation vii, the remaining terms being unaltered. In the latter case it is these terms that are changed, the H_2O_2 concentration being unaltered. While improved reproducibility in the peroxide determinations would be desirable, the results for three mixtures, two of quite different hydrogen concentration, indicate a close correlation between rate and H_2O_2 concentration, thus supporting reaction 11 rather than 11a.

(*d*) *Re-combination of* HO_2 *radicals*—A competition between the gas phase reaction 11 and the surface process 5 would result in a diameter dependence of the reaction rate, particularly at the highest hydrogen mole fractions where the operation of reaction 11 increases the rate by a factor of nearly 100 per cent. No such diameter effect is apparent, and it seems certain, therefore, that the HO_2 radicals form H_2O_2 in the gas phase, rather than by surface re-combination. This conclusion is also required by the second limit mechanism developed later. It also explains why reaction 8 appears to

play no part in the slow reaction, since at the higher relative concentration of HO_2 in the slow reaction, the rate of reaction 10 increases faster than the reaction 8; quantitative calculations support this conclusion that 8 can be neglected in the slow reaction.

(*e*) *The reaction between* H *and* H_2O_2—Two alternative forms of this reaction can be written, namely 14a and 14:

$$H + H_2O_2 = H_2O + OH \qquad (14)$$

The kinetic effects of these two reactions are almost identical in the slow reaction, though the equation using 14 gives slightly better agreement between observed and predicted results. More striking confirmation is provided by the fact that the mechanism developed later for the explosion limit clearly requires reaction 14 rather than 14a.

(*f*) *The choice between* $OH + H_2O_2$ *and* $O + H_2O_2$ (13)—These two reactions, which become important at low hydrogen concentrations, have rather similar kinetic effects. If, for example, reaction 15 is replaced by 13 in the mechanism used to deduce equations vii and viii, vii is unaltered, but the peroxide concentration is modified to

$$[H_2O_2] = \frac{k_3[H_2]k_2[O_2]}{k_{13}k_2[O_2] + k_{14a}k_3[H_2]} \qquad (ix)$$

At a fixed pressure, equation ix differs from viii only because of the variation of M with mixture composition, but whereas the stationary H_2O_2 concentration from ix is proportional to the first power of the pressure, in equation viii this power is less than unity. The difference between reaction 15 and 13 is thus revealed in the prediction of the effect of pressure and of N_2 addition, and the results favour reaction 15 rather than 13.

(*g*) *Complete mechanism*—The full scheme, involving reactions 1–4, 7, 10, 11, 14 and 15 gives a rate expression

$$\frac{d[H_2O]}{dt} = \frac{2dP}{dt} = 2R$$

$$= \frac{2k_7[H_2O_2]M'(k_4[O_2]M + k_2[O_2] + k_{14}[H_2O_2])}{(k_4[O_2]M - k_2[O_2] - k_{14}[H_2O_2])} \qquad (x)$$

where

$$[H_2O_2] = \frac{k_1[H_2]k_2[O_2](1 + \beta k_4M/k_2)}{k_{15}k_4[O_2]M(1 - \beta) + k_{14}k_1[H_2]} \qquad (xi)$$

and $$\beta = \frac{k_{11}[H_2](1 + k_2/k_4M)}{(4k_{10}R)^{1/2}} \qquad (xii)$$

Although equation x contains the rate on both sides of the equation, it can be used to predict the variation of rate with experimental variables either by using successive approximation methods, or by using the experimental rate as a sufficient approximation to elucidate the value of β.

By selecting suitable values of the ratios $k_{14}k_1/k_{15}k_4$, $k_7k_1k_2/k_{15}k_4$ and $k_{11}/k_{10}^{1/2}$ the rates predicted in *Figures 2–6* have been obtained. The remarkable agreement between observed and predicted rates over a very wide range of experimental conditions provides a convincing demonstration in support of the suggested mechanism. The inert gas effects are particularly striking, since the rates at 210 mm pressure in the absence of nitrogen have been predicted from constants obtained by using the variation of rate with mixture composition at a fixed pressure of 500 mm.

SECOND LIMIT MECHANISM

The failure to detect any evidence for reaction 6 between HO_2 and H_2O_2 indicates that significant modifications are necessary to previously suggested mechanisms[9,11] for the quadratic branching mechanism in boric acid vessels, since these mechanisms have incorporated 6 as the reaction determining the stationary concentration of H_2O_2. For the purpose of the present paper, it will be assumed that this controlling reaction now becomes 14, since this reaction predominates at normal O_2/H_2 ratios, and is even more likely to do so at the low O_2/H_2 ratios at which the quadratic branching effect becomes particularly marked. Introducing the quadratic branching reaction 8, and omitting 11, which can be shown to be almost negligible, then with the remaining reactions used for the slow reaction mechanism the stationary concentration of HO_2 is given by the equation

$$k_8[HO_2]^3 - \phi[HO_2]^2 - \alpha[HO_2] + \alpha\gamma = 0$$

where $$\phi = k_4[O_2]M - 2k_2[O_2]$$

$$\alpha = k_2k_7k_8[O_2]M'/k_{10}k_{14}$$

$$\gamma = k_4[O_2]M/k_8$$

By expressing the limiting condition for this cubic equation to have a positive root for all positive values of HO_2, the explosion boundary is obtained as

$$(9k_8\alpha\gamma - \alpha\phi)^2 = 4(\phi^2 + 3\alpha k_8)(\alpha^2 + 3\alpha\gamma\phi)$$

By making reasonable assumptions, which can later be shown to be justified, this reduces to

$$(9k_8\alpha\gamma)^2 = 12\alpha\gamma\phi^3$$

from which

$$M = \frac{2k_2}{k_4} + \left(\frac{27k_2k_7k_8^2MM'}{4k_4^2k_{10}k_{14}[O_2]}\right)^{1/3} \qquad (xiii)$$

This can be written in the form

$$mP = D + E(mm'P/y)^{1/3} \qquad (xiv)$$

To test this equation, second limits were measured

at 500°C in a 36 mm diameter vessel over a wide range of oxygen mole fractions (0·72–0·0044) at a constant hydrogen mole fraction of 0·28, using both fresh and aged vessels. With the aged vessels a mixing time of 15 sec was used to eliminate any possibility of water formation during the mixing period; with the fresh coating the same mixing time was also used, though the limit proved to be independent of mixing time between 15 and 120 sec.

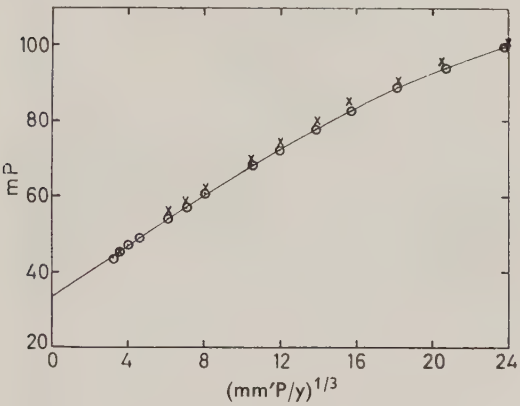

Figure 9. Second limits in boric acid coated vessels.
x = 0·28 ⊙ 36 mm *diameter aged*
× 36 mm *diameter fresh coating*

The plot of mP against $(mm'P/y)^{1/3}$ is shown in *Figure 9*. For the aged vessel, a good straight line is obtained over most of the oxygen concentration range. The falling off at very low oxygen concentrations may well be due to some contribution from surface destruction of H atoms, and in any case is slightly less than the curvature (*Figure 10*) of the plot of $mP - (1/Py)^{1/2}$ derived from the Egerton–Warren mechanism. Moreover, if the limits for mixtures of varying hydrogen mole fraction (0·07–0·86) are also plotted on *Figure 10*, they lie in a skew manner across the curve. This skew feature is almost entirely eliminated if equation xiii is modified[14] by introducing the reaction between OH + H_2O_2 to an extent consistent with the slow reaction studies.

The intercept on the mP axis in *Figure 9* gives a value of $D = 2k_2/k_4$ of 34 mm Hg. This is in close agreement with the value of 36–37 obtained from second limit studies in KCl coated vessels at 500°C, on the assumption that the mechanism in these vessels involves reactions 1–4 and 5a. The limits in the two vessels are thus consistent, and the difficulty raised by Warren[10] is avoided.

If reaction 14 is replaced by 14a, the value of D in equation xiv now becomes k_2/k_4. This is clearly inconsistent with the above data, and convincing evidence that H atoms react with H_2O_2 according to reaction 14 is thus obtained.

The results obtained with a fresh boric acid coating are also plotted in *Figure 9* and are effectively identical with the aged coating. While this would appear to suggest that the mechanism is exactly the same with both fresh and aged coatings, the authors would prefer to delay drawing this conclusion until evidence obtained by studying the effect of withdrawal rate on the limits in freshly coated vessels has been fully assessed.

CONCLUSION

The suggested mechanism, involving reactions 1–4, 7, 10, 14 and 15, with the addition of 11 for the slow reaction and 8 for the second limit, accounts extremely well for both the slow reaction and second limit observations in the aged boric acid coated vessel. No evidence has been found for reaction 6, though this does not necessarily exclude the occurrence of this reaction at the higher peroxide concentrations used by Satterfield and Stein[23] in studying the thermal decomposition of H_2O_2. Of the conclusions (*a*)–(*g*) summarized earlier, (*c*) and (*f*) may be regarded as less firmly established than the rest. The evidence for the nature of reaction 11 is based on peroxide determinations and improved reproducibility is desirable here, while the distinction between

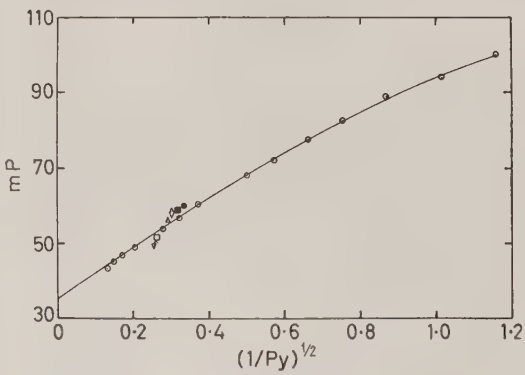

Figure 10. Egerton–Warren plot of second limits with aged coating.
36 mm *diameter vessel* ⊙ *x* = 0·28, *y* variable
y = 0·14 *x* = 0·86 ● 0·72 ■ 0·56 ◇ 0·42 △
0·28 ⊙ 0·14 ⊡ 0·10 × 0·07 ▽

OH + H_2O_2 and O + H_2O_2 rests on relatively small improvements in the prediction of total pressure and inert gas effects.

Assistance in the limit determinations by Mr. P. Doran, and in the peroxide determinations by Mr. C. Higgens is gratefully acknowledged. The authors wish to thank Professors Brynmor Jones and N. B. Chapman for the generous provision of facilities, the Royal Society and Imperial Chemical Industries for grants for the purchase of equipment, and the Preston Education Committee for the award of a research grant to Mr. L. Mayor.

REFERENCES

[1] Hinshelwood, C. N. *Proc. Roy. Soc. A* 188 (1947) 1

[2] Baldwin, R. R., Corney, N. S. and Simmons, R. F. *5th International Combustion Symposium*, p. 502. 1955. New York; Reinhold

[3] Baldwin, R. R. and Simmons, R. F. *Trans. Faraday Soc.* 51 (1955) 680

[4] — — *Trans. Faraday Soc.* 53 (1957) 955, 964

[5] Lewis, B. and von Elbe, G. *J. chem. Phys.* 10 (1942) 366

[6] — — *Combustion, Flames and Explosions of Gases.* 1951. New York; Academic Press

[7] Hinshelwood, C. N. and Willbourne, A. H. *Proc. Roy. Soc. A* 185 (1946) 353, 369, 376

[8] Lewis, B. and von Elbe, G. *3rd Symposium on Combustion, Flame and Explosion Phenomena*, p. 484. 1949. Baltimore; Williams and Wilkins

[9] Egerton, A. C. and Warren, D. R. *Proc. Roy. Soc.* 204 (1951) 465

[10] Warren, D. R. *Proc. Roy. Soc.* 211 (1953) 96

[11] Dixon-Lewis, G., Linnett, J. W. and Heath, D. F. *Trans. Faraday Soc.* 49 (1953) 766

[12] Baldwin, R. R. and Mayor, L. Unpublished results

[13] — — *XVIth International Congress of Pure and Applied Chemistry*, published in *Rev. Inst. franc. Pétrole*, April 1958.

[14] — — Papers submitted for publication.

[15] Hinshelwood, C. N. and Gibson, C. H. *Proc. Roy. Soc. A* 119 (1928) 591

[16] — and Thompson, H. W. *Proc. Roy. Soc. A* 118 (1928) 170

[17] — and Williamson, A. T. *The Reaction between Hydrogen and Oxygen.* 1934. Oxford

[18] Cullis, C. F. and Hinshelwood, C. N. *Proc. Roy. Soc. A* 186 (1946) 462

[19] Ashmore, P. E. and Dainton, F. S. *Nature, Lond.* 158 (1946) 416

[20] Chirkov, N. M. *Acta Phys. chim. U.R.S.S.* 6 (1937) 915

[21] Egerton, A. C., Everett, A. J., Minkoff, G. J., Rudrakanchana, S. and Salooja, K. C. *Analyt. chim. acta* 10 (1954) 422

[22] Semenoff, N. N. *Chemical Kinetics and Chain Reactions.* 1935. Oxford

[23] Satterfield, C. N. and Stein, T. W. *J. phys. Chem.* 61 (1957) 537

3

THE MERCURY PHOTOSENSITIZED HYDROGEN–OXYGEN REACTION AT LOW OXYGEN CONCENTRATIONS

J. S. WATSON

INTRODUCTION

The early investigations[1–6] on the mercury photosensitized hydrogen–oxygen reaction showed that hydrogen peroxide could be an important product although water was found in considerable amounts. There was some doubt however whether or not the quantum yield was greater than unity. Volman[7] in a careful study has concluded that hydrogen peroxide is the initial product and may be obtained in yields above 90 per cent. He has also shown that no chain reaction takes place and, in his work, obtained quantum yields varying from 0·29 to 0·54 depending on conditions. Volman's mechanism is essentially

$$Hg^3P_1 + H_2 \rightarrow 2H\cdot + Hg^1S_0 \quad (I)$$

$$H\cdot + O_2 \rightarrow HO_2\cdot \quad (1d)$$

$$HO_2\cdot + HO_2\cdot \rightarrow H_2O_2 + O_2 \quad (4)$$

$$H\cdot + M \rightarrow HM \quad (5)$$

$$HM + HM \rightarrow H_2 + M \quad (5a)$$

He considered that water was obtained either catalytically or photochemically from hydrogen peroxide.

Recently the question as to whether a chain can occur in the hydrogen–oxygen mercury sensitized reaction at room temperature has been raised by Callear and Robb[8]. They find that it will occur under special conditions, for example, in a mixture of 99·8 per cent H_2 and 0·2 per cent O_2 at a pressure of 45–50 mm Hg as many as ten molecules of water may be formed per photon absorbed. At higher and lower pressures the quantum yield falls to below unity however. These authors consider that a chain is propagated in the following manner

$$H\cdot + HO_2 \rightarrow 2OH\cdot \quad (2)$$

$$OH\cdot + H_2 \rightarrow H_2O + H\cdot \quad (3)$$

Another possible way to obtain the H atoms required to sustain the chain has been shown by Volman[7] to be

$$H_2O_2 + h\nu \rightarrow 2\cdot OH \quad (I) \text{ followed by}$$

$$\cdot OH + H_2\cdot \rightarrow H_2O + H\cdot \quad (3) \text{ as before}$$

In other words the hydroxyl radicals come from the photolysis of the hydrogen peroxide formed in reaction 4 and not directly from the reaction between H atoms and $HO_2\cdot$ radicals as envisaged by Callear and Robb.

The results of Callear and Robb were deduced from the thermal effects of the reaction of hydrogen and oxygen in a quartz cell when illuminated by a low-pressure mercury lamp. Since they were unable to measure the rates of consumption of H_2 or O_2 and the rate of production of products it was considered of interest to measure these quantities directly and obtain further proof that a chain mechanism is possible. This work confirms that at very low oxygen concentrations a chain reaction does occur and while results are not completely in agreement with those of Callear and Robb the mechanism of reaction is not incompatible with that of these authors.

EXPERIMENTAL

Materials

Hydrogen and oxygen were usually taken from commercial cylinders, roughly purified by passing through traps cooled in liquid nitrogen and stored in large glass flasks. Where high purity oxygen was required this was made by heating solid potassium permanganate *in vacuo*. Butane and ethylene used were research grade from the Phillips Petroleum Company. They were purified by the usual trap to trap distillations and the middle fraction taken.

Apparatus

A closed system in which the gases were circulated by a suitable pump[9] was used to enable the rates of disappearance of hydrogen and oxygen to be measured. The apparatus is similar to that described by Watson and Darwent[10]. It included a quartz spiral reaction vessel *Q* of 19 c.c. capacity separated by a cylindrical metal shutter *S* from an axially placed low-pressure mercury lamp *L* all enclosed in an electrically heated furnace. The gases were circulated over a mercury surface *SAT* maintained at 80°C by passing a suitable amount of current through heating coil *HC*, through the reaction vessel and traps which could be cooled to −180°C to freeze out products, and then through a Beckman Oxygen Analyser *A* in order to measure the concentration of oxygen throughout the experiment. The total volume of the system was

about 600 c.c. but this could be increased to about 1,800 c.c. by the inclusion of a 1,200 c.c. flask in the system. The flow rate used was normally about 4 litres per minute, allowing a contact time of 0·3 sec. Pressure changes during the experiment were noted on manometer M_1. Also attached to the system was an oxygen reservoir R the flow of oxygen into the system being controlled by needle

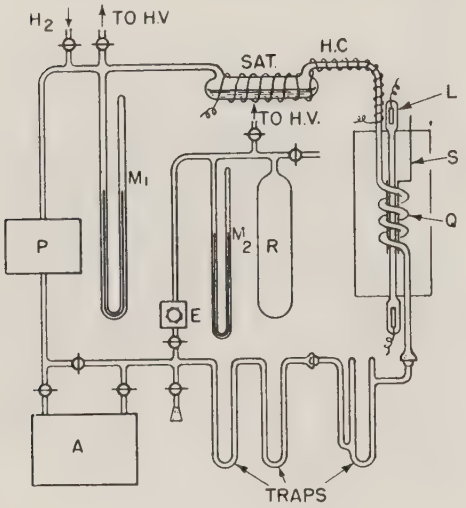

Figure 1. Diagram of apparatus

valve E. This valve is manufactured by W. Edwards and Co., England. The amount of oxygen admitted to the system could be easily computed since the volume of the reservoir was known and the pressure of gas registered on manometer M_2. The trap on the right hand side was of special design recommended by Volman[7]. It is effective in trapping out fogs since the outside is cooled in liquid nitrogen while the well is kept at room temperature by directing on it a stream of air. This trap was detachable so that the contents could be analysed.

Procedure

Before starting an experiment the whole apparatus was thoroughly evacuated. In experiments where there was always a finite amount of oxygen present, this was then admitted to the system via E until the desired pressure was obtained; it was not usually greater than 40 mm. This amount was checked against the Beckman Oxygen Analyser, the total oxygen admitted also being computed from the amount taken from the reservoir. Hydrogen was then admitted to the system to give the desired pressure, traps were normally cooled to $-180°C$ and the gases allowed to mix by circulating them for half an hour. During this time the lamp was switched on and allowed to come to a steady condition, the shutter being closed. The reaction was started by opening the shutter, and allowed to proceed for a measured time, usually until about 500 μmoles oxygen had reacted, during which time the total pressure and oxygen pressures were measured. At the end of the experiment the contents of the trap were usually analysed.

Some dexterity was required for the experiments where oxygen was fed into the system at such a rate that its consumption was complete on passing through the cell. Hydrogen was put into the system and photolysed for some time to ensure that no oxygen was present, then oxygen was slowly admitted via valve E while the reading on the Oxygen Analyser was carefully observed. The flow of oxygen was increased until a small reading was obtained on the Oxygen Analyser; when this happened there was a sudden rise in the oxygen concentration and the experiment had to be repeated. However by a series of experiments it has been possible to arrive at a figure for rate of oxygen consumption which must approach very closely to that required for maximum chain length.

Analysis

Water was estimated by gas–liquid partition chromatography; an 18 foot column containing glass spheres (passing 270 mesh) saturated with dioctyl phthalate was used. Experiments with known amounts of water showed that the area of the peak obtained was directly proportional to the amount of water passed through the column. This technique of course estimated the total water including that from any hydrogen peroxide which decomposed on passage through the column. In order to estimate the amount of peroxide a separate hydrogen oxygen experiment was required. Hydrogen peroxide was estimated by N/10 $KMnO_4$ solution. In experiments where ethylene was added to the mixture of hydrogen and oxygen the products were also analysed by gas chromatography.

Light intensity

The intensity of light at 2,537 Å was measured by observing the rate of production of hydrogen from propane or butane[12] and adopting the values of the quantum yields for these reactions as found by the authors. Since there is some doubt about the exact value of the figures[13] the intensity has been calculated to be of the order $1{\cdot}6 \pm 0{\cdot}1 \times 10^{-3}$ Einsteins per hour. This figure varied of course with the aging of the lamp and had to be checked from time to time. The intensity of the lamp was varied by altering the current through it and the relationship between current and intensity estimated with butane.

RESULTS

At room temperature somewhat erratic results were obtained due to the formation of a thin film, presumably of mercuric oxide, in the cell. This has been noticed by other workers[7,13] on hydrogen oxygen sensitized reactions. However at 45–50°C this complication was eliminated and experiments were done at this temperature. In order to obtain good yields of hydrogen peroxide certain other precautions had to be taken. These included cleaning the cell by photolysing butane in it at about 500 mm pressure for about one hour, or by flaming out the cell before reaction. It was also necessary to keep the reaction cell well saturated with mercury vapour and it was advantageous to keep the traps cooled in liquid nitrogen.

The course of typical experiments with an oxygen–hydrogen mixture (initial pressure about 500 mm Hg) containing initially about 4 per cent oxygen is shown in *Figure 2*. The flow rate was

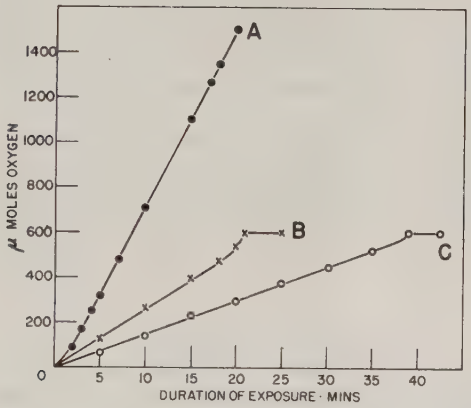

Figure 2. Consumption of oxygen under different conditions. Initial pressure of hydrogen about 500 mm Hg *in all cases. A, all* O_2 *consumed in passage through cell, trap at* −180°C; *B, initial* O_2 *pressure* 20 mm (600 μmoles), *trap at* − 180°C; *C, initial* O_2 *pressure* 20 mm (600 μmoles) *trap at room temperature*

about 4 litres per minute. When the trap was cooled in liquid nitrogen hydrogen peroxide was the main product and the rate of oxygen consumption equalled the rate of hydrogen consumption. On the other hand if the cooling were omitted only water was found and the oxygen consumption was then about half the hydrogen consumption. It is of interest to note that the rate of oxygen consumption remained constant until it had nearly all been consumed, then there was a slight increase in rate (curves *B* and *C*, *Figure 2*).

On the other hand when initially only hydrogen was present in the system and oxygen was fed in at such a rate that it disappeared completely on reaction the rate of consumption increased markedly (curve *A*, *Figure 2*). In contrast also to the first set of experiments the rate of oxygen consumption was found to be dependent on the total gas pressure (curve *A*, *Figure 3*). These rates

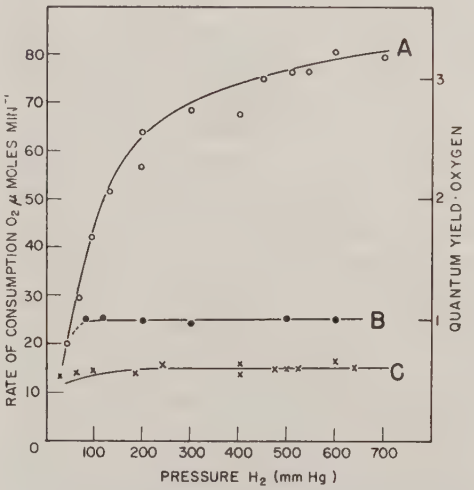

Figure 3. Effect of hydrogen pressure on the quantum yield. A, fast flow rate; B, slow flow rate; oxygen consumed completely on passage through the cell; C, results of experiments with hydrogen–oxygen mixtures containing not more than 10 per cent *oxygen initially*

increased from about 15 μmoles per minute at 50 mm pressure to about 80 μmoles per minute at 700 mm pressure. Rates for the non-chain reaction remained at about 15 μmoles per minute over this range when water was the product. In no experiment where a chain reaction occurred was hydrogen peroxide found; the sole product was water.

Packed cell

In order to determine if the surface of the cell were influencing the reaction rate the cell was packed with Pyrex glass beads 3 mm in diameter. These doubled the effective area of the cell but the volume was reduced to half. Apart from reducing the rates of reaction slightly this treatment appeared to have little effect on the general course of the reaction.

Effect of reducing flow rate

Reducing the flow rate from 4 litres per minute to 0·1 litres per minute had a marked effect on the rate of reaction when oxygen was admitted at a rate where it was entirely consumed (curve *B*, *Figure 3*). The effect was very much less on the non-chain reaction however.

Effect of added ethylene

This effect is illustrated in Table 1. It will be noted that the rate of oxygen consumption is the same whether the mixture of hydrogen and

oxygen contained initially oxygen or not. In both cases the rate was about 29 μmoles per minute, about the same rate as when hydrogen peroxide was the only product from the oxygen-hydrogen reaction. The ethylene added had evidently

TABLE 1

Effect of Ethylene on the Hydrogen–Oxygen Reaction (Initial hydrogen pressure about 500 mm Hg in all cases)

$P_{C_2H_4}$ mm Hg	P_{O_2} mm Hg	R_{O_2} μmoles min^{-1}	R_{H_2O} μmoles min^{-1}
25	25	29	—
25	0*	29	—
nil	25	15†	30
nil	25	28‡	—
nil	0*	75	150

* Oxygen consumed as fast as it enters reaction cell.
† Rate when water is produced.
‡ Rate when hydrogen peroxide is produced (Trap at −180°C).

stopped any chain reaction. The products of this reaction were ethyl alcohol, acetaldehyde, a little water but the main product was ethyl hydroperoxide. The results agree with those of Turner, Callear and Cvetanovic[14] who have investigated this reaction recently.

Quantum yield

From the results of repeated experiments with hydrogen–oxygen mixtures and by constantly checking the intensity of the light from the lamp, it is reasonably certain that the quantum yield for the non-chain reaction is 0·6 ± 0·05 and not 1·00 as would be expected if reaction I were completely efficient. This figure leads to a maximum quantum yield for the oxygen disappearance in the chain reaction to be of the order 3·0 ± 0·25 at a pressure of 500 mm Hg. This means that about six molecules of water are formed per quanta absorbed.

Effect of light intensity

Reducing the intensity to about a quarter of its value reduced the rates of reaction about the same amount whether the reaction was a chain or not.

DISCUSSION

The following mechanism is a simplified version of that used by Callear and Robb to explain their results,

$$H_2 + Hg^3P_1 \rightarrow 2H\cdot + Hg^1So \quad (I)$$
$$H\cdot + O_2 + H_2 \rightarrow HO_2\cdot + H_2 \quad (1)$$
$$H\cdot + HO_2\cdot \rightarrow 2OH\cdot \quad (2)$$
$$\cdot OH + H_2 \rightarrow H_2O + H\cdot \quad (3)$$
$$HO_2\cdot + HO_2\cdot \rightarrow H_2O_2 + O_2 \quad (4)$$
$$H\cdot \rightarrow \text{wall} \quad (5)$$

the reactions $H\cdot + O_2 \rightarrow HO_2^{\star}\cdot$, 1a, $HO_2^{\star}\cdot \rightarrow H\cdot + O_2$, 1b, and $HO_2^{\star}\cdot + M \rightarrow HO_2\cdot + M$, 1c, being replaced by reaction 1. When no chain is produced the reaction may be explained simply by reactions I, 1, 4 and 5, this being essentially the mechanism proposed by Volman.

For the chain mechanism reactions I and 1 are the initiating steps and reactions 2 and 3 are chain carriers. Other possible propagating steps such as

$$HO_2\cdot + H_2 \rightarrow H_2O_2 + H\cdot \quad (3a)$$
$$HO_2\cdot + H_2 \rightarrow H_2O + OH\cdot \quad (3b)$$

are not considered likely; both would lead to a chain reaction in the normal mercury sensitized reaction, that is when the oxygen concentration is appreciable, and this has been shown not to be the case from the present work and from the results of Volman. In any case step 3a requires an activation energy[15] of about 17 kcal and is endothermic[16] to about 14 kcal. Callear and Robb[8] also consider that H_2O_2 formed by reaction 3a would decompose immediately into two ·OH radicals as happens with reaction 2. Reaction 3b is, however, exothermic to the extent of 54 kcal[16,17] (with a third body) and may be a possibility. However the present results show that a chain occurs only when all oxygen is consumed in passing through the cell so that there must be an excess of H atoms present. Further evidence of this is obtained by noting the effect of ethylene on the reaction; the chain is completely stopped. There does not seem to be much doubt that reaction

$$C_2H_4 + H\cdot \rightarrow C_2H_5\cdot \quad (7)$$

consumes the excess H· atoms produced, thus suppressing reaction 2 completely. In addition reaction 3 has a small activation energy of the order 7 kcals (the figures in the literature are divergent however[18]) and the reaction is exothermic by 15 kcal.

There is a further possible manner by which a chain reaction may occur. There is no doubt that hydrogen peroxide formed in reaction 4 may decompose either catalytically, on mercury for example, or by absorbing light. The mechanism[14] generally accepted is

$$H_2O_2 \rightarrow 2OH\cdot \quad (I')$$
$$\cdot OH + H_2O_2 \rightarrow H_2O + HO_2 \quad (6)$$
$$HO_2\cdot + HO_2 \rightarrow H_2O_2 + O_2 \quad (4)$$
$$HO_2\cdot + \cdot OH \rightarrow H_2O + O_2 \quad (4a)$$

Volman[20] has found that the photolysis of hydrogen peroxide even when present in small quantities can initiate the non-sensitized hydrogen–oxygen reaction and gives reaction 3 as the chain carrier

$$\cdot OH + H_2 \rightarrow H_2O + H\cdot \quad (3)$$

This mechanism has also been used to account for the reduced amount of hydrogen peroxide in the photolysis of water vapour when hydrogen is added[21]. There seems no doubt that OH radicals are produced from hydrogen peroxide in the non-chain reaction since only water is found when the traps are not cooled, and the question is, why do these not initiate a chain when it has already been shown that OH radicals are chain carriers when the oxygen concentration is very small? A possible explanation is that reaction 6 may occur when H_2O_2 is initially present and will compete with reaction 3, also reaction 2 is exothermic to the extent[22] of 85 kcal so that the OH radicals may be sufficiently 'hot' to react in 3. However it is possible, as will be seen in the next section, that no peroxide at all is formed in the chain reaction so that a reaction initiated by this mechanism is not applicable.

Incidentally from the mechanism postulated by Volman it will be evident that, even when no chain occurs, one molecule of hydrogen peroxide should react with H_2 to give eventually two molecules of water. No oxygen would be regenerated. If this were so, the rate of consumption of oxygen would be the same whether or not water or hydrogen peroxide is produced. That the rate of consumption of oxygen when water is the sole product is half that when hydrogen peroxide is the only product is a strong indication that reaction 3 does not occur in the non-chain reaction.

Terminating steps

A stationary state treatment of equations I to 5 using 4 as the terminating step and omitting equation 5 gives the rate of production of water as

$$R_{H_2O} = \frac{4I\,k_3\left(\frac{2I}{k_4}\right)^{1/2}}{K_1[O_2][H_2] - k_2\left(\frac{2I}{k_4}\right)^{1/2}} \qquad \text{(a)}$$

whereas utilizing 5 and omitting 4 the rate becomes

$$R_{H_2O} = 4I \cdot \frac{k_1}{k_5}[H_2]^2[O_2] \qquad \text{(b)}$$

From equation 2 it will be seen that if reaction 4 is the important terminating step it would be expected that the rate of production of water, or, what is the same thing, the rate of consumption of oxygen would depend on the reciprocal of the hydrogen concentration and on some power of the light intensity greater than one, whereas if reaction 5 were the only terminating step the rates would depend on the square of the hydrogen concentration and on the first power of the light absorbed, equation b. Callear and Robb deduced that up to about 40 mm pressure the mechanism where H atoms are removed by the wall is important but that at greater pressures the main terminating step is reaction 4 and it reduces the chain very quickly to zero. In this work a maximum chain reaction at some particular hydrogen pressure was not observed, the rate of oxygen consumption increasing rapidly as the pressure increased to about 200 mm, and at greater pressures increasing at a slower rate (curve *A*, *Figure 3*). An important difference in the experimental technique is that the experiments of Callear and Robb were carried out in a static system using a cell of comparatively large volume where H atoms had to diffuse to the walls, while in this work a small cell was used and the gases were passed through it at a comparatively fast rate. From this it would be expected that wall reactions would be less important since a wall reaction is directly proportional to contact time and inversely proportional to flow rate. However the proximity of the walls would offset the effect of the fast flow rate. Reducing the flow rate from 4 litres per minute to 0·1 litres per minute has a marked effect on the rate of reaction as will be seen from *Figure 3*. Volman in his work also noticed a considerable alteration in the rate of reaction on altering the flow rate. A further test for a wall reaction is that of altering the surface/volume ratio. In the packed cell used the surface area was doubled but the volume was halved so that the effects would cancel each other out and thus this cell had little effect on the rates. It is thus apparent that reaction 5 is an important terminating step.

Since these results are at variance with those of Callear and Robb another reason for studying the reaction at reduced flow rates was to attempt to approach their conditions in the hope that a maximum quantum yield might be obtained in the region between 50 and 700 mm pressure. However, as already noted the effect of reducing the flow rate was merely to reduce the rate of reaction over the whole range of pressure. The most likely explanation of the difference in results is that reaction 4 is not such an important terminating step in this work. Some weight is given to this idea from the fact that no hydrogen peroxide is found when there is a chain reaction and appreciable amounts would be expected since the chain is short. It seems possible that the $HO_2\cdot$ radicals formed will react with H atoms rather than with each other since the oxygen is deficient. Furthermore, their rate of reaction with hydrogen atoms is about nine times faster than the re-combination reaction 23. However there is not much doubt that there must be other terminating steps in addition to step 5 since the reaction rate falls off

with increasing pressure at least in the range investigated. Terminating steps such as

$$H\cdot + H\cdot + H_2 \rightarrow H_2 + H_2 \qquad (5a)$$

$$H\cdot + OH\cdot + H_2 \rightarrow H_2O + H_2 \qquad (5b)$$

are possible, the hydrogen present acting as third body. Reaction 4a is also a possible terminating step.

It must be concluded therefore that while the evidence concerning the propagating steps is strongly in support of reaction 2 followed by reaction 3, the nature of the terminating steps is rather obscure.

REFERENCES

[1] Dickinson, R. G. *Proc. nat. Acad. Sci., Wash.* 10 (1924) 409

[2] Marshall, A. L. *J. phys. Chem.* 30 (1926) 1078; *J. Amer. chem. Soc.* 49 (1927) 2763

[3] Bates, J. R. and Taylor, H. S. *J. Amer. chem. Soc.* 49 (1927) 2438

[4] — and Salley, D. J. *J. Amer. chem. Soc.* 55 (1933) 110

[5] — *J. chem. Phys.* 1 (1933) 457

[6] Frankenburger, W. and Klinkhardt, H. *Z. phys. Chem.* 1315 (1932) 421

[7] Volman, D. H. *J. chem. Phys.* 14 (1946) 707

[8] Callear, A. B. and Robb, J. C. *Trans. Faraday Soc.* 51 (1954) 649

[9] Watson, J. S. *Canad. J. Tech.* 34 (1956) 373

[10] Watson, J. S. and Darwent, B. deB. *J. phys. Chem.* 61 (1957) 577

[11] Bywater, S. and Steacie, E. W. R. *J. chem. Phys.* 19 (1951) 319

[12] Cvetanovic, R. J. *J. chem. Phys.* 23 (1955) 143

[13] Evans, M. G. *J. chem. Phys.* 2 (1934) 726

[14] Turner, A. H., Callear, A. B. and Cvetanovic, R. J. To be published

[15] Lewis, B. and von Elbe, G. *Combustion, Flames and Explosions of Gases*, p. 59. 1951. New York; Academic Press

[16] Schumb, W. C., Satterfield, C. N. and Wentworth, R. L. *Hydrogen Peroxide*, p. 39. 1955. New York; Reinhold

[17] Schwab, G. M. *Catalysis*, p. 43. 1937. London; Macmillan

[18] See refs. 8, 16, 21 also Hardwick, T. J. *Atomic Energy of Canada Ltd. Publ. No.* 459 (May 1957)

[19] Giguère, P. A. and Liu, I. D. *Canad. J. Chem.* 35 (1957) 283

[20] Volman, D. H. *J. chem. Phys.* 23 (1955) 2458; 25 (1956) 288

[21] Taylor, H. A. and Chen, M. C. *J. chem. Phys.* 27 (1957) 857

[22] Calculation using the dissociation energy $D(H—O_2) = 2{\cdot}04$ eV given by Foner, S. N. and Hudson, R. L. *J. chem. Phys.* 23 (1955) 1364–5, and the data of Weiss, J. *Advances in Catalysis IV*, p. 362. 1952. New York; Academic Press

[23] Robb, J. C. Private communication

4

PRODUCTION OF HYDROGEN PEROXIDE IN REACTING MIXTURES OF HYDROGEN AND OXYGEN

J. W. LINNETT and C. P. TOOTAL

INTRODUCTION

Our object was to study the production of hydrogen peroxide in hydrogen–oxygen mixtures under conditions between the second and third explosion limits. A flow method was used, the temperature being 566°C. Pease[1] and Holt and Oldenberg[2] have made observations of this type. Pease, using a flow system with chemical analyses of the exit gases showed that hydrogen peroxide was formed under his conditions. From experiments at 1 atmosphere and 540°C using a Pyrex reaction vessel 1·7 cm in diameter and 10 cm long ($v = 20$ c.c.) he concluded that: (*a*) a stationary concentration of hydrogen peroxide had been reached (residence times: 6 to 20 seconds), and (*b*) that the formation of water and hydrogen peroxide is greater with hydrogen in excess than with oxygen in excess. However conclusions (*a*) and (*b*) each rest on a single experiment.

Holt and Oldenberg using a reaction vessel 130 cm long and 5·5 cm in diameter showed spectroscopically that hydrogen peroxide was actually present in the reacting gases. Their experiments were carried out at 530 to 540°C with residence times of 3 to 7 sec. The total pressure is not stated but it seems likely that it was 1 atm. The results of 13 experiments showed that the ratio of the quantity of hydrogen peroxide determined spectroscopically to that determined chemically in the exit gases was approximately constant. The latter was greater; perhaps because an average content of the reaction vessel was determined spectroscopically whereas it was the 'end gases' which flowed out of the reaction vessel and were analysed chemically. Holt and Oldenberg also concluded that the amount of hydrogen peroxide obtained was very dependent on the surface conditions of the tube and therefore the results lacked reproducibility. They did not seem to have reached conditions in which the hydrogen peroxide had attained a stationary concentration, and state that a longer heating time leads to a higher concentration of hydrogen peroxide. It is doubtful therefore whether their results are relevant to discussions of stationary concentrations.

Holt and Oldenberg conclude that the 'formation of hydrogen peroxide is enhanced by a large hydrogen to oxygen ratio'. They quote three sets of results in support of this, but in two, increasing the hydrogen to oxygen ratio is accompanied by an increase in the residence time which, by itself, is known to increase the quantity of hydrogen peroxide produced under Holt and Oldenberg's conditions. Moreover as regards the first set (experiments 8 and 10) one could equally quote experiments 15, 16 and 17 which do not support the conclusion. A further difficulty in interpreting Holt and Oldenberg's results is that no measurements were made of the amount of water formed; that is of the extent of reaction.

These two papers provide the only information regarding the production of hydrogen peroxide from hydrogen and oxygen reacting isothermally at temperatures between 500 and 600°C. Since this information is most important when considering the reaction mechanism it was proposed to make a systematic study of the production of hydrogen peroxide under similar conditions and this paper describes our first results.

EXPERIMENTAL METHOD

Hydrogen and oxygen, from cylinders, were dried and their flow rates measured on flow-meters. The gases were mixed, passed through a control valve, and then down a narrow-bore tube into the cylindrical silica reaction vessel which they entered tangentially at the bottom. They flowed out of the reaction vessel from the centre of the top via a straight tube of 2 mm internal diameter. From this they passed to two consecutive *U* tube traps cooled in liquid oxygen in which the water and hydrogen peroxide were frozen out. The gases then passed via another control valve to the pumps. The water condensed in the traps was determined by weighing, and the hydrogen peroxide by titrating with a standard ceric solution using ferroin as indicator. By using two traps it was possible to be sure that, in most experiments, virtually all the hydrogen peroxide and water had been condensed. In a few experiments at the highest flow rates all had not been condensed, but by using the results for the two *U* tubes it was possible to make an allowance for what had not been condensed. Before use the reaction vessel had been washed

with hot nitric acid and 12 times with distilled water. The temperature, measured with a thermocouple, was 565–567°C in all experiments. A third tube was connected directly to the reaction vessel and this led to a mercury manometer.

EXPERIMENTAL RESULTS AND DISCUSSION

The first set of experiments was designed to examine the effect of residence time (i.e. flow rate). A mixture of a fixed composition ($2H_2 + O_2$) at a fixed pressure (230 mm) was passed through the vessel at various rates and the water and hydrogen peroxide in the traps determined. The results are shown in *Figures 1* and *2* in which the amounts of water and hydrogen peroxide are expressed as partial pressures in the gases flowing from the reaction vessel. From *Figure 1* it will be seen that the results appear to fall into two sets. For both, the partial pressure of water in the exit gases is proportional to the residence time. Points for experiments 17, 20, 27, 28, 29, 30, 31, 32, 34 and 38 lie on the upper line, while points for experiments 23, 24, 25, 26, 35, 36 and 37 lie on the lower one. That for 33 lies between the two lines. Experiments 18, 19, 21 and 22 were not concerned with this set. It seems therefore that for certain periods the vessel showed one behaviour and for others another. This is probably associated with the condition of the surface. Explosions sometimes took place in the vessel but we could not correlate the changing behaviour with the occurrence of explosions. Apparently the surface changes its nature (if that is the true explanation) as a consequence of conditions we have not controlled.

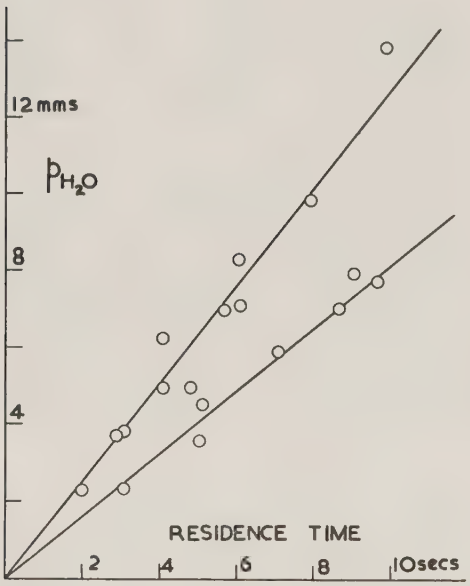

Figure 1. Variation of partial pressure of water formed with residence time for a $2H_2 + O_2$ *mixture at* 230 mm

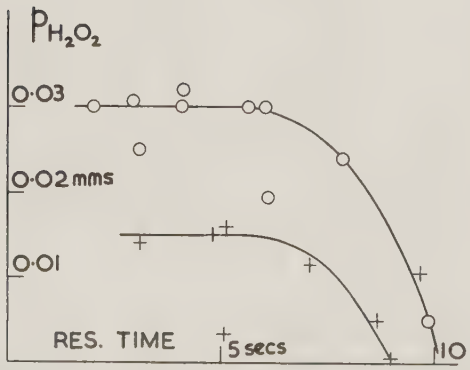

Figure 2. Variation of partial pressure of hydrogen peroxide formed with residence time for a $2H_2 + O_2$ *mixture at* 230 mm

In *Figure 2* the results for hydrogen peroxide are presented, the results for the upper set in *Figure 1* being marked by circles and those for the lower set in *Figure 1* by crosses. These also form two sets though there are here one or two more random points. Nevertheless it appears, for both sets, that the partial pressure of hydrogen peroxide remains constant for residence times up to 5 or 6 seconds, then falls off rapidly at longer residence times. Since the results in *Figure 1* show that for residence times from 2 to 5 or 6 seconds the water produced increases steadily with time it does seem that a stationary concentration of hydrogen peroxide has been reached. The fall off at longer residence times might be due either to a destruction of hydrogen peroxide in the reaction vessel as the reaction proceeds (e.g. by water) though this seems unlikely if account is taken of the results of Pease[1]; alternatively it may be due to the decomposition of hydrogen peroxide in the tubes between the reaction vessel and the traps. This would be expected to be greater the slower the flow rate though it is surprising that the fall off is so rapid. To account for this it would appear to be necessary to suppose in addition that the reaction is autocatalytic perhaps on the walls of the tube which carries the mixture out of the furnace and which is therefore warm.

Because of the above results the next experiments were all carried out at a constant residence time of about 4 seconds. The pressure was kept constant at 230 mm and the hydrogen to oxygen ratio varied. The results for water and hydrogen peroxide produced are given in *Figures 3* and *4*. It will be seen that the partial pressures of both decrease as the hydrogen/oxygen ratio (R) is increased. The results are surprisingly consistent, and since the sequence of experiments with increasing hydrogen/oxygen ratio was 41, 39, 47, 42,

46, 40, 45, 48 it seems that here the behaviour of the surface must have remained very constant even though 6 days elapsed between experiments 42 and 45. (Experiment 43 followed two explosions in the vessel and the amount of hydrogen peroxide produced was very small; 44 was not a member of this set; the point off the line in *Figure 4* is for experiment 46.) There seems little doubt therefore that under these conditions (566°C, 230 mm, residence time 4 sec) the extent of reaction and the concentration of hydrogen peroxide decrease with increasing hydrogen/oxygen ratio.

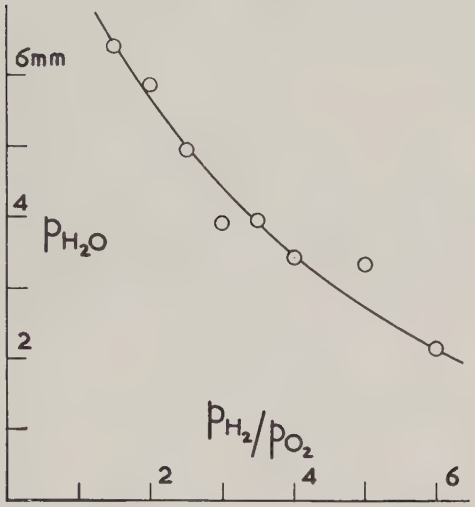

Figure 3. Variation of partial pressure of water formed with the ratio p_{H_2}/p_{O_2} *for a total pressure of* 230 mm *and a residence time of* 4 sec

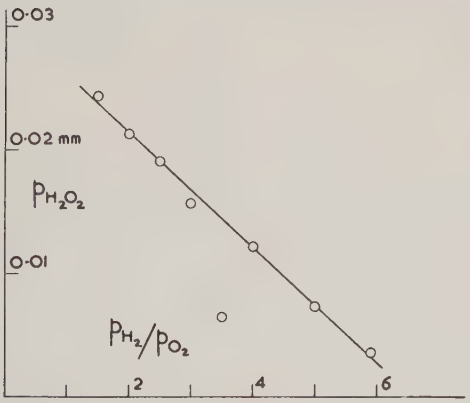

Figure 4. Variation of partial pressure of hydrogen peroxide formed with the ratio p_{H_2}/p_{O_2} *for a total pressure of* 230 mm *and a residence time of* 4 sec

The results summarized in *Figure 3* are surprising because all workers on this reaction have agreed that the rate of reaction increases more rapidly with increasing hydrogen pressure than with increasing oxygen pressure. However a closer examination of the literature shows that all data on rates have been obtained for conditions well above the second limit whereas it was realized that the present data are for conditions very close indeed to the second limit. To test this a few measurements were made of second limits in the same flow apparatus by reducing the pressure in the reaction vessel by opening the exit control valve until explosion occurred.

The results for a 50 : 50 mixture are shown in *Figure 5*. It was found that the measured limits were dependent on flow rate (F) and in *Figure 5* the measured limit is plotted against the reciprocal of the flow rate. The fall in the limit pressure on passing to lower flow rates (longer residence times) suggests that at lower flow rates there is an increased production of water which presumably, by virtue of its known large third-body coefficient for the reaction $H + O_2 + M \rightarrow HO_2 + M$, lowers the second limit. Extrapolation to $1/F = 0$ will give some idea of the limit for dry gases. This is considerably higher than the limits recorded in the literature. Since these have been obtained by the withdrawal method it appears that in such determinations some water may have been present. It should be noted that the results in *Figure 5* were for residence times of 3 to 6 sec and those in *Figure 3* for a residence time of 4 sec.

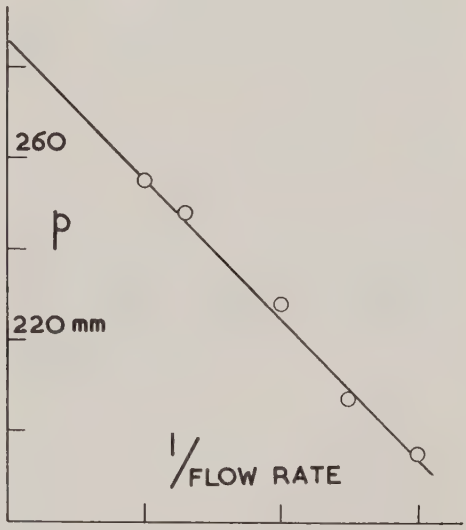

Figure 5. Variation of second limit explosion pressure for an $H_2 + O_2$ *mixture with the reciprocal of the flow rate (at* 567°C)

From a curve analogous to *Figure 5* the extrapolated limit for a $2H_2 + O_2$ mixture was found to be 255 mm; but in the set of experiments, the results of which are summarized in *Figures 3* and *4*, a $2H_2 + O_2$ mixture was studied at 230 mm.

Since this did not explode and indeed the extent of reaction was quite small it must have been rendered non-explosive by the water produced and present in the vessel. These figures show that our experiments were carried out at pressures very near the second limit. Since it is difficult to know exactly what allowance to make for the water in the reaction vessel it is difficult to deal with our data quantitatively. However it can be stated quite certainly that qualitatively the form of *Figure 3* is due to the fact that an increase in the H_2/O_2 ratio moves the mixture away from the limit conditions because the third-body coefficient of hydrogen is greater than that of oxygen. The result of this is that, as the mixture moves further from the limit, the rate of reaction decreases. An approximate calculation shows this to be reasonable, but the difficulty regarding the water makes a precise treatment too uncertain to be worth while.

Under these conditions it can be seen from *Figure 4* that the curve for the production of hydrogen peroxide is similar in form to that in *Figure 3* for water; that is it runs roughly parallel with the rate of reaction. This suggests that the hydrogen peroxide may be produced from HO_2, the stationary concentration of which will increase as the limit is approached. A stationary concentration of hydrogen peroxide could be achieved as a result of a balance between production from HO_2 and destruction, perhaps at the wall.

It will be noted in *Figure 3* that the decrease in hydrogen peroxide production from $R = 1{\cdot}5$ to $R = 6$ is relatively greater (sevenfold) than the decrease in the production of water over the same range (threefold). Since, on passing from $R = 1{\cdot}5$ to 6 the mixture is moving away from the limit (*cf.* above) and therefore presumably the chain length is decreasing, the bulk of initiation cannot arise from the stationary concentration of hydrogen peroxide under these conditions. If it did, the production of water would be expected to decrease more than sevenfold from $R = 1{\cdot}5$ to $R = 6$.

It is proposed to carry out more measurements in the region near the second limit and to extend them to conditions more distant from that limit. The effect of surface coatings will also be studied.

REFERENCES

[1] Pease, R. N. *J. Amer. chem. Soc.* 52 (1930) 5107
[2] Holt, R. B. and Oldenberg, G. O. *J. chem. Phys.* 17 (1949) 1091
[3] Lewis, B. and von Elbe, G. *Combustion, Flames and Explosions of Gases*, p. 42. 1951. New York; Academic Press.

5

THE RATE AND MECHANISM OF THE THERMAL DISSOCIATION OF OXYGEN

K. F. HERZFELD

INTRODUCTION

The rate of any elementary forward reaction (like a dissociation) is connected with that of the corresponding back reaction (e.g. re-combination) by the equilibrium constant which is thermodynamically determined.

Making use of this relationship and assuming that every collision of two atoms leads to re-combination, the rate constant for the dissociation of a diatomic molecule was first deduced[1] to be

$$[k] = \nu \exp\left(-\frac{D}{kT}\right) \tag{1}$$

where ν is the vibrational frequency and D the dissociation energy per molecule. This is valid if the temperature is so high that the vibrational specific heat is R. If only the vibrational ground state is present, expression 1 has to be multiplied with the reciprocal ratio of the partition functions, and one gets[2]

$$[k] = \frac{kT}{h} \exp\left(-\frac{D}{kT}\right) \tag{2}$$

At the time these formulae were deduced it had not been realized that a triple collision is necessary for re-combination, to remove the energy set free. When this became clear[3] it was thought that every triple collision would lead to re-combination[4]. Therefore, both the rate of re-combination and of dissociation were multiplied with the factor σ/Λ (σ molecular diameter, Λ mean free path). The equilibrium constant is of course unchanged. If one introduces the time τ_c between collisions, this can be set approximately

$$\tau_c = \Lambda/\bar{w}$$

where $\bar{w}$ is the mean thermal speed, so that

$$[k] = \sigma/\Lambda\, \nu \exp\left(-\frac{D}{kT}\right) = \frac{1}{\tau_c}\frac{\sigma}{\bar{w}}\nu \exp\left(-\frac{D}{kT}\right) \tag{3}$$

The factor $\sigma\nu/\bar{w}$ is of the order unity for standard density.

Since recent experiments, discussed farther on, seem to indicate a rate higher than that calculated from equation 3, Logan[5] has assumed that an equation of the form 3, or rather of the corresponding form

$$[k] = \frac{\sigma}{\Lambda}\frac{kT}{h} \exp\left(-\frac{D}{kT}\right) \tag{4}$$

is valid for every vibrational state of the molecule separately, so that to get the overall rate of dissociation one should multiply equation 2 with the total number of possible excited states (30–40). Such an assumption would however imply a very large re-combination cross-section, one 30–40 times the classical one.

It should be pointed out that in the dissociation of diatomic molecules the rate of the energy supply is decisive, while in polyatomic molecules, if the pressure is not too low, the energy supply is considered sufficiently fast, so that the reaction rate is determined by the rate of transition through an 'activated' state[2].

Equations 3 and 4 are based on the assumption —although this was not recognized at the time— that the efficiency of energy removal by the third partner in re-combination and the efficiency of energy supply by collision in dissociation is unity. The recent experimental and theoretical[6,7] determinations of this efficiency, which were occasioned by ultrasonic investigations, have shown[8,9] that on the contrary this efficiency is small if the energy transferred is high. This paper is concerned with the application of these results to the problem of dissociation rates.

The classical model for the quantum theoretical calculations based on the fundamental ideas of Landau and Teller[10] is then as follows:

A particle A hits a molecule O_2—which may be vibrating—in an arbitrary direction. The first effect is that the directly hit O atom receives additional velocity towards his partner and bounces back. The efficiency of the collision depends on the question whether it can return part of the excess energy to the hitting particle. If yes (adiabatic collision) no dissociation occurs; if no—because particle A has already moved away —the outward motion of the O atom continues

and, if the energy is sufficient, ends in dissociation of the molecule into atoms.

Bodenstein and Lütkemeyer[11] have first tested equation 3, or rather the rate of re-combination, by measuring indirectly the stationary concentration of Br atoms produced by photodissociation, and found good agreement. More recent measurements on iodine with similar methods have been made by Davidson and his co-workers[12,13] and by Norrish[14]. Comparison with the theory has not been made.

The use of the shock tube at high Mach numbers has made possible the determination of the rate of dissociation of oxygen and nitrogen at high temperatures[15,16]. It was found that within a factor 3–10 the rate is that given by equation 3. Eckerman[17] has determined the rate by measurements made on the shock detachment distance ahead of a sphere moving at high Mach numbers. He can represent the oxygen dissociation between 4,000°K and 6,000°K by the expression

$$[k] = 0{\cdot}105 \times 7{\cdot}23 \times 10^{-12}(T)^{\frac{1}{2}} \times \left(\frac{D}{kT}\right)^2 \times \exp\left(-\frac{D}{kT}\right) \frac{\text{c.c.}}{\text{molecules second}} \quad (5)$$

GENERAL ASSUMPTIONS AND PREVIOUS RESULTS

(1) The interaction between the dissociating and the 'hitting' oxygen molecule is given by a Lennard-Jones formula

$$H' = 4\varepsilon\left[\left(\frac{r_0}{r}\right)^{12} - \left(\frac{r_0}{r}\right)^{6}\right] \quad (6)$$

For this is substituted an expression which is equivalent in the important region of r

$$H' = -\varepsilon + H_{00}\exp(-r/l) \quad (7)$$

l is equal to 0·1824 Å for $O_2 - O_2$ collisions.

(2) The mutual interaction energy between the two atoms of the dissociating oxygen molecule is given by a Morse function[18]

$$H'_{\text{osc}} = -D + D(e^{-2Ku} - 2e^{-Ku}) \quad (8)$$

where u is the difference of the momentary internal O–O distance and of its equilibrium value. The vibrational energy levels are given by

$$E_v = -D + h\nu(v + \tfrac{1}{2}) - \frac{1}{4D}(h\nu)^2(v + \tfrac{1}{2})^2 \quad (9)$$

ν is the vibrational frequency near the bottom of the potential well, in practice the vibrational frequency of the ground state, and is given by

$$(2\pi\nu)^2 = \frac{2DK^2}{\tilde{m}}$$

$\tilde{m}$ is the effective mass, in our case half the mass of an atom.

It is convenient to introduce, with Strachan[19], a dimensionless quantity d, defined by

$$d = \left(\frac{8\pi^2\tilde{m}D}{K^2h^2}\right)^{\frac{1}{2}} = \frac{2D}{h\nu} \quad (10)$$

In oxygen, $D/h = 41{,}000$ wave numbers[20], $\nu = 1{,}580$, therefore $d = 53{\cdot}2$. The energy levels can then be written

$$E_v = -\frac{D}{d^2}[d - (v + \tfrac{1}{2})]^2 \quad (11)$$

The highest level has therefore the quantum number

$$v_m = d - \tfrac{1}{2} - \delta \quad (12)$$

where δ is a positive number less than unity. This level is below the dissociation energy by an amount

$$+\frac{D}{d^2}\delta^2 = \frac{h\nu}{d}\delta^2$$

i.e. in oxygen less than 0·01 $h\nu$ or less than 16 wave numbers.

The qth vibrational level below the highest, i.e. the one with $v = v_m - q = d - \tfrac{1}{2} - \delta - q$, has an energy

$$E_v = -\frac{h\nu}{d}(q + \delta)^2 \quad (13)$$

Actual potential curves deviate[21] for large v from the Morse curve, and have fewer levels than given by expression 12. For lack of anything better, we will keep the expressions for the Morse curve. The energy necessary to produce dissociation from any vibrational state is, of course, $-E_v$.

For temperatures such that $h\nu < kT < D$, the vibrational partition function is found to be approximately

$$\frac{kT}{h\nu}\left(1 + \frac{kT}{2D} + \ldots\right) + 0{\cdot}88\frac{(DkT)^{\frac{1}{2}}}{h\nu}\exp\left(-\frac{D}{kT}\right) \quad (14)$$

i.e. approximately equal to that of the simple harmonic oscillator.

(3) Transition probability. We call Z the number of collisions necessary to produce a certain effect in the O_2 molecule, in particular Z_d the number necessary to produce dissociation. The corresponding transition probability is $(Z_d)^{-1}$. One can show[8] that Z is made up of three factors.

(*a*) The first factor, Z_0, is determined by the mutual orientation of the molecules, or more precisely[9], by the rotational transitions accompanying the main process.

Originally, Z_0^{-1} was put equal to $\overline{\cos^2\theta} = \frac{1}{3}$, however the newer calculation shows that

$$Z_0^{-1} = l/L$$

where l is the length appearing in expression 7, and L the distance between the nuclei.

(*b*) Z_{tr} is determined by the change in velocity (or rather the momentum) of the relative motion of the hitting and the dissociating molecule.

It is convenient to introduce two characteristic temperatures

$$\theta = \frac{h\nu}{k} \tag{15}$$

$$\theta' = \frac{16\pi^4 \tilde{\tilde{m}} \nu^2 l^2}{k} \tag{15a}$$

where $\tilde{\tilde{m}}$ is the effective mass of the relative motion (i.e. m_O).

The energy transfer ΔE in a process where an oxygen molecule in the vibrational state v is dissociated and the resulting atoms have the relative kinetic energy E_{kin} is

$$\Delta E = -E_v + E_{\text{kin}} \tag{16}$$

Strachan[19] introduces a quantity μ, defined by

$$\mu^2 = \frac{8\pi^2 \tilde{\tilde{m}} E_{\text{kin}}}{K^2 h^2} \tag{17}$$

or

$$\mu^2 = d^2 \frac{E_{\text{kin}}}{D} \tag{17a}$$

so that

$$\Delta E = \frac{D}{d^2}(d - v - \tfrac{1}{2})^2 + \frac{D}{d^2}\mu^2$$

$$= \frac{h\nu}{2d}[(d - v - \tfrac{1}{2})^2 + \mu^2] \tag{17b}$$

One has then as one can easily see by following the deduction given in reference 8 that the probability of removing the energy ΔE is

$$Z_{tr}^{-1} = \left(\frac{2\pi}{3}\right)^{\frac{1}{2}} \frac{1}{2\pi^2} \left(\frac{\theta'}{\theta}\right)^2 \left(\frac{\theta'}{T}\right)^{\frac{1}{3}} \left(\frac{\Delta E}{h\nu}\right)^{\frac{1}{3}}$$

$$\times \exp\left[-\frac{3}{2}\left(\frac{\theta'}{T}\right)^{\frac{1}{3}} \left(\frac{\Delta E}{h\nu}\right)^{\frac{2}{3}} + \frac{\varepsilon}{kT} + \frac{\Delta E}{2kT}\right] \tag{18}$$

This formula is valid if the energy transfer is large. If, on the other hand,

$$\frac{1}{2\theta}(\theta')^{\frac{1}{2}} \left| \left[\left(\frac{E}{k}\right)^{\frac{1}{2}} - \left(\frac{E \pm \Delta E}{k}\right)^{\frac{1}{2}}\right] \right|$$

$$\sim \frac{1}{4\theta}\left(\frac{k\theta'}{E}\right)^{\frac{1}{2}} \left|\frac{\Delta E}{k}\right| \ll 1 \tag{18a}$$

(18) is to be replaced by

$$Z_{tr}^{-1} = \frac{4}{\pi^2}\frac{\theta'}{\theta^2} T \tag{18b}$$

Table 1 shows, for oxygen at 5,000°K, the ratio of 18 to 18b, as a function of $\Delta E/h\nu$.

TABLE 1

Ratio of Effectiveness of Energy Transfer for Oxygen at 5,000°K

$\Delta E/h\nu$	0	0·33	0·5	0·7	1
$\Delta E/k$ °K	0	740	1,110	1,550	2,220
Ratio of efficiency	1	0·675	0·139	0·026	0·0027

(*c*) A factor Z_i^{-1} takes care of the internal transition probability within the dissociating molecule.

In case of vibrational de-excitation of a simple harmonic oscillator, only single steps $v \to v - 1$ are possible. One gets then, for a molecule BC

$$Z_i^{-1} = 8\pi^2 \frac{m_B^2 + m_C^2}{(m_B + m_C)^2} \frac{\tilde{\tilde{m}}}{\tilde{m}} \frac{\theta}{\theta'} \tag{18c}$$

This follows from a perturbing energy, which contains the factor

$$H_i'' = \frac{m_B}{m_B + m_C} u/l$$

In the present case we have a Morse potential which, if developed, contains higher powers of u than the first and therefore allows transitions with quantum jumps larger than unity, since the amplitudes are not small any more.

The perturbing interaction potential for 'hard' collisions follows, from equation 7, as

$$H_i'' = \exp\left(-\frac{m_B}{m_B + m_C} u/l\right) - 1$$

$$= \exp\left(-\frac{m_B}{m_B + m_C}\frac{1}{Kl} Ku\right) - 1$$

Because of the orthogonality of the wave functions, the summand -1 does not contribute to the transition probability.

For O_2, $\frac{m_B}{m_B + m_C} = \frac{1}{2}$, $l = 0{\cdot}1824$ Å for energies of the order D, K is[15] $2{\cdot}34 \times 10^8$ cm^{-1}, so that

$$\frac{m_B}{m_B + m_C}\frac{1}{Kl} = 0{\cdot}855$$

This will be replaced by unity. Therefore the perturbing interaction energy, which causes transitions, is

$$H_i'' = \exp(-Ku) = \frac{1}{2d}\eta \tag{19}$$

where[19]

$$\eta = 2d \exp(-Ku)$$

In the later part of this paper the internal transition probability belonging to the Morse function

and the perturbation interaction 19 will be calculated.

(*d*) The rate constant of dissociation from the state v is finally

$$\frac{1}{\tau_c}(Z_0 Z_{tr} Z_i)^{-1}\frac{N_v}{N}\exp\left(-\frac{\Delta E}{RT}\right) \qquad (20)$$

Here τ_c is the time between collisions, which can be calculated from the expression[8,22]

$$\text{Coefficient of viscosity} = 1{\cdot}271\, p\tau_c$$

N_v/N is the fraction of molecules in the state v. This is

$$N_v/N = (\text{partition function})^{-1}\exp\left(-\frac{D+E_v}{kT}\right) \qquad (20a)$$

Using equation 14 and 20a, one has as rate of dissociation from state v

$$[O_2]\frac{1}{\tau_c}(Z_0 Z_{tr} Z_c)^{-1}\frac{h\nu}{kT}\exp\left(-\frac{D+E_{kin}}{kT}\right) \qquad (20b)$$

This has to be integrated over all kinetic energies E_{kin} of the dissociated atoms, and then summed over the states v.

VIBRATIONAL TRANSITION IN A DISSOCIATING DIATOMIC MOLECULE

Transition probabilities for a Morse potential have been partly calculated by Lennard-Jones and Strachan[23] and by Strachan[19], whose notation we use. The normalized vibrational wave function has the following form[19]

$$\left[K\frac{2d-2v-1}{\Gamma(2d-v)}v!\right]^{\frac{1}{2}}\eta^{d-\frac{1}{2}}\times \sum_0^v \frac{\Gamma(2d-v)}{\Gamma(2d-v-n)}\frac{(-1)^n}{n!(v-n)!}\eta^{-n} \qquad (21)$$

The vibrational transition probability from a state v into a dissociated state with a kinetic energy within the limits dE_{kin} is

$$(Z_i)^{-1} = \frac{\bar{m}}{K^2\hbar^2}2\pi\frac{dE_{kin}}{\mu}\frac{2d-2v-1}{\Gamma(2d-v)}v!\times \frac{\Gamma(\frac{1}{2}-d+i\mu)\Gamma(\frac{1}{2}-d-i\mu)}{\Gamma(2i\mu)\Gamma(-2i\mu)} \times \frac{1}{4d^2}\left|\int_0^\infty W(d,-i\mu,\eta)e^{-\frac{1}{2}\eta}\eta^{d-1}(\Sigma)\,d\eta\right|^2 \qquad (22)$$

where (Σ) signifies the sum in equation 21.

We multiply and divide 22 by

$$\Gamma(d+\tfrac{1}{2}+i\mu)\Gamma(d+\tfrac{1}{2}-i\mu)$$

and use expressions given in references 19, 23. Then

$$(Z_i)^{-1} = \frac{d^2}{2\pi}\frac{dE_{kin}}{D}\frac{2d-2v-1}{\Gamma(2d-v)}\times \frac{\sinh(2\mu\pi)}{\cosh(2\mu\pi)-\cos(2d-1)\pi}\times \frac{1}{4d^2}\left\{\frac{\Gamma(2d-v)}{\{\Gamma(d+\frac{1}{2}+i\mu)\Gamma(d+\frac{1}{2}-i\mu)\}^{\frac{1}{2}}}\sum\frac{(-1)^n}{n!} \times \frac{\Gamma(d+\frac{1}{2}-n+i\mu)\Gamma(d+\frac{1}{2}-n-i\mu)}{\Gamma(2d-v-n)\Gamma(v-n+1)}\right\}^2 \qquad (23)$$

The factor

$$\frac{\sinh(2\mu\pi)}{\cosh(2\mu\pi)-\cos(2d-1)\pi}$$

goes to zero for $\mu = 0$ (except in the special case $2d-1$ equal to an even integer, when it becomes infinite, but the integral over dE_{kin} still converges). For $2\mu > 1$, the factor approaches unity quickly. Since it will be seen later that in the integration the range of μ from zero to about $(d)^{\frac{1}{2}} \sim 7$ is important, the above factor will be replaced by unity in the integration but for the sake of completeness will be carried in the formulae with the abbreviation

$$S = \frac{\sinh(2\mu\pi)}{\cosh(2\mu\pi)-\cos(2d-1)\pi} \qquad (24)$$

DISSOCIATION FROM THE GROUND STATE, $v = 0$

According to equations 23, 3A, and 10A, one gets

$$(Z_i)^{-1} = \frac{2d-1}{8\pi}S(\mu)\frac{[\Gamma(d+\frac{1}{2})]^2}{\Gamma(2d)}\times \frac{dE_{kin}}{D}\exp\left(-\frac{4d^2}{2d+1}\frac{E_{kin}}{D}\right)$$
$$= \frac{1}{4(2\pi)^{\frac{1}{2}}}(2d-1)^{\frac{3}{2}}\frac{1}{2^{2d}}S(\mu)\times \frac{dE_{kin}}{D}\exp\left(-\frac{4d^2}{2d+1}\frac{E_{kin}}{D}\right) \qquad (25)$$

This has to be multiplied with $(Z_{tr})^{-1}$. The exponent in the latter is approximately

$$-\frac{3}{2}\left[\frac{\theta'}{T}\left(\frac{D+E_{kin}}{h\nu}\right)^2\right]^{\frac{1}{3}}-\frac{D+E_{kin}}{2kT}+\frac{\varepsilon}{kT}$$
$$= -\frac{3}{2}\left[\frac{\theta'}{T}\left(\frac{D}{h\nu}\right)^2\right]^{\frac{1}{3}}\left(1+\frac{E}{D}\right)^{\frac{2}{3}}-\frac{D+E_{kin}}{2kT}+\frac{\varepsilon}{kT}$$
$$= -\frac{3}{2}\left[\frac{\theta'}{T}\left(\frac{D}{h\nu}\right)^2\right]^{\frac{1}{3}}-\frac{D}{2kT}+\frac{\varepsilon}{kT} -\left\{\left[\frac{\theta'}{T}\left(\frac{D}{h\nu}\right)^2\right]^{\frac{1}{3}}+\frac{D}{2kT}\right\}\frac{E_{kin}}{D} \qquad (26)$$

For O_2 ($\theta' = 2{\cdot}27 \times 10^6$) and $T = 5{,}000°K$, the first summand in { } is 68·5, the second is 5·7.

Therefore the dependence on E_{kin} of expressions 25 and 26 combined is given by

$$\exp(-178E_{kin}/D)$$

This means that the range up to about $E_{kin} = 3(D/178) \sim D/60 \sim k \times 1{,}000°K$ is significantly present; in μ this is the range up to

$$\mu = d(3/178)^{\frac{1}{2}} \sim 7$$

It is now possible to perform the integration over dE_{kin}/D which introduces a factor 1/178 into the rate.

After integration we have

$$(Z_i)^{-1} = 7 \times 10^{-33} \quad (Z_{tr})^{-1} \sim 10^{-36} \exp\left(-\frac{D}{kT}\right)$$

at 5,000°K.

Therefore the probability of direct dissociation from the ground state is negligible for two reasons: the vibrational transition probability is very small and the efficiency of transferring such a large amount of energy by collision is very small.

DISSOCIATION FROM AN EXCITED VIBRATIONAL STATE NEAR THE TOP OF THE MORSE CURVE

Consider now the dissociation from a state near the top of the Morse curve, $v = v_m - q$. According to equations 23 and 5A one has

$$(Z_i)^{-1} = \frac{1}{4\pi}\frac{q+\delta}{e^2} S(\mu) \frac{dE_{kin}}{D} \exp\left(-\frac{4d^2}{2d+1}\cdot\frac{E_{kin}}{D}\right) \tag{27}$$

(*a*) From the top state, $q = 0$.

Condition 18a requires, if we put $E = 3/2k \times 5{,}000°K$

$$\frac{\Delta E}{k} \ll 4\frac{2{\cdot}2 \times 10^3}{1{\cdot}5 \times 10^3}(7{,}500)^{\frac{1}{2}} \sim 520°K$$

Since the exponent in 27 is

$$-\frac{E}{D} \times 105 \sim -\frac{E}{k}\frac{k}{D} \times 105 \sim \frac{E_{kin}}{k}\frac{1}{540}$$

values of E_{kin}/k up to several times 540°K contribute to $(Z_i)^{-1}$, so that expression 18a is not really fulfilled in the whole range and a smaller $(Z_{tr})^{-1}$ should be used for the larger values of E_{kin}/k. Nevertheless, we will use the constant value (18b) for $(Z_{tr})^{-1}$.

Integrating 25 and multiplying with (Z_0^{-1}) and 18b one gets $(Z)^{-1}$; this is to be multiplied with the fraction of particles in the top vibrational state,

$$\frac{h\nu}{kT}\exp\left(-\frac{D}{RT}\right)$$

and one has finally for the rate of dissociation from the top excited state

$$\frac{1}{\tau_c}\frac{1}{4\pi}\frac{\delta}{e^2}\frac{2d+1}{4d^2}\frac{4}{\pi^2}\frac{\theta'}{\theta^2}T\frac{l}{L}\frac{\theta}{T}\exp\left(-\frac{D}{kT}\right) = \frac{1}{\tau_c}\frac{1}{2\pi^3e^2}\frac{\delta}{d}\frac{l}{L}\frac{\theta'}{\theta}\exp\left(-\frac{D}{kT}\right) \tag{28}$$

(*b*) States near the top of the Morse function. Two changes have to be made; δ is to be replaced by $q + \delta$, and the kinetic energy interval into which the dissociated particles can efficiently be emitted is decreased because the colliding particles have also to supply the energy $-E_v$ with which the particles are still bound. Call the function represented in Table 1 $f\left(\frac{\Delta E}{h\nu}\right)$. Then the transition probability from state v is (after replacing $2d + 1$ with $2d$)

$$Z^{-1} = \frac{1}{\pi^3e^2}\frac{l}{L}\frac{\theta' T}{\theta^2}(q+\delta)\exp\left(-2d\frac{E_v}{D}-\frac{E_v}{kT}\right) \times \int_{-E_v}^{\infty} f\left(\frac{\Delta E}{h\nu}\right)\exp\left[-\frac{\Delta E}{D}\left(2d+\frac{D}{kT}\right)\right]\mathrm{d}\frac{\Delta E}{D}$$
$$= \frac{1}{\pi^3c^2}\frac{l}{L}\frac{\theta' T}{\theta^2}(q+\delta)\exp\left(-4\frac{E_v}{h\nu}\right) \times \frac{2}{d}\int_{-E_v}^{\infty} f\left(\frac{\Delta E}{h\nu}\right)\exp\left[-\frac{\Delta E}{h\nu}\left(4+\frac{h\nu}{kT}\right)\right]\mathrm{d}\frac{\Delta E}{h\nu} \tag{29}$$

and the reaction rate constant is

$$[k] = \frac{1}{\tau_c}\frac{l}{L}\frac{\theta'}{\theta}\frac{2}{\pi^3e^2} \left\{\sum_q \frac{q+\delta}{d}\exp\left\{\left[\frac{2(q+\delta)^2}{d}\right]\left(1+\frac{h\nu}{4kT}\right)\right\}\right. \left.\int_Z^{\infty} f(y)\exp\left[-4y\left(1+\frac{h\nu}{4kT}\right)\right]\mathrm{d}y\right\}\exp\left(-\frac{D}{kT}\right)$$

with

$$y = \frac{\Delta E}{h\nu}, \quad Z = \frac{(q+\delta)^2}{2d} \tag{30}$$

If the summation over q is replaced by integration

$$[k] = \frac{1}{\tau_c}\frac{2}{\pi^3e^2}\frac{l}{L}\frac{\theta'}{\theta}\exp\left(-\frac{D}{kT}\right) \int_0^{\infty}\mathrm{d}z\exp(4{\cdot}4z)\int_Z^{\infty} f(y)\exp(-4{\cdot}4y)\mathrm{d}y \tag{30a}$$

$$1 + \frac{h\nu}{7kT} = 1{\cdot}1$$

The double integral can be transformed by partial integration into

$$\frac{1}{4{\cdot}4}\int_0^\infty f(y)(1-\mathrm{e}^{-4{\cdot}4y})\mathrm{d}y$$

which gives approximately 0·030 so that

$$[k]=\frac{1}{\tau_c}\frac{0{\cdot}06}{\pi^3e^2}\frac{l}{L}\frac{\theta'}{\theta}\exp\left(-\frac{D}{kT}\right) \qquad (31)$$

Comparison with equation 28 shows, if one puts roughly

$$\frac{1}{2d}\sum(q+\delta)=\frac{(qm+\delta)^2}{4d}=0{\cdot}06$$

that in effect the four top states co-operate. This is in qualitative agreement with an old prediction of Rice[24].

COMPLEX COLLISIONS

There is one other mechanism possible in which two vibrationally *excited* molecules meet and the energy of dissociation is supplied by the combined vibrational energy.

We will only consider the case where one molecule has only a few quanta v' and the other is near the top of the Morse curve. The first molecule, being near the bottom of the potential curve, is so closely a simple harmonic oscillator that only jumps by unity are permissible. The transition probability for all such transitions is then, according to equation 18c,

$$8\pi^2\frac{\theta}{\theta'}\sum v'\frac{\theta}{T}\exp\left(-\frac{hv}{kT}v'\right)\sim 8\pi^2\frac{\theta}{\theta'}\frac{\theta}{T}\frac{T^2}{\theta^2}$$

$$=8\pi^2\frac{T}{\theta'} \qquad (32)$$

The resultant probability is found by multiplying expression 32 with 28, after replacing δ with $q+\delta$, and summing over all the states q with an energy less than hv below dissociation. Therefore

$$[k]=\frac{1}{\tau_c}\frac{8\pi^2}{2\pi^3e^2}\frac{l}{L}\frac{T}{\theta}\left(\sum\frac{q+\delta}{d}\right)\exp\left(-\frac{D}{kT}\right)$$

$$=\frac{1}{\tau_c}\frac{4}{\pi e^2}\frac{l}{L}\frac{T}{\theta}\frac{(q_m+\delta)^2}{2d}\exp\left(-\frac{D}{kT}\right) \qquad (33)$$

where (see equation 13)

$$hv\frac{(q_m+\delta)^2}{d}=hv$$

$$q_m+\delta=(d)^{\frac{1}{2}}\sim 7$$

Therefore

$$[k]=\frac{1}{\tau_c}\frac{2}{\pi e^2}\frac{l}{L}\frac{T}{\theta}\exp\left(-\frac{D}{kT}\right) \qquad (34)$$

DISCUSSION OF RESULTS

In the following the factor preceding $\exp\left(-\frac{D}{kT}\right)$ in the rate constant will be discussed.

Eckerman's empirical equation, gives, at 5,000°K, $7{\cdot}7\times10^{-9}$ and this factor is proportional to $T^{-\frac{3}{2}}$.

The classical formula 3 results in $5{\cdot}9\times10^{-9}$, which agrees sufficiently with Eckerman, but is practically independent of temperature.

We have treated two parallel mechanisms: transfer of kinetic energy (31), which gives $2{\cdot}6\times10^{-11}$, and transfer of vibrational energy (34), which leads to $1{\cdot}9\times10^{-11}$. The sum, $4{\cdot}5\times10^{-11}$, is too small by a factor 170. This is an unexplained problem which has been discussed before[8,25]. It is of interest that re-combination should occur preferentially among slow atoms. B. Lewis tells me that he has drawn such a conclusion previously.

I wish to thank Drs. Z. I. Slawsky and J. Eckerman, both of the U.S. Ordnance Laboratory, for many enlightening discussions and for the use of the N.O.L. facilities.

APPENDIX

The first term in expression 23 contains the factor

$$\frac{v!}{\Gamma(2d-v)}\frac{[\Gamma(2d-v)]^2\,\Gamma(d+\frac{1}{2}-i\mu)\,\Gamma(d+\frac{1}{2}+i\mu)}{[\Gamma(2d-v)]^2\,[\Gamma(v+1)]^2}$$

$$=\frac{1}{\Gamma(2d-v)\Gamma(v+1)}\,\Gamma(d+\tfrac{1}{2}-i\mu)\,\Gamma(d+\tfrac{1}{2}+i\mu) \qquad (1A)$$

Assuming $\mu>d$ and using the approximation

$$\Gamma(d+\tfrac{1}{2}-i\mu)\,\Gamma(d+\tfrac{1}{2}+i\mu)=[\Gamma(d+\tfrac{1}{2})]^2\exp\left(-\frac{2\mu^2}{d+\frac{1}{2}}\right)$$

one can re-write the factor

$$\frac{[\Gamma(d+\frac{1}{2})]^2}{\Gamma(2d-v)\,\Gamma(v+1)}\exp\left(-\frac{4\mu^2}{2d+1}\right) \qquad (2A)$$

For the ground state, $v=0$, one gets therefore

$$\frac{[\Gamma(d+\frac{1}{2})]^2}{\Gamma(2d)}\exp\left(-\frac{4\mu^2}{2d+1}\right) \qquad (3A)$$

For a state near the top of the Morse curve, we write

$$v=v_m-q=d-\tfrac{1}{2}-\delta-q \qquad (4A)$$

and assume v to be still large enough for the application of the Stirling formula. Then

$$\frac{[\Gamma(d+\tfrac{1}{2})]^2}{\Gamma(2d-v)\,\Gamma(v+1)}$$

$$= \frac{(d-\tfrac{1}{2})^{2d}}{(2d-v-1)^{2d-v-\frac{1}{2}}\,v^{v+\frac{1}{2}}}$$

$$\exp(-2d+1+2d-v-1+v)$$

$$= \frac{(d-\tfrac{1}{2})^{2d}}{(d-\tfrac{1}{2}+\delta+q)^{d+\delta+q}(d-\tfrac{1}{2}-\delta-q)^{d-\delta-q}}$$

$$= \frac{(d-\tfrac{1}{2})^{2d}}{[(d-\tfrac{1}{2})^2-(\delta+q)^2]^{2d}}\left(\frac{d-\tfrac{1}{2}-\delta-q}{d-\tfrac{1}{2}+\delta+q}\right)^{\delta+q}$$

$$\sim 1-\frac{1}{d}(q+\delta)^2 \sim 1 \qquad (5A)$$

The remaining sum in expression 23 which has to be squared, is, after the first term has been taken out as factor

$$\sum \frac{(-1)^n}{n!}\left[\frac{\Gamma(d+\tfrac{1}{2}-n)}{\Gamma(d+\tfrac{1}{2})}\right]^2 \frac{\Gamma(2d-v)}{\Gamma(2d-v-n)}\,\frac{\Gamma(v+1)}{\Gamma(v-n-1)} \qquad (6A)$$

The factor $n!$ in the denominator is 6×10^5 for $n=10$, so that terms with $n>10$ will contribute only negligibly to the sum, i.e. we can set

$$\frac{\Gamma(d+\tfrac{1}{2}-n)}{\Gamma(d+\tfrac{1}{2})} \sim \frac{1}{(d-\tfrac{1}{2})^n}$$

$$\frac{\Gamma(2d-v)}{\Gamma(2d-v-n)} \sim (2d-v-1)^n$$

$$\frac{\Gamma(v+1)}{\Gamma(v-n+1)} \sim v^n$$

Therefore the sum is

$$\sum \frac{(-1)^n}{n!}\left[\frac{(2d-v-1)v}{(d-\tfrac{1}{2})^2}\right]^n$$

$$= \sum \frac{(-1)^n}{n!}\left[\frac{(d-\tfrac{1}{2}+\delta+q)(d-\tfrac{1}{2}-\delta-q)}{(d-\tfrac{1}{2})^2}\right]^2$$

If we now extend the sum to infinity, we have

$$\sum = \exp\left[-\frac{(d-\tfrac{1}{2})^2-(q+\delta)^2}{(d-\tfrac{1}{2})^2}\right]$$

$$= \exp\left[-1+\left(\frac{q+\delta}{d-\tfrac{1}{2}}\right)^2\right] \sim e^{-1} \qquad (7A)$$

The factor 1A therefore takes the form for the qth state down from the dissociation energy if $q \ll d$

$$\exp\left[-2-\frac{4\mu^2}{2d+1}\right] \qquad (8A)$$

Actually a slightly more complicated form

$$\left[1-\frac{(q+\delta)^2}{d}\right]\exp\left[-2+2\left(\frac{q+\delta}{d}\right)^2-\frac{4\mu^2}{2d+1}\right] \qquad (9A)$$

is probably approximately valid down to $q \sim \tfrac{1}{2}d$.

According to expression 17a,

$$\frac{4\mu^2}{2d+1}$$

in the exponent of 8A and 9A is

$$\frac{4d^2}{2d+1}\,\frac{E_{kin}}{D}$$

REFERENCES

[1] Herzfeld, K. F. *Ann. d. Phys.* 59 (1919) 635
[2] Glasstone, S., Laidler, J. K. and Eyring, H. *Theory of Rate Processes.* 1941. New York; McGraw-Hill
[3] Polanyi, M. *Z. Phys.* 1 (1920) 337
[4] Herzfeld, K. F. *Z. Phys.* 8 (1922) 132
[5] Logan, J. G. *Preprint 728,* Inst. of Aeronaut. Sciences. Jan. 1957
[6] Schwartz, R. N., Slawsky, Z. and Herzfeld, K. F. *J. chem. Phys.* 20 (1952) 1591
[7] — and Herzfeld, K. F. *J. chem. Phys.* 22 (1954) 767
[8] Herzfeld, K. F. Chapter H, Relaxation phenomena in gases, in F. Rossini, *Thermodynamics and Physics of Matter.* 1955. Princeton University Press
[9] — and Litovitz, T. A. *Dispersion and Absorption of Ultrasonic Waves.* 1958. New York; Academic Press
[10] Landau, L. and Teller, E. *Phys. Z. Soviet Union* 10 (1936) 34
[11] Bodenstein, M. and Lütkemeyer, H. *Z. phys. Chem.* 114 (1924) 208
[12] Britton, D., Davidson, N. and Schott, G. *Disc. Faraday Soc.* 17 (1954) 58
[13] Marschall, R. and Davidson, N. *J. chem. Phys.* 21 (1953) 659
[14] Christie, M. I., Harrison, A. J., Norrish, R. G. W. and Porter, G. *Proc. Roy. Soc. A* 231 (1955) 446
[15] Camac, M., Kamm, J., Feldmann, S., Keck, J. and Petty, C. *Reprint 802,* Inst. of Aeronaut. Sciences. Jan. 1958
[16] Glick, H. S. and Wurster, W. H. *J. chem. Phys.* 27 (1957) 1224
[17] Eckerman, J. *Ph. D. diss.* Catholic University, 1958
[18] Morse, P. M. *Phys. Rev.* 34 (1929) 57
[19] Strachan, C. J. *Proc. Roy. Soc. A* 150 (1935) 456
[20] Gaydon, A. G. *Dissociation Energy and Spectra of Diatomic Molecules.* 1947. New York; Wiley
[21] Herzberg, G. *Spectra of Diatomic Molecules,* 2nd ed. 1950. New York; van Nostrand
[22] Kohler, M. *Z. Phys.* 125 (1949) 715
[23] Lennard-Jones, J. E. and Strachan, C. J. *Proc. Roy. Soc. A* 150 (1935) 442
[24] Rice, O. K. *J. chem. Phys.* 9 (1941) 258
[25] Griffing, V. and Herzfeld, K. F. *J. phys. Chem.* 61 (1957) 844

6

ON SOME REACTIONS OCCURRING DURING THE EXPLOSION INDUCTION PERIOD

V. V. VOEVODSKY

Auto-acceleration observed in the oxidation of many combustible gases is connected either with thermal factors[1], or with a chain branching mechanism[2]. The branching may be rapid, on interaction of chain carriers with a molecule of the initial product, or degenerate. In the latter case acceleration is due to radicals being formed by dissociation of molecules or stable intermediates (peroxydes, aldehydes and others). In both cases the autocatalytic increment φ is connected with the explosion induction period τ_i by relation

$$\varphi \times \tau_i = \text{const} \qquad (1)$$

where τ_i is 10^{-2}–10^{-3} sec for rapid branching, whilst for degenerate branching it may attain very high values up to many minutes and even hours.

The nature of auto-acceleration during the induction period plays an important part in investigations on the explosion mechanism and on the ways of its control. This question can be solved by rigorous analysis of the reaction mechanism and by establishing the nature of elementary processes, occurring at initial stages of the reaction. Apart from the mechanisms outlined above, branching processes such as

$$R + M \rightarrow n\dot{R}^1$$

where M is a molecule of an intermediate or of an end product, could also conceivably take place. This paper is concerned with two processes of this type.

COMBUSTION OF HYDROGEN NEAR THE THIRD LIMIT

As has already been pointed out[3–5] pre-treatment of vessel walls considerably affects the rate of hydrogen oxidation within upper and third limits. In clean vessels the reaction rate is much higher (according to Pease[4] by a factor of 1,000), the reaction proceeds by an autocatalytic mechanism[5] and the explosion has been shown to be thermal. On the other hand Willbourn and Hinshelwood[9] have observed that in vessels treated with KCl the reaction proceeds without deviation from normal kinetics and the explosion occurs by a chain mechanism. Oldenberg and Sommers have pointed out[10] that the explosion induction period in pre-treated vessels can attain considerable values and depend on the pressure of the combustion mixture. Most authors were at first inclined to think that these differences could be explained by different values for the efficiency of HO_2 destruction on various surfaces; this hypothesis proved, however, to be insufficient. Von Elbe and Lewis[4] suggested an additional reaction of chain initiation by molecules of hydrogen peroxide formed at the wall. It should be pointed out that the mechanism proposed could not account for the autocatalytic acceleration of the reaction in clean vessels, observed by Chirkov[7]:

$$-\frac{d(H_2)}{dt} = k(H_2)^2(H_2O) \qquad (2)$$

The best way to find out the nature of these inconsistencies was thought to be a parallel study of explosion limits and slow kinetics in treated and untreated vessels under identical conditions, and the working out of an overall chain scheme that would fit all data available.

Kinetics and the explosion limit were studied by Poltorak and Voevodsky[11] in spherical Pyrex and silica vessels with a diameter of 4 cm, either clean (washed by cold concentrated HNO_3 and distilled water) or treated with a water solution of KCl. At first hydrogen was admitted into the heated vessel (up to pressures above the upper limit), then oxygen was added and the flash was observed or kinetic measurements of the fall of pressure were made by a mercury manometer to within an accuracy of 1 mm Hg. In experiments with the addition of water, water vapour was admitted first, and after that hydrogen and oxygen. The furnace temperature was measured by means of a thermocouple iron-constantan to within an accuracy of 1°. Gases were obtained by electrolysis. The mixture was stoichiometric throughout all the runs.

A modified technique was used to check the data obtained. A silica vessel containing the mixture at room temperature and under a known pressure was introduced into a thermostat with molten tin. The rise of pressure due to increase in temperature could be estimated from the ideal gas law. The occurrence of a flash indicated that the explosion limit was surpassed. Results obtained by both methods were in good agreement.

The explosion limit was obtained by drawing a smooth curve between the points corresponding to explosion (even with induction periods as high as 20–30 sec) and the points corresponding to absence of explosion*.

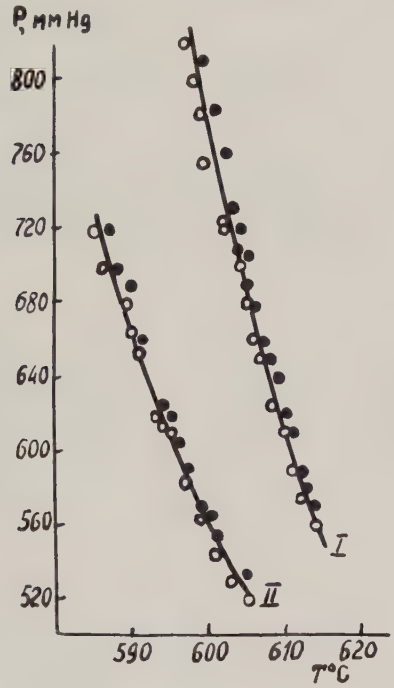

Figure 1. Third explosion limit for clean vessels (II) *and for vessels treated with* KCl (I)

Explosion in vessels treated with KCl was reported to occur at much higher temperatures and pressures (*Figure 1*).

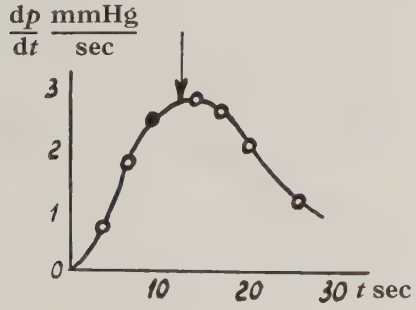

Figure 2. Kinetic curve for a clean vessel

Very important differences are also observed in pre-explosion kinetics. In a clean vessel the explosion occurs after considerable acceleration on attainment of a certain critical value (*Figure 2*).

* Willbourn and Hinshelwood[9] denote by P_3 the pressure leading to explosion in 4–5 sec after hydrogen was admitted.

This is in full agreement with the thermal explosion theory. The explosion limit was calculated from Frank-Kamenetskii's equations, making use of our experimental values for reaction rates and taking $E = 75{,}000$[5] and $\lambda = 3 \times 10^{-4}$ in accordance with reference 12, due allowance being made for temperature. Calculated values appeared to be in good agreement with experiment (Table 1).

TABLE 1

T°C	P mm Hg	W_p mm Hg/sec	$(P_3)_{obt}$	$(P_3)_{calc}$
588	680	2·8	700	685
590	640	2·7	675	670
591	650	2·8	660	655
595	610	3	614	620
597	585	3	590	588

In vessels treated with KCl the explosion is of a quite different nature—the flash occurs after a certain period of induction during which the reaction rate remains constant (*Figure 3*). Thus it

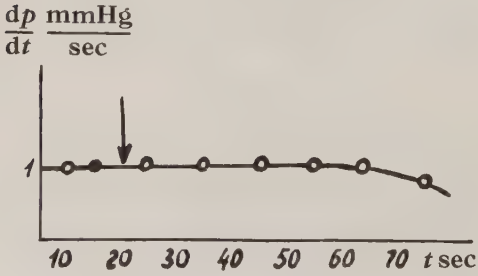

Figure 3. Kinetic curve for a vessel treated with KCl

could be conceived that once a certain amount of the product leading to a chain explosion is formed the explosion is practically immediate. Since water is the only stable product capable of accumulating at the given constant reaction rate, some reactions between radicals and water resulting in an explosion at critical P_{H_2O} values would be supposed to occur in the system. A shorter period of induction was in fact observed on the addition of small amounts of water vapour in experiments making use of vessels treated with KCl; as these amounts were too small as compared to the whole amount of water formed, lowering of the limit could not have been observed.

Several years before these experiments were commenced a suggestion was made by Voevodsky[13] that peculiarities of hydrogen combustion might be considered as the result of reaction

$$H\dot{O}_2 + H_2O \xrightarrow{(9)} H_2O_2 + \dot{O}H$$

regenerating active OH from an inactive HO_2 radical*.

Inclusion of 9 into the von Elbe and Lewis hydrogen oxidation scheme[15] explained the auto-acceleration in terms of a law similar to reaction 2 for vessels where the concentration of HO_2 was very high, owing to very small values of the efficiency of HO_2 heterogeneous re-combination (ε_{HO_2}). These values being small the reaction rate in this case depends through ε_{HO_2} upon the nature of the surface. In vessels where ε_{HO_2} are high (for instance in those treated with salts) the re-combination rate is limited by diffusion and the reaction appears to be much more reproducible. This has been pointed out by several authors[3–6].

After including 9 into the reaction scheme (due allowance being made for accumulation of considerable amounts of water), the overall equation for explosion limits becomes

$$\left\{\frac{[P + 6{\cdot}3\ (H_2O)]k_6}{2k_2} - 1\right\} \times \frac{k_7^0}{[P + (H_2O)][\frac{2}{3}k_8 P + k_9(H_2O)]} = 1 \qquad (3)$$

where P is the limiting pressure, and k_2, k_6, k_8 and k_9 are reaction rate constants of processes

$$H + O_2 \xrightarrow{(2)} OH + H$$

$$H + O_2 + M \xrightarrow{(6)} HO_2 + M$$

$$HO_2 + H_2 \xrightarrow{(8)} H_2O + OH \text{ (or } H_2O_2 + H)$$

and of reaction 9; $k_7 = k_7^0/P$ is the rate constant for destruction of HO_2 on the wall in the diffusion limited case. According to Semenov[16], for a spherical vessel

$$k_7^0 = \frac{39{\cdot}9 \times D_0}{d^2} \qquad (4)$$

where $D_0 = D \times P$.

The higher root of 3 corresponds to the third explosion limit.

As has been noted P_3 was measured at the moment when nearly all the combustible mixture was converted into water. Consequently 3 may be rewritten in a simplified form, without k_8:

$$P_3 = 2{\cdot}36 \times \frac{k_7^0}{k_9} \times \frac{k_6}{k_2}\left[1 + \left(1 - 0{\cdot}44\frac{k_2^2}{k_6^2} \times \frac{k_9}{k_7^0}\right)^{1/2}\right] \qquad (5)$$

The value of ratio k_2/k_6 and its dependence on temperature are known with a reasonable degree of accuracy[14]. Thus ratio k_9/k_7^0 could have been found from P_3 values at different temperatures and k_9 was derived from 4

$$k_9 = 2 \times 10^{-16} e^{-(8{,}000/RT)}\ cm^3/sec \qquad (6)$$

Good linear dependence obtained in coordinates $1\ g k_9 - 1/T$ appears to warrant the suggestion that introduction of 9 into the reaction scheme enables us to determine explosion limits and reaction kinetics both for clean vessels and for vessels treated with salts.

Accurate checking of numerical values for k_9 was of great interest, especially in connection with the determination of HO_2 characteristics. It is pointed out that the expression for the reaction rate constant of 8 obtained before[17]

$$k_8 \simeq 2 \times 10^{-13} e^{-(24{,}000/RT)}\ cm^3/sec \qquad (7)$$

was confirmed in this work from the reaction rate below the explosion limit. The results of Willbourn and Hinshelwood[9] on slow kinetics and third limit measurements below the explosion limit in vessels treated with KCl were used for checking the values obtained. Since these authors assumed an explosion limit value slightly different from that measured in our experiments (see above), their P_3 values would obviously depend upon k_3. As 9 was not included in their reaction scheme, the observed dependence of P_3 on addition of water vapour could not have been explained. Allowing for 9 and substituting $[k_8 + k_9\{(H_2O)/(H_2)\}]$ for k_8 in the Willbourn and Hinshelwood equations, the empiric value of C used by these authors becomes proportional to

$$\left[1 + \frac{k_9}{k_8} \times \frac{(H_2O)}{(H_2)}\right]^{-1}$$

C values given by Willbourn and Hinshelwood for a temperature $T = 586°C$ are plotted in *Figure 4* as C_0/C *versus* $(H_2O)/(H_2)$. The linear

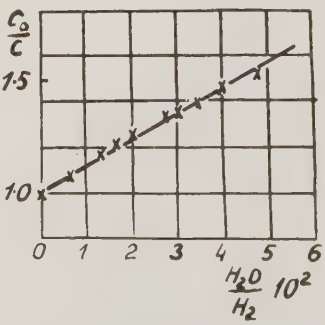

Figure 4. Curve for dependence of constant C on relationship H_2O/H_2

nature of this relationship appears to confirm the proposed suggestion on the reaction mechanism. As can be seen from above the slope tangent of the straight line is equal to k_9/k_8. The value of this

* Elementary reactions are numbered in accordance with reference 14.

ratio obtained from figure 9 is approximately 9·5. A calculation making use of 6 and 7 at $T = 586°C$ gives a value of 11·3.

A similarly good agreement with experiment is obtained on dependences of the explosion limit and of the slow reaction rate upon the hydrogen–oxygen mixture composition[18], allowance being made for 9.

Thus from kinetic considerations the introduction of 9 into the reaction scheme seems to be fully justified. The possibility of interaction between HO_2 and a water molecule is also confirmed by great efficiency of water molecules in the thermomolecular reaction of HO_2 formation[17]. This efficiency is known to depend on the life time of $[H \times H_2O]$, suggesting the possibility of a considerable decrease in activation energy of process 9.

On the other hand absence of detailed information on the energy of HO_2 formation appears to be a serious handicap. Bodenstein[19] suggested a value of 40–45 kcal/mole for the energy of the $H—O_2$ bond. Foner and Hudson[20] have recently obtained mass-spectrometrically a value $Q_{H—O_2}$ equal to 47 $\pm$ 2 kcal/mole. Incidentally the radical HO_2 was obtained by reaction

$$\dot{R} + H_2O_2 \rightarrow RH + HO_2$$

This value $Q_{H—O_2}$ being accepted, 9 would become endothermic by some 20 kcal/mole, which does not agree with the value obtained before: $E_9 = 8{,}000$ kcal/mole.

At the same time the suggestion that the HO_2 radical formed in interaction between H and O_2 atoms immediately acquires a structure corresponding to the position of H and O atoms in the H_2O_2 molecule, cannot be considered as unequivocal. Geib and Harteck have already pointed out[21] that in investigating the reaction $H + O_2$ they observed at first the formation of some isomeric compounds, which were converted into H_2O_2 only after warming up of the condensate at a temperature near to $-115°C$, the conversion being accompanied by abundant foaming. It is pointed out that the same was observed in flow experiments on slow hydrogen oxidation, on warming up of the products condensed in liquid nitrogen, at very small degrees of conversion. Geib and Harteck propose a value for this primary and more active form of HO_2

$$Q_{H—O_2} \cong 10{,}000 \text{ kcal/mole}$$

similar to that obtained by Bodenstein[19] for the lower limit of this quantity. Dainton and Norrish[22] also suggested the possible existence of two forms of HO_2 radicals converting into each other with release of energy. Finally it should be pointed out that in another work Foner and Hudson[23] tried to obtain the HO_2 radical not from H_2O_2 but by interaction between H atoms and O_2 molecules. They did not succeed in observing this radical in the gas phase and this might be due to the weakness of the $H—O_2$ bond in the case under question, diminishing the possibility of observing appropriate ions mass-spectrometrically. Summing up, it may be concluded that reaction 9 permits us to connect quantitatively and convincingly a variety of effects observed in hydrogen oxidation below the third limit, as well as the basic characteristics of explosion under various conditions. On the other hand such a process would occur only in case the labile form of HO_2 with a bond energy not exceeding 25 kcal/mole actually exists. The best way to prove it would be to work out appropriate methods for direct measurements of HO_2 concentration in the autocatalytic reaction in clean vessels, thus following under experimental conditions the reactions involving this radical.

DETAILED CHAIN BRANCHING MECHANISM OF HYDROCARBON OXIDATION

Two basic mechanisms of chain branching reactions[2] are given schematically by

$$R + M_{in} \rightarrow n \times \dot{R}^1 \qquad (8)$$

and

$$M_{st} \rightarrow 2\,\dot{R}^1 \qquad (9)$$

where $\dot{R}$ and $\dot{R}^1$ are free radicals, M_{in} and M_{st} are molecules of initial and stable intermediates respectively, and n is more than unity. Von Elbe and Lewis[15] suggest a third mechanism

$$\dot{R} + M_{st} \rightarrow n\dot{R}^1 \qquad (10)$$

but they give no detailed analysis of its kinetic consequences.

The after-effect observed by Stern and Sergeev[25] was confirmed by Kalinenko and the author several years ago in investigations on propane oxidation photosensitized by bromine[24]. After the illumination was switched off the reaction kept going, and even auto-acceleration was sometimes observed for several minutes*. Detailed evidence allowed us to state that this reaction was preceded by a homogeneous mechanism with branching of chains at the wall. The degenerate nature of this branching can be seen from small values of the logarithmic increment (10^{-3}–10^{-1} sec). The linear dependence of the photosensitized reaction rate upon $(I_0)^{1/2}$ shows that chain rupture occurs

* It will be noted that *iso*propyl peroxide and acetone are principal reaction products at initial stages, their relationship remaining constant throughout the process.

homogeneously by a second order reaction. Therefore the free radical concentration will be represented by the differential equation

$$\frac{d(\dot{R})}{dt} = W_0 + k_p(M_{st}) - k(\dot{R})^2 \qquad (11)$$

if branching occurs by reaction 9 or by

$$\frac{d(\dot{R})}{dt} = W_0 + k_p^1(M_{st}) \times n - k(\dot{R})^2 \qquad (12)$$

if branching occurs by 10.

The choice between these two possibilities can be made from evidence on slow acceleration of the process once the light had been switched off.

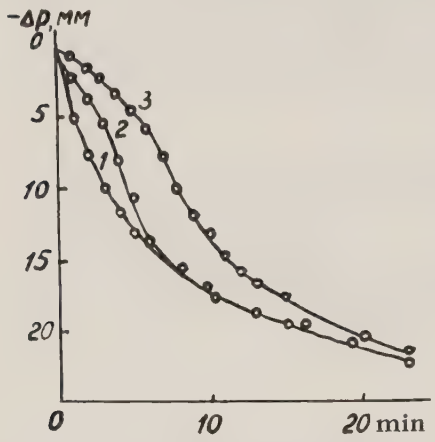

Figure 5. Kinetic curves for photosensitized propane oxidation: curve 1, under constant illumination; curve 2, for light switched off after an interval of 1 min*; curve 3, for light switched off after an interval of* 15 min

Results obtained with a vessel pre-treated first with fluoric and then with sulphuric acid are given in *Figure 5*. The autocatalytic nature of the processes is evident from initial parts of curves 2 and 3, e.g.

$$-\Delta P \sim (M_{st}) \sim e^{\varphi t} \qquad (13)$$

Taking that

$$\frac{d(M)}{dt} = a(\dot{R}) \qquad (14)$$

and on the conventional assumption that $\{d(\dot{R})/dt\} \ll \{d(M)/dt\}$, e.g. $\{d(\dot{R})/dt\} \simeq 0$, kinetics of the reaction after the light was switched off become in case of 11

$$(\dot{R}) = \left(\frac{k_p}{k}\right)^{\frac{1}{2}} (M)$$

and consequently

$$(M) = \left[(M)_{t=0} + \frac{1}{2}\left(\frac{k_p}{k}\right)^{\frac{1}{2}}(t - t_0)\right]^2 \qquad (15)$$

where t is the time when the light was switched off.

The same assumptions being made we find from 12 that $(\dot{R}) \simeq k_p^1/k\,(M)$ and

$$(M) = (M)_{t=0}\, e^{\frac{ak_p^1}{k}t} \qquad (16)$$

Thus the dependence of (M) and Δp on time obtained experimentally appears to be a direct evidence of chain branching by reaction 10.

In this connection it seems desirable to make a general estimation of kinetic consequences that would result from including equation 10 into the mechanism of slow hydrocarbon oxidation. For simplification Vedeneev and Voevodsky[26] considered a less complex scheme than that described above, namely a process with branching 10 occurring homogeneously. In hydrocarbon oxidation where RO_2 is the most stable radical capable of interaction by 10 and peroxides or aldehydes can be formed as intermediates, processes

$$R\dot{O}O + R^1CHO \rightarrow R\dot{O} + \dot{O}H + R^1\dot{C}O$$
$$- \sim 20 \text{ kcal/mole}$$

$$R\dot{O}O + R^1OOH \rightarrow R\dot{O} + R^1\dot{O} + H\dot{O}_2$$
$$- \sim 9 \text{ kcal/mole}$$

are possible on thermodynamic grounds*. This can be exemplified by the conventional scheme of aldehyde formation in gas reactions of hydrocarbon oxidation, including a branching process of the type of 10:

$$RH \xrightarrow{(0)} 2\dot{R}^1 \qquad \dot{O}H + RH \xrightarrow{(3)} H_2 + R$$

$$\dot{R} + O_2 \xrightarrow{(1)} ROO \qquad RO_2 \xrightarrow{(4)} \text{destruction}$$

$$R\dot{O}O \xrightarrow{(2)} A + \dot{O}H \qquad RO_2 + A \xrightarrow{(5)} 3\,\dot{R}^1$$

$$\dot{R}^1 + RH \xrightarrow{(6)} R + R^1H$$

where A denotes aldehydes and RH hydrocarbons.

It will be assumed that processes 3, 6 and 1 are so rapid that radicals $\dot{R}$, $\dot{R}^1$ and $\dot{O}H$ practically do not accumulate in the system. As we are going to consider only the initial reaction period, consumption of RH and A can be neglected. Reaction 4 was assumed in connection with the results of Fok and Nalbandyan[28] on photosensitized oxidation of propane in the presence of mercury vapour. Inclusion of a chain rupture reaction of the second order has no direct bearing on final conclusions but considerable mathematical difficulties would arise through its use.

* Thermal effects are calculated on the assumption that the dissociation energy of the O—O bond in peroxide is 30 kcal/mole[27].

On these assumptions kinetics of the oxidation scheme will be represented by differential equations:

$$W = \frac{d(RH)}{dt} = \frac{d(A)}{dt} \cong k_2(RO_2) \quad (17)$$

$$\frac{d(RO_2)}{dt} = W_0 + [2k_5(A) - k_4](RO_2) \quad (18)$$

By rather cumbersome substitution of variables[26] the system is transformed to the Eyrie equation

$$\frac{d^2\psi}{dS^2} = \psi S \quad (19)$$

where

$$2k_5(A) - k_4 = 2\rho \frac{d \ln \psi}{dS} \quad (20)$$

$$S = \frac{1}{4}\frac{k_4^2}{\rho^2} - \rho t \quad (21)$$

and $\rho = (k_2 k_5 W_0)^{1/3}$.

The solutions of equation 19 are tabulated[29]. For

$$\mu = \frac{1}{4}\frac{k_4^2}{\rho^2} \geqslant 2$$

the value of

$$\frac{k_5}{\rho^2}\frac{d(A)}{dt}$$

proportional to the reaction rate may be computed as a function of $S = \mu - \rho t$ (*Figure 6*). It

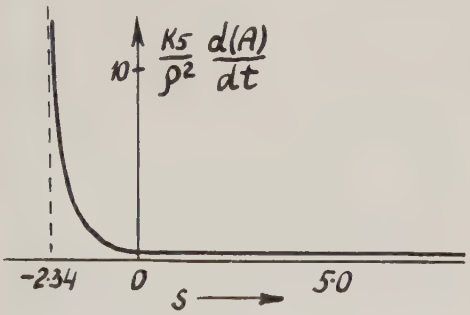

Figure 6. Theoretical dependence of the reaction rate on $S = \mu - \rho t$

follows from the plot that a marked acceleration is taking place within the range from $S = 0$ to $S = -2{\cdot}34$ and the explosion will occur at the moment

$$\tau = \frac{\mu + 2{\cdot}34}{\rho} \quad (22)$$

Expressing the plot in conventional coordinates $W = f(t)$ we get a kinetic curve of the autocatalytic type with a markedly prolonged induction period (*Figure 7*, curve 2). The results of Chirkov and Entelis[30] represented by circles are given for comparison. A slight deviation in the range of high rates is quite natural, since consumption of initial products is not allowed for in the given calculation. The broken line 1 is obtained in accordance with

$$W = N_0 e^{\varphi t} \quad (23)$$

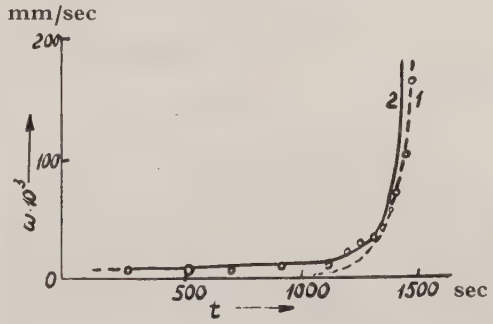

Figure 7. Comparison of the theoretical curve (2) with experimental results of Chirkov and Entelis[30] (circles) *and with approximate equation 23 (curve 1)*

from experimental points for high rates. As can be seen from the above, the scheme allowing for 5 fits autocatalytic kinetics with a prolonged induction period much better. It will be pointed out that difficulties arising from computing N_0 from 23 are not encountered with this mechanism. However in computing N_0 by 23 from the kinetic curves of the type described this value appears to be so small that it has no physical sense.

Making use of a relationship of the 23 type to describe the region $2{\cdot}34 \leqslant S \leqslant 0$ of the theoretical curve, it can be computed that

$$\frac{k_5}{\rho 2}\frac{d(A)}{dt} \cong B\, e^{2{\cdot}18\rho t} \quad (24)$$

and that value φ in 23 can consequently be approximated as

$$\varphi = 2{\cdot}18\rho \quad (25)$$

From this and 22 we derive

$$\varphi\tau_i \simeq 2{\cdot}18(\mu + 2{\cdot}34)^* \quad (26)$$

It follows that at $\mu \ll 2{\cdot}34$

$$\tau \simeq 2{\cdot}18 \times 2{\cdot}34 = \text{const} \quad (27)$$

This relationship is not very accurate, since at $\mu < 2$ the shape of the theoretical curve of *Figure 6* is slightly altered. More rigorous calculations show, however, that the change is very slight, being only several units of the constant value. Thus at $\mu \ll 2{\cdot}34$

$$\varphi\tau \simeq 2 - 5 \quad (28)$$

* Value τ represents time very near to the explosion induction period (τ_i). Generally τ and τ_i are not similar, but at high values of τ_i

$$\tau - \tau_i \ll \tau_i$$

This result is in perfect agreement with a great number of experimental facts, described within the limits of the classic theory of degenerate branching (equation 1, reference 2).

On the other hand at $\mu \gg 2{\cdot}34$ equation 26 becomes

$$\varphi^3\tau_i = 2{\cdot}5 \times k_4^2 \qquad (29)$$

or, since k_4 does not substantially depend on temperature

$$\varphi^3\tau_i = \text{const} \qquad (30)$$

This equation is related to another extreme case derived from the theory discussed. Since for degenerated branching $\varphi \ll 1\ \text{sec}^{-1}$, the relationship between τ_i and φ for a reaction with a prolonged induction period should be well described by this expression. Values φ and τ_i, taken from the results of Chernyak, Antonovsky, Revsin, and Stern[31] on propane oxidation at $T \sim 300°$, are listed in Table 2.

TABLE 2

T°C	φ sec^{-1}	τ sec	$\varphi\tau$	$\varphi^3\tau$
285	$7{\cdot}7 \times 10^{-3}$	9,850	76	$4{\cdot}5 \times 10^{-3}$
300	$12{\cdot}7 \times 10^{-3}$	2,425	31	$5{\cdot}0 \times 10^{-3}$

As can be seen, equation 30 is more satisfactory than 28.

Finally I would like to draw upon the physical sense of the results obtained. Considering the degenerated branching mechanism suggested by von Elbe and Lewis [15], Semenov[32] has pointed out that if branching occurs with free radicals involved the period of auto-acceleration will be much less than 0·1 sec. In the case under question the prolonged period of induction is due to τ_i being, strictly, not an induction period of explosion, but the time interval required for accumulation of a certain amount of A, necessary for attainment of the chain branching explosion limit. Since this accumulation occurs below the limit, this process may proceed very slowly, in full accordance with the theory of chain branching. This is indeed observed in experiments.

Thus reaction 5 is shown to have the same importance for the hydrocarbon oxidation mechanism as that of 9 in hydrogen oxidation. It is a reaction between a radical with small activity and a molecule of the product by which the chain reaction is reactivated. The accumulation of the product ultimately leads up to concentration values necessary for a chain branching explosion.

REFERENCES

[1] Semenov, N. N. *Usp. fiz. Nauk* 23 (1940) 251
Frank-Kamenetskii, D. A. *Zh. fiz. Khim.* 13 (1939) 738

[2] Semenov, N. N. *Chain reactions.* 1934. Moscow; ONTI

[3] Gibson, G. and Hinshelwood, C. N. *Proc. Roy. Soc. A* 119 (1928) 591

[4] von Elbe, G. and Lewis, B. *J. chem. Phys.* 10 (1942) 366

[5] Oldenberg, O. and Sommers, H. S. *J. chem. Phys.* 9 (1941) 432
—— *J. chem. Phys.* 10 (1942) 193

[6] Pease, R. N. *J. Amer. chem. Soc.* 52 (1930) 5106

[7] Chirkov, N. M. *Acta Physicochim. U.R.S.S.* 6 (1937) 915

[8] Frank-Kamenetskii, D. A. *Zh. fiz. Khim.* 14 (1940) 1653

[9] Willbourn, A. H. and Hinshelwood, C. N. *Proc. Roy. Soc. A* 185 (1946) 353, 369
—— *Proc. Roy. Soc. A* 188 (1947) 1

[10] Oldenberg, O. and Sommers, H. S. *J. chem. Phys.* 9 (1941) 114

[11] Poltorak, V. A. and Voevodsky, V. V. *Zh. fiz. Khim* 24 (1950) 299

[12] *Technical Encyclopedia* (Russian) Vol. VII, p. 449

[13] Voevodsky, V. V. *Zh. fiz. Khim.* 20 (1946) 1285

[14] Nalbandyan, A. B. and Voevodsky, V. V. *The mechanism of hydrogen oxidation and combustion* (Russian), Ed. by the Acad. Sci. of the USSR, 1949

[15] von Elbe, G. and Lewis, B. *Combustion, Flames and Explosions in Gases*, 1st ed. 1938. New York; Academic Press

[16] Semenov, N. N. *Acta Physicochim. U.R.S.S.* 18 (1943) 93

[17] Voevodsky, V. V. and Tal'rose, V. L. *Zh. fiz. Khim.* 22 (1948) 1192

[18] —— *Zh. fiz. Khim.* 22 (1948) 457; see also reference 14

[19] Bodenstein, M. and Schenk, P. *Z. phys. Chem. B* 20 (1933) 420

[20] Foner, S. N. and Hudson, R. L. *J. chem. Phys.* 23 (1955) 1364

[21] Geib, K. H. and Harteck, P. *Ber.* 65 (1932) 1551
—— *Erg. exakt. Naturwiss.* 15 (1936) 44

[22] Dainton, F. S. and Norrish, R. G. W. *Proc. Roy. Soc. A* 177 (1941) 393

[23] Foner, S. N. and Hudson, R. L. *J. chem. Phys.* 23 (1955) 1974

[24] Kalinenko, R. A. and Voevodsky, V. V. *Zh. fiz. Khim.* 30 (1956) 537

[25] Sergeev, G. B. and Stern, V. Ya. *Doklady Akad. Nauk S.S.S.R.* 91 (1953) 1357

[26] Voevodsky, V. V. and Vedeneev, V. I. *Doklady Akad. Nauk S.S.S.R.* 106 (1956) 679

[27] Thomas, J. R. *J. Amer. chem. Soc.* 77 (1955) 246

[28] Fok, N. V. and Nalbandyan, A. B. *Doklady Akad. Nauk S.S.S.R.* 86 (1952) 589

[29] For instance Fok, V. A. *Diffraction of radiowaves around the earth surface* (Russian), ed. by the Acad. of Sci. of the U.S.S.R., 1946

[30] Chirkov, N. M. and Entelis, S. G. *Zh. fiz. Khim.* 22 (1948) 930

[31] Chernyak, N. Ya., Antonovsky, V. A., Revsin, R. F. and Stern, V. Ya. *Zh. fiz. Khim.* 28 (1954) 251

[32] Semenov, N. N. *Usp. Khim.* 20 (1951) 702

7

REACTIONS OF SOME RADICALS AND THEIR CONCENTRATION IN FLAMES

V. N. KONDRATIEV

The fact that the concentration of radicals in flames is much in excess of their equilibrium concentrations can be considered now as well established. Therefore in determining the concentration of radicals in burnt gases, rate constants of elementary chemical processes, involving free radicals and determining the concentration of these radicals in the reaction zone, will have an importance similar to that of equilibrium constants.

Thus various authors tried to obtain the rate constant of process

$$O + H_2 = OH + H \qquad (I)$$

but it should be recognized that these efforts were unsuccessful.

Kistiakowsky[1] seems to be the first to have evaluated this constant. He has found that at room temperature reaction 1 occurs with a probability of 10^{-4}. However this value was obtained for a reaction of a metastable oxygen atom $O(^1D)$, the reaction of a normal atom $O(^3P)$ would be less probable*.

The energy activation of reaction I for $O(^3P)$ was obtained by Harteck and Kopsch[3] by measuring the yield of water produced by interaction between oxygen containing 25–30 per cent of O atoms and hydrogen, at temperatures 27, 100 and 189°C. It was found to be $E = 6 \pm 1$ kcal. Various authors[4,5,6] have tried to derive the absolute constant of I from this value. Thus taking the steric factor as equal to unity it is possible to calculate the upper limit of k_I

$$k_I = 9{\cdot}5 \times 10^{-10} e^{-(6{,}000/RT)} \text{ cm}^3 \text{ molecule}^{-1} \text{ sec}^{-1}$$

This limiting value leads to a value for oxygen atom concentration in rarefied hydrogen flames 50 times lower than that for hydroxyl concentration and 10,000 times lower than the concentration of H atoms (stoichiometric mixture, $T = 1{,}000°K$).

* It should be noted that this conclusion is in agreement with the results of Bear and Eyring[2], who had found that the activation energy of reactions

$O(^3P) + H_2 \rightarrow H_2O$ and $O(^1D) + H_2 \rightarrow H_2O$

is 8 and 2–3 respectively. Assuming that the activation energy of I is near to these values and taking $E = 2{\cdot}5$ kcal for reaction $O(^1D) + H_2 = OH$ the steric factor of this reaction is 0·01.

Assuming that process

$$O + H_2 + M = H_2O + M$$

competes with process (I) in photosensitized oxidation of hydrogen at low temperatures ($T < 250°C$) and under pressures high enough ($p > 15$ mm Hg), Nalbandyan and Voevodsky derived an equation for the chain length

$$\nu = 2 + \frac{\dfrac{k(M)}{k_I}}{1 + \dfrac{k(M)}{k_I}} \qquad (1)$$

where k is the rate constant of $O + H_2 + M = H_2O + M$. They suggested that the best agreement for chain length values both calculated by this equation and measured by Nalbandyan[7] can be obtained if

$$\frac{k}{k_I} = 4{\cdot}6 \times 10^{-21} e^{-(6{,}000/RT)} \text{ cm}^3 \text{ molecule}^{-1}$$

Hence, assuming $k = 2{\cdot}1 \times 10^{-32}$ cm^6 molecule^{-1} sec^{-1} they get

$$k = 2 \times 10^{-13} (T)^{1/2} e^{-(6{,}000/RT)} \text{cm}^3 \text{molecule}^{-1} \text{sec}^{-1}$$

However the reaction rate constant of $O + H_2 + M = H_2O + M$ suggested by Nalbandyan and Voevodsky does not seem to be very probable as this reaction proceeds without spin conservation. From this point of view the reaction rate constant of (I) which is by three orders lower would be more probable. This would give a value for the k_1 pre-exponential factor of the order of 10^{-14} molecule^{-1} sec^{-1}.

A value of this order can be obtained also if process

$$O + O_2 + M = O_3 + M$$

is substituted for $O + H_2 + M = H_2O + M$.

Then, under the experimental conditions of Nalbandyan and Voevodsky, we get an expression for the chain length

$$\nu = \frac{2 + \dfrac{k(M)\ (O_2)}{k_1(H_2)}}{1 + \dfrac{k(M)\ (O_2)}{k_I(H_2)}} \qquad (2)$$

where k is the rate constant of $O + O_2 + M = O_3 + M$.

Inserting the value of k obtained from equation

$$k = (7{\cdot}3 \pm 0{\cdot}4) \times 10^{-35} e^{(6{,}000/RT)} \text{ cm}^6 \text{ molecule}^{-2} \text{ sec}^{-1}$$

derived by Benson and Axworthy[8] for M = O_2, we get

$$k_I = 7{\cdot}9 \times 10^{-15} e^{-(6{,}000/RT)} \text{ cm}^3 \text{ molecule}^{-1} \text{ sec}^{-1}$$

A near value for k_I can be obtained from the results of Harteck and Kopsch[3].

Lewis and von Elbe[6] have also evaluated k_I. As has been shown by these authors the empirical dependence of the pressure of mixture $2CO + O_2 + xH_2$ upon p_{H_2} at the second combustion limit and at a temperature of 545°, obtained by Buckler and Norrish[9], is given by the following equation derived from the reaction mechanism

$$p' = p\left(1 + \frac{kpp_{O_2}}{k_I p_{H_2}}\right) \qquad (3)$$

where p' is the critical pressure at high hydrogen content in the mixture and k is the reaction rate constant of $O + O_2 + M = O_3 + M$.

According to Lewis and von Elbe, at a temperature of 545°C $k : k_I$ is $1{\cdot}16 \times 10^{-20}$ cm^3 molecule^{-1}. Hence $k_I = 8{\cdot}6 \times 10^{19} k$ cm^3 molecule^{-1} sec^{-1}. Evaluating k and assuming the steric factor for k_I to be 10^{-1}–10^{-3}, Lewis and von Elbe obtained $k_I = 10^{-13}$–10^{-15} cm^3 molecule^{-1} sec^{-1}. The value of k_I calculated from the constant k obtained by Benson and Axworthy[8] is $k_I = 9 \times 10^{-15}$ cm^3 molecule^{-1} sec^{-1}, e.g. the mean of the values of Lewis and von Elbe (and by an order lower than that reported by Nalbandyan and Voevodsky[5]).

However the above calculation also does not seem to be very convincing. In fact from the five curves plotted by Buckler and Norrish for the dependence of the critical pressure of mixture $2CO + O_2 + xH_2$ upon hydrogen pressure, at temperatures of 445, 475, 515, 545 and 565°C, Lewis and von Elbe have used only that for 545°, whilst considering all these curves it is easy to see that they are quite unappropriate to equation 3.

For instance the ratio k/k_I of this equation would not obey the Arrhenius law, as the effective activation energy changes from 20 kcal for the temperature range 475–515°C to 120 kcal for 545–565°C. It follows that either it is impossible to use equation 3 for the dependence of critical pressure on hydrogen pressure as important corrections would have to be made in the reaction mechanism, or—and this seems to be more probable—that the results of Buckler and Norrish are not accurate enough to be evaluated quantitatively from the reaction mechanism*. In both cases the possibility of deriving the reaction rate constant I from 4 on the basis of the results of Buckler and Norrish should be excluded.

Thus ignoring the values of reaction rate constants k_I, obtained both by Lewis and von Elbe and by Nalbandyan and Voevodsky, on account of their being improbable or contradictory to experimental data, we derive from expression 2 a value having a certain experimental basis

$$k_I = 10^{-14} e^{-(6{,}000/RT)} \text{ cm}^3 \text{ molecule}^{-1} \text{ sec}^{-1}$$

As can be seen from comparison of k_I with its maximum value (page 41) the steric factor for k_I should be 10^{-5}. However apart from this small steric factor being improbable in case of a reaction such as expression I, it is easy to see that the low k_I value obviously contradicts existing information on hydrogen combustion reactions.

Indirect evidence, namely measurements of OH[4] and H[10] concentrations in the rarefied flame zone as well as measurements of the second hydrogen ignition limit as a function of composition of hydrogen-oxygen mixtures, actually confirmed the following relationship obtained by Lewis and von Elbe from the mechanism for hydrogen combustion

$$k_V(H_2)(OH) = 2k_{IV}(O_2)(H) = 2k_I(H_2)(O) \qquad (4)$$

where k_V and k_{IV} are the rate constants of processes

$$OH + H_2 = H_2O + H$$

and

$$H + O_2 = OH + H$$

Since respective values of partial pressures of OH and H in rarefied hydrogen flames (stoichiometric mixture, T = 1,000°K) are approximately 0·01 and 0·1 of the total pressure, partial pressure of O should be less than $100 p_{OH}$ and $10 p_H$.

Inserting into expression 4 these p_O values together with those for constants

$$k_V = 2{\cdot}2 \times 10^{-10} e^{-(10{,}000/RT)} \text{ cm}^3 \text{ molecule}^{-1} \text{ sec}^{-1}$$

$$k_{IV} = 8{\cdot}8 \times 10^{-11} e^{-(14{,}900/RT)} \text{ cm}^3 \text{ molecule}^{-1} \text{ sec}^{-1}$$

and E_1 = 6,000 kcal/mole we obtain for the lower limit of the pre-exponential factor in the expression for k_I a value of the order of $A_I = 10^{-13}$ cm^3 molecule^{-1} sec^{-1}. Thus $10^{-13} A\ 10^{-9}$, the upper limit being obtained from the pre-exponential factor value with a steric factor close to unity (page 41). From calculation of the mean value for upper and lower A_I we find that $A_I = 10^{-11}$ and consequently

$$k_I = 10^{-11} e^{-(6{,}000/RT)} \text{ cm}^3 \text{ molecule}^{-1} \text{ sec}^{-1} \qquad (5)$$

It should be noted that this value is very near to that reported by Nalbandyan and Voevodsky, which was in fact arbitrary. Since the most probable steric factor is scarcely higher than 0·1

* Apparently water formation preceding ignition accounts for errors caused by use of this method.

and the partial pressure of oxygen atoms is certainly less than 0·1 of the total pressure, the true value for k_I would be near to that given in expression 5.

Other important constants are those for interaction both of OH radicals and of O atoms with a CO molecule. Rate constant values of reaction

$$OH + CO = CO_2 + H \qquad (II)$$

obtained by various authors[6,12,13] will not be mentioned here and we shall only state that the rate constant estimated from the results of Avramenko and Lorenzo (Kolesnikova)[13] seems to be the most reliable

$$k_{II} = 4{\cdot}8 \times 10^{-12} e^{-(5,700/RT)} \text{ cm}^3 \text{ molecule}^{-1} \text{ sec}^{-1} \qquad (6)$$

Trimolecular mechanism $O + CO + M = CO_2 + M$ is usually accepted for reaction

$$O + CO \rightarrow CO_2 \qquad (III)$$

though for the range of high temperatures some authors have also proposed a bimolecular mechanism $O + CO \rightarrow CO_2$. Zeldovitch and Semenov for instance[14], on the basis of kinetic investigations on flame propagation in mixtures of carbon monoxide with oxygen and with air, came to the conclusion that CO_2 is produced from O and CO by a bimolecular mechanism. Gaydon[15] suggested that the CO flame continuum observed for hot flames and absent in the low-temperature atomic flame of CO is connected with the bimolecular process $O + CO = CO_2 + h\nu$*.

Dixon-Lewis and Linnett[18] suggest that the appropriate expression for dependence of the upper ignition limit of oxygen–hydrogen–carbon monoxide mixtures upon mixture composition can be obtained only by including into the reaction mechanism the bimolecular process $O + CO = CO_2$†. Similarly Gordon and Knipe[19] are of the opinion that chain branchings observed in explosion of a CO—O_2 mixture are due to comparatively long-living excited molecules of CO_2 formed in a bimolecular interaction of CO and O.

The rate constant for formation of CO_2 from O atoms and from CO at relatively low temperatures (T = 420–550°K) was obtained by Avramenko and Kolesnikova at the Institute of Chemical Physics. Since their experiments were carried out under constant pressure they suggested that the value obtained may have been both a bimolecular constant (k_2) and a trimolecular constant multiplied by O_2 (=M), e.g. $k_2 = k_3(M)$. However the value derived from their results

$$k_{III} = k_2 = 1{\cdot}6 \times 10^{-13} e^{-(3,800/RT)} \text{ cm}^3 \text{ molecule}^{-1} \text{ sec}^{-1} \qquad (7)$$

should rather be considered as appropriate to a bimolecular mechanism. For instance by calculating the ratio of k_2 to the rate constant of a trimolecular process $O + O_2 + O_2 = O_3 + O_2$ multiplied by oxygen concentration under pressure of 1 atm and at room temperature T = 290°K, we obtain a value 1 : 25 which is near to that measured by Groth[20] (1 : 40), whilst the ratio of k_3 to the constant of ozone formation rate appears to be 10 (instead of 1 : 40).

Gordon and Knipe suggest that bimolecular formation of comparatively long-living CO_2 molecules is accounted for by possible crossing of potential energy surfaces of the CO · O complex, leading to increase of life-times of triplet excited states of CO_2 molecules. Under their experimental conditions CO_2 molecules will obey the bimolecular law only if the life-time of an excited CO_2 molecule exceeds by several orders the value 10^{-11} sec common to simple molecules such as CO_2.

In fact using the steady-state condition $\{d(CO_2^*)\}/dt = 0$ we obtain from the mechanism of CO_2 formation

$$O + CO = CO_2^* \qquad k_2$$
$$CO_2^* = CO + O \qquad k_{-2}$$
$$CO_2^* + M = CO_2 + M \qquad k_4$$

a reaction rate

$$\frac{d(CO_2)}{dt} = \frac{k_2(CO)(O)}{1 + \dfrac{k_{-2}}{k_4(M)}} \qquad (8)$$

Since under the experimental conditions mentioned $k_4(M)$ is of the order of 10^9 sec^{-1}, the reaction will be governed by the bimolecular law only if the life-time of an excited CO_2 molecule defined by $1 : k_{-2}$ is not less than 10^{-8} sec. Consequently it would exceed the normal value by at least three orders, which can scarcely be due to crossings of potential energy surfaces of CO_2 molecules for the triplet states, as suggested by Gordon and Knipe.

However the long life-time of an excited CO_2 molecule, formed from CO and O by the bimolecular law, can also have a different explanation. From evidence on monomolecular dissociation of N_2O having a structure near to that of CO_2 we obtain for the life-time of an activated molecule, dissociating by the reaction scheme $N_2O \rightarrow N_2 + O$, a value of 10^{-8} sec which is by three orders higher than that for triatomic molecules (such as F_2O). As can be seen this is in agreement with the above mentioned upper value for the life-time of an excited CO_2 molecule. Since the

* See also References 16 and 17.

† According to Dixon-Lewis and Linnett the ratio of $k_2 = k_{III}$ to k_I is given by

$$\frac{k_{III}}{k_I} = 1{\cdot}26 \times 10^{-2} e^{-(700/RT)}$$

Taking into account that the estimated energy activation for process III (and also for I) can be erroneous by 1·5–2 kcal/mole, the values for k_I and k_{III} given in this paper cannot be considered as contradictory to the above expression.

long life-time of an activated N_2O molecule should be accounted for by small probability of intercombination transition $N_2O(^1\Sigma) \rightarrow N_2(^1\Sigma) + O(^3P)$ it would also be reasonable to connect the long life-time of CO_2 with violation of the intercombination rule in transition $CO + O \rightarrow CO_2^*$. In other words the excited state of the CO_2 molecule produced by bimolecular interaction of CO and O should be considered not as a triplet but as a singlet state. This conclusion is in a certain sense confirmed by the steric factor of the rate constant k_2 (expression 7) which is of the order of 10^{-3}. Assuming that k_2 is equal to $10^8\,sec^{-1}$ we obtain the bimolecular law for formation of CO_2^* under the conditions of Gordon and Knipe.

The bimolecular law is also fulfilled in the experiments of Avramenko and Kolesnikova. Since under their experimental conditions the pressure is low (4 mm Hg) process

$$CO_2^* = CO_2 + h\nu$$

having a rate constant of the order of $10^8\,sec^{-1}$ (equal to k_{-2} as well) and being by an order higher than $k_4(M)$, should be accepted together with other processes mentioned earlier, and the rate of CO_2 formation becomes

$$\frac{d(CO_2)}{dt} = \frac{k_2}{2}(CO)(O)$$

e.g. the bimolecular law is obeyed and the effective rate constant has the same order of magnitude as k_2.

It is obvious that the mechanism of formation of CO_2 from CO and O discussed above requires further more detailed investigations.

The thermal dissociation of molecules is also of great importance in connection with kinetics of flame reactions. Theoretical treatment of this process has hitherto been handicapped by difficulties due to the impossibility of using the simple collision theory in estimating the dissociation constant (k_D) as it often had led to values by two orders lower than those obtained from the re-combination rate constant of process $A + B + M = AB + M(k_p)$ and from the equilibrium constant $A + B \rightleftharpoons AB(K)$, $k_D = k_pK$. Rice[21] was the first to note this difficulty and proposed an explanation for discrepancies in theoretical and measured values of k_D. Analogous investigations were made by other authors*. The only convincing suggestion seems to be made by Nikitin (Institute of Chemical Physics) who emphasized the role played by deviations from Boltzmann energy distribution and has shown the importance of rotational energy of thermally dissociating molecules taking part in their activation together with vibrational energy.

* See for instance references 22 and 23.

The dissociation constant of a bromine molecule obtained by Nikitin from quantum statistical calculations can be defined by equation

$$k_D = 5 \times 10^{-2}\left(\frac{D}{RT}\right)^{1.5} z_0 e^{-(D/RT)}$$

(valid at $h \simeq RT$, which is just the case here). This equation is in good agreement with the empirical formula

$$k_D = 3 \times 10^{-2}\left(\frac{D}{RT}\right)^{1.97} z_0 e^{-(D/RT)}$$

obtained by Palmer and Hornig[23] for M = Ar. This permits us to suggest that in other cases quantum statistical calculations will also give good results.

REFERENCES

[1] Kistiakowsky, G. B. *J. Amer. chem. Soc.* 52 (1930) 1868

[2] Bear, R. S. and Eyring, H. *J. Amer chem. Soc.* 56 (1934) 2020

[3] Harteck, P. and Kopsch, U. *Z. phys. Chem. B*12 (1931) 327

[4] Kondratiev, V. *Spectroscopic investigations on chemical reactions in the gas phase* (in Russian). M.-L. 1944

[5] Nalbandyan, A. N. and Voevodsky, V. V. *Mechanism of oxidation and combustion of hydrogen* (in Russian). M.-L. 1949

[6] Lewis, B. and von Elbe, G. *Combustion, Flames and Explosions of Gases* 1951. New York; Academic Press

[7] Nalbandyan, A. B. *Zh. fiz. Khim.* 20 (1946) 1259

[8] Benson, S. W. and Axworthy, A. E. *J. chem. Phys.* 26 (1957) 1718

[9] Buckler, E. J. and Norrish, R. G. W. *Proc. Roy. Soc. A*167 (1938) 318

[10] Kondratieva, E. and Kondratiev, V. *Zh. fiz. Khim.* 20 (1946) 1239

[11] Ischireov, N. M. *Acta physicochim.* U.R.S.S. 6 (1937) 915

[12] Avramenko, L. I. *Zh. fiz. Khim.* 21 (1947) 1135

[13] — and Lorenzo, R. V. *Zh. fiz. Khim.* 24 (1950) 207

[14] Zeldovitch, Ya. B. and Semenov, N. N. *Zh. Exp. Teor. Fiz.* 10 (1940) 1427

[15] Gaydon, A. G. *Proc. Roy. Soc. A*183 (1944) 111

[16] Laidler, J. and Shuler, K. *Chem. Rev.* 48 (1951) 153

[17] Marr, G. V. *Canad. J. Phys.* 35 (1957) 1265, 1275

[18] Dixon-Lewis, G. and Linnett, J. W. *Trans. Faraday Soc.* 49 (1953) 756

[19] Gordon, A. S. and Knipe, R. H. *J. phys. Chem.* 59 (1955) 1160

[20] Groth, W. *Z. phys. Chem. B* 37 (1937) 315

[21] Rice, O. K. *J. chem. Phys.* 9 (1941) 258

[22] Careri, G. *Nuovo Cimento* 6 (1949) 94
— *Nuovo Cimento* 7 (1950) 155
— *J. chem. Phys.* 21 (1953) 749

[23] Palmer, H. B. and Hornig, D. F. *J. chem. Phys.* 26 (1957) 98

8

FURTHER STUDIES OF INDUCTION PERIODS IN MIXTURES OF H_2, O_2 AND NO_2

P. G. ASHMORE and B. P. LEVITT

INTRODUCTION

In 1928, H. B. Dixon found that traces of nitrogen dioxide could lower the ignition temperature of certain mixtures of hydrogen and oxygen by more than 200°C, and so initiated a long series of researches by various investigators[1–5] upon the 'sensitization' of ignitions by nitrogen dioxide. By 1941, these careful investigations had established the principal conditions of temperature, vessel size, and concentrations of reactants and sensitizer which lead, after an induction period which may last tens of seconds, to slow reaction or ignition. Ignition occurs only if the pressure of nitrogen dioxide lies between a lower and an upper sensitizer limit of ignition; these limits change with total pressure so as to enclose an ignition region[4]. Several suggestions about the kinetic mechanisms of the sensitization had been proposed, but none was completely satisfactory. Thus in 1951, Lewis and von Elbe wrote[6] 'The suggestion that

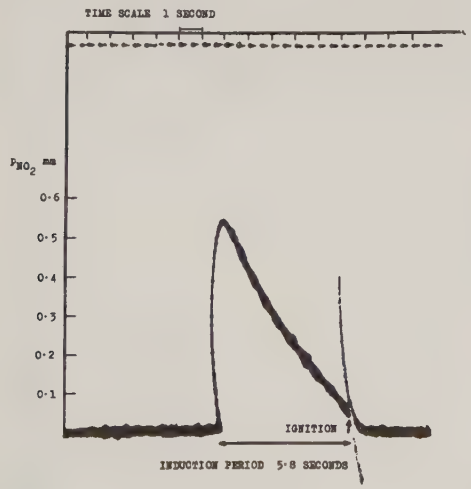

Figure 1. The concentration of NO_2 *against time during the induction period of a sensitized ignition.* 376°C, 0·6 mm NO_2, 100 mm H_2, 50 mm O_2 *initially. Photograph of pen recorder trace of photometer output*

the NO_2 sensitization is due to the development of branched chains is generally accepted, but its implementation by a specific mechanism is a matter of great difficulty and cannot be regarded as solved at this time. It is not even clear what the relative roles of NO and NO_2 might be, both of which may be present more or less in equilibrium with oxygen.' Since then, a good deal of indirect[7] and direct[8] evidence has been presented which shows that the induction periods represent the time taken for the nitrogen dioxide to react with hydrogen to yield nitric oxide[9]. For example, *Figure 1* is typical of results obtained in a preliminary photometric study[8] of the changes of p_{NO_2} during the induction periods before ignitions. The pressure of nitrogen dioxide fell from 0·6 mm on admission to less than 0·1 mm at the end of six seconds. This extensive decomposition (~80 per cent) cannot be due to the bimolecular reaction $2NO_2 \rightarrow 2NO + O_2$, which would lead to only 0·06 per cent decomposition in six seconds[10]. At the end of the induction period, the trace takes a sharp downward kick due to the ignition flash. Experiments with mixtures of the same composition showed that the concentration of nitrogen dioxide immediately before this downward kick is reproducible from run to run, and it was suggested[8] that the attainment of this limiting pressure, p_e, could be taken as a condition for ignition appropriate to the original mixture. It was expected that the relationship between p_e and the corresponding values of p_{NO}, p_{H_2}, p_{O_2}, etc., would give information about the relative roles of nitric oxide and nitrogen dioxide in branching and terminating steps, and could be used to test various theories of the branching mechanism which have been proposed[7,11]. The work described in this paper set out to investigate how p_e is influenced by the initial pressure of the sensitizer, the total pressure of a stoichiometric mixture, the partial pressure of hydrogen or oxygen, the temperature, and the pressure of inert gas added. The photometer described previously[12] was modified to follow lower concentrations of nitrogen dioxide and to allow better time resolution. The significant observation was made that a rapid (but continuous) increase in the rate of removal of nitrogen dioxide occurs at the end of the induction period when p_e is reached. The bearing of this observation and the other results upon the conditions postulated for the end of the induction period and the occurrence of ignition or slow reaction is discussed in detail.

EXPERIMENTAL

The gases were prepared and stored as described elsewhere[9]. Reactant mixtures were prepared in mixing vessels, and then delivered through a conventional Pyrex glass vacuum system to a Pyrex or quartz reaction vessel heated in an electric furnace. The bulk of this work was carried out in a quartz reaction vessel, a plane-ended cylinder of length 20 cm and diameter 3·5 cm. Pressure changes were measured with a Bourdon gauge. The concentration of nitrogen dioxide in the reaction vessel was followed continuously with a modification of a photometer described previously[12]. A tungsten lamp was viewed by two separate logarithmic photometers[12], using photomultiplier tubes which are matched as nearly as possible in sensitivity. The reaction vessel lies between the source and one photomultiplier ('measure') and an adjustable slit between the source and the other ('dummy'). The difference in potential between the photomultiplier cathodes is directly proportional to the concentration of nitrogen dioxide in the vessel; it was measured on a microammeter, or amplified to operate a short period 'Record' pen recorder, a Kelvin-Hughes high-speed pen recorder, or an oscilloscope. The double beam circuit reduced drift due to variations in light intensity by a factor of 40; the overall drift of the photometer was reduced by a factor of 5; the sensitivity was doubled; and the 50 cycle noise considerably reduced.

The detailed study of the changes of concentration of nitrogen dioxide near the end of the induction periods was started, using the oscilloscope. A device was constructed to trigger the oscilloscope time base for a single sweep (1·5 or 0·5 seconds) when the concentration of nitrogen dioxide fell to a selected level. By choosing this level just above p_e, photographs could thus be taken of the oscilloscope trace near the end of the induction periods.

RESULTS

Variation of p_{NO_2} near p_e

(*a*) *Before ignition*—Although the rate of removal of nitrogen dioxide during the induction period would be expected[9] to fall as the first power of the concentration, and traces like those in *Figure 1* show some decrease in the rate as nitrogen dioxide disappears, some traces taken at low total pressures showed an increasing rate towards the end of the induction period (see below). Closer examination of traces like those in *Figure 1* showed that there was a clear increase in the rate of disappearance of nitrogen dioxide after the attainment of p_e and immediately before the ignition flash. To make sure that this was not due to the finite time response of the recorder, photographs of an oscilloscope trace of the output from the photometer were taken during the last second of the induction period. A typical trace is shown in *Figure 2*. After p_e is reached, the rate of removal of nitrogen dioxide increases rapidly, and ignition occurs only after the pressure of nitrogen dioxide has

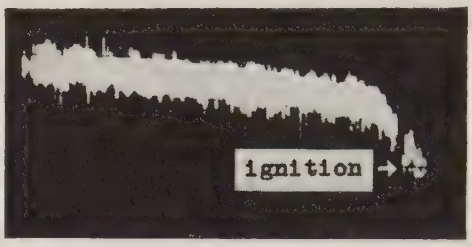

Figure 2. Photograph of oscilloscope trace near the end of an induction period

fallen to a lower but definite concentration, p_i. The rate of disappearance of nitrogen dioxide accelerates thirtyfold for a fall in p_{NO_2} of only 10 per cent.

(*b*) *Above the upper sensitizer limit*—Immediately above the upper sensitizer limit the same rapid acceleration is observed when p_e is attained. However, the acceleration falls off rapidly, and instead of reaching a very low value, p_{NO_2} falls to a nearly stationary value, p_s. The onset of the slow hydrogen–oxygen reaction was followed by the pressure change on a Bourdon gauge. It occurred, as closely as could be judged, immediately after p_e was attained when p_{NO_2} fell rapidly; the coincidence was within a small fraction of a second after an induction period of a minute or more.

As p_0 was increased further in successive runs, p_s rises rapidly, and the acceleration of the removal

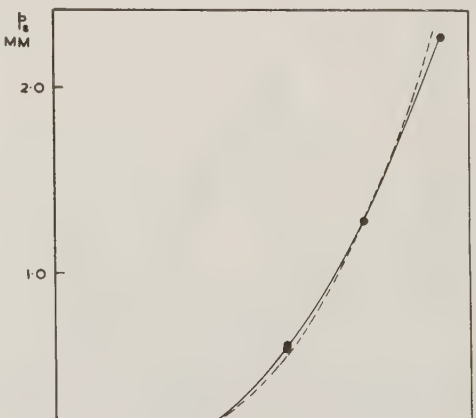

Figure 3. Pseudo-stationary concentration of nitrogen dioxide in mixtures with initial concentrations of 33·3 mm O_2, 66·7 mm H_2 *and* p_0 mm NO_2 *at* 370°C *plotted against* p_0

of NO_2 becomes less and less pronounced. Eventually, with high p_0, p_{NO_2} falls smoothly to p_s and there is no observable onset of the hydrogen–oxygen reaction. The points in *Figure 3* show how p_s varies with p_0.

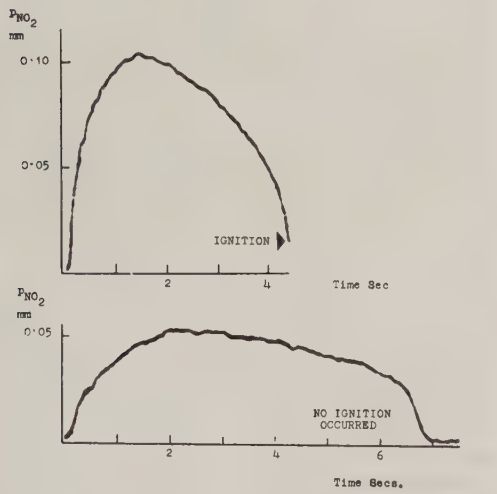

Figure 4. The concentration of nitrogen dioxide during the induction period of the sensitized hydrogen–oxygen reaction. Photograph of pen recorder trace; 372°C. *Trace A:* 34 mm ($2H_2 + O_2$), 0·13 mm NO_2 *initially*; *Trace B:* 16 mm ($2H_2 + O_2$), 0·07 mm NO_2 *initially*

(*c*) *Below the lower sensitizer limit*—At 370°C and moderate pressures, the induction periods become very short near the lower sensitizer limit. It was found to be convenient to cross the limit by successive runs with mixtures of constant composition but lower and lower total pressure. *Figure 4* shows photographs of pen recorder traces for two runs in a series of this type; the pen recorder used here is of longer period than that used for *Figure 1*. Mixture A lies above the limit of ignition. At these low pressures the rate of removal of nitrogen dioxide appears to increase almost continuously, though this appearance is in part due to the finite radius of the pen recorder. Mixture B lies below the ignition limit. Here the concentration of nitrogen dioxide falls steadily until the rate suddenly accelerates. The concentration at which the rate accelerates can be identified with p_e. *Figure 5* shows p_e and the induction period plotted against total pressure for the whole series. Both are continuous across the limit. The phenomena continue, as the initial pressure is reduced, to the lowest point at which photometry is possible.

The experiments detailed above show that each induction period can be divided into two very unequal portions. In the longer initial part, often lasting tens of seconds, p_{NO_2} falls steadily to the critical value p_e at which a substantial acceleration in $-dp_{NO_2}/dt$ occurs; this acceleration, over a few hundredths of a second, leads to ignition or slow reaction of the reactants. Thus the time at which p_e is reached virtually determines the end of the induction period. Although the ignition is detected when p_{NO_2} reaches p_i, and not p_e as was previously thought[8], p_e as the point of commencement of the acceleration is of great importance. The

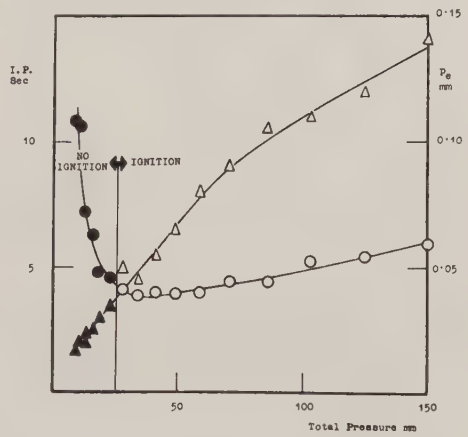

Figure 5. Plots showing the variation of: (i) *the concentration of nitrogen dioxide, p_e, at the end of the induction period* (*R.H. scale, triangles*), (ii) *the length of the induction period* (*L.H. scale, circles*) *against total pressure of a mixture of the composition:* $H_2 : O_2 : NO_2 = 167 : 83 : 1$ *in each run initially,* 372°C. *Induction period measured to the sensitized ignition or to the rapid disappearance of nitrogen dioxide where no ignition occurs*

observed dependence of p_e upon certain variables will therefore be described.

Variation of p_e with p_0 and with p_T

The variation of p_e with the initial pressure p_0 of nitrogen dioxide was investigated for three different total pressures p_T of a 2 : 1 mixture of hydrogen and oxygen at 370°C, using the high-speed pen recorder. The results are shown in *Figure 6*. For most of the ignition region, p_e falls linearly as p_0 is increased, particularly at the higher pressures; the slope $-(dp_e/dp_0)_{p_T}$ appears larger at higher values of p_T. For all the plots, p_e is greater the higher the total pressure, and dp_e/dp_T decreases somewhat as p_0 increases but is approximately constant for each value of p_0. Towards the upper sensitizer limit of ignition, the curve of p_e against p_0 flattens but is continuous across the limit. Eventually p_e is replaced by p_s as explained earlier.

The induction period τ, the time p_{NO_2} takes to fall from p_0 to p_e, increases rapidly as p_0 approaches and crosses the upper limit as found by other investigators[1–5].

Variation of p_e with p_{H_2} and with p_{O_2}

Figure 7 shows the variation of p_e and of τ for constant p_0 when the partial pressure of hydrogen

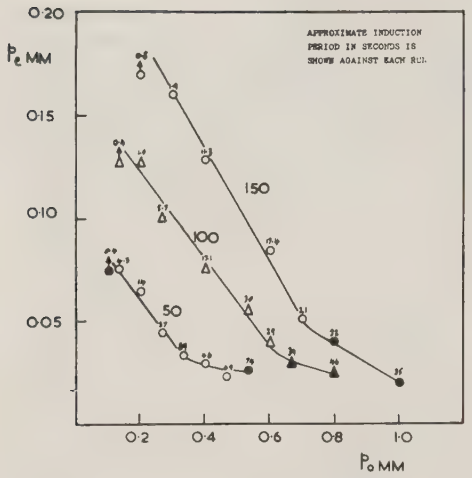

Figure 6. Plots of p_e against p_0 for ignitions of hydrogen and oxygen sensitized by p_0 mm *nitrogen dioxide, total pressure of stoichiometric mixture shown in* mm *against each plot,* 370°C. *Open circles, ignition; filled circles, no ignition*

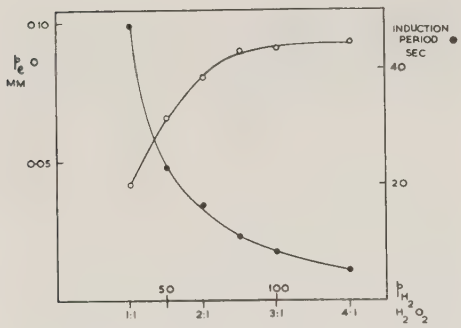

Figure 7. Plots of p_e and induction period against partial pressure of hydrogen for sensitized ignitions at 370°C. 33·3 mm O_2 *and* 0·4 mm NO_2 *initially in each run*

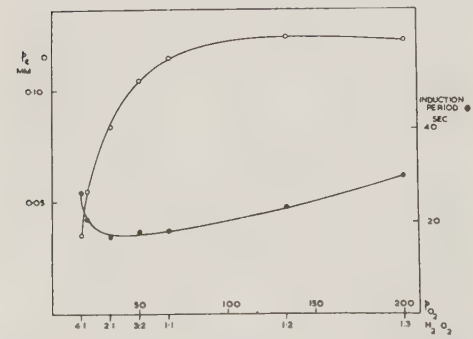

Figure 8. Plots of p_e and induction period against partial pressure of oxygen for sensitized ignitions at 370°C*:* 66·7 mm H_2 *and* 0·4 mm NO_2 *initially in each run*

p_{H_2} is altered, and *Figure 8* shows the changes when the partial pressure of oxygen p_{O_2} is altered. In both cases p_e rises rapidly as the concentration of added gas rises through the stoichiometric ratio, but well above this it becomes nearly constant. The behaviour of the induction periods, however, are in marked contrast: those for added hydrogen decrease steadily even when p_e is nearly constant, whereas those for added oxygen fall sharply until the stoichiometric point is reached and then rise slowly.

The mixture X containing 0·4 mm NO_2, 33·3 mm O_2 and 66·7 mm H_2 is common to *Figures 6–8*. If dp_e/dp_T is constant for $p_0 = 0{\cdot}4$ mm, the identity

$$\left(\frac{dp_e}{dp_T}\right)_{p_0} = \left(\frac{dp_{H_2}}{dp_T}\right)\left(\frac{dp_e}{dp_{H_2}}\right)_{p_{O_2}} + \left(\frac{dp_{O_2}}{dp_T}\right)\left(\frac{dp_e}{dp_{O_2}}\right)_{p_{H_2}}$$

provides a useful check on the experimental technique. It is found to hold within the error of measuring the slopes. At first sight, the plots in *Figures 7* and *8*, with the above identity, suggest that $(dp_e/dp_T)_{p_0}$ tends to zero at higher values of p_T; but further consideration shows that this is not a correct inference from the curves; dp_e/dp_{O_2} may be very large when dp_e/dp_{H_2} is close to zero, and vice versa.

p_e and temperature

The variation of p_e with temperature has not been extensively investigated because it is difficult to find mixtures which remain within the ignition region, and have a finite induction period, over a wide range of temperature. However, it is clear that, other things being constant, p_e rises rapidly with increasing temperature.

TABLE 1

Values of p_e and τ for $2H_2 + O_2 = 100$ mm for Various Values of p_0

370°C	p_0	0·4	0·6	0·8 mm
(Quartz vessel)	p_e	0·07	0·04	0·02 mm
$2H_2+O_2 = 100$ mm	τ	17	29	46 sec
412°C	p_0	0·5	1·0	2·0 mm
(Pyrex vessel)	p_e	0·12	0·06	0·04 mm
$2H_2+O_2 = 100$ mm	τ	4	15	49 sec

Cross checks available for 150 mm of reactants at 370°C show that p_e does not change much with the nature of the vessel surface.

p_e and added inert gas

If inert gas is added to the mixture X, the effect is similar to that observed when p_0 is raised. As nitrogen is added p_e falls steadily; 125 mm reduces it by 50 per cent and just suppresses ignition. The acceleration is still observed when p_e is reached,

and p_e is continuous across the ignition limit. If more nitrogen is added, the acceleration disappears (175 mm), and p_{NO_2} falls steadily to a nearly stationary value. This sequence shows a remarkable similarity to that observed when p_0 is increased above the upper sensitizer limit.

DISCUSSION

Length of the induction period

This experimental work has substantiated previous ideas[7,8] that the induction period represents the time τ taken for a substantial portion of the nitrogen dioxide originally present to be removed by reaction with hydrogen. The rate of this reaction is given[9] by expression 1.

$$-\frac{dp_{NO_2}}{dt} = \frac{k_1 p_{NO_2} p_{H_2}^{1.5}}{p_{NO} + k_2 p_{NO_2}} \qquad (1)$$

The rate is slowed[9] by adding inert gases such as nitrogen. k_2 is close to one at temperatures near 400°C. The observed effect on the induction periods of changing p_{NO_2}, p_{H_2}, p_{O_2} and p_{N_2} can be explained as follows:

(1) as the initial pressure p_0 of NO_2 is increased across the ignition region, τ increases rapidly. *Figure 6* shows that p_e decreases, so the extent of reaction is increased whereas equation 1 shows that the initial rate is independent of p_0 and is in fact slower for each given p_{NO_2} the higher p_0—for then p_{NO} is higher. Hence the time taken before ignition increases, as observed, when p_0 is increased.

(2) as p_{H_2} is increased, τ falls rapidly (*Figure 7*). Not only does p_e increase, so reducing the extent of reaction required, but the rate increases, as shown by equation 1.

(3) as p_{O_2} is increased, the induction period first falls sharply and then rises slowly. The fall corresponds to a rapid rise in p_e (*Figure 8*) and can be attributed to the greatly decreased extent of reaction necessary, for the effect of oxygen on the rate of the nitrogen dioxide + hydrogen reaction is slight—it acts as an inert gas and slows the reaction somewhat. However, once p_e levels off, this slowing will account for the region where τ increases slowly.

(4) the addition of nitrogen lowers p_e (note the contrast here with oxygen) and slows the rate of the hydrogen + nitrogen dioxide reaction; hence the extent of decomposition required is increased, and the rate decreased, and these effects explain why nitrogen increases the induction periods much more strongly than does oxygen (*cf. Figure 8* of reference 4).

Our observations also agree with the explanations put forward[3,4] to account for the shortening of the induction periods upon photolysis; any reaction which hastens the decomposition of NO_2 will shorten the induction periods.

The quantitative agreement of the length of the induction periods with values calculated from the kinetics of the hydrogen + nitrogen dioxide mixture is fairly good at high total pressures. For example, at 370°C the rate of fall of NO_2 with 0·6 mm NO_2 and 100 mm H_2 can be calculated from published results[9] to be 1/11 mm/sec; the effect of 50 mm oxygen on this ratio is small, so that p_{NO_2} would be reduced from 0·6 to 0·1 mm in 0·5 × 11 or 5·5 seconds if the rate remained constant. As it falls slightly (*Figure 1*) the calculation is in excellent agreement with the observed value of 5·8 seconds. However, the kinetics of the NO_2/H_2 reaction have not been investigated at very low pressures, and it is not possible to account quantitatively for results like those shown in *Figure 4*. It appears, therefore, that most of the investigations of induction periods in these systems can be explained in terms of the reaction between nitrogen dioxide and hydrogen. There is, however, one feature reported in the literature[3,4] which cannot be explained by our present interpretation. This is the substantial increase in τ reported at lower sensitizer concentrations, below the lower sensitizer limit of ignition, with constant pressure of hydrogen and oxygen. (The effect is not the same as that shown in *Figure 5*, which can be explained by the fall in p_{H_2}.) All our work suggests an increase rather than a decrease in the rate of removal of NO_2 at very low concentrations, which would lead to shorter induction periods as $p_0 \to 0$. At present, we can only suggest that what was taken at low p_0 to be the end of an induction period was actually the attainment of a finite pressure change due to an extremely slow reaction which began upon admission of the mixtures to the reaction vessel (*cf.* Dainton[13]). This point requires further investigation.

Ignition boundaries

(*a*) *Upper sensitizer limit*—The observations upon p_e, p_i and p_s described earlier allow a rational explanation of the upper sensitizer limit of ignition, and the behaviour of mixtures of composition just above this limit. *Figure 3* (points) shows that p_s increases rapidly as p_0 increases; on the other hand *Figures 6* and *2* show that p_e falls as p_0 increases and that p_i lies below p_e for each value of p_0. Hence a point will come, as p_0 is increased, when p_{NO_2} can fall to p_e, but reaches p_s before p_i; there should be an acceleration of the removal of nitrogen dioxide and the hydrogen + oxygen reaction should begin, but there will be no ignition. The upper sensitizer limit of ignition has been reached. At still higher values of p_0, p_s will be reached before p_e; hence no acceleration and no hydrogen–oxygen reaction should occur. This is exactly what is observed.

The mechanism which establishes p_s seems to be extremely simple. As p_0 is increased, the pressure p_{NO} which is built up as the nitrogen dioxide reacts

with hydrogen is increased and the reaction $2NO + O_2 \xrightarrow{k_t} 2NO_2$ becomes important. When its rate equals that of the removal of nitrogen dioxide,

$$\frac{k_1 p_{NO_2} p_{H_2}^{1.5}}{p_{NO} + k_2 p_{NO_2}} = k_t p_{NO}^2 p_{O_2}$$

Now $k_2 \sim 1$ at 300°C, and as long as $p_s \ll p_0$,

$$\frac{k_1 p_s p_{H_2}^{1.5}}{p_0} = k_t p_0^2 p_{O_2}$$

$$\therefore \quad p_s \propto p_0^3$$

The dotted curve in *Figure 3* is a cubic in p_0, passing through $p_s = 1{\cdot}3$, $p_0 = 8{\cdot}0$. It is a close fit to the full curve through the experimental points. Moreover, absolute calculations of p_s from appropriate values[9,10] of k_1 and k_t agree well with the experimental values.

It may be concluded that the upper sensitizer limit occurs because a stationary state concentration of nitrogen dioxide is set up by the reactions

$$H_2 + NO_2 = NO + H_2O$$
$$2NO + O_2 = 2NO_2$$

We thus return to a modification of the ideas of Crist and Wertz[14].

(*b*) *The lower sensitizer limit*—The experiments described here throw little light on the problem of the lower sensitizer limit of ignition. Experiments[7] on the ignition boundary found with nitric oxide as sensitizer suggest that a minimum amount of nitric oxide is necessary, and that this minimum corresponds with the lower sensitizer limit with nitrogen dioxide. Our experiments support this view, and further investigations of p_e and p_i at lower values of p_0 may be helpful.

Conditions for ignition

There are several reasons[11] for believing that the reactions leading to ignition involve branched chains, and that the phenomena observed at the end of the induction periods cannot be explained by an increased rate of initiation (by nitric oxide) and reduced rate of termination (by nitrogen dioxide). The behaviour shown in *Figure 2* provides the strongest support for these conclusions; the rate accelerates by some thirtyfold over a small change of concentration of nitrogen dioxide. Further strong support comes from: (*a*) our observation that the rate of reaction immediately below ignition boundaries like those shown in *Figure 1* of reference 3 is very slow—in marked contrast to the behaviour in non-branching systems[11], (*b*) the very great difficulty of devising any rapid initiating steps with nitric oxide, (*c*) the evidence[9] from the hydrogen + nitrogen dioxide reaction that nitric oxide is rather more effective than nitrogen dioxide in terminating chains involving OH and H. The argument that positive branching reactions are present is strong, and it seems very likely that the net rate of branching (the rate of production of centres by positive branching minus the rate of removal of centres by termination reactions) increases from some low negative value at the beginning of the induction period towards zero at the end of the induction period. The increase in chain centre concentration inferred from *Figure 2* could occur as the net rate of branching approaches zero, however, and does not require the net rate to be zero; most arguments advanced previously on these points have wrongly assumed a constant net rate of branching. Until further studies of p_i have been made, such as the effect[4] of adding inert gases of different heat capacities and different thermal conductivities, it is not possible to assert that the ignitions are 'thermal' or 'isothermal' in character.

On the other hand, it is worth while to investigate whether a reasonable branching chain mechanism, combined with the simple assumption that the net rate of branching is zero at the point $p_{NO_2} = p_e$, can explain the variations found in p_e. The problem of finding an exclusive mechanism is far from solved, but the one now proposed accounts for most of the observations on p_e, and avoids certain unsatisfactory features[11] of a mechanism suggested earlier[7]. The mechanism now proposed takes reactions 1–7 which are important in the hydrogen + oxygen reaction[15] at higher temperatures, and those which have been postulated in studies[9] of the hydrogen + nitrogen dioxide reaction (reactions 8–11). Three further reaction steps 12, 13, 14 are postulated, and their roles are discussed briefly.

The kinetic scheme

$$H + O_2 = OH + O \qquad (1)$$
$$O + H_2 = OH + H \qquad (2)$$
$$OH + H_2 = H_2O + H \qquad (3)$$
$$H + O_2 + M = HO_2 + M \qquad (4)$$
$$HO_2 + \text{wall} = \text{end} \qquad (5)$$
$$H + \text{wall} = \text{end} \qquad (6)$$
$$OH + \text{wall} = \text{end} \qquad (7)$$
$$H_2 + NO_2 = HNO_2 + H \qquad (8)$$
$$H + NO_2 = OH + NO \qquad (9)$$
$$OH + NO_2 + M = HNO_3 + M \qquad (10)$$
$$OH + NO + M = HNO_2 + M \qquad (11)$$
$$O + NO_2 = NO + O_2 \qquad (12)$$
$$HO_2 + NO = NO_2 + OH \qquad (13)$$
$$HO_2 + NO = HNO_2 + O \qquad (14)$$

Reactions 12, 13, and 14

Reaction 12 is known[4] to be rapid, and early in the induction periods it will effectively stop branching by competing with reaction 2 for oxygen atoms. Reaction 13 has been suggested before[7]; its importance will increase during the induction

period, and it will reduce the rate of termination of chains through removal of HO_2 by 5 at a time when 4 and 5 would be competing successfully with 9 for hydrogen atoms. As has been explained, however, it is unlikely that the reduction of chain termination is sufficient to explain the observations, especially in view of the additional termination step 11. Reaction 14 provides a possible branching step, representing an attack of NO on the HO– group of HO_2 rather than on the –O as in 13. The two transition complexes might be formulated as

(13) ON·····O(OH) (14) ON·····O(H)

If 14 is followed by 2, the chain will have branched; of course, this is only likely when p_{NO_2} becomes small and 12 less important. Previous estimates of the heat of formation of gaseous HNO_2 suggest that reaction 14 will be endothermic unless the HO_2 carries over some of the energy of reaction 4; this will often happen—in fact, Robb has recently given reasons[16] for believing that HO_2 formed in the binary collision $H + O_2$ can have a long life. Another possible branching step might be the ternary reaction

$$H + O_2 + NO = HNO_2 + O$$

which would be equivalent to reaction 4 followed by reaction 14, and would begin to be important in comparison with 4 as p_{NO} builds up. However, it seems better to keep the successive steps at present.

Rates of terminating and of branching

The net branching rate has been worked out for the full kinetic scheme, but for the present purpose a great simplification can be made by ignoring reaction 1, because this is acknowledged to be slow at these temperatures compared with reaction 4; it will therefore be assumed that branching occurs via reactions 4 and 14 followed by 2. The terminating and branching reactions can then be shown schematically as follows:

This scheme leads to an expression for dH/dt which will hold up to the point where the net rate of branching becomes zero. If the velocity constants are allowed to stand for the full rate expression for each of the reaction steps, the equation can be written

$$(1 + \alpha)\frac{dH}{dt} = (1 + \alpha)R_i + \frac{k_4 k_{14}}{k_5 + k_{13} + k_{14}} \cdot \frac{k_2(1 + \alpha) - k_{12}}{k_2 + k_{12}} - \alpha(k_4 + k_6 + k_9) - \left(k_6 + \frac{k_4 k_5}{k_5 + k_{13} + k_{14}}\right)$$

where α stands for $\frac{k_7 + k_{10} + k_{11}}{k_3}$, and R_i for the rate of initiation (reaction 8).

Inspection of the above equation will show that the terms after $(1 + \alpha)R_i$ each contain the H atom concentration once, within k_4, k_6, and k_9; the other rate expressions occur as ratios in which any chain centre concentrations cancel. These terms represent the net rate of branching. Now it is likely that the surface terms k_5, k_6, and k_7 are small compared with other terminating steps; we found that p_e did not change much in going from a quartz to a Pyrex vessel, and Dainton and Norrish[4] found that the surface had little effect on the sensitizer limits if the vessel diameter was above 20 mm. There is also evidence[9] that $\alpha \ll 1$. With these simplifications, the condition that the net rate of branching becomes zero is

$$\frac{k_4 k_{14}(k_2 - k_{12})}{(k_{13} + k_{14})(k_2 + k_{12})} = \frac{k_{10} + k_{11}}{k_3}(k_4 + k_9)$$

The work[9] on the reaction between hydrogen and nitrogen dioxide has shown that $k_{10} \sim k_{11}$, so that $k_{10}p_{NO_2}p_M + k_{11}p_{NO}p_M$ can be replaced by $k_{10}p_0p_M$. If the pressure of nitrogen dioxide falls to p_e when the net rate of branching becomes zero, then

$$\frac{k_4 p_{O_2}(k_2 p_{H_2} - k_{12}p_e)k_{14}}{(k_2 p_{H_2} + k_{12}p_e)(k_{13} + k_{14})} = \frac{k_{10}p_0}{k_3 p_{H_2}}(k_4 p_{O_2} p_M + k_9 p_e) \qquad (2)$$

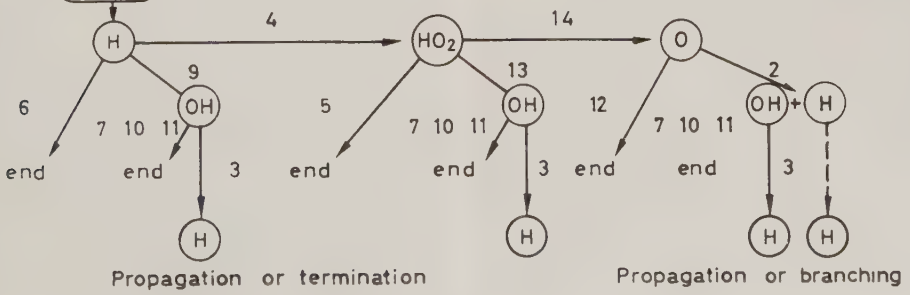

is the equation representing the variation of p_e with the initial pressure p_0 of nitrogen dioxide, p_{H_2} of hydrogen, p_{O_2} of oxygen, and p_M the total pressure. It will be seen that the pressure of nitric oxide does not occur in the equation under the conditions postulated.

Equation 2 is successful in accounting for most of the observed variations of p_e.

(1) It is clear that the left-hand side of the equation could not become positive until $p_e < k_2 p_{H_2}/k_{12}$. The need for the pressure of nitrogen dioxide to fall *below* a critical value is apparent, and the competition between 2 and 12 for O atoms obviously plays a vital part in the mechanism.

(2) Under conditions where the pressure of oxygen is high, the second term on the right-hand side becomes negligible in comparison with the first towards the end of the induction periods. Thus for a stoichiometric mixture, $p_{H_2} = 2p_M/3$, and it can be shown that

$$p_e = \frac{a(1 - bp_0)}{1 + bp_0}$$

where $$a = 2k_2 p_M / 3k_{12}$$

and $$b = \frac{3k_{10}(k_{13} + k_{14})}{2k_3 k_{14}}$$

This equation predicts that p_e is proportional to the total pressure p_M or p_T, and this was found experimentally. Also, the equation predicts that p_e falls linearly with p_0, provided that p_{O_2} is not low, and that the slope will increase as p_M is increased; both these predictions are correct, as shown by *Figure 6*.

(3) The equation predicts that when p_{O_2} is not low, the effect of adding an inert gas such as nitrogen should be the same as increasing p_0, for p_M and p_0 occur together as the product $p_M p_0$ on the right-hand side of equation 2, the other terms in p_M cancelling. This is exactly what was found experimentally.

(4) That p_e must be independent of p_{O_2} at high values of the latter is obvious from what has been said and from inspection of equation 2. However, at low values of p_{O_2}, the right-hand side may become independent of p_{O_2}; when this occurs, further *decrease* of p_{O_2} will have the same effect on the resulting equation as *increasing* p_0 has on equation 2—i.e. it decreases p_e. This was observed (*Figure 8*).

(5) It is easily seen from equation 2 that increasing p_{H_2} will mean that p_e has not got to be so low in order to make the left-hand side positive, so that p_e will rise as p_{H_2} is increased. This does occur at low values of p_{H_2} (*Figure 7*) but at high values p_e tends to a maximum value. Unfortunately, no manipulation of equation 2 seems to predict this maximum value, and this point remains a weakness of the scheme put forward.

On the whole, however, this comparatively simple treatment seems very successful in explaining the observed variations in p_e, as well as giving a clear reason for the need for p_{NO_2} to fall below some critical value, identified with p_e, before any branching can become effective. The powerful effect of reaction 12 in restricting branching has been noted before[2,3,4]; it is now plain that it would effectively prevent branching in most mixtures of hydrogen, oxygen, and nitrogen dioxide were the nitrogen dioxide not removed by reaction with hydrogen.

The authors would like to express their gratitude to the Royal Society for a grant which defrayed part of the cost of the photometer, to the Director, R.A.E., M.O.S., Westcott, for the temporary loan of a high speed recorder, and to the Director, E.R.D.E., M.O.S., Waltham Abbey, for the temporary loan of an oscilloscope and camera.

REFERENCES

[1] Hinshelwood, Sir Cyril, and Thompson, M. S. *Proc. Roy. Soc. A* 124 (1929) 214

[2] Griffiths, J. G. A. and Norrish, R. G. W. *Proc. Roy. Soc. A* 139 (1933) 147

[3] Foord, S. G. and Norrish, R. G. W. *Proc. Roy. Soc. A* 152 (1935) 196

[4] Dainton, F. S. and Norrish, R. G. W. *Proc. Roy. Soc. A* 177 (1941) 393, 411

[5] Lewis, B. and von Elbe, G. *Combustion, Flames, and Explosions of Gases*, p. 56 *et seq.* 1938. Cambridge Univ. Press; and *J. Amer. chem. Soc.* 59 (1937) 2022, and *J. Amer. chem. Soc.* 61 (1939) 1350

[6] Lewis, B. and von Elbe, G. *Combustion, Flames, and Explosions of Gases*, p. 71. 1951. New York; Academic Press

[7] Ashmore, P. G. *Trans. Faraday Soc.* 51 (1955) 1090

[8] Ashmore, P. G. and Levitt, B. P. *Advances in Catalysis and Related Subjects*, p. 367 Vol. IX. 1957

[9] Ashmore, P. G. and Levitt, B. P. *Trans. Faraday Soc.* 52 (1956) 835; 53 (1957) 945

[10] Bodenstein, M. and Lindner. *Z. phys. Chem.* 100 (1922) 106; Ashmore and Levitt, *Research, Lond.* (Corresp) 9 (1956) S25; Wise and Rosser, *J. chem. Phys.* 24 (1956) 493

[11] Ashmore, P. G. *Chem. Soc. Spec. Publ. No. 9.* In course of publication

[12] Ashmore, P. G., Levitt, B. P. and Thrush, B. A. *Trans. Faraday Soc.* 52 (1956) 830

[13] Dainton, F. S. *Chain Reactions*, p. 34. 1956. London; Methuen

[14] Crist, R. H. and Wertz, J. E. *J. chem. Phys.* 7 (1939) 719

[15] Lewis, B. and von Elbe, G. *Combustion, Flames, and Explosions of Gases*, chap. 1. 1951. New York; Academic Press

[16] Robb, J. C. *Chem. Soc. Spec. Publ. No. 9.* In course of publication

9

REACTIONS OF ATOMIC OXYGEN AND ATOMIC NITROGEN WITH OXIDES OF NITROGEN

F. KAUFMAN and J. KELSO

INTRODUCTION

The present renaissance in the study of atom and radical reactions at low temperatures has derived its impetus from three different fields: (*a*) combustion and flame work, (*b*) radical stabilization, and (*c*) upper atmosphere research. This investigation was undertaken primarily because of its applicability to problems in combustion and high-temperature reaction kinetics. The method used is a variant of the Wood-Bonhoeffer method. The atoms were generated in microwave discharges, pumped through a long tube and the second reactant added past the discharge[1–3]. The extent and rate of reaction was determined by the decay of chemiluminescence associated with the atomic species, the air afterglow for O and the nitrogen afterglow for N. Other recent investigators have used the stirred flow reactor technique in conjunction with mass spectrometry[4,5], low concentration photolysis of NO_2[6,7], and other methods. Most of the reactions which are described here had been studied qualitatively by early investigators, among them particularly Spealman and Rodebush[8].

EXPERIMENTAL

High frequency electrodeless discharges were produced by Raytheon microtherm units (2,450 mc/sec, up to 100 W of microwave power), and later by a larger Raytheon magnetron oscillator, type QK 390, 2,450 mc/sec, powered by a Radarange power supply W-7000 which had been extensively modified to permit C.W. operation of the magnetron. Though C.W. operation reduced the power output somewhat, it was possible to generate 5–600 W of microwave power. The power was transmitted through a wave guide to a tapered resonant cavity which was traversed by the quartz discharge tube. A water attenuator was placed between the magnetron and the discharge. It consisted of a quartz tube through which water was made to flow at 10 to 20 c.c./sec. A differential iron-constantan thermocouple measured the temperature rise of the water between inlet and outlet. The whole attenuator could be lowered into the wave guide mechanically. Between the magnetron and the water attenuator a standing wave ratio meter was inserted and standing wave ratios were repeatedly checked for the protection of the magnetron.

The quartz discharge tube (8 mm o.d.) was followed by a light trap and then by a Vycor tube, 100 cm long and 2·2 cm o.d. along which a photomultiplier could be moved. The photomultiplier output was amplified by a Leeds and Northrup amplifier and recorded on a Speedomax recorder.

Reactants could be added to the discharged gases at the upstream end of the main tube through a small Vycor jet. Their flow rates could be measured by noting the pressure drop in a variable closed system on a Hg manometer, a calibrated oil manometer, or by measuring directly the weight loss of the liquid in a suitable thermostat.

Large flows of O_2 or N_2 were regulated by a stainless steel needle valve and measured on Matheson universal flow meters. A calibrated McLeod gauge was used to measure the pressure at the upstream and downstream end of the main tube. Most experiments were run with total flows of 4 to 12 c.c./sec, at pressures of 1 to 3 mm Hg and linear flow rates of around 10 m/sec. All experiments were carried out at room temperature.

Nitrogen (Matheson, pre-purified) and oxygen (Burdette Oxygen Co.) were used without purification. Cylinder nitric oxide (Matheson) was purified over ascarite, condensed in liquid nitrogen, and distilled. Nitrogen dioxide was prepared from purified nitric oxide with excess oxygen and slowly pumped through a dry ice-acetone trap. Nitrous oxide was distilled after pumping off all non-condensable gases.

RESULTS and DISCUSSION

Atomic oxygen

Reaction with nitrogen dioxide—The study of O atom reactions was made possible by an investigation of the kinetics of the greenish-yellow air afterglow[1,2]. Its intensity had been found to be proportional to (O)(NO) and independent of the nature or amount of added gases unreactive to atomic oxygen. Moreover, the concentration of O could be measured quickly and accurately by a titration with NO_2 in which the extinction of the glow supplies the endpoint. This is made possible

by the great speed and simple stoichiometry of the reaction

$$O + NO_2 \rightarrow O_2 + NO \qquad (1)$$

Reaction 1 also assures that the NO which is necessary to give the afterglow remains at constant concentration in the flowing gas, because it is regenerated so rapidly from NO_2. Only a lower limit for k_1 could be obtained: judging from the complete disappearance of the glow within a small mixing region, it must be greater than 10^{11} c.c. mol^{-1} sec^{-1}, but it is probably around 10^{12} c.c. mol^{-1} sec^{-1}. This result is supported by values of 1 to 2 $\times$ 10^{12} c.c. mol^{-1} sec^{-1} recently reported by other investigators[7,9].

Reaction with nitric oxide—There are two reactions between O and NO. The bimolecular association which produces the glow, and a termolecular re-combination without light emission. The rate constant, $k^\star$, of the light producing process

$$O + NO \rightarrow NO_2 + h\nu$$

was found to be about 10^7 c.c. mol^{-1} sec^{-1} by photometry under known conditions of concentration and geometry. The ternary reaction

$$O + NO + M \rightarrow NO_2 + M$$

has a rate constant, k_2, of 2 to 3 $\times$ 10^{16} c.c.^{2} mol^{-2} sec^{-1} when M = O_2, N_2 or A and a somewhat larger k of around 4 $\times$ 10^{16} when M = CO_2 or N_2O. The details of this investigation are reported elsewhere[2]. A comparison of these two rates of removal of atomic oxygen by NO shows that the chemiluminescent process accounts for less than 1 per cent of the total rate at 300°K when the total pressure is 1 mm, as it was in much of this work. At 0·1 mm total pressure, less than 10 per cent is due to $k^\star$ and only at 0·01 mm does $k^\star$ contribute 50 per cent to the overall rate. In all of the experiments described here, the light-producing reaction therefore adds negligibly to the removal of O and represents a good indicating process for the measurement of the concentration of atomic oxygen.

Reaction with nitrous oxide—No direct reaction between O and N_2O was ever found. This puts a lower limit of 8 to 10 kcal on the activation energy of the bimolecular reaction. Henriques, Duncan, and Noyes[10] have deduced a lower limit of 14 kcal from photochemical work and Kaufman, Gerri, and Bowman[11] found a value of 15·5 kcal from measurement of the initial formation of NO in the thermal decomposition of N_2O. More recently still, Fenimore and Jones[12] suggested a much higher activation energy of 32 kcal from a study of flame reactions which makes it necessary to assign the reverse reaction

$$2NO \rightarrow N_2O + O$$

as the major path for the homogeneous thermal decomposition of NO[13]. Though it appears that the activation energy for O + N_2O is greater than 14 kcal, more work is needed to determine its value.

Atomic nitrogen

Reaction with nitric oxide—Just as NO_2 serves in the titration of atomic oxygen because of its fast reaction and simple stoichiometry, NO fulfills the same purpose for atomic nitrogen. The reaction

$$N + NO \rightarrow N_2 + O$$

is extremely fast, its rate constant is at least 10^{11} to 10^{12} c.c. mol^{-1} sec^{-1} and probably about 4 $\times$ 10^{12} c.c. mol^{-1} sec^{-1}. The evidence for this is manifold. The nitrogen afterglow can be brought sharply to extinction with added NO. There are several important differences between this extinction and that of the air afterglow with NO_2. Though the nitrogen afterglow is weakened by less than equimolar amounts of NO, the β, γ and δ bands of NO are emitted with increasing intensity to a maximum and then with decreasing intensity coming to extinction together with the nitrogen afterglow. This produces the characteristic sequence of colours from the orange-yellow N afterglow through pink, purple, and blue to extinction. When still more NO is added, the greenish-yellow air afterglow is emitted, since much atomic oxygen has been formed in the above reaction. Experiments[3] with added ^{15}NO have shown that the band spectra of excited NO in the pink to blue stages are due to ^{14}NO which undoubtedly arises by a re-combination process such as

$$^{14}N + O + M \rightarrow {}^{14}NO + M$$

long after the fast titration reaction has gone to completion.

By mass-spectrometer methods, Kistiakowsky and Volpi[5] have recently set a lower limit of 4 $\times$ 10^{11} c.c. mol^{-1} sec^{-1}. From the effect of oxygen on the high temperature thermal decomposition of NO, Kaufman and Decker[14] have obtained a value of 4 $\times$ 10^{12} c.c. mol^{-1} sec^{-1}. These estimates resulting from widely different experimental work leave no doubt that the reaction has no activation energy and proceeds with a collision yield of 10^{-1} to 10^{-2}.

Reaction with nitrogen dioxide—The reaction between atomic nitrogen and nitrogen dioxide is also extremely fast, but its stoichiometry is more complicated. Kistiakowsky and Volpi[5] found N_2O as a major product and suggested

$$N + NO_2 \rightarrow N_2O + O \qquad (2)$$

as the major primary reaction though the steps

$$N + NO_2 \rightarrow 2NO \qquad (3)$$

$$N + NO_2 \rightarrow N_2 + O_2 \qquad (4)$$

were necessary to describe some of the results. They also reported that the mol ratio of atomic nitrogen and NO_2 consumed was unity ± 20 per cent.

Our technique permits us to show that this is due to the inclusion of subsequent steps after all N atoms have reacted. Observation of the main tube downstream from the added gas jet gave the following qualitative results when increasing amounts of NO_2 were added. A change from orange-yellow through pink, purple and blue to the first extinction, entirely analogous to NO addition; then into the air afterglow increasing and decreasing to a second extinction, beyond which no further emission could be produced by increasing the NO_2 flow rate. This can be understood as follows: at flow rates of added NO_2, less than that which produces the first extinction, the rapid reaction between N and NO_2 produces some O which with excess unreacted N gives rise to the blue NO glow. In this regime neither NO nor NO_2 can persist beyond the zone of mixing, because they would rapidly react with N or O or both. The first extinction represents exhaustion of N, but not of O. The further increment of NO_2 between the first and second extinction represents the familiar titration of O with NO_2 (reaction 1), which was described above. It seems clear that for the purpose of elucidating the stoichiometry of the N—NO_2 reaction the first extinction must be used. Though NO_2 persists unreacted only after the second extinction, all atomic nitrogen is used up at the first extinction as is shown by the absence of the nitrogen and nitric oxide glows.

Many quantitative experiments were run in which the following critical flow rates were measured: NO to extinction, F_{NO}; NO_2 to first extinction, $F^{I}_{NO_2}$; NO_2 to second extinction, $F^{II}_{NO_2}$. Of these, F_{NO} merely titrates atomic nitrogen, because the N + NO reaction is of simple stoichiometry. Our results show that

$$\frac{F^{I}_{NO_2}}{F_{NO}} = 0{\cdot}6 \pm 0{\cdot}1; \qquad \frac{F^{II}_{NO_2}}{F^{I}_{NO_2}} = 1{\cdot}8 \pm 0{\cdot}1$$

that is, it takes much less NO_2 than NO to titrate N. This rules out reactions 2 and 4 as the major processes. Though N_2O undoubtedly is a product of the reaction and step 2 must occur, the above ratios demand that step 3 plays an important part. Step 4 seems doubtful as a very fast reaction on structural grounds and will be disregarded.

If 2 occurred exclusively and O would react with NO_2 only after exhaustion of N,

$$\frac{F^{I}_{NO_2}}{F_{NO}} = 1; \qquad \frac{F^{II}_{NO_2}}{F^{I}_{NO_2}} = 2$$

If 2 occurs exclusively and a fraction, α, of O were to react before all N is exhausted

$$\frac{F^{I}_{NO_2}}{F_{NO}} = 1 + \alpha; \qquad \frac{F^{II}_{NO_2}}{F^{I}_{NO_2}} = \frac{2}{1 + \alpha}$$

The first of these ratios cannot be less than unity if reaction 2 is the only primary step.

Should reaction 3 be the exclusive first step, the product NO would continue to react with N,

$$N + NO_2 \rightarrow 2NO$$
$$2N + 2NO \rightarrow 2N_2 + 2O$$
$$3N + NO_2 \rightarrow 2N_2 + 2O$$

and

$$\frac{F^{I}_{NO_2}}{F_{NO}} = \frac{1}{3}; \qquad \frac{F^{II}_{NO_2}}{F^{I}_{NO_2}} = 3$$

It is clear that no combination of steps 2 and 3 can match the experimental second ratio unless some atomic oxygen reacts with NO_2 before the first extinction is reached. This is not unreasonable in view of the great speed of the O + NO_2 reaction. It seems futile, moreover, to inquire into the details of the overall mechanism since it is certain that all of the following reactions are extremely fast,

$$N + NO_2 \rightarrow N_2O + O$$
$$N + NO_2 \rightarrow 2NO$$
$$N + NO \rightarrow N_2 + O$$
$$O + NO_2 \rightarrow NO + O_2$$

and that diffusion and mixing must in part be rate-determining. The peculiarities of the N_2O and O_2 *versus* NO_2 plots in reference 5 are then due to concentration gradients within the stirred flow reactor which enable slightly slower, but still very fast, reactions to become important when the local concentration of certain species is high.

The small value of the first ratio, $F^{I}_{NO_2}/F_{NO}$, plus the fact that O + NO_2 must occur to some extent before the first extinction, indicate that reaction 3 is the main primary step as would be expected for structural reasons. Reaction 2 is fairly unimportant and accounts for only 10 to 20 per cent of the products. Certainly, N_2O does not react rapidly with any of the species present and will persist when formed.

Reaction with nitrous oxide—In agreement with the stirred flow reactor study we find no reaction between N and N_2O, undoubtedly because of its potential violation of spin selection rules. There is much evidence, however, that vibrationally excited ground state N_2 is present in active nitrogen[15],

and that N_2O is very efficient in bringing about its relaxation. The direct, bimolecular reaction

$$N + N_2O \rightarrow N_2 + NO$$

is at least 10^4 times slower than N + NO, but it may be much slower still.

REFERENCES

[1] Kaufman, F. *J. chem. Phys.* 28 (1958) 352
[2] — Communicated to *Proc. Roy. Soc., London*
[3] — and Kelso, J. R. *J. chem. Phys.* 27 (1957) 1209
[4] Berkowitz, J., Chupka, W. A. and Kistiakowsky, G. B. *J. chem. Phys.* 25 (1956) 457
[5] Kistiakowsky, G. B. and Volpi, G. G. *J. chem. Phys.* 27 (1957) 1141
[6] Ford, H. W. and Endow, N. *J. chem. Phys.* 27 (1957) 1277
[7] — — *J. chem. Phys.* 27 (1957) 1156
[8] Spealman, M. L. and Rodebush, W. H. *J. Amer. chem. Soc.* 57 (1935) 1474
[9] Kistiakowsky, G. B. and Kydd, P. H. *J. Amer. chem. Soc.* 79 (1957) 4825
[10] Henriques, F. C., Jr., Duncan, A. B. F. and Noyes, W. A., Jr. *J. chem. Phys.* 6 (1938) 518
[11] Kaufman, F., Gerri, N. J. and Bowman, R. E. *J. chem. Phys.* 25 (1956) 106
[12] Fenimore, C. P. and Jones, G. W. *J. phys. Chem.* 62 (1958) 178
[13] Kaufman, F. and Kelso, J. R. *J. chem. Phys.* 23 (1955) 1702
[14] — and Decker, L. J. This volume, page 57
[15] — and Kelso, J. R. *J. chem. Phys.* (1958)

10

EFFECT OF OXYGEN ON THERMAL DECOMPOSITION OF NITRIC OXIDE AT HIGH TEMPERATURES

F. KAUFMAN and L. J. DECKER

INTRODUCTION

An earlier investigation[1] had shown that the thermal decomposition of NO is a homogeneous, bimolecular reaction above about 1,400° K and that its rate is unaffected by added N_2 or He, or by changes in the surface to volume ratio. That study had been carried out in a static system, with very good reproducibility, and free from the ambiguities of flow systems. In the temperature range 1,370 to 1,530° K, the rate constant was found to be $2{\cdot}6 \times 10^{12}\ e^{-63{\cdot}8 \pm 0{\cdot}6/RT}$ c.c. mol^{-1} sec^{-1}. This value of the activation energy now supersedes a considerable array of earlier ones whose great range was due to questionable experimental work or over-simplification of results obtained under highly complicated conditions. In view of Vetter's results[2] it was clear that a catalysis by O_2 was to be expected at still higher temperatures and the beginnings of such an effect were barely observed[1] at 1,473° K. Recent work by Fenimore and Jones[3] on the decomposition of NO in flames at 2,200 to 2,400° K showed inhibition by O_2, but did not lead to a satisfactory mechanism.

The decomposition of NO at flame temperatures is of much interest in propellant chemistry and in flame studies[4] where the mechanism of certain fuel–NO flames has precipitated some controversy[5]. There is little doubt that the oxygen effect is due to atom reactions of the type

$$O + NO \underset{-2}{\overset{2}{\rightleftarrows}} O_2 + N \qquad H_o^o = + 32{\cdot}1 \text{ kcal}$$

$$N + NO \underset{-3}{\overset{3}{\rightleftarrows}} N_2 + O \qquad H_o^o = - 75{\cdot}05 \text{ kcal}$$

Two points must be stressed. (*a*) The ΔH of these steps is now settled[6], i.e. $D_o^o\ [N_2] = 225{\cdot}1$ kcal, $D_o^o\ [O_2] = 117{\cdot}96$ kcal, which means that this 'chain' reaction scheme is not a chain at all, but, as Fenimore and Jones have pointed out[3], a slow, endothermic reaction of atomic oxygen whose ultimate regeneration by reaction 3 is immaterial since thermal equilibrium is likely to exist between O and O_2. (*b*) There is independent information on the rates of these oxygen and nitrogen atom reactions [7–9] which can be applied directly.

This paper describes experiments in a static system up to 1,690° K with initial $[O_2]/[NO]$ ratios from zero to 40. A very satisfactory account of all experimental results can be given within a simple mechanism and in agreement with the available information on the rates of atom reactions.

EXPERIMENTAL

The decompositions were carried out in cylindrical porcelain reaction flasks (McDanel Refractory Porcelain Company) fitted with an inlet tube and a thermocouple well. Their volume was approximately 350 c.c. The furnace consisted of an alundum tube (Norton) wound with heavy Kanthal wire, B. and S. 13, 6 turns per inch. The winding extended $3\frac{1}{2}$ in. beyond the tapered end of the reaction vessel on both ends to ensure temperature uniformity. The furnace tube was housed in a larger cylindrical enclosure made of sheet aluminium and transite, and filled with fine alumina powder. The furnace resistance was about 9 ohms. At a reactor temperature of 1,690° K it dissipated 1,000 W. Temperature uniformity was very good, about $\pm$ 1° C over the main volume. A capillary insert in the inlet tube kept the cold volume to a minimum of 1 to 2 per cent of total volume.

Spectrophotometric analyses for unreacted NO were carried out by conversion to NO_2 with large excess of O_2 in a 10 cm absorption cell and determination of the optical density at 3,200 and 4,000 Å. In runs with little decomposition, O_2 was converted to an $NO_2 - N_2O_3$ equilibrium mixture with large excess of NO and analysed at several wavelengths between 3,450 and 3,600 Å. Details of the method are presented in reference 1.

NO was prepared from cylinder gas (Matheson) by slow passage through a large tube filled with ascarite and through a trap at dry-ice temperature, followed by condensing at – 195° C. It was distilled once, then repeatedly sublimed until infra-red analysis showed no trace of higher oxides of nitrogen and an N_2O content of 0·01 per cent or less. Nitrogen (Matheson, pre-purified)

and oxygen (Burdett Oxygen Co., 99·5 per cent O_2) were used without purification.

The procedure of kinetic experiments was so designed to cancel errors that may have been due to variable addition of oxygen or nitrogen. NO was admitted to the reactor to the desired pressure (15 to 50 mm Hg) and measured to 0·1 mm Hg. The reactor was isolated, the line pumped out, and 30 to 50 seconds later, a known $N_2 - O_2$ mixture ranging from pure N_2 to pure O_2 was admitted to the reactor in large excess to give a total pressure of about 60 mm Hg. The reaction was then allowed to proceed to about 40 to 70 per cent completion (usually 6 to 15 min.) and was stopped by expansion into the absorption cell. The expansion was done in a way to minimize the accumulation of gas from the cold volume in the cell as previously described[1]. This procedure eliminated all variability due to cold volume, compression and mixing with added gases, and other effects of large changes in total pressure. It was justified by the experimental fact that added N_2 had no effect on the rate over the entire temperature range.

RESULTS

One hundred kinetic runs were carried out. Of these, 47 were done in the first reaction flask which failed at 1,580° K. The remaining 53 were done in the second flask from 1,575 to 1,690° K. The last 25 runs were done using the above procedure at 1,575, 1,606, 1,637, 1,663, and 1,690° K. At 1,690° K the furnace failed.

The first 30 experiments were performed at 1,378 to 1,530° K to overlap with the earlier investigation. Several runs at 1,378° K gave a bimolecular $k_1 = 190 \pm 10$ c.c. mol^{-1} sec^{-1} and at 1,476° K, $k_1 = 850 \pm 40$ c.c. mol^{-1} sec^{-1}. The earlier results[1], $k_1 = 2{\cdot}6 \times 10^{12} e^{-63.8/RT}$ give 198 at 1,378° K, and 910 at 1,476° K. This represents excellent agreement when it is considered that the present results were obtained in a flask 1/5 the size, of a different material (porcelain *versus* quartz), and geometry (cylindrical *versus* spherical) of that used before. No oxygen effect was found at 1,378 and 1,476° K, but a small increase of k_1 was observed at 1,530° K giving a range of 2,000 to 2,700 c.c. mol^{-1} sec^{-1} for k_1 when oxygen addition was varied from zero to an eightfold excess over $[NO]_0$. Some of these experiments also showed a slight increase of k_1 with increasing time of reaction, indicating catalysis by the oxygen formed in the decomposition.

The results of the last 25 runs, at the highest temperatures, and with variable amounts of added O_2, are shown in *Figure 1*. The fictitious second-order rate constant, k, is here plotted *versus* $(pO_2)^{1/2}$ and its increasing dependence on added oxygen is clearly shown. There is seen to

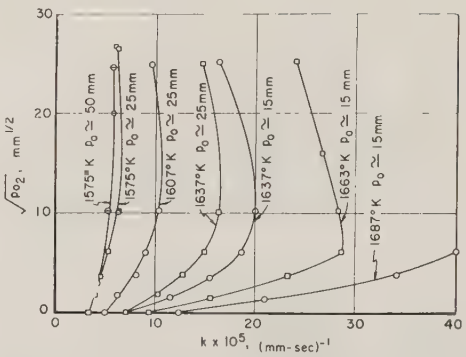

Figure 1. Second order rate constants for NO *decomposition with added oxygen*

be strong catalysis by small amounts of O_2, but when the initial pO_2/p_{NO} is about 4, the effect is near its maximum, and for much higher ratios, it decreases again. This is particularly pronounced at the highest temperatures, where the peak k is three times k_1 and where the decrease at high pO_2 is clearly evident. These runs ranged from 40 to 70 per cent decomposition and enough O_2 was formed to raise k well above k_1 even in the absence of added O_2. The decomposition runs of pure NO are therefore entered in *Figure 1* for the average value of pO_2 present during the experiment. The values for $pO_2 = 0$ are extrapolated from lower temperatures using $k_1 = 2{\cdot}4 \times 10^{12} e^{-63{\cdot}8/RT}$. *Figure 1* is only a graphical summary of the results and is not further used in the calculations.

CALCULATION AND DISCUSSION

We use the following set of assumptions. Concurrent with the simple, bimolecular decomposition of NO, there is reaction by steps 2, −2, and 3. Reaction −3 is negligibly slow in this temperature range, i.e. the equilibrium concentration of NO is very small and no N_2 effect was ever observed. Atomic oxygen is in thermal equilibrium, with O_2, and N is in steady state by steps 2, −2, and 3. This leads to the rate expression

$$\frac{-\,\mathrm{d}\,[NO]}{\mathrm{d}t} = k_1\,[NO]^2 + \frac{2k_2K\,[NO]\,[O_2]^{1/2}}{1 + \dfrac{k_{-2}}{k_3}\dfrac{[O_2]}{[NO]}} \qquad (1)$$

where $K = [O_2]^{1/2}/[O]$. It is clearly of the correct form to explain the data if the ratio k_2/k_3 is small. For $k_{-2}/k_3 \cong 0{\cdot}07$, the denominator of the second term is approximately 1 as long as $[O_2]/[NO] <\sim 1$, i.e. small amounts of added O_2 give rise to catalysis of magnitude proportional to $[O_2]^{1/2}$. Further increase of $[O_2]$ will make the second term of the rate expression reach a maximum and then decrease again. For very large

$[O_2]$, it will be proportional to $[O_2]^{-1/2}$ and there will be inhibition by added oxygen. Since it was not possible to measure the rate of decomposition over small increments of NO, the rate expression must be integrated. This presents difficulties when $[O_2]_o$ is small because the exact differential equation is of the form

$$\frac{-\,dx}{dt} = Ax^2 + \frac{Bx\,(C-x)^{1/2}}{1 + D\,\frac{C-x}{x}}, \qquad (2)$$

$x = [NO]$. The integration was therefore carried out only for those runs where $[O_2]$ could be considered constant, i.e. the runs with 30 mm Hg or more initially added O_2. In most cases, 4 to 6 mm Hg of O_2 were formed during the run and an error of 2 to 3 per cent at most was made by setting the oxygen concentration equal to the amount added initially plus one-half the O_2 formed in the decomposition. The simplified equation now becomes

$$\frac{-\,dx}{dt} = k_1 x^2 \left[1 + \frac{\beta}{x+\alpha}\right] \qquad (3)$$

where $\beta = 2k_2/k_1 \cdot K[O_2]^{1/2}$ and $\alpha = k_{-2}/k_3[O_2]$, and it was integrated to give the relation

$$k_1(t_1 - t_o) - \frac{1}{x_1} + \frac{1}{x_o} = \frac{\beta}{\alpha+\beta}\left[\frac{1}{x_o} - \frac{1}{x_1} + \frac{2{\cdot}303}{\alpha+\beta}\log\left(\frac{x_1+\alpha+\beta}{x_o+\alpha+\beta}\cdot\frac{x_o}{x}\right)\right] \qquad (4)$$

Initial calculations of experiments at constant T with various $[O_2]_o$ showed that in order to give the desired dependence of α and β on $[O_2]$, the ratio k_{-2}/k_3 would have to lie between 0·05 and 0·1. A value of 0·070 was chosen at 1,575° K and slowly increasing ratios of 0·072, 0·075, and 0·079 used at the higher temperatures. This choice is discussed further below.

Each run was corrected for the short time (30 to 50 sec) after admission of NO but before addition of the $N_2 - O_2$ mixture to the reaction vessel. After all preliminary corrections, each experiment supplied a set of $(t_1 - t_o)$, x_o, and x_1. With α known, β was determined by iteration. An approximate β was guessed and used in equation 3 as $(\alpha + \beta)$ and $(x + \alpha + \beta)$ to solve for an improved value of β. This was repeated until no further improvement was obtained.

From the definition of β and k_β,

$$\beta \equiv \frac{2k_2}{k_1} K\,[O_2]^{1/2} \equiv k_\beta\,[O_2]^{1/2}$$

it is seen that k_β should be a constant at constant T. With increasing T there should be a rise in k_β. This is indeed observed. Table 1 shows the data of two of the five temperatures. k_β is independent of $[O_2]$ and rises with T.

The graph of log k_β *versus* $1/T$ is shown in *Figure 2*. The highest temperature is represented by a single point which lies too high. From the graph, $k_\beta = 15 \times e^{-35 \pm 1/RT}$ (mol/c.c.)$^{1/2}$.

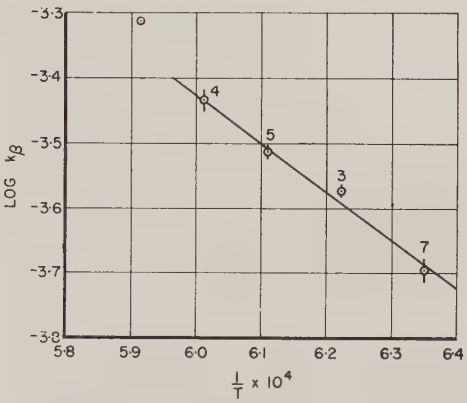

Figure 2. Temperature dependence of K_β

In the range T = 1,500 to 1,700° K, the equilibrium constant $K = 5{\cdot}015 \times e^{-59{\cdot}3/RT}$ (mol/c.c.)$^{1/2}$, corrected for the new, slightly higher $D[O_2]$. Using $k_1 = 2{\cdot}4 \times 10^{12}e^{-63{\cdot}8/RT}$ c.c. mol^{-1} sec^{-1}, we evaluate $k_2 = 3{\cdot}6 \times 10^{12}e^{-39{\cdot}5 \pm 1/RT}$.

The results that $E_2 = 39{\cdot}5 \pm 1$ kcal is a most reasonable one. Taken together with the endothermic ΔH of 32·1 kcal of reaction 2, it implies that reaction -2 has an activation energy of about 7·5 kcal. Recent experiments with active nitrogen by Kistiakowsky and Volpi[8] and in our laboratory[9] have shown that reaction 3 is extremely fast and has no activation energy and that reaction 2 is slow at room temperature[8], $k_{-2} = 2 \times 10^{12}e^{-6{\cdot}2/RT}$. Extrapolating k_2 to the temperature range 1,500 to 1,700° K and combining with the experimental finding that k_{-2}/k_3 is about 0·07 makes $k_3 \simeq 4 \times 10^{12}$ c.c. mol^{-1} sec^{-1}, a normal value for a fast, bimolecular reaction. The ratio, k_{-2}/k_3, therefore has an activation energy of 6·2 kcal and rises slowly between 1,575 and 1,690° K as stated above.

The agreement of the direct experimental $E_{-2} = 6{\cdot}2$ kcal with the value of 7·5 kcal in this work is also quite good, since it actually represents agreement between the calculated $E_2 = 38{\cdot}2$ kcal and our experimental $E_2 = 39{\cdot}5 \pm 1$ kcal. The pre-exponential factor of k_2, $3{\cdot}6 \times 10^{12}$ c.c. mol^{-1} sec^{-1} is high. Using $k_{-2} = 2 \times 10^{12}e^{-6{\cdot}2/RT}$ and the known equilibrium constant, K_2, $k_2 = 4{\cdot}2 \times 10^{11}e^{-38{\cdot}2/RT}$. This discrepancy of a factor of 9 is reduced to one of a factor of 5 when the activation energies are matched. Considering the great extrapolation of k_{-2} from the range 400 to 500° K in which it was measured, to 1,500 to 1,700° K, this factor is not serious.

The above analysis thus yields a consistent interpretation of all runs with much added oxygen and provides rate constants which agree with other work.

Because of its dependence on $[O_2]^{1/2}$ for low $[O_2]$, the second term in the differential rate expression 1 should become appreciable when only very little O_2 is added. At 1,663° K, the fictitious second order rate constant when no O_2 is added was found to be $1{\cdot}54 \times 10^4$ c.c. mol^{-1} sec^{-1} for 55 per cent decomposition, whereas k_1, the extrapolated bimolecular rate constant in the absence of any O_2 effect is only 0·94. It appeared that the small amount of oxygen formed during the decomposition raised the overall rate constant 60 per cent. This was verified in the following manner. The time interval of this experiment, No. 177, was 8 minutes. It was subdivided into 8 one-minute intervals and the amount of NO decomposed was calculated for each minute using the rate constants obtained with large O_2 addition. An average value for [NO] and $[O_2]$ was used for each minute interval. It was found that the contribution of the second term in the differential rate expression grew so quickly that during the eighth minute it was equal to that of the first term. The calculated amount of NO decomposed in the entire run, 7·86 mm Hg, agreed perfectly with the experimental value, 7·84 ± 0·15 mm Hg. The kinetic scheme is thus also able to explain the experimental results with little or no added oxygen. It is in good agreement with Vetter's experimental findings[2]. An earlier re-interpretation of some of his high temperature results[1] had given $k_2 = 8{\cdot}3 \times 10^{12}e^{-40{\cdot}5/RT}$. This was slightly in error because $K = 8{\cdot}5 \times e^{-60{\cdot}5/RT}$ was used instead of $5{\cdot}0 \times e^{-59{\cdot}3/RT}$. The corrected $k_2 = 14 \times 10^{12}e^{-41{\cdot}7/RT}$ is in satisfactory agreement with our present $k_2 = 3{\cdot}6 \times 10^{12}e^{-39{\cdot}5/RT}$.

We cannot explain Fenimore and Jones' results, but believe that the application of the O and N atom scheme to flames with excess H_2 does not seem justified, as it neglects entirely any direct reaction with H_2. Their results with excess O_2 suggest that the presence of H_2O and OH may be partly responsible for their high rate of decomposition and its inverse square root dependence on O_2.

The behaviour of NO at still higher temperatures, in flames and explosions, can now be predicted with greater confidence. In the absence of H_2, CO, or other reactants whose high temperature reaction with NO has not yet been cleared up, the second term in rate expression 1 will overshadow the first with increasing temperature. Because of the low activation energy of reaction −2, the ratio k_{-2}/k_3 will rise only very slowly, and so the decomposition of NO will retain some of the characteristics observed here; a rate proportional to [NO] $[O_2]^{1/2}$ for low $[O_2]$, becoming independent of $[O_2]$ and inhibited by O_2 at high $[O_2]$. The second term of equation 1 is at its maximum when

$$\frac{[O_2]}{[NO]} = \frac{1 + \sqrt{2}}{3\ (k_{-2}/k_3)}$$

With $k_{-2}/k_3 = 0{\cdot}07$ to 0·08, $[O_2]/[NO] = 11{\cdot}5$ to 10. Since $[O_2]/[NO]$ increases as each run progresses and NO is decomposed, the maximum overall rate constant should be observed for somewhat lower initial $[O_2]/[NO]$ ratios. This is indeed the case, the maxima in *Figure 1* occur at initial ratios of 6 to 8. At flame temperatures of about 2,500° K and 3,000° K, this maximum instantaneous rate should be found at ratios of 5·5 and 4·5, respectively, and the maximum overall rates nearer initial ratios of 3.

The results of this work can also be easily extended to provide information on the rate of formation of NO from N_2 and O_2 at high temperatures.

TABLE 1

Calculated values of $k\beta = 2k_2K/k_1$

Run	T °K	p_0NO mm	p_0O_2 mm	$k_1 \times 10^6$ mm/sec^{-1}	$k\beta$ mm$^{1/2}$
160	1574·7	52·8	96·0	33·85	1·88
161	1571·9	52·9	597·4	32·51	1·90
156	1573·4	25·7	33·6	33·23	1·81
153	1573·4	26·2	98·4	33·23	2·02
155	1573·9	25·8	100·7	33·47	1·94
154	1574·0	25·9	702·9	33·52	2·16
152	1572·5	25·4	708·2	32·80	2·05
			$k\beta$ average at 1,575° K—1·997		
170	1640·1	25·4	99·4	73·35	3·29
171	1638·2	25·6	618·8	71·74	3·06
175	1637·5	15·0	33·0	71·14	3·13
174	1637·6	16·2	101·6	71·23	3·09
176	1640·4	15·2	628·2	73·60	3·14
			$k\beta$ average at 1,637° K—3·10		

REFERENCES

1 Kaufman, F. and Kelso, J. R. *J. chem. Phys.* 23 (1955) 1702

2 Vetter, K. *Z. Elektrochem.* 53 (1949) 369, 376

3 Fenimore, C. P. and Jones, G. W. *J. phys. Chem.* 61 (1957) 654

4 Adams, G. K., Parker, W. G. and Wolfhard, H. G. *Disc. Faraday Soc.* 14 (1953) 97

5 Rozlovskii, A. I. *Zh. fiz. Khim.* 30 (1956) 912, 1444

6 Brix, P. and Herzberg, G. *Canad. J. Phys.* 32 (1954) 110

7 Kaufman, F. *J. chem. Phys.* 28 (1958) 352

8 Kistiakowsky, G. B. and Volpi, G. G. *J. chem. Phys.* 27 (1957) 1141

9 Kaufman, F. and Kelso, J. R. *J. chem. Phys.* 27 (1957) 1209

11

RECENT STUDIES OF THE OXIDATION AND DECOMPOSITION FLAMES OF HYDRAZINE

P. GRAY and J. C. LEE

INTRODUCTION

Flames involving hydrazine have attracted considerable attention in recent years. Three factors particularly have contributed to this. First, hydrazine is an endothermic compound and even in decomposition can support a flame[1–6]; its correspondingly more vigorous combustion[1,7–9] with oxygen, ozone, fluorine or nitric acid offers some of the most powerful chemical propellent systems known. Secondly, hydrazine flames have received much attention from theoreticians[10–13]. The decomposition flame is one of the systems whose measurable properties have been a yardstick of success of the theories of flame as these have advanced from the primitive treatments in terms of ignition temperatures through those based on a single chemical reaction to the stationary state non-branching chain and finally to the general branched chain reaction. The process continues and this paper comments on its progress. Thirdly, by its very difference from the hydrocarbon–oxygen systems to which so much work has been devoted, the study of hydrazine both widens experience and offers novel systems for assessing the success of proposed interpretations of flames. An example is the role of pyrolysis in flames. In recent years the idea that, in combustion, pyrolysis of the fuel is no less important than its oxidation has received growing support. In hydrazine combustion there are extreme interpretations; either that pyrolysis is a trivial consequence of exothermic oxidation or that the controlling reactions are those of decomposition, subsequent oxidation serving only to produce a hotter flame.

We have here examined the combustion flames of hydrazine supported by oxygen, by nitrous oxide and by nitric oxide; we have determined flame speeds S_B and derived flame temperatures and burning velocities S_U. We have discovered the decomposition of excess reactants in non-stoichiometric mixtures and have examined the conditions governing the transition, which occurs in increasingly rich mixtures, from the oxidation flame to the decomposition flame. All these oxidation flames are more exothermic, hotter and much faster than the decomposition flame of pure hydrazine studied previously. For flames in hydrazine and oxygen or nitrous oxide mixtures, speeds are a maximum at the stoichiometric proportions ($N_2H_4 + O_2$ and $N_2H_4 + 2N_2O$). For mixtures with nitric oxide, the speed is a maximum in a hydrazine-rich mixture ($N_2H_4 + NO$).

We have also examined the decomposition flame of hydrazine and correlated our results with those of other workers. While there is agreement on the independence of pressure of flame speed (corresponding to overall kinetic order two) and on the dependence of flame speed on final flame temperature (corresponding to overall activation energy near to 35 kcal mole^{-1}) there are significant discrepancies between absolute values of burning velocities.

The decomposition of hydrazine in a flame produces considerable amounts of ammonia as well as hydrogen and nitrogen. This production of ammonia furnishes a striking example of the non-equilibrium conditions which may prevail even in hot, fast flames.

EXPERIMENTAL

Materials

Concentrated hydrazine, containing *ca.* 98 per cent N_2H_4, was dehydrated by refluxing for 2 to 3 hours over fused caustic soda at 120 to 150 mm Hg in an atmosphere of nitrogen and by distillation under similar conditions. Analysis by the iodate method gave 99·9 to 100·2 per cent N_2H_4. This high degree of purity which is readily attained with small samples but is a nuisance to achieve with larger amounts of material is very important. Product analyses, in particular, are available only when all water is absent: previous workers[1,2,6] who have used hydrazine even of 97 per cent purity have failed to obtain accurately reproducible product analyses.

Nitric oxide was prepared by reducing sodium nitrite with ferrous sulphate. It was first freed from nitrogen dioxide and water and then purified by distillation *in vacuo*.

Nitrous oxide and oxygen were taken from cylinders.

Apparatus and procedure

The combustion vessel was a glass cylinder 20 cm in diameter and 20 cm long. Electrodes of 1 mm diameter tungsten were projected horizontally from side arms leaving a spark gap of 4·6 mm at the centre of the vessel. The vessel was enclosed in an air thermostat at 62°C to prevent condensation of the hydrazine.

The movement of the flame was followed by the schlieren technique. The field of view was restricted to a narrow section of the flame along its vertical diameter. The progress of the flame in this direction was recorded as a *V* shaped trace on a film moving horizontally in a drum camera. The spark used to ignite the gas was obtained from an induction coil; the spark energy was never greatly in excess of the minimum required.

The photographic record showed that, in most cases, after a short acceleration period, the movement of the flame was uniform until it reached a diameter of about 10 cm. Measurements of flame speed were made at points corresponding to a flame diameter of 6 cm, i.e. where the radius of the flame sphere r_B was 0·3 R, where R is the radius of the vessel. There was no significant difference between the slopes of the upper and lower traces; the estimated error is about 2 per cent.

In traces where the acceleration period extended to larger diameters and where the duration of the uniform motion was briefer, the measured value of the speed may be a few per cent lower than the true value. The size of these errors shows that the flame speeds measured here by the closed vessel technique are the most accurate available at present. Three factors peculiar to hydrazine contribute to this.

(1) The purity (100 ± 0·2 per cent) of the hydrazine—the large amounts of hydrazine needed for the burner method has deterred its users from making the essential though tedious purification.

(2) The reproducibility of experimental conditions. The flame traces give a continuous record of flame speed through the vessel. Burner methods suffer from the difficulty of metering the relatively involatile fuel accurately and this is probably their most serious defect; furthermore, at low pressures, temperature and pressure control are very hard to achieve.

(3) Curvature of the flame front. All burner methods so far used have involved flames much more curved than the 6 cm flame sphere photographed in these closed vessel measurements. Hydrazine is not easy to burn safely on a wide burner.

Interpretation of the traces[14]

After a gas is ignited at the centre of a closed vessel and the flame travels towards the walls, the pressure rises and both the burned and unburned gases are compressed. As a result, the movement of the flame depends on the gas flow as well as on the burning rate. However, during the initial phase of the combustion the increase in pressure is small and the linear speed of the flame, S, is very nearly equal to the speed of the flame relative to the burned gas, S_B. Even when the radius of the flame sphere r_B is 0·3 R, where R is the radius of the vessel, the pressure has risen by only 3 per cent and the speed S differs from S_B by only 2 per cent. The speed of the flame measured at this point is therefore essentially the speed relative to the burned gas at the initial pressure.

RESULTS

Decomposition flame of pure hydrazine

The speed of the decomposition flame of pure hydrazine shows little variation as the initial pressure is altered from 20 to 80 mm Hg; in fact the apparent fall off (see *Figure 1*) at low pressure may be merely a result of the method of measurement. At 50 mm Hg the speed is 1,330 cm sec^{-1}. Since the thermal theory[10–12] of flame propagation predicts that flame speed will vary with pressure according to $S_B \propto P^{n/2-1}$ where n is the kinetic order of the chemical reaction controlling the flame, this behaviour indicates that $(n/2)-1 = 0$ i.e. that overall reaction is *second order*.

The products of the pure hydrazine decomposition flame correspond closely with the equation:

$$N_2H_4 \rightarrow 1{\cdot}00\ NH_3 + 0{\cdot}50\ N_2 + 0{\cdot}50\ H_2$$
$$\Delta H = -33{\cdot}74 \text{ kcal mole}^{-1} \qquad (1)$$

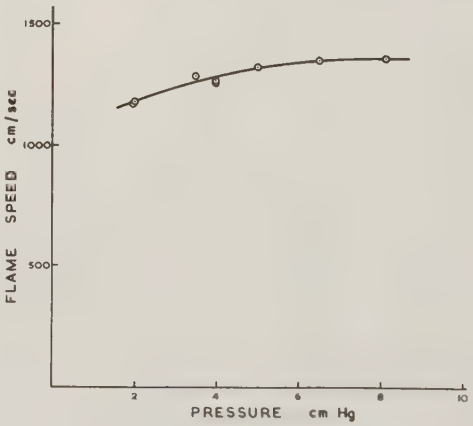

Figure 1. Effect of pressure on the speed, S_B, of the decomposition flame in pure hydrazine

Thus the calculated final flame temperature is 1,904°K, the expansion ratio S_B/S_U is 11·37 and a speed S_B of 1,330 cm sec^{-1} corresponds to a fundamental flame speed S_U of 117 cm sec^{-1}. When the initial pressure is 40 mm, S_B is 1,270 cm sec^{-1} and S_U 112 cm sec^{-1}.

When diluents are added the speed of the decomposition flame is decreased (*Figure 2*). Two factors operate and their contributions have been assessed[5]. The first is the heat capacity; the diluent lowers the final flame temperature—in this respect, nitrogen and hydrogen, with higher heat capacity, have a greater effect than argon and helium. The second is the thermal conductivity—when diluents have essentially the same heat capacities (e.g. helium and argon; hydrogen and nitrogen) flame propagates most rapidly in the systems with the higher thermal conductivity.

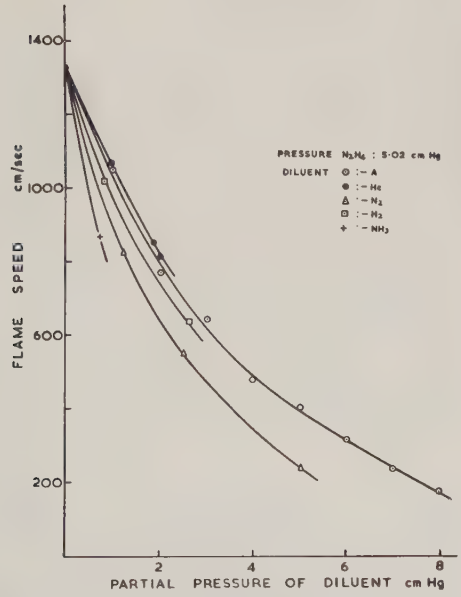

Figure 2. Effect of diluents on the speed, S_B, of the decomposition flame of hydrazine

pressure are 62°C and 40 mm Hg. The results are illustrated by *Figure 3*. They show that at this pressure the flame speed S_B has its maximum value of 4,020 cm sec^{-1} in the stoichiometric mixture 1 N_2H_4 + 1 O_2 although at atmospheric pressure the maximum speed occurs in slightly lean mixtures (excess oxygen). The speed of the *slowest* flame examined is only 555 cm sec^{-1}. It

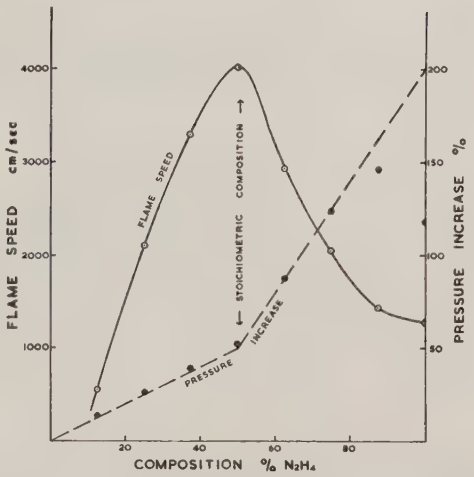

Figure 3. Flames in hydrazine–oxygen mixtures. Dependence of flame speed S_B on composition

Flames in oxygen + hydrazine mixtures

Flame speeds, S, in mixtures of hydrazine with oxygen have been determined over a range of composition. The initial temperature and was obtained in a lean mixture containing 1 N_2H_4 + 8 O_2. The speed in pure (100 per cent) hydrazine is 1,270 cm sec^{-1}.

In the stoichiometric mixture the final products are represented by equation 2 and the equilibrium composition of the burned gases before cooling by equation 2a.

$$N_2H_4 + O_2 \rightarrow N_2 + 2H_2O$$
$$\Delta H \ldots -138{\cdot}3 \text{ kcal mole}^{-1} \quad (2)$$

$$N_2H_4 + O_2 \rightarrow 0{\cdot}98_5\, N_2 + 1{\cdot}32\, H_2O + 0{\cdot}41\, H_2 + 0{\cdot}14\, O_2 + 0{\cdot}25\, OH + 0{\cdot}30\, H + 0{\cdot}12\, O + 0{\cdot}03\, NO \quad (2a)$$

Equations 2 and 2a correspond to a final flame temperature of 2,700°K ± 5°K and to a value of burning velocity S_U of 280 cm sec^{-1}.

In lean mixtures containing *less* hydrazine than the stoichiometric proportion, oxidation is complete and excess oxygen survives unchanged. However, in rich mixtures containing *more* than the stoichiometric proportion of hydrazine, the pressure increase observed indicates that the stoichiometric proportion is oxidized and that the excess hydrazine is decomposed. Between stoichiometric and 75 per cent hydrazine, decomposition yields only nitrogen and hydrogen while oxidation yields nitrogen and water. The final products can be represented by a combination of equation 2 with equation 3

$$N_2H_4 \rightarrow N_2 + 2H_2$$
$$\Delta H = -22 \text{ kcal mole}^{-1} \quad (3)$$

The broken line in *Figure 3* represents the percentage pressure rise in combustion predicted on this basis (i.e. from equations 2 and 3) and the points on it the pressure increases actually

observed. The expectations are borne out up to about 75 per cent hydrazine when combustion begins to be displaced by the decomposition flame (equation 1) and ammonia is found among the products.

Flames in nitrous oxide + hydrazine mixtures

Flame speeds, S_B, in hydrazine combustion supported by nitrous oxide, have been determined over a range of composition. The initial temperature is 62°C and the initial pressure 40 mm Hg. Results are illustrated in *Figure 4*. They show that

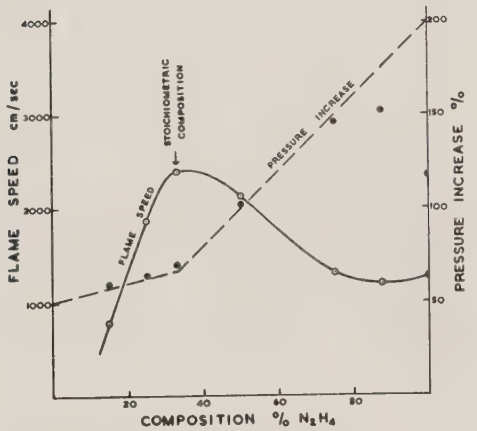

Figure 4. Flames in hydrazine–nitrous oxide mixtures. Dependence of flame speed S_B on composition

the flame speed is a maximum in the stoichiometric mixture 1 N_2H_4 : $2N_2O$ with S_B = 2,400 cm sec^{-1}. In these flames the final products of complete oxidation correspond to equation 4 and the equilibrium composition of the burned gases before cooling to equation 4a. These equations correspond to a final flame temperature of 2,655 ± 5°K and to a burning velocity S_U of 164 cm sec^{-1}.

$$N_2H_4 + 2N_2O \rightarrow 3N_2 + 2H_2O \qquad \Delta H = -177{\cdot}5 \text{ kcal mole}^{-1}$$

$$N_2H_4 + 2N_2O \rightarrow 2{\cdot}97_5\ N_2 + 1{\cdot}30\ H_2O + 0{\cdot}42\ H_2 + 0{\cdot}14\ O_2 + 0{\cdot}24\ OH + 0{\cdot}31\ H + 0{\cdot}12\ O + 0{\cdot}05\ NO \qquad (4a)$$

Not only, as before, is the excess hydrazine of rich mixtures decomposed, but in lean mixtures the excess nitrous oxide is decomposed also, yielding nitrogen and oxygen. We may thus distinguish three ranges of composition: (a) lean mixtures, in which all the hydrazine oxidized to nitrogen and water and the excess nitrous oxide is decomposed to nitrogen and oxygen; (b) stoichiometric and slightly rich mixtures (up to 75 per cent N_2H_4), in which all the nitrous oxide is reduced to nitrogen and water and the excess hydrazine decomposes to nitrogen and hydrogen; and (c) very rich mixtures (containing from 75 to 100 per cent hydrazine), in which decomposition to ammonia becomes gradually more important.

This analysis of the system is illustrated in *Figure 4* in which the expected pressure rise in combustion is drawn as a broken line. The points on it represent the experimental results and agreement is again complete until the decomposition flame begins to play the chief role.

Flames in nitric oxide + hydrazine mixtures

Flame speeds, S_B, in hydrazine combustion supported by nitric oxide have been determined over a range of composition. The initial temperature and pressure are 62°C and 40 mm Hg. Results are illustrated in *Figure 5*. They show

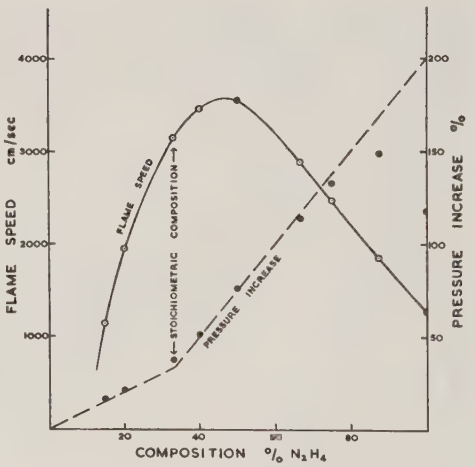

Figure 5. Flames in hydrazine–nitric oxide mixtures. Dependence of flame speed S_B on composition

that the flame speed in the stoichiometric mixture (1 N_2H_4 : 2 NO) is 3,150 cm sec^{-1}. Complete oxidation is represented by equation 5 and the equilibrium composition, before cooling, of the burned gases to equation 5a. These equations correspond to a final flame temperature of 2,745 ± 5°K; and the speed S_B of 3,150 cm sec^{-1} thus implies a burning velocity S_U of 245 cm sec^{-1}.

$$N_2H_4 + 2NO \rightarrow 2N_2 + 2H_2O \qquad \Delta H = -181{\cdot}5 \text{ kcal mole}^{-1} \quad (5)$$

$$N_2H_4 + 2NO \rightarrow 1{\cdot}97_5\,N_2 + 1{\cdot}16\,H_2O + 0{\cdot}48\,H_2 + 0{\cdot}16\ O_2 + 0{\cdot}29\ OH + 0{\cdot}43\ H + 0{\cdot}18\ O + 0{\cdot}05\ NO \qquad (5a)$$

The fastest flames occur not at the stoichiometric composition ($N_2H_4 + 2NO$) but in hydrazine-rich mixtures. *Figure 5* shows that the flame speed S_B has its maximum 3,550 cm sec^{-1}, in the equimolecular mixture ($N_2H_4 + NO$). For this mixture the calculated adiabatic flame temperature, $T_B = 2{,}645 \pm 5°K$ together with the equilibrium composition of the hot burned gases represented by equation 5b, corresponds to $S_U = 238$ cm sec^{-1}. The flame speed S_U has its maximum at a composition intermediate between stoichiometric and equimolecular. In the mixture ($N_2H_4 + 1{\cdot}5\ NO$) the calculated adiabatic flame temperature $T_B = 2{,}725°K$ together with the (equilibrium) product composition represented by equation 5c corresponds to $S_U = 252$ cm sec^{-1} when S_B is 3,460 cm sec^{-1}.

$$N_2H_4 + NO \rightarrow 1{\cdot}49_5\,N_2 + 0{\cdot}86_5\,H_2O + 0{\cdot}91\,H_2 + 0{\cdot}01\,O_2 + 0{\cdot}09\,OH + 0{\cdot}37\,H + 0{\cdot}02\,O + 0{\cdot}01\,NO \qquad (5b)$$

$$N_2H_4 + 1{\cdot}5\,NO \rightarrow 1{\cdot}73_5\,N_2 + 1{\cdot}06\,H_2O + 0{\cdot}62\,H_2 + 0{\cdot}06\,O_2 + 0{\cdot}20\,OH + 0{\cdot}44\,H + 0{\cdot}09\,O + 0{\cdot}03\,NO \qquad (5c)$$

In lean mixtures (containing excess nitric oxide) pressure measurements will not reveal nitric oxide decomposition. Chemical analysis revealed its decomposition. Thus, we again have three composition ranges to distinguish: (a) lean mixtures, in which all the hydrazine is oxidized and the excess nitric oxide is decomposed; (b) stoichiometric and rich mixtures (33 to 75 per cent N_2H_4), in which all the nitric oxide is reduced and any excess hydrazine yields nitrogen and hydrogen; and (c) very rich mixtures, in which the decomposition flame of hydrazine eventually supplants the combustion flame and ammonia is found among the products. Expectation and experiment are illustrated in *Figure 5*.

DISCUSSION

Decomposition flame of hydrazine

The propagation of a flame is controlled by the diffusion of matter, the conduction of heat and the kinetics of the chemical reactions occurring in it. Simple thermal theories of flame[15,16] permit us to express the relationships between thermal and kinetic properties and flame speeds explicitly and either (1) to predict the speed of the flame from the transport properties and the flame-reaction kinetics (when these are reliably known) or (2) to infer the salient properties of the kinetics from the observed properties of the flame. The first approach is that made hitherto by the theoreticians[10–13]. It involves postulating the reaction mechanism, assuming the validity of extrapolating both kinetic and transport properties from ordinary temperatures to those of the flame in order to predict the speed of the flame. The second approach is that made here. We have chosen to supply accurate experimental data on the speed of the flame and its dependence on pressure and temperature, to make inferences from these data and also to test the validity of the earlier assumptions.

The results are clear. The burning velocity S_B is independent of pressure over the range 2 cm to 8 cm when the initial temperature is 62°C. This implies a kinetic order two in the overall reaction and not unity as postulated by earlier workers.

Support for this result and the conclusion comes from two sources. The first source is work on burner flames by Hall and Wolhard[6]. Their results, obtained by a different experimental method, lead them to the same conclusion; that, within their experimental errors the speed of the flame is independent of pressure over the range 3 to 15 cm Hg. If a correction is applied to these results, which were obtained when the initial temperature was 120°C, on the basis of the temperature dependence of flame speed discovered here (viz. an overall activation energy of 36 kcal $mole^{-1}$) we have, for these two sets of work at low pressures:

Closed vessel (Gray and Lee)
S_U *ca.* 120 cm sec^{-1} ($T_B = 1{,}904°C$)

Bunsen flame (Hall and Wolfhard)
S_U *ca.* 155 cm sec^{-1} (T_B corrected to 1,904°C)

The second source is recent work on the burning of liquid hydrazine in tubes. The interpretation of this type of work is made difficult by the influence of the tube walls on the flame. When this quenching effect is taken into account (as was not done in earlier[2,4] investigations) and when flame speeds at different pressures are measured in tubes which are always the same multiple of the quenching diameter, it is possible to use the tube technique to discover the manner in which burning velocity depends on pressure. The burning velocity is constant from 15 cm to 1 atm, confirming the previous results and the inference that the effective kinetic order of the flame reaction is two.

Murray and Hall's pioneering measurements of flame speed at atmospheric pressure[1] are not easy to compare with the low pressure flames, because the initial temperatures (150°, 120° and 60°C) are different. The temperature dependence at atmospheric pressure to which these authors' results lead[2] corresponds to an effective activation energy, E, of approximately 36,500 cal $mole^{-1}$.

TABLE 1

Summarized Comparison of Exothermicities, Flame Temperatures and Flame Speeds in Hydrazine Decomposition and Combustion

System $P = 40$ mm $T = 62°C$		$-\Delta H_{298}$ kcal mole^{-1}	T_B °K	S_B cm sec^{-1}	S_U cm sec^{-1}
Decomposition					
N_2H_4	$\rightarrow NH_3 + \frac{1}{2}N_2 + \frac{1}{2}H_2$	33·7	1,904	1,270	110
Oxidation					
$N_2H_4 + O_2$	$\rightarrow N_2 + 2H_2O$	138·3	2,700	4,020	280
$N_2H_4 + 2N_2O$	$\rightarrow 3N_2 + 2H_2O$	177·5	2,655	2,400	164
$N_2H_4 + 2NO$	$\rightarrow 2N_2 + 2H_2O$	181·5	2,745	3,150	245
$N_2H_4 + 2NO + N_2$	$\rightarrow 3N_2 + 2H_2O$	181·5	2,665	1,670	150
$N_2H_4 + NO$	$\rightarrow \frac{3}{2}N_2 + H_2O + H_2$	122·1	2,645	3,550	238

The measurements reported here on flame speeds in mixtures with diluents lead to a value of $E = 35{,}000$ cal mole^{-1} and they are confirmed by van Tiggelen's recent work[8].

Combustion flames of hydrazine

The table summarizes some of the important features of oxidation flames. These are all about five times as exothermic as decomposition: $-\Delta H_{298}$ (kcal mole^{-1}) ranging from 140 to 180 in oxidation compared with 34 in decomposition. However, flame speeds and final flame temperatures show a much narrower range. This is only partly due to increased heat capacity of the products of oxidation: the chief cause for the levelling down is the onset of dissociation above 2,000°K. The flame speeds in stoichiometric mixtures S_U (cm sec^{-1}) vary from 164 to 280 (110 in decomposition), oxygen flames being fastest despite the more favourable energy balance and flame temperature of the others.

An interesting comparison is afforded by the fortuitously close heats of reaction of hydrazine with nitric oxide and nitrous oxide. The heat capacities of the reaction products of the two systems can be made the same by adding nitrogen to the nitric oxide one. Then we have two mixtures—$N_2H_4 + 2N_2O$ and $N_2H_4 + 2NO + N_2$—giving identical products $3N_2 + 2H_2O$ at almost identical temperatures. The flame speed S_U (cm sec^{-1}) in the former is 164 and in the latter *ca.* 115: thus the nitric oxide is the least ready of the three oxidants to react.

None the less this system, $NO + N_2H_4$, is of great interest as one of the few in which nitric oxide reacts with any readiness at all. Nitric oxide is unusually difficult to react in flames and tends to burn with rather low velocities both with hydrocarbons and with hydrogen, apparently requiring temperatures for its own pyrolysis to be rapid enough to precede oxidation; here, however, it reacts fast and readily. This reactivity with hydrazine resembles and even surpasses its behaviour with ammonia. The reason may be that nitric oxide is attacked by $\cdot NH_2$ radicals which are known to be present even in ammonia flames and are probably abundant in the hydrazine systems.

The question of prior pyrolysis preceding combustion of a fuel has been raised in this connection by Hall[1,6], who considers the hydrazine of oxygen–hydrazine mixtures to decompose more readily than it oxidizes, and by van Tiggelen[8] who has suggested the extreme view (possible in this hydrazine system) that the oxygen serves only to burn the decomposition products and the oxidation flames are faster than the decomposition flames simply because they are so much hotter. Such a two-stage process is not, in our opinion, as likely with oxygenated mixtures as with nitric oxide mixtures. In fact, as we find a continuous increase in burning velocity as either oxygen or nitric oxide is added to hydrazine, we think it clear that both oxidations proceed more rapidly than pyrolysis. However, as indicated in the table above, the disparity in rates is not so great as to preclude simultaneous oxidation and decomposi-

tion even in the earliest zones. Some of Hall's spectroscopic evidence[6] also supports this suggestion: hydroxyl band emission, characteristic of oxidation, occurs as early in the flame as the NH and NH_2 bands which are found in both decomposition and oxidation flames. Simultaneous oxidation and pryolysis seem the most likely processes in the early stages of the flame.

When flames are maintained by nitric oxide or nitrous oxide the pattern of behaviour revealed as the proportions of reactants is altered reflects the unstable character of both fuel and oxidant. In lean mixtures (excess NO or N_2O) combustion and decomposition are complete, only the thermodynamically stable constituents surviving. In stoichiometric mixtures there are no excess decomposition products to consider. In slightly rich mixtures, decomposition is complete and combustion is not: hydrogen remains. Then, in very rich systems as the oxidant is removed the hydrazine decomposition flame becomes preeminent and ammonia is found. The occurrence of so much ammonia in this flame (with a flame speed S_U of more than 100 cm sec^{-1} and a final temperature more than 1,600°C) affords a most striking example of failure to reach equilibrium conditions in a flame front.

We thank Dr. G. K. Adams of E.R.D.E., Waltham Abbey, Dr. A. R. Hall of R.P.D., Westcott, and Dr. A. van Tiggelen of the Université de Louvain, for interesting discussions.

REFERENCES

1 Murray, R. C. and Hall, A. R. *Trans. Faraday Soc.* 47 (1951) 743

2 Adams, G. K. and Stocks, G. W. *Fourth Symposium on Combustion*, p. 239. 1953. Baltimore; Williams and Wilkins

3 Pannetier, G. and Guedeney, F. *Compt. rend.* 238 (1954) 898

4 Gray, P. and Kay, J. C. *Research, Lond.* 8 (1955) S3

5 — Lee, J. C., Leach, H. A. and Taylor, D. *Sixth Symposium on Combustion.* 1956. New York; Reinhold

6 Hall, A. R. and Wolfhard, H. G. *Trans. Faraday Soc.* 52 (1956) 1520

7 Gray, P. and Lee, J. C. *International Union of Pure and Applied Chemistry.* 1957. Paris

8 van Tiggelen, A. *International Union of Pure and Applied Chemistry.* 1957. Paris

9 Gray, P. and Lee, J. C. *Fifth Symposium on Combustion.* 1954. New York; Reinhold

10 Hircshfelder *et al. J. phys. Chem.* 57 (1953) 403

11 von Karman *et al. Selected Combustion Problems I.* 1954. London; Butterworths

12 — To be published.

13 Spalding, D. B. *Phil. Trans. Roy. Soc. A* 249 (1956) 1

14 Lewis, B. and von Elbe, G. *Combustion, Flames and Explosions in Gases*, p. 448. 1951. New York; Academic Press

15 Semenov, N. N. *Prog. Phys. Sci. U.S.S.R.* 24 (1940) 433 (*N.A.C.A. Tech. memo.* 1026)

16 Zeldovich, Y. B. and Frank-Kamenetskii, D. A. *Acta Physiochim. U.R.S.S.* 9 (1938) 341

12

MECHANISM INVOLVED IN THE PHOTOCHEMICALLY INITIATED COMBUSTION OF H_2S

A. P. ZEELENBERG

INTRODUCTION

The combustion of hydrogen sulphide has not been investigated as intensively as that of other combustibles and only a few papers have appeared which deal with the mechanism of the reaction. In Russia some work has been done on the slow combustion in connection with the kinetics of the overall reaction[1]. The occurrence of an intermediate in the slow combustion was detected spectroscopically and after some controversy, which even now is not settled, this absorption has been attributed[2] to the molecule S_2O_2. The reactions occurring in the flame of hydrogen sulphide have been studied by Fowler and Vaidya[3] by means of the emission spectra. They observed emission by OH, S_2, SO and a continuous emission in which the absorption bands of SO_2 appeared. The SH spectrum was not detected by these authors and was found only much later, in 1947, by Gaydon and Whittingham on introducing SO_2 or H_2S in a hydrocarbon flame. Other investigations dealt with the influence of addition of H_2S to flames in relation to carbon formation or corrosion[4,5] and spectroscopic and other data led to the postulation of certain reaction steps. Harteck and Kopsch[6] have investigated the reaction of O atoms with H_2S and observed a continuous emission from 3,000 to 4,700 Å.

This paper summarizes the work of Norrish and Zeelenberg who studied the mechanism of the combustion of H_2S with the method of flash photolysis and kinetic spectroscopy[7] and investigated the homogeneous fast combustion in a static system. From the absorption spectrum of the reactants and an observed continuous light emission a complete mechanism for the combustion could be derived.

EXPERIMENTAL

The method by which the absorption spectra of the reactants during the fast homogeneous combustion were taken makes use of flash lamps as spectrographic source[8]. A discharge of 350 J (14 μF, 7 kV) gave the background density on Ilford Selochrome plates and an E1 Hilger spectrograph was employed. The homogeneous initiation of the combustion was achieved by the irradiation of the reaction vessel by a photoflash tube which could dissipate up to 3,000 J/flash. An electronic delay unit was employed to fire the second (spectroscopic) flash at the desired time. As an alternative to the photographic method, it was also possible to use photoelectric cells for following the reaction; they were mounted in the focal plane of the spectrograph. By shifting the photomultiplier cells slightly after each experiment and repeating the experiments several times the wavelength dependence of the emission could be studied.

RESULTS

The flash irradiation of a mixture of H_2S and O_2 in the first instant acts only on the H_2S. The photochemical dissociation of H_2S into SH and H which is known to occur both with high and with low intensities is here the first reaction, as is evidenced by the occurrence of the SH absorption spectrum. The SH is formed in the ground state with no excess vibrational energy[9]. The presence of oxygen manifests itself by the subsequent disappearance of the SH absorptions; this occurs much faster in the presence of oxygen than in its absence. This stage of the reaction can be investigated best at a pressure of 1 mm Hg. At higher pressures, e.g. 20 mm H_2S, the SH spectrum is present during a longer time but the continuous absorption which also occurs interferes with the observations. Only the 0,0 transition is then visible because the 1,0 band is obscured. Consequently, the further experiments were done at the lower pressure.

The next stage in the reaction depends on the prevailing macroscopic conditions. It is possible to distinguish between two kinds of combustion: (*a*) the quasi-isothermal, and (*b*) the quasi-adiabatic case. In the former the temperature is kept low throughout the reaction by the addition of a large excess of inert gas (Ar, N_2, CO_2), while in the latter the temperature can rise freely as a result of the irradiation and of the reaction, which in this case can be characterized as an explosion.

Quasi-isothermal combustion

The SH radicals formed by the flash disappear after about 100 μsec, but already earlier, shortly after the flash, the intense absorption bands of S_2O_2 can be discerned. An excess of oxygen is useful to prevent the formation of S_2 which finally

results in a sulphur deposit in the reaction vessel. The intensity of the S_2O_2 bands increases rapidly in the beginning but continues to rise at a slower rate for a long time. Even with less than 1 mm H_2S the final extinction below 3,000 Å is almost complete. An absorption band of S_2O_2 at the place where the 0,0 band of the $^2\Sigma$–$^2\Pi$ transition of OH occurs makes it difficult to decide whether absorption by OH is present or not, especially since SH has also an overlying band. Any pressure change accompanying the reaction does not exceed 0·05 mm Hg and we found that the reaction did not go to completion. Absorption by SH again became visible when the photolytic flash was fired a second or even a third time. The flash irradiation of the reaction products also influences the S_2O_2: its absorption bands disappear temporarily but regain the same intensity in less than 1 msec. A small amount of sulphur dioxide is also formed. The S_2O_2 is the final product; no change in intensity of its absorption bands was observed after hours, not even when the experiment was performed at a higher temperature.

Quasi-adiabatic combustion

After the same first step, the photochemical dissociation, the following reaction steps are quite different from those encountered in the quasi-isothermal combustion. Our spectrographic observations (*Figure 1*) reveal that for a mixture of 1 mm H_2S and 3 mm O_2 the SH spectrum is replaced completely by the OH spectrum within 100 μsec after the photoflash. The radical SH remains of importance, as can be deduced from observations on a mixture with relatively less oxygen. The 0,0 absorption band of SH is then visible for several msec, especially if the pressure is raised somewhat. Another feature of the combustion is the occurrence of a continuous absorption: this is present immediately after the flash, reaches its maximum after about $\frac{1}{2}$ msec and disappears much later.

The last stage of the reaction is the formation of SO_2, which again can be followed by its absorption spectrum. At low pressure of the initial reactants the bands can be observed from 2 msec onwards; at higher pressure the overlying continuum makes a determination in the early stage impossible. Even after 0·1 sec the SO_2 bands still increase in intensity. At low pressure and with a large amount of oxygen the SO_2 bands appear quite soon. No indication was found of quenching by excess oxygen and S_2O_2 is always absent.

A very interesting feature of the combustion was the emission of light during the reaction. This emission was studied in its dependence on pressure, oxygen concentration, flash energy and wavelength. Especially at low pressures the emission of light is very brief. Higher pressures increase its duration and the total amount of emitted radiation. The maximum intensity of the light emission is not affected greatly by the pressure and is

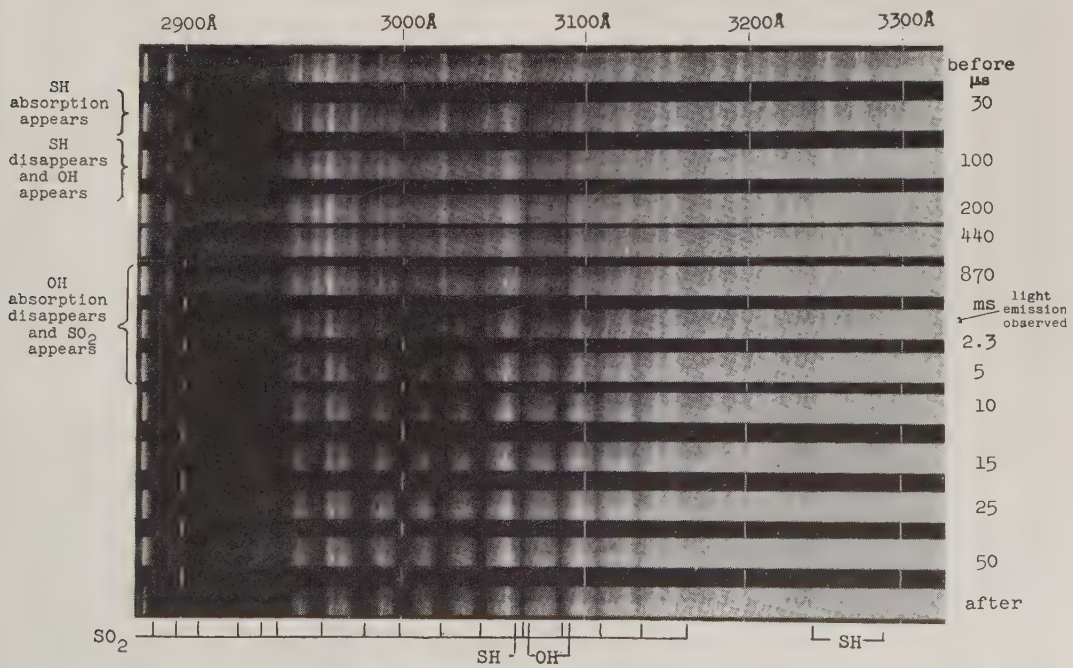

Figure 1. Spectra against time. 1 mm H_2S + 3 mm O_2. *Flash energy* 1,500 J

always reached after about the same time. An increase in the oxygen concentration and in the flash energy have the same phenomenological effect on the length of the initial period during which no light is emitted. In both cases this initial period shortens if one of these parameters is increased. Addition of inert gas to the mixture decreases the amount of radiation. The distribution of the radiation over the various wavelength regions was measured photoelectrically. An attempt to photograph the emission was not successful although multiple exposures were used. As far as could be judged from the signal from the multiplier cells the emission was continuous with a maximum response at about 3,300 Å and extending to 5,000 Å. The behaviour towards small wavelengths could not be investigated exactly but the signal fell off more rapidly than could be explained by the decreasing sensitivity of the photocell.

Transition from isothermal to adiabatic combustion

It was of interest to investigate which conditions determine whether S_2O_2 or SO_2 is formed. For this purpose mixtures with increasing amounts of added gas (Ar, N_2, CO_2) were flash irradiated under standardized conditions and examined spectroscopically for the presence of S_2O_2 and SO_2 after the flash irradiation. It was found that the transition from one product to the other took place between certain mixture ratios. It seems that the composition of the mixtures between which the transition takes place for a certain gas is dependent on the specific heat of the gas.

Within the experimental accuracy the product of specific heat and limiting pressure is a constant. In order to investigate whether the temperature is a deciding factor the experiments were repeated at higher initial temperatures, because then more diluent gas should be required for the formation of S_2O_2. This proved to be actually the case but no quantitative data could be deduced from the experiments since the transition was not sharp. The influence of the flash energy is also important; when a large energy was used for the initiation, again a larger amount of inert gas was needed to secure the production of S_2O_2. A slight increase in oxygen concentration also favoured the production of SO_2 above S_2O_2 and it was necessary to add much more coolant gas to obtain S_2O_2.

Flash irradiation of SO_2

The fact that the spectrum of S_2O_2 disappeared temporarily on flash irradiation was a reason to investigate whether such an effect also could be noticed with SO_2. When the pressure of the SO_2 was 1 mm or less the absorption spectrum of SO_2 indeed disappeared completely on irradiation but came back after about 1 msec. While in the case of S_2O_2 the presence of inert gas does not influence the disappearance of the bands, addition of inert gas to SO_2 has an important influence; flash irradiation of SO_2 in the presence of a tenfold excess of inert gas only results in a weakening of the absorption bands.

DISCUSSION

To explain the observed facts the following reactions are assumed to take place.

Initiation:

$$H_2S + h\nu \rightarrow SH + H \quad (1)$$

$$H + H_2S \rightarrow SH + H_2 \quad (2)$$

Quasi-isothermal, chain termination:

$$SH + O_2 \rightarrow SO + OH \quad (3)$$

$$OH + SH \rightarrow SO + H_2 \quad (4)$$

$$SO + SO \rightarrow S_2O_2 \quad (5)$$

Flash irradiation of S_2O_2:

$$S_2O_2 + h\nu \rightarrow SO + SO \quad (6)$$

$$SO + SO \rightarrow S_2O_2 \quad (5)$$

Quasi-adiabatic case;

chain propagation:

$$SH + O_2 \rightarrow SO + OH \quad (3)$$

$$OH + H_2S \rightarrow SH + H_2O \quad (7)$$

chain branching:

$$SO + O_2 \rightarrow SO_2 + O \quad (8)$$

$$O + H_2S \rightarrow OH + SH \quad (9)$$

chain termination and light emission:

$$SO + O \rightarrow SO_2^+ \rightarrow SO_2 + h\nu \quad (10)$$

Flash irradiation of SO_2:

$$SO_2 + h\nu \rightarrow SO_2^+ \quad (11)$$

$$SO_2^+ + SO_2^+ \rightarrow SO + SO + O_2 \quad (12)$$

$$SO + O_2 \rightarrow SO_2 + O \quad (8)$$

$$O + SO \rightarrow SO_2 \quad (10)$$

The postulation of these reaction steps is based on the following considerations.

The photochemical dissociation of H_2S into SH and H, reaction 1, is well known in photochemical work and is proved directly by the spectroscopic observation of the SH radical after flash irradiation. The subsequent step is added to account for the H atoms formed in reaction 1. A reaction involving oxygen is not included as it is probably of less importance during the early stages. The fact that OH absorption, if present, is extremely weak in the quasi-isothermal case combined with the renewed formation of SH when the reaction products are flash irradiated indicates

that the reaction does not go to completion. Probably the produced radicals start no chain reaction but react only in processes which require a very low activation energy. This can explain why reaction 4 is important in the quasi-isothermal combustion, but is replaced by reaction 7 in the quasi-adiabatic case. The same reactions can also take place in the slow combustion at low temperatures and Kondratieva and Kondratiev[10] indeed observed the formation of S_2O_2 under these conditions. These reactions also explain the absence of any pressure change. The postulated entity SO has not been detected spectroscopically but the fast formation of S_2O_2 is sufficient explanation for this. After the flash irradiation of S_2O_2 similar considerations prevail.

In the quasi-adiabatic case we found direct proof for the occurrence of step 3 in the spectroscopic observation of OH. SO could be detected for reasons similar to those mentioned above. Recently it has been reported that the SO absorption spectrum was detected by a flash technique during the explosion of CS_2 and O_2, but higher pressures were employed there[11]. The fast disappearance of SH at low H_2S/O_2 ratios and the longer persistence of the SH spectrum at higher ratios suggest the reaction 7 as supplementary to reaction 3. The combination of both reactions ensures a certain balance between the radicals OH and SH.

It is possible that the strong continuous absorption is due to hot H_2S molecules, since for hot molecules the absorption spectrum is often shifted to longer wavelengths[12]. The fact that now no S_2O_2 is produced and that the reaction goes to completion suggest that SO is consumed in another reaction than in the quasi-isothermal case. Steps 8 and 9 are consistent with the final products and give a branching character to the reaction.

The light emission is so remarkably simultaneous with the first observation of the SO_2 absorption that these phenomena must be connected by reaction 10 which is an inverted pre-dissociation, similar to the light emission which occurs when NO reacts with O atoms.

About the reactions induced by flash irradiation of SO_2 a certain controversy is possible. The light emitted by the flash has not enough energy to dissociate the SO_2 molecule in a single step. Instead of step 12 which involves the reaction between two excited molecules, another mechanism may be postulated in which a hot SO_2 molecule absorbs a quantum of light and is dissociated. The reaction is then followed by the reaction:

$$O + SO_2 \rightarrow SO + O_2$$

Both descriptions are equivalent in result, provided that the reactions take place very rapidly. The addition of inert gas results in a suppression of the reactions following the irradiations.

The author wishes to thank Professor R. G. W. Norrish, F.R.S. (under whose supervision this work was carried out) for the facilities offered in his laboratory and for his stimulating interest. He also wishes to thank the management of the Koninklijke/Shell-Laboratorium, Amsterdam (N. V. De Bataafsche Petroleum Maatschappij) for providing the opportunity which made this work possible.

REFERENCES

1 Emanuel, N. M. *Zh. fiz. Khim.* 19 (1945) 15
2 Jones, A. V. *J. chem. Phys.* 18 (1950) 1263
3 Fowler, A. and Vaidya, W. M. *Proc. Roy. Soc. Lond. A* 132 (1931) 320
4 Gaydon, A. G. and Whittingham, G. *Proc. Roy. Soc. Lond. A* 189 (1947) 313
5 Kurz, P. F. *Industr. Engng Chem. (Industr.)* 45 (1953) 2072
6 Harteck, P. and Kopsch, U. *Z. phys. Chem. B* 12 (1931) 327
7 Norrish, R. G. W. and Zeelenberg, A. P. *Proc. Roy. Soc. Lond. A* 240 (1957) 293
8 — and Thrush, B. A. *Quart. Rev. chem. Soc. Lond.* 10 (1956) 149
9 Ramsay, D. A. *J. chem. Phys.* 20 (1952) 1920
10 Kondratieva, E. and Kondratiev, V. *Zh. fiz. Khim.* 14 (1940) 1528
11 Myerson, A. L., Taylor, F. R. and Hanst, P. L. *J. chem. Phys.* 26 (1957) 1309
12 Franck, J., Sponer, H. and Teller, E. *Z. phys. Chem. B* 8 (1932) 88

13

FIRST LIMIT INDUCTION TIME STUDIES OF CS_2–O_2 EXPLOSIONS

F. R. TAYLOR and A. L. MYERSON

INTRODUCTION

In an extensive study of thermally initiated CS_2–O_2 explosions involving ignition limit and spectroscopic investigations[1,2], relatively long and reproducible induction times were obtained along the low pressure or first limit. That long induction times can be observed with CS_2–O_2 mixtures has been known for some time[3,4]. However, the results of previous investigations were erratic and the pattern of the variation of induction time with pressure or temperature difficult to perceive. It has been concluded from these past studies that the greatest deterrent to reproducibility is the sensitivity of the reaction to surface conditions. In the present study, considerable care was exercised in: (*a*) stabilizing the reaction vessel surface by coating it with the products of numerous explosions, (*b*) carefully regulating reaction vessel temperature, (*c*) precise measurement of pressure, and (*d*) guarding reactants and apparatus from contaminants. This procedure has resulted in orderly relationships between induction time and temperature, and induction time and pressure for various mixture ratios and reaction vessel volumes.

EXPERIMENTAL

Explosions between carbon disulphide and oxygen were produced by rapidly introducing thoroughly mixed mixtures of these gases into various sizes of spherical Pyrex and quartz vessels which were maintained at desired temperatures in an air-stirred thermostat ($\pm 0{\cdot}2$°C). Explosion, if it took place, was evidenced by a brilliant violet flash. Induction times were measured automatically by an accurate timer which was actuated by a sensitive Bourdon tube pressure gauge when the CS_2–O_2 mixture passed into the reaction vessel. The timer was then stopped by the detection of the emission from the explosion by a sensitive electron multiplier phototube and associated circuit.

It was found possible to control the surface of the reaction vessels and achieve satisfactory reproducibility of induction times in two ways. The first was by meticulously cleaning the reaction vessels by flaming. In this procedure, after an explosion, the flask was removed from the thermostat and cleaned of all surface impurities by repeatedly evacuating, filling with oxygen, and flaming to a red heat with a gas–oxygen flame. This treatment, which removed all products as SO_2 and CO_2, caused some distortion of Pyrex flasks but had very little effect upon quartz ones in which most of the experiments were carried out. After flaming, the flask was returned to the thermostat and maintained at 300°C and a few tenths of a micron of pressure for three hours. The vessel was then ready for another explosion, which occurred under almost identical conditions.

The second method employed for obtaining reproducible induction times consisted of building up a stable and constant coating of non-volatile explosion products on the vessel wall by allowing a dozen or more preliminary explosions to take place in the flask. This method was used by Ritchie, Brown, and Muir[5] to obtain a constant surface for spark ignition limit studies of CS_2–O_2 mixtures. This technique allows a large number of explosions to be carried out successively, the only treatment necessary between experiments being the evacuation of the reaction vessel. The surface provided by the deposit of explosion products is presumably a coating of $(CS)_n$ polymer and sulphur. The chain-breaking efficiency of the coating appeared to change gradually as the deposit increased, but at a rate which was slow enough to permit some data to be obtained under essentially constant conditions.

DISCUSSION AND RESULTS

Typical pressure–temperature ignition boundaries obtained for CS_2–O_2 mixtures for various sizes of Pyrex and quartz flasks have previously been published (*Figure 1* of reference 1) and is repeated here for convenience as *Figure 1*. All of these curves are seen to possess first and second limits, which are characteristic of chain-branching explosive reactions. It is also seen from this figure that a third limit was also found for each of the smaller flasks in the pressure region explored.

According to generally accepted theory, at lower pressures in the region of the first limit, increase of pressure linearly decreases the probability of an active centre diffusing to and being destroyed at the reaction vessel wall. Explosion may then result from a faster propagation rate, and hence at a lower temperature. At higher

pressures, as the pressure is increased, active centres are prevented by other molecules or atoms from diffusing to the wall and perishing there. It should be possible then to attain a pressure where the generation of chains can proceed with only a small fraction of the chains being terminated at the wall. When this pressure is reached, the critical explosion temperature and pressure should become independent of surface and hence vessel size. This region, where the reaction becomes a supposedly gas phase one, is known as the second limit. Finally the third boundary is believed to be principally the manifestation of the increasing

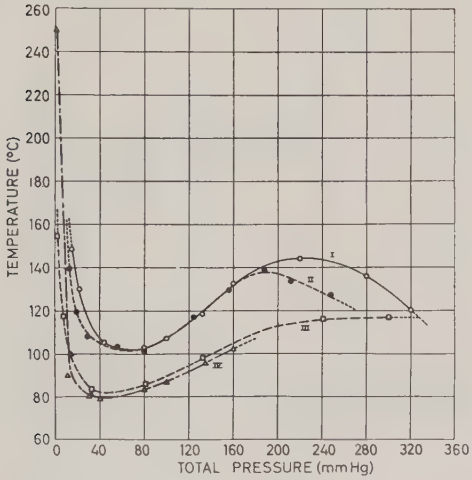

Figure 1. Ignition limits of $CS_2 + 3O_2$ *as a function of total pressure and temperature. Curve I* = 38 c.c. *spherical quartz flask, curve II* = 64 c.c. *spherical quartz flask, curve III* = 116 c.c. *spherical quartz flask, curve IV* = 100 c.c. *spherical Pyrex flask*

importance of thermal explosions with increasing gas densities. As the pressure increases, the amount of heat that must be dissipated by a given surface area increases. Therefore, the temperature required for ignition decreases as the pressure increases.

As was just discussed, the conditions for explosion at the first limit are defined in terms of the competing factors of chain-branching propagation in the gas phase and chain breaking, or destruction of chain carriers, at the wall and in the gas phase. Where the balance between chain carrier propagation and destruction is not too sensitive to changes in total pressure and temperature, it should be possible to observe long induction times. In the present experimentation, such induction times have been obtained. *Figures 2–7* present the results of our induction time studies which utilized several reaction vessel volumes and mixture compositions. Note that the points fall on practically smooth hyperbolic curves. The asymptotes

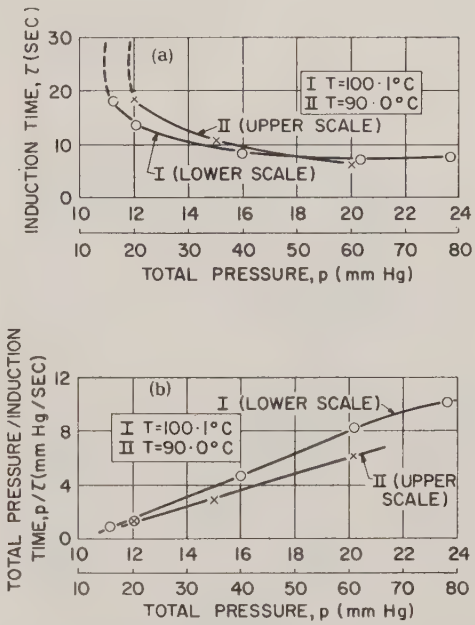

Figure 2. (a) Induction time as a function of total pressure for 1:3 mixtures of CS_2 : O_2 (100 c.c. *spherical Pyrex flask)*

(b) Total pressure/induction time as a function of total pressure for 1:3 mixtures of CS_2 : O_2 (100 c.c. *spherical Pyrex flask)*

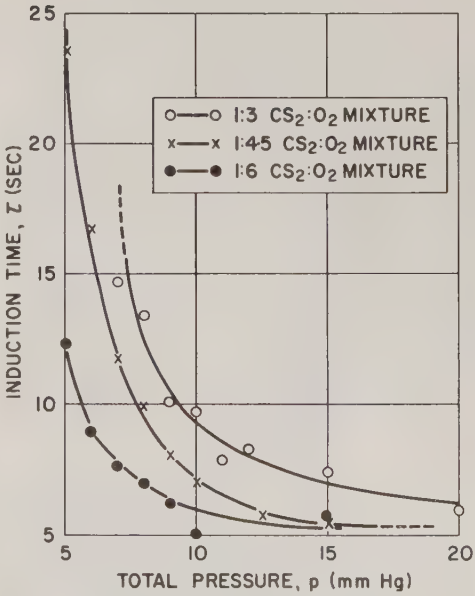

Figure 3. Induction time as a function of total pressure for various mixtures of CS_2 *and* O_2 *at* 125°C (116 c.c. *spherical quartz flask)*

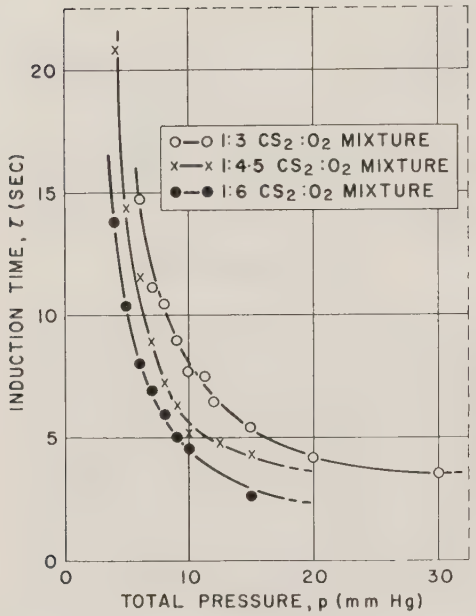

Figure 4. Induction time as a function of total pressure for various mixtures of CS_2 *and* O_2 *at* 134°C (116 c.c. *spherical quartz flask*)

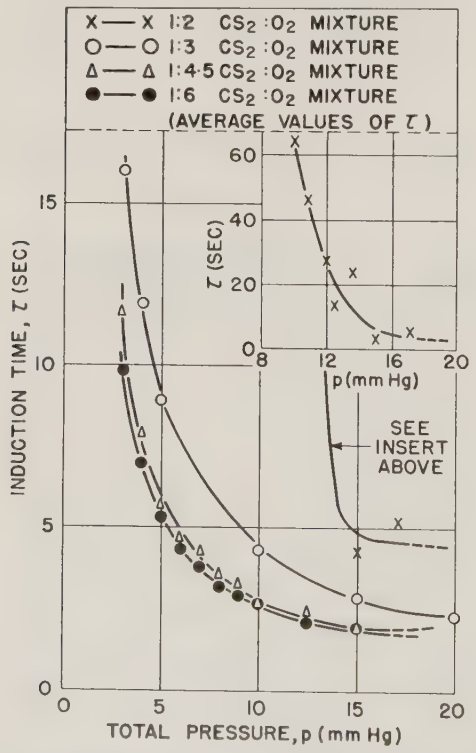
x—x 1:2 CS_2 : O_2 MIXTURE
o—o 1:3 CS_2 : O_2 MIXTURE
Δ—Δ 1:4·5 CS_2 : O_2 MIXTURE
●—● 1:6 CS_2 : O_2 MIXTURE
(AVERAGE VALUES OF τ)
τ (SEC)
p (mm Hg)
SEE INSERT ABOVE
INDUCTION TIME, τ (SEC)
TOTAL PRESSURE, p (mm Hg)

Figure 5. Induction time as a function of total pressure for various mixtures of CS_2 *and* O_2 *at* 160°C (116 c.c. *spherical quartz flask*)

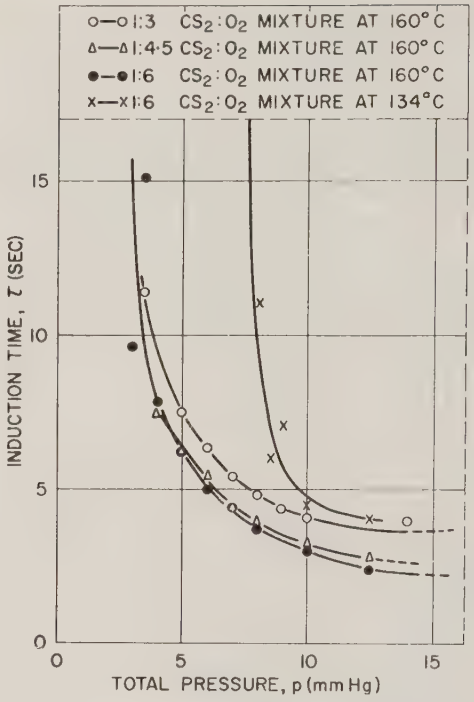
o—o 1:3 CS_2 : O_2 MIXTURE AT 160° C
Δ—Δ 1:4·5 CS_2 : O_2 MIXTURE AT 160° C
●—● 1:6 CS_2 : O_2 MIXTURE AT 160° C
x—x 1:6 CS_2 : O_2 MIXTURE AT 134° C
INDUCTION TIME, τ (SEC)
TOTAL PRESSURE, p (mm Hg)

Figure 6. Induction time as a function of total pressure for various mixtures of CS_2 *and* O_2 *at* 160°C *and* 1 : 6 *mixture at* 134°C (64 c.c. *spherical quartz flask*)

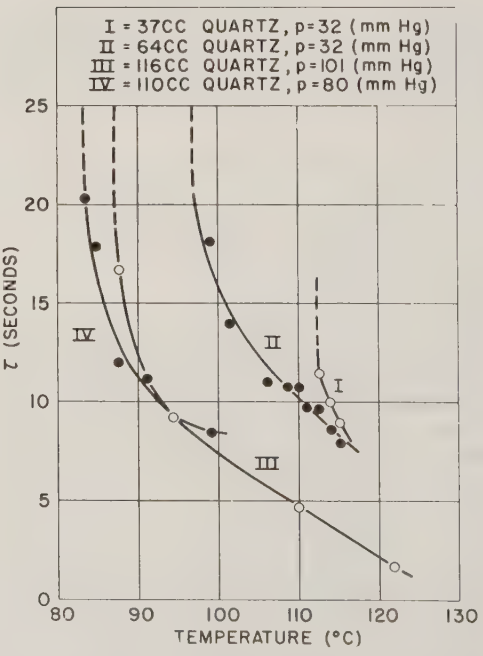

Figure 7. Variation of induction time with temperature for 1 : 3 *mixtures of* CS_2 : O_2 *in spherical flasks*

at low pressures are, of course, the ignition limits. The levelling off at high pressures would seem to indicate that a minimum rate of chain carrier destruction at the wall has been reached. If the experiments were carried out to still higher pressures, the induction times would begin to increase as the second limit was approached, so that a U shaped curve would result in the overall picture.

Induction time as a function of pressure

The equation expressing the growth of chain carriers or active centres with time, under first ignition limit conditions, is as follows:

$$\frac{\partial n}{\partial t} = D\,\frac{1}{r^2}\,\frac{\partial}{\partial r}\left(r^2\,\frac{\partial n}{\partial r}\right) + \alpha n + n_0 \qquad (1)$$

Here, n is the number of chain carriers per c.c. of gas, D is the gaseous diffusion constant, r is the radial distance of any given chain carrier at time t from the centre of the flask and α is the specific branching rate constant. Alpha does not represent one particular elementary reaction as is usually the case with the specific rate constant, k, as used in kinetics. Rather it must be considered as an empirically determined constant which is effectively an average of many k's and expresses the net effect of propagation of chain carriers. It is often separated into the difference of two terms: a branching rate constant β minus a chain breaking rate constant δ that is characteristic of the reactions which take place in the gas phase (i.e. $\alpha = \beta - \delta$). The last term, n_0, is the constant rate of spontaneous generation of chain carriers associated with the initiation reaction. In the following considerations its value will not matter. While the steady state form of equation 1, where $\partial n/\partial t$ is set equal to zero, has received considerable attention[6], only one publication[7] has been found in the literature which treats the non-steady state form representing the course in time of a chain branching reaction ($\partial n/\partial t \neq 0$). However, the latter paper carries the solution to a series expansion only for a one-dimensional case. This solution is not applicable to the present purpose, which requires n as a function of time, t, at $t = \tau$ (induction time), and the initial pressure, p. Also, a relationship between τ and p that is obtained by Semenoff[8] involves considerable approximation in its final stages and does not yield a finite value for the critical explosion pressure at $\tau \to \infty$. Therefore it seemed in order to derive a function which would relate these variables accurately and which might be directly and simply applied to our data. This has been accomplished, for the three-dimensional case, in a rigorous time-dependent solution of equation 1 by Wachtell[9] of The Franklin Institute Laboratories. Assuming $n = 0$ at $t = 0$ and the boundary condition representing chain initiation and breaking at the surface of the container, the following solution was obtained:

$$\frac{p}{\tau} = \frac{\alpha p}{K} - \frac{pDc}{K} \qquad (2)$$

Here K is a constant if, as is most likely for free radicals such as SO, monatomic S, etc., the chain breaking efficiency, ε, is greater than approximately 3×10^{-5}. The constant, c, depends on the radius of the chamber, but is practically independent of pressure. As pD is a constant for a given temperature, p/τ is evidently linear with respect to p.

It has been possible to obtain similar results by direct integration of an approximate form of equation 1. It is necessary to consider n as representing the space average value of the chain carrier concentration, as determined by the value of n_0, and the rate of loss by diffusion and surface destruction (reference 10, section 7). Then the rate of change of n is proportional to n and we may set

$$D\,\frac{1}{r^2}\,\frac{\partial}{\partial r}\left(r^2\,\frac{\partial n}{\partial r}\right) = DK_1 n \qquad (3)$$

Equation 1 then becomes

$$\frac{\mathrm{d}n}{\mathrm{d}t} = -DK_1 n + \alpha n \qquad (4)$$

and its solution is

$$\ln n_c = -DK_1\tau - \alpha\tau + K_2 \qquad (5)$$

where K_2 is a constant of integration. The value n_c is taken as an arbitrary constant giving the concentration of active centres at the time of explosion, $t = \tau$. It is obvious from a consideration of the exponential nature of $n = f(t)$ for a delayed chain-branching explosion that a negligible portion of the induction time (seconds) is involved in the explosion itself. During the brief duration (milliseconds) of the explosion n becomes very large—say of the order of magnitude of 10^{10}. Therefore by selecting one appropriately large value of $n = n_c$ for all pressures and their corresponding induction times, only a small error will be introduced. Incorporating constants and rearranging, we obtain as in equation 2

$$\frac{p}{\tau} = \frac{\alpha p}{K_3} - \frac{K_1}{K_3} \qquad (6)$$

where $K_3 = \ln n_c - K_2$.

Both equations 2 and 6 indicate that a plot of p/τ against p should yield a straight line, at least if the αn term of equation 1 does not contain a factor with the dimensions of pressure. *Figures 8* and *9* show such graphs for the data of the preceding *Figures 2–6*. It will be noted that the

points follow a straight line rather closely at lower pressures, and begin to deviate from this law by curving upwards at higher pressures. This effect seems to become more pronounced for higher

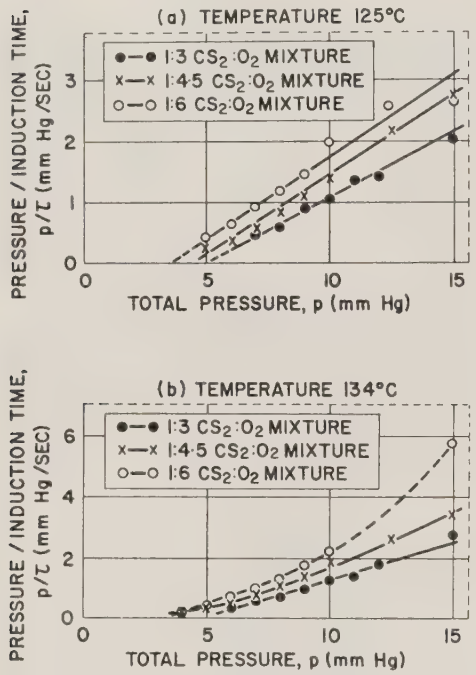
(a) TEMPERATURE 125°C
●—● 1:3 CS_2:O_2 MIXTURE
x—x 1:4·5 CS_2:O_2 MIXTURE
○—○ 1:6 CS_2:O_2 MIXTURE
PRESSURE / INDUCTION TIME, p/τ (mm Hg/SEC)
TOTAL PRESSURE, p (mm Hg)
(b) TEMPERATURE 134°C
●—● 1:3 CS_2:O_2 MIXTURE
x—x 1:4·5 CS_2:O_2 MIXTURE
○—○ 1:6 CS_2:O_2 MIXTURE
PRESSURE / INDUCTION TIME, p/τ (mm Hg/SEC)
TOTAL PRESSURE, p (mm Hg)

Figure 8. Total pressure/induction time as a function of total pressure for various mixtures and temperature of CS_2 *and* O_2 (116 c.c. *spherical quartz flasks*)

temperatures as evidenced by successively greater curvatures for 125, 134 and 164°C, when used with the 116 c.c. flask. Such deviation might well be expected with higher pressures where factors other than the two simple ones on which the equation is based become important. In any case, the data seem to follow the solution of equation 2 closely enough to imply that the rate equation 1 is a reasonably accurate description of the phenomena involved.

Effect of mol ratio of $CS_2 : O_2$ *mixtures on induction times*

Thus far the concentration or partial pressures of CS_2 and O_2 have not been considered. However it is readily apparent from the presented induction time data, as well as the ignition limits previously presented in *Figure 1*, that the relative partial pressures of the reactants are important both to the duration of the induction period and in determining whether or not explosion will take place. It can be seen in every case in *Figures 3–6* that for a given pressure the induction time becomes shorter with increasing proportions of O_2. This is in complete agreement with the results of the ignition limit studies. In all cases, first limits were depressed to lower temperatures by increasing proportions of oxygen. In the case of the induction times, this effect seems to be true for the entire temperature range studied, from 134 to 160°C. Although the data are not sufficiently precise to make such a conclusion final, it would seem that the effect becomes much more pronounced for richer mixtures of $CS_2 : O_2$. Thus, in *Figure 5*, it will be noted that the induction times increase tremendously in going from a 1 : 3 to a 1 : 2 mixture.

Apparently, the quantities p_{CS_2} and p_{O_2} should enter the αn term of equation 1, but not as $\alpha n p_{CS_2} p_{O_2}$ as would be expected in the usual case of bi- or ter-molecular reaction. That is, it is *not* true that the rate of the chain-carrier propagation reaction leading to explosion is proportional to both p_{CS_2} and p_{O_2}. For example, a 3 : 1 mixture of $CS_2 : O_2$

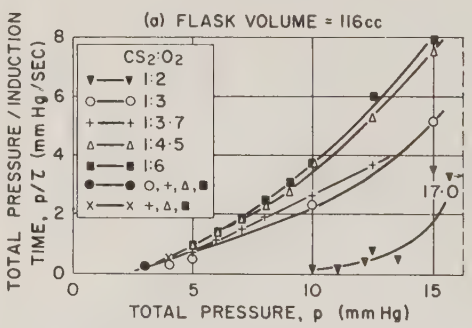

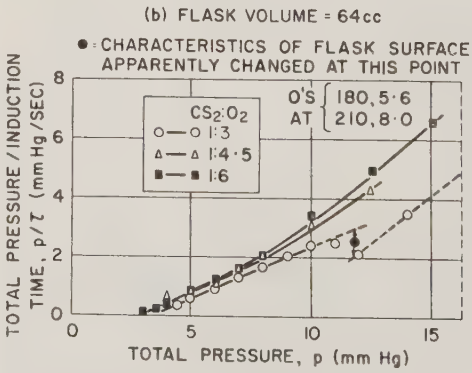
(b) FLASK VOLUME = 64cc
● : CHARACTERISTICS OF FLASK SURFACE APPARENTLY CHANGED AT THIS POINT
O'S AT 180, 5·6
210, 8·0
CS_2:O_2
○—○ 1:3
△—△ 1:4·5
■—■ 1:6
TOTAL PRESSURE / INDUCTION TIME, p/τ (mm Hg/SEC)
TOTAL PRESSURE, p (mm Hg)

Figure 9. Total pressure/induction time as a function of total pressure for various mixtures of CS_2 *and* O_2 *at* 160°C (116 *and* 64 c.c. *spherical quartz flasks*)

will have an enormously longer induction time than a 1 : 3 mixture according to the induction time data cited. It can be concluded that since the rate is increased by increasing the mol ratio of

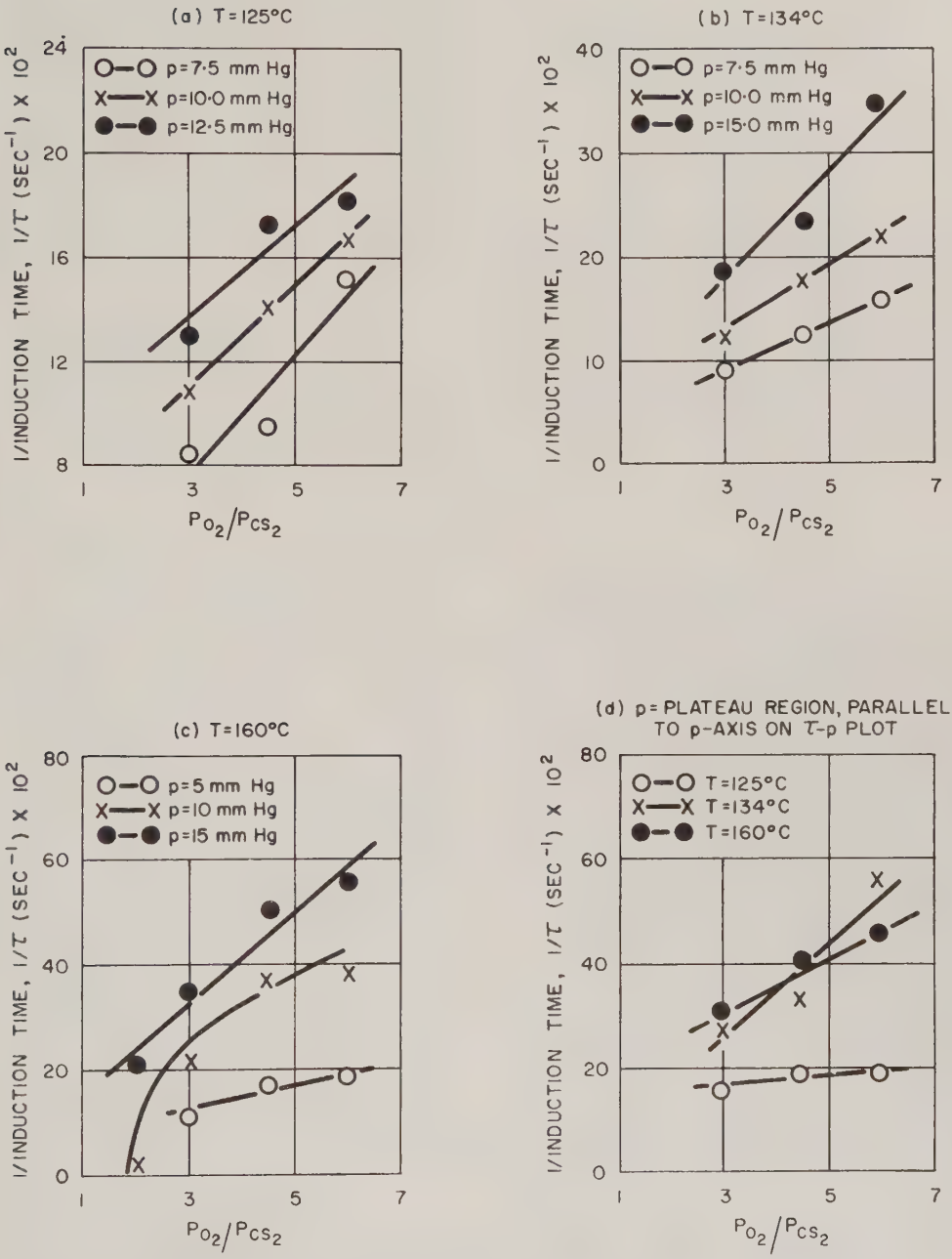

Figure 10. Reciprocal of induction time as a function of the ratio of the partial pressure of O_2 to that of CS_2, at constant pressure and temperature

$(O_2)/(CS_2)$ the ratio p_{O_2}/p_{CS_2} should appear in this term:

$$\frac{\partial n}{\partial t} = D\nabla^2 n + \frac{\alpha n p_{O_2}}{p_{CS_2}} + n_0 \qquad (7)$$

It would not seem, from a general inspection of the presented $\tau - p$ data, that the latter are quite precise and mutually consistent enough to warrant further quantitative analysis of this point. For example, it might be expected that comparison of 1 : 3 with 1 : 6 data might be subject to some error due to 'drifting' of the wall efficiency. Opportunity for such changing of chain-breaking characteristics would be afforded by the observations of 1 : 4·5 mixture explosions made in the interim. However, since all trends seem to be always in the correct direction, it was thought worthwhile to briefly examine the mathematical nature of the relationship. The latter can be accomplished by inserting $R_p (= p_{O_2}/p_{CS_2})$ in equation 2 or 6 so that we have

$$\frac{p}{\tau} = \frac{\alpha p R_p}{K} + \frac{pDc}{K} \qquad (8)$$

Then at constant pressure, flask size, and temperature, $1/\tau$ should be linear in R_p. Using the $\tau - p$ data for the 116 c.c. flask, a series of plots of this nature has been made and is shown in *Figure 10*. Since only three mol ratios were used, only three points are available for each line, corresponding to values for $CS_2 : O_2$ of 1 : 3, 1 : 4·5 and 1 : 6, at selected pressures and temperatures as indicated. The fourth graph, in the lower right-hand corner, presents pressure points corresponding to the plateau portion of the $\tau - p$ curve where it begins to run parallel to the p-axis. Here the diffusion effect should become very small, so that the second term in equation 8 can be set equal to zero. Then only the homogeneous gas phase reaction need be considered.

It can be seen that the data follow a strict linear relationship in approximately 50 per cent of the cases studied, so that one cannot conclude with any degree of certainty that this relation is theoretically true. However, the trend is unmistakeable —there can be no question that for a limited region $\partial n/\partial t$, the rate of propagation of chain carriers is approximately linear with respect to the ratio of p_{O_2}/p_{CS_2}.

As previously mentioned, it definitely seems that the rate increases with R_p much more rapidly than linearly for mixtures richer than stoichiometric, as can be noted for the 1 : 2 ratios at 160°C.

Induction time as a function of temperature

In the course of obtaining ignition limits in our early experiments where CS_2 and O_2 were mixed in the reaction vessel[1], several series of values for induction time as a function of temperature were obtained at constant pressure. These values are presented in graphical form in *Figure 7*. It is possible, however, to interpret with greater significance the much more extensive $\tau - p$ data herein presented in the following manner. The relationship between α/K, which is the slope of the line formed by plotting p/τ *versus* p from equation 2, and the temperature, can be obtained by means of an Arrhennius plot. In this case the logarithm of α/K, (α/K is proportional to the specific reaction rate constant), was plotted against the reciprocal of the absolute temperature. *Figure 11* shows such

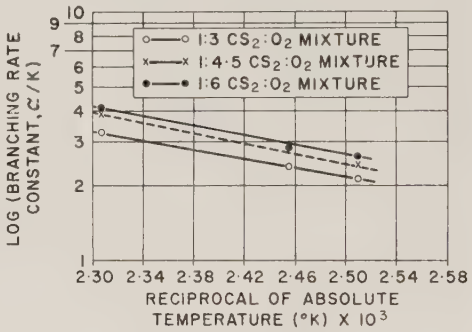

Figure 11. Initial slope (α/K) *of* p/τ versus p *curves, as a function of reciprocal of absolute temperature for various mixtures of* CS_2 *and* O_2 (116 c.c. *quartz flask*)

plots for the three ratios of $CS_2 : O_2$ studies. Unfortunately, it was impossible to determine an unequivocal slope for the 1 : 4·5 mixture at 134°C. However, it is apparent that the data, though sparse, follow the relationship quite precisely.

From the slopes of *Figure 11*, the activation energy was calculated and found to be 4,100 cal per mole for the 1 : 3 mixture, and 3,900 for the 1 : 6 mixture. Since there are only two points for the 1 : 4·5 data, there is little justification for calculating a slope from them. However, for the two points obtained, $E_{act} = 4{,}800$ cal per mole.

This research was performed under Contract No. AF 33(038)-20863 *with Wright Air Development Center, Dayton, Ohio.*

REFERENCES

[1] Myerson, A. L. and Taylor, F. R. *J. Amer. chem. Soc.* 75 (1953) 4348
[2] —— and Hanst, P. L. *J. chem. Phys.* 26 (1957) 1309–1320
[3] Thompson, H. W. *Z. phys. Chem.* 10B (1930) 273
[4] — and Kearton, C. F. *Z. phys. Chem.* 14B (1931) 359

[5] Ritchie, A., Brown, R. R. H. and Muir, J. J. *Proc. Roy. Soc. A* 137 (1932)
[6] Lewis, B. and von Elbe, G. *Combustion, Flames and Explosions*, Chap. II. 1951. New York; Academic Press
[7] Bursian, V. and Sorokin, V. *Z. phys. Chem.* 12B (1931) 247
[8] Semenoff, N. *Chemical Kinetics and Chain Reactions*, pp. 85–87. 1935. Oxford; Clarendon Press
[9] Myerson, A. L., Taylor, F. R., Hanst, P. L. and Trevethan, D. H. Franklin Institute Laboratories, *WADC Technical Report* 54–377 to Wright Air Development Center. Contract No. AF 33(038)-20863, October, 1954
[10] See Reference 8, section 7

14

A STUDY OF VIBRATIONAL RELAXATION IN CARBON MONOXIDE BY SHOCK WAVES AND INFRA-RED EMISSION

M. WINDSOR, N. DAVIDSON and R. TAYLOR

INTRODUCTION

The interchange of energy between external degrees of freedom (translation) and the internal degrees of freedom (vibration and rotation) of a molecule when it undergoes a collision is a subject of great importance, because of its intrinsic interest, because of its significance in the general field of chemical kinetics, and because of its bearing on various gas dynamical and combustion problems. When a gas is suddenly heated, as for example, by a shock wave, or suddenly cooled, as by a rapid expansion, it undergoes a rapid change in temperature. In our normal usage of the term 'temperature' we mean that the kinetic energy of translation of the molecules has changed. If the change is sudden, the new distribution of molecular velocities may instantaneously no longer follow the Maxwell–Boltzmann law. A new Boltzmann distribution is established in the time of a few collisions. To achieve complete thermodynamic equilibrium, it is now necessary for the energies of the rotational and the vibrational degrees of freedom to become adjusted. This will involve a further change of temperature as interchange of energy between translation and rotation and vibration takes place. The collisional processes by which this equilibration is effected are called rotational and vibrational relaxation.

Rotational relaxation usually takes only a few to a few tens of collisions, corresponding to a time of about 10^{-9} sec at s.t.p. Rotation and translation may, for most purposes therefore, be grouped together as external degrees of freedom. The transfer of energy between vibrations and external degrees of freedom, on the other hand, often turns out to be a very inefficient process. This is especially so for simple stiff diatomic molecules such as nitrogen, where many hundreds of thousands or even millions of collisions may be required. The relaxation time is long enough to make the question of vibrational relaxation assume practical importance. It affects, for example, the state of a gas undergoing rapid expansion in a rocket nozzle or suffering rapid compression behind a shock wave.

With increasing molecular complexity, vibrational relaxation is more rapid, less than 90 collisions being required for propane at 20°C and 1 atm. It is still not uncommon, however, to find several thousand collisions necessary and in special cases, as in CO_2 at room temperature, the relaxation time may still be as long as several microseconds.

These statements apply to the pure gas. The study of molecules with long relaxation times is almost always complicated by the fact that polyatomic molecules usually make much more efficient collision partners for relaxation than another molecule of the pure gas. Minute amounts of polyatomic impurities may therefore reduce the observed times by several orders of magnitude. The commonest contaminant is water vapour and the problem of its removal will be discussed later on.

A number of methods have been employed for measuring relaxation times. These include: (1) the dispersion and absorption of ultrasonic waves[1], (2) the impact tube[1], (3) interferometric measurements of density changes behind shock waves[1,2], (4) a direct method involving infra-red radiation, called the spectrophone technique[3], and (5) the infra-red emission method described here.

In the present work a new technique for measuring vibrational relaxation times has been developed[4]. The rate of population of a particular vibrationally excited state in a gas that has been rapidly heated by the passage of a shock wave is followed by observing the emission of infra-red radiation from this state with a detector of short response time.

In the particular application described here, we observe the rate of population of the second vibrational state ($v = 2$) of CO from the time dependence of the emission of the first overtone ($2 \rightarrow 0$) radiation at $2{\cdot}335\ \mu$. (To some extent, of course, one is also looking at the transitions, $3 \rightarrow 1$, $4 \rightarrow 2$, etc., and hence at the population of these upper states.) The radiative life-time for the $2 \rightarrow 0$ transition is 1·1 sec[5]. At equilibrium, 1 atm at 1,500°K, the calculated emission is $7{\cdot}2 \times 10^{-3}$ watts c.c.$^{-1}$, which, in the experimental arrangement, is readily detected. It is difficult to calculate self-absorption accurately, but approximate calculations according to the method of Penner and Weber[6] indicate that it is small or negligible. (Actually, the amount of radiation is proportional to the population of the $v = 2$ state even if there is self-absorption provided that the

amount of self-absorption is fairly constant; and specifically if it is not large in the boundary layer where the density and temperature are quite different from that of the bulk gas.) The radiative life-time for the $2 \rightarrow 1$ transition is 0·015 sec[5]; in our experiments, the life-time for the $2 \rightarrow 0$ overall transition by collision is 10^{-3} sec or less. Therefore, the radiative processes serve to indicate the population of the state without significantly affecting it.

EXPERIMENTAL

Shock tube

The use of the shock tube in this laboratory as a tool for studying chemical reactions at high temperatures has already been described[7]. In all of our previous work the progress of a chemical reaction has been followed by the absorption of visible or ultraviolet light.

The length of our shock tube has been increased in order to improve the quality of the shocks and to increase the time available for observations. The diameter is 15 cm; the driving section is a 270 cm length of aluminium pipe; the shock wave section consists of a 140 cm length of aluminium pipe and two 150 cm lengths of Pyrex pipe.

Part of the motivation to lengthen the tube was the desire to make observations in the region behind the reflected shock front which would have previously been terminated far too soon by the arrival of disturbances from the driving section. Reflected shock studies have several advantages. In the first place, the gas behind the reflected shock is stationary, so that the time-compression effect associated with the fact that the gas behind the incident shock is moving, does not occur. The removal of this penalty was important since our detector was already a limiting factor and we could ill afford to sacrifice any of its limited response time. Secondly, almost a millisecond was available before the arrival of the cold front. Finally, due to the double compression and heating, high temperatures and pressures could be reached without excessively high driving pressures and using less carbon monoxide. All of the experimental results presented here were made using the reflected shock technique. The observation station was set up as close as possible to the end-plate to minimize disturbances due to the growth of the boundary layer and to get the maximum observation time. The distance chosen was 3 cm. With the optical system employed, this was enough to prevent the detector seeing possible radiation from the end-plate.

Infra-red cell

A lead sulphide photo-conductive detector made by The Electronics Corporation of America was used. The sensitive element was 3 mm by 3 mm. The response time was 12 ± 3 μsec; the cell resistance was 6 megohms; the sensitivity was $1{\cdot}5 \times 10^4$ V/W; and the noise equivalent power (at 5 c/s) was *ca.* 3×10^{-11} W. The associated electronics did not increase the rise time. The output of the detector was fed into a pre-amplifier and then to an oscilloscope. The cell was mounted in a turret setting with three-way movement for focusing. A germanium filter cut off radiation below 2·0 μ and the Pyrex wall of the shock tube absorbed radiation longer than 2·8 μ.

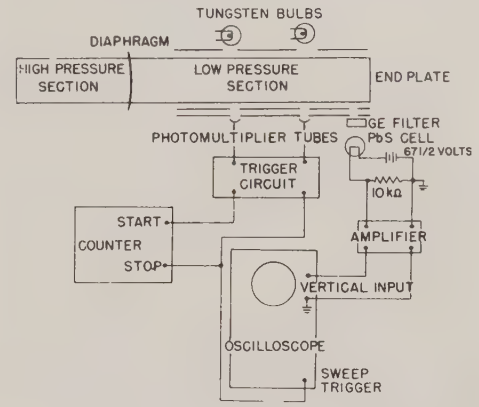

Figure 1. Schematic diagram of equipment

In addition, a Corning filter No. 3484 with a long wavelength cut-off at 2·6 μ was used. This effectively isolated radiation from the $0 \rightarrow 2$ transition in carbon monoxide which is centred at 2·335 μ. In control experiments with dry nitrogen, less than 4 per cent emission was observed. The experimental layout is shown in *Figure 1*. This also shows schematically the schlieren systems which were used for starting and stopping the timer and triggering the oscilloscopes.

Removal of impurities

Early work served to emphasize the importance of excluding water vapour and other impurities from the system due to the very high efficiency of these molecules as collision partners for the relaxation process. Two measures were necessary: (*a*) the use of carbon monoxide of very high purity, (*b*) the reduction of the static pressure of H_2O or CO_2 in the shock tube, caused by desorption from the walls, to as low a level as possible.

One series of experiments was made with Matheson Assayed Reagent Grade CO. Mass spectrometric analyses were supplied, and listed the main impurities in two samples as carbon dioxide, 0·04 and 0·27 mole per cent, and hydrogen, 0·03 and 0·02 mole per cent. Most of the work was done with samples prepared by fractional distillation of Matheson C.P. grade carbon monoxide in a good low-temperature column with a reflux head refrigerated with pumped-down liquid

nitrogen. This gave quite pure CO. A typical mass spectrometer analysis (Consolidated Electrodynamics Co.) is: O_2, 10^{-4} mole per cent, H_2O, less than 0·015 mole per cent, all other impurities less than 0·005 mole per cent.

The other source of impurities was the walls of the shock tube. To combat this three measures were adopted. (*a*) The whole low-pressure section of the shock tube, except for the observation area, was wound with a heating element. A temperature of 50 to 70°C could then be maintained while pumping out the tube to facilitate outgassing. (*b*) A false end-plate was designed fitted with a re-entrant cold finger which could be refrigerated with liquid nitrogen or other coolant. During evacuation a hole in the false end-plate gave access from the main volume of the tube to the cold finger which lay between the true end and the false end. Before starting a run, this hole was filled by pushing in a plug, the shaft of which extended through the tube end-plate via a hole sealed with an *O* ring. The end-plate also carried a mounting for a Phillips ionization gauge. (*c*) The pumping arrangements for the tube, which now has a volume of about 80 litres, were improved by installing a three-stage oil diffusion pump connected to the tube via a high-speed, one in. aperture baffle valve.

With the aid of these improvements it was possible to achieve a pressure of about 10^{-5} mm Hg with liquid nitrogen in the cold finger. The pressure rise with the shock tube isolated was less than 10^{-6} mm per minute. Since a run takes about ten minutes after closing off the pumps, this is negligible with the amounts of gas used. For experiments with added CO_2, the cold finger was filled with dry ice and trichlorethylene, and a control experiment was made under these conditions without added CO_2. Mixtures of CO and CO_2 were made up beforehand in a storage bulb. For experiments with added H_2O, either dry ice as above or methylene bromide at its freezing point was employed. The technique adopted was to admit excess water vapour to the tube first and then let in the CO. About 15 minutes was allowed for the H_2O to come to equilibrium with the ice on the cold finger and to mix with the CO. The vapour pressure of H_2O is 0·56 μ at −78°C (dry ice) and about 50 μ at −50°C (melting methylene bromide). Control runs without added H_2O were done at each temperature.

Calculation of temperature and pressure

The temperature and density of a shocked gas can be calculated from the shock velocity and the initial conditions if the enthalpy of the gas is known as a function of temperature. As vibrational relaxation occurs behind a strong shock, the temperature decreases and the density increases. The situation is more complicated for reflected shocks. We have calculated the conditions behind the reflected shock from the measured velocity of the incident shock. We assume, in accordance with the evidence, that the gas behind the incident shock is unrelaxed. Calculations have been made for the unrelaxed incident–unrelaxed reflected condition. This is strictly applicable to the reflected shock very close to the end-plate. Calculations could also be made for the unrelaxed incident–relaxed reflected conditions. This would be appropriate for the steady state shock after a long period of time. One is however observing the process of vibrational relaxation close to the end-plate. Neither of the above limiting steady flow conditions therefore applies. The gas behind the shock is contracting and the resulting rarefaction wave is moving out to merge with and slow down the shock. A correct calculation would be very complicated. We have therefore used the unrelaxed–unrelaxed calculations of temperature and density. Fortunately, the vibrational enthalpy is not too large and the uncertainties are small.

Examples of reflected shock calculations are given in Table 1.

TABLE 1
Typical Shock Parameters in CO

T_i °K	S_i cm/msec	π_i	Δ_i	T_r °K	S_r cm/msec	π_r	Δ_r	π_t	Δ_t
500	69·97	4·44	2·65	739	35·13	3·31	2·24	14·7	5·93
600	83·47	6·39	3·18	965	37·72	4·05	2·52	25·9	7·99
700	95·23	8·37	3·57	1,192	40·42	4·59	2·70	38·4	9·61
800	105·8	10·36	3·86	1,420	43·06	5·01	2·82	51·9	10·89
900	115·4	12·36	4·09	1,648	45·61	5·33	2·91	65·9	11·92
1,000	124·0	14·36	4·28	1,886	48·28	5·60	2·97	80·4	12·70
1,100	132·3	16·34	4·43	2,120	50·84	5·83	3·02	95·4	13·36
1,200	140·2	18·35	4·56	2,340	53·77	6·00	3·07	110·0	14·00
1,300	147·6	20·36	4·67	2,560	54·91	6·14	3·11	124·8	14·50
1,400	154·8	22·40	4·77	2,800	56·20	6·28	3·14	140·5	14·98
1,500	161·6	24·40	4·85	3,020	58·38	6·40	3·17	156·0	15·38

T, temperature of heated gas behind shock; S, shock velocity; π, pressure ratio across shock; Δ, density ratio across shock. Subscript i refers to incident shock, subscript r refers to reflected shock, and subscript t refers to total change.

RESULTS

The vibrational relaxation time of carbon monoxide has been measured between 1,400°K and 3,000°K and over a range of final pressures from 1 to 3·5 atm. A preliminary study of the effect of small amounts of CO_2 and H_2O has also been made.

A typical experimental record of infra-red emission due to the $2 \rightarrow 0$ transition is shown in *Figure 2.*

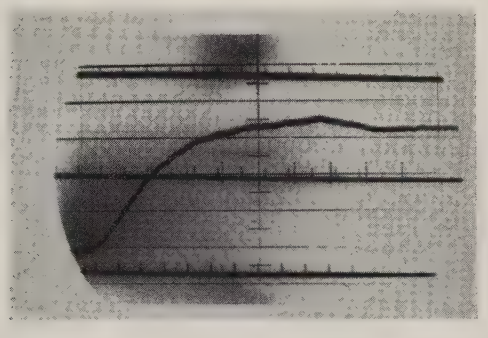

Figure 2. Typical oscillograph record of emission from CO *heated by shock. Initial condition;* $T = 298°K$; $P = 0{\cdot}056$ atm. CO. *Final condition,* $T = 1{,}446°K$, $P = 3{\cdot}01$ atm. *Time is the horizontal coordinate. The three horizontal sweeps at the top, middle, and bottom of the picture are time calibration marks with* 100 μsec *pips. Emission of* CO *increases vertically*

As indicated previously, it is believed that the intensity of the emission is directly proportional to the concentration of molecules in the upper state. After a small initial region of gradually increasing slope, the trace rises almost linearly for about half the total amplitude and then approaches the equilibrium value asymptotically.

Interpretation

One may conceive of any one of three possibilities as being the most important path for populating the state $v = 2$.

There is the direct $0 \rightarrow 2$ excitation

$$CO + CO \underset{k_{20}}{\overset{k_{02}}{\rightleftharpoons}} CO + CO^{**} \qquad (1)$$

There is a two-step process, $0 \rightarrow 1 \rightarrow 2$

$$CO + CO \underset{k_{10}}{\overset{k_{01}}{\rightleftharpoons}} CO^{*} + CO \qquad (2)$$

$$CO^{*} + CO \underset{k_{21}}{\overset{k_{12}}{\rightleftharpoons}} CO^{**} + CO$$

There is also the possibility (hypothesis 3), in which two CO^{*} molecules react to give CO^{**} + CO, in which no conversion of translational energy to vibrational energy occurs, but in which the vibrational energy is re-distributed. For this process the forward and reverse rate constants, e, are equal.

$$CO + CO \underset{k_{10}}{\overset{k_{01}}{\rightleftharpoons}} CO^{*} + CO \qquad (3)$$

$$CO^{*} + CO^{*} \underset{e}{\overset{e}{\rightleftharpoons}} CO^{**} + CO$$

For simplicity, make the approximation $(CO^{**}) \ll (CO^{*}) \ll (CO)$.

Hypothesis 1 gives a simple exponential growth of (CO^{**}).

$$(CO^{**}) = (CO^{**})_{\infty} \{1 - \exp [-k_{20}(CO)t]\} \qquad (1a)$$

In the harmonic oscillator approximation, $k_{12} = 2k_{01}$, $k_{21} = 2k_{10}$. Then hypothesis 2 gives

$$(CO^{**}) = (CO^{**})_{\infty} \{1 - \exp [-k_{10}(CO)t]\}^2 \qquad (2a)$$

If in hypothesis 3 we assume e is very large, expression 2a again results. Thus, hypothesis 1 gives a simple exponential growth, beginning with a finite slope, whereas 2 and 3 give growth beginning with zero slope, then rising steeply, with a rise time of the order of $1/k_{10}(CO)$, namely the relaxation time of the first vibrational state.

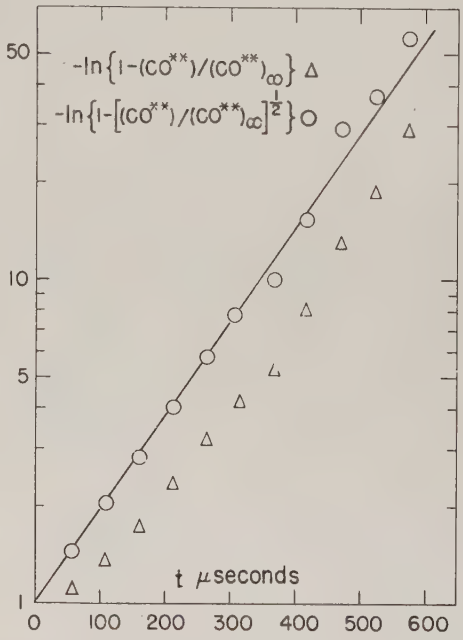

Figure 3. One-step versus *two-step relaxation processes*

Hypothesis 3 can be discussed in further detail as follows. Reactions like 3a are 'energy transfers at exact resonance'. The complete set of such

TABLE 2

Relaxation Time Measurements

Initial pressure of CO atm	T_i °K	T_τ °K	π_t	Δ_t	P_τ atm	τ μsec	τP_τ μsec atm
0·0560	810	1,446	53·7	11·01	3·01	278	836
0·0488	810	1,446	53·7	11·01	2·62	246	645
0·0718	787	1,395	50·6	10·77	3·63	168	610
0·0469	814	1,453	54·2	11·04	2·54	237	601
0·0311	811	1,447	53·7	11·01	1·67	352	588
0·0484	805	1,433	52·9	10·95	2·56	224	573
0·0318	815	1,455	54·5	11·05	1·73	327	565
0·0317	810	1,445	53·6	11·00	1·70	325	552
0·0403	812	1,451	54·0	11·03	2·18	248	540
0·0306	835	1,500	57·0	11·28	1·74	234	407
0·0248	930	1,724	70·3	12·19	1·74	183	319
0·0182	1,112	2,150	97·6	13·54	1·78	132	234
0·0216	1,012	1,916	82·3	12·84	1·78	98	174
0·0215	1,015	1,921	82·7	12·87	1·78	97	172
0·0179	1,122	2,170	98·9	13·60	1·77	67	119
0·0181	1,100	2,117	95·4	13·45	1·73	66	104
0·0062	1,485	2,985	153·0	15·33	0·95	37	35
0·0060	1,485	2,985	153·0	15·33	0·92	37	34

reactions do not create vibrational energy, but they re-distribute it in such a way that the population of the nth level, $(CO^{n\star})$, is related to the population of the first excited level by

$$(CO^{n\star}) = (CO^{\star})^n \left(\frac{E_{v1b}}{h\nu + E_{v1b}}\right)\left(\frac{h\nu}{h\nu + E_{v1b}}\right)$$

That is, there is a Boltzmann-like distribution determined by the total amount of vibrational energy, E_{v1b}, in the system. Given such a Boltzmann-like distribution, reactions like 3a will be proceeding backwards and forwards at equal rates and will not further affect the distribution. Now, Montroll and Shuler[9] have shown that if one considers the complete set of equations like 2 in the harmonic oscillator approximation, then a system which starts with a Boltzmann distribution of vibrational states appropriate to one temperature relaxes to the Boltzmann distribution appropriate to the translational temperature via a set of Boltzmann distributions appropriate to intermediate temperatures. Under these circumstances, the reaction system 3a makes no contribution to the vibrational distribution even though its rate constant may be large.

Plots of $\ln\{1 - (CO^{\star\star})/(CO)^{\star\star}_{\infty}\}$ *versus* t and of $\ln\{1 - [(CO^{\star})/(CO^{\star})_{\infty}]^{\star\star 1/2}\}$ *versus* t are shown in *Figure 3*. The latter relation gives a better straight line, thus favouring hypothesis 2 or 3. The situation is not perfectly clear cut however because the finite rise time of the detector tends to make a curve like 1a look like 2a. We believe this effect is small. A more detailed examination of this point will be made in a later paper.

Accept equation 2a. Define the relaxation time τ, as $1/k_{10}(CO)$. From the equation there is a point of inflection, $d^2(CO^{\star\star})/dt^2 = 0$ at $(CO^{\star\star}) = (CO^{\star\star})_{\infty}/4$. On both sides of this point, the curve is almost linear and the slope is $2/\tau$. Values of τ so obtained are presented in Table 2.

The mean value of the measurements in the vicinity of 1,400°K, converted to 1,400°K and 1 atm pressure is

$$\tau = 650 \pm 50\ \mu\text{sec}$$

The form of pressure and temperature dependence used in making these conversions will be discussed below. τ may also be obtained from the slope of the straight line in *Figure 3* which has the advantage of using the whole curve. Within the limits of accuracy both methods gave the same results in several cases and the less laborious inflection point method was therefore adopted.

Pressure dependence of τ

For a collisional process, a simple inverse pressure dependence is to be expected. A graph of τp *versus* p for those experiments close to 1,400°K is shown in *Figure 4*. The values of τ have been converted to 1,400°K. A reasonable fit to a straight line is obtained.

Temperature dependence of τ

The relaxation times are observed to decrease with increasing temperature as expected. The usual theories of vibrational relaxation lead to an expression of the form,

$$\log \tau = AT^{-1/3} + B \qquad (4)$$

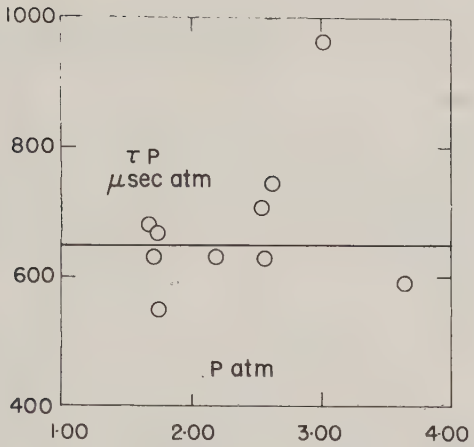

Figure 4. Pressure dependence of vibrational relaxation in CO

where A and B are constants. Values of log τ *versus* $T^{-1/3}$ for the present observations are plotted in *Figure 5.* The best straight line that can be drawn through the experimental points leads to $A = 64{\cdot}45$ and $B = -2{\cdot}943$.

Equation 3 and the above value of A were used in making the conversions of τ to 1,400°K mentioned earlier.

Effect of impurities

The effect of small amounts of added H_2O or CO_2 on the relaxation time of CO is shown in Table 3. Water causes a marked increase in the rate of relaxation even in trace amounts. At a relative concentration of three parts in 10^3 the value of τ is reduced by at least a factor of six. The reduction may be somewhat greater because the observed time is close to the response time of the detector. For CO_2 a ratio of one part in 10^3 reduces τ by a factor of about 1·5. The experiment with the Matheson Reagent Grade CO gave relaxation times of about half those observed with the fractionally distilled samples. Since

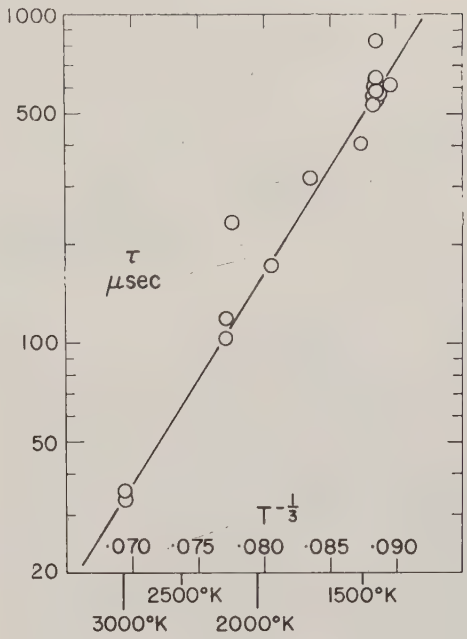

Figure 5. Temperature dependence of vibrational relaxation in CO

the CO_2 impurity was removed by the −196°C trap, this may be due to the hydrogen impurity.

CONCLUSIONS

The value reported here, $\tau = 550$ μsec at 1470°K, is thirty times greater than that given in our preliminary report[4]. The value at 2,200° (150 μsec) is greater than the value of 10 μsec given in a preliminary report by the Princeton group[8]. This is presumably a matter of the removal of impurities. It is of course possible that even the present results are affected by impurities.

At present one may say that CO has the longest vibrational relaxation times known at any given temperature.

TABLE 3

Effect of Impurities on Vibrational Relaxation of CO

Composition of gas	*Coolant in trap*	T_τ °K	P_τ atm	τ μsec	τP μsec atm
pure CO*	dry ice	1,437	1·74	198	344
pure CO*	melting methylene bromide	1,437	1·72	210	361
CO + 0·002% H_2O	dry ice	1,393	1·61	212	341
CO + 0·3% H_2O	melting methylene bromide	1,430	1·70	35	60
CO + 0·1% CO_2	dry ice	1,431	1·70	150	255
CO + 0·03% H_2 with <0·04% CO_2	liquid N_2	1,404	1·24	178	220

* Control runs with pure gas.

The experimental data favour hypotheses 2 and/or 3 over 1. Theory very strongly seconds the motion[1], in that the interconversion of a large amount of energy between vibration and translation, as in reaction 1, is predicted to be extremely improbable ($\sim 10^{-7}$ less probable than process 2 in the present instance).

We have made preliminary calculations of the rate constants k_{10} and e for equations 2 and 3 above according to the Schwartz, Slawsky, Herzfeld theory[1] as amended by Tanczos[10]. For the Lennard-Jones parameter, σ, for CO, we use[11] 3·59 Å. We calculate, at 1,400°K, $k_{10} = 1{\cdot}9 \times 10^{-6}Z$, $k_{01} = 2{\cdot}1 \times 10^{-7}Z$, $e = 4{\cdot}3 \times 10^{-3}Z$. Z is the gas kinetic theory collision number. The experimental τ at 1,400°K corresponds to $k_{10} = 5 \times 10^{-7}Z$. The agreement between theory and experiment is as good as can be expected. Note that although e is calculated to be about 10^3 greater than k_{10}, the discussion given earlier indicates that the energy transfer at exact resonance probably does not affect the kinetics of the population of the various vibrational states significantly.

The vibrational relaxation time of CO is greatly diminished by the impurities H_2O and CO_2. These molecules have shorter vibrational relaxation times, and we suggest that the principal process is the highly efficient transfer of vibrational energy from one species to the other:

$$H_2O^{\star} + CO \rightleftharpoons H_2O + CO^{\star}$$

The infra-red method for measuring vibrational relaxation times has the advantage of looking, at least to some extent, at the rate of excitation of particular states. The limitations as to rise time and sensitivity of detectors at present available are such that the method is applicable only to infra-red active molecules with rather long relaxation times.

We are indebted to the ONR for support. Dr. Russ Duff of Los Alamos generously performed many of the reflected shock calculations.

One of us (M. W.) is indebted to the Commissioners for the Exhibition of 1851 for a Senior Studentship, and one of us (R. T.) is indebted to the duPont Co. for a fellowship.

Contribution No. 2330 from the Gates and Crellin Laboratories of Chemistry.

REFERENCES

1 Herzfeld, K. *Thermodynamics and Physics of Matter*, Section *H*. 1955. Princeton University Press

2 Blackman, V. *J. Fluid Mech.* 1 (1956) 61

3 Slobodskaya, P. V. *Izvest. Akad. Nauk S.S.S.R., Ser. Fiz.* 12 (1948) 656

4 Windsor, M. W., Davidson, N. and Taylor, R. *J. chem. Phys.* 27 (1957) 315

5 Penner, S. and Weber, D. *J. chem. Phys.* 19 (1951) 807, 817

6 — — *J. chem. Phys.* 19 (1951) 1351, 1361

7 Britton, D., Davidson, N. and Schott, G. *Disc. Faraday Soc.* 17 (1954) 58

8 Greenspan, W. D. and Blackman, V. H. *Bull. Amer. phys. Soc.* 112 (1957) 217 (April 1957, Washington meeting)

9 Montroll, E. and Shuler, K. E. *J. chem. Phys.* 26 (1957) 454

10 Tanczos, F. I. *J. chem. Phys.* 25 (1956) 439

11 Hirschfelder, J. O., Curtiss, C. F. and Bird, R. B. *Molecular Theory of Gases and Liquids*, p. 1111. 1954. New York; Wiley

15

ON THE PERTURBATION OF THE VIBRATIONAL EQUILIBRIUM DISTRIBUTION OF REACTANT MOLECULES BY CHEMICAL REACTIONS

K. E. SHULER

INTRODUCTION

Any rate process occurring in finite time involves a disturbance of equilibrium. This is true for scalar processes such as chemical reactions as well as for vector processes such as diffusion or heat conduction. The question then is not whether a chemical reaction perturbs the initial equilibrium Maxwell-Boltzmann distribution in the reaction system, but how much of a perturbation is introduced by the reaction and how serious will be its effect on the rate of the reaction.

In previous papers[1,2] the status of this problem has been reviewed. The conclusion which can be drawn from the work of Kramers[3], Zwolinsky and Eyring[4], and Prigogine[6,7] is that the perturbation of the initial Maxwell-Boltzmann distribution and the corresponding deviation from the equilibrium rate is quite small when $E_{act}/kT > 5$ and that the use of the equilibrium theory of chemical reaction is justified under these conditions. When $E_{act}/kT < 5$, there is a pronounced perturbation of the initial equilibrium distribution. Curtiss[5] and Prigogine[6,7] who investigated the perturbation of an initial Maxwell velocity distribution by a chemical reaction were able to obtain explicit expressions for the perturbed velocity distribution function. Analogous expressions for the perturbation of the distribution function of the internal degrees of freedom are not available and cannot readily be obtained from the work of the authors referred to above.

In a recent paper on the application of the theory of stochastic processes to chemical kinetics[2] the departure from equilibrium in certain types of dissociation reactions has been investigated. The methods developed in that paper lend themselves readily to a study of the perturbation of the *vibrational* distribution function, i.e. the population distribution over the vibrational energy levels, during such reactions. In this paper we report on the results of such a study.

THE MODEL

This approach to the study of the perturbation of the initial vibrational equilibrium Boltzmann distribution by a chemical reaction is a discrete quantum mechanical analogue of Kramers' Brownian motion model[3]. It is an extension of a model which has been used previously in a discussion of the relaxation of vibrational non-equilibrium distributions[8].

We consider an ensemble of reactant molecules with quantized energy levels to be immersed in a large excess of (chemically) inert gas which acts as a constant temperature heat bath throughout the reaction. The requirement of a constant temperature T of the heat bath implies that the concentration of reactant molecules is very small compared to the concentration of the heat bath molecules. The reactant molecules are initially in a Maxwell-Boltzmann distribution appropriate to a temperature T_0 such that $T_0 < T$. By collisions with the heat bath molecules the reactants are excited *in a stepwise process* into their higher vibrational energy levels until they reach 'level' $N + 1$ where they dissociate irreversibly and are thus removed from the reaction system. The collisional transition probabilities per unit time W_{nm} which govern the rate of transfer of the reactant molecules between levels with energies E_n and E_m are functions of the vibrational quantum numbers n and m and can, in principle, be calculated in terms of the interaction of the reactant molecules with the heat bath.

The model described above corresponds to a bimolecular activation followed by dissociation

$$\mathrm{M} + \mathrm{A}_0 \underset{k_{10}}{\overset{k_{01}}{\rightleftharpoons}} \mathrm{M} + \mathrm{A}_1 \underset{k_{21}}{\overset{k_{12}}{\rightleftharpoons}} \mathrm{M} + \mathrm{A}_2 \rightleftharpoons$$

$$\ldots \mathrm{M} + \mathrm{A}_N \xrightarrow{k_{N,N+1}} \mathrm{M} + \mathrm{A}^{\star}_{N+i}$$

$$\mathrm{A}^{\star}_{N+i} \xrightarrow{k_D} \text{dissociation products} \qquad \text{(I)}$$

where M represents the heat bath molecules, A_i the reactant molecules in the vibrational quantum state i, and $\mathrm{A}^{\star}_{N+i}$ the reactants with energy greater than E_N. Since it has been assumed that the concentration $\mathrm{M} \gg \mathrm{A}$, the activating and deactivating collisions suffered by the molecules A will take place predominantly with the heat bath molecules M so that the activation and dissociation processes are first order in A and the differential

equations governing the rate of activation will be linear in the concentration of the reacting species A.

The relevant stochastic process corresponding to this model of a chemical reaction is that of a one-dimensional random walk with an absorbing barrier. In this random walk, the probability per unit time W_{mn} that a 'walker' will take a step from level n to m is a function of the distance from the origin, $n = 0$. The time dependent distribution of the reactant molecules among the vibrational energy levels $n = 0, \ldots, N$ is then given by the fractional population $x_n(t)$ of walkers n levels from the origin at time t. The distribution is normalized such that $\sum_n x_n(0) = 1$.

If the reactant molecules are treated as simple harmonic oscillators, and if it is assumed that only weak interactions exist between the oscillators and the heat bath molecules, the collisional transition probabilities per unit time, W_{mn}, can be calculated explicitly. This was first done by Landau and Teller[9] who showed that the transition probabilities per collision, P_{nm}, are given by

$$P_{n,m} = [(m+1)]\delta_{n-1,m} + [m\delta_{n+1,m}]P_{10} = P_{m,n} \tag{1}$$

where

$$\delta_{n\,m} = \begin{cases} 1 & \text{if } n = m \\ 0 & \text{otherwise} \end{cases} \tag{1a}$$

and where P_{10} is the transition probability per collision for the transition $0 \leftarrow 1$. It is to be noted that these transition probabilities are identical with those for the optical transitions of a harmonic oscillator in a radiation bath. *Transitions in this harmonic oscillator model are possible only between adjacent levels.*

The transition probabilities per collision P_{mn} are related to the transition probabilities per unit time W_{mn} (for transitions $n \rightarrow m$) by

$$W_{n+1,n} = ZM\,e^{-\theta}P_{n,n+1}$$

$$W_{n,n+1} = ZMP_{n+1,n} \tag{2}$$

The quantity Z is the collision number, i.e. the number of collisions per unit time suffered by the oscillator when the gas density is one molecule per unit volume, M represents the total concentration of heat bath molecules, and $\theta = h\nu/kT$, where ν is the natural frequency of the oscillator and T is the temperature of the heat bath. From equation 3 one obtains $W_{n,n+1}/W_{n+1,n} = \exp\theta = \exp(h\nu/kT)$ as required by the principle of detailed balancing.

The potential energy curve for such a 'dissociating harmonic oscillator' reactant is shown in *Figure 1.* It is a truncated harmonic oscillator potential with a finite number of equally spaced energy levels such that the level N is the last discrete level of the oscillator and the energy $E_{N+1} = h\nu(N+1)$ is the dissociation energy.

THE DISTRIBUTION FUNCTION

The temporal variation of the fractional population $x_n(t)$ in the vibrational level system $n = 0, 1 \ldots N+1$ is described by the transport equation 10

$$\frac{dx_n(t)}{dt} = \sum_{\substack{m=0,1,2\ldots \\ m\neq n}} (W_{nm}x_m - W_{mn}x_n) \tag{3}$$

The positive terms represent the increase in the population in the nth level by transitions $m \rightarrow n$ while the negative sum corresponds to the loss

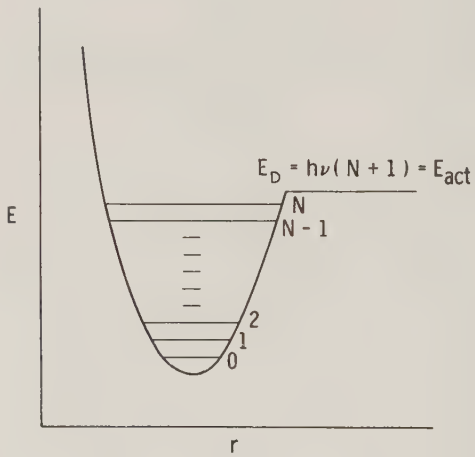

Figure 1. Potential energy for a harmonic oscillator reactant with a dissociation 'cut-off'. The energy $E_D = h\nu(N+1)$ is the dissociation energy

associated with transitions $n \rightarrow m$. Under the restriction that transitions can take place only between neighbouring levels, equation 1, and with the assumption that the level $(N+1)$ is a completely absorbing state, i.e. all oscillators which reach this level dissociate and none of them return to the initial ensemble of oscillators, equation 3 becomes

$$\frac{dx_n(t)}{dt} = W_{n,n-1}x_{n-1} - (W_{n-1,n} + W_{n+1,n})x_n + W_{n,n+1}x_{n+1} \qquad n = 0, 1, \ldots (N-1) \tag{4a}$$

$$\frac{dx_N(t)}{dt} = W_{N,N-1}x_{N-1} - (W_{N-1,N} + W_{N+1,N})x_N \tag{4b}$$

Equation 4b is the boundary condition for the top of the energy level system shown in *Figure 1.*

Substitution of equation 2 into equation 4 finally leads to the transport equations

$$\frac{dx_n(t)}{dt} = \kappa\{ne^{-\theta}x_{n-1} - [n + (n+1)e^{-\theta}]x_n + (n+1)x_{n+1}\};\ n = 0, 1, \ldots (N-1) \quad (5a)$$

$$\frac{dx_N(t)}{dt} = \kappa\{Ne^{-\theta}x_{N-1} - [N + (N+1)e^{-\theta}]x_N\} \quad (5b)$$

with $\kappa = P_{10}ZM$.

As has been shown previously[2,8] the solution of this set of differential difference equations can be obtained through the use of the Gottlieb polynominals $l_n(\mu)$[11]. A brief development of this solution is presented here. One assumes $x_n(t)$ to be a linear combination of terms $l_n \exp(\mu\tau)$ where

$$\tau = \kappa t(1 - e^{-\theta}) \quad (6)$$

is a dimensionless time. Substitution of these terms into equations 5a and 5b shows that l_n satisfies the difference equations

$$(e^{-\theta} - 1)\mu l_n = ne^{-\theta}l_{n-1} - [n + (n+1)e^{-\theta}]l_n + (n+1)l_{n+1};\ n = 0, 1, \ldots N \quad (7a)$$

where μ is a root of the boundary condition

$$l_{N+1}(\mu) = 0 \quad (7b)$$

The Gottlieb polynominals $l_n(\mu)$ which are defined by

$$l_n(\mu) = e^{\theta\mu}\Delta^n\left\{\binom{\mu}{n}e^{-\theta\mu}\right\} \quad (8a)$$

or

$$l_n(\mu) = e^{-n\theta}\sum_{\nu=0}^{n}(1 - e^{\theta})^{\nu}\binom{n}{\nu}\binom{\mu}{\nu} \quad (8b)$$

satisfy the recursion formula 7a. Hence the boundary condition 5b is satisfied by choosing μ to be a root of equation 7b. The general solution of equation 5a is then

$$x_n(\tau) = \sum_{j=0}^{N} a_j l_n(\mu_j) \exp(\mu_j\tau) \quad (9)$$

where the coefficients a_j are given in terms of the initial distribution $x_n(0)$ and with the aid of the orthogonality condition

$$\sum_{n=0}^{N} e^{n\theta}l_n(\mu_j)l_n(\mu_k) = 0 \quad \text{if } j \neq k \quad (10)$$

by

$$a_j = \sum_{n=0}^{N} x_n(0)l_n(\mu_j)e^{n\theta} \Big/ \sum_{n=0}^{N} l_n^2(\mu_j)e^{n\theta} \quad (11)$$

For an initial Boltzmann distribution of the oscillators in the vibrational energy level system at temperature T_0 one has

$$x_n(0) = (1 - e^{-\theta_0})e^{-n\theta_0} \quad (12)$$

where $\theta_0 = h\nu/kT_0$. For this initial distribution one finds, under the assumption that θ_0 is sufficiently large so that $e^{-n\theta_0} \simeq 0$ when $n > N$,

$$a_j \simeq (1 - e^{-\theta_0})\sum_{n=0}^{\infty} e^{-n(\theta-\theta_0)}l_n(\mu_j) \Big/ \sum_{n=0}^{N} l_n^2(\mu_j)e^{n\theta} = \left[\frac{1 - e^{-(\theta_0-\theta)}}{1 - e^{-\theta_0}}\right]^{\mu_j} \Big/ \sum_{n=0}^{N} l_n^2(\mu_j)e^{n\theta} \quad (13)$$

The distribution function $x_n(\tau)$ is then given by

$$x_n(\tau) = \sum_{j=0}^{N}\left\{l_n(\mu_j)\left[\frac{1 - e^{-(\theta_0-\theta)}}{1 - e^{-\theta_0}}\right]^{\mu_j} \Big/ \sum_{m=0}^{N} l_m^2(\mu_j)e^{m\theta}\right\}e^{-\mu_j\tau} \quad (14)$$

It can readily be shown by means of the asymptotic formulae for large N derived in reference 2 that for large N, i.e. for a high activation energy and a consequent slow rate of reaction, equation 14 reduces to

$$x_N(\tau) \simeq [(1 - e^{-\theta})e^{-\mu_0\tau}](1 - e^{-\theta})e^{-N\theta} \quad (15)$$

This corresponds to a Boltzmann distribution at the temperature T of the heat bath at all times. The rate of removal of the oscillators from the reaction system is described by the terms in the square brackets.

It has been shown previously[2] that a rate process of the type considered here is governed by two time scales. As the ensemble of oscillators at the temperature T_0 is introduced into the heat bath at the temperature T, the initial vibrational Boltzmann distribution of the oscillators relaxes to the new Boltzmann distribution at the temperature of the heat bath. The characteristic time for this process is $\sim 1/\mu_1$. The dissociation process, i.e. the excitation of the oscillators to the $(N+1)$st vibrational level, is associated with the characteristic time $1/\mu_0$. Since $\mu_0 < \mu_1$ the vibrational relaxation process is more rapid than the dissociation process and the initial state of the oscillators for the dissociation process is essentially the equilibrium vibrational Boltzmann distribution at the temperature T of the heat bath. A behaviour of the type described here would be expected to be observed in the passage of a shockwave through a diatomic gas with a final temperature sufficiently high for dissociation of the shocked gas. Experimental work has shown[12,13] that this is indeed the case and that the vibrational relaxation precedes the onset of dissociation.

RESULTS AND DISCUSSION

To evaluate the distribution function 14 it is necessary to obtain the roots μ_j of the Gottlieb polynomials from the boundary condition 7b.

This calculation has been carried out on the IBM 704 electronic computer at the National Bureau of Standards using the definition of the Gottlieb polynominals in equation 8, the recursion formulae 7a, and the relation $l_0(\mu) = 1$. The set of roots of the Gottlieb polynominals $l_n(\mu)$ for $n = 0, 1 \ldots 10$ obtained here will be published shortly. We have used the values $\theta_0 = 10$ and $\theta = 1$ in the numerical evaluation of the distribution function 14. These values of θ correspond to temperatures of about 300°K for the initial Boltzmann distribution of the oscillators and of about 3,000°K for the heat bath. Using these values of θ_0 and θ, and the roots μ_j computed as indicated above, equation 14 was then evaluated for a sequence of

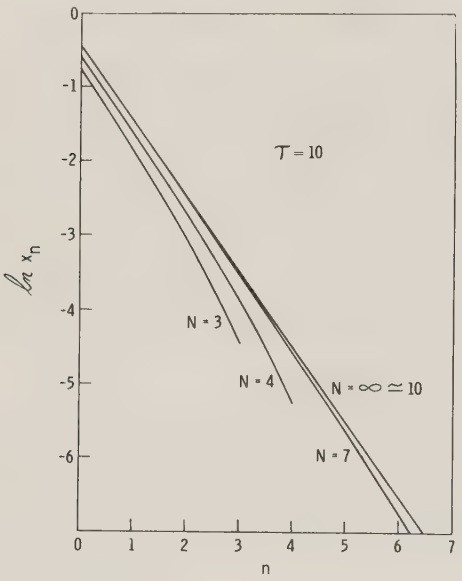

Figure 2. A plot of $\ln x_n$ versus n *at* $\tau = 10$ *for* $N = 3, 4, 7,$ *and* 10 *showing the deviation of the reactant distribution from the Boltzmann distribution at* $N = \infty$. *The vertical displacement relates to the loss of reactant molecules from the system by dissociation*

times τ ranging from $\tau = 1 \times 10^{-2}$ to 1×10^{3} and for values of $N = 0, 1, \ldots 10$. It should be recalled that $(N + 1)\theta = (N + 1)\, h\nu/kT = E_{act}/kT$. For the value of $\theta = 1$ used here the quantity $(N + 1)$ is a direct measure of E_{act}/kT.

Some of the results of these calculations are presented in *Figures 2–4*. *Figures 2* and *3* show graphs of $\ln x_n$ *versus* n at $\tau = 10$ and $\tau = 100$ for several values of N. If the reactant oscillators had remained in their 'initial' vibrational Boltzmann distribution (at the temperature T of the heat bath) during the dissociation reaction, *Figures 2* and *3* would have displayed a series of parallel straight lines. The slopes of these lines would have been equal to $-\theta(= -h\nu/kT)$ with a vertical displacement of the lines increasing with decreasing N from the 'base line' at $N = \infty$ (corresponding to no reaction) owing to the decreased concentration of reactant molecules after any given time τ at the

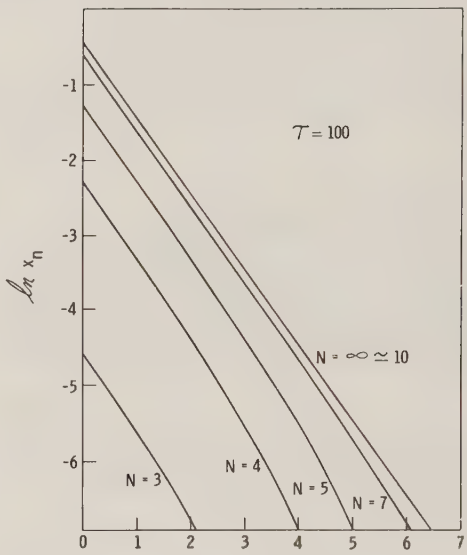

Figure 3. A plot of $\ln x_n$ versus n *at* $\tau = 100$ *for* $N = 3, 4, 5, 7,$ *and* 10 *showing the deviation of the reactant distribution from the Boltzmann distribution at* $N = \infty$. *The vertical displacement relates to the loss of reactant molecules from the system by dissociation*

lower dissociation energies $(N + 1)\theta$. The deviations shown in *Figures 2* and *3* from such a straight line relationship confirm that *the initial vibrational equilibrium Boltzmann distribution is perturbed by the chemical reaction.*

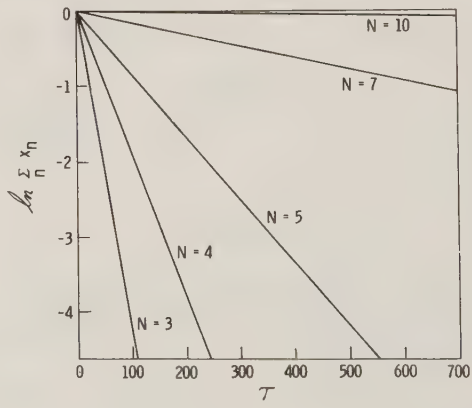

Figure 4. A plot of $\ln \sum_n x_n(\tau)$ versus τ *for several values of* N. *The slopes of these lines are proportional to the first order rate constants for the dissociation reaction*

The perturbation of the initial vibrational Boltzmann distribution increases with decreasing N, i.e. increases with lower values of E_{act}/kT. For $N = 10$, corresponding to $E_{act}/kT = 11$, the vibrational distribution of the reactant molecules remains

(within the accuracy of this calculation) a Boltzmann distribution with the temperature T of the heat bath. For $E_{act}/kT < 10$, i.e. for $N \leq 10$, the perturbation becomes noticeable. This is in good agreement with the results of the authors referred to above[3–7] on the influence of the magnitude of E_{act}/kT on the deviation of the calculated rate from the equilibrium rate. The perturbation of the initial equilibrium vibrational distribution by the chemical reaction manifests itself, as is seen from the shape of the lines, as a depletion below the equilibrium value of the oscillator population in the upper vibrational energy levels. For the model considered here then, the rate of re-supply of high energy molecules by inelastic collisions between the oscillators and the heat bath molecules is not sufficiently high to keep up with the irreversible dissociative loss of molecules from level N into 'level' $N + 1$. For a more detailed discussion of this aspect of the problem, reference may be made to Kramers' paper[3].

The actual extent of the deviation from equilibrium is quite small as can be seen from the small curvature of the lines in *Figures 2* and *3*. For the most extreme cases, i.e. for curves $N = 3$ and $N = 4$, the population of oscillators in vibration levels $n = 3$ and $n = 4$, respectively, has been reduced to only about 85 per cent of the equilibrium value at both $\tau = 10$ and $\tau = 100$. This percentage reduction is essentially constant for all times τ.

In *Figure 4* a plot of $\ln \sum_{n=0}^{N} x_n(\tau)$ *versus* τ has been presented for various values of N. For the set of bimolecular activation reactions followed by dissociation (reaction I), one would expect a rate law, under equilibrium conditions, of the form

$$[A]_t = [A]_0 e^{-kt} \tag{16}$$

which becomes, in the notation of this paper,

$$\sum_{n=0}^{N} x_n(\tau) = e^{-\lambda\tau} \tag{17}$$

with $\sum_{n=0}^{N} x_n(0) = 1$. If the initial equilibrium distribution is not perturbed by the reaction, one would then expect that a plot of $\ln \sum_{n=0}^{N} x_n(\tau)$ *versus* τ should give a straight line with slope equal to $-\lambda$.

In view of the very small perturbation of the equilibrium distribution found above, it is not surprising that *Figure 4* does indeed show such straight line relationships. The following analysis indicates the basis of this behaviour. According to equation 14, the quantity $\sum_{n=0}^{N} x_n(\tau)$ is given by an equation of the form

$$\sum_{n=0}^{N} x_n(\tau) = \sum_{n=0}^{N} \sum_{j=0}^{N} A_{jn} e^{-\mu_j \tau} \tag{18}$$

As has been discussed earlier $\mu_0 < \mu_1 < \mu_2 \ldots$ etc. If $\mu_0 \ll \mu_1$ corresponding to a process with very rapid vibrational equilibration, equation 18 can be rewritten as

$$\sum_{n=0}^{N} x_n(\tau) \simeq \sum_{n=0}^{N} A_{0n} e^{-\mu_0 \tau} \simeq e^{-\mu_0 \tau} \tag{19}$$

since $\sum_{n=0}^{N} A_{0n} = 1$ from the initial condition at $\tau = 0$. The slope of the lines in *Figure 4* should then be equal to $-\mu_0$ where μ_0 is the lowest root of the boundary condition 7b.

Table 1 shows a comparison between the slopes

TABLE 1

Comparison Between the Slopes and the Calculated Values of μ_0

N	*Slope* (*Figure 4*)	$\mu_0(704)$	$\mu_0(N \to \infty)$
3	$4{\cdot}18 \times 10^{-2}$	$4{\cdot}22 \times 10^{-2}$	$4{\cdot}63 \times 10^{-2}$
4	$1{\cdot}87 \times 10^{-2}$	$1{\cdot}90 \times 10^{-2}$	$2{\cdot}13 \times 10^{-2}$
5	$8{\cdot}33 \times 10^{-3}$	$8{\cdot}35 \times 10^{-3}$	$9{\cdot}40 \times 10^{-3}$
7	$1{\cdot}51 \times 10^{-3}$	$1{\cdot}54 \times 10^{-3}$	$1{\cdot}69 \times 10^{-3}$
10	$1{\cdot}08 \times 10^{-4}$	$1{\cdot}10 \times 10^{-4}$	$1{\cdot}16 \times 10^{-4}$

obtained from *Figure 4* and the values of μ_0 calculated by two different methods. The values of μ_0 obtained from the slope, which are shown in column 2, are based on the approximation that the slope can be equated to μ_0 owing to the inequality $\mu_0 \ll \mu_1 < \mu_2 \ldots$. The values of μ_0 shown in column 3 and labelled $\mu_0(704)$ are exact and were obtained on the IBM 704 computer as the roots of the boundary condition 7b. The values of μ_0 shown in the last column are the approximate solution for the lowest root of equation 7b as $N \to \infty$ and are given by[2]

$$\underset{(N \to \infty)}{\mu_0} \simeq (1 - e^{-\theta})(N + 1)e^{-(N+1)\theta} \tag{20}$$

It will be noted that the slopes of the lines of *Figure 4* are in excellent agreement with the exact roots μ_0. This shows that the approximation $\mu_0 \ll \mu_1 < \mu_2 \ldots$ is a valid one. It is further to be noted that the approximate roots μ_0 obtained in reference 2 for large N do not differ from the exact roots μ_0 by more than 10 per cent even for very small values of N such as $N = 3$. The results obtained for $N \to \infty$ pertain to equilibrium conditions since large values of N are equivalent to high values of E_{act}/kT and consequent low rates of reaction. The close agreement, even for low values of N, between the μ_0's obtained for $N \to \infty$ and the exact roots μ_0 is thus a further indication that the perturbation of the equilibrium distribution which develops during the reaction is quite small.

A final word is in order concerning the very small perturbation from equilibrium found in these and similar calculations by other workers[3–7]. In all of these studies, the model considered is one in which there are initially a large number of particles in the reaction system. By one mechanism or another, i.e. collisions, diffusion, or dissociation, a fraction of these particles is then allowed to leak out of the initial system of reactants. The rate with which this leakage is allowed to occur is always such that in a time interval characteristic of the leakage process, e.g. the time between collisions, only a very small fraction of the reactants are removed from the reactant pool. The studies, including this one, on the perturbation of initial distributions have, therefore, always been concerned with small leaks from a large reservoir rather than with the conditions one would find if one blew up the restraining dam which contained the reservoir. For models of this type it is not at all surprising, owing to the large inertia of the large pool of reactants, that the perturbation due to the small leak is very small. It should be emphasized that there is nothing special about the Maxwell-Boltzmann distribution, with which one is usually dealing, in its resistance to, or recovery from, a small perturbation. The same results would be obtained for any other initial distribution of reactant molecules. The small perturbation of the initial distribution is due to the high inertia of the usually large and densely populated initial system of reactants rather than to any special property of the initial distribution.

Most chemical reactions fall in the category of the large pool with the small leak. For these types of reactions, it can by now be considered as firmly established that the perturbation of the initial equilibrium distribution due to the chemical reaction is quite small and that the use of equilibrium theories of chemical kinetics is, therefore, justified. Still unanswered, however, is the question as to the nature and the extent of the departure from equilibrium of the initial distribution when the time scale for the transformation of reactants to products is comparable with the time scale for the relaxation of the initial distribution, i.e. when one is dealing with a torrent rather than a leak. This problem may become of importance as the study of reaction rates is pushed to higher and higher temperatures.

This work was supported by the U.S. Atomic Energy Commission.

The author wishes to acknowledge with thanks many helpful discussions with E. W. Montroll about various aspects of this problem. Particular thanks are due to Mr. William F. Cahill of the Computation Section, Applied Mathematics Division, National Bureau of Standards, who carried out with great skill the computations described in this paper on the IBM 704 computer at the National Bureau of Standards.

REFERENCES

[1] Shuler, K. E. *Fifth Symposium (International) on Combustion*, p. 56. 1955. New York; Reinhold
[2] Montroll, E. W. and Shuler, K. E. *Advances in Chemical Physics*, Vol. 1. 1958. New York; Interscience
[3] Kramers, H. A. *Physica* 7 (1940) 284
[4] Zwolinsky, B. J. and Eyring, H. *J. Amer. chem. Soc.* 69 (1947) 2702
[5] Curtiss, C. F. *University of Wisconsin, Naval Research Laboratory, CM-476*, June 8, 1948
[6] Prigogine, I. and Xhrouet, E. *Physica* 15 (1949) 913
[7] — and Mahieu, M. *Physica* 16 (1950) 51
[8] Montroll, E. W. and Shuler, K. E. *J. chem. Phys.* 26 (1957) 454
[9] Landau, L. and Teller, E. *Phys. Z. Sowjet.* 10 (1956) 34
[10] A critical discussion of the derivation and validity of transport equations such as equation 4 (the Master Equation) has been given recently by Van Hove, L. *Physica* 21 (1955) 517; 23 (1957) 441
[11] Gottlieb, M. J. *Amer. J. Math.* 60 (1938) 455
[12] Logan, G. J. *J. Aero. Sci., Preprint No.* 728 (January, 1957)
[13] Glick, H. S. and Wurster, W. H. *J. chem. Phys.* 27 (1957) 1224

16

ON THE ANALYSIS OF RE-COMBINATION REACTIONS IN AN EXPANDING GAS STREAM

F. T. SMITH

INTRODUCTION

The expanding gases leaving the combustion chamber of a reaction motor often contain atomic, radical, or ionic species in a mobile equilibrium of the type $A + B \rightleftarrows C$. In the course of the expansion, the pressure and temperature fall, and the equilibrium shifts, generally in the direction of re-combination. If the reaction rate is fast enough, the concentrations of A, B, and C tend to follow the shifting equilibrium, with a lag which is small if the rate constants and the concentrations of A and B are large enough. Shifting equilibrium, and the near-equilibrium case where the lag is small, can be handled by known analytical methods[1,2]. Another extreme case, where the rates are so slow that the reaction is completely or almost frozen, can also be treated by a simple theory[1], as can the case where the reaction is essentially irreversible (because the reverse rate is insignificant). There is, however, a domain of transitional behaviour, where shifting equilibrium no longer applies and simple irreversible re-combination has not yet been attained, where these simple approximations do not apply. The region of temperature and pressure in which this transition occurs depends upon the concentrations, the reaction rate constants, and the rate of expansion. Knowledge of the behaviour of this transition as a function of the various parameters would be of considerable utility for the prediction and correlation of experimental results.

The effect of the transition from shifting equilibrium has been examined by a numerical integration in the case of hydrogen expanding through a deLaval nozzle, assuming a three-body re-combination process, $H + H + M \rightleftarrows H_2 \rightleftarrows M$, with a temperature-independent re-combination rate constant[3], $k_f = 10^{16}$ cm^3 mol^{-2} sec^{-1}. The results of an approximate treatment, using several re-combination rates, are given by Wilde[4]. In both these investigations, attention was focused on the effect of the reaction rates on the thrust of a rocket motor. Deviations from chemical equilibrium could also be studied by observation of the concentration of various species in the exhaust gases—the concentration of electrons in a rocket exhaust has recently been studied in this way[5]. The possibility of further studies of this type has motivated the present investigation on the theory of the transition from shifting equilibrium to slow re-combination in a conical nozzle.

While the situation is potentially complex, the number of independent parameters turns out to be small if attention is confined to the three-body collision mechanism appropriate for re-combination in the high-pressure region, and if the concentrations are such that the chemical reaction does not greatly affect the flow. A case which fits these restrictions is the ionization of an impurity in the gas. If we assume that $x_A = x_B \ll 1$ and x_c are mole fractions, it will be shown that over a wide range of parameters it is possible to express x_A in the downstream region of the nozzle in terms of $x_0 = x_A + x_C$ by an approximation of the form

$$\ln x_A = \alpha \ln x_0 + b \tag{1}$$

where a and b depend on the rate constants, the dissociation energy, and the rate of expansion.

THEORETICAL ANALYSIS

Formulation of the problem

It is convenient to use as a variable the degree of dissociation (or ionization), β, defined in terms of the concentrations [A], [B], and [C] by

$$n_0 \equiv [A] + [C], \quad \beta \equiv [A]/n_0, \quad \delta \equiv ([B] - [A])/n_0 \tag{2}$$

with $x_0 \equiv n_0 kT/p$ a mole fraction. δ is a constant, often equal to 0. The equilibrium value of β, β_e, is given as a function of temperature and pressure by

$$\frac{\beta_e(\beta_e + \delta)}{1 - \beta_e} = \frac{F_A(T)F_B(T)}{n_0 F_c(T)} \, e^{D/kT} \cdot \frac{K_c(T)}{n_0} \tag{3}$$

where the F's are partition functions per unit volume, D is the dissociation or ionization energy, and it is assumed that an ideal gas approximation is adequate. In the case of ionization, $F_A/F_C = F(C^+)/F(C)$ is equal to the ratio of the ground-state electronic multiplicities, to a close approximation, and $F_B = F(e^-) = 2(2\pi m_e kT/h^2)^{3/2} = 4{\cdot}83 \times 10^{15} T^{3/2}$. Unless there are other ionizing species charge balance requires δ to be 0 in this case.

The rate coefficient, α, for the re-combination reaction can be defined by

$$\left(\frac{\partial[\mathrm{A}]}{\partial t}\right)_{\text{re-combination}} = -\alpha[\mathrm{A}][\mathrm{B}] \qquad (4)$$

The dissociation rate is then

$$\left(\frac{\partial[\mathrm{A}]}{\partial t}\right)_{\text{dissociation}} = \alpha K_c[\mathrm{C}] \qquad (5)$$

The rate equation is more conveniently set in terms of β, which is independent of density changes in the gas flow except as it responds through chemical reaction,

$$\frac{\mathrm{d}\beta}{\mathrm{d}t} = -\alpha n_0\left[\beta(\beta + \delta) - (1 - \beta)\frac{K_c(T)}{n_0}\right] \qquad (6)$$

The coefficient α will vary with T and p, in general (and perhaps with composition), and T and p will in turn be known functions of the time t. We shall assume that the re-combination process does not involve an energy of activation, but it may require a three-body collision and thus depend on the density as well as on some small power of the temperature. For electron-ion re-combination at fairly low pressures, where the Thomson process prevails[6], we have

$$\alpha = \alpha_i\left(\frac{\rho}{\rho_i}\right)\left(\frac{T}{T_i}\right)^{3/2} \qquad (7)$$

where the index i refers to some standard state—we shall take it to refer to conditions in the combustion chamber before expansion.

In order to complete the formulation of the problem it is necessary to introduce in equation 6 the explicit functional dependence of T, n_0, and α on the time. n_0 as well as α depends on the density,

$$n_0 = n_i\frac{\rho}{\rho_i}, \qquad n_i = \frac{x_0 p_i}{kT_i} \qquad (8)$$

We shall assume that the approximation of one-dimensional flow with constant γ is adequate; then,

$$\frac{\rho}{\rho_i} = \left(\frac{T}{T_i}\right)^{1/\gamma - 1} \qquad (9)$$

The relationship between these quantities and the time depends on the shape of the nozzle. For a simple conical nozzle, with throat diameter r_0 and half-angle Φ, it is useful to introduce a reduced time τ by the equation

$$t = \frac{r_0}{a_i \tan\Phi}\tau = g\tau \qquad (10)$$

where a_i is the sound velocity in the combustion chamber,

$$a_i = \left(\frac{\gamma_i R T_i}{M_i}\right)^{1/2} \qquad (11)$$

and M_i is the average molecular weight. If v is the local flow velocity and $A/A^\star$ is the area ratio, the reduced time can be calculated by numerical integration from

$$\tau = \int\frac{a_i}{v}\,\mathrm{d}\left(\frac{A}{A^\star}\right)^{1/2*} \qquad (12)$$

τ can be tabulated as a function of the Mach number, from which we can find $T_i/T = f(\tau)$; for $\gamma = 1{\cdot}28$ the result is plotted in *Figure 1.*

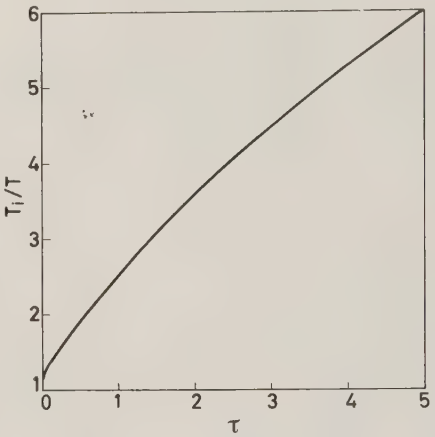

Figure 1. The relation between temperature and reduced time, τ: $T_i/T = f(\tau)$, for a conical nozzle with $\gamma = 1{\cdot}28$

A useful approximation over a region not too close to the throat is

$$\frac{T_i}{T} = f(\tau) \cong 1{\cdot}5 + \tau \qquad (13)$$

It is now possible to express the differential equation 6 using τ and $f(\tau)$. The equilibrium constant becomes

$$K_c(T) = K_c(T_i)\mathrm{e}^{D/kt_i}\,.f^{-m}(\tau)\mathrm{e}^{-Df(\tau)/kT_i} \qquad (14)$$

(for ionization, $m = 3/2$). With the definitions,

$$w = \frac{D}{kT_i}, \quad A_i = \alpha_i n_i g, \quad B_i = \alpha_i g K_c(T_i)\mathrm{e}^{D/kT} \qquad (15)$$

equation 6 becomes

$$\frac{\mathrm{d}\beta}{\mathrm{d}\tau} = -A_i f^{-p}(\tau)\beta(\beta + \delta) + B_i f^{-q}(\tau)\mathrm{e}^{-wf(\tau)}(1 - \beta) \qquad (16)$$

where $p - q = -m + [1/(\gamma - 1)]$.

For ionization with Thomson re-combination, $p = 2/(\gamma - 1) - 3/2$ and $q = 1/(\gamma - 1)$.

The analytical problem is now to solve equation 16, subject to a suitable initial condition. Since the gases have resided at the high temperature and pressure of the combustion zone for a comparatively long time, they have essentially reached

* See Appendix.

equilibrium under these conditions, so that the initial condition is

$$\frac{\beta(0)[\beta(0) + \delta]}{1 - \beta(0)} = \frac{B_i}{A_i} e^{-D/kT_i} \qquad (17)$$

For specific values of the parameters, the solution of equations 16 and 17 may be obtained by numerical integration, but the general behaviour of the solution as the parameters are varied can be better understood through examining some analytical approximations. These will now be considered. To simplify the discussion, δ will be assumed to vanish.

An approximate solution

Two limiting cases of equation 16 or 6 are well-known approximations: shifting equilibrium and pure re-combination. The case of shifting equilibrium applies when the rate of re-combination is fast enough that the degree of dissociation follows closely the equilibrium value that would be applicable at the local conditions of temperature and pressure. In this case (neglecting δ),

$$\beta \approx \beta_e(\tau), \quad \text{where} \quad \frac{\beta_e^2}{1 - \beta_e} = \frac{B_i}{A_i} f^{p-q}(\tau) e^{-wf(\tau)} \qquad (18)$$

A sufficient condition for the validity of this approximation is that the rate of change of β by re-combination be large compared to the rate of change of the equilibrium value itself:

$$\frac{\partial \beta}{\partial t} = -A_i f^{-p}(\tau)\beta_e^2(\tau) \gg \frac{d\beta_e}{d\tau} \qquad (19)$$

As τ increases, the exponential decline of the equilibrium constant causes greater and greater deviation between the true degree of dissociation and the equilibrium value. Ultimately, the re-combination term in equation 16 completely dominates the dissociation term, and the equation takes the asymptotic form

$$\frac{d\beta}{d\tau} \sim -A_i f^{-p}(\tau)\beta^2 \qquad (20)$$

This can be integrated to

$$\frac{1}{\beta_\sim} = \frac{1}{\beta_\sim(\tau^\star)} + A_i \int_{\tau^\star}^{\tau} f^{-p}(\sigma)\, d\sigma$$

$$= \frac{1}{\beta_\sim(\tau^\star)} + A_i[F(\tau) - F(\tau^\star)] \qquad (21)$$

Equations 20 and 21 represent the case of pure re-combination.

An approximation, $\beta_1(\tau)$, to the solution of equation 16 can be made by joining the functions of equations 18 and 21, using the conditions

$$\beta_1(\tau) = \beta(\tau) \quad \text{for} \quad \tau < \tau^\star$$
$$\beta_1(\tau) = \beta_\sim(\tau) \quad \text{for} \quad \tau > \tau^\star$$
$$\beta_\sim(\tau^\star) = \beta_e(\tau^\star) \qquad (22)$$

The junction point, $\tau^\star$, is appropriately chosen to be where the rate of change of β_e is equal to the re-combination rate,

$$\left(\frac{d\beta_1}{d\tau}\right)_{\tau^\star} = -A_i f^{-p}(\tau^\star)\beta_e^2(\tau^\star) = \left(\frac{d\beta_e}{d\tau}\right)_{\tau^\star}$$

$$= \beta_e(\tau^\star)\frac{1 - \beta_e(\tau^\star)}{2 - \beta_e(\tau^\star)}\left[\frac{p - q}{f(\tau^\star)} - w\right]\left(\frac{df}{d\tau}\right)_{\tau^\star} \qquad (23)$$

If $\beta_e(\tau^\star) \ll 1$, as will usually be the case, $\tau^\star$ is a root of the equation:

$$wf(\tau^\star) + (p + q)\ln f(\tau^\star) + 2\ln\left(\frac{df}{d\tau}\right)_{\tau^\star}$$

$$+ 2\ln\left[\frac{w}{2} - \frac{p - q}{2f(\tau^\star)}\right] - \ln(A_iB_i) = 0 \qquad (24)$$

Thus, for fixed p, q, and w, $\tau^\star$ will be a smoothly varying function of $\ln(A_iB_i)$. Furthermore, the value of β_1 at some large value of τ, say τ_f, depends on $\tau^\star$ (see equation 21), and thus on $\ln(A_iB_i)$.

Actually it can be shown that the approximation $\beta_1(\tau)$ lies everywhere below the true solution $\beta(\tau)$, and at different distances for different values of the parameters. Nevertheless it is to be expected that the exact solution will retain the qualitative form of the dependence of β_1 (at large τ) on $\ln(A_iB_i)$. The situation can be more thoroughly examined in a special case in which an exact analytical solution is available.

Analytical solution in a special case

We now consider a special case of equation 16 in which we can find an analytical solution. We shall assume $\delta = p = q = 0$, and $B_i/A_i \ll 1$ so that $\beta \ll 1$ everywhere. In addition, we take f as a linear function of τ, $f(\tau) = R + S\tau$. The equation 16 then is

$$\frac{d\beta_2}{d\tau} = -A_iB_2^2 + B_i e^{-wR_e - wS\tau} \qquad (26)$$

with the initial condition,

$$\beta_2^2(0) = \frac{B_i}{A_i} e^{-w} \qquad (27)$$

To solve equation 26, we first change variables, putting

$$y \equiv \frac{A_i}{wS}\beta_2, \quad r \equiv wS\tau, \quad \lambda^2 \equiv \frac{A_iB_i}{(wS)^2} e^{-wR} \qquad (28)$$

Then,

$$\frac{dy}{dr} = -y^2 + \lambda^2 e^{-r}, \quad y^2(0) = \lambda^2 e^{w(R-1)} = \lambda^2\varepsilon^2 \qquad (29)$$

With the further change of variable $u = 2\lambda e^{-r/2}$, equation 29 becomes a Riccati equation, soluble

in terms of Bessel functions[7,8]. The solution is

$$y = \frac{u}{2}\frac{Kh_1(u) - \psi I_1(u)}{Kh_0(u) + \psi I_0(u)} \qquad (30)$$

where ψ depends upon the initial condition:

$$\psi = \frac{Kh_1(2\lambda) - \varepsilon Kh_0(2\lambda)}{I_1(2\lambda) + \varepsilon I_0(2\lambda)} \qquad (31)$$

ψ depends on λ, but it is negligibly small if λ is large enough—i.e., if the initial reaction rate is fast.

The behaviour of y (or β) as a function of τ can be found readily from equations 30 and 31, using tabulated values of the Bessel functions or their expansions; a numerical solution of equation 29 has also been tabulated[9]. At large values of τ, u is small, and an expansion of equation 30 gives

$$\frac{1}{y} = \frac{wS}{A_i\beta_2} = \pi\psi + 0{\cdot}846 + r - \ln(\lambda^2) + \lambda^2 e^{-r}(\ldots) + \ldots = a + r - \ln(A_iB_i)\ldots \qquad (33)$$

This substantiates the expectation of a smooth relationship between (e) $= n_0\beta$ and $\ln(A_iB_i)$, which varies as $\ln x_0$ when other conditions (α_i, T_i, w) are constant. Numerical analysis of a more realistic case of equation 16 confirms this conclusion.

The case of ionization: a numerical treatment

In order to find the effect of a more realistic variation of the coefficients of equation 16 with τ than is given in the artificial case just considered, it is necessary to integrate equation 16 numerically. This we have done for the case of ionization with Thomson re-combination, where we have used $\gamma = 1{\cdot}28$, so that $p = 5{\cdot}64$ and $q = 3{\cdot}57$. We have used $w = 16{\cdot}1$, which corresponds to ionization of potassium at about 3,130°K, or sodium at about 3,700°K. For a number of values of A_i and B_i, integral curves have been obtained. (Integration was by machine computation, using Euler's method with one corrector[10], with a varying interval.) Representative curves are plotted in *Figure 2*. These curves show that the change in β is negligibly slow for $\tau > 2$ in all the cases considered—i.e., the degree of ionization is essentially frozen at some point in the expansion.

The analogy with equation 33 suggests that for large values of τ_f, $A_i\beta(\tau_f) = \alpha_i g n_i \beta(\tau_f)$ should depend primarily on $A_iB_i = \alpha_i^2 g^2 n_i K_c(T_i)e^w$. This is tested, for $\tau_f = 6{\cdot}5$, in Table 1, which shows that

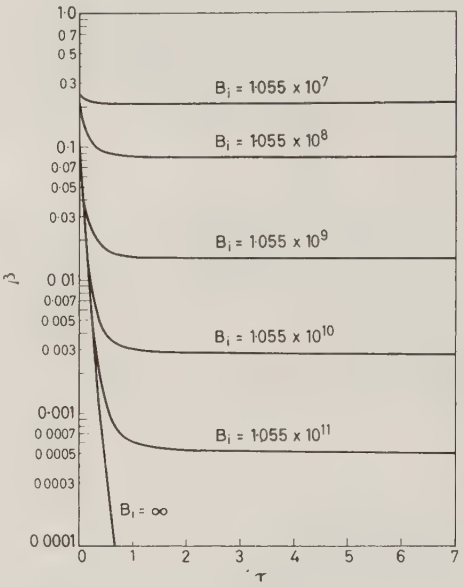

Figure 2. Representative integral curves. The degree of ionization, β as a function of reduced time, τ, for $A_i/B_i = 1{\cdot}185 \times 10^{-6}$ and various values of B_i

the expectation is confirmed, except at small values of $A_i = \alpha_i g n_i$. A log-log plot, *Figure 3*, of $A_i\beta(\tau_f)$ *versus* A_iB_i for various values of B_i, shows curves with a common envelope which can be represented quite well by

$$\log[A_i\beta(\tau_f)] = 0{\cdot}129 \log(A_iB_i) - 0{\cdot}262 \qquad (34)$$

if $A_i > 10^3$. Thus for a wide range of parameters, equation 34 provides a simple description of the behaviour of the system. For cases with different values of $w = D/KT_i$, a similar relation would be expected with other values of the numerical constants.

TABLE 1

$A_i\beta(\tau_f)$ as a Function of A_iB_i and B_i

B_i	A_iB_i									
	$1{\cdot}32 \times 10^8$	$1{\cdot}32 \times 10^9$	$1{\cdot}32 \times 10^{10}$	$1{\cdot}32 \times 10^{11}$	$1{\cdot}32 \times 10^{12}$	$1{\cdot}32 \times 10^{13}$	$1{\cdot}32 \times 10^{14}$	$4{\cdot}05 \times 10^{14}$	$1{\cdot}32 \times 10^{15}$	$1{\cdot}32 \times 10^{16}$
$1{\cdot}055 \times 10^7$	2·62	6·41	10·8	14·1						
$1{\cdot}055 \times 10^8$		4·98	10·4	14·0	18·1	25·1				
$1{\cdot}055 \times 10^9$			6·54	13·2	18·0	25·0	34·5		46·9	
$3{\cdot}37 \times 10^9$								40·2		
$1{\cdot}055 \times 10^{10}$				7·24	16·7	24·8	34·5		46·9	62·6
$1{\cdot}055 \times 10^{11}$						22·4	34·1		46·8	62·6
$1{\cdot}055 \times 10^{12}$									46·0	62·4

A plot such as *Figure 3* can be used as a nomogram to determine the effective re-combination rate constant if data are available on the variation of the degree of dissociation in the expanded gas as a function of the initial concentration of the dissociating species, provided other conditions do not

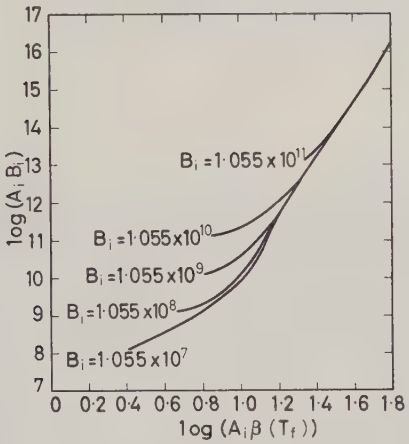

Figure 3. The dependence of the ionization at large τ, $A_i\beta(\tau_f)$, *on the combined parameter* A_iB_i. *Curves for various values of* B_i, *with a common envelope*

vary. The curves of *Figure 3* can be represented in general by the equation

$$\log [A_i\beta(\tau_f)] = G(\log (A_iB_i)) + H(A_i,B_i) \quad (35)$$

where $H(A_iB_i) \to 0$ for large enough A_i. From the experimental data, it is possible to plot

$$\log \frac{A_i}{B_i} = \log \left(\frac{n_i}{K_c(T_i)e^w} \right)$$

versus

$$\log Z = \log \left(\frac{n_i\beta(\tau_f)}{K_c(T_i)e^w} \right)$$

Since

$$\log [A_i\beta(\tau_f)] = \log Z + \log B_i$$
$$= G(\log A_iB_i) + H(A_i, B_i)$$
$$= G\left(\log \frac{A_i}{B_i} + 2 \log B_i\right) + H(A_i,B_i) \quad (36)$$

a shift of the experimental data along the line $\log Z = 2 \log (A_iB_i) + \text{const}$ until the points are brought into juxtaposition with one of the calculated curves gives a good means of measuring $\log B_i$ and thus α_i.

APPENDIX

For a nozzle of arbitrary shape, the axial distance downstream from the throat, z, is related to the corresponding radius, r, by

$$z = r_0 h \frac{r}{r_0} \quad (A1)$$

For a conical nozzle,

$$h \frac{r}{r_0} = \cot \Phi \left(\frac{r}{r_0} - 1 \right) \quad (A2)$$

If $A/A^\star$ is the area ratio,

$$\frac{r}{r_0} = \left(\frac{A}{A^\star} \right)^{1/2} \quad (A3)$$

If time is measured from passage of an element of the gas past the throat, and the local flow velocity is v, t can be obtained by integration of

$$\mathrm{d}t = \frac{\mathrm{d}z}{v} = r_0 \frac{\mathrm{d}h(r/r_0)}{v} = \frac{r_0}{a_i} \frac{\mathrm{d}h}{v/a_i} \quad (A4)$$

For a conical nozzle, then,

$$t = \frac{r_0}{a_i \tan \Phi} \int \frac{a_i}{v} \mathrm{d} \left(\frac{A}{A^\star} \right)^{1/2} \quad (A5)$$

The integral, $\tau = \int (a_i/v)\, \mathrm{d}(A/A^\star)^{1/2}$, is a function only of the Mach number, M, and γ, because

$$\frac{v}{a_i} = M \left[1 + (\gamma - 1) \frac{M^2}{2} \right]^{-1/2}$$

and

$$\frac{A}{A^\star} = \frac{1}{M} \left[\frac{2 + (\gamma - 1)M^2}{\gamma + 1} \right]^{(\gamma+1)/2(\gamma-1)} \quad (A6)$$

The lower limit of integration is $M = 1$, corresponding to conditions at the throat.

Assuming a particular value of γ, $\tau = \tau(M)$ is obtained by numerical integration. Since

$$\frac{T_i}{T} = 1 + \frac{\gamma - 1}{2} M^2 \quad (A7)$$

we can find the functional dependence $T_i/T = f(\tau)$, which is shown in *Figure 1* for $\gamma = 1{\cdot}28$.

This work was performed under contract with the U.S. Air Force, Air Research and Development Command.

REFERENCES

[1] Penner, S. S. *Chemical Reactions in Flow Systems*, 1955. London; Butterworths

[2] Wegener, P. P. *Bull. Amer. phys. Soc.* II 1 (1956) 362

[3] Krieger, F. J. *J. Amer. Rocket Soc.* 21 (1951) 179

[4] Wilde, K. A. *Jet Propulsion* 28 (1958) 119

[5] Dauguet, A. *Ann. Telecomm.* 12 (1957) 243

[6] Massey, H. S. W. and Burhop, E. H. S. *Electronic and Ionic Impact Phenomena*. 1952. Oxford

[7] Watson, G. H. *A Treatise on the Theory of Bessel Functions*, p. 90. 1922. Cambridge Univ. Press

[8] Jeffreys H. and Jeffreys, B. N. *Methods of Math. Physics*. 1950. Cambridge Univ. Press

[9] Rothstein, J. *J. chem. Phys.* 28 (1958) 153

[10] Scarborough, J. B. *Numerical Mathematical Analysis*. 1950. Johns Hopkins Press

17

SHOCK TUBE STUDIES OF REACTION KINETICS OF ALIPHATIC HYDROCARBONS

H. S. GLICK

INTRODUCTION

The pyrolysis of aliphatic hydrocarbons has been extensively studied and a large literature, too bulky to be discussed here, has accumulated. It is well known, for instance, that the nature and distribution of the reaction products is influenced by the length of time the hydrocarbon is allowed to remain at high temperature. Thus, for long reaction times, solid carbon and CO (if oxygen-bearing components are present in the original mixture) are the principal carbon-bearing products while C_2H_2 and C_2H_4 appear in large concentrations, if the reaction is immediately quenched.

Kinetic properties of the decomposition of aliphatic hydrocarbons at very short reaction times (0·25 to 4 milliseconds) have been recently studied at Cornell Aeronautical Laboratory, and are reported in the present paper. The experiments, which covered a temperature range varying from 1,000 to 3,500°K, were designed: (1) to determine the identity and distribution of the intermediate products of the decomposition as a function of temperature, pressure, and reaction time; (2) to correlate the product distributions with estimates based on equilibrium calculations in which the species assumed were those found experimentally; and (3) to determine the kinetics of the various steps.

Since the transformation of aliphatics into C_2H_2 and C_2H_4 requires high reaction temperatures and short reaction times, the single-pulse shock tube, which had been developed several years ago at C.A.L., appeared to be a useful tool for the proposed investigation. This shock tube technique[1,2] had previously been employed in the study of the kinetics of reaction: $N_2 + O_2 \rightleftharpoons 2NO$ between 2,000–3,000°K. The experimental techniques developed during that study were believed to be sufficiently advanced so that the more complex kinetics of aliphatic hydrocarbon decomposition might also be studied with this shock tube method. However, several problems arose that were not present in the nitric oxide study, and their solutions are discussed in later sections.

In the present studies, reactant gas mixtures were processed by a single, high-temperature pulse of controlled amplitude, shape, and duration. To do this, a shock wave was formed ahead of a 'piston' of high pressure 'driver' gas suddenly released by the breaking of the diaphragm adjoining the reactant section of the tube (*Figure 1*). This shock, upon being reflected at the closed end of this section, brings the reactant gas to rest at a temperature and pressure which can be calculated from the measured initial shock speed. Meanwhile, at a controlled time after the shock has been initiated, the diaphragm adjoining the evacuated tank (*Figure 1*) is shattered, so that the bulk of the driver gas flows back into the tank. This flow generates a non-steady expansion wave which quenches the reacting gases. The 'debris' formed during the high-temperature pulse is then withdrawn through a sample port at the reflecting end of the tube and analysed by gas chromatography.

EXPERIMENTAL TECHNIQUES

The experimental methods employed in the present work were largely those developed previously and described in references 1 and 2. Several modifications were necessary, however, due to the large number of chemical species in the product gas and the highly endothermic nature of the reactions.

Vapour phase gas chromatography was used for almost all the analyses, although a mass spectrometer was employed when a more detailed analysis was desired.

Obtaining an uncontaminated gas sample was a problem of special importance in our shock tube work because during the time the reactant gas is at high temperature it is in contact on one bounding surface with the cold driver gas, and even during the few milliseconds that this occurs appreciable mixing takes place. The temperature history of the reactant gas in the region affected by mixing differs from that in the rest of the reactant gas, and the distribution of chemical species is, therefore, generally far different. The amount of contamination was determined by measuring the concentration in the sample of an inert tracer gas—usually neon—which had been added to the reactant mixture before the experiment. It was found that contamination in excess of 20 per cent by driver gas

made the analysis of the breakdown products inaccurate.

If the initial pressure ratio between driver and reactant sections (*Figure 1*) is adjusted to insure that the mixed gas, or interface, region is finally swept into the large damping tank by the wave processes, almost no driver gas will be found in the gas sample. If, on the other hand, the final position of the interface is allowed to move toward the other end of the shock tube, the driver gas concentration increases, and can easily become of the order of 95 per cent of the sample. Experience shows that the primary parameters which

Another problem associated with the decomposition of aliphatic hydrocarbons is the heat of formation of the reaction products. The shock waves process the reactant gas to an initial temperature, pressure, and enthalpy[3,4], and the reaction then proceeds essentially at constant total enthalpy and pressure. Due to the energy changes associated with the chemical reactions, the temperature will change, and often drastically. For example, if methane is heated to 3,500°K, and if 50 per cent of the CH_4 is converted to C_2H_2, the temperature drop is about 1,500°K! Such large temperature changes make kinetic analyses very

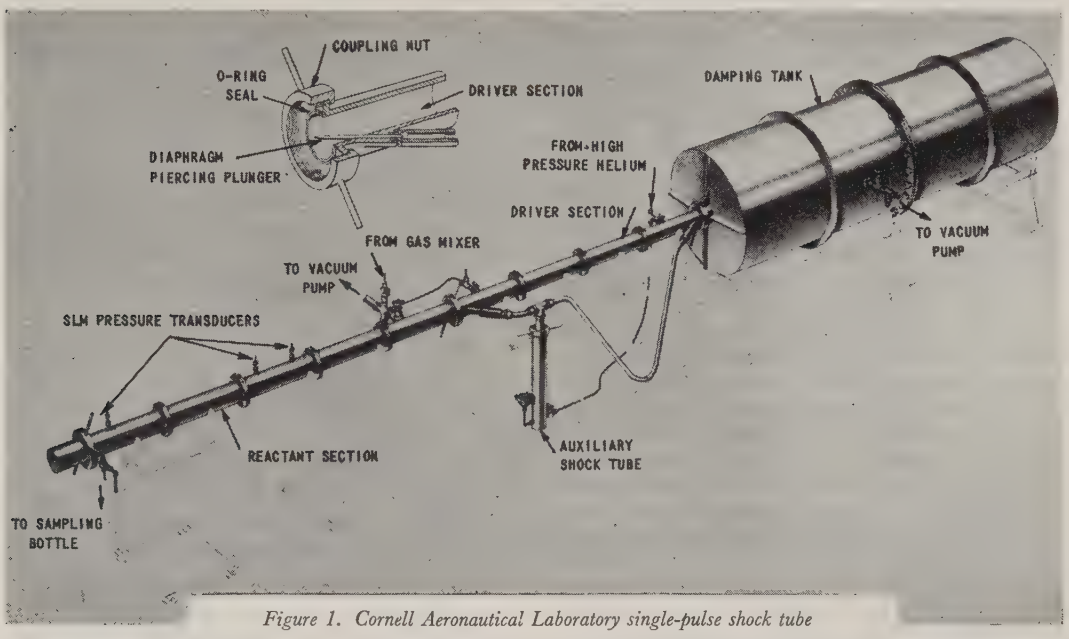

Figure 1. Cornell Aeronautical Laboratory single-pulse shock tube

govern the mixing process are the pressure ratio across the main shock tube diaphragm, the ratio of damping tank volume to driver section volume, the specific heat of the reactant gas mixture, and the entropy increase produced in the reactant gas by the shock waves. It was found that by keeping the diaphragm pressure ratios below 100, good samples were achieved in the present experiments. By restricting the pressure ratio to values below 100, high reaction temperatures could be obtained only by increasing the dilution of the reactant gas or by increasing the initial speed of sound of the driver gas. Increasing the dilution of the reactant gas tends to reduce the accuracy of the chemical analyses, and increasing the initial driver gas speed of sound, for a given shock tube geometry, restricts the range of reaction times. However, by varying these parameters properly, it has been possible in the present experiments to cover a large range of temperature, dilution, and reaction time, while obtaining good samples.

difficult. In order to prevent such temperature variations, the reactant gas contained large amounts of noble gases (A, He, Kr, Ne, Xe). Noble gases were used because they are chemically inert, easily heated to high temperatures by shock waves[5], and have desirable properties from a boundary layer viewpoint[6].

Instrumentation, sampling, and analytical techniques

The shock tube used in the present experiments was very similar to that employed in the nitric oxide study[2]. However, the driver and low pressure sections were equipped with heating elements which permitted initial reactant gas temperatures up to 100°C. A heated stainless steel gas mixing tank with a volume of about 30 litres was fabricated, and was used primarily to pre-mix samples for experiments in which water vapour was a reactant gas constituent.

In most of the experiments, two gas samples were taken and analysed. The samples were obtained

by first evacuating two 300 c.c. glass sampling bottles, arranged in series. Immediately after the wave processes were completed, a valve connecting the shock tube with the sampling bottles was opened, and the reacted gas products flowed into the sampling bottles. The gas samples were then analysed by two vapour fractometers. These chromatographs were used with Brown recorders which had one millivolt full-scale sensitivities and one second pen speeds. Hydrogen was generally employed as the carrier gas. The chromatographs were calibrated every day with known gas mixtures that contained component concentrations in the range of those expected in the experiments. Standards were prepared by the partial pressure method using a 0–100 lb./in.^{2} absolute pressure gauge, whose scale could be read to 0·01 lb./in.^{2} It is estimated that the errors in the measured concentrations of the major components of the gas sample were less than 2 per cent.

In order to accurately measure the chemical changes that occurred in the experiments, a small amount of tracer gas, generally helium or neon, was added to the reactant gas. Carbon balances, based on the tracer gas, generally accounted for over 90 per cent of the carbon, especially in the ethane studies, and thereby indicated that no gross errors were being made in the chemical analyses, and that no important constituent was being overlooked. Mass spectrometer analyses, which were performed from time to time, showed that in addition to the major components found in the gas chromatographic analyses, small amounts of allene, benzene, methyl acetylene, diacetylene, etc., were also produced.

The electronic instrumentation was similar to that described in reference 2. Shock velocity records were taken using a camera-equipped oscilloscope. The oscilloscope was operated with a raster sweep, and the estimated error in shock velocity is $\pm$ 0·2 per cent. The pressure of the reacting gas mixture was monitored by a high frequency pressure transducer, which served both to give the time history of the enthalpy and pressure of the reactant gas and to provide a cross-check on the velocity measured by the shock velocity pickups. The output of the pressure transducer was also recorded on an oscilloscope.

METHANE STUDIES

Methane pyrolysis experiments

The first aliphatic hydrocarbon studied was methane. Pyrolysis experiments using 1:1:8 CH_4–He–A mixtures showed that CH_4 starts to decompose at temperatures of about 1,400°K for reaction times of the order of milliseconds (*Figure 2*). As the temperature was increased, appreciable quantities of C_2H_2 and C_2H_4 were formed. At an initial reaction temperature of 2,500°K, for example, over 90 per cent of the CH_4 was decomposed, with about 45 per cent forming C_2H_2 and C_2H_4, and the other 45 per cent appearing as solid carbon, which was found as a dense coating on the inside walls of the shock tube. The data were quite reproducible and the specific reaction rate constants for the decomposition of CH_4 were calculated from the experimental data assuming a first order reaction. The

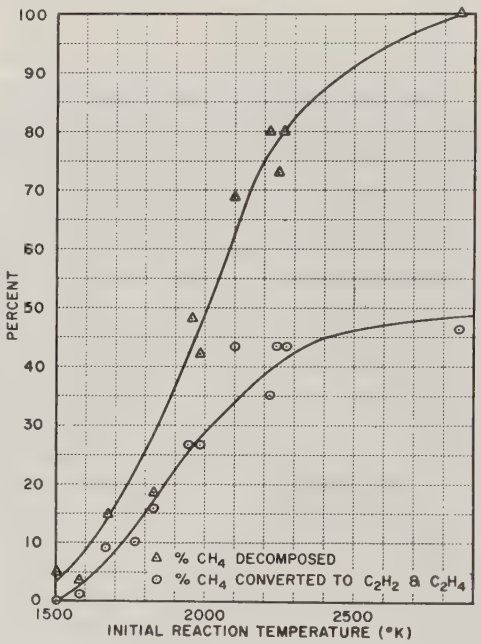

Figure 2. Per cent methane decomposed and per cent methane converted into C_2H_2 *and* C_2H_4 *for* 1:1:8 CH_4–He–A *mixtures as a function of initial reaction temperature for reaction times of the order of a millisecond*

kinetic data is given in *Figure 3*, together with the lower temperature data published by Kassel[7] and Rudder and de Biedermann. The data, as monitored by the pressure transducer, were obtained at constant enthalpy and pressure. Although the reactant gas was diluted with large amounts of argon and helium, the temperature drops due to changes in chemical species were appreciable when the degree of CH_4 decomposition was large. For example, if the reactant mixture had an initial reaction temperature of 2,200°K and had a final product distribution of 25 per cent unreacted CH_4, 35 per cent solid carbon, 20 per cent C_2H_2, and 20 per cent C_2H_4, the final temperature was about 1,800°K. In view of the non-isothermal nature of the experiments in which the CH_4 was strongly decomposed, the agreement of the present kinetic data with that of Kassel and Rudder and de Biedermann is remarkably good. However,

at temperatures below 1,900°K where the decomposition of CH_4 is less than 35 per cent, the temperature drop due to the chemical reactions is less than 150°K, and isothermal reaction conditions are approached.

Methane–water vapour–argon experiments

A series of experiments employing CH_4–H_2O–A mixtures was carried out to determine the

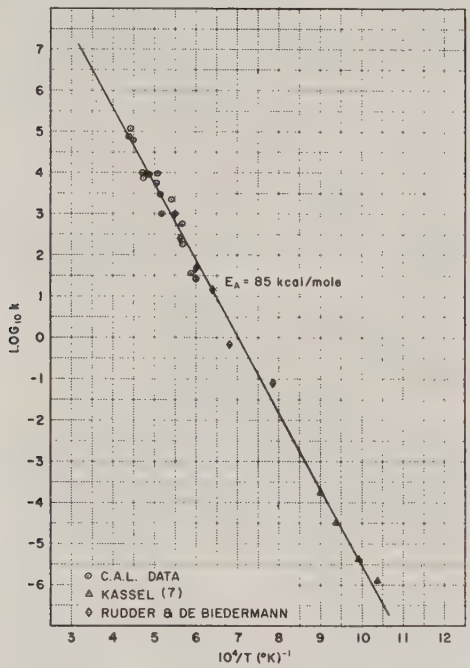

Figure 3. First order specific rate constant for the decomposition of methane as a function of reciprocal temperature

reactivity of water vapour with CH_4 and/or its decomposition products. Experiments using 1:4:5 parts by volume CH_4–H_2O–A mixtures, in which the reaction times were of the order of one millisecond, were performed first. The conversion of CH_4 into C_2H_2 reached a maximum at an initial reaction temperature of about 2,000°K. CO becomes the dominant carbon-bearing substance at higher temperatures. It therefore appeared that at initial reaction temperatures below 2,000°K, the decomposition of CH_4 into C_2H_2 and C_2H_4 is either more rapid than the reaction between the hydrocarbons and H_2O, or that a sufficient concentration of C_2H_2 and/or C_2H_4 must be present to start CO formation.

In order to investigate this point, a series of experiments was performed with 1:1:8 CH_4–H_2O–A mixtures over the same temperature range. It was found that, at the same temperature, total reaction pressure and reaction time, CO formation was substantially reduced, and higher C_2H_2 concentrations were achieved. It was also found that the data obtained in the 1:1:8 CH_4–H_2O–A experiments were in good agreement with those obtained in the CH_4–He–A series over that temperature range where CO formation was small, indicating that H_2O acts as an inert diluent until CO formation begins, and that the nature of the diluent is not critical.

Methane–oxygen and methane–oxygen–hydrogen experiments

The next series of experiments was designed to determine the reaction of molecular oxygen with CH_4. Experiments using 8:2:90 CH_4–O_2–A mixtures were performed at total reaction pressures of 80 lb./in.^{2} (*Figure 4*). The relatively small conversions to C_2H_2 and C_2H_4 were due to strong CO formation, which occurred even at low reaction temperatures. Increasing reaction pressure and reaction time tend to increase CO formation.

Since the data obtained in the methane–oxygen experiments suggested that O_2 combines with hydrocarbons giving CO and H_2 rather than CO and H_2O, a series of experiments using CH_4–O_2–H_2–Kr mixtures was carried out. The

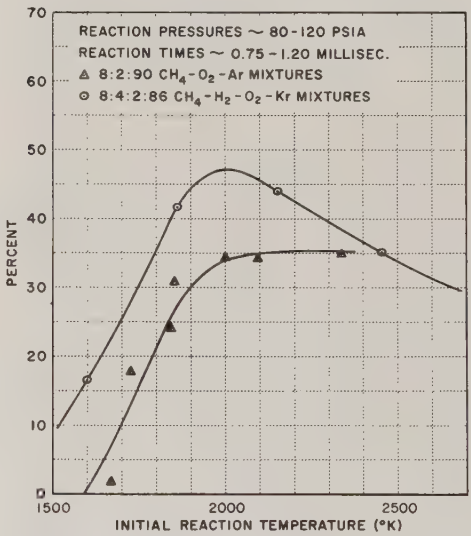

Figure 4. Per cent methane converted into C_2H_2 *and* C_2H_4 *for* 8:2:90 CH_4–O_2–A *and* 8:4:2:86 CH_4–H_2–O_2–K_r *mixtures as a function of initial reaction temperature. Reaction times were about* 0·75 milliseconds

results of these experiments are also shown in *Figure 4*. It is seen that the concentrations of C_2H_2 and C_2H_4 were raised approximately 10 to 15 per cent by the introduction of hydrogen into the reactant mixture. The lower temperature at which C_2H_2 and C_2H_4 production started suggests that energy was evolved by a chemical reaction between oxygen and hydrogen.

ETHANE AND BUTANE STUDIES

Product distributions

The second major phase of the work dealt with studies of the reactive properties of ethane and butane at high temperatures and in the presence of water vapour. A series of experiments with gas mixtures having a $H_2O:C_2H_6$ ratio of approximately 2 was carried out initially. The results of this series showed surprisingly large concentrations of C_2H_2 and C_2H_4 before the deleterious effects of CO formation became significant (*Figure 5*). Similar results were found with a $H_2O:C_2H_6$ ratio of 8 (*Figure 6*), except that CO formation occurred at temperatures about 400°K lower, which is similar to the results observed in the CH_4–H_2O experiments.

Next, the effect of reaction time was investigated. The results shown in *Figure 7* show that CO formation occurred at temperatures about 200°K lower when the reaction time was increased approximately fourfold. The formation of CO therefore tended to increase with larger $H_2O:C_2H_6$ ratios and with longer reaction times.

A similar series of experiments was carried out using C_4H_{10}–H_2O–A mixtures, and the results are given in *Figures 8, 9, 10,* and *11*. As in the ethane case, the temperature at which CO formation began decreased with increasing $H_2O:C_4H_{10}$ ratio. Also, comparing the data in *Figures 10* and *11*, in which the main parameter varied was the reaction time, it is seen that the temperature at which CO formation began was reduced by about 150°K for a fourfold increase in reaction time. Therefore, for C_4H_{10}–H_2O mixtures, CO formation also tends to be enhanced by increasing the $H_2O:C_4H_{10}$ ratio and by increasing the reaction time.

In addition, ethane and butane studies were carried out using proportions of steam similar to those mentioned above, but with much less argon. Since the concentration of steam was 2·5 to 5 times greater, the formation of CO was enhanced. However, in the reaction zone where CO did not appear, no significant difference in the distribution of products was found, indicating once again that, within this range, H_2O acts as an inert diluent.

Equilibrium correlations

Comparison of the data obtained in the methane, ethane, and butane experiments showed that these aliphatic hydrocarbons have similar decomposition product distributions. Also, it was observed that at the same temperature, composition and reaction time, increasing the reaction pressure tended to increase the $C_2H_4:C_2H_2$ ratio. These observations suggested that equilibrium correlations might prove fruitful. Calculations of the equilibrium distributions were carried out assuming that only C_2H_2, C_2H_4, H_2 and the original hydrocarbon were present in the product gas sample. The results of one such calculation for ethane are shown in *Figure 12*. The general character of the species distribution is qualitatively similar to the experimental results shown in *Figures 5, 6,* and *7*.

A more detailed analysis of the data has been carried out, and the results are presented in *Figures 13* and *14*. The temperatures, T_1 and T_2, were calculated from the measured product distributions of experiments in which no CO was formed, by means of the equilibrium equations

$$K_1(T_1) = \frac{[C_2H_2][H_2]^2}{[C_2H_6]}$$

corresponding to the reaction

$$C_2H_6 \rightleftharpoons C_2H_2 + 2H_2$$

where $K_1(T_1)$ is the equilibrium constant for this reaction, and

$$K_2(T_2) = \frac{[C_2H_2][H_2]}{[C_2H_4]}$$

corresponding to the reaction

$$C_2H_4 \rightleftharpoons C_2H_2 + H_2$$

where $K_2(T_2)$ is the equilibrium constant for this reaction.

If the reactant gas is in equilibrium just before the cooling by the expansion waves begins, T_1 and T_2 should both be equal to the final reaction temperature, T_f, which is calculated from the Rankine–Hugoniot normal shock relations and the temperature drop due to the measured changes in chemical species. In *Figure 13* it is seen that $T_2 = T_1 + 50$°K, which is fairly good agreement. However, *Figure 14* shows that $T_f = T_2 + 150$°K, which means that the reaction cannot be strictly assumed to equilibrate in stages even if the species are chosen *a posteriori*. The data indicate, however, that there are tendencies which can be described by equilibrium considerations even at these extremely short dwell times.

Kinetics of CO *formation*

If CO is allowed to be a component in the product distribution, equilibrium calculations show that almost all the oxygen atoms present will unite with carbon atoms to form CO. The data gathered in the experiments in which water vapour was a major constituent of the reactant gas showed that the degree of CO formation was considerably below the values computed assuming equilibrium, and therefore the concentration of CO is determined by reaction kinetics.

The observation that the tendency for CO formation increases with reaction time and H_2O: hydrocarbon ratio prompted a kinetic analysis based on the assumption that the rate of CO

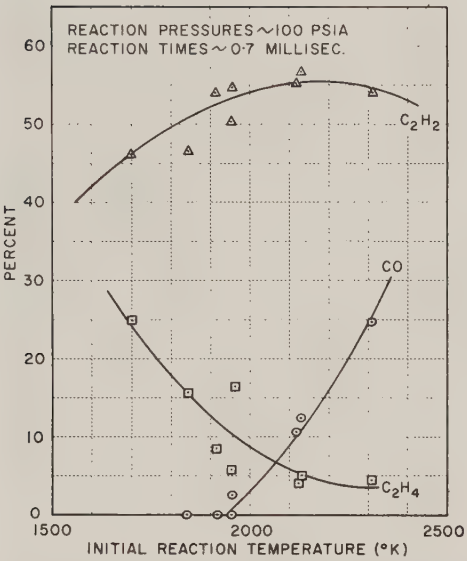

Figure 5. Per cent carbon converted into C_2H_2, C_2H_4 *and* CO *as a function of initial reaction temperature for reactant gas mixtures of* 3·92 per cent C_2H_6, 8·00 per cent H_2O *and* 88·1 per cent (A + He)

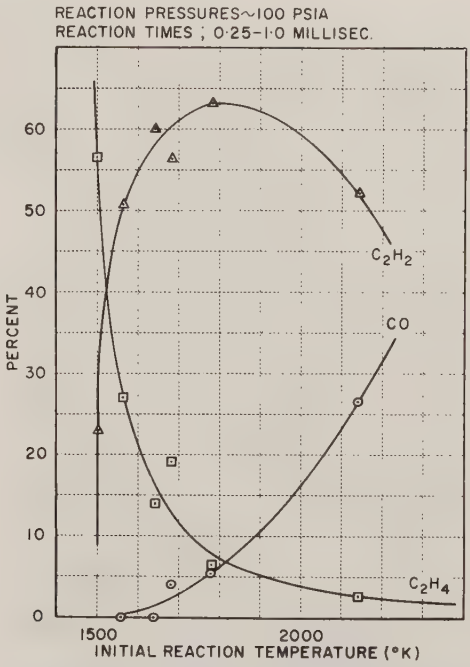

Figure 6. Per cent carbon converted into C_2H_2, C_2H_4 *and* CO *as a function of initial reaction temperature for reactant gas mixtures of* 2·06 per cent C_2H_6, 16·5 per cent H_2O *and* 81·5 per cent (A + He)

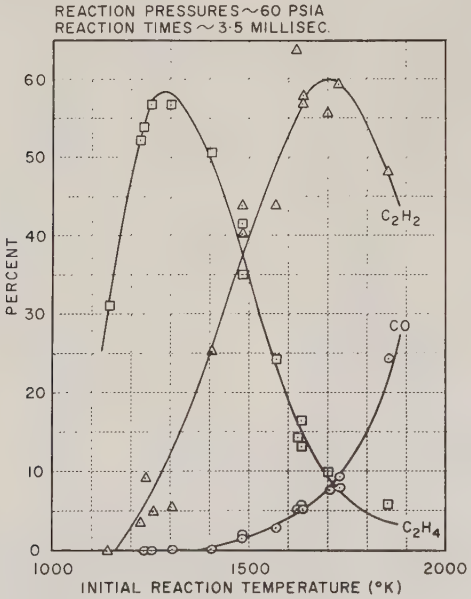

Figure 7. Per cent carbon converted into C_2H_2, C_2H_4 *and* CO *as a function of initial reaction temperature for reactant gas mixtures of* 2·06 per cent C_2H_6, 16·6 per cent H_2O *and* 81·5 per cent (A + He)

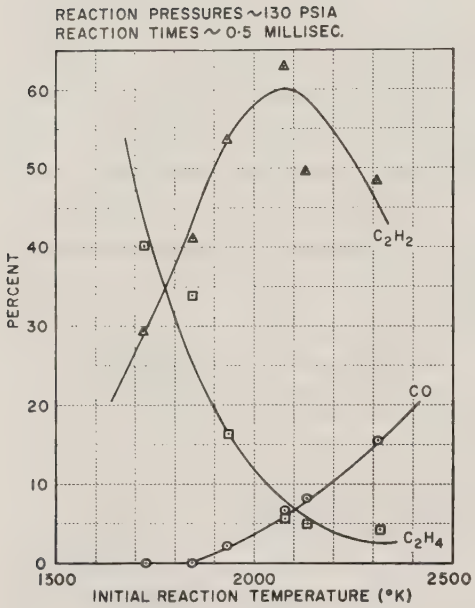

Figure 8. Per cent carbon converted into C_2H_2, C_2H_4 *and* CO *as a function of initial reaction temperature for reactant gas mixtures of* 1·94 per cent C_4H_{10}, 7·4 per cent H_2O *and* 90·6 per cent (A + He)

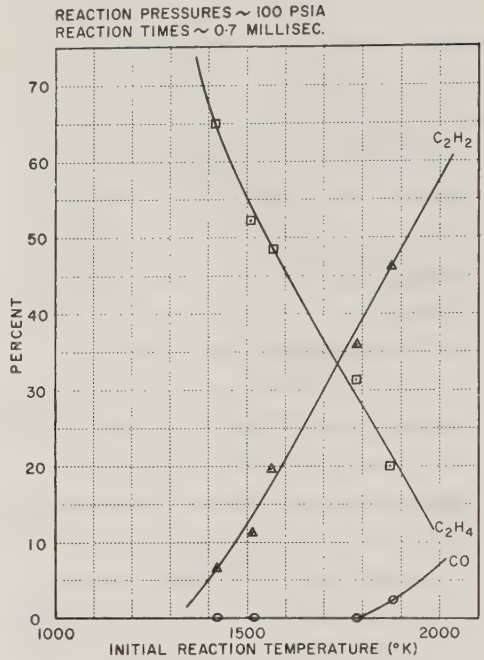

Figure 9. Per cent carbon converted into C_2H_2, C_2H_4 *and* CO *as a function of initial reaction temperature for reactant gas mixtures of* 2·01 per cent C_4H_{10}, 16·2 per cent H_2O *and* 81·8 per cent (A + He)

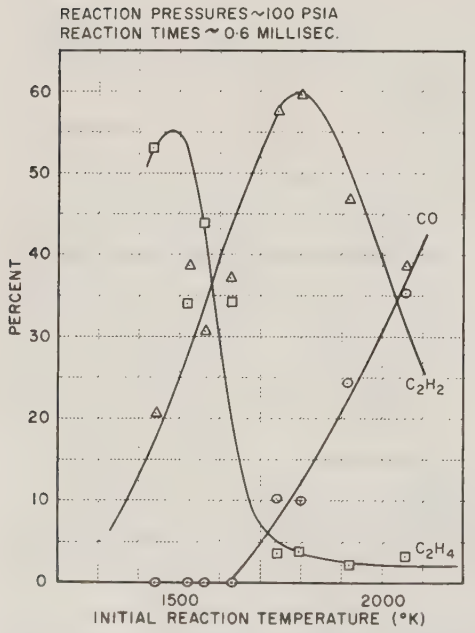

Figure 10. Per cent carbon converted into C_2H_2, C_2H_4 *and* CO *as a function of initial reaction temperature for reactant gas mixtures of* 1·04 per cent C_4H_{10}, 16·6 per cent H_2O *and* 82·4 per cent (A + Ne)

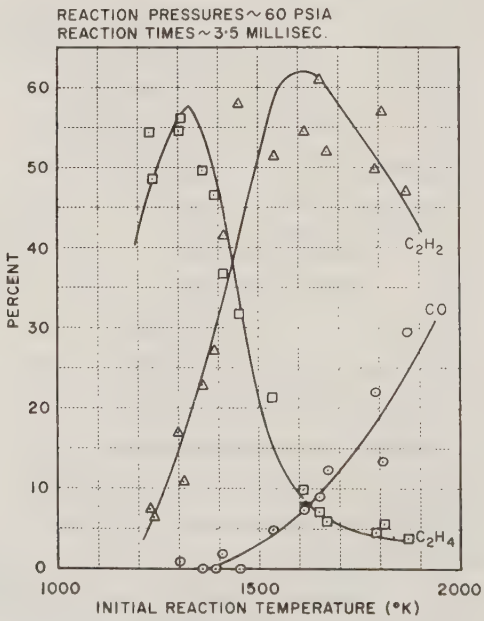

Figure 11. Per cent carbon converted into C_2H_2, C_2H_4 *and* CO *as a function of initial reaction temperature for reactant gas mixtures of* 0·97 per cent C_4H_{10}, 16·7 per cent H_2O *and* 82·3 per cent (A + Ne)

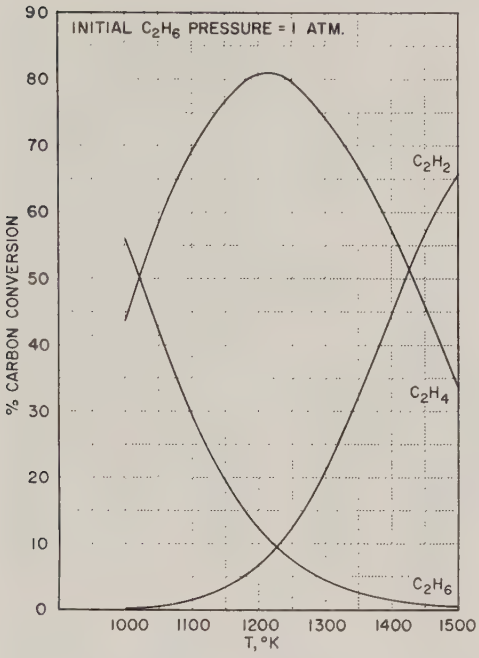

Figure 12. Equilibrium percentages of the original carbon found as C_2H_2, C_2H_4 and C_2H_6 assuming that ethane is heated to temperature, T, and only C_2H_2, C_2H_4, C_2H_6 and H_2 are present in the product gas

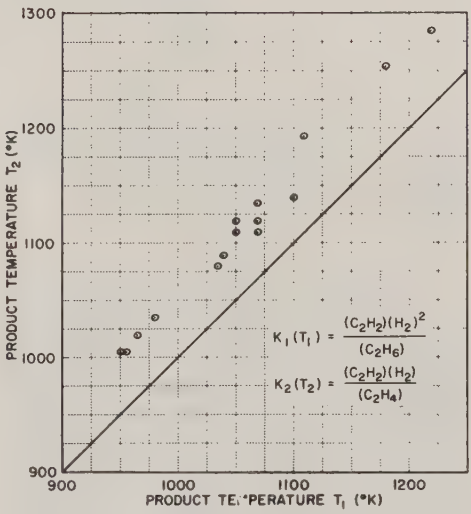

Figure 13. Comparison of temperatures computed from the measured product distribution, using the known variation of the equilibrium constants, K_1 and K_2, with temperature for C_2H_6–H_2O–A mixtures in which no CO formed

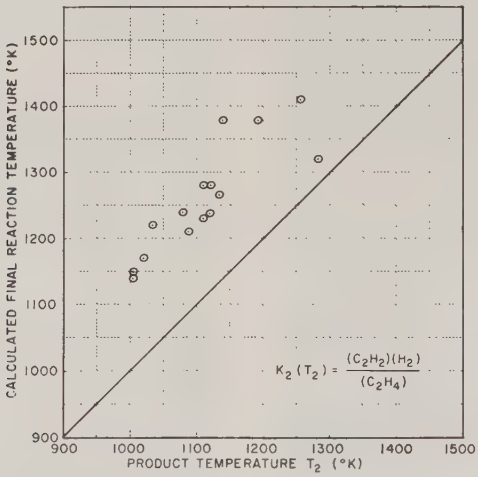

Figure 14. Comparison of temperatures computed from the measured product distribution, with final reaction temperatures calculated from the Rankine–Hugoniot normal shock relations, corrected for the endothermicity of the measured changes in chemical species, for C_2H_6–H_2O–A mixtures in which no CO formed

formation is first order with respect to both steam and hydrocarbon concentration. An Arrhenius plot of all the ethane and butane data in which CO formation occurred showed that the data points fell near a single curve, with a scatter corresponding to $\pm$ 40°K in the reaction temperature. The equation for the CO kinetic data was found to be

$$\log_{10} k = 7{\cdot}80 - \frac{8{,}250}{T_f}$$

where T_f is the final reaction temperature and k is the specific rate constant in $(\text{atm-sec})^{-1}$ for the formation of CO according to the rate law

$$\frac{dx}{dt} = k[H_2O]$$

where x = fraction of initial carbon appearing as CO. Since it was assumed that CO forms after the formation of C_2H_2 and C_2H_4, and since the energy change due to CO formation is small, the kinetic step in which CO is formed is very nearly isothermal at the final reaction temperature.

To check this assumption, the kinetics of CO formation in C_2H_2–H_2O mixtures were studied (*Figure 15*). Since the magnitude and activation

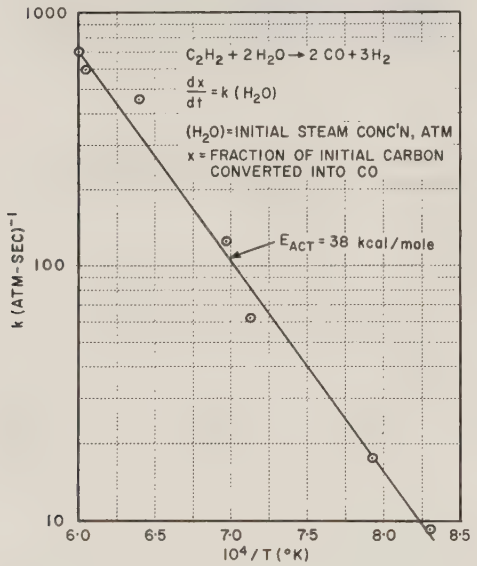

Figure 15. Specific rate constant, k, as a function of reciprocal temperature for the reaction $C_2H_2 + 2H_2O \rightarrow 2CO + 3H_2$, *assuming* $\frac{dx}{dt} = k(H_2O)$, *where* x = *fraction of initial carbon appearing as* CO, *and* (H_2O) = *steam concentration, atm partial pressure*

energy of the specific rate constant for CO formation from C_2H_2 agreed with that from C_2H_6 and C_4H_{10}, it is believed that the breakdown of the latter into C_2H_2 precedes their subsequent oxidation by steam.

Kinetics of acetylene formation from ethylene

The data obtained in the present experiments indicated also that C_2H_6 and C_4H_{10} pyrolyse to form C_2H_4 first, followed by the formation of

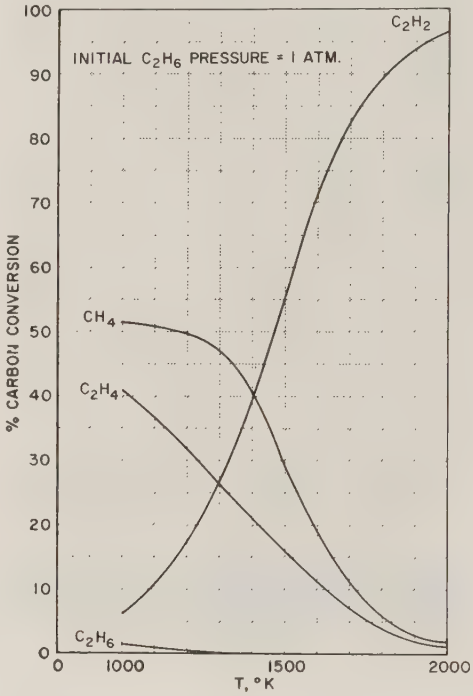

Figure 16. Equilibrium percentages of the original carbon found as C_2H_2, C_2H_4, C_2H_6 *and* CH_4 *when ethane is heated to temperature, T, and only* C_2H_2, C_2H_4, C_2H_6, CH_4 *and* H_2 *are present in the product gas*

C_2H_2. A kinetic analysis, based on this hypothesis, was carried out assuming the kinetic rate law

$$\frac{d[C_2H_2]}{dt} = k[C_2H_4] = -\frac{d[C_2H_4]}{dt}$$

Upon integration, we have

$$k = \frac{2{\cdot}3}{\Delta t} \log_{10} \frac{[C_2H_4]_i}{[C_2H_4]_f}$$

where Δt is the measured reaction time, and $[C_2H_4]_i$ and $[C_2H_4]_f$ are the initial and final ethylene concentrations obtained from the measured product distributions. The heat absorbed by the reaction $C_2H_4 \rightarrow C_2H_2 + H_2$ is such that the temperature drop due to reaction is always below 50°K, and often only a few degrees.

The kinetic analysis gave an activation energy of 30 kcal, in agreement with the work of Fischer and Pichler[8] and Tropsch and Parrish[9]. However, certain discrepancies in our data indicate a basic uncertainty in the whole approach used above, since it was assumed that $[C_2H_4]$ was present at the beginning of the time interval Δt,

while actually it probably forms and partially decomposes into C_2H_2 during Δt.

Kinetics of ethylene formation

Preliminary experiments on C_2H_4 formation have been carried out using C_2H_6–H_2O–A mixtures. The results are not complete, but one interesting fact has been observed. In most of the ethane experiments, small amounts of CH_4 were present, as well as larger quantities of C_2H_4. The product distributions of several experiments performed at low temperatures (about 1,000°K) showed appreciable quantities of C_2H_4, but no CH_4. It is interesting to note that, from an equilibrium point of view, CH_4 and C_2H_4 should both occur in large concentrations at such temperatures (*Figure 16*). The absence of CH_4 when large concentrations of C_2H_4 were present suggests that hydrogen stripping of C_2H_6 is a kinetically favoured process compared with the breaking of the carbon-carbon bond.

CONCLUDING REMARKS

The C.A.L. single-pulse shock tube has been used to study the reactions which take place when three aliphatic hydrocarbons (methane, ethane, and butane) are heated to high temperatures, either alone or in the presence of oxygen-bearing substances such as water vapour.

The kinetics of the decomposition of methane were investigated and the data agree closely with those of Kassel and Rudder and de Biedermann. Studies with CH_4–O_2 and CH_4–O_2–H_2 mixtures indicate that the addition of hydrogen enhanced C_2H_2 formation in the kinetic zone where CO formation did not dominate. Experiments with CH_4–H_2O mixtures showed that for certain conditions, water acts essentially as an inert diluent, and that fairly large conversions to C_2H_2 and C_2H_4 could be achieved before CO formation began. It was found that CO formation in CH_4–H_2O mixtures was strongly enhanced by increasing the water vapour concentration.

The studies of ethane and butane decomposition revealed many similar characteristics. It was found, for example, that the introduction of large amounts of water vapour does not necessarily cause CO formation if the temperature, pressure and reaction time are properly controlled. Correlation of the product distributions that were found in experiments in which no CO was formed showed trends that may be deduced from equilibrium considerations, such as the C_2H_4:C_2H_2 ratio. However, the equilibrium temperatures computed from the product distributions were about 150°K lower than the final reactant gas temperatures calculated from the Rankine–Hugoniot normal shock relations and the temperature drop due to the measured changes in chemical species. Therefore, the assumption of equilibrium is not strictly valid.

Kinetic studies of CO formation in C_2H_6–H_2O, C_4H_{10}–H_2O, and C_2H_2–H_2O mixtures have been carried out assuming

$$\frac{dx}{dt} = k[H_2O]$$

x is the fraction of initial carbon appearing as CO, and it has been found that all the data fall near a single curve, which is given by

$$\log_{10} k = 7{\cdot}80 - \frac{8{,}250}{T_f}$$

where T_f is the final reaction temperature.

In addition to the study of CO formation, the kinetics of the formation of C_2H_4 and C_2H_2 have been investigated for the C_2H_6–H_2O and C_4H_{10}–H_2O experiments in which no CO was found in the gas sample.

The work presented in this paper was performed at the Cornell Aeronautical Laboratory. The author gratefully acknowledges the contributions of Mr. James Klein and Dr. George Markstein of the Aerodynamic Research Department of the Cornell Aeronautical Laboratory, Dr. Margaret Carncrose of Niagara University and Drs. Gordon Skinner, Clarence Dulaney, and George Barker of the Monsanto Chemical Company. The author is also pleased to acknowledge the advice, encouragement and co-operation provided by Dr. F. K. Moore and A. Hertzberg of the Cornell Aeronautical Laboratory, as well as the assistance and co-operation of the engineering and scientific staffs of the Monsanto Chemical Company who participated in this programme.

The work reported in this paper was supported by the Monsanto Chemical Company.

REFERENCES

[1] Glick, H. S., Squire, W. and Hertzberg, A. *Fifth (International) Symposium on Combustion*, p. 393. 1955. New York; Reinhold

[2] — Klein, J. J. and Squire, W. *J. chem. Phys.* 27 (1957) 850

[3] Gordon, J. S. *Thermodynamics of High Temperature Gas Mixtures, WADC tech. Rep. Nos. 57–33* (January 1957)

[4] *Selected Values of Physical and Thermodynamic Properties of Hydrocarbons and Related Compounds.* American Petroleum Institute, Carnegie Press (1952)

[5] Resler, E. L., Lin, S. C. and Kantrowitz, A. R. *J. appl. Phys.* (1952) 1930

[6] Mark, H. *J. aero. Sci.* 24 (1957) 304

[7] Kassel, I. S. *J. Amer. chem. Soc.* 54 (1932) 3949

[8] Fischer, F. and Pichler, H. *Brennst. Chemie* 13 (1932) 406

[9] Tropsch, H., Parrish, C. and Egloff, G. *Industr. Engng Chem.* (*Industr.*) 28 (1936) 581

18

THE POINT OF ATTACK IN HYDROCARBON OXIDATION—I. PROPANE

R. BURT, C. F. CULLIS, R. LARSEN and G. J. MINKOFF

INTRODUCTION

Studies of the reactions of hydrocarbons with reagents other than oxygen indicate clearly that the reactivity of C—H bonds decreases in the order: tertiary > secondary > primary. Thus, for example, analysis of the pyrolysis products of different hydrocarbons[1] shows that the relative probabilities of alkyl radical attack at primary, secondary and tertiary centres are 1 : 2 : 10 at 600°C and 1 : 3 : 33 at 300°C. A similar order of reactivity of CH_3, CH_2 and CH groups towards attack by chlorine atoms also determines the rates of chlorination of hydrocarbons[2]. It has indeed been suggested[3] that, since all free radicals are electrophilic, the same order of reactivity of C—H bonds should be observed in other radical reactions, the point of attack being governed primarily by the attraction of radicals to local accumulations of negative charge.

The factors controlling the point of oxygen attack in hydrocarbon combustion are, however, somewhat less clearly defined[4,5]. Thus the observed correlation between resistance to oxidation and the number and proximity of methyl groups in a hydrocarbon molecule[6] suggests that branching of the carbon chain and the consequent introduction of tertiary C—H bonds decreases vulnerability to oxidative attack. Furthermore, there is some evidence to show that attack at CH_3 groups is not unimportant. Pope, Dykstra and Edgar[7] for example deduced, from measurements of the ratio of CO to CO_2 formed, that the slow oxidation of large hydrocarbon molecules involves end-attack followed by stepwise degradation of the carbon chain. Newitt and Thornes[8] who followed the slow combustion of propane by ultraviolet absorption, observed the spectrum of propionaldehyde, thus proving the occurrence of at least some end-attack. More recently, Bailey and Norrish[9] have reported the formation of all aldehydes from caproaldehyde to formaldehyde during the slow oxidation of *n*-hexane; this result indicates some end-attack followed by stepwise degradation in the combustion of this hydrocarbon also.

It is evident therefore that the factors which control the vulnerability to oxidative attack of different parts of hydrocarbon molecules are by no means straightforward and that the normal order of reactivity of C—H bonds is not as strongly in evidence in combustion processes as in the other reactions cited. More direct methods are thus clearly required of determining the point of oxygen attack in the combustion of hydrocarbons and the present paper represents an attempt to obtain the required information.

In order to reduce the number of extraneous factors, the smallest paraffin hydrocarbon was selected for study which had more than one type of C—H bond, namely propane. It was thought that, if satisfactory results were obtained with this compound, extensions could be made, with the application of appropriate safeguards, to more complex hydrocarbons. One requirement was that the chemical process investigated should be, as nearly as possible, the first reaction between fuel and oxygen. For this reason, labelling parts of the hydrocarbon skeleton with isotopically enriched carbon was not employed in this study since the relationship between the products and the point of oxygen attack was considered to be too complicated. It was therefore decided to label the different types of C—H bond by replacing the hydrogen by deuterium. One advantage of this approach is that deductions can, in principle, be made not only from the nature of the products formed but also from the effect of isotope substitution on the rate of reaction.

The oxidation conditions should preferably be such that the carbon skeleton is retained, since the formation of small reactive fragments might lead to less selective attack on other hydrocarbon molecules. According to Satterfield and Reid[10] such conditions exist for propane in the high temperature region where in the presence of excess hydrocarbon the products consist mainly of propylene and hydrogen peroxide. The first method examined therefore involved the preparation of d_1- and d_2-propanes and the measurement of the rate of disruption of C—D bonds in the presence of a deficit of oxygen at different temperatures. The oxidations were followed *in situ* by recording as a function of time the intensity of the infra-red absorption band corresponding to the C—D bond. The information obtained should have led to an estimate of the difference in activation energy for attack at the primary and secondary positions.

It was found, however, that the C—D frequency was affected even when a different part of the molecule was attacked. When in order to overcome this difficulty wide slits were used, interference was experienced from the absorption of carbon monoxide, which was one of the combustion products.

Another method of approach was therefore investigated; this involved measurement of the rate of formation of propylene, first from ordinary propane and then from d_1- and d_2-propanes. The formation of propylene should be more markedly reduced when the more reactive position is deuterated and vice versa. An *in situ* method was therefore developed for recording the intensity of the =C—H band of propylene as a function of time. Interference by the C—H bond of propane[11] however made this technique suitable only for determination of the optimum working conditions.

The method finally adopted therefore involved measurement of the deuterium content of the water and hydrogen peroxide in the products. The slow combustion of the labelled hydrocarbons was allowed to proceed to completion and after a period long enough for the peroxide to decompose to water but not sufficiently long to permit appreciable oxygen-sensitized pyrolysis to take place, the products were expanded and frozen in a trap. The deuterium content of the condensable products, which contained only small amounts of alcohols and aldehydes[10], was measured from the intensity of the O—D infra-red absorption band.

EXPERIMENTAL

Materials

Propane—For preliminary studies, this was prepared from 96 per cent Propagas by fractional distillation through a low temperature packed column. The composition was checked by mass spectrometry (Dr. Powell, British Petroleum Co. Ltd.) and not more than 3 per cent of propylene was found to be present. For accurate work pure propane was kindly made available by the British Petroleum Co. Ltd.

Mono-deuterated propanes—These compounds were prepared by a modification of the method described by Schissler, Thompson and Turkevitch[12], in which the *d*-acetic acid required for the reduction is made *in situ* by addition of heavy water to a mixture of zinc and acetic anhydride in the presence of the appropriate halide.

d_1-propane: *n*-propyl iodide (170 g), acetic anhydride (200 g) and zinc (100 g) were mixed, and heavy water (20 g) was slowly added with shaking. Reaction occurred at room temperature and some cooling was required to avoid a rise in temperature. Yield: 98 per cent.

d_2-propane: *iso*propyl iodide (170 g) was reduced under similar conditions. Yield: 98 per cent.

2,2-dideuteropropane—2,2-dichloropropane (prepared by the action of dry acetone on cooled phosphorus pentachloride) (23 g), acetic anhydride (80 g) and zinc (40 g) were allowed to react with heavy water (4 g) in a manner similar to that described for the mono-deutero compounds. Yield: 90 per cent.

1,1,1-trideuteropropane—The first stage of the preparation of this compound involved the deuteration of nitromethane[13,14]. The exchange was carried out by shaking nitromethane (8 g), heavy water (5·5 g), sodium acetate (0·25 g) and glacial acetic acid (0·01 ml) at 80°C for 20 hours. The mixture was then distilled through a drying tube (K_2CO_3) and the nitromethane was collected. The exchange was found to be complete after four operations. The deuterated nitromethane (6·4 g) was reduced in the usual way to the amine hydrochloride (5·8 g) which was benzoylated by the Schotten-Baumann procedure. The benzoyl derivative (11 g) was mixed with phosphorus pentachloride (20 g) and the mixture was gently heated. Phosphorus oxychloride distilled over first, and, when the rate of heating was increased, the deuterated methyl chloride was driven over in a slow stream of nitrogen. It was washed (*aq.* KOH), dried ($CaCl_2$) and then added to an ethereal solution of ethyl magnesium chloride. The gases evolved were frozen out and later distilled. Yield: 40 per cent.

$$CH_3NO_2 \xrightarrow[\text{acetate buffer}]{D_2O} CD_3NO_2 \xrightarrow{Fe/HCl} CD_3NH_2{\cdot}HCl$$

$$\xrightarrow[(2)\ PCl_5]{(1)\ C_6H_5COCl} CD_3Cl \xrightarrow{C_2H_5MgCl} CD_3CH_2CH_3.$$

1,1,1.3,3,3-hexadeuteropropane—This compound was synthesized by the method of Condon[15]. Acetone (2 g) and heavy water (2 g) were distilled under reflux for 20 hours in the presence of a trace of potassium carbonate. Exchange was found to be complete after ten operations. The deuterated acetone (2 g) was reduced with lithium aluminium hydride (0·6 g) in ether (25 ml). The *iso*propanol formed (2 g) was allowed to react with hydrochloric acid (10 g) and zinc chloride (8 g). The Grignard reagent was prepared from the resulting 2-chloropropane (1·9 g) and magnesium (0·75 g) in ether (50 ml). The solution was distilled under reflux for 1 hour to eliminate by-product hydrocarbons. Excess water was slowly added and the evolved gas was frozen out and distilled. Yield: 55 per cent.

$$CH_3{\cdot}CO{\cdot}CH_3 \xrightarrow[K_2CO_3]{D_2O} CD_3{\cdot}CO{\cdot}CD_3 \xrightarrow{LiAlH_4}$$

$$CD_3{\cdot}CH(OH){\cdot}CD_3 \xrightarrow{ZnCl_2/HCl}$$

$$CD_3{\cdot}CHCl{\cdot}CD_3 \xrightarrow{Mg} CD_3{\cdot}CH{\cdot}CD_3$$

$$CD_3{\cdot}CH_2{\cdot}CD_3 \xleftarrow{H_2O} \mid MgCl$$

Oxidation conditions

The rate of formation of propylene was measured semi-quantitatively by the *in situ* infra-red method already referred to[11]. The minimum rate of oxidation in the region of negative temperature coefficient occurred at *ca.* 400°C; only 30–40°C separated this from the explosion limit and most combustions were therefore carried out at 423°C. Equal volumes of propane and purified air were admitted at a total pressure of 1 atmosphere to a cylindrical Pyrex reaction vessel of *ca.* 250 ml capacity; the fuel : oxygen ratio was thus *ca.* 5 : 1. Under the conditions used, oxidation was complete after *ca.* 1 min. The products were therefore withdrawn, after 5 min., through heated tubing and were frozen out in a trap cooled to −26°C. The products of four separate combustions gave a large enough liquid sample for the direct estimation of the deuterium content.

Deuterium estimation

A procedure for the infra-red analysis of deuterium in aqueous solution was developed by Thornton and Condon[16] and their method was modified to suit the spectrometer available[17]. Approximately 0·03 ml of liquid was sufficient to fill the calcium fluoride cell, the operative thickness being 0·05 mm. The transmission was measured at 3·97 μ. A double-beam technique was employed, the comparison beam being initially balanced against a solution containing no isotope. More sensitivity could then be obtained by opening the slits and increasing the gain. Calibration against standard H_2O—D_2O mixtures was always carried out before and after each estimation.

The advantage of this method was that at 3·97 μ the liquid product from non-deuterated propane had almost negligible absorption, which was easily compensated for by introduction of a neutral filter in the comparison beam. There was thus no need to convert the products to pure water or to pure hydrogen for the estimation of the deuterium. Tests were made to ensure that products such as methanol did not cause interference.

RESULTS

In Table 1 are given the mean values for a number of determinations of the deuterium content of the water formed during the slow combustion of various labelled propanes; the corresponding H/D ratios in the water formed are also included. Control experiments show that the error in the estimation of deuterium is less than 1 per cent.

In order to deduce from the results in Table 1 the relative rates of oxygen attack at the various positions in the propane molecule, it is necessary to make several assumptions, the validity of which will be considered later. One possible source of error can however be eliminated at this stage,

TABLE 1

Temperature 423°C; Propane Pressure 380 mm; Air Pressure 380 mm

Compound oxidized	% D_2O (*obs.*)	H/D (*obs.*)	H/D (*calc.*)
$CH_2D{\cdot}CH_2{\cdot}CH_3$	4·7	22·4	22·1
$CH_3{\cdot}CHD{\cdot}CH_3$	8·9	11·3	9·6
$CD_3{\cdot}CH_2{\cdot}CH_3$	18·9	4·8	5·7
$CH_3{\cdot}CD_2{\cdot}CH_3$	25·5	3·2	3·6
$CD_3{\cdot}CH_2{\cdot}CD_3$	36·5	1·8	1·7

for the different H/D ratios obtained with d_1- and d_2-propanes show that randomization does not occur at the temperatures used.

The principal assumption is that oxygen removes from the propane molecule only the first of the two hydrogen atoms required for the formation of propylene, and that the second atom is removed by some reaction which does not lead to its appearance in the water collected for analysis. Considerable support to this is given by the H/D ratios observed which are significantly different from the ratios predicted for a mechanism in which both hydrogen atoms appear in the water.

Another assumption is that the rate of attack at a secondary carbon atom is x times greater than the rate of attack at a primary carbon atom irrespective of whether hydrogen or deuterium is attached to the carbon. In the same way it is assumed that attack of a C—D bond is y times faster than attack at a C—H bond and that y does not depend appreciably on the type of centre attacked. Although in practice x and y probably vary slightly, only second-order errors will be caused by assuming their constancy.

With these assumptions in mind then, let us now consider the composition of the water formed by oxidation of propane with a deficit of oxygen. The contributions of each hydrogen or deuterium atom in the propane molecule is clearly dependent on the relative rates of oxidation at primary and secondary centres and on the nature of the atoms attacked to these centres.

Let the contribution of a 1° C—H be a

then the contribution of a 1° C—D is ay

and the contribution of a 2° C—H is ax

and the contribution of a 2° C—D is axy.

If allowance is made for the numbers of bonds of each type in the various labelled propanes, the contributions to the hydrogen and deuterium

contents of the water can readily be deduced. Thus, for example, with d_1-propane, the contribution of H atoms is $5a + 2ax$ and that of D atoms is ay, and the observed H/D ratio is then equated to the ratio $(5a + 2ax)/ay$. This is done for the five labelled compounds studied, five simultaneous equations being obtained. These can be conveniently solved by expressing x in terms of y for each set. The intersection of five curves then gives the required values of x and y.

The mean results obtained in this way were:

$$x = \frac{\text{Rate of removal of H from a 2° CH}}{\text{Rate of removal of H from a 1° CH}} = 2{\cdot}1 \text{ (at 423°C)}$$

$$y = \frac{\text{Rate of removal of D}}{\text{Rate of removal of H}} = 0{\cdot}41 \text{ (at 423°C)}.$$

The H/D ratios calculated for the five deuterated propanes using these values of x and y are given in the last column of Table 1 and may be compared with the corresponding observed values.

Some experiments were also carried out with the mono-deuterated propanes at 360°C, at which temperature considerable amounts of oxygenated products are formed. The results were less reproducible, since under these conditions the surface has more influence on the early stages of reaction. However, x has almost exactly the same value at this temperature, while y decreases by an amount which suggests a difference of *ca.* 2 kcal mole^{-1} between the bond strengths of C—H and C—D.

DISCUSSION

The significance of the values obtained for x and y depends largely on the validity of the assumption that only the first of the hydrogen atoms removed from propane appears in the water produced. Some support for this is provided by the negligible effect of temperature on the value of x; for, if the second hydrogen atom removed also made an appreciable contribution to the composition of the aqueous products, considerable differences would be expected due to the marked variation with temperature of the extent of C—C bond fission. The closely similar values of x deduced from comparisons of the behaviour of mono-, di-, tri- and hexa-deuterated propanes also appears to support the above assumption.

The fate of the second hydrogen atom removed from propane is not immediately obvious. For example the reaction

$$C_3H_7 + O_2 \rightarrow C_3H_6 + HO_2 \qquad (1)$$

will occur to some extent[10] and this will tend to reduce the value of x. However, since the oxygen concentration is initially low, and since it rapidly diminishes as reaction proceeds, reaction 1 must decrease in importance. When the overall concentration of radicals reaches its peak, some interaction of propyl radicals with oxygenated radicals will take place, e.g.

$$C_3H_7 + HO_2 \rightarrow C_3H_6 + H_2O_2 \qquad (2)$$

$$C_3H_7 + OH \rightarrow C_3H_6 + H_2O \qquad (3)$$

thus affecting the calculated value of x. If this were the only important factor, however, the H/D ratio would have been considerably different from that observed. It is therefore necessary to assume that at least as important as reactions 2 and 3 are processes which do not result in the second hydrogen atom removed from propane appearing in the aqueous products; such reactions might include dimerization, disproportionation and decomposition[18–20].

The ratio for the relative ease of oxidation of primary and secondary groups is in broad agreement with that suggested elsewhere[3]. However, since propane contains three times as many primary as secondary C—H bonds, the oxidation products will clearly include to comparable extents those expected from both 'end-attack' and from attack on the central group. Thus, for example, Burt, Ebeid and Minkoff[21] showed that at 280°C, the slow oxidation of *n*-heptane gives rise mainly to propionaldehyde and butyraldehyde. On the other hand, at a somewhat higher temperature, all aldehydes from C_6 to C_2 are found among the combustion products. While, therefore, at the lower temperature, initial oxidation occurs preferentially at the secondary centres, at higher temperatures the radicals formed by initial attack at these centres tend to be less selective in their subsequent reaction with the hydrocarbon.

The present results thus no doubt explain why apparently conflicting data were found by some of the earlier workers and also make it understandable why the protagonists of the various opposing theories were able to find the products expected from different modes of initial attack.

The authors gratefully acknowledge the receipt of financial support from the North Thames Gas Board and the Salters Institute (R. B.) and from the Hydrocarbon Panel of the Institute of Petroleum (R. L.). They would also like to thank Imperial Chemical Industries for gifts of heavy water and Dr. J. H. Burgoyne for helpful discussions.

REFERENCES

[1] Rice, F. O. *J. Amer. chem. Soc.* 53 (1931) 1958; 55 (1933) 3035
[2] Steiner, H. and Watson, H. R. *Disc. Faraday Soc.* 2 (1947) 87
[3] Walsh, A. D. *Trans. Faraday Soc.* 42 (1946) 269
[4] Boord, C. E. *Third Symposium on Combustion*, p. 416. 1949. Baltimore; Williams and Wilkins
[5] Cullis, C. F. *Petroleum* 21 (1958) 49

[6] Hinshelwood, Sir Cyril N. *J. chem. Soc.* (1948) 531
[7] Pope, J. C., Dykstra, F. J. and Edgar, G. *J. Amer. chem. Soc.* 51 (1929) 1874, 2203, 2213
[8] Newitt, D. M. and Thornes, L. S. *J. chem. Soc.* (1937) 1656
[9] Bailey, H. C. and Norrish, R. G. W. *Proc. Roy. Soc. A* 212 (1952) 311
[10] Satterfield, C. N. and Reid, R. C. *Fifth Symposium on Combustion*, p. 511. 1955. New York; Reinhold
[11] Burt, R. and Minkoff, G. J. *Anal. Chim. Acta* 16 (1957) 259
[12] Schissler, D. O., Thompson, S. O. and Turkevitch, J. *Disc. Faraday Soc.* 10 (1951) 46
[13] Noether, H. D. *J. chem. Phys.* 10 (1942) 664
[14] Wilson, T. P. *J. chem. Phys.* 11 (1943) 361
[15] Condon, F. E. *J. Amer. chem. Soc.* 73 (1951) 4675
[16] Thornton, V. and Condon, F. E. *Anal. Chem.* 22 (1950) 690
[17] Minoff, G. J. *Fuel* 29 (1950) 228
[18] Whiteway, S. G. and Masson, C. R. *J. chem. Phys.* 25 (1956) 233
[19] Heller, C. A. and Gordon, A. S. *J. phys. Chem.* 60 (1956) 1315
[20] McNesby, J. R. and Gordon, A. S. *J. Amer. chem. Soc.* 79 (1957) 4593
[21] Burt, R., Ebeid, F. B. and Minkoff, G. J. *Nature, Lond.* 180 (1957) 188

19

PRODUCTS OF COOL FLAME OXIDATION OF PROPANE-2-^{13}C

R. E. FERGUSON and C. R. YOKLEY

INTRODUCTION

The products of slow oxidation of propane have been studied intensively, beginning with the work of Pease and co-workers[1] and Harris and Egerton[2]; and much of the information available was summarized by Lewis and von Elbe[3]. Among recent papers on the products of oxidation both of propane and of intermediates important in the reaction should be mentioned those of Knox and Norrish[4] on the cool flame oxidation of propane, and of Cullis and Newitt[5,6] on the oxidation of ethanol, in which acetaldehyde is an intermediate as it is in the oxidation of propane. Grumer[7] has published detailed analyses by mass spectrometry of the products of propane and acetaldehyde oxidation. A paper by Satterfield and Reid[8] has given an extensive outline of elementary steps thought to occur in the reaction and a useful bibliography.

The major products are now well known and plausible mechanisms have been put forward to explain their information and also, in a qualitative way, the kinetic features of the autocatalytic reaction, which is believed to involve chain branching via aldehydes, especially acetaldehyde, as essential intermediates.

At this stage of investigation the application of isotopic tracer methods can be expected to furnish additional information on the mechanism, and some work using tracer techniques has been published recently. Burt, Ebeid and Minkoff[9] and Braude, Cullis, Hardy and Turner[10] have studied the point of initial attack problem in this way, the former authors with deuterated propane and the latter using a variety of ^{14}C labelled 2-methylpentanes. Byrko, Kryuglakova and Lukovnikov[11] have reported results of experiments with ^{14}C marked propane in which the ^{14}C content of the products acetaldehyde, formaldehyde, and the carbon oxides were determined. A study of the oxidation of propane-2-^{13}C was contemplated some time ago by Grumer and co-workers[7] but methods were not then available to make such an experiment practicable.

With the advent of gas chromatography, detailed tracer studies of the products of complex reactions have become feasible. This paper reports the results of an investigation of the cool flame oxidation of propane-2-^{13}C in which the major products were isolated by low-temperature distillation and gas chromatography and the isotopic composition of each was determined by mass spectrometry.

The findings give evidence to support many of the currently postulated modes of formation of the products. There was little isotopic mixing in the reaction of the kind which would obscure the meaning of the results (e.g., random re-synthesis of the starting material) and the interpretation to be given to the data is fairly obvious. For this reason (and also to avoid an exercise in mechanism writing) the discussion to follow will involve mainly some of the general conclusions that can be drawn from the data directly.

Only one unfamiliar reaction is postulated, and that from apparent necessity.

EXPERIMENTAL

Conditions

After a preliminary survey of the products of slow and cool flame oxidation of ordinary propane in a static vessel, conditions were selected for the tracer experiments, represented by a point on the pressure–temperature diagram inside the multiple cool flame region (12,4), where in our apparatus the induction period was conveniently short and reaction was extensive.

Three separate experiments were carried out with equimolar propane-2-^{13}C oxygen mixtures in a 120 c.c. Vycor bulb at 318°C and 421 mm Hg initial temperature and pressure. The induction period varied from one to two minutes and in each case the cool flame reaction exhibited seven sharp pressure pulses, spaced about 2 sec apart, after which the pressure rise sensibly ceased. As many as 11 successive pulses of reaction were sometimes observed in preliminary experiments. Under these conditions, 30 to 45 per cent of the propane and 70 to 90 per cent of the oxygen were consumed. The induction period and the extent of reaction varied in the three runs with marked propane between the limits indicated, probably owing to variations in the condition of the vessel surface which was not, for economic reasons, aged in the usual manner to obtain reproducibility. The intermediate product distribution does not change markedly with an increase in the extent of reaction, although the intermediates left

unconsumed decrease and the end products (carbon oxides and water) increase.

Procedure

The procedure used for separation of the cool flame product mixture has been described in detail elsewhere[13]. The products were withdrawn from the reaction vessel immediately after the final cool flame and the fraction condensable at liquid nitrogen temperature was transferred to a LeRoy–Ward still. Non-condensable gases, except hydrogen, were separated by gas chromatography and isolated by trapping on silica gel at −196°C. The condensable products were then divided by low-temperature distillation into fractions, each of which could be separated into the pure components on an appropriate gas chromatography column. Individual products were trapped near the column outlet and in some cases were passed through the column again to remove small amounts of impurities. The samples were transferred on the vacuum line to sample bulbs and were usually analysed by mass spectrometry during the same day.

Formaldehyde was oxidized to carbon monoxide for isotopic analysis[13].

Materials

Oxygen for the first two runs was a sample from the Linde Company stated to be 99·99 per cent oxygen. That used for the third run was ordinary tank oxygen supplied by the Southern Oxygen Company.

TABLE 1

Composition of Marked Propane

Component	*Concentration,* mole per cent
C—^{13}C—C	61·6
C—^{13}C—^{13}C	1·4
C—C—^{13}C	0·8
C—C—C	36·2

The propane-2-^{13}C used was a sample of that prepared in a previous study[14]. It contained 63 atomic per cent ^{13}C in the 2-position and the natural abundance of ^{13}C (1·1 atomic per cent) in the end positions. The preparation and analysis of the sample are described in the earlier paper.

No impurities were detectable in the sample by gas chromatography or mass spectrometry; in particular, the amount of any single lower hydrocarbon impurity introduced into the reaction vessel with the 33 c.c. of propane used per run could not have exceeded 0·02 c.c. of gas (n.t.p.). The composition is given in Table 1.

The isotopic composition of the starting material is probably known more accurately than that of some of the products, and for present purposes it is unnecessary, if not unwarranted, to treat the data on product composition very exactly. Accordingly a three-carbon product found to contain 62 to 65 mole per cent of the ^{13}C labelled species will be said to have the original propane-2-^{13}C skeleton. Similarly, a two-carbon product, 62 to 65 mole per cent of which contains one ^{13}C atom, will be called an intact two-carbon fragment of the original propane chain. A single carbon product from the middle carbon atom will be 63 atomic per cent labelled with ^{13}C; one from the end will have the natural abundance of 1·1 atomic per cent ^{13}C. Examination of the composition of the sample shown in Table 1 and of the ways it can break up will show that this approximate way of treating the results cannot be seriously misleading.

Isotope analyses and purity of the separated products

The products isolated were analysed first by mass spectrometry using 70 V electron energy. This confirmed the identity of the sample, furnished an estimate of purity, and enabled calculation of the isotopic composition in cases where there was not enough sample also to obtain the molecule–ion spectra at low electron energy. In most cases, however, it was possible to make low voltage measurements (only the molecule–ions present) on the same sample, and the latter were used for the calculation of isotopic composition. Molecule–ion intensity measurements should give accurate results since the isotope effect in the formation of molecule–ions by electron impact is small or absent if no fragmentation occurs[15].

The purity of the individual products was greater than 99 mole per cent as shown by the gas chromatograms and the mass spectra obtained in this and the preliminary studies.

RESULTS

Table 2 shows the results of three separate experiments and their simplest interpretation in terms of the origin of the products from parts of the isotopic propane molecule.

Amounts isolated

The amount of each product *actually isolated* in Run 3 is shown in the second column of Table 2. These figures are presented to give a rough indication of the relative amounts present in the product mixture. Carbon and hydrogen balances calculated from them, taking into account the water produced, are unsatisfactory. Formaldehyde was recovered as carbon monoxide by an inefficient method[13], and other losses occurred owing to the difficulty of separating acids (0·1 to 0·2 c.c. of gas by titration) and acetals from water.

Isotopic composition

The data in Table 2 are the figures calculated directly from the mass spectra, giving the mole per cent of each product which is marked with one ^{13}C. Data are available showing the C—^{13}C—^{13}C and ^{13}C—^{13}C content for some of the products, which is small and about what one would expect considering the propane composition (see the discussion of the starting material above).

DISCUSSION

The interpretation of the results in terms of the origin of the products is obvious in most cases. The products will be discussed first by groups according to the length of the carbon chain.

Three-carbon species

The three-carbon compounds, except acetone, contain substantially the carbon skeleton of the

TABLE 2

Isotopic Composition of Cool Flame Products of Propane-2-^{13}C

Product	*Isolated in run* 3, c.c. gas (n.t.p.)	*Mole per cent product labelled with one* ^{13}C			*Interpretation*
		Run 1	*Run* 2	*Run* 3	
Propane (unreacted)	18·0	60·1	61·4	60·1	About 60 per cent ^{13}C in the 2-position (small isotope effect?)
Propylene	1·5	(60·5)	65·2	65·9*	Contain carbon skeleton of parent propane
Propylene oxide	0·30		66·1	63·3*	
Propionaldehyde	0·05		64·3	64·5*	
*Iso*Propyl alcohol	0·08			63·3*	
Acetone	0·4		46·8	46·4*	At least 50 per cent from propane skeleton
Ethane	0·1	(23·9)	53·4	53·5	80 per cent a propane fragment
Ethylene	0·7	(59·5)	69·6	65·3*	Intact two-carbon fragments of propane
Ethylene oxide	0·06		59·8	62·7	
Acetaldehyde	0·6	66·6	64·6	63·5*	
Methane	0·9	1·9	2·2	2·7*	95 per cent from end methyl groups of propane
Methanol	4·0	2·7	3·6	2·9	
Formaldehyde	0·5		19·3	15·5	Approx. 25 per cent from 2-position
Carbon monoxide	15·0	25·3	25·5	24·4	Approx. 39 per cent from 2-position
Carbon dioxide	2·8	(1·1)	38·3	40·3	Approx. 61 per cent from 2-position

* Computed from low voltage molecule–ion spectra.

The figures in parentheses in the third column, Run 1, are in error; in this experiment a heated activated charcoal chromatography column was used for the separation of hydrocarbons and carbon dioxide and exchange appears to have taken place, most extensive with carbon dioxide. A silica gel column was used for this separation in Runs 2 and 3. Run 3 gives the best data: no separated products contained impurities sufficient to interfere with mass spectrometric analysis.

The paper by Byrko, Kryuglakova and Lukovnikov[11] referred to earlier gives data for acetaldehyde and the last three compounds listed in Table 2. They find that acetaldehyde is a fragment of the propane, and report formaldehyde 22·6 per cent, carbon monoxide 22 per cent, and carbon dioxide 52 per cent from the 2-position in propane-2-^{14}C. Our figures are in rough agreement; differences may be expected because the reaction conditions were not the same in the two studies.

original propane. The propane left unconsumed has a slightly lower ^{13}C content than the starting material which indicates that the rate of initial attack on the propane molecule is slightly higher for ^{13}C labelled species. This is shown by noticeable isotope enrichment of several of the products.

The acetone composition presents an unexpected problem. Acetone might be supposed to arise rather directly from oxygen attack on propane, but if the isotopic composition found is correct, at least 20 to 30 per cent comes from some other reaction not involving the parent carbon chain. A possible explanation will be given below.

Two-carbon products

The two-carbon species, with the exception of ethane, are identifiable as intact fragments of the parent molecule. In particular, this is true of acetaldehyde, and the acetaldehyde has been shown by mass spectrometric analysis to contain

the ^{13}C in the $-CHO$ group. Approximately 20 mole per cent of the ethane is not a two-carbon fragment of the original propane. This fraction most likely is formed by methyl radical re-combination in the cool flame.

Methane and methanol

The isotopic composition of these products shows that nearly all the methane and methanol formed come from the end methyl groups of the propane. This leads to the conclusion that nearly all the methyl and methoxy radicals participating in the reaction are from the 1- and 3-positions, which is a most useful result when applied to the problem of the origin of other products.

Formaldehyde

This product has a mixed origin, with the end positions favoured slightly (about 1·5 to 1). The appreciable content of formaldehyde-^{13}C indicates definitely that there are modes of formation other than via methyl radical oxidation or hydrogen abstraction from the methoxy radical. Plausible mechanisms have been suggested previously[16], for example

$$CH_3{}^{13}CH_2O \rightarrow CH_3 + {}^{13}CH_2O$$

The ethoxy radical is undoubtedly present in the reaction, for ethanol (about 0·02 c.c., not enough for isotopic analysis) is present in the products.

Carbon monoxide

Carbon monoxide also comes from all three carbon atoms of the propane, but the 2-position is favoured (about 1·3 to 1), indicating the probable importance of acetyl radical decomposition as a source:

$$CH_3{}^{13}CO \rightarrow CH_3 + {}^{13}CO$$

Approximately 60 per cent then must arise through end attack on the propane or via methyl radical oxidation.

Carbon dioxide

The middle atom is strongly favoured (3 to 1) as the point of origin of carbon dioxide, showing the likelihood of its formation by the oxidation of acetaldehyde followed by decomposition of the acetoxy (or the peracetyl) radical[17]:

$$CH_3{}^{13}CO_2 \rightarrow CH_3 + {}^{13}CO_2$$

The rest, from the ends, presumably is produced by the oxidation of formaldehyde and possibly propionaldehyde by a similar mechanism.

These results give little information on whether carbon monoxide is oxidized in the cool flame, although there is some evidence in the literature[18] that this should be expected. It is clear, however, from the large difference in isotopic composition of the carbon oxides found, that the oxidation of carbon monoxide can be a source of only part of the carbon dioxide produced in the cool flame under these conditions.

Acetone

Mass spectrometric analysis indicates that only about 46 mole per cent of the acetone is labelled with ^{13}C whereas it should be 63 mole per cent labelled if it has the carbon chain of propane. We have looked unsuccessfully for sources of error and are reasonably sure of the result. The gas chromatographic separation seemed to be clean and the molecule–ion mass spectra were clear and simple to interpret.

It is easily seen that a middle-labelled three-carbon chain must be broken completely and re-assembled in order for the concentration of the species containing one ^{13}C to be lowered appreciably. Thus the reaction, commonly postulated in the photolysis of acetone,

$$CH_3CO + CH_3 \rightarrow CH_3COCH_3 \qquad (1)$$

alone would not explain the result obtained unless the acetyl radical itself were formed by combination of methyl radicals and carbon monoxide present in the reaction mixture. If the acetyl radical comes from acetaldehyde (which contains the ^{13}C in the $-CHO$ group) acetone having the parent propane skeleton would result from reaction 1. Therefore it seems reasonable to postulate the occurrence of

$$CH_3 + CO \rightarrow CH_3CO \qquad (2)$$

followed by reaction 1 to explain the formation of an appreciable fraction of the acetone. If the carbon monoxide involved has the isotopic composition of that isolated at the end of the reaction (25 atomic per cent ^{13}C), it can be estimated that nearly half of the acetone is produced by reactions 2 plus 1.

There is good indirect evidence for reaction 1; Grumer has found 'acetone or propionaldehyde' in the products of oxidation of acetaldehyde[7] and we have recently found both as minor products of the same reaction (unpublished work). Faltings[19] has reported the formation of acetone in the photolysis of ethane in the presence of carbon monoxide, giving some experimental support to the occurrence of reaction 2; however, Porter and Benson[20] have looked unsuccessfully for products of reaction 2 in the decomposition of *di-t*-butyl peroxide in the presence of ^{14}CO.

We hope soon to add ^{13}CO to a reaction mixture of ordinary propane and oxygen and to examine the acetone produced. If reactions 2 and 1 occur, ^{13}C will turn up in the carbonyl group. A second goal of the experiment will be to find whether carbon monoxide is oxidized to carbon dioxide in the cool flame.

SUMMARY AND COMMENT

The most useful general conclusions to be drawn from the experiments with propane-2-^{13}C completed at this writing are the following:

(1) Nearly all the methyl and methoxy radicals participating in the cool flame reaction come from the end methyl groups of propane.

(2) Acetaldehyde, an important intermediate, is a two-carbon fragment of the propane and the carbon atom in the —CHO group is from the 2-position of the parent molecule.

(3) Formaldehyde arises from all three carbon atoms of the propane. Since its exclusive formation via methyl radical oxidation would produce formaldehyde containing mostly the end carbon atoms of the reactant, a second mechanism of production is indicated. This may be the decomposition of ethoxy radicals, as postulated by others.

(4) The isotopic compositions of the carbon oxides differ considerably, showing that only a fraction of the carbon dioxide produced can result from the oxidation of carbon monoxide. Most of the carbon dioxide comes from the 2-position in propane; this supports the view that much of it is formed via decomposition of the acetoxy or peracetyl radical.

(5) Evidence for the combination of methyl radicals to form ethane, and for reactions of methyl radicals and carbon monoxide to give acetone has been obtained. These processes occur in the presence of large concentrations of reactive stable species, indicating that the methyl radical population may be quite high in the cool flame.

More detailed conclusions can be drawn from the data in Table 2, but since this report is intended mainly as a communication of experimental results, the interpretation will not be carried further here.

It is interesting to find that tracer techniques using carbon isotopes work reliably in studies of slow oxidation reactions. The application here has been to the 'worst' case, that of multiple cool flames with associated sudden temperature rises of perhaps 100°C or more above the furnace temperature, and with extensive reaction taking place. Since isotopic mixing was slight under these circumstances, it is very unlikely to be a problem where less drastic conditions obtain.

Much more can be learned using these techniques. For example, a better quantitative analysis of the product mixture, taken together with the data presented here, would tell something about the relative importance of the reaction paths via acetaldehyde and formaldehyde oxidation. Determination of the isotope content of the one-carbon products at several points during the induction period would also yield informative results.

We wish to thank Dr. F. L. Howard for his support and encouragement of this work, and Mrs. Mary Joslyn and others of the Mass Spectrometry Section of the National Bureau of Standards for the mass spectrometric analyses and for their considerable patience with small samples.

This work was supported by the United States Air Force Office of Scientific Research of the Air Research and Development Command under Contract CSO-680-56-33.

REFERENCES

[1] Pease, R. N. *Chem. Rev.* 21 (1937) 279
[2] Harris, E. J. and Egerton, A. *Chem. Rev.* 21 (1937) 287
[3] Lewis, B. and von Elbe, G. *Combustion, Flames and Explosions of Gases.* 1951. New York; Academic Press
[4] Knox, J. H. and Norrish, R. G. W. *Proc. Roy. Soc. Lond. A* 221 (1954) 151
[5] Cullis, C. F. and Newitt, E. J. *Proc. Roy. Soc. Lond. A* 237 (1956) 530
[6] — — *Proc. Roy. Soc. Lond. A* 242 (1957) 516
[7] Grumer, J. *Fifth Symposium (International) on Combustion,* p. 447. 1955. New York; Reinhold
[8] Satterfield, C. N. and Reid, R. C. *Fifth Symposium (International) on Combustion,* p. 511. 1955. New York; Reinhold
[9] Burt, R., Ebeid, F. B. and Minkoff, G. J. *Nature, Lond.* 180 (1957) 188
[10] Private communication from C. F. Cullis
[11] Byrko, B. M., Kryuglakova, K. E. and Lukovnikov, A. F. *Dokl. Akad. Nauk SSSR* 108 (1956) 1093
[12] Newitt, D. M. and Thornes, L. S. *J. chem. Soc.* (1937) 1656
[13] Yokley, C. R. and Ferguson, R. E. *Combustion and Flame* 2 (1958) 117
[14] Ferguson, R. E. *Combustion and Flame* 1 (1957) 431
[15] Field, F. H. and Franklin, J. L. *Electron Impact Phenomena,* p. 214. 1957. New York; Academic Press
[16] Rust, F. F., Seubold, F. H. and Vaughan, W. E. *J. Amer. chem. Soc.* 73 (1951) 15
[17] Blanchard, L. P., Farmer, J. B. and Ouellet, C. *Canad. J. Chem.* 35 (1957) 115
[18] Mardles, E. W. J. *Trans. Faraday Soc.* 27 (1931) 686
[19] Faltings, K. *Ber.* 72B (1939) 1207
[20] Porter, G. B. and Benson, S. W. *J. Amer. chem. Soc.* 75 (1953) 2773

20

SOME PROBLEMS OF ELEMENTARY REACTIONS IN GAS-PHASE SLOW COMBUSTION

Z. G. SZABÓ

In this paper—which is intended to be a supplement to Tipper's[1] excellent treatise—I should like to add some remarks on three main problems: (1) the wall-effect and its role in the reaction; (2) conclusions drawn from the examination of the bond strength; and (3) interpretation of the strange shape of the kinetic curve.

So far the wall-effect has been considered both in the starting and breaking processes of oxidation reactions, especially in the case of oxidation of hydrocarbons, although it can be stated beyond doubt that in recent work its role in the rupturing reactions has been examined in more detail. The relationships are extremely complicated in such a complex process as the oxidation of hydrocarbons so that some effects may be screened by others; therefore, if we want to reach more or less unambiguous conclusions the complicating factors must be excluded as far as possible. Our experiments[2] carried out in extremely clean vessels and with materials of extreme purity exhibited just such an analysis of the wall-effect.

When the experiments on oxidation of hydrocarbons were carried out in a fresh vessel which had been treated with hydrofluoric acid, this gave the most rapid reaction which then in the aged vessel took place more and more slowly and at last the process was the slowest in vessels treated at high temperature. On the other hand, in vessels not treated with hydrofluoric acid the reaction started slowly and measurable reaction rates could be obtained only after a series of experiments[3]. This behaviour might suggest that the common glass wall is contaminated and thus poisoned for the primary reaction and this is the reason why the reaction takes place at a slower rate, whereas a surface treated with hydrofluoric acid is active and the reaction starts easily on it.

In my opinion the situation is quite different. Two different kinds of surface must be distinguished, the apparent effect of which can be the same; namely, the fresh surface which has not been treated and the surface conditioned at high temperature and in high vacuum. In the contaminated vessel the subsequent experiments accelerate because meanwhile the wall gets clean; similarly, in a very clean vessel not treated with hydrofluoric acid the reaction is also slow and it becomes quicker in the subsequent experiments.

These phenomena can be interpreted by assuming that the wall-effect refers especially to chain breaking. The contaminated surface ruptures the chain with great efficiency, therefore the process is slower. After repeated experiments the surface becomes clean and the process quicker. The extremely pure surface is uncovered, hence it is very active, and it also breaks the oxidation chains to a great extent. In the course of the subsequent experiments the surface becomes slowly covered, its chain-breaking activity decreases, consequently the overall process accelerates. This is supported by the fact that in a vessel not treated with hydrofluoric acid the increase of the rate in subsequent runs is very similar to the acceleration of subsequent reactions which take place in a vessel evacuated for a long time and at high temperature, but not treated with hydrofluoric acid[4].

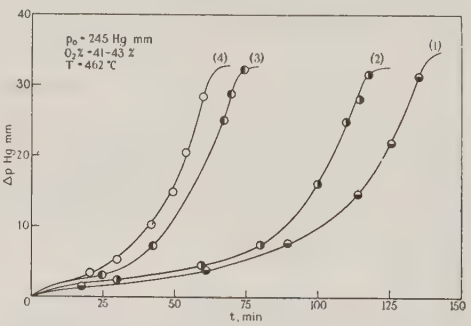

Figure 1. Gradual acceleration of reactions of $2C_2H_6 + O_2$ *in Pyrex vessel evacuated first strongly at high temperature*

Thus in very clean vessels the gradual acceleration of reactions shows the characteristics of the wall-effect of the Bodenstein–Bernreuter type. According to this opinion treatment with hydrofluoric acid does not activate but, on the contrary, deactivates the wall by dissolving of its edges and peaks which first of all represent the active centres. Thus the chain breaking is less frequent and the process quicker. The correctness of this point of view is further proved by the following two facts.

A wall treated with hydrofluoric acid keeps its activity more or less even when after the experiment it stands in air for a long time, e.g. in the experiments of Egerton and his co-workers[3]

(*Figure 3*) where it was standing in air for 20 weeks under such conditions that common glass surfaces would be contaminated and become inactive in general. In their experiments the activity—the smaller extent of breaking—did not change considerably. On the other hand it is interesting to note that the experiments carried out in a silica vessel are very similar to experiments carried out in a Pyrex vessel treated with hydrofluoric acid[3]. The silica surface is smooth and inactive from the point of view of breaking. That the wall plays the most important role in the breaking is shown by the fact that on introduction of acetylene–oxygen mixture into the reaction vessel an explosion occurs in every case except when the surface is covered with basic substances, as for example with tertiary phosphates[5].

In our opinion the wall does not exert any effect in initiating the reaction chain. This has not been, as far as we know, until now explicitly stressed. There is some reaction in vessels covered by different substances but it is extremely slow. Should the wall play any role in the initiating of the reaction no slow reaction could be observed, only explosion. It is a well known fact in reaction kinetics that an appreciable conversion may evolve from very few primary acts, too, supposing that the chains be long enough. As an example the kinetics of thermal decomposition of chlorine dioxide may be mentioned.

From the fact that the slowing down of the reaction becomes especially strong in the case of such a covering which decomposes the peroxides, the assumption becomes very probable that the chain-breaking effect of the wall becomes effective in determining the fate of the radical HO_2. In consequence, in processes influenced less by the wall a greater role must be attributed to this radical than has been done till now, as can be seen from the discussion in the paper of Egerton and his co-workers[3].

It is very likely that the wall has no role in the primary process. Apart from the characteristics of the wall reaction this is mainly supported by energetic calculations. Opinions are not yet unequivocal as far as the heat of reaction of the process $H + O_2 = HO_2$ is concerned but the reaction $RH + O_2 = HO_2 + R$, even in the case of methane, is endothermic to such an extent only that the activation energy secures richly the heat of the reaction. In order to estimate the relationships we must know the bond dissociation energy of some R–H bonds, then we can calculate exactly such and similar bond strengths[6]. For example it can be easily established that the bond dissociation energy of the hydrogen atom referring to the hydrogens of CH_4, C_2H_6, C_3H_8 (secondary) and C_4H_{10} (tertiary) are: 103, 101, 99 and 97 kcal. The change of the bond strength shows well the increasing probability of the dissociation of hydrogen, in other words, the place of the primary attack. Knowing the bond strengths it can be easily estimated that, due to the decreasing of the activation energy, the ratios of the probabilities of dissociations of the tertiary, secondary and primary hydrogens are: 20 : 3 : 1. Some other bond strengths are:

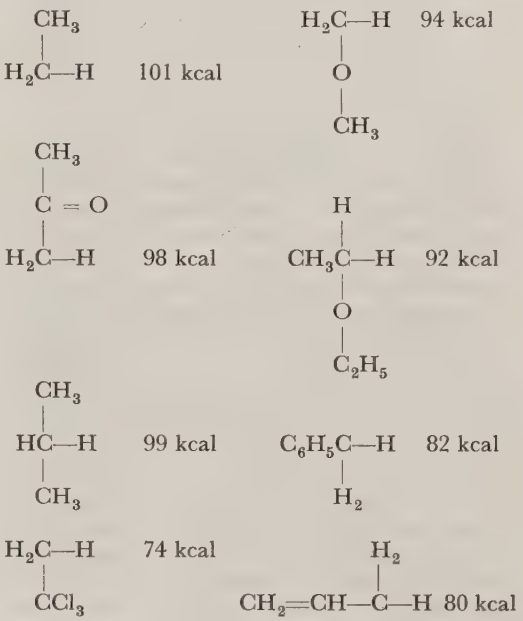

The process of dehydrogenation in the case of ethylene and even of acetylene means the bond dissociation of a more stronger C–H bond than in the case of aliphatic hydrocarbons, these values being 104 and 131 kcal respectively. It is thus evident that in these unsaturated hydrocarbons the dehydrogenation reaction would require greater activation energy, but the activation energy—which can be best estimated from the temperature coefficient of the running up time, τ_{max}, as we have already stressed[2]—varies in the case of ethane between 60 to 75 kcal, depending on the oxygen content, but in the case of ethylene it is only 31 kcal. In connection with this we must stress that in the oxidation of ethylene in a clean vessel no wall-effect has been observed. A process which needs a great activation energy could take place with a lower activation energy only on the wall and the very opposite is true. The measured activation energies essentially supply the endothermic reaction heat of the dehydrogenation steps, even if the enthalpy of formation of the reaction $H + O_2 = HO_2$ is taken only as 50 kcal.

In the case of unsaturated hydrocarbons the oxygen does not react by dehydrogenation but by an addition reaction. An interaction occurs

between the π electrons of the double bond and the oxygen atom or molecule, respectively, which can be considered as a bi-radical. The oxide and peroxide thus formed reacts in different ways by breaking off different bonds. In the oxidation reactions of hydrocarbons the examination of the bond strengths may give us further interesting information. For example it can be demonstrated that in hydroperoxides formed after the dissociation of a tertiary hydrogen the O–O bond and the neighbouring C–C bond will break most easily with respect to the intervening decrements.

The kinetic curve of the oxidation of hydrocarbons differs to a great extent from those of other chemical processes. It is the very analysis of this peculiar shape which may promise that we shall be able to obtain an insight into the mechanism of the process. In the previous investigations the rate–time curves passing their maximum descend almost symmetrically. This fact is reflected by the ξ function of Semenoff[8]. Such an asymmetry of the rate–time curve was shown by the investigations of Tschirkov and Entelis[9]. In our investigations on the oxidation of ethane under extremely clean conditions the rate–time curve accelerates gradually up to the maximum and then descends in a very abrupt slope[10]. The statement that the process suddenly finishes at its maximum rate is true to a good approximation. This circumstance allows us to draw the conclusion that the extremely pure conditions conserve a carrier which is able to cause this peculiar course of reaction.

The time lag, i.e. the period during which no pressure change in the reaction mixture can be observed, does not mean that nothing happens in the mixture. The time lag may occur if the processes take place without any change in the molar number. This is possible because the initial steps of the hydrocarbon oxidations—in different mechanisms suggested by different authors—are mostly such bimolecular reactions, the products of which are also two molecules. The rise after the time lag reaches the maximum with acceleration in general, and the rate curve breaks at this point.

This type of reaction is in accordance with Semenoff's[11] recent assumption referring to the zoning of the hydrocarbon oxidation processes. We think it is necessary to add to this hypothesis that in the process a self-inhibition is also present. The rise of the rate curve begins only when the concentration of the burning substance drops under a certain ratio and the concentration of some of the intermediates increases above a certain ratio. The phenomenon of the self-inhibition, which can be regarded as the contrary of the autocatalytic effect, has been given less attention in the reaction kinetics until now, although its presence can be established beyond doubt in the degenerate explosion of chlorine monoxide, for example. In this reaction, as is known, chlorine dioxide is formed, and it may reach a fairly high concentration. The chlorine dioxide formed does not explode until chlorine monoxide is present, although it would be expected under the experimental conditions. A new and sudden increasing of the kinetic curve—agreeing with the explosion curve of the pure chlorine dioxide—begins when the concentration of the chlorine monoxide drops below 5 per cent of its initial value[12].

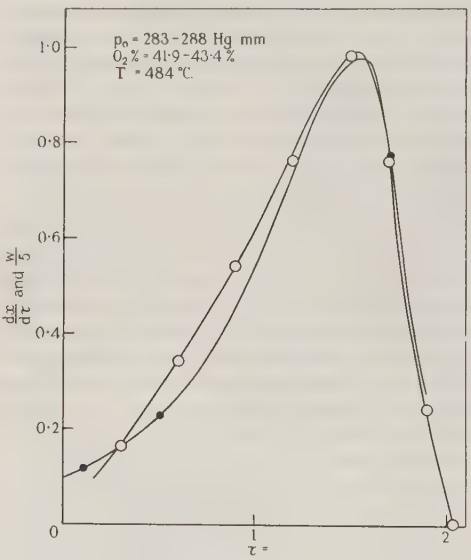

Figure 2. Approximation of the rate–time curve of a reaction $A = 0{\cdot}18$, $B = -4{\cdot}00$, $C = -0{\cdot}60$, $D = 6{\cdot}00$, $E = 0{\cdot}10$

Not much can be said about the chemistry of the process of self-inhibition in hydrocarbon oxidation; nevertheless, we have tried to describe formally the peculiar shape of the kinetic curve. As a first step, we tried to connect this peculiar behaviour with the autocatalytic effect of an intermediate product. The scheme of the reactions is the following:

(1) $A + B \rightarrow X + E$

(2) $A + X \rightarrow I + X'$ followed by the fast $B + X' \rightarrow I + X$

(3) $A + X \rightarrow 2X + I$

(4) $X + X \rightarrow E$

(5) [Au] $I + X \rightarrow 2X$

This scheme contains, besides the formal equations[13] of the starting, propagating, branching

and rupturing processes, an autocatalytic step designated with [Au]. Its rate must be considered in the velocity equation by the term $k_5(c_0-c)n$. The system of the rate equations is the following:

$$\frac{dn}{dt} = k_1c^2 + k_3cn + k_5(c_0 - c)n - k_4n^2$$

$$-\frac{dc}{dt} = k_1'c^2 + k_2cn$$

This system of equation can be formulated with the substitutions $c = c_0x$, $k_2n = c_0y$ and $0{\cdot}125\ t = \tau$ and further by separating the rate component $k_5(c_0-c)n$ into two parts, as follows

$$\frac{dy}{d\tau} = Ax^2 + Bxy + Cy^2 + Dy$$

$$-\frac{dx}{d\tau} = Ex^2 + xy$$

By the variation of A, B, C, D and E we have succeeded in obtaining rate curves which approximate the peculiar form of the rate curve of the oxidation of ethane.

REFERENCES

[1] Tipper, C. F. *Quart. Rev.* 11 (1957) 313
[2] Szabó, Z. G. and Gál, D. *Combustion and Flame* 1 (1957) 404
[3] Egerton, A. C., Minkoff, G. J. and Salooja, K. C. *Combustion and Flame* 1 (1957) 25; *cf.* also Cheaney, D. E. and Walsh, A. D. *Fuel* 35 (1956) 258
[4] Gál, D. and Szabó, Z. G. *Acta Chim. Hung.* 16 (1958) 16
[5] Szabó, Z. G. and Gál, D. *Acta Chim. Hung.* 11 (1957) 263
[6] — *Z. Elektrochem.* 61 (1957) 1083
[7] Walsh, A. D. *J. chem. Soc.* (1948) 331
[8] Semenoff, N. N. *Chemical Kinetics and Chain Reactions*, p. 301. 1935. Oxford
[9] Tschirkov, N. and Entelis, G. *Zhurnal Fizitsheszkoj Himii* 22 (1948) 930; *Chemical Abstracts* 43 (1949) 473
[10] Szabó, Z. G. and Gál, D. *Acta Chim. Hung.* 10 (1957) 395
[11] Semenoff, N. N. *On Some Problems of Chemical Kinetics and Reactivity.* 1954. Moscow (In Russian) (Revised edition published in English, 1958)
[12] Beaver, J. J. and Stieger, G. *Z. phys. Chem. B* 12 (1931) 93
[13] Szabó, Z. G. *Z. Elektrochem.* 59 (1955) 1038

21

RATE CONSTANTS OF ELEMENTARY REACTIONS IN HYDROCARBON OXIDATION—LOW TEMPERATURE OXIDATION OF LOWER HYDROCARBONS

J. H. KNOX

The slow oxidation reactions of aliphatic hydrocarbons are among the best examples of degenerately branching chain reactions[1]. Such reactions proceed through the agency of free radical chains of finite length which produce a product, I, of intermediate stability which can react after a delay of the order of minutes to initiate new chains. Provided that any one chain eventually initiates at least one new chain the reaction will accelerate exponentially[2]. Normally the pressure rise gives a reasonably good measure of the extent of reaction[3] (see *Figure 1*) and one accordingly expects that the pressure will increase during the reaction according to the equation

$$\Delta p = A \,.\, e^{\phi t} \quad \text{or} \quad \rho = d(\Delta p)/dt = \phi \,.\, \Delta p$$

where ϕ is the net branching factor or acceleration constant of the reaction. ϕ is thus obtained from a

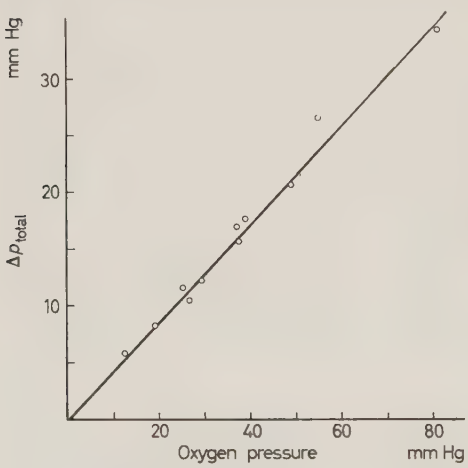

Figure 1. Total pressure rise as a function of initial oxygen pressure in the oxidation of propane at 318°C

plot of rate of pressure rise, ρ, against pressure rise, Δp. Experimentally such plots are straight over the greater part of the acceleration of the reaction as shown in *Figure 2*.

The acceleration constant ϕ may be evaluated in terms of the rates of the individual steps in any degenerate branching mechanism as follows. Let the length of the basic chains be ν and let a proportion α of the chain steps produce the active intermediate I. Let a fraction β of these molecules

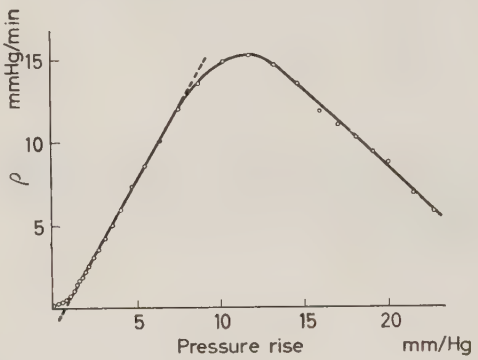

Figure 2. Rate versus *pressure rise curve for oxidation of propane at* 318°C [C_3H_8] = 54·6 mm Hg [O_2] = 77·2 mm Hg. $\phi = 1{\cdot}80\ min^{-1}$

of intermediate I actually react to form free radicals which initiate new chains, and let θ be the lifetime of I with respect to *all* the reactions destroying it, whether or not they finally initiate new chains. The net number of additional chains produced by any one chain is then

$$n = (2\alpha\beta\nu - 1)$$

and the acceleration constant is

$$\phi = n/\theta = (1/\theta)(2\alpha\beta\nu - 1)$$

The number 2 enters into the equations since each molecule of I will generally yield two free radicals in the branching reaction. If it is assumed that the termination of the reaction chains involves the same radical, X, as normally attacks the hydrocarbon, Hy, the actual rates of the various reactions may be expressed generally as:

Propagation	$R_p = k_p[\text{Hy}][\text{X}]$
Termination	$R_t = k_t[\text{X}]$
Branching	$R_b = k_b[\text{I}]$
Non-branching destruction of intermediate	$R_d = k_d[\text{I}]$

then

$$1/\theta = (k_b + k_d)$$

$$\beta = k_b/(k_b + k_d)$$

$$\nu = k_p[\mathrm{Hy}]/k_t$$

and

$$\phi = (k_b + k_d)\left\{2\alpha \frac{k_b}{k_b + k_d} \times \frac{k_p[\mathrm{Hy}]}{k_t} - 1\right\}$$

$$= k_b\left\{2\alpha \frac{k_p[\mathrm{Hy}]}{k_t} - 1\right\} - k_d$$

In this expression the generalized rate constants may themselves contain concentration factors. If, for example, the branching reaction were second order and of the form

$$\mathrm{I} + \mathrm{O_2} = 2 \text{ free radicals}$$

then the branching rate constant would be $k_b = k_b'[\mathrm{O_2}]$ where k_b' is independent of reactant

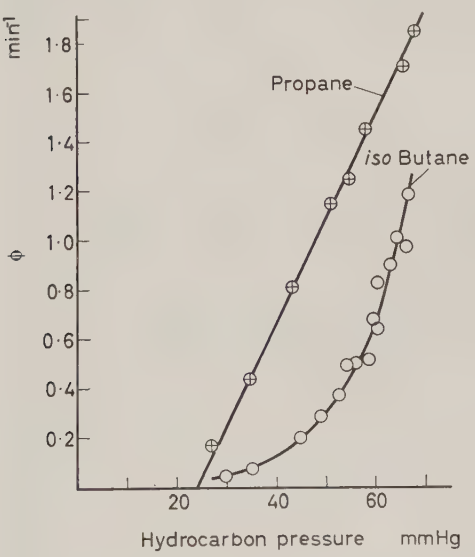

Figure 3. Plots of ϕ against [Hy] *for oxidations at* 318°C. C_4H_{10}/O_2 *mixtures equimolecular;* C_3H_8/O_2 *mixtures contained* $[O_2] = 54$ mm Hg

concentration. In the simplest case where $k_d = 0$, α is constant and ν is proportional to [Hy], a plot of ϕ against [Hy] should be a straight line whose negative intercept on the ϕ axis gives k_b and whose gradient gives $2\alpha k_b k_p/k_t$. Such straight lines are obtained for ethane and propane but not for *iso*butane where the dependence is more complex (see *Figures 3* and *4*).

The maximum rate of reaction, which is a more widely measured reaction parameter than the acceleration constant, is more difficult to interpret. The maximum rate may result either from the consumption of the reactants or from the destruction of the intermediate I by radical attack[3–5]. It appears that both factors are important in most oxidation systems but that to a first approximation the former may be ignored in oxygen rich mixtures. Two pieces of evidence support this conclusion (*a*) that ϕ does not decline until a considerable degree

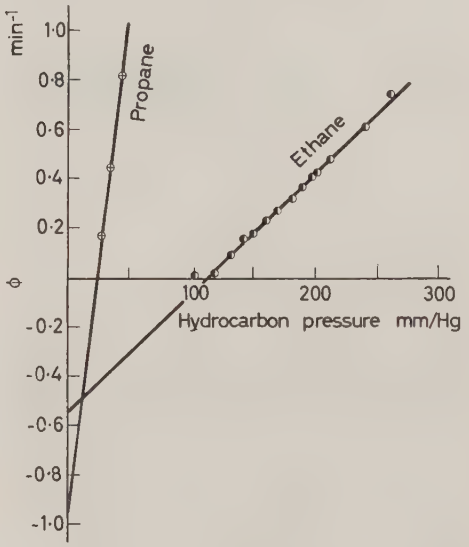

Figure 4. Plots of ϕ against [Hy] *for oxidations at* 318°C. C_3H_8/O_2 *mixtures as in Figure 3;* C_2H_6/O_2 *mixtures equimolecular*

of reaction has occurred (see *Figure 2*) and that the products of reaction are therefore as effective in propagating the reaction as the original reactants, and (*b*) that a 'negative induction period' may often be induced by the addition of sufficient chain initiating substances such as aldehydes[4]. With propane the addition of excess propionaldehyde, as shown in *Figure 5*, causes the reaction to start at a

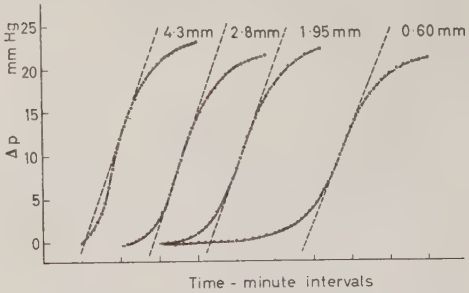

Figure 5. Effect of added propionaldehyde on pressure-time curves for oxidation at 318°C *of mixtures containing* $[C_3H_8] = 50$ mm Hg; $[C_3H_6] = 5$ mm Hg; $[O_2] = 54$ mm Hg. *Propionaldehyde pressures are given on individual lines*

greatly enhanced rate, but the rate of reaction finally achieved is found to be only slightly increased by the addition of the aldehyde. There is therefore a maximum rate of reaction which can be

tolerated by the system in the later stages of reaction. This rate is not dependent upon the rate at which the reaction commences.

When free radical removal of the intermediate limits the maximum rate of reaction we may write

$$R_d = k_d[\mathrm{I}] = k'_d[\mathrm{X}][\mathrm{I}]$$

where it is assumed that the radical attacking and destroying I is the same as normally attacks the hydrocarbon. Thus for any stage in the reaction

$$\phi = k_b \left\{ 2\alpha \frac{k_p[\mathrm{Hy}]}{k_t} - 1 \right\} - k'_d[\mathrm{X}]$$

At maximum rate of reaction $\phi = 0$ and therefore rearranging

$$[\mathrm{X}] = \frac{k_b}{k'_d} \left\{ 2\alpha \frac{k_p[\mathrm{Hy}]}{k_t} - 1 \right\} = \phi_0/k'_d$$

where ϕ_0 is the value of ϕ at the beginning of the reaction when [X] is small. The maximum rate of removal of the hydrocarbon is then

$$R_{\max} = k_p[\mathrm{X}][\mathrm{Hy}] = \frac{k_p \times \phi_0[\mathrm{Hy}]}{k'_d}$$

$$\frac{R_{\max}}{\phi_0[\mathrm{Hy}]} = k_p/k'_d$$

$R_{\max}$ is however the rate of removal of the hydrocarbon while the quantity measured experimentally is the rate of pressure rise. The two are simply

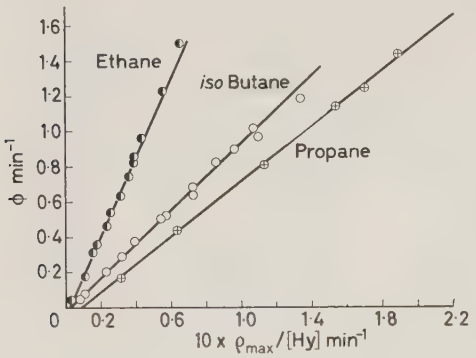

Figure 6. Plots of ϕ against $\rho_{\max}/[\mathrm{Hy}]$ for ethane, propane and isobutane oxidations at 318°C. Mixtures as for Figures 3 and 4. For ethane, ordinates and abscissae should be halved

connected. The total pressure rise in the reaction is proportional to the initial oxygen pressure (*Figure 1*), that is $\Delta p_{\max} = B \times [\mathrm{O_2}]$ where B is found experimentally to be independent of hydrocarbon concentration. It is therefore almost certain that the rate of pressure rise during the reaction is proportional to the rate of disappearance of oxygen. In the mechanisms so far proposed for low temperature oxidations[6–9] one molecule of oxygen is initially consumed for each molecule of hydrocarbon used and it is therefore reasonable to identify the rate of disappearance of oxygen with the rate of disappearance of hydrocarbon. Thus $\rho_{\max} = B \,.\, R_{\max}$ and

$$\frac{\phi_0[\mathrm{Hy}]}{\rho_{\max}} = \frac{k'_d}{B \,.\, k_p}$$

This relation holds well for ethane, propane and *iso*butane (see *Figure 6*) provided that the $[\mathrm{O_2}]/[\mathrm{Hy}]$ ratio is not less than unity. For lower ratios the maximum rate is largely limited by the consumption of oxygen and the reaction ceases suddenly when all the oxgyen is consumed. The experimental values of $\phi_0[\mathrm{Hy}]/\rho_{\max}$ then increase with decreasing oxygen concentration. However, for oxygen rich mixtures, where the ratio is constant and independent of oxygen pressure, the rate constant ratio k'_d/k_p may be obtained. The values obtained for k_b, $2\alpha k_p/k_t$, B and k'_d/k_p for ethane, propane and *iso*butane at 318°C are given in Table 1.

TABLE 1

	k_b min^{-1}	$2\alpha k_p/k_t$ (cm Hg)$^{-1}$	B	k'_d/k_p
Ethane*	0·55	0·089	0·245	5·4
Propane	0·98†	0·425‡	0·415	2·9†
*Iso*butane §	—	—	0·40	4·1

* Equimolecular ethane/oxygen mixtures.
† Oxygen pressure larger than 50 mm Hg.
‡ Oxygen pressure 54 mm. Hg.
§ Equimolecular *iso*butane/oxygen mixtures.

The values for the rate constants of branching do not vary as much as might have been expected from ethane to propane, the half-lives of the intermediates being of the order of 2 and 1 minutes respectively. The values appear to be almost independent of oxygen pressure although preliminary results with propane indicate that k_b falls off when the oxygen pressure falls below 50 mm Hg. From *Figures 3* and *4* it can be seen that the number of branches per chain under the experimental conditions used was always small and never exceeded about three. This implies that either the reaction chains are very short or that the quantity α is very much less than unity. It appears unlikely that the chains can be as short as say ten units and therefore likely that α is small and that only a fraction of the chain steps actually produce branching intermediate. This is contrary to most of the theories so far put forward where the branching intermediate is formed in every complete chain cycle.

It is also of note that k'_d/k_p does not vary widely from one hydrocarbon to another. This is in agreement with the results presented in another

paper[10] where the rates of radical attack on ethane, propane and *iso*butane are shown to differ by much less than the overall reactivity of the hydrocarbons. These results can be combined with those of the present paper to give the relative rates of attack of the radicals on the branching intermediates in the oxidations of the three hydrocarbons, and also the relative values of α/k_t. The results are presented in Table 2.

TABLE 2

	Ethane	*Propane*	Iso*butane*
Propagation rate constant relative to k_p for ethane	1·0	2·3	3·4
k'_d/k_p	5·4	2·9	4·1
Rate constant for destruction of I by radicals relative to k_p for ethane	5·4	6·7	14·0
α/k_t relative to value for ethane	1·0	2·1	—

They show that there are only moderate differences in the reactivity of the intermediates with respect to the radicals present and probably only moderate differences in the efficiency of production of branching intermediate, α.

The differences in reactivity of various hydrocarbons are therefore probably due not to major differences in the rates of any one critical reaction such as branching or chain propagation. There appear, in fact, to be at least five factors which are important in determining the overall reactivity of a hydrocarbon towards oxygen: (1) the rate of the branching reaction, (2) the chain length of the basic chain, (3) the fraction of chain steps which produce branching intermediate, (4) the fraction of molecules of I which, once formed, react to initiate new chains, and (5) the rate at which radicals attack the branching intermediate compared to the rate at which they attack the hydrocarbon. The contribution of each factor to the overall reactivity as measured by ϕ or R_{max} may vary only slightly from one hydrocarbon to another but their cumulative effect can very well result in the very large differences in reactivity observed in practice from one hydrocarbon to another.

REFERENCES

[1] Semenov, N. N. *Chemical Kinetics and Chain Reactions*, p. 68. 1935. Oxford University Press

[2] Prettre, M. *Third Symposium on Combustion, Flame and Explosion Phenomena*, p. 397. 1949. Baltimore; Williams and Wilkins

[3] McEwan, A. C. and Tipper, C. F. H. *Proc. Roy. Soc. A* 216 (1953) 280

[4] Harding, A. J. and Norrish, R. G. W. *Proc. Roy. Soc. A* 212 (1952) 291

[5] Bell, K. M. and Tipper, C. F. H. *Proc. Roy. Soc. A* 238 (1956) 256

[6] Norrish, R. G. W. *XVI International Colloquium*, p. 16. 1948. Paris; C.N.R.S.

[7] Walsh, A. D. *Trans. Faraday Soc.* 42 (1946) 269

[8] Cullis, C. F. and Hinshelwood, Sir Cyril. *Disc. Faraday Soc.* 2 (1947) 117

[9] Cullis, C. F. and Newitt, E. J. *Proc. Roy. Soc. A* 237 (1956) 530

[10] Knox, J. H., Smith, R. F. and Trotman-Dickenson, A. F. This volume, p. 126

22

RATE CONSTANTS OF ELEMENTARY REACTIONS IN HYDROCARBON OXIDATION—COMPETITIVE OXIDATION OF LOWER HYDROCARBONS

J. H. KNOX, R. F. SMITH and A. F. TROTMAN-DICKENSON

Although there are considerable differences between the various current theories of the low temperature oxidation of hydrocarbons, they are in agreement in assigning the main consumption of hydrocarbons to the chain-propagating steps. The present work was carried out to throw light on the nature of these steps. As there did not appear to be any way of measuring the rates of these reactions directly, a competitive method of measuring their relative rates was employed. This could be done either by measuring the relative rates of disappearance of the two hydrocarbons from a mixture with oxygen or by the measurement of the rates of appearance of characteristic products formed from them. The latter method has the disadvantage that it is not easy to select products that are truly characteristic of each hydrocarbon and which may be presumed to provide an accurate measure of the rates of reaction. This presumption can only be accepted if it is backed up by a full analytical study of the products. We have accordingly employed the former and more direct method.

In the oxidation of the pure hydrocarbons R_1H and R_2H, the chain-propagating reactions may be written:

$$X_1 + R_1H \rightarrow X_1H + R_1 \quad k_{11}$$

$$X_2 + R_2H = X_2H + R_2 \quad k_{22}$$

where X_1 and X_2 are oxygenated radicals such as OH, HO_2, RO or RO_2. When a mixture of the two hydrocarbons is oxidized, two further propagating reactions will occur:

$$X_2 + R_1H = X_2H + R_1 \quad k_{12}$$

$$X_1 + R_2H = X_1H + R_2 \quad k_{21}$$

If we define the overall rate constants for the removal of the two hydrocarbons as k_1 and k_2, then the ratio k_1/k_2 can be obtained from analysis of the amounts of each hydrocarbon present at the beginning and end of the reaction from the relation

$$\frac{k_1}{k_2} = \frac{\log ([R_1H]_{\text{initial}}/[R_1H])_{\text{final}}}{\log ([R_2H]_{\text{initial}}/[R_2H])_{\text{final}}}$$

If $k_{11} \neq k_{12}$ and $k_{22} \neq k_{21}$, the experimental value of k_1/k_2 will depend upon the composition of the mixture.

In the present experiments known amounts of two hydrocarbons were mixed with oxygen in the reaction vessel. After a convenient time, which was usually close to the time required for the increase in pressure to cease, the mixture was analysed by gas chromatography. An alumina column was used with carbon dioxide as the carrier gas. The gases were estimated by the Janak technique. Ethane, propane, *iso*butane, ethylene and propylene were all cleanly separated.

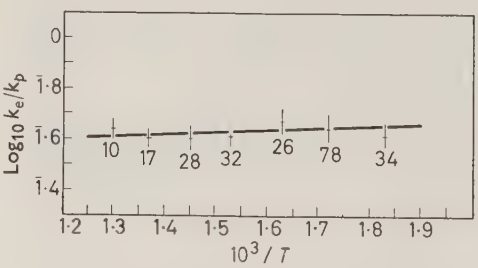

Figure 1. The variation of the ratio k_e/k_p with temperature

Extensive work was carried out on ethane/propane mixtures. It was found at each temperature investigated that the value of k_e/k_p did not vary for ethane/propane ratios between 1/3 and 3/1. This indicates that the attacking radical X_e produced by the reaction of oxygen with an ethyl radical has the same reactivity and is therefore probably the same substance as the radical X_p produced from propyl. k_e/k_p was also found to be independent of the hydrocarbon/oxygen ratio between 5 and 1·3 and of the total pressure in the system between 100 and 600 mm. The dependence of k_e/k_p upon temperature is shown in *Figure 1* (the numbers beside each point give the number of values averaged to obtain the plotted point).

Similar though less extensive experiments were carried out with propane/*iso*butane mixtures at 310° and 420°. Again no change in k_b/k_p was found for variations in the *iso*butane/propane ratio

from 3/1 to 1/3 or for hydrocarbon/oxygen ratios between 2 and 4 to 1.

The remarkable constancy of the ratios

$$k_p/k_e = 2{\cdot}27 \pm 0{\cdot}05 \quad \text{and} \quad k_b/k_p = 1{\cdot}5$$

strongly indicates that the same radical X carries the chains in all three oxidations. The results show that the differences in the activation energies for attack on the three hydrocarbons are very small indeed; the slope of the line in the Arrhenius plot shown in *Figure 1* corresponds to $E_e - E_p = -300 \pm 46$ cal mole^{-1}. It is reasonable to conclude from this small difference that the absolute activation energies must also be very small, probably not more than two or three kcal mole^{-1} at the most.

If the assumption is made that all primary hydrogen atoms react with X at the same rate, it can readily be shown that the values of k_{primary} : $k_{\text{secondary}}$: k_{tertiary} are in the ratio 1 : 3·8 : 11. Since the primary hydrogens in propane and *iso*-butane are probably more reactive than those in ethane, these figures probably overestimate the differences in the reactivities.

Recently, two papers have been published[1,2] in which the relative rates of attack of X on the different positions in propane and 2-methylpentane have been estimated. The estimates are only reliable if the assumed reaction schemes are correct in every detail. The authors recognize that both types of scheme appear doubtful on a number of counts and that the results cannot be accepted without reserve until full detailed analyses of the products have been made.

The comparatively small differences in the reactivities of the hydrocarbons and the apparent absence of activation energy differences make it extremely unlikely that X is a radical of the type ROO. Work on autoxidations in solution indicates that these radicals are markedly selective and react with activation energies of 6 or more kcal mole^{-1} even with olefins. Their reactions with alkanes would probably be considerably endothermic. Furthermore it might be expected that C_2H_5OO would have a detectably different reactivity from C_3H_7OO. Much the same type of argument serves to rule out alkoxy radicals.

The highly reactive radical OH might be expected to have the attributes of X, but it is difficult to explain the results on several oxidations, particularly those at high temperatures, on the assumption that OH is the main chain carrier, whereas an HO_2 chain fits the facts most satisfactorily. For instance, it explains the formation of propylene without hydrogen as the major product of the oxidation of propane above 400°C, and the formation of acetaldehyde and hydrogen peroxide in equal quantities as the only products in the oxidation of ethyl alcohol[3,4] as low as 300°C. However, the presently accepted value of 89·5 $\pm$ 3 kcal mole^{-1} for D(HOO–H) makes it very difficult to accept it as the universal chain carrier. It seems that the problem of the nature of X will only be settled by the study of further hydrocarbons and the acquisition of further knowledge of the properties of the different kinds of oxygenated radicals.

REFERENCES

[1] Burt, R., Ebeid, F. B. and Minkoff, G. J. *Nature* (*Lond.*). 180 (1957) 188

[2] Cullis, C. F., Hardy, F. R. F. and Turner, D. W. *Proc. Roy. Soc. A* 244 (1958) 573

[3] Cullis, C. F. and Newitt, E. J. *Proc. Roy. Soc. A* 237 (1956) 530

[4] Falconer, J. W. and Knox, J. H. Unpublished results

APPLICATION OF RADIOACTIVE ISOTOPES TO STUDY THE MECHANISM OF SOME OXIDATION PROCESSES

D. GÁL, F. DUTKA, L. GUCZI and I. KENDE

We investigated four different reactions: the oxidation of (*a*) mercaptoacetic acid and (*b*) styrene, both in solution; (*c*) acetaldehyde and (*d*) hexane, both in gas phase.

OXIDATION OF MERCAPTOACETIC ACID

The kinetics of the oxidation of mercaptoacetic acid, as a model compound of carboxylic acids containing a sulph-hydril group, have been studied by a great number of authors. Among them the papers of Harrison, Schöberl, and Schöberl and Graefje are the most outstanding[1–3]. They discussed the character of the kinetic curves (oxygen uptake during the reaction time) at different pH values and on the basis of these experimental results they suggested a hypothetical mechanism. The essence of the latter is, that in the first step dithiodiacetic acid is formed from the starting material.

1. $HS—R—COOH \rightarrow$
   $HOOC—R—SS—R—COOH \rightarrow$
   $HOOC—R—SH + HOOC—RSOH \rightarrow$
   $HOOC—RSO_2H \xrightarrow{HOOC—R'SH}$
   $HOOC—R'SSR'COOH$[1]

2. $HS—R—COOH \rightarrow$
   $HOOC—RSS—R—COOH \rightarrow$
   $HOOC—RSH + HOOC—RSOH \rightarrow$
   $HOOC—RSH + HOOC—R—COOH + H_2S \rightarrow$ [2]

3. $HS—R—COOH \rightarrow$
   $HOOC—RSS—RCOOH \rightarrow$

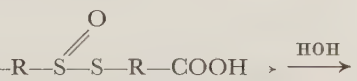

   $2HOOC—R—SOH \rightarrow H_2S + \ldots \rightarrow$ [3]

Present experiments were carried out at 50°C temperature in water solution at pH = 8. Concentration of the mercaptoacetic acid was 0·1867 mol/l. To eliminate the effect of heavy metal trace catalysis, we introduced 0·001 mol/l. 1-2-diamino*cyclo*hexane-tetracetic acid into the system.

The kinetic curves (O_2 uptake in ml plotted against *t*, time in hours) show the ordinary exponential course.

As shown by *Figure 1*, in presence of Na_2S, taken

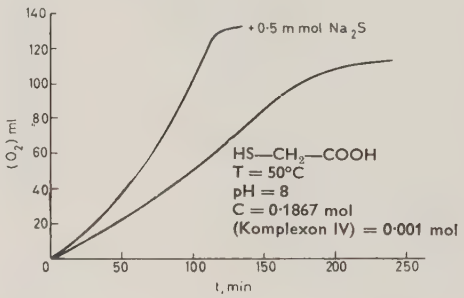

Figure 1

into the system in a very small amount (0·5 mmol/l) at the start of the reaction, the oxygen uptake could be much more swiftly compared with the 'pure oxidation'. So Na_2S has a very pronounced catalytic effect on the reaction.

To explain the role of the Na_2S intermediate product, we used the so-called 'kinetic isotopic method' elaborated by Neuman and co-workers[4]. We have introduced Na_2S labelled with ^{35}S and determined the changes in its specific activity (*Figure 2*, curve 1) and concentration during the reaction (*Figure 2*, curve 2).

From these data we got the amount of the sulphide formed in course of the reaction (*Figure 2*, curve 3).

$$[X] = \int_{t_1}^{t_2} W_1 \, dt = \int_{\alpha_1}^{\alpha_2} c \, d \ln \alpha$$

where α means the specific activity and c the concentration at given time.

From these data we can calculate the rate of sulphide formation:

$$W_1 = -c \frac{d \ln \alpha}{dt}$$

and the rate of its further oxidation:

$$W_2 = W_1 - \frac{dc}{dt}$$

The resulting curves are shown in *Figure 3*.

It can be seen that the formation of sulphide begins at the start of the reaction but its further

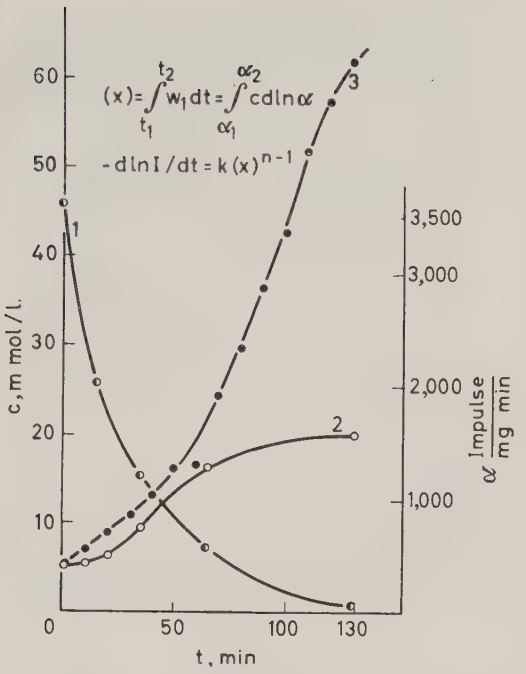

Figure 2

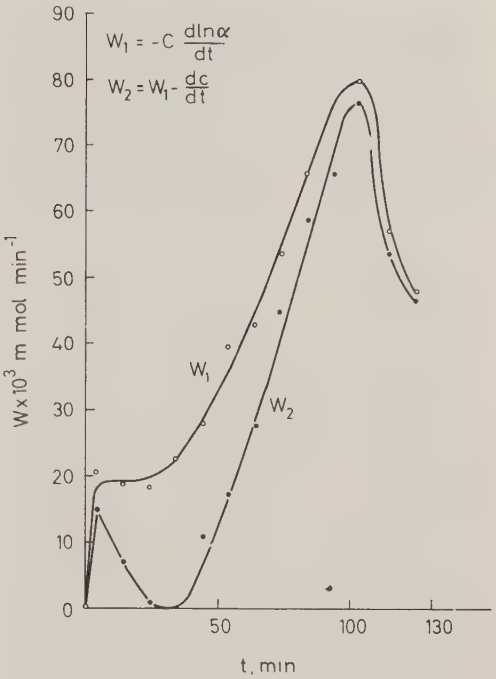

Figure 3

oxidation becomes significant only after a certain period of time. Taking into consideration the fact that the oxygen uptake is considerably catalysed by the little amount of sulphide taken into the system, we can draw the conclusion that the formation of sulphide has a decisive role in this chain reaction.

The oxidation order with respect to sulphide is:

$$-\frac{\mathrm{d}\ln I}{\mathrm{d}t} = k[\mathrm{X}]^{n-1}$$

where I represents the total activity. The further oxidation of sulphide is of first order with respect to the concentration of sulphide. The experimental and calculated data mentioned above are summarized in Table 1.

By intake of inactive sulphate in addition to the kinetic data, the sequence of the intermediate products can also be determined.

OXIDATION OF STYRENE

Oxidation of styrene was studied in detail by Miller and Mayo[5], and Medvedev and Zeitlin[6]. These authors investigated the oxygen uptake in solution and analysed the products. On the basis of the results, they suggested that during the

TABLE 1

Time min	$c = [Na_2S]$ mmol/l	α *Counts*/ mg/min	$w_1 = -c\,\frac{\mathrm{d}\ln\alpha}{\mathrm{d}t}$	$\mathrm{d}c/\mathrm{d}t$	$w_2 = w_1 - \frac{\mathrm{d}c}{\mathrm{d}t}$	$X = \int c\,\mathrm{d}\ln\alpha$ mmol/l
0	0·59	3,620	0·027	0·0025	0·0242	0
5	0·61	2,850	0·0250	0·005	0·0200	0·13
15	0·69	2,030	0·0218	0·011	0·0108	0·36
25	0·81	1,540	0·0204	0·015	0·0054	0·58
35	1·00	1,212	0·0240	0·020	0·0040	0·79
45	1·22	950	0·0281	0·025	0·0031	1·04
65	1·63	571	0·0428	0·0150	0·0278	1·60
95	1·91	202	0·0705	0·0050	0·0655	3·45
105	1·95	150	0·0790	0·0030	0·0760	4·20
125	1·99	80	0·0474	0·0010	0·0464	5·47

reaction two parallel processes are taking place: polymerization and oxidation. The former leads to polymerperoxide, and the latter to benzaldehyde, formaldehyde and peroxides.

We measured the oxidation both in bromobenzene solution and in pure styrene at a temperature of 70°C. *Figure 4* shows the data of oxygen uptake (curve 1, styrene dissolved in

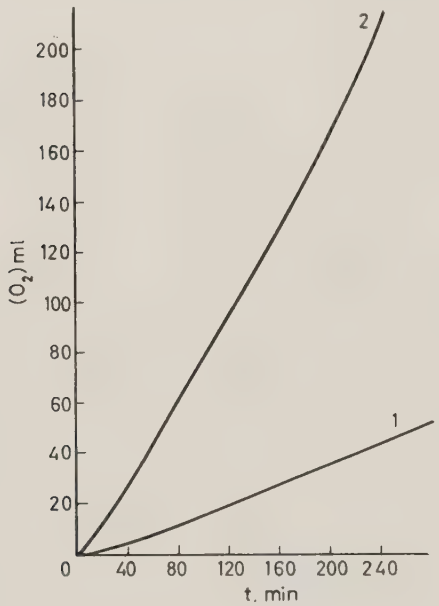

Figure 4

bromobenzene; curve 2, pure styrene). It was necessary to work in the dark because the reaction is very photosensitive.

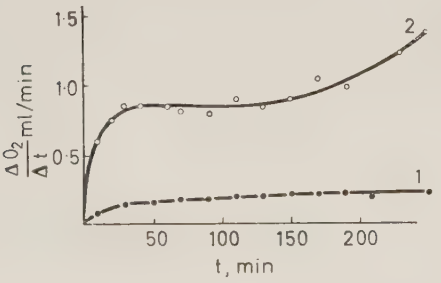

Figure 5

The corresponding rate curves are represented by *Figure 5*. The curves are typical for the oxidation of unsaturated hydrocarbons. It can be seen that in this case also the equation

$$y = Ae^{\varphi t}$$

is not valid, as suggested by Neuman. In its place we suggest

$$y = At^n (n \approx 1)$$

(the φ autocatalytic factor is very small compared to the rate of the initial reaction) see *Figure 6*.

We synthesized in the laboratory 1-^{14}C–styrene from acetic acid labelled with ^{14}C in its carboxyl group. After the oxidation we separated the chief products (polymerperoxide, formaldehyde as dimedonate, benzaldehyde as dinitrophenylhydrazone) and measured their specific activity together

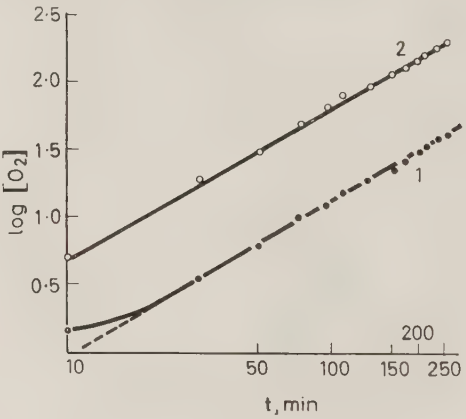

Figure 6

with the starting material. We found among the products labelled formaldehyde, consequently formaldehyde is also formed from the C atom next to the benzol ring. The detailed experimental data will be published elsewhere.

EFFECT OF ACETIC ACID ON OXIDATION OF ACETALDEHYDE IN THE GAS PHASE

Aldehydes play a key role in the oxidation of hydrocarbons. The conclusion to be drawn from more recent papers is that aldehydes—and among them acetaldehyde—are the chief intermediate products in hydrocarbon oxidation and ensure the degenerated branching[7,8]. In a recent paper one of the authors referred to the fact that the appearance of cool flames in lower hydrocarbon oxidation is connected with the accumulation of acetaldehyde[9].

The kinetics of the oxidation were measured at a temperature of 180°C and at 120 mm Hg initial pressure, with 1,1-acetaldehyde–oxygen mixture. In similar circumstances acetic acid catalyses the oxidation in quartz reaction vessel, as explained by Emanuel[10]. This fact is very interesting, because in published data there are only four well known gas reactions in which the end-product plays the role of a catalyst. We investigated this effect in 'Razotherm' reaction vessel among the experimental conditions mentioned above and found, that with an increasing proportion of acetic acid (from 0 to 13 mm Hg) the catalytic effect increases too.

As we can see from *Figure 7*, the time necessary to reach the minimum of the change of pressure diminishes with increasing acetic acid pressure, and the rate of both the rise and decrease of pressure increases also.

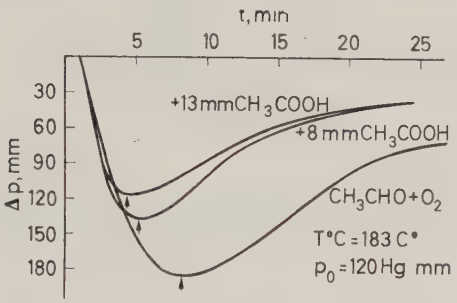

Figure 7

In the next series we made eight reactions under identical conditions and introduced in the system eight times 13 mm Hg acetic acid labelled with ^{14}C in its carboxyl group. After the reactions were completed, the products were frozen out with

TABLE 2

Amount of $CH_3{}^{14}C$ OOH introduced	104 mm Hg = $4{\cdot}42 \cdot 10^{-2}$ g
Specific activity of $CH_3{}^{14}C$ OOH	365 μc/mmol
Total activity introduced	$5{\cdot}92 \cdot 10^{8}$ counts/min
Measured CO_2	$4{\cdot}21 \cdot 10^{-2}$ g
Total activity of CO_2	Series I: $2{\cdot}88 \cdot 10^{5}$ counts/min; Series II: $3{\cdot}08 \cdot 10^{5}$ counts/min

liquid air and their activity was measured. The more important results are summarized in Table 2.

From this table it follows that CO_2 can be formed not only from peracetic acid or acetaldehyde as assumed by Neuman and Feklisow[11] but from acetic acid too. So we can say, that the acetic acid gets further oxidized and the C—C linkage is disrupted. We can assume that the further oxidation of acetic acid is catalysed by the oxidation of acetaldehyde. From these facts we can form an understanding of the catalytic effect of acetic acid on the oxidation of acetaldehyde.

EFFECT OF ACETOPHENONE AND STYRENE ON THE OXIDATION OF HEXANE

Inhibitors and catalysts are of great importance in the oxidation of hydrocarbons. Among them the aromatic compounds have very great effect in small amounts, as is shown by the investigations of Chamberlain and Walsh[12] in case of oxidation of di*iso*propylether-benzene, toluene, styrene, aniline, acetophenone and so on.

Oxidation of hexane is a typical degenerated branching-chain-reaction[13]. We investigated its kinetics at a temperature of 226°C and at an initial pressure of 250 mm Hg (70 mm Hg hexane, 180 mm Hg oxygen). The reaction starts after 1·5 min and the kinetic curves show the ordinary exponential course. In the presence of acetophenone (0·6 mm Hg) the pressure change becomes faster (although in the case of di*iso*propylether, acetophenone acts as an inhibitor). Styrene, on the contrary, inhibits the oxidation. The inhibiting effect increases with the pressure of styrene (from 0 to 6 mm Hg) as in the case of other inhibitors[14] (see *Figure 8*).

The inhibition affects not only the rate, but the total pressure change also: it decreases linearly with the pressure of styrene (*Figure 9*).

If $p_{\text{styrene}} > 4$ mm Hg, the form of the kinetic and rate curves is changed: in the presence of more styrene we get typical curves for the oxidation of unsaturated hydrocarbons and we do not find rate maximums, but after a given time a constant rate (*Figure 10*).

The autocatalytic factors φ in the presence of acetophenone and styrene respectively are summarized in Table 3.

TABLE 3

Styrene mm Hg	*Acetophenone* mm Hg	φ min^{-1}
0	0	0·142
2·6	0	0·079
4·0	0	0·051
6·0	—	0·037
—	0·6	0·228

We synthesized acetophenone labelled with ^{14}C in the oxo group and investigated whether its activity could be measured in the products obtained by the hexane oxidation. We proved that carbon dioxide shows activity. From this fact it follows that CO_2 is formed from the oxo group. The object of our further investigations is to measure the activity of the other end-products and intermediate products at different reaction times, in the presence of labelled styrene.

The activity of sulphur was measured by a G.M. tube of 1 mg/cm^2 end-window; measurements of ^{14}C were carried out with the gas counter shown in *Figure 11*.

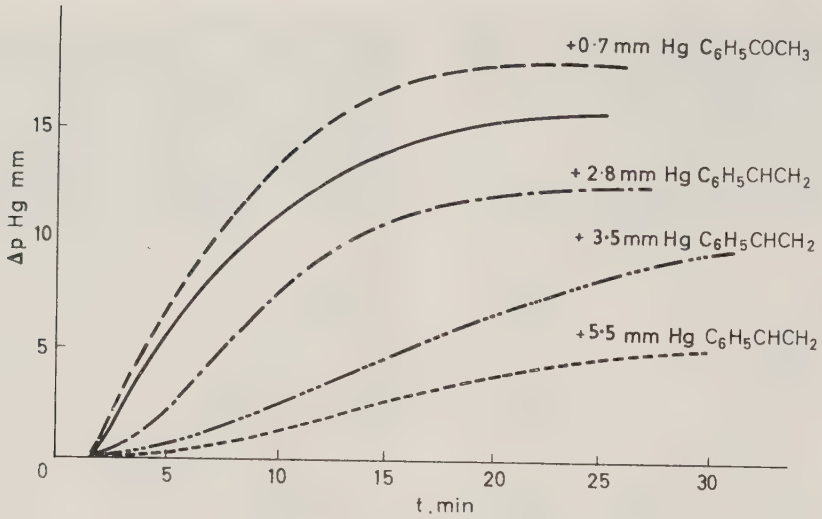

Figure 8

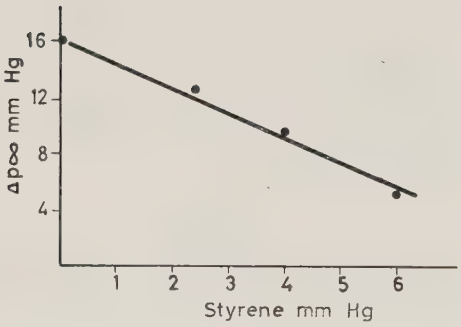

Figure 9

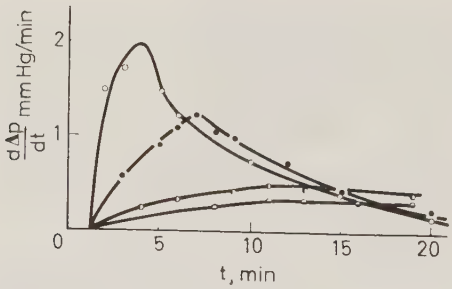

Figure 10

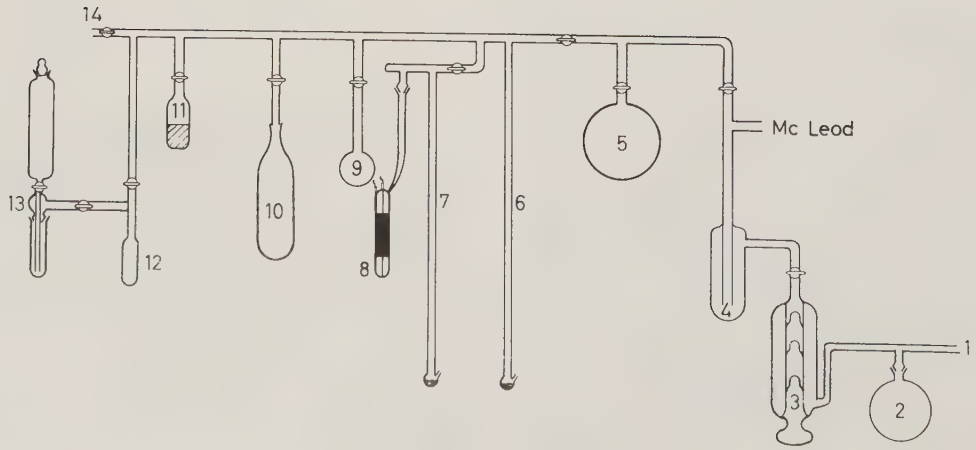

Figure 11

It is to be noticed that the organic compounds were transformed into carbon dioxide and $BaCO_3$ respectively and the evolving CO_2 was led with ethanol as self-quenching gas into the system.

REFERENCES

[1] Harrison, D. C. *Biochem. J.* 21 (1927) 1404
[2] Schöberl, A. *Liebigs. Ann.* 507 (1933) 111
[3] Schöberl, A. and Graefje, H. *Proc. Inst. Wool. Text. Res. Conf.* C 157 (1955)
[4] Neuman, M. B. *J. phys. Chem. Moscow* 28 (1954) 1235
[5] Miller, A. A. and Mayo, F. R. *J. Amer. chem. Soc.* 78 (1956) 1017
[6] Medvedev, S. and Zeitlin, P. *J. phys. Chem. Moscow* 18 (1944) 13
[7] Pollak, S. S. and Stern, J. V. *J. phys. Chem. Moscow* 27 (1953) 631
[8] Stern, J. V. and Pollak, S. S. *C. R. Acad. Sci. URSS* 65 (1949) 311
[9] Gál, D. and Szabó, Z. G. *Acta chim. hung.* 16 (1958) 39
[10] Emanuel, N. M. *Kinetics of oxidation chain reactions*, p. 167. 1954. Akademiai Kiadó; In Hungarian
[11] Neuman, M. B. and Feklisow, G. I. *C. R. Acad. Sci. URSS* 90 (1953) 583
[12] Chamberlain, G. H. N. and Walsh, A. D. *Trans. Faraday Soc.* 45 (1949) 1032
[13] Cullis, C. F. and Hinshelwood, C. N. *Disc. Faraday Soc.* 2 (1947) 117
[14] Szabó, Z. G. and Gál, D. *Acta chim. hung.* 11 (1957) 205

SOME PROCESSES IN GASEOUS SLOW COMBUSTIONS. FORMATION OF CARBON MONOXIDE AND CARBON DIOXIDE

G. SKIRROW and C. F. H. TIPPER

SUMMARY

A general mechanism is proposed to account for the formation of carbon monoxide, carbon dioxide, and incidentally carboxylic acids, in the slow combustion of hydrocarbons and their simple derivatives in the gas phase. It is suggested that with most fuels CO and CO_2 are produced solely from aldehydes, which are intermediates in oxidation.

$$RCHO \xrightarrow{-H} RCO \xrightarrow{O_2} \begin{cases} R + CO \\ CO_2 + \text{products} \end{cases}$$

The overall picture, the steps of which are discussed in detail, can account for the variation of the relative yields of CO and CO_2 with conditions given in the literature, although in a few cases it is necessary to assume that the above is not the only method of formation.

INTRODUCTION

Despite the large amount of work on combustion there is still no general agreement about many of the processes involved, and there exists a need to examine oxidation systems in detail in order to attempt to detect generalizations. The purpose of this paper is to suggest a general mechanism for the production of CO and CO_2 in slow combustion reactions of paraffins, olefins and saturated aldehydes. In addition possible reasons for the failure of certain systems to comply with the proposed scheme are examined.

An attempt to explain CO production in slow combustion reactions has been made previously by Walsh[1]. He postulated the direct breakdown of intermediate aldehydes formed by peroxy-radical decomposition according to

$$RCH_2OO \rightarrow RCHO \rightarrow RH + CO$$

but offered no suggestion for the origin of carbon dioxide or carboxylic acid. In the theory which we propose an intermediate aldehyde is still recognized as the source of the carbon monoxide, although we suggest that actual attack on the aldehyde must precede CO formation. A second, and more important, aspect of our treatment is that an intimate relationship between the production of carbon monoxide, carbon dioxide and carboxylic acid is suggested.

Before examining the theory in detail it is pertinent to consider to what extent carbon dioxide produced in gaseous oxidations may be regarded as a product of the direct oxidation of carbon monoxide.

Very dry carbon monoxide[2] does not react at an appreciable rate with oxygen much below 1,000°C. Water vapour may depress this temperature[3] to about 400°C, and in the oxidation of simple hydrocarbons at temperatures in excess of this a proportion of the carbon dioxide must be regarded as being produced via the monoxide. For example, in the oxidation of methane in static systems at 670° the CO–time curve passes through a maximum[4]. Van Meerssche[5] has shown that in this reaction both CO and CH_4 are subject to attack by the same active centres. Bell and Tipper[6] showed that the addition of CO to the CH_3OH–O_2 system at 440° increased the yield of dioxide.

Below 400–440°C it is unlikely that direct oxidation of carbon monoxide plays a significant part in hydrocarbon combustion reactions although a few studies designed to test this point have been made. However, by the addition of ^{14}CO to butane–oxygen and propylene–oxygen mixtures Neiman and his co-workers[7] were able to show that in the low temperature range less than 5 per cent of the dioxide was derived from the monoxide.

In Table 1 are collected data showing approximate CO/CO_2 ratios for a large range of systems and conditions. Oxidation systems are notorious for the difficulty of precise comparison of the results of different groups of workers. To some extent this is because of the influence of vessel shape, size and surface and the disproportionate effect of adventitious impurities on branched chain reactions. For those reasons any comparisons drawn from Table 1 cannot be better than semi-quantitative, but nevertheless certain generalizations can be made.

(*i*) For paraffins, olefins and aldehydes, if the relative reactant concentrations are fixed CO/CO_2 ratio increases with increasing temperature.

(*ii*) If the temperature is fixed the ratio decreases as the oxygen/fuel ratio is increased.

(*iii*) Certain classes of compounds (esters, *cyclo*paraffins higher than *cyclo*propane and crotonaldehyde) on oxidation may give anomalous CO/CO_2 ratios.

(*iv*) High CO/CO_2 ratios are observed for oxidation of formaldehyde.

Statement of the mechanism

In the proposed mechanism it is suggested that from a hydrocarbon one of the first formed molecular products is an aldehyde. This may be the successor to an earlier peroxide, hydroperoxide or peroxy-radical, but for the present purpose the important postulate is that the production of this aldehyde precedes the formation of CO or CO_2. That is, for paraffins and their simply substituted derivatives, CO and CO_2 do not come directly from reactions of the radical R (fuel = RH) with oxygen but from the intermediate aldehyde, R′CHO, by the steps

1 $R'CHO + X \rightarrow R'CO + XH$ (X = radical or O_2)

2 $R'CO \rightarrow R' + CO$

3 $R'CO + O_2 \rightarrow CO_2 +$ products.

Steps 1 and 2 are elementary reactions; stage 3 is a summary of a series of reactions *q.v.*, although the initial step of this series is probably the combination of R′CO and O_2 to give a peracid radical.

Examination of the mechanism

There is abundant evidence for the formation of aldehydes as intermediates in oxidation systems[8], and for the ease of attack on aldehydes according to step 1. The dissociation energy of the aldehydic C—H bond in acetaldehyde (approximately 80 kcal)[9] is less than that of the methyl C—H bonds by about 20 kcal and H abstraction will most probably occur at this point. The energy of activation for H abstraction by CH_3 radicals is

TABLE 1

CO/CO_2 and CO_2/acid ratios (s, static method; f, flow method)

Fuel	*Fuel*/O_2 mm mm	*T* °C	*Method*	CO/CO_2	CO_2/acid	*Comments*	*Ref.*
HCHO	502 : 238	275	s	7	0·5–0·9		60
	100 : 100	294	s	6	—		44
		328	s	7·6	—		
		376	s	12	—		
	155 : 75	337	s	7	1–2	CO/CO_2 ratio influenced by surface	45
	100 : 100	337	s	8·3	—		43
CH_3CHO	210 : 205	120	s	0·125	1·5–2	Pyrex vessel	32
	83 : 78	197	s	0·40	1·0		
	31 : 45	230	s	0·33	0·55	Silica vessel, nitrogen present	31
		355	s	5·7	—		
C_2H_5CHO	36 : 81	235	s	1·1	—	Silica vessel, nitrogen present	31
		360	s	10·0	—		
n-C_3H_7CHO	≈30 : 180	200 to 550	f	1·0–4·0	—	Nitrogen present to 1 atm. Complete results too detailed for inclusion but increase of CO/CO_2 ratio with temperature clearly shown	54
n-$C_6H_{11}CHO$	≈15 : 150	200–550	f	1–3	—		54
CH_4			s	—	—	Acetone sensitized. CO/CO_2 increases with temperature. Total CO_2 independent of temperature	46
	66 : 133	460	s	1·8	—		
	100 : 100		s	3·0	—	Pyrex vessel	47
	133 : 66		s	3·2	—		

TABLE 1—*continued*

Fuel	*Fuel*/O_2 mm mm	*T* °C	*Method*	CO/CO_2	CO_2/acid	*Comments*	*Ref.*
C_2H_6	530 : 230	~600	f	10–20	—	Cool-flame region(?)	48
	482 : 241	316	s	5·5	—		49
	360 : 360		s	5·0	—		
	241 : 482		s	2·7	—		
	230 : 230	274	s	2·1	3		34
	180 : 180	400	s	7·0	—	No acids formed	
	380 : 380	330	s	5·8	—	Silica vessel	50
	506 : 253	340	s	7·2	—		
	608 : 152	331	s	7·8	—		
	380 : 380	337	s	3·3	—	KCl surface	
C_3H_8	100 : 300	375	f	5·1	—	CO/CO_2 increases with increasing temperature	51
	200 : 200		f	6·8	—		
	300 : 100		f	9·8	—		
	20 atm	260	s	0·95	—	Steel vessel. 1:3·6 C_3H_8/air ratio. Total pressure as indicated	53
	60 atm		s	0·46	—		
	100 atm		s	0·37	—		
	150 : 150	230	s	1·0	—	Azomethane-induced oxidation-quartz vessel	52
		250	s	3·0	—		
n-C_4H_{10}	300 : 100	350	f	4·0	—		
i-C_4H_{10}	300 : 100	350	f	6·1	—	Reaction tube coated with KCl	51
	100 : 300		f	4·4	—		
	300 : 100	450	f	6·0	—		
n-octane	≈13 : 150	250 to 650	f	~1–3	—	Other isomeric octanes give similar results. Nitrogen added to 1 atm. Complete results too detailed for inclusion. See lines 13 and 14	54
					—		
3,4 dimethyl hexane		346	f	7·3	2		55
C_2H_4	100 : 100	400	s	8–11	—		56
	630 : 125	300	s	13·3	—		57
	500 : 250		s	5·8	—		
	250 : 500		s	4·1	—		

TABLE 1—*continued*

Fuel	*Fuel*/O_2 mm mm	*T* °C	*Method*	CO/CO_2	CO_2/acid	*Comments*	*Ref.*
C_3H_6	70 : 350	291	s	—	7	No CO determination	58
	50 : 70	340	s	4·1	—	Total acid changed little with reactant concentrations	59
	50 : 140		s	2·6	—		
	100 : 70		s	2·7	—		
*cyclo*propane	200 : 200	405	s	7	—		42
	200 : 100	428	s	7	—		
*cyclo*pentane	40 : 80	370	s	1·49	—	Pyrex vessel	23
		400	s	1·58	—		
		438	s	1·68	—		
	25 : 80	400	s	1·39	—		
	50 : 80		s	1·76	—		
	40 : 80		s	5·48	—	Boric acid coated vessel	
methyl-*cyclo*-pentane	200 : 200	232	s	2·1	~1		24
	50 : 50	465	s	2·6	~15		
	1 : 1 ratio	300	f	~6	~2		
		365	f	~8	~7		
methyl formate	100 : 100	380	s	0·77	—		
ethyl formate	100 : 200	280	s	0·58	—		22
ethyl formate		340	s	0·73	—		
ethyl formate		380	s	1·0	—		
ethyl formate		425	s	1·1	—		
methyl acetate		380	s	3·5	—		
methyl propionate			s	2·0	—		
acrolein	100 : 100	240	s	~1·5	—	Lower slow combustion zone–cool-flame zone—gas temperature probably higher than 325	31
	34 : 34	325	s	~1·7	—		
		350	s	~2·5	—	Upper slow combustion zone	
croton-aldehyde	95 : 95	166	s	0·9	—		20
	38 : 38	292	s	2·0	—		
	25 : 25	347	s	2·9	—		
	25 : 9·2		s	3·2	—		
	25 : 20		s	2·7	—		

small[10] $\approx$10 kcal and acetaldehyde readily undergoes chain decomposition on photolysis[10], and will decompose by a chain reaction in presence of traces of oxygen[11] at temperatures as low as 150°C.

The instability of R′CO radicals implicit in step 2 is a relative concept and it has been emphasized[12] that in systems in which oxygen is present in great excess, a zero activation energy for combination with oxygen will cause the radical to appear stable. However, even in the presence of oxygen it is to be expected that at more elevated temperatures the importance of decomposition, i.e. step 2, relative to combination will increase, and an increasing CO/CO_2 ratio with temperature should be observed.

Published data suggest that the stability of the radical R′CO decreases slightly on passing from R = CH_3 to R = C_2H_5. The activation energy for the dissociation of the acetyl radical has been given by Steacie[10] as approximately 16 kcal, and recent investigations of the photochemical decomposition of acetone in the presence of butadiene[13] and its pyrolytic decomposition by the toluene carrier method[14] support a value of this magnitude. Jolley[15] has deduced from his results on the photo-oxidation of diethylketone that the difference in E for decomposition of C_2H_5CO and oxygen addition is approximately 13 kcal. A comparative study of the photo-decomposition of acetic and propionic anhydrides[16] in the temperature range 30–195°C showed RCO and RCO_2 radicals to be produced. The CO yield increased with temperature with acetic anhydride while remaining constant with propionic anhydride, suggesting CH_3CO to be more stable than C_2H_5CO. Even qualitative information on the dissociation energies of carboxyl radicals higher than propionyl does not appear to be available, but it seems probable that they are even less stable.

Examination of the available data for the oxidation of saturated aldehydes (Table 1) shows that the predictions of the theory—increase of CO/CO_2 ratio with temperature, and a decrease of the ratio with increasing oxygen/aldehyde ratio—appear to be upheld. Furthermore, the relative CO/CO_2 ratios for acetaldehyde and propionaldehyde oxidations at 230°C are in keeping with the order of stability of the CH_3CO and C_2H_5CO radicals noted above. Hoare[17], studying the photo-oxidation of acetone, showed the CO/CO_2 yield to decrease with increasing oxygen pressure, and a similar observation has been reported by Marcotte and Noyes[18]. Finkelstein and Noyes[19] have been able to show by the use of ^{14}C that in the photo-oxidation of diethyl ketone the CO produced originated in the carbonyl CO group, while the CO_2 resulted from C_2H_5CO–O_2 collisions.

If, as was postulated earlier, the CO and CO_2 produced during the oxidation of paraffins arise mainly from reactions of the intermediate aldehydes, then here also the CO/CO_2 ratio should increase both with increasing temperature and decreasing oxygen/fuel ratio. The lower reactivity of the paraffins compared with aldehydes towards initial attack does not permit oxidation studies to be made much below 250°, but the results given in the literature give strong support to the theory (Table 1). Because of the higher temperatures the intermediate aldehyde tends on attack to give radicals which favour decomposition according to step 2 rather than addition by step 3, this tendency being reflected in high values for the CO/CO_2 ratio.

Anomalous systems

Table 1 shows that certain systems—notably crotonaldehyde, certain esters and *cyclo*paraffins higher than *cyclo*propane—do not produce CO and CO_2 in amounts compatible with the suggested scheme. The behaviour of crotonaldehyde[20] is probably explained by the mesomeric character of the radical derived from it by hydrogen abstraction. Volman and Brinton[21] studying the CH_3 initiated decomposition of acrolein and acetaldehyde found acrolein to yield only insignificant amounts of ethylene whereas acetaldehyde under similar conditions gave a copious yield of methane. Thus the radical $CH_2{=}CH{-}CO$ must be more stable than the CH_3CO radical. It is reasonable to suppose that the crotonyl radical $CH_3{\cdot}CH{=}CH{\cdot}CO$ is similarly stabilized, and that step 2 is infrequent in the oxidation of this substance. There is no evidence for any marked increase in the CO/CO_2 ratio with temperature for crotonaldehyde oxidation and it seems likely that CO may be produced by the sequence

$$CH_3CH{=}CH{\cdot}CO \xrightarrow{O_2} CH_3{\cdot}\underset{\displaystyle O{-}O{\cdot}}{\underset{|}{C}}H{-}CH{\cdot}CO \longrightarrow CH_3CHO + HCO + CO$$

Check experiments showed the acetaldehyde produced to be subject to only slight degradation presumably because of the ease with which active radicals are removed from the system by reaction with the crotonaldehyde. The high yields of CO_2 from the oxidation of esters[22], particularly methyl formate, are probably due to direct breakdown of the radical produced by hydrogen abstraction

$$CH_3OOCH \xrightarrow{-H} CH_3OOC{\cdot} \longrightarrow CH_3^{\cdot} + CO_2$$

Even so it seems probable that a proportion of the CO and CO_2 must be derived by the general mechanism since the CO/CO_2 ratio tends to increase with temperature.

In the oxidation of *cyclo*pentane[23] and methyl-*cyclo*pentane[24] at around 400°C it seems probable

that the low CO/CO_2 yield (e.g. 1·5 for *cyclo*pentane compared with 4–5 for propane under roughly equivalent conditions) is a consequence of peroxy-radical decomposition, e.g.

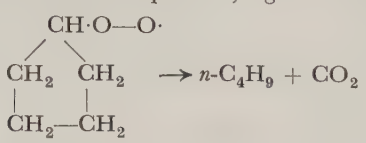

This reaction is probably heterogeneous in the *cyclo*pentane oxidation since at 400°C coating the Pyrex reaction vessel with boric acid increased the ratio from 1·5 to 4 while the total CO yield remained unaltered.

Mechanism of CO_2 *formation*

Beyond noting that stage 3 is undoubtedly complex, so far nothing has been said of the details of the CO_2-producing reactions. It is now necessary to examine this stage of the reaction more closely since it is here that CO_2 and carboxylic acids are probably produced and it is important to ascertain the factors governing the relative amounts of each formed. At the moment of its formation the peroxy-radical is potentially unstable since it contains the excess energy of the association. However complex entities may have appreciable life-times due to the spread of this vibrational energy over several bonds[25].

RO_2 radicals may disappear by unimolecular decomposition, by a second order process as suggested for termination in the oxidation of acetaldehyde[26], or by a H abstraction reaction giving a peracid which may subsequently decompose. Of these various possibilities those which concern us here may be summarized.

4	$R'CO_3^{\cdot}$	$\rightarrow R'O\cdot + CO_2$
4a	$R'CO\cdot + O_2$	$\rightarrow R'O\cdot + CO_2$
5	$R'CO_3^{\cdot} + RH$	$\rightarrow R'CO_3H + R\cdot$
6	$R'CO_3H$	$\rightarrow R'OH + CO_2$
7	$R'CO_3H$	$\rightarrow R'CO_2^{\cdot} + OH\cdot$
8	$R'CO_2^{\cdot}$	$\rightarrow R'\cdot + CO_2$
9	$R'CO_2^{\cdot} + RH$	$\rightarrow R'CO_2H + R\cdot$

Reaction 4 or 4a has been postulated as a possible process in the photo-oxidation of acetone[27], biacetyl[28] and diethyl ketone[15], and has been suggested as the source of alcohol in the oxidation of acetaldehyde[29]. However, although alcohols are among the products of hydrocarbon oxidation[30], their formation can be explained without invoking reaction 4 or 4a and the observed trend of the CO_2/alcohol ratio in the oxidation of acetaldehyde[31] (1·75 at 230 to 0·33 at 350°C) seems to be evidence of some process other than either 4 or 6 as the source of CH_3OH.

Evidence for peracid formation during the slow combustion of aldehydes at low temperatures is indisputable[32], and reaction 5 is now universally accepted. The mode of decay of peracids is less well established. Farmer and McDowell[26] were able to explain satisfactorily the kinetics and autocatalytic nature of the acetaldehyde oxidation on the assumption that the latter is due to 7. There is good evidence for believing that $R'CO_2$ radicals are unstable in the gas phase, and Rembaum and Szwarc[33] investigating the thermal decomposition of diacetyl peroxide in presence of toluene found yields of CO_2, CH_4 and C_2H_6 which are compatible with

$$(CH_3CO_2)_2 \rightarrow 2CH_3CO_2^{\cdot} \rightarrow 2CH_3^{\cdot} + 2CO_2$$

The photo-decomposition of acetic anhydride already discussed[16] showed the $CH_3CO_2^{\cdot}$ radical to be less stable than $CH_3CO\cdot$, consequently if the temperature is high enough for reaction 2 to be significant, it must also favour 8.

The condition normally employed for the study of slow combustion reactions, i.e. high fuel concentration, gives $RCO_2^{\cdot}$ radicals a reasonable chance of abstracting H atoms according to reaction 9. The yield of carboxylic acids produced in this manner would be expected to be much less for oxidation of paraffins than for aldehydes since at the higher temperatures necessary for appreciable oxidation of the former both $RCO\cdot$ and $RCO_2^{\cdot}$ are unstable.

In general these predictions are supported by experimental findings. Thus at the completion of the oxidation of propane at 274° and *iso*butane at 291° the CO_2/acid ratios were 3 and 4 respectively[34,35]. At 400°C no acids were detectable in the products of propane oxidation[34]. Although Garner and Petty[36] do not consider acids to be produced via intermediate aldehydes in heptane slow combustion, nevertheless their observations and those of Raine and Garner[37] on the relative amounts of the different acids formed are consistent with this route and emphasize the importance of reaction 8 relative to 9 as the temperature is increased.

Production of CO *and* CO_2 *from formaldehyde*

So far only aldehydes higher than HCHO have been considered as sources of CO and CO_2 since this compound is a special case. Although formaldehyde is somewhat more resistant to oxidation than its higher homologues there is no reason to believe that the energy of activation of the reaction

$$H_2CO + X \rightarrow XH + HCO$$

is very high.

Tipper[38] and also Calvert[39] have recently discussed the activation energy of decomposition of the formyl radical. Although the latter favours a value of about 15 kcal/mole, D H–CO may well be

higher—26–28 kcal/mole. The recovery of glyoxal from hydrocarbon flames quenched by excess fuel suggests that HCO radicals must have an appreciable life-time even at quite high temperatures[40], 500–800°C. The reaction

$$10 \qquad HCO + O_2 \rightarrow HO_2 + CO$$

probably occurs at temperatures in excess of 400°C. Thus H_2CO retards the H_2–O_2 reaction just above the second limit[41], probably by replacing the active H atoms by HO_2, viz.

$$11 \qquad H + HCHO \rightarrow H_2 + HCO$$

this being followed by 10.

Reaction 10 has been suggested as an important reaction step in the oxidation of CH_3OH[6] and *cyclo*propane[42] at 400° where H_2CO is a branching intermediate. Little CO_2 is formed in these systems and is probably the result of CO oxidation and the very small hydrogen yield supports reaction 10 as opposed to HCO decomposition.

High CO/CO_2 ratios are a feature of the results of studies of HCHO oxidation (Table 1). This emphasizes that formaldehyde does not appear to have access to a ready route of CO_2 production such as we have suggested for higher aldehydes, and that in the oxidation of higher hydrocarbons probably only a small proportion of the carbon dioxide is derived from intermediate formaldehyde.

The authors believe that, although other schemes for CO and CO_2 production could be devised, the suggestions outlined in this paper do appear to correlate and explain a mass of results in a reasonable way.

REFERENCES

[1] Walsh, A. D. *Trans. Faraday Soc.* 43 (1947) 297
[2] Burgoyne, J. H. and Hirsch, H. *Proc. Roy. Soc. A* 227 (1954) 73
[3] Hoare, D. E. and Walsh, A. D. *Trans. Faraday Soc.* 50 (1954) 37
[4] Vanpee, M. *Ann. Min. Belg.* 47 (1948) 1053
[5] Van Meerssche, M. *Ann. Min. Belg.* 48 (1949) 643
[6] Bell, K. M. and Tipper, C. F. H. *Proc. Roy. Soc. A* 238 (1956) 256
[7] Neiman, M. B., Efremov, V. Ya., Serdyok, N. K. and Lokovnikov, A. F. *Izvest. Akad. Nauk. SSSR Otdel Khim. Nauk.* (1956) 408; Lokovnikov, A. F. and Neiman, M. B. *Zhur. fiz. Khim.* 29 (1955) 1410
[8] Lewis, B. and von Elbe, G. *Combustion, Flames and Explosion of Gases.* 1951. New York; Academic Press
[9] Szwarc, M. *Chem. Rev.* 47 (1950) 75
[10] Steacie, E. W. R. *Atomic and Free Radical Reactions.* 1954. New York; Reinhold
[11] Niclause, M. *Thesis,* 1953. Nancy
[12] Nicholson, A. J. C. *J. chem. Phys.* 20 (1952) 1811
[13] Volman, D. H. and Graven, W. M. *J. chem. Phys.* 20 (1952) 919
[14] Szwarc, M. and Taylor, J. W. *J. chem. Phys.* 23 (1955) 2310
[15] Jolley, J. E. *J. Amer. chem. Soc.* 79 (1957) 1537
[16] Ausloos, P. *Canad. J. Chem.* 34 (1956) 1709
[17] Hoare, D. E. *Trans. Faraday Soc.* 49 (1953) 1292
[18] Marcotte, E. B. and Noyes, W. A. *Disc. Faraday Soc.* 10 (1951) 236. *J. Amer. chem. Soc.* 74 (1952) 783
[19] Finkelstein, A. and Noyes, W. A. *Disc. Faraday Soc.* 14 (1953) 76, 81
[20] Osborne, A. D. *Thesis,* 1957. Liverpool
[21] Volman, D. H. and Brinton, R. K. *J. chem. Phys.* 20 (1952) 1764
[22] Parsons, B. I. and Danby, C. J. *J. chem. Soc.* (1956) 1795
[23] McGowan, I. R. and Tipper, C. F. H. *Proc. Roy. Soc. A* 246 (1958) 64
[24] Burgoyne, J. H. and Silk, J. A. *J. chem. Soc.* (1951) 572
[25] Small, N. J. H. and Ubbelohde, A. R. *J. appl. Chem.* 3 (1953) 193
[26] Farmer, J. B. and McDowell, C.A. *Fifth Symposium on Combustion,* p. 453. 1955. New York; Reinhold
[27] Hentz, R. R. *J. Amer. chem. Soc.* 75 (1953) 5810
[28] Taylor, R. P. and Blacet, F. E. *Industr. Engng. Chem. (Industr.)* 48 (1956) 1505
[29] Neiman, M. B. and Feklisov, G. I. *Dokl. Akad. Nauk. SSSR.* 90 (1953) 583
[30] Satterfield, C. N. and Reid, R. C. *Fifth Symposium on Combustion,* p. 511. 1955. New York; Reinhold
[31] Newitt, D. M. and Baxt, L. M. *J. chem. Soc.* (1939) 1711
[32] McDowell, C. A. and Thomas, J. A. *J. chem. Soc.* (1949) 2208, 2217
[33] Rembaum, A. and Szwarc, M. *J. Amer. chem. Soc.* 76 (1954) 5975
[34] Newitt, D. M. and Thornes, L. S. *J. chem. Soc.* (1937) 1656
[35] Batten, J. J., Gardner, F. H. and Ridge, A. D. *J. chem. Soc.* (1955) 3029
[36] Garner, F. H. and Petty, D. S. *Trans. Faraday Soc.* 47 (1951) 877
[37] Raine, T. L. and Garner, F. H. *Trans. Faraday Soc.* 47 (1951) 896
[38] Tipper, C. F. H. *Quart. Rev. chem. Soc., Lond.* 11 (1957) 313
[39] Calvert, J. G. *J. phys. Chem.* 61 (1957) 1206
[40] Malmberg, E. W. *J. Amer. chem. Soc.* 76 (1954) 890
[41] Baldwin, R. R., Corney, N. S. and Simmons, R. F. *Fifth Symposium on Combustion,* p. 502. 1955. New York; Reinhold
[42] McEwan, A. C. and Tipper, C. F. H. *Proc. Roy. Soc. A* 216 (1953) 266
[43] Axford, D. W. E. and Norrish, R. W. G. *Proc. Roy. Soc. A* 192 (1948) 518
[44] Summers, D. *Thesis,* 1939. London; Kings College
[45] Scheer, M. D. *Fifth Symposium on Combustion,* p. 435. 1954. New York; Reinhold
[46] van Tiggelen, A. *Ann. Min. Belg.* 43 (1942) 117

[47] Egerton, A., Minkoff, G. J. and Salooja, K. C. *Proc. Roy. Soc. A* 235 (1956) 158
[48] Gray, J. A. *J. chem. Soc.* (1953) 741
[49] Bone, W. A. and Hill, S. G. *Proc. Roy. Soc. A* 129 (1930) 434
[50] Harris, E. J. and Egerton, A. *Chem. Rev.* 21 (1937) 287
[51] Pease, R. N. *J. Amer. chem. Soc.* 51 (1929) 1839
[52] Scheer, M. D. and Taylor, H. A. *J. chem. Phys.* 20 (1952) 653
[53] Newitt, M. D. and Schmidt, W. G. *J. chem. Soc.* (1937) 1665
[54] Pope, J. C., Dykstra, F. J. and Edgar, G. J. *J. Amer. chem. Soc.* 51 (1929) 1875, 2203, 2213
[55] Beatty, H. A. *Chem. Rev.* 21 (1937) 328
[56] Harding, A. J. and Norrish, R. G. W. *Proc. Roy. Soc. A* 212 (1952) 291
[57] Bone, W. A., Haffner, A. E. and Rance, H. F. *Proc. Roy. Soc. A* 143 (1934) 16
[58] Mulcahy, M. F. R. and Ridge, A. D. *Trans. Faraday Soc.* 44 (1953) 906
[59] Mullen, J. D. and Skirrow, G. *Proc. Roy. Soc. A* (1958)
[60] Bone, W. A. and Gardner, J. B. *Proc. Roy. Soc. A* 154 (1936) 297

25

ON HIGH-TEMPERATURE OXIDATION OF METHANE

G. I. KOZLOV

INTRODUCTION

The solution of many problems related to the inflammability and burning of gases, as well as to the calculation of the more complex combustion phenomena, requires knowledge of the overall kinetic equation, owing to the fact that the process of heat liberation is related to the overall reaction rate. These equations are interesting in connection with the present-day engineering trend of employing forced conditions of burning in high-speed gas flows. So far, however, the only field in which some clarity has been achieved with regard to the kinetic relationships of the process is the high-temperature oxidation of carbon monoxide. As to other gases, hydrocarbons included, extensive material has accumulated in the literature on the kinetic regularities of low temperature (300 to 600°C) oxidation, but these relationships cannot be extrapolated into the regions of higher temperatures.

This paper will deal with an experimental derivation of the overall kinetic equation of the high temperature (700 to 1,100°C) oxidation of methane. The investigation of carbon monoxide burning involved was of auxiliary interest and was carried out, first, for the purpose of testing the experimental procedure, inasmuch as the principal kinetic characteristics of this process are already known from the literature[1–6] and are considered, besides, in other papers of this Symposium[7–9]; secondly, because an important factor in the oxidation of methane is the oxidation of the carbon monoxide formed during the oxidation of methane[10]; and thirdly, because of the ambiguity of available data on the absolute values of the rate of oxidation of carbon monoxide and its temperature dependence in the above-indicated temperature range.

EXPERIMENTAL PROCEDURE

A dynamic procedure was employed. A gas–air mixture of definite composition was saturated with water vapour at room temperature. Then it passed through a coil immersed in melting ice to condense the excess moisture. Thus, on leaving the cooler the concentration of water vapour in the mixture corresponded to the concentration of saturated water vapour at 0°C, namely, 0·6 per cent by volume. This was checked for all rates of the mixture by passing a measured volume of the mixture over phosphorus pentoxide and then determining the moisture content gravimetrically. From the cooler the mixture passed into a three-section quartz reaction vessel (reactor). The first section the gas entered served as the pre-heater and had an independent electric heater. Here, depending on the conditions of the experiment, the mixture was heated to a temperature between 500 and 800°C, that is about 200 or 300°C below the temperature of the reaction. In the second section, the ante-reactor, which was a quartz tube 1·5 mm in diameter and 60 mm long and equipped with an independent electric heater, the mixture was heated rapidly to the temperature of the reaction. The temperature of the walls of the ante-reactor was maintained at a level high enough to ensure that the reacting mixture should enter the first probe of the reactor at the temperature of the reaction. The third section, the reaction section, was made of 2·0 mm quartz tubing and consisted of four probes through which the gas passed to be analysed. In addition, these probes served as ducts through which thermocouples were inserted into the reactor to measure the temperature of the reacting mixture. In the published literature the general opinion is that quartz is inert to the high-temperature oxidation of methane and carbon monoxide. The use of a reactor of small diameter ensured a large surface-to-volume ratio in the reactor, making it possible to conduct the process isothermically right up to temperatures of the order of 1,100°C. A constant temperature was tested by means of seven platinum-platino-rhodium thermocouples made of 0·15 mm wire. The beads of the four inner thermocouples were glazed with a thin layer of porcelain to avoid catalysis. The three outer thermocouples were inserted under a heat isolating layer so that they should measure the temperature of the outer wall over the length of the reaction section. The reactor had a compensation-type platinum electric winding by means of which the temperature of the reaction section could be regulated. The length of the reaction zone in the experiments with this reactor, which in the following will be referred to as reactor A, varied from 107 to 160 mm depending on the section

selected, between the probes of which the process would proceed isothermically.

Owing to the high-temperature gradient along the probes (about 100°C per 1 mm) the gas samples were frozen almost instantly. The cooled reaction products were analysed by means of two type GIP-5 infra-red absorption gas analysers selectively sensitive to CO_2 and CO respectively.

In the experiments with methane, carried out with the same apparatus, other reactors were used which will be referred to in the following as reactors B and C. Reactor B had an inner diameter of 1 mm and two probes with inner diameters of 0·5 mm, through which the gas passed to be analysed. Isothermic conditions were controlled by means of two inner thermocouples inserted through special side tubes and three outer thermocouples. The length of the reaction zone was 75 mm. Reactor C was made of 5·0 mm quartz tubing, the length of the reaction zone being 297 mm. It had two probes, one on each side, similar to those of reactor A, through which the gas passed on its way to be analysed. Isothermic conditions were controlled by means of three inner thermocouples, two of them stationary, inserted through the probes, and one sliding thermocouple capable of moving over the entire length of the reaction zone. If the deviation of the temperature from its mean value over the length of the reaction zone did not exceed $\pm$ 5°C, the temperature field was considered as satisfactory.

EXPERIMENTAL RESULTS, TREATMENT AND ANALYSIS

Determination of absolute rates of high-temperature oxidation of carbon monoxide

It has been established[1–4, 6–8], that in the case of lean mixtures of carbon monoxide and oxygen the overall order of the reaction with respect to carbon monoxide equals 1·0. The overall order of the reaction with respect to water vapour equals 0·5. The order of the reaction with respect to oxygen equals 1·0 and 0·25 respectively for mixtures containing over and under 5·0 per cent oxygen.

On the basis of these data the kinetic equation of the overall reaction of oxidation of carbon monoxide may be written as follows

$$-\frac{d[CO]}{dt} = K_0\left(\frac{\rho_0 T_0}{\mu T}\right)^{1.5}[CO][O_2][H_2O]^{0.5}e^{-E/RT}$$

for $[O_2] < 0{\cdot}05$ (1)

and

$$-\frac{d[CO]}{dt} \quad K_0(0{\cdot}05)^{0.75}\left(\frac{\rho_0 T_0}{\mu T}\right)^{1.5}[CO]\,[O_2]^{0.25}[H_2O]^{0.5}e^{-E/RT}$$

for $[O_2] > 0{\cdot}05$ (2)

where K_0 is the specific rate constant of overall reaction; ρ_0 is the density of gas at s.t.p. (g/cm³); T_0 is the initial temperature of the mixture, 273°K; μ is the molecular weight of gas at s.t.p. (g/cm³); E is the activation energy of overall reaction (cal/mole); R is the gas constant (cal/mole°K); and T is the absolute temperature (°K).

As the oxygen concentration in our experiments was over 5 per cent, the data were treated according to equation 2. Neglecting the change in concentration of the oxygen, integration of equation 2 gives

$$\log \phi' = \log [K_0(0{\cdot}05)^{0.75}\left(\frac{\rho_0 T_0}{\mu T}\right)^{1.5}[O_2]^{0.25}[H_2O]^{0.5}] - \frac{E}{RT}\log e \qquad (3)$$

where

$$\phi' = -\frac{\ln (1 - n')}{l/w}$$

where ϕ' is the reaction rate (sec^{-1}); n' is $([CO]_0 - [CO])/[CO]_0$, degree of burning out; l is the length of reaction zone (cm); and w is the rate of flow in reactor (cm/sec).

The change in temperature under the logarithm sign may be neglected. Then, plotting the results of treatment of the experimental data as $\log \phi'$ *versus* $1/T$, we find the value of the overall kinetic parameters E and K_0 by the conventional method from the slope of the straight line.

The experiments were carried in reactor A. The concentration of carbon monoxide in the CO–air mixture varied from 2 to 6 per cent. Simultaneously, the initial concentration of oxygen in the mixture varied insignificantly and could be considered to equal 20 per cent in all experiments. The reaction temperature in the experiments ranged from 600 to 1,100°C.

It was established that the rate of flow does not affect the reaction rate, and therefore in the experiments this parameter was varied in such a way as to make the difference in concentration of carbon monoxide in the samples range from 0·7 to 1·5 per cent.

The results of treatment of the experimental data are shown in *Figure 1*. Within the temperature range 750–1,100°C the activation energy was found to equal 32,000 cal/mole. At lower temperatures the activation energy rises insignificantly up to a value of 35,000 cal/mole. The results of these experiments are well described by the following kinetic equation

$$\phi = 1{\cdot}04 \,.\, 10^{12}\,\frac{[CO][O_2]^{0.25}[H_2O]^{0.5}}{T^{2.5}}\,e^{-32{,}000/RT} \qquad (4)$$

In *Figure 2* the absolute rate values obtained by us for the overall reaction of oxidation of carbon

monoxide are compared with the data of other authors. Besides corrections related to various water vapour content in mixtures were not introduced. Attention is drawn to the good agreement of our data as concerns absolute reaction rates with the values determined by Zeldovich and Semenov[2,3] obtained by computation on the basis of the treatment of the data of various authors on the normal velocity of flame propagation.

Besides this our data are in good agreement with the results of computation of the kinetics of carbon monoxide carried out by Tsukhanova[8]. However, as can be seen from *Figure 2*, the activation energy calculated by her for the overall reaction is somewhat lower than the data of other authors. Our data agree also with the calculations of Sobolev[7] who determined the kinetic relationships of the combustion of carbon monoxide proceeding from measurements of normal velocities and flame temperatures; and also with other experimental data[9].

Regarding the experiments of Karzhavina[4], there is a certain indefiniteness in her experiments, as is known, with respect to the rate of flow in the reaction section, and therefore in *Figure 2* the data obtained by her are represented calculated for the greatest and smallest possible flow rates under

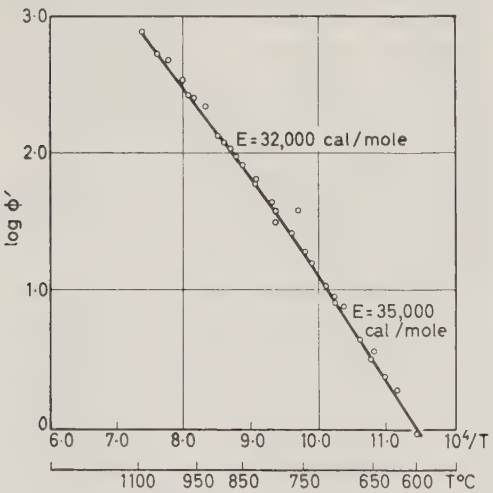

Figure 1. Temperature dependence of overall rate of carbon monoxide oxidation

the conditions of her experiments. Our data (see *Figure 2*) fall within the region bounded by these limit curves.

Mention should be made of the considerable divergence, almost two orders between our data, on absolute values, and the data obtained in the temperature range 600–750°C by Chukhanov[5] and that in the region just behind the flame front by Sobolev[7]. The reasons for such a large discrepancy are not clear so far, and special experiments will have to be made to find them out.

Thus, the absolute values obtained by us experimentally and the temperature dependence of the overall rate of oxidation of carbon monoxide is in general agreement with the calculated and experimental data found in the literature.

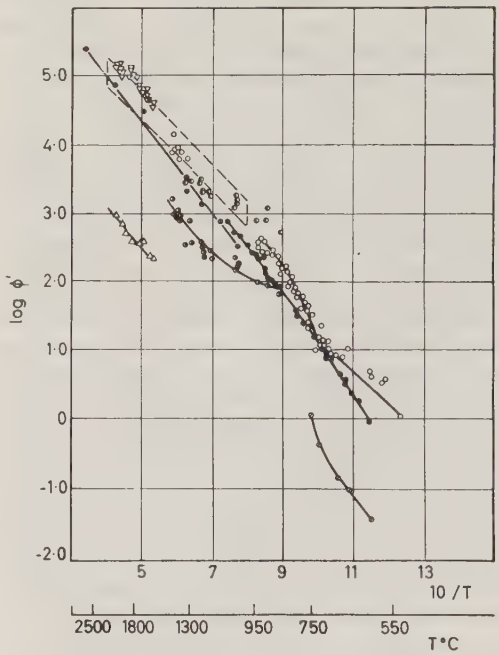

Figure 2. Comparison of data of various authors on temperature dependence of carbon monoxide oxidation. ⊘—Chukhanov; ◐◑—Karzhavina; ○—Solovyova; △ ▽—Sobolev; ⊙—Kozlov; ●—Zeldovich and Semenov; - - -—Tsukhanova; ⊗—Friedman and Cyphers

Determination of overall kinetic equation of high-temperature oxidation of methane

There are many papers in the literature devoted to elucidation of the mechanism and kinetic relationships of the oxidation of methane at temperatures below 750°C, when the walls of the reaction vessels influence the kinetics, and the rate of reaction permits the use of static methods for investigation. We know of only one paper[10] in which the kinetics of oxidation of methane was investigated in the region of 1,000°C. The authors of that paper gave no general kinetic equation but their paper contains a great deal of information concerning the specific features of the course of the reaction, as well as the concentrations of intermediates. It follows from their paper, first, that the oxidation of methane takes place, as it were, in two stages—oxidation of the methane to carbon monoxide and combustion of the latter; secondly, in the course of the oxidation

of methane the concentration of the chief intermediate, formaldehyde, is stationary and insignificant; thirdly, the concentrations of the other intermediates are also small; fourthly, methane retards its own oxidation to carbon monoxide; and finally, methane retards the oxidation of the carbon monoxide formed during its oxidation, especially effectively in the initial stage of oxidation of the methane. Taking the above into

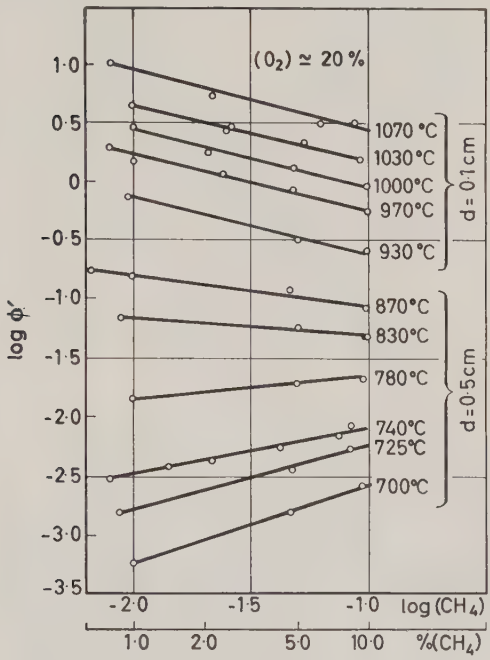

Figure 3. Dependence of reaction rate on methane concentration in mixtures at various temperatures

account, and also owing to the fact that we did not undertake to establish the mechanism of oxidation of methane, but just to determine the overall rate of oxidation of methane to CO and of combustion of the latter, the reaction products were analysed only for CO and CO_2. The reaction rate was calculated from the difference between the concentrations of CO and CO_2 in the probes according to the formula

$$\phi' = -\frac{d[CH_4]}{dt} = \frac{d([CO] + [CO_2])}{dt}$$

$$= \frac{\Delta([CO] + [CO_2])}{\Delta t} = \frac{4QT\Delta([CO] + [CO_2])}{\pi d^2 l T_0} \qquad (5)$$

where Q is the rate of flow of mixture (cm^3/sec); and d is the inner diameter of reactor (cm).

In the temperature range 700–900°C the experiments were carried out in reactor C, but at higher temperatures it was impossible to maintain isothermal conditions in this reactor. Therefore, in experiments involving reaction temperature between 900 and 1,100°C we made use of reactor B. In contradistinction to reference 11 there was evidently no activation of the walls in time in our experiments. This is borne out by the fact that the process was stationary and by the good reproducibility of the experiments. The reaction rates, as in the experiments with carbon monoxide, were virtually independent of the rate of flow in the reactor. Assuming that the overall rate of oxidation of methane can be approximated by the following function

$$\phi = K_0 \left(\frac{\rho_0 T_0}{\mu T}\right)^{n+m} [CH_4]^n [O_2]^m e^{-E/RT} \qquad (6)$$

where n is the overall order of reaction with respect to fuel; and m is the overall order of reaction with respect to oxygen. The task was to determine the values of the kinetic parameters K_0, n, m, E.

Determination of n—In the experiments for determining the order of the reaction with respect to methane the oxygen concentration in the mixture was kept constant and equal to 20 per cent in all cases. Several series of tests were run at various temperatures ranging from 700 to 1,070°C. The methane concentration in all series was varied between 1·0 and 10·0 per cent, the reaction rate in some of the series being determined for only three methane concentrations, namely 1, 5 and 10 per cent. The results are shown in *Figure 3*, an examination of which suggests that the dependence of the reaction rate on the methane concentration

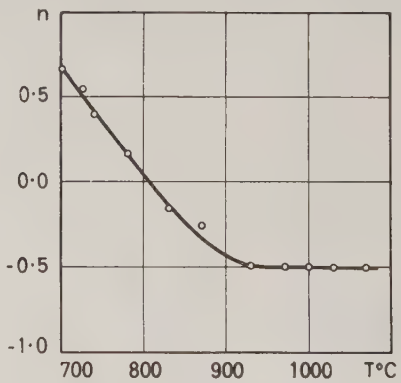

Figure 4. Variation of order of reaction with respect to methane with the temperature

is linear in each series, the slope varying with the temperature. *Figure 4* gives the temperature dependence of the order of the reaction with respect to methane. Over the temperature range 700 to 930°C it varies almost according to a rectilinear law from 0·65 to − 0·5. With temperatures of 930°C and higher, up to 1,070°C, the order of the reaction with respect to methane remains constant and equal to $n = -0{\cdot}5$.

To determine the possible influence of the effective oxygen concentration in mixtures rich in oxygen on the order of the reaction with respect to methane, a series of experiments was made with mixtures containing 30 per cent oxygen. *Figure 5* shows the dependence of the rate of methane oxidation on the methane concentration for effective oxygen concentrations of 18 and 30 per cent, obtained at 1,030°C. The lines have identical slopes, showing that the oxygen concentration does not influence the order of the reaction with respect to methane at this temperature.

Determination of m—Experiments for determining the order of the reaction with respect to oxygen were carried out at temperatures of 740°C, 970°C and 1,030°C. The effective methane concentration in the experiments at 740°C was kept equal to 4·5 per cent. The effective oxygen concentration was varied from 7 to 50 per cent. The results of these experiments, represented in *Figure 6a*, are well expressed by a straight line corresponding to $m = 2{\cdot}0$, illustrating the great influence of the oxygen concentration on the rate of reaction. Similar data obtained at 970°C for an effective methane concentration of 4 per cent and oxygen concentrations ranging from 10 to 30 per cent indicate a reaction order with respect to oxygen of 1·5. The value $m = 1{\cdot}5$ remains invariable at higher temperatures as well, as can be seen by examining *Figure 6b*, where the dependence of the rate of oxidation of methane on oxygen concentrations between 10 and 30 per cent at 1,030°C is represented for effective methane concentration of 3 and 8 per cent. Besides, the fact that the lines are parallel indicates that the methane concentration does not affect the order of the reaction with respect to oxygen at these temperatures.

Determination of K_0 and E—To determine the temperature dependence of the rate of methane oxidation the concentrations of methane and oxygen in the mixture were kept constant. The effective oxygen concentration equalled 20 per cent in all experiments. The temperature ranged from 700 to 1,120°C. *Figure 7* demonstrates the temperature dependences of the rate of methane oxidation for effective methane concentrations of 1, 5 and 10 per cent. However, the curves reflect

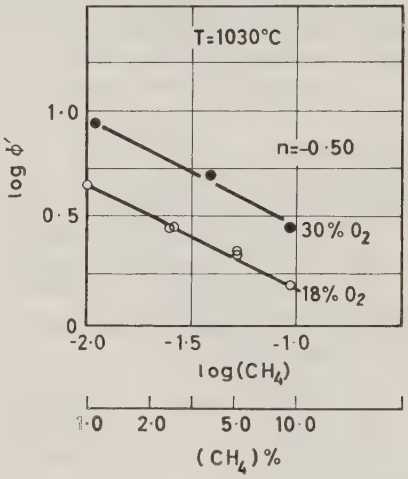

Figure 5. Dependence of reaction rate on methane concentration at $T = 1{,}030$°C

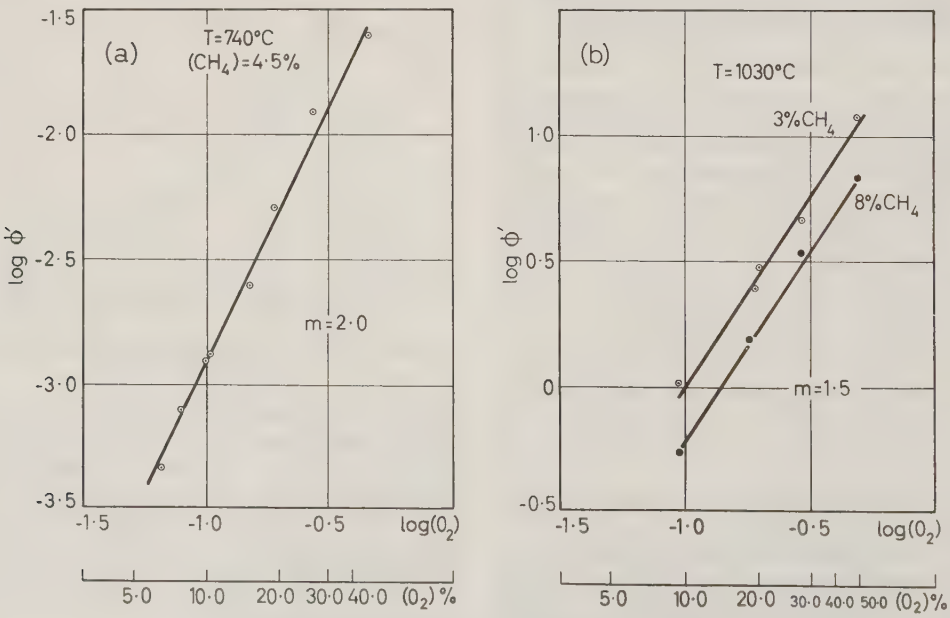

Figure 6. Dependence of reaction rate on concentration of oxygen in mixture

not only the action of the Arrhenius dependence of the reaction rate on the temperature but also a weaker temperature dependence of the reaction orders with respect to methane and oxygen. The influence of the latter factors could have been excluded in order to determine the value of the activation energy over the entire range of temperatures studied, but this would hardly have

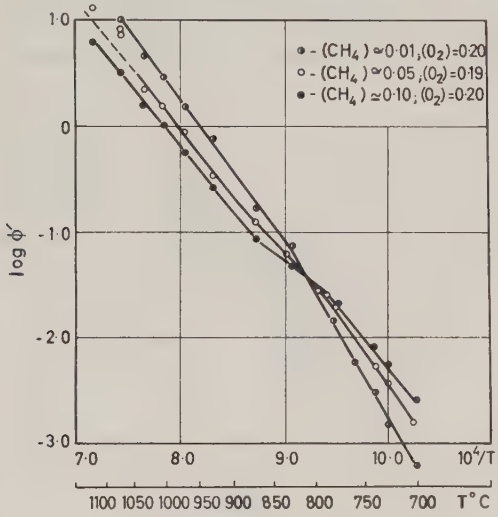

Figure 7. Temperature dependence of overall rate of oxidation of methane to carbon monoxide

been advisable as we do not know the value of the reaction rate constant over the temperature range 700–900°C. It has been shown above that the values of n and m are constant at temperatures between 930 and 1,120°C. The mean value of the activation energy for effective methane concentrations from 1 to 10 per cent in the mixture over this temperature range equals approximately 60,000 cal/mole on the basis of *Figure 8*. Accordingly, the following overall kinetic equation can be written for the overall reaction rate of methane oxidation to carbon monoxide within the temperature range 930–1,120°C

$$\phi = 7{\cdot}10^8 \frac{[CH_4]^{-0{\cdot}5}[O_2]^{1{\cdot}5}}{T} e^{-60{,}000/RT} \qquad (7)$$

ϕ being the reaction rate (mole/cm^3 sec).

It is evident that to understand the combustion of methane to its end products we must have data on the process of combustion of carbon monoxide which forms according to relationship 7. For this purpose we attempted to determine experimentally the rate of oxidation of the carbon monoxide formed during the oxidation of methane when the retarding action of the latter disappears. However, in these experiments, the carbon monoxide would ignite, as a rule, before the methane had disappeared completely, this apparently being due to the large difference between the rates of methane oxidation and of carbon monoxide oxidation at the temperatures employed. Estimations of the rate of this process showed that after the retarding influence of methane had disappeared the rate of oxidation of the carbon monoxide formed from the methane was close to the rate of oxidation of ordinary carbon monoxide. A comparison of the rates of the overall reactions of methane oxidation and carbon monoxide oxidation, presented in *Figure 9* for 5 per cent mixtures of these gases with air, shows that approximately up to 1,500°C the overall rate of burning of methane is limited by the reaction of its oxidation, while at higher temperatures the burning of carbon monoxide should become the limiting factor, provided, of course, that the extrapolation of relationships 4 and 7 into the region of higher temperatures is correct.

The kinetic relationships obtained for methane oxidation are in agreement with the experimental data of Burgoyne and Hirsh[10]. However, our kinetic equation 7 does not agree with the kinetic equation proposed by Norrish[15] on the basis of a theoretical examination of the possible mechanism of methane oxidation, employed by Bartholomé[16] and Sandri[13] in their calculations of the normal rate of flame propagation.

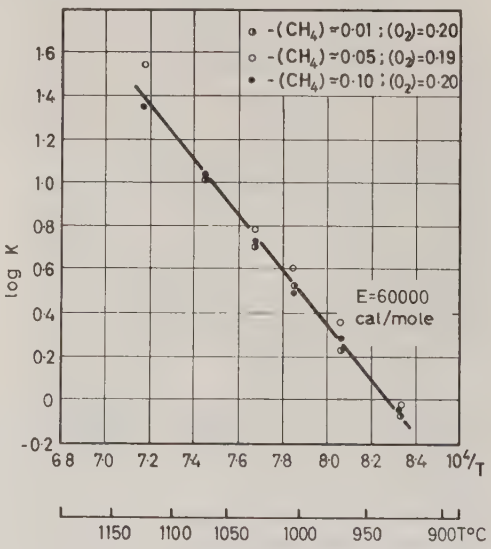

Figure 8. Temperature dependence of reaction rate constant

The good agreement obtained by Sandri between the calculated values of the normal rate of flame propagation and the experimental values for mixtures containing 8 and 9·5 per cent methane in air cannot serve as an evidence of the correctness of Norrish's mechanism. At all events Gaydon[17] came to the conclusion on the basis of

spectroscopic measurements that the inner cone of the methane flame contains no atomic oxygen, which is the basic active particle in the mechanism suggested by Norrish.

CALCULATION OF ABSOLUTE VALUES OF NORMAL RATE OF FLAME PROPAGATION IN CH_4–AIR MIXTURES

As the temperature conditions of the above-described experiments are close to those in the flame front near the lower limit of flame propagation, the relationships obtained may serve as a starting point for establishing the mechanism of chain reactions taking place in the methane flame, if the overall kinetics determined by us are actually realized in the flame front. The latter idea can be verified at present only indirectly by a calculation (based on the kinetic equations obtained above) of the absolute values of the normal rate of flame propagation in CH_4–air mixtures. Such a calculation was carried out on the basis of the theory developed by Zeldovich,

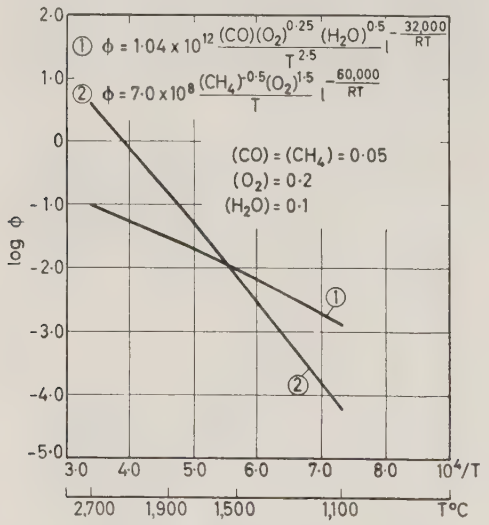

Figure 9. Comparison of overall rates of decomposition of methane to carbon monoxide (equation 2) and of oxidation of latter (equation 1) calculated by equations 7 and 4 for concentrations $[CH_4] = [CO] = 0{\cdot}05$; $[O_2] = 0{\cdot}2$; $[H_2O] = 0{\cdot}1$

Frank-Kamenetskii and Semenov[3,12]. The following expression was employed in calculating the normal velocity of flame propagation

$$u = \frac{1}{\rho_0(T_m - T_0)} \left[2 \int_{T_0}^{T_f} \frac{\lambda}{C_P^2} \cdot q\phi dT \right]^{\frac{1}{2}}$$

where u is the normal rate of flame propagation (cm/sec); T_m is the temperature at which ϕ function reaches maximum (°K); T_f is the temperature of reaction products (°K); λ is the heat conductivity of gas (cal/cm sec°K); C_p is the specific heat of gas at constant pressure (cal/g°K); and q is the thermal effect of reaction (cal/mole).

This expression was obtained by neglecting thermal diffusion and on the assumption that similarity exists between the temperature and concentration fields.

This formula may be considered sufficiently accurate, according to estimates made by Sandri[13], the error in the value of the normal rate of flame

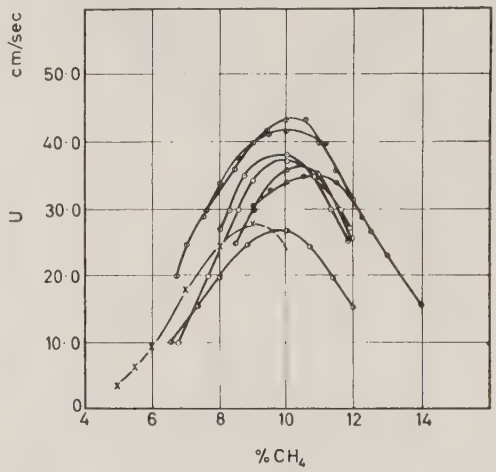

Figure 10. Comparison of calculated curve with experimental data of various authors for dependence of u on CH_4 *concentration in methane–air mixtures.* ◑—*Coward and Hardwell;* ○—*Egerton;* ◐—*Hartman;* ●—*Jan;* ⊙—*Swith;* ⊗—*Klingman;* ⓘ—*Andreyer;* ×—*calculated*

propagation calculated according to formula 8 does not exceed 5 per cent in comparison with the method of exact numerical integration. The absolute values of the normal rate of flame propagation in methane–air mixtures were calculated according to formula 8 by graphical integration. It was assumed that the overall combustion rate of methane is limited by its oxidation to carbon monoxide, and therefore the overall kinetic equation 7 obtained in this paper was employed as the source of heat. However, the calculation met with a difficulty in connection with the fact that, as it follows from equation 7, the value of the reaction rate tends towards infinity as the effective methane concentration drops to 0. Therefore we were obliged to 'cut off' the source at very small effective methane concentrations in the mixture (concentrations of the order of 0·05 per cent); this, however, could hardly produce any substantial error in calculating u. On the other hand, it is quite clear that kinetic equation 7 can hardly be true for very low methane concentrations in the mixture.

In *Figure 11* the calculated curve is compared with the experimental data of various authors

who measured u in methane–air mixtures. It can be seen from *Figure 11* that the calculated curve agrees rather well with experimental results up to methane concentrations of approximately 8 per cent in the mixture. For methane concentrations exceeding 8 per cent the calculated curve deviates from the experimental ones. Especial note should be made of the surprisingly good agreement between the calculated values of u at the lower limit of flame propagation with the precision experimental data of Egerton and Thabet[14] (see *Figure 11*) obtained with a flat burner.

CONCLUSIONS

Analysis of the results of this study suggests the following conclusions:

(1) The additional information obtained by direct experiment on the absolute values and

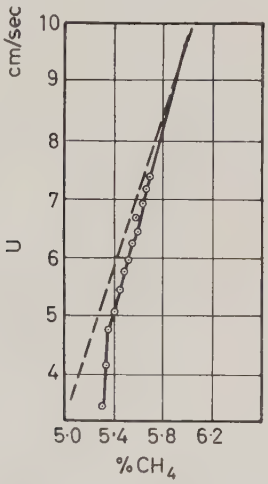

Figure 11. Comparison of calculated values of u with experimental data of Egerton and Thabet: ⊙—experimental; - - - -—calculated

temperature dependence of the reaction rate of the high-temperature oxidation of carbon monoxide agrees on the whole with the material available in the literature. The temperature dependence of the rate of carbon monoxide oxidation at temperatures between 750 and 1,100°C corresponds to an activation energy of 32,000 cal/mole.

(2) The overall kinetic equation of high-temperature methane oxidation to carbon monoxide has been determined. For the temperature range 930–1,120°C it has the following form

$$\phi = 7 \cdot 10^8 \frac{[CH_4]^{-0.5}[O_2]^{1.5}}{T} e^{-60{,}000/RT}$$

At temperatures below 930°C the values of the kinetic parameters vary with the temperature.

(3) It has been shown that the overall rate of methane combustion is most probably limited approximately up to 1,500°C by the oxidation of methane to carbon monoxide, whereas at higher temperatures the limiting factor must be the combustion of the carbon monoxide formed from the methane; provided that the extrapolation of the above determined kinetic equations of methane oxidation and carbon monoxide oxidation is correct.

(4) The absolute values of the normal rate of flame propagation calculated on the basis of the Zeldovich–Frank-Kamenetskii–Semenov theory, with the aid of the overall kinetic equation of methane oxidation obtained in this paper, agrees well with experiment in the vicinity of the lower limit of flame propagation.

The author wishes to express his special thanks to Professor L. N. Khitrin for valuable advice and continued interest in this work.

REFERENCES

[1] Barsky, G. A. and Zeldovich, Y. B. *Zh. fiz. Khim., Mosk.* 25, Part 5 (1951)
[2] Zeldovich, Y. B. and Semenov, N. N. *J. Exp. teor. Phys., Moscow* 10, Part 10 (1940)
[3] Semenov, N. N. *Adv. phys. Sci., Moscow* 24, Part 4 (1940)
[4] Karzhavina, N. A. *Zh. fiz. Khim., Mosk.* 19, Part 10 (1945)
[5] Chukhanov, Z. F. *Zh. tekn. Fiz., Mosk.* 8, Part 2 (1938)
[6] Friedman, R. and Cyphers, J. *J. chem. Phys.* 25, No. 3 (1956)
[7] Sobolev, G. K. *High Temperature Oxidation and Burning of Carbon Monoxide.* This volume, Paper No. 57
[8] Tsukhanova, O. A. *Calculation of the Overall Reaction Kinetics for Carbon Monoxide with Oxygen and Methane with Oxygen.* To be published
[9] Khitrin, L. N. and Solovyova, L. S. *Homogeneous-Heterogeneous Combustion of Carbon Monoxide in Narrow Tubes (Channels).* This volume, Paper No. 74
[10] Burgoyne, J. H. and Hirsh, H. *Proc. Roy. Soc. A* 227 (1954) 73
[11] Kovalsky, A. A., Sadovnikov, P. Y. and Chirkov, N. M. *Zh. fiz. Khim., Mosk.* 4, Part 1 (1938)
[12] Zeldovich, Y. B. and Frank-Kamenetskii, D. A. *Zh. fiz. Khim., Mosk.* 12, Part 1 (1938)
[13] Sandri, R. *Canad. J. Chem.* 34, No. 3 (1956)
[14] Egerton, Sir Alfred and Thabet, S. K. *Proc. Roy. Soc. A* 228 (1955) 1174
[15] Norrish, R. G. W. *Proc. Roy. Soc. A* 150 (1936) 36
[16] Bartholomé, E., Dreyer, H. J. and Leseman, K. J. *Z. Elektrochem.* 54 (1950) 246
[17] Gaydon, A. G. *Trans. Faraday. Soc.* 42 (1946) 295

26

A MASS SPECTROMETRIC INVESTIGATION OF THE METHANE–OXYGEN REACTION AT LOW PRESSURES

D. J. FABIAN and W. A. BRYCE

The foundations for the use of the mass spectrometer as a means of studying decomposition and combustion reactions, with particular reference to the kinetics of the primary processes, were laid by Eltenton[1]. He studied the thermal decomposition of some lower hydrocarbons and also their combustion in low-pressure flames. In this work Eltenton showed that the mass spectrometer can be used for detecting and identifying free radicals in such systems.

The mass spectrometer has since been applied by several workers to the study of a variety of heterogeneous and homogeneous reactions. Low-pressure oxidations of hydrogen and of lower hydrocarbons have been studied by Robertson[2] and by Foner and Hudson[3], and considerable emphasis has been given to the study of the HO_2 radical by these workers.

A discussion of the problems involved in measuring radical concentrations is given by Robertson[5], and by Lossing *et al.*[6] who stress the experimental difficulties involved in the measurement of rates of radical reactions.

The present work was undertaken in an attempt to elucidate the primary steps in the oxidation of methane. With this in view a system has been employed whereby high temperatures could be obtained, but with reactant pressures insufficient to support a flame. The concentration of the intermediates then obtained is extremely low, but their analysis is greatly simplified.

EXPERIMENTAL

The mass spectrometer

The mass spectrometer was similar to that described by Lossing and Tickner[7] and used by Ingold and Bryce[8], but with the ion source and pumping arrangements modified to give preferential attention to the detection of the more unstable radicals of the type OH, HO_2, CH_3O_2, etc. As pointed out by Eltenton[1] and described by Robertson[9,5], fast pumping through the ion source is of considerable importance when studying radicals that are sensitive to surface collision.

The ion source housing was evacuated directly through a 5 cm diameter pumping line, as shown in *Figure 1*, giving a pumping speed in the ion source region of 6·5 l. per sec for oxygen. Pressure measurements within the chamber were obtained by both a McLeod gauge and an ion gauge. In order to take advantage of the faster pumping, the ionization box was made open in construction, and gas, sampled through a 6 mm hole in the top plate, was pumped away from between the first and second plates. This arrangement results in less overall sensitivity than that obtained with the unmodified ionization chamber, but a considerable advantage is gained when studying unstable free radicals since the ion source partial pressure of these becomes greater relative to that of stable molecules.

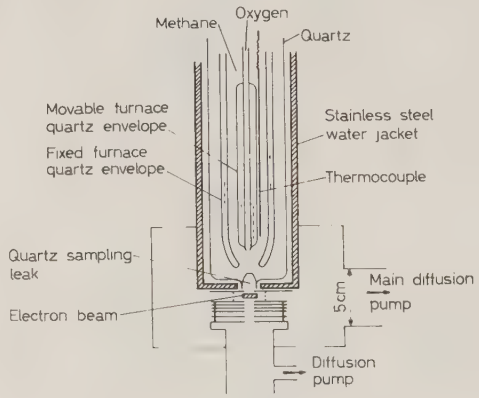

Figure 1. Reactor and ion source (schematic)

A second diffusion pump was attached, as shown, to the mass spectrometer tube and the design of the ion source plates was such that this pump produced differential pumping for the electron filament box. Provision was made for isolation of the main diffusion pump and evacuation solely via the electron box; thus two greatly different pumping rates for the ion source were available. This facility was incorporated in order that measurements of the sensitivity to surface reaction of a radical could be made, when desired, by the method described by Fabian and Robertson[10]. Under the lower pumping speed conditions 0·54 l. per sec for oxygen were obtained at the ion source.

The reactor

The quartz reactor, shown schematically in *Figure 1*, was similar to that employed by Bryce and Ingold, but with several improvements in design. A double-walled stainless steel jacket was constructed such that a water-cooled lining screened the ion source entirely from the hot reactor except for a 1 cm hole which allowed for sampling. The water inlet tube ran within the double wall and carried the water to the bottom of the jacket.

The reactor consisted of two furnaces both entirely enclosed in quartz envelopes so that no hot surface other than quartz was available to the reactants, thus minimizing the possibility of heterogeneous reaction. The furnace filaments were of molybdenum ribbon. One reactant flowed down the inside, and the second reactant down the outside, of the central movable furnace. The reactants, pre-heated in this manner, came together below the central furnace and the reaction temperature was maintained by means of the second fixed furnace. Reactants and products flowed past the tip of the sampling thimble which projected up into the hot one. Sampling occurred in the usual manner through a pin-hole leak, 20 μ diameter and 10 μ deep, located in the tip of the quartz thimble. The leak was made by blowing the quartz to a flat tip about 3 mm across and 100 μ thick, etching a portion 1 mm in diameter with hydrofluoric acid to 10 μ thickness, and sparking with a tesla coil. This procedure enabled the accurate location of the hole in the centre of the tip which, being flat, facilitated the measurement of depth and diameter. Such leaks were found capable of standing atmosphere pressure without fracture.

By measuring the rate of fall of pressure in an enclosed volume above the leak for a variety of gases of differing molecular weight, it was established that molecular flow conditions held up to pressures of 10 mm and more in the reactor. This property is of considerable importance since it ensures first that the sample path is predominantly collision-free and secondly that the partial pressures of components in the ion source, and hence peak intensities, are directly related to the respective partial pressures in the reactor. This permits quantitative results on product concentrations to be obtained.

Temperature measurement

To the outside of the movable furnace was attached a quartz enclosed platinum–platinum rhodium thermocouple which recorded the temperature at the lower end of this furnace, i.e. just above the mixing point. The thermocouple moved with the furnace and allowed measurement of any temperature gradient existing in the reactor. The temperature was found to be quite uniform along the reactor length when one or both furnaces were operating. The central furnace could be retracted to a distance of 8 cm from the sampling leak.

Pressure measurement and reactor flow rates

The methane and oxygen flow systems were controlled with needle valves and monitored with calibrated flow meters. A McLeod gauge was attached to the gas inlet tube leading to the inside tube of the central furnace. With the gas flow in this tube shut off and with gas flowing into the reactor around the outside of the central furnace, the steady-state pressure in the reactor could be read directly with the McLeod. For each reactant in turn it was shown that the reactor pressure was directly related to the flow-meter reading, and that viscous flow conditions obtained. Since the McLeod sampling point was movable, the pressure gradient in the reactor could be measured.

Raising the reactor temperature to 1,100°C was shown to have negligible effect on the steady-state pressure for a given gas flow. The inside tube of the central furnace had, in some experiments, an internal diameter of 1 mm. This tube is the sampling tube for the McLeod which is at room temperature, while the gas whose pressure is being measured is at 1,000 to 1,100°C, therefore the possibility that a thermal transpiration correction[11] is necessary must be considered.

We can estimate the magnitude of the effect using the equation of Liang[12],

$$R = \frac{P_1}{P_2} = \frac{\alpha_{He}(\phi_g X)^2 + \beta_{He}(\phi_g X) + R_m}{\alpha_{He}(\phi_g X)^2 + \beta_{He}(\phi_g X) + 1}$$

where $R_m = (T_1/T_2)^{1/2}$, P_1 = pressure (mm Hg) at lower temperature T_1, P_2 = pressure (mm Hg) at higher temperature T_2, $X = P_2 d$, d = internal diameter of tubing under consideration, α_{He}, β_{He} = constants; Liang gives these the values 2·52 and 7·68 $(1 - R_m)$, for $R_m \leqslant 1$, respectively, and ϕ_g = constant factor, dependent on the gas and defined such that $\phi_{He} = 1$.

Using this equation P_1/P_2 can be calculated for helium, for which the effect would be greatest. With a reactor temperature of 1,000°C, a pressure of 3 mm, and for tubing 1 mm in diameter, the result obtained indicates that a 1 per cent correction to the pressure reading is necessary. This is only a very approximate estimation, however, since Liang was considering much lower temperatures than we are dealing with and further, as pointed out by Bennett and Tompkins[13], Liang assumed that α_{He} and ϕ_g are invariant with temperature. The treatment of Bennett and Tompkins leads to a modified form of the Liang equation, but an examination of their considerations reveals

its non-applicability to large temperature differences such as those in our apparatus. We can conclude, however, that the pressure correction necessary is considerably less than 5 per cent and can therefore be neglected in our measurements.

With a 30 l./min rotary oil pump a 400 c.c./sec gas flow in the reactor was obtained. By interposing constrictions in the large diameter pumping line between reactor and pump, it was shown that the limiting factor was the pump capacity. Three pumps were therefore used in parallel; each could be isolated, and by operating one, two or three at a time, three different gas flow rates of 400 c.c./sec, 725 c.c./sec, and 870 c.c./sec could be obtained through the reactor. The linear flow rates, dependent upon reactor tube diameter, were in most experiments respectively, 390 cm/sec, 715 cm/sec and 850 cm/sec.

Materials

Methane used in the experiments was research grade product. Oxygen was the standard compressed gas dried over phosphorous pentoxide. Analysis of the two reactants with the mass spectrometer showed a high grade of purity of each.

Procedure

In most experiments oxygen flowed through the reactor via the central tube of the movable furnace and methane from around the outside of this furnace. Flow rates were adjusted to give oxygen and methane pressures of the order of 3 mm and 5 mm respectively. Products of reaction were searched for with electrons of low energy, at various temperatures, and with different flow rates and contact times in the reactor. The presence of a detected product was confirmed by shutting off the reactants in turn. Attempts were made to measure the concentration of a detected product with high energy electrons.

RESULTS

The homogeneous reaction between oxygen and methane, in the absence of catalysts and of flame, proved to be fairly slow, with HO_2 and CH_3 radicals forming the primary products. Both these radicals were detected in low concentration in mixtures of 5 mm of methane and 3 mm of oxygen at temperatures of 1,070 to 1,100°C. The temperature at which reaction was observed seemed to be quite critical. No products were detected below 1,070°C and the yield of HO_2 radicals appeared to fall off slightly as the temperature approached 1,100°C. No experiments were performed above 1,100°C since this was the limiting temperature to which the reactor could be raised. H_2O_2 was also observed in low concentration. No convincing evidence for CH_3O_2 was obtained. With short contact times, when CH_3 radicals were present in only low concentration, ethane was not detected conclusively. At higher contact times, greater than 10^{-2} sec, the mass spectra of products became increasingly complex and a detailed study was not made. Measurements were taken under conditions where CH_3, HO_2 and H_2O_2, although in very low concentration, were the only observable products. CH_3OH was presumably present also, but could not be detected due to the large excess of O_2^+ of the same mass. Hydrogen atoms, CH_2, CH_3O and OH radicals, were sought but not detected. Oxygen atoms were difficult to study due to the large O^+ contribution from O_2.

HO_2 radicals were observed at both low and high electron energies. It was found more convenient, however, due to the greater stability of mass spectra when using electrons of higher energy, to take measurements with 40 eV electrons. The CH_3 radical was detected at low electron energies but, due to the large contribution to mass 15 from methane, measurements on CH_3 radical concentration with 40 eV electrons were not possible. Hence the extent of reaction was estimated from the HO_2 radical concentration after subtracting the contributions to the mass 33 peak from the $^{16}O^{17}O$ isotopic molecule of oxygen, and from H_2O_2. With a 3·2 mm partial pressure of oxygen in the reactor, measurements were made on mass peaks 32, 33 and 34 both before and after the methane stream was switched on. In this way the isotope contributions and any background peaks at mass 33 and 34 were cancelled directly. When the methane stream was introduced, the oxygen partial pressure in the reactor would drop slightly, due to the decreased pressure drop across the needle valve controlling the flow of this gas. That this was not caused by reaction taking place was determined with the furnaces cold. It was necessary, therefore, to relate the 33/32 and 34/32 ratio to the same 32 peak. For these experiments the reactor temperature was kept at 1,090°C and the central furnace fixed at a pre-determined position which was the optimum found for the observation of HO_2 radicals in the system.

Figure 2 shows the typical mass spectra obtained in one such experiment, with a gas flow of 390 cm/sec and oxygen and methane partial pressures of 3·2 and 5·0 mm respectively.

Table 1 gives the 32, 33 and 34 peak intensities related to the same 32 peak height. The measurements were made using 40 eV electrons and with the bottom of the central furnace set 3·6 cm above the sampling leak.

If we assume about the same ionization cross-section for the formation of HO_2^+ from HO_2 as for O_2^+ from O_2, these figures represent a 0·05 per cent conversion of O_2 to HO_2. The contribution to

HO_2^+ from H_2O_2 was taken as 10 per cent of that part of the 34 peak that can be attributed to H_2O_2. This is in agreement with the correction found necessary by Ingold and Bryce[8] at 50 eV.

Figure 2. Mass spectra obtained at 40 eV, *for* (a) 3·2 mm *pressure of* O_2 *and no methane; and* (b) 3·2 mm *of* O_2 *with* 5·0 mm *of methane. Reactor temperature was* 1,090°C *in both cases.* 32 *peak is recorded with* 1/10th *the sensitivity of* 33 *and* 34

The effect, observed by Lossing, Ingold and Tickner[14], of peak intensities falling off as the reactor temperature was raised, was encountered with the present apparatus. Since no fall-off in ion source pressure was observed, the phenomenon was attributed to the temperature sensitivity of the mass spectra, probably due in part to decreased ionization cross-section of the heated gas molecules entering the ionization chamber. Extending the water-cooled jacket so as to come below the reactor and screen, the latter as much as possible, as in the apparatus described here, reduced the effect considerably; but at 1,100°C the peaks would still fall off to about one-third of the value with the reactor cold. A calibration of the fall-off with temperature was not necessary in the present work since it did not affect the measurements described above.

With the HO_2 radical observable in the reaction mixture, the establishment of low pumping speed conditions at the ion source increased the oxygen pressure in the ionization region to the order of 10^{-4} mm, and this resulted in too much instability for quantitative measurement of peak intensities. The HO_2 radical could then no longer be observed with any certainty, even with low electron energies. A direct measurement of the sensitivity of HO_2 to surface reactions was therefore not possible. However, due to the instability at these high ion source pressures, a partial pressure of HO_2 radicals in the ion source would not have been detected at low electron energies unless it was greater than 1/4 to 1/3 of that observed when fast pumping was used. The importance of this result in setting a lower limit to the HO_2 sensitivity to surface reactions is discussed later.

TABLE 1

Peak Intensities Obtained in the CH_4—O_2 Reaction at 1,090°C Using 50 eV Electrons. Peak Heights Relative to Mass 32 Intensity

Mass	CH_4 *stream on* cm	CH_4 *stream off* cm	*Difference* cm
32	204·0	204·0	—
33	0·26	0·12	0·14
34	0·90	0·64	0·26

An attempt to elucidate further the kinetics of the reaction, by relating HO_2 concentration to the position of the central furnace, and hence to position of the mixing point and to contact time, was not successful. The position of the central furnace for radicals to be observed was somewhat critical. In the above experiments it was set at 3·6 cm from the sample leak. When moved nearer to the leak, the HO_2 concentration quickly fell off while it could be withdrawn to 5·5 cm without appreciably affecting the observed concentration. Above this it fell off once more, presumably due to the radicals being used up. The concentration of HO_2 was too low for a quantitative study of the effect. The setting of 3·6 cm was that at which the highest observable HO_2 concentration occurred with lowest contact time.

Changing the flow rate in the reactor did, however, give a qualitative picture of the primary processes of the reaction. H_2O_2 was found to be a secondary product as indicated in *Figure 3.* In each case when the pumping rate on the reactor

was increased, the gas flows were increased in the same proportion in order to keep the reactor pressure the same. The partial pressure of methane, only, required accurate adjustment, since any discrepancy in the O_2 pressure cancelled out when

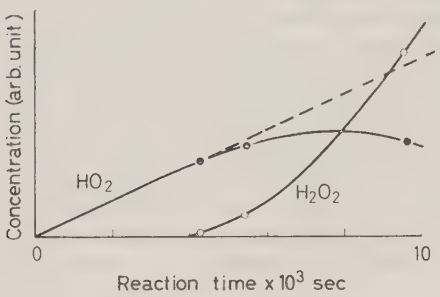

Figure 3. Relative concentrations of HO_2 *and* H_2O_2 *after different reaction times*

the peak heights were related to mass 32 intensity. The 33/32 ratios were measured in each case, with the reactor temperature and furnace position left unaltered.

DISCUSSION

It is observed that the reaction of oxygen with methane, at temperatures from 1,070 to 1,100°C, is quite slow; however, this is in accordance with the relatively high endothermicity of $CH_4 + O_2 \rightarrow CH_3 + HO_2$. Using 100 kcal for the dissociation energy of the C—H bond and the result of Foner and Hudson[15] and of Robertson[16], that $D(H—O_2) = 47$ kcal, we obtain a value of the endothermicity of the $CH_4—O_2$ reaction as 53 kcal. If we consider this endothermicity as being the major barrier to the process occurring when an oxygen molecule collides with one of methane, we can calculate an order of magnitude for the steric factor P of the reaction.

At 1,090°C it was observed that 0·05 per cent of the oxygen was converted to HO_2 radicals in a partial pressure of 5 mm of methane. The reaction time required for this conversion was 10^{-2} sec, and in this time every oxygen molecule will collide with approximately 2×10^6 molecules of methane. Hence 1 in 4×10^9 collisions is effective at 1,090°C. The collision yield S of the reaction is therefore $(4 \times 10^9)^{-1}$ or $10^{-9·6}$. Since $S = Pe^{-E/RT}$, if we take E as 53 kcal we obtain $P = 5 \times 10^{-2}$.

This figure must be treated as an order of magnitude value only since the observed 0·05 per cent conversion of oxygen to HO_2 is calculated first on an assumption for the unknown ionization cross-section for the formation of HO_2^+ from HO_2, and secondly without taking account of any loss of HO_2 radicals by decomposition or by surface reactions within the ion source.

HO_2 radicals formed at these high temperatures are likely to decompose readily to give H atoms and oxygen molecules. Such decomposition occurring within the reactor will be offset by the very fast reaction $H + O_2 \rightarrow HO_2$, so that any H atoms produced will quickly reform HO_2 radicals in the large excess of oxygen present. Reaction of H atoms with methane, $H + CH_4 \rightarrow H_2 + CH_3$ will be relatively slow, since a C—H bond has to be broken while for the H and O_2 addition there is a plentiful supply of third bodies.

We need consider, therefore, only the decomposition of HO_2 in its path between sampling and ionization. This distance was approximately 1 cm in the present apparatus. Each radical will traverse the electron beam several times before it is ionized, but intermediate collisions with surfaces will cause it to be cooled quickly; hence a fair approximation is obtained by considering the extent of decomposition in a path of 1 cm. The radicals will have a temperature of about 1,000°C when they enter the ion source. Free from collision their thermal velocity at this temperature will be approximately 10^5 cm/sec, and 1 cm will be traversed in 10^{-5} sec. Assuming for the unimolecular decomposition of HO_2, that $K \sim 10^{13} e^{-E/RT}$, and using $E = 47$ kcal, we obtain for the life-time of the radical a value of 10^{-5} sec. Thus the life-time is of the same order of magnitude as the interval in which decomposition can occur. Some loss by decomposition after sampling and before ionization is therefore to be expected. Moreover, calculation shows that, whilst a 50°C increase in reactor temperature slightly more than doubles the concentration of HO_2 radicals formed, and causes the radical life-time for decomposition within the ion source to be just halved, the same temperature increase brings about only a 2 per cent reduction in the time interval required for the radical to traverse 1 cm. Thus it would appear that an optimum temperature for the observation of HO_2 should occur in the range of 1,000 to 1,100°C. Beyond this optimum, as the temperature is increased, the HO_2 concentration observed should gradually fall off. This is in agreement with the results obtained.

A further loss of HO_2 radicals, after entering the ionization region, is caused by reaction at surfaces. To investigate this, HO_2 was sought with slow pumping at the ion source. The radical was no longer detected, but, as already observed, a concentration of HO_2, relative to O_2, equal to about 1/3 to 1/4 of that found before the pumping speed was reduced, would not have been conclusively detectable. This was due to ion source instability at the higher pressures caused by the lowering of pumping rate. Therefore, though it is not possible to obtain the sensitivity of HO_2 to surface reactions directly, we can apply the equation of Fabian and Robertson[10] to obtain a value for the lower limit of this sensitivity.

We use the equation,

$$\frac{P_r}{P_m} = \frac{N_r M_r^{1/2}}{N_m M^{1/2}} \frac{S/L}{S/L + KAk_r} \qquad (1)$$

where P_r = steady-state partial pressure of radicals in the ion source in mm of mercury, P_m = partial pressure of stable molecules in the ion source (in the present case these are oxygen molecules since the HO_2 concentration is related to per cent conversion of oxygen), N_r = flow of radicals per sec entering ion source, N_m = flow of stable molecules per sec entering ion source, M_r = mass of each radical in atomic weight units, M = mass of each stable molecule, S = pumping speed at the ion source, for particles of unit molecular weight, in l. per sec, L = constant = $3{\cdot}03 \times 10^{-20}$ at 20°C (we can assume that the radicals are cooled to room temperature before being pumped away), K = constant = $2{\cdot}05 \times 10^{21}$ at 20°C, A = area of surfaces at which radical can be lost, and k_r = probability of reaction of an HO_2 radical at a single surface collision.

Since P_r/P_m is reduced by at least 1/3 when S is lowered from 34·5 l./sec to 2·9 l./sec with N_r, N_m, M_r and M remaining constant, we obtain $Ak_r > 1{\cdot}25 \times 10^{-1}$.

We must consider what value to assign to A. When the pumping rate is reduced the radicals whose loss by surface reaction will affect P_r, as recorded by the ionizing electron beam, are those radicals within the ionization region. In the present apparatus, where all particles to be ionized approach the electron beam through a hole in the top ion source plate, and are pumped away at the perimeter of the gap between the first and second plates, it may be considered that the radicals in question are almost entirely confined to the region between the first two plates. The surface area available to these radicals is thus approximately 25 cm². Hence, $k_r > 5 \times 10^{-3}$.

An upper limit to the value of k_r may be obtained from an examination of equation 1, and from the experimental result for the steric factor P of the reaction. The possibility exists that, even at the higher pumping speed, a considerable proportion of the radicals that enter the ion source are lost by surface reaction. Then P_r would not be representative of N_r. However, the steric factor cannot exceed the theoretical value $P = 1$, therefore, in the extreme limit, P_r cannot have been reduced to less than 5×10^{-2} of its value, had none been removed by surface reaction. Hence $(P_r/P_m)/(N_r/N_m) < 5 \times 10^{-2}$. Applying this to equation 1,

$$\frac{S/L}{S/L + KAk_r} \frac{M_r^{1/2}}{M^{1/2}} > 5 \times 10^{-2}$$

for $S = 34{\cdot}5$ l. sec. Thus $k_r < 4 \times 10^{-1}$.

In these calculations we have assumed for the value of K that the radicals are at 20°C. The constant K is a measure of the rate of collision of particles at unit pressure with unit surface area. At 1,000°C, K would be lower by a factor of about 2. However, the radicals make numerous surface collisions before being either ionized, or pumped away, and after a relatively small proportion of these collisions they should be cooled to room temperature.

Thus, for the HO_2 radical we obtain the result $5 \times 10^{-3} < k_r < 4 \times 10^{-1}$. The extreme limits calculated in this way for k_r are generous limits and it is likely, therefore, that k_r is of the order of 4×10^{-2}. It is clear that HO_2 is considerably more sensitive to reaction at surfaces than most non-oxygen containing hydrocarbon radicals[6,10]. The result also lends support to the observations of Robertson[2], confirmed by Foner and Hudson[4], that HO_2 is formed from hydrogen atoms and oxygen molecules by three body collisions in the gas phase; but it is not entirely in agreement with the proposed reaction mechanisms of Badin[17], and Foner and Hudson[18], which involve formation of HO_2 at the wall of the reaction vessel.

Experiments performed with different flow rates in the reactor resulted in only a qualitative picture of the primary kinetics of the reaction. The difficulties involved in measurement of reaction kinetics, as described by Lossing[6] for a similar apparatus—unknown concentration gradients, indefinite initiation point for the reaction, etc.—apply more particularly in the present case where very low radical concentrations were obtained. From *Figure 3* it is evident that H_2O_2 is a secondary product. The ionization cross-section for the formation of $H_2O_2^+$ from HO_2 is unknown, hence the curves shown indicate relative concentrations only. If we assume that, in the absence of secondary reactions of HO_2, its concentration would be proportional to reaction time, it is seen from *Figure 3* that about one-half of the HO_2 radicals are lost by secondary processes after 10^{-2} sec. On the average every HO_2 radical formed during this time interval will have 5×10^{-3} sec in which to undergo reaction. Thus, since no other secondary products were observed after a contact time of 10^{-2} sec, we conclude that about 50 per cent of HO_2 would be converted to H_2O_2 after 5×10^{-3} sec, in 5 mm of methane at 1,090°C. Under these conditions each HO_2 radical would collide with approximately 10^6 molecules of methane in 5×10^{-3} sec. Hence the collision yield for the reaction $HO_2 + CH_4 \rightarrow H_2O_2 + CH_3$ is about $(2 \times 10^6)^{-1}$ or $10^{-6{\cdot}3}$, which leads to a value of 39 kcal for the activation energy of the reaction if we assume a steric factor of the order of 1. This value is probably in error by more than ± 10 kcal and must therefore be

treated with considerable reserve; however, it is evident that the activation energy for the reaction is somewhat higher than its endothermicity of approximately 11 kcal.

We conclude, from the present work, that when reactions are studied under conditions that lead to very low product concentrations, provided that these concentrations can be observed with a fair degree of accuracy, much advantage is gained from the considerable simplification of the kinetics. When a primary product is present in such low concentration, only those secondary reactions that occur between a primary product and an original reactant present in excess become important. Thus the absence of CH_3O_2 does not suggest that this radical will not be formed after longer reaction times, or at greater reactant pressures, but does imply that the reaction $CH_3 + O_2 \rightarrow CH_3O_2$ occurs at a lesser rate than $HO_2 + CH_4 \rightarrow H_2O_2 + CH_3$. This agrees with the observations of Hoare and Walsh[19] that $CH_3 + O_2 \rightarrow CH_3O_2$ requires a three body collision. The absence of CH_3O radicals and of hydrogen atoms indicate the very small extent, if any, of the reactions $CH_3 + O_2 \rightarrow CH_3O + O$, and $CH_3 + CH_4 \rightarrow C_2H_6 + H$ respectively; while the reaction $CH_3 + CH_4 \rightarrow CH_4 + CH_3$ would only be detectable using isotopically substituted reactants, since the occurrence of this reaction would not affect any of the present observations. The formation of H_2O_2 by the reaction $CH_4 + O_2 \rightarrow CH_2 + H_2O_2$ which would require an activation energy of at least 66 kcal, would be extremely slow at these temperatures and reactant concentrations. Thus CH_2 radicals were not detected, though the presence of a large CH_2^+ peak from methane made their absence not absolutely conclusive.

This work was supported by the Defence Research Board under Grant DRB 5001–10. One of us (D. J. F.) is indebted to the Board for a Research Associateship.

We are indebted to Professor C. A. McDowell for his encouragement, to Dr. A. J. B. Robertson for helpful discussions, and to Mr. A. J. Hawkins for his glass-blowing skill.

REFERENCES

[1] Eltenton, G. C. *J. chem. Phys.* 15 (1947) 455
[2] Robertson, A. J. B. *Conference on Mass Spectrometry*, Paper No. 11. 1953. London; Institute of Petroleum
[3] Foner, S. N. and Hudson, R. L. *J. chem. Phys.* 21 (1953) 1374
[4] — *J. chem. Phys.* 21 (1953) 1608
[5] Robertson, A. J. B. *Mass Spectrometry*. 1951. London; Methuen
[6] Lossing, F. P., Ingold, K. U. and Henderson, I. H. S. *Conference on Mass Spectrometry*, Paper No. 9. 1953. London; Institute of Petroleum
[7] — and Tickner, A. W. *J. chem. Phys.* 20 (1952) 907
[8] Ingold, K. U. and Bryce, W. A. *J. chem. Phys.* 24 (1956) 360
[9] Robertson, A. J. B. *Mass Spectrometry*, p. 47. 1952. London; Institute of Petroleum
[10] Fabian, D. J. and Robertson, A. J. B. *Trans. Faraday Soc.* 53 (1957) 363
[11] Tompkins, F. C. and Wheeler, D. E. *Trans. Faraday Soc.* 29 (1953) 1248
[12] Liang, S. C. *Can. J. Chem.* 33 (1955) 279
[13] Bennett, M. J. and Tompkins, F. C. *Trans. Faraday Soc.* 53 (1957) 185
[14] Lossing, F. P., Ingold, K. U. and Tickner, A. W. *Disc. Faraday Soc.* No. 14 (1953)
[15] Foner, S. N. and Hudson, R. L. *J. chem. Phys.* 21 (1955) 1364
[16] Robertson, A. J. B. *Trans. Faraday Soc.* 48 (1952) 228
[17] Badin, E. J. *J. Amer. chem. Soc.* 70 (1948) 3651
[18] Foner, S. N. and Hudson, R. L. *J. chem. Phys.* 23 (1955) 1974
[19] Hoare, D. E. and Walsh, A. D. *Trans Faraday Soc.* 53 (1957) 1102

27

KINETICS AND MECHANISM OF METHANE OXIDATION

N. S. ENIKOLOPYAN

Despite many investigations that have been carried out, there is no detailed evidence on the mechanism of methane oxidation. Many reaction schemes for the chain oxidation of methane were proposed by various authors[1–4], but quantitative estimation of these schemes is greatly handicapped by bad reproducibility and lack of kinetic evidence on consumption and accumulation of reaction products in vessels with steady surface condition. A happy exception to this is the recent work of Egerton with co-workers[5], unfortunately not involving methane oxidation.

This paper is concerned with detailed kinetic studies of intermediate and end-products of methane oxidation at steady surface condition of the reaction vessel. A possible mechanism is proposed based on the evidence obtained. All experiments were carried out by static methods.

The reaction vessel consisted of a tube with a diameter of 40 mm and a volume of 203 cm^3. Good reproducibility was obtained in an 'aged' vessel, in which successive experiments had been carried out for over a year. The runs were conducted at temperatures from 423 to 513°C and under pressures from 100 to 375 mm Hg using various mixture compositions ($CH_4 : O_2 = 1 : 2$, $1 : 1$, $2 : 1$).

PART PLAYED BY FORMALDEHYDE IN METHANE OXIDATION

Considerable auto-acceleration is known to be characteristic of methane oxidation reactions. According to Semenov[6] this is due to stable intermediary products generating active centres at a rate exceeding that of initial products. Most authors consider formaldehyde as responsible for chain branching in methane oxidation reactions. This conclusion is usually based on observed parallelism between formation of formaldehyde and change of pressure of a reaction, and also on a marked dependence of the induction period upon formaldehyde as has been observed by Bone[7], Norrish[8], Vanpée[9] and others. But these conclusions cannot be considered as unequivocal, since a considerable though perhaps a slightly less marked effect on the induction period was also observed on addition of methyl alcohol, formic acid and water.

The fact that a certain product is actually responsible for degenerate branching can be considered to be well established[10], if on addition of this product to the reaction mixture in amounts equal to its maximum value at the maximum rate without additives, the induction period becomes zero. Moreover there must be a strong correlation between the product concentration and the reaction rate.

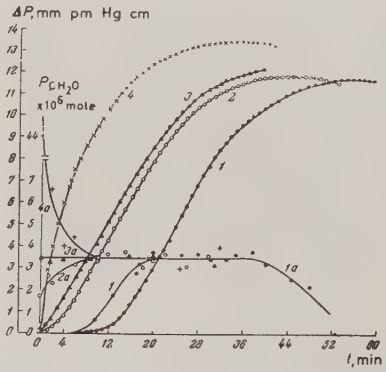

Figure 1. Effect of formaldehyde on kinetics of methane oxidation (in experiments with addition of CH_2O*) at* $T = 423°C$, $P_0 = 235$ mm Hg

Experimental evidence on the effect of formaldehyde on methane oxidation is given in *Figure 1*. Formaldehyde was added in amounts of 0·5 and 12·6 per cent of its steady concentration (3·6 $\times 10^{-6}$ mole). It will be pointed out that qualitatively similar results (*cf.* curves *1* and *3* of plot 1) were obtained by Vanpée at $T = 520°C$, $P = 300$ mm Hg for a mixture $2CH_4 + O_2$.

The behaviour of formaldehyde accumulation and methane consumption was estimated from theoretical calculations and kinetic formulae for degenerate branching chain reactions and from the methane oxidation mechanism proposed, comparison being made with experimental results.

If at $t = 0$ the concentration of CH_2O is also zero (without additions being made), then the expression for its change with time, obtained from integrating equation 4, will be

$$\xi = \frac{e^{\alpha\tau}\sqrt{e^{2\alpha\tau} + a^2} - a}{e^{2\alpha\tau} + a^2} \qquad (1)$$

where $\xi = \left[\frac{k_1'k_5'}{k_2k_5}\right]^{\frac{1}{2}} \frac{[CH_2O]}{[CH_4]}$;

$$a = \frac{k_3(O_2)}{h} \cdot \frac{CH_4}{\left[\frac{k_2'k_5'}{k_2k_5}\right]^{\frac{1}{2}}}; \quad \tau = \frac{2k_3h_0}{k_p}\left[\frac{k_2'k_5'}{k_2k_5}\right]^{\frac{1}{2}} t$$

This is shown in *Figure 2* by a full curve *1* plotted from equation 1. One of the points indicated by + has been taken for determining the value of n_0 (included in a). The points correspond to experimental values.

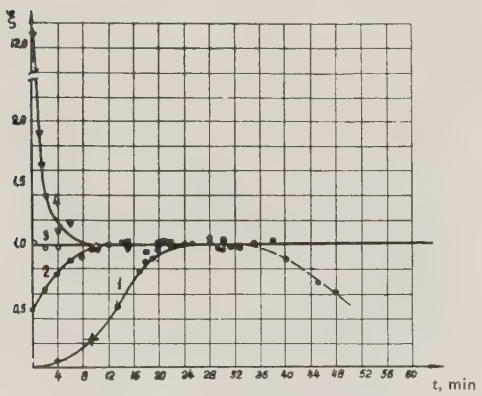

Figure 2. Theoretically calculated kinetic curves for CH_2O *accumulation in experiments with addition of* CH_2O *into the reacting mixture: 1 is the curve for a mixture without additives, 2, 3, 4 are mixtures with addition of* CH_2O *in amounts of* 0·5, 1 *and* 12·6 per cent *of the steady concentration*

If at $t = 0$ ($[CH_2O] \neq O$), then integrating equation 4 we obtain

$$\xi = \frac{e^{\alpha\tau}\sqrt{\theta_0^2\, e^{2\alpha\tau} + a^2\theta_0 - \theta_0} - a}{\theta_0\, e^{2\alpha\tau} + a^2} \qquad (2)$$

where

$$\theta_0 = \frac{(1 + a\,\xi_0)^2}{1 - \xi_0^2}$$

ξ_0 is the dimensionless concentration of formaldehyde added to the initial mixture. Curves *2*, *3* and *4* in *Figure 2* were calculated from equation 2.

The rate of methane consumption (see equation 6) in dimensionless coordinates will be

$$\frac{d\xi}{dt} = 1 + a\xi \qquad (3)$$

where

$$\xi = \frac{P_{CH_4}^{\circ} - P_{CH_4}}{\left[\frac{k_2k_5}{k_2'k_5'}\right]^{\frac{1}{2}} P_{CH_4}^{\circ}}$$

The kinetics of methane consumption with time at the initial stage, when the concentration of initial products can be considered constant, can be calculated by inserting ξ values from equations 1 and 2 into equation 3 and integrating.

Variations in methane concentration with time on addition of various amounts of CH_2O are shown in *Figure 3*, where the experimental results

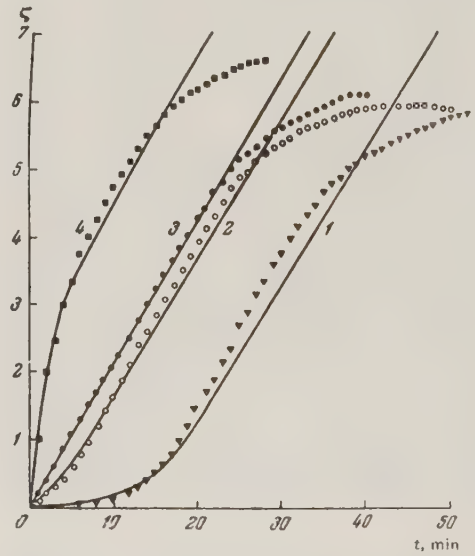

Figure 3. Theoretical curves for methane consumption in mixtures $CH_4 : O_2 = 1 : 2$ *with different* CH_2O *content* (*1*, 0; *2*, 0·5; *3*, 1·0; *4*, 12·6). *Points represent experimental values.* $T = 423°C$; $P_0 = 235$ mm Hg

are represented by points. Discrepancies in experimental and theoretical results observed at high values of time of contacts are due to consumption of initial products not being allowed for in integrating equation 3. Thus it was shown that formaldehyde is the only intermediate responsible for degenerate branching[11]. The validity of the mechanism proposed is also confirmed by good agreement of theoretical and experimental results.

It has also been shown that another intermediate product, the methyl alcohol, does not affect degenerate branching. Decrease of the induction period on addition of methyl alcohol is due to additional formation of formaldehyde.

KINETICS OF METHANE OXIDATION

Reaction kinetics at various temperatures

Investigations of the kinetics of consumption of initial products and accumulation of intermediate and end-products were carried out at temperatures within 423–513°C. Characteristic kinetic curves for variation of pressure, consumption of methane and oxygen and accumulation of reaction products (CO, CO_2, H_2O and H_2) in a stoichiometric methane–oxygen mixture at an initial pressure 235 mm Hg, are given in *Figures 4–7.* The kinetics of intermediate product accumulation (CO_2O and H_2O_2) are plotted in *Figures 8–11.*

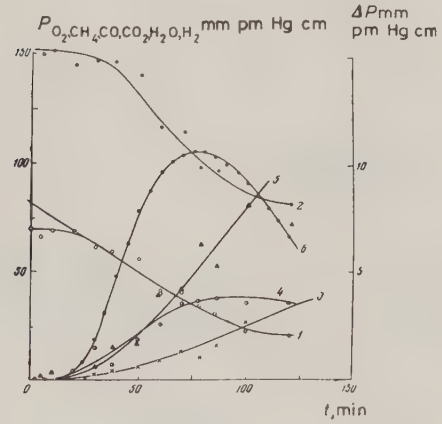

Figure 4. Kinetics of consumption: 1, CH_4 *and 2,* O_2 *and of accumulation of reaction products at* $T = 423°C$ *and* $P_0 = 235$ mm Hg *for a mixture without additions: 3,* CO_2; *4,* CO; *5,* H_2O; *6, Δp*

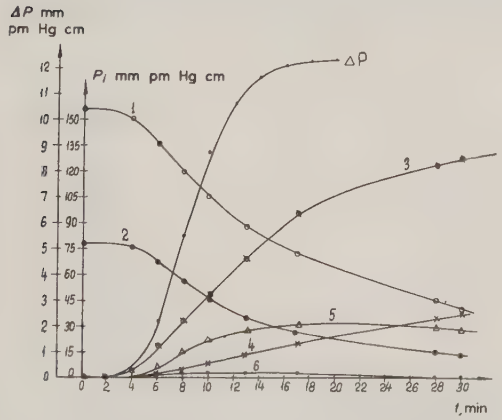

Figure 5. Kinetics of methane oxidation and accumulation of reaction products in mixture $CH_4 + 2O_2$ *at* $T = 472°C$, $P_0 = 235$ mm Hg. *Curves 1 and 2 represent consumption of* O_2 *and* CH_4 *respectively and curves 3, 4, 5 and 6 accumulation of* H_2O, CO_2, CO *and* H_2 *respectively*

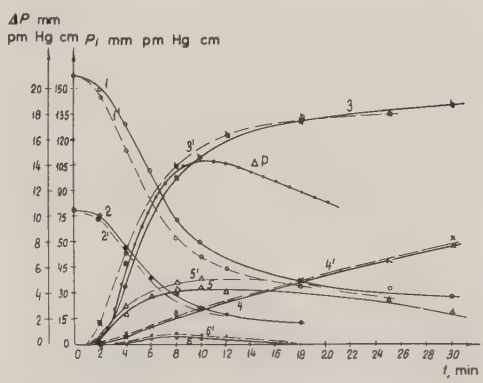

Figure 6. Kinetics of methane oxidation in mixture $CH_4 + 2O_2$ *at* $T = 491·5°C$ *and* $P_0 = 235$ mm Hg. *1,* O_2; *2,* CH_4; *3,* H_2O; *4,* CO_2; *5,* CO; *6,* H_2. *Broken lines represent mixtures diluted by* N_2 (140 mm Hg)

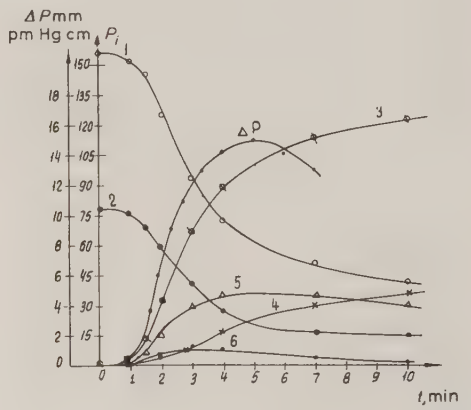

Figure 7. Kinetics of methane oxidation in mixture $CH_4 + 2O_2$ *at* $T = 513°C$ *and* $P_0 = 235$ mm Hg. *1,* O_2; *2,* CH_4; *3,* H_2O; *4,* CO_2; *5,* CO; *6,* H_2

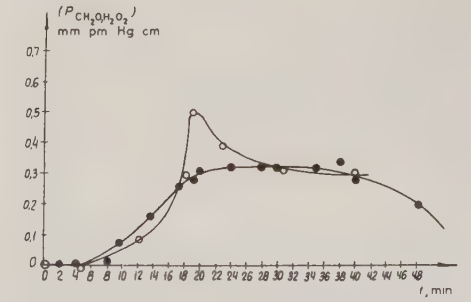

Figures 8–11. Kinetics of CH_2O *and* H_2O_2 *accumulation in products of methane oxidation at different temperatures.* $CH_4 : O_2 = 1 : 2$; $P_0 = 235$ mm Hg. *Figure 8 refers to temperature* 423°C, *9 to* 472°C, *10 to* 491·5°C, *11 to* 513°C

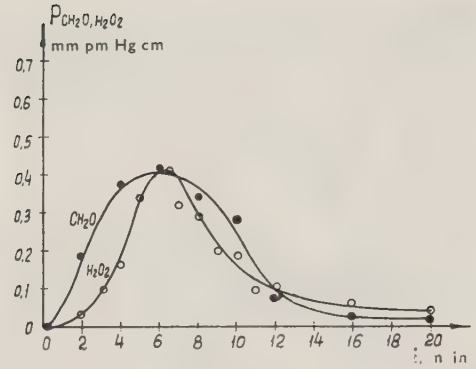

Figure 9

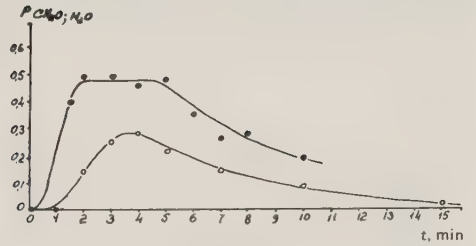

Figure 10

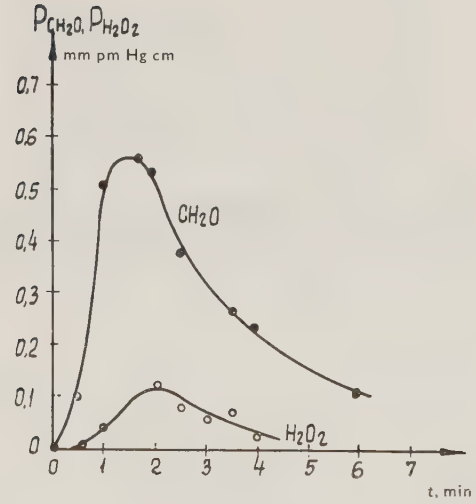

Figure 11

Maximum rate values were obtained from slopes of the straight parts of kinetic curves. The logarithmic anamorphose of the maximum rate is given in *Figure 12*. The activation energy obtained was of the order of 43 ± 1 kcal/mole.

It will be noted that maximum rates of methane consumption and of CO accumulation are quite similar within the whole range of temperatures observed, the maximum rate of oxygen consumption being approximately 1·5 times that of methane, the latter twice the rate of the pressure change and 0·5 times the rate of water accumulation.

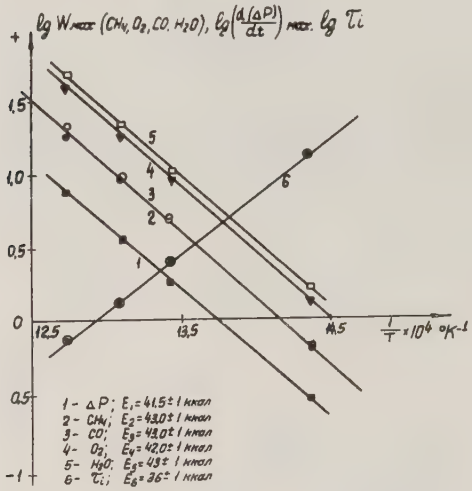

Figure 12. Temperature dependence for maximum rates of pressure change $(d\Delta P/dt)_{max}$. *(1), methane consumption* $(W_{CH_4})_{max}$; *(2), oxygen consumption* $(W_{O_2})_{max}$; *(4), CO accumulation* $(W_{CO})_{max}$ H_2O *accumulation* $(W_{H_2O})_{max}$; *(5), induction period and* τ_i; *(6) in methane oxidation* ($CH_4 + 2O_2$; P = 235 mm Hg)

The straight line *6* of *Figure 12* represents variations of the induction period with temperature, the effective activation energy being $E_6 = 36 \pm 1$ kcal/mole.

Dependence of the maximum formaldehyde yield $(CH_2O)_{max}$ on temperature is given in *Figure 13*. E_{eff} was calculated from the slope of the straight line and was found to be 7·8 kcal/mole.

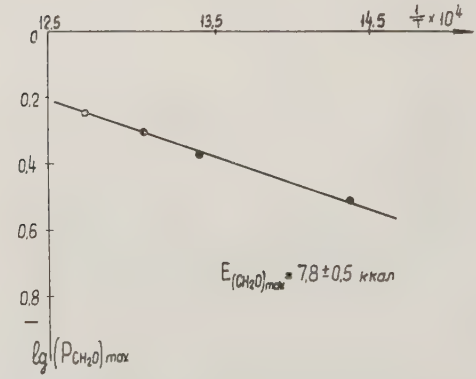

Figure 13. Temperature dependence for maximum formaldehyde yield in methane oxidation in a stoichiometric mixture with oxygen at P_0 = 235 mm Hg

Effect of initial mixture composition and of initial pressure on kinetics of methane oxidation

A series of experiments using methane–oxygen mixtures was carried out to determine the reaction order from the total pressure and from partial pressures of initial components at $T = 491{\cdot}5°C$ and under different initial pressures. The ratio of components CH_4 and O_2 varied within 2 to 0·5.

Kinetic curves for a stoichiometric mixture at initial pressures of 117 and 375 mm Hg are shown in *Figures 14* and *15*. Corresponding curves for $P = 235$ are given in *Figure 4*. The dependence of the maximum methane consumption rate upon pressure is well described by equation $W_{max} = CP^n$, n being 2·7.

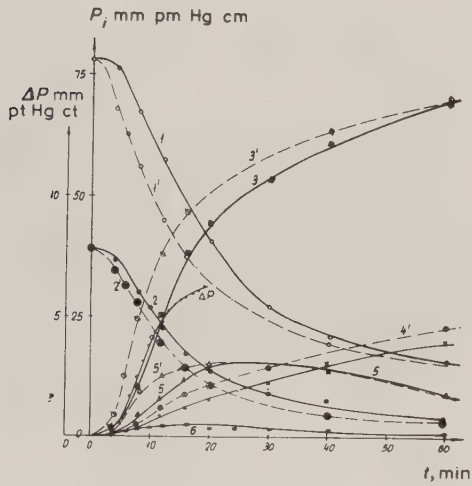

Figure 14. Kinetics of methane oxidation in a stoichiometric mixture with oxygen. $P = 117$ mm Hg, $T = 491{\cdot}5°C$. *1*, O_2; *2*, CH_4; *3*, H_2O; *4*, CO_2; *5*, CO; *6*, H_2. *Broken lines represent a mixture diluted by* N_2 (258 mm Hg)

In order to differentiate between the effect of pressure on active centre diffusion and the effect of concentration, the stoichiometric mixture was diluted by inert gas (N_2) under constant pressure $P_{CH_4 + O_2} + P_{N_2} = 375$. The results obtained are given by broken lines in *Figures 4, 14 and 15*. Dependence of W_{max} on P_0 is not connected with mixture composition and is well described by equation

$$W_{max} = C \times P_0^{\gamma}$$

γ was found to be $\sim 0{\cdot}1$.

Mixtures with high methane content ($CH_4 : O_2 = 1 : 1$ and $2 : 1$) were used in investigating the reaction order for methane and oxygen. Corresponding kinetic curves are given in *Figures 16* and *17*. The reaction order for methane, α, and for oxygen, m, was obtained from the empiric formula

$$W_{max} = [CH_4]_0^{\alpha} [O_2]_0^{\beta} p_0^{\gamma}$$

Experiments have shown that $\alpha = 1{\cdot}62$, $\beta = 0{\cdot}96$, $\alpha + \beta + \gamma = 2{\cdot}68$, which is near to $n = 2{\cdot}7$.

At an induction period $\tau = ap^m$, m was found to be unity.

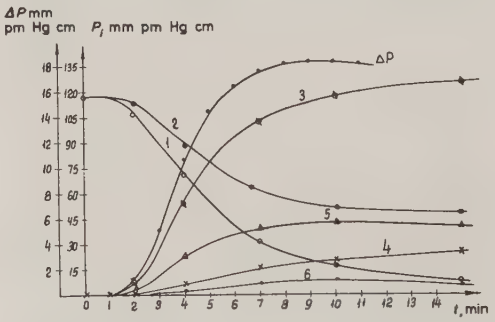

Figure 16. Kinetics of methane oxidation in an equimolecular mixture with oxygen ($CH_4 + O_2$). $P = 235$ mm Hg, $T = 491{\cdot}5°C$. *1*, O_2; *2*, CH_4; *3*, H_2O; *4*, CO_2; *5*, CO; *6*, H_2

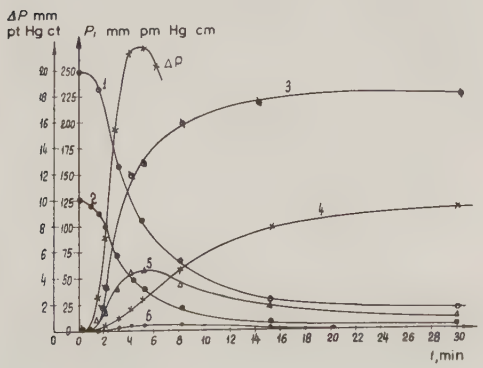

Figure 15. Kinetics of methane oxidation in a stoichiometric mixture with oxygen. $P_0 = 375$ mm Hg, $T = 491{\cdot}5°C$. *1*, O_2; *2*, CH_4; *3*, H_2O; *4*, CO_2; *5*, CO; *6*, H_2

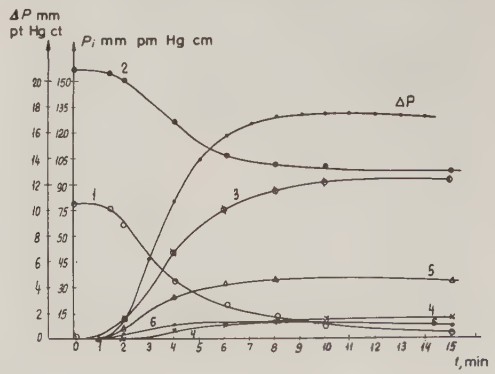

Figure 17. Kinetics of methane oxidation in a mixture $2CH_4 + O_2$. $P_0 = 235$ mm Hg, $T = 491{\cdot}5°C$. *1*, O_2; *2*, CH_4; *3*, H_2O; *4*, CO_2; *5*, CO; *6*, H_2

The dependence of the maximum yield of formaldehyde on total pressure at $T = 491{\cdot}5°C$ is shown in *Figure 18.*

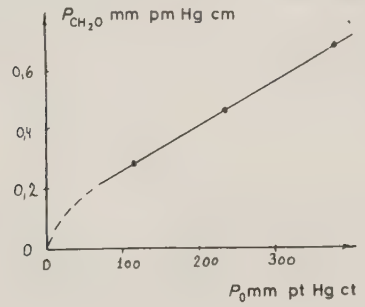

Figure 18. Effect of initial pressure on maximum yield of CH_2O *in methane oxidation.* $T = 491{\cdot}5°C$. $CH_4 : O_2 = 1 : 2$

The dependence of the maximum yield of formaldehyde on methane concentration was studied in a mixture with constant pressure of oxygen ($P_{O_2} = 55$ mm Hg). The results obtained are shown in *Figure 19.* It was found that beyond 55–60 mm Hg the yield of formaldehyde hardly depends on oxygen concentration (*Figure 20*).

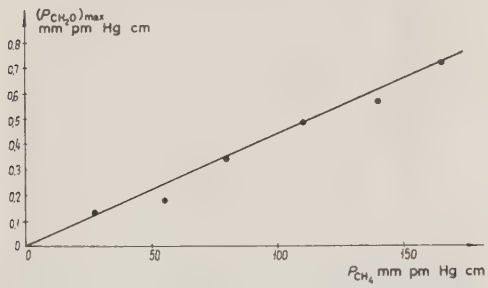

Figure 19. Dependence of maximum formaldehyde yield on methane content. $P_0 = 235$ mm Hg, $P_{CH_4} = 78$ mm Hg. $T = 491{\cdot}5°C$

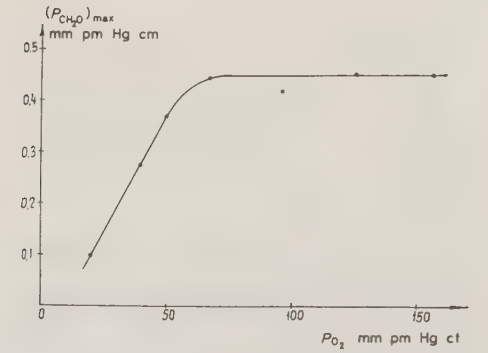

Figure 20. Dependence of maximum formaldehyde yield on oxygen content. $P_0 = 235$ mm Hg; $P_{CH_4} = 78$ mm Hg; $T = 491{\cdot}5°C$

On the mechanism of methane oxidation

A probable and well grounded mechanism of methane oxidation will be proposed here, leaving aside detailed discussion of separate elementary processes and comparison of various reaction routes possible. This is discussed in detail in the article by Karmilova, Enikolopyan and Nalbandyan[12] and in a monograph by Semenov, soon to be published. The following scheme is proposed:

(0)	CH_4	$+ O_2$	$\rightarrow$	CH_3	$+ H\dot{O}_2$
(1)	CH_3	$+ O_2$	$\rightarrow$	CH_2O	$+ \dot{O}H$
(2)	OH	$+ CH_4$	$\rightarrow$	H_2O	$+ CH_3$
(2′)	OH	$+ CH_2O$	$\rightarrow$	H_2O	$+ \dot{C}HO$
(3)	CH_2O	$+ O_2$	$\rightarrow$	$H\dot{C}O$	$+ H\dot{O}_2$
(4)	$H\dot{C}O$	$+ O_2$	$\rightarrow$	CO	$+ H\dot{O}_2$
(5)	HO_2	$+ CH_4$	$\rightarrow$	H_2O_2	$+ CH_3$
(5′)	HO_2	$+ CH_2O$	$\rightarrow$	H_2O_2	$+ CHO$
(6)	OH	+ wall	$\rightarrow$	destruction	

where 0 is the formation of primary radicals from initial products; 1, 2, 4 and 5 are chain propagation reactions in methane oxidation; 3 is a degenerate branching process; 2′ and 5′ are chain propagation reactions on formaldehyde oxidation. The mechanism does not allow for conversion of carbon oxide into CO_2 and hydroperoxide into water, and also for the presence of small amounts of methyl alcohol[4].

Making use of the quasi steady-state method for the determination of formaldehyde accumulation rate, we obtain

$$\frac{d\,[CH_2O]}{dt} = 2a_2\left(1 - \frac{a_2'a_5'}{a_2a_5}\right)\frac{a_0 + a_3}{k_6} \qquad (4)$$

where $a_0 = k_0[CH_4]\,[O_2]$ is the rate of formation of active centres, $a_3 = k_3\,[CH_2O]\,[O_2]$ is the rate of degenerate branching, a_2 is the product of the corresponding elementary process constant on the concentration of initial and intermediate products.

Formaldehyde concentration is maximum at the maximum reaction rate. From equation 4 we get

$$[CH_2O]_{max} = \left[\frac{k_2k_5}{k_2'k_5'}\right]^{\frac{1}{2}}(CH_4) \qquad (5)$$

The rate of methane consumption is

$$-\frac{dCH_4}{dt} = 2a_2\frac{a_0 + a_3}{a_6} \qquad (6)$$

The maximum rate of methane consumption is

$$-\left(\frac{dCH_4}{dt}\right)_{max} = \frac{2a_2a_3}{k_6}$$

$$2 = \frac{k_2k_3}{k_6}\,[CH_4]\,[O_2]\,[CH_2O]_{max} \qquad (7)$$

Maximum rates of O_2 consumption and CO and H_2O accumulation will consequently be

$$-\frac{d[O_2]}{dt} = \frac{3a_2a_3}{k_6} \quad (8)$$

$$\frac{d[CO]}{dt} = \frac{2a_1'a_5'}{a_5} \cdot \frac{a_3}{a_6} = \frac{2a_2a_3}{a_6} \quad (9)$$

$$\frac{d[H_2O]}{dt} = \frac{4a_2a_3}{a_6} \quad (10)$$

The rate of pressure change in the methane oxidation reaction is

$$\frac{d\Delta p}{dt} = -\frac{dCH_4}{dt} - \frac{dO_2}{dt} + \frac{dCO}{dt} + \frac{dH_2O}{dt} = \frac{a_2a_3}{a_6} \quad (11)$$

As can be seen from comparison of equations 7, 8, 9, 10 and 11

$$\frac{d\Delta p}{dt} = \frac{1}{2}\frac{dCH_4}{dt} = \frac{1}{3}\frac{dO_2}{dt} = \frac{1}{2}\frac{dCO}{dt} = \frac{1}{4}\frac{dH_2O}{dt} \quad (12)$$

This relation was indeed confirmed by experimental results.

It follows from equation 5 that the maximum formaldehyde concentration $[CH_2O]_{max}$ does not depend on oxygen concentration and is proportional to that of methane. These same relations were observed in investigations on the dependence of $[CH_2O]_{max}$ on oxygen and methane.

Equation 5 may be rewritten to read

$$\frac{[CH_2O]_{max}}{CH_4} = \left(\frac{k_2k_5}{k_2'k_5'}\right)^{\frac{1}{2}} \quad (13)$$

From the results of Avramenko[15] and theoretical conceptions[12,13] it follows that

$$\left(\frac{k_2k_5}{k_2'k_5'}\right)^{\frac{1}{2}} = e^{-8500/RT} \quad (14)$$

$E_{[CH_2O]_{max}}$ obtained experimentally was found to be 7·8 ± 1 kcal/mole, which is in fairly good agreement with theoretical results. The maximum amount of methane converted into formaldehyde at $T = 491{\cdot}5°C$ was calculated from equation 14 and found to be

$$\alpha = \frac{[CH_2O]_{max}}{CH_4} = \left(\frac{k_2k_5}{k_2'k_5'}\right)^{\frac{1}{2}} = e^{-\frac{8500}{2{\cdot}7645}} = 3{\cdot}8 \times 10^{-3}$$

As can be seen from the straight line of *Figure 9* the experimental value for α was $4{\cdot}4 \times 10^{-3}$. Accounting for the values of some reaction constants being approximate, this can be considered to be in good agreement with theory.

In accordance with equation 7 the maximum rate of methane consumption depends on methane concentration. Inserting the value $[CH_2O]_{max}$ from equation 5 into 7 we obtain

$$-\left(\frac{dCH_4}{dt}\right)_{max} = \frac{2k_2k_3}{k_6}\left(\frac{k_2k_5}{k_2'k_5'}\right)^{\frac{1}{2}}[CH_4]^2[O_2] \quad (15)$$

As can be seen the maximum rate of methane consumption depends on methane concentration in the second power, and on that of oxygen in the first power.

The reaction order of the maximum rate by total pressure is $n = 3$.

The values obtained experimentally were: $n = 2{\cdot}7$; $\alpha = 1{\cdot}62$; and $\beta = 0{\cdot}96$, which is in good agreement with theoretical values.

The energy activation value of the methane oxidation reaction can be calculated from the mechanism proposed. It follows from equation 15 that the overall activation energy is the sum of the activation energy of the branching chain reaction 3 equal to 32 kcal (the activation barrier being zero and the heat of reaction − 32 kcal), of the activation energy of reaction 2 equal to 8·5 kcal (results of Avramenko) and of the temperature ratio of expression $\left(\frac{k_2k_5}{k_2'k_5'}\right)^{\frac{1}{2}}$ equal to 8·5 kcal, the total being $E_{eff} \sim 49$ kcal/mole, on condition that k_6 is not dependent upon temperature. However, since OH destruction occurs in the kinetic region, as can be seen from small dependence of the reaction rate on the inert gas pressure ($\gamma \sim 0{\cdot}1$) and by strong dependence on the surface condition of the reaction vessel, the probability of OH destruction would depend on temperature. The activation energy of this dependence is known to be 4–6 kcal[15]. On accounting for this value the effective activation energy of methane oxidation will be lowered down to 43–45 kcal. The experimental value of the effective activation energy calculated from methane and oxygen consumption, from accumulation of CO and H_2O and from the maximum rate of pressure rise, was found to be 43 ± 1 kcal.

To obtain the maximum rate of methane consumption it is necessary to know the steric factor f_3 of reaction 3 and the value a_2/a_6 (see equation 15). According to Nalbandyan[17] at $T = 500°C$ $a_2/a_6 = 100$. f_3 was computed from $(dCH_4/dt)_{max} = 0{\cdot}01$ mm/sec at $T = 423°C$ and was found to be $\sim 0{\cdot}01$. Maximum methane consumption rates at different temperatures were obtained from these data, making use of equation 15. Comparison of experimental and theoretical results is given in Table 1.

TABLE 1

Rates of Methane Oxidation Calculated from the Mechanism Proposed and Obtained Experimentally

T°C	$[W_{CH_4}]_{max}$ mm/sec *calculated*	$[W_{CH_4}]_{max}$ mm/sec *obtained experimentally*
472	0·07	0·088
491·5	0·14	0·15
513	0·33	0·31

The value of the induction period and its dependence on temperature can be estimated from the mechanism proposed:

$$\tau = \frac{\text{const} \cdot k_6}{2k_2^{\circ}k_3^{\circ}\,[CH_2O]\,[O_2]}\, e^{\frac{E_3 + E_2 - E_6}{RT}} \qquad (16)$$

Since $E_2 - E_6 \simeq 4$ kcal and the activation energy of degenerate branching is $E_3 = 32$ kcal, it follows that $E \simeq 36 \pm 1$ kcal.

Comparison of calculated quantitative parameters for methane oxidation kinetics with those obtained experimentally is given in Table 2.

Good agreement of experimental and theoretical values seems to show that the mechanism proposed fits the methane oxidation reaction fairly well.

REFERENCES

[1] Semenov, N. N. *Usp. Khim.* 20 (1951) 673

[2] Norrish, R. *Disc. Faraday Soc.* 10 (1951) 296

[3] Lewis, B. and von Elbe, G. *Combustion, Flames and Explosions of Gases.* 1951. New York; Academic Press

[4] Karmilova, L. V., Enikolopyan, N. S. and Nalbandyan, A. B. *Zh. fiz. Khim.* 30 (1956) 798

[5] Egerton, A. C., Minkoff, G. I. and Salooja, K. C. *Proc. Roy. Soc. A* 235 (1956) 158; *Combustion and Flame* 1 (1957) 25

[6] Semenov, N. N. *Chain Reactions* (Russian) 1934. ONTI

[7] Bone, W. and Gardner, J. *Proc. Roy. Soc. A* 134 (1932) 578

[8] Norrish, R. and Ford, S. *Proc. Roy. Soc. A* 157 (1936) 503

[9] Vanpée, M. and Grand, F. *Fuel* 34 (1955) 433

[10] Enikolopyan, N. S. *Zh. fiz. Khim.* 30 (1956) 769

[11] Karmilova, L. V., Enikolopyan, N. S. and Nalbandyan, A. B. *Zh. fiz. Khim.* 31 (1957) 851

[12] — — — and Semenov, N. N. *Zh. fiz. Khim.* In course of publication

[13] Semenov, N. N. On some problems of chemical kinetics. In course of publication

[14] Avramenko, L. I. and Lorenzo, R. V. *Dokl. Akad. NaukSSSR* 69 (1949) 205

[15] — and Kolesnikova, R. V. *Dokl. Akad. Nauk SSSR* 91 (1953) 107

[16] Nalbandyan, A. B. and Voevodsky, V. V. *On the Mechanism of Hydrogen Oxidation and Combustion.* 1949. USSR Academy of Sciences

[17] — *Dokl. Akad. Nauk Armyanskoi SSSR*

TABLE 2

Calculated and Experimental Values of the Kinetic Parameters for Methane Oxidation Reactions

Item	*Theory*	*Experiment*
(1) Reaction order $[CH_2O]_{max}$		
by CH_4	1	1
by O_2	0	0
(2) Activation energy $[CH_2O]_{max}$	8·5 kcal	7·8 ± 1 kcal
(3) $\frac{[CH_2O]_{max}}{CH_4} = \alpha$ at $T = 491{\cdot}5$°C	$3{\cdot}8 \times 10^{-3}$	$4{\cdot}4 \times 10^{-3}$
(4) Reaction order at the maximum rate by CH_4	2	1·62
by O_2	1	0·96
by p_{tot}	3	2·7
(5) Activation energy at the maximum rate	46 kcal	43 ± 1 kcal
(6) $\left(\frac{dCH_4}{dt}\right)_{max} : \left(\frac{dO_2}{dt}\right)_{max} : \left(\frac{dCO}{dt}\right)_{max} : \left(\frac{dH_2O}{dt}\right)_{max} : \left(\frac{d\Delta P}{dt}\right)_{max}$	$1 : \frac{3}{2} : 1 : 2 : \frac{1}{2}$	$1 : \frac{3}{2} : 1 : 2 : \frac{1}{2}$
(7) Absolute reaction rate		
at $T = 472$	0·07 mm Hg/sec	0·088 mm Hg/sec
at $T = 491{\cdot}5$	0·14 mm Hg/sec	0·15 mm Hg/sec
at $T = 513$°C	0·33 mm Hg/sec	0·31 mm Hg/sec
(8) Activation energy of the induction period τ	36 kcal	36 ± 1 kcal

28

INHIBITION OF DIETHYL ETHER–OXYGEN FLAMES BY ALIPHATIC AMINES

D. J. WADDINGTON

Aliphatic amines are among the most powerful inhibitors of combustion processes. Several observations have been reported on the effect of aliphatic amines on the combustion of hydrocarbons[1,2] and other fuels[3,4]. Secondary amines inhibit certain reactions involved in the oxidation of trimethylamine[5], triethylamine[6] and other tertiary amines[7].

A detailed study of their effect on the slow oxidation of acetaldehyde showed that they are the most powerful inhibitors of the reaction yet reported[8]; thus ethylamine is over 20 times more effective than either ethane[9] or ethanol[10]. It was found that secondary and tertiary amines are even more powerful inhibitors than the primary compounds.

However, the study of the action of amines on the combustion of acetaldehyde is made complicated because amines and acetaldehyde react together to form complex condensation products[8,11,12].

For example:

$$RNH_2 + CH_3CHO \rightleftarrows RN{=}CHCH_3 + H_2O$$

It is impossible to assess whether inhibition is due to condensation products or to the amines themselves.

An investigation has been made into the action of amines on the combustion of diethyl ether. There is no interaction between inhibitor and fuel molecules, even at elevated temperatures; inhibition will be due to the amines and not to derivatives formed by intermolecular side reactions. Moreover, diethyl ether oxidizes at temperatures at which most amines are relatively stable to attack by oxygen[5–7]; there is, therefore, little possibility that inhibition is caused by products of amine oxidation.

Although the action of some aromatic amines and other compounds on the oxidation of ethers has been reported[13,14], no detailed study has been made on the action of aliphatic compounds. An account of the way in which the low temperature oxidation of diethyl ether is affected by aliphatic amines will be described elsewhere; this paper is concerned with their influence, and that of other nitrogen containing substances, on the occurrence of flames in the diethyl ether–oxygen system.

EXPERIMENTAL

A static type vacuum apparatus of conventional design was constructed. Reactants were introduced into cylindrical Pyrex reaction vessels (8 cm length; 6 cm diameter) maintained at a constant temperature. The vessels were rinsed with pure nitric acid, washed thoroughly with water and heated under vacuum at 450°C for several hours. The progress of reaction was followed by measurements of pressure change, using a capillary mercury manometer; results, with uninhibited mixtures of ether and oxygen, were in close agreement with those obtained with other types of gauge[13–16].

Diethyl ether was obtained in a high state of purity (80 per cent transmission at 2,500 Å). Samples were dried and repeatedly fractionated before use; the middle fractions were stored in previously evacuated globes. Oxygen and oxygen-free nitrogen, from cylinders, were dried by passage through magnesium perchlorate and through traps surrounded by solid carbon dioxide freezing mixtures, and stored in globes.

Methylamine was prepared by dropping strong aqueous solutions on to solid potassium hydroxide; the gas was dried by passage over magnesium perchlorate and condensed. Diethylhydroxylamine was prepared by dry distillation of its oxalate with calcium oxide. Other additives were obtained in the anhydrous state.

All additives were carefully fractionated before use. Middle fractions of the condensed products were allowed to evaporate into storage globes. As only small amounts were needed to inhibit reaction between ether and oxygen, the vapour of the additive was diluted with nitrogen. Larger amounts of gas could be admitted into the reaction vessel, the pressure of additive being known with an accuracy of $\pm$ 0·1 mm.

RESULTS

Relatively reproducible results were obtained in a reaction vessel after about 100 runs; there was then a coating of carbonaceous material inside the vessel. Results were found to be more reproducible if a standard procedure for the evacuation of

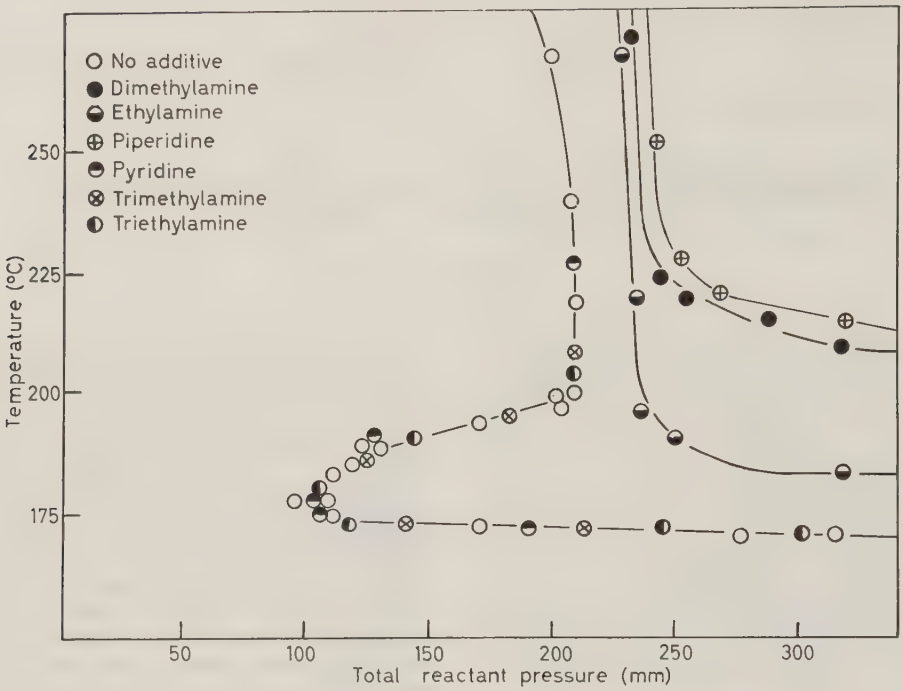

Figure 1. The influence of additives on the explosion limits of a (1:3) *diethyl ether–oxygen mixture. Additive added* 4 per cent

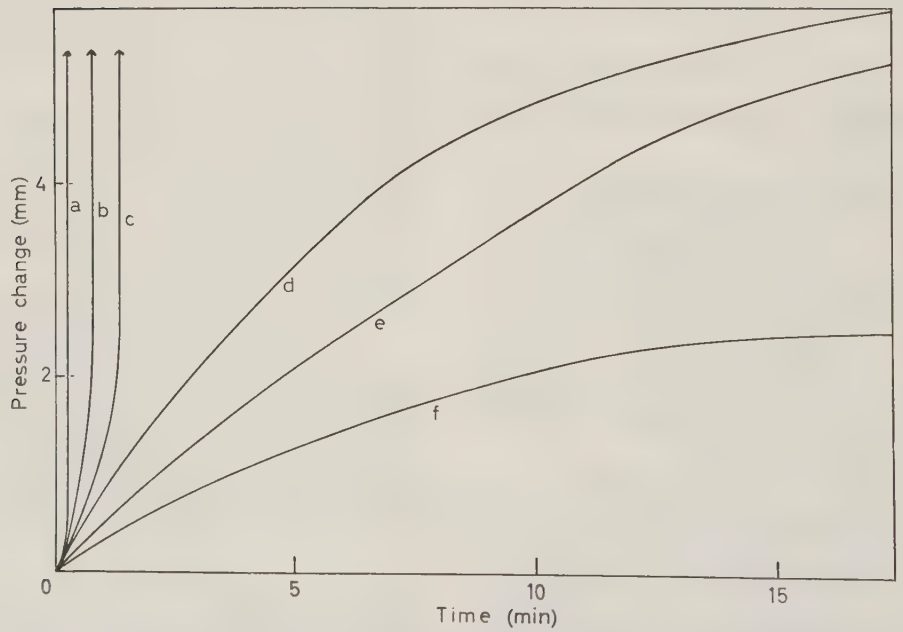

Figure 2. The influence of methylamine on the pressure–time curves for the oxidation of diethyl ether. Diethyl ether pressure 50 mm*; Oxygen pressure* 150 mm, *Methylamine added* (*a*) 2·0 mm, (*b*) 2·3 mm, (*c*) 3·8 mm, (*d*) 5·7 mm, (*e*) 6·1 mm, (*f*) 9·3 mm, *Temperature* 183°C

products from the vessel was used. It was found essential to allow each reaction to come to completion before evacuation.

Ignition diagrams

A pressure–temperature ignition diagram for an ether-rich mixture is shown in *Figure 1*. Flames

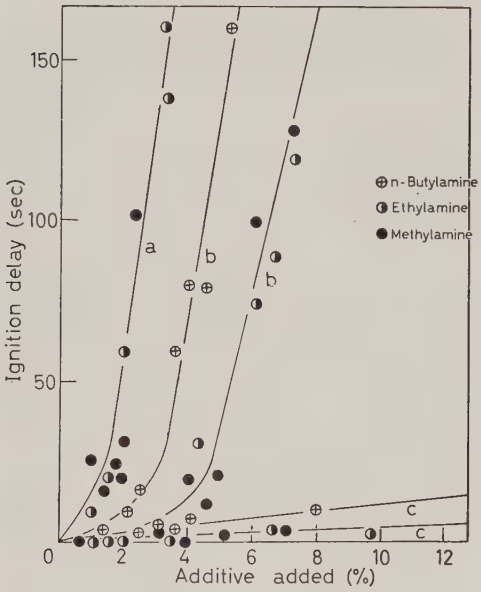

Figure 3. The influence of primary aliphatic amines on the ignition delay for a diethyl ether–oxygen mixture. Diethyl ether 50 mm*; Oxygen pressure* 150 mm*; Temperature* (*a*) 183°C, (*b*) 193°C, (*c*) 205°C

are observed above 170°C; there is a 'peninsula' at 180°C. Cool flames occur, under certain conditions, above 170°C. These results are in agreement with those of other workers[13–16].

Conditions necessary for explosion are altered markedly by additions of certain organic compounds. *Figure 1* shows how the limits of instantaneous ignition change when mixtures contain 4 per cent additive. Thus, ignition is not observed below 185°C, in the presence of 4 per cent ethylamine, even with increased reactant pressures; there is, moreover, no peninsula. On the addition of secondary aliphatic amines, and other compounds containing an imino group, both temperature and pressure, necessary for explosion, are further increased. For example, with diethylamine, instantaneous ignition does not take place below 210°C; with piperidine, the temperature limit is even higher.

Conditions for ignition do not seem to be altered by the addition of tertiary aliphatic amines or by pyridine (*Figure 1*).

A more detailed study of the effect of the additives was made.

Influence of primary aliphatic amines

At lower temperatures (170–195°C) primary amines delay the explosion of ether–oxygen mixtures when the concentration of amine is less than 3 per cent; ignition is inhibited above this concentration (*Figure 2*).

The structure of the alkyl group in the primary amine molecule has a little influence on its inhibitory power (*Figure 3*). *n*-Butylamine is a slightly more effective inhibitor than either methylamine or ethylamine.

The inhibitory power of primary amines decreases rapidly as the temperature is raised (*Figure 3*).

Influence of secondary aliphatic amines

Secondary amines are considerably more powerful inhibitors of ether oxidation than either primary or tertiary compounds (*Figures 1* and *4*). The relationship between ignition delay and the amount of secondary amine added is shown in *Figure 5*; above a critical amount of amine the passage of flames was completely inhibited. At

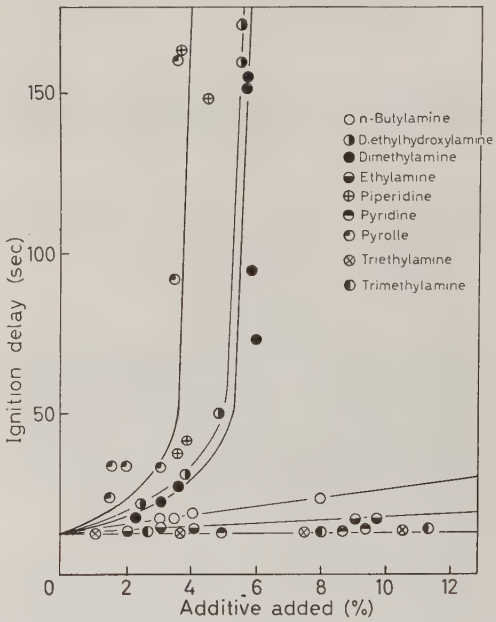

Figure 4. The influence of some compounds, containing a nitrogen atom, on the ignition delay for a diethyl ether–oxygen mixture. Diethyl ether 50 mm*; Oxygen* 150 mm, *Temperature* 205°C

205°C, 35°C above the normal ignition limit of the ether–oxygen mixture, 3 per cent secondary amine inhibits the passage of flames.

The nature of the alkyl groups attached to the imino group of the inhibitor would seem to be relatively unimportant (*Figure 5*).

Unlike primary amines, secondary amines do not lose their effectiveness above 210°C. Thus the difference in inhibitory power between these compounds and the other alkylamines increases with increasing temperature (*Figures 3* and *5*).

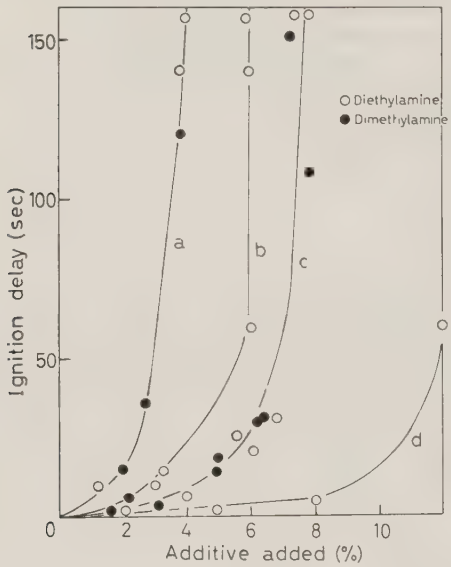

Figure 5. The influence of secondary aliphatic amines on the ignition delay for a diethyl ether–oxygen mixture. Diethyl ether 50 mm; *Oxygen* 150 mm, *Temperature* (*a*) 193°C, (*b*) 205°C, (*c*) 215°C, (*d*) 230°C

Compounds containing an imino group are the only organic compounds studied that are effective above 230°C as inhibitors (*Figure 5*).

Influence of tertiary aliphatic amines

Trimethylamine and triethylamine have little or no influence on either temperature or total reactant pressure necessary for the ignition of ether–oxygen mixtures (*Figures 1* and *4*). Ignition delays of less than 20 seconds are observed when over 10 per cent tertiary amine is present in the reactant mixture.

Influence of other compounds containing one nitrogen atom

From the foregoing results it would appear that compounds containing an imino group are the most powerful, and that the tertiary amines are the least effective inhibitors of the reaction. This conclusion is supported by studies on the action of other compounds having similar nitrogen-containing groups, but with widely differing groups attached to them.

The inhibitory powers of piperidine and pyrrole are remarkably alike (*Figures 1* and *6*). These compounds are more effective than the dialkylamines studied.

Pyridine, like trimethylamine and triethylamine, does not affect the explosion limits (*Figures 1* and *4*).

Diethylhydroxylamine has an inhibitory power comparable with secondary aliphatic amines (*Figure 4*).

Influence of other compounds

Several aliphatic compounds which do not contain a nitrogen atom were tested as inhibitors of the ether–oxygen reaction. Although ethane thiol and ethanol retard reaction, they are less powerful than either primary or secondary amines (*Figure 7*), and lose their effectiveness above 200°C.

Chlorethane has no effect on the explosion limits (*Figure 7*).

DISCUSSION

The oxidation of diethyl ether is probably initiated by a bimolecular reaction forming a reactive species, the ether radical[14]:

$$CH_3CH_2OC_2H_5 + O_2 \rightarrow CH_3\dot{C}HOC_2H_5 + \cdot HO_2 \quad (1)$$

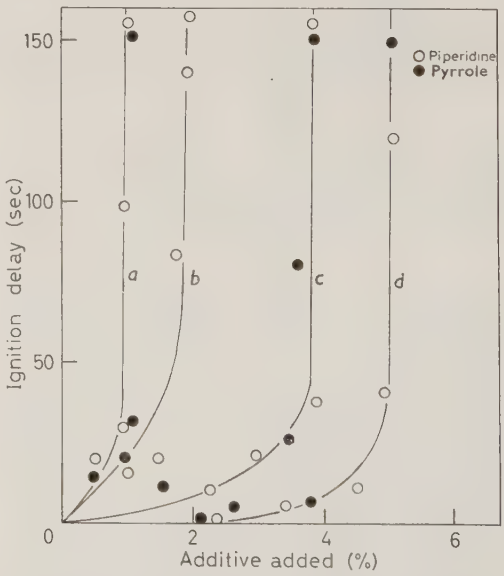

Figure 6. Influence of piperidine and pyrrole on the ignition delay for a diethyl ether–oxygen mixture. Diethyl ether 50 mm; *Oxygen* 150 mm, *Temperature* (*a*) 188°C, (*b*) 193°C, (*c*) 205°C, (*d*) 215°C

The ether radicals react with oxygen, and a chain cycle is set up:

$$CH_3\dot{C}HOC_2H_5 + O_2 \rightarrow CH_3CH(O\dot{O})OC_2H_5 \quad (2)$$

$$CH_3CH(O\dot{O})OC_2H_5 + CH_3CH_2OC_2H_5 \rightarrow CH_3CH(OOH)OC_2H_5 + CH_3\dot{C}HOC_2H_5 \quad (3)$$

The supply of chain initiators is reinforced by the decomposition of ether radicals, expression 4, and ether peroxide molecules, expression 5.

$$CH_3\dot{C}HOC_2H_5 \rightarrow CH_3CHO + C_2H_5\cdot \quad (4)$$

$$CH_3CH(OOH)OC_2H_5 \rightarrow CH_3CHO + \cdot OH + C_2H_5O\cdot \quad (5)$$

There is little doubt that the rate of reaction is greatly influenced by the concentration of peroxides and aldehydes formed in the early stages of reaction[15].

The effect of amines on the ether–oxygen system may result from their interfering with the 'build-up' of chain initiators. There are three ways in which this may occur: first, amines may prevent the initiation reaction (1) taking place; secondly, amines may interfere with the propagating steps (expressions 2 and 3); and finally, they may destroy peroxides as they are formed, producing stable products which will not act as chain carriers[17].

The initiation reaction, 1, is unlikely to be affected by small concentrations of additive, unless it is a heterogeneous process, and amines poison the surface. However, there is little kinetic evidence that the initiation reaction takes place on the surface[18].

Amine molecules may interfere with the propagation of chain carriers, expressions 2 and 3, by allowing the radicals to abstract hydrogen, and thus become stable. There may be competition between amine and oxygen for the ether radicals formed by reaction 1:

$$CH_3\dot{C}HOC_2H_5 + O_2 \rightarrow CH_3CH(O\dot{O})OC_2H_5 \quad (2)$$

$$CH_3\dot{C}HOC_2H_5 + \text{Inhibitor} \rightarrow CH_3CH_2OC_2H_5 + \text{Inhibitor radical} \quad (2a)$$

Similarly, if the ether radicals decompose, expression 4, there may be competition between amine and oxygen for the radicals formed.

The build-up of the critical concentration of radicals necessary for explosion would thus be hindered. For effective inhibition, reaction 2a must be considerably easier than reaction 2; the difference in activation energies of the two reactions must be significant. This scheme also pre-supposes that the inhibitor radicals, produced by reaction 2a, are relatively stable and will not take part in the reaction as chain carriers.

There are two parts of the amine molecule at which hydrogen may be abstracted by radicals; abstraction may take place either at the hydrocarbon part of the molecule or at the nitrogen-containing group. This was not possible in the inhibition of oxidation of acetaldehyde, for the amino and imino groups were masked by alkyl groups[8,11,12], the amines having condensed with acetaldehyde. The considerable influence of secondary and tertiary amines[8] gave every indication that the abstraction must be at the hydrocarbon part of the molecule.

However, in the ether–oxygen system the nitrogen-containing groups are free, and both parts of the amine molecule are open to attack by radicals. There is a complete lack of influence of the groups attached to the nitrogen-containing group. Thus, all compounds containing the imino group are efficient inhibitors, whether they

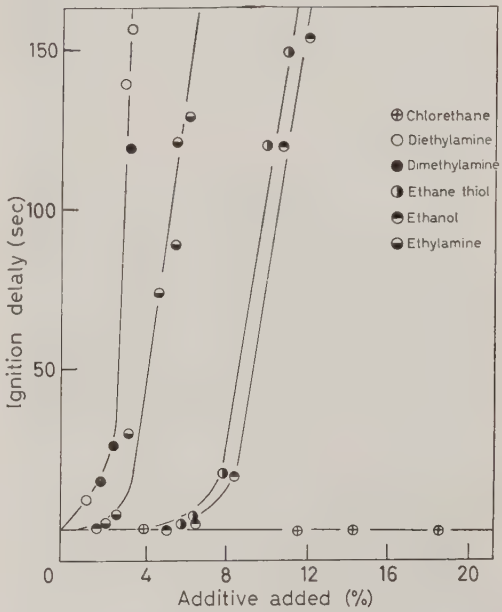

Figure 7. Influence of other compounds on the ignition delay for a diethyl ether–oxygen mixture. Diethyl ether 50 mm*; Oxygen* 150 mm, *Temperature* 193°C

be aliphatic or heterocyclic. All compounds containing an amino group exert some influence, but the tertiary amines were comparatively ineffective.

Abstraction of hydrogen may thus come from both ends of the amine molecule, but predominantly from the nitrogen-containing group. This is in direct contrast with the action of amines in the oxidation of acetaldehyde, because in this reaction the amino and imino groups were masked.

Tests with scaled molecular models support the experimental evidence; the models show that acetyl and other small radicals, formed during the combustion of acetaldehyde, can be stabilized by hydrogen abstraction from the α-carbon atoms of the amine molecules, even if the amine has undergone condensation with acetaldehyde. It is less easy for the larger radicals formed during the combustion of diethyl ether to take part in this

process; however, stabilization from the amino or imino groups is possible.

The weak inhibitory power of tertiary amines may be deceptive, as they are prone to attack by oxygen at these temperatures[5,6], and may be prevented from exerting their true influence. In fact, tertiary amines are more powerful inhibitors at lower temperatures, although they are still considerably less effective than secondary amines[18].

Although amines and related compounds are basic, there is no correlation between basic strength and inhibitory power. For example, pyrrole and piperidine have similar inhibitory powers, yet pyrrole is a compound whose basic properties are extremely weak[19] while piperidine is a strong base[20]. It is unlikely, therefore, that amines form hydroxides which then act as inhibitors. Furthermore, such hydroxides[21] are unstable above 100°C.

Inhibition may be enhanced by the interaction between amines and peroxides, formed in the early stages of ether oxidation (expression 3), to produce stable products which cannot take further part in the chain reactions. Amines do catalyse the decomposition of certain peroxides in solution; in most instances, reaction does not involve radicals[22]. The effect of amines on the thermal decomposition of peroxides in the gas phase is now being studied. Preliminary results indicate that this reaction plays a small part in the inhibition of ether flames.

No direct comparison of results between the action of amines as inhibitors in the acetaldehyde–oxygen and in the diethyl ether–oxygen systems can usefully be made. The latter system is likely to give more fruitful information as there is no chance of condensation between fuel and inhibitor. However, in both systems inhibition is probably due to the facile abstraction of hydrogen by free radicals. This can take place at both ends of the molecule in ether oxidation but only at the hydrocarbon part of the molecule in the combustion of acetaldehyde. In both systems the presence of a nitrogen atom in the inhibitor molecule is essential for strong inhibition, especially at temperatures above 200°C. If nitrogen is replaced by other atoms of small atomic weight, for example oxygen, sulphur or chlorine, the inhibitory power of the compound is considerably decreased. The nitrogen atom would seem to facilitate hydrogen abstraction from the inhibitor molecule.

There is a striking similarity between the power of amines to delay and inhibit formation of ether flames, and their power to prevent knock in the combustion of hydrocarbons[23]. Similar types of radical are probably formed during both combustion processes. These results would appear to give additional support to the theory that effective anti-knock agents must have the power to stabilize free radicals in the gas phase.

The author wishes to thank Shell Petroleum Company for their most generous assistance towards the purchase of apparatus. He is grateful to the Governors, Master, and Head of the Science Department of Wellington College for the facilities they have provided, and to several boys who have helped in preparative work.

REFERENCES

1 Gerber, M. I. and Neiman, M. B. *Zhur. fiz. Khim.* 27 (1953) 1572
2 Mullins, B. P. *Fuel* 32 (1953) 451
3 Sieg, L. *Angew. Chem.* 63 (1951) 143
4 Dixon-Lewis, G. and Linnett, J. W. *Proc. Roy. Soc. A* 210 (1951) 48
5 Cullis, C. F. and Waddington, D. J. To be published
6 — — *Proc. Roy. Soc. A* 244 (1958) 110
7 — — *Proc. Roy. Soc.* To be published
8 — — *Trans. Faraday Soc.* 53 (1957) 1317
9 Small, N. J. H. and Ubbelohde, A. R. *J. Chem. Soc.* (1950) 723
10 Farmer, J. B. and McDowell, C. A. *Trans. Faraday Soc.* 48 (1952) 624
11 Mannich, C. and Roth, K. *Arch. Pharm.* 274 (1936) 527
12 — and Davidsen, H. *Bericht* 69 (1936) 2106
13 Chamberlain, G. H. N. and Walsh, A. D. *Trans. Faraday Soc.* 45 (1949) 1032
14 — — *Third Symposium on Combustion*, p. 368. 1949. Baltimore; Williams and Wilkins
15 Lemay, A. and Ouellet, C. *Can. J. Chem.* 33 (1955) 1316
16 — — *Can. J. Chem.* 35 (1957) 124
17 Ubbelohde, A. R. Private communication
18 Waddington, D. J. To be published
19 Fischer, H. and Orth, H. *Die Chemie des Pyrrols.* Vol. 1 (1934) Leipzig
20 Sidgwick, N. V. *Organic Chemistry of Nitrogen Compounds*, p. 478. 1937. Oxford; Clarendon
21 Latimer, W. M. and Rodebush, W. H. *J. Amer. chem. Soc.* 42 (1920) 1419
22 Horner, L. and Schwenk, E. *Angew. Chem.* 61 (1949) 411
23 British Patents Specification. 592,966

29

STABILIZATION BY ALIPHATIC AMINES OF FREE RADICALS IN OXIDATION SYSTEMS

C. F. CULLIS and B. A. KHOKHAR

INTRODUCTION

Among simple organic compounds, amines are the most powerful inhibitors of gaseous oxidation reactions. Recent studies of the effect of aliphatic amines on slow combustion processes[1] suggest that the inhibiting action may be ascribed, at any rate in part, to the ability of the inhibitor to stabilize free radicals by hydrogen donation. This paper describes some work designed to elucidate further the mode of action of aliphatic amines and to extend the measurements previously reported on the inhibition of slow oxidation to the prevention of explosive combustion.

EXPERIMENTAL

Materials

The purest available commercial samples of triethylamine, diethylamine and ethylamine were carefully fractionated and after being introduced into storage bulbs were freed from dissolved gases by repeated freezing and melting under vacuum. Trimethylamine was prepared by dropping a strong aqueous solution on to solid potassium hydroxide, and the middle fraction of the condensate was distilled into a storage globe. The purified amines were examined by gas–liquid chromatography and were found to be free from related basic compounds.

Acetaldehyde was freshly distilled in a current of nitrogen and was then fractionated *in vacuo*; the vapour was stored in a black-lacquered glass vessel to prevent photo-decomposition. Oxygen from a cylinder was dried by passage over magnesium perchlorate and was then passed through a cold trap (— 183°C) into a storage globe.

NN-diethylhydroxylamine (used for calibration in chromatographic analysis of combustion products) was prepared by pyrolysis of triethylamine oxide[2].

Apparatus

The apparatus consisted essentially of a spherical Pyrex reaction vessel, *A*, of 200 ml capacity, suspended in an electric furnace and connected both to a mercury manometer and to a pre-mixing vessel, *B*, of 1,500 ml capacity, maintained at 25°C. The sharing factor between *A* and *B* was accurately determined under a wide series of conditions of temperature and pressure, so that if the pressure in *B* before sharing were known, that developed in *A* after sharing could readily be calculated.

To determine the ignition diagrams for triethylamine and trimethylamine, amine–oxygen mixtures of known composition were prepared manometrically in *B*. A wide-bore tap connecting *A* and *B* was then momentarily opened and closed again. Explosion in *A* was denoted by a sudden depression of the meniscus of the mercury manometer accompanied by a bright flash of light. A much milder pressure pulse indicated the passage of a cool flame. After evacuation of *A*, the combustible mixture remaining in *B* could again be admitted to *A* giving progressively lower pressures until slow reaction was observed.

In the determination of the effect of amines on the explosive combustion of acetaldehyde, it was first necessary to carry out many 'trial' runs (by addition of acetaldehyde to pure oxygen) in order to establish reproducible conditions. 50 mm oxygen was introduced into *A* and acetaldehyde vapour was admitted to *B* to such a pressure that, on opening the connecting tap, 50 mm acetaldehyde vapour flowed into *A*. After the reaction vessel had become acclimatized it was found that at 218°C, for example, explosive combustion of the above equimolar acetaldehyde–oxygen mixture took place *ca.* 15 sec after mixing. The presence of amines greatly delays, or even prevents, the onset of explosion, but in general concentrations of less than 3 per cent gave conveniently measurable delays. Lean amine–oxygen mixtures containing the required concentration of amine were therefore prepared manometrically by dilution in another vessel, *C*, and the required pressure (*ca.* 50 mm) was then admitted to *A*. Acetaldehyde vapour was then admitted to *B* to such a pressure that on momentarily connecting *A* and *B*, 50 mm was introduced into *A*.

With the three ethylamines, the induction period was taken as the time between admission of acetaldehyde to *A* and the occurrence of explosion. Since with trimethylamine, explosion is

completely prevented, although slow combustion nevertheless takes place, the induction period with this compound was taken as the time between the introduction of acetaldehyde to *A* and the attainment of a pressure decrease of 5 mm.

The reaction between acetaldehyde and oxygen is highly sensitive to impurities[3] and it was therefore found necessary to standardize rigidly the

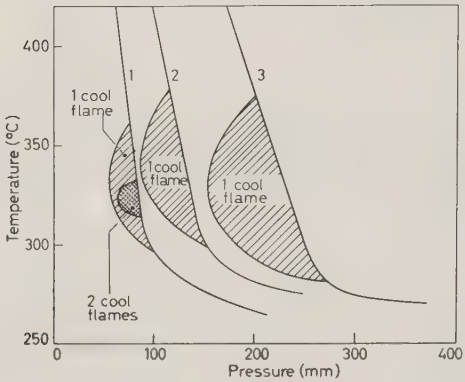

Figure 1. Ignition diagrams for triethylamine–oxygen mixtures. Curve 1, 16·7 per cent *triethylamine; curve 2,* 9·1 per cent *triethylamine; curve 3,* 4·8 per cent *triethylamine*

procedure used when experiments were carried out with this compound. The reaction vessel was therefore always evacuated for an hour after each run and was then flushed with oxygen for a further hour before the next run was carried out.

RESULTS AND DISCUSSION

Explosive combustion of triethylamine and trimethylamine

The ignition diagrams for three different triethylamine–oxygen mixtures (*Figure 1*) indicate the occurrence of regions of slow combustion, of single and multiple cool flames and of true explosion. Two successive cool flames are observed only between 315 and 330°C and with the richest mixture investigated. Explosion is generally preceded by a measurable induction period during which an increase in pressure is noted. The length of this induction period decreases markedly with temperature and with the proportion of oxygen in the mixture. Explosion is, however, more violent in rich than in lean mixtures.

Figure 2 shows the corresponding ignition diagrams for a number of trimethylamine–oxygen mixtures. Under comparable conditions of temperature and pressure, explosion occurs at considerably lower temperatures and is much more violent than with triethylamine. The chief difference in the behaviour of the two amines is that trimethylamine, in common with the first members of many other homologous series of aliphatic compounds[4], does not give rise to cool flames.

Examination of *Figures 1* and *2* shows that, with both tertiary amines, lean systems are generally less prone to explosion than rich systems. The compositions of the mixtures studied have been varied over a wide range, and if it is borne in mind that for complete combustion 1 molecule of trimethylamine and triethylamine requires approximately 6 and 11 molecules of oxygen respectively, it will be seen that mixtures with both a stoichiometric deficit and excess of amine have been used. The fact that the tendency to explosion increases continuously with the amine concentration is somewhat surprising in view of the well known inhibiting effect of tertiary amines. A possible explanation is however that unchanged tertiary amine is not the only inhibitor but that even more effective inhibition may be caused by reaction products which are formed more readily in lean than in rich mixtures. To investigate the possibility further, it was necessary to introduce a third component into the system and to study the inhibiting effect of amine–oxygen mixtures and their reaction products on the explosive combustion of another fuel. Acetaldehyde is particularly suitable for this purpose since it is oxidized explosively in a temperature region convenient for studies of the slow oxidation of triethylamine and trimethylamine.

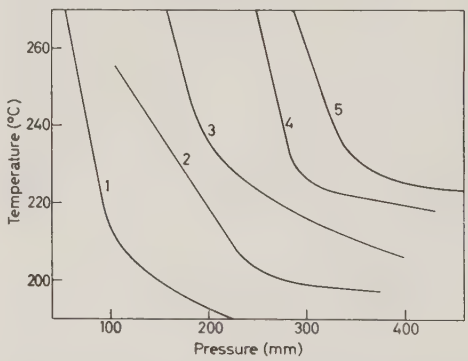

Figure 2. Ignition diagrams for trimethylamine–oxygen mixtures. Curve 1, 50·0 per cent *trimethylamine; curve 2,* 16·7 per cent *trimethylamine; curve 3,* 9·1 per cent *trimethylamine; curve 4,* 6·2 per cent *trimethylamine; curve 5,* 5·4 per cent *trimethylamine*

Inhibition of explosive combustion of acetaldehyde

Figure 3 shows that the length of the induction period preceding explosion is directly proportional to the initial pressure of triethylamine present. This result is the same as that found for the inhibition of slow oxidation of acetaldehyde[1], and suggests that a similar underlying mechanism is in operation for both slow and explosive combustion.

It is found, however, that if the concentration of triethylamine is raised above 3 per cent, reaction is more or less indefinitely inhibited.

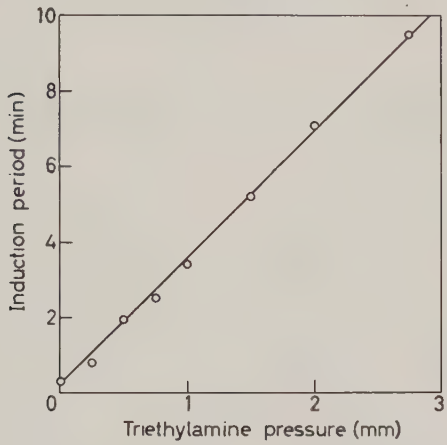

Figure 3. The influence of the pressure of added triethylamine on the induction period preceding explosive combustion of acetaldehyde. Temperature, 218°C*; acetaldehyde pressure,* 50 mm*; oxygen pressure,* 50 mm

For a given initial pressure of triethylamine the length of the induction period is markedly dependent on the time for which the amine–oxygen mixture is heated prior to admission of the

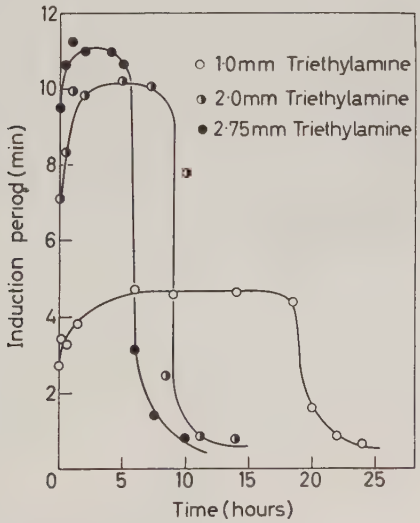

Figure 4. The influence of the time of pre-heating of triethylamine–oxygen mixtures on the explosive combustion of acetaldehyde. Temperature, 218°C*; acetaldehyde pressure,* 50 mm*; oxygen pressure,* 50 mm

acetaldehyde. The results in *Figure 4* show that, as the time of pre-heating of triethylamine–oxygen mixtures is increased, the induction period at first increases, then remains effectively constant for some time and finally decreases again quite sharply. Similar behaviour is also in evidence with trimethylamine–oxygen mixtures (*Figure 5*), although at 218°C trimethylamine appears to cause slow reaction rather than to delay explosive combustion. The observed effect of pre-heating is less pronounced with the lower amine, probably

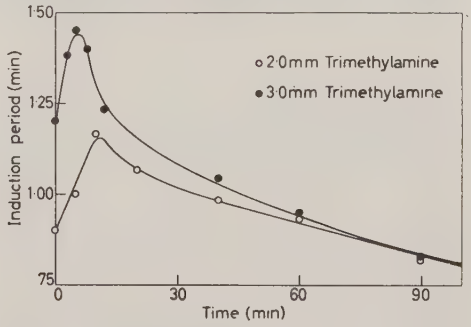

Figure 5. The influence of the time of pre-heating of trimethylamine–oxygen mixtures on the combustion of acetaldehyde. Temperature, 218°C*; acetaldehyde pressure,* 50 mm*; oxygen pressure,* 50 mm

on account of more rapid oxidation of the methyl compound at the temperatures used. The ratio

$$\frac{\text{maximum induction period}}{\text{initial induction period}} = \phi$$

clearly constitutes a measure of the inhibiting power of the reaction products, and the results in Table 1 show that for both amines this ratio is greatest in lean mixtures. It is evident from these findings that certain products formed during the oxidation of triethylamine and trimethylamine

TABLE 1

Temperature 218°C; Acetaldehyde Pressure 50 mm; Oxygen Pressure 50 mm

Inhibitor	*Pressure* (mm)	ϕ
Triethylamine	1·0	1·77
	2·0	1·44
	2·75	1·17
Trimethylamine	2·0	1·30
	3·0	1·19

have an even greater inhibiting power than the parent tertiary amines, and that the formation of these products is favoured by a large excess of oxygen.

The oxidation of tertiary aliphatic amines has been fully studied[5]. With triethylamine, for example, the main nitrogen products are diethylamine and ethylamine[6]. This result was confirmed in the present work by gas–liquid chromatography

and there was no evidence for the formation of appreciable amounts of oxygenated compounds such as NN-diethylhydroxylamine, which is known to be a powerful inhibitor. Experiments were however carried out to determine the inhibiting power of mixtures of primary, secondary and tertiary amines in order to see whether their combined effect was greater than would be expected from the sum of their separate effects.

Inhibiting effect of mixtures of amines

The results in *Figure 6* show how the induction period varies with composition for mixtures of

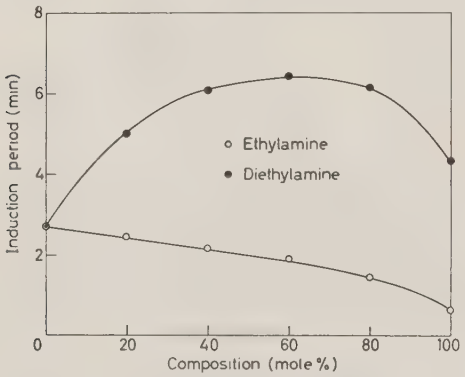

Figure 6. The dependence of the induction period preceding explosive combustion of acetaldehyde on the composition of mixtures of triethylamine with diethylamine and with ethylamine. Temperature, 218°C*; acetaldehyde pressure,* 50 mm*; oxygen pressure,* 50 mm*; total amine pressure,* 1·0 mm

triethylamine with diethylamine and with ethylamine. Diethylamine is indeed found to be a more powerful inhibitor than triethylamine, but the maximum inhibiting effect is observed for approximately equimolar mixtures of the two amines. This somewhat unexpected result suggests that for maximum inhibition two types of free radicals must be destroyed, one being stabilized by reaction with triethylamine and the other by reaction with diethylamine.

On the other hand, ethylamine is a much less powerful inhibitor than either triethylamine or diethylamine and the inhibiting power decreases continuously as ethylamine is substituted for triethylamine in binary mixtures of the two compounds (*Figure 6*). The results in *Figure 4* may thus well be explicable on the basis of a series of reactions involving oxidation of at least some triethylamine to diethylamine followed by oxidation of the latter to ethylamine which is stable at the temperatures used. In accordance with this hypothesis it is found that the final values attained by the induction period in the triethylamine–oxygen mixtures studied (*Figure 4*) correspond closely with those which would be expected if the triethylamine were completely converted to ethylamine.

The authors wish to express their gratitude to the Central Government of Pakistan for the award of a Research Scholarship to one of us (B. A. K.) and to the Shell Petroleum Company for valuable financial assistance in the purchase of apparatus.

REFERENCES

[1] Cullis, C. F. and Waddington, D. J. *Trans. Faraday Soc.* 53 (1957) 1317
[2] Rogers, M. A. T. *J. chem. Soc.* (1955) 769
[3] McDowell, C. A. and Thomas, J. H. *J. chem. Soc.* (1949) 2208
[4] See e.g. Prettre, M. *Bull. Soc. chim. Fr.* 51 (1932) 1132
[5] Cullis, C. F. and Waddington, D. J. *Fifth Symposium on Combustion*, p. 545. 1955. New York; Reinhold
[6] — — *Proc. Roy. Soc. A* 244 (1958) 110

30

MECHANISM OF COMBUSTION INHIBITION BY COMPOUNDS CONTAINING HALOGEN

W. A. ROSSER, H. WISE and J. MILLER

INTRODUCTION

Volatile compounds containing halogen atoms, in particular bromine and iodine, are unusually effective inhibitors of hydrocarbon combustion. Flammability studies have shown, for instance, that on a mole basis methyl bromide is five times as effective as carbon dioxide and eight times as effective as nitrogen in rendering methane–air mixtures non-flammable[1]. Observations such as these suggest that the effectiveness of extinguishing agents such as methyl bromide is chemical in origin and involves the destruction of reactive intermediates essential to the combustion process. Neither the manner of destruction nor the identity of the intermediates is known, although a recent study[2] of CH_4–air–CH_3Br flammability limits indicates that CH_3Br is only a precursor of the actual inhibitor.

While a few per cent of a halogen inhibitor will prevent ignition, smaller quantities significantly reduce flame speed, as shown by Simmons and Wolfhard[2] and by Garner *et al.*[3] The ability of an inhibitor to reduce flame speed, a convenient and significant measure of the effectiveness of an inhibitor, can be measured near the limit of zero concentration of inhibitor and therefore refers to a situation uncomplicated by gross changes in mixture properties. For this reason, and because little can be gained from further attention to flammability limits, this study of combustion inhibition is devoted to an investigation of the influence of various halogen-containing inhibitors on flame speed, and to the effect of halogen inhibitors on flame temperatures and on flame spectra.

EXPERIMENTAL

Flame speed measurements

Flame speed may be measured by various methods. Of these, the bunsen burner method is the simplest and best suited for comparative measurements involving a large number of flame speed determinations. For this study an average burning velocity is defined as the ratio of the volumetric gas flow rate to the area of the visible flame surface.

The burners used were Pyrex tubes $\frac{1}{2}$ and $\frac{3}{4}$ in. inside diameter and about 30 diameters long; a Pyrex cylinder 4 in. in diameter enclosed the burner. During the course of an experiment a stream of nitrogen flowing upward through this outer tube prevented the entry of secondary air into the system. Fuel, oxidizer and inhibitor were metered into a mixing chamber before passing through a flame trap into the burner tube. For a given series of measurements the flows of fuel and of oxidizer were held constant while the flow of additive was varied. The flame associated with each mixture was photographed and the flame area evaluated numerically from the flame photograph. All measurements were made at ambient temperature and pressure (25°C and 1 atm).

Gas flows were metered with rotameters (Fischer and Porter Co., Harboro, Penn.) calibrated where necessary by displacement of water or of mercury. Those inhibitors which are liquids at room temperature were introduced into the combustible mixture as gases by means of an electrically heated vaporizer. The liquid was supplied to the vaporizer from a syringe the piston of which advanced at a known rate controlled by a servo mechanism. The gaseous inhibitor so produced was swept away by a stream of air or of nitrogen which was then admixed to the fuel-oxidizer mixture. The partial pressure of inhibitor in the resultant mixture was always much less than its saturation vapour pressure at ambient temperature.

Chemical substances used in this study included a number of gases and liquids of varying degrees of purity. Most of the gases were obtained commercially and are listed in Table 1. Compressed laboratory air was dried by passage over $CaCl_2$. Liquid inhibitors included CCl_4, Br_2, CH_2Br_2, CH_2BrCl, CH_3I, i-C_3H_7I and $CHBr_3$.

Flame speeds of methane–air mixtures measured in the absence of inhibitors are presented graphically in *Figure 1* over a range of mixture ratios. This curve is compared with the flame speed data reported in reference 4.

The effect of different inhibitors on burning velocity was determined for various fuel–air

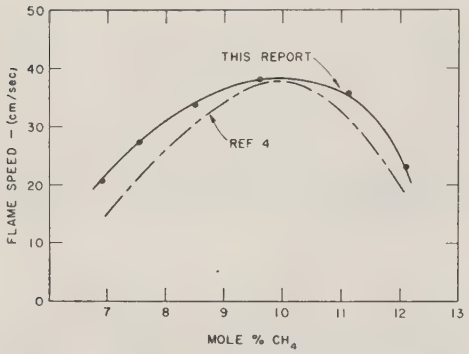

Figure 1. Flame speed of methane–air mixtures

compositions. In the range of inhibitor concentrations used, the measured flame speed varied linearly with the mole fraction of inhibitor, X_I, added to the combustible mixture ($X_I < 0{\cdot}005$). Typical curves are shown in *Figure 2*. The negative slopes, $-dS/dX_I$, of such curves are used as a measure of the effectiveness of an inhibitor or other additive and are presented for the following substances:

TABLE 1

Substance	*Stated purity %*
NH_3	> 99
CH_4	> 99
H_2	99·8
CH_3Br	99·4
CF_2Br_2	Unknown
Cl_2	> 99·3
CF_3Br	94
HBr	99·1
CH_3Cl	99 5
NO	> 99
N_2	Industrial grade
O_2	Industrial grade

All gases except N_2 and O_2 were obtained from the Matheson Company, Inc., Joliet, Illinois.

Figure 3 CCl_4, CH_3Cl, Cl_2

Figure 4 CH_3I, i-C_3H_7I

Figure 5 Br_2, CH_3Br, CH_4

Figure 6 HBr, H_2

Figure 7 CF_2Br_2, CF_3Br

Figure 8 CH_2Br_2, $CHBr_3$, CH_2BrCl

For comparison, the results obtained with Br_2 as an inhibitor are superimposed on figures for Br-containing substances.

Other measurements showed that NO, although it inhibits many low temperature decomposition and oxidation reactions[5], has an insignificant effect on flame speed ($-ds/dX_I < 0{\cdot}1 \times 10^3$).

The experimental data show that the effectiveness of most inhibitors varies markedly with mixture composition. Of interest is the empirical observation that for methane–air mixtures near the point of maximum flame speed (10 vol per cent CH_4) the effectiveness of bromine-containing inhibitors is essentially equal to that of an equivalent amount of bromine (*Figure 9*). It is apparent that bound bromine, such as in CH_3Br, must be released by decomposition or oxidation in order to be effective. Since neither the effectiveness of Br_2 nor of HBr, two possible decomposition products, varies appreciably with mixture composition it may be surmised that the variation in effectiveness observed for other substances containing bound bromine is due to decomposition products other than Br_2 or HBr or to failure of the inhibitor to decompose prior to some critical stage of combustion.

The extent to which the decomposition products of a given inhibitor supply additional fuel can be estimated by inspection of the molecular formula of the original inhibitor. For example, consideration of the experimental data for CH_4, CH_3Br and Br_2 reveals that CH_3Br reduces flame speed to about the same extent as an equivalent amount of $CH_4 + \frac{1}{2}Br_2$.

An interpretation of the effectiveness of CF_3Br by a formal partition into a bromine part plus a non-bromine part of the molecule requires a contribution by the CF_3 radical to the process of flame inhibition in order to account for the superior effectiveness of CF_3Br compared to that of an equivalent amount of Br_2. On the other hand, the peak effectiveness of CF_2Br_2, although

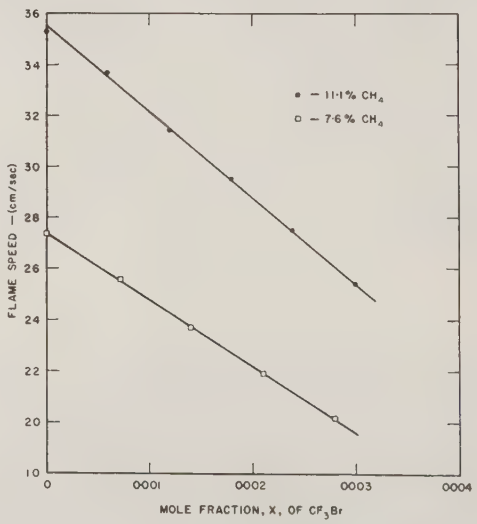

Figure 2. Methane–air: flame speed as a function of CF_3Br *concentration*

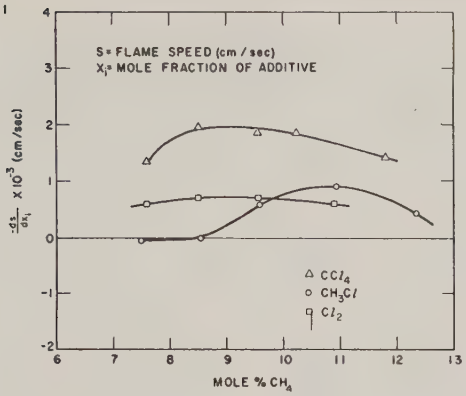

Figure 3. Methane–air: rate of flame speed reduction by CCl_4, Cl_2 *and* CH_3Cl

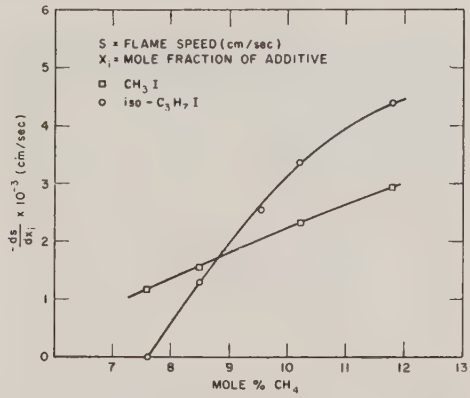

Figure 4. Methane–air: rate of flame speed reduction by CH_3I *and* i-C_3H_7I

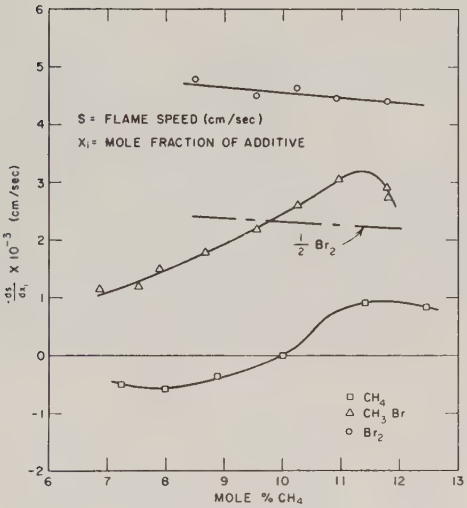

Figure 5. Methane–air: rate of flame speed reduction by Br_2, CH_3Br *and* CH_4

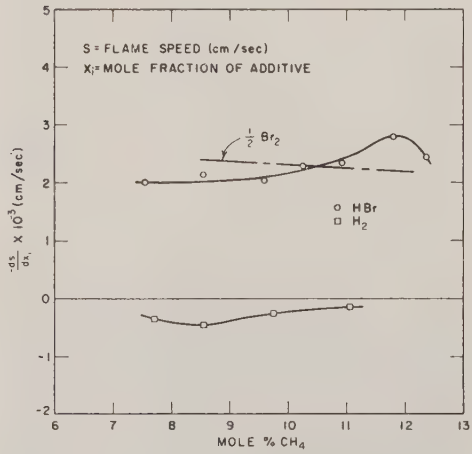

Figure 6. Methane–air: rate of flame speed reduction by HBr *and* H_2

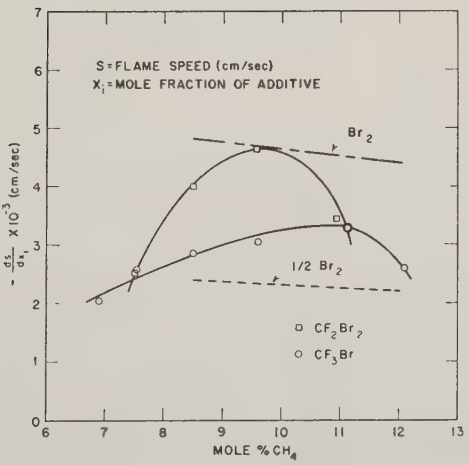

Figure 7. Methane–air: rate of flame speed reduction by CF_2Br_2 *and* CF_3Br

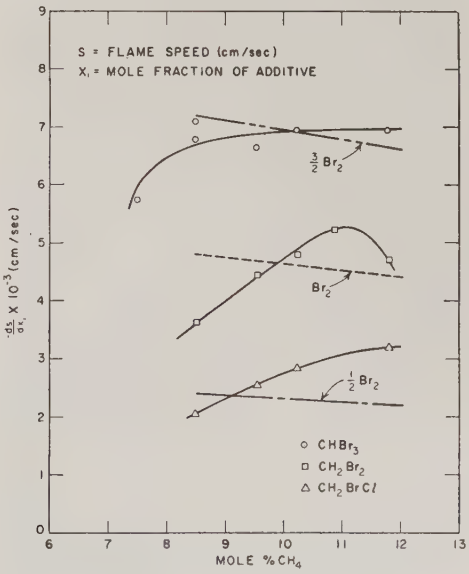

Figure 8. Methane–air: rate of flame speed reduction by $CHBr_3$, CH_2Br_2 *and* CH_2BrCl

larger than that of CF_3Br, does not exceed that of Br_2. The pronounced decrease in effectiveness of CF_2Br_2 in lean and rich mixtures presumably reflects the thermal stability of the difluoro derivatives of methane[6].

The analysis can be extended to include the other inhibitors tested. A comparison of the

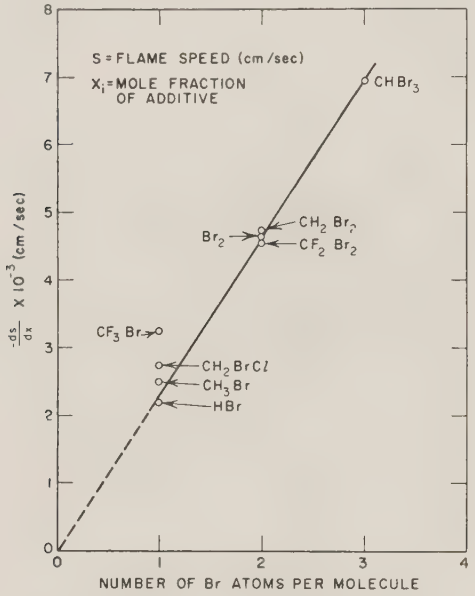

Figure 9. Rate of flame speed reduction by various substances for a 10 per cent CH_4*–air mixture*

results for Br_2 and Cl_2 indicates an overall ratio of effectiveness of 7/1, while the data for CH_3I and CH_3Br suggest near equality for I_2 and Br_2. The relative effectiveness of CH_3I and i-C_3H_7I is consistent with their relative fuel contents.

Less detailed but similar flame speed measurements were carried out using NH_3–O_2–N_2 mixtures with a fixed oxidizer ratio $O_2/(O_2 + N_2) = 0{\cdot}4$. The flame speeds associated with such mixtures are comparable to those observed for CH_4–air flames. In general, the various inhibitors reduce the flame speed of NH_3–O_2–N_2 mixtures (*Figure 10*) at rates smaller than but comparable to those observed for CH_4–air flames. The experimental data show that inhibition by halogen-containing compounds is not limited to carbonaceous systems. As in the case of CH_4–air flames, inhibition by CH_3I or CH_3Br is qualitatively consistent with a formal partition into fuel and inhibitor, and the effectiveness of CF_3Br relative to CH_3Br suggests a contribution by the CF_3 portion of the molecule to flame inhibition.

Flame temperature measurements

Flame temperatures were measured by the sodium D-line reversal technique[7] for fuel compositions containing from 8·6 to 11·2 per cent CH_4 and up to 0·7 mole per cent CH_3Br. The $\frac{1}{2}$ in. burner was modified by inserting just above the flame trap (about 20 diameters from the mouth of the burner) a nichrome loop coated with borax. Electrical heating of the nichrome wire introduced sufficient salt into the gas mixture to colour the flame. The optical apparatus consisted of a tungsten ribbon lamp, an optical system and a Bausch and Lomb 1·5 metre stigmatic grating spectrograph with 14·8 Å/mm dispersion in the first order. An achromatic eyepiece focused on the image plane of the spectrograph exit in the region near 5,890 Å was used for visual observation of the reversal point. The brightness temperature of the tungsten ribbon lamp at various current settings was determined with a Leeds and Northrup optical pyrometer. Flame reversal temperatures could be determined with an r.m.s. deviation of 5°K.

By means of a position selector in front of the spectrograph slit it was possible to determine the maximum flame temperature from a series of measurements made along the vertical axis of the flame. Changes in flame height with inhibitor concentration could be compensated for in this way. A slit width of 20 μ was used in order to obtain sharp reversal contrast.

Measured flame temperatures for methane–air mixtures with and without inhibitor are shown in Table 2. Theoretical adiabatic flame temperatures[8] have been corrected for the addition of fuel.

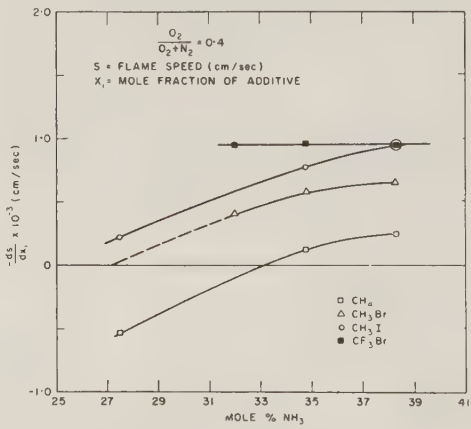

Figure 10. NH_3–O_2–N_2*: rate of reduction of flame speed by* CF_3Br, CH_3I, CH_3Br *and* CH_4

Inspection of the data reveals that the addition of inhibitor does not significantly affect the maximum temperature attained by the system. The temperature increase observed in the case of CH_3Br for the fuel-lean mixture (8·6 per cent CH_4) is comparable to that expected from the addition of fuel. Similarly, on the fuel-rich side a small decrease in flame temperature is noted. It is concluded from these temperatures that the addition of small

TABLE 2

Methane–Air Flame Temperatures in the Presence of Methyl Bromide and Hydrogen Bromide

Inhibitor	CH_4, mole %	*Inhibitor*, mole %	*Flame temperature*	
			Experimental °K	*Theoretical* °K
CH_3Br	8·60	0	2,135	2,120
	8·60	0·37	2,154	2,165
	8·60	0·51	2,196	2,180
	11·15	0	2,123	2,125
	11·15	0·49	2,104	2,055
	11·15	0·72	2,108	2,015
HBr	8·60	0	2,110	2,120
	8·60	0·09	2,123	2,120
	8·60	0·18	2,155	2,120

quantities of inhibitor markedly reduces flame speed without producing a corresponding decrease in the maximum flame temperature.

Flame spectroscopy

The intensity of the light emitted by OH*, C_2^*, and CH* was studied at selected wavelengths[9]—3,064 Å for OH*, 5,165 Å for C_2^* and 4,315 Å for CH*. For this purpose the 1·5 m spectrograph

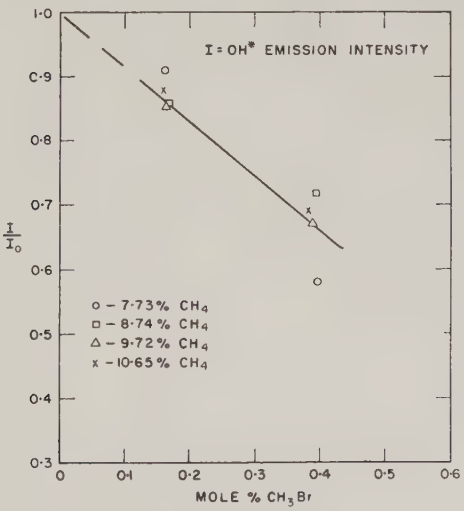

Figure 11. Methane–air: the effect of CH_3Br *on the intensity of* OH* *emission*

was fitted with a scanning photomultiplier. Entrance and exit slits of 1 mm were employed in order to sum the radiation over the most intense portion of the (0,0) bands near the listed wavelengths. An inverted, *V* shaped flame, rather than a normal bunsen flame, was used for spectroscopic study in order to avoid the presence of cool reaction products in the light path, particularly of bromine which absorbs radiation in the wavelength region of interest. The inverted flame, held by a nichrome wire placed perpendicular to the direction of gas flow, was viewed from the side.

The addition of 0·5 mole per cent CH_3Br to a combustible mixture of CH_4 and air increased the

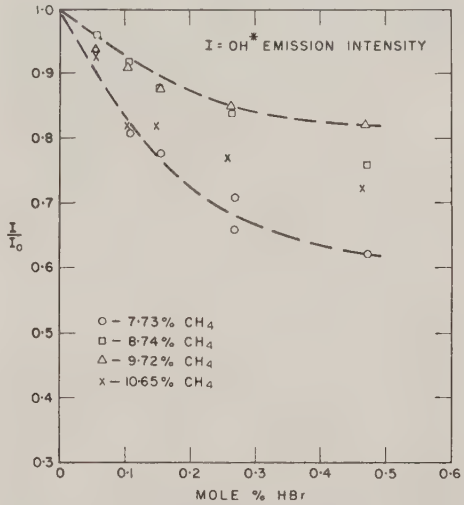

Figure 12. Methane–air: the effect of HBr *on the intensity of* OH* *emission*

CH* emission by as much as 50 per cent. Increases in intensity were observed for a wide range of CH_4–air compositions. Emission by C_2^* varied in a less consistent manner. As CH_3Br, HBr or Br_2 was added to a lean mixture C_2^* emission first decreased by as much as 20 per cent, passed through a minimum and finally increased. When using near stoichiometric or rich mixtures C_2^* emission increased more or less linearly with inhibitor content. Since the variation in flame propagation velocity is a monotonic function of inhibitor concentration, these results suggest that neither C_2^* nor CH* is related to flame speed.

In contrast, OH* emission decreased on addition of inhibitor at all fuel–air ratios investigated in this study (see *Figures 11*, *12* and *13*). Before discussing these results one should note the following factors.

(1) The observed radiation includes a contribution from the flame products as well as from the reaction zone itself. The two regions are probably not affected by inhibitor to the same extent since the concentration of OH* in the flame zone has a value partly determined by kinetics while that in the products is determined by chemical equilibria. (2) The radiation observed in this study originates primarily from excited OH with low and medium rotational quantum numbers. The relationship between this population and the concentration of other critical species is not known. (3) No correction has been applied for self-absorption. (4) The

increase in CH* emission with inhibitor concentration may reflect a similar increase in the concentration of unexcited CH radicals which may react with O_2 as shown

$$CH + O_2 \rightarrow CO + OH^* \qquad (1)$$

Such a reaction tends to oppose the reactions responsible for the observed decrease in OH* concentration and emission. Despite these limitations it is noteworthy that the relative intensity I/I_0 decreases with increasing inhibitor concentration at about the same rate as the relative flame speed S/S_0. We do not wish to imply that flame speed is proportional to the concentration of a species as scarce as OH* but rather that OH* and S are each proportional to some third quantity.

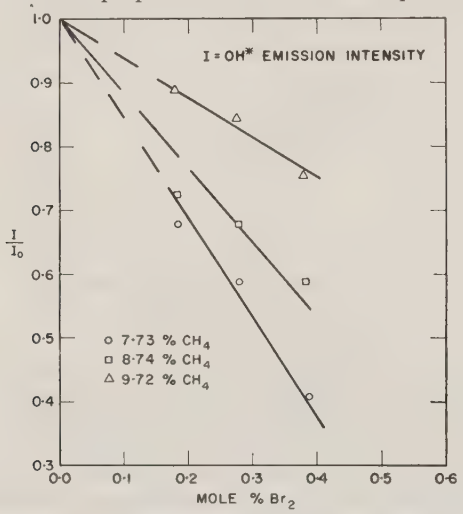

Figure 13. Methane–air: the effect of Br_2 *on the intensity of* OH* *emission*

Although no conclusive identification of the third quantity is possible, the simplest explanation is that both S and OH* are each proportional to the concentration of unexcited OH in the region of the flame from which the bulk of the radiation originates. Analogous relationships may also exist between S and any species coupled to OH by a main propagation reaction. The assumed relationship between S and OH requires at the very least that the inhibiting reactions do not distinguish between excited and unexcited OH.

DISCUSSION

The general proportionality between the square of the flame speed and the mean rate of heat release per unit volume in the reaction zone[10] implies that an inhibitor which reduces flame speed reduces the reaction rate where it is high, that is at temperatures near the adiabatic flame temperatures. The theoretical adiabatic flame temperature of the CH_4–air mixtures studied varies from about 1,800 to 2,200°K. Accordingly, the temperature region in which significant inhibition occurs may be taken to be above about 1,500°K.

The importance of high temperature reactions in producing inhibition is also suggested by the correlation between inhibitor efficiency and bromine content. Such a relationship would not be expected unless common halogen-containing species, produced where necessary by decomposition or oxidation of the original molecule, were responsible for the inhibition. The species resulting from decomposition and probably responsible for inhibition are the halogen atoms X and the halogen acids HX.

In order to proceed further it is necessary to determine the time available for flame reactions. In the case of CH_4–air flames at atmospheric pressure this residence time is about 10^{-4} sec as suggested by the ratio of the thickness of the visible flame (about 0·02 cm) to the spatial velocity in the flame zone (about 200 cm/sec). At flame temperature only a few of the substances which might result from the presence of a halogen inhibitor are stable with respect to decomposition for a time of this length. In particular, consideration of Table 3 reveals that the decomposition rates of bromine and iodine are rapid enough to insure near equilibrium composition in the flame zone. For the concentrations used in this study, equilibrium dissociation is virtually complete and the molecular species cannot be responsible for the observed inhibition. Similar considerations apply to molecular fluorine. For Cl_2 with its higher bond strength some undissociated molecules may be present in the flame. The presence of significant quantities of the species X–O is precluded by the rapid decomposition of such compounds.

In a similar way one can compare the residence time to the times required for cleavage of the carbon–bromine bond in molecules such as CH_3Br, CH_2Br_2, $CHBr_3$ and CF_3Br. Consideration of bond energies suggests that in the decomposition rates of this group of compounds the slowest is that of CH_3Br. The data in Table 3 indicate that a temperature of at least 1,500°K is necessary to result in essentially complete destruction of CH_3Br during its residence time in the flame. Since the decomposition of CH_3Br is probably catalysed by Br

$$CH_3Br \rightarrow CH_3 + Br \qquad (2)$$

$$Br + CH_3Br \rightarrow CH_3 + Br_2 \qquad (3)$$

$$Br_2 \rightleftarrows 2Br \qquad (4)$$

the temperature restriction may be less severe than noted. Also, early in the flame such substances as CH_3Br may be subject to preferential oxidation or decomposition induced by oxidation.

TABLE 3

Species	*Unimolecular rate constant* (sec^{-1})	τ (sec) 1,500°K	τ (sec) 2,000°K
Br–Br	$10^{13}e^{-46,000/RT}$	$10^{-6.4}$	10^{-8}
I–I	$10^{13}e^{-36,000/RT}$	$10^{-7.8}$	$10^{-9.1}$
CH_3–Br	$2 \times 10^{13}e^{-67,500/RT}$	$10^{-3.5}$	10^{-6}
H–Br	$10^{13}e^{-87,000/RT}$	$10^{-0.4}$	$10^{-3.6}$
H–I	$10^{13}e^{-71,500/RT}$	$10^{-2.7}$	$10^{-5.2}$
Br–O	$10^{13}e^{-54,000/RT}$	$10^{-5.2}$	$10^{-7.1}$
I–O	$10^{13}e^{-44,000/RT}$	$10^{-6.6}$	$10^{-8.2}$

(Residence time in flame $\approx 10^{-4}$ sec)

Rate constants all refer to unimolecular decomposition by splitting of the bond indicated. Except in the case of CH_3Br the rate constants are assumed to be given by the product of a more or less normal pre-exponential times an exponential in which the activation energy equals the bond strength in calories. For unimolecular decompositions the time $\tau = 1/k$ is time required to reduce concentration of species to $1/e$ of initial value and is a measure of the average life time of the species. The rate expression for CH_3Br was obtained from reference 11, the bond strengths for Br_2, I_2, HBr and HI from reference 12, and the bond strength for IO from reference 13. The bond strength for Br–O is an assumed value midway between that for IO and that for ClO.

Presumably, any chain initiation caused by a free radical produced in reactions such as 2 or 3 is outweighed by subsequent inhibition reactions. The decomposition rates of the remaining bromides and of the iodides are faster than that of CH_3Br and need not be considered further. Decomposition rates for the corresponding chlorine compounds are slower because of the greater carbon–chlorine bond strength and may in some cases limit the degree of inhibition.

The exceptional stability of HBr with respect to decomposition is reflected in its life time which becomes comparable to the residence time in the flame only at temperatures near 2,000°K. In view of this thermal stability and inasmuch as the bimolecular decomposition of HBr is too slow to dispose of the few tenths of a per cent HBr added to the various CH_4–air mixtures, the observed inhibition effectiveness of HBr suggests that HBr as a molecule participates in the flame reactions which result in inhibition. By analogy, the other halogen acids, HX, may be considered to participate in inhibition reactions.

The free halogen atoms F, Cl and Br produced by decomposition of a carrier molecule will rapidly abstract hydrogen from the fuel and ensure the presence of the corresponding halogen acids in the flame. Abstraction from CH_4 by I is much slower than that of the other halogens but is still sufficiently rapid to produce some HI during transit through the flame. More rapid reactions between I and hydrogen containing intermediates (e.g. CH_2O) may add to the available supply of HI.

Such considerations suggest that an inhibition mechanism can be formally represented by the reactions

$$H\alpha + X \rightarrow HX + \alpha \quad (5)$$

$$\beta + HX \rightarrow X + H\beta \quad (6)$$

where X represents a halogen atom, HX a halogen acid, $H\alpha$ the fuel or other hydrogen-containing species, and β such abstracting species as H, OH, O, CH_3, etc. The mechanism may be regarded as a means of substituting X for β. Inhibition, while originating in this substitution, results from a reduction in the rate of (*a*) the transfer of reactivity upstream by the diffusion of species β such as H, O, OH, of (*b*) the exothermic propagation reaction

$$OH + CO \rightarrow CO_2 + H \quad (7)$$

of (*c*) chain branching by

$$H + O_2 \rightarrow OH + O \quad (8)$$

or by

$$O + CO \rightarrow CO_2^* \quad (9)$$

$$CO_2^* + O_2 \rightarrow CO_2 + 2O \quad (10)$$

The reduction in the rate of diffusion of such species as H, OH, and O may not be a major feature of combustion inhibition but is included for completeness. The substitution of X for H, OH and O tends to restrict such species to their region of origin. At the same time diffusion upstream by Br or I involves diffusion constants appreciably smaller than those of the removed radicals and is opposed by the concentration gradient resulting from the large, positive temperature coefficient for the abstraction reactions

$$CH_4 + I \text{ or } Br \rightarrow CH_3 + HI \text{ or } HBr \quad (11)$$

Reactions 7 and 8 undoubtedly occur in hydrocarbon–air flames and a reduction in the concentration of OH and H will clearly reduce their contribution to the rate of heat release and to flame speed.

The inhibition mechanism does not directly reduce the concentration of hydrocarbon fragments. For instance, the removal of a methyl radical by reaction

$$CH_3 + HX \rightarrow CH_4 + X \quad (12)$$

is nullified by the reverse reaction

$$X + CH_4 \rightarrow CH_3 + HX \quad (13)$$

However, the partial substitution of X for a radical like OH as the abstracting species involves some secondary features. The spectrum of hydrocarbon fragments resulting from abstraction by OH will in general differ from that resulting from abstraction by X. In the particular case of abstraction by Br atoms compared to abstraction by OH the decrease in bond strength from CH_4 to fragments containing less hydrogen favours the production of stripped species such as CH and C at the expense of fragments richer in hydrogen. The increase in CH emission observed when a few tenths of a per cent bromine is added to a burning

CH_4–air mixture is assumed to reflect such an increase in the CH population.

The extent of inhibition is proportional to the rate (for critical β such as H, OH and O) of reaction 6 since the rate of this reaction determines the degree of reduction of β. The effectiveness of a given degree of β reduction either does not depend on which of the halogens produced the effect (chemical inhibition) or increases in the order F, Cl, Br and I (diffusion inhibition). Accordingly, if the bulk of the added halogen is present in the flame as HX, the observed order of effectiveness will be in the same order as the rate constants for reactions 6 of a given type, i.e.

$$k_6(\mathrm{HF}) < k_6(\mathrm{HCl}) < k_6(\mathrm{HBr}) < k_6(\mathrm{HI})$$

Estimates of the rates of reactions 5 and 6 indicate that a deviation from the condition $X/HX < 1$ is unlikely for HF, HCl and HBr but may occur in the case of HI unless I abstracts primarily from molecules with CH bonds substantially weaker than those of CH_4. The observed equivalence of CH_3I and CH_3Br, rather than $CH_3I > CH_3Br$, is assumed to originate in this way.

A number of miscellaneous factors may reduce the effectiveness of halogen inhibition. Among them are (*a*) the decomposition of the halogen acids

$$\mathrm{HX} \rightarrow \mathrm{H} + \mathrm{X} \qquad (14)$$

(*b*) the oxidation of the halogen acids

$$\mathrm{HX} + \mathrm{O_2} \rightarrow \mathrm{HO_2} + \mathrm{X} \qquad (15)$$

and (*c*) the failure of the carrier to decompose (e.g. CF_2Br_2).

Factors (*a*) and (*b*), while probably negligible in hydrocarbon–air flames, will increase in magnitude from HF to HI and may in unusually hot flames become important. The inclusion of factor (*a*) underlines a critical factor in the mechanism—the strength of the HX bond. If too strong the rate of reaction 6 is correspondingly reduced. If too weak HX will decompose rather than react. The almost unique ability of iodine and of bromine compounds to reduce the flame speed of hydrocarbon flames reflects this balance of strength and weakness.

This research was supported by the Engineer Research and Development Laboratories, U.S. Army, Corps of Engineers, under contract DA–44–009–Eng–2863.

REFERENCES

[1] Friedman, R. and Levy, J. B. *WADC Technical Report* 56–568, Astia Document No. AD 110685

[2] Simmons, R. F. and Wolfhard, H. G. *Trans. Faraday Soc.* 51 (1955) 1211

[3] Garner, F. H., Long, R., Graham, A. J. and Badakhsham, A. *Sixth Symposium (International) on Combustion*, p. 802. 1957. New York; Reinhold

[4] Egerton, H. C. and Lefebvre, A. H. *Proc. Roy. Soc. A* 222 (1954) 215

[5] Steacie, E. W. R. *Atomic and Free Radical Reactions*, Chap. IV. 1954. New York; Reinhold

[6] Noller, C. R. *Chemistry of Organic Compounds*, p. 678. 1951. Philadelphia; Saunders

[7] Broida, H. P. *Temperature, Its Measurement and Control in Science and Industry*, Vol. 2, p. 265. 1955. New York; Reinhold

[8] Clingman, W. H. *et al. Fourth Symposium (International) on Combustion*, p. 310. 1953. Baltimore; Williams and Wilkins

[9] Gaydon, A. G. *The Spectroscopy of Flames*, Chap. VII. 1957. New York; Wiley

[10] — and Wolfhard, H. G. *Flames, Their Structure, Radiation and Temperature*, p. 89. 1953. London; Chapman and Hall

[11] Schon, A. H. and Szwarc, M. *Proc. Roy. Soc. A* 209 (1951) 110

[12] Pauling, L. *The Nature of the Chemical Bond*, p. 59. 1948. Ithaca, New York; Cornell University Press

[13] Cottrell, T. L. *The Strengths of Chemical Bonds*, p. 281. 1954. London; Butterworths

31

EFFECTS OF SURFACES ON COMBUSTION OF METHANE AND MODE OF ACTION OF ANTI-KNOCKS CONTAINING METALS

D. E. CHEANEY, D. A. DAVIES, A. DAVIS, D. E. HOARE, J. PROTHEROE and A. D. WALSH

EFFECTS OF SURFACES ON COMBUSTION OF METHANE

Hoare and Walsh[1] discovered that the kinetic law governing the maximum rate of pressure rise in methane slow oxidation at *ca.* 500°C in a silica vessel was sharply different according to whether, on the one hand, the surface was new or had been HF-treated or, on the other hand, had been 'aged', 'heat-treated' or PbO-coated. There were thus two categories of surface. Cheaney and Walsh[2] showed that HF-treatment of a silica vessel produced a surface film of silicic acid (*cf.*[3]); and pointed out that new vessels probably possessed such a surface film. They also[4] extended the lists of surfaces in the two categories. Category I included silicic acid, boric acid, phosphoric acid, germanium dioxide and titanium dioxide. Category II included metallic oxides (and, probably, hydroxides) and salts in general. Other things being equal, the rate of pressure rise varies little from one category I vessel to another, but is always much less for category II than for category I vessels and varies considerably from one category II vessel to another. The kinetic law (referred to as type II) governing the maximum rate of pressure rise in a category II vessel differs from that (referred to as type I) associated with a category I vessel in showing: (i) a much higher total order of the rate; (ii) a considerably higher order with respect to the concentration of inert gas present; (iii) a much higher activation energy of the rate; and (iv) a much greater dependence of the rate upon vessel diameter. This division of surfaces into two fundamentally different classes is of outstanding importance.

Surfaces may also be divided into two classes by a study of the second explosion limit of hydrogen–oxygen mixtures[5–8]. Surfaces in the first class yield an expanded explosion region and a first kinetic law relating the partial pressures of hydrogen and oxygen at the explosion limit; surfaces in the second class yield a sharply different, second, kinetic law governing the explosion limit. The evidence is strong[4] that the empirical division of surfaces into two categories is essentially the same whether made by a study of the slow oxidation of methane or by a study of the second explosion limit of hydrogen.

Now the accepted, basic, mechanism of the hydrogen–oxygen reaction at the second explosion limit means that the two types of surface must differ in the fate that they accord to HO_2 radicals which become adsorbed upon them. Taken in conjunction with arguments developed by Chamberlain, Hoare and Walsh[9] as to which radicals are likely to reach the surface in methane combustion under normal conditions, it becomes practically certain that the two types of surface affect the slow oxidation of methane differently because they mete out a different fate to HO_2 radicals which reach them.

What is the fate of an HO_2 radical on a category I surface? All the category I surfaces are acidic. Moreover, it appears that under the experimental conditions used for their study, none of them is completely anhydrous[4]. When an HO_2 radical becomes adsorbed on a category I surface, the first step is very plausibly therefore donation of a proton by the surface to the radical. Category I surfaces are indeed of the kind known to bring about such reactions as cracking or isomerization of hydrocarbons and their derivatives, i.e. reactions which are thought to occur via the formation of carbonium or oxonium ions. Such reactions are generally considered to have the same mechanism whether brought about heterogeneously or homogeneously in strong acid solution. Cheaney and Walsh[4] argued therefore that if the fate of HO_2 radicals in strong acid solution were known this could also be expected to be the ultimate fate of HO_2 radicals on category I surfaces. The fate of HO_2 radicals in strong acid solution is almost certainly reduction to H_2O_2 molecules[10]. If such molecules were formed in sufficient numbers on category I surfaces, H_2O_2 would be released to the gas phase since it is known that category I surfaces are such as to preserve H_2O_2[11]. One is thus led to the hypothesis that, on category I surfaces,

$$HO_2 + H^+ \rightarrow \ldots \overset{\uparrow}{\tfrac{1}{2}H_2O_2} + \overset{\uparrow}{\tfrac{1}{2}O_2} + H^+ \quad (1)$$

where the . . . line stands for some cycle of reactions eventually returning a proton to the surface*.

In order to test this hypothesis, H_2O_2 was sought for in the products of methane combustion. It was found[4] that peroxide was readily detectable in the products of combustion carried out in a category I vessel but not in a category II vessel. Further, it was shown[4] that addition of H_2O_2 had profound catalytic effects on methane combustion carried out in a category I vessel. It follows, therefore, that if reaction 1 occurs on a category I, but not on a category II, surface, an explanation is immediately available for the two outstanding facts that the maximum rate of pressure rise is so much greater in a category I than in a category II vessel and obeys a different kinetic law in the two vessels. With category I vessels, the catalogue of important reactions has to include reaction 1 and the subsequent steps by which H_2O_2 accelerates the combustion; with category II vessels, reaction 1 has to be replaced by some other reaction and the subsequent steps referred to presumably omitted.

What is the fate of an HO_2 radical on a category II surface? That the ultimate products have to be different to those of reaction 1 makes it very probable that they are H_2O and O_2. The inertness of these products is of course compatible with the failure to detect H_2O_2 in the products of combustion carried out in a category II vessel and helps to explain the slower maximum rate of pressure rise in category II than in category I vessels. Cheaney and Walsh[4] postulated that, on a category II surface, the first reaction step is the donation of an electron to the adsorbed HO_2 radical:

$$HO_2 + \varepsilon \rightarrow . . . \tfrac{1}{2}\overset{\uparrow}{H_2O} + \tfrac{3}{4}\overset{\uparrow}{O_2} + \varepsilon \qquad (2)$$

where the . . . line stands for some cycle of reactions eventually returning an electron to the surface. The evidence in support of this postulate includes the fact that it provides a simple explanation of why there are just two fundamental types of surface—an adsorbed HO_2 radical can receive either a positive or a negative charge—but the strongest evidence in favour of the postulate is that there is a linkage[4] between the effectiveness of a category II surface as an inhibitor of methane combustion and simple expectations as to the availability of electrons in the surface for donation. Thus the inhibiting efficacy increases from NaCl to KCl to CsCl and from KF to KCl to KBr to KI and as the H atoms of H_3PO_4 are progressively replaced by more electropositive metal atoms. So far as is known, there is no exception to the rule that the inhibiting efficacy increases as the electronegativity of the cations and anions in the surface decreases. There is suggestive evidence[4,12] of a link between inhibiting efficacy and non-stoichiometry of the surface, the latter property being expected to be linked in turn with the availability of electrons.

Further, it may be argued that if electron availability determines the effectiveness of a surface as an inhibitor, then, since all anions may be described as electronegative, metal surfaces should be much more effective inhibitors than oxide or hydroxide or salt surfaces. Because of this argument Davies and Walsh[13] and Davis and Walsh[14] tested the effectiveness of noble metal surfaces as inhibitors of methane combustion. It was found as expected that both gold and silver were much more effective inhibitors than oxide or salt surfaces.

However, it was also found that the kinetic law governing the rate of pressure rise in methane combustion in, say, a silvered vessel was neither type I nor type II, but of a third type. In particular, the type III law revealed a much greater order of the rate with respect to total pressure or to pressure of added inert gas. Because of the existence of a third type of kinetic law, it was apparent that, although there was strong evidence supporting the occurrence of reaction 2 on all inhibiting surfaces (i.e. on surfaces in category II and on pure metals), the theory of the action of inhibiting surfaces was not complete.

Two other arguments showed also the incompleteness of the theory at this stage. The first was as follows. The rate in a category II vessel varied greatly from one surface to another, the kinetic law governing the rate remaining approximately the same. The rate, as already implied, also increased considerably when the impedance to diffusion was increased by the addition of inert gases. Now the termination of chains on a surface involves: (i) diffusion of a chain carrier to the surface, (ii) adsorption or reaction of the chain carrier on the surface, and whichever is the slower of these two steps will be rate-controlling for the chain-ending process as a whole. If only a single species of chain carrier is involved, it is impossible to explain, over the whole range of category II surfaces, the simultaneous occurrence of kinetically important surface nature and diffusion effects. Yet reaction 2 deals only with a single species of chain carrier.

The second indication of an incompleteness in the theory was as follows. Under the conditions used in our work, the gaseous reaction

$$HO_2 + CH_4 = H_2O_2 + CH_3 \qquad (3)$$

would not be expected to be negligible. The

* That HO_2 on a boric acid surface is converted into H_2O_2 was first postulated by Egerton and Warren[5] in order to explain certain features of the kinetics of the hydrogen–oxygen reaction.

failure to detect H_2O_2 in the products of combustion carried out in a category II vessel is therefore only partly explained by the occurrence of reaction 2 as opposed to reaction 1.

The last argument suggested to us that the following reaction was also occurring on category II surfaces

$$H_2O_2 + \varepsilon \rightarrow \ldots \overset{\uparrow}{H_2O} + \tfrac{1}{2}\overset{\uparrow}{O_2} + \varepsilon \qquad (4)$$

where the line . . . stands for a cycle of reactions (such as that proposed by Weiss[15] for the destruction of H_2O_2 on metal surfaces) eventually returning an electron to the surface. Occurrence of reaction 4 could explain the failure to detect the specific ways listed above), which at first was disturbing, turns out to be a natural consequence of the postulation of reaction 4 in addition to reaction 2.

The postulates above, however, lead to another corollary which can be decisively tested by experiment. The corollary is that, since removal of HO_2 by surfaces in categories II and III is postulated always to be diffusion-controlled under our experimental conditions, the observed variation of the rate of pressure rise from one vessel to another in categories II and III should be entirely due to varying ability of the surfaces concerned to destroy H_2O_2. Hoare, Protheroe and Walsh[16] therefore carried out experiments to determine the relative abilities of various surfaces to destroy

TABLE 1

Surface	*Category I*	*Category II*	*Category III*
Fate of HO_2	*Either* preserved *or* $HO_2 \xrightarrow{H^+} \frac{1}{2}H_2O_2 + \frac{1}{2}O_2$	$HO_2 \rightarrow (HO_2)_{ads.} \xrightarrow{\varepsilon} \frac{1}{2}H_2O + \frac{3}{4}O_2$ Diffusion-controlled	$HO_2 \rightarrow (HO_2)_{ads.} \xrightarrow{\varepsilon} \frac{1}{2}H_2O + \frac{3}{4}O_2$ Diffusion-controlled
Fate of H_2O_2	Preserved	$H_2O_2 \rightarrow (H_2O_2)_{ads.} \xrightarrow{\varepsilon} H_2O + \frac{1}{2}O_2$ Not diffusion-controlled	$H_2O_2 \rightarrow (H_2O_2)_{ads.} \xrightarrow{\varepsilon} H_2O + \frac{1}{2}O_2$ Diffusion-controlled

H_2O_2 formed by reaction 3. It could also explain the simultaneous occurrence of kinetically important surface nature and diffusion effects; for now surface destruction of *two* species of chain carrier would be involved and the one chain-ending process could be supposed to be diffusion-controlled while the other is not diffusion-controlled. Of the two species HO_2 and H_2O_2, it would be natural to suppose that it is the *radical* HO_2 that is readily adsorbed and that is therefore destroyed by an overall process which is diffusion-controlled; while the *molecule* H_2O_2 is less readily adsorbed and is therefore destroyed by an overall process which is not diffusion-controlled. The corollary follows that, if the combustion of methane is carried out in a vessel whose surface adsorbs and destroys H_2O_2 extremely readily, the destruction of *both* HO_2 and H_2O_2 should be diffusion-controlled. In other words, a third category of surface should exist, associated with a kinetic law governing the maximum rate of pressure rise that shows an even greater dependence on factors that affect diffusion than does the type II law. This third category would be expected to contain those metallic surfaces, such as silver, which are known to be extremely effective heterogeneous catalysts for the decomposition of H_2O_2. The experimental finding that a silvered vessel yielded not only a very strongly inhibited reaction but also a third type of kinetic law (differing from the type II law in gaseous H_2O_2. Taken in conjunction with the similar work of Satterfield and Stein[11], the results leave no doubt that if the surfaces of categories II and III are arranged in their order of effectiveness as catalysts for the heterogeneous destruction of H_2O_2, this order is exactly the same as the order of effectiveness of those surfaces as inhibitors of the slow combustion of methane. Strong evidence is thus provided for the above postulates.

It should be noted, however, that the probable occurrence of reaction 3 and, on surfaces other than those in category I, of reaction 4 weakens somewhat the argument that reaction 1 occurs on category I surfaces because H_2O_2 is detected only in category I vessels; the possibility that category I surfaces merely preserve or reflect HO_2 radicals is not eliminated.

Summarizing, it appears that the three categories of surface yield different kinetic laws governing the slow oxidation of methane because they are associated with the reactions in Table 1. The statements concerning diffusion-control of the chain-ending processes refer of course to the conditions used in our experiments. It is of interest that Lewis and von Elbe[17], from quite different evidence derived from a study of the hydrogen–oxygen reaction, have earlier arrived at a rather similar classification of surfaces with respect to chain-breaking by surface destruction of HO_2 and H_2O_2.

MODE OF ACTION OF ANTI-KNOCKS CONTAINING METALS

It is a remarkable fact that although anti-knocks containing metals have been known for many decades, there has hitherto been little understanding of their mode of action.

Downs, Walsh and Wheeler[18,19,20,21] established that, with normal fuels, knock occurs by a two-stage process characteristic of what has come to be called 'low' temperature ignition of paraffins. During the first stage, peroxides increase in concentration. The first stage culminates in the appearance of a cool flame in the engine, during the passage of which the peroxide concentration falls sharply. During the second stage, aldehydes increase in concentration and peroxides again increase rapidly. It was later shown[22], by chromatographic techniques, that the peroxides in the first stage are mainly organic, while the peroxide in the second stage is mainly hydrogen peroxide. Addition of lead tetraethyl markedly affects only the second stage, greatly reducing the hydrogen peroxide concentration. Under some conditions the aldehyde concentration is also reduced[20], under others[23] it is not affected by lead tetraethyl, so that it appears that the reduction of hydrogen peroxide concentration is the more fundamentally important. It is significant that Withrow and Rassweiler[24], by spectroscopic methods applied to an engine, found that the only end-gas product whose concentration was markedly reduced by additions of lead tetraethyl was a material which gave strong continuous absorption from *ca.* 3,000 Å towards shorter wavelengths. Hydrogen peroxide possesses just such absorption.

Chamberlain and Walsh[25,26] showed that lead tetraethyl acutely inhibits the second stage of 'low' temperature ignition of the higher paraffins and their derivatives; and also acutely inhibits the slow combustion of methane. It is well established[27] that the reactions occurring in the second stage of 'low' temperature ignition are akin to those occurring in the slow oxidation of methane. Chamberlain and Walsh[25] also found the acute inhibition to persist after prolonged evacuation of the apparatus, even though no more lead tetraethyl was added, and traced this to the deposition of lead monoxide in the reaction vessel. Lead monoxide was shown to cause acute inhibition similar to that caused by lead tetraethyl. By a study of the effects of inert gases on the PbO-inhibited slow oxidation it was proved that the inhibition was due to the surface of solid PbO.

In engines it was not possible to suppose that lead tetraethyl acted by deposition of a PbO surface on the cylinder walls since one can readily show that under the high pressure conditions of an engine end-gas there is not time for chain carriers to diffuse to the walls in the short relevant period of the engine cycle. Direct experiments wherein the cylinder walls and piston head were deliberately coated with PbO confirmed this. It was only possible for lead tetraethyl to act in an engine in the same essential way as it appeared to act in the non-engine slow combustion experiments (viz. by formation of a surface of PbO) if, on oxidation, the lead tetraethyl produced a fog of PbO particles distributed throughout the end-gas region of the engine cylinder, so making the necessary diffusion path very short. Chamberlain and Walsh[25] therefore studied the oxidation of lead tetraethyl and showed, in non-engine apparatus, by the use of a Tyndall beam method, that the process did produce a fog and that the deposits from this fog consisted of PbO. The experiment opened the way for the supposition that lead tetraethyl acted in both engine and non-engine apparatus in essentially the same way, viz. by creation of a PbO surface able to cause acute inhibition. To make matters doubly certain, however, it was then shown[28] that in an engine the scattering of light by the end-gas (but only in the second stage of the two-stage knock process) markedly increased when lead tetraethyl was added to the fuel. There is no doubt therefore that lead tetraethyl does produce a fog in an engine cylinder and, in view of the known acute inhibition by PbO surfaces, there can be little doubt that it is the surfaces of the fog particles that cause the acute anti-knock action.

The conclusion that a fog is involved is hardly surprising when one considers the known metallic derivatives that act as anti-knocks (e.g. lead tetraethyl, tellurium diethyl, iron pentacarbonyl, nickel tetracarbonyl—see Walsh[26]); the common feature of them all is that they are known, or strongly expected, to produce on oxidation fogs of solid particles. It is significant that the alkyls of bismuth, lead and thallium are anti-knocks, but the alkyls of mercury are not[29]; the abrupt change is explicable because the temperatures at which mercuric oxide decomposes and mercury boils are such that, alone of the above alkyls, those of mercury cannot give rise to solid particles in the end-gas of an engine.

If metallic derivatives *do* all act as the metallic oxide fogs that they are known or confidently expected to produce in the engine, then we should expect the characteristic effects of these anti-knocks to be those associated with category II surfaces as set out in the first part of this paper. In agreement, if the various metallic derivatives that act as anti-knocks are arranged in an order of effectiveness then, as far as is known, this order is the same as that of the expected metal oxide category II surfaces as inhibitors of methane combustion. Further, it should be clear from what has been said that the data relating to the action

of lead tetraethyl in an engine *are* just what would be expected if its action is ascribed to its known production of a category II surface. Inhibition is not apparent until an oxide surface has been produced. It is then acute (as expected, with short diffusion paths, for the heavy metal oxide PbO), and is associated with a marked reduction in hydrogen peroxide concentration; and it occurs with methane as well as with the higher paraffins. It is significant too that the anti-knock action occurs also with hydrogen as fuel[20], the relevant mode of ignition of hydrogen is known to be associated with the presence of HO_2 radicals and H_2O_2 molecules and has indeed been shown directly[26] to be inhibited by PbO surfaces.

To be sure, there are one or two cases known (e.g. the glow of phosphorus[26]) where inhibition by lead tetraethyl occurs under conditions such that the action is probably one of unchanged lead tetraethyl molecules rather than of PbO. Inhibition in such processes is probably to be connected with the fact that hydrocarbons in general act as inhibitors of the processes; it is not difficult to suggest mechanisms for the inhibition which could apply to lead tetraethyl as well as to hydrocarbons. In engines, however, there appears to be no important inhibiting effect of unchanged lead tetraethyl molecules, since the first stage of the two-stage knock process is hardly lengthened.

Certain statements, out of line with our conclusions concerning the mode of action of lead tetraethyl as an anti-knock, have recently appeared[30]. These statements have arisen from flash photolysis work under conditions extremely different from those of engines. The conditions include the use of: (i) fuels which are not typical for spark ignition engines, e.g. amyl nitrite added to smaller quantities of acetylene; (ii) temperatures far in excess of those under which the reactions leading to knock are known to develop; and (iii) pressures (e.g. 4 mm $C_5H_{11}ONO$ + 3·3 mm C_2H_2 + 20 mm O_2) far below those of engine end-gases. It appears to us dangerous to assume, as is done implicitly by the authors concerned, that the results obtained are directly relevant to anti-knock action in engines. Our own conclusions have been checked, whenever possible, by direct engine work. The essential observation in the flash photolysis experiments is that lead tetraethyl additions increase the delay period before the growth of OH radical concentration. Part of the increased delay is admitted, on good evidence, to be due to an action of unchanged lead tetraethyl molecules; radicals generated by the photolysis of amyl nitrite attack lead tetraethyl molecules in preference to acetylene molecules. The possibility that the whole of the increase in delay period is due to such action (i.e. to an action which is of only minor importance to engine knock) does not appear to be eliminated. It should be noted that the increase in delay period is not large in comparison with, say, what can be caused by merely changing the fuel/oxygen ratio.

REFERENCES

[1] Hoare, D. E. and Walsh, A. D. *Fifth Symposium on Combustion*, pp. 467, 474. 1955. New York; Reinhold

[2] Cheaney, D. E. and Walsh, A. D. *Fuel* 35 (1956) 258

[3] Holt, P. F. and King, D. T. *J. chem. Soc.* (1955) 773

[4] Cheaney, D. E. and Walsh, A. D. In course of publication

[5] Egerton, Sir Alfred and Warren, D. R. *Proc. Roy. Soc. A* 204 (1951) 465

[6] Warren, D. R. *Proc. Roy. Soc. A* 211 (1952) 86, 96

[7] Dixon-Lewis, G., Linnett, J. E. and Heath, D. F. *Trans. Faraday Soc.* 49 (1953) 766

[8] Warren, D. R. *Trans. Faraday Soc.* 53 (1957) 199

[9] Chamberlain, G. H. N., Hoare, D. E. and Walsh, A. D. *Disc. Faraday Soc.* No. 14 (1953) 89

[10] Latimer, W. M. *Oxidation Potentials*, 2nd ed., p. 47. 1952. New York; Prentice Hall

[11] Satterfield, C. N. and Stein, T. W. *Industr. Engng. Chem.* (*Industr.*) 49 (1957) 1173

[12] Protheroe, J. and Walsh, A. D. To be published

[13] Davies, D. A. and Walsh, A. D. In course of publication

[14] Davis, A. and Walsh, A. D. In course of publication

[15] Weiss, J. *Trans. Faraday Soc.* 31 (1935) 1547

[16] Hoare, D. E., Protheroe, J. and Walsh, A. D. In course of publication

[17] Lewis, B. and von Elbe, G. *Combustion, Flames and Explosions of Gases*, p. 67. 1951. New York; Academic Press

[18] Wheeler, R. W., Downs, D. and Walsh, A. D. *Nature, Lond.* 162 (1948) 893

[19] Downs, D. and Walsh, A. D. *Nature, Lond.* 163 (1949) 370

[20] — — and Wheeler, R. W. *Phil. Trans.* 243 (1951) 463

[21] — *Six Lectures on the Basic Combustion Process*, p. 127. 1954. Detroit; Ethyl Corporation

[22] Wheeler, R. W. Unpublished work

[23] Withrow, L. and Rassweiler, M. *Industr. Engng Chem.* (*Industr.*) 26 (1934) 1256

[24] — — *Industr. Engng Chem.* (*Industr.*) 27 (1935) 872

[25] Chamberlain, G. H. N. and Walsh, A. D. *Proc. Roy. Soc. A* 215 (1952) 175

[26] Walsh, A. D. *Six Lectures on the Basic Combustion Process*, p. 103. 1954. Detroit; Ethyl Corporation

[27] Chamberlain, G. H. N. and Walsh, A. D. *Rev. Inst. franc. Pétrole* 4 (1949) 301

[28] Downs, D. and Walsh, A. D. Unpublished work

[29] Cramer, P. L. and Campbell, J. M. *Industr. Engng Chem.* (*Industr.*) 41 (1949) 893

[30] Erhard, K. H. L. and Norrish, R. G. W. *Proc. Roy. Soc. A* 234 (1956) 178

DISCUSSION

HYDROGEN–OXYGEN REACTION

Papers 1, 2, 3, 4, 8

V. Voevodsky (*Moscow*) said: These most interesting results communicated in the paper of Baldwin and Mayor may from my point of view indicate that a new third case is found for the influence of surface on the hydrogen oxidation. The two already known cases ('clean' and 'salt-coated' vessels) differ evidently in the great differences in the effectivity of chain breaking in these vessels (ε_{HO_2} is very small in the first case and near to unity in the second). The quite different relationships obtained in a boric acid-coated vessel may indicate the possibility of a surface chain branching reaction in this case.

In connection with the paper by Linnett and Tootal I would like to mention work done several years ago by Talrose and myself. In this work it was shown that in vessels with sufficiently great values of the ratio d/ε_{HO_2} in a fast flow system and eliminating traces of water, the limit must be governed by the equation

$$p_2 = \frac{p_2^0}{1 - p_2^0 \dfrac{dk_8}{\varepsilon_{HO_2} v_{HO_2}} \cdot \dfrac{p_{H_2}}{p_{H_2} + p_{O_2}}}$$

where p_2^0 is the second limit value extrapolated from the low-temperature data and k_8 is the rate constant of the reaction

$$HO_2 + H_2 \rightarrow H_2O_2 + H$$

Our equation leads evidently to values of p_2 greater than p_2^0 which is in accordance with the data given in the paper.

D. R. Warren (*Melbourne*), referring to the paper of Baldwin and Mayor, said: It is certainly a relief to me and also, I imagine, to Dixon-Lewis and Linnett to see the $2k_2/k_4$ *versus* $3k_2/k_4$ anomaly resolved. Whether the dissociation of H_2O_2 is or is not monomolecular at these pressures will probably be decided ultimately by direct experiment, if such has not already been done; but my only objection to the mechanism is that it includes no surface reaction, postulating that H_2O_2 is produced in the gas phase. Experiments* in a vessel coated partly with B_2O_3 and partly with KOH seemed to indicate that H_2O_2 was being produced on the B_2O_3 surface. The paper by Walsh *et al.* at this Symposium seems to support this view, and I would like to know whether Baldwin can reconcile it with his mechanism.

R. R. Baldwin (*Hull*) made the following comments on points raised during the discussion of his paper:

(*a*) Direct tests have shown that the aged boric acid surface is remarkably inefficient for the surface destruction of hydrogen peroxide. We have, in fact, used this surface successfully for a study of the homogeneous decomposition of hydrogen peroxide. In confirmation of the mechanism suggested in our paper, we find that the velocity constant k_7 obtained in this way agrees with that estimated from our slow reaction studies.

(*b*) Careful tests (our paper, reference 13) gave no evidence either for instantaneous or slow adsorption of water vapour on the aged surface at 500°C.

(*c*) In regard to the experiments described by Warren using vessels coated with both boric acid and potassium hydroxide, I would first say, as emphasized in our paper, that the mechanism given applies strictly to the aged vessel; for fresh boric acid surfaces, as well as clean Pyrex, we think that some small modifications may be necessary and these would account for the observations described by Warren. Secondly, owing to the volatility of boric acid, I am not certain that the initial alkali surface would be permanent.

(*d*) With regard to the reaction

$$H_2O + HO_2 = H_2O_2 + OH$$

suggested by Voevodsky in an earlier session, we made repeated tests on the effect of water vapour in our aged vessels. These tests were carried out particularly to eliminate a possible poisoning action of water on the surface destruction of HO_2, suggested by Lewis and von Elbe (our paper, reference 6) to account for the auto-acceleration observed in Pyrex vessels. Addition of up to 22 mm of water was found to have no significant effect on either the maximum rate or the time to reach maximum rate. This would appear to eliminate Voevodsky's reaction at 500°C, and while it may occur at 600°C (the temperature of Voevodsky's experiments), I wonder whether the alternative explanation of surface poisoning has been entirely eliminated in his case.

In connection with the paper of Darwent and Krasnansky, the coefficients for oxygen and carbon dioxide in the reaction

$$H + O_2 + M = HO_2 + M$$

* Warren, D. R. *Trans. Far. Soc.* 53 (1957) 199, 206.

determined by second-limit measurements of the hydrogen–oxygen reaction are certainly quite different, carbon dioxide being about three times more effective than oxygen. I would like to ask Darwent whether, in evaluating his term *m* used in *Figures 2, 3* and *5*, he has simply added together the pressures of oxygen, hydrogen sulphide and carbon dioxide, or whether he has made allowance for different coefficients. If he has not, the difficulty arises that allowance for these coefficients, for example in *Figure 5*, gives gradients that are no longer in the theoretical ratios of 1:2:4.

Sir Alfred Egerton (*London*) in making some general remarks about the hydrogen–oxygen reaction said: Owing to the necessity to investigate reactions in vessels there is always the bugbear of the surface effects which make unnecessary complications. For practical purposes we want mainly to know what the reactions are in the free gas. Following Poliakov in hydrogen–oxygen explosions, Minkoff and I found that we could deposit up to nearly 30 per cent H_2O_2 by condensing in liquid air. My efforts now with Pratt are to investigate reactions in flowing streams of gas trying to wean away the surface effects.

W. Forst (*Quebec*) said: I would like to make three remarks about the paper of Baldwin and Mayor. The first one concerns the behaviour in boric acid-coated vessels. Giguère and Liu* have tried to measure the homogeneous decomposition of hydrogen peroxide in a boric acid-coated vessel and found that pressure in the system *decreased* instead of increasing, indicating that adsorption of water must have been taking place at their experimental temperature (about 450°C). For this reason it seems to me that pressure measurements in boric acid-coated vessels might easily lead to erroneous results.

The second remark deals with the reaction of hydrogen peroxide with OH and H. We have recently published some work† on the inhibiting action of hydrogen peroxide in the hydrogen–oxygen reaction. The analysis of experimental results consisted of taking the simplest mechanism for the uninhibited limit (reactions 1–4 of Baldwin's paper), and then starting to add to it all the *a priori* conceivable reactions of H_2O_2 with the chain particles H (three reactions), OH (one reaction) and O (two reactions). It turned out that the simplest way to explain our results was to add the reactions

$$H + H_2O_2 \rightarrow OH + H_2O \qquad (a)$$

$$OH + H_2O_2 \rightarrow HO_2 + H_2O \qquad (b)$$

to the mechanism for the uninhibited limit. These two reactions happen to be the same two reactions as selected by Baldwin and Mayor, and the agreement may be taken as further proof that reactions a and b have their place in the hydrogen–oxygen reaction under certain conditions.

In my last comment I am afraid I have to disagree with Baldwin on the molecularity of the hydrogen peroxide decomposition. We have done some work on this recently* (sponsored by the Office of Scientific Research of the U.S. Air Force) and the results show that the decomposition is unimolecular, although second order around 10–20 mm Hg. I have time here to mention the evidence only briefly:

(1) The reaction is first order with respect to time up to about 15 or 20 mm Hg.

(2) The apparent first-order rate constant increases linearly with peroxide pressure at least up to 15 mm Hg. The straight line does not go through the origin due to the simultaneous occurrence of a heterogeneous reaction.

(3) In the presence of an inert gas, at fixed peroxide concentration the apparent first-order rate constant increases linearly with inert gas pressure for all inert gases tested (water, oxygen and helium, the latter at five different temperatures). Such behaviour is typical of a unimolecular reaction in its second-order region. The activation energy and the number of classical oscillators involved all have reasonable values.

O. Reitlinger (*Washington*) said that hydrogen peroxide is decomposed in the liquid and in the gaseous phase at all surfaces with the exception of Pyrex glass when previously conditioned by fuming nitric acid and subsequently cleaned and kept humid, and provided that the surface is void of scratches.

ATTAINMENT OF EQUILIBRIUM IN COMBUSTION REACTIONS

Papers 5, 7, 14, 15, 16

In opening the discussion, *B. L. Crawford* (*Minneapolis*) said: This group of papers shows our growing realization of the importance—both practical and theoretical—of the details of the processes going forward in a reacting gas mixture. Smith's paper, the sole really practical representative, is an interesting step forward into the middle region where reactions in a nozzle are neither frozen nor following, but something in between. He shows us both how significant these effects can be, and how hard to handle even in an artificially simple case; there is thus compelling practical urgency for us to understand the intimate details of the reactions going forward.

* Giguère, P. A. and Liu, I. D. *Can. J. Chem.* 35 (1957) 283.

† Forst, W. and Giguère, P. A. *J. phys. Chem.* 62 (1958) 340.

* Forst, W. *Can. J. Chem.* In press.

It is interesting to note that at the recent Gordon Conference on infra-red spectroscopy a half-day was devoted to relaxation effects. It seems to me that this coming together of kineticists and spectroscopists is timely. Kineticists are realizing more and more that a species is not sufficiently designated by its chemical individuality; its reactivity will be affected also by its electronic and even vibrational state; so the information and understanding to be gained from the spectroscopist's approach should be useful. Spectroscopists on the other hand are beginning to realize that kinetics is a branch of normal vibration theory, dealing to be sure with unusual vibrations of large excursion and a high degree of anharmonicity, but still amenable to the same approach.

There are some questions in my mind arising from specific points in these papers. Windsor implies that complex collisions in which vibrational energy is transferred (his constant e) are faster than simple collisions (his constant k_{01}). Herzfeld, on the other hand, finds these two processes comparable in rate. Is this a real discrepancy?

As regards agreement with experiment on the anomalous dissociation rate, Herzfeld finds an error of a factor of 200. Kondratiev quotes results of Nikitin in which agreement is obtained when (1) one allows for a deviation from a Boltzmann distribution, and (2) includes the effect of rotation. Now Shuler's paper shows that the effects of deviation from the Boltzmann distribution should be very small; and my recollection is that both Shuler and Herzfeld have, in discussions, indicated that the contribution of rotational energy transfer must be small. I should like very much to hear some discussion on these points.

K. F. Herzfeld (Washington): In reply to Crawford's question concerning an apparent contradiction between Windsor's and my statements: If the vibrational energy to be transferred is large—as in the paper by Windsor *et al.*—the resonance transfer is much faster than the direct transfer to translation. If the vibrational energy is very small—as is the case for the small quanta at the top of the Morse function, which I discussed—the rates are comparable.

A. G. Gaydon (London): In a hot gas the molecules will normally possess considerable rotational energy; the effective potential energy curve for a rotating molecule will differ markedly from the Morse curve assumed by Herzfeld. In particular, it will possess a maximum. I suggest that a predissociation process, through this maximum, may occur, greatly increasing the rate of dissociation.

W. Jost (Goettingen): We are acquainted, in the decomposition of ozone, with the reaction

$$O_3 + O = O_2 + O_2 \qquad (1)$$

From the value of the rate constant for this reaction and that of the equilibrium constant, one can calculate the rate constant of the reverse reaction

$$O_2 + O_2 = O_3 + O \qquad (2)$$

(which would be followed by a rather rapid decomposition of O_3) ΔH for reaction 2 is some 25 kcals smaller than that for

$$O_2 + O_2 = O_2 + O + O \qquad (3)$$

Thus it is possible that a quantitative calculation would show that oxygen dissociation proceeds via reaction 2; then both Herzfeld's calculations and the observed rates of oxygen decomposition could be correct.

F. Kaufman (Aberdeen Proving Ground, Md.): Referring to the paper by Windsor *et al.*, we have recently observed by indirect physical evidence that much vibrationally excited N_2 is present in active nitrogen. In comparing the relaxation of these two isoelectronic molecules, CO and N_2, it is interesting to note that we have found CO_2 and N_2O most efficient in bringing about relaxation, and H_2O much less so, indicating that near-resonance of vibration frequencies is the most important factor for N_2. Windsor's results show that this order is strongly reversed for CO, perhaps because of dipole interactions with H_2O.

J. W. Linnett (Oxford): In his paper Kondratiev has discussed processes which involve a change of multiplicity. It seems to me that, at the moment, our knowledge of the extent to which a change of multiplicity makes a process difficult is most uncertain. Surely this is a problem on which theoretical and experimental chemists could help one another and one hopes that, in the near future, some progress will be made here. However, I would like to draw the attention of the meeting to a paper by Stearn and Eyring* on the dissociation of nitrous oxide in its ground state to a nitrogen molecule and an oxygen atom both in their ground states. This paper which is usually overlooked discusses just this problem.

R. G. W. Norrish (Cambridge): In connection with the problem of transfer of energy from vibrational to other degrees of freedom, I should like to draw attention to exothermic reactions of the type

$$A + BCD = AB + CD$$

where A is an atom. We have been able to show that in such cases a large proportion (*ca.* 50–90 per cent) of the energy of the reaction may remain unequilibrated in vibration of the newly formed bond, A–B, while the molecule remains rotationally quite cold. Such reactions are

$$H + O_3 = OH^{\star} + O_2$$

* Stearn, A. E. and Eyring, H. *J. chem. Phys.* 3 (1935) 778.

discovered by Boudart and his colleagues, in which the vibrationally excited hydroxyl may take up to 90 per cent of the energy of reaction. In the following cases, using the method of flash photolysis, we have been able to photograph the vibrationally excited species in absorption—in the case of $O_2^\star$ as an extension of the Schumann Runge bands towards the visible.

$$O + NO_2 = O_2^\star + NO$$
$$O + ClO_2 = O_2^\star + ClO$$
$$O + O_3 = O_2^\star + O_2$$
$$Cl + O_3 = ClO^\star + O_2$$
$$Br + O_3 = BrO^\star + O_2$$

In the case of ozone, oxygen molecules vibrating with up to 17 quanta in the ground state are observed, quite cold with respect to rotation.

Thus we see that high energy of vibration may remain located in newly formed molecules, and the possibility of chain propagation by excited molecules is made obvious.

This method of kinetic spectroscopy provides a means for observing the rate of decay of such excited species, and Lipscomb, Thrush and I have made preliminary measurements on the deactivation of the $O_2^\star$ molecule. It is found for example that while some 10^7 collisions with argon or nitrogen are necessary for one deactivation, from the sixth to the fifth *vibrational* level, only about 10^3–10^4 are required if carbon dioxide or nitric oxide is the deactivating molecule. It is concluded that resonance between the vibrational levels of the two molecules is necessary for easy deactivation. Development of the method should provide a unique means of studying the transfer of vibrational energy.

S. L. Bragg (Derby): I would like to refer the analysis of Smith's paper to a specific case. The gases in the combustion chamber of a typical rocket engine have probably had sufficient time to approach an equilibrium composition of, for example, 35 per cent CO, 32 per cent H_2O, 12 per cent CO_2, 12 per cent H_2, 4 per cent OH, 4 per cent H, 1 per cent O_2, and 1 per cent O, at a temperature of about 3,500°K. They then expand, in a time of about 1 msec, over a pressure ratio of over 50 : 1 to a temperature below 2,000°K. Under equilibrium conditions at this temperature only CO, H_2O, CO_2 and H_2 would still exist, though in what proportions is immaterial, since the water gas reaction involves so little energy. The question is, therefore, are the reaction rates of the active species OH, O and H sufficiently high for them to re-associate and give up their energy—which is nearly 10 per cent of the total calorific value of the fuel—in the short time available during expansion? If the rates *are* sufficiently high then the thrust potentially available from the expanding gases is some 5 per cent higher than if they are not.

A rather approximate 'engineer's' calculation performed at Rolls-Royce by M. Lemon and based on the assumption that the overall reactions taking place, and therefore the available heat release rates, were similar to those occurring for example in Longwell's 'stirred reactor' experiments, led us to expect that at least 90 per cent of the dissociation energy should be recovered during expansion. If this were true, all assessments of rocket engines should be based on the performance theoretically obtainable with shifting equilibrium, rather than with 'frozen' composition. Would Smith confirm that practical values of the parameter B_i in his computations substantiate this conclusion?

A. S. Gordon (Naval Ordnance Test Station) (communicated): I should like to refer the following points to Kondratiev.

(1) I agree with him that just the crossing of potential energy surfaces would not increase the life-time of the $CO_2^\star$ molecule by three orders of magnitude. In our paper Knipe and I pointed out that the crossing could place the configuration in a triplet state with vibrational excitation. As long as the life-time of the excited state is about that for collision probability, collisions will lower the $CO_2^\star$ further into the well of the curve, and thus stabilize it.

(2) What clear-cut evidence exists that spin multiplicity is not conserved for chemical processes involving simple molecules?

R. H. Tourin (New York) (communicated): Under equilibrium conditions, the velocities of combustion gas molecules follow the Maxwellian velocity distribution, and the combustion engineer can confidently write

$$\overline{\tfrac{1}{2} mv^2} = \tfrac{3}{2} kT$$

for the mean translational kinetic energy of the gas molecules, lacking equilibrium, the temperature T loses its significance, and the use of ordinary thermodynamic equations becomes questionable. It would be of great value in practical combustion work if the various studies of non-equilibrium conditions in combustion gases could be extended to estimate quantitatively the extent to which the molecular velocity distribution departs from Maxwellian form, and the time dependence of such departures.

M. Boudart (Princeton University): We have studied the effect of water vapour on vibrational relaxation in oxygen. The presence of water should affect the mechanism of relaxation and this should show up in the relaxation curve. Has Windsor observed any effect on the shape of the curve?

M. W. Windsor (Washington): The effectiveness of water vapour in our experiments is so high that

even very small amounts markedly reduce the observed relaxation time. It is not easy to introduce known small amounts of water with sufficient control to get a measurable effect but not an overwhelming one. Our technique was to admit excess water vapour and rely on a suitable coolant mixture to determine the temperature of the cold finger and hence the vapour pressure of water in the shock tube. From the limited number of experiments we were able to do with water vapour present, we can say that 2 parts in 10^5 has no appreciable effect while 3 parts in 10^3 has a very pronounced effect (see Table 3). Since the observed relaxation time in the latter case is comparable with the response time of the detector, it would not be justified to make any inferences regarding change of mechanism from the shape of the experimental curve.

L. F. Allbright (*Lafayette, Ind.*): Windsor mentions the difficulty of removing adsorbed water vapour from the walls of your shock tube. Does he think that the effect of impurities could be attributed to a surface effect?

M. W. Windsor (*Washington*): Under the conditions of our experiments (1,400°K and 1 atm and a shock-tube diameter of 15 cm), the rate of molecular diffusion is too low for more than a very small fraction of the gas molecules to make a collision with the surface during the observed time of relaxation (less than 1 msec).

It is conceivable that wall effects might become important at much lower pressures or with smaller shock tubes, but it is safe to rule them out in the present experiments.

I wish to draw attention to some changes which we have made in our paper which do not appear in the set of pre-prints but which will appear in the printed book. The main change concerns our appraisal of the contribution of the complex collision process

$$CO^{\star} + CO^{\star} \underset{e}{\overset{e}{\rightleftharpoons}} CO^{\star\star} + CO \qquad (3a)$$

to the rate of population of the level $v = 2$. In the pre-print version we concluded that since e is about 10^4 greater than k_{10}, the rate constant involved in the conversion of energy from translation to vibration,

$$CO + CO \underset{k_{10}}{\overset{k_{01}}{\rightleftharpoons}} CO^{\star} + CO$$

$$CO^{\star} + CO \underset{k_{21}}{\overset{k_{12}}{\rightleftharpoons}} CO^{\star\star} + CO \qquad (2)$$

then the former would predominate when $(CO^{\star})/(CO)$ exceeded 10^{-4} which occurs at an early stage in the relaxation for the temperature range studied. This argument turns out to be invalid and for the following reason. It can be shown that a system which starts off with a Boltzmann distribution of vibrational states relaxes to the distribution appropriate to the translational temperature via a set of Boltzmann distributions appropriate to intermediate temperatures. Under these conditions processes like 3a proceed backwards and forwards at equal rates and serve only to commute molecules back and forth between two vibrational levels.

Such processes neither affect the distribution further nor do they affect the rate of energy transfer between translation and vibration.

A more detailed discussion of this point is given in the corrected version of our paper.

The high efficiency of impurities, such as H_2O and CO_2, in inducing vibrational relaxation, may be explained as follows. Complex collisions of the type,

$$CO + H_2O^{\star} \rightleftharpoons CO^{\star} + H_2O$$

in which vibrational quanta are exchanged are relatively efficient, since only the balance of energy appears as (or must be supplied from) translation. The smaller is this energy balance, that is the closer the system approaches to resonance, the higher the probability becomes. The probability is in fact determined, more than by any other factor, by the size of the change in translational energy. In the presence of impurities then, the rate of relaxation depends on two factors: (*a*) the rate of vibrational relaxation of the impurity molecule itself; and (*b*) the rate of vibrational energy exchange by complex collision. One or the other of these will be the rate-determining step.

MECHANISM OF COMBUSTION REACTIONS—NON-HYDROCARBONS

Papers 6, 9, 10, 11, 12, 13

G. Porter (*Sheffield*) opened the discussion: Both sessions this morning are concerned with the mechanism of combustion reactions and this afternoon combustion in practical systems is discussed. It is a disturbing fact that a *practical* combustion system apparently involves no chemistry or alternatively that our endeavours in the field of combustion mechanism have not yet reached the point where they are of practical value. The ultimate objective of our work is presumably to be able to predict the gross behaviour of a combustion system from accurately known rate constants of a limited number of elementary reactions, i.e. reactions which cannot usefully be resolved into simpler steps. Just what we are up against in this problem is illustrated by the fact that, after over 30 years of intensive study, the mechanism of the H_2/O_2 reaction is still open to substantial modifications and the rate constants of many of the elementary reactions are, to say the least, uncertain.

The new reaction proposed by Voevodsky, viz.

$$HO_2 + H_2O \rightarrow H_2O_2 + OH$$

to explain the effect of water seems necessary to fit his data but raises the question of the value of this remote approach to reaction kinetics. Are the mechanism of the H_2/O_2 reaction—especially in the third explosion limit region—and the rate constants of the elementary steps and their dependence on temperature so reliably known that one can place any reliance on predictions which conflict violently with energetic and structural considerations? Voevodsky apparently believes so and accounts for an energetic discrepancy of the order of 20 kcal by postulating a second structural form for HO_2.

The fact that explanations of this kind cannot readily be disproved illustrates how the science of combustion kinetics is retarded by our inadequate knowledge of transient intermediates and their elementary reactions. A combustion reaction is one of the least suitable systems for the study of elementary reactions and in this sense the proper study of combustion is not always combustion.

Important data of the kind which are so urgently required are given in the paper of Kaufman and Kelso. Photochemical methods, which have proved most useful for the study of excited states, atoms and radicals are not readily applicable to oxygen and nitrogen atoms and the elegant method using the chemiluminescence of the reaction

$$O + NO \rightarrow NO_2$$

developed by these authors is therefore particularly valuable. The rate constants of some of their reactions are remarkably high, particularly the metathetical reactions involving two radicals, where the activation energies are very nearly zero. Presumably the bonding which is always possible in the transition state of this type of reaction produces a deep well in the potential energy surface with a consequent lowering of the activation energy barriers. (Incidentally why use units of mole c.c.$^{-1}$? There is some justification for molecules c.c.$^{-1}$, which are readily related to collision cross-sections and also for mole litre^{-1}, which are used almost universally by chemists, particularly in solution; but two sets of units are already too many in this field and three become a real nuisance.)

One of the many new factors which may appear in high-temperature combustion, such as flames and explosions, compared with low-temperature oxidation, is thermal decomposition of the fuel which may precede oxidation. If thermal decomposition has high A and E factors compared with oxidation processes—as will usually be the case—we must always expect it to become predominant first step when the temperature is high enough. There is much evidence for this in some hydrocarbon flames and explosions, e.g. even in oxygen-rich mixtures carbon radicals such as CH and C_2 are formed and there is often a suggestion that the decomposition proceeds in some cases to the point of incipient carbon formation. The system studied by Gray and Lee is interesting in this connection since hydrazine alone has its own well known decomposition flame and therefore one can proceed continuously by addition of oxidants such as O_2 and NO, from decomposition to combustion. The authors believe that their burning velocity measurements indicate that the two-stage process is not predominant and that in both cases oxidation proceeds more rapidly than pyrolysis though, since the increased burning velocity is accompanied by increasing temperature, the extreme view of van Tiggelen does not seem to me to be excluded.

Combustion processes involving sulphur are attractive in that most of the important intermediate radicals are readily observed spectroscopically. The CS_2/O_2 system was studied spectroscopically by Myerson, Taylor and Hanst and the present work on the first explosion limit by Taylor and Myerson provides a step towards an integration of overall explosion studies with direct observation of the reactions of intermediates.

The H_2S/O_2 system studied by Zeelenberg and Norrish and reported here by Zeelenberg is quite complex even when the intermediates are observed directly, as they are in these flash photolysis experiments. One of the uncertainties in this system is the assignment of the 3,000 Å system to S_2O_2. This is by no means certain and even if the assignment is correct the work of Vallance Jones indicates that it would have to have the structure

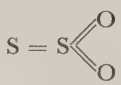

which makes its ready formation by dimerization of SO somewhat improbable. The observation on pure SO_2 is very interesting. When the system is kept isothermal by the addition of excess inert gas no change is observed on flashing, a fact which I can substantiate on the basis of my own observations. However, when the temperature is allowed to rise—the 'adiabatic' case—the SO_2 spectrum disappears and all returns after a few msec. Such an effect is commonly observed with many substances and is often to be attributed to an effect of temperature and concentration gradient. This effect is worth mentioning here because its importance is not generally appreciated and it is present in all systems, such as flash photolysis, shock-tube work and explosions in closed vessels, where a gas is heated very rapidly by some means not involving heating of the vessel. If the gas temperature is

raised instantaneously from T_0 to T, the wall temperature being T_0, a temperature gradient is set up in the vessel, and a short time afterwards the concentration along the axis of a cylindrical vessel will be less than that near the wall. If spectra are recorded along the axis the apparent concentration will fall and, for high gas temperatures, will be reduced to a small fraction of the original concentration. The temperature and concentration profiles are time dependent and quite complex, making quantitative measurements in this type of system very difficult.

Zeelenberg has not discussed this possibility and I wonder whether it can be invoked to explain his observations on SO_2. I understand from Norrish that an increased absorption appears at shorter wavelengths which does suggest that SO_2 is replaced by a new species but could not this be due to a greatly increased extinction of SO_2 in this region owing to the higher temperature and population of higher vibrational levels? The small amount of SO_2 which remains in the light path makes this rather unlikely but not as unlikely as the mechanism proposed by Zeelenberg involving photodissociation of SO_2 with the overall result

$$SO_2 \rightarrow SO + \tfrac{1}{2}O_2 \qquad (1)$$

Since there is no permanent change this must be followed exclusively by

$$SO + O_2 \rightarrow SO_2 + O \qquad (8)$$

but the concentration of O_2 approaches zero towards the end of this reaction and, in the isothermal case, even in excess O_2 the reaction

$$2SO \rightarrow S_2O_2 \qquad (5)$$

proceeds very efficiently. The complete absence of S_2O_2 in the products of SO_2 photolysis under all conditions is a very strong argument against this mechanism.

R. G. W. Norrish (Cambridge): Since the work of Zeelenberg and myself on the flash photolysis of hydrogen sulphide–oxygen mixtures, Oldershaw and I have carried out further work on the flash photolysis of SO_2. We have confirmed that when flashed adiabatically so that temperatures of up to 1,000°C are momentarily generated the normal SO_2 spectrum disappears *completely* and is replaced by a new continuous spectrum in the far ultraviolet. This disappears as the original spectrum is regenerated after a few msec. If a comparatively large amount of inert gas is added to keep the system isothermal, the effect is entirely eliminated. We have been able to show definitely that the effect is not photolytic but thermal, and are of the opinion that a thermal isomer of the type postulated by Myerson and his colleagues, e.g. SOO, is generated reversibly. The exact nature of the isomer must await elucidation but we have concluded that it may dissociate photolytically by absorption in the far ultraviolet (*ca.* 2,200 Å) to give SO molecules whose spectrum in absorption becomes visible for the first time, as a series connecting with the SO emission spectra described by Martin. The SO spectrum is not produced by normal SO_2 molecules under the same conditions of irradiation since the limiting quantum for photolysis lies outside our range.

The partial fading of the SO_2 spectrum on heating to *ca.* 500°C in a furnace was also described by Wieland some years ago and is undoubtedly the same phenomenon.

Finally, in connection with his scheme of reaction for the combustion of H_2S, I think Zeelenberg should have included the reaction

$$O + H_2S = OH + HS$$

to allow for branching in the explosive reaction under adiabatic conditions.

V. Voevodsky (Moscow): Several of Porter's questions have already been considered in my paper, but I should like to deal with one new criticism. Porter finds it difficult to imagine two different forms of the HO_2 radical. I think that I can make some suggestions on this point now, although experimental investigation must be delayed for some time. For instance, one may assume that, apart from the usual H–O–O radical produced by hydrogen atom abstraction from the H_2O_2 molecule, a hydrogen atom may also form a bond with the π-electrons of an oxygen molecule, leading to a triangular radical

$$\begin{array}{c} O \underset{H}{=} O \end{array}$$

These two structural forms of HO_2 may be compared to the carbonium ion and π-complex which are often considered in organic chemistry.

Perhaps I may even go further and postulate that such a π-type complex may be formed in the first stage of an interaction between hydrogen atoms, or possibly even more complicated radicals, and unsaturated molecules such as olefines and acetylenes.

A. R. Ubbelohde (London): In commenting upon the paper by Voevodsky, I should like to mention some results relating to the efficiency of the H_2O molecule in energy-transfer by gaseous collision.

Various authors have commented on the need to establish firm experimental facts about many of the individual steps that have to be, or that are, postulated about complicated oxidation mechanisms. One such step which we have been studying intensively, because of its bearing on reaction kinetics, refers to the transfer of internal energy in gaseous collisions. For example, vibrators such as ethylene, nitrous oxide, or carbon dioxide are comparatively inefficient in exchanging vibrational

energy in self-collisions. Various polyatomic molecules are found to be much more efficient as energy transfer catalysts in hetero-collisions; but amongst examples where the atoms in the collision partner with one of these vibrators are reduced to 2 or 3, it is found that H_2O is outstanding for its efficiency with a diversity of vibrators. H_2O is markedly more efficient for example than the isoelectronic molecule CH_4. We have attributed this to the fact that the dipole in H_2O is associated with a comparatively small van der Waals repulsion envelope, so that in a collision with a vibrator molecule the H_2O dipole can exert high local electrostatic perturbations before the repulsion potential prevents any closer approach. Although this explanation is not necessarily in conflict with assumptions about loose complex formation during a collision, it seems more general.

J. H. Knox (Edinburgh): Voevodsky has suggested that the failure of the equation $\phi\tau = \text{const}$ to hold in degenerate branching chain reactions such as hydrocarbon oxidations may be due to the occurrence of quadratic degenerate branching reactions which may be generally represented as

$$R + M_{st} = 3 \,.\, R'$$

where M_{st} is a stable intermediate product of the reaction.

In the oxidation of propane at 320°C this explanation does not account for the results obtained. It is found for example:

(1) that the dependence of $1/\tau$ and of ϕ on reactant concentrations are completely different and cannot be accommodated by any simple product relationship of the form

$$\phi^m \tau^n = \text{const}$$

(2) that $1/\tau$ is strongly increased by the addition of inert gases such as N_2 or CO_2 while ϕ is only very slightly affected.

It appears that these results may most readily be interpreted in terms of the diffusion of molecules of the chain-branching intermediate (say an aldehyde or peroxide) to the walls of the reaction vessel where they are destroyed. It is then possible for each chain in the early stages of the reaction to produce less than the single branch necessary for the autocatalytic acceleration of the reaction. However, as the reaction proceeds the surface of the reaction vessel appears to become less reactive with respect to this destruction reaction and by the end of the induction period its activity has reached a steady state so that the reaction can accelerate uniformly. Any wall reaction which then destroys the branching intermediate is no longer diffusion controlled.

Quadratic branching does not therefore appear to be necessary in order to explain the slowly increasing acceleration of the reaction during the induction period.

Z. G. Szabó (Szeged): It is very interesting that Voevodsky assumes a reaction between the end-product, water, and an intermediate radical in order to explain the autocatalytic effect resulting in an explosion at pressure P_3. Later he remarks that P_3 was measured at the moment when nearly all the combustible mixture was converted into water. I should like to ask whether instead of assuming an autocatalytic effect to interpret the explosion, one could not explain the delay of the acceleration by a removal of an inhibition at this moment? This would be another mechanism, the removal of an inhibition by the initial gases. This concept is somewhat similar in result to the point of view of Lewis and von Elbe* according to which the chain-termination properties of the surface are cancelled by the water vapour.

What the nature of this inhibition may be is an open question.

V. Voevodsky (Moscow): Knox, in his comment, proposed the possibility of a diffusion process involving an intermediate (M_{st}) governing the duration of the induction period (τ_i). I should like to point out that the diffusion process by itself cannot be the limiting factor because τ_i is many times larger than the average diffusion time.

D. R. Warren (Melbourne): The postulation which Voevodsky has made both in this and in his earlier work that water is involved in pre-combustion chain reactions is of fundamental interest both in the H_2/O_2 reaction and in the oxidation of hydrocarbons. There is other evidence to suggest that some such reactions involving water might well be revealed.

For many years now it has been passed on from father to son that the main activity of water is as a third body of extraordinary efficiency (14·3 relative to H_2 as compared with a calculated value of 0·6–0·9). On tracing the source of this data one finds that while most of the early third-body efficiency measurements (O_2, N_2, A) were checked at varying H_2/O_2 ratios and temperatures and found to be constant, in the case of water only stoichiometric H_2/O_2 proportions were used†, and it was assumed by analogy with the other gases that the whole of its enormous inhibiting effect was due only to its activity as a third body. Had part of this effect been due to some other kinetic process involving one or other of the chain carriers, either by a gas phase reaction as postulated in this paper or by some modification of surface efficiency by adsorption, then it would have shown up as a

* von Elbe, G. and Lewis, B. *Third Symposium on Combustion, Flame and Explosion Phenomena*, p. 787. 1949. Baltimore; Williams and Wilkins.

† von Elbe, G. and Lewis, B. *J. chem. Phys.* 10 (1942) 366.

variation of the apparent third-body constant with temperature or mixture ratio. It is worth our notice, therefore, that a value of 10·4 was reported in the same paper for a measurement at a slightly lower temperature. Other subsequent workers have reported different values again, as low, I believe, as 5.

Occasionally evidence from other directions raises the same suspicions. In Baldwin's early paper* on the action of inhibitors, water shows an anomalous effect on the apparent activation energy, possibly due to some hitherto unrecognized kinetic activity.

In spite of this predisposition I am not at all happy about the present method of derivation or the feasibility of reaction 9 to explain auto-acceleration. I cannot agree that 'water is the only stable product capable of accumulating' since both H_2O_2 (as in Baldwin's paper in this present Symposium) and even HO_2 must be considered sufficiently stable to accumulate. I am sure more feasible conclusions would have arisen had the treatment included our current views of chain initiation by self-generation of H_2O_2 and of the contributions of quadratic branching which have been shown to be considerable near the third limit even in a KCl vessel†.

Our knowledge of the slow reaction in this region is still too much in a state of flux to make deductions of new fundamental reactions with much confidence. I would suggest that for a consideration of the possible activities of water a more reliable starting point would be to go back and re-examine the anomalies in those third-body efficiency values. Variation with fuel $/O_2$ ratio, temperature and surface coating might well give us some exciting and valuable new lead.

P. Gray (Leeds): I should like to mention the following points in replying to Kaufman's comments. In *constant pressure* flame systems, from a few cm to 76 cm Hg, we find the stoichiometry of decomposition is adequately represented by the equation:

$$N_2H_4 \qquad NH_3 + 0{\cdot}5\ N_2 + 0{\cdot}5\ H_2$$

where the *exact* values of the coefficients depart only a little from the simple ratios above (which have no especial virtue beyond their mnemonic property). *In constant volume* systems, such as Kaufman describes, high transient pressures are reached and the final temperatures are considerably greater. We have examined the products remaining after both spontaneous ignition (Gray, lecture at Aberdeen Proving Ground, Md., 1954) and spark ignition (also studied by Pannetier) of pure hydrazine in constant volume systems and the figures quoted by Kaufman confirm and extend our early work. A typical analysis appropriate to spark ignition in a closed vessel, which was quoted at the Sixth Combustion Symposium (1956) is:

$$N_2H_4 \rightarrow 0{\cdot}72\ NH_3 + 0{\cdot}64\ N_2 + 0{\cdot}93\ H_2$$

I look forward to a fuller account of Kaufman's work and in particular to hearing whether he has produced analyses corresponding to the stage of reaction immediately preceding ignition.

Porter raises a central point when he draws attention to the role of *pyrolysis* in the hydrazine oxidation flames. An extreme view is that oxidation flames are chemically no more than decomposition flames maintained by subsequent energetic oxidation, the oxidant reacting only with the *final* products, ammonia and hydrogen. My own view is that all oxidants (oxygen, nitrous oxide, nitric oxide) intervene at a much earlier stage and that they may accompany hydrazine breakdown by bond fission. Two points may be mentioned which bear on this. (1) The decomposition flame of *pure* hydrazine shows NH and NH_2 emission. So does the oxidation flame; it also emits OH radiation and the OH emission accompanies and is not preceded by the NH and NH_2 bands. (2) When oxygen, nitrous oxide and nitric oxide are added to hydrazine it is ammonia formation which is first supplanted while hydrogen remains. Ammonia *decomposition* is favoured by the higher temperatures of combustion but I feel an important contribution to its disappearance is made by participation of the oxidants among the reactions involving the NH_2, NH and possibly N_2H_3 radicals.

G. Porter (Sheffield): As regards the comments of Voevodsky and Herzfeld I agree that one cannot calculate third-order re-combination coefficients on the basis of collision diameters—this is made quite obvious by the results of the extensive work on halogen atom re-combination. On the other hand, water is not particularly unusual as a third body and falls into the general scheme if one interprets the three-body process in terms of the consecutive reactions

$$X + H_2O \rightarrow XH_2O$$
$$X + XH_2O \rightarrow X_2 + H_2O$$

A. L. Myerson (Philadelphia): With reference to the matter of inhomogeneities in the density of free radicals in an absorption tube, as mentioned by Porter, one should take careful cognizance of the time–temperature relationships as follows.

If the gas in a cylindrical absorption tube is heated to a high temperature quickly and homogeneously and then allowed to cool, the temperature will first decrease more quickly near the walls than in the centre, but the final temperature of the gas in the tube will be uniform and equal to the wall temperature. The result is that the density

* Baldwin, R. R. *Fuel* 31 (1952) 313.
† Warren, D. R. *Proc. Roy. Soc. A* 211 (1952) 86.

of the gas in the centre of the tube will first decrease and then increase, the final density being the same as the initial one. Thus, when observing free radicals under such conditions, if the time under observation is less than that for minimum density, the correction should be made in terms of a *decrease* rather than an increase in density. We are making a rigorous analysis of this at the present time.

May I make a second comment. From observations made by flash spectroscopy of thermally induced CS_2—O_2 explosions, a reasonable mechanism for the formation of S_2O_2 would seem to be the following: The thermal isomer of SO_2, SOO (called sulphur superoxide) may also be formed by abstraction of a sulphur atom from CS_2:

$$CS_2 + O_2 = CS + SOO$$

Further reaction of SOO with CS_2 could produce S_2O_2

$$CS_2 + SOO = CS + S_2O_2$$

Both S_2O_2 and SOO were observed during induction periods.

MECHANISM OF COMBUSTION REACTIONS—HYDROCARBONS

Papers 17, 18, 19, 20, 21, 22, 23, 24, 25, 26, 27

The discussion was opened by *A. D. Walsh (Dundee)*.

V. Voevodsky (Moscow): I do not think that the conclusion given in the paper by Szabó, that the effects obtained by treating the vessel with hydrofluoric acid are due to a change in the effectivity of the chain rupture rate at the wall is the only possible explanation. Some results obtained by Poltoran and myself, while investigating the thermal cracking of propane in the presence of small quantities of oxygen, give sufficient evidence that chains are not only broken but also initiated at the wall. If the chain breaking is the only efficient heterogeneous process in the chain reaction, then quite a different dependence on the S/V ratio would be obtained.

I do not think, further, that the data given by Szabó for the C–H bond dissociation energies in propane (99 kcal/g mol, secondary atom) and in *iso*butane (97 kcal/g mol, tertiary atom) are quite reliable. If they were true, it would mean that the coefficients of hydrogen abstraction given by Rice, that are in very good accordance with most of the known experimental data, are incorrect; I see no reason to reach such a conclusion.

I should like to make a small remark about the paper by Enikolopyan. It must be pointed out that it is, as far as I know, the first case where direct computation, on the basis of a simple oxidation mechanism (that was given in its essentials in the literature long ago), and data on rate constants of elementary reactions, lead to value of an overall activation energy, temperature dependence of the maximum of the intermediate compound (formaldehyde), etc., quite close to the experimental values. The mechanism does not include however heterogeneous stages, that are, in some experimental conditions, of very significant interest. It would be interesting to see how these results could be reconciled, for example, with the data of Hoare and Walsh.

G. J. Minkoff (London): I think my colleagues and I agree that the term 'active surface' in Szabó's paper is misleading, in that the surface is then mainly failing to destroy radicals which propagate the chain. With regard to the difference between chain initiation and continuation, a striking illustration is provided by Ridge*. During the slow oxidation of *iso*butane, this author showed that the induction period varied inversely as the concentration of inert gas. Clearly the active intermediates were being saved during the early growth of the chains. The maximum rate, on the contrary, was independent of the inert gas pressure.

J. H. Knox (Edinburgh): Walsh's somewhat partisan criticisms of our paper are fortunately in the main unsound. We fully realize that the concentrations of the radicals X_1 and X_2 vary widely throughout the reaction. This, however, is irrelevant in the present instance since we are concerned with rate constant ratios and it is only the ratio $[X_1]/[X_2]$ which is important. This ratio, presuming for the moment that X_1 and X_2 are not identical, will probably vary rather slowly throughout the reaction. It was with this possibility specifically in mind that we carried out experiments in which the ratio of total hydrocarbon to oxygen varied. From the constancy of k_e/k_p in these experiments we deduced either that little change in the above concentration ratio took place or that if there was any change, such changes had no influence on k_e/k_p. Further experiments, as detailed in the paper, then led us to conclude that X_1 and X_2 were, in fact, identical. A more detailed analysis of the reaction scheme will be given elsewhere†.

The logarithmic expression used for the determination of k_1/k_2 from the analytical results is, in fact, mathematically correct for the ratio of the rate constants of two competing reactions, first order with respect to the hydrocarbon. For very small consumption of the reactants it reduces to

$$\frac{k_1}{k_2} = \frac{\Delta[R_1H] \times [R_2H]}{\Delta[R_2H] \times [R_1H]}$$

where Δ denotes the change in a given concentration. Both expressions have already been used by

* Ridge, M. J. *Trans. Faraday Soc.* 52 (1956) 858.

† Knox, J. H., Smith, R. F. and Trotman-Dickenson, A. F. *Trans. Faraday Soc.* In press.

the authors*†. The criticism that the use of the logarithmic expression minimizes any variation of k_1/k_2 is quite unsound.

The third point raised by Walsh is a more important one. We thought initially that the trend observed in *Figure 1* of our paper, which is similar to that observed in the overall rates of oxidation of hydrocarbons, was within the experimental uncertainty. However, it is possible that the trend, though slight, may be real and as such may represent a secondary variation of k_e/k_p superimposed upon an overall constancy. The slopes of the end portions of the curve yield activation energy differences of $E_e - E_p = 1{,}000$ cal mole^{-1}. This is still a very small difference comparable with that found for chlorine atoms, so that our general conclusions and arguments are not altered.

In connection with the paper by Burt, Cullis, Larsen and Minkoff I should like to mention some results obtained by Falconer and myself (in course of publication) in support of the reaction

$$C_3H_7 + O_2 = C_3H_6 + HO_2 \qquad (1)$$

as the main source of propylene in the oxidation of propane, even in mixtures very weak in oxygen. *Figure 1* shows the product yields as a function of

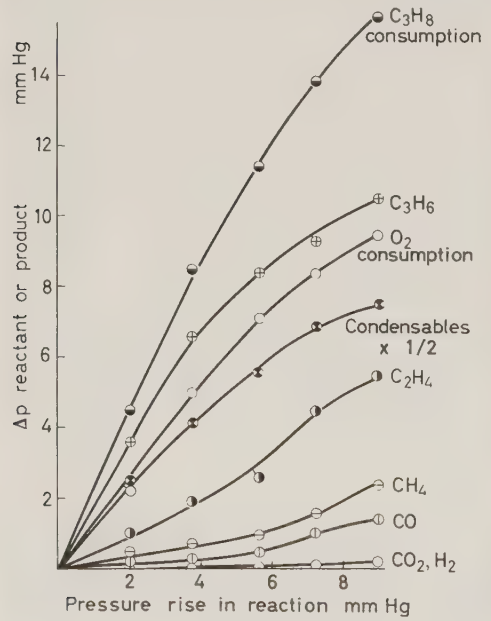

Figure 1

pressure rise for the oxidation of a mixture containing 9·5 mm of oxygen and 100 mm of propane at 435°C in a 500 ml Pyrex reaction vessel. It is seen that throughout the reaction there is an almost equimolar appearance of propylene and disappearance of oxygen while the only important oxygen-containing products are condensables (mainly water). This can be explained simply only if propylene is formed as a result of a chain reaction comprising reactions 1 and

$$C_3H_8 + HO_2 = C_3H_7 + H_2O_2 \qquad (2)$$

followed by the decomposition of most of the hydrogen peroxide to give water.

Further support for reaction 1 is found in the observation that the relative rates of formation of propylene and ethylene increases with oxygen concentration. Since ethylene is almost certainly formed largely by

$$C_3H_7 = CH_3 + C_2H_4 \qquad (3)$$

the propylene must be formed by a reaction involving oxygen. There can be little doubt that this reaction is 1 above.

It is, however, clear that the results reported by the authors cannot be explained on the basis of the reactions 1 and 2 only: the deuteropropanes $CH_3CD_2CH_3$ and $CD_3CH_2CD_3$, for example, would necessarily form water or hydrogen peroxide containing exactly equal amounts of H and D. It therefore appears that the results obtained must arise from the particularly selective attack of the radicals OH and HO_2 on the products of the initial reaction which offer a much greater choice of CH and CD bonds. It, therefore, appears most unlikely that the authors have, in fact, determined the relative rates of attack of radicals at different points in the propane molecule.

A. R. Ubbelohde (London): It seems to be desirable to arrive at more concrete ideas about 'clean' and 'dirty' surfaces, in order that these ideas in Szabó's paper can be tested by experiment. For example, when a glass surface is 'cleaned' by treatment with hydrofluoric acid, does this serve to convert the hydroxyl groups, or oxygen bridges attached to the glass network, into fluoride groups, or does it remove chemi-absorbed metal atoms, or what? In a study of the chlorination of hydrocarbons which has problems parallel to those in oxidation, we were recently able to show that changes in the surface produced by reaction were remarkably permanent. Starting with a surface 'cleaned' with hot nitrating mixture, the progress of reaction converted this into a stabilized surface which could be washed or treated in various ways and still give very reproducible behaviour. Only treatment with gaseous oxygen at fairly high temperatures or with hot alcoholic potash restored the original activity, making it likely that 'stabilization' in this instance involved methylation of free hydroxyl or labile oxygen bridges attached to the glass network. Can changes of similar permanence be stabilized in oxidation reactions?

* Knox, J. H., Smith, R. F. and Trotman-Dickenson, A. F. *J. Amer. chem. Soc.* 77 (1955) 2629.
† — — — *Chem. and Ind.* (1955) 1631.

Z. G. Szabó (Szeged): I have always emphasized that the activation energy calculated from the temperature coefficient of the running-up time is an approximate value. As we cannot measure directly the activation energy of the primary step we must use another quantity. According to a vigorous criticism this proved the best approach to the activation energy of the primary step*.

In answer to the remark of Voevodsky I would say that it is extremely difficult to draw conclusions concerning the wall effect from experiments carried out under different conditions. The generally accepted view that treating the wall with hydrofluoric acid favours the chain initiation leads to some discrepancies in the uniform interpretation of the experimental results. I do not know the state of the wall in Voevodsky's investigations and can only state that, from our experiments, the conclusion mentioned in my paper was to be drawn. Just the S/V ratio has led to the establishment of this conclusion.

As to his second remark: The C–H bond dissociation energies in propane and *iso*butane are not only calculated by my method but also found experimentally and are in the line of the hydrogen abstraction probability given by Rice (*cf.* also the paper presented by Minkoff in this Symposium). I think that there must be some mistake on this point.

In answer to the remarks of Ubbelohde, 'clean' surface means, in our experiments, a reaction vessel connected with a quartz manometer, separated from other parts of the apparatus by Bodenstein all-glass valves, which secure a good separation without traces of grease, and pumped out to high vacuum by means of a mercury diffusion pump for many days (not less than 2 or 3). The reaction vessel was previously washed with either chromic or hydrofluoric acids and thereafter rinsed thoroughly by distilled water. A vessel prepared in this way represented the initial stage which was altered in the course of subsequent experiments. The experimental substances have been purified by low-temperature distillation in several runs (at least 5 or 6). This means that the alteration of the surface can originate only from the molecules of the reaction mixture adsorbed on the surface. The oxidation experiments carried out under such circumstances have shown that the influence of the wall must be attributed to the breaking of chains. Of course, other reactions such as chlorinations may show a wall effect at the initiation step too. This was demonstrated in the experiments concerning the thermal formation of hydrochloric acid and carried out under the same conditions in Bodenstein's Institute in 1938 (Kornfeld and Khodsharian).

* *Cf.* Szabó, Z. G. and Gál, D. *Combustion and Flame* 1 (1957) 404.

The paper of Burt, Cullis, Larsen and Minkoff is an interesting one and proves not only that the attack in hydrocarbon oxidation happens in positions of decreasing bond strength, but it proves also that steric (i.e. statistical) points of view are not dominating in the process. Each part of the propane molecule is equally open to attack.

Regarding the remark of Walsh, I should like to note that the point of attack in the later stages of a chain reaction should also be governed by the same rule.

The postulate, in the paper of Skirrow and Tipper, that the formation of CO and CO_2 originates from the intermediately formed aldehydes seems to me to be strongly supported by our investigations (till now unpublished) that the corresponding acids themselves can be oxidized only at much higher temperatures than those at which the hydrocarbon oxidations are running down, and are always preceded by a heterogeneous decomposition. If the oxidation of a hydrocarbon produces some acid this happens at the decomposition of the peracids formed from aldehydes. Such a decomposition, however, can take place only under very favourable fuel conditions.

As regards the paper by Fabian and Bryce, the very good agreement between the measured and theoretically calculated values of the kinetic parameters proves very convincingly that the hydrogen abstraction process by an oxygen molecule may proceed homogeneously still under such experimental conditions where a wall effect would be, otherwise, very probable. To the remark of the authors that HO_2 is considerably more sensitive to reaction at surfaces than most non-oxygen containing hydrocarbon radicals, I would like to add that the coating by KCl, as well as other salts, does not influence the decomposition of ethane or of such substances in which no oxygen occurs. This means, in turn, that the coating destroys the oxygen containing radicals, especially the HO_2.

The detailed kinetic study of the oxidation of methane by Enikolopylan seems to settle to a great extent the problems of this reaction. I was very glad to see that in his reaction scheme no wall effect occurs at the initiating, only at the termination, reaction. This is in agreement with the point of view of the paper I have presented at this Symposium. As to the elementary reactions of the scheme I would like to remark that the wall destruction of the radical HO_2 should also be considered, further that the decomposition of hydrogen peroxide may govern the mechanism as well.

C. F. H. Tipper (Liverpool): As regards the paper by Szabó, I think that it is somewhat dangerous to deduce the activation energies of the initiation reactions of hydrocarbon slow combustion from the temperature coefficients of the induction period deduced from the pressure-time curve. For

instance McGowan and myself* have found that the overall activation energy of the reciprocal of the induction period in the oxidation of *cyclo*pentane by the static method is about 18 kcals mole^{-1}. This can hardly be the activation energy of the reaction

$$C_5H_{10} + O_2 = C_5H_9 + HO_2$$

in the gas phase.

H. S. Glick (Pasadena): The question has been raised by Windsor as to whether the difference between the final reaction temperature, T_f, and the product temperature, T_z, can be explained on the basis of non-uniform reaction times. It should be pointed out that the single pulse shock-tube technique employed in the present study actually minimizes non-uniform reaction times by employing reflected shocks to heat the reactant gas to reaction conditions. This feature of the technique is explained in detail in earlier papers where this method was used to determine the kinetic of nitric oxide formation.

G. Skirrow (Liverpool): Although the scheme suggested by Tipper and myself deals specifically with the production of carbon monoxide, carbon dioxide and carboxylic acids, it may be noted that it has the additional merit of offering an explanation of the frequently reported negative temperature coefficient of the rate of oxidation of hydrocarbons. Thus the reactions suggested in our paper which lead to the production of carbon dioxide and carboxylic acid radicals are essentially branching reactions whereas the reaction leading to carbon monoxide formation may be regarded as non-branching. Increase of temperature will, as pointed out in our paper, lead to increased CO/CO_2 ratios but will also result in decreased branching and a consequent falling off of reaction rate. In many systems branching may occur by breakdown of hydro-peroxides, but in those systems in which aldehydes are known to function as degenerately branching intermediates it may be that the change of CO/CO_2 ratio with temperature and a negative coefficient of rate have a common origin.

G. J. Minkoff (London): Walsh has stated, when opening the discussion, that we do not propose any branching reactions. In fact, our communication is concerned with the point of attack, and not with a complete discussion of the mechanism of the oxidation of propane. We therefore quoted only that part of Satterfield's mechanism which was directly relevant to our theme.

The remainder of his comments could be discussed at length. For the sake of brevity, however, we shall merely emphasize the point he has apparently overlooked. This, as stated in the paper, consists of the observation of H/D ratios, with five separate deuterated propanes, which differ markedly from those predicted for the mechanism in which both H atoms appear in the water analysed for its D content. Speculation as to the mechanism of the removal of the second H atom will be deferred until the conclusion of a detailed experimental study. We may, nevertheless, draw attention to the results presented at this Symposium which show that, at these high temperatures, radicals such as CH_3 cannot be regarded as being instantaneously removed by reaction with O_2.

The comments of Voevodsky were concerned with the nature of the products, and with the effect of the presence of alkyl radicals. The experimental evidence regarding the preponderance of propylene in the oxidation products above the region of the negative temperature coefficient has been published by Satterfield* and is supported by the work of Ferguson, Knox and ourselves. There is no disagreement with the low-temperature observations of Stern and Polyak. As for the propyl radicals 'randomizing' the labelled positions, it is not likely that this will be an important effect because: (*a*) the majority of such radicals will have been formed by abstraction at the more reactive carbon; and (*b*) they will attack fresh molecules in the most reactive positions. Thus the eventual indication of the point of attack will not be seriously affected.

Finally, there is Knox's query, based on the propylene formed and the initial correlation between the oxygen content. Without a detailed knowledge of the subsequent reactions, a definite explanation cannot be given. Qualitatively, two cases may be considered. In the first, no sensitized decomposition is assumed to take place. It can then be shown that the propylene formed could readily be linked to the number of oxygen molecules present initially. Secondly, if sensitized decomposition does occur, the two quantities must still be mechanistically related, although the connection may be less obvious. The first case, however, seems the more probable.

INHIBITION OF OXIDATION REACTIONS

Papers 28, 29, 30, 31

N. P. W. Moore (London): In opening the discussion I propose to treat the four papers in what may turn out to be the inverse order of reactivity. Before dealing with the papers, I will make the following four points: (1) all four papers treat inhibition, but in different systems; (2) inhibition is in all cases a trace effect; (3) inhibition is only explicable on chain theory; and (4) hydrocarbons

* McGowan, I. R. and Tipper, C. F. H. *Proc. Roy. Soc. A* 246 (1958) 52.

* Satterfield, C. N. *Industr. Engng. Chem.* (*Industr.*) 46 (1954) 1002.

themselves also show a similar mode of inhibition; this recalls the work of Baldwin.

Turning now to the papers, first those of Waddington and of Cullis and Khokar, may I pause to congratulate and encourage Waddington, who has succeeded in carrying out an important piece of research as a schoolmaster. This is an important development, but it is not the first time that a major research contribution has been made in the laboratory of a school; shortly after the discovery of X-rays, Porter, in England, demonstrated the finding to his pupils.

The two papers on closed vessel inhibition studies demonstrate the stabilization of free radicals in the gas phase, which is clearly important to the mechanism of knock. Both papers have studied kinetics by pressure change and by the observation of limits, and it is timely to ask if it is not important to introduce other measurements, if possible of the concentrations of reactants and products, in a similar experiment.

The paper by Rosser, Wise and Miller is an entirely different study; inhibition is detected by the influence of halogens on the laminar flame speed of various mixtures. In introducing the discussion I urge that we should not discuss the validity of the flame speed measurements (which question we are considering in other sections), but that we should concentrate on the mechanism which is responsible for the inhibition. An important point is that these authors have considered at the same time variations in burning velocity, OH emission, temperature and reaction rate; the study is considerably more valuable for having simultaneous information on these quantities. May we, however, ask if observations were made at the same time of the effect on propagation limits.

Finally I turn to the paper by Walsh and his colleagues at the University of St. Andrews, who claim to tie up the evidence relating to metallic anti-knocks; by way of discussion I propose to untie their evidence, but with the kindest of intentions. They are to be congratulated in that they have attempted an overall statement of the mechanism and also in that they have not lacked the courage to test their theory in an engine. I think we can best introduce discussion on their paper by suggesting related work; it is important that we should consider side by side with these proposals evidence that appeared some years ago from studies at the Ethyl Corporation concerning the decomposition of tetra-ethyl lead and the kinetics of the related processes. I refer to the work of Rifkin and Walcutt; perhaps we may draw out Lovell and Griffiths on this work.

Norrish and Erhard have, I know, strong views on the subject of this paper, which they will, no doubt, put forward in succeeding contributions. The discovery of the importance of hydrogen peroxide is referred to; this would also seem to have been clear from the earlier work of Cohen, Sturgis and Pahnke, in which the relative importance of organic and hydrogen peroxides was deduced from a motored engine experiment. It is also noteworthy that the importance of hydrogen peroxide was suspected by Sir Alfred Egerton and others in this City of Oxford as early as 1935.

The observations of spectral absorption at 3,000 Å, and below, in the earlier work of Rassweiler and Withrow is particularly interesting; it will, however, be valuable to hear from Gaydon if there is not another possible interpretation for this evidence. Concerning the evidence of cool flames in engines, we can, perhaps, draw out Ferguson from Washington, who recorded some observations on this subject some years ago: my own work has also touched on this aspect of the paper. The observation of a fog attributed to the decomposition of tetra-ethyl lead into PbO particles is a key in the argument; it is perhaps unfortunate that this experimental observation rests in unpublished work by Walsh. I think it is most important that this experiment be discussed in the open literature so that we can examine and if necessary repeat the experimental observation. I think it is important at this stage to mention that a fog during hydrocarbon oxidation in the absence of lead, was recorded some years ago by Friedlander and Grundberg, and quite independently by Vanpée in Belgium.

Let us finally list what appears to be still in doubt: We cannot be content that a theory of anti-knock action can rest wholly on vessel experiments, nor entirely on flash photolysis studies, since, as was stated, both methods involve conditions far removed from those in the engine. The vital question is to decide and to justify by further experimental work, ultimately in the engine, whether the mechanism involves gas phase or surface termination.

C. F. H. Tipper (*Liverpool*) commenting on the paper by Waddington: Although amines are moderately efficient anti-knocks in engines with hydrocarbon fuels, Bell and I* have found that addition of small amounts ($\sim$ 1 mm) of *o*-toluidine had very little effect on the slow combustion of methanol, *cyclo*propane, *n*-butane and *n*-hexane, in a static system at temperatures which varied from 255 to 444°C. However, at 300 to 400°C with diethyl- or di*iso*propyl-ether as the fuel, addition of the amine increased the time to the maximum rate considerably, and reduced p_{max} somewhat, the retarded reaction being complicated by irreproducible surface effects. Even if, as is suggested by Waddington, the amine oxidizes at these higher

* Bell, K. M. and Tipper, C. F. H. *Research, Lond.* 10 (1957) 121.

temperatures, it seems odd that the retarding effect was only noted with ethers, especially as it is not likely that the general mechanism of slow combustion varies from fuel to fuel.

J. H. Knox (Edinburgh): *Figure 2* of Waddington's paper shows the striking result that the addition of between 3·8 and 5·7 mm of methylamine to a mixture of 50 mm ether and 150 mm oxygen brings about a change from a branching chain reaction to a non-branching chain reaction. If, as is suggested, the role of the amine is to remove free radicals from active participation in the reaction chains this result is readily explained. The reaction of any chain propagating radical with a molecule of amine may be formally regarded as a chain termination reaction, and as such it will shorten the basic reaction chain (Knox, Paper 21). By the addition of sufficient amine the chain will be shortened to such an extent that it produces exactly one branch per chain, that is, each chain will simply regenerate itself but will not initiate any net additional chains. This critical condition corresponds to the cross-over point from branching to non-branching reaction.

If the radical which is removed by the amine is the $C_2H_5OC_2H_4$ radical, the basic chain length is determined by the rates of the two competing reactions:

Propagation

$$C_2H_5OC_2H_4 + O_2 \xrightarrow{k_p} C_2H_5OC_2H_4OO$$

Inhibition

$$C_2H_5OC_2H_4 + A \xrightarrow{k_{in}} \text{Inactive products}$$

Ignoring the normal chain termination reaction in face of chain termination by the amine, the chain length of the inhibited reaction is given by:

$$\nu = k_p[O_2]/k_{in}[A]$$

The cross-over point occurs at the particular $[O_2]/[A]$ ratio where ν is such that the chain produces exactly one new chain as a result of degenerate branching. The cross-over point will thus occur at the same $[O_2]/[A]$ ratio, irrespective of the ether concentration, [E].

If, however, the radical which reacts with the amine is the radical which normally attacks the ether (here assumed to be $C_2H_5OC_2H_4OO$), the chain length will be given by:

$$\nu' = k'_p[E]/k'_{in}[A]$$

Here the cross-over point will occur at a given [E]/[A] ratio and will be independent of the oxygen concentration. An investigation of the dependence of the cross-over point on mixture composition would thus give important information on the nature of the radical reacting with the amine, and indirectly as to the mode of action of the amine as an inhibitor.

Z. G. Szabó (Szeged): The papers presented by Waddington, by Khokar, as well as by Rosser are examples of the classical homogeneous chain catalysis. The results reported here have shown a more or less pronounced inhibiting effect. Now, I should like to draw attention to the fact that such homogeneous catalysts may have a double effect, i.e. the sense of the influence can change with the concentration of the influencing substance. An inhibition at greater concentration may change into catalysis at small concentration and vice versa. In a theory of these catalytic effects, which was presented at the Philadelphia Symposium two years ago, I was able to show that the influence may not be a simple increase in catalysis or in inhibition with an increase in the concentration of the influencing substance, but that also there may be a maximum catalytic effect after which increasing concentration of the influencing substance leads to a decrease in catalytic effect ending in an inhibition, or there may be a maximum inhibiting effect after which increasing concentration leads to decreased inhibition turning into catalysis. This last type was found by Hinshelwood and Staveley in reactions with nitric oxide.

Of course, the variation of the concentration of the influencing substance must be made very cautiously in the proximity of maximum or minimum catalysis.

D. J. Waddington (Wellington College): The comments made by Tipper on my paper are very interesting. In the present work, the temperature was lowered to just above the lower ignition limit for the diethyl ether–oxygen mixture in order that the amine inhibitors were not themselves destroyed by molecular oxygen. In Tipper's work, higher temperatures were used, and it is probable that the amines were destroyed by direct oxidation.

In the present work, there was poor reproducibility for over 100 runs; the conditioning of the reaction vessel seems to be an essential prerequisite in these investigations.

The suggestion by Knox can well be developed, and such tests should be relatively simple to make.

J. H. Burgoyne (London): Moore has suggested that the effect of halogen derivatives upon limits of inflammability might profitably be brought into the discussion, and has mentioned our work and that of Wolfhard on this subject. It has been found that in the presence of such additives as methyl bromide, both upper and lower limits of fuels are affected, so that the adiabatic flame temperature at the limit is very substantially increased. Inert diluents, such as nitrogen or carbon dioxide, have, of course, no such effect. Similarly, the limit flame temperatures for the halogen derivatives themselves, for example trichlorethylene, are abnormally high compared with fuels containing only carbon, hydrogen and oxygen.

R. G. W. Norrish (Cambridge): Walsh refutes our experiments on anti-knock action on the grounds that they are unrealistic in relation to the conditions obtained in the engine cylinder: I will show that this is far from the case. The criticism could, with more point, be levelled at his own experiments, for he bases his conclusion on the study of the slow oxidation of methane in vessels with PbO-coated walls—surely about as far from the conditions obtaining in the engine cylinder as one could devise.

The point at issue is whether PbO operates as an anti-knock in the form of a particulate smoke, as is contended by Walsh, or, as we believe, in the gas phase as a vapour. The explosion engendered by flash photolysis is a homogeneous one occurring nearly simultaneously throughout the vessel; it therefore simulates the homogeneity of detonation. In our experiments we have flashed mixtures of a normal aliphatic hydrocarbon, amyl nitrite, and oxygen; the nitrite group of the amyl nitrite acts as a photosensitizer, absorbing radiant energy, raising the temperature, and dissociating to give initial centres (O atoms) for the development of the reaction.

Our results with *n*-heptane show that the spectrum of amyl nitrite disappears immediately on flashing. In the absence of tetra-ethyl lead, explosion occurs 200 μsec after the flash, as shown by the first appearance of the OH absorption spectrum; with added TEL, the induction period is extended to 630 μsec, and during this period there is a steady growth of the absorption spectrum of PbO, reaching its maximum at about the point of explosion, at which instant it is converted to atomic lead by the reducing gases (CO, etc.) produced by the flame. There is no question that under the conditions of our experiment the PbO is steadily produced throughout the induction period in the gas phase as a vapour, for otherwise one should not see its absorption spectrum; there is no light scattering due to smoke. That the PbO does not result from the photolysis of the amyl nitrite, as suggested by Walsh, is shown by the fact that the nitrite is destroyed instantaneously (less than 20 μsec) by the flash, while the PbO develops slowly over 600 μsec.

The initial temperature in our tube immediately after the flash is about 400°C; it rises in times of the order of 1 or 2 msec to 800–900°C as a result of pre-flame reactions; immediately after this the mixture explodes. This is about the same as occurs in the 10–1 compression engine of, say, a racing car at 10,000 rev/min during the latter half of the stroke to top-dead-centre—time 1 msec, temperature rise about 400 to 850°C. During this time the TEL is decomposed unimolecularly (Rifkin and Walcutt) and oxidized to PbO. Our experiments show that under these conditions the PbO is formed in the gas phase; there can be no time to form smoke, and at 850°C the vapour pressure of PbO, *ca.* 0·25 mm, is ample to hold the whole of the change in the gaseous condition. The main difference in conditions is that the total pressure of the end gas in the engine is higher than in our case (though it is largely made up by nitrogen). The condition for the formation of PbO smoke in the engine cylinder would be more difficult than in our case, since less TEL is involved, and also the higher total pressures would hinder aggregation to form solid particles. Thus, since smoke is not formed under our conditions, it is still less likely that it will be formed in the engine. A claim to observe heterogeneity by light scattering without identification is no evidence.

We believe that the anti-knock action of TEL is twofold: first, it decomposes thermally and reacts with the oxygenated intermediates in the flame, so reducing the number of centres of autogeneration; secondly, the PbO so formed may react with chain centres as follows:

$$\mathrm{PbO + R = Pb + RO}$$
$$\mathrm{Pb + OH = PbOH}$$
$$\mathrm{PbOH + OH = PbO + H_2O}$$

the latter two reactions shortening the chains and reducing the rate of release of energy and thus the tendency to detonation. In this connection it is significant that in the ignition of benzene, TEL shows no effect; no PbO is formed; there is no effect on the induction period; there are no oxygenated precursors to the reaction of the type found with aliphatic hydrocarbons.

The anti-detonant action of TEL in our experiments is well shown in explosions of hexane, amyl nitrite and oxygen, with or without TEL, by the fact that, in our photographs, the peaks characteristic of the formation of shock waves are absent in the presence of TEL, and the induction period between flash and explosion is increased some threefold.

J. W. Linnett (Oxford): Recently J. C. Greaves, K. R. Jennings, M. Green, D. Schofield and I have produced oxygen and hydrogen atoms in a discharge tube and investigated their re-combination on surfaces. With oxygen atoms a large number of oxides has been studied, and it is found that, broadly speaking, the more 'acidic' surfaces are less active and the more 'basic' surfaces more active. With hydrogen atoms, washing a silica surface with ammonia increases its activity, while washing it with strong acid decreases its activity. These results are interesting in relation to the results of Walsh and his colleagues, since they run parallel to the activity they have found, and which they presume to be related to the destruction of hydrogen peroxide and HO_2.

S. T. Griffiths (Bletchley): I have been asked by N. P. W. Moore to report on the mechanism of anti-knock action of tetra-ethyl lead as indicated in engine experiments, in-so-far as this may throw some light on the controversial points of view of the Walsh and Norrish schools of thought.

I need not stress the difficulties involved in undertaking engine work in order to investigate reaction mechanisms *in situ*, since the system is very complex with respect to pressure, temperature and concentration of the reactants. It is not surprising, therefore, that differences of opinion occur when the results of 'all-glass' laboratory experiments are extrapolated to provide mechanisms under engine conditions.

We have investigated the decomposition of tetra-ethyl lead in a fired engine by a series of sampling experiments in the end-gas zone. This work closely parallels that of Rifkin and Walcutt (A.C.S. Division of Petroleum Chemistry, September 1955), who derived the following Arrhenius equation for the rate constant (k) for tetra-ethyl lead decomposition under motored engine conditions:

$$\log k = -4{\cdot}124\ 10^3/T + 7{\cdot}617$$

where k is in sec^{-1} and T in °K.

We have substituted the rate constants for tetra-ethyl lead decomposition obtained from our own experiments in the above expression, and have thus calculated end-gas temperatures under fired engine conditions. The end-gas temperatures obtained during tetra-ethyl lead decomposition justify the contention that PbO particles can exist under engine conditions.

The second point that I wish to make concerns an extremely interesting implication arising from the paper by Walsh and his colleagues. The authors have designated PbO as a category 2 surface, and as such the destruction of the active entity HO_2 is diffusion controlled. Accepting Walsh's PbO fog theory for engine operation, one may suppose that the diffusion path of HO_2 to a PbO particle is tremendously reduced, and the overall destruction of HO_2 will be surface controlled. Under these conditions both HO_2 and H_2O_2 are destroyed by processes independent of diffusion rates. This suggests that if it were possible to render the PbO surface more active by some physical modification then an increase in overall effectiveness in the destruction of HO_2 and H_2O_2 would result.

It may well be for this type of argument that the effect of a metal oxide may be promoted by the addition of small quantities of a second metal oxide.

A. R. J. P. Ubbelohde (London), commenting on the paper by Walsh *et al.*, said: If the anti-knocks are acting as solid inhibitors with a definite crystal structure, then: (1) the co-operative effects in the crystal lattices lead to a different order of basicity or acidity from that established for isolated molecules; and (2) mixed oxides should be formed under certain conditions, when mixed anti-knocks are used. Because of the well known promoter action in solid catalysts whose crystal structure is disturbed by the inclusion of foreign atoms in solid solution, marked 'promoter action' should be observable, in some cases, with anti-knocks, if these act as fogs of solids in the engine.

Until there is definite evidence of these two characteristic differences between solid and gaseous catalysts, arguments for the action of anti-knocks as crystals lack some vital evidence.

PART II

SPECTROSCOPY OF FLAMES

EMISSION SPECTRA FROM MIXTURES OF ATOMIC NITROGEN AND ORGANIC SUBSTANCES

N. H. KIESS and H. P. BROIDA

INTRODUCTION

Reactions at low pressures of the gaseous discharge products of nitrogen with organic compounds were studied first by Strutt (later Lord Rayleigh)[1,2,3], and hydrogen cyanide was found to be the main product of these reactions. More recently, Winkler and his collaborators[4,5] have made extensive chemical studies of such reactions. They concluded from a careful examination of the experimental evidence that the major reactive species in the discharge products is atomic nitrogen in its ground state (^4S). Some evidence also was given for the presence of another active species, perhaps vibrationally excited molecular nitrogen[5].

These reactions are accompanied by bright 'lilac' flames. However, the brightness and the colour change considerably with changes in pressure and in chemical composition of the reacting substance. Strutt and Fowler[6] obtained the spectra of these flames and showed that the predominant emission was due to the red ($A^2\Pi$-$X^2\Sigma$) and the violet ($B^2\Sigma$-$X^2\Sigma$) systems of CN. They also showed that this spectrum differed in several respects from CN emission observed in the carbon arc. Later Herzberg[7], Beutler and Fred[8], and Wager[9] showed that intensity anomalies in the violet bands originating in the $v' = 0$ level of the $B^2\Sigma$ state are caused by perturbations with the $v' = 10$ level of the $A^2\Pi$ state. Jennings and Linnett[10] recently have made a survey of spectra emitted when organic substances are introduced downstream from a discharge through nitrogen.

The present study was undertaken to determine the effects of pressure and of organic material on the electronic, the vibrational, and the rotational intensity distributions in the CN emission from these 'active' nitrogen flames. The relative intensity of CH emission also has been measured.

EXPERIMENTAL

The nitrogen afterglow was produced by passing nitrogen through an electrodeless discharge maintained by a 2,450 megacycle magnetron power supply (rated at 125 W). *Figure 1* is a sketch of the apparatus: it was made of Pyrex glass except for a 10 cm section of quartz in the discharge region. The discharge products contained about 1 per cent nitrogen atoms, as determined by mass spectroscopic measurements[11]. Organic materials were introduced 35 cm downstream from the discharge in a reaction chamber 25 mm in diameter. Flames were formed immediately on contact of the afterglow with the organic material and often extended the 20 cm length of the tube. The emission was observed by viewing the flame end-on

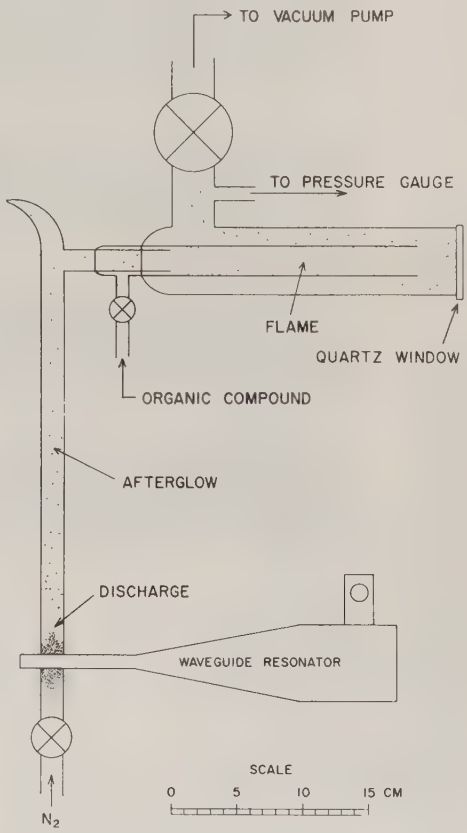

Figure 1. The discharge and atomic 'flame' apparatus

through a quartz window sealed at the end of the tube. Other types of burners, or methods of mixing the gases, were tried. The one selected gave the shortest exposure times over a wide range of burning conditions.

Special 'pre-purified' nitrogen containing less than 0·01 per cent impurities was used. Gaseous

and liquid organic materials were of the purest grade obtainable from commercial sources. Flow rates of nitrogen varied from 1 to 50 cm^3/sec (n.t.p.) and were measured with conventional float type flow meters. Flow rates of organic gases were measured with similar meters while flow rates from liquids were estimated from the rate of loss of the liquid. Although the flow rate ratios of nitrogen to organic substances were varied by several orders of magnitude, no appreciable effect was found on the relative intensity of spectral features due to this change. However, the brightness was affected and a flow rate ratio of nitrogen to organic substance of about 100 gave the brightest flame. This ratio indicates that the brightest flames are obtained when there are as many reacting organic molecules as there are nitrogen atoms. Pressures were varied from 0·1 to 40 mm Hg; pressure measurements were made with a sensitive Bourdon type manometer.

Spectra were recorded photographically by means of medium glass and medium quartz prism spectrographs ($f/10$) and photoelectrically by means of a grating monochromator[17]. Exposure times ranged from a few seconds to a few hours. Only the brightest flames were recorded with the high resolution equipment.

RESULTS

Fuel effect

Twenty-nine organic compounds were burned in

TABLE 1—Special Intensities in Various Atomic Nitrogen Flames

Compound	CN (0,0) $B^2\Sigma$–$X^2\Sigma$ *Pressure,* mm Hg				CN (10,4) $A^2\Pi$–$X^2\Sigma$ *Pressure,* mm Hg				CH (0,0) $A^2\Delta$–$X^2\Pi$ *Pressure,* mm Hg			CN ratio 9,4/4,0 $A^2\Pi$–$X^2\Sigma$ *Pressure,* mm Hg			
	1	4	10	30	1	4	10	30	1	4	10	1	4	10	30
CH_4		5				<1				1					
CH_3Cl		70	70			7	2			2					
CH_2Cl_2	500	500	500		50	50	25		7	2	1	2·0	1·5	1·0	
$CHCl_3$	500	1,000	1,000	1000	100	100	25	7				2·0	1·5		0·5
CCl_4	70	1,000	1,000		7	100	50						1·5	1·0	
CHF_3		50				5									
$CHBr_3$		200				20							4		
CH_2I_2	10				1				<1						
$CHClF_2$	500	1,000	1,000		100	100	25						1·0	0·7	
CCl_2F_2		500				50									
$CClF_3$		50				5									
C_2H_6		10				1				2					
CH_2ClCH_2Cl		200				20				4					
$C_2Cl_3F_3$		500				50							0·7		
CH_3CHF_2		100	100			10	2			7	1				
CH_3CH_2Br		20	10			2	1			<1	<1				
CH_2BrCH_2Br		70				5				<1					
CH_3CH_2I		40				2				7					
C_2H_4		20				2				2					
$CHClCHCl$		100											1·5		
$CHClCCl_2$		500											1·5		
CCl_2CCl_2		500											1·5		
C_2H_2		500	200			50	5			4	<1				
CH_2CHCH_3		30				3				7					
$CH_2CH_2CH_2$		10				1				2					
$CH_3CH_2CH_3$		10				1				2					
$CH_2C(CH_3)CH_3$		30				3				7					
$CH_3(CH_2)_2CH_3$		20				2				2					
$(C_2H_5)_2O$		10				<1				1					
CO		30				2									

order to ascertain the effect of chemical composition on the observed spectra. A summary of the spectral intensity measurements is given in Table 1, Several other compounds were used for which spectra were not obtained. With estimates of brightness on the scale of column 2 of Table 1, these are: CH_3CCl_3 (500), C_2ClF_3 (300), CH_3CClCH_2 (100), and C_5H_5N (10). The first column of the table gives the chemical formula of the compound used. Column 2 gives an estimate of the brightness of the various flames at different pressures as determined by the relative exposure times to obtain the 0,0 band of the violet ($B^2\Sigma$–$X^2\Sigma$) transition of CN. The brightest flame, rated at 1,000, just gave this band with an exposure of 4 sec on a 103a-G Eastman plate with the glass spectrograph. Column 3 lists the relative brightness of the red ($A^2\Pi$-$X^2\Sigma$) transition of CN as obtained by comparison of the 10,4 band with the violet system on a 103a-G Eastman plate taken with the glass spectrograph. CH intensities are given in column 4. Since there is a marked change in vibrational distribution of the red system, the fifth column gives a measure of this change for some compounds by giving the ratio of intensities of the 9,4 vibrational transition to the 4,0 transition. In general, hydrocarbons gave weaker flames than halogen-substituted hydrocarbons. Brightest flames were obtained from compounds containing chlorine. The chemical composition of the hydrocarbon had a strong effect on the flame intensity as well as on the relative intensities of the red and violet CN systems. Hydrocarbons with a high ratio of hydrogen to carbon atoms produced weak flames. Thus, the flame of C_2H_2 was bright, that of C_2H_4 faint, and that of CH_4 very faint.

The vibrational distribution of the red CN system showed a rather high vibrational 'temperature' for all hydrocarbons. However, in the halogen substituted hydrocarbons the vibrational 'temperature' was strongly dependent on the particular halogen. At a constant pressure the vibrational 'temperature' varied with halogen substitution from 'cool' to 'hot' as follows; fluorine compounds, chlorine compounds, hydrocarbons, bromine compounds, and iodine compounds. This effect is illustrated in *Figure 2* which compares the 'hot' flame of $CHBr_3$ (*Figure 2a*) with the cooler flame of $CHCl_3$ (*Figure 2c*). Within one group of halogen-substituted hydrocarbons there was little difference in the vibrational distribution. For

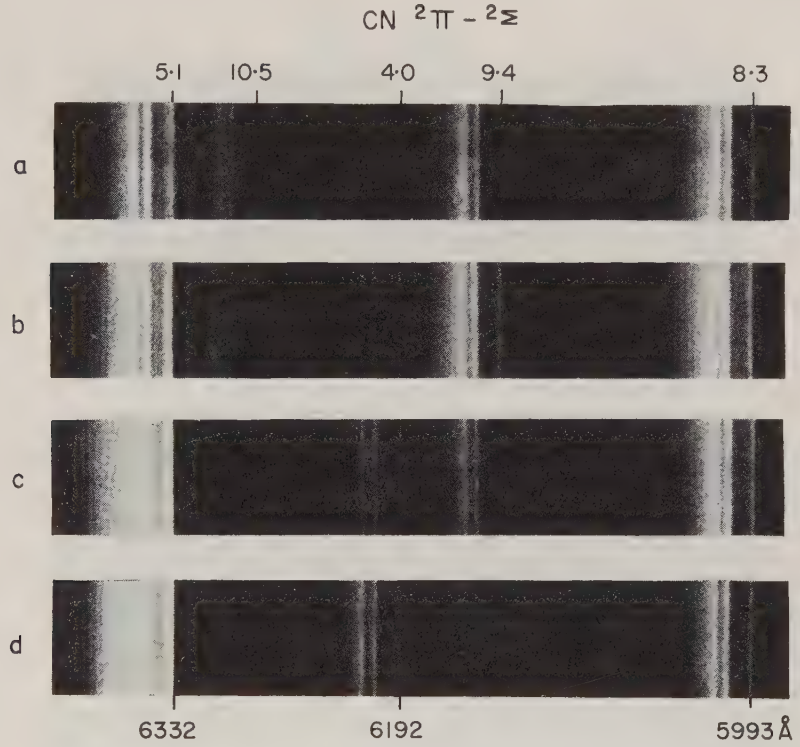

Figure 2. Spectra of part of the red CN ($A^2\Pi$–$X^2\Sigma$) *system in atomic nitrogen 'flames' obtained with the glass prism spectrograph on III-F (3) Eastman Kodak plates*
(*a*) $CHBr_3$ *at* 4 mm; 5 min *exposure;* (*b*) $CHCl_3$ *at* 1 mm; 1 min *exposure;* (*c*) $CHCl_3$ *at* 4 mm; 30 sec *exposure;* (*d*) $CHCl_3$ *at* 30 mm; 5 min *exposure*

example, although the flame of CCl_2CCl_2 was much brighter than that of CHClCHCl it had nearly the same vibrational distribution.

The violet system of CN also showed changes of vibrational distribution with different organic materials. The 'tail' bands were observed in substituted as well as non-substituted hydrocarbons. A high vibrational 'temperature' was observed in bromine- and iodine-substituted hydrocarbons, and in some chlorine- and fluorine-substituted hydrocarbons as well. To some extent, vibrational 'temperature' in the violet system was high when it was high in the red system.

Pressure effect

Brightest flames occurred at pressures between 3 and 10 mm Hg. This was also the pressure range in which the brightest 'active' nitrogen afterglows occurred. At low pressures the red CN system was more intense than the violet system while at high pressure the violet system was more intense. In $CHCl_3$ flames the ratio of intensity in the red to the violet system changed by a factor of 8 between 30 mm and 1 mm Hg.

Pressure also had a large effect on the vibrational intensity distributions. In particular, with decreasing pressure the vibrational 'temperature' of

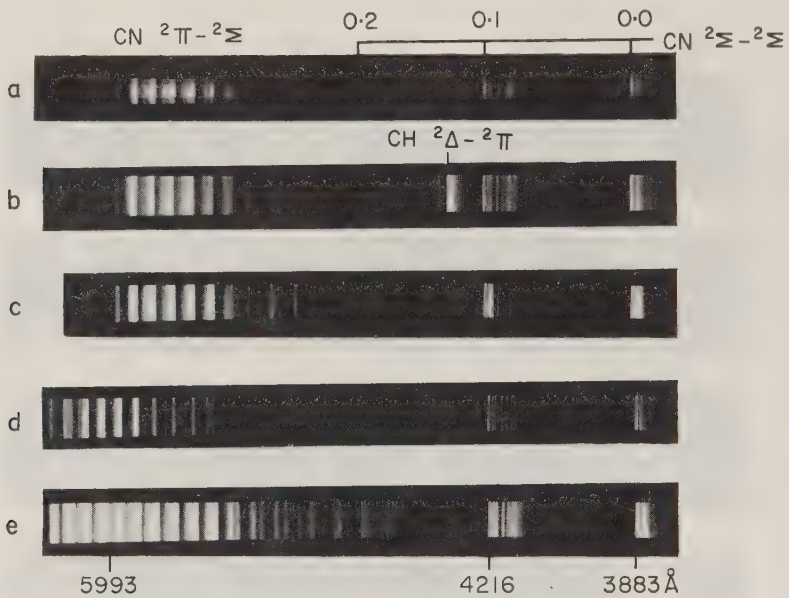

Figure 3. Spectra of atomic nitrogen 'flames' obtained with the glass prism spectrograph

(*a*) C_2H_2 *at* 4 mm; 2 min *exposure*; 103a–G *plate*; (*b*) $CH_2C(CH_3)CH_3$ *at* 4 mm; 30 min *exposure*; 103a–G *plate*; (*c*) $CHCl_3$ *at* 4 mm; 2 min *exposure*; 103a–G *plate*; (*d*) $CHBr_3$ *at* 4 mm; 1 min *exposure*; 103a–B *plate*; (*e*) $CHBr_3$ *at* 4 mm; 4 min *exposure*; 103a–B *plate*

Although CN was always the most prominent feature of the spectra of these flames, the CH band ($A^2\Delta$–$X^2\Pi$) at 4,315 Å was strong under conditions of large hydrogen to carbon atom ratio. Thus, the spectrum of $CH_2C(CH_3)CH_3$ in *Figure 3* shows stronger CH than that of C_2H_2. A trace of the $^2\Sigma^-$–$^2\Pi$ transition of CH at 3,872 Å was observed in a long exposure of the $CH_2C(CH_3)CH_3$ flame. NH($^3\Pi$–$^3\Sigma$) at 3,360 Å usually followed the CH emission, being stronger with increasing hydrogen to carbon ratio. C_2 bands (Swan system at 5,165 Å) were usually masked by strong CN emission; we found them only in C_2H_2 flames at high pressure (10 mm Hg). Small oxygen impurities in the nitrogen greatly enhanced both CH and C_2 emission.

the red system greatly increased. This effect is illustrated in *Figure 2*, which shows part of the red system for three pressures in flames with $CHCl_3$. The intensity ratio of the 9,4 band to the 4,0 band changes from 0·5 at 30 mm to 2·0 at 1 mm Hg. A similar temperature effect was found in the 1,0 and 2,1 bands at 9,198·1 Å and 9,392·5 Å respectively. A 15 minute exposure on a hypersensitized I-M Eastman plate was sufficient to record the two bands. At a pressure of 30 mm Hg, the 1,0 band is 3 times as intense as the 2,1 band while at 1 mm the two bands are of equal intensity.

Pressure also affected the violet system as shown in *Figure 4*. At high pressure the 'tail' bands are very much developed and the vibrational 'temperature' is increased. At low pressure the

violet system is very weak and shows mainly the perturbed rotational levels in the $v' = 0$ bands. CH intensity relative to the CN increases with decreasing pressure.

Rotational intensity distribution of the violet system

Herzberg[7] first noticed the rotational intensity anomalies shown in *Figure 5*. Beutler and Fred[8] suggested that the anomalously high intensity of levels $K' = 4, 7, 11$ and 15 is caused by interaction of these rotational levels of the $v' = 0$ level in the $B^2\Sigma$ state with corresponding rotation levels of the $v' = 10$ level[12] in the $A^2\Pi$ state. This suggestion was confirmed by Wager[9] with measurements on the 10,4 band of the red system. The perturbed levels are characterized by a small displacement (0·02 to 0·2 cm^{-1}) and the occurrence of an extra line. For non-equilibrium, the intensities of these lines are greater than the surrounding lines.

At higher pressures the intensity of the perturbed lines does not greatly exceed that expected for equilibrium. In fact at a pressure of 20 mm Hg the usual logarithm plot[13] (*Figure 7*) for determining the rotational temperature of the 0,0 band of the violet CN gives a reasonably good straight line and a 'temperature' of 315 $\pm$ 15°K. Under similar conditions Dixon and Nicholls[16] find a somewhat higher rotational 'temperature' in the red CN system. The rotational 'temperature' is in good agreement with the rotational 'temperature' found for the NO_β system in a similar source[14] as well as that estimated for CN by Birge[15] from plates of Strutt and Fowler[6]. This temperature is about that of the glass walls of the reaction vessel and indicates that the gas is near rotational equilibrium. However, with decreasing pressure there is no longer any sensible rotational 'temperature'. At the lowest pressures measured near 0·1 mm, the highly perturbed lines are as much as 6 times nearby lines. Moreover lines adjacent to the highly perturbed lines appear to be abnormally intense (*Figure 5*, top tracing). The doubling of lines for $K' > 15$ (*Figure 5*, bottom tracing) was pointed out by Wager[9]. We find that the intensity of the short wavelength component increases relatively with increasing pressure.

The anomalous rotational intensity distribution does not appear to depend upon the particular organic material used. However, detailed high resolution spectra such as those in *Figure 5* were obtained only for a few of the brighter flames. CH_2Cl_2 was found to be bright at pressures down to 0·1 mm and was used for this figure. Photographic spectra such as those in *Figure 3* show that at low pressure in flames of all compounds the CN

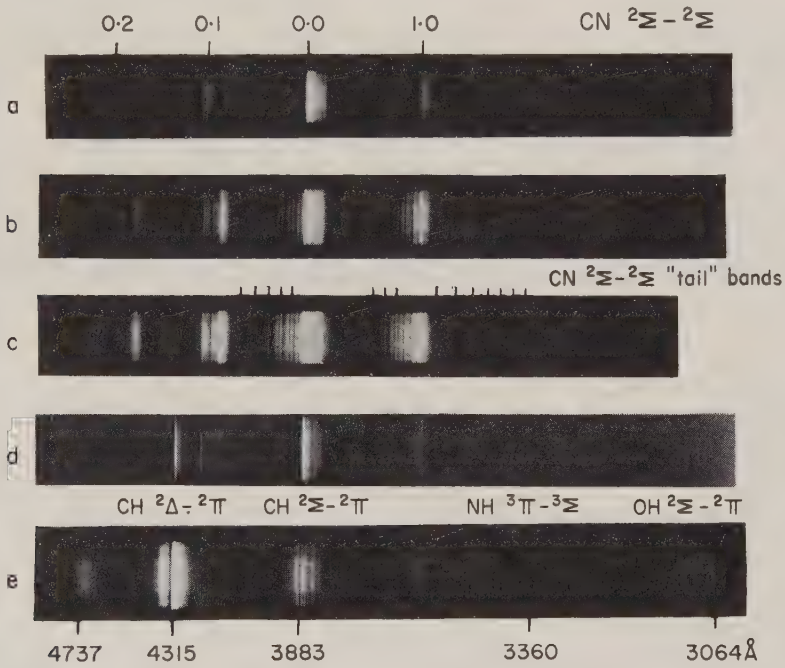

Figure 4. Spectra of atomic nitrogen 'flames' obtained with the quartz prism spectrograph

(*a*) CH_3CHF_2 *at* 5 mm; 30 sec *exposure;* 103–0 *plate;* (*b*) CH_3CHF_2 *at* 10 mm; 30 sec *exposure;* 103–0 *plate;* (*c*) CH_3CHF_2 *at* 10 mm; 2 min *exposure;* 103–0 *plate;* (*d*) $CH_2C(CH_3)CH_3$ (*isobutylene at* 3 mm); 2 min *exposure;* I–0 *plate;* (*e*) *Air through discharge and* C_2H_2 *at* 2·3 mm; 2 min *exposure;* 103a–0 *plate*

violet emission is caused predominantly by the perturbed lines.

To show that the rotational distribution is characteristic of atomic nitrogen flames, the intensity distribution of the afterglow flame was compared to that found in a low pressure discharge of benzene and nitrogen in an excess of argon. *Figure 6* shows these distributions and also are relatively much weaker in the discharge than in the atomic flame source of the same pressure.

SUMMARY AND CONCLUSIONS

(1) In flames of atomic nitrogen with organic molecules, at pressures near 1 mm Hg, the red system ($A^2\Pi$–$X^2\Sigma$) of CN is much brighter than the violet ($B^2\Sigma$–$X^2\Sigma$) system. With increasing

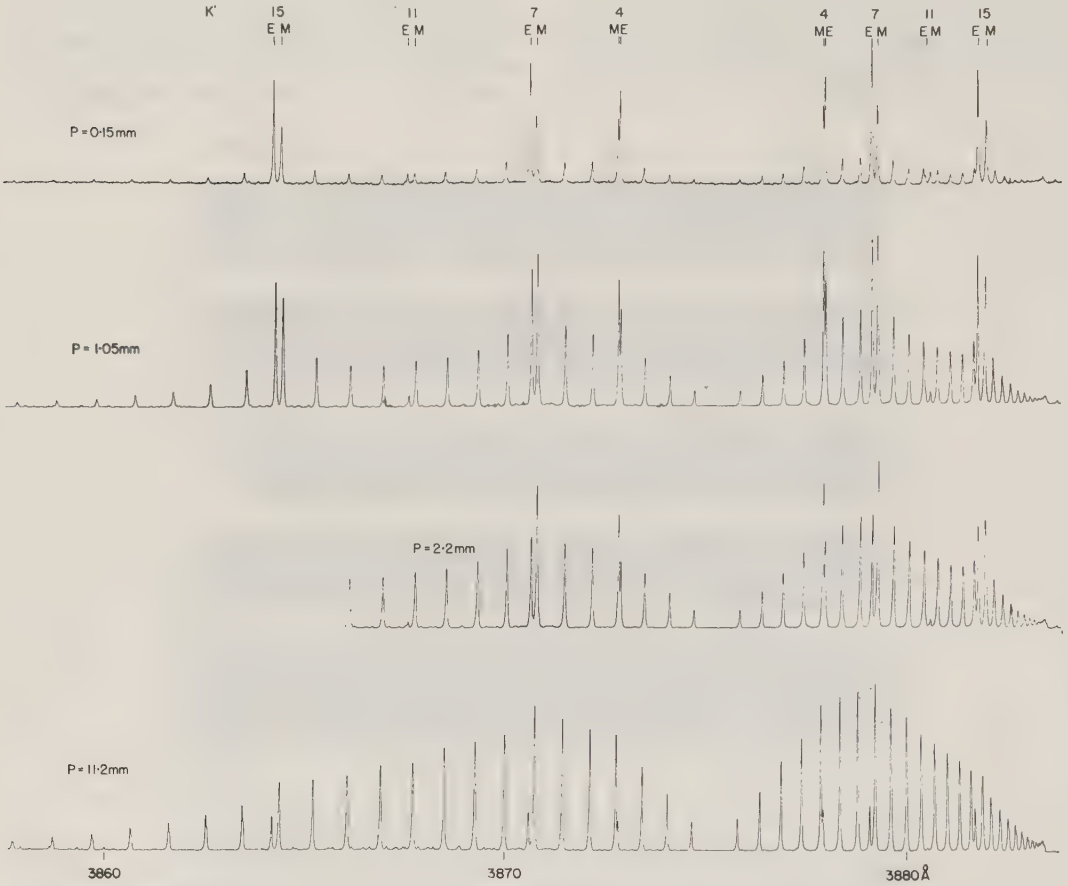

Figure 5. Spectral tracings of the 0,0 *band of the violet* ($B^2\Sigma$–$X^2\Sigma$) *system of* CN *in the atomic nitrogen 'flame' of* CH_2Cl_2 *obtained with the grating monochromator. Vertical displacements are directly proportional to intensity. The perturbed lines are marked M and the extra lines E*

that in the white mantle of an atmospheric acetylene–oxygen flame burning in air with about equal flow rates of acetylene and of oxygen. A comparison of these spectra shows that the discharge source has a slightly higher rotational 'temperature' than the afterglow and a considerably greater vibrational 'temperature'. It is interesting to note that the vibrational 'temperature' of the discharge is as great as or greater than that of the atmospheric pressure flame. The ratio of intensities of the 0,0 head at 3,883 Å and the 1,1 head at 3,872 Å (*Figure 6*) gives an indication of the vibrational 'temperature'. The perturbed and 'extra' lines

pressure the violet system increases rapidly in intensity as compared to the red system. In organic, atmospheric pressure flames containing nitrogen, the red system is very weak compared to the violet system. This indicates that: (*a*) CN is formed preferentially in the $A^2\Pi$ state at low pressures, and/or (*b*) electronically excited CN in the $A^2\Pi$ state is increasingly de-activated by collisions as the pressure is increased.

(2) The recent work of Dixon and Nicholls[16] on the red system of CN shows that at a pressure of 8 mm Hg with CCl_4 in 'active' nitrogen, bands arising from vibrational levels have intensities

in excess of those predicted by an equilibrium. This 'temperature' can be increased at a given pressure by substitution of heavier halogens (bromine or iodine). Moreover the vibrational 'temperature' can be increased by lowering the pressure. These effects substantiate the first hypothesis mentioned above, that CN is formed with an excess population in the $A^2\Pi$ state.

relative intensities of the two CN systems leads to the conclusion that at least two mechanisms are involved in the production of electronically excited CN. This conclusion is confirmed by the relative intensity increase of the perturbed and extra rotational lines in the violet system with decreasing pressure and by the weakening of these lines at the same pressure in a discharge source.

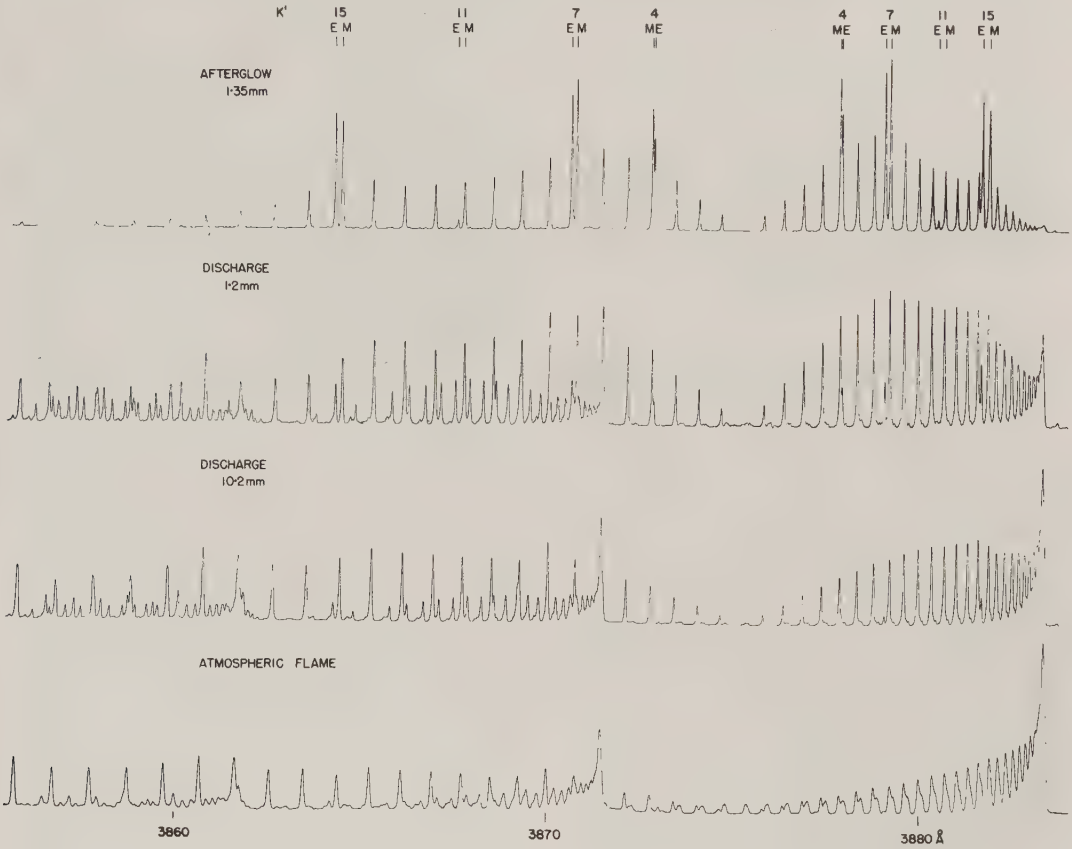

Figure 6. Comparison of the $\Delta v = 0$ sequence of the violet system of CN in the atomic nitrogen 'flame' of CH_2Cl_2, *a discharge through benzene and nitrogen in a large excess of argon, and a fuel-rich acetylene oxygen/flame at* 1 atm

(3) The vibrational distribution in the violet system is affected differently by pressure. The vibrational 'temperature' increases with increasing pressure.

(4) The rotational anomaly appears to be independent of the fuel. Therefore it is likely that the ratio of populations of the $v' = 10$ level of the $A^2\Pi$ state and the $v' = 0$ level of the $B^2\Sigma$ state is not greatly changed by a change of organic material. This result indicates that the effect of substituting heavier halogens is to decrease the population of the lower vibrational levels of the $A^2\Pi$ state, causing an apparent increase in vibrational 'temperature'.

The effect of pressure on the vibrational 'temperatures' and the effect of pressure on the

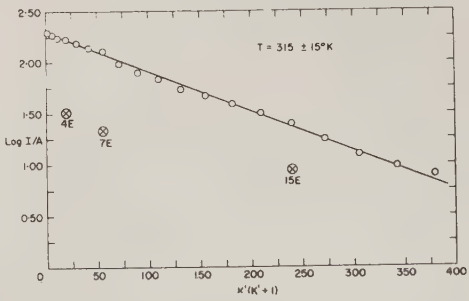

Figure 7. Rotational 'temperature' determination for atomic nitrogen 'flame' of CH_2Cl_2 *at a pressure of* 20 mm Hg. *Plot of the logarithm of the ratio of intensity (I) to the transition probability (A) as a function of $K'(K'+1)$, which is proportional to the energy of the upper level.* Log I/A *for the extra lines are marked E*

From the relative intensities of the $K' = 15$ lines at $p = 0{\cdot}15$ mm (in *Figure 5*) and the relative transition probabilities given by Wager[9] the ratio of the population of the $A^2\Pi$ to the $B^2\Sigma$ state is about 11. Apparently there are different mechanisms operating to produce the red $A^2\Pi$ state and the violet $B^2\Sigma$ state. However, the data presented in this paper are not sufficient for suggesting specific reactions leading to electronically excited CN.

It is a pleasure to acknowledge the assistance of Mr. J. deGroot in obtaining some of the preliminary spectra and of Mr. G. E. Beale for building and maintaining the apparatus.

We also wish to thank Professor G. H. Dieke, Johns Hopkins University, for kindly giving one of us (N.H.K.) permission to complete this work while holding a fellowship at his department.

REFERENCES

[1] Strutt, R. J. *Proc. Roy. Soc. Lond. A* 85 (1911) 219
[2] — *Proc. Roy. Soc. Lond. A* 88 (1913) 539
[3] — *Proc. Roy. Soc. Lond. A* 91 (1914) 303
[4] Evans, H. G. V. and Winkler, C. A. *Canad. J. Chem.* 34 (1956) 1217
[5] — Freeman, G. R. and Winkler, C. A. *Canad. J. Chem.* 34 (1956) 1271
[6] Strutt, R. J. and Fowler, A. *Proc. Roy. Soc. Lond. A* 86 (1911) 105
[7] Herzberg, G. *Z. Phys.* 52 (1929) 815
[8] Beutler, H. and Fred, M. *Phys. Rev.* 61 (1942) 107
[9] Wager, A. T. *Phys. Rev.* 64 (1943) 18
[10] Jennings, K. R. and Linnett, J. W. *Nature, Lond.* 180 (1957) 1272
[11] Herron, J. T., Franklin, J. L. and Dibeler, V. H. Private communication
[12] The numbering of vibration levels in the $A^2\Pi$ state was revised by Herzberg, G. and Phillips, J. G. *Astrophys. J.* 108 (1948) 163
[13] Broida, H. P. *Temperature, Its Measurement and Control in Science and Industry*. Vol. 2, p. 265. 1955. New York; Reinhold
[14] Barton, H. A., Jenkins, F. A. and Mulliken, R. S. *Phys. Rev.* 30 (1927) 175
[15] Birge, R. T. *Astrophys. J.* 55 (1922) 273
[16] Dixon, R. N. and Nicholls, R. W. *Canad. J. Phys.* 36 (1958) 127
[17] This monochromator was constructed by Leeds and Northrup Company and loaned to the National Bureau of Standards on a field trial basis

SPECTROPHOTOMETRIC STUDIES OF LAMINAR FLAMES—I THE DECAY OF RADICAL RADIATION

E. T. CHILD and K. WOHL

The spectrophotometric studies of the structure of laminar flame fronts which had been undertaken by Wohl and Welty[1] have been continued in various directions. The procedure consists in viewing a flat flame edge-wise by an instrument with a very small aperture, and moving the flame front perpendicularly to the optical axis. The flame was established above a water-cooled porous metal plate (which was theoretically treated[2] and used for quenching experiments[3]; see also Botha and Spalding[4]). This has the advantage over the flame described in reference 1 that it is more stable so that distances of 0·01 mm are meaningful and radiation gradients can for the first time be measured close to the flame front. Besides it is now possible to vary the pressure since the flame remains flat down to at least 1/3 atm.

The flame is not a free one since it loses heat to the porous plate. This, however, is turned to advantage: By varying the velocity with which the combustible mixture passes through the porous plate the maximum flame temperature can be varied at constant composition and pressure. On the other hand, flames of different concentration and pressure can be burned at such velocities that they reach the same maximum temperature so that the effects of isothermal variations can be studied. The addition of an inert gas to the combustible mixture would not be equivalent to cooling, neither with respect to the temperature profile nor, because of the increased chance for ternary collisions, with respect to chemical kinetics.

The flame front being horizontal, the spectrophotometer had to be turned 90 degrees so that the slits were in a horizontal position. Visible and ultraviolet radiation was measured by a quartz-enclosed photomultiplier tube. The mean thickness of the flame slice seen by the instrument was chosen as 0·13 mm in the range of steep radiation gradients and larger at larger distances from the flame front. The band peaks studied are shown in Table 1. The continuous background radiation which is probably caused by the process[5] CO + O and is designated by the symbol CO_2^* has been measured mostly only at the wavelength of 4,500 Å which is free from band spectra. Since the shape of the continuum in the post-combustion zone is very constant[1] the intensity at this wavelength is proportional to that of the whole continuum.

TABLE 1

Representative Wavelength

Emitter	*Transition*		*Wavelength*, Å	*Resolution*
CC*	$^3\Pi_g \rightarrow {}^3\Pi_u$,	(0, 1)	5,565	98 Å
CC	$^3\Pi_g \rightarrow {}^3\Pi_u$,	(0, 0)	5,163	80
CC*	$^3\Pi_g \rightarrow {}^3\Pi_u$,	(1, 0)	4,685	63
CO_2*	Continuum		4,500	57
CH	$^2\Delta \rightarrow {}^2\Pi$,	(0, 0)	4,310	51
CH*	$^2\Sigma \rightarrow {}^2\Pi$,	(0, 0)	3,895	39
CHO			3,503	29
OH	$^2\Sigma \rightarrow {}^2\Pi$,	(0, 0)	3,100	20

* These band peaks have only been studied at the flame points of maximum intensity.

The temperature profiles were determined from the intensity ratio of two water-vapour band peaks in the near infra-red (see Bernath *et al.*[6]). The flame width seen by the instrument had to be increased for these measurements to 0·75 mm. By comparison with the radiation from a standard tungsten-in-quartz lamp the absolute intensity of the signals in W/c.c. micron was obtained at all wavelengths. Since the distances from the porous plate which were of interest were nearly always smaller than 1/3 of the plate diameter the flow could be considered one-dimensional; the temperature profiles thus permitted us to convert distances quite accurately into time.

The flames studied and some of their characteristics are given in Table 2. It is seen that two flames have equal pressures and different temperatures, and two different pressures and equal temperatures. The latter conditions were achieved by a variation of the degree of cooling of the porous plate.

TABLE 2

Conditions for Decay Studies. Stoichiometric Butane–Air Flame. Burner Diameter 2 in.

Pressure, atm	1	1	1/3
Cold gas velocity, cm/sec (70°C)	30	10	30
Maximum temperature, °K	2,100	1,805	1,805
Temperature at place of maximum CH-radiation	~1,850	~1,630	~1,630
Distance of CH-radiation maximum from plate, msec	0·39	3·2	0·93
Distance of point of 99 per cent of temperature rise from plate, msec	3·1	6·2	4·5
msec per 1 mm travel at high temperature	~0·53	~1·8	~0·60

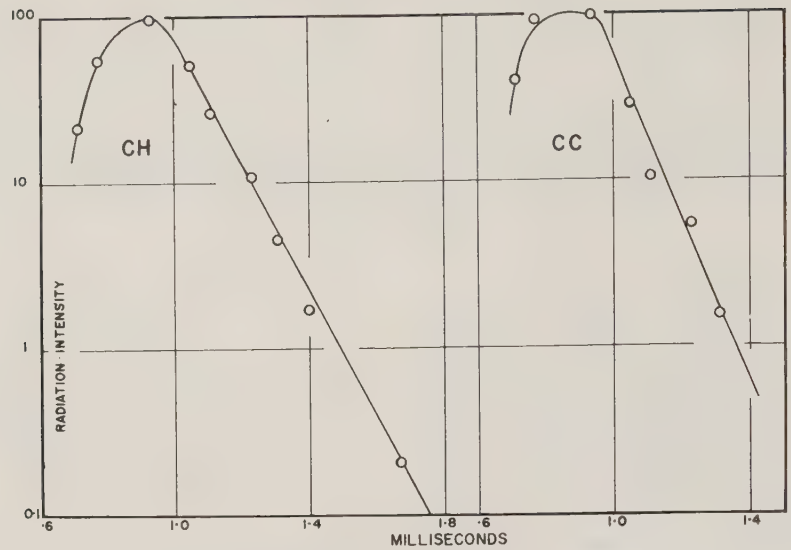

Figure 1. Traverse through flame front, CC-*radiation* (5,163 Å) *and* CH-*radiation* (4,130 Å). 3·13 per cent *butane,* 1/3 atm, 30 cm/sec *gas velocity at* 70°C

TABLE 3

Evaluation of the Rate of Decay of CH, CC and OH

Pressure, atm	*Cold gas velocity,* cm/sec		*Slope,* $msec^{-1}$	*Average temperature* °K	*Collision number*	*Correction factor*	*Activation energy* kcal/mole
1	30	*Figure 1,*	13·3	1,875	$6·7 \times 10^{8}$	$8·2 \times 10^{-5}$	5
1	10	Average of	3·0	1,650	$7·1 \times 10^{8}$	$9·2 \times 10^{-5}$	11
1/3	30	CH and CC, 1st order	3·9	1,650	$2·4 \times 10^{8}$	$9·2 \times 10^{-5}$	6
1	30	*Figure 3,* OH, 2nd order	71·3	2,100	$2·7 \times 10^{9}$	$2·9 \times 10^{-4}$	11

RADICALS CH AND CC

The curves of the CH- and CC-radiation are shown for one flame in *Figure 1.* In this and the following six figures the time zero is the one at which the gas emerges from the porous plate. The space resolution in *Figure 1* is much better than that achieved by Wohl and Welty[1]. The new curves terminate at about 1/100 or 1/1,000 of the maximum intensity I_{max}. The slow decay from 1/1,000 to 1/1,000,000 of I_{max} which had been reported[1] could not be reproduced in the new apparatus. The radiation curves of CH and CC are very similar to each other in all the three flames, and are of the same type in all of them. The straight lines on a semi-logarithmic plot indicate that the radiation decay is of the first order.

The interpretation of these curves is probably complex since they lie within what may be called the main reaction zone. Here the decrease of radiation is partly caused by a decrease of the rate of production of radicals, and of excited radicals above the level of thermal equilibrium with the fundamental state, and only partly by a disappearance of the created radicals—inclusive of those in the radiative state—through chemical processes.

It may, however, be pointed out that the order of magnitude of the decay rates of CH and CC fits the interpretation of decay by purely chemical processes: If the excitation of the two radicals is taken as thermal and the temperature as constant (there is a slight rise of temperature which is negligible; see Tables 2 and 3) the radiation

intensity is a measure of the total radical concentration. The first order then probably means that CH and CC disappear by reaction with H_2O and CO_2 both of which hardly change their concentration within the decay range. The negative straight slope in *Figure 1*, times 2·303, is the rate constant in $msec^{-1}$. It is largest at the high temperature as expected. The accuracy, however, is not sufficient to calculate an activation energy

TABLE 4
Time after Emerging from Porous Plate, msec

Pressure atm	*Cold gas velocity,* cm/sec	*Kink in* OH *curve*	*Drop to* 0·5% *of maximum intensity*	
			CH	CC
1	30	0·6	0·56	0·59
1	10	4·0	4·2	3·8
1/3	30	1·6	1·6	1·4

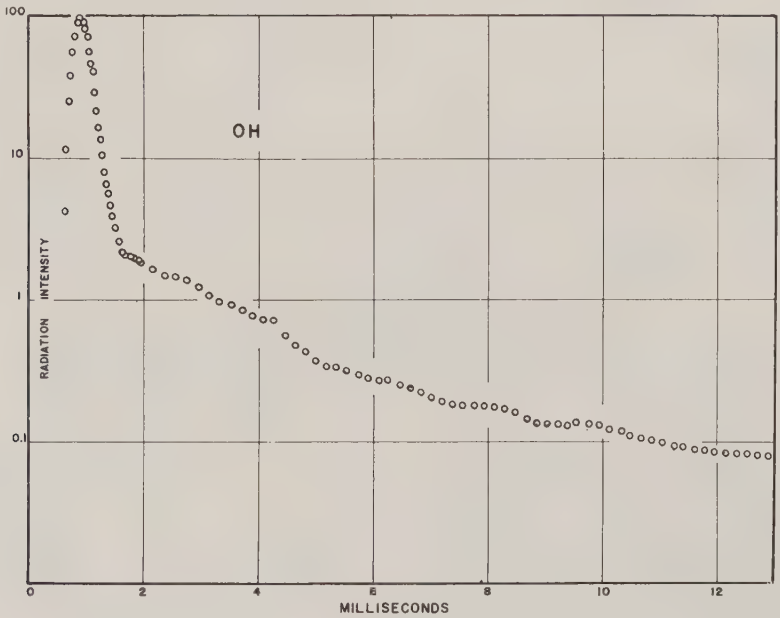

Figure 2. Traverse through flame front, OH-*radiation.* 3·13 per cent *butane,* 1/3 atm, 30 cm/sec

from the temperature dependence of the rate. In order to show that the rates have a plausible order of magnitude, activation energies have been calculated by an approximate version of the theory of absolute reaction rates, as shown in Table 3. The method of computation has been taken from Frost and Pearson[7]. The partial pressures of the reaction partner of the radicals have been estimated to be 30 per cent of the total pressures. The values of 5–11 kcal obtained for the activation energy are in a plausible range.

THE RADICAL OH

In all the three flames the decay of the OH-radiation is first rapid and slows down abruptly at a point very close to those at which the CH- and CC-radiations have dropped to 0·5 per cent of maximum value as can be seen from *Figure 2* and Table 4. This point terminates the main reaction zone in which the OH radiation is luminescent (i.e. above thermal) and in which OH may react rapidly with CH, CC, and possibly with fragments of fuel which are precursors of CH and CC.

Immediately following the kink in the radiation curve, the OH-decay at 1 atm becomes of the second order. This is shown for the hotter flame in *Figure 3* where the ratio of maximum intensity to intensity at the time t is plotted *versus* t. A straight line indicates a second order. The temperature in this range remains about constant; beyond it the rate shifts to lower order, and finally the temperature begins to drop. Here the radiation varies[1] as the equilibrium concentration of OH. Data on the flame of lower temperature and atmospheric pressure (Table 2) are also best fitted by a second order curve but are less accurate.

Beyond the kink in *Figure 2* thermal radiation and absence of significant OH-creating processes can safely be assumed. The second order of the OH-decay is then obviously due to a re-combination of two OH-radicals. The second order decay of OH-radiation may be expressed by the equation for the slope of the line in *Figure 3*

$$\frac{\Delta(H_{max}/H)}{\Delta t} = \frac{\Delta\left(\frac{c_{max}}{c}\right)}{\Delta t} = c_{max}k$$

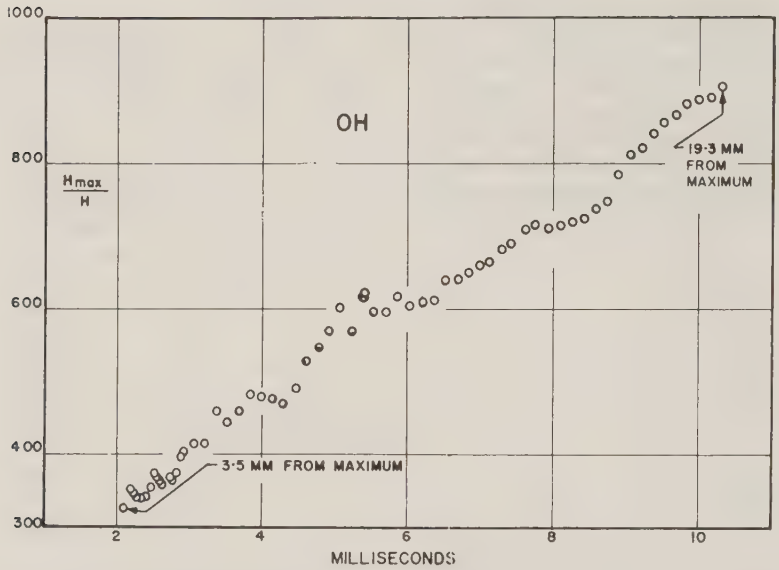

Figure 3. Second order correlation for OH*-radiation.* 3·13 per cent *butane,* 1 atm, 30 cm/sec *H = height of signal, proportional to radiation intensity.* H_{max} *= height of maximum signal in flame front. This applies also to Figures 4–7*

where c is the concentration of OH and c_{max} is the calculated value of c for the point of maximum intensity. The value for c_{max} is estimated by multiplying the equilibrium concentration of OH at a point in the far downstream region with the ratio of the maximum radiation intensity to that at the equilibrium point far downstream. One finds a value of c_{max} which corresponds to a partial pressure of OH of 1·28 atm. This result is, of course, fictitious and demonstrates the existence of an excess of excited OH radicals at the radiation peak. For our purpose this is irrelevant. It is then possible to calculate k. If a binary collision is assumed, an activation energy can be obtained by the same method which was used for CH and CC. The correction factor is chosen for the case that two linear molecules form a non-linear complex $[H_2O_2]$. The last line of Table 3 shows an activation energy of 11 kcal which appears somewhat high (disappearance by re-combination in a ternary collision would make the activation energy negative).

The OH-radiation in the low-pressure flame yields a straight line over a remarkably long distance or period if $[H_{max}/H]^{0·5}$ is plotted *versus* time (see *Figure 4*). This corresponds to a decay of the 1·5th order. Though the constancy of this order cannot be explained it is suggested that at lower pressure the order of the reaction becomes smaller than 2 because the reaction OH + CO prevails over OH + OH. This agrees with the relatively high value for the activation energy of the latter reaction. The decay curves of the

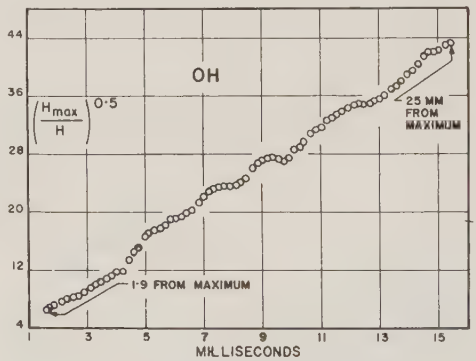

Figure 4. 1·5th order correlation for OH*-radiation.* 3·13 per cent *butane,* 1 atm, 30 cm/sec

CO_2^*- and OH-radiation indicate that CO disappears much more slowly than OH so that the reaction order of the OH-decay approaches that of a pseudomolecular reaction. CO has then to exist in the low-pressure flame at a higher concentration than OH. This would also favour the shift from the reaction OH + OH to OH + OC with decreasing pressure.

CONTINUOUS BACKGROUND (CO_2^*-) RADIATION

The intensity of the CO_2^*-radiation follows in all cases (*Figures 5, 6* and *7*) with high precision a constant order of decay from shortly after the point of maximum intensity throughout the measurable extension of the flame. The observed orders of

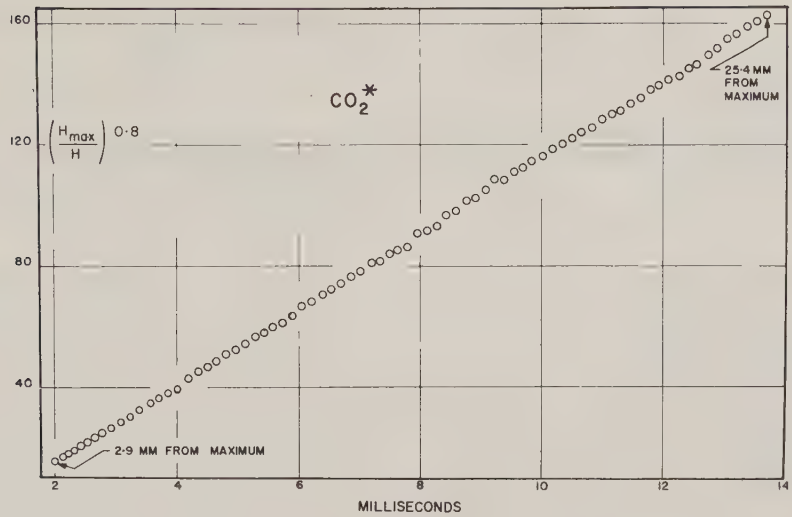

Figure 5. 1·8*th order correlation for* CO_2^**-radiation.*
3·13 per cent *butane*, 1 atm, 30 cm/sec

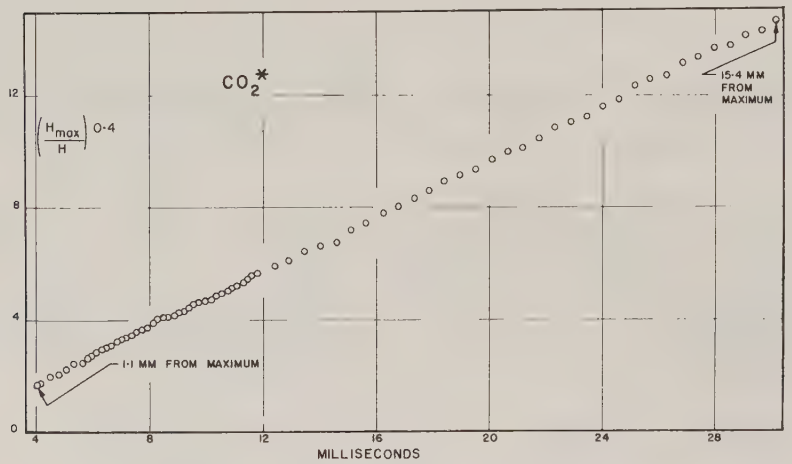

Figure 6. 1·40*th order correlation for* CO_2^**-radiation.*
3·13 per cent *butane*, 1 atm, 10 cm/sec

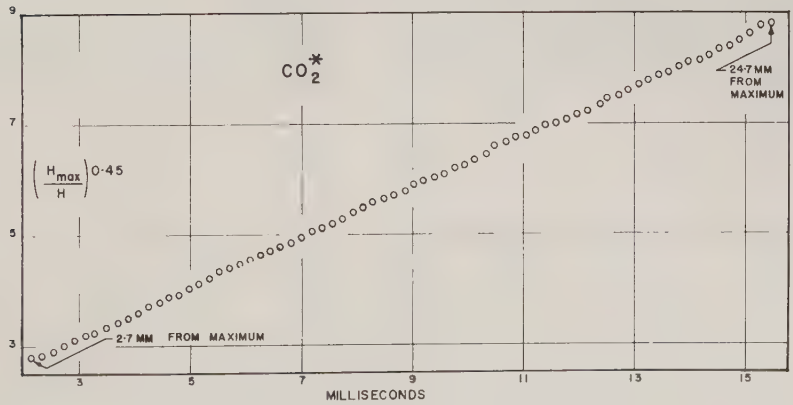

Figure 7. 1·45*th order correlation for* CO_2^**-radiation.*
3·13 per cent *butane*, 1/3 atm, 30 cm/sec

decay are 1·8 for the high-temperature and 1·4 and 1·45 for the two low-temperature flames, the 1 atm-10 cm/sec flame and the 1/3 atm-30 cm/sec flame, respectively (see Table 2).

A reaction order close to that found for the low-temperature flames can be explained as follows: Intensity of CO_2^*-radiation:

$$I = k[O]\,[CO] \tag{1}$$

Concentration of O-atoms:

$$[O] = K[O_2]^{1/2} \tag{2}$$

In the stoichiometric flame:

$$[CO] = 2[O_2] \tag{3}$$

The decay of CO is mainly given by

$$-\frac{d[CO]}{dt} = k_4[CO][O][M] \tag{4}$$

There follows

$$\frac{I}{I_0} = (1 + k_4 KM(O_2)_0^{1/2} t/2)^{-3}$$

(The subscript 0 refers to the time zero),

or

$$-\frac{dI}{dt} \sim I^{4/3}$$

The reaction order is thus 1·33 instead of 1·4 or 1·45. If CO disappears in the low-pressure flame mainly by reaction 4 the concentration of [CO] compared with that of [OH] would have to be still higher than follows from the argument at the end of the last section.

For the high temperature equation 4 is to be replaced by

$$-\frac{d[CO]}{dt} = k_4'[CO][OH] \tag{4'}$$

This may be so because the reaction of equation 4[1] has a higher activation energy than that of equation 4, and because at high temperature there may exist in the range of interest a high excess of OH above the equilibrium level. The disappearance of OH, according to the previous section, is given mainly by the equation

$$-\frac{d[OH]}{dt} = k_5[OH]^2 \tag{5}$$

Integration of equation 5, insertion into equation 4 and further integration gives a term for $[CO]/[CO]_0$ from which there follows, with the help of equations 1 to 3:

$$\frac{I}{I_0} = (1 + k_5[OH]_0 t)^{-1{\cdot}5 k_4'/k_5}$$

This expression finally yields

$$\frac{-dI}{dt} \sim I^{(1+0{\cdot}667 k_5/k_4')}$$

i.e. a reaction order of $(1 + 0{\cdot}667 k_5/k_4')$. This would agree with the experimental order 1·8 if k_5 were slightly larger than k_4'. Since reaction 5 is assumed to be more rapid than reaction 4′ this leads to the conclusion that in the high-temperature flame the concentration of OH exceeds that of CO.

This work was sponsored by Project SQUID which is supported by the Office of Naval Research, Department of the Navy, under contract Nonr 1858 (25) NR-098-038. Reproduction in full or in part is permitted for any use of the United States Government.

REFERENCES

[1] Wohl, K. and Welty, F. *Fifth Symposium (International) on Combustion*, p. 746. 1955. New York; Reinhold

[2] — *Fourth Symposium (International) on Combustion*, p. 68. 1953. Baltimore; Williams and Wilkins

[3] *Semi-Annual Progress Report*, April 1 and October 1, 1954, *Project Squid*. New Jersey; Princeton University, Princeton

[4] Botha, J. P. and Spalding, D. B. *Proc. Roy. Soc. A* 225 (1954) 71

[5] Gaydon, A. G. and Broida, H. P. *Trans. Faraday Soc.* 49 (1953) 1190

[6] Bernath, L., Powell, H. N., Robison, G. A., Welty, F. and Wohl, K. *Proc. Gen. Discussion on Heat Transfer*, p. 315. 1951. London; Institution of Mechanical Engineers

[7] Frost, A. A. and Pearson, R. G. *Kinetics and Mechanism*. 1953. New York; Wiley

34

SPECTROPHOTOMETRIC STUDIES OF LAMINAR FLAMES—II THE FLAME FRONT

R. KUSHIDA and K. WOHL

In the preceding paper, No. I, spectrophotometric measurements have been reported of the decay of the banded radiation emitted by the radicals CH, CC and OH, and of the continuous-background- or CO_2^* radiation from the intensity maxima in the main reaction zone or flame front far into the post-combustion zone.

The wavelengths of the band heads, and of the place in the continuous spectrum, chosen for observation are listed in Table 1 of reference 1. Local temperatures were measured with the help of the infra-red H_2O-radiation. A very stable flat flame which was established above a cooled porous metal disc was viewed edge-wise by the instrument and moved past its optical axis. By varying the flow rate through the porous disc the flame temperature could be varied.

The same types of radiation have now been investigated in detail with essentially the same arrangement for the flame front proper. The experimental conditions are shown in Table 1. It is seen that, besides the stoichiometric butane–air flame (3·13 per cent fuel), one lean and two rich flames have been studied at pressures of 1 atm and 1/3 atm, and in the case of atmospheric pressure at three different velocities of the cold gas and correspondingly three different flame temperatures. For the atmospheric flames, the diameter of the porous disc was 1 inch, for flames at 1/3 atm 2 inches. The discs were mounted in a vacuum chamber of 6 inches diameter which was purged by a slow stream of air or, with fuel-rich flames, of nitrogen. Cooling water was circulated at 70°C. Two thermocouples were embedded in each disc. The surface temperature as found by extrapolation never exceeded 83°C. For the flame front

TABLE 1

Flame Conditions: Intensities of Flame Radiation at Points of Maximum Intensity (watts/cm³ micron) × 10^5

Mole per cent butane	*Pressure,* atm	*Gas velocity,* 70°C	*Maximum temp.* °K	*Flame front temp.* °K	*Maximum intensities*			
					OH 3,100 Å	CC 5,163 Å	CH 4,310 Å	CO* 4,500 Å
2·60		30	1,958	1,715	4·3	75	480	92
		20	1,870	1,670	1·13	32	160	54
		10	1,738	1,610	0·083	2·9	14·1	7·1
3·13		30	2,053	1,750	5·9	470	1160	120
		20	1,980	1,690	2·0	196	420	72
	1	10	1,780	1,560	0·42	31	85	14·6
3·40		30	1,996	1,715	6·5	610	1560	186
		20	1,906	1,665	3·4	500	610	64
		10	1,740	1,590	0·40	126	85	16·1
4·00		30	1,996	1,860	7·2	3,700	1,510	210
		20	1,878	1,790	1·81	1,660	560	64
		10	1,755	1,700	0·039	370	29	17·6
2·60			1,829	1,635	2·06	19·5	175	9·37
3·13			1,925	1,740	3·52	180	327	27·5
3·40	1/3	30	1,898	1,720	3·96	394	474	33·4
4·00			1,953	1,860	2·88	1,950	699	84·3

studies the measurement of distances was carried to an accuracy of better than 0·005 mm. The entrance slit was 0·05 mm wide against 0·1 mm in reference 1; the exit slit (0·3 mm) and the aperture (f/100) were the same as in reference 1. An analysis showed that through these conditions the true value of the maximum point intensity was reduced by no more than 15 per cent while the half-width of the radiation range (Table 3) was practically unaffected.

Continuous background-(CO_2^*-)*radiation*

Spectral traverses from about 2,800 to 6,800 Å have been taken for all the flames studied at numerous points in order to determine the background continuum and thus the true intensity of the band peaks. *Figure 1* represents a spectrum for a point right in the flame front and shows the assumed curve for the background radiation. The CHO-band system visible in the figure will not be treated in this paper. At the amplification chosen the main peak of the CH-band far exceeds the width of the strip chart. As was stated[1,2] Child found that the shape of the CO_2^*-radiation curve in the post-combustion is the same for mixtures of CO, CH_4, or C_4H_{10} with air, and is independent of fuel-air ratio, pressure and temperature within the experimental range. The shape is characterized in Table 2 by the ratio of the intensity at a number of wavelengths to that

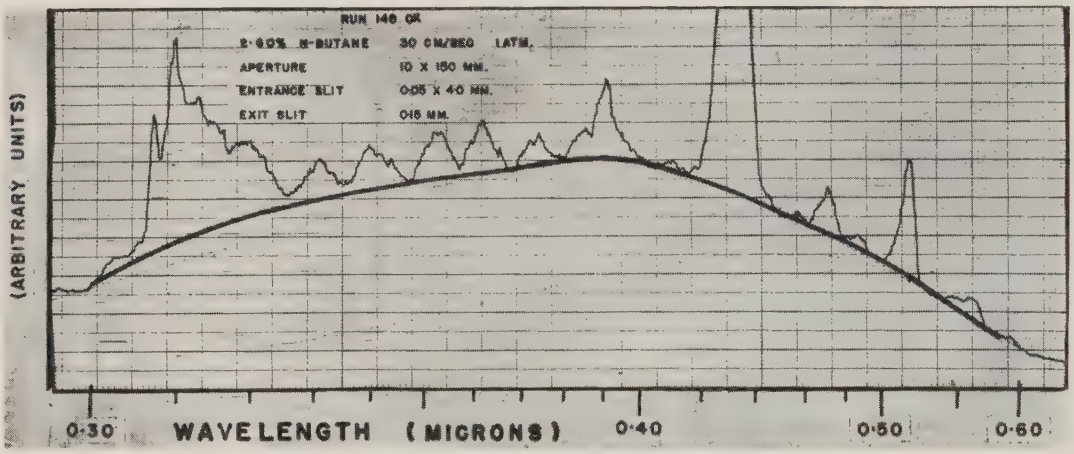

Figure 1. Spectral traverse at point of maximum CH-*intensity*

TABLE 2

Ratio of the Intensities Per Unit of Wavelength of the CO^*-continuum at Various Wavelengths to that at 4,500 Å

Wavelength Å				5,163	4,500	4,310	3,503	3,100
Post-combustion zone				0·80	1	0·99	0·15	0·013
Point of maximum intensity of free stoichiometric CO-*air flame*, 1 atm				0·735	1	0·99	0·14	0·008
Points of maximum CH-*intensity of butane air-flames*	*Mole per cent fuel*	*Pressure* atm	*Cold flow velocity* cm/sec					
	2·60	1	30	0·645	1	1·09	0·30	0·042
	3·13	1	30	0·74	1	1·07	0·26	0·043
	3·40	1	30	0·85	1	1·00	0·22	0·035
	4·00 (?)	1	30	1·21	1	0·90	0·14	0·021
	3·13	1	10	0·68	1	1·06	0·29	0·043
	2·60	1/3	30	0·70	1	1·06	0·30	0·048
	3·13	1/3	30	0·86	1	1·00	0·20	0·031
	3·40	1/3	30	0·95	1	0·96	0·17	0·026
	4·00 (?)	1/3	30	1·15	1	0·87	0·10	0·015

at 4,500 Å where, due to the absence of noticeable bands (except possibly at 4 per cent butane, see below), the CO_2^*-radiation is usually measured. It is seen that the shape in the reaction zone of the CO-flame is quite similar to that in the post-combustion zone while the shape in the butane–air flame front shows peculiarities which depend significantly on the butane concentration, somewhat on the pressure and least on temperature.

The shapes found in the flame fronts at atmospheric pressure and highest gas velocity (i.e. temperature, see Table 1) are presented in *Figure 2* together with the shape found in the post-combustion zone. In the lean flame there is a strong shift of the background intensity in favour of shorter wavelengths. The same holds to a lesser degree

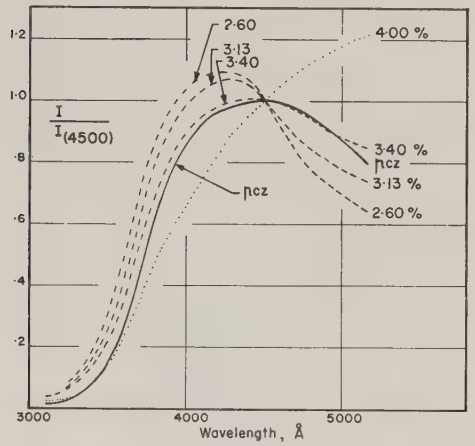

Figure 2. Intensity per unit of wavelength of CO_2^**-continuum relative to that at* 4,500 Å. 1 atm, *cold gas velocity* 30 cm/sec. *pcz = post-combustion zone*

for the stoichiometric flame while in the rich flame of 3·4 per cent butane the effect is obscured by a general broadening of the spectral range covered by the CO_2^*-radiation. The data for the richest flame (4 per cent) are not reliable since here the CC-radiation in the flame front is too strong for permitting a fixation of the background curve beyond 4,200 Å. (This does not affect perceptibly the accuracy of the peak intensities of radical radiation.)

A shift of the radiation curve to short wavelengths might be assumed to indicate that the particles CO and O which are supposed to produce by collision the background radiation (see, for example, reference 1) possess more energy in the flame front than in the post-combustion zone. Such a view would be plausible if the radiation could be created by excited $O(^1D)$ atoms. This, however, appears to be excluded for spectroscopic reasons[3]. This line of reasoning, moreover, seems at variance with the observation that the shape of the CO_2^*-radiation curve in the post-combustion zone does not depend on temperature, while in the flame front (Table 2, velocity of 10 cm/sec) it depends on temperature 'in the wrong way', if at all. A reduction of pressure tends to shift the CO_2^*-radiation intensities towards longer wavelengths.

Sequence of intensity maxima

The order in which the maxima of radiation appear in the flame front has so far not been reported for atmospheric flames though it is known for flames burning at very low pressures. These maxima are, at 1 atm, indeed separated by very small distances only, ranging from 0·1 to less than 0·01 mm. From Table 3 in which the data

TABLE 3

Characteristic Distances

Mole per cent butane	*Pressure* atm	*Cold gas velocity* cm/sec	*Distance of point of maximum intensity ahead of* CH-*maximum* mm			*Half width*, mm			
			OH (3,100)	CC (5,163)	CO_2 (4,500)	OH (3,100)	CC (5,163)	CH (4,310)	CO_2^* (4,500)
2·60	1	30	0·004	0·037	−0·007	0·144	0·134	0·153	0·225
	1	10	0·016	0·055	−0·095	0·356	0·306	0·398	0·750
3·13	1	30	0·024	0·025	0	0·153	0·132	0·111	0·195
	1	10	0·029	0·034	−0·016	0·198	0·135	0·190	0·290
3·40	1	30	0·027	0·021	0·011	0·170	0·131	0·144	0·190
	1	10	0·056	0·038	0·010	0·225	0·170	0·222	0·302
4·00	1	30	0·034	0·002	0·006	0·195	0·138	0·160	0·210
	1	10	0·052	0·004	0·013	0·250	0·244	0·315	0·340
2·60	1/3	30	0·046	0·068	−0·020	0·458	0·340	0·424	0·558
3·13	1/3	30	0·056	0·060	0·018	0·478	0·360	0·430	0·495
3·40	1/3	30	0·082	0·062	0·033	0·504	0·388	0·430	0·482
4·00	1/3	30	0·178	0·048	0·048	0·584	0·386	0·532	0·512

are collected it can be seen that in rich flames of this pressure the OH-radiation appears before the CC-radiation, presumably because the hydrogen from a hydrocarbon is earlier attacked than the carbon. In lean flames the order is inverted. This ties in with the fact that in lean flames the maximum CC-radiation is much weaker while CC- and the OH-maxima. This pattern of radiation distribution remains essentially unchanged if the pressure is reduced to 1/3 atm and, according to previous experience, to even much lower values.

The points of incipient radiation have on the whole the same order as those of maximum

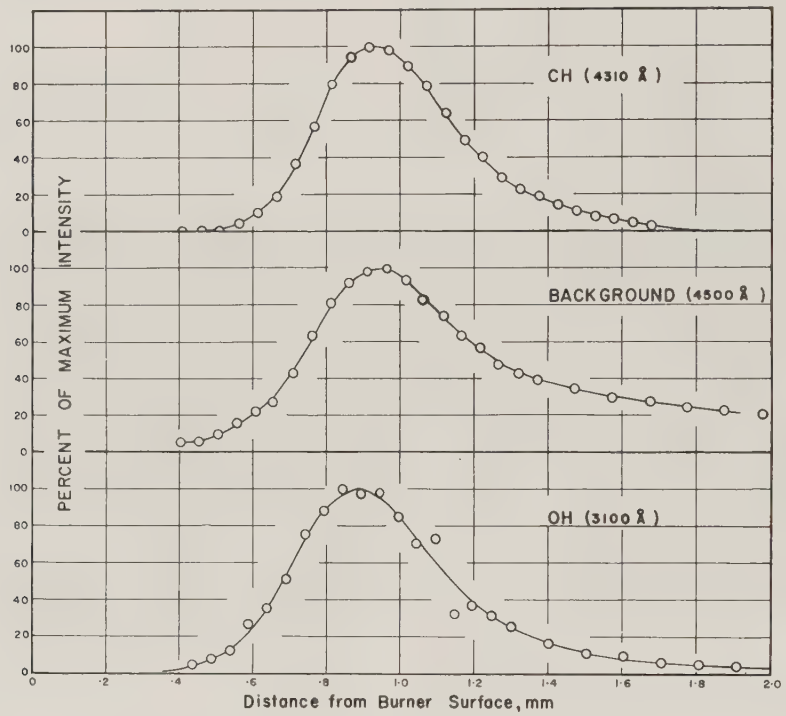

Figure 3. Spatial traverses through flame front. 2·60 per cent *butane*, 1/3 atm, *cold gas velocity* 30 cm/sec

that of OH has hardly changed (see Table 1), and that the decay of CC-radiation is much more rapid in lean flames than in rich ones (see reference 1). Thus, even if the situation for the creation of CC- and OH-radicals is the same in both mixtures the CC-radical will form its weak maximum in the lean flame ahead of the point at which the strong maximum appears in the rich flame. The CH-radiation always follows that of OH and CC. This lends support to the idea that excited CH is formed by a reaction between OH and CC, if one takes into consideration that the maximum overall concentrations of OH and CO—which would almost coincide with the maximum CH-radiation—will occur later than the maximum concentrations of excited OH- and CC-radicals or the maxima of the OH- and CC-radiation. The maximum of the CO_2^*-radiation is observed in lean flames slightly downstream of the CH-maximum, and in rich flames further upstream, between the intensity, with a few exceptions which are related to the values of the half-widths of the radiation ranges listed in Table 3.

Half-widths of radiation range

Spatial traverses through the flame front have been measured for all the conditions and types of radiation listed in Table 1. An example of such a traverse is presented in *Figure 3.* Most of the data obtained for the half-widths of the radiation range are assembled in Table 3. The product of half-width and pressure has been plotted as a function of maximum temperature. *Figure 4* shows the situation for the CO_2^*-radiation. From such figures it is possible to find, besides the effects of temperature, the effects of the type of radiation, of concentration, and of pressure on the half-width for the 'isothermal' case, i.e. for a constant maximum temperature. For a medium temperature

of 1,900°K the half-widths at various per cent butane are as follows:

CO_2^*: ~0·21 mm at all concentrations

OH: ~0·16 mm at 2·6 and 3·1 per cent, ~0·185 mm at 3·4 and 4 per cent

CH: ~0·16 mm at 2·6—3·4 per cent, 0·22 mm at 4 per cent

CC: ~0·14 mm at 2·6—3·4 per cent, 0·18 mm at 4 per cent

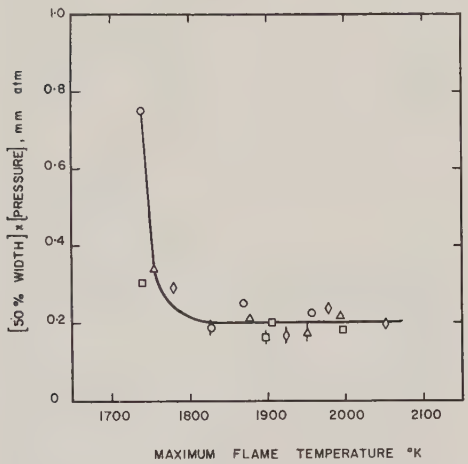

Figure 4. Half-width of the CO_2^*-continuum at 4,500 Å, multiplied by pressure

Conditions and Symbols						
	Mole per cent butane				Velocities at 70°C	Burner
	2·60	3·13	3·40	4·00	cm/sec	diameter
1 atm	○	◇	□	△	30, 20, and 10	1 inch
1/3 atm	○	◇	□	△	30	2 inches

CO_2^* has the largest half-width; the radicals show an increase with increasing butane concentration, but all the differences are small, and one may, broadly speaking, ascribe to a butane–air flame of medium temperature a half-width of the reaction zone of 0·18 mm.

A temperature drop corresponding to a change of gas velocity from 30 to 20 cm/sec (73–118°C according to Table 1) has practically no effect on the half-width, except for CH and CC in the 4 per cent butane–flame. A transition to 10 cm/sec causes an increase of half-width which is substantial only for the mixtures of extreme composition, especially the lean flame. Since the temperature change is coupled with a velocity change the 'half-time' increases strongly with decreasing temperature. In the low temperature range the half-times change more strongly than the reciprocal of cold stream velocities. The situation at 1/3 atm is quite similar to that at 1 atm.

The 'isotherm' increase of half-width with decreasing pressure is surprisingly uniform at all conditions (see, for example, *Figure 4*). Assuming an exponential pressure dependence of the half-width, the average exponent n varies from −0·81 (CO_2^*) to −0·92 (OH) with a tendency to increase from lean to rich. An approximate translation of these observations into values for half-time yields a complex picture, probably because this procedure requires more accurate temperature data. No consistent relationship has been noted between half-width and maximum radiation intensity.

Maxima of radiation intensity

The dependence of the directly observed maximum intensities on butane concentration presents the familiar features (see Table 1): there is generally an increase with increasing fuel content which is smallest for OH and largest for CC. The most strongly cooled flame (10 cm/sec velocity) shows the peculiarity of a reduction of intensity at the two extreme compositions which is strongest for OH (and non-existent for CC in the richest flame). It is plausible that the heat losses to the porous disc have the strongest quenching effect on the weakest flames. The 'isotherm' concentration effect in 1 atm flames can be seen from *Figures 5–8* in which the logarithm of maximum intensity is plotted *versus* the reciprocal of the maximum flame temperature. One finds that only CC shows the same features as Table 1. Otherwise two regimes are noticed: at low temperature the dependence on concentration is similar insofar as at least the lowest intensity occurs in the lean flame. At high temperature the lowest intensity appears invariably in the stoichiometric flame.

The dependence of maximum radiation intensity on flame temperature is shown in *Figures 5–8* as mentioned. Similar plots have been made for two more CC-band peaks and one CH-band peak (see reference 4 and Table 4). The maximum temperature $T_{\max}$ rather than the flame front temperature T_{fr} has been chosen as abscissa. The differences between $T_{\max}$ and T_{fr} form a consistent pattern (with one exception, 2·6 per cent butane, 1/3 atm), but in view of the relatively wide aperture used for temperature measurement, (see reference 1), the steep temperature gradient in the flame front, and the low water vapour radiation at 1/3 atmosphere, the flame front temperature was nevertheless considered not sufficiently reliable for this purpose. Of the 28 $\log I_{\max}$–$1/T$ curves plotted, 75 per cent are quite straight, four convex in downward direction and three convex in upward direction. The average slopes of these curves have been presented in Table 4 by way of 'activation energies' whenever the curvature of the lines was not excessive. Though a strict interpretation of these energy values is not possible it is presumed that their

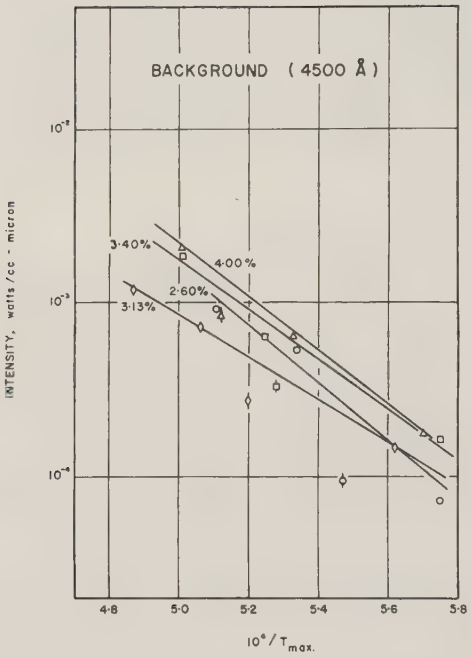

Figure 5. Absolute intensity of the CO_2^*-continuum at 4,500 Å at points of maximum intensity. Conditions and symbols as in Figure 4

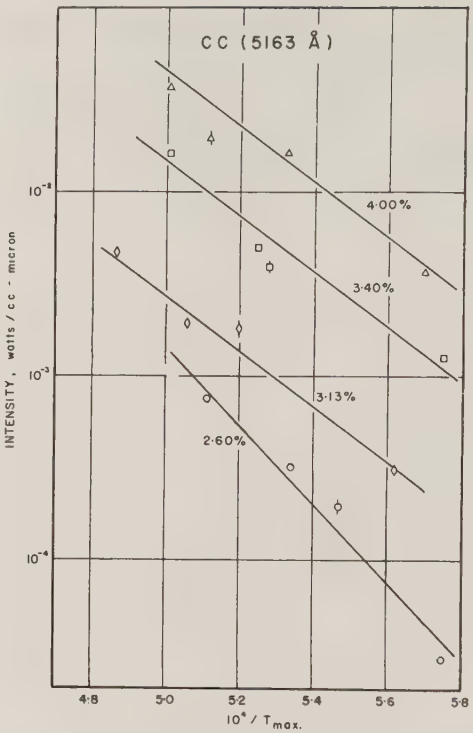

Figure 6. Absolute intensity of the CC-radiation at 5,163 Å at points of maximum intensity. Conditions and symbols as in Figure 4

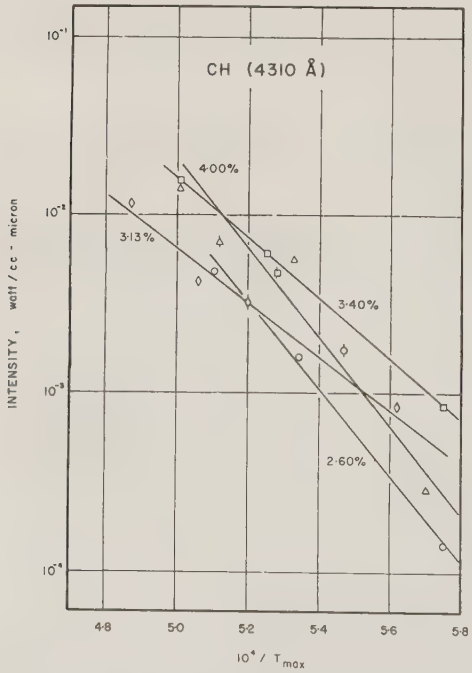

Figure 7. Absolute intensity of the CH-radiation at 4,310 Å at points of maximum intensity. Conditions and symbols as in Figure 4

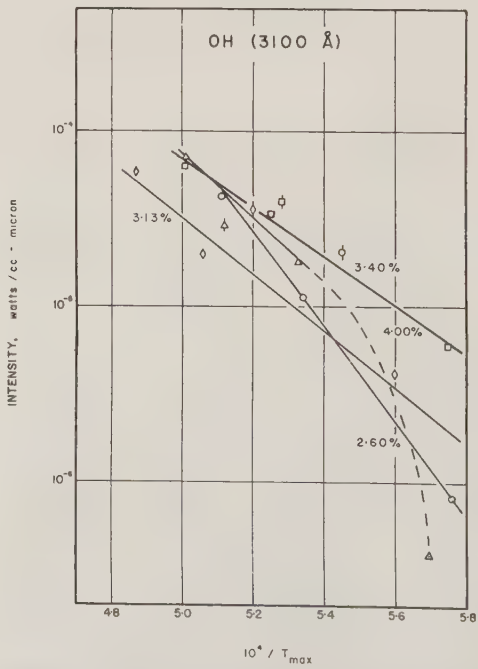

Figure 8. Absolute intensity of the OH-radiation at points of maximum intensity. Conditions and symbols as in Figure 4

TABLE 4

Apparent Activation Energy for Creating Excited Radicals, Obtained from *Figures 5–8* and Similar Figures

Emitter	*Wavelength* Å	*Spectral excitation energy* kcal	*Activation energy*, kcal, *at various mole per cent of fuel*			
			2·60%	3·13%	3·40%	4·00%
CC	5,565	51·2		77	76	56
CC	5,163	55·1	101	72	69	67
CC	4,688	60·9	129	83	83	72
$CO_2^\star$	(4,500)		80	56	67	72
CH	4,310	66·0	104	71	60	
CH	3,895	73·2	140	77	88	70
OH	3,100	92·0	121	74	74	

order of magnitude as well as their mutual relationship is of interest.

The energy values are mostly larger than the energies of excitation of the radiating radicals, and since the values would rise further (on the average by a factor 1·4) if the flame front temperature instead of the maximum temperature were used for their computation it may be said that all of them are larger. For the weakest mixtures, i.e. those of extreme composition, the cooling of the flame causes the strongest quenching as mentioned. This explains why most of the energy values at 2·6 per cent are excessively high. For two cases at 4 per cent an extreme degree of quenching occurs only in the flame of lowest temperature so that no activation energies can be assigned to the whole range. All the other energy values in Table 4 are not too different from each other. The two CC-band peaks at 5,163 and 4,688 Å differ by the vibrational excitation in the upper state (see Table 1 in reference 1). The two CH-peaks differ by their upper electronic state. In either case the activation energy is larger for the state of higher energy.

Pressure dependence of maximum radiation intensity

Figures 5–8 and similar ones which have not been reproduced here[4] permit us to determine the 'isotherm' pressure dependence of the maximum radiation intensities in the flame front. It is found that, broadly speaking, all the three types of CC-radiation listed in Table 1 are independent of pressure at all conditions. For the CH-radiation at 4,310 Å this is true from 3·13 to 4·00 per cent butane, and for the CH-radiation at 3,895 Å as well as for the OH-radiation it holds at 3·4 and 4·00 per cent. At lower butane content the intensities increase with decreasing pressure. In contrast to these types of radiation which are banded and emitted by excited radicals, the continuous $CO_2^\star$-radiation which is emitted as the result of a collision decreases invariably with decreasing pressure. The pressure exponent varies between 1 for the leanest mixture and 0·5 for the richest.

The pressure independence of radical radiation can be made plausible for chemiluminescent as well as for thermal radiation if use is made of the steady state hypothesis. In the case of chemiluminescence, assume the creation of the excited radiating radical R* by collision of two other radicals:

$$\frac{dR^\star}{dt} = k_1 R' R'' \tag{1}$$

R* is mainly destroyed by

$$\frac{-dR^\star}{dt} = k_2 R^\star M \tag{2}$$

R′ is created by

$$\frac{dR'}{dt} = k_3 AB \tag{3}$$

(A and B are molecules the concentration of which is proportional to the total pressure) and destroyed by

$$\frac{-dR'}{dt} = k_4 (R')^2 M \tag{4}$$

If reactions analogous to 3 and 4 are assumed for radical R″ there follows

$$R^\star \sim p^0, \quad \text{i.e.} \quad I \sim p^0$$

In case of thermal radiation we may have for the radiating radical in the fundamental state

$$\frac{dR}{dt} = k_5 CD \tag{5}$$

where C and D are molecules like A and B above.

$$\frac{-dR}{dt} = k_6 R R' M \tag{6}$$

$$\frac{dR'}{dt} = k_7 EF \tag{7}$$

$$\frac{-dR'}{dt} = k_8 R' G \tag{8}$$

There follows $I \sim R^\star \sim R \sim p^0$.

A positive pressure exponent n of radical radiation could be explained very easily but no substantial positive value of n has been observed. A negative pressure exponent for chemiluminescent radiation will occur if for R^* we have reactions 1 and 2, for R' reaction 3 and 4, and for R'' reactions 5 to 8. The result is $I \sim p^{-1/2}$. If reactions 5 to 8 apply to R' and R'' there follows $I \sim p^{-1}$. With thermal radiation $n = -1/2$ is obtained if D in reaction 5 is not a molecule which is proportional to the pressure but an atom or radical which is in equilibrium with D_2 so that $D \sim p^{1/2}$. If instead of equation 5, one would have $dR/dt = k_5' C$, the result would be $n = -1$. An example for equation 1 is the reaction $CC + OH \rightarrow CH^* + CO$. Also, a reaction of the type $CH + O_2 \rightarrow OH^* + CO$, in which a radical reacts with a molecule whose concentration may be proportional to p, can yield a value zero or a negative value for n if the proper scheme, out of those mentioned, is applied to the radical.

If the CO_2^*-radiation is produced by a collision of CO and O, and if O is taken to be in equilibrium with O_2 we have $I \sim (CO)(O_2)^{1/2}$ which can be written, at least for the lean flame, $I \sim (CO)p^{1/2}$. In order to make the pressure exponent for I vary from 1 (lean) to 1/2 (rich) (see above) the pressure exponent of CO would have to vary from 1/2 to O. The exponent zero follows if CO is formed by a monomolecular reaction (of an aldehyde?) and destroyed by a bimolecular reaction. The average value 1/2 for the exponent will appear if part of the CO is created and destroyed by bimolecular reactions.

This work was sponsored by Project SQUID which is supported by the Office of Naval Research, Department of the Navy, under Contract Nonr 1858(25) NR-098-038. Reproduction in full or in part is permitted for any use of the United States Government.

REFERENCES

[1] Child, E. and Wohl, K. This volume, p. 215
[2] Wohl, K. and Welty, F. *Fifth Symposium (International) on Combustion*, p. 746. 1955. New York; Reinhold
[3] Laidler, K. J. *The Chemical Kinetics of Excited States*, p. 72. 1955. Oxford; Clarendon Press
[4] Kushida, R. *Ph. D. Dissertation*, 1957. University of Delaware

35

EMISSION AND ABSORPTION SPECTRA OF FLAT FLAMES

G. N. SPOKES

Emission spectra of pre-mixed and bunsen-type flames of the majority of the common organic liquids and gases are fairly well known, and their study has improved our knowledge of combustion phenomena. Study of the absorption spectra of these types of flame, however, has failed to reveal much of further value. Short-lived radicals, such as C_2 and CH, which have high emission intensity, have never been seen in absorption in steady flames, but OH, which has a fairly high equilibrium concentration, is readily obtained in absorption. In slow combustion experiments, various intermediates have been detected by their absorption spectra[1,2]. The observation of intermediate pyrolysis or oxidation products in flames had not until quite recently been made[3].

The invention of the flat flame burner[4,5] has enabled steady combustion of gases at mixture strengths close to the limit of combustion. The flame is of large diameter and almost flat, and is thus ideal for spectroscopic investigation. Weak mixture flames of all common organic fuels with air are blue in colour, but the flames of rich mixtures of fuel with air vary greatly in appearance depending on the mixture strength. Thabet[6] has described the changes in colour and appearance of some of these flames. It is well known that some fuels, such as ethyl-ether and acetaldehyde, show a two-stage flame under very fuel-rich conditions. The first stage flame is the cool flame and propagates some distance under the second stage or main flame, the separation between the two flames increasing with increase in the fuel–air ratio. Under fuel-rich conditions, the characteristic yellow glow of carbon particle formation occurs with most hydrocarbons and ethers. Below the luminous volume of the carbon glow is a flat reaction zone, which is usually blue or blue-grey in colour. The reaction zone is separated from the carbon glow by a dark space in most of the cases investigated when air is used as oxidant (this dark space is not present when running the very sooty flame of methane with oxygen instead of air). The blue reaction zone is, of course, separated from the burner top by a small distance, usually between 1 and 2 cm; this distance may be varied by variation of the total flow rate or by adjustment of the fuel–air ratio. One further way in which the burner may be used is to burn flames of nitrogen-diluted mixtures of otherwise fast burning mixtures. The dilution reduces the flame speed to 7–10 cm per second, and stabilization of a flame of this speed is possible.

By using the Egerton–Powling burner, some of the difficulties in the way of observation of absorption spectra are overcome. It will be worth while to set out the main difficulties so that they may be more completely appreciated.

(1) The reaction zone, where oxidation or pyrolysis products may be expected to occur, is usually extremely thin and often curved; it is thus very difficult to confine the optical beam to the region where the intermediaries of interest might be expected to be found, and impossible to obtain long path lengths through such a region.

(2) It is necessary to have a background source, the brightness temperature of which exceeds the effective excitation temperature in the flame (which may be higher than the equilibrium temperature of the flame).

(3) The beam of light must not be thrown out of the region under investigation by schlieren effects.

(4) The concentration of absorbing species may be low because of instability or reactivity.

Some of these difficulties have been overcome in this work by use of: (*a*) a flat flame burner of the Egerton–Powling type which gives a flat flame of fairly large diameter, the reaction zone of which is much thicker than that of the normal bunsen type of flame; (*b*) a very bright high pressure xenon arc lamp (Osram XBO 162) as background source; (*c*) a system of mirrors, similar to that designed by White[7], to reflect the beam of light backwards and forwards through the flame gases a number of times.

Refractive index gradients are low in this type of flame and the deflection of the light beam out of the region under investigation was not found to be serious for up to 24 traverses; however, some trouble was experienced during the investigation of the cool flame region of rich ether, using about this number of traverses.

For this work, a modification was made to the normal circular burner, the one used being rectangular in shape and largely of metal construction. Side tubes contain the mirror system, and shutters are provided to isolate the mirrors from the flame during start-up conditions under which they are

most likely to be spoilt by deposits of various condensates or carbon. The rectangular matrix is 8 cm long by 3 cm wide and gives a flame about 8 cm long. Front surface mirrors were found to tarnish when exposed to some types of flame gases and back surfaced aluminized quartz mirrors have therefore been used. The curvatures of the mirror surfaces are so designed that the images formed by the reflections from the front and back surfaces coincide.

Absorption spectra were recorded photographically on a medium quartz Zeiss Q24 spectrograph. Exposures of usable intensity were obtained in 30 min in the 2,500 Å region with 24 traverses of the flame gases, and in 10 min in the visible region with 36 traverses, using the xenon arc as background. It is possible to increase the spatial resolution in the flames by reducing the vertical aperture of the system, but this, of course, increases the exposure times. The mirrors were 1 cm in height and had a radius of curvature of about 15 cm. To ensure good focus throughout the visible and ultraviolet, good quartz–lithium fluoride achromats were used.

Emission spectra of these rather weakly emitting flames were recorded with small quartz or glass Raman spectrographs. Ilford Astra III plates were used in view of their flat spectral response throughout the visible and ultraviolet.

Gases used were of commercial quality from cylinders and their flows were regulated by needle valves and monitored by rotameter flow meters. Liquid fuels were introduced by passing some of the air into a saturating device in which the liquid was contained at constant temperature. The air–fuel mixture from the saturator was mixed at a *T* piece with the remainder of the air and the mixture led off to the burner. Saturation was fairly good, but since only a qualitative indication of the fuel–air ratio was needed, exact knowledge of the saturation efficiency was unnecessary. Nitrogen was passed through the saturators when acetaldehyde was used as fuel to prevent oxidation. Nitrogen was also used in this capacity when running rich flames of methanol which has rather low vapour pressure at room temperature. No attempt was made to add extra oxygen to compensate for this nitrogen, which may represent up to 15 per cent of the air flow.

Some preliminary work has been done on the emission and absorption spectra of flames on a porous plate burner of the type described by Botha and Spalding[8], and some attempts have been made to detect absorption in low pressure flames.

ABSORPTION SPECTRA OF EGERTON–POWLING FLAMES

Ether and acetaldehyde under two-stage flame conditions

As the fuel–air ratio is increased, a cool flame is seen to separate from the underside of the blue reaction zone. The luminous region of carbon formation is seen to diminish in brightness and finally only the two blue flames remain. In the case of acetaldehyde, the cool flame increases in brightness as the richness increases until the cool flame is as bright or brighter than the second stage flame. In the case of ether, however, the cool flame does not exhibit any such brightness changes and it always appears appreciably less bright than the second stage flame.

With a path length of about 30 cm through the rich flame of ether, the ultraviolet formaldehyde absorption system was quite strong. It was found in all the cases recorded that the formaldehyde absorption commences below the cool flame, becomes strongest between the cool and main flames and is somewhat weaker above the main flame.

Acetaldehyde flames

It has been found possible to observe the disappearance of the acetaldehyde absorption continuum with distance through the rich acetaldehyde flame. The banded system above 2,800 Å is masked by formaldehyde absorption in the region of the cool flame, but the continuous absorption is strong. The acetaldehyde continuum fades out between the cool and second stage flames and is not detectable above the second stage flame. Formaldehyde is present above the second stage flame but is rather weaker than between the cool and second stage flames.

Ether flames under carbon-forming conditions

Under these conditions it is found that the formaldehyde absorption is still present but that with path lengths of nearly 200 cm some weak benzene absorption ($\lambda\lambda$ 2,589, 2,528) is detectable above the main reaction zone. With these long path lengths, using the full aperture of the system, some doubt must exist as to the exact place of origin of the benzene.

Hexane under carbon-forming conditions

With hexane as the fuel, no cool flame was apparent (this condition is only obtained with pre-heated burners at atmospheric pressure). The hexane–air flame was run under carbon-forming conditions, and observations with 12 traverses showed that benzene absorption first appeared about 1 cm below the blue reaction zone, together with an unassigned absorption band at about 2,750 Å. The bands all persist through to the carbon zone with almost unchanged intensity. This new band is a few angstroms wide, of diffuse appearance, and seems weakly degraded to longer wavelengths, the head being at 2,750 Å. With benzene introduced into the original fuel, the absorption appeared to be weaker above the blue

reaction zone than below it. With a path length of nearly 200 cm, weak formaldehyde absorption was detected in the carbon formation region. In the dark space between the reaction zone and the yellow carbon glow, using a path length of about 100 cm, a weak continuous absorption extending below 2,600 Å, was detected.

Other fuels

Weak formaldehyde absorption has been observed in the flames of rich methanol, propane, and methyl-ether. It has not been found in the case of the rich methane flame. The flame of methyl-ether is similar to ethyl-ether in respect of emission spectrum, absorption spectrum, carbon formation and low-pressure flame emission spectrum.

Carbon monoxide (Egerton-Powling and Spalding burners)

Attempts to obtain the absorption spectrum of the triplet and third positive systems in flames of rich mixtures of carbon monoxide using the Egerton–Powling and Spalding burners have been unsuccessful. Up to 36 traverses through the Egerton–Powling burner flame have been used in the search for the Triplet system, and up to 12 have been used in the search for the Third Positive system. Only four traverses of the Spalding flame have been tried. Only OH absorption has been detected in these attempts with the Spalding flame. OH absorption was also weakly present in the Egerton–Powling flame. No attempt was made to dry the gases.

LOW-PRESSURE FLAMES

Some work on the absorption by OH in the reaction zone of a low-pressure ethylene/oxygen flame with the xenon arc as background source has failed to give sufficiently strong absorption to enable a rotational temperature to be obtained. The measured absorption was about 5 per cent for the biggest peaks with four traverses of a 3·5 cm diameter flame, using a quartz Littrow spectrograph. With more traverses through the flame, the absorption was apparently less owing to the drop in the effective brightness temperature of the emergent beam, and the very strong emission of OH from the flame.

It was found possible to obtain weak NH absorption in the reaction zone of an N_2O–ethylene flame at a pressure of about 2·5 cm Hg, with only four traverses of the 3·5 cm diameter flame. An attempt to obtain C_2 and CH absorption from these reaction zones using the xenon arc as background source has been unsuccessful.

EMISSION SPECTRA OF FLAT FLAMES

Weak mixtures

The emission spectra of flames burning at the weak limit have been investigated for several fuels such as methane, butane and ethyl-ether. It has been found that the spectrum under these conditions is very similar to that of the corresponding weak bunsen flame, and in these cases the main features are CH, OH, the hydrocarbon flame bands, attributed by Vaidya[9] to the radical HCO, and the usual CO flame bands with their accompanying continuum. The emission spectra of the rich flames, however, show considerable differences from the richest flame of the pre-mixed kind which it is possible to run on a bunsen type of burner.

Rich mixtures

The blue reaction zone of the carbon-forming hydrocarbon or ether flame is found to show as its strongest feature, the HCO bands, the bands of CH and OH being somewhat weaker. For some fuels, e.g. methane or propane, it is still possible to detect some C_2 radiation. In those cases where it is possible to proceed to mixtures richer than those giving carbon formation, e.g. in the case of ether–air, then it is found, in accordance with the findings of Agnew and Agnew[10], that the HCO emission of the second stage flame gives place to HCHO as the richness increases. OH and CH also fade out as the mixture gets richer but these two features persist to richer mixtures than does the HCO. A two-hour exposure of the second stage flame of a very rich diethyl-ether flame using the glass Raman spectrograph showed some very feeble structure in the region 5,000–6,000 Å, but owing to the weakness of the source no identification was possible. The spectrum of the cool flame of both rich ethyl-ether and acetaldehyde/air flames have been obtained and both were shown to give the cool flame bands of HCHO. It was noted that the HCO bands emitted by rich limit flames of all the organic fuels studied (including methane, butane, methyl-ether, etc.) did not give that part of the HCO system denoted by Vaidya[9] as the B system, whereas the weak limit mixtures all gave the B system in addition to the remaining systems which were also found in the rich flames.

The emission spectra of flames of some fuels with air burnt on a porous plate burner of the type described by Botha and Spalding[8] have been examined. It has been found that for ethyl-ether the HCO bands remain very prominent throughout the whole range of mixture strengths which it is possible to stabilize on this type of burner. The OH, CH, and C_2 systems appear to follow similar variations in intensity with fuel–air ratio to those found in the case of a bunsen flame, but the HCO bands are relatively much stronger than in the case of the bunsen flame. As mixture strength increases so the B bands of the HCO system weaken and finally with the richest stabilizable flame on this type of burner they have disappeared. Under

these conditions the spectrum of the flame closely resembles the spectrum of the rich mixture Egerton-Powling flame, the richest ether flames, for example, show cool flame bands.

DISCUSSION OF RESULTS

Formaldehyde in flames

The occurrence of formaldehyde absorption under the experimental conditions described is not surprising. Some previous workers (for example, Foresti[11]) have indicated that the concentration of formaldehyde is greater above the second stage flame than that between the cool and the second stage flames whereas the work here reported suggests that the concentration of formaldehyde is greatest between the two flames. The reason for this is probably that previous experiments were carried out at richer mixture strengths than those used in the present case. The presence of a greater relative proportion of oxygen will increase the oxidation efficiency and raise the final flame temperature, thereby reducing the efficiency of the formaldehyde-forming mechanisms and causing combustion of some of the formaldehyde present. It was not found possible to stabilize the very richest flames as flat flames, the second stage flame being badly curved under these conditions. In consequence of this no spectral records have been obtained for which the formaldehyde concentration has been greatest above the second stage flame.

Formaldehyde absorption has been recorded for rich-limit flames of methanol above the reaction zone, and this is to be expected from a study of its normal oxidation processes.

Sensitivity for formaldehyde absorption is considerably greater than for acetaldehyde detection. Foresti[11] obtains considerable acetaldehyde formation in the case of a diethyl-ether flame but under similar conditions in the present case none was detected, due to masking by HCHO.

Benzene in flames

Benzene absorption in flames of rich limit mixtures of hexane with air begins in the pre-heat region, apparently, and extends through to the carbon zone.

It has been found (Campbell and Johnson[12]) that the absorption spectrum of benzene undergoes considerable change on heating the benzene to only 500°C, the characteristic banded spectrum changing to a strong continuous absorption extending from the shortest quartz ultraviolet to the near u.v. In view of this it is possible that the banded benzene absorption observed was due to the presence of benzene in cooler regions of the burner. Vortices at the ends of the burner could be responsible for bringing the benzene down to a level with the pre-heat region from the higher regions of the flame, in which case the apparent position of origin of the benzene bands would be lowered considerably, and such possibilities as this must be borne in mind when interpreting the results obtained.

The continuous absorption observed between the reaction zone and the yellow carbon zone may be caused, in part at least, by benzene. Other possible absorbers are acids or peracids. It is possible that in regions of pyrolysis in this flame considerable numbers of molecules of a cyclic nature are formed by ring closure processes and benzene is a likely product. Processes of build-up of carbon particle nuclei from smaller molecules are not ruled out, and many fragments will probably be produced in the reaction zone which may 'seed' the carbon-forming process.

The observation of very feeble benzene absorption (apparently) in the region of yellow luminosity of the ethyl-ether flame is rather unexpected. The benzene may be formed during a stage in the pyrolysis. In this flame, oxidation processes are competing strongly with carbon formation and soot is not usually deposited. The yellow particles are presumably limited in size by a surface oxidation process, and pass out of the burner without growing sufficiently to leave a deposit of soot. Processes of carbon formation are discussed in detail by Gaydon[13] and Street and Thomas[14].

The unassigned band obtained in the hexane flame at 2,750 Å could be due to absorption by a molecule or radical of cyclic nature. This seems most likely as the position of earliest detection in the flame is close to that of the benzene absorption system. This band seems to follow the intensity variations of the benzene, and occurs in a similar spectral region (see *Figure 1*).

Emission spectra of some flat flames

The emission spectra recorded for the rich diethyl–ether flames seem largely in accord with the findings of Agnew and Agnew except that in the present case the method of recording spectra is rather more sensitive in the near ultraviolet and rather less sensitive to the longer wavelengths in the visible. Thus in the present case the HCO emission has been observed to 2,716 Å. This is due to the use of an all-quartz optical system.

In discussing the emission spectrum of the rich diethyl-ether flame, Agnew and Agnew[10] have suggested a relationship between the disappearance of the HCHO and the appearance of the HCO emission as the mixture is made leaner. They suggest that the reaction $O + HCHO = HCO + OH$, could account for the HCO emission. The reaction of atomic oxygen with formaldehyde is known to give OH emission and possibly some CO flame band emission at room temperatures. Even if this reaction does give $HCO^{\star}$ radicals, it is

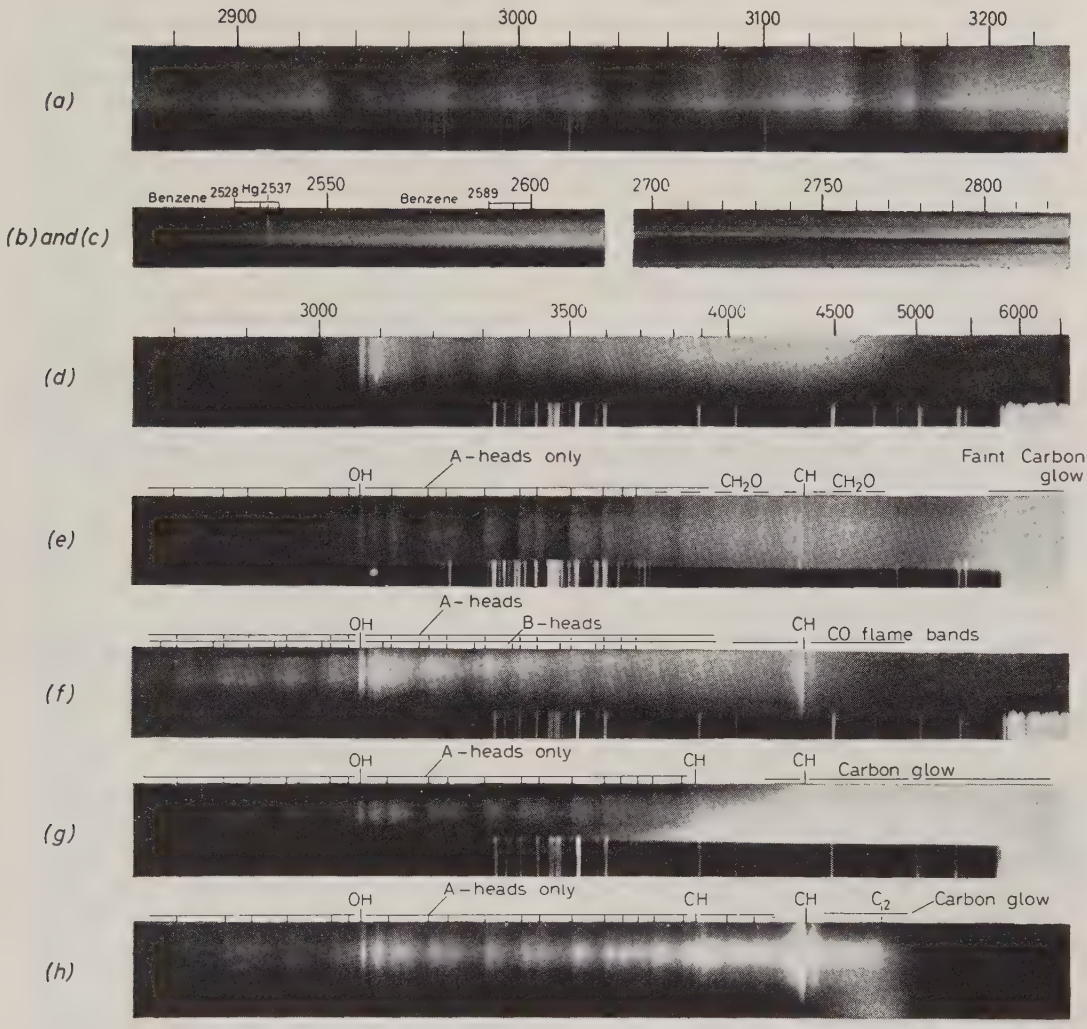

Figure 1. Description of spectra

(a) Formaldehyde absorption in the region of the cool flame of a diethyl/air fuel-rich Egerton–Powling flame, using 12 traverses. About 14 per cent ether by volume, flame speed about 4 cm/sec.

(b) Benzene absorption in the pre-heat region of a carbon forming rich hexane flame. Flame speed about 6 cm/sec.

(c) 2,750 Å absorption under the same conditions as (b).

(d) Weak diethyl-ether/air flame showing *A* and *B* heads of Vaidya's hydrocarbon flame bands.

(e) Rich diethyl-ether/air flame showing *A* heads only of the hydrocarbon flame bands. Yellow carbon formation is in evidence. Flame speed about 5 cm/sec.

(f) Weak butane/air flame. Flame speed about 7 cm/sec. Note the strong *B* heads in addition to the *A* heads of the HCO system. Flame speed about 7 cm/sec.

(g) Rich butane/air flame with strong carbon formation. Only *B* bands of the HCO system are present. Flame speed about 7 cm/sec.

(h) Rich methane/air flame, with very weak carbon formation. Flame speed about 8 cm/sec. Only *A* heads present.

Plates used for exposures (*a*), (*b*), (*c*) and (*h*) were Ilford Zenith. Plates used for exposures (*d*), (*e*), (*f*) and (*g*) were Ilford Astra III.

difficult to see where the atomic oxygen can come from when the final flame temperature is only of the order of 1,000°C. Reactions to give the atomic oxygen are not easy to specify and considerable quantities would be needed to account for the strength of the HCO system. It is possible that, as suggested by Agnew and Agnew, the formaldehyde burnt in the flame front of these flames does give rise to these HCO bands, other possible reactions being:

$$(1) \qquad HCHO + OH = HCO + H_2O$$

$$(2) \qquad HCHO + R = HCO + RH$$

The first reaction does not seem much more likely to give HCO emission than the reaction involving atomic oxygen, because HCO emission should be found in the normal flame of formaldehyde which is not the case. The second reaction is more probable as various alkyl radicals R will be found in these flames which will not be found in the

formaldehyde flame. Replacement of HCHO by HCHO* in these equations would give reactions which are more energetically acceptable. The HCHO* would naturally tend to radiate, but as the mixture is made leaner the energy release rate in the reaction zone increases, the combustion processes become faster, and the reactions involving the excited formaldehyde more likely. The HCHO* could react with less reactive species than OH or alkyl radicals to give HCO*, in view of the considerable energy carried by the HCHO*. More exact details of the radiative life of HCHO* are needed.

The HCO emission given by the rich flames of methane and butane is very similar to that in the case of diethyl–ether, the B bands being absent in each case. It has been suggested by Gaydon[15] that the B bands may be due to the appearance of heads in the rotational structure brought out by a higher rotational temperature. The similarity of emission of the HCO bands could be due to an effective low rotational temperature in each case. It is possible that there is a basic similarity in the processes leading up to HCO emission in the three cases quoted. In this case, mechanisms involving the use of HCHO or HCHO* will be somewhat less likely than others not using them, as it seems unlikely that they will be found in the reaction zones of methane and butane flames.

A further suggested mechanism for the production of HCO emission is

(3) $C_2 + HO_2 = HCO + CO$ (Gaydon[16])

This is a mechanism which is energetically adequate, and appears fairly apt for the conditions of rich mixtures under discussion. The C_2 emission, however, is rapidly diminishing with increase in mixture strength for those fuels studied, and for ether is quite absent.

Absorption spectra of carbon monoxide flames

For explosion flames of carbon monoxide, Knipe and Gordon[17] have given evidence that part of the structure of the carbon monoxide flame bands may be due to absorption, possibly by molecules of excited carbon monoxide in the $a^3\Pi$ state. The experiments reported here, using undried carbon monoxide–air flames at atmospheric pressure, do not lend support to this, no absorption from the $a^3\Pi$ state having been detected under the experimental conditions reported earlier in this paper.

SUMMARY

The multiple reflection absorption technique has been applied to flat flames. The presence of oxidation and pyrolysis intermediates in rich-limit flat flames has been shown by their ultraviolet absorption spectrum. Formaldehyde and benzene have been detected in flames of ether and hexane with air. There is also weak absorption in the region 2,750 Å in the case of the hexane flame. This could be attributed to absorption by a cyclic radical or molecule. Early results of the application of the multiple reflection technique to low-pressure flames have given the absorption bands due to OH and NH.

The emission spectra of the Egerton–Powling flames of various fuels near the rich and weak limits of combustion are recorded. It is found that the emission spectrum of the rich diethyl–ether flame varies in a similar way to that indicated by Agnew and Agnew but some details of a qualitative nature are added. The occurrence of the hydrocarbon flame bands and the possible relationship with the conditions of occurrence of the cool flame bands are briefly discussed.

Observations of the emission and absorption spectra of flames burnt on a porous plate burner are mentioned.

The author wishes to acknowledge the continued help and encouragement of Dr. A. G. Gaydon, F.R.S.; also financial assistance from a United States A.R.D.C. contract.

REFERENCES

[1] Egerton, Sir Alfred C. and Pidgeon, L. M. *Proc. Roy. Soc. A* 142 (1933) 26
[2] Newitt, D. M. and Baxt, L. M. *J. chem. Soc.* (1939) 1711
[3] Spokes, G. N. and Gaydon, A. G. *Nature, Lond.* 180 (1957) 1114
[4] Powling, J. *Fuel* 28 (1949) 25
[5] Egerton, Sir Alfred C. and Thabet, S. K. *Proc. Roy. Soc.* 211 (1952) 445
[6] Thabet, S. K. *Ph.D. Thesis* (1951) London
[7] White, J. U. *J. opt. Soc. Amer.* 32 (1942) 285
[8] Botha, J. P. and Spalding, D. B. *Proc. Roy. Soc.* 225 (1954) 71
[9] Vaidya, W. M. *Proc. Roy. Soc.* 147 (1934) 513
[10] Agnew, W. G. and Agnew, J. T. *Ind. Eng. Chem.* 48 (1956) 2224
[11] Foresti, R. J. *5th Symposium on Combustion*, p. 582. 1954. New York; Reinhold
[12] Campbell, C. E. and Johnson, I. *J. chem. Phys.* 27 (1957) 316
[13] Gaydon, A. G. *The Spectroscopy of Flames*, p. 189. 1957. London; Chapman and Hall
[14] Street, J. C. and Thomas, A. *Fuel* 34 (1955) 4
[15] Gaydon, A. G. *The Spectroscopy of Flames*, p. 119. 1957. London; Chapman and Hall
[16] Gaydon, A. G. *The Spectroscopy of Flames*, p. 199. 1957. London; Chapman and Hall
[17] Knipe, R. H. and Gordon, A. S. *J. chem. Phys.* 23 (1955) 2097

36

CHEMILUMINESCENCE AND RADICAL RE-COMBINATION IN HYDROGEN FLAMES

P. J. PADLEY and T. M. SUGDEN

INTRODUCTION

Although it has been known for some time that line-reversal measurements of temperature made on the spectral lines of certain elements, present as traces, in a wide variety of flames indicate abnormally high electronic excitation of those elements in the reaction zone[1,2], no completely satisfactory explanation has hitherto been suggested for the phenomenon, nor has it been studied in great quantitative detail. Previous work has been conducted primarily with the elements iron, lead, and thallium, in acetylene–oxygen or hydrogen–oxygen mixtures, near stoichiometry, burning either at low pressure (in order to broaden the reaction zone) or at atmospheric pressure. In the case of acetylene, lines requiring up to 173 kcal/mole for their excitation have been reported as appearing with abnormal intensities in the reaction zone, but not in the interconal gases. Hydrogen, on the other hand, has hitherto been regarded as giving rise to an essentially thermal distribution of electronic energy, even in the reaction zone.

The present authors have recently given an account of work in which evidence of marked chemiluminescence from sodium was observed in hydrogen–oxygen flames heavily diluted with nitrogen, at atmospheric pressure[3]. With relatively small amounts of nitrogen, and consequently higher temperatures, this effect was overshadowed by the higher thermal excitation. Gaydon and Wolfhard[1] suggest that the excitation observed in hydrocarbon and other flames arises through three-body collisions between the metal atom and unspecified free radicals, whereas Broida and Shuler[2] favour a collision scheme of the type

$$CH(CH_2) + O + M \rightarrow CO + M^{\star} + H(H_2)$$

where M is H_2O, O_2, H_2 or C_2H_2, followed by the efficient bimolecular exchange

$$M^{\star} + Fe\ (e.g.) \rightarrow Fe^{\star} + M$$

The observations of Padley and Sugden[3] were made on a wide variety of fuel-rich hydrogen–oxygen–nitrogen flames, with a burnt gas temperature range of over 1,000°C (*ca.* 1,400–2,500°K), with traces of added sodium. The results, some of which are presented here for completeness, in *Figure 2*, were discussed in detail and interpreted briefly as follows:

(i) At the high final temperatures (T_f) the excitation is considered to be predominantly thermal at all points above the reaction zone, the rise during the first millisecond (corresponding with about 1 cm above the reaction zone) being due to a rise in the bulk temperature of the gases, which tends towards T_f. This rise is occasioned by the heat released during re-combination of the radicals H and OH, which are produced in amounts exceeding the equilibrium ones in the main combustion, towards their equilibrium concentrations. This has been shown to be reasonable on a quantitative basis.

(ii) At the lower final temperatures, where the thermal level of the intensity of the *D* lines in emission is correspondingly much lower, there is an almost instantaneous rise of intensity at the reaction zone, followed by a steady decay towards the thermal level, which corresponds with T_f. This is a chemiluminescent effect, arising from excitation of sodium by reactions I and II.

$$Na + H + H \rightarrow Na^{\star} + H_2 \qquad (I)$$

$$Na + OH + H \rightarrow Na^{\star} + H_2O \qquad (II)$$

This excitation diminishes with height above the reaction zone on account of the fall of radical concentrations because of the re-combination reactions

$$H + H + M \rightarrow H_2 + M \qquad (III)$$

$$H + OH + M \rightarrow H_2O + M \qquad (IV)$$

where M is a third body—usually a molecule of one of the major constituents of the burnt gas—H_2O, H_2, or N_2. The contribution of reactions I and II to the total re-combination is negligible, the amount of sodium being very small. This chemiluminescent effect is almost independent of temperature. Velocity constants have been deduced for reactions I–IV, and shown to have reasonable values. For example, $k_I \sim 2 \times 10^{-32}$ molecules^{-2} cm^6 sec^{-1} and $k_{II} \sim 6 \times 10^{-32}$ molecules^{-2} cm^6 sec^{-1} at 1,500°K. These values are of the same order of magnitude as the collision

frequencies, which suggests that nearly all ternary encounters are effective in promoting excitation.

(iii) At intermediate temperatures, the results are an obvious combination of those described in (i) and (ii) above.

In the work to be reported here, an extension of the observations has been made to include the elements Ga, In, Tl, Fe, Co, Ni, K, Cs, Cu, Ag, Cd, Mn, and Pb. In most cases the resonance lines were used, but not in all. The results are discussed in the light of the concentrations of the radicals H and OH, which have been determined by the flame photometric methods developed in this laboratory[4,5].

EXPERIMENTAL

The burner used for producing flames of pre-mixed hydrogen, oxygen, and nitrogen is shown in *Figure 1.* The central 'experimental' flame, of

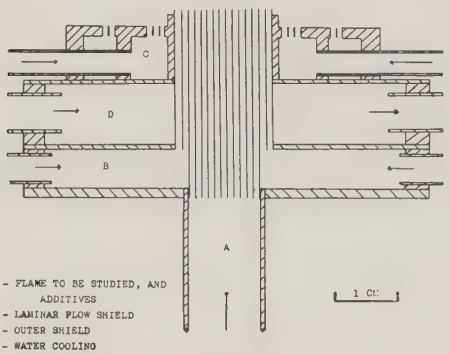

Figure 1. Diagrammatic cross-section of the burner; A, central 'experimental' flame, containing additives; B, laminar flame shield; C, outer flame shield; D, water cooling

diameter 1 cm, is burnt above a core of 100 stainless steel hypodermic tubes, tightly soldered together. This gives primary cones not more than $\frac{1}{2}$ mm in height, and an excellent laminar flame. It is surrounded by a laminar shielding flame, which serves to eliminate discontinuities at the boundary of the inner flame; this shield has the same mixture composition, and is shown as B in *Figure 1.* Additional shielding from entrained air is provided by an outer flame, also of the same composition, supplied from C, excellent protection of the inner flame being obtained up to heights of about 10 cm above the burner.

The flames were classed in 'families', as in previous work[3], based on the composition of the unburnt gas. Each family was characterized by a subscript numeral giving the unburnt N_2/O_2 ratio by volume; this varied from 2 to 9. A family contained five flames, with unburnt H_2/O_2 ratios of 2·5, 3·0, 3·5, 4·0, 4·5, denoted by F, K, P, U, Z respectively. The final temperatures (called T_f) of the burnt gases were measured several centimetres above the reaction zone by the sodium *D* line reversal method[6]; these correspond with the horizontal parts of the curves of *Figure 2.* The rate of supply of gas to the burner was changed progressively through the range of flames so as to compensate for a sixfold change in the burning velocity. Maximum unburnt gas flow to the central flame was $\frac{1}{2}$ ft.^{3}/min, and the shielding flames consumed four times as much mixture as the central flame.

The flame photometric system for measuring the intensity of the emitted light was similar to that described by James and Sugden[7]. An image of the inner flame was focused on to a sector disc, giving a 600 c/s signal. Two front-surfaced mirrors (plane) were arranged in conjunction with a second lens so as to form a further image, rotated through 90°, on the vertical entrance slit of either a Hilger E.3 Medium Quartz spectrometer, or a Rutherford prism monochromator constructed in the laboratory. By control of the entrance slits or by alteration of the conjugate points of the optical system the light from a horizontal strip of the flame gases as narrow as 0·1 mm could be examined. Detection was by an IP 28 photomultiplier tube, the signal being converted into a d.c. micro-ammeter reading by a low-noise homodyne amplifier synchronized by the chopping disc. Spectral resolution was of the order of 1 Å in the region of 5,000 Å. The resolution obtainable in terms of time in the flowing column of burnt gas was about 100 μsec for the lowest burning velocities, and about 25 μsec for the highest ones.

The range of elements for the survey was based largely on those which have fairly strong transitions in the accessible region of the spectrum, preferably away from the strong OH band system at 3,060 Å, and as far as possible on those which do not form large proportions of compounds with the flame gases, such as hydroxides and oxides. The ones best satisfying these requirements are Cu, Ag, Fe, Co, Ni, Mn, Pb, Tl and Na. Results given below for other elements have been corrected or the proportion of the element known to be combined.

These metallic elements were added as fine sprays of dilute solutions of their salts, from a calibrated atomizer, in amounts small enough for self-reversal of the lines to be negligible—usually less than 1 part in 10^6 of the total gases. Nitrates and chlorides were used, since they are known[3] to be completely fragmented in the reaction zone, in contrast with the more stable sulphates and phosphates, which persist for some little distance into the burnt gas.

RESULTS

Using a constant addition of salt to the supply to the central flame, the light emission from a section

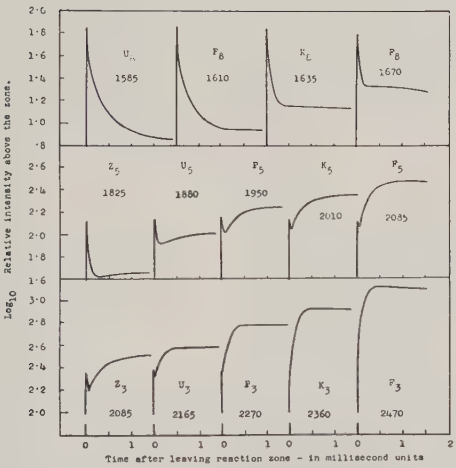

Figure 2. Variation of sodium D line intensity with time after primary combustion at the reaction zone for three 'families' of flames. A family is denoted by a subscript numeral giving the unburnt N_2/O_2, by volume, in the gases, and contains five flames, denoted F, K, P, U, Z, with unburnt H_2/O_2, by volume, of 2·5, 3·0, 3·5, 4·0, 4·5 respectively. The temperatures given are T_f in °K—the sodium D line reversal temperature where the curves become horizontal

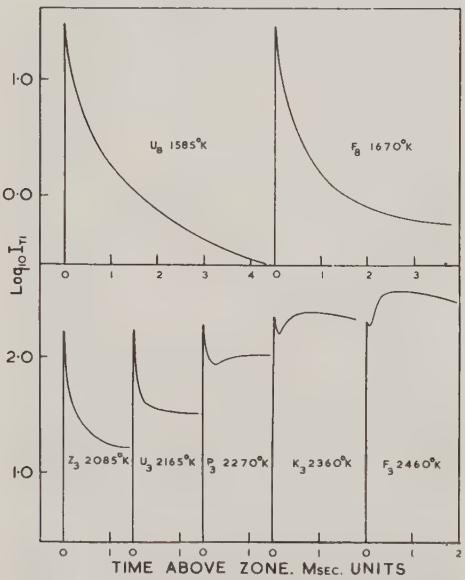

Figure 3. Variation of the intensity of the thallium 5,350 Å line with time from the reaction zone for a number of flames. The temperatures on the diagrams are the sodium D line reversal temperatures T_f (see Figure 2)

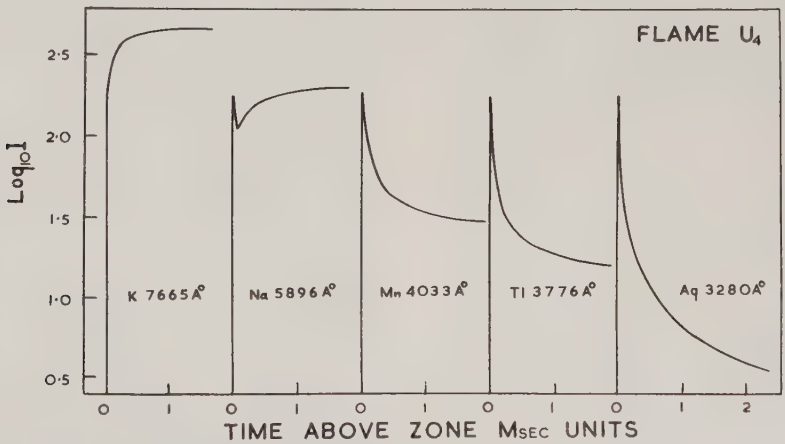

Figure 4. Variation of intensity with time for lines with different excitation energies in a given flame (U_4). All are resonance lines, so that the wavelength is simply related to the excitation energy

of the burnt gas ½ mm in height was examined as a function of the time from leaving the reaction zone for all flames. A selection of the results for sodium and thallium is shown in *Figures 2* and *3* respectively. In the case of sodium, a reasonably steady intensity is always reached after about 1 msec from the reaction zone. The emission here has been shown to be thermal[7], and the corresponding D line reversal temperatures are given in the figures, and will be denoted by T_f. The analysis of these curves for sodium has been given in the introduction; it is the low-temperature effect (chemiluminescence) which will be considered here. This effect is more clearly marked for thallium than for sodium, the thermal level for thallium not being reached at the lowest temperatures, and the chemiluminescence persisting towards much higher temperatures. Thus, for given excitation energy E, the predominance of chemiluminescence is favoured by a low level of thermal emission. A similar conclusion holds for variation of E with a given flame: this is shown in *Figure 4* for a selection of elements. The same trend is shown in a different way in *Figure 5*, in which the peak intensity (identified with the reaction zone) is plotted as I_{cz}/I_f against the

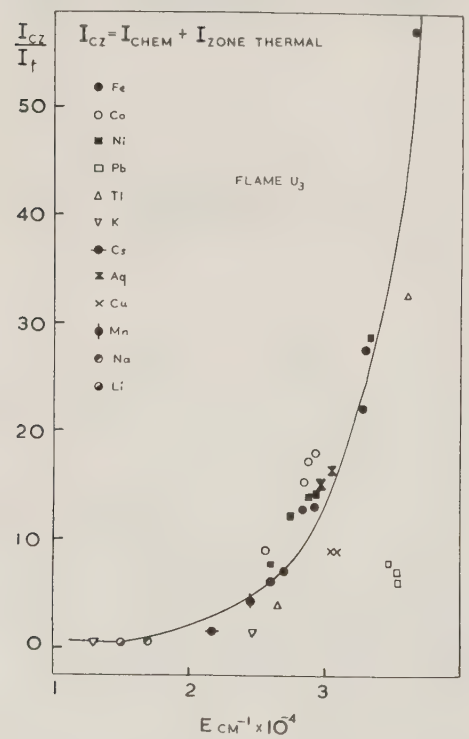

Figure 5. The degree of over-excitation in a given flame (U_3) for various lines, plotted as I_{cz}/I_f against the excitation energy of the upper state of the transition. I_{cz} is the observed intensity, and I_f the thermal value corresponding with the ultimate temperature T_f

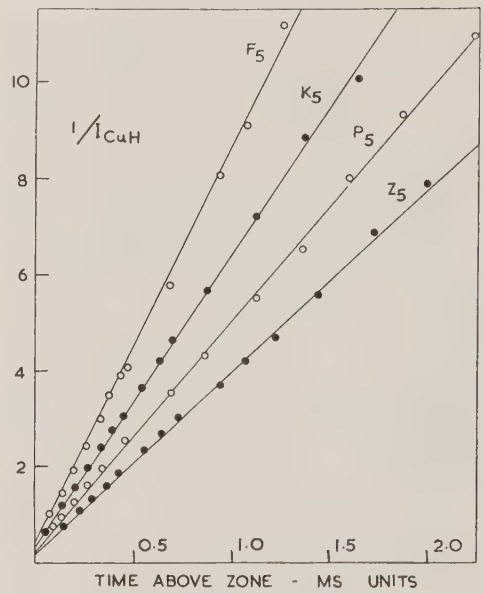

Figure 6. Plots of $1/I_{CuH}$ for four flames; I_{CuH}, the intensity of the CuH 0,0 *band at* 4,280 Å, *is proportional to the concentration of atomic hydrogen. The graphs show that this concentration diminishes with time according to a second order law. This holds effectively right to the reaction zone*

excitation energy of the upper level of the transition (assessed from the electronic ground state). I_{cz} is the total intensity observed, and can be regarded as made up of the sum of I_c (the chemiluminescent intensity) and I_{tz} (the thermal intensity); I_f is the thermal intensity corresponding with T_f, the final temperature. A fairly smooth curve is obtained, particularly if various lines of one element (e.g. Fe) are considered. The outstanding exception is lead—which will be discussed below. These results are in conformity with those of Gaydon and Wolfhard[1], and are in some ways an extension of them. They have been considered with respect to the concentrations of the free radicals H and OH in the flame gases. The concentration of atomic hydrogen has been shown[4] to correlate directly, apart from a small temperature effect, with the intensity of the CuH 0,0 band in emission at 4,288 Å: similarly the concentration of hydroxyl has been shown by James and Sugden[5] to correlate with the intensity of the continuum emitted in the visible region of the spectrum when sodium is present in the flame. Examples of the results are shown in *Figures 6* and *7*, plotted as reciprocals of intensity against time. They are good straight lines almost to the reaction zone, with finite intercepts. They suggest very strongly that re-combination of the radicals by reactions III and IV takes place from the reaction zone onwards. These methods for obtaining

relative H and relative OH may be calibrated from observations made some distance above the burner with very hot flames[8], where there is good reason to suppose that the radicals approach their equilibrium concentrations. It is thus possible to estimate, without any great error, what the concentrations of these radicals are in the reaction zone itself: the values obtained are set out for several families of flames in *Figure 8*. They are seen to exhibit clearly marked 'family' effects—i.e. they show isothermal variations dependent on the flame gas composition.

DISCUSSION

The discussion will take as starting point the supposition that reactions I and II, generalized from sodium to any metallic element A, are responsible for the excitation. This has already been shown to be very reasonable in the case of sodium[3]. 104 kcal/mole are available from re-combination of hydrogen atoms, and 118 kcal/mole from re-combination of H and OH. Only one line has been observed with an energy of excitation greater than 118 kcal/mole, and that was an Fe line requiring 122 kcal/mole. The small increment required might well be taken up from translational or rotational energy. The intensity of chemiluminescent emission at any point is then given by an equation of the form

$$n(1 + \phi\tau) = c_1[\mathrm{H}]^2 + c_2[\mathrm{H}][\mathrm{OH}] \qquad (1)$$

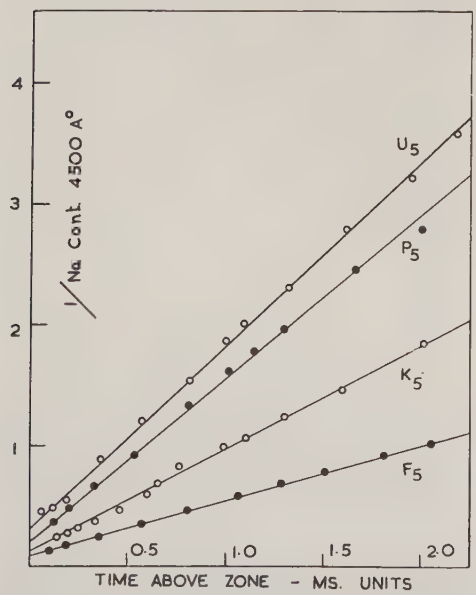

Figure 7. Plots of 1/(intensity of sodium continuum) for four typical flames; the intensity of the continuum is proportional to the concentration of hydroxyl radicals. The graphs show that hydroxyl obeys a similar kinetic law to atomic hydrogen (cf. Figure 6)

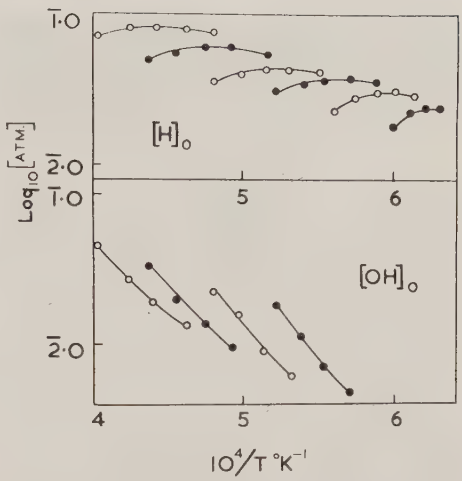

Figure 8. $[\mathrm{H}]_0$ and $[\mathrm{OH}]_0$ at the reaction zone for various families of flames, estimated from short extrapolations of CuH *and sodium continuum measurements respectively*

where n is the number of quanta emitted per second, $(1 + \phi\tau)$ is a Stern-Volmer factor to allow for collisional deactivation, τ being the radiative life-time of the excited atom and ϕ the number of quenching collisions per second. The parameters c_1 and c_2, apart from a constant factor, are products of the concentrations of atoms of metal and the velocity constants of reactions I and II respectively. This equation will be considered from two points of view—the decay of chemiluminescence with time in the burnt gas, and the peak intensity at the reaction zone. In the former case it should be possible to relate the effect to the known decay of the concentrations of atomic hydrogen and hydroxyl, according to reactions III and IV, and in the latter case to the data of *Figure 8*.

The decay of chemiluminescence in the burnt gas

It has been shown[8] that in these flames the reactions

$$\mathrm{H} + \mathrm{H_2O} \rightleftharpoons \mathrm{H_2} + \mathrm{OH};\ \text{eq. const. K}$$

are effectively equilibrated at all points in the burnt gases, and since $\mathrm{H_2}$ and $\mathrm{H_2O}$ are bulk constituents of these gases, they will have concentrations independent of time from leaving the reaction zone. Hence equation 1 can be written

$$n(1 + \phi\tau) = c_f[\mathrm{H}]^2 \qquad (2)$$

where
$$c_f = c_1 + c_2\frac{[\mathrm{H_2O}]\mathrm{K}}{[\mathrm{H_2}]} \qquad (3)$$

The decrease of [H] with time may be represented by equation 4

$$\frac{1}{[\mathrm{H}]} - \frac{1}{[\mathrm{H}]_0} = \left(k_1 + k_2\frac{[\mathrm{H_2O}]\mathrm{K}}{[\mathrm{H_2}]}\right)t = k_f t \qquad (4)$$

where k_1 and k_2 are the mean velocity constants for reactions III and IV respectively (including the concentrations of third bodies). The chemiluminescent intensity I may be related to n by $n = rI$, where r depends only on the measuring

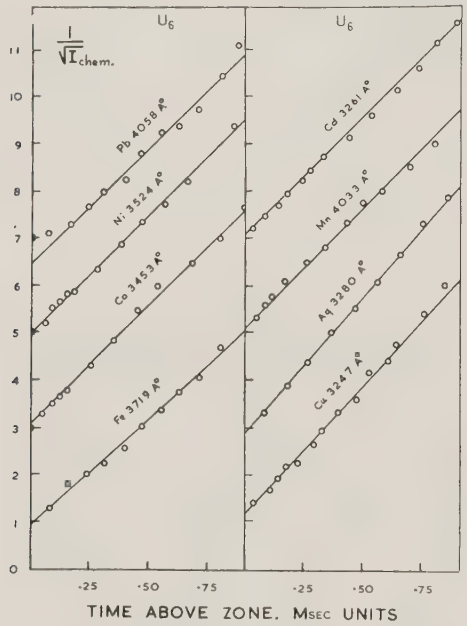

Figure 9. The variation of chemiluminescence with time from the reaction zone for various elements in a typical flame, plotted as $1/\sqrt{I}$. The upper three lines of each half of the diagram have been shifted along the ordinate axis by successive amounts of 2 units

apparatus. Equations 2 and 4 may be combined to give

$$\frac{1}{(I)^{\frac{1}{2}}} = r^{\frac{1}{2}} \left(\frac{1 + \phi\tau}{c_f}\right)^{\frac{1}{2}} \left(\frac{1}{[\mathrm{H}]_0} + k_f t\right) \qquad (5)$$

Thus plots of $1/(I)^{\frac{1}{2}}$ against t should be straight lines. This law has been shown to hold for sodium[3], and is strikingly confirmed by other elements, the results for eight of them being shown in *Figure 9*.

As described in the caption, the ordinates have been shifted for clarity of presentation. The ratio (intercept/slope) of the lines of *Figure 9* is very nearly constant, as would be expected from equation 5, since k_f depends only on the re-combination reactions III and IV, and is independent of the additive. The corresponding third order mean velocity constants k_f are of order of magnitude 10^{-31} molecules^{-2} cm^6 sec^{-1}. This is in good agreement with independent determinations[3,9]. *Figure 9* presented data for one flame; *Figures 10* and *11* show the effect for copper and thallium respectively for a particular family of flames. These are of interest in that they show that the ratio of slope to intercept remains almost constant. The conclusion is that k_f does not vary much within a family.

Equation 5 is essentially an equation giving the variation of 1/[H] with time, and as a final confirmation of the general correctness of the present viewpoint, *Figure 12* is included, showing the variation of 1/[H] and 1/[OH] with time, as determined from the intensity of the CuH band and the sodium continuum respectively for the flame U_6. The results are quantitatively similar to those depicted for U_6 in *Figure 11*. The absolute values of c_1 and c_2 will not be discussed at length here. They may, however, be deduced from the results if the quenching factor is known. The main quenching molecules will be H_2O, H_2 and N_2, of which the first is probably the most effective.

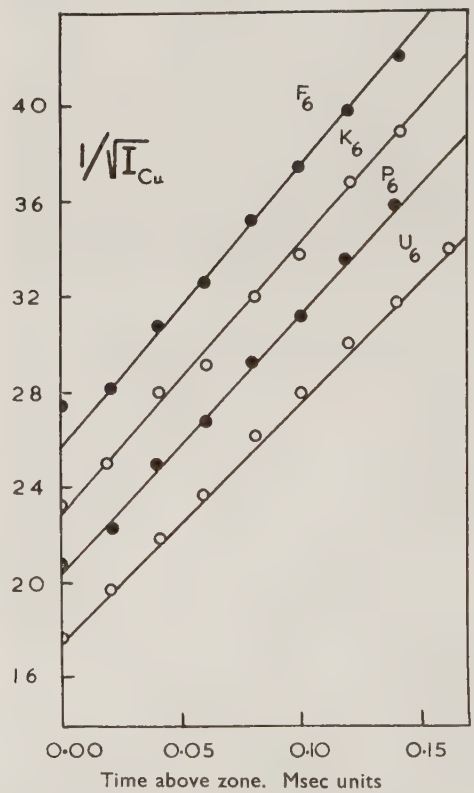

Figure 10. The chemiluminescence of the copper resonance line as a function of time from the reaction zone for one family of flames. Ordinates of upper three lines shifted upwards successively by 3 units

Unfortunately, there are insufficient data available, but on the quenching data given by Mitchell and Zemansky[10] and Laidler[11] little or no isothermal composition (family) effect is to be expected for ϕ, and the whole factor $(1 + \phi\tau)$ to have a value in the region of 10. These assumptions were used in obtaining the values of c_1 and c_2 for sodium[3],

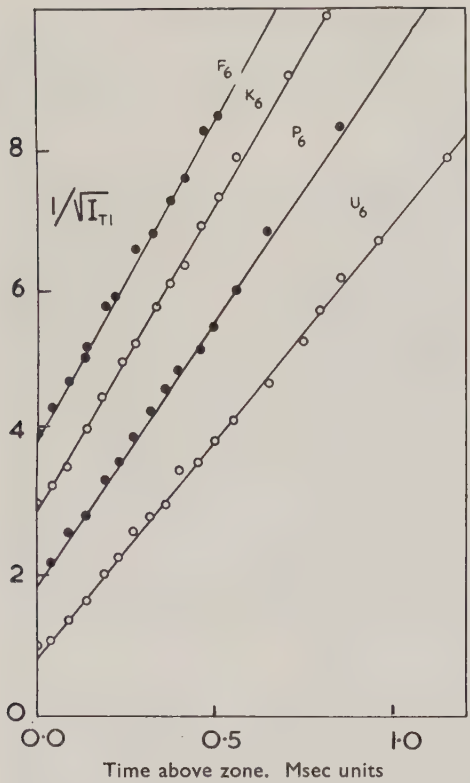

Figure 11. The chemiluminescence of the thallium resonance line as a function of time from the reaction zone for one family of flames. Ordinates of upper three lines shifted upwards successively by 1 unit

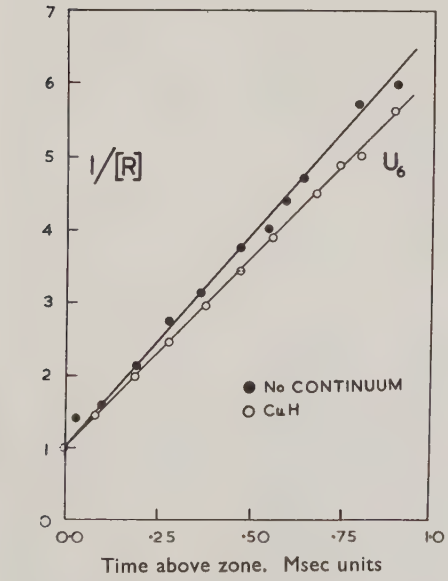

Figure 12. Reciprocals of intensities of the CuH *0,0 band and the sodium continuum for one of the flames shown in Figures 10 and 11*

quoted in the introduction. If ϕ shows negligible variation with composition for given temperature, some interesting conclusions about the ratio c_1/c_2 can be drawn. This may be done most easily by considering the peak intensities.

The peak intensities of chemiluminescence

The position of peak intensity, for present purposes, has been identified with that of the reaction zone, which cannot be far from true.

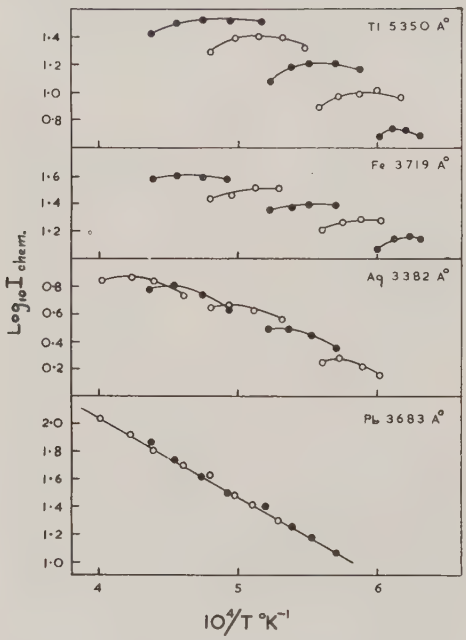

Figure 13. The peak intensity of chemiluminescence for various families of flames plotted for lines of thallium, iron, silver, and lead. The cases of thallium and lead are the extreme types observed

Peak intensities for four elements are shown for various families of flames in *Figure 13*. There is, in general, a characteristic 'family' effect for each element, ranging between the extreme cases of thallium and lead depicted in *Figure 13*. All the other elements studied fall between these two cases. If I_0 is the peak intensity, corresponding with $t = 0$ in equation 5, that equation may be re-arranged to give

$$I = \frac{[\mathrm{H}]_0^2 c_f}{r(1 + \phi\tau)} \qquad (6)$$

or

$$I = \frac{1}{r(1 + \phi\tau)} (c_1[\mathrm{H}]_0^2 + c_2[\mathrm{H}]_0[\mathrm{OH}]_0) \qquad (7)$$

the subscript zero denoting values at the reaction zone. Plots of $[\mathrm{H}]_0^2$ and $[\mathrm{H}]_0[\mathrm{OH}]_0$, computed from the data of *Figure 8*, are shown in *Figure 14*. Their respective resemblances to the plots for

thallium and lead of *Figure 13* are outstanding. They imply that these extreme cases are governed by

$$Tl + H + H \rightarrow Tl^{\star} + H_2 \quad (c_1 \gg c_2)$$

and

$$Pb + H + OH \rightarrow Pb^{\star} + H_2O \quad (c_1 \ll c_2)$$

respectively. The factors determining the ratio of these two parameters c_1 and c_2 obviously merit detailed investigation from the chemical kinetic point of view in future work. From the point of view of combustion research, the use of thallium and lead to study concentrations of atomic hydrogen and hydroxyl may be of some value. The fact that the extreme cases seem to appear in the above way goes some distance in justifying the assumption that the quenching factor shows no family effect.

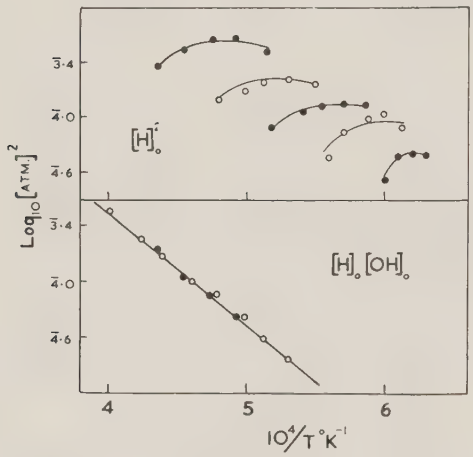

Figure 14. The functions $[H]_0^2$ *and* $[H]_0[OH]_0$ *estimated for the reaction zone from the data of Figure 8*

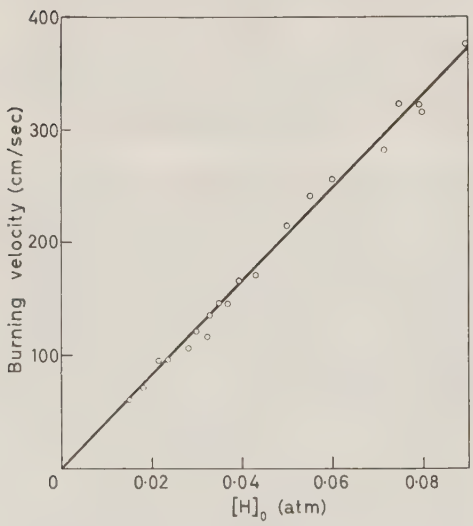

Figure 15. Burning velocities of hydrogen–oxygen–nitrogen flames as a function of $[H]_0$*, the concentration of atomic hydrogen in the reaction zone*

The relationship of $[H]_0$ *to the burning velocity*

One last point is worthy of mention here. The above results suggest that reasonably accurate values of the concentration of atomic hydrogen in the reaction zone have been obtained. In *Figure 15* these are plotted against the burning velocities for $H_2/O_2/N_2$ flames given by Jahn[12]. An excellent straight line passing through the origin is obtained. This is a very much more striking correlation than any which can be obtained from the considerations of Tanford and Pease, based on equilibrium concentrations of atomic hydrogen[13]. No theoretical explanation of this straight line is offered here, but it is felt that the correlation with actual concentrations of atomic hydrogen, estimated both from CuH and chemiluminescence measurements, is too significant to be overlooked.

One of us (P. J. P.) is grateful to the Ministry of Education for a Studentship. The authors wish to extend their thanks to their colleagues, in particular Miss E. M. Bulewicz, for interesting discussions in the course of this work.

REFERENCES

[1] Gaydon, A. G. and Wolfhard, H. G. *Proc. Roy. Soc. A* 205 (1951) 118
[2] Broida, H. P. and Shuler, K. E. *J. chem. Phys.* 27 (1957) 933
[3] Padley, P. J. and Sugden, T. M. *Proc. Roy. Soc. A* 248 (1958) 248
[4] Bulewicz, E. M. and Sugden, T. M. *Trans. Faraday Soc.* 52 (1956) 1475
[5] James, C. G. and Sugden, T. M. *Proc. Roy. Soc. A* 248 (1958) 238
[6] Gaydon, A. G. and Wolfhard, H. G. *Flames*, Chap. X. 1953. London; Chapman & Hall
[7] James, C. G. and Sugden, T. M. *Proc. Roy. Soc. A* 227 (1955) 312
[8] Bulewicz, E. M., James, C. G. and Sugden, T. M. *Proc. Roy. Soc. A* 235 (1956) 89
[9] — and Sugden, T. M. To be published
[10] Mitchell, A. C. G. and Zemansky, M. W. *Resonance Radiation and Excited Atoms.* 1934. Cambridge University Press
[11] Laidler, K. G. *The Chemical Kinetics of Excited States.* 1955. Oxford; Clarendon Press
[12] Jahn, G. *Der Zündvorgang in Gasgemischen.* 1934. Berlin; Oldenbourg
[13] Tanford, C. and Pease, R. N. *J. chem. Phys.* 15 (1947) 431, 861

DISCUSSION

A. G. Gaydon (London): In opening the discussion, I should like to welcome the trend towards quantitative measurements and note that these have resulted from developments in experimental techniques, especially the burners for flat flames. Even with these, care must still be taken to avoid disturbances due to schlieren-type effects.

Intensities of lines and bands depend not only on concentrations and excitation processes, but also on de-activation processes. Recent work at Imperial College on shock tubes, in which the temperature has been measured by sodium-line reversal, suggests that the excitation of sodium lines may follow the effective vibrational temperature of nitrogen molecules. It is, therefore, important that detailed energy transfer processes should be taken into account in interpreting quantitative observations of flame spectra.

A. R. Ubbelohde (London): It seems at first sight rather surprising that the vibrational degrees of freedom in a collision, such as that between nitrogen and excited sodium atoms, or the reverse process, should prove so much more efficient than collisions between sodium atoms and argon atoms. In general, vibrational degrees of freedom do not appear to be particularly effective in the exchange of internal energy, because of quantum restrictions. Is it possible that the further possibility of changes of rotational quanta in a collision, when nitrogen is substituted for argon, makes it much easier to satisfy the dynamical and quantum restrictions for efficient interchange? The bulk of the energy exchange may always be located in the process electronic $\rightleftharpoons$ vibrational energy. Coupled with the differences in repulsion potential energy in different excitation states of the sodium atoms, the possibilities for adjusting rotational energy and angular momentum may lead to very significant differences between, say, nitrogen and argon in collisions where a transfer of internal energy is required.

J. W. Linnett (Oxford): Gaydon mentioned, in his introduction to the discussion, that it seems from his shock-tube experiments that the sodium-line reversal method follows the vibrational temperature of nitrogen as it is heated by the shock. This seems to be most surprising but I wonder whether the necessary interaction between the nitrogen vibration and the electron cloud of the sodium atom exists because the sodium atom has a different size in the ground and excited states.

M. Boudart (Princeton) spoke of the importance of vibrationally excited molecules, including those of HCl in the reaction between hydrogen and chlorine.

B. A. Thrush (Cambridge): As Boudart suggests, vibrationally excited HCl produced by the reaction, $H + Cl_2 = HCl^{\star} + Cl$, is probably important in producing chain branching in the H_2/Cl_2 flame. In recent work at the National Bureau of Standards, Washington, we have observed emission by HF molecules with up to nine quanta of vibrational energy from the H_2/F_2 flame. The intensity distribution of this vibration-rotation spectrum suggests strongly that vibrationally excited HF is produced by the reaction $H + F_2 = HF^{\star} + F$. This reaction is more than 90 kcal exothermic and can provide more than twice the energy needed for the chain-branching reaction $HF^{\star} + F_2 = HF + F + F$. In these circumstances, I also feel that the agreement between Boudart's suggestion and van Tiggelen's activation energy for the H_2/Cl_2 flame is fortuitous, as van Tiggelen finds that the activation energy for the H_2/F_2 flame is only about 2 kcal less than for the H_2/Cl_2 flame, whilst the energy surplus of the branching reaction would suggest a much bigger difference.

E. M. Bulewicz (Cambridge): In their paper on the decay of radical radiation, Child and Wohl attribute the second-order decay of OH radiation above the reaction zone to the re-combination of two OH radicals in a bimolecular process with an activation energy of about 19 kcal/mole.

This interpretation is not the only possible one. In a system containing water vapour and hydroxyl radicals, molecular hydrogen and hydrogen atoms will also be present. [H] and [OH] will not be independent, because of the rapid reactions:

$$H + H_2O \rightleftharpoons H_2 + OH$$

The re-combination of two hydrogen atoms or a hydrogen atom and a hydroxyl radical may lead to the same apparent order of OH radiation decay.

We have made measurements on radical re-combination in the burnt gases of hydrogen/oxygen/nitrogen flames and have found that the re-combination is termolecular and proceeds through the reactions

$$H + H + X \rightarrow H_2 + X \qquad (1)$$

$$H + OH + X \rightarrow H_2O + X \qquad (2)$$

the third body, X, being mainly H_2O (which might be expected for a system in which the bulk constituents are H_2O, N_2 and H_2). We have

measured the rate constants in the range 2,200–1,600°K and have found that they both increase with decreasing temperature, which is characteristic of many radical re-combination reactions. The values of the rate constants at 1,600°K are, approximately,

$$k_{1(X=H_2O)} = 5 \times 10^{-32} \text{ cm}^6 \text{ molecule}^{-2} \text{ sec}^{-1}$$
$$k_{2(X=H_2O)} = 1 \times 10^{-30} \text{ cm}^6 \text{ molecule}^{-2} \text{ sec}^{-1}$$

It is not unreasonable to suggest that the results for butane/air flames could perhaps be interpreted along similar lines.

G. N. Spokes (London): Since my paper was submitted, some further experimental results have been obtained.

Qualitative examination of the absorption band of the OH radical in the reaction zone of a low-pressure flame has been made. The rotational temperature in absorption has been shown to be appreciably lower than the rotational temperature in emission for flames of acetylene and ethylene with oxygen.

With fuel-rich oxy-acetylene flames at low pressures, absorption in the region 3,143 Å has been found. The diffuse absorption band appears in the reaction zone, and is attributed to that of the Q branch of the (0, 0) transition of CH. No rotational structure was resolved. A quartz Littrow spectrograph was used for these observations, with a flash tube as background source.

R. H. Tourin (New York), commenting on the papers by Kiess and Broida, and Child and Wohl: In both of these papers mention is made of flame temperature determinations obtained from the flame spectra. Child and Wohl, using an infra-red brightness method, report quite reasonable temperatures for the butane–air flame (their Table 2). On the other hand, Kiess and Broida found gross anomalies in their temperature determinations, which were obtained from Boltzmann equation plots of the rotational and vibrational energy distributions in electronic band spectra. While such anomalous 'temperatures' are undoubtedly useful in the study of flame kinetics and reaction mechanisms, their value as indications of the thermal state of the flame is very limited. It seems desirable that anomalous 'temperature' determinations obtained from Boltzmann plots be supplemented by infra-red brightness temperatures, measured by techniques such as the one described by Child and Wohl.

H. P. Broida (Washington) in reply to Tourin: The measured rotational 'temperature' of 315°K is, as stated in the paper, the temperature of the glass walls of the reaction vessel. The walls feel slightly warm when touched. Whereas the high vibrational 'temperature' ($\sim$ 3,000°K) found in the discharge shows a non-equilibrium in the vibrational degrees of freedom, the rotational 'temperature' ($\sim$ 350°K) is nearly an order of magnitude less and is more likely near the wall temperature.

Cook asked whether, in the paper by Kiess and Broida, the OH 'temperatures' were measured in emission or in absorption.

H. P. Broida (Washington) in reply: In emission, OH emission 'temperatures' have been shown* to be a chemiluminescent phenomena characteristic of the reactions producing the excited OH radical. Essentially, in every collision of the excited OH, the electronic excitation is removed and thus the rotational distribution has no direct relation to the temperature of the bulk of the gas.

K. R. Jennings (Oxford): We have recently carried out work similar to that described in this paper and our results are in general agreement with those presented here. One point of especial interest was the fact that the CH 4315 Å system, due to the transition $^2\Delta \rightarrow {}^2\Pi$, was always observed in flames in which carbon and hydrogen were present, but the 3,900 Å system, due to the transition $^2\Sigma \rightarrow {}^2\Pi$, was never observed.

In hydrocarbon–oxygen flames, CH radicals are thought to be formed in the reaction

$$C_2 + OH \rightarrow CH + CO \quad \Delta H = -122 \text{ kcal}$$

By analogy, in atomic nitrogen flames, the CH radicals may be formed in the reaction

$$C_2 + NH \rightarrow CH + CN \quad \Delta H = -67 \text{ kcal}$$

The energy released in these reactions can account for radiation at wavelengths longer than about 4,270 Å, but is insufficient to excite CH radicals to the $^2\Sigma$ state. It is thought that this may account for the non-appearance of the CH 3,900 Å system in atomic nitrogen flames.

* Broida, H. P. and Carrington, T. *J. chem. Phys.* 23 (1955) 2202.

PART III

IONIZATION IN FLAMES

37

MASS SPECTROMETRY OF THE IONS PRESENT IN HYDROCARBON FLAMES

P. F. KNEWSTUBB and T. M. SUGDEN

Although the subject of ionization in flames has received much attention in recent years from the point of view of the interpretation of conductivity measurements, based on both high-frequency absorption and probe techniques, these measurements are essentially of the concentration of free electrons, and the exact nature of the positive ions has remained doubtful. A useful summary of much of the work in this field has recently been given by Calcote[1]. It is already known that the reaction zone of pre-mixed flames of hydrocarbons with oxygen shows marked ionization (i.e. electrical conductivity), and since this is most probably related to some of the highly energetic processes occurring in combustion, it might be hoped that a more detailed examination would throw some light on such processes. This paper is concerned with mass spectrometric observations which have been made of the ions occurring in the reaction zones of pre-mixed flames of hydrocarbon and oxygen. In contrast with the work of Eltenton[2], the ions are sampled directly from the flame, and not produced from the flame gases by subsequent ionization by an electron beam. All our work has been done with flames at atmospheric pressure; rather similar work appears to be in progress, for flames at lower pressures, as shown by Deckers and van Tiggelen[3]; their results will be compared with ours below.

A detailed description of the apparatus will not be given here, but is to be published later; preliminary mention of it has already been made[4]. The chief experimental problem lies in the sampling process, and has been solved in this case by a kinetic differential pumping system of adequate capacity. The flame under examination is directed against a thin (0·002 in.) platinum disc, in which a hole approximately 0·002 in. in diameter admits a sample of about $\frac{1}{4}$ c.c. sec^{-1} at atmospheric pressure from the flame. A pumping speed of about 250 litres sec^{-1} on the opposite side of this disc reduces the pressure here to about 10^{-3} mm Hg. Any ions contained in the sample are accelerated along the axis of the instrument through a slit, into a second chamber which is continuously pumped to a lower pressure, and likewise into a third chamber, where a pressure of 3×10^{-6} mm Hg is reached. This pressure is suitable for the operation of a fairly conventional sector type of magnetic analyser. After leaving the vicinity of the first sampling hole, the ions should not suffer further collisions, or at least will not reach the detector if they do so. Ions present at any selected mass/charge ratio are detected by a multiplier device, the pulses being counted on a scaling unit. The sensitivity is such that concentrations of ions of the order of 10^7 cm^{-3} in the flames may be observed. The analyser is capable of dealing with masses in the range 1–400 atomic units, but in this work has been restricted to the range 12–150 atomic units.

Pre-mixed flames have been used in these experiments, burnt in the end of a Pyrex tube so as to give a single primary reaction cone about 6 mm high, the tip of which was directed against the hole. Provision was made for small controlled movements of the burner in an axial direction, so that concentration profiles through the tip of the reaction zone could be plotted. The fuels used were in the main hydrogen, acetylene, ethylene, ethane, methane and acetone, mixed with oxygen and nitrogen in proportions such as would give burnt gas temperatures in the vicinity of 2,500°K. The mixture strength is defined by the parameter λ thus:

$$\lambda = \frac{\text{(stoichiometric fuel/oxygen ratio)}}{\text{(actual fuel/oxygen ratio)}}$$

Thus, values of $\lambda < 1$ correspond to fuel-rich mixtures. Mixtures rich enough to give visible permanent carbon formation have not been used, as the deposition of carbon tends to clog the entry to the analysing system. The greater part of this paper will be given over to a survey of the results for acetylene, with discussion of their implications, which will be followed by a brief comparison of results for other fuels.

THE IONS IN ACETYLENE FLAMES

At the time of writing the most complete survey has been made with acetylene as a fuel, and a typical mass spectrum is shown in *Figure 1*. This spectrum was taken in the reaction zone

of the flame. With very few exceptions the ions appeared and disappeared again within a distance of about 0·3 mm at the reaction zone. A certain amount of discrimination could be made about the relative positions in which various ions gave peak concentrations, and will be referred to below: the most important point to note is that mass standpoint, there being no other ionizing source than the flame reactions themselves.

(2) The ions at masses 18, 19, 21 and 37 persist into the burnt gas beyond the reaction zone, and also occur in hydrogen flames[4]; they have been ascribed with considerable certainty to H_2O^+, H_3O^+, $H_3{}^{18}O^+$ and $H_5O_2^+$ respectively.

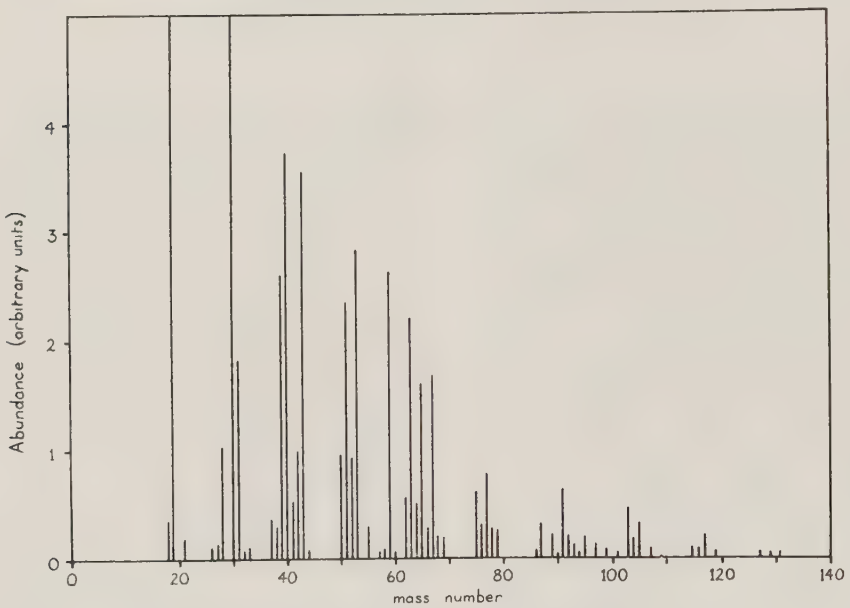

Figure 1. Mass spectrum of the positive ions in the reaction zone of an acetylene–oxygen–nitrogen flame; $\lambda = 0{\cdot}80$

39 was the earliest (i.e., nearest the burner) to appear. The data plotted in *Figure 1* show the peak intensities reached, irrespective of the position in or near the reaction zone. The most evident feature is the richness of the flame both in kinds and amounts of positive ions. The largest peaks shown correspond with about 10^9 ions cm^{-3}, and the total ionic concentration falls into the region of 10^{10} ions cm^{-3}. This is broadly in line with conductivity data of the type presented by Calcote and King[5], and is many orders of magnitude greater than could correspond with thermal ionization. The absence of alkali impurities is shown by the absence of a peak at mass 23 (sodium being the most likely, readily ionizable impurity).

Although it is not possible at this stage to give a complete analysis of this spectrum, a partial one will be attempted, and extended and justified by consideration of further results below. The following points may be made about *Figure 1*.

(1) Since no half integral peaks appear, it will be assumed that ions of unit charge only appear. This is very reasonable from an energetic The only other peak persisting in this manner is mass 30, which in some cases is indeed the major ionic constituent. This peak disappears when argon is substituted for nitrogen, and is thus most probably due to NO^+.

(3) Certain peaks are conspicuous by their absence—in this case $CH^+(13)$, $C_2^+(24)$ and $CH_2^+(14)$, although the parent bodies CH and C_2 are known from their electronic spectra to exist in an excited state in the reaction zone, and in contrast with the results of Deckers and van Tiggelen[3], who find the CH^+ and CH_2^+ to be abundant in acetylene flames at lower pressures ($\sim$50 mm Hg).

(4) The pattern of all the peaks above mass 38 bears, with certain exceptions, a great similarity to the cracking patterns obtained for many hydrocarbons obtained by more conventional mass spectrometry, using ionization by electrons of about 100 eV energy. It is considered that the bulk of them arise from hydrocarbon ions $C_nH_m^+$. One notes

(*a*) A broad subdivision into groups corresponding to hydrocarbons based on from

3 to 10 atoms of carbon, with varying, although rather low, degrees of hydrogenation.

(*b*) An alteration of abundance in the groups, the odd masses predominating; this is also found in cracking patterns. It is clearly linked with the stabilities of the ions as compared with the parent molecules, of which the latter are always free radicals for odd mass numbers. Some light is thrown on this interpretation by consideration of *Figure 2*, in which mass spectra of acetylene flames of different mixture strengths are shown.

All are for flames which did not give rise to permanent formation of carbon particles (which occurs for $\lambda < 0{\cdot}4$), although *Figure 2a* ($\lambda = 0{\cdot}43$) is a flame in which the reaction zone, with its

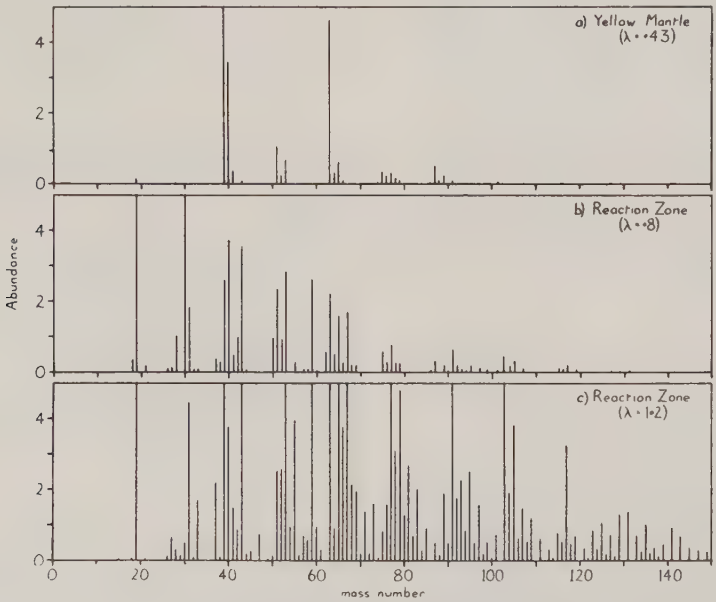

Figure 2. Mass spectra of positive ions in various acetylene–oxygen–nitrogen flames. (a) Luminous mantle of a flame with $\lambda = 0{\cdot}43$; *(b) reaction zone of a flame with* $\lambda = 0{\cdot}80$; *(c) reaction zone of a flame with* $\lambda = 1{\cdot}2$

(*c*) The C_3 group are the most abundant, with a broad maximum at about the C_5 group for the remaining ones.

(*d*) The large peak at mass 59 stands out of the pattern, and is believed to be an oxygenated ion $C_2H_3O_2^+$.

(*e*) The earliest ions to appear were at masses 39 ($C_3H_3^+$) and 65 ($C_5H_5^+$), followed by 53 ($C_4H_5^+$) and 77 ($C_6H_5^+$), and later by all the others. An accurate time resolution is not yet possible, but the ions noted had clearly reached their peak values while most of the others were just appearing. The average time spent by the flame gases in crossing the region in which ions occur is of the order of 100 μsec.

(5) The ions at mass numbers 26, 27, 28, 31, 32, 33 present certain difficulties, but the following seems most likely, since none of them disappeared in the argon experiments.

26; $C_2H_2^+$	31; CH_3O^+
27; $C_2H_3^+$	32; CH_4O^+, O_2^+
28; $C_2H_4^+$	33; HO_2^+

characteristic C_2 radiation, is surmounted by a luminous mantle. The following points may be noted.

Figure 2a ($\lambda = 0{\cdot}43$). This spectrum was taken in the luminous mantle above the reaction zone of a flame on the verge of carbon formation. Here the ionization, although much reduced, persists for much longer (about 10 times as long as for the flame of *Figure 2c*). All the oxygenated peaks, including $H_2O^+(18)$ and $H_3O^+(19)$, have disappeared or become very small, leaving a simple pattern of hydrocarbon ions. The alteration of intensities is still discernible, but generally it is the lowest mass number of each group which is most abundant. The very large value for $C_5H_3^+(63)$ is most noteworthy, as is also the high value for $C_7H_3^+(87)$.

Figure 2b ($\lambda = 0{\cdot}8$). An intermediate case, discussed on the basis of *Figure 1*.

Figure 2c ($\lambda = 1{\cdot}2$, an oxygen-rich flame). Very large ionization, amounting to at least 10^{11} ions cm^{-3}. The hydrocarbon families, with alternating intensities in each family, are clearly visible from the C_3 to the C_{12} group, the largest

peaks being for C_nH_n (n odd) or $C_nH_{n\pm1}$ (n even). There is again a broad maximum of concentration in the C_5 group, with C_3H_3(39) standing out as very high. The C_2 group is now more clearly defined and extended, and there is definite indication of CH_3^+(15), which occurred as the merest trace in *Figure 1* ($\lambda = 0{\cdot}8$). The duration of the ionization was found to be shortest in this flame, despite the high level of the ion peaks.

The large ionization observed is well out of line with the thermal ionization of the hydrocarbon molecules and radicals likely to be present, as may be seen from the figures presented by Calcote[1], even in the cases of radicals such as $CH_2{-}C{\equiv}CH$ (C_3H_3) with low ionization potentials (8·25 eV). The ion of this radical is of great interest in that it appears earliest, and may well be in some ways a parent ion. It must be produced by some process involving only small endothermicity. Gaydon[6] presents strong evidence for the reaction

$$C_2 + OH \rightarrow CO + CH \ (\Delta H = -122 \text{ kcal}) \quad (1)$$

The heat quoted is for ground state molecules. This reaction is sufficiently exothermic to give electronically excited CH (> 70 kcal/mole required); if the OH were itself excited much more energy would be liberated, with the possibility of dissociating the CH. Highly excited (electronically or otherwise) CH radicals, diffusing backwards, could attack C_2H_2 to give direct ionization

$$HC{\equiv}CH + CH^* \rightarrow H_2^+C{-}C{\equiv}CH + \epsilon \quad (2)$$

since the direct combination of C_2H_2 and CH (ground state) to give the corresponding propargyl radical ($H_2C{-}C{\equiv}CH$) would not be far from 100 kcal/mole exothermic, and the ionization potential of the radical is 190 kcal/mole. This reaction would not be more than about 20 kcal endothermic. Alternatively CH^+ might be produced by reaction 3

$$C_2 + OH^* \rightarrow CO + CH^+ + \epsilon \quad (3)$$

followed by direct attachment

$$C_2H_2 + CH^+ \rightarrow H_2^+C{-}C{\equiv}CH \quad (4)$$

Reaction 3 is only about 30 kcal endothermic. It might be noted, however, that CH^+ has not been detected in our work, although Deckers and van Tiggelen[3] have found it very important at lower pressures. Processes involving the simultaneous production of a positive and a negative ion (such as OH^-) might also be involved, as suggested by Tverdokhlebov[7,8]. It is hoped in the future to modify the instrument to allow of examination of negative ions. This ion, $C_3H_3^+$, once made, could readily grow by processes of polymerization, possibly involving dehydrogenation, as follows:

$$H_2^+C{-}C{\equiv}CH + HC{\equiv}CH \rightarrow H_2^+C{-}C{\equiv}C{-}C{\equiv}CH + H_2$$

$$H_2^+C{-}C{\equiv}CH + HC{\equiv}CH \rightarrow H_2^+C{-}CH{=}CH{-}C{\equiv}CH$$

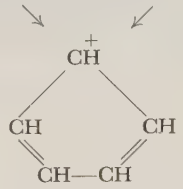

and similarly $C_7H_3^+$ (linear), $C_7H_7^+$ (a 7-ring structure), etc. The high values of $C_5H_3^+$(63) and $C_7H_3^+$(87) in *Figure 2a* are of interest in this connection.

This would only account for the ions with odd numbers of carbon atoms. These are clearly favoured in flames which are on the margin of carbon formation (*Figure 2a*). Even numbered ones might be obtained by a variety of processes between which no distinction can be made at the present. Among these the reaction with excited hydroxyl radicals to give two ions, as postulated by Tverdokhlebov[7,8], seems very reasonable.

$$C_nH_m + OH^* \rightarrow C_nH_m^+ + OH^-$$

In *Figure 2a* should also be noted the tendency for the ions $C_nH_3^+$ to be the largest in each group. It is difficult to see how these could have a ring structure with so little hydrogen, and a linear skeleton of carbon atoms seems more probable. They could, however, rapidly condense together to give highly active radicals of graphitic (or at least benzenoid) structure, which could then build up to give carbon particles of similar type. C_2 might be formed in this process, as suggested by Gaydon and Wolfhard[9].

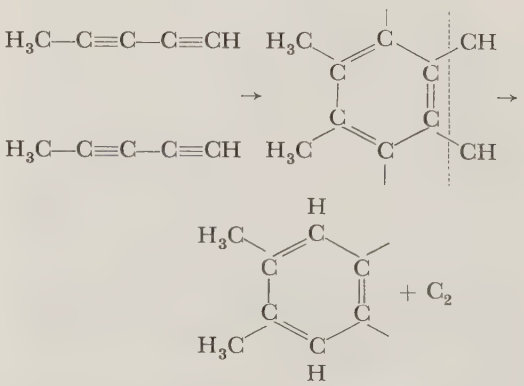

Whether this occurs with ions or parent molecules would seem to be immaterial. As the molecules become sufficiently large to be considered as particles their work functions (ionization potential)

will approach that of graphite, and their ionization can be dealt with along the lines suggested by Sugden and Thrush[10], and by the more rigorous treatment of Einbinder[11]. It is uncertain whether the final process in the above equation would release enough energy to provide excited C_2.

Another way in which C_2 might be produced in an electronically excited state, however, is by re-combination of positive hydrocarbon ions with electrons. This will release at least 7 eV (165 kcal/mole). The total concentration of ions of type $C_nH_3^+$ (for example) is of the order of 10^{10} cm^{-3} in the flame of *Figure 2c*. These disappear very rapidly in the reaction zone, and presumably by collision with negative ions or electrons. Collision of an electron with a linear $C_nH_3^+$ would yield a radical in a high vibrational level. As pointed out by Ubbelohde[12], and from a somewhat different aspect by Thomas[13], such a state of affairs might lead to rapid dissociation.

$$H_2^+C—C{\equiv}CH + \epsilon \rightarrow CH_3 + C_2^*$$

or a similar reaction with a longer chain giving rise to at least one excited C_2. This process has the merit of providing ample energy for excitation of C_2, and being capable of producing the amounts required to explain the observed intensity in emission.

This discussion for acetylene, hypothetical and incomplete though it must necessarily be, has shown how the ions may be involved in carbon formation, and in the production of C_2^*. The results themselves provide very strong evidence of what is essentially a polymerization of the fuel in the reaction zone. This polymerization is associated with anomalously high ionization, possibly reflecting the importance of ionic species in the reaction chain. In its early stages, at least, it would appear to be much more rapid in oxygen-rich flames, in which, however, it is superseded by an equally rapid depolymerization —or at least rapid oxidation of polymer with accompanying breakdown. It is not possible to say what the detailed roles of oxygen-containing molecules or radicals are. The variation of the peaks at 31, 43 and 59 with mixture strength, however, marks them down as different from those ascribed to hydrocarbon ions, and it seems likely that they arise from CH_3O^+, and $C_2H_3O^+$ and $C_2H_3O_2^+$ respectively.

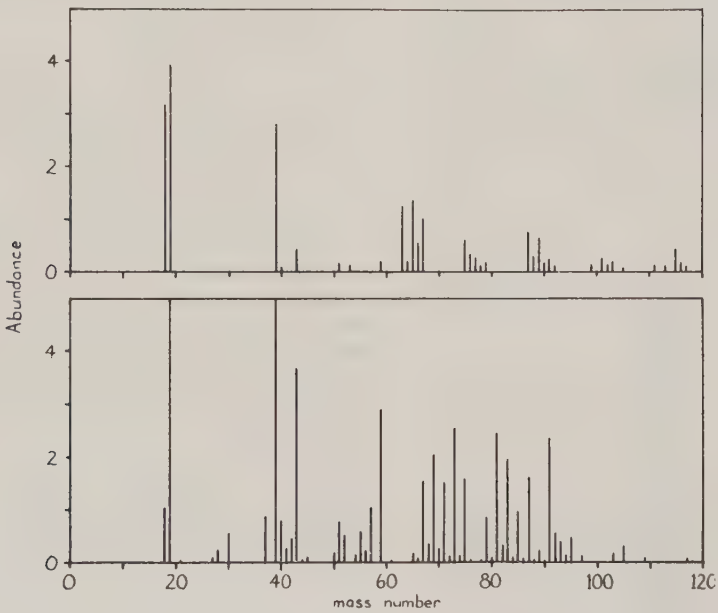

Figure 3. Comparative mass spectra of reaction zones of flames of acetylene (above) and of ethylene (below) pre-mixed with oxygen and nitrogen. In both cases $\lambda \sim 0{\cdot}6$

Further progress awaits more detailed results, including work on C_2D_2 as a fuel. Interesting features, however, are shown by a number of runs made with other fuels.

ETHYLENE

Figure 3 shows a comparison of ethylene and acetylene at similar mixture strengths. A similar extensive polymerization is noted.

Special interest attaches here to the C_5, C_6, C_7 groups, which for ethylene are clearly more hydrogenated than for acetylene. That some dehydrogenation occurs, probably with production of acetylene, as suggested by Porter[14], is shown by appearance of ions with rather high carbon/hydrogen ratios, but this is far from

complete. The processes of polymerization, at least as reflected in the ionic distribution, do not require complete breakdown to acetylene as a preliminary step. Masses 43 ($C_2H_3O^+$) and 59 ($C_2H_3O_2^+$) are present in large amounts, but mass 31 (CH_3O^+) is absent.

ETHANE

Figure 4 shows results for an ethane flame. The mass pattern is strikingly different from any previous one. The ions are concentrated in the C_3 group, with some, but rather small, evidence of polymerization to give C_4, C_5, C_6 hydrocarbons. The distribution of these last resembles that for acetylene more than that for ethylene.

As far as any conclusions can be drawn, it would seem to be likely that dehydrogenation occurs

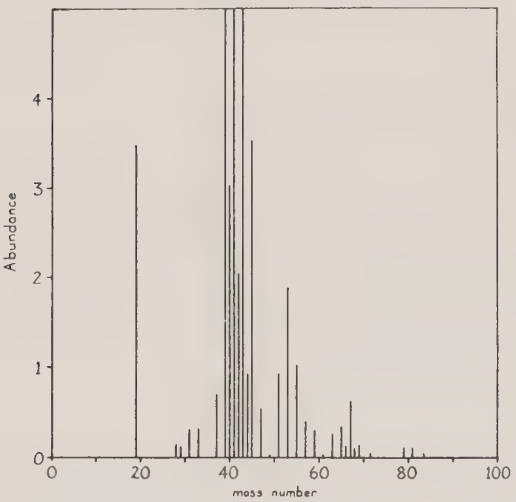

Figure 4. Mass spectrum of the positive ions in the reaction zone of an ethane–oxygen–nitrogen flame; $\lambda \sim 1$

rather rapidly to C_2H_4 and C_2H_2, and that these give rise to $C_3H_5^+$ and $C_3H_3^+$ ions by reaction with CH* or CH^+. The concentration of C_2H_2 built up, however, does not appear to remain sufficiently high for long enough to give much polymerization, rapid oxidation taking place.

METHANE

From the foregoing, a rather poor crop of ions might be expected from the reaction zone of methane flames, and this appears to be the case—as is seen in *Figure 5.*

A remarkable feature is the very large concentration of both H_2O^+ and H_3O^+, there being in this a strong resemblance to the behaviour of hydrogen flames[4]. There is also a large peak at 31 (CH_3O^+). Hydrocarbon ions are poorly represented, with medium strength at $C_3H_3^+$,

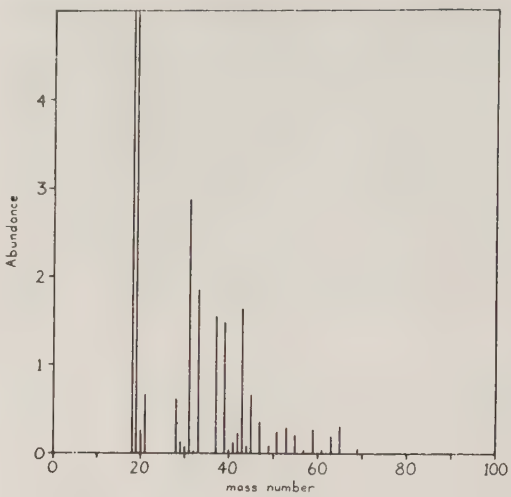

Figure 5. Mass spectrum of the positive ions in the reaction zone of a methane–oxygen–nitrogen flame; $\lambda \sim 1$

and small groups for the types C_4 and C_5, again of somewhat acetylenic distribution. The evidence again favours a certain amount of dehydrogenation to give acetylene, followed by a little polymerization. It is clearly desirable, however, to investigate ranges of mixture strengths for these last three fuels.

ACETONE

The last example chosen for depiction is that of an acetone flame with oxygen. This is remarkable in a number of respects—see *Figure 6.*

The 59 peak becomes very large, providing strong evidence for the ascription $C_2H_3O_2$, while all the hydrocarbon peaks above the C_3 group have vanished, with one minor exception. The other

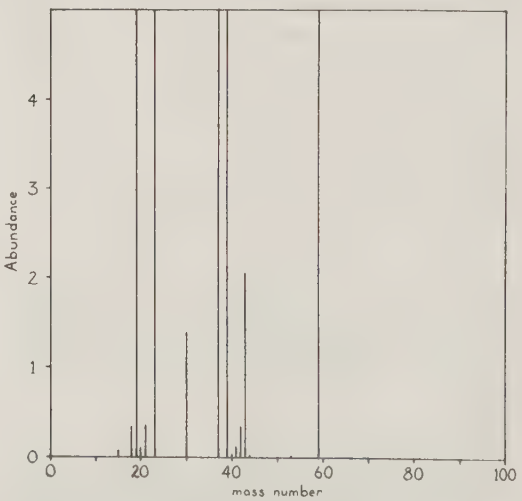

Figure 6. Mass spectrum of the positive ions in the reaction zone of an acetone–oxygen–nitrogen flame

large peaks are H_3O^+(19), Na^+(23) impurity, $H_5O_2^+$(37) and $C_3H_3^+$(39). The last may derive from a trace of potassium impurity, since sodium at least is visibly present. If acetylene is formed here, it is certainly under circumstances where further polymerization is not possible. The CH_3^+ peak (15) is unusually large, as is also the 43 peak (CH_3CO^+), which is not surprising in view of the nature of the fuel. Other fuels which have been examined are benzene, which gave very similar results to acetylene; formaldehyde, which gave no hydrocarbon ions at all, but only those characteristic of hydrogen; and carbon monoxide, which gave a trace of CO^+ only.

GENERAL CONCLUSIONS

This rapid survey has sufficed to show the power of the mass spectrometric method, in revealing not only the large variety and concentration of positive ions in the reaction zones of various fuels but also some of the very characteristic variations of pattern with the nature of the fuel and the mixture strength. The general conclusion that can be drawn is that some polymerization of fuel occurs in the early part of the reaction zone, this being more rapid in oxygen-rich flames; this has been shown to give rise to molecules containing at least 12 atoms of carbon. Such molecules are then rapidly broken down—except in flames rich enough in fuel to give visible carbon formation. Tentative mechanisms for the production of some of the important ions, such as $C_3H_3^+$, by chemical reaction are suggested, as are mechanisms by which these can add on further molecules of fuel (acetylene). The neutralization of such ions by electrons can provide sufficient energy to give C_2*, and thereby possibly give an explanation of the anomalously high intensity of the Swan bands. All these points suggest further extensive experimentation.

The authors wish to express their gratitude to the Research Laboratory of the General Electric Company (Schenectady, N.Y.) for a grant in support of this work.

REFERENCES

1 Calcote, H. F. *Combustion and Flame* 1 (1957) 385
2 Eltenton, G. C. *J. chem. Phys.* 15 (1947) 455
3 Deckers, J. and van Tiggelen, A. *Bull. Soc. Chim. Belg.* 66 (1957) 664
4 Knewstubb, P. F. and Sugden, T. M. *Nature, Lond.* 181 (1957) 474
5 Calcote, H. F. and King, I. R. *Fifth Symposium (International) on Combustion*, p. 423. 1955. New York; Reinhold
6 Gaydon, A. G. *The Spectroscopy of Flames*, p. 197. 1957. London; Chapman and Hall
7 Tverdokhlebov, V. I. *Dokl. Akad. Nauk S.S.S.R.* 103 (1955) 1049
8 — *Chem. Abstr.* 50 (1956) 7569
9 Gaydon, A. G. and Wolfhard, H. G. *Proc. Roy. Soc. A* 201 (1950) 570
10 Sugden, T. M. and Thrush, B. A. *Nature, Lond.* 168 (1951) 703
11 Einbinder, H. *J. chem. Phys.* 26 (1957) 948
12 Ubbelohde, A. R. *Fifth Symposium (International) on Combustion*, p. 74. 1955. New York; Reinhold
13 Thomas, N. *J. chem. Phys.* 20 (1952) 899
14 Porter, G. *Fourth Symposium (International) on Combustion*, p. 248. 1953. Baltimore; Williams and Wilkins

38

ION IDENTIFICATION IN FLAMES

J. DECKERS and A. VAN TIGGELEN

The complete study of the ionization in flames involves the solution of four problems: (1) measurement of ion concentration; (2) extraction of the ions from the flame front; (3) identification of the ions; and (4) mechanism of their formation in the flame. A solution to the first problem is proposed in another paper presented in this symposium.

To the extraction device, which has been described elsewhere[1], a mass spectrometer has now been adapted in order to proceed to the identification of the ions which are formed in the flame.

The purpose of this paper is to give a description of our equipment and to relate the results which we have obtained in the identification of the ions in some flames[2].

EXPERIMENTAL

The schematic description of the mass spectrometer including the ion extraction device is given in *Figure 1*; it consists of four successive chambers. The flame is run in the first chamber at a pressure of about 40 mm Hg; a hole in the bottom of this chamber is periodically opened during 1/1300 of a second by means of a rotating perforated disc. A system of electrodes in the following two chambers creates an electrostatic field which retains and accelerates the ions present in the gases entering in the chamber during each opening. The retained ions are brought from chamber II at a vacuum of 10^{-2} mm Hg into chamber III at a vacuum of 10^{-4} mm Hg; the ion beam is projected on to a slit (1 mm broad and 15 mm high) which is used as the entrance slit of chamber IV which is placed between the polar pieces of an electromagnet.

Both electrostatic and magnetic fields can be changed in order to register the different masses caught on the collector which is placed at the end of chamber IV. The total accelerating field is divided between the different electrodes, which are represented separately in *Figure 1*.

The ionic current is measured by means of a vibrating reed electrometer; scanning can be achieved by varying the electromagnetic field.

RESULTS AND DISCUSSION

Calibration of mass scale

Our experiments have all been made on a rich (75 per cent N_2, 8·75 per cent C_2H_2 and 16·25 per cent O_2) $C_2H_2/O_2/N_2$ flame burning at a pressure of about 40 mm Hg.

In these calibration experiments the total accelerating potential (1,080 V) was divided between the different electrodes represented in *Figure 1* as follows:

D_1 :	1080	L_2 :	1010
L_1 :	1055	L_3 :	540
D_2 :	1045	Slit :	O (grounded)

The first results reported[2] are highly objectionable: they were obtained when the vacuum in chambers III and IV was insufficient (about 10^{-4} mm Hg); and the observed peaks were generally very diffuse and even in some cases did not seem to correspond to entire mass units. Evidently a vacuum of 10^{-4} mm Hg corresponds to working conditions where the possibility of charge exchange is no more negligible: it is well known in mass spectrometry that diffuse peaks are observed as soon as the vacuum becomes insufficient. Therefore all efforts were made to improve the vacuum in chamber IV up to 10^{-5} mm Hg.

In order to identify without doubt the different observed peaks which will be described below, the first difficulty was to calibrate the mass spectrometer scale with some internal standard giving well defined and known ions. In order to achieve this some lithium, sodium and potassium salts were introduced in the flame: the applied technique therefore consisted in using a Na(Li or K) borate bead electrically heated on a Pt wire placed in the nitrogen stream feeding the burner. The Li (or K) borate was prepared by fusing the carbonate with boric acid; sodium borate was used in the Na borate bead.

As soon as the Pt wire was heated very intense peaks ($>10^{-13}$ amps) were observed: they correspond of course to the masses 7 (Li^+), 23 (Na^+) or 39 and 41 (K^+), depending on the alkali metal, which is introduced in the flame. The alkali ions disappear completely when the heating of the Pt wire is turned out.

Most abundant ions in the $C_2H_2/O_2/N_2$ flames

After the calibration of the mass scale as explained above, the identity of the ions has been further checked by burning also deuterated acetylene and observing the shift of the peaks towards higher mass units whenever a hydrogen-containing ion is concerned; not only is a shift to

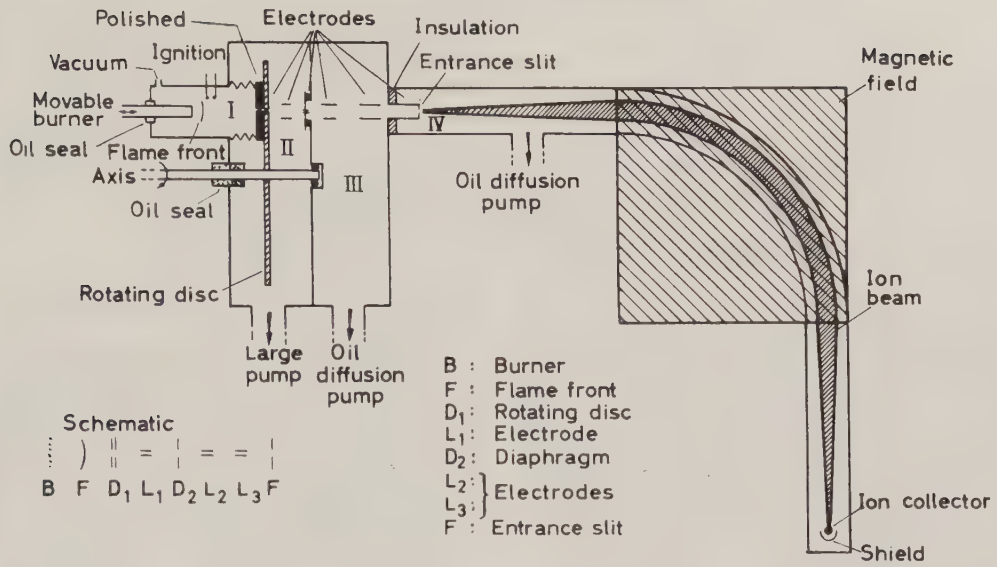

Figure 1

be observed but even a splitting when partially deuterated acetylene is burning.

A description of the most important peaks which have been observed follows.

(1) The most important peak ($\sim 10^{-13}$ amps) corresponds to mass 19. Its identity H_3O^+ is shown by the splitting in four peaks with partially heavy acetylene: 19, 20, 21 and 22 (this 22 peak comes next to the Na^+ peak at a distance of one mass unit when Na salt is also introduced in the flame).

(2) Next to mass 19 a weaker peak ($\sim 10^{-14}$ amps) appears at mass 18–H_2O^+). Using partially deuterated acetylene its splitting overlaps with the splitting of peak 19; but considered both together they are split in five different peaks 18, 19, 20, 21 and 22.

(3) Two weak peaks ($\sim 10^{-14}$ amps) are also observed at masses 28 and 30; the corresponding ions do not contain hydrogen and are most probably CO^+ and NO^+.

Charge transfer phenomena

It should be noted that the intensity of all peaks is profoundly decreased and even reduced to zero when an increasing amount of alkali salt is introduced in the flame (by increasing the temperature of the borate bead).

Another interesting observation concerns some experiments which have been made on a $H_2/N_2O/N_2$ flame: this flame was chosen instead of a $H_2/O_2/N_2$ flame because it was easier to run and to control a yellow coloured than a colourless flame. As could be expected from such an ion poor flame, we did not observe any important peak except a weak maximum (10^{-14} amps) corresponding to mass 30 (NO^+); however as soon as some Na salt is introduced in this flame this maximum disappears while peak 23 appears with an intensity about ten times weaker than with the acetylene flame.

CONCLUSIONS

We do not have in the actual state of our research definite indications concerning the influence of flame composition and pressure on the relative concentration of the identified ions. Furthermore the intensity ratios seem to depend also on the experimental conditions, i.e. on the distance between the flame and the extraction opening in chamber I.

The eventual dependence of relative peak intensity on the applied electric field needs also to be studied before it will be possible to decide whether the ions, which have been identified, are really formed in the flame or if they might result from charge transfer; secondary ions might also be formed in chamber II where the vacuum reaches only the value of 10^{-2} mm Hg.

Much is to be expected from the study of hydrocarbon structure on the nature or the abundance of the different ions.

The authors express their thanks to the Fonds National de la Recherche Scientifique and to the European Office of the Air Research and Development Command (U.S.A.F) for financial support (Contract No AF61(514)–1099).

REFERENCES

[1] DECKERS, J. and VAN TIGGELEN, A. *Combustion and Flame* 1 (1957) 281

[2] — — *Bull. Soc. chim. Belg.* 66 (1957) 664

COMPARATIVE STUDY OF IONIZATION IN ACETYLENE–OXYGEN AND ACETYLENE–NITROUS OXIDE FLAMES

J. PONCELET, R. BERENDSEN and A. VAN TIGGELEN

INTRODUCTION

Some difficulties are encountered in the experimental measurement of ion concentration in flames and the applicability of the usual methods is always restricted by some inherent limiting factors. The method of flame deflection in an external electric field[1–3], involves a rather complex interpretation of results which are perhaps altered by the interaction of the electric field on the burning velocity[4].

The microwave attenuation method gives very valuable data concerning equilibrium and ionization processes in flames; it has been successfully applied by Sugden and his co-workers[5]. The method however requires a minimum volume of the investigated flame (dimension at least equal to the wavelength) and it is therefore not appropriate to an investigation which is to be limited to the flame front itself, except, perhaps, in the case of low pressure flames.

The use of Langmuir probes[6,7] is able to furnish interesting data on the distribution of the ions in the flame. However this method has the two main disadvantages of all techniques which involve the use of probes: cooling of the explored region by the probe and deformation of the flame front due to a quenching effect. Furthermore the thermo-emission by the probe material greatly restricts the applicability of the method[8].

DESCRIPTION OF NEW METHOD

In order to overcome the difficulties and to avoid the limitations of the classical methods mentioned above, we have developed a new method which fulfills the following requirements:

(1) It should enable us to measure exclusively the ionization in the flame front alone and not in the whole flame (including burnt gases).

(2) It should be applicable to any flame, even to very hot flames.

(3) The flame front (reaction zone) should not be perturbed by the introduction of probes.

All these conditions seem to be realized in the present method. The essential part of the apparatus is the burner, schematically represented in *Figure 1*. It is made of two coaxial tubes which are electrically insulated from each other; the premixed flammable mixture flows in the space between the two tubes and a flame is maintained which is annular in shape.

First orientation experiments with a burner made of two rather narrow tubes (diameter 4 and 10 mm) have shown an important deformation of the reaction zone due to the dynamic pressure of the burnt gases. The burner with which all the experiments reported here have been performed (*Figure 1*) was constructed with broader

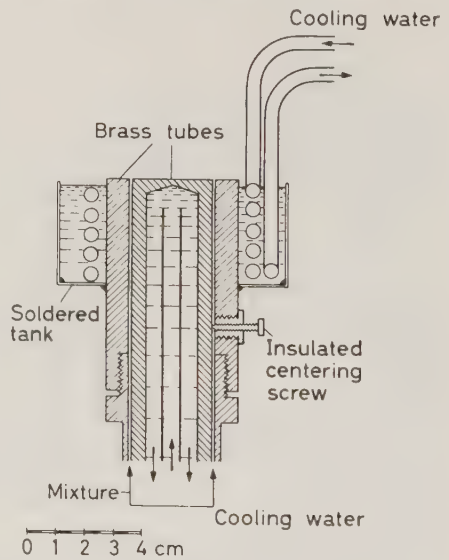

Figure 1

tubes: external tube, diameter 2·99 cm; internal tube, diameter 2·79 cm; thickness of annular space, 1 mm; total length of tubes, ~50 cm. The centring of the inner tube was achieved by means of three insulated screws placed at 120° from each other and at about 5 cm from the top of the external tube. At the bottom a polystyrene conical joint completed the closing and centring of the annular space. Water circulates in the inner tube which is closed at the upper part and earthed. The outer tube carries at the top a circular reservoir filled with water which in turn is kept cool by means of cold water circulating in a Pyrex spiral plunged in the reservoir. This arrangement ensures the cooling of the whole burner while the two tubes remain perfectly insulated.

The bottom of the burner is fitted with a system to obtain a homogeneous distribution of the gas flow. In order to prevent oxidation of the burner rim, a thin rhodium deposit was formed on the upper parts of the tube edges.

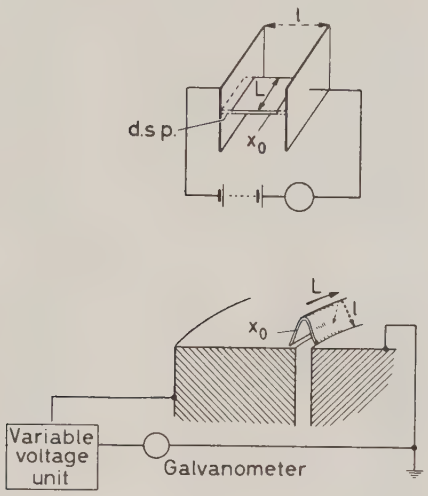

Figure 2

The electrical equipment is very simple; a stabilized direct current source is used and the current intensities measured with a galvanometer (sensitivity up to 10^{-9} amp). The applied voltage is adjustable from 1·5 up to 1,200 volts.

INTERPRETATION OF MEASUREMENTS

General considerations

An ideal flat flame between two conducting plates is represented schematically in the upper part of *Figure 2* and we shall admit, as a first approximation, that our annular flame can be assimilated to the ideal case with the corresponding flame dimensions reported in the lower part of *Figure 2*.

As long as the potential E applied to the plates remains sufficiently low, the value of current intensity (I) can be written

$$I = \frac{E}{R_a + R_f + R_c}$$

R_a and R_c have the meaning of a 'contact resistance' between flame and the conducting plates at the positive and negative sides respectively; they correspond to the voltage drop in the dead spaces. R_a and R_c are constant for a given flame. R_f is the resistance of the flame and its value may be given as a function of the flame dimensions (l, L and x_0) and of its specific resistance ρ.

$$R_f = \frac{\rho l}{L x_0}$$

Therefore

$$I = \frac{E}{(R_a + R_c) + \frac{\rho l}{L x_0}} \qquad (1)$$

L remains constant for all flames and is equal to the perimeter of the annular flame

$$L = 2\pi \frac{(r_1 + r_2)}{2} = 2\pi r$$

$2r_1$ being the external diameter of the inner tube, $2r_2$ the internal diameter of the outer tube, and $2r = 2{\cdot}89$ cm.

From the definition of the burning velocity (V_0) (gas flow D divided by flame surface S), l is related to D with a good approximation according to

$$V_0 = \frac{D}{S} = \frac{D}{2\pi r l} \qquad (2)$$

Substitution in equation 1 gives

$$I = \frac{E}{(R_a + R_c) + \frac{\rho D}{(2\pi r)^2 V_0 x_0}} \qquad (3)$$

In this equation R_a, R_c, ρ, x_0 and V_0 vary when the composition of the flammable mixture changes but, for a given mixture, the current intensity varies only with gas flow D.

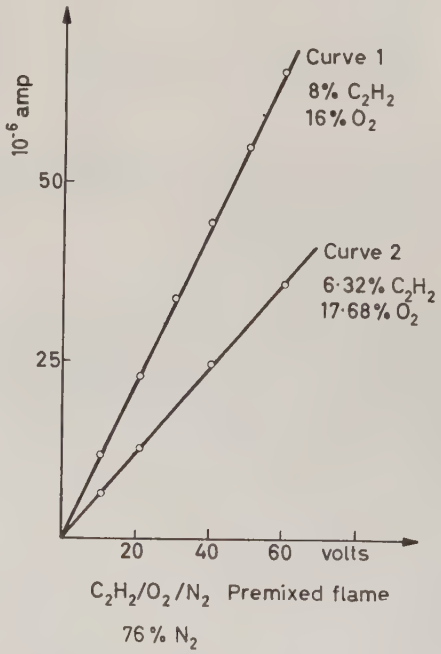

Figure 3

The validity of equation 3 can easily be tested. (*a*) For constant mixture composition and gas flow but increasing potential E, a straight line, passing through the origin, must be obtained when I is plotted in function of E. This is illustrated in *Figure 3* for two mixtures $C_2H_2/O_2/N_2$.

When potential E increases, the linearity fails above a critical value E_s; saturation occurs and the current is space charge limited (*Figure 4*). For this reason all our experiments were made at a potential of 30 V which is much lower than the value at which equation 3 should be modified.

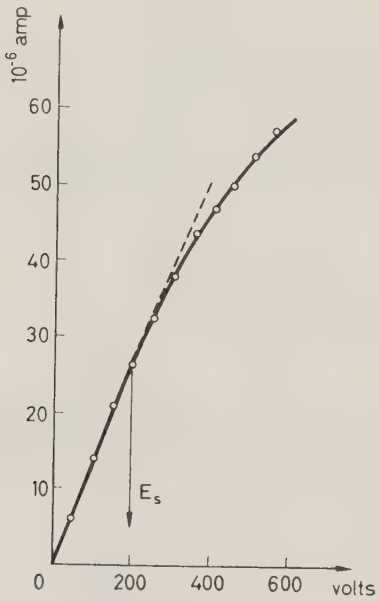

Figure 4

(*b*) For a given gas mixture (fixed dead spaces) a plot of $1/I$ *versus* D also gives a straight line (*Figure 5*); its slope is equal to:

$$\rho/E(2\pi r)^2 V_0 x_0 = \tan\alpha \qquad (4)$$

Flame conductivity and ion concentration

In previous work it has been shown theoretically[9] and experimentally[10] that the product of the flame velocity and flame front thickness $V_0 x_0$ is proportional to the square root of the mean temperature T of the flame front

$$V_0 x_0 = 0{\cdot}96 \times 10^{-2}(T)^{1/2} \qquad (5)$$

A good estimation of T is given by[11]

$$T = T_0 + 0{\cdot}74\,(T_f - T_0) \qquad (6)$$

where T_0 and T_f are respectively the temperatures of the fresh and burnt gases (T_f = flame temperature).

The slope ($\tan\alpha$) of the straight lines obtained by plotting $1/I$ as a function of D (as illustrated in *Figure 5*) enables us to calculate for each mixture the specific resistance ρ of the flame. Replacing $V_0 x_0$ in equation 4 by its value given in equation 5 we obtain

$$\rho = \tan\alpha \,.\, 0{\cdot}96 \,.\, (2\pi r)^2 E(T)^{1/2} \,.\, 10^{-2} \qquad (7)$$

The specific resistance of the flame is related to the ion concentration R according to

$$\frac{1}{\rho} = ne(k_+ + k_-)$$

where e is the electron charge, and $n = n_+ = n_-$, the flame front being electrically neutral. k_+ and k_- are the mobilities of positive and negative ions (electrons).

Since $k_- \gg k_+$ we shall neglect k_+ as compared to k_- for which a value of 2,500 will be accepted[12].

Finally the number (n) of ions per c.c. in the flame front can be calculated from

$$n = 1/0{\cdot}96 \,.\, 10^{-2} \,.\, (2\pi r)^2 \,.\, \tan\alpha \,.\, ek_- E(T)^{1/2} \qquad (8)$$

$$n = 5{\cdot}36 \,.\, 10^{16}/E \,.\, \tan\alpha \,.\, (T)^{1/2}$$

This last equation was obtained using suitable units:

I in amps and D in l./min (for $\tan\alpha$) $2\pi r = 9$; $e = 4{\cdot}8 \,.\, 10^{-10}$ (v.e.s.) E in volts (in our experiments $E = 30$ V).

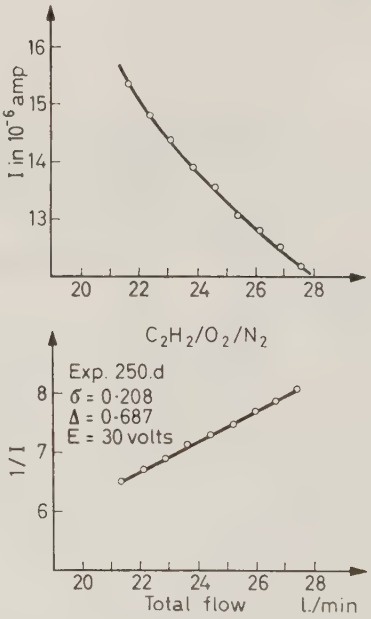

Figure 5

EXPERIMENTAL RESULTS AND DISCUSSION

The method described in the previous sections has been applied to $C_2H_2/O_2/N_2$ and to $C_2H_2/N_2O/N_2$ flames. The values of flame temperatures and of the burning velocities were taken from previous publications[10]. (A few values are extrapolated.)

Results are given in Tables 1 and 2 with the following data:

TABLE 1

$C_2H_2/O_2/N_2$ Flames

$C_2H_2/C_2H_2 + O_2$	N_2 per cent	V_0	T_f°K	T°K	tan $\alpha \times 10^{-3}$	ρ ohms 10^{-5}	$n \times 10^{-10}$/cm^3
0·200	71	114	2150	1665	2·74	27·35	1·52
	73	101	2095	1623	7·94	74·20	0·56
	76	75	2010	1558	45·20	416·00	0·10
0·233	71	141	2270	1755	0·79	7·75	5·38
	73	123	2200	1700	1·44	13·80	3·02
	76	93	2135	1655	3·91	36·30	1·12
	79	67	2015	1565	31·20	287·00	0·14
0·263	71	153	2355	1818	0·37	3·68	11·23
	73	133	2290	1770	0·63	6·17	6·76
	76	109	2215	1715	1·32	12·90	3·24
	79	81	2100	1626	6·55	61·40	0·68
0·294	71	165	2446	1886	0·25	2·48	17·00
	73	147	2350	1814	0·40	3·90	10·47
	76	114	2255	1745	0·80	7·77	5·37
	79	83	2140	1580	2·20	20·80	1·99
0·313	71	162	2460	1895	0·22	2·21	18·63
	73	144	2370	1830	0·36	3·55	11·75
	76	111	2270	1755	0·73	7·08	5·89
	79	81	2155	1668	1·62	15·40	2·69
	81	60	2025	1569	6·22	57·30	0·73
0·333	71	159	2470	1905	0·24	2·38	17·38
	73	137	2375	1835	0·36	3·55	11·75
	76	106	2270	1755	0·73	7·08	5·89
	79	75	2165	1675	1·52	14·40	2·88
	81	54	2065	1600	5·24	48·80	0·85
0·357	71	149	2490	1920	0·30	3·08	13·50
	73	122	2390	1845	0·47	4·68	8·91
	76	92	2290	1770	0·89	8·71	4·79
	79	58	2135	1653	1·83	17·30	2·40
0·385	71	123	2480	1905	0·50	5·08	8·13
	73	91	2380	1837	0·81	8·24	5·13
	76	58	2280	1763	1·91	18·70	2·24

Ratio $C_2H_2/C_2H_2 + O_2$ or $C_2H_2/C_2H_2 + N_2O$
Concentration of inert gas N_2 given by the ratio: 100(inert)/(inert + fuel + oxidant)
Burning velocity V_0
Flame temperature T_f
Mean temperature of flame front $T = T_0 + 0{\cdot}74(T_f - T_0)$ $(T_0 = 293°K)$
tan α
Specific resistance of flame front ρ
Ion concentration n (per c.c.)

It should be noted that the maximum ion concentration corresponds approximately to the maximum burning velocity (slightly shifted toward richer mixtures).

For the interpretation of our results it is preferable to express the concentration of ions in molar fractions instead of concentration per unit volume. Therefore, in order to compare all flames, all n values must be multiplied by the ratio T/T_0 because of the expansion of the gases in the flame front.

If the formation of the ions results from a chemical process, it seems plausible to admit a proportionality relation between the concentration of normal and ionized radicals. This relation has been accepted in a previous investigation on the intensity of spectral emission in C_2H_2 flames[13].

Therefore we shall use here analogous relations to those which were used in the last mentioned work

$$\log\left(\frac{nT}{T_0}\right) = K'' + \log T + 2\log V_0 + \frac{0{\cdot}4343E_p}{RT}$$

(E_p represents the activation of a propagating step: only a few kcal.)

For a series of mixtures with constant fuel/oxidant ratio but increasing dilution

$$\log V_0 = K' + \frac{i}{2}\log Y - \frac{1}{2}\log T - \frac{0{\cdot}4343E}{2RT}$$

where E represents the overall activation energy of the chain branching process, Y is equal to

TABLE 2
$C_2H_2/N_2O/N_2$ Flames

$C_2H_2/C_2H_2 + N_2O$	N_2 per cent	T_f°K	T°K	tan $\alpha \times 10^{-3}$	ρ ohms $\times 10^{-5}$	$n \times 10^{-10}$/cm^3
0·15	47	2528	1932	2·14	21·96	1·62
	50	2480	1911	3·54	36·20	1·00
	52	2428	1873	5·13	51·98	0·71
	54	2376	1834	7·59	76·01	0·48
	56	2328	1799	11·74	116·53	0·32
0·18	43	2654	2040	0·66	6·99	1·52
	47	2590	1993	1·17	12·26	1·30
	50	2540	1956	1·95	20·17	1·18
	52	2492	1920	2·82	28·89	1·13
	54	2440	1882	5·49	55·81	0·84
	56	2392	1846	6·60	66·48	0·55
	58	2342	1809	11·48	114·23	0·32
0·205	50	2560	1971	1·48	15·36	1·24
	52	2515	1937	1·78	18·31	1·20
	54	2470	1904	2·24	22·85	1·16
	56	2425	1871	2·88	29·16	1·13
	58	2380	1837	4·17	41·76	0·83
0·230	52	2548	1962	1·55	16·06	1·23
	54	2504	1929	1·95	19·89	1·18
	56	2455	1893	2·63	26·72	1·14
	58	2405	1856	3·63	36·55	1·00
	60	2345	1811	5·37	53·44	0·68

Burning velocities V_0 have not been measured

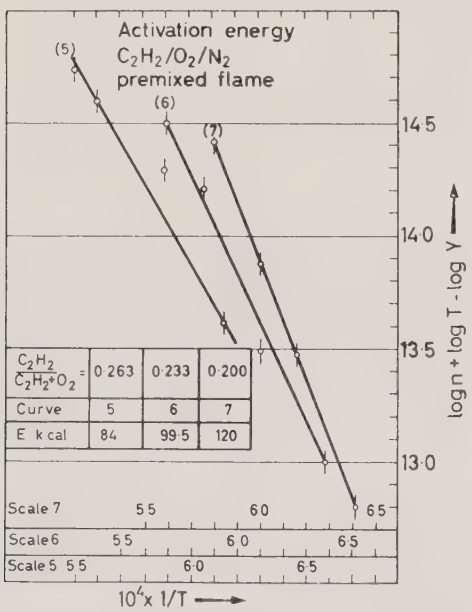

Figure 6

(100 — percentage diluent/100) and i represents the overall order of the branching process minus unity; $i = 1$ for C_2H_2 flames[10].

Combining the two last equations, since T_0 is constant in all our experiments, one obtains for each series of experiments with the same fuel/oxidant ratio but varying dilution

$$\log n + \log T - i \log Y = K - \frac{0{\cdot}4343(E - E_p)}{RT}$$

Plots of the first member of this equation *versus* $1/T$ for C_2H_2/O_2 mixtures are given in *Figures 6* (rich mixtures) and *7* (lean mixtures). The corresponding graphs for C_2H_2/N_2O mixtures are given in *Figure 8*. The obtained activation energies are assembled in Table 3; there is striking evidence

TABLE 3
Apparent Activation Energies for Ion Formation in Acetylene/Oxygen and Acetylene/Nitrous-Oxide Flames

Ratio $C_2H_2/C_2H_2 + O_2$	*E* kcal	*Ratio* $C_2H_2/C_2H_2 + N_2O$	*E* kcal
0·200	120	—	—
0·223	100	—	—
0·263	84	0·150	77
←	stoichiometry	→	
0·294	50	0·180	74
0·313	45	0·205	57
0·333	42	0·230	52
0·357	40	—	—

that the apparent activation energy tends, in both cases, towards a lower value on the rich side. A fairly constant value is reached which differs by only a few kcal from the activation energy which has been found when similar calculations are applied to the measured intensities of the C_2 and

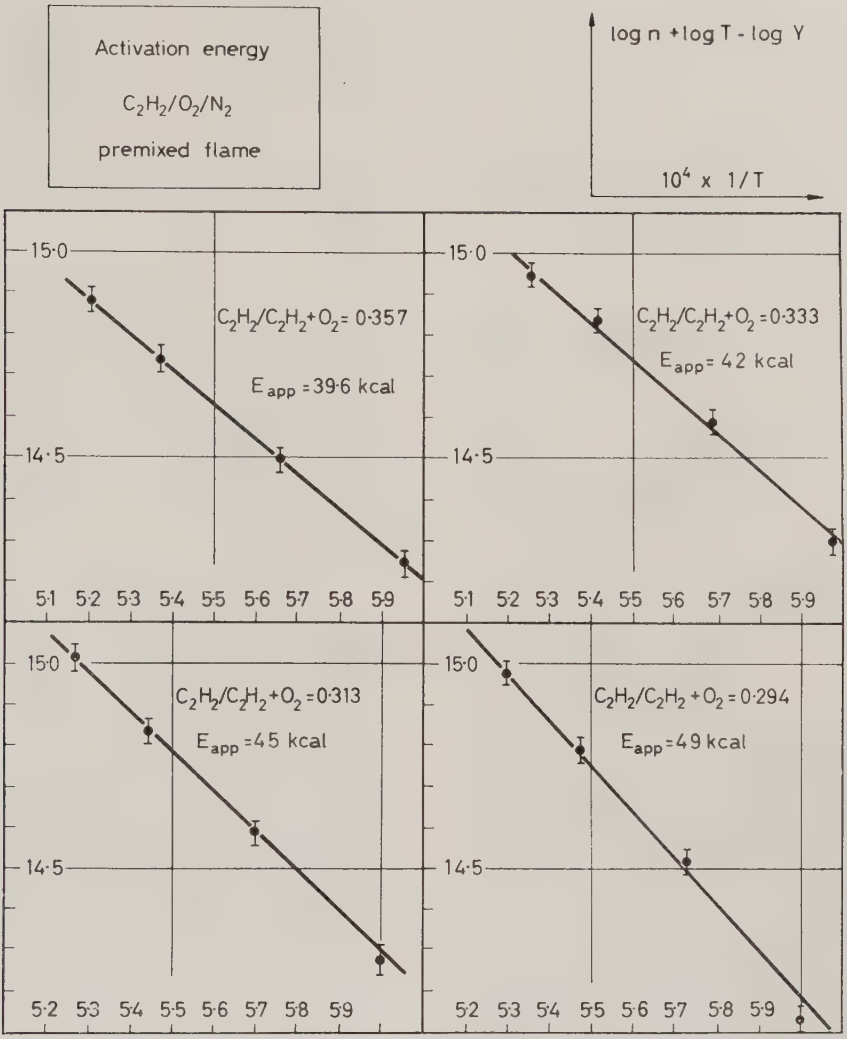

Figure 7

CH spectra in C_2H_2 flames[13]. The low activation energy is comparable (10 kcal higher) to the activation energy derived from burning velocities data[10]: 31 kcal for C_2H_2/O_2 flames and 40 kcal for C_2H_2/N_2O flames.

It should be mentioned that the formation of a carbonaceous deposit on the burner rim reduces the reproducibility of our measurements of the acetylene flames, especially with rich mixtures. The relatively low values of E in both cases prove not only that the ions are really formed in a chemical process but that their formation results from the reaction of some radicals which are normal intermediate species appearing in the successive steps of the chain reactions. The abnormally high values of the activation energy on the lean side in both flames suggest that the ion forming radicals are fragments of the fuel molecule whose presence is less probable when the O_2(or N_2O) content increases; the lifetime of the different alternating species whose formation alternates in the chain is inversely proportional to the concentration of the initial component with which it reacts[11]. This explains also that in the work on chemiluminescence[13], constant values for activation energies from OH emission can only be found on the lean side and not by very rich mixtures: the OH radical has in this case a longer lifetime when the mixture contains more oxidant. Furthermore it seems quite probable that an excess of O_2(or N_2O)does not act as an ordinary diluent as soon as ions are concerned. Our measurements involve only the current transported by the electrons: all electrons captured by molecules to

form negative ions, owing to their low mobility, participate to a negligible degree in the measured conductivity. The presence of much O_2 or N_2O, and consequently of O atoms and OH radicals helps in the formation O_2^-, O^- and OH^- which are precisely among the few stable negative ions at the flame temperature. As a consequence it seems reasonable to disregard the high activation energies obtained with lean mixtures; at least their interpretation seems to be premature in the present state of the problem.

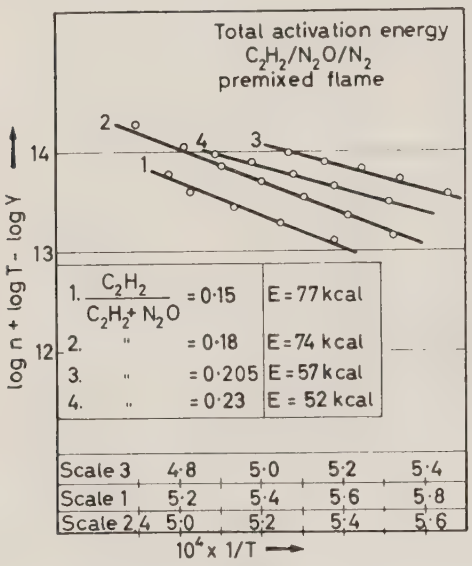
Total activation energy
$C_2H_2/N_2O/N_2$
premixed flame
log n + log T - log Y
14
13
12
1. $\frac{C_2H_2}{C_2H_2+N_2O}$ = 0·15 E = 77 kcal
2. " = 0·18 E = 74 kcal
3. " = 0·205 E = 57 kcal
4. " = 0·23 E = 52 kcal
Scale 3 4·8 5·0 5·2 5·4
Scale 1 5·2 5·4 5·6 5·8
Scale 2,4 5·0 5·2 5·4 5·6
$10^4 \times 1/T$

Figure 8

A very interesting discussion of the different possible steps by which chemi-ions could be formed is made in a recent paper[14]. There are two main processes to consider. (*a*) Cumulative excitation: two excited molecules (or radicals) are colliding. A process results with the liberation of an amount of energy which exceeds the ionization energy of one of the departing particles; examples are given in the original paper. (*b*) True chemi-ionization: the heat of reaction (plus, eventually, the excitation energy carried by one of the colliding species) exceeds the ionization energy of one of the reaction products. A few examples are given as an illustration.

$$C_2^*(^3\pi g) + O_2 \rightarrow CO + CO^+ + e^-$$

$$CO(^1\pi) + O \rightarrow CO_2^+ + e^-$$

In our opinion true chemi-ionization seems the more likely process since only one excited species is involved in the collision. Before it is possible to choose between different chemi-ionization processes, it is first essential to obtain data concerning the identification of the ions which are present in the flame; without absolute certainty of the exact nature of these ions, all considerations about their formation process could only be speculative.

This work has been sponsored in part by the Air Research and Development Command, United States Air Force, under contract No. AF 61(514)–1099, through the European Office (A.R.D.C.).

The authors express their thanks to the Fonds National de la Recherche Scientifique and to A.R.D.C. (U.S.A.F.) for financial support. J. Poncelet and R. Berendsen are respectively indebted to the European Research Associates (E.R.A.) and to the I.R.S.I.A. for post-graduate fellowships.

REFERENCES

[1] Lewis, B. *J. Amer. chem. Soc.* 53 (1931) 1304

[2] Calcote, H. F. *Third International Symposium on Combustion*, p. 245. 1949. Baltimore; Williams and Wilkins

[3] — and Pease, R. *Industr. Engng. Chem.* (*Industr.*) 43 (1951) 2726

[4] Gaydon, A. G. and Wolfhard, H. G. *Flames*, p. 281. 1953. London; Chapman and Hall

[5] Sugden, T. M. *Fifth International Symposium on Combustion*, p. 406. 1955. New York; Reinhold

[6] Loeb, L. B. *Basic Processes of Gaseous Electronics*, p. 332. 1955. Univ. California Press

[7] Calcote, H. F. and King, I. R. *J. chem. Phys.* 23 (1955) 2203; *Fifth International Symposium on Combustion*, p. 423. 1955. New York; Reinhold

[8] Poncelet, J. and Van Tiggelen, A. *Bull. Soc. chim. Belg.* 67 (1958) 49

[9] Van Tiggelen, A. and Vaerman, J. *Bull. Soc. chim. Belg.* 62 (1953) 653

[10] Van Wonterghem, J. and Van Tiggelen, A. *Bull. Soc. chim. Belg.* 63 (1954) 235; 64 (1955) 780

[11] Van Tiggelen, A. *Mem. Acad. Roy. Belg. Cl. Sci.* 27 (1952) 1

[12] Wilson, H. A. *Rev. mod. Phys.* 3 (1931) 156

[13] Vaerman, J., Nenquin, G. and Van Tiggelen, A. *Bull. Soc. chim. Belg.* 65 (1956) 435

[14] Calcote, H. F. *Combustion and Flame* 1 (1957) 385

40

DISTRIBUTION OF IONS IN LOW-PRESSURE FLAMES

T. KINBARA, J. NAKAMURA, and H. IKEGAMI

INTRODUCTION

Although many theories have been proposed for the mechanism of formation of ions in flames, nothing decisive has been established up to the present[1]. Not only the mechanism of formation, but also the very nature of positive ions has not yet been clarified. Since it is quite a difficult matter to directly identify ions as they exist in flames, some other indirect methods such as observation of mobility have been adopted and the nature of the ions has been presumed from the results.

It is also important, in the study of the mechanism of ion creation, to know in which part of a flame most of the ions are produced. Now, as is well known, the combustion process in a hydrocarbon flame can be divided into three stages: i.e., the first stage in which the free radical C_2 is produced, the second stage in which CH is produced, and the third stage following after the above. This is clearly demonstrated by a low-pressure flat flame[2]. One can observe a thin green layer (due to C_2-band emission) at the lowest part of the flame and a blue zone (due to CH-band emission) just above it, followed by a faint purple region. In the lower part of usual diffusion flames of city gas or of liquid fuels one can also observe these C_2- and CH-layers, although the separation is not so clear. The authors measured roughly the specific conductivity of each layer and tentatively concluded that most ions in flames are possibly produced in the C_2-layer[3].

To make sure of this deduction, the authors planned to study a low-pressure flat flame of propane, because it has a combustion zone of great thickness and is quite suitable for the study of ions from layer to layer. The distribution of ions among layers was studied by a probe method, applying Langmuir's theory.

In our experiment we could choose either of two kinds of low-pressure flames, i.e. a pre-mixed flame or a diffusion flame. The pre-mixed flame was preferable in a sense, but the bottom of this flame adhered, under all conditions, to the burner-port and it became impossible to probe the lowest boundary of the flame as well as the pre-flame region. That was the reason that we chose the diffusion flame.

In this case it was quite easy to make the flame float about 1 cm above the port, by adjusting the total pressure or the mixing ratio of C_3H_8 and air. Moreover, the flame had a distinct boundary at its bottom.

Two conditions can be considered in the region of the port: (*a*) the amount of heat absorbed by the burner is sufficiently great that it is difficult to keep the flame temperature high enough for maintaining combustion; and (*b*) the mixing of C_3H_8 and air in this region is not sufficient to make the mixture combustible. These may be the reasons why a diffusion flame floats at a distance from the burner port.

It was indispensable, however, to keep the total pressure as large as 5 cm Hg in order to make the flame stable and unaffected by insertion of the probe. As a natural result, the combustion zone was contracted, and the C_2 region was just a thin layer not more than 0·5 mm thick, the CH portion was of the order of 1 mm and the faint purple portion was less than several mm. Thus, precise determination of ion concentration from layer to layer could not be expected, but from our results it seems quite reasonable to consider that most ions are created in, or at least in the region nearest to the C_2-layer, in agreement with the previous supposition.

This is also consistent with either of the following mechanisms of ion-formation which are considered most probable at the present[1].

$$CO(^1\Pi) + C_2(^1\Sigma_u^+) \rightarrow CO(^1\Sigma^+) + C_2^+ + e^-,$$

$$C_2(^3\Pi_g) + O_2 \rightarrow CO(^1\Sigma^+) + CO^+ + e$$

THEORETICAL

Double-probe method

Let us consider that a probe is inserted in a plasma composed of positive ions and electrons. Its potential should be lower than that of the ambient gas except for the case where the probe is charged positively at a voltage high enough to cause discharge phenomena in the gas. This is due to the fact that the mass of the electron is extremely small compared with that of a positive ion, i.e. electrons have far more chances to meet the probe than do positive ions.

Thus, when a pair of probes connected to a cell is inserted in a plasma, the potential around the probes would be like *Figure 1*, provided E, the voltage of the cell, is not exceedingly large[4].

Near each of the probes P_1 and P_2 there are narrow regions called sheaths where the potential drops by the amounts $V^{(1)}$ and $V^{(2)}$. V_c in *Figure 1* is the potential difference in the gas. But in our experiment, both probes were kept apart only about 4 mm and always laid in a horizontal plane near the flame axis, so V_c should be the potential drop due to the current I and could be neglected in comparison with E.

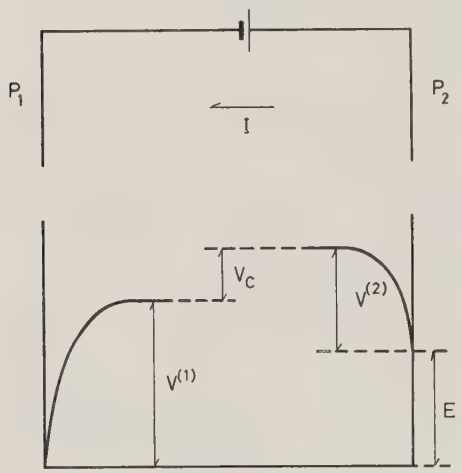

Figure 1. Distribution of potential around probes

One of the results for the I–E relation for a spherical double probe is shown in *Figure 2*. The curve should be symmetric to the origin O if the probe spheres are made exactly equal in size and positioned symmetrically with respect to the flame axis.

This relation is explained in the following way. Since there is no field outside of the sheath (*Figure 1*), both types of ions diffuse into the sheath only by their diffusive heat motions. All of the positive ions which diffuse into the sheath can reach the probe, while only a part of the electrons having more kinetic energy than $eV^{(1)}$ ($eV^{(2)}$) can reach the probe P_1 (P_2) against the potential drop $V^{(1)}$ ($V^{(2)}$). Thus the current into P_1 (from P_2) is

$$I = I^{(1)} - \mathcal{J}^{(1)} = \mathcal{J}^{(2)} - I^{(2)} \qquad (1)$$

where $I^{(1)}$ and $\mathcal{J}^{(1)}$ are the electric charges per sec conveyed to P_1 by the streams of positive ions and electrons; and the same holds for $I^{(2)}$ and $\mathcal{J}^{(2)}$.

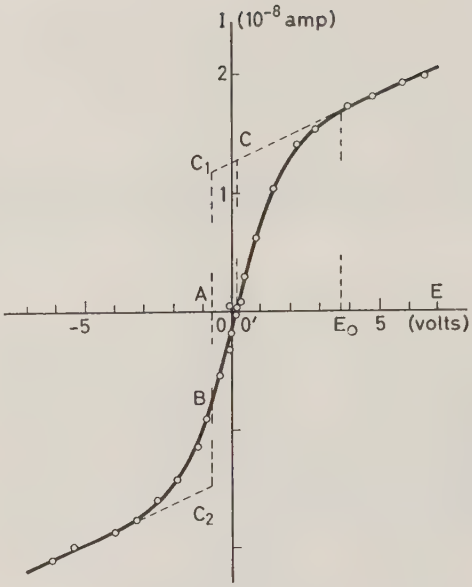

Figure 2. Characteristic curve of spherical double probe
$AC_1 = I^{(1)}$ $\quad AC_2 = I^{(2)}$
$BC_1 = \mathcal{J}^{(1)}$ $\quad BC_2 = \mathcal{J}^{(2)}$
$O'C = I_w^{(1)}$

Let i and j be the currents through unit area of the gas carried by free diffusions of positive ions and electrons respectively. Then

$$i = e\mathcal{N}_+ \sqrt{\frac{\overline{KT_+}}{2\pi M}}, \quad j = e\mathcal{N}_- \sqrt{\frac{\overline{KT_-}}{2\pi m}} \qquad (2)$$

where $\mathcal{N}_+$, $\mathcal{N}_-$ are the numbers of positive ions and electrons per unit volume; T_+, T_- are the ion- and the electron-temperature; and M, m are the masses of an ion and an electron.

If we denote the surface areas of the sheaths around the probes by $S^{(1)}$ and $S^{(2)}$,

$$\left.\begin{aligned} I^{(1)} &= S^{(1)} i, \quad \mathcal{J}^{(1)} = S^{(1)} j \exp\left(-\frac{eV^{(1)}}{KT_-}\right) \\ I^{(2)} &= S^{(2)} i, \quad \mathcal{J}^{(2)} = S^{(2)} j \exp\left(-\frac{eV^{(2)}}{KT_-}\right) \end{aligned}\right\} \qquad (3)$$

The electron current $\mathcal{J}^{(1)}$ ($\mathcal{J}^{(2)}$) decreases quickly with the increase of $V^{(1)}$ ($V^{(2)}$) and practically vanishes when $V^{(1)}$ ($V^{(2)}$) exceeds a certain value. This is the reason that I in *Figure 2* changes its rate of increase at $E = E_o$ ($= E_o'$).

Thus, for $E > E_o$ (or $< E_o'$),

$$\left.\begin{aligned} I &= I^{(1)} = S^{(1)} \mathcal{N}_+ e \sqrt{\frac{\overline{KT_+}}{2\pi M}} \quad (E > E_o), \\ I &= I^{(2)} = S^{(2)} \mathcal{N}_+ e \sqrt{\frac{KT_+}{2\pi M}} \quad (E < E_o'). \end{aligned}\right\} \qquad (4)$$

Now, as is shown in *Figure 2*, $I^{(1)}$ ($I^{(2)}$) varies linearly with E for $E > E_o$ ($E < E_o'$), which fact means that the sheath surface $S^{(1)}$ ($S^{(2)}$) around the spherical probe increases linearly with E for its wide range. Then it would not be unreasonable to extend this linearity to point C_1 (*Figure 2*) a little beyond $E = O$.

For $I = O$, positive ion current just balances electron current. In this case,

$$\left.\begin{aligned} I^{(1)} = I_w^{(1)} &= S_w^{(1)}\ \mathcal{N}_+\ e\sqrt{\frac{\overline{KT_+}}{2\pi M}} \\ I^{(2)} = I_w^{(2)} &= S_w^{(2)}\ \mathcal{N}_+\ e\sqrt{\frac{\overline{KT_+}}{2\pi M}} \end{aligned}\right\} \quad (5)$$

where $S_w^{(1)}$, $S_w^{(2)}$ mean the areas of the sheath-surfaces at the state $I = O$.

In order to determine $\mathcal{N}_+$ from 5, it is necessary to know in advance $S_w^{(1)}$ ($S_w^{(2)}$), T_+ and M, all of which are quite hard to be observed in our present experiment.

Our present purpose is to know the position of the layer in which ions are produced most, and it is not impossible to know it even only by using 5.

From 3,

$$\frac{\mathcal{J}^{(1)}}{\mathcal{J}^{(2)}} = \frac{I^{(1)}}{I^{(2)}} \exp\left(-\frac{eE}{KT_-}\right) \quad (6)$$

where $I^{(1)}$, $I^{(2)}$, $\mathcal{J}^{(1)}$, $\mathcal{J}^{(2)}$, E are given by AC_1, AC_2, BC_1, BC_2, OA in *Figure 2*. The electron temperature T_- is calculated from this. On the other hand, the actual temperature T can be observed with a thin thermocouple.

As it is sure that $T_- \geqslant T_+ \geqslant T$ at every point, let us consider the cases where $T_+ = T$ and $T_+ = T_-$. The true layer of maximum concentration of ions should lie between the two maximum layers which are found on the supposition that $T_+ = T$ and $T_+ = T_-$.

Now $V^{(1)}$ ($V^{(2)}$) at the state $I = O$ is the so-called wall potential and is deduced from $I^{(1)} = \mathcal{J}^{(1)}$ ($I^{(2)} = \mathcal{J}^{(2)}$), assuming $| \mathcal{N}_+ - \mathcal{N}_- | \ll \mathcal{N}_+$, as:

$$V_w^{(1)} = V_w^{(2)} = \frac{-KT_-}{2e} \ln \frac{T_+}{T_-}\ \frac{m}{M} \quad (7)$$

As $V_w^{(1)}$ ($V_w^{(2)}$) is the potential drop in the sheath, it is quite reasonable to suppose that the larger is $V_w^{(1)}$ ($V_w^{(2)}$), the larger is the corresponding value of $S_w^{(1)}$ ($S_w^{(2)}$). Thus we know easily if the gradient of $S_w^{(1)}$ at any point is positive or negative. This contributes to giving some corrections to the position of the layer of the maximum ion-concentration which has been found assuming $S_w^{(1)}$ to be constant. The details will be treated later on.

Single-probe method

At most parts of the flame there is an unbalance of $\mathcal{N}_+$ and $\mathcal{N}_-$, which gives rise to the space potential V_s given by

$$\frac{d^2V_s}{dx^2} = -4\pi e\ (\mathcal{N}_+ - \mathcal{N}_-) \quad (8)$$

where x is the distance measured perpendicularly to the flame surface.

If a single-probe is inserted in a flame and its potential to the burner is observed electrostatically, V_s can be given as the observed potential plus the wall potential given by 7. Then $(\mathcal{N}_+ - \mathcal{N}_-)$ will be calculated by 8. We postulated in our theory that $| \mathcal{N}_+ - \mathcal{N}_- | \ll \mathcal{N}_+$, and so the single-probe method will answer the purpose of checking our assumption.

EXPERIMENTAL

Low-pressure flame

The apparatus for the low-pressure flame was that commonly used in such studies and the essential parts are shown in *Figure 3*. The combustion chamber was a Pyrex glass cylinder 40 cm long and of 10 cm dia. Burned gases were exhausted by a vacuum pump from the top, through a large condenser tank, which served to make the gas flow free from pulsations. A mercury manometer was connected to the exhaust tube.

The burner consisted of concentric double tubes of brass, 40 cm long, the diameters of which were 4·8 cm and 3·0 cm respectively. Propane and air were supplied to the chamber respectively through the inner and the outer tube. The flow rate of each gas was measured by a flow meter showing the pressure difference at both ends of a capillary tube. These supply rates as well as the exhaust rates were controlled by gas-cocks.

The mixed gas was ignited by electric sparks inside the chamber (the spark gaps are not shown in *Figure 3*). The diffusion flame assumed varied forms according to the pressure and it became just like a usual diffusion flame of 1 atmosphere when the pressure was more than several decimeters of Hg and sufficient fuel was supplied. When the pressure was about 4–6 cm Hg and the flow rates of C_3H_8 and air were about 0·1–0·3 (l.min^{-1}) and 10–30 (l.min^{-1}) respectively, the flame had the appearance shown in *Figure 3* and was quite stable even when a probe was inserted in it.

This flat flame was composed of three parts: green (G), blue (B) and faint purple (P). The corresponding thicknesses were 0·5 mm, 1 mm and more than 1 mm. The lower the pressure was made, the thicker each part became, but the flame became more and more sensitive to disturbances and soon was extinguished by insertion of a probe.

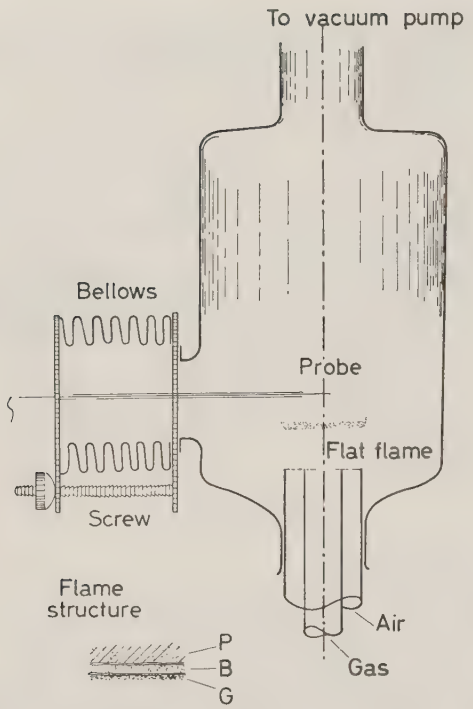

Figure 3. Apparatus (P = purple part, B = blue part, and G = green part)

Probe and thermocouple

The single probe was made of a Pt-wire of 0·1 mm dia., covered with a fused-silica tube of 0·4 mm dia. except for about 3 mm at its end. When it was used as a double probe, its end was made into a ball of 0·5 mm dia. by melting and was covered with the fused-silica tube except for the ball. Two of these probes were fixed side by side at a spacing between centres of about 4 mm. So the double probe used could be regarded practically as a spherical one.

The thermocouple was made of Pt and Pt–Rh (13 per cent) wires of 0·1 mm dia. Since no special compensation was made for the heat lost by conduction through the wires or by radiation from their surfaces the temperature read by this thermocouple should be considered lower than the true gas temperature by a small quantity which we neglected in our study. The two wires of it were also covered with fused-silica tubes of 0·4 mm dia. except for 3 mm near the junction.

When the probe and the thermocouple were inserted in a point of the flame at the same time the flame was distorted severely at that point owing to the large heat capacity of the probe and couple. Thus, it was preferable to make observations by the probe and by the couple separately, because it was found comparatively easy to maintain the flame in just the same state by keeping the pressure and mixture ratio constant.

The position of the probe or the couple was varied by a bellow-and-screw system shown in *Figure 3* and its vertical distance from the bottom surface of the flame was read by a cathetometer to within 0·1 mm. Thus the distance x in the following figures means the distance measured upwards from the bottom surface of the flame.

RESULTS

N_+ distribution

The characteristic curve of the double probe at one of the points of the flame is shown already in *Figure 2.* From similar curves for various points, the electron temperatures T_- at those points could be calculated. The results obtained, together with those of gas temperature T measured by the thermocouple, are shown in *Figure 4.* The rise of T_- in the region $x > 1{\cdot}5$ cm is quite remarkable and strange, but it will be discussed later on.

From *Figure 4* the distribution of wall potential V_w is calculated for $T_+ = T$ and $T_+ = T_-$ assuming $M = 30 \times 1{,}800 \times m$, and its variation is shown in *Figure 5.* The absolute value of M exerts no influence on determining the position of the layer of N_+-maximum.

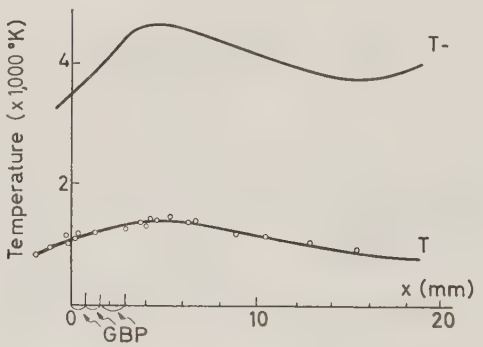

Figure 4. Distribution of gas-temperature (T) and electron-temperature (T_-)

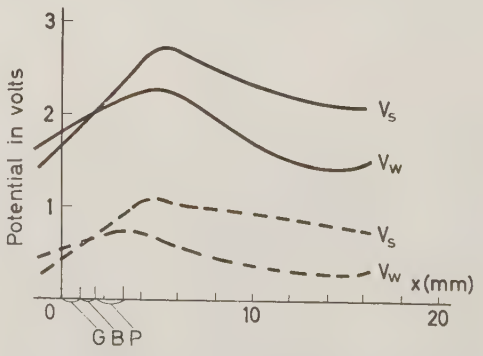

Figure 5. Distribution of space potential (V_s) and wall potential (V_w). Solid lines correspond to $T_+ = T$ and dotted lines to $T_+ = T_-$

On the other hand, from the positive-ion-current $I_w^{(1)}$ observed at various points of the flame, the distributions of $S_w^{(1)} N_+$ for $T_+ = T$ and $T_+ = T_-$ were deduced and are shown in *Figure 6*.

As $S_w^{(1)} N_+$ is expressed in arbitrary units, *Figure 6* shows only the relative values of $S_w^{(1)} N_+$, but it is obvious that, in both cases where $T_+ = T$ and $T_+ = T_-$, $S_w^{(1)} N_+$ has a remarkable peak at a point in the blue part.

At this point, V_w (*Figure 5*) is still increasing with x. This means, according to our former consideration, that if the graph for $N_+ - x$ were given, the maximum for N_+ should be nearer to the flame boundary ($x = 0$) than the maximum for $S_w^{(1)} N_+$ in *Figure 6*.

Thus it can be at least concluded from our results that N_+ attains its maximum at a point in the blue, rather close to the green part.

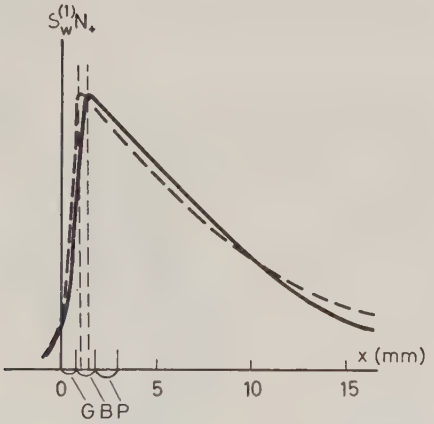

Figure 6. Distribution of $S_w^{(1)} N_+$. Solid and dashed lines correspond to $T_+ = T$ and $T_+ = T_-$ respectively

N_- distribution

As was mentioned formerly, the space potential V_s was obtained from the observed electrostatical potential of the probe and the wall potential. The results are shown in *Figure 5*. The remarkable rise of V_w at higher points of the flame, as well as that of T_-, should not be accepted as it is and will be discussed later.

$N_+ - N_-$ could be deduced by getting $\frac{d^2 V_s}{dx^2}$ graphically from *Figure 5*, but the result will be accompanied by a great deal of error, because a small deviation of V_s would cause a considerable effect in the result. But we can at least conclude from *Figure 5* that $N_+ - N_-$ is of the order of 10^5 cm^{-3} at the parts in question.

On the other hand, N_+ can be roughly estimated from 5, assuming $T_+ = T$, $M = 30 \times 1{,}800 \times m$, and S_w = surface area of the probe sphere. The result is $N_+ \simeq 10^8$ cm^{-3}, showing that our assumption $N_+ \gg | N_+ - N_- |$ holds as was expected.

DISCUSSION AND CONCLUSION

There are several problems about the application of the probe method to find the ion concentration.

We supposed from the beginning that the sheath around the probe, when the probe current $I = 0$, is very thin. If this were not the case, the sheath would stretch over several layers of various concentrations of ions, and N_+ obtained in our experiment would mean only the average value of N_+'s of these layers. It was impossible to find the thickness of the sheath, but it seems reasonable to consider that the thickness is very small because $S_w^{(1)} N_+$ varies quite rapidly with x, as is shown in *Figure 6*.

Our theory was based on the supposition that all the negative charge carriers are pure electrons ; but as the authors have reported[5] already, electrons in a flame have a tendency to attach themselves to molecules or radicals as they ascend in the flame, and our theory is no longer applicable to the upper part of the flame. As to the negative charge carriers in the lower part of the flame, we assumed that most of them were electrons, but this assumption should be left for further investigations.

The most serious problem in our experiment was that the flame was disturbed to some degree by the insertion of the probe or the couple. To keep the flame from being disturbed, it is necessary to make the probe and the couple as small as possible. The diameter of the wire used for the thermocouple was 0·1 mm and that of the silica tubes was as great as 0·4 mm. Some inevitable errors due to this ought to be expected, but it can at least be concluded that N_+ attains its maximum value at a point in the blue part.

The catalytic action of the Pt-wire for chemical process of combustion should also be taken into consideration. In order to study this effect, Pt- and W-wire probes of the same size were inserted side by side in the low-pressure diffusion flame and the *I–E* characteristics of these two probes were compared. But no distinguishable difference was seen between them, from which fact we could conclude that the catalytic action of Pt is not serious.

The surface area of our probe was so small that the thermion current from the probe surface was only of the order of 10^{-10} amp even when the temperature was 1,700° K and all thermions emitted were supposed to be removed. It is quite weak compared with the current due to ions in the flame which amounted to 10^{-8} amp. Therefore,

it is not necessary to take into account the effect of thermionic emission upon the probe current.

Now we shall consider the location of the layer in which ions are mostly produced. Let $q(x)$ be the rate of creation of ions at the point x, v the velocity of ascending burnt gas (assumed to be constant), D_+ the diffusion coefficient of positive ion through the flame, and α the re-combination coefficient. Then the equation for $\mathcal{N}_+$ is

$$q = \alpha \mathcal{N}_+^2 + v \frac{d\mathcal{N}_+}{dx} - D_+ \frac{d^2\mathcal{N}_+}{dx^2} \qquad (9)$$

If the gas velocity v were zero, the point where $\mathcal{N}_+$ is maximum would be just where q is maximum. On the contrary, if v were very large, q would be maximum at $\frac{d\mathcal{N}_+}{dx} = \text{maximum}$, which would be very close to the flame boundary (*Figure 6*). Thus the point where q is maximum should be somewhere between these two extremes.

Equation 9 may be regarded as the equation for $\mathcal{N}_-$ if we put D_- in place of D_+. In our experiment, however, it was shown that the difference between $\mathcal{N}_+$ and $\mathcal{N}_-$ was quite small in spite of D_- being much larger than D_+. This means that the last term of the right-hand side is comparatively small and the comparison of the first two terms is important.

In the blue region just adjacent to the green layer, $\mathcal{N}_+ \simeq 10^8$ cm^{-3}, $\frac{d\mathcal{N}_+}{dx} \simeq 10^9$ cm^{-4}; α is known[2, 4, 6, 7] to be of the order of 10^{-10} cm^3·sec^{-1} and $v \simeq 10^2$ cm·sec^{-1}. Accordingly, $\alpha \mathcal{N}_+^2 \simeq 10^6$ and $v \frac{d\mathcal{N}_+}{dx} \simeq 10^{11}$ showing that $v \frac{d\mathcal{N}_+}{dx}$ predominates over $\alpha \mathcal{N}_+^2$.

Thus we can safely conclude that the layer in which most ions are created is located very close to, or almost certainly in, the green part. This agrees with our original expectation.

It merits attention also that the electron temperature in *Figure 4*, and accordingly the wall potential in *Figure 5*, rises again in the upper part of the flame. This arises probably because we applied our theory to the regions where a great deal of negative ions are expected to exist. And so T_- thus obtained does not mean the true electron temperature.

It is not unreasonable, however, to suppose that the second chemical process associated with production of ions begins after the first processes producing C_2 and CH have begun to decline. In fact, Tverdokhlebov[8] considered that the active CO which appears in the second process is easily ionized by a weak electric field. As to this point, further investigations should be undertaken.

REFERENCES

[1] Calcote, H. F. *Combustion and Flame* 1 (1957) 385

[2] Gaydon, A. G. and Wolfhard, H. G. *Flames: Their Structure, Radiation and Temperature.* 1953. London ; Chapman and Hall

[3] Kinbara, T. and Nakamura, J. *Fifth Symposium on Combustion*, p. 285. 1955. New York; Reinhold

[4] Loeb, L. B. *Basic Processes of Gaseous Electronics.* 1955. Berkeley; University of California Press

[5] Kinbara, T. and Ikegami, H. *Combustion and Flame* 1 (1957) 199

[6] Matton, G. *Sixth Symposium on Combustion*, p. 77. 1956. New York; Reinhold

[7] Longwell, J. P., Frost, E. E. and Weiss, M. A. *Industr. Engng. Chem.* (*Industr.*) 45 (1953) 1629

[8] Tverdokhlebov, B. I. *J.E.T.P.* 30 (1956) 2.

THE PREDOMINANT PROCESS OF ELECTRON DECAY IN THE MANTLE OF AN ACETYLENE-AIR FLAME

H. WILLIAMS

INTRODUCTION

Little is known concerning the decay of ionization in hot flame gases. There are two possible processes, re-combination and attachment, and both may exist together or ionization may decay, controlled first by one process and then, as time proceeds, by the other. It was in order to obtain experimental information enabling a decision to be made on the process responsible for electron decay in the mantle of flames that this experiment was designed.

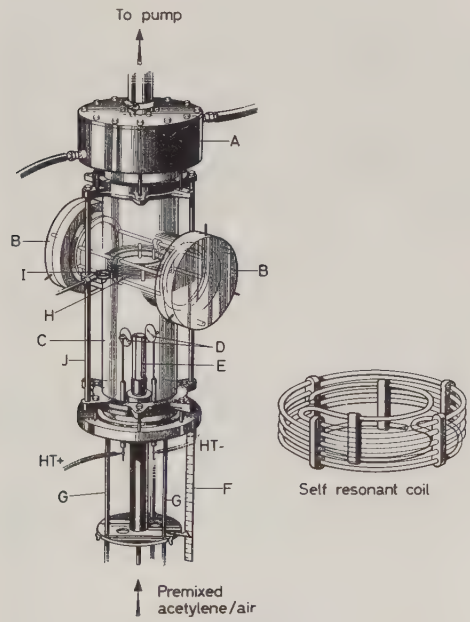

Figure 1. General view of apparatus

A watercooled head, *B* Perspex window, *C* Pyrex low-pressure vessel, *D* ignition discharge electrodes, *E* burner tube assembly, *F* burner position scale, *G* burner guide rods, *H* self-resonant coil, *I* generator coil, *J* coil supports (polystyrene)

Following the assumption[1] that an excessively high concentration of electrons exists in the reaction zone of an acetylene–air flame, the decay of this excessive ionization with distance, and therefore time, above the reaction zone is detected by its damping effect on a self-resonant electrical circuit. This principle is identical to that described by Smith and Sugden[2]. The self-resonant circuit comprises a coil of copper wire, the ends being looped about the coil axis and set facing each other as shown in *Figure 1*; in this way a capacitor is formed which along with the stray capacities present tunes the coil to a frequency of approximately 30 Mc/sec. The flame gases pass through the two loops thus affecting a fraction of the tuning capacity; the coil is excited into oscillation by a signal generator and its Q measured. The necessary theory is developed in the following section. This system was chosen because it does not interfere with the flame. Probes are known to cool the flame considerably[1] and under the condition of low electron concentration thermal emission by the probe may add still further complication. It is this fact of low electron concentration which eliminates the possibility of using microwave attenuation techniques; they are not sensitive enough.

The rather preliminary results quoted here favour strongly the process of attachment whereby an electron attaches to a neutral molecule to form a negative ion. An estimate is made of the overall probability that an electron will attach on a single impact.

THEORY OF SELF-RESONANT COIL

The self-resonant coil when excited as shown in *Figures 1* and *3* by a generator coil only very loosely coupled to it, the same condition applying to the detector coil, may be described by the equivalent circuit diagram of *Figure 2*.

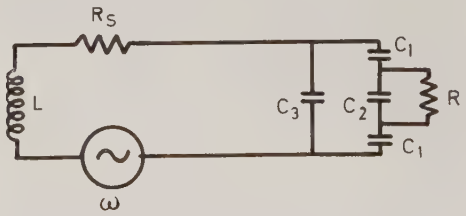

Figure 2. Equivalent circuit diagram of self-resonant coil

The fraction of the total capacitance affected by the flame is C_2. As the flame does not touch the end loops we must add C_1 either side of C_2. C_3 describes the remaining stray distributed capacitance. When the flame is burning a resistance R,

due to its finite conductivity, is presented across C_2. At the electron densities likely to exist in the mantle of the flame without additives the dielectric constant is unity. The total series inductance is L and the series resistance with flame off, R_s.

In the flame off condition

$$Q_0 = \frac{w_0 L}{R_s} = \frac{1}{w_0 C_0 R_s} \tag{1}$$

where w_0 is the resonant frequency (rads sec^{-1}), and C_0 the total series capacitance given by

$$C_0 = C_3 + \frac{C_1 C_2}{C_1 + 2C_2} \tag{2}$$

With flame on:

$$\frac{1}{Q} = \frac{1}{Q_L} + \frac{1}{Q_C} \tag{3}$$

where Q_L refers to the inductance and Q_C to the series capacitance. If all loss in the flame off condition is associated with the series inductance and the added loss with flame on with the series capacitance then

$$\frac{1}{Q_L} = \frac{1}{Q_0}$$

and

$$\frac{1}{Q} - \frac{1}{Q_0} = \frac{1}{Q_C} \tag{4}$$

With flame on the effective series reactance of the capacitive side of the circuit becomes

$$X_{sc} = \frac{w_1 R^2 C^2 (2C_2 + C_1) + \dfrac{4C_3}{w_1} + \dfrac{2C_1}{w_1}}{w_1^2 R^2 C^4 + (2C_3 + C_1)^2}$$

and the effective series resistance

$$R_{sc} = \frac{RC_1^2}{w_1^2 R^2 C^4 + (2C_3 + C_1)^2}$$

where $C^2 = 2C_2C_3 + C_1C_2 + C_1C_3$

Thus

$$\frac{1}{Q_C} = \frac{R_{sc}}{X_{sc}} = \frac{RC_1^2}{w_1 R^2 C^2 (2C_2 + C_1) + \dfrac{4C_3}{w_1} + \dfrac{2C_1}{w_1}}$$

Under the conditions of no easily ionizable additives in the flame R is very large and we may assume

$$w_1 R^2 C^2 (2C_2 + C_1) \gg \frac{4C_3}{w_1} + \frac{2C_1}{w_1}$$

and thus

$$\frac{1}{Q_C} = \frac{C_1^2}{w_1 RC^2 (2C_2 + C_1)}$$

which may be written

$$\frac{1}{Q_C} = \frac{1}{w_1 RC_2} \frac{(C_0 - C_3)^2}{C_0 C_2}$$

Substituting in 4

$$\frac{1}{Q} - \frac{1}{Q_0} = \frac{1}{w_1 RC_2} \frac{(C_0 - C_3)^2}{C_0 C_2} \tag{5}$$

It can be shown that for any condenser completely filled with a dielectric of dielectric constant ε and conductivity σ ohm^{-1} cm^{-1} the product of the capacity in cm and its effective parallel resistance in ohms is given by

$$CR = \frac{\varepsilon}{4\pi\sigma} \text{ ohm cm}$$

This is independent of the geometry of the condenser. Substituting in 5 we have:

$$\frac{1}{Q} - \frac{1}{Q_0} = \frac{4\pi\sigma}{w_1} \frac{(C_0 - C_3)^2}{C_0 C_2} \frac{1}{1 \cdot 11 \cdot 10^{-12}}$$

$$[1 \text{ cm} = 1 \cdot 11 \cdot 10^{-12} \text{ F}]$$

The conductivity of a gaseous medium containing free electrons is closely described by

$$= \frac{Ne^2 w_e}{m(w^2 + w_e^2)} 1 \cdot 11 \cdot 10^{-12} \text{ ohm}^{-1} \text{ cm}^{-1}$$

Thus

$$\frac{1}{Q} - \frac{1}{Q_0} = \frac{4\pi Ne^2}{m(w_1^2 + w_e^2)} \frac{w_e}{w_1} \frac{(C_0 - C_3)^2}{C_0 C_2} \tag{6}$$

where N is the electron density (cm^{-3}), e the electronic charge (e.s.u.), m the electronic mass (g) and w_e the collision frequency (sec^{-1}) of free electrons with heavy molecules. w is the applied radio frequency (rads sec^{-1}).

It is interesting to note that the resonant frequency under the assumption of high R is given by

$$w_2 L = \frac{w_2 R^2 C^2 (2C_2 + C_1)}{w_2^2 R^2 C^4} = \frac{2C_2 + C_1}{w_c C^2} = \frac{1}{w_2 C_0}$$

$$\therefore \quad w_2^2 = \frac{1}{LC_0}$$

This is also the resonant frequency with the flame off and therefore one of the necessary conditions for our assumption to be valid is that there should be no change of resonant frequency on introducing the flame into the coil. This is always found to be the case to better than 0·1 per cent.

The opposite assumption that $R \to 0$ leads to

$$w_3 L = \frac{\dfrac{4C_3}{w_3} + \dfrac{2C_1}{w_3}}{(2C_3 + C_1)^2} = \frac{2}{w_3(2C_3 + C_1)}$$

$$\therefore \quad w_3^2 = \frac{2}{L(2C_3 + C_1)}$$

This is also the resonant frequency one obtains if C_2 is assumed shorted out. It is worth pointing out that as $R \to 0$ the above theory will fail due to eddy currents in such a medium and its effect on field distribution in the coil. It is not surprising therefore that the introduction of a copper cylinder through both end loops which, on the simplest theory, might be considered to short out

C_2 and give a resonant frequency w_3 does not in fact do so. The resonant frequency does not decrease as the theory says but in fact increases.

At points between the two assumptions as for instance with flames containing ionizable additives the full theory must be employed. Calibration of the system is required.

APPARATUS AND METHOD

Low-pressure burner

This is shown in *Figure 1* and comprises a 2 ft. length of 6 in. diameter Q.V.F. Pyrex pipeline with side arms. It is a symmetrical structure, sealed at top and bottom by means of P.V.C. gaskets and metal flanges as shown. The two side windows are Perspex in this case, but can be anything suitable, and sealed on to a greased, ground-glass flange by the positive external pressure. This was found satisfactory. The top P.V.C. gasket is cooled by means of a watercooled head.

The burner itself consists of two concentric tubes, the inner one being Pyrex glass and the outer mild steel. The glass tube protrudes some 10 cm above the steel one, a seal between the two being made by an overlapping short length of wide bore rubber tubing. The whole burner tube assembly is some 50 cm in length and enters the low-pressure vessel through the base plate and two *U* ring seals mounted in the base plate. The region between the two *U* rings is continuously evacuated. This seal is sufficient to allow movement of the burner up and down whilst maintaining the low pressure in the apparatus. The burner assembly is guided by means of three guide rods which pass through a plate to which the burner assembly is fixed as shown in the diagram. Locking nuts in this plate which clamp on to the guide rods enable the burner to be clamped at any vertical position as measured on the burner scale.

The pre-mixed gases of acetylene and air are admitted at the base of the burner tube. Ignition is achieved at low pressure by means of an electrical discharge between the two ignition electrodes.

The self-resonant coil is shown positioned in the apparatus and also in detail in this illustration. It is manufactured of 12 s.w.g. copper wire. The self-resonant coil is mounted rigidly on PTFE supports, the two side arms being employed to carry the assembly. PTFE was used because of its low dielectric loss in order to maintain a high *Q* for the circuit. The two end rings of the coil assembly are centred and clamped by means of three screws made of unplasticized P.V.C. The whole coil assembly can be removed as a complete unit through one of the windows.

On either side of the glass envelope of the low-pressure vessel are mounted two small coils on polystyrene supports. One is excited by a signal generator and, by transformer coupling, excites the inner self-resonant coil when the signal generator frequency is near or equal to its resonant frequency, whilst the other detects the current flowing in the inner coil in order that its *Q* may be determined.

The whole vessel is continuously evacuated by means of a large rotary oil pump.

Electrical apparatus

In *Figure 3* is shown a block diagram of the electrical side of the apparatus. The master oscillator produces two outputs, one sine wave and the other square wave. These are synchronized, as shown inset in *Figure 3*, such that the leading edge of the square wave corresponds to the peak of the sine wave. The reason for this will become evident. The signal generator is frequency modulated by the sine wave output of the master oscillator, the output of the signal generator being fed to the generator coil through an amplitude modulator. To this is fed the square wave output of the master oscillator, which is of such an amplitude as to switch the signal at the generator coil on and off alternately. The resultant oscillations in the inner self-resonant coil, as seen by the detector coil, are detected by a small germanium crystal diode (C.V.425) and presented via the *Y* amplifier of the oscilloscope on the cathode ray screen. The time base is driven by the sine wave output of the master oscillator.

Since the frequency modulation of the signal generator and the time base of the C.R.T. are driven by the same sine oscillation, the C.R.T. time base may be directly calibrated in terms of frequency and will be linear. Thus the time base may be assigned a calibration in kc/sec/cm. The synchronization of the square wave is such that the exciting signal is switched off as the time base returns after each traverse and thus the zero is drawn. If the centre frequency of the signal generator is now tuned to the resonant frequency of the self-resonant coil, then we have the frequency response characteristic of the coil along with the zero base line presented on the C.R.T. screen. This type of picture is illustrated in *Figure 3*. Not shown in *Figure 3*, because of possible confusion but used for calibration purposes, is another signal generator not capable of the modulations of the first signal generator but having an extremely accurately calibrated output in terms of frequency. The frequency scale can be calibrated every interval of 1 Mc/sec by beating against the harmonics of a crystal oscillator accurate to 2 parts in 10^4.

If the output of this generator is now mixed with the f.m./a.m. output of the driving signal generator, then whenever the two generator frequencies coincide a beat will be seen on the C.R.T. trace.

Thus not only can the time base be calibrated in terms of kc/sec/cm but the resonant frequency of the coil determined accurately.

The method employed in determining the circuit Q from the presented frequency response characteristic depends on the fact that the breadth of the response curve[3] at half power equals the resonant frequency divided by the circuit Q, or

$$\frac{1}{Q} = \frac{\Delta fo}{fo} \qquad (7)$$

where fo is the resonant frequency in c/sec and Δfo the breadth of the curve in c/sec at the half power points.

As mentioned previously the generator and detector coils are only very loosely coupled to the resonant coil and thus the crystal detector is dealing with very small signal voltages and may be considered to have a square law characteristic. Thus what is presented on the screen of the C.R.T. is effectively the square of the current in the resonant circuit. A transparent mask placed over the C.R.T. screen carrying three equally spaced horizontal lines, the centre line being marked in mm, enables the width at half power to be determined by lining up the peak of the curve and the zero base with the upper and lower lines, the width of the curve then being read on the centre line. If the time base is calibrated then the width in c/sec is readily determined.

Substitution of this and the measured resonant frequency in 7 allows the immediate determination of Q.

Apparatus for particle track velocity measurements

This technique is described fully elsewhere[4] and under optimum conditions is capable of considerable accuracy. Small particles of MgO are introduced into the gas stream and, if light enough, travel at the gas velocity. The particles are illuminated by an intermittent source of light and the reflected light from the particle imaged by a camera on to a photographic plate. The particle track therefore appears on the plate as a series of dots, each dot corresponding to a flash of the intermittent illuminating source. Knowing the repetition frequency of this source and the image/object ratio of the camera the velocity of the particle and therefore the gas velocity can be determined by measuring the separation of the dots on the photographic plate.

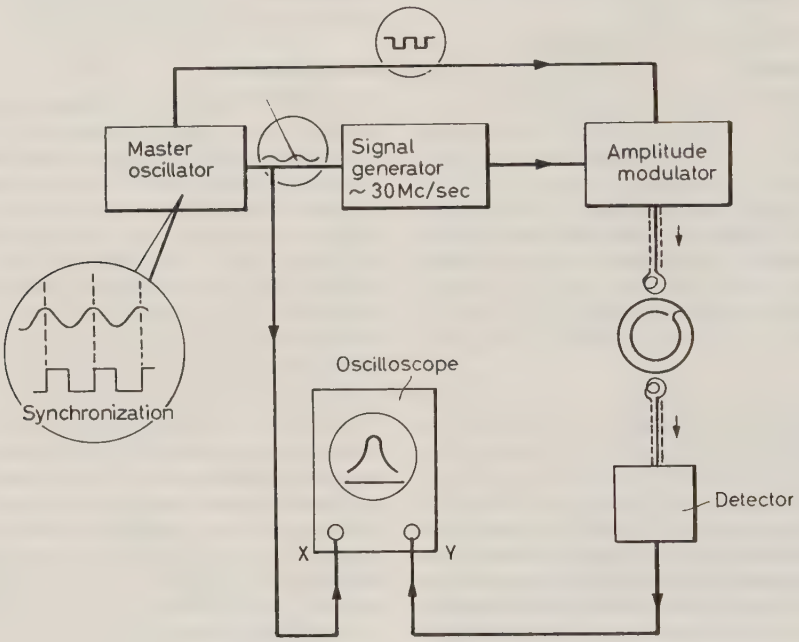

Figure 3. Block diagram of electronic apparatus

The optical system used is shown in *Figure 4*. The intermittent source of light is shown on the left. It is an S.F.E. 1 flash tube driven at 2 joules per flash and 4,000 flashes per sec for a total of 2,000 flashes by a stroboscopic unit which is described elsewhere[5]. The light from this source is condensed by means of an F 1–0 cylindrical lens to form a strip image on the axis of the burner tube. Light reflected from particles in the flame is imaged by a camera as shown. The lens was an f 5·6 and image to object ratio 0·57 for an object on

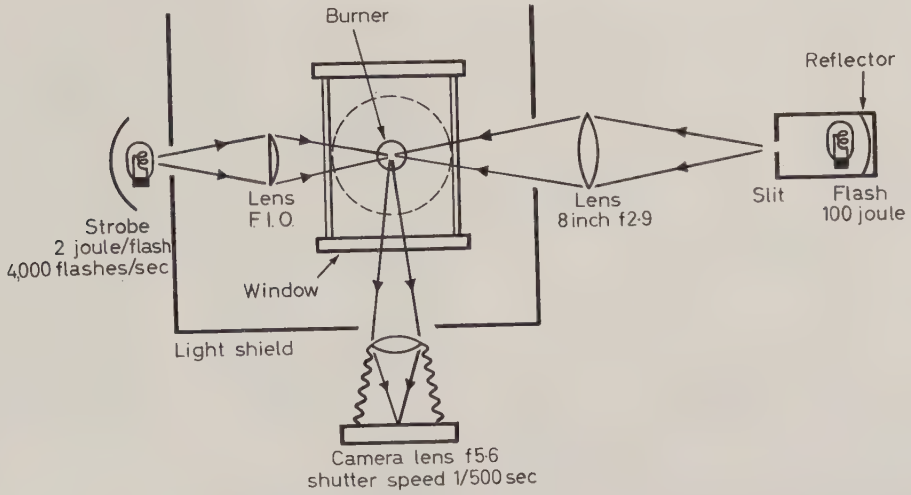

Figure 4. Optical system for particle track photography

the burner tube axis. The depth of field of the camera lens was such as to render particle tracks in focus some ± 6 mm off the flame diameter normal to its line of sight. In order to define a diameter of the flame the illuminating system on the right was added. A slit is illuminated by a single flash and imaged by an $f2{\cdot}9$ lens on to the flame axis, defining a region about 1 mm in width. Consequently only particles in this region will carry a 'tag' produced by reflection of light from this flash: this is shown in *Figure 7*.

The 'tag' flash was a normal photographic flash unit (100 joule), initiated by means of the synchronizing contacts on the shutter. This shutter was operated at 1/500 sec, thus allowing approximately eight individual exposures of the particle, some time during the half second duration of the stroboscopic flash. It was quite satisfactory if the synchronization of this shutter and the strobe were performed manually.

From the particle track images at various heights above the burner the gas velocity/distance curve may be determined by use of a travelling microscope.

TABLE 1

Results of Two Separate Runs on a Stoichiometric Flame

Burner scale reading	*Circuit Q*		$\frac{1}{Q}-\frac{1}{Q_0}$		$\mathrm{Log}_{10}\left(\frac{1}{Q}-\frac{1}{Q_0}\right)$	
	Run 1	*Run* 2	*Run* 1	*Run* 2		
7	560	556	5×10^{-5}	6×10^{-5}	$\times -4{\cdot}3$	$\times -4{\cdot}2$
8	550	550	8×10^{-5}	8×10^{-5}	$-4{\cdot}1$	$-4{\cdot}1$
9	540	540	$1{\cdot}1 \times 10^{-4}$	$1{\cdot}1 \times 10^{-4}$	$-3{\cdot}96$	$-3{\cdot}96$
10	528	532	$1{\cdot}5 \times 10^{-4}$	$1{\cdot}4 \times 10^{-4}$	$-3{\cdot}82$	$-3{\cdot}85$
11	518	510	$1{\cdot}9 \times 10^{-4}$	$1{\cdot}8 \times 10^{-4}$	$-3{\cdot}75$	$-3{\cdot}75$
12	494	496	$2{\cdot}3 \times 10^{-4}$	$2{\cdot}2 \times 10^{-4}$	$-3{\cdot}64$	$-3{\cdot}66$
13	454	454	$2{\cdot}9 \times 10^{-4}$	$2{\cdot}9 \times 10^{-4}$	$-3{\cdot}54$	$-3{\cdot}54$
14	474	474	$3{\cdot}7 \times 10^{-4}$	$3{\cdot}7 \times 10^{-4}$	$-3{\cdot}43$	$-3{\cdot}43$
15	446	446	$5{\cdot}0 \times 10^{-4}$	$5{\cdot}0 \times 10^{-4}$	$-3{\cdot}30$	$-3{\cdot}30$
16	408	410	$7{\cdot}1 \times 10^{-4}$	$7{\cdot}0 \times 10^{-4}$	$-3{\cdot}15$	$-3{\cdot}16$
17	362	362	$1{\cdot}03 \times 10^{-3}$	$1{\cdot}03 \times 10^{-3}$	$-2{\cdot}987$	$-2{\cdot}987$
18	296	296	$1{\cdot}64 \times 10^{-3}$	$1{\cdot}64 \times 10^{-3}$	$-2{\cdot}785$	$-2{\cdot}785$
19	238	242	$2{\cdot}46 \times 10^{-3}$	$2{\cdot}39 \times 10^{-3}$	$-2{\cdot}609$	$-2{\cdot}622$
20	228	—	$2{\cdot}65 \times 10^{-3}$	—	$-2{\cdot}566$	—

$Q_0 = 576$, $\frac{1}{Q_0} = 1{\cdot}74 \,.\, 10^{-3}$, $f_o = 28{\cdot}85$ Mc/sec

C_2H_2 flow = 1·5 c.c./sec, Air flow = 18 c.c./sec Pressure = 22 mm Hg

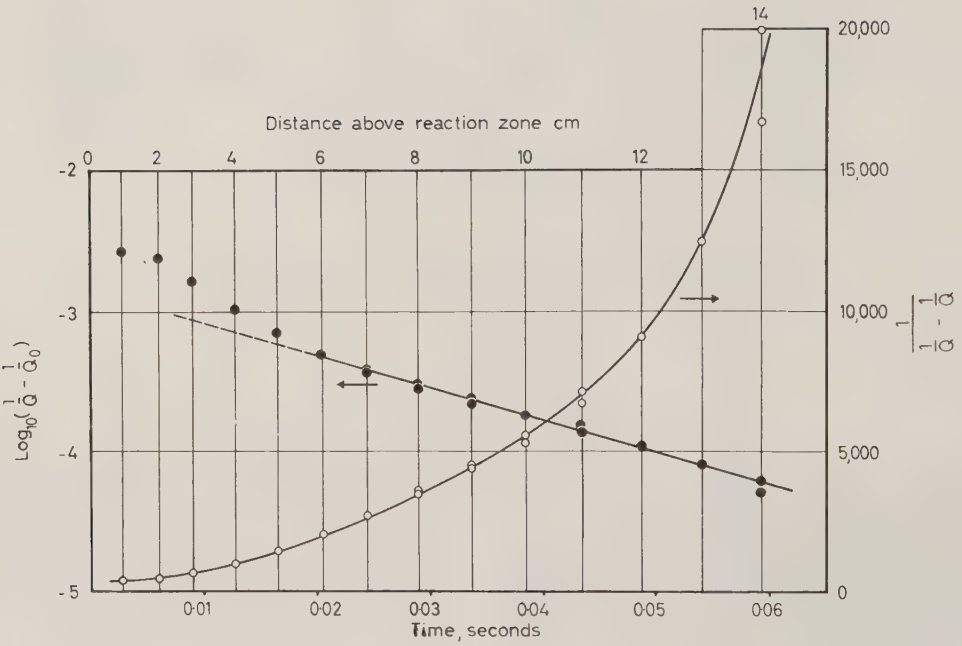

Figure 5. $Log_{10}\left(\frac{1}{Q}-\frac{1}{Q_0}\right)$ *and* $\frac{1}{(1/Q)-(1/Q_0)}$ versus *time*

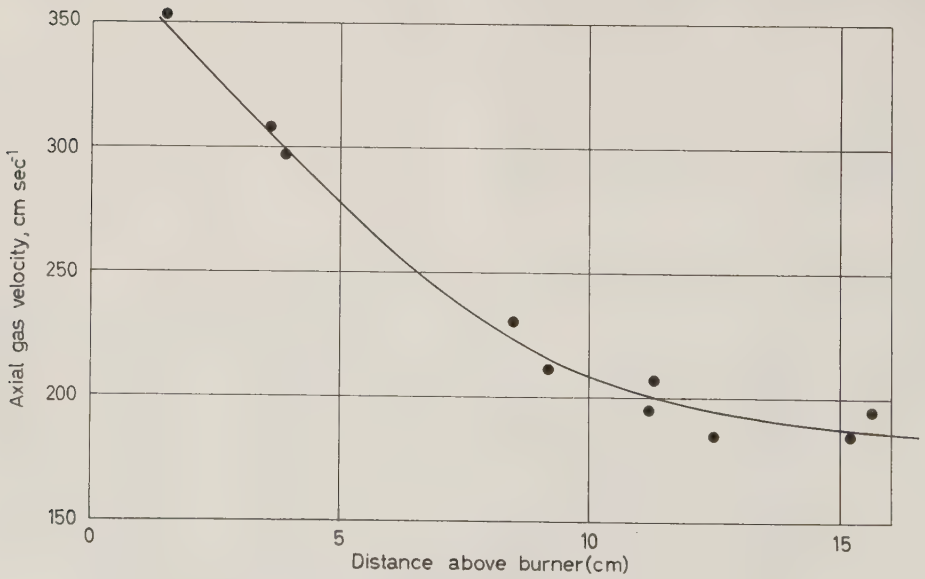

Figure 6. Axial gas velocity versus *distance above burner*

RESULTS

A stoichiometric flame of acetylene/air was burnt at a total pressure of 22 mm Hg absolute. The absolute flow rates were 1·5 c.c./sec for acetylene and 18 c.c./sec for air measured at 1 atmosphere and room temperature. With the burner diameter of 30 mm the reaction zone appeared as a flat disc under the above conditions.

In Table 1 are presented the results of two separate runs on the flame, the circuit Q being recorded at various readings of the burner height as recorded on the burner position scale. The reaction zone appeared in the centre of the coil at a reading of 21 cm on this scale.

In *Figure 5* are shown plotted the results of Table 1. The time scale, derived from particle velocity measurements, the results of which are shown in *Figure 6*, cannot be relied upon to any great degree of accuracy as to absolute time (reaction zone = 0) mainly because of the high

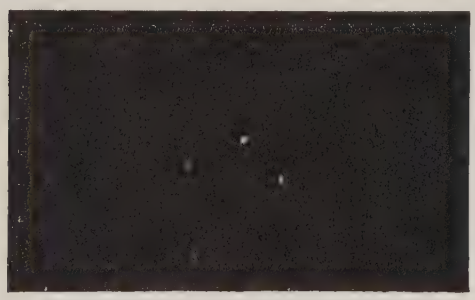

Figure 7. Particle tracks

velocities and accelerations in the neighbourhood of the reaction zone. The method, as used here, did not have the 'resolving power' to follow the velocities at all accurately in this region of high accelerations. The time intervals, however, particularly in the regions of the flame farthest removed from the reaction zone, may be relied upon, the accelerations here being much lower. In this particular application of estimating the decay constants for free electron densities it is the time intervals alone that matter.

CONCLUSIONS

As mentioned in the introduction there are two possible processes of electron decay. In recombination the electron combines with a positive ion with mutual neutralization. The fractional decrease in electron density in a time dt is given by

$$dN = -\alpha N^2 \, dt$$

where α is a constant of proportionality.
On integration

$$\frac{1}{N} - \frac{1}{N_0} = \alpha t \qquad (8)$$

where N_0 is the density at an arbitrary time $t = 0$.

In attachment the electron attaches to a neutral molecule to form a negative ion. Let h be the chance that an electron attaches to a giv n molecular species on a single impact. The average random velocity of the electron is $\bar{C}_1$ (Maxwellian) and its average free path λ. It will therefore make $\bar{C}_1/\lambda \, dt$ collisions in a time dt and the number which attach becomes:

$$dN = -hN\frac{\bar{C}_1}{\lambda} \, dt$$

On integration

$$N = N_0 \, e^{-(h\bar{C}_1/\lambda)t} \qquad (9)$$

From the above it can be seen that a plot of $1/N$ against t is a straight line if re-combination predominates whereas a plot of log N against t is a straight line if attachment predominates. The results of Table 1 are plotted in these two forms in *Figure 5*. As can be seen, attachment appears the predominant process at distances greater than 6 cm above the reaction zone. The curvature close to the reaction zone may be due to a number of things such as changing flame geometry and lack of resolution of the detecting system. There may also be an effect due to the process here being re-combination. As re-combination depends upon N^2 whereas attachment depends only on N then one might expect the former to predominate at high electron concentrations.

These results however do not allow of any decision on this question. From 9 and 6

$$\log_{10}\left(\frac{1}{Q} - \frac{1}{Q_0}\right) = \frac{-h}{2{\cdot}3}\frac{\bar{C}_1}{\lambda} t + \text{constant}$$

Thus the slope of the plot in *Figure 5* gives

$$\frac{h}{2{\cdot}3}\frac{\bar{C}_1}{\lambda}$$

If we consider the overall possibility of attachment then we may write

$$\bar{h}\frac{\bar{C}_1}{\lambda} = \bar{h}w_e$$

where $\bar{h}$ is the possibility of attachment at a single impact averaged over all impacts.

From the graph

$$\frac{\bar{h}w_e}{2{\cdot}3} = 23$$

$$\therefore \qquad \bar{h}w_e - 53$$

From a measurement of Belcher and Sugden[6] the electron collision frequency in a coal gas/air flame at 1 atm and 2,200°K is $8{\cdot}8 \, . \, 10^{10}$ sec^{-1}.

Correcting for pressure and neglecting temperature as only second order we obtain $w_e = 2{\cdot}5 \,.\, 10^9$ sec^{-1}

$$\therefore \qquad \bar{h} = 2 \,.\, 10^{-8}$$

and may be taken to indicate the order of magnitude.

The actual species operative in attachment cannot be decided from the results quoted here. This is left till a later date.

Crown Copyright Reserved

The author is indebted to Dr. A. R. Hall who obtained the photographs of particle tracks necessary in the determination of the gas velocity.

REFERENCES

[1] Calcote, H. F. and King, I. R. Studies of ionisation in flames by means of Langmuir probes. *Fifth Symposium (International) on Combustion.* 1955. New York; Reinhold

[2] Smith, H. and Sugden, T. M. *Proc. Roy. Soc. A* 211 (1952) 31

[3] Terman, F. E. *Radio Engineers Handbook.* New York; McGraw Hill

[4] Fristrom, R. M., Prescott, R., Newman, R. K. and Avery, W. H. Temperature profiles in propane-air flame fronts. *Fourth Symposium (International) on Combustion.* 1953. Baltimore; Williams and Wilkins

[5] Chesterman, W. D., Glegg, D. R., Peck G. T. and Meadowcroft A. J. A new power stroboscope for high-speed flash photography. *Proc. Instn. Elec. Engrs.* 98 Part II (1951) 65

[6] Belcher, H. and Sugden, T. M. Studies on the ionisation produced by metallic salts in flames. I The determination of the collision frequency of electrons in coal gas/air flames. *Proc. Roy. Soc. A* 201 (1950)

42

IONIZATION IN DETONATION WAVES

S. BASU and J. A. FAY

INTRODUCTION

In recent years ionization in flames and shock waves has been the subject of several investigations. Calcote[1] has studied *n*-butane–air flames at 2,170°K by subjecting them to transverse electric fields and estimating the ion density from the deflection of the flames. He obtained densities of the order of 10^{12} ions/c.c. in the inner cone and, since the value was much higher than that predicted by thermodynamic equilibrium calculations, concluded that non-equilibrium conditions existed in the flame front. In a later paper[2] he reported measurements with Langmuir probes of ion densities in carbon disulphide, hydrogen sulphide and propane–air flames, and came to the same conclusion. Sugden and his co-workers[3–5] have examined coal gas–air and hydrogen–air flames with added alkali salts at temperatures of about 2,100°K. Using a microwave attenuation technique, they found electron densities of the order 10^{10}–10^{11} ions/c.c., in good agreement with calculations based on thermodynamic equilibrium. More recently Shuler and Weber[6] have studied the ionization in oxy-hydrogen flames at temperatures up to 2,900°K and in oxy-acetylene flames at temperatures up to 3,300°K. Employing a similar microwave attenuation technique they obtained densities of the order 10^{9} ions/c.c. for the oxy-hydrogen and 10^{10} ions/c.c. for the oxy-acetylene flames, in agreement with the results of appropriate thermodynamic equilibrium calculations. However, in the case of rich oxy-acetylene flames the measured ion densities were well in excess of those computed assuming C^+ as the chief source of ions. They suggested that the discrepancy was due to the ionization of solid carbon aggregates or polymers with an ionization potential intermediate between the work function of graphite and the ionization potential of gaseous monatomic carbon.

Lin *et al.*[7,8] have studied the ionization behind shock waves in argon and air in the temperature range 4,000°K to 14,000°K. They measured the electrical conductivity of the gas behind the shock wave by a magnetic field interaction technique and obtained results in good agreement with thermodynamic equilibrium calculations.

The research reported in this paper was undertaken to study ionization in detonation waves. The electrical properties of ionized gases depend partly upon the electron density and hence it is of considerable interest to determine whether or not thermodynamic equilibrium with respect to ion formation is established behind the wave. Using a simple d.c. probe technique, measurements have been made of the electrical conductance of stoichiometric oxy-hydrogen detonation waves with initial pressures of $\frac{1}{10}$ to 1 atm, and of oxy-acetylene detonation waves at 1 atm initial pressure with mixture composition varying from 30 per cent C_2H_2 to 80 per cent C_2H_2. The measured values were compared with theoretical results based on thermodynamic equilibrium calculations.

APPARATUS AND EXPERIMENTAL PROCEDURE

Detonation waves were generated in a steel tube 3 in. i.d., and 17 ft long, by spark initiation. In low pressure (below $\frac{1}{4}$ atm) oxy-hydrogen mixtures

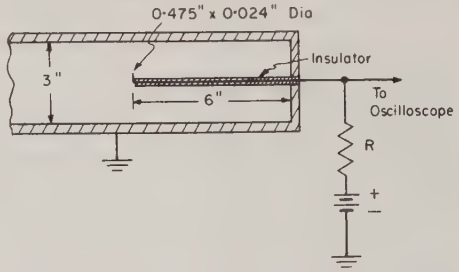

Figure 1. Schematic diagram of circuit for measuring electrical conductance of detonation waves

and rich (above 60 per cent C_2H_2) oxy-acetylene mixtures spark initiation was not sufficient to produce detonation waves. In these mixtures apparently stable detonation waves were initiated by the use of a driver ($2H_2$–O_2 or C_2H_2–O_2 at 1 atm) which occupied 3 ft of the tube and was separated from the test mixture by a Cellophane diaphragm.

Figure 1 shows schematically the circuit used to measure the electrical conductance of the waves. A d.c. probe made of 0·024 in. diameter steel wire is supported by the end-plate of the tube and all

but the tip is insulated by a coating of glyptal. The uninsulated portion of the probe is 0·475 in. long and is placed on the tube axis with the probe axis normal to the tube axis. The tube is grounded, and a voltage of about 20 V is applied to the probe (anode) through an external resistance R. As the detonation wave sweeps past the probe, the probe current builds up from zero to a steady value (which is measured) in about 10 μsec or less, corresponding to a distance behind the front of

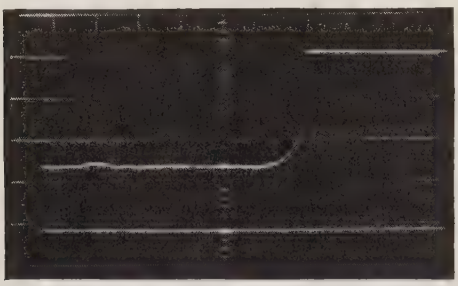

Figure 2. Photograph of typical oscilloscope record. Time runs from right to left, with a scale of 20 μsec per cm. *The bottom horizontal line corresponds to zero voltage and the top horizontal line to an open circuit voltage of about* 20 V. *The gas mixture was* $2H_2$–O_2 *at* $\frac{1}{4}$ atm *initial pressure*

about 3 cm. The voltage drop across the ionized gas is measured with an oscilloscope. The photograph of a typical oscilloscope record (*Figure 2*) shows the voltage across the gas as a function of time, which proceeds from right to left. From the voltage drop and the known resistance, R, the probe current and consequently the resistance of the gas between the probe and the tube wall is easily determined.

The probe potential was varied from about 10 to 100 V and it was found that the gas resistance was independent of probe current in this range within experimental scatter, thus showing that surface effects were probably negligible in the measurement of the gas resistance. This may be due to the fact that the probe is the anode and is stationary, so that the plasma flowing by it at a high velocity supplies enough electrons to the boundary layer to neutralize any space charge built up around the probe.

THEORETICAL ESTIMATION OF THE GAS CONDUCTANCE

For purposes of comparison with the experimentally measured values of gas conductance, theoretical values were computed as follows:

(*a*) The equilibrium concentrations of ionic species were computed at the temperature and pressure given by the Chapman–Jouguet theory of detonation waves.

(*b*) From the electron density the specific conductivity σ (mho/cm) was calculated by making use of suitable electron-molecule collision cross-sections.

(*c*) The gas conductance Σ (mhos) was computed from the conductivity, σ, and the probe geometry.

The specific assumptions involved in each of the above steps are as follows:

(*a*) For a given initial mixture composition, pressure and temperature, the pressure, temperature and composition of the gas behind the detonation wave can be calculated from the Chapman–Jouguet[9] theory. For the oxy-hydrogen waves these calculations were carried out by us, whereas for the oxy-acetylene waves the results were computed by the Gibbs Chemical Laboratory of Harvard University. With these data the electron density can be computed with the help of Saha's equation[10]. Table 1 gives the values of ionization potentials and ratio of statistical weights of the molecules needed in the calculation.

It was found that the N_2 impurity in the O_2 (0·1 per cent) was sufficient to mask the ionization of the other species present in the oxy-hydrogen waves by producing NO, which ionizes more easily. To eliminate the effects of NO, the initial N_2 mole fraction would have to be lowered below 10^{-6}. Instead, $\frac{2}{3}$ mole per cent of N_2 was added to the stoichiometric H_2–O_2 mixture to give a controlled impurity level.

TABLE 1

Species	*Ionization potential* eV	*Ratio of statistical weights* $\frac{g_A + g_e}{g_A}$
O_2	12·075	$\frac{8}{3}$
H_2O	12·590	2 (?)
NO	9·25	$\frac{1}{2}$
C_2H_2	11·41	2 (?)
CH	11·1 (?)	2 (?)
C_{gas}	11·265	2

Smith and Sugden[5] have suggested that OH^- ions may be formed in flames and estimated the electron affinity to be 63 kcal/mole. Two values of the electron density were therefore calculated, one neglecting and the other including OH^- formation. Table 2 gives the temperature and pressure of the gas behind the oxy-hydrogen waves, the mole fractions of the ion-contributing species present, and the electron density.

Kistiakowsky and Zinman[11] have measured the velocities of oxy-acetylene detonation waves and found that in the range 60 to 70 per cent acetylene in the initial mixture the measured velocities corresponded to homogeneous rather than total equilibrium behind the detonation wave, i.e. solid carbon was not formed. Therefore, for rich

oxy-acetylene mixtures in the above range, calculations of electron density were made assuming complete equilibrium and also partial equilibrium without the formation of solid carbon. Table 3 gives the temperature and pressure of the gas behind the oxy-acetylene waves, the mole fractions of the ion-contributing species present and the electron density.

Sugden and Thrush[12], and more recently Einbinder[13] and Smith[14], have presented methods of computing the electron density due to the ionization of solid particles, taking into account the electrostatic attraction between the electrons and the charged solid particles and their size. For oxy-acetylene detonations with more than 60 per cent initial acetylene, electron densities were computed following the method of Smith[14] with particle radii 100, 500, 1,000, and 2,000 Å, covering approximately the range of particle radii observed experimentally in rich hydrocarbon flames[15].

(*b*) For a slightly ionized gas the electrical conductivity, in mhos/cm is given in reference 16:

$$\sigma = \frac{0{\cdot}532}{9 \times 10^{11}} \cdot \frac{\alpha e^2}{(m_e k T)^{\frac{1}{2}}} \cdot \frac{1}{S}$$

where α is n_e/n, the fraction ionized; n_e is the number density of electrons per c.c.; n is the number density of gas molecules per c.c.; e is the charge of an electron; m_e is the mass of an electron; k is Boltzmann's constant; T is the absolute temperature in degrees K; and S is the effective electron-molecule collision cross-section in cm^2.

For the H_2–O_2 waves it was assumed that the electron–H_2O collision cross-section was appreciably larger than any other, and had the value 3×10^{-15} cm^2. This value is given by Bailey and Duncanson[17] for H_2O vapour at an electron temperature of 3,500°K and also corresponds to the collision frequency measured by Belcher and Sugden[3] in a coal gas–air flame with the assumption that H_2O vapour has a much larger collision cross-section than the other molecules. The latter is true for O_2 and N_2 but nothing is known regarding the cross-sections of OH, O, and N.

In the C_2H_2–O_2 waves the main constituents present were CO and H_2 and both molecules have collision cross-sections of about 10^{-15} cm^2 at electron temperatures of[18] 3,500°K: hence this value was used in the computation of σ. The

TABLE 2

Properties of Stoichiometric Oxy-hydrogen Detonation Waves at Initial Temperature 296°K with $\frac{2}{3}$ per cent N_2

Initial pressure (atm)	*Final pressure* (atm)	*Final temperature* (°K)	*Mole fraction of ion contributing species*				*Electron density (curve C, Figure 1)* $n_e \times 10^{12}$ (per c.c.)	*Specific electrical conductivity (curve C, Figure 1)* $\times 10^4$ (mhos/cm)
			H_2O	O_2	NO	OH		
0·0180	0·2793	3,000	0·4764	0·0619	0·0024	0·1083	0·010	1·715
0·0611	1·3117	3,200	0·4920	0·0585	0·0029	0·1161	0·064	2·670
0·4038	7·1106	3.500	0·5178	0·0532	0·0037	0·1251	0·750	4·960
1·5468	28·7303	3,750	0·5420	0·0498	0·0043	0·1288	4·320	6·980

TABLE 3

Properties of Oxy-acetylene Detonation Waves at 1 atm Initial Pressure and 296°K Initial Temperature

Initial C_2H_2 (per cent)	*Final pressure* (atm)	*Final temperature* (°K)	*Mole fraction of ion contributing species*				*Electron density* $n_e \times 10^{12}$ (per c.c.)	*Specific electrical conductivity* $\times 10^4$ (mhos/cm)
			H_2O	O_2	C_2H_2	C_{gas}		
30	34·7	4,240	0·0589	0·01650	—	—	7·24	16·80
40	41·0	4,460	0·0870	0·0973	—	—	9·43	19·00
53	40·6	4,275	—	—	0·0367	0·0032	8·45	16·80
60	35·2	3,975	—	—	0·1027	0·0014	3·65 (I)	8·31
60	34·1	3,900	—	—	0·1360	0·0012	3·41 (II)	7·66
65	32·8	3,845	—	—	0·1079	0·0007	2·08	4·85
70	30·9	3,722	—	—	0·1111	0·0004	1·14 (I)	2·75
70	25·0	3,177	—	—	0·3056	0·0001	0·735 (II)	0·21
75	28·65	3,615	—	—	0·1131	0·0001	0·639	1·65
80	26·6	3,515	—	—	0·1141	0·0001	0·364	1·00

variation in cross-section with temperature in the range under consideration was negligible.

The last columns of Tables 2 and 3 show the values of σ (mhos/cm) computed under the above assumptions.

(*c*) The probe was assumed to be an ellipsoid of revolution with major axis to minor axis ratio equal to the probe length to diameter ratio, and such that its surface area was the same as that of the probe. With this geometry the total gas conductance Σ (mhos) worked out to $2{\cdot}36\sigma$.

RESULTS

Theoretical and experimental values for the gas conductance are compared in *Figures 3* and *4*. *Figure 3* shows a log-log plot of the total gas conductance Σ (mhos) against the initial pressure of the mixture (atm) for stoichiometric oxy-hydrogen detonation waves. Curve *A* corresponds to the hypothetical case in which no N_2 is present

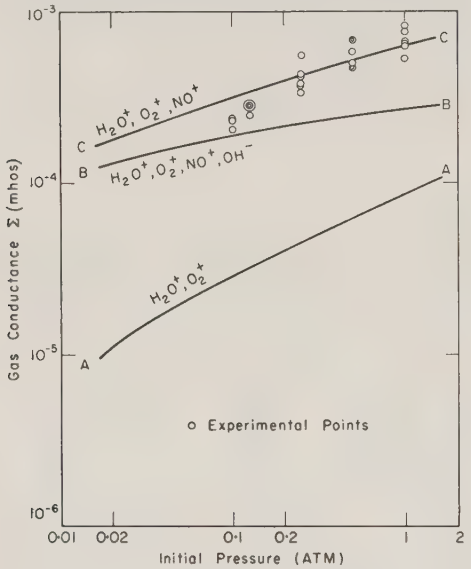

Figure 3. Comparison between experimental and theoretical electrical conductance of stoichiometric oxy-hydrogen detonation waves. Curve A corresponds to the hypothetical case in which no N_2 *is present in the system in which case the important ions are* H_2O^+ *and* O_2^+. *Curve B corresponds to the experimental condition in which* $\frac{2}{3}$ mole per cent N_2 *is present in the system, in which case the important ions are* H_2O^+, O_2^+, NO^+ *and* OH^-. *Curve C denotes the same condition as Curve B except that* OH^- *formation is neglected, so that the important ions are* H_2O^+, O_2^+ *and* NO^+

in the system in which case the important ions are H_2O^+ and O_2^+. Curve *B* corresponds to the experimental condition in which $\frac{2}{3}$ mole per cent N_2 is present in the system, in which case the important ions are H_2O^+, O_2^+, NO^+ and OH^-. Curve *C* denotes the same condition as curve *B* except that OH^- formation is neglected, so that the important ions are H_2O^+, O_2^+ and NO^+. An increase in initial pressure causes an increase in the temperature of the gas behind the detonation wave and this results in increased ionization.

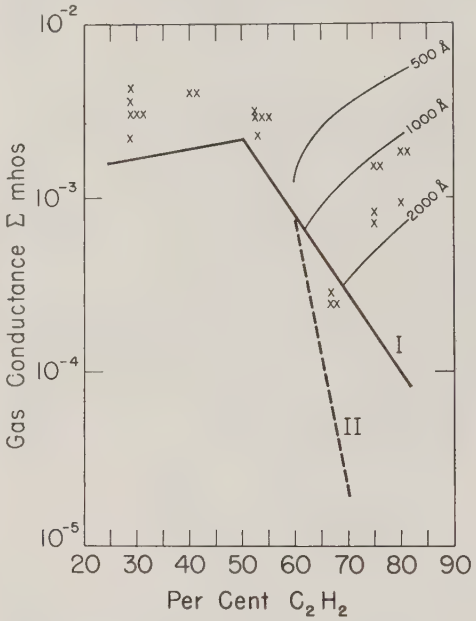

Figure 4. Comparison between experimental and theoretical electrical conductance of oxy-acetylene detonation waves at 1 atm *initial pressure.* × *denotes an experimental point. Curve I corresponds to complete equilibrium, while curve II corresponds to partial equilibrium without the formation of solid carbon. Below* 50 per cent C_2H_2 *the important ions are* H_2O^+ *and* O_2^+, *whereas above* 50 per cent C_2H_2 *the important ions are* $C_2H_2^+$ *and* C^+. *The curves marked* 500, 1,000, *and* 2,000 Å *correspond to conductivities obtained when the ionization of solid carbon is taken into account, the particle radii being* 500, 1,000, *and* 2,000 Å *respectively*

Figure 4 shows a semi-logarithmic plot of the gas conductance Σ (mhos) against the concentration of acetylene in the initial mixture for oxy-acetylene waves. Up to about 50 per cent acetylene, the important ions were H_2O^+ and O_2^+. In richer mixtures C_2H_2 and C contributed most of the ions. As the concentration of acetylene increases beyond stoichiometric, the temperature of the gas rises until about 50 per cent acetylene is reached, with a corresponding rise in conductivity. As the mixture gets richer the temperature (and thus conductivity) falls continuously. Between 60 and 70 per cent acetylene there are two curves, I and II, corresponding to total equilibrium, and partial equilibrium without the formation of solid carbon, respectively. For a certain initial composition, curve I corresponds to a higher temperature than does curve II due to the condensation of carbon (in the case of curve I) and the consequent liberation of its heat of sublimation. The three

curves marked 500, 1,000, and 2,000 Å correspond to conductivities obtained when the ionization of solid carbon particles is taken into account, the size of the particles being 500, 1,000, and 2,000 Å, respectively.

DISCUSSION

For the oxy-hydrogen detonation waves it is clear that the formation and subsequent ionization of NO are the dominant factors in determining the electron density behind these waves. From *Figure 3* it would also seem that OH^- ions are not formed behind these detonation waves. This may be due to the fact that the time involved in these experiments is of the order of 100 μsec and this may not be sufficient for the formation of OH^- by a three-body collision process. In the flames studied by Sugden[5], the time available, which is about 10^3 times as long as that for the detonation, may be sufficient for the formation of OH^-.

Shuler and Weber[6] neglected the formation of NO^+ and OH^- in their ionization calculations for oxy-hydrogen flames, but their theoretical electron densities were in good agreement with their measurements. It is found that good agreement is also obtained between equilibrium calculations taking account of the formation of NO^+ and OH^- ions and the experimental results of Shuler and Weber. This is because the formation of NO^+ and OH^- produce opposing effects which almost cancel each other at the flame temperatures under consideration, thus causing little net change in the calculated electron densities. Therefore, there appears to be no discrepancy between theory and experiment for these flames if OH^- ions are formed.

In the case of oxy-acetylene detonation waves, the agreement between theory and experiment is not so good. However, at 30, 40, and 53 per cent C_2H_2 the experimental values are uniformly about a factor of two higher than the theoretical. This may be due to an uncertainty in the collision cross-sections used, as these are not known very accurately. If this is indeed the case, then at 66 per cent C_2H_2 the conductance is found to correspond to homogeneous equilibrium behind the detonation wave in agreement with the observation of Kistiakowsky and Zinman[11]. At richer mixtures the measured conductance is higher than the theoretical by as much as a factor of about ten if the ionization is assumed to be gaseous. This high conductivity may possibly be due either to the ionization of solid carbon or the formation and ionization of other hydrocarbons with lower ionization potentials than C_2H_2, e.g. benzene (9·3 eV).

If the ionization of solid carbon particles is taken into account following the method of Smith[14] then it is seen from *Figure 4* that the measured conductance corresponds to an average particle size of 2,000 Å radius.

The presence of excessive ionization in rich C_2H_2–O_2 flames has been reported by Shuler and Weber[6]. They found that measured electron densities were as much as a factor of 30 times higher than calculations based on thermodynamic equilibrium. They suggested that this may be due to the formation of small carbon aggregates and polymers in the flame and their subsequent ionization at an ionization potential intermediate between that of graphite (4·35 eV) and atomic carbon (11·265 eV). However, it appears that they did not take into account the ionization of C_2H_2 (11·41 eV). If the formation of $C_2H_2^+$ is considered, it is estimated that the discrepancy would be considerably reduced.

Working with the data of Shuler and Weber, Einbinder[13] has arrived at a carbon particle radius between 55 and 85 Å to obtain agreement between theoretical and experimental electron densities. Experiments[15] indicate that carbon particles formed in rich hydrocarbon flames vary from 100 to 2,000 Å in diameter. The average value of 2,000 Å radius obtained theoretically to satisfy the measured values of gas conductance behind rich oxy-acetylene detonations corresponds, therefore, to particles which are twice the size of the largest carbon particles observed in flames.

The whole question of excessive ionization in rich oxy-acetylene flames and detonations remains an unsolved problem. To obtain high conductance in these waves due to the ionization of carbon aggregates, it is necessary to suppose that these aggregates are so finely dispersed that the electron clouds around them overlap (i.e. that the distance between aggregates is less than the Debye distance) and thus maintain a current through the gas.

In the experiments with rich C_2H_2–O_2 detonation waves the distance between aggregates is of the same order as the Debye distance for particles 2,000 Å in radius; for smaller particle size the inter-particle distance is smaller than the Debye distance. Since particles larger than 2,000 Å in radius do not contribute appreciably to the electron density, it is possible that the observed conductance is due to the ionization of fine particles 100 to 2,000 Å in diameter which, however, constitute only a fraction of the total solid carbon present, the rest being in the form of particles larger than 2,000 Å radius. An experimental determination of particle size in the gas behind rich C_2H_2–O_2 detonations would help immensely in clearing up this matter.

CONCLUSIONS

(1) In view of the general agreement between theory and experiment, it appears that equilibrium

ionization is achieved in detonation waves in the mixtures tested.

(2) The formation of NO^+ ions dominates the ionization in oxy-hydrogen detonation waves.

(3) OH^- ions are probably not formed in these waves due to lack of time.

(4) The measured gas conductance for oxy-acetylene waves with 66 per cent C_2H_2 in the initial mixture corresponds to homogeneous rather than total equilibrium in agreement with the results of Kistiakowsky and Zinman[11].

(5) In C_2H_2–O_2 waves with more than 70 per cent C_2H_2 the measured conductance is about a factor of 10 higher than theoretical, if gaseous ionization only is considered. If the ionization of solid carbon particles is considered, the measured gas conductance corresponds to an average particle size of 2,000 Å radius.

(6) On the basis of experiments performed up to now, the d.c. probe seems to be an adequate tool for the measurement of electrical conductivities of detonation waves.

This work was sponsored by Project SQUID which is supported by the Office of Naval Research, Department of the Navy, under contract Nonr 1858(25) NR-098-038.

REFERENCES

[1] Calcote, H. F. *Third Symposium on Combustion, Flame and Explosion Phenomena*, p. 245. 1949. Baltimore; Williams and Wilkins
[2] — and King, I. R. *Fifth Symposium (International) on Combustion*, p. 423. 1955. New York; Reinhold
[3] Belcher, H. and Sugden, T. M. *Proc. Roy. Soc. (Lond.) A* 201 (1950) 480
[4] — — *Proc. Roy. Soc. (Lond.) A* 202 (1950) 17
[5] Smith, H. and Sugden, T. M. *Proc. Roy. Soc. (Lond.) A* 211 (1952) 31, 58
[6] Shuler, K. E. and Weber, J. *J. chem. Phys.* 22 (1954) 491
[7] Lin, S. C., Resler, E. L. and Kantrowitz, A. *J. appl. Phys.* 26 (1955) 95
[8] — and Lamb, L. *J. appl. Phys.* 28 (1957) 754
[9] Lewis, B. and von Elbe, G. *Combustion, Flames and Explosions of Gases*, p. 606. 1951. New York; Academic Press
[10] Saha, M. N. and Saha, N. K. *A Treatise on Modern Physics*, p. 630. 1934. Allahabad and Calcutta; The Indian Press
[11] Kistiakowsky, G. B. and Zinman, W. G. *J. chem. Phys.* 23 (1955) 1889
[12] Sugden, T. M. and Thrush, B. A. *Nature (Lond.)* 168 (1951) 703
[13] Einbinder, H. *J. chem. Phys.* 26 (1957) 948
[14] Smith, F. T. *J. chem. Phys.* 28 (1958) 746
[15] Wolfhard, H. G. and Parker, W. G. *Proc. phys. Soc. (Lond.) B* 62 (1949) 523
[16] Chapman, S. and Cowling, T. G. *The Mathematical Theory of Non-Uniform Gases*, Sec. 18.12 and 14.2, and Table 6, Sec. 10.53. 1952. London; Cambridge University Press
[17] Bailey, V. A. and Duncanson, W. E. *Phil. Mag.* 10 (1930) 145
[18] Massey, H. S. W. and Burhop, E. H. S. *Electronic and Ionic Impact Phenomena*, p. 206. 1952. Oxford

DISCUSSION

M. Gerstein (Cleveland): There are four questions which immediately come to mind with respect to a subject such as Ions in Flames. First, are there ions in a flame; second, which ionic species are present; third, what is their concentration; and finally, what is their role and influence?

The first question can be dismissed immediately. Certainly there is ample evidence that ions exist in the flames which are usually encountered, although they may possibly be absent in some low-temperature decomposition flames.

The second question is one of the most difficult to answer and some of the papers in this Symposium have made praise-worthy contributions on this problem. The ions reported to be present differ somewhat from those predicted on the basis of calculated ionization potentials and this raises the question of the mechanism of the ionization process. There also appears to be a difference between the species found in highest concentration at low pressure and those found at high pressure. It would be interesting to know if the change is due to pressure alone and a series of experiments with the same system at various pressures should help answer this question. The identification of H_3O^+ suggests some interesting research. It has been reported that the ion concentration in CS_2/air flames is low. The change in H_3O^+ concentration with water addition to the CS_2/air mixture might add some useful knowledge about this particular ion. The other experiment has nothing to do with combustion. H_3O^+ is the Bronsted acid in aqueous solution. The existence of this ion in the gas phase should make possible acid-base studies in a molecular beam uncomplicated by the presence of a solvent.

There seems to be qualitative agreement concerning the total ion concentration in a flame. It would be desirable to use the same flame system to determine if the various techniques used to measure ion concentration are in quantitative agreement. The validity of the techniques and interpretation of ion formation mechanisms cannot be made until it is known if the various methods are in agreement. The validity of the measurements must be determined before a positive statement can be made concerning whether or not the number of ions is equal to or different from that calculated from thermal equilibrium considerations alone. In this Symposium there seems to be fair agreement that the ion concentration is greater than that expected from thermal equilibrium considerations alone and chem-ionization is suggested. The literature contains a few suggestions that the ions can be accounted for on an equilibrium basis. In the papers included here, one wonders why the ion concentration should be in apparent thermal equilibrium in the much faster processes occurring in a detonation wave and not in a flame.

Finally, what is the role and influence of the ions present in a flame. The total concentration, of the order of 10^{12} ions per cm^3, is certainly lower than the concentration of the free radicals considered important in flame reaction mechanisms. Are the ions, then, just minor species present whose influence is of little concern except under special conditions, such as the presence of strong electric or magnetic fields, or do they play an important role in either the chemical or energy processes in a flame? It has been suggested that the ions can be used as tracers to assist in determining the changes in certain neutral species which are not as easily detected or measured. There would seem to be some risk in such interpretations. If, as has been suggested, the ions are not in thermal equilibrium with their parent species, it would be questionable to estimate the concentration of the parent species or even their exact nature since the ions may have been formed by some minor side reactions. It would seem that much more must be known about the mechanism of ion formation before confidence could be placed in the interpretations of combustion mechanisms based on the ions detected.

J. Deckers (Princeton): Since our paper (J. Deckers and A. van Tiggelen) was submitted for pre-printing other types of flames have been investigated; the results which have been obtained in undiluted rich mixtures (except where otherwise stated) are given in the table on page 284.

Concerning the concentration of the different ions in a flame an estimation, based on the hypothesis that the NO^+ ions are thermal ions, gives for a 10·5 per cent acetylene, 19·5 per cent oxygen and 70 per cent nitrogen mixture the following number of ions per c.c.

NO^+	10^7 ions/CC
COH^+	2×10^7
H_3O^+	3×10^9
$C_3H_3^+$	3×10^9
$H_5O_2^+$	5×10^8

The maximum value for each ion, as given here, does not occur at the same point of the flame.

All the new results were obtained with a total accelerating potential of 750 V. Between electrodes

D_1 and L_2 only a potential drop of 10 to 15 V was applied. Even with a potential drop of only 7 V between these electrodes the ratios of the different peaks were not markedly altered.

Mixture	*Mass units*	*Hydrogen content*	*Identity of ion*	*Remarks*
	19	3	H_3O^+	
	37	5	$H_5O_2^+$	Only in flames diluted with nitrogen and at a rather higher pressure (at least 25 mm Hg).
C_2H_2/O_2	39	3	$C_3H_3^+$	Only in fuel-rich flames
	29	1	COH^+	
	30	0	NO^+	Does not appear when no nitrogen is added to the flame
Very weak peaks are noticed at mass numbers 13, 14, 17, 18, 24, 26, 28, 43; less than 0·1% of H_3O^+ max.				
	30	0	NO^+	At least 90%
	18	4	NH_4^+	
	19	3	H_3O^+	
	28	2	H_2CN^+	
C_2H_2/N_2O	39	3	$C_3H_3^+$	Only in fuel-rich mixtures
	29	1	COH^+	
	43	?	?	Too weak to check hydrogen content
Very weak peaks at mass number 26, 31, 41, 44; less than 0·1%.				
C_2H_2/O_2 with about 1% NH_3 or 2% HCN	More or less the same mass spectrum as in the case of acetylene-nitrous oxide flames but the NO^+ peak is only about 50% of the total number of ions The ratio H_2CN^+/NO^+ is about the same in both cases NH_4^+ is less pronounced with the addition of HCN than of NH_3			
CH_4/O_2	19 29	3 1	H_3O^+ COH^+	about 1%
H_2/N_2O	30	0	NO^+	

H. F. Calcote (Princeton): I have several remarks in answer to the questions raised by Gerstein and pertaining to the papers presented in this section. Gerstein asks why is equilibrium observed in detonation (Basu and Fay) and not in deflagration. In all cases where equilibrium ionization is observed, including the experiments of Shuler and Weber* the temperature has been high, approximately 3,000°K; while non-equilibrium ionization is observed at lower temperatures, less than 2,400°K. At the higher temperatures thermal ionization evidently masks non-thermal ionization. In this regard we might observe that the concentration of ions is determined by the relative rates of ion production and removal. The process of removal is fast† and is second order with respect to the concentration of ions so that it becomes increasingly difficult to build-up large concentrations of ions downstream from a combustion wave producing non-thermal ionization. Equilibrium ionization would, of course, continue to produce ions downstream from the combustion wave so long as the concentration of species ionized does not decay.

The different techniques of measuring ionization in flames measure different chemical species. Some, e.g. mass spectrometry and Langmuir probes, respond to positive ions, while others, e.g. conductivity measurements and microwave attenuation, respond to electrons. The number of positive species has to equal the number of negative species, at least in most cases. However, the negative species may be either electrons or negative ions. Caution must therefore be exercised in comparing the degree of ionization arrived at by different investigators employing different tools.

With respect to the question 'what kinds of ions are formed?'—there have been two interesting programmes reported on at this Symposium. The ions observed may not be the ions first produced in the combustion process and it is my personal belief that the majority, particularly the large hydrocarbon ions observed by Knewstubb and Sugden, are formed by subsequent ion reactions. Both charge–exchange processes and the growth of larger hydrocarbon ions from smaller ions are efficient processes and could account for much of what is observed. The large concentration of H_3O^+ is difficult to account for energetically by a reaction of neutral species. However, it is not difficult to write down equations which are both energetically and kinetically feasible for forming H_3O^+ from other ions. The large quantities of water present make these processes especially easy. For example, if we assume that either CO^+ or OH^+ are formed initially (Calcote†), then the following reactions are energetically and kinetically possible:

$$CO^+ + H_2O \rightarrow (H_2O\ CO^+)$$
$$\xrightarrow{+H_2O} H_3O^+ + (HOC=O)$$
$$\downarrow$$
$$OH + CO$$

* Shuler, K. E. and Weber, H. C. *J. chem. Phys.* 22 (1954) 491.

† Calcote, H. F. *Combustion and Flame* 1 (1957) 384.

or $$OH^+ + H_2O \rightarrow H_3O^+ + O$$

Once H_3O^+ is formed reactions such as:

$$H_3O^+ + C_nH_m \rightarrow H_2O + C_nH^+_{m+1}$$

are energetically reasonable for producing hydrocarbon ions.

The most important problem remaining is the identification of the ion which is first produced. After that a whole new field of gas-phase chemical kinetics opens up.

Gerstein's last question was—if the ions are produced non-thermally are they chain carriers in the combustion process and what information can we get from them about the kinetics of flame reactions? I know of no reliable evidence that ion reactions play a significant role in combustion reactions although the possibility has been considered on numerous occasions in the past. The relatively low ion concentration makes this seem improbable although it is worth noting that the ion concentration is simply a steady-state value determined by the relative rates of ion production and removal. Recent mass spectrometer studies indicate that ion reactions are very fast so that the question of their significance in combustion process should be re-opened. It may be just a coincidence but, in general, flame inhibiting agents also reduce the electron concentrations in flames. Certainly studies of ionization in flames will lead to a better understanding of high temperature chemical kinetics.

A. L. Thompson (Montreal): Have the authors (P. F. Knewstubb and T. M. Sugden) studied the stability of the hydrated ions?

P. F. Knewstubb (Cambridge): Regarding the stability of the hydrated ions which we observed, I can only say that these ions appear later in the flame process than the parent ions. This may be related to the falling temperature, or entirely to the necessity of producing the parent ion before the hydrated form can appear. So far these ions have merely been observed with interest, and we have not made any careful observations on their appearance in flames at different temperatures.

F. T. Smith (Stanford Research Institute): I should like to suggest to Basu and Fay that the ion H_3O^+, which figures so prominently in the reported mass-spectrometer studies, may be important in the thermal ionization behind the detonation wave of hydrogen and oxygen. Its heat of formation has been deduced from appearance potential measurements* and the equilibrium constant for the reaction

$$H + H_2O \rightleftharpoons H_3O^+ + e$$

can be estimated. The temperature dependence will simulate that of an ionization potential much lower than that of H in the absence of water.

On the question of the binding energy of hydrated ions in general, it should not be forgotten that this energy may be large if the ion is small. With a sodium ion, for example, a purely classical estimate of the ion-dipole binding of $Na^+.OH_2$ gives an energy of about 45 or 50 kcal/mole.

A. G. Gaydon (London): The observations, by Knewstubb and Sugden, of the formation of relatively large polymer molecules is most valuable and points to a possible mechanism of formation of large concentrations of ions in the reaction zones of organic flames. W. C. Price and colleagues recently reported, at the Institute of Petroleum Hydrocarbon Research Group's Conference on Molecular Spectroscopy in February, 1958, that some of the larger hydrocarbon molecules have surprisingly low ionization potentials, e.g. methyl naphthalene 7·96 eV. Unsaturated ones tend to have lower ionization potentials than saturated ones. Large unsaturated free radicals would tend to have even lower ionization potentials, and might cause the high ionization found in flames.

T. M. Sugden (Cambridge): I would like to make one or two points in connection with ionization in the reaction zones of flames in general, and in particular with reference to the paper by Knewstubb and myself. In the first place, it is a matter of extreme difficulty at this stage to infer much about the concentrations of the parent neutral species from measurements on the positive ions. Undoubtedly the ionization is much too high for thermal equilibrium, even with the rather low ionization potentials of some hydrocarbon radicals. That there is some relationship between ionization potential and ionic concentration seems likely, however, for two reasons: first C_3 hydrocarbons and higher ones, which appear strongly in our results, have in general much lower ionization potentials than the C_1 and C_2 hydrocarbons (molecules or radicals), which appear only very weakly: secondly, within a hydrocarbon group there is an alternation in ion intensities as the number of hydrogen atoms increases, those with odd numbers of hydrogen atoms (i.e. the free radicals) being generally more abundant than their immediate neighbours.

Another point which should be stressed is that, despite the richness in variety of ion-types which has been disclosed in acetylene and other flames, the total ion population is never much more than 10^{11} ions/c.c., and that is concentrated in a relatively small number of species. This is a very small fraction of the total gases (about 4×10^{18} molecules/c.c.). It may not be presumed therefore that ions play any major part in the overall flame reaction, but it is suggested that a connection between ionization and chemiluminescence might

* Field, F. H. and Franklin, R. E. *Electron Impact-Phenomena and the Reactions of Gaseous Ions.* 1957. New York.

exist. In particular the release of energy produced by re-combination of an electron with a large unsaturated hydrocarbon ion is capable of ejecting excited molecules of C_2 from the resulting molecule in sufficient amount to explain the observed intensity of C_2 radiation.

Lastly, one might briefly consider the processes by which ionization can occur fairly readily. In hydrogen flames, in which H_3O^+ is produced in fair amount, it is not impossible that collisions between three radicals can occur in the reaction zone.

$$H + H + OH \rightarrow H_3O^+ + e$$

Such a process should not be far from thermoneutral. The work of Padley and Sugden discussed in another paper at this Symposium shows that the concentrations of H and OH may reach a few per cent of the total gases in the reaction zone, making a sufficient number of such ternary collisions feasible. In the case of hydrocarbons, the problem is basically more simple, since smaller ionization potentials are involved for some of the intermediates in the early stages of reaction, if a partial polymerization occurs.

A. R. Ubbelohde (London): The problem of whether ions play any essential part in one or other of the many steps in combustion can be usefully considered in the light of some fundamental gas-kinetic considerations.

(1) Those ions that are actually isolated are not likely to be the most reactive, for the same reasons as apply to other labile intermediates.

(2) A collision between a neutral group with marked electron affinity such as OH, or O_2, and a neutral molecule such as a hydrocarbon, might lead to separation of positive and negative ions, rather than a mere bond rearrangement, when the probability factors favour it. One favorable factor for ion separation is that the directions of relative approach of, say, $R - H$ and OH are likely to be much less restricted, for effective transfer of an electron $RH + OH \rightarrow RH^+ + OH^-$ than for bond rearrangement,

$$RH + OH \rightarrow R + H_2O$$

leading to a higher temperature independent factor in the rate constant. If the electron affinity is sufficiently high, it can partly compensate for the comparatively high ionization energy of most of the neutral molecules taking part in the reaction.

(3) Once reactive ions have been formed in some way, their effective collision diameters are likely to be very considerably larger than those of the neutral molecules whose gas-kinetic collision diameters are known from a variety of experimental studies. This increases their collision frequency relatively to the neutral molecules.

Though none of these considerations guarantees that ionized species have an essential part to play in combustion, it is especially at high temperatures that the greater temperature independent factors may outweigh the larger activation energies and may permit ionic reactions to overtake neutral reactions in combustion.

PART IV

STRUCTURE AND PROPAGATION OF FLAMES

43

COMPOSITION TRAVERSES IN CURVED LAMINAR FLAME FRONTS

G. H. MARKSTEIN

INTRODUCTION

The large majority of recent investigations of laminar flames dealt with one-dimensional plane flame fronts. This comparative neglect of two- and three-dimensional flame structure has been criticized[1] on the grounds that practical problems always involve curved flame fronts. The lack of knowledge of the properties of highly folded flame fronts, for example, contributes much to the difficulties associated with the current controversy regarding the wrinkled flame front and the distributed flame zone models of turbulent flame structure[2].

The study of non-planar flames would seem to be also of fundamental significance because it may ultimately provide information about transport processes that could not be derived from one-dimensional flame structure alone. The occurrence of transport processes across flow lines is indeed the feature that distinguishes two- and three-dimensional flames from one-dimensional ones. This phenomenon must occur whenever the temperature and concentration gradients are not parallel to the flow velocity. It is of interest to note that curved shape of the flame front is neither a sufficient nor a necessary condition for transport across the flow. In flames of spherical or cylindrical symmetry the flow lines are everywhere normal to the flame front and cross-gradients are absent while, on the other hand, they are present in a plane flame front approached by converging or diverging flow.

Among the effects of transport across flow lines, shifts of composition due to preferential diffusion have attracted particular interest and have been linked with anomalous values of ignition energies[3], flammability limits[4] and of turbulent burning velocities[5] and with cellular flame structure[6,7]. However, surprisingly few previous measurements of composition shifts attributable to preferential diffusion have been carried out on laminar flames[8–10], although these effects have been definitely established in wake regions behind flame-holders[12–14].

In the present work sampling methods similar to those developed by others[10,15–17] have been applied to steady, essentially two-dimensional cellular flames. These flames were selected because they contain curved regions in which pronounced transport across flow lines should occur, while, nevertheless, their geometry is fairly simple. It is by no means implied by this choice, however, that cellular flames are the only ones in which transport across flow lines may be significant.

EXPERIMENTAL

The burner and sampling probe set-up is shown in *Figure 1*. The slot burner designed for the purpose of obtaining steady, almost two-dimensional, cellular flames has been described previously[18,19], but a minor modification of the burner was required in order to facilitate introduction of the sampling probe into the flame from the burned-gas side: previously, an enclosure of 5 cm height was used for preventing entrainment of air into the burned gas. For the present work the enclosure of 2 cm height, shown in *Figure 1*, was employed; this height was found to be adequate for preventing air entrainment.

A further modification of the burner was needed for eliminating the tendency of the flame cells for irregular lateral motion along the slot. It had been found earlier that a ridge between two flame cells would attach itself to a wire inserted into the flame near its base. The cells near the sampling probe could therefore be immobilized by means of wires placed a short distance from the probe on either side. Two steel wires of 0·16 cm diameter, mounted on supports that could be moved along the slot and clamped in any position, were used for this purpose, as shown in *Figure 1*. As discussed more fully elsewhere[20], increase or decrease of the distance between the two wires expanded or compressed the cells located between them, respectively, unless limit cell widths were exceeded at which cell splitting or collapse occurred. For the present work, the distance of the wires was chosen so that it contained five or six cells of widths about half-way between the limit widths.

The sampling probes were prepared from fused-quartz tubing of 1 mm i.d. and 2 mm o.d., similar to those used by others[15–17]. The diameter of the orifice was in the range of 50 to 100 μ. Occasionally, some difficulty was encountered owing to the tendency of some probes to close

off gradually under continuous exposure to flame gases, but by using probes with rather short tapers of the tip this difficulty was eliminated satisfactorily.

The problems associated with flame sampling by small probes have been extensively studied[15–17,21]. These authors showed that under the conditions prevailing in their work the sample withdrawn by the probe was representative of the local gas composition, and that the probe was effective in quenching the chemical reactions except for reactions involving unstable chemical species. The use of gas chromatography for chemical analysis in the present work required higher pressures in the probe and larger sampling rates than those used by the above workers; the conditions are thus not as favourable for obtaining a representative sample. However, the sampling rate was still below that assumed in calculations that showed very small distortion of the concentration field in the vicinity of the probe[21]. The pressure drop across the probe tip was sufficient to ensure sonic flow at the orifice, so that it appears likely that the reactions were quenched in the probe. This quenching is borne out by the results presented below.

A further question of importance in the present work concerns the lateral space resolution of the probe. Based on the relationships derived by Westenberg *et al.*[21] a width of the stagnation stream tube at infinity upstream of the probe of the order of 0·03 cm was computed.

The probe was shaped so that it could be inserted into the flame from the burned-gas side, with its axis aligned with the gas flow. The probe was mounted on a slide compound provided with micrometer screws that permitted traverses normal to the flame front and parallel to the burner slot. Micrometer settings for which the probe touched the luminous flame zone from the burned-gas side were determined visually and were used as reference settings during sampling traverses.

The analysis of the gas samples was carried out by means of gas chromatography[22,23]. Details of chromatographic technique are summarized in Table 1. The only components of the flame gases that could not be separated were argon and oxygen. Since the argon mole fraction could be calculated from that of nitrogen under the reasonable assumption that the argon–nitrogen ratio was not affected by diffusion phenomena, the oxygen mole fraction could be computed from the combined A + O_2 chromatogram peak. Of the two instruments (Perkin–Elmer Vapour Fractometer 154B) used, one served for determining water concentration, the other for analysing the remaining constituents of the gas samples. Except for the purpose of water analysis, the gas was pumped from the probe through a tube filled with drierite and into two glass flasks of 250 c.c. capacity. After pumping for several minutes at full rate the pressure was allowed to rise to 200 mm Hg, and, by regulating the pumping rate, was maintained for several minutes at this value before the flasks were closed off. The samples were then pressurized with mercury and introduced into the sample valve of the chromatograph at atmospheric pressure and room temperature.

A different technique had to be developed for

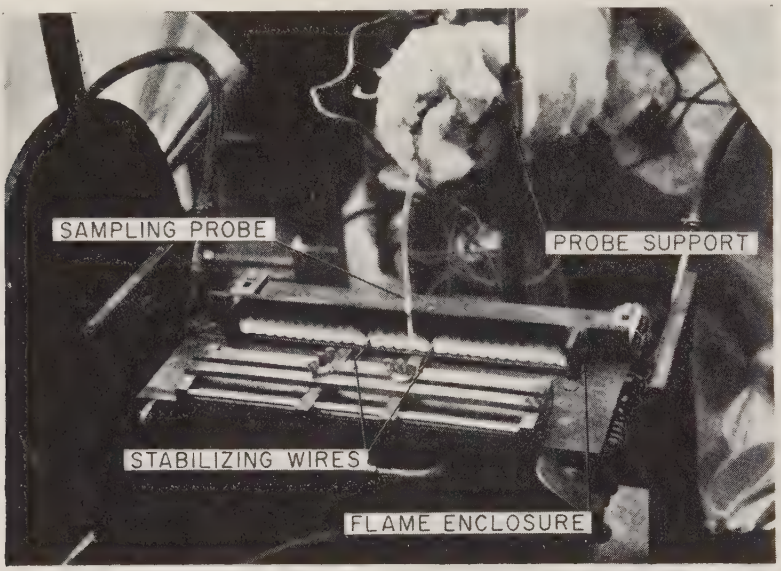

Figure 1. Burner and probe assembly

TABLE 1

Details of Gas-Chromatographic Technique

Gases to be separated	*Column material*	*Column length*, m	*Column temperature*, °C	*Carrier gas*	*Carrier gas flow* c.c./min	*Sample volume*, c.c.
H_2	Molecular sieve 5A	2	46	N_2	20	1
A + O_2, N_2, CO, CH_4	Molecular sieve 5A	2	46	H_2	50	1
CO_2, C_2H_6, C_2H_4, C_2H_2, C_3H_8, C_3H_6	Silica gel + 1 % octoil S	2	110	H_2	50	1
H_2O	30% 2-amino-biphenyl on fire-brick C 22	1	110	He	50	5

water analysis in order to avoid adsorption and condensation of water vapour in the apparatus. The gas to be analysed was pumped for this purpose at constant flow rate from the probe directly into the sample valve of the chromatograph. The probe and connecting hose, the sample valve, and a portion of the hose from the sample valve to the vacuum pump were thermally insulated and maintained at about 120°C by electrical heating. The insulation and heating wire on the probe can be seen in *Figure 1*. The temperature of the tubing on the sample valve that forms the sample volume was monitored with an iron–constantan thermocouple. The pumping rate was regulated for maintaining a pressure of 200 mm Hg in the sample valve.

In addition to the problem of adsorption and condensation, which was overcome by the above technique, a difficulty arises in the chromatographic analysis of water and other highly polar substances owing to the non-linearity of the distribution isotherm[24]. This phenomenon causes highly asymmetric chromatogram peaks ('tailing'); moreover, since low concentrations move slower through the column than high ones, some vapour is retained by the column for appreciable times. Therefore, consecutive peaks corresponding to samples of the same vapour concentration taken at constant time intervals tend to increase and approach constant heights and areas only asymptotically. In the present work samples were introduced at 8 minute intervals until the peak heights became reasonably constant; usually, from the fourth sample on the increases became negligible.

The chromatographs were calibrated on every day on which samples were analysed. Calibration standards were prepared by partial pressure measurement except for the water vapour standard that was made up by introducing a weighed amount of water into a gas cylinder of known volume that was subsequently filled with nitrogen at known pressure. The mole fractions of the components of the calibration standards were selected close to those encountered in the flame gas samples in order to minimize errors due to deviation from linear response of the instruments. Calibration procedures duplicated those for sample analysis in every respect. A conservative estimate of the accuracy of the analysis would be about ± 2 per cent. It is felt, however, on the basis of the consistency of the results presented below, that better accuracy was usually achieved with the possible exception of the water analysis.

The present work was carried out on fuel-rich propane–air flames. Dried air from the Laboratory compressed-air supply, and CP grade propane were used. Fuel and air flows were determined with calibrated rotameters, and, moreover, the composition of the unburned gas was checked by chromatographic analysis. Composition profiles were determined along traverses across the flame front at regions of maximum curvature, that is, at a ridge (convex towards burned gas) and at a valley (concave towards burned gas). Another traverse was carried out along the wavy flame front in the burned gas.

RESULTS AND DISCUSSION

The composition profile of a traverse across a ridge of a fuel-rich propane–air flame is shown in *Figures 2a* and *b*. The corresponding profile across a valley is presented in *Figures 3a* and *b*. The profiles are qualitatively similar to those determined by others[16–17], and the sequence of appearance and disappearance of the intermediate hydrocarbons in space agrees with the sequence with increasing temperature encountered in shock tube studies[25]. As in other work, no oxidation products other than CO, CO_2 and H_2O were found. The completeness of the analysis, at least

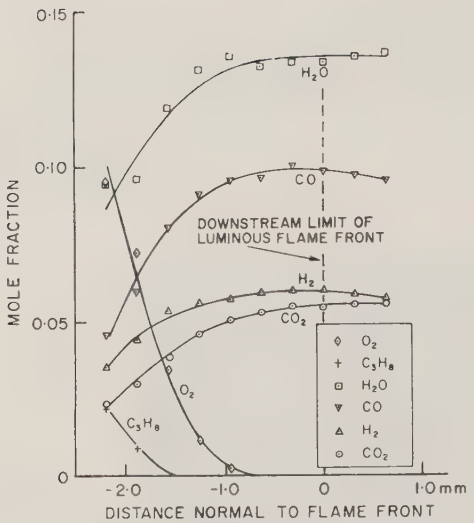

Figure 2a. Composition traverse across a ridge of propane–air flame of equivalence ratio 1·44. Reactants and final products

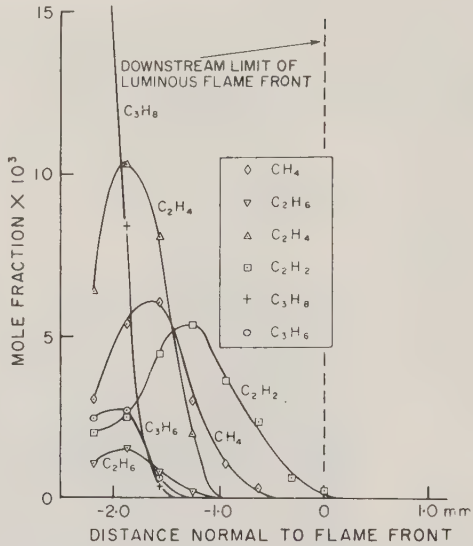

Figure 2b. Composition traverse across a ridge of propane–air flame of equivalence ratio 1·44. Hydrocarbon fuel and intermediates

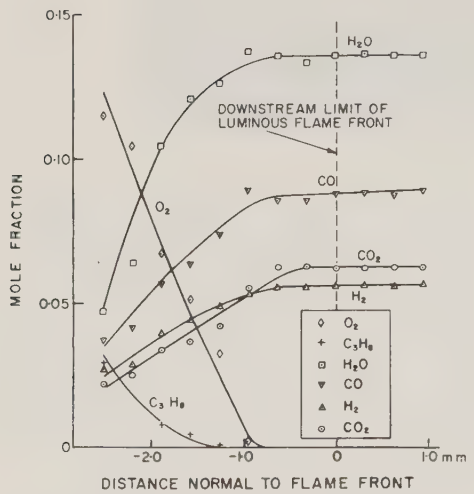

Figure 3a. Composition traverse across a valley of propane–air flame of equivalence ratio 1·44. Reactants and final products

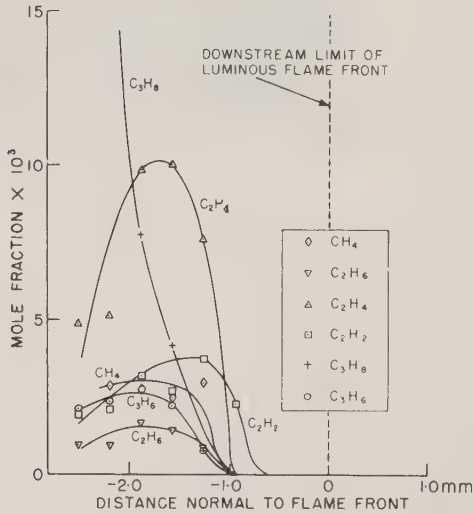

Figure 3b. Composition traverse across a valley of propane–air flame of equivalence ratio 1·44. Hydrocarbon fuel and intermediates

as far as non-condensible components are concerned, was borne out by the fact that the sum of the mole fractions of the components of the dry gas was always equal to one within ± 1 per cent. The present results, obtained with fuel-rich flames, differ from those obtained with stoichiometric composition[16–17] by the absence of the pronounced maxima of the CO and H_2 profiles.

The main interest of the present work centres on the differences between the profiles determined at a ridge and at a valley. Such differences are apparent, both regarding the distribution of pyrolysis products and the final composition of the burned gas. At the valley, propylene, ethane and ethylene peaks are rather broad, the methane and acetylene peaks are low, and only acetylene remains for a short distance beyond the point at which the other hydrocarbons disappear. At the ridge, propane, propylene, ethane and ethylene disappear farther from the luminous flame front,

but, on the other hand, the acetylene and methane peaks are higher, and these two pyrolysis products persist for a longer distance beyond the point where the others disappear; some acetylene remains present even in the luminous zone. It is not entirely clear what causes this appreciable difference between the ridge and the valley. It seems, however, that one may interpret the longer persistence of acetylene and methane at the ridge

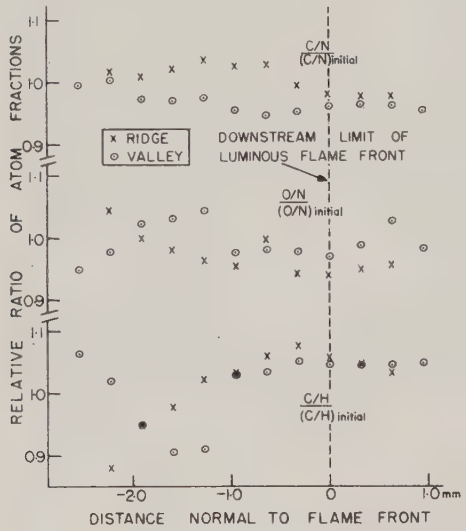

Figure 4. Ratios of atom fractions, relative to their initial values, along traverses across a ridge and a valley of propane–air flame of equivalence ratio 1·44

as an indication that in this region of sharp concave curvature towards the unburned gas pyrolysis can proceed further before oxidation is completed.

In order to detect shifts of composition owing to preferential diffusion, the results were evaluated in terms of the ratios C/N, O/N and C/H of the local atom fractions. Diffusion effects should become apparent as deviations of these ratios from their values in the initial gas mixture. These deviations include effects of diffusion in the direction of the flow that are also present in plane flame fronts, as well as the effects of transport across flow lines that are specific for two- and three-dimensional flames. The differences between the relative ratios $(C/N)/(C/N)_{initial}$, etc., determined from the composition profile at the ridge and at the valley, may be regarded as measures of the effects of preferential diffusion across the flow.

A plot of the relative ratios of atom fractions is shown in *Figure 4*. In view of the fairly large irregular fluctuations of the data points, no curves were drawn through them. It is obvious that the fluctuations due to random errors of measurement are almost of the same order of magnitude as the diffusion effects that are to be determined. This is particularly apparent for the ratios involving oxygen and hydrogen that depend on the analysis for water vapour, which was less reliable than the determination of the other components.

In spite of the random fluctuations, definite trends that must be due to preferential diffusion are readily discernible. The carbon–nitrogen ratios are larger at the ridge than at the valley throughout the profile, their maximum difference being about 8 per cent and their mean difference 4 per cent. It is not clear whether the sudden drop of C/N ratio near the luminous flame front at the ridge is a real effect or merely due to inherent measurement inaccuracy. An obvious explanation would be the formation of solid carbon, which is known to occur preferentially at flame ridges. There was no visible indication of carbon formation in the slot burner flame, but a faint yellow glow was visible above the ridge at the flame tip when the same combustible mixture was burned on a rectangular nozzle burner. This explanation becomes even more plausible since the formation of carbon would coincide with the disappearance of acetylene, which, at the ridge, occurs in a region where no oxygen for its combustion is present (see *Figures 2a* and *b*). If this interpretation is correct, the actual shift of C/N ratio owing to preferential diffusion would be at least about 8 per cent.

Although the irregularities of the O/N ratios are larger than those of the C/N ratios, a definite shift between ridge and valley is also noticeable. On the average, the O/N ratios are about 3 per cent lower at the ridge than at the valley. No definite conclusion can be drawn regarding the C/H ratios, owing to the fluctuations of the data. There seems to be a slight excess of C/H at the ridge, compared to the valley. Again, if the drop of C/H ratio at the ridge near the luminous flame front is due to carbon formation, this excess may be larger in reality than indicated by the data. A preferential diffusion shift of the C/H ratio cannot be excluded on theoretical grounds, since pyrolysis of the fuel and formation of free hydrogen occur early enough in the reaction zone for this effect to take place.

The shifts of composition observed in the present work are thus similar to those reported by Jost and Krischer[10,11] for polyhedral flames. A further effect, noted first by these authors, becomes apparent when the temperature corresponding to the water–gas equilibrium, $CO_2 + H_2 \rightleftarrows CO + H_2O$, is computed. The results, shown in *Figure 5*, indicate an appreciably higher temperature at the ridge than at the valley. The apparent rise of temperature upstream of the luminous flame zone is, of course, due to non-equilibrium. It is at present not known, however, whether

the fairly constant temperatures downstream of the luminous zone may be regarded as true equilibrium temperatures. Measurement of temperature distribution by means of fine-wire

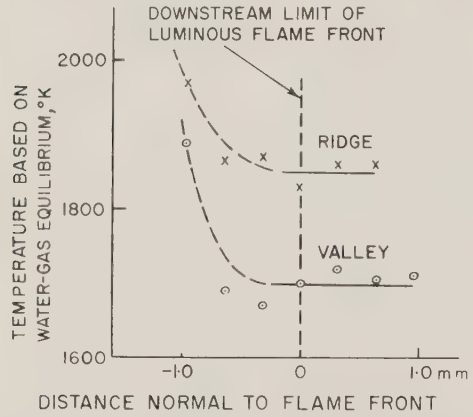

Figure 5. Temperatures based on water–gas equilibrium along traverses across a ridge and a valley of propane-air flame of equivalence ratio 1·44

thermocouples[26] was attempted, but was prevented thus far by rapid burn-out of the thermocouples in these rich flames. (The author is greatly indebted to Dr. Walter Kaskan of the General Electric

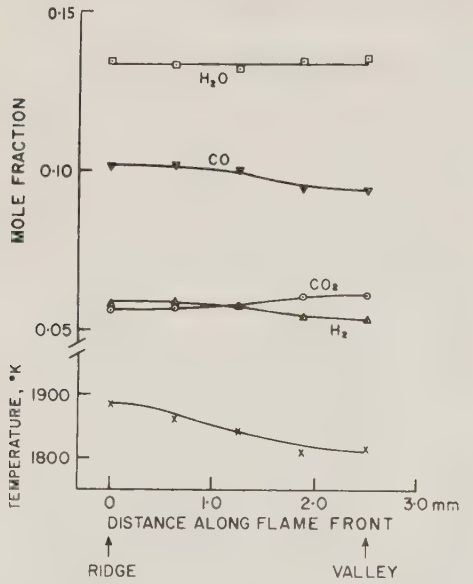

Figure 6. Composition profile and temperature based on water–gas equilibrium along flame front of propane–air flame of equivalence ratio 1·46. *Traverse was carried out* 1·3 mm *downstream of luminous flame front*

Research Laboratory for detailed instructions regarding preparation of fine-wire thermocouples.)

The results discussed above are confirmed by measurements of composition along a traverse in the burned gas at a distance of 1·3 mm downstream of the luminous flame front. The composition profile, and the temperature obtained from the water–gas equilibrium, are shown in *Figure 6.* The composition shifts and the temperature change are somewhat smaller than those determined for the traverses across the flame front, presumably owing to fairly rapid equalization of composition by lateral diffusion in the burned gas.

Results very similar to those obtained with propane–air mixtures were also obtained with butane–air flames. Since the technique for determining water vapour concentration had not been developed at the time when these measurements were performed, the results are incomplete and will not be reported here.

The present results are in qualitative agreement with expected effects of diffusion and heat conduction across flow lines. The influences of composition shift and of temperature change on burning velocity oppose each other, the former causing a decrease, and the latter an increase of the velocity at the ridge. Since the flow lines upstream of a valley diverge and upstream of a ridge converge, the burning velocity at the valley should be smaller than at the ridge. This qualitative conclusion is confirmed by the requirements of linearized[7] as well as higher-order[20] analysis of cellular flame structure. It is, however, not necessary that the effect of temperature change alone over-compensate the effect of composition change, since a further increase of burning velocity at the ridge may be caused by preferential diffusion of chain carriers.

CONCLUSION

Measurements of composition profiles in curved regions of laminar flame fronts have indicated shifts of composition and temperature in qualitative agreement with predictions based on transport processes across flow lines. The results are compatible with the changes of burning velocity required by fluid dynamics analysis. The lack of an adequate theory of the structure of two-dimensional flame fronts precludes at present a quantitative evaluation of the results in terms of transport processes.

The author is greatly indebted to H. M. Preston and H. Charleson for performing and evaluating the gas analyses, and to L. M. Somers and R. Phibbs for their participation in the experimental work. The invaluable advice of Dr. G. E. Barker of the Monsanto Chemical Company regarding techniques of gas chromatography is gratefully acknowledged.

This work was sponsored by Project SQUID which is supported by the Office of Naval Research, Department of the Navy, under Contract Nonr 1858(25) NR–098–038. Reproduction in full or in part is permitted for any use of the United States Government.

REFERENCES

[1] Spalding, D. B. *Sixth Symposium (International) on Combustion*, p. 12. 1957. New York; Reinhold

[2] Richmond, J. K., Donaldson, W. F., Grumer, J. and Burgess, D. S. *Paper* 517–57, American Rocket Society Annual Meeting, New York (December 1957)

[3] Lewis, B. and von Elbe, G. *Combustion, Flames and Explosions of Gases*, pp. 427–428. 1951. New York; Academic Press

[4] Goldmann, F. *Z. phys. Chem. B* 5 (1929) 307

[5] Wohl, K. and Shore, L. *Ind. Eng. Chem.* 47 (1955) 828

[6] Manton, J., von Elbe, G. and Lewis, B. *J. chem. Phys.* 20 (1952) 153

[7] Markstein, G. H. *Fourth Symposium (International) on Combustion*, p. 44. 1953. Baltimore; Williams and Wilkins

[8] Bubnoff, N. *Z. phys. Chem.* 88 (1914) 641

[9] Haber, F. *Z. phys. Chem.* 88 (1914) 670

[10] Jost, W. and Krischer, B. *Z. phys. Chem.* (N.F.) 5 (1955) 398

[11] Krischer, B. *Z. Elektrochem.* 60 (1956) 1017

[12] John, R. R., Wilson, E. S. and Summerfield, M. *Jet Propulsion* 25 (1955) 535

[13] Wilson, E. S., John, R. R. and Summerfield, M. *Jet Propulsion* 27 (1957) 892

[14] Williams, G. C., Woo, P. T. and Shipman, C. W. *Sixth Symposium (International) on Combustion*, p. 427. 1957. New York; Reinhold

[15] Friedman, R. and Cyphers, J. A. *J. chem. Phys.* 23 (1955) 1875

[16] Fristrom, R. M., Prescott, R. and Grunfelder, C. *Combustion and Flame* 1 (1957) 102

[17] — and Westenberg, A. A. *Combustion and Flame* 1 (1957) 217

[18] Markstein G. H. and Somers, L. M. *J. chem. Phys.* 21 (1953) 941

[19] — and Schwartz, D. *Proceedings of the Gas Dynamics Symposium on Aerothermochemistry*, p. 83. 1956. Evanston, Illinois; Northwestern University

[20] — *Heat Transfer and Fluid Mechanics Institute Preprints*, p. 295. 1957. Pasadena; California Institute of Technology

[21] Westenberg, A. A., Raezer, S. D. and Fristrom, R. M. *Combustion and Flame* 1 (1957) 467

[22] Phillips, C. *Gas Chromatography*. 1956. New York; Academic Press

[23] Keulemans, A. I. M. *Gas Chromatography*. 1957. New York; Reinhold

[24] Reference 22, pp. 17–18

[25] Glick, H. This volume, p. 98

[26] Kaskan, W. *Sixth Symposium (International) on Combustion*, p. 134. 1957. New York; Reinhold

44

OPTICAL FLAME STRUCTURE STUDIES: SOME CONCLUSIONS CONCERNING THE PROPAGATION OF FLAT FLAMES

A. LEVY and F. J. WEINBERG

INTRODUCTION

The work here presented forms part of an investigation of laminar flame structure designed for the study *in situ* of the mechanism and chemical kinetics of flame propagation.

The usefulness of predictive theories in combustion has been vitiated by the lack of directly relevant kinetic information. Extrapolation from conventional 'slow kinetics' studies to the extreme conditions prevailing in combustion zones is unreliable: indeed, it is no longer unusual to find that whilst reaction-rate studies at more leisurely conditions are treated entirely in terms of detailed radical processes, the theory of combustion 'hardware' is based on the premise of a single overall reaction. The examination of the validity of the latter concept was one of the principal aims of this work. Thus, although the present project is in continuation of the earlier analytical work[1] based on certain optical properties of flames[2] it differs from it to some extent, both in aim and method.

The aim towards high temperature kinetics implies that analysis of a number of flames, connected by some simple variable, is desirable, since deductions from the analysis of a single flame (being tied to a particular temperature—composition relationship) affords no means of cross checking. Variation of the initial gas temperature was chosen as the simplest parameter. Modifications in method are largely directed towards improvement in accuracy to conform to the exacting demands of subsequent analysis.

The resulting deductions of profiles of temperature, heat release rates, etc., are of relevance to such a variety of aspects of combustion and flame propagation phenomena that some selection for discussion in this account has proved necessary. It was felt that a summary of those conclusions concerning the flat flame burner and the mechanism of flame propagation would probably be the more relevant to the subjects of this symposium.

APPARATUS

The flames investigated were burned on a modified version of the Powling–Egerton flat flame burner. In this a bed of glass beads randomizes the gas flow which is then rendered uniform by a stream-lining 'matrix'. The principles of the burner system have been described previously by a number of workers[4,5]. Here only a brief account is given of the modifications introduced.

The initial temperature of the gas mixture was controlled in magnitude and uniformity by two cylindrical and coaxial electric heaters. The inner consisted of a winding of eureka strip upon a cylindrical former of asbestos paper. The whole was hermetically sealed with refractory cement, to prevent contact between hot metal and reactants, and embedded in the glass beads. The outer heater was wound on the outside of the burner tube and lagged. The two heaters were independently controlled so that the variable initial temperature could be rendered uniform over the cross-section of the burner. In practice it was found possible, by this means, to keep the maximum variation from the mean always below $\pm$ 3°C.

The temperature of the gas leaving the matrix has been shown to be very close to the local temperature of the matrix[1] and was measured by means of eight thermocouples distributed over the surface of the matrix, the leads being taken down through the fine passages to the base of the burner.

The brass 'chimney' was provided with a cylindrical window of selected thin mica sheet which maintained its good optical properties at the temperatures attained. The top cover was of $\frac{1}{4}$ in. thick asbestos sheet, perforated by 2 mm or 4 mm holes at 1 cm centre spacing, which proved rather more effective than the conventional metal gauze in insulating the flame from external draughts.

The reactants to be burned were ethylene from a cylinder and air, suitably dried and cleaned, pumped from the laboratory. The comparatively small range of the flat flame burner, in terms of mixture strength, necessitates very accurate measurement of the initial composition in order to keep any error introduced to a small fraction of the total range. The mixture strength was calculated from measurements made of the

individual air and ethylene flows by capillary flow meters. To obtain the accuracy desired the meters were designed to work to a high sensitivity and the effects of line pressure, ambient pressure and temperature were determined and allowed for. After calibration, the maximum error of either flow meter was $\pm$ 0·2 per cent, giving a mixture strength accurate to $\pm$ 0·4 per cent of the nominal value.

through the flame it was ensured that the temperature traverses obtained by the optical method were not liable to error due to the presence of solid bodies in the flame. The particles were illuminated by a stroboscopically interrupted Tyndal beam passing horizontally above the matrix. The light source was an a.c. mains operated arc so that interruptions in the photographically recorded tracks corresponded to twice mains frequency and

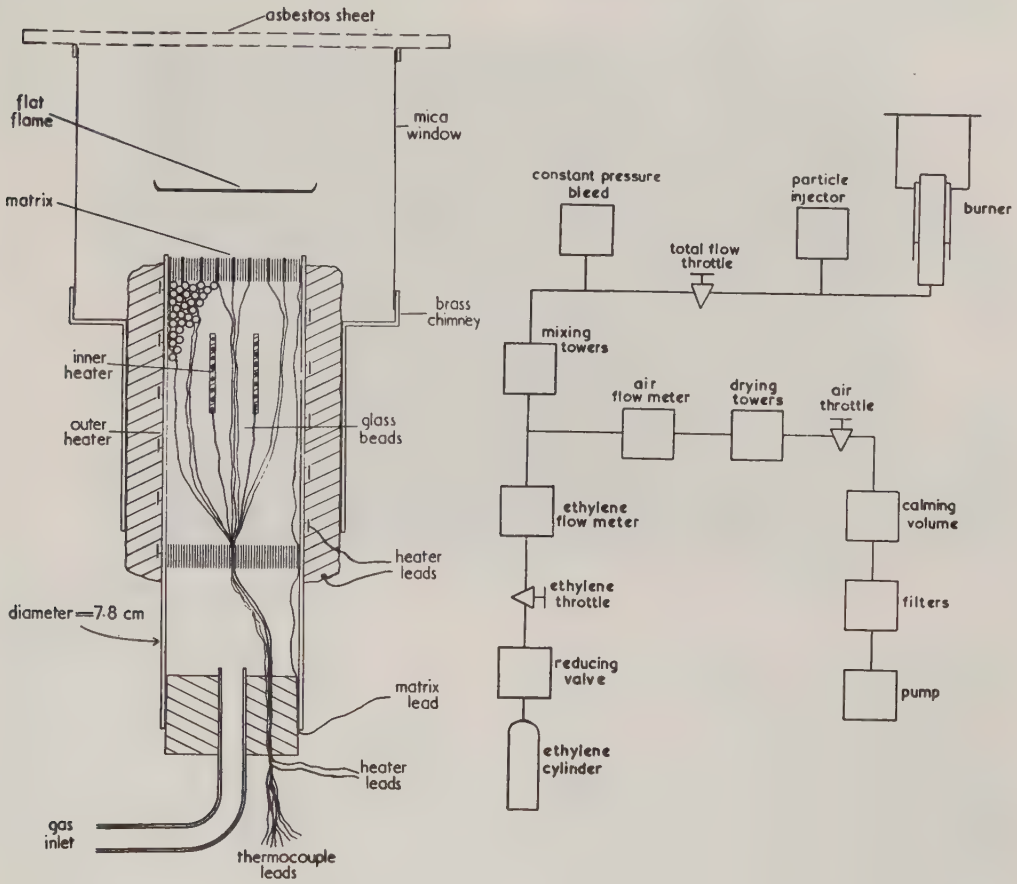

Figure 1

Independent control of mixture strength and total flow-rate was achieved by including a rotating float flow-meter as a bleed to the atmosphere, followed by a throttle immediately before the burner (*Figure 1*). This combination acted as a variable, recording leak, the adjustment of which did not affect flow meter pressure and hence mixture composition.

The flow regime of the flame was investigated by a particle track method. A simple arrangement for injecting a burst of particles (of Bentonite, mean particle diameter 4 microns) into the flow system immediately prior to the burner was devised. By avoiding a continual flow of particles both the direction and velocity of flow could be deduced in each region.

The distribution of temperature through the flame was determined by the ray deflection method described previously[1,2] in which the distorted image of a parallel-light illuminated inclined slit is photographed beyond the flame. Its shape is, in effect, an instantaneous graph of a calculable function of the refractive index distribution. In practice a screen of slits is used to provide data for edge corrections.

Modifications, the detail and theory of which will be reported elsewhere, consisted mainly of the introduction of a second lens beyond the burner

(*Figure 2*), and a change in the procedure of interpretation. The effects of the former are increased sensitivity and sharpness due to control of the diffraction pattern, and of the latter that analysis is no longer based on flame flatness but merely upon symmetry about the vertical axis. This results in a refractive index profile at the axis of the flame, which is also the point at which burning velocity is measured, and avoids use of an average result over the whole of the flame.

RESULTS

A large number of flames have been studied, full use being made of the range of the burner in terms of burning velocity, mixture strength and initial temperature. The lower limit of initial temperature was set by the self-pre-heating characteristics of the burner used (this is further discussed below), and the upper limit was dictated by a tendency to cusp formation, possibly associated with the onset of pre-reaction in the matrix. The actual ranges were confined to between 130° and 347°C for initial temperature and 2·39 to 1·89 per cent for initial ethylene concentration. Because of the labour and time involved in the full interpretation, only four of these flames were selected for complete analysis involving calculation of volumetric heat release rate distribution. Selection of these flames was such that three were close to the limit of propagation and two were of equal initial ethylene concentration (differing only in initial temperature). At the same time the four flames utilized the full range of the burner in terms of mixture strength, initial temperature and burning velocity.

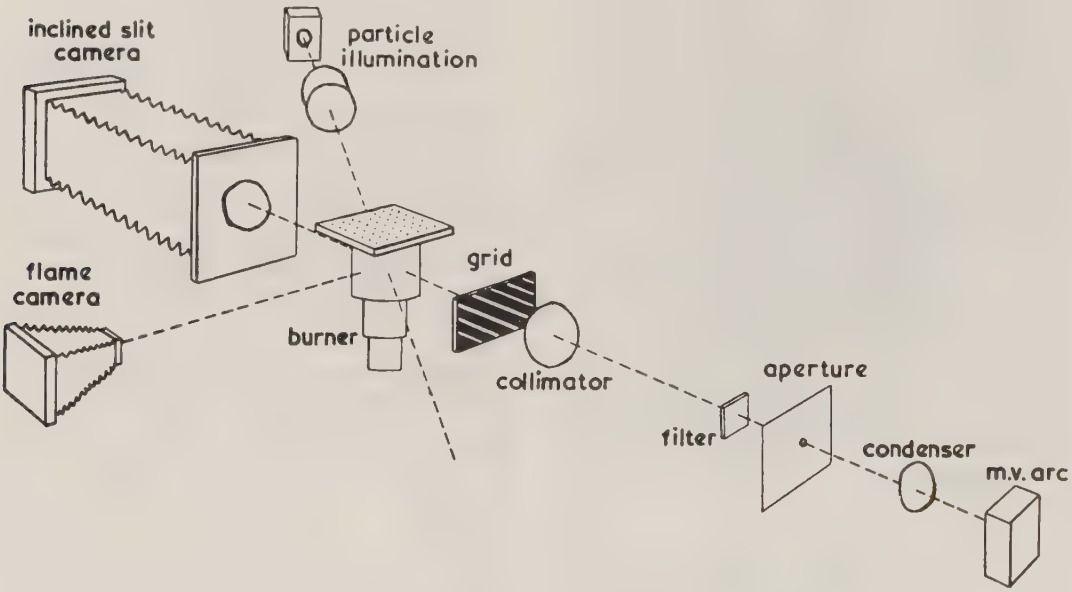

Figure 2

Interpretation of the data obtained may be sub-divided under:

(1) The aerodynamics of the flat flame with particular reference to the use of the burner for the accurate measurement of burning velocity.

(2) The measurement of burning velocity of lean ethylene/air mixtures as a function of initial temperature and fuel concentration.

(3) The calculation of the distribution through the flame zones of the volumetric heat release rate by the substitution of the measured burning velocities and temperature profiles in the steady state flame equations.

(4) Testing the validity of the concept of effective 'overall' kinetics by calculation of reactant concentration profiles based upon such a model and intercomparison of resulting rate laws within each flame and between different flames.

(5) Analysis of the distribution within each flame of the effective reaction order referred to reactants and of the distribution of fraction of successful bimolecular collisions. The latter yielded profiles of effective activation energies which could then be compared with those characteristic of radical reactions, those obtained in 'slow' kinetic studies, and the effective overall value calculated from variation of burning velocity with initial temperature.

(6) An investigation of the concept of 'normal' diffusion, i.e. of the assumption of diffusion coefficients equal to the thermal diffusivity of the mixture for various molecular components, and its comparison with neglect of diffusion.

(7) A test of recent flame propagation theory

using measured heat release profiles in place of assumed kinetic laws.

The large number of results necessitates some selection and it is considered that the conclusions concerning the mechanism of flame propagation and the operation of the flat flame burner are more relevant to this symposium. The experimental details and the kinetic studies in sections (3), (4), and (5) are therefore dealt with elsewhere[3].

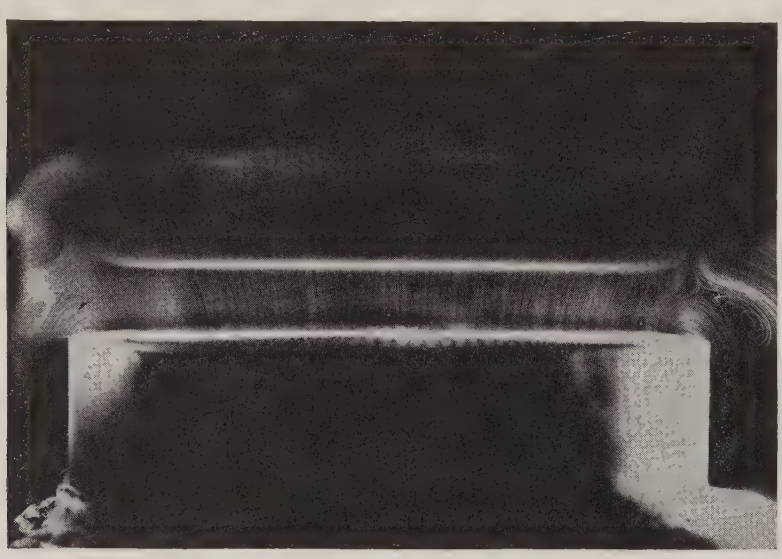

Figure 3

THE FLAT FLAME BURNER AND BURNING VELOCITY

The flow field of the flat flame is clearly illustrated by particle track photographs such as that shown

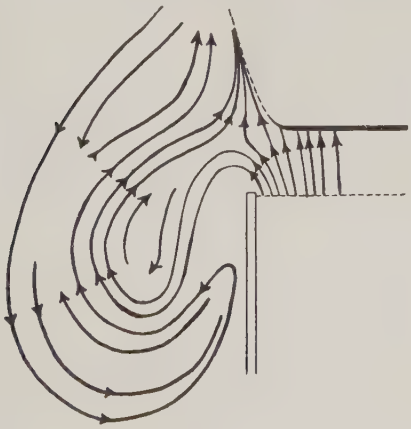

Figure 4

in *Figure 3*, when used in conjunction with a sketch (*Figure 4*) of the directions of flow observed.

The records of the flow patterns suggest solutions to hitherto unexplained aspects of flat flame behaviour. Examples are the up-turned flame edge, the observation[8] that the use of a stream of inert gas as an outer sheath to the flame gases results in reduced stability, and the fact that the normal temperature distribution over the matrix, due to the self-pre-heating effect, shows a maximum at the edge of the matrix.

Analysis of the product gases has shown[8] that no part of the reactants escapes complete combustion in the flat flame. The present work shows that the reactant stream emerging within 3 mm of the burner periphery is diverted through a system of vortices before entering the flame to burn at a level rather higher than that of the central part of the flame, thus producing the familiar rim.

If, as seems probable, these toroidal vortices play some part in anchoring the flame, then stability should be diminished in the presence of an outer sheath of flowing inert gas. A similar effect might be expected when too narrow a 'chimney' is used. Both are observed in practice.

The finding by earlier workers that the temperature distribution across the matrix under normal 'self-pre-heat' conditions manifests a strong maximum at the edge with, occasionally, a much smaller secondary peak at the centre proved difficult to explain so long as conduction and radiation were regarded as the only possible modes of heat transfer from the hotter parts of the burner and flame gases. The former is unlikely to contribute appreciably, since the temperature gradient in the gas attains measurable magnitudes only well above the burner port, whilst the greatest effect due to the latter would be expected to occur where the angle subtended by the hot

regions is greatest, i.e. at the centre. Flow visualization, however, now shows that convection also contributes, in that part of the hot product gases is re-circulated due to the vortex ring around the port periphery. Combination of this effect with that of radiation satisfactorily explains observed temperature distributions. In the present work, of course, this distribution was almost entirely eliminated by balancing inputs to the two heaters to compensate for such inhomogeneity.

Although elucidation of the flow pattern answered some questions, it raised its own problems. Thus the conclusion that, for accurate work, the flame may no longer be regarded as truly unidimensional led to the modifications in interpretation mentioned above. Furthermore, the form of the flow pattern suggested the need for re-examining the procedure for accurate burning velocity measurement. The Powling burner was originally designed for burning velocity measurement and has, within its range, shown itself to be reasonably satisfactory for this purpose. However, for the detailed analysis of the flame zones it became essential to establish the limits of error incurred in the measurement of burning velocity as deduced by the normal method of dividing volumetric flow rate by luminous flame area.

A direct test became possible on the present burner system since volumetric flow rate could be varied at constant mixture strength and uniform initial temperature (and hence constant burning velocity). At given constant initial conditions it was found that a certain volume flow rate through the burner gave the best flat flame. A small increase in the flow rate produced a slightly domed flame while a small decrease led to a 'saucer-shaped' flame (*Figure 5*).

Several criteria, including those suggested by previous workers, were used to estimate an effective diameter as a basis for the calculation of flame areas: (1) The diameter of the flat region alone (this comprised by far the greatest fraction of the flame area); (2) the diameter of the flat region plus $(2)^{\frac{1}{2}}$ times the base projection of the upturned edge; (3) the diameter of the projection of the whole flame on to a horizontal plane.

The area observed did vary somewhat with flow rate but agreement was not quantitative. It was found that the apparent burning velocity for the domed flame was 10 per cent greater than for the saucer-shaped flame as compared with a variation of 25 per cent in flow rate.

These results were compared with burning velocities determined by the particle track measurements at the flame centres. It was found that the burning velocity calculated from measurement of these tracks did not vary with the burner flow and that the value obtained was close but not identical (within 2 per cent) to the value obtained for the best flat flames when criteria (2) or (3) were used. The cause of these differences may lie in the uncertainty of defining a precise boundary to the luminous flame surface. Due to this residual uncertainty in the determination of burning velocity by area measurement the particle track method was used throughout subsequent experimental work.

The variation of burning velocity as a function of initial temperature and composition was investigated. Burning velocity, S, is given corrected to s.t.p. by the ideal gas laws so that S is proportional to the mass burning rate, the constant of proportionality being the reciprocal of the reactant density at s.t.p. The mixture strength, C, is the percentage by volume of ethylene initially present in the mixture.

(1) *At constant mixture strength*—A series of four flames with an initial ethylene concentration of

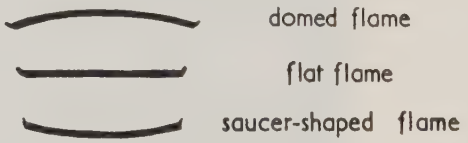

Figure 5

$(2{\cdot}315 \pm 0{\cdot}010)$ per cent were burned at initial temperatures, T_o, of 151°, 193°, 223°, and 245°C. It was found that the burning velocity increased linearly (average scatter 0·03 cm/sec) with initial temperature over the range investigated. The law relating the two within this region is

$$S = 0{\cdot}0473(T_o) - 2{\cdot}97 \qquad (1)$$

(2) *At constant initial temperature*—It was not experimentally convenient to burn a series of flames at a single initial temperature. However, the results obtained for a variety of initial temperatures and compositions were corrected to a standard initial temperature of 300°C by equation 1, since $(\partial S/\partial T_o)$ is unlikely to vary appreciably over the small range of composition considered. Plotting burning velocity against composition again gave a straight line of small scatter, the equation being

$$S = 16{\cdot}30(C) - 26{\cdot}73 \qquad (2)$$

(3) *At constant burning velocity*—As $S = f(T_o C)$

$$\mathrm{d}S = \left(\frac{\partial S}{\partial T_o}\right)_C \mathrm{d}T_o + \left(\frac{\partial S}{\partial C}\right)_{T_o} \mathrm{d}C$$

Hence, at constant S

$$\left(\frac{\partial C}{\partial T_o}\right)_S = -\frac{\left(\frac{\partial S}{\partial T_o}\right)_C}{\left(\frac{\partial S}{\partial C}\right)_T}$$

Thus, from equations 1 and 2

$$\left(\frac{\partial C}{\partial T_o}\right)_S = -0{\cdot}00290 \text{ per cent/°C}$$

This value may be regarded as the equivalent of the pre-heat temperature in terms of the chemical energy of the fuel. Its magnitude is of practical importance in correcting for the effect of pre-heat in normal flat flame burning velocity work. Data for some other fuels have recently been published[6]. Hitherto it had been assumed[4,5], following a suggestion of White[7], that the effect of pre-heating may be considered identical with the effect of that addition of fuel producing the same increase in final flame temperature.

The flames for which present results were obtained were all sufficiently near the lower limit of propagation for comparison with previous experimental investigations of the variation of the lower limit with temperature to be valid. Two previous values for ethylene are available: — 0·0027 by White[7], and — 0·0030 by Burgoyne and Smith[9]. Agreement is seen to be reasonable considering the differences in approach.

EXAMINATION OF CONCEPTS RELATING TO THEORY OF FLAME PROPAGATION

General—Although results furnished by the present investigation lend themselves to testing any particular hypothesis relating to either reaction kinetics or the mechanism of flame propagation, it has been general policy in this work to keep the interpretation deductive and analytical. In particular, considerations of flame propagation theory are designed to examine individual concepts which form the basis of comprehensive theories in general, rather than their ultimate predictive success.

Aside from minor assumptions resulting in imperfections the likely magnitude of which can be assessed without flame analysis, the main steps constituting a comprehensive theory may be expressed as follows: (1) assumption of kinetics expressing volumetric heat release rate as a function of local composition and temperature; (2) expression of heat release rate in terms of a single variable (usually the fractional temperature rise) by assuming a relationship linking composition and temperature within the flame; and (3) the mathematical procedure leading to solution of the steady state equation in terms of this single variable to yield the profile of the latter and the burning velocity as the eigenvalue of the equation for given boundary conditions.

Present results have been used as a test of individual steps rather than their end-product; thus, substitution of experimental heat release profiles into the mathematical procedure bypasses steps 1 and 2 and tests 3 alone (see above). Similarly, the assumptions underlying step 2 which are normally based on a relationship between diffusion coefficients and thermal conductivity can be examined alone (see above). Concerning (1) detailed results for the present series of ethylene/air flames are presented elsewhere[3]. As a background indicating the flame system discussed in this section, however, the general findings may be outlined as follows: For all the flames analysed the distribution of activation energy starts at values typical of radical reactions but reaches, by the point of maximum heat release, values comparable to those obtained both in vessel and in rapid mixing studies. Order of reaction profile leads to similar conclusions.

Burning velocity from heat release profile—To assess progress in methods of obtaining solutions two extreme approaches have been considered—the early treatment of Semenov, Zeldovich and Frank-Kamenetskii[10], and the recent theory of Spalding[15]. The former is based upon the assumption that reaction proceeds principally at the final flame temperature, whilst the latter suggests a simple modification taking into account the true shape of the heat release profile in terms of the position of its centroid.

Following Spalding's treatment the mass burning rate is given by

$$M^2 = -\frac{(T_f - T_o)}{\lambda (H_f - H_o)^2} \int_0^1 kq^{\cdot\prime\prime\prime}\, dh \qquad (3)$$

In this expression the original assumption of constant specific heat has been replaced by using as variable the fractional increase in thermal enthalpy, h, instead of the fractional temperature rise. Other symbols are:

$(T_f - T_o)$ = total temperature rise across flame.

$(H_f - H_o)$ = total thermal enthalpy rise across flame.

k = local thermal conductivity.

$q^{\cdot\prime\prime\prime}$ = local volumetric heat release rate.

λ is the parameter of the shape of the heat release profile for which Spalding proposes

$$\lambda = \tfrac{1}{2} - 0{\cdot}6604(1 - h_c) - 0{\cdot}4283(1 - h_c)^2 \qquad (4)$$

where h_c is the centroid of the $kq^{\cdot\prime\prime\prime}$ versus h diagram.

i.e.
$$h_c = \frac{\int_0^1 hkq^{\cdot\prime\prime\prime}\, dh}{\int_0^1 kq^{\cdot\prime\prime\prime}\, dh}$$

Thus, in the terms of Zeldovich and Frank-Kamenetskii's theory $h_c = 1$ and $\lambda = \frac{1}{2}$.

The experimental distribution of q''' was obtained from the conservation equation:

$$\mathrm{d}/\mathrm{d}x\left(M \cdot \int_{T_o}^{T} C_p \,\mathrm{d}T - k(\mathrm{d}T/\mathrm{d}x)\right) - q''' = 0$$

the variation of k with temperature from the data of Stops[11] being used throughout. Graphs of this quantity are shown in *Figure 6*. The results of the calculation are shown in the table above.

Flame	*Initial temp.* T_o°K	402	424	520	620
	Fuel %	2·39	2·31	2·31	1·89
Mass burning rate M	*Experimental*	0·00540	0·00539	0·01106	0·00804
	Calculated for $\lambda = \frac{1}{2}$ (Zeldovich, Frank-Kamenetskii[10])	0·00421	0·00403	0·00726	0·00522
	Calculated for $\lambda < \frac{1}{2}$ (Spalding[15])	0·00522	0·00501	0·01083	0·00691

It is seen that when theory is divorced from kinetics and attendant assumptions, agreement is good and the improvement occasioned by Spalding's treatment considerable.

Diffusion—Expression of reaction rate in terms of a single variable (i.e. reduction of the number of conservation equations to one) is generally achieved by assuming a relationship between the diffusion coefficients D_j of each rate controlling species, j, and the thermal conductivity, k, of the mixture at all points in the flame. The diffusion coefficient divided by the thermal diffusivity has been termed the Lewis number, δ.

'Thermal' theories involving neglect of diffusion may then be summarized by $\delta = 0$, whilst 'comprehensive' theories have frequently made use of the assumption $\delta = 1$ for all species; it can readily be shown from the conservation equations that for $\delta = 0$ the fractional change* in reactant mass fraction at any point and the fractional heat released are the same and equal to the local fractional heat flow,

$$\frac{M(H - H_o) - k(\mathrm{d}T/\mathrm{d}x)}{M(H_f - H_o)}$$

For $\delta = 1$, on the other hand, the fractional concentration is equal to the fractional rise in heat content of the gas $(H - H_o)/(H_f - H_o)$.

These simple consequences of the two hypotheses have been compared directly with the fractional species distributions calculated from the reaction rate profile and individual diffusion coefficients. The latter were obtained in part by calculation[12], and in part from the experimental work of Klibanov[13]. Distributions of major species were obtained by numerical integration of the species conservation equations from the hot boundary.

Comparison is necessarily confined to the major species on an overall reaction model. However, radical concentrations are likely to be relatively small and, in any case, the comparison is mainly one of δ's, the analytical results merely playing the part of providing an authentic reaction rate profile for the purpose of the test.

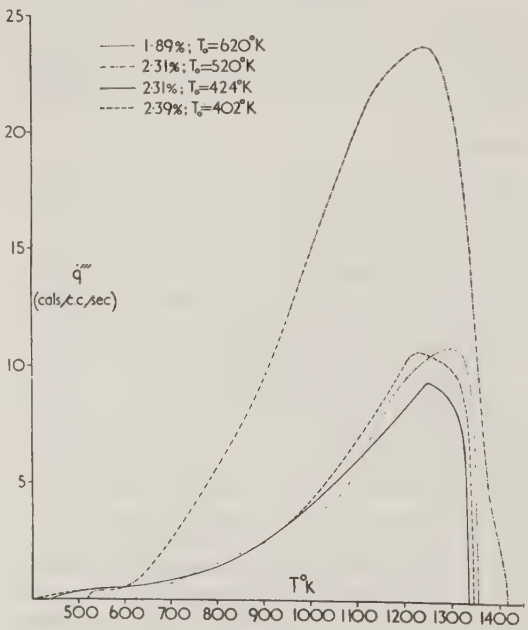

Figure 6

These results, for oxygen, ethylene, carbon dioxide and water vapour, are given in dimensionless form against distance in *Figure 7* (the curves for carbon dioxide and ethylene are so similar

* All the quantities are given in the dimensionless form as fractions of their maximum variation across the flame.

that they cannot be distinguished) and compared with the profiles of the fraction of thermal enthalpy rise and the fraction of heat released. The similarity between the curves for the oxygen concentration and the fraction of enthalpy rise shows clearly how near δ is to unity for this species in the case of flames with excess air. For ethylene and carbon dioxide the agreement is also good and if oxygen and ethylene are considered to be the

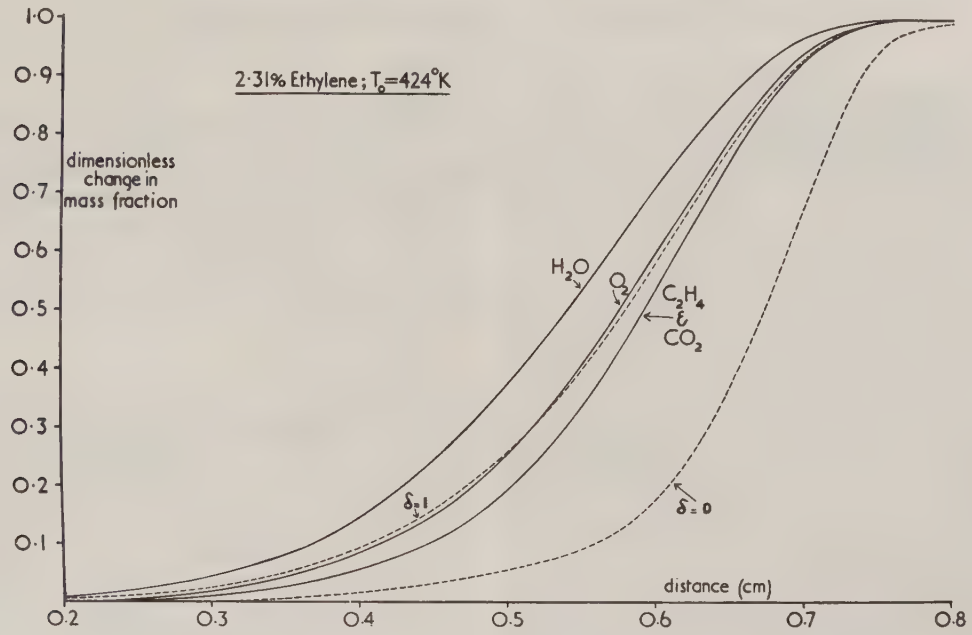

Figure 7

reactants then the assumption of normal diffusion is a reasonable approximation. For water vapour agreement is not quite so good, and much worse results may be expected in the case of radicals of large D_j. The assumption of no diffusion, however, in agreement with the results of recent sampling studies[14] is seen to be untenable for all species.

REFERENCES

[1] Burgoyne, J. H. and Weinberg, F. J. *Proc. Roy. Soc. A* 224 (1954) 286

[2] Weinberg, F. J. *Sixth Symposium (International) on Combustion*, p. 765. 1956. New York; Reinhold

[3] Levy, A. and Weinberg, F. J. In course of preparation

[4] Powling, J. A. *Fuel* 28 (1949) 25

[5] Egerton, Sir Alfred and Thabet, S. K. *Proc. Roy. Soc. A* 211 (1952) 445

[6] Dixon-Lewis, G. and Isles, G. L. *Trans. Farad. Soc.* 53 (1957) 193

[7] White, A. G. *J. Chem. Soc.* 177 (1925) 672

[8] Egerton, Sir Alfred and co-workers. Private communication

[9] Smith, I. E. *Ph.D. Thesis*, University of London, 1955

[10] Evans, M. W. *Chem. Rev.* 51 (1952) 363

[11] Stops, D. W. *Nature, Lond.* 146 (1949) 966

[12] Hirschfelder, J. O., Curtiss, C. F. and Bird, R. B. *Molecular Theory of Gases and Liquids*. 1954. New York; Wiley

[13] Klibanov, T. M., Pomerantsev, V. V. and Frank-Kamenetskii, P. A. *J. Tech. Phys. USSR* 12 (1942) 14

[14] Fristrom, R. M. and Westenberg, A. A. *Combustion and Flame* 1 (1957) 217

[15] Spalding, D. B. *Combustion and Flame* 1 (1957) 287

REACTIONS OF SIMPLE HYDROCARBONS IN FLAME FRONTS—MICROSTRUCTURE OF C_2 HYDROCARBON–OXYGEN FLAMES

R. M. FRISTROM, W. H. AVERY and C. GRUNFELDER

INTRODUCTION

The chemistry of hydrocarbon flames is a complex subject involving reactions which are rapid and occur at relatively high temperatures. Recently, methods have become available which allow quantitative studies to be made of such reacting systems[1,2]. The composition history of a reacting gas can be determined as a function of the distance through the flame front. The details of the techniques for making these measurements have been discussed critically in other publications[3,4] and will not be repeated here. This paper is a preliminary survey of the chemistry of three lean C_2 hydrocarbon–oxygen flames. The data available at this time are presented to record the species observed in these flames and the relationships between the species. The precision of the flame sampling method permits quantitative interpretation of the concentration profiles.

Conditions were chosen for these flames to minimize chemical complications and to match physical properties closely. Oxygen-diluted lean flames were chosen so that the number of intermediates would be minimized and the concentration of oxygen would vary only slightly (<10 per cent). Physical conditions were matched by adjusting flows to equivalent burning velocities, therefore, initial fuel concentration varies with species, and final adiabatic temperatures differ by 400°C.

EXPERIMENTAL

Burner

The flat flame burner used in these studies is of the screen type[5](see *Figure 1*). It has a diameter of 1·24 in. and uses 100-mesh screens of the 'Lektromesh' type. Such a burner has very high flow uniformity; temperature distribution across the flame varied less than 2°C over the inner centimetre radius. The burner was housed in a glass chamber and flows were regulated $\pm 0{\cdot}2$ per cent so that the flame remained in a stable position in space ($\pm 50\,\mu$ over a 3-hour period), and the temperature of a fixed point in the flame ($Z \simeq 0{\cdot}025$ mm) remained $\pm < 1$°C during the sampling period. The details of techniques for producing these stable flames are discussed elsewhere[6].

Materials

To permit a study of reaction mechanisms, gases of the highest available purity were used. Our analyses of these gases are given in Table 1. Analyses were made with both a mass spectrometer and a gas chromatograph. The major impurities, argon (0·4 per cent), water (0·1 per cent), and carbon dioxide (0·2 per cent), did not interfere with the course of the reaction or the analysis of the flame gases.

Method of sampling

Samples were removed from the flame front continuously (by use of a quartz microprobe) and passed into a mass spectrometer for analysis. Two probes were used in these studies with diameters of 10 and 30 microns, respectively. Pressure within the probe was maintained at 200 microns. Position of the probe was adjusted using a micrometer drive (see *Figure 2*). The relative position of the burner and probe could be read on a dial micrometer to $\pm 0{\cdot}0005$ in. This position and the relative position of the luminous region were confirmed directly with a cathetometer and by photographic measurements. In the first set of runs the 10 micron probe was held in a fixed position and the burner was moved. In the second set of runs the burner was fixed and the 30 micron probe was moved. There was no dependence of results in the reaction zone either on probe diameter or on method of positioning the probe.

The analyses were made with a mass spectrometer (CEC#21-610), by techniques previously described. The principal difference between these measurements and previous studies[2,3] is the use of a Teflon flow system instead of the batch analytical system. This technique greatly improves the reproducibility of the analyses since it solves two of the major problems: adsorption, and contamination and loss of the hydrocarbons in stopcock grease. With the sampling rate used, the flow system came to equilibrium in less than 100 seconds. Analyses were usually run until peak readings agreed to the least count of the instrument (this usually required only two runs).

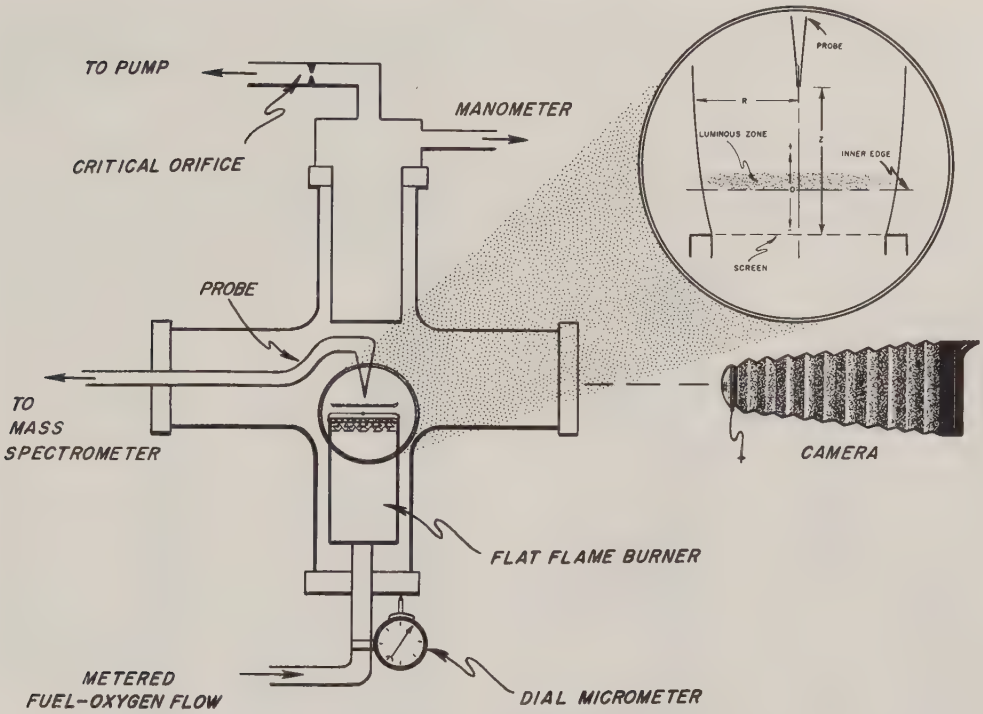

Figure 1. Flame sampling apparatus—flame diagram and coordinates

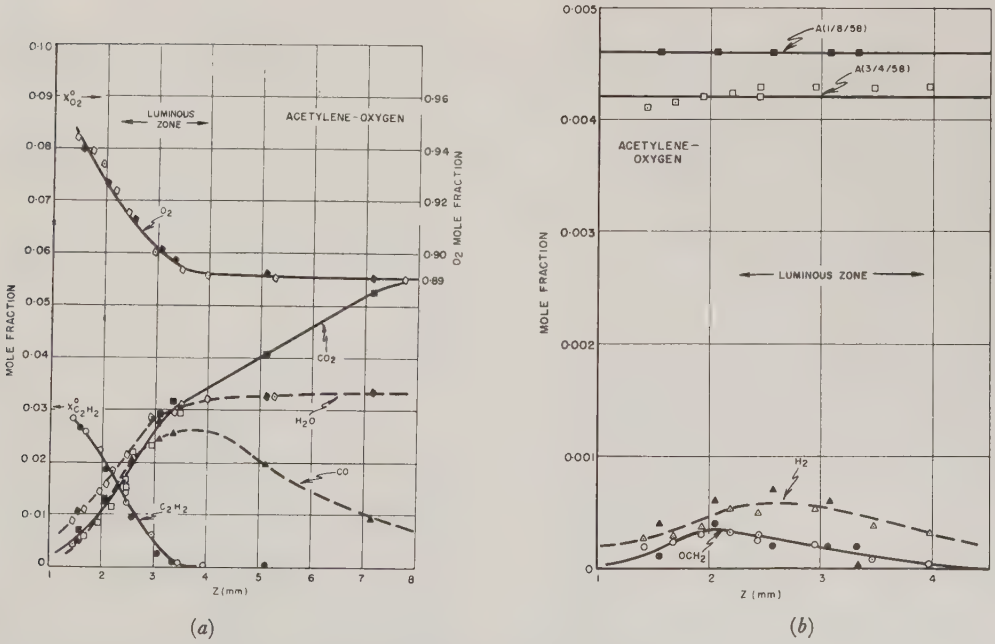

(*a*) (*b*)

Figure 2. Mole fraction versus *distance* (mm) (*See Table 1 for initial compositions*).
(*a*) C_2H_2—O_2 *flame, major constituents;* (*b*) C_2H_2—O_2 *flame, minor constituents*

TABLE 1

Initial and Final State of C_2 Flame Gases

	Units	C_2H_2		C_2H_4		C_2H_6	
		Calculated	*Experimental*	*Calculated*	*Experimental*	*Calculated*	*Experimental*
T_0	°K	300		300		300	
P_0	Atm	0·1		0·1		0·1	
X (Fuel)	M.F.	0·03102		0·0390		0·0429	
X_0 (O_2)	M.F.	0·9674		0·9555		0·950	
X_0 (H_2O)	M.F.	0·0093		0·002		0·005	
X_0 (CO_2)	M.F.	0·002		0·001		0·002	
X_0 (A)	M.F.	0·00463		0·00452		0·00440	
$\bar{\gamma}_0$		1·42		1·40		1·40	
$\bar{M}_0$	g/mole	32·21		31·93		32·04	
V_0	cm/sec	70·5		71·0		71·3	
T_f	°K	1451		1691		1889	
$\bar{\gamma}_f$		1·2788		1·2658		1·2552	
$\bar{M}_f$	g/mole	32·307		31·869		31·233	
C_{pf}	cal/c.c./°K	9·114		9·460		9·769	
X_f (CO)	M.F.	0·000	0·000	0·00002	—	0·00017	0·005
X_f (CO_2)	M.F.	0·06509	0·062	0·07821	0·074	0·08547	0·0807
X_f (H)	M.F.	0·0	—	0·0	—	0·00002	—
X_f (H_2)	M.F.	0·0	0·000	0·0	0·000	0·00005	0·000
X_f (H_2O)	M.F.	0·03649	0·0338	0·07800	0·079	0·12597	0·117
X_f (O)	M.F.	0·0	—	0·00015	—	0·00089	—
X_f (O_2)	M.F.	0·89371	0·889	0·83822	0·831	0·77972	0·795
X_f (OH)	M.F.	0·00006	—	0·00062		0·00270	—
X_f (A)	M.F.	0·00463	0·0046	0·00452	0·0045	0·00440	—

Coordinate origins

The choice of origin for coordinate systems is important in comparing composition profiles from different probes, in comparing composition with luminosity profiles, and in comparing the profiles of several flames. No convenient absolute reference system is available since, although in any single run the variables can be closely enough controlled so that very high resolution is attained (±50 microns), a duplicate run may show a displacement of profiles relative to the burner coordinate system as high as several hundred microns. The source of this irreproducibility is those variables which are inconvenient to regulate precisely from day to day, in particular, mass flow and room temperature. Differences of several tenths per cent in total mass flow occur between runs on different days, but the equivalence ratio stays constant since fuel and oxygen flows are equally affected. Mass flow could be held constant to within ±0·1 per cent during the time taken to run a complete profile.

The most convenient absolute reference in the flame is the upstream edge of the luminous zone. This point can be located in these flames both visually and photographically. In the most favourable of these cases, the acetylene flame*, two observers could locate this position reproducibly with an average dispersion of 30 microns (the difference in judgment between two observers was 50 microns). During any particular run the distance between the burner surface and the inner edge of the luminous zone appeared to remain fixed within the limits of error (50 microns).

A confirmation of this invariance is given by the temperature readings of a small fixed thermocouple suspended just above the burner screen. Because of the steep temperature gradients in the flames, this reading gives a very sensitive indication of flame front movement. It is estimated that a movement of a few microns could be easily detected with this thermocouple. This is particularly valuable in detecting flame oscillations which are invisible to the eye (because they correspond to excursions smaller than 50 microns). Oscillations of this kind occur irregularly in almost all closed burner systems; their cause usually being traced to poor flow regulation or acoustic coupling[9]. In the runs presented, there was no evidence of short period fluctuations (i.e. with

* Visual error in the ethane or ethylene flame might be as much as three times this value.

period between 0·1 sec and 5 sec); fluctuations with frequency higher than ten cycles would not be detected because of the galvanometer period, and fluctuations due to a long period drift and excursions did not exceed 40 microns.

EXPERIMENTAL RESULTS

Duplicate composition profiles were obtained for ethylene and acetylene, and a single profile was obtained for ethane. The data are presented in *Figures 2–4*. As pointed out in the section on method of sampling, the internal consistency of the data is considerably better than the reproducibility from run to run, so that gradients and curvatures should be estimated from a single run and then averaged.

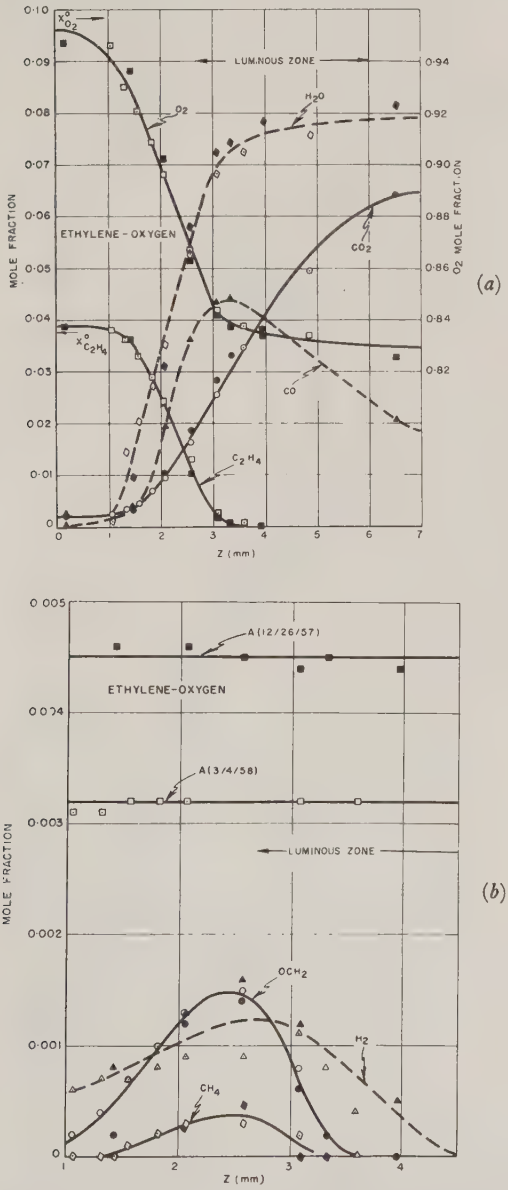

Figure 3. Mole fraction versus *distance* (mm) (*See Table 1 for initial compositions*). (*a*) C_2H_4—O_2 *flame, major constituents;* (*b*) C_2H_4—O_2 *flame, minor constituents*

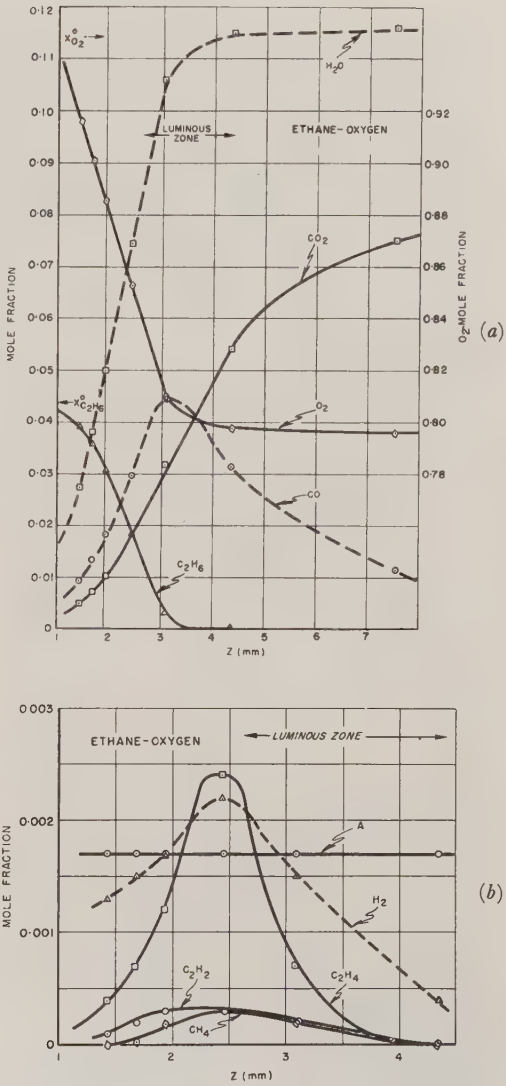

Figure 4. Mole fraction versus *distance* (mm) (*See Table 1 for initial compositions*). (*a*) C_2H_6—O_2 *flame, major constituents;* (*b*) C_2H_6—O_2 *flame, minor constituents*

Inspection of the profiles brings out the following facts:

(1) The relative rate of disappearance of initial fuel and oxygen is the same for the three hydrocarbons, within experimental error (see *Figure 5a* and *b*). (Note that the fuel concentrations were adjusted to make the flame speeds the same.)

(2) The rate of oxygen disappearance decreases sharply when hydrocarbon is consumed, although

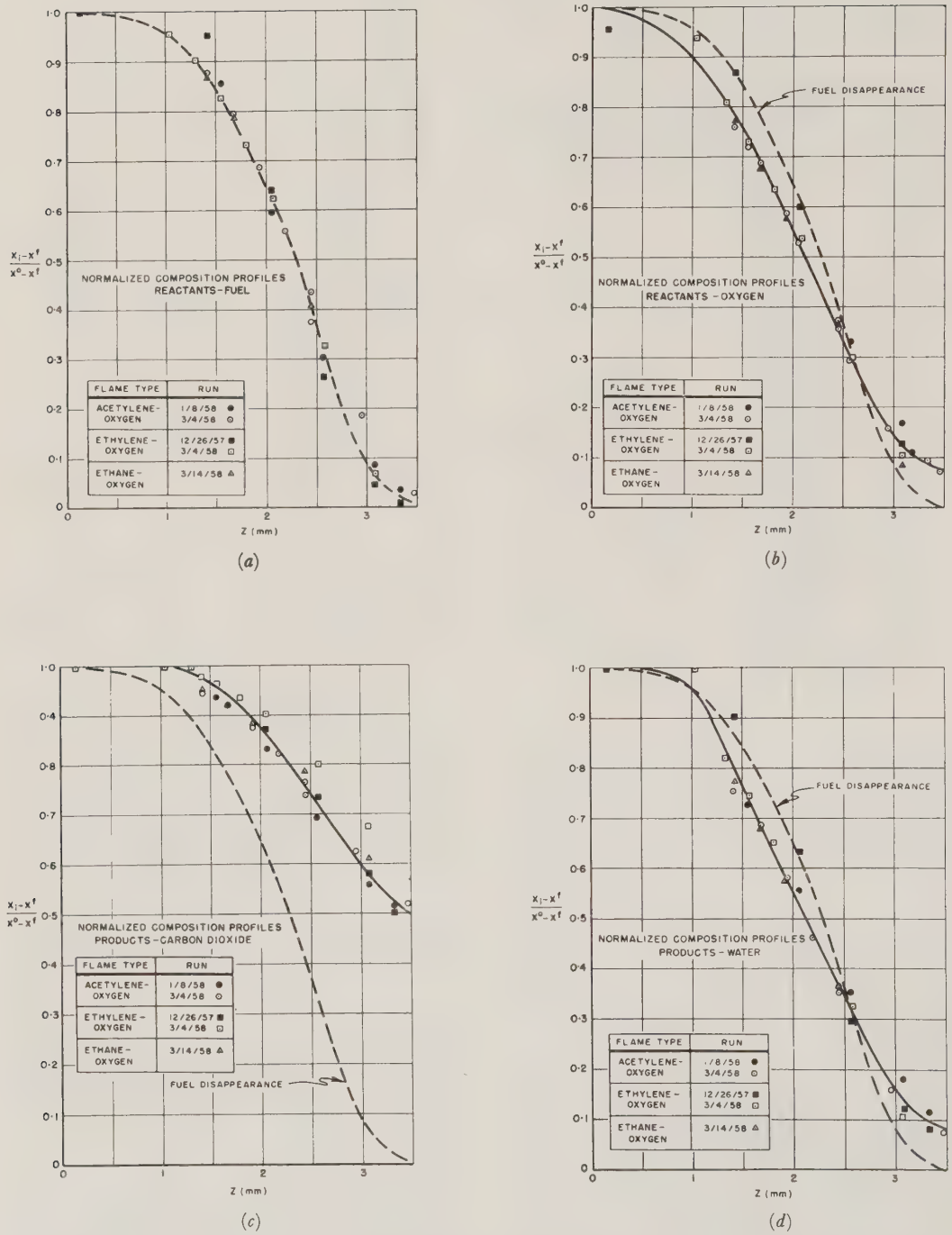

Figure 5. Composite composition profiles. (*Normalized concentration* $(X_i - X^f)/(X^o - X^f)$ versus *distance* (mm).)
(*a*) *fuel*; (*b*) *oxygen*; (*c*) CO_2; (*d*) H_2O

an appreciable concentration of CO remains to be oxidized.

(3) The CO concentration is maximum at the position of apparent final disappearance of hydrocarbon.

(4) The concentrations of the other intermediates are maximum at roughly the position of maximum slope of the hydrocarbon profile.

(5) Numbers as well as maximum concentrations of intermediates increase with the number of hydrogen atoms in the molecule. Absolute values of the intermediate concentrations are very small—of the order of a tenth of a mole per cent.

Maximum luminosity occurs at about the point of disappearance of initial hydrocarbon for all three flames. (*c*) The point of apparent initial luminosity (which is dependent on intensity or exposure time) occurs between the points at which 55 and 65 per cent of the initial fuel has disappeared.

(8) All hydrogen is oxidized by the time the initial hydrocarbon concentration reaches zero. Thus, no measurable concentration of hydrogen results from reaction of CO with water in the downstream region of the flame.

(9) The absence of a number of intermediates is also significant. Hydrocarbons higher than the

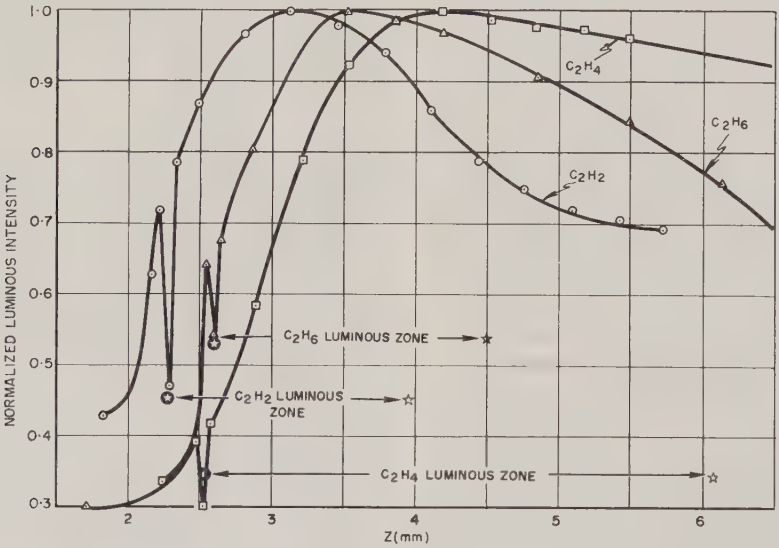

Figure 6. Luminosity profiles—photographic luminous intensity versus *distance* (mm)

(6) With regard to the composition of intermediates, it is noteworthy that formaldehyde is the most important compound not apparently the result of simple dehydrogenation or cracking reactions.

(7) Comparison of the regions of luminosity of the flames with the composition profiles brings out several points of interest (see *Figure 6*): (*a*) The luminous regions of the flames are distinctly different in character, that of acetylene being sharply defined, ethane being fairly sharp, and ethylene thick and diffuse. These differences in luminosity are not reflected in the composition profiles which for the fuel disappearance are congruent on a normalized basis, within experimental accuracy. This suggests that the major part of the luminosity may be attributable to a specific excitation of ethylene or a primary reaction product of ethylene. Thus the ethane flame which contains ethylene as an intermediate shows this to a lesser extent, while the acetylene flame does not show to any significance diffuse luminosity. (*b*) initial one are quantitatively absent (usual limits are 2×10^{-4} mole fraction). Stable oxygen-containing compounds such as alcohols, aldehydes, ketones, and acids (excluding formaldehyde) are also quantitatively absent (2×10^{-4} mole fraction). Peroxy compounds are also absent, but this result is not necessarily significant since the metal in the spectrometer leak might destroy such compounds. Ozone and hydrogen peroxide were also absent (5×10^{-3}). Limits for the detection of these two compounds are affected because they are partially decomposed by the metal spectrometer inlet. Other studies[7] support the view that hydrogen peroxide and ozone are unimportant in hydrocarbon flames. Because of specific interferences in the mass spectral analysis, several of the minor species curves are subject to greater error than those usually quoted. In our systems these are: (1) formaldehyde, ethylene, and acetylene and methane in the presence of ethane possible error equals $\pm 0{\cdot}04\ X_{C_2H_6}$; (2) methane and acetylene in the presence of ethylene possible error

equals $\pm 0{\cdot}04\ X_{C_2H_4}$. As indicated previously, derivatives should be taken from individual runs. However, for purposes of comparison and economy in presentation, the data for individual flames are grouped together and a single average curve drawn. To show the relationships among the three flames, the reactants and products have been cross-plotted in terms of reduced concentration variables. Since the coordinate origin is somewhat arbitrary, it was decided to choose a system in which the fuel disappearance profiles for the flames were made congruent (see *Figure 5*). Zero distance on the abscissa then corresponds roughly to the position of the screen. As would be expected, the relationship between the various composition profiles and the luminosity profiles, both of which are flame fixed, are invariant. The relation of these curves and coordinates to the laboratory fixed position of the burner screen depends upon total mass flow which varied from run to run as discussed above. These variations had no apparent effect on the reproducibility of the profiles or the relations of the flame fixed coordinates. The intermediates showed no simple relationship among the different hydrocarbons and are shown only in terms of mole fractions plotted as a function of distance.

DISCUSSION

The internal consistency of the single run results assures reasonable precision in the derivation of reaction rates from the profiles, but the concentration curves presented here must be corrected quantitatively for diffusion and mass flow[3]. This calculation will be the subject of a later report. The apparent simplicity of the acetylene flame should make possible definitive conclusions about the reaction mechanism. The number of possible intermediate steps can be greatly restricted by consideration of the fact that only rapid reactions, i.e. those with low activation energy and small steric factors, can lead to appreciable concentration changes in the fraction of a millisecond available[8]. Information on the acetylene flame reaction mechanism should then be applicable to elucidation of ethylene, and so on.

It is hoped that the data presented here will demonstrate the utility of the flame sampling technique for study of flame reactions and will encourage others to supplement the small amount of quantitative information available on reaction kinetics at high temperature.

We wish to acknowledge the interest and helpful suggestions of Dr. A. A. Westenberg of the Applied Physics Laboratory; the courtesy of Dr. D. R. Lide of the National Bureau of Standards who analysed several flame gas samples for formaldehyde on his microwave spectrometer; the careful work of Mr. Stanley Favin of the Applied Physics Laboratory in reducing and compiling the data; and the work of Roger Simmons of the Applied Physics Laboratory Art Department who prepared the figures.

This work was supported by the Bureau of Ordnance, U.S. Navy, under contract NOrd 7386, *at the Applied Physics Laboratory, The Johns Hopkins University, Silver Spring, Maryland.*

REFERENCES

[1] Fristrom, R. M., Avery, W. H., Prescott, R. and Mattuck, A. Flame zone studies by the particle track technique—I, *J. chem. Phys.* 22 (1954) 106

[2] — Prescott, R. and Grunfelder, C. Flame zone studies III—Techniques for the determination of composition profiles of flame fronts. *Combustion and Flame* 1 (1957) 102

[3] — and Westenberg, A. A. Flame zone studies IV—Micro structure and material transport in a laminar propane–air flame front. *Combustion and Flame* 1 (1957) 217

[4] Westenberg, A. A., Raezer, S. and Fristrom, R. M. Interpretation of the sample taken by a probe in a laminar concentration gradient. *Combustion and Flame* 1 (1957) 467

[5] Powling, J. A flat flame burner. *Fuel* 28 (1949) 25

[6] Fristrom, R. M. and Raezer, S. Design of a low pressure burner system for laminar flame studies. *Johns Hopk. Univ. Rep. APL/JHU CM–912* (August, 1957)

[7] Foner, S. and Hudson, R. Private communication. (See also p. 106, Ref. 2)

[8] Fristrom, R. M., Westenberg, A. A. and Avery, W. H. An experimental study of propane–air reactions based on flame front analyses. *Johns Hopk. Univ. Rep. APL/JHU CM–925* (November, 1957)

46

FLAME STRUCTURE STUDIES—IV. PRE-MIXED CARBON MONOXIDE COMBUSTION

R. FRIEDMAN and R. G. NUGENT*

INTRODUCTION

The flat-flame burner first devised by Powling provides a geometry especially convenient for the study of flame structure. Friedman and co-workers[1–3] have utilized this technique for a series of studies of lean hydrocarbon air–flames. Fine-wire thermocouple and sample-withdrawal techniques applied to these flames on a 25 cm burner at low pressure have shown that even in the presence of excess oxygen the carbon monoxide formed as a combustion intermediate is slow to oxidize completely to carbon dioxide. In order to learn more about this slow step it seemed worth while to study flames in which carbon monoxide is the primary fuel.

Preliminary to the present flame-structure investigation, Friedman and Cyphers[4] have measured burning velocities of a series of CO—O_2—N_2—H_2O mixtures at low pressure with a flat-flame burner, partly to determine which mixtures could be stabilized on such a burner and partly to obtain the relatively easily measurable relations between burning velocity, mixture composition, and pressure before approaching the much more difficult structure measurements. In that study, for a series of flames at the same temperature (2,010°K), burning velocity was found to be directly proportional to $[CO]_u^{0.5}\,[H_2O]_u^{0.25}$ and independent of $[O_2]$. Symbols $[CO]_u$ and $[H_2O]_u$ denote mole fractions in unburned gas.

In the present study temperature and composition traverses have been made in lean carbon monoxide–oxygen flames with small proportions of added hydrogen or water vapour. A large excess of oxygen, rather than air, has been used to dilute the flame to temperatures sufficiently low to permit traversing because the mass 28 of N_2 coincides with that of CO, interfering with mass-spectrometric analysis.

EXPERIMENTAL

The general features of the apparatus and techniques have already been described[2,3] and hence will be reviewed only very briefly here, except in-so-far as changes have been made.

It was found possible to stabilize flames of a reasonable range of compositions at 30 mm Hg abs., so this pressure was chosen for all tests. At this pressure the thickness of the flame was of the order of 4–5 cm, which was considered optimum in relation to burner diameter, window size, and travel of traverse mechanism.

The flames in appearance were pale blue and quite free of flutter. Carbon monoxide was obtained from cylinders (Matheson C. P. grade) each of which was analysed mass-spectrometrically and found to be free of hydrogen. Iron carbonyl was removed by passage over heated glass beads[4]. Water vapour was added by a two-stage bubbler, or hydrogen was added from a cylinder. Critical-flow orifices were calibrated with wet-test gas meters.

Temperature traverses were made with thermocouples fabricated from 13 micron platinum and platinum 10 per cent rhodium wire, coated with[1] National Bureau of Standards Ceramic A-418. Gas samples for analysis were withdrawn into an evacuated quartz tube drawn to a capillary tip. The pressure drop was more than sufficient to ensure sonic flow at the inlet, which was small enough so that 2 minutes were required to obtain a sufficient sample (about 0·3 c.c. at s.t.p.). An earlier discussion of aerodynamic disturbances produced by the probe and reaction-quenching within the probe[3] is still applicable. The low pressure within the probe (always below 1 mm Hg) and the short residence time in the 5 cm uncooled portion were primarily responsible for quenching the carbon monoxide oxidation, although it was not of course possible to isolate radicals. Samples were collected in a series of bottles previously evacuated below 1 micron and were analysed immediately thereafter with a Consolidated Electrodynamics Corporation Model 21-620 mass-spectrometer. Bottles were generally filled to 700–800 μ pressure, as shown by a McLeod gauge.

Position of the thermocouple or sampling probe was measured relative to the beginning of luminosity by means of a cathetometer readable to 0·01 cm. Tests were made with the room in darkness to permit dark-adaptation of the observer's eye.

* This work was sponsored by Project SQUID, which is supported by the Office of Naval Research, Department of the Navy, under Contract Nonr 1858(25)NR-098-038. Reproduction is permitted for any use of the United States Government.

RESULTS

In spite of the large size of the flame and the smallness of the probes, flame-probe interactions revealed as flame-front distortion were observed to occur when the probe (of either type) was brought down from above so that it extended completely through the luminous zone. However, as long as the probe was kept in the last two-thirds of the reaction zone, where the gradients

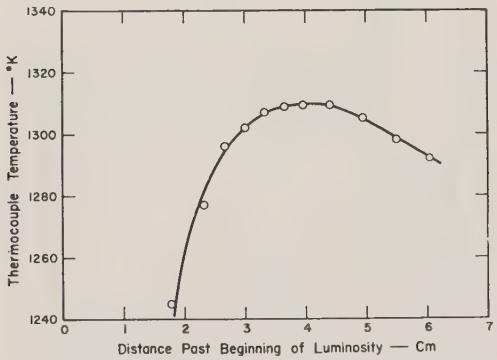

Figure 1. Measured temperature versus *distance through flame* (*run* CO—O_2—H_2O—1)

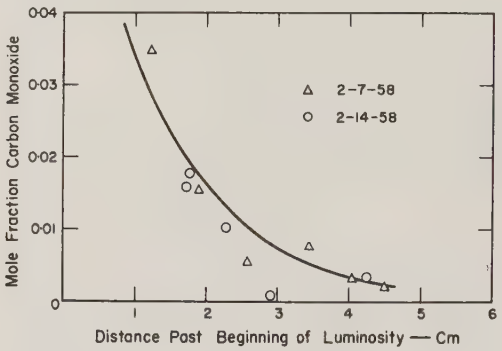

Figure 2. Carbon monoxide content versus *distance through flame* (*run* CO—O_2—H_2O—1)

are less steep, no flame-front distortion could be observed, so data taking was limited to this region.

A set of typical temperature-traverse results is plotted in *Figure 1.* The carbon monoxide distribution for the same flame is shown in *Figure 2.* No hydrogen was found in the data taking region described above, for either this or other flames traversed, including those containing hydrogen in the initial mixture. The estimated limit of sensitivity of the analytical technique was one or two parts per thousand of hydrogen. (Maintenance of equilibrium between CO, CO_2, H_2, and H_2O in the reaction zone would have required a proportion of hydrogen ranging from a trace up to three parts per thousand for the various compositions sampled. Accuracy of the gas analyses was probably not adequate to yield firm conclusions on this point.) Results for other constituents (CO_2, O_2) conformed quite well with stoichiometric expectations. Water vapour was not measured directly.

Table 1 summarizes results based on both temperature and composition traverses for four

TABLE 1

Summary of Flame-Traverse Results

Run number	CO—O_2—H_2—1	CO—O_2—H_2—2	CO—O_2—H_2O—1	CO—O_2—H_2O—2
Initial composition (mole fr.)				
CO	0·1298	0·1445	0·1800	0·1822
O_2	0·8395	0·8251	0·7898	0·7633
H_2	0·0307	0·0304	—	—
H_2O	—	—	0·0302	0·0545
Test pressure (mm Hg)	30·0	30·0	30·0	30·0
Initial temp. (°K)	330	330	330	330
Calcd. flame temp. (°K)	1,590	1,732	1,780	1,790
Burning velocity (cm/sec)	32·0	42·2	29·4	36·1
Overall rate constant $k(sec^{-1})$				
Detd. from CO traverse	267 (0·9–3·3)*	608 (1·3–3·0)*	185 (1·3–4·5)*	
Detd. from temp. traverse	357 (1·5–3·5)*	489 (1·1–3·1)*	262 (2·4–5·0)*	196 (2·5–4·4)*
		901 (3·2–4·2)*		

* (0·9–3·3), for example, signifies that the portion of the traverse between 0·9 and 3·3 cm beyond the beginning of the luminous zone was utilized in the anaylsis.

experimental compositions. It is desired to compare values of flame reaction rate by these two methods of measurement; hence the rather involved data treating process outlined below was followed for each traverse result.

(1) A plot was prepared of ln [CO] *versus* distance, since the carbon monoxide disappears more or less exponentially. The slope s of the best straight line through the data points was measured. This treatment implies a reaction rate first-order with respect to carbon monoxide; this is consistent with the finding that the burning velocity varies with $[CO]^{0.5}$, while burning velocity theoretically should vary with the square root of reaction rate.

(2) To transform this slope to a rate constant k (sec^{-1}), it is necessary to know the rate of motion of the CO molecule through the flame, which is determined by the diffusive flow superimposed on the mass flow. The use of average values for k (sec^{-1}), diffusion coefficient D (cm^2/sec) and velocity v (cm/sec) over the region traversed leads to the following derived equation [3] relating s (cm^{-1}, always a negative number) and k:

$$k = -s\,(v - sD) \qquad (1)$$

In one example, v was 224 cm/sec, s was $-1{\cdot}59$ cm^{-1}, and D was 100 cm^2/sec. Neglect of the sD term would have caused the result to be 43 per cent low. Note that k as obtained from equation 1 is a first-order decay constant for CO. Nothing has been assumed in regard to its dependence on concentrations of other species or on pressure.

(3) Kinetic information is obtainable also from the temperature distribution, by computing the rate of heat release, Q (cal/cm^3-sec), at a given point in the flame from the energy equation:

$$Q = v\rho C_p\,\mathrm{d}T/\mathrm{d}x - \mathrm{d}(\lambda\,\mathrm{d}T/\mathrm{d}x)/\mathrm{d}x \qquad (2)$$

where v is gas velocity, ρ is density, C_p is specific heat, T is gas temperature, λ is thermal conductivity, and x is distance. The equation is rigorous except that λ and C_p actually vary with composition. In this application all mixtures contained at least three-fourths oxygen, the other gases in the traversed region (CO, CO_2, H_2O) having a mean molecular weight not too different from oxygen, so, to simplify computation, thermal conductivity and specific heat were taken to be that of oxygen at the appropriate temperature. Thermal conductivity was extrapolated above 600°K by assuming a variation with the 2/3 power of absolute temperature.

(4) Before equation 2 is used, the thermocouple temperatures T_c must be converted to gas temperatures T. To a good approximation, $T - T_c$ is proportional to $T_c^4/(T + T_c)$, the numerator being due to radiative heat loss and the denominator to temperature dependence of thermal conductivity through the gas film. The proportionality constant might be established from heat-transfer correlations, which would be difficult because a Knudsen-number effect is just beginning to come in, or from the calculated flame temperature. The latter method was used.

(5) Using T values determined in 4, the equation of 3 was solved numerically with each set of data, the distance interval being arbitrarily taken as 0·05 cm. Smoothing procedures were used at various stages in the computation which will not be detailed here. One finally obtains Q *versus* x.

(6) The Q thus obtained is a *net* Q, the difference of Q_C, the chemical heat generation rate, and Q_L, the radiant heat-loss rate from gas to walls. In the extreme downstream portion of the traversed zone, the temperature was generally observed to be dropping and this was taken to be a measure of a radiant heat-loss rate Q_L, presumably from CO_2 and H_2O molecules. Q_L is, of course, much smaller than Q_C except in the region where Q_C goes to zero, but this is part of the region of interest. Hence, Q_L was added to Q to yield Q_C.

(7) Upon plotting ln Q_C *versus* x, a curve is obtained (*cf. Figure 3*) which may be roughly

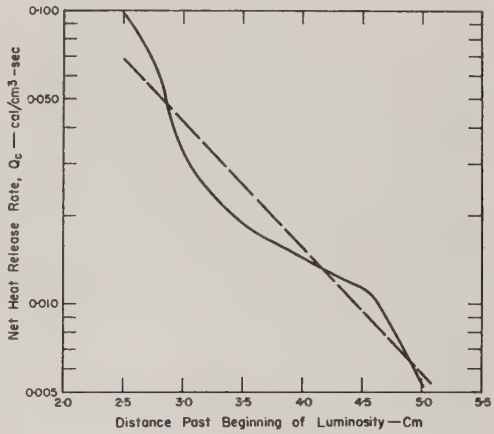

Figure 3. Calculated heat-release rate versus *distance* (*run* CO—O_2—H_2O—1)

approximated by a straight line in certain regions. The significance of the slope of this line is that if Q_C is proportional to [CO] in any zone, the proportionality constant being invariant with x in this zone, then d ln Q_C/dx must be equal to d ln [CO]/dx, which in turn leads to a value of k, by equation 1. Thus, an independent method for checking the value of k is available. Note that if Q_C were proportional to $[CO]^n$, then d ln Q_C/dx would equal n d ln [CO]/dx. From the agreement

in the results of Table 1 for k determined by the two methods, it is evident that n cannot differ enormously from unity.

DISCUSSION

Certain trends of interest may be discerned by a study of Table 1.

First, a comparison of the two hydrogen runs shows that the mixture containing the greater proportion of carbon monoxide, and hence giving the higher flame temperature (1,732 *versus* 1,590°K) has a higher burning velocity (42·2 *versus* 32·0 cm/sec) and a higher rate of carbon monoxide decay in the tail of the flame. Qualitatively, this is what would be expected, of course. The inconsistencies of the k values determined in various ways, as shown in the table, do not permit a good quantitative measure of the increase of the reaction rate with flame temperature. The ultimate reason for these inconsistencies is that fantastically accurate traverse data and knowledge of flame properties would be required to yield entirely satisfactory rate constants after differential analysis such as has been described.

The table also shows the effect of replacement of hydrogen by water vapour. Run CO—O_2—H_2—2, with 3·04 per cent hydrogen, has a calculated flame temperature of 1,732°K, while run CO—O_2—H_2O—1, with 3·02 per cent water vapour, is at 1,780°K; however, the hotter flame, with the water vapour, has a burning velocity only 70 per cent of that of the hydrogen flame. Also, the CO decay rate constant is roughly three times as great in the tail of the water-vapour flame as in that of the hydrogen flame. It is recalled that gas-sampling in the pertinent region of the CO—O_2—H_2 flame did not reveal any free hydrogen, the hydrogen apparently being entirely consumed early in the luminous zone. If one considers that the burning velocity is controlled primarily by the reaction rate at the point of most intense reaction (i.e. the early part of the luminous zone, corresponding to the region of most intense luminosity), as Eyring *et al.*[5] have proposed, then the greater flame speed in the hydrogen case might be attributed to acceleration of the carbon monoxide combustion in this region by intermediates in the hydrogen oxidation, such as hydroxyl. Alternatively, the more rapid second-stage reaction in the hydrogen case may act to feed more heat back to the rate-controlling primary step, thus accelerating it. In any event, however, one is left with a difficulty in explaining how the gas in the tail of the flame knows that in one case its water-vapour content came from hydrogen burning in the primary zone and in the other case from water added originally. If the results are correct, some long-lived species must be carried several cm downstream from the intensely luminous zone through the tail, where it accelerates the rate. The time involved here is of the order of 20 msec, which is sufficient for a molecule at these flame conditions to undergo roughly 10^6 collisions.

To return to a study of the table, comparison of runs CO—O_2—H_2O—1 (3·02 per cent water vapour) and CO—O_2—H_2O—2 (5·45 per cent water vapour), with flame temperatures virtually identical (1,780 *versus* 1,790°K), shows an increase of burning velocity of 23 per cent with increasing water vapour content. The correlation of the earlier burning-velocity study would have predicted a 17 per cent increase, which constitutes agreement within the experimental error. The temperature-traverse result indicates that the rate of CO decay is of the same magnitude for the two water-vapour concentrations; the precision of these results is not sufficient to permit any firmer statement.

There is more information to be gained simply from the magnitudes of the burning velocities in these tests. First, it is recalled that the earlier burning-velocity study[4], which led to an empirical correlation of v_u with $[CO]_u^{0.5}\,[H_2O]_u^{0.25}\,P^{-0.12}$, involved mixtures containing substantial proportions of nitrogen as diluent, the mole fraction of oxygen ranging from 0·101 (rich) to 0·167 (lean). Within this range $[O_2]_u$ was not required as a correlating variable. In the present tests, excess oxygen was used as diluent, $[O_2]_u$ being 0·7898 in run CO—O_2—H_2O—1. It is of interest to determine if the measured burning velocity of 29·4 cm/sec is in agreement with the above-mentioned correlation. If it is, it would show that the correlating group, which indicates CO burning velocity to be independent of O_2 concentration, is valid over a twentyfold range of CO/O_2 ratios. It turns out that the correlation would have predicted a value of 25·6 cm/sec, which compares quite satisfactorily with the measured value of 29·4 cm/sec.

A second important result may be deduced from the magnitude 29·4 cm/sec. It is obviously of interest to convert this number to a reaction constant for the rate of decay of CO by means of a theory relating burning velocity to reactivity. A decay constant obtained in this way could then be compared with values already measured in the tail of the flame. To accomplish this computation, the Zeldovich, Frank-Kamenetskii and Semenov theory was used, the detailed form of which is presented in the earlier paper[4]. Spalding[6] has shown that results obtained with this theory do not differ by any substantial factor from those obtained from a half-dozen other theories of the overall-reaction type with various mathematical refinements.

On the basis of burning-velocity correlations,

the reaction rate is assumed to be represented by the law:

moles CO reacting/cm^3-sec

$$= (n_{CO})(n_{H_2O})^{0.5} A e^{-E/RT} = k(n_{CO}) \quad (3)$$

Hence, $$k = (n_{H_2O})^{0.5} A e^{-E/RT} \quad (4)$$

From equation 4 above and equation 2 of the earlier paper[4], for lean mixtures, one may eliminate A and partly eliminate exp $(-E/RT)$, obtaining:

$$k = \frac{\beta^{1/2} v_u^2 \rho_u^2 C_p^2 (T_b - T_u)^3 E^2}{2\lambda_b q R^2 T_b^3 T_u (n_{CO})_u} \left(\frac{T_b}{T}\right)^{0.5} \times \exp\left[\frac{-E}{RT_b}\left(\frac{T_b}{T} - 1\right)\right] \quad (5)$$

The symbols are defined as follows, with numerical values corresponding to run No. CO—O_2—H_2O—1: β is moles reactant gas per mole product (1·10), v_u is burning velocity (29·4 cm/sec), ρ_u is density of unburned gas (0·0000465 g/c.c.), C_p is heat capacity at constant pressure (0·278 cal/g-°K), T_b is burned-gas temperature (1,780°K), T_u is unburned-gas temperature (330°K), E is activation energy (20,000 cal/mole, from correlation of earlier paper), λ_b is thermal conductivity of burned gases (0·000239 cal/cm-sec-°K), q is heat of combustion of CO (67,000 cal/mole), R is the gas constant (1·987 cal/mole-°K), $(n_{CO})_u$ is the concentration of CO in the unburned gas (2·62 × 10^{-7} moles/c.c.), and T is a temperature in the reaction zone.

For $T/T_b = 0{\cdot}95$ and $E = 20{,}000$ cal, k comes out to be 2,339 sec^{-1}; for $T/T_b = 0{\cdot}90$ and $E = 20{,}000$ cal, k comes out to be 1,725 sec^{-1}. These k values are seen to be enormously larger than those in Table 1 determined from the traverses (185–262 sec^{-1}). Before considering the significance of this, the sensitivity of equation 5 to the somewhat uncertain value of E must be studied. This may be seen from the plot of *Figure 4*, which is based on solutions of equation 5 for various assumed values of E and T/T_b.

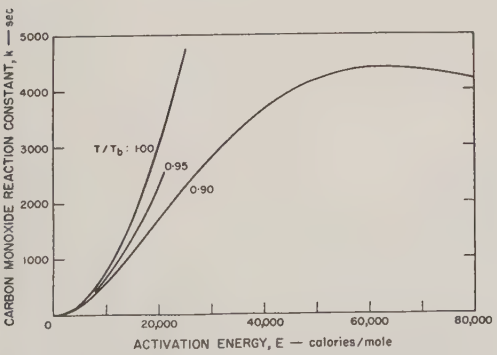

Figure 4. Solution of equation 5, with parameters corresponding to run CO—O_2—H_2O—1 *as a function of E and T/T_b*

Clearly, the equation can give a k value of the order of 200 sec^{-1} only if E were of the order of 5,000 cal/mole. This is far too low to account for the variation of carbon monoxide burning velocity with flame temperature, which requires about 20,000 cal/mole according to Friedman and Cyphers[4] and 22,000 cal/mole according to Slootmaekers and van Tiggelen[7]. Thus, the results suggest that a qualitatively different process occurs in the intensely luminous primary reaction zone and the tail of the flame. To shed further light on this, an attempt will soon be made to measure character and relative intensity of the light emitted from the two regions.

As a final topic of discussion, the results will be compared with those of another investigation. Fenimore and Jones[8] have made gas-sampling traverses in atmospheric-pressure carbon monoxide flames, the present investigation having been carried out at 30 mm Hg. It is pertinent to compare the two sets of results. For one of their mixtures (28·6 per cent CO, 1·67 per cent H_2O, 69·7 per cent air, $T_b = 1{,}909$°K) they find d ln [CO]/dt (which is defined as k in this paper) to be 30 sec^{-1}. This number would be multiplied by a factor of 0·68 to convert from 1,909 to 1,780°K according to an exp. $(-20{,}000/RT)$ law. If one uses their activation energy of 24,000 cal instead, the factor becomes 0·62. In either case, k at 1,780°K would be roughly 20 sec^{-1}. In the present study, k was found to be ten times this large, it will be recalled. The influence of pressure remains to be discussed, the present study being conducted at 1/25 the pressure of Fenimore and Jones' study. They propose that k (as defined in this paper) is roughly proportional to water-vapour partial pressure. The effect of water vapour on burning velocity[4] suggests that k varies with the square root of water vapour partial pressure. According to the latter rule, their k value extrapolated to the conditions of run CO—O_2—H_2O—1 would be about 5 sec^{-1}, which is lower than the value actually found by about a factor of 40. The assumption of first-power dependence on water-vapour partial pressure would lead to an even greater discrepancy, of course. No detailed explanation can be offered for this large difference at this time, except for the comment that Fenimore and Jones were apparently sampling in the zone where the last one per cent of the fuel was burning while the present data were not obtained this far downstream.

SUMMARY AND CONCLUSIONS

Traverses of lean carbon monoxide–oxygen flames with hydrogen or water added, at 30 mm Hg abs., indicate the following:

(1) The flame reaction consists of a rapid step,

associated with intense luminosity, followed by a much slower process in which the last of the carbon monoxide is consumed. An assumption that the reaction rate decreases linearly with decreasing carbon monoxide concentration does not account for this effect, although the variation of burning velocity with carbon monoxide concentration indicates a proportionality between reaction rate and carbon monoxide concentration. Traverses show the temperature to be rising through the region in question, so the effect cannot be attributed to cooling, but must have a chemical explanation, the details of which are unknown.

(2) Values for the rate of consumption of carbon monoxide in the final stages of combustion, expressed as first-order decay constants, are listed in Table 1.

(3) Hydrogen and water vapour are not interchangeable as additives for lean carbon monoxide–oxygen flames, even though mixture compositions are adjusted to give the same flame temperature. The hydrogen additive gives a higher burning velocity and a more rapid second-stage reaction, although gas analysis indicates that hydrogen is converted to water in the first stage.

(4) Burning velocity may be correlated with $[CO]_u^{0.5}\,[H_2O]_u^{0.25}$ for a series of mixtures with the same flame temperature in which the oxygen concentration is varied twentyfold.

REFERENCES

[1] Friedman, R. *Fourth Symposium (International) on Combustion*, pp. 259–263. 1953. Baltimore; Williams and Wilkins

[2] — and Burke, E. *J. chem. Phys.* 22 (1954) 824

[3] — and Cyphers, J. A. *J. chem. Phys.* 23 (1955) 1875

[4] — — *J. chem. Phys.* 25 (1956) 448

[5] Eyring, H., Giddings, J. C. and Tensmeyer, L. G. *J. chem. Phys.* 24 (1956) 857

[6] Spalding, D. B. *Combustion and Flame* 1 (1957) 296

[7] Slootmaekers, P. J. and van Tiggelen, A. *Bull. Soc. chim. Belg.* 65 (1956) 425

[8] Fenimore, C. P. and Jones, G. W. *J. phys. Chem.* 61 (1957) 651

47

STUDY OF THE CHEMISTRY OF DIFFUSION FLAMES

A. S. GORDON, S. R. SMITH and J. R. McNESBY

INTRODUCTION

The quantitative chemical mechanism of hydrocarbon flames has been a stumbling block to the quantitative formulation in the theory of burning rates of fuels. It has been assumed that these mechanisms could hardly be made tractable quantitatively and much ingenuity has gone into avoiding the chemistry involved in formulations of these theories. Recent studies in our laboratories on diffusion flames[1–4] as well as propane–air premixed flames in other laboratories[5] indicate that the pyrolysis of the fuel molecule is a most important reaction. This conclusion was also arrived at on the basis of spectroscopic studies[6], although in these studies it is not possible to state what percentage of the reaction goes via this path. Satterfield[7] has studied the slow oxidation of hydrocarbons over a temperature range. At every temperature there were two concurrent reactions, a pyrolysis and an oxygenate producing reaction. As the temperature increases the pyrolysis reaction dominates.

APPARATUS AND PROCEDURES

A conical flame about 1 in. diameter at the port was used for flame studies of gaseous fuels. The height of the cone was controlled by the flow rate. The sampling probe was a quartz tube drawn out so that it was 5 mils o.d. and 3 mils i.d. The end of the probe was first flame sealed and then ground open so that a diaphragm type of probe resulted with an opening of less than 1 mil diameter. In this way the sample stayed in the hot region of the probe for less than 1 msec and was at very low pressure during this time. The burner was mounted on a micro manipulator so that various regions of the flame could be conveniently probed. The probe was attached to a manifold which was continuously evacuated. When the flame was completely stable and undisturbed, a stopcock was turned so that two samples could be taken simultaneously into two previously evacuated flasks. The samples were taken to a total pressure of about 2 cm mercury; one sample was then analysed by mass spectrometric techniques and the other sample was analysed by gas chromatography. Peaks on the gas chromatography unit which could not be readily identified were trapped and the fraction then identified by the mass spectrometer. With these qualitative data the complex mass spectra can be broken down and

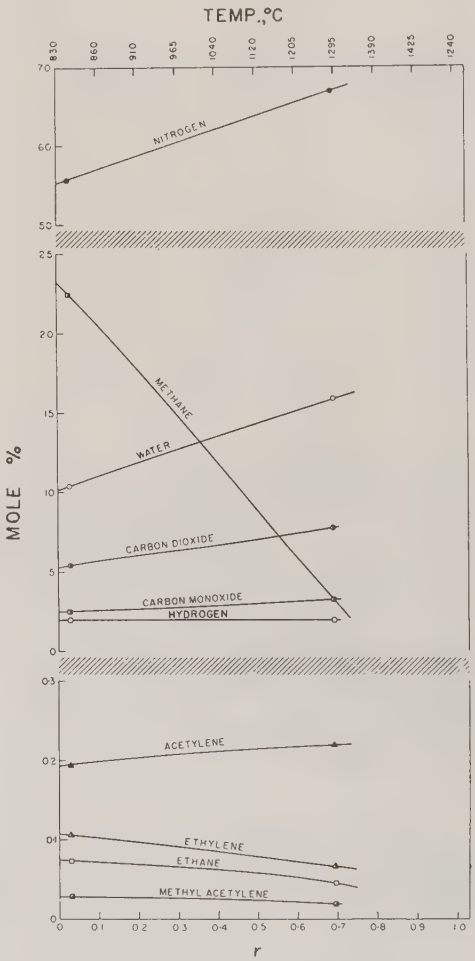

Figure 1. Composition of sample probed from flame 20 mm *above port. (r = ratio of distance of probe to central axis to radius of flame)*

it is possible to analyse mixtures containing more than 20 constituents, some as low as 0·01 per cent of the total. Liquid fuels were burned on a glass wick and probed in the same manner as the gaseous fuel flames.

The studies of free radical reactions were done mainly with photochemical techniques in which acetone or acetone d_6 was mixed with the hydrocarbon under study and the mixture photolysed at various temperatures. CH_3 and CD_3 radicals were thereby generated *in situ*. Studies also were made using other radical sources, generated by photolysis of the appropriate ketone–hydrocarbon mixture.

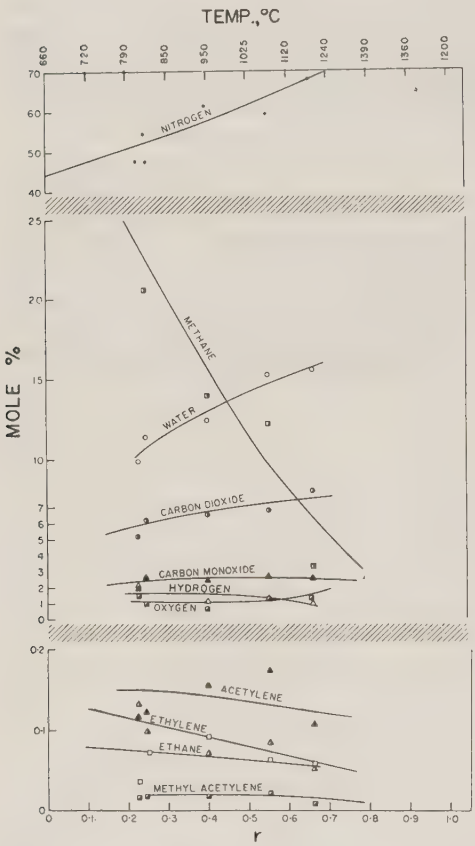

Figure 2. Composition of sample probed from flame 11 mm *above port. (r defined in Figure 1)*

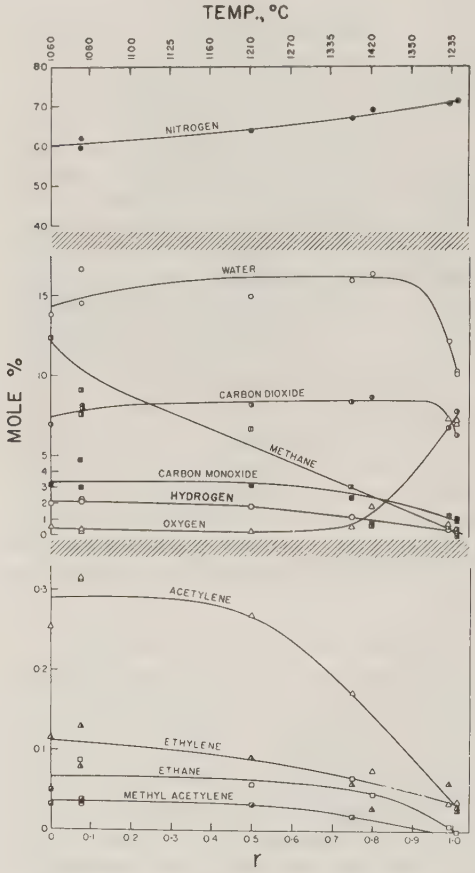

Figure 3. Composition of sample probed from flame 7 mm *above port. (r defined in Figure 1)*

RESULTS AND DISCUSSION

The methane diffusion flame and the methanol diffusion flame will be discussed as examples of the pyrolysis reactions inside the flame mantle.

Methane diffusion flame

In *Figure 1* the major constituents inside the methane diffusion flame cone are plotted against the ratio of the distance of the probe to the axis of the flame and the total distance from the axis to the edge of the luminous zone. At the same time temperatures were recorded at the same point that the samples were taken. A 1 mil platinum–platinum rhodium thermocouple which was coated with a very thin layer of quartz 1–2 mils in thickness was employed. On other occasions uncoated platinum–platinum rhodium thermocouples were employed and no significant difference in the temperatures was noted inside the luminous region. However, in a very narrow region at the edge of the flame, temperature gradients were so steep that no success in measuring these temperatures was had even when a 0·1 mil thermocouple was employed. The temperatures inside the flame cone are also included in *Figures 1*, *2* and *3* where the composition in each figure is for a constant distance above the port. A number of points emerge from an examination of these figures. (1) Methane disappears very rapidly and is at zero concentration level at the edge of the flame. (2) On the other hand water and carbon dioxide concentrations are a maximum close by the edge of the flame. (3) Nitrogen is at an extremely high concentration at all points in the flame increasing towards the edge; on the axis, 7 mm above the

port it is almost 45 mol per cent of the sample. (4) There is always some oxygen in the samples. Extreme precautions were taken to guard against air contamination of the samples so that we feel that this oxygen is really present in the flame and plays an important role in the pyrolysis process. A diffusion flame may thus be regarded as a very rich pre-mixed flame. (5) The total oxygen, both in the combined and uncombined form, inside the flame cone compared to the nitrogen at the same flame point is higher than the O_2/N_2 ratio in air. This would indicate that the weighted average diffusion coefficient of H_2O, CO, and CO_2 is greater than the diffusion coefficient for nitrogen. (6) Equilibrium constants for the water gas reaction were calculated from the concentration of CO, CO_2, hydrogen and water in the samples. All these concentrations were reliable except water, which is a minimum value. When the temperatures corresponding to these equilibrium constants inside the flame cone were compared with the observed temperatures they were always found to be hundreds of degrees too high. Since water is a minimum value here, the calculated temperatures are minimum temperatures and we must conclude that water gas equilibrium is not set up inside the flame mantle.

If pure methane is pyrolysed in a furnace 800–900°C its rate of disappearance is very small. In the flame at the same temperature we find that methane disappears at a rate which is orders of magnitude larger. It is well known that small amounts of oxygen strongly increase the rate of pyrolysis of hydrocarbons and this same mechanism must operate inside the flame cone. The intermediate products of the pyrolysis inside the cone are everywhere found at quite low concentration and these concentrations do not change very much inside the flame cone except near the edge. The only intermediate product of the pyrolysis which appears in a reasonably high concentration is hydrogen, which is also a product of the pyrolysis of methane. There is no evidence of the fate of the carbon in the methane from our gas analyses and we must conclude it appears as carbonaceous particles. Of particular interest is the observation that no oxygenated hydrocarbons are present. We tried especially hard to find formaldehyde in the flame. Using wet methods of great sensitivity some reducing material was present not over one part in 10^5. The question can arise as to whether formaldehyde could persist in the flame if it were formed. To answer this question we volatilized *para*formaldehyde pellets into the flame from the port of the burner. Under these conditions large quantities of formaldehyde were easily detected.

TABLE 1

Samples Probed from Methanol Flame

Sample No.	1	2	3	4	5
Carbon dioxide	7·56	6·98	8·17	9·04	11·21
Argon	0·55	0·51	0·55	0·61	0·63
Methyl alcohol	16·29	14·76	6·03	3·04	0·04
Oxygen		0·03	0·04		0·06
Formaldehyde	0·51	0·52	0·27	0·27	0·02
Ethylene	0·05	0·02	0·03	0·03	0·03
Acetylene	0·04	0·03	0·02	0·03	
Water	14·08	19·61	25·09	21·18	26·59
Methane	0·28	0·24	0·21	0·06	0·01
Carbon monoxide	8·58	7·93	7·51	9·19	4·61
Nitrogen	46·09	43·41	47·23	51·33	54·71
Hydrogen	5·97	5·94	4·83	5·23	2·07
	100·00	100·00	100·00	100·00	100·00
Temperature °C	350	375	980	1,150	1,300

Methanol diffusion flame

In Table 1 the analysis of samples probed from a methanol flame are shown. The temperatures of these samples in the flame are also shown. Samples Nos. 1 and 2 were probed from the zone near the wick of the flame while 3, 4 and 5 were sampled along the central axis going towards the tip of the flame. The analyses show: (1) Formaldehyde is an important intermediate in this flame and is relatively stable so that even at temperatures of 1,150° it is still easily detected. (2) No ethane was detected in the flame samples although small concentrations of ethylene and acetylene were noted. Methane is present indicating the presence of methyl radicals. (3) Carbon monoxide and

hydrogen are present in larger concentrations than in the methane diffusion flame, showing that they are more readily formed from the pyrolysis of the parent molecule. Carbon monoxide is easily formed by the pyrolysis of methanol whereas in the methane diffusion flame it results only from oxidation of a pyrolysis product. The small concentration of methyl radicals which must be the precursor for the methane, as well as for ethylene and acetylene (via an undetectably low ethane precursor) is reasonably understood since methyl radicals can occur only by two difficult processes: (1) The breaking up of the C—OH bond of 115 kcal, and (2) the H atom attack on methanol to form H_2O and CH_3.

Carbon formation

One of the most interesting features of flames is the formation of carbon particles by processes which must be very efficient. In many of the flames which we have studied the acetylene concentration increases with the ability of the flame to form soot, in conformity with the mechanism postulated by Porter. However, there are some exceptions, the most glaring of which is the benzene diffusion flame. This flame is a most efficient soot former, yet it has an acetylene concentration about the same magnitude as that found in a methane diffusion flame, and the temperature distribution inside the flame is, if anything, somewhat lower than for the methane flame. Therefore, there must be materials other than acetylene which can form carbon particles. Unsaturated species must be present for carbon formation. In a methanol flame where there is only a small percentage of any unsaturated hydrocarbon no soot is formed. The most likely way that carbon particles can be formed is via free radical addition to unsaturates, ultimately forming a polymer which does not depolymerize but rather dehydrogenates at higher temperatures. Ethylene found in the flame will certainly add radicals but at flame temperatures these radicals should be very unstable, and break down to ethylene and a small free radical. Acetylene offers a better path since the larger radical formed by the addition of acetylene and the radical is probably more stable to the inverse reaction. Also by addition of two more acetylene molecules, benzene can be formed and the original radical regenerated. The benzene so formed is readily converted to a phenyl radical. Phenyl radicals can also be formed when the acetylene free radicals add two acetylene molecules and form a ring. These phenyl radicals add to benzene and produce large condensed rings with concurrent loss of H_2. The polynuclear aromatics can carbonize further by loss of hydrogen in the hotter regions of the flame. Indeed in a study of the pyrolysis of methane, one of the authors was able to detect evidence for the existence of many polynuclear aromatic hydrocarbons in the products. This mechanism would also account for the excellent ability of benzene to carbonize since the phenyl radical would be able to add to the benzene parent forming a large free radical which in turn would add more benzene, and rapidly form a large polynuclear configuration with concurrent loss of H_2.

It should be noted that the free electron in the phenyl *cyclo*hexadienyl free radical can be in the *ortho* position or in the *para* position, and the radical is thus resonance stabilized. If another benzene molecule adds to the phenyl *cyclo*hexadienyl radical

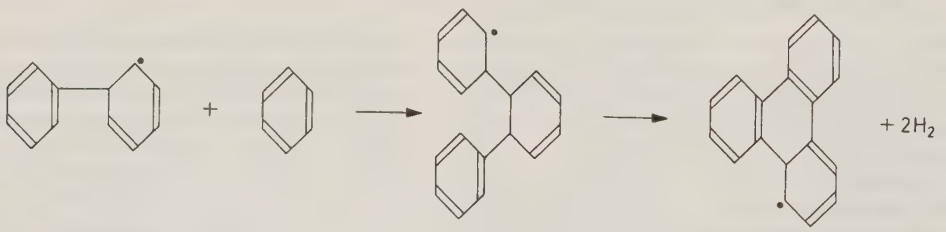

This configuration can eliminate two hydrogen molecules during the process and form a new aromatic ring in the molecule which lowers the activation energy for the elimination of H_2. Acetylene can take the place of a benzene molecule in these reactions, and an acetylenyl free radical can replace a phenyl radical. Thus the carbonaceous particle is probably a copolymer of benzene and acetylene. Large free radicals can combine. In a highly condensed ring system, the free electron is mobile so that the steric factor for the re-combination reaction between two large radicals should not be much smaller than for methyl radical re-combination. This reaction must be important in forming soot particles, since the maximum size of soot particle occurs in the part of the flame where all the small precursor molecules have almost entirely disappeared.

Study of free radical reactions

The results of the diffusion flame work have led us to study free radical reactions. We have studied the Arrhenius factors for the abstraction of various types of hydrogen mostly by methyl radicals. Recently we have determined the abstraction of H by the allyl radical. The pyrolysis of large free radicals has been studied. Lastly we will report on some addition reactions of free radicals to unsaturates.

The abstraction of H by methyl radicals was accomplished by a technique originally introduced by Trotman-Dickenson, Birchard and Steacie[8]. A mixture of acetone d_6 and the hydrocarbon to be studied is irradiated at a particular temperature. The CD_3 radicals formed in the primary process stabilize themselves as CD_3H and CD_4 by reacting with the hydrocarbon and the parent acetone respectively. The CD_3H/CD_4 ratio measures the product of the ratio of the rate constants and the ratio of the concentration of hydrocarbon and Ad_6. Since we react only one or two per cent of the material, the value of this ratio does not change appreciably during the course of the reaction. The relative rate constants of reaction are determined over a temperature range and the relative pre-exponential factors and activation energies are obtained since,

$$\ln CD_3H/CD_4 = \ln A_H/A_D + (E_D - E_H)/RT$$

The energy of activation, E_D, for the abstraction of D from Ad_6 by CD_3 has been determined by studying the $CD_4/(C_2D_6)^{\frac{1}{2}}$ ratios over a temperature range and assuming that the re-combination of CD_3 radicals has zero energy of activation[9]. This value has been cross checked with the value for CH_3 abstracting H from normal acetone and the energy of activation difference for CD_3 abstracting H and D from normal acetone and acetone d_6 respectively[10]. The absolute value of the rate constant for CD_3 abstracting D from acetone d_6 makes it possible to transform all the relative values of abstraction from hydrocarbons and Ad_6 into absolute values for abstraction of H by CD_3.

This method has the advantage that the variation of light flux in the reaction vessel has no effect on the accuracy. In Table 2 some results obtained by this method with various compounds are listed. Of especial interest is the extension of the method to the determination of the Arrhenius factors for the abstraction of primary and secondary hydrogen in butane. This was done by synthesizing $CH_3CD_2CD_2CH_3$ butane where the primary and secondary hydrogens are clearly differentiated.

TABLE 2

Energies of Activation for Abstraction of H or D by Methyl Radicals*

System	*Temp. range of studies*	E_{act} (kcal)	$A_{reactant}/A_{acetone}$
CH_4	350–430	14·0	0·48
Ethane-d_0	250–525	11·5	1·21
Ethane-d_6	250–510	14·8	0·20
D_2	140–425	11·9	0·44
$CH_3CD_2CD_2CH_3$ (D abstraction)	350–450	11·4	1·00
$CH_3CD_2CD_2CH_3$ (H abstraction)	350–450	11·4	0·93
$CH_3CH_2CH_2CH_3$ (sec H abstraction)	250–450	9·3	0·62
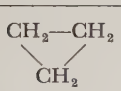	250–400	13·1	1·3
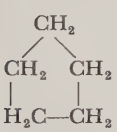	250–400	9·3	1·65

* These energies are based on the abstraction of a D atom from acetone d_6 by a CD_3 radical. The pre-exponential factors are given as a ratio of the rate of attack on reactant molecules and the rate of attack on the acetone used for the methyl radical source extrapolated to infinite temperature.

If the photolysis of acetone d_6 is a source of CD_3 radicals the only reactions which generate methane are

$$(1)\ CD_3 + CH_3CD_2CD_2CH_3 \rightarrow CD_3H + CH_2CD_2CD_2CH_3$$

$$(2)\ CD_3 + CH_3CD_2CD_2CH_3 \rightarrow CD_4 + CH_3CDCD_2CH_3$$

$$(3)\ CD_3 + CD_3COCD_3 \rightarrow CD_4 + CD_2COCD_3$$

Since very little reaction occurs, as previously noted, the ratio of reactants stays constant, and $CD_4/CD_3H = k_2/k_1 + k_3/k_1(Ad_6/Bd_4)$. The Ad_6/Bd_4 ratios have been varied at constant temperature and the resulting CD_4/CD_3H ratios plotted against the Ad_6/Bd_4 ratios. The slope of the resulting straight line is k_3/k_1 and the intercept is k_2/k_1. If the reaction is studied over a range of temperatures these ratios permit the evaluation of A_3/A_1, A_2/A_1, E_2/E_1, E_3/E_1 to be made. In this way the energy of activation for H and D abstraction from butane d_4 as well as the corresponding Arrhenius pre-exponential factors have been obtained relative to the reaction of CD_3 abstracting deuterium from acetone d_6. Now if a similar study is done using normal butane in place of the marked butane then the energy of activation for the abstraction

TABLE 3

Ratios of CD_3H/CH_4 for Photolysis of Equimolar Mixtures of Acetone and Acetone d_6

Temperature °C	CH_4/CD_3H
188	0·98
188	1·01
219	0·95
253	1·04
253	1·01

from the secondary hydrogen of the butane is determined since the abstraction of the primary H is known from the previous work. Two assumptions are implicit in this work. (1) The presence of deuterium on a carbon atom does not influence the abstraction of hydrogen from an adjacent carbon. (2) CD_3 will abstract in exactly the same way as CH_3. We have checked this second assumption in the photolysis of equimolar mixtures of acetone and acetone d_6. It has been shown by Benson[12] that the molar extinction coefficients for acetone and acetone d_6 are equal. We have investigated the abstraction reaction in the temperature range where there are no chain processes. Here the rate of generation of CH_3 and CD_3 radicals are equal. By examining the CH_4/CD_3H ratio we have examined the relative rates of abstraction of hydrogen by CH_3 and CD_3 radicals. As can be seen in Table 3 the ratio stays very close to unity over a wide temperature range. Thus CH_3 and CD_3 show no difference in their ability to abstract H from the same source.

In general our results show that the greater the carbon hydrogen bond strength the higher the energy of activation for abstraction of the hydrogen. This is not correlated with the heat of the overall reaction, since for hydrogen abstraction from methane by methyl radical, $\Delta H = 0$, but the $E_{act} = 14$ kcal. Although the Evans–Polanyi[13] relation between bond strength and energy of activation was not derived for hydrocarbons, some of our results are in very good accord with it.

We have recently been able to determine the hydrogen abstraction by the allyl radical, a highly resonance stabilized configuration, and we could compare this directly with that for the methyl radical in the same system. This was shown by a photolysis and pyrolysis of a mixture of acetone d_6 and *cyclo*pentane. *Cyclo*pentane is quite stable against pyrolysis. However, the CD_3 radicals can easily abstract an H forming a *cyclo*pentyl radical which breaks down readily at temperatures over 250°C, forming ethylene and an allyl radical. The allyl radical in this system can stabilize itself by abstracting hydrogen from its parent or deuterium from the acetone d_6 as well as by reaction with another free radical. The two abstraction processes are differentiated by the dueterium content of the resulting propylene. All the hydrogens in *cyclo*propane are equivalent and all the deuteriums in Ad_6 are also equivalent. At the same time there are CD_3 radicals as well as allyl radicals in the reaction system, which has been studied over a wide temperature range to over 500°C. At temperatures up to about 430° the allyl radical does not appreciably abstract hydrogen or deuterium since the product gases contain no propylene. As the temperature is increased, however, the propylene/ethylene ratio rapidly increases, until at temperatures of over 500° this ratio is about 0·5, showing that the allyl radical generated at the same time as the ethylene is abstracting hydrogen at a rate equal to the rate of disappearance via radical-radical processes.

The abstraction of H by allyl in the temperature range of organic free radical pyrolysis reactions has another consequence. Propylene is often employed as a radical trap for free radical organic pyrolysis reactions. It acts by virtue of an easily abstractable H, and it forms an allyl radical as a result. It is usually assumed that this resonance stabilized radical is so unreactive that it disappears exclusively via radical-radical processes. Our work has shown that the allyl radical can abstract H in these temperature ranges and is a chain carrier, although a less efficient chain carrier than,

say, the methyl radical. Any quantitative evaluation of chain length from propylene inhibition must take the abstraction by allyl into account.

The propylene/methane ratio increases strongly with temperature, indicating the E_{act} for abstraction of hydrogen by allyl is considerably greater than that for methyl. The peak areas in the *cyclo*pentane–Ad_6 reaction were determined by the products butene–1, methane, and propylene. The methane fraction was analysed for CD_3H and CD_4 and the propylene for d_1 and d_0 content. These data were recorded over a temperature range which permitted us to calculate that the E_{act} for abstraction of H from *cyclo*pentane by allyl radical is 32 $\pm$ 3 kcal. Methyl radical abstracts the same hydrogen with an E_{act} of 9·3 kcal[14].

The two butyl radicals generated from butane 2, 2, 3, 3-d_4 have been shown to decompose in the temperature range 350–500°C. The decomposition products are ethylene and an ethyl radical from the primary butyl radical, and propylene and methyl from the secondary butyl radical. The D content of the ethylene and propylene fractions shows that no migration of H or D along the carbon skeleton took place[15]. However, hydrogen can migrate along a carbon skeleton, although reluctantly. When *cyclo*propane and deuterium mixtures are pyrolysed, all the propylene is light, indicating that the process for propylene formation from *cyclo*propane is intramolecular and that a hydrogen atom must migrate along the carbon skeleton prior to C—C bond rupture.

We have also looked at the addition of radicals to the olefins. If CD_3 radicals are added to butane–1, at temperatures ranging from 300 to 500°C, much of the methane is formed by CH_3 radicals.

(4) $CD_3 + CH_3CH_2CH = CH_2 \rightarrow CH_3CH_2CH - CH_2CD_3$

$CH_3 + CH_2 = CHCH_2CD_3$

(5) $CH_3CH_2CH - CH_2CD_3 \rightarrow CD_3 + CH_2 = CHCH_2CH_3$

The mechanism was substantiated by the butene–1 d_3 in the product. Using the above interpretation it is possible to calculate roughly the rate of addition of CD_3 to the terminal carbon atom of butene–1 relative to the rate of abstraction of D from Ad_6. At 250° this ratio is about 2, and at 400° it is almost 12.

The addition of methyl radicals to the non-terminal carbon atom in butene–1 can be represented by

(6) $CD_3 + CH_3CH_2CH = CH_2 \rightarrow CH_3CH_2CHCH_2CD_3$

(7) $CH_3CH_2CHCH_2CD_3 \rightarrow CD_3 + CH_3CH_2CH = CH_2$

$CH_3CH_2CHCH_2CD_3 \rightarrow CH_3CH_2 + CD_3CH = CH_2$

If we assume that the two rate constants for reaction 7 are equal to each other and that every pentyl radical formed in 6 decomposes via 7, the rate of formation of propylene d_3 may be used as a measure of reaction 6. On this basis the rate of terminal addition of methyl radicals to the butene–1 is seven times the rate of non-terminal addition at 400°.

The reaction of methyl, ethyl, and hydrogen atoms with ethylene has been studied over a temperature range. In the case of methyl radicals the temperature range was from less than 200 to over 500°C, and in the case of ethyl and H atom the temperature was about 300°C. We have found that the major hydrocarbon product for all these radicals reacting with ethylene at temperatures over 300°C is propylene. It is probably formed via the reactions:

(8) $CH_3 + C_2H_4 \rightarrow CH_3CH_2CH_2$

(9) $CH_3CH_2CH_2 + CH_2CH_2 \rightarrow CH_3CH_2\ CH_2CH_2CH_2$

The pentyl radical can abstract H intramolecularly

(10) $CH_3CH_2CH_2CH_2CH_2 \rightarrow CH_3CHCH_2\ CH_2CH_3$

(11) $CH_3CHCH_2CH_2CH_3 \rightarrow CH_3CH = CH_2 + CH_3CH_2$

The ethyl radical then reacts with ethylene:

(12) $CH_3CH_2 + CH_2 = CH_2 \rightarrow CH_3\ CH_2CH_2CH_2$

(13) $CH_3CH_2CH_2CH_2 + CH_2 = CH_2 \rightarrow CH_3CH_2CH_2CH_2CH_2CH_2$

The hexyl radical abstracts H intramolecularly and forms

$CH_3CHCH_2CH_2CH_2CH_3$

which breaks down

(14) $CH_3CHCH_2CH_2CH_2CH_3 \rightarrow CH_3\ CHCH_2 + CH_3CH_2CH_2$

thus forming a chain. It is readily seen that ethyl radicals would go through the same chain process. For H atoms the reaction is

(15) $H + C_2H_4 \rightarrow C_2H_5$

so that the common major product is understood. The mechanism is also in accord with the fact that ethane, propane, and butane are common products of reaction of all three radicals with

ethylene. Also, when CD_3 reacts with ethylene, most of the propylene is light, showing a chain mechanism to be operative.

It is surprising at first sight to note that saturated free radicals add so readily to ethylene to form larger radicals at temperatures of over 500°. Normally we have noted that these large radicals already break down at temperatures of 250° because there is no competitive reaction of addition to unsaturates available. In the special case where a large excess of ethylene or butene is present, it is clearly seen that the addition reactions are very favourable compared to the abstraction processes.

REFERENCES

[1] Smith, S. R. and Gordon, A. S. *J. chem. Phys.* 22 (1954) 1150
[2] — — *J. phys. Chem.* 80 (1956) 759
[3] — — *J. phys. Chem.* 60 (1956) 1059
[4] — — and Hunt, M. H. *J. phys. Chem.* 61 (1957) 553
[5] Fristrom, R., Prescott, R. and Grunfelder, C. *App. Phys. Lab. Johns Hopkins Univ.* (1955) 858
[6] Wolfhard, H. G. and Parker, W. G. *Proc. phys. Soc. A* 65 (1952) 2
[7] Satterfield, C. *et al. Fifth Symposium (International) on Combustion.* 1956. New York; Reinhold
[8] Trotman-Dickenson, A. F., Birchard, J. R. and Steacie, E. W. R. *J. chem. Phys.* 19 (1951) 163
[9] Whimple, E. and Steacie, E. W. R. *J. chem. Phys.* 21 (1953) 993
[10] McNesby, J. R. and Gordon, A. S. *J. Amer. chem. Soc.* 76 (1954) 1416
[11] — — *J. Amer. chem. Soc.* 78 (1956) 3570
[12] Private communication
[13] Evans, M. and Polanyi, M. *Trans. Faraday Soc.* 34 (1938) 11
[14] McNesby, J. R. and Gordon, A. S. *J. Amer. chem. Soc.* 79 (1957) 825
[15] — Drew, C. M. and Gordon, A. S. *J. chem. Phys.* 24 (1956) 1260
[16] — and Gordon, A. S. *J. chem. Phys.* 25 (1956) 582

MASS ANALYSIS OF FLAMES AND FLUE GASES

E. A. BUNT

INTRODUCTION

The physical determination of the composition of flames, whether burning freely or confined in engine combustion chambers, has in the past relied heavily on emission or absorption spectroscopy[1]; an associated problem is that of the analysis of exhaust products, for which infra-red spectroscopy has been employed[2]. In internal combustion engine research, however, the difficulties of interpretation of transient spectra are such that it is as well that the emphasis has now largely passed from the cyclic to the constant pressure unit. One modern approach to the problem of analysis of flame gases is to freeze such particles as OH, O, H, and N in a liquid helium trap for subsequent identification[3]. Another is the possibility of collecting the thermal ions known to be present in a flame by means of a probe connected to an amplifier. A typical record of the random currents flowing in a bunsen flame is shown in *Figure 1.*

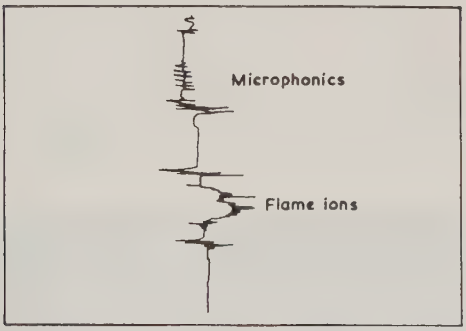

Figure 1. Recorder trace of random ion currents

Since such ions are formed at atmospheric pressure and cannot be directly formed into a molecular beam for analysis, further work leads either to the use of a mass spectrometer employing a viscous flow probe and one or more pressure-dropping stages in series, or to limiting analyses to low-pressure phenomena. The first fast reaction mass analyses at pressure heads up to 4 mm Hg were performed by Eltenton[4–6]; the nature of this apparatus placed a severe limitation on the permissible range of flame pressures, however. Later investigations included those of Foner and Hudson[7,8], Leger and Ouellet[9,10], and Lossing, Tickner and Ingold[11–14]; another report refers to the extraction of gases from flames burning in a vacuum chamber at low pressure[15].

This report is concerned mainly with some investigations into the potentialities of the former aspect, i.e. the analysis of gases withdrawn from flames burning at atmospheric pressure. This application is essentially that of Longwell and Weiss[16], whereby samples for H_2 analysis were withdrawn from a spherical pressurized reactor.

INSTRUMENTATION

The instrument built incorporated a conventional 60 degree sector field. Following a suggestion by Nier[17], the source was simplified, as shown in *Figure 2*, giving somewhat lower resolution. A

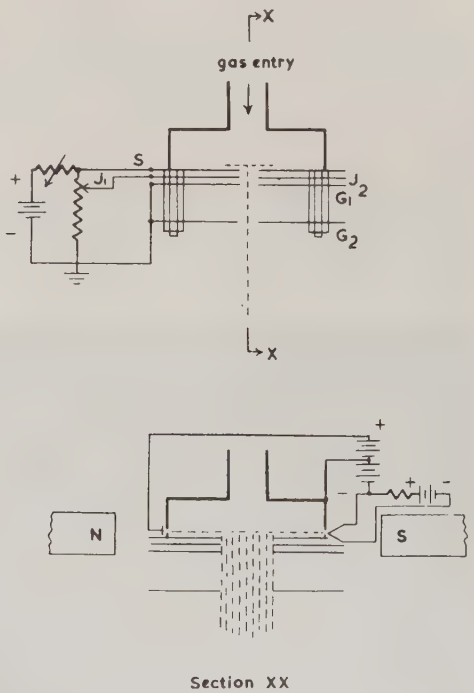

Figure 2. Simplified Nier-type ion source used

single collector slit was employed and spectra were recorded on a Brown Electronic recorder equipped with an automatic range selector[18], using voltage scanning. The sample was expanded

through a viscous flow leak valve and a molecular flow diaphragm leak in series with a hypodermic needle flame probe (for accurate positioning, as well as for avoidance of undue disturbance of the flame, such as is caused by the type of water-cooled probe used in conventional sampling of gas turbine combustion chambers). Various diaphragm leaks were used. *Figure 3* shows a micrograph of a

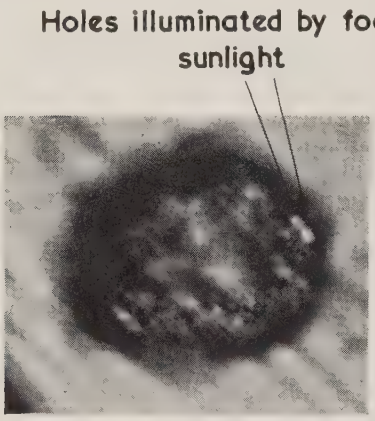

Figure 3. Micrograph of small leak holes

parallel (double) leak developed that had an effective diameter of only $2{\cdot}5 \times 10^{-4}$ cm, corresponding to downstream molecular flow from a pressure head of 2 cm Hg. When discharging gas of high water content, however, these leaks tended to corrode, and larger glass capillaries of the Dibeler type[19] were more satisfactory. No arrangements were made to focus the H_2 peak, and its abundance was partly deduced from the magnitude of the water peaks in the combustion spectra.

TEST PROCEDURE

Two types of test were run: in the first, gases were withdrawn direct from flames for analysis as in the 'process monitor' procedure of chemical plant operation; secondly, analytical sampling of stored products was carried out. With most samples withdrawn from flames, the method of analysis did not permit air to be excluded from the analysis. On account of the partial pressure distribution of each constituent in the ionization chamber, one result of this was the reduction of signal strength for other species of low abundance, particularly combustion products of high molecular weight. The total response time of the gas inlet system was estimated at 30 msec. Where possible, high energy (70 V) ionizing electrons were used, as the sensitivity did not then vary so much with changes in the energy. Spectra shown reproduced were run at the most suitable scale range.

DIRECT FLAME SAMPLING

Oxy-acetylene flames

Spectrogram 1 shows the result of sampling the outer sheath of an oxy-acetylene flame burning in air, using a conventional burner ('analytical' samples are described in this instance as the flame temperature was too great to allow a probe to remain intact long enough to permit direct scanning). The sensitivity in this case is too low to show the three characteristic water peaks. Although the $^{44}CO_2^+$ peak appears, this showed wide variation in height over otherwise identical runs. A small peak at mass 16 was also visible, and is mostly accounted for by oxygen drawn in with the sample. The measured 28/32 peak ratio provided evidence to show that at least 50 per cent of the mass 28 peak was due to CO, pointing to far

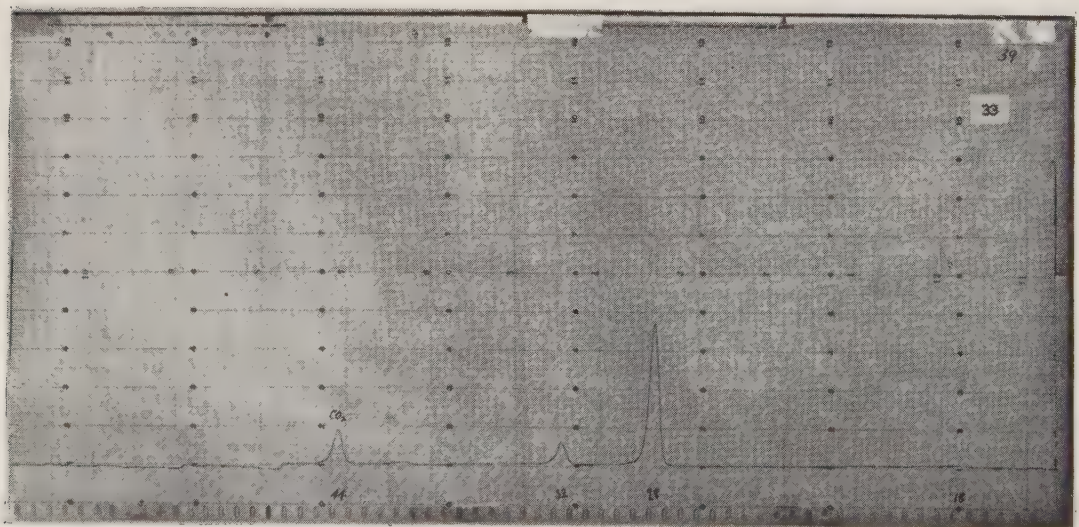

Spectrogram 1

from complete combustion. Other records from the outer sheath of such a flame showed larger water peaks, indicating more complete combustion here.

Other runs illustrated the changes brought about when the oxygen supply was cut off. In this type of sooty flame the water peaks were considerably reduced, and a large peak at mass 26 indicated unburnt C_2H_2; this was supported by the presence of a small $^{12}C^+$ peak, suggesting that only a small portion of fuel had been burnt.

of a peak at mass 12, indicating that the latter may have partly resulted from the breakdown of $^{28}CO^+$, the second largest constituent of the fuel, as the contribution to peak 12 by methane is less than its contribution to peak 13, which was seen to be small. The reduction of the peak at mass 14 was considered to be due to a change in the ionizing conditions in the source resulting from the use of a lower (25 V) ionizing voltage, as this was the only change of variable. (It was previously observed as a characteristic of the instrument that the size of

Table of Mass 12–18 System for Coal Gas/Air Flame

Type of flame	*Probe station*	*Spectrogram No.*	*Relative intensity of mass*							*Ionizing voltage*
			12	13	14	15	16	17	18	
↑	(Fuel only)	2	10	3	24	19	29	3	12	70
	At fuel entry	3	—	—	5	29	45	3	18	25
	Dark zone (inner radius of annular space)	4	2	—	6	21	24	5	42	25
	Dark zone (outer radius of annular space)	5	2	3	6	30	40	4	15	25
Blue	Base of inner cone	6	—	9	12	—	9	9	61	25
	Upper part of inner cone	7	5	2	66	3	19	—	5	70
		8*	11	—	52	5	16	—	6	70
	Outer zone	9	5	—	52	—	16	5	22	70
↓		10*	1	—	14	—	6	15	64	70
Yellow	Yellow zone	11	12	3	44	6	13	5	17	70

In the absence of a single parent, the proportionality is adjusted so that peak height = 100, in place of making say, *m/e* $18(H_2O)^+ = 100$.

* 'Live' sample.

Coal gas flames

The considerably cooler pre-mixed coal gas*/ compressed air flames examined enabled more attention to be given to the potentialities of 'live' sampling. The burner used in these tests is shown in *Figure 4*, which also illustrates typical spectra observed at various sampling stations. Air entered up the central pipe. Some characteristics of various flame zones are given in the table above showing the mass 12–18 system, and in *Figures 4* and *5*. In the spectrum of entering fuel (spectrogram 3) peak 28 is largely due to CO, in consequence of the small amount of oxygen entering with the fuel. This run differed from a spectrum of unburnt fuel particularly in respect of its much reduced mass 14 peak, and in the absence

* A representative analysis of the coal gas was: CO_2, 5·4; O_2, 0·6; CN, HN, 1·9; CO, 16·1; CH_4, 21·2; H_2, 41·2; H_2O, 1·8; N_2 (by difference), 11·9 per cent.

the air dissociation peaks $^{44}N^+$ and $^{16}O^+$ was a strong function of the ionizing voltage, as the ratio of these to their parents could be made to differ considerably from the values noted in the literature. This fact was therefore taken into account when assessing the respective contributions of N_2 and CO to the mass 28 peak. As compared with exhaust gas analyses, however, flame sampling yielded considerably greater $^{14}N^+$ and $^{16}O^+$ peaks, and this points to these being the result of thermal dissociation in the outer parts of the flame.) In general it appeared that the CO_2 combustion efficiency was very low; under conditions of sampling with different flames, it often proved very difficult to record sufficiently representative $^{44}CO_2^+$ peaks, and this pointed to a variation of instrumental sensitivity. Heating of the gas inlet line to minimize sorption of hydrocarbons and OH groups has previously been followed[20] and some improvement attended this practice here. Such

sorption may be a factor in the reduction of the CO_2 peak, coupled with absorption by stopcock greases.

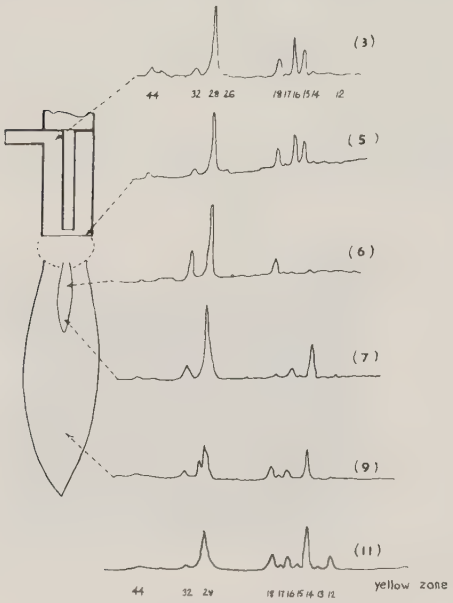

Figure 4. Characteristic spectra associated with coal gas/air flame

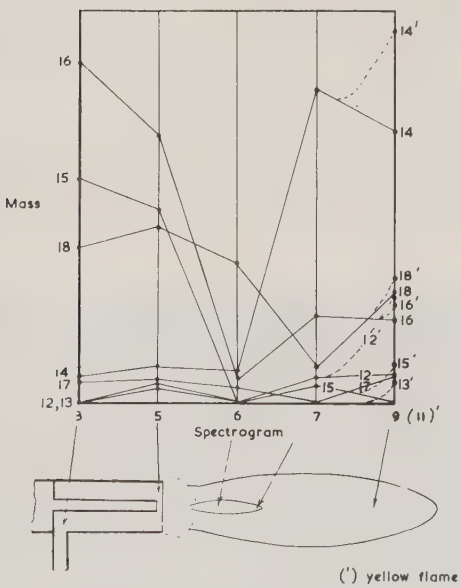

Figure 5. Progressive mean pattern change through coal gas/air flame

Significant changes occurred between the luminous and non-luminous parts of the flame. Runs 4 and 5 (see Table) using the same ionizing conditions record samples withdrawn from the faintly luminous, almost spherical, zone at the base of the flame; the large peaks at masses 15 and 16 due to CH_4 still persist, little reaction having occurred, as found by Byrne[21]. A spectrogram showing the analysis of a sample taken from near the base of the inner bright blue reaction zone formed around the entering air jet emphasizes that CO no longer represents a major contributor to the mass 28 peak, on account of the more normal 32/28 ratio. The water peaks appear to remain almost constant throughout the reaction zone, but an actual increase in the quantity of water in the flame would be obscured by the greater partial pressure now exerted by the air jet. Absence of a mass 15 peak points to complete combustion of methane at this level.

Analysis of samples obtained from the upper part of the inner cone, as represented by other spectrograms (7 and 8), closely resemble those obtained from the outer light blue zone (9 and 10). Although 32/28 peak ratio is small, it is unlikely that this is due to CO, and the sample is not influenced to the same extent by the entering air jet. Only a very small peak now remains at 15 to indicate remaining methane in this region, and this disappeared in samples taken from the outer zone. Comparing inner zone and outer zone records it was found that the use of direct sampling gave rise to no significant differences as compared with stored sampling procedures. Spectrogram 10, however, represented a somewhat special case, and underlines one difficulty of combustion product analysis: the disproportionately large water peaks were no doubt due to elution within the instrument. A small peak at mass 30—which may be due to formaldehyde HCHO[22] or NO[23]—is to be seen in further spectrograms (8 and 10).

The yellow gas flame pattern also varied. A strong $^{12}C^+$ peak is to be seen in spectrogram 11, together with a high peak at mass 14. In a run at lower sensitivity the proportion of water shown was greater. Peaks also appeared at mass 31 and 27 in the latter case; these may have been CH_3O or C_2H_3. In the above, the peaks at mass 44 were in general smaller than those at, say, mass 12, due perhaps to dilution. *Figure 5* attempts to show the progressive pattern change through the flame. In this the significant emergence of mass 14 has been stressed.

COMBUSTION PRODUCTS SAMPLING

The procedure was also applied to the analysis of samples from exhaust ducts to determine its degree of suitability thereto. This is partly illustrated in *Spectrograms 12–14.* Some spectra depicting products withdrawn from the exhaust pipe of an automobile at idling did not confirm the finding by Shepherd and others[24] of acetylene but merely pointed to a large proportion of CO present. An unsuccessful attempt was made to obtain a picture of the efflux of a Ricardo E5 variable compression

Spectrogram 12

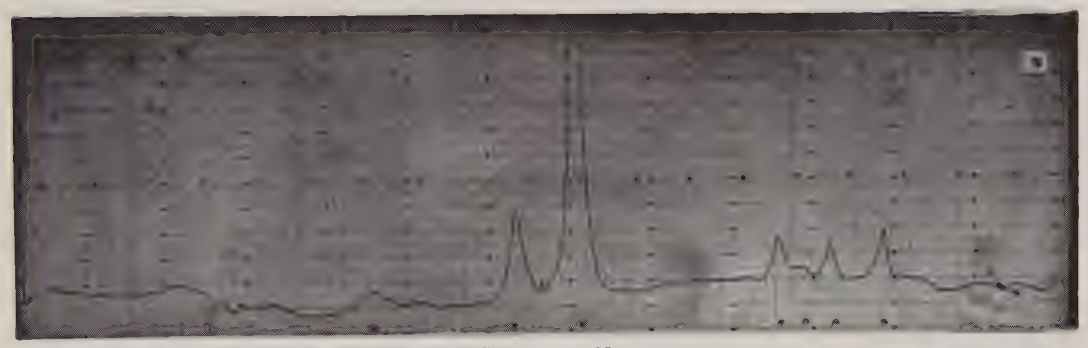

Spectrogram 13

Spectrogram 14

engine running on a rich mixture. The manner of sampling in this instance was by drawing the sample for some time through a concentration bottle containing glass wool, as suggested by Shepherd and others[24], but it was clear that this procedure was mainly effective only in trapping water. The strong dissociation peaks of $^{14}N^+$ and $^{16}O^+$ were absent, although considerable air was present: this suggested the presence of these particles as thermal ions in flames, but not persisting long enough to be detected in exhaust products. The results suggested that the exhaust gas largely comprised O_2, H_2O and CO, as might be expected, the relatively large proportion of CO being confirmed by supplementary tests with an Orsat apparatus, but the high proportion of water present in the sample unfortunately led to difficulty in assessing the amount of nitrogen present.

Flue gases from a steam boiler were also sampled, but owing to its remoteness from the spectrometer, no 'live' sampling was possible. Samples were taken from a point away from the duct wall, in front of the economizer, using an existing probe. As seen in *Spectrogram 12*, the sensitivity of the sampling suffered, as it did in the previously mentioned case, from excessive dilution of the products of combustion by air. In consequence only small $^{44}CO_2^+$ and $^{18}H_2O^+$ peaks can be positively identified, apart from the usual contribution of atmospheric oxygen and nitrogen to the peaks at 14 and 16

The size of the oxygen and nitrogen peaks also indicated a contribution by CO to mass 28. The water peaks were in all cases relatively smaller than those observed in flames. In addition, a peak at mass 12 was seen in one case when a lower ionizing voltage was used. It was thought interesting to compare this analysis with that of a human respiratory sample, as has previously been done with a special mass spectrometer[25]. As shown in *Spectrogram 13*, using 25 V electrons, the scan of a collected breath sample closely resembles a flue gas sample, excepting that the absence of a contribution of CO to the peak at mass 28 is certain. Little decrease in the height of the O_2 peak was evident, and it appeared that the proportion of O_2 used up during respiration was small. Apart from the small peak at mass 44 due to CO_2, and the contribution of water vapour to peaks 16, 17 and 18, the other main peaks were due to the usual dissociation of O_2 and N_2 in the ion source. As expected, this spectrum was relatively 'clean', resulting from the analysis of simple products.

The exhaust duct sampling method was also applied to draw products from the wall of a model combustion chamber, formed by extending the coal gas burner by about 12 diameters, the flame being stabilized opposite the sampling tapping by critical adjustment of gas and air pressures. Dilution of flame products with secondary air was also evident as shown in *Spectrogram 14*. The peaks were similar to those previously found for flue gas sampling, but relatively larger at 16 and 18, and smaller at masses 12 and 14. Other runs confirmed the presence of a water peak at mass 17, and the main difference with the flue gas samples was seen to lie in the presence of a peak mass 15, as given by the analysis of some of the collected samples withdrawn from the inner cone of the open coal gas/air flames. This indication of unburnt fuel, taken with the disproportionate sizes of the 32/28 peak ratio, pointed to a turbulent spread of the blue region of incomplete combustion throughout the lower part of the flame tube.

CONCLUSIONS

No significant differences were observed between the analyses of 'dead' and 'live' samples, indicating that short-lived intermediates were not susceptible to collection under the imposed conditions of relatively long response time. High mass 14 and 16 peaks in the records of samples withdrawn direct from flames appeared to indicate that $^{14}N^+$ and $^{16}O^+$ ions persisted long enough to record. Various instrumental limitations were observed, e.g. absolute peak heights were critically dependent on the emission current setting and the sensitivity to CO_2 was low. Under optimum conditions it proved possible to largely dispense with the collimating magnetic field in the ion source, the use of which only increased the trap current without materially altering the ion beam strength.

Considerable variation in flame samples of each particular type occurred. While certain patterns are known to be unstable, in that sensitivity is not a linear function of partial pressure—as with the NO_2 reaction with Hg in the presence of water[24]—the presence of water as a combustion product in large measure was almost certainly a major cause of this variation. (The presence of water in the fuel was ignored.) The main problems were those of absorption and elution, the most offending surface being between the leak and the ion source, which was therefore made as short as possible. The water present also shortened the life of the filaments from months to hours, and in certain cases to minutes; under conditions of frequent filament changes consistent results were difficult to obtain. Sample variation was also undoubtedly due to the length of time required to record complete scans. The spectra taken proved particularly suitable for the identification of a parent molecule, say CH_4, in a region where unburnt fuel was present. Although the mass spectrometer was only equipped for handling the gas phase, analyses—particularly those performed with yellow luminous flames—clearly demonstrated its ability to record unburnt carbon. An evident disadvantage in the

work was the coincidence of important peaks, such as those of N_2 and CO.

It was noted that the mass spectrometer seemed more suited to routine analysis of simple compounds, with reproducible ionization diagrams, than to the complex mixtures it was forced to accept. The similarity of the 'broken' spectra of combustion products to those of multi-component analyses suggested the presence of a number of reaction products all contributing dissociation species, thus pointing to the complicated nature of hydrocarbon reactions. For this reason investigators have often concentrated on one peak at a time, say CH_3. In short, the records emphasized an apparent low sensitivity of the mass spectrometer to combustion products, compared with greater sensitivity for 'straight' compounds. Sampling the relatively cool contents of a flue afforded less information than direct withdrawal of products from a flame zone.

In view of so many instrumental variations a quantitative result cannot be claimed for combustion analyses obtained under the above conditions. Under more controlled conditions, however, there is no reason why the flue gas type of analysis should not be fully representative of flue contents in spite of possible stratification, as in ordinary process monitoring. It appeared that the greatest technical improvement is to be expected from a wider use of kinetic scanning[7,8] in order to present a complete instantaneous scan of conditions at any point. Non-steady variations are then observed by focusing on one peak.

SUGGESTIONS FOR FURTHER WORK

Work suggested by the results are the combination of a mass spectrometer and a shock tube for the recording of dissociation data and the further application of the mass spectrometer to obtaining analyses in gas turbine or ramjet combustion chambers, or the investigation of the mechanism of fouling of turbine blades. Although the mass spectrometer can apparently detect free carbon, it might not distinguish between the soft carbon (soot) that accumulates inside the combustion chamber and the microscopic hard carbon cenospheres that go straight into the exhaust.

The author would like to thank Professors W. J. Walker and S. F. Gimkey for providing laboratory facilities, and the Council for Scientific and Industrial Research, Pretoria, for subventing a portion of this work.

REFERENCES

1 Rassweiler, G. M. and Withrow, L. *Industr. Engng. Chem.* (*Industr.*) 24 (1932) 528
2 — — *Industr. Engng. Chem.* (*Industr.*) 24 (1932) 195
3 Anon. *Nat. Bur. Stand. News Bull.* 40 (1956) 112
4 Eltenton, G. C. *J. chem. Phys.* 10 (1942) 403
5 — *J. chem. Phys.* 15 (1947) 455
6 — *J. phys. Colloid Chem.* 52 (1948) 463
7 Foner, S. N. and Hudson, R. L. *J. chem. Phys.* 21 (1953) 1374
8 — — *J. chem. Phys.* 21 (1953) 1608
9 Leger, E. G. and Ouellet, C. *J. chem. Phys.* 21 (1953) 1310
10 — *Can. J. Phys.* 33 (1955) 74
11 Tickner, A. W. and Lossing, F. P. *J. chem. Phys.* 18 (1950) 148
12 Lossing, F. P. and Tickner, A. W. *J. chem. Phys.* 20 (1952) 907
13 — Ingold, K. U. and Tickner, A. W. *Disc. Faraday Soc.* 14 (1953) 34
14 Ingold, K. U. and Lossing, F. P. *J. chem. Phys.* 21 (1953) 1135
15 Anon. *Westinghouse Engineer* p. 48. Jan. 1955
16 Longwell, J. P. and Weiss, M. A. *I.M.E.—A.S.M.E. Joint Conference on Combustion*, 1955
17 Nier, A. O. Private communication
18 Bunt, E. A. *Rev. sci. Instrum.* 22 (1951) 57
19 Dibeler, V. H. and Taylor, T. I. *Science* 108 (1948) 686
20 Kelley, H. M. *Anal. Chem.* 23 (1951) 1081
21 Byrne, J. F. *Proc. Sixth Symposium* (*International*) *on Combustion*, p. 120. 1957. New York; Reinhold
22 Shepherd, D. G. *An Introduction to the Gas Turbine*, p. 340. 1949. London; Constable
23 Benedict, M. and Williams, C. *Engineering Developments in the Gaseous Diffusion Process*, p. 13. 1949. New York; McGraw-Hill
24 Shepherd, M. and others. *Anal. Chem.* 23 (1951) 1431
25 Pratt, A. W. *Rev. sci. Instrum.* 22 (1951) 694

DEVIATION FROM THE KINETIC STEADY-STATE APPROXIMATION IN A FREE-RADICAL FLAME

E. S. CAMPBELL, J. O. HIRSCHFELDER and L. M. SCHALIT

INTRODUCTION

Any understanding of the simultaneous roles of diffusion, thermal conduction, and reaction kinetics in flames pre-supposes an understanding of the effect of deviations from the steady-state hypothesis of reaction kinetics. This paper reports the first part of a study which seeks to disclose how such deviations affect the flame.

Campbell[2] reported that the deviations were serious for the Br atom in the hydrogen–bromine system. His conclusion was based upon (*a*) an integration of the hydrodynamic equations which included diffusion and thermal conduction but which assumed the steady-state for [H] and [Br]; (*b*) a preliminary study of the hydrodynamic equations which did not assume the steady-state. Giddings' approximate method[7] also predicted the failure of the steady-state approximation. In contradiction to this conclusion, Gilbert and Altman[9] reported that the deviations were insignificant. They derived their conclusion from an approximate solution of the flame equations based on an illuminating treatment of ways in which deviations from the steady-state might arise.

This controversy over the effect of the steady-state approximation can be resolved by integrating the complete hydrodynamic equations without *a priori* assumptions. For this purpose a general method for solving a set of differential equations subject to the asymptotic boundary conditions employed in flame studies has been developed[4]. However, since the solution for hydrogen–bromine depends upon two eigenvalues, the use of the proposed method for numerical integration will be feasible only if we first develop an understanding of how the solutions to the flame equations depend upon these eigenvalues.

In order to elucidate the effect of the two eigenvalues, it is desirable to study first an idealized flame which will contain a simulated free-radical and include the effect of both diffusion and thermal conduction. Such studies of idealized systems are gradually laying a basis for an understanding of the physical processes in flames[7,8,10,11,14,16]. A simplified model can be used to determine the effects of diffusion and kinetic parameters upon deviations from the steady-state and, therefore, to obtain a physical interpretation of these deviations. In addition, the effect of the failure of the steady-state upon the flame-speed, the mole-fractions, and the mass-rates of flow can be determined and the role of the two eigenvalues can be investigated.

Recent theoretical studies[7,8] suggest the proper beginning for an investigation of the steady-state. These calculations have led to new criticism of the diffusion theories of flame propagation. In the case of one model for a branched chain free-radical flame[7], an increase in the binary diffusion coefficient involving the free-radical by a factor of two had little effect upon the deviation from the steady-state in the temperature range for rapid reaction and decreased the flame velocity from 55·1 to 54·8 cm/sec. Conversely, diffusion theories would have predicted an increase by $(2)^{\frac{1}{2}}$. This result suggests that if the ratio of the specific-rate for the free-radical to that for the main combustion reaction is sufficiently high, then the flame will maintain the steady-state and will be relatively insensitive to variation of the diffusion coefficients over the range of possible values. A later study[8] showed that in other cases where there was a deviation (in the region of rapid reaction) from the steady-state of the order of 20 per cent, an increase in the free-radical diffusion coefficient by a factor of two decreased the flame velocity by about 2 per cent. It is, therefore, desirable to determine first how low this ratio must be to yield significant deviations from the kinetic steady-state in the region of rapid flame reaction and, second, the effect of the diffusion coefficient. Hence the first stage in our study consists in determining how the $X_\beta(T)$, $G_\beta(T)$ and the flame velocity depend upon ω, the ratio of the frequency factor for the main combustion reaction to that of the free-radical reaction, where $G_\beta(T)$ is the fractional mass rate of flow of species β at temperature $T(G_\beta = n_\beta m_\beta v_\beta / \Sigma_\gamma n_\gamma m_\gamma v_\gamma)$ (*cf.* equations 3, 8 and 27).

THE ABC FLAME MODEL

Kinetic model

Consider a flame produced by the burning of a pure fuel, A, to give a product, C, with the

liberation of Q cal/gmol A. Suppose that the conversion of A to C can only occur in the presence of an active intermediate B and that B is really an activated state of A produced by the expenditure of E cal/gmol A. Then the kinetics of the four flame reactions are:

Reaction

$$(1) \qquad X + A \rightleftarrows X + B \tag{1}$$

$$(2) \qquad A + B \rightleftarrows B + C$$

where X is any constituent of the gas mixture. Let $R_i^f(R_i^r)$: rate of the i-th forward (reverse) reaction

$$R_i = R_i^f - R_i^r \tag{2a}$$

f_i^f, f_r^i : specific rate constants for concentrations expressed as mole fractions.

Then

$$R_1^f = f_1^f x_A; \quad R_1^r = f_1^r x_B; \quad R_2^f = f_2^f x_A x_B; \quad R_2^r = f_2^r x_C x_B \tag{2b}$$

The specific rates are frequently approximated by the functional forms[6]

$$f_i^f(T) = a_i^f T^{b_i^f} \exp[-\varepsilon_i^f/T]; \quad f_i^r(T) = a_i^r T^{b_i^r} \exp[-\varepsilon_i^r/T] \tag{3}$$

where T = temperature °K.

Approximations for physical properties of the model

The following assumptions were introduced to simplify the calculations:

(*a*) The kinetic schema itself introduces the approximation of equal masses:

$$m = m_A = m_B = m_C \tag{4}$$

(*b*) Since B is to simulate a free-radical and since the energy of re-combination of free-radicals is frequently small compared with other activation energies, the re-conversion of B to A proceeds without energy of activation

$$\varepsilon_1^r = 0 \tag{5}$$

(*c*) Several approximations are introduced not because they are physically reasonable but because they simplify the calculations. Thus:

(1) The heat, Q, released by the reaction is set equal to the energy of activation, E.

$$Q/R = E/R = \varepsilon_1^f \tag{6}$$

(2) In the presence of the active intermediate, B, the reaction $A \rightarrow C$ proceeds without additional activation and we suppose

$$\varepsilon_2^f = 0; \quad \varepsilon_2^r = Q/R = \varepsilon_1^f \tag{7}$$

$$a_1^f = a_1^r = a_1; \quad a_2^f = a_2^r = a_2 \tag{8}$$

(3) The characteristics of collisions which give rise to each of the reactions[6] are the same so that

$$b_1^f = b_1^r = b_2^f = b_2^r = b \tag{9}$$

(4) The heat capacities are the same and are constant and the binary diffusion coefficients are all equal

$$C_A = C_B = C_C = C; \quad D_{AB} = D_{AC} = D_{BC} = D \tag{10}$$

Flame equations

Subject to these simplifications, the flame equations derived by Hirschfelder and Curtiss[12] can be written as

$$\frac{dG}{dZ} \equiv \frac{d(G_A + 2G_B)}{dZ} = \frac{m}{M}(R_1 - R_2) \tag{11}$$

$$\frac{dG_B}{dZ} = \frac{m}{M} R_1 \tag{12}$$

$$\frac{dx}{dZ} \equiv \frac{d(x_A + 2x_B)}{dZ} = \frac{M}{mnD}(x - G) \tag{13}$$

$$\frac{dx_B}{dZ} = \frac{M}{mnD}(x_B - G_B) \tag{14}$$

$$\frac{dT}{dZ} = \frac{M}{\lambda} \sum_\alpha \left[\frac{H_\alpha G_\alpha}{m_\alpha} - \lim_{Z \to \infty} \frac{H_\alpha G_\alpha}{m_\alpha} \right] = \frac{M}{\lambda}\{C[T - T_m] + 2Q[G - G_m]\} \tag{15}$$

where x and G are linear combinations of the flame variables introduced to simplify the equations, n is number of particles per c.c., Z is distance coordinate, M is total mass rate of flow $\sum_\alpha n_\alpha m_\alpha v_\alpha$, H_α is the enthalpy of species α, m_α is mass of species α, λ is coefficient of thermal conductivity, G_m is limit of $G(Z)$ as $Z \rightarrow \infty$ and T_m is temperature of the hot boundary.

For purpose of calculation the equations in Z were transformed to equations in a reduced temperature, t, as an independent variable,

$$t = (T - T_m)/T_m \tag{16}$$

Then the functions from the numerators and denominators of the equations in t were regrouped and written in terms of dimensionless variables:

$$du(t)/dt = F(u)/F(t) \tag{17}$$

$$F(G) = \mu(\mathscr{R}_1 - \mathscr{R}_2), \; F(G_B) = \mu\mathscr{R}_1 \tag{18}$$

$$F(x) = \delta^{-1}(x - G), \; F(x_B) = \delta^{-1}(x_B - G_B) \tag{19}$$

$$F(t) = t + h(G - G_m) \tag{20}$$

$$\mu = [m^2 \lambda a_1 T^b]/[M^2 C] \tag{21}$$

$$\delta = \lambda/[nDC] \tag{22}$$

$$h = Q/[CT_m] \tag{23}$$

$$\mathscr{R}_1 = f(t)x_A - x_B,\ \mathscr{R}_2 = \omega x_B[x_A - f(t)x_C] \tag{24}$$

$$x_A = x - 2x_B,\ x_C = 1 - x_A - x_B \tag{25}$$

$$f(t) = \exp(-a)\exp(+g),\ g = at/(1+t),$$
$$a = \varepsilon_1^f/T_m{}^* \tag{26}$$

$$\omega = a_2/a_1 \tag{27}$$

where u = a flame variable.

Boundary values and values for parameters

The general assumptions about the hot and cold boundaries have been discussed previously[5a]. They require that all variables approach equilibrium as $t \to 0$, that the G_α be continuous at the cold boundary temperature t_c, and that the $x_\alpha(t_c)$ are not precisely determined, where x_α is mole fraction of the molecular species α:

$$\lim_{t\to 0} F(u) = 0;\quad G(t_c) = 1,\ G_B(t_c) = 0 \tag{28}$$

The parameter ω [defined as the ratio of the frequency factor for the main combustion reaction 2 to that for the free-radical reaction 1], is the parameter whose effect upon deviations from the steady-state is being studied.

To obtain an idea of the possible temperature dependence of the function μ, recall that for hard spheres $\lambda \sim T^{\frac{1}{2}}$, and that subject to certain assumptions about the approach of two molecules for a collision, $b = -1{\cdot}5$[6]. For this crude model, $\mu \sim T^{-1}$. Actually, μ is treated as a constant function. However, it is a function of the eigenvalue, M, which represents a parameter to be determined by fitting the cold boundary condition, $G = 1$ [*cf.* equation 28].

For the sake of simplicity, the function δ has been assumed to be constant. This approximation is suggested, but by no means justified, by the fact that this would be true if the molecules behaved like hard spheres ($\lambda \sim T^{\frac{1}{2}}$, $D \sim T^{\frac{3}{2}}$, $n \sim T^{-1}$).

The parameter values have been selected as

$\delta = 1$,† $a = 4{\cdot}5882\ 98828$,‡
$h = 0{\cdot}91765\ 97656$,§ $t_c = -0{\cdot}908$‖

* It is convenient to factor out $\exp[-a]$ as a constant function since a is large compared with unity whereas $(at/[1+t])$ is less than one in the region of most rapid flame reactions.

† This value was chosen since when $\delta = 1$ the flame equations assume a simpler form as discussed in the next section.

‡ This is based on a related value used in previous studies of this system. There is no particular reason for choosing exactly this number. However, it is in a reasonable range, since if $T_m = 3{,}000°\text{K}$, $\varepsilon_1{}^f = \Delta E/R \simeq 1{\cdot}4 \times 10^4\ \text{deg}^{-1}$.

§ This is the value of $h = a/[C/R]$ if $C = 5R$.

‖ For a discussion of the cold boundary temperature see reference 5*a*.

SOLUTION OF THE FLAME EQUATIONS

Simplification when $\delta = 1$

The equation for the second derivative of $x(t)$ is

$$\frac{d^2x(t)}{dt^2} = \frac{d}{dt}\left[\frac{\delta^{-1}(x-G)}{t + h(G - G_m)}\right]$$
$$= \frac{-\left(1 + \frac{h\,dG}{dt}\right)\frac{dx}{dt} + \delta^{-1}\left(\frac{dx}{dt} - \frac{dG}{dt}\right)}{t + h(G - G_m)} \tag{29}$$

Therefore, for $\delta = 1$ the second derivative vanishes identically if $dx/dt = -h^{-1}$. Since this value for dx/dt satisfies the hot boundary conditions, x is the linear function

$$x(t) = x(t_0) - h^{-1}t \tag{30}$$

This leaves three differential equations in G, G_B, x_B to be solved.

Method used

A method has been developed for solving a set of differential equations subject to asymptotic boundary conditions when the solutions depend upon more than one eigenvalue[4]. This method will be applied to the two eigenvalue *ABC* problem. However, whenever the parameter values are such that the steady-state is approximately obeyed, previous studies[2] have supported the view that to the accuracy we require a solution for physical purposes, a flame such as *ABC* will depend essentially on only one eigenvalue. Therefore, for that part of this study which concerns moderate deviations from the steady-state, previously developed techniques[5b] were used to construct a twentieth-order power series about t_0. The series in t were summed to give starting values for point by point numerical integration.

Whenever x_B approximately follows the steady-state, numerical indeterminacy prevents standard integration techniques from following the solutions[1,3]. Therefore, the equations were solved by a method which integrates a sequence of successive approximating equations. For this step the two equations for x_B and G_B were replaced by a single second-order equation for R_1. [*Cf.* equation 32.] Let k denote the level of approximation. At the k-th level we integrate for all t, $t_c \leqslant t < t_0$, the k-th approximating equation for $dG^{(k)}/dt$, using $(k-1)$-st approximations for x_B:

$$x_B^{(k-1)} = x_B^{(0)} - [\mathscr{R}_1^{(k-1)}/(1+2f)] \tag{31}$$
$$x_B^{(0)} = xf/(1+2f)$$

[the function which describes the steady-state].

Here $\mathscr{R}_1^{(0)}$ is taken to be zero and $\mathscr{R}_1^{(k)}$ is computed from successive approximations to its second-order differential equation:

$$\mathscr{R}_1^{(k)} = -\mu^{-1}[F_t^{(k)}]^2\left[\frac{d^2x_B^{(0)}}{dt^2} - \frac{d^2}{dt^2}\left(\frac{\mathscr{R}_1^{(k-1)}}{1+2f}\right)\right] - h[\mathscr{R}_2^{(k)} - \mathscr{R}_1^{(k-1)}]\left[\frac{dx_B^{(0)}}{dt} - \frac{d}{dt}\left(\frac{\mathscr{R}_1^{(k-1)}}{1+2f}\right)\right] \quad (32)$$

The first derivatives, the $d[\mathscr{R}_1^{(k-1)}/(1+2f)]/dt$, are computed by numerical differentiation of the $[\mathscr{R}_1^{(k-1)}/(1+2f)]$ and the second derivatives by numerical differentiation of the first. Two different schema, denoted by I and II, were used to obtain the zero-th approximations for the derivatives. In schema I, the derivatives were equated to zero. This is consistent with the equation $\mathscr{R}_1^{(0)} \equiv 0$. Schema II can be described as follows. If the successive approximation schema I is to converge, then in general, apart from isolated points for which dx_B^0/dt, $d^2x_B^0/dt^2$ vanish,

$$|dx_B^0/dt| > d[\mathscr{R}_1/(1+2f)]/dt|,$$
$$|d^2x_B^0/dt^2| > d^2[\mathscr{R}_1/(1+2f)]/dt^2| \quad (33)$$

As ω increases and μ decreases, $\mathscr{R}_1$ and therefore its derivatives increase. Then it is necessary to obtain better zero-th approximations for the derivatives in computing $\mathscr{R}_1$. The method used is described in Appendix A.

To initiate the integration for any k level it was convenient to use the six-point Runge–Kutta formulae which do not require any information from backward points[15a]. The solution was then continued by either the Runge–Kutta or the six-point backward difference formulae[15b].

RESULTS

Qualitative

The assumption $\delta = 1$ so simplifies the flame equations for *ABC* that we can obtain explicit equations which show relations which hold exactly in this special case and approximately in more complex flames. For example, although the method used to compute first derivatives[5c] for *ABC* in general requires the solution of a quintic equation, for $\delta = 1$, it requires only the solution of a quartic which possesses a simple algebraic solution. The equations of Appendix B show that in this case the first derivatives of the mole-fractions at the hot boundary, t_0, depend explicitly on ω but not on the flame velocity. The magnitude of the quantities involved in the equations shows that they vary less than 10 per cent as ω changes from 1 to 1,000. At $\omega = 1{,}000$ the steady-state is no longer followed even approximately.

Consider now the effect of ω when the deviations from the steady-state are not too great. In the case of the *ABC* flame, this would mean that $|(x_B - x_B^{(0)})/x_B|$ is less than $\simeq 5$ per cent through the region of rapid chemical reaction. First let us see how the $G_\alpha(T)$ and $x_\alpha(T)$ depend upon M. Results on both H_2–Br_2 and *ABC* have shown that in this case the $x_\alpha(T)$ are comparatively

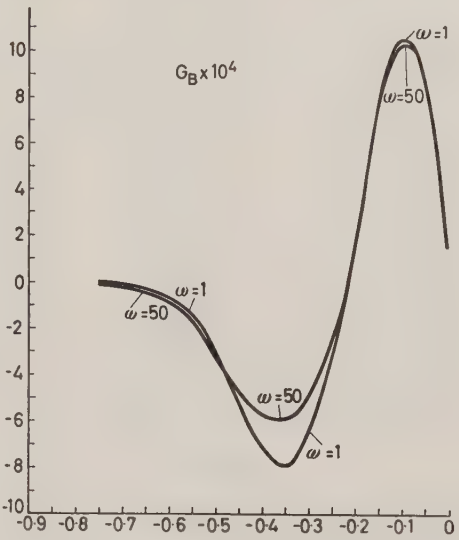

Figure 1

less sensitive to M and that for a non-free-radical, α,

$$\{M[G_\alpha(t_c) - G_\alpha(t_0)]\}_{M=M_1} \simeq \{M[G_\alpha(t_c) - G_\alpha(t_0)]\}_{M=M_2} \quad (34)$$

This comparison is consistent with the observations that: (*a*) dx_α/dT has no explicit dependence on M, each term of $F(x_\alpha)$ involves a G_β as a factor, and the dominant terms in $F(t)$ contain $[G_\alpha(t) - G_\alpha(t_0)]$ as factors; (*b*) dG_α/dT depends explicitly on M^{-2}, $F(G_\alpha)$ is independent of the G_β, and the dominant terms in $F(t)$ contain $[G_\alpha(t) - G_\alpha(t_0)]$ as factors.

We can use the relation between M and $[G(t_c) - G(t_0)]$ to interpret how $\mathscr{R}_1$ is related to ω. For the steady-state [in which $\mathscr{R}_1 = 0$], the relation $\mu =$ constant is replaced by the relation $\mu\omega =$ constant. Since the eigenvalue μ is determined by fitting $G(t_c)$, it is clear that deviations from the steady-state will appreciably affect μ only when $|x_B - x_B^{(0)}|$ is sufficiently large in the region of rapid reaction [i.e. the region of large values for $|dG/dT|$] to alter significantly dG/dT and therefore $G(t_c) - G(t_0)$. Consider equation 32 for $\mathscr{R}_1$. Since: (*a*) the dominant term in $F(t)$ is $G - G(t_0)$, and, therefore, $F_{(t)}^2 \sim M^{-2} \sim \mu\omega$;

(*b*) in the region where the steady-state is approximately followed,

$$|d^2x_B^{(0)}/dt^2| > |d^2[\mathscr{R}_1/(1 + 2f)]/dt^2|;$$

(*c*) $x_B^{(0)}$ does not depend on μ, it follows that the first term is approximately $\sim \omega$. Furthermore, since: (*a*) $|\mathscr{R}_2| > |\mathscr{R}_1|$; (*b*) $\mathscr{R}_2 \sim \omega$; (*c*) $|dx_B^{(0)}/dt| > d[\mathscr{R}_1/(1 + 2f)]/dt|$, it follows similarly that

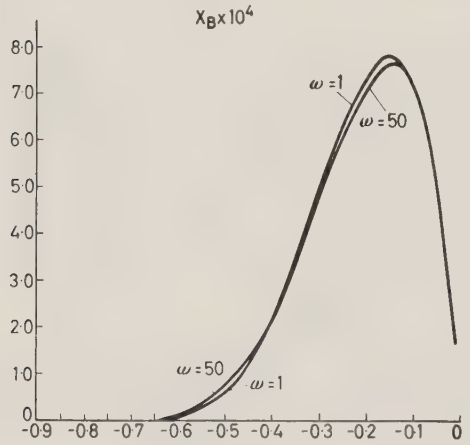

Figure 2

the second term is approximately $\sim \omega$. Therefore $\mathscr{R}_1$ is approximately $\sim \omega$. This approximate proportionality should hold for $\omega < 100$, since for $\omega = 1$, $|(x_B - x_B^{(0)})/x_B| < \simeq 10^{-3}$ in the region of rapid flame reaction. It is interesting that when Klein[13d] expressed a solution for the *ABC* flame as a polynomial in powers of ω, he first introduced as a hypothesis the assumption, $\mathscr{R}_1 \sim \omega$; then he showed that the approximate equations which included only terms in the first power of ω were those for the steady-state approximation. The preceding discussion supports the relation in the reverse direction, that when the steady-state holds, then $\mathscr{R}_1 \sim \omega$.

Quantitative

Klein[13d] obtained a neat solution to the *ABC* problem for the case of moderate deviations from the steady-state by assuming that all functions could be expressed as a power series in ω and that the constant term in the expansion of $\mathscr{R}_1$ vanished. He included terms up to ω^3. The coefficients in his expansion are functions of temperature which were determined by numerical integration and whose values he tabulated. Since in his expansion,

$$x_B - x_B^{(0)} = a_1\omega + a_2\omega^2 + a_3\omega^3 \qquad (35)$$

the ratios of the successive coefficients are of the order of 100 in the region of rapid reaction, one would hope that his solution would be valid up to about $\omega = 50$.

The object of the present study is to develop methods which can be generalized for more complex flame systems. Additional techniques are needed since Klein's requires as input initial approximations for the mol-fractions. These are difficult to guess for non-steady-state free-radical flames.

We now comment briefly on the results for smaller ω. The steady-state free-radical mole-fraction, which is independent of ω, is given in Table 1. The relative deviations of the actual mole-fraction from its steady-state value are listed for $\omega = 1$, 20, and 50 in Table 2. Finally, there are graphs of the actual free-radical mole-fraction and fractional mass rate of flow.

TABLE 1

Steady-State Free-Radical Mole-Fraction

t	$x_B^{(0)}$	t	$x_B^{(0)}$
− 100 (− 2)	+ 202 (− 4)	− 395 (− 1)	+ 224 (− 4)
− 200 (− 2)	+ 292 (− 4)	− 459 (− 1)	+ 106 (− 4)
− 310 (− 2)	+ 380 (− 4)	− 507 (− 1)	+ 511 (− 5)
− 350 (− 2)	+ 410 (− 4)	− 555 (− 1)	+ 205 (− 5)
− 410 (− 2)	+ 452 (− 4)	− 603 (− 1)	+ 638 (− 6)
− 510 (− 2)	+ 515 (− 4)	− 651 (− 1)	+ 140 (− 6)
− 107 (− 1)	+ 736 (− 4)	− 699 (− 1)	+ 185 (− 7)
− 147 (− 1)	+ 779 (− 4)	− 747 (− 1)	+ 110 (− 8)
− 203 (− 1)	+ 727 (− 4)	− 795 (− 1)	+ 167 (− 10)
− 251 (− 1)	+ 618 (− 4)	− 859 (− 1)	+ 698 (− 15)
− 299 (− 1)	+ 482 (− 4)	− 891 (− 1)	+ 513 (− 19)
− 347 (− 1)	+ 344 (− 4)		

The reduced temperature t is defined as $t = (T - T_m)/T_m$. The numbers in parentheses are the powers of ten. Thus + 167 (− 10) is + 1·67 × 10^{-10}.

Apparently Klein's method[13d] does not converge in the neighbourhood of the cold boundary. The present results indicate large deviations produced by back diffusion of the free-radical in the lower temperature region followed by a decrease in the vicinity of the cold boundary, whereas it has been assumed that the relative deviations approached infinity[7]. The present result agrees with the prediction of equation 32. Thus,

$$(x_B - x_B^{(0)})/x_B^{(0)} = -[\mathscr{R}_1/(1 + 2f)]/x_B^{(0)} \qquad (36)$$

Since $\mathscr{R}_2 \gg \mathscr{R}_1$, $\mathscr{R}_2 \sim x_B^{(0)}$ and dx_B/dt decreases rapidly for t near t_c, it follows that the second term of equation 32, after division by $x_B^{(0)}$, becomes small in the vicinity of the hot boundary. Furthermore $F_t \to 0$ as $t \to t_c$ and $|d^2x_B/dt| \geqslant |d^2x_B/d^2t|t_c$. Therefore, after division by $x_B^{(0)}$, which is non-zero, the first term $\to 0$ as $t \to t_c$. This implies that $(x_B - x_B^{(0)})/x_B^{(0)}$ must again become small in the neighbourhood of the cold boundary.

TABLE 2

Relative Deviation from the Steady State

t	$\omega = 1$	$\omega = 20$	$\omega = 50$	$\omega = 100$
− 5·00 (− 3)	5·001 (− 5)	1·005 (− 3)	2·535 (− 3)	5·142 (− 3)
− 1·00 (− 2)	9·358 (− 5)	1·887 (− 3)	4·776 (− 3)	9·762 (− 3)
− 2·00 (− 2)	1·615 (− 4)	3·265 (− 3)	8·306 (− 3)	1·709 (− 2)
− 4·10 (− 2)	2·252 (− 4)	4·525 (− 3)	1·136 (− 2)	2·231 (− 2)
− 5·10 (− 2)	2·215 (− 4)	4·400 (− 3)	1·083 (− 2)	1·977 (− 2)
− 7·90 (− 2)	1·141 (− 4)	2·014 (− 3)	3·983 (− 3)	3·259 (− 3)
− 1·03 (− 1)	− 6·454 (− 5)	− 1·723 (− 3)	− 6·063 (− 3)	− 1·294 (− 3)
− 1·51 (− 1)	− 5·373 (− 4)	− 1·082 (− 2)	− 2·673 (− 2)	− 4·350 (− 2)
− 2.07 (− 1)	− 1·024 (− 3)	− 1·902 (− 2)	− 4·220 (− 2)	− 7·870 (− 2)
− 2·55 (− 1)	− 1·154 (− 3)	− 2·064 (− 2)	− 4·420 (− 2)	− 8·275 (− 2)
− 3·03 (− 1)	− 8·575 (− 4)	− 1·537 (− 2)	− 3·373 (− 2)	− 5·638 (− 2)
− 3·51 (− 1)	− 4·212 (− 5)	− 1·904 (− 3)	− 8·355 (− 3)	− 2·866 (− 2)
− 4·15 (− 1)	1·889 (− 3)	3·110 (− 2)	5·797 (− 2)	5·670 (− 2)
− 4·47 (− 1)	3·192 (− 3)	5·504 (− 2)	1·114 (− 1)	1·507 (− 1)
− 4·63 (− 1)	3·747 (− 3)	6·913 (− 2)	1·448 (− 1)	2·187 (− 1)
− 5·11 (− 1)	6·371 (− 3)	1·200 (− 1)	2·776 (− 1)	5·360 (− 1)
− 6·07 (− 1)	1·243 (− 2)	2·758 (− 1)	7·324 (− 1)	1·562 (0)
− 7·03 (− 1)	2·092 (− 2)	5·651 (− 1)	2·149 (0)	6·202 (0)
− 7·67 (− 1)	3·018 (− 2)	9·751 (− 1)	5·685 (0)	4·371 (+ 1)
− 8·37 (− 1)	—	1·294 (0)	1·016 (+ 1)	1·259 (+ 2)
− 8·63 (− 1)	—	9·555 (− 1)	5·674 (0)	5·856 (+ 1)
− 8·93 (− 1)	—	1·840 (− 1)	3·856 (− 1)	5·965 (0)

The columns give the relative deviation $(x_B - x_B^{(0)})/x_B^{(0)} = -[\mathscr{R}_1/(1 + 2f)]/x_B^{(0)}$.

APPENDIX A

Equations of schema II for $\mathrm{d}[\mathscr{R}_1^{(0)}/(1 + 2f)]/\mathrm{d}t$ *and* $\mathrm{d}^2[\mathscr{R}_1^{(0)}/(1 + 2f)]/\mathrm{d}t^2$

If the superscript (k) and $(k - 1)$ are omitted, then equation 32 is the second-order differential equation for $\mathscr{R}_1$. A single differentiation of this equation gives an equation for $\mathrm{d}\mathscr{R}_1/\mathrm{d}t$ as a function of $\mathscr{R}_1$, $\mathrm{d}^2\mathscr{R}_1/\mathrm{d}t^2$ and $\mathrm{d}^3\mathscr{R}_1/\mathrm{d}t^3$. A second differentiation gives an equation for $\mathrm{d}^2\mathscr{R}_1/\mathrm{d}t^2$ as a function of $\mathscr{R}_1$, $\mathrm{d}\mathscr{R}_1/\mathrm{d}t$, $\mathrm{d}^3\mathscr{R}_1/\mathrm{d}t^3$, and $\mathrm{d}^4\mathscr{R}_1/\mathrm{d}t^4$. Equations for the third and fourth derivatives were derived in a similar way. When the fifth and sixth derivatives of $[\mathscr{R}_1/(1 + 2\delta)]$ are neglected in comparison with $\mathrm{d}^5x_B^{(0)}/\mathrm{d}t^5$ and $\mathrm{d}^6x_B^{(0)}/\mathrm{d}t^6$ respectively, then we have five equations which are non-linear in the unknown $\mathscr{R}_1^{(1)}$, $\mathrm{d}\mathscr{R}_1^{(0)}/\mathrm{d}t$, $\mathrm{d}^2\mathscr{R}_1^{(0)}/\mathrm{d}t^2$, $\mathrm{d}^3\mathscr{R}_1^{(0)}/\mathrm{d}t^3$ and $\mathrm{d}^4\mathscr{R}_1^{(0)}/\mathrm{d}t^4$ and depend upon the previously computed $G^{(1)}$ and known functions of t. These equations can be solved by a suitable numerical approximation schema.

APPENDIX B

Equations for the ABC flame at the hot-boundary, t_0

It has been shown that the first derivatives for the flame variables can be determined in two steps[5c]:

(*a*) Solve for the roots of the characteristic equation

$$\left| \frac{\partial F(u_j)}{\partial u_k} - \alpha\delta_k^j \right| = 0, \; 1 \leqslant j \leqslant M, \; 1 \leqslant k \leqslant M \quad (37)$$

$$u_M = t$$

(*b*) Select the negative root of smallest absolute value and solve any $(M - 1)$ of the dependent linear equations:

$$\left(\frac{\partial F(u_j)}{\partial u_k} - \alpha\delta_k^j \right) \frac{\mathrm{d}u_k}{\mathrm{d}t} + \frac{\partial F(u_j)}{\partial t} - \alpha\delta_M^j = 0, \qquad 1 \leqslant j \leqslant M \quad (38)$$

In the case of the general *ABC* problem, the characteristic equation 37 is a quintic. For $\delta = 1$, this reduces to the quartic equation:

$$-\frac{1}{h}\left[\frac{\alpha(1-\alpha)}{\mu}\right]^2 + \left[\frac{1}{h}\frac{\partial \mathscr{R}_1}{\partial x_B} - \frac{\partial \mathscr{R}_1}{\partial t} + \frac{\partial \mathscr{R}_2}{\partial t}\right]\left[\frac{\alpha(1-\alpha)}{\mu}\right] - \left[\frac{\partial \mathscr{R}_1}{\partial x_B}\frac{\partial \mathscr{R}_2}{\partial t} - \frac{\partial \mathscr{R}_1}{\partial t}\frac{\partial \mathscr{R}_2}{\partial x_B}\right] = 0 \quad (39)$$

Equation 39 has the solutions:

$$[\alpha(1-\alpha)]/\mu = A \pm B$$

$$A = (h/2)A_0 + A_1\omega$$

$$B = -\frac{h}{2}\{(A_0)^2 + b_1\omega + b_2\omega^2\}^{\frac{1}{2}} \tag{40}$$

$$\alpha = -\frac{1 \pm \{1 - 4\mu(A + B)\}^{\frac{1}{2}}}{-2}$$

$$A_0 = \frac{1}{h}\frac{\partial \mathscr{R}_1}{\partial x_B} - \frac{\partial \mathscr{R}_1}{\partial t}, \quad A_1 = \frac{h}{2}\frac{\partial[\mathscr{R}_2/\omega]}{\partial t}$$

$$b_1 = \frac{1}{h}\left\{-2\frac{\partial \mathscr{R}_1}{\partial x_B}\frac{\partial[\mathscr{R}_2/\omega]}{\partial t} + \frac{\partial \mathscr{R}_1}{\partial t}\left[+4\frac{\partial[\mathscr{R}_2/\omega]}{\partial x_B} - 2h\frac{\partial[\mathscr{R}_2/\omega]}{\partial t}\right]\right\}$$

$$b_2 = \left[\frac{\partial[\mathscr{R}_2/\omega]}{\partial t}\right]^2$$

Here A_0, A_1, b_1, b_2 are independent of μ and ω. Then it can be shown that $(\mathrm{d}x_B/\mathrm{d}t)_{t_0}$ is independent of μ.

$$\left(\frac{\mathrm{d}x_B}{\mathrm{d}t}\right)_{t_0} = \frac{\partial \mathscr{R}_1/\partial t}{A \pm B - \partial \mathscr{R}_1/\partial x_B} \tag{41}$$

and that

$$(\mathrm{d}G/\mathrm{d}t)_{t_0} = (\alpha - 1)/h \tag{42}$$

$$(\mathrm{d}G_B/\mathrm{d}t)_{t_0} = (1 - \alpha)(\mathrm{d}x_B/\mathrm{d}t)_{t_0} \tag{43}$$

This research has been supported in part by the Naval Bureau of Ordnance under Contract NOrd 15884 with the University of Wisconsin Naval Research Laboratory and in part by the Air Force Office of Scientific Research under Contract AF 49(638)–169 with New York University. Reproduction in whole or in part is permitted for any purpose of the United States Government.

REFERENCES

1 Campbell, E. S. *CM 847, University of Wisconsin Naval Research Laboratory*, July 1955

2 — *Sixth International Symposium on Combustion*, pp. 213, 219. 1957. New York; Reinhold

3 — *Math. Tab., Wash.* 11 (1957) 229

4 — Unpublished work

5 — Hughes, D. R. and Buehler, R. J. *CF–2109, University of Wisconsin Naval Research Laboratory;* (*a*) pp. 4*ff*; (*b*) pp. 12*ff*; (*c*) pp. 12–17

6 — and Fristrom, R. M. *Chem. Rev.* April 1958

7 Giddings, J. C. *Sixth International Symposium on Combustion*, p. 199. 1957. New York; Reinhold

8 — and Hirschfelder, J. O. *J. phys. Chem.* 61 (1957) 738 (*cf.* p. 743)

9 Gilbert, M. and Altman, D. *Sixth International Symposium on Combustion*, p. 222. 1957. New York; Reinhold

10 Hirschfelder, J. O., Curtiss, C. F. and Campbell, D. E. *Fourth International Symposium on Combustion*. 1953. Baltimore; Williams and Wilkins

11 — and Campbell, E. S. *CM 784, University of Wisconsin Naval Research Laboratory*, May 1953

12 — Curtiss, C. F. and Bird, R. B. *The Molecular Theory of Gases and Liquids*, Chap. 11. 1954. New York; Wiley

13 Klein, G. (*a*) *ONR–8*, June 1954; (*b*) *ONR–13*, September 1954; (*c*) *Squid* (*1*), February 1955; (*d*) *Squid* (*2*), February 1955; (*e*) *Squid* (*4*), August 1955, *University of Wisconsin Naval Research Laboratory*

14 — *Phil. Trans.* 249 (1957) 389

15 Milne, W. E. *Numerical Solution of Differential Equations*, (*a*) p. 73; (*b*) equation 20.5, p. 50. 1953. New York; Wiley

16 Schatzki, T. F. *CM–853, University of Wisconsin Naval Research Laboratory*, September 1955

50

AN ACTION PRINCIPLE FOR THE LAMINAR FLAME

G. ROSEN

FORMULATION OF THE ACTION PRINCIPLE

An adiabatic, inviscid, constant-pressure deflagration, in one-dimensional steady propagation, can be represented by the coupled equations

$$\frac{d^2\tau}{dy^2} - \frac{d\tau}{dy} = -\lambda\Phi(\tau, \mu) \tag{1}$$

$$N_L \frac{d^2\mu}{dy^2} - \frac{d\mu}{dy} = -\lambda\Phi(\tau, \mu) \tag{2}$$

where μ is the weight fraction of the product specie, N_L is the non-dimensional ratio of mass diffusivity to thermal diffusivity, assumed constant, and all other notation is the same as employed by Spalding[1]. The boundary conditions for equations 1 and 2 are

$$\left.\begin{aligned} &\tau = \mu = 0 \quad \text{at} \quad y = -\infty \\ \text{and} \quad &\\ &\tau = \mu = 1 \quad \text{at} \quad y = +\infty \end{aligned}\right\} \tag{3}$$

Under the change of independent variable,

$$y = \ln \xi \tag{4}$$

this system becomes,

$$\ddot{\tau} = -\frac{\lambda\Phi(\tau, \mu)}{\xi^2} \tag{5}$$

$$\xi\left(\frac{\dot{\tau}}{\xi}\right)^{\cdot} = N_L \xi^{1/N_L} \left(\frac{\dot{\mu}}{\xi^{(1/N_L)}}\right)^{\cdot} \tag{6}$$

$$\left.\begin{aligned} &\tau = \mu = 0 \quad \text{at} \quad \xi = 0 \\ &\tau = \mu = 1 \quad \text{at} \quad \xi = \infty \end{aligned}\right\} \tag{7}$$

where a dot differentiation with respect to ξ, and 6 has been obtained from 1 and 2 by subtraction and an integration. Since the original system makes no mention of the y origin, the equations 5, 6 and 7 will have equivalent solutions if ξ is replaced everywhere by $c\xi$, with c a positive constant.

The relationship 6 can be used to express $\mu(\xi)$ in terms of the non-dimensional temperature distribution $\tau(\xi)$.

$$\mu(\xi) = \frac{1}{N_L}\tau(\xi) + \frac{1}{N_L}\left(1 - \frac{1}{N_L}\right)\xi^{1/N_L}\int_\xi^\infty \frac{\tau(\xi)\, d\xi}{\xi^{1+(1/N_L)}} \tag{8}$$

Physical considerations dictate that $\tau(\xi)$ should be monotonic—increasing through the active region of the flame, implying the existence of $\xi = \xi(\tau)$ for $0 < \tau < 1$—so that equation 8 gives

$$\mu = f(\tau) \tag{9}$$

after elimination of ξ. Setting

$$\Phi(\tau, f(\tau)) \equiv \Phi(\tau) \tag{10}$$

the problem we study then takes the form

$$\ddot{\tau} = -\frac{\lambda\Phi(\tau)}{\xi^2} \tag{11}$$

$$\left.\begin{aligned} &\tau = 0 \quad \text{at} \quad \xi = 0 \\ &\tau = 1 \quad \text{at} \quad \xi = \infty \end{aligned}\right\} \tag{12}$$

with λ the burning velocity eigenvalue grouping, fixed under the normalization

$$\int_0^1 \Phi(\tau)\, d\tau = 1 \tag{13}$$

It is possible to re-phrase this problem in the compact form of an action principle. Moreover, this can be accomplished without the introduction of any non-physical mathematical artifice which one might suppose to be necessitated by the irreversible composite processes of a deflagration. For the class of all continuously differentiable functions satisfying the boundary conditions, 12, we define the functional

$$\Lambda = \Lambda[\tau] \equiv \frac{\int_0^\infty \tfrac{1}{2}(\dot{\tau})^2\, d\xi}{\int_0^\infty V\, d\xi} \tag{14}$$

in which

$$V = \frac{1}{\xi^2}\int_0^\tau \Phi(\tau)\, d\tau \tag{15}$$

The lower limit in the integral of 15 has been chosen in a way which guarantees the existence of the denominator in 14. We now demand that

under a variation of $\tau(\xi)$ to a neighbouring member of the class of functions, the physical $\tau(\xi)$ must be such that

$$\delta\Lambda = 0 \tag{16}$$

Inasmuch as

$$\delta\Lambda = -\frac{\int_0^\infty \left\{\ddot{\tau} + \frac{\Lambda}{\xi^2}\Phi(\tau)\right\}\delta\tau\,\mathrm{d}\xi}{\int_0^\infty V\mathrm{d}\xi} \tag{17}$$

the condition 16 requires that $\tau(\xi)$ satisfy 11, and with the assumption of uniqueness for the eigenvalue, that the number

$$\Lambda = \lambda \tag{18}$$

A more detailed investigation of 14 reveals that the stationary value will be a minimum[2]. Hence we can formulate the following action principle for the laminar flame:

The non-dimensional temperature distribution $\tau(\xi)$ must be such that the action functional 14 assumes its smallest possible value; this number is the eigenvalue proportional to the inverse square of the burning velocity.

Variational principles are often useful starting points for approximate solutions of physical problems[3]. For instance, we could represent

$$\tau(\xi) = g(\xi;\ \alpha_1 \ldots \alpha_i) \tag{19}$$

where the $\{\alpha_i\}$ are shape parameters. By virtue of 8, 9 and 10, we can express

$$\mu(\xi) = h(\xi;\ \alpha_1 \ldots \alpha_i) \tag{20}$$

and

$$\Phi(\tau) = \Phi\{g(\xi;\ \alpha_1 \ldots \alpha_i)\} \tag{21}$$

Then, by 14,

$$\Lambda = \Lambda(\alpha_1 \ldots \alpha_i) \tag{22}$$

and the best approximation for $\tau(\xi)$, according to 16, gives the i conditions on the $\{\alpha_i\}$

$$\frac{\partial\Lambda}{\partial\alpha_i} = 0 \tag{23}$$

If these equations are solved for the $\{\alpha_i\}$, and the resulting quantities inserted into 22, we shall arrive at an estimate for λ. Since Λ is stationary for neighbouring $\tau(\xi)$, this value for λ will be only slightly above the true value, even if 19 is not a very flexible description of $\tau(\xi)$. These remarks will be illustrated in the following section.

THEORETICAL CONFIRMATION OF THE CENTROID RULE

Without aid of a variational principle, Spalding[1] has succeeded in writing down a relationship between the eigenvalue and the rate function $\Phi(\tau)$, verifiable for a large class of reactions

$$\lambda = \tfrac{1}{2} - 0{\cdot}6604(1 - \tau_c) - 0{\cdot}4283(1 - \tau_c)^2 \tag{24}$$

in which the 'centroid temperature'

$$\tau_c \equiv \int_0^1 \tau\Phi(\tau)\,\mathrm{d}\tau \tag{25}$$

We are able to get a somewhat more general form of Spalding's 'centroid rule' from the action principle formulated above. Let the temperature distribution be simulated by

$$\tau(\xi) = \begin{cases} \dfrac{\xi}{1+\alpha\xi}, & 0 \leqslant \xi \leqslant \dfrac{1}{1-\alpha} \\ 1\quad , & \xi \geqslant \dfrac{1}{1-\alpha} \end{cases} \tag{26}$$

where α (<1) is a shape parameter which remains at our disposal. From 14 and 15, a brief calculation establishes

$$\Lambda(\alpha) = \frac{(1 - \alpha + \frac{1}{3}\alpha^2)}{2(1 - \alpha + q)} \tag{27}$$

in which the number

$$q \equiv \int_1^\infty \left\{\int_0^{\frac{1}{\eta}} \Phi(\tau)\,\mathrm{d}\tau\right\}\mathrm{d}\eta \tag{28}$$

is computed entirely from the rate function, in the same manner as 25.

Expression 27 has its acceptable minimum value at

$$\alpha = 1 + q - (1 - q + q^2)^{\frac{1}{2}} \tag{29}$$

and by virtue of the action principle 16 and 18, 29 substituted into 27 yields

$$\lambda = \tfrac{1}{6} + \tfrac{1}{3}\{(1 - q + q^2)^{\frac{1}{2}} - q\} \tag{30}$$

This is a theoretically deduced version of the 'centroid rule' 24. We test 30 on a class of rate functions studied by Spalding, namely

$$\left.\begin{aligned} &\text{(i)}\ \Phi(\tau) = (n+1)(n+2)(1-\tau)\tau^n \\ &\text{and} \\ &\text{(ii)}\ \Phi(\tau) = \tfrac{1}{2}(n+1)(n+2)(n+3) \\ &\qquad\qquad \times (1-\tau)^2\tau^n \end{aligned}\right\} \tag{31}$$

for which 28 is simply

$$\left.\begin{aligned} &\text{(i)}\ q = \frac{2}{n} \\ &\text{(ii)}\ q = \frac{3}{n} \end{aligned}\right\} \tag{32}$$

or in terms of Spalding's parameter 25

$$\left.\begin{aligned} &\text{(i)}\ q = \frac{2(1-\tau_c)}{3\tau_c - 1} \\ &\text{(ii)}\ q = \frac{3(1-\tau_c)}{4\tau_c - 1} \end{aligned}\right\} \tag{33}$$

The Maclaurin expansion of 30 is

$$\lambda = \tfrac{1}{2} - \tfrac{1}{2}q + \tfrac{5}{24}q^2 + \mathrm{O}[q^3] \qquad (34)$$

so that if we write 33 as

$$\left.\begin{aligned} &\text{(i)}\ q = (1-\tau_c) + \tfrac{3}{2}(1-\tau_c)^2 \\ &\qquad\qquad + \mathrm{O}[(1-\tau_c)^3] \\ &\text{(ii)}\ q = (1-\tau_c) + \tfrac{4}{3}(1-\tau_c)^2 \\ &\qquad\qquad + \mathrm{O}[(1-\tau_c)^3] \end{aligned}\right\} \qquad (35)$$

then it follows,

$$\left.\begin{aligned} &\text{(i)}\ \lambda = \tfrac{1}{2} - \tfrac{1}{2}(1-\tau_c) - \tfrac{13}{24}(1-\tau_c)^2 \\ &\qquad\qquad + \mathrm{O}[(1-\tau_c)^3] \\ &\text{(ii)}\ \lambda = \tfrac{1}{2} - \tfrac{1}{2}(1-\tau_c) - \tfrac{11}{24}(1-\tau_c)^2 \\ &\qquad\qquad + \mathrm{O}[(1-\tau_c)^3] \end{aligned}\right\} \qquad (36)$$

These relations 36 agree with 24 within about 1 per cent in the range of greatest physical interest, for which

$$(1-\tau_c)^3 < 0{\cdot}005 \qquad (37)$$

Of course a better theoretical estimate is available to us in the form of 30 and 32.

I wish to express my appreciation to Professor Martin Summerfield for his stimulating suggestions concerning this problem and his survey of the manuscript.

REFERENCES

[1] Spalding, D. B. *Combustion and Flame* 1 (1957) 287

[2] Courant, R. and Hilbert, D. *Methods of Mathematical Physics*, p. 214. 1953. New York; Interscience

[3] Morse, P. M. and Feshbach, H. *Methods of Theoretical Physics*, p. 1106. 1953. New York; McGraw-Hill

51

EXCESS ENTHALPY AND THE INITIATION AND STABILITY OF COMBUSTION WAVES

G. VON ELBE and B. LEWIS

It is the purpose of this paper to review the question of excess enthalpy in combustion waves in the light of recent work on combustion theory and experiment. No final conclusions are presented; instead, the review is intended to point out experimental facts and theoretical considerations that should be given attention in future studies of the ignition problem.

The concept of excess enthalpy has been proposed by the authors as a means of interpreting measured values of minimum ignition energies of electric sparks. Such minimum ignition energies are represented, within limitations discussed below, by the equation

$$H = \pi d^2 \frac{\lambda}{S_u} (T_b - T_u) \qquad (1)$$

where H is the minimum ignition energy; d is the distance to which the electrodes must be separated in order to have no quenching effect on the incipient spark-initiated flame; and the factor

$$\frac{\lambda}{S_u} (T_b - T_u) \qquad (2)$$

approximately represents the sensible heat that is imparted by conduction to the gas within the hot and cold boundaries of a combustion wave, per unit area of the wave; λ is the heat conductivity; S_u is the burning velocity; and T_b and T_u are the temperatures of the burned and unburned gas, respectively. The term 2 is obtained from an approximate integration of the energy equation for the combustion wave, and under certain assumptions it represents an enthalpy excess of the gas within the wave, above its enthalpy outside the wave. The model of the ignition process thus envisages that the initial flame consists of a spherical combustion wave which has received its excess enthalpy from the energy of the source. As the diameter increases the additional excess enthalpy required by the increased wave surface is obtained by retention of some of the heat liberated within the wave, so that the temperature T_b behind the wave is lower than the adiabatic flame temperature. Since the loss of temperature decreases as the diameter increases (in view of the decreasing curvature), the wave continues to grow if, at the critical diameter d, its enthalpy requirement is satisfied by the source energy. If the source energy is insufficient the temperature loss extinguishes the flame.

The energy equation may be written for the purpose of illustration in the form given below, using a simple one-dimensional model of the combustion wave such as has been treated in a recent paper by Spalding[1]:

$$\left(\lambda \frac{\mathrm{d}T}{\mathrm{d}x} + HD_A \rho \frac{\mathrm{d}m_A}{\mathrm{d}x} \right) \rho_u S_u = c(T - T_u) - H(m_{A,\,u} - m_A) \qquad (3)$$

Here ρ and c denote density and specific heat, respectively; m_A is the mass, per unit mass of mixture, of a reactant A that is completely consumed at the hot boundary; H is the heat of reaction of A per unit mass, and D_A is the diffusion coefficient for A. The right-hand side represents the difference between sensible heat and heat produced by the reaction, per unit mass, at plane x in the wave; if this difference is positive the wave carries excess enthalpy. It is readily shown[1,2] that this is the case only when

$$\lambda/c > D_A \rho \qquad (4)$$

When λ/c is equal to or smaller than $D_A \rho$ there is no excess enthalpy or a deficiency of enthalpy, respectively.

In a recent discussion of the problem, Penner and Williams[3] compute the excess enthalpy for the case of a $(O_3 + 3O_2)$ mixture, using Hirschfelder's[4] numerical solution for this system. According to Hirschfelder, the best values of the transport coefficients obtained from theory and experiment indicate that $\lambda/c > D_A \rho$, so that an excess enthalpy exists; however, the numerical value of the excess enthalpy is found to be only about one-fifth of the value $(\lambda/S_u)(T_b - T_u)$ used by Lewis and von Elbe in their equation of minimum ignition energy. Penner and Williams suggest that this large discrepancy reflects the fact that enthalpy changes produced by heat conduction, rather than total enthalpy changes, are of dominant importance in ignition processes; they point out that this is in accord with conclusions reached by Linnett[5] after critical examination of arguments in favour of excess enthalpy by Lewis

and von Elbe and by Burgoyne and Weinberg[6] and objections raised by Spalding[7]. Penner and Williams[3] also show that for the case of negligible diffusion of chemical energy Lewis and von Elbe's minimum energy equation and Spalding's computed critical dimensions for flame extinction are consistent with the following postulate: 'Thermal ignition will occur if the rate of energy transfer per unit area by thermal conduction equals the rate of enthalpy change per unit area'.

The latter postulate is in accord with the concept advanced by the present authors. However, whether in the general case of non-negligible diffusion of chemical energy the enthalpy change by heat conduction rather than total enthalpy change is dominant, cannot be decided on the basis of the above analysis. This is so because actual measurements of the minimum ignition energy have not yet been carried out for the ozone–oxygen system. Possibly when this is done the experimental values will be found to be consistent with values computed on the basis of total enthalpy change rather than values computed from Lewis and von Elbe's equation. The following compilation, taken from an earlier publication[8], shows that in many instances the experimental values of minimum ignition energies are much smaller than the values computed from Lewis and von Elbe's equation, so that for a number of systems the agreement may be expected to improve substantially if the computation were made on the basis of total enthalpy change. The compilation demonstrates that this is particularly the case for systems with large content of diluents and thus may well apply to the system $(O_3 + 3O_2)$ which Williams and Penner have selected for their study.

In formulating the ignition energy equation 1, it has been assumed that the spark-generated flame which is just capable of self-propagation consists of a core of substantially burned gas, surrounded by the combustion wave in the form of a comparatively thin shell. It is possible to compare the flame diameters d in Table 1 with the characteristic width

$$\eta = \frac{\lambda}{c\rho_u S_u} \qquad (5)$$

for the pre-heat zone of the combustion wave[9]. This comparison leads throughout to ratios of η/d smaller than 0·05, and is thus consistent with the adopted model of the combustion wave constituting a thin shell around a core of burned gas. The ignition energy is thought to supply the excess enthalpy which is required by the combustion wave, and which cannot be furnished by the heat of the flame core without excessively lowering the temperature levels and hence the reaction rate. Indeed, calculations, using the data of Table 1, show that the heat $\pi d^2(\lambda/S_u)(T_b - T_u)$ stored in the wave is always of the order of the heat contained in a burned-gas volume of diameter d, so that such heat could not be abstracted from the burned core and stored in the wave without substantially decreasing the temperature levels throughout the incipient flame. The demand on the original heat source, viz. the spark, for furnishing the heat required by the wave is decreased by the diffusion of chemical species from the ambient (unburned) medium into the flame core and by the reaction of these chemical species in the reaction zone of the flame sphere; in this way the minimum ignition energy may become substantially smaller than the energy calculated from equation 1. However, within the framework of the model it is thought that in all real combustion waves the inequality 4 (or a corresponding inequality formulated in terms of a more sophisticated theory of the combustion wave) is fulfilled; that is, the transport rate of sensible heat is larger, even if only slightly larger, than the transport rate of the countercurrent chemical enthalpy. For the case that inequality 4 is not fulfilled or reversed, the model predicts that no ignition energy is required at all and the medium would in effect be 'hypergolic', i.e. igniting spontaneously.

It is readily seen that the latter prediction is an unwarranted extrapolation of the model. It rests on the supposition that if an extremely small spark were passed through such medium, i.e. one in which inequality 4 is not fulfilled or reversed, an extremely narrow reaction zone would instantly form around the spark volume, permitting chemical enthalpy to flow towards the origin and be converted into heat at such rate that in the burned core the temperature would never drop below the adiabatic flame temperature. This would ensure the continued growth of the flame but also would require extremely high reaction rates in the initial flame stages, far in excess of the reaction rate in the steady-state wave. For a vanishingly small spark the reaction rate would have to be virtually infinite, and since the Arrhenius-type temperature dependence of the rate does not permit this to happen, even if the spark temperature were virtually infinite, it is readily seen that even for media in which $\lambda/c < D_A\rho$ a finite spark size and therefore spark energy is required.

Whether this admission of the existence of a minimum ignition energy even for the case of $\lambda/c < D_A\rho$ invalidates the previous concept based on excess enthalpy is another matter. Here it may be stated that although reaction rates cannot grow to infinity, they would nevertheless in the case under consideration be in excess of normal near the origin. This is so because the temperature

TABLE 1

Comparison of Experimental and Calculated Minimum Ignition Energies *H*.
(Atmospheric Pressure and Room Temperature)

Fuel content fraction of stoichiometric	S_u cm/sec	$T_b - T$ °C	$\lambda \times 10^5$ cal/cm sec °C CH_4—O_2	d, cm	*Min. ign. energy* cal × 10^6 $H_{calcd.}$	$H_{exp.}$	*Ratio* $H_{calcd.}/H_{exp}$
			CH_4—O_2				
0·3	80	1,900	6·3	0·072	24	10	2·4
0·45	175	2,350	6·4	0·050	6·7	3·1	2
0·75	304	2,700	6·5	0·027	1·4	1·4	1
1·2	305	2,700	6·7	0·058	4·9	5·0	1
1·5	122	2,350	6·9	0·165	109	110	1
			C_3H_8—O_2				
0·4	240	2,200	6·1	0·038	2·5	1·7	1·5
0·6	335	2,550	6·0	0·028	1·1	0·68	1·6
0·8	382	2,700	5·9	0·024	0·77	0·50	1·5
0·8	382	2,700	5·9	0·024	0·77	0·50	1·5
1·0	375	2,750	5·9	0·022	0·65	0·48	1·3
1·2	320	2,700	5·8	0·024	0·88	0·63	1·4
1·4	235	2,500	5 7	0.028	1·5	1·0	1·5
1·9	30	1,300	5·6	0·045	15	6	2·5
			1,1 $CH_4 + O_2$, Nitrogen Added				
$N_2/O_2 =$ 0·5	240	2,640	6·3	0·045	4·5	5·3	0·9
1·0	170	2,510	6·4	0·053	8·4	9	0·9
1·86	110	2,320	6·5	0·079	2·6	20	1·3
air	42	1,900	6·5	0·25	590	110	5
			H_2—Air				
0·67	100	1,610	7·2	0·071	18	6·2	3
1·01	195	2,000	8·0	0·064	10	4·5	2
1·35	265	1,940	9·0	0·076	12	6·6	1·8
1·92	190	1,550	9·0	0·165	63	49	1·3
			C_3H_8—Air				
0·7	28	1,570	6·5	0·42	2,000	530	4
0·9	35	1,870	6·5	0·24	630	140	4
1·0	40	1,940	6·5	0·19	360	92	4
1·28	27	1,820	6·5	0·17	400	59	7
1·40	17	1,730	6·5	0·20	820	62	13
1·50	12	1,530	6·5	0·25	1,620	70	23
			CH_4—Air				
0·7	15	1,600	6·5	0·29	1,800	180	10
0·8	27	1,700	6·5	0·22	610	100	6
0·9	35	1,850	6·5	0·20	430	72	6
1·0	43	1,950	6·5	0·21	410	72	6
1·1	42	1,900	6·5	0·25	590	110	5
1·25	25	1,800	6·5	0·45	2,900	400	7

in the burned core is higher than the adiabatic flame temperature, being the sum of flame temperature and residual source temperature, and because the temperature coefficient of a typical flame reaction is extremely large. Hence one would expect, in the case $\lambda/c < D_A\rho$, the minimum flame diameter d to be small compared to the normal width of the combustion wave, and the minimum ignition energy to be correspondingly relatively small compared to the value computed from equation 1. The experimental facts compiled in Table 1 show on the contrary, as pointed out before, d to be substantially larger than the normal wave width and the minimum ignition energy to be equal to or comparable with the computed value. It thus appears that although the case under consideration is theoretically admissible, there is no experimental example at hand which demonstrates its actual existence, and perhaps it does not in fact occur in real explosive media.

Although the evidence that has been cited in favour of the excess enthalpy hypothesis is suggestive rather than substantive, there is likewise no compelling evidence against the suggestion that excess enthalpy is in fact a property of real combustion waves. In the final analysis this question can be decided only by precise studies of the various diffusivities in such waves. At present no such studies appear to be on record, except for the ozone–oxygen flame studied by Hirschfelder, and Penner and Williams. In the meantime there is no reason to abandon the simple interpretation of ignition energy data afforded by the excess enthalpy concept. Beyond the problem of incipient flames, however, the existence or non-existence of excess enthalpy does not seem to be an important consideration. In computations of burning velocities and temperature and concentration profiles of steady-state combustion waves, any reasonable choice of values of the diffusivities leads to acceptable results. Likewise, no reference to excess enthalpy is required in treating problems of quenching or inflammability limits.

REFERENCES

1 Spalding, D. B. *Proc. Roy. Soc. A* 240 (1957) 83
2 Lewis, B. and von Elbe, G. *Combustion, Flames, and Explosions of Gases*, p. 346. 1951. New York; Academic Press
3 Penner, S. S. and Williams, F. *Jet Propulsion* 27 (1957) 544
4 Hirschfelder, J. O., Curtis, C. F. and Campbell, D. E. *Fourth Symposium on Combustion*, p. 190. 1953. Baltimore; Williams and Wilkins; Univ. of Wisconsin Report CM-756, November 24, 1952
5 Linnett, J. W. *Selected Combustion Problems II* (AGARD), p. 139. 1956. London; Butterworth
6 Burgoyne, J. H. and Weinberg, F. J. *Proc. Roy. Soc. A* 224 (1954) 286
7 Spalding, D. B. *Fuel* 34 (1955) 100
8 Lewis, B. and von Elbe, G. *Advances-in-Chemistry Series, No. 20*, p. 15. 1958. American Chemical Society
9 Karlovitz, B., Denniston, D. W., Jr., Knapschaefer, D. H. and Wells, F. E. *Fourth Symposium on Combustion*, p. 613. 1953. Baltimore; Williams and Wilkins

Note added to proof—Independent of the above considerations, we may make reasonable order-of-magnitude estimates of the heat contained in an incipient flame, which we take to be spherical and of diameter d, and compare this estimated heat with the experimental minimum ignition energy. Evidently, the latter should not exceed the estimated total heat of the flame but conceivably may be much smaller. In order to estimate the heat of the flame, we may make use of equation 1, above; this equation applies to a spherical combustion wave and yields an approximate value of the heat which the gas within the wave has acquired by conduction. Another equation is based on the total heat within the flame sphere, which is represented by the integral

$$\int_0^{d/2} 2\pi r\rho c_p(T_u - T_u)dr; \qquad (6)$$

taking $\rho \sim 1/T$, an upper bound of the value of this integral is found to be

$$\frac{\pi}{\sigma}d^3\rho_u c_p T_u\left(1 - \frac{T_u}{T_b}\right) \qquad (7)$$

For the data in Table 1, computed values of the latter quantity are listed below. The units are 10^6 cal, and the sequence corresponds to the sequence of mixture compositions in Table 1.

CH_4–O_2	C_3H_8—O_2	$1{\cdot}1CH_4 + O_2$	H_2–Air	C_3H_8–Air	CH_4–Air
21	3·0	N_2 added	16	3,170	1,120
8	1·3	6·3	12	626	580
1·4	0·86	9·5	40	319	387
15	0·71	28	580	226	455
360	0·97	780	—	378	780
—	1·6	—	—	752	4,670
—	6·6	—	—	—	—

On comparing these values with the values derived from equation 1 (see Table 1), one notes a consistent order-of-magnitude agreement. Comparison of these calculated values with the experimental minimum ignition energies shows that a similar order-of-magnitude agreement exists whenever the burning velocity is not very low, i.e. whenever the mixture is not strongly diluted with inerts such as atmospheric nitrogen and excess of one of the reactants. In contrast, for weak mixtures the experimental minimum ignition energy is found to be only a small fraction of the computed approximate value of total flame heat.

It thus appears that in strong mixtures an incipient flame, viz. a flame of the size of the quenching diameter d, derives most of its sensible heat from the spark energy, whereas in weak mixtures the sensible heat residing within the flame is largely contributed by chemical reaction of the gas within the flame.

For an interpretation of this conclusion we consider the processes taking place during the time interval between spark discharge and establishment of the minimum-diameter flame. During this time, reactants diffuse to the flame core and are chemically converted there, thus contributing to the total heat release. The amount of diffusion and reaction depends, however, on the 'sink strength' of the flame core, viz. on the reaction rate in the flame core. If this rate does not substantially exceed the rate existing in the reaction zone of the normal steady-state combustion wave, the concentration gradients formed during the stated time interval are relatively flat and heat liberation by reactants diffusing into the flame core is relatively insignificant. On the other hand, if during the stated time interval the chemical reaction rate in the flame core is much larger than in the normal flame, concentration gradients are relatively steep and reactant diffusion makes an effective contribution to the total heat release. In strong mixtures, the normal flame reaction proceeds at high temperatures and high free-radical concentration so that the additional contribution of the spark to these principal agents of chemical reaction appears to be comparatively minor. In the normal flame of weak mixtures the temperatures and free-radical concentration are comparatively low, so that the contribution furnished by the spark may be expected to become important. It may therefore be suggested that the described relation between total flame heat and spark ignition energy is governed by the promotion of the chemical reaction by the spark, the promoting effect being small in strong mixtures and large in weak mixtures.

REACTION ORDER IN THE HYDROGEN–BROMINE FLAME FROM THE PRESSURE DEPENDENCE OF QUENCHING DIAMETER

A. E. POTTER, Jr. and E. ANAGNOSTOU

INTRODUCTION

The mechanism and rate constants for the low-temperature reaction between hydrogen and bromine are fairly well known[1]. The low-temperature kinetic data have been used for calculation of burning velocity[2,3]. However, the extrapolation of low-temperature mechanisms and rate constants to high temperatures is always open to question, since new reaction paths, unimportant at low temperatures, may become important at high temperatures. For example, Campbell[1] has suggested that the bimolecular H_2–Br_2 reaction might be important in the flame; thus, experimental tests of the applicability of the low-temperature data to the flame are desirable. The major test is, of course, the comparison of calculated and observed burning velocity. The agreement is good, indicating that the kinetic data do apply to the flame. Another test is a comparison of observed and calculated overall orders for the flame reaction. The purpose of this research is to make such a comparison.

The overall order of the flame reaction may be determined by measurements of the pressure dependence of either burning velocity or quenching diameter as shown by Potter and Berlad[4], where global orders from burning velocity and quenching distance were found to be in good agreement with one another. The former is preferable from a rigorous theoretical viewpoint, but the latter is preferable from an experimental viewpoint, since the quenching diameter lends itself very well to precise measurement at low pressures. Consequently, the quenching diameter for hydrogen–bromine flames was measured as a function of pressure.

APPARATUS AND PROCEDURE

The apparatus used to measure the quenching diameter of H_2–Br_2 mixtures is similar to that described by Simon, Belles and Spakowski[5], and is shown in *Figure 1*. It consists of a testing section, a mixture preparation and storing section, a pressure measuring and balancing section, and a vacuum system.

The testing section consists of a glass tube about 8·5 cm in diameter containing a spark gap and connected at the lower end to a glass tube 36·5 cm long and 8·05 cm in diameter (the quenching section). At the upper end, the tube connects to a 47 litre carboy, which serves as a plenum, through a ground glass joint and a 35 mm bore stopcock. Tubes of varying diameters are nested into the quenching section. In order to change the quenching diameter tubes are added to or removed from this nest, the tubes ranging from 6·63 to 1·84 cm in diameter. The quenching tubes are closed off at the bottom with a rubber stopper covered with a brass plate.

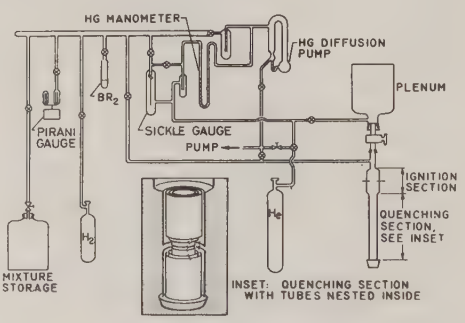

Figure 1. Apparatus

The pressure measurement section consists of a glass sickle gauge used in conjunction with a mercury manometer. This set-up must be used to prevent reaction between bromine and mercury. The plenum is also connected to the manometer so that the sickle gauge can be used for equalizing the pressure in the plenum to that in the test section. Helium is used to pressurize the plenum.

The parts of the apparatus in contact with bromine are glass or Teflon, except the brass valve at the storage tank. This valve had to be replaced periodically because of corrosion. Kel–F stopcock grease was used for stopcocks in contact with bromine.

The mixtures were made to an approximate composition by partial pressures in the mixture reservoir. The exact composition was determined by measurement of the vapour density of the mixture, after standing 24 to 48 hours. This procedure was necessary since bromine tended to

condense as hydrogen was introduced into the mixture reservoir.

For each run the procedure was as follows: the test section was filled to the desired pressure from the mixture reservoir after being evacuated to approximately 0·5 mm. Then helium was bled into the plenum until the plenum pressure was equal to that in the test section. The test section was then closed off from the mixture reservoir, the stopcock to the plenum was opened and the mixture ignited with a spark.

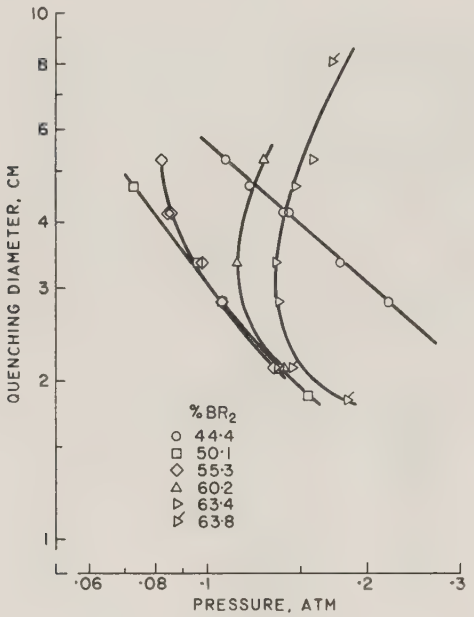

Figure 2. Variation of quenching diameter with pressure for several H_2–Br_2 mixtures

For every mixture, especially at low pressures, there were some flames which entered the tube, but were extinguished after traversing a third or half of the tube. These flames were considered to be quenched. The quenching pressure was taken to be the mean between the pressure at which a flame propagated the entire length of the tube, and the pressure at which the flame was quenched. The difference between these pressures was 3 mm of mercury or less.

Most of the measurements were made with the tubes vertical, so that flames propagated downwards. For a few measurements the plenum and quenching tubes were turned 90 degrees, so that flames propagated horizontally.

To avoid accumulation of systematic errors in the measurement, quenching distances for a given mixture were measured at intervals from low to high pressures, then from high back to low pressures.

All measurements were made at room temperature, which varied from 25 to 30°C.

ORDER OF THE FLAME REACTION

The first series of measurements was made with the quenching tubes vertical so that flames propagated downwards. The results are shown in *Figure 2*, where quenching diameter is plotted against pressure for H_2–Br_2 mixtures ranging from 44·4 to 63·4 per cent Br_2. The data points for the bromine-lean mixture (44·4 per cent Br_2) fall on a straight line within experimental error; the data points for stoichiometric and bromine-rich mixtures describe curves—a regular increase in the amount of curvature can be seen as the concentration of bromine is increased. The amount of curvature is almost negligible for the stoichiometric mixture, but for mixtures containing 60·2 and 63·4 per cent Br_2 the curvature becomes so large that the lines reverse direction at large tube diameters. As a result of this reversal a low-pressure limit for downwards flame propagation exists for these flames; no matter how large the tube, flames will not propagate downwards below a certain pressure.

In an effort to eliminate this effect the quenching tubes were turned 90 degrees so that flames propagated horizontally. The results of quenching measurements made in this way for one bromine-rich and one bromine-lean mixture are shown in *Figure 3*. For purposes of comparison interpolated results for downwards propagation are also plotted in this illustration. Examination of the results for the bromine-rich flame shows that the curvature observed for downwards propagation disappears

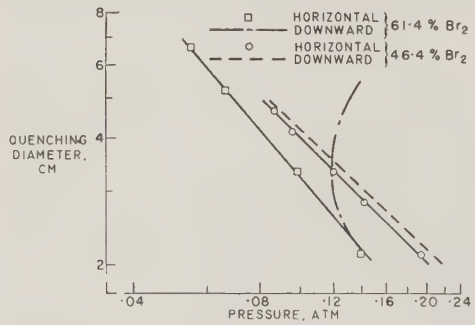

Figure 3. Effect of direction of propagation on the quenching H_2–Br_2 flames

completely when the flames are allowed to propagate horizontally; this can only mean that convective effects are the cause of the curvature. This subject is discussed at greater length in a later section of the paper. In contrast to the bromine-rich flame, the bromine-lean flame is seen to be little affected by convection—the slope is hardly changed by the direction of propagation. There appears to be about a 5 per cent difference between quenching diameters for the two directions. This is in agreement with the results of

Belles and O'Neal[6] who observed a difference of about 10 per cent between quenching diameters of propane–air flames for upwards and downwards propagation.

The principal purpose of this research is to compute the overall reaction order in the hydrogen–bromine flame from the pressure dependence of quenching diameter. From the preceding discussion it is clear that bromine-rich flames are not suitable for this purpose since they are strongly affected by convection. The results for bromine-lean flames are suitable since they are affected little, if at all, by convection. Presumably this is because burning velocity is highest for bromine-lean flames. Anderson[7] has observed that the maximum burning velocity occurs for mixtures containing about 40 per cent bromine.

The information required for calculation of the reaction order is the exponent describing the pressure dependence of quenching diameter. This was calculated by the method of least squares from the data for 44·4 per cent (*Figure 2*) and 46·5 per cent (*Figure 3*) Br_2 mixtures. The results are given in Table 1, along with the extrapolated quenching

TABLE 1

Quenching Diameters and Pressure Exponents for some H_2–Br_2 Flames

Per cent Br_2	n	*Quenching diameter*, 1 atm	*Quenching diameter*[10], 1 atm
44·4	0·87	0·75	0·6, 0·42
46·4	0·98	0·42	0·40

diameters at one atm. Included in Table 1 are Anderson's quenching diameters[7] at one atm and about 90°C. The agreement between the data of this research and that of Anderson is probably as good as can be expected considering the differences in technique and the long extrapolation.

It is shown by Potter and Berlad[4] that the pressure exponent n for quenching diameter is related to the overall order m of the flame reaction and the pressure dependence of the flame temperature by the following expression:

$$n = \frac{1}{2}\left(r - \frac{E}{RT_q}\right)\frac{\mathrm{d}\ln T_q}{\mathrm{d}\ln P} - \frac{m}{2} \qquad (1)$$

Here, r is an exponent describing the overall temperature dependence of all factors which affect quenching distance, except the Arrhenius exponential term. E is the activation energy for the flame reaction, T_q is the temperature of the 'about-to-be' quenched flame, and P is the pressure. It was found empirically for a number of flames (Potter and Berlad[8]), including the H_2–Br_2 flame, that T_q, T_f (the adiabatic flame temperature) and T_0 (the initial temperature), are related as follows:

$$\frac{T_q - T_0}{T_f - T_0} = 0{\cdot}78 \qquad (2)$$

The initial temperature in this experiment was about 300°K, and flame temperature for the 44·4 per cent Br_2 mixture in the pressure range of measurement is about 1,600°K.

Thus,

$$T_q \approx 1{,}300°\mathrm{K} = 0{\cdot}82\,T_f \qquad (3)$$

Assuming[4] that r is about 1·5, equation 1 becomes, after substitution of 3 and rearrangement,

$$m = \left(1{\cdot}5 - \frac{1{\cdot}22E}{RT_f}\right)\frac{\mathrm{d}\ln T_f}{\mathrm{d}\ln P} - 2n \qquad (4)$$

Two more factors must be evaluated before equation 4 can be used for calculation of m. These are the activation energy E and the pressure dependence of flame temperature. For the former, the value of 40·0 kcal/mole was used. For the latter, flame temperatures were calculated at three pressures using thermodynamic data[9] and assuming the concentration of hydrogen atoms in the flame to be negligible. The results are shown in Table 2. From these results

TABLE 2

Variation of Flame Temperature with Pressure for Some H_2–Br_2 Mixtures (initial temp. = 300°K)

Per cent Br_2	P, atm	T_f, °K
45	0·05	1,566
	0·10	1,592
	1·0	1,662
50	0·05	1,555
	0·10	1,584
	1·0	1,671
55	0·05	1,341
	0·10	1,350
	1·0	1,480

$\mathrm{d}\ln T_f/\mathrm{d}\ln P$ was calculated. It varies slightly with pressure so that it must be evaluated at each pressure that one wishes to use equation 4. When this is done and the results combined with the experimental value of n, equation 4 yields the overall order m at several pressures. The variation with pressure is insignificant, so that an average value is given here. The results are:

Per cent Br_2	Overall order
44·4	1·47
46·4	1·64

We shall now compute the overall order predicted from low-temperature kinetic data. At low

temperatures the important reaction steps are as follows[1]:

$$M + Br_2 \xrightarrow{k_1} 2Br + M$$
$$Br + H_2 \xrightarrow{k_2} HBr + H$$
$$H + Br_2 \xrightarrow{k_3} HBr + Br$$
$$H + HBr \xrightarrow{k_4} H_2 + Br$$
$$M + 2Br \xrightarrow{k_5} Br_2 + M$$

For the case that both bromine and hydrogen atoms obey the steady state assumption, the overall reaction rate is given by:

$$\frac{d[HBr]}{dt} = \frac{2k_3k_2\left[\frac{k_1}{k_5}\right]^{\frac{1}{2}}[H_2][Br_2]^{\frac{1}{2}}}{k_3 + k_4\frac{[HBr]}{[Br_2]}}$$

Inspection of this equation reveals that the overall order of the reaction is 1·5. Thus, the experimental results are in reasonable agreement with the order predicted from low-temperature kinetics. This indicates that the low-temperature reaction path is also the path followed by the reaction in the flame.

The question may be asked, does agreement of observed reaction order with the order predicted from assumption of the steady state argue for the correctness of that assumption? This question was considered for the case that bromine atoms did not obey the steady state assumption with the following results.

For large deviations from the steady state the overall order depends on two factors; the pressure, and the exponent s, describing the pressure dependence of $d[Br]/dt$, the deviation from steady state. The following chart can be constructed, showing limiting values of the overall order at very high and very low pressures for various values of s.

s	*Overall order*	
	High pressure	*Low pressure*
0	1·5	0·5
1	1·5	1·0
2	1·5	1·5
3	2·0	1·5
4	2·5	1·5

For large deviations from the steady state it is conceivable that one would observe an overall order different from the steady state value. The order should be pressure dependent, and should increase with pressure. However, it is quite possible that large deviations from the steady state could occur with no observable effect on the overall order. This is especially true if $d[Br]/dt$ varies as P^2. If one assumes that $[Br]^2$ throughout the flame varies approximately as $[Br_2]$, a variation as P^2 for $d[Br]/dt$ is to be expected. Thus, agreement of the experimental results with the order predicted from steady state considerations is evidence neither for nor against the steady state assumption.

CONVECTIVE EFFECTS IN BROMINE-RICH FLAMES

As mentioned in the previous section, log-log plots of quenching diameter against pressure for bromine-rich flames propagating downwards are curved (*Figure 2*). In some cases the curvature is so great as to produce a low-pressure limit for downwards propagation. At first radiation losses from the burned gases were thought to be the cause of this anomaly, since Spalding[10] has predicted a low-pressure limit for flame propagation resulting from radiation losses. However when the flame was made to propagate horizontally the curvature disappeared (*Figure 3*). This seems to indicate that convection rather than radiation loss is the

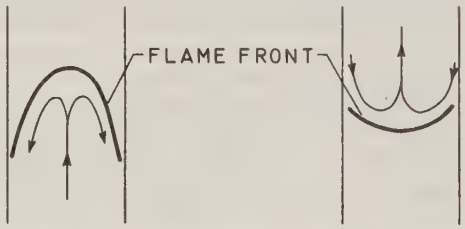

Figure 4. Convective flows which tend to exist behind flames in tubes: (a) upwards propagation; (b) downwards propagation

cause of the curvature. Convective effects have long been recognized as important in flame propagation. Linnett[11] has pointed out the importance of convection in determining flammability limits. Let us consider what effect convection has on a flame in a tube. The burned gases behind the flame in a tube are cool near the walls and hot near the axis; as a result, convection tends to make the gas near the axis rise, and gas near the wall fall. The convective forces thus alter the flame shape and the velocity profile in the burned gases behind the flame. The convective forces become noticeable for slow flames in large tubes, where upwards propagating flames have elongated bullet shapes, and downwards propagating flames are roughly hemispherical[11]. These changes are illustrated in *Figure 4* where flame shapes and the convective flows which tend to exist for upwards and downwards flame propagation are sketched. These flows are superimposed on the usual flows which always accompany flame propagation in tubes (not shown in the illustration). Now let us consider how convection might affect heat loss from the flame to the wall.

For a given tube and combustible mixture the rate of heat loss from the burned gas to the tube walls by conduction is quite independent of the direction of flame propagation, however, as shown in *Figure 4*, the flame area is not (when convection is important); consequently, the rate of heat loss experienced by the flame per unit area is greatest for downwards propagation where the flame area is smallest. In this connection it must be remembered that heat loss to the wall does not occur to any appreciable extent in front of the flame front, because the flame is propagating just as fast as heat conduction will allow; as a result, all heat loss to the wall occurs through the burned gases, behind the flame front.

Consider now a flame propagating downwards as tube diameter is increased. The convective forces increase with tube diameter, so that the flame becomes flatter: as a result, large tubes remove heat from the flame more effectively than if the flame shape had not changed, and consequently the flame in a large tube is quenched at a higher pressure than it would have been if the flame had not been flattened. This explains the observed trend of the experimental data for bromine-rich flames. For upwards propagation convective forces should have the opposite effect. Flames in large tubes should be quenched at a lower pressure than expected if no change in flame shape took place; thus, the experimental data should curve in the opposite direction to that observed for downwards propagation. For horizontal propagation one might expect a cancellation of the two opposing effects, so that no curvature at all would be observed, and this is precisely the case, as seen from *Figure 3*.

One further observation is of interest in connection with the bromine-rich flames. In large tubes the flames were cellular for downward propagation: this has also been observed by Kokochashvillii[12]. However, the flames were smooth, exhibiting no sign of cellularity, for horizontal propagation. This seems to indicate that convective forces play a part in the formation of the cellular flames. It would be interesting to observe whether or not the cellular flames of rich hydrocarbon flames are similarly affected by the direction of propagation.

SUMMARY OF RESULTS

(1) The pressure dependence of quenching diameter for bromine-lean hydrogen–bromine flames is consistent with an overall order of 1·5 predicted from low-temperature kinetics. This strongly indicates that the flame reaction follows the same path as does the low-temperature reaction.

(2) Bromine-rich hydrogen–bromine flames are anomalous in that log-log plots of quenching diameter against pressure are curved for downwards propagation. The effect was shown to be a result of convection, since the curvature disappeared when measurements were repeated with horizontal flame propagation.

REFERENCES

[1] Campbell, E. S. and Hirschfelder, J. O. *CF 2108, Univ. of Wisconsin*, Nov. 17, 1953

[2] Campbell, Edwin S. *Sixth Symposium (International) on Combustion*, p. 213. 1957. New York; Reinhold

[3] von Karman, T., Penner, S. S. and Millan, G. *Tech. Rept. No. 16, Contract DA–04–495–Ord–446*, Calif. Inst. of Tech., Pasadena, 1956

[4] Potter, A. E., Jr. and Berlad, A. L. *Sixth Symposium (International) on Combustion*, p. 27. 1957. New York; Reinhold

[5] Simon, Dorothy M., Belles, Frank E. and Spakowski, Adolph E. *Fourth Symposium (International) on Combustion*, p. 126. 1953. Baltimore; Williams and Wilkins

[6] Belles, Frank E. and O'Neal, Cleveland. *Sixth Symposium (International) on Combustion*, p. 806. 1957. New York; Reinhold

[7] Phillips, Victor D., Brotherton, Tom D. and Anderson, Robbin C. *Fourth Symposium (International) on Combustion*, p. 701. 1953. Baltimore; Williams and Wilkins

[8] Potter, A. E., Jr. and Berlad, A. L. A relation between burning velocity and quenching distance. *Nat. adv. Comm. Aero. Tech. Note 3882*, Nov. 1956

[9] *Selected Values of Chemical Thermodynamic Properties*. National Bureau of Standards, Series III. June 30, 1948

[10] Spalding, D. B. *Proc. Roy. Soc. A* 240 (1957) 83

[11] Linnett, J. W. and Simpson, C. J. S. M. *Sixth Symposium (International) on Combustion*, p. 20. 1957. New York; Reinhold

[12] Kokochashvillii, V. *Zhur. fiz. Khim.* 25 (1951) 444

53

FLAME PROPAGATION IN TWO-PHASE MIXTURES

I. N. SUNDUKOV and A. S. PREDVODITELEV

INTRODUCTION

As a rule, when liquid fuel is ejected into the combustion chamber the drops formed in the course of atomizing do not have sufficient time to evaporate by the moment of ignition. As a result the fuel ignited and burnt inside the chamber is not a homogeneous mixture but a two-phase system consisting of vapour and drops. The combustion of such mixtures is the object of investigation of many researchers who study this process—in most cases, during the actual tests of combustion chambers. However, there does not exist any consistent conception which can help to describe the phemonena occurring in engine combustion chambers. There have been very few attempts to establish some kind of theoretical foundation of the process of two-phase combustion in these conditions.

The task of the present paper is to discuss one of the possible conceptions of combustion of the above-mentioned mixtures.

The work by Predvoditelev devoted to the investigation of automodelling processes in chemically active mixtures, describes the mechanism of two-phase mixture combustion. While keeping to this mechanism of combustion in the present paper, we shall try to give some additional data pertaining to the formation and travel of the flame front. Apart from this we shall describe some of the experiments undertaken to confirm the proposed conception. We shall begin with the description of experiments.

EXPERIMENTAL

The two-phase mixture designed for combustion was produced with the aid of a special burner-atomizer which is shown schematically in *Figure 1.*

The stream of air washing the injector mouth, 6, ejected gasoline and hit the spherical baffler, 5, thus ensuring finer atomization of the fuel. On mixing, the air and atomized fuel were delivered to the burner, 1, 13·3 mm in diameter. The mixture there was initiated by a continuous duty gas-oxygen ignition device, 2. The fuel consumption was controlled by an adjusting needle valve, 7. It was noticed that in a burner of this design the variations in the fuel consumption did not much affect the size of drops in the heterogeneous mixture. This is explained by intensive separation of bigger-sized drops in the mixing chamber and in the burner proper.

The mixing chamber, in this case, is the space between the injector mouth, 6, and the burner, 1.

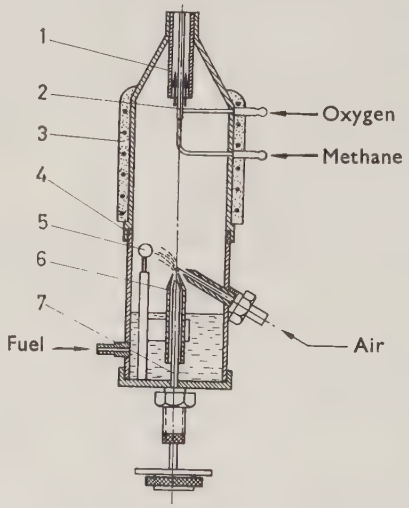

Figure 1. Design of burner-atomizer

The figure shows an electric heater, 3, installed on the mixing chamber. By raising the temperature of the chamber walls from 5°C to 50°C the volume of the liquid phase in the mixture could be varied from zero to 60 per cent.

The lower part of the burner-atomizer made of Plexiglass, 4, bore two marks notched at a definite distance from each other.

Since we knew the vessel volume between the two marks and the consumption time of the gasoline filling that volume we could determine the fuel consumption per unit of time.

A special device was made to determine the proportion of liquid phase relative to the total amount of gasoline in the combustible mixture. This device could measure the above-mentioned ratio with the precision of up to 12 per cent in each particular experiment.

The flame velocity was measured by the angle of spread of flame wedges photographed on plates.

Figure 2 shows the flame wedge diagram. The spread angle was determined from a considerable number of photographs by means of a measuring microscope. If we knew the angle of spread of the

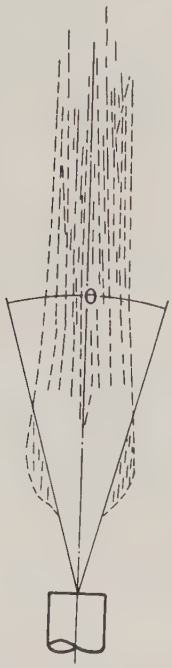

Figure 2. Flame wedge diagram

flame wedge and the average velocity of mixture flow we could calculate flame velocity g by the following formula

$$g = W \sin \frac{\theta}{2}; \qquad g - W_n = 0 \qquad (1)$$

The main results of the investigation are shown in *Figure 3.* This figure shows that flame velocity determined by formula 1 depends on the total fuel-air ratio. Flame velocity g is plotted on the Y axis, and total fuel-air ratio on the X axis.

During the experiments the proportion of the gasoline liquid phase in relation to its total volume (phase characteristic) varied from zero to 60 per cent. By way of comparison this figure also contains a diagram showing the co-relation of flame velocity and fuel-air ratio in homogeneous mixtures. The experimental data are marked in the figure by circles. These data sum up the results obtained on the basis of numerous repeated experiments. Therefore we consider them quite reliable. As is clearly seen from the figure the presence of liquid phase in combustible mixture greatly affects the velocity of flame propagation.

The experiments carried on in a rich mixture involved considerable difficulties. The fact is that as soon as the mixture was enriched, the liquid phase started creeping along the wall of the burner. It ran over the brim thus making it difficult to determine the fuel-air ratio. In spite of all this, numerous visual observations enable us to form the conclusion that the upper limit for the ignition of a two-phase mixture, as compared with that for

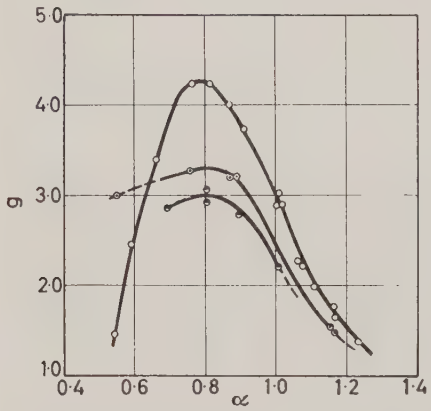

Figure 3. Relation of flame velocity to total fuel-air ratio. ◓ *proportion of liquid phase to total amount of fuel* Φ = 40–60 per cent per cent; ○ Φ = 20-30 per cent per cent; ○ Φ = 0–10 per cent per cent

a homogeneous mixture, tends to shift towards greater gasoline concentrations. To stress the tentative character of the experimental data the curve in this region is dotted (*Figure 3*).

By raising the temperature of the walls we could reduce the volume of liquid phase in the mixture down to 10 per cent of the total amount of gasoline. In this case the curve characterizing the dependence of flame velocity upon the fuel-air ratio tends to approach the similar curve for homogeneous mixtures.

Now we are facing a serious question—what is the physical meaning of the value which we measured in accordance with formula 1?

Most researchers identify the velocity found with the aid of formula 1 with the normal velocity determined by Guy-Michelson in homogeneous mixtures in which, in the case of laminar flows, there is always a narrow zone of combustion. Moreover, the researchers seek to establish a functional relationship between these two velocities, attempting in this way to prove the identity of both phenomena, as if they were both completely comprehended.

In our opinion such unqualified identification of the two above-mentioned concepts can hardly be considered well-grounded from the scientific point of view. Consequently, prior to proceeding to the discussion of the results obtained we must establish the physical meaning of the concept which we introduce for the description of the process.

However, this can be done only after we choose between one or the other pattern of the process. Our intuition cannot be fed upon indiscriminately accumulated empiric data obtained through the medium of physically uncomprehended notions.

THEORY

Let us assume that we have a chain of drops and we have found means to ignite one of them. The drop will begin to evaporate and burn in the homogeneous region whose distance from the drop surface is determined by the ignition point.

The thermal front will travel through the gas mixture, and when this front with a temperature equalling the ignition point reaches the neighbouring drops the latter will also be initiated. This will cause further movement of the thermal front and hence further ignition of the neighbouring drops, etc. The observer may find himself under the impression that the flame front is in the state of continuous movement, though during certain periods of time no combustion may actually take place. In this case it would be more correct to speak of flash movement rather than of flame movement. The velocity of flash movement can be determined in an ordinary way by the increase of the surface normal (per time unit) on which flashes are located. The movement of the thermal front in homogeneous mixtures will be expressed by the integral of the equation of thermal conductivity. This integral could be used for determining the velocity of flash movement. However, we shall follow a different course, bearing in mind the following circumstance. The moment the drops are ignited, all the temperature derivatives are subject to discontinuity. Consequently, in this case we can apply Adamar's mathematical method to the equation of thermal conductivity. Thus, let us perform pass-through-flash-front operation on the equation of thermal conductivity. Before passing the front we shall have

$$\left|\frac{\partial T}{\partial t}\right|_1 = \alpha\,|\Delta_2 T|_1$$

After passing the front we have

$$\left|\frac{\partial T}{\partial t}\right|_2 = \alpha\,|\Delta_2 T|_2$$

By subtracting the first equality from the second one we have

$$\left(\frac{\partial T}{\partial t}\right)_2 - \left(\frac{\partial T}{\partial t}\right)_1 = \delta\,\frac{\partial T}{\partial t};$$

$$(\Delta_2 T)_2 - (\Delta_2 T)_1 = \delta\Delta_2 T$$

$$\delta\,\frac{\partial T}{\partial t} = \alpha\delta\Delta_2 T \qquad (2)$$

We regard temperature conductivity as continuously varying value.

According to conditions of compatibility which Adamar deduced for discontinuity functions, in case of continuous jumps, the following co-relations will be true

$$\delta\,\frac{\partial T}{\partial t} = \frac{\lambda_{1T}}{H}\,\frac{\partial f}{\partial t};$$

$$\delta\Delta_2 T = \frac{\lambda_2}{H^2}\left[\left(\frac{\partial f}{\partial x_1}\right)^2 + \left(\frac{\partial f}{\partial x_2}\right)^2 + \left(\frac{\partial f}{\partial x_3}\right)^2\right] = \lambda_{2T} \qquad (3)$$

Here f expresses discontinuity surface, H the differential parameter, and λ_{1T} and λ_{2T} the arbitrary constants which we shall term discontinuity parameters.

We shall define flame velocity as the relation of infinitely small increase of the surface normal to infinitely small time period.

Let us give the exact differential for the discontinuity surface. We shall have

$$\frac{\partial f}{\partial n}\mathrm{d}n + \frac{\partial f}{\partial t}\mathrm{d}t = 0; \quad H\mathrm{d}n + \frac{\partial f}{\partial t} = 0$$

Hence

$$\frac{\mathrm{d}n}{\mathrm{d}t} = g = -\frac{\partial f}{\partial t}\,\frac{1}{H} \qquad (4)$$

If we transform equation 2 by means of Adamar's compatibility conditions 3 and co-relation 4, we shall have

$$g = -\,a\,\frac{\lambda_{2T}}{\lambda_{1T}} \qquad (5)$$

To make the problem more definite, i.e. to exclude indefinite parameters of discontinuity λ_{1T} and λ_{2T} from formula 4, we should have additional physical correlation. We may take for the purpose the relation of average distance between drops to ambient temperature.

There is no single solution of the problem of average distance between drops. For example we may proceed along the following line of argument: let us assume that we have volume V filled with two-phase mixture, with L expressing the average distance between drops and σ the drop diameter.

Then the volume occupied by one drop will be equal to

$$(L + \sigma)^3$$

The number of drops will obviously be equal to the ratio of volume V to the volume of one drop. Thus we have

$$N_1 = \frac{V}{(L + \sigma)^3}$$

Hence

$$L = \frac{V^{1/3}}{N_1^{1/3}} - \sigma$$

If we let N represent the number of drops per volume unit we shall have

$$L = \frac{1 - \sigma N^{1/3}}{N^{1/3}} \qquad (6)$$

The formula thus obtained will be sufficiently exact in case of cubic arrangement of drops. In the event of spheric symmetry of drop arrangement the calculations made should be corrected as follows

$$N = \frac{3}{4\pi\left(\frac{L+\sigma}{2}\right)^3} = \frac{6}{\pi(L+\sigma)^3}$$

Hence

$$L = \left(\frac{6}{\pi N}\right)^{1/3} - \sigma$$

But these last arguments are not quite correct either, for they do not show what law causes the variations in the density of the drops on the surface of the sphere formed by any radius whose centre may be located on any of the drops. Incidentally, the uniform distribution of the drops over the space implies equal density of all drops located within the sphere formed by any radius drawn from the centre of the drop. This density can be easily calculated with the help of the following obvious equation

$$N_s S = 1$$

with S in this case representing minimum surface corresponding to one drop. N_s expresses surface density of a number of drops.

The equation thus obtained gives the following

$$N_s = \frac{1}{S}$$

The volume of the sphere formed by the radius equal to the average distance between drops will contain the following number of drops

$$\frac{4}{3}\pi L^3 N$$

The number of drops on the surface of the sphere will be equal to

$$\frac{4\pi L^2}{S}$$

The latter two values should differ from each other by 1. Therefore we have

$$\frac{4}{3}\pi L^3 N = \frac{4\pi L^2}{S} + 1$$

Hence

$$L^3 - \frac{3}{SN} L^2 - \frac{3}{4\pi N} = 0$$

The third addend is so small that it may be disregarded. Thus, we shall have the following final formula

$$L = \frac{3}{SN} \qquad (7)$$

Generally speaking, the above co-relation is a temperature function, for every mixture is characterized by a certain degree of expansion when its temperature is being changed. Therefore we shall make use of the obtained co-relation to find the indefinite parameters of discontinuity λ_{1T} and λ_{2T}. This can be done as follows: let us differentiate the obtained co-relation with regard to time twice. As a result we shall have

$$\left.\begin{aligned} \frac{\partial L}{\partial T}\cdot\frac{\partial T}{\partial t} &= -\frac{3}{S^2 N}\frac{\partial S}{\partial t} = -A \\ \frac{\partial^2 L}{\partial T^2}\left(\frac{\partial T}{\partial t}\right)^2 + \frac{\partial L}{\partial T}\frac{\partial^2 T}{\partial t^2} &= \frac{6}{S^3 N}\left(\frac{\partial S}{\partial t}\right)^2 \\ &= \frac{2A}{S}\frac{\partial S}{\partial t} \end{aligned}\right\} \qquad (8)$$

When differentiating co-relation 7 we considered derivative $\partial S/\partial t$ to be constant according to the law of Sreznevskey.

In crossing the front these equations are subject to discontinuity.

Applying Adamar's operations to them we shall have

$$\left.\begin{aligned} \dot{L}\lambda_{1T} g &= \delta A \\ -2\ddot{L}\overline{\frac{\partial T}{\partial t}}\lambda_{1T} g + \dot{L}\lambda_{2T} g^2 &= \frac{2\sigma A}{S}\cdot\frac{\partial S}{\partial t} \end{aligned}\right\} \qquad (8a)$$

The bar above the derivative means that the arithmetical mean should be taken. We should add equation 5 to these equations. Now the set of simultaneous equations is quite closed. By excluding discontinuity parameters λ_{1T} and λ_{2T} we can easily obtain the formula of flame velocity. Thus, we shall have

$$g^2 = -a\left[\overline{\frac{\partial S}{\partial t}}\frac{1}{S} + 2\frac{\ddot{L}}{\dot{L}}\cdot\overline{\frac{\partial T}{\partial t}}\right]$$

Let β represent the linear expansion coefficient of the mixture. If we assume that it depends on temperature to a very small extent, we shall have

$$\frac{\ddot{L}}{\dot{L}} = \beta$$

Therefore the last equation can be written as follows:

$$g^2 = -a\left[\overline{\frac{\partial S}{\partial t}}\frac{1}{S} + 2\beta\overline{\frac{\partial T}{\partial t}}\right]$$

Temperature distribution before the flame front remains constant during the latter's movement.

Consequently, we shall have

$$\frac{\left(\frac{\partial T}{\partial t}\right)_2 - \left(\frac{\partial T}{\partial t}\right)_1}{2} = -\left(\frac{\partial T}{\partial t}\right)_1 \cdot \frac{1}{2}$$

Since the drop surface can only diminish in the course of time, derivative $(\partial T/\partial t)_1$ is positive, derivative $\partial S/\partial t$ is negative. Therefore the formula found for the square of travel velocity can finally be written as follows:

$$g^2 = a\left[\frac{1}{S}\left|\frac{\partial S}{\partial t}\right| + \beta\left(\frac{\partial T}{\partial t}\right)_1\right] \qquad (9)$$

The meaning of the second addend in the given formula is quite obvious. If no combustion is taking place, i.e. derivative $\partial S/\partial t$ equals zero, the value g^2 will be this:

$$g^2 = a\beta\left(\frac{\partial T}{\partial t}\right)_1$$

This means that instead of the flame front we shall have the propagation of the varying concentrations of liquid fuel vapours.

Let us try to apply formula 9 to the interpretation of the experiments described above. With this aim in view let us transform formula 9. From Sreznevskey's law it follows

$$S = At + S_0 \qquad (10)$$

We shall estimate combustion process from the point of view of fuel-air ratio. We shall express the reaction rate as follows:

$$\frac{\partial \alpha}{\partial t} = f(\alpha)$$

According to Predvoditelev this process is automodelling. Let us transform the last equation in relation to the co-ordinate ξ determined in this way

$$\xi = \frac{S}{t}$$

As a result we shall have

$$-\frac{\mathrm{d}\alpha}{\mathrm{d}\xi}\frac{\xi}{t} = f(\alpha)$$

With regard to steady-state process Predvoditelev proved

$$-\frac{\mathrm{d}\alpha}{\mathrm{d}\xi} = \text{const} = B; \quad \xi = g$$

Thus, we have

$$B\frac{g}{t} = f(\alpha)$$

Hence:

$$t = \frac{Bg}{f(\alpha)}$$

Now, let us subtract time t from equation 10 with the help of this equation. Then we shall have

$$S = \frac{ABg}{f(\alpha)} + S_0$$

Now we can write the following co-relation

$$\left|\frac{\partial S}{\partial t}\right|\frac{1}{S} = \frac{Af(\alpha)}{ABg + S_0 f(\alpha)}$$

The co-relation thus obtained enables the formula for front velocity to be written as follows:

$$g^2 = a\left[\frac{Af(\alpha)}{ABg + S_0 f(\alpha)} + \beta\left(\frac{\partial T}{\partial t}\right)_1\right]$$

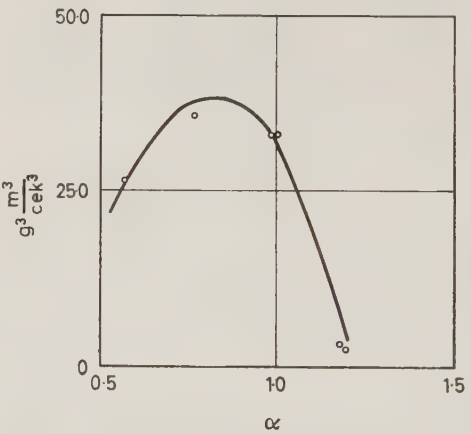

Figure 4. Relation of flame velocity to total fuel-air ratio (theoretical curve). ⊙ Φ = 20–20 per cent (experimental points)

If we disregard the last addend and consider that the drops are of a sufficiently small size to leave out product $S_0 f(\alpha)$ as compared with product ABg, then the last formula will turn into

$$g^3 = \frac{af(\alpha)}{B} \qquad (11)$$

In *Figure 4* the values of the cubes of flame front velocity are plotted along the Y axis, and fuel-air ratio along X axis. As seen from the figure we have a dome-shaped curve which can be expressed by the following function

$$g^3 = \frac{a}{B}f(\alpha) = \frac{a}{B}(b - \alpha)(\alpha - c)$$

The block curve is drawn according to the following formula

$$g^3 = 232(1{\cdot}2 - \alpha)(\alpha - 0{\cdot}4) \qquad (13)$$

Consequently, the combustion of two-phase mixture can be regarded as a chemical process with a reaction rate of the second order as far as the fuel-air ratio is concerned. In all analysed experiments the mixture used contained 20–30 per cent liquid phase of the total amount of the fuel.

CONCLUSIONS

The calculations made above refer only to cases in which the drop relative velocity in the two-phase mixture was equal to zero. However, it is not at all difficult to extend these calculations to a two-phase mixture with the relative velocity of drops differing from zero. This will be observed in the combustion of two-phase mixtures in turbulent flows. Our main guiding principle boils down to the conclusion that the process is automodelling. But in such processes, pointed out by Predvoditelev in the work quoted above, the reaction rate expressed by fundamental variable ξ is a constant value. This conclusion leads to Sreznevskey's law which holds good in conditions where relative velocity of drops is not equal to zero, i.e. in turbulent flows.

The formulae deduced in the present paper can also be applied to turbulent combustion in homogeneous mixtures. In fact the role of drops in homogeneous mixtures will be played by gas globules which are liable to stray motion. It is well known that the theory of turbulent movement can be based strictly on a conception of special hydrodynamic formations (globules) which travel in accordance with the law of stray motion.

Such problems can be solved by generalizing the equation of thermal conductivity and finding the formula for the average path of globule's stray motion. Consequently the method of calculation proposed at the beginning of the present paper is permissible here as well. No detailed knowledge of kinetics of chemical transformation is required in such a case.

As we have shown in our paper, this difficulty can be coped with by studying the travel velocity of isothermal surface of combustion.

Apart from this some additional data pertaining to the kinetics of chemical transformations can be obtained by studying the process of after-burning.

As is shown in one of the papers by Predvoditelev, true kinetics of chemical transformations are distorted in turbulent flows of gas mixtures. The distortion is chiefly caused by non-uniformity of temperature and concentrations resulting from turbulence of the flow.

We hope that the ideas expressed in this paper may find practical application.

GENERALIZED FLAME STABILITY DIAGRAM FOR THE PREDICTION OF INTERCHANGEABILITY OF GASES

D. W. VAN KREVELEN and H. A. G. CHERMIN

INTRODUCTION

The variety of gases that have become available in the last few years has created the problem of interchangeability of gases which may be formulated as follows: to what extent may the combustion properties of a new gas deviate from those of the gas to which the burners are adjusted, without experiencing hindrance from the change in gas composition. The solution to this problem demands a deeper knowledge of the combustion properties of gases. These properties are varied in nature and the difficulty arises that the phenomena observed are determined not only by the nature of the gas but also by the burner design and the surroundings.

Characteristic combustion properties are:

(1) rate of heat production (with gas velocity and calorific value as parameters),

(2) flame stability (including the phenomena of flashback, blow-off and blow-out),

(3) completeness of combustion (including the phenomena of yellow tipping, sooting and carbon monoxide formation).

The object of this paper is to describe a generalized method of predicting the interchangeability of arbitrary gas mixtures concerning the flame stability only. The numerical data in this paper apply to long circular tubes.

Townend *et al.*[1] and Lewis and von Elbe[2] have shown that instability phenomena are governed by the combined effect of normal burning velocity and a characteristic phenomenon known as 'dead space', 'quenching distance' or a similar term. A parameter for this combination is the critical velocity gradient at the burner wall.

According to Lewis and von Elbe both flashback and blow-off are exclusively governed by the boundary velocity gradient and the air–gas ratio. This theory has been confirmed experimentally: it has been found, for example, that the two stability limits are independent of the burner diameter (provided the latter is greater than the quenching diameter). Grumer[3] determined these characteristics for a large number of gases and gas mixtures.

Typical flame stability diagrams are shown in *Figure 1*, viz. for the gases methane and hydrogen which, more or less, can be considered as extremes. When the flame stabilities are plotted on the same scale, the large difference in behaviour between the two gases becomes very obvious.

Hydrogen with its extremely high combustion rate may flash back already at a boundary velocity gradient of 10,500 sec^{-1} but can hardly

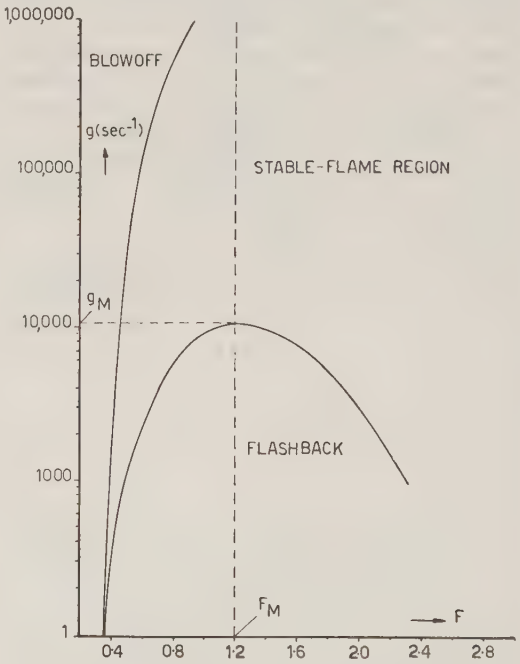

Figure 1a. Flame stability diagram of hydrogen

be blown off; methane on the other hand can flash back only when the boundary velocity gradient has fallen to the low value of 400 sec^{-1}, whereas blow-off already occurs at 2,000 sec^{-1} (at the stoichiometric gas concentration).

A schematic representation of the flame stability diagram is shown in *Figure 2*. This diagram is characterized by the following data:

(1) the coordinates of the peak (T) of the flashback curve (g_M, F_M),

(2) a quantity providing a measure of the width of the flashback curve,

(3) the distance of the blow-off curve from the peak of the flashback curve characterized, for example, by the distances *TP* and *TQ*.

In principle, the flame stability diagram for any given gas or gas mixture (burning in air) is completely characterized by these three quantities.

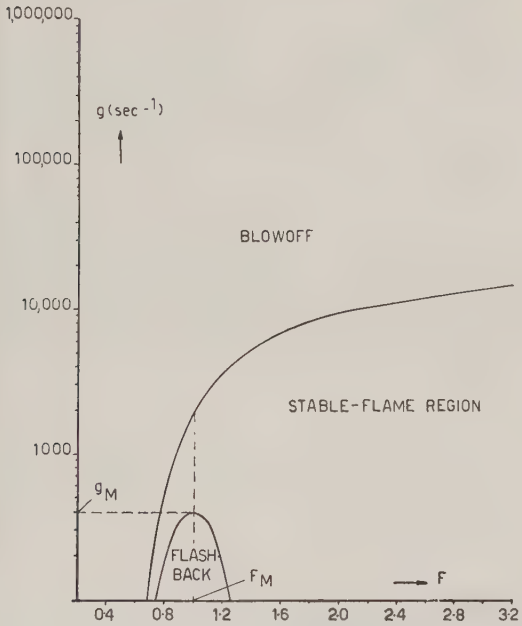

Figure 1b. Flame stability diagram of methane

GENERALIZED (OR REDUCED) FLAME STABILITY DIAGRAM

It has been found possible now to reduce all individual stability diagrams (both for pure gases and for mixtures) to a generalized diagram by using the following coordinates: (*a*) the dimensionless reduced boundary velocity gradient, (*b*) the reduced gas concentration.

(*a*) *Reduced boundary velocity gradient*

It is rather obvious to use the following relationship for this quantity

$$g_R = g/g_M \qquad (1)$$

i.e. the gradient divided by the gradient in the peak of the flashback curve.

(*b*) *Reduced gas concentration*

For the reduced gas concentration we chose

$$F_R = 1 + \phi(F - F_M) \qquad (2)$$

where F is the fuel gas concentration, fraction of stoichiometric; F_M is the F-value, corresponding to the position of the peak of the flashback curve; and ϕ is the reduction factor—this is a reciprocal measure of the width of the flashback curve and has been normalized in such a way that for methane $\phi = 1$.

The generalized stability diagram is represented in *Figure 3*. This comprises a bundle of blow-off curves which are exclusively determined by the percentage hydrogen in the inert-free mixture.

TABLE 1

Fuel gas	g_M (sec^{-1})	F_M	ϕ
CH_4	400	1·00	1·00
C_2H_6	650	1·13	0·80
C_3H_8	580	1·12	0·60
C_2H_4	1,400	1·10	0·63
C_3H_6	800	1·14	0·68
C_6H_6	720	1·09	0·63
H_2	10,500	1·20	0·46
CO (pure gas)*	(100)	(1·39)	

* See also Table 3, page 362.

The numerical values of g_M, F_M and ϕ of pure fuel gases are given in Table 1. In a following section we shall go into the problem of calculating the parameters of gas mixtures from those of pure gases.

Grumer's data[3] were used as far as possible in our calculations. Supplementary measurements were done in the authors' laboratory*.

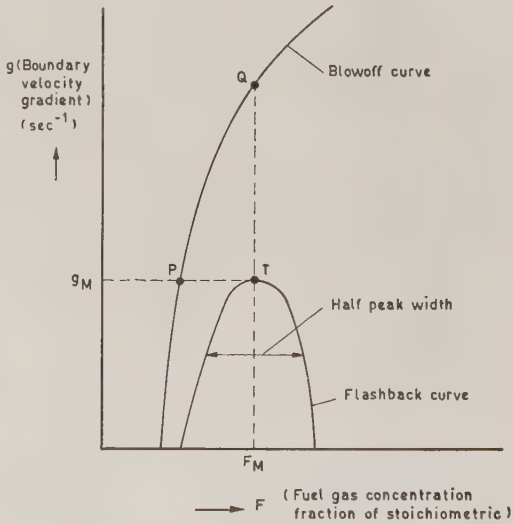

Figure 2. Typical flame stability diagram

With regard to the three characteristic quantities mentioned in the introduction we may point out that in the generalized diagram:

(1) the position of the peak of the flashback curve has in all cases been normalized to $g_R = 1, F_R = 1$;

* We thank Dr. Th. G. Scholte and Mr. P. B. Vaags for carrying out the necessary experiments.

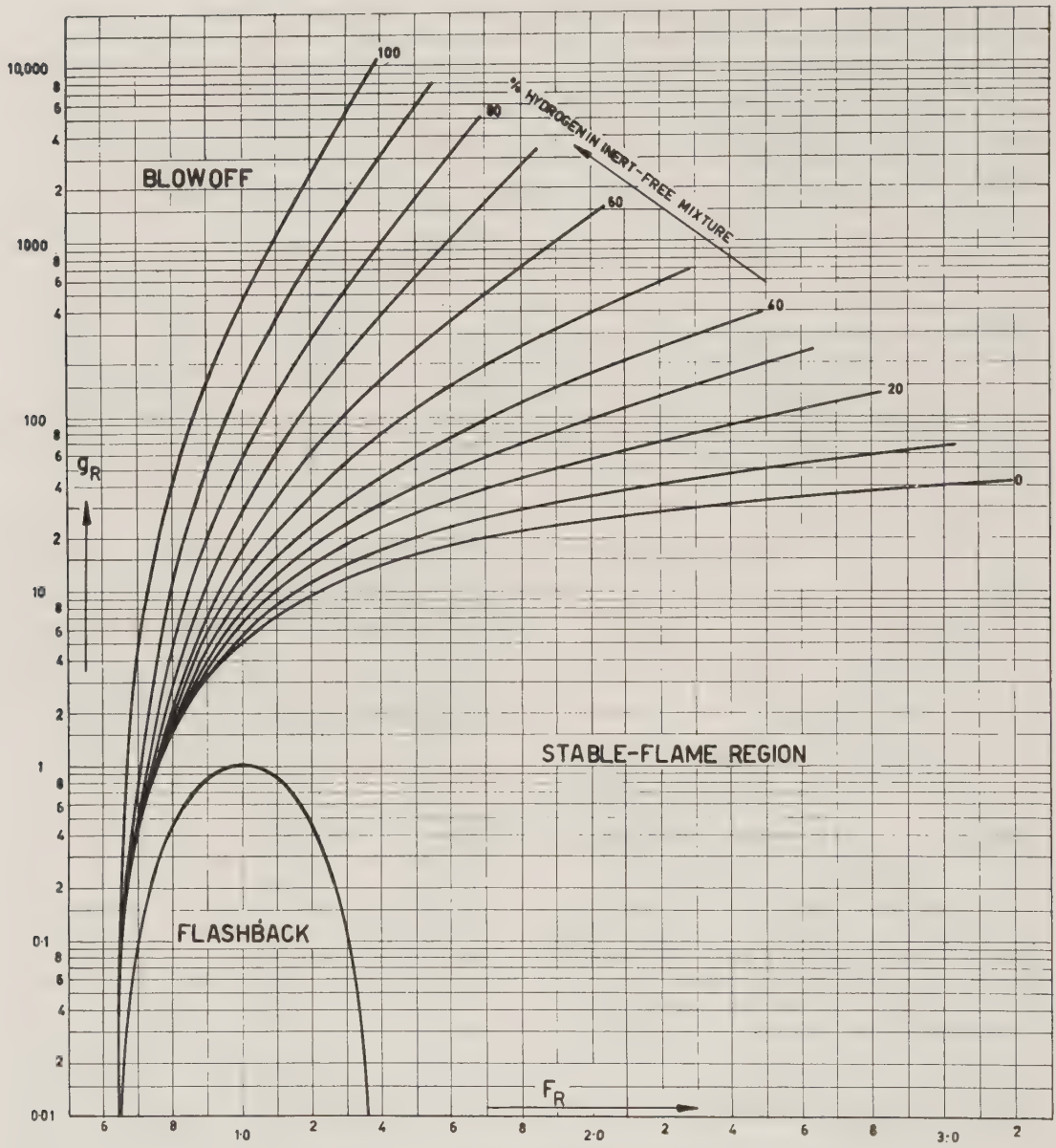

Figure 3. Generalized flame stability diagram

(2) the half-value width of the flashback curve has been characterized by the reduction factor ϕ;

(3) the position of the blow-off curve in relation to the peak of the flashback curve is determined by the hydrogen content as parameter.

Influence of inert gases on the combustion properties

The influence of inert gases, such as nitrogen and carbon dioxide, on the critical boundary velocity gradient was derived mainly from experiments made in the authors' laboratory. It was found that up to a concentration of 50 volumes per cent of inert gas the maximal boundary velocity gradient at flashback can be calculated, as a first approximation, with the formula:

$$g_M = g_M^\circ(1 - Ax) \qquad (3)$$

where x is the volume fraction of inert gas (see e.g. *Figure 4*).

The reduced gas concentration at the maximum can be calculated, as a first approximation, from a similar relationship:

$$F_M = F_M^\circ(1 - Bx) \qquad (4)$$

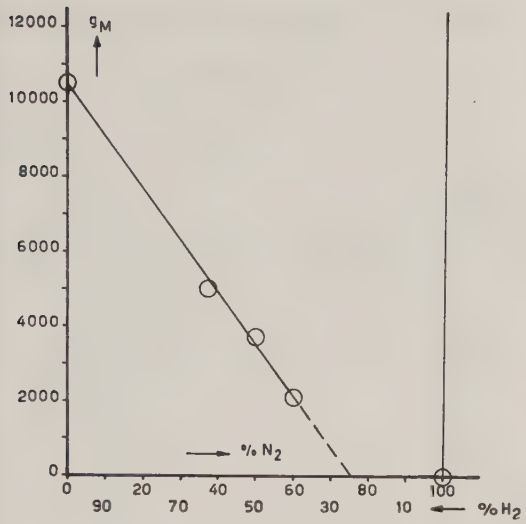

Figure 4. H_2–N_2 *mixtures*

TABLE 2

Inert Corrections

Fuel gas	$g_M = g^\circ_M(1 - Ax)$		$F_M = F^\circ_M(1 - Bx)$	
	A		*B*	
	Inert gas			
	N_2	CO_2	N_2	CO_2
H_2	1·343	1·562	0·167	0·225
CO	1·40	2·80	0·570	0·747
CH_4	0·857	1·525	0·000	0·000
C_2H_6	0·431	0·928	0·115	0·115
C_2H_4	0·360	0·790	0·091	0·055
C_3H_6	0·590	0·975	0·065	0·092

x = volume fraction inert gas.

The constants A and B for the binary, fuel gas-inert, mixtures examined are given in Table 2. For multi-component mixtures the constants A and B can be calculated as follows:

Influence of N_2

$$A_{N_2} = A_{N_2\text{–}H_2}\bar{x}_{H_2} + A_{N_2\text{–}CO}\bar{x}_{CO} + \ldots \quad (5)$$

$$B_{N_2} = B_{N_2\text{–}H_2}\bar{x}_{H_2} + B_{N_2\text{–}CO}\bar{x}_{CO} + \ldots \quad (6)$$

Influence of CO_2

$$A_{CO_2} = A_{CO_2\text{–}H_2}\bar{x}_{H_2} + A_{CO_2\text{–}CO}\bar{x}_{CO} + \ldots \quad (7)$$

$$B_{CO_2} = B_{CO_2\text{–}H_2}\bar{x}_{H_2} + B_{CO_2\text{–}CO}\bar{x}_{CO} + \ldots \quad (8)$$

where $\bar{x}_{H_2}$, etc., is the volume fraction H_2, etc., in the inert-free fuel gas.

For a multi-component gas mixture containing nitrogen and carbon dioxide the formulae become:

$$g_M = g^\circ_M(1 - A_{N_2}x_{N_2} - A_{CO_2}x_{CO_2}) \quad (9)$$

and

$$F_M = F^\circ_M(1 - B_{N_2}x_{N_2} - B_{CO_2}x_{CO_2}) \quad (10)$$

N.B. The latter formula is an approximation; F_M never becomes smaller than 1. (In the case that $F_M < 1$ is calculated, $F_M = 1$ should be used.)

As far as is known the value of the reduction factor ϕ approaches more to one as the inert content is higher. When the reduction factor of the inert-free mixture is represented by ϕ° the following relationship holds as a good approximation:

$$\phi = (1 - x_{inert})\phi^\circ + 1{\cdot}00x_{inert} \quad (11)$$

N.B. It should be pointed out that $F_M = 1{\cdot}00$ always goes with $\phi = 1{\cdot}00$, irrespective of the result of the calculation.

Fuel gas mixtures

Of the characteristic parameters the reduction factor ϕ is the only additive one. The other two, g_M and F_M, are only additive for mixtures of hydrocarbons (*Figure 5*) and approximately for

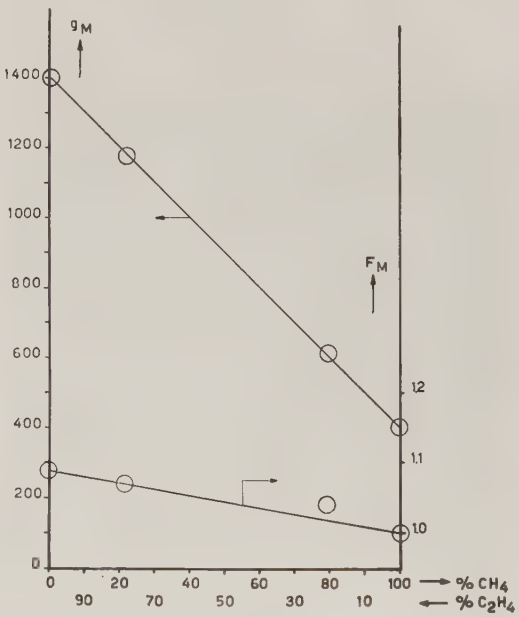

Figure 5. C_2H_4–CH_4 *mixtures*

mixtures of hydrogen and carbon monoxide (*Figure 6*). The behaviour of carbon monoxide appears to be abnormal in many respects. Completely purified carbon monoxide has a low combustion velocity and, as is indicated in Table 1, a

correspondingly low 'boundary velocity gradient' (g_M = 100 cm^{-1})*. With carbon monoxide these two quantities may be strongly influenced by adding small amounts of hydrogen and hydrocarbons[4]. Consequently, when considering gas mixtures we shall always make use of the so-called 'practical' g_M and F_M values for carbon monoxide, i.e. of the values which correspond as closely as possible with the experiments with industrial gases.

TABLE 3

Fuel gas	g_M (sec^{-1})	F_M	ϕ
CO ('practical' value for the calculation of mixtures)	1,500	1·7 (flashback) 1·0 (blow-off)	0·37 (flashback) 1·0 (blow-off)

For mixtures of CO or H_2 with hydrocarbons it appears to be necessary to introduce *depression factors*, which are defined as:

$$\psi = \frac{g_M \text{ (measured)}}{g_M \text{ (calculated additively)}} \qquad (12)$$

and

$$\psi' = \frac{F_M \text{ (measured)}}{F_M \text{ (calculated additively)}} \qquad (13)$$

As Grumer's measurements do not give sufficient information on the depression factors of binary mixtures of hydrocarbons with H_2 or CO, the calculations are chiefly based on supplementary measurements in our laboratory. A few examples of the results of these measurements are plotted in *Figure 7*. The measurements proved to agree well with a few earlier experiments performed by Grumer. The depression factors for binary mixtures were calculated from these measurements as represented in *Figures 8 a–d* and *9 a–d*.

With multi-component mixtures of hydrogen and carbon monoxide with hydrocarbons the depression factors can be calculated as follows:

The depression factors read from the *total hydrocarbon content* being given by $\psi_{H_2\text{–}CH_4}$; $\psi_{H_2\text{–}C_2H_6}$ or $\psi_{CO\text{–}CH_4}$; $\psi_{CO\text{–}C_2H_6}$, etc., the total depression factor is:

$$\psi_{H_2\text{–}hc} = \sum_i \bar{\bar{x}}_i \cdot \psi_{H_2\text{–}i} \qquad (14)$$

or

$$\psi_{CO\text{–}hc} = \sum_i \bar{\bar{x}}_i \cdot \psi_{CO\text{–}i} \qquad (15)$$

respectively, where $\bar{\bar{x}}_i$ is the volume fraction of hydrocarbon i in the inert-, CO- and H_2-free mixture.

* Measurement in the authors' laboratory.

Similarly the depression factors ψ' are found, so that:

$$\psi'_{H_2\text{–}hc} = \sum_i \bar{\bar{x}}_i \cdot \psi'_{H_2\text{–}i} \qquad (16)$$

or

$$\psi'_{CO\text{–}hc} = \sum_i \bar{\bar{x}}_i \cdot \psi'_{CO\text{–}i} \qquad (17)$$

respectively.

If the inert-free mixture contains, in addition to the hydrocarbons, the volume fractions $\bar{x}_{H_2}$

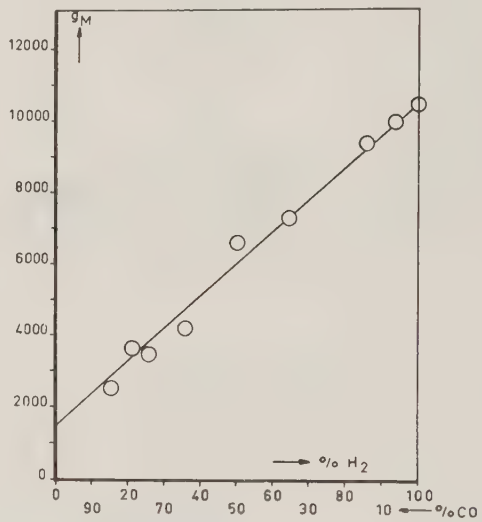

Figure 6. H_2–CO *mixtures*

hydrogen and $\bar{x}_{CO}$ carbon monoxide, the maximal boundary velocity gradient is calculated by means of the formula:

$$g^{\circ}_M = \psi_{H_2\text{–}hc} \cdot \bar{x}_{H_2} \cdot g_{MH_2} + \psi_{CO\text{–}hc} \cdot \bar{x}_{CO} \cdot g_{MCO} + \frac{\bar{x}_{H_2} \cdot \psi_{H_2\text{–}hc} + \bar{x}_{CO} \cdot \psi_{CO\text{–}hc}}{\bar{x}_{H_2} + \bar{x}_{CO}} \cdot \sum_i \bar{\bar{x}}_i \cdot g_{Mi} \qquad (18)$$

and the fuel gas concentration ('fraction of stoichiometric') at maximal boundary velocity gradient, by means of:

$$F^{\circ}_M = \psi'_{H_2\text{–}hc} \cdot \bar{x}_{H_2} \cdot F_{MH_2} + \psi'_{CO\text{–}hc} \cdot \bar{x}_{CO} \cdot F_{MCO} + \frac{\bar{x}_{H_2} \cdot \psi'_{H_2\text{–}hc} + \bar{x}_{CO} \cdot \psi'_{CO\text{–}hc}}{\bar{x}_{H_2} + \bar{x}_{CO}} \cdot \sum_i \bar{\bar{x}}_i \cdot F_{Mi} \qquad (19)$$

These equations show the additivity of CO- and H_2-free hydrocarbon mixtures as well as the additivity of hydrocarbon-free H_2 + CO mixtures.

Both equations hold for inert-free fuel gas mixtures. When inert gases are present a correction is made by means of equations 9 and 10.

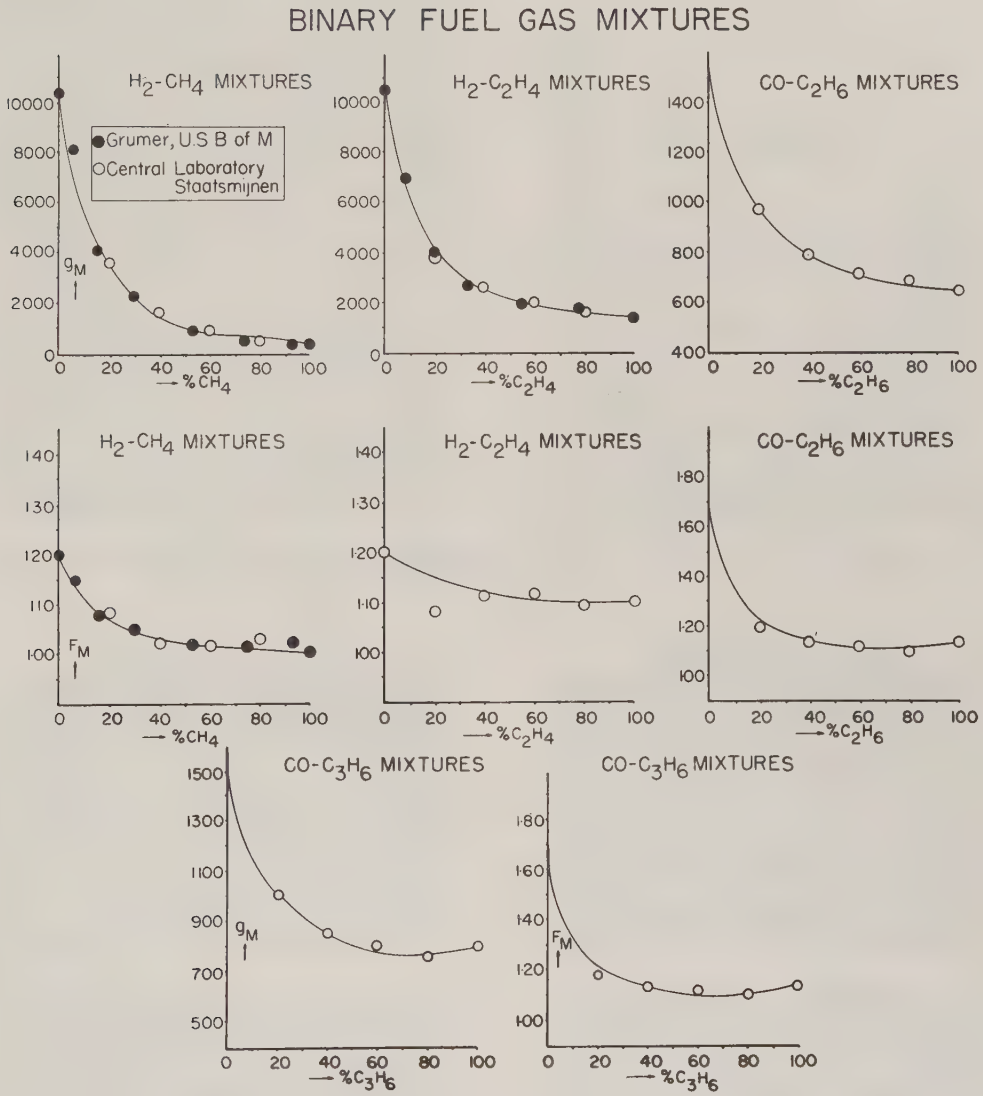

Figure 7. Binary fuel gas mixtures

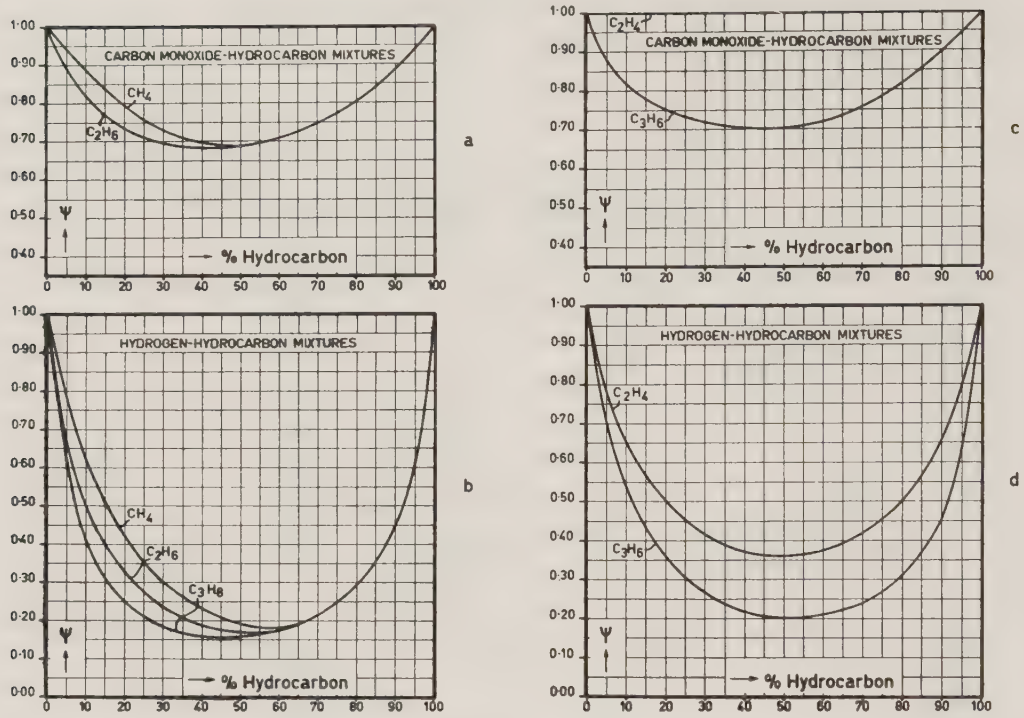

Figure 8. Calculation of g_M: a and b, depression factors ψ for saturated hydrocarbons; c and d, depression factors ψ for unsaturated hydrocarbons

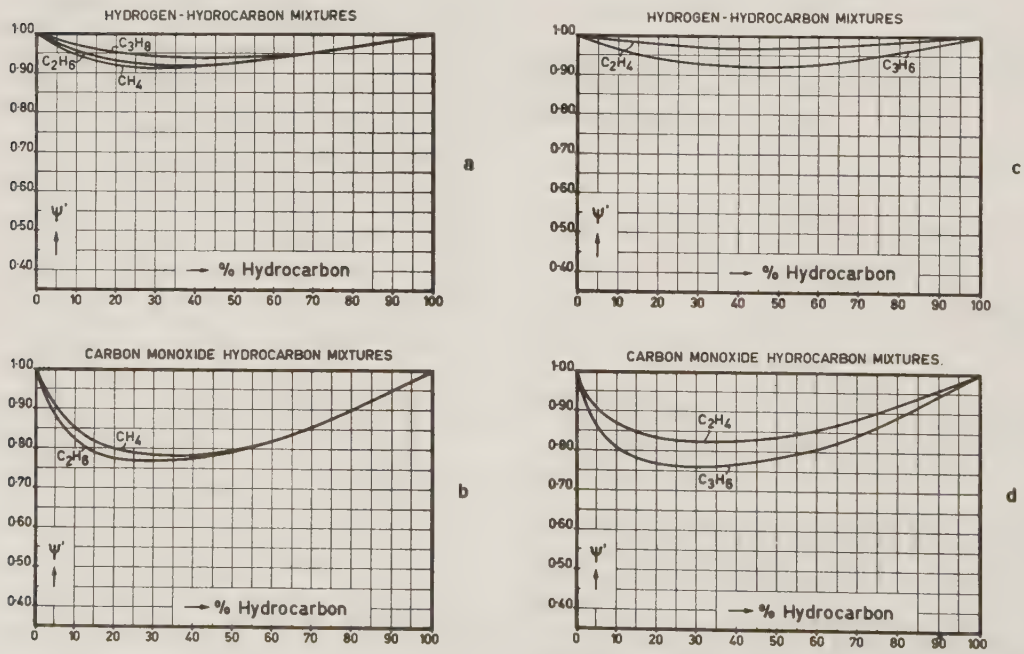

Figure 9. Calculation of F_M: a and b, depression factors ψ' for saturated hydrocarbons; c and d, depression factors ψ' for unsaturated hydrocarbons

Calculation of a Flame Stability Diagram of a Fuel Gas Mixture from the Reduced Diagram

Components	CH_4	C_2H_6	C_3H_8	C_2H_4	C_3H_6	H_2	CO	N_2	CO_2
Gross gas (% by volume)	42·6	2·2	2·1	18·1	0·3	17·0	9·1	3·4	5·2
Inert-free (% by volume)	46·6	2·4	2·6*	19·8		18·6	10·0		
Inert- and CO- and H_2-free (% by volume)	65·3	3·4	3·6	27·7					
ψ_{H_2-hc}	0·223	0·223	0·223	0·424					
ψ_{CO-hc}	0·757	0·757	0·757	1·000					
ψ'_{H_2-hc}	0·956	0·956	0·956	0·979					
ψ'_{CO-hc} flashback	0·860	0·860	0·860	0·887					
ψ'_{CO-hc} blow-off	1·000	1·000	1·000	1·000					

* C_3H_8 and C_3H_6 are taken together.

Hence:

$$\psi_{H_2-hc} = 0{\cdot}653 \times 0{\cdot}223 + 0{\cdot}034 \times 0{\cdot}223 + 0{\cdot}036 \times 0{\cdot}223 + 0{\cdot}277 \times 0{\cdot}424 = 0{\cdot}288$$

$$\psi_{CO-hc} = 0{\cdot}653 \times 0{\cdot}757 + 0{\cdot}034 \times 0{\cdot}757 + 0{\cdot}036 \times 0{\cdot}757 + 0{\cdot}277 \times 1{\cdot}000 = 0{\cdot}824$$

$$\psi'_{H_2-hc} = 0{\cdot}653 \times 0{\cdot}956 + 0{\cdot}034 \times 0{\cdot}956 + 0{\cdot}036 \times 0{\cdot}956 + 0{\cdot}277 \times 0{\cdot}979 = 0{\cdot}962$$

$$\psi'_{CO-hc} = \begin{cases} 0{\cdot}653 \times 0{\cdot}860 + 0{\cdot}034 \times 0{\cdot}860 + 0{\cdot}036 \times 0{\cdot}860 + 0{\cdot}277 \times 0{\cdot}887 \\ \quad = 0{\cdot}868 \text{ (for flashback)} \\ 0{\cdot}653 \times 1{\cdot}000 + 0{\cdot}034 \times 1{\cdot}000 + 0{\cdot}036 \times 1{\cdot}000 + 0{\cdot}277 \times 1{\cdot}000 \\ \quad = 1{\cdot}000 \text{ (for blow-off)} \end{cases}$$

With formulae 18 and 19 we then find for the inert-free mixture:

$$g^\circ_M = 0{\cdot}288 \times 0{\cdot}186 \times 10{,}500 + 0{\cdot}824 \times 0{\cdot}100 \times 1{,}500 + \frac{0{\cdot}288 \times 0{\cdot}186 + 0{\cdot}824 \times 0{\cdot}100}{0{\cdot}186 + 0{\cdot}100} \times (0{\cdot}466 \times 400 + 0{\cdot}024 \times 650 + 0{\cdot}026 \times 580 + 0{\cdot}198 \times 1{,}400)$$

$$g^\circ_M = 937 \text{ sec}^{-1}$$

$$F^\circ_M = 0{\cdot}962 \times 0{\cdot}186 \times 1{\cdot}20 + 0{\cdot}868 \times 0{\cdot}100 \times 1{\cdot}70 + \frac{0{\cdot}962 \times 0{\cdot}186 + 0{\cdot}868 \times 0{\cdot}100}{0{\cdot}186 + 0{\cdot}100} \times (0{\cdot}466 \times 1{\cdot}00 + 0{\cdot}024 \times 1{\cdot}13 + 0{\cdot}026 \times 1{\cdot}12 + 0{\cdot}198 \times 1{\cdot}10)$$

$$F^\circ_M = 1{\cdot}050 \text{ (for flashback)}$$

$$F^\circ_M = 0{\cdot}962 \times 0{\cdot}186 \times 1{\cdot}20 + 1{\cdot}000 \times 0{\cdot}100 \times 1{\cdot}000 + \frac{0{\cdot}962 \times 0{\cdot}186 + 1{\cdot}000 \times 0{\cdot}100}{0{\cdot}186 + 0{\cdot}100} \times (0{\cdot}466 \times 1{\cdot}000 + 0{\cdot}024 \times 1{\cdot}13 + 0{\cdot}026 \times 1{\cdot}12 + 0{\cdot}198 \times 1{\cdot}10)$$

$$F^\circ_M = 1{\cdot}037 \text{ (for blow-off)}$$

The constants in the correction formulae 9 and 10 for the influence of inert gases are found as follows:

$$A_{N_2} = 0{\cdot}466 \times 0{\cdot}857 + 0{\cdot}024 \times 0{\cdot}431 + 0{\cdot}026 \times 0{\cdot}431 + 0{\cdot}198 \times 0{\cdot}360 + 0{\cdot}186 \times 1{\cdot}343 + 0{\cdot}100 \times 1{\cdot}40 = 0{\cdot}882$$

$$A_{CO_2} = 0{\cdot}466 \times 1{\cdot}525 + 0{\cdot}024 \times 0{\cdot}928 + 0{\cdot}026 \times 0{\cdot}928 + 0{\cdot}198 \times 0{\cdot}790 + 0{\cdot}186 \times 1{\cdot}562 + 0{\cdot}100 \times 2{\cdot}80 = 1{\cdot}474$$

$$B_{N_2} = 0{\cdot}466 \times 0{\cdot}000 + 0{\cdot}024 \times 0{\cdot}115 + 0{\cdot}026 \times 0{\cdot}115 + 0{\cdot}198 \times 0{\cdot}091 + 0{\cdot}186 \times 0{\cdot}167 + 0{\cdot}100 \times 0{\cdot}570 = 0{\cdot}112$$

$$B_{CO_2} = 0{\cdot}466 \times 0{\cdot}000 + 0{\cdot}024 \times 0{\cdot}115 + 0{\cdot}026 \times 0{\cdot}115 + 0{\cdot}198 \times 0{\cdot}055 + 0{\cdot}186 \times 0{\cdot}225 + 0{\cdot}100 \times 0{\cdot}747 = 0{\cdot}134$$

Hence for the total mixture:

$$g_M = 937(1 - 0{\cdot}034 \times 0{\cdot}882 - 0{\cdot}052 \times 1{\cdot}474) = 837 \text{ sec}^{-1}$$

$$F_M = \begin{cases} 1{\cdot}050(1 - 0{\cdot}034 \times 0{\cdot}112 - 0{\cdot}052 \times 0{\cdot}134) = 1{\cdot}041 \text{ (for flashback)} \\ 1{\cdot}037(1 - 0{\cdot}034 \times 0{\cdot}112 - 0{\cdot}052 \times 0{\cdot}134) = 1{\cdot}029 \text{ (for blow-off)} \end{cases}$$

The reduction factor for flashback is given by:

$$\phi = 0{\cdot}426 \times 1{\cdot}000 + 0{\cdot}022 \times 0{\cdot}799 + 0{\cdot}021 \times 0{\cdot}597 + 0{\cdot}181 \times 0{\cdot}628 + 0{\cdot}003 \times 0{\cdot}680 + 0{\cdot}170 \times 0{\cdot}460 + 0{\cdot}091 \times 0{\cdot}365 + 0{\cdot}034 \times 1{\cdot}000 + 0{\cdot}052 \times 1{\cdot}000 = 0{\cdot}770$$

and for blow-off:

$$\phi = 0{\cdot}426 \times 1{\cdot}000 + 0{\cdot}022 \times 0{\cdot}799 + 0{\cdot}021 \times 0{\cdot}597 + 0{\cdot}181 \times 0{\cdot}628 + 0{\cdot}003 \times 0{\cdot}680 + 0{\cdot}170 \times 0{\cdot}460 + 0{\cdot}091 \times 1{\cdot}000 + 0{\cdot}034 \times 1{\cdot}000 + 0{\cdot}052 \times 1{\cdot}000 = 0{\cdot}827$$

By combining these data with the reduced diagram, the stability diagram can be calculated

TABLE 4*a*

Calculation of the Flashback Curve

$g_M = 837$ sec^{-1}, $F_M = 1{\cdot}041$, $\phi = 0{\cdot}770$

F_R	$F_R - 1$	$F - F_M$ (from (2))	F	g_R *Figure 3*	g (sec^{-1})
1·000	0·000	0·000	1·041	1·000	837
0·900	— 0·100	— 0·130	0·914	0·850	711
0·850	— 0·150	— 0·195	0·849	0·655	548
0·800	— 0·200	— 0·260	0·784	0·450	376
0·750	— 0·250	— 0·325	0·719	0·260	218
0·700	— 0·300	— 0·390	0·654	0·115	97

The flashback curve is assumed to be symmetrical, hence only one side is to be calculated.

TABLE 4*b*

Calculation of the Blow-off Curve

$g_M = 837$ sec^{-1}, $F_M = 1{\cdot}029$, $\phi = 0{\cdot}827$, % H_2 in inert-free gas = 18·6

F_R	$F_R - 1$	$F - F_M$ (from (2))	F	g_R *Figure 3*	g (sec^{-1})
0·700	— 0·300	— 0·363	0·666	0·43	360
0·800	— 0·200	— 0·242	0·787	1·65	1,383
0·900	— 0·100	— 0·121	0·908	3·5	2,930
1·000	0·000	0·000	1·029	6·3	5,280
1·200	0·200	0·242	1·271	13	10,900
1·400	0·400	0·484	1·513	21·5	18,010
1·600	0·600	0·726	1·755	30	25,100
1·800	0·800	0·968	1·997	39	32,700
2·000	1·000	1·209	2·238	50·5	42,300
2·400	1·400	1·693	2·722	71	59,500

as is represented in Table 4*a* and *b* and *Figure 10*. Grumer's experimental results are also represented in this illustration. The agreement appears to be good.

The interchangeability problem

If a given gas, or gas mixture A, is burning with a stable flame on a burner port, the coordinates relating to this burner-fuel gas combination (the 'performance point' of the burner for gas A) naturally lie within the stable-flame region of the stability diagram, or the reduced stability diagram, respectively. This gas is interchangeable with another gas (B) only if the coordinates of the performance point of the burner-fuel gas B combination also come within the stable-flame region.

If we know the performance point of a burner with adjustment gas A, the performance of the same burner with a substitute fuel B can be calculated. The equations needed for this calculation have been derived by von Elbe and Grumer[5]. They can be approximated as follows

$$g_B \approx g_A(P_B/P_A) \tag{20}$$

$$F_B \approx F_A(W_B/W_A) \tag{21}$$

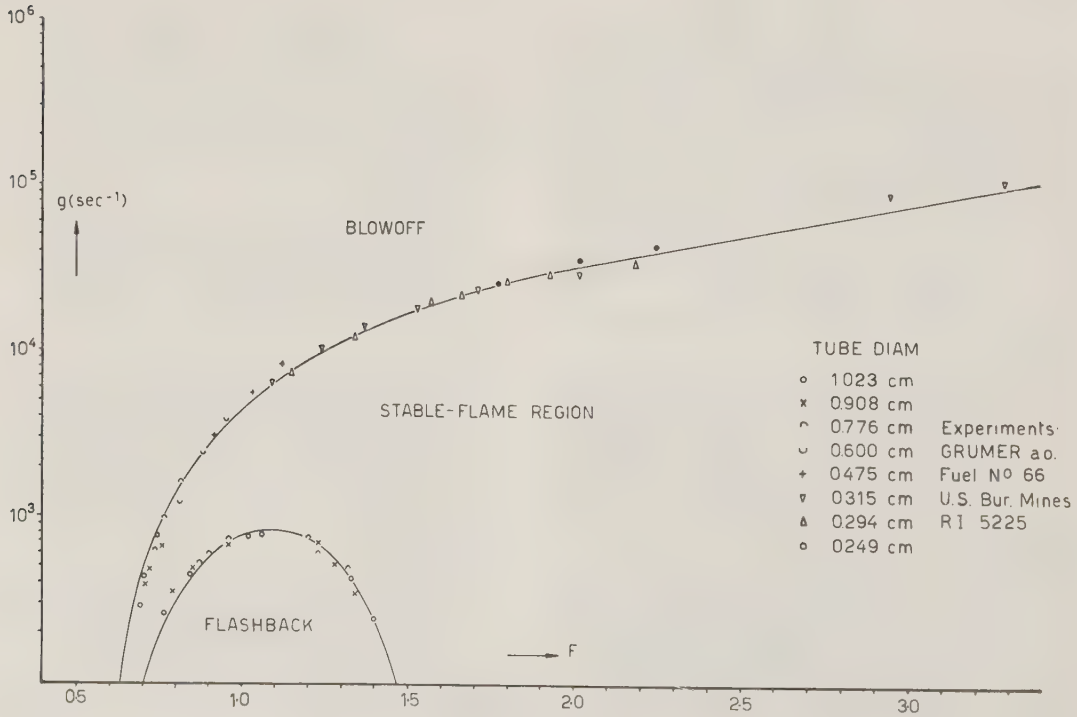

Figure 10. Flame stability diagram. Comparison of calculated curves and experimental points

where P is the gas-line pressure and W is the Wobbe index of the gas ($W = H/(d)^{\frac{1}{2}}$ = calorific value/root of fuel gas specific gravity). The derivation of these equations is given in the Appendix.

Supposing that both the composition of the adjustment gas A with Wobbe index W_A and the coordinates of the performance point (g_A and F_A) are known, the position of the performance point in the reduced stability diagram can be calculated.

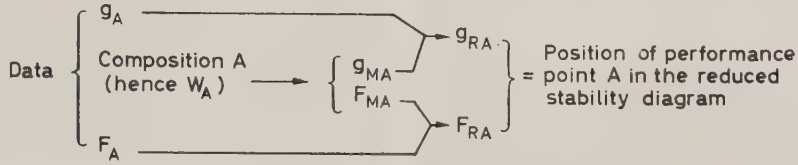

Using equations 20 and 21, mentioned above, the performance point for the same burner with the substitute fuel gas can now also be calculated.

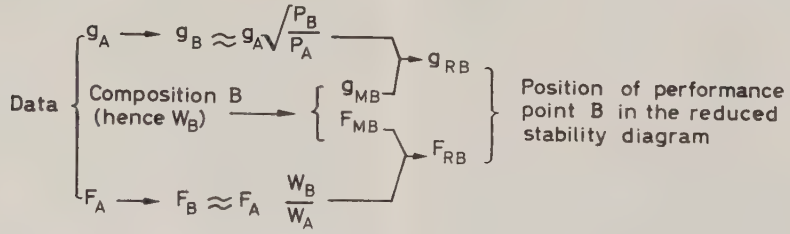

If the performance point B in the reduced diagram lies in the stable-flame region, the gases A and B are interchangeable.

It appears therefore that the question whether two gases are interchangeable depends mainly on the boundary velocity gradient, the Wobbe index and the gas-line pressure.

Example—A burner has been adjusted for methane (A) and the coordinates of the performance point are

$$g_A = 750 \text{ sec}^{-1},\ F_A = 1{\cdot}2,\ P_A = 1 \text{ cm Hg}$$

The performance point in the reduced diagram becomes

$$g_{RA} = \frac{750}{400} = 1{\cdot}88 \text{ and } F_{RA} = 1{\cdot}2$$

The Wobbe index $W_A = 12{,}780$.

Now let us see whether this gas is interchangeable with a mixture (B) of 60 per cent propane and 40 per cent hydrogen or with a mixture (B') of 40 per cent propane and 60 per cent hydrogen (at equal gas-line pressures).

Mixture B. The calorific values of propane and hydrogen are 24,120 and 3,050 respectively, the densities being 1·56 and 0·07 respectively.

For mixture B we thus find

$$H_B = 0{\cdot}60 \times 24{,}120 + 0{\cdot}40 \times 3{,}050 = 15{,}690$$
$$d_B = 0{\cdot}60 \times 1{\cdot}56 + 0{\cdot}40 \times 0{\cdot}07 = 0{\cdot}954$$

Hence, the Wobbe index (W_B) is 16,070.

Mixture B′

$$H_{B'} = 0{\cdot}40 \times 24{,}120 + 0{\cdot}60 \times 3{,}050 = 11{,}480$$
$$d_{B'} = 0{\cdot}40 \times 1{\cdot}56 + 0{\cdot}60 \times 0{\cdot}07 = 0{\cdot}666$$

Similarly we find for the Wobbe index ($W_{B'}$) = 14,070.

Performance point of mixture B—The parameters are

$$\begin{cases} g_{MB} = (0{\cdot}60 \times 580 + 0{\cdot}40 \times 10{,}500) \times 0{\cdot}18 \\ \quad = 820 \\ F_{MB} = (0{\cdot}60 \times 1{\cdot}12 + 0{\cdot}40 \times 1{\cdot}20) \times 0{\cdot}94 \\ \quad = 1{\cdot}08 \\ \phi_B = 0{\cdot}60 \times 0{\cdot}60 + 0{\cdot}40 \times 0{\cdot}46 = 0{\cdot}544 \end{cases}$$

$$\begin{cases} g_B = 750 \\ F_B = 1{\cdot}2\,\dfrac{16{,}070}{12{,}780} = 1{\cdot}51 \end{cases}$$

hence:

$$\begin{cases} g_{RB} = \dfrac{750}{820} = 0{\cdot}91 \\ F_{RB} = 1 + 0{\cdot}544 \times (1{\cdot}51 - 1{\cdot}0) = 1{\cdot}23 \end{cases}$$

In the reduced diagram this performance point lies just within the limits of the stable-flame region. Consequently gas B can be substituted for gas A, although it should be noted that the critical limit has almost been reached.

Performance point of mixture B′. Here we have

$$\begin{cases} g_{MB} = (0{\cdot}40 \times 580 + 0{\cdot}60 \times 10{\cdot}500) \times 0{\cdot}16 \\ \quad = 1{,}045 \\ F_{MB} = (0{\cdot}40 \times 1{\cdot}12 + 0{\cdot}60 \times 1{\cdot}2) \times 0{\cdot}93 \\ \quad = 1{\cdot}10 \\ \phi_B = (0{\cdot}40 \times 0{\cdot}60 + 0{\cdot}60 \times 0{\cdot}46) = 0{\cdot}516 \end{cases}$$

$$\begin{cases} g_B = 750 \\ F_B = 1{\cdot}2\,\dfrac{14{,}070}{12{,}780} = 1{\cdot}32 \end{cases}$$

hence:

$$\begin{cases} g_{RB} = \dfrac{750}{1{,}045} = 0{\cdot}71 \\ F_{RB} = 1 + 0{\cdot}515(1{\cdot}32 - 1{\cdot}10) = 1{\cdot}11 \end{cases}$$

This performance point lies in the flashback region. Consequently, gas A and gas B' are not interchangeable.

APPENDIX

Derivation of formulae 20 and 21

Most atmospheric burners contain Venturi ducts which serve to transform kinetic energy into the pressure, necessary to overcome the pressure loss over a multi-hole port. Neglecting energy losses and neglecting the transfer of momentum for the entrained air against the transfer of momentum by the fuel gas, one can write for a given apparatus 5, that

$$\frac{dV^2}{d_0 V_0^2} = \text{constant}$$

where the index 0 refers to the fuel gas and the quantities without index to the air-gas mixture.

When the fuels A and B are interchanged on a single burner without adjustment, one can write

$$\left(\frac{dV^2}{d_0 V_0^2}\right)_A = \left(\frac{dV^2}{d_0 V_0^2}\right)_B$$

Since $V_0/V = FS$ and in practice $(d)_B/(d)_A \approx 1$, we get

$$(F^2 S^2 d_0)_A = (F^2 S^2 d_0)_B$$

With a good approximation $S \sim 1/H$, so that the following relationship holds:

$$\frac{F_A^2}{F_B^2} = \frac{(H^2/d_0)_A}{(H^2/d_0)_B} \quad \text{or} \quad \frac{F_A^2}{F_B^2} = \frac{W_A^2}{W_B^2}$$

The change in the boundary velocity gradient caused by the interchange of gases can be calculated as follows. Generalizing Poiseuille's law, we suppose that even for a not fully developed laminar flow profile, one may approximately write

$$g \sim V$$

The outflow of the fuel through the orifice is, for a given apparatus, determined by:

$$P = \text{const. } d_0 V_0^2$$

hence:

$$\frac{P_B}{P_A} = \frac{(d_0 V_0^2)_B}{(d_0 V_0^2)_A}$$

Since:

$$\frac{(d_0 V_0^2)_B}{(d_0 V_0^2)_A} = \frac{(dV^2)_B}{(dV^2)_A}, \text{ where } \frac{d_B}{d_A} \approx 1$$

we can write, substituting $g \sim V$:

$$\frac{P_B}{P_A} = \frac{g_B^2}{g_A^2}$$

or

$$\frac{G_B}{G_A} = \left(\frac{P_B}{P_A}\right)^{\frac{1}{2}}$$

NOMENCLATURE

A = constant
B = constant
c = constant
d = specific gravity (of gas-air mixture)
F = fuel-gas concentration, fraction of stoichiometric
g = boundary velocity gradient $(= \lim_{r \to R} (-\,\mathrm{d}U/\mathrm{d}r))$
H = calorific value of fuel gas
P = fuel gas-line pressure
R = radius of burner tube
S = stoichiometric fuel-gas concentration
U = stream velocity at distance r from the axis of the burner tube
V = volumetric flow in burner tube
W = Wobbe index $\{= H/(d)^{\frac{1}{2}}\}$
x = volume fraction
$\bar{x}$ = volume fraction in inert-free fuel gas
x = volume fraction in inert-, H_2- and CO-free hydrocarbon mixture
ϕ = reduction factor
ψ = depression factor
ψ' = depression factor

Indices

o = inert-free fuel gas
M = top of flashback curves
R = reduced quantity

REFERENCES

[1] Townend, D. T. A., Davies, D. G. R. and Forsyth, J. S. *Trans. Inst. Gas Engrs.* 91 (1941–42) 47
[2] Lewis, B. and von Elbe, G. *J. chem. Phys.* 11 (1943) 75
[3] Grumer, J. *et al. Industr. Engng Chem.* (*Industr.*) 41 (1949) 2756; 44 (1952) 1547, 1554; 46 (1954) 2424. *Rep. Invest. No. 5225* (July 1956) *U.S. Bur. Min.*
[4] Scholte, Th. G. and Vaags, P. B. In press
[5] von Elbe, G. and Grumer, J. *Industr. Engng Chem.* (*Industr.*) 40 (1948) 1123

55

A STUDY OF THE KINETICS OF CYANOGEN FLAMES

K. SCHELLER and W. E. McKNIGHT

INTRODUCTION

Cyanogen flames have recently attracted some interest by virtue of their extraordinarily high adiabatic flame temperatures[1]. Brokaw and Pease[2] found that the burning velocities of cyanogen–oxygen mixtures are greatly increased by the addition of small amounts of water vapour. Work in this laboratory on cyanogen–air flames[3] has suggested that cyanogen burns in a two-stage process, cyanogen being oxidized to carbon monoxide in the first stage of the flame and the carbon monoxide then oxidizing to CO_2 downstream of the primary reaction zone. The present investigation was undertaken to explore further the hypothesis of the two-stage nature of the cyanogen flame.

The low burning velocities of cyanogen–air flames (*ca.* 10 cm/sec)[3,4] coupled with their high flame temperatures (at least 200°K higher than saturated hydrocarbon–air mixtures), suggests that the oxidation of CO to CO_2 in the assumed second stage of the flame is very loosely coupled to the primary oxidation of cyanogen to CO, and has little influence upon the temperature of the primary reaction zone. On this view it was reasoned that an increase of the rate of combustion in the second stage would raise the temperature of the first stage reaction, and thereby increase the burning velocity of the mixture. It is known that the burning rate of rich moist CO–air flames may be accelerated without increase in flame temperature by replacing the nitrogen in the mixture with CO[5]: accordingly, a series of burning velocity determinations was made on mixtures of cyanogen, oxygen, and nitrogen in which the nitrogen content of the mixture was progressively replaced by carbon monoxide. Elementary kinetic theory indicates that to a very good first approximation the flame temperature, thermal conductivity, and diffusivity of these mixtures are unaffected by the substitution of CO for nitrogen. Furthermore, slow oxidation studies of cyanogen–oxygen mixtures[6] have demonstrated that CO has little or no influence upon the oxidation of cyanogen. Thus it appears that the addition of carbon monoxide to cyanogen–oxygen–nitrogen mixtures will affect only the kinetics of the CO oxidation.

EXPERIMENTAL

Materials

Cyanogen was prepared by the thermal decomposition of AgCN under vacuum at 400°C. The cyanogen was condensed at liquid-air temperatures as it evolved and subsequently fractionated into breakseals. Mass spectrographic analysis of the material produced in this manner indicated that it contained traces of O_2 and N_2 and no detectable quantities of H_2O or HCN. Its purity was estimated to be 99+ per cent of C_2N_2.

The oxygen and carbon monoxide gases were obtained from commercial cylinders supplied by the Matheson Company. Moisture was removed from the gases by passage through traps containing magnesium perchlorate and ascarite. No other purification was attempted. The manufacturer's analysis of the carbon monoxide quoted a hydrogen and nitrogen content of 1·0 per cent each and less than 0·5 per cent of CO_2 as impurities. Preliminary experiments with the stored CO indicated that it did not contain significant quantities of iron pentacarbonyl.

Apparatus and procedure

An all-Pyrex vacuum system was used for transferring and mixing the gases in the desired proportions. To prepare the mixtures, a breakseal containing C_2N_2 was sealed to the vacuum system which was then evacuated to a pressure of 0·01 mm Hg. The breakseal was broken and the cyanogen was allowed to sublime into a 5 litre storage flask. The system was then pumped down, flushed with air and re-evacuated to remove all cyanogen in the lines. Next, appropriate quantities of air and O_2 were admitted to the system at a calculated pressure (measured by a mercury manometer) after passage through magnesium perchlorate and ascarite. A separate 5 litre mixing flask was filled with the oxygen-enriched air to a pre-determined sub-atmospheric pressure. After removal of air from the lines, cyanogen was added to the mixing vessel from the storage flask until the total pressure rose to 1 atm. In the absence of experimental difficulties, the mixing vessel contained a quantity of combustible mixture of a specified composition sufficient for several determinations of the burning velocity.

Burning velocities were measured by the latex balloon method of Price and Potter[7] modified so that mixtures could be exploded without exposure to moisture. This was accomplished by the use of the vacuum mixing system and an electrode system constructed so that the balloon could be flushed and evacuated after it had been placed on the electrode. The electrode consisted of a hollow steel tube, 3·2 mm in diameter, through which was inserted a ceramic insulated wire of 0·38 mm diameter. The free end of the wire was flush with one end of the tube while the other end was connected to a high voltage source, the end of the

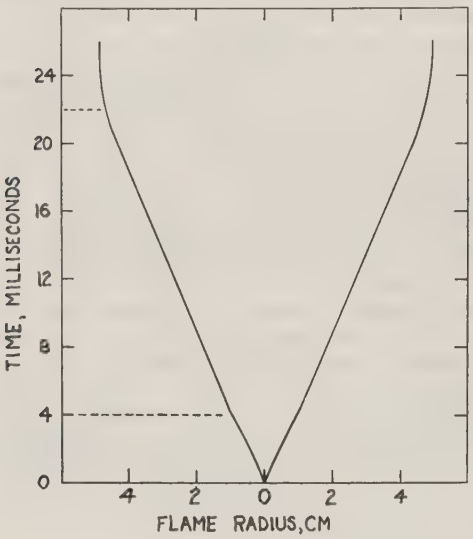

Figure 1. Flame trace for a 13 per cent *cyanogen-enriched air mixture*

tube and wire being sealed with black wax into glass tubing and connected to the vacuum system. The balloon was firmly attached to an aluminium sleeve 10 mm long which slid over the electrode in a friction fit. In practice, the friction fit proved to be a quite satisfactory seal, allowing negligible leakage from the inflated balloon during the preparation time required prior to the ignition of the combustible mixture.

Before embarking upon a systematic study of the burning velocities, a few exploratory determinations were made with cyanogen–air mixtures over their range of flammability. Ignition was found to be unreliable with the present spark system, but completely reliable ignitions were obtained with slightly enriched air containing 25 per cent O_2 and 75 per cent N_2. Hence this mixture was employed as the oxidant for the entire series of experiments.

In making a run, the balloon was first flushed with the combustible mixture by repeated inflation and evacuation and then inflated to a diameter of approximately 10 cm. The inflated balloon was carefully centred on the electrode and subjected to a spark discharge from an 0·01 μF condenser. Spark energy was controlled by limiting the output (5,000 to 10,000 V) of a Hivolt Power Supply used to charge the condenser. Balloon ignition was accomplished approximately 0·5 sec after a high-speed streak camera (a modified Wollensak Fastax 16 mm) trained upon the balloon was started. This delay time was set by an Industrial Timer Corporation automatic control, adjusted to allow the camera time to accelerate to a constant speed before ignition occurred. A spotlight illuminated the balloon to permit photographs of its initial and final dimensions so that the expansion ratio could be determined. A metal cylinder of accurately known diameter was placed in the proximity of the balloon to serve as a standard length for the determination of the magnification of the film trace. The film speed was obtained from msec timing marks, imprinted upon the film by a Potter 1,000 cycle signal generator which activated a neon flash lamp within the camera case. Several runs were made for each mixture composition in order to allow for explosions in which the data were not usable due to asymmetric expansion of the balloon.

The fundamental burning velocity, U_f, was calculated from the observed spatial flame speed, S_f, and expansion ratio, E, by the following simple relation:

$$U_f = S_f/E = S_f \left(\frac{d_o}{d_t}\right)^3$$

in which d_o = initial diameter of balloon and d_t = final diameter of balloon.

The spatial flame speed is equal to the rate of growth of the diameter of the flame. It was determined by examining the film of each explosion, frame by frame, in a microreader to obtain the flame diameter as a function of time. A plot of a typical run is shown in *Figure 1*, zero on the time origin being the point of ignition. This particular trace is for a 13 per cent cyanogen-enriched air mixture. The flame attained a constant spatial velocity about 4 msec after ignition, which did not vary appreciably until the flame reached the balloon wall 22 msec after ignition. The spatial velocity is given by the slope of the flame radius trace, 212 cm/sec for this example. From the observed expansion ratio of 6·21, one calculates a fundamental burning velocity of 34·2 cm/sec for this mixture.

RESULTS

The compositions of the experimental mixtures, measured expansion velocities and spatial flame speeds are recorded in Table 1. The derived

TABLE 1
Compositions of Experimental Mixtures and Observed Flame Parameters

Per cent *cyanogen*	*Oxidant composition*, per cent			*Expansion ratio*	*Spatial flame speed*, cm/sec
	O_2	N_2	CO		
10	25	0	75	8·00	1,002
				8·71	1,003
				8·40	1,002
10	25	25	50	8·72	953
				8·00	936
				8·25	920
				9·00	961
10	25	50	25	8·25	596
				7·61	596
				8·26	626
				8·00	533
13	25	0	75	8·50	1,002
				8·94	1,068
				9·64	1,102
				9·19	1,103
13	25	25	50	8·46	871
				8·48	920
				9·06	920
13	25	50	25	8·23	687
				7·55	636
13	25	75	0	6·29	221
				6·16	212
				6·21	212
16	25	0	75	8·74	878
				8·98	962
				9·10	1,028
				8·37	935
16	25	25	50	8·12	690
				8·47	669
				7·86	669
16	25	50	25	6·96	463
				7·56	502
				8·99	553
16	25	75	0	8·15	218
				8·00	268
				8·28	268
				8·05	254
19	25	0	75	7·77	502
				8·84	617
19	25	25	50	6·84	401
				7·44	426
				7·77	429
19	25	50	25	8·24	462
				7·67	365
				9·85	402
19	25	75	0	9·73	339
				10·90	391
				9·88	330
				9·88	363
22	25	0	75	7·26	401
				7·58	485
22	25	25	50	9·46	401
				8·50	436
				8·00	430
				7·76	376
22	25	50	25	7·66	352
				6·98	279
				5·49	233
				6·66	277
22	25	75	0	10·70	423
				10·30	379
				9·49	374
				10·70	423

normal burning velocities are plotted in *Figure 2*, as a function of cyanogen content, for the four oxidant mixtures containing the indicated quantities of carbon monoxide. Curves were faired in through the averaged values of the burning velocity for each mixture. For the cyanogen-enriched air flames (0 per cent CO), the burning velocity is noticeably insensitive to cyanogen content over the entire composition range investigated, slightly lean to very rich mixtures. (The stoichiometric mixture ratio corresponds to a cyanogen content of 11·11 per cent, at 20 per cent C_2N_2 the stoichiometric products are CO and N_2.) However, when one-third of the nitrogen in the 'air' is replaced by carbon monoxide, the burning velocity curve assumes a typical dependence upon fuel concentration, attaining a maximum value of 85 cm/sec for the 13 per cent cyanogen mixtures.

Further replacement of nitrogen by CO again changes the shape of the burning velocity curve, the highest burning velocities now being achieved at a cyanogen content of 10 per cent. It is possible that these curves may also pass through a maximum at lower cyanogen concentrations, but our data did not indicate such a trend. The substitution of CO for N_2 has effected a really remarkable increase in the burning velocity of the moderately rich cyanogen mixtures. Total replacement of nitrogen produced more than a threefold increase in burning velocity for the slightly lean and near-stoichiometric rich mixtures. This effect appears to be well outside the range of possible experimental error.

The maximum spread in burning velocity between the highest values and lowest values in any given set of data for a specified mixture

composition was generally less than 10 cm/sec, corresponding to a reproducibility of 10 per cent in the case of the lowest burning mixtures and 5 per cent for the mixtures of highest burning velocity. Though the absolute error in our measurements cannot be ascertained with certainty, the relative error is certainly no greater than 10 per cent. The genuineness of the maximum in the burning velocity curve for the 25 per cent CO 'air' mixtures may be open to some question in view of the marked difference in trend between this curve and

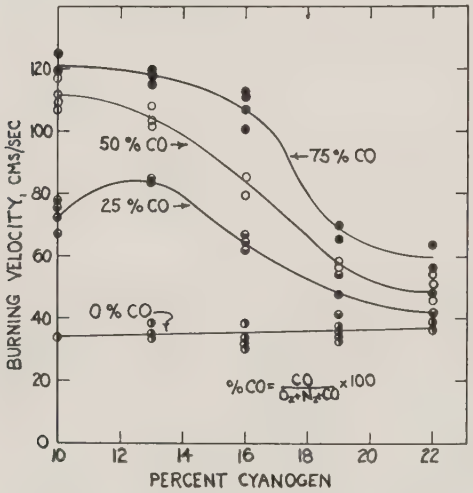

Figure 2. Burning velocities of cyanogen–oxygen–nitrogen mixtures with varying amounts of carbon monoxide substitution for nitrogen $O_2/(O_2 + N_2 + CO) = 0{\cdot}25$

the others for CO substituted mixtures. However, the experimental scatter in the data for the 10 per cent cyanogen point gives us no reason to suspect an abnormally large error in the burning velocity values for this mixture.

DISCUSSION

At first glance the burning velocity results appear to provide very convincing evidence for our hypothesis regarding the two-stage nature of the cyanogen flame. In mixtures containing no added carbon monoxide we assume that the cyanogen burns to CO in the primary zone of the flame, and that the further oxidation of CO to CO_2 occurs so far downstream of the primary region of reaction that it contributes little to the burning velocity. Evidence for such a phenomenon in hydrocarbon flames is afforded by the work of both Fristrom[8] and Friedman and Burke[9]. In particular, Fristrom has shown that for propane–air flames, the rate of propagation is determined principally by the primary oxidation of propane to CO, heat conduction and diffusion from the secondary zone in which CO is oxidized to CO_2 have a negligible influence upon the fundamental burning velocity. We now suppose that with the addition of some carbon monoxide to cyanogen mixtures the oxidation of CO to CO_2 is accelerated, coupling the secondary zone of the flame more closely in space and time to the primary region. It is further postulated that heat conduction from the secondary zone now begins to play a part in the flame propagation process, increasing the temperature of the reaction zone in which cyanogen is oxidized to CO. This rise in temperature in turn increases the rate of conversion of C_2N_2 to CO, producing an overall increase in the burning velocity of the mixture. With the further substitution of CO for N_2, the coupling between the cyanogen and CO oxidation processes becomes stronger, generating further increases in the rate of cyanogen conversion to carbon monoxide and in the burning velocity. This effect would be expected to vary with the cyanogen content of the combustible mixtures, being greatest in the leaner mixtures in which greater quantities of CO_2 are produced. Gratifyingly enough, our data confirm these expectations. Progressive substitution of CO for N_2 results in progressive increases of burning velocity. Thus, in the 13 per cent cyanogen mixtures, the burning velocity increases from 35 cm/sec for the initial C_2N_2–O_2–N_2 mixtures, to 85 cm/sec for mixtures in which one-third of the nitrogen has been replaced by CO, to 100 cm/sec for two-thirds replacement of the nitrogen, and finally to 118 cm/sec when all of the nitrogen is replaced. Furthermore, the effect is much greater for the leaner mixtures than for the richer ones. In the 19 per cent cyanogen mixtures, for example, the burning velocity rises to a value of only 69 cm/sec for total replacement of the nitrogen by carbon monoxide.

Of course the picture we have drawn of the mechanism of the cyanogen flame is open to a number of immediate objections. One might ask, for instance, for more convincing evidence that CO is not readily oxidized to CO_2 in cyanogen flames, and that the replacement of nitrogen by carbon monoxide increases the temperature of the zone in which C_2N_2 is converted to CO. It might be argued that since the carbon monoxide used in these experiments contained 1 per cent of hydrogen, the observed increases in burning velocity resulted simply from the addition of hydrogen to the cyanogen mixtures. One might further inquire as to whether the increases in burning velocity could arise from the preferential oxidation of CO in the substituted mixtures. Finally, even if one concedes some validity to the proposed mechanism for the action of CO on cyanogen flames, its applicability to rich mixtures containing 20 per cent or more of cyanogen

(where stoichiometry predicts only CO as an oxidation product) may certainly be questioned. The answer to these arguments requires a more critical analysis of our experimental results than has been presented thus far.

Berl and Barth[10] have shown that CO_2 is not produced in explosions of moderately rich C_2N_2–air mixtures for compositions in which it would be expected from stoichiometric considerations. Our experimentally determined expansion ratios also indicate that the carbon monoxide is not oxidized to CO_2 in dry cyanogen-enriched air flames. This can be demonstrated by comparing the measured expansion ratios with the theoretical expansion ratios calculated upon two different premises, one that the maximum amount of CO_2 permitted by the available oxygen is produced and the other that no CO_2 is formed. The expansion ratio is equal to the density ratio of the unburned to the burned gases and is given by the relationship:

$$E = \frac{T_b M_u}{T_u M_b}$$

in which T_b and T_u are the temperatures and M_b and M_u are the molecular weights of the burned and unburned gases respectively. The equilibrium flame temperatures and burned gas

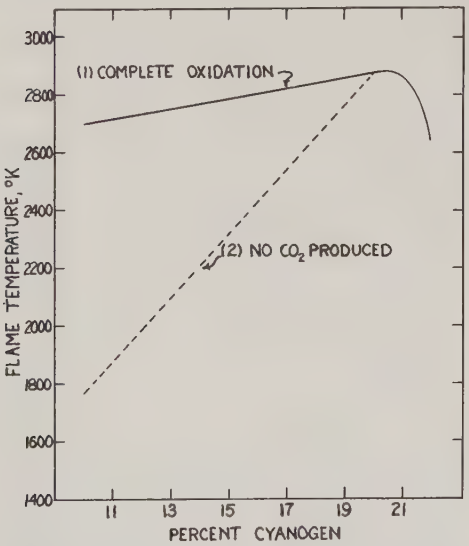

Figure 3. Calculated flame temperatures of cyanogen-enriched air (25 per cent O_2) *mixtures assuming: (1) complete oxidation, and (2) no* CO_2 *produced*

composition required for the evaluation of the ideal expansion ratios were calculated, using the equilibrium constants and thermochemical data tabulated by Lewis and von Elbe[11] and the thermodynamic functions for C_2N_2 and CN determined by Rutner, McLain, and Scheller[12]. Since there was no experimental evidence of carbon formation in these flames its presence was neglected in the rich side calculations (C_2N_2 > 20 per cent). The calculated flame temperatures are presented in *Figure 3* for the cases of both complete oxidation and no CO_2 formation. The two assumptions lead to a very considerable difference in adiabatic flame temperatures in the

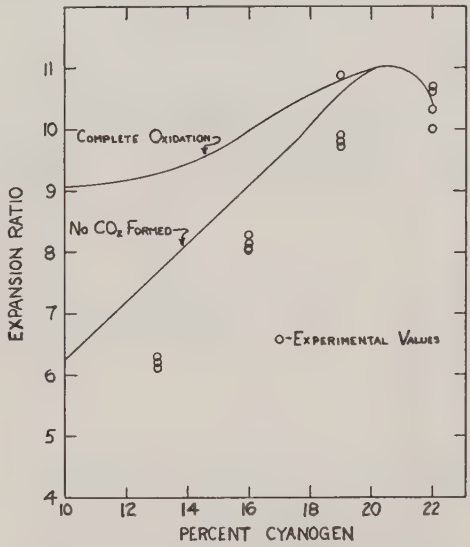

Figure 4. Comparison of calculated and observed expansion ratios for cyanogen-enriched air mixtures

leaner mixtures, which naturally decreases with increasing C_2N_2 content and vanishes at the 20 per cent value. In *Figure 4*, the calculated expansion ratios for the two conditions (solid curves) are shown, together with the plotted experimental values for C_2N_2-enriched air mixtures. Both the trend and magnitude of the observed expansion ratios indicate quite clearly that CO_2 is not being formed in these flames. In the leaner mixture, combustion even to CO appears to be incomplete, as these values lie well below the lower theoretical curve. However, calculations of the effect of unburned cyanogen or the expansion ratio reveal that a relatively large change in the expansion ratio can be produced by small amounts of unburned cyanogen. Combustion is more complete in the richer mixtures (19–22 per cent C_2N_2) and the experimental values are in satisfactory agreement with the calculated ones.

Accepting as fact the evidence that cyanogen burns only to CO in air mixtures, we are faced with a rather puzzling aspect of these flames. Consider again the calculated flame temperatures depicted in *Figure 3*. It is seen that there is a difference of approximately 1,000°K between the adiabatic flame temperature of the 10 and 19

per cent cyanogen mixtures. Despite the much higher flame temperature and greater fuel concentration of the 19 per cent mixtures, it apparently possesses the same burning velocity as the 10 per cent mixture, surely a most curious situation. Assuming a reasonable overall activation energy (*ca.* 40,000 cal/g mole) and a first order dependence upon fuel concentration, one would expect approximately a tenfold difference in the burning velocity of the two mixtures. The fact that such a difference is not observed demands some sort of an explanation. It might be argued that the activation energy of the cyanogen flame is very nearly zero, and that temperature has no effect on burning velocity on this account. However, this proposition does not appear to be tenable in view of the very low burning velocity of these flames. It could also be argued that our measurements are very badly in error and that large differences in burning velocity do in fact exist between the two mixtures. We refuse to concede that an order of magnitude relative error was possible in our experiments. Failing these two alternatives, it might be postulated that the reactivity of cyanogen mixtures is extraordinarily susceptible to their oxygen content, and that this factor is of overwhelming importance in determining the burning velocity of cyanogen flames. The latter supposition as well as the validity of our measurements can be examined with the aid of other experimental results. In *Figure 5* are reproduced burning velocity data for cyanogen with various oxidant mixtures obtained by different experimental techniques. The data on cyanogen–oxygen–nitrogen mixtures is from our present work with a balloon. Values for cyanogen–oxygen–argon mixtures were obtained in a bunsen burner by Brokaw and Pease[2]. Flame tube determinations for cyanogen–air mixtures were taken from reference 3. All the data exhibit the same independence of burning velocity on fuel concentration. It is significant to note that the cyanogen–oxygen–nitrogen and cyanogen–oxygen–argon mixture, which have the same oxygen content, appear to have equal burning velocities within the limits of experimental error, despite the higher theoretical flame temperatures of the argon containing mixtures. The most convincing demonstration of the influence of oxygen is afforded by a comparison of the cyanogen–air and cyanogen–oxygen–nitrogen flames. The burning velocity curves for both mixtures are quite parallel to one another over the entire composition range plotted. Upon the basis that only CO is formed in the flame, the two mixtures will have the same calculated flame temperatures up to a cyanogen concentration of 17·35 per cent (the stoichiometric value for CO formation in air mixtures). However, the burning velocity of the 25 per cent O_2 mixtures is more than three times as great as that of the air mixtures over this range, a result we may assume of the 4 per cent difference in oxygen content. Work is in progress in the laboratory to explore the effect of oxygen upon cyanogen flames in greater detail. For the present, we may conclude that our experimental data are reasonably valid, at least in a relative sense, and that oxygen plays a dominant role in the cyanogen combustion process.

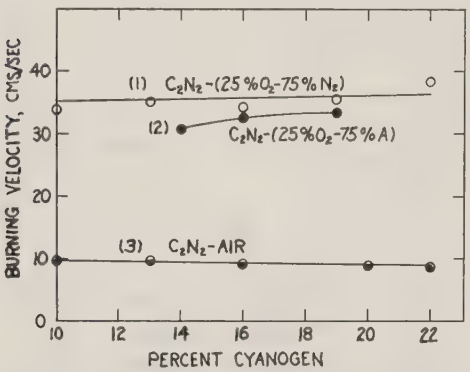

Figure 5. Influence of cyanogen content on burning velocity for various oxidant mixtures, obtained by: (1) balloon, (2) bunsen burner, and (3) flame tube methods

We had supposed, in our explanation of the influence of added carbon monoxide on the burning velocity of cyanogen mixtures, that its principal effect was to increase the temperature of the primary zone of the flame in which cyanogen is converted to CO. In the light of our findings that CO apparently is not oxidized at all in cyanogen–air flames, we may now postulate that the effect of added CO is to increase the flame temperature as a whole by inducing the previously unreacted CO to oxidize to CO_2 within the time available for reaction within the flame. The measured expansion ratios permit an examination of this premise. For this purpose, the variation of observed expansion ratio with increasing CO content has been recorded in *Figure 6* for 13 per cent cyanogen mixtures. A solid curve has been drawn through the averaged experimental data for each oxidant mixture composition. The trend of the data shows an unmistakable approach to the theoretical expansion ratio for complete oxidation to CO_2 as nitrogen is progressively replaced by CO. It seems fairly certain that the flame temperatures of these mixtures are increased by the substitution of CO for nitrogen. This effect is of course not attributable to the difference in specific heats between nitrogen and carbon monoxide, since the calculated flame temperatures for the two mixtures will differ by less than 1 per cent.

The analysis of the expansion ratios for the 10 per cent cyanogen mixtures is complicated by the fact that they are somewhat lean and the added

CO may burn with the excess oxygen to increase the flame temperature. The combustion of the carbon monoxide simultaneously produces a decrease in the molecular weight ratio of the unburned to burned gases; the net result may be a decrease in the expansion ratio for the mixtures richest in CO. Actually, the observed expansion ratios for these mixtures did not vary greatly over the entire range of CO substitution. Since in the 13 per cent cyanogen mixtures the theoretical flame temperatures would be the same for all CO contents, these were selected to illustrate the kinetic effect of CO substitution on the CO_2 oxidation.

Measurements of the expansion ratio in the richer mixtures (16–22 per cent cyanogen) were more uncertain than those in the leaner mixtures due to the greater luminosity of the richer flames. Nevertheless, it may be of interest to discuss them briefly. In the 16 per cent cyanogen mixtures the increase in expansion ratio with greater CO content was less marked than was the case for the 13 per cent mixtures. For total replacement of N_2 by CO, the expansion ratio rose to a value of 8·8 as compared with an initial value of 8·1 for C_2N_2–O_2–N_2 mixtures and a theoretical ratio of 10·0 for complete oxidation to CO_2. It may be that in this instance some of the CO was oxidized to CO_2 at the expense of unburnt cyanogen. This tendency was still more pronounced in the richer mixtures, in which the expansion ratio actually fell as N_2 was replaced by CO. To explore this situation further, the flame temperature and expansion ratio were calculated for a 19 per cent cyanogen mixture, in which all of the nitrogen had been replaced by CO, assuming that none of the cyanogen burned. Under these conditions the theoretical flame temperature falls to 2,500°K from a value of 2,750°K for the cyanogen-enriched air mixture and the expansion ratio is 6·6, as compared with a theoretical value of 10·7 and an observed average value of 10·1 for the initial air mixture. Since the measured average expansion ratio for the fully substituted CO mixture was 8·3, it appeared that a partial preferential oxidation of CO may have occurred. It is interesting to note that even in this case an increase in burning velocity is possible upon CO substitution. Let us assume that none of the cyanogen burns and that it acts merely as an inert diluent in the CO–O_2 mixture. An equivalent CO–O_2–N_2 mixture composition can be calculated which has the same flame temperature as the cyanogen mixture (2,500°K) and the same CO to O_2 ratio. From Jahn's work[13] the burning velocity of such a mixture is estimated to be 45 cm/sec. If the cyanogen burns to any extent it will raise the flame temperature and the estimated burning velocity of an equivalent nitrogen containing mixture.

It has already been pointed out that the carbon monoxide used in these experiments contained 1 per cent of hydrogen and that the burning velocities of cyanogen flames are greatly increased by the addition of small amounts of water vapour. A question naturally arises regarding the effect of hydrogen in increasing the burning velocity of CO substituted mixtures. Information bearing on this

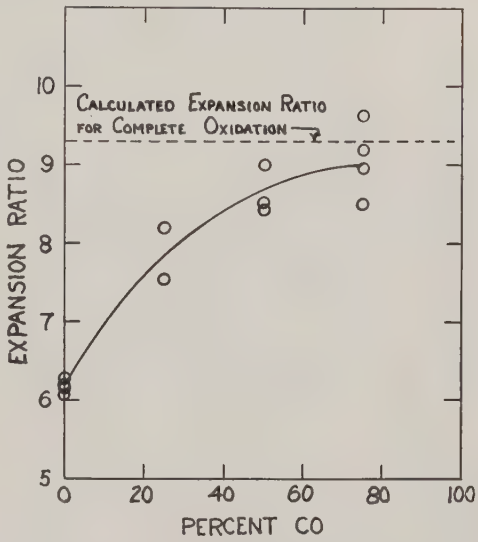

Figure 6. Variation of observed expansion ratio with CO *content of oxidant for* 13 per cent *cyanogen mixtures.* Per cent CO = $[CO/(O_2 + N_2 + CO)] \times 100$

matter is afforded by the previously referenced study of Brokaw and Pease[2]. They found the burning velocity of a dry 13 per cent cyanogen–oxygen–argon mixture to be approximately 30 cm/sec. The addition of 1 per cent of water vapour raised the burning velocity of this mixture to 50 cm/sec, an increase of some 67 per cent. This is to be compared with the increase of over 300 per cent obtained for the 13 per cent cyanogen–oxygen–carbon monoxide containing an estimated 0·6 per cent of hydrogen (since hydrogen is rapidly converted to water on an equimolal basis in the flame, the two substances may be considered to be equivalent in effect at low concentrations). Brokaw and Pease further observed that the effect of water was greater for the richer cyanogen mixtures. In their 19 per cent cyanogen mixtures, for example, the addition of 0·35 per cent of water increased the burning velocity from 34 to 44 cm/sec, corresponding to a rise of about 85 per cent in burning velocity for a 1 per cent water addition. In our experiments, on the other hand, the effect of CO decreased with increasing cyanogen content. In the 19 per cent cyanogen–oxygen–carbon monoxide mixtures, the burning

velocity rose by 100 per cent for an estimated hydrogen content of 0·6 per cent. Considering these facts, it does not appear that the effect of carbon monoxide in increasing the burning velocity can be attributed to the hydrogen it contained.

It remains now to discuss the possibility that the preferential oxidation of carbon monoxide might be responsible for the burning velocity increase in the moderately rich ($C_2N_2 < 16$ per cent) substituted mixtures. This contingency will be examined with respect to the 13 per cent cyanogen–oxygen–carbon monoxide mixtures. Assuming that none of the cyanogen burns, the flame temperature for the mixture is calculated to be 2,650°K and the expansion ratio 7·26, as compared with values of 2,750°K and 9·30 respectively for a C_2N_2–O_2—N_2 mixture. The measured average expansion ratio of 9·07 is in pronounced disagreement with the assumption of preferential oxidation. The burning velocity of an equivalent CO–O_2–N_2 mixture (same flame temperature and CO/O_2 ratio) is estimated to be 55 cm/sec from Jahn's data[13], a value to be compared with the observed one of 118 cm/sec. On the foregoing grounds the assumption that preferential oxidation occurs in these flames is clearly inadmissible. These calculations reveal an interesting synergistic effect produced by the substitution of carbon monoxide. The burning velocity of moderately rich C_2N_2–O_2–CO mixtures is twice as great as the flame speed of either fuel burned alone with the same amount of oxygen and an equivalent quantity of inert diluent.

CONCLUSIONS

The burning velocities of cyanogen-enriched air mixtures are markedly increased by the substitution of carbon monoxide for nitrogen. This effect is greatest for the leaner mixtures in which the production of greater quantities of CO_2 may be expected upon a stoichiometric basis.

Analysis of the observed expansion ratios indicates that cyanogen does not oxidize to CO_2 in dry, moderately rich C_2N_2–O_2–N_2 mixtures containing sufficient oxygen for its production. It is suggested that the effect of added CO on these mixtures is to increase the flame temperature by inducing the previously unreacted carbon monoxide to oxidize to CO_2 within the time available for reaction within the flame. There was evidence that in the richer mixtures the added carbon monoxide promotes preferential oxidation to CO_2 at the expense of unburned cyanogen.

The burning velocity of cyanogen mixtures appears to be extraordinarily sensitive to their oxygen content. Comparison of our 25 per cent O_2–N_2 mixtures with air mixtures reveals a threefold difference in burning velocity for the same theoretical flame temperature.

It does not seem reasonable to attribute the burning velocity increase obtained in the CO substituted mixtures to the small amount of hydrogen they contained.

It is quite improbable that the effect of carbon monoxide on moderately rich cyanogen mixtures is due to its preferential oxidation to CO_2.

The present work indicates quite clearly that cyanogen burns in a two-stage process. In dry air mixtures the second stage, involving oxidation to CO_2, is entirely suppressed. The second stage is believed to be activated by the addition of carbon monoxide. It is postulated that small quantities of added water or hydrogen act in a similar manner.

REFERENCES

[1] Conway, J. B., Wilson, R. H., Jr. and Grosse, A. V. *J. Amer. chem. Soc.* 75 (1953) 499

[2] Brokaw, R. S. and Pease, R. N. *J. Amer. chem. Soc.* 75 (1953) 1454

[3] Rutner, E., Scheller, K. and McLain, W. H., Jr. In press

[4] Edse, R., Strauss, W. A. and Fong, M. C. *Quart. Progr. Rep.* No. 10 on Contract AF 33(616)–2833 with Ohio State University

[5] Scheller, K. *Sixth Symposium (International) on Combustion*, pp. 280–288. 1957. New York; Reinhold

[6] Hadow, H. J. and Hinshelwood, C. N. *Proc. Roy. Soc. A* 132 (1931) 375

[7] Price, W. T. and Potter, J. H. *Fourth Symposium (International) on Combustion*, pp. 363–368. 1953. Baltimore; Williams and Wilkins

[8] Fristrom, R. M. *J. chem. Phys.* 24 (1956) 888

[9] Friedman, R. and Burke, E. *J. chem. Phys.* 22 (1954) 824

[10] Berl, E. and Barth, K. *Z. phys. Chem. Bodenstein Festband* 211 (1931)

[11] Lewis, B. and von Elbe, G. *Combustion, Flames and Explosion of Gases*. 1951. New York; Academic Press

[12] Rutner, E., McLain, W. H., Jr. and Scheller, K. *J. chem. Phys.* 24 (1956) 173

[13] Jahn, G. *Der Zündervergang in Gasgemisch.* 1934. Berlin; Oldenbourg

BURNING VELOCITY MEASUREMENTS BY THE CONSTANT-PRESSURE BOMB METHOD

W. A. STRAUSS and R. EDSE

INTRODUCTION

The effect of pressure on the burning velocity of combustible gas mixtures has been established for a number of systems by the bunsen burner method[1]. To substantiate these results, measurements were made using the constant-pressure bomb method. It was felt that this investigation was needed for the following reasons: (1) to extend previous results to the maximum operating pressure of 90 atm since for some systems stable flames at pressures above 21·4 atm could not be established at all or in some cases only on extremely small burner tubes; (2) flame fronts of high-energy flames were very difficult to see and photograph because of a halo of intense light surrounding the cone. It was also considered desirable to check burner tests by an entirely independent method.

APPARATUS AND METHOD

The method used to measure the burning velocities of gas mixtures was similar to the atmospheric pressure constant-pressure bomb method developed by Stevens[2]. Explosions of the gas mixtures were photographed by a high-speed strip film camera built in this laboratory. Since the gas expands as it burns, the unburned gases have an initial velocity; therefore, the actual burning velocity (S_u) is obtained from the photographically determined spatial velocity, S_t, according to the following expression:

$$S_u = \frac{S_t}{E}$$

where E represents the ratio of burned gas volume to unburned gas volume. The expansion ratios may be obtained from direct measurements of initial and final bubble size or from calculations of adiabatic flame temperature and combustion gas composition assuming that complete chemical and thermodynamic equilibrium prevails in the burned gas. Since it was found to be difficult to photograph the bubble wall and since any error in the determination of the diameter is cubed in calculating the volume expansion ratio, it was decided to derive E from thermodynamic calculations of adiabatic flame temperature and combustion gas composition. The results of these calculations are to be published later[3]. According to Simon and Wong[4] the calculated expansion ratios are in general very close to the observed values.

The apparatus used to measure burning velocities of gas mixtures by the constant-pressure bomb method is shown in *Figure 1*. It consists of: (1) a large-volume, high-pressure combustion chamber, (2) a remote control apparatus to position the constant-pressure spheres in the chamber at high pressures, (3) a device to ignite the high-pressure gases, (4) a device for producing the desirable gas mixture which forms the contents of the bubble, and (5) a high-speed strip film camera to record the explosion.

The design of the high-pressure chamber is shown schematically in *Figure 2*. It was made of a 10 ft length of 12 in. pipe. It has four 7/8 in. quartz windows which are used to project light into the chamber, to observe during bubble manufacture, and to photograph the propagation of the flame.

Two types of constant-pressure bombs were used for these studies. These were: (1) the non-aqueous soap solution bubble, and (2) the transparent thin-walled latex balloon. Whenever possible the non-aqueous soap solution bubble was used. However, at present, experiments with cyanogen–air and ammonia–oxygen are made with rubber balloons since these gases are readily absorbed by the soap solution. The soap bubble firing column apparatus employs two pneumatically operated electrodes to produce a spark. A 3·5 cm diameter bubble is positioned in such a fashion that the tips of the two electrodes make contact in the centre of the bubble. A spark is produced by passing a current through the electrodes and separating them shortly thereafter. The non-aqueous soap bubbles were blown with a flat blower tip. Various types of soap solutions were tested[5]; however, best results were obtained with a glycerine solution containing from 10 to 15 per cent by volume of Maypon 4C Special No. 2 detergent (Maywood Chemical Works, Maywood, New Jersey). This mixture is both temperature and age sensitive.

The rubber balloon firing column apparatus produces a spark in the same manner as the soap bubble apparatus. The rubber balloons (closed

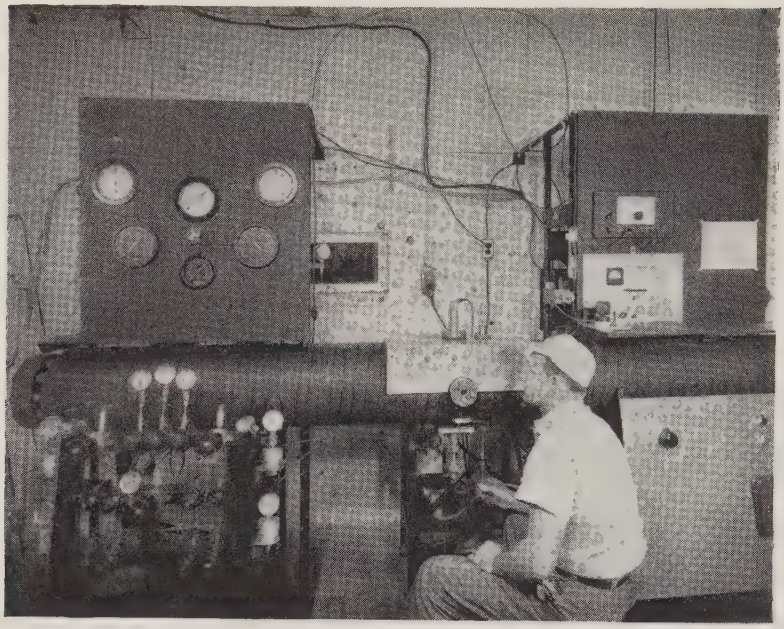

Figure 1. Photograph of high-pressure constant-pressure bomb apparatus

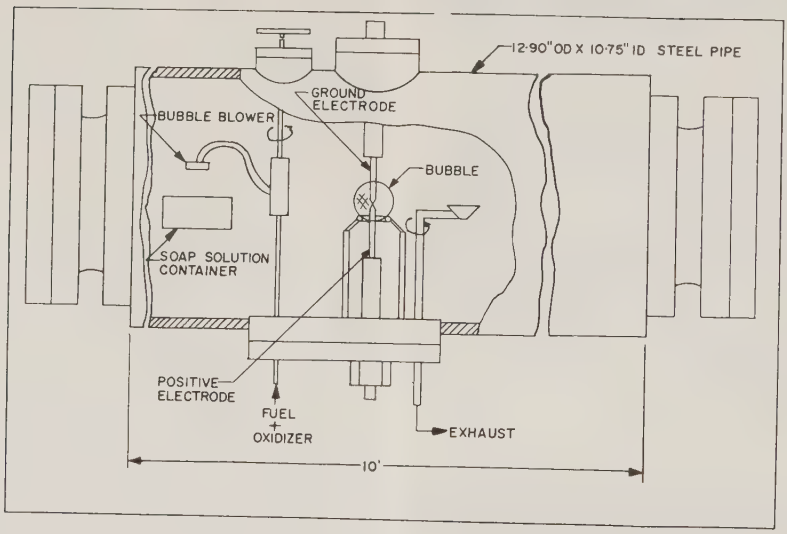

Figure 2. Sketch of constant-pressure bomb combustion chamber

at one end) are mounted in a collar, the open end of which is inserted on the firing column apparatus. All pressure seals are made with rubber *O* rings. The balloon is purged by successively pressurizing and depressurizing it with the desired gas mixture. To facilitate the conduction of the experiments, a conveyor with an asbestos belt was installed inside the high-pressure combustion chamber. This conveyor was used to deliver the collars (with rubber balloons) to a yoke which is subsequently used to attach the collars to the firing column apparatus. The thin-walled, transparent latex balloons were washed in a mixture of carbon tetrachloride and alcohol to remove the talcum powder.

A flow diagram of the apparatus for manufacturing the desirable gas mixtures is shown in *Figure 3.* A continuous flow of the gas mixture is produced from which a small amount of gas is withdrawn to blow the bubble.

A high-speed strip film camera (designed and constructed at this laboratory) was used to photograph progression of the flame front within the bubble. The film is attached to the periphery of a 10 in. diameter drum and held in place by a cam-locking device. The drum speed was made continuously variable from a maximum of 7,200 rev/min to a minimum of 6 rev/min. The timing mark light pulses are generated by a 1B59 glow

Carbon monoxide (Matheson): 96·8 per cent carbon monoxide, 0·36 per cent carbon dioxide, 0·97 per cent hydrogen, 1·0 per cent nitrogen, and 0·8 per cent saturated hydrocarbons

Nitric oxide (Matheson): 99·61 per cent nitric oxide, 0·37 per cent carbon dioxide, 0·02 per cent water

The air compressed at this laboratory was dried by activated silica gel. Iron penta carbonyl,

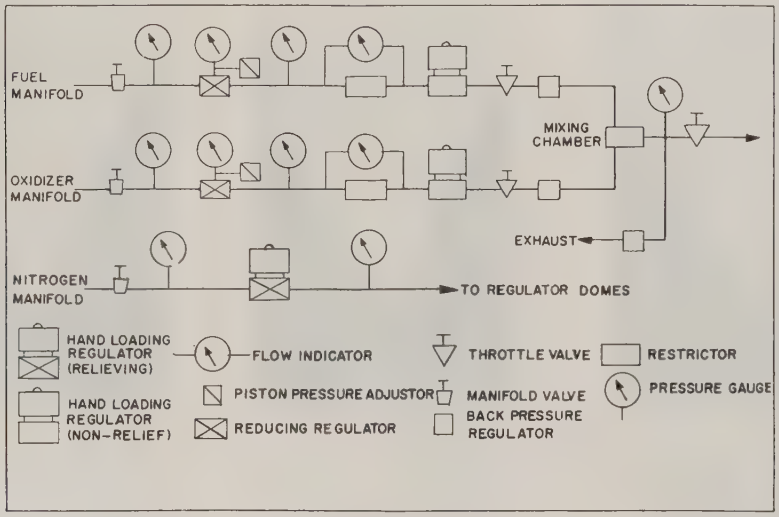

Figure 3. Flow diagram of constant-pressure bomb gas mixture apparatus

modulator tube which is excited by an RC oscillator[6] whose frequency is variable within the range of 40 to 20,000 c/s. The frequency of the oscillator is adjusted to give reasonable spacing of the timing marks for a given film speed, and the frequency is measured by an AN/UAM-26 frequency meter, the rated accuracy of which is $\pm 0{\cdot}1$ c/s. Non-perforated 35 mm Kodak Tri-X and Dupont SX-Pan films were used. Both were processed in Kodak D-19 which was activated by adding Kodak 'Solution A' to give maximum emulsion speed.

The gases used for the experiments were purchased from commercial manufacturers with the exception of the high-pressure air which was compressed at this laboratory. Typical analyses of the commercial gases as given by the manufacturer are as follows:

Oxygen (Linde): 99·5 per cent oxygen, 0·3 per cent argon, 0·02 per cent nitrogen

Hydrogen (Air Reduction): 99·92 per cent hydrogen, 0·08 per cent oxygen

Methane (Matheson): 93 per cent methane, plus ethane, propane, and small amounts of nitrogen and oxygen

carbon dioxide, and the saturated hydrocarbons were removed from the carbon monoxide gas by passing it over an activated charcoal trap cooled by dry ice.

Operation of the constant-pressure bomb apparatus described above is as follows: The fuel and oxidizer gas flows are adjusted to give the desired mixture by means of the flow control apparatus (*Figure 3*); the constant-pressure sphere mechanism and auxiliary lines are then purged with this mixture. The purged gas is not permitted to accumulate in the chamber but is exhausted directly to the atmosphere. During the purging time, the timing light frequency and strip film camera speed are adjusted to the desired values. A constant-pressure sphere of approximately 3-1/2 cm was then blown with the gas mixture. Next, the positive electrode piston is pressurized causing this electrode tip to contact the ground electrode at the centre of the sphere. The mixture within the bubble is exploded remotely by a switch which: (1) sends current through the electrodes, (2) actuates a solenoid valve which depressurizes the positive electrode piston, and (3) energizes two solenoids which trip both the shutter

of the timing mark lens and that of the taking lens of the strip film camera. The shutter of the taking lens is opened just before the electrodes separate.

RESULTS

Carbon monoxide–oxygen flames

The burning velocities of the carbon monoxide–oxygen system were measured at 1, 5·1, 21·4, 52 and 90 atm. *Figure 4* contains a series of photographs showing typical records of explosions of a carbon monoxide–oxygen mixture of approximately 80·25 per cent carbon monoxide at 1, 52 and 90 atm. Explosion traces at 1 and 5·1 atm pressure were similar. The spatial flame speed was constant as indicated by the sharp, straight-line burning trace (after a short initiation period). However, in some of the 21·4, 52 and 90 atm pressure tests the burning fronts oscillated. The amplitude of the oscillations increased both with the radius of burning and also with increasing pressure. For very rich and very lean mixtures no oscillations were observed. The wavy flame traces for these experiments were evaluated at both the initial and the final portions of the burning trace. The final portion was evaluated by drawing an average line through the oscillations and considering this as the front along which an average flame would advance. For about 30 per cent of the experiments at 52 atm and for most of those at 90 atm two values of the burning velocity were obtained as shown in *Figure 5.* According to these results the burning velocity increases with pressure for the final stage of burning, whereas it decreases with pressure for the initial propagation of the flame. Since the low values of burning velocity of the double valued experiments (based on initial portion of explosion trace) fall along the same curve which is defined by experiments whose fronts did not oscillate, it was assumed that the lower values at both pressures are most valid. Strehlow and Stuart[6] observed high-frequency oscillations in flames burning at atmospheric pressure. In the present investigation this type of oscillation did not occur at atmospheric pressure

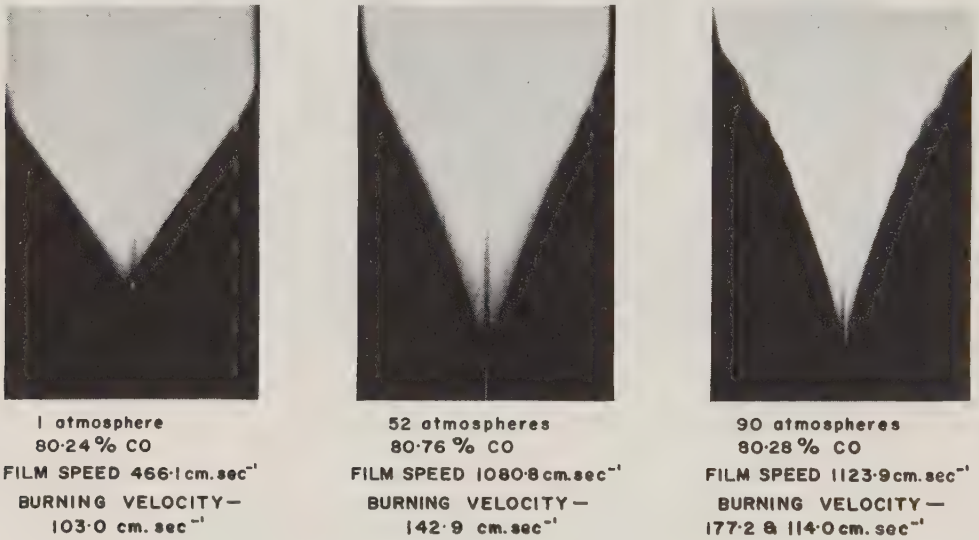

Figure 4. Typical record of explosion of carbon monoxide–oxygen mixtures at various pressures

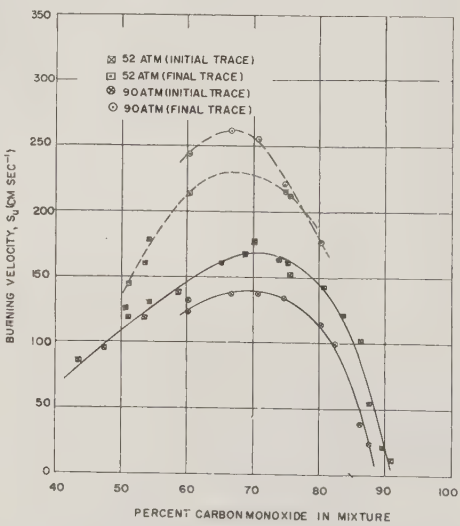

Figure 5. Comparison of carbon monoxide–oxygen burning velocities evaluated from initial and final portions of explosion trace

possibly because of the large volume of the combustion chamber. However, the low-frequency oscillations encountered in some experiments were found to be related to the time required for sound waves to move across the chamber diameter. The oscillations are therefore believed to be caused by pressure waves reflecting from the chamber wall.

The results of the measurements of the carbon monoxide–oxygen burning velocities are graphically depicted in *Figure 6.* This graph shows

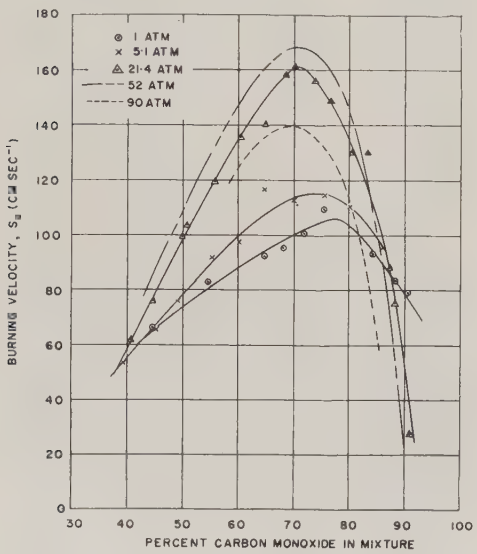

Figure 6. Burning velocities of carbon monoxide–oxygen flames

clearly that the burning velocity increases with rising pressure up to 52 atm and thereafter decreases.

Carbon monoxide–air and methane–air flames

The carbon monoxide–air and methane–air systems were investigated at 1, 21·4 and 90 atm. Burning velocities of these mixtures are plotted in *Figures 7* and *8,* respectively. As seen from these graphs the burning velocities of these mixtures decrease with increasing pressure. This result is in agreement with the observations obtained by the bunsen burner method for similar systems. However, for the carbon monoxide–air flames the maximum value of the burning velocity as determined by the bubble method is approximately 75 per cent above that obtained by the burner method while the maximum values of the burning velocity for given pressures occurs at the same mixture ratio. For methane–air mixtures the peak burning velocities also occur at approximately the same mixtures; however, at 21·4 and 90 atm

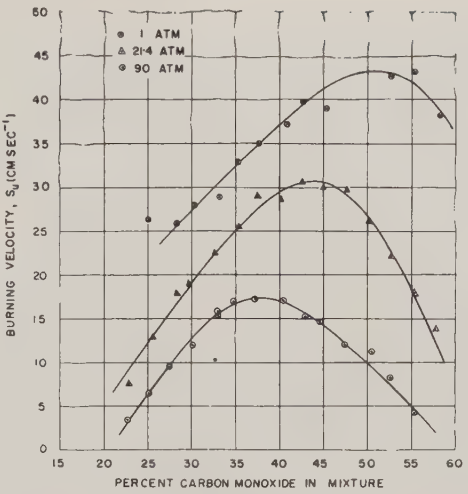

Figure 7. Burning velocities of carbon monoxide–air flames

the burning velocities derived by the constant-pressure bomb method are approximately 50 per cent higher than those obtained with the burner method. The dip in the curve representing the burning velocities of methane–air mixtures burning at 90 atm cannot be explained at this time. Simon and Wong[4] pointed out that the bubble method is not suitable for the determination of low burning

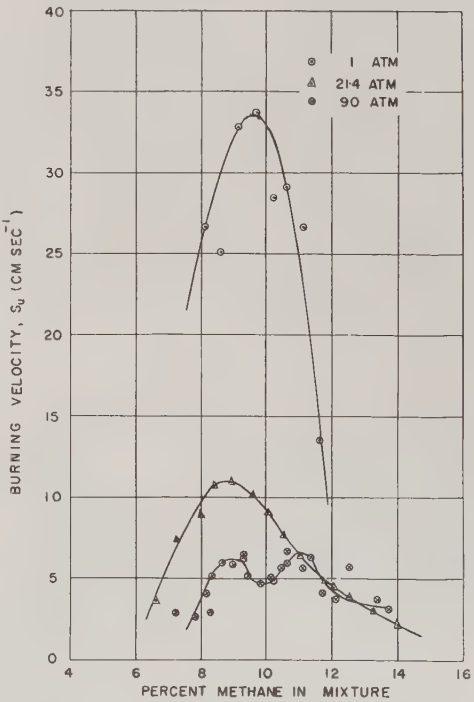

Figure 8. Burning velocities of methane–air flames

velocities because of the convective rise of the burned gases. This effect of the burned gas is particularly serious at elevated pressures. Since the flame traces were obtained by photographing the horizontal component of the spreading flame, the buoyancy would tend to yield lower burning rates. However, for these systems the burning velocities derived from the bubble method are above those of the burner method.

Methane–oxygen, hydrogen–oxygen, and hydrogen–nitric oxide flames

The burning velocities of methane–oxygen and hydrogen–oxygen mixtures were investigated at 1, 21·4 and 90 atm while the hydrogen–nitric oxide system was investigated at 5·1, 21·4 and 52 atm. The results of these investigations are shown in *Figures 9, 10* and *11*. These graphs indicate that

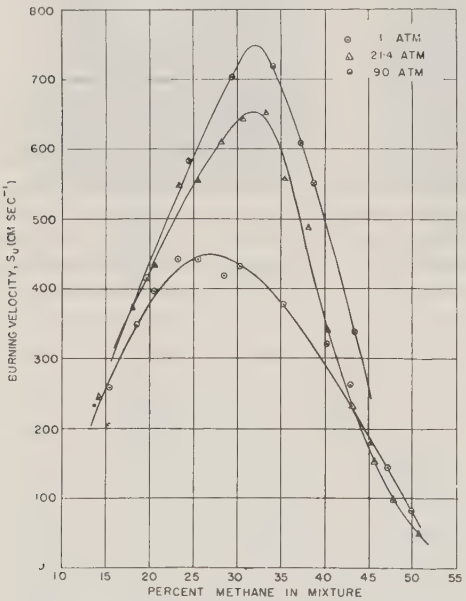

Figure 9. Burning velocities of methane–oxygen flames

the burning velocities of these mixtures increase with increasing pressure. This observation is in exact agreement with the measurements obtained with the bunsen burner method. Whereas the maximum burning velocities obtained by the constant-pressure bomb method at atmospheric pressure for the methane-oxygen and hydrogen-oxygen systems are again above those obtained by the burner method, at 21·4 atm the reverse is true. The burning velocities of hydrogen-oxygen mixtures measured by the bubble method at atmospheric pressure are not very accurate since the explosion traces on the film were very faint and, therefore, difficult to evaluate.

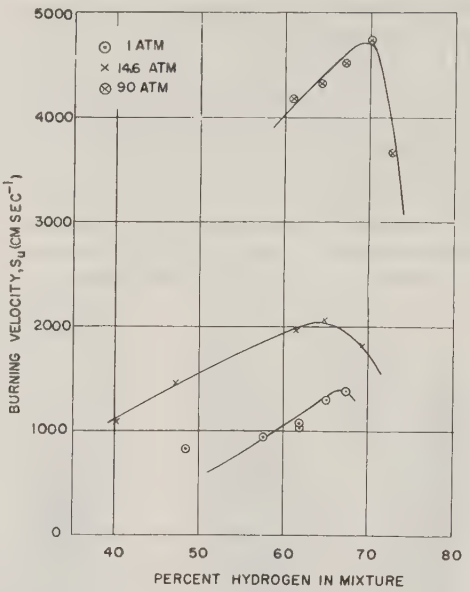

Figure 10. Burning velocities of hydrogen–oxygen flames

DISCUSSION OF RESULTS

The preceding discussion has shown that qualitative agreement exists between the results obtained for the effect of pressure on the burning velocities of various combustible gas mixtures according to two entirely different methods of measurement. In general, it can be stated that the burning

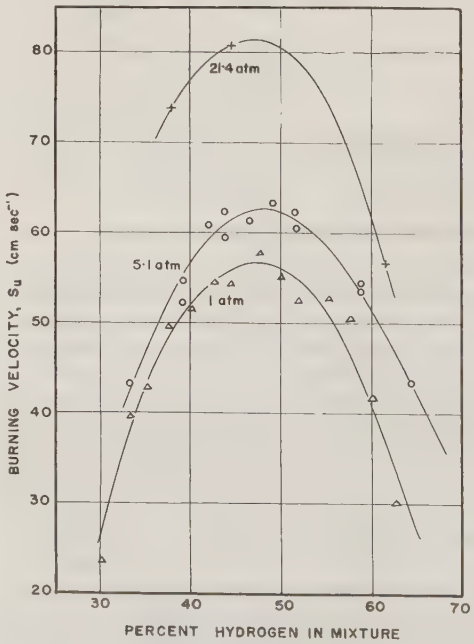

Figure 11. Burning velocities of hydrogen–nitric oxide flames

velocities of low-energy systems such as fuel–air flames decrease with increasing pressure whereas those of most high-energy systems such as fuel–oxygen mixtures increase with rising pressure for pressures between 1 and 90 atm. At the present only two major exceptions to this rule are known: (1) the burning velocities of carbon monoxide–oxygen mixtures reach a maximum at 52 atm, and (2) the burning velocities of hydrogen–nitric oxide mixtures are only moderately affected by pressure.

The quantitative relationships between burning velocity and pressure for all systems that have been investigated by the constant-pressure bomb method in this laboratory up to this time are graphically shown in *Figure 12.* In order to

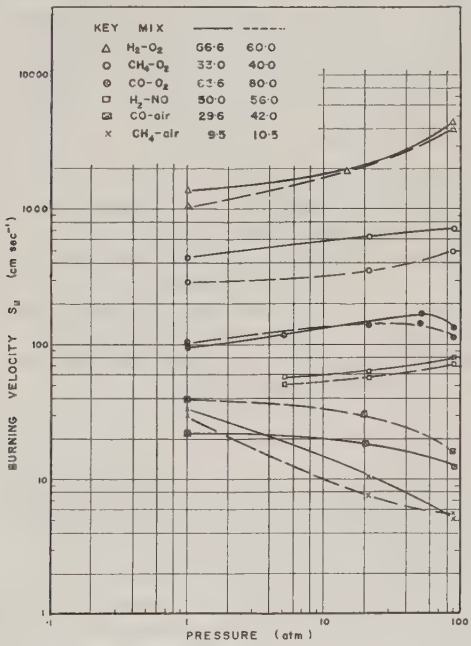

Figure 12. The effect of pressure on the burning velocity of various gas mixtures

explain these relationships theoretically it is necessary to consider all factors which contribute to the propagation of a flame front through a combustible gas mixture. For laminar flames these factors are: (1) composition of gas mixture, (2) initial temperature and pressure of gases, (3) transport properties of initial gases and reactants (heat and particle transfer rates), (4) chemical reaction rates, and (5) flame radiation.

For a given gas mixture at a fixed initial temperature a change in pressure will have an effect on the transport phenomena, on the chemical reaction rates and on the radiation properties in the flame zone. In traversing the reaction zone of a steady state flame normal to its plane we pass from the initial state of the unburned gas through regions of different composition until we reach the burned gas. It may be assumed that for most flames at a certain point this burned gas is in a state of complete thermodynamic and chemical equilibrium at a temperature which is only slightly below the adiabatic flame temperature. In any zone upstream of this plane such equilibrium does not exist. Therefore, according to the laws of thermodynamics, reactions leading to eventual equilibrium occur in these zones. The rates of these reactions depend on the gas temperature and on the concentrations of the reactants. Because of these variations of concentrations of particles and temperature in a direction normal to the flame front, diffusion and heat transfer occur. To formulate the contribution of the heat transfer is rather difficult because the hot molecules are also chemically different from the cold molecules. Therefore, heat transfer may be considered to be partially dependent on diffusion of reactants and intermediates. In any event the rates of these transport processes will depend predominantly on the gradients of temperature and concentration. When the pressure is increased, these gradients may change for two reasons: (1) the thickness of the flame zone decreases, and (2) the temperature and the absolute concentrations of particles in the burned gas may increase. Unfortunately, very little is known about the effect of pressure on the flame thickness. Only the adiabatic flame temperature and the equilibrium composition of the burned gas are amenable to exact theoretical calculations at present. According to these calculations the maximum flame temperatures of high-energy fuel-oxidizer mixtures such as methane–oxygen, hydrogen–oxygen, hydrogen–nitric oxide, and carbon monoxide–oxygen amount to approximately 3,000°K at atmospheric pressure while at 90 atm they[3] approximate 3,600°K. The absolute concentrations of radicals (n_i) such as OH, O and H in all high-energy systems are practically of equal order of magnitude. For a given mixture ratio they depend on pressure according to the following relationships:

$$n_{OH} \approx\!\propto p^{0.9}, \qquad n_O \approx\!\propto p^{0.8}, \qquad n_H \approx\!\propto p^{0.8}$$

For an estimate of the contribution of diffusion of particles from the burned to the unburned gas, however, the mole fractions of these particles have to be considered. According to the thermodynamic calculations of the equilibrium composition of the burned flame gases the mole fractions, γ, of OH, O and H decrease with increasing pressure as follows:

$$\gamma_{OH} \approx\!\propto p^{-0.09}, \qquad \gamma_O \approx\!\propto p^{-0.06}, \qquad \gamma_H \approx\!\propto p^{-0.17}$$

Spectroscopic measurements made at The General Electric Co.[7] have shown that the actual

radical concentrations in the flame zone are higher than those derived from the equilibrium composition of the burned gas. Assuming that the effective flame thickness practically does not depend on pressure, it appears that on the basis of the calculations of the equilibrium conditions in the burned gas the rate of diffusion in high-energy flames is reduced only slightly while the rate of heat transfer is increased by a fair amount. Therefore, it might be expected that the burning velocities of these systems increase with increasing pressure. This trend has been observed for a number of fuel-oxidizer flames as shown in the previous section. Since the adiabatic flame temperature does not increase indefinitely with pressure and since at very high pressures the mole fractions of the active radicals will decrease at a rate greater than that indicated by the equations for the 1 to 90 atm pressure range, the burning velocities of these systems should eventually decrease with rising pressure. Such a trend was observed only for the carbon monoxide–oxygen flames.

In general, for flames of low-energy systems such as fuel–air flames the adiabatic flame temperatures are practically independent of pressure while the mole fractions of active radicals decrease rather sharply with pressure[3]. Therefore, the burning velocities of such mixtures should decrease with rising pressure if it is again assumed that the effective flame thickness is practically independent of pressure and that the chemical reaction rates are not so low as to become the rate determining link. In the previous section it was shown that the burning velocities of all fuel–air systems decrease with rising pressures for all mixture ratios. From *Figures 6* and *9* it can be seen that for rich mixtures of the high-energy systems the burning velocities also decrease with increasing pressure. This observation is in agreement with the fact[3] that the adiabatic flame temperatures of these mixtures do not increase with rising pressure.

It is true that the effect of pressure on the burning velocities of pre-mixed combustible gases may be explained by suitable assumptions concerning the mechanism of the chemical reactions in the various regions of the flame. However, it is believed that sufficient information on these mechanisms is not available at present to justify formulation of a theory including any possible contribution of the reaction mechanism to the effect of pressure on the burning velocity of flames of pre-mixed gases. It might be argued that in most cases the rates of the chemical reactions occurring in flames are rapid enough to disqualify them from being the rate-determining factor for the burning velocity. In order to investigate the contribution of the chemical reactions to the mechanism of flame propagation we have started a series of experiments with binary fuel systems following a suggestion made by Karl Scheller of the Aeronautical Research Laboratory at the Wright Air Development Centre, Wright-Patterson Air Force Base, Ohio.

In the present study of the mechanism of flame propagation the influence of the chemical reactions on the rate of flame propagation became strongly apparent only in the case of hydrogen–nitric oxide flames. Although the adiabatic flame temperature and the radical concentrations in the burned gas of this system are of the same order of magnitude as those of corresponding hydrogen–oxygen mixtures, the burning velocities of hydrogen–nitric oxide mixtures are only about 1/20 of those of hydrogen–oxygen flames. Furthermore, the burning velocity of hydrogen–nitric oxide flames increases only very moderately with pressure. According to the bunsen burner method it was found to be independent of pressure. The most obvious reason for the great difference in the behaviour of these two systems may be seen in the large activation energy of the initiation reaction of the hydrogen–nitric oxide reaction which probably is represented by the homogeneous bimolecular decomposition of nitric oxide. The activation energy for this reaction has been reported as 75 kcal by Kaufman and Kelso[8]. However, Roslovskii[9] finds the activation energy to be only 50·7 kcal. He derived this value from measurements of the burning velocities of hydrogen–nitric oxide mixtures burning at pressures between 1·8 and 19 atm in constant-volume bombs assuming a third-order reaction. For a mixture containing 55 per cent nitric oxide Roslovskii found that the burning velocity depends greatly on pressure whereas for a mixture containing 33·8 per cent nitric oxide the burning velocity was described by him as being pressure independent. His numerical values for the burning velocities are much lower than those measured in this laboratory. The very small pressure dependence of the burning velocities of hydrogen–nitric oxide flames found in this laboratory must be considered as evidence against the assumption of termolecular initiation reaction in the flame.

That the low burning velocity of hydrogen–nitric oxide mixtures is not caused by the presence of nitrogen in the reacting gas can be seen from the fact that the burning velocities of hydrogen–oxygen–nitrogen flames[10] whose gas compositions correspond to those of hydrogen–nitric oxide flames are approximately 8 times faster than those of the hydrogen–nitric oxide flames. The possible influence of nitric oxide on the burning velocity was investigated in this laboratory by adding 1 per cent nitric oxide to a stoichiometric hydrogen–oxygen mixture. The burning velocity of this mixture was about 5 per cent lower than that of a pure hydrogen–oxygen flame.

In conclusion it can be stated that the effect of pressure on the burning velocities of pre-mixed gas mixtures can be explained by the effects of pressure on the rate of diffusion of active radicals, on the rate of heat transfer from burned to unburned gas, and in cases where a chemical reaction is the rate determining process it can be explained by the effect of pressure on this chemical reaction. To some extent all these factors, including probably the flame radiation which increases greatly with pressure, are inter-related. Since they depend on temperature and pressure in a very complicated fashion, the problem of finding an analytical expression for the burning velocity as a function of pressure over a large range of pressures appears to be practically insurmountable.

This research was supported in part by the United States Air Force under Contract No. AF 33(616)-2833, monitored by the Aeronautical Research Laboratory, WCLJC, Wright Air Development Centre, with The Ohio State University Research Foundation.

REFERENCES

[1] Strauss, W. A. and Edse, R. Investigation of flames burning at pressures up to 100 atmospheres, *WADC Technical Report* 56–49, 1956, *ASTIA No. AD* 103 095

[2] Stevens, F. W. A constant pressure bomb, *NACA Report* 176, 1923

[3] Strauss, W. A. and Edse, R. *Adiabatic Flame Temperatures, Combustion Gas Composition and Expansion Ratios of Combustible Gas Mixtures at Various Pressures.* In press, WADC

[4] Simon, D. M. and Wong, E. L. Evaluation of the soap bubble method for burning velocity measurements using ethylene-oxygen-nitrogen and methane-oxygen-nitrogen mixtures, *NACA Technical Note* 3106, *February* 1954

[5] Kaufman, F. and Cook, H. J. Non-aqueous soap bubbles for flame studies, *B.R.L., Aberdeen Proving Grounds, Technical Note* 575, *January* 1952

[6] Strehlow, R. A. and Stuart, J. G. An improved soap bubble method of measuring flame velocities, *Aberdeen Proving Grounds, Report No.* 835, *October* 1952

[7] *General Electric Review* 61 (1958) 8

[8] Kaufman, F. and Kelso, J. R. Kinetics and mechanism of high temperature reactions of nitric oxide, *B.R.L., Aberdeen Proving Grounds, Report No.* 923, *August* 1954

[9] Roslovskii, A. I. *Combustion of Mixtures of Nitric Oxide With Hydrogen*, Translation No. 656, 1957. Royal Aircraft Establishment, Ministry of Supply

[10] Jahn, G. *Der Zündvorgang in Gasgemischen.* 1934. Berlin; Oldenbourg

57

HIGH-TEMPERATURE OXIDATION AND BURNING OF CARBON MONOXIDE

G. K. SOBOLEV

The chemical transformation of carbon monoxide into carbon dioxide is a very complicated process. We have as yet no quite definite idea either of the mechanism of the elementary reactions which, in the long run, determine the overall characteristics of the process or of the dependence of that mechanism on the physicochemical and possibly the 'historical' conditions under which the reactions take place.

A large number of papers have been devoted to the study of the kinetics of burning of carbon monoxide, however, the results obtained up till now do not make it sufficiently clear whether the mechanism of burning of CO in the flame front is identical to the mechanism of its oxidation in the reaction zone just before and just beyond the front. The purpose of this study was to measure the rate of burning of CO in the flame front, using the results of normal flame velocity measurements for this purpose, and simultaneously to make direct measurements of the rate of oxidation of CO in the after-burning zones of the same flames. A comparison of the data obtained by these two independent methods will evidently be not only of theoretical but of practical value as well.

PROCEDURE

The tests were carried out at normal pressure with round cylindrical bunsen burners 7, 10 and 14 mm in diameter. Moist mixtures of CO, O_2 and N_2 were investigated. In studying the dependence of the reaction rate on the carbon monoxide or oxygen concentration the combustible mixtures were made up so as to keep the theoretical burning temperature approximately constant. For this purpose the excess component in the mixture was substituted by a corresponding quantity of nitrogen and the concentration of the substance in deficiency with respect to stoichiometry in the mixtures of each given series of experiments was kept the same. The theoretical burning temperatures were varied by changing the concentrations of the deficient component in the mixture[1]. The moisture concentration in the initial mixtures was kept approximately at 2 per cent in all experiments. Normal flame velocity was measured by the Guy–Michelson method.

The composition of the combustion products in the central zone of the flame was determined by chemical analysis of gas samples taken by means of a water-cooled gas sampling pipe. The position of the end of the pipe with respect to the apex of the luminous cone was recorded photographically.

The temperature of the combustion products was measured by the reversal method of sodium spectral lines. Streamline 'colouring' of the flame was carried out with a finely dispersed mist of a saturated aqueous solution of NaCl only along the axis of the central zone.

To determine the linear velocity of flow of the gases the gas streams were traced by means of tiny stroboscopically illuminated particles of magnesium oxide.

The data obtained as a result of direct measurements in the after-burning zone of the bunsen flame were treated by means of the general kinetic relation:

$$w = \frac{\Delta(CO_2)}{\Delta t} = K_0(CO)^n(O_2)^m \exp(-E/RT) \tag{1}$$

where w (mole/cm³ sec) = chemical reaction rate, (CO), (O_2) (mole/cm³) = molar concentration of carbon monoxide and oxygen in the reaction zone at the moment t and $\Delta(CO_2)$ = number of moles of carbon dioxide formed in Δt(sec) in 1 cm³, n and m = numbers corresponding to the order of the reaction rate with respect to carbon monoxide and to oxygen, $K_0\left(\frac{1}{\text{sec}}\left(\frac{\text{cm}^3}{\text{mole}}\right)^{m+n-1}\right)$ = overall reaction rate constant, E (cal/mole) = overall activation energy, R (cal/mole degr) = universal gas constant, T(°K) = temperature in reaction zone.

The reaction time $\Delta t = \Delta h/v$, where Δh (cm) = travel of the tip of the gas probe, and v (cm/sec) = linear rate of flow, was taken small enough (200–700 μsec) to allow use of kinetic equation 1 written in finite differences with sufficient accuracy.

The thermal theory of burning developed by Zeldovich, Frank-Kamenetskii[2] and Semenov[3] relates the heat release rate Q (cal/cm³ sec) to the normal flame velocity (cm/sec) as follows:

$$u = \frac{1}{\rho_0 L}\left(2\lambda\int_0^{T_1} Q\,dT\right)^{\frac{1}{2}} \tag{2}$$

where ρ_0 (g/cm³) = density, L (cal/g) = calorific value of the initial mixture, λ (cal/cm sec degr) = thermal conductivity, T_1 (°K) = theoretical burning temperature. The rate of heat release can be expressed as the product of the reaction heat q (cal/mole) by the reaction rate w:

$$Q = q \cdot w \qquad (3)$$

and an expression analogous to relation 1 can be used for determining the rate of reaction w in the

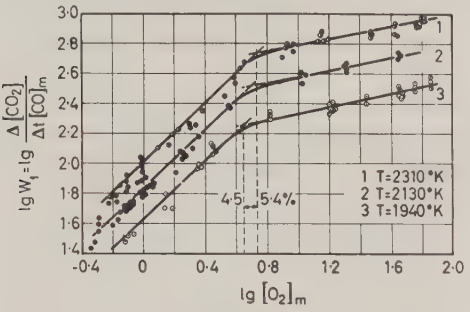

Figure 1. Dependence of CO *oxidation rate on oxygen concentration*

flame front. Therefore this theory makes it possible to establish indirectly the principal overall kinetic characteristics of burning (in the sense of the properties of Q) in the flame front.

EXPERIMENTAL RESULTS

Dependence of reaction rate on oxygen concentration

Preliminary experiments showed that with minor variations of the carbon monoxide concentrations when the oxygen concentration and the temperature in the reaction zone remain practically constant, the order of the oxidation rate n with respect to CO lies between 0·94 and 1·14. As these results were obtained at various temperatures and over almost the entire range of CO concentrations studied, the reaction rate value employed in establishing the dependence of the rate of CO oxidation on the oxygen concentration was referred to unity concentration of carbon monoxide and in first approximation it was assumed that $n = 1{\cdot}0$.

The experiments for determining the dependence of the rate of CO oxidation on the oxygen concentration were made at 1,940°, 2,140° and 2,310°K and covered the region of O_2 concentrations in the reaction zone from 0·5 to 73 per cent. The results of the measurements are given in *Figure 1*. The curves show that the rate of CO oxidation is in complex relationship to the oxygen concentration. All three curves have a distinct break in the concentration range 4·5–5·4 per cent. At low oxygen concentrations (below 5 per cent) the reaction rate may be considered proportional within the limits of experimental error to the first power of the oxygen concentration. At the same time, in the region of oxygen concentrations above 5 or 6 per cent the reaction rate is proportional to the 0·20 power of the oxygen concentration*.

In the experiments for determining the dependence of the normal flame velocity on the oxygen concentration the mixtures employed had theoretical burning temperatures of 2,100°, 2,150°, 2,240° and 2,650°K, the actual oxygen concentrations in the flame front $(O_2)_a$ being varied from 66 to 4·6 per cent. Further reduction of the oxygen concentration was accompanied by a considerable drop in the temperature measured above the apex of the luminous cone. This was an indication of substantial deviation of the processes characterizing that series of tests from isothermal conditions. The actual oxygen concentration in the flame front $(O_2)_a$ (in per cent by volume) was calculated on the assumption that this concentration exceeded the excess oxygen concentration in the initial mixture $\{(O_2)_0 - \frac{1}{2}(CO)_0\}$ by the value of $\frac{1}{2}(CO)_a$, corresponding to under-burning in the flame front. The under-burning in the flame front or rather the CO concentration in the reaction zone corresponding to the beginning of the characteristic temperature interval $T_1 - T$ was determined from the relationship

$$(CO)_a = (CO)_0 \frac{T_1 - T}{T_1 - T_0}$$

under the assumption that the interval

$$T_1 - T \simeq \frac{RT_1^2}{E}$$

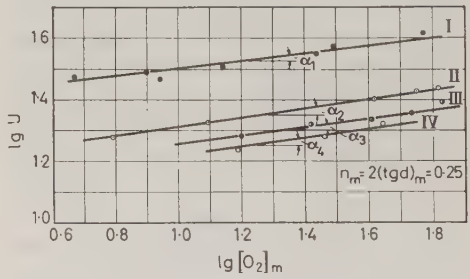

Figure 2. Dependence of normal flame velocity on excess oxygen concentration

The results of the measurements are given in *Figure 2*. These curves show that the normal flame velocity in the temperature and concentration range in question depends slightly on the concentration of oxygen contained in the mixture in excess of the stoichiometric amount. The

* Karzhavina concluded that the order of CO burning rate on oxygen is equal to unity up to 5 per cent of oxygen content in the mixture, and is equal to zero when the oxygen concentration is more than 5 per cent.

experimental points fall with sufficient accuracy on straight lines, the slopes of which with regard to the abscissa axis range from 0·11 to 0·14. The mean value of the order of the burning rate with respect to oxygen m, determined according to these data, equals approximately 0·25. This value is a little higher than, but agrees quite satisfactorily with, the above value $m = 0{\cdot}20$, determined by direct measurements in the after-burning zone of the bunsen flame*.

It can be seen from the results given above that when burning lean mixtures of carbon monoxide it is not rational to attempt to increase the after-burning rate by enriching the atmosphere with oxygen up to concentrations exceeding 4 to 6 per cent, owing to the very low efficacy of this measure. When rich mixtures were burnt, increasing the oxygen in the atmosphere to concentrations above 4 to 6 per cent raised the reaction rate considerably but this was due not so much to the influence of the oxygen on the reaction as to a substantial rise in the temperature.

Dependence of reaction rate on carbon monoxide concentration

The experiments for determining the dependence of the CO oxidation rate on the carbon monoxide concentration were carried out at 1,950°, 2,140° and 2,420°K. The results of the measurements are given in *Figure 3*, where the

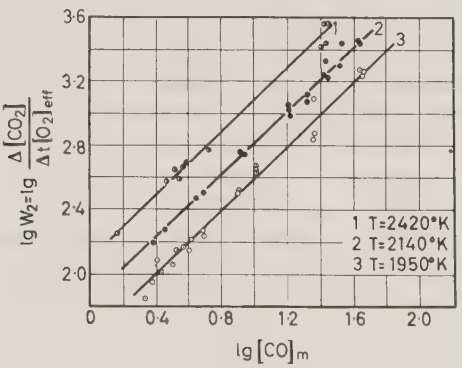

Figure 3. Dependence of CO *oxidation rate on carbon monoxide concentration*

logarithms of the CO oxidation rates referred to unit concentration of 'effective' oxygen are plotted along the ordinate axis. The concentration of 'effective' oxygen was calculated from the approximate relationship:

$$(O_2)_{\text{eff}} = \begin{cases} (O_2) & \text{at } (O_2) \leqslant 5 \text{ per cent} \\ 5\left[\dfrac{(O_2)}{(5)}\right]^{0{\cdot}20} & \text{at } (O_2) \geqslant 5 \text{ per cent} \end{cases} \qquad (4)$$

* Barsky concluded that the flame velocity does not depend on the concentration of the excess oxygen.

obtained on the basis of the above results of the dependence of the CO oxidation rate on the O_2 concentration. On the basis of these curves it may be considered that the rate of CO oxidation at constant temperatures and constant concentrations of other active components in the after-burning zone of the bunsen flame is directly proportional to the carbon monoxide concentration.

In the experiments for studying the dependence of the normal flame velocity on the carbon

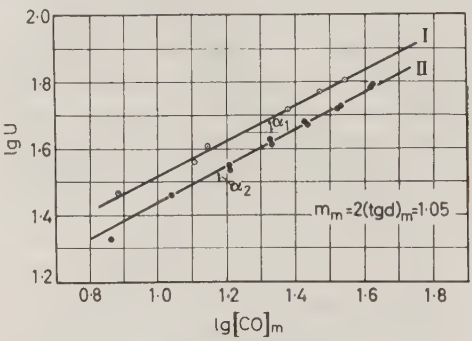

Figure 4. Dependence of normal flame velocity on excess carbon monoxide concentration

monoxide concentration the mixtures employed had theoretical burning temperatures of 2,300° and 2,540°K. The actual carbon monoxide concentrations in the flame front $(CO)_a$ were varied in these experiments from 42 to 7 per cent. As in the case of excess oxygen it was assumed that here also the actual concentration of carbon monoxide in the flame front $(CO)_a$ exceeds the excess CO concentration in the initial mixture $\{(CO)_0 - 2(O)_0\}$ by the value of $2(O_2)_a$. The relative oxygen concentration in the flame front $(O_2)_a$ was also calculated on the assumption of similarity between the temperature field and the concentration distribution of the deficient component in the reaction zone. In other words it was assumed that

$$(O_2)_a = (O_2)_0 \frac{RT_1^2}{E(T_1 - T_0)}$$

The results of the measurements are given in *Figure 4*. The tangent of the angle of slope of the curves to the abscissa axis equals approximately 0·525. The order of the burning rate n, with respect to carbon monoxide when the latter is in excess of the stoichiometric quantity in the mixture, turns out according to these data to be close to unity*. Thus, the result obtained coincides sufficiently well with the result found in studying the dependence of the oxidation rate on the CO concentration in the after-burning zone of the bunsen flame.

* The same results were obtained in papers given as references 5 and 6.

TEMPERATURE DEPENDENCE OF REACTION RATE

The temperature dependence of the CO oxidation rate in the after-burning zone of an open bunsen flame was investigated over a temperature range of 1,910° to 2,400°K. The results of this investigation are presented in *Figure 5* (points indicated by 0) as log K_1 *versus* $1/T$. The values of the rate constant of the monomolecular reaction were calculated from the relationship:

$$K_1 = \frac{\Delta(CO_2)}{\Delta t(CO)_m} \qquad (5)$$

i.e. the reaction rate was assumed to be independent of the oxygen concentration. As this

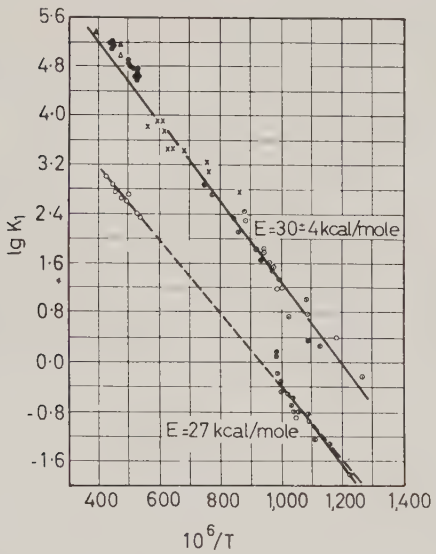

Figure 5. Temperature dependence of reaction rate

× *data of Karzhavina*[6]; ⊙ *data of Solovyeva*[7];
⊗ *data of Kozlov*[8]; ◑ *data of Chukhanov*[4];
△ *data of Barsky*[5]; ○, ● *author's data.*

assumption is approximately true for the burning of lean mixtures, only those experiments were taken into account in which oxygen was present in great excess. The mean value of the activation energy E determined according to these data equals 27 ± 3 kcal/mole. Attention is drawn to the fact that the mean value of the activation energy of CO oxidation determined according to the data of Chukhanov[4] (E = 28·8 kcal/mole) for the temperature range 820°–1,020°K approximately equals the value (E = 27 kcal/mole) calculated by us for temperatures of 1,910°–2,400°K. The absolute values of the pre-exponential factors K_{0_1} (1/sec) found from the relationship:

$$K_1 = K_{0_1} e^{-E/RT} \qquad (6)$$

agree sufficiently well with each other, this being borne out also by the fact that the data of Chukhanov ($K_{0_1} = 6{\cdot}9 \times 10^5$ 1/sec) fall rather closely around the continuation of the straight line drawn through our experimental points ($K_{0_1} = 2{\cdot}7 \times 10^5$ 1/sec). The values of the burning rate constant determined according to the results of normal flame velocity measurements were calculated by the approximate relationship:

$$K_1 = \frac{u^2(CO)_0^2}{T_m(CO)_a} \frac{(5)}{(O_2)_{eff}} \frac{qE}{2{\cdot}27 \cdot 10^6 \cdot 2\lambda \cdot RT_0} \qquad (7)$$

This relationship was derived on the basis of the thermal theory of burning (see above) and the assumption that the temperature T_m measured in the direct vicinity of the flame front is a more accurate characteristic of the processes taking place in the flame reaction zone than the theoretical burning temperature T_1, which is practically never attained in the open bunsen carbon monoxide flame. Preliminary experiments show that the temperature T_m agrees sufficiently well with the condition of similarity between the temperature and concentration fields, so that in the case of the lean mixtures dealt with in this paper the concentration value $(CO)_a$ in the flame front can be calculated by means of the relationship:

$$(CO)_a = (CO)_0 \frac{T_1 - T_f}{T_1 - T_0} \qquad (8)$$

where $T_f = T_m - RT_m^2/E$. The value of $(O_2)_{eff}$ in expression 7 was calculated by means of expression 4. The factor $(5)/(O_2)_{eff}$ is included in expression 7 to reduce K_1 to the corresponding value for a conditional combustible mixture containing 5 per cent oxygen.

In calculations of K_1 the value of q was accepted as equalling 67,600 cal/mole and the value of the thermal conductivity λ was taken equal to $2{\cdot}2 \times 10^{-4}$ cal/cm sec degr, which was calculated for a mean burning temperature T = 2,100°K by the Sutherland formula:

$$\lambda = \lambda_0 \frac{T_0 + B}{T + B} \left(\frac{T_0}{T_0}\right)^{\frac{3}{2}} \qquad (9)$$

where T_0 = 380°K, $\lambda_0 = 7{\cdot}4 \times 10^{-5}$ cal/cm sec degr and the constant B = 120. The results of this calculation are given in *Figure 5* (points designated by •). The mean value of E determined according to these data equals 30 ± 4 kcal/mole. The data of other authors[4–8] have also been plotted in this illustration, and they can quite readily be connected by a single straight line whose slope with respect to the abscissa axis corresponds to a mean activation energy of approximately 30 kcal/mole. However, the mean value of the constant resulting from these data and corresponding evidently to the conditions

of flame combustion of CO, equals $9{\cdot}5 \times 10^7$ 1/sec, whereas the value of K_{0_1} determined according to the lower line corresponding to oxidative conditions of formation of carbon dioxide equals $2{\cdot}7 \times 10^5$ 1/sec. Thus, the oxidation of CO in a large excess of oxygen in the after-burning zone of a laminar bunsen flame can be described by the kinetic equation:

$$\frac{d(CO)}{dt} = -2{\cdot}7 \cdot 10^5 (CO)\, e^{-(13{,}500/T)} \quad (10)$$

and in the case of the burning of lean mixtures the dependence of the normal flame velocity u on the carbon monoxide concentration and the temperature measured in the direct vicinity of the flame front is described sufficiently well by the relationship

$$u = \left\{2{\cdot}8 \cdot 10^4 \frac{(CO)_a T}{(CO)_0^2} e^{-(15{,}000/T)}\right\}^{\frac{1}{2}} \quad (11)$$

Comparison of the data obtained shows that the overall kinetic parameters of the process of formation of carbon dioxide, such as the order of the reaction rate with respect to oxygen (m), the order of the reaction rate with respect to carbon monoxide (n) and the activation energy of the process E determined by the two methods described above, agree sufficiently well within the limits of experimental error. However, the absolute values of the rate constants (K_{0_1}) determined from the data of these independent measurements differ by two orders. The rate constant of the chemical reaction taking place in the flame front turns out to be 300 to 400 times larger than the rate constant of the chemical reaction taking place in the after-burning zone.

That the rates of these reactions differed was pointed out also by Friedman and Cyphers[9].

Studying the oxidation of CO, they found that the carbon monoxide formed in the after-burning zone of a propane–air flame reacts 5·6 times more slowly than a CO–air mixture burns. The reason for this phenomenon is not quite clear as yet. It may probably be assumed that the different rates are due to the specific conditions governing the course of the elementary reactions in the flame front. The constancy of the principal overall kinetic parameters (m, n, E), though far from unambiguous, probably indicates that the mechanism of transformation of carbon monoxide does not undergo substantial changes on passing from the flame front into the after-burning zone. It is quite possible that owing to the sharp deviation of the system from conditions of thermal and chemical equilibrium, exceedingly high concentrations of those active centres which mainly determine the numerical value of the overall reaction rate may build up in the front reaction zone, while their concentrations under the quasi-equilibrium conditions arising in the after-burning zone is comparatively low.

A study of the mechanisms of the elementary reactions taking place under various conditions will evidently throw more light on this question.

CONCLUSIONS

(1) It has been established that under conditions of high-temperature CO oxidation in the after-burning zone of the bunsen flame the order of the overall reaction rate with respect to oxygen m at low concentration of the latter equals 1, and at a higher concentration (above 6 per cent) equals 0·20; the order of the reaction rate with respect to CO n equals 1 over the entire range of carbon monoxide concentration studied; the value of the activation energy of the overall monomolecular oxidation process equals 27 ± 3 kcal/mole, and the absolute value of the monomolecular reaction rate constant K_{0_1} equals $2{\cdot}7 \times 10^5$ 1/sec.

(2) It has been established that under conditions of flame combustion of carbon monoxide the order of the overall reaction rate with respect to the excess oxygen m equals 0·25; the order of the reaction rate with respect to the excess carbon monoxide n equals 1; the value of the activation energy E of the overall monomolecular process is 30 ± 4 kcal/mole and the absolute value of the overall monomolecular process constant K_{0_1} is $9{\cdot}5 \times 10^7$ 1/sec.

(3) It is pointed out that the principal kinetic parameters (m, n, E) of CO_2 formation taking place in the flame front agree sufficiently well with the characteristics of the process of formation of CO_2 in the after-burning zone of the same flames. It is emphasized, however, that the absolute values of the rates of these processes differ by two orders.

(4) The assumption is put forth that the reason for the difference in the rates of these processes is probably due to the specific conditions of the reactions taking place in the flame front, these conditions possibly being related to the substantial deviation of the system from conditions of thermal and chemical equilibrium.

The author wishes to express his gratitude to Professor L. N. Khitrin for his aid and interest in the work.

REFERENCES

[1] Zeldovich, Y. B. and Barsky, G. A. Burning kinetics of carbon monoxide. *Zh. fiz. Khim.* (*U.S.S.R.*) 25 (1951) 523

[2] Zeldovich, Y. B. and Frank-Kamenetskii, D. A. Thermal theory of flame propagation. *Zh. fiz. Khim.* (*U.S.S.R.*) 12 (1938) 100

[3] Semenov, N. N. Thermal theory of burning and explosion. *Uspekhi fiz. nauki* (*U.S.S.R.*) 24 (1940) 4

[4] Chukhanov, Z. F. Burning of carbon. *Zh. Tekh. Fiz.* (*U.S.S.R.*) 8 (1938) 147
— *Zh. Tekh. Fiz.* 8 (1938) 621

[5] Barsky, G. A. Investigation of the burning of carbon monoxide. *Thesis, Inst. of Chemical Physics, U.S.S.R. Academy of Sciences*, 1945

[6] Karzhavina, N. A. Burning of carbon monoxide. *Zh. fiz. Khim.* 19 (1945) 551

[7] Khitrin, L. N. and Solovyeva, L. S. Homogeneous-heterogeneous combustion of carbon monoxide in narrow tubes (channels). Paper 74

[8] Kozlov, C. I. On high-temperature oxidation of methane. This volume, Paper 25

[9] Friedman, R. and Cyphers, J. S. On the burning rate of carbon monoxide. *J. chem. Phys.* 25 (1956) 448

THE VERTICAL TUBE REACTOR—A TOOL FOR STUDY OF FLAME PROCESSES

K. G. WILLIAMS, J. E. JOHNSON and H. W. CARHART

INTRODUCTION

Studies of flame development in a heated vertical tube have shown it is possible to separate and stabilize in a single apparatus the various stages which lead to normal flames in the autoignition process. The first clearly marked phase in this process is the development of a low intensity combustion wave known as a cool flame. The cool flame, which gives off some heat and a pale bluish light, spectrally characteristic of activated formaldehyde, has been examined by many investigators, a few of which are cited[1,2,3,4].

The cool flame is self-inhibiting and never releases the total available chemical enthalpy of the system so the final products contain partially oxygenated materials such as aldehydes and peroxides. While the mechanism of the inhibition is not yet unambiguously understood, it seems to be related to a negative temperature coefficient of reaction which operates to reduce the extent of reaction in the cool flame as the temperature is raised beyond a critical zone[5,6]. This effect is not always easy to observe because reactions subsequent to the cool flame are not similarly inhibited. Nevertheless it often serves to confine the cool flame to a relatively low percentage of the available reactants so that oxidizing gas, unaltered fuel, and cool flame products are available for further reaction.

The maximum temperature attained by the cool flame is seldom more than 100–150°C above its initiation temperature (250–400°C) and is not sufficient to initiate directly a normal combustion wave. The necessary additional temperature increase arises from a second chain-branching process, separated in time from the cool flame. This delay, like the cool flame induction period, seems to arise from the necessity of generating a sufficient concentration of chain initiators.

The development of the second stage culminates in a blue flame of sufficiently great luminosity so it can readily be seen in subdued light. Emission from this blue second-stage flame, under fuel rich conditions where subsequent thermal reactions do not complicate the spectrum, is nearly identical to that of the cool flame[7,8].

The temperature rise in the blue flame depends primarily on the availability and proportions of reactants. When conditions are favourable, normal combustion is initiated. The fully developed combustion wave is characterized spectrally by emission from fragmentary particles such as OH, C_2 and H_2O.

Under many conditions, where autoignition occurs, the controlling induction period is that of the cool flame. Once this has been initiated the subsequent transitions occur with such rapidity and inhomogeneity that the stepwise nature of the process is obscured.

To study details of the discrete stages, they may be separated in either time or space. While each approach is subject to inherent disadvantages, both have been used with success.

This paper deals with an experimental technique based on a vertical reactor for separating the stages leading to normal combustion so that each can be examined in either the presence or absence of the next succeeding stage.

The vertical reactor was designed originally to determine the temperature at which the autoignition process was superseded by normal combustion. There are indications from studies of Levedahl[11] and from Johnson, Crellin and Carhart[12] that this transition occurs at a temperature of 550–600°C, regardless of the cool flame susceptibility of the fuel.

Because of the extremely rapid transition from second stage to normal combustion in static systems, a flow system in which the oxygen concentration could be raised gradually to the critical level was believed to offer the best chance of success. Flat flame burners operated on this principle provide a clean distinction between the cool and second-stage flames[13,14], but it was believed that wider separation could be achieved in a heated tube. Successful separations have been reported in horizontal heated tubes[7,15], but temperature variations across the vertical diameter of the tube lead to oddly shaped flames having only bilateral symmetry. Since vertical mounting of the tube would provide a flame having axial symmetry, this was tried.

The separations obtained with the vertical reactor were satisfactory and gradual increase of

the oxygen concentration was found to provide an excellent precession of flame stages. The method is reported below.

EXPERIMENTAL

Apparatus

The initial apparatus (*Figure 1*) consisted of a vertically mounted Pyrex glass tube, 42 mm i.d. and 20 in. long. The tube was heated electrically by means of a transparent conductive coating of tin oxide fused on to the outer surface. The

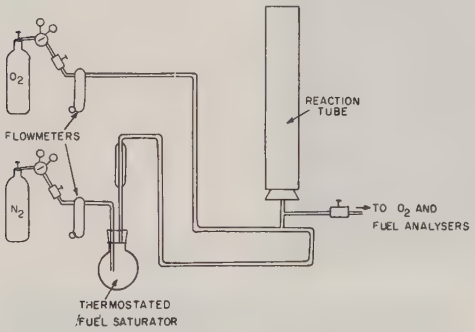

Figure 1. Sketch of apparatus

bottom of the tube was closed with a rubber stopper supporting a bed of glass beads ($\frac{1}{8}$ in. diam) 2 in. in depth to disperse the gas entering through an axial hole in the stopper. A loose plug of glass wool prevented random air currents from disturbing flow at the top of the tube and the tube was shielded from draughts by a glass jacket.

Ancillary equipment was limited to the pressure reducing and throttling valves and flow meters necessary to meter separate streams of oxygen and nitrogen into a mixing 'Tee' at the bottom of the reactor, a temperature controlled fuel bubbler in which the nitrogen stream was saturated with fuel vapour, a para-magnetic oxygen analyser and an infra-red absorption meter to monitor the reactant concentrations.

Procedure

The tube was heated to the desired temperature while the fuel bubbler temperature and nitrogen valves were adjusted to give the desired flow conditions. Then, while observing the tube in total darkness (15–20 min were usually allowed for dark adaptation of the observer's eyes), the oxygen flow was started and gradually increased.

Visual observations

The first visible reaction appeared near the top of the tube as a diffuse cloud of luminosity several in. in length. As the oxygen flow was increased this moved downwards in the tube and coalesced into a clearly defined cool flame. Additional oxygen caused a slight additional movement downwards and decreased the apparent thickness of the luminous zone. A second diffuse cloud of luminosity then appeared near the top of the tube (usually also along the walls) and as the oxygen flow continued to increase, coalesced into the second-stage flame which was clearly separated from the cool flame and was considerably brighter.

Additional oxygen decreased the separation of the two stages and led very gradually to a column of orange luminosity in the wake of the second-stage flame. This increased in intensity and spread out to form a sooty candle-like flame bright enough so that the cool flame could no longer be seen. Additional oxygen caused this flame to break up into a hollow cylinder made up of several cusps which rotated slowly in the tube.

Up to this point the flame structure was completely stable and could be retrograded smoothly by decreasing the oxygen flow. Beyond this point the cusps elongated and probed erratically towards the bottom of the tube, eventually pulling the whole flame structure down to the beads. Additional oxygen increased the intensity and whiteness of this stabilized flame. Still more oxygen caused the flame to flash back abruptly through the bed of glass beads and to burn vigorously in the $\frac{1}{8}$ in. diam passages of the mixing 'Tee'.

Sketches of these steps are shown in *Figure 2* and photographs are shown in *Figure 3*. The stability of the cool flame was such that colour photographs taken with a 10 min exposure showed no appreciable movement.

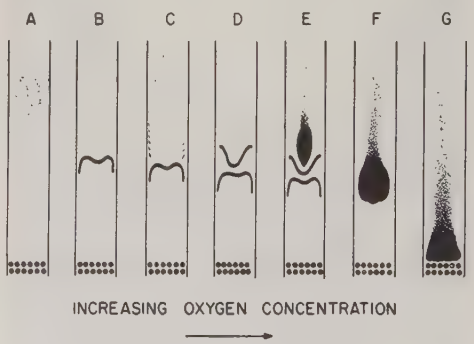

Figure 2. Sketch of observed flame stages. (A) Diffuse pre-cool flame luminosity; (B) coalesced cool flame; (C) cool flame plus wall luminescence and diffuse luminosity; (D) cool flame and blue second-stage flame; (E) developing orange flame; (F) cylindrical, cusped flame; (G) thermally self-sustaining flame stabilized at bottom of tube

Temperature measurement

To determine the position of the various flame stages a thermocouple was mounted so that it could be moved along the axis of the tube. The

couple was made of platinum and platinum-rhodium wire about 0·003 in. diam covered with a thin sheath of glass to minimize catalytic effects. It was supported on a yoke which maintained its axial positioning and the lead wires were brought out along the walls to minimize their influence on the flame. The output was fed into a potentiometric function plotter which recorded thermocouple output against its position. Replicate runs made with the couple moving upward through the flame at rates not exceeding 5 cm/min gave results agreeing within the reading error of the potentiometer and could be reproduced by moving the couple downwards but at a greatly reduced rate. Corrections were not applied to the reported temperatures.

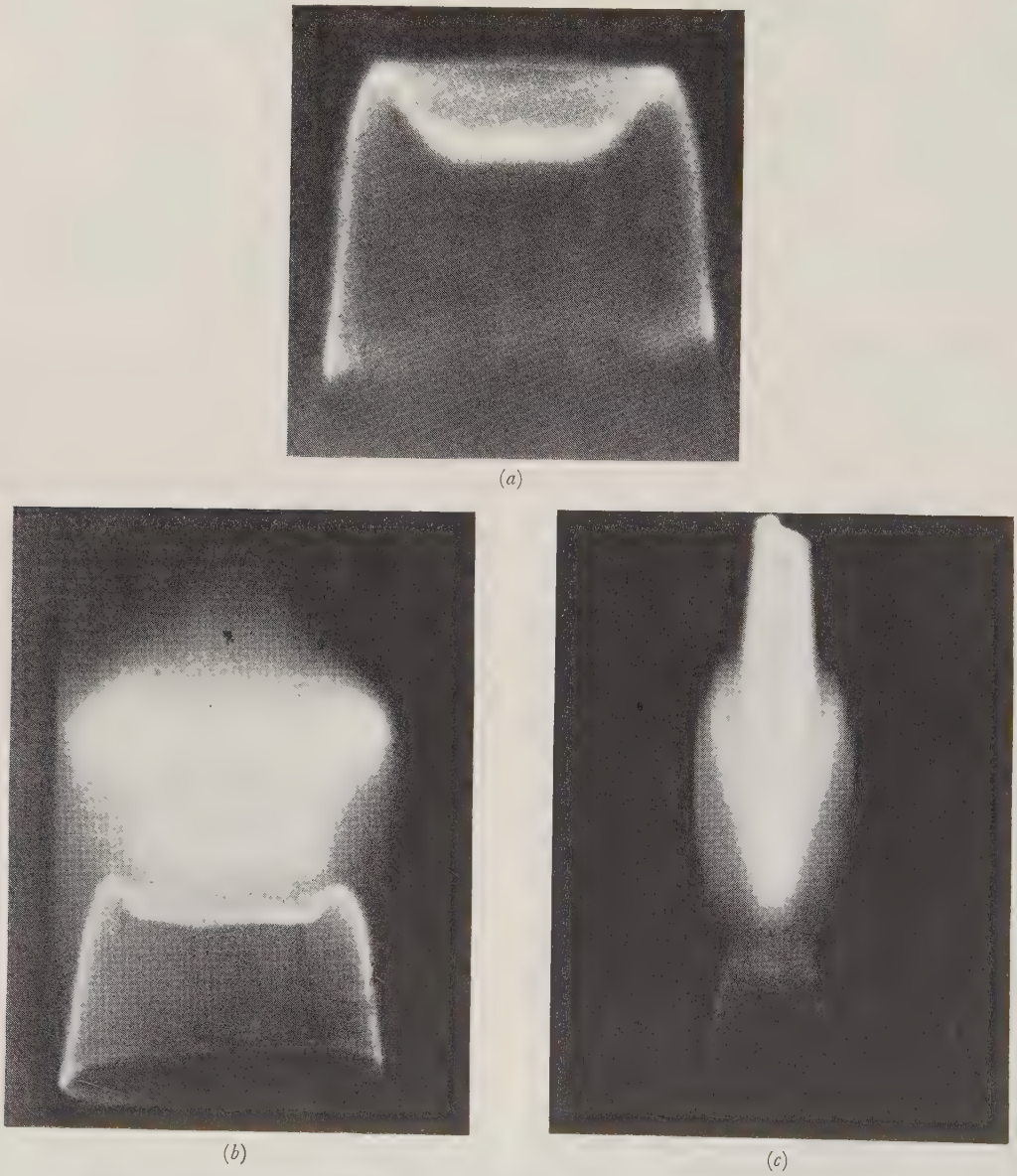

Figure 3. Photographs of flame stages. (a) Cool flame; (b) cool plus second-stage flame; (c) cool plus second-stage flame with orange luminosity. (Photographs were not taken under same flow conditions)

To give a comprehensive picture of the developing flame structure, temperature profiles at several oxygen levels were plotted on the same sheet. A tracing of such a record is shown in

Figure 4. The luminous zones correspond to the zones of maximum rate of temperature rise with the exception of the orange luminosity which arises in the wake of the second-stage flame. This orange luminosity leaves no specific indication of its existence on the thermocouple trace. It may be seen in *Figure 4* that the temperatures in both the cool and second-stage flames increase linearly with distance. In the space between these stages the

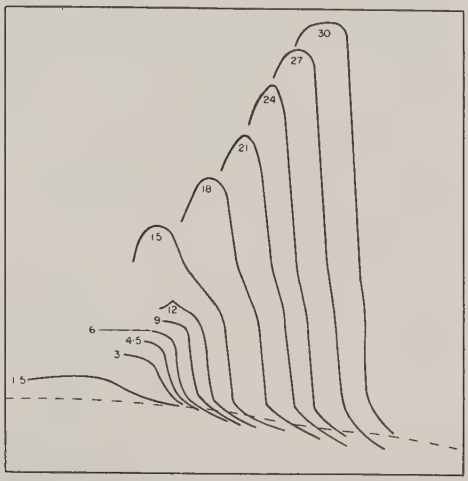

Figure 4. Temperature profiles along axis of reactor at successive oxygen levels traced from potentiometer record. Thermocouple position is plotted horizontally and millivolt output vertically. Tube diameter 62 mm. *Total distance represents about* 40 cm. *Direction of gas flow is from right to left. Figures on curves denote present oxygen. Initial tube temperature* 350°C *with no oxygen flow (dashed line). Basic flow—* 4 l./min. *Fuel—n-hexane* (15 per cent *of basic flow)*

temperature also increases linearly. This is most easily seen at the lower oxygen concentrations. When the curves in *Figure 4* are expanded and corrected for the base-line temperature profile, a zone of linear temperature rise becomes apparent just ahead of the cool flame.

Effects of operating variables

Following the development of the temperature plotting system, studies were made of several operating parameters. The observations were limited to oxygen concentrations which permitted good control of the flame (Phases *A* through *E* in *Figure 2*); these are discussed individually below.

A. Flow rate

For a given tube, the basic flow (N_2 + fuel) could be varied satisfactorily by a ratio of at least 5 to 1, corresponding to linear flow rates of 2·1 to 10·5 cm/sec (calculated for 350°C). The upper limit was imposed by the onset of turbulence which disturbed the flame structure. At low rates the flame structure became compressed and approached the glass beads at the bottom too closely to permit meaningful temperature measurements with the thermocouple used.

Changes in flow rate had a marked effect on the shape of the flame. At low flows both the cool and second-stage flames were quite flat and approximated the configuration of published photographs of two-stage flames obtained on flat flame burners[13,14]. At higher flows, the cool flame assumed a dimpled button shape which elongated into a truncated re-entrant cone at the highest flows. This folded structure seemed to arise from a disturbance of the parabolic Poisseuille distribution of velocity characteristic of isothermal cylindrical flow as a result of convective rise as heat is transferred inward from the walls. This folding process contributes to the stability of the flame position by providing a means of adjusting the flame area to the flow rate so that the characteristic propagation velocity of the mixture can be maintained.

The second-stage flame, flat at very low flows, develops into an increasingly steep cone as the flow is increased. This shape arises from the necessity of maintaining a flame area in equilibrium with the flow rate and burning velocity and at the same time compensating for energy losses to the walls. The reality of these losses was demonstrated by displacing the thermocouple from the axis to a position near the wall. Vertical probing under these conditions showed a temperature drop up to 50°C between the cool and second-stage flames.

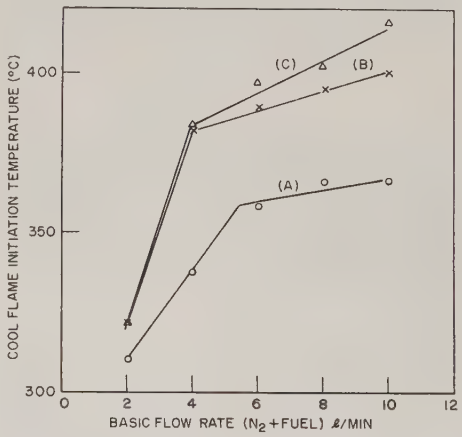

Figure 5. Effect of basic flow rate on initiation temperature of cool flame. Plots A, B and C were made at tube temperatures of 300, 350 *and* 400°C *respectively. Oxygen* 27 per cent. *Fuel n-hexane* (15 per cent *of basic flow). Tube diameter* 62 mm

At high oxygen levels the heat developed by the flame causes excessive convective velocity increases along the tube axis where energy losses to the walls are minimal. The formation of the hollow cylindrical structure would seem to arise

from attainment of an axial linear velocity which exceeds the burning velocity of the mixture. Cusps at its lower edge provide the necessary area to support the flame in a stable position.

The basic flow rate also has a considerable influence on the temperature at which the cool flame arises. This is shown in *Figure 5*.

B. Tube diameter

Tubes of 62, 42, 25 and 16 mm internal diameter have been used successfully. At similar

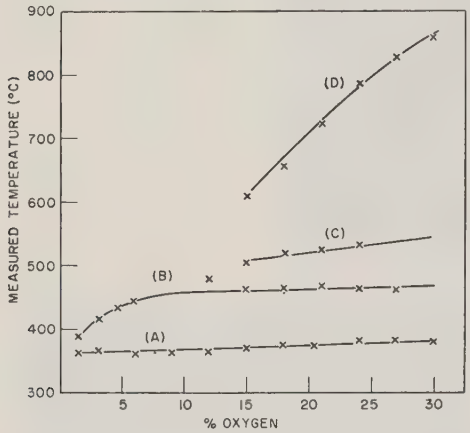

Figure 6. Transition temperatures in flames as a function of oxygen concentration. (A) Initiation temperature of cool flame; (B) maximum temperature reached in cool flame; (C) initiation temperature of second-stage flame; (D) maximum temperature reached in second-stage flame. Basic flow 4 l./min. *Fuel—n-hexane* (15 per cent *of basic flow*). *Tube temperature* 350°C. *Tube diameter* 62 mm

linear flow rates and tube temperature the principal effect of reducing the tube size was to increase the separation between the cool and second-stage flames. This effect was most pronounced in going from the 25 to the 16 mm tube. Higher oxygen levels were required to initiate second-stage flames in the smaller tubes.

C. Oxygen concentration

Since oxygen concentration was used as a parameter in all the studies, its gross effects on the flame structure are those shown in *Figure 4*. Reduction of data relating oxygen concentrations to the cool flame initiation temperature, the maximum temperature attained by the cool flame, the initiation temperature of the second-stage flame and the maximum flame temperature are shown in *Figure 6*. The data used to plot *Figure 6* were taken from curves such as those shown in *Figure 4*. Curves *A* and *B* represent the beginning and end of the steep rate of temperature rise associated with the cool flame. Curve *C* represents the beginning of the second-stage flame and curve *D* the maximum temperature observed in the tube. It may be noted in *Figure 6* that the initiation and maximum temperatures of the cool flame do not seem to be affected by the presence or absence of the second stage. Also to be noted in *Figure 6* is the fact that the maximum temperature (curve *D*) shows no break in the vicinity of 24 per cent oxygen where the orange luminosity first appears.

D. Fuel concentration

Although most of the work reported was done with 15 per cent *n*-hexane, a few runs were made

TABLE 1

Effect of Fuel Concentration on Oxygen Requirements

% *n-Hexane*	*Approximate % oxygen necessary*		
	cool flame	*second-stage*	*loss of control*
15	3	15	30–32
12·5	3	18	27–28
10	3	24	24–25

in the 25 mm tube at *n*-hexane concentrations of 15, 12·5 and 10 per cent. As the fuel concentration was reduced, no drastic variation in the cool flame was noted. On the other hand, the percentage of oxygen required for second-stage initiation increased markedly. At the same time the additional oxygen necessary to carry the flame to its point of instability decreased. Approximate limits are shown in Table 1.

This relationship may account for the difficulties mentioned by Prettre[16] in establishing stable flames in upwards flow in vertical tubes. Using

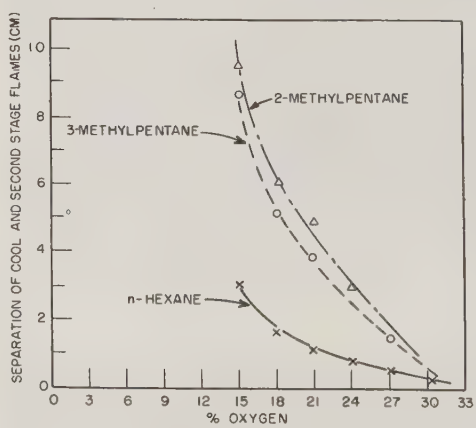

Figure 7. Separation between cool and second-stage flames of three hydrocarbons as a function of oxygen concentration. Basic flow 4 l./min. *Fuel*—15 per cent *of basic flow. Tube temperature* 350°C. *Tube diameter* 62 mm

low fuel concentrations, the development of the second-stage flame occurs only at oxygen levels high enough to establish immediately a thermally self-sufficient flame which over-rides the controls inherent in the cool flame mechanism and propagates more or less violently downwards.

E. Nature of the fuel

Similar flame patterns were observed for *n*-hexane, 2-methylpentane, 3-methylpentane, *cyclo*-hexane and hexene-1. The separation of the cool and second-stage flames of two hexane isomers as a function of oxygen concentration is illustrated in *Figure 7*. Other illustrative data are given in Table 2.

TABLE 2

Separation of Cool and Second-stage Flames*

Fuel	*Separation (cm)*
n-Hexane	1·03
2-Methylpentane	4·1
3-Methylpentane	4·0
Hexene-1	1·2
*Cyclo*hexane	4·3

* Conditions: Tube diameter, 62 mm. Tube temperature, 350°C. Total flow, 5·1 l./min.

Composition, 11·9 per cent fuel, 21·0 per cent oxygen, 67·1 per cent nitrogen.

As shown in *Figure 8*, the transition temperatures were similar for the hexane isomers despite the significantly different delay times. 2,3-Dimethylbutane did not ignite at tube temperatures up to 500°C and oxygen concentrations up to 35 per cent.

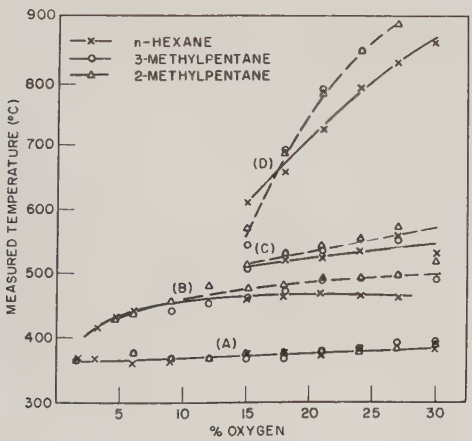

Figure 8. Transition temperatures in flames of three hydrocarbons as a function of oxygen concentration. (A), Initiation temperature reached in cool flame; (B), maximum temperature reached in cool flame; (C), initiation temperature of second-stage flame; (D), maximum temperature reached in second-stage flame. Basic flow 4 l./min. *Fuel*—15 per cent *of basic flow. Tube temperature* 350°C. *Tube diameter* 62 mm

F. Tube temperature

Temperature distribution within the tubes with only fuel and nitrogen flowing is characterized by the dotted line of *Figure 4*. Addition of oxygen modified this pattern by cooling the lower end of the tube and heating the tube near any ensuing exothermic reactions.

Because of the inverse relationship between the ignition temperature and induction delay of cool flames, the most obvious effect of tube temperature was in establishing the initial equilibrium position of the cool flame. Once a flame was established, energy transfer forwards from the combustion wave reduced the relative contribution of the tube, and beyond the transition to a thermally self-sufficient flame, the tube temperature became irrelevant.

Up to the transition point, cutting off the heater current caused the flame to migrate slowly upwards to extinction. In the case of one cool flame (4 per cent O_2, 15 per cent *n*-hexane) the extinction temperature was measured and found to be 278°C. Beyond the transition point the flame, stabilized on the beads, continued to burn indefinitely.

Initial tube temperatures of 300–500°C were employed and all permitted successful flame development. At the higher temperatures the cool flame formed well down in the tube while at lower temperatures they tended to form at the top of the tube. At low tube temperatures the cool flame initiated at temperatures appreciably lower than those required with higher tube temperatures (see *Figure 5*).

G. Miscellaneous observations

The heavy deposit of soot laid down on the walls of the tube by fully developed flames (stage *F*, *Figure 2*) could be removed by establishing a cool flame in the tube; 15 min was usually sufficient to remove all traces. Since the wall temperatures were as low as 300°C it was believed that free radicals or some other highly reactive species were responsible. To test this qualitatively, a lead film was deposited on the outside of a test tube which was then suspended over a cool flame in the vertical reactor. Within 25 min the lead film had been removed.

DISCUSSION

While the experimental results attained to date provide a fertile field for speculation on the interrelation of flame stages, the authors feel that any extended theoretical discussion of their observations should be deferred. The method is offered in its present state of development as a tool which offers certain advantages in studying the early phases of the autoignition reactions.

The principal advantage of the method seems to lie in its ability to separate widely in space the stages involved in the spontaneous ignition process. By proper manipulation of a single variable, various combustion phases which have been observed in widely different apparatuses can be presented for leisurely observation. These phases, developed in a single very simple apparatus, are stable enough to permit temperature measurements, sampling studies and spectrographic or other photographic observations. The various stages appear in coherent relationship to each other and provide unambiguous orientation. Since separation of the flame stages can be controlled over wide limits by the choice of experimental conditions it is suggested that the vertical reactor might provide a rapid technique for studying the effect of additives, fuel structure and the like.

REFERENCES

[1] Lewis, B. and von Elbe, G. *Combustion, Flames and Explosions of Gases*, pp. 172–188. 1951. New York; Academic Press

[2] Jost, W. *Explosion and Combustion Processes in Gases*, pp. 367–500. 1946. New York

[3] Walsh, A. D. *Trans. Faraday Soc.* 42 (1946) 269.

[4] Boord, C. *Third Symposium on Combustion, Flame and Explosion Phenomena*, p. 416. 1949. Baltimore; Williams and Wilkins

[5] Williams, K., Woods, F., Johnson, J. and Carhart, H. *Dynamic Studies in Cool Flames* presented at Minneapolis Meeting (ACS) Sept. 1955

[6] Jost, W. *Explosion and Combustion Processes in Gases*, p. 428. 1946. New York

[7] Topps, J. and Townend, D. *Trans. Faraday Soc.* 42 (1946) 345

[8] Agnew, J., Agnew, W. and Wark, K., Jr. *Sixth Symposium (International) on Combustion*, pp. 894–902. 1957. New York; Reinhold

[9] Gaydon, A. *The Spectroscopy of Flames*, pp. 113–135. 1957. New York

[10] Fristrom, R., Prescott, R. and Grunfelder, C. *APL/JHU CM 858* (1955)

[11] Levedahl, W. *Fifth Symposium (International) on Combustion*, pp. 372–85. 1955. New York; Reinhold

[12] Johnson, J. E., Crellin, J. W. and Carhart, H. W. *Industr. Eng. Chem. (Industr.)* 46 (1954) 1512

[13] Powling, J. *Fuel* 28 (1949) 25

[14] Foresti, R. *Fifth Symposium (International) on Combustion*, pp. 582–85. 1955. New York; Reinhold

[15] Bailey, H. and Norrish, R. *Proc. Roy. Soc. A* 212 (1952) 311

[16] Prettre, M. Discussion appended to reference 7

59

EXPERIMENTAL TEMPERATURE GRADIENTS IN BURNING DROPS

A. R. HALL

As studies progress into the burning of drops and sprays it becomes ever more important to know the temperatures and the heat flow into the interior of the drops during combustion.

Thus, in the past, rates of burning of single drops have been obtained by measurement of the change in drop dimensions[1,2,3] but this is not strictly sufficient to give the true mass rate of burning; for that the mean density of the drop, and therefore the temperature situation in the drop, and any variation in it during burning, are also required.

Again, theoretical expressions for the rate of burning of drops[3,4] indicate that the rate is a function of heat transferred to the drop per unit mass vaporized. The value of this quantity will depend on the rate of heat conduction into the drop.

Some calculations have been made of the distribution of temperature with time within burning drops[5,6,7] and the general conclusion has been reached that the temperature at the centre of hydrocarbon drops burning under natural convection becomes comparable to the surface temperature at least in the later stages of burning.

To provide experimental data on this question some temperature measurements have been made with a fine thermocouple within drops of tetrahydronaphthalene (tetralin) and decane suspended on a silica filament and burning in air at atmospheric pressure. Simultaneous measurements were made of the change in drop dimensions.

Heat conduction considerations provide good evidence for the general reliability of the gradients so obtained, and these confirm the theoretical expectation mentioned above. Values could therefore be obtained for the rate of heat conduction into the drop, the true mass rate of burning and the heat transfer to the drop per g of fuel burnt, Q. The so-called evaporation 'constant' increases in the early stages of burning in a way that is qualitatively explicable by the corresponding change in Q.

METHODS

Approximate temperature gradients within a drop on ignition and combustion

Experimental—Temperatures were measured at two points within drops of tetralin and decane, suspended on a silica filament, during their ignition and the initial burning in air at atmospheric pressure, as follows.

The junction of a fine iron-constantan thermocouple (0·025 mm diam) was placed first at the centre and then 0·12 mm from the surface of the drop (1·0 mm diam) in separate experiments. This couple was held taut by soldering both wires, half an inch from the junction, on to 1/8 in. diam rods of iron and constantan, respectively; the rods were clamped in terminals mounted on the opposing limbs of a V shaped insulating mount, so that the wire stretched horizontally between the limbs (see *Figure 1*). To carry the drop a thin silica filament was suspended vertically downward from a unit, giving fine screw movements in three dimensions, which was attached to the base of the V mount (C, *Figure 1*). The filament was curved slightly near the tip to leave room for the couple junction to occupy the centre of the drop; *Figure 1* shows the arrangement schematically.

The drop was ignited by passing a small diffusion flame of gas immediately beneath it. To prevent the couple wires adjacent to the drop from becoming unduly heated by the ignition or droplet flames they were each sheathed with a short length of fine bore ceramic tubing at a fixed distance from the drop. Heat transfer along the wires into the drop was thus reduced.

To ensure that the couple junction was sited correctly in the drop, and to check that it remained so during the experiment, it was observed by a low power microscope. The couple tended to move appreciably upwards when the ignition flame passed beneath the drop but it was found that it could be kept quite steady by pressing the silica filament against it.

It was found desirable to extinguish the drop flame about 1/2 sec after ignition to prevent it melting the wires. The following prodecure was therefore adopted. The burner bearing the ignition flame was supported on an arm which pivoted on the shaft of a clockwork motor. Also attached to this arm was a flat tube from whose slit-orifice nitrogen gas issued at a rate just sufficient to extinguish the drop flame when it passed immediately beneath it (*Figure 1*). This extinguisher was arranged to reach the drop at a definite, short time-interval (0·44 sec) after the igniter flame.

The thermocouple electromotive forces were recorded, photographically, throughout the experiments, with oscillograph equipment. It was noted that the results were about 5 per cent too low because of the non-instantaneous response of the electronic circuits. The error due to this was not taken into account in deducing the temperature records.

tures of the wires outside the drop at a short, known distance from the drop surface, during the burning. This was done by siting the couple junction at this distance, on each side of the drop in turn. As the corresponding temperatures of the drop surface were known approximately from the normal experiments the rate of heat transfer along the wires could be computed.

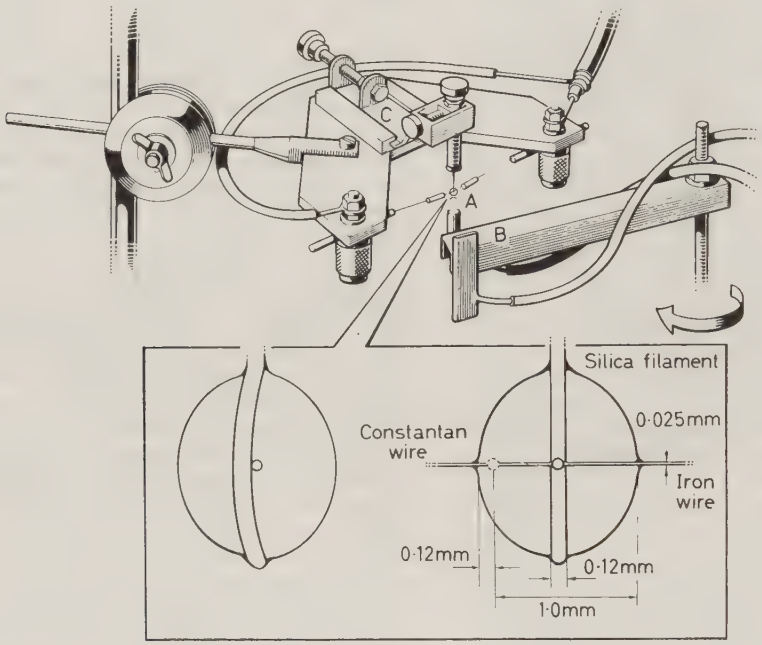

Figure 1. Measurement of temperature in burning drops with thermocouple. A, igniting flame; B, extinguisher (flow of nitrogen) for drop flame

The temperature records for the centre and 'surface' positions of the couple were correlated by determining the time interval between the moments of initial rise of temperature in the two cases. This was done by putting the normal couple junction at the centre of the drop and forming a second junction on the constantan wire 0·12 mm from the drop surface. This was produced by simply hooking on at that point another length of fine iron wire, a satisfactory electrical connection being achieved by momentarily wetting the temporary junction with acid. The electromotive forces from both couples could be recorded simultaneously, with the usual time base.

The thermal diffusivities of constantan and iron are respectively about 70 and 200 times greater than those of the hydrocarbons used. The presence of such highly conducting wires must tend to affect the results in two main ways.

First there must be an enhanced rate of heat flow into the drop during combustion by conduction along the wires. This was roughly measured by obtaining the approximate tempera-

Secondly the wire must tend to decrease the temperature gradient in the liquid in its vicinity. However, even suspended drops rotate quite readily and it was considered that quite a low rate of incidental rotation would both strongly counter this effect and also lead to a more uniform temperature over the drop surface and thus to a more spherosymmetrical temperature distribution within the drop. To help to ensure that the couple junction recorded the temperature of the adjacent liquid, rather than a temperature imposed on it by heat flow along the adjacent wires, the diameter of the spot welded junction was made slightly larger than that of the wires; in that way the area across which heat could be transmitted between the wires and the junction was only some 10 per cent of the total surface area of the junction.

Theoretical—It was desired to provide a rough theoretical check on the order of the experimental temperature gradients in the drops.

As a first approximation to the initial thermal gradient produced on ignition a value has been estimated for tetralin by a two-step process.

For the first step the 'film-cooling' effect of the evaporation was ignored. The drop was assumed to be instantaneously immersed in a hot gas with a temperature (2,000°K) and conductivity (0·00018 cal sec^{-1} cm^{-1} (deg C)$^{-1}$) estimated to obtain in the ignition conditions in this work. (Other physical quantities adopted for calculations in the paper are listed in the Appendix.) A Nusselt number of 2 was adopted and heat transfer with the drop was taken to be by conduction alone, i.e. the effect of possible convection or other currents was not considered and radiation was regarded as negligible. The temperature gradient was computed for the instant when the surface temperature reached the boiling point (205°C for tetralin). This was done by means of Grober's charts[8]. As the cooling effect of the evaporation was not taken into account in this step the value of the gradient obtained at this stage does not represent any practical condition.

After this point, and for the second step, the surface temperature was taken to be constant and the temperature gradient was allowed to change according to heat conduction requirements and was calculated for an overall ignition time of 0·2 sec, i.e. before much reduction in drop diameter could have taken place. This was done by a step method of calculation due to Ingersoll and Zobel[9] as this method, although approximate, was also found suitable for use when the drop diameter was decreasing (see below).

It will be seen in the experimental records that the surface temperature of the drop is still appreciably below the boiling point after the overall ignition time of 0·2 sec. This makes it difficult to use the above theoretical gradient as a direct check on the general reliability of the experimental one. However, where the temperature gradient is known the approximate heat content of the drop can readily be worked out. The heat contents of the drop were thus obtained and compared for the experimental and theoretical cases.

Correlation of temperature gradient and drop size during burning. Rate of burning of drops

The change in drop size during burning was obtained simultaneously with the recording of its internal temperature, by the photographic method described in an earlier paper[3]. The two measurements could be correlated.

The apparent rates of combustion were computed from these measurements of the drop size. The latter were also obtained in the absence of the thermocouple.

RESULTS

Approximate temperature gradients

Experimental: correlation with drop size—The diameter, measured horizontally, of all the drops used in this work was arranged to be exactly 1·0 mm but the drops were ellipsoidal with a volume equal to that of a sphere with a diameter of 1·06 mm. A slight change of shape sometimes occurred on ignition but this did not materially affect the relative positions of drop and thermocouple.

The temperatures indicated by the thermocouple are plotted against time in *Figure 2* for

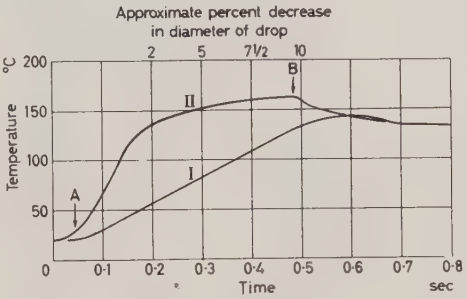

Figure 2. Temperature recorded by thermocouple at centre (I) and 0·12 mm from surface (II) of a drop of tetralin (diam. 1·06 mm) on ignition and burning. A, igniter flame immediately beneath drop; B, drop flame extinguished

tetralin; occasional angularities have been smoothed out. The zero of the time scale here and throughout this paper, unless otherwise stated, is taken as the instant of first temperature rise recorded by the couple junction when sited near the drop surface. These temperature/time records were fairly well reproducible where the ignition flame had a fixed size and route beneath the drop, except for the brief period between 0·05 and 0·15 sec; here the steepness of the temperature rise recorded near the drop surface could vary from one experiment to another. The interval between the moments of temperature rise recorded near the surface and at the centre of the drop was of the order of 0·04 sec for both tetralin and decane. The two temperature records could thus be correlated to the same time base.

The moment when the ignition flame was immediately beneath the drop (see *Figure 2*) could be approximately assessed from the moment the extinguisher was beneath the drop (manifested by the abrupt check in the temperature rise of the 'surface' couple), as the time interval between these two agents (0·44 sec) was known.

The change in drop size corresponding to these temperature records is indicated on the abscissa of *Figure 2*.

Although values for temperatures were thus obtained at only two points within the drop it was possible to draw the implied temperature gradient between the points, for any time, as it was clearly fairly linear. *Figures 3* and *4* show some of these gradients, drawn as continuous lines, for the drops of tetralin and decane respectively. In order to

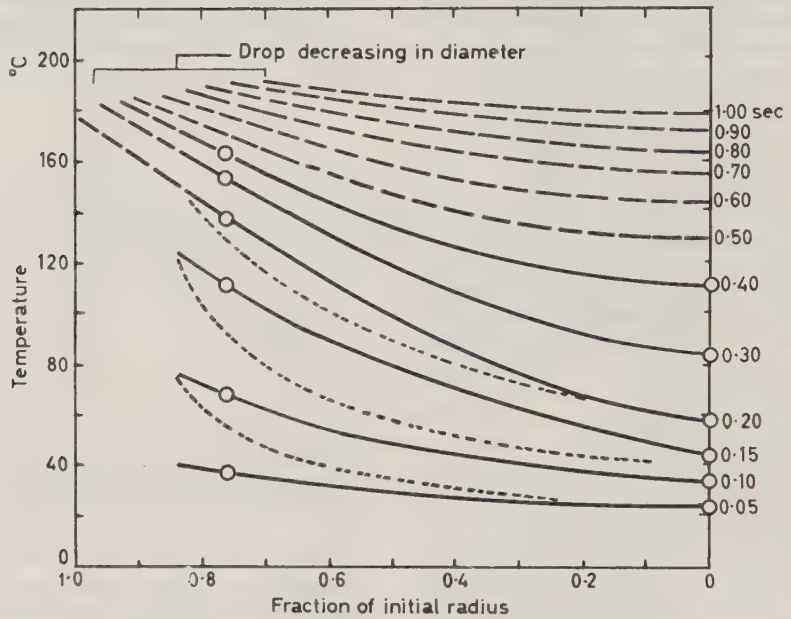

Figure 3. Temperature gradients in a burning drop of tetralin (initial diameter 1·06 mm). *——experimental; – – – – semi-empirical (see text regarding dotted curves)*

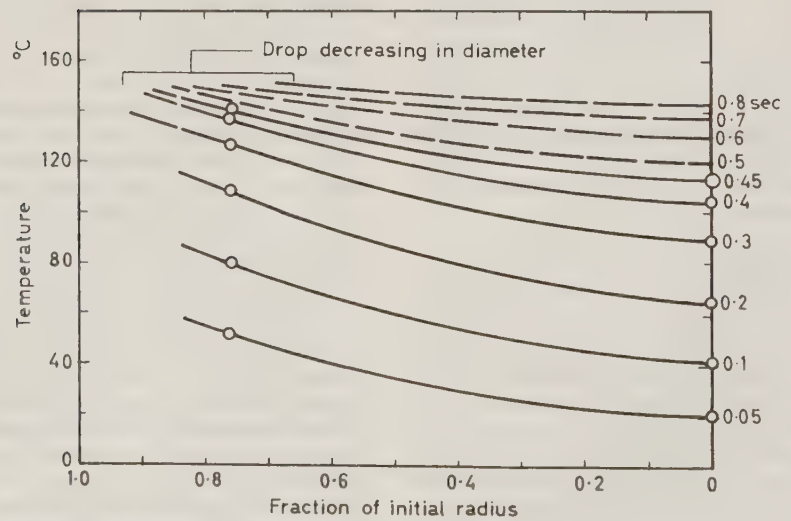

Figure 4. Temperature gradients in a burning drop of decane (initial diameter 1·06 mm). *——experimental; – – – – semi-empirical*

see if the change in gradient with time conformed to heat conduction requirements, they were examined in the following manner.

Each gradient in turn was taken as a datum line and by Ingersoll and Zobel's method[9] the theoretical change in this gradient resulting from heat conduction was determined for the known time interval between the datum gradient and the next experimental gradient drawn above it in *Figures 3* and *4*. For this calculation it was necessary to take the rise in temperature at the upper end of the gradient, over this time interval, as that recorded experimentally. It was found that the changes in the experimental gradients obtained on and after 0·2 sec for tetralin and 0·3 sec for decane agree fairly closely with those theoretically resulting from heat conduction. This was not the case in the preceding periods: here the experimental gradients indicate a far more rapid rise of the temperature than may be explained by conduction. These theoretical curves are dotted in *Figure 3*; there is some indication that the changeover between the two regimes is a fairly smooth one.

The gradients between the experimental points have been extrapolated to the drop surface in such a way that they continue to satisfy the requirements of heat conduction. The extrapolations are rendered as discontinuous lines in *Figures 3* and *4*. Some values for the gradients subsequent to the last measured values were calculated for the sake of completeness, the slight rise in the surface temperature indicated by the preceding experimental values being assumed to continue. These semi-empirical gradients are drawn as discontinuous lines in *Figures 3* and *4*.

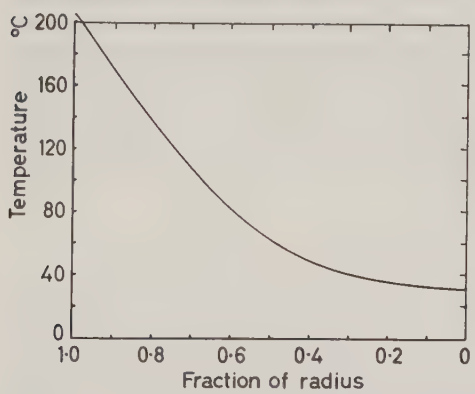

Figure 5. Theoretical temperature gradient in tetralin drop (diameter 1·06 mm) *after* 0·21 sec *under ignition conditions*

Theoretical—The theoretical gradient for a 1·06 mm diameter drop of tetralin at an overall ignition time of 0·21 sec is shown in *Figure 5*. It was computed that under the ignition conditions the temperature at a point 0·12 mm from the drop surface would begin to rise after about 0·01 sec. The theoretical state at 0·21 sec may thus be compared with the experimental one at 0·2 sec. Unfortunately it is not feasible to compare the experimental and theoretical temperature gradients directly as the surface temperatures differ appreciably in the two cases, but the rises in heat contents of the drops were calculated from the gradients and both were found to be 0·029 cal. The exactness of this agreement is, of course, fortuitous.

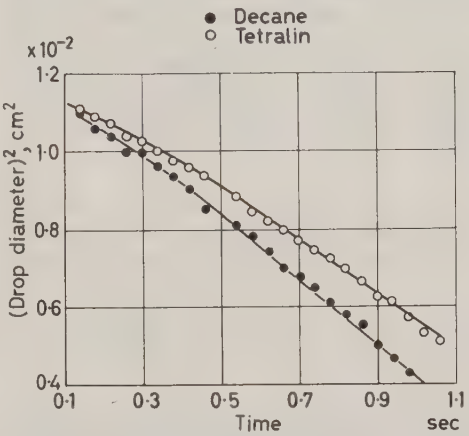

Figure 6. (*Drop diameter*)^2 versus *time for burning drops* (*initial diameter* 1·06 mm)

The rise in heat content in this period corresponds to a mean rate of heat transfer of 0·15 cal/sec. The mean rate of heat transfer into the drop along the wires was found to total only 0·008 cal/sec.

Rate of burning of drops: apparent and real

In previous work with burning drops, plots of the square of the diameter (d) against time (t) were found to be linear for most of the burning time[1,2,3], giving the relationship

$$d^2 = d_0^2 - \lambda t \qquad (1)$$

or

$$\frac{dv}{dt} = -\frac{\lambda \pi d}{4} \qquad (2)$$

where λ is a constant, termed the evaporation constant, and v is the volume of the drop.

A similar plot with the results in the present work gave a slight curve for the period in which the first 15 per cent decrease in drop diameter took place, as noted by Kumagai and Isoda[1]; thereafter the results could be reasonably well accommodated on a straight line. This is shown for tetralin and decane in *Figure 6*. Furfuryl alcohol was also examined and found to give a similar result. The results were fairly well reproducible. The diameter used here, and elsewhere in this

paper unless otherwise stated, was that of the sphere which had a volume equal to the volume of the ellipsoidal drop concerned.

The rate of decrease of drop diameter was not found to differ within experimental error whether the thermocouple was present or not, up to the time the flame was extinguished at 0·44 sec.

The evaporation 'constant', λ, is given by the slope of the line in these graphs. It is clearly gradually increasing in the early period of the burning to reach a constant value later. Some values for λ are given in Table 1.

Using the thermal gradients in *Figures 3* and *4*, i.e. the experimental ones up to 0·45 sec and the semi-empirical ones thereafter, some values for the apparent and true rates of burning have been calculated; those for tetralin are given in Table 1.

Table 1 shows the appreciable increase in λ in the period up to 0·6 sec, during which the mass of the drop decreases by nearly half. By definition (see equation 2), λ is a direct index of the rate of burning of a fuel for a given size of drop. However it is also clear that λ is not a reliable index of this

TABLE 1

Apparent and Real Mass Rates of Burning, etc., of a Drop of Tetralin (initial diam 1·06 mm)

*Time** sec	*Drop diameter* cm	*Evaporation 'constant' λ* $cm^2\ sec^{-1}$	*Apparent mass rate of burning* g/sec	*Rate of mass evaporation hidden by decreasing density of drop* g/sec	*Real mass rate of burning* g/sec
0·2	$1·04 \times 10^{-1}$	$5·2 \times 10^{-3}$	$3·5 \times 10^{-4}$	$0·9 \times 10^{-4}$	$4·4 \times 10^{-4}$
0·3	1·01	5·4	3·6	0·7	4·3
0·4	0·99	5·9	3·8	0·6	4·4
0·5	0·97	6·7	4·2	0·4	4·6
0·6	0·92	6·9	4·1	0·3	4·4
0·7	0·88	6·9	4·0	0·2	4·2
0·8	0·85	6·9	3·8	0·15	4·0
0·9	0·8	6·9	3·6	0·1	3·7
1·0	0·75	6·9	3·4	0·05	3·4

* Measured from the moment of the first rise in temperature of the 'surface' couple.

Where λ is known the apparent volume rate of burning is obtainable from equation 2. However, where the density is decreasing because the drop is heating up, as in the present work, the density decrease represents a quantity of liquid whose evaporation is not detected by measurement of the decrease in drop size. A correction is therefore required to the apparent mass rate of burning as given by the product of the apparent volume rate of burning and the density of the drop. Straightforward considerations show that this correction, in mass per unit time for the particular drop, is given by the expression

$$\frac{\left(\frac{\partial T}{\partial r}\right)_{r=R} Ak\beta}{\bar{c}}$$

where $(\partial T/\partial r)_{r=R}$ is the thermal gradient at the surface
k is the thermal conductivity at the surface
A is the area of the surface
β is the mean coefficient of cubical expansion
$\bar{c}$ is the mean specific heat
} of the drop

kind in this particular period, for as has been pointed out the apparent rate of burning deduced from change in drop size must be corrected for evaporation which is not detected by size measurement, because of the decrease in density of the drop on heating up, and Table 1 shows that this correction remains an appreciable proportion of the total rate up to 0·6 sec. The true index of the mass burning rate certainly increases over the same time but not as much as λ does.

Total heat transferred to drop per unit mass of liquid burnt

Where the temperature gradients in the drop, at the surface, are known the rate of heat conduction into the drop may be obtained. Where the true mass rates of burning are also known this permits the calculation of the total heat transferred to the drop per g burnt, Q. Some values for Q for tetralin are given in Table 2 and *Figure 7*; the latter also contains the corresponding values for decane.

The big change in Q in the period up to about 0·7 sec (see *Figure 7*) provides a qualitative explanation of the change in λ over the same period.

TABLE 2

Heat Transfer Rates to a Drop of Tetralin (initial diam 1·06 mm) During Burning

Time sec	*Drop diameter* cm	*Surface area of drop* cm^2	*Temperature gradient in drop at surface* °C/cm	*Rate of heat conduction into drop* cal/sec	*Rate of heat transfer to drop for latent heat of evaporation* cal/sec	*Total rate of heat transfer to drop* cal/sec	*Heat transferred to drop per* g *of tetralin evaporated** cal/g
0·2	$1·04 \times 10^{-1}$	$3·39 \times 10^{-2}$	$4·0 \times 10^{3}$	$4·3 \times 10^{-2}$	$3·5 \times 10^{-2}$	$7·8 \times 10^{-2}$	175
0·3	1·01	3·2	3·4	3·5	3·4	6·9	160
0·4	0·99	3·05	2·8	2·7	3·5	6·2	140
0·5	0·95	2·85	2·3	2·0	3·6	5·6	120
0·6	0·92	2·65	1·7	1·4	3·5	4·9	112
0·7	0·88	2·45	1·3	0·95	3·3	4·3	100
0·8	0·85	2·25	0·9	0·65	3·1	3·8	95
0·9	0·8	2·0	0·7	0·45	2·9	3·4	90
1·0	0·75	1·7	0·5	0·25	2·7	3·0	88

* Latent heat of tetralin 79 cal/g.

CONCLUSIONS

The validity of the general order and rate of change of the experimental temperature gradients found here for the burning drops of tetralin and decane, apart from those in the earliest stage of combustion, seems to be confirmed by heat conduction requirements. This implies that there is no significant internal motion in the drops in the periods in question. Convection and other currents arise fairly readily in large drops[10,11] but it is thought that they are much less likely to occur with small droplets[6,10].

If this is so, and if the mass rate of burning varies directly with the drop diameter, then it may be shown that the temperature gradients found hold for any (smaller) size of drop, of the fuels concerned and for the particular experimental conditions, if the temperatures are plotted against the fraction of the drop radius, as in *Figures 3* and *4*, the times to reach the gradients being proportional to (diameter)^2. It follows from this that the same is true of the variation in the heat transferred to the drop per unit mass burnt (Q) and in the evaporation 'constant' (λ) if these are plotted against, say, the fraction of the original radius.

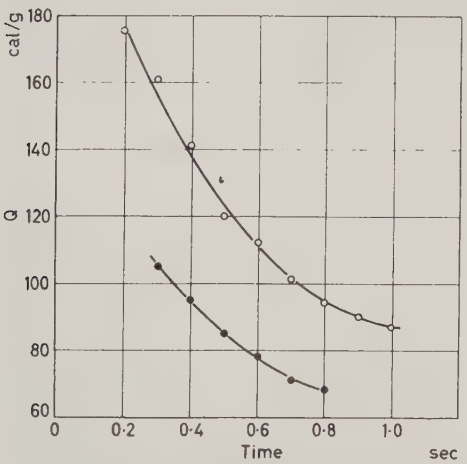

Figure 7. Decrease of heat transferred to drop per g *burnt.* ○ *tetralin (latent heat* 79 cal g^{-1}); ● *decane (latent heat* 60 cal g^{-1})

Even if there is significant internal motion in the drops in the earliest stage of burning, the main features of the results may be expected to obtain for other sizes of drop. Thus, although the resistance to such motion is presumably greater the smaller the diameter, the initial thermal gradient in the drop is inversely proportional to its diameter, for given heating conditions, and so the convectional forces presumably increase as the drop size is decreased. The main results must also apply to most other liquid fuels as the variation in their relevant properties is of a low order.

The general order of the temperature gradients found in the drops has two main implications.

First, the order is such that initially over half the heat transferred to the drop is conducted into the interior of the drop, as predicted by Hottel, Williams and Simpson[6], and this component remains a significant proportion of the total heat transferred until appreciably more than half the mass of the drop has been burnt. In other words the value of Q is at first over twice that of the latent heat and does not approach the latent heat until a much later stage of the combustion of the drop. This explains qualitatively why the evaporation 'constant' increases appreciably to a steady value in the period following ignition. All this may be theoretically shown to apply, in general, to any greater rate of combustion, for example in oxygen.

Secondly, by the time λ has reached a relatively

constant value (which was the value measured in past experimental work) the temperature level within the drop has been raised appreciably and the density is much less than it was originally. This must be taken into account when deducing mass rates of burning, especially at elevated pressure, for then the boiling point, and thus the mean temperature of the drop, may be raised considerably. For this reason it must be concluded that the effect of pressure on the burning rate is even less than was apparently found experimentally[3].

Crown Copyright Reserved

REFERENCES

[1] Kumagai, S. and Isoda, H. *Science of Machine* 4 (1952) 337

[2] Gödsave, G. A. E. *Fourth Symposium (International) on Combustion*, p. 818. 1953. Baltimore; Williams and Wilkins

[3] Hall, A. R. and Diederichsen, J. *Fourth Symposium (International) on Combustion*, p. 837. 1953. Baltimore; Willliams and Wilkins

[4] Spalding, D. B. *Fuel* 29 (1950) 2, 25; and later papers

[5] Godsave, G. A. E. Unpublished British Ministry of Supply Report (1952)

[6] Hottel, H. C., Williams, G. C. and Simpson, H. C. *Fifth Symposium (International) on Combustion*, p. 101. 1955. New York; Reinhold

[7] Wise, H. and Ablow, C. M. *J. chem. Phys.* 27 (1957) 389

[8] Jakob, M. *Heat Transfer*, Vol. 1, p. 278. 1949. New York; Wiley

[9] Ingersoll, L. R., Zobel, O. J. and Ingersoll, A. C. *Heat Conduction*, p. 228. 1948. New York; McGraw-Hill

[10] Garner, F. H. *Trans. Instn. chem. Engrs. Lond.* 28 (1950) 88

[11] El Wakil, M. M., Priem, R. J., Brikowsky, H. J., Myers, P. S. and Uyehara, O. A. *Nat. Adv. Comm. Aero. Tech. Note* 3490 (1956)

APPENDIX

Physical Constants used in Calculations

	Tetralin	*Decane*
Density at surface temperature of drop during combustion, g c.c.$^{-1}$	0·85 (180°C)	0·63 (150°C)
Mean* density, g c.c.$^{-1}$	0·92	0·68
Mean specific heat, cal g^{-1}	0·46	0·55
Mean thermal conductivity, cal sec^{-1} cm^{-1} (deg. C)$^{-1}$	0·00033	0·00033
Mean coefficient of cubical expansion, c.c./c.c. (deg. C)	0·00096	0·00131
Boiling point, °C	206	174
Latent heat at the b.p. cal g^{-1}	79	60·2

* i.e. mean value between room temperature and surface temperature of drop during combustion.

Note added to proof—The observation of fine particles suspended in the drops burning in the present conditions does not reveal internal motion with tetralin, and suggests it is possibly not present to any effective extent with decane, in the time periods in question (0·2 to near 1 sec with tetralin and 0·3 to 0·45 sec with decane).

It is true that with decane, which is less viscous and more volatile than tetralin, appreciably random motion is detectable within the drop before ignition. However, on ignition, and after the brief disturbance to the whole drop when the igniting flame passes beneath it, this internal motion generally appears to be suddenly checked, at least appreciably and possibly almost completely, for about a quarter of a second or so.

The fact that droplets heat up to near the boiling point during combustion has an interesting implication for sprays burning at elevated pressure, for it has been pointed out that as surface tension forces disappear when the fluid temperature reaches the critical point, drops will no longer exist but will presumably give place to sheets or filaments.

DISCUSSION

STRUCTURE OF FLAMES

Papers 43, 44, 45, 47, 48, 58, 59

H. G. Wolfhard (Pittsburgh), opening the discussion said: Markstein's paper is of great interest for the understanding of unstable and cellular flames. Looking at such a flame one sees quite large differences in colour between the ridges and valleys, and for fuel-rich flames carbon formation occurs preferentially in the ridges. It is therefore a great surprise to see that he (as indeed did Jost in a similar arrangement) finds such small differences in the overall O/H, C/H and C/N ratios between ridges and valleys. Is it that we need only such small differences in fuel–air ratio to cause the distortion of the flame, or may it be that the differences in O/H, etc., ratios are only a secondary effect and we do not really understand the primary causes of flame distortion? The temperature differences between ridges and valleys are quite large if calculated from the water–gas equilibrium. It would be preferable, however, to use other methods of temperature measurement, as the water–gas equilibrium seems to be notorious for being slow in adjusting itself to the temperature of the flame.

It has become customary to postulate simplified theories of flame propagation using overall or global reaction rates. Weinberg is to be congratulated on starting experimental work to find out whether such concepts are justified.

The paper by Fristrom, Avery and Grunfelder throws important new light on the detailed structure of flame fronts. It is interesting that the luminous zone does not necessarily coincide with the chemical zone as determined by probing, especially for ethylene flames. This divergence needs further investigation as these facts may throw new light on the mode of excitation of radicals in the flame front. It is becoming increasingly clear that reactions are not complete directly behind the flame front and this has been proved now to be the case for fuel-lean flames, where it may be least expected. Although the time for this delay may be short, it may be long enough to be of importance in fast explosions and certainly we can no longer expect to find theoretical temperatures directly behind the flame front. It would be important to establish whether this phenomenon is restricted to fuel-lean flames only or whether it is of general significance. Experimental material to date does not seem sufficient to decide on this question.

Gordon stresses the importance of small amounts of oxygen on the fuel side of diffusion flames. The rates of pyrolysis are not explainable without the accelerating influence of O_2. The question now arises as to how oxygen gets on to the fuel side of diffusion flames as the reaction zone is supposed to use up O_2 and thus prevent any penetration. Two possibilities arise: First, oxygen may penetrate through the base of the diffusion flame where the burner causes a 'dead space'. If this is so, spherical diffusion flames* should be quite different from upright flames, as they have no base. This point may be worth investigating. The second possibility is that oxygen *does* penetrate in small amount through the reaction zone, probably because diffusion rates are too fast for reactions to follow completely. This idea would be contrary to accepted theories on the structure of diffusion flames, at least for undiluted flames far removed from their limit of burning.

The probing of flames in connection with analysis by a mass spectrometer is discussed by Bunt. He finds higher mass 14 and 16 peaks, when sampling directly from the flame instead of taking probes from the exhaust gases. He assumes that these mass peaks are indicative of atomic nitrogen and oxygen. Considerable doubt should be expressed in this interpretation, however, as he finds the same high peaks (when sampling directly from the flame) if a sampling vessel is used and the probe is thus stored for a considerable time.

A new burner arrangement is presented by Williams *et al.* which allows the very stable burning of cool and second-stage rich flames. Such flames are normally stabilized on an Egerton–Powling type flat-flame burner and this latter arrangement will indeed be used if flat or nearly flat flames are necessary. However, the interdiffusion of air or nitrogen cannot be prevented and probing is thus difficult. It is here that the new arrangement will prove useful and ought to be used.

Hall has gone to infinite pains to measure temperature differences in burning droplets. The temperatures and temperature gradients within the drop seem to be consistent with theory. It is shown that the increase of surface temperature with increasing pressure is a factor which has to be considered in evaluating the true pressure dependence of the consumption rate of droplets.

J. Grumer (Pittsburgh): Concerning the diffu-

* WOLFHARD, H. G. *Selected Combustion Problems II*, p. 344. 1956. London; Butterworths.

sional process whereby composition changes occur in the vicinity of flame zones due to diffusion of burnt and unburnt gases along their concentration gradients across the flame zone, this can be observed by considering carbon–nitrogen ratios in enclosed slow burning flames. For example, the carbon–nitrogen ratio in the original mixture is often found to be lower than the local value in the upstream zone of enclosed conical and flat flames*† of very rich hydrocarbon–air mixtures.

G. H. Markstein (Buffalo): In reply to Wolfhard's remarks, I should like to say that we also expected somewhat larger preferential diffusion effects than those observed. As pointed out in the paper, the probe unavoidably averages the composition over a finite width so that the actual variation may be somewhat larger than observed. This averaging effect is most serious at the flame ridge where the radius of curvature is a minimum and varies rapidly. It seems encouraging that our results are quite similar to those obtained by Jost and Krischer (references 10 and 11 of the paper). The temperature variation along the flame front was confirmed by Krischer, using the sodium line reversal method, and it would therefore appear that the temperatures computed on the basis of the water–gas equilibrium are not entirely fictitious. Perhaps one should not expect preferential diffusion effects to be very large in view of the fact that they must vanish if the Lewis numbers of all species are equal to unity. The effects should therefore be proportional to (Lewis No. -1), which, for most species, is a small quantity.

G. Dixon-Lewis (Leeds): Concerning the paper of Levy and Weinberg, we have, in another paper‡ compared weak ethylene–air flat-flame burning velocities, as determined by the luminous area method by Badami and Egerton, and by Egerton and Thabet, with those obtained by ourselves on the modified burner. In the region of overlap of the results the systems behave similarly. Nevertheless our own burning velocities are considerably lower than those given by Sir Alfred Egerton and co-workers. Further, if in determining the area we neglect what we had normally regarded as the upturned edge of the flame, our results in this region agree very well with those of Egerton and Thabet. On the other hand, for the weaker mixtures in our range the upturned edges of the flames assume a more definite appearance, and in this region the total flame areas as measured by us gave burning velocities in reasonable agreement with our temperature profiles. Clearly, however, as Levy and Weinberg point out, there is some considerable uncertainty in defining the flame boundary. For this reason we have been investigating the use of the particle track technique for measuring the flat-flame burning velocities.

In the course of these experiments we have investigated the effect on the flame and the flow field around the burner of gradually introducing an outer sheath of air to the flame gases. It was observed that, on gradually increasing the sheath velocity from zero to a value only about half the main stream velocity, the vortex originally around the burner mouth gradually disappeared. At the same time the flame lifted to a position higher above the burner and became somewhat saucer-shaped. Detailed results will be published in due course.

Lastly, if the curves of *Figure 6* of Levy and Weinberg's paper end on the hot side at the adiabatic flame temperature, there is in these cases very little indication of a slower after-burning region such as has been observed in hydrocarbon–air flames at lower pressures, or such as our own results* using thermocouples at atmospheric pressure may indicate, even allowing for the thermal effect of the surface above the flame. A direct comparison of the two methods of measuring temperature profiles, such as we are currently carrying out, should clarify this situation.

F. J. Weinberg (London): Dixon-Lewis and Isles can easily check the magnitude of any errors introduced into their burning velocity results, due to various criteria for defining the flame edge, by the use of our equations 1 and 2 which are based on particle track measurements.

Concerning their second point, the original burner, as described by Powling in 1949, incorporated such a 'guard ring' of flowing gas. The stability range improved on its removal. The observations of Dixon-Lewis and Isles tend to confirm our suspicions that the position of the flame may be affected by that of the vortex.

Finally, our temperature–distance curves indeed do manifest the 'tail' referred to. No comparison of methods is necessary, however, to elucidate the reason for its absence in *Figure 6* (a plot of volumetric heat release rate against *temperature*):

$$\mathrm{d}\dot{q}'''/\mathrm{d}T = \frac{\mathrm{d}\dot{q}'''/\mathrm{d}x}{\mathrm{d}T/\mathrm{d}x}$$

so that as long as $\mathrm{d}\dot{q}'''/\mathrm{d}x$ is not zero, our gradient, $\mathrm{d}\dot{q}'''/\mathrm{d}T \to \infty$ as $\mathrm{d}T/\mathrm{d}x \to 0$.

Sir Alfred Egerton (London): The flat pre-mixed flame has been useful in determining the chemical reactions in, and physical state of, flames. When Powling and I first used it, we thought it was going to give a perfect method of determining the velocity

* Grumer, J. and Harris, M. E. Smoke limits of bunsen burner ethylene–air flames. *Industr. Eng. Chem. (Industr.).* In press.

† Singer, J. M. and Grumer, J. *Carbon Formation in Very Rich Hydrocarbon–Air Flames—I. Studies of Chemical Content, Temperature, Ionization and Particulate Matter.* This volume, Paper 78.

‡ Dixon-Lewis, G. and Isles, G. L. Paper 68.

* Dixon-Lewis, G. and Isles, G. L. Paper 68.

of burning but it was soon apparent that there were 'snags': chiefly the edge effect. Some photographs taken along with Sen showed the swirl at the edge very clearly. I am very glad that its physical significance on the stability of the flame and the further exploration of the reacting flame gases has been in Weinberg's competent hands, and have led to a closer understanding of the rate of release of energy in the flame.

I would like to further comment on the interesting mass spectrograph sampling of the gases in the flat flame by Fristrom, Avery and Grunfelder. The production of formaldehyde in the propane flame particularly interested me and it will be still more interesting to learn what happens in this respect in the methane flame. Following on Burgoyne and Hirsch's work on burning of weak methane mixtures, I thought that this method might be developed to study the reactions in a flame front and to separate to some extent the wall influence. That is what I am trying to do now along with Pratt at Imperial College; but in the preliminary work (already published) Roy and I found that formaldehyde was very important in the methane combustion. The other point of importance which agrees with Burgoyne and Hirsch's results with methane, and which we have confirmed, is that the CO does not burn until the methane is nearly completely burnt and I was interested to note that with propane in Avery's mass spectrographic analysis, a similar delayed combustion of the CO occurs.

F. J. Weinberg (London): With regard to the luminosity profiles shown by Fristrom, Avery and Grunfelder, any quantitative evaluation should involve consideration of the optical properties of the flame. It has been shown in a recent publication* that, due to the ray deflections occasioned by the flames' refractive index fields, the apparent thicknesses and positions of luminous zones are always, in part, optical illusion. The magnitude of this effect varies from flame to flame but is calculable, and its dependence on the properties of the reactants can be expressed in the form of a simple equation.

W. H. Avery (Silver Spring, Md.): In reply to the remarks of Wolfhard and Weinberg, the profiles of luminosity presented are to be interpreted only in a roughly quantitative sense, to show differences among the three compounds. Precise values for the thickness of the zones would require evaluation of errors arising from the finite extent of the flame and of bending of the light due to gradients in the index of refraction.

G. J. Minkoff (London): Cole and I agree with the deduction of Gordon, Smith and McNesby that in diffusion flames, acetylene is not the major precursor of carbon formation. Using narrow-angle infra-red absorption spectroscopy we* found that although acetylene was detected (in a flat-flame burner of the Parker and Wolfhard type) in the region between the fuel and the oxygen, the intensity of the band could not be correlated with the sooting of the flame when the fuel properties were varied. We are now starting a corresponding examination of pre-mixed flat flames.

A. S. Gordon (London and China Lake, Calif.): I agree with Wolfhard that oxygen can penetrate a diffusion flame. The penetration is, of course, more efficient near the port, since the temperature there is much lower. The important point is that a small amount of oxygen does penetrate the flame mantle and that it plays a vital role in the flame chemistry.

MECHANISM OF FLAME PROPAGATION

Papers 46, 49, 50, 51, 52, 53, 54, 55, 56, 57

Marjorie W. Evans (Menlo Park, Calif.), opening the discussion said: This session, devoted to the subject Mechanism of Flame Propagation, in previous years in numerous combustion symposia would have been titled instead Theory of Flame Propagation: I suggest that this slight alteration of the word *theory* to the word *mechanism* is significant and hopeful.

In previous years the time allotted to this session was devoted to discussion of the merits of various theories, the various points doubtless being familiar to you. The test of merit was without exception the ability of the theory to predict a value for flame velocity which corresponded to the experimental value. Now, occasionally, in those days one heard in justification of the effort being expended on flame propagation theory the assertion that success would allow us to predict burning velocities for various gaseous systems. The truth of the matter was, and still is, that with no exception that occurs to me, it is easier to *measure* the burning velocity than to predict it. In addition, the predicted value of burning velocity turned out to be quite insensitive to the type of theory or the class of assumptions. Its use as a standard of merit was little more than a matter of convenience. Five years ago it was the only quantity characteristic of a flame which could be universally measured and agreed upon.

However, if justification for these efforts were required, in addition to our article of faith that it is always desirable to know more about natural processes, such justification did exist. An almost ripe plum, called chemical kinetics, hung on the tree. Five years ago it was chiefly an obstacle in the path of those who sought to predict flame

* Weinberg, F. J. *Proc. Roy. Soc. A* 243 (1957) 107.

* Minkoff, G. J. and Cole, T. *Proc. Roy. Soc. A* 239 (1957) 280.

velocity. I am persuaded today, however, that the reaction kinetics of gaseous processes at high temperatures is coming into its own, the fruit of the efforts of these past years.

This subject of kinetics at high temperatures is being approached from several directions, many of them not represented by papers at this Symposium. The approach with which we are chiefly concerned in this meeting is the coupling of flame propagation theory with experimental measurements of burning velocity *and* of composition and temperature profiles. This marriage had to await the invention of the Powling–Egerton flat-flame burner and the various ingenious methods for measuring temperature and composition. The success, or hope of success, is demonstrated by the number of papers devoted in whole or in part to these topics. In addition to the papers of this session there have been presentations in the session on Structure of Flames, particularly the beautiful Levy and Weinberg work, and Gerstein's paper in the session on special fuels, which could equally well have been included in this session.

If we are to extract from a theory coupled with experiment a nugget of information on chemical kinetics, we must be certain (a), that the experiments are correctly performed and interpreted, (b) that the theory correctly treats the other processes involved in propagation—heat conduction and diffusion. I wish to say a few words on the second point. It is natural that the preference of the chemist studying kinetics in a flame should be for analytical expressions through which he may deduce his kinetics. This accounts for the popularity of the Zeldovich type of equations which use a single overall reaction mechanism and single and constant coefficients of heat conduction and diffusion. This Symposium makes it clear that interesting results can be obtained in this way. You have heard the Friedman and Nugent paper on the kinetics of carbon monoxide burning, which utilized this type of analysis. There is an unread paper by Sobolev on a similar subject. The paper given on Saturday by Levy and Weinberg presented a treatment of ethylene–air flames using Spalding's modification of Zeldovich's equation. Levy and Weinberg make it clear that using these methods we are not only able to a certain extent to deduce chemical kinetics but to check theoretical assumptions with respect to heat conduction and diffusion.

Should we then, in this flush of optimism, be content with theory as it presently is, interpreting our data in terms of analytical expressions which take diffusion into account but use a Lewis number of 1, assume single and constant coefficients of heat conduction and diffusion, assume a single overall reaction? Surely not, for our knowledge of heat transfer and diffusion tells us that we may for certain systems fall into error, and our lengthy experience with chemical kinetics warns us that reactions usually turn out to be more rather than less complicated than we had at first suspected. We are obliged then to pursue the detailed study of the simultaneous roles of diffusion, thermal conduction, and kinetics for cases which are more and more complicated. True, the results often do not yield analytical expressions. They can at the very least, however, be used as checks of analytical formulae derived for a given situation. We have come to look particularly to Hirschfelder and his colleagues for this work, and the paper presented by Campbell *et al.*, which studies the degree of validity of the steady-state approximation, perfectly illustrates my point.

Now I wish to comment on the papers presented but not read. Sobolev's work on high-temperature oxidation and burning of carbon monoxide is on the same subject as the Friedman and Nugent paper, and the two taken together offer some interesting material for debate. The two papers agree on a major point, that the flame has two parts, a fast burning zone at the front and a zone of slower kinetics downstream. The rate of the fast zone is computed in both papers from the measured flame velocity and the Zeldovich, Frank-Kamenetskii, Semenov equation relating flame velocity to the integral of heat release which in turn is related to the rate of heat release and thus the chemical reaction rate. The rate in the slow zone in each case was computed from composition traverses, and by Friedman and Nugent from a temperature traverse as well. Sobolev measured and analysed the data as a function of temperature, thus obtaining an activation energy. Friedman and Nugent felt the differential analysis scheme was not of sufficient accuracy to warrant this treatment. Certain experimental details such as pressure, composition, and type of burner differ in the two works. This may account for the fact, as I interpret the data, that although the two papers agree on the rate in the slow zone, they disagree by an order of magnitude in the fast zone, that found by Sobolev being the faster.

Strauss and Edse have carried us into new experimental regions. They have measured the burning velocities of various gaseous mixtures at pressures up to 90 atm, using the constant pressure bomb method. Their results show the same qualitative trends as results from the burner method, but quantitatively the values are different, in some instances the bomb measurements being high by a factor of two. This disagreement between values obtained by the two techniques has been observed before, and suggests that the quasi-theories used to interpret observation in terms of burning velocity may be incorrect. Fuel–oxygen systems showed an increase of burning

velocity with pressure; fuel–air systems showed an inverse behaviour. The authors showed qualitatively that such results may be expected from the known dependence of diffusion and heat conduction on pressure. They take care to observe, however, that chemical kinetics may in some instances be the dominant factor.

Sundukov and Predvoditelev present experimental results obtained from burner measurements, relating flame velocity to gasoline–air ratio for two-phase mixtures. The velocity was found to be, in general, less for the two-phase mixture than for a homogeneous mixture, and the velocity decreased as the proportion of liquid phase to total amount of fuel increased. They present a theoretical treatment of the velocity of motion of a thermal front through these mixtures. Interpreting their data in terms of this theory leads them to the conclusion that the combustion of the two-phase mixture can be regarded as a chemical process with a reaction rate of second order.

Rosen presents a mathematical treatment of the one-dimensional laminar flame problem for a one-step reaction, uniting an action functional in terms of non-dimensional temperature and an independent space variable. He shows that the non-dimensional temperature distribution must be such that this functional assumes its smallest possible value. The value of the function obtained by variational methods is then the eigenvalue proportional to the inverse square of the burning velocity. Rosen shows that Spalding's centroid rule may be arrived at from this general form which embodies a more detailed dependence on the rate function.

Van Krevelen and Chermin have correlated data on flame stability on burners in order to make it possible to predict the interchangeability of hydrocarbons for a given burner. The coordinates of their generalized diagram are a reduced boundary velocity gradient and a reduced gas concentration. For a burner with a known performance point for a given gas mixture, the stability of performance for another mixture can be predicted.

Now, in closing, I am going to make the following general assertions which you perhaps may wish to attack or defend in the subsequent discussion:

(1) Our chief interest in flame propagation theory at the present time lies in the opportunity of coupling it with experimental data to obtain information on high-temperature reaction kinetics.

(2) In-so-far as reaction kinetics and flame propagation mechanism is concerned, we shall not learn a great deal by simply measuring flame velocity and attempting to adjust the data to a theory. We must take more subtle data to gain our ends, data such as the temperature and composition profiles which have been described.

(3) We can now afford to forgo what Spalding has called 'shortcut theories,' those which assume a single process to be dominant, including not only the well-worn thermal and diffusion theories, but Eyring's recent theory which lets chemical reaction be dominant. The comprehensive theories which permit analytical solutions through judicious simplifications, such as those of Zeldovich, Spalding, and Karman and Penner, are sufficiently simple to permit ready use and yet sufficiently sophisticated to include the major phenomena involved.

(4) We must allow these analytical solutions constantly to be checked for validity of assumptions by methods which make no assumptions, as we extend the studies to higher pressure, higher temperatures, and more complicated chemical systems.

G. K. Adams (Waltham Abbey): On the subject of the paper by Campbell, Hirschfelder and Schalit, we* have made some calculations of radical concentration distribution in flames and its influence on the propagation constants by a method which appears to work equally well for conditions under which the distribution is close to, or far removed from, the steady-state values. The method follows that of Spalding† in solving the time-dependent flame equations written in finite difference form. The equations have been programmed for an electronic digital computer, enabling the progress of the solutions from the initial ignition conditions to those close to steady-state flame propagation to be followed with reasonable accuracy and computation time.

The reaction scheme examined corresponded to a formal non-branching chain reaction with the initiating reaction first order, propagating reaction second order and terminating reaction third order respectively, in terms of total pressure. The kinetic steady state is then the limiting solution at high pressures. The curves shown reveal the way in which deviations from the steady-state radical concentration increase with decreasing pressure. The concentration in the high-temperature regions of the flame is less, and in the low-temperature regions greater, than the steady-state value. For the steady-state distribution the overall reaction rate is first order with respect to pressure, but the effect of the varying degree of deviation with pressure is to cause the apparent overall order to fall to a value of about two-thirds as the pressure is decreased, before increasing, at low pressures, to a value which may at high flame temperatures approach two.

* Adams, G. K. and Cook, G. B. *Combustion and Flame* (to be published).

† Spalding, D. B. *Phil. Trans. Roy. Soc.* 249 (1956) 1.

A. L. Berlad (San Diego, Calif.): Rosen's very beautiful paper presents a variational principle for an adiabatic, steady-state laminar flame. The starting point in the derivation of this principle involves the usual conservation equations. Yet, there appears to be no 'difficulty' associated with *cold* boundary conditions, even though the 'adiabatic' assumption prevents a solution of the steady-state conservation equations*. Here, in spite of the adiabatic assumption, an appropriate value of Λ may be determined by the variational technique. In this connection, it is significant that the variational technique is, by its very nature, an approximation technique. Thus, the error incurred in $\dot{\tau}$ by the adiabatic assumption is minimized by the variational process. However, the existence of a stationary value for Λ should not be interpreted as implying the existence of an adiabatic steady-state deflagration wave.

G. Rosen (Princeton): With regard to Berlad's remarks, the cold boundary difficulty still remains somewhat latent in the action principle presented here. To see this, notice that the denominator of the action functional (14),

$$\int_0^\infty V \mathrm{d}\xi = \int_0^\infty \left(\frac{1}{\xi^2} \int_0^\tau \Phi(\tau) \mathrm{d}\tau \right) \mathrm{d}\xi = \int_0^1 \frac{1}{\xi(\tau)} \Phi(\tau) \mathrm{d}\tau$$

where the last step results from a change of the limits of the double integral, followed by a performance of the ξ integration. In the vicinity of the cold boundary ($\tau = 0$), we have the direct preheat proportionality,

$$\xi \propto \tau$$

and thus the denominator of the action principle will be finite only if

$$\int_0^1 \frac{1}{\tau} \Phi(\tau) \mathrm{d}\tau$$

is finite, or, equivalently, only if $\Phi(0) = 0$. This obviously physical condition of a vanishing rate expression at the cold boundary is hardly new to us and is indeed necessary if the Klein iteration procedure and Spalding's recent work is to be meaningful.

In accordance with Berlad's remark, however, it is actually possible to refine the action principle so that we need *not* require $\Phi(0) = 0$ and this has been done by the author.

J. W. Linnett (Oxford): It seems to me that Lewis and von Elbe would obtain the equations they do if they considered only the transport of thermal energy and ignored the transport of material by diffusion. This is, in effect, what they do but they imply that it is necessary to say that diffusion is small. In fact, all that is necessary is to ignore the effects of diffusion because the effect of temperature on the rate of chemical reaction is so much greater than the effect of changes in concentration. If this is so, then the term 'excess enthalpy' is a misleading one and should be replaced by something like 'excess thermal energy'. Moreover, if this is the correct interpretation, Lewis and von Elbe's treatment is not incompatible with finding some flames for which there is a decrease in enthalpy in the flame front, for, in such flames, there would be an increase in thermal energy in the flame front even though there was a decrease in enthalpy.

F. J. Weinberg (London): The 'excess enthalpy' hypothesis can be neither proved nor disproved on theoretical grounds alone. The summation, from flame structure data, of the enthalpies of the detectable species may well be irrelevant, if the criteria for ignition must be satisfied before any concentration gradients and hence diffusion flows are established. The authors' expression which constitutes the 'thermal excess enthalpy' may then be the relevant component if not the full quantity. (For this reason also we have preferred to refer to the concept as the 'energy hump'*.)

On the other hand, this proves nothing of a causal relationship. Consider a 'continuous waterfall' such that the flow velocity is constant, the potential energy being degraded to heat, or indeed any system in which a 'non-diffusible' type of potential energy is being so converted. The resultant temperature distribution leads to reverse heat conduction and a simple calculation (formally identical to the flame case) leads to the at first sight somewhat surprising conclusion that 'waterfalls' manifest excess enthalpies. It does not, however, follow that a waterfall may be established by heating up water. The analogy can perhaps be pressed too far, but it seems advisable, as suggested earlier* to defer discussion until relevant further data allow full assessment of the hypothesis on empirical grounds alone.

J. Grumer (Pittsburgh): With regard to the work of van Krevelen and Chermin, it is often helpful in developing new avenues of investigation to emphasize fundamentals. With this in mind, let us note that the Wobbe index is not a fundamental aspect of the problem of fuel gas interchangeability. As stated in an earlier publication,† the interchangeability of fuel gases can be predicted when the specific gravities, stoichiometric fuel gas percentages, flame stability diagrams and gas line pressures are known.

N. Manson (Poitiers): Concerning the paper by

* Berlad, A. L. and Yand, C. H. *On the Existence of Steady-state Flames.* Western States Section of the Combustion Institute, June, 1958 (to be published).

* Burgoyne, J. H. and Weinberg, F. J. *Fuel* 33 (1954) 436.
— — *Fuel* 34 (1955) 351.

† Grumer, J. *Industr. Eng. Chem.* (*Industr.*) 41 (1949) 2756.

Strauss and Edse, the observation that in relating flame velocity to pressure by the law

$$S_n \propto p^n$$

n can be negative or positive, is due perhaps to the fact that the propagation of flame in a soap bubble and in a bomb does not necessarily occur in a laminar regime.

Troshin and Shchelkin* have shown, by strioscopic photography, that in acetylene–oxygen flames the flame became turbulent very rapidly. Goldenberg and Pelevin† in their work on flame velocity measurement by a burner method, showed clearly that in the turbulent regime n is negative if one works at a constant Reynolds number, but that n is positive at constant flow velocity.

In the soap bubbles as used by Strauss and Edse there is never a constant Reynolds number, either during a single experiment or from experiment to experiment, because the pressure varies. In consequence it is probable that there are two situations: (*a*) when the flame front is smooth (laminar) and n is negative; and (*b*) when after short travel the front becomes wrinkled or turbulent and n is positive.

Dorothy M. Simon (Lawrence, Mass.): I wish to discuss the validity of the measurement of burning velocity of fast flames by the constant pressure bomb method. In *Figure 4* of the paper by Strauss and Edse, the third flame trace shows considerable curvature. The authors state that burning velocities were measured from such traces by using the linear portion of the trace to establish a spatial velocity, S_t. The burning velocity, S_u, was then calculated by dividing this velocity by the calculated equilibrium expansion ratio, E. Thus $S_u = S_t/E$. Wong and I‡ also observed curved traces and studied the cause. By photographing expanding flames in soap bubbles with a Fastax Camera at 8,000 frames per sec we observed that the flame front became disturbed or roughened, and the flame area increased. Faster flame velocities resulted. *Figure 1* shows some selected frames from schlieren photographs for a methane, oxygen, nitrogen mixture with an initial velocity of 2,500 cm/sec.

The observed flame roughening is not dependent upon preferential diffusion as are the non-isotropic flames discussed by Lewis and von Elbe§. Markstein‖ has suggested that the cause of the flame roughening is an interaction of the flame generated pressure wave reflected from the soap bubble-gas interface with the advancing flame front. If this is so, the effect is inherent in the pressure bomb method and limits its usefulness.

For flames with spatial velocities of less than 2,500 cm/sec an initial portion of smooth flame propagation was usually observed. However, it is necessary to have photographic evidence other than the strip films to establish the length of smooth flame travel in order to determine burning velocities accurately.

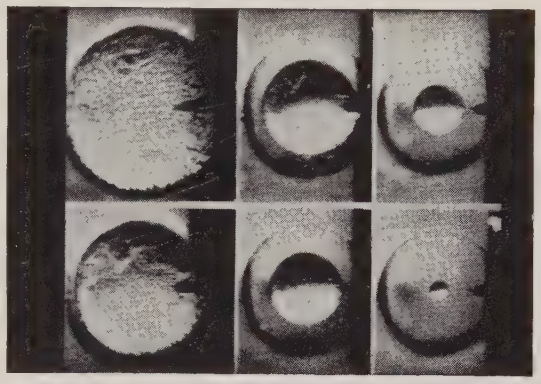

Figure 1

As the initial velocity increases from 2,500–3,500 cm/sec, transition was observed earlier and earlier until the flame was rough from the first photograph or $1{\cdot}5 \times 10^{-4}$ sec after ignition. We observed errors in burning velocity for fast flames measured from the initial slope of the trace as high as 100 per cent.

In *Figure 12* of the paper by Strauss and Edse the pressure effects on burning velocities for various systems are given. The top curves were probably influenced by flame roughening. These curves show the results for hydrogen–oxygen and for methane–oxygen. The third curve, the one for carbon monoxide–oxygen, is near the borderline and may be affected. I suggest that the influence of flame roughening on the measurement of burning velocity by these methods be investigated before theoretical conclusions are based on quantitative effects of pressure on burning velocity.

N. P. W. Moore (London): A comment in support of Dorothy Simon's remarks. We have also observed marked disturbances of confined flames by pressure wave reflections. In our work the flames were of simple shape (approximating to plane waves).

M. R. Barusch (Richmond, Calif.): Phenomena of simultaneously stabilized cool flames, blue second-stage flames and orange flames, virtually identical to those discussed in the paper by

* Troshin, Ya. K. and Shchelkin, K. I. *Dokl. Akad. Nauk, U.R.S.S. Otdel. tekh. Nauk* 9 (1955) 160.

† Goldenberg, S. A. and Pelevin, V. C. Paper 81.

‡ Simon, M. and Wong, E. *NACA Technical Note* 3106, February 1954.

§ Lewis, B. and von Elbe, G. *Combustion, Flames and Explosions*, p. 310. 1951. New York; Academic Press.

‖ Markstein, G. H. Private communication.

Williams, Johnson and Carhart, have been observed in a horizontal tube during experiments carried out at the California Research Corporation. We have conducted analyses of samples obtained through probes, as well as of the effluent gases. The gases obtained through a probe positioned between the cool and blue flame were similar in composition to the effluent gases from a mixture producing only the cool flame. However, limited efforts to obtain a sample of the product between the intense blue and orange flames were unsuccessful; only the products of the cool or orange flames were obtained.

It is probable that the orange flame rested on the blue flame in our horizontal tube. It seems somewhat unlikely that the orange flame could be stabilized in a relatively slow flowing gas stream without a flame-holder and it is suggested that the blue flame functions as a flame-holder for this intense flame.

PART V

IGNITION AND LIMITS OF INFLAMMABILITY

60

SOME FACTORS GOVERNING THE IGNITION DELAY OF A GASEOUS FUEL

R. E. MILLER

INTRODUCTION

The possibility that spontaneous ignition might be a rate determining step in the processes occurring in a gas turbine combustion chamber was first discussed by Lloyd[1]. Since then much work on this subject has been done at the National Gas Turbine Establishment by Mullins who has described the development of a combustion chamber test rig for measuring ignition delays[2].

In this rig the temperature and composition of the 'hot air stream' could not be varied independently because the air was heated by burning fuel in it. It seemed that valuable information could be obtained from an apparatus in which high temperatures could be realized without vitiation. Such an apparatus has been developed, the air being heated electrically, and the dimensions being reduced thus making it convenient to study the effect of atmospheres other than air.

The reactions leading to spontaneous ignition are undoubtedly complex and one might expect several factors, apart from those predicted by the simple Arrhenius equation, to affect the results for a given fuel.

The effect of temperature has been studied by Mullins for a large number of fuels.

The effect of oxygen index or fractional concentration of oxygen by volume has never been investigated over a wide range by the N.G.T.E. method. Mullins[3] reported that the ignition delay was inversely proportional to the square of the oxygen index for a restricted range of oxygen index below 0·21. The method of obtaining this relationship was, however, rather indirect. Jackson and Brokaw[4] found a relationship of the type

$$\tau \propto a^{-\frac{1}{2}} \qquad (1)$$

where τ is the ignition delay and a is the oxygen index.

The same authors[4] found that the ignition delay was inversely proportional to the fuel concentration, whereas most of the N.G.T.E. results showed no variation of ignition delay with fuel concentration for weak mixtures[5].

The nature of the diluents present might also be expected to have some effect on the ignition delay. Since triatomic molecules like water and carbon dioxide occur in practical combustion systems the effect of water on ignition delay has been investigated in the present paper.

Other possible factors influencing spontaneous ignition are the scale of the apparatus and the presence of free radicals. The former has been studied in the present paper by comparing results for the same fuel obtained in rigs of different scale. It is hoped to investigate the latter problem at some time in the future.

EXPERIMENTAL

The apparatus is shown in *Figure 1*. In general character it is similar to that described by Mullins[2]

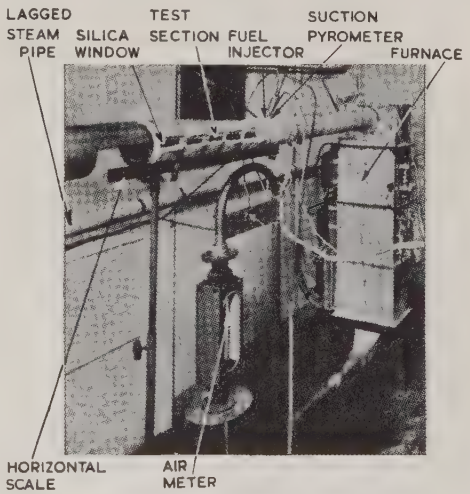

Figure 1. Spontaneous ignition rig

except that it is smaller and the air is heated electrically. The rig has so far only been used with a gaseous fuel, calor gas. This fuel was chosen in order to compare the results with those obtained by Mullins for the same fuel.

The main air flow was measured by a Solway Flowrator covering the range 6 to 32 ft.^{3}/min. Oxygen, nitrogen and calor gas were all measured by means of air rotameters, corrections being applied for pressure and molecular weight. A flow of steam was obtained from a Bastian and

Allen electrode boiler which produced a steady flow of steam in steps of 10 per cent of the maximum output. Once calibrated this was used without a steam meter.

Air heating was carried out by means of an electric furnace which contained three sections. The bottom section consisted of five 2 kW nichrome coils. The middle section contained six crusilite rods as heating elements. These were arranged in two groups of three rods in series, the two groups being connected in parallel. Each rod had a resistance of 4·4 ohms. The top section contained five globars, each of 2·25 ohms resistance connected in series. Air temperatures of over 900°C could be obtained.

Temperatures were measured by means of a suction thermocouple and it was found that the temperature profile across the working section was reasonably flat to within $\frac{1}{4}$ in. of the walls ($\pm$ 5° at the working temperature).

The test section was situated just downstream of the furnace. Into this section calor gas was added by means of a small ring injector and the mixture then entered a 3° diffuser. The diffuser was about 2 ft. long and contained five rectangular silica windows through which observations of the flame front could be made. The diameter of the diffuser was 2 in. at the narrower end. A thermocouple was placed just upstream of the injector.

A number of different injectors were used. These were all 1 in. diameter rings of hypodermic but the number and diameter of the holes were varied. The results did not change significantly from one injector to another.

Experiments have been carried out to determine the quality of the mixing. Experimental conditions could be simulated quite closely by injecting carbon dioxide into the airstream; the flows of both air and simulated fuel were kept as close to the experimental conditions as possible. The tests were done at room temperature so that the airstream momentum was lower than that of most of the tests by a factor of 2 or 3. However, by examining the mixing over a range of airstream momentum it was possible to estimate the degree of mixing at the working temperature. Typical results suggested that C_{max}/C_{mean} (a measure of the quality of mixing, the ratio of the maximum concentration to the mean concentration in a given plane) had dropped to about 1·7 one in. downstream of the injector.

The distance of the flame front from the injector was measured on a scale mounted beside the diffuser and the calculation of ignition delay was carried out in a manner similar to that described by Mullins[2]. In this treatment it is assumed that the velocity profile is flat and measurements have indicated that this is true to within a very short distance of the duct walls. The calculation also involves a mixture temperature which is obtained on the assumption that complete mixing of air and fuel occurs.

RESULTS

The variation of ignition delay with temperature has been investigated; the variation of temperature being quite independent of secondary composition changes. It was found that the logarithm of the ignition delay varied in a linear manner with the reciprocal of the absolute mixture temperature.

The variation of ignition delay with temperature has been obtained for various oxygen–nitrogen mixtures. Typical plots are shown in *Figure 2*. Each line in *Figure 2* corresponds to a particular air–nitrogen or air–oxygen mixture. These varied from a mixture of 40 per cent nitrogen and 60 per cent air having an oxygen index of 0·12 up to pure oxygen ($a = 1$). For each mixture a linear plot was obtained and there appeared to be no change in slope with increasing oxygen index other than that due to experimental scatter. The slope of each line was obtained by the method of least squares and the average value taken as the correct one. All the ignition delay measurements were consistent with the equation

$$\tau a^{1\cdot02} = 4\cdot88 \times 10^{-13} \exp \frac{32{,}400}{T} \qquad (2)$$

where T is absolute temperature. The oxygen index exponent is very close to unity, the difference being well within the experimental error. In future it will be assumed that the difference is in fact due to scatter and the exponent will be taken as unity.

Ignition delay *versus* temperature curves have been obtained over a wide range of equivalence ratios. It is found that when allowance is made for the drop in mixture temperature caused by increasing the fuel concentration the ignition delay is independent of fuel concentration. This result was found to hold for weak mixtures having equivalence ratios between 0·009 and 0·20. The variation of ignition delay with mixture temperature for fuel-air mixtures over this fairly wide range of equivalence ratios is shown in *Figure 3*. It can be seen that all the points lie close to one line despite the fact that ϕ has been varied by a factor of more than 20 on the weak side.

If the fuel concentration is increased too far a certain critical fuel flow is reached. Beyond this point the results obtained are not consistent with those obtained in weaker mixtures and the nature of the spontaneous ignition process seems to change. It is accompanied by a good deal of noise and the results are not reproducible. This may possibly be due to fuel hitting the walls and undergoing premature ignition.

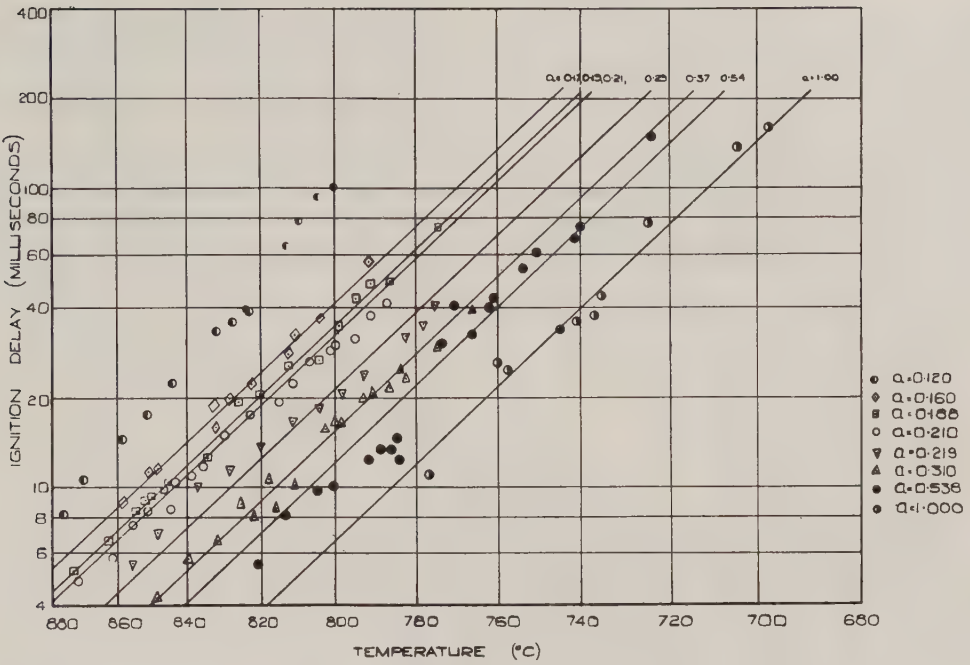

Figure 2. Ignition delay measurements at varying oxygen concentration in a range of oxygen–nitrogen mixtures

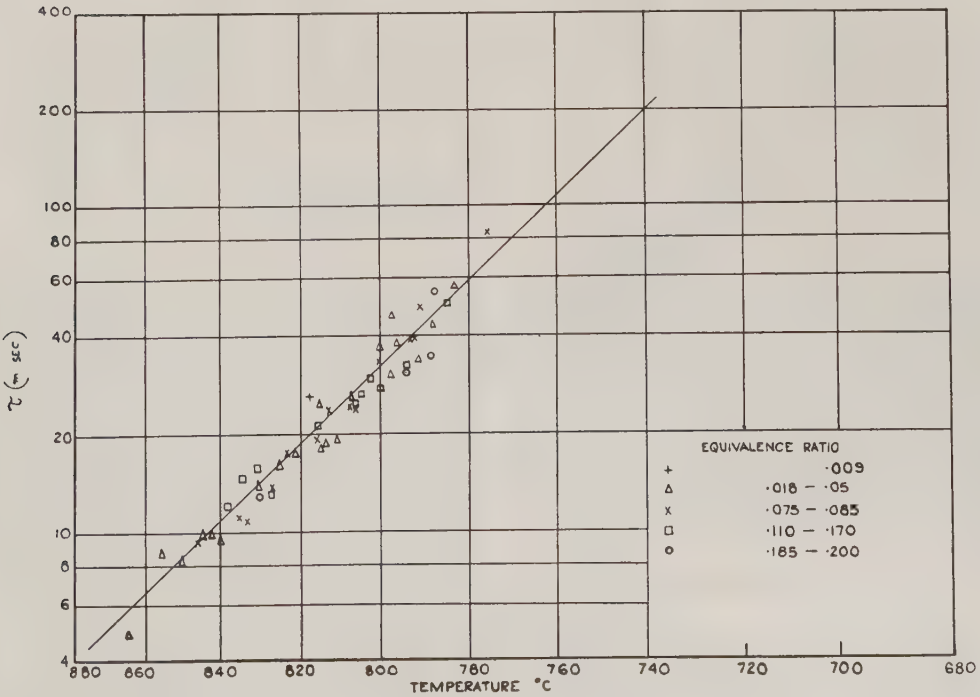

Figure 3. Ignition delay data for calor gas over a wide range of equivalent ratios

The effect of steam on ignition delay is shown in *Figure 4*. Early measurements show that steam increased the ignition delay for calor gas–air mixtures and it was found convenient to add small amounts of oxygen together with the steam. The mixtures investigated varied from air to a mixture containing about 3 volumes of steam to 1 of oxygen. The reproducibility of results in mixtures containing steam was not as good as that in oxygen–nitrogen mixtures, but nevertheless there is an unmistakable trend towards increased airstream, whereas the laboratory scale apparatus has a 2 in. diameter working section. Equation 3 may be used to bring all the data obtained on the laboratory scale apparatus to one unique curve. If the scale effect is negligible Mullins' data should also lie close to this curve.

Strictly speaking the situation is complicated by the fact that Mullins' vitiated airstream contained carbon dioxide and no allowance is made for this constituent in equation 3. Just as equation 3 is a more general form of equation 2 it should be

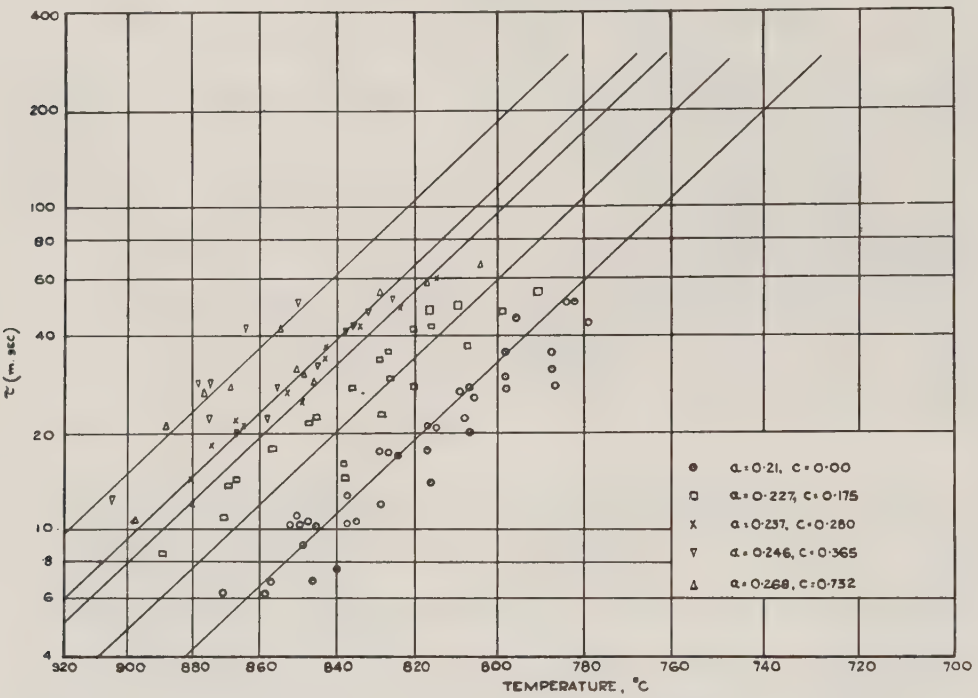

Figure 4.- Ignition delay data in steam–air–oxygen mixtures

ignition delay with increasing steam content of the mixture. This is not merely a dilution effect such as that obtained by adding nitrogen to the air, since those mixtures containing large quantities of steam also contain more oxygen than air. It was found that equation 2 could be modified to include the results shown in *Figure 4* by including a term to account for c, the fractional concentration by volume of water vapour. The following equation was found applicable,

$$\frac{\tau a}{(8{\cdot}5c + 1)} = 4{\cdot}88 \times 10^{-13} \exp \frac{32{,}400}{T} \qquad (3)$$

The results described above are comparable with ignition delay data obtained by Mullins for calor gas[6]. The main difference between the two sets of results lies in the fact that Mullins' data were obtained in a 6 in. duct using a vitiated

possible to obtain an even more general equation taking into account variation in the concentration of all the species likely to be present. In the absence of such an equation it seems reasonable to treat carbon dioxide as though it were an equivalent amount of steam especially as under the conditions of Mullins' experiments the concentration of carbon dioxide was quite small (about 5 to 7 per cent by volume). Since carbon dioxide is unlikely to have a very large effect on ignition delay the above treatment is unlikely to involve large errors.

Equation 3 must now be re-written

$$\frac{\tau a}{(8{\cdot}5c' + 1)} = 4{\cdot}88 \times 10^{-13} \exp \frac{32{,}400}{T} \qquad (4)$$

where c' is the total fractional concentration by volume of water vapour and carbon dioxide.

A plot of $\log \tau a/(8{\cdot}5c' + 1)$ against $1/T$ is

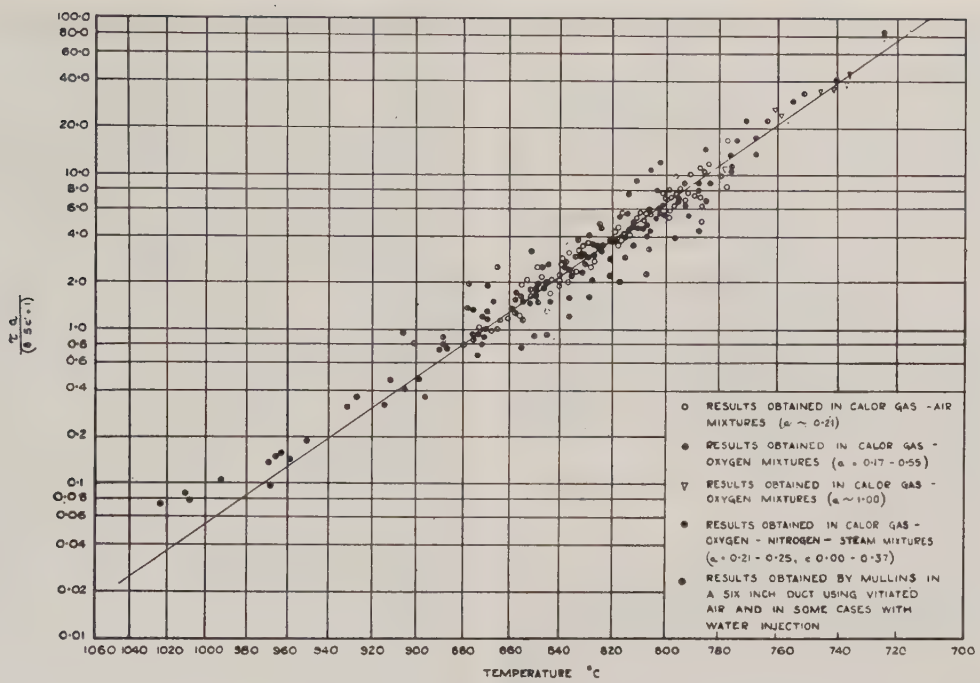
100·0
80·0
60·0
40·0
20·0
10·0
8·0
6·0
4·0
2·0
1·0
0·8
0·6
0·4
0·2
0·1
0·08
0·06
0·04
0·02
0·01
1060 1040 1020 1000 980 960 940 920 900 880 860 840 820 800 780 760 740 720 700
TEMPERATURE °C
RESULTS OBTAINED IN CALOR GAS - AIR MIXTURES (a ~ 0·21)
RESULTS OBTAINED IN CALOR GAS - OXYGEN MIXTURES (a = 0·17 - 0·55)
RESULTS OBTAINED IN CALOR GAS - OXYGEN MIXTURES (a ~ 1·00)
RESULTS OBTAINED IN CALOR GAS - OXYGEN - NITROGEN - STEAM MIXTURES (a = 0·21 - 0·25, c 0·00 - 0·37)
RESULTS OBTAINED BY MULLINS IN A SIX INCH DUCT USING VITIATED AIR AND IN SOME CASES WITH WATER INJECTION

Figure 5. Correlation of ignition delay data (1)

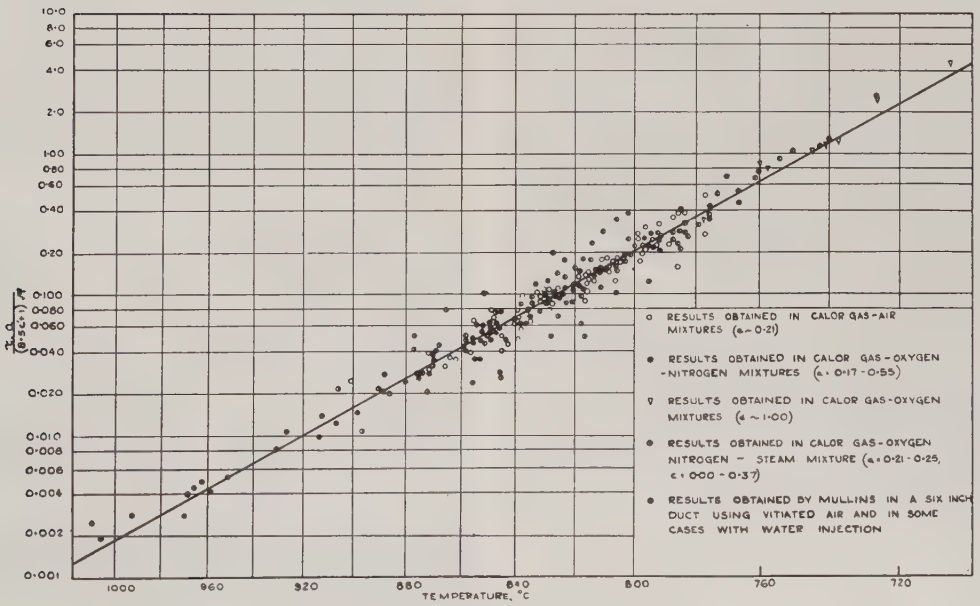

Figure 6. Correlation of ignition delay data (2)

shown in *Figure 5*. This plot contains the following data:

(1) Spontaneous ignition results for calor gas–air mixtures over a wide range of equivalence ratios ($\phi = 0{\cdot}009$ to $0{\cdot}20$) obtained on the laboratory apparatus having a 2 in. diameter working section.

(2) Results obtained in the same apparatus for a wide range of calor gas–oxygen–nitrogen mixtures ($a = 0{\cdot}17$ to $1{\cdot}00$).

(3) Results obtained in the same apparatus for a wide range of calor gas–steam–oxygen–nitrogen mixtures ($c = 0{\cdot}00$ to $0{\cdot}73$, $a = 0{\cdot}21$ to $0{\cdot}27$).

(4) Results obtained by Mullins using a rig having a 6 in. diameter working section for calor gas-vitiated air mixtures with, in some cases, extra water injected.

The results 1 to 4 above cover a temperature range of some 350°C.

DISCUSSION

The correlation of results given in *Figure 5* is a useful one covering both the high-temperature range work of Mullins (850 to 1,050°C) and the lower temperature range results (700 to 900°C) obtained by the present author. The correlation strongly suggests that the essential mechanism leading to spontaneous ignition remains the same over a considerable temperature range without sharp discontinuities.

The points in *Figure 5* would be better fitted by a slight curve than by the straight line. It could be argued that Mullins' data tend to fall on a line corresponding to a rather lower activation energy than the laboratory results and this separation into two lines might possibly be due to a change in fuel. Mullins believes that the calor gas which he used contained a higher proportion of unsaturateds than that used in the laboratory, and he observes that the introduction of a double bond may reduce the apparent activation energy by as much as 20 per cent[7].

However, if the two sets of results do in fact lie on different lines it is remarkable that these lines should coincide so closely over the temperature range 840 to 920°C. It seems much more likely that the falling away at the high temperature end is due to the points in fact fitting a smooth curve.

A suggestion by Mullins[5] that the correct relationship should be of the form

$$\frac{\tau a(T)^{\frac{1}{2}}}{(8{\cdot}5c' + 1)} \propto e^{E/RT} \qquad (5)$$

leads to no improvement and has been criticized on general grounds. It should be stressed that the correlation given in *Figure 5* is merely an empirical attempt to account for the observed facts and does not represent an attempt to force a simple kinetic law, second order or otherwise, on the experimental data.

The lack of effect of fuel concentration is at first sight surprising and has frequently aroused disbelief. The view has been put forward that any fuel effect which occurs is masked by poor mixing and that under the conditions of Mullins' experiments ignition of stoichiometric pockets is always observed. The same lack of effect of fuel concentration has been observed in the laboratory over quite a wide range of equivalence ratios and it can be argued that in the laboratory apparatus the ignition observed is always due to an optimum pocket*. Such an argument will not stand up to more detailed investigation, however.

The mixing experiments quoted in the second section suggest that the mixing time is relatively small compared with the ignition delay time in most cases. However, if an optimum pocket were formed factors governing the conditions in such a pocket would be the initial air temperature, the initial fuel temperature and the local fuel/air ratio relevant to the pocket. These quantities govern the pocket temperature and the reactant concentrations and therefore the ignition delay. The fuel/air ratio of an optimum pocket would be independent of the fuel added to the airstream and if the initial fuel temperature remained constant we would expect to correlate ignition delay with *airstream temperature*. This, however, does not give a good correlation and it is found that ignition delay is best correlated with the mixture temperature T_m. This quantity is calculated on the supposition that cold fuel and hot air are uniformly mixed so that if the above arguments are correct T_m would have no physical significance. The argument may be clarified by a numerical example.

At an airstream temperature of 820°C and an airflow of 25·9 ft.^{3}/min calor gas was added and the ignition delay measured at fuel flow rates of 0·021 and 0·21 ft./min respectively. If bad mixing occurred we might expect the delay times to be the same in each case since only the number of optimum pockets would differ. In fact the ignition delay in the latter case, that is in the richer mixture, is approximately twice the delay found in the former case (32 and 16·9 msec respectively). This is in accordance with the calculated values of the mixture temperature (817 and 788° respectively). The 30° difference corresponds to the temperature increment required to change the ignition delay by a factor of two. Both this argument and the mixing results set out in the second section suggest that the lack of dependence of ignition delay on fuel concentration is a real effect and not due to poor mixing.

* Such a pocket need not in general be stoichiometric however.

The observation of Jackson and Brokaw[4] that ignition delay varies inversely with the fuel concentration is suspect. These authors found that their results could be accounted for in terms of a second order surface reaction.

It has been pointed out in the previous section that if the fuel flow is increased beyond a certain critical amount a sharp discontinuity in the results occurs, and the spontaneous ignition process is accompanied by considerable noise. It has always been assumed that this is due to a wall effect and care has been taken to keep the fuel flow below the critical condition. The fact that Jackson and Brokaw have interpreted their results in terms of a surface reaction suggests that they have not observed this transition or perhaps ignored it and are consequently measuring a different aspect of the spontaneous ignition process from that investigated at N.G.T.E.

If an attempt is to be made to find a theoretically acceptable correlation for ignition delay data it is necessary to define precisely what is meant by ignition delay. This is an extremely difficult thing to do since although the ignition delay is a perfectly definite and measurable quantity the conditions necessary for the onset of visible flame are not known.

Bragg and Holliday[8] suppose that fuel and air react in the pre-flame zone thereby raising the temperature to a point at which ignition occurs. They suggest that 'practically the entire delay period is spent in raising the temperature by the first few degrees'. This suggests that it is only necessary to raise the inlet temperature by 'a few degrees' to cut out 'practically the entire delay period' but this is not found in practice. Mullins[9] has recently published some temperature measurements in the pre-flame zone which suggest that for weak mixtures the pre-flame zone might be almost isothermal. The results established that there is no unique temperature at which ignition occurs.

Jackson and Brokaw[4] suggest that ignition occurs in propane–oxygen–nitrogen mixtures when the fractional rate of propane consumption reaches a critical value characteristic for a given temperature and pressure. The assumption seems to be rather arbitrary and does not fit their results very well. For these reasons it will not be considered further here.

Mullins[5] suggested that the ignition delay may be taken to represent the time for a given fraction of the reaction to be completed. This assumption appears at first sight to be more reasonable than that of Jackson and Brokaw without necessarily being the final answer. If the fraction of reaction completed is small the reactant concentrations throughout the flame zone remain effectively constant and from Mullins' temperature measurements we may assume, at any rate for very weak mixtures, that the temperature also remains constant. Under these conditions it is interesting to note that if the ignition process were governed by second order kinetics a relation of the form of those developed above can be explained. If the initial concentration of fuel and oxygen are p and q respectively the reaction rate may be written

$$\frac{\mathrm{d}x}{\mathrm{d}t} = k(p - x)(q - x) \tag{6}$$

where x refers to the concentration of product and k is velocity constant. On re-arranging this equation and integrating it we find that

$$\frac{1}{k(q - p)} \ln \frac{p(q - x)}{q(p - x)} = t \tag{7}$$

If we now assume with Mullins that the induction period corresponds to the time required for the completion of a definite fraction of reaction we may say that when $t = \tau$ $x = k'p$ where k' is a constant less than unity.

Thus

$$\frac{1}{k(q - p)} \ln \frac{(q - k'p)}{q(1 - k')} = \tau \tag{8}$$

Under the conditions of most of the laboratory experiments it is possible to neglect p in comparison with q without introducing too much error so that

$$\tau = \frac{1}{kq} \ln \frac{1}{(1 - k')} \tag{9}$$

The concentration of oxygen (measured in moles per litre or similar units) is related to the oxygen index, a, by the expression

$$q = \frac{a}{RT} \tag{10}$$

at one atmosphere and the velocity constant k is given by the expression

$$k = A(T)^{\frac{1}{2}} \mathrm{e}^{-E/RT} \tag{11}$$

where A is a constant. Combining we find that

$$\tau = \frac{RT}{A(T)^{\frac{1}{2}} \mathrm{e}^{-E/RT} a} \ln \frac{1}{1 - k'}$$

$$= \left(\frac{R}{A} \ln \frac{1}{1 - k'} \right) \frac{(T)^{\frac{1}{2}} \mathrm{e}^{E/RT}}{a} = \text{const} \frac{(T)^{\frac{1}{2}} \mathrm{e}^{E/RT}}{a} \tag{12}$$

This expression is similar in form to those developed above (equations 2, 3 and 4). It predicts that ignition delay decreases exponentially with

temperature, is inversely proportional to the oxygen index and is independent of fuel concentration, all of which are found experimentally. It also suggests that a better correlation than that obtained in *Figure 5* would be obtained by plotting $\log \tau a/\{(8{\cdot}5c' + 1)(T)^{\frac{1}{2}}\}$ against $1/T$. Such a plot is shown in *Figure 6*. This plot does in fact give a rather better straight line relationship than *Figure 5*, although some curvature is still present.

The treatment outlined above does not of course explain the increase of ignition delay with increasing steam concentration. Indeed the assumption of a simple second order process cannot tell us anything about the effect of diluents. It may well be that the second order scheme is only a special case of a more general reaction rate equation. For instance Satterfield and Wilson[10] have suggested a mechanism for the rate of oxidation of propane

$$\frac{-d[C_3H_8]}{dt} = \left(1 + \frac{k_2}{k_3O_2}\right)(k_1[C_3H_8][O_2] + k_4[C_3H_8][HO_2]) \quad (13)$$

It can be seen that under certain conditions this reduces to a second order reaction rate equation; the fuel propane is an important constituent of calor gas studied in the present work. It may well be that the addition of water would modify such a mechanism and the only method of investigating the effect is by direct experiment.

Figure 6 shows a slight curvature. This may possibly be due to the fact that at high temperatures the mixing time becomes an appreciable fraction of the total delay time. However, it may be due to changes in the activation energy and it should be remembered that this latter quantity is not strictly independent of temperature even for simple reactions.

In the case of complex activation processes the total energy of the colliding molecules cannot be represented adequately in two quadratic terms. The simple Arrhenius equation will not then be a good approximation to the observed behaviour and the variation of velocity constant with temperature will be given by the expression

$$\frac{d \log k}{dT} = \frac{E - \frac{1}{2}(n-1)RT}{RT^2} = \frac{E'}{RT^2} \quad (14)$$

instead of

$$\frac{d \log k}{dT} = \frac{E}{RT^2} \quad (15)$$

where n is the number of degrees of freedom.

Thus the apparent activation energy E' must decrease as the temperature increases

$$E' = E - \tfrac{1}{2}(n-1)RT \quad (16)$$

$$= E + RT - \bar{U} \quad (17)$$

where $\bar{U}$ is the average energy of all the molecules.

It is interesting to note that the activation energy quoted by Mullins is about 12 kcal/mole less than that quoted by the present author (52 and 64 kcal/mole respectively) whereas the change in $\bar{U}$ for butane over this temperature level difference is about 10 or 11 kcal/mole in the expected direction. In this connection it is possible that activation energies derived from spontaneous ignition measurements at relatively low temperatures can be reconciled with the activation energy for *iso*octane reported by Longwell[11]. It is not very clear to what temperature this latter activation energy would correspond since it is an empirical value designed to account for the observed behaviour over a wide temperature range. The suggestion is merely advanced tentatively as an argument against the idea that the values are incompatible.

Crown Copyright Reserved

REFERENCES

[1] Lloyd, P. Combustion losses in gas turbines. *Unpublished M.O.S. Report*

[2] Mullins, B. P. Studies on the spontaneous ignition of fuels injected into a hot airstream. Part I. *Fuel* 32 (1953) 218

[3] —Combustion in vitiated atmospheres III; Effect of oxygen concentration on ignition induction period. *Fuel* 28 (1949) 205

[4] Jackson, J. L. and Brokaw, R. S. Variation of spontaneous ignition delays with temperature and composition for propane–oxygen–nitrogen mixtures at atmospheric pressure. *N.A.C.A. RM. E54B19*

[5] Mullins, B. P. *Spontaneous ignition of liquid fuels. AGARDograph No. 4.* 1955. London; Butterworths

[6] — Studies on the spontaneous ignition of fuels injected into a hot airstream. Part IV. *Fuel* 32 (1953) 343

[7] — Studies on the spontaneous ignition of fuels injected into a hot airstream. Part V. *Fuel* 32 (1953) 363

[8] Bragg, S. L. and Holliday, J. B. The influence of altitude operating conditions on combustion chamber design. *Selected Combustion Problems II*, p. 270. 1955. London; Butterworths

[9] Mullins, B. P. and Miller, R. E. Unpublished work at N.G.T.E. 1957

[10] Satterfield, C. N. and Wilson, R. E. Partial oxidation of propane. *Rep. No. 37 D.I.C. 6552 Div. Ind. Co-operation, M.I.T.*, 1953

[11] Longwell, J. P. and Weiss, M. A. High temperature reaction in hydrocarbon combustion. *Industr. Engng. Chem.* (*Industr.*) 47 (1955) 1634

61

THE THERMAL THEORY OF INDUCTION PERIODS AND IGNITION DELAYS

P. GRAY and M. J. HARPER

INTRODUCTION

Thermal theories of ignition delays are set out in examination of the conditions in an exothermally reacting medium: thermal and kinetic properties of the system are the starting point. Solutions are sought in terms of position and time if the medium is stationary, and in terms of position along and transverse to the lines of flow if it is in streamline motion. Ideally, the form of the solution is an explicit function of the various parameters which is both simple and exact. Because of the form of the differential equations for heat transfer and the presence in them of strongly non-linear terms representing chemical reaction rate this ideal is unattainable. Since, in principle, numerical analysis can lead to a solution of any specified accuracy if sufficient labour is expended, an alternative approach is made possible by modern electronic computing engines and, in practice, these methods are limited as much by the reliability of the physical data and the correctness of the physical model rather than by difficulties of computation. A third possibility lies in the use of approximations which make the equations more tractable without reducing their exactness beyond the present-day errors in experimental data.

In this paper the fundamental heat conduction equation and two approximations employed (exponential and quadratic) are set out and explained. The approximations are then employed to obtain explicit solutions of a number of problems. *Steady state* conditions corresponding to those derived by Semenov and by Frank-Kamenetskii are obtained as limiting examples of a general case. The *general non-steady state* equation is integrated by means of the quadratic approximation to give explicit functions for ignition delays in a uniformly heated medium. Finally, both functional and numerical solutions are obtained for a *particular non-steady state* problem, which can also be solved exactly, and compared with the exact solutions. Agreement is highly satisfactory and the approximations employed should have useful application to further problems of this type.

NOMENCLATURE

C_p	molar heat capacity	cal mole^{-1} deg^{-1}
E	activation energy of reaction	cal mole^{-1}
k	velocity constant	sec^{-1}
$Q(-\Delta H)$	heat of reaction	cal mole^{-1}
S	surface area of container	cm^2
V	volume of container	cm^3
z	frequency factor	sec^{-1}
λ	thermal conductivity	cal cm^{-1} sec^{-1} deg^{-1}
ρ	density	mole cm^{-3}
χ	heat exchange coefficient	cal cm^{-2} sec^{-1} deg^{-1}
T	temperature	deg
$\overline{T}$	mean temperature	deg
θ	dimensionless temperature	$(T - T_0)E/RT_0^2$
$\bar{\theta}$	mean dimensionless temperature	$(\overline{T} - T_0)E/RT_0^2$

THE FUNDAMENTAL EQUATION AND THE APPROXIMATIONS

When heat is transferred solely by conduction the variation of temperature in an isotropic, homogeneous, reactive medium is governed by the following equation

$$C_p V\rho(\partial T/\partial t) = V\nabla \cdot \lambda\nabla T + Q\rho Vz \exp(-E/RT)$$

net rate of evolution of heat | loss of heat by conduction | heat generation by chemical reaction

Ignoring the variation of λ with temperature and dividing throughout by V we have

$$C_p\rho(\partial T/\partial t) = \lambda\Delta T + Q\rho z \exp(-E/RT) \quad (1)$$

Owing to the presence and form of the non-linear term $\exp(-E/RT)$, a solution of the above equation in closed form is not possible. A numerical solution to any specified accuracy is possible if sufficient labour be expended but most methods are limited by the reliability of the physical data and the correctness of the physical model. We therefore attempt to make approximations to one or more of the terms of the equations so that an analytic solution may be obtained. We require the solution of such an approximate equation to be as accurate as is

consistent with the accuracy with which we know the physical magnitudes in equation 1; A, E, λ, etc.

EXPONENTIAL APPROXIMATION

The exponential approximation is obtained by replacing the argument of the exponential term in expression 1 by a Taylor expansion in $T - T_0$

$$E/RT \simeq E/RT_0 - (T - T_0)E/RT_0^2 + (T - T_0)^2E/RT_0^3 \ldots$$

Omitting all but the first two terms of the expansion since $(T - T_0) \ll T_0$, as will be shown later,

$$E/RT \simeq E/RT_0 - E/RT_0^2(T - T_0)$$

Hence on substitution into the exponential term

$$\exp(-E/RT) \simeq \exp(-E/RT_0)\exp\{(T - T_0)E/RT_0^2\}$$

or, in terms of the dimensionless variable θ,

$$\exp(-E/RT) \simeq \exp(-E/RT_0)\exp\theta$$

This is the approximation used by Frank-Kamenetskii[1–4] in his treatment of the steady state. Its accuracy can be seen from Table 1.

QUADRATIC APPROXIMATION

The quadratic approximation replaces the exponential term by a quadratic expression in the variable θ

$$\exp\theta\exp(-E/RT_0) \simeq \exp(-E/RT_0)\{\alpha + \beta\theta + \gamma\theta^2\}$$

To determine the coefficients α, β, γ we write

$$\exp\theta_i\exp(-E/RT_0) = \exp(-E/RT_0)\{\alpha + \beta\theta_i + \gamma\theta_i^2\}\ i = 1, 2, 3$$

Any three values θ_i may be substituted into the above equation and the resulting simultaneous equation in α, β, γ solved. In the present paper however we have fitted the approximate expression at $\theta = 0$, 1 with the added condition that the point of contact at $\theta = 1$ is second order. This gives $\alpha = 1$, $\beta = (e - 2)$, $\gamma = 1$.

TABLE 1

Numerical Comparison of Approximations

θ	$\exp(-E/RT)$	$\exp(-E/RT_0)\exp\theta$	$\exp(-E/RT_0)(1 + 0{\cdot}72\theta + \theta^2)$
0·0	$3{\cdot}139 \times 10^{-17}$	$3{\cdot}139 \times 10^{-17}$	$3{\cdot}139 \times 10^{-17}$
0·5	5·123	5·176	5·054
1·0	8·281	8·532	8·538
1·5	13·250	14·066	13·592
2·0	20·987	23·194	20·215
3·0	50·598	63·050	38·170

It will be seen from Table 1 that both these approximations are quite good in the interval $\theta\langle 0, 2\rangle$ but fall off very badly outside. This is not serious however as we are not concerned with values of θ lying outside this region.

STEADY STATE THEORY

When, in equation 1 $(\partial T/\partial t) = 0$, an equation is obtained which describes the conditions in the steady state—i.e. when the temperature distribution is independent of time

$$\lambda\Delta T = -Q\rho z\exp(-E/RT) \qquad (2)$$

Solutions to this equation are possible only under certain conditions. By assuming that the temperature at the boundary equalled the temperature of the surroundings, Frank-Kamenetskii[1–4] showed that these conditions could be expressed in the form $\delta \leqslant \delta_{crit}$, where δ is the group

$$(Q/\lambda)(E/RT_0^2)r^2\rho z\exp(-E/RT_0)$$

If this inequality is not satisfied, there is no solution to equation 2 and hence no steady state is possible. The temperature of the system described would increase indefinitely.

The earliest description, due to Semenov[5], ignored the spatial variation of temperature and replaced it by a mean value $\overline{T}$ and represented heat loss by a heat-transfer coefficient of the type familiar in newtonian cooling with a finite temperature difference across the boundary:

$$\chi S(\overline{T} - T_0) = -Q\rho zV\exp(-E/R\overline{T})$$

The mean value is taken in such a way that

$$\overline{\rho}\exp(-E/R\overline{T}) = \overline{\rho\exp(-E/RT)}$$

This is equivalent to the condition that the same amount of reaction takes place in either case.

From this treatment one obtains for the critical temperature rise for explosion to occur: $\Delta T_{crit} = RT^2/E$. Semenov argued that since $(T - T_0) \ll T$ then this relation can be replaced by $\Delta T_{crit} = RT_0^2/E$. This is the result one obtains directly by using the exponential approximation, $\Delta T_{crit} = RT_0^2/E$ or $\bar{\theta}_{crit} = 1$.

The relationship between this treatment and Frank-Kamenetskii's has received two interpretations.

The first, given by Frank-Kamenetskii himself, regards the introduction of the mean temperature as a mathematical trick to evade the difficulties inherent in the non-linear differential equation 2, and as a justifiable approximation to the same physical problem. On this basis χ_{eff} was evaluated in terms of δ_{crit}, λ, and a factor depending on the shape and size of the vessel.

Recently, the work of Thomas[6] has made it clear that the two treatments are better considered as the exact solutions to two physically

different problems. The differences arise from the boundary conditions. These have been combined by Thomas into

$$\chi(T - T_0) + \lambda(\partial T/\partial x) = 0 \text{ at the boundary}$$

Substituting $x = rz$, where r is the radius, or half-width, of the vessel this condition becomes:

$$(\chi r/\lambda)(T - T_0) + (\partial T/\partial z) = 0$$

at the boundary.

The relative importance of the $(T - T_0)$ term depends on the value of the parameter $(\chi r/\lambda)$. When this parameter is zero the solution of the equation gives a temperature distribution identical with that assumed by Semenov; T is independent of the spatial coordinates. When $(\chi r/\lambda)$ increases indefinitely the form of the temperature distribution approaches that obtained by Frank-Kamenetskii; $T = T_0$ at the boundary.

Observed cases fall between the two extremes. *Figure 1* shows the critical steady state temperature profiles as a function of $(\chi r/\lambda)$.

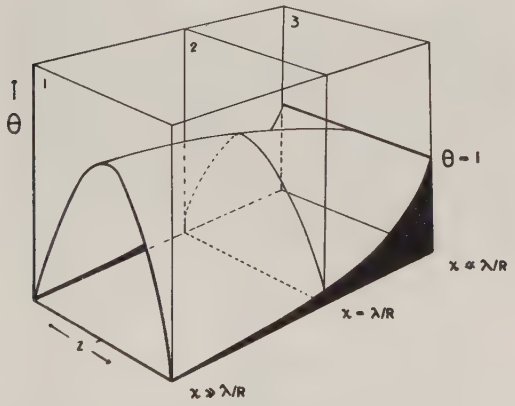

Figure 1. Temperature-position profiles in the critically explosive condition as a function of $(\chi r/\lambda)$

NON-STEADY STATE: CALCULATION OF INDUCTION PERIODS

It has already been pointed out that equation 1 presents great mathematical difficulties if one wishes to obtain the temperature time course of the reaction. Rice[7] avoided some of these difficulties by ignoring the spatial variation of temperature, replacing it by an average temperature which is equal at all points inside the container. This leads to equation 3:

$$V\rho C_p(\mathrm{d}\bar{T}/\mathrm{d}t) = VQ\rho z \exp(-E/R\bar{T}) - \chi S(\bar{T} - T_0) \quad (3)$$

rate of production of heat	rate of production of heat by chemical reaction	rate of loss of heat to surroundings

This still cannot be integrated in closed form. Rice has integrated the equation numerically (with the introduction of a consumption of reactants term) and has obtained solutions of the form shown in *Figure 2*. The curves marked 1

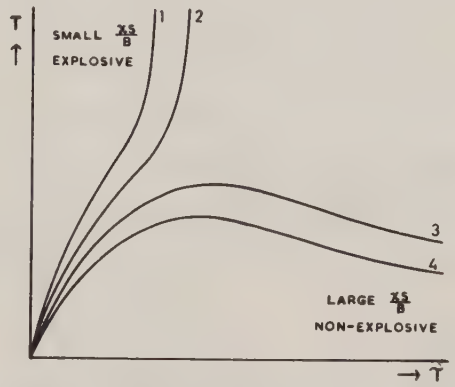

Figure 2. Variation of temperature with time during exothermic reaction $B = Q\rho zV$
(after Rice)

and 2 represent conditions when the rate of self-heating is always in excess of the rate of loss of heat to the surroundings, i.e. χS is small, and ignition finally results: in curves 3 and 4 χS is large and as the temperature rises the rate of loss of heat approaches the rate of production of heat by the chemical reaction and finally equals it. A steady state then results. Owing to the consumption of reactants the temperature, after reaching a maximum value, slowly decreases with time.

An attempt has been made by Eyring *et al.*[8] to solve the non-steady state problem by point to point graphical integration of equation 1 with the inclusion of reactant consumption. The method was so excessively laborious that it was abandoned.

Of the two approximations considered the quadratic form is more suitable since it contains a linear term into which the heat loss term in equation 3 can be absorbed. This problem is first attempted without taking into account the consumption of reactants.

In equation 3 substitute $\bar{\theta} = (\bar{T} - T_0)E/RT_0^2$ and introduce the quadratic approximation $\exp(-E/RT_0)(1 + 0{\cdot}72\bar{\theta} + \bar{\theta}^2)$. This gives:

$$(\mathrm{d}\bar{\theta}/\mathrm{d}t) = (Qz/C_p)(E/RT_0^2) \exp(-E/RT_0)(1 + 0{\cdot}72\bar{\theta} + \bar{\theta}^2) - (\chi S/VC_p\rho)\bar{\theta}$$

Dividing throughout by

$$(Qz/C_p)(E/RT_0^2) \exp(-E/RT_0):$$

$$(C_p/Qz)(RT_0^2/E) \exp(E/RT_0)(\mathrm{d}\bar{\theta}/\mathrm{d}t) = 1 + 0{\cdot}72\bar{\theta} + \bar{\theta}^2 - (\chi S/V\rho)(1/Qz)(RT_0^2/E) \exp(E/RT_0)\bar{\theta}$$

Put $(\chi S/V\rho)(1/Qz)(RT_0^2/E)\exp(E/RT_0) = \tau_r$,

then

$$\tau_\infty(\mathrm{d}\bar{\theta}/\mathrm{d}t) = 1 + (0{\cdot}72 - \tau_r)\bar{\theta} + \bar{\theta}^2$$

Integrating this equation with initial conditions $t = 0$, $\bar{\theta} = 0$, we obtain $\bar{\theta}$ as a function of τ,

$$\tau = \int_0^\tau \mathrm{d}t = \tau_\infty \int_0^{\bar{\theta}} \frac{\mathrm{d}\bar{\theta}}{1 + (0{\cdot}72 - \tau_r)\bar{\theta} + \bar{\theta}^2} \quad (4)$$

where τ_∞ stands for the group:

$$(R\bar{T}_0^2/E)(C_p/Qz)\exp(E/R\bar{T}_0)$$

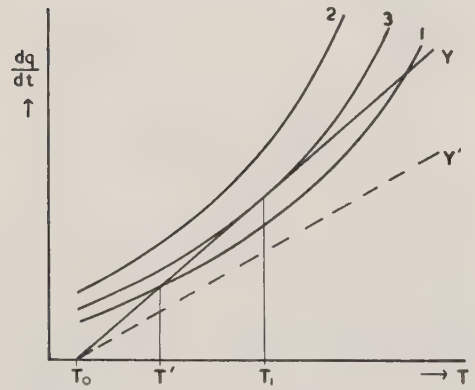

Figure 3. Heat generation and heat loss in an exothermic reaction

The integral on the R.H.S. of equation 4 has three different solutions corresponding to the three distinct physical situations represented in *Figure 3*. The first case where the heat production, curve 2, always exceeds the heat loss, represented by the line *Y*, has its mathematical counterpart in the solution when the quadratic has no real roots; corresponding to explosion conditions. In mathematical form the discriminant of the quadratic is negative

$$(0{\cdot}72 - \tau_r)^2 < 4$$

i.e.

$$\tau_r < 2{\cdot}72 \text{ (actually } < e)$$

$\therefore$ the condition for a steady state is

$$(\chi S/V\rho)(1/Qz)(RT_0^2/E)\exp(E/RT_0) \geqslant 2{\cdot}72$$

When the straight line *Y*, of heat removal, cuts curve 1, the quadratic has two distinct roots. The mathematical form of the solution then corresponds to a steady state. In the critical case where the line is tangent to curve 3, the quadratic has two equal roots and the solution represents the temperature variation in the critical case. Performing the integration in each of the three cases:

case I—explosion occurs, discriminant negative

$$\tau = \frac{2\tau_\infty}{(4 - (0{\cdot}72 - \tau_r)^2)^{\frac{1}{2}}}\left\{\tan^{-1}\frac{2\bar{\theta} + (0{\cdot}72 - \tau_r)}{(4 - (0{\cdot}72 - \tau_r)^2)^{\frac{1}{2}}} + \tan^{-1}\frac{\tau_r - 0{\cdot}72}{(4 - (0{\cdot}72 - \tau_r)^2)^{\frac{1}{2}}}\right\}$$

case II—no explosion, discriminant positive

$$\tau = \frac{2\tau_\infty}{\{(0{\cdot}72 - \tau_r)^2 - 4\}^{\frac{1}{2}}}\left\{\coth^{-1}\frac{0{\cdot}72 - \tau_r}{\{(0{\cdot}72 - \tau_r)^2 - 4\}^{\frac{1}{2}}} - \coth^{-1}\frac{2\bar{\theta} + (0{\cdot}72 - \tau_r)}{\{(0{\cdot}72 - \tau_r)^2 - 4\}^{\frac{1}{2}}}\right\}$$

case III—critical conditions, discriminant zero,

$$\tau = 2\tau_\infty\{1/\tau_r - 1/(2\bar{\theta} + \tau_r)\}$$

These solutions give curves of the type shown in *Figure 4*.

These show a close similarity to the curves obtained by Rice using numerical methods in the solutions of the unsteady state equation. The main difference is that in his treatment the temperature falls after reaching a maximum value whereas in *Figure 4* it approaches a maximum asymptotically. This difference of behaviour is expected: it arises from the omission of the consumption of reactants term in the above treatment.

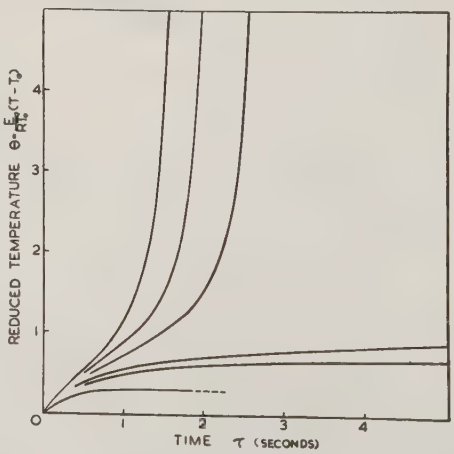

Figure 4. Variation of temperature with time in an exothermic reaction (ignoring reactant consumption)

Substitution of a consumption of reactants term, e^{-kt} into the equation gives an expression which cannot be integrated analytically. If we omit the heat loss term $\chi S(\bar{T} - T_0)$, i.e. assume

the explosion to occur adiabatically, then the equation becomes integrable.

$$\rho(\mathrm{d}\bar{T}/\mathrm{d}t) = n_0(Qz/C_p)\exp(-E/R\bar{T})\exp(-kt)$$

$$(\rho/n_0)(C_p/Qz)\int_{T_0}^{T}\exp(E/R\bar{T})\mathrm{d}\bar{T} = \int_0^{\tau}\exp(-kt)\mathrm{d}t = (1/k)[1-\exp(-k\tau)]$$

k is a function of temperature, the error in assuming it to be a constant is, however, small; or we may we wish replace it by a mean value $k^{\star}$.

NON-STEADY STATE: ADIABATIC SYSTEMS

The problem we discuss below is that of the non-steady state; the solution of this problem involves the determination of the variation of temperature as a function of both the time and the spatial coordinates, which involves integration of the fundamental equation. As we are concerned in this section only with those systems which are potentially explosive we can make the following simplifying approximation. We will assume that the heat loss during the development of an explosion is negligible compared with the production of heat by the chemical reaction. This will be very nearly true in systems which are remote from the critical state. The heat conduction term can be omitted from equation 1 giving

$$\rho C_p(\mathrm{d}\bar{T}/\mathrm{d}t) = Q\rho z\exp(-E/R\bar{T}) \qquad (5)$$

i.e.

$$(\mathrm{d}\bar{T}/\mathrm{d}t) = (Q/C_p)z\exp(-E/R\bar{T})$$

$\bar{T}$ is the mean temperature as defined in the previous section.

We wish to calculate the ignition delay or induction period of the system described by equation 5. This is usually taken to be the time corresponding to the critical temperature rise of the exothermic reaction, which is a small multiple (between 1 and 2) of the dimensionless temperature unit RT_0^2/E. In fact, the actual value of the factor is of no great concern as examination of *Figure 2* will show. We shall in the following text use the value nRT_0^2/E so that any value of n may be substituted in the result.

To illustrate the usefulness of the exponential and quadratic approximations we shall compare solutions obtained by employing them with the approximate solution found by Todes[9] and with the complete solution in terms of the exponential integral. The comparison is made first in terms of explicit functions and then numerically for a typical case.

Complete solution

The differential equation 5 with initial conditions $t = 0$, $T = T_0$ yields:

$$\tau_n = \int_0^{\tau_n}\mathrm{d}t = \int_{\bar{T}_0}^{\bar{T}_0+nR\bar{T}_0^2/E}(C_p/Qz)\exp(E/R\bar{T})\mathrm{d}\bar{T}$$

$$= \tau_\infty\{1-\mathrm{e}^{-n}+2(R\bar{T}_0/E)[1-\overline{n+1}\,\mathrm{e}^{-n}] + O(R^2\bar{T}_0^2/E^2)\}$$

This formula gives a rough division of the terms composing τ_n into those characteristic of the system such as E, Q, $\bar{T}_0$, and those depending on the terms of inquiry, viz. what is the rise in temperature defining the induction period.

Todes' result is obtained by omitting all but the first term in the brackets.

Exponential approximation

Replacing $\exp(-E/R\bar{T})$ by $\exp(-E/R\bar{T}_0)\exp\bar{\theta}$, we obtain

$$(\mathrm{d}\bar{T}/\mathrm{d}t) = (Q/C_p)z\exp(-E/R\bar{T}_0)\exp\theta$$

$$\therefore\int_{\bar{T}_0}^{\bar{T}_0+nR\bar{T}_0^2/E}\exp[(\bar{T}-T_0)E/R\bar{T}_0^2]\,\mathrm{d}\bar{T} = (Q/C_p)z\exp(-E/R\bar{T}_0)\int_0^{\tau_n}\mathrm{d}t$$

On integrating and substituting the limits we have

$$\tau_n = (R\bar{T}_0^2/E)\exp(E/R\bar{T}_0)(C_p/Qz)(1-\mathrm{e}^{-n})$$

or for convenience

$$\tau_n = \tau_\infty(1-\mathrm{e}^{-n})$$

This expression differs from the result obtained by Todes by the presence of the factor $(1-\mathrm{e}^{-n})$.

Quadratic approximation

Replacing the exponential term by the approximate value $\exp(-E/R\bar{T}_0^2)(1+0{\cdot}72\bar{\theta}+\bar{\theta}^2)$, we obtain

$$(\mathrm{d}\bar{\theta}/\mathrm{d}t) = (Qz/C_p)(E/R\bar{T}_0^2)(\exp-E/R\bar{T}_0)(1+0{\cdot}72\bar{\theta}+\bar{\theta}^2)$$

Integrating

$$\tau_n = \int_0^{\tau_n}\mathrm{d}t = \tau_\infty\int_0^n\frac{\mathrm{d}\bar{\theta}}{1+0{\cdot}72\bar{\theta}+\bar{\theta}^2}$$

which gives

$$= 1{\cdot}112\tau_\infty\left\{\tan^{-1}\frac{2n+0{\cdot}72}{1{\cdot}807}-0{\cdot}3744\right\}$$

Comparison of results

From *Figure 2* it is seen that for all practical purposes the value of the critical temperature rise may be taken anywhere in the region $\theta\ \langle 1, 2\rangle$. This is precisely the region in which both the

exponential and quadratic approximations have the best fit to $\exp(-E/RT)$. We expect our approximate solutions in this case to be very near that given by the exact expression. The results are set out in Tables 2 and 3 confirming this.

To obtain a better comparison of these results the induction period has been calculated assuming the critical temperature rise as $R\bar{T}_0^2/E$ (i.e. $n = 1$). The following values of the constants have been used: $C_p = 23$ cal mole^{-1} deg^{-1}; $Q = 33{,}000$ cal mole^{-1}; $z = 5 \times 10^{13}$ sec^{-1}; $T_0 = 500°$K; $E = 38{,}000$ cal mole^{-1}.

The authors wish to thank Dr. P. H. Thomas of the Fire Research Station for his comments; they are also grateful to the Ministry of Education for a scholarship to M.J.H.

TABLE 2

	(τ/τ_∞)
Exponential approximation	$1 - e^{-n}$
Quadratic approximation	$1{\cdot}112 \left\{\tan^{-1} \dfrac{2n + 0{\cdot}72}{1{\cdot}807} - 0{\cdot}3744\right\}$
Complete solution (neglecting terms of $0(R^2T_0^2/E^2)$	$1 - e^{-n} + 2(R\bar{T}_0/E)$ $\{1 - \overline{1+n}\exp(-n)\}$
Todes' solution	1

TABLE 3

Numerical Comparison of Calculated* Induction Periods

	τ/τ_∞	
Exponential approximation	0·632	3·69 sec
Quadratic approximation	0·678	3·96 sec
Complete solution		
(*a*)	—	3·71 sec
(*b*) omitting $0(R^2\bar{T}_0^2/E^2)$	0·646	3·77 sec
Todes' solution	1·0	5·84 sec

* Calculations refer to adiabatic reaction with $C_p = 23$ cal. deg^{-1} mole^{-1}, $Q = 33{,}000$ cal mole^{-1}, $z = 5 \times 10^{13}$ sec^{-1}, $T_0 = 500°$K, $E = 38{,}000$ cal mole^{-1}.

REFERENCES

[1] Frank-Kamenetskii, D. A. *Zh. fiz. Khim.* 13 (1939) 738
[2] — *Acta Physicochim., U.R.S.S.* 10 (1939) 365
[3] — *Acta Physicochim., U.R.S.S.* 16 (1942) 357
[4] — *Acta Physicochim., U.R.S.S.* 20 (1945) 729
[5] Semenov, N. N. *Z. phys. Chem.* 48 (1928) 571
[6] Thomas, P. H. *Trans. Faraday Soc.* 54 (1958) 60
[7] Rice, O. K., Allen, A. O. and Campbell, H. C. *J. Amer. chem. Soc.* 57 (1935) 2212
[8] Eyring, H., Powell, R. E., Duffey, G. H. and Parlin, R. D. *Chem. Rev.* 45 (1949) 69
[9] Todes, O. M. *Acta Physicochim., U.R.S.S.* 5 (1936) 785

62

IGNITION DELAY OF PROPANE IN AIR BETWEEN 725–880°C UNDER ISOTHERMAL CONDITIONS

C. J. CHANG, A. L. THOMPSON and R. D. WINSHIP

INTRODUCTION

When a suitable hydrocarbon–oxygen–nitrogen mixture is flowing in a tube a chemical reaction commences if the molecules possess enough energy to combine upon collision. If this reaction is an accelerating exothermic reaction it results in combustion accompanied by the formation of a visible flame. Ignition delay is the time between the first contact of the reactants and the formation of a visible flame.

This laboratory has a small programme on ignition delay studies which has resulted in a series of theses for the M.Eng. degree[1]. There has been a gradual refinement of technique in the attempt to investigate the effect of changing one parameter at a time.

The main parameters affecting ignition delay are: temperature, pressure, fuel concentration, composition of the fuel, oxygen concentration, type of surface of the tube, physical characteristics of the tube, condition of the mixture flow, method of fuel injection and insulating properties of the surrounding medium. These factors may be placed in three categories: (1) physical delay; (2) chemical diffusion delay; (3) delay due to the chemical properties of the fuel called chemical delay.

The physical properties of the flow tube and the condition of the mixture (turbulence) were varied in this investigation to indicate that in a lean homogeneous mixture in a turbulent system the physical delays are insignificant. The chemical diffusion delay is proportional to the concentration of the reactants and in the apparatus used, with a mixing screen and then 16 injection points spread over the tube area, the delay is assumed to be small compared with the chemical delay. Therefore in this paper the ignition delay is considered to be chemical ignition delay. This has been investigated using propane injected into a hot air stream where there was only a very small temperature gradient along the tube before the fuel was injected. There was a complication with regard to the temperature of the fuel but this has been resolved reasonably well except for the higher air temperatures.

The effect of the following parameters on chemical ignition delay are included in this paper: turbulence, confining tube size (25–54 mm i.d.), fuel–air ratio (up to one-half stoichiometric), and oxygen concentration (12–30 per cent) in a temperature range from 725–880°C at atmospheric pressure.

APPARATUS

A diagram of the equipment is shown in *Figure 1*. The air is supplied from the laboratory compressed air supply through a constant pressure valve. The oxygen concentration could be varied by the addition of either nitrogen or oxygen from cylinders. The flow rates were controlled by needle valves and measured by thin plate orifices. The air was pre-heated in a gas-fired counterflow heat exchanger made from type 310 stainless steel tubes. It passed from the heat exchanger through a stainless steel adaptor which could be changed to fit the diameter of the Vycor tube.

The test gas* was injected through 8 or 16 holes in two stainless steel tubes inserted at right angles into the adaptor which also held the turbulence screen and two chromel-alumel thermocouples. Attempts were made in some experiments to measure the test gas temperature with fine thermocouples inserted in the injection tubes. The adaptor was covered with loose Fibrefrax and an electrically heated stainless steel screen to prevent heat loss. The Vycor tube was supported in the centre of a horizontal stainless steel pipe, 4 in. i.d. and 9 ft. long. This was covered with a layer of Fibrefrax cloth and then a 100-mesh type 316 stainless steel screen which was welded to the pipe at the end near the heat exchanger. The electrical connections to the arc welding transformer were made at the other end. The screen was insulated with Fibrefrax leaving only a narrow slit with a mica window covered with asbestos cloth which could be raised to observe the flame. Chromel-alumel thermocouples were welded to the stainless steel pipe at 18 in. intervals. A long thermocouple could be inserted in the Vycor tube to measure the air temperature and to determine the current setting required to maintain the temperature with a decrease of only 3–5°C over

* The test gas was usually commercial grade propane but pure propane (Matheson) was also used.

the whole length of the tube. The thermocouples were calibrated by comparison with a standard platinum–platinum rhodium thermocouple.

EXPERIMENTAL PROCEDURE

Following the initial warm-up period, the air flow was set to the lowest mass flow that had been selected, and the temperature of the air and the test section was stabilized at the lowest temperature to be investigated. The test gas flow was then varied over a suitable range (limited by tube length, temperature and flashback point) and readings were recorded at specific settings across the range. Flashback was the condition where the reaction accelerated and the flame velocity increased rapidly and the flame front moved back to and remained at the injectors. At each test gas setting for which a flame could be obtained, the mean flame front position was observed and the delay distance from the injectors was recorded. On completion of the test gas settings up to flashback the air mass flow was increased to the next pre-selected setting and the temperature was stabilized at the same value as before. Another series of flame measurement was then made. When this had been repeated for each air mass flow at the initial temperature, the temperature was raised to the next pre-selected level and the procedure was repeated. Thus the temperature was increased step-wise across the range and readings were taken for each mass flow at a particular temperature.

For each reading the test gas flow was established in the exhaust line with an equivalent flow resistance and then switched by a solenoid valve to the injectors (*Figure 1*). A short stabilizing period for both test gas flow and flame was allowed and readings of air temperature, air mass flow, test gas flow and flame front distance were then recorded. The test gas was then switched off and the injectors were purged immediately with nitrogen to prevent decomposition of propane in the hot tubes and subsequent carbon fouling.

Approximate temperature corrections were applied for the cooling effect of the injected fuel (as measured by the traversing thermocouple for a mixture temperature just below the formation of flame or with fuel injected into pure nitrogen). Later attempts to eliminate this correction by pre-heating the fuel to the test air temperature have not been too successful for this delay region of a few milliseconds.

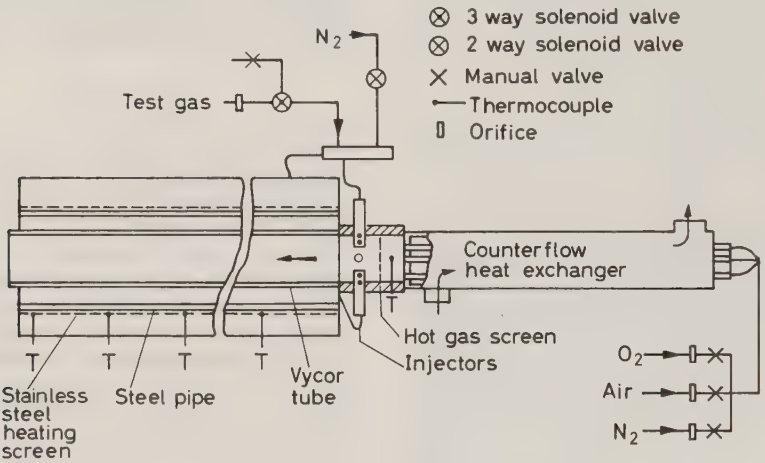

Figure 1. Diagram of ignition delay rig

The ignition delay time γ was calculated from the formula

$$\gamma = \frac{pA}{mR}\frac{x_f}{T_0}$$

where p is the absolute pressure, A the cross-sectional area of the tube, m the mass flow, R the gas constant, x_f the distance from the injectors to the flame front, and T_0 is the absolute temperature of the air stream.

The value of p was nearly constant since in this investigation the pressure drop across the tube was negligible.

RESULTS

The effect of the intensity of turbulence on ignition delay in an air stream having a Reynolds Number of 2,000–14,000 was negligible. This turbulence was induced by placing different mesh screens (4, 10 and 20 mesh) just before the injectors. As an indication of the turbulence induced, the pressure drop across the 4 mesh and 10 mesh screens was measured for the temperature range 800–900°C. The maximum was found to be about 2 in. of water using the 10 mesh screen and 1·6 in. of water for the 4 mesh screen, with a variation of roughly 10 per cent across the temperature range.

It is realized that there was additional turbulence induced from the injection of the fuel and it was difficult to assess the value of this parameter.

The variation of the tube size from 30 mm to 61 mm (nominal) (25 mm to 54 mm i.d.) did not change the ignition delay. However, the fuel–air ratio at which flashback occurred varied with the tube size. In the 30, 51 and 61 mm tubes, flashback occurred at approximately a fuel–air ratio of 15×10^{-3}, while in the 38 mm flashback occurred at a fuel–air ratio of 30×10^{-3}. The stoichiometric fuel–air ratio is 65×10^{-3} (*Figures 2* and *3*). These figures could be reproduced from day to day quite readily.

Studies with four different sizes of Vycor tubes indicated that the ignition delay did not vary with the fuel–air ratio in the temperature range 750–825°C until the flashback point. In the temperature range 825–880°C in the 38 mm tube, where higher fuel–air ratios were achieved, the ignition delay did not change with fuel–air ratio until a value of 25×10^{-3} was reached. At higher fuel–air ratios the ignition delay decreased slightly with the increase in fuel–air ratio until flashback occurred. As the temperature was increased flashback occurred at a lower fuel–air ratio.

It was observed (*Figure 3*) that for an air mass flow of 0·012 lb./sec in the 45 mm i.d. (50 mm nominal) Vycor tube (air velocity approximately

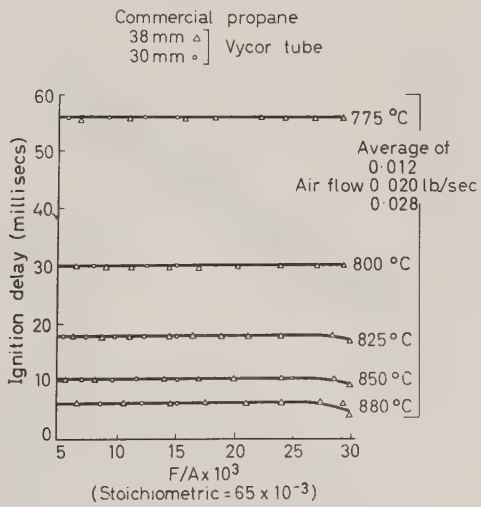

Figure 2

18 ft./sec) the ignition delay was about 10 per cent less than for the other flow rates. The flashback point occurred at about one-half the fuel–air ratio of the other flow rates. It would appear that there was a delicate balance between flame speed and velocity of the air stream. Otherwise in this study the ignition delay time was independent of air velocity (in the range of about 25–150 ft./sec) when other parameters were kept constant.

Ignition delay decreased with the increase of air temperature according to the Arrhenius type of equation

$$\gamma = Ae^{E/RT}$$

where γ is the ignition delay, A the constant, E the activation energy, R the universal gas constant, and T is the absolute temperature.

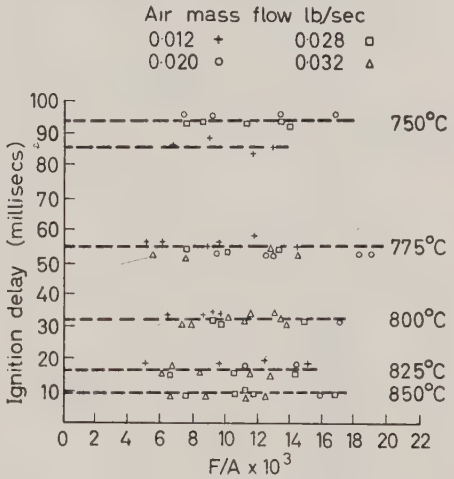

Figure 3. Ignition delay curves for propane–air in 50 mm o.d. *Vycor tube*

The value of the 'global' activation energy determined from these tests was approximately 47 kcal/g mole for the temperature range 750–880°C. If log k (where k is a rate constant $= 1/\gamma$) was plotted against the reciprocal of the temperature the value for A in the Arrhenius equation was about 1×10^{12} litres/g mole/sec.

In studies on the effect of oxygen concentration (from 12 to 30 per cent by weight) in the 45 mm i.d. (50 mm nominal) Vycor tube it has been observed that the flashback occurred at slightly higher fuel/$(O_2 + N_2)$ ratio for the lower oxygen concentration at 775°C and lower. There was not much difference in the flashback at 800°C and higher (*Figure 4*). With the increase in oxygen concentration the flame became progressively shorter; the flame shape became more clearly defined, the colour was more intense and the noise was louder.

There was a linear relationship between log γ and log $[O_2]$, when the temperature of the $(O_2 + N_2)$ mixture was 775°C (*Figure 5*). For the other temperatures and for the oxygen concentration lower than 20 per cent by weight there was a slight departure from linearity.

In general

$$\gamma = \frac{\text{constant}}{[O_2]^n} e^{E/RT}$$

where n was a constant with a value of 0·74 (from 725–850°C) (see *Figure 5*). The value of the

'global' activation energy E apparently changed from 47 kcal for an $[O_2]$ of 30 per cent by weight to approximately 50 for 12·5 per cent (see *Figure 6*). This might be due to experimental difficulties of measurement at the lower $[O_2]$ since the flame front was more diffuse. There might be changes in the reaction characteristics or it might be a real effect. Further studies are necessary before a reliable explanation can be made.

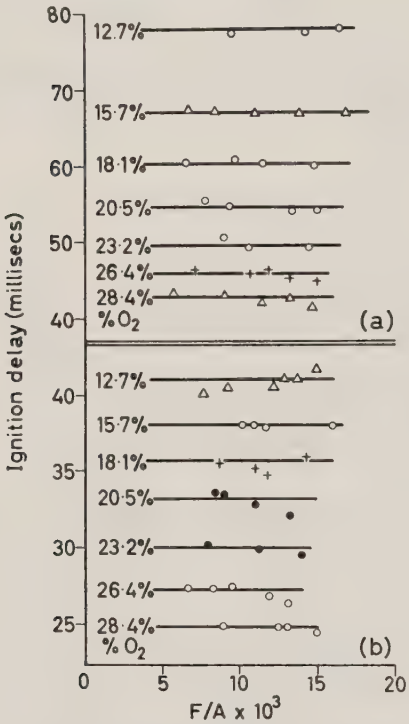

Figure 4. 50 mm *Vycor tube* 0·012 lb./sec *total mass flow, commercial propane mixture: (a) temperature* 775°C*; (b) temperature* 800°C

DISCUSSION

These results have extended the work of Brokaw[2] and have commenced the approach to the investigation recommended recently by Mullins[3] to ignition delay studies at high temperatures. They are really still preliminary and serve to point up certain technical difficulties. The tests to date have been carried out without pre-heating the fuel and this approximates more closely to conditions in practice. However, pre-heating the fuel as high as possible would reduce the uncertainty in the temperatures of the mixture and would possibly improve the kinetic value of the results. Preliminary tests indicate that the ignition delay time is reduced by about 10 or 20 per cent when the temperature of the air stream is 800°C and the fuel temperature is 750°C.

The authors are grateful to Dean D. L. Mordell, Director of the Gas Dynamics Laboratory for his interest, encouragement and procurement of financial assistance for this work through D.R.B. Grant 5001. The assistance of Mr. Jean Gravel in instrumentation and helpful

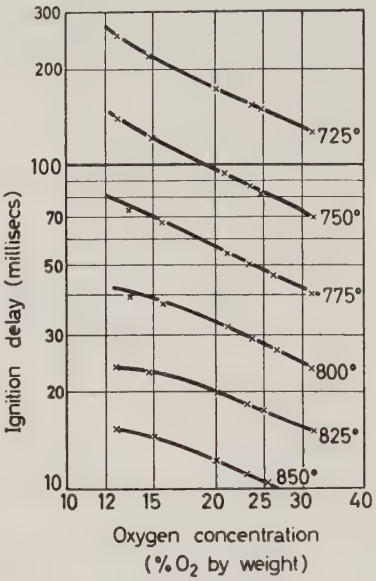

Figure 5

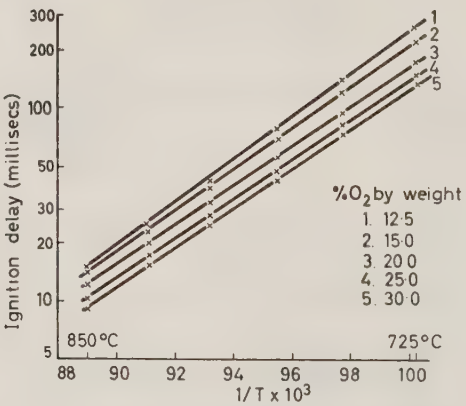

Figure 6. Plot of log γ versus $1/T$ *for a flowing propane:* O_2–N_2 *mixture*

discussion is appreciated. Other members of the Gas Dynamics Laboratory staff have helped in various ways. The financial assistance of the Defence Research Board of Canada is gratefully acknowledged.

REFERENCES

1 *Theses (M.Eng.) on Combustion.* Gas Dynamics Laboratory. McGill University.
Adams, G. N. Measurement of recirculation in flame stabilization. Ph.D. 1953

Balakrishna, N. H. Some aspects of the spontaneous ignition delay of propane injected into a hot air stream. 1956

Bernard, E. A. Spontaneous ignition delays of propane injected into a hot air stream. 1956

Bula, P. J. The effect of oxygen concentration on flame propagation at elevated temperatures. 1954

Dodis, N. G. Spontaneous ignition measurements of some gaseous fuels injected into a hot air stream. 1955

Fang, S. K. Spontaneous ignition delays of propane injected into a hot air stream. 1956

Irwin, R. E. A study of the spontaneous ignition delay of hot lean mixtures of gaseous hydrocarbon fuels and air in a flow system. 1957

Gupta, M. C. Studies on turbulent flames. 1955

Levine, S. The effect of turbulence on the spontaneous ignition delay and combustion of liquid hydrocarbon fuels in a hot gas stream. 1950

Srinivasan, M. R. Flame propagation at elevated temperatures. Ph.D. 1954

Winship, R. D. Spontaneous ignition delay of lean hydrocarbon mixtures. 1957

[2] Brokaw, R. S. and Jackson, J. L. *Fifth Symposium (International) on Combustion*, p. 563. 1955. New York; Reinhold

[3] Mullins, B. P. *The Applicability of Kinetic Data to Engine Combustion.* AGARD Meeting, Washington, November 1957

63

IGNITION PHENOMENA IN HYDROGEN-AIR MIXTURES

H. E. ROSE and T. PRIEDE

INTRODUCTION

Spark discharges have widely been used for the study of initiation phenomena in the ignition of fuel-oxidant mixtures and for the experimental determination of minimum ignition energies for such mixtures. These investigations have, however, almost invariably revealed very pronounced effects arising from variations in the shape of the electrodes, in the characteristics of the electrical discharge and from other factors which vary with small differences in the layout of the experimental equipment.

In order to explain the observed phenomena a number of theories of ignition have been developed, the principal of these being: (*a*) the thermal theory; and (*b*) the electrical theory.

The position relating to these controversial theories was considerably clarified by Lewis and Von Elbe[1,2] who discovered pronounced flame quenching effects produced by the electrodes themselves; the ignition energies measured by Lewis and Von Elbe, for electrode distances larger than the quenching distance of the mixture, being, in general, of the order of 1/100 of the minimum values measured by previous investigators, who almost invariably worked below the quenching distance. This enormous discrepancy arises from the cooling effects of the electrodes themselves and so the data relating to the earlier tests have little significance.

Even when working with gap distances greater than the quenching distance, however, the phenomena are complicated for, although in such cases it appeared that the effects of the electrodes are small, subsequent work by Calcote[3] has shown that the use of a flanged negative electrode leads to consistently higher ignition energies than are measured with plain hemispherical electrodes.

The present work deals with the study of various parameters, such as electrode configuration, electrode material and the rate of energy release, as determined by high-speed oscillographic technique, which affect the ignition energy; the experiments being carried out to cover electrode separation greater and less than the quenching distance of the mixture.

THE APPARATUS

The essential features of the high-speed oscillograph, and the associated measuring circuits, have already been described.

The design of the ignition bomb was controlled, largely, by the need for high-speed oscillographic measurements of the spark discharge characteristics; the design being derived from the results of extensive investigations of the factors controlling the spark discharge characteristics.

The ignition bomb, shown in *Figure 1*, is made entirely from insulating material. It consists of a quartz cylinder 2 in. diameter and 2 in. long clamped between the end plates of insulating material; a quartz tube being chosen so that ultraviolet irradiation of the gap, from an auxiliary spark gap which is also connected in such a way as to trigger the cathode ray tube, initiates the spark. Only by this means was it possible to obtain, with a reasonable certainty, a record of the spark discharge on the tube.

The positive high-voltage electrode holder is made of brass and is screwed into one of the end plates.

The earthy electrode holder is made movable for easy adjustment of the gap distance. This holder consists of a plunger and barrel with lapped surfaces, the plunger being spring loaded against the micrometer which thus provides means of a precise adjustment of the gap distance and for the accurate measurement of the distance.

The two end plates are fitted with terminal mounting legs which can be either directly connected to terminals of the capacitor or secured to the porcelain stand; the mounting legs also furnish a clamping arrangement for the series and measuring resistances.

In the end plate on the earthy side of the gap is fitted two $\frac{1}{2}$ in. brass gas unions. One of these unions serves as a gas inlet and the other is connected to the pressure relief valve; this pressure relief valve consists of a small cylindrical chamber with spring loaded lid. The spring force is adjusted such that the valve opens at a pressure of about 1/10 atm.

The different types of electrodes investigated are shown in *Figure 2*.

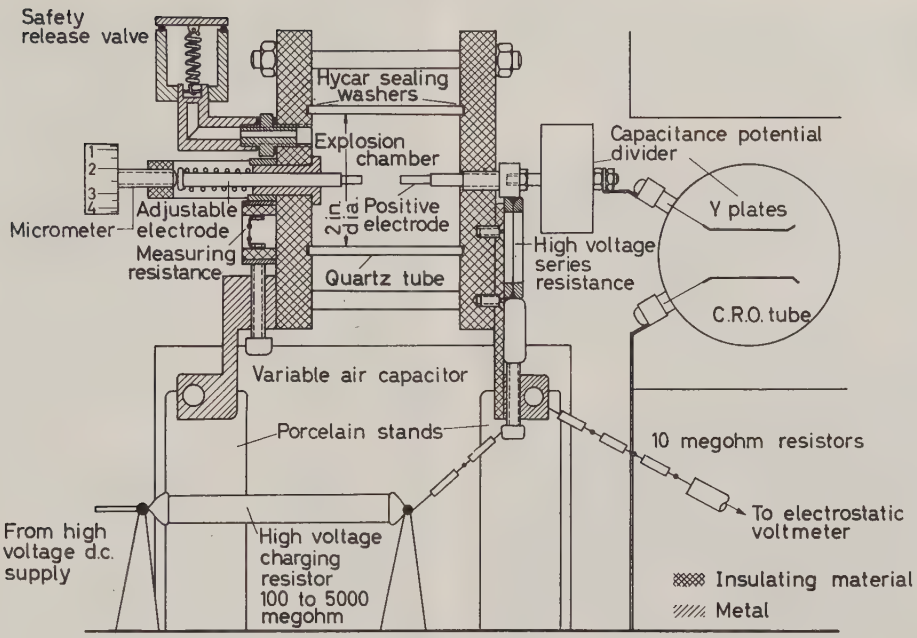

Figure 1

Capacitors were provided to cover the range from 1μμF to 1,000μμF. For values up to 21μμF the capacitors were of fixed air type employing polythene insulation, from 21μμF to 200μμF a variable air capacitor was employed and from 200μμF upwards the capacitances were Micalex type.

The capacitor is charged through a high resistance of the order of 100 to 5,000 megohm. The higher resistance value is normally chosen when capacitances of smaller values are used. To minimize the capacitance effect of the end connection of the charging resistor, the connection to the discharge capacitance is made through two ½ W 10 megohm resistances in series, these resistors having been specially selected with a view to their having a minimum capacitance.

The static voltage of the capacitor is measured with an electrostatic voltmeter and, since the internal capacitance of the voltmeter was of some 18μμF, the effect of this capacitance on the spark discharge was eliminated by connecting it through three 10 megohm resistances connected in series. The high voltage arm of the discharge capacitor is connected with the positive electrode holder by a straight copper strip, but when the effects of the series resistance is to be investigated this strip is replaced by the relevant resistance. The current through the spark gap is recorded as a voltage developed across a measuring resistance which is connected, by means of a coaxial cable, to the *Y* plates of the cathode ray tube. The gap voltage is measured by a capacitance voltage divider which is formed by interposing a small high voltage air capacitor between the positive electrode holder and the *Y* plate terminal of CRO tube. Thus the capacitance of the *Y* plates of the tube form the low voltage arm of the divider.

The gaseous mixtures were prepared in a separate mixing chamber of 300 in.³ capacity in which the mixture was prepared at a total

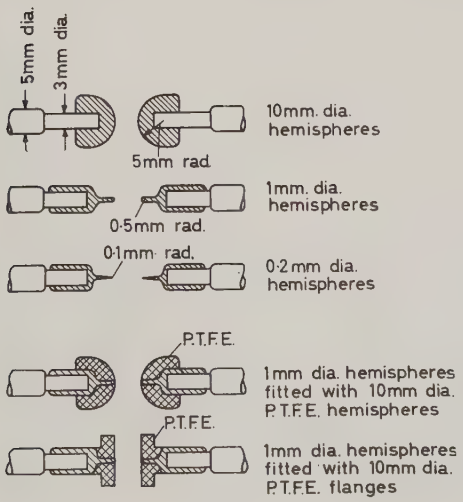

Figure 2

pressure of 2 atm absolute. The composition of the mixture was determined by measurement of partial pressures of the component gases by means of a mercury manometer.

TEST PROCEDURE

The ignition experiments were carried out with hydrogen–air mixtures of 10, 20, 30, 40, 50 and 60 per cent hydrogen concentration at 760 mm Hg pressure. All these experiments were made over a wide range of spark discharge characteristics, which were obtained by varying the electrode configuration, electrode material and the series resistances incorporated in the discharge circuit.

The following tests were made.

After the ignition bomb was filled with hydrogen–air mixture the voltage of the d.c. supply was raised by a Variac control unit, thus slowly charging the capacitor through a high resistance, until a single spark passed between the electrodes. The value of the charging resistance was chosen such as to practically fully charge the capacitor in some 6 to 10 sec; thus ensuring that a second spark could not occur in a shorter time interval than this.

When dealing with small capacitances, up to 21μμF, the ignition experiments were carried out with a fixed capacitance but with varying gap distance, until the ignition and non-ignition regions were well defined. When using variable air capacitor (i.e., 21μμF to 200μμF) the tests were made at a fixed gap distance but with varying capacitance.

Ignition of the mixture was defined as the appearance of flame and of an increase of pressure sufficient to actuate the pressure relief valve.

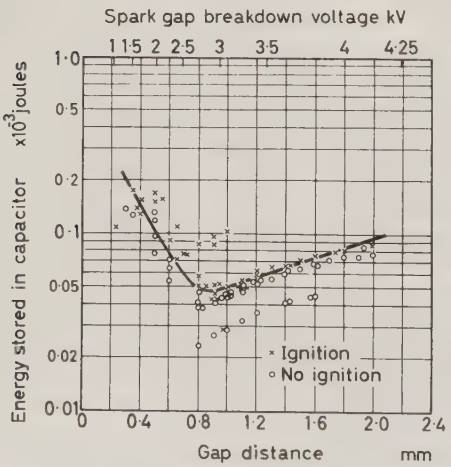

Figure 3

Ignition was also assumed to occur when the mixture was ignited by, at least, the third successive spark; although in these circumstances the test was normally repeated.

For each of the experiments, whether producing ignition or not, the *circuit energy* was computed from the relationship $E=\frac{1}{2}CV^2$ where C is capacity in farads and V the capacitor voltage prior to breakdown. The points of the calculated energy specifically designated as 'non-ignition' and 'ignition points' were plotted on graphs, such as that of *Figure 3*.

As can be seen when large numbers of points are recorded, the ignition limits are clearly defined and a curve can be drawn defining the minimum ignition energy as a function of gap distance.

After defining the minimum ignition circuit energy curve, the spark discharge characteristics were recorded at a number of points by the oscillograph, these data then supplying information as to the discharge characteristics of the spark, e.g. of the time for discharge, maximum current, voltage waveform, the rate of electrical energy release and the total electrical energy released at the electrodes.

RESULTS

Although a number of tests were made at various mixture concentrations, the most detailed work was related to ignition of 50 per cent H_2 air mixture, which will be fully described.

Effect of electrode configuration

In *Figure 4b* is shown the effect of electrode configuration on the minimum ignition energy in the spark for the 50 per cent hydrogen–air for various gap distances; the electrodes used being aluminium hemispheres of 10, 1 and 0·2 mm diameter.

Apart from the very pronounced differences produced by electrodes below the quenching distance, marked effects on minimum ignition energy also are found above the quenching distance. The effect is generally that ignition energy decreases with decreasing electrode size. *Figure 4a*, *c* and *d* also show the corresponding curves of gap voltage and capacitance *versus* gap distance, and also data such as discharge time, peak current and gap resistance, which have been obtained by the use of the oscillograph. These curves show that both with different electrode configurations and with different gap resistances, pronounced changes in spark discharge characteristics are produced. These changes can account for the measured differences in the minimum ignition energy which have been encountered. Nevertheless it is of interest to know, when large

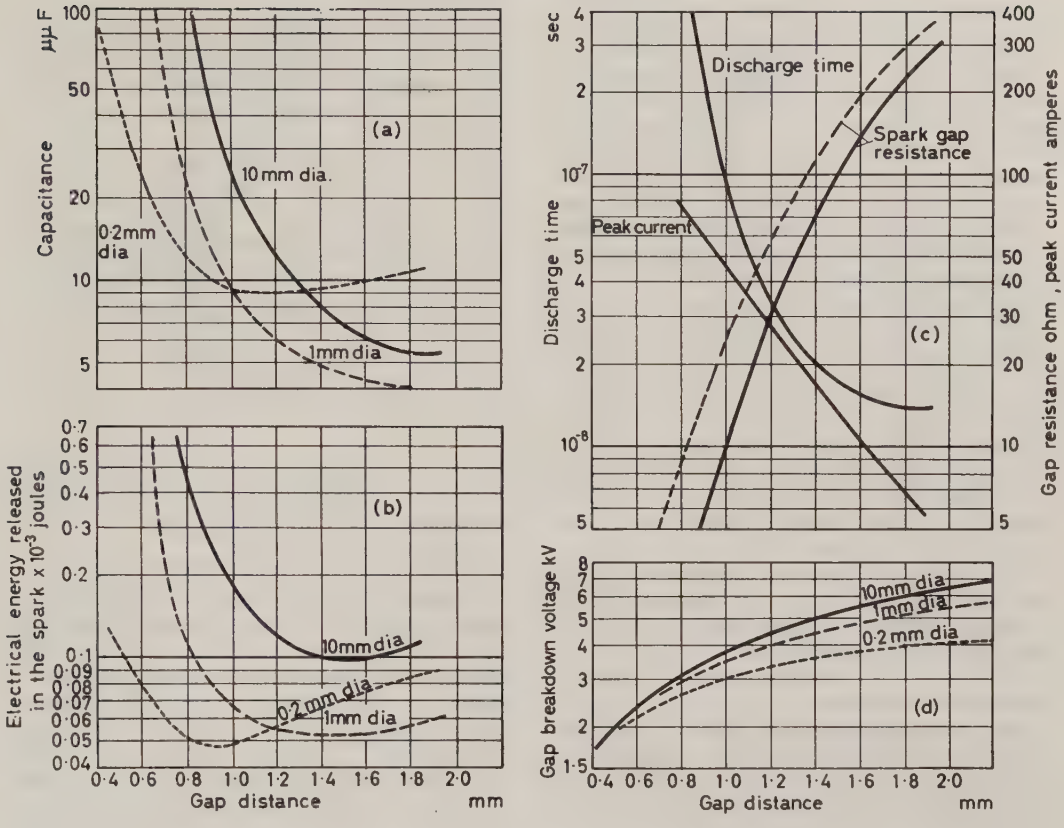

Figure 4

electrodes are used, if any physical quenching of the flame occurs when the gap distance is greater than the quenching distance.

This has been studied experimentally by the use of electrodes which are electrically equivalent to electrodes of 1 mm diameter but of which the physical size is equivalent to 10 mm diameter hemisphere. This was accomplished by fitting to the 1 mm diameter electrodes a hemisphere made of insulating material (PTFE) of 10 mm diameter.

This, of course, follows from the work oi Friedman[4], who has shown that the nature of the material of the solid boundary does not affect the quenching distance, because the heat conductivities of solids exceed heat conductivities of gases by order of magnitude. Electrically these composite electrodes are found to be identical with plain 1 mm diameter hemispheres, i.e. the breakdown voltage was the same and no difference was found in discharge characteristics.

Test results with these electrodes as compared with plain 1 mm hemispheres are shown in *Figure 5*. As can be seen, above the quenching distance they gave exactly the same results as the plain 1 mm hemispheres, but at or below the quenching distance more energy was required to ignite the mixture. Thus evidence is provided, by this test, that the larger electrodes do not produce any extra quenching effect at distances in excess of the quenching distance of the mixture, and

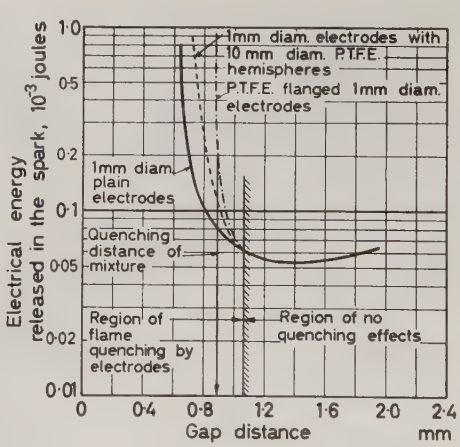
1mm diam. electrodes with 10 mm diam. P.T.F.E. hemispheres
P.T.F.E. flanged 1mm diam. electrodes
1mm diam plain electrodes
Quenching distance of mixture
Region of flame quenching by electrodes
Region of no quenching effects
Electrical energy released in the spark, 10⁻³ joules
Gap distance
mm

Figure 5

that the higher ignition energy required with larger electrodes must arise from other causes.

Similarly when 1 mm diameter hemispherical electrodes were fitted with PTFE flanges of 10 mm diameter, it was found that at distances much above the quenching distance these also did not produce detectable effect on minimum ignition energy. However, they clearly defined the quenching distance of the particular mixture, and below this distance it was impossible to ignite the mixture.

Tests were also made with electrodes of identical physical size but different in electrical respect. This was accomplished, in one instance, by using as a positive electrode a 10 mm aluminium hemisphere and as the negative electrode a 1 mm hemisphere fitted with 10 mm insulated PTFE hemisphere, whilst in the other case the polarity of the composite electrodes was reversed. The minimum ignition energy curves show pronounced differences, thus supporting the view that it is the influence of the electrode geometry on the spark discharge and not the physical shape of the electrodes which produces these changes in minimum ignition energy.

Effect of electrode material

This was investigated, for 50 per cent hydrogen–air mixtures, by use of 10 mm hemispherical electrodes made of platinum, aluminium, silver and cadmium. The curves of minimum ignition energy *versus* gap distance for these electrodes are shown in *Figure 6*. As can be seen, the effect of electrode material on minimum ignition energy is very marked. For electrodes set beyond the quenching distance platinum electrodes require the highest ignition energy, and the energies required with other materials follow in the same order as the boiling temperature of the materials; the lowest recorded ignition energies being with cadmium electrodes.

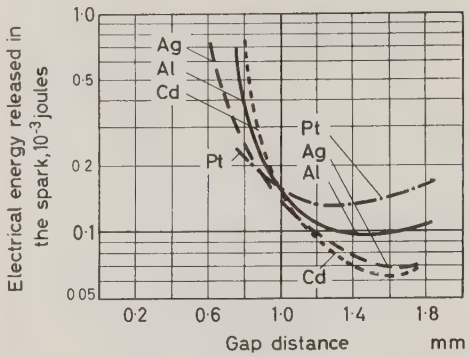

Figure 6

Effect of series resistance on minimum ignition energy

In general, a series resistance incorporated in the discharge circuit reduces the rate of the energy release and, for above critically damped circuit conditions, also increases the discharge time: in addition to these effects an appreciable amount of energy is dissipated in the resistance during the discharge.

The minimum ignition energy curves (expressed as energy stored in the capacitor) *versus* gap distance for a 50 per cent hydrogen–air mixture, with series resistances of 0, 220, 1,000, 5,025, 15,000 and 100,000 ohm in conjunction with aluminium hemispheres electrodes of 10, 1 and 0·2 mm diameter are shown in *Figure 7*. These graphs also show lines of constant capacitance and gap breakdown voltage, and thus at any

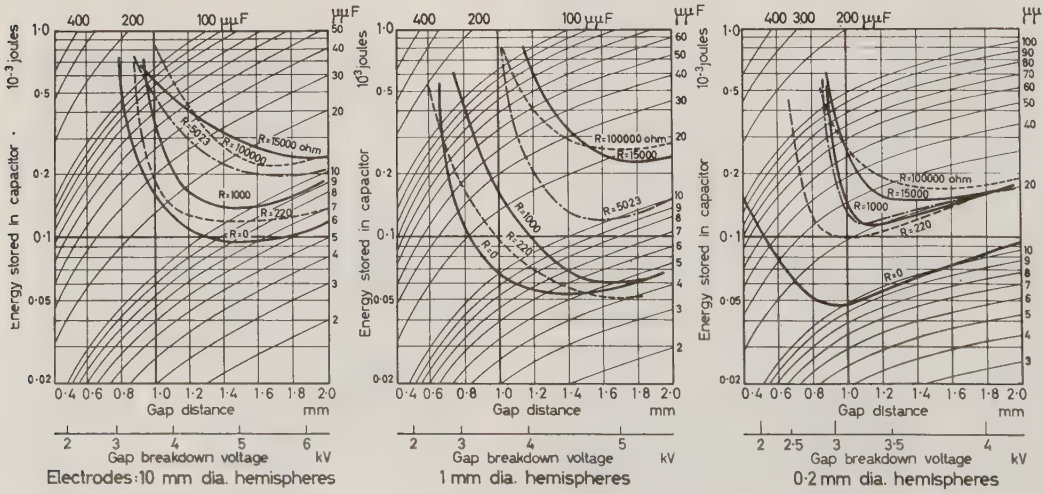

Figure 7

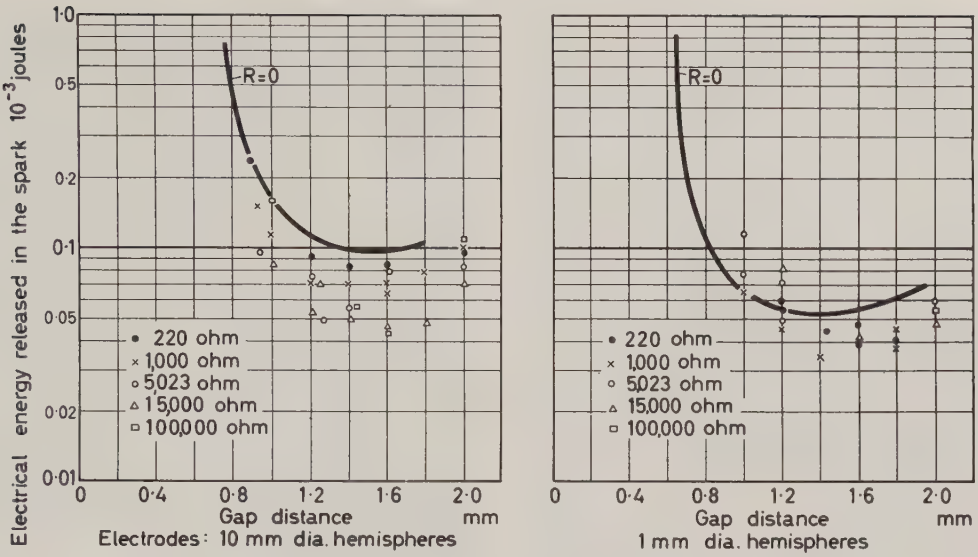

Figure 8

point all the circuit parameters can be readily assessed.

As can be seen, in all cases where resistance is incorporated in the discharge circuit the energy required to be stored in the capacitor in order to produce ignition is increased; but, when the electrical energy released at the spark gap is considered (calculated from the current and gap voltage diagrams) it is found, as shown in *Figure 8*, that the electrical energy required at the gap to produce ignition decreases considerably with increasing circuit resistance.

With 1 mm diameter hemisphere the greatest reduction (up to 40 per cent) was recorded with 1,000 ohm circuit resistance and with 10 mm diameter hemisphere the reduction was greater (up to 60 per cent) with 100,000 ohm resistance. With electrodes of 0·2 mm diameter hemisphere

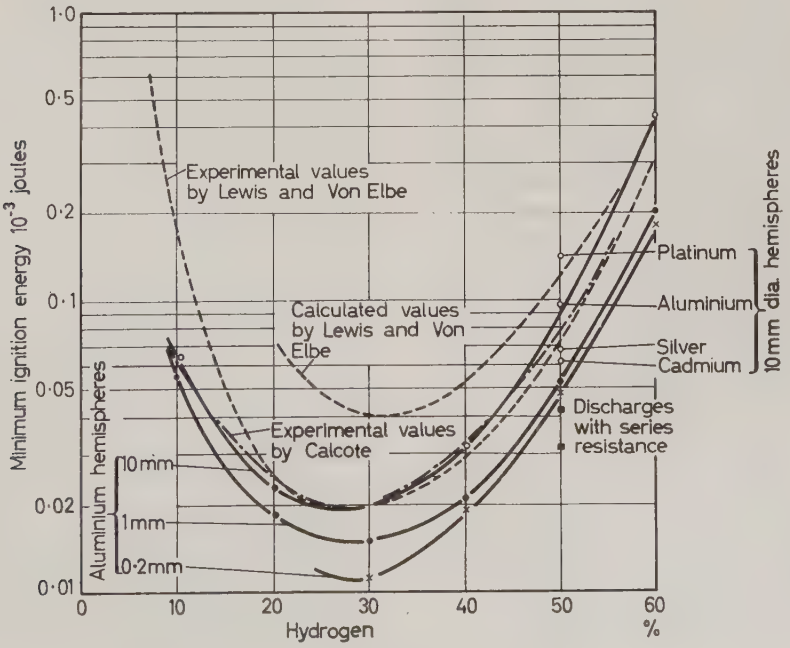

Figure 9

it was impracticable to obtain the oscillograms due to difficulties of initiating the spark by ultra-violet irradiation; a phenomenon which is generally observed when the electrode size is reduced.

These results, summarized in *Figure 9* together with data published by Lewis and Von Elbe and by Calcote, show the minimum ignition energies *versus* mixture concentration. In addition to the data showing the effects of electrode configuration, which were obtained over the whole range of mixture concentration, points are entered showing the effect of electrode material and of series resistance on the ignition of a 50 per cent hydrogen–air mixture. The variation in the measured minimum energy in the spark gap may have, according to experimental conditions of the test, a fivefold difference of value.

DISCUSSION OF TEST RESULTS

Whilst it is not claimed that the investigation presented here is in any way complete, or that a generalized consistent account of the spark ignition processes can be given, it is believed that some significant observations which may form a basis for further investigations aimed at deriving a mechanism of ignition have been made.

There have been a number of phenomena observed which can be explained on a thermal basis, but there are other phenomena where electrical influences appear to play a prominent part.

In this discussion it is assumed that with the three-electrode configurations shown in *Figure 4* all the electrical energy released at the spark gap is imparted to the gas mixture. Since in these experiments additional circuit resistance was not incorporated, all the discharges are of an oscillatory nature and the electrical energy released at the gap is practically equal to that charged in the capacitor.

When considering the minimum ignition curve (*Figure 4*) obtained with 0·2 mm diameter electrodes, it will be seen that it follows exactly the trends one would expect by reasoning on a thermal hypothesis.

(*a*) The minimum of this curve is at the quenching distance of the flame, i.e. when the energy is supplied to a minimum length of the spark channel.

(*b*) For distances greater than the quenching distance, the ignition energy increases with the gap length in more or less uniform manner, which indicates that the energy which is supplied in a spark channel having a length in excess to that of the minimum flame diameter does not usefully participate in the ignition process.

(*c*) For gap lengths of less than the quenching distance the ignition energy increases with decreasing length, but this is due to quenching of the flame by the electrodes themselves.

However, the minimum ignition curves derived with other electrodes, namely 1 and 10 mm diameter hemispheres, show entirely different trends. The energy required to ignite the mixture continues to decrease with gap distance, even beyond the point at which quenching must cease. (The critical distance at which any physical quenching of electrodes may take place is indicated by a hatched line (*Figure 5*) which has been experimentally derived with 1 mm diameter electrodes fitted with PTFE flanges and hemispheres of 10 mm diameter.)

An explanation of these trends does not follow directly from the simple thermal reasoning advanced for the 0·2 mm diameter electrodes, and thus one is compelled to take into consideration the appropriate changes which take place in the spark discharges.

With increasing gap distance the discharges are at progressively higher gap breakdown voltages (which is fixed purely by the physical nature of the discharge process and thus cannot be altered at will) which permits a progressive reduction of the capacitance (*Figure 4a* and *d*), whilst still allowing ignition to occur.

According to the investigation carried out on spark discharges the reduction of capacitance produces: (*a*) a reduction in the discharge time and in the peak current; and (*b*) an increase in the gap resistance, which results in a reduction of the diameter of the spark channel.

These observations comply with the reasoning of the thermal model of ignition, i.e. that energy is supplied in a shorter time and to the smaller volume of gas. These effects may be so marked that, despite the energy being supplied to a gap length in excess of the minimum flame diameter, a decrease of minimum ignition energy with increasing gap distance is observed. Furthermore, the observations offer an explanation of the differences of ignition energy, for any fixed gap distance, observed with different sizes of electrode, and of the pronounced effect which a series resistance has in reducing the energy required for ignition; an effect which could be the result of a marked reduction of the spark channel diameter.

The calculation of the magnitude of these effects is impossible at this stage, however, since such calculations require information concerning the spark channel structure and dimensions, which are not available and would require a substantial investigation, involving the use of high-speed photographic and similar techniques.

The considerations which have been advanced above do not explain the effects produced by different electrode materials. The changes of the

spark channel produced by the use of different electrode materials would not be so large as to reasonably be the source of the discrepancies measured in minimum ignition energies. When, therefore, the nature of the spark discharge processes are considered, it follows that not all the electrical energy released at the spark gap (the quantity to which the ignition energy is related in this paper) participates in initiation of the flame; in fact, some of the energy can as far as ignition is concerned be regarded as lost.

One of these losses can be the energy imparted to electrodes. It is generally agreed that breakdown and the sudden rise of the discharge current is followed by the establishment of cathode and anode spots, of very high current density (order of 10^5 to 10^6 amperes/cm^2), from which metal is evaporated.

Llewellyn-Jones[5] has given a theoretical treatment of the energy lost to electrodes from the amount of erosion of the electrode material. Unfortunately not enough data are available to predict an exact solution for discharges such as those employed in the ignition experiments. Nevertheless some approximate calculations were made, from which it is deduced that with the discharge times encountered in ignition experiments carried out in the neighbourhood of the minimum ignition energy, the formation of the cathode spots is unlikely since the discharge times hardly exceed 10^{-7} sec, but establishment of anode spots is certain for all the discharges encountered in this work.

When a current density of 10^6 amp/cm^2 in the channel is assumed, and the diameter of the channel is taken as being the same for all the electrode materials, it is found, using an expression derived by Llewellyn-Jones, that in heating a specified area of electrode surface to a specified depth to the boiling temperature of the material the greatest energy loss will be that of the platinum electrodes; the losses to aluminium, silver and cadmium following in that order. This order is the same as found by experiments in the present research.

An eightfold ratio of the losses was found between platinum and cadmium electrodes. It has not been possible to determine the actual energy loss, however, since this would require the data as to the spark channel diameter and the erosion loss of electrode material per spark, which are not available.

As a conclusion to this discussion of the thermal theory of the ignition process it is of interest to illustrate graphically the relationship between the size of the spark, the electrodes and the minimum flame diameter; this is done in *Figure 10* for 50 per cent H_2–air mixture with 1 mm diameter electrodes at 1·2 mm distance. As can be seen, the spark is a very narrow cylindrical channel

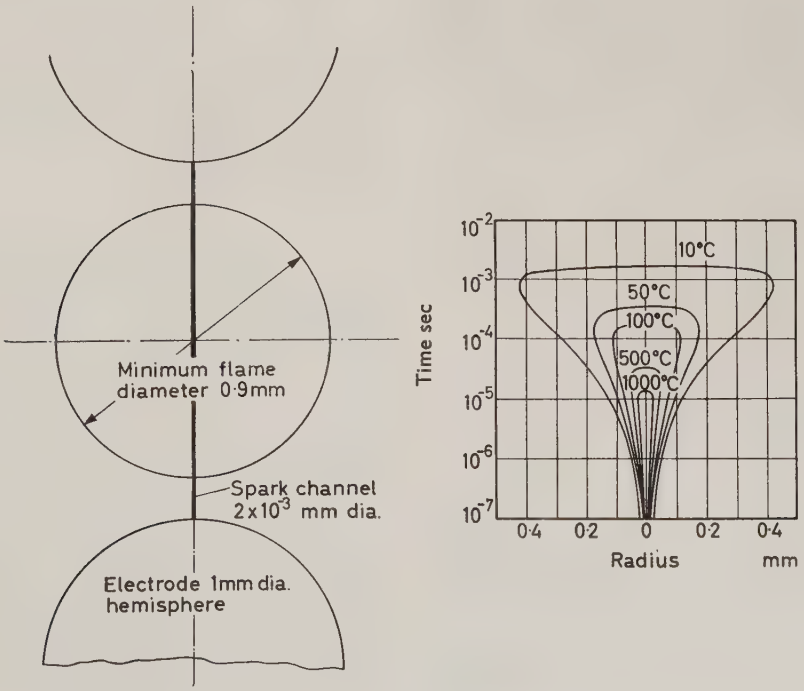

Figure 10

compared with the electrode dimensions, and with the minimum flame diameter. If an energy release of $0{\cdot}1 \times 10^{-3}$ joules is assumed, the calculated temperature distribution from a cylindrical line source is also shown.

It is apparent that with this amount of energy released, only a small cylindrical volume of a diameter of $0{\cdot}6 \times 10^{-2}$ mm (7·5 times smaller than minimum flame diameter) can be brought to ignition temperature. The flame propagation can thus only be initiated from such narrow cylindrical sources and not from the spherical volume of minimum flame diameter. The schlieren photographs taken by Lewis and Von Elbe[2] illustrate clearly the initial reaction taking place from the cylindrical source.

The above discussion shows that the thermal effects are prominent in determining the minimum ignition energies, but there are indications that the electrical phenomena can produce effects which may lower the minimum ignition energy. One of these may be mentioned: the striking difference in discharge characteristics between electrodes of 10 and 1 mm diameter.

The oscillatory discharges with 10 mm hemispheres show, after the energy charged in the capacitor is released, a very distinct extinction of the spark. With 1 mm hemispheres, and particularly with 0·2 mm diameter electrodes, at low breakdown potentials, the extinction of the spark channel is delayed for a considerable period; that is, the channel remains in a conducting state after most of the energy stored in the capacitor has been discharged. This effect follows from the persistent oscillations following the main discharge. Table 2 shows a comparative time of discharge of a 55$\mu\mu$F capacitor between different electrodes.

TABLE 1

	Energy released in	*Oscillation persists*
10 mm electrodes	$3{\cdot}8 \times 10^{-7}$ sec	—
1 mm electrodes	$1\text{–}1{\cdot}5 \times 10^{-7}$ sec	Up to 6×10^{-7} sec
0·2 mm electrodes	2×10^{-7} sec	Up to 10^{-6} sec

Since the conductive condition is associated with an ionized state of the channel it may be assumed that ionization has some significant effect in lowering the minimum ignition energy.

Finally, when considering the effect of the series resistance in the lowering of the ignition energy, the same factor, namely, increasing the discharge time, that is maintaining the channel in the ionized state, would give further support to the considerations advanced above for oscillatory discharges. Furthermore, a factor which may influence the ignition when the circuit contains a series resistance is the voltage level at which the energy is released. Some of these values, which can be only approximately stated, are shown in Table 2, the data relating to 10 mm diameter hemispheres at a distance of 1·4 mm.

TABLE 2

Series resistance	*Minimum ignition energy in gap* (joule)	*Maximum rate of energy release* W	*Total discharge time*	*Voltage level and time interval*
0	$0{\cdot}1 \times 10^{-3}$	120,000	10^{-8} sec	2 kV over $0{\cdot}5 \times 10^{-8}$ sec
220	$0{\cdot}085 \times 10^{-3}$	7,000	2×10^{-8} sec	2 kV over $0{\cdot}8 \times 10^{-8}$ sec
1,000	$0{\cdot}07 \times 10^{-3}$	2,000	7×10^{-8} sec	1 kV over 3×10^{-8} sec
5,025	$0{\cdot}055 \times 10^{-3}$	500	4×10^{-7} sec	1·5 kV over 3×10^{-7} sec
15,000	$0{\cdot}05 \times 10^{-3}$	300	$1{\cdot}2 \times 10^{-6}$ sec	1 kV over 3×10^{-7} sec
100,000	$0{\cdot}055 \times 10^{-3}$	200	4×10^{-6} sec	1 kV over 4×10^{-7} sec

As can be seen it is possible that when the discharge is maintained for a considerable time, at a reasonably high potential, the ignitability of the mixture is improved due to higher activation levels in the gas mixture.

CONCLUSIONS

It has been found that for capacitive discharges, with a gap distance greater than the quenching distance of the mixture, changes in the gap geometry and in the circuit conditions can produce two to fivefold changes in the experimentally derived values of the minimum energy to be liberated in the gap in order to produce ignition. Thus the prevailing opinion that minimum ignition energy is independent of the experimental details of the test cannot be supported.

The minimum ignition energy, expressed as electrical energy released at the spark gap, decreases with the following factors: (*a*) a reduction of the electrode size; (*b*) with the electrode material in the order platinum, aluminium, silver cadmium; (*c*) the increase in the value of the series resistance in the discharge circuit.

Most of the factors which influence the electrical

energy required for ignition can be explained qualitatively, according to thermal considerations: (*a*) Only a proportion of the electrical energy released at the spark gap takes part in the ignition process, since some of the energy is lost to the electrodes. The energy imparted to electrodes decreases with the reduction of energy required to being a critical area of the electrode material to boiling temperature and with the electrode size. (*b*) The ignition energy decreases with a reduction of the spark channel diameter and discharge time; both of which depend upon the electrical characteristics of the test circuit.

Electrical influences affecting ignition are the time intervals during which the spark channel remains in a conducting state, after the energy release, and the voltage level at which the energy is being released; both these factors also being dependent upon the parameters of the circuit.

The authors acknowledge their indebtedness to the Delegacy of King's College, London, for making available facilities for the research and to Messrs. C.A.V. Ltd., for assistance to carry out the work. Thanks are also due to Professor S. J. Davies, formerly Professor of Mechanical Engineering at King's College, for his interest and encouragement.

REFERENCES

[1] Blanc, H. V., Guest, P. G., von Elbe, G. and Lewis, B. L. *J. chem. Phys.* 15 (1947) 798

[2] Lewis, B. L. and von Elbe, G. *Combustion, Flames and Explosions of Gases.* 1951. New York; Academic Press

[3] Calcote, H. F., Gregory, C. A., Burnett, C. M. and Gilmer, R. B. *Industr. Engng. Chem.* (*Industr.*) 44 (1952) 2656

[4] Friedman, R. *Third Symposium on Combustion and Explosion Phenomena.* 1949. Baltimore; Williams and Wilkins

[5] Llewellyn-Jones, F. *Brit. J. app. Phys.* 1 (1950) 60

IGNITION OF FUEL-AIR MIXTURES BY HOT GASES AND ITS RELATIONSHIP TO FIREDAMP EXPLOSIONS

H. G. WOLFHARD and M. VANPÉE

INTRODUCTION

The ignition of explosive mixtures by jets of hot gases has been investigated in a previous paper[1]. A gas such as nitrogen or air was heated in a furnace and injected as a 4 mm diameter jet into a cold combustible mixture. Luminous reactions were observed within the jet and, under favourable conditions, ignition of the outside mixture occurred at the end of the luminous jet at distances up to 30 cm from the furnace. In the experiments reported earlier[1], conditions were standardized and 35 c.c./sec gas flows were used for the hot jet. When ignition occurred downstream the ignition temperature was taken as the temperature at which the gas jet left the furnace. Temperatures were measured for two conditions: (*a*) ignition of a diffusion flame when hot air flows into pure cold fuel—the resulting flame either floats on top of the jet or strikes down to form a conventional diffusion flame resting on the furnace exit; (*b*) ignition of an explosive mixture by hot nitrogen—fuel and air diffuse into the hot jet, heating it by slow reactions until ignition occurs. Ignition temperatures are lower for (*a*), where the physical conditions are more favourable because only fuel must diffuse into the jet, whereas in (*b*) both fuel and air must diffuse into a hot region to start a reaction. It has been noted[1] that these 'hot-gas ignition temperatures' do not correlate with other known flame characteristics. The differences are especially marked when the values are compared with 'spontaneous ignition temperatures', measured in furnaces. For example, hydrogen and carbon monoxide have high 'spontaneous ignition temperatures', whereas their relative 'gas ignition temperatures' are low.

The purpose of the present paper is to extend the earlier work to conditions that may be expected to prevail in the ignition of firedamp by hot spent detonation gases. Detonation of an explosive in a shothole is accompanied by a shock wave that issues from the shothole and may ignite the firedamp atmosphere into which it emerges. This source of ignition will not be considered here. Ignition by hot particles is also outside the scope of this paper. We are concerned with the jet of hot gases that succeeds the shock wave. It is this jet which usually ignites the firedamp atmosphere, although the details of the process are not well understood. It was the purpose of the present investigation to reproduce the conditions of this ignition process on a smaller scale, so that it could be studied in detail, varying such parameters of the hot jet and the firedamp atmosphere as they might vary in practice. Factors to be studied included: the composition of the firedamp atmosphere and its influence on ignition; the oxygen index of the ambient atmosphere as this value has been proposed as a measure for the incendivity of the explosive; the influence of turbulence of the hot jet on ignition; and changes in ignition that occur if the expelled hot gases contain either oxygen or residual fuel, to simulate conditions of detonation gases from explosives that are either under- or over-oxidized, e.g., the detonation gases from certain commercial explosives contain up to 20 per cent carbon monoxide and 30 per cent hydrogen. Many ignition processes must be studied with hydrocarbons other than methane which has a much higher ignition temperature than any other fuel and thus introduces experimental difficulties. It should be noted that this investigation uses hot jets which are continuously running, whereas firedamp ignition is by a short burst of hot gas. The time factor involved certainly is very important and it is conceivable that some of the conclusions advanced below may need revision. This problem is now under study.

EXPERIMENTAL SET-UP

The experimental set-up is essentially the same as that described earlier[1]. However, a longer platinum furnace (2 ft. long) was used so that faster gas jets could be utilized. The inner diameter of the ceramic furnace tube was unchanged (4 mm), and insulation by additional ceramic tubes has been as described[1]. The outer vessel into which the hot gas jet emerged had an inner diameter of about 10 cm and was 50 cm long (*Figure 1*). As this volume was sufficiently large to lead to quite violent explosions, the vessel was made of brass and provided with a window. A platinum–platinum rhodium thermocouple measured the temperature of the hot gas jet immediately above the furnace before and after each ignition experiment. No values are reported here unless both

measurements coincided, showing that the furnace condition was steady. No radiation corrections were made; they are difficult to assess accurately. Outside gases were introduced as shown[1] in *Figure 1*. A flow of 200 c.c./sec was usually adequate to purge the vessel and prevent appreciable dilution

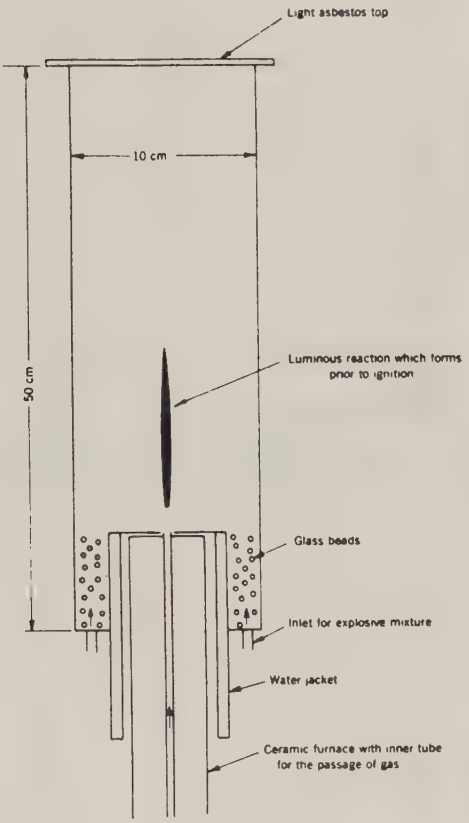
Light asbestos top
10 cm
50 cm
Luminous reaction which forms prior to ignition
Glass beads
Inlet for explosive mixture
Water jacket
Ceramic furnace with inner tube for the passage of gas

Figure 1. Experimental arrangement

by the inert gases of the hot jet. The outside gases used were drawn directly from cylinders. Unless otherwise stated, the CP grade of carbon monoxide (Matheson Company) was used, instead of the commercial grade used in earlier work[1] which contains about 1·5 per cent hydrogen.

RESULTS AND DISCUSSION

In the earlier work it had been found[1] that the gas ignition temperature depended somewhat on the design of the furnace and its history. To establish continuity the ignition temperatures were measured again with the new longer furnace, using hot air to ignite a diffusion flame in pure fuel (type a) ignition. The results are given in Table 1.

The values reported in Table 1 were reproducible to ±20°C. They are intermediate between the values reported for an aged and a new furnace[1].

TABLE 1

Ignition Temperatures Measured with Hot Air (35 c.c./sec) Going into Cold Pure Fuel (new 2 ft. long furnace)

Fuel	*Ignition temperature* °C*
Methane	1,190
Ethane	945
Propane	1,010
n-Butane	1,025
Ethylene	875
Propylene	1,060
*iso*Butylene	1,070
Acetylene	755
Carbon monoxide (commercial)	765
Hydrogen	670

* Temperatures uncorrected for radiation losses of thermocouple (see reference 1)

The 2 ft. furnace showed no sign of aging, due mainly to the fact that temperatures above 1,200°C were avoided as much as possible. Thus, ignition with a jet of hot nitrogen into an explosive fuel–air mixture was not repeated for all the gases. However, it should be noted that although hot-nitrogen ignition temperatures are higher than 'hot-air ignition temperatures', the sequence of the fuels is the same as in Table 1 (see reference 1).

Influence of jet velocity on ignition

The influence of the velocity of the hot jet on ignition temperature was measured next. Unfortunately no precise values could be derived because the temperature profile of the hot gas jet is not uniform at low velocities, as the last 5 mm of the furnace carry no heating wire and the layers of the jet closest to the wall lose heat. As the velocity of the jet increases this effect becomes smaller and at flow rates around 100 to 130 c.c./sec the temperature appears very uniform across the furnace exit, as far as can be ascertained over such a small area. For higher flows the layers closest to the wall are hotter than at the centre because the furnace is too short to heat such flows uniformly. It is of course to be expected that a jet of uniform high temperature will be a better source of ignition than a jet which reaches the highest temperature only at the centre, the highest temperature within the jet being considered as the ignition temperature.

Table 2 shows that the ignition of an ethylene diffusion flame by hot air is quite independent of jet velocity. The small increase between 20 and 60 c.c./sec air can be explained by the fact that the thermocouple approaches the true gas temperature more closely at high velocities for which heat transfer to the couple becomes more efficient.

TABLE 2

Ignition of Pure Ethylene by a Jet of Air (variation of jet velocity expressed by mass flow of jet)

Mass flow of jet, c.c./sec (n.t.p.)	*Temperature of jet* °C		*Remarks*
	At centre	*At wall*	
20	840		Jet hottest at centre
35	865		Jet hottest at centre
60	865		Jet hottest at centre
100	860		Temperature very uniform
150	840	870	Jet hotter at wall
200	780	900	Jet hotter at wall

Beyond 150 c.c./sec the data allow no conclusions as the temperature is lower at the centre of the jet. For high velocities ignition is not accompanied by the sudden appearance of a small diffusion flame floating on the jet, but has the character of an explosion. The jet becomes turbulent at the point where ignition occurs. No coherent flame forms but small self-igniting eddies seem to sputter in all directions.

Table 3 gives the ignition temperatures for ethylene–air mixtures ignited by hot nitrogen.

TABLE 3

Ignition of Optimum Ethylene–Air Mixture (close to stoichiometric) by a Jet of Nitrogen (variation of jet velocity expressed by mass flow of jet)

Mass flow of jet, c.c./sec (n.t.p.)	*Maximum temperature within jet* °C	*Remarks*
25 nitrogen	1,020	Jet hottest at centre
35	1,035	Jet hottest at centre
50	1,040	Jet hottest at centre
70	1,050	Jet hottest at centre
100	1,100	Temperature very uniform
130	1,140	Temperature very uniform

This nitrogen jet is luminous and is turbulent for mass flows above 70 c.c./sec. In this region the ignition temperature increases steeply, probably because it is more difficult for a small eddy to cause ignition than for a large coherent body of hot gas. However there is no sputtering such as is observed for hot air jets into pure fuel. The turbulence of the luminous nitrogen jet shows up as a rapid growth and decrease of the length of the luminous column.

Ignition temperatures of fuel mixtures

The ignition temperatures differ markedly for different fuels and it is of interest to know at what temperature a fuel mixture will ignite. Firedamp for instance, is not pure methane, but contains ethane which ignites much more readily. *Figures 2* to *4* show ignition temperatures of methane–ethane, ethane–propylene, hydrogen–methane, carbon monoxide–propane, and hydrogen–carbon monoxide systems ignited by jets of hot air. The fuel percentages mean direct ratios by volume of the corresponding fuel flows ignited by a jet of hot air (60 c.c./sec). There is no linear relationship between ignition temperature and fuel mixture,

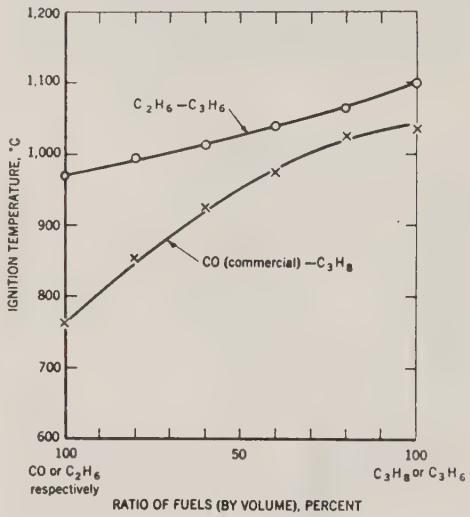

Figure 2. Ignition of diffusion flames of mixed fuels by 60 c.c./sec *hot air. The ratio of the fuels is expressed as direct ratio (by volume)*

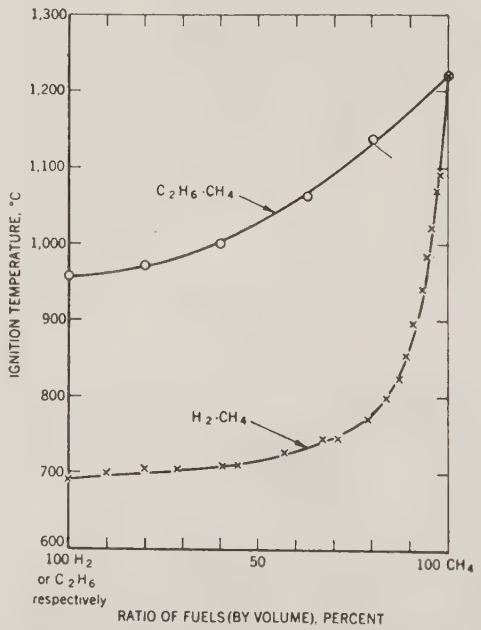

Figure 3. Ignition of diffusion flames of mixed fuels by 60 c.c./sec *hot air. The ratio of fuels is expressed as direct ratio (by volume)*

but deviations from linearity are not marked for the hydrocarbon mixtures. In mixtures with hydrogen and carbon monoxide (CP) the deviations are very pronounced. For example, a

90 : 10 mixture of methane and hydrogen ignites 300°C lower than pure methane. This may be due to the rapid diffusion of hydrogen into the air jet. It clearly demonstrates the danger of hydrogen

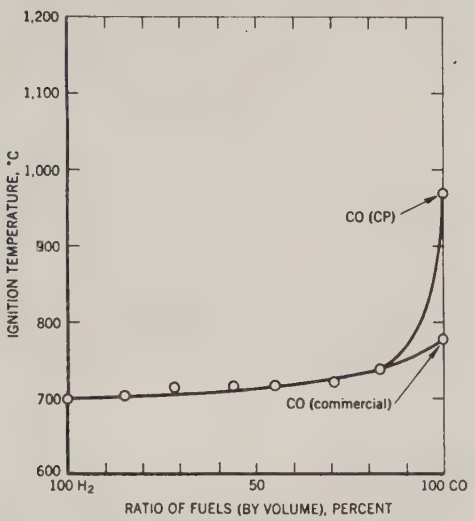

Figure 4. Ignition of diffusion flame of mixed fuel by 60 c.c./sec *hot air. The ratio of fuels is expressed as direct ratio (by volume)*

when added to hydrocarbon fuels even in small quantities. Carbon monoxide is essentially free from this influence when it is not pure, as in commercial grades. However, the Matheson CP grade

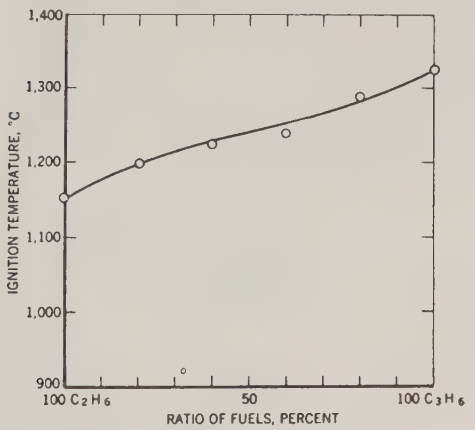

Figure 5. Ignition of mixed ethane–propylene fuel with stoichiometric air by 60 c.c./sec N_2 *jet*

clearly shows the influence of small additions of hydrogen, an effect well known in flame propagation.

Ignition of mixed fuel–air mixtures by a jet of 60 c.c./sec hot nitrogen also was studied. In these experiments hot nitrogen flowed into an atmosphere of CO_2 and the two fuels were admitted in the required ratio. The carbon dioxide was then replaced by air and ignition observed. The overall mixture was always kept stoichiometric after the admittance of air. Unfortunately, methane could not be used because of the very high ignition temperature[1] (about 1,400°C).

For mixtures of ethane and propylene the ignition temperature is roughly a linear function of the fuel ratio (*Figure 5*). The stoichiometry of the fuel must of course be considered in this experiment. Thus 100 per cent ethane as represented in *Figure 5* means 200 c.c./sec air and 12 c.c./sec ethane for the outside mixtures, whereas 100 per cent propylene stands for 200 c.c./sec air and 9·35 c.c./sec propylene. A 50 : 50 mixture thus represents 200 c.c./sec air + 6 c.c./sec ethane + 4·7 c.c./sec propylene. *Figure 6* represents ignition

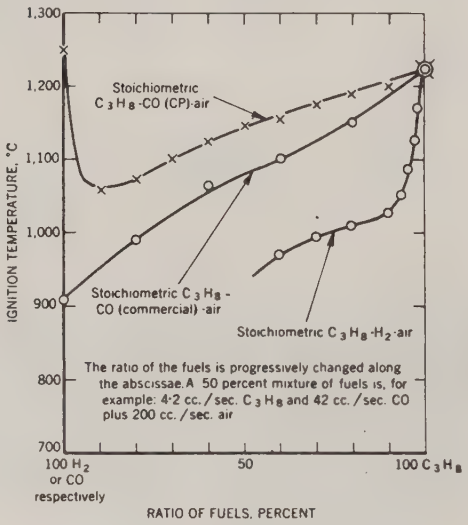
1,300
1,200
1,100
1,000
900
800
700
IGNITION TEMPERATURE, °C
Stoichiometric C3H8-CO (CP)-air
Stoichiometric C3H8 - CO (commercial) -air
Stoichiometric C3H8-H2-air
The ratio of the fuels is progressively changed along the abscissae. A 50 percent mixture of fuels is, for example: 4·2 cc./sec. C3H8 and 42 cc./sec. CO plus 200 cc./sec. air
100 H2 or CO respectively
50
100 C3H8
RATIO OF FUELS, PERCENT

Figure 6. Ignition of mixed fuel–air mixtures by 60 c.c./sec N_2

temperatures for stoichiometric propane–hydrogen air mixtures. The influence of hydrogen on the ignition of propane is again evident. Unfortunately data could not be obtained for hydrogen-rich mixtures as the explosions became too violent. Mixed carbon monoxide–propane–air mixtures are especially interesting (*Figure 6*). Whereas the ignition temperatures of commercial carbon monoxide–propane mixtures show little deviation from linearity, CP grade carbon monoxide–propane mixtures cause the ignition temperatures to go through a minimum. It would probably be expected that both curves coincide except the region close to the CO point, but it seems that the hydrogen in the commercial grade carbon monoxide is much more efficient in lowering ignition temperature than the addition of propane to the CP grade (see for comparison, *Figure 4*).

Influence of the oxygen index on ignition

Variations of the oxygen index (defined by $O_2/(O_2 + N_2)$) of natural gas–air mixtures have been proposed for the testing of permissible explosives. It is therefore of interest to establish a relationship between hot-gas ignition and the oxygen index. *Figure 7* shows ignition temperatures of hot 'air' jets (60 c.c./sec) igniting pure fuel.

Ignition temperatures were also measured with a hot nitrogen jet into a fuel–'air' mixture, using ethane, propane and commercial carbon monoxide as fuels (*Figure 8*). In general, explosions became too violent for oxygen indices around 0·40, however carbon monoxide could be ignited when mixed with pure oxygen. For oxygen indices below 0·21, i.e. air, the ignition temperature rises

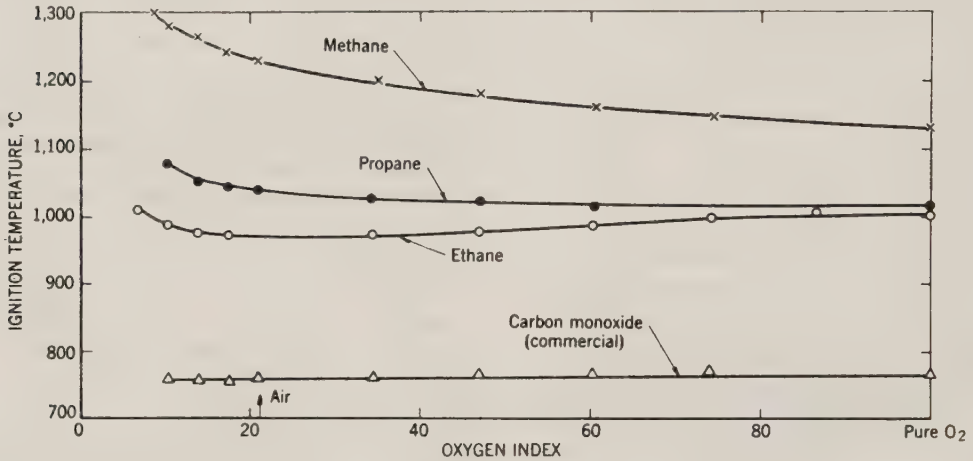

Figure 7. Ignition of pure fuels by a jet of hot 'air' with change of oxygen index of 'air'. Mass flow of 'air', 60 c.c./sec

The oxygen index of the 'air' was varied from about 0·10 to 1·00 (pure O_2). Commercial carbon monoxide showed no change whatsoever between these extreme limits. The ignition temperature of ethane was higher with pure oxygen than with air. The variation was small for propane. Methane was the only fuel for which the ignition temperature decreased significantly as the oxygen index increased.

steeply. However this is partially due to dilution by the nitrogen jet itself, as evidenced by the fact that a 35 c.c./sec nitrogen jet leads to a flatter curve than that observed for the 60 c.c./sec jet. On the whole, changes of ignition temperature with oxygen index are not very large considering the sensitivity of other flame characteristics to oxygen index, e.g. burning velocity, minimum ignition energy, quenching diameter. It is possible

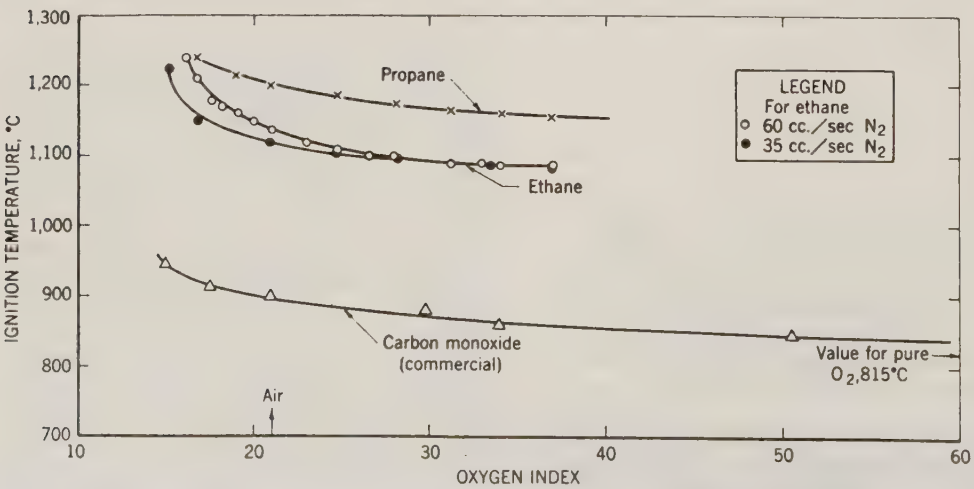

Figure 8. Ignition of most favourable fuel–'air' mixtures by 60 c.c./sec N_2. *Change of oxygen index of the outside 'air'*

that the relationship of the ignition temperature to the oxygen index is affected by the jet diameter, and that it may be even smaller for large jets. This remains to be investigated.

Ignition temperatures measured with hot jets containing a fuel or an oxidizer

An explosive may be under- or over-oxidized, although in practice they are usually under-oxidized. The hot gases of detonation will not always be inert gases such as CO_2, H_2O and N_2 but may contain oxygen or a fuel such as hydrogen or carbon monoxide. The influence of residual oxygen in the propellant gases is already clear. Hot air ignites stoichiometric fuel–air mixtures slightly better than hot nitrogen. More important is that hot air ignites rich fuel–air mixtures much better than stoichiometric mixtures (see reference 1). Thus the most ignitable fuel–air mixtures are those near the rich limit if the hot jet contains oxygen.

The presence of hydrogen or carbon monoxide in the hot jet lowers the ignition temperature appreciably, because hydrogen and carbon monoxide are the most ignitable gases. This holds not only for ignition by a hot air jet into hydrogen or carbon monoxide but also by a hot hydrogen or carbon monoxide jet into cold air (see reference 1). *Figure 9* shows the ignition temperature of hot

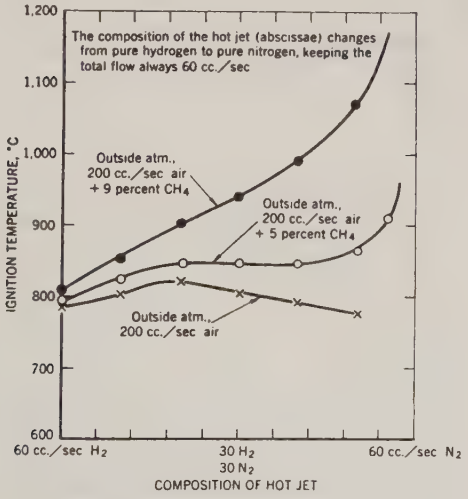
The composition of the hot jet (abscissae) changes from pure hydrogen to pure nitrogen, keeping the total flow always 60 cc./sec
Outside atm., 200 cc./sec air + 9 percent CH4
Outside atm., 200 cc./sec air + 5 percent CH4
Outside atm., 200 cc./sec air
IGNITION TEMPERATURE, °C
1,200
1,100
1,000
900
800
700
600
60 cc./sec H2
30 H2
30 N2
60 cc./sec N2
COMPOSITION OF HOT JET

Figure 9. Hot $(H_2 + N_2)$ *jets,* 60 c.c./sec *into air + methane atmospheres*

hydrogen (60 c.c./sec) into cold air, the hydrogen being gradually replaced by nitrogen. In each case the resulting flame is a diffusion flame, which gradually becomes weaker as less hydrogen is available for burning. Increasing dilution of the hydrogen with nitrogen first raised, then lowered the ignition temperature. In the next curve 5 per cent methane was added to the outside air, representing the lean limit. Pure hot hydrogen ignited this methane–air mixture just as efficiently as air, except that ignition was followed by a methane–air explosion instead of by a hydrogen–air diffusion flame. Dilution of the hot hydrogen jet with nitrogen raises the ignition temperature only slightly. A hot jet containing less than 10 per cent hydrogen in nitrogen gives an ignition temperature of only 900°C. This must be contrasted with an ignition temperature of above 1,400°C for pure hot nitrogen into a stoichiometric methane–air mixture and even higher temperatures for lean mixtures. Ignition temperatures for hot hydrogen–nitrogen mixtures into 9 per cent methane–air (representing near stoichiometric mixtures) are also shown. Even for stoichiometric amounts of methane–air the ignition temperature remains low with hot hydrogen. However, increasing dilution of hydrogen with nitrogen rapidly raises the ignition temperature. Thus, it is clear that ignition temperatures of methane–air mixtures are drastically reduced even by small amounts of hydrogen in inert hot gas jets and that the most ignitable mixture is no longer the stoichiometric mixture, but the lean limit. The reason for this drastic reduction of ignition temperature seems to be that hydrogen ignites with the surrounding air as a first step and that the resulting flame triggers the methane–air explosion. Methane itself seems to inhibit the first step and this is the reason for greater ignitability near the lean limit.

Figure 10 shows similar curves obtained with 50 : 50 hydrogen–carbon monoxide jets diluted incrementally with nitrogen. With cold air alone outside dilution of the jets again leads to a reduction of

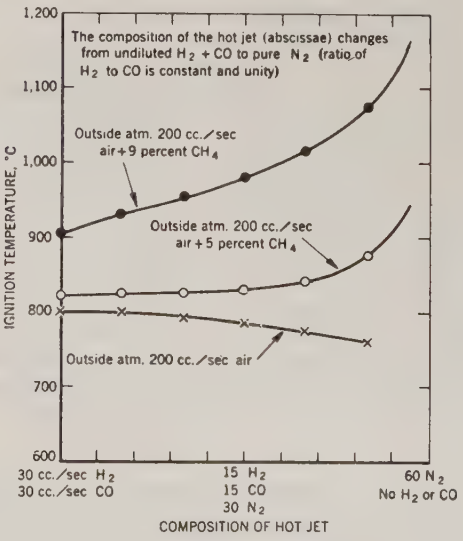
The composition of the hot jet (abscissae) changes from undiluted H2 + CO to pure N2 (ratio of H2 to CO is constant and unity)
Outside atm. 200 cc./sec air + 9 percent CH4
Outside atm. 200 cc./sec air + 5 percent CH4
Outside atm. 200 cc./sec air
IGNITION TEMPERATURE, °C
1,200
1,100
1,000
900
800
700
600
30 cc./sec H2
30 cc./sec CO
15 H2
15 CO
30 N2
60 N2
No H2 or CO
COMPOSITION OF HOT JET

Figure 10. Hot $(H_2 + CO + N_2)$ *jet;* H_2/CO *ratio 1. Total jet flow* 60 c.c./sec *into air + methane atmosphere*

ignition temperature. With 5 per cent methane in the air, the ignition temperature is largely independent of dilution up to very dilute jets for which the ignition temperature rises slowly. Stoichiometric methane–air mixtures are more difficult to ignite even without dilution. *Figure 11*

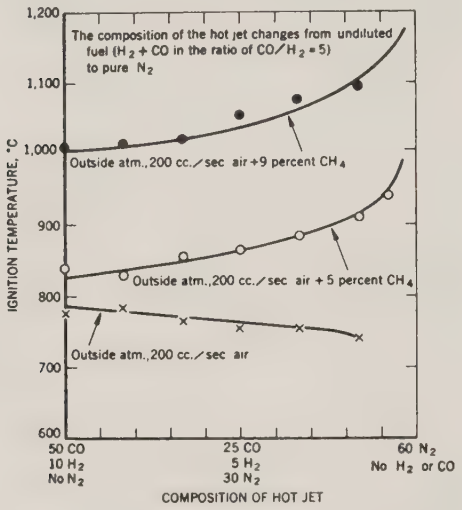

Figure 11. Hot (H_2 + CO + N_2) *jet;* CO/H_2 *ratio 5. Total jet flow* 60 c.c./sec *into air + methane atmosphere*

gives curves for a 50 : 10 carbon monoxide–hydrogen mixture. Methane inhibits ignition drastically, especially without nitrogen dilution of the CO—H_2 jet, but a lean methane–air mixture can still be ignited at around 900°C, when only 10 per cent combined H_2 and CO are present in hot nitrogen.

Carbon monoxide (CP grade) itself gives less reproducible results, as unavoidable traces of moisture can occur in the fuel supply lines. However, *Figure 12* is representative of the main effects. Curve 1 shows ignition by hot carbon monoxide (CP) into cold air to which methane is added gradually (methane concentrations as the abscissae). Small amounts of methane in the air at first lower the ignition temperature, but subsequently the ignition temperatures increase rapidly, reaching almost 1,200°C at the lean methane limit, and about 1,400°C at the stoichiometric point, which is the same value as for ignition by hot nitrogen. The remaining curves show how hydrogen added to carbon monoxide flattens the curve and counteracts the inhibiting effect of methane.

CONCLUSIONS

It should be stressed again that the experiments in this paper cannot simulate all the facets of firedamp ignition, but only the part played by the jet of hot gases emerging from a shothole. The jet velocities and diameters used here are quite small, but they are about the largest which can be used safely in the laboratory without going into outside gallery tests. A more serious objection is the fact that the ignitions investigated here are produced by a continuous jet instead of by short bursts of hot gases. Consequently, the recommendations resulting from the present investigation are to be considered only as an indication of what may happen in firedamp ignition and where it may be useful to investigate actual firedamp ignitions in more detail.

The first interesting information concerns the mode of ignition itself. Under ideal conditions and for laminar hot jets, the ignition process is extremely reproducible, whereas in explosives

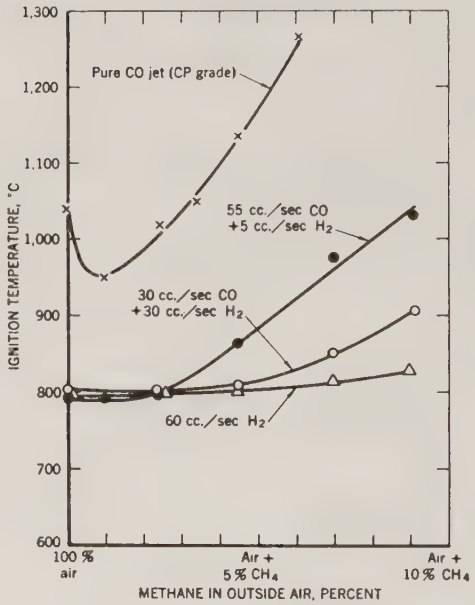

Figure 12. The influence of methane in the outside atmosphere on the ignition by hydrogen and carbon monoxide jets

testing, results must always be expressed in a statistical manner. Although explosive testing facilities cannot be expected to give as reproducible results as a laboratory set-up it is believed that the turbulence of the hot jet emerging from the shothole introduces an element of uncertainty as the breakup of the jet into eddies is not reproducible. This is also the case with our small-scale hot jets. Turbulence raises the ignition temperatures, as small eddies may be expected to be less efficient igniting agents than large volumes of laminar hot gas.

The presence of 9 per cent ethane in methane (which is about the composition of firedamp) reduces the ignition temperature by some 30°C, and this is in line with testing practice where the

composition of natural gas is closely watched. The use of the oxygen index of the firedamp atmosphere to control the incendivity of explosives is somewhat ambiguous. It is true that the ignition temperatures of methane–air mixtures are much more sensitive to oxygen indices than those of other fuels, but this raises the suspicion that this effect is tied up with geometrical consideration. For example, it was found that the dependence of ethane–air ignition temperatures on oxygen indices itself was a function of the mass flow of the hot jet. More basic experiments are needed to evaluate the significance of the oxygen index text, especially as the oxygen-index test as proposed for explosives testing does not only change the oxygen index but also the mixture strength, as methane is kept constant at 8 per cent[2]. However, it should be pointed out that a mixed fuel, such as methane–ethane or preferably methane–carbon monoxide which is always kept at stoichiometric or at a given mixture strength would be an excellent criterion for the safety of explosives. For example, an explosive that does not ignite a 50 : 50 methane–carbon monoxide mixture may be considered 'safe' in firedamp.

The most important conclusion is that the concept of a 'most ignitable mixture' (e.g. to use an 8 per cent natural gas–air mixture for all testing) is useful only if the hot jet is inert; i.e. consists of CO_2, H_2O and N_2. If oxygen is present in the hot jet the most ignitable mixture may be close to the rich limit. When small amounts of hydrogen and/or carbon monoxide are present in the products, this may reduce the ignition temperatures by as much as 500°C. It also makes fuel–air mixtures near the lean limit (which are much more probable in a mine) the most ignitable. Large amounts of hydrogen and carbon monoxide in the detonation products of explosives not only decrease the ignition temperature but also the temperature of the detonation products, as such explosives will be rather cool. This means that the really dangerous explosives may be those that liberate small amounts of H_2 and CO. Further controlled experiments with short bursts of hot gases into explosive mixtures are needed. The degree of turbulence in the hot jet also requires further investigation, as the scale of turbulence may conceivably alter some of the current results. Such experiments are now being conducted at the Bureau of Mines.

REFERENCES

[1] Wolfhard, H. G. The ignition of combustible mixtures by hot gases *Jet Propulsion* In press

[2] Brinkley, R. F. and van Dolah, R. W. *Bureau of Mines Information Circular* 7804, 1957

65

AN INVESTIGATION OF THE CHARACTERISTICS OF SPARK DISCHARGES AS EMPLOYED IN IGNITION EXPERIMENTS

H. E. ROSE and T. PRIEDE

INTRODUCTION

The investigation of the characteristics of spark discharges is a very wide field of inquiry, since the number of circuit parameters which can be varied is very large and, furthermore, the possible test conditions can be varied widely. Although a large amount of information on the subject is available in the published literature, very few investigations have been made on capacitive spark discharges and their energy release characteristics in relation to the ignition of explosive gaseous mixtures. The most substantial work on spark discharge is that which has been carried out by Electrical Research Association and published in a number of reports by Nethercot[1] and Riddlestone[2-4]. The discharges investigated by these workers, however, were at larger energy levels (capacitances 100$\mu\mu$F and larger) than are normally encountered in ignition experiments; the capacitance values at which minimum ignition energies are encountered, for example by Lewis and Von Elbe[5] and Calcote[6], being found to be normally of the order of 1 to 10$\mu\mu$F.

The investigation presented here and in Paper 63 concerns a detailed inquiry into the characteristics of spark discharges in relation to the ignition of gaseous mixtures; the experiments covering the range of capacitance from 1,000$\mu\mu$F down to a few $\mu\mu$F. The study of discharges was made in air and in hydrogen-air mixtures, the results of the latter being correlated also with ignition data presented in another paper. In this paper the effects produced by the series resistance on spark discharges and upon their energy release characteristics is explored.

INSTRUMENTATION

The measurement of the spark discharge characteristics is in itself a problem of considerable difficulty, since many important phenomena occur in extremely short intervals of time (say 10^{-9}–10^{-6} sec) and a considerable amount of work upon measuring techniques, only, was carried out.

It is beyond the scope of this paper to give a full account of this work and therefore only a limited account of essential features will be presented.

The two parameters, the current and the gap voltage largely define the characteristics of the spark; the product of the two also gives the rate of release of electrical energy in the gap, while the time integral of this quantity gives the total electrical energy released in the spark gap.

Both the current through the gap and gap voltage were recorded by means of a high-speed oscillograph which has a resolution capable of distinguishing time intervals of the order of 10^{-9} sec; this instrument having been specially built by the authors since, when the research was commenced, there was no suitable commercial instrument available.

The method of measurement is as follows:

(1) The current through the gap is measured by the interposition of a resistance in the earthy side of the circuit; the voltage developed across this resistance being proportional to the current.

(2) The voltage across the gap was measured by means of a capacitance potential divider employing a capacitance of the Y plates of the cathode ray tube as the low voltage arm of the divider.

As will be shown later, it is not always possible to insert the necessary measuring equipment into the spark circuit without significantly altering the parameters of the test circuit. For this reason it is not possible, for every set of experimental conditions, to measure both the current through the gap and the gap voltage and, in these cases, the measurement which involved the minimum disturbance of the circuit conditions was made.

Thus, the measurement to be made has to be decided by consideration of each individual set of circumstances.

These difficulties can be summarized thus:

(a) Measurement of spark discharges with negligible circuit resistance

Current measurement is ruled out since the addition of the measuring resistance in the circuit alters the characteristics of the circuit. In this

instance it is theoretically possible to measure either the capacitor voltage or the gap voltage. Unfortunately this is also impracticable since, due to distributive inductance in the practical layout of the circuit, it is impossible to define a point which can be taken as the capacitor terminal and that as the spark gap terminal. For example a voltage waveform measured at the electrode holder, some $1\frac{1}{4}$ in. from the electrode tip, is markedly different, due to inductance of this holder, to that measured at the tip.

Nevertheless, from a voltage oscillogram recorded at any point in the circuit, the current and the gap voltage diagrams can, on the basis of certain reasonable assumptions, be calculated with reasonable precision.

(b) Measurement of spark discharge characteristics with incorporated series resistance

In this instance the current measurements are simple since part of the series resistance can be placed on the earthy side of the circuit and so the current oscillogram obtained.

The measurement of the gap voltage, however, can produce a very pronounced effect on the discharge, since the potential divider connected to the positive electrode increases the capacitance of this electrode. The discharge of this capacitance is not limited by the series resistance but only by the measuring resistance placed on the earthy side of the circuit. Nevertheless effects produced by the potential divider can be tolerated for discharges employing capacitances 50$\mu\mu$F and larger.

For capacitances below 50$\mu\mu$F, the capacitance of the potential divider becomes progressively greater in comparison with that of the main discharge capacitor and the spark discharge is no longer representative. Thus for spark discharges employing small capacitances 4 to 50$\mu\mu$F, current measurements only were made and from these the gap voltage and energy was calculated.

TEST RESULTS

The discharge circuit as normally employed in ignition experiments consists essentially of two elements, namely, the capacitor and the spark gap. Besides these two elements there are elements which are present in the layout of any practical electrical circuits, namely, inductance, resistance and stray capacitance. These latter are distributed throughout the circuit in leads, connections, electrodes, etc. The resistance of a circuit can be normally kept very low, of the order of 0·01 ohm, but it was found that, even by taking special precautions in the design of the ignition bomb and the choice of capacitances, the inductance of the circuit cannot be reduced much below about 0·15 to 0·3μH.

Thus the discharges normally obtained are of oscillatory nature and these will be considered first. Aperiodic discharges, which are obtained by incorporation of series resistances in the discharge circuits, will be considered later.

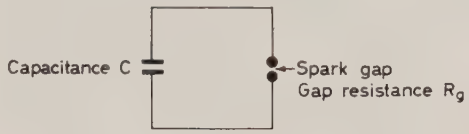

Figure 1

Spark discharge characteristics with 'zero' series resistance

The schematic diagram for this circuit is that shown in *Figure 1* and, as previously stated, in this case, only voltage measurements are practicable.

The curves of current and rate of energy release plotted against time, shown in *Figure 2*, are fairly representative of the results of tests upon this circuit; these diagrams are obtained for discharges between aluminium hemispheres of 10 mm diameter, set at such a distance that the breakdown voltage in air is 5,000 V.

All these discharges are of damped oscillatory nature and when the amplitudes of successive positive and negative peaks are plotted on a semi-logarithmic scale, in *Figure 3*, a relationship which is linear over a considerable range, is obtained.

This relationship indicates that the gap resistance, for these discharges, remains sensibly constant during the greater part of the discharge period and, furthermore, this resistance can be calculated with reasonable accuracy from the slope of this line.

The gap resistance so calculated is found to increase markedly with the decrease of capacitance, the oscillation of the discharge being increasingly damped with decreasing capacitance. Thus, for very low capacitance values, 4$\mu\mu$F or less, the discharges approach heavily damped conditions.

Examination of the curves of *Figure 2* also shows that a reduction of capacitance markedly reduces the maximum value of the discharge current (e.g., 80-fold; from about 400 amperes when $C = 1{,}000\mu\mu$F to about 5 amperes when $C = 4{\cdot}2\mu\mu$F) and also reduces the maximum rate of energy release (about 10-fold over the same range of variation of capacitance). The reduction in the maximum rate of energy release is less than the reduction of the maximum current because, due to the high resistance of the gap, when the circuit capacitance is reduced the energy is released at a higher voltage level.

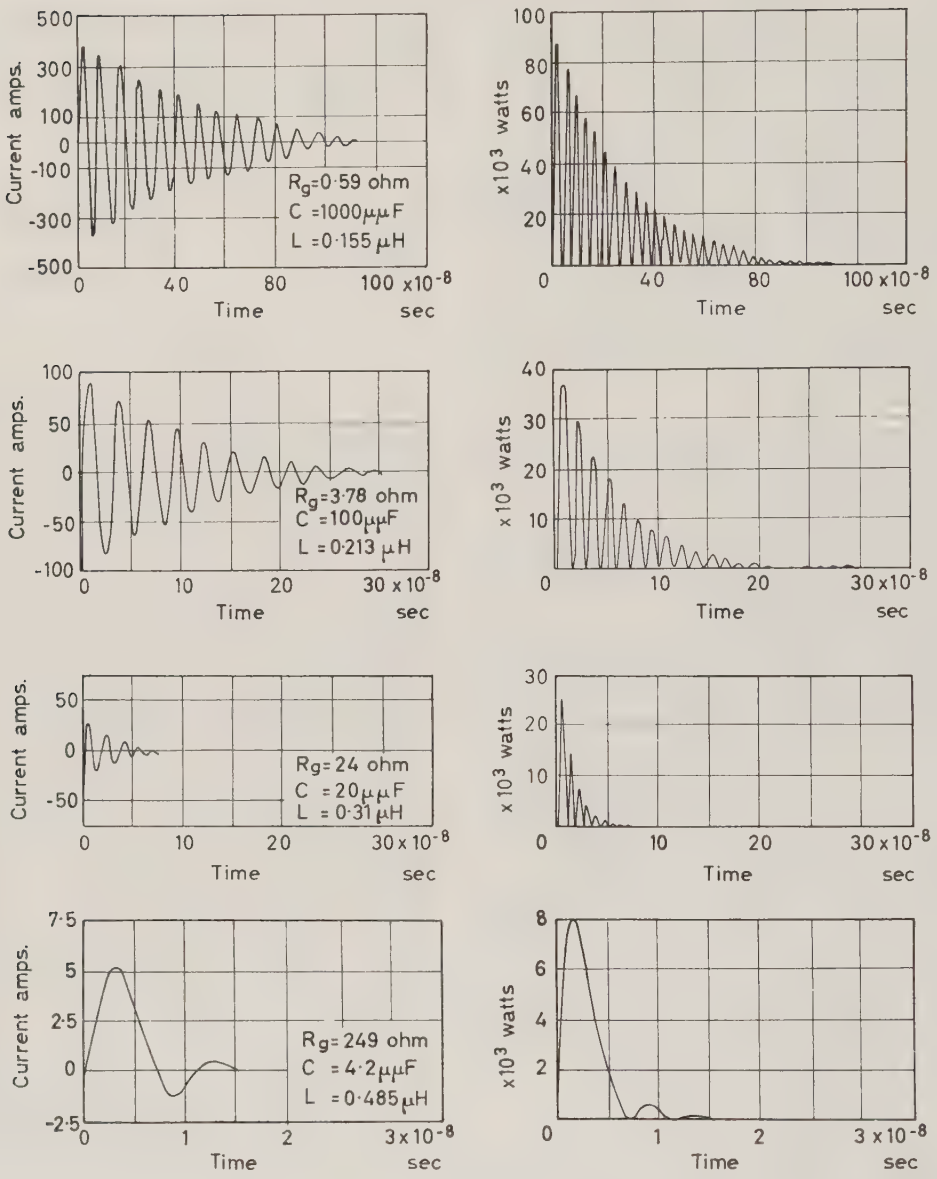

Figure 2

This essentially constant gap resistance is also found for oscillatory discharges with series resistance incorporated in the discharge circuit but in this instance the circuit resistance produces an increase of the gap resistance.

Examination of the numerous oscillograms revealed that the gap resistance itself was determined primarily by the initial rise of the current following the breakdown and, furthermore, this current rise is mainly governed by the characteristics of the circuit, i.e. the capacitance, inductance and series resistance. Hence it is logical to expect that the spark gap resistance will be a function of the circuit impedance Z, where $Z=(L/C)^{\frac{1}{2}}+R$ and L is the inductance in henries, C is the capacitance in farads and R is the series resistance in ohms.

The resistance of a spark gap, consisting of aluminium hemispheres of 10 mm diameter, set to break down at 5 kV in air, plotted against circuit impedance, is shown in *Figure 4*.

As can be seen, the points form a reasonably

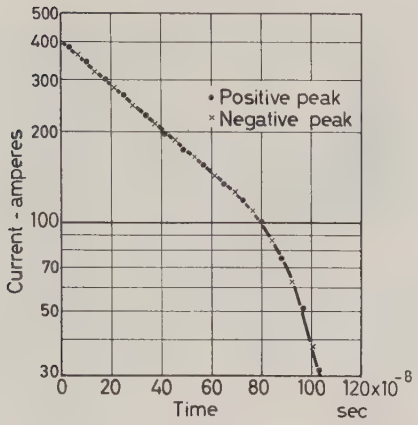

Figure 3

good straight line and so it follows that the gap resistance is given by an empirical equation of the form

$$R = Ke^{aZ} \qquad (1)$$

In the present case the expression is

$$R_g = 0{\cdot}4e^{3{\cdot}4\times10^{-2}Z} \qquad (2)$$

Following the obtaining of this relationship between gap resistance and circuit impedance, an attempt was made to generalize the treatment to include other conditions.

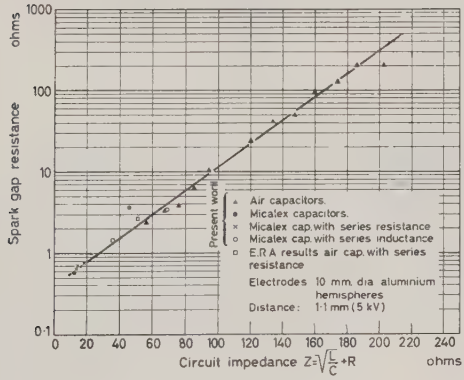

Figure 4

In this analysis it was found that for breakdown voltages greater than 4 kV the gap resistance increases slightly with increasing gap distance.

A very pronounced difference in gap resistance was found, however, with hydrogen and hydrogen-air mixtures, when the gap breakdown voltage was set to the same value as in air. Nevertheless when these results (at each breakdown voltage) were compared on the basis of specific gap resistance (resistance per unit length of gap), the values were found the same. This suggests that the correlation should be on the basis of specific resistance of the gap.

The slope of the gap resistance curve with circuit impedance was found to be unaffected by variations of either the gap distance or gap composition. Thus the spark discharge characteristics can be predicted with sufficient accuracy for most purposes by use of the expression, above,

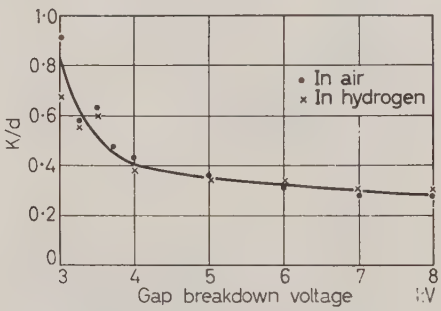

Figure 5

with the value of K obtained from *Figure 5* and a knowledge of the breakdown voltage of the gap.

Experiments were also carried out in which electrodes made of platinum, silver and cadmium were used. These tests showed some variations in the gap resistance but the trends were not well defined and the use of the expression above, for the calculation of the resistance of a spark gap, between electrodes of these materials, will lead to errors which are not significantly greater than the scatter of the points on the original graph.

Spark discharge characteristics with incorporated series resistance

The experiments were made in air, hydrogen and 50 per cent hydrogen–air mixtures covering the same range of capacitance, namely from 4 to 1,000$\mu\mu$F; the equivalent circuit being shown in *Figure 6*.

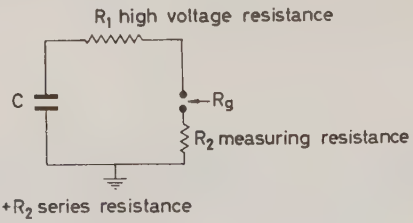

Figure 6

In *Figure 7* is shown a series of oscillograms obtained by variation of the value of the resistor which is placed in series with a capacitor of

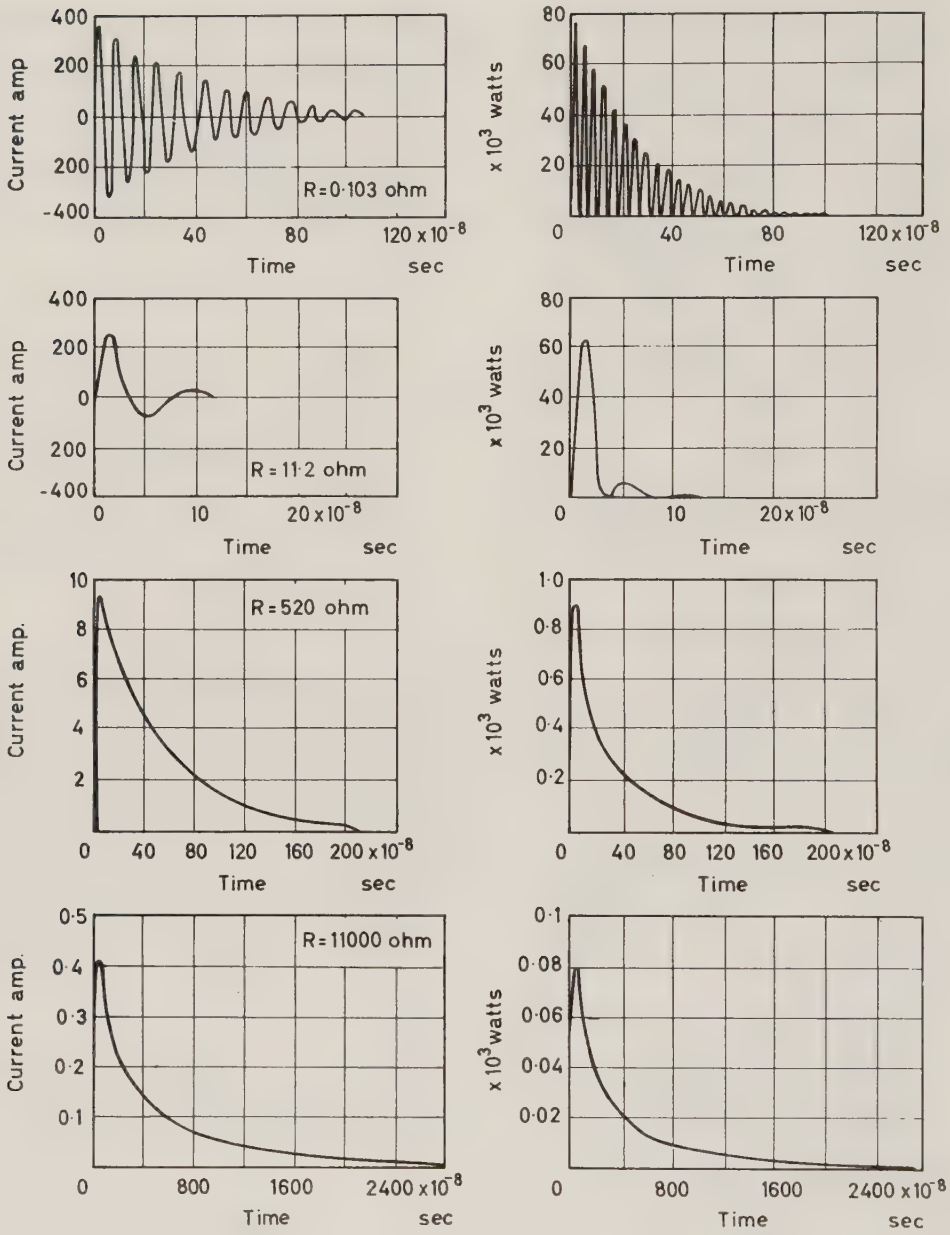

Figure 7

1,000$\mu\mu$F and a spark gap; the gap, again, consisting of aluminium hemispheres of 10 mm diameter set to break down at 5 kV in air.

From these curves it will be seen that, for small values of circuit resistance, the discharge is oscillatory in nature and shows the characteristic of an essentially constant gap resistance. For increasing values of circuit resistance, however, the discharge becomes aperiodic.

For the oscillatory range a marked reduction of discharge time is obtained; accompanied by only a slight reduction of the peak current and the peak rate of energy release.

The diagrams taken beyond the critically damped condition resemble closely discharges of a capacitor through an ohmic resistance.

Following the breakdown the gap voltage falls to a very low value due to establishment of an

arc-like discharge and since the gap resistance is then normally only a small fraction of the total circuit resistance, the energy release at the spark gap becomes very small.

With reference to the gap resistance it was also found that it is primarily determined by the initial current rise following the breakdown. Following this initial period the gap resistance tends to be constant for a short period until the arc conditions are established.

The characteristics of these aperiodic spark discharges were found to be of similar nature for capacitances down to some 100$\mu\mu$F; the gap resistance being in all these cases determined by the current flow.

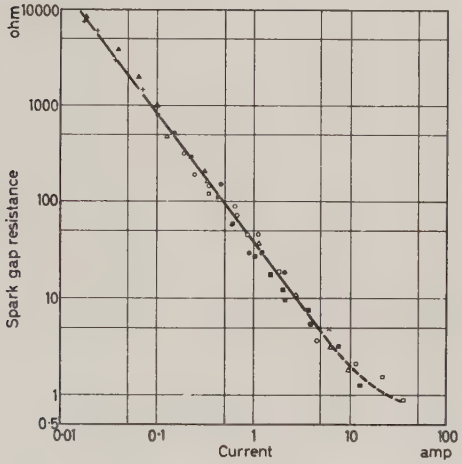

Figure 8

In *Figure 8* is shown, for capacitances covering the range from 100 to 1,000$\mu\mu$F, the gap resistance as a function of discharge current, these data being plotted on logarithmic scales.

From this plot it is seen that the relationship

$$R_g \times I^n = \text{const} \qquad (3)$$

holds well for a wide range of variables, the index n having the value of about 1·36.

It also follows that

$$V_g \times I^{n-1} = \text{const} \qquad (4)$$

This expression is the well known general equation for steady arc discharges.

Thus, it follows that the characteristics of a non-oscillatory spark discharge may be predicted with reasonable accuracy by use of the published data relating to steady arcs.

The effects produced by series resistance on the spark discharge characteristics are summarized in *Figure 9;* the following data of spark discharges from a 1,000$\mu\mu$F capacitor being plotted as a function of the series resistance: time of discharge,

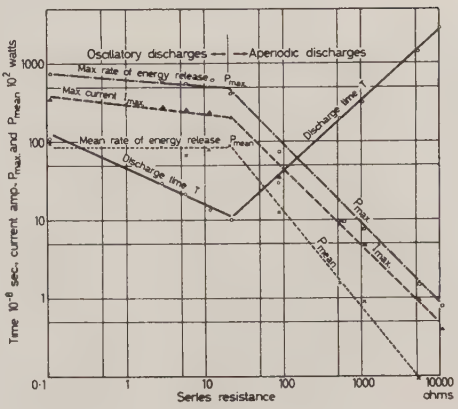

Figure 9

peak current, maximum rate of energy release, mean rate of the energy released. As can be seen all these variables follow a straight line law when plotted on the logarithmic scale and, therefore, all these can be expressed by a single equation of the form,

$$Y \times R^k = \text{const} \qquad (5)$$

where Y is one of the quantities listed above and k is positive for all quantities; except for the case of the discharge time with aperiodic discharges. All the variables have a discontinuity at the value of resistance corresponding to a critically damped circuit condition; the exponent k having different values for oscillatory and aperiodic discharge conditions.

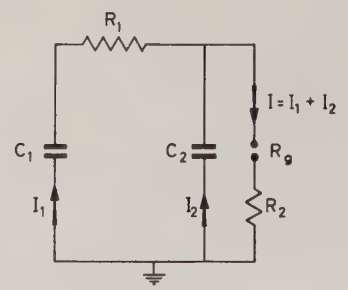

C_1 - Discharge capacitor
C_2 - Electrode capacitance
$C = C_1 + C_2$ - Total circuit capacitance

I_1 - Discharge current of capacitance C_1
I_2 - Discharge current of capacitance C_2
$I = I_1 + I_2$ - Current in the spark gap

R_1 - Main series resistance
R_2 - Measuring resistance

Figure 10

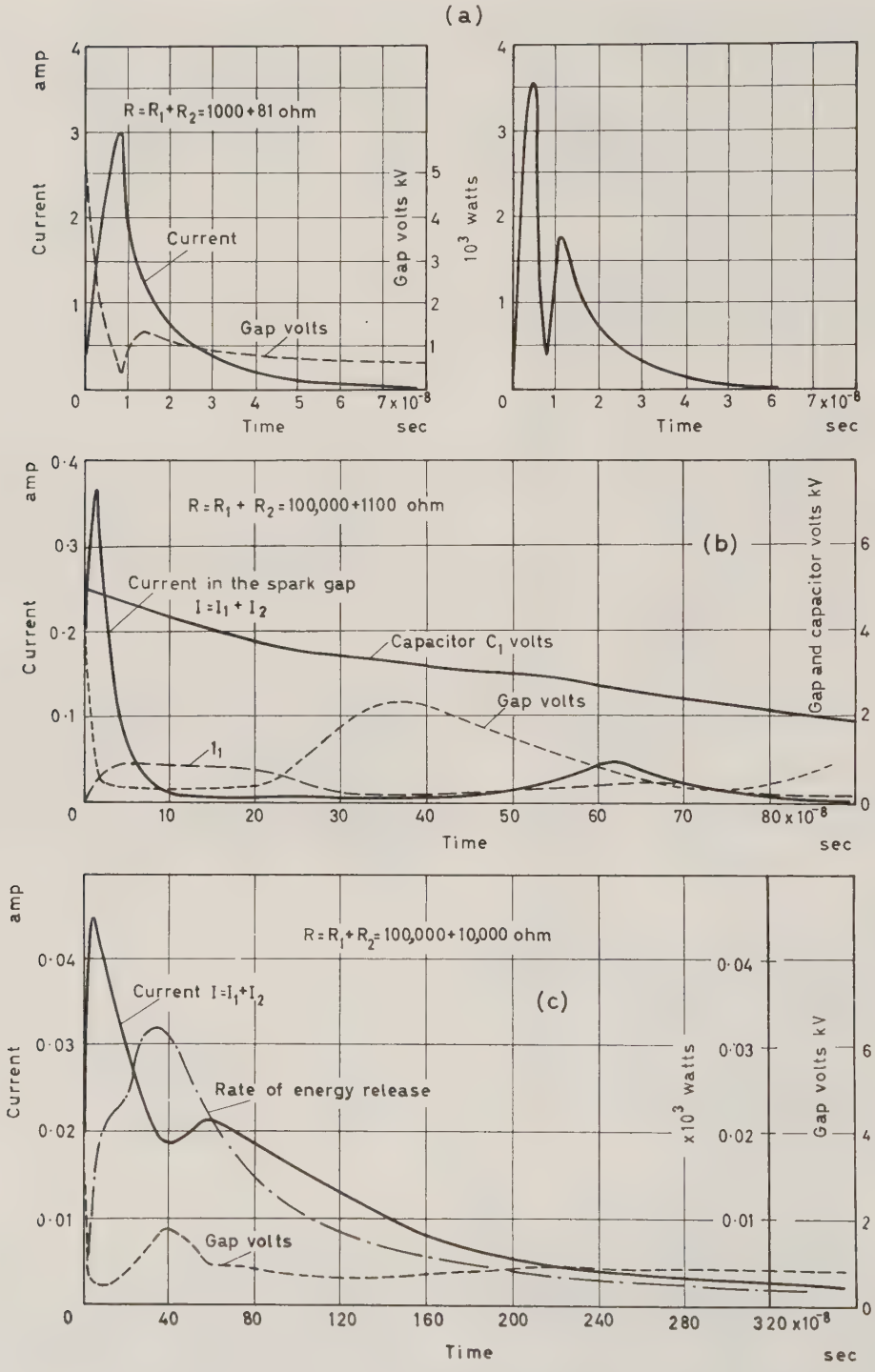
(a)
amp
Current
R = R1 + R2 = 1000 + 81 ohm
Current
Gap volts
Gap volts kV
Time
sec
10^3 watts
Time
sec
(b)
R = R1 + R2 = 100,000 + 1100 ohm
Current in the spark gap
I = I1 + I2
Capacitor C1 volts
Gap volts
I1
Gap and capacitor volts kV
Time
sec
(c)
R = R1 + R2 = 100,000 + 10,000 ohm
Current I = I1 + I2
Rate of energy release
Gap volts
x10^3 watts
Gap volts kV
Time
sec

Figure 11

The foregoing analysis relates to the case when the capacitance is not too small; for example greater than, say, 100μμF.

Great divergencies, however, occur when the discharge of small capacitances is considered, the pronounced effect in this case being produced by the electrode capacitance itself, which then becomes appreciable in relation to that of the whole circuit.

In a practical layout it is extremely difficult to reduce the electrode capacitance below about 1μμF, and the discharge of this capacitance has a profound effect upon the discharge characteristics.

The theoretical circuit diagram for this case is as shown in *Figure 10*.

In *Figure 11* are shown some representative diagrams for the discharge of a capacitor of 9μμF capacity through a spark gap consisting of aluminium hemispheres of 10 mm diameter set to break down at 5 kV, the values of the series resistor and measuring resistor being varied.

A notable feature in these discharges is the high level of the gap voltage at which the energy is released. A further point of interest is the pronounced hump, of the order of 1,000 to 2,000 V in the gap voltage curve following the rapid drop of the gap voltage during the breakdown period. The energy release is also at an appreciably higher level than with corresponding discharges in which capacitances of above 100μμF are used.

The various events of the discharge can be analysed clearly by consideration of the diagrams in *Figure 11b*, i.e. that based on 1,105 ohm measuring resistance. As can be seen the electrode capacitance is rapidly discharged, in a time of the order of 10^{-7} sec, following the breakdown of the gap. During this interval the gap voltage drops to a low value, of about 250 V; also the voltage of the electrode capacitance C_2 relative to earth remains very low, due to a low value of current attained. The spark channel contracts following this initial discharge, but is maintained in a conductive state by a small flow of current of constant magnitude (0·01 amperes). The current from the main capacitor C, however, increases to a maximum value which is limited by the 100,000 ohm series resistance. This current I_1 can be greater than the total current I_1+I_2 (I_2 can be negative) which indicates that electrode capacitance is being gradually charged, while the spark channel remains in its contracted form. The gap voltage, however, gradually increases during this charging process until after a time interval of some 40×10^{-8} sec, a voltage of about 2,300 V is attained. This increase of the gap voltage is accompanied by a pronounced increase of the current until again the electrode capacitance is rapidly discharged. This process continues until the energy initially charged in the circuit is dissipated.

It should perhaps be emphasized that, while the above analysis describes the phenomena with fair accuracy, in fact there are appreciable differences between different oscillograms, some diagrams showing several sharp current peaks resembling the initial breakdown of the gap.

The discharge processes are of a similar nature when the resistance ratio R_1/R_2 has a greater value (normally R_1/R_2 is taken as 0·1) but the discharge processes are, on the whole, of more continuous nature (*Figure 11a* and *c*). The mechanism, however, of the pronounced high voltage peaks following the breakdown are essentially the same as described above.

Effect of series resistance on energy release

All the results, in terms of percentage of energy released in a spark gap in air, are shown in *Figure 12*, these data being plotted *versus* series

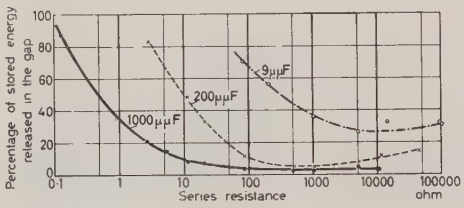

Figure 12

resistance for the capacitances examined, namely, 1,000, 200 and 9μμF.

For a given resistance value the percentage of released energy, in general, increases with the decrease of capacitance. On the basis of the results of the investigation into the characteristics of discharges, which has been described before, the important factors producing this effect are as follows.

The gap resistance, as it was shown before, for oscillatory discharges increases with the decrease of capacitance. Thus for a certain series resistance the ratio R_g/R increases with the reduction of capacitance and therefore greater proportion of the energy is released in the spark gap. For example, with 1,000μμF capacitor the gap resistance, R_g, was 0·585 ohm but with a 9μμF capacitor it was 110 ohm. Assuming a series resistance of 10 ohm and that energy released is as the ratio of R_g/R; in the first instance only 6 per cent of the total energy can be expected to be released at the spark gap, while in the second instance 90 per cent would be released. As can be seen these orders of magnitudes are not very different from the values obtained experimentally.

The effect of the change of gap resistance with

capacitance, described above, also applies for aperiodic discharges; but in this case the proportion of the energy released during the initial stages of discharge increases markedly with the reduction of capacitance Tests made at different gap distances also show that with an increase of gap distance (i.e., increasing breakdown voltage) there is an approximately proportional increase in the current, in the gap voltage and in the rate of the energy release. However, the general characteristics of the discharge remain essentially the same. The percentage of the stored energy which is released in the spark gap, in air, is practically independent of the gap distance.

In hydrogen the percentage of the stored energy which is released in the gap increases slightly with gap distance. The percentage of energy released in hydrogen was also found to be higher than that for air for the same gap distance, an effect which is due mainly to the somewhat higher gap voltage.

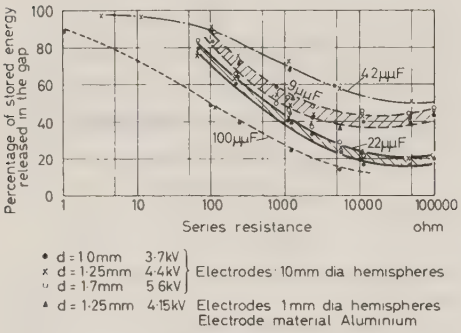

Figure 13

The same applies for discharges in hydrogen–air mixtures. In *Figure 13* are summarized the electrical energy release in 50 per cent hydrogen–air mixtures, as a function of series resistance, for capacitances 4·2, 9, 22 and 100μμF. As can be seen a greater proportion of the energy is released at a fixed series resistance with decreased values of the capacitance, whilst an increase in the gap distance produces only slight increase in the proportion of the energy released.

CONCLUSIONS

From the foregoing analysis the following tentative conclusions appear to be justified:

The capacitance spark discharges normally employed in ignition experiments (4 to 1,000μμF capacitance and 0·4 to 2 mm gap distance) are of an oscillatory nature, due to the distributed inductance inescapable in any practical layout of the discharge circuit.

Under such conditions the gap resistance is found to be sensibly constant over the greater part of the discharge, this resistance being to some extent dependent on the electrode configuration but depending mainly upon the impedance of the electrical circuit.

The empirical equation for the gap resistance, R_g,

$$R_g = Ke^{\alpha Z}$$

(where K and α are functions of the electrode configuration and Z is the circuit impedance) enables the current, voltage and energy release during the spark discharge to be predicted with reasonable accuracy.

The discharge can be damped by the addition of resistance in the external circuit to give, beyond the critically damped condition, an aperiodic discharge. In the case of capacitances of the order of 4 to 10μμF, however, the discharge is in any case very nearly critically damped by the resistance of the gap itself. The empirical equation given above is applicable up to the point of critical damping and is also to discharge circuits containing lumped inductances and series resistance. Beyond this point, however, the character of discharge changes.

In the aperiodic discharge of capacitances of 100 to 1,000μμF the gap resistance is constant at a value determined by the circuit impedance, only for a very short period of the discharge; this phase is followed by an arc-like discharge. The period of constant resistance is so brief, however, that for the purpose of calculation it may be treated as part of the arc-like discharge and the whole process can therefore be calculated by use of the conventional treatment for an arc discharge.

The aperiodic discharge of smaller capacitances (less than 100μμF) is of a more complex nature and is easily affected by minor changes in the circuit parameters. It is unlikely, therefore, that analytical treatment of these discharges would be practicable.

The proportion of the total stored energy which is released at the spark gap depends upon the ratio of the gap resistance to other resistance in the circuit and so it means that for small capacitances (gap resistance high—of the order of 150 to 300 ohm) resistances up to 10 ohm have an almost negligible effect on the energy release. In many experimental circuits a circuit resistance of below 0·1 ohm is practicable and for such cases the expression $\frac{1}{2}CV^2$ can be accepted as a good criterion for the electrical energy released at the spark gap.

With circuit resistances of 10 ohm and upwards, the proportion of the total stored energy that is released at the spark gap decreases with increasing series resistance, with increasing capacitance and with increasing hydrogen concentration.

The authors acknowledge their indebtedness to the Delegacy of King's College, London, for making available facilities for the research and to Messrs. C.A.V. Ltd., for assistance to carry out the work. Thanks are also due to Professor S. J. Davies, formerly Professor of Mechanical Engineering at King's College, for his interest and encouragement.

REFERENCES

[1] Nethercot, W. and Bruce, C. E R. *E.R.A. Report L/T*205 (1948)

[2] Riddlestone, H. G. *E.R.A. Report G/T*253

[3] — *E.R.A. Report G/T*293 (1954)

[4] — *E.R.A. Report G/T*278 (1953)

[5] Lewis, B. L. and von Elbe, G. *Combustion, Flames and Explosions of Gases.* 1951. New York; Academic Press

[6] Calcote, H. F., Gregory, C. A., Burnett, C. M. and Gilmer, R. B. *Industr. Engng. Chem.* (*Industr.*) 44 (1952) 2656

66

AN ATTEMPT AT MEASURING HOMOGENEOUS IGNITION TEMPERATURES

J. A. SAGE and F. J. WEINBERG

INTRODUCTION

The criterion for ignition upon which this work is based is as follows: that if the temperature of an infinite volume of the reactants at constant pressure is instantaneously and homogeneously raised to above some critical value, T_i, and maintained thereat, then an explosion will occur homogeneously throughout the volume, thus forestalling flame propagation. If the temperature, however, is raised to a value less than T_i, no explosion will occur no matter how long the gases are maintained at that temperature. This is the original 'auto-ignition temperature' concept and irrespective of its significance as an absolute ignition criterion, measured values of T_i are of obvious theoretical interest. Available data, however, are based upon results of experiments far removed from the postulates of the definition.

Rapid ignition by small sources (e.g. electric sparks) is fundamentally different in that the criteria governing inflammation of a large volume are those of flame propagation rather than those of ignition. Even ignition of reactants by extended sources, such as hot vessel walls, however, is not to be expected to occur homogeneously. The combination of steep dependence of reaction rate on temperature and strong exothermicity, together with the necessity of temperature gradients as preliminary to any heat transfer within the gas, would be expected to lead to localized ignition in a layer in which there has been some heat release and change in composition near the walls, even without regard to any chemical effects of the wall surface. Such local ignition followed by flame propagation to the rest of the volume would then give rise to low values of T_i.

Homogeneous conditions are more closely approached in ignition by flash photolysis or adiabatic compression; however, a propagating detonation wave has been shown to be associated with the former (Thrush[1]) whilst in both the process of temperature development and ignition is associated with a particular pressure-time relationship which bears little resemblance to the constant pressure case. Considerations such as these have prompted the present attempt at establishing a method of measuring ignition temperatures conforming to the requirements of the above definition.

BASIS OF METHOD

The principle (Weinberg[2]) of the method investigated lies in supplying the ignition energy in two steps. In the first stage the gas is heated homogeneously to a known temperature, T_g ($< T_i$), and in the second the additional energy, E, required to effect ignition is supplied and measured. As T_g is increased from room temperature to that at which pre-reaction is first detected, E falls. Extrapolating a graph of E against T_g to zero E gives the temperature, T_i, at which no further energy would be necessary to ignite the gas.

This process is essentially a null point method (even though the null point is an extrapolated one) in that any imperfections of the igniting system are extrapolated out of its conclusions as E tends to zero. Similarly any function of E, tending to zero as E tends to zero, may be used to facilitate the extrapolation.

There are two points on which the method may fail. The first is the onset of pre-reaction, with attendant change in reactant composition, at a value of temperature T_g, so far below T_i as to make extrapolation from the ideal region unreliable. The extent of pre-reaction may be reduced by minimizing the residence time at the pre-heat temperature. Analysis for pre-reaction of the uniformly heated reactants, however, becomes an essential part of the investigation of the method.

The second point of possible failure can arise only when the igniter is a solid body for which zero energy supply may not correspond to thermal equilibrium between gas and igniter. This may occur either if catalysis occurs on the igniter surface with consequent heat release (in which case the surface temperature is above that of the gas even at $E = 0$) or if the igniter can radiate to outside the system (in which case, on the contrary, energy must be supplied to the igniter merely to maintain it at the temperature of the gas).

Both difficulties can be overcome by a simple modification of the extrapolation technique. Instead of recording the additional energy required for ignition, the surface temperature, T_s, of the igniter is measured and plotted against T_g. On such a graph the straight line through the origin at 45 degrees to both axes ($T_s = T_g$) is the locus of states of thermal equilibrium between gas

and igniter. The experimental relationship is thus extrapolated from the region of no pre-reaction to its point of intersection with this line, yielding T_i, the temperature at which no temperature difference between gas and igniter is necessary for ignition to occur. This method of extrapolation equally satisfies the criteria discussed above.

In either case the ultimate test of the method must be independence of the ignition temperature deduced of the nature of the igniter.

APPARATUS

Experimentally, a flow system was chosen in order to allow some latitude in varying residence times by flow rate variation and to maintain pressure constant.

The reactants, bottled commercial ethylene and air compressed into a buffer volume by a laboratory compressor, were metered separately after drying, in silica gel packed towers, by capillary flow meters working at a constant pressure (atmospheric plus line pressure) of 80 cm mercury. As discussed later, in some experiments it was found necessary to introduce into the explosive mixture a small but controllable quantity of water vapour. This was carried out by saturating a variable part of the air supply (after metering) in a bubbler maintained at constant temperature. The fuel and air flows were mixed in a tower packed with glass beads before entering the ignition tube.

The latter consisted of a translucent silica tube, having an internal diameter of 9 cm, wall thickness 0·7 cm and overall length 46 cm. The tube was mounted vertically and contained both stages in the supply of the igniting energy, the mixture passing direct from the first to the second.

A circular electrically heated grid fitting the ignition tube and having no metal parts exposed to the gas stream (in order to minimize catalysis) was developed for use in the first stage. This heater, which was capable of dissipating approximately 560 W at 140 V was situated 11 cm below the top surface of a bed of silica chips with its plane normal to the gas stream and its covered leads cemented through holes in the tube. The bed of silica chips, extending over 18 cm, commencing 9 cm above the inlet, ensured that the velocity of the mixture through the heating element was random, thus aiding homogeneous heating over the entire width of the tube.

All metallic parts of the apparatus that could not conveniently be encased in quartz were covered with asbestos cement.

The second, or igniting, stage consisted of an electrically heated cylinder situated with its axis horizontal 5·5 cm above the silica chips. This was constructed of a Mullite tube heated over its central section by passing current through nickel-chrome resistance wire wound upon it, the whole, including leads being sealed with asbestos cement, resulting in a cylinder of 0·7 cm diameter. Igniters of differing heated surface areas were obtained by varying the length of the heated section, and at least two such igniters were employed under each set of conditions.

To measure T_s, the surface temperature, a platinum/platinum-rhodium thermocouple was cemented to each igniter. To avoid catalysis it was necessary to cover the thermocouple so that the temperature just under the surface was actually recorded. It can be shown, however, that differences between the true surface temperatures and those recorded by the thermocouple are small and that, in any case, the difference tends to zero as the surface temperature tends to the pre-heat temperature, i.e. that the extrapolation is free from error.

To minimize the heat losses to outside the system another heater was wound on the outside of the ignition tube, the whole being suitably lagged. The power supplies to this heater, to the pre-heater and to the igniter were each derived from the a.c. mains via independently and continuously variable transformers.

The pre-heat temperature, T_g, of the reactants was measured at the position occupied by the igniter by means of a suction pyrometer in which the gas was drawn over the coated junction of a platinum/platinum-rhodium thermocouple contained in a constriction. It was found that the temperature indicated by the thermocouple became independent of the aspirated gas flow velocity over it at flow rates greater than 1·5 litres per min at room temperature, and this was taken as the criterion for rendering radiation losses from the couple negligible. In use, a suction rate of approximately 3 litres per min was applied by means of a water pump. In operation the pyrometer was free to move along a diameter of the ignition tube with the intake hole pointing downwards to face the oncoming gas stream so that the temperature distribution across the tube could be measured.

To ascertain the lowest temperature at which detectable pre-reaction occurred it was necessary to analyse the various mixtures after the first heating stage. Samples for this purpose were withdrawn through an inverted funnel placed over the exit of the ignition tube.

Extensive calibrations were carried out to match electrical inputs to the external and internal heaters, for various constant temperature regions within the ignition tube. Employing a suction pyrometer capable of both vertical and horizontal traverses of the tube it was found that, if the top was covered by a perforated asbestos lid, the temperature over a region extending from the top of the silica chips to 5 cm above the igniter stage

could be maintained constant to within ±2°C transversely and ±4°C axially along the tube at all points and pre-heat temperatures. Differential thermocouples across the walls of the tube were employed as a further aid in obtaining correct heater settings such that no temperature gradients, and thus no heat losses, occurred across the tube walls.

The arrangement of the apparatus is shown schematically in *Figure 1.*

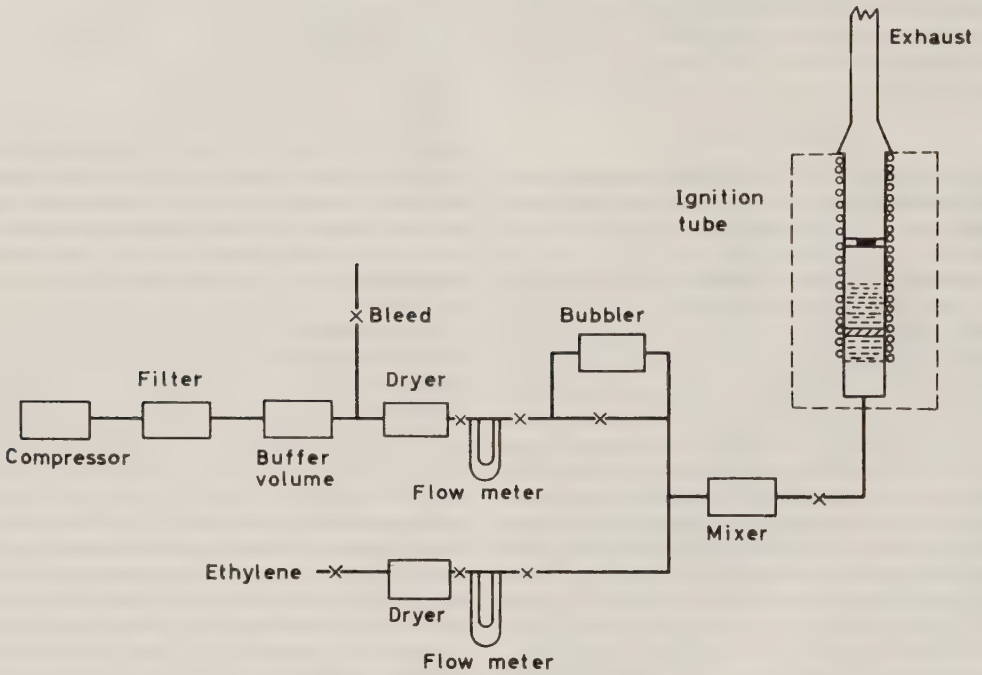

Figure 1. Schematic arrangement of apparatus

PRELIMINARY EXPERIMENTS

Pre-reaction

The aims of the work demanded sensitive detection of the onset of pre-reaction rather than exhaustive quantitative analysis. Accordingly increases in the concentration of carbon dioxide and formaldehyde were detected qualitatively, the latter by a modified form of a test (due to Bricker and Johnson[3]) and for which sensitivity of 1 part in 10^6 has been claimed) employing chromotropic acid reagent. The carbon monoxide content was measured by means of a non-dispersive infra-red analyser and the temperature rise due to pre-reaction was recorded. The latter was obtainable directly by comparison of T_g for the mixture with that for pure air at the same heater settings and flow rate (the difference in specific heats having been computed and shown small).

Typical results are shown in *Figure 2.* Changes in both flow rate and mixture composition altered the extent of pre-reaction but did not affect the temperature of its onset appreciably. The temperature at which pre-reaction became appreciable (460°C) was close enough to the hot vessel auto-ignition temperature (540°C, Kane and Townend[4]) to suggest that no great difficulty in extrapolation was to be expected due to this cause.

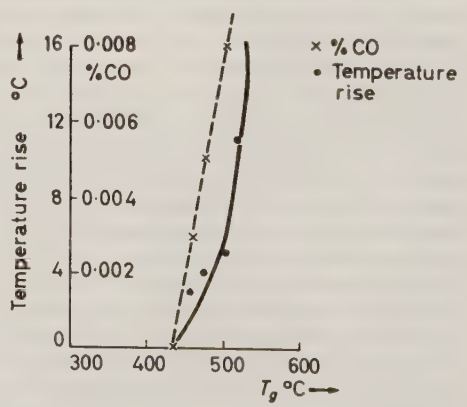

Figure 2. Carbon monoxide content and temperature rise due to pre-reaction in the first stage heating for a 6·5 per cent *ethylene–air mixture having a cold flow rate of* 500 c.c. per sec

Effect of flow rate

The design of the apparatus was based on an assumed flow rate of about 500 c.c. per sec at room temperature, corresponding to a linear cold flow velocity of approximately 8 cm per sec, and this proved a suitable choice. To investigate effects of varying residence time trials were carried out at one half and twice this rate. It was found that at the lower flow rate the extent of pre-reaction increased, whilst at the higher, ignition data of the smaller of the two igniters used showed considerable scatter. The latter effect may be due to the onset of turbulence in the wide ignition tube and results of the kind observed might be expected if the scale of turbulence were comparable to the igniter dimensions.

Accordingly, all subsequent work was carried out at a cold flow rate of 500 c.c. per sec.

Energy-temperature variation

The extrapolation tested initially was of the first type described in the second part. Two

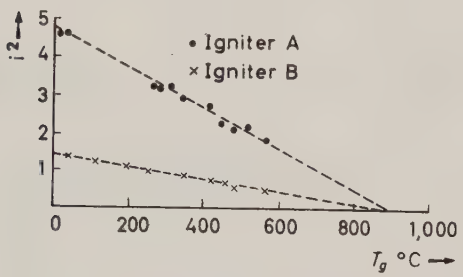

Figure 3. E–T_g relationship for 5 per cent *ethylene–air mixture at a cold flow rate of* 500 c.c. per sec. *Igniter A, heated surface area* 1·25 cm²; *igniter B, heated surface area* 8·25 cm²

igniters, having heated surface areas of 1·7 and 7·7 cm², were used during these preliminary investigations. The square of the steady state igniter current was chosen as the function of igniter energy plotted against T_g.

The initial results were promising. Occasional runs in fact appeared to make superfluous the tests of any other form of extrapolation. It was shown later, however, that some of their desirable features were fortuitous. A typical example is shown in *Figure 3* which represents results for a 5 per cent ethylene/air mixture obtained at a cold flow rate of 500 c.c. per sec. It is seen that:

(a) The relationship between T_g and E appeared approximately linear.

(b) This trend, rather surprisingly, was maintained above the temperature at which pre-reaction set in.

(c) The results for both igniters extrapolated to very nearly the same temperature.

(d) This extrapolated ignition temperature (1,125°K) is close to the final flame temperature of limiting mixtures (1,140°K for 2 per cent ethylene/air mixture).

(e) The temperatures at which ignition occurred in the tube without use of a second stage agreed well with auto-ignition temperatures for the same mixtures (e.g. 830°K as compared with 820°K, Kane and Townend[4]).

(f) There was a large difference (300°C) between this temperature and the extrapolated ignition temperature.

In spite of their occasional apparent success results based on this form of extrapolation were used only for the purpose of the tests described in this section, for reasons given below.

Reproducibility

Before comparing results of the two forms of extrapolation it was considered necessary to test the reproducibility of the method and accordingly repeated measurements were carried out at each

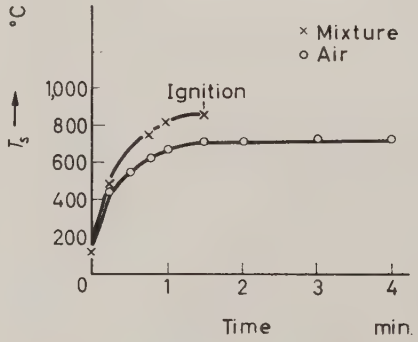

Figure 4. Surface temperature–time relationship during heating of igniter, C, having heated surface area 4·4 cm². *Pre-heat temperature,* 100°C; 5 per cent *ethylene–air mixture*

of a series of fuel–air ratios. It was then found that although individual runs frequently showed as little scatter as that illustrated in *Figure 3*, repetition after a period of days did not produce the same results. Furthermore, even within a single run, scatter was small only if readings were taken in sequence. Re-determination of any one point usually led to a value lying well off the curve.

Gradually increasing chemical contamination of the igniter surface was considered the most likely cause of the latter irreproducibility. The degree of surface reaction on the igniter was investigated by observing the surface temperature–time relationship in the period following the energizing of the igniter for similar flows of air and of inflammable mixture. The current passed was just adequate to cause ignition in the mixture. *Figure 4* shows typical results, in this case of a 5 per

cent mixture pre-heated to 200°C, both relationships being plotted on the same graph. The effect of changes in thermal properties due to added ethylene was computed and found negligible below a mixture strength of 10 per cent. The results leave little doubt as to the existence of such a heat-releasing reaction.

The only plausible cause of irreproducibility from day to day was considered to be the variation in the water vapour content of the gas stream. Burgoyne and Hirsch[5] investigated the effect of small concentrations of water vapour on the ignition of carbon monoxide–air mixtures and found that below 0·35 per cent the amount of water vapour had a marked effect on the ignition temperature. It seemed possible that similar considerations applied to the case of ethylene. Accordingly, the water vapour content of the air stream was determined and found to vary over a period of days between 0·03 and 0·24 per cent, depending on the state of the silica gel drying agent occasioned by the varying relative humidity of the atmosphere.

To test these possible causes of irreproducibility, the igniters were heated to 700°C in a stream of oxygen before each ignition and, by means of the bubbler described above, 1 per cent water vapour was introduced into the gas stream in order to bring the moisture content into the region where it no longer exercises an appreciable effect on ignition characteristics.

These measures proved successful. Concerning reaction on the surface of the igniter, results now obtained for the temperature–time relationships indicated not only that the igniter was brought to the same condition before each ignition, but also, rather surprisingly, that surface reaction on the igniter was greatly reduced. Typical results are shown in *Figure 5*, which may be compared

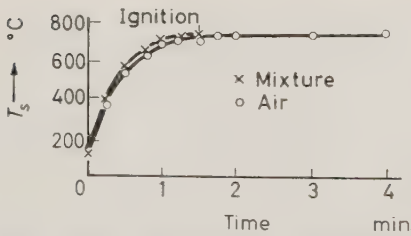

Figure 5. Surface temperature–time relationship as in Figure 3 with the addition of 1 per cent *water vapour and after heat treating the igniter in* O_2

directly with those in *Figure 4*. Day-to-day reproducibility also improved and results remained consistent over periods of weeks.

The pre-heat temperature-energy relationship could now be re-examined and compared with results obtained by the second type of extrapolation. All subsequent results were obtained with 1 per cent water vapour added to the reactants, the igniters being heated to 700°C in oxygen before each ignition.

RESULTS

Repetition of all the pre-heat temperature-ignition energy measurements showed that whilst results

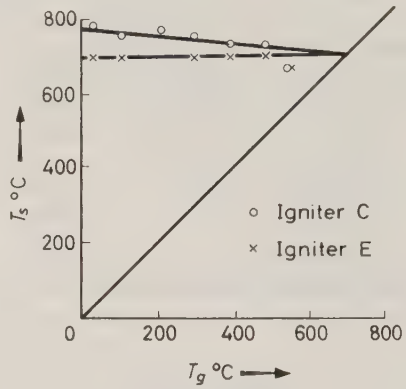

Figure 6. Variation of surface temperature with pre-heat temperature for 6·5 per cent *ethylene–air mixture. Igniter C heated surface area* 4·4 cm^2; *igniter F heated surface area* 2·2 cm^2

were reproducible, the graphs were no longer straight lines and their extrapolation did not lead to the same temperature for igniters of different areas. The trend with igniters areas, moreover, suggested this discrepancy to be due entirely to the radiation effect mentioned previously.

The second type of extrapolation described above was, therefore, tested using two igniters having heated surface areas of 2·2 and 4·4 cm^2 (data for the two types of extrapolation were obtained from the same experiments). Results for each igniter were plotted on a separate graph so that the extrapolated ignition temperature for one igniter should in no way influence the extrapolation made for the other. A typical example (in which, for convenience, both igniters are included on the same graph) is shown in *Figure 6* which represents results for a 6·5 per cent mixture. It was found that, within experimental error, the two igniters always extrapolated to the same temperature.

Comparison of the two methods showed not only that values obtained by energy extrapolation were not independent of the igniter (the higher values being obtained consistently with the larger igniter), whereas those obtained by temperature extrapolation were independent, but also that the latter were always smaller than either of the former.

The first method of extrapolation, therefore,

appears to fail due to some radiation from the igniter which is lost to the system and necessitates energy supply to the igniter merely in order to maintain it at the gas temperature. An approximate assessment of this effect is possible. Neglecting heat losses along leads and radiation and absorption of the gas, the steady state energy transfer equation for the igniter may be expressed as:

$$E = K_i(T_s - T_g) + A_i\sigma\varepsilon_i T_s^4 - \sigma \int T^4 \varepsilon \, dA$$

where K_i is the appropriate heat transfer coefficient, σ = Stephan's constant, ε = emissivity, A = area, the suffix i denotes the igniter and the integration in the last term extends over the entire effective enclosure in which the igniter is situated. This may be written as

$$E = K_i(T_s - T_g) + K(T_s^4 - \bar{T}_w^4)$$

where K is a constant for a given igniter and $\bar{T}_w$ is the effective mean wall temperature of the enclosure as defined by the two equations.

Only if $\bar{T}_w = T_g$ does the above equation give $E \to 0$ as $T_s \to T_g \to T_i$; i.e. only if the igniter 'sees' no surface area at a temperature below that of the gas do the two methods of extrapolation become identical. In fact, however, $\bar{T}_w < T_g$ and, therefore, $E > 0$ when $T_s = T_g = T_i$.

Approximate calculations, correcting for radiation losses, on the above model gave reasonable agreement between the two igniters in the energy extrapolation method as well as between the two methods.

The variation of ignition temperature deduced from the temperature extrapolation, with composition in the range 2·8 to 10 per cent is shown in *Figure 7*. Plotted on the same graph, for comparison, are calculated final flame temperatures of near lower limit mixtures, temperatures at which ignition occurred in the tube without use of second stage igniter and auto-ignition temperatures obtained by Kane and Townend[4].

CONCLUSIONS

It is concluded that the method has been established in the T_s–T_g extrapolation and that its use presents no serious obstacle, at least in the case of the reactants used. Values of ignition temperatures have been measured over a range of ethylene–air ratios.

Inspection of the results (*Figure 7*) shows that these ignition temperatures are about 150°C higher than the accepted values of auto-ignition temperature for ethylene–air mixtures and follow a somewhat different form. The temperatures at which ignitions occur in the tube without additional energy being supplied agree closely with the previous values, in spite of the very different experimental arrangement used. At the limit, values of T_i approach calculated final flame temperatures.

Work is in hand to examine the ignition process in the neighbourhood of a hot surface, in detail, by optical means as part of the extension of the present investigation to other reactant mixtures.

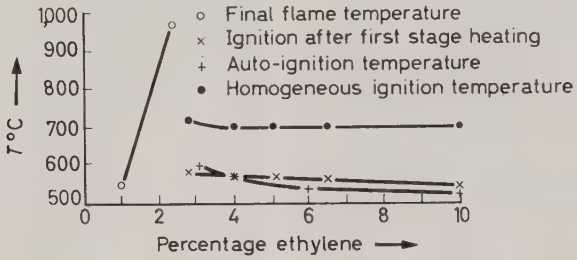

Figure 7. Variation of ignition temperature with mixture strength

One of the authors (J. A. S.) is indebted to the Gas Council for the award of a Research Scholarship.

REFERENCES

[1] Thrush, B. A. *Proc. Roy. Soc. A* 233 (1955) 147
[2] Weinberg, F. J. *Proc. Roy. Soc. A* 230 (1955) 331
[3] Bricker, C. E. and Johnson, H. R. *Ind. engng Chem. (Anal)* 17 (1945) 400
[4] Kane, G. P. and Townsend, D. T. A. *Proc. Roy. Soc. A* 160 (1937) 174
[5] Burgoyne, J. H. and Hirsch, P. B. *Proc. Roy. Soc. A* 227 (1954) 73

67

ON SOME CONSEQUENCES OF THE THERMAL THEORY OF IGNITION IN A FAST FLOW

L. N. KHITRIN

The thermal theory of ignition by a hot body developed earlier[1] and the equation for the concentration limits of motionless and flowing combustible gas mixtures which follow from the theory were based on a simplified thermal scheme of the phenomenon. It was assumed that the rate of heat loss was uniform over the entire surface of the body and that it was described by the mean heat transfer coefficient. It is evident that, strictly speaking, such an assumption is justified only for cases involving stationary or slowly moving gases.

At high rates of flow the rate of heat transfer varies widely for various parts of a body. Consequently the critical conditions necessary for the appearance of a flame do not need to exist at all points of the body simultaneously and this may, correspondingly, effect the properties of the ignition process.

In this paper an attempt is made to supplement existing views on the ignition of flowing gas mixtures so as to take into account the non-uniform heat transfer rate in various parts of a hot body.

The scheme of the phenomenon which served as the basis for the conclusions drawn earlier[1] remains unchanged; it is assumed that the reaction takes place in a thin layer of thickness ξ in the immediate vicinity of the hot wall at a temperature close to that of the wall (body) T_s. Ignition of the mixture (appearance of flame) occurs when the amount of heat q_2, developed in the layer, becomes larger than the heat which must inevitably be lost by the zone and which is given by $q_1 = \alpha\,(T_s - T_0)$, where α is the heat transfer coefficient.

Obviously such simplification of the phenomenon, aimed at obtaining in the most simple manner some basic relations for ignition in a flowing gas, is not at all in contradiction to, and does not compete with more accurate and detailed considerations of the phenomenon of flame formation in a flowing gas contained in a number of recent interesting papers[2, 3].

A method which might have been used in solving this problem would be the application of experimental relations for local coefficients of heat transfer by various bodies. However there are few data available and, furthermore, using such a method it would not be possible to arrive at conclusions of a more general nature. It seemed more expedient to utilize the possibilities of an analytical consideration of the heat transfer process from hot bodies, in particular, to make use of the results obtained in classical investigations by Boussinesq[4] and King[5] of the laws of heat transfer during cooling of bodies in a flowing stream. It is well known that in spite of the extreme idealization of the process involved (potential flow of an ideal and incompressible fluid) this method of solving the heat transfer problem makes it possible by simple analytical means not only to derive all the basic properties of the process but also to obtain numerical results showing good agreement with experimental data. The application of the method to problems of combustion of solid bodies in flowing streams[6–9] turned out to be no less fruitful.

In the case under consideration, of non-uniform heat loss from the surface of a body, it is necessary to introduce the local value of the heat flux into the conditions for ignition. The case will be analysed where the surface of the body is maintained at a constant temperature, T_s, and where the surrounding atmosphere of temperature, T_0, is moving at a velocity ω, with vectoral projections on the x, y and z axes of ω_x, ω_y and ω_z. If the temperature difference $\theta = T_s - T_0$ is considered, then the heat propagation equation has the following well known form:

$$\omega_x \frac{\partial \theta}{\partial x} + \omega_y \frac{\partial \theta}{\partial y} + \omega_z \frac{\partial \theta}{\partial z} = a\left(\frac{\partial^2 \theta}{\partial x^2} + \frac{\partial^2 \theta}{\partial y^2} + \frac{\partial^2 \theta}{\partial z^2}\right) \qquad (1)$$

where $a = \dfrac{\lambda}{c_p \rho}$, and λ is the heat transfer coefficient, c_p is the specific heat and ρ is the density.

The equation becomes more simple if the flow velocity is directed along the x-axis and its magnitude is such that $\partial^2\theta/\partial x^2 < \partial\theta/\partial x$.

For such a case equation 1 will be:

$$\omega_x\frac{\partial\theta}{\partial x}+\omega_y\frac{\partial\theta}{\partial y}=a\left(\frac{\partial^2\theta}{\partial y^2}+\frac{\partial^2\theta}{\partial z^2}\right) \qquad (1')$$

IGNITION FROM A PLANE WALL OR THIN PLATE IN CROSS FLOW

A plate of heated band situated on an endless flat surface (semi-limited body) is of infinite length in the direction of the z-axis and of width a along the x-axis. The plate is located in plane $y = 0$ and its front edge coincides with the z-axis. Then, according to equation 1′:

$$\frac{\partial\theta}{\partial x}=\frac{a}{\omega}\frac{\partial^2\theta}{\partial x^2}=\kappa\frac{\partial^2\theta}{\partial x^2} \qquad (2)$$

and the conditions are

(a) at $y = 0$ $\quad\theta(x) = 0$ if $x \leqslant 0$

$\qquad\qquad\theta(x) = \theta_s$ if $0 < x \leqslant a$

(b) far from the body: $\theta(x) = 0$

The solution is

$$\theta=\frac{2}{\sqrt{\pi}}\int_{\frac{y}{2\sqrt{\kappa x}}}^{\infty}\theta\left(x-\frac{y^2}{4\kappa a^2}\right)e^{-a^2}da \qquad (3)$$

It follows that the heat flux is

$$q_1=-\lambda\left(\frac{\partial\theta}{\partial y}\right)_{y=0}=\left(\frac{\lambda c_p\rho}{\pi}\omega\right)^{\frac{1}{2}}\frac{\theta_s}{\sqrt{x}} \qquad (4)$$

At the ignition limits

$$q_1 = q_2$$

Since q_2 is given by

$$q_2=\left(2Q\lambda\int_{T_\xi}^{T_S}W(c,T)\,dT\right)^{\frac{1}{2}}$$

where $W(c, T)$ is the reaction rate, then

$$\frac{\omega}{x}=\frac{\pi}{\lambda c_p\rho}\frac{2Q\lambda}{\theta_s^2}\int_{T_\xi}^{T_S}W(c,T)\,dT \qquad (5)$$

If the concentration limits of ignition (flame propagation) are considered, then according to reference 1 $T_s \approx T_f$ where T_f is the flame temperature, and, approximately:

$$\frac{\omega}{x}\approx\frac{\pi c_p{}^2}{\lambda c_p\rho}m^2 \qquad (6)$$

where m is the mass velocity of the flame, $\bar{c}_p$ the mean specific heat of the combustion products in the interval $\theta_f = T_f - T_0$; $\bar{c}_p$ is close in value to c_p and, therefore, it is simpler to use

$$\frac{\omega}{x}\approx\frac{\pi}{\lambda/c_p\rho}u^2 \qquad (6')$$

where u is the normal velocity of the flame.

From equation 6 or 6′ there follows an important conclusion, which is a result of the variable rate of heat transfer along the length of the plate: if a mixture of constant composition is undergoing ignition, i.e. m = const, then ignition takes place so that when ω increases, x changes correspondingly, but their ratio remains constant. The displacement of the flame along the length of the plate proceeds until the flame reaches the edge of the plate at $x = a$. The flow velocity corresponding to this moment is the limiting one up to which ignition is still possible. It follows that the point of complete blow-out of the flame is determined not by the mean rate of heat loss or the mean heat transfer coefficient, but by the rate of heat loss in the vicinity of point a.

The following conclusion is also of considerable importance. It is known that $m \sim \exp(-E/2RT_f)$ from which it follows that

$$\frac{\omega}{x}\sim\exp(-E/RT_f) \qquad (7)$$

and, consequently, when the composition of the mixture changes the ratio ω/x must vary as a function of T_f according to the Arrhenius equation. The value of a is included in this expression as the limiting value of x and it follows that the ratio ω/x, i.e. the characteristic of full flame blow-out must also obey equation 7.

The case considered above of ignition from a plane plate can be realized in practice, for instance, by means of an electrically heated band or by creating a hot strip on a flat wall along which the stream is moving.

IGNITION BY A BODY OF FINITE THICKNESS

An infinite cylinder in a cross flow

A cylinder of infinite length in the direction of the z-axis has an elliptical cross-section (semi-axis a lies along the x-axis, semi-axis b lies along the y-axis). As above, its surface is maintained at a temperature T_s. By transforming the coordinate according to Boussinesq, differential equation 1′ is converted to the form of equation 2, however x and y are now replaced by another system—an orthogonal system of lines of equal potential, ψ and a system of current traces φ:

$$\frac{\partial\theta}{\partial\psi}=\kappa\frac{\partial^2\theta}{\partial\varphi^2} \qquad (2')$$

As far as the geometry of the system is concerned, the cylinder is converted by the transformation to the φ, ψ, z coordinates to a band of infinite length in the direction of the z-axis and of width $\psi_1 = 2(a + b)$, i.e. to a problem identical with the one discussed above. Correspondingly, the solution assumes the form of equation 3

$$\theta = \frac{2}{\sqrt{\pi}} \int_{\frac{\varphi}{2\sqrt{\kappa\psi}}}^{\infty} \Phi \left(x - \frac{\varphi^2}{4\kappa a^2} \right) e^{-a^2} da \qquad (3')$$

with the difference, however, that the function $\Phi(x)$ is not similar to the function $\theta(x)$ and does not reduce, generally speaking, to θ_s as $\varphi = 0$. This is due to the fact, arising from the properties of the coordinate system transformation, that for the class of bodies of elliptical shape being considered the flux

$$q_1 = -\lambda \left(\frac{\partial\theta}{\partial n} \right)_0 = -\lambda \left(\frac{\partial\theta}{\partial\varphi} \right)_0 \left(\frac{\partial\varphi}{\partial n} \right)_0$$

will always have a value of 0 at the ends of a body $(\partial\varphi/\partial n)_0 = 0$, which is in contradiction to the actual conditions. It follows that no assumption regarding the form of the function $\Phi(x)$ may be made beforehand, in particular, the assumption that it is constant and has a value of θ_s as was done above. The problem of determining the form of the function $\Phi(x)$ is not a simple one and must be considered specially. Therefore, the more simple but particular case where the use of solution 3 is practically permissible will be considered, i.e. the case where $(\partial\varphi/\partial n)_0 \approx 1$. This holds at points far from the ends of an ellipse, in its central part, and the more elongated it is in form, the larger is the part of the surface of the ellipse for which this is true (i.e. when $a \gg b$). In this case, when $\varphi = 0$ (on the surface of the ellipse) we obtain $\psi = x + a$, inasmuch as $\psi = (a + b)(x/a + 1)$. If moreover only the half of the ellipse from $x = 0$ to $x = a$ is assumed to be heated, then $\psi = x$ and therefore once again

$$q_1 = \left(\frac{\lambda c_p \rho}{\pi} \omega \right)^{\frac{1}{2}} \frac{\theta_s}{\sqrt{x}}$$

The case for such a cylinder having a strongly elongated elliptical profile may be considered as an approximation of that of ignition from a hot plate of finite thickness. Also, such a 'flattened' cylinder, only one half of which is heated, may be viewed as a sort of prototype of a pilot flame created by a narrow split type burner.

Ignition from a body of rotation

Let us consider a body of rotation in the form of an ellipsoid whose major axis lies along the x-axis. As above, equation 1 when transformed to ψ, φ — coordinates may be reduced to an equation of type 2′, if the member $\frac{2}{(\Delta_1\psi)^2} \frac{\partial\psi}{\partial x} \cdot \frac{\partial\theta}{\partial\varphi}$ is neglected and the variable $\psi' = fr^2 d\psi$ is introduced, where $r^2 = y^2 + z^2$ and $\Delta_1\psi$ is the first differential parameter:

$$\frac{\partial\theta}{\partial\psi'} = \kappa \frac{\partial^2\theta}{\partial\phi^2}$$

The remarks made in regard to the properties of the transformation of the boundary conditions for q_1 remain valid for this case also. In this connection let us again consider the most simple case of a very elongated ellipsoid. For an ellipsoid of rotation the value of ψ depends on the x-coordinate and on the size of the ellipsoid axes, a and b, in a special fashion

$$\psi = 2x/(ab^2B) + \text{const}$$

where

$$B = \frac{2}{a^2 - b^2} \left[\frac{a^2}{b^2} - \frac{1}{(a^2 - b^2)^{\frac{1}{2}}} \log \left\{ \frac{a + (a^2 - b^2)^{\frac{1}{2}}}{a - (a^2 - b^2)^{\frac{1}{2}}} \right\}^{\frac{1}{2}} \right]$$

Moreover, inasmuch as $\psi' = \int r^2 d\psi$, therefore

$$\psi' = \frac{2}{ab^2B} \left[b^2 (a + x) - b^2 \left(a + \frac{x^3}{za^2} \right) \right]$$

When $a > b$, i.e. when the ellipsoid is strongly elongated in the direction of the x-axis and approaches the form of a rod, then $b^2B \approx 2/a$, and if also only the half of the ellipsoid from $x = 0$ to $x = a$ is heated, then

$$\psi' = b^2x - b^2 \frac{x^3}{za^2} \approx b^2x$$

and again

$$q_1 = \left(\frac{\lambda c_p \rho}{\pi} \omega \right)^{\frac{1}{2}} \frac{\theta s}{b\sqrt{x}}$$

Thus in all the cases, that of a plate, of an elliptical cylinder and of an elongated ellipsoid of rotation, an expression of the general type is found for q_1, and accordingly, equations 6 and 7 should be applicable.

In all the cases full blow-out of the flame is determined by the velocity at which x corresponds to the point where the stream leaves the surface

of the body. It follows, that this, the length of the hot body, is the value which determines complete extinction of the flame. In the terms used in earlier considerations of the ignition problem, where the mean value of q_1 for the whole body and, accordingly, the mean heat transfer coefficient were used, the determining value was the transverse dimension of the body, i.e. b (or for the case of a sphere, its diameter). The conclusions arrived at here show that this is not correct, since bodies of the same cross-section but of different length will indicate different flame blow-out limits. Evidently because of this, flame-holders of various shapes, discs, plates, spheres, cones, etc., of the same dimensions in cross-section, show, in general, different flame extinction limits since the length of the re-circulation zone differs somewhat for them. As far as the basic laws of flame extinction are concerned, obviously they remain unchanged regardless of whether the mean heat transfer coefficient or the local one (for complete blow-out) are used in the calculations.

ON THE EFFECT OF TURBULENCE

The conclusions formed up till now were based on the assumption that in the reaction zone and the bordering gas layer, where the principal heat transfer takes place, the values λ and u correspond to laminar flow and, therefore, do not depend on the flow rate. For the case of turbulence of the bordering gas layer, if it is assumed that it is of the type which is usually named the state of small scale turbulence, the conclusions drawn above and the final results remain valid, with the exception that for turbulent flow λ_T must be used instead of the molecular value λ and, correspondingly, u_T, the flame velocity for small scale turbulence, in place of u, the velocity of the laminar flame.

u_T can be found from $u_T = u\left(\frac{\lambda_T}{\lambda}\right)^{\frac{1}{2}}$, and,

therefore, according to equation 6′:

$$\frac{\omega}{x} = \frac{\pi}{\lambda_T/c_p\rho}\, u_T^2$$

or

$$\frac{\omega}{x} = \frac{\pi}{\lambda_T/c_p\rho}\,\frac{\lambda_T}{\lambda}\,u^2 = \frac{\pi}{\lambda/c_p\rho}\cdot u^2$$

i.e. the final result turns out to be absolutely identical with that for laminar flow. In other words, the presence of small scale turbulence in the reaction zone does not lead to a change either in the main equation for the flow ignition limits or in the numerical values. A similar conclusion can also be arrived at using the more general equation[1] $\alpha = \bar{c}_p\rho u$, where α is the mean heat transfer coefficient. If it is assumed, in agreement with experimental data, that $\alpha \sim \lambda_T \sim \omega$, the law $\omega \sim u^2$ is again obtained. This interesting result explains why using the dimensionless form of the condition for the limits, $Re = AS^2$ where $S = ud/a$ (ref. 1) gives satisfactory correlation for the large amount of experimental data regarding flame blow-out from bluff body stabilizers.

ON THE LIMITS OF IGNITION FOR MIXTURES OF COMBUSTIBLE GASES

One of other interesting consequences of the general relationship for the concentration limits of ignition both for flowing and stationary mixtures is an equation for the ignition limits in mixtures of several combustible gases.

It will be assumed in the following derivations that the chemical process follows a first order rate equation with respect to the deficient component, which is close to the actual behaviour for limits mixtures, and that the combustible components do not react with each other or with the combustion products, i.e. that for the chemical reaction additivity is the case. For the sake of simplicity a two-component mixture will be considered although the derivation can be carried out for any number of mixed gases.

According to equation 6 or the more general condition $\alpha = \bar{c}_p m$, for each value of α there is a corresponding definite limiting value of m_{lim}. If the dimension of the ignitor (d or a) is given, then the m^{lim} value is a function of only the flow velocity. For a fixed value of the flow velocity, and in particular for $\omega = 0$, $m_{lim} = \text{const}$. However the m_{lim} value depends on the composition of the mixture and its kinetic characteristics; $m_{lim} \sim L_x\kappa_{ox}e^{-E_x/RT_x}$ where L_x is the concentration of the deficient component at the limit for combustible x in the absence of other combustible gases, κ_{ox} and E_x are the constants for that combustible, and T_x is the flame temperature at the limit of ignition for combustible x in the absence of other combustibles.

From the condition $m_{lim} = \text{const}$ it follows that

$$L_1\kappa_{01}e^{-E_1/RT_1} = L_2\kappa_{02}e^{-E_2/RT_2} = \ldots = \text{const} \qquad (8)$$

The assumption is now made that the mixture contains two components of content n_1 and n_2 ($n_1 + n_2 = 1$). From the assumption that the chemical properties are additive in nature

$$L\,(n_1\kappa_{01}e^{-E_1/RT} + n_2\kappa_{02}e^{-E_2/RT}) = \text{const} \qquad (8')$$

where L is the concentration at the limit in the complex mixture; in general T differs from T_1 and T_2.

It follows that

$$L = \frac{\text{const}}{n_1\kappa_{01}e^{-E_1/RT} + n_2\kappa_{02}e^{E_2/RT}}$$

or using equation 8

$$L = \frac{1}{\frac{n_1}{L_1}e^{-\frac{E_1}{R}\left(\frac{1}{T}-\frac{1}{T_1}\right)} + \frac{n_2}{L_2}e^{-\frac{E_2}{R}\left(\frac{1}{T}-\frac{1}{T_2}\right)}}$$

Rearranged this yields

$$\frac{1}{L} = \frac{n_1}{L_1}e^{\frac{E_1}{R}\left(\frac{1}{T}-\frac{1}{T_1}\right)} + \frac{n_2}{L_2}e^{\frac{E_2}{R}\left(\frac{1}{T}-\frac{1}{T_2}\right)} \qquad (9)$$

If T_1 and T_2 are close in value, condition 9 can be simplified to

$$\frac{1}{L} = \frac{n_1}{L_1} + \frac{n_2}{L_2} \qquad (9')$$

This condition is known as the Le Chatelier rule. It follows from the conclusions drawn that this rule is only a particular case of the general relations of the theory of ignition and its applicability is not limited to only a narrow field of limiting phenomenon in stationary gas mixtures; its use should be equally justified with respect to ignition limits (flame stabilization limits) in moving mixtures.

It is interesting to note that the sequence of the Le Chatelier condition is the linear relation between the content of one combustible gas at the boundary and the content of the other added combustible gas in the mixture. Indeed if the limit value of the content in the mixture of one gas is N_1 and the content of the other N_2 ($N_1 + N_2 = L$) then as $n_1 = N_1/L$ and $n_2 = N_2/L$ from equation 9

$$N_1 = L_1 - \frac{L_1}{L_2}N_2 \qquad (10)$$

that is, the equation of a straight line. The form of boundary curves, and the inflammability zones are shown on *Figure 1* for the case of adding CO and CH_4 to the H_2/air mixture. The experimental data are shown by points (after Coward, Carpenter and Pyman).

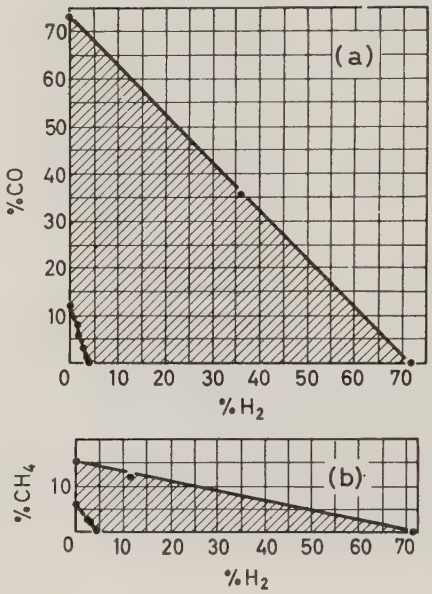

Figure 1

REFERENCES

[1] Khitrin, L. N. and Goldenberg, S. A. *Sixth Symposium on Combustion*, p. 545. 1957. New York; Reinhold

[2] Cheng, S. I. and Kovitz, A. A. *Sixth Symposium on Combustion*, p. 418. 1957. New York; Reinhold

[3] Tan-Yi-Toong. *Sixth Symposium on Combustion*, p. 523. 1957. New York; Reinhold

[4] Boussinesq, M. J. *J. Math. pur. appl.* (1905) 285

[5] King. *Phil. Trans. A.* 214 (1915) 373

[6] Predvoditelev, A. S., Khitrin, L. N., Tzukhanova, O. A. *et al. Burning of Carbon.* 1949. USSR Academy of Science, Publishing House

[7] Blinov, V. I. *Bull. Heat Eng. Inst.* (USSR) No. 7 (1934)

[8] Tu, C. M., Davies, M., Hottel, H. C. *Industr. Engng. Chem.* (*Industr.*) 26, No. 8 (1934)

[9] Khitrin, L. N. *Sixth Symposium on Combustion*, p. 565. 1957. New York; Reinhold

68

LIMITS OF INFLAMMABILITY

G. DIXON-LEWIS and G. L. ISLES

INTRODUCTION

None of the steady-state theoretical treatments of the propagation of an infinite planar flame front is able to account for the existence of inflammability limits, and there is at present no agreed explanation of why such limits occur. Until comparatively recently there has been a marked tendency to regard the observed limits as fundamental properties of the inflammable mixtures to which they refer, and a number of attempts have been made[1–4] to relate the limits to some feature of the internal structure of the flames. The alternative view is that the observed limits, which are measured for finite flames, are essentially quenching phenomena, arising from some interaction of the flames with their environment. Yet another possibility is that although the observed limits may be essentially quenching phenomena, a fundamental limit is nevertheless required by some internal condition in the flame; but such a fundamental limit has never been obtained in practice due to masking by the observed limit. The position at the time of the Yale Symposium was very ably reviewed by Linnett and Simpson[5], who concluded that the dependence of observed limits on experimental conditions favoured the opinion that these limits were not fundamental, and that there was probably a considerable difference between the observed limit and any possible fundamental limit. Some of the major evidence for this conclusion lies in the comparison of limits observed in tubes with limits obtained by the flat flame method of Egerton and co-workers[6–8]. The flat flame lower limit mixtures for hydrocarbons in air are considerably weaker than the corresponding tube limit mixtures[9], the difference in limit flame temperature frequently amounting to 100–200°C.

The paper describes some work which has been aimed at clarifying the position of limits of inflammability. The properties of ethylene–air flames near the lower limit were investigated on a modified flat flame burner in which the top of the chimney was closed by an electrically heated, perforated stainless steel plate[10]. The experiments are divided into two parts. In the first the burning velocities of the mixtures are determined as a function of mixture composition. In the second part the temperature profiles in some of the near limit systems have been investigated in order to try to evaluate the action of the heated plate.

EXPERIMENTAL METHOD

Apparatus

The modified flat flame burner has been described in a previous publication[10]. Essentially, the flame burns between two fixed planes, the burner matrix at a fixed temperature upstream and the top plate at a controllable and measured temperature downstream. The distance between the top plate and matrix could be varied over wide limits. Most of the heating of the matrix occurs by radiation from the top plate and this depends on the distance between plate and matrix. It is clear therefore that with this arrangement the effect of the heated plate above the flame can be studied independently of the effect of the pre-heat at the matrix. In this way possible quenching or similar effects due to the solid surface above and downstream of the flame could be examined. Top plate temperatures up to 900–950°C could be obtained.

In the present set-up the matrix temperature was taken to be the temperature of the 30-mesh stainless steel gauze at its top. This temperature was measured as before[10] by four thermocouples placed spirally at distances of 0, 1, 2 and 3 cm from the centre of the gauze, but these thermocouples were now actually silver-soldered to the gauze. It was found that the previous system[10] where the thermocouples were simply pushed into close thermal contact with the gauze did not give sufficiently good heat transfer between the two solids, so that erroneous matrix temperatures were obtained[11]. The temperature in the body of the top plate was measured by a platinum/platinum 13 per cent rhodium thermocouple inserted in a hole at its centre.

Both the ethylene and air supplies were controlled by valves and measured by calibrated capillary flow gauges, the calibrations being corrected to give the flows at 18°C and 760 mm. Corrections were applied for variations in the static conditions on the assumption of frictionless Venturi flow. Periodic checks showed the reproducibility to be well within 1 per cent. Both the ethylene and air were dried by calcium chloride

and magnesium perchlorate. The two samples of ethylene used in the burning velocity determinations had purities of 98·5 and 98·7 per cent respectively. The ethylene used for the temperature measurements was 98·8 per cent pure. The compositions quoted are all expressed in terms of the actual C_2H_4 content.

Measurement of burning velocity

The technique for measuring the burning velocity has been described elsewhere[10] and involves division of the area of the luminous disc of flame into the total flow rate. Following Badami and Egerton[8] a simple form of correction is applied for the effect on the area of the upward curvature at the edge of the circular flames by adding $2a\sqrt{2}$ to the diameter of the flat section, where a is the average distance between the visible edge of the flame and the point where the inclination from the horizontal commences. This gives an area usually 1–2 per cent higher than if the sloping portion were regarded as the slant surface of a cone frustum. The difference is not serious in view of the uncertainty in the visual determination of the outer edge. For the slower flames studied the velocities are consistent with flame zone thicknesses obtained from rough temperature profile measurements (see later).

Temperature profile measurements

The temperature profiles in some of the near limit flame systems when the top plate temperature was in the region of 800–900°C were investigated by means of thermocouple traverses. The technique, and the reduction of the errors involved to a minimum, has been fully discussed by Friedman[12].

The thermocouples were made by gas welding 0·01 mm platinum and platinum 13 per cent rhodium wires, giving a junction of 0·05 mm diameter. Each wire was about 5 mm long, and was attached at its other end to a thicker support wire (s.w.g. 28) of the same material. The support wires, insulated from each other, were enclosed for about 10 cm in a ceramic tube leading through a hole in the top plate of the burner. The whole thermocouple assembly could be moved in a vertical direction by a traversing mechanism. The position of the thermocouple bead relative to the lower surface of the top plate was measured by a × 10 power microscope fitted with a vertical traverse and scale.

To avoid catalytic effects at the thermocouple, the junction and exposed leads were coated with the ceramic coating A418 developed by the National Bureau of Standards. The efficiency of the coating depends primarily on its completeness, and under the conditions of use several consistent traverses could be made before renewal. Deterioration in the coating led to unsteady readings being obtained even in an unignited ethylene–air stream flowing towards the heated plate: at the same time it could be observed that the platinum wire periodically became much hotter than the platinum–rhodium, thus showing the platinum to be primarily responsible for the catalysis.

An important correction which must be applied to temperatures measured by thermocouples in systems such as the present is that for radiational heat transfer between the thermojunction and its surroundings. Assuming (*a*) unit emissivities for both the top plate and the thermocouple bead, and (*b*) that only insignificant amounts of radiation are received by the bead from anywhere other than the top plate, the heat balance at the thermocouple bead immersed axially in the gas stream with Reynolds number less than one, would be given approximately by:

$$T_g - T_c = \frac{\sigma d}{2\lambda} T_c^4 - \frac{\sigma d}{4\lambda} T_p^4 \left\{ 1 - \left(\frac{y^2}{a^2 + y^2} \right)^{\frac{1}{2}} \right\} \qquad (1)$$

where T_g, T_c and T_p are the absolute temperatures of the gas, thermocouple bead, and top plate respectively, σ is the Stefan-Boltzmann constant, λ is the thermal conductivity of the gas, d is the bead diameter, y is the distance of the bead from the plate and a is the radius of the plate. The radiation correction $T_g - T_c$ decreases with decreasing bead diameter. With $T_p = 1{,}126$°K, $d = 5 \times 10^{-3}$ cm, and $a = 6{\cdot}25$ cm, T_c at the lowest point in a traverse carried out on an airstream approaching the heated plate was 678°K, with $y = 3{\cdot}0$ cm. The value of $T_g - T_c$ from equation 1 is then − 8°K. With $T_c = 1{,}213$°K and $y = 1{\cdot}0$ cm, $T_g - T_c = +\ 28$°K. This last correction is in very good agreement with a value obtained experimentally by comparing readings on two thermocouples which were identical except for the bead diameters which were respectively 0·05 mm and 0·20 mm. With T_c for the smaller bead equal to 1,245°K, the temperature given by the larger bead was 1,158°K. Since, according to equation 1 the radiation correction is directly proportional to the bead diameter, this corresponds to a correction of + 29°K for the smaller junction under these conditions. The value of T_p for each set of readings was obtained from the value of T_c at $y = 0$ by assuming that at this position $T_p = T_g$. The values of T_p so obtained were a few degrees below the value given by the thermocouple in the body of the heated plate.

EXPERIMENTAL RESULTS

Burning velocity measurements

The burning velocities of weak ethylene–air mixtures under various conditions are shown in *Figure 1* (flow rates corrected to 18°C and 760 mm).

In *Figure 2* the burning velocity curves for all the matrix temperatures studied are brought to an initial temperature of 18°C by applying the pre-heat correction method of Egerton and collaborators[7,8]. This assumes that for a given burning velocity on the steeper parts of the curves the sum of the pre-heat and the heat provided by the combustion is constant. Thus, a given burning velocity corresponds to a fixed adiabatic flame temperature. *Figure 2* shows that for the ethylene–air mixtures studied the correction is valid. The corrected burning velocity curves obtained by Egerton and Thabet[7] and by Badami and Egerton[8] for ethylene–air mixtures are also shown in *Figure 2*. The differences between the curves may be due to errors in measuring the flame area.

The burning velocity measurements have been extended towards considerably lower burning velocities (*ca.* 1·5 cm/sec) and adiabatic flame temperatures (900°C) than have previously been obtained in hydrocarbon–air mixtures. Thus, Burgoyne and Williams-Leir[9] obtained a lower limit adiabatic flame temperature of *ca.* 1,230°C for ethylene–air mixtures by the tube method; whilst Badami and Egerton[8], by the flat flame method without the heated plate, obtained a limit adiabatic flame temperature of 1,105°C coupled with a burning velocity of 3·74 cm/sec. The work of Egerton and co-workers first cast doubt on the fundamental nature of tube limits. It now seems probable that none of the limits previously

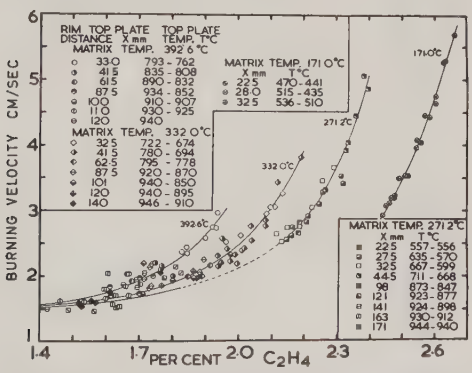

Figure 1. Curves of burning velocity of weak ethylene–air mixtures against composition

measured can be regarded as fundamental in the sense that it depends only on the internal properties of the flame.

The extension of the burning velocity curves is due to the influence of the heated top plate. For every combination of matrix temperature and top plate temperature a composition limit can be obtained; and as the top plate becomes hotter, so lower burning velocities and flame temperatures become possible. Nevertheless, under some conditions the flames may become aerodynamically unstable. Hence the broken line portion of the 271·2°C curve in *Figure 1*.

Behaviour of flames

For a given matrix temperature and top plate temperature the slower flames had a larger diameter and took up a higher stable position in the chimney. The general behaviour in a given set-up strongly suggests that flame stability in this type of

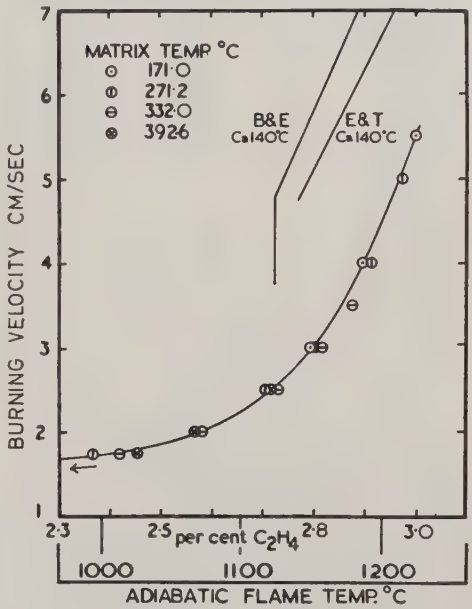

Figure 2. Burning velocity curves with pre-heat correction applied. E & T, Egerton and Thabet[7]; B & E, Badami and Egerton[8]

system is governed by a competition between convection effects (which tend to accelerate the gases through the flame front, producing convergence of the gas stream) and the effect of the top plate (which tends to produce divergence by slightly restricting the outlet for the gases). The convection effects are clearly shown by photographing the tracks of powder particles entrained in the flame gases[18]. The closer approach to the top plate as the burning velocity decreases may be necessary to counteract these effects and to produce flame stability. Eventually quenching by the plate becomes important, and for plate temperatures below about 800°C a limit is obtained which depends on the plate temperature.

For these low top plate temperatures the flames also tend to become less stable aerodynamically as the distance between matrix and top plate increases, and flame oscillations may be obtained[10] which may become violent enough to produce a stability limit by blowing the flame into or through the quenching region of the top plate. It is this phenomenon which causes the instability

region in the 271·2°C curve of *Figure 1*. In the 332·0 and 392·6°C curves suitable combinations of top plate temperature and distance from the matrix do not occur.

At plate temperatures above about 850°C, and particularly at 900°C and higher, the top plate could re-ignite an oscillating flame which had

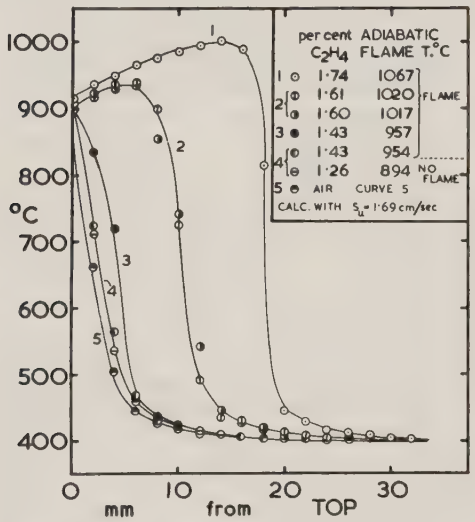

Figure 3. Temperature profiles in near limit ethylene–air flames. Matrix temperature, 394·1°C; plate temperature ca. 905°C

blown off. On weakening the mixture the oscillations became less pronounced, and at 900°C and above fairly stable flames could again be obtained. These took up positions very close to, and even apparently touching, the top plate. Due to difficulty in seeing the flame zone for the very weakest mixtures in contrast with the intense radiation from the hot plate, it is impossible to quote specific composition limits. The very weakest flames studied were all in this region, in which the hot top plate, with its reduced quenching action, is the stabilizing factor. Indeed, a comparison of the adiabatic flame temperatures of the weakest mixtures for which measurements could be made (882°C on 271·2°C curve and 953°C on 392·6°C curve) indicates that the matrix temperature is now relatively unimportant, and that the hot plate controls the combustion. More generally, it seemed that at high values of the plate temperature the adiabatic flame temperature became relatively less important compared with the actual mixture composition in determining both the burning velocity and the accessibility of the flame to area measurement.

Temperature profile measurements

Ethylene–air mixtures—It must be presumed that as the top plate becomes hotter it abstracts less heat from the flames; and indeed, due to the possibility of receipt of energy from the hot plate by the gases after they have left the burner matrix, it is possible for actual flame temperatures in the apparatus to exceed the adiabatic values. Clearly we cannot, without actual temperature measurements in the flames, establish what the temperature and heat transfer conditions are. These in turn may be important in explaining an apparent anomaly. The virtual control of the system by the top plate when this is hot enough is attained in spite of the fact that with the exception of only two mixtures (the two weakest when the matrix temperature T_m was 271·2°C) the adiabatic flame temperature T_{ad} was always above the plate temperature T_p.

Figures 3–6 show a series of temperature profiles in near-limit ethylene–air flames, determined by means of thermocouple traverses with radiation correction as previously described. Due to flame oscillations the precision of the steep parts of the profiles is not sufficient for detailed analysis; but care was exercised to ensure that the maximum temperature, together with its approximate position, was measured. The graphs show that the maximum temperatures T_f actually obtained in

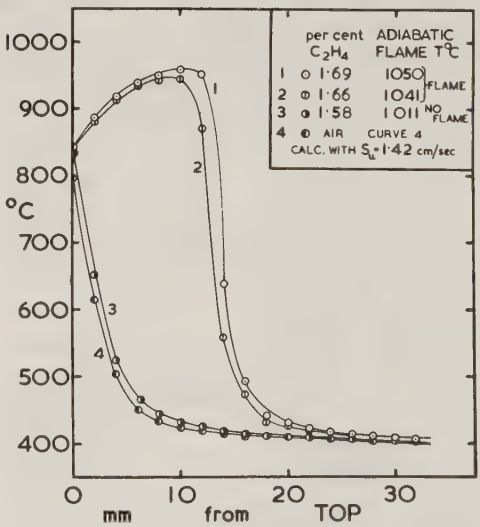

Figure 4. Temperature profiles in near limit ethylene–air flames. Matrix temperature, 394·1°C; plate temperature, ca. 840°C

the flames are always below the calculated T_{ad} (except of course if $T_{ad} < T_p$, but this did not in fact occur in any of the mixtures for which profiles were measured). The immediate result is that some flames having a calculated T_{ad} not much greater than T_p in fact may receive considerable amounts of energy from the plate, and have T_p as their maximum temperature. This explains the increasing importance of T_p when its value is sufficiently high.

Figures 3 and *4* show the effect on the flames of varying T_p from *ca.* 900°C to *ca.* 840°C. In the first case no really well-defined limit of flame propagation can be measured. In *Figure 4*, however, curve 2 represents the profile of the limit mixture. Clearly in this case quenching by the top plate has become important.

Figure 5 shows a series of profiles for some limit ethylene–air flames with decreasing values of T_p. For the two highest values of T_p the flame went right up to the plate. For T_p = 870°C the limit flame was intermittent and very close to the plate. 870°C was also the minimum value for T_f. As the top plate was cooled further, so definite limits were obtained and the limit values for both T_f

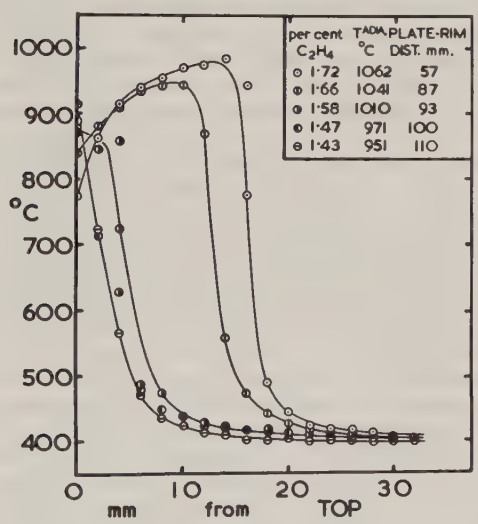

Figure 5. Temperature profiles in limit ethylene–air flames. Matrix temperature, 394·1°C

and T_{ad} increased, the flame moving further from the now quenching region of the plate.

Figure 6 refers to profiles for a lower matrix temperature of 334·3°C, the top plate temperature T_p being *ca.* 900°C as in *Figure 3*. The influence of the high top plate temperature in fixing T_f is clear.

Conditions at surface of heated plate—With T_m = 394·1°C and a plate-rim distance of 110 mm, the values of the gas temperature T_p at the plate for a number of mixture compositions are shown in *Figure 7*. The initial linear temperature rise with ethylene composition indicates that the heat of combustion of the ethylene is liberated even in the absence of a visible flame zone. Similar results were obtained with a plate-rim distance of 87 mm, where a definite limit flame occurs. Catalytic action on the thermocouple itself was not observed either before or after the measurements; so that the observed dependence of T_p on ethylene concentration must probably be attributed to catalytic reaction on the plate surface when no flame is present. At least at the higher values of T_p in this system therefore, the transition at the visible flame limits may probably be regarded as only one of reaction path, and not as a transition from

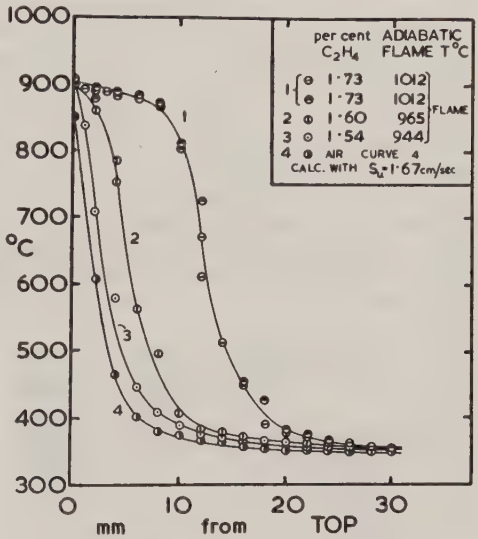

Figure 6. Temperature profiles in near limit ethylene–air flames. Matrix temperature, 334·3°C*; plate temperature ca.* 900°C

rapid to zero reaction. This could be further investigated by analysis of the products leaving the system. Such analyses have not, however, yet been carried out.

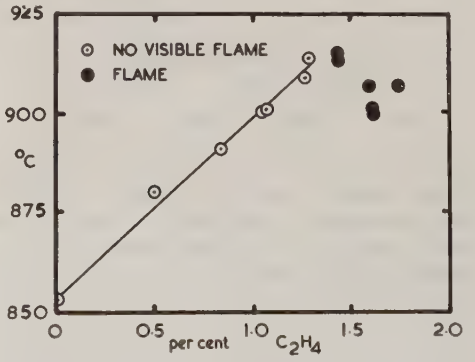

Figure 7. Gas temperatures at top plate for mixtures of ethylene and air. Matrix temperature, 394·1°C. *Total flows constant at* 141 c.c./sec. *Plate-rim distance,* 110 mm

Temperature profiles in air streams—Figure 8 shows some temperature profiles obtained using air instead of ethylene–air mixtures. The experimental data are compared with some calculated conductivity curves using conductivity data obtained from Spiers[13] and assuming the conductivities to be constant over 100° intervals. This procedure considerably simplifies calculation and

introduces an error of less than 1 per cent over the temperature range calculated compared with the assumption of constancy over 50° intervals. The agreement, for the linear flow velocities quoted, is good; and although the initial temperatures T_i were higher than the matrix temperatures T_m the experimental data themselves between 30 and 40 mm from the plate suggest the higher values. The possibility of using the method for measuring by means of a single experiment the thermal conductivities of gases and gaseous mixtures over a temperature range is therefore being investigated. Friedman and Burke[14] have pointed out the importance in the analysis of flame temperature profiles of accurately knowing the temperature dependence of the thermal conductivity of the gases entering the flame zone. It may be possible

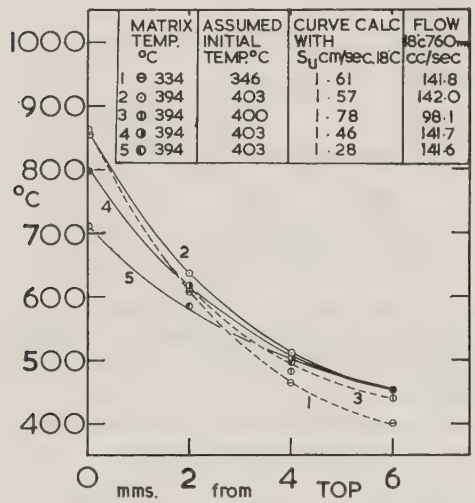

Figure 8. Temperature profiles for air flowing towards top plate

by this method to carry out in some cases both flame measurements and associated conductivity measurements on the mixture without the flame present in the same apparatus.

From the point of view of limits, the important data are the approach velocities S_u which must be assumed in order to obtain agreement with experiment. Firstly, at least for a given top plate geometry, S_u is determined primarily by convection, and not volumetric flow rate, even in the absence of a flame zone (curves 2 and 3). Secondly, in the case examined S_u is not affected by altering T_m from 394 to 334°C (curves 1 and 2). Lastly, on reducing the plate temperature, lower approach velocities can be obtained (curves 2, 4 and 5). Thus the importance of convection in these systems is again apparent, and it becomes clear firstly why in this particular system burning velocities below about 1·5 to 1·6 cm/sec are not obtained, and secondly why the burning velocity curves for all the matrix temperatures level off at about this value.

DISCUSSION

Flat flame burner limits

The results confirm those of a previous investigation on methane–air mixtures[10], that in this type of system convection plays an important part in determining the flame behaviour near the inflammability limits. Due to the greater ease of oxidation of ethylene as compared with methane, however, it has been possible within the practical temperature limits of operation of the top plate to extend the burning velocity curves and to obtain flames which appear to sit actually touching the top plate. Such behaviour was not found with the methane–air flames. For the latter a definite limit occurred for each top plate condition, but with ethylene–air mixtures there was no really well defined limit when the top plate was very hot (900°C and above). Now even in the absence of a flame the hot top plate has been shown to cause convection effects which impose a lower limit on the linear approach velocity of an air stream. This in turn places a lower limit on the burning velocity when ethylene is present. In addition, the reaction velocity, and hence the burning velocity, is far more dependent on temperature than on composition (*cf.* Dixon-Lewis[15]); and in these cases, as opposed to most limit flames, the maximum temperatures are the plate temperatures T_p which are independent of composition. Hence the comparative lack of sharpness in the composition limit. Similarly, due to variation of approach velocity with plate temperature, and probably also with some aspects of the plate geometry, there is unlikely to be a unique burning velocity curve which is absolutely independent of the top plate conditions. This may account for some of the scatter at the weak end of the burning velocity curves.

At lower top plate temperatures $T_f > T_p$ at the limit, sharper composition limits are obtained, and the limit burning velocity starts to increase. This is in contrast with the behaviour of an air stream, whose minimum approach velocity decreases at lower T_p. As the mixtures become weaker and the burning velocity decreases, the flames approach closer to the top plate in order to stabilize themselves against their own convection effects. Eventually they reach a position where, due presumably to quenching by the top plate, they are unable to recover from chance disturbances. This occurs at a sharp composition limit. The behaviour of the flames with $T_p < 870$°C (*Figure 5*) is consistent with the sharp limits being caused by a quenching action of the plate, and these limits are therefore brought into line with

the low pressure 'tube' limits studied by Simon, Belles and Spakowski[16]. The top plate clearly stabilizes the flame against a convection limit caused by itself: depending on the plate temperature it may then either produce a quenching limit or its own convection limit.

The significance in ethylene–air flames of the temperature of 870°C, above which the top plate loses its quenching properties, is not quite clear. It is possible to speculate that the situation may be compared with the transition from slow reaction to explosion in a corresponding static system. The temperature itself may be compared with initial temperatures of 1,021 and 789°C required for the oxidations of 1 per cent mixtures of methane and ethane respectively in air in the flow apparatus used by Burgoyne and Hirsch[17] using a 4·8 msec residence time, and 966°C for methane with a 15·3 msec residence time. The flow velocities in our system at 870°C were about 1 mm per 15 msec.

Application to theory of limits

The modified flat flame limits show that much weaker mixtures than had previously been thought are able to support self-propagating flames, and very plausible explanations of all these limits can be advanced which involve environmental effects. Moreover, all the flames obtained, with the exception of the two mentioned earlier, are on balance quenched to some degree (*Figures 3–6*). It is therefore unlikely on these grounds alone that any of the 'inflammability' limits so far found experimentally should be explained in terms of instability to small disturbances from the steady state (Lewis and von Elbe[1]; Rosen[2]) or in terms of the kinetic properties of the mixtures (van Tiggelen[3]; Weinberg[4]). In contrast with Rosen's result[2] that instability to perturbations may exist in certain circumstances, Layzer[18] has analysed the case of a single-step constant-enthalpy reaction, and has concluded that such disturbances always die away without flame extinction.

In an extended volume of gas, in which the flame moves with respect to the stationary medium, convection effects in themselves will only modify the apparent flame velocity. They seem to us to be unlikely to produce inflammability limits in these circumstances unless they occur in a non-uniform manner so as to cause distortion of the flame front in such a way as to render it unstable.

Spalding[19] has recently examined the effect of introducing a heat loss or quenching term into the steady-state flame equations. He finds that if the reaction rate decreases with decreasing temperature more rapidly than the heat loss rate, then a composition limit of inflammability is obtained, and there is a small but finite burning velocity at the limit. The explanation in this way, by means of radiational heat loss, of the limits in an infinite planar flame front appears to us at present to represent the most plausible approach.

Temperature profiles

The temperature profiles showed that the maximum temperatures T_f actually obtained in the flames were always below the adiabatic flame temperatures T_{ad}. The magnitude of the discrepancies is given for some of the flames in Table 1. $T_{ad} - T_f$ varies in these mixtures

TABLE 1

Temperature Relationships in some Near Limit Ethylene–Air Flames

Per cent C_2H_4	T_p °C	T_{ad} °C	$T_{ad} - T_f$ °C	*Distance of* T_f *from top* mm
1·74	907	1,067	65	14
1·72	762	1,062	77	14
1·61	899	1,020	83	6
1·69	842	1,050	92	10
1·66	838	1,041	97	10
1·58	870	1,010	140	0
1·73	900	1,012	112	0

between 65 and 140°C, its value being somewhat larger as T_p decreases, and appearing to increase considerably in the early stages of the approach of the flame to the top plate. With the plate in a non-quenching condition it reached a maximum when T_f just became equal to T_p. Thereafter T_f and T_p were always equal, $T_{ad} - T_f$ decreased, and the combustible gases appeared to receive increasing amounts of energy from the plate during their approach to the latter. This transfer of energy occurred even though T_{ad} was still above both T_p and T_f.

It is unlikely that the observed effects are due to inaccuracies in the temperature profiles for two reasons. Firstly, the system appeared to give consistent and reasonable values for the air profiles. Secondly, the readings at both ends of the flame profiles compared well with independent values, so that it is then reasonable to suppose that in a case such as curve 3 in *Figure 6* where $T_{ad} - T_f = 44$°C, the thermocouple will not give a reading 100° or so lower than the plate temperature when it should be reading higher.

It is also unlikely that the observed effects are due to sideways heat losses, or to interdiffusion with re-circulating burnt gas and resulting dilution of the combustible mixture, since again there is little evidence from the air curves for such a major contribution of these effects, and further, little reason to suppose that they would increase as they do when the flame approaches the top plate. Leah and Carpenter[20] ascribed rather similar

discrepancies in carbon monoxide–oxygen flames to a failure of the gases to reach chemical and thermodynamic equilibrium in the visible flame zone, equilibrium only being reached at some later stage. This sort of explanation would account for the increasing discrepancies observed here as the visible flame approaches the top plate, since then the time allowed for the attainment of equilibrium becomes less. The catalytic action of the plate surface presumably hastens the attainment of equilibrium, so that in fact the flame gases probably repay to the plate the energy they may have borrowed from it during their approach.

There is now an increasing body of evidence that thermodynamic equilibrium is not always attained in visible flame zones. Leah and Carpenter[20] assumed their temperature readings using a quartz-coated resistance wire to be low immediately after the flame zone, due to the slowness of removal of oxygen atoms by $O + CO + M = CO_2 + M$. In pre-mixed weak propane–air flames at low pressure, Friedman and Burke[14] found that the temperature continued to rise for 1 to 2 cm after the luminous zone, suggesting a two-stage oxidation process. Composition profile measurements on the same flame by Friedman and Cyphers[21], as well as measurements by Fristrom *et al.*[22–25] on richer propane–air flames again indicate that the combustion may be a two-stage process—a fast reaction region extending from the beginning of the reaction to the outer edge of the luminous zone, and a more extended after-burning region beyond this zone. The first region is normally associated with the flame propagation. The reactions in this region are essentially cracking of the hydrocarbon and partial oxidation to form primarily CO and H_2O with some CO_2 and H_2. The second stage involves primarily the oxidation of CO to CO_2, and it is this second extended stage which is probably incomplete in our system.

It is noteworthy that Fristrom *et al.* found no oxygenated compounds such as alcohols, aldehydes, etc., in their primary reaction region. In this their results resemble those of Smith and Gordon[26,27] and Wolfhard and Parker[28] on hydrocarbon–air diffusion flames, where cracking of the hydrocarbon in the absence of oxygen is the primary process. They differ, however, from the results of Burgoyne and Hirsch[17] who found formaldehyde as an intermediate in the oxidation of methane at up to 1,000°C, and similarly acetaldehyde in the oxidation of ethane at *ca.* 800°C. Burgoyne and Hirsch found in the oxidation of weak methane–air mixtures that no CO oxidation occurred until all the methane was used up, but with ethane the separation of the reaction in this way was much less pronounced. The pattern of behaviour with methane thus seems to be very similar to that observed in the propane–air flames, although the primary oxidation mechanisms are dissimilar. The modified flat flame burner system corresponds fairly closely in temperature conditions with those of Burgoyne and Hirsch, so that some analysis of the course of reaction in the burner would be most instructive.

In conclusion, the work with the modified flat flame burner system has shown that limits of inflammability in the burner are essentially functions of the apparatus and environment. Either convection limits or quenching limits of inflammability may be obtained depending on the conditions, and there is as yet no evidence for the occurrence of any fundamental limit depending only on the internal properties of the flame. Analysis of the temperature conditions in the systems has yielded some supporting evidence for the view that hydrocarbon oxidation in flames is not complete at the end of the luminous zone. Further work on this aspect is planned.

Crown Copyright Reserved

It is a pleasure to thank Professor A. L. Roberts and the Joint Research Committee of the Gas Council and the University of Leeds for their encouragement during the course of this work.

REFERENCES

1 Lewis, B. and von Elbe, G. *Combustion, Flames and Explosions*, p. 369. 1951. New York; Academic Press

2 Rosen, J. B. *J. chem. Phys.* 22 (1954) 733, 743. *Sixth Symposium (International) on Combustion*, p. 236. 1957. New York; Reinhold

3 Van Tiggelen, A. *Bull. Soc. chim. belg.* 55 (1947) 202

4 Weinberg, F. J. *Proc. Roy. Soc. A* 230 (1955) 331

5 Linnett, J. W. and Simpson, C. J. S. M. *Sixth Symposium (International) on Combustion*, p. 20. 1957. New York; Reinhold

6 Powling, J. *Fuel* 28 (1949) 25

7 Egerton, A. C. and Thabet, S. K. *Proc. Roy. Soc. A* 211 (1952) 445

8 Badami, G. N. and Egerton, A. C. *Proc. Roy. Soc. A* 228 (1955) 297

9 Burgoyne, J. H. and Williams-Leir, G. *Proc. Roy. Soc. A* 193 (1948) 525

10 Dixon-Lewis, G. and Isles, G. L. *Trans. Faraday Soc.* 53 (1957) 193

11 — — To be published

12 Friedman, R. *Fourth Symposium (International) on Combustion*, p. 259. 1953. Baltimore; Williams and Wilkins

13 Spiers, H. M. *Technical Data on Fuel.* 1950. London; British National Committee, World Power Conference

14 Friedman, R. and Burke, E. *J. chem. Phys.* 22 (1954) 824

[15] Dixon-Lewis, G. *Selected Combustion Problems*, Vol. 2. London; Butterworths
[16] Simon, D. M., Belles, F. E. and Spakowski, A. E. *Fourth Symposium (International) on Combustion*, p. 126. 1953. Baltimore; Williams and Wilkins
[17] Burgoyne, J. H. and Hirsch, H. *Proc. Roy. Soc A* 227 (1954) 73
[18] Layzer, D. *J. chem. Phys.* 22 (1954) 222, 229
[19] Spalding, D. B. *Proc. Roy. Soc. A* 240 (1957) 83
[20] Leah, A. S. and Carpenter, N. *Fourth Symposium (International) on Combustion*, p. 274. 1953. Baltimore; Williams and Wilkins
[21] Friedman, R. and Cyphers, J. A. *J. chem. Phys.* 23 (1955) 1875
[22] Prescott, R., Hudson, R. L., Foner, S. N. and Avery, W. H. *J. chem. Phys.* 22 (1954) 145
[23] Fristrom, R. M. *Sixth Symposium (International) on Combustion*, p. 96. 1957. New York; Reinhold
[24] — Prescott, R. and Grunfelder, C. *Combustion and Flame* 1 (1957) 102
[25] — and Westenberg, A. A. *Combustion and Flame* 1 (1957) 217
[26] Smith, S. R. and Gordon, A. S. *J. chem. Phys.* 22 (1954) 1150
[27] — — *J. phys. Chem.* 60 (1956) 759
[28] Wolfhard, H. G. and Parker, W. G. *Proc. phys. Soc. A* 65 (1952) 2

69

FLAME TEMPERATURES OF LIMIT MIXTURES

M. G. ZABETAKIS, S. LAMBIRIS, and G. S. SCOTT

INTRODUCTION

Most combustible-oxidant systems have two limits of flammability, or limits, at any specified temperature and pressure. These limits are ordinarily defined in such a way that all included mixture compositions are flammable.

Burgess and Wheeler[1] showed that the heat liberated by a mole of a lean limit mixture is nearly constant for many combustible-air-mixtures at ordinary temperatures and pressures (law of Burgess and Wheeler). In a re-evaluation and extension of this work, Egerton and Powling[2] found that the amount of heat liberated by such limit mixtures of the paraffins was not constant but increased with increasing molecular weight so that the corresponding adiabatic flame temperature also increased, approaching the value 1,600°C asymptotically. Further, since the lean limit mixture compositions are dependent on the temperature and pressure, the above 'law' is also violated if the initial temperature and pressure are varied. However, while investigating the effect of initial temperature on the limits of flammability, White[3,4] found that the adiabatic flame temperatures of many limit mixtures were essentially constant, i.e. they were independent of the initial temperature. Similarly, Egerton and Powling[2] showed that the addition of an inert diluent to a limit mixture did not appreciably alter the limit flame temperature. Accordingly, this temperature would appear to be an important quantity in determining the composition of the limit mixture for a particular combustible-oxidant-inert system. However, Burdon, Burgoyne and Weinberg[5] noted that a 'non-flammable' gas such as methyl bromide does not necessarily behave as an inert in a flame; the addition of such a gas to a flammable mixture essentially changes the nature of the combustible and therefore the limit flame temperature.

In the present study, additional data are presented on the effects of temperature and inert diluents on the adiabatic limit flame temperatures. In addition, the effect of pressure is considered.

Flame temperatures were calculated by the trial and error method; the heat of combustion of each limit mixture was equated to the enthalpy change required to increase the temperature of the combustion products to that of the flame. Because of the relatively low temperatures encountered, dissociation of the products was neglected. The data of Rossini *et al.*[6] and of Knowlton and Rossini[7] were used for these calculations.

APPARATUS AND TEST PROCEDURES

The apparatus and test procedures used to obtain the data utilized in this study have been discussed in detail[8–11]. A 2 in. explosion tube and upward propagation of flame were used in all cases. At ambient temperatures and one atmosphere pressure the ignition source (a high voltage discharge between platinum electrodes spaced 0·25 in. from a 15,000 V, 30 mA luminous tube transformer) was located at the open end of a 2 in. glass tube 48 in. long. At elevated temperatures and one atmosphere pressure, the same ignition source was used at the closed end of a similar 2 in. glass tube; the upper end of this tube was open to the atmosphere. At elevated pressures both ends of a 2 in. steel tube, 12 in. long (inside dimensions) were closed; the ignition source consisted of two or more strands of 36 gauge platinum wire each 1·5 cm long mounted between vertical electrodes and fused by the application of a voltage surge from a.c. power mains. In some cases, guncotton was used in addition to the platinum wire where the wire was found to be inadequate when used alone.

EFFECT OF INITIAL TEMPERATURE

As noted above, while investigating the effect of initial mixture temperature on the limits of flammability, White[3,4] found that the corresponding adiabatic limit flame temperatures remained essentially constant. For example, he found the limit flame temperatures of ammonia–air mixtures were 1,620 $\pm$ 10°C for both the lower and upper limit mixtures over the initial temperature range 20 to 450°C. These experiments were conducted in closed vertical 5 cm glass tubes, 1·5 metres long using upward propagating flames. A similar set of experiments conducted with six other gases showed that over a rather wide temperature range, limit flame temperatures were independent of the initial temperature. However, since these latter data were obtained with downward propagating

flames they cannot be compared directly with the other data to be considered here.

The adiabatic limit flame temperatures, T_f, obtained for the lower limit mixtures of six paraffins over the temperature range 27 to 200°C and one atmosphere pressure[11] are given below:

Combustible	T_f (°C)
n-hexane	1,410 ± 20
n-heptane	1,370 ± 20
n-octane	1,410 ± 20
*iso*octane	1,430 ± 40
n-nonane	1,365 ± 25
n-decane	1,345 ± 15

Contrary to Egerton and Powling's findings[2], T_f does not increase with increase in molecular weight.

Since T_f is essentially constant for any particular combustible over a range of initial mixture temperatures, the law of Burgess and Wheeler may be modified as follows to show the effect of temperature on the heat liberated by lower limit mixtures (*cf.* reference 4):

$$L \cdot C + \Delta H = k \qquad (1)$$

where L is the lower limit composition,

C is the heat of combustion of the combustible involved, and

ΔH is the heat energy added to the limit mixture to raise its temperature from the reference temperature (e.g. 27°C) to the test temperature.

In this equation, k depends on the combustible and the direction of flame propagation.

EFFECT OF INITIAL PRESSURE

Since the lower limit of flammability is decreased by an increase in pressure at a fixed initial temperature, the heat liberated by the limit mixtures and the corresponding adiabatic flame temperatures also decrease. The effect of pressure on the adiabatic flame temperature of natural gas–air mixtures is shown in *Figure 1*, in which the limit flame temperature is given as a function of pressure between 0 and 10,000 lb./in.² gauge. Three sets of data are given. Two were obtained by assuming a constant pressure and the third a constant volume process. The same limit data were used to calculate the closed tube constant volume (closed tube, C_v) and constant pressure (closed tube, C_p) process flame temperatures; the flammability experiments were conducted in closed tubes, however, the volume of unburned gas did not remain constant but decreased as the flame propagated up the tube. Similarly, the pressure did not remain constant during these experiments. However, it is interesting to note that the adiabatic flame temperature of a limit mixture obtained in an open tube at one atmosphere pressure lies much nearer the value obtained in a closed tube at one atmosphere initial pressure if a constant pressure rather than a constant volume process is assumed. Thus, although flame propagation does not occur under constant pressure or constant volume conditions in closed tubes, use of the former condition results in flame temperatures that are more nearly correct as a first approximation. Additional examples of this are given in Table 1 for several hydrocarbon–air mixtures at an initial pressure of one atmosphere:

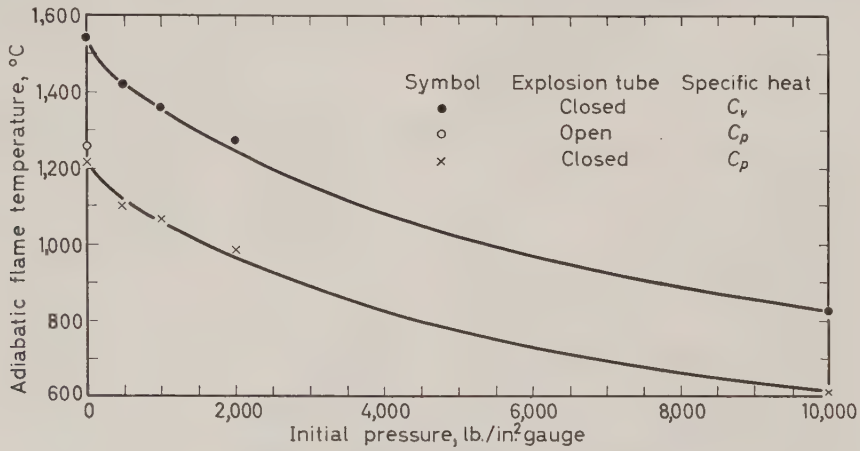

Figure 1. Adiabatic flame temperatures of lower-limit natural gas–air mixtures as a function of pressure

TABLE 1

Combustible	L (vol. per cent)		T_f (°C)		
	Closed tube	*Open tube*	*Closed tube* (C_v)	*Closed tube* (C_p)	*Open tube* (C_p)
Methane	5·00	5·23	1,540	1,210	1,260
Ethane	2·85	2·90	1,540	1,210	1,230
Propane	2·15	2·20	1,630	1,280	1,310
n-Butane	1·75	1·83	1,700	1,340	1,390

Flame temperatures of upper limit mixtures are approximately the same as those of the corresponding lower limit mixtures at atmospheric pressure. However, they appear to decrease quite rapidly with pressure yielding extremely low values at moderate pressures. For example, the upper limit flame temperature of a natural gas–air mixture at 2,000 lb./in.^{2} gauge pressure is less than 400°C.

EFFECT OF DILUENT COMPOSITION

The substitution of an inert diluent for part or all of the nitrogen in the 'air' used to make up a limit mixture does not appear to affect the limit flame temperature appreciably unless the thermal conductivity, specific heat and molecular weight of the substituted diluent vary appreciably from those of nitrogen. Egerton and Powling[2] calculated the limit flame temperatures for a number of combustible-inert gas–air mixtures. They found little variation in flame temperatures except for mixtures in which helium was used as the diluent. Limit-of-flammability data obtained with *cyclo* propane- and with methane-oxidant mixtures in which the nitrogen in the air was replaced by an inert diluent[12] showed essentially the same effect. These data and the corresponding limit flame temperatures are listed in Table 2.

TABLE 2

Diluent	*L* (vol. per cent C_3H_6)	T_f (°C)
CO_2	3·7	1,430
N_2	2·4	1,370
He	2·0	1,550
Ne	1·7	1,350
A	1·7	1,350
Kr	1·8	1,400
Xe	1·8	1,400
Diluent	*L* (vol. per cent CH_4)	T_f (°C)
CO_2	8·3	1,360
N_2	5·2	1,250
He	4·7	1,500
Ne	4·3	1,390
A	3·8	1,240

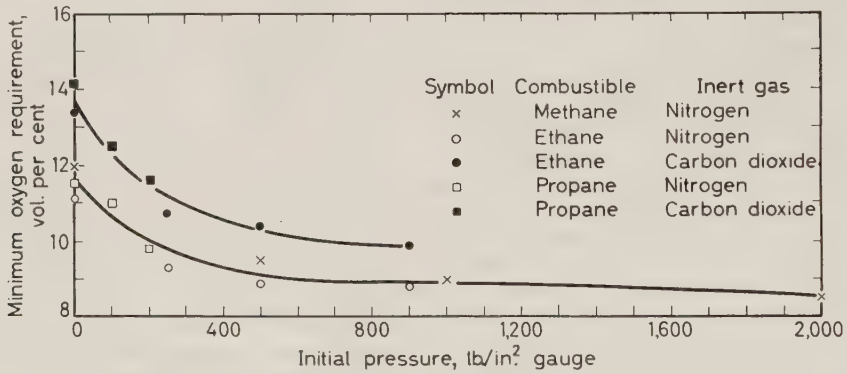

Figure 2. Minimum oxygen requirements for flame propagation through various combustible-inert gas–air mixtures at 27°C as a function of pressure

In each set of data the effect of helium is most pronounced. Because of the high thermal conductivity of this gas, the amount of heat lost from the flame is greater than that involving the other inerts, therefore the adiabatic flame temperature is raised since additional fuel must be added to the corresponding lower limit mixture to obtain a propagating flame.

The effects of added diluents and elevated pressures can be evaluated by determining the effect of pressure on the minimum quantity of oxygen required for flame propagation. This quantity is plotted as a function of pressure in *Figure 2* for fiv combustible-inert gas–air systems. It decreases quite markedly with pressure up to about 500 lb./in.^{2} gauge. The corresponding adiabatic flame temperatures also decrease with increase in pressure, again the rate of decrease being greatest at low pressures. As an example, the flame temperatures (closed tube, C_p) corresponding to the methane–nitrogen–air minimum oxygen values in *Figure 2* are given in Table 3.

TABLE 3

Pressure lb./in.^{2} gauge	T_f (°C)
0	1,390
500	1,110
1,000	1,040
2,000	980

DISCUSSION

Adiabatic flame temperatures of limit mixtures appear to be relatively independent of initial mixture temperature for many combustibles. However, they are dependent on initial pressure, direction of flame propagation and combustible and inert gas compositions. For any particular combustible-inert gas–air system, the limit flame temperatures decrease with increase in pressure; upper limit flame temperatures decrease more rapidly with increase in pressure than lower limit flame temperatures.

Since the initial mixture temperature does not affect the lower limit flame temperature of many combustibles appreciably, the effect of temperature on the lower limit can be determined by assuming a constant flame temperature or by using a modified Burgess-Wheeler law. The effect of pressure cannot be assessed in the same manner although some trends in the lower limits, minimum oxygen requirements and limit flame temperatures have been noted.

REFERENCES

[1] Burgess, M. J. and Wheeler, R. V. *J. chem. Soc.* 99 (1911) 2013

[2] Egerton, A. C. and Powling, J. *Proc. Roy. Soc.* 193 (1948) 190

[3] White, A. G. *J. chem. Soc.* 121 (1922) 1688

[4] — *J. chem. Soc.* 127 (1925) 672–684

[5] Burdon, M. C., Burgoyne, J. H. and Weinberg, F. J. *Fifth Symposium (International) on Combustion*, pp. 647–651. 1955. New York; Reinhold

[6] Rossini, F. D. *et al. Circular of the National Bureau of Standards C461*, 1947

[7] Knowlton, J. W. and Rossini, F. D. *Research Paper RP2012*, National Bureau of Standards. 43 (1949) 113

[8] Coward, H. F. and Jones, G. W. *Bull. U.S. Bur. Min.* 503 (1952) 9

[9] Jones, G. W., Kennedy, R. E. and Spolan, I. *Rep. Invest. U.S. Bur. Min.* 4557 (1949)

[10] Hanna, N. E., Zabetakis, M. G., Van Dolah, R. W. and Damon, G. H. *Rep. Invest. U.S. Bur. Min.* 5223 (1956)

[11] Zabetakis, M. G., Scott, G. S. and Jones, G. W. *Industr. Engng Chem. (Industr.)* 43 (1951) 2120

[12] Jones, G. W. Unpublished data

DISCUSSION

W. H. Avery (Silver Spring): The papers on ignition cover too wide a range of subjects to permit detailed discussion in the seven minutes allotted. It seems more appropriate, therefore, to discuss them according to the method of approach to solution of the problems of ignition. Two of the papers—Gray and Harper, and Khitrin—are theoretical treatments in which simplifying assumptions are made to permit analytical solutions to be found. Such treatments are valuable if the factors neglected are in fact unimportant, otherwise they are of value only as mathematical exercises. In this connection I should like to ask Gray whether there are any examples of pure thermal explosions apart from those treated by Rice, Allen and Campbell.

A second group of the papers presented deals with attempts to obtain data which will be basic to the understanding of ignition phenomena. The papers of Miller, Sage and Weinberg, Priede and Rose, and Thompson *et al.*, are in this category. The value of such studies depends on whether sufficient insight—i.e. recognition of fundamental principles and significant parameters—is employed in designing the experiments so that the data may be regarded as 'true facts', not correlations valid only for the particular experimental equipment used. The first paper of Priede and Rose is an excellent example of a thoroughly well documented experimental study that should be of considerable importance in understanding of spark ignition phenomena. It will supplement and support studies of such phenomena by schlieren techniques, e.g. Olsen and Gayhart's work in this field.

Finally, there is one example of a study with a directly applied objective, that of Wolfhard and Vanpée. These authors have secured information of direct practical value predicting conditions under which firedamp explosions may be prevented. If such studies are to be of maximum value the authors should relate the results of their particular experiment to work that may be of more fundamental or broader significance. I would like to ask Wolfhard in this connection if his ignition data may be related to those of Miller and Thompson. The relationship of Weinberg's interesting experiment to other work is not apparent. Perhaps there will be an opportunity for him to enlarge on this point.

J. H. Burgoyne (London): In the study of limits of inflammability two kinds of approach are useful: (1) measurement of limit values for practical use, usually in connection with the avoidance of explosion hazards; (2) observations which improve understanding of the fundamental significance of limits.

I feel that the investigations reported by Zabetakis, Lambiris and Scott on the one hand, and by Dixon-Lewis and Isles on the other fall respectively into these two categories.

Zabetakis, Lambiris and Scott base their discussion on measurements made in the 2 in. vertical tube, and the justification for its use is that the values thus obtained appear in most cases to approach limits ruling in the larger spaces encountered in practice. With this background, they have examined the effect of certain factors upon the adiabatic flame temperature T_f at the limit, and have concluded that:

(1) T_f is relatively independent of the initial temperature in many cases, and therefore the effect of initial temperature on the limit can be calculated.

(2) T_f decreases with increase of initial pressure, especially as referred to the upper limit.

(3) T_f for closed tube limits is more appropriately calculated on a basis of constant pressure combustion than constant volume.

(4) Inert diluents have little effect on T_f, except in the case of helium when T_f is somewhat raised. (No doubt the higher thermal conductivity of helium is important, but its effect upon the temperature structure of the pre-heat and reaction zones may be at least as important as its effect upon heat losses from the flame front.)

I would like to express my appreciation of the immense amount of work done over many years at the Bureau of Mines on the measurement of inflammability limits. The work of the late G. W. Jones and his colleagues forms the major source of information on this subject for most practical purposes, and often one would have been at a loss without them.

It does seem to be clear, however, that limits as they are encountered in the ordinary way are dictated by several factors of different kinds, and in these circumstances it would seem unprofitable to seek any fundamental correlations between such limit values at the present stage.

Dixon-Lewis and Isles have sought to strip off some of the environmental factors in an endeavour to simplify the picture. They have confirmed, what had previously been indicated from other quarters, that if a planar flame is removed from the influence of surrounding walls and protected

against convective disturbance, the lower limit value is greatly reduced. Their technique has, however, imposed other environmental restrictions and a fresh approach seems necessary if the stripping process is to be pursued further. I feel, however, that any further steps in this direction should be accompanied by close observation of the manner in which the limit flame fails under the conditions employed. Some indication might be obtained, for example, as to whether the flame is failing due to the spread of a local disturbance or whether it is failing as a whole, as it might be expected to do on arriving at the point considered by Spalding, where heat loss is the only factor opposing flame propagation.

Alternatively, what possibility is there of developing the theory of, for example, limitation by heat loss to the stage where sufficiently accurate predictions of numerical limit values can be made for purposes of comparison with experimental observation? It would appear to me that accurate temperature analyses through near-limit flame reaction zones, such as can be made by the methods described elsewhere in this Symposium by Weinberg and Levy, might provide a factual basis which would greatly facilitate such predictive calculations.

P. Gray (Leeds): I agree with Avery's point that the implications of approximate methods should receive more careful scrutiny and interpretation than has sometimes been the case in flame propagation theory. Here we are on firmer ground as we are dealing with only small departures from isothermal conditions and we have been able to make numerical assessment of the approximations before (Table 1) and after (Table 3) their application.

On the point of real systems describable in this way let me first draw attention to a necessary shift of emphasis. The fact is that *all* exothermic reactions must depart from isothermal conditions and the real value of this introductory paper and of our more sophisticated investigations is that the *extent of this departure is assessable.* A recent illustration is offered by Groocock's work on lead azide; an older but no less dramatic one is the prediction of the explosion (P *vs.* T) limits of gaseous nitrous oxide (spontaneous ignition) before its experimental determination (Yakovlev).

Voevodsky has suggested that Frank-Kamenetskii's picture of the temperature distribution is a more refined one than Semenov's. I offer the suggestion that although their relationship *may* be regarded in this light an alternative view is also helpful, viz. that both treatments are legitimate but refer to physically different situations. The point is illustrated by *Figure 1* of our paper and elaborated in reference 6.

G. von Elbe (Pittsburgh): In Mullin's method of measuring ignition lags, the induction period is set equal to the time of travel of the mixture from the point of formation to the flame front. If the position of the flame front were determined by some extraneous stabilization mechanism, the time of travel would in general not coincide with the induction period. On what evidence do the authors conclude that no such stabilization is operative in their experiments?

B. P. Mullins (Farnborough): In his remarks relating to Miller's paper, which describes test results using the smaller scale N.G.T.E. ignition apparatus, von Elbe has asked what was the nature of the residence time measured. I shall attempt to answer this question.

The residence time is calculated from the observed distance between the plane of fuel injection into the test section and the plane nearest this at which flame is observed to be continuously present in the duct. This latter plane has been loosely referred to by myself and other people as a 'flame front' but it is in no sense a flame front of the type observed in flame propagation processes. In fact, in the present flow regime where velocities are of the order of 25 ft./sec (2 in. rig) or 250 ft./sec (6 in. rig) there is no flame stabilization in the test section, but flame appears spontaneously in the duct and away from the walls after the fuel–air mixture has existed for a sufficient time at the elevated temperature. This residence time computed from the distance between the plane of fuel injection and the plane at which steady flame is first observed represents the chemical delay time for a weak fuel-vitiated air mixture. In the cases where fuel is injected either as liquid or vapour through a single central orifice the effective mixture strength which creates this flame position is smaller indeed than the nominal overall mixture strength obtained by dividing the total fuel flow by the vitiated air flow. This is because only a portion of the injected fuel volatilizes and mixes very quickly (in a time of the order of 0·1 msec). In calculating the residence time it is assumed that the very rapidly formed weak mixture is present from the fuel injector plane and moves downstream with the velocity of the general stream.

Some unpublished tests which I have made, in which special care was taken to distribute and mix the added fuel very quickly—by the use of a multiple-drilled double ring injector manifold and perforated plates and gauzes—have shown that the ignition delay is insensitive to variation of equivalence ratio, ϕ, in the range 0·001 to 0·5; hence it is not necessary to create a precisely determined mixture ratio, so long as we require $\phi < 0{\cdot}5$, when testing fuel sprays or gaseous fuels using a single-hole injector or any other injector which by its very nature cannot produce a uniform mixture at once. I have some experimental

evidence that in these flow experiments the ignition delay time is reduced by some 30–50 per cent as the stoichiometric mixture ratio is approached from the weak side.

In the standard experiments which I have described* I always took care to ignore, for purposes of ignition delay calculation, the occasional 'flame flashes' observed between the plane of fuel injection and the plane of steady flame appearance which I tentatively ascribed to near-stoichiometric pockets of gas mixture which were created by the diffusion of fuel from the spray into the turbulent airstream. This flame flashing, which corresponded to a shorter residence time than that which I plotted in my curves, may indeed have been due to the creation of such more easily ignitable pockets of gas mixture of which there would be less than of the weak pockets of gas mixture which are responsible for the establishment of the steady flame position; alternatively, the flame flashing may have been due to some turbulence-dependent phenomenon such as an intermittent yet rapid fluctuation of gas stream velocity or temperature. The second reference describes in more detail this phenomenon of 'flame flashing'.

When liquid fuel is used the coarser spray droplets are seen to burn behind, that is, downstream of the steady flame position, and the same applies to that part of a gaseous fuel injected through a single orifice which takes longest to mix with the airstream.

So, summarizing, the residence time as measured very closely approximates to the true chemical delay time for a weak mixture of the fuel and vitiated air and this is borne out by the linearity of curves of 'log residence time *versus* reciprocal absolute temperature'; in the case of Miller's results the airstream was not vitiated but was either pure air or a synthetic atmosphere.

S. L. Bragg (Derby): Miller suggests that his results disprove the method of correlating 'spontaneous ignition' data which was suggested by, among others, Holliday and myself: we do not agree that this is necessarily so.

Our simplifying assumption was to suppose that the local reaction rate in any part of the apparatus was principally determined by the concentrations of fuel, oxygen and already burnt products, and the corresponding temperature: there would then be a unique relationship between the 'degree of reactedness' and the corresponding temperature, and the heat release rate, independent of the initial test conditions. (Incidentally, if such an assumption is *not* made, then it is very difficult to see any practical application of these comparatively low-temperature results to engineering systems.) Reaction would then start immediately the combustibles were mixed and would continue at an accelerating rate until the flame became visible and 'ignition' was said to occur. Most of the delay period would be spent in raising the reactants through the first few degrees, as is well shown by Miller's *Figure 3*—on our interpretation, out of a delay time of 60 msec at 780°C, half is spent in raising the temperature by 20 degrees to 800°C.

Miller, however, rejects our hypothesis, primarily because the supposed rise in temperature has not been measured. Now our second hypothesis was that the fuel did *not* mix completely immediately on injection, but that the flow tended to be striated. Reaction then proceeded fastest, and so ignition was apparent, in those streams where the mixture ratio was near stoichiometric: thus the apparent ignition delay corresponded always to a near-stoichiometric mixture whatever the overall ratio of injected fuel to airstream flow. This seems the only possible reason why, as *Figure 2* shows, the oxygen concentration has a big effect on the delay while the overall fuel: mixture ratio has none at all. In this respect it would be very interesting to do the inverse test—injecting oxygen into a hot mixture of fuel and nitrogen: one might well find that the fuel concentration was then of importance but that delay was independent of the overall oxygen concentration.

On the same argument, if only the near-stoichiometric streams are reacting appreciably in the early stages after injection, the average temperature rise is small. The fact that no rise is measured does not therefore discount the theory.

Furthermore, although the author claims that the time average concentration at points just downstream of the injection plane varies only by a factor of two, this is no proof that there is not considerable time-wise variation of mixture ratio along a given stream, so the above arguments may still hold.

R. E. Miller (Newcastle-upon-Tyne): My results certainly do not disprove the method of correlating spontaneous ignition data supported by Bragg. The results which are relevant to the discussion are some temperature measurements obtained by Mullins at N.G.T.E. some years ago. Even with these I prefer not to use the word 'disprove'.

I have examined some simple criteria for spontaneous ignition suggested by various authors in order to determine whether any of them are capable of explaining my own ignition delay results and those of Mullins for calor gas. Of the three suggestions mentioned in my paper I have rejected one as being improbable. The other two (those of Bragg and Mullins) seem to be equally promising starting points although both must be regarded as extreme simplifications since the chemistry of this process is undoubtedly complex. My assumptions

* Mullins, B. P. *Fuel* 32 (1953) 218, 234, 327, 343, 363, 451, 467, 481.

are similar to those outlined above by Bragg. I assume that the reaction rate is determined by fuel concentration, oxygen concentration and temperature. At this point one asks the question 'When does ignition occur?' Mullins has suggested that it occurs after a definite fraction of the reaction has been completed while Bragg prefers the idea of a constant temperature rise between the mixing of the combustibles and the appearance of flame. In choosing between these two suggestions I have been guided by the temperature measurements mentioned above. These seem to contradict the assumption of either a constant ignition temperature or of a constant temperature rise before ignition. To my knowledge this is the only existing piece of experimental evidence which is relevant to a choice between the two alternatives. Using Mullins' suggestion and assuming that the pre-flame zone can be represented as an isothermal region (this is probably not too far from the truth when one remembers that the largest group of measurements were made over a range of equivalence ratios of 0·018 to 0·05) it is then possible to account for the observed effects for the weak mixtures which have been studied. The object of the paper, however, is merely to show that a simple criterion such as that discussed above is capable of explaining these facts and certainly not to disprove any alternative mechanism. Such an alternative must be regarded as equally valid provided that it is capable of explaining all the experimental facts.

I am not completely in agreement with Braggs' arguments on mixing. The production of a completely homogeneous fuel–air mixture immediately on injection is of course an ideal which can never be reached in any practical system. However, arguments set out in the paper suggest that the results can be explained more easily by assuming complete mixing. It must be remembered that under our experimental conditions cold fuel is added to a hot air stream. Under these conditions if we have bad mixing there will be a range of pockets varying from very weak mixtures at temperatures near that of the air stream to very rich ones at very low temperatures. If a stoichiometric pocket were formed this would be at a temperature lower than that of the ideal homogeneous fuel–air mixture for most of the experiments by more than 100 degrees. In view of the exponential temperature dependence of ignition delay it is not at all obvious that a near-stoichiometric mixture would ignite first. Bragg regards the hypothesis of poor mixing as being the 'only possible reason why' the mixture ratio has no effect on ignition delay. It cannot be too strongly stressed here that the ignition delay is not the same thing as a reaction *rate*. The fact that one of these quantities apparently depends on fuel concentration while the other does not is therefore no contradiction. Indeed all the ignition delay measurements have been explained on the assumption that the overall reaction rate is proportional to the first power of both the oxygen concentration and the fuel concentration. Starting from this assumption equation 8 is obtained which involves terms of the form $(q-p)$. For weak mixtures, which are the only ones studied on our laboratory scale apparatus, it is possible to neglect p, the fuel concentration, so that the expression for τ (equation 9 and subsequent equations) turns out to be independent of equivalence ratio. This approximation is obviously strictly valid only for infinitely weak mixtures. For the weak mixtures considered here (where the equivalence ratio for most of the mixtures is below 0·1 and for all the mixtures is below 0·2) the assumption is a reasonably good approximation. If one could explain results over the entire range of mixture strengths by a second-order equation one should, as Bragg suggests, find that, on adding *small amounts* of oxygen to a stream of hot fuel and nitrogen, the ignition delay was independent of oxygen concentration. For the purpose of this argument we shall ignore the experimental difficulties involved in preparing such a hot fuel stream. However, when we approach a stoichiometric mixture either from the weak or the rich side the treatment outlined above cannot be used since it is no longer possible to neglect one concentration with respect to the other. There is the added complication that in such mixtures a fairly large temperature rise might occur in the pre-flame zone if the fraction of reaction completed there is appreciable. The assumption of an isothermal pre-flame zone will not then be correct and treatment of any such results must be considered in rather more detail.

F. J. Weinberg (London): In reply to Avery's question, the temperature at which ignition occurs without the use of a second stage corresponds to conventional auto-ignition. This value, however, is not a constant, since it depends on the amount of heat released by the gas in contact with the surface and hence on time of contact, surface area, etc. The smaller the heat release the higher is the ignition temperature. Our T_i gives the upper limit of the range of 'ignition temperatures'.

E. A. Watson (Birmingham): The two papers by Priede and Rose form a valuable contribution to our knowledge of the initiation of ignition by electric sparks and are notable for the very remarkable technique applied to a difficult problem.

My remarks are based on the statement that it is assumed that all the energy released at the gap is imparted to the gas mixture. In some work which has been carried out over the last few years

on the ignition of fuel sprays at low densities and pressures, where relatively large amounts of energy are involved, it became very clear that this was by no means the case. In our experiments we found that a large portion of the energy actually released at the gap was imparted to the electrode surfaces and only released to the gas relatively slowly, but apart from this the discharges were accompanied by very appreciable radiation, a flash and a bang and this radiant energy would be ineffective as an igniting source. It can be argued that even if the energy is released comparatively slowly some 70 per cent will appear as heat, the rest doing mechanical work on the surrounding gas, but if the energy is released very rapidly to produce a hot core at a high pressure which then expands adiabatically the amount of residual energy in the hot kernel is still further reduced, the balance appearing as a shock wave. It is true that the energy in this shock wave is converted into heat ultimately but this will be comparatively low-grade heat and ineffective as an igniting source.

In our high energy sources we were only able to account for a small fraction of the total—some 10 per cent at most which could be really effective —and the question arises as to whether a similar condition can prevail in these low energy sources. It is true that visible and audible radiation is difficult to detect but at the same time the momentary rates of energy dissipation are high and a rough calculation would indicate that the instantaneous temperature of the spark channel in *Figure 10* could be of the order of 30,000°C or more.

This supposition is supported by the results of the authors' experiments which showed that the introduction of resistance into the circuit reduced the amount of liberated energy required to produce ignition. The introduction of resistance by reducing the instantaneous rate of energy release could of course easily reduce the relative amount of radiated and ineffective energy.

Although in most cases occurring in practice the energy required for ignition is so small that these losses are of no great significance, this is not the case under certain conditions of low pressure and also of fuel–air mixtures bordering on the limit of inflammability, and particularly so in the case of fuel sprays as opposed to homogeneous gaseous mixture.

G. von Elbe (Pittsburgh): Reference has been made to energy loss during ignition of inflammable gases by electric sparks. Such loss is mainly caused by the shock wave which radiates from the spark without contributing to the ignition process. In a private communication, Clarke has informed us of some experiments on sparks in argon which showed rather large losses of energy. However, the spark energies in these experiments were very large compared to those usually required for ignition; the ratio of heat loss to heat retained decreases with decreasing spark energy; and in diatomic or polyatomic gases the fraction of heat retained in the spark centre is substantially larger than in argon. It appears therefore that the ignition energy data reported by various investigators, including ourselves, are not very greatly in error and are certainly correct within the order of magnitude.

M. G. Zabetakis (Pittsburgh): If we assume, as noted by Dixon-Lewis and Isles for their burner, that the lower limit of inflammability at a specified (mixture) temperature can actually be decreased by increasing the wall temperature of a conventional cylindrical limit of inflammability apparatus, one would expect to find a non-linear relationship between the lower limit and the (mixture and wall) temperature at a fixed pressure. However, all the data obtained to date in cylindrical apparatus indicate a linear relationship actually exists between these quantities.

A. L. Berlad (San Diego): Dixon-Lewis and Isles have strikingly called attention to the dependence of 'limits of inflammability' upon apparatus. It is significant to note that steady-state flames are *always* non-adiabatic, and therefore must depend upon the apparatus (boundary conditions). Strictly speaking, then, 'inflammability limits independent of apparatus' is a self-inconsistent concept. In fact, examination of the well known solution of the time dependent heat conduction equation shows that a finite temperature gradient is *immediately* established at the boundaries of an initially isothermal (arbitrarily large, but finite) domain. It is thus impossible, even if one (improperly) excludes the importance of radiation losses, for a steady-state flame to be unaware of the boundaries. A detailed examination of the fact that 'steady-state' flames must be non-adiabatic is presented elsewhere*. One must therefore conclude that distinctions between 'quenching limits' and 'inflammability limits' are somewhat arbitrary. Thus, *conduction* as well as radiation losses are operative in defining 'inflammability limits'†.

The authors particularly noted that limits in tubes and on flat-flame burners are different. That this is generally so follows from the discussion presented in the preceding paragraph and from the fact that extinction limits depend upon the *manner* in which energy is abstracted from flames. Thus, the question 'how much heat must we abstract

* Berlad, A. L. and Yang, C. H. *On the Existence of Steady-State Flames.* Paper presented at the Western States Section of The Combustion Institute (U.S.A.), June 1958 (to be published).

† — — *A Theory of Non-adiabatic Flame Propagation.* Paper presented, in part, at the Western States Section of The Combustion Institute (U.S.A.), June 1958 (to be published).

from a flame to extinguish it?' is *not* a generally valid one. For example, a freely propagating, non-adiabatic, steady-state flame (in a long, cold tube) may be considered to be semi-infinite in extent. It thus gives up *all* its heat of combustion to the surroundings. *Everywhere* within this semi-infinite domain, the energy conservation equation must be balanced, if the steady-state flame is to exist. It can be shown* that extinction limits (quenching *and* inflammability) are predictable from limits of applicability of the conservation equations which describe the non-adiabatic flame structure in the neighbourhood of the reaction zone. This follows from the facts that:

(*a*) energy conservation is easy to satisfy in the neighbourhoods of very low reaction rates (near the 'cold boundary' and on the 'hot' side of the maximum flame temperature).

(*b*) The energy conservation equation is very sensitive to heat abstraction in regions of high chemical reactivity. Thus it follows that different boundary conditions (heat sinks) will affect the flame structure in different ways. Hence extinction limits resulting from the use of different kinds of apparatus (boundary conditions) *should* be expected to differ.

J. Grumer (Pittsburgh): The observation of Dixon-Lewis and Isles, that leaner flames can be generated in special flat-flame burners than in tubes, does not exclude the possibility that fundamental limits exist which depend on the properties of the unburned mixture. Apparatus effects should be unimportant in gas explosions in huge vessels as in mines. With reference to such explosions, experience indicates that fundamental flammability limits exist and though a mixture may not be hazardous in the mine, the combustibles in it can be reacted on a red hot coil in gas analysis equipment.

G. Dixon-Lewis and G. L. Isles (Leeds): We wish to emphasize that the 'limits of inflammability' and minimum burning velocities quoted by us are not to be regarded as fundamental to the ethylene–air flame, but as environmental limits produced by the apparatus. By studying the effect of the temperature of the stabilizing medium (hot plate) above the flame it has been possible to show that the limits obtained in this particular apparatus can very probably be associated with convection effects due to the flame itself together with the quenching properties of the plate when the latter is at temperatures below about 870°C. At higher plate temperatures the quenching properties of the plate disappear, but its convectional properties become important. In the latter case the limit burning velocity is controlled by the convectional approach velocity, and a visible flame is only obtained when the mixture composition is sufficient under the conditions prevailing to give the limit burning velocity. Whilst it has been suspected for some time that convection may be very important in determining the limits in this type of system, the interplay between convection and quenching, and the two different types of limit, have not, so far as we are aware, previously been shown.

During the discussion Zabetakis referred to the constancy of adiabatic limit flame temperatures in tubes as the initial mixture temperature is varied over quite wide range, and suggested that it is difficult to explain this on the basis of a quenching theory of the limits. Similarly, it was not until the top plate in our experiments reached almost 700°C that the adiabatic 'limit' flame temperature commenced to decrease at all rapidly. The effect in our experiments may be partly due to the steepness of the burning velocity curve in the region corresponding to the low-temperature limits. In this region the decrease in burning velocity due to a slight lowering of the adiabatic flame temperature may sufficiently increase the quenching effect per unit volume of gas that it offsets the reduced quenching due to the higher temperature of the surface near the flame. A similar type of approach might help to explain the above aspect of tube limits, though again it may be that such limits are determined by effects of the tube other than quenching.

In reply to Grumer's points, our observations, indeed, do not exclude the possibility that fundamental limits exist which depend only on the internal properties of the flame burning under adiabatic conditions. It nevertheless seems most likely to us that such limits, if they do exist, have not yet been reached; and that the observed limits so far obtained are not fundamental in this sense. In the case of mine explosions and explosions in large, but finite, vessels the possibilities of flame instability produced by convectional deformation of the flame front or of limits caused by radiation losses have been mentioned.

Lastly, we should like to draw attention to our observation that even in the absence of a flame catalytic reaction occurs at the hot surface of the top plate. We are inclined to compare this, rather than our visible flames, with the type of reaction occurring on the red-hot wire of the gas analysis apparatus. In our view the close approach to the heated plate is necessary to stabilize the flame aerodynamically. This does seem to result in a conversion of the later stages of the flame reaction into a catalytic action on the plate, and the problem then becomes one of how far this catalytic reaction will affect the propagation of

* Berlad, A. L. and Yang, C. H. *A Theory of Non-adiabatic Flame Propagation.* Paper presented, in part, at the Western States Section of The Combustion Institute (U.S.A.), June 1958 (to be published).

the main flame zone. There is no obvious change in the appearance of the luminous zone as it approaches the plate; and in the absence at present of further experimental evidence we are inclined to believe that, even if the luminous zone is only separated from the plate by a millimetre or so, the effect is small, due to the high values of the reaction rates and radical concentrations actually in the luminous zones of most flames compared with the values behind them.

PART VI

INTERACTION OF FLAMES AND SURFACES

THE QUENCHING OF FLAME BY WIRE GAUZES

K. N. PALMER

INTRODUCTION

Flame arresters are devices which are able to prevent or quench the passage of flame; their main use is in industrial plant for preventing the propagation of explosion through combustible gas mixtures in ducts or other systems. Although flame arresters of various types have long been used, as in the Davy safety lamp, recent reviews[1,2] have shown that their use is on an empirical basis. There has been little fundamental work to relate the performance of the arresters with the properties of the flames, the nature of the explosive gas mixtures, and the dimensions of the systems in which the arresters were installed. Research is therefore being carried out to provide the necessary fundamental information and in the present paper an account is given of some experiments with wire gauze arresters. Wire gauze was used because it was readily available in a wide range of sizes of aperture and could be built up into packs.

EXPERIMENTAL

Materials and apparatus

Details of the meshes and the materials of the gauzes are listed in Table 1.

TABLE 1

Characteristics of the Wire Gauzes

Material of gauze	*Nominal mesh*	*Nominal wire gauge* s.w.g.	*Mesh width* (m) cm	*Wire diameter* (D) cm	*Surface area of wire in unit area of gauze* (A) cm^2	*Proportion of area of gauze blocked by wires*
Brass	4	20	0·551	0·0838	0·829	0·246
Brass	6	20	0·329	0·0940	1·40	0·395
Steel	6	20	0·330	0·0935	—	—
Brass	10	24	0·198	0·0559	1·39	0·392
Steel	10	24	0·199	0·0546	—	—
Brass	18	28	0·106	0·0356	1·58	0·437
Steel	28	28	0·0531	0·0376	—	—
Brass	30	32	0·0572	0·0267	2·00	0·663
Brass	40	34	0·0404	0·0231	2·29	0·595
Steel	40	34	0·0399	0·0236	—	—
Brass	60	37	0·0248	0·0175	2·60	0·656
Steel	60	37	0·0251	0·0173	—	—
Brass	80	39	0·0192	0·0130	2·54	0·645
Steel	80	39	0·0212	0·0122	—	—
Phosphor bronze	120	43	0·0125	0·0089	2·61	0·659
Phosphor bronze	200	46	0·0065	0·0061	3·04	0·734

The following approximate relations may be derived from the values given.

$$m = 13{\cdot}2D^{1{\cdot}5}$$

$$AD^{0{\cdot}35} = 0{\cdot}535$$

Three fuels were used in the preparation of the explosive gas mixtures: propane, ethylene, and town gas. The propane was specified by the manufacturers as being at least 97 per cent pure; the ethylene was specified as being 98·2 per cent pure. The town gas was used from the mains supply and samples of the gas were taken from the mains before and after the series of tests. The two samples gave the analyses shown in Table 2. With each of the fuels fast flames were obtained by enriching the fuel/air mixture with oxygen; the oxygen was of normal commercial purity.

TABLE 2

Analysis of Town Gas

Constituent	*Percentage by volume*	
	initial sample	*final sample*
CO_2	4·9	4·3
C_nH_m	4·2	5·5
O_2	0·3	0·4
CO	20·5	23·7
H_2	46·4	43·8
C_nH_{2n+2}	17·5	17·8
N_2 (by difference)	6·2	4·5

The tube in which the explosions were produced was of Perspex; the length of the tube was 170 cm, the internal diameter was 6·4 cm, and the wall thickness was 0·6 cm. The tube was cut into two sections, the shorter section being 58·5 cm in length, and the two sections were held vertically so that they butted end-wise on to each other; the arrester was sandwiched tightly between the two sections and was held in position by friction only. In all experiments the gas mixture was ignited at an open end of the tube, with the other end of the tube closed. The apparatus could be adapted to permit experiments with either upward or downward propagation of flame and for the propagation

of the flame along either the shorter or the longer section of the tube before reaching the gauze. Measurements of flame velocities near the gauze were made using a rotating drum camera; the speed of the drum was calibrated by means of a signal generator in conjunction with a cathode ray oscilloscope.

Procedure

In each experiment with single gauzes a fresh sample was cut to form a circular disc whose diameter equalled that of the outside of the tube, and after the gauze had been washed in carbon tetrachloride it was dried and then sandwiched horizontally between the ends of the two sections of tube. When multiple layers of coarse gauzes were used the gauze circles were bolted together so that the meshes were aligned, the edges of the gauzes were then soldered and the bolts were removed before cleaning and insertion of the gauze assembly in the tube. As packs containing three or more layers of coarse gauze gave no sign of distortion by the flame they were each used for several experiments. Combinations of fine and coarse gauzes were assembled by soldering the circles together at the edges; the building of packs of fine gauzes was not attempted because of the difficulty in obtaining alignment of the meshes. After the gauze was inserted in the tube the system was made gas-tight by binding the junction with transparent adhesive cellulose tape.

The explosive gas mixture was then metered through the tube, allowing about ten changes of the gas in the tube, and the supply was then cut off. The quiescent gas mixture in the tube was ignited by a small gas flame applied to the open end of the tube, and the movement of the flame near the gauze was recorded by the drum camera. The velocity of the flame was measured at the following positions relative to the gauze: (1) at about 1·5 cm from the gauze surface on the approach side (initial velocity) and, if the flame passed through the gauze, (2) at about 1·5 cm from the gauze surface on the departure side (final velocity).

The velocity of the flame was calculated from measurements of the slope of the flame front on the photographic record and the speed of rotation of the camera drum. With fast flames vibrations developed in the flame front and hence the camera record was wavy; in such cases the maximum value of the flame velocity at or near the point 1·5 cm from the gauze was taken as the local flame velocity, the photographic record for the maximum value was usually clearly defined and measurement could be made with the minimum of subjective error. When the photographic record was obscure, so that definite measurements were not possible, the record was rejected.

RESULTS

Observation of the flames

The velocity of propagation of the flame in the tube could be altered by changing either the composition of the explosive mixture, or the length of the tube between the igniting flame and the gauze (the run-up length), or the direction of propagation; these results were similar to those described by other workers for flames propagating in tubes without gauzes. A sufficiently wide range of flame velocities was produced by using gas mixtures whose compositions ranged from near-limit fuel/air mixtures to a stoichiometric mixture containing fuel, air and additional oxygen (e.g. propane 1 part by volume, oxygen 5 parts, nitrogen 7·6 parts).

If the flame did not pass the gauze the damage suffered by the gauze was small, the greatest damage being slight discoloration of the very fine gauzes. If the flame passed through the gauze little damage was caused to gauzes coarser than 18-mesh, but gauzes finer than 60-mesh were usually destroyed. Gauzes of intermediate mesh were often split. The destruction of gauzes was frequently accompanied by the emission of light from the molten metal; this emission was particularly marked with the fine steel gauzes and was often sufficient to affect the photographic record and to interfere seriously with the measurement of flame velocities. The interference could be reduced by introducing a blue light filter into the camera.

Experiments with single gauzes

The arresting of propane flames by brass or phosphor-bronze gauzes was investigated using a run-up length of 58·5 cm, the flame propagating upwards, and the results are given in *Figure 1*. The initial flame velocity is plotted against the width of the gauze mesh on logarithmic axes and distinction is made whether or not the flame passed the gauze; no account is taken of variation in the composition of the explosive mixture even though both lean and rich mixtures were used to produce slow flames. It was possible to draw a straight line which, with a few exceptions, separated the results of experiments in which the gauze quenched the flame from those results for which the flame passed through the gauze. The line was arranged so that equal numbers of the exceptional results fell on each side of it. The results of experiments with propane flames under similar conditions with steel gauzes are shown in *Figure 2*. Further experiments with propane flames propagating upwards, with brass or phosphor-bronze gauzes, were carried out using a longer run-up length (111·5 cm) and the results are given in *Figure 3*. The behaviour of propane flames propagating downwards was

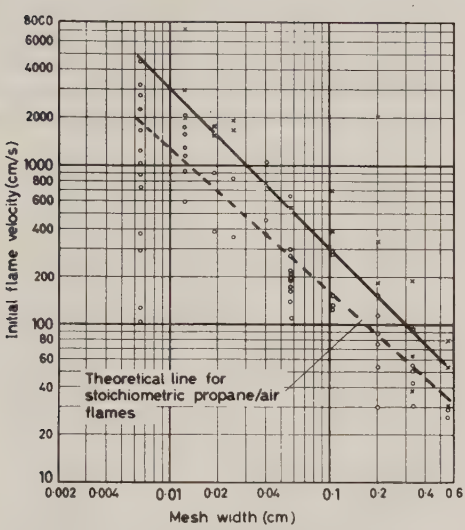

Figure 1. The arresting of propane flames by single layers of brass and phosphor-bronze gauze. (Upward propagation; run-up, 58·5 cm; × gauze passed flame; ○ gauze stopped flame)

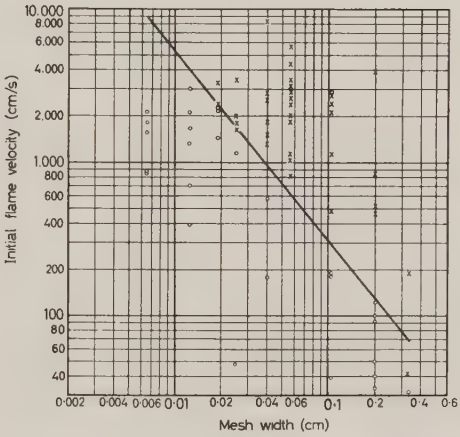

Figure 3. The arresting of propane flames by single layers of brass and phosphor-bronze gauze. (Upward propagation; run-up, 111·5 cm; × gauze passed flame; ○ gauze stopped flame)

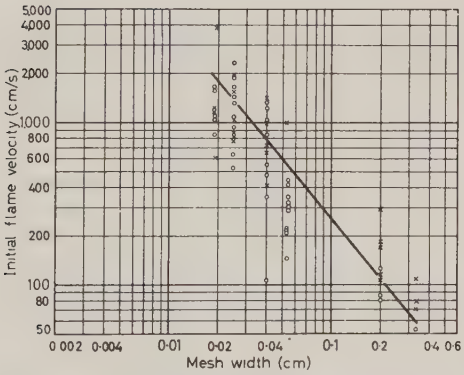

Figure 2. The arresting of propane flames by single layers of steel gauze. (Upward propagation; run-up, 58·5 cm; × gauze passed flame; ○ gauze stopped flame)

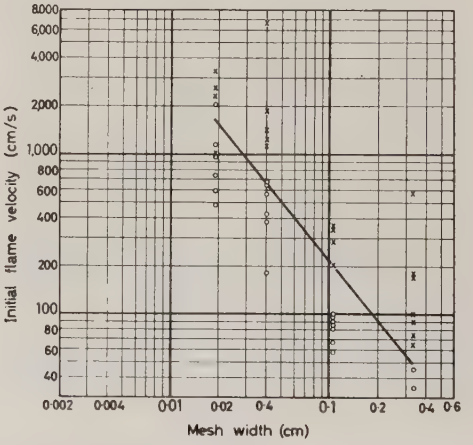

Figure 4. The arresting of propane flames by single layers of brass and phosphor-bronze gauze. (Downward propagation; run-up, 58·5 cm; × gauze passed flame; ○ gauze stopped flame)

studied using a 58·5 cm length of tube between the igniting source and the gauze, and the results are shown in *Figure 4*.

The results for ethylene and town gas flames propagating upwards, and with a run-up length of 58·5 cm, are shown in *Figures 5* and *6* respectively. The gauzes used were brass or phosphor-bronze.

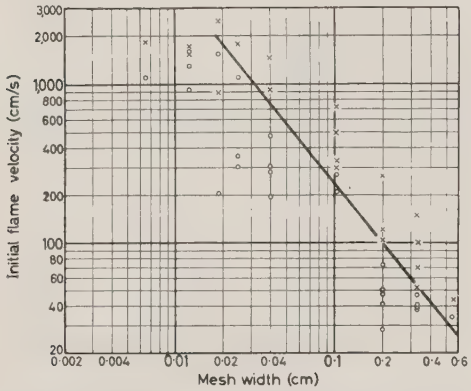

Figure 5. The arresting of ethylene flames by single layers of brass and phosphor-bronze gauze. (Upward propagation; run-up, 58·5 cm; × gauze passed flame; ○ gauze stopped flame)

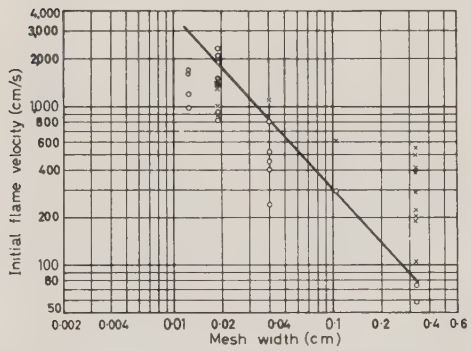

Figure 6. The arresting of town gas flames by single layers of brass and phosphor-bronze gauze. (Upward propagation; run-up, 58·5 cm; × gauze passed flame; ○ gauze stopped flame)

Experiments with combinations of gauzes

The effect of increasing the number of layers of gauze in the arrester was studied with 10-mesh gauzes, with up to ten layers arranged so that the meshes were accurately aligned. The fuel used was propane and the flames propagated upwards with either a 58·5 cm or a 111·5 cm run-up. The results are given in *Figure 7*, where the initial flame velocity is plotted on logarithmic axes against the number of gauzes in the pack. A further set of experiments was carried out with packs of 6-mesh gauze, using ethylene flames propagating upwards, with a run-up length of 58·5 cm. Similar results were obtained.

In an attempt to devise an arrester with the quenching ability of a fine gauze but with the mechanical strength of a coarse gauze experiments were carried out with a 120-mesh phosphor-bronze gauze soldered to a 6-mesh brass gauze. The combined gauzes were inserted in the tube,

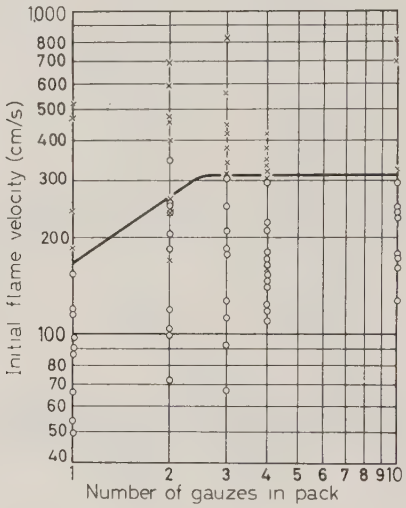

Figure 7. The arresting of propane flames by packs of 10-mesh gauze (brass). (Upward propagation; run-up, 58·5 or 111·5 cm; × gauze passed flame; ○ gauze stopped flame)

with a 58·5 cm run-up length, and were exposed to propane flames travelling upwards. The results are given in Table 3 for experiments with the finer gauze on the underside, the finer gauze was

TABLE 3

Experiments with Combined 6- and 120-mesh Gauzes

Initial flame velocity cm/sec	*Behaviour of flame*
1,091	Passed
831	Passed
800	Quenched
622	Quenched
555	Quenched
388	Quenched

thus the first reached by the flame. With a reverse arrangement of gauzes the results were erratic and evidence was obtained that the centre of the finer gauze was lifted by the slight pressure developed as the flame approached, so that when the flame neared the arrester the two gauzes were no longer in contact over their whole area. With neither arrangement of gauzes was the combined arrester

as effective as a single layer of 120-mesh gauze (*Figure 1*).

In a further attempt to construct a robust arrangement capable of stopping fast flames packs were made up in which a finer brass or phosphor-bronze gauze was sandwiched between two 6-mesh brass gauzes. Propane flames propagating upwards were again used, with the run-up length of

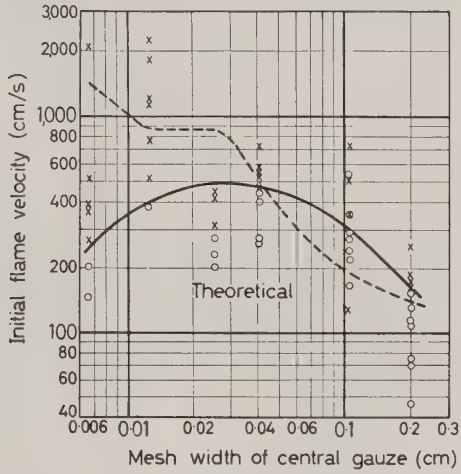

Figure 8. The arresting of propane flames by single gauzes sandwiched between two 6-mesh brass gauzes. (Upward propagation; run-up, 58·5 cm*; × gauze passed flame; ○ gauze stopped flame)*

58·5 cm; the results are shown in *Figure 8*. In no instance was the combination markedly more effective than the central gauze alone, and with the finer gauzes the effectiveness was considerably reduced.

DISCUSSION

The arresting of flames by single gauzes

With each of the fuels tested, and under each set of experimental conditions, there were critical values of the initial flame velocity below which the flames were arrested, and above which they propagated through the arrester. In each of the sets of results shown in *Figures 1–6* a line can be drawn to separate the results of experiments in which the gauze quenched the flame from those results in which the flame was not quenched, apart from a relatively small number of results. It may be seen from *Figures 1–6* that the lines connecting the critical flame velocities were approximately straight, and that each set of results may be represented approximately by an equation of the form

$$V = \frac{C}{m^n} \qquad (1)$$

where V is the critical value of the initial flame velocity, m is the width of the mesh of the gauze (Table 1), and C and n are constants. Values of the two constants corresponding to the various fuels and experimental conditions are given in Table 4. The relation between the critical velocity of the flame and the width of the mesh of the gauze, equation 1, was only slightly influenced by variation of the composition of the fuel, the material of the gauze, the direction of propagation, and the length of the run-up of the flame. The effectiveness of gauze arresters under the conditions of test thus appears to depend largely on the velocity of the flame as it nears the gauze, and factors such as the direction of propagation and the length of the run-up from the point of ignition to the gauze appear to be of secondary importance except in so far as they affect the flame velocity.

TABLE 4

Values of the Constants in Equation 1

Fuel	*Material of gauze*	*Direction of propagation*	*Run-up length* cm	*n*	*C*
Propane	Brass and phosphor-bronze	Upwards	58·5	1·00	30·0
Propane	Steel	Upwards	58·5	1·22	14·9
Propane	Brass and phosphor-bronze	Upwards	111·5	1·24	17·5
Propane		Downwards	58·5	1·21	13·2
Ethylene		Upwards	58·5	1·27	12·8
Town gas		Upwards	58·5	1·10	23·3

Theoretical aspects of flame arresting by single gauzes

By assuming that the quenching of the flame was caused by heat transfer from the flame to the gauze, so that if more than a certain critical amount of heat were removed the flame would be quenched, it was possible to derive a theoretical equation of the form of equation 1. A curved flame was assumed to be propagating through a stationary gas mixture with velocity V and approaching a gauze arrester of wire diameter D. Then as the flame passes the gauze, the amount of heat absorbed by unit area of gauze in unit time is equal to $hA(T_h - T_g)$, where h is the heat transfer coefficient, T_h is the mean bulk temperature of flame gases through the gauze, and T_g is the temperature of the gauze.

Now, let there be a zone of flame, of thickness x, from which a critical amount of heat must be removed in order to quench the flame. Then the flame is in contact with the gauze for a time x/V approximately.

Thus the total amount of heat absorbed from the flame by unit area of gauze

$$= q = hA(T_h - T_g)x/V$$

Now, the velocity of the flame is proportional to its surface area, and a flat flame propagates at the adiabatic burning velocity S. If, therefore, the

flame velocity is V, each square centimetre of gauze is opposed, on the average, by V/S cm² of flame. So the total amount of heat lost by unit area of flame is

$$Q = q \cdot \frac{S}{V} = hA(T_h - T_g)\frac{xS}{V^2}$$

The thickness of the flame, x, is governed by the velocity of the chemical reactions in the flame. If the flame is propagating at velocity V, greater than S, the thickness of the flame is increased by a factor V/S, i.e.

$$\frac{x}{V} = \frac{x_0}{S}$$

So $$Q = hA(T_h - T_g)x_0/V$$

If it is assumed that the convection is non-transient and that the gauze may be treated as an array of cylinders whose boundary layers do not interact, then an approximate value for h may be derived from the Nusselt number. This is given for laminar flow over cylinders at low Reynolds numbers by[3],

$$N_u = \frac{hD}{k} = 0{\cdot}32 \text{ approximately}$$

Thus

$$Q = 0{\cdot}32\frac{kA}{D}(T_h - T_g)\frac{x_0}{V}$$

$$= \frac{0{\cdot}32 \times 0{\cdot}535 \times (13{\cdot}2)^{0{\cdot}9}}{m^{0{\cdot}9}} k \cdot (T_h - T_g)\frac{x_0}{V}$$

or

$$V = \frac{0{\cdot}32 \times 0{\cdot}535 \times (13{\cdot}2)^{0{\cdot}9} k(T_h - T_g)}{m^{0{\cdot}9} \quad Q/x_0} \quad (2)$$

For simplicity, in the following calculation the composition of the unburnt mixture was taken as constant (4 per cent propane in air) and the flame velocity was assumed to have been varied by changing the area of the flame. The following information is available on adiabatic flame temperature[4] and other thermal properties[5]:

Flame temperature of 4 per cent propane/air mixture = 2,260°K
Flame temperature of 2·4 per cent propane/air mixture = 1,750°K
} T_h = 2,000°K approximately

$$T_g = 290°\text{K}$$

$$\text{Mean film temperature} = \frac{2{,}000 + 290}{2} = 1{,}145°\text{K}$$

k, for nitrogen (the major constituent of the flame) at 1,145°K = $2{\cdot}90 \times 5{\cdot}8 \times 10^{-5}$ c.g.s.u.

If it is further assumed that, for quenching, the burning velocity must be reduced to that at the lower flammability limit (2·4 per cent propane/air) then Botha and Spalding[6] showed in their experiments with a water-cooled flat flame burner that a total of 5·0 cal/c.c. propane measured at n.t.p. must be removed from the flame. Thus, for a 4 per cent propane/air flame, whose flame temperature is 2,260°K, the amount of heat to be removed from unit volume of flame = $25/26 \times 273/2{,}260 \times 0{\cdot}04 \times 5$ cal approximately, since 25 mol of reactants yields 26 mol of products.

Thus the amount of heat to be removed from unit volume of flame in order to quench it $= 2{\cdot}32 \times 10^{-2}$ cal $= \frac{Q}{x_0}$ from equation 2.

Thus equation 2 becomes

$$V = \frac{21{\cdot}6}{m^{0{\cdot}9}} \quad (3)$$

This relation is represented by a broken line in *Figure 1*. This theoretical line lies lower than the experimental line, and part of the discrepancy arises from the omission in the theory of the effect of changes in the mixture composition. It can be shown that the theoretical line is displaced upwards for slower burning and downwards for faster burning mixtures.

The arresting of flames by packs of gauzes

The results given in *Figure 7* for multiple layers of coarse gauze showed that the benefit obtained by increasing the number of layers tailed off fairly quickly so that comparatively little was obtained by increasing the number of gauzes of the same mesh above five.

A combination of fine and coarse gauzes was less effective in flame quenching than the fine gauzes alone. This behaviour may be explained on the basis that flame cannot pass through the area of the fine gauze that is covered by the wires of the coarse gauze. Thus, some of the surface area of the wire in the fine gauze is lost for quenching, being to some extent replaced by the smaller surface area of the wire in the coarse gauze; the efficiency of the combination as an arrester ought to be less than that of the fine gauze, in proportion to the loss of surface area of wire. The calculated velocity for a single 6- and 120-mesh combination (820 cm/sec) is in excellent agreement with the experimental results (Table 3), but with the alternative arrangement the experimental results were too scattered for comparison. From the theoretical viewpoint, both arrangements should be equally effective in arresting flames. When a gauze was sandwiched between two coarser gauzes the predicted behaviour of the combination was in reasonable agreement with the experimental results (*Figure 8*), if it were assumed that the faces of the coarse gauze in contact with the fine gauze made a negligible contribution to the quenching of the flame. The central flat portion

of the curves in *Figure 8* arises because with the 60- and 120-mesh gauzes the surface areas of wire in unit area of gauze are approximately equal (Table 1).

CONCLUSIONS

(1) Using wire gauze arresters, mounted in a short vertical tube and with explosions initiated at the open end of the tube, there was a critical velocity of approach of a flame below which the flame was quenched and above which the flame passed through the arrester.

(2) With single layers of gauze this critical velocity was approximately inversely proportional to the width of the mesh of the gauze, over a wide range of mesh sizes. The relation between the critical velocity and the mesh width was similar for propane, ethylene, and town gas flames and was very little affected by change in the direction of propagation and length of the run-up of the flame to the gauze. Both brass and steel gauzes gave similar results.

(3) If coarse gauzes were built into packs the critical flame velocity for quenching increased slightly, but the effect did not increase indefinitely as packs containing more than five layers of gauze did not show further increase in effectiveness.

(4) Combinations of coarse gauzes and a fine gauze were less effective than the fine gauze alone.

(5) A simple theory based on the assumption that the quenching of the flame results from the abstraction of heat by the wire of the gauze is in broad agreement with the experimental results for propane flames.

Crown Copyright Reserved

Miss J. S. Hall, Mr. P. S. Tonkin, and Miss S. E. Townshend assisted in the experimental work.

The work described in this paper forms part of the programme of the Joint Fire Research Organization of the Department of Scientific and Industrial Research and Fire Offices' Committee; the paper is published by permission of the Director of Fire Research.

REFERENCES

[1] Palmer, K. N. *J. Inst. Fuel* 29 (1956) 293
[2] Massey, B. S. and Lindley, B. C. *J. R. aero. Soc.* 62 (1958) 32
[3] McAdams, W. H. *Heat Transmission.* 1942. London; McGraw-Hill
[4] Smith, R. W., Edwards, H. E. and Brinkley, S. R. *U.S. Bur. Min. Rep. No. 4938.* 1953
[5] Hilsenrath, J. *et al.* Tables of thermal properties of gases. *U.S. Nat. Bur. Stand. Circ. 564.* 1955
[6] Botha, J. P. and Spalding, D. B. *Proc. Roy. Soc. A* 225 (1954) 71

71

SUPPRESSION OF EXPLOSION WAVES IN GASEOUS MIXTURES BY MEANS OF FINE POWDERS

P. LAFFITTE and R. BOUCHET

SUPPRESSION OF DEFLAGRATIONS

It has been known for a long time that certain flames can be extinguished by pulverized metallic salts and in particular by alkaline metal salts. Fifty years ago Dautriche[1] was the first to mention the influence of sodium and potassium salts on the combustion of the various gaseous products (viz. hydrogen, carbon monoxide) of the incomplete combustion of explosives. He has also shown that a cloud made of finely divided potassium or sodium salt inhibits the combustion of gases and of combustible dusts.

More recently van der Deussen[2] has shown that the material used must be very finely divided in order to extinguish methane; later still Matla[3] has shown that potassium salts are better extinguishers than sodium salts. As a part of the history of this field of research one must also mention particularly the work of Dufraisse and associates[4,5] who have studied the extinction of flames of various gases (town gas, hydrogen, methane, carbon monoxide) with air, by more than 250 pulverized samples. Their work has led them to draw a classification of the material studied according to the effectiveness of their extinguishing power. Given in order of increasing effectiveness they found potassium bicarbonate, picrate and oxalate were the best. As far as the mechanism of extinction was concerned they concluded that there was a specific suppression power not related to mechanical or chemical mass action but on the contrary related to anti-oxygen catalysis.

Quite recently Dolan and Dempster[6,7] have studied the suppression of ignition of a methane/air mixture in a dust suspension in a flowing known mixture which was artificially ignited. Amongst the salts studied, alkali halides are between the most effective in quenching methane/air ignitions. Aluminium chloride proved the most effective out of all the materials investigated.

Investigations carried out so far relate to deflagrations and in most cases to stationary flames. No data appear in connection with the extinction of flames propagating at high velocities measured in particular just before quenching occurs. We have undertaken a series of investigations on these questions and prior to the study of detonations we have carried out a set of experiments on deflagrating flames propagating in cylindrical tubes.

In these experiments the flame propagation was followed by the chronophotographic recording method of Mallard and Le Chatelier. The extinguishing material was placed on a small brass plate introduced inside the horizontal glass tube at a given distance from the ignition end[8].

Experiments carried out under these conditions on methane/air or propane/air mixtures have shown that suppression can never be obtained during the uniform movement of the flame. In the case of deflagrations with a variable velocity (and in particular for vibratory flames) the extinction can be obtained provided a satisfactory material is chosen and the quantity, though relatively small, is sufficient. Under these conditions the compression wave preceding the flame front raises a cloud of the pulverized material which leads immediately to the extinction of the flame. For instance in a glass tube 120 cm long and 3 cm diameter a flame of 5·4 per cent propane/air mixture is extinguished by less than 0·200 g of potassium oxalate at a point where the velocity reaches 150 m/s.

The influence of the particle size of the quenching material has been studied in the case of methane/air mixtures. The extinction was obtained in a part of the tube where the flame was vibratory (mean velocity 3 m/s). A large number of sodium and potassium salts and also metal oxides have been studied. A number of tests were carried out for average particle diameter ranging from 25 μ to 100 μ. The experiments have not only confirmed that the extinguishing power increases when particle size is reduced but also that for very small diameters (25 μ) samples which were poor extinguishers become good ones. The minimum quantity necessary to extinguish the flame varies little for all the salts studied. In particular, sodium salts with a very small particle size become as good extinguishers as the corresponding potassium salts.

SUPPRESSION OF DETONATIONS

We have attempted with the apparatus described to suppress the explosion wave in various methane/oxygen or propane/oxygen mixtures containing various amounts of nitrogen. The extinguishing salt used was potassium oxalate of 25 μ size. It has never been possible to obtain the result desired.

However, using mixtures capable of detonating, a flame can be extinguished in the pre-detonation period (between the igniting spark and the point where the explosion wave starts)[9]. For instance, with a mixture of C_3H_8 (10 per cent)—O_2 (45 per cent)—N_2(45 per cent) with a detonation velocity of 2,100 m/s, suppression is obtained at 30 or 40 cm from the ignition end with 115–120 mg of potassium oxalate at a point where the flame velocity is approximately 400 m/s. In another case with the mixture CH_4 (20 per cent)—O_2 (40 per cent)—N_2 (40 per cent) suppression is obtained at distances of 25, 40, 45 or 50 cm from the igniting spark with quantities of potassium oxalate ranging from 0·100 to 0·365 g and for flame velocities ranging from 135 to 430 m/s at the stopping point. In one more instance with the mixture $C_4H_{10} + 6{\cdot}5\ O_2 + 13\ N_2$ whose detonation velocity is 1,650 m/s the flame was extinguished at a point where the velocity reached was 320 m/s.

It has therefore been possible to obtain the suppression of a flame propagating at relatively high velocities of a few hundred metres per second in the period of pre-detonation. In this series no quenching could be obtained if the velocity was higher than 450 m/s. This might be due to the fact that during the progress of the flame with the velocity increasing continuously, the distance separating the shock wave from the flame front following it is progressively reduced. The case might occur where the shock wave has no longer the time to lift up the cloud of dust before the passage of the flame. For the same reason it appears impossible to extinguish a detonation since the flame front is in that case immediately behind the shock wave front. If this hypothesis is correct it is reasonable to suppose that an explosion wave can be suppressed provided that the cloud is raised before the passage of the explosive phenomenon. Bearing this point in mind an experimental device was set up in which the gaseous mixture likely to detonate was contained in a vertical glass tube of 16·4 mm diameter and 1·40 m long, the mixture being at atmospheric pressure and at ambient temperature. At two-thirds of its length (measured from the lower end) a convenient device allows the dropping of a known quantity of dust. A cloud is thus formed towards which travels the explosion wave ignited simultaneously at the bottom end. The propagation of the explosive phenomenon is recorded chronophotographically on the rotating drum of a film recorder. In this way the velocity of the wave after propagating through the cloud can be determined together with the precise distance where the quenching occurs.

With this device we have always been able to obtain the suppression of detonations in all the mixtures studied. Suppression has been obtained with various materials whatever the wave velocity, provided the substance was in sufficient quantity, though this remained in all cases relatively small. When extinction occurs this is always obtained after the wave progresses through the cloud by a few centimetres only. If the quantity of powder is below the minimum then the detonation can be observed to propagate either at a reduced velocity or even to become a deflagration.

After obtaining the suppression of detonation with fine powders we have studied more particularly a number of factors related in some cases to the extinguishing material and in others to the detonating mixtures.

As far as the extinguishing material is concerned we have studied the influence of the surface area of the particles in two cases, namely those of vitreous silica and potassium chloride. The detonating mixture chosen was $CH_4 + 2\ O_2 + N_2$ for which the wave velocity is 1,850 m/s. The average particle size of the extinguishing material was after reducing, determined by a Roller type air elutriator, the surface area being measured by the Rigden air permeability method[10]. Table 1 shows the results obtained.

TABLE 1

Material	*Average particle diameter* μ	*Specific surface area* cm²	*Extinguishing quantity* g	cm²
Silica	5–10	7,800	0·440	3,420
	10–20	3,950	0·825	3,260
Potassium chloride	5–10	5,400	1·180	6,380
	10–20	2,790	2·150	600

It would appear from these results that, within the limits imposed by the precision of experiments, for the particle size used, the minimum quantity of material producing extinction is inversely proportional to the surface area of the particles.

However, this conclusion cannot be taken as general; it has not been verified in the case of salts of organic acids (such as potassium bitartrate)

for which melting and decomposition occur at relatively low temperatures.

The comparable effectiveness of different materials of same particle size (10–20 μ) has been studied in respect of the same mixture, namely $CH_4 + 2\,O_2 + N_2$. Table 2 summarizes the results obtained and shows for each case the minimum quantity of material used (by weight and surface area) to produce the extinction of the explosion wave.

TABLE 2

Material	*Surface area* cm²/g	*Weight* g	*Surface* cm²
Silica	3,950	0·825	3,260
Potassium chloride	2,790	2·150	6,000
Potassium bicarbonate	4,150	0·835	3,470
Potassium oxalate	5,220	0·920	4,800
Potassium bitartrate	7,650	0·460	3,520
Sodium bitartrate	7,400	0·930	6,900

These results show that in the case of detonation the order of increasing effectiveness is entirely different from that of deflagrations. For instance, silica which is a poor and even bad extinguishing agent of deflagrations becomes a good extinguisher of detonations. Its effectiveness is as good as, if not better than, that of potassium bicarbonate and practically the same as that of potassium oxalate which for the same particle size is a far better extinguisher of deflagrations.

In order to study the influence of the nature and composition of the detonating mixture we have used potassium bitartrate (particle size 10–20 μ) for which the particles are well defined and do not stick together to form aggregates. Its extinguishing power has been studied on the explosion wave of different mixtures of hydrogen, methane, propane, *iso*butane, acetylene, and diethyl ether.

Tables 3 to 8 show the results obtained. In each case mixture composition, velocity v of the explosion wave together with the minimum quantity (in weight and in surface area) of potassium bitartrate for the suppression of the detonation wave, are given.

TABLE 3

H_2—O_2 Mixtures

Mixture composition	$H_2 + 2\,O_2$	$H_2 + O_2$	$2\,H_2 + O_2$	$4\,H_2 + O_2$
Extinguishing quantity g	0·970	1·280	1·370	0·415
Extinguishing quantity cm²	7,400	9,800	10,300	3,180
Velocity m/s[11]	1,927	2,328	2,821	3,268

TABLE 4

CH_4—O_2 Mixtures

CH_4 per cent	20	25	33·3	40	45
Extinguishing quantity g	0·900	1·050	1·415	1·340	·390
Extinguishing quantity cm²	6,900	8,000	11,100	10,250	2,980
Velocity m/s[12]	1,980	2,145	2,322	2,465	2,510

TABLE 5

C_3H_8—O_2 Mixtures

C_3H_8 per cent	10	16·6	22·2	31	34
Extinguishing quantity g	0·750	1·330	0·750	0·310	0·240
Extinguishing quantity cm²	5,750	10,150	5,750	2,370	1,685
Velocity m/s[13]	2,059	2,336	2,500	2,648	2,537

TABLE 6

IsoC_4H_{10}—O_2 Mixtures

C_4H_{10} per cent	8	10	13·3	18·2	25
Extinguishing quantity g	1·180	1·340	1·280	0·970	0·425
Extinguishing quantity cm²	9,000	10,250	9,800	7,400	3,250
Velocity m/s[13]	2,095	2,180	2,324	2,552	2,570

TABLE 7

C_2H_2—O_2 Mixtures

C_2H_2 per cent	9·1	28·3	50	66·6	75
Extinguishing quantity g	0·560	1·680	1·060	0·610	0·390
Extinguishing quantity cm²	4,290	12,850	8,050	4,660	3,000
Velocity m/s[13]	1,850	2,482	2,960	2,300	2,117

TABLE 8

$(C_2H_5)_2O$—O_2 Mixtures

$(C_2H_5)_2O$ per cent	6	9·1	14·3	20	26	30
Extinguishing quantity g	0·630	0·805	1·140	0·910	0·670	0·540
Extinguishing quantity cm²	4,810	6,150	8,720	6,960	5,130	4,130
Velocity m/s[13]	1,950	2,140	2,400	2,542	2,555	2,400

As has been already said it appears that, for all the mixtures studied, the suppression of a detonation has been obtained whatever the wave velocity (ranging in our experiments from 1,850 to 3,270 m/s).

The minimum quantities of potassium bitartrate vary in fairly large proportions with the nature and composition of the detonating mixture. The quantities although small are, however, larger than those used in deflagrations; but it must be borne in mind that the experimental device is not the same in the two cases and comparison may not be entirely justified.

Figures 1 to *6* show the minimum quantities of

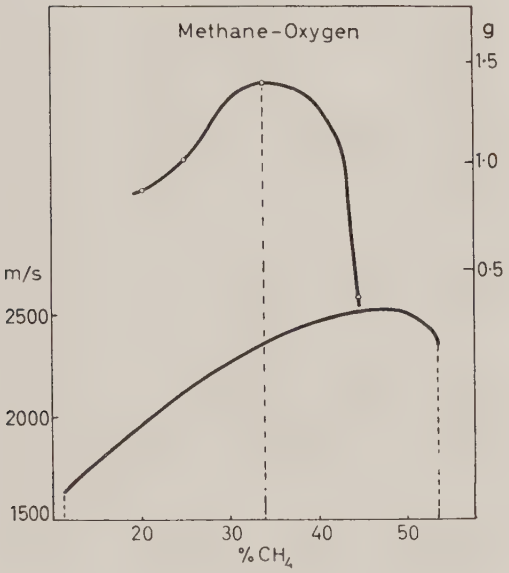

Figure 1

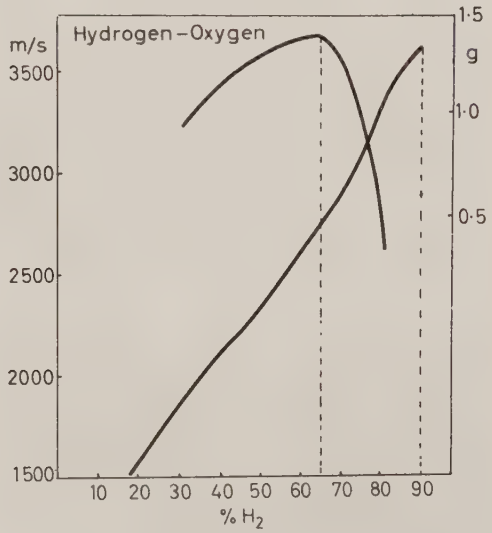

Figure 2

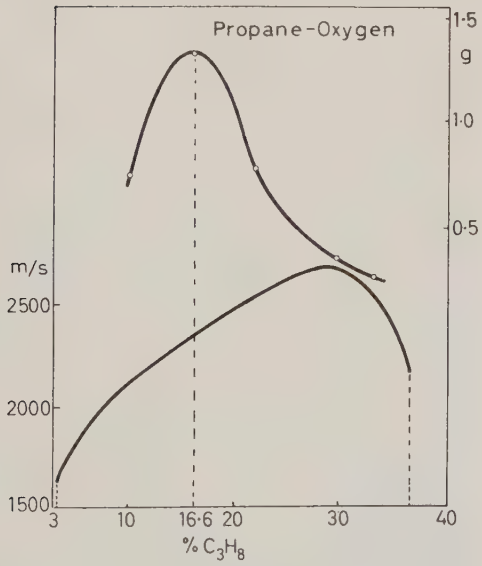

Figure 3

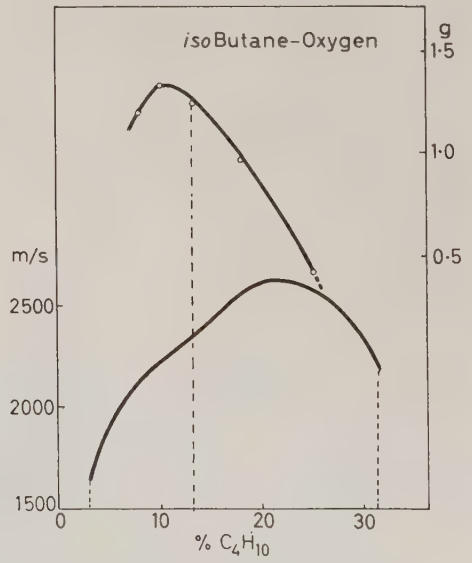

Figure 4

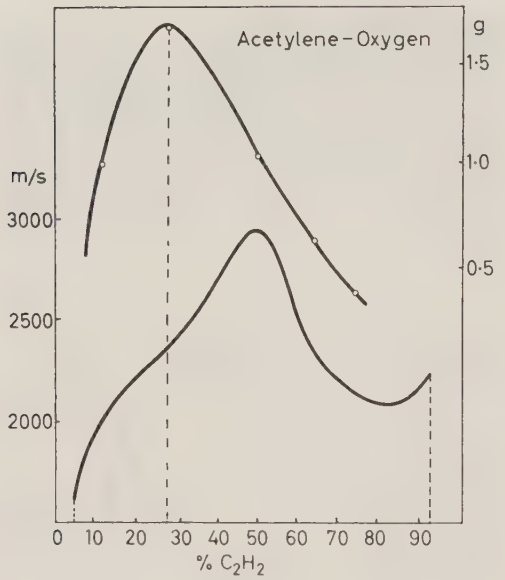

Figure 5

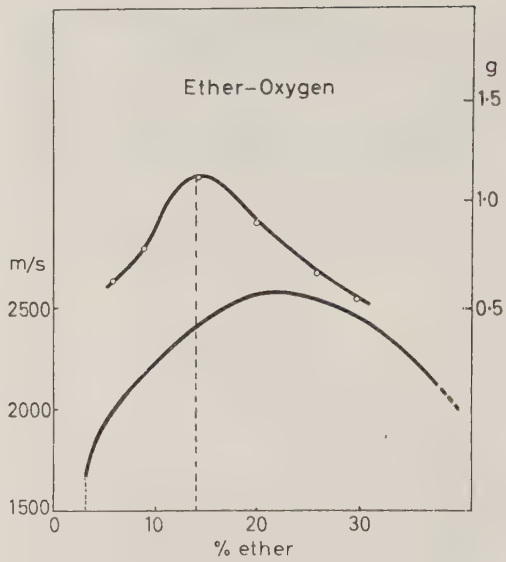

Figure 6

potassium bitartrate leading to extinction as a function of mixture composition, together with the wave velocity curves. It appears that it is the stoichiometric composition leading to complete combustion that requires the larger amount of extinguishing substance. Mixtures of *iso*butane and oxygen show a slight shift towards rich mixtures. In all cases mixtures close to the detonation limits are the more easily extinguished. In the case of hydrogen–oxygen mixtures, those close to the upper limit of detonation call for relatively small quantities of extinguishing substance. It so happens that these mixtures have the highest wave velocity (3,268 m/s). In any case the maximum wave velocity always occurs for mixtures richer than stoichiometric even in the case of acetylene–oxygen mixtures where the maximum velocity is followed by a minimum. This is due to the fact that in the case of mixtures relatively poor in oxygen the dissociation reaction of acetylene progressively overlaps the combustion reaction. This dissociation also propagates as a detonation.

In the case of hydrogen–oxygen mixtures no maximum appears in the detonation velocities. The curve rises regularly as hydrogen concentration increases. The minimum quantity curve and the detonation velocity as a function of mixture composition are therefore not parallel. The same remark can be made in the other cases where the two curves show a maximum without, however, corresponding. The curves showing the minimum extinguishing quantities can also be usefully compared to the curve of the temperature on the detonation wave front.

In conclusion it appears that the extinguishing properties of potassium bitartrate in respect of detonations are not directly related to the wave velocity nor to the temperature of the wave front.

Investigations at present in progress concern the relation between the extinguishing properties and the thermal energy developed by the detonation of gaseous mixtures. Other experiments are also needed under conditions where the dust suspension can be considered homogeneous and of known distribution and density.

REFERENCES

[1] Dautriche, *C.R. Acad. Sci., Paris* 146 (1908) 535

[2] Van der Deussen, A. *Rec. Trav. chim. Pays-Bas* 54 (1935) 873

[3] Matla, W. P. M. *Rec. Trav. chim. Pays-Bas* 55 (1936) 182

[4] Dufraisse, C. and German, M. *C.R. Acad. Sci., Paris* 207 (1938) 1221

[5] — Le Bras, J. and German, M. *C.R. Acad. Sci., Paris* 236 (1953) 164

[6] Dolan, J. E. and Dempster, P. B. *J. appl. Chem.* 5 (1955) 510

[7] — *Sixth Symposium (International) on Combustion*, p. 787. 1957. New York; Reinhold

[8] Bouchet, R., Delbourgo, R. and Laffitte, P. *C.R. Acad. Sci., Paris* 242 (1956) 2152

[9] — — — *C.R. Acad. Sci., Paris* 244 (1957) 606

[10] Tranchant, J. *Mémor. Serv. chim. État.* 30 (1948) 155

[11] Dixon, H. B. *Phil. Trans.* 184 (1893) 97

[12] Payman, W. and Walls, N. S. *J. chem. Soc.* 123 (1923) 420

[13] Breton, J. *Thesis.* 1936. Nancy: *Ann. Off. Comb. liq.* 11 (1936) 487

72

EVAPORATION AND COMBUSTION OF A DROP CONTACTING WITH A HOT SURFACE

Z. TAMURA and Y. TANASAWA

INTRODUCTION

The first aim of the present paper is to clarify the behaviour of impinged fuel drops on the flame tubes of ordinary turbo-jet engines, and the vaporizing action of the fuel poured into the *U* shaped vaporizing burner such as made by the Armstrong Siddeley Motors Ltd.

The second aim is to find the optimum operating condition of the so-called 'Meurer's process' in diesel engines, in which the fuel is injected into the combustion chamber in the form of a high-speed liquid column rather than in the form of a spray, in order to obtain more extensive spreading of the film on the combustion chamber wall to facilitate very rapid vaporization of the fuel.

APPARATUS AND PROCEDURE

In *Figure 1*, a concave fused quartz plate 7 placed on a flat quartz plate 6 is heated by the hot air in the aluminium oxide cylinder, which is also heated with silicone carbide heating elements 4.

The concavity of the hot surface prevents the vaporizing drop splashing out of the field of view of the camera.

The surface temperature of the fused quartz plate 7 can be measured with a Pt/Pt–Rh thermocouple of diameter 0·06 mm, embedded in a slit etched by hydrogen fluoride solution on the surface. The surrounding air temperature above the hot quartz plate 7 is measured with several fine Ni·Cr alloy thermocouples 10, 11, and 12.

A fuel drop 21 is suspended from a fine special steel wire 20, and is dropped to the hot surface of 7 by a shock, which is produced when the supporter 18 of the wire 20 is moved to the right on a bed and a projection 19 drops over the end of the bed.

To obtain the drops of the diameters required, the fuel is either fed from fine hypodermic tubes or nickel rings.

A film of fuel is artificially formed on the nickel ring, and is transmitted to the tip of the steel wire 20.

Large drops can also be fed directly on to the hot surface from fine hypodermic tubes; the drops falling from these tubes are not accompanied by any satellite drop under a certain value of the outer diameter[2].

The modes of evaporation, vaporization, and combustion of drops are photographed using a single filament lamp 1, condenser lenses 2, a prism 15, a telephoto-lens 16, and a standard 16 mm ciné-camera 17, with varying speeds from single-shot to 64 frames per sec.

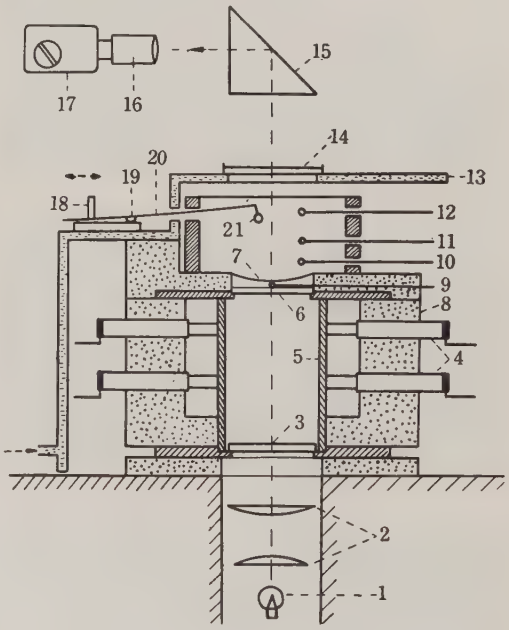

Figure 1. Experimental apparatus

The optical system is protected from heating by both the water jacket 13 and the fused quartz plates 3 and 14.

The determination of the surface temperature of the hot surface is very important, and the use of fused quartz is not suitable since its thermal conductivity λ is rather low, say $\lambda \cong 1$ kcal/m-h-°C, which causes the sudden drop of the surface temperature θ_s when the drop makes contact with the surface.

Therefore, instead of the fused quartz plate, a massive stainless steel cylinder of diameter 160 mm and of height 100 mm with a concave surface is used to get more accurate and quantitative results.

In these cases, photographs are taken by reflected light.

Comparing the results obtained with the fused quartz plate (which is now only used for photographic purposes) and the stainless steel cylinder, the equivalent surface temperatures θ_s of the fused quartz plate is determined.

The surrounding air temperature θ_a above the hot surface, which has proved to have a great

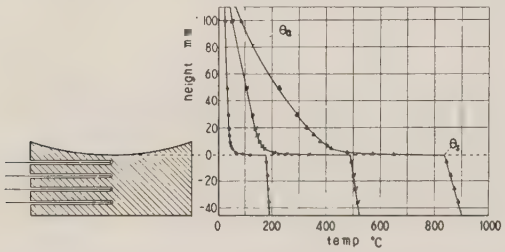

Figure 2. Temperature distribution in and above the cylinder

influence on the ignition point of the fuel drop, is measured in detail as shown in *Figure 2* and correlated with the surface temperature θ_s.

The surface temperature θ_s is determined by averaging the temperatures measured at several points in the stainless steel block.

RESULTS FOR A TYPICAL PURE FUEL

Figure 3 shows a typical life curve obtained with benzene C_6H_6.

In the figure, the time t required from the beginning of contact of a drop with the hot surface to the complete extinction of the drop is plotted against the surface temperature θ_s of the hot surface.

When θ_s is below the boiling point of the liquid, the drop rests on the surface in the shape of a lens and gradually evaporates as shown by the curve *a–b*.

If the surface temperature reaches the boiling point of the liquid, a vapour bubble arises at the central part of the drop, and vaporization occurs. A slight increase in gradient appears in the life curve and the time decreases as θ_s increases, as shown by the curve *b–c*.

But when θ_s is superheated above the boiling point as much as 40–50°C, the lens-shaped drop flattens into a film and a sudden and violent vaporization occurs everywhere in the film. Thus the drop disappears at a high rate as shown by the minimum point *c*.

This surface temperature obviously corresponds to the so-called 'maximum boiling rate point' found by Nukiyama[3].

Above the maximum boiling rate point *c*, the flattened drop splits into several main and satellite drops and dances to and fro, and up and down on the hot surface lengthening the life until the so-called 'Leidenfrost point *d*' is reached, where the evaporation in one spheroidal form on a thin seat of vapour occurs.

The transition from the maximum boiling rate point to the Leidenfrost point is very unstable.

In the spheroidal state, the evaporation takes place rather slowly and the lives of drops become long, though they may decrease with the increasing surface temperature as shown by the curve *d–e*.

If the temperature and the concentration of the mixture of fuel vapour and air reach a sufficient value, the ignition initiates between the hot surface and the floating drop, but the spheroidal state is maintained nevertheless.

A slight decrease of the life is observed after the ignition as shown by the curve *e′–f′*.

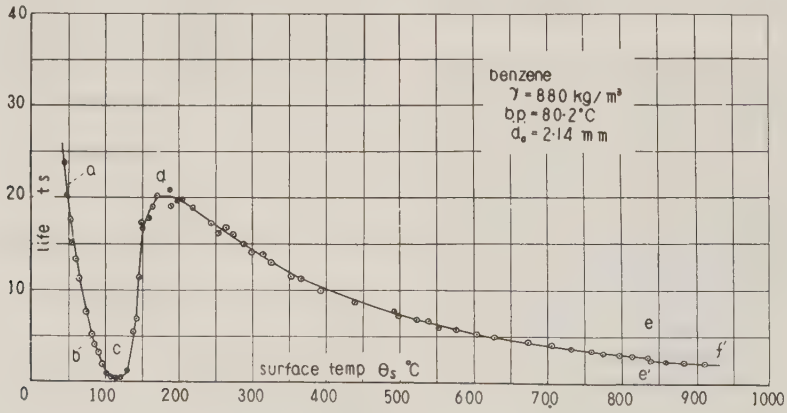

Figure 3. A typical curve for benzene

Figure 4 shows typical photographs of the benzene drop at every stage. The time t measured from the instant when the drop touches the hot surface corresponds to the middle frame of the photograms, and Δt denotes the time interval of each frame.

Figure 4a indicates the evaporation stage (*a–b*

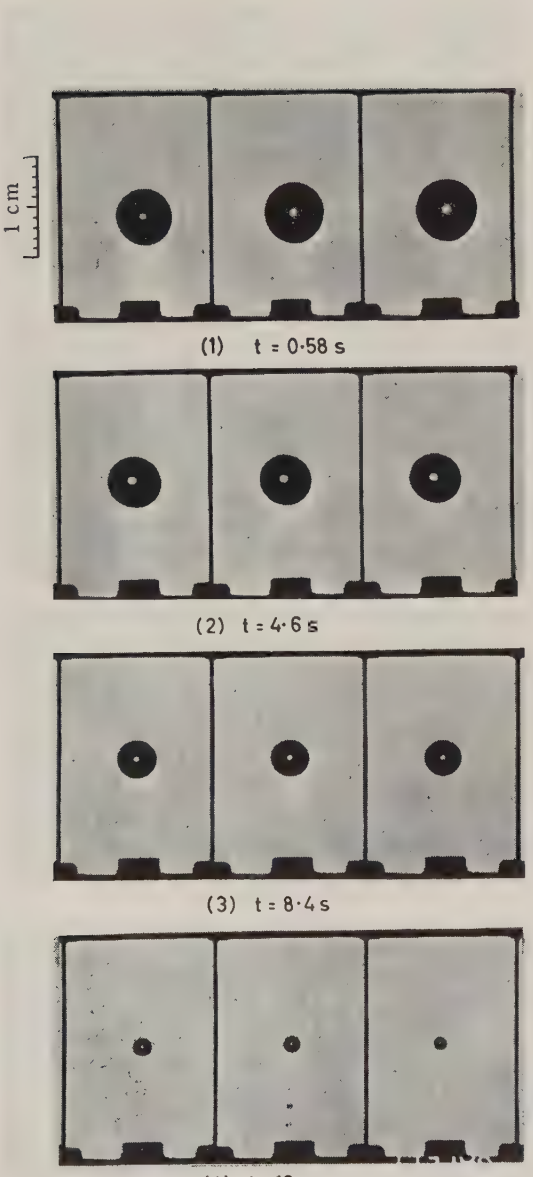

Figure 4a. Evaporation of a lens-shaped benzene drop

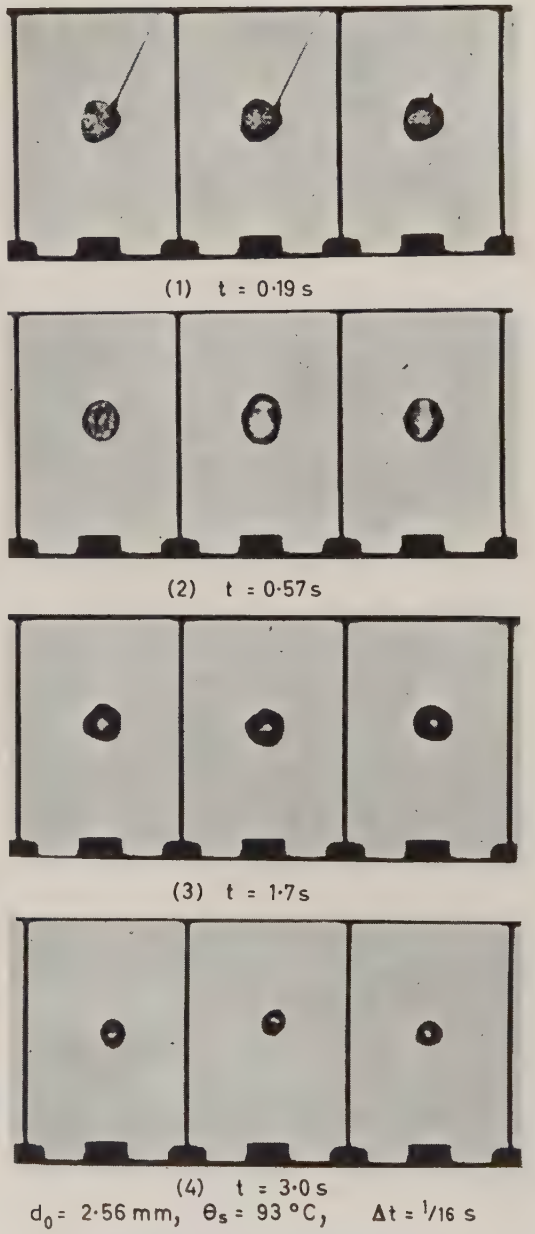

Figure 4b. Vaporization of a benzene drop near its boiling point

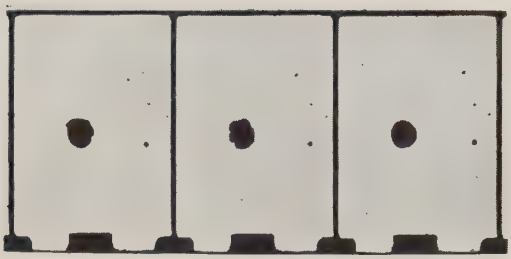

(1) t = 0·30 s

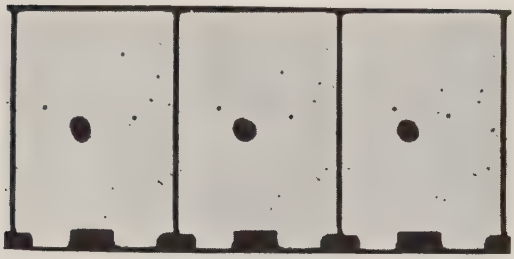

(2) t = 0·44 s

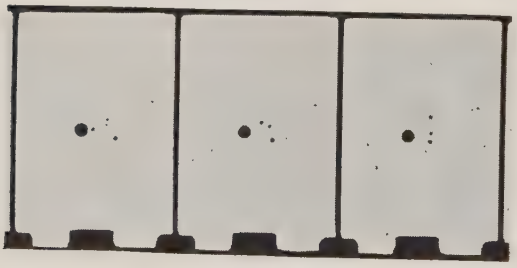

(3) t = 0·80 s

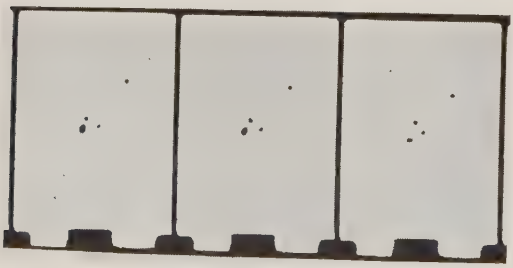

(4) t = 0·94 s

d_0 = 2·56 mm, θ_s = 115 °C, Δt = 1/64 s

Figure 4c. Vaporization of a benzene drop near its maximum boiling rate point

(1) t = 0·25 s

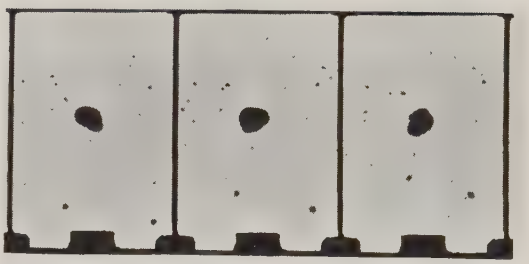

(2) t = 0·47 s

(3) t = 0·66 s

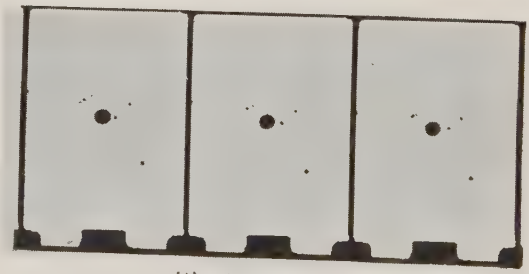

(4) t = 0·97 s

d_0 = 2·56 mm, θ_s = 128 °C, Δt = 1/64 s

Figure 4d. A benzene drop at its transition stage

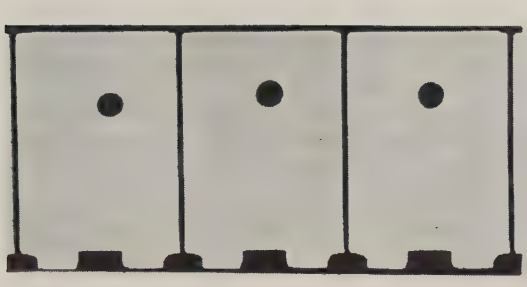

(1) t = 0·50 s

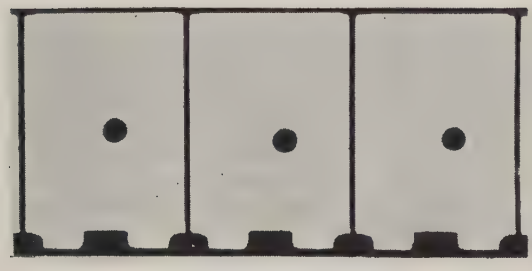

(2) t = 1·4 s

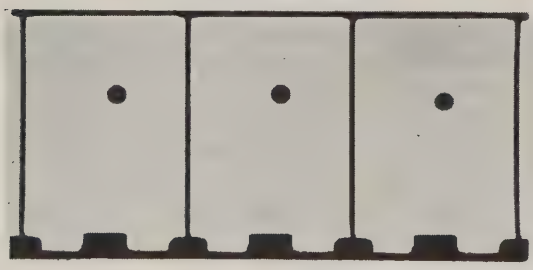

(3) t = 3·0 s

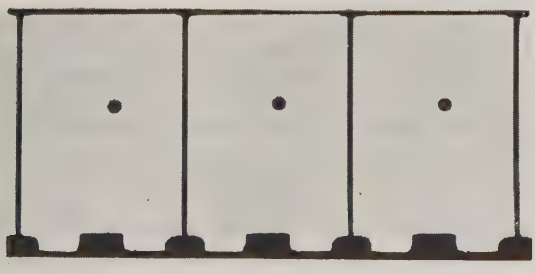

(4) t = 4·8 s
d_0 = 2·56 mm, Θ_s = 550 °C, Δt = 1/16 s

Figure 4e. A benzene drop at its spheroidal evaporation stage

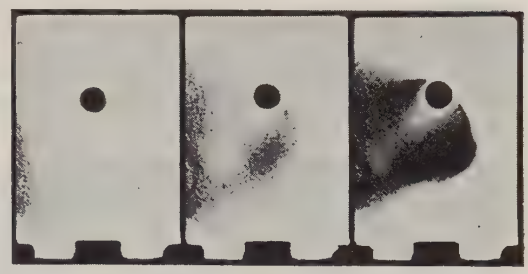

(1) t = 0·44 s

(2) t = 0·69 s

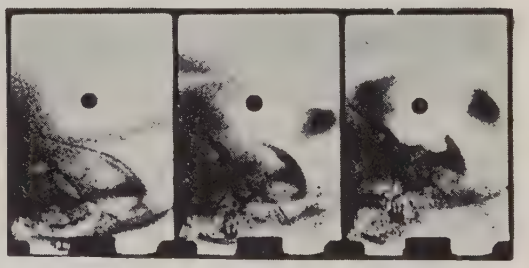

(3) t = 2·8 s

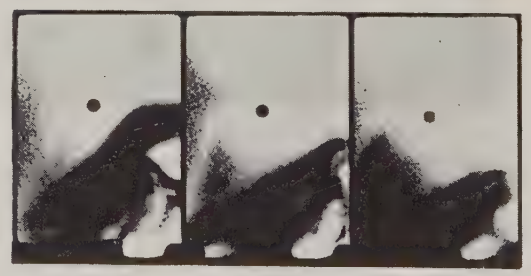

(4) t = 3·5 s
d_0 = 2·56 mm, Θ_s = 850 °C, Δt = 1/16 s

Figure 4f. A benzene drop at its spheroidal combustion stage

in *Figure 3*) and *Figure 4b* shows the vaporization at the boiling point (*b* in *Figure 3*). A vapour bubble is seen at the centre of the lens-shaped drop.

Figure 4c shows the state of violent vaporization near the maximum boiling rate point (*c* in *Figure 3*).

The lens-shaped drop flattens into a thin film, and the nucleate boiling starts at several points of the contacting surface.

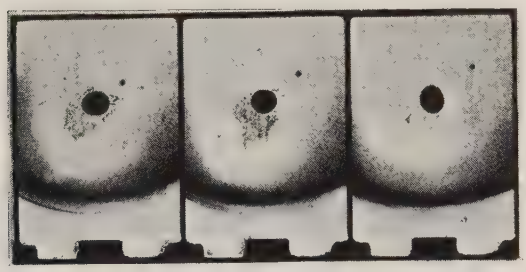

(1) t = 0·22 s

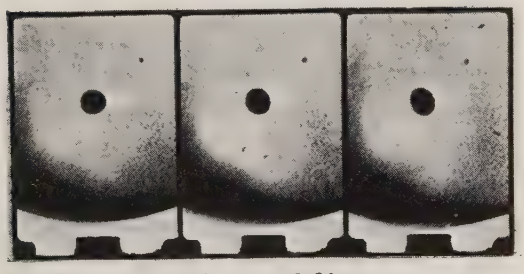

(2) t = 0·31 s

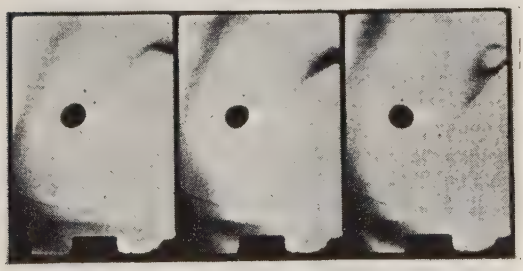

(3) t = 0·44 s

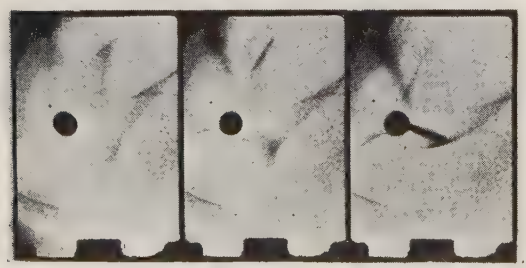

(4) t = 0·56 s

d_0 = 2·56 mm, Θ_s = 850 °C, Δt = 1/64 s

Figure 4g. Ignition has started from the surrounding mixture of a benzene drop

Figure 4d shows the transition stage from the maximum boiling rate point to the Leidenfrost point (*c–d* in *Figure 3*). The flattened film splits into several main and satellite drops which are made to dance about by the periodic generation of vapour between the drops and the hot surface.

Figure 4e shows the spheroidal evaporation stage (*d–e* in *Figure 3*).

If we plot the value of the square of the diameter d^2 of the drop against the time t, a nearly linear relation will be observed as shown in *Figure 5*.

That is

$$-d(d^2)/dt = \text{const} \tag{1}$$

Or if we put the constant as C_e and call it the constant of the evaporation velocity, we can write

$$d^2 = d_1^2 - C_e t \tag{2}$$

where d_1 indicates the initial diameter of the drop just before the spheroidal evaporation begins.

From equations 1 and 2, we can conclude that the spheroidal evaporation of a drop obeys the same law, as a drop suspended in a hot gas with a fine fused silica filament also does.

Figure 4f shows the spheroidal combustion stage (*e′–f′* in *Figure 3*).

A spheroidal drop surrounded with a flame, just like the candle flame, vibrates vertically with the periodic generation of the vapour.

The plot of the values of the square of the diameter d^2 of the drop against the time t also gives a straight line as shown in *Figure 6*, from which we can deduce the relation

$$-d(d^2)/dt = \text{const} = C_b \tag{3}$$

or

$$d^2 = d_2^2 - C_b t \tag{4}$$

where d_2 denotes the initial diameter of the drop just after the ignition and C_b the constant of the combustion velocity.

Figure 4g shows the flame front just after the ignition has taken place.

In *Figure 7*, typical modes of evaporation, vaporization and combustion of a volatile liquid drop touching a hot surface are given schematically.

RESULTS FOR VARIOUS PURE FUELS

From *Figures 8–11* the life curves for various reference fuels for gasoline and diesel engines such as normal heptane, *iso*octane, normal cetane and α-methyl-naphthalene are given.

To know the effect of the initial diameter d_0 of the drop on the life-time, drops of various diameters are dropped from the height $z \simeq 20$ mm.

The ethyl alcohol which does not belong to the petroleum series is also tested as shown in *Figure 12*. Its life-time curve shows a similarity to that of the gasoline.

As a reference, the life-time curve of water is

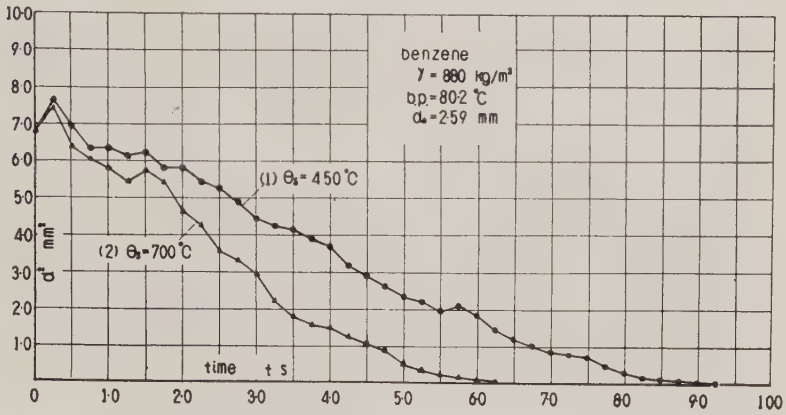

Figure 5. A linear relation exists between d^2 and t during the spheroidal evaporation

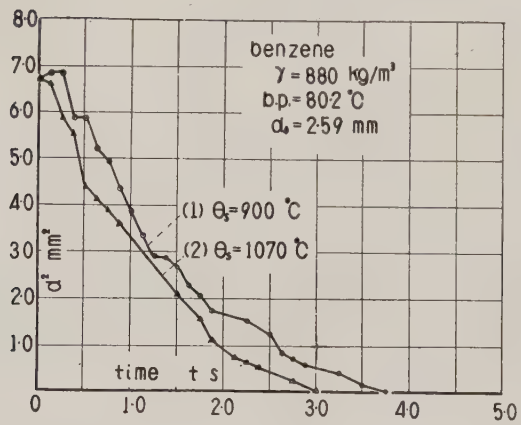

Figure 6. A linear relation also exists between d^2 and t during the spheroidal combustion

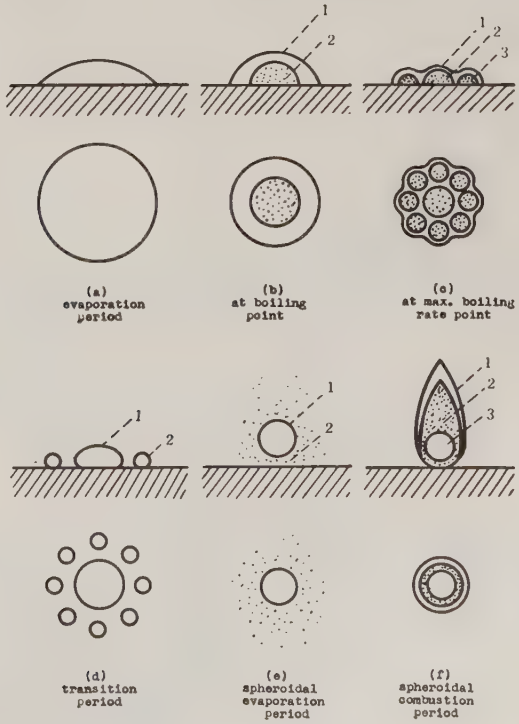
(a) evaporation period
(b) at boiling point
(c) at max. boiling rate point
(d) transition period
(e) spheroidal evaporation period
(f) spheroidal combustion period

Figure 7. Sketch of the form of drop at various stages for a volatile fuel

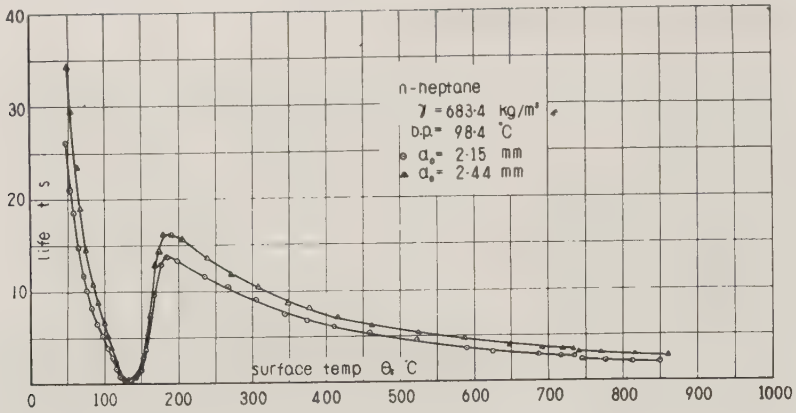

Figure 8. Life curves for normal heptane

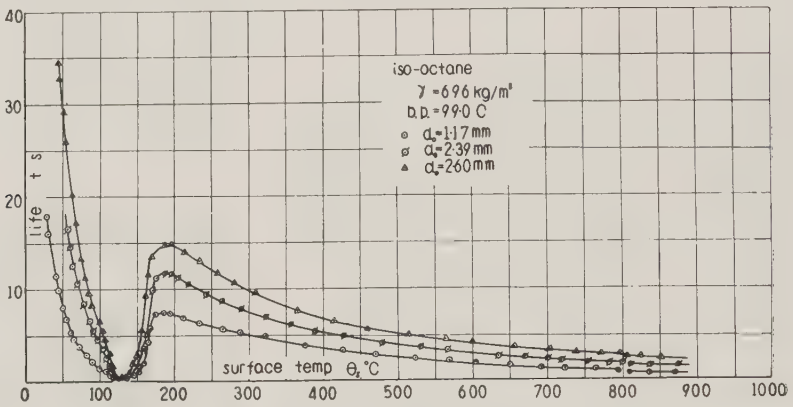

Figure 9. Life curves for isooctane

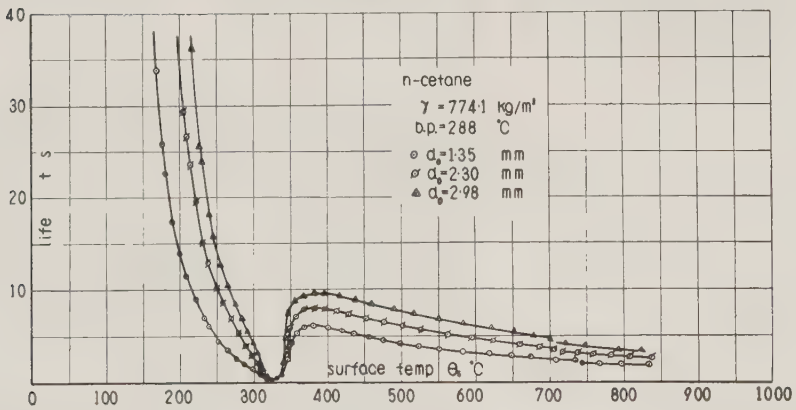

Figure 10. Life curves for normal cetane

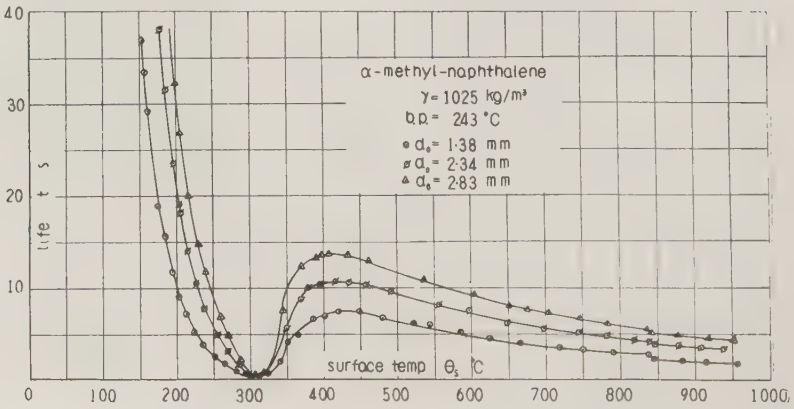

Figure 11. Life curves for α-methyl-naphthalene

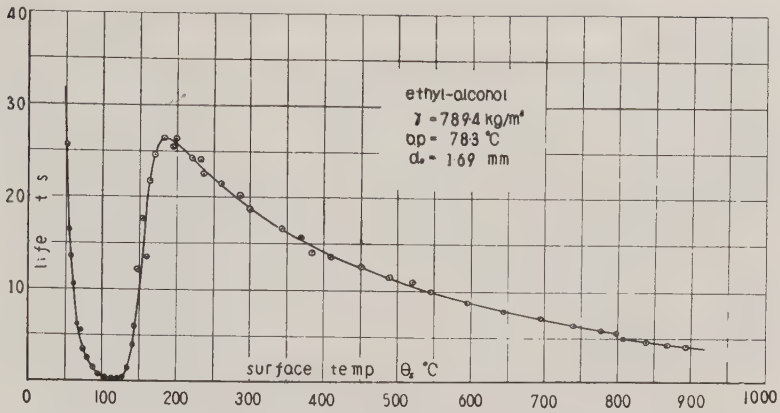

Figure 12. Life curve for ethyl alcohol

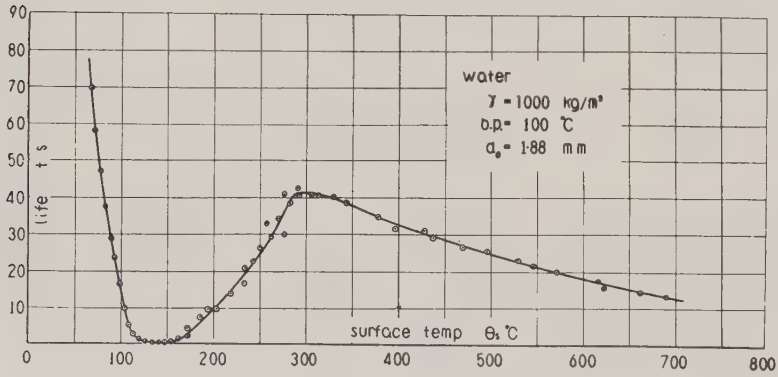

Figure 13. Life curve for water

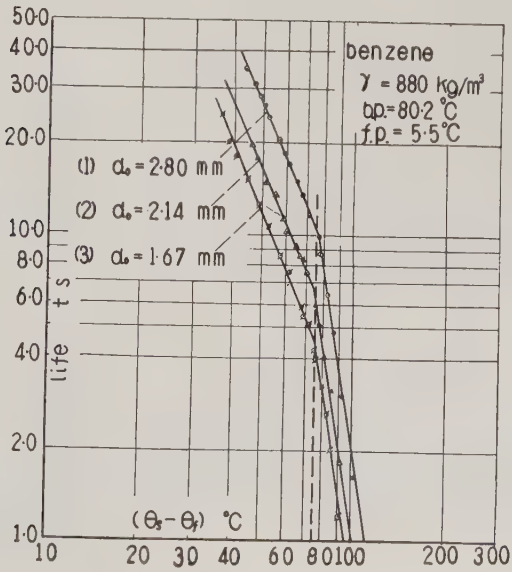

Figure 14. Effect of the diameter on the evaporation and the vaporization time of lens-shaped drops

obtained as shown in *Figure 13*. It has no ignition point of course.

In *Figure 14*, the effects of the initial diameter d_0 on the evaporation and vaporization of the lens-shaped drops are examined from logarithmic plots.

From these graphs, we can express the life-time t for benzene as

$$t = k_b d_0^{1.5}\{(\theta_b - \theta_f)/(\theta_s - \theta_f)\}^m = 2{\cdot}1 d_0^{1.5}\{(\theta_b - \theta_f)/(\theta_s - \theta_f)\}^{2{\cdot}3} \quad (5)$$

for the range of evaporation, and

$$t = k_m d_0^{1.5}\{(\theta_m - \theta_f)/(\theta_s - \theta_f)\}^n = 0{\cdot}13 d_0^{1.5}\{(\theta_m - \theta_f)/(\theta_s - \theta_f)\}^{6{\cdot}9} \quad (6)$$

for the range from the boiling point to the maximum boiling rate point.

In the above expression, k_b and k_m denote the life-time at the boiling point and the maximum boiling rate point respectively for a drop of 1 mm in diameter, and θ_f°C the freezing point of the fuel.

The maximum boiling rate point θ_m°C is generally obtained by the relation

$$\theta_m = \theta_b + (30 \sim 70) \quad (7)$$

for the ordinary non-viscous liquid, the boiling point of which is θ_b°C.

For the unstable transition stage, which lies between the maximum boiling rate point and the Leidenfrost point, we cannot deduce any definite relation. Volatile liquids such as water, alcohol, benzene, heptane, and octane, split violently into several drops marking a wide and definite range of transition, while less volatile liquids, such as cetane and α-methyl-naphthalene, do not separate, showing a very narrow transition range.

For the spheroidal evaporation stage, we can express the evaporation characteristics by the value of the constant for the evaporation velocity C_e. The values of C_e in the case of drops contacting with hot surfaces become rather large compared with those obtained from the suspended drops as shown in Table 1.

For the spheroidal combustion stage, the combustion characteristics can be expressed by the constant of the combustion velocity C_b. The values of C_b for drops contacting with hot surfaces also shows larger values compared with those of the suspended drops.

RESULTS FOR VARIOUS PRACTICAL BLENDED FUELS

In *Figure 15* and *Figure 16*, the life curves for motor gasoline and kerosine are given. These practical distillate fuels do not show the clear boiling points, but show the similar tendency obtained for the pure fuels. Therefore the relations 1 and 3 can also be applied.

The residual fuel such as the heavy oil A shows quite different characteristics as shown in *Figure 17*. No definite maximum boiling rate point or Leidenfrost point is visible, but there are very faint indications of them.

At first, the volatile part in the fuel evaporates along curve 1 and ignites at the point *e*. But the tarry matter remains on the hot surface and it vanishes along curve 2 coinciding with curve 1 at about 1,000°C.

Even though they burn along the curve *e–f*, we can see various kinds of carbon skeletons, deposits, and ashes on the hot surface after the completion of the combustion, from which we can clearly examine the character of the residual fuels.

In *Figure 18a*, the mode of evaporation of a heavy oil drop is shown. The tarry matter spreads like a halo from the periphery of the lens-shaped volatile part, which diminishes in diameter with the time as shown from equations 1 to 3. The remaining tarry matter gradually carbonizes and evaporates very slowly as shown in equation 4.

Figure 18b shows the behaviour during combustion. The drop splashes into one main and several satellite drops, and ignites in the last frame of the photogram (1).

The honeycomb structure of the drop shown in (3) shows the bubbling of the volatile part of the fuel. The tarry matter remaining on the hot surface gradually vanishes maintaining its original shape as shown in (8).

Lubricating oil, such as the mobile oil, shows a similar tendency to that of heavy oil. The tarry matter spreads also like a halo, and ignites at rather low temperatures of 700 ∼ 800°C.

CONCLUSION

From the above results, we can make the following conclusions.

(1) The time required for vaporizing the fuel can be shortened, if the maximum boiling rate points are used (as Meurer probably intended) in preference to the ignited sprayed drops. It must be noted, however, that a narrower range of surface temperature is required together with a wider projected area of vaporization.

(2) The maximum boiling rate point must be used also for the vaporizing burners of the turbo-jet engines.

(3) No fuel condensation or quenching occurs in the flame tubes of the turbo-jet combustors when the wall temperature of the flame tubes is maintained above the Leidenfrost point.

(4) For pure fuels, there exist five stages—evaporation, vaporization, transition, spheroidal evaporation, and spheroidal combustion; and these stages are distinctly divided by the boiling points, maximum boiling rate points, Leidenfrost points, and ignition points.

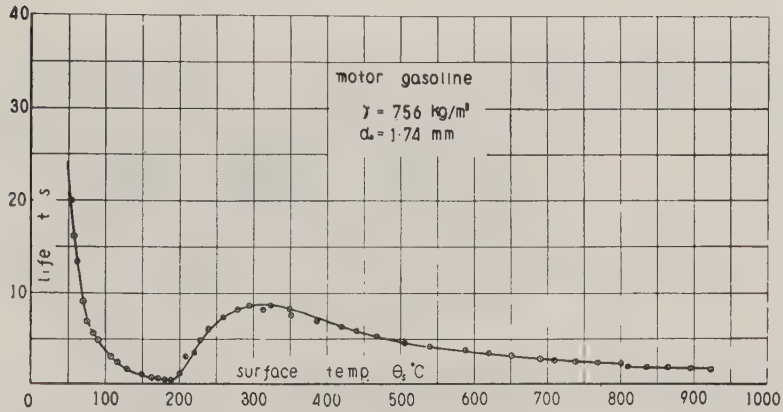

Figure 15. Life curve for motor gasoline

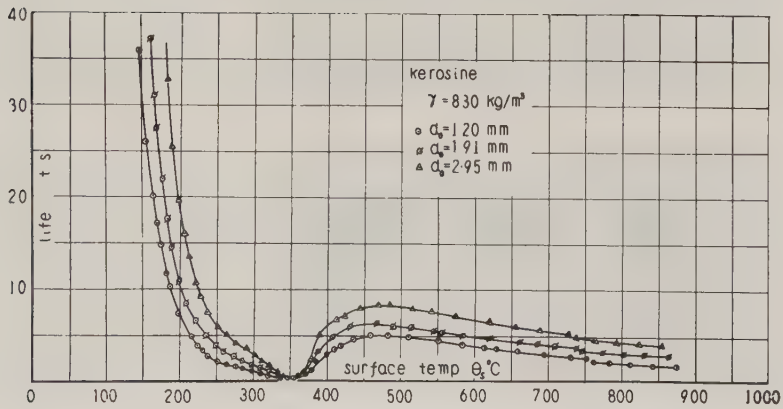

Figure 16. Life curves for kerosine

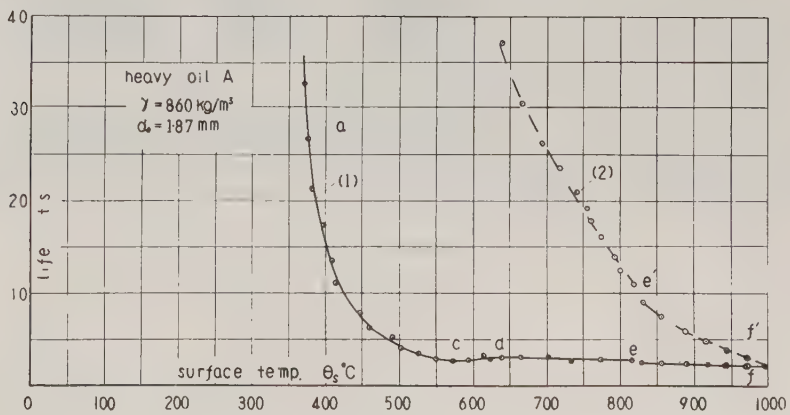

Figure 17. Life curves for heavy oil A

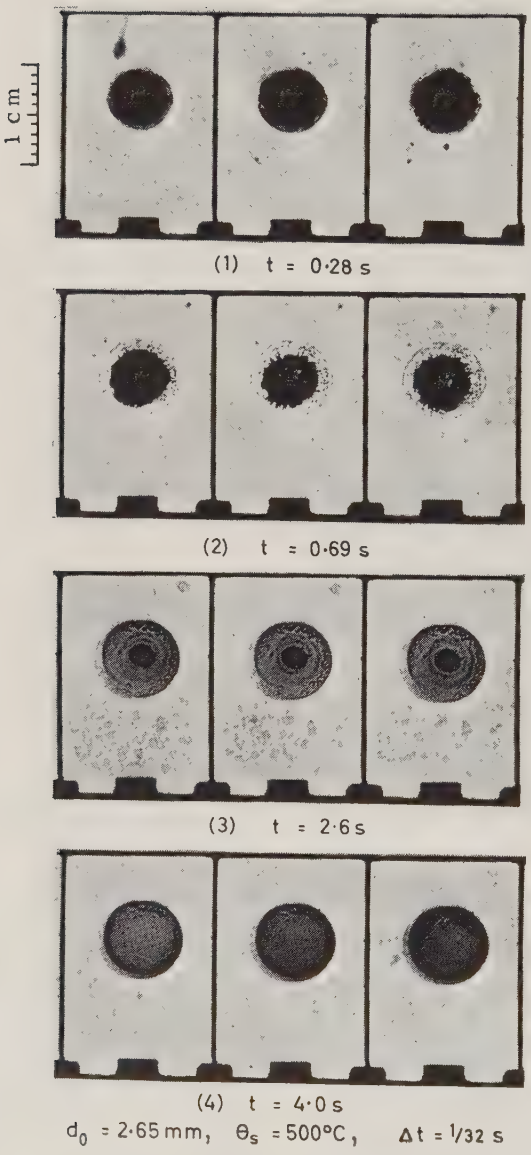

Figure 18a. Evaporation of a heavy oil drop

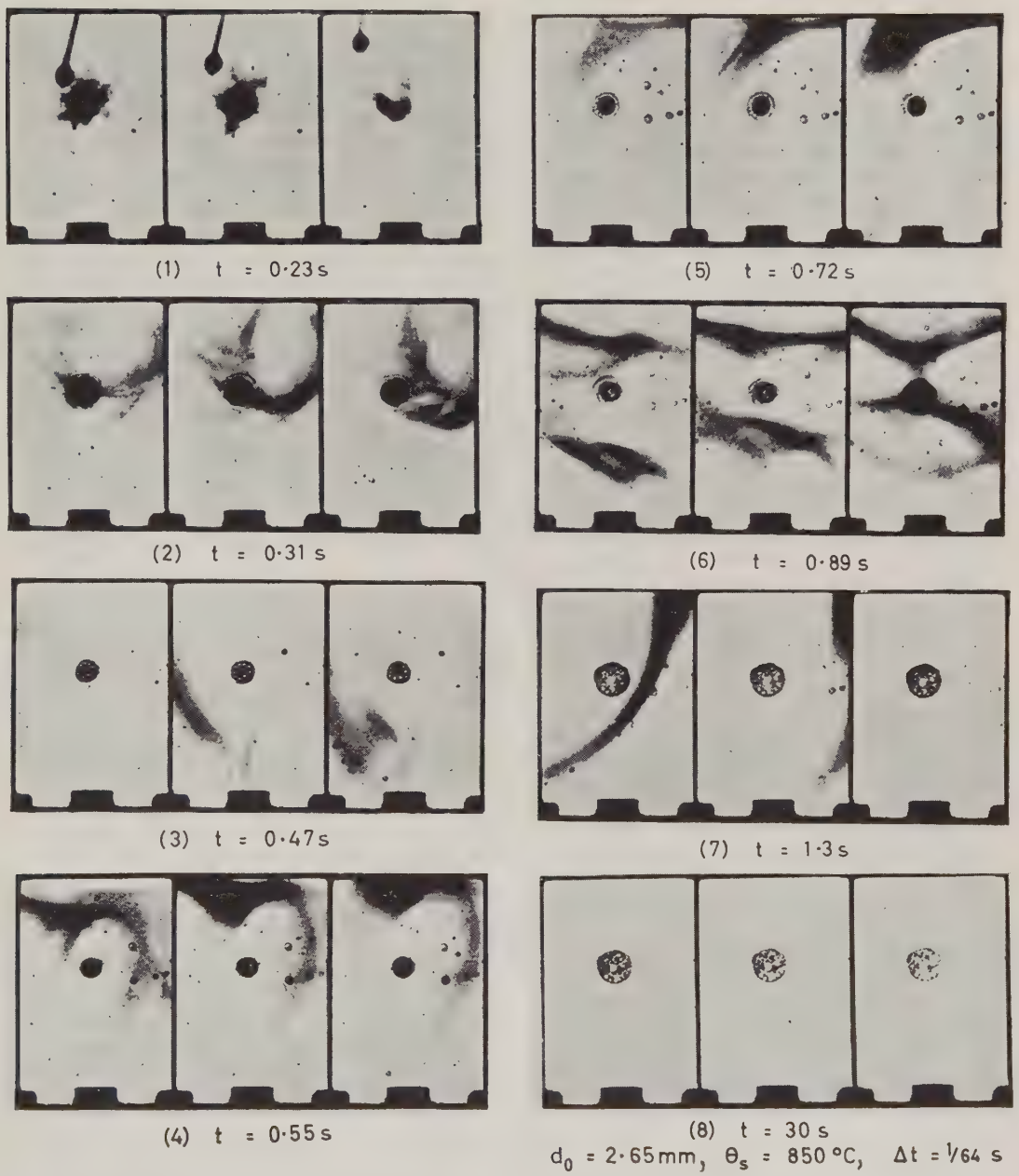

Figure 18b. Combustion of a heavy oil drop

Up to the maximum boiling rate point, the relations 5 and 6 exist. For the spheroidal evaporation and combustion, the relations 1 and 3 hold.

(5) The blended distillate fuel has no definite boiling point, but has the same tendency as the pure fuel.

(6) The residual fuels have very different characteristics, which must be examined individually. These fuels cannot be used for either Meurer's process or the vaporizing combustor.

(7) As the present experimental apparatus is very simple in construction and shows clearly the behaviour of the fuel drops in the various stages of evaporation, vaporization, ignition and combustion, it can be used for measuring these characteristics. For example, the effect of various kinds of additives may be clarified.

(8) Table 1 summarizes the characteristics of the fuels discussed in this paper.

We wish to express our heartfelt thanks to Messrs Susumu Goto, Kozi Hayakawa, Yosiyuki Yamaya and Takao Hayasi for their zealous help throughout the experiment, to Professor Takemaru Sakurai for preparing the concave fused quartz plate and to Professor Hirosi Tokuhisa for the preparation of the pure fuels. We also thank the Toyota Motor Car Company and the Ministry of Education for their financial aid.

REFERENCES

[1] Schweitzer, P. H. *Fifth Symposium (International) on Combustion*, p. 7. 1955. New York; Reinhold
[2] Tanasawa, Y. and Toyoda, S. *Technological Report of Tohoku University* 19, No. 2 (1955) 135
[3] Nukiyama, S. *J. Soc. Mech. Engrs Japan* 37, No. 206 (1934) 367

TABLE 1

Evaporation, Vaporization and Combustion Characteristics of Fuel Drops Contacting with a Hot Surface

No.	*Name of fuel*	*Chemical formula*	*Specific wt.* (20°C) r kg/m³	*Freezing point* θ_f°C	*Boiling point* θ_b°C	*Max. boiling rate point* θ_m°C	*Leidenfrost point* θ_l°C	*Ignition point* θ_i°C
1	benzene	C_6H_6	880	5·5	80·2	118	195	840
2	*n*-heptane	C_7H_{16}	683	— 90·6	98·4	134	182	738
3	*iso*octane	C_8H_{18}	696	— 108·0	99·0	132	184	800
4	*n*-cetane	$C_{16}H_{34}$	774	20·0	288·0	327	380	720
5	α-methyl-naphthalene	$C_{10}H_7 \cdot CH_3$	1,025	— 22·0	243·0	310	420	852
6	ethyl alcohol	$C_2H_5 \cdot OH$	789	— 115·0	78·3	117	185	800
7	water	H_2O	1,000	0·0	100·0	148	302	
8	gasoline		756			190	300	806
9	kerosine		830			352	470	735
10	heavy oil A		860			570	645	750

No.	$k_b s$/mm$^{1.5}$ *at* b.p.	*Index* m	$k_m s$/mm$^{1.5}$ *at* m.b.r.p.	*Index* n	*Initial diam.* d_0 mm	C_e mm²/s *at*		C_b mm²/s *at*	
						$\theta_s = 450$°C	$\theta_s = 700$°C	$\theta_s = 900$°C	$\theta_s = 1{,}070$°C
1	2·1	2·3	0·13	6·9	2·56	1·0	1·6	2·0	2·7
2	1·8	5·2	0·13	23	2·52	1·5	2·5	3·4	4·7
3	1·6	6·0	0·12	23	2·50	1·5	2·5	4·2	5·2
4	1·3	4·9	0·17	17	2·59	1·4	2·4	3·5	4·9
5	2·1	5·8	0·15	16	2·61	1·2	1·8	2·2	2·7
6	2·8	6·4	0·16	15	2·98	0·8	1·1	1·7	2·0
7	7·4	4·0	0·14	8·2	3·28	0·3	0·4		
8					2·57	1·2	1·7	3·0	3·6
9					2·58	1·4	2·4	2·9	3·3
10					2·65				

The values given are approximate. Initial temperature of fuel drops = 5–30°C.
Air temperature °C at $z = 5$ mm: $\theta_a = 165$ ($\theta_s = 450$), $\theta_a = 330$ ($\theta_s = 700$), $\theta_a = 485$ ($\theta_s = 900$), $\theta_a = 660$ ($\theta_s = 1{,}070$).

NEW ASPECTS OF DROPLET COMBUSTION

H. ISODA and S. KUMAGAI

INTRODUCTION

Single droplets have been extensively investigated in relation to combustion in gas turbines, jet engines and rocket motors, by Godsave[1], Spalding[2], Goldsmith and Penner[3,4], Okazaki and Gomi[5], Kobayashi[6], Wise, Lorell and Wood[9], Agoston, Wise and Rosser[10], Miesse[11], and the present authors[7,8]. The efforts to use the known relationships determined from the studies on stationary droplets to predict the burning characteristics of sprays have been made by Probert[12] and Tanasawa[13], but modifications may be needed because the combustion of sprays differs apparently from that of stationary single droplets in the influence of convection and in the interfering effect by adjacent droplets.

The purpose of this paper is to present some new aspects of droplet combustion. In the first place, the burning of stationary droplets accompanied with free convection and its effect on the combustion are investigated. Secondly, spherical diffusion flames of droplets in a zero-gravity field are observed. These experimental results are compared with the results of the spherical diffusion theories derived by Godsave, and Goldsmith and Penner. Some disagreements in this comparison suggest that the combustion process is in a transient state, and a further theoretical approach is presented.

COMBUSTION OF STATIONARY DROPLETS

It has been known that the burning rate of stationary droplets is proportional to the first power of the droplet diameter, namely the following relationship holds between the droplet diameter D_l and the time t: $D_{l_0}^2 - D_l^2 = kt$, where D_{l_0} is the initial droplet diameter and k is the evaporation constant. The burning rate of stationary droplets is considerably accelerated by free convection. According to our recent experiment, the values of k in the combustion without convection are about 60 per cent of those under the stationary condition.

The effect of convection appears sensitively in the flame shape, and therefore the strength of convection can be estimated from the flame shape after the treatment presented by Kumagai and Kimura[14].

Observation of the flame shape

In a quiescent atmosphere the droplet is suspended from a silica filament of about 0·11 mm in diameter and is ignited by an electric spark. A 16 mm motion picture camera is used to photograph the droplet and its flame. Fuels used in this experiment are *n*-heptane and ethyl alcohol. From the photographs, as shown in *Figure 1* for example, the dimensions of droplets and their flames are measured. Using the system of measurement shown in *Figure 2*, the dimensions of the flame boundary *versus* the droplet diameter are given in *Figures 3* and *4*. The values of a and b, from which 'flame radius' has been determined, are nearly proportional to the square root of the droplet diameter*, and the values of h are directly proportional to the droplet diameter. The lines for a and b, and for h in *Figures 3* and *4* are those proportional to $(D_l)^{\frac{1}{2}}$ and D_l, respectively.

Analysis of the flame shape

A theoretical treatment of the combustion of single droplets under free convection has been presented by Kumagai and Kimura[14,8]. Assuming that the droplet is a point source of fuel vapour and the convective current is a uniform upward flow of air, they concluded that the lower part of the flame boundary is nearly equal to the contact surface of the vapour flow and the air flow. Then, a and b are given by the expressions,

$$a = (\dot{m}/4\pi U)^{\frac{1}{2}} \tag{1}$$

$$b = (\dot{m}/2\pi U)^{\frac{1}{2}} \tag{2}$$

where $\dot{m}$ is the volume flow rate of fuel vapour, and U is the velocity of upward flow of air. The mean values of b/a observed are 1·6 and 1·3 for *n*-heptane and ethyl alcohol, respectively, which show fairly good agreement with the theoretically predicted value $(2)^{\frac{1}{2}}$.

An appropriate mean value for the gas density inside of the flame, ρ_1, being taken, we get

$$\dot{m} = \frac{\dot{m}_f}{\rho_1} = \frac{\pi\rho' k D_l}{4\rho_1} \tag{3}$$

* In Kumagai and Kimura's early work, the values of a and b were taken to be independent of D_l. This may be the result of the fact that they observed the values of a and b for larger D_l, where the variation of these values is small.

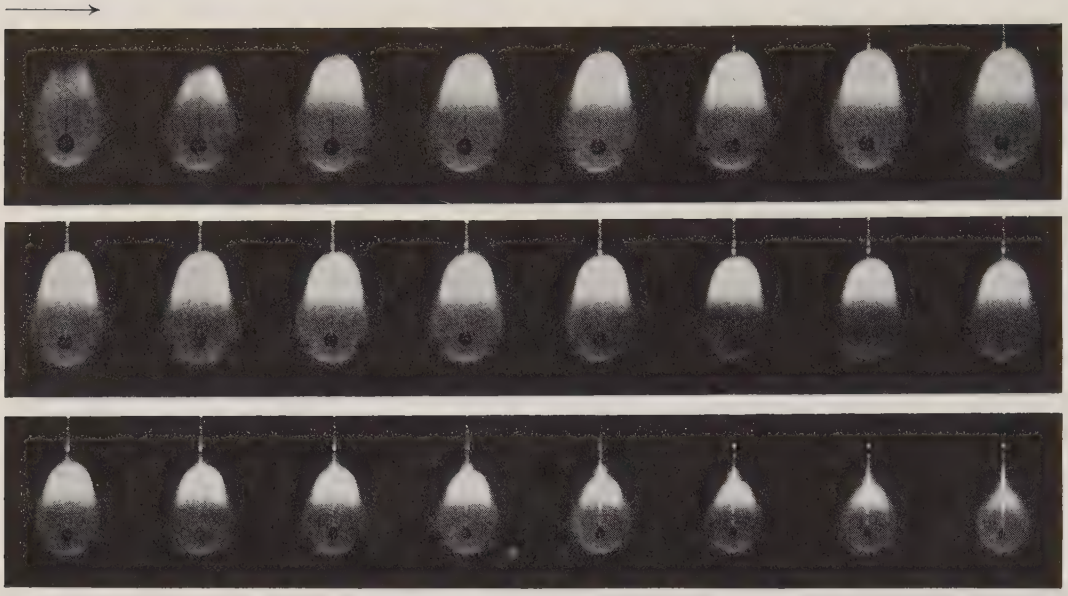

Figure 1. Direct photographs of burning stationary droplet (n-heptane). Initial diameter; 1·05 mm, *camera speed; 24 frames per sec*

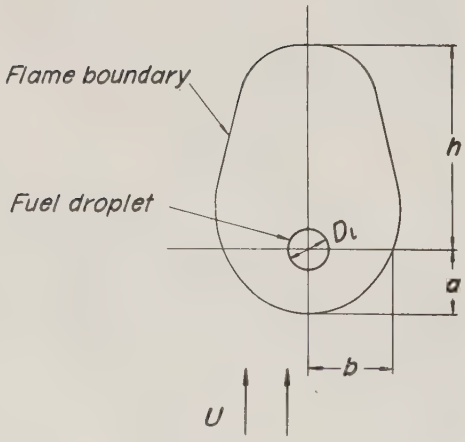

Figure 2. Schematic presentation of burning droplet

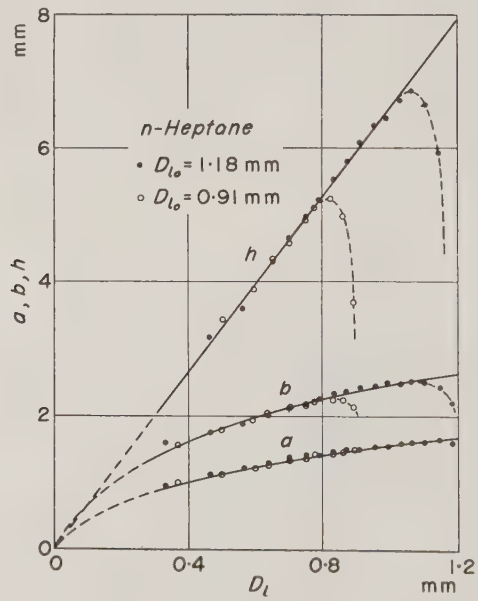

Figure 3. Dimensions of flames of stationary n-heptane droplets versus *droplet diameter*

where $\dot{m}_f$ is the burning rate and ρ' is the density of the liquid. As the value of a can be expressed as $a = A(D_l)^{\frac{1}{2}}$ from the experiment, equations 1 and 3 lead to

$$U = \frac{k\rho'}{16\rho_1 A^2} \tag{4}$$

where A is a constant; thus, the velocity of upward flow of air is independent of the droplet diameter or the time. The values of k and A being given

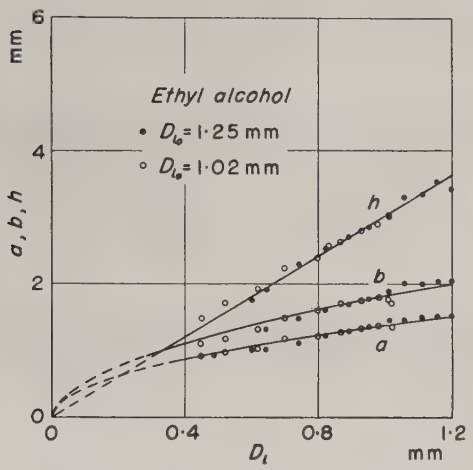

Figure 4. Dimensions of flames of stationary ethyl alcohol droplets versus droplet diameter

from the experiment, and the values of ρ_1 being reasonably estimated, the flow velocities are given as 1·4 cm/sec for *n*-heptane and 3·2 cm/sec for ethyl alcohol. The flow patterns of the convective current are visualized by photographing the dust particles suspended in the flow by side illumination (*Figure 5*). As the time of exposure is known, the flow velocity is determined from the length of streaks of the dust particles on the photograph. The flow pattern under the droplet may be roughly regarded as that predicted by Kumagai and Kimura's treatment, but the flow velocity increases rapidly at the vicinity of the flame, owing to the increase in temperature. Though the observed air velocity varies with the measuring position it is independent of the droplet diameter at a fixed position, as predicted by the theory. The observed values of the air velocity at a sufficiently lower position from the droplet, corresponding to the theoretical presentation of U, are 1·3 cm/sec for *n*-heptane and 1·6 cm/sec for ethyl alcohol (at 10 mm below the droplet), being in agreement with the calculated values in the order. This shows the validity of the theory.

Kumagai and Kimura have also shown that the combustion process at the upper part of the flame can be approximated by a concentric cylindrical diffusion flame analysed by Burke and Schumann[16]; thus the height of the flame, h, is determined by the volume flow rate of the vapour which burns in the upper part of the flame $\dot{m}_1$. The volume of the vapour which burns in the lower part of the flame per unit time, $\dot{m}_2$, may be only a small part of $\dot{m}$, and considered to decrease as the droplet diameter decreases because the surface area of the lower part of the flame boundary is directly proportional to D_l. Since $\dot{m}$ is known to be proportional to kD_l, the volume of the vapour which burns in the upper part of the flame per unit time, $\dot{m}_1 = \dot{m} - \dot{m}_2$, can be considered approximately to be proportional to kD_l, namely

$$\dot{m}_1 \propto kD_l$$

The average velocity of upward vapour flow, u, is expressed as

$$u = \dot{m}_1/\pi b^2 \propto kD_l/b^2 \tag{5}$$

As b^2 is proportional to D_l, u becomes independent of D_l. As U is independent of D_l from equation 4, u/U is naturally independent of D_l, and from equations 4 and 5 they are virtually equal for the cases where the values of $\dot{m}_1/\dot{m}$ are similar to each other.

On the other hand the height of a fuel jet, h', under similar conditions has been given by Hawthorne, Weddel and Hottel[15] as

$$h' \propto b'^2u'/K_d$$

where b' is the radius of the fuel jet, u' is the flow velocity, and K_d is the diffusion coefficient.

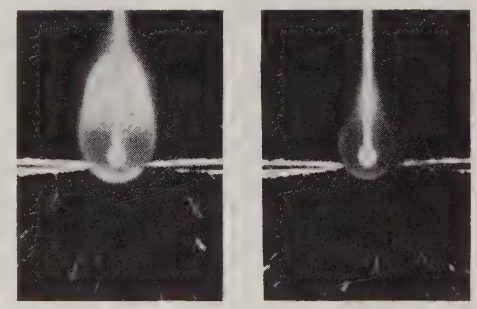

(*a*) (*b*)

Figure 5. Particle tracks in convective current of burning stationary droplets; (a) n-heptane, (b) ethyl alcohol

Making h', b', and u' to correspond with h, b and u, respectively, we get the following expression for the combustion of fuel droplets:

$$\frac{hK_d}{D_l k} = \text{constant} = C \tag{6}$$

For a given fuel K_d is constant, then h should be directly proportional to D_l: this is confirmed by the experimental results (*Figures 3* and *4*). In order to estimate the flame height of droplets of various fuels, the values of K_d and C must be given. The value of K_d adopted here is that for

the arithmetical mean temperature between the flame and the ambient gas. Taking the values of k and h/D_l obtained from the experiment, we get the value of C in equation 6 as $6{\cdot}0 \times 10^3$ for both n-heptane and ethyl alcohol.

COMBUSTION OF DROPLETS WITHOUT CONVECTION

Experiment in a zero-gravity field

When a closed chamber falls freely the gravity is not felt in the chamber, and consequently the burning droplet fixed to the falling chamber does not suffer the influence of free convection, thus the spherical combustion process can be observed. The falling apparatus, which is schematically shown in *Figure 6*, is assembled as compactly as possible to reduce experimental difficulties. A 16 mm ciné camera is fixed on a base board together with the combustion chamber. All controls of the apparatus are by remote switches, and ignition is automatically made when the apparatus leaves the suspension. The height of fall is about 5 m, and the time of observation is about 1 sec. As the falling speed reaches to about 10 m/sec the apparatus must be converted into a stream-line shape, otherwise, as a result of deceleration by the air drag, weak convection starts and the flame shape is visibly influenced. The shock of fall is absorbed by feather cushions piled about 1 m high.

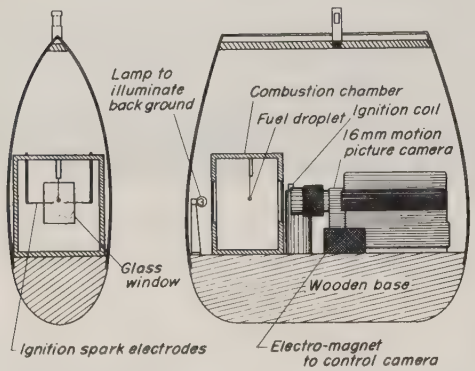

Figure 6. Schematic diagram of falling apparatus

Fuels used are n-heptane, ethyl alcohol and benzene. The photographs of burning droplets are shown in *Figure 7*. The flame boundary is completely spherical and concentric with the droplet; but in the case of benzene droplets, a brilliant zone of carbon particles appears inside the flame boundary, as shown in *Figure 7c*, and owing to this obstruction the dimensions of flames of benzene droplets cannot be measured from the photographs. The dimensions of droplets and their flames of n-heptane and ethyl alcohol, measured from the photographs, are shown in *Figures 8* and *9*. The relationship, $D_{l_0}^2 - D_l^2 = kt$ holds again, and the observed values of k for n-heptane and ethyl alcohol are 0·60 mm²/sec and 0·46 mm²/sec, respectively, the corresponding values of k under the stationary condition being 0·84 mm²/sec and 0·70 mm²/sec, respectively.

The ratio of flame and droplet radius, which is predicted to be constant by the former theories, varies with time as shown in *Figure 10*, where the calculated values by Goldsmith and Penner[3] are also shown for comparison. Schlieren photographs reveal that a hot air zone, which appears around the flame, expands with time as shown in *Figures 11* and *12*. These experimental results of flame radii and hot air zones suggest that heat and mass transfer outside of the flame is in a transient state.

On the other hand, the temperature distribution inside the flame boundary may rapidly approach that of a steady state, because the heat capacity of gas inside the flame is very small. Under such conditions the burning rate is little influenced by the variation of the flame radius, according to the former theories, and therefore the change in the value of k may be as small as experimental errors.

Theoretical analysis of spherical combustion in transient state

The former theoretical analyses of the droplet combustion have been based on a spherically symmetric model in which steady state conditions are assumed. The experimental results, however, indicate that the combustion process is in a transient state, as described above. Then we attempt to analyse the transient droplet combustion on the basis of the following assumptions: the system is spherically symmetric; the fuel and the oxygen in air react instantaneously at the flame boundary in stoichiometric proportion; appropriate mean values of physicochemical properties are used; the pressure is uniform throughout the system.

The experimental results have shown that the burning rate is directly proportional to the droplet radius, r_l, namely

$$\dot{m}_f = \pi k \rho' r_l / 2 \tag{7}$$

and the combustion life of the droplet, t_1, is

$$t_1 = 4r_{l_0}^2 / k \tag{8}$$

Combining equations 7 and 8

$$r_l = r_{l_0}(1 - t/t_1)^{\frac{1}{2}}$$

The heat and mass transfer outside of the flame is expressed by the following equations:

$$\frac{\partial T}{\partial t} = \alpha \frac{\partial^2 T}{\partial r^2} + \frac{2\alpha}{r}\frac{\partial T}{\partial r} - v\frac{\partial T}{\partial r} \tag{9}$$

$$\frac{\partial Y}{\partial t} = K_d \frac{\partial^2 Y}{\partial r^2} + \frac{2K_d}{r}\frac{\partial Y}{\partial r} - v\frac{\partial Y}{\partial r} \tag{10}$$

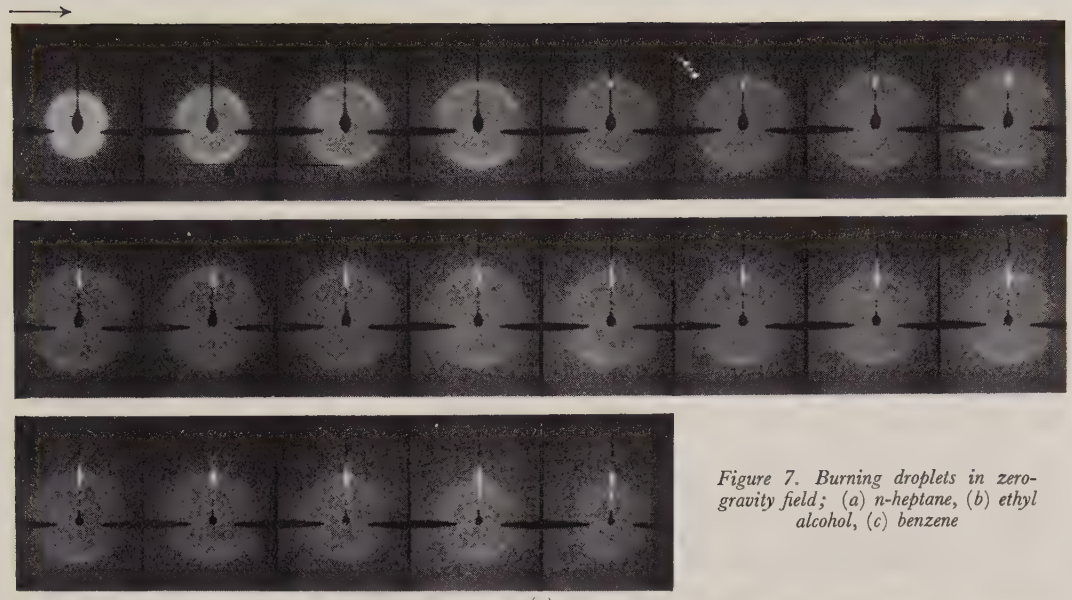

(a)

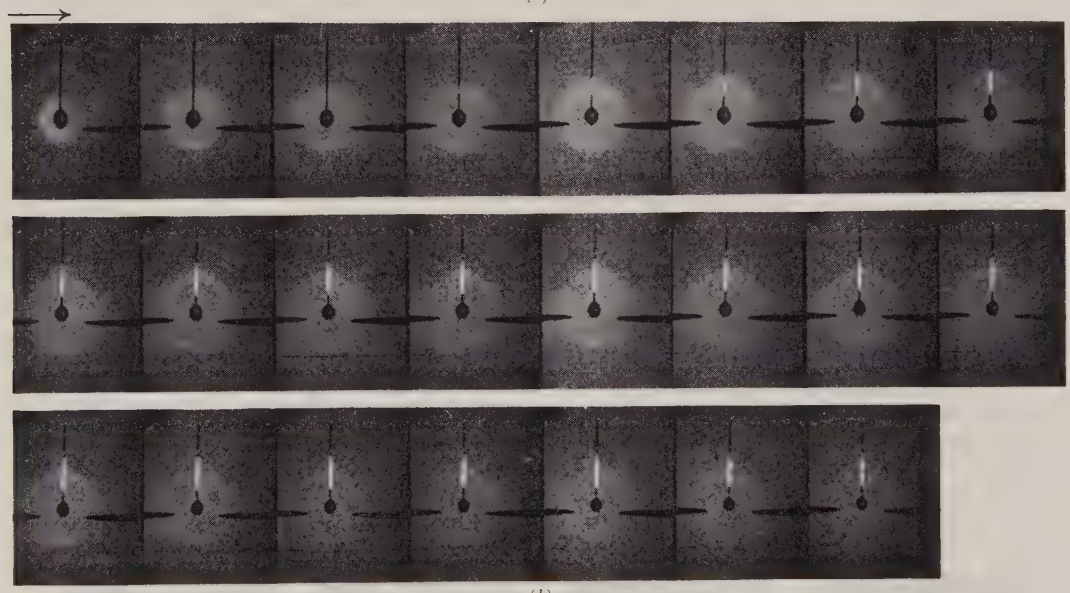

(b)

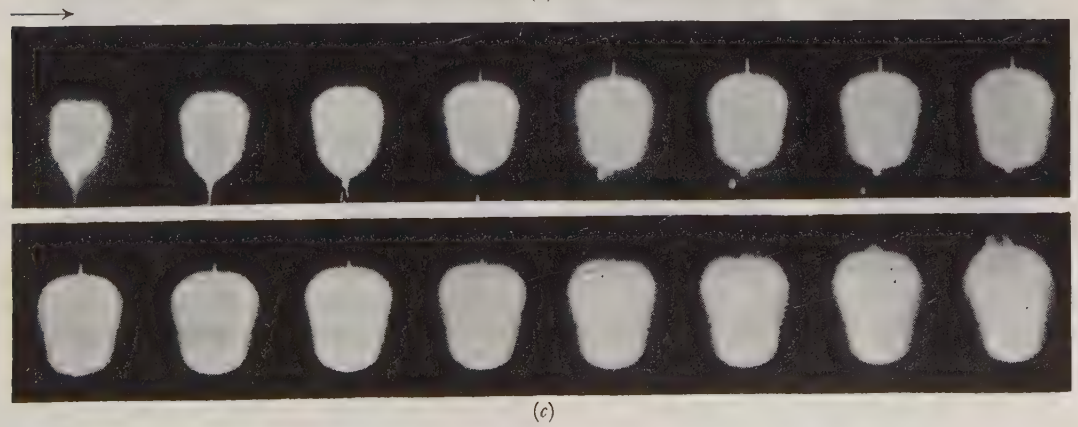

(c)

Figure 7. Burning droplets in zero-gravity field; (a) n-heptane, (b) ethyl alcohol, (c) benzene

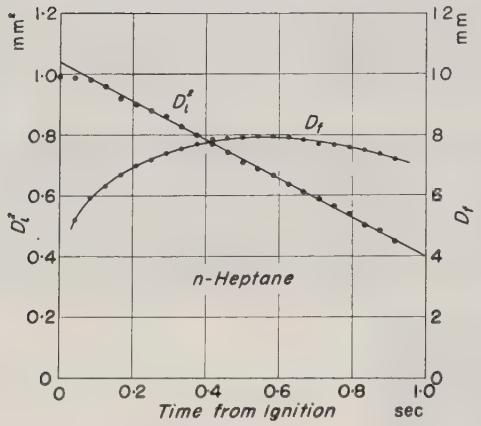

Figure 8. Variation of droplet diameter and flame diameter of spherically burning n-heptane droplet

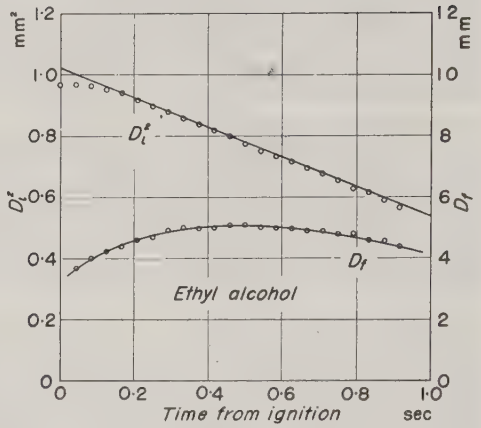

Figure 9. Variation of droplet diameter and flame diameter of spherically burning ethyl alcohol droplet

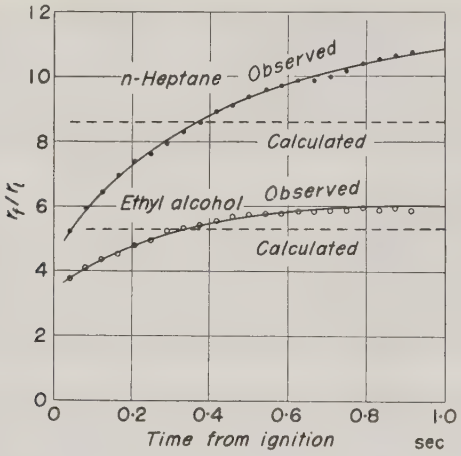

Figure 10. Observed values of r_f/r_l versus time

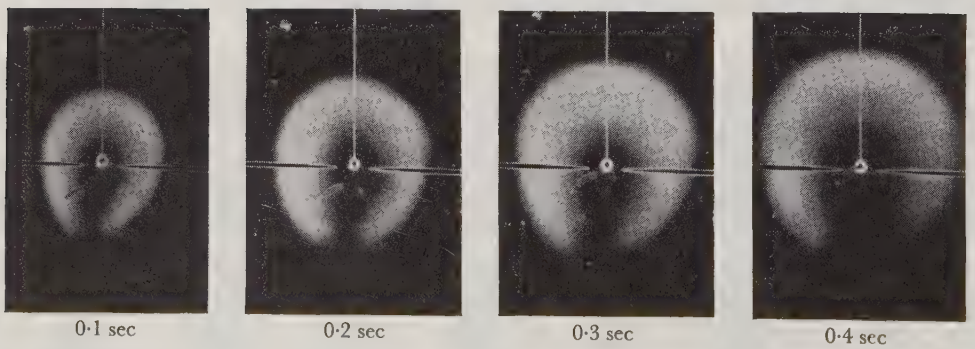

0·1 sec 0·2 sec 0·3 sec 0·4 sec

Figure 11. Schlieren photographs of hot air zones of n-heptane droplet burning in zero-gravity field

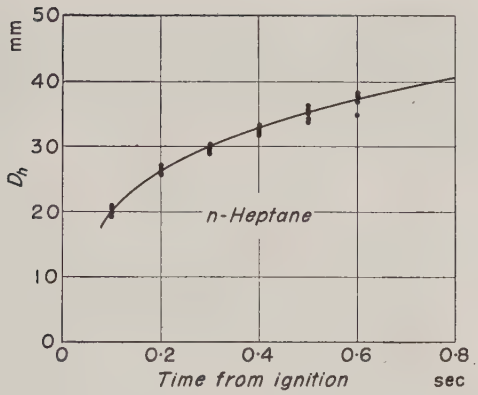

Figure 12. Observed diameters of hot air zones versus *time (n-heptane)*

where T and Y are the temperature and the oxygen concentration, respectively, at a distance r from the droplet centre at the time t, and α is the thermal diffusivity and v is the velocity of radial flow. The boundary conditions are $T = T_f$ or $Y = 0$

and

$$\left[\frac{dT}{dr}\right]_{r=r_f} = \frac{(H-L)\dot{m}_f}{4\pi r_f^2 \lambda}$$

or

$$\left[\frac{dY}{dr}\right]_{r=r_f} = \frac{n\dot{m}_f}{4\pi r_f^2 K_d \rho}$$

at the flame boundary, and $T = T_\infty$ or $Y = Y_\infty$ in the ambient gas, where H is the heat of reaction, L is the latent heat of fuel, λ is the thermal conductivity, n is the mass ratio of oxygen and fuel in stoichiometric reaction, and ρ is the density of gas. The initial conditions are then

$$r_f = r_{f_0} = r_{l_0}$$
$$T = T_f, \quad Y = 0 \quad \text{at } r = r_{f_0}$$
$$T = T_\infty, \quad Y = Y_\infty \text{ at } r > r_{f_0}$$

For the values $2\alpha/r \gg v$ or $2K_d/r \gg v$ so that v may be neglected with respect to $2\alpha/r$ or $2K_d/r$, equations 9 and 10 are re-written as follows:

$$\frac{\partial T}{\partial t} = \alpha \frac{\partial^2 T}{\partial r^2} + \frac{2\alpha}{r}\frac{\partial T}{\partial r} \qquad (11)$$

$$\frac{\partial Y}{\partial t} = K_d \frac{\partial^2 Y}{\partial r^2} + \frac{2K_d}{r}\frac{\partial Y}{\partial r} \qquad (12)$$

Introducing

$$\xi = -1/r$$

equations 11 and 12 are transformed into the forms to which the method of finite difference can be applied. The solutions of the transformed equations satisfying the boundary conditions can be readily obtained by using a graphical method, when the appropriate mean values of α, K_d, ρ and λ are taken.

Since α and K_d have nearly equal values at any temperature, we may put $\alpha = K_d$ in equations 11 and 12, then they become quite similar equations having similar boundary conditions. From this similarity $T_f - T_\infty$ can be derived as about 2,300°K for each fuel. This treatment contains no consideration for thermal dissociation, so that the actual flame temperature may be appreciably lower than this calculated value.

In *Figure 13* the plots are the experimental results and the curves represent the calculated results of variation of flame radius with respect to time, when the values of physicochemical properties at 1,000° and 850°C are adopted as mean values for *n*-heptane and ethyl alcohol, respectively.

A simplified treatment of droplet combustion

As it is rather difficult to solve equations 9 and 10 exactly, we propose a simplified model for the transient combustion of droplets. In the transient heat transfer the temperature outside of a certain finite zone at a certain time may be virtually unchanged; this is also proved by the fact that the outside boundary of the hot air zone appears distinctly on the schlieren photograph. Based on this, in the combustion model shown schematically in *Figure 14* the temperature and the oxygen concentration are assumed to remain unchanged outside of the hot air zone; the distributions of temperature and oxygen concentration in the hot air zone are approximated to those of heat conduction and diffusion in steady state in which the temperature and the oxygen concentration at the flame boundary are fixed to T_f and 0, and at the outside boundary of the hot air zone to T_∞ and Y_∞; the fuel and the oxygen in the air are assumed to react in stoichiometric proportion.

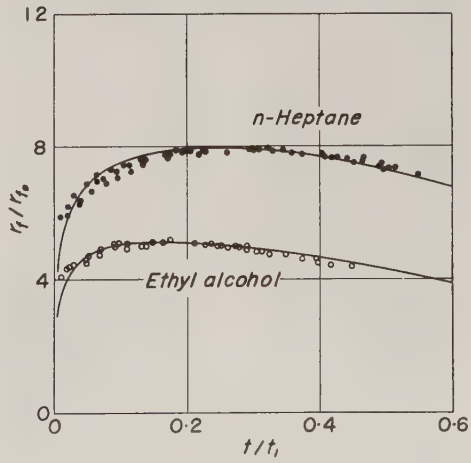

Figure 13. Calculated values of flame radii versus *time, from equations 11 and 22*

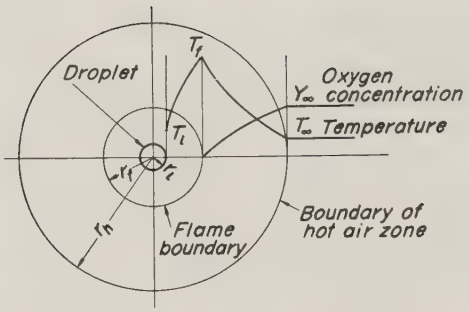

Figure 14. Schematic diagram of combustion model

The values of λ and $K_d\rho$ in the hot air zone can be estimated by the following approximate expressions: $\lambda = \lambda_s T/T_s$ and $K_d\rho = K_s T/T_s$ where λ_s and K_s are the values of λ and $K_d\rho$ for the standard temperature, $T_s = 300°K$, respectively. Thus, the temperature in the hot air zone, which is approximated to that in steady state, is

$$T/T_\infty = \{1 + (\gamma^2 - 1)(r_h/r - 1)/(\beta - 1)\}^{\frac{1}{2}} \tag{13}$$

where $\gamma = T_f/T_\infty$, $\beta = r_h/r_f$, and r_h is the radius of the outside boundary of the hot air zone. The values of T_f and r_h can be estimated by the following expressions:

$$T_f - T_\infty = \frac{(H - L)K_s Y_\infty}{\lambda_s n} \tag{14}$$

$$\frac{r_h}{r_l} = \frac{k\rho' n(\beta - 1)T_s}{4K_s Y_\infty(\gamma + 1)T_\infty} \tag{15}$$

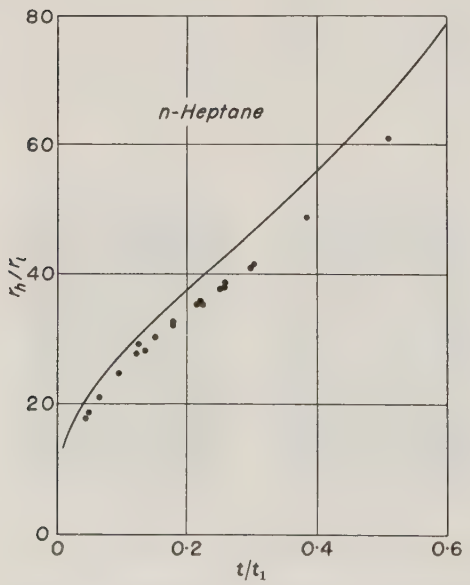

Figure 15. Calculated values of r_h/r_l versus t/t_1 from combustion model in Figure 14 (n-heptane)

According to the experimental results, the heat and mass transfer inside of the flame boundary may be fairly approximated to that in steady state. Goldsmith and Penner have presented the steady state solution for the evaporation constant as the following expression:

$$k = \Phi/(1 - r_l/r_f) \tag{16}$$

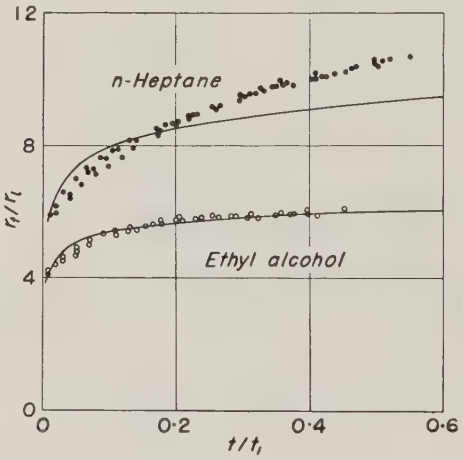

Figure 16. Calculated values of r_f/r_l versus t/t_1 from combustion model in Figure 14 (n-heptane and ethyl alcohol)

where Φ is a function of the flame temperature, the droplet temperature and the physicochemical properties inside of the flame boundary. Then equations 15 and 16 lead to

$$\frac{r_h}{r_l} = \frac{\Phi n\rho'(\beta - 1)T_s}{4K_s Y_\infty(\gamma + 1)T_\infty} + \beta \tag{17}$$

The heat released by combustion should be accumulated in the hot air zone, because the temperature outside of the hot air zone is assumed unchanged. Thus,

$$\left(\frac{r_{l_0}}{r_l}\right)^3 = \frac{c\rho_s T_s}{\rho'(H - L)}\left(\frac{r_h}{r_l}\right)^3\left(1 - \frac{1}{\beta^3} - 3I\right) \tag{18}$$

where

$$I = \int_{r_f}^{r_h} \frac{r^2}{r_h^2}\frac{T_\infty}{T}\,\mathrm{d}\left(\frac{r}{r_h}\right)$$

c is the specific heat, and ρ_s is the gas density at $T = T_s$.

From equations 16, 17 and 18, we can obtain the relationships between r_h/r_l and t/t_1, and between r_f/r_l and t/t_1, by the numerical calculation taking β as a parameter. The calculated results are shown in *Figures 15* and *16*. In this combustion model the temperature in the hot air zone is over-estimated with increasing flame radius, namely in the early period of the combustion, and is under-estimated with decreasing flame radius,

namely in the later period. This tendency results in giving too large values for r_h/r_l and too small for r_f/r_l, as the value of t/t_1 approaches to unity, as contrasted with the experimental plots in *Figures 15* and *16*.

CONCLUSIONS

(1) The combustion of stationary droplets accompanied with free convection is observed. The average velocity of the convective current under the droplet remains constant during combustion, as predicted by Kumagai and Kimura's theory, and its value is about a few cm per sec for *n*-heptane and ethyl alcohol droplets.

(2) The flame shape of a stationary droplet is influenced seriously by free convection and the greater portion of evaporated fuel burns at the upper part of the flame, where the combustion process is more likely to be a cylindrical diffusion flame. Hence, the combustion of stationary droplets is not very similar to the combustion of fine droplets, in which the convective effect is considered to be negligible.

(3) The spherically symmetric combustion is realized in a freely falling chamber. The results obtained from the experiment using such a device are as follows: the burning rate is directly proportional to the droplet diameter; the flame diameter increases at first and begins to decrease later; the hot air zone outside of the flame expands with time during combustion.

(4) An attempt to solve the differential equations of the heat and mass transfer in transient state for the spherical combustion of a droplet is presented. The values of flame radius calculated by making some modifications on the equations agree well with the observed values.

(5) A simplified treatment based on the experimental results is suggested, in which the temperature outside of the hot air zone is assumed to remain constant and the temperature distribution in the hot air zone is assumed to take a given form. The results calculated by such a treatment also agree well with the experimental results.

REFERENCES

[1] Godsave, G. A. E. *Fourth Symposium (International) on Combustion*, p. 818. 1953. Baltimore; Williams and Wilkins

[2] Spalding, D. B. *Fourth Symposium (International) on Combustion*, p. 847. 1953. Baltimore; Williams and Wilkins

[3] Goldsmith, M. and Penner, S. S. *Jet Propulsion* 24 (1954) 245

[4] — *Jet Propulsion* 26 (1956) 172

[5] Okazaki, T. and Gomi, M. *Trans. Japan Soc. Mech. Engr.* 19 (1953) 1

[6] Kobayashi, K. *Fifth Symposium (International) on Combustion*, p. 141. 1955. New York; Reinhold

[7] Kumagai, S. and Isoda, H. *Fifth Symposium (International) on Combustion*, p. 129. 1955. New York; Reinhold

[8] — — *Sixth Symposium (International) on Combustion*, p. 726. 1957. New York; Reinhold

[9] Wise, H., Lorell, J. and Wood, B. J. *Fifth Symposium (International) on Combustion*, p. 132. 1955. New York; Reinhold

[10] Agoston, G. A., Wise, H. and Rosser, W. A. *Sixth Symposium (International) on Combustion*, p. 708. 1957. New York; Reinhold

[11] Miesse, C. C. *Sixth Symposium (International) on Combustion*, p. 732. 1957. New York; Reinhold

[12] Probert, R. P. *Phil. Mag.* 37 (1946) 94

[13] Tanasawa, Y. *Technology Reports of Tohoku University (Sendai, Japan)* 18 (1954) 195

[14] Kumagai, S. and Kimura, I. *Science of Machine (Japan)* 3 (1951) 431

[15] Hawthorne, W. R., Weddell, D. S. and Hottel, H. C. *Third Symposium on Combustion and Flame and Explosion Phenomena*, p. 266. 1949. Baltimore; Williams and Wilkins

[16] Burke, S. P. and Schumann, T. E. W. *Ind. Eng. Chem.* 20 (1928) 998

HOMOGENEOUS-HETEROGENEOUS COMBUSTION OF CARBON MONOXIDE IN NARROW TUBES (CHANNELS)

L. N. KHITRIN and L. S. SOLOVYEVA

INTRODUCTION

It is well known that on the surface of some solid bodies (catalysts) gas reactions proceed with great intensity. The oxidation reaction, i.e. combustion, is no exception; however, observations on the phenomenon can be carried out only in the relatively low-temperature region, and there are, therefore, very few data on the course and characteristics of surface (catalytic) combustion at high temperatures, which is the area of greatest practical interest. Industrial experience in gas combustion has in many cases seemed to lead to the conclusion that incandescent (refractory) surfaces act most positively on the completeness and the rate of combustion. This has given rise, among other things, to a new expression (and combustion method), to the so-called flameless combustion of gases (see for example Ravich[1]). In many other cases, however, on the basis of an analysis of this kind of combustion investigators have come to the conclusion that the surface reaction plays no significant part in high-temperature combustion and that, probably, some purely physical factors and even the specific geometric configuration of the apparatus (burners) were items of greater significance.

An example showing that this is true in many cases may be found in the so-called (in Russia) 'tunnel burners'; the combustion process in such burners has often been studied, recently most fully in the investigation by Ievlev[2].

The principal reason for the many uncertainties and contradictory data in regard to the part played by active surfaces in the high-temperature combustion of gases is that combustion under such conditions comprises a complex homogeneous-heterogeneous process. It is therefore necessary in investigating and analysing combustion under such conditions to take into account the transfer of the substances taking part in the reaction to the active solid wall; however, this was not always done. Mass transfer must be taken into account both in establishing the basic laws governing the process and in determining the kinetic characteristics of the surface combustion reactions for any concrete system gas-wall.

Consequently, the aims of this investigation were:

(1) To obtain in the simplest possible form the basic equations describing combustion under conditions where the chemical process can occur both in the gas volume (homogeneously) and on the surface of a solid active wall (heterogeneously).

(2) On this basis, to establish the necessary conditions for the determination by experiments and calculations of the kinetic constants of a surface process.

(3) To apply the results obtained to a concrete case of complex volume-surface combustion.

BASIC RELATIONSHIPS

Heterogeneous-combustion theory, which has been quite fully developed[3,4] can serve as an excellent basis for developing a theory of the more complex homogeneous-heterogeneous combustion processes. It follows from the heterogeneous combustion that a considerable simplification of calculations and analysis is often obtained by applying the so-called average equations of heterogeneous combustion[5].

These equations can also be used in the case at hand, where combustion can proceed both in the gas volume and on a solid surface. Let us assume that combustion of a uniform mixture takes place either in a straight channel (tube) of diameter d or in a bed of uniform particles of dimension (diameter) d. If the gas flow is along the x-axis (cm) at a filtration rate of w (cm/sec), and the reaction takes place in a large oxygen excess and follows the kinetic law for a first order reaction with respect to the combustible component (such an assumption can be made in many actual cases) then the average equation for the fuel consumption reduces to a very simple expression:

$$-w\frac{dc}{dx} = k_v C + S_i k C = (k_v + S_i k)C \qquad (1)$$

where C is the fuel concentration, k_v is the reaction velocity constant for the volume reaction (1/sec), k is the corresponding constant for the surface process (cm/sec) and S_i is the specific reaction surface of the catalyst (cm^2/cm^3). The constant k is of a complex nature:

$$k = \frac{1}{\frac{1}{k_s} + \frac{1}{\beta}} \quad \text{or} \quad k = \frac{k_s}{1 + \frac{k_s}{\beta}}$$

where k_s is the velocity constant of the reaction at the surface (cm/sec) and β is a diffusion coefficient[4] ($\beta = \frac{D}{d} Nu_{\text{dif}}$); β is an analogue of the heat transfer coefficient, and it obeys the well-known laws governing heat-transfer.

The solution of equation 1 is

$$\frac{C}{C_o} = e^{-(k_v + S_i k)\frac{x}{w}} = e^{-k_v \frac{x}{w}} \cdot e^{-S_i k \frac{x}{w}} \qquad (2)$$

where C_o is the initial fuel concentration value.

If C/C_o is replaced by $\kappa = 1 - C/C_o$, a factor characterizing the efficiency of combustion, then equation 2 reduces to

$$\kappa = 1 - e^{-k_v \frac{x}{w}} \cdot e^{-S_i k \frac{x}{w}} \qquad (2')$$

In this equation $e^{-k_v(w/x)}$ depends on volume combustion, whereas $e^{-S_i k(x/w)}$ depends on the process on the surface of the solid catalyst. In tests the factor x is usually fixed (it is the length of the channel or the thickness of the particle bed). The values of k_v and k_s, the velocity constants, depend on the temperature and are given by the Arrhenius equation:

$k_v = k_{vo} \exp(-E_v/RT)$; $k_s = k_{so} \exp(-E_s/RT)$

The chief differences of homogeneous-heterogeneous combustion result from the existence of various possible ratios of the constants k_v and k (k in turn being dependent on k_s and β). It is known[4] that k may be in agreement with the so-called 'kinetic regime of surface combustion' when k_s is small and $k \approx k_s$, and with the 'diffusion regime' when $k \approx \beta$. In the latter case the heterogeneous process is governed by the purely physical process of diffusion and its value is determined by the value of the diffusion-rate index β.

There must, evidently, exist the following possible special cases of the complex homogeneous-heterogeneous process.

(1) The heterogeneous (surface) process is negligible or absent, i.e. $S_i k \ll k_v$.

In this case

$$\kappa = 1 - e^{-k_v \frac{x}{w}} \qquad (3)$$

and from measurements of the degree of combustion of the fuel over a given length of a channel, x, it is possible to determine both the value of the overall velocity constant, k_v, for the volume reaction $k_v = -\ln(1 - \kappa)/(x/w)$ and the activation energy, E_v.

(2) The heterogeneous (surface) process proceeds with high intensity, the volume process is negligible or absent, i.e. $k_v \ll S_i k$. In this case

$$\kappa = 1 - e^{-S_i k \frac{x}{w}} \qquad (4)$$

There are two extreme modes by which the process can take place, depending on the character of the variable k. They are the kinetic mode ($k_s \ll \beta$), using which it is possible to determine the values of $k_s = -\ln(1 - \kappa)/S_i(x/w)$ and of E_s, and the diffusion mode ($k_s \gg \beta$), through which it is possible to determine the value of β.

For the first mode, as in the case of a homogeneous process, the reaction rate should depend very much on the temperature; for the second mode there will be a much slighter dependance on the temperature.

(3) The general case of the homogeneous-heterogeneous process corresponds to conditions where $S_i k$ and k_v are of comparable magnitude. The role of the heterogeneous process in this the most probable case will be the larger the greater the value of S_i, i.e. the smaller the value of d. It follows, that in channels (tubes) of large diameter the surface combustion process should be insignificant even though the value of the constant k_s may be very great. Thus, in the general case the process is described by the equation:

$$\kappa = 1 - e^{-(k_v + S_i k)\frac{x}{w}} = 1 - e^{-K \frac{x}{w}} \qquad (5)$$

where $K = k_v + S_i k$.

It follows from the above that for determining the rate constants k_s and E_s for the surface process it is desirable to use such a temperature region where combustion will be of type 2 and conditions corresponding to the kinetic mode. Nevertheless, if there be some participation of the volume process in the combustion, then special tests should be made to determine the value of k_v for the temperature range investigated, after which for the conditions of the test the magnitude of $e^{-k_v(x/w)}$ in the complex process can be estimated.

EXPERIMENTAL

A cylindrical tube was chosen as the reaction vessel and materials of varying catalytic power were used for the tube wall material: quartz, which may be regarded to be a surface-inactive material, at least in the temperature range 500–900°C, platinum, a material of high catalytic activity, and copper, an intermediate material.

Carbon monoxide was chosen as the fuel. This choice was based on a number of considerations, mainly because quite detailed and reliable overall kinetic characteristics are available for that gas, i.e. the overall reaction order according to carbon monoxide and to oxygen and the activation energy

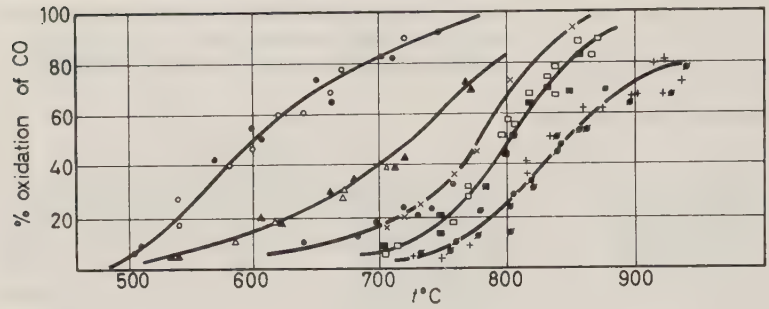

Figure 1. Percentage of carbon monoxide oxidation as a function of the temperature in a quartz tube

W — 1 m/sec ○ ●
W — 4 m/sec △ △
W — 8 m/sec ⊙ ×
W — 17 m/sec □ ■
W — 34 m/sec + ◪

over a wide range of temperatures[6–9]. On the basis of the available data, it may be considered that the reaction is of the first order with regard to carbon monoxide.

The mixture was obtained by adding carbon monoxide from a gasometer to air fed by a blower. The entering air had a constant humidity value, obtained by saturating the air at room temperature and condensing excess water vapour in coils immersed in a water-filled thermostatically controlled bath with a temperature of 10°C. For preliminary heating of the uniform gas-air mixture it was passed through a quartz tube located in an electrically heated tube oven. The mixture was heated to the temperature of the test in a narrow electrically heated 2 mm quartz tube. This tube entered directly into the reaction tube (channel), 2 mm in diameter and 150 mm long and equipped with a variable electric heater.

Samples of the fuel mixture and of the reaction products were collected simultaneously in gas-pipettes through nipples located at the entrance and exit of the reaction channel. Sampling was conducted at a rate low enough not to disturb the pattern of flow in the channel.

Temperatures were measured by means of platinum-platinum-rhodium thermocouples 0·15 mm in diameter. Two of the thermocouples were located inside the reaction tube, near the gas exit and near the gas entrance; the wires were passed out through the nipples used for taking the gas samples for analysis. Three thermocouples were fastened to the outer wall of the reaction tube. These outside thermocouples were used for recording the temperature change along the length of the reaction tube. The junctions of the thermocouples inside the tube were provided with thin porcelain protective layers to prevent a catalytic surface reaction from taking place there.

The temperature was controlled so as to yield nearly isothermal conditions in all points of the tube.

Test in the quartz tube

The experiments in the quartz tube served for obtaining data on homogeneous combustion of carbon monoxide and for determining the value of k_y. The temperature was varied within the range 520–950°, and the initial carbon monoxide concentration from 2 to 5 per cent. The flow rate was varied over the wide range of from 1 to 34 m/sec.

The results of the experiments are given in *Figure 1*. The mean of the temperature inside the tube near the entrance of the gas mixture and that inside the tube near the gas exit was considered to be the temperature of the test. Usually the temperature difference, measured with the thermocouples, did not exceed 10°.

The percentage of carbon monoxide oxidized, κ, was found to be independent of the initial carbon monoxide concentration, which is in agreement with an expected first order reaction with respect to carbon monoxide.

The results are given in the coordinate system $\ln \frac{1-\kappa}{x/W}$ *versus* $\frac{1}{T}$ in *Figure 2* (black dots and crosses). For comparison, data of other authors (named below the figures) were also plotted. The good agreement with parallel data obtained by the same method[9] should be noted, some difference is observed in the data for temperatures below 700°C, where the accuracy of the measurements is lower and where, also, differences as yet not explainable are sometimes found.

There are indications of good agreement between the data obtained in this study and data for higher temperatures[8] calculated by the Zeldovich method on the basis of specially made measurements of the normal flame velocity. *Figure 2* also contains results of earlier tests[6] (curves *a* and *b*), for which two extreme possible values are given due to the uncertainty of the mean velocity determination; the two extreme positions are almost symmetrically located with respect to the curve for the data of this investigation.

Thus, our data are in satisfactory quantitative agreement with available data on the value of the reaction-rate constant for the combustion of carbon monoxide; this confirms the validity of the assumption that in quartz capillary tubes surface combustion is practically absent and that

for more complex cases data obtained in such tests can be used for estimating the value of the homogeneous factor in the general equation 2.

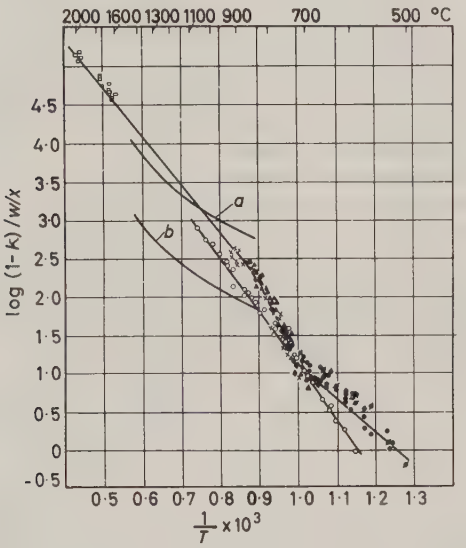

Figure 2. Rate of carbon monoxide oxidation as a function of temperature

W — 1 m/sec
W — 4 m/sec
W — 8 m/sec
W — 17 m/sec
W — 34 m/sec ×
Data of N. A. Karzhavina—curves a *and* b
Data of G. I. Kozlov ○
Data of G. K. Sobolev □

Tests in a platinum tube

The tests carried out in the platinum tube (channel) had a twofold aim: to determine the value of β under the conditions of the test, and then to calculate the characteristics of the reaction on a platinum surface from the data obtained for a wide-as-possible temperature range. As above, the initial carbon monoxide concentration was varied from 3 to 5 per cent; the rate of the gas flow was varied from 3 to 70 m/sec, and the temperature over a range of 300–600°C.

The experimental data obtained are plotted in *Figure 3*.

Beforehand a check was made (at two flow rates) of the degree to which the carbon monoxide combustion follows the first order reaction equation with respect to carbon monoxide within the range of carbon monoxide concentration tested (see *Figure 4*).

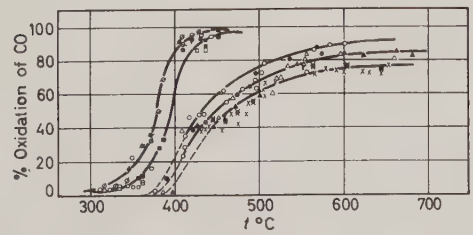

Figure 3. Percentage of carbon monoxide oxidation as a function of the temperature in a platinum channel

W — 3 m/sec ∅
W — 6 m/sec □
W — 34 m/sec ○
W — 55 m/sec △
W — 70 m/sec ×

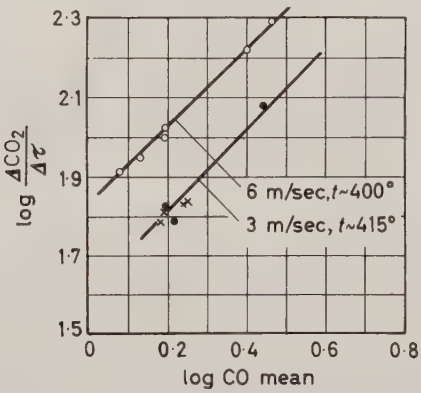

Figure 4. Rate of carbon monoxide oxidation in a platinum tube as a function of the initial concentration

Figure 3 shows that for all the flow rates used oxidation of carbon monoxide in the platinum tube commences at a temperature of approximately 320°C (w = 3 m/sec), after which it proceeds at a very high rate, so that the range in which oxidation lies below 50 per cent is very difficult to realize.

The pattern of the data at the highest temperatures for large flow velocities differs from that for the tests in the quartz tube: instead of approaching 100 per cent, clearly tends to approach another, lower, extreme value; this indicates that in spite of a rise in the temperature there is no increase in the rate of the combustion process in a platinum tube.

The overall data on the relationship between carbon monoxide combustion in a platinum tube and temperature are given in *Figure 5* by the log K *versus* $1/T$ curve, where K, as was pointed out above, in the general case can be expressed as $K = k_v + S_i k$. However, the value of interest here was k_s, contained in the expression

$$k = \frac{1}{\frac{1}{k_s} + \frac{1}{\beta}}$$

From the k_v data obtained in the tests in the quartz tube, the value of $e^{-k_v x/w}$ for the tests in the platinum tube could now be calculated.

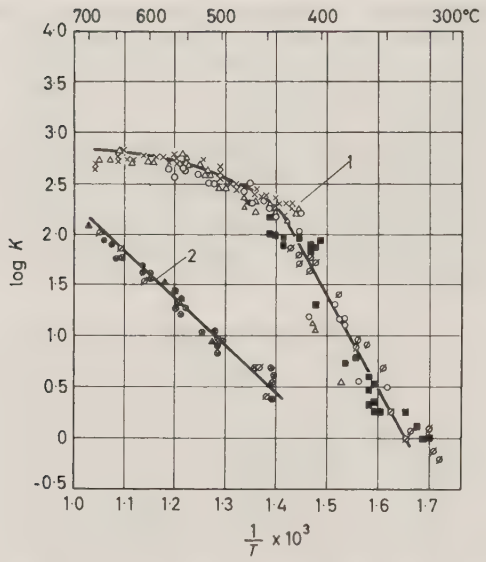

Figure 5. Overall carbon monoxide combustion velocity constant as a function of the temperature: for platinum, curve 1; for copper, curve 2

Figure 6 contains the corresponding relationship, showing the change with temperature in the sought constant for the surface process, i.e. for the heterogeneous interaction between carbon monoxide and platinum. It can be seen in *Figure 6* that the curve giving the relationship between log k and $1/T$ at first shows a sharp increase in k with a rise in the temperature, which can be described by an equation of the Arrhenius type with a value of activation energy of about 45,000 cal/mole. However, at temperatures above 420°C the growth of k slows down sharply and k clearly tends to approach a limit. The character of the curve in this range points toward a typical case of slowing down of a combustion process by diffusion of the reagents to an active surface. An estimate of the limit made on the basis of heat transfer data shows close agreement between the expected value of β and the experimental k values.

The dotted-line curve of *Figure 6* is a plot of β values obtained from heat transfer data.

It follows that beginning with temperatures of the order of 450°C the combustion process in the platinum channel used in our studies reaches the limiting diffusion regime. This explains why the rate of the process is nearly independent of temperature over the high temperature range. It is therefore erroneous in this case to explain the phenomenon from the purely chemical point of view and to point to a low activation energy for the 'reaction' as evidence of very high activity of the catalyst. As the tests show, it is precisely because of the large, and not small, activation energy on platinum that the process changes over to one of the diffusion mode type at temperatures only slightly above 400°C.

From the values of k as determined from the test data and the roughly estimated β values the sought value of k_s can be determined using the equation

$$\frac{1}{k_s} = \frac{1}{k} - \frac{1}{\beta}$$

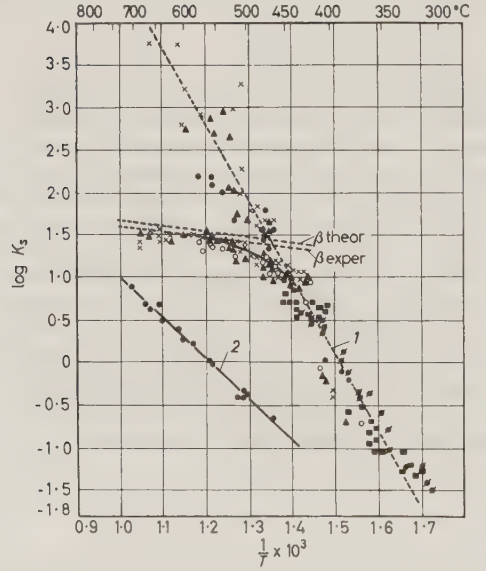

Figure 6. Velocity constant of surface reaction in carbon monoxide combustion as a function of temperature: for platinum, curve 1; for copper, curve 2

The theoretical value of β (according to heat transfer) differs somewhat from the values estimated on the basis of experimental values of k at the extreme higher temperatures. Consequently, an empirical coefficient, a, was found correlating the values of β obtained from the test data with the value calculated from the corresponding data of the Nu and $Pe\ d/x$ relationship for the case of heat transfer. A value of 0·88 was found for a. The calculated values of k_s are also plotted in *Figure 6*.

The calculated values show considerably more scattering than the initial experimental data; this is due to the nature of the equation used for the calculations (containing a difference of the reciprocals of k and β). This part of the straight line was, consequently, given by a dotted line.

For the entire temperature range tested there seems to be a generally linear relationship, corresponding to an activation energy for the surface reaction of carbon monoxide on platinum of $E_s \approx 45{,}000$ cal/mole (the corresponding value of k_{so} is approximately 10^{15}). On this basis, the kinetic equation for the reaction of carbon mon-

oxide on platinum can be expressed as follows (for small carbon monoxide concentrations):

$$-\frac{dCO}{dt} = 10^{15} \cdot CO \cdot e^{-\frac{45{,}000}{RT}} \frac{\text{mole}}{\text{cm}^3\text{sec}}$$

where CO is the molar carbon monoxide concentration.

The case of homogeneous-heterogeneous carbon monoxide combustion, where the parts played by volume combustion and by surface combustion are of comparable magnitude, was to have been studied in a tube of stainless steel. However, preliminary tests yielded the same results as were obtained with the quartz tube, and further tests were therefore made with a copper tube. The investigation of the oxidation of carbon monoxide in a copper tube was carried out over a temperature range of 450–730°C at rates of flow of the mixture in the channel equal to 6–15 m/sec and for initial carbon monoxide concentrations of 3–5 per cent.

The experimental data and final calculated values are also given in *Figure 6*. In this case $E_s \approx 22{,}000$ cal/mole and $k_{s0} = 10^6$, which characterize the copper surface as a catalyst of low activity.

SOME RESULTS

The analysis of the complex homogeneous-heterogeneous process of gas combustion, the basic features of which are expressed by equation 2, thus leads to the conclusion that the properties of such combustion processes may differ very widely. Depending on the relative values of k_v and k, and, especially, on the value of the determining dimension, d, the catalytic properties of a solid wall in an oxidation or combustion zone may or may not be felt. One and the same material may under certain conditions exert an effect on the combustion process and in other conditions may not be evident at all, although the temperature conditions were the same in both cases.

If, as an example, the combustion of carbon monoxide flowing through tubes (cylindrical chamber) of various diameters be considered, then under optimum conditions, when the rate of the surface reaction is very high ($k_s \gg \beta$), the role of surface combustion ($S_i k$) in the overall process ($k_v + S_i k$) is found to be extremely small (at 1,400°C) even for a tube of a diameter of about 10 mm, and only when the tube diameter is much less does a sharp increase in ratio occur (see *Figure 7*, continuous curve *1*). For practical purposes this means that in all real combustion chambers, even when made of an active refractory material, there is practically no catalytic effect by the walls on the combustion of the gas mixture flowing through the chamber.

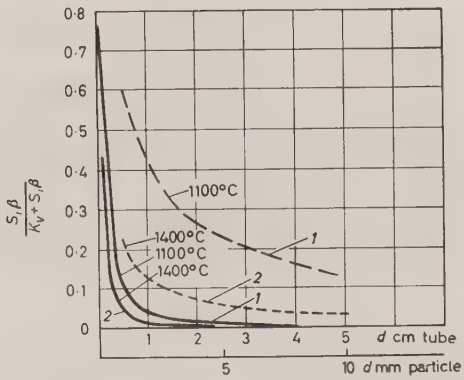

Figure 7. Surface combustion ratio as a function of tube (chamber) diameter and bed-particle size
Tube, 30 m/sec (*curve 1*, 1,100°C; *curve 2*, 1,400°C)
Bed, 3 m/sec (*curve 1*, 1,100°C; *curve 2*, 1,400°C)

Qualitatively, the laws of combustion in a bed of particles of a catalytically active material (a form of flameless combustion) are of the same nature (*Figure 7*, dashed curves). There is, however, a significant practical difference between a channel and a bed. Combustion in the latter case can be carried out practically using a small-grain bed, for which the d value is small; this is not true for the case of a tube. It can be seen that for the bed, due to the somewhat different value of β, the surface process begins to become unnoticeable for a dimension of 5 mm, and at $d = 0{\cdot}5$–$1{\cdot}0$ mm, it predominates completely in the overall process. Thus, for a small-grain bed, of course, when the material represents a very active catalyst, surface, catalytic or, as it is also called, flameless combustion may play a very important part and may lead to a significant increase in the intensity of combustion of a gas. This follows from the fact that the combustion zone in a bed is much shorter than in a tube of the same determining dimension and that in a bed the length of the combustion zone does not change noticeably, when the blasting rate is changed, so that the value of the volume rate of heat release increases roughly linearly with an increase in the flow rate.

These above considerations refer to the extreme case of a very high activity catalyst. However, if the characteristics of the surface combustion are known, an estimate can also be made of the part played by that process in the case when extreme surface-combustion conditions do not exist and when the mass transfer characteristics are known.

The authors are indebted to Professor M. B. Ravich and Dr. O. A. Tsukhanova for their kind interest in this investigation and for valuable suggestions on carrying out the experiments described above.

REFERENCES

[1] Ravich, M. B. *Surface Flameless Combustion.* 1949. Academy of Sciences, USSR

[2] Ievlev, V. N. *Sixth Symposium (International) on Combustion,* p. 317. 1957. New York; Reinhold

[3] Predvoditelev, A. S., Khitrin, L. N., Tsukhanova, O. A., *et al. Burning of Carbon.* 1949. Academy of Sciences, USSR

[4] Khitrin, L. N. *Sixth Symposium (International) on Combustion,* p. 565. 1957. New York; Reinhold

[5] Tsukhanova, O.A. *Sixth Symposium (International) on Combustion,* p. 573. 1957. New York; Reinhold

[6] Karzhavina, N. A. *J. phys. Chem.* (in Russian) 19 (1945) 551

[7] Zeldovich, Ya. B., and Barsky, G. A. *J. phys. Chem.* (in Russian) 25 (1951) 52

[8] Sobolev, G. K. This volume, page 386

[9] Kozlov, G. I. This volume, page 142

COMBUSTION OF A GAS INJECTED INTO A HYPERSONIC BOUNDARY LAYER

G. W. SUTTON

INTRODUCTION

One of the central problems of hypersonic flight within the earth's atmosphere is that of keeping the structure of the vehicle cool, since the gases in the shock layer which surround the vehicle are at temperatures between 4,000 and 8,000°K. One novel heat protection method is the use of area mass-transfer cooling, in which a cool gas is forced through a porous skin on the exterior of the vehicle surface, see *Figure 1.* This procedure has two effects: first, the boundary layer is thickened thus reducing the temperature gradient in the boundary layer and hence reducing the energy flux to the surface; secondly, the gas as it passes through the wall absorbs the energy flux to the surface by virtue of temperature increase. Thus, it may be possible to keep the exterior of the porous wall at a temperature well below that of the gas in the inviscid shock region, so that the wall material retains its structural integrity.

In this paper, the use of combustible coolant gas is considered. Such a gas may result in a diffusion flame, where the high-temperature oxygen in the shock layer, which surrounds the vehicle, diffuses through this boundary layer which is adjacent to the vehicle surface, and reacts chemically with the combustible gas which is being injected. It is, therefore, necessary to analyse this flame and its effect on the heat transfer.

This problem is similar to that of the burning of a liquid fuel droplet in a stream[1,2].

In the present analysis, the combustion process is explored in detail at the stagnation point of an axially symmetric body at hypersonic speeds. The parameters which govern the combustion process will be presented, first by a calculation of the transit times through the boundary layer of the injected combustible gas, and secondly by a calculation of the diffusion flame front for a first-order reaction rate with an Arrhenius dependence upon temperature. The effect due to subsequent dissociation of the products of combustion is calculated.

Finally, the preceding results are applied to determine the required injection rate of coolant in order to maintain the wall temperature at a specific temperature; for example, a temperature at which the vehicle surface still retains its structural integrity.

ASSUMPTIONS

Since the present purpose is to evaluate qualitatively the effect of combustion of the injected species, only the simplest analysis will be presented. It is therefore desirable to make assumptions which allow solutions to be found in terms of previously obtained solutions to the boundary layer equations. These assumptions are[3]:

(1) The product of density and viscosity is constant.

(2) The diffusion coefficient and molecular weight of each chemical species is equal.

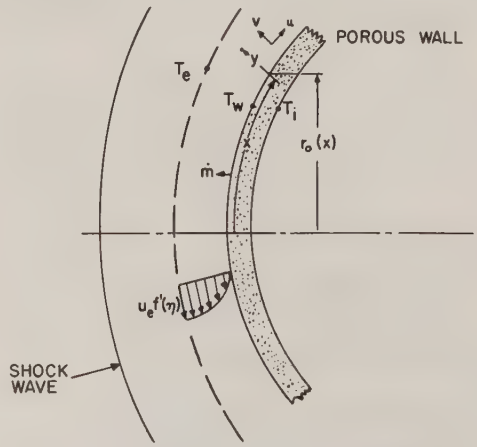

Figure 1. Schematic diagram of area injection of a combustible gas

(3) The Prandtl and Schmidt numbers are equal to unity.

(4) The specific heats of all chemical species are equal and constant.

(5) Chemical reactions do not take place on the surface of or within the porous wall.

(6) The system is in quasi-steady state. The effect of dissociation of oxygen and nitrogen is neglected.

EQUATIONS

The boundary layer equations at a stagnation point are as follows (see *Figure 1*):

Continuity

$$\frac{\partial}{\partial x}(\rho u r_o) + \frac{\partial}{\partial y}(\rho v r_o) = 0 \qquad (1)$$

Momentum

$$\rho\left(u\frac{\partial u}{\partial x}+v\frac{\partial u}{\partial y}\right)=-\frac{\mathrm{d}p}{\mathrm{d}x}+\frac{\partial}{\partial y}\left(\mu\frac{\partial u}{\partial y}\right) \quad (2)$$

Energy

$$C_p\left(u\frac{\partial T}{\partial x}+v\frac{\partial T}{\partial y}\right)=\frac{\partial}{\partial y}\left(k\frac{\partial T}{\partial y}\right)-w_f Q_f \quad (3)$$

where Q_f is evaluated locally. Note that the pressure work term $u\,\mathrm{d}p/\mathrm{d}x$ and the dissipation function $\mu(\partial u/\partial y)^2$ are negligible at a stagnation point and are therefore omitted from equation 3.

Diffusion of ith species

$$\rho u\frac{\partial c_i}{\partial x}+\rho v\frac{\partial c_i}{\partial y}-\frac{\partial}{\partial y}\left(\rho D\frac{\partial c_i}{\partial y}\right)=w_i \quad (4)$$

A stream function ψ is next introduced so that

$$\rho u r_o=\partial\psi/\partial y \quad (5)$$
$$\rho v r_o=-\partial\psi/\partial x$$

Finally, the following similarity variables are utilized in order to reduce the above equations to ordinary differential equations in which η is the independent variable[4]:

$$\eta=\frac{\rho_e u_e}{(2\tilde{S})^{\frac{1}{2}}}\int_o^y r_o\frac{\rho}{\rho_e}\,\mathrm{d}y \quad (6)$$

$$\tilde{S}=\int_o^x \rho_e\mu_e u_e r_o^2\,\mathrm{d}x \quad (7)$$

$$\psi=(2\tilde{S})^{\frac{1}{2}}f(\eta) \quad (8)$$

At a stagnation point,

$$\left(\frac{\partial\eta}{\partial y}\right)_w=\left\{2\left(\frac{\partial u_e}{\partial x}\right)_s\rho_w/\mu_w\right\}^{\frac{1}{2}} \quad (9)$$

Note that $u/u_e=f'(\eta)$, while

$$v_w=-f(0)\left\{2\mu_w\left(\frac{\partial u_e}{\partial x}\right)_s/\rho_w\right\}^{\frac{1}{2}} \quad (10)$$

and

$$m_w=\rho_w v_w=-f(0)\left\{2\rho_w\mu_w\left(\frac{\partial u_e}{\partial x}\right)_s\right\}^{\frac{1}{2}} \quad (11)$$

When equations 6–8 are substituted into equations 1–4, there results:

Momentum

$$f'''+ff''+\tfrac{1}{2}\left(\frac{\rho_e}{\rho}-f'^2\right)=0 \quad (12)$$

Energy

$$T''+fT'=-W_f\frac{Q_f}{c_p}=W_o\frac{Q_o}{C_p} \quad (13)$$

Diffusion

$$c_i''+fc_i'=+W_i \quad (14)$$

where

$$W_i=\frac{-w_i 2\tilde{S}}{\rho\rho_e\mu_e u_e^2 r_o^2}=\frac{-w_i}{2\rho(\mathrm{d}u_e/\mathrm{d}x)_s}\ \text{at a stag. pt.} \quad (15)$$

The last term in equation 12 has only a small effect[4] on the resulting temperature and concentration profiles; hence it is dropped from the analysis. The resulting error is of the same order of magnitude as caused by the other assumptions. The appropriate boundary conditions for equation 12 are then

$$\begin{aligned} f'(0)&=0\\ \lim_{\eta\to\infty}f'(\eta)&=1\\ f(0)&=\text{various values, depending upon the injection rate, see equation 11}\end{aligned} \quad (16)$$

Equation 12 with the boundary conditions given by equation 16 has been solved by Emmons and Leigh[5] for a large number of the injection parameter, $f(0)$. Use will be made of those solutions in the remainder of this report.

BOUNDARY LAYER TRANSIT TIMES

Thus far, the chemical source term, w_i, has not been defined. Before doing so it is of interest to determine the average time it takes for the injected species to traverse the laminar boundary layer by convective and diffusion processes, but in the absence of combustion. Then by comparison of the time, density, and temperature history to that which is required for reaction to occur, it may be possible to determine whether combustion is likely for the particular set of conditions.

For the calculation W_i is taken as zero, in which case the solution to the diffusion equation for the injected species is:

$$c_f(\eta)=c_f(0)[1-f'(\eta)] \quad (17)$$

The time history $t(\eta)$ is obtained from:

$$t=\int_0^y\frac{\mathrm{d}y}{v_i(x,y)_i} \quad (18)$$

At a stagnation point $\mathrm{d}\eta=(\partial\eta/\partial y)\mathrm{d}y$, while

$$v_i=v+V_i=v-\frac{D}{c_i}\frac{\partial c_i}{\partial\eta}\frac{\partial\eta}{\partial y} \quad (19)$$

Substitution of equations 9, 17 and 19 into equation 18 yields:

$$t(\eta)=\frac{1}{2(\mathrm{d}u_e/\mathrm{d}x)_s}\int_0^\eta\frac{\mathrm{d}\eta}{-f(\eta)+\dfrac{f''(\eta)}{1-f'(\eta)}} \quad (20)$$

The equation of the streamline for the injected species, $x(\eta)$ is obtained from:

$$\mathrm{d}\eta=\frac{\partial\eta}{\partial x}\mathrm{d}x+\frac{\partial\eta}{\partial y}\mathrm{d}y$$
$$=\left(\frac{\partial\eta}{\partial x}+\frac{\partial\eta}{\partial y}\frac{v_i}{u_i}\right)\mathrm{d}x \quad (21)$$

Now at a stagnation point $\partial\eta/\partial x = 0$. Substitution of equation 19 and $u_i \doteq (\mathrm{d}u_e/\mathrm{d}x)_s\, xf'(\eta)$ into equation 21 and integration yields:

$$x(\eta) = x(0) \exp\left[\tfrac{1}{2}\int_0^{\eta} \frac{f'(\eta)\mathrm{d}\eta}{-f(\eta) + \dfrac{f''(\eta)}{1 - f'(\eta)}}\right] \tag{22}$$

where $x(0)$ is the x coordinate of the origin of a particle path. In a similar manner it may be shown that on a flat plate

$$\left[\frac{x(\eta)}{x(0)}\right]_{\text{flat plate}} = \left[\frac{x(\eta)}{x(0)}\right]^4_{\text{st. pt.}} \tag{23}$$

and the time history is given by:

$$t(\eta)_{\text{flat plate}} = \frac{2x(0)}{u_e}\int_0^{\eta} \frac{x(\eta)}{x(0)} \cdot \frac{\mathrm{d}\eta}{-f(\eta) + \dfrac{f''(\eta)}{1 - f'(\eta)}} \tag{24}$$

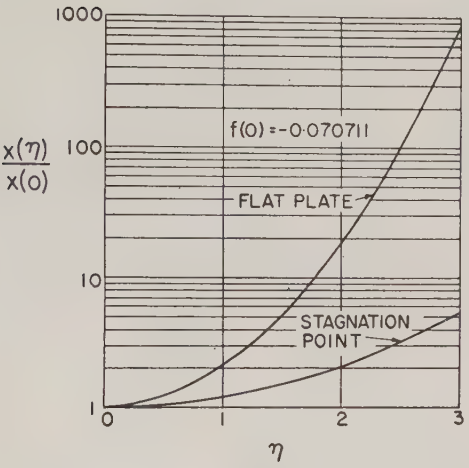

Figure 2. Path of injected species. Stagnation point, equation 22; flat plate, equation 23

The streamlines are shown in *Figure 2*, while the time histories are shown in *Figure 3* for a stagnation point and in *Figure 4* for a flat plate for the case $f(0) = -0{\cdot}070711$. The temperature profile is given by:

$$T = (T_e - T_w)f'(\eta) + T_w \tag{25}$$

as may be verified by substitution into the energy equation, while the density of injected gas is:

$$\rho_f = \rho c_f = c_{f_w}[1 - f'(\eta)]T_e\rho_e/T(\eta) \tag{26}$$

As an example, an injection parameter of $f(0) = -0{\cdot}070711$, nose radius of 1 ft., Mach No. = 20, and an altitude of 10^5 ft., it takes 0·6 msec for the injected gas to pass through the boundary layer. If the time required for combustion for the densities and temperatures given by equations 26 and 25 is greater than 0·6 msec, it is unlikely that combustion will take place within the boundary layer.

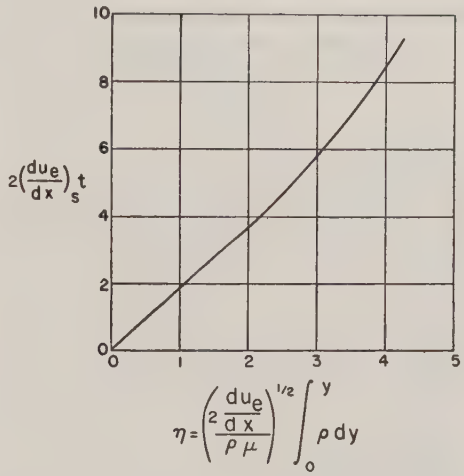

Figure 3. Time history of injected species near a stagnation point, equation 20

STRUCTURE OF DIFFUSION FLAME

The flame front itself may be calculated directly for various reaction kinetics, in order to determine whether combustion will occur. If a first-order reaction rate law is assumed:

$$w_f = -\rho_f \tau^{-1} \mathrm{e}^{-E/RT} \tag{27}$$

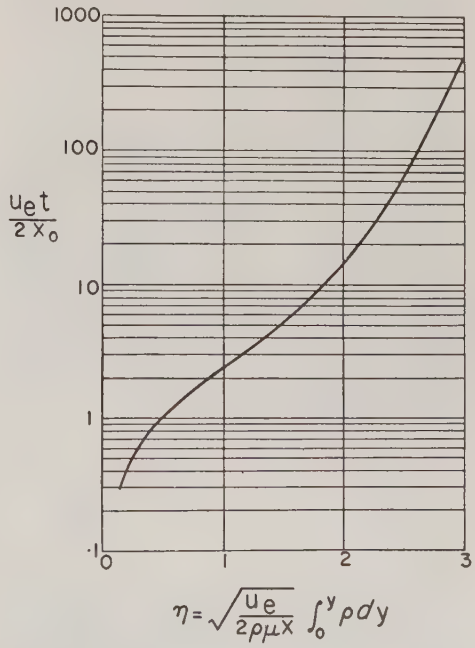

Figure 4. Time history of injected species on a flat plate, equation 24

Then the diffusion equation becomes

$$c_f'' + f c_f' - \frac{c_f \, e^{-E/RT_e \theta(\eta)}}{2(du_e/dx)_s \tau} = 0 \qquad (28)$$

and, combining equations 13 and 14 it can be shown that:

$$\theta(\eta) = \frac{T(\eta)}{T_e} = (1 - \theta_w) f'(\eta) + \theta_w + \frac{Q_f}{C_p T_e} \times \{c_{f_w}[1 - f'(\eta)] - c_f(\eta)\} \qquad (29)$$

Equation 28 has been solved for several values of $(du_e/dx)_s\tau$, Q_f/C_pT_e, and E/RT_e, for a wall temperature and mass transfer, of $T_w/T_e = 0{\cdot}25$, and

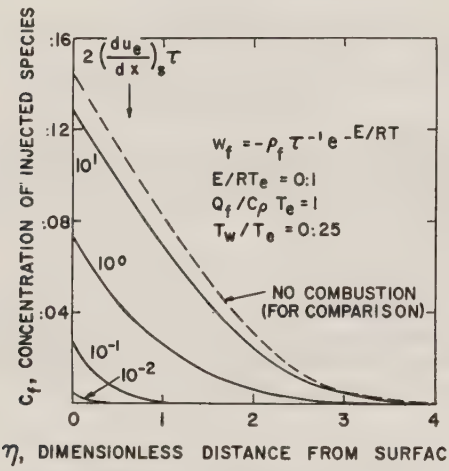

Figure 5. Effect of characteristic combustion time, τ, on combustion within the boundary layer

$-f(0) = 0{\cdot}070711$, respectively. The effect of decreasing the product $2(du_e/dx)_s\tau$ can be seen in *Figure 5*. For a value of 10, the combustion reaction is slow, as indicated by the proximity of the curve to the dashed line, which represents the zero-combustion case. As $2(du_e/dx)_s\tau$ decreases, the local rate of consumption of injected gas is increased, which decreases the local concentration. For a value of 0·01, the combustion takes place adjacent to the wall. For this last case, $f(\eta)$ can be taken as $f(0)$ and $\theta(\eta)$ as θ_w, and equation 28 can be integrated to obtain:

$$c_f(0) = c_{f_w} = [0{\cdot}5 - G^{\frac{1}{2}} f(0)^{-1}]^{-1} \qquad (30)$$

$$c_f(\eta) = c_{f_w} \exp\{-[f(0)/2 + G^{\frac{1}{2}}]\eta\} \qquad (31)$$

where

$$G = [2(du_e/dx)_s\tau]^{-1} \exp(-E/RT_w) \qquad (32)$$

The above equations apply when $G \gg f(0)^2$ and for $-f(0) < c_{o_e} f''(0)/r_{o/f}$. The temperature gradient at the wall, from equation 29 is then given by:

$$\theta_{\eta_w} = (1 - \theta_w) f''(0) - \frac{Q_f}{C_p T_e} f(0) \left\{ \left[1 + \frac{f(0)}{2G^{\frac{1}{2}}} \right]^2 - \frac{f''(0)}{G^{\frac{1}{2}}} \left[1 + \frac{f(0)}{G^{\frac{1}{2}}} \right] \right\} \qquad (33)$$

which shows that as $G/f(0)^2$ increases all of the combustion energy, equal to $m_w Q_f$, is returned to the wall.

The effect of increasing the activation energy is shown in *Figure 6*, for a value of $E/RT_e = 1$. The effect is to decrease the rate of combustion, which increases the concentration of combustible gas in the boundary layer. For a value of $2(du_e/dx)_s\tau = 10$ very little of the gas combusts, as can be seen by comparison of this curve with the dashed curve of *Figure 5*. For $E/RT_e = 10$, no combustion takes place for $10^{-2} < 2(du_e/dx)_s\tau$.

It should be noted that the value of $2(du_e/dx)_s\tau$ depends not only on the value of the characteristic time, τ, but on the nose radius of the vehicle, since this affects the velocity gradient $(du_e/dx)_s$. Thus, for a given injected gas, combustion may not take place for a small nose radius, when $(du_e/dx)_s$ is large, but can take place on a vehicle with a large nose radius when $(du_e/dx)_s$ is small.

Since small activation energies, E, and combustion times, τ, result in the maximum energy

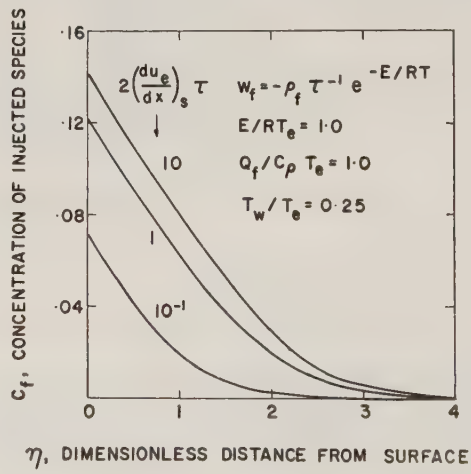

Figure 6. Effect of activation energy, E, on combustion; compare with Figure 5

transfer to the porous surface, this is the situation of most interest. Since the combustion takes place in a narrow zone, W_f can be taken as:

$$W_f = \tilde{W}_f \delta(\eta - \eta_c) \qquad (34)$$

DISSOCIATION OF PRODUCTS OF COMBUSTION

The effect of dissociation of the products of combustion is next calculated for a gas such that the products of dissociation is the same as the injected

species, f. The model, see *Figure 7*, is similar to that in reference 6 in which only the dissociation and re-combination of the injected species is considered. At a plane, c, the combustion takes place, and at a plane, d, the products of combustion dissociate such that in zone III there exists only nitrogen, oxygen, and the injected species. It is assumed that the reactions are frozen except at the planes, c and d. For this case, equation 13 becomes:

$$T''' + fT'' = \frac{Q_o}{c_p}\left\{\tilde{W}_{o_c}\delta(\eta - \eta_c) + \tilde{W}_{o_d}\delta(\eta - \eta_d)\right\} \tag{35}$$

Integration of equation 35 yields:

$$T'_{c+} - T'_{c-} = \tilde{W}_{o_c}Q_o/c_p \tag{36}$$

$$T'_{d+} - T'_{d-} = \tilde{W}_{o_d}Q_o/c_p \tag{37}$$

The solution to equation 35, in terms of T_c and T_d, is:

$$\text{I}\quad T = (T_c - T_w)f'(\eta)/f'_c + T_w \tag{38a}$$

$$\text{II}\quad T = (T_d - T_c)(f' - f'_c)/(f'_d - f'_c) + T_c \tag{38b}$$

$$\text{III}\quad T = (T_e - T_d)(f' - f'_d)/(1 - f'_d) + T_d \tag{38c}$$

If one can now evaluate T_c, the temperature gradient and hence the heat transfer can be evaluated from equation 38a. Substitution of equation 38 into equations 36 and 37 yields two simultaneous algebraic equations in terms of T_c and T_d, from which T_d may be eliminated to obtain:

$$T_c - T_w = f'_c\left\{T_e - T_w - \frac{Q_o}{C_p}\left[\frac{\tilde{W}_{o_c}(1 - f'_c)}{f''_c} + \frac{\tilde{W}_{o_d}(1 - f'_d)}{f''_d}\right]\right\} \tag{39}$$

It is next necessary to determine $\tilde{W}_{o_c}$ and $\tilde{W}_{o_d}$. This may be done from the diffusion equation for oxygen which becomes:

$$c''_o + fc'_o = -\tilde{W}_{o_c}\delta(\eta - \eta_c) - \tilde{W}_{o_d}\delta(\eta - \eta_d) \tag{40}$$

the solution to which is given by

$$\text{I}\quad c_o = (c_{o_c} - c_{o_w})f'/f'_c + c_{o_w} \tag{41a}$$

$$\text{II}\quad c_o = (c_{o_d} - c_{o_c})(f' - f'_c)/(f'_d - f'_c) + c_{o_c} \tag{41b}$$

$$\text{III}\quad c_o = (c_{o_e} - c_{o_d})(f' - f'_d)/(1 - f'_d) + c_{o_d} \tag{41c}$$

Substitution of equation 41 into equation 40 and integration yields:

$$-\frac{\tilde{W}_{o_c}}{f''_c} = \frac{c_{o_d} - c_{o_c}}{f'_d - f'_c} - \frac{c_{o_c} - c_{o_w}}{f'_c} \tag{42}$$

and

$$-\frac{\tilde{W}_{o_d}}{f''_d} = \frac{c_{o_e} - c_{o_d}}{1 - f'_d} - \frac{c_{o_d} - c_{o_e}}{f'_d - f'_c} \tag{43}$$

c_{o_e} can be determined from the boundary condition that the rate of mass transfer of oxygen through the porous wall is zero, that is:

$$0 = m_w c_{o_w} - \left(\rho D \frac{\partial c}{\partial \eta}\frac{\partial \eta}{\partial y}\right)_w$$

or

$$0 = -f(0)c_{o_w} - [c_{o_c} - c_{o_w}]f''(0)/f'_c \tag{44}$$

Substitution of equations 42, 43 and 44 into equation 39 yields T_c. Use of T_c in equation 38a gives the result:

$$q_w = k_w\left(\frac{\partial \eta}{\partial y}\right)_w f''(0)\left\{T_e - T_w + \frac{Q_o}{C_p}\left[c_{o_e} - c_{o_w}\left(1 - \frac{f(0)}{f''(0)}\right)\right]\right\} \tag{45}$$

Equation 45 is identical to the result which is obtained if no allowance had been made for dissociation[3], hence for the assumptions which were made, there is no effect upon the heat transfer due to subsequent dissociation of the products of combustion. This result is consistent with that of reference 7.

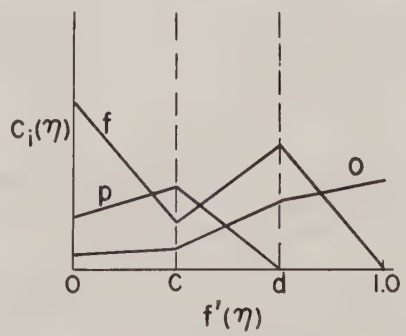

Figure 7. Model for combustion and dissociation of injected gas. c, combustion zone. d, dissociation zone. f, injected species. O, oxygen. p, product of combustion

The conditions under which c_{o_w} may be greater than zero are twofold: (1) the reaction kinetics are very slow; (2) the reaction kinetics are rapid, but the rate of injection is small. In the latter case,

$$(\rho v)_{f_w} = -(\rho v)_{o_w} r_{o|f} \tag{46}$$

which becomes

$$-\frac{f(0)}{f''(0)} r_{o|f} = c_{o_e} - c_{o_w}\left[1 - \frac{f(0)}{f''(0)}\right] \tag{47}$$

Thus, for rapid reaction kinetics, the combustion will take place adjacent to the wall as long as $c_{o_w} > 0$, or for

$$-f(0) < c_{o_e} f''(0)/r_{o|f} \tag{48}$$

Substitution of equation 47 into equation 45 yields:

$$q_w = k_w \frac{\partial \eta}{\partial y_w} \left\{ f''(0)(T_e - T_w) + f(0) Q_f \right\} \quad (49)$$

Equation 49 states that for combustion adjacent to the porous surface, the heat transfer is the sum of the convective heat transfer in the absence of combustion, plus the product of the injection rate times the heat of combustion. In this case, all of the energy of combustion is returned to the wall. When $-f(0) > c_{o_e} f''(0) r_{o/f}$, the flame front is pushed away from the porous surface, and since

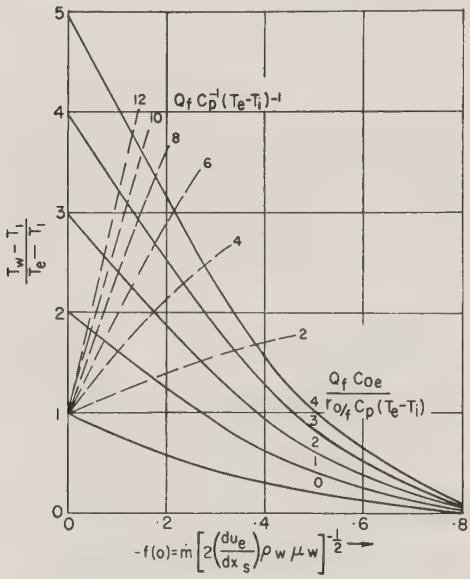

Figure 8. Dependence of adiabatic wall temperature on mass transfer rate, $f(O)$, and heat of combustion, Q_f

$f''(0)$ decreases rapidly with increasing injection rate, the effect of combustion is minimized, see equation 45.

APPLICATION TO TRANSPIRATION COOLING

If it is assumed that no energy is transferred to the injected gas prior to its passage through the porous wall, then the integral form of the energy equation requires that

$$m_{fw} c_p (T_w - T_i) = q_w \quad (50)$$

One may now use equations 11, 45 and 49 and solve for the wall temperature ratio

$$(T_w - T_i)/(T_e - T_i)$$

which is the solution to the problem. The following cases may be examined:

(1) Reaction zone adjacent to the surface with rapid reaction kinetics. For this case the wall temperature ratio is given by:

$$\frac{T_w - T_i}{T_e - T_i} = \frac{1 - \dfrac{f(0)}{f''(0)} \cdot \dfrac{Q_f/C_p}{T_e - T_i}}{1 - f(0)/f''(0)} \quad (51)$$

Thus, if $(Q_f/C_p)(T_e - T_i)^{-1} > 1$, the wall temperature will exceed the temperature of the gases at the edge of the boundary layer, and will increase with increasing injection rate. The flame will remain adjacent to the surface until the mass transfer is increased above that required to decrease the concentration of oxygen at the surface to zero, as given by equation 48. This effect is shown as the dotted lines in *Figure 8.*

(2) Flame blown off surface. This applies when $-f(0) > c_{o_e} f''(0)/r_{o/f}$, and the wall temperature ratio is obtained from equations 45 and 50:

$$\frac{T_w - T_i}{T_e - T_i} = \frac{1 + \dfrac{Q_o \left\{ 1 - \dfrac{c_{o_w}}{c_{o_e}} \left[1 - \dfrac{f(0)}{f''(0)} \right] \right\}}{C_p (T_e - T_i) c_{o_e}}}{1 + \dfrac{f(0)}{f''(0)}} \quad (52)$$

For $c_{o_w} = 0$, the wall temperature ratio decreases rapidly with increasing mass transfer, $f(0)$. This is shown as the solid lines in *Figure 8.* The intersection of the proper dotted curve and the solid line gives the maximum possible wall temperature. Note that in order to maintain low wall temperature ratios, appreciable mass transfer is required, but the effect of combustion on the required mass transfer is small.

On the other hand, for

$$(T_w - T_i)/(T_e - T_i) \sim 1$$

the effect of combustion is to increase the required mass transfer appreciably. This effect of an increase in the required injection rate has been demonstrated previously for a turbulent boundary layer by Crocco[7].

The effect of incomplete combustion is to increase the concentration of oxygen at the wall. The required mass transfer, as a function of oxygen concentration at the wall, c_{o_w} may also be deduced from *Figure 8,* if c_{o_e} is replaced by $c_{o_e} - c_{o_w}[1 - f(0)/f''(0)]$. Again it is evident that the effect of combustion on the required mass transfer $f(0)$ is minimized for small wall temperature ratios. Note that when

$$(c_{o_w}/c_{o_e})[1 - f(0)/f''(0)] = 1$$

none of the combustible gas has been consumed. This case is equivalent to the case of $Q_o = 0$; that is, this case is identical to the case of no combustion, and equation 52 reduces to the usual equation for the injection of an inert gas.

CONCLUSIONS

When a combustible gas is used for mass transfer cooling, the required mass transfer rate is greater than for a non-combustible gas. The percentage increase becomes smaller as the required wall temperature decreases, so that for very small wall temperatures, the effect of combustion can be neglected.

If the products of combustion dissociate, this has no effect on the rate of energy transfer to the wall as long as the concentration of oxygen at the wall is unchanged, for the assumptions made.

Finite reaction kinetics increases the thickness of the diffusion flame front, and decreases the rate of energy transfer to the surface.

The effect of the assumptions is to introduce an error in the absolute magnitude of energy transfer, but this does not invalidate the conclusions.

NOMENCLATURE

c_i	local mass fraction of ith species $= \rho_i/\rho$
C_p	specific heat
du_e/dx	inviscid velocity gradient
D	diffusion coefficient
E	activation energy
h	total enthalpy of mixture, including chemical
K	reaction rate, see equation 17
k	thermal conductivity of gaseous mixture
$f(\eta)$	similarity stream function; $f'(\eta) = u/u_e$
m	mass transfer rate per unit area $= \rho v$
m_i	mass flux rate of species $i = \rho_i v_i = \rho_i(v + V_i)$
p	pressure
q	heat transfer rate to surface per unit area $= K(\partial T/\partial y)$
Q_o	heat of combustion at constant pressure per unit mass of oxygen
Q_f	heat of combustion at constant pressure per unit mass of fuel $= Q_o r_{o/f}$
R	gas constant
$r_o(x)$	radius of cross section of body at body station x
$r_{o/f}$	mass of oxygen consumed per mass of fuel consumed
$\tilde{S}$	similarity variable in x direction
t	time
T	temperature
u	macroscopic stream velocity in x direction
v	macroscopic stream velocity in y direction
v_i	absolute velocity of ith species $= v + V_i$
V_i	diffusion velocity of ith species $= -\rho D \nabla c_i$
w_i	mass rate of production of ith species per unit volume
W_i	see equation 15
$\tilde{W}_i$	see equation 34
x	distance from stagnation point along surface
y	distance normal to surface
Z	fraction of combustion energy returned to the wall
μ	viscosity of gaseous mixture
θ	T/T_e, dimensionless temperature
η	similarity variable in y direction
ψ	stream function
δ	Dirac delta function, $\lim_{\varepsilon \to 0} \int_{-\varepsilon}^{\varepsilon} \delta(\eta) d\eta = 1$
ρ	mass density of gaseous mixture
τ	characteristic combustion time

Subscripts

c	point in the boundary layer at which combustion takes place
d	point in the boundary layer at which dissociation takes place
e	at outer edge of boundary layer
f	fuel (injected species)
i	initial
o	oxygen (molecular and atomic)
p	product of combustion
s	stagnation point
w	at the outer surface of the porous wall

Superscript

$'$	differentiation with respect to η

The author would like to thank Dr. S. M. Scala and Dr. H. G. Lew for their many suggestions and for reviewing the manuscripts, S. Blecher for checking the equations, and Dr. Joseph Farber for suggesting this problem.

REFERENCES

1 Spalding, D. B. *Some Fundamentals of Combustion.* 1955. New York; Academic Press

2 Emmons, H. W. Film combustion of liquid fuels. *Z. angew. Math. Mech.* 36 (1956) 60

3 Sutton, G. W. Combustion of a gas into a hypersonic laminar boundary layer. *Amer. Rocket Society preprint* 621–58

4 Lees, L. Laminar heat transfer over blunt-nose bodies at hypersonic flight speeds. *Jet Propulsion* 26, No. 4 (1956) 259

5 Emmons, H. W. and Leigh, D. *Tabulation of the Blasius Function with Blowing and Suction.* Division of Applied Sciences, Combustion Aero. Lab., Interim Technical Report No. 9, Harvard University, 1953

6 Cohen, C. B., Lipkis, R. and Bromberg, R. Boundary layers with chemical reactions due to mass additions. *Paper GM-TR-268,* Ramo-Wooldridge Corp., Los Angeles, Calif., October 1957. (To be published in *Jet Propulsion*)

7 Crocco, L. An approximate theory of porous, sweat, or film cooling with reactive fluids. *Jet Propulsion,* November/December (1952) 331

FORMATION OF DISPERSED CARBON BY THERMAL DECOMPOSITION OF HYDROCARBONS

P. A. TESNER

Though carbon black is formed during many of the processes of thermal decomposition and combustion of hydrocarbons and though much research has been done on the subject, this process has been studied insufficiently[1]. This paper gives a new approach to the study of the process and presents experimental data confirming its validity.

GENERAL

From a physical point of view the formation of carbon black is an example of the formation of a solid dispersed phase from a gas, and therefore this process should obey the general laws governing all processes of formation of a new dispersed phase.

The formation of a dispersed phase is a complex and insufficiently studied process determined by two different but simultaneous processes, viz. the formation of primary nuclei and the growth of those nuclei. These two processes may have very different mechanisms.

The most characteristic features of processes of dispersed phase formation are, first, their extreme sensitivity to supersaturation of the system and, secondly, their autocatalytic, 'avalanche' nature.

Relative to the formation of carbon particles by the thermal decomposition of hydrocarbons a supersaturated condition is one remote from thermodynamic equilibrium as determined by the hydrocarbon concentration and temperature. And since the formation of carbon black has been found to be possible only at relatively high concentrations of the hydrocarbon, supersaturation of the system depends mainly on the temperature, i.e. on the extent of 'superheating' of the system with respect to the temperature of thermodynamic equilibrium.

Carbon black can form only at high temperatures and its formation is so rapid that it cannot be separated from the process of heating the gas to the reaction temperature. It is therefore natural to conclude that the rate of carbon black formation and the degree of dispersion of the resulting product must depend not only on the maximum temperature attained by the system but on the rate of rise of the temperature as well. Indeed, the higher the temperature, the greater the supersaturation and the higher the rate of formation of primary nuclei and their rate of growth. But the higher the temperature, the higher the overall velocity of decomposition, i.e. the higher the rate of fall of supersaturation of the system owing to decreasing hydrocarbon concentration. Therefore with slowly rising temperature complete decomposition of the hydrocarbon will occur on the relatively small number of nuclei formed long before the system reaches its maximum temperature. In such a case the dispersity of the product will not be high, because the temperature of formation of the nuclei was relatively low. The greater the rate of rise of the temperature, the higher the temperature at which the formation of primary nuclei will cease and the higher the dispersity of the resulting carbon black should be.

Mathematical analysis shows that if the gas is heated in an externally heated reaction tube the absolute rate of heating of the gas, i.e. the rate of rise of its temperature in deg/sec depends on the conditions of flow, the linear velocity of the gas and the diameter of the reaction tube. The ratio of absolute heating rates (ω) for two cases differing in reaction tube diameter (d' and d'') and in linear gas velocity (w' and w'') can be expressed as follows:

(1) Laminary flow: $$\frac{\omega'}{\omega''} = \left(\frac{w'}{w''}\right)^{0.2} \cdot \left(\frac{d''}{d'}\right)^{1.5}$$

(2) Turbulent flow: $$\frac{\omega'}{\omega''} = \left(\frac{w'}{w''}\right)^{0.8} \cdot \left(\frac{d''}{d'}\right)^{1.2}$$

Therefore, the degree of dispersion of the carbon black formed by the thermal decomposition of hydrocarbons in an externally heated reaction tube should be the higher, the greater the linear velocity of the gas and the smaller the diameter of the reaction tube, independent of the chemical mechanism by which the nuclei form and afterwards grow.

CARBON SURFACE GROWTH

In accordance with the general considerations set forth above, the processes of growth of the carbon surface and of formation of the primary carbon

black nuclei were studied in separate sets of experiments.

It was proved that conditions of thermal decomposition of any hydrocarbons could always be found where thermal decomposition occurred only on the surface, and no carbon black nuclei formed. This enabled development of a special procedure for studying the kinetics of growth of the carbon surface. Two methods were employed for this purpose: electron microscopy and a weight method.

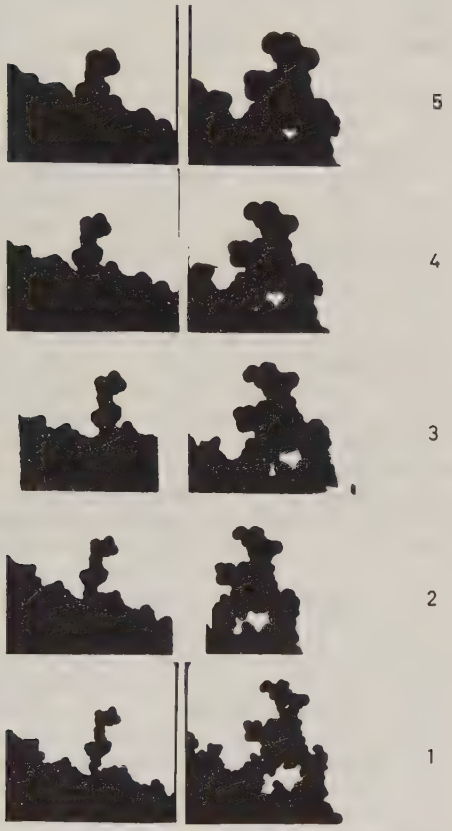

Figure 1. Successive electron photographs of the same carbon black particle aggregates after being covered with a carbon layer

By means of the electron microscope the actual growth of carbon black particles introduced into an atmosphere of a heated hydrocarbon was measured[2]. *Figure 1* shows a group of carbon black particles after such treatment. In the weight method the amount of carbon formed on the surface of a sample of substance having a strictly definite surface was determined[3]. The most convenient substance for this purpose was carbon black.

Kinetic measurements showed that growth of the carbon surface during the thermal decomposition of the hydrocarbon is due to direct decomposition of hydrocarbon molecules on the surface. This involves decomposition of active hydrocarbon molecules at the most active points of the carbon surface, the carbon atoms of the decomposed hydrocarbon molecule not migrating along the surface, as is usually the case in the growth of a crystal lattice, but remaining at the point of the surface where the reaction occurred. The peculiarity of this process is that it is not preceded by any chemical process in the bulk of the hydrocarbon. In other words, it is the molecules of the initial hydrocarbon that decompose on the carbon surface and not carbon radicals or bulk-polymerization products. This was proved by special experiments in which the amount of hydrogen corresponding to the carbon formed on the surface was determined. In all cases this amount was in agreement with the stoichiometric ratios between the carbon and the hydrogen in the molecules of the decomposed hydrocarbons. If the carbon surface grew due to decomposition of radicals or polymers, which are lower in hydrogen than the initial molecules, the quantity of hydrogen formed would have been smaller. Of course, molecules of the various intermediates and resultants of the pyrolysis reaction in the bulk of the hydrocarbon decompose simultaneously on the surface, but these processes occur in parallel with the main process of decomposition of hydrocarbon molecules on the surface.

The kinetics of growth of the carbon surface obeys simple laws. The rate of growth is proportional to the hydrocarbon concentration, has a high temperature factor and is greatly retarded by the hydrogen formed during the reaction.

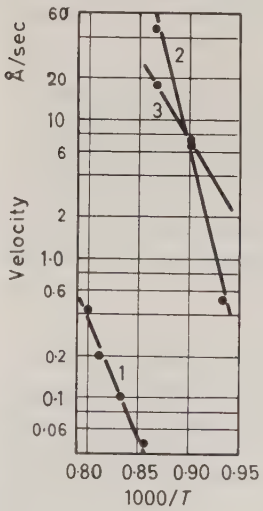

Figure 2. Rate of carbon surface growth during decomposition of methane (1), benzene (2) and cyclohexane (3) by electron microscope measurements

This retardation is due to chemisorption of the hydrogen by the carbon surface. *Figure 2* shows the temperature dependence of the growth rate

of the carbon surface in Arrhenius co-ordinates, plotted on the basis of electron microscope measurements. According to these measurements the apparent activation energy of growth for benzene, methane and cyclohexane were, respectively, 138, 78 and 55 cal/mole. *Figure 3* shows the dependence between the growth rate of the carbon surface during the thermal decomposition of methane on platinum and the hydrogen content, plotted from data obtained by the weight method.

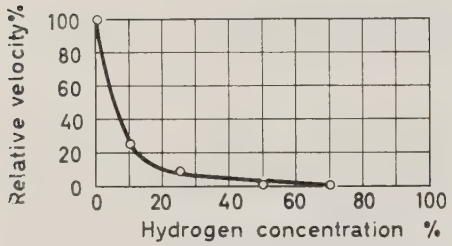

Figure 3. Relative rate of carbon formation during decomposition of methane over platinum at various hydrogen concentrations in a methane-hydrogen mixture. Temperature, 950°C

On the whole, the formation of the carbon surface is a purely heterogenic or, rather, topochemical process and therefore its velocity depends substantially on the physical and chemical properties of the growing surface. In this connection the rate of growth of a carbon layer on various non-carbon surfaces (say, platinum, aluminium oxide, aluminosilicates, etc.) is different, and, as a rule, lower than that of a carbon surface. Therefore, as the non-carbon surface becomes coated with the carbon layer, the rate of formation of the carbon rises until it reaches a velocity corresponding to the rate of growth of a carbon surface.

It should be pointed out that growth rates measured by the weight method developed by us are so perfectly reproducible that the method can be used to measure the specific surface area of dispersed carbonaceous materials. This led to the development of the so-called kinetic method of measurement of specific surface areas of carbon blacks[4] which has been of great use in our investigations.

FORMATION OF DISPERSED CARBON

The formation of dispersed carbon by the thermal decomposition of a hydrocarbon was studied under dynamic conditions in an externally heated reaction tube[5]. The carbon black formed was collected quantitatively and its degree of dispersion was determined.

In agreement with the results obtained in our study of the growth of a carbon surface we found that when a hydrocarbon is thermally decomposed in a flow system the spontaneous formation of nuclei of new carbon black particles in the bulk of the gas is accompanied by the simultaneous surface formation of a surface layer of solid carbon on the walls of the reaction chamber, this process limiting the carbon black yield.

Mathematical analysis of the formation of carbon particles and of the growth of the solid carbon layer on the wall revealed the relation between the mean rate of growth of the carbon layer and the degree of dispersion of the carbon black particles.

The simple relationship arrived at, viz. $V = K \frac{r_{max}}{\tau}$ was confirmed by experiment. In this relation V is the mean linear rate of growth of the carbon surface over the length of the reaction tube, Å/sec; K is a proportionality factor depending mainly on the physical properties of the surface of the growing particles and of the surface of the reaction tube wall; r_{max} is the radius of the largest particle of carbon black obtained, Å; τ is the time (sec) the largest particle remains within the reaction zone.

Despite the fact that solid carbon forms in the same parts of the reaction chamber as the carbon black, the lustrous carbon layer was never found to be covered with a layer of carbon black after the experiment; the carbon black begins to settle on the walls of the reaction tube only at the end of the reaction zone, where the solid carbon hardly forms at all.

It was found that carbon black does not settle in the hottest zone, the zone of intensive formation of lustrous carbon and carbon black. This is due to the fact that hydrogen is evolved simultaneously with the formation of the lustrous carbon layer on the walls, and this hydrogen flows inwards from the walls hindering the free diffusion of the carbon particles towards the wall. Only at the end of the reaction zone where the formation of lustrous carbon becomes sufficiently slow on account of the low concentration of the hydrocarbon and the high concentration of the hydrogen, does the flow of hydrogen become insignificant, and the carbon particles are then able to settle on the walls. Such a flow is observed in all cases where the volume of the gas arriving at the wall due to diffusion increases as a result of the chemical reaction taking place at the wall. As the decomposition of methane and benzene to carbon and hydrogen involves an increase in volume the decomposition of these hydrocarbons gives rise to a hydrogen flow from the walls which accounts for the fact that carbon black does not settle in the zone of intense formation of the lustrous carbon layer. Indeed, in control

experiments made by decomposing acetylene, which takes place without any change in volume ($C_2H_2 = 2C + H_2$), the carbon black was observed to settle at all points of the reaction tube.

These considerations suggested that coagulation of carbon black particles is impossible in the zone of their intensive formation and growth, i.e. that each of the growing particles is surrounded by a stream of hydrogen directed outwards from the surface of the particle and serving as a protective atmosphere. It follows therefore that the number of carbon black particles leaving the reaction tube must equal the number of particles formed in the reaction zone.

In connection with this the number of particles forming per unit time and determined by the yield and degree of dispersion of the carbon black was accepted as the principal kinetic characteristic of the process. Hereafter this constant will be termed the mean rate of particle formation, as it characterizes the rate of particle formation throughout the entire reaction zone. The degree of dispersion of the carbon black was determined mainly by the kinetic method, the results being corrected by measurements made with the electron microscope.

The above-described procedure was employed in a study of the kinetics of formation of carbon black particles by the thermal decomposition of methane, natural gas and benzene. It was found that to form carbon black nuclei by the decomposition of a hydrocarbon the latter must be 'superheated' with respect to the process of carbon formation on the walls.

For instance, on the thermal decomposition of methane in a flow system a carbon layer begins to appear on the walls at 900°C whereas carbon black particles are observed to form only at 1,050°C. On the decomposition of the benzene the carbon layer begins to form at a measurable rate at 750°C, while carbon black particles appear only at 950°C.

Thus, to form carbon black nuclei by the decomposition of a hydrocarbon, the latter must be 'superheated' at 150 to 200°C. Taking into account the high temperature factors of carbon surface growth, the absolute 'superheating' observed should be regarded as very high. This shows how difficult it is for carbon particle nuclei to form.

The rate of particle formation was measured at various temperatures, hydrocarbon concentrations and various linear rates of flow.

However, the results obtained did not fit in with any simple kinetic scheme. For instance, it was found that increasing the temperature in the reaction zone at a constant rate of flow of the hydrocarbon affects the rate of particle formation very little, while with constant rate of decomposition of the hydrocarbon, the effect of the temperature is, on the contrary, very high, this being in line with the high apparent activation energy values of the process (*Figure 4*). It was also found that the rate of particle formation increases sharply when the hydrocarbon is diluted with hydrogen. Whereas the retardation of carbon surface growth is greatest at low hydrogen concentrations, the rate of the new particle formation begins to increase perceptibly only at a high hydrogen concentration (*Figure 5*).

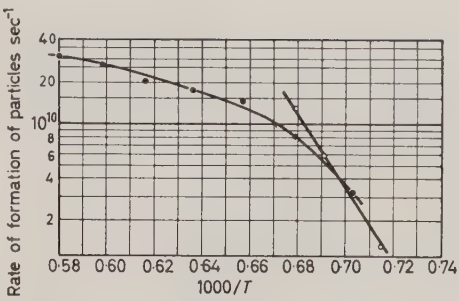

Figure 4. Mean rate of formation of carbon black particles by decomposition of methane depending on the temperature in the reaction chamber in Arrhenius co-ordinates.
- • *Rate of gas flow* 500 ml/min
- ○ *Degree of decomposition* 50 per cent

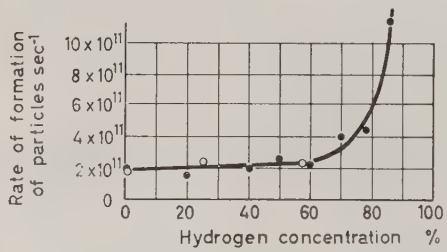

Figure 5. Mean rate of formation of carbon black particles by decomposition of natural gas depending on hydrogen concentration in natural gas-hydrogen mixture.
- • *Vertical furnace arrangement*
- ○ *Horizontal furnace arrangement*

It was discovered that if the hydrocarbon is diluted with hydrogen and the linear velocity of the gas is increased the zone of carbon black particle formation shifts towards higher temperatures.

Thus, it proved that actually hydrogen does not accelerate but, on the contrary, slows down the formation of carbon black particles; the considerable acceleration observed is due to the specific conditions of heating the gas in stream. Owing to the retardation of the process in the initial stages of decomposition carbon black formation begins and goes on in the hotter part of the reaction chamber. This increases the

heating rate, which, in its turn, causes the increase in the rate of particle formation and in the dispersity of the carbon black. These results account for the well known fact that the degree of dispersion of thermal carbon black made from natural gas increases if the gas is diluted preliminarily with hydrogen.

Analysis of electron photographs of carbon black samples obtained by us showed that the carbon black does not contain particles below a certain minimum size. This shows that particle formation ceases earlier than the process of particle growth. Mathematical treatment made it possible to calculate the hydrocarbon concentration at the moment the carbon black nuclei ceased to form, and the relative length of time the gas takes to pass through the zone where new carbon black particles are being formed and through the zone where the particles are only growing.

Calculations carried out for the thermal decomposition of natural gas showed that at the moment the nuclei stopped forming in the gaseous phase, from 25 to 40 per cent of undecomposed methane still remained. The fact that the nuclei stop forming though the concentration of hydrocarbon is still high, while the carbon surface continues to grow intensively under the same conditions, illustrates the great 'difficulty' of nucleus formation relative to nuclear growth. This is manifested also in the fact that surface growth begins at a much lower temperature than spontaneous nucleus formation.

These calculations also show that the higher the temperature and the greater the linear velocity of the gas, the shorter the time the gas takes to pass through the zone of new carbon particle formation.

With rates of flow of natural gas of 200, 500 and 2,000 ml/min (tube diameter 19 mm, temperature 1,350°C) the gas passes through the zone in 0·52, 0·29 and 0·084 sec, respectively. The considerable increase in the rate of the process when the linear velocity of the gas is raised is due to the increase in the rate of heating of the gas as a result of which the process is actually going on at a higher temperature. The thermal decomposition of flowing hydrocarbons to form carbon black particles and a carbon layer on the walls may be represented by the diagram in *Figure 6.*

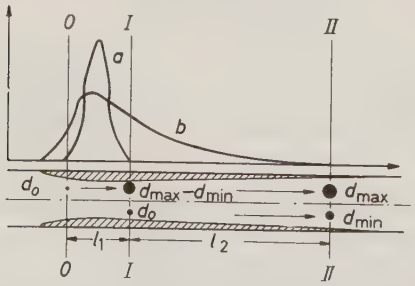

Figure 6. Diagram of the processes of nucleus formation and growth of carbon black particles and solid carbon layer during thermal decomposition of flowing hydrocarbons
l_1 *zone of new nucleus formation*
l_2 *zone of particle growth*
a rate of appearance of nuclei
b rate of particle growth

To verify the theoretical reasoning with respect to the influence of the rate of heating of the gas on the process, tests were made with various linear gas velocities as well as with reaction tubes of various diameters.

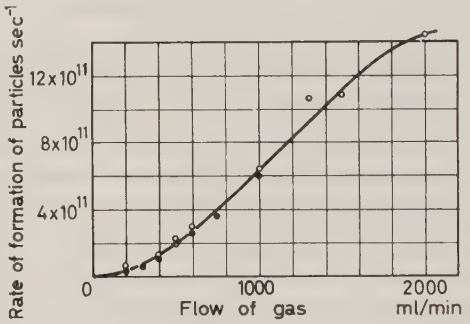

Figure 7. Rate of formation of carbon black particles by decomposition of natural gas depending on rate of flow.
• *Vertical furnace arrangement*
○ *Horizontal furnace arrangement*

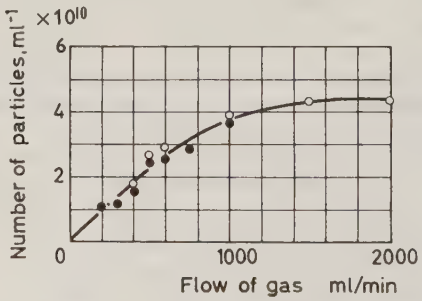

Figure 8. Number of carbon black particles formed per unit volume of gas by decomposition of natural gas depending on rate of flow.
• *Vertical furnace arrangement*
○ *Horizontal furnace arrangement*

The experiments in which the rate of gas flow was varied were made with natural gas at 1,350°C. The results are shown in *Figures 7* and *8.* The carbon black yield remains practically constant over the entire interval of gas velocities studied. The specific surface of the carbon black increases with the rate of gas flow up to 1,000 ml/min, beyond which it remains practically constant with increasing rates of flow. The mean rate of carbon black particle formation rises from 0·6 × 10^{11} sec^{-1} at a flow rate of 200 ml/min to 14·5

TABLE 1

Experiment No.	*Temperature* °C	*Tube diameter* mm	*Rate of flow of gas* ml/min	*Linear velocity of gas at 20°C* cm/sec	*Yield of carbon black (per cent to carbon in gas throughput)*	*Specific surface of carbon black* m^2/g	*Rate of particle formation* 10^{10} sec^{-1}	*Number of particles,* 10^{10} ml^{-1}
50/1	1,350	10	137	2·28	41·3	16·5	7·62	3·34
50/2	1,350	10	260	5·52	41·9	18·4	20·4	4·74
26/1–2	1,350	19	500	2·28	43·9	14·0	18·3	2·19
31/9–13	1,350	19	2,000	11·7	46·7	17·6	145	4·36
62/3	1,350	3	300	70·8	26·7	72·4	825	165·0
63/1	1,380	3	300	70·8	—	73·2	—	—
63/2	1,380	3	300	70·8	—	74·8	—	—

$\times 10^{11}$ sec^{-1} at a rate of 2,000 ml/min, i.e. 24-fold with a 10-fold increase in the rate of flow.

Thus, the mean rate of carbon black particle formation rises with increasing rate of gas flow, i.e. with growing linear velocities or with diminishing contact times. This is illustrated also by the curve in *Figure 8* showing the number of carbon black particles formed per ml of gas input.

To determine the influence of the reaction tube diameter experiments were carried out in tubes 19, 10 and 3 mm in diameter. The results are given in Table 1.

Difficulties were experienced in carrying out the 3 mm tube experiments owing to settling of the carbon black formed on the walls. For this reason the only tests made in this tube were with a rate of flow of 300 ml/min, this corresponding to a considerably higher linear velocity than in the experiments in the 19 mm tubes.

As the linear velocities differed in different tubes, the relative rate of carbon black particle formation was compared by the number of particles formed per unit volume of gas, rather than by the mean rate of particle formation.

The values of this factor, given in the last column of the table, show that the rate of formation of carbon black particles rises considerably with decreasing reaction tube diameter. Thus, at equal linear gas velocities $2·19 \times 10^{10}$ particles are formed per ml in the 19 mm tube (experiment 26/1–2) and $3·34 \times 10^{10}$ particles in the 10 mm tube (experiment 50/1). At a linear velocity of 5·52 cm/sec the number of particles formed in the 10 mm tube was $4·74 \times 10^{10}$ per ml, while in the 19 mm tube at a linear velocity twice as high (11·7 cm/sec) the number of particles was $4·36 \times 10^{10}$ per ml. Accordingly, the specific surface of the carbon black obtained in the 10 mm tube is higher than that of the carbon black obtained at the same linear velocity in the 19 mm tube.

At a linear velocity of 2·28 cm/sec the carbon black from the 10 mm tube has a specific surface area of 16·5 m^2/g while that from the 19 mm tube has 14·0 m^2/g.

The acceleration of carbon black particle formation in the 3 mm tube was still greater. The number of particles formed per ml of gas throughput in this tube was from 83 to 165×10^{10}, which is more than a whole order higher than the largest values obtained in the 10 and 19 mm tubes. Accordingly, the degree of dispersion of the resulting carbon black is also much higher, equalling 57·6 to 72·4 m^2/g according to measurements made by the kinetic method.

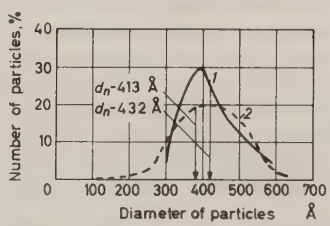

Figure 9. Particle size curves of various carbon blacks. (1) Carbon black obtained by thermal decomposition of natural gas in 3 mm tube. (2) Channel carbon black

Figure 9 shows the particle size curves of carbon black obtained in a 3 mm tube, compared to channel carbon black. The curves show that the two samples obtained by entirely different methods are very similar.

Mean diameters and specific particle numbers calculated from the distribution curves show these values to be very close too in both cases:

	Carbon black	
	Experimental thermal	*Channel*
Mean arithmetical diameter Å . . .	432	413
Mean surface diameter Å	455	447
Specific number of particles g^{-1} . .	$11·9 \times 10^{15}$	$12·75 \times 10^{15}$

Attempts to establish a relationship between the mean rate of particle formation or the specific number of particles formed and the rate of heating

of the gas in experiments with different linear gas velocities and different reaction tube diameters were fruitless. The trouble was that the necessary temperature conditions could not be accomplished in experiments with laboratory-type high-temperature furnace.

In particular, when the velocity of the gas was increased the maximum heating temperature of the gas had to be lower on account of the shortness of the reaction zone (200–250 mm) which, taking into consideration the high temperature factors of the rates of the processes under study, must have distorted the results considerably. Besides, experiments in the 3 mm tube could be carried out for one gas velocity only.

DISCUSSION OF RESULTS

It seems to us that the results obtained are quite convincing and prove that the formation of dispersed carbon by the thermal decomposition of hydrocarbons possesses all the characteristic features of processes of formation of a dispersed phase and obeys the laws peculiar to such processes. Owing to the specific features of these laws the most important factor, determining both the kinetics of the process and the degree of dispersion of the resulting product, proved to be not the chemical mechanism of the process but the purely physical process of heating of the hydrocarbon.

Our results can explain why papers devoted to studies of the kinetics of thermal decomposition of hydrocarbons to carbon and hydrogen have been contradictory and not very convincing. These studies have always employed conventional methods of chemical kinetics, the rate of decomposition being estimated both in dynamic and static conditions by the amount of hydrogen formed during the reaction. The carbon formed during the reaction was usually left without sufficient attention; its quantity was not measured, and in most studies even the form in which it was formed could not be established. This is the only explanation for the fact that up till now even the kinetics of thermal decomposition of methane, which has been the subject of dozens of special studies, has remained insufficiently clear and that investigators still disagree as to whether this reaction is homogeneous or heterogeneous in nature.

The thermal decomposition of a hydrocarbon is a complicated set of processes. At a comparatively low temperature two processes take place simultaneously: heterogeneous thermal decomposition on a solid surface with the formation of a solid layer of carbon, and homogeneous transformation in the bulk. The overall rate of decomposition depends on the surface-to-volume ratio in the reaction space. At higher temperatures, after a certain minimum 'supersaturation' has been achieved, spontaneous formation of carbon black nuclei sets in and autocatalytic decomposition begins on their growing surface. From this moment the process acquires the features of process of formation of a new solid dispersed phase. It is clear that all attempts to express this complex process within the terms of chemical kinetics will fail.

Of course, the results so far obtained are not sufficient to build up a quantitative theory of the process. However, they give a qualitative picture of it and indicate the way for further experimentation. Such experimentation should first of all clear up the physical aspects of the process and give a quantitative relation between the rate of formation of the dispersed phase and the principal physical parameters, which are the determinative parameters of the process as a whole.

The chemical mechanism is of secondary importance. In this study the question of mechanism was not investigated specially, but the results obtained make it possible to suggest some general ideas. First, the formation of carbon black particles takes place in two stages (nucleus formation and particle growth), each of which has an entirely different mechanism. The mechanism of particle growth is probably similar to the mechanism of growth of a macroscopic carbon surface. Therefore, this is a process of direct decomposition of the initial hydrocarbon molecules on the particle surface, requiring no intermediate stage in the bulk of the hydrocarbon.

As to the mechanism of nucleus formation we know nothing about it. The only thing that can be stated is that its chemical mechanism would have to be rather complex to overcome the thermodynamic difficulty of forming a nucleus of a new phase. From our point of view the numerous papers in which the mechanism of formation of carbon black particles is discussed actually deal with the mechanism of formation of the nuclei. Since a nucleus is four to five orders smaller in volume than a particle, and hence only an insignificant proportion of the decomposing hydrocarbon goes to form the nuclei, the question as to the mechanism governing nucleus formation seems very complex to us.

In any case, the presence of any definite hydrocarbons in the zone preceding that of carbon black particle formation can in itself hardly be considered to prove those hydrocarbons participate in the formation of the nuclei.

The results of an investigation of carbon black formation by thermal decomposition should be of interest for combustion processes as well. In any case, the formation of carbon black during the turbulent or diffusional combustion of streams of hydrocarbon and air which have not been mixed preliminarily takes place in an atmosphere of

unburnt hydrocarbon in the absence of oxygen and is essentially of a thermal nature. The difference between this process and the thermal process is only that in the former case the hydrocarbon is diluted with combustion products diffusing from the combustion front.

CONCLUSIONS

(1) The formation of carbon black by thermal decomposition of hydrocarbons is a process of formation of a dispersed phase and takes place in two stages: nucleus formation and particle growth. These stages have different mechanisms. The temperature needed to form carbon black nuclei is much higher than that necessary for particle growth or for decomposition of the hydrocarbon on the walls to form a layer of solid carbon. This 'superheating' is analogous to the 'supersaturation' of systems required for the formation of a new dispersed phase during condensation.

(2) The course of the formation of dispersed carbon, in the time when a flowing hydrocarbon is heated, is determined by the velocity ratios of the following three processes: (*a*) heating of the hydrocarbon, (*b*) formation of carbon black nuclei, (*c*) particle growth. The rates of nucleus formation and of particle growth depend essentially on the temperature, and therefore the rate of heating of the hydrocarbon is the most important factor, determining the overall rate of the decomposition and the degree of dispersion of the resulting carbon black. The higher the rate of heating of the hydrocarbon, the higher the rate of decomposition and the higher the degree of dispersion of the resulting product.

(3) When heating a flowing gas the rate of heating is the higher, the greater the linear velocity of the gas and the smaller the diameter of the reaction tube. Therefore, the rate of particle formation and the degree of dispersion of the carbon black increase with growing linear gas velocities and especially with diminishing reaction tube diameters.

The author acknowledges his great indebtedness to S. Z. Roginsky, Corresponding Member of the Academy of Sciences of the USSR, for discussions and a number of valuable suggestions.

REFERENCES

[1] *Fifth Symposium on Combustion.* Panel discussion, p. 799. 1955. New York; Reinhold

[2] TESNER, P. A. and YECHEISTOVA, A. I. *Dokl. Akad. Nauk SSSR* 87, No. 6 (1952) 1029

[3] TESNER, P. A. and RAFALKES, I. S. Treatment and transport of natural gas. *VNIIGAS Proceedings*, p. 3. 1953. Gostoptekhizdat (in Russian)

[4] TESNER, P. A. and RAFALKES, I. S. *Dokl. Akad. Nauk SSSR* 80 (1951) 401

[5] RAFALKES, I. S. and TESNER, P. A. Treatment of natural gas. *VNIIGAS Proceedings*, Issue 3 (II), p. 3. 1958. Gostoptekhizdat (in Russian)

[6] TESNER, P. A. Treatment of natural gas. *VNIIGAS Proceedings*, Issue 3 (II), p. 34. 1958. Gostoptekhizdat (in Russian)

77

FORMATION AND GASIFICATION OF CARBON IN AN ATMOSPHERE OF COMBUSTION PRODUCTS

E. F. M. VAN DER HELD

INTRODUCTION

The transfer of heat from a flame to the objects to be heated can take place in two ways, viz. by direct contact, that is to say by conduction to the surface in the flame gases, and by radiation. It is also possible for the surface to have an accelerating effect on the chemical reactions, whereby heat is produced at or in the immediate vicinity of the surface. In this case the reacting substances have to be carried to the surface by diffusion. In general, gases are poor radiators, at least for layer thicknesses such as occur in practice. The presence of solid matter therefore greatly increases the heat emitted by radiation. Hot gases in which finely dispersed solid matter is suspended are known as luminous flames (*Figure 1*). We should

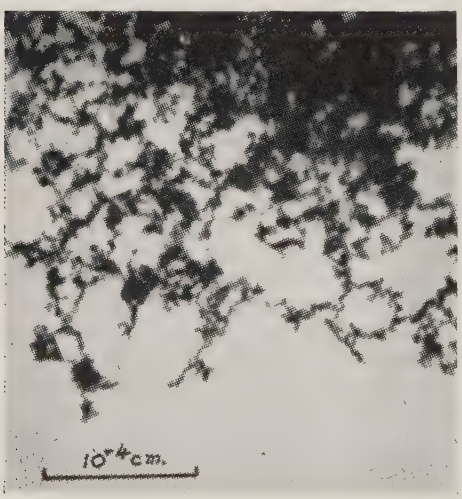

Figure 1

realize, however, that much heat is also radiated in the infra-red. It is therefore better to speak of carbon bearing flames. The form in which the carbon occurs as appears from *Figure 1*, viz. in flakes, makes the falling velocity of these flakes so slight that it need not be taken into account in any of the following considerations (compare for instance the falling velocity of snow and rain, flake and drop having the same weight).

Investigations by Ornstein and his students have shown that with few exceptions (e.g. pure H_2 gas) equilibrium is established in non-luminous flames so quickly after leaving the first reaction zone (the 'green' cone of the town-gas flame) that the temperatures of the gases can be measured with intensity measurements of lines and bands in the spectrum.

If, however, finely dispersed solid carbon is present in the flame, equilibrium will take so long to establish that the outermost reaction zone is reached before equilibrium is attained.

Among the following processes—the endothermic reactions $C + CO_2 \rightarrow 2CO$ and $C + H_2O \rightarrow CO + H_2$, the transport of CO_2 and H_2O to the carbon surface by diffusion, the transport of CO and H_2 away from the surface and the supply of heat to the surface for the endothermic reactions—there must be at least one which sufficiently retards the gasification process to allow the flame to remain carbon bearing.

Contrary to the observations, the flame should in many cases be non-luminous in equilibrium (watergas equilibrium). The carbon particles must therefore have originated earlier, viz. before establishment of the pseudo gas equilibrium, and have no time to gasify completely thereafter. By pseudo gas equilibrium we understand the state of the gas which is attained when all the rapid pre-reactions are complete and only one or more very slow processes with their post-reactions remain.

There are various possible ways in which the soot particles that may occur in many types of flame, e.g. candle, gas and oil flames, can originate. If, in the case of oil, its boiling point is high enough free carbon may already occur in this phase owing to cracking. In most cases, however, the oil will not be cracked until the gas phase. Once the reaction zone is reached incomplete combustion may leave free carbon behind. Condensation of over-saturated carbon vapour is then possible. In this event the gas mixture tends towards the Boudouard equilibrium, the excess of carbon condensing to a mist. Which of these solid carbon producers is the supplier will depend upon the fuel and the burner.

If strong radiation is desired, the formation of finely dispersed solid carbon will be allowed to occur as early as possible and in order to prevent sooting of the flame complete combustion in the outermost reaction zone will be aimed at. The possibility of non-homogeneity of the gases will also have to be allowed for. For if the concentrations are strongly non-homogeneous there may (although on the average the conditions require a non-luminous flame) be islands in which the gases must be luminous owing to the higher concentrations of hydrocarbons present. In such a case the flame will radiate all the same. Diffusion and turbulence may then be the cause of the luminous flame becoming non-luminous further up.

We see from this that the consideration of equilibria should precede every other consideration since after every intervention the gases will tend towards equilibria, however far they may appear to be from these at the moment of observation.

EQUILIBRIA

Boudouard's equilibrium conditions

$$K_B = \frac{(p_{CO})^2}{p_{CO_2}} \tag{1}$$

apply at a carbon surface. At the surface the carbon has a saturation pressure p_{Cs} which is a function of the temperature only*, therefore

$$K_C = p_{Cs} \tag{2}$$

Dividing equation 1 by equation 2 gives the formula

$$\frac{K_B}{K_C} = \frac{(p_{CO})^2}{p_{Cs}p_{CO_2}} \tag{3}$$

K_B/K_C is a function of the temperature only. In the absence of a carbon surface equilibrium may exist between the gas pressures p_{CO_2}, p_{CO} and p_C (atomic carbon gas) when $p_C \leqslant p_{Cs}$, with an equilibrium constant

$$K_H = \frac{(p_{CO})^2}{p_C p_{CO_2}} \tag{4}$$

in which K_H is again a function of the temperature only. On the other hand if there is a carbon surface in equilibrium with the surrounding gases p_C must equal p_{Cs} and the following must apply

$$K_H = K_B/K_C \tag{5}$$

In the following considerations we shall be concerned also with the water gas equilibrium

$$K_g = \frac{p_{CO}p_{H_2O}}{p_{CO_2}p_{H_2}} \tag{6}$$

and the dissociation equilibrium of CO_2

$$K_o = \frac{p_{O_2}(p_{CO})^2}{(p_{CO_2})^2} \tag{7}$$

We ignore the equilibria relating to those components of the flame gases which, though observed, should occur only in slight quantities under normal equilibrium conditions, such as hydrocarbons. This makes for greater clarity in the result without detracting much from its accuracy.

We assume that the composition of the mist (both the solid matter and the gas in which this solid matter is suspended) is known by analysis. We therefore know the total quantity of oxygen in the gas mixture, and convert this to pressure of oxygen molecules $p_{O_2,a}$

$$p_{O_2} + p_{CO_2} + \tfrac{1}{2}p_{CO} + \tfrac{1}{2}p_{H_2O} = p_{O_2,a} \tag{8}$$

We also convert the total quantity of hydrogen to pressure of hydrogen molecules $p_{H_2,a}$

$$p_{H_2} + p_{H_2O} = p_{H_2,a} \tag{9}$$

We now wish to know how much carbon is present in gasified form. This is

$$p_k = p_C + p_{CO} + p_{CO_2} \tag{10}$$

For this, we express p_{CO} and p_{CO_2} as p_C.

From equations 4 and 7 it follows that

$$p_{O_2} = \frac{K_o}{(K_H p_C)^2}\ (p_{CO})^2 \tag{11}$$

from equation 4 that

$$p_{CO_2} = \frac{1}{K_H p_C}\ (p_{CO})^2 \tag{12}$$

and from equations 4 and 6 that

$$p_{H_2} = \frac{K_H p_C}{K_g}\ \frac{p_{H_2O}}{p_{CO}} \tag{13}$$

Inserting equation 13 in 9 we find

$$p_{H_2O} = \frac{K_g p_{H_2,a}}{K_H p_C + K_g p_{CO}}\ p_{CO} \tag{14}$$

Finally, inserting equations 11, 12 and 14 in equation 8 gives us the formula

$$\frac{K_o}{(K_H p_C)^2}\ (p_{CO})^2 + \frac{1}{K_H p_C}\ (p_{CO})^2 + + \frac{K_g p_{H_2,a}}{2(K_H p_C + K_g p_{CO})}\ p_{CO} = p_{O_2,a} \tag{15}$$

Regarding $\dfrac{p_{CO}}{K_H p_C}$ as a new variable, say y, equation 15 becomes

$$K_o y^2 + y\,p_{CO} + \tfrac{1}{2}\,p_{CO} + \frac{K_g p_{H_2,a}}{2(1 + K_g y)}\ y = p_{O_2,a} \tag{15a}$$

* Here we carry out the proof with carbon atoms. A reasoning allowing for C_2 molecules gives the same results, as the numbers of C atoms and C_2 molecules are likewise bound by an equilibrium condition and in the result p_C and p_{C_2} can be ignored relatively to the other pressures.

or

$$p_{CO} = \frac{2(p_{O_2,a} - K_o y^2)\,(1 + K_g y) - K_g p_{H_2,a}\, y}{(2y + 1)\,(1 + K_g y)} \qquad (15b)$$

wherewith the correlation between p_{CO} and y is known and, with the aid of $y = p_{CO}/K_H p_C$, also the correlation between p_{CO} and p_C, all for a given temperature.

We have thus found the correlations

$$p_{CO} = F_1\,(p_C, p_{H_2,a}, p_{O_2,a})$$

and

$$p_{CO_2} = F_2\,(p_C, p_{H_2,a}, p_{O_2,a})$$

We can insert these in the formula for p_k and thus solve the problem.

THE BOUNDARY CURVES

The change from non-carbon bearing ($p_C \leqslant p_{Cs}$) to the carbon bearing flame takes place when $p_C = p_{Cs}$. But then according to equations 2 and 5: $p_{Cs} K_H = K_B$ and equation 15 becomes a cubic equation in p_{CO}:

$$K_g (K_o + K_B)\,(p_{CO})^3 + \\ + K_B (K_o + K_B + \tfrac{1}{2} K_g K_B)\,(p_{CO})^2 + \\ + K_B{}^2 \{ \tfrac{1}{2} K_B + K_g (\tfrac{1}{2} p_{H_2,a} - p_{O_2,a}) \} \\ p_{CO} - K_B{}^3 p_{O_2,a} = 0 \qquad (16)$$

In the range that is technically important, $K_o \ll K_B$ (see Table 1), and we can thus neglect K_o as against K_B.

Equation 16 then becomes

$$K_g (p_{CO})^3 + K_B (1 + \tfrac{1}{2} K_g)\,(p_{CO})^2 + \\ + K_B \{ \tfrac{1}{2} K_B + K_g (\tfrac{1}{2} p_{H_2,a} - p_{O_2,a}) \} \\ p_{CO} - K_B{}^2 p_{O_2,a} = 0 \qquad (16a)$$

If we start with a certain temperature and a certain value for $p_{H_2,a}$ we can calculate for various values of p_{CO} in succession: the corresponding values of $p_{O_2,a}$ with formula 16a, of p_{H_2O} with 14, of p_{H_2} with 9, of p_{CO_2} with 1 and of p_{O_2} with 11 or, by combining 1 and 11, with

$$p_{O_2} = \frac{K_o}{K_B}\, p_{CO_2} \qquad (17)$$

From Table 1 it will be seen that below 3,000°K K_o/K_B is never greater than 10^{-6}. We need not therefore allow for oxygen in the form of molecules. This is also the case with oxygen atoms. For, if K_D is the equilibrium constant for the dissociation of oxygen then, according to formula 11:

$$(p_O)^2 = K_D p_{O_2} = \frac{K_D K_o}{K_B{}^2}\,(p_{CO})^2$$

or

$$p_O = \frac{K_D{}^{\frac{1}{2}} K_o{}^{\frac{1}{2}}}{K_B}\, p_{CO} \qquad (18)$$

Even at 3,000°K, $K_D{}^{\frac{1}{2}}\, K_o{}^{\frac{1}{2}}/K_B$ is only about 3×10^{-8}.

The results of calculating $p_{k,a}$ (value of p_k at the boundary curve) in relationship with $p_{O_2,a}$ with various values of $p_{H_2,a}$ as parameter at 1,000°K and 1 atmosphere are collated in *Figure 2*. If the calculation is repeated at 2,000°K all other partial pressures are found to be very small compared with the pressures of carbon monoxide and hydrogen, so that all curves coincide in the straight line $p_{ks} = p_{CO} = 2\, p_{O_2,a}$. It is only at much higher pressures that the 1 atmosphere assumed for the calculation that the curves will deviate from this line and from one another. Even at 1 atmosphere and 1,700°K the curves were still found to coincide with $p_{ks} = 2\, p_{O_2,a}$.

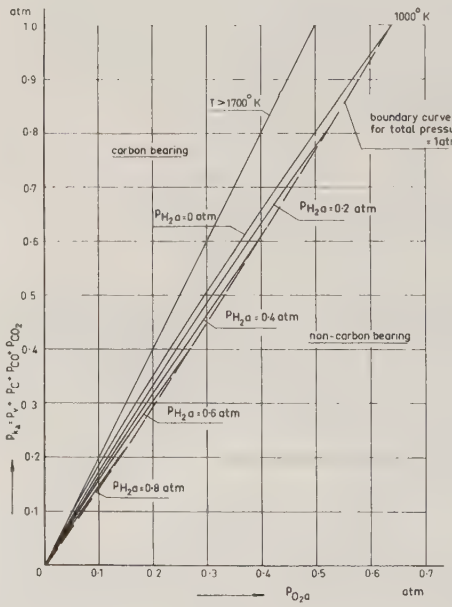

Figure 2

USE OF THE GRAPH

Starting with the measured composition of a flame gas we calculate $p_{O_2,a}$ (total oxygen content expressed in atmospheres as if all oxygen were present in the form of O_2 gas), $p_{H_2,a}$ (total hydrogen content, under a parallel assumption) and $p_{k,a}$ (total carbon content, including solid carbon, expressed in atmospheres as if all carbon were present either in the form of atoms or in the form of gas molecules with only one carbon atom). In *Figure 2* we plot by direct calculation or interpolation the boundary curve appertaining to the measured gas temperature and the calculated $p_{H_2,a}$ (in our *Figure 2* there are still too few data for this, but we assume that these have been calculated). If the point ($p_{O_2,a}$, $p_{k,a}$) is above this curve the flame gas is carbon bearing and if it

is below it the flame gas is not carbon bearing under *equilibrium conditions*, but outside the equilibrium it may be !

We now make *Figure 2* usable in practice by plotting along the ordinate also the gaseous carbon present in reality. This quantity p_e following from experiments, again expressed in atmospheres of atomic carbon, is the sum of the experimental values for p_C, p_{CO}, p_{CO_2} and p_{CH_4}. The carbon p_v present as solid matter thus amounts to $p_v = p_{k,a} - p_e$. For $p_{k,a}$-values above the boundary curve appertaining to the conditions, p_C as the equilibrium value of the gasified carbon will be located on the boundary curve with the same abscissa values, and for $p_{k,a}$-values below this curve p_e will coincide with $p_{k,a}$. But in general, $p_e \leqslant p_{k,a}$. Only with oversaturated carbon vapour will this not necessarily be the case.

p_e too belongs to the same abscissa value as $p_{k,a}$. The greater the deviation from the equilibrium state the greater p_v can be. If there is no equilibrium, p_e need not in the first case be located on the boundary curve and in the second case need not coincide with $p_{k,a}$, but will almost certainly be lower. Then the gas is carbon bearing ! p_e will move towards the equilibrium point along its ordinate. It follows from the observations that this process proceeds slowly. Many flames are therefore carbon bearing, although their composition in equilibrium requires a non-luminous flame.

RESULTS

As a demonstration we will now discuss several measurements made by the Gas Institute with outlet gases from an oven oil-fired with a shortage of air*. Table 2 shows some measured values and the magnitudes calculated therefrom. In Table 3 are compiled the magnitudes from all the tests which are necessary for using *Figure 2*.

The $2p_{O_2,a} - p_{k,a}$ row indicates how far below the line $p_k = 2p_{O_2,a}$ the equilibrium point is located. At 1,500°K the boundary curve at $p_{H_2,a} = 25$ to 30 is still close to this line, and it can thus be concluded that in equilibrium all the flames investigated would have to be non-luminous. It will be seen from Table 2 that about 30 per cent of the carbon is free. There is thus a strong deviation from equilibrium. It must be deduced from this:

(1) That the gasification reaction proceeds so slowly that in the time during which the gases remain in the oven complete gasification does not occur and

(2) That the carbon originates before, in or immediately after the first combustion zone. There are flames in which the origin of carbon before the first reaction zone can be seen distinctly because the gases bear no carbon after passing the front. The carbon formed by cracking starts glowing before reaching the reaction zone, but in the reaction zone it finds sufficient oxygen to be gasified again[1]. (See *Figure 3a*.)

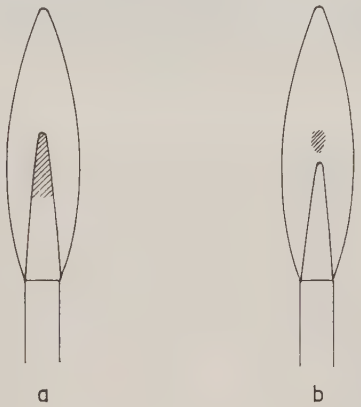

a) formation of carbon before the gases have passed the first combustion zone

b) formation of carbon after the gases have passed the first combustion zone

Figure 3

There are also flames in which the carbon does not become visible until just after it has passed the front (observed for instance with butane by Egerton and Powling[2], see *Figure 3b*). There are two possible explanations:

(1) The flames are carbon bearing in equilibrium. The existence of a transparent field just past the front may be due to the carbon particles still being small—small relatively to the wave lengths of visible light. But they grow quickly and then become visible, i.e. a typical condensation phenomenon.

(2) In the first instance gases may occur, such as CH_4, C_2H_2, etc., which are not cracked until later. From the tests by the Gas Institute this explanation seems to be very probable. For even in sampling, CH_4 is still present. The thickness of the transparent layer gives an idea of the time necessary for the carbon particles to attain sufficient density for them to be observed. A generally satisfactory explanation of the phenomenon has in my opinion not yet been found, however. Further investigation is therefore very desirable.

The influence of the pressure has been investigated by various workers. The soot invariably occurs with the same composition, but grows more easily at higher pressures. At low pressure the

* We should like to record our gratitude to the Gas Institute for kindly making these data available and for their permission to publish the same.

influence of the walls becomes noticeable. Moreover in the latter case the boiling point is lower and there will thus be less cracking in the liquid phase.

REFERENCES

[1] GAYDON, A. G. and WOLFHARD, H. G. *Flames: Their Structure, Radiation and Temperature*, Plate 1b. 1953. London; Chapman and Hall

[2] EGERTON, A. C. and POWLING, J. *Proc. Roy. Soc.* 193 (1948) 172, 190

TABLE 1

Temperature, °K	log K_o	log K_B	log K_g
298	− 89·5	− 21·42	− 4·9
500		− 8·98	− 2·3
750		− 2·81	− 0·8
1,000	− 20·5	+ 0·26	− 0·14
2,000	− 5·6	+ 4·72	+ 0·66
3,000	− 1·0	+ 6·06	+ 0·85

TABLE 2

Conditions, Measured Values and Calculated Magnitudes of Outlet Gases from Oil-fired Oven with Shortage of Air

Item	*No steam* T = 1,200°C		0·25 kg *Steam* per kg *oil* T = 1,200°C		0·44 kg *Steam* per kg *oil* T = 1,220°C	
	(a)	(b)	(a)	(b)	(a)	(b)
% CO_2	3·9	3·6	6·0	5·25	6·0	4·95
% CO	16·3	14·9	14·3	12·5	12·5	10·3
% H_2	16·9	15·5	12·0	10·5	14·7	12·15
% CH_4	0·4	0·35	2·1	1·85	0·5	0·4
% N_2	62·5	57·3	65·6	57·55	66·3	54·8
% H_2O		8·35		12·35		17·4
O converted to % O_2	12·05		13·15		12·25	
21/79 × % N_2	16·6		17·45		17·6	
% H_2O formed in gas	9·1		8·6		10·7	
Total H_2 in gas		24·55	21·75*	26·55	21·75*	30·35
Total C vol. % (1·58 : 1·345 × % H_2*) = 100 $p_{k,a}$		28·85		25·5		25·5
As total pressure 1 atm. C present in gaseous form = 100 p_C as total pressure 1 atm.		18·85		19·6		15·65
Free carbon vol. % p_v		10·0		5·9		9·85
$K_g = (p_{H_2O} \cdot p_{CO})\,(p_{H_2} \cdot p_{CO_2})$		2·24		2·80		2·98
K_g according to measured temperature		2·58		2·58		2·66
temperature corresponding to K_g (°C)		1,120		1,255		1,300
deviation from measured temperature		− 80		+ 55		+ 80
$n_1 = \dfrac{21/79 \times \%\ N_2 + \frac{1}{2}\%\ H_2O \text{ steam}}{\text{total C} + \frac{1}{2} \text{ total } H_2}$		0·370		0·456		0·462
$n = \dfrac{21/79 \times \%\ N_2}{\text{total C} + \frac{1}{2}\ \%\ H_2 \text{ oil}}$		0·370		0·420		0·399

(a) Columns without water vapour; (b) columns with water vapour

* Without steam, but expressed as percentage in composition *with* water vapour

TABLE 3

Number	1	2	3	4	5	6	7	9
$p_{k,a}$	28·7	28·85	28·55	28·7	25·5	24·5	25·5	23·95
$p_{O_2,a}$	15·5	15·2	17·15	17·45	17·65	18·3	18·8	18·8
$p_{H_2,a}$	24·4	24·55	28·2	29·9	26·55	27·0	30·35	28·35
$2p_{O_2,a} - p_{k,a}$	2·3	1·85	5·75	6·2	9·8	12·1	12·1	13·65
Temperature °C	1,280	1,200	1,160	1,140	1,200	1,200	1,220	1,240

CARBON FORMATION IN VERY RICH HYDROCARBON–AIR FLAMES—I. STUDIES OF CHEMICAL CONTENT, TEMPERATURE, IONIZATION AND PARTICULATE MATTER

J. M. SINGER and J. GRUMER

INTRODUCTION

Flat and conical flames of very rich propane–air and ethylene–air mixtures have been examined to determine the identity of smoke precursors and the mechanism of carbon formation, chemical composition, temperature and ionization, carbonaceous matter was examined by electron microscopy. Observations were made in the region extending from the initial blue zone to late in the yellow zone. Results were as follows.

Analysis of flame gases

The main reaction products in rich flat flames of propane–air and ethylene–air were carbon monoxide, carbon dioxide, hydrogen and water. Only small concentrations of other gases were detected. Acetylene, ethylene and methane were generally present in amounts of 1 to 1·5 per cent. Traces of diacetylene, methyl acetylene, benzene, toluene, aldehydes and peroxides were detected but there was no indication that their concentrations were steady. The oxygenated intermediates totalled less than 0·01 per cent, which is in marked difference with cool flames. Except for propane, the C_3 and above hydrocarbon content of the flames was less than 0·06 per cent. These traces were consumed in the initial regions of the yellow zone. No compound of molecular weight greater than toluene was observed even in concentrated samples.

The small quantities of low molecular weight aromatics and unsaturated hydrocarbons and their absence in the smokier regions of the flame indicate that carbon is not formed mainly by polymerization. Carbon formation may involve direct splitting of C–C and C–H bonds.

Conical diffusion flames and flat pre-mixed flames contained essentially the same compounds but in different concentrations. The CO_2/CO ratios were approximately five times larger in diffusion flames than in pre-mixed flames. Both oxygen and nitrogen were present in the yellow of diffusion flames, indicating diffusion of secondary air into the yellow flame through the outer blue mantle.

Rich propane–air and ethylene–air flames were not in thermochemical equilibrium. Observed concentrations of hydrogen and carbon monoxide were lower than the theoretical composition, indicating that carbon monoxide may be involved in carbon growth in a manner not yet identified. The water–gas equilibrium constant based on experimental data was larger than theoretical in the initial blue zone and lower in the yellow zone.

Temperature profiles

Thermocouple temperatures through a rich flat propane–air flame were higher than theoretical in the vicinity of the initial blue flame zone and lower in most of the yellow zone. Flame temperatures depended on initial fuel–air composition, decreasing for richer mixtures, and always in excess of usual 'cool' flame temperatures.

Ionization profiles

The ionization maximum in flat flames occurred a short distance beyond the start of the yellow flame zone, at a position where temperatures were falling and most of the overall reaction had occurred. This suggested carbon nuclei or carbon precursors of unknown identity were ionizing.

Electron microscope studies

Electron micrographs revealed that particulates within rich ethylene–air and propane–air flames differ in physical appearance. The shape of ethylene–air carbons was granular-spherical. The shape of propane–air carbons was filamentary near the start of the yellow zone, and partly filamentary and partly granular-spherical in the rest of the yellow flame. The filaments appeared to be hollow and similar to those obtained by other investigators from heated carbon monoxide in contact with metal catalysts.

EXPERIMENTAL RESULTS AND DISCUSSION

Chemical analysis of gases in yellow-forming conical flames and flat propane–air and ethylene–air flames

Flat flames—Figure 1 shows the burner equipment and typical flame structure. The flames were stabilized above a water-cooled 7·6 cm i.d. cylindrical water-cooled tube packed with a coil made

of alternating corrugated and flat brass sheets (0·0076 cm thick). Steady flames were produced when a wire nichrome ring heated electrically was placed at the burner rim. A slight flow of N_2 was

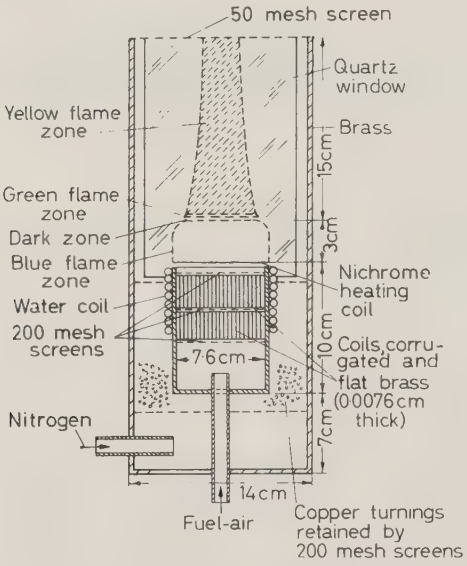

Figure 1. Flat flame burner with typical flame structure

maintained coaxially around the burner. The entire flame and burner were enclosed in a 14 cm square duct either 17·5 or 35 cm high; the top of each duct was covered by a 50 mesh wire screen. Duct height affected the flame appearance, flames in the shorter duct being more luminous than those in the long one. Burning started with a thin blue zone rising vertically from the burner rim and forming a horizontal 5 cm diameter disc at a distance of 3 cm above the hot wire stabilizer. The yellow region started 3 mm downstream of the flat blue flame, so that a transitional dark zone existed between the yellow and blue flames. A green colour appeared at the onset of yellow, disappearing within a distance of 1 mm. The yellow region was 15 cm in height when the flame was contained in the longer (35 cm) duct, gradually tapering from 4 cm diameter at the base to a downstream diameter of 2 cm. In the shorter (17·5 cm) duct the yellow flame extended only to a height of 5 cm. The yellow colour in both ducts decreased in intensity with increasing distance from the blue zone, changing finally to a dark yellow-red colour near the retaining top screen. This equipment and flame geometry permitted point-wise sampling and the exclusion of secondary air.

Samples were withdrawn from various axial flame positions through horizontal quartz probes of different diameters. In the region near the blue flame zone, small diameter probes (0·013 cm) were used. However, in the yellow forming zone, the probe diameter was increased to 0·061 and 0·125 cm to avoid clogging with carbon. Preliminary testing at variable pressures and flow rates within the probe manifold systems revealed no dependence of the resultant mass spectrometric chemical analysis on probe material, total sampling pressure (from 1 cm Hg to atmospheric pressure) or rate of sampling (from sonic velocity to burner fuel–air velocity). These experiments do not rule out the possibility that reactions occur within the probe, but indicate that this possibility is unlikely.

Table 1 contains a survey of the appearance and disappearance of products in a flat 8·0 per cent propane–air flame as a function of time spent in the flame. Samples were taken from the region 1 cm upstream of the blue flame; in this region no reaction was discernible. Samples were also taken 1 mm below the blue flame (columns 1 and 2), then from the dark space following the blue flame (column 3), and finally from the yellow zone of the flame (columns 4 and 5). This sequence should tend to separate initial products, intermediates and final products. Columns 1 and 2 showed almost all of the original propane unreacted. The main initial products of reaction were H_2, CO, CO_2 and water*. Only small quantities of other hydrocarbons and oxygenated hydrocarbons were present. Column 3 shows that almost all of the original fuel was consumed in passing through the blue zone; additional methane ethylene and acetylene appeared along with traces of a few complex hydrocarbons. The composition of the flame gases did not change materially at the stations corresponding to columns 4 and 5 except for the slight decrease of the C/N_2 ratio in the yellow zone (column 5). Falling of the C/N_2 ratio has been taken as a measure of the formation of particulate carbonaceous matter.

Column 3 in Table 1 and *Figure 2* show that between the blue flame and 1 mm into the dark zone, 3·4 per cent oxygen, 0·5 per cent propane and 4·0 per cent other hydrocarbons have survived 0·01 sec residence at temperatures of 1,500–1,800° K. Similarly, columns 4 and 5 and *Figure 2* show 3·06 per cent hydrocarbons remain after a total residence time of 0·02 sec at temperatures no lower than 1,500°K, and 1·95 per cent after a total residence time of 0·2 sec at temperatures between 1,900 and 1,300°K. These temperatures and residence times are sufficient for pyrolysis of hydrocarbons to occur. The decrease from 0·337 to 0·29 (Table 1) in the ratio of carbon atoms to nitrogen molecules in the gas phase may be due to such pyrolysis.

* Table 1 is presented on a water-free basis. Water concentrations were obtained by means of a hydrogen balance.

TABLE 1

Propane–Air Flat-flame Composition at Various Axial Sampling Positions, 8·0 per cent Propane–Air, 0·061 cm Probe Inlet Diameter

	1	2	3	4	5
	1 mm *below blue* flame zone*	1 mm *below blue† flame zone*	1 mm *above blue in dark space*	2 mm *above blue, in green flame zone*	1·5 cm *above blue, in yellow flame zone*
Argon	0·1	0·1	0·6	0·8	0·8
Nitrogen	70·7	71·7	67·3	67·5	67·7
Oxygen	17·1	16·8	3·4	0·9	0·06
Hydrogen	2·7	1·8	9·7	10·2	10·9
Carbon monoxide	1·3	2·0	11·9	14·2	14·3
Carbon dioxide	0·3	0·5	2·8	3·3	4·3
Methane	0·2	0·1	1·5	1·2	0·9
Ethylene	0·0	0·2	1·0	0·4	Trace
Acetylene	0·1	0·1	1·1	1·4	1·03
Methyl acetylene	0·0	0·0	0·04	0·04	0·01
Propane	7·5	6·7	0·5	0·0	0·0
Benzene	0·0	0·0	0·0	Trace	0·0
Diacetylene	0·0	0·0	0·01	0·02	0·01
Propylene	0·0	0·0	0·2	0·0	0·0
Ethane or formaldehyde	0·0	0·0	0·1	0·0	0·0
CO_2/CO	0·23	0·25	0·235	0·232	0·299
CO/H_2	0·481	1·11	1·23	1·39	1·31
(C/N_2) orig.	0·328	0·328	0·328	0·328	0·328
(C/N_2) exp.	0·346	0·324	0·337	0·333	0·29

* Flame not held by probe; small probe, 0·013 cm inlet diameter
† Flame was held by the probe in a *V* shape

In order to further concentrate trace constituents in the flame gases, condensed and non-condensed fractions were collected at liquid nitrogen temperatures. A typical analysis is presented in Table 2. A variety of high molecular weight compounds and oxygenates did not appear, in further support of the conclusion that most of the carbon in flames was not formed by progressive formation of high molecular weight compounds.

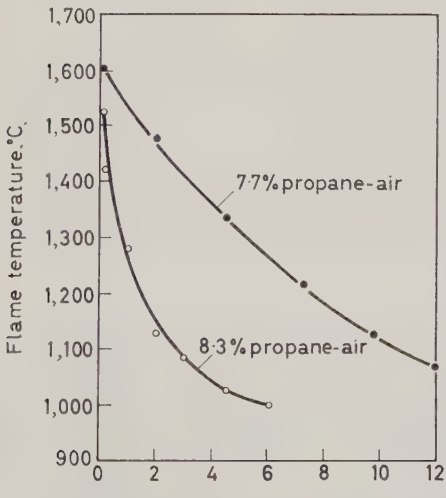

Figure 2. Axial flame temperature profiles in yellow zones of flat propane–air flames

TABLE 2

Analysis of Condensed and Non-condensed Fractions of Reaction Products Collected at Liquid Nitrogen Temperatures, 1 mm above the Blue Zone of a Flat 7·7 per cent Propane–Air Flame

	Condensed	*Non-condensed*
CO_2	1·8	
Benzene	0·1	
H_2O	95·1	
Diacetylene	0·2	
Methyl acetylene	0·1	Trace
Methanol	0·1	
O_2	0·1	4·5
C_2H_4	0·4	
C_2H_2	0·4	
CH_4	0·1	1·0
CO	0·7	12·6
H_2	0·2	11·1
Argon		0·8
N_2		70

TABLE 3

Propane–Air and Ethylene–Air Flat-flame Compositions, 1·5 cm Above the Blue Zone, 0·061 cm Probe Inlet Diameter

	Original mixture	
	A 16·8 *per cent ethylene–air* % *composition*	B 8·0 *per cent propane–air* % *composition*
Argon	0·7	0·8
Nitrogen	57·8	67·7
Oxygen	0·6	0·06
Hydrogen	15·7	10·9
Carbon monoxide	18·3	14·3
Carbon dioxide	2·2	4·3
Methane	1·3	0·9
Ethylene	0·2	Trace
Acetylene	2·8	1·03
Methyl acetylene	0·04	0·01
Benzene	0·02	—
Diacetylene	0·1	0·01
Ethane or formaldehyde	0·2	—
CO_2/CO	0·120	0·299
CO/H_2	1·17	1·31
(C/N_2) orig.	0·509	0·328
(C/N_2) exp.	0·494	0·29

In Table 3 the product compositions of a 16·8 per cent ethylene–air and an 8·0 per cent propane–air flame are compared, the samples having been taken in the luminous yellow carbon zone, at an axial position 1·5 cm above the blue flat flame. No gross difference existed between the products of a rich unsaturated and saturated hydrocarbon–air flame.

Table 4 compares theoretical and experimental composition ratios for propane–air flames at different initial compositions and flame temperatures. The theoretical calculations were based on the water–gas equilibrium and were performed in accord with the method of Brinkley and Lewis[1]. Table 5 contains a like comparison of calculated values and experimental values of a number of composition ratios for rich ethylene–air flames. The ethylene–air flame temperatures were assumed to fall within the range of temperatures listed in the table. Tables 4 and 5 show that the propane–air and ethylene–air flames contained less than theoretical quantities of carbon monoxide and hydrogen. Non-equilibrium burning was indicated especially in the blue flame zone. This finding will be discussed below.

Peroxides, aldehydes, and oxides of nitrogen were analysed by wet chemical techniques*, since minute quantities of these materials could not be detected by mass spectroscopy. No oxides of nitrogen were found in any position throughout the flat propane–air flame. Only traces of peroxide were found in the flame gases, the maximum being about 2×10^{-4} per cent in the region from 1 mm beneath the blue to 3 mm above it. Thereafter the concentration of peroxides decreased progressively until it vanished about 15 mm above the blue zone. Approximately 0·008 per cent total aldehyde concentration was indicated in the yellow region near the blue flame zone.

Conical flames—Chemical analyses were made of the flame gases in a conical diffusion and conical pre-mixed flame to determine whether reversal of the sequence of blue and yellow flame zones alters the combustion products. In a pre-mixed rich conical or flat flame the blue flame zone to be discussed is located upstream of the yellow zone; in a diffusion flame, the blue zone is downstream of the yellow flame. In the pre-mixed flat flame, yellow flame combustion feeds on the products of blue flame combustion. In the diffusion flame, this does not occur.

Samples were drawn from three positions in a propane diffusion flame of 18·5 c.c./sec flow which was stabilized on a 2·5 cm i.d. Pyrex tube. These positions were: (1) 0·5 cm above the burner rim and at the interface of the blue and yellow flame zones; (2) 1·5 cm above the rim and in the blue; (3) 1·5 cm above the rim and in the yellow. The analyses of these samples are given in Table 6.

The compounds found were the same as observed in pre-mixed yellow flat flames and conical flames. The main difference was that the CO_2/CO ratio was larger in diffusion flames, even in the yellow zone. The CO_2/CO ratio* in the yellow of the diffusion flame was about five times that in the enclosed flat flame.

The reactant mixture burning in the diffusion flame at the point of sampling may be reconstituted by making carbon and nitrogen balances, assuming the reactants to be propane and air. The results of such a calculation are given in Table 6. It is interesting to note that the equivalent propane–air concentrations in the flame zones were not stoichiometric (4·02 per cent propane).

Temperature profiles

A butt-welded platinum and platinum–10 per cent rhodium thermocouple of 0·015 cm diameter was used to measure temperatures through the yellow region of a flat propane–air flame. The thermocouple was coated with N.B.S. A–418 ceramic coating to eliminate catalytic effects on

* Oxides of nitrogen by means of phenol-disulphonic acid analysis[2]; aldehydes by means of aldehyde-bisulphite analysis[3]; peroxides by starch iodide tests.

* The CO_2/CO ratios of methane diffusion flames as experimentally determined by Smith and Gordon[5] were approximately the same as these CO_2/CO ratios of the propane diffusion flame.

TABLE 4

Comparison of Theoretical Equilibrium Compositions and Experimental Values in Rich Propane–Air Flames

Concentration, per cent propane	*Temp.*, °K	CO_2/CO		H_2/N_2		CO/N_2		CO_2/N_2		H_2O/N_2		$\frac{(CO)\,(H_2O)}{(CO_2)\,(H_2)}$		*Apparent temp.*, °K
		Calc.	*Exp.*	*Calc.*	*Exp.*	*Calc.*	*Exp.*	*Calc.*	*Exp.*	*Calc.*	*Exp.*	*Calc.**	*Exp.*	
7·5	1,900	0·166		0·241		0·264		0·044		0·180		4·42		
7·6	1,900	0·161		0·242		0·270		0·043		0·176		4·42		
7·7	1,900	0·152		0·248		0·275		0·042		0·169		4·42		
7·7	1,700	0·176		0·260		0·269		0·047		0·162		3·40		
8·3	1,700	0·132		0·309		0·304		0·040		0·149		3·40		
Sampling positions in 8·0 per cent propane–air flame														
1·5 cm above blue zone	1,800			0·299		0·161		0·209		0·063		0·192		3·94	1,820
2 mm above blue zone				0·232		0·152		0·211		0·049		0·223		6·33	2,200
1 mm above blue zone				0·235		0·142		0·176		0·041		0·172		5·15	2,150
1 mm below blue zone				0·23		0·038		0·0184		0·004		0·024		2·75	1,550

* Reference 4.

TABLE 5

Comparison of Theoretical Equilibrium Compositions and Experimental Values in Rich Ethylene–Air Flames

Concentration, per cent ethylene	*Temp.*, °K	CO_2/CO		H_2/N_2		CO/N_2		CO_2/N_2		H_2O/N_2		$\frac{(CO)\,(H_2O)}{(CO_2)\,(H_2)}$		*Apparent temp.*, °K
		Calc.	*Exp.*	*Calc.*	*Exp.*	*Calc.*	*Exp.*	*Calc.*	*Exp.*	*Calc.*	*Exp.*	*Calc.**	*Exp.*	
16·8	1,100	0·0308		0·463		0·494		0·015		0·015		1·01		
	1,300	0·0245		0·491		0·497		0·012		0·018		1·76		
	1,500	0·0182		0·488		0·500		0·009		0·021		2·57		
	1,900	0·0121		0·485		0·502		0·006		0·024		4·42		
Sampling position:														
3 mm above blue zone				0·124		0·199		0·249		0·031		0·100		4·05	1,840
1·5 cm above blue zone				0·120		0·268		0·313		0·038		0·133		4·13	1,870

* Reference 4.

TABLE 6

Analyses of Flame Gases in a Propane Diffusion Flame

	Position 0·5 cm above burner (in initial yellow zone) Per cent	*Position 1·5 cm above burner (in blue zone) Per cent*	*Position 1·5 cm above burner (in yellow zone) Per cent*
CO_2	6·4	10·6	8·2
O_2	4·9	1·9	0·1
CO	4·4	3·0	5·4
N_2	72·8	81·3	71·0
CH_4	1·1		1·8
H_2	3·2	1·3	4·5
C_2H_6	0·2		0·5
C_3H_8	4·1	2·0	4·2
C_2H_4	1·9		2·4
C_2H_2	1·2		1·9
C_3H_6	0·4	0·1	0·5
CO_2/CO	1·44	3·52	1·52
$O_2/O_2 + N_2$	0·062	0·022	0·001
Reconstituted reactants, per cent C_3Hg_8	8·2	6·0	13·2

the surface of the wire. The thermocouple wires were mounted on *U* shaped platinum and platinum–10 per cent rhodium prongs so that only the thermocouple wire was in the flame region. At least 1 cm of the wire on either side of the welded junction was in a constant temperature zone. The thermocouple-supporting prongs were connected to a traversing mechanism which permitted graduated movements of the junction in both vertical and horizontal directions.

Figure 2 shows the axial temperature traverses through the yellow region of a 7·7 and an 8·3

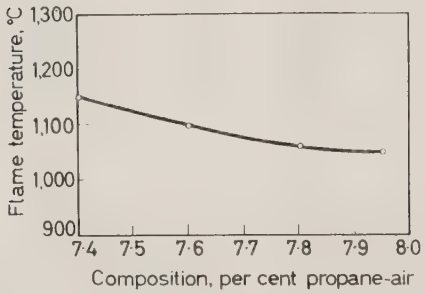

Figure 3. Axial flame temperatures at a fixed distance of 12 cm *above the blue zone of flat propane–air flames*

per cent propane–air flame. The latter traverse was made with a 0·003 cm diameter thermocouple. The flame temperature decreased rapidly downstream of the blue zone. In another experiment, the 0·015 cm thermocouple was placed in a fixed position, 12 cm above the blue zone, while the fuel concentration was varied. The flame temperature at this position was dependent on fuel–air composition to the extent shown in *Figure 3*. The theoretically computed flame temperature for a 7·6 per cent propane–air flame, based on the water–gas equilibria and the dissociation of water, hydrogen and carbon dioxide, is 1,700°K. The experimental maximum temperatures for the flat propane–air flames were higher, approximately 1,900°K for the 7·7 per cent mixture and 1,800°K for the 8·3 per cent mixture. This comparison indicates non-equilibrium burning in these fuel-rich flames.

Ionization profiles

Other investigators[6–8] have supported the view that carbon particles can be responsible for ions observed in flames. They based this suggestion partly on a comparison of ionization potentials of materials in flames. The ionization potential of carbon particles lies between 4·35 eV, the work function of solid carbon, and 11·3 eV, the ionization potential of gaseous carbon. Reaction intermediates and products of flames, namely H_2O, CO, CO_2, OH, O and H have ionization potentials between 12 and 16 eV, and the radicals CH and C_2 have potentials of 11·1 and 12 eV, respectively. Other radicals which may be present in rich flames have lower ionization potentials (such as $CH_2{=}CH$, 8·16 eV, and $CH{\equiv}C{-}CH_2$, 8·25 eV); however, they do not usually exist in flames in sufficient concentration to account for the observed high ionization values[9].

Relative ionization currents within the flames were measured by means of an electronic probe of the following description. The probe consisted of a bare tungsten wire, 1 cm long and 0·063 cm in diameter, protruding from a water-cooled metallic jacket. The probe was biased negatively with voltages ranging from 6 to 90 V. The negative electrode was electrically insulated. Both outer jacket ground terminal and tungsten wire were in direct contact with the flame so that a complete electrical circuit was made through the flame plasma. The probe permitted unrestricted collection of space charge at the negatively biased wire.

Response of the probe to positive flame ionization was measured with a sensitive mirror galvanometer. Only relative values of ionization conductivity were determined. Using a negative probe bias of 90 V, ionization in the yellow zone of a flat 7·8 per cent propane–air flame built up to a maximum at a distance of 1·5–2·5 cm from the blue zone and then levelled off. When the bias voltages were lowered, the direction and trend of ionization current changed but always reached a

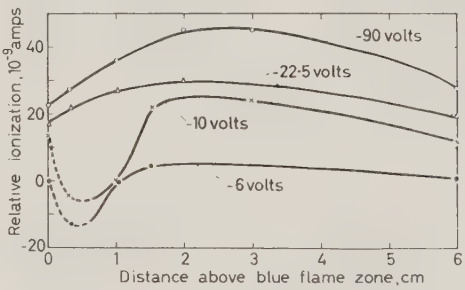

Figure 4. Relative ionization above the blue flame zone of a 7·8 per cent *propane–air flame*

maximum at the same distance of 1·5–2·5 cm above the blue flame zone in the yellow zone. *Figure 4* compares the relative ionization profiles for a flat 7·8 per cent propane–air flame for different bias voltages. The dashed curves represent a region where galvanometer readings fluctuated considerably. A second probe consisting of two tungsten wires, 1 cm long by 0·063 cm in diameter protruding divergently from a water-cooled metallic jacket, substantiated the appearance of maximum ionization in the yellow zone. The present experiments served qualitatively to locate the appearance of maximum ionization in the yellow zone. Since in this region temperatures are

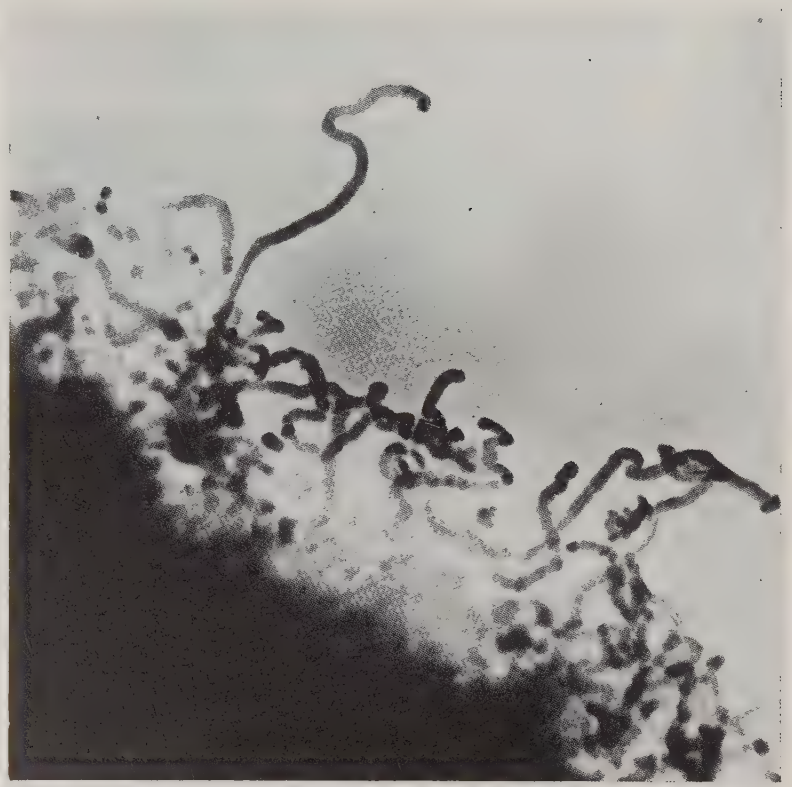

Figure 5. Electron photomicrograph of particulate matter withdrawn from the green-yellow zone of a 7·8 per cent *propane–air flat flame. Position A. Stainless steel grid held in flame* 3 mm *above blue flame zone. Magnification* 61,000 × *; reduced on reproduction* 4/7

Figure 6. Electron photomicrograph of particulate matter withdrawn from the yellow zone of a 7·8 per cent *propane–air flat flame. Position B. Stainless steel grid held in flame* 2·5 cm *above blue zone. Magnification* 61,000 × *; reduced on reproduction* 4/7

Figure 7. Electron photomicrograph of particulate matter withdrawn from the yellow zone of a 7·8 per cent *propane–air flat flame. Position C. Stainless steel grid held in flame* 3·75 cm *above blue zone. Magnification* 38,000 × *; reduced on reproduction* 4/7

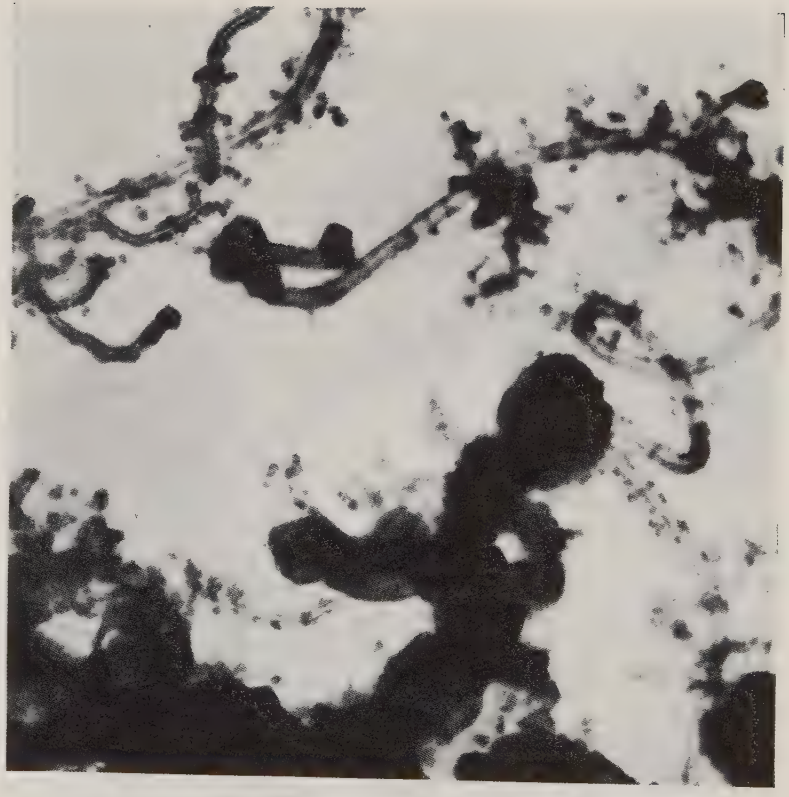

Figure 8. Electron photomicrograph of particulate matter withdrawn from the yellow zone of a 7·8 per cent *propane–air flat flame. Position D. Stainless steel grid held in flame* 6·5 cm *above the blue zone. Magnification* 61,000 × *; reduced on reproduction* 4/7

falling (*Figure 2*) and most of the oxidation reaction has been completed (Table 1), the ionization must be caused by accumulating species which are probably carbon nuclei or carbon precursors of low ionization potential*.

Examination of carbonaceous particulate matter collected from rich flat flames of propane–air and ethylene–air

A rich flat propane–air flame was examined for the form of particulate matter present at several heights in the flame. Carbon was deposited on stainless steel screens at four positions above the blue flame zone: *A*, 3 mm above the blue zone, between the green and yellow zones; *B*, 2·5 cm above the blue zone in the yellow zone; *C*, 3·75 cm above the blue zone in yellow; *D*, 6·5 cm above the blue zone in yellow. Electron microscope photographs of carbon deposited at these positions are shown in *Figures 5–8*. An instrument with resolution of 10 to 20 Å was utilized. Magnification is 61,000-fold, except for *Figure 7*, which has a magnification of 38,000†. These views are of particulate matter caught in the interstices of a 200 mesh stainless steel screen. The particulate structure is marked by long filaments with opaque granules at the tips or bends of the filaments and a typical carbon black structure (spherical-granular) surrounding the filaments. Few granules are evident at position *A* either within or between the filaments. The structure is mostly granular at position *B*, possibly due to the bursting or shattering of filaments. Indeed, the two broad filaments in *Figure 6* seem like swollen versions of the filaments in *Figure 5*. At position *C*, granular and filamental structure of particulates is again indicated. The observed hollow filamental structure in *Figures 5–8* is similar to the structure of carbon deposited on iron, nickel and cobalt catalysts by heated carbon monoxide[10] and also to the structure of carbon deposited on fire brick from heated CO and iron oxide[11]. Tesner and Echeistova[12] obtained filamental carbon growth when heating methane, benzene or *cyclo*hexane with carbon black. They did not report the appearance of hollow filaments. It may be suspected that the stainless steel screen in the flame gases acted as an iron catalytic surface in hot carbon monoxide. To test this possibility particulate matter was collected from the yellow zone of a rich propane–air flame on a mica screen (*Figure 9*). Again hollow filaments developed. The yellow zone of a rich ethylene–air flame on a mica screen (*Figure 10*) and on a stainless steel screen (*Figure 11*) did not show filaments. Strings of light granules, decked with dark granules, were obtained. No real difference was found between particulate matter collected on stainless steel or mica. Absence of filaments in *Figures 10* and *11* and their appearance in *Figures 5–9* may be due to the different fuel or fuel–air ratio employed.

* The flat flame has the advantage of being completely isolated from atmospheric air. A peak in the ionization curve was not observed with two other flames which were in free air. Ionization measurements were made along the outer surfaces of a propane diffusion flame and a 7·8 per cent propane–air flame in free air. In both cases, the level of ionization fell continuously from the base to the top of the flame and was always orders of magnitude greater than the values obtained in the flat flame.

† *Figures 5–8* reduced 4/7 on reproduction.

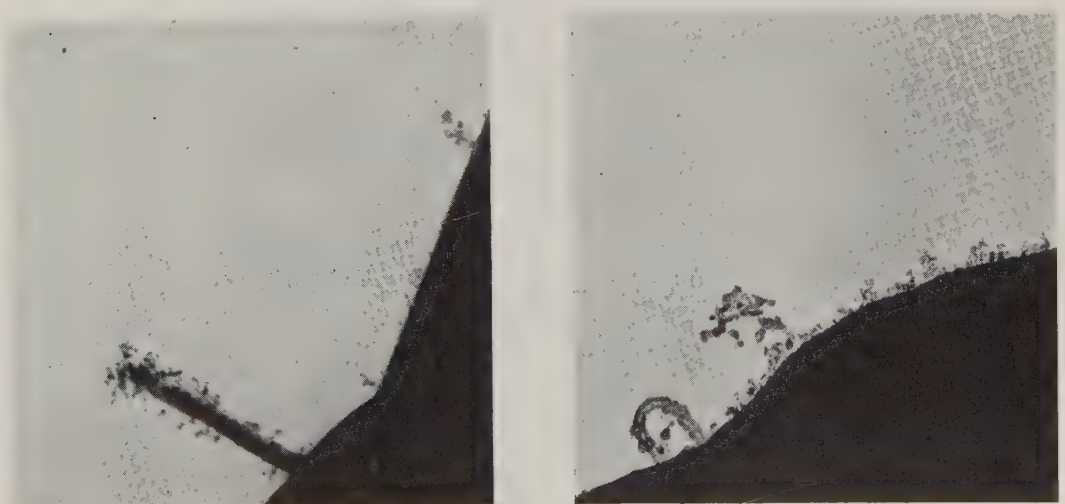

Figure 9. Electron photomicrographs of particulate matter drawn from the yellow zone of a 7·8 per cent *propane–air flat flame. Mica grid held in flame* 1·5 cm *above blue zone. Magnification* 61,000 ×

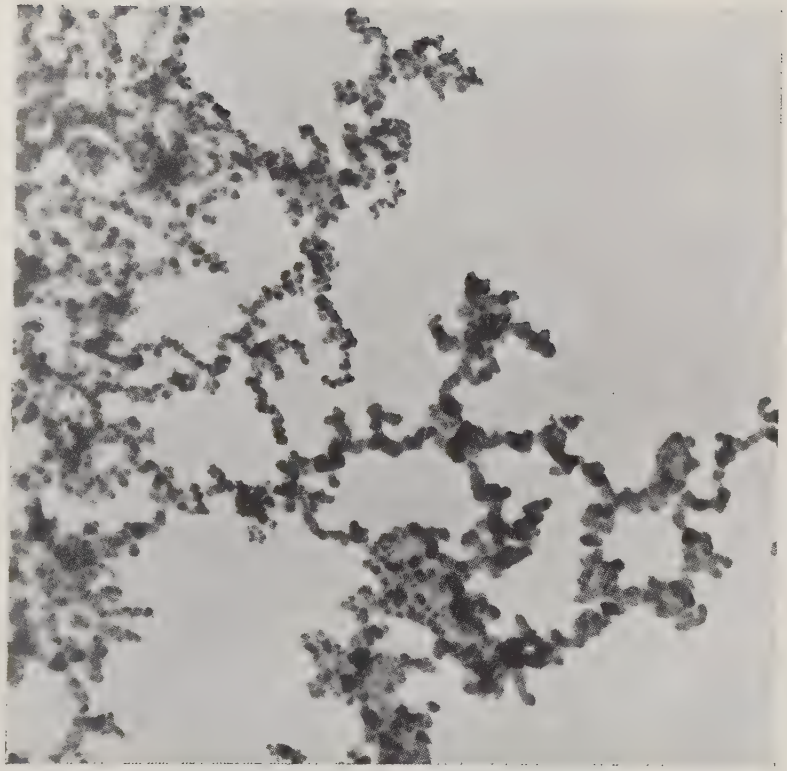

Figure 10. Electron photomicrograph of particulate matter withdrawn from the yellow zone of a 16·8 per cent *ethylene–air flat flame. Mica grid held in flame* 1 cm *above the blue zone. Magnification* 61,000 ×*; reduced on reproduction* 4/7

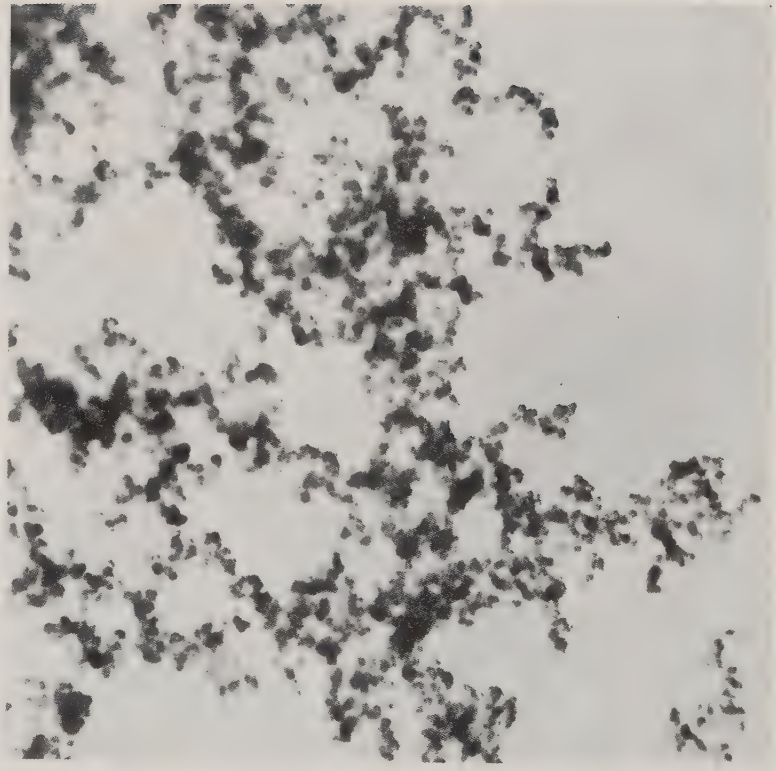

Figure 11. Electron photomicrograph of particulate matter withdrawn from the yellow zone of a 16·8 per cent *ethylene–air flat flame. Stainless steel grid held in flame* 1 cm *above the blue zone. Magnification* 61,000 ×*; reduced on reproduction* 4/7

TABLE 7

Size of Carbon Deposits from Flames and Pyrolysis or Reduction of Various Gases

Source	*Diameter,* Å	*Filament length, microns*
Filaments from 8·0 per cent propane–air	490–4,700	1·5–5
Granules from 8·0 per cent propane–air	165–490	
Granules from 16·5 per cent ethylene–air	83–490	
Filaments from heated CO on nickel, cobalt and iron[10]	100–1,000	2
Filaments from heated hydrocarbons[12] on (platinum grid + carbon black)	2,000–5,000	10–100
Granules from 30 per cent acetylene–air flames[13]	400	
Granules from (acetylene + additive) explosions, without air[14]	280–3,300	
Carbon from amyl acetate diffusion flames[15]	100–500	

Particulate sizes of carbons observed in *Figures 5–11* are given in Table 7 along with measurements obtained by other investigators. Sizes of filamentary carbonaceous deposits from the propane–air flames and from CO on catalysts were similar, but different from the filament sizes of carbons from heated hydrocarbons in contact with a platinum grid covered with carbon black. Carbon granule sizes from propane–air, ethylene–air and acetylene–air flames were similar, but different from the granular size of carbons from (acetylene + additive) explosions containing no air.

The results of these particulate examination experiments, as well as the chemical analysis experiments, indicate that carbon monoxide is involved in the flame processes leading to carbon growth. Carbon deposits may possibly grow through a mechanism occurring on surfaces of carbon nuclei and in the presence of hydrogen and carbon monoxide. This postulate has not yet been properly supported and contrary evidence exists[16]. Carbon may also be formed in both diffusion and pre-mixed flames by pyrolysis and dehydrogenation in the presence of oxygen as has been suggested by our experiments and others[5].

The authors are indebted to Dr. R. Friedel, Mr. A. G. Sharkey, Jr., and Miss J. Schultz of the Bureau of Mines for the mass spectrometer analyses; and to Mr. J. McCartney of the Special Coal Research Section of the Bureau of Mines, who prepared the electron micrographs.

This research is supported by the American Gas Association (Project ZC–20).

REFERENCES

[1] Brinkley, S. R. Jr. and Lewis, B. The thermodynamics of combustion gases: general considerations. *Bureau of Mines Rept. of Investigations* 4806 (1952)

[2] Beatty, R. L., Berger, L. B. and Shrenk, H. H. Determination of oxides of nitrogen by phenol-disulfonic acid method. *Bureau of Mines Rept. of Investigations* 3687 (1943)

[3] Goldman, F. H. and Yagoda, H. *Industr. Engng. Chem. (Anal.)* 15 (1943) 377

[4] *American Petroleum Institute Tables, Research Project* 44, 1953. Carnegie Press

[5] Smith, S. R. and Gordon, A. S. *J. phys. Chem.* 60 (1956) 759

[6] Lewis, B. and von Elbe, G. *Combustion, Flames and Explosions of Gases*, pp. 206–207. 1951. New York; Academic Press

[7] Shuler, K. E. and Weber, J. *J. chem. Phys.* 22 (1954) 491

[8] McNeely, J. K., Brown, O. A. and Crosno, C. D. *Iowa St. Coll. J. Sci.* 5 (1931) 269; 6 (1931) 1

[9] Calcote, H. F. *Combustion and Flame* 1 (1957) 385

[10] Hofer, L. J. E., Sterling, E. and McCartney, J. T. *J. phys. chem.* 59 (1955) 1153

[11] Davis, N. R., Slawson, R. J. and Rigby, G. R. *Nature, Lond.* 171 (1953) 756

[12] Tesner, R. A. and Echeistova, A. I. *Dokl. Akad. Nauk. SSSR* 87 (1952) 1029

[13] Sugden, T. M. and Thrush, B. A. *Nature, Lond.* 168 (1951) 703

[14] Jones, G. W., Kennedy, R. E., Spolan, I. and Scott, G. S. Carbon blacks formed by decomposition of mixtures of acetylene with a hydrocarbon or other gas at elevated pressures. *Bureau of Mines Rept. of Investigations* 4695 (1950)

[15] Parker, W. G. and Wolfhard, H. G. *Chem. Soc. J.* (1950) 2038

[16] Ferguson, R. E. *Combustion and Flame* 1 (1957) 431

DISCUSSION

D. B. Spalding (*London*) said: The linking together of boundary layer theory and combustion is often fruitful; Sutton's paper is therefore welcome. The problem is similar in essence to that of liquid-fuel combustion studied by others. In the latter problem, the surface temperature is fixed (approximately at boiling temperature) and the mass transfer rate has to be calculated; in the wall-cooling problem, the effusion rate is fixed and the surface temperature must be calculated. The two essential parts of the calculation are: (1) Determination via thermodynamics of the relationship between surface temperature and the 'transfer number'; this is conveniently performed on an enthalpy-composition diagram. (2) Determination via boundary layer theory of relationship between the 'transfer number' and (dimensionless) effusion rate.

Under (2), the author's neglect of $\frac{1}{2}(\rho e/\rho - f'^2)$ in equation 12 seems unwise and unnecessary. It amounts to assuming that the stagnation-point boundary layer is similar to that on a flat plate. This is known to be untrue quantitatively, and may not even be qualitatively correct; for it is not certain that the effusion rate approaches an asymptotic value, for the stagnation point, as the transfer number tends to infinity. I hope the author will obtain the exact solution in future work.

J. F. Alcock (*Shoreham*): Tamura and Tanasawa have made a happy choice of subject, for it is now known that the 'Meurer process,' impact of the fuel spray on the hot chamber wall, followed by evaporation, is not peculiar to the Meurer engine, but occurs in almost all small diesels.

The conditions of the authors' experiments differ widely from those in the diesel, where the fuel impinges on the hot wall with a velocity of hundreds of ft. per sec and, even with impact normal to the surface, spreads laterally for a considerable distance. I think that the authors were right in starting with their simplified system, which is easier to understand, but I hope they or others will carry on the good work to cover diesel conditions.

The drop-life curves, *Figure 3* and onwards, are on too small a scale to give accurate life figures in the maximum boiling rate region, this latter is of major interest, since in high-speed diesels only a few msec are available for evaporation. If the authors have reasonably accurate figures in this region they would form a useful addition to the final paper.

Figure 3 and onwards appear to have been taken with the stainless steel plate. When a drop or spray strikes the plate, the metal surface will be locally chilled, and the heat of evaporation must be conducted to the surface from the bulk of the metal, at a rate which will depend on the metal conductivity. In many engines the fuel strikes a piston of aluminium alloy, whose conductivity is many times that of stainless steel. It would be useful to know what effect this has.

R. J. Priem (*Cleveland*): Tamura and Tanasawa have again made a worthwhile contribution to science. The results presented in *Figures 3, 8, 9, 10, 11, 12* and *13* could be made more general by plotting the life of the drop against the temperature difference (surface temperature minus the boiling temperature). This seems logical as the authors explain the phenomenon in terms of the boiling rate curve which is usually given in terms of the temperature difference. It also agrees with the data, as the shortest life-time, corresponding to the 'maximum boiling rate point' of Nukiyama always occurs between 40 and 50°C above the boiling point for all fluids used in the investigation. If the phenomenon is a function of the temperature difference, rather than the surface temperature, this would introduce a pressure dependency, i.e. at higher pressures the boiling point is raised which would require a corresponding higher surface temperature. For a diesel engine with a 20 atm chamber pressure, this would raise the surface temperature required for minimum life-time about 200°C. This is a considerable increase in wall temperature.

I have a second question regarding the effect of a velocity component of the liquid perpendicular to the flat surface. A crude experiment that I conducted while at the University of Wisconsin indicated that with a velocity component the liquid will bounce off the wall, atomizing in the process. This velocity condition is closer to those existing in the 'Meurer's process' engine. Therefore, I wonder if drop shattering at the hot surface is not responsible for the high vaporization rate in the Meurer engine.

T. Urbanski (*Warsaw*): Referring to the paper by Tamura and Tanasawa, I would like to mention that Rychter and myself have published a paper* on behaviour of a drop of nitroglycerine contacting a hot metallic surface.

The shape of curve, induction-period against temperature, was very similar to that given by

* Rychter, S. and Urbanski, T. *C.R. Acad. Sci., Paris* (1938).

Tamura and Tanasawa. Below 300° the drop remains on the hot surface in the shape of a lens and violently detonates after an induction period. This behaviour of nitroglycerine was of course known—but what was unknown so far was the behaviour of nitroglycerine at temperatures much above 300° when the drop acquires a spheroidal shape. Here the substance burned quietly without any explosion.

If we draw a line parallel to the abscissa we find two induction-periods τ_1 (below 300°) and τ_2 (above 300°) for violent decomposition and quiet burning respectively.

We calculated the activation energy of quiet combustion of nitroglycerine in spheroidal shape and found it to be *ca.* 8,000 kcal. This is much below the activation energy of the induction reactions preceding detonation (*ca.* 20,000 kcal according to Roginsky and ourselves).

Y. Tanasawa (Sendai): We appreciate the remarks of Alcock and Priem as indicating a future direction for this research.

We are, of course, continuing our work to find the effects of the impinging velocity of the drop, of the temperature and pressure of the surrounding air, which will probably be published in the future.

The life-times near the maximum boiling rate region were measured carefully with a high-speed camera, and these values are to be represented in semi-empirical formula in the future, too.

The effect of the thermal conductivity on the chilling effect is measured using several materials of different conductivity, and the so-called equivalent surface temperature for infinitely large conductivity is adopted, correcting the actual values.

As to the discussion of Urbanski, we are sorry that we did not find and mention his literature; but we are glad to hear that he also obtained an induction-time curve for nitroglycerine similar to our life-time curves.

The transition from explosion to quiet burning will surely involve the heat transfer problem, and we are interested in his success in explaining the phenomenon using both the activation energy and heat transfer coefficient.

A. K. Oppenheim (California): I have a question regarding Laffitte's paper. Although it might be premature with respect to the research programme I would appreciate it if Laffitte would state his present views on the mechanism of suppression of explosion curves produced by fine powders. In particular: why do certain substances suppress detonation, but do not affect deflagration waves?

In connection with the paper of Palmer I would like to point out that, by the time the flame reaches a velocity of a few hundred msec the gas in front of the flame can be set in motion by the action of compression waves generated at the flame front even in the case of ignition at the open end.

F. Powell (Buxton): With reference to the paper by Laffitte and Bouchet, and the question raised by Oppenheim, the effectiveness of any powder in quenching deflagration by the particular experimental method described may be to some extent dependent on how easily the powder is dispersed into a cloud by the gas flow preceding the flame.

With regard to Palmer's paper, it may be of interest to note that a few tests have been made at S.M.R.E. with crimped ribbon flame arresters under conditions visualized by Oppenheim; that is, with the gas mixture in motion. This type of arrester, made by winding together around a central core two metal ribbons, one plain and the other crimped, is in effect a matrix of triangular channels. The arresters were used with methane–air mixtures in a horizontal tube of 2·75 in. diameter. A range of flame speeds was obtained by varying the point of ignition and by the use of restrictions in the tube. Although only a few results were obtained it appears that the critical flame speeds depend to a much greater extent on the crimp height than did those observed by Palmer on the mesh of his gauzes.

Assumption of a very simplified mechanism of quenching, similar to that given by Palmer, by cooling the flame gases to some critical temperature allied to the ignition temperature, but with the mode of heat-transfer which occurs in turbulent pipe flow, suggests that the critical flame speed, V, would be related to the crimp height, h, by a relation of the form $Vh^6 = C$, where C is a constant for a given gas mixture and thickness of arrester: the available results are not inconsistent with this relationship.

K. N. Palmer (Boreham Wood): In reply to verbal comments: The work of Holm and of Minchin is reported in reference 1, which is a review paper. These workers suggested that with perforated plate arresters the loss of heat from the flamelets emerging from the perforations was the cause of the quenching. The effect of transfer of heat by radiation between neighbouring flamelets was also discussed. On this theory it would be expected that alteration of the thickness of the plate would not affect its quenching ability. In some recent experiments both perforated metal plates and metal blocks with the same configuration of holes have been tested in a similar apparatus to that described in the paper; under these conditions the critical flame velocity at which quenching just occurs is directly proportional to the thickness of the arrester over the range investigated (0·1–5·0 cm). It therefore appears unlikely that the flamelet theory can hold for the present system.

During these tests no appreciable heating of the arresters occurred.

The reason for the difference in behaviour on increasing the thickness of metal-block arresters and packs of wire gauze is not clear, but it may arise from the pockets of gas mixture contained between the wires of the gauze, whereas the metal block is an array of straight smooth-walled tubes.

The quenching of the flame was assumed to result from heat transfer from the flame gases to the gauze. The main thermal resistance to the flow of heat is then the boundary layer of gas around the wire of the gauze; this resistance is independent of the thermal properties of the gauze. Also, as the thermal capacity of the flame gases is small, the amount of heat to be withdrawn from the flame to quench it is also small. The differences in the thermal properties of the various metals are not therefore important. This conclusion is substantiated by the lack of damage to even the finest gauze if the flame is quenched and does not pass through it.

The reasons for the behaviour of combined coarse and fine gauzes are discussed in the paper.

I agree with Oppenheim that the propagation of fast flames up the tube will lead to some gas movement through the arrester ahead of the flame. This gas movement will increase the heat transfer coefficient and will reduce the disparity between the theoretical prediction and the experimental results (*Figure 1*).

D. W. Gill (*Leatherhead*): Concerning Tesner's very interesting paper, I was particularly impressed by the concept that there will be no coagulation of carbon particles in a zone in which these are growing rapidly by surface decomposition of hydrogen, owing to the flow of hydrogen away from the surface, and the corresponding idea that soot particles will not settle on the wall of a containing vessel while surface decomposition of hydrocarbons is occurring thereat.

It seems to me that the whole problem of the coagulation of carbon particles is one which merits a great deal more attention than it at present receives.

While I have no disagreement in substance with Tesner's paper, there are one or two points of detail which I should be glad if he would clear up. The first is a slight inconsistency which may have arisen in translation of the paper. In connection with increase in hydrogen concentration, it is stated that this retards the process of carbon particle formation, which therefore goes on in a hotter part of the reaction chamber. This increases the heating rate, which, in its turn, causes an increase in the rate of particle formation. Later on in the paper, however, while discussing variation in gas flow rate, a different order of events is given: there is an increase in the rate of heating of the gas, as a result of which the process is going on at a higher temperature, which causes an increase in the rate of particle formation. Since one of the main conclusions of the paper is that the rate of heating of the hydrocarbon is the most important factor determining the course of formation of dispersed carbon, I think it is important to get this point clear. It seems to me that the degree of 'superheating' of the system is the direct controlling factor, so that the second sequence of events is the more logical.

Secondly, he refers in his discussion of the experimental results to the fact that a nucleus is four to five orders smaller in volume than a particle. I should be very interested to hear any information he has regarding size of the nuclei, and any theory he may have about the mechanism of their formation.

Finally, I would like to ask one question of Van der Held and of Singer and Grumer. Do they believe that the carbon flakes and filaments referred to in their papers actually exist as such in the flame, or do they think that perhaps these might be built up on the sampling grid from smaller, more or less spherical, particles present in the flame?

PART VII

TURBULENCE IN FLAMES

79

FLAME TURBULENCE

A. G. PRUDNIKOV

INTRODUCTION

There exist many problems, such as the problems of turbulent combustion, the solutions of which require extensive studies of air flow and flame turbulence. At present these studies are, in the main, conducted by two methods: thermo-anemometric and diffusion. The complexity of the first method and the vast amount of labour involved in the second method greatly limit the opportunities for such investigations and are therefore a serious obstacle in solving the problems.

This paper outlines the results of some research on the turbulence of air flows and flames by means of a new method, which being a modification of the diffusion method combines its simplicity and clearness with the rapidity of the thermoanemometric method.

METHOD OF MEASUREMENT

The method essentially consists of the following: the turbulence characteristics are measured by

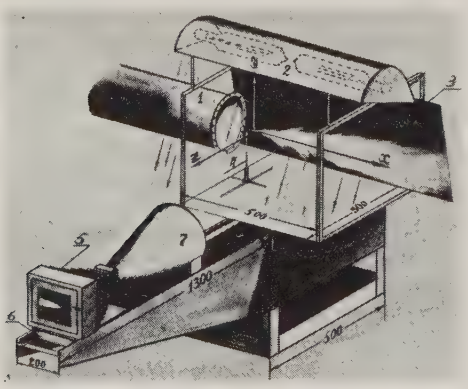

Figure 1. Diagram of experimental installation
1, tube; 2, illuminating lamps; 3, background (black velvet); 4, source; 5, photographic apparatus; 6, sliding carriage; 7, lens hood

means of the photographs of the diffusion wake of luminous particles behind the point source placed in a flow[11]. For cold flows a point source of tobacco smoke (dia = 1–2 mm) was used. A diagram of the installation is shown in *Figure 1*. A tiny stream of smoke was photographed with a conventional 9 × 12 cm camera against a dark background, with side illumination. For flames, a syringe needle (dia = 1 mm) with NaCl pressed in it was used as a source, one end of the needle being clamped in a holder cooled with water. The dimensions of the orifice from which the NaCl vapours were discharged were by far less than 0·1 mm.

By using the results of the statistical theory of turbulent diffusion it can be shown that the following condition is met in the case of small concentrations of luminous particles:

$$I(x,y) = I(x,0)e^{\frac{-y^2}{2\overline{Y^2}}} \tag{1}$$

where $I(x,y)$ is the intensity of light at a point of the photographic plate; $I(x,0)$ is the intensity of light getting on to the axis of the image of the diffusion wake in cross-section x; and $\overline{Y^2_{(x)}}$ is the dispersion of the turbulent transfer of particles in cross-section x.

Axis ox is directed along the flow, the origin of the coordinates is located in the source, and a flat image is photographed in coordinates xy. It can also be shown that with the total number of the luminous particles along the wake being constant, the following condition is fulfilled:

$$I(x,0) \sim \frac{1}{(\overline{Y^2_{(x)}})^{\frac{1}{2}}} \tag{2}$$

By applying the two conditions and the well-known property of photographic plates:

$$\frac{dS}{d(\log I)} = \gamma \tag{3}$$

it is easy to deduct an equation independent of the individual characteristic of the photographic plate:

$$\frac{1}{2}\frac{d\overline{Y^2}}{dx} = \left(\frac{\dfrac{\partial S}{\partial x}}{\dfrac{\partial S}{\partial (y^2)}}\right)_{y=0} \tag{4}$$

where $S(x,y)$ is the logarithm of blackening in the examined point of the image of the wake; and γ is the coefficient of the plate contrast.

The method of computing by formula 4 is simple (see *Figure 2*). For a number of cross-sections of the wake image: x_i $(i = 1, 2, 3, \ldots n)$ the series of $S(x_i y)$ curves is determined with the aid of a microphotometer, by which $\partial S/\partial x$ values are determined as tangents to the curve $S(x, 0)$ and the values $\partial S/\partial(y^2)$ as coefficients of the parabolas inscribed in the curves $S(x_i y)$.

Equation 4 may be applied only provided the luminous particles along the wake are constant, as, for instance, in the case of sufficiently stable latter included measurements in flame with gradients of mean temperatures.

Equations 4 and 5 may be used for determining not only the desired function $\overline{Y^2_{(x)}}$ by the photographic plate of the diffusion wake but also the value γ of the photographic plate contrast coefficient; it can be compared with the real value γ determined by conventional marking of the photographic plate. When the required condition of constancy of luminous particles along the wake is set up, both values of the contrast coefficient

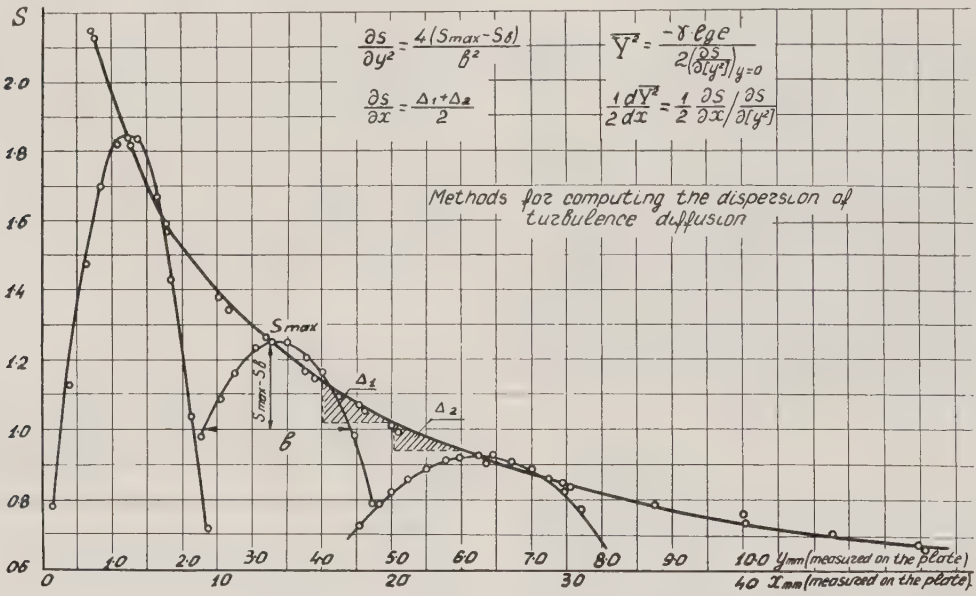

Figure 2. Methods for computing the dispersion of turbulence diffusion $\overline{Y^2_{(x)}}$

dispersion properties of the smoke along a stream in a cold flow, or in the case of constant temperature of NaCl vapours along the stream in a hot flow. If the requirement is not met another equation should be employed, obtained only from the condition 1.

$$\overline{Y^2_{(x)}} = \frac{-\gamma \log e}{2\left(\frac{\partial S}{\partial(y^2)}\right)_{y=0}} \quad (\log e = 0{\cdot}4343) \qquad (5)$$

This equation is simpler but the coefficient of the plate contrast has to be known. Apparently it is inapplicable only when the temperature gradients along y are large. We say 'apparently' to provide for the case of a 'micro-volumetric' mechanism of combustion; in the case of a 'surface' mechanism of combustion, the influence of the gradient of mean temperatures is negligibly small. This influence is manifested, above all, in an 'asymmetry' of curve $S(y)$. No asymmetry was recorded in any of our measurements, though the prove to be identical. *Figure 3* shows the results of such a comparison for various types of photographic plate, and for the sources employed in the 'cold' and 'hot' flows. Such a satisfactory coincidence of the theoretical and experimental values testifies to the reliability of measurements by the given method. Apart from this the trustworthiness of measurement by this method was checked through numerous measurements of the diffusion of carbonic acid (CO_2) in a cold flow. Equations 4 and 5 were used for measurements in a cold flow, while equation 5 alone was used for measurements in flame.

The intensity, the diffusion coefficient and the Lagrangian scale of turbulence were determined with the aid of equations which are an apparent result of G. I. Taylor's well-known equation:

$$\frac{(\overline{u^2})^{\frac{1}{2}}}{V} = \left(\frac{1}{2}\left(\frac{d^2\overline{Y^2}}{dx^2}\right)_{x=0}\right)^{\frac{1}{2}};$$

$$\frac{D}{V} = \frac{1}{2}\left(\frac{d\overline{Y^2}}{dx}\right)_{x=\infty} l_L = \frac{D}{(\overline{u^2})^{\frac{1}{2}}}$$

where $(\overline{u^2})^{\frac{1}{2}}$ is the mean quadratic lateral turbulence velocity; V is the mean velocity of the flow; D is the coefficient of turbulence diffusion; and l_L is the Lagrangian scale of turbulence.

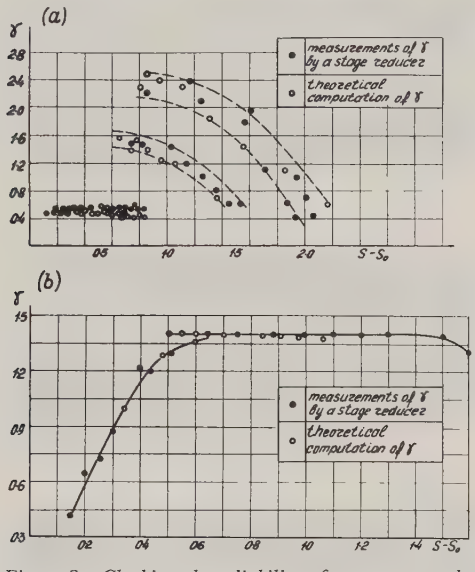

Figure 3. Checking the reliability of measurements by the given method. (a) Comparison of values of contrast coefficients γ for a 'cold' flow. (b) Comparison of values of contrast coefficients γ for a 'hot' flow

The exactness of the method is mainly limited by the locality of the source: for turbulence with an intensity of ~ 5 per cent and a Lagrangian turbulence scale $\geqslant 2$ mm, all the characteristics were measured with an average error of ~ 5 per cent.

With an error of ~ 10 to 15 per cent the turbulence intensity $(\overline{u^2})^{\frac{1}{2}}/V$ may be appraised 'by sight', using the catalogue of printed photographs compiled in the course of research. A sample of such a catalogue is shown in *Figure 4*.

RESULTS OF MEASUREMENTS

Reference 11 is devoted to detailed studies of turbulence of cold flows by means of the given method, but here we shall confine ourselves to the findings relevant to the measurements of turbulence in flame.

(1) For natural turbulence on the axis of a tube, similar conditions of velocity are observed, as well as those of geometrical similarity, i.e.

$$\frac{(\overline{u_1^2})^{\frac{1}{2}}}{V_1} 100 \simeq 4{\cdot}5 \text{ to } 5 \text{ per cent}; \qquad \frac{D_1}{V_1 d_p} \simeq 0{\cdot}001 \tag{6}$$

by measurements with CO_2 diffusion and with the aid of the given method, with: $d_p = 45$; 100; 145; 200; 400 mm and $V_1 = 20$ to 65 m/sec, $T_1 = 300°\text{K}$, $R_e = 10^5$ to 10^6. The value $(\overline{u_1^2})^{\frac{1}{2}}/V_1$ coincides with the commonly known values measured by thermoanemometers. The value $D_1/V_1 d_p$ coincides with that obtained for $R_e \geqslant 10^5$ by Goldenberg[12] who reduced to a mean Nikuradze's well-known data for the whole cross-section of the tube. It can be seen from equation 6 that the real value of the scale of mixing (the Lagrangian turbulence scale) is three or four times less than the Prandtl's scale of mixing on the axis of the flow, as computed by Nikuradze.

Measurements of turbulence in a hot flow (far behind the combustion zone) and in flame (in the combustion zone and directly behind it) were mainly taken in a 100 mm tube. Measurements behind a 60 mm flame-holder were taken in a 400 mm tube. The flame was stabilized in four different ways: (1) by a burner, 2 mm in diameter; (2) by a grid of flame-holders with the meshes and crosspieces ~ 18 mm in size; (3) by a grid of flame-holder, with the meshes and crosspieces ~ 6 mm in size; and (4) by a single flame-holder, 60 mm in diameter.

The grid of flame-holders represents a perforated iron sheet, the meshes 18 mm (6 mm) in diameter being disposed in rows one below the other in such a way that a roughly square crosspiece of the same typical size was obtained between four meshes. The range of velocities and temperatures in front and behind the combustion zone equalled respectively:

$$V_1 = 12 \text{ to } 30 \text{ m/sec}; \quad T_1 = 400°\text{K};$$
$$V_2 = 20 \text{ to } 120 \text{ m/sec};$$
$$T_2 \simeq 1{,}400 \text{ to } 2{,}200°\text{K}$$

A homogeneous mixture of benzene and air was used in the experiments.

Now a few words regarding the necessity of measuring turbulence in flame. The need for such measurements has arisen because of the great discrepancy between the theoretical estimates of the velocity of turbulent combustion and experimental findings. There arose a suspicion that the speed of combustion is determined not only by the turbulence of the upstream flow, but also by the one which occurs during combustion. This suspicion has grown particularly strong following the appearance of the well-known theoretical works by Landau[1], Markstein[2,3], Scurlock[4,5], Karlowitz[6,7] and others, who have proved that an increase in turbulence in the combustion zone is possible in principle.

It was necessary, first, to ascertain the lowest level of turbulence which becomes established in a tube, far behind the combustion zone. Measurements have shown that the intensity of stable

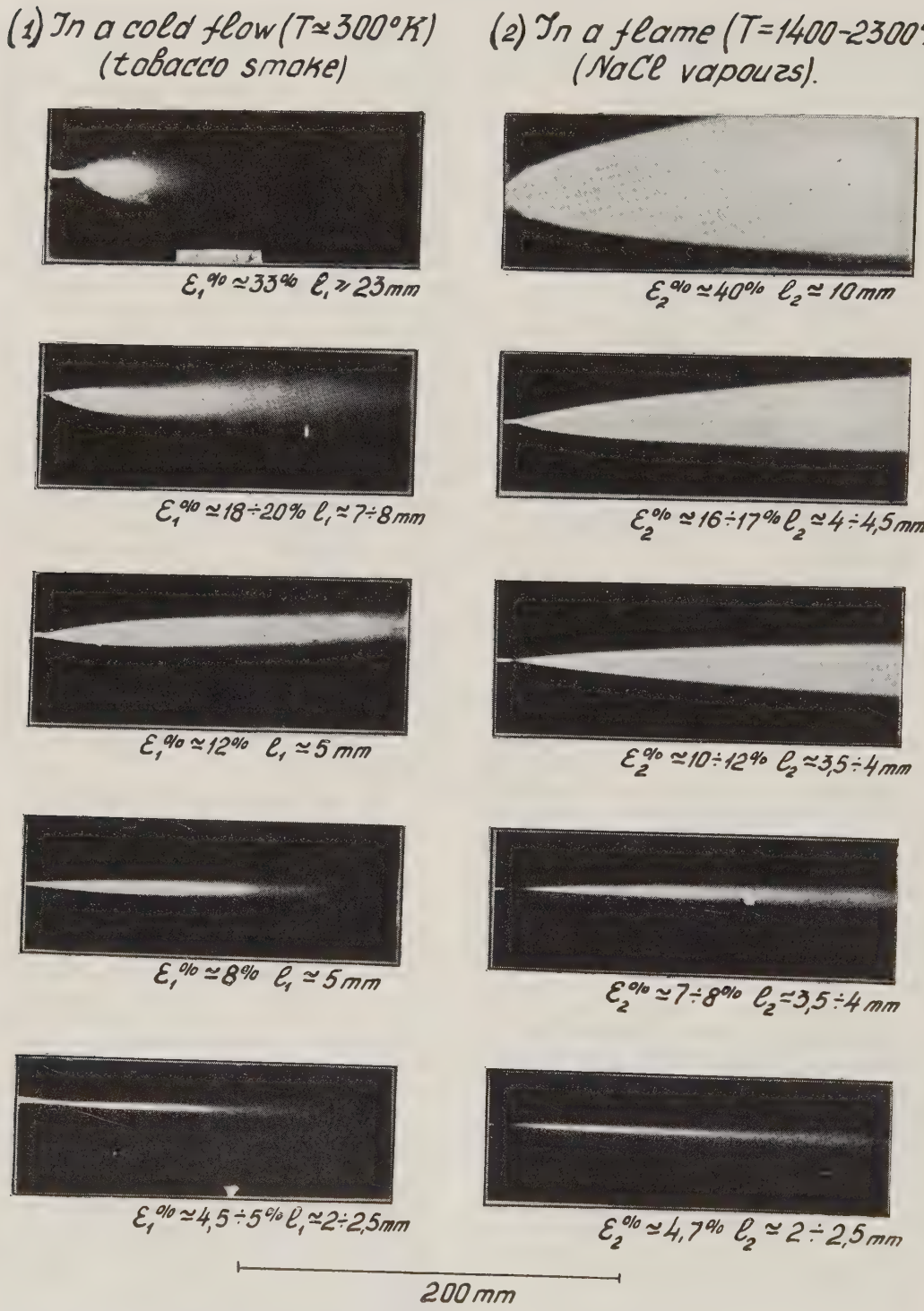
(1) In a cold flow (T≈300°K)
(tobacco smoke)
(2) In a flame (T=1400-2300°K)
(NaCl vapours).
ε1% ≈ 33% l1 ≈ 23mm
ε2% ≈ 40% l2 ≈ 10mm
ε1% ≈ 18÷20% l1 ≈ 7÷8mm
ε2% ≈ 16÷17% l2 ≈ 4÷4,5mm
ε1% ≈ 12% l1 ≈ 5mm
ε2% ≈ 10÷12% l2 ≈ 3,5÷4mm
ε1% ≈ 8% l1 ≈ 5mm
ε2% ≈ 7÷8% l2 ≈ 3,5÷4mm
ε1% ≈ 4,5÷5% l1 ≈ 2÷2,5mm
ε2% ≈ 4,7% l2 ≈ 2÷2,5mm
200mm

Figure 4. Samples of photographs of the diffusion wake of luminous particles in flows with different levels of turbulence

turbulence on the axis of a hot flow, far behind the combustion zone, amounts to $100(\overline{u_2^2})^{\frac{1}{2}}/V_2 \simeq 5$ per cent.

Exact measurements of the turbulence scale encountered difficulties as the measurements of the scale were taken on the end of the tube, beyond the boundaries of the region of constant turbulence*. It can only be said that the scale of turbulence appeared 1·5 to 2 times greater than that of the cold flow. It should be noted incidentally that in every measurement, both in flames

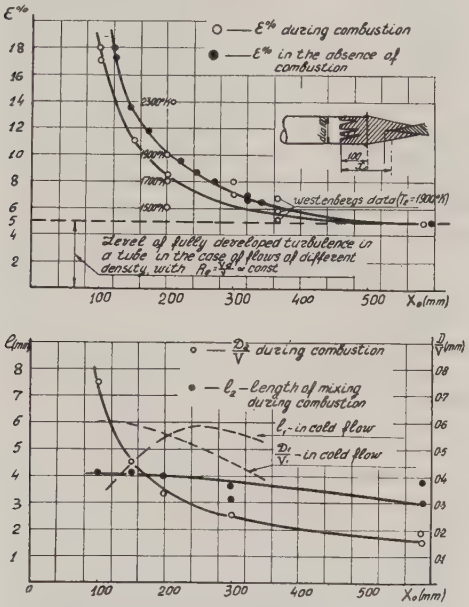
ε%
o — ε% during combustion
• — ε% in the absence of combustion
250 m/s
200 m/s
150 m/s
westenbergs data (T₂=1900°K)
Level of fully developed turbulence in a tube in the case of flows of different density, with Re = const
X₀(mm)
l₂(mm)
o — 2l₂/V during combustion
• — l₂ – length of mixing during combustion
l₂ – in cold flow
D₂/V₂ – in cold flow
X₀(mm)

Figure 5. Distribution of intensity, diffusion coefficient and turbulence scale in flame behind an 18 mm *grid*

and in 'hot' flows, other things being equal, the values $(\overline{u_2^2})^{\frac{1}{2}}/V_2$; D_2/V_2; l_2 are independent of the absolute value of the mean flow velocity V_2 (see, for example, *Figures 8* and *9*).

From the limited amount of data on turbulence in flame[7, 8–10], Westenberg's data appear to be generally accepted. Westenberg measured the intensity of turbulence in flame behind the flame-holders of three typical dimensions (12·5; 25; 37·5 mm) with the aid of diffusion of helium with the same ratio of mixture and at one and the same point, and derived two conclusions:

(1) the intensity of turbulence depends but little on the shape and the typical dimensions of the flame-holder;

(2) the increase in turbulence during combustion is negligible.

We took measurements of the decay of turbulence during combustion behind a grid of flame-holders of approximately the same dimensions as Westenberg's flame-holders. The comparison given in *Figure 5* shows that Westenberg took measurements at a distance where the turbulence intensity practically equals tube turbulence; hence the slight dependence on the dimensions of the flame-holders he obtained and the value of turbulence intensity, approximating 5 per cent.

On the basis of a theoretical solution of the hydrodynamics of a flame behind the burner, Scurlock predicted and theoretically computed the anticipated effect of increased turbulence in a torch owing to the appearance of a gradient of mean velocities. Our measurements behind the burner in a 100 mm tube, behind a single flame-holder, 60 mm in diameter, in a 400 mm tube and behind the grid of flame-holders, $\sim$ 18 mm in size, in a 100 mm tube have shown that Scurlock's effect does not practically manifest itself there where it might be expected; more frequently the reverse effect is manifested, a decrease in the intensity of turbulence due to a reduced gradient of mean velocities during combustion behind a bluff body. See, for example, *Figures 5* and *7*. *Figure 5* presents charts of the decay of turbulence behind the grid (18 mm) in a 100 mm tube in the absence of combustion ($T_1 = 300°$K) and during combustion ($T_2 = 1{,}700$ to $1{,}800°$K).

Such a peculiarity of the behaviour of turbulence in flame behind bluff bodies has made it possible to observe the influence of self-turbulence of flame behind an 18 mm grid of flame-holders. *Figure 6* shows the variation of turbulence intensity with temperature at a fixed depth of the combustion zone stabilized behind the 18 mm grid of flame-holders. The source of NaCl vapours was placed at a distance of 200 mm from the grid, in the wake behind one of the flame-holders, since at such a distance the field of mean temperatures and velocities was still quite non-uniform. It can be seen from *Figure 6* that in lean mixtures the intensity of turbulence during combustion is several times less than that in the absence of combustion, but as the temperature grows it begins to rise markedly, and at maximum temperatures it attains greater values than in the absence of combustion. Such an increase in turbulence may be accounted for only by an increase in self-turbulence of the flame, following the rise in temperature, since the gradients of mean velocities only diminished in this case.

No such effect was recorded in a turbulent flame behind a single flame-holder in the range of temperatures under investigation: the intensity of turbulence only diminished (as the gradients of mean velocities decreased) (see *Figure 7*). The following unexpected fact is worth noting: unlike the case of the grid of flame-holders, the minimum value of turbulence intensity behind the single

* An increase in turbulence velocities on the axis of a hot flow ($T_2 = 1{,}700°$K) was observed already at a distance less than the diameter from the end of the tube.

flame-holders during combustion was by far larger than that measured under the same conditions, but in the absence of combustion.

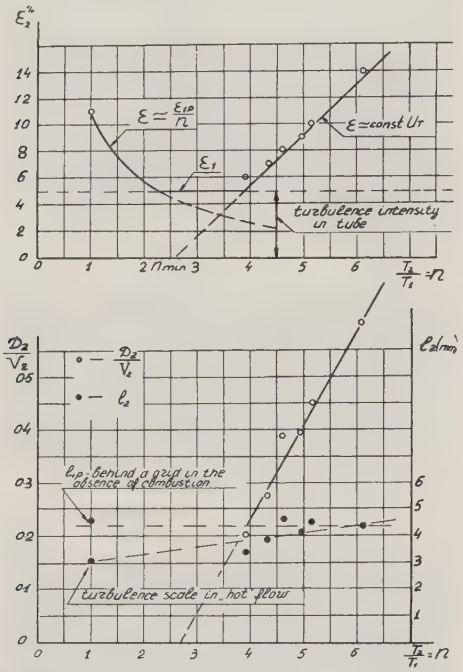

Figure 6. Dependence of flame turbulence characteristics behind an 18 mm *grid of flame-holders on the temperature of combustion products*

The difference in the hydrodynamics of the stream during the combustion in the tube and in an open flow leads to the assumption that turbulence in the two cases may be different: experimental findings have corroborated this assumption. *Figures 8* and *9* show the change in turbulence in the flame behind the burner and the grid of flame-holders (6 mm) as the function of velocity ratio V_2/V_1 behind and in front of the combustion zone*. It can be seen that turbulence in flame possesses quite different properties, depending on the fact whether the flame is located in the tube or in an open flow.

The transition of turbulence from the condition of 'open flame' to that of 'closed flame' depends only on the ratio V_2/V_1 and takes place in a very abrupt manner: with $V_2/V_1 < 2$, it is an 'open flame', and with $V_2/V_1 > 3$, it is a 'closed flame' (with any T_2/T_1 and with any method of stabilizing the flame). The greatest difference is obtained in the case of monodimensional zone of combustion, set up behind small-scale grid (6 mm) (see *Figure 9b*).

During combustion in the tube the flow is accelerated along the tube and consequently the effect of eddy distortion could be expected: decreasing in lateral scales and increasing in longitudinal ones. The lateral scale should, notably, be by far greater in an open flame than in a closed one. The effect of distortion was most distinctly observed during combustion behind a 6 mm screen in which case there was continuous transition from an open to a closed flame. It can be seen from *Figure 9b* that the scales diminished uninterruptedly as V_2/V_1 increased to reach the scale of tube turbulence.

The results so obtained also demonstrate that with regard to flames in tubes the scale of turbulence practically coincides with the scale of tube turbulence of the hot flow in every case of measurement in the zone and behind the zone of combustion.

The turbulence intensity $(\overline{u_2^2})^{\frac{1}{2}}/V_2$ measured directly behind the combustion zone equals by magnitude not only the intensity of a hot flow tube turbulence, but also the turbulence measured in a cold flow. Hence the following condition is derived:

$$\frac{(\overline{u_2^2})^{\frac{1}{2}}}{(\overline{u_1^2})^{\frac{1}{2}}} = \frac{V_2}{V_1}$$

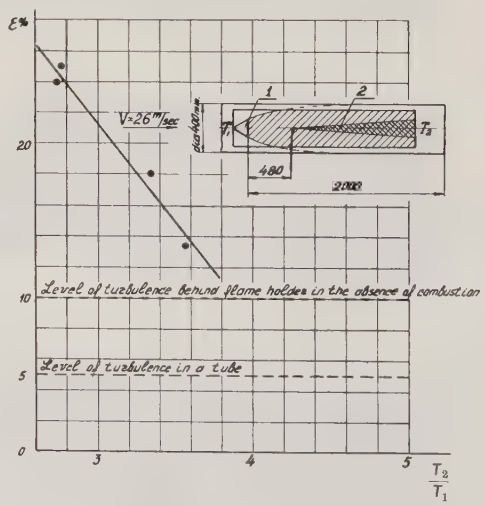

Figure 7. Dependence of flame turbulence characteristics behind a single flame-holder on the temperature of combustion products: (*1*) *flame-holder;* (*2*) NaCl *vapours*

For example, in the case of a stoichiometric mixture turbulence velocity increases sixfold (*Figure 9*), consequently the remarks of some researchers as to the slight change in turbulence during the transition of the flow through the

* The ratio V_2/V_1 was determined by means of a Pitot tube and the thermocouple. The ratio V_2/V_1 could be varied by moving the flame-holder inside the tube; in the given measurements it was varied either by increasing velocity V_1 (for the burner), or by by-passing a part of the air through the grid in the absence of combustion.

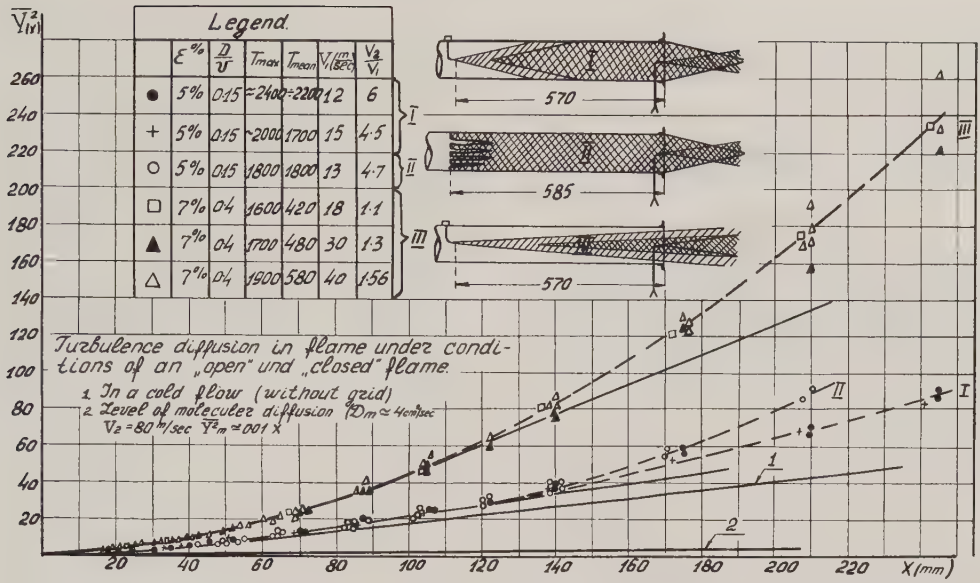
Legend
Turbulence diffusion in flame under conditions of an „open" und „closed" flame
1 In a cold flow (without grid)
2 Level of molecular diffusion
X (mm)

Figure 8. Turbulence diffusion in flame under conditions of an 'open' and 'closed' flame

combustion zone do not prove to be justified even in this case of a minimum level of turbulence in flame. It should, however, be noted that such a 'stability' of the turbulence level can be accounted for not only by the nature of self-turbulence of closed flames alone. In studying the turbulence of cold flows in tubes we observed a great velocity of regeneration of the level of tube turbulence during any artificial raising (or lowering) of the level of turbulence in the tube. The stability so recorded may also be accounted for by this effect, if it is admitted that this effect appears far sooner in the flames.

CONCLUSIONS

Three major conclusions may be drawn on the basis of the results so obtained:

(1) Turbulence in flame, as in a cold flow, is similarly related to velocity, i.e. $(\overline{u_2^2})^{\frac{1}{2}}/V_2$; D_2/V_2; l_2 does not depend on the magnitude of V_2;

(2) Combustion in a turbulent flow substantially changes not only the values of the mean velocities, but also of turbulent ones. The least value of turbulence intensity $(\overline{u_2^2})^{\frac{1}{2}}/V_2$ measured in flame was not below 5 per cent. Turbulence velocity $(\overline{u_2^2})^{\frac{1}{2}}$ in flame behind the grid of flame-holder may be even smaller than turbulence velocity $(\overline{u_1^2})^{\frac{1}{2}}$ behind the same grid in the absence of combustion, due to a great decrease in the gradients of the mean velocities during combustion. Turbulence velocity behind the combustion zone is, however, always greater than that of an upstream flow;

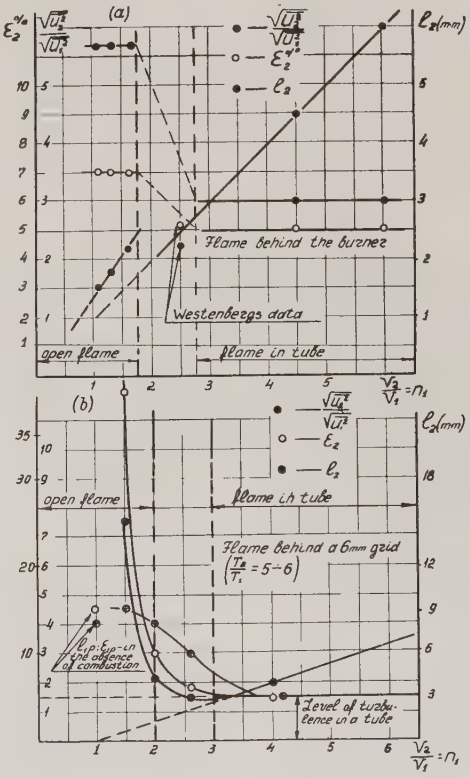

Figure 9. Dependence of flame turbulence characteristics on the acceleration of the flow in the combustion zone

(3) Turbulence parameters greatly differ in value, depending on their being measured in an open flame or in a flame in a tube.

This work was carried out at the Moscow Physico-Technical Institute, under the guidance of Professor E. S. Schetinkov, Doctor of Science (Technology).

REFERENCES

[1] Landau, L. D. *J. exp. theor. Phys.* 14 (1944) 240
[2] Markstein, G. H. *J. chem. Phys.* 17 (1949) 428
[3] — *Fourth Symposium (International) on Combustion*, 1953. Baltimore; Williams and Wilkins
[4] Scurlock, A. E. *Meteor Report No. 19.* July 1948. Fuels Research Laboratory
[5] — *Third and Fourth Symposiums (International) on Combustion*, p. 21, 1949; and p. 645, 1953. Baltimore; Williams and Wilkins
[6] Karlovitz, B. *J. chem. Phys.* 19 (1951)
[7] — *Fourth Symposium on Combustion*, p. 60. 1953. Baltimore; Williams and Wilkins
[8] Westenberg, A. *J. chem. Phys.* 22 (1954) 814
[9] Gross, R. A. *Jet Propulsion* 25 (1955) No. 12
[10] Jensen, W. P. *Jet Propulsion* 26 (1956) No. 6
[11] Prudnikov, A. G. Measurements of the turbulence of air flows and flames by the optical-diffusion method. *Master of Science Thesis.* 1956. Moscow Physico-Technical Institute
[12] Goldenberg, S. A. *Izvestiya of the U.S.S.R. Academy of Sciences, Department of Technical Sciences*, Nos. 4, 5, April 1950

80

CALCULATION OF FLAME VELOCITY IN TURBULENT STREAM

E. S. SHETINKOV

TURBULENT FLAME MODEL

Despite the considerable amount of research work that has been carried out up to the present there is still no clear understanding of the nature of turbulent burning, owing to the exceptional complexity of the phenomenon. For this reason it would be more correct to speak not of the theory but of the conception or model of turbulent flame. The construction of a proper model is one of the most important present-day tasks.

The wrinkled laminar flame model has been widely recognized. The model was first formulated by Damkoehler and later developed by Shelkin and a number of other research workers.

It is based on the assumption that laminar flame which has initially originated cannot be extinguished. The flame is mechanically split into parts or wrinkled by turbulent fluctuations, attended with a proportional increase in the total flame surface.

It is, however, known from experiments that the free flame globules of limited dimensions are extinguished under the effect of strong turbulence, and further propagation of the flame ceases[1].

Theoretical analysis of the laminar flame in a stream with a gradient of velocity points to possible extinction of flame under such conditions[2]. The paper by Kovaznay[3] likewise acknowledges the break-up of laminar flame at sufficiently high velocity.

Proceeding from the above, it is quite likely that in a turbulent brush the laminar flame need not necessarily appear as the boundary between individual moles consisting of combustion products and a fresh mixture*.

If this is so, the mutual diffusion of the combustion products and of the fresh mixture, occurring on the boundaries of and inside individual moles, acquires great importance: the micro-diffusion proceeds at a sufficiently rapid rate and the laminar flame has no time to start. Instead, a homogeneous chemical reaction may begin in the mixture of the combustion products, the fuel and the oxidant, which has been formed inside the mole.

* Turbulent moles are assumed to represent individual volumes whose motion during a fixed period of time within a certain accuracy may be considered as motion of a solid body.

In general, it may be assumed that both surface and homogeneous volume burning may take place in a turbulent brush.

The development of a method for calculating such a complex model appears, however, quite difficult. At the present stage of development of the combustion theory, the model should be considerably simplified so that it might be defined quantitatively.

Simplification may be effected in two directions: (1) We may disregard the homogeneous reaction and consider that the basic mass of fuel burns out according to the surface mechanism—this is the way chosen by most investigators; (2) the model of the phenomenon may be simplified in another direction, namely, by disregarding the amount of fuel consumed according to the surface mechanism and considering that the bulk of fuel burns out in volume reactions occurring inside individual moles. This paper deals with the second method.

For the sake of brevity, such a simplified model is to be subsequently termed the model of micro-volume burning.

TURBULENCE MODEL

For a quantitative calculation of the speed of flame propagation on the basis of a micro-volume model a turbulence model must be elaborated in which: (*a*) the conception would be applied regarding the turbulent stream as consisting of individual turbulent moles which constantly appear and disappear; (*b*) a connection would be established between the characteristics of the selected model and the generally accepted characteristics of turbulence: intensity $\varepsilon = v'_m/u$ the Lagrangian scale l_d as well as the spectrum of speeds and scales.

Owing to the absence of necessary data it is difficult at present to set up a model meeting all the requirements.

The number of possible turbulence models may be as large as desired, and the selection of any of them is somewhat arbitrary. The concrete model described below should, therefore, be considered merely as an example illustrating the calculation.

Considering turbulence as being uniform and isotropic let us divide the flat stream into squares I, II, III . . . (*Figure 1*) and analyse the diffusion of a foreign substance out of square I.

Let us assume that under the influence of 'intramolar' diffusion the concentration of the substance inside the square is similar at each of its points. Let us further assume that every square consists of

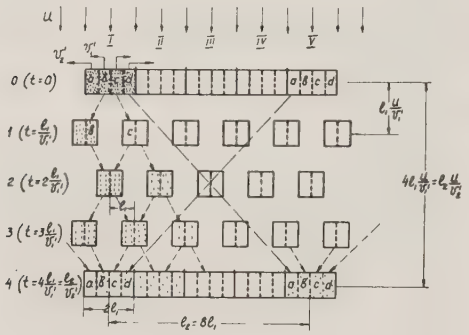

Figure 1. Model of turbulent diffusion

moles of two kinds: 'small-scale moles' b and c moving in a transverse direction to the left and right to a distance l_1 at speed v_1', and 'large-scale ones' a and d moving to distances $l_2 = 8l_1$, at speed $v_2' = 2v_1'$.

The mean concentration of substance is calculated in those squares, downstream, where moles a, b, c and d move, and the procedure is then repeated.

It follows from the above that the following correlation between l and v' underlies the model under investigation:

$$l^{1/3} = \text{const} \cdot v'$$

As shown by calculations[5], the above model is equivalent by its diffusion characteristics to the stream which has $v_m' = 1{\cdot}46v_1'$ and $l_d = 2{\cdot}91l_1$.

It is natural that by complicating the model (for instance, by introducing not two, but three or more scales, etc.), it is possible to obtain any desired approximation of the calculation results to the 'cold' experiment at short and long distances from the source.

METHOD OF CALCULATION

In accordance with the turbulent flame model, calculation of flame propagation is reduced to computing the mean volume mole temperature and fuel concentration, and the amount of fuel which burns up during the 'life-time' of the mole under examination. For the sake of simplification, we shall disregard the thermal expansion of the combustion products and flame turbulence.

Let the 'life-time' of the mole under examination equal $t_p = l/v'$.

Then the time during which the reaction of burning proceeds in the given mole is determined from $t_b = t_p - t_s$, where t_s is the time of delay of ignition equal at first approximation to the sum of intramolar mixing time periods t_m, and induction lag t_i. For numerical calculations it was assumed that $t_m = 0$ and $t_i = 10^{-5}e^{10,000/RT_{\text{in}}}$ sec where T_{in} is the initial mean temperature of the mole. The combustion reaction speed $V = -\,\mathrm{d}C_f/\mathrm{d}t$ was computed by the usual kinetic equation of the second order reaction, with the energy of activation $E = 25{,}000$ and the sterical factor amounting to 1*.

The initial mean fuel concentration $C_{f\,\text{in}}$ and temperature T_{in}, which were obtained at the formation of the mole under investigation, were calculated as mean values of the temperature and concentration of the volumes a, b, c, d from which the given mole was obtained.

T_{in} being known, it is possible to determine t_b and, where $t_b > 0$, to compute the final concentration of fuel in the given mole C_{ff} by formula:

$$t_b = \int_{C_{ff}}^{C_{f\,\text{in}}} \frac{\mathrm{d}C_f}{V}$$

The temperature of mole T_f at the end of its life-time may be determined from the balance equation:

$$(T_f - T_{\text{in}})c_p = H_u(C_{f\,\text{in}} - C_{ff})$$

where H_u is the heating value of the fuel.

Then the mole (square) is divided into its elements, the latter are moved in accordance with the selected model of turbulence to new places and mixed in new moles (squares).

Figure 2 shows a typical diagram obtained in calculating the propagation of flame from a combustion products jet, moving parallel to the stream of a fresh mixture.

The shaded areas denote the squares where the reaction of burning takes place, the area being approximately proportional to the difference between the initial and final temperature of the given mole.

The shaded squares define on the whole the burning zone. The shape of the burning zone contours near the ignition source is determined by the chosen conditions of igniting the mixture; but when the process of flame propagation is sufficiently remote from the initial point in the field of homogeneous isotropic turbulence it becomes stabilized, and the position of the front boundary of the flame may be approximated by a straight line. The incline of the line determines the turbulent burning velocity u_t. The rear boundary of the flame area may be approximated in the same way, and consequently the width of the burning zone may be similarly determined.

* The magnitude of activation energy $E = 25{,}000$ was taken on the assumption that the normal speed of burning, calculated by formulae of the thermal theory, proved to equal 35 cm/sec with $T_0 = 288°\text{K}$.

As can be seen from the diagram, the front boundary of the flame has an uneven 'ragged' appearance which to some extent resembles the

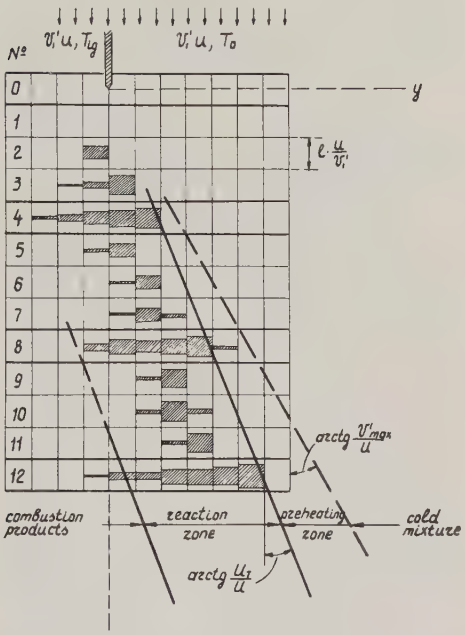

Figure 2. Structure of turbulent brush in a micro-volume burning model

actual shape of a turbulent brush photographed at a short exposure.

The steps noticeable on the diagram in the 'full' lines 4, 8, 12 . . . result from the effect of the large-scale component of fluctuation speed v_2' (*cf. Figure 1*).

RESULTS OF CALCULATIONS

In numerical computations, small-scale component of turbulence was assumed as $l_1 = 0{\cdot}9$ mm.

The conditions of ignition are the same as in *Figure 2*. The temperature of the igniting jet was assumed to equal 1,800°K*.

As a rule, the calculation was made up to $X = (20 \text{ to } 24) l_1/\varepsilon_1$.

Taking into account some arbitrariness in drawing tangential straight lines through a limited number of points, two possible variants of incline of the straight lines (double points) are sometimes given on the computed diagrams.

Figure 3 shows the results of calculations dealing with the influence of fluctuating velocity v_1' on u_t.

* Computations were likewise made for other temperatures within the range of 1,300–2,400°K. It appeared that u_t was the same in every case, and it was only the length and the shape of the transition section that underwent a change.

The same illustration contains plotted approximating curves for every air ratio number e (reciprocal of equivalence ratio), which accord with equation $u_t \sim v_1'^{0{\cdot}67}$.

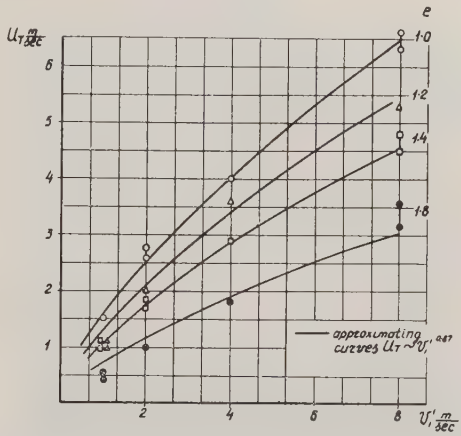

Figure 3. Influence of v' and e on u_t with $T_0 = 400$°C, $p = 760$ mm Hg

Owing to the reasons stated above it is difficult to compare directly the calculation with experiment. It can only be pointed out that some experimental results[6] testify to a similar functional dependence of u_t on v' with $e = \text{const}$.

Figure 4 shows the results of calculating u_t at

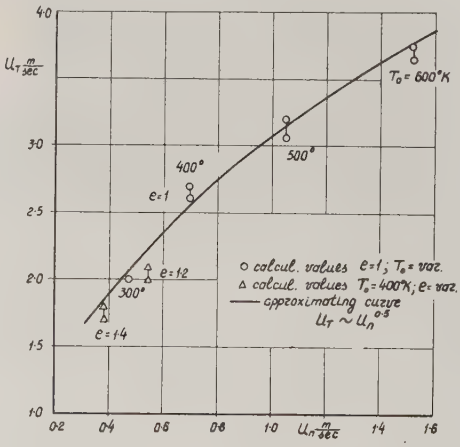

Figure 4. Influence of u_n on u_t with $v_1' = 2$m/sec, $p = 760$ mm Hg

various normal flame velocities u_n. The magnitude of u_n changed both due to a change in the temperature of the fresh mixture T_0 with $e = 1$, and to e with $T_0 = 400$°K. The connection between u_n, T_0 and e was obtained from experiments[7]. It can be seen from the diagram that the connection between u_t and u_n is approximately the same: $u_t \sim u_n^{0{\cdot}5}$, irrespective of the method of changing u_n (by means of e or T_0).

As is well known, experimental results do not supply an unambiguous answer. Vlasov[6] and others point to a 0·2 to 0·3 power, while Bollinger[8]

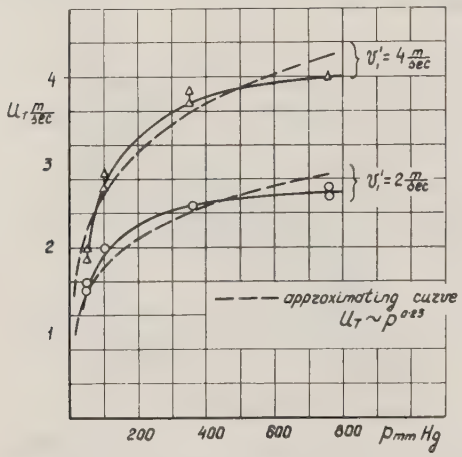

Figure 5. Influence of p on u_t with $e = 1$; $T_0 = 400$°K

refers to a substantially greater value (up to 1).

Figure 5 shows the influence of pressure p on u_t with two values of $v_1' = 2$ and 4 m/sec. It was assumed in the calculation that p does not affect the period of induction or turbulence intensity. The full lines were drawn directly between the computed points, while the approximating curves $u_t \sim p^{0.23}$ are represented by dashed lines.

It has been shown in experimental work[9] that $u_t \sim p^{0.12}$. The same paper indicates, however, that pressure influences turbulence intensity $\sim p^{0.34}$.

Therefore, if account is taken of the decrease in v_1', n in equation $u_t \sim p^n$ should grow. However, t_i decreases in proportion to p and the surmised reaction order for hydrocarbons is not 2, as assumed in the calculation, but somewhat less. The result is that curves u_t plotted against p in *Figure 5* should not change greatly.

The above method for calculating burning velocities also permits a quantitative analysis of the ignition of a combustible mixture from a jet source of ignition and flame blow-out.

It is known from experiment that ignition depends on the power of the ignition source (temperature and dimensions), the kinetics of burning reaction and on the characteristics of turbulence.

The calculation indicates, in agreement with the experiment, that at a sufficiently high speed of the stream, the flame (burning reaction) appears not immediately behind the ignition source but at some distance x_f from it.

Figure 6 shows the computed dependence x_f on the temperature and the width of the ignition source. It can be seen from the diagram that the width of the source considerably influences ignition if it becomes less than a certain magnitude (in the case under investigation, $2H < 8l_1$).

When the width of the source is adequate, it is

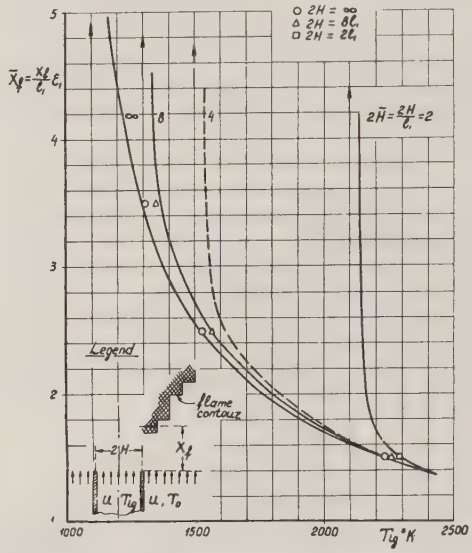

Figure 6. Influence of the ignition source temperature and width on the distance from the flame to the source, with $u = 40$ m/sec; $\varepsilon_1 = 5$ per cent, $T_0 = 400$°K

the ignition temperature that acquires importance. The less the width, the higher the minimum temperature at which ignition becomes possible.

Figure 7 represents the flame contours obtained

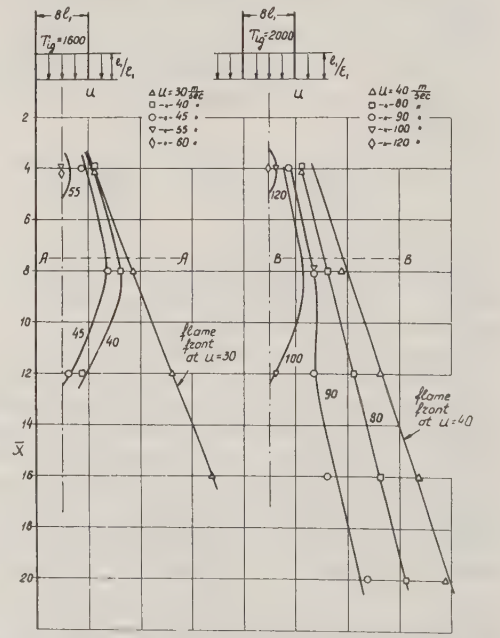

*Figure 7. Contours of flame for two ignition sources ($T_0 =$ 1,600 *and* 2,000°K), *with different u and with* $T_0 = 400$°K, $e = 1$, $p = 760$ mm Hg*

by computation in the various stages of velocity blow-out (with $\varepsilon_1' = 5$ per cent). Two cases were computed, differing only by the temperature of the igniting jet: 1,600 and 2,000°K. As can be seen from the diagram, with an increase in the velocity of the stream, there first occurs a decrease in the incline of the straight-line contours of the flame.

Then, at some distance there appears a local narrowing of the brush (the 'neck', with $u = 90$ m/sec and $T_0 = 2{,}000$°K). When the speed of the stream further increases the propagation of the flame into the fresh mixture ceases, and burning is confined to a closed region near the ignition source. When the speed attains 160 m/sec this region disappears as well, as the heat conduction becomes so great that it exceeds the inflow of heat from combustion.

Analysis of such factors as T_0, e, E, p, etc. on the blow-out, by means of similar calculations, appears to present no difficulty whatsoever.

The above results of the numerical calculations lead to the following general conclusion. Although the micro-volume model does not comprise the notion of laminar (surface) burning, the theoretically computed influence of individual factors (v_1', u_n, e, etc.) on u_t and the stability of burning agree qualitatively with experimental observations. Hence, it follows that microdiffusion processes appear to play an important part in turbulent burning.

SOME EXPERIMENTAL PREMISES OF THE PROPOSED MODEL

When experimental data are compared with the combustion model, the conditions of the experiments should be taken into account.

It may be assumed that with weak though large-scale turbulence ($l_d > \delta_l$ and $v' < u_n$) there exists a laminar flame in the flame brush. In the case of such a brush, the wrinkled laminar flame model is quite justified. When, however, turbulence intensity increases, the laminar flame fronts begin to 'dissolve'.

A criterion defining this phenomenon has been suggested[3]

$$\Gamma = \frac{v_m' \delta_l}{\lambda u_n}$$

where λ is the microscale of turbulence and δ_l is the thickness of the laminar flame.

Regretfully enough, the criterion Γ has not as yet been checked experimentally and it is therefore difficult to assert at which value of $\Gamma = \Gamma_{cr}$ the existence of laminar flame fronts really becomes unlikely. It may only be assumed that, beginning with $\Gamma > \Gamma_{cr}$, combustion is supposed to proceed, in the main, according to the micro-volume model.

With a further increase in v_m', there comes a time when the duration of one fluctuation l_d/v_m' proves to be small as compared with the laminar burning time*, i.e.

$$\beta = \frac{v_m' \delta_l}{l_d u_n} \gg 1$$

It may be expected that turbulent diffusion will prevail over kinetics. Then the distributed reaction zone model would be justified[4]. To some extent the model at small pressure has been confirmed experimentally[10].

In view of the above, let us analyse some experimental data which are difficult to account for if one proceeds from the model of surface burning.

(1) *Figure 8* shows the diagrams of temperature T and ionization probe current i recorded on a 'combined probe' on a loop oscillograph[5]. The

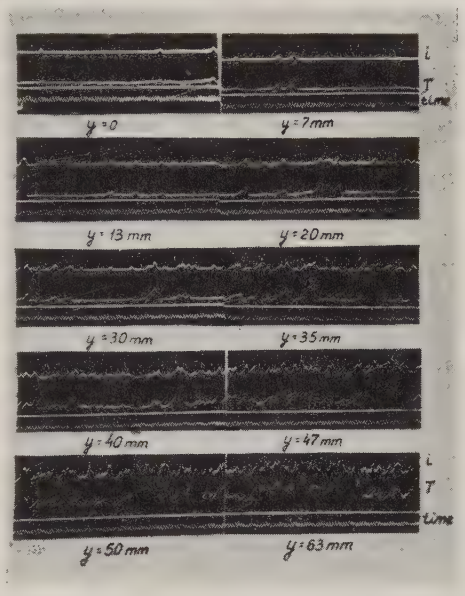

Figure 8. Oscillograms of ionization current (i) and temperature (T) at various points y along the depth of the burning zone, with $u = 15$ m/sec; $e = 1{\cdot}2$; $\varepsilon = 5$ per cent. Diameter of tube: 220 mm; *time marks:* 1/500 sec

combined probe consisted of a small-inertia resistance thermometer (length of filament: 6·5 mm, diameter: 0·018 mm) combined with an ionization-gap probe (gap: 0·5 mm).

Analysis of the oscillograms points to a singular analogy between the temperature curves and the ionization current: each 'splash' of T is attended in every case with a similar 'splash' of i.

The length of every splash is quite considerable and amounts to 15–60 mm. Unfortunately it has not been possible to record the oscillogram in the depth (in the second part) of the burning zone because of the insufficient strength of the resistance thermometer.

* See also reference 10 for criterion β.

The analogy between T and i so obtained might be explained from the viewpoint of the wrinkled laminar flame model by inadequate locality and resolving power of the equipment, assuming that all the volumes 15–60 mm in size are filled in a similar way with a dense network of laminar flames. As a matter of fact, the density of the network should be random, and combustion will, therefore, end in some moles earlier than in others. As a result, the analogy between T and i can be confused.

On the other hand, proceeding from the micro-volume burning model, the analogy between T and i can be explained if one makes the probable assumption that the processes of mixing and combustion inside individual moles are continuous*. It is only in the depth of the burning zone where the fresh mixture is to be encountered relatively seldom that the similarity between the T and i curves can be confused.

(2) *Figure 9* presents a comparison[10] of the contours of turbulent flame, measured by the

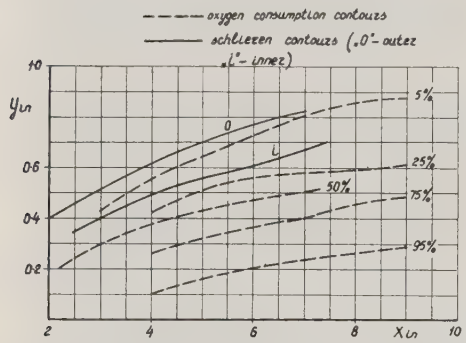

Figure 9. Contours of stoichiometric flame according to the schlieren picture and consumption of oxygen. x is the distance from the flame-holder along the stream. y is the distance from the flame-holder axis across the stream

schlieren picture, and chemical analysis. The experiments were conducted in an air–propane mixture jet, 2 × 1·5 in., with $u = 60$ ft./sec.

As can be seen from *Figure 9*, combustion does not start in the zone of the schlieren front characterized by the presence of numerous 'wrinkles' (consumption of $O_2 < 5$ per cent); this points to the presence of a large number of small globules with a high temperature. The absence of noticeable remnants of laminar flame fronts in the depth of the zone, where the consumption of O_2 amounts to 25–95 per cent, hardly agrees, however, with the wrinkled laminar flame model.

In the case of a micro-volume burning model such a pattern may be accounted for by insufficient contrast of the schlieren pictures (in this model the gradients of density between the individual moles should, generally speaking, diminish in proportion to the depth of the zone).

(3) Theoretical analysis of the wrinkled flame model leads to computing formulae of the kind $u_t = f(u_n, v', u, T_b/T_0)$, the last two factors taking account of the influence of flame turbulence[2,11]. By varying e, p, u_n and the other factors, it is possible to arrange two experiments in such a way that u_n and v' undergo no change. As a rule, however, various values are obtained for u_t. For example, if u_{t_1} is measured, with $e_1 = 1$ and u_{t_2}, with $e_2 < 1$, so that $u_{n_1} = u_{n_2}$, the result of the experiment is that: $u_{t_2} > u_{t_1}$. This difference cannot be accounted for by flame turbulence as $T_{b_2} < T_{b_1}$.

It is to be regretted that all the above proofs of the 'inconsistency' of the wrinkled laminar flame model at developed turbulence are indirect and not direct, and further experimental research should be welcomed, aimed at studying the fine structure of turbulent brush, so as to clarify the conditions in which the existence of laminar flame fronts proves impossible.

CONCLUSIONS

(1) A number of numerical calculations of turbulent burning were made on the basis of a micro-volume burning model without using the notion of laminar flame. The influence of v', e, T, u_n and p on the velocity and stability of the flame were analysed in the calculations. The results of the latter are in qualitative agreement with experimental observations.

(2) Theoretical considerations and some experimental data point to the slight likelihood of the existence of laminar flame fronts in a strongly turbulent stream. Together with (1), this confirms the presence of a region along v'_m where combustion may chiefly occur in micro-volumes as a homogeneous reaction. With a decrease in v'_m and other conditions being constant, there is an increase in the fraction of fuel which burns up in wrinkled laminar flame fronts (Damkoehler–Shelkin's model), and with an increase in v'_m, transition to homogeneous distributed burning becomes likely (model by Summerfield and his associates).

(3) It is advisable that further study of the model of turbulent combustion and of the methods of calculation should be made in the following directions: (*a*) investigating experimentally the fine structure of the turbulent brush and establishing statistical regularities between the characteristics of the combustible mixture and those of the flame; and (*b*) determining the initial computing data (structural characteristics of turbulence, summary kinetics of the burning reaction) so as to compare quantitatively the computed and experimental results.

* The turbulence model shown in *Figure 1* is a computing scheme. No 'division' or 'stops' of moles in a real stream exist.

REFERENCES

[1] Olsen, H. and Gayhart, F. *Jet Propulsion* 25 (1955) 276

[2] Karlowitz, B. in *Combustion Processes*, chapter H 1956. Princeton; University Press

[3] Kovaznay, L. *Jet Propulsion* 26 (1956) 485

[4] Summerfield, M., Reiter, S., Kebely, V. and Mascolo, R. *Jet Propulsion* 25 (1955) 377

[5] *Proceedings of the Moscow Seminar on Combustion.* Paper read by E. S. Shetinkov. USSR Academy of Sciences Publishing House (in press)

[6] Vlasov, K. P. *J. Tech. Phys.* No. 2 (1957)

[7] Dugger, G. *NACA Techn. Note, No. 2170*, 1950

[8] Bollinger, L. and Williams, D. *Third Symposium (International) on Combustion*, p. 176. 1949. Baltimore; Williams and Wilkins

[9] *Proceedings of the Moscow Seminar on Combustion.* Paper read by V. A. Khramtsov. USSR Academy of Sciences Publishing House (in press)

[10] Wohl, K. *et al. Sixth Symposium (International) on Combustion*, p. 333. 1957. New York; Reinhold

[11] Scurlock, A. O. and Grover, J. V. *Selected Combustion Problems* (AGARD). 1954. London; Butterworths

81

INFLUENCE OF PRESSURE ON RATE OF FLAME PROPAGATION IN TURBULENT FLOW

S. A. GOLDENBERG and V. S. PELEVIN

In contradistinction to flame propagation in stationary mixtures or in a laminar flow, the turbulent propagation of flame, both experimentally and theoretically, has been investigated very little.

To date the main objects of study have been the effect of the rate of flow (W) on the turbulent flame velocity (U_T), the turbulence characteristics of the approach stream ($U' = (\overline{U^2})^{\frac{1}{2}}$)—the root mean square value of fluctuation velocity ; l scale of turbulence), the nature of the fuel and its concentration in the mixture, and the influence of the initial temperature of the mixture. Up to the time our investigations were started no papers had been published on the experimental study of the effect of pressure on the velocity of a flame in a turbulent flow.

Meanwhile, investigations of the effect of pressure on the rate of flame propagation in a turbulent flow are not only practically important but of definite theoretical interest as well.

The first-order task in solving the fundamental questions of flame propagation in a turbulent flow is to accumulate a sufficient quantity of extensive and reliable experimental data on the influence of various external factors on the process of flame propagation. The present paper is devoted to the study of one of these factors, namely, the pressure.

APPARATUS AND PROCEDURE

The most convenient method for studying the effect of pressure on the rate of flame propagation and on the size of the combustion zone behind a flame front in a turbulent flow is probably the burner method. Choice of this method was stipulated, besides, by the necessity of establishing the effect of pressure on flame propagation in both laminar and turbulent flow under comparable conditions. In both cases the experiments were conducted with gasoline–air mixtures using a 16 mm cylindrical burner. The pressure was varied over a range of 760 to 100 mm Hg. To exclude the influence of the burner size on the laminar velocity of the flame under low pressures and to stabilize the flame at high rates of flow the ignition source used was in the form of a small flame ring at the end of the burner. It was established by special experiments that the ignition source does not affect the flame velocity, which was determined in all cases by the inner luminescent cone by direct photographing of the flame.

EFFECT OF PRESSURE ON LAMINAR FLAME VELOCITY

The results of experiments carried out over a wide range of fuel concentrations in the mixture show that as the pressure (P) drops the laminar flame velocity or normal flame velocity, as it is usually called, (U) increases regularly. However, the concentration limits within which the flame can spread become narrower. Treatment of our data gave the following relationship:

$$U \sim P^{-n}$$

where $n = 0{\cdot}23$ to $0{\cdot}26$ in the interval of gasoline concentrations in the mixture $C = 1{\cdot}5 - 2{\cdot}4$ per cent. Our experimental data (methane–air mixtures were studied besides the gasoline–air mixtures mentioned above) and analysis of published papers[1] testify to the fact that for a wide class of hydrocarbon–air mixtures at low pressures the exponent in expression 1 varies within narrow limits:

$n = 0{\cdot}25$ to $0{\cdot}3$. It follows that the effective order of the reactions with respect to the pressure is a fractional value between $1{\cdot}4$ and $1{\cdot}5$.

For practical calculations the following relationship is eligible:

$$U \sim P^{-0{\cdot}25} \qquad (1)$$

INFLUENCE OF PRESSURE ON TURBULENT FLAME VELOCITY

In these experiments, conducted only with gasoline–air mixtures, the R_e numbers were varied from 4×10^3 to 20×10^3. In most experiments R_e was kept constant. In other experiments the pressure was varied, keeping the rate of flow constant (i.e. W = const.) and varying the R_e numbers. The experiments were carried out without turbulizing screens. The intensity of turbulence ($\epsilon = U'/W100$), 4 to 5 per cent, which is the value characteristic of tubes, did not vary along the axis within the internal cone

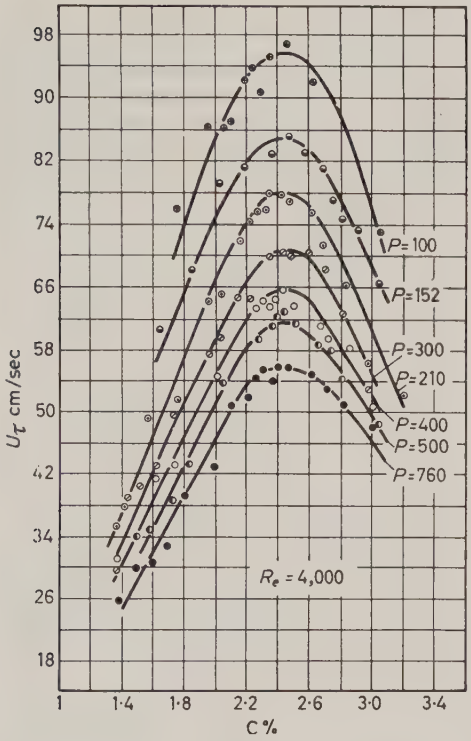

Figure 1

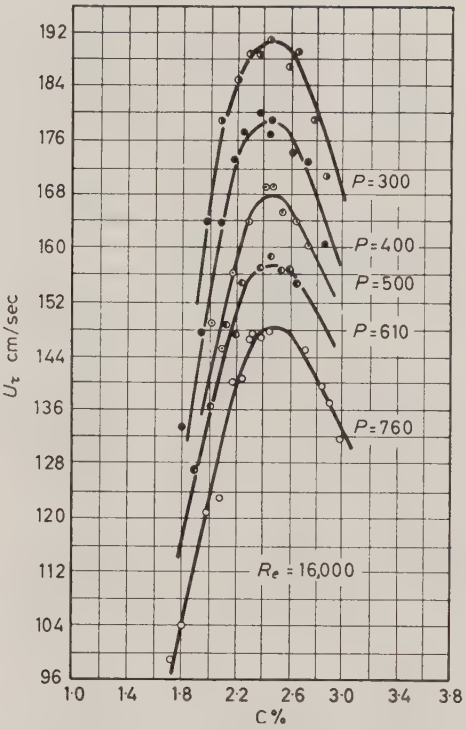

Figure 3

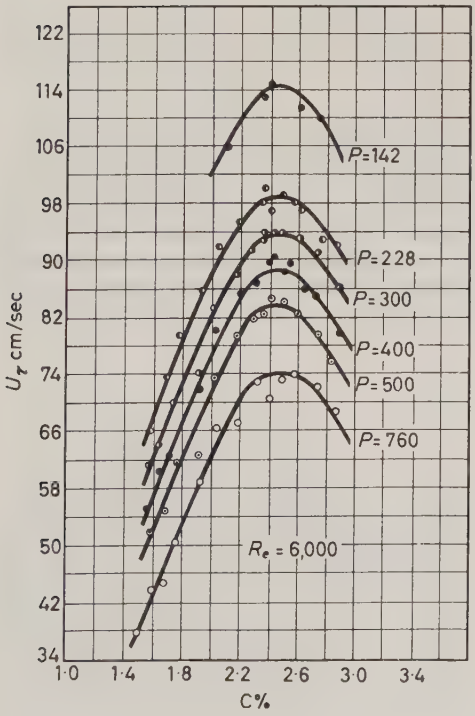

Figure 2

of the flame. It was established by preliminary experiments that, with a flame burning, the core length of the jet cold fuel mixture becomes much longer than that of an ordinary unburning jet issuing from the burner. Thus the experiments were carried out at a constant turbulence intensity over the length of the inner luminescent cone.

Figures 1, *2* and *3* show several typical curves illustrating the dependence of the flame velocity (U_T) on the pressure and the fuel concentration in the mixture at definite constant R_e numbers.

It is clear from the shape of these curves that with constant R_e numbers the effect observed over the entire range studied is the same: as the pressure falls off, the linear flame velocity (U_T) in turbulent flow increases. Thus with constant R_e numbers the general tendency of the process due to pressure changes is the same in turbulent as in laminar conditions.

It is important to point out that the position of the maximum on the flame velocity curves remains practically constant with changes in pressure, just as in the experiments under laminar conditions. The position of the maximum at atmospheric and lower pressures corresponds to a concentration of 2·4 to 2·5 per cent and is displaced into the region of rich mixtures. At low

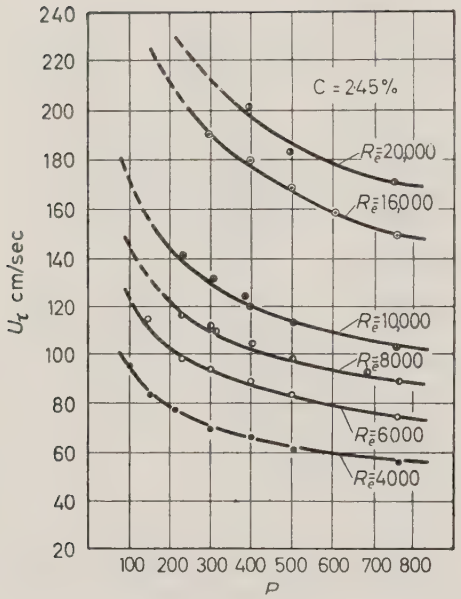

Figure 4

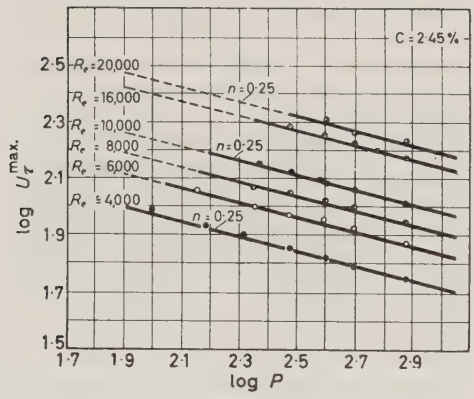

Figure 5

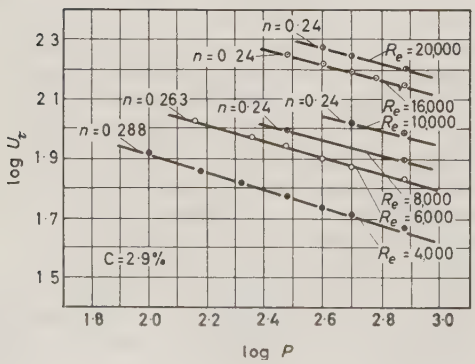

Figure 6

pressures the limits of inflammability become somewhat narrower.

It is interesting to trace the nature of the changes in U_T with the pressure at various concentrations. *Figure 4* demonstrates the typical shape of the curves at a given concentration. The exponent can be established with sufficient accuracy by plotting these data on logarithmic coordinates (see *Figures 5 and 6*). On the average it may be considered that the exponent $n = 0{\cdot}25$ to $0{\cdot}28$.

Thus for practical calculations the following relationship may be established:

$$U_T \simeq U_{To} \Big/ \left(\frac{P}{P_o}\right)^{0{\cdot}25}, \text{ or} \qquad (2)$$

$$U_T \sim P^{-0{\cdot}25} \qquad (3)$$

where U_{To} and P_o are respectively the flame velocity and the pressure at normal conditions.

These results suggest that at a constant mass velocity of flow of the fuel mixture issuing from the burner (R_e = const) the regularities relating to pressure changes will be identical for laminar and turbulent flame velocities.

At the same time it was interesting to ascertain the effect of the pressure at a constant rate of flow at the burner exit but with variable R_e. The fairly exhaustive experimental material obtained by us allows selection of pressure values and corresponding R_e numbers from a series of curves, some of which are shown in *Figures 1–3*, at which the rate of flow of the mixture at the burner exit was constant.

Figure 7 shows the relationship between U_T and P for a constant rate of flow W = 1,960 cm/sec at various concentrations. Experimental points are plotted on the same curves for flow rates close to that indicated (the numerical values of the corresponding flow of W are indicated at each point). It is clear from these data that lowering the pressure is connected primarily with a decrease in the R_e number. To establish the dependence

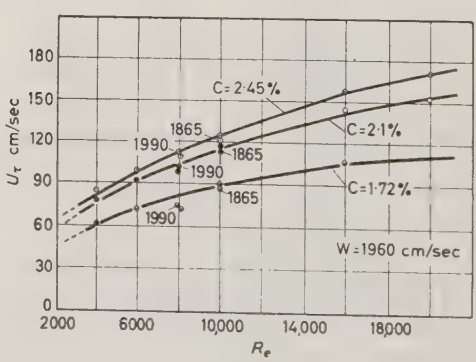

Figure 7

between U_T and P at a constant flow rate the experimental curves of *Figure 7* are plotted in *Figure 8* on a logarithmic scale. These curves

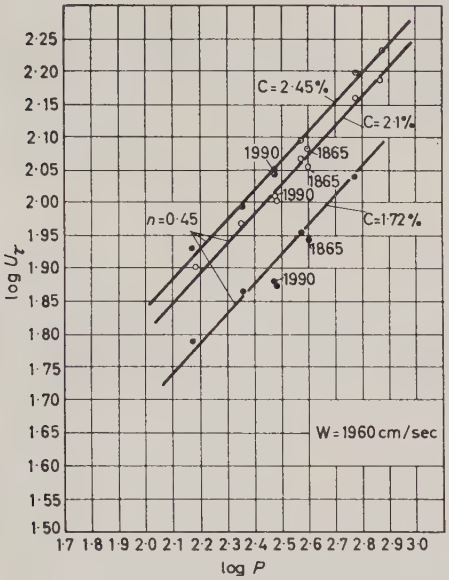

Figure 8

coincide sufficiently well with straight lines approximating the following relationship

$$U_T = AP^n \tag{4}$$

where $n = 0{\cdot}455$ and the coefficient $A = f(c)$, c = concentration. We may write approximately

$$U_T \sim P^{0{\cdot}45} \tag{5}$$

Thus our experiments have established that a change in pressure at a constant mass velocity (R_e = const) causes the turbulent flame velocity to increase according to a law similar to that by which the normal flame velocity changes ($U_T \sim P^{-0{\cdot}25}$) while at constant flow rates the turbulent flame velocity decreases with increasing pressure approximately according to the following law

$$\cdot U_T \sim P^{0{\cdot}5}$$

ANALYSIS OF RESULTS

To analyse the above results it is evidently necessary to refer to the present day conceptions of the process of turbulent flame propagation. It must, however, be remembered that there is not a single theory which allows analytical examination of the relationship between the turbulent velocity of flame propagation and the pressure without the use of experimental data.

Owing to these circumstances the theory of flame propagation cannot be expected to establish more than the general tendency of the process due to pressure changes.

According to various theories and experimental studies the velocity of flame propagation in turbulent flow depends in general on the following parameters

$$U_T = f(U, U', l) \tag{6}$$

In the particular case of the flame being propagated in a stabilized flow issuing from a cylindrical burner in the absence of screens for generating turbulence, expression 6 can obviously be replaced by

$$U_T = \varphi(U, R_e^n, d^m) \tag{7}$$

According to reference 2 in the case of small-scale turbulence

$$\frac{U_T}{U} \sim \left(\frac{A_T}{A}\right)^{\frac{1}{2}} \tag{8}$$

where A_T = turbulent thermal diffusivity, or eddy diffusivity.

A = molecular thermal diffusivity. Accordingly, in the case of large-scale turbulence

$$\frac{U_T}{U} \sim \frac{A_T}{A} \tag{9}$$

In reference 3 the following dependence was established:

$A_T \sim AR_e^{0{\cdot}84}$ for R_e numbers $R_e \leqslant 100 \times 10^3$. Therefore instead of expression 9 the following may be written

$$U_T \sim UR_e^{0{\cdot}84} \tag{10}$$

With large R_e numbers ($R_e > 100 \times 10^3$), as has been established in reference 3

$$A_T \sim AR$$

Thus in the two limit cases of small-scale and large-scale turbulence, we get different relationships between the velocity of flame propagation and the R_e number. Actually, in a real flow, especially with small R_e numbers, there is always a spectrum of scales and a spectrum of pulsation velocities.

On the strength of this, coincidence between the calculated and experimental U_T *versus* R_e dependences can hardly be expected.

Experimentally we established the following relationship between U_T and R_e under normal conditions (P = 760 mm Hg) with an accuracy equal to that of the constant factor

$$U_T \sim UR_e^{0{\cdot}715} \tag{11}$$

The scale of turbulence is included in the constant factor because in our experience the burner diameter did not vary.

It should be pointed out that the difference

between the exponents of R_e obtained in a number of studies is due particularly to the fact that in those studies the rate of propagation of the flame was determined not by the inner cone but by the mean enveloping surface between the inner and outer cones of the flame. Under such conditions the value of U_T depends on the width of the combustion zone, even when the true rate of propagation of the turbulent flame remains invariable.

The experimental data we have obtained supply a basis for analysis of the effect of the pressure on the rate of turbulent flame propagation.

Evidently the pressure influences the turbulent velocity of the flame according to relation 6 through the parameters which determine U_T, i.e. U, U', l.

As indicated above, in our case $U_T = f(U, R_e^n)$ and $l \sim d$.

Therefore our experimental data can be analysed either according to relation 10, obtained by calculation, or to 11, obtained experimentally.

Let us consider the influence of the pressure on the turbulent velocity of flame propagation under the condition that $R_e = \text{const}$. In both cases, evidently, $U_T \sim U$. Therefore the dependence of U_T on the pressure under such conditions should follow the relationships established for the normal flame velocity. As indicated in reference 1, it was established that $U \sim P^{-0.25}$; therefore the following relationship should hold: $U_T \sim P^{-0.25}$, which is actually observed in agreement with experiment (see relation 3).

Now let us consider the conclusions that follow from relation 10 or 11 when the pressure varies at a constant rate of flow.

According to our experimental data, if the rate of flow is kept constant but the pressure is varied, the R_e number decreases, which involves an increase in the kinematic viscosity when the density of the medium decreases.

It is clear from elementary considerations that the R_e number is a hydrodynamic characteristic of the flow under a given set of conditions, $R_e \sim P$ at a constant rate of flow and invariable burner diameter. Therefore relation 11 should lead to the following dependence of U_T on the pressure if we take into account that $U \sim P^{-0.25}$.

$$U_T \sim P^{-0.25}\, P^{0.715}$$
$$\text{or approximately: } U_T \sim P^{0.46} \qquad (12)$$

which is very close to the experimentally derived formula 5.

Thus the general tendency of the process can be established quite definitely within the limits of the existing conceptions of turbulent flame propagation.

In this connection it is interesting to examine the question of flame propagation under conditions differing from ours, namely, under conditions approaching isotropic turbulence caused by screens. It is common knowledge that in such a case the R_e number is not a hydrodynamic characteristic of the flow, the latter being determined by the values U' and l. The task is to find the direct functional relationship between U', l and ν. According to the theory of damping of isotropic turbulence beyond a screen[4]

$$U' \sim \frac{\text{const}}{(\nu t)^{5/4}}$$

where t = time, ν = kinematic viscosity.

When the pressure is varied at a constant rate of flow the fluctuation velocity for any given point of space will evidently depend on ν as follows

$$U' \sim \frac{\text{const}}{\nu^{5/4}} \qquad (13)$$
$$\text{(or)}$$
$$U' \sim P^{5/4} \qquad (14)$$

In this case the relationship between U_T and U, U' is usually established experimentally as

$$U_T \sim (U')^{\gamma}\,(U)^{\delta} \qquad (15)$$

Substituting the relationships $U' \sim P^{5/4}$ and $U \sim P^{0.25}$ into 15, we get

$$U_T \sim (P^{-0.25})^{\gamma}\,(P^{5/4})^{\delta} \qquad (16)$$

Particularly with $\gamma \simeq \delta \simeq 0.5$ we should have obtained:

$$U_T \sim (P)^{\frac{1}{2}} \qquad (17)$$

A relationship of this kind should be expected at the last stages of damping of turbulence beyond the screens, i.e. under conditions close to isotropic turbulence.

Thus, when the pressure is varied the determining factor of flame propagation in a turbulent flow is the density of the medium and therefore the kinematic viscosity, which influences the characteristics of turbulence and normal flame velocity.

REFERENCES

[1] Goldenberg, S. A. and Pelevin, V. S. *Izvestia Akad. Nauk SSSR, Otd. tekh. nauk. No. 2*, 1958

[2] Damkohler, G. *Z. Electrochem.* 46, No. 11 (1940)

[3] Goldenberg, S. A. *Izvestia Akad. Nauk SSSR, Otd. tekh. nauk. No. 4*, 1950

[4] Landau, L. D. and Lifschitz, E. M. *Mechanics of Continuous Media*, 1953 (in Russian)

THEORY OF RATE OF SPREAD OF CONFINED TURBULENT PRE-MIXED FLAMES

D. B. SPALDING

THE PROBLEM

Scope of paper

The type of flame considered is that which spreads from the wake of a flame stabilizer mounted in a steady stream of pre-mixed combustible gas, flowing at high speed through a duct of constant area (*Figure 1*).

The question considered is: What governs the axial distance, l, between the flame-holder and the section where the flame reaches the wall?

No new experimental data are put forward, but old data are re-examined. It is shown that these exhibit features which contradict current theories of turbulent flame propagation.

A new theory is presented which postulates that over an important range of conditions the rate of flame spread is governed by the rate of entrainment of cold gas by hot. This rate of entrainment is predicted from data on the mixing of parallel fluid streams, by assuming that jets 'forget' their origin.

The consequences of the theory are compared with the experimental data and a fair agreement is demonstrated.

Experimental data about rate of flame spread

The first extensive study of the spread of flame behind baffles in two-dimensional flow was that of Scurlock[1], who used city gas and propane mixed with atmospheric-pressure air. Rod-like baffles

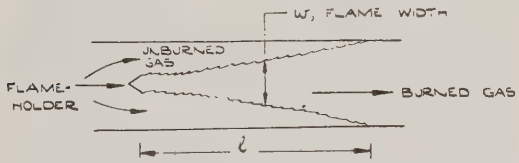

Figure 1. Turbulent flame spreading from flame-holder; two-dimensional flow

were mounted centrally in a rectangular duct of width 3 in. normal to the baffle axis. Typical results for the width of the city gas flame, w (*Figure 1*), at a distance 4 in. downstream of the flame-holder axis, are shown in *Figure 2*. Flame width is of course a measure of the speed of propagation of the flame into the unburned stream.

Figure 2 demonstrates that the effect of air–fuel ratio on flame speed is much less marked at low velocity than at high. At a stream velocity of 50 ft./sec, for example, the flame width is twice as great at the stoichiometric ratio (6·5 to 1) as it is at the weak ratio of 13 to 1; this behaviour is in

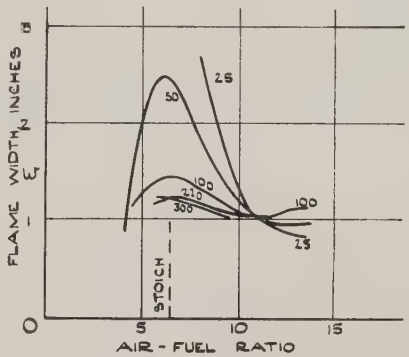

Figure 2. Typical results for flame width versus *mixture ratio at various velocities, fixed downstream position (Scurlock); numbers represent velocities in* ft./sec

line with, although less pronounced than, that which could be expected were the flame a laminar one. At a stream velocity of 220 ft./sec, on the other hand, the flame width is almost independent of mixture ratio.

The effect of mixture ratio at low velocity is easy to understand; in the present paper therefore only the high-velocity behaviour will be discussed. Explanations will be sought also for the facts, reported by various workers[1,2,3], that the speed of flame propagation in this regime is comparatively uninfluenced by the stream turbulence level, by the flame-holder dimension, or by the static pressure, but is proportional to the stream velocity.

Existing theories about rate of turbulent flame spread

A number of authors have proposed ways in which the turbulent flame speed might depend on chemical and aerodynamic factors[4,5,6]. Although differing considerably in their starting-points and conclusions, their theories have in common the implication that the turbulent flame speed depends upon the volumetric-reaction rate characteristics of the gas mixture. According to the theory of Damköhler, for example, turbulence is accounted for by replacing the laminar conductivity, k, by the eddy conductivity, k_t, in the usual formula for

flame speed; this can be taken (for simplicity) as:

$$S = \{2k\overline{\dot{q}'''}/(T_b - T_u)\}^{1/2}/c\rho \qquad (1)$$

where S = flame speed; $\overline{\dot{q}'''}$ = average volumetric reaction rate on a temperature basis; $T_b - T_u$ = adiabatic temperature rise of gases on combustion; c = mean specific heat at constant pressure; and ρ = density under conditions at which S is measured.

Since, for a fully turbulent stream of velocity, u, in a duct of width, d, the eddy conductivity is proportional to $c\rho ud$, the Damköhler theory would give a turbulent flame speed, S_t, of

$$S_t = \text{const.}\ \{ud\overline{\dot{q}'''}/c\rho(T_b - T_u)\}^{1/2} \qquad (2)$$

This implies that S_t is proportional to the square root of the stream velocity and to the inverse square root of the pressure, and, like the laminar flame speed, exhibits a pronounced maximum around the stoichiometric mixture ratio. All these predictions are falsified by the facts mentioned above.

The theories of Karlovitz *et al.*[5], Scurlock and Grover[6], and others cannot be expressed so simply as Damköhler's, but they also indicate that the turbulent flame speed depends on the laminar flame speed of the mixture. Their predictions are therefore also in conflict with the facts about confined turbulent flames.

There is clearly a need for a new theory which can explain the facts.

OUTLINE OF PRESENT APPROACH

Existing knowledge of the aerodynamics of confined flames

Scurlock[1] was the first to note that as a consequence of the confinement of the gases in a constant-area duct, the velocity distribution across the duct is bound to become non-uniform. The

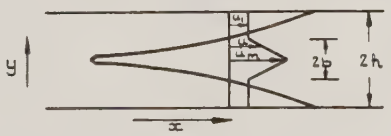

Figure 3. Illustrating typical velocity distribution in confined flame, and notation used

reason is clear: because of the density decrease caused by combustion, the gases must accelerate as they move downstream; so the pressure falls in the direction of flow; burned gases and as-yet-unburned gases are subjected to the same pressure fall, but the former accelerate more rapidly because of their lower density; so the velocity is highest in the middle of the duct. *Figure 3* shows a typical velocity distribution.

The velocity profiles can be calculated. Scurlock did this numerically; Tsien[7] used a more elegant approximate method; Fabri *et al.*[8], and Iida[9] have taken account of compressibility. The latter author has also compared the theoretical profiles with experimental ones; the agreement is fairly good.

These theories have a common shortcoming: although they predict reasonably well the velocity distribution along lines normal to the duct walls, they are silent about the velocity variation along lines parallel to the walls. The turbulent flame speed which appears in the equations is, and remains, an unknown.

These theories are however the jumping-off point for the present work; for the peaked velocity distributions disclosed by them are suggestive of those in turbulent jet systems. Information about these is available from other sources.

Existing knowledge of jet mixing

Cross-stream velocity profiles such as that shown in *Figure 3* are encountered downstream of the plane where fast-moving fluid from a slot-shaped nozzle enters a slower surrounding stream. Turbulent mixing in such systems has been studied by many workers, and, fortunately from the present point of view, particular attention has been focused on stream-wise velocity variations. The flow in the central region of elevated velocity is known as a jet.

A striking characteristic of a turbulent jet is that it tends to draw in fluid from its surroundings, so that the mass flow rate in the jet increases with distance downstream. The amount of entrainment per unit length has been determined experimentally; it is of course intimately associated with the rate of fall-off of peak velocity.

There is reason to suppose that jets have short memories, that is that the change in jet properties from one plane to the next downstream depends only on the local velocity and density distribution and not on how the jet originated. If this is the case, we may suppose that if a velocity distribution such as that in *Figure 3* is built up as a result of the processes described in the last section, the central jet of hot gas will entrain cold gas from its surroundings just as if the hot gas had been ejected from a nozzle. This hypothesis forms the first step in the present theory.

The 'entrainment-control' hypothesis

Turbulent-jet studies have shown that the entrainment is accompanied by a mixing process in which composition and energy interchanges occur. Now it is precisely such interchanges, occurring between hot products and unburned combustible, which are necessary if the latter is to burn at an appreciable rate. Entrainment in the situation of *Figure 3* therefore encourages the spread of flame.

Having arrived at this point, the next step is

obvious: suppose that the reaction rate of the mixture is sufficiently high for the fresh gas entrained by the central jet to be almost instantly burned, but not so high that the laminar flame speed is comparable with the stream velocity. Then the entrainment rate will *control* the rate of burning. The rest of the paper is devoted to examining the consequences of this hypothesis.

The procedure will be to deduce the missing length-scale of confined-flame aerodynamics from measurements made on mixing in non-reacting jets; the 'jet-forgetfulness' and 'entrainment-control' hypotheses form the connecting links. It is evident however that care will be needed to distinguish what is similar in the jet and flame situations from what is different and, it is hoped, irrelevant. For example, the peak velocity in the flame increases with distance downstream; in the jet system the peak velocity decreases with distance downstream. Clearly we cannot use the rate of change of peak velocity directly as the connecting link.

Outline of the calculation procedure

The jet-mixing data to be used are those of Förthmann[10], and of Weinstein, Osterle and Forstall[11]. For our purposes their data must first be replotted to give a test of the 'jet-forgetfulness' hypothesis. Then an entrainment law must be deduced in differential form; this is a relationship between the increment in mass flow rate per unit length and the jet properties at that plane.

It will be found convenient to derive the velocity profiles in the flame system in a slightly different way from that of Tsien *et al.* When this has been done it is found to be possible to express all the terms in the differential entrainment law as functions of flame width, or fraction of gas burned. All that remains, therefore, is to solve the equation, which is a first-order differential one with axial distance as independent variable, by numerical means. The result is a predicted variation of flame width with axial distance; in other words, a theory of turbulent propagation rate.

DERIVATION OF THE ENTRAINMENT LAW

Data on two-dimensional jet mixing: stagnant surroundings

Förthmann[10] has measured the velocity field when a fluid emerges steadily from a slot of width, d, into a large volume of stagnant fluid of equal density. His results for the variation of peak velocity, u_m (*Figure 4*), with distance, x, from the orifice, can be expressed as

$$\frac{u_m}{u_0} = 2{\cdot}4\left(\frac{d}{x}\right)^{1/2} \qquad (3)$$

where u_0 is the uniform velocity of the entering fluid on emergence from the slot; u_1, representing the velocity of the surrounding fluid in *Figure 4*. is of course zero in this case.

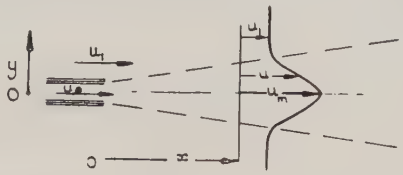

Figure 4. Illustrating typical velocity distribution in constant pressure jet mixing, and notation used

Since we wish to suppose that the jet 'forgets' the conditions of its origin, it is desirable to replace u_0, d, and x in equation 3 by quantities which can be evaluated without knowledge of the origin. To do this a momentum flux, $\dot{M}'$, is introduced and equation 3 is differentiated with respect to x.

The momentum flux is defined by

$$\dot{M}' = \int_{-\infty}^{+\infty} \rho u(u - u_1)\mathrm{d}y \qquad (4)$$

where ρ is the fluid density, y is the distance normal to the direction of flow, and u is the x-wise velocity at any point. $\dot{M}'$ is important because, for the constant-pressure experiments in question, Newton's second law of motion leads to

$$\dot{M}' = \rho d u_0(u_0 - u_1)$$
$$= \text{constant for all } x \qquad (5)$$

For expression 5 to hold it is necessary that u_1 should be invariant with x; but it need not be zero, as it is in Förthmann's case.

The aforesaid procedures enable equation 3 to be re-written as

$$\frac{\mathrm{d}u_m}{\mathrm{d}x} = -0{\cdot}0868\,\frac{\rho {u_m}^3}{\dot{M}'} \qquad (6)$$

which indicates that the rate of fall-off of peak velocity can be calculated when the local values of u_m and $\dot{M}'$ are specified.

Data on two-dimensional jet mixing: finite secondary velocity

Weinstein, Osterle and Forstall[11] have conducted experiments in which the surrounding fluid is moving parallel to the injected fluid with the uniform velocity u_1. They have presented their results in a form similar to that of expression 3, albeit with constants depending on the initial velocity ratio u_0/u_1.

These data can furnish at once a test of the 'forgetfulness principle' and an empirical entrainment law if they are re-plotted in the light of dimensional analysis. Consideration of expression 6 shows that it is no longer to be expected that the

numerical coefficient is a constant: the coefficient must be influenced by the fact that the surrounding fluid is moving. Since it is still desired to allow only local quantities to appear in the velocity-decay law, we suppose that there exists a single law governing such jets, having the form:

$$-\frac{\dot{M}'}{\rho u_m^3}\frac{\mathrm{d}u_m}{\mathrm{d}x} = f\left\{\frac{u_m}{u_1}\right\} \tag{7}$$

If this law exists, then, when u_1 and $\dot{M}'$ are constant as in the experiments of Weinstein *et al.*, integration leads to

$$\frac{u_m}{u_1} = F\left\{\frac{\rho u_1^2 x}{\dot{M}'}\right\} \tag{8}$$

If plotted with the variables of expression 8 as ordinate and abscissa therefore, Weinstein's data should fall on a single curve.

This is put to the test in *Figure 5*, which actually has $u_m/u_1 - 1$ as ordinate and $u_1^2 x/u_0(u_0 - u_1)d$ as abscissa; this amounts to the same as the above. It is evident that if the horizontal regions, representing flow in the 'potential core' of the jets, are disregarded, the three sets of Weinstein's data form a fairly continuous curve with those of Förthmann. With sufficient approximation for our purposes, this curve can be represented by the dotted line in *Figure 5*, that is by the equation

$$\frac{u_m}{u_1} = 1 + 2{\cdot}4\left\{\frac{\dot{M}'}{\rho u_1^2 x}\right\}^{1/2} \tag{9}$$

This expression has the form required by expression 8. Insertion of expression 5 shows that 9 has 3 as an asymptotic form for small u_1.

The fact that the four sets of data on *Figure 5* nearly form a single curve suggests that the loss-of-

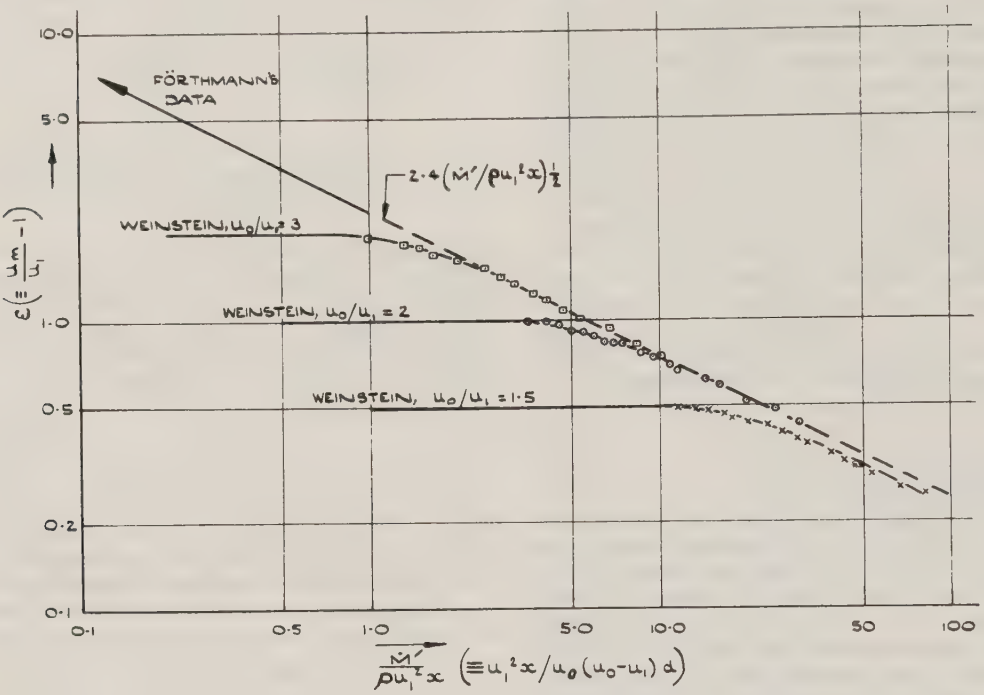

Figure 5. Two-dimensional jet mixing data plotted to test 'jet-forgetfulness'

memory hypothesis is nearly correct. Equation 9 can therefore lead to a universal entrainment law for two-dimensional jets.

Definition of mass flux, $\dot{m}'$

First it is necessary to define what is meant by the mass flow rate in the jet. When $u_1 = 0$, the integral $\int_{-\infty}^{+\infty} \rho u \, \mathrm{d}y$ has a finite value and represents the total mass flux; however when u_1 is finite this integral is infinite. The integral therefore cannot serve as a measure of the amount of fluid which has been significantly influenced by the jet. It would also be possible to define the entrainment rate as

$$\frac{\mathrm{d}}{\mathrm{d}x}\left\{2\int_0^H \rho u \, \mathrm{d}y\right\}$$

where H is some fixed dimension much larger than the wake. This expression would measure the inclination of the outer streamlines. However, this definition would also be inappropriate because, for very small relative velocity, the expression tends to zero; but the zone of influence of the jet increases by turbulent diffusion at a rate which is

not zero: it is this rate which is the important one for flame propagation.

An arbitrary definition is therefore used, involving prescription of definite boundaries between what fluid is to be regarded as in the jet and what as in the surrounding stream. The procedure used below is as follows:

The real jet is considered to be replaced by an ideal one with a triangular velocity profile (*Figure 6*), and with sufficient width, $2b$, to have the same momentum as the real jet. Then the mass flux, in the jet, $\dot{m}'$, is defined as

$$\dot{m}' = \int_{-b}^{+b} \rho u \, dy \tag{10}$$

This definition implies a relationship between $\dot{m}'$, $\dot{M}'$, u_m and u_1. It is

$$\dot{m}' = \frac{3\dot{M}'(u_m + u_1)}{(u_m - u_1)(u_1 + 2u_m)} \tag{11}$$

A check on the realism of this formula is obtained by considering the case $u_1 = 0$. Then $\dot{m}'$ defined by expression 11 is about 6 per cent less than the true total mass flux. The definition appears satisfactory.

Derivation of entrainment law

Dimensional analysis combined with the memory-loss hypothesis leads to the conclusion that there exists an entrainment law, i.e. a relationship between the variation of mass flow with distance, and other variables, of the form

$$\frac{\dot{m}'}{\rho\dot{M}'}\frac{d\dot{m}'}{dx} = f\left\{\frac{\dot{M}'}{\dot{m}'u_1}\right\} \tag{12}$$

The unknown function $f(\ )$ has to be determined from the experimental data embodied in expression 9. Combining this relationship with 11, we find

$$\left.\begin{aligned} \frac{\dot{m}'}{\rho\dot{M}'}\frac{d\dot{m}'}{dx} &= 1{\cdot}56\,\frac{(\varepsilon+1)(\varepsilon+2)(\varepsilon+3)}{(2\varepsilon+3)3} \\ \frac{\dot{M}'}{\dot{m}'u_1} &= \frac{\varepsilon(2\varepsilon+3)}{3(\varepsilon+2)} \end{aligned}\right\} \tag{13}$$

where $$\varepsilon \equiv u_m/u_1 - 1 \tag{14}$$

Equation 13 can be regarded as a parametric form of 12, and is the required universal entrainment law for two-dimensional jets. It is plotted in *Figure 6*, wherein it is seen that $(\dot{m}'/\rho\dot{M}')d\dot{m}'/dx$ varies only between 0·347 for $\dot{M}'/\dot{m}'u_1 = 0$ ($\varepsilon = 0$; peak jet velocity = surrounding stream velocity), and 0·195 for $\dot{M}'/\dot{m}'u_1 = \infty$ ($\varepsilon = \infty$; surroundings at rest).

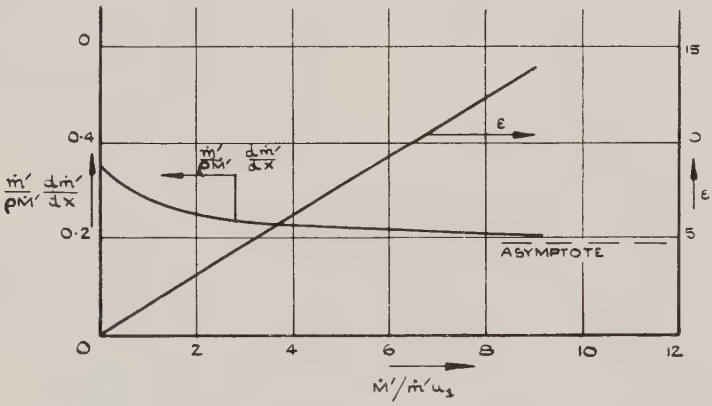

Figure 6. The entrainment law for two-dimensional jets, deduced from experiment

The effect of density differences

The experiments cited were carried out with fluids of substantially uniform density; we wish to apply the entrainment law to systems in which the density of fluid in the jet is much smaller than that of the surroundings. We therefore assume that, in expression 13, ρ is to be evaluated at the surrounding temperature. The justification is that it is fluid of surrounding density, ρ, which is being entrained, and that a similar procedure seems to fit some data for round jets[12]. This assumption is the weakest link in the chain of argument and requires experimental support. However if a different assumption for ρ were made, the conclusions would only be altered in a secondary fashion.

CALCULATION OF RATE OF FLAME SPREAD

Results deducible from conservation of mass and momentum

In the present section relationships are found between u_m, u_1, the flame width $2b$, the fraction burned ψ, and the density ratio (unburned/burned) λ. The results differ slightly from those of Tsien because of a somewhat different approximation procedure. The present assumptions are: (1) the velocity profiles in the y direction are triangular (Tsien introduced this); (2) the flow external to the flame (jet) is inviscid and incompressible (Tsien made this assumption about the central stream

line as well); (3) the mass and momentum conservation equations may be applied to the whole duct, the pressure being uniform in the y direction at any x; the drag due to the flame-holder is neglected. (Tsien did not need the integral momentum equation.)

The following relationships are then easily derived:

$$u_m = \frac{3}{8} - \frac{u_1}{8} + \frac{1}{2}\left\{u_1^2\left(6\lambda - \frac{15}{16}\right) + u_1\left(\frac{21}{8} - 6\lambda\right) + \frac{9}{16}\right\}^{1/2} \tag{15}$$

$$\frac{b}{h} = \frac{u_1 - 1}{u_1 - (u_1 + u_m)/2\lambda} \tag{16}$$

$$\psi = \frac{u_m + u_1}{2u_0} \cdot \frac{b}{h\lambda} = \frac{\dot{m}'}{2\rho_1 u_0 h} \tag{17}$$

where h = half duct width (*Figure 3*).

It will be noted that axial distance x is absent from these relationships. *Figure 7, a, b,* and *c* contains results obtained from their evaluation. The differences from Tsien's values are slight. ε, the parameter in expression 13 is also plotted.

Integration of the entrainment equation

Combining expressions 13, 14, 11 and 17, the

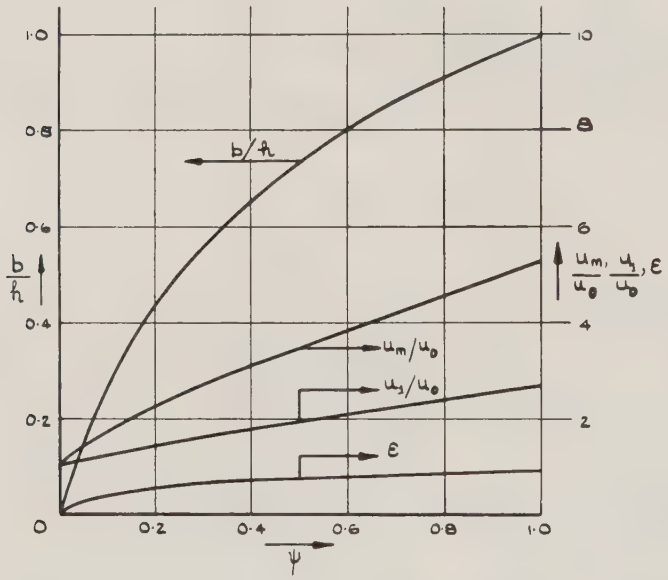

Figure 7a. Velocity ratios and flame width versus *fraction burned, determined from momentum and mass conservation:* $\lambda = 4$

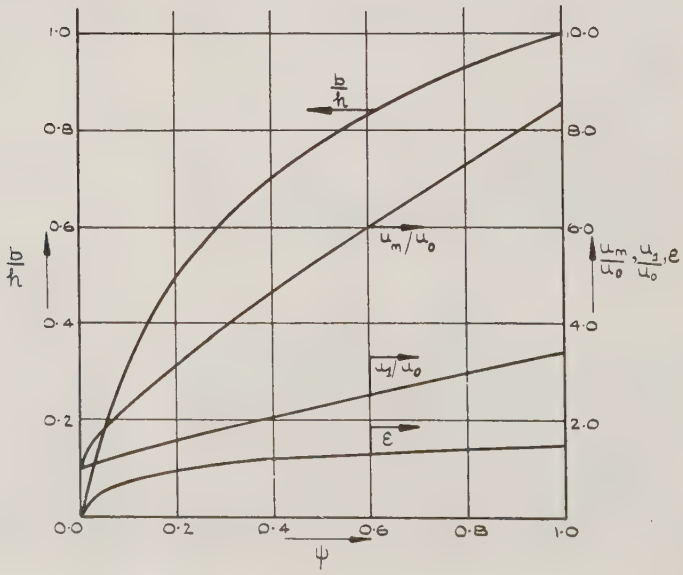

Figure 7b. Velocity ratios and flame width versus *fraction burned, determined from momentum and mass conservation:* $\lambda = 6{\cdot}0$

entrainment law reduces to

$$\frac{d\psi}{d(x/2h)} = 0{\cdot}52\,\frac{\varepsilon(\varepsilon+1)(\varepsilon+3)}{(2\varepsilon+3)^2} \qquad (18)$$

Now *Figure 7 a*, *b*, and *c* contains values of ε for any value of ψ. We therefore merely have to solve expression 18 numerically in order to obtain values of ψ, the fraction burned, as a function of $x/2h$, the dimensionless distance.

the x axis, signifying that, for a very small flame holder, the flame must travel a very large distance downstream before it 'gets started' in its propagation across the duct.

This is contrary to experience, although the initial rate of spread is certainly often lower than the later rate. The reason is clearly that the entrainment-control assumption does not hold in the region just downstream of the baffle. For at the downstream end of the re-circulation zone a

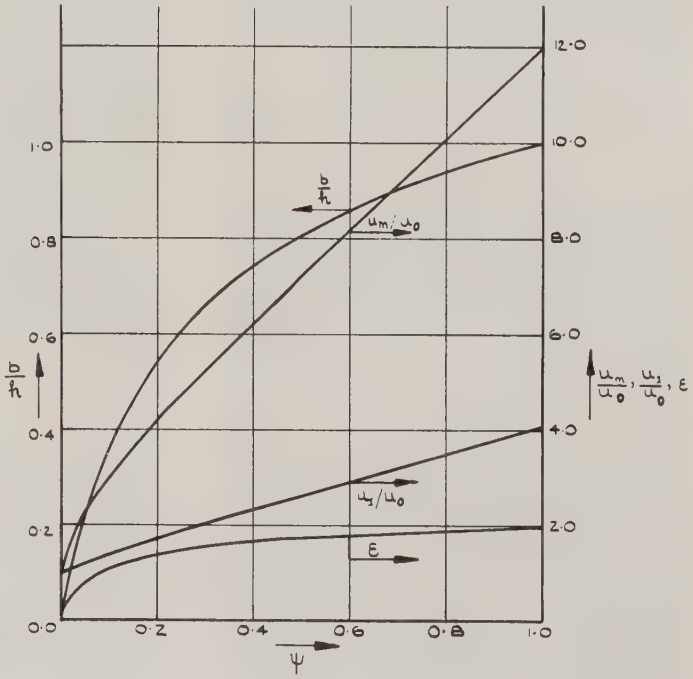

Figure 7c. Velocity ratios and flame width versus *fraction burned, determined from momentum and mass conservation:* $\lambda = 8{\cdot}0$

This has been done; then ψ has been replaced with the appropriate b/h value from *Figure 7*. The results are contained in *Figure 8* for each of the three λ values. The origin of the axial distance has been taken as the point where the flame (jet boundary) hits the wall.

Interpretation of the result

The scales of *Figure 8* are such that the shapes of the curves should be identical with the shapes of the flames. However, each curve is asymptotic to

section exists at which both hot and cold gas are flowing at the same velocity; no entrainment will therefore occur. At this section, flame propagation depends on laminar transport processes, augmented by the random turbulence of the stream; only when the flame has got away from this 'dead-point' can entrainment-control take over.

It should be noted that the drag of the flame-holder, neglected in the calculations presented, can be included in the equation with little extra difficulty. A finite drag results in a reduction in

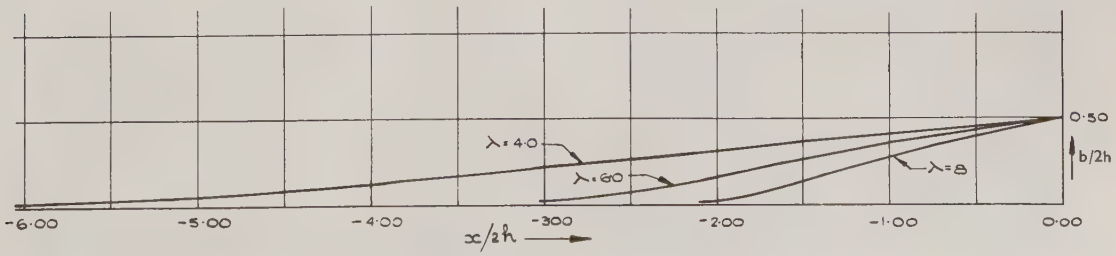

Figure 8. Predicted flame shapes; to scale for one half of duct

the rate of spread because it causes the 'dead-point' to move farther downstream. This will usually be compensated in practice by the larger width of the wake region, meaning that the flame has less far to travel.

Despite the difficulty about the start of the flame, *Figure 8* can be interpreted as showing that the flame spreads to the wall from a central flame-holder in about 5 duct widths if $\lambda = 4$, 3 duct widths if $\lambda = 6$, and 2 duct widths if $\lambda = 8$. The increased rate associated with high λ results of course from the large velocity differences which result from large temperature ratios.

COMPARISON WITH EXPERIMENT

Results of Scurlock[1]

The flame lengths obtained by this author can be estimated from the photographs published by him. For a typical flame in the fully turbulent regime (evidenced by the slight influence of fuel–air ratio), the flame reached the walls about 4 duct widths from the baffle for a λ of about 6, irrespective of the stream velocity.

The rate of spread is therefore about 25 per cent lower than predicted.

Results of Barrère and Mestre[2]

These authors used a duct of 100 mm width, a central flame-holder, and a combustible gas stream pre-heated to 500°C. The flame length, judged from static pressure measurements, was about 500 mm, i.e. 5 duct widths. Since in this case the density ratio must have been somewhat below 4, the agreement with the prediction is fairly good.

It is noteworthy that although the high pre-heat must have increased the chemical reactivity of the mixture, the flame spread rate was smaller than in Scurlock's experiments without pre-heat. This is inexplicable by previous theories of flame spread but is correctly predicted by the present theory, which attributes the reduction in rate to the lowered value of the density ratio λ.

Results of Petrein, Longwell and Weiss[3]

These authors used a 9 in. wide duct of low aspect ratio, with baffles of between 0·5 and 2·25 in. width. The combustible mixture was pre-heated to 235°F, giving a λ of about 6. The turbulence level in the approach stream was high. The static pressure level in the approach stream was varied from 8 up to 30 in. Hg; the stream velocity was varied, but was in the region of 150 ft./sec. Velocity and oxygen profiles downstream of the flame-holder were reported.

The results indicate that, in most cases, combustion was complete at about 50 in. downstream of the baffle, with the first 10 in. contributing little to the lateral flame growth. Thus the length for flame spread to the walls was about $4\frac{1}{2}$ duct widths, which roughly agrees with Scurlock's results and with the present theory.

The authors report little effect of either baffle width or approach stream velocity on the flame shape, and a slight effect of mixture ratio. The first of these may be attributed to a counter-balancing of the bad effect of increased drag and the good effect of a reduction in the lateral distance which must be travelled. The last may be associated with the effect on λ. It appears that all the changes in conditions had more effect on the region immediately downstream of the flame-holder than on that farther downstream.

The pressure effect was also most noticeable in the first 10 in. of flame length. The magnitude of the effect varied; pressure exponents of effective flame velocity are reported as between 0·1 and 0·6.

Generally speaking the results of the Petrein investigation are understandable in terms of the present theory, whereas they were hardly explicable before. However it seems likely that the measurements show an influence of chemical reactivity; the way in which this fits into the entrainment theory will now be discussed.

Influence of insufficiently rapid chemical reaction

The assumption that fresh gas burns as soon as it is entrained must certainly be wrong when the pressure is low and the mixture ratio far from stoichiometric. How will this influence the propagation rate?

In order to consume the entrained gas, the mean temperature in the jet must fall; for this gives (at first) an increased reaction rate, because of the well known shape of the reaction-rate curves near the upper temperature limit: but a lowered temperature means a lowered density ratio λ. According to the entrainment theory the rate of flame spread will therefore also fall.

Oxygen concentration profiles reported by Petrein *et al.* for a pressure of 10 in. Hg confirm that, at least under these conditions, combustion is not as immediate as has been supposed above. The highest central 'oxygen efficiency' is not much above 90 per cent; close to the baffle it is only 70 per cent. Again the special sensitivity of the upstream part of the flame is revealed.

Evidently the effect of pressure on flame velocity will not be a straightforward one: it will be zero at high pressures, while at low pressures it will become so great as eventually to extinguish the flame. Qualitatively at least, the Petrein results fit this prediction.

Results of Iida[9]

This investigation is mentioned merely in order to emphasize that the present theory only

holds at stream velocities higher than, say, 50 times the laminar flame speed. This condition was apparently not fulfilled in Iida's work, which therefore exhibits phenomena more akin to those of laminar flame propagation than to entrainment-controlled propagation.

CONCLUSIONS

Validity of theory

It appears that the experimental data on the propagation of flame from central baffles in two-dimensional flows at high stream velocities agree qualitatively with the predictions of a theory employing two hypotheses: that the flame region entrains fluid from its surroundings just as though it were a turbulent jet; and that the rate of entrainment controls the rate of burning.

Quantitative agreement with theory is fairly good. The most likely cause of the discrepancies is that only jet-mixing data for streams of uniform density are available. Experimental studies of entrainment in the presence of density differences are needed. Crucial tests of the theory should also be devised.

Consequences of the theory

A practical implication of the theory is that little can be done about increasing the rate of flame spread from baffles. Pre-heating the gas stream decreases the rate, whereas even adding oxygen only increases it as a secondary result of the decrease in density of the burned gases. It would be interesting to test this prediction practically.

The simple rule which emerges is that an axial length of three to five duct widths should be provided if the flame anchored to a central baffle is to hit the wall.

Possible extensions of the theory

A treatment of the axially symmetrical turbulent flame is possible along the lines of the present paper, and has been made. The results, which are qualitatively similar, will be published elsewhere. The author does not know of experimental data for this flame system, although the corresponding jet-mixing experiments have been done.

It is also possible to study in the present manner the flow in a converging or diverging duct. Such calculations may suggest ways of reducing flame length by varying the duct cross-section.

The importance of confined flows with non-uniform velocity of course reaches far beyond the flame propagation problems discussed here. If applied to flows without combustion, for example, the present methods would predict the onset of re-circulation; the theory would in fact become very similar to those of Langer[12], and of Craya and Curtet[13], who discuss the re-circulation problem. To take another example, we could predict the flow pattern in a duct of which only the central portion was supplied with fuel; there the possibility exists of an initial acceleration of the gases, followed by re-circulation of the outer stream.

REFERENCES

[1] Scurlock, A. C. *Meteor Report No. 19*, Massachusetts Inst. Tech., 1948. See also Williams, G. C., Hottel, H. C. and Scurlock, A. C. *Third Symposium on Combustion*, p. 21. 1949. Baltimore; Williams and Wilkins

[2] Barrère, M. and Mestre, A. *Selected Combustion Problems*, p. 426. 1954. London; Butterworth

[3] Petrein, R. J., Longwell, J. P. and Weiss, M. A. *Jet Propulsion* 26 (1956) 81

[4] Damköhler, G. *Z. Elektrochem.* 46 (1940) 601

[5] Karlovitz, B., Denniston, D. W. and Wells, F. E. *J. chem. Phys.* 19 (1951) 541

[6] Scurlock, A. C. and Grover, J. H. *Selected Combustion Problems*, p. 215. 1954. London; Butterworth

[7] Tsien, H. S. *J. appl. Mech.* 18 (1951) 188

[8] Fabri, J., Siestrunck, R. and Foure. *Fourth Symposium on Combustion*, p. 443. 1953. Baltimore; Williams and Wilkins

[9] Iida, H. *Sixth Symposium on Combustion*, p. 341. 1958. New York; Reinhold

[10] Förthmann, E. *Ingenieur Archiv.* 5 (1934) 42

[11] Weinstein, A. A., Osterle, J. F. and Forstall, W. *A.S.M.E. Paper 55-A-60*

[12] Langer, G. Flow reversal in a constant-area jet system. *International Flame Research Foundation Doc. No. G.02/C/1*, 1955

[13] Craya, A. and Curtet, R. *C. R. Acad. Sci. Paris*, T.241 (1955) 621

[14] Sunavala, P. D., Hulse, C. and Thring, M. W. *Combustion and Flame* 1 (1957) 179

THE GROWTH AND BURN-OUT OF FLAME SURFACE IN A TURBULENT STREAM

B. KARLOVITZ

INTRODUCTION

Turbulent flames which show a definite configuration, such as flames stabilized in a simple stream by pilot flames or flame-holders, can be characterized by the usual concepts of turbulent burning velocity and flame brush thickness. These quantities can be derived from the laminar burning velocity and the turbulence parameters without the direct calculation of the combustion wave area. In contrast to this, flames in many practical applications fill the available space with distributed luminosity without exhibiting a discernible geometrical configuration. Although such flames also consist of randomly fluctuating combustion waves within almost the entire range of practical applications, they cannot be described by the simple concept of turbulent burning velocity. These flames can be characterized by the distribution of the combustion wave surface per unit volume only.

In this paper, the principles of a theory are presented which permits the direct calculation of the combustion wave area from the turbulence parameters and the laminar burning velocity. The paper is also concerned with the limits within which the combustion wave concept may be applied, and presents a numerical example as an illustration of the theory.

THEORY

Generation of combustion wave area by turbulent motion

In a medium which is in turbulent motion the distance between two points, which are carried by the turbulent fluctuations, is continually increased on the average by the random turbulent motion. Consequently, the area of any surface, made accessible for observation by some marking, increases with time. The combustion wave in a turbulent explosive mixture constitutes such an observable surface. Its rate of growth per unit surface area can be calculated from the following consideration. A small rectangular section of the combustion wave with the side length l will change in $\mathrm{d}t$ time into a rectangle with the side length $l + \mathrm{d}l$. If l is equal, or larger, than the Lagrangian scale of turbulence then $\mathrm{d}l = u'\mathrm{d}t$, where u' is the intensity of turbulence. The surface area of the small rectangle increases from l^2 to $l^2 + 2l\,u'\,\mathrm{d}t$. The rate of surface area increase is therefore

$$\frac{\mathrm{d}A}{\mathrm{d}t} = \frac{2lu'\,\mathrm{d}t}{\mathrm{d}t} = 2lu' \tag{1}$$

and the rate of area increase per unit surface area

$$\frac{1}{A}\frac{\mathrm{d}A}{\mathrm{d}t} = \frac{2lu'}{l^2} = 2\frac{u'}{l} \tag{2}$$

On the average two points move apart during half the time, and towards each other during the other half. The area is increased when neighbouring points move apart, but the increase is not annihilated by the backward motion, because due to the random motion in the direction normal to the surface the points do not move back on the original surface. The flame surface bends out in the third dimension, and in general its area is not reduced by the return motion. Nevertheless, the exact value of the numerical coefficient in equation 2 may be smaller than two. As the exact value of the coefficient is not known, we assume a coefficient of one, and write

$$\frac{1}{A}\frac{\mathrm{d}A}{\mathrm{d}t} = \frac{u'}{l} \tag{3}$$

Annihilation of combustion wave area by burn-out

A small volume occupied by a highly turbulent flame contains a comparatively large combustion wave area, which is distributed within this volume at random. Such a flame can be characterized by (A/V_u), the combustion wave area per unit volume of unburned gas. In general (A/V_u) will have a definite average value at every point of a combustion system, which will vary from point to point. Because of the random distribution of the combustion wave within any small volume we may assume that the consumption of a small volume of explosive mixture eliminates a proportional area of the combustion wave.

That is

$$\mathrm{d}A = \left(\frac{A}{V_u}\right)\mathrm{d}V_u \tag{4}$$

The volume of mixture burned in $\mathrm{d}t$ time is

$$\mathrm{d}V_u = AS_u\,\mathrm{d}t \tag{5}$$

where A is the combustion wave area, cm^2; V_u is the volume of unburned mixture, cm^3; and S_u is the laminar burning velocity, cm/sec. Therefore

$$\frac{1}{A}\frac{dA}{dt} = -\left(\frac{A}{V_u}\right) S_u \tag{6}$$

The net rate of change of combustion wave area is the sum of the rate of surface production and of annihilation.

$$\frac{1}{A}\frac{dA}{dt} = \frac{u'}{l} - \left(\frac{A}{V_u}\right) S_u \tag{7}$$

The growth of the combustion wave area becomes zero when the rate of surface annihilation equals the rate of surface generation. That is

$$\frac{dA}{dt} = 0 \quad \text{when} \quad \frac{u'}{l} = \left(\frac{A}{V_u}\right) S_u \tag{8}$$

At this condition

$$\left(\frac{A}{V_u}\right)^{\star} = \frac{u'}{l}\frac{1}{S_u} \tag{9}$$

Flame surface area per unit volume of unburned gas

Equation 7 gives the rate of change of combustion wave area per unit area present. With the aid of this relationship one can calculate the variation of the combustion wave area per unit volume of unburned gas.

The rate of change of combustion wave area per unit volume of unburned gas mixture is

$$\frac{d}{dt}\left(\frac{A}{V_u}\right) = \frac{V_u\frac{dA}{dt} - A(dV_u/dt)}{V_u^2} \tag{10}$$

where A is the combustion wave area in an arbitrary volume V_u of unburned gas. V_u itself is variable in time, due to the burn-out of the mixture.

Inserting dA/dt from equation 7 and dV_u/dt from equation 5 into equation 8, we have

$$\frac{d}{dt}\left(\frac{A}{V_u}\right) = \left(\frac{A}{V_u}\right)\frac{u'}{l} - \left(\frac{A}{V_u}\right)^2 S_u + \left(\frac{A}{V_u}\right)^2 S_u \tag{11}$$

or

$$\frac{d}{dt}\left(\frac{A}{V_u}\right) = \left(\frac{A}{V_u}\right)\frac{u'}{l}$$

Integration of equation 11 gives the combustion wave area per unit volume of unburned gas as a function of time

$$\left(\frac{A}{V_u}\right) = \left(\frac{A}{V_u}\right)_0 e^{t/T} \tag{12}$$

where $T = l/u'$ is characteristic time, defined by the scale and intensity of turbulence; $(A/V_u)_0$ is the combustion wave area per unit volume of unburned gas at time zero; and t is time.

According to equation 12 the combustion wave area contained in unit volume of unburned gas mixture should increase exponentially with time. This result is strictly true only at low values of (A/V_u) where the volume of the combustion wave due to its finite thickness takes up only a small fraction of the volume of the unburned gas. At large (A/V_u) the above analysis which is based on constant laminar burning velocity loses its validity. The limiting value of (A/V_u) will be discussed in a later section of this paper.

Combustion wave area per unit mass of gas flow

The variation of the combustion wave area per unit mass of gas flow with time is given by

$$\frac{d(A/G)}{dt} = \frac{1}{G}\frac{dA}{dt} = \left(\frac{A}{G}\right)\frac{u'}{l} - \left(\frac{A}{G}\right)\left(\frac{A}{V_u}\right) S_u \tag{13}$$

from which

$$\frac{1}{(A/G)}\frac{d(A/G)}{dt} = \frac{u'}{l} - \left(\frac{A}{V_u}\right)_0 S_u e^{t/T} \tag{14}$$

Integration gives

$$\left(\frac{A}{G}\right) = \left(\frac{A}{G}\right)_0 e^{t/T} - \left(\frac{(A/V_u)_0}{(A/V_u)^{\star}}\right)(e^{t/T} - 1) \tag{15}$$

The combustion wave area per unit mass of gas has a maximum at $t^{\star}$

$$t^{\star} = T \ln \frac{(A/V_u)^{\star}}{(A/V_u)_0} \tag{16}$$

The value of this maximum is

$$\left(\frac{A}{G}\right)_{max} = v_u\left(\frac{A}{V_u}\right)^{\star} e \frac{(A/V_u)_0}{(A/V_u)^{\star}} - 1 \tag{17}$$

or with good approximation

$$\left(\frac{A}{G}\right)_{max} = \frac{v_u}{S_u}\frac{u'}{l}\frac{1}{e} \tag{18}$$

Combustion wave area per unit volume of combustion space

The most important quantity for the design of combustion systems is the combustion wave area

per unit volume of combustion space. This quantity is given by

$$\left(\frac{A}{V}\right) = \left(\frac{A}{V_u}\right)\frac{V_u}{V_u + V_b} \tag{19}$$

The quantity $V_u/(V_u - V_b)$ is the fraction of volume occupied by unburned gas mixture. In the following this quantity will be denoted by ϕ. To calculate ϕ as a function of time, first the variation of V_u and V_b is calculated. Here V_u and V_b denote volumina of unburned and burned gas corresponding to an arbitrary initial volume of V_{u_0}.

The unburned gas volume decreases in dt time by

$$\mathrm{d}V_u = -\left(\frac{A}{V_u}\right)V_u S_u \,\mathrm{d}t \tag{20}$$

inserting (A/V_u) from equation 10

$$\mathrm{d}V_u = -\left(\frac{A}{V_u}\right)_0 V_u S_u e^{t/T}\,\mathrm{d}t \tag{21}$$

from which

$$\ln\left(\frac{V_u}{V_{u_0}}\right) = -\left(\frac{A}{V_u}\right)_0 S_u T(e^{t/T} - 1) \tag{22}$$

The burned gas volume increases in dt time by

$$\mathrm{d}V_b = -\alpha\,\mathrm{d}V_u \tag{23}$$

from which

$$\left(\frac{V_b}{V_{u_0}}\right) = \alpha\left(1 - \frac{V_u}{V_{u_0}}\right) \tag{24}$$

here $\alpha = v_b/v_u$ is the expansion ratio due to combustion; v_b is the specific volume of burned gas; and v_u is the specific volume of unburned gas. With the above values of V_u and V_b we obtain

$$\phi = \frac{V_u}{V_u + V_b} = \frac{\left(\frac{V_u}{V_{u_0}}\right)}{\left(\frac{V_u}{V_{u_0}}\right) + \left(\frac{V_b}{V_{u_0}}\right)}$$

$$= \frac{\left(\frac{V_u}{V_{u_0}}\right)}{(1 - \alpha)\left(\frac{V_u}{V_{u_0}}\right) + \alpha} \tag{25}$$

Closely related to the fraction ϕ is the average specific volume of the randomly mixed parcels of burned and unburned gas. The average specific volume is defined as

$$v = \frac{V}{G} = \frac{V_b + V_u}{G_b + G_u} \tag{26}$$

where V is a small volume, and G the average weight of gas contained in this volume.

The original volume occupied by the gas of weight G is

$$V_{u_0} = v_u G$$

The volume $V = V_u + V_b$ for any given ϕ is

$$V = \frac{1}{\phi}V_u$$

Therefore

$$v = \frac{V}{G} = \frac{V}{V_{u_0}}v_u = \frac{v_u}{\phi}\left(\frac{V_u}{V_{u_0}}\right) \tag{27}$$

Inserting ϕ from equation 25

$$v = v_u\left[\alpha - (\alpha - 1)\left(\frac{V_u}{V_{u_0}}\right)\right] \tag{28}$$

Equation 28 gives a convenient formula for the calculation of

$$\phi = \frac{(V_u/V_{u_0})}{v/v_u} \tag{29}$$

Degree of completion of combustion

The degree of completion of the combustion may be defined as the fraction of the weight of the gas burned.

$$\psi = \frac{G_b}{G_u} = \frac{v_u V_b}{v_b V_{u_0}} = 1 - (V_u/V_0) \tag{30}$$

Heat release rate

The local heat release rate is

$$q = 3{,}600\left(\frac{A}{V}\right)S_u H \,\frac{\mathrm{kcal}}{m^3 h} \tag{31}$$

where q is the heat release rate per unit volume of combustion space and H the heat of combustion per unit volume of mixture.

Limitations of usefulness of combustion wave concept

In the above analysis only the surface area of the combustion wave was considered, and no attention was paid to the thickness of the wave. In reality the finite thickness of the combustion wave introduces important limitations for the applicability of the normal combustion wave concept. If, for example, combustion waves approach each other on the average within the thickness of the pre-heat zone, then the waves are moving into mutually pre-heated gas mixture and the laminar burning velocity increases rapidly. Therefore, the above derivations, pre-supposing constant laminar burning velocity, are valid only in a range where

$$\left(\frac{A}{V_u}\right) < \frac{1}{\eta_0} \tag{32}$$

Here $\eta_0 = \lambda/c_p\rho S_u$ is a measure of the thickness of the pre-heat zone; c_p is the specific heat of the gas mixture; ρ is the density of the gas mixture; and λ is the heat conductivity of the gas mixture.

Another important limitation arises from the intermittent velocity gradients produced by the turbulent fluctuations. The average magnitude of these velocity gradients is in the order of u'/l. A combustion wave in a turbulent medium is continually exposed to these velocity gradients. As is well known (see p. 613, *Fourth Symposium on Combustion*) moderate velocity gradients do not affect the stability and the propagation velocity of combustion waves. But relatively strong velocity gradients scatter the heat flowing from the wave into the unburned gas thereby reducing the propagation velocity of the wave, and may even extinguish the combustion wave. These effects become noticeable when

$$\frac{\eta_0}{U}\frac{\mathrm{d}U}{\mathrm{d}y} \geqslant 1 \tag{33}$$

Where η_0 is the thickness of the pre-heat zone; U is the flow velocity relative to the wave; and y is the distance in direction normal to U. Equation 33 states that the combustion wave is disrupted by the steep velocity gradient if the flow velocity approximately doubles its value within the thickness of the pre-heat zone. The smaller the flow velocity U the smaller velocity gradients can the combustion wave tolerate. The velocity U cannot be smaller than the laminar burning velocity S_u, therefore, for turbulent fluctuations the condition given in equation 33 becomes

$$\frac{\eta_0}{S_u}\frac{u'}{l} \geqslant 1 \tag{34}$$

According to equation 9,

$$\left(\frac{A}{V_u}\right)^{\star} = \frac{u'}{l}\frac{1}{S_u}$$

If

$$\{(\eta_0/S_u)(u'/l)\} < 1$$

then

$$\left(\frac{A}{V_u}\right)^{\star} = \frac{u'}{l}\frac{1}{S_u} < \frac{1}{\eta_0}$$

and, therefore, the combustion wave area per unit volume of unburned gas can reach, and even exceed the value $(A/V_u)^{\star}$. Such flames will have the tendency to accelerate rapidly and eventually to go over into detonation. On the other hand if $(\eta_0/S_u)(u'/l) > 1$ the heat of the combustion wave is rapidly scattered and the flame is likely to blow out.

Numerical example

The following numerical example describes the development and burn-out of flame surface in a constant cross-section straight duct. High intensity approach flow turbulence is assumed, corresponding to 2 per cent pressure drop, but the additional turbulence generated by the flame is not taken into consideration. The initial combustion wave surface is assumed to be established by some means and distributed at random, but on the average uniformly, over the entrance cross-section of the duct.

Assumed data:

$$U_0 = 100 \text{ ft./sec} = 3{,}050 \text{ cm/sec}$$

$$u' = 3{,}600 \text{ cm/sec}$$

$$l = 1 \text{ cm}$$

$$S_u = 40 \text{ cm/sec}$$

$$\alpha = 7$$

$$\eta_0 = 0{\cdot}55 \times 10^{-2} \text{ cm}$$

$$\left(\frac{A}{V_u}\right)_0 = 0{\cdot}01 \text{ cm}^2/\text{cm}^3$$

From which

$$T = \frac{l}{u'} = 0{\cdot}278 \times 10^{-3} \text{ sec}$$

$$\left(\frac{A}{V_u}\right)^{\star} = \frac{u'}{l}\frac{1}{S_u} = 90 \text{ cm}^2/\text{cm}^3 < \frac{1}{\eta_0} = 180 \text{ cm}^2/\text{cm}^3$$

$$\frac{t^{\star}}{T} = \ln\frac{(A/V_u)^{\star}}{(A/V_u)_0} = 9{\cdot}1$$

The variation of (A/V_u), ϕ, (A/V) and (V_u/V_{u0}) along the duct is shown in *Figure 1.*

Assuming 795 kcal/cm³ heat of combustion for the mixture, the average specific heat release rate amounts to

$$q = 3{\cdot}65 \times 10^8 \text{ kcal/m}^3\, h \text{ atm}$$

or

$$4{\cdot}07 \times 10^7 \text{ B.Th.U./ft.}^3 h \text{ atm}$$

in the entrance region of the combustion chamber because of the relatively small combustion wave area present, nevertheless the magnitude of the initial combustion wave area has only small effect on the total flame length. Reaction rate is small again in the outlet region of the combustion system because of the remaining small volume of combustible mixture.

The analysis presented here can be considered

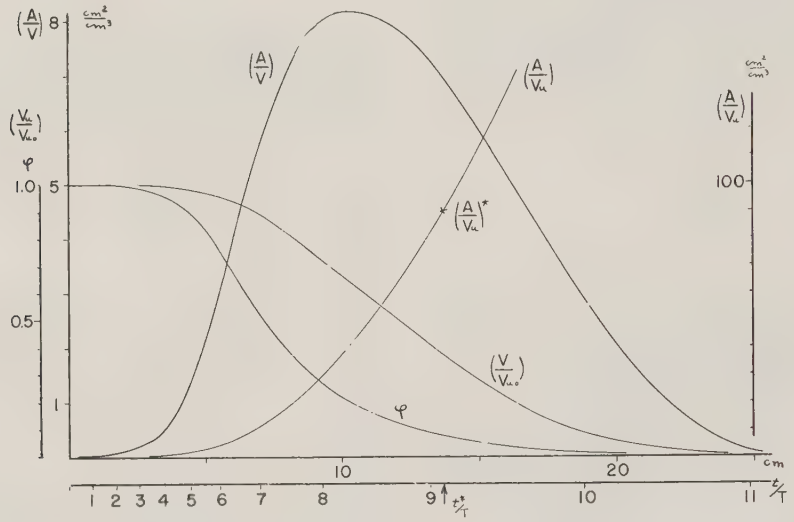

Figure 1. Variation of combustion wave area per unit volume of unburned gas (A/V_u), per unit volume of combustion space (A/V); of fraction of unburned gas remaining (V/V_{u_0}), and of fraction of volume of unburned gas ϕ along a duct containing a turbulent flame

and the maximum of the local heat release rate $q_m = 9{\cdot}16 \times 10^8$ kcal/m³ h atm.

CONCLUSIONS

It is interesting to note that the time-scale of flame development and burn-out is determined by the characteristic time T, which is a function of the turbulence parameters only. Reaction rate is low as a first approach to the problem of turbulent flames enclosed in a chamber. Nevertheless it reveals the main characteristics of such flames and the effect of various parameters on the flame. Future work will have to clarify further the effect of high intensity turbulence on the combustion wave, and apply the results developed here to flow configurations containing return eddies.

INVESTIGATION OF PRESSURE EFFECT ON THE PARAMETERS OF TURBULENCE AND ON TURBULENT BURNING

V. A. KHRAMTSOV

INTRODUCTION

Most papers on combustion at pressures below atmospheric have dealt with the effect of pressure on the laminar burning velocity. It is only in recent years that the first papers have appeared, devoted to determining experimentally the effect of pressure on the turbulent burning velocity and the thickness of the turbulent zone of combustion, the work being carried out by study groups headed by Goldenberg and Doroshenko[3].

Due to this research, the qualitative picture of turbulent combustion at reduced pressure has now become more or less clear: as pressure diminishes, the turbulent burning velocity U_t decreases and the thickness of the turbulent zone of combustion δ_t (with W = const) increases. However, the problem of the parameters through which pressure influences U_t and δ_t still remains largely unsolved.

In order to determine the dependence of turbulent burning velocity and the thickness of the turbulent zone of combustion on pressure, it is necessary to investigate the effect of pressure on the pulsation velocity, the scale of turbulence and the normal burning velocity.

The present research was devoted to an experimental study of the effect of pressure on the characteristics of turbulence (ϵ, l, D) and on turbulent combustion (U_t and δ_t). In this case the plan was to eliminate the effect of pressure on U_t through pulsation velocity U'. This presupposed that the hydrodynamic conditions of stream should remain invariable at every pressure.

EXPERIMENTAL INSTALLATION

The tests were conducted with an experimental installation whose key diagram is given in *Figure 1*. The installation operates in the following way: by scavenging the air from the receiver, the vacuum pump sets up rarefaction in the system. The air sucked into the system passes through the heat exchanger and then enters the operating burner placed in the pressure chamber. From the pressure chamber the products of combustion pass into the cooler and further on through the receiver to the vacuum pump. The working pipe is included in the heated pipe along which the

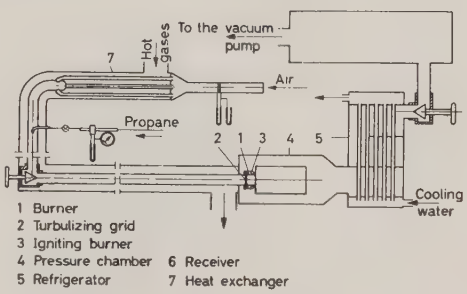

Figure 1. Key diagram of the installation

products of combustion move from a special heating chamber. Such heating prevents the air passing along the working pipe from the heater to the burner being cooled and makes it possible to use heated combustible mixtures. Burners, 45 and 36 mm in diameter, were used in the experiments. *Figure 2* shows turbulizing grids behind which were determined the intensity turbulence of the flow, the coefficient of turbulent diffusion and the Lagrangian scale of turbulence (length of mixing).

Ignition of the basic combustible mixture and stabilization of the brush of flame at any rarefaction in the pressure chamber were provided by a special annular igniting gas and oxygen burner. Propane was used as fuel.

All the major experiments on determining ϵ, l, D, U_t and δ_t were carried out at constant flow velocity of 40 m/sec, and at pressures of 0·6, 0·3 and 0·1 atm.

METHODS FOR DETERMINING THE TURBULENT PARAMETERS OF FLOW

The turbulence parameters of the flow were determined by the optical-diffusion method theoretically substantiated and practically developed by Prudnikov[1].

The method essentially consists in photographing the diffusion wake of luminous particles (smoke, atoms of Na, Li, etc.) behind a point source in the turbulent flow and determining from the distribution of blackening across the image of the wake the distribution of intensity of the

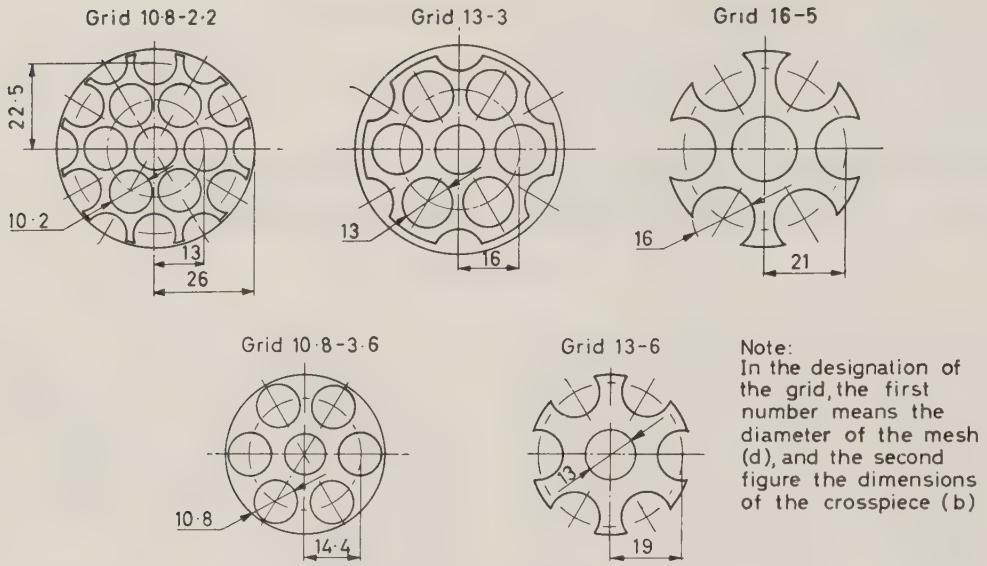

Figure 2. Turbulizing grids

incident light and that of the concentration of particles which emitted light in the given direction. Then the dispersion of turbulent transfer $\overline{Y^2}$ is computed which, as is well known, is given by the two following limit equations:

$$\overline{Y^2} = \epsilon^2 x^2 \tag{1}$$

$$\overline{Y^2} = 2\frac{D}{W}(x - x_1) \tag{2}$$

Here x_1 is the value of abscissa x at the point where the axis ox crosses the continuation of the rectilinear section of the curve $\overline{Y^2} = f(x)$.

Equation 1 permits the turbulence intensity $\epsilon = U'/W$ to be found while the equation 2 determines the coefficient of turbulent diffusion D. The knowledge of the turbulence intensity and of the coefficient of turbulent diffusion is sufficient to find the Lagrangian scale of turbulence from the well-known equation:

$$\frac{D}{W} = \epsilon l \tag{3}$$

METHODS FOR DETERMINING THE TURBULENT BURNING VELOCITY AND THE THICKNESS OF THE TURBULENT ZONE OF COMBUSTION

The turbulent burning velocity was determined from the measured flame front area and from the given flow rate of the combustible mixture. The surface of the inner cone of the turbulent front on which the temperature differed from that of the initial mixture by 20°C was assumed as the flame front area. The rise in temperature was determined by the fields of the temperature, taken in the cross-sections of the flame brush with the aid of a thermocouple with an open juncture.

The distance along the axis of the brush on which the temperature rose from the initial temperature of the mixture to the maximum temperature of the products of combustion was assumed as the thickness of the turbulent zone of combustion δ_t.

RESULTS OF EXPERIMENTS

Effect of pressure on the dispersion of turbulent transfer of smoke particles $\overline{Y^2}$, on the intensity of turbulence ϵ, the coefficient of turbulence diffusion D and the scale of turbulence l

Figure 3 presents experimental data on the change in the dispersion of turbulent transfer of smoke particles ($\overline{Y^2}$), depending on the distance from the source (x) placed in a fixed section behind grid 13–3 (see *Figure 2*) at varying pressure in the flow. From the charts it follows that the turbulent transfer behind grid 13–3 at $x_0 = 55$ mm considerably diminishes as the pressure changes from 0·6 to 0·1 atm. Similar results were obtained behind grids 10·8–2·2 and 16–5.

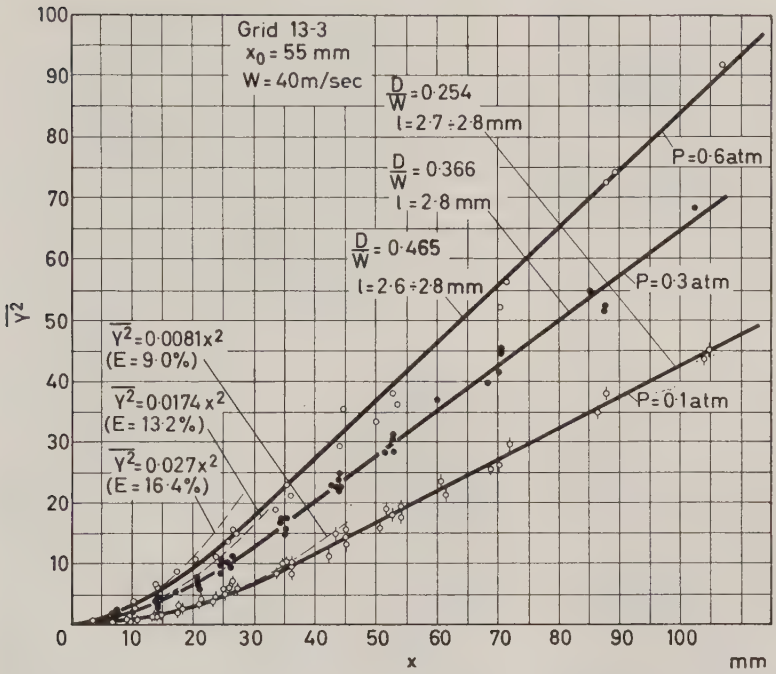

Figure 3. Dependence of the mean square of the turbulent transfer (dispersion) of smoke particles ($\overline{Y^2}$) on the distance (x) from the source in a fixed section (x_0) behind grid 13–3 at low pressure in the flow

Analysis of the experimental curve $\overline{Y^2} = f(x)$ at various pressures has allowed the dependence of turbulence intensity, the coefficient of turbulent diffusion and the scale of turbulence on pressure to be found: the turbulence intensity ϵ and the coefficient of turbulence diffusion D change as $P^{0.34}$, while the scale of turbulence l does not depend on pressure (see *Figure 4*). The experimental data so obtained on the effect of pressure on the scale of turbulence proved to be rather unexpected. It had been assumed that with a drop of pressure the scale of turbulence would grow, due to the increase in kinematic viscosity, and this should result in the disappearance of small-scale eddies and a corresponding increase in the mean scale of turbulence. The result so obtained is, however, in satisfactory agreement with Laurence[2] which comprises an experimental chart demonstrating that the scale of turbulence does not depend on Reynolds number (in the range $192 \cdot 10^3$–$725 \cdot 10^3$). A change in the R_e number in the given paper was achieved by changing the velocity, while in the present experiment the R_e number was changed approximately in the same range owing to a drop of density with the velocity of the flow held constant.

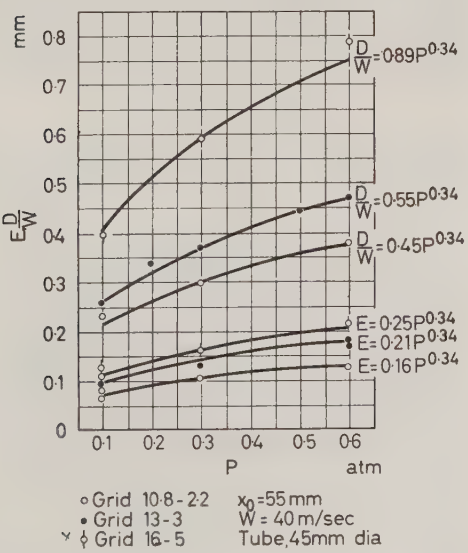

Figure 4. Experimental dependence of turbulence intensity ϵ and the coefficient of turbulence diffusion D on pressure P

Keeping invariable the conditions of stream at low pressures

The construction of turbulizing grids which produce one and the same intensity of turbulence at different pressures was an important task in these experiments. By way of illustration, the method can be shown for computing grid 10·8–3·6 which with $P = 0{\cdot}1$ atm should have generated the same intensity ϵ as grid 10·8–2·2 with $P = 0{\cdot}6$ atm. It can be seen from *Figure 4* that as the pressure diminishes sixfold (from 0·6 to 0·1 atm), turbulence intensity behind grid 10·8–2·2 drops approximately 1·65 times. To compensate for this

drop of intensity, a grid was selected which under conditions of initial pressure ($P = 0{\cdot}6$ atm) sets up an intensity 1·65 greater than grid 10·8–2·2. This was achieved by correspondingly increasing the width of crosspiece of the grid, since it was found from experiments that at the initial pressure $P = 0{\cdot}6$ atm the turbulence intensity behind the given grids at the region of decay was connected with the dimensionless magnitude x/b by the empirical equation:

$$\epsilon = \frac{3{\cdot}1}{\frac{x}{b}}$$

The dispersion of turbulent transfer $\overline{Y^2}$ determined behind the equivalent grid 10·8–3·6 in the section $x_o = 55$ mm with $P = 0{\cdot}1$ atm, coincided with those behind the grid 10·8–2·2 with pressure $P = 0{\cdot}6$ atm (*Figure 5*). Similar experimental data

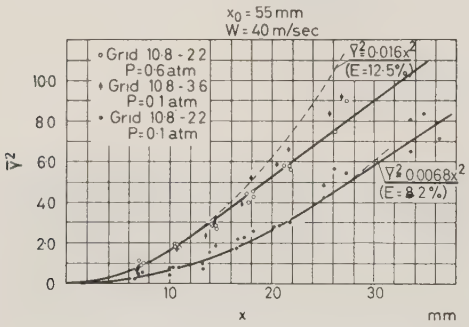

Figure 5. Dependence $\overline{Y^2} = f(x)$ behind grid 10·3–2·2 with $P = 0{\cdot}6$ and 0·1 atm and behind grid 10·8–3·6, equivalent to it, with $P = 0{\cdot}1$ atm

were obtained at various distances of the source of smoke from the grids. The values of turbulence intensity behind the corresponding grids were computed according to these data. It follows from the charts given in *Figure 6* that these values ϵ behind the equivalent grids with pressure $P = 0{\cdot}1$ atm coincide in a satisfactory manner with the experimental values ϵ obtained behind the initial grids (10·8–2·2 and 13–3) with the initial pressure $P = 0{\cdot}6$ atm. For the sake of comparison, two experimental points were plotted in *Figure 6*, which illustrate the drop of turbulence intensity behind the initial grid 10·8–2·2 as pressure changes from 0·6 to 0·1 atm.

Dependence of turbulent burning velocity on pressure with $U' = var$ and $U' = const$

Combustion behind one and the same grid with $W = const$ and varying pressure takes place in a flow where with a change in pressure the pulsation velocity changes. According to the present experiments, the turbulent burning velocity with $U' = var$ changes in proportion to pressure at

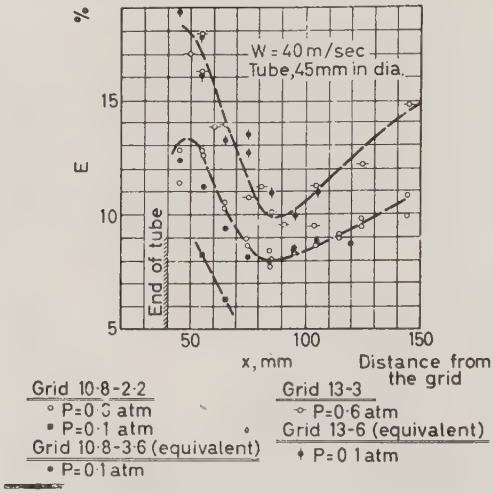

Figure 6. Variation of turbulence intensity behind the grids

a degree of 0·4 (the lower curve in *Figure 7*):

$$U_t \sim P^{0{\cdot}4}.$$

In this case the pressure affects U_t through the kinetics of combustion and through the pulsation velocity. The construction of turbulizing grids producing one and the same turbulence intensity at varying pressure precludes the effect of pressure on U_t through the pulsation velocity. In this case pressure influences U_t only through the kinetics and the microstructure of turbulence.

Had it been possible to reduce the effect of pressure on turbulent burning velocity U_t through kinetics to the influence of the normal burning velocity, as is done in research on turbulent combustion at atmospheric pressure, the dependence of U_t on P would have appeared in the following way:

$$U_t \sim P^{-0{\cdot}12}$$

This expression was obtained from the formula referred to by many researchers, namely :

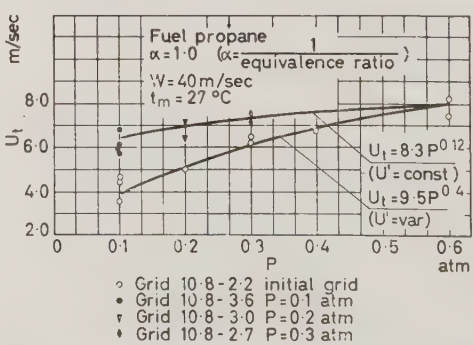

Figure 7. Experimental dependence of the turbulent burning velocity on pressure with $U' = var$ and $U' = const$

$U_t \sim (U')^{0.6} \cdot (U_n)^{0.4}$, where the relationship $U_n = 0.5 \cdot P^{-0.3}$ found for the propane–air mixture used in the given experiments had been substituted.

As a matter of fact, U_t with $U' = \text{const}$ proved to be proportional to $P^{0.12}$ (see upper curve in *Figure 7*). This leads to the conclusion that under conditions of reduced pressure it does not suffice to take into account the effect of the kinetics of chemical processes on U_t only by means of U_n. It should be noted that the same conclusion was reached even before that by Schetinkov[3], proceeding from theoretical considerations.

Effect of pressure on the thickness of the turbulent zone of combustion δ_t

The value δ_t assumed in this paper as the thickness of the turbulent zone of combustion (see above) is not quite the thickness of the turbulent zone of combustion since air must be added to the open brush of flame in the pressure chamber. The change in the assumed value δ_t, resulting from pressure and temperature, defines, however, a change in the real thickness of the turbulent zone of combustion, and a qualitative study of the influence of P and T on δ_t is therefore of some interest.

Figure 8 shows the experimental dependence of δ_t on pressure. It can be seen from the charts in question that the thickness of the turbulent zone of combustion δ_t increases as the pressure diminishes:

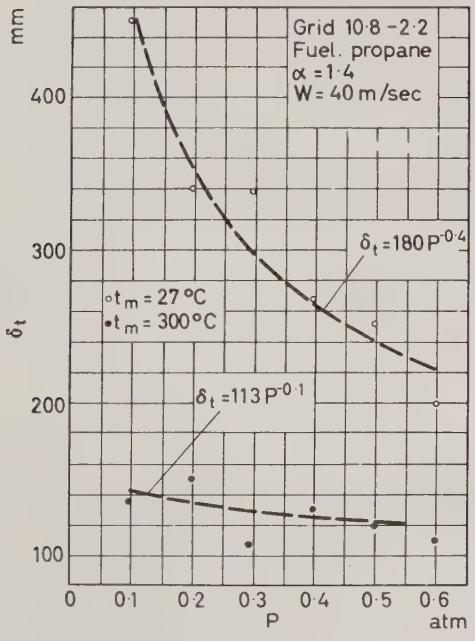

Figure 8. Dependence of the thickness of the turbulent combustion zone on pressure

the lower the initial temperature of the fresh mixture, the greater the increase:

At $t_m = 27°C$ $\quad \delta_t \sim P^{-0.4}$
At $t_m = 300°C$ $\quad \delta_t \sim P^{-0.1}$

The influence of the temperature of a heated combustible mixture on U_t *and on* δ_t *at pressure below atmospheric*

The initial temperature of the combustible mixture has but little effect on U_t : U_t increases as the temperature rises. The nature of this effect is the same in every pressure used in this study (*Figure 9*)

$$U_t \sim T^{0.25}$$

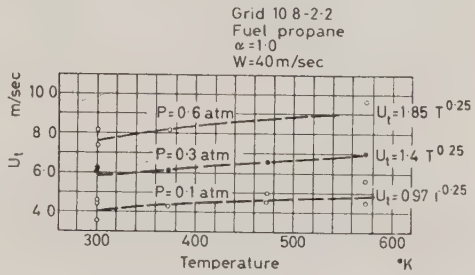

Figure 9. Influence of the temperature of the combustion mixture on the turbulent burning velocity at low pressure

The temperature exercises a great influence on the thickness of the turbulent zone of combustion. As the initial temperature of the mixture rises, δ_t diminishes. In this case the degree of influence of the temperature depends on pressure (*Figure 10*)

With $P = 0.6$ atm $\quad \delta_t \sim T^{-0.9}$
With $P = 0.4$ atm $\quad \delta_t \sim T^{-1.2}$
With $P = 0.1$ atm $\quad \delta_t \sim T^{-1.8}$

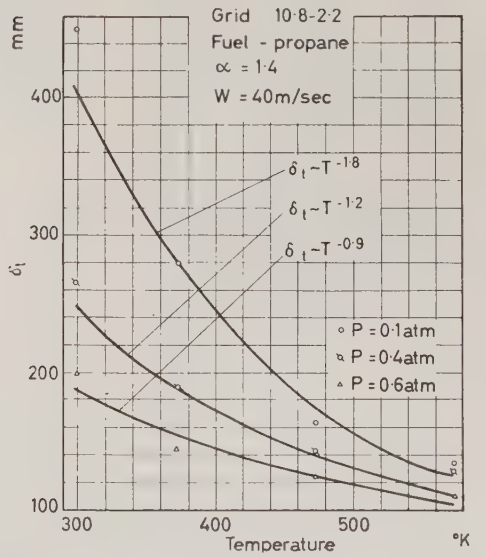

Figure 10. Dependence of the thickness of the turbulent combustion zone on the temperature of the combustible mixture

CONCLUSIONS

(1) It has been experimentally established that the intensity of turbulence and the coefficient of turbulent diffusion change as $P^{0.34}$ (P = absolute pressure).

(2) The scale of turbulence behind the grids of the investigated geometrical dimensions does not depend on pressure (in the examined range of pressures: 0·6 to 0·1 atm).

(3) The turbulent burning velocity during combustion behind one and the same grid, i.e. with U' = var, is proportional to 0·4 power of pressure, and with U' = const is proportional to 0·12 power of pressure.

(4) At reduced pressure it is not sufficient to take into account the effect of the kinetics of chemical processes on U_t only by means of the normal burning velocity.

(5) Experimental data prove qualitatively that as pressure diminishes, the thickness of the turbulent zone of combustion δ_t increases, and the lower the initial temperature of the combustible mixture, the greater the increase.

NOMENCLATURE

W = velocity of flow
U_n = the normal burning velocity
U_t = the turbulent burning velocity
U' = $(U^2)^{\frac{1}{2}}$ = the mean quadratic flateral turbulence velocity
ϵ = U'/W = turbulence intensity
l = scale of turbulence
D = coefficient of turbulence diffusion
$\overline{Y^2}$ = mean statistical square of displacement (turbulent transfer) of smoke particles in a turbulent field
x = distance from the point source of smoke to the current section
x_o = distance from the grid to the point source of smoke
b = width of cross-piece between the meshes in the grid
d = diameter of the mesh of the grid
δ_t = thickness of the turbulent zone of combustion
t_m = temperature of the combustible mixture
P = pressure in the flow

REFERENCES

[1] Prudnikov, A. G. Measurements of the turbulence of air flows and flames by the optical-diffusion method. *M.Sc. Thesis, Moscow Physical Technical Institute, 1956*

[2] Laurence, J. C. Intensity, scale and spectra of turbulence in the mixing region of free subsonic jet. *Report of NACA No. 1292*, 1956

[3] *Proceedings of the Moscow Seminar on Combustion.* Publishing House of the U.S.S.R. Academy of Science (in print), 1958

TURBULENT FLAME PROPAGATION BY LARGE-SCALE WRINKLING OF A LAMINAR FLAME FRONT

J. K. RICHMOND, J. GRUMER and D. S. BURGESS

INTRODUCTION

From work with bunsen type flames affected by pipe-flow turbulence it appears that a useful distinction may be drawn between flames that burn: (1) in the turbulent core of the approach flow; and (2) in the wake of the burner rim, in what is commonly known as the 'mixing zone'. A schematic illustration appears in *Figure 1*. The dashed line represents a conical surface within which the average gas flow velocities, turbulent fluctuation velocities, and presumably scales of turbulence, are close to their values at the mouth of the burner; a flame at low Reynolds number is shown to lie almost entirely within this core. Near dot-dash line there are steep velocity gradients, and in the tall flame illustrated at high Reynolds number gas approaches the flame position with perhaps half its average velocity in the burner. The scale of turbulence in this wake zone* is markedly larger than in the core.

Flames within the central core may have large burning velocities which increase generally with increasing turbulence, laminar burning velocity, burner diameter and height in the flame. These are probably the flames of practical importance. Unfortunately there are unresolved controversies over their structures, which may depart from the traditional model of a wrinkled laminar flame front.

For this reason it is useful to study flames in the wake zone where one may speak most confidently of a wrinkled flame structure; by learning quite definitely what to expect from a wrinkled laminar flame, one is then equipped to study departures from this structure.

CHARACTERISTICS OF FLAMES IN THE WAKE ZONE

A typical example of such flames is obtained at 50,000 R_e using a $1\frac{1}{4}$ in. diameter burner with stoichiometric natural gas–air. The salient characteristics of this flame are summarized in *Figure 2*.

The strongest argument for a continuous laminar flame structure is shown in *Figure 2a*, which presents an oscillogram of a small pencil of light from the flame brush[1]. The minimum instantaneous signal is in the range of the signal from a laminar flame seen broadside (and of the same equivalence ratio) as indicated by the arrow. The maximum

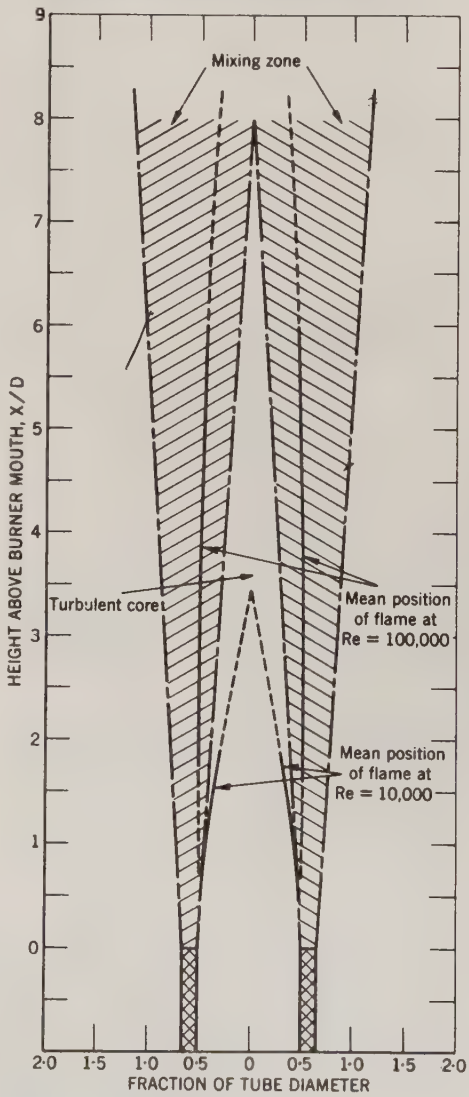

Figure 1. Representative average positions of turbulent flames on $1\frac{1}{4}$ in. bunsen burner

* We avoid the term 'mixing zone' because of a possible connotation of mixing of unburned gas with surrounding air.

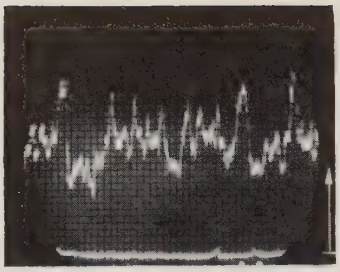

(a)

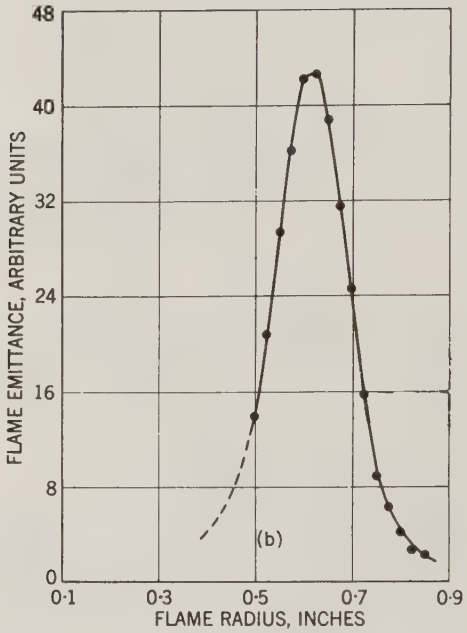

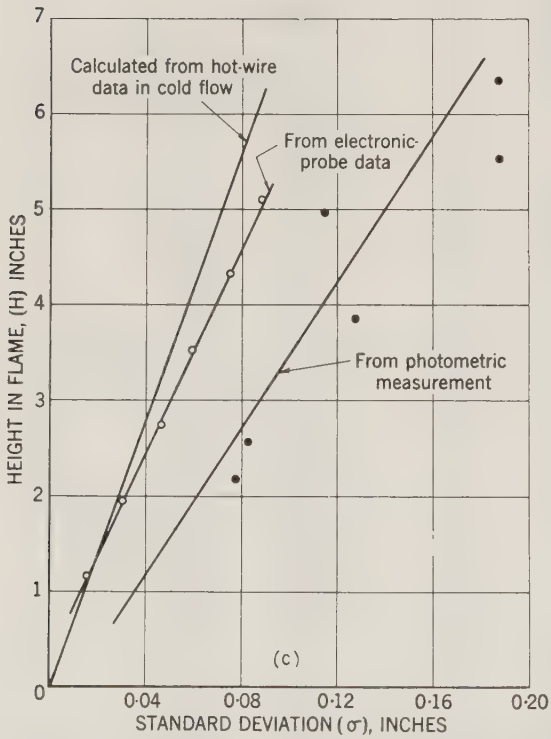

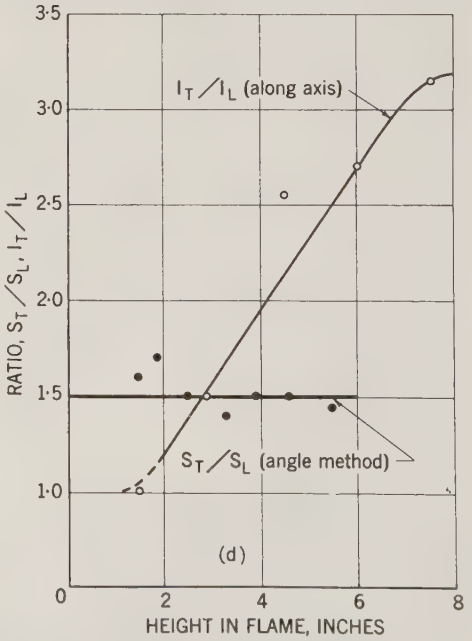

Figure 2. Salient features of a wake zone flame, stoichiometric natural gas–air at $R_e = 50{,}000$, $1\frac{1}{4}$ *in. diameter burner. (a) Transient light from unit flame surface, compared to value (arrow) obtained from laminar flame; (b) horizontal distribution of radiation at* 4,325 Å; *(c)* r.m.s. *displacement of wrinkled flame front from its mean position; (d) local turbulent burning velocities and average levels of flame radiation, ratios to laminar values (By courtesy of Bureau of Mines, U.S. Department of the Interior)*

fluctuation of signal increases with height in the flame.

The spatial distribution of this flame front within the flame brush is indicated by *Figure 2b*, which portrays a radial, time average distribution of radiation at 4,325 Å. The curve was found to fit a Gaussian probability function and its symmetry indicates that flame front fluctuations are symmetrical about a mean position[2]. A similar argument has been derived from electronic probe data[3].

The r.m.s. displacement of fluctuations, as obtained from *Figure 2b*, is shown to grow almost linearly with height in the flame in *Figure 2c*. The linearity is regarded as significant in that it suggests that fluctuations grow continually, that is, without much chance of a reversal of direction. Photometric data and electronic probe data are compared in the graph with predictions based on hot wire anemometer measurements in cold flow*, and assuming $\sigma/H = v'/U$.

Figure 2d presents a crucial problem for the wrinkled flame concept. The turbulent burning velocity, as determined by the flame's average position in a measured velocity of approach flow ($S_T = U \sin \alpha$), is shown to be independent of height in the flame[2]. On the other hand, the time-average radiation from unit surface of the flame brush is shown to rise sharply to a peak at the intersection of the flame brushes; barring a drastic change in the photon yield of the combustion process, this radiation should also be a measure of burning velocity. The reality of these two apparently contradictory findings is examined below.

In the two flames of this type that were intensively studied, burning velocities were not only constant with height but were closely represented by

$$S_T = U \sin \alpha = S_L + v' \qquad (1)$$

The literature was searched for burning velocity data that were clearly representative of comparable flames; a flame height/burner diameter ratio of 10 or more was used as a criterion for distinguishing such flames from those burning wholly or in part within the turbulent core; this criterion excludes all but a few of the measurements by Bollinger and Williams[4]. *Figure 3* presents these data along with our own as a function of approach gas velocity. The lines drawn represent equation 1 with $S_L = 40$ for natural gas– and propane–air, $S_L = 70$ for ethylene–air, and $v' = 0{\cdot}007U$. The Bollinger and Williams data represent the total flame area while our own measurements represent about 35 per cent of the gas flow close to the base of the flame; agreement even as good as shown in *Figure 3* can only exist in-so-far as burning velocity is constant with height in the flame.

A roughly quantitative test of radiation from a wrinkled surface is represented in *Figure 4*. A tall, slender laminar flame was obtained at $R_e = 4{,}000$ on a 9/16 in. burner, the centre line approach velocity being 840 cm/sec. Since the flame surface has a very small radius of curvature in the upper in. or so of the flame (corresponding to extreme

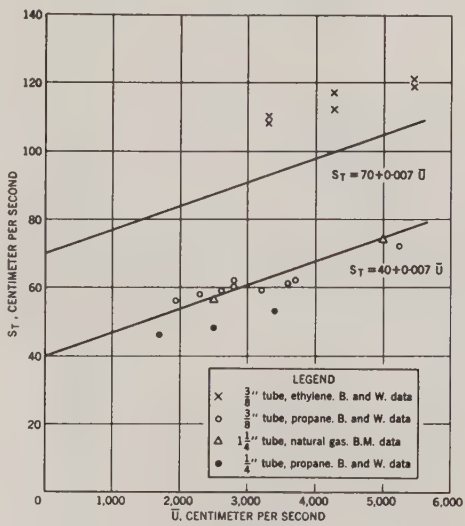
S_T, CENTIMETER PER SECOND
$\bar{U}$, CENTIMETER PER SECOND
$S_T = 70 + 0{\cdot}007\ \bar{U}$
$S_T = 40 + 0{\cdot}007\ \bar{U}$
LEGEND
$\frac{3}{8}$" tube, ethylene. B. and W. data
$\frac{3}{8}$" tube, propane. B. and W. data
$1\frac{1}{4}$" tube, natural gas. B.M. data
$\frac{1}{4}$" tube, propane. B. and W. data

Figure 3. Summary of turbulent burning velocity data for flames burning in the wake zone

wrinkling in a turbulent flame) conditions are highly favourable to pre-heating of the unburned gas, with any consequent increase of emittance. As shown by the photocurrent curve of *Figure 4*, no such increase was observed below the rounded flame tip*. Correspondingly, no significant change of burning velocity was observed in the same region. We conclude that the photometric results of *Figure 2d* may be taken as a rough measure of burning rate, that is, of volume rate of mixture burned per unit average surface of flame. Assuming laminar combustion throughout the flame, the photocurrent curve of *Figure 2d* is a relative measure of specific flame surface.

PHYSICAL MEANING OF 'TURBULENT BURNING VELOCITY'

Figure 5 presents schematically the factors necessary to reconcile the experimental data shown in *Figure 2d*. An arbitrary disturbance in the approach flow is shown acting upon a laminar flame

* The electronic probe measurements were contributed by Mr. W. F. Donaldson.

* When the entire stream was pre-heated in the burner over a range of temperatures from about 50 to 360°C, an increase in photocurrent was obtained for all parts of the flame.

front. The half-period of the resulting fluctuation was chosen as 1 cm by reason of electronic probe data (counts per second, 1,400; stream velocity, 1,200 cm/sec). As the wrinkle moves downstream, a certain distortion occurs because of laminar

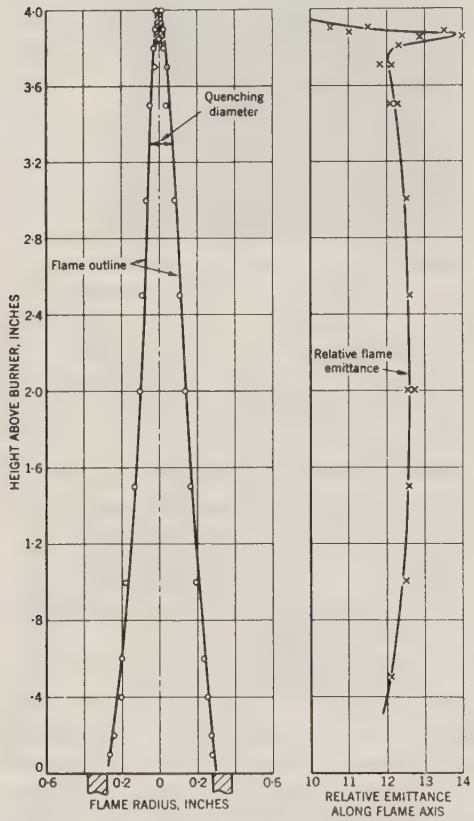

Figure 4. Photometric outline and relative axial emittance of a laminar flame. Flame of stoichiometric natural gas–air at $R_e = 4{,}000$ *on a* 9/16 in. *diameter burner*

burning, but the specific flame surface increases continuously. This is in accord with the photometric data of *Figure 2d*. It was postulated by Karlovitz[5] that the net flame advancement was produced by burning out of fluctuations towards the burned gas. As a result of this 'phase velocity' effect he obtained a constant burning velocity of $S_L + v'$ for short downstream distances*. However, the illustration shows that the scale of turbulence is too large in this flame for this burning out of wrinkles to be significant. Moreover, as shown by *Figure 2b*, the distribution of luminous emission in the flame brush is nearly symmetrical with respect to the mean position; in the Karlovitz model, asymmetry is required for flame advancement.

Scurlock and Grover[6] correctly postulated that the specific flame surface would increase with height; but as a consequence of this increased surface they predicted an increase of turbulent burning velocity with height in the flame, in contradiction to the experimental evidence.

The point that is not clearly brought out by these theories is that unburned gas (shaded area) is being continuously stored in the growing wrinkles as they progress upwards in the flame and across the average stream tubes of approach flow.

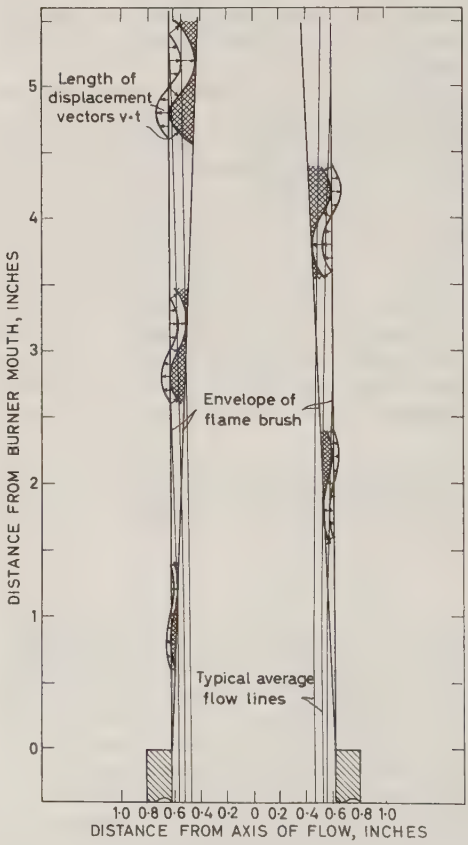
Length of displacement vectors v·t
Envelope of flame brush
Typical average flow lines
DISTANCE FROM BURNER MOUTH, INCHES
DISTANCE FROM AXIS OF FLOW, INCHES

Figure 5. Model of wrinkled laminar flame structure, applied to a flame at $R_e = 50{,}000$ *on a* $1\frac{1}{4}$ in. *diameter burner. Cross-hatch represents unburned gas in flame brush*

* As shown by *Figure 5*, this effect of increased specific surface is not restricted to wrinkles on the burned gas side of the mean position. All of the unburned gas (shaded areas) is susceptible to burning out from the sides. In extreme cases, S_T could very much exceed $S_L + v'$, as discussed in a later section.

Within a particular stream tube, U and sin α may be estimated and U sin α defines the linear flow normal to the mean flame position; one must not assume that this flow passes through the flame front. Instead, a portion of the flow is caught

up in pockets which grow at the average rate* $U \cos \alpha(\sigma/H)$. Since $\cos \alpha$ is nearly 1·0 and $\sigma/H = v'/U$, the linear flow rate corresponding to wrinkle formation is v'. Thus, in the absence of a significant phase velocity, a net flame advancement still occurs at all flame heights as indicated by

$$U \sin \alpha - v' = S_L \qquad (2)$$

where the three terms represent gas mixture entering the flame brush, being stored in the brush, and passing through the flame front, respectively. Up to a certain point, the existence of a phase velocity serves merely to decrease the unburned gas stored in the flame brush while increasing the amount of gas burned, until equation 2 approaches equation 1. This has no effect on the term $U \sin \alpha$, the turbulent burning velocity. Eventually, of course, the flame brush becomes significantly unsymmetrical, thus contributing an additional advancement of the mean position.

The physical meaning of *Figure 2d* is that for this flame the phase velocity is virtually non-existent in the first in. or two above the burner rim; thereafter it catches up to the rate of storage of unburned gas at about the third in. At this point the Scurlock–Glover burning velocity should correctly predict the measured value (their prediction, excluding flame-generated turbulence, about 50 cm/sec, as compared with the experimental value, 56–57 cm/sec). Since the flame surface is increased to some extent on both sides of the mean flame position, the brush remains symmetrical and the burning velocity constant for at least 5 or 6 in. of flame height.

To summarize this section, a distinction must be drawn between burning velocities defined by fuel–oxidant consumption rate and by mean flame position. Experimental values, always determined from the mean flame position, are not tested by the Scurlock–Grover theory, the predictions of which are more closely represented by the photometric results of *Figure 2d*.

DISCUSSION

From the foregoing discussion of specific surface effects, it is clear that turbulent scale may not be neglected in consideration of burning rates except in those cases (such as shown in *Figure 5*) where the scale is so large that the phase velocity is insignificant. Historically, the distinction between 'fine scale' and 'large scale' is based on its value, l, relative to the laminar flame thickness, θ. However, a further distinction should be based on its value relative to $S_L \cdot t$, where t is the age of the wrinkle, H/U, which is a matter of a few milliseconds. When $0 < l < S_L \cdot t$, that is, when l is of the order of a millimeter and S_L about 40 cm/sec, most small wrinkles will have been completely burned out; the net flame advancement is then determined primarily by the occasional large fluctuation towards the unburned gas; S_T then exceeds $S_L + v'$.

Based on the turbulent scales to be expected in 'core-burning' flames, one may predict flame characteristics contrasting with those of the 'wake-zone' flame of *Figure 2*.

(*a*) The transient light level should be generally higher, with less frequent occurrence of the minimum level representing a single laminar front seen broadside to the photometer's axis.

(*b*) The time-average radial distribution of light emission should rapidly become asymmetrical.

(*c*) The rate of flame-brush thickening should decrease with height, and the flame brush thickness must now be determined by the occasional large fluctuation velocity rather than by average or r.m.s. values.

(*d*) The burning velocity will increase with height in the flame; this follows not only from specific surface considerations but also from the increase of eddy diffusivity as one moves from the burner wall towards the axis of flow.

These predictions have been verified in a qualitative way at low Reynolds number with measurements comparable to those shown in *Figure 2*.

Examples of flames burning in the two zones are shown in *Figure 6*. The tall flame at the left is

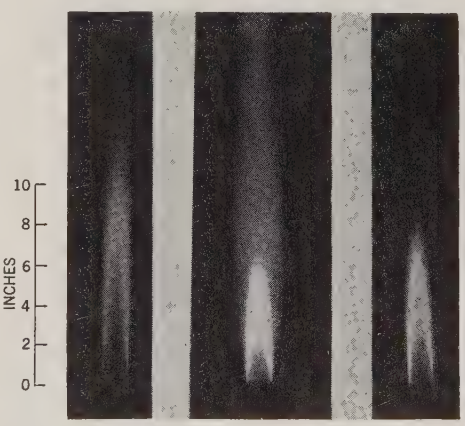

Figure 6. Time-exposure photographs of flames on a $1\frac{1}{4}$ in. *diameter burner. Reading from left to right,* $R_e = 50{,}000$ *natural gas–air;* $R_e = 50{,}000$ *natural gas–air enriched to* 30 per cent O_2*; and* $R_e = 25{,}000$ *natural gas–air*
(*By courtesy of Bureau of Mines, U.S. Department of the Interior*)

* Strictly speaking, the r.m.s. quantities v' and σ should be replaced by average absolute fluctuation velocities and displacements. Turbulent burning velocities have been measured by average volume flows and average surface areas. However, the differences involved are small and equation 1 has had a long and useful history.

the wake-zone flame at $R_e = 50{,}000$, the data for which were summarized in *Figure 2*. The flame on the right ($R_e = 25{,}000$) burns almost entirely within the turbulent core; its burning velocity is about 50 per cent higher, presumably because of the smaller scale in the core and a resultant large effect of phase velocity. To test the effect of scale on wake-burning flames, it is probably useless to change the burner diameter since the scale existing in the flame zone is surely influenced by such things as burner tube wall thickness and surrounding air flow. The desired effect can be produced by varying the value of S_L, keeping all other parameters substantially constant. The central flame in *Figure 6* was produced at the same approach flow as the one on the left, but the oxygen index was increased to 0·3, so that the laminar burning velocity was approximately doubled (increased by about 40 cm/sec). For a wake-burning flame, the turbulent burning velocity should have been increased by only the same amount but the net effect here was to bring the flame over into the core region and to increase the turbulent burning velocity by a much larger amount with a corresponding increase in flame brush thickness. The increase in total turbulent burning velocity (total area method) was estimated to be more than 140 cm/sec.

CONCLUSIONS

There is considerable evidence that pre-mixed open turbulent flames can operate in two distinct modes. For flames burning in the wake of the burner tube, the 'classical' model of a wrinkled laminar flame explains the salient features of structure and propagation rate. For flames burning in the turbulent core, this simple model may still give useful predictions, even though the complexity of the flame brush structure is enormously greater.

The authors wish to acknowledge the helpfulness of Mr. J. C. Laurence of the Lewis Flight Propulsion Laboratory, NACA, in discussions of turbulence.

This research was supported in part by the United States Air Force through the Air Force Office of Scientific Research of the Air Research and Development Command, under contract CSO-680-58-10. Reproduction in whole or in part is permitted for any purpose of the United States Government.

REFERENCES

[1] Richmond, J. K., Donaldson, W. F., Burgess, D. S. and Grumer, J. *Evidence for the Wrinkled Continuous Laminar Wave Concept of Turbulent Burning.* Presented at Meeting of American Rocket Society. December 1957. *Jet Propulsion* 28 (1958) (*AFOSR TN* 57–676, *ASTIA No.* 136 666)

[2] — Singer, J. M., Cook, E. B., Oxendine, J. R., Grumer, J. and Burgess, D. S. *Sixth Symposium (International) on Combustion,* pp. 303–311. 1957. New York; Reinhold

[3] Denniston, D. W., Jr., Oxendine, J. R., Knapschaefer, D. H., Burgess, D. S. and Karlovitz, B. *J. appl. Phys.* 28 (1957) 70

[4] Bollinger, L. M. and Williams, D. T. *NACA Report No.* 932, 1949

[5] Karlovitz, B., Denniston, D. W., Jr. and Wells, F. E. *J. chem. Phys.* 19 (1951) 541

[6] Scurlock, A. C. and Grover, J. H. *Fourth Symposium (International) on Combustion,* pp. 645–58. 1953. Baltimore; Williams and Wilkins

TURBULENT FLAME BLOW-OFF STABILITY. EFFECT OF AUXILIARY GAS ADDITION INTO SEPARATION ZONE

F. FETTING, A. P. R. CHOUDHURY and R. H. WILHELM

As is well known, a flame in a high velocity stream of a pre-mixed combustible gas may be anchored spacially by means of a bluff-body holding device. Present work concerns blow-off limits at a 5 mm o.d. cylindrical flame-holder as the velocity of a pre-mixed propane–air stream of different compositions is caused to increase

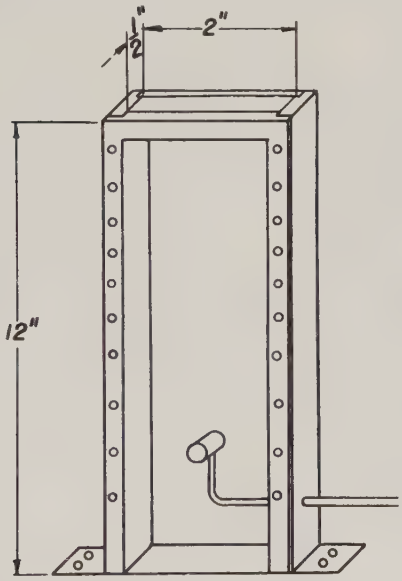

Figure 1. Combustion chamber with flame-holder in position

to the condition of flame blow-off within a rectangular combustion chamber, 12 × 2 × ½ in. *Figure 1* shows the position of the holder within the duct and *Figure 2* illustrates the parts of the flame as seen through Vicor glass windows. By perturbing conditions experimentally near the flame-holder it is sought to explore the blow-off process and to gain insight regarding the location of the seat of blow-off stability, relationships between the different parts of the flame structure in the stabilization processes and possibly contributions of chemistry in the process. System disturbances were geometric and gas compositional in nature. In some experiments the normal, cylindrical holders are replaced by streamlined

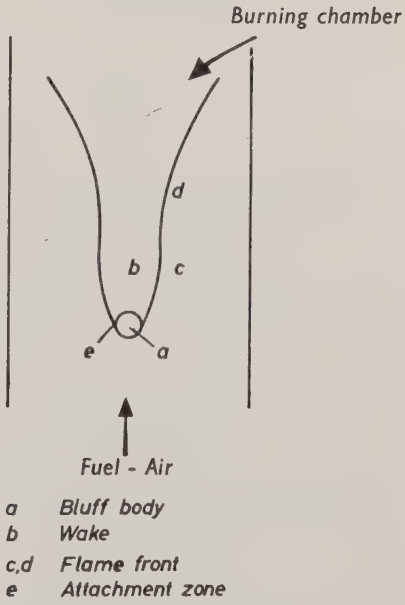

Figure 2. Flame and flame-holder in combustion chamber

shaped bodies which protrude into and fill the wake region to different extents. In other experiments local gas compositions in the immediate vicinity of the holder surface are modified from those existing because of normal contributions from the primary propane–air stream and from the re-circulating wake gas. These modifications are made by adding, in turn, small, controlled quantities of various pure combustible, oxidizer and inert gases through small holes from within hollow flame-holders in one of three directions, downstream, upstream and at the separation positions.

The particular experiments in turbulent flame blow-off here reported are an extension of previous work on blow-off stability in laminar flames[13]. In laminar flames blow-off characteristics were found to be affected markedly in a modified bunsen burner by the introduction of small continuous quantities of auxiliary gas into the immediate vicinity of the burner lip attachment zone. In this background study, auxiliary combustible

gases were found to raise the blow-off limit substantially for lean mixtures of the main pre-mixed gas stream; oxygen acted in a like manner for rich mixtures. Inert gases tended to depress blow-off limits. The rate of supply of auxiliary gas was insufficient to change measurably the adiabatic burning velocity as determined in the combustion wave distant from the burner lip. It was concluded that a stabilizing ignition zone in a laminar flame is resident in the region near the burner lip in which streams of pre-mixed combustible gases and convective streams of the gas surrounding the burner (air in most instances) join and mix. The resulting intermediate gas composition is characteristic only of the local zone and not of the adiabatic combustion wave farther distant. These results suggested that a similar local laminar boundary layer juncture zone be sought also in relation to blow-off stabilization of turbulent flames and that the relative roles of pre-mixed combustible gas stream and surrounding atmospheric gas of the bunsen burner may be analogous to combustible gas and re-circulating wake gas streams, respectively, in the case of turbulent flames.

Flame attachment and blow-off in high velocity pre-mixed gas streams have become classic areas of study and the literature is extensive. Recent summaries of the literature are given by John and Mayer[3] and by Childs[1]. References pertinent to the present work will be given in connection with the discussion of results.

EXPERIMENTAL

In this section experimental apparatus and procedures are described.

Apparatus

The combustion chamber (*Figure 1*) is the same as that used and described by John and Summerfield[1,3]. The chamber was provided with a gas mixing section, calming screens and a converging nozzle designed to give a flat velocity profile at the combustion chamber entrance. The flame-holder was positioned as shown in *Figure 1*. An auxiliary hydrogen pilot flame was introduced through a side port to ignite a flame at the holder position, the port being closed after this operation.

The majority of experiments were conducted with hollow, stainless steel cylindrical flame-holders, 5 mm in diameter. Three variants of the holders were prepared with rows of small holes drilled through the cylinder surface parallel to the axis to permit flow of small streams of auxiliary gas from within the holder into various regions surrounding the holder. Radius angle positioning of holes in the three holders is indicated in *Figure 3* for upstream, downstream and sidestream injection. In the last case, rows of holes are provided

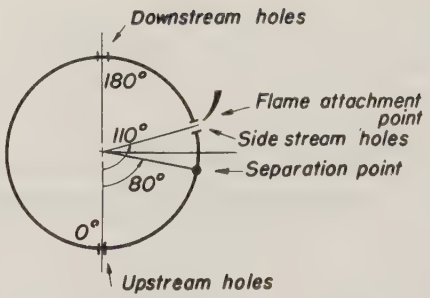

Figure 3. Radial angle positions of rows of auxiliary injection gas ports in three cylindrical flame-holders, providing for upstream, downstream and sidestream gas introduction

on both sides of the holder. The figure shows also relative positions of the free layer separation point and the location of the end of the luminous flame tip. The size and numbers of holes are as follows: upstream, 6 holes, 1·07 mm in diameter; sidestream, 6 holes in each row, 0·275 mm in diameter; downstream, 3 holes, 0·8 mm in diameter. Holes were uniformly spaced in the axial direction. However, because of the presence of a 1·68 mm diameter stainless steel lead-in tube at the upstream location, injection holes were drilled laterally on either side of the tube.

Certain experiments were performed with flame-holders having approximately streamlined shapes. Relative sizes of the three elongated holders are shown in *Figure 4*; all were 5 mm in projected diameter, this dimension being common between the cylindrical holders and the present set. Holder I was provided with sidestream holes for auxiliary gas introduction with radius angle placement the same as in the corresponding cylindrical holder. Some blow-off experiments were performed prior to drilling these parts to determine whether the surface roughness caused by the presence of the holes might affect blow-off properties (it did not). Holders II and III were fitted with a means for internal water cooling but none for auxiliary gas introduction.

The primary, pre-mixed gas stream consisted of propane–air mixtures of various compositions. Propane was of commercial purity, about 95 per cent propane and 5 per cent other hydrocarbons. Propane flow was measured with a calibrated standard orifice and air flow, with a Koerting Rotameter. Normal corrections for pressure and temperature were performed in determining flow rates of the individual gas streams, and through these, the mixture composition.

Small streams of auxiliary gas were introduced into the flame-holder directly from gas cylinders after being measured with a calibrated capillary flow meter or a small Rotameter. Purities and sources of the auxiliary gases were as follows:

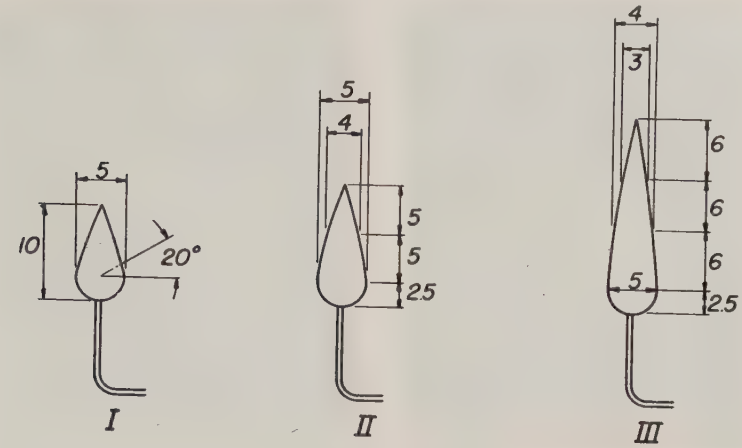

Figure 4. Flame-holders with approximately streamlined shapes. Holder I in two variants had smooth surfaces in one and drilled auxiliary gas port holes in the other. Holders II and III were provided with internal water cooling

Gas	*Purity*	*Source*	
N_2	99·9%	American Oxygen Co.,	water pumped
O_2	99·5%	ditto	electrolytic
He	99·9%	ditto	
H_2	99·8%	ditto	electrolytic
CH_4	99·0%	The Matheson Co., Inc.	c.p.
C_3H_8	99·6%	ditto	instrument grade
C_4H_{10}	99·6%	ditto	,, ,,
CO	99·6%	ditto	,, ,,

Schlieren photographs as well as normal pictures of the region of the flame-holder were taken. The schlieren assembly consisted of a tungsten arc light source, a small aperture, a lens, two parabolic mirrors, a razor knife edge and a Speed Graphic Camera with ground glass viewer.

Analyses of the CO content of the wake were performed quantitatively with a Perkin-Elmer Infra-red Analyser, using the rotational banks of CO in the vicinity of 4·67μ. Gas samples were taken in evacuated bulbs and were dried with calcium chloride.

Procedure

An initial step towards determining a blow-off velocity was to establish an equilibrium propane–air flame at a pre-determined total gas flow rate and with a composition close to the stoichiometric. A hydrogen pilot light initiated the combustion at the flame-holder. After one or two minutes of operation, to achieve thermal equilibrium at the flame-holder, the propane flow rate was increased or decreased, until blow-off occurred, air rate remaining constant. Through this procedure, gas composition and total gas flow rate are varied simultaneously. Use of the opposite procedure, namely, varying air flow rate at constant propane rate gave equivalent blow-off results. When auxiliary gases were introduced, constancy in flow rate of these gases was maintained by successive adjustments to allow for pressure changes near the holder as main gas stream flow changes were made.

Blow-off limits ordinarily were abrupt and clearly defined. Some uncertainty in definition of blow-off limits occurred, however, in the case of lean propane–air mixtures when auxiliary fuel was introduced locally, and also for rich propane–air mixtures when auxiliary oxygen was introduced. In either condition for low blow-off velocities, small residual flames tended to remain in the wake region after the main flame lobes had become extinguished. In all cases, the gas velocity required for extinction of the main flame was taken as the blow-off velocity. On various blow-off velocity-gas composition curves the approximate velocity beyond which the residual flame is not stable is marked R.F.O. (residual flame out).

Standard experiments of blow-off velocity *versus* propane composition, expressed as fraction of stoichiometric, were determined at intervals over the period of one year, as shown in a composite curve in *Figure 5*. The random variations of data points about the mean curve represent contributions due to the use of a succession of propane cylinders and also due to normal measurement errors in gas flow and composition. In preparing the standard curve it was necessary to close the inlet tube, intended ultimately for supplying auxiliary gases. Particularly in the case of the flame-holder with downstream injection ports, the higher-than-ambient pressure in the wake caused a backflow of wake gases into the holder, with subsequent overheating, unless the entry tube was closed.

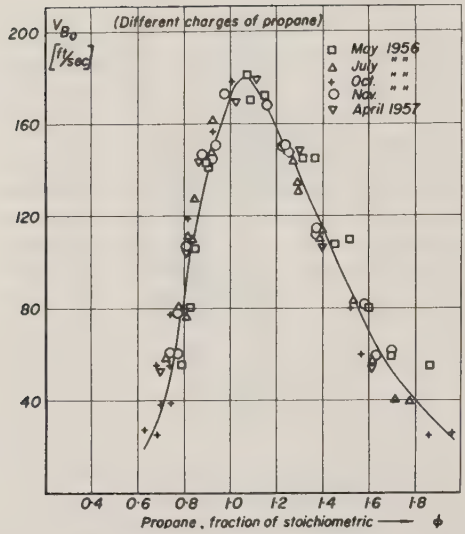

Figure 5. Standard propane–air blow-off curve, blow-off velocity versus *propane composition expressed as fraction of stoichiometric. Data were taken at intervals over a period of one year and with different supplies of propane*

RESULTS

Experimental results fall into two categories: geometric, relating to the location of the flame anchoring and stabilization region, and chemical, relating to effect of local gas compositional changes in that region on the gross stability limit as measured by flame blow-off.

Geometric results

The region near the free-layer separation point and the wake region immediately downstream of this point was studied photographically by means of schlieren and direct image photography. Geometric considerations also appear in blow-off measurements as these are affected by the shape of the holder, progressing from the cylindrical to shapes I, II and III, as illustrated in *Figure 4*.

For ready photography a solid cylindrical holder 12·5 mm in diameter was used, rather than the normal 5 mm size. By sighting on the end of the holder the thermal free layer is rendered visible in a schlieren photograph while a steady flame is anchored to the holder. The density gradient to which schlieren photography is sensitive arises through the heating of pre-mixed gas in a boundary layer contact with the flame-heated holder prior to separation. *Figure 6a* shows such a layer at a Reynolds number of 4×10^3. The thermal free layer was found to persist as much as one minute after flame extinction because sensible heat in the holder continued to be transferred to the upstream boundary layer. A schlieren photograph taken 10 seconds after flame extinction is shown in *Figure 6b*, all other conditions being the same as in *6a*. The location of the thermal free boundary layer is seen to be substantially the same, whether or not the flame is present. The approximate separation point of 80° is consistent with past studies[11]. *Figures 6c* and *6d* present schlieren and direct photographs of a flame for a Reynolds number of 16×10^3. The luminous flame is observed to lie directly adjacent to the wake side of the thermal boundary layer and to lean inwards, away from the thermal layer in the immediate vicinity of the holder. These effects are shown in *Figure 6e* in which corresponding flame schlieren and direct photographs are superimposed. The final photograph in *Figure 6* shows the development of a density-gradient free layer through the introduction of butane into the wake of a cylindrical holder at N_{Re} of 4×10^3, in the absence of flame, the main stream being air. The circulation path in the wake carries the butane from the point of introduction high in the wake (the tube tip shows in the photograph) well into the fillet formed by the free layer with the surface of the holder, but not completely back to the point of separation.

The use of streamlined flame-holders which protrude into the wake region was intended as an inquiry regarding the effect on blow-off limits as the re-circulating gas flow pattern in the wake is modified by the introduction of these geometric obstacles. It was found that Holder I (see *Figure 4*) with a length-to-diameter ratio of 2 and straight sides, gave a closely similar blow-off curve to that for the standard cylinder of equal diameter. These results are shown in *Figure 7*. It was found that the addition of auxiliary gases from side ports also gave quantitatively similar effects between these two holders. Thus Holder I and cylindrical holders are concluded to have similar flame stabilization properties. Holder II, with a length-to-diameter ratio of 2·5 and rounded sides, on the other hand, was shown to decrease flame stability substantially, as shown in *Figure 7*. These results are for an uncooled device. Furthermore the flame did not appear to maintain a steady base, but it oscillated on the surface of the final, i.e. trailing third of the holder length, leading to the appearance of a brushy flame. When Holder II was water-cooled, it was not possible to stabilize a flame on it, as was also the case, under all circumstances, for Holder III, which had a length-to-diameter ratio of 4·05 and rounded sides.

Effect of auxiliary gas addition on stability limits

In *Figures 8–15* effects on the characteristic blow-off curve are given as the result of introducing small flows at different radial holder positions of inert, of oxidizing and of combustible

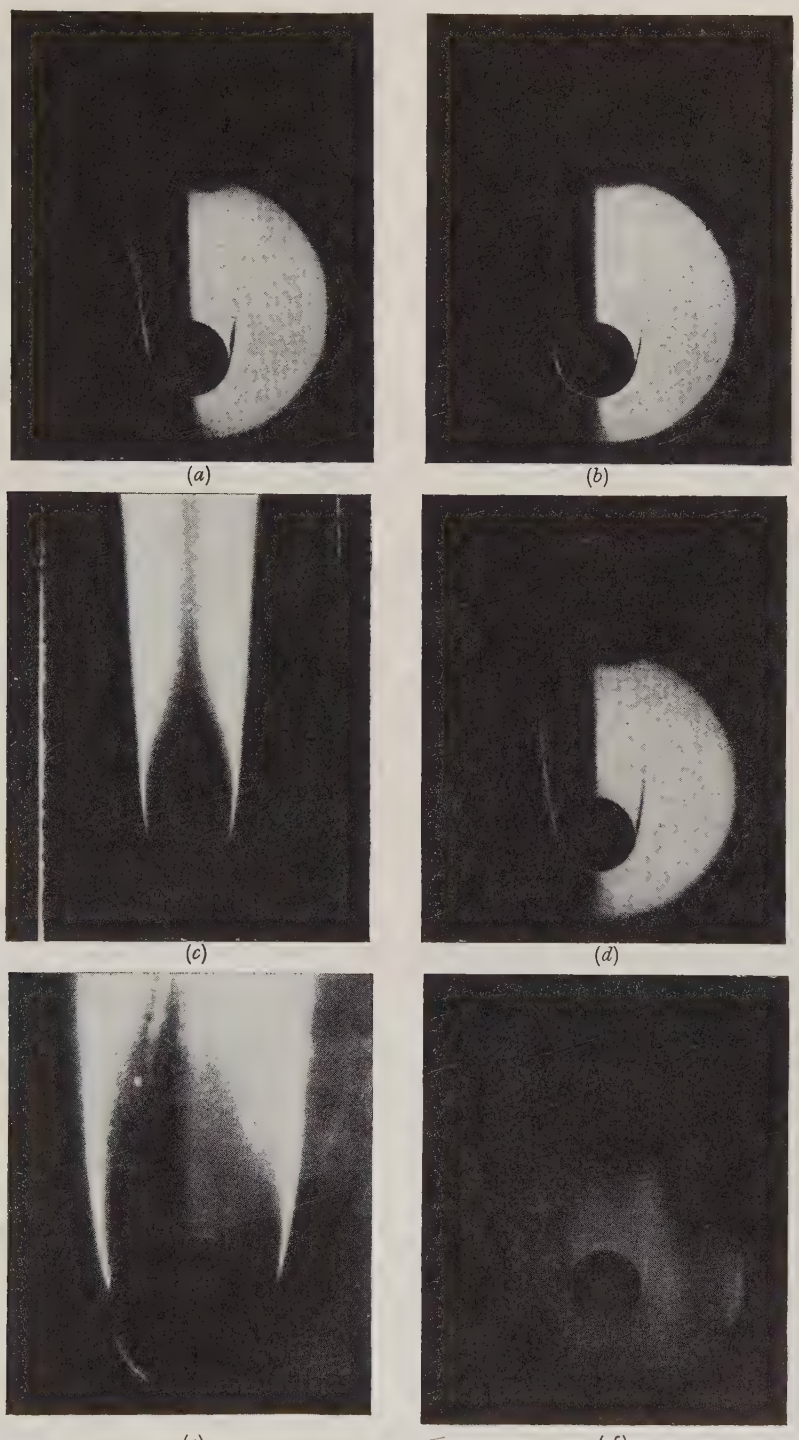

Figure 6. Schlieren and direct photographs of 12·5 mm *cylindrical flame-holder. (a) Schlieren photograph showing thermal free layer with flame in position* $N_{Re} = 4 \times 10^3$. *(b) Schlieren photograph showing thermal free layer 10 seconds after flame extinction. (c) Direct flame photograph* $N_{Re} = 16 \times 10^3$. *(d) Schlieren photograph showing thermal free layer with flame in position,* $N_{Re} = 16 \times 10^3$. *(e) Superimposed schlieren and direct photographs. (f) Schlieren photograph showing free layer through introduction of butane into wake of holder in absence of flame,* $N_{Re} = 4 \times 10^3$

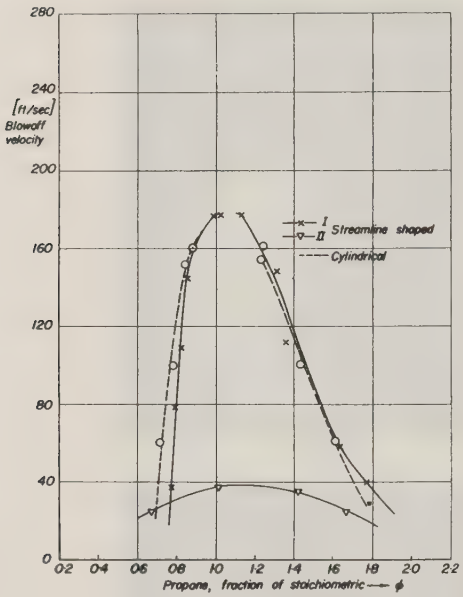

Figure 7. Comparison of blow-off limits of streamlined flame-holders compared to standard cylindrical holders. Holder geometrics are recorded in Figure 4

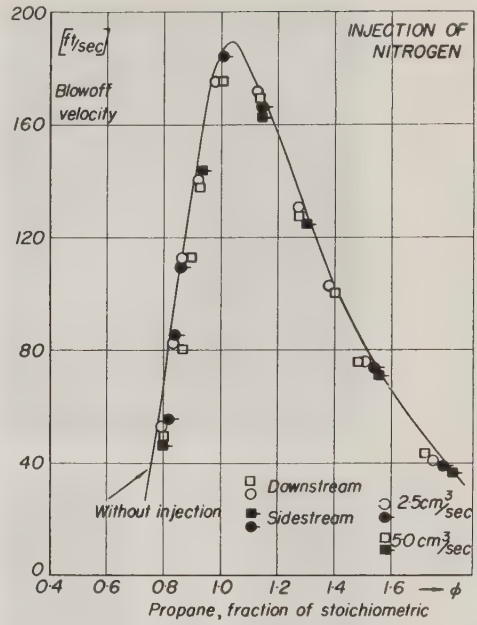

Figure 8. Blow-off velocity versus *propane equivalence ratio. Parameters are nitrogen injection position on flame-holder and rate*

gases. The reference blow-off curve in each figure presents a base for judgment, it having been determined in the absence of auxiliary gas injection and with the same propane supply as the remainder of the data in that plot. Curves representing different constant auxiliary gas rates were secured by interpolation of data relating gas injection rate, equivalence ratio and blow-off velocities. During measurements, the rates of auxiliary gas were between 1·5 and 6·5 cm³/sec for all gases except H_2 and He, for which the rates were between 2 and 18 cm³/sec.

It is observed that the addition of inert gases, N_2 and He (*Figures 8 and 9*) decreases the blow-off velocity only slightly with an approximately uniform decrease at all equivalence ratios. Aside from dilution, inert gases seem to play a small role in the attachment-stabilization process. The addition, on the other hand, of O_2, H_2, CH_4, C_3H_8, C_4H_{10} and CO had certain similar effects which occur to varying extents. The entire blow-off curve is shifted with a change in the maximum towards a richer main-gas composition in the case of O_2 addition, and towards leaner compositions in the case of all combustible gas additions. For all auxiliary gases the maximum of the blow-off curves is increased to larger values by auxiliary gas addition. In all cases, also, the addition of auxiliary gases in larger rates led to larger effects on blow-off limits. The positive effects on blow-off of introducing auxiliary gases in upstream or sidestream positions were closely similar in magnitude. However, the addition of auxiliary gas from the holder in a downstream direction, into the wake, led to greater increases in blow-off limits than did additions either in the upstream or sidestream directions.

Very substantial increases in blow-off limits were achieved on the addition of auxiliary oxygen, at 2·5 and 5·0 cm³/sec rates, especially into the wake region. It is noted that the lean lobe of the normal blow-off curve is but little affected by oxygen addition whereas the rich lobe blow-off limits are increased for all modes of addition. The composition of CO in the wake during normal combustion of rich propane–air mixtures was

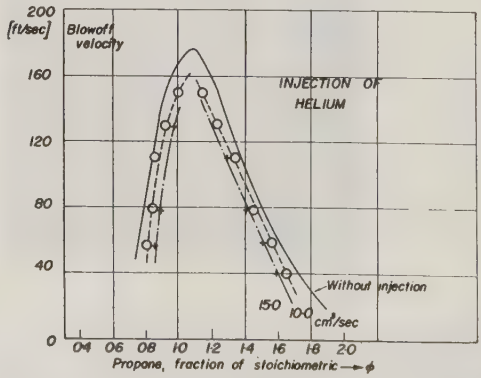

Figure 9. Blow-off velocity versus *propane equivalence ratio. Parameter is local injection rate of helium*

measured by means of infra-red analysis and is recorded on a water-free basis in *Figure 16*. Thus surplus fuel is available for combustion in the wake by means of the auxiliary oxygen. At lower free stream velocities and in the case of oxygen introduction into the wake small flame cups could be observed within the wake attached at the three points of oxygen introduction. These small flames were present especially for stoichiometric and richer free stream compositions, but they persisted, more weakly, for a small equivalence interval into the lean side of the gross propane–air combustion. High main stream velocities caused the separated cups to join in forming a single flame front within the wake. It seems evident that one contribution of auxiliary oxygen addition is to increase the temperature of the wake by means of the auxiliary flame within the wake, thereby affecting ultimately the blow-off limits of the main flame.

In regard to the introduction of auxiliary hydrogen on blow-off, it is observed that this gas is particularly effective in increasing the blow-off limit and that major increase occurs in lean propane–air main stream mixtures. In connection with downstream addition experiments, it should be recalled that lean flames commonly contain oxygen in the wake. The addition of hydrogen (or other combustible) to the wake thus serves to increase the value of the wake gas as a low-grade pre-mixed fuel which may release heat

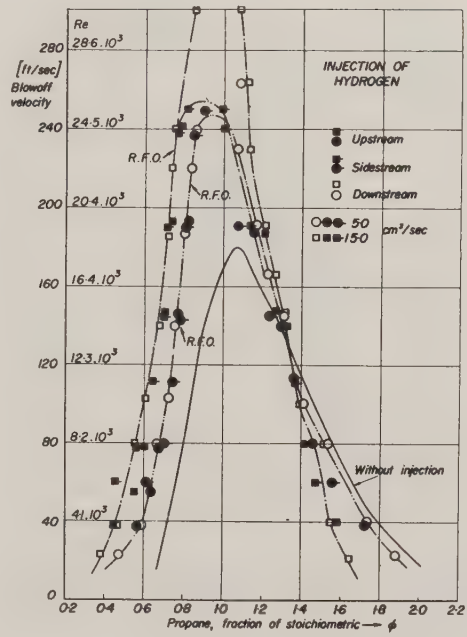

Figure 11. Blow-off velocity versus *propane equivalence ratio. Parameters are hydrogen injection position on flame-holder and rate*

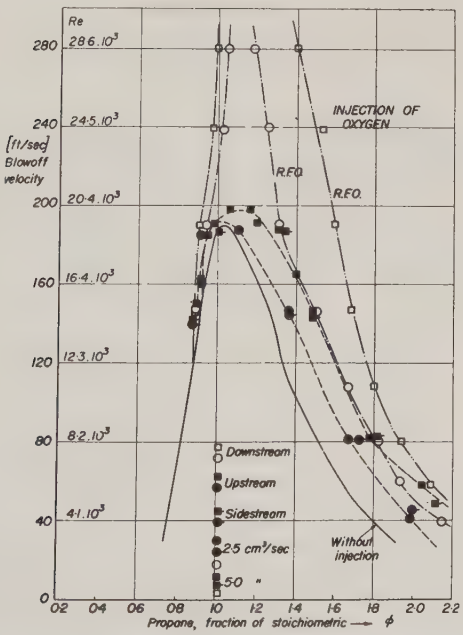

Figure 10. Blow-off velocity versus *propane equivalence ratio. Parameters are oxygen injection position on flame-holder and rate*

energy in an ignition-stabilization zone of the primary flame.

The shifted blow-off curves resulting from addition of methane, propane and butane are noted, respectively, in *Figures 10*, *11* and *12*. All follow the pattern of a shift of maximum to lean values of the main stream propane composition as well as an increase in the maximum. Equal volume rates of auxiliary gas additions are compared. The smallest effect on extending blow-off velocity is that of methane, next is butane and highest effect is due to propane. This order corresponds to the order of adiabatic flame temperatures for these auxiliary gases when burned individually in air.

The introduction of CO into the holder vicinity led to positive changes, characteristic of active chemical species, but the extent of change was small.

Although the number depends upon the dimensions of the burner duct and it is not basic, it is of interest to estimate the amount of auxiliary gas employed compared to the propane flow in the combustion chamber. Considering propane as the auxiliary gas as well as the free-stream gas, at maximum blow-off conditions of 280 ft./sec and $\phi = 0{\cdot}8$, a propane injection rate of 2·5 cm³/sec corresponds to 1/1,000 of the main stream propane flow rate.

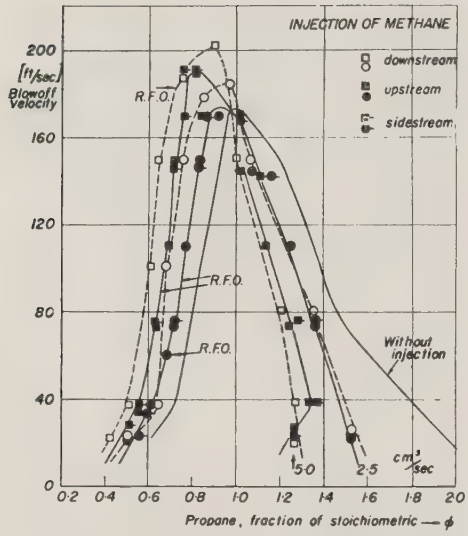

Figure 12. Blow-off velocity versus *propane equivalence ratio. Parameters are methane injection position on flame-holder and rate*

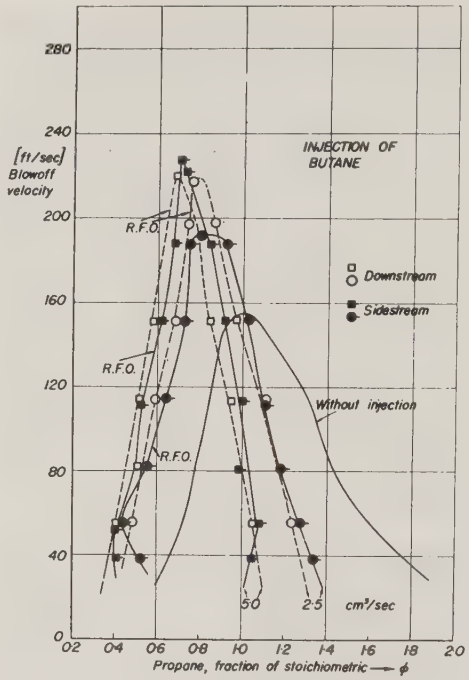

Figure 14. Blow-off velocity versus *propane equivalence ratio. Parameters are butane injection position on flame-holder and rate*

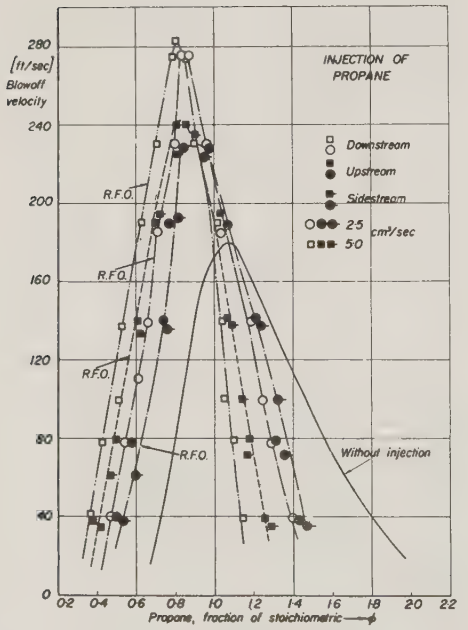

Figure 13. Blow-off velocity versus *propane equivalence ratio. Parameters are auxiliary propane injection position on flame-holder and rate*

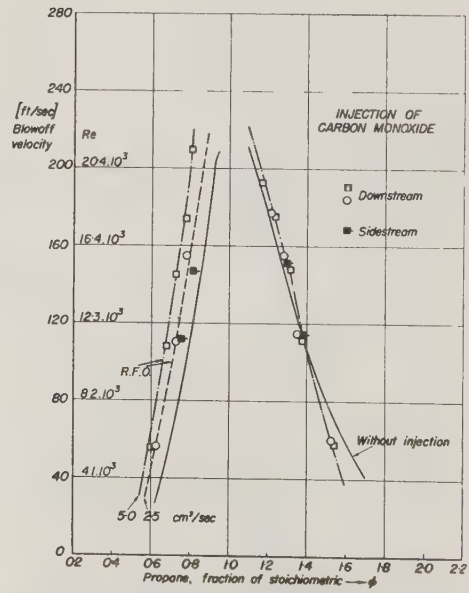

Figure 15. Blow-off velocity versus *propane equivalence ratio. Parameters are carbon monoxide injection position on flame-holder and rate*

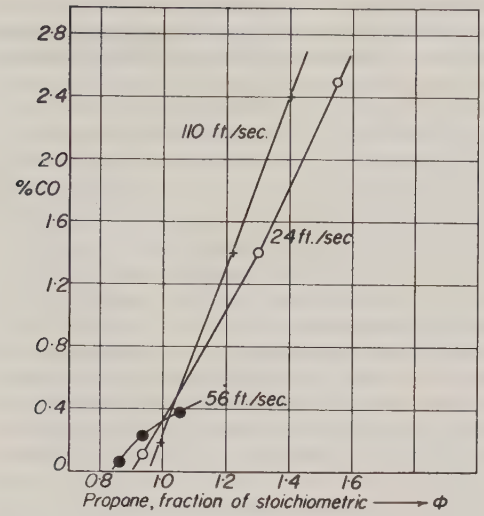

Figure 16. Composition of wake during combustion of pre-mixed propane air. Per cent CO (H_2O-free) versus *propane equivalence ratio*

DISCUSSION

A representation of the visual flame location near the holder in *Figure 17*, together with *Figure 2* and photographs in *Figure 6*, provide a basis for discussing present results.

Two streams of gas flow around the holder and converge in the region of flame attachment. One of these is the pre-mixed gas, which, starting at the forward stagnation point forms a boundary layer that separates from the cylinder at about 80° to form a free layer. The steep velocity gradients in such a layer for the same Reynolds number range (N_{Re} between 10^3 and 10^4) have been detailed by Schiller and Linke[11]. The other stream is the well-known re-circulation eddy system in the wake which causes a local flow near the surface from the downstream stagnation point back towards the separation point, finally changing direction, tending to become parallel to the free layer. The flame is observed to be attached closely to the inner, wake side of the free boundary layer (*Figure 6*). However, the flame attachment tip is noted to lean in towards the holder and away from the free layer, an elongated triangle being formed between the flame, the free layer and the holder surface. As has been photographed by Prandtl[9] and others, the region of discontinuity for a cylinder lying between the stagnation-separation point and the region of gross re-circulation pattern is populated by small eddies which have shed from the free layer directly after separation. Transport within this triangle region of eddying motion presumably is substantially larger than for molecular processes, thereby providing a rapid diffusive means for transporting heat and reactants from the free layer of pre-mixed gases to the flame tip and ignition region. The location of the flame is suggested to be at an interface between gross flow patterns of hot re-circulating wake gas on the one side and a region of fine grained eddy patterns on the other. The flame stabilization region thus is linked spacially to the stagnation-separation point on the holder surface through the zone of discontinuity. *In effect, this model represents the flame as lying along a highly porous septum through which reactants diffuse and along which a hot gas flows.*

Stabilization of the flame is considered to reside in a small volume-element that lies on an extension of the flame in the direction of the holder surface, well beyond the visible tip. The properties of the fluid in the elementary volume are fixed in space in relation to the holder position by the hydrodynamic situation described above. The volume element is supplied with reactants and heat through various flow and transport processes. A heat production rate by reaction is maintained continuously such that a finite positive temperature gradient will exist at the element, the size of which increases continuously with position along a trace between the ignition volume-element and the luminous flame tip. This is suggested to be ignition in a flow system.

It will be of interest now to trace various transport paths in *Figure 17* by which the ignition zone and the adjacent flame tip are likely to be supplied

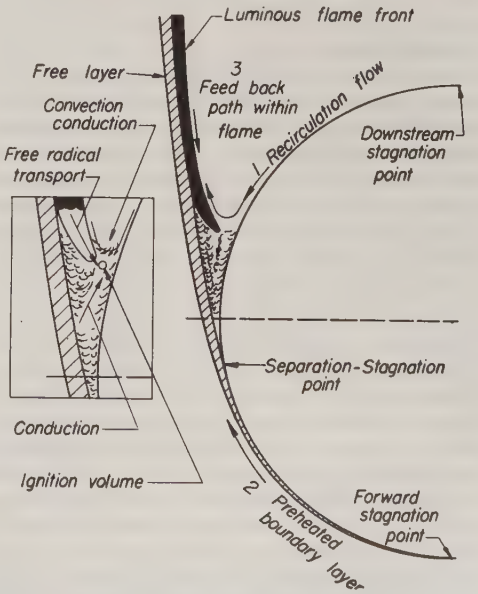

Figure 17. Diagrammatic representation of the flame attachment zone showing various flow and heat and mass transport paths

with reactants and heat. There are suggested to be three such paths, the re-circulation flow of wake gases, the boundary layer formed by the approaching pre-mixed gases at the holder surface together with its extension as a free layer and finally a feedback path from the flame proper to the zone of ignition.

Part of the burnt gases from the flame circulate in the wake and in so doing provide heat by conduction-convection to the ignition zone from the circulating stream. According to Zukoski and Marble[15] the measured temperature in the wake is quite uniform throughout the wake and it does not change appreciably as the blow-off limit is approached. At the same time the wake stream tends to dilute the composition of the reactant gases in the critical ignition volume with inert combustion gases, the resultant steady-state composition at that location being different than that of the pre-mixed main-stream gas to which blow-off velocity commonly is related empirically. As dictated by the detailed processes of mixing and burning in the turbulent flame, at a distance from the holder, there may be small quantities of excess oxygen or combustible in the wake when main-stream compositions are lean or rich, respectively. Such reactant components in the wake contribute to reaction and heat release rates in the critical ignition volume. Also, the hot circulating vortex, in flowing over the exposed surface of the holder transfers heat to it. This heat is conducted by the holder to the upstream surface where it serves to heat a layer of pre-mixed gas that is in process of forming a boundary layer as it flows over an 80° arc from the forward stagnation point to the point of separation. A thermal boundary layer is formed as a result, which, separating with the velocity boundary layer, forms an associated combination of free heat and velocity layers. *Figure 6a* and *b* shows a schlieren photograph of the density gradient in the thermal free layer and it gives evidence that the position of the layer, starting at the separation point, is not different in the presence or absence of the flame. A slight thickening of the schlieren image during combustion is noted, however, in the vicinity of the luminous flame tip. The broadened density or temperature gradient is suggested to be the result of a local thermally induced enhancement of mixing and heat transport rate in the triangular, fine-vortex mixing zone. As discussed above, this transition zone is presumed to be a high conductivity region by means of which combustible reactants at the inner temperature of the boundary layer are curled off that layer and transferred to the part of the flame axis lying between the ignition point and the luminous flame tip.

In considering the third path, the feedback flux of energy along the flame axis in the direction towards the holder, progressing from the luminous zone, through the flame tip to the ignition volume-element, a number of possible energy carriers may be contemplated, such as radiant energy, electrons, protons, free radicals and atoms and charged radicals. Electrons and protons are present in extremely small concentrations, radicals have relatively low mobility and radical-radical collisions as chain breakers tend to limit chain lengths. These entities therefore are not considered of likely importance in the process. The absorption of radiant energy is a slight possibility, but strongest immediate experimental evidence concerns a likely re-combination of hydrogen atoms which have high mobility and which, in comparison with other radicals, can travel relatively far before a third body collision permits release of energy by re-combination. H — H re-combination releases 103 kcal/mol. Hydrogen atoms also initiate combustion chains in a pre-mixed gas at non-flame temperatures, releasing heat. Hydrogen atom diffusion and re-combination has been considered one of the component mechanisms in determining the velocity with which a flame progresses into unburned gas; it is here suggested also as a mechanism by which heat is introduced into the ignition volume-element and so effecting blow-off stability. Support for this view comes from a study of Lapidus, Rosen and Wilhelm[6] who found experimentally that the rate of flame ignition and travel from one end to another of a slot burner changed measurably and reproducibly as the catalytic nature of the burner lip was varied. On the assumption that the different rates of flame propagation were due to a change in free radical concentration at the flame front because of re-combination at the surface a theoretical model was proposed which led to quantitative values of surface re-combination coefficients relative to platinum surfaces. For dry surface the relative coefficients were these: platinum, 10^{-1}; brass, 10^{-3}; magnesium oxide, 10^{-4}. When humidified, all surfaces gave re-combination coefficients smaller than 10^{-4}. Thus, if radicals can reach the surface of a flame-holder, as is indicated above, then such radicals will certainly reach the ignition volume-element which lies between the surface and the luminous flame, i.e. the source.

The simultaneous diffusion of radicals and heat from the flame attachment tip to the ignition zone may be regarded as contributory to blow-off stability as the same phenomena in a direction lateral to the surface commonly is considered to be contributory to flame propagation.

The various experimental results are now discussed in terms of the model of flame attachment presented above. Broadly speaking, blow-off is considered to occur when the equations of

change for the ignition volume-element representing all physical and chemical processes of reaction, diffusion and flow become unstable to perturbations in temperature, flow rate or composition as the mean velocity is increased.

Stabilization appears to be associated in its positioning with a stagnation point resulting from the counterflow of the combustible gas and a second, stabilizing gas stream. The latter commonly is induced by the flame itself, as in the vortex motions of bluff body stabilizers. In a bunsen burner also a stabilizing flow of air, induced by the rising combustion gases, meets the combustible gas at the burner lip at a stagnation point where stabilization takes place. Schaffer and Cambel[12] showed that stabilization can occur using an opposing, stabilizing jet. At a cylindrical holder such as was studied here, the actual stabilization point is some distance removed from the stagnation point in question, which is the separation point. When streamlined holders, such as I, II, III are used the re-circulation flow is slowed with increasing length of holder. The size of the transition triangle increases and the flame tends to stabilize farther away from the separation point, calling for a diffusion of reactants over longer distances from the free layer to the stabilization point. Eventually, a completely unstable situation ensues when heat and mass balances can no longer be maintained. This occurred between the geometric configurations represented by Holders II and III.

That the path for heat supply from the wake vortex stream to the ignition volume is important is shown experimentally, first by the fact that Holder body II when cooled with water did not stabilize a flame, whereas it did so, although to low degree, when no coolant was provided and the holder became heated. A small difference in the heat balance at the ignition volume-element spelled the difference in behaviour. A second item of evidence is given in *Figure 10* on the effect of auxiliary oxygen in greatly increasing stability limits. Since the oxygen burned with carbon monoxide in the wake in a small, auxiliary flame, the temperature of the wake was raised directly thereby favouring the heat balance at the ignition point.

The addition of chemically active gases shifted the position of the blow-off curve on the propane–air main stream gas composition. It is suggested that the auxiliary gases simply served to modify the composition for reaction at the ignition point which normally consists of some proportion of main stream and wake gases. In principle, blow-off velocities should be related to the ignition volume-element composition, were it accessible, rather than main stream composition. The important compositional contribution that the stabilizing gas has to the blow-off process is illustrated also[7,13] in laminar combustion blow-off when conducted in a surrounding (stabilizing gas) atmosphere of air, compared to an inert atmosphere.

The differences in blow-off curves when auxiliary gases were introduced into the wake, compared to introduction through upstream or sidestream ports, are consistent with the model portrayed above. Visual observation and photographs showed the flame tip in the vicinity of the holder surface to lean away from the free layer and towards the re-circulation zone. Thus gases introduced into the wake are within a short diffusion-flow path of the stabilization volume-element. Those gases, on the other hand, that are introduced exterior to the wake must traverse by diffusive means through the triangular region of discontinuity. The latter path evidently has a higher transport resistance than does the former.

That the nature of the chemical species of auxiliary gas may be important in the blow-out process is suggested by the differing values of blow-off maxima achieved with different gases. The large effect of hydrogen gas, with its high burning velocity and heat of combustion, is evident in this regard and the relative ordering of blow-off with the hydrocarbon additive, methane, butane and propane, in accordance with flame temperatures, is indicative of ordered contributions to the heat balance in the critical region.

In the present experimental paper it is not proposed to review theories of blow-off, which has been done recently[1,3], but only to comment briefly on these in relation to the discussion above. Because of the manifest difficulty of including all pertinent chemical kinetic, heat and mass transport and fluid mechanical terms in a mathematical analysis, selections of terms have been made by various authors, for example, by placing emphasis on fluid mechanical aspects, on heat transfer aspects or on chemical rate aspects, or on certain combinations as being critical in determining stabilization and blow-off criteria. In one mode of approach, chemical kinetics is embodied in flame velocity, in another, fluid mechanics are simplified by assuming complete stirring. Some of the problems encountered in determining whether a system may or may not be stable in relation to the selection or rejection of terms in the equations of change are illustrated in recent papers on stability limits of a laminar combustion wave[14,10].

A recent direct approach in stabilization analysis is that of Cheng and Kovitz[4,5] in an adjacent paper. This paper is a generalization of that by Marble and Adamson[8]. A simple geometry is adopted, that of a cold combustible gas joining with a hot inert gas beyond a separating plane.

In a boundary layer approximation for the full set of equations of change, simple chemistry as well as mass and heat fluxes are introduced in detail. There is no *a priori* selection of classes of terms to be included in the formulation. Solution leads to the definition of a characteristic length x_i, a distance beyond the point of stream confluence, at which a temperature bulge in the lateral profile begins to appear. The bulge results from the increasing importance of reaction heat release compared to heat removal processes. The distance, which is estimated to be very small, corresponds to the ignition volume-element in the present discussion. Details of heat transfer by vortex re-circulation at a gutter-type holder are included in the model and blow-off criteria are given in terms of kinetic and heat balance equations. Present experiments suggest that a somewhat modified model (see page 629) may be more appropriate for the ignition region of the attachment zone than the parallel boundary layer model of Cheng and Kovitz.

This research was supported by the United States Air Force through the Air Force Office of Scientific Research of the Air Research and Development Command under Contract AF33(038)-23976.

The authors wish to acknowledge the contribution of Professor Martin Summerfield in making available the combustion chamber in his laboratory. Our thanks go as well to Dr. Richard John who, having used the equipment previously, offered material assistance in the early stages of the present work. Stimulating discussions with Professors Sin-I Cheng and Martin Summerfield were most helpful.

REFERENCES

[1] Childs, J. H. *High Speed Aerodynamics and Jet Propulsion*, XI. Section E. Princeton University Press (scheduled, 1958)

[2] Fage. *Phil. Mag.* 7 (1929) 253

[3] John, R. R. and Mayer, E. *ARDE Associates Tech. Note 4555–5, ASTIA No. 126526* (1957)

[4] Kovitz, A. and Cheng, S. I. This volume, paper 93

[5] Kovitz, A. *Aero. Eng. Report 335–d*, Princeton University

[6] Lapidus, L. L., Rosen, J. B. and Wilhelm, R. H. *Industr. Engng Chem.* (*Industr.*) 49 (1957) 1181

[7] Lewis, B. and Von Elbe. *Combustion, Flames and Explosions.* 1951. New York; Academic Press

[8] Marble, F. E. and Adamson, T. C. *Jet Propulsion* 24 (1954) 85

[9] Prandtl and Tietjens. *Hydro- and Aeromechanics*, 1934. New York; McGraw-Hill

[10] Rosen, J. B. *J. chem. Phys.* 22 (1954) 750

[11] Schiller, L. and Linke, W. *Z. Flugtech.* 24 (1933) 193

[12] Schaffer, A. and Cambel, A. B. *Jet Propulsion* 25 (1955) 284

[13] Thomas, A. L. and Wilhelm, R. H. *Sixth Symposium* (*International*) *on Combustion*, p. 111. 1956. New York; Reinhold

[14] Wehner, F. and Rosen, J. B. *Combustion and Flame* 1 (1957) 339

[15] Zukoski, E. E. and Marble, F. E. *Proc. Gas Dynamics Symposium*, p. 205. 1956. Northwestern University

DISCUSSION

G. C. Williams (Massachusetts): To the engineer one notable deficiency in this session is the complete lack of material on turbulent diffusion flows in spite of their practical importance. It is gratifying, however, to note that there is no evidence of the earlier disagreement as to whether or not turbulent systems could give rise to combustion performance in which apparent flame speed need not necessarily bear any relationship to laminar or flame velocity. Spalding's ingenious treatment of enclosed stabilized flame and Khramtsov's experiments on grid-stabilized flame both show this independence. It is interesting to note that the Khramtsov data showing turbulent flame velocity proportional to $P^{0.4}$ and apparent flame thickness proportional to $P^{-0.4}$ may be treated to produce a loading factor similar to that for the well-stirred reactor, the feed rate per unit of turbulent flame area being expressed as PU and the flame volume per unit of flame area being δ_t so that the loading factor is $PU/\delta_t \approx PP^{0.4}/P^{-0.4} = P^{1.8}$, an apparent order of reaction generally associated with stirred reactors.

Khramtsov's measurements of cold turbulent diffusion as a function of pressure show increasing values of eddy diffusivity with increase in pressure at constant velocity. Since the turbulence scale presumably remains fixed, it seems clear that turbulence intensity must increase with pressure level (possibly a Mach No. effect), an observation which appears to be in accord with some M.I.T. studies on turbulent jet mixing.

The paper by Fetting, Choudhurry and Wilhelm presents some excellent information on flow near the stabilizer. The large effect of injection of small amounts of fuel and oxidizer near the stabilizer seems at first remarkable, until it is recalled that molecular diffusion can also give rise to similar effects, resulting in a relatively large change in the oxidant-fuel ratio in the re-circulation zone. Since it seems reasonable that the molecular diffusion process occurs over the entire length of laminar wake, and thus affects the composition of the entire re-circulation zone, it does not appear clear that the present experiments offer support for the stabilization theory of Cheng and Kovitz.

The papers of Prudnikov and Shetinkov offer experimental and theoretical treatments of turbulent flames complementary to the papers of Spalding and Karlovitz, respectively.

It is to be noted that substantially all theoretical papers on turbulent flames based on a treatment of the data as a turbulent diffusion process use a mathematical analysis based on isotropic turbulence of fixed scale and intensity. Although values of these parameters so determined have engineering utility, the reader is cautioned against assuming validity of the separate values of U' and l_2.

Richmond, Grumer and Burgess rightly point out that their measurements of turbulent wake flames may have little practical utility. Their ingenious technique of measurement may, however, be useful in other applications.

A. A. Westenberg (Maryland): Regarding the paper of Prudnikov, it is certainly true that, if we are ever to solve the problems of turbulent combustion, one of the first requirements will be the ability to measure accurately the statistical properties of the turbulent flow in the combustion zone. For this reason I was very glad to see this work which, as far as I know, represents only the second set of such data ever reported. Some years ago I reported on some flame zone turbulence measurements performed by the method of helium diffusion from a point source, while this paper by Prudnikov contains results obtained by a similar technique using a sodium tracer with optical detection. I have three specific comments to make on his paper: (1) The author makes comparisons of flame and cold flow turbulence by way of values for the *relative* intensity $(u^2)^{\frac{1}{2}}/V$. I think this basis is apt to be misleading since, due to the acceleration of the mean flow velocity in flame zones, the relative intensity will change even though nothing happens to the fluctuating velocity component. (2) I hope the author has been very careful in correcting his results for molecular diffusion, as the latter contribution he shows for his sodium tracer seems quite low. Molecular diffusion can be very appreciable in many turbulent flames. (3) I would be very interested to know whether or not the author made a comparison of his smoke-tracer technique in cold flow with results of a standard technique such as hot-wise anemometry. We were not in a position to do this in the helium diffusion work, and it is an important type of verification of these diffusion methods which really should be attempted.

E. E. Zukoski (Pasadena): Spalding has made an interesting attempt to extend the work of Scurlock, Tsien, etc., on flame spreading by postulating that the entrainment of gas in the flame front is similar to the entrainment of gas in a turbulent jet.

In comparing his theory with experiment, Spalding concludes that data which show little

variation of flame width with fuel–air ratio are in agreement with the theory. However, this is clearly not the case. Consider results of theory presented in *Figure 8*. As fuel–air ratio is varied, the density ratio, λ, also changes; hence the illustration demonstrates that the flame width should also change rapidly with fuel–air ratio. To illustrate the degree of disagreement between theory and measurement, consider the data of Scurlock, *cf. Figure 2*, for 220 ft./sec velocity. The reduction in wake width due to a change of fuel–air ratio from stoichiometric value, $\lambda \approx 6$, to a value about half of stoichiometric, $\lambda \approx 4$, is less than 20 per cent. However, *Figure 8* indicates that a change of the order of 100 per cent can be expected in wake width for a similar variation of λ. Therefore it must be concluded that the theory is in strong disagreement with the experimental data at present available and that some new approach must be made to properly account for the lack of dependence of flame width on the density ratio.

I would also like to suggest that a more realistic model of flame spreading would take into account several additional features of the flow: First, the combustion front, in a turbulent flame, stabilized by a bluff body, is not a thin region but rather is a thick turbulent flame burning in a shear layer. The thickness of the flame is often of the order of magnitude of the flame half-width for practical flame-holder–duct configurations. Hence, the approximation that this complex zone is of negligible thickness is a poor one. Secondly, spreading theories are usually based on the assumptions that the flame-holder is infinitesimal and that the velocity field is that presented in *Figure 3* with the boundary condition that $u_m = u_1$ at the holder. However, in reality the flame-holder is itself important in fixing the initial flow field and near the downstream end of the re-circulation zone the velocity on the centre line, u_m, is zero. An extension of Tsien's theory to include these more accurate upstream boundary conditions is easy to make* and may produce a more realistic theory.

A. H. Lefebvre (Derby): It is difficult to reconcile Spalding's assumption that fresh gas burns instantaneously upon entrainment with the well known influence of pressure on after-burner combustion efficiency. Certainly at high pressures the reaction time is short enough to be considered instantaneous for most practical purposes, but with reducing pressure the zone of reaction increases and, at very low pressures, can extend downstream of the jet pipe. Under these conditions the 'flame front' merely indicates the upstream boundary of the reaction zone. Admittedly the author confines his arguments to high pressures but here there is no combustion problem.

The mechanism of flame-spreading has so far received comparatively little attention and, in view of its controlling influence on after-burner combustion efficiency, it is hoped that the author will enlarge the scope of his studies to include the important, low-pressure case.

D. B. Spalding (London): Regarding Zukoski's remarks, the main support for the theory lies in the predicted and measured lack of dependence of flame width on pressure, gas velocity, and baffle size over a considerable range. These results were previously inexplicable by theories assuming that chemical reaction rate played an important part. The weakest part of the argument, specifically pointed out in the paper, is the necessity, due to lack of information, to use data obtained with uniform-density jets to predict entrainment rates when there are large differences of density. It is therefore not surprising that the absolute prediction of the effect of density ratio is poor. Experimental research on variable-density jets appears to be what is wanted, rather than an entirely new approach.

The particular integrations of the equations reported in the paper were for small baffles. Application of the theory to baffles of large drag is easy, and predicts the stagnation point referred to by Zukoski. The theory cannot, however, predict the local propagation rate in this region because other factors (molecular diffusion, stream turbulence) over-ride mixing due to shear stresses.

Lefebvre correctly notes that the theory is deliberately restricted to regimes in which chemical reaction rate is not controlling. But I disagree that there is no combustion problem in such regimes, for the designer would often like to have a greater angle of flame spread than experiments (and the present theory) show to be possible in ducts of uniform area.

One way in which the theory can be extended to low pressures is indicated in the paper, in the section 'Influence of insufficiently rapid reaction'. This extension can be made quantitative if chemical reaction rate data are assumed; it demonstrates the finite flame thickness pointed out by Zukoski. At low pressures the region of the stagnation point also becomes more important; further assumptions regarding the turbulence level must be introduced to predict how the flame gets away from this point.

G. H. Markstein (Buffalo): I should like to call attention to the fact that in high-speed compressible flows, as Kovasznay and others have shown, one must consider three modes of random disturbances, namely, the shear or vorticity mode, the pressure or 'noise' mode, and entropy spottiness. Only the shear mode has been considered in

* Wright, F. H. and Zukoski, E. E. Report in preparation. Jet Propulsion Laboratory, California Institute of Technology.

current theories of turbulent flames. While these three modes are coupled only in second order in a fairly uniform flow, they become strongly coupled in first order at flame fronts, shock waves, screens or other regions of discontinuity or of steep gradients of the mean flow, therefore, all three modes should be taken into account in theories of turbulent flames. In particular, with flames enclosed in ducts the noise mode may become of great importance: pressure waves corresponding to resonance frequencies of the duct may rise to large amplitudes, and might have a larger effect on flame structure than the shear-flow disturbances that reach the flame from the upstream side.

PART VIII

COMBUSTION IN PRACTICAL FLOWING SYSTEMS

87

USE OF AERODYNAMIC MODELS IN THE STUDY OF INDUSTRIAL FURNACES, PARTICULARLY OPEN HEARTH FURNACES

A. HOGG, C. HOLDEN and R. G. SIDDALL

INTRODUCTION

The distribution pattern of the fuel, air and waste gases is the predominant factor determining the efficiency of combustion in many industrial processes. This is particularly the case when a turbulent diffusion flame is used as in the open hearth furnace. However, because of the high operating temperature and large volume of the furnace chamber it is extremely difficult and laborious to measure gas analysis, velocity and temperature. Small scale models have therefore been developed[1,2] for studying both the general flow pattern throughout the furnace system and the rate of mixing of fuel and air.

Flow visualization is better carried out with water as the fluid since the velocities are lower than with air and suitable tracers are easy to obtain, e.g. polystyrene, which has a good reflectivity and a specific gravity of almost unity. On the other hand it is much easier to make quantitative measurements, such as the mixing rate of fuel and air and velocity surveys, when air is used as the flow medium. In all models an attempt is made to achieve aerodynamic similarity by arranging that the Reynolds number in the model is the same as that at one particular section in the furnace. Since there is a large variation of temperature and hence Reynolds number within the furnace, similarity can only be approximate. The validity of any quantitative model results is therefore in doubt until a comparison has been made with full scale to check the similarity theory. Gas analyses along the assumed axis of the flame in an oil fired open hearth furnace were compared with the mixing in a 1/24th scale model in the I.S.I. Special Report 59[3] and reasonable agreement was obtained at three reference points. However, as the trial was not primarily concerned with the mixing rate of fuel and air, the number of gas samples taken and reference points used were insufficient to substantiate the similarity theory. Hence a further trial was undertaken in which a more comprehensive survey was made of the rate of mixing in and around the flame of an oil fired open hearth furnace. These results are compared in this paper with the mixing results obtained in a 1/24th scale model.

MIXING MEASUREMENTS IN THE FURNACE

The furnace, *Figure 1*, on which the measurements were made was oil fired at a rate of 375 gal./h, 2,600 lb./h of steam at a pressure of 120 lb./in.^{2} gauge were used to atomize the fuel oil, but the main purpose of the steam was to provide forward momentum. The burner nozzle had a convergent-divergent profile with a 13/16 in. diameter throat which gives the most efficient conversion of pressure into kinetic energy for these flow rates[4]. The routine measurements made on this furnace were oil and steam flow, furnace pressure, roof temperature and stack draught. During the trials the air supply to the furnace was calculated from Pitôt tube traverses in the duct between the fans and the reversing valves and it was found to be about 15 per cent in excess of stoichiometric. The volume flow of air in this duct, however, may not necessarily be the same as that in the uptake because of air infiltration. Using 2,000 ft.^{3}/h of oxygen as a tracer it was found that on a similar furnace the volume of air in the uptake was approximately the same as that metered at the fans, so it would seem reasonable to suppose that for this furnace the Pitôt tube traverses gave a good estimate of the quantity of combustion air. Gas analysis of samples taken in the downtake indicated that there was 40 per cent air in excess of stoichiometric requirements. Thus the infiltration of air between the inlet and outlet of the furnace chamber was approximately 25 per cent.

Gas sampling in and about the flame

The number of samples taken in any one heat was limited by the personnel available for sampling and analysing. Samples were therefore taken for one firing direction only as it was considered better to obtain a consistent set of data for one flame rather than an average for two, and in any case the combustion system is symmetrical. The period chosen for the measurements was the two or three hours immediately following the end of charging, when the bath was melted flat and yet firing rates were still reasonably constant. Water cooled probes were inserted through holes in any

one of the three doors or two wickets, the positions of which are shown in *Figure 1.*

Details of the probe used are shown in *Figure 2.* The choice of 3/16 in. bore tubing for the 2 in. long quenching zone was a compromise between the necessity to cool the hot gases rapidly and the desirability of a minimum pressure drop. In practice it was found that when sampling near to the bath the probe was prone to blockage by slag droplets which were very difficult to remove. When filled with water the probe sagged owing to its considerable length, therefore in order to position the tip of the probe accurately it was necessary to 'calibrate' the probe before use. The accuracy of the positioning was ± 3 in. horizontally and ± 1 in. vertically. The sampling patterns for each of the five points of entry of the probe are shown in *Figure 3* but because of variations in the position of the sampling hole caused by door changes and slag on the sill, there were small variations in this pattern from day to day. Samples were withdrawn by a 1/3 h.p. vacuum pump, capacity $3\frac{1}{2}$ ft.^{3}/min, and delivered via glass wool filters to butyl rubber inner tubes of $3\frac{1}{2}$ ft.^{3} capacity. To save time these were not purged when sampling. The procedure adopted was to exhaust them as flat as possible before the trial, and then having purged the sampling line, to fill the inner tubes to capacity with the gas sample. Thus, any errors in gas composition due to stale gas remaining in the tubes were negligible. The time required for sampling was of the order of one to three minutes. Samples were analysed in a modified Orsat apparatus[5] but a number of analyses were checked on a Bone and Wheeler.

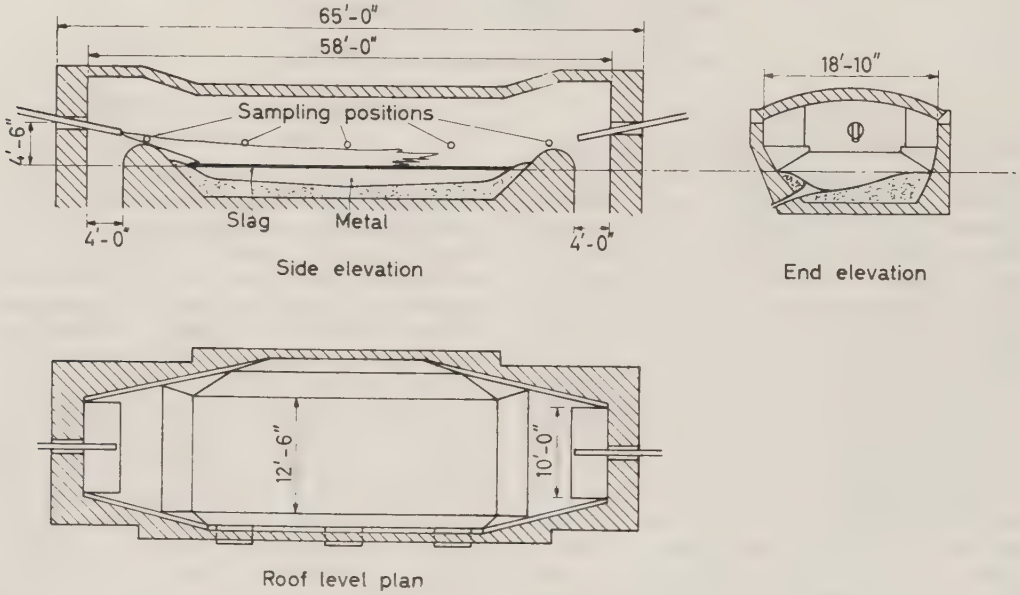

Figure 1. Plan and elevations of trial furnace

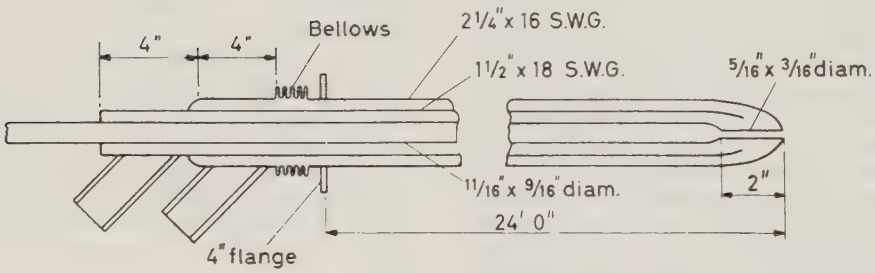

Figure 2. Sketch of probe used for gas sampling on furnace

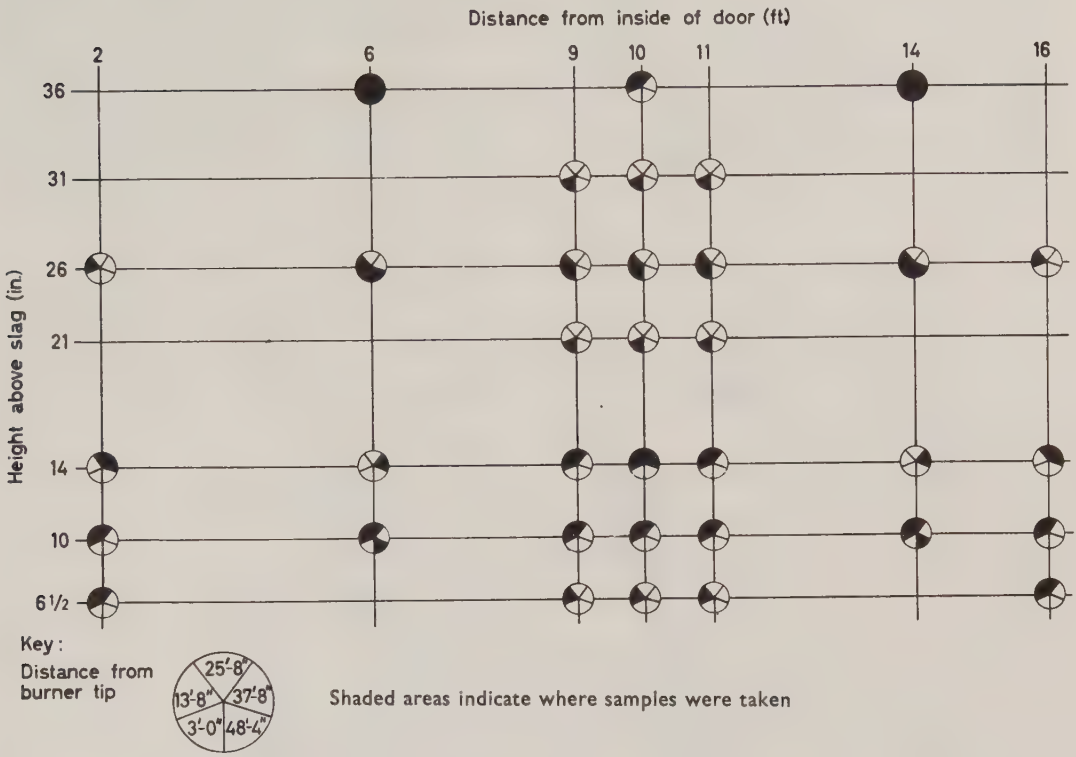

Figure 3. Sampling patterns using 24 ft. *probe*

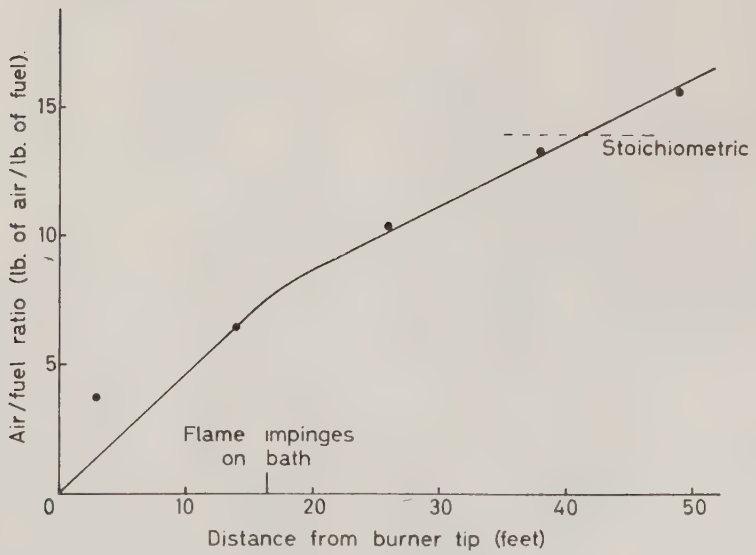

Figure 4. Axial mixing curve for the trial furnace

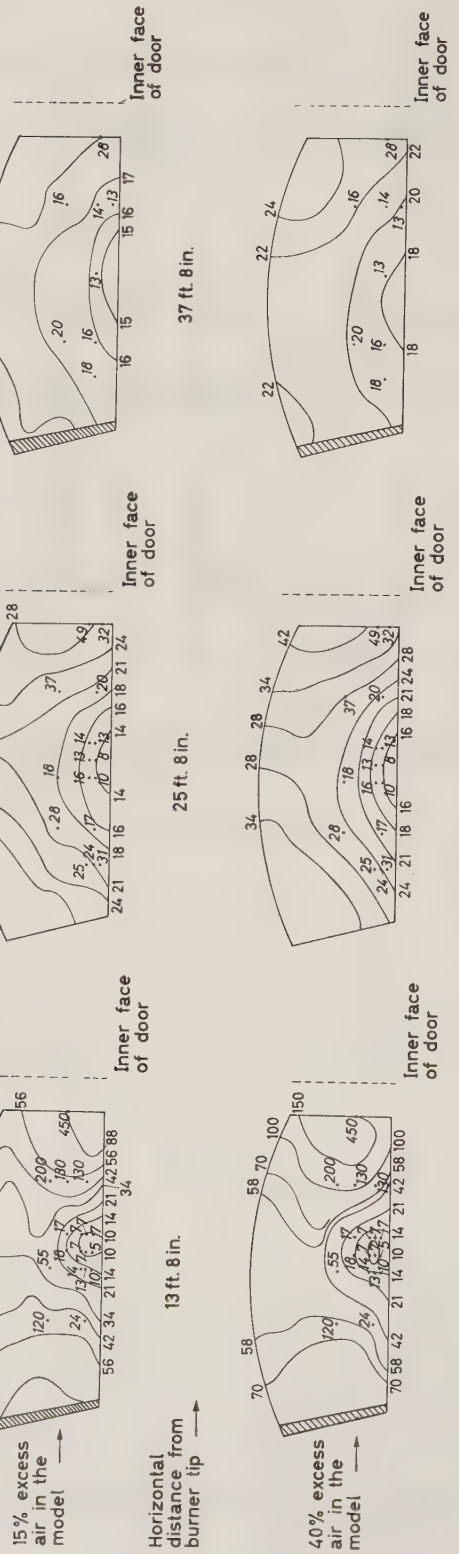
15% excess air in the model
40% excess air in the model
Horizontal distance from burner tip
13 ft. 8 in.
25 ft. 8 in.
37 ft. 8 in.
Inner face of door
Key: Model results shown as contours of the air/fuel ratio, furnace results are in italics

Figure 5. Comparison of mixing in furnace and model

Table 1 gives typical analyses for points on or near the axis of the flame. These are actual sample analyses for the points nearest the axis since interpolation to find an axial value was considered to be unsatisfactory.

The air/fuel ratios calculated for these analyses have been plotted to give the axial mixing curve shown in *Figure 4*. Less weight has been given to the gas analysis at 3 ft. from the burner since it was suspected that when sampling at this point, unburnt oil was left behind in the probe giving too high a value of air/fuel ratio.

Gas sampling under the roof

Gas samples were also taken at eleven positions just under the roof by means of alumina tubes protruding 2 in. into the furnace. Each tube was connected by 1/4 in. o.d. copper tubing to a small air pump which delivered the gas to a 250 c.c. sampling bottle. Preliminary experiments showed that it was necessary to pass through the bottle five times its own volume in order to change the atmosphere completely. This required two minutes at the sampling rate used but in practice five minutes were allowed. The samples were analysed with an Orsat apparatus.

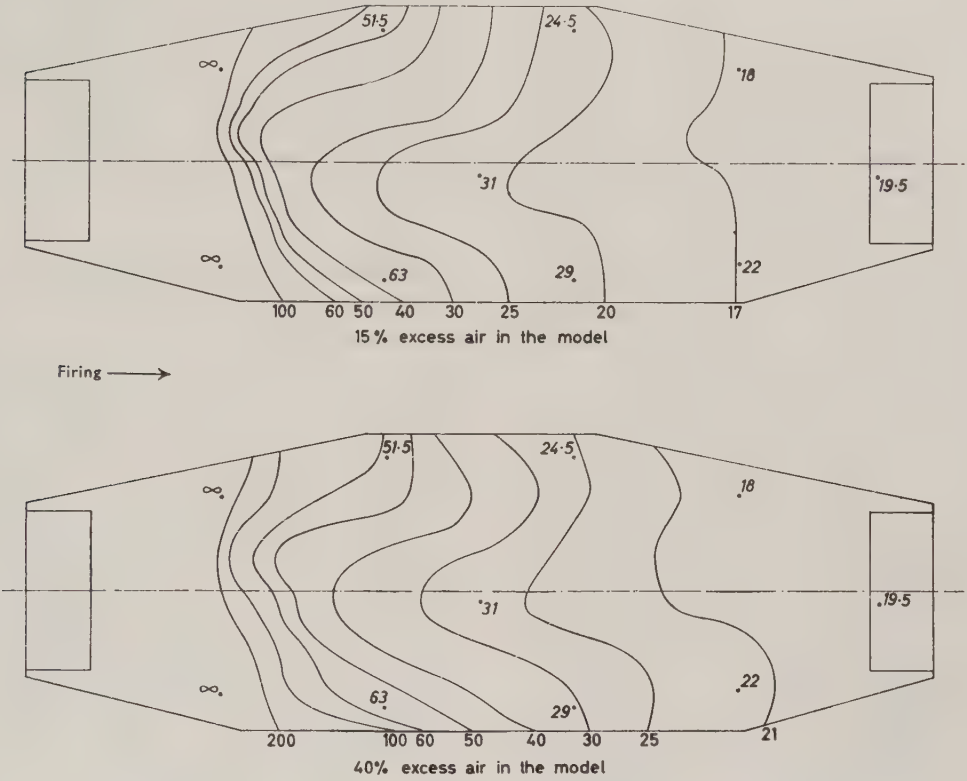

Figure 6. Comparison of mixing under the roof for furnace and model

TABLE 1

Horizontal distance from burner tip	CO_2	*Unsaturated*	O_2	CO	H_2	CH_4	N_2	*Air/fuel ratio*
3 ft. 0 in.	5·1	6·2	2·4	11·5	10·3	3·1	61·4	3 . 18
13 ft. 8 in.	5·4	0·1	0·4	15·1	12·4	0·5	66·1	6 . 46
25 ft. 8 in.	7·5	nil	2·4	2·7	2·1	nil	82·3	10 . 42
37 ft. 8 in.	12·9	nil	2·7	nil	0·6	nil	83·8	13 . 33
48 ft. 4 in.	14·6	nil	1·0	1·3	0·1	0·1	82·9	15 . 6

Discussion of results

The mean values of the air/fuel ratio for each position, calculated from oxygen and hydrogen balances, are shown in *Figures 5* and *6*. As the flow rates were not stabilized and routine practice was observed throughout it is not surprising that for the same position there were differences in the air/fuel ratio from day to day. These variations were most noticeable in positions where the air/fuel ratio gradient was steepest, i.e. at the

boundary of the flame. A further source of error may have arisen in the choice of the formula for the unsaturated hydrocarbons. It was suggested[6] that the best approximation was to assume that all the unsaturated hydrocarbons were in the form of propylene (C_3H_6).

MIXING MEASUREMENTS IN THE MODEL

Experimental details

In order to determine the mixing pattern in an aerodynamic model it is necessary to measure the amount of 'fuel' at any point. This can be achieved by heating the burner fluid and measuring the local temperature, assuming similar transport properties for temperature and mass. For this experiment, the burner fluid (steam plus oil) was represented by compressed air at a pressure of just over 20 lb./in.^{2} gauge heated by an electric heater to 260°C. The model was constructed from Perspex sheet, the inside contours being built to 1/24th scale of the full size furnace. To reduce heat losses, i.e. 'fuel', through the Perspex walls the model was insulated with a layer of cotton wool 1 in. thick.

The flow rates for combustion air and nozzle fluid were determined on the basis of similarity of Reynolds number[7,8]. It was expected that the mixing in the furnace would be complicated by the air infiltration into the combustion chamber which was 25 per cent of the stoichiometric requirements. The results should, however, lie somewhere between those which would be obtained if there were no air infiltration and those which would be obtained if all the air infiltration occurred before the burner. Therefore, two rates of combustion air, 15 per cent and 40 per cent excess, were used in the model. The area of the nozzle in the model was calculated initially from data given by Jamison and Mordell[9], but as a check the thrust of this nozzle was measured by determining the force on a large plate placed in front of it. The measured value, 1·13 lb. weight, was found to agree closely with the theoretical value, 1·10 lb. weight.

Temperature measurements were made with 36 s.w.g. chromel alumel thermocouples sheathed with vitreosil and recorded on a 12 point Honeywell-Brown potentiometer. A survey of the downtake showed an even temperature distribution indicating that mixing was complete at the section where the outlet temperature was measured. The air/fuel ratio at any point in the model was estimated from the temperatures at that point, in the uptake and in the downtake. Traverses were made of the model at six sections and the air/fuel ratios at other points estimated by interpolation.

Discussion of results

The total error in the model measurements, due to differences in the thermocouple calibrations, heat losses through the Perspex, errors in the rates of flow, and positioning of thermocouples has been estimated at less than 6 per cent of the value of the air/fuel ratio obtained.

The mixing patterns obtained for the two values of excess air used are shown as contours of the air/fuel ratio, for transverse sections at each of the three doors and under the roof, in *Figures 5* and *6*. It can be seen that the mixing patterns are fairly similar, although with 15 per cent excess air the front wall region at the roof tends to be slightly richer in fuel than the back wall, whereas with 40 per cent excess air the higher air/fuel ratios were found above the back wall. As might be expected the higher excess air gives a shorter 'flame length'.

COMPARISON OF MIXING RESULTS FOR MODEL AND FURNACE

It can be seen from *Figures 5* and *6* that the model results do not, in general, agree with the results obtained from the furnace. In the furnace the air/fuel ratios are lower inside and higher outside the flame than at corresponding positions in the model which indicates that the rate of mixing in the furnace is slower than would be predicted from the model. This fact is also evident from the axial mixing curves for the model and the furnace shown in *Figure 7*. However, there is reasonable agreement at roof level when the model is run with 40 per cent excess air. The difference is probably best illustrated by regression curves fitted to the results when the fuel/air ratios in the model are plotted against the fuel/air ratios in the furnace for similar positions, *Figures 8a* and *8b*. These do not include the roof results which have been examined separately.

There are at least three reasons why the model results should not be in exact agreement with those of the furnace even if the similarity theory used is completely valid:

(*a*) Because of lack of data it was not possible to simulate air infiltration through the furnace doors and brickwork. Although the model was run with two values of excess air to try to determine the effect of this, the actual position of entry of the infiltrating air may be important.

(*b*) Carbon monoxide evolution from the charge was not simulated in the model. This should not affect the values of air/fuel ratio obtained on the furnace as the calculations were based on hydrogen, oxygen and nitrogen balances only. It is reasonable to assume that the oxygen liberated from the bath in form of CO is compensated for by the fact that oxidation of the bath

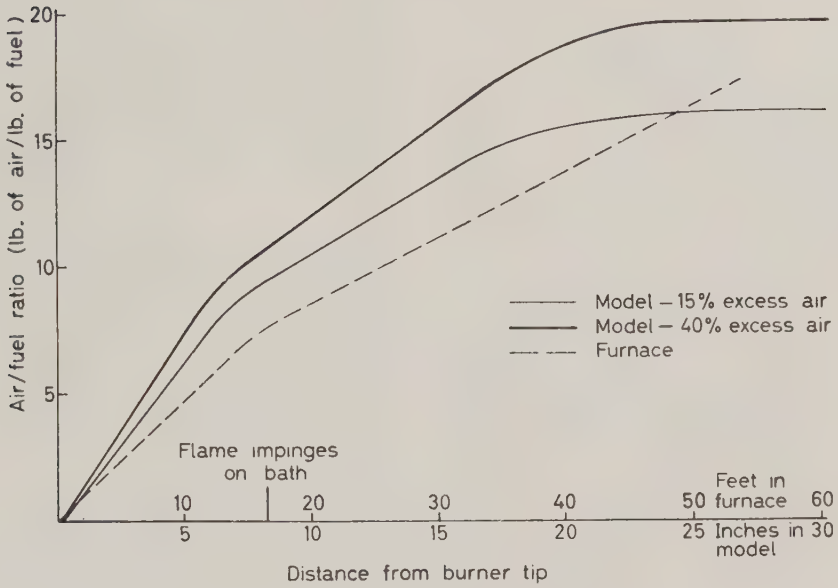

Figure 7. Comparison of axial mixing in model and furnace

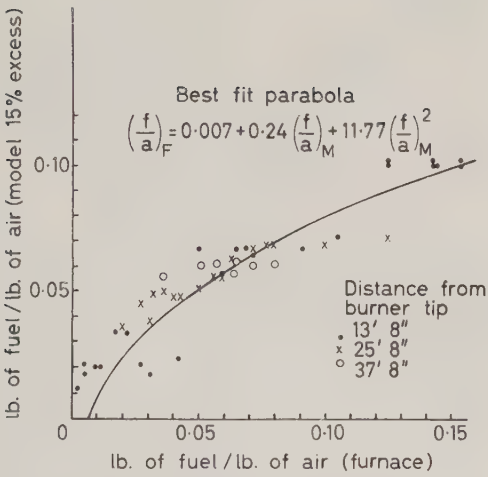

Figure 8a. Comparison of fuel/air ratio for model (15% excess air) and furnace

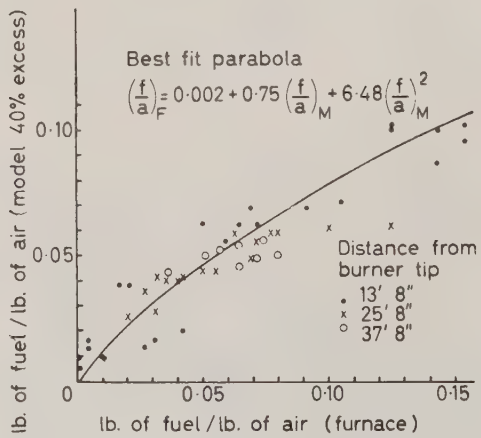

Figure 8b. Comparison of fuel/air ratio for model (40% excess air) and furnace

is taking place at a similar rate. This carbon monoxide may, however, affect the mixing pattern by lowering the rate of entrainment of combustion air. The weight of carbon monoxide liberated, however, is only about 2 per cent of that of the air passing through the furnace.

(*c*) A stabilized control system was not available so that some variations in the flow rates occurred. The effect on air/fuel ratio of variations in fuel flow is obvious whilst that of steam flow causes changes in burner thrust and hence rate of entrainment. Also the amount of air infiltration varies considerably with changes in furnace pressure.

It has already been stated that gas analysis in the downtake indicated that there was about 40 per cent excess combustion air and that the air infiltration through the doors and brickwork of the furnace chamber was of the order of 25 per cent. Most of this infiltrating air was presumably drawn in around the first door which was 13 ft. 8 in. from the burner tip. Flow pattern observations in a water model showed that the recirculating gases from the outgoing end met the clean

combustion air from the uptake at about this point. Thus the mixing for the first 14 ft. of the flame should be independent of the air infiltration, and should therefore be in good agreement with the model results with 15 per cent excess air, even if air infiltration and its position of entry is important for the rest of the furnace. However, neither set of model results gives a good correlation.

Beyond the first door the flow pattern in the furnace is complicated by air infiltration which is increasing the excess air. The furnace results of 25 ft. 8 in. and 37 ft. 8 in. should therefore lie somewhere between the values of 40 per cent excess air and 15 per cent excess air in the model. However, as the initial mixing rate in the furnace was much slower than that in the model, it is not surprising that the air/fuel ratios at these positions were even lower than those in the model with 15 per cent excess air.

At the roof the air/fuel ratios are mainly determined by recirculating gases. The results obtained indicated much closer agreement with 40 per cent excess air (*Figure 9*) which is to be

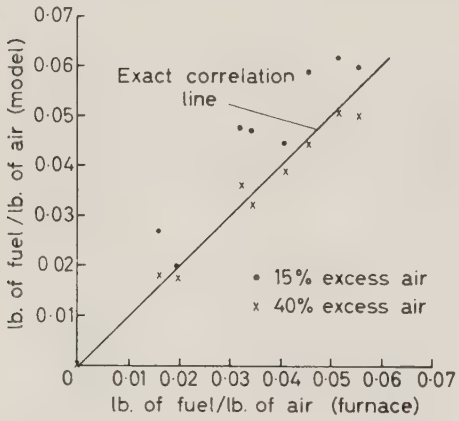

Figure 9. Correlation of gas samples at the roof of S furnace with the mixing results obtained in a model

expected since the majority of the recirculating gases have originated from the end of the flame.

The effects of variations in input conditions on the furnace results were examined by the authors, but although these explain some of the scatter in the results at any one position they do not account for the shape of the best fit regression curves. They have, therefore, not been included.

Since good agreement was not found at the incoming door where the best correlation was expected, some doubt must exist as to the validity of the similarity criteria used. The basic assumptions used in setting up an aerodynamic model are:

(*a*) That Reynolds number is the parameter controlling flow patterns. The values of this throughout the furnace system are well above critical so that it is possible to run the model at a fraction of the full Reynolds number and still obtain the same flow pattern.

(*b*) The oil steam jet in the furnace entrains in a similar manner to the hot air jet in the model, i.e. the ratio of the entrainment coefficients is unity.

Reynolds' criterion for similarity is well established for isothermal models. In a furnace, where combustion is taking place, there is a continual change in Reynolds number which cannot be simulated in a geometrically similar model. Even so it is doubtful whether this variation produces more than a second order effect since, as previously stated, the Reynolds numbers throughout the furnace are well above the critical value.

It would appear therefore that the oil and steam jet in the furnace does not entrain in the same way as the hot air jet used in the model. The difference is such that the flame entrains more slowly than the air jet which might suggest that too high a thrust was used on the model, although on the basis of the similarity theory the thrust actually used in the model was equivalent to that in the furnace. It can be seen from the Appendix that if model thrust is too high the coefficient of $(f/a)_M$ is always greater than 1 and neglecting the squared term introduces an error of approximately 2 per cent. For example, if the thrust in the model is 23 per cent too high then

$$\left(\frac{f}{a}\right)_F = 1{\cdot}18\left(\frac{f}{a}\right)_M + 0{\cdot}24\left(\frac{f}{a}\right)_M^2 \qquad (1)$$

The best fit regression curves obtained for 15 per cent and 40 per cent excess air respectively

$$\left(\frac{f}{a}\right)_F = 0{\cdot}007 + 0{\cdot}24\left(\frac{f}{a}\right)_M + 11{\cdot}77\left(\frac{f}{a}\right)_M^2 \qquad (2)$$

and

$$\left(\frac{f}{a}\right)_F = 0{\cdot}002 + 0{\cdot}75\left(\frac{f}{a}\right)_M + 6{\cdot}48\left(\frac{f}{a}\right)_M^2 \qquad (3)$$

In neither case is the coefficient of $(f/a)_M$ greater than 1 nor can the squared term be neglected. Therefore the difference in mixing cannot be explained on the basis of too high a thrust in the model.

The most likely explanation of the discrepancy is that, in the furnace, the jet fluid does not diffuse outwards as fast as it does in the model. For the first several feet of the flame, the inertia of the fuel droplets results in an effective eddy diffusion coefficient which is lower than it would be if all the fuel were vaporized. Large reductions have been observed with diesel fuels[10] where the spreading of a spray indicated an effective eddy diffusion coefficient as low as half that of

the vapour. Even after the droplets have evaporated so that the fuel can be considered to be gas, experimental evidence suggests[11,12,13] that the effective rate of diffusion during the combustion of gaseous fuel is less than that for an air jet. It is therefore to be expected that the initial angle of spread of the flame is less than that of the air jet used in the model.

Assuming that a difference exists between the jet angles in model and furnace but that the radial distributions of concentration are similar, the Substituting for values of $(f/a)_M$ and r from the model the curve shown in *Figure 10* was obtained which, it can be seen, is in good agreement with the best fit parabola for the experimental data.

Using the model burner, measurements were made of the free jet angle with the same input conditions as were used for the model experiments. The semi half jet angle was found to be 6° 20′ (±10′) from which it was concluded that the full jet angle was about 25°. From the value of Y, 1·6, the equivalent jet angle for the furnace was

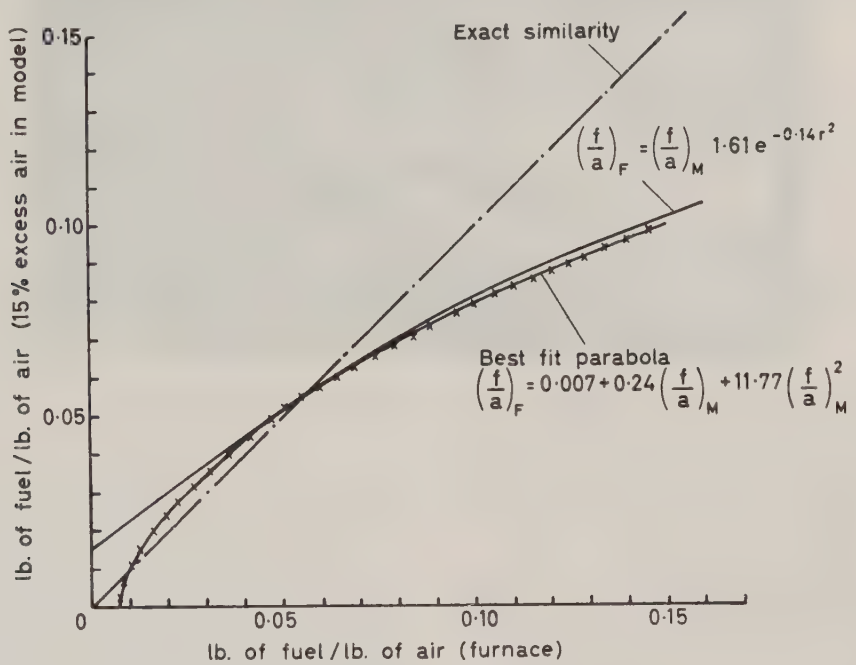

Figure 10. Comparison of best fit parabola for 15% excess air in the model, with curve predicted by assuming a difference in jet angles

fuel/air ratio at any point in the furnace is related to that at a similar position in the model by the approximate equation

$$\left(\frac{f}{a}\right)_F = \left(\frac{f}{a}\right)_M Y\, e^{-pr^2} \qquad (4)$$

where Y is the ratio of the tangent of the half-angle of jet in the model to the tangent of the half-angle of the flame, p is a constant, and r is the radial distance in feet at full scale from the axis to the point considered.

The values of Y and p were determined by substituting two values of $(f/a)_F$ and $(f/a)_M$ from the best fit correlation curve for 15 per cent excess air in equation 4—one on the axis and one at the edge of the jet. This gave the following equation

$$\left(\frac{f}{a}\right)_F = 1{\cdot}6\left(\frac{f}{a}\right)_M e^{-0{\cdot}14r^2} \qquad (5)$$

calculated to be about 16°. *Figure 11* shows a photograph of a heavy fuel oil flame on a similar furnace. It can be seen that visual jet angle is about 17°. Angles have also been estimated by the authors from gas analysis and velocity measurements for the flames examined during Combustion Mechanism Trials II of the International Flame Research Foundation. The values for five different flames (two gas, two light oil and one heavy oil) were all in the range 15–19°. It should be noted that these values were all obtained from enclosed turbulent diffusion flames.

Yagi and Saji[12] report that the angle of spread of gas and pulverized fuel flames is substantially constant and equal to about 12° and that their observations are supported by Hawthorne[11] and by Kunugi[14]. Most of their observations, however, were made on vertical free jets. These conclusions are not in agreement with the results of Sunavala[15] who not only found that the axial

decay of a town's gas jet was 30 per cent faster than for an equivalent air jet but also put forward evidence which suggested that jet angle was not affected by temperature.

There are theoretical grounds which support the conclusions that the jet angle, which is determined by the eddy diffusivity, is greater for the model than for the furnace. Yagi and Saji have developed equations for the eddy diffusivity in isothermal, non-isothermal and burning free jets. Using their equations it may be shown that

$$\left(\frac{\epsilon_M}{\epsilon_F}\right) = \left(\frac{G_M}{G_F}\right)^{1/2} \left(\frac{\rho_F}{\rho_M}\right)^{1/2}_{273°K} \left(\frac{\bar{T}_M}{\bar{T}_F}\right) \quad (6)$$

where ϵ = eddy diffusivity and G = momentum of jet.

When calculating the flow rates and thrust in the model it is assumed that there are average temperatures in both the model and the furnace which are typical of both systems. This gives rise to the inherent assumption that ϵ_M/ϵ_F is constant. *Figure 12* shows the variation in $(\epsilon_M/\epsilon_F) \times (G_F/G_M)^{1/2}$ against distance from the burner tip for four possible sets of model conditions in which the ambient temperature is approximately 50°C. The values for the mean flame temperature in the furnace have been interpolated from the theoretical data of Thring[3] and the Schmidt temperatures reported by Copland and Holden.

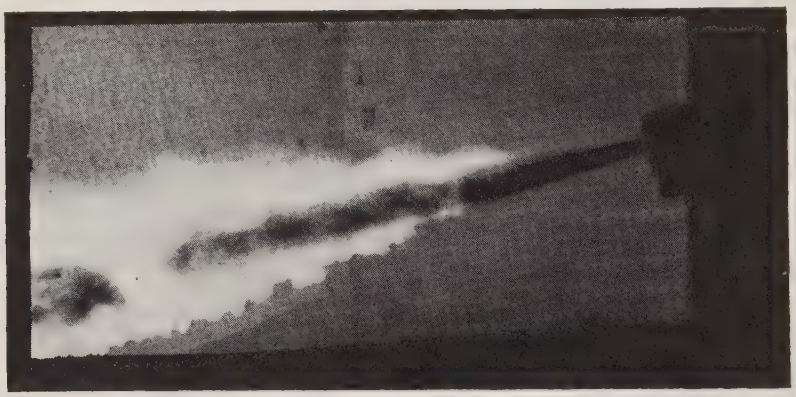

Figure 11. Photograph of flame in open hearth furnace (oil flow 235 gal./h, *steam flow* 1,650 lb./h, *nozzle throat* 13/16 in.)

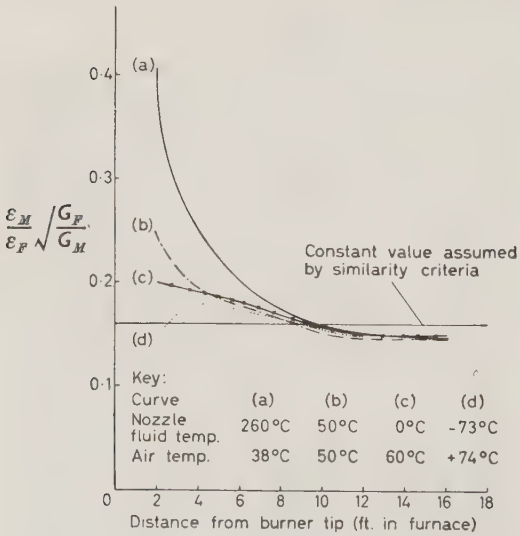

Figure 12. Variation in $(\epsilon_M/\epsilon_F)(G_F/G_M)^{1/2}$ *for the early part of the flame*

It can be seen, *Figure 12* curve (a), that there is a large variation in the ratio of the eddy diffusivities and that the average value of $(\epsilon_M/\epsilon_F) \times (G_F/G_M)^{1/2}$ for the first 14 ft. of the flame is about 40 per cent greater than the value assumed by the model criteria. It is not surprising, therefore, that the model has a greater jet angle than the furnace.

Curves (b) (c) and (d) show the effect of changing the nozzle fluid and 'combustion air' temperatures in the model, keeping the average ambient temperature at about 50°C. The isothermal model, curve (b), still shows a greater eddy diffusivity for the initial mixing zone than is assumed by the similarity criteria. However, if the nozzle fluid temperature is lowered to about −73°C and the 'combustion air' raised to +74°C, then $(\epsilon_M/\epsilon_F)(G_F/G_M)^{1/2}$ is approximately constant for the first 16 ft. of the flame. This model setting should, therefore, give good agreement with the actual furnace.

CONCLUDING REMARKS

A survey has been made of the mixing of fuel and air in an open hearth furnace during normal production and has been compared with a

similar survey made on a 1/24th scale geometrically similar model.

The air infiltration above stage level for this furnace was of the order of 25 per cent of the total combustion air, and when allowance was made for this in the model a good correlation was obtained for the gas analysis immediately under the roof.

The rate of entrainment in the furnace is less than would be predicted by the model. A probable explanation has been put forward that the effective eddy diffusivity in the flame is less than that in the air jet used in the model. This implies a smaller jet angle for the furnace than for the model. If the model results are corrected on this assumption a good correlation is obtained.

If model work is to be of the utmost aid to furnace design a further similarity criterion must be added, namely, similarity of jet angle. This could probably be achieved by choosing different flow media, for example, a cold air jet entraining hot air. If this is not possible an approximate comparison can be made by correcting the results by the method outlined in the report.

The authors wish to express their thanks to Mr. F. H. Saniter, Director of the Research and Development Department of the United Steel Companies Ltd., for permission to publish this paper.

They also acknowledge the assistance given by Dr. J. H. Chesters, United Steel Companies Ltd.; Professor M. W. Thring, Department of Fuel Technology and Chemical Engineering, University of Sheffield; Mr. J. A. Chapman and Mr. H. H. England, Messrs. Steel, Peech & Tozer; Professor D. B. Spalding of Imperial College of Science and Technology and Dr. N. P. Bacon of Messrs. Guest Keen Iron & Steel Co.; members of the Furnace Design Section of United Steel Companies Ltd., and the Department of Fuel Technology and Chemical Engineering of the University of Sheffield.

APPENDIX

Comparison of the mixing of two free jets

The equation governing the fully developed region of a free jet may be written as

$$\frac{C}{C_A} = e^{-c(r/r_b)^2} \tag{7}$$

and

$$\frac{C_A}{C_n} = \frac{d_n}{x} \cdot K_1 \left(\frac{\rho_n}{\rho_a}\right)^{1/2} \tag{8}$$

where C, C_A and C_n are the concentrations at any point, on the axis and at the nozzle respectively

r is the radial distance of any point from the axis

r_b is the total jet radius at any section

K_1 is the entrainment constant which is proportional to $1/\tan\frac{1}{2}\theta$

θ is the total jet angle

d_n is the nozzle diameter

x is the distance along the axis from the nozzle

ρ_n and ρ_a are the nozzle and ambient densities respectively

C is a constant which may be different for different jets.

The concentration at any point (x, r) is given by

$$\frac{C}{C_n} = \frac{d_n}{x} K_1 \left(\frac{\rho_n}{\rho_a}\right)^{1/2} e^{-c(r/r_b)^2} \tag{9}$$

If a comparison is made of two jets, in the present case model and furnace, the resulting correlation is

$$\frac{C_M}{C_F} = \frac{C_{nM}}{C_{nF}} \frac{K_{1M}}{K_{1F}} \frac{d_{nM}}{d_{nF}} \frac{x_F}{x_M} \times \left(\frac{\rho_{nM}}{\rho_{nF}} \frac{\rho_{aF}}{\rho_{aM}}\right)^{1/2} e^{-\left(\frac{C_M r_M^2}{r_{bM}^2} - \frac{C_F r_F^2}{r_{bF}^2}\right)} \tag{10}$$

The equivalent nozzle diameter[8] $d' = d_n(\rho_n/\rho_a)^{1/2}$. Therefore if the entrainment constants and jet angles are equal, and the equivalent nozzle diameters are in the same ratio as the scaling factor, then for a similar position

$$\frac{C_M}{C_F} = 1 \tag{11}$$

If there is a difference in thrusts there is a difference in the equivalent nozzle diameters such that

$$\frac{C_M}{C_F} = \frac{d'_M}{d'_F} \cdot \frac{x_F}{x_M} = P \text{ (say)} \tag{12}$$

(If the thrust in the model were 23 per cent too high then $P = 0{\cdot}9$)

$$\therefore \frac{\left(1 + \frac{a}{f+s}\right)_F}{\left(1 + \frac{a}{f+s}\right)_M} = P$$

$$\left(\frac{f+s}{a}\right)_F = \frac{1}{(P-1) + p\left(\frac{a}{f+s}\right)_M}$$

$$= \left(\frac{f+s}{a}\right)_M \cdot \frac{1}{P}\left\{1 - \frac{P-1}{P} \cdot \left(\frac{f+s}{a}\right)_M\right\} \tag{13}$$

neglecting third powers of $\left(\frac{f+s}{a}\right)_M$

The steam (s) is proportional to the fuel (f).

Let $s_F = \alpha_F f_F$ and $s_M = \alpha_M f_M$

Therefore

$$(1 + \alpha_F)\left(\frac{f}{a}\right)_F = \frac{(1 + \alpha_M)}{P}\left(\frac{f}{a}\right)_M \times \left\{1 - \left(\frac{P-1}{P}\right)(1 + \alpha_M)\left(\frac{f}{a}\right)_M\right\} \quad (14)$$

Now assuming too high a thrust such that $P = 0{\cdot}9$, $\alpha_F = 0{\cdot}65$, $\alpha_M = 0{\cdot}75$

$$\left(\frac{f}{a}\right)_F = 1{\cdot}18\left(\frac{f}{a}\right)_M\left\{1 + 0{\cdot}2\left(\frac{f}{a}\right)_M\right\} \quad (15)$$

It can be seen that neglecting the squared term for $(f/a)_M < 0{\cdot}1$ only introduces an error of 2 per cent. Thus the only effect of difference in thrust would be to give an approximate straight line whose slope depends on the difference in thrust.

If now the thrust is assumed to remain constant but the jet angles differ, then as the equivalent nozzle diameters are in the same ratio as the scaling factor

$$\frac{C_M}{C_F} = \frac{K_{1M}}{K_{1F}} \cdot e^{-pr^2} = Q \text{ (say)} \quad (16)$$

where $p = \left\{\frac{c_M}{r_{bM}{}^2}\frac{L_M{}^2}{L_F{}^2} - \frac{c_F}{r_{bF}{}^2}\right\}$

$$\therefore \quad \left(1 + \frac{a}{f+s}\right)_F = Q\left(1 + \frac{a}{f+s}\right)_M$$

$$\left(\frac{a}{f+s}\right)_F = (Q - 1) + Q\left(\frac{a}{f+s}\right)_M$$

$$\therefore \quad \left(\frac{f+s}{a}\right)_F = \left(\frac{f+s}{a}\right)_M \times \frac{1}{Q}\left\{1 - \frac{Q-1}{Q}\left(\frac{f+s}{a}\right)_M\right\} \quad (17)$$

neglecting third-order powers.

Let $s_F = \alpha_F f_F$ and $s_M = \alpha_M f_M$

$$\therefore \quad (1 + \alpha_F)\left(\frac{f}{a}\right)_F = \left(\frac{1 + \alpha_M}{Q}\right)\left(\frac{f}{a}\right)_M \times \left\{1 - \frac{Q-1}{Q}(1 + \alpha_M)\left(\frac{f}{a}\right)_M\right\}$$

As the thrusts are assumed equal $\alpha_F = \alpha_M \simeq 0{\cdot}75$

$$\therefore \quad \left(\frac{f}{a}\right)_F = \frac{1}{Q}\left(\frac{f}{a}\right)_M - \left(\frac{Q-1}{Q^2}\right)1{\cdot}75\left(\frac{f}{a}\right)_M^2 \quad (18)$$

Assuming *axial* points only ($r = 0$) and $C_M/C_F = Q = 1{\cdot}5$

$$\left(\frac{f}{a}\right) = 0{\cdot}67\left(\frac{f}{a}\right)_M - 0{\cdot}37\left(\frac{f}{a}\right)_M^2$$

Thus when $(f/a)_M < 0{\cdot}1$, neglecting the squared term introduces an error of less than 6·5 per cent. To a first approximation therefore the relationship between similar positions for two jets with different jet angles is

$$\left(\frac{f}{a}\right)_F = Y\,e^{-pr^2}\left(\frac{f}{a}\right)_M \quad (19)$$

where

$$Y = \frac{K_{1F}}{K_{1M}} = \frac{\tan \tfrac{1}{2}\theta_M}{\tan \tfrac{1}{2}\theta_F}$$

REFERENCES

1. Groume-Grjimailo, W. E. *The Flow of Gases in Furnaces.* 1923. London; Chapman and Hall
2. *Some Aspects of Fluid Flow.* 1951. London; Edward Arnold and Co.
3. Pearson, S. W., Thring, M. W. and Chesters, J. H. Combustion and heat transfer in an open hearth furnace. *Iron Steel Inst. Spec. Rep. No. 59* (1956)
4. McInerney, M. J., Mattocks, G. R. and Newby, M. P. *I.M.E. and A.S.M.E. Combustion Conference*, paper No. 21, section 3, 1955
5. International Flame Research Foundation. *Doc. Nr. C. 72/a/4, Part VII*
6. Romanska, Mrs. J. Private communication
7. Bacon, N. P. *Joint Symposium on the Scaling up of Chemical Plant and Processes.* May 1957. London; Institution of Chemical Engineers
8. Thring, M. W. and Newby, M. P. Combustion length of enclosed turbulent jet flames. *Fourth Symposium (International) on Combustion.* 1953. Baltimore; Williams and Wilkins
9. Jamison, R. R. and Mordell, D. L. The compressible flow of fluids in ducts. *A.R.C. Tech. Rep.* 1945. London; H.M.S.O.
10. Longwell, J. P. and Weiss, M. A. Mixing and distribution of liquids in high-velocity air streams. *Industr. Engng. Chem.* (*Industr.*) 45 (1953) 667
11. Hawthorne, W. R., Weddell, D. S. and Hottell, H. C. Mixing and combustion in turbulent gas jets. *Third Symposium (International) on Combustion*, p. 266. 1949. Baltimore; Williams and Wilkins
12. Yagi, S. and Saji, K. Problems of turbulent diffusion and flame jet. *Fourth Symposium (International) on Combustion*, p. 771. 1953. Baltimore; Williams and Wilkins
13. Sawai, I., Kunugi, M. and Jinno, H. Turbulent diffusion flames. *Fourth Symposium (International) on Combustion*, p. 806. 1953. Baltimore; Williams and Wilkins
14. Kunugi, M. *Chem. Eng.* (*Japan*) 15 (1951) 125
15. Sunavala, P. D., Hulse, C. and Thring, M. W. Mixing and combustion in free and enclosed turbulent jet diffusion flames. *Combustion and Flame* 1 (1957) 179

88

SIMULATION OF COMBUSTION CHAMBER PERFORMANCE: EXAMINATION OF THE PREDICTIONS OF AN ANALOGUE OF A HIGH INTENSITY COMBUSTION CHAMBER

D. G. MARTIN and J. D. WEBB

INTRODUCTION

The design of combustion chambers is at the present time a matter of trial and error guided by experience. The development process is usually protracted and tends to be expensive, particularly when the effects of altitude have to be examined, and thus any device which promises a reduction of full-scale testing is to be welcomed. Such a device appears to be an analogue of the combustion chamber as recently described by Spalding[1]. The use of such an analogue permits a large proportion of the preliminary development to be performed in a model of the combustion chamber in which the temperature rise is not large and in which the flow rates can be relatively moderate.

Obviously the validity of the analogue requires careful experimental verification before it can safely be used in development, particularly since it is not easy to fulfil simultaneously all the conditions for similarity between analogue and combustion chamber. A considerable number of comparisons between analogue and combustion chamber are required in order that a careful appraisal of the virtue of the analogue may be made, and, of this number, the work described in the present paper forms a small part. It is the purpose of the present paper to describe a comparison between the predictions of an analogue and the performance of the comparable combustion chamber.

APPARATUS

The comparison is made between a burner of variable geometry, but of a single design, and a geometrically similar analogue.

The combustion chamber is of the 'one stream' type and consists of a cylindrical duct containing an annular baffle, extending from the wall of the duct and of variable internal diameter. Premixed propane and air enter the combustion chamber through a conical diffuser approach section, and, disposed symmetrically relative to the axis of the duct, there is a second baffle, conical in shape, supported on a spider in the entry diffuser. The annular baffle is held in a sliding carrier and can be moved axially relative to the conical baffle.

A sketch of the burner is given in *Figure 1*. The streams of propane and air are metered by sharp-edged orifices before careful mixing some distance upstream of the burner. A flow diagram is given in *Figure 2*.

The analogue is supplied with a stream of air, which simulates the combustible mixture, and contains a number of small heated elements, the current to which is related to the local temperature and simulates the effect of reaction. The analogue has been described in detail by Senior[2] and the analogue results used in this paper are given in the reference.

MEASUREMENTS

The effects of various changes in the geometry of the burner on the limit of flame stability have been investigated. Stability limit *versus* fuel–air ratio curves have been obtained (within the limits of available air mass flow) for various values of the internal diameter of the annular baffle and for various axial positions of a given annular baffle with respect to the fixed conical baffle. The limit of flame stability at a given air mass flow was approached by varying the fuel flow rate gently and continuously until the flame blew out from within the combustion chamber. It was noticed that under all conditions the flame detached from the conical baffle first, and that further change in the fuel flow rate was necessary to cause the flame to blow off the annular baffle.

The effect of variations of the annular baffle diameter on the flame stability is shown in *Figure 3* in which stability limit *versus* fuel–air ratio curves are shown for various internal diameters of the annular baffle. The effect of variation of the axial position of the annular baffle is shown in *Figure 4* in which stability limit *versus* fuel–air ratio curves are shown for two different values of the distance between conical and annular baffle.

The analogue results with which these data are compared are summarized in *Figure 5*.

DISCUSSION

The conditions for similarity between the analogue and the combustion chamber have been

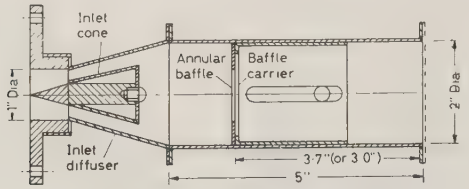

Figure 1. Sketch of combustion chamber

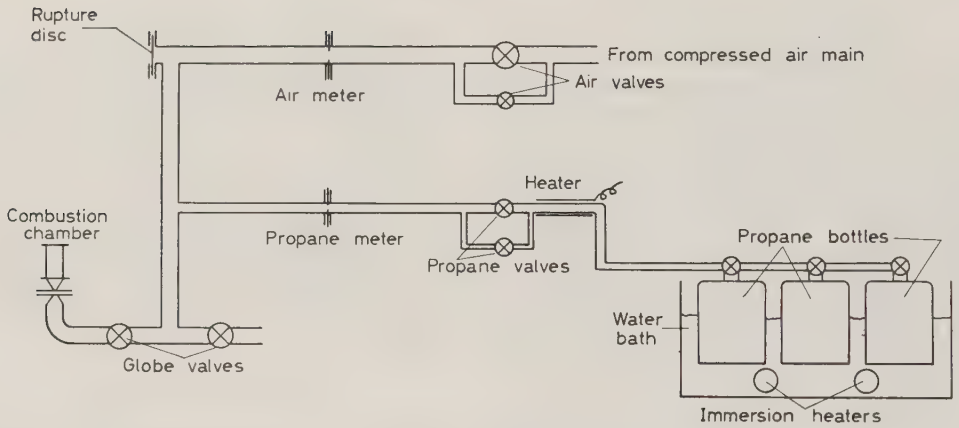

Figure 2. Flow diagram

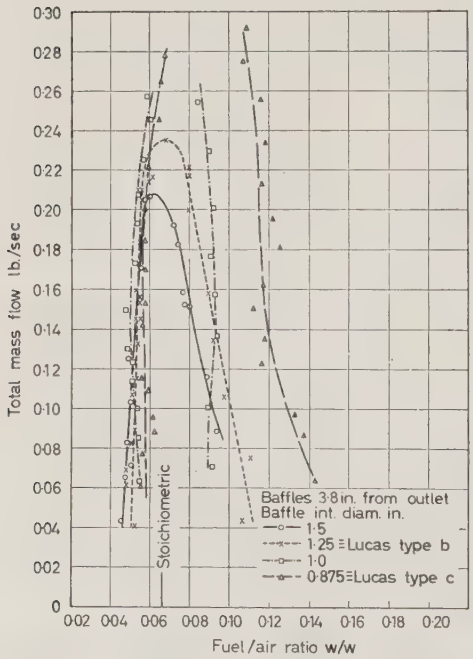

Figure 3. Effect of varying inner diameter of annular baffle on the stability of flame

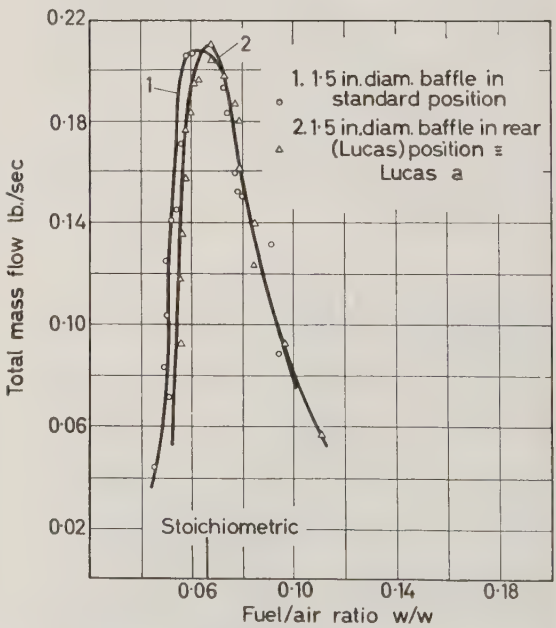
Total mass flow lb./sec
Fuel/air ratio w/w
1. 1·5 in. diam. baffle in standard position
2. 1·5 in. diam. baffle in rear (Lucas) position ≡ Lucas a
Stoichiometric

Figure 4. Effect of varying position of annular baffle relative to conical baffle

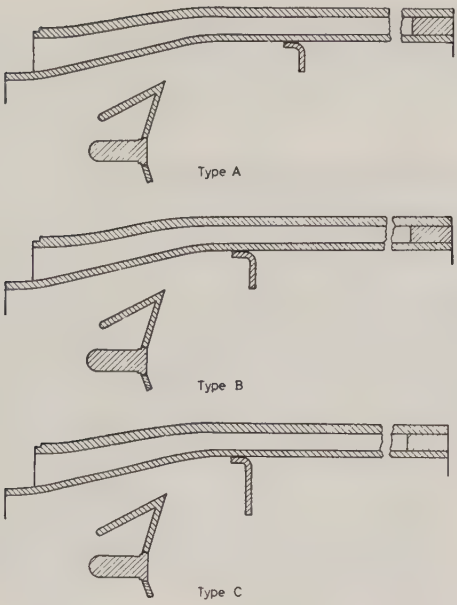

Figure 5. Type C more stable than type B and type B more stable than type A. (By courtesy of Proc. Instn. mech. Engrs, Lond.)

summarized by Senior[2] and derived by Spalding[3]. The important conditions are: (1) geometrical similarity; (2) equal fuel–air ratio; (3) equal loading factors.

Other factors of rather less importance are: (4) equal $\Delta T/T_u$; (5) similar $\dot{q}''' - x$ curves; (6) equal Reynolds numbers; and (7) equal Mach numbers.

The conditions of equal Reynolds numbers and equal Mach numbers need not be fulfilled if the former is high and the latter is low.

In the above list the symbols and nomenclature are as follows: loading factor: defined by $\dot{m}c\Delta T/\dot{q}'''_m v$; m = mass flow rate; c = specific heat at constant pressure; ΔT = temperature rise for complete combustion; $\dot{q}'''$ = volumetric rate of heat release (suffix m = maximum); v = volume of combustion chamber; T_u = initial unburned temperature; x = reactedness = $T - T_u/\Delta T$, where T = gas temperature.

The conditions for similarity are not fulfilled in the present comparison in two respects: first, the volumetric heat release rate *versus* reactedness curves are not similar; second, the ratio $\Delta T/T_u$ is not similar. The failure to fulfil the second of these conditions is probably more severe than failure to fulfil the first, and means, in effect, that the flow patterns in the analogue are dissimilar to those in the combustion chamber in-so-far as they are a consequence of changes of density. Neither of these departures from complete similarity would be expected to invalidate a qualitative comparison, but they are likely to affect the results of a quantitative comparison. The magnitude of the errors thereby induced, the extent to which they can be eliminated by modifications to the analogue, and the extent to which they can be rendered unimportant by analytical consideration must receive careful consideration in the light of a considerably larger body of data than we have at our disposal. The authors, therefore, propose to confine themselves to a qualitative comparison.

The results obtained with the analogue predict that decreasing the internal diameter of the annular baffle causes an increase in the limiting mass flow for which a flame can be stabilized. That is to say, in *Figure 5*, that combustion chamber *C* is more stable than combustion chamber *B*, which is in turn more stable than combustion chamber *A*. Furthermore, the results quoted by Senior[2] predict that the combustion, as the mass flow rate increases, should become unstable first on the conical baffle, and, only at an appreciably higher mass flow rate, subsequently become unstable on the annular baffle.

Figure 3 shows that decreasing the internal diameter of the annular baffle in the combustion chamber improves the stability of the combustion within the burner. This is obviously true for those baffle sizes for which the peak of the stability limit fuel/air rates curves could be reached; it may be surmised to be true for the other baffles tested in that at a given mass flow rate, the smaller the internal diameter of the baffle, the wider the band of fuel/air ratios for which the flame can be stabilized. As has already been mentioned, the flame was in every case observed to blow off from the conical baffle first, and only at an appreciably higher mass flow rate was complete blow out from within the combustion chamber obtained. There is thus complete accord between the qualitative predictions of the analogue and the performance of the combustion chamber.

CONCLUSIONS

The comparison has shown that the predictions of the analogue and the performance of the burner are in good qualitative agreement. Further work is necessary before the degree of quantitative agreement can be examined, but, at least for single-stream combustion chambers (to which the present investigation has been confined), there is in the comparison effected here good confirmatory evidence of the validity of the analogue.

REFERENCES

[1] Spalding, D. B. *Proc. Instn mech. Engrs., Lond.* 171 (1957) 383

[2] Senior, K. B. Discussion contributed to reference 1

[3] Spalding, D. B. *Aircraft Engineering* 28 (1956) 110, 168

89

SIMULATION OF LOW COMBUSTION PRESSURES BY WATER INJECTION

A. H. LEFEBVRE and G. A. HALLS

INTRODUCTION

The characteristics of aircraft gas turbines are such that at constant engine speed the mass flow of air delivered to the combustion system is roughly proportional to its pressure. Chemical reaction rates, however, are proportional to $(\text{pressure})^n$ where n probably lies between 1·5 and 2 for the types of fuel currently employed. This means that as the pressure is reduced the rate of supply of combustibles falls off less rapidly than does the chemical rate of reaction; the result is a deterioration in combustion performance. In testing a combustion system, therefore, only at its lowest operating pressure are its performance limitations fully exposed; in aircraft combustion systems this corresponds to a few lb./in.^{2} abs.

Unfortunately the cost of installing and operating low pressure plant is extremely high and is virtually prohibitive for universities and other academic institutions. The cheapest air by far is that supplied from a fan and for this reason a large proportion of the experimental research on combustion in flowing systems has utilized fan air. This is essentially at atmospheric pressure, so that where the combustion systems tested have been of a practical size, the results, often in the form of stability or ignition data, have usually been confined to very weak or very rich fuel/air mixtures. Where tests have been carried out in the most interesting fuel/air ratio range, i.e. near stoichiometric, either velocities have been very high or dimensions very small. In either event extrapolation to practical velocities or practical dimensions has been a somewhat dubious process. It is difficult to extrapolate dimensions because any such extrapolation must also take into account effects arising from a change in 'blockage'. It is equally difficult to extrapolate velocities because at high velocities compressibility effects can change the flow pattern in and around the combustion zone.

The method to be described is free from these objections. It allows the complete performance testing of full-scale combustion systems operating within their normal range of velocities and fuel/air ratios. Fan air is used and low pressures are simulated by introducing water into the combustion zone. The essence of the method is the theoretical equivalence, on a reaction rate basis, between a reduction in reaction pressure and a reduction in reaction temperature which, in this instance, is accomplished by the addition of water.

In a paper to the Sixth Symposium the water injection technique was put forward as an interesting idea with practical possibilities. The main object of the present paper is to demonstrate, by means of examples, how the technique has developed into a powerful tool for both research and development purposes.

APPLICATION OF WATER INJECTION TECHNIQUE TO SYSTEMS SUPPLIED WITH UNIFORM FUEL/AIR MIXTURES

Stability tests

The most important practical examples of combustors in which the fuel distribution approaches uniformity are after-burner and ramjet systems. One of the most useful applications of this technique, therefore, is in obtaining blow-off data for various designs of stabilizer. A standard method of obtaining such data is to feed the stabilizer with a uniform combustible mixture and increase the flow velocity until extinction occurs. This is experimentally a difficult and tedious process. Any increase in velocity necessitates adjustment of the fuel flow to maintain a constant mixture strength. If, as is usual, a slave pre-heat chamber is employed, a further adjustment of fuel flow is required in order to restore the pre-heat temperature. Because the final extinction point cannot be accurately predicted the above procedure is performed cautiously and in small steps.

In an actual after-burner system, however, as the altitude is increased extinction eventually takes place, not because the velocity has increased (it remains, in fact, practically constant) but because the rate of heat release at the gutter has fallen with decreasing pressure until it can no longer cope with the input of fresh combustibles. In the proposed method the heat release at the gutter is gradually reduced in a manner simulating a decrease in pressure (i.e. an increase in altitude) by the addition of water which lowers the combustion temperature. When extinction finally occurs

it does so by a mechanism which corresponds closely to an actual after-burner extinction. It is thus a more realistic method of testing gutter stability. Moreover the test procedure is very much easier and the testing time considerably shorter.

The stabilizer under test is mounted in a pipe which is connected to the outlet of a fan via a pre-heat combustion chamber. Upstream of the stabilizer are manifolds designed to inject fuel or fuel/water mixture uniformly across the gas stream. Although not essential to the method, fuel and water are thoroughly mixed before entering the manifolds by means of a Duple atomizer in which the pilot spray is formed by fuel and the main spray by water. The arrangement is shown schematically in *Figure 1.*

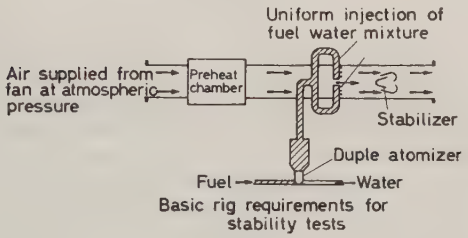

Figure 1

The test procedure is quite simple. The velocity and temperature of the gas flowing over the stabilizer are adjusted to actual engine values; the fuel is turned on and a flame established in the re-circulation zone downstream of the stabilizer. Water is then gradually admixed with the fuel in increasing amounts until extinction occurs. This process is repeated at a sufficient number of fuel flows for a complete stability loop to be drawn. A typical stability loop is shown in *Figure 2* in

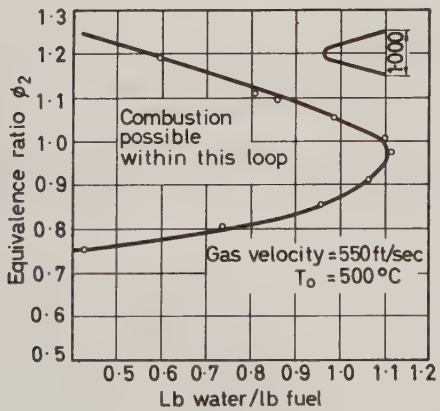

Figure 2

which the ordinate represents the equivalence ratio of the kerosine/air mixture (including pre-heat fuel) and the abscissa denotes the mass ratio of water flow to kerosine flow. This figure illustrates how easily and clearly defined is the point of peak stability, a most useful characteristic of stability loops obtained by the water injection technique.

Ignition tests

The application of the technique in establishing ignition limits may be illustrated by reference to some tests that were carried out to determine the relative ignitability of various designs of High Energy plug. The test rig is shown in *Figure 3*;

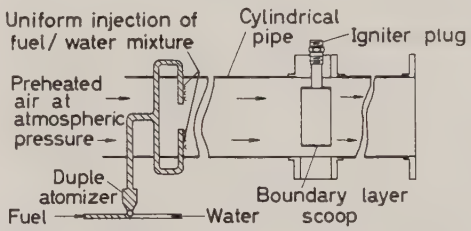

Figure 3

it is identical to the stability rig except in the working section which consists of a length of 4 in. diam. piping with the igniter located about 1 ft. from its open end. The igniter face is arranged to be 'flush' with the inside surface of a short cylindrical tube which is mounted concentrically within the 4 in. pipe and is incorporated in order to present the plug face to midstream gas where composition and velocity are near to the measured mean values (i.e. boundary layer effects are avoided). Initial pre-heating of the air to 500°C ensures that the fuel and water are completely vaporized in the plane of the igniter. The test procedure is similar to that employed in measuring stability. Water is gradually admixed with the fuel until passage of the spark no longer produces a streak of flame downstream of the plug.

Ignition loops for three widely different designs of plug are shown in *Figure 4.* Again results are plotted as graphs of equivalence ratio *versus* water/fuel ratio. In the same figure, for comparison, are plotted ignition loops for the same three plugs when operating in an actual combustion chamber at a constant sub-atmospheric pressure. These loops are plotted in the conventional manner as graphs of overall equivalence ratio *versus* mass flow. Comparison of the two sets of curves shows good qualitative agreement.

The technique has also been used to examine the influence on ignition performance of changes

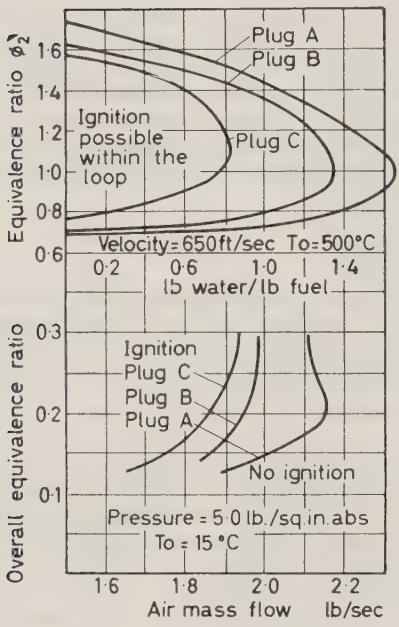

Figure 4

in the operating variables of inlet temperature and velocity. Curves illustrating the adverse effect of high velocity on ignition are illustrated in *Figure 5.*

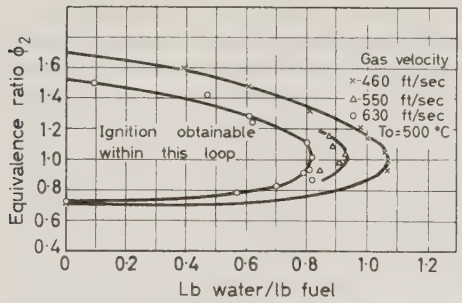

Figure 5

APPLICATION TO SYSTEMS OPERATING WITH NON-UNIFORM FUEL/AIR MIXTURES

All conventional combustion chambers fall into this category. There are two possible methods whereby the water injection technique may be applied in evaluating the main performance criteria of combustion efficiency, stability and ignition; these methods are illustrated schematically in *Figure 6.*

In one method the water is injected through manifolds located upstream of the combustion chamber under test. The pre-heat temperature

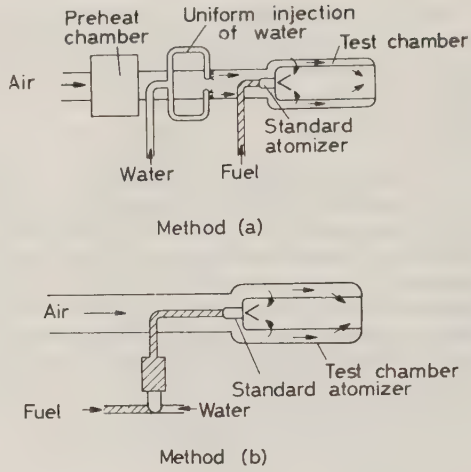

Figure 6

must again be sufficiently high to ensure that the water is fully vaporized at entry to the test chamber. Fuel is supplied to the test chamber through its own atomizer in the normal manner. An alternative method which avoids the use of pre-heat is simply to add water to the fuel at some point upstream of the atomizer. This method, however, introduces the difficulty of trying to compress a fuel/water mixture to the high pressure required for adequate atomization. A further disadvantage is that the addition of water to the fuel increases the ratio of liquid/gas momentum in the primary zone and thereby changes the pattern of fuel distribution. This effect could be important in systems where fuel atomization and distribution set the limit on performance at low pressures. For this reason all experience has so far been gained using the first method.

Combustion efficiency

If combustion efficiency is used as the yardstick in comparing the performance of various designs of combustion system, or any given combustion system before and after some design modification, then the test conditions must be such that the level of combustion efficiency is always less than 100 per cent. This usually entails rig testing at sub-atmospheric pressures.

In applying the water injection technique the combustion chamber is operated at normal engine velocities and with a high inlet temperature (usually 400°C) to ensure complete evaporation of the injected water. If an adequate supply is available steam may be used in preference to water since it entails little or no pre-heat. The addition of water or steam to the inlet air reduces

combustion efficiency in the manner illustrated in *Figure 7*, where the two curves represent the performance of a tubular chamber at two values of equivalence ratio.

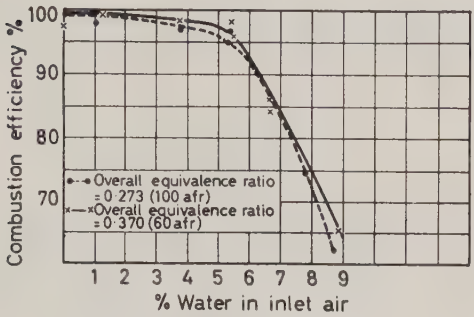

Figure 7

Stability and ignition

The test procedure follows that described above for pre-mixed fuel/air systems. With the chamber operating at constant velocity, inlet temperature and equivalence ratio the flow of water is gradually increased until either extinction occurs or the system fails to ignite. The procedure is repeated at sufficient equivalence ratios to enable stability and/or ignition loops to be drawn. Typical ignition and stability loops obtained from a single tubular chamber are shown in *Figure 8*. The

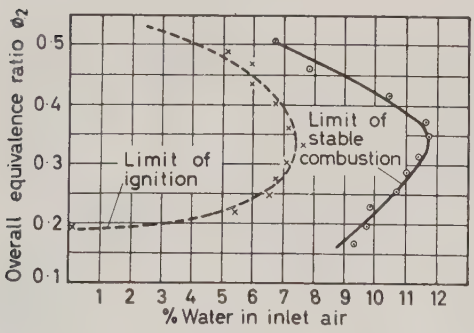

Figure 8

results are plotted, as in *Figure 7*, with equivalence ratio as ordinate and the percentage by weight of water contained in the inlet air as abscissa.

APPLICATION TO COMBUSTOR DEVELOPMENT

The water injection technique can considerably reduce the amount of time and money normally expended in low-pressure rig testing of new combustor designs. Consider, for example, the case where a design modification has been made in order to improve the mechanical reliability of the flame tube. Should the modification prove mechanically sound at high pressure it is then normally required to determine its effect on combustion performance at low pressures. This often necessitates transferring the combustor and its associated equipment to a separate low-pressure rig; in any event low-pressure air is always expensive. In the proposed method, after the high pressure testing is complete, the combustor is operated on the same rig at atmospheric pressure and at stipulated conditions of inlet temperature and velocity. Water or steam is then injected into the inlet air and curves obtained of stability, ignition and combustion efficiency, as illustrated in *Figures 7* and *8*. These curves are then compared with those obtained prior to the design modification in order to assess the effect of the modification on low-pressure performance.

It is not suggested, at this stage, that the water injection technique can completely replace low-pressure combustion testing. The main advantage of the method is that it allows cheap and rapid performance testing of numerous new designs or design modifications which would normally be prohibited by the time and expense involved in the standard low-pressure method. After testing by the water injection technique only those designs which show performance gains need be considered further.

THEORETICAL RELATIONSHIP BETWEEN QUANTITY OF ADDED WATER AND EQUIVALENT FALL IN PRESSURE

Discussion has so far been confined to the application of the water injection technique in comparing combustion systems from various performance aspects. Its value would obviously be increased by a relationship between the quantity of added water and the equivalent fall in pressure.

Now the effect of adding water to a reaction zone is twofold. First, by its presence, it reduces the concentration of reacting species. Secondly, by virtue of its heat capacity, it lowers the reaction temperature. The combined effect may be evaluated quantitatively using reaction rate theory with assumed values of overall reaction order and activation energy. Reaction rate equations for kerosine burning in fresh or vitiated air were presented in reference 1 for an assumed overall reaction order of 2. For many practical combustion systems, however, the effective reaction order is less than 2 and a second set of equations has been derived based on a value of n of 1·75.

For lean mixtures ($\phi_2 > 1$)

$$\frac{M}{V P^{1.75}} \propto \frac{(1-B)^{0.75}\,[1-\phi_1-B\,(\phi_2-\phi_1)]\,(\phi_2-\phi_1)^{-0.25}}{T^{1.25}\exp.\,21{,}000/T.B.\,[85{\cdot}7+6\,\phi_2-5\,(1-1{\cdot}87K-B)\,(\phi_2-\phi_1)]^{1.75}}$$

For rich mixtures ($\phi_2 < 1$)

$$\frac{M}{V P^{1.75}} \propto \frac{(1-B)^{1.75}\,(1-\phi_1)\,(\phi_2-\phi_1)^{-0.25}}{T^{1.25}\exp.\,21{,}000/T.B.\,[85{\cdot}7+6\,\phi_1-18B\,(1-\phi_1)+(\phi_2-\phi_1)\,(1+23B+9{\cdot}34K)]^{1.75}}$$

where M = air mass flow, lb./sec; V = reaction volume, ft.^{3}; P = static pressure, atm; T = reaction temperature, °K; and B = fraction of fuel burned (combustion efficiency).

The above equations describe the performance of a homogeneous reactor supplied with fresh or vitiated air plus kerosine fuel of which a fraction (1–B) leaves the reactor unburned. ϕ_1 is the equivalence ratio of combustion processes occurring upstream of the reactor; it is assumed that any such process takes place with 100 per cent combustion efficiency. ϕ_2 is the overall equivalence ratio. The reacting species are unburned fuel and oxygen, and the effect of water in reducing their concentration is taken into account in the above equations where the quantity of added water is expressed as a fraction K of the fuel supplied to the reactor.

Reaction temperature, T, is obtained by a heat balance. The heat lost by the completely burned products in falling from flame temperature to reaction temperature is equated to the heat absorbed in raising the unburned fuel and air to reaction temperature and in converting water or steam at inlet temperature to steam at reaction temperature. Full allowance is made for the effects of chemical dissociation.

By substituting appropriate values of ϕ_1, ϕ_2, and B into the above equations, together with the corresponding calculated values of T, relationships may be obtained between the quantity of added water and the equivalent fall in gas pressure. Several such relationships were provided in the reference.

The effect of water in reducing reaction rates is illustrated in *Figure 9*, where curves of $M/(VP^{1.75})$ are shown plotted against B for various values of K. The dashed line in this figure corresponds to halving P. It is observed to follow closely the line drawn for $K = 1$ and demonstrates that, for the conditions quoted, adding a pound of water to each pound of fuel is roughly equivalent to halving the gas pressure. This relationship was shown in reference 1 to hold over a wide range of inlet temperatures and equivalence ratios.

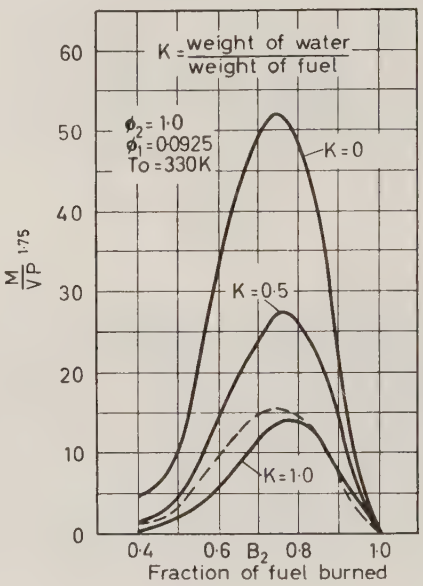

Figure 9

CONCLUSIONS

(1) Water injection is a cheap and rapid method of assessing and comparing combustion systems operating with either pre-mixed or separate fuel/air injection.

(2) A theoretical relationship between the amount of water required to simulate any given reduction in pressure has been evaluated using simple reaction rate theory. The addition of a pound of water to each pound of kerosine is roughly equivalent to halving the gas pressure. This relationship has been verified for systems supplied with uniform fuel/air mixtures[1].

(3) The technique cannot be applied to systems whose low-pressure performance is limited by mixing or fuel atomization or any process other than chemical reaction. This restriction does not usually apply to most practical forms of gas turbine combustion equipment.

The authors' thanks are due to Messrs Rolls-Royce, Ltd., for permission to write and publish this paper.

REFERENCE

GREENHOUGH, V. W. and LEFEBVRE, A. H. Some applications of combustion theory to gas turbine development. *Sixth Symposium (International) on Combustion*, p. 858. 1956. New York; Reinhold

90

A NON-ACOUSTIC THEORY OF OSCILLATIONS IN PRESSURE-JET OIL-FIRED COMBUSTION CHAMBERS

M. W. THRING

OCCURRENCE OF OSCILLATIONS

It is a definite experimental fact that stable oscillations of a well defined frequency are often established in the combustion chamber of pressure-jet oil-firing systems[1]. The absolute pressure in the combustion chamber oscillates sometimes with a sufficient amplitude to cause the flame to blow back out of the air inlet. Observation by A. M. Brown on large boiler flames shows that the ignition plane of the oil projected into the flame oscillates, and it is clear that the rate of air supply into the combustion chamber must oscillate because the amplitude of the pressure oscillations in the combustion chamber is of the same order, as these oscillations have a frequency of the order of 10 per sec, probably rising to the order of 100 per sec on smaller combustion chambers. These frequencies may correspond to acoustic sound waves in the combustion chamber but as the fractional amplitude of the absolute pressure fluctuations is small it is interesting to see whether they can be due to oscillations in which the whole pressure throughout the combustion chamber oscillates simultaneously and affects the instantaneous rate of air supply. These oscillations are analogous to 'chugging' in rocket motors rather than 'screaming'[2]. Chugging in rocket motors is definitely associated with oscillations in the rate of supply of liquid propellants to the combustion chamber caused by oscillations in the absolute pressure in the combustion chamber[3].

Other facts about these oscillations in atmospheric pressure combustion chambers are as follows: (1) the occurrence of the oscillations is definitely dependent on the design of the air register, but it is not yet known which is the best design from this point of view; (2) supplying the combustion air at a higher pressure through a smaller register reduces the tendency to oscillate; (3) increasing the resistance to gas flow out of the combustion chamber increases the tendency to oscillate; (4) increasing the gas and air supply rates together so as to shorten the dwell time of the gases in the combustion chamber increases the tendency to oscillate; (5) increasing the amount of excess air to values over 50 per cent reduces the tendency to oscillate; (6) connecting the combustion chamber direct to the atmosphere by opening a door always stops the oscillation.

A THEORY OF OSCILLATIONS

The existence of stable oscillations necessarily requires: (*a*) a tuned circuit or a system with a natural stable frequency which can arise if there are two delay times in the system of the same order of magnitude which interact on each other, and (*b*) a power feed-back mechanism which replaces the energy absorbed by the natural damping of the system.

In the present system one natural time period is the average dwell time (t_c sec) of the combustion gases in the combustion chamber which is of the order of a half to two seconds (it is approximately related to the combustion intensity by the formula

$$CI = \frac{3 \times 10^7}{t_c \cdot T_c} \, CHU/\text{ft.}^3\,\text{h}$$

where T_c is the mean absolute temperature of the gases in the combustion chamber °K). The only other delay time of the same order of magnitude would appear to be the delay time (T_a sec) of the air in passing through the combustion air tube between the supply inlet or fan and the register, and the delay time (t_e sec) of the combustion gases after leaving the combustion chamber and before leaving the end of the stack. It is therefore postulated that the other delay time is one of these two. The feed-back mechanism that supplies the power to maintain the oscillations must clearly come from the heat release on combustion. Since the oil supply rate is very unlikely to be affected by a swing in the absolute pressure in the combustion chamber of the order of a few in. of water gauge, it is postulated that the oil supply rate is constant. Two possible assumptions could be made as to the effect of a change in the instantaneous rate of air entry ($\dot{m}_a$ lb./sec) from the time mean value ($\bar{\dot{m}}_a$). The first is that this produces a proportional change in the instantaneous space mean temperature T of the gases in the combustion chamber, i.e.

$$T - \bar{T} = k(\dot{m}_a - \bar{\dot{m}}_a)$$

The equations resulting from this assumption are given in the third section which shows that they can correspond to sustained oscillations (terms in d/dt zero) when k is chosen at a sufficiently great negative value. This would correspond physically

to a system in which an increase in air flow rate produced an immediate contraction of the whole of the gases in the combustion chamber.

Another plausible assumption in the third section, is that the change in instantaneous air entry rate produces a time rate of change in the space mean gas temperature so that

$$\frac{\mathrm{d}T}{\mathrm{d}t} = k(\dot{m}_a - \bar{\dot{m}}_a)$$

where the new k has the dimensions (°K/sec)/(lb./sec) and the calculations show that if it has a sufficiently large negative value sustained oscillations are possible.

In order to develop a simple theory it is also assumed that the inlet and outlet gas flow rates

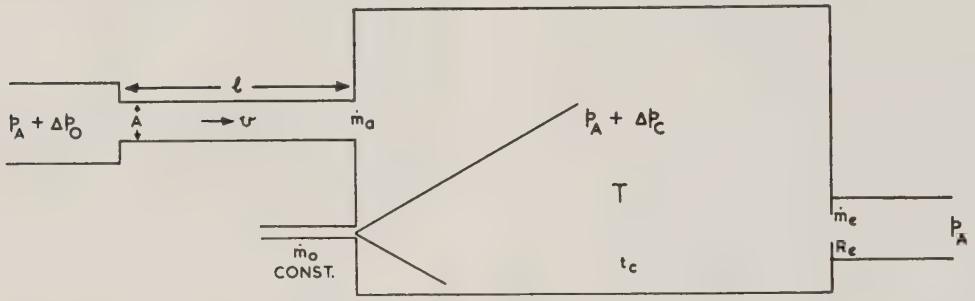

Figure 1. Assumed system for inlet air momentum

are linearly proportional to the pressure drop across the inlet and outlet resistances. This makes the mathematics simpler and does not obscure the essential physics of the process.

MATHEMATICAL THEORY

Inertia of the inlet air

It can be postulated that the air inlet supply rate at the register is related to the pressure drop between the combustion chamber and a constant upstream pressure Δp_0 by a delay equation of the type

$$\dot{m}_a + t_1 \frac{\mathrm{d}\dot{m}_a}{\mathrm{d}t} = \frac{\Delta p_0 - \Delta p_c}{R_a} \qquad (1)$$

(which means that the mass flow of air across the register starts to respond immediately to a change in combustion chamber pressure but only completes the change exponentially with a decay time t_1). The term containing t_1 is by the electrical analogy an inductance term and must arise from the finite momentum of the air in the inlet pipe. To interpret t_1 physically consider the Navier-Stokes equation for the fluid in the inlet pipe. If we neglect the viscous terms which give rise to the term in $\dot{m}_a$ in expression 1 this may be written

$$\frac{\mathrm{d}}{\mathrm{d}t}(\rho v) = \frac{\mathrm{d}\Delta p}{\mathrm{d}x}$$

or $\dfrac{\mathrm{d}}{\mathrm{d}t}\left(\dfrac{\dot{m}_a}{A}\right) = \dfrac{\mathrm{d}\Delta p}{\mathrm{d}x}$ where A is the area of the inlet pipe.

So

$$\Delta p_0 - \Delta p_c = \int_0^l \frac{\mathrm{d}}{\mathrm{d}t}\left(\frac{\dot{m}_a}{A}\right)\mathrm{d}x = l\frac{\mathrm{d}}{\mathrm{d}t}\left(\frac{\dot{m}_a}{A}\right) = \frac{l}{A}\frac{\mathrm{d}\dot{m}_a}{\mathrm{d}t}$$

if the area of the inlet is constant along its length l and is too small for fluid to accumulate when the pressure changes. Thus, comparison with expression 1 shows that $t_1 R_a = l/A$

$$t_1 = \frac{l}{A}\cdot\frac{\bar{\dot{m}}_a}{\Delta p_0 - \overline{\Delta p_c}} = \frac{l}{A}\cdot\frac{\rho A v}{C\,.\,\frac{1}{2}\rho v^2} = \frac{2l}{C\,.\,v}$$

where C is the resistance coefficient. Thus, since C is a number of the order of unity, t_1 is a time of the order of the dwell time of the air in the high velocity region of the air inlet. It will not however necessarily vary exactly with this time for changes in l and A because a square law of resistance has been introduced in the interpretation. In this case it is possible to have stable oscillations with the simple linear combustion equation

$$T - \bar{T} = k(\dot{m}_a - \bar{\dot{m}}_a) \qquad (2)$$

in which the space-mean combustion chamber temperature responds at once to a change in air inlet rate.

The other two equations required are the mass storage equation for the combustion chamber

$$\dot{m}_0 + \dot{m}_a - \dot{m}_e = \frac{\bar{M}\,.\,\bar{T}}{\bar{p}}\frac{\mathrm{d}}{\mathrm{d}t}\left(\frac{p_c}{T}\right) = \bar{\dot{m}}_e\,.\,t_c\,.\,\frac{\bar{T}}{\bar{p}} \times \left(\frac{1}{T}\frac{\mathrm{d}p_c}{\mathrm{d}t} - \frac{p}{T^2}\frac{\mathrm{d}T}{\mathrm{d}t}\right) \qquad (3)$$

where $\bar{M}$ is the mean total mass of gas in the combustion chamber, $\dot{m}_0$ is the oil input rate assumed unaffected by changes in instantaneous chamber pressure and the equation for the instantaneous gas exit mass flow

$$\dot{m}_e = \frac{\Delta p_c}{R_e} \qquad (4)$$

These equations can be combined to give a second order differential equation for $\dot{m}_a$, the instantaneous mass flow rate of air into the combustion chamber, as follows:

$\dot{m}_e$ is eliminated between expressions 4 and 3; $\mathrm{d}T/\mathrm{d}t$ is obtained by differentiating 2 and substituted in the equation obtained from 4 and 3. Then Δp_c is eliminated using 1. The differential equation is:

$$t_c t_1 \frac{\mathrm{d}^2\dot{m}_a}{\mathrm{d}t^2} + \left\{\frac{\bar{p}t_1}{R_e\,\bar{\dot{m}}_e} + t_c\left(1 + \frac{k\bar{p}}{R_a\bar{T}}\right)\right\}\frac{\mathrm{d}\dot{m}_a}{\mathrm{d}t} + \dot{m}_a\left(1 + \frac{R_a}{R_e}\right)\frac{\bar{p}}{R_a\bar{\dot{m}}_a} = \text{constant}$$

In the case where $R_e \ll R_a$ this may be simplified to

$$\tau \doteq 2\pi(t_c t_1)^{1/2}\left(\frac{R_e\bar{\dot{m}}_a}{\bar{p}}\right)^{1/2}$$

Thus $\tau = 0{\cdot}014$ sec and $0{\cdot}09$ sec in the low and high loading cases discussed.

Delay volume on the air inlet side (inlet delay time t_1 sec)

The equations relating the instantaneous pressure $p_A + \Delta p_c$ in the combustion chamber (p_A = atmospheric pressure in w.g.), the instantaneous pressure ($p_A + \Delta p_1$) in the air inlet volume, the instantaneous mass flow rate of air into the combustion chamber ($\dot{m}_a$) and the instantaneous rate of gas flow out of the combustion chamber ($\dot{m}_e$), and the instantaneous value (T°K) of the space mean temperature of the gases in the combustion chamber based on these assumptions are as follows:

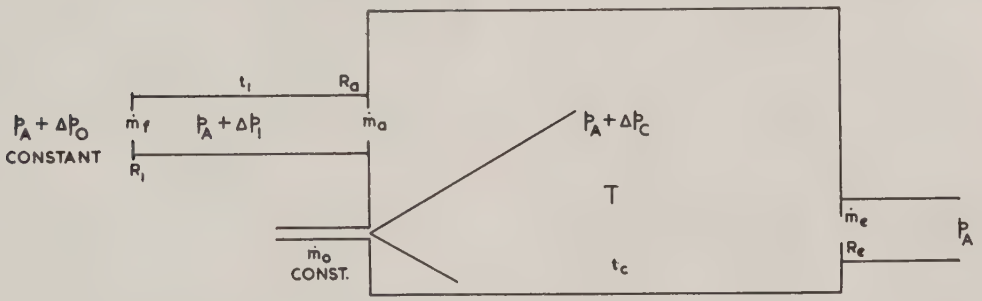

Figure 2. Assumed system for inlet delay volume

This implies sustained oscillations in the air mass flow ($\dot{m}_a$) across the register if

$$-k \geqslant +\frac{R_a\overline{T}}{\bar{p}} + \frac{t_1}{t_c}\cdot\frac{R_a}{R_e}\cdot\frac{\overline{T}}{\bar{\dot{m}}_e}$$

Thus on this theory stable oscillations are less likely because the value that $(-k)$ must exceed for stable oscillations becomes larger if:

(1) R_a is increased, i.e. the cross-sectional area of the air register is reduced while the fan pressure Δp_0 is increased to keep $\dot{m}_a$ constant. This is the biggest factor as it comes into both terms in k.

(2) t_1/t_c is increased, i.e. the volume of the combustion chamber is reduced in relation to the volume of the high velocity region of the air inlet.

(3) R_e is reduced, i.e. the combustion chamber is more widely open to the atmosphere.

(4) $\dot{m}_e$ is reduced, i.e. the mass flow through the system is reduced. However the best way of avoiding stable oscillations is to reduce $(-k)$ by reducing the fraction of the volume of the combustion chamber that is occupied by unmixed air.

The oscillation cycle period is

$$\tau = \frac{2\pi(t_c t_1)^{1/2}}{\left[\left(\frac{1}{R_a} + \frac{1}{R_e}\right)\frac{\bar{p}}{\bar{\dot{m}}_a}\right]^{1/2}}$$

$$\frac{\Delta p_0 - \Delta p_1}{R_1} = \dot{m}_1 \tag{5}$$

$$\bar{\dot{m}}_a\, t_1 \cdot \frac{1}{\bar{p}}\frac{\mathrm{d}p_1}{\mathrm{d}t} = \dot{m}_1 - \dot{m}_a \tag{6}$$

$$\frac{\Delta p_1 - \Delta p_c}{R_a} = \dot{m}_a \tag{7}$$

$$\bar{\dot{m}}_e t_c\left\{\frac{1}{\bar{p}}\frac{\mathrm{d}p}{\mathrm{d}t} - \frac{1}{\overline{T}}\frac{\mathrm{d}T}{\mathrm{d}t}\right\} = \dot{m}_a + \dot{m}_0 - \dot{m}_e \tag{8}$$

$$\frac{\mathrm{d}T}{\mathrm{d}t} = k(\dot{m}_a - \bar{\dot{m}}_a) \tag{9}$$

$$\frac{\Delta p_c}{R_c} = \dot{m}_e \tag{10}$$

$\bar{p}$ is the time mean pressure in the region which may be taken as p_A.

Note that: $\dot{m}_0 = \bar{\dot{m}}_0$ as the oil inlet rate does not vary with time; $\bar{\dot{m}}_a + \dot{m}_0 + \bar{\dot{m}}_e = 0$ (Conservation of mass); $\bar{\dot{m}}_a$ = 16–20 times $\bar{\dot{m}}$.

Equation 5 is the flow equation into the air supply space across the first inlet resistance, 7 the flow equation into the combustion chamber, 6 the change in storage of air in the air supply space due to change in pressure, 8 the change in storage of gas in the combustion chamber due to changes in temperature and pressure, 9 the assumption about the relationship of temperature change rate to the instantaneous air supply rate, and 10 is the equation for gas exit from the combustion chamber. These equations can be solved by eliminating the fluctuating variables $\dot{m}_1$, $\dot{m}_a$, $\dot{m}_e$, $\mathrm{d}T/\mathrm{d}t$ and Δp_c, to give a differential equation for the fluctuating variable Δp_1 the pressure in the air inlet volume. This equation is as follows:

$$\frac{\bar{m}_a}{\bar{p}^2} t_1 t_c \frac{\mathrm{d}^2 p_1}{\mathrm{d}t^2} + \frac{1}{\bar{p}} \frac{\mathrm{d}p_1}{\mathrm{d}t} \left\{ \left(\frac{1}{R_a} + \frac{1}{R_1} + \frac{k\bar{m}_a t_1}{\bar{T} R_a} \right) t_c + \frac{\dot{m}_a}{\bar{m}_e} t_1 \left(\frac{1}{R_A} + \frac{1}{R_c} \right) \right\} + \Delta p_1 \left\{ \frac{k t_c}{\bar{T} R_1 R_a} + \frac{1}{\bar{m}_e} \left(\frac{1}{R_1 R_a} + \frac{1}{R_c R_a} + \frac{1}{R_1 R_e} \right) \right\} = \text{constant}$$

This equation shows that if k is negative, that is an increase in the instantaneous rate of air flow into the combustion chamber causes the space mean combustion gas temperature to begin to fall and has the value

$$k = -\bar{T} \left\{ \frac{1}{t_1 \bar{m}_a} \left(1 + \frac{R_a}{R_1} \right) + \frac{1}{t_c \bar{m}_e} \left(1 + \frac{R_a}{R_e} \right) \right\}$$

then stable oscillations can be set up. These oscillations have the time of oscillation

$$\tau = \frac{2\pi (t_1 t_c)^{1/2} \bar{m}_a}{\bar{p} \left(\frac{\bar{m}_a}{\bar{m}_e} \frac{1}{R_e R_a} - \frac{t_c}{t_1} \left(\frac{1}{R_1 R_a} + \frac{1}{R_1^2} \right) \right)^{1/2}} \text{ sec}$$

Since $\bar{m}_a$ and $\bar{m}_e$ do not differ much and t_c is usually greater than t_1 stable oscillations can only occur if R_1 and R_a are both much larger than R_e, while t_c is not very much greater than t_1.

To give reasonable numerical values, two cases are considered: a lightly loaded combustion chamber, and a heavily loaded one with suitable air inlet resistances. The conditions for stable oscillations in these cases and the corresponding frequencies are given in Table 1.

TABLE 1

Lightly loaded combustion chamber

$\bar{T}_c = 1{,}000°\mathrm{K}$

$t_c = 2$ sec

$CI = 15{,}000$ CHU/ft.^{3}-h

$T_1 = 0{\cdot}1$ sec

$$R_1 = R_a = 200\, R_e = \frac{\bar{p}}{200\, \bar{m}_a}$$

i.e. pressure drop across each inlet resistance = 2 in. w.g., pressure drop across outlet resistance = 0·01 in. w.g.

Value of k for stable oscillations

$$= -\frac{1{,}000}{\bar{m}_a} \{10(1 + 1) + \tfrac{1}{2}(1 + 200)\} = -\frac{1{,}000}{\bar{m}_a} 120$$

This means that a change of 1 per cent in the instantaneous air inlet rate must produce a drop in combustion chamber space mean temperature at the rate of 1 per cent in 1/120 sec, a value compatible with the rate of movement of the oscillating flame front observed by Brown.

Frequency of stable oscillations

$$\tau = \frac{2\pi (0{\cdot}2)^{1/2}}{(200^2 \,.\, 200 - 20 \,.\, 200^2 \,.\, 2)^{1/2}} = \frac{2\pi (0{\cdot}2)^{1/2}}{200 (160)^{1/2}} = 0{\cdot}0011 \text{ sec}$$

Heavily loaded combustion chamber

$T_c = 1{,}000°\mathrm{K}$

$t_c = \frac{1}{4}$ sec

$CI = 120{,}000$ CHU/ft.^{3}-h

$t_1 = \frac{1}{12}$ sec

$$2R_1 = R_a = 20\, R_e = \frac{\bar{p}}{50\, \bar{m}_a}$$

i.e. pressure drop across first inlet resistance 4 in. w.g., across register 8 in. w.g., across tube bank 0·45 in. w.g.

$$k_{st} = -\frac{1{,}000}{\bar{m}_a} \{12(3) + 4{\cdot}21\} = -\frac{1{,}000}{\bar{m}} 120$$

$$\tau_{st} = \frac{2\pi (1/200)^{1/2}}{(50{,}000 - 3(5000 + 10{,}000))^{1/2}} = 0{\cdot}006 \text{ sec}$$

Case when second delay volume is on exit side

Making exactly similar assumptions to the previous case, but letting $p_A + \Delta p_2$ represent the instantaneous pressure in the exit delay volume and R_f the resistance to gas flow at the other side of this, the equations of the oscillations in this case are as follows:

$$\frac{\Delta p_0 - \Delta p_c}{R_a} = \dot{m}_a$$

$$\bar{m}_e t_c \left\{ \frac{1}{\bar{p}} \frac{\mathrm{d}p_c}{\mathrm{d}t} - \frac{1}{\bar{T}} \frac{\mathrm{d}T}{\mathrm{d}t} \right\} = \dot{m}_a + \dot{m}_0 - \dot{m}_e$$

$$\frac{\mathrm{d}T}{\mathrm{d}t} = k(\dot{m}_a - \bar{m}_a)$$

$$\dot{m}_e - \dot{m}_f = \bar{m}_e \frac{t_c}{\bar{p}} \frac{\mathrm{d}p_2}{\mathrm{d}t}$$

$$\frac{\Delta p_c - \Delta p_2}{R_e}$$

$$\frac{\Delta p_2}{R_f} = \dot{m}_f$$

Here the solution obtained is:

$$\frac{d^2p_2}{dt^2} t_c t_e \frac{\bar{m}_e^2}{\bar{p}^2} + \frac{\bar{m}_e}{\bar{p}} \frac{dp_2}{dt} \left\{ t_c \left(\frac{1}{R_e} + \frac{1}{R_f} + \frac{k}{R_a \bar{T}} \bar{m}_c t_e \right) + t_e \left(\frac{1}{R_e} + \frac{1}{R_a} \right) \right\} + \Delta p_2 \cdot \left\{ \frac{k t_c \bar{m}_e}{\bar{T} R_a} \left(\frac{1}{R_e} + \frac{1}{R_f} \right) + \left(\frac{1}{R_a R_e} + \frac{1}{R_a R_f} + \frac{1}{R_f R_e} \right) \right\} = \text{constant}$$

At first sight it looks as though stable oscillations could be obtained in this case also, but if k had a sufficiently large negative value eliminating the d/dt term and thus the damping of the oscillations, then the coefficient of the Δp_2 terms becomes negative and the system is no longer an oscillating system, but becomes a simple unstable system.

CONCLUSIONS

It is of considerable interest that two sets of hypotheses based on (1) a negative effect of the instantaneous air inlet flow rate on the space mean combustion temperature and (2) a negative effect of small rises in combustion chamber pressure on the instantaneous air inlet flow rate can give rise to stable oscillations. Of the two mechanisms discussed in section 3 the first seems the most likely. The practical importance of such a theory lies in the possibility it suggests of eliminating pressure pulsations in the combustion chamber without using the methods which are bad fuel technology (reducing the rate of firing or the gas exit resistance which is required for good convective heat transfer, or increasing the excess air proportion or the gas inlet resistance). Thus improvement of the mixing conditions in the chamber towards the fully pre-mixed condition and stabilizing the flame more closely to the burner nose should both reduce the absolute value of $(-k)$ and hence reduce the possibility of stable oscillations.

APPENDIX

The equations for inlet control with linear temperature assumption.

$$\frac{\Delta p_0 - \Delta p_1}{R_1} = \dot{m}_1$$

$$\dot{m}_a \frac{t_1}{\bar{p}} \frac{dp_1}{dt} = \dot{m}_1 - \dot{m}_a$$

$$\frac{\Delta p_1 - \Delta p_c}{R_a} = \dot{m}_a$$

$$\dot{m}_e \cdot t_c \left\{ \frac{1}{\bar{p}} \frac{dp_c}{dt} - \frac{1}{\bar{T}} \frac{dT}{dt} \right\} = \dot{m}_a + \dot{m}_0 - \dot{m}_e$$

$$T - \bar{T} = k(\dot{m}_a - \bar{m}_a)$$

$$\frac{\Delta p_c}{R_e} = \dot{m}_e$$

The solution is

$$\frac{d^2p_1}{dt^2} \cdot \frac{t_c t_1}{\bar{p}} \bar{m}_a \left(\frac{R_a}{\bar{p}} + \frac{k}{\bar{T}} \right) + \frac{dp_1}{dt} \times \left\{ \frac{t_c}{\bar{p}} \left(1 + \frac{R_a}{R_1} + \frac{k\bar{p}}{\bar{T} R_1} \right) + \frac{\bar{m}_a}{\bar{m}_e} \frac{t_1}{\bar{p}} \left(1 + \frac{R_a}{R_e} \right) \right\} + \frac{\Delta p_1}{\bar{m}_e} \left\{ \frac{1}{R_1} + \frac{1}{R_e} + \frac{R_a}{R_e R_i} \right\} = \text{constant}$$

If k is given a sufficiently large negative value to make the coefficient of the dp_1/dt term vanish, then the coefficient of the d^2p_1/dt^2 term becomes negative. Thus stable oscillations are not possible with this set of assumptions.

REFERENCES

[1] Putman A. A. and Dennis, W. R. *Pulsations in Residential Heating Equipment, Heating Piping and Air Conditioning*, p. 131. 1956

[2] Ross, C. C. and Datner, P. P. Combustion instability in liquid propellant rocket motors. AGARD *Selected Combustion Problems I*, p. 352. 1955. London; Butterworths

[3] Crocco, R. and Cheng, S. I. *Theory of Combustion Instability in Liquid Propellant Rocket Motors* (Agardograph, No. 8). 1956. London; Butterworths

COMBUSTION STABILITY IN A SPHERICAL COMBUSTOR

A. E. CLARKE, A. J. HARRISON and J. ODGERS

INTRODUCTION

The theory of a well stirred spherical combustor was first enunciated by Longwell[1], and the combustion rates attained are so high as to suggest that they are limited by reaction kinetics. These rates represent the maximum which can be obtained in a practical appliance and as such they merit particular study since they may provide pointers for the improvement of applied combustion processes. Such high output combustion systems give evidence that the burning rate is due largely to the intense re-circulation of the hot products of combustion with the unburnts entering the system.

In an applied combustion system this re-circulation and mixing has to be provided by the aerodynamic pressure loss across the flame tube, and normally a pressure loss of the order of 5 per cent $\Delta P/P$ is available. Experiments of the Longwell type, however, had involved calculated pressure losses as high as 90 per cent $\Delta P/P$ and hence direct use of the fundamental work was difficult.

The object of the present work was to investigate this pressure drop and mixing effect, and the experiments described here represent the initial stage in the investigation.

In order to simplify these early stages of the work, gaseous propane was employed as fuel; also, to achieve correlation with other workers in the field the system as a whole was made as similar as possible to existing spherical combustors.

THEORETICAL

Previous work by Longwell and Hottel has shown that the blow-out curves of fuel air mixtures in a spherical combustor may be related to a semi-empirical kinetic equation of the type

$$\mathcal{N}/VP^n = \frac{k\,(m+1)}{\epsilon\varnothing\,.\,R^n}\ {}^zO\ {}^zF.\ \frac{e^{-E/RT}}{T^{n-\frac{1}{2}}}$$

Where

$\mathcal{N}$ = air mass flow, g moles/sec
V = combustor volume, litres
P = pressure, atm
n = reaction order
k = 'collision factor'
m = the ratio $\frac{\text{moles inert}}{\text{moles oxygen in the mixture}}$
ϵ = fractional oxygen consumption efficiency
$\varnothing$ = equivalence ratio
R = gas constant
${}^zO$ = molar fraction—oxygen
${}^zF$ = molar fraction—fuel
E = activation energy cals/g mol
T = adiabatic flame temperature, °K

This relationship assumes that the system is perfectly homogeneous and it follows that blow-out should be limited purely by chemical kinetics. The characteristic curves of temperature *versus* generalized rate for a well stirred reactor have been considered by Hottel[2] and it will be sufficient here to say that only those reactions possessing a high value of activation energy will give rise to the characteristic blow-out curves experienced in these experiments.

For propane one may derive the following fundamental relationship based upon simple collision theory and an nth order reaction.

$$\mathcal{N}/VP^n = \frac{(m+1)\times 1{\cdot}2618\times 10^{13}}{R^n}\times \frac{e^{-E/RT}}{T^{n-\frac{1}{2}}}\ \frac{[2\,(\varnothing-\epsilon\varnothing)]^{\alpha}\,[1-\epsilon\varnothing]^{\beta}}{\epsilon\varnothing\,[m+1+1{\cdot}4\,\varnothing-\epsilon\varnothing]^{n}} \tag{2}$$

The terms are as before except that α represents the reaction order for fuel and β represents the reaction order in oxygen. The above equation is limited to weak mixtures since it has been derived by assuming that the only unburnt product is carbon monoxide.

For rich mixtures the unburnt products are more diverse and carbon monoxide, hydrogen and propane have all been detected, and it seems likely that at very rich mixtures some unsaturated compounds may be produced. If the carbon dioxide, carbon monoxide, hydrogen and water are assumed to obey the water-gas equilibrium it is possible to derive an equation in which the only unburnt substance considered is the residual propane. By doing this the following equation may be derived:

$$\mathcal{N}/VP^n = \frac{(m+1)\times 1{\cdot}2618\times 10^{13}}{R^n}\times \frac{e^{-E/RT}}{T^{n-\frac{1}{2}}}\ \frac{1}{\epsilon}\ \frac{[0{\cdot}2\varnothing\,(1-\epsilon)]^{\beta}\,[1-\epsilon]^{\alpha}}{[m+1-\epsilon+0{\cdot}2\varnothing\,(1+6\epsilon)]^{n}} \tag{3}$$

Equations 2 and 3 are purely theoretical. As will be seen, the values of E, α and β were later chosen to give the best experimental fit. The theoretical value of k was also modified by including what can only be tentatively described as a 'steric factor'.

In the present series of experiments early results showed a wide scatter due to the presence of varying amounts of water and water vapour in the compressor line. Theoretical calculations have been carried out to obtain the effect of water upon the volumetric heat release rate. Because of its different thermal capacity compared with air, water vapour reduces considerably the reaction temperature and since the reaction rate is exponentially related to the flame temperature a comparatively small reduction of the latter will give rise to a large reduction in reaction rate. The position is further aggravated by the fact that water vapour also acts as a diluent. Table 1 gives the calculated effect of water vapour at various equivalence ratios and for various inlet temperatures. It will be seen that the presence of as little as 1 per cent of water vapour could reduce the reaction rate by as much as 24 per cent. With this in mind, an air drier was incorporated in the system as shown in *Figure 1*.

Hottel[2] has suggested that for similar mass flows the limiting value of N/VP^n at any given equivalence ratio is dependent upon the degree of mixing. He demonstrated this in his experiments by varying the hole sizes in the fuel injectors and suggested that his combustor, and indeed that used by Longwell, might not have been perfectly stirred, particularly in the case of very weak or very rich mixtures. It was thought that the result of this would be an alteration of the pressure exponent n, and the argument was illustrated by means of dimensional analysis.

One of the aims of the present series of experiments was to investigate this mixing effect. It was hoped that by a careful analysis of the results it would be possible to incorporate a 'factor of mixedness' in the derived semi-empirical expression. Previous combustion experience[3] had suggested that specific heat release rates are related to the ratio $(\Delta P/P)^{\frac{1}{2}}$, where P is the injection total pressure and ΔP is the difference between P and the pressure of the combustion space.

Thring[4], from dimensional analysis considerations, has also suggested that combustion intensity should be proportional to $(\Delta P/P)^{\frac{1}{2}}$.

TABLE 1

Per cent Decrease in Reaction Rate Caused by the Presence of 1 per cent Water Vapour in the Air

Inlet Temp. \ ϵ	0·99	0·95	0·90	0·85	0·80	∅
300°K	10·5	11·3	12·4	13·0	15·0	
400°K	11·1	10·9	11·9	12·5	13·2	1·0
600°K	8·3	10·1	10·1	10·4	12·7	
300°K	10·1	11·8	12·0	14·2	15·8	
400°K	12·7	13·1	13·6	14·0	14·0	0·9
600°K	12·1	12·2	12·5	12·4	14·1	
300°K	8·8	11·9	13·7	14·0	16·9	
400°K	11·5	12·5	13·4	14·7	16·2	0·8
600°K	8·1	10·0	12·0	13·3	15·2	
300°K	14·3	16·1	17·1	16·4	17·8	
400°K	18·1	16·2	14·9	14·0	13·6	0·7
600°K	11·4	13·2	13·2	14·0	14·1	
300°K	17·8	19·9	19·6	22·1	24·2	
400°K	8·6	10·8	12·6	15·5	18·1	0·6
600°K	13·1	13·4	14·0	14·5	15·0	

APPARATUS

The apparatus used is shown diagrammatically in *Figure 1*. Air from a compressor or from the atmosphere (depending upon the required conditions) passes through a silica gel drier to the metering section and thence to the variable electrical pre-heater and the pebble bed chamber, where it mixes intimately with metered and vaporized fuel. The resultant fuel/air mixture

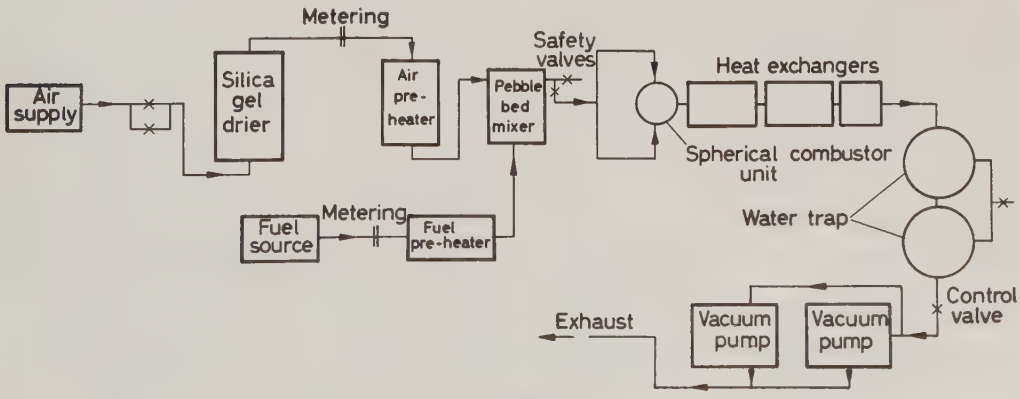

Figure 1

flows into both sides of the injector which is placed in the centre of the spherical combustion chamber.

After combustion the exhaust is cooled in the heat exchangers—sometimes with additional water sprayers—and then flows through the water separators to the exhaust vacuum pumps.

It should be noted that in these experiments with atmospheric inlet temperature and propane gas neither the air pre-heater nor the fuel pre-heater were in operation.

The spherical combustion chamber is virtually identical to that of Longwell and Weiss[1] and is shown diagrammatically in *Figure 2*. Plimanite Superall refractory was used for the 1 in. thick insulation to the 3 in. i.d. combustion chamber, this material having a specified limiting temperature of 1,970°K. The exhaust gases left the chamber via 60 equi-spaced $\frac{1}{4}$ in. diameter holes.

Three different types of injectors were used (see *Figure 2*) :

(1) Spherical injectors (0·75 in. diameter or 1·0 in. diameter).

(2) Cylindrical injectors (0·375 or 0·75 in. diameter by 1 in. length). In this type of injector the holes were drilled in banks equi-spaced and at right angles to the surface of the cylinder.

(3) Cylindrical injector (0·375 diameter by 1 in. length). In this type the holes were drilled radially as from the centre of the sphere used in type (1).

The injectors were supported in the centre of the combustion chamber by two stainless steel

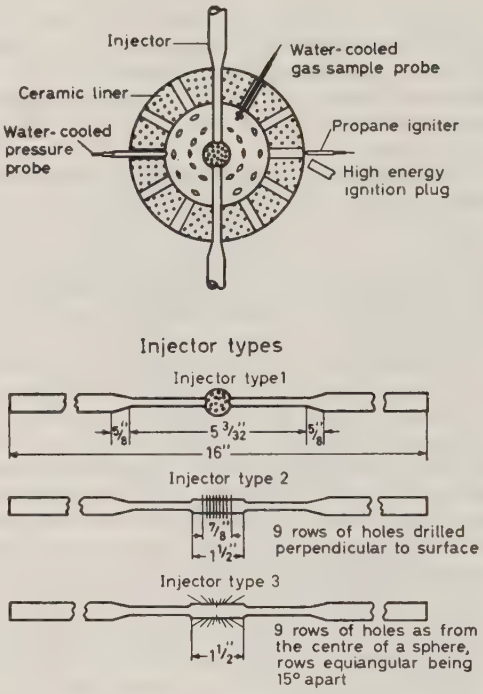

Figure 2

tubes which acted as feeds for the pre-mixed air and fuel. The diameter of these feed tubes was varied from 0·125 i.d. to 0·4375 in. i.d.—the specifications for the various injectors being given in Table 2.

TABLE 2

Combustor and Injector Details

*Combustor or injector**	*Burning volume*	*Injector hole diameter*	*Number of holes*	*Total hole area*	*Inlet tubes diameter*	*Total inlet area*	*Injector type see Figure 2*
	Litres	In.		In.²	In.	In.²	
A	0·226	0·0465	68	0·1156	$\frac{1}{4}$ OD × $\frac{1}{8}$ in. ID	0·02454	Spherical $\frac{3}{4}$ in. diam type (1)
B	0·228	0·0465	68	0·1156	$\frac{1}{4}$ OD × $\frac{1}{8}$ in. ID	0·02454	Cylinder $\frac{3}{8}$ in. diam type (3)
C	0·228	0·0465	68	0·1156	$\frac{1}{4}$ OD × $\frac{1}{8}$ in. ID	0·02454	Cylinder $\frac{3}{8}$ in. diam type (2)
D	0·226	0·0625	68	0·2086	$\frac{1}{4}$ OD × $\frac{1}{8}$ in. ID	0·02454	Spherical $\frac{3}{4}$ in. diam type (1)
E	0·228	0·0625	68	0·2086	$\frac{1}{4}$ OD × $\frac{1}{8}$ in. ID	0·02454	Cylinder $\frac{3}{8}$ in. diam type (2)
F	0·226	0·0935	68	0·4669	$\frac{1}{4}$ OD × $\frac{1}{8}$ in. ID	0·02454	Spherical $\frac{3}{4}$ in. diam type (1)
G	0·228	0·0935	68	0·4669	$\frac{1}{4}$ OD × $\frac{1}{8}$ in. ID	0·02454	Cylinder $\frac{3}{8}$ in. diam type (2)
H	0·220	0·111	68	0·6580	$\frac{1}{4}$ OD × $\frac{1}{8}$ in. ID	0·02454	Cylinder $\frac{3}{4}$ in. diam type (2)
K	0·218	0·120	48	0·5429	$\frac{7}{16}$ OD × 0·432 in. ID	0·2931	Spherical 1 in. diam type (1)
L	0·222	0·1285	68	0·8819	$\frac{1}{2}$ OD × $\frac{7}{16}$ in. ID	0·3007	Cylinder $\frac{3}{4}$ in. diam type (2)

* All combustors are 5 in. OD × 3 in. ID with 60 equi-spaced holes $\frac{1}{4}$ in. diameter.

FUEL

The fuel used throughout was commercial propane, for which a typical analysis is shown in Table 3. It will be seen that the fuel contains some 98 per cent of saturated hydrocarbons, of which 92 per cent is propane. In view of this and the nature of the experiments, no attempt was made accurately to control the chemical composition throughout the test series.

TABLE 3

Typical Fuel Composition

	Volumetric Percentage
Propane	92
Unsaturated C_3 compounds	1·5
Saturated C_2 compounds	5·0
Unsaturated C_2 compounds	Nil
Saturated C_4 compounds	1·3
Unsaturated C_4 compounds	0·2

PROCEDURE

Two different procedures were used to obtain the blow-out values. At mixture strengths close to stoichiometric the air and fuel flows were set and maintained constant, while the combustion chamber pressure was slowly reduced. Close to extinction the pressure was reduced in steps of less than 0·1 in. Hg, the conditions being allowed to settle at each step until extinction occurred.

For blow-outs away from the peak of the curve the chamber pressure and the air mass flow were set and maintained constant, while the fuel flow was slowly increased or decreased until extinction took place. Changing the air mass flow at constant chamber pressure and fuel flow was equally successful.

At each extinction the inlet static pressure and the combustion chamber pressure were noted, the appropriate instrumentation being illustrated in *Figure 3*. For convenience the static pressure measurement was made at a point *A*, after showing that the pressure losses from *A* to *B* were negligible over the range of mass flows employed.

Although no comprehensive gas analysis has been carried out, regular tests have been done with a modified Orsat apparatus as a check on the air and fuel metering.

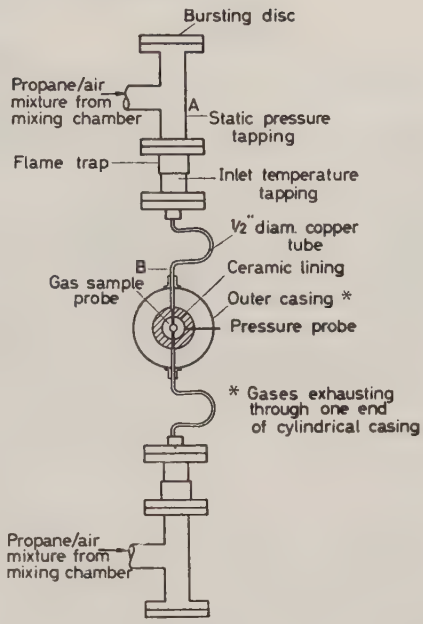

Figure 3

TEST DATA

The range of variables studied is shown in Table 4, and the results in Table 5.

Temperature correction has been made to 300°K and in some cases to 400°K, using data by Longwell[1], although as the present work is concerned with a different fuel the correction is not strictly valid.

TABLE 4

Range of Variables Studied

Air flow rate, g mols/sec	0·061–0·248
Fuel flow rate, g mols/sec	0·00159–0·0122
Combustor pressure, atm	0·117–1·044
Equivalence ratio,	0·437–2·067
Inlet temperature, °K	273–289
Burning volume, litres	0·218–0·228
Injector feed holes, in. diam	0·0465–0·1285

DISCUSSION

Effect of fuel type upon the value of $N/VP^{1\cdot8}$ at blow-out conditions

From Table 2 it will be seen that combustor *A* is identical in size and geometry to the 3 in. i.d. combustion chamber used by Longwell, having a ¾ in. spherical injector containing 68 holes each

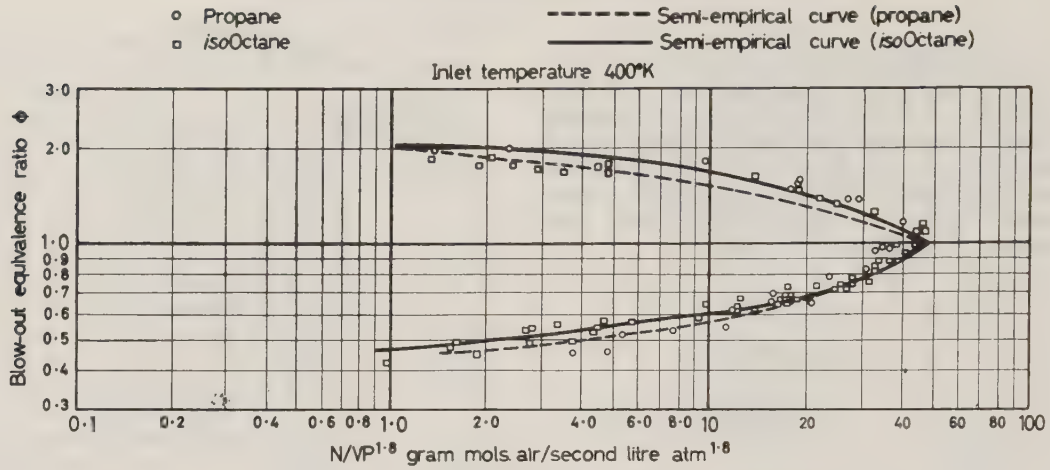

Figure 4

of 0.0465 in. diam. *Figure 4* compares the values of $N/VP^{1\cdot8}$ at blow-out for the experimental points cited by Longwell[1] for *iso*octane and those obtained in these experiments for propane corrected to 400°K—no account being taken of heat losses in the latter case. It will be seen that the semi-empirical curves based on the data are very similar. Taking the actual test points for propane at $\varnothing = 1{\cdot}0$, it will be noted that they give a peak some 29 per cent less than the peak of the Longwell curve, although the difference between the actual test data is somewhat less. This would suggest that for saturated hydrocarbons of the paraffin type similar heat release rates can be expected. The reaction rates and the volumetric heat release rates given by the systems at stoichiometric conditions are compared below.

Heat release rate or reaction rate at 1 atm	*Iso*octane	*Propane*	
	Semi-empirical equation	*Semi-empirical equation*	*Best experimental curve*
$\frac{\text{Millions CHU's}}{(\text{ft.}^3)\ (\text{R})\ (\text{atm})^{1\cdot8}}$	185	177	131
$\frac{\text{mols. fuel burnt}}{(\text{cm})^3\ (\text{sec})}$	$8{\cdot}14 \times 10^{-4}$	$19{\cdot}43 \times 10^{-4}$	$14{\cdot}36 \times 10^{-4}$

This condition (that is, $\varnothing = 1$) is assumed to be the one at which the maximum volumetric heat release rate is obtained. Theoretical work has shown that the above maximum should be attained at slightly rich conditions. Because of inherent experimental error it is difficult to detect this practically.

Reaction order

The comparison made above can only be justified if the reaction order for propane is 1·8. Work done by Hottel[2] using a propane/carbon dioxide/oxygen mixture suggests that the pressure exponent n, which may be taken as indicative of the apparent reaction order, varies from 1·3 to 1·7. Both Longwell and Hottel are agreed that the value of activation energy, E, is of the order of 40,000 cals/g mol. The results for combustor A have been plotted as (a) N/VP^2, (b) $N/VP^{1\cdot8}$ and (c) $N/VP^{1\cdot3}$ *versus* $\varnothing$. The root mean square deviation from the best experimental line was 6·7 per cent in the case of N/VP^2, 5·7 per cent for $N/VP^{1\cdot8}$ and 6·3 per cent for $N/VP^{1\cdot3}$. The values are similar but on the whole it would appear more justifiable to take 1·8 as the pressure exponent.

On the basis of the above values, equations 2 and 3 were respectively modified to:

$$N/VP^{1\cdot8} = 8{\cdot}919 \times 10^{15} \times \frac{e^{-21{,}137/T}}{T^{1\cdot3}} \frac{[2\,(\varnothing - \epsilon\varnothing)]^{\alpha}\,[1-\epsilon\varnothing]^{\beta}}{\epsilon\varnothing\,[m+1+1{\cdot}4\varnothing-\epsilon\varnothing]^{n}} \qquad (4)$$

$$N/VP^{1\cdot8} = 8{\cdot}919 \times 10^{15} \times \frac{e^{-21{,}137/T}}{T^{1\cdot3}} \frac{1}{\epsilon} \frac{[0{\cdot}2\varnothing\,(1-\epsilon)]^{\beta}\,[1-\epsilon]^{\alpha}}{[m+1-\epsilon+0{\cdot}2\varnothing\,(1+6\epsilon)]^{n}} \qquad (5)$$

Since no vitiation of the air occurred the value of m was taken as 3·76. Into the above equations a 'steric factor', c, was introduced in the following manner: The maximum value of $N/VP^{1\cdot8}$ given by the best experimental curve was inserted in the LHS of equations 4 and 5. Since this value was obtained at $\varnothing = 1$ the only remaining unknown was ϵ. Differentiation of a modified version of equations 4 and 5 indicated that at $\varnothing = 1$ the values of ϵ to be expected were approximately those quoted by Longwell[1]. Hence, the values given in his paper (that is $\epsilon = 0{\cdot}83$ for weak mixtures and $\epsilon = 0{\cdot}75$ for rich mixtures) have been used. The value of α was taken as 0·8 and

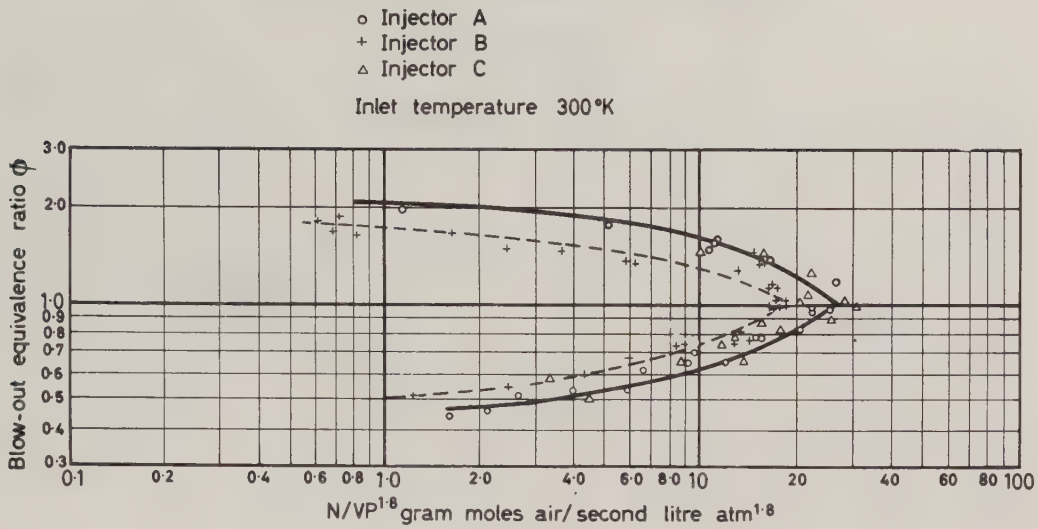

Figure 5

that of β as 1·0. Assuming that the values of the LHS and RHS of the equations 4 and 5 may be made compatible by introducing a constant, c, the values of c obtained were 1/786 and 1/236 for weak and rich mixtures respectively. The derived semi-empirical curve is plotted in *Figure 4*.

Effect of injector configuration

It was decided to investigate the effect of injector shape upon volumetric heat release rates. For this purpose three injectors were designed having the same inlet injector tubes, the same number of holes and the same total injector hole area. They are listed in Table 2 with combustors *A*, *B* and *C*, and the results corrected to 300°K are illustrated in *Figure 5*. It will be seen that whilst a reasonable curve can be drawn through the points obtained for combustors *A* and *C* the results given by combustor *B* lie within the envelope of the other two, and the maximum value is appreciably reduced. Further results using similar type injector systems to *C* and *A* showed little difference, if any, in the values of $N/VP^{1.8}$ measured under the same conditions. A comparison is drawn below of the maximum values of $N/VP^{1.8}$ obtained by Longwell, Hottel and those given by combustors *A*, *B* and *C*, correction having been applied to adjust all the values of $N/VP^{1.8}$ to an inlet temperature of 400°K.

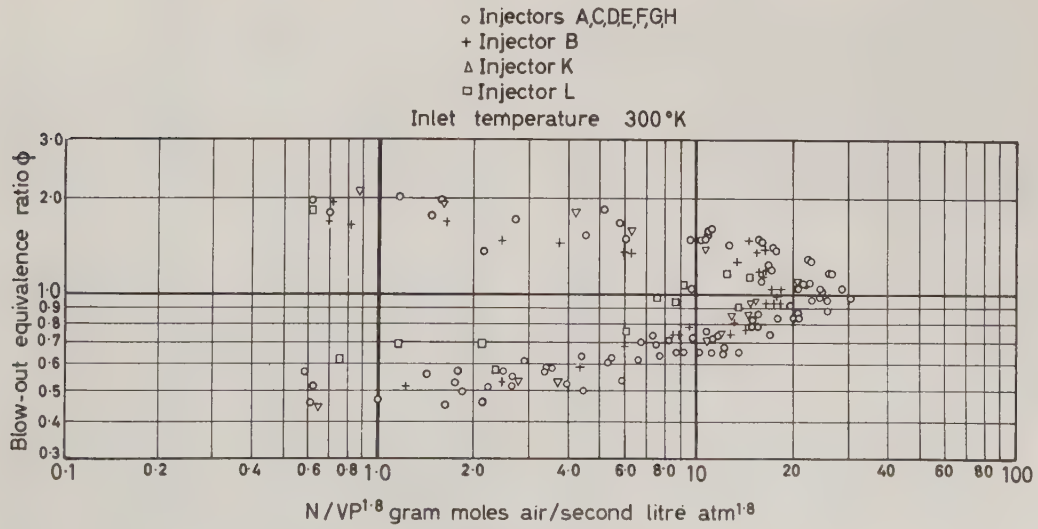

Figure 6

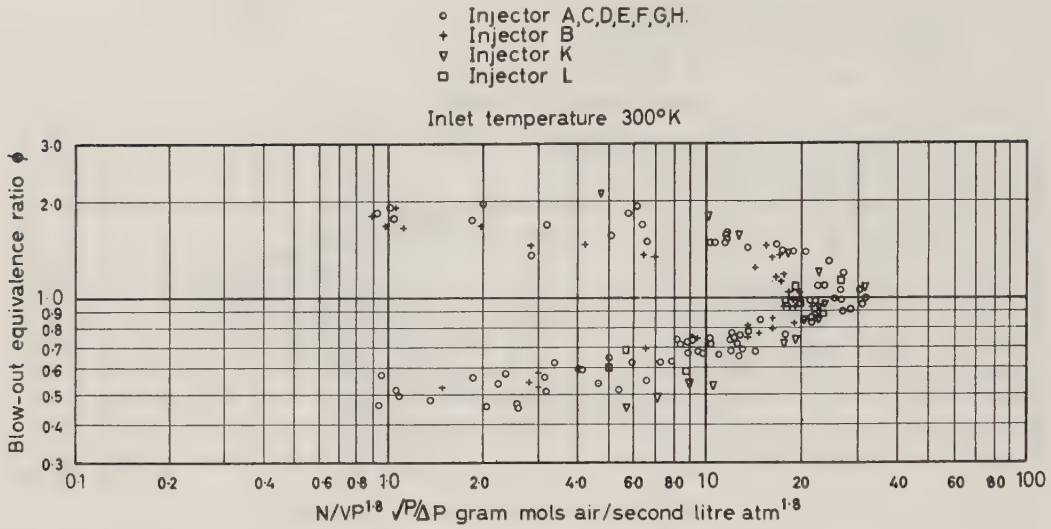

Figure 7

Longwell (semi-empirical equation-*iso*octane/air)
$$\mathcal{N}/VP^{1.8} = 48 \ (\varnothing = 1.0)$$

Hottel (experimental curve—57·7 per cent C_3H_8, 31 per cent CO_2, 11·3 per cent O_2)
$$\mathcal{N}/VP^{1.8} = 32 \ (\varnothing = 0.9)$$

Injector *A* (experimental curve—C_3H_8/air)
$$\mathcal{N}/VP^{1.8} = 34 \ (\varnothing = 1.0)$$

Injector *B* (experimental curve—C_3H_8/air)
$$\mathcal{N}/VP^{1.8} = 28 \ (\varnothing = 1.0)$$

Injector *C* (experimental curve—C_3H_8/air)
$$\mathcal{N}/VP^{1.8} = 37 \ (\varnothing = 1.0)$$

Mixing effects

In order to investigate the effect of different degrees of mixing upon the blow-out values, experiments have been performed in which the total hole area of the injector was varied from 0·1156 to 0·8819 in.^{2}. All these data, corrected to 300°K, are illustrated in *Figure 6*. It will be seen that there is appreciable scatter, for example at $\varnothing = 1.0$ the value of $\mathcal{N}/VP^{1.8}$ varies from 7·5 to 30.

In view of the previous suggestions that heat release is related to the ratio $(\Delta P/P)^{\frac{1}{2}}$, the data in *Figure 6* were 'corrected' by dividing by this factor and the results are shown in *Figure 7*. It is clear that the scatter from *Figure 6* is now reduced and at $\varnothing = 1.0$ the value of $\mathcal{N}/VP^{1.8}\ (P/\Delta P)^{\frac{1}{2}}$ varies from 18 to 31.

It should be pointed out that the pressure loss (ΔP) measured is that for the complete injector and not the loss across the injector holes. It would appear that the latter is more desirable, since the loss across the holes is more directly connected with mixing in the combustion chamber. However, in view of the geometry of the injectors and the fact that sonic velocities occur at certain conditions, an analysis of the pressure loss is a matter of considerable difficulty. This analysis has not been effected at the present time.

Thus the pressure loss term lacks precision and hence no attempt has been made to obtain a better correlation. Hence all that can be said pending a full analysis of the pressure loss term, is that the scatter of experimental data is appreciably improved by the inclusion of a pressure loss term of the type $(\Delta P/P)^{\frac{1}{2}}$.

CONCLUSIONS

(1) Volumetric heat release rates have been compared for propane and *iso*octane at the same conditions of inlet temperature, and the maximum rates have been shown to be similar. A comparison of the rate of molecular destruction of the fuel shows that the propane decomposes approximately twice as fast as *iso*octane.

(2) Careful examination of the experimental data suggests that a reaction order of 1·8 can be assigned to the combustion of propane air mixtures. This agrees with the order suggested by Longwell for *iso*octane combustion.

(3) The results obtained with a spherical injector were similar to those given by an equivalent cylindrical injector having holes drilled normally to the surface of the cylinder.

(4) An improvement in the scatter of results is obtained when the parameter $(\Delta P/P)^{\frac{1}{2}}$ is intro-

duced as a mixing term into the correlation. It is felt that the parameter lacks precision due to the different relative geometries of the injectors and further work is proceeding in an endeavour to break down the pressure loss components.

This work has been carried out in the Combustion Research Laboratories of Joseph Lucas (Gas Turbine Equipment) Ltd., Burnley, and thanks are due to the Company for permission to publish this paper.

REFERENCES

1 LONGWELL, J. P. and WEISS, M. A. *Industr. Engng. Chem.* (*Industr.*) 47 (1955) 1634

2 HOTTEL, H. C., WILLIAMS, G. C. and BAKER, M. L. *Sixth Symposium* (*International*) *on Combustion*, pp. 398–411. 1957. New York; Reinhold

3 CLARKE, J. S. *Joint Conference on Combustion*, pp. 354–361. 1955. London; Inst. Mech. Eng.

4 THRING, M. W. *Trans. Inst. Chem. Eng.* 35 (1957) 234

TABLE 5

Results

Combustor	ø	N g mol/sec	P atm	T_i °K	$\{N/VP^{1\cdot8}\}$ 300	$\Delta P/P_1$	$\{N/VP^{1\cdot8}\}300\left(\frac{P_1}{\Delta P}\right)^{\frac{1}{2}}$
K	0·437	0·116	1·00	277·0	0·653	0·0133	5·66
A	0·447	0·206	0·807	278·5	1·62	0·617	2·06
A	0·455	0·200	0·682	278·5	2·13	0·677	2·59
E	0·457	0·148	1·04	283·5	0·609	0·425	0·934
D	0·467	0·191	1·00	281·0	0·980	0·521	1·36
E	0·486	0·144	1·04	281·5	0·691	0·398	1·10
K	0·487	0·171	0·669	278·0	1·87	0·068	7·16
C	0·497	0·248	0·487	283·2	4·48	0·710	5·32
F	0·505	0·128	1·01	284·0	0·621	0·350	1·07
A	0·509	0·203	0·593	278·5	2·66	0·722	3·13
E	0·510	0·148	0·539	284·5	2·19	0·500	3·10
B	0·513	0·243	1·00	286·6	1·23	0·678	1·49
A	0·524	0·208	0·485	278·0	3·93	0·730	4·60
K	0·525	0·164	0·524	277·7	2·78	0·096	8·96
F	0·526	0·140	0·598	284·0	1·76	0·608	2·25
K	0·529	0·162	0·433	283·0	3·75	0·126	10·6
A	0·534	0·197	0·377	278·0	5·90	0·823	6·50
B	0·537	0·234	0·659	278·2	2·48	0·769	2·83
G	0·552	0·134	0·658	279·0	1·41	0·581	1·85
D	0·553	0·202	0·579	281·0	2·67	0·726	3·14
G	0·562	0·116	1·00	279·0	0·579	0·364	0·960
H	0·567	0·111	0·525	278·5	1·79	0·561	2·39
C	0·570	0·172	0·459	288·0	3·36	0·714	3·97
G	0·570	0·140	0·494	279·5	2·47	0·689	2·98
L	0·580	0·065	0·328	285·0	2·37	0·076	8·64
H	0·581	0·113	0·370	278·5	3·39	0·693	4·08
D	0·582	0·204	0·498	283·0	3·53	0·764	4·03
B	0·596	0·208	0·445	278·5	4·40	0·824	4·85
L	0·605	0·062	0·593	282·0	0·799	0·025	5·05
H	0·610	0·112	0·288	279·5	5·45	0·759	7·25
D	0·613	0·164	0·480	282·5	2·88	0·726	3·38
D	0·614	0·181	0·367	283·2	5·37	0·815	5·94
A	0·619	0·218	0·365	278·0	6·66	0·718	7·86
F	0·634	0·140	0·350	284·7	4·44	0·771	5·06
A	0·644	0·191	0·242	280·0	12·1	0·887	12·9
E	0·645	0·152	0·226	287·0	10·3	0·875	11·0
D	0·646	0·084	0·198	276·7	7·72	0·791	8·68
A	0·656	0·194	0·294	278·0	9·12	0·861	9·83
C	0·656	0·212	0·304	283·7	8·68	0·873	9·52
C	0·657	0·163	0·202	284·0	13·7	0·934	14·2
D	0·658	0·156	0·226	281·7	11·1	0·863	12·0
D	0·670	0·169	0·223	282·7	12·1	0·870	13·0
B	0·677	0·193	0·356	279·7	6·04	0·853	6·54
L	0·683	0·063	0·484	280·5	1·16	0·041	5·72
D	0·691	0·085	0·202	276·5	7·45	0·787	8·40
D	0·695	0·179	0·234	285·2	11·8	0·882	12·5
H	0·695	0·109	0·248	280·0	6·72	0·788	7·57

TABLE 5 (*continued*)

Combustor	∅	$\mathcal{N}$ g mol / sec	P atm	T_i °K	$\{\mathcal{N}/VP^{1.8}\}$ 300	$\Delta P/P_1$	$\{\mathcal{N}/VP^{1.8}\}$ 300 $\left(\frac{P_1}{\Delta P}\right)^{\frac{1}{2}}$
L	0·695	0·062	0·340	281·5	2·15	0·052	9·43
A	0·697	0·194	0·280	276·7	9·62	0·867	10·3
D	0·698	0·161	0·250	282·0	9·45	0·857	10·2
G	0·704	0·137	0·268	279·5	8·06	0·830	8·85
K	0·709	0·163	0·233	279·5	11·4	0·389	18·2
H	0·712	0·108	0·224	280·0	8·19	0·809	9·10
E	0·724	0·148	0·231	286·0	9·66	0·869	10·4
C	0·726	0·168	0·228	285·0	11·4	0·859	12·3
D	0·726	0·153	0·277	281·5	7·42	0·842	8·09
H	0·726	0·111	0·190	280·5	11·1	0·839	12·2
K	0·734	0·159	0·223	276·7	12·0	0·384	19·4
B	0·742	0·201	0·295	285·5	8·54	0·875	9·13
B	0·744	0·173	0·270	280·0	8·91	0·878	9·51
D	0·744	0·107	0·178	277·2	11·8	0·844	12·8
G	0·748	0·135	0·163	280·0	17·0	0·895	18·0
B	0·755	0·213	0·249	274·6	12·8	0·906	13·5
C	0·758	0·129	0·183	284·2	12·9	0·887	13·7
D	0·759	0·083	0·161	277·2	11·0	0·824	12·1
L	0·769	0·062	0·188	285·7	6·13	0·163	15·2
B	0·777	0·212	0·227	287·5	14·2	0·913	14·9
B	0·788	0·211	0·288	282·7	9·51	0·881	10·1
A	0·789	0·209	0·224	278·0	15·3	0·899	16·1
A	0·793	0·164	0·198	274·5	15·1	0·986	16·0
B	0·806	0·200	0·235	275·8	13·2	0·911	13·8
C	0·824	0·139	0·160	282·7	18·0	0·898	19·0
H	0·826	0·147	0·188	277·2	15·0	0·877	16·1
A	0·833	0·210	0·189	277·0	20·5	0·912	21·4
D	0·837	0·171	0·157	279·0	20·6	0·909	21·6
K	0·839	0·150	0·206	277·5	13·1	0·396	20·8
H	0·841	0·143	0·191	278·5	13·9	0·874	14·9
D	0·842	0·155	0·161	278·2	20·1	0·907	21·1
K	0·850	0·144	0·189	276·0	14·6	0·411	22·8
D	0·857	0·112	0·135	274·2	20·5	0·881	21·9
C	0·863	0·126	0·164	282·0	15·5	0·897	16·3
C	0·890	0·158	0·139	285·5	25·8	0·910	27·1
L	0·895	0·117	0·172	278·2	13·6	0·345	23·2
G	0·896	0·130	0·121	282·7	27·1	0·921	28·2
D	0·915	0·166	0·157	280·2	19·7	0·908	20·7
K	0·929	0·151	0·189	277·5	15·0	0·423	23·1
G	0·933	0·135	0·118	280·5	29·8	0·924	31·0
B	0·937	0·191	0·193	279·5	17·4	0·912	18·2
B	0·940	0·169	0·186	278·8	16·7	0·906	17·5
L	0·940	0·063	0·155	280·0	8·75	0·206	19·3
B	0·942	0·195	0·191	279·5	18·1	0·915	19·0
A	0·945	0·161	0·154	282·2	22·8	0·922	23·7
K	0·953	0·143	0·182	276·0	15·4	0·420	23·7
D	0·954	0·151	0·154	278·0	21·0	0·907	22·0
D	0·958	0·088	0·117	277·2	20·1	0·876	21·5
A	0·962	0·200	0·162	278·2	25·5	0·924	26·5
L	0·972	0·063	0·168	280·5	7·60	0·179	18·0
A	0·975	0·203	0·169	277·3	24·2	0·924	25·2
C	0·975	0·144	0·121	281·5	30·4	0·926	31·6
B	0·981	0·169	0·178	279·5	17·9	0·912	18·7
D	0·985	0·167	0·161	281·5	20·4	0·902	21·5
C	1·017	0·162	0·159	282·6	20·6	0·916	21·6
C	1·018	0·155	0·128	289·0	28·9	0·921	30·1
B	1·019	0·190	0·186	279·2	18·7	0·918	19·5
D	1·020	0·093	0·108	275·5	24·9	0·894	26·4
B	1·023	0·169	0·181	279·5	17·4	0·909	18·2
C	1·064	0·120	0·131	281·7	21·9	0·919	22·8
L	1·070	0·610	0·145	289·0	9·17	0·231	19·1
H	1·081	0·095	0·140	278·7	16·1	0·870	17·3
E	1·082	0·137	0·138	280·2	22·9	0·922	23·8
K	1·094	0·144	0·175	278·5	21·0	0·441	31·6

TABLE 5 (*continued*)

Combustor	∅	$\frac{N}{\text{g mol}/\text{sec}}$	P atm	T_i °K	$\{N/VP^{1.8}\}\,300$	$\Delta P/P_1$	$\{N/VP^{1.8}\}\,300\left(\frac{P_1}{\Delta P}\right)^{\frac{1}{2}}$
L	1·111	0·063	0·118	280·0	14·8	0·311	26·5
B	1·124	0·168	0·187	277·0	16·4	0·918	17·2
L	1·159	0·070	0·135	278·2	12·7	0·308	22·9
A	1·170	0·152	0·138	276·0	26·1	0·922	27·2
B	1·174	0·140	0·169	287·2	16·0	0·913	16·7
B	1·185	0·138	0·162	288·0	16·9	0·917	17·6
D	1·186	0·152	0·172	280·5	17·4	0·899	18·3
H	1·239	0·096	0·137	278·5	17·2	0·877	18·4
B	1·250	0·144	0·191	283·5	13·4	0·898	14·2
C	1·284	0·111	0·179	279·7	22·8	0·872	24·4
C	1·311	0·106	0·446	284·7	2·16	0·570	2·86
B	1·319	0·145	0·293	280·2	6·35	0·838	6·94
B	1·330	0·153	0·184	278·5	15·4	0·914	16·1
B	1·354	0·146	0·310	278·9	5·93	0·832	6·50
B	1·360	0·143	0·171	279·5	16·3	0·910	17·1
K	1·366	0·146	0·223	278·0	11·0	0·360	18·3
G	1·367	0·125	0·145	280·5	19·5	0·907	20·4
A	1·375	0·170	0·188	282·7	16·6	0·904	17·4
A	1·383	0·147	0·169	276·0	18·0	0·905	18·9
D	1·403	0·165	0·210	285·0	13·0	0·894	13·7
C	1·438	0·111	0·153	279·5	15·9	0·886	16·9
B	1·450	0·145	0·400	279·0	3·71	0·776	4·22
B	1·451	0·161	0·197	273·2	14·8	0·906	15·6
C	1·451	0·110	0·200	280·5	9·69	0·853	10·5
D	1·454	0·188	0·268	284·0	10·3	0·923	10·8
B	1·455	0·143	0·496	278·7	2·45	0·726	2·88
D	1·466	0·142	0·303	279·5	5·95	0·817	6·58
A	1·472	0·177	0·249	276·7	10·8	0·882	11·5
F	1·512	0·140	0·343	286·5	4·50	0·772	5·12
A	1·517	0·146	0·220	275·5	11·1	0·880	11·8
E	1·527	0·135	0·204	285·2	11·1	0·884	11·8
K	1·547	0·127	0·283	280·0	6·34	0·243	12·9
A	1·589	0·145	0·217	275·7	11·2	0·879	11·9
B	1·618	0·161	1·00	274·2	0·811	0·529	1·12
E	1·663	0·136	0·308	280·0	5·81	0·825	6·40
B	1·680	0·132	0·967	282·5	0·69	0·494	0·982
B	1·684	0·132	0·600	278·0	1·64	0·674	2·00
D	1·695	0·135	0·469	277·7	2·70	0·703	3·22
D	1·719	0·141	0·670	280·2	1·47	0·626	1·86
K	1·774	0·124	0·358	280·0	4·12	0·165	10·1
D	1·783	0·139	1·00	280·0	0·698	0·443	1·05
A	1·798	0·146	0·341	278·5	5·13	0·812	5·69
B	1·800	0·127	1·02	282·2	0·613	0·468	0·896
E	1·808	0·130	1·00	287·7	0·623	0·443	0·936
K	1·890	0·120	0·594	279·5	1·60	0·069	6·09
B	1·900	0·139	1·00	275·1	0·710	0·430	1·08
F	1·915	0·126	1·01	288·0	0·602	0·350	1·02
D	1·932	0·132	0·625	279·2	1·57	0·614	2·00
A	1·991	0·146	0·788	279·0	1·14	0·565	1·52
K	2·067	0·106	0·777	280·2	0·873	0·034	4·73

92

STABILIZATION OF FLAME IN HIGH SPEED FLOW BY PILOT FLAMES

W. P. JENSEN and C. W. SHIPMAN

Most studies of flame stabilization in high velocity streams have been concerned with the action of bluff-body or can-type flame-holders. In those cases where an auxiliary pilot was used, it has usually been associated with bluff-body stabilizers and influenced by the re-circulation zone created thereby. Stability limits of piloted flames have been expressed as functions of the pilot heat supplied to the system.

There is a similarity between the action of an unaided pilot and the action of an unaided bluff-body flame-holder. Those who have studied bluff-body stabilizer action agree that the re-circulation zone immediately downstream of the stabilizer serves as a pilot and that energy and mass transport between the burned gases of this zone and the main stream of unburned combustible, across the free vortex layer separating them, is essential for ignition of the main stream and establishment of a propagating flame.

This interaction between parallel burned and unburned streams has been studied extensively in connection with bluff-body stabilization. Williams and Shipman[1] noted that the free vortex layer surrounding the wake of a bluff-body flame-holder is the locus of incipient flame and concluded that failure of the flame to propagate, and ultimately to be stabilized, is due to quenching of the hot gases by rapid mixing with the cold, unburned feed, the rapid mixing being due to turbulence generated by shear between the cold, main-stream gases and the hot gases in the wake region. Zukoski and Marble[2], using similar techniques, concluded that a critical time, τ, of contact between the cold and hot gases is required for propagation of the incipient flame. According to these authors the time of contact is given by the ratio of the length of the eddy region to the feed velocity, and so long as this ratio L/U is greater than τ, the system is stable. The gradual change in the character of the free vortex layer (from laminar to turbulent) with increasing feed velocity is not considered by Zukoski and Marble to affect τ, except that a change in the correlating curve is required when the vortex layer becomes completely turbulent.

A related theoretical study is that of Marble and Adamson[3], who used boundary layer theory to analyse ignition and laminar flame-front development in the laminar mixing zone between parallel streams of combustible gas and combustion products. This analysis takes account of both thermal and diffusional effects and shows that the distance required for ignition is an exponential function of the hot-stream temperature. This ignition distance is measured from first contact of the two streams to the point where heat loss by conduction equals heat gain due to chemical reaction, and it appears as the first local maximum in the temperature profile. In their analysis Marble and Adamson assumed equal velocities for the two streams and uniform velocity profiles. In a subsequent paper Cheng and Kovitz[4] again treated the case of equal stream velocities but allowed for non-uniform velocity fields, i.e. for velocity boundary layers. Their refinement shows the distance to the first local temperature maximum reduced by as much as tenfold. This ignition distance is found to be proportional to the 3/2 power of the stream velocity, and to the slope of the velocity profiles at the point of initial contact between the two streams. No analysis of the case involving turbulent transport between cocurrent streams has yet been reported.

The experimental studies of the mixing region between hot-product and cold-combustible streams cited above were close examinations of the region downstream of bluff-body flame-holders. The study of controllable, initially separate, streams is quite uncommon. Barrère[5], however, has briefly reported work at O.N.E.R.A. in which a combustor having separate, parallel streams was used. In half the duct fresh combustible flowed, and in the other hot, burned gas. The device was used to study ignition-distance variables, temperature distributions, and the diffusion process.

Typical of the studies of ignition of flowing streams are those of Khitrin and Goldenberg[6], who presented a thermal theory of ignition; Kumagai and Kimura[7] who studied ignition by heated wires; and Swett[8] who studied ignition by long duration spark discharges.

Studies of ignition by pilot streams have been made by Archer and Jacobi[9] who measured ignition limits of flowing butane–air mixtures by oxy-hydrogen pilots, and by Wolfhard and Burgess[10] who studied ignition of slow-moving CH_4–NO mixtures by various pilot mixtures, pilot tube diameter and flow rate not being independently controlled. An experimental study closely related to that reported herein was that of Wright and Becker[11] who used a device which provided for the smooth junction of a hot, inert-gas stream and a cooler coaxial stream of combustible mixture. They found that with appropriate conditions, ignition occurred and an 'initial' flame similar to the familiar 'residual' flame of bluff-body stabilization developed in the mixing region. Under some conditions, an extension of this flame propagated into the whole stream of cool combustible. Using several different fuels, these workers measured 'detachment' distances from the point of initial contact to points of initial-flame and propagating-flame development. Detachment distances were found to decrease (as expected) with increasing inert stream temperature, equivalence ratio (below stoichiometric) and inert/main-stream velocity ratio, and with decreasing main-stream absolute velocity. In all of this work the velocity ratio, u_o/u_i, of the cold and hot streams was between 0·02 and 0·29, with the maximum cold-stream velocity about 43 ft./sec. Wright and Becker, while recognizing that the calculations for the case of uniform stream velocities is not strictly applicable, pointed out the analogy between their experiments and the analytical work of Marble and Adamson and, using the Zukoski–Marble concept of critical time of contact, contend that τ 'depends only on the chemical characteristics of the combustible mixture and on the temperature field, not on other flow properties'.

It was the objective of the work herein reported to study the problem of ignition by pilot flames at velocities approximating those found in high output burners, with the system idealized by insuring a low turbulence level and flat velocity profile in an annular main stream surrounding a central stream of completely burned gases. Ignition of the main stream requires raising the temperature and/or providing sufficient chain carriers to a sufficient portion of the main stream. One additional requirement is that, having provided these conditions, the resulting mixture must not be dispersed too rapidly into the cold gas, or quenching of the flame will result.

From the work of Williams and Shipman[1] and of Zukoski and Marble[2] it is apparent that, for given compositions and temperatures of the pilot and main streams, ignition is dependent on the patterns of mixing between the hot and cold gases, i.e. rapid mixing can result in concentrations of energy and chain carriers in the main stream which are too small to initiate self-propagation. It seems unreasonable to describe 'the correct pattern' in terms of a time of contact based solely on feed velocity and length of the eddy region, since by causing the boundary between hot and cold gases to be partly turbulent (as by impressed sound or other disturbance) the 'time of contact' computed in this way would be the same while the character of the zone of contact would be altered.

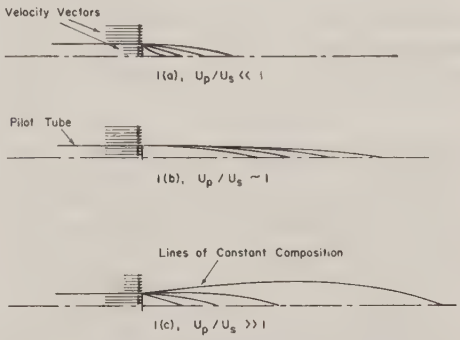

Figure 1. Patterns of mixing between co-axial streams

Qualitatively speaking, three conditions of mixing between the hot and cold streams may be imagined: (1) the velocity of the hot, pilot gases is much less than the stream velocity, (2) the hot-gas velocity is about the same as the stream velocity, and (3) the hot-gas velocity is much greater than the stream velocity. These three cases are illustrated in *Figure 1, a–c*, respectively, for the case where the mass flow of the pilot stream is a negligible fraction of the main stream. The lines of constant composition illustrate the rapid dissipation of the pilot by the main stream for the cases $u_p/u_s \ll 1$ and $u_p/u_s \gg 1$. In both of these cases the difference in velocity between the pilot and main streams causes development of turbulence which in turn causes rapid mixing. In *Figure 1* (*c*) the high pilot stream flow rate means that the pilot jet retains its identity for a greater downstream distance. For the case $u_p/u_s \sim 1$, it would be expected that mixing would take place largely by molecular processes, so that the 'jet length' may be expected to increase with pilot flow rate.

A quantitative description of the mixing process up to the condition where chemical reaction becomes significant is given by the equation of continuity for the pilot gas, viz.

$$\rho \vec{u} \cdot \nabla \chi - \nabla \cdot \mathscr{D} \nabla \chi = 0 \qquad (1)$$

where χ is the mass fraction of pilot gas, $\mathscr{D}$ is the sum of the molecular and turbulent coefficients of

material transport, and the difference between mass and mol linear velocities has been ignored. By adopting the dimensionless parameters:

$$\begin{aligned} \rho^+ &= \rho/\rho_s & \nabla^+ &= d\,\nabla \\ \mathscr{D}^+ &= \mathscr{D}/\mathscr{D}_o & r^+ &= r/r_s \\ u^+ &= u/u_s \end{aligned} \qquad (2)$$

and dividing by the coefficient of the left-hand term, one obtains from equation 1:

$$\rho^+ u^+ \cdot \nabla^+ \chi - \left(\frac{\mathscr{D}_o}{\rho_s u_s d}\right) \nabla^+ \cdot \mathscr{D}^+ \nabla^+ \chi = 0 \qquad (3)$$

The boundary conditions for the mixing problem may be written:

$$\text{at } r^+ < 1, \quad z^+ = 0; \quad \chi = 1, \text{ and } u^+ = u_p/u_s \qquad (4)$$

$$\text{at } r^+ > 1, \quad z^+ = 0; \quad \chi = 0, \text{ and } u^+ = 1$$

The solution of equation 3 is obviously a function of the coefficient $(\mathscr{D}_o/\rho_s u_s d)$ and of the boundary conditions, viz.

$$\chi\,(r^+, z^+) = f\,(\mathscr{D}_o/\rho_s\, u_s\, d,\, u_p/u_s) \qquad (5)$$

It should be noted that for equal values of the independent parameters of equation 5, similar composition patterns will be obtained. It is apparent, however, that the absolute size of the mixing region must be important for ignition. Therefore, it may be expected that for given main stream conditions, fixed values of the independent parameters of equation 5 will be required to insure ignition, but these values will be different for geometrically similar pilots of different characteristic dimension.

$\mathscr{D}_o$ is defined as the sum of eddy and molecular transport coefficients based on the parameters at the junction of the pilot and main streams. There are two principal sources of velocity gradient which will result in eddy transport, the boundary layer on the outside of the pilot tube and the difference between the pilot and the main stream velocities. The boundary layer inside the pilot tube and the wake at the downstream edge of the tube are regarded as negligible. From purely dimensional considerations one may write:

$$\mathscr{D}_o = k_1\, \rho_s\, d\,(u_p - u_s) + k_2\, \rho_s\, d\, u_s + D \qquad (6)$$

The second term on the right-hand side is the eddy transport due to the boundary layer, and D is the molecular diffusion coefficient. By use of equation 6 there is obtained:

$$\frac{\mathscr{D}_o}{\rho_s\, u_s\, d} = k_1\, \frac{u_p}{u_s} - k_1 + k_2 + \frac{D}{\rho_s\, u_s\, d} \qquad (7)$$

Stating the solution, 5, in terms of the quantities controlled,

$$\chi\,(r^+, z^+) = f\left(\frac{u_p}{u_s}, \frac{D}{\rho_s\, u_s\, d}\right) \qquad (8)$$

If molecular transport is negligible, the result is simply:

$$\chi\,(r^+, z^+) = f\,(u_p/u_s) \qquad (9)$$

APPARATUS AND PROCEDURE

Determinations of lean ignition limits in high velocity streams with coaxial pilots were made with the apparatus shown diagrammatically in *Figure 2*. Air was fed to the system from an oil-free air compressor through a pressure regulating valve, a 0·813 in., square-edged orifice installed in a 2 in. pipe in accordance with ASME

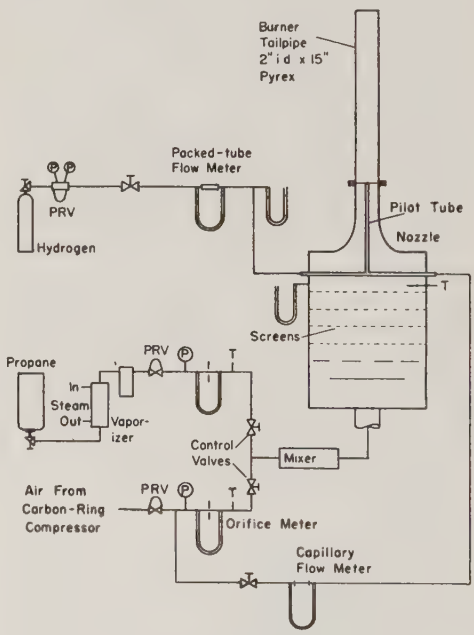

Figure 2. Ignition study apparatus

recommendations, and a pair of parallel control valves. The main-stream fuel used was natural gas propane (about 97 per cent pure) fed from an inverted cylinder through a vaporizer, a pressure regulating valve, a square-edged metering orifice (either 0·187 in. or 0·413 in.), and parallel flow control valves. Air and fuel were mixed in a 4 ft. section of 4 in. pipe packed with Berl saddles, and fed to the burner through a calming chamber which contained four 200-mesh screens to reduce stream turbulence. Surmounting the calming chamber was a nozzle that provided a 25 : 1

area-contraction ratio to ensure a flat velocity profile at the entrance to the 2 in. i.d. combustion chamber. A Pyrex glass tail-pipe, 15 in. long by 2 in. i.d., was mounted on a flange at the plane of the pilot-burner exit, a point 3 in. downstream of the nozzle throat. Temperatures of the air, propane, and the mixture were measured at the points indicated in *Figure 1*, the measuring points for the air and fuel being far enough downstream to assure recovery after the orifices.

The pilot tubes were located coaxially with the combustion chamber, the downstream end being in the plane of the nozzle exit. The pilot tubes were supported at the upstream end inside the plenum chamber, upstream of the nozzle and downstream of the final screen. The supporting members were the hydrogen and air feed tubes which entered from opposite sides of the plenum chamber.

The three stainless steel pilot tubes were 0·25, 0·135, and 0·063 in. inside diameter and were 0·314, 0·165, and 0·083 in. o.d. respectively. These are hereinafter called $\frac{1}{4}$, $\frac{1}{8}$, and $\frac{1}{16}$ in. pilots. In order to prevent flashback of the pilot flames when operating at low velocities, a nest of 21-gauge stainless steel tubes about 1 in. long was inserted into each pilot tube so that the downstream end of the nest was one pilot tube internal diameter from the pilot tube exit. The internal diameter of the 21-gauge tubing is 0·020 in., and the quenching distance reported for 30 per cent (by volume) hydrogen in air is 0·026 in.[12]. The arrangement proved entirely satisfactory.

The hydrogen and air were metered by means of porous-plug and capillary flow meters, respectively. The porous-plug meters were made by packing steel wool into polyethylene tubing, and the capillary flow meters were fabricated from stainless steel tubing; all these meters were calibrated by means of a dry gas meter. The pressure on the downstream side of the hydrogen meter was used to correct the flow rate to conditions at the tip of the pilot, pressure drop through feed lines being entirely negligible.

The pilot flow rates were selected to give a mixture of 31·6 volume per cent hydrogen and superficial hot gas velocities from 50 to 450 ft./sec in 50 ft./sec intervals. The $\frac{1}{4}$ and $\frac{1}{8}$ in. pilots were stable at all of the velocities selected, but the $\frac{1}{16}$ in. pilot was unstable at velocities of 300 ft./sec and higher. The hot gas velocity was computed for a mol ratio of products to reactants of 0·852 and an adiabatic flame temperature[13] of 2,318°K. More recent calculations of flame temperature and more accurate calculations of the equilibrium composition[14] give an estimated mol ratio on complete combustion of 0·865 and an adiabatic flame temperature of 2,400°K, resulting in an error of about 3·7 per cent in the hot gas velocity. Errors in metering and in neglecting lateral expansion are probably greater than this so that the correction is not worth while. Further, since this study was concerned only with the effects of relative velocities of pilot and main stream for varying pilot diameters, this error, being constant for all pilot velocity calculations, is unimportant.

The character of the pilot flames was not the same for all operating conditions. At low pilot feed rates the flame burned from the top of the tube nest, and the tip of the pilot tube was red hot. At higher pilot feed rates the flame burned from the top of the tube as a normal bunsen flame. The point of transition from one condition to the other was a function of pilot feed rate, main stream velocity, and pilot tube diameter. These differences in character of the pilot flames had no observable effect on the results.

The experimental procedure consisted in setting first the pilot flow rate so that the calculated mean velocity of the pilot combustion products was an integral multiple of 50 ft./sec (generally within $\pm$ 5 per cent), similarly adjusting the air flow rate of the cold main stream, and finally admitting propane to the system until ignition was sufficient to cause a flame to propagate beyond the 15 in. tail-pipe. This determination of the ignition limit was in some respects a subjective measurement. As the fuel flow rate was gradually increased, its presence was first made apparent as a blue border along the pilot product stream. Eventually propagation of flame into the entire stream occurred. In most cases this development occurred over only a small increase in fuel/air ratio. Usually, if the propagating flame was strong enough to reach the end of the 15 in. tail-pipe, it also extended several burner diameters into the free atmosphere before being quenched by the aspirated ambient air. In all cases the condition of ignition was taken as that where the flame did extend into the free region beyond the burner exit. This had to be a subjective judgment because the flame character changed somewhat depending on pilot size, pilot/main stream velocity ratio and the absolute flow velocities. Flames varied from soft, laminar brushes to sharply pulsing bursts at low frequency. In some cases, especially with the smallest pilot, the flame was a very thin string of luminous emitters until at the end of the tail-pipe the reduced velocity that accompanied jet spreading allowed quite complete propagation to occur. In order to make the measurement as objective as possible, flow adjustment was made in such a way that the operator could not see the flow-indicating instruments. It was found that judgments of the ignition limit were reproducible within the accuracy of metering. Independent judgments by a second observer were not consistently different.

RESULTS AND DISCUSSION

A priori it is reasonable to assume that both the composition pattern and the absolute pilot size (or time of contact between hot and cold gases) must be important in determining whether ignition will occur. If it is assumed, however, that the composition patterns alone determine the ignition, then the mixture ratio required to obtain ignition is a function of the composition pattern. This relationship is tested together with the assumptions of equation 9 in *Figure 3* (a few points at high

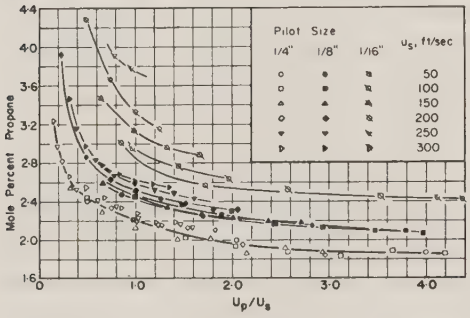

Figure 3. Lean-limit ignition by co-axial pilots

values of u_p/u_s have been omitted). It is clearly evident that for a given pilot diameter, u_p/u_s does not provide complete correlation. It is also apparent that the variations in lean ignition limit with stream velocity at fixed u_p/u_s decrease with increasing pilot diameter, suggesting that the molecular diffusion term is important. For a given pilot diameter it was assumed that the functional relationship of equation 8 could be represented by:

$$\chi\,(r^+, z^+) = \phi\left(\frac{u_p}{u_s} + \frac{K}{u_s}\right) \qquad (10)$$

The values of K were found empirically, and are 164 and 30·4 for the $\frac{1}{16}$ and $\frac{1}{8}$ in. pilots, respectively. Because of the close correlation for the

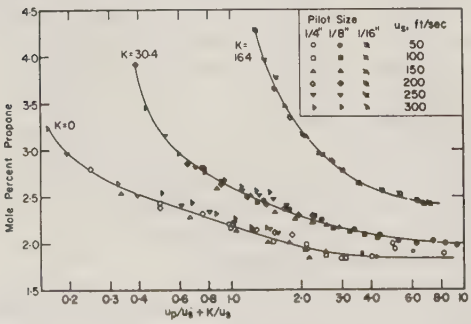

Figure 4. Lean-limit ignition of high-speed streams by co-axial pilots

$\frac{1}{4}$ in. pilot shown in *Figure 3* it was not possible to obtain an accurate value of K, and while there is some segregation of the '$\frac{1}{4}$ in.' data with stream velocity, the separation is not large. The results are shown in *Figure 4*. Semi-logarithmic co-ordinates have been used in order to expand low values of the abscissa.

It was found empirically that a reasonable correlation of the data for higher equivalence ratios could be obtained by plotting mole per cent propane at ignition against the product $(u_p/u_s)d$. Such a correlation implies that total pilot energy per unit of pilot perimeter is a correlating factor. It is clear from *Figure 3* that such a correlation is deceptive, because it does not take proper account of variations in the stream velocity.

Turning now to a consideration of the effect of pilot diameter, it was pointed out earlier that the functional relationship indicated by equation 8 implies similarity of composition patterns, but that ignition of the main stream is dependent on the absolute amounts of material and energy transport, and consequently on the absolute size of the mixing region. This means that the larger the pilot diameter, the more favourable the possibility of ignition at given values of the variables u_p/u_s and u_s. This is supported by the data, *Figure 4*. Because of the character of the mixing process, it should be possible to offset the effect of larger pilot diameter by increasing pilot gas velocity. At high values of u_p/u_s, however, the system must behave like a turbulent jet issuing into ambient atmosphere, at least for several pilot diameters downstream from the point of initial contact with the main stream. Studies of jet mixing[14] show that at sufficiently high values of jet velocity, or u_p/u_s in the present case, the mixing patterns become independent of u_p/u_s. This means that the composition patterns for large and small pilots at high values of u_p/u_s would be similar, and it would not be possible to offset a decrease in absolute size of the mixing region by an increase in pilot feed rate.

It follows that the ignition limits would tend to a constant value at high pilot feed rates and that the asymptote would be different for different pilot sizes. These conclusions are supported by the data. No simple relation was found for bringing the curves of *Figure 4* together.

It will be noted that with large values of u_p/u_s for the $\frac{1}{4}$ in. pilot, some of the data points indicate ignition of propane–air mixtures leaner than the literature values of flammability limits. This is readily explainable on the grounds that 'limit' determinations depend strongly on the nature of the burner used, and on the temperature of the mixture being tested.

Values of the lean ignition limit for propane–air mixtures have been reported in the literature[16–18]

as about 2·0 to 2·4 per cent propane. Linnett and Simpson[19] point out that the limits determined by the flat flame method[17] are good evidence of the absence of any 'absolute' limit of inflammability.

Increased temperature of a hydrocarbon–air mixture causes the apparent lean limit composition to change by 6 to 8 per cent for each 100°C of temperature rise[20,21]. Egerton and Thabet[17] studied the effect of temperature on the lean inflammability limits of propane–air mixtures, and found the limit (expressed as per cent of propane) to be nearly linear in temperature. They found values varying from 1·82 per cent propane at 148°C to 1·38 per cent propane at 380°C. In the present work the leanest limit found was 1·83 per cent propane with the $\frac{1}{4}$ in. pilot, u_p/u_s about 3, and main stream velocities of 50 and 100 ft./sec. These results are compatible with those of Egerton and Thabet[17] if pre-heating by the pilot is taken into account. Specifically, the pilot heat would be sufficient to raise the average temperature of a $\frac{3}{4}$ in. diameter core of the main stream from its initial temperature of 15°C to the pre-heat temperature required, 141°C. That pre-heating by the pilot was indeed confined to a relatively small core of the total main-stream cross-section was confirmed by rough temperature traverses of the burner exit. Once flame is established in this narrow core, the thermal energy generated is sufficient to supply the required pre-heat to the remainder of the stream.

Finally, examination of *Figure 4* shows that there are three fairly distinct sections in the curves for the two larger pilots. It may be assumed that these correspond to the three conditions mentioned earlier, $u_p/u_s \ll 1$, $u_p/u_s \approx 1$, and $u_p/u_s \gg 1$.

Some conclusions of practical interest may be drawn from these data. To achieve ignition at a given mixture ratio, say 2·6 mole per cent propane, the energy supplied by the $\frac{1}{4}$ in. pilot needs to be almost twice that required with the $\frac{1}{8}$ in. pilot, and almost four times that required with the $\frac{1}{16}$ in. pilot. This indicates that in one sense there is a disadvantage in using too large a pilot for some ranges of operation, bearing in mind that the maximum breadth of ignition limit (high u_p/u_s) is greater for larger pilots.

In general, it may be stated that while absolute size of the mixing region is of importance, the nature of the flow in the region of contact between burned and unburned gas plays a major role in determining the limits of ignition (or stability). It is also clear, from the asymptotic character of the curves of *Figure 3*, that for pilots larger than a minimum (between $\frac{1}{8}$ and $\frac{1}{4}$ in.), there is substantially no advantage to be gained in increasing pilot feed rate beyond the point where u_p/u_s is about 3·0. More generally, assuming stability of the pilot flame, there is a value of u_p/u_s beyond which no decrease in lean stability limit results from increased pilot feed rate at fixed pilot diameter.

The co-operation of the Fuels Research and Gas Turbine Laboratories of the Massachusetts Institute of Technology in the use of their facilities is gratefully acknowledged.

NOMENCLATURE

D	Molecular diffusivity, (mass)/(length) (time)
$\mathscr{D}$	Coefficient of diffusion equal to the sum of molecular and turbulent transport coefficients
$\mathscr{D}_o$	Normalizing diffusion coefficient, based on conditions at the point of initial contact between pilot gases and main stream
d	Pilot diameter
K	Empirical constant
k_1, k_2	Constants of proportionality
r^+	Reduced radial coordinate, pilot diameters from axis of the pilot tube
u	Velocity
u_p	Velocity of the hot pilot gases based on pilot tube cross-section
u_s	Velocity of the main stream
z^+	Reduced longitudinal coordinate, pilot diameters from tip of pilot tube
ρ	Density
ρ_s	Density of the main stream
χ	Mass fraction of pilot gas
∇	Vector operator $\vec{i}\frac{\partial}{\partial x} + \vec{j}\frac{\partial}{\partial y} + \vec{k}\frac{\partial}{\partial z}$

REFERENCES

1 Williams, G. C. and Shipman, C. W. *Fourth Symposium (International) on Combustion*, p. 733. 1953. Baltimore; Williams and Wilkins

2 Zukoski, E. E. and Marble, F. E. Experiments concerning the mechanism of flame-blow-off from bluff bodies. *Gas Dynamics Symposium*, Evanston, Ill. Aug. 22-24, 1955

3 Marble, F. E. and Adamson, T. C., Jr. *AGARD, Selected Combustion Problems*, p. 111. 1954. London; Butterworths

4 Cheng, S. I. and Kovitz, A. A. *Sixth Symposium (International) on Combustion*, p. 418. 1957. New York; Reinhold

5 Barrère, M. Discussion 'Flame stabilization in fast streams', *Sixth Symposium (International) on Combustion*, p. 941. 1957. New York; Reinhold

6 Khitrin, L. N. and Goldenberg, S. A. *Sixth Symposium (International) on Combustion*, p. 545. 1957. New York; Reinhold

7 Kumagai, S. and Kimura, I. *Sixth Symposium (International) on Combustion*, p. 554. 1957. New York; Reinhold

8 Swett, Jr., C. C. *Sixth Symposium (International) on Combustion*, p. 523. 1957. New York; Reinhold

9 Archer, D. A. and Jacobi, W. Unpublished work, Univ. of Delaware, 1953

[10] Wolfhard, H. G. and Burgess, D. S. *Combustion and Flame* 2 (1958), 3
[11] Wright, F. H. and Becker, J. L. *Jet Propulsion* 26 (1956) 973
[12] Lewis, B. and von Elbe, G. *Combustion, Flames, and Explosions of Gases*, p. 411. 1951. New York; Academic Press
[13] — — *Combustion, Flames, and Explosions of Gases*, p. 766. 1951. New York; Academic Press
[14] Drell, I. and Belles, F. E. *Nat. Adv. Comm. Aero. RM E57D24*, July 26, 1957
[15] Hawthorne, W. R., Weddell, D. S. and Hottel, H. C. *Third Symposium on Combustion and Flame and Explosion Phenomena*, p. 266. 1949. Baltimore; Williams and Wilkins
[16] Coward, H. F. and Jones, G. W. Limits of flammability of gases and vapors. *Bull. U.S. Bur. Min.* (1952) 503
[17] Egerton, A. C. and Thabet, S. K. *Proc. Roy. Soc. A* 211 (1952) 445–471
[18] Biedler, W. T. III, and Hoelscher, H. E. *Jet Propulsion* 27 (1957) 1257
[19] Linnett, J. W. and Simpson, C. J. S. M. *Sixth Symposium (International) on Combustion*, p. 20. 1957. New York; Reinhold
[20] White, A. G. *J. chem. Soc.* (*Lond.*) 127 (1925) 672
[21] Zabetakis, M. G., Scott, G. S. and Jones, G. W. *Industr. Engng. Chem.* (*Industr.*) 43 (1951) 2120

THEORY OF FLAME STABILIZATION BY A BLUFF BODY

S. I. CHENG and A. A. KOVITZ

INTRODUCTION

There are two fundamental aspects of flame stabilization, the chemical kinetic aspect and the fluid mechanical (including heat transfer) aspect. Existing theories of flame stabilization differ only in the degree of simplification of the two fundamental aspects and are primarily concerned with prediction of the blow-off limits.

The fundamental concepts of these theories are quite similar. They differ basically in the simplifying assumptions used to bring about a mathematical formulation of the blow-off criterion. They are formulated explicitly either based upon energy balance (Williams, Hottel and Scurlock[1], Khitrin and Goldenberg[2,3]) or on mass balance (Longwell, Frost and Weiss[4]) or on purely kinetic considerations (Zukoski and Marble[5]). However, in the process of reasoning or the evaluation of each term entering the final equation, other aspects of the blow-off limit are inherently assumed. For example, the introduction of ignition temperature, ignition lag, the analogy of blow-off and ignition, etc., are included in many theories. It is rather difficult to evaluate the relative merits of these theories purely on soundness of reasoning. Attempts to justify the different theories by experiment are rather difficult because of the necessity of introducing further quantitative assumptions in the theoretical results and because of the scarcity and lack of agreement between experimental data.

From the point of view of fundamental understanding, it appears that one should first endeavour to understand: (*a*) how a flame is stabilized on a bluff body wake under steady state conditions; (*b*) how a flame selects its equilibrium position; and (*c*) what are the essential roles of chemical kinetics and fluid mechanics. These questions should be answered without initial assumption of the preponderance of chemical kinetics or fluid mechanics. The equilibrium configuration must be the result of a balance between two or more competitive processes. Once an understanding is obtained for the steady state, the blow-off limit as a marginal steady state configuration should fall out as a natural corollary of the steady state formulation. It is this approach that will be followed in the subsequent discussion.

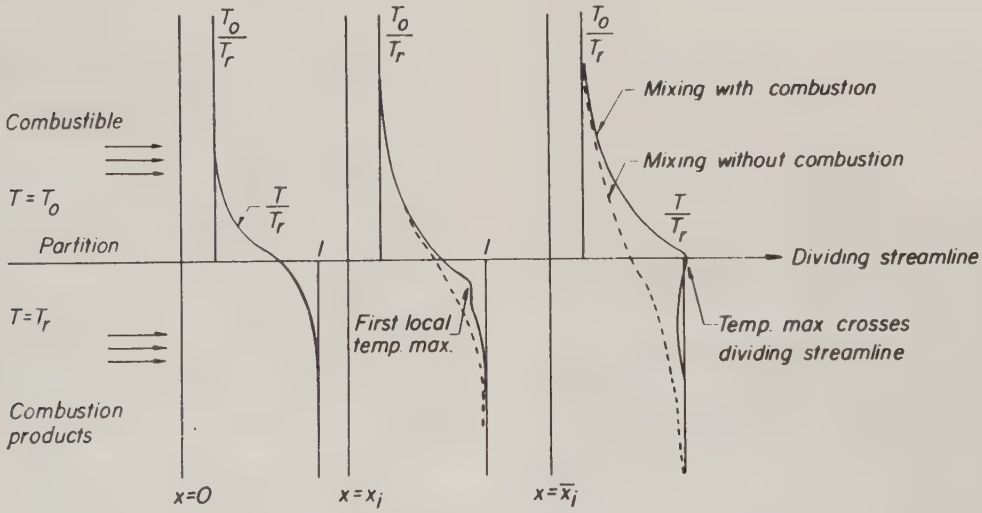

Figure 1. Temperature distribution in the initial mixing zone

PHYSICAL DESCRIPTION OF MODEL

The theory of bluff body flame stabilization presented here is based upon consideration of the

mixing zone between cool combustible and hot inert gas. This process was first analysed by Marble and Adamson[6] for the case of uniform velocity profiles in the two streams before mixing, and it has been extended by the authors[7,8] to include symmetric Blasius velocity profiles at the initial contact point between the two streams. A detailed description of these idealized mixing processes will not be given here. The salient feature of each of both investigations refers to the development of an initial local temperature maximum due to chemical reaction. This local maximum or 'bulge' appears in the hot inert gas downstream of the initial contact point between the two flows assuming, of course, that the initial temperature of the hot gas is less than the adiabatic flame temperature of the cool combustible. The process is schematically shown in *Figure 1.*

The authors[7,8] have shown that the distance to the 'bulge' depends upon various parameters in the following way

$$x_i/l \propto \left[\frac{u_{\mathrm{I}}\tau}{l}\frac{c_p(T_{\mathrm{II}}-T_{\mathrm{I}})}{\Delta H}\exp\left(-A/RT_{\mathrm{II}}\right)\right]^{3/2} \qquad (1)$$

where x_i is distance to initial local temperature maximum in cm, l is the length of the flat plate separating the two streams, assuming first order chemical kinetics and T_{I} and T_{II} are temperatures of combustible and hot inert gas, respectively, u_{I} is free stream velocity, cm/sec, ΔH is heat of combustion, cal/g, A is activation energy, cal/mole, and τ is pre-exponential factor in chemical rate law, sec. Higher order kinetics are not expected to change this result fundamentally. Other restricting assumptions are to be found in references 6 and 7.

The hot gas stream is at a temperature somewhat lower than the adiabatic flame temperature of the combustible. If somewhere in the downstream region of the mixing zone a laminar flame is to be established, the distributed combustion source must develop a sufficient amount of heat not only to overcome the conductive loss under the heat diffusion mechanism but also to heat the gas mixture to a temperature such that the gradient vanishes with respect to the direction perpendicular to the flow. Thus a necessary condition prior to the establishment of a laminar flame is the presence of a temperature maximum in the mixing zone which propagates rapidly towards the unburned combustible with a steepening front and eventually approaches a nearly discontinuous flame front.

Consider next the situation of anchoring a flame on a bluff body wake. There are two fundamental differences. First, the hot gas supply is the previously burned gas which comes back into the flame-holding zone through the re-circulating flow in the wake with its thermodynamic state unknown. Secondly, the re-circulating hot gas is not an infinite heat source or reservoir, but a finite mass of inert, though hot, gas not able to generate heat itself. The mass of re-circulating gas is essentially trapped at least on the time-wise average. If this limited amount of mass is called upon to heat up the incoming cool combustible continuously in steady state operation it must receive heat from its surroundings, that is, the hot burned gas from the flame zone (*Figure 2*).

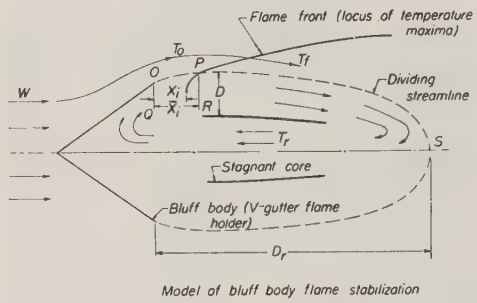

Figure 2. Schematic diagram of bluff body flame stabilization

The average temperature T_r of the gas in the re-circulation zone should therefore be slightly lower than the temperature of the gas immediately behind the flame front which is itself somewhat smaller than T_f (the adiabatic flame temperature in the stagnant condition). A steady flame front can be established and maintained when the rate of heat transfer into the re-circulation zone, across the dividing streamline (PS) downstream of the flame front, together with chemical heat release within the re-circulation zone, is just enough to balance the heat loss from the re-circulation zone to the unburned gas stream across (OP). This balance establishes and maintains the flame front at the designated position*, and determines the average temperature of the re-circulation zone.

A general solution to the aerothermochemical problem of bluff body flame stabilization is at present not possible. A rigorous approach to the solution would demand knowledge of the governing equations, together with their boundary conditions. Even these cannot be written down explicitly. However, if they could be, the mathematical difficulties would indeed be formidable and in all probability demand an iterative procedure analogous to that employed for solving the Navier-Stokes equations in certain viscous flow problems.

In further amplification of this point the following remarks should clarify the point of view taken

* In steady state operation the flame-holder is maintained at constant temperature. The heat supplied by the re-circulating hot gas to the flame-holder will eventually appear in the unburned combustible that comes into contact with the upstream end of the flame-holder.

in this paper. Associated with a given flame stabilization occurrence is a certain aerothermochemical flow field satisfying the governing equations and boundary conditions. In order to determine this flow field analytically one could consider two flow regions: (1) that where chemical reaction is dominating, and (2) that where chemical reaction is negligible. A first approximation would assume a certain flow-temperature distribution in region (2) and calculate, according to the governing equations, the resultant flow in region (1). Naturally, all quantities at the boundary between these two regions must match so that the solutions make sense physically. In general this first approximation will result in a solution for region (1) that does not satisfy the boundary conditions in that region; thus, second and higher approximations are constructed until all constraints are satisfied and the two solutions are completely compatible. It is obvious to those familiar with the field that the analogy to boundary layer flow problems is quite strong.

As expressed above, the approach in this paper will be to formulate the energy balance and chemical kinetic aspects separately, but with strong coupling between them. That is, even though chemical heat release is the primary phenomenological agent it can be assumed to have little effect on the functional form of the overall energy balance, to first approximation. This is distinctly analogous to the role of viscosity in producing flow separation, in which a certain 'frictionless' free stream flow is caused to separate from a surface. The chemical heat release producing the flow (the separating effect of viscosity) is completely determined by the velocity-temperature distribution in the bluff body wake (the adverse pressure gradient of the external frictionless flow). Conversely, the velocity-temperature distribution completely determines the distribution of chemical heat release.

ANALYSIS OF THE MODEL

The rate of heat loss from the re-circulation zone may be written qualitatively as

$$\text{Heat loss} = \Lambda_1 \bar{x}_i (T_r - T_0)$$

where $\bar{x}_i$ is the length of common boundary (OP), $T_r - T_0$ is the average temperature difference across the boundary, and Λ_1 is a film coefficient.

The rate of heat gain by the re-circulation zone may be written qualitatively as

$$\text{Heat gain} = \Lambda_2 (D_r - \bar{x}_i)(T_f - T_r)$$

Here D_r is the arc length along the dividing streamline (OS), *Figure 2*, and $(D_r - \bar{x}_i)$ the length of common boundary between the re-circulation zone at temperature T_r and the flame zone at temperature T_f. Λ_2 is analogous to Λ_1. In view of the remarks preceding this section a term for chemical heat release does not appear explicitly in the heat gain relation, to the approximation considered.

The downstream portion of the re-circulation zone is usually turbulent for flame-holders of practical sizes: moreover the wake boundary is vague. It is indeed not possible to say very much, but it appears certain that Λ_2 is likely to be larger than Λ_1. Even if the downstream portion of the wake is laminar, the local conductivity coefficient will still be much larger than that in the upstream portion because of the higher temperature. Thus $\Lambda = \Lambda_2/\Lambda_1$ can be expected to be large under most circumstances. The statement that $\Lambda \geqslant 1$ is of great importance in the later argument.

The heat balance of the re-circulating mass may therefore be written as:

$$\bar{x}_i/D_r = \frac{\Lambda(1 - \theta_r)}{\Lambda(1 - \theta_r) + \theta_r - \theta_0} \tag{2}$$

where θ_r, non-dimensional re-circulation zone temperature, $= T_r/T_f$, $\theta_0 = T_0/T_f$.

In terms of $\bar{x}_i/D_r$ the condition for the development of the temperature bulge, or the flame, may be written as

$$\bar{x}_i/D_r = \Theta_1 \left[\frac{C_p(T_r - T_0)}{\Delta H}\right]^n \left(\frac{D}{D_r}\right) \cdot \left(\frac{D}{l}\right)^{n-1} \left(\frac{W_\tau}{D}\right)^n \exp\left(\frac{nA}{RT_f}\frac{1}{\theta_r}\right). \tag{3}$$

where Θ_i = non-dimensional constant, W = flow velocity upstream of flame-holder, cm/sec, and D is representative length of bluff body, cm.

The exponent 3/2 has been replaced by n since this exponent will probably vary between 3/2 and 4/3 depending upon the flame-holder geometry and whether the viscous boundary layer is separated or unseparated before entering the wake. Furthermore, x_i has been replaced by $\bar{x}_i$ because the analysis shows (references 7 and 8) that the bulge, once developed, propagates upwards along a line initially normal to the mixing boundary. Thus it can be expected to cross that boundary at an $\bar{x}_i$ not substantially different from or at least closely related to x_i.

The two equations that must be satisfied for a steady state to exist are then equations 2 and 3, one for the heat balance, and the other the kinetic requirement for development of the initial local temperature maximum. The function $(D/D_r)(D/l)^{n-1}$ will be considered as purely fluid mechanical. Thus

$$\bar{x}_i/D_r = \delta\left(\frac{\theta_r - \theta_0}{1 - \theta_0}\right)^n \exp\left(\frac{nA}{RT_f}\frac{1}{\theta_r}\right) \tag{4}$$

with

$$\delta = \Theta_1 [c_p(T_f - T_0)/\Delta H]^n \times (D/D_r)(D/l)^{n-1}(W_\tau/D)^n \tag{5}$$

For the following qualitative discussion, we shall regard Λ and δ to be constant once the flow parameters and the combustible mixture are prescribed.

The determination of $\bar{x}_i/D_r$ and θ_r will be most

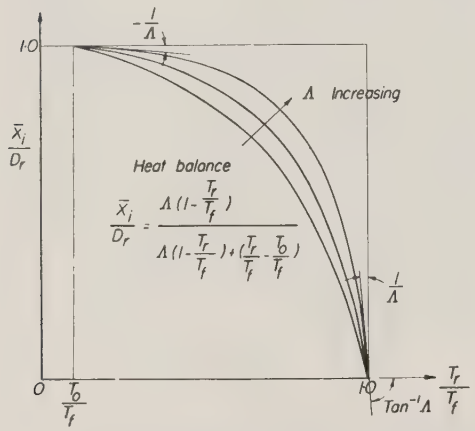

Figure 3. Approximate location of initial local temperature maximum, $\bar{x}_i/D_r$, as a function of θ_r for various values of Λ, from the energy balance

conveniently discussed graphically in the plane of $\bar{x}_i/D_r$ and θ_r. The heat balance equation, 2, provides a family of curves for different values of the ratio of the initial temperature T_0 of the cool combustible to the adiabatic flame temperature T_f as shown in *Figure 3*. $\bar{x}_i/D_r$ clearly decreases with increasing $\theta_r = T_r/T_f$ and vanishes when $T_r = T_f$. The fact that $\Lambda \geqslant 1$ requires the curvature to be negative. Starting from unity, the slope of the curve is $-1/\Lambda$. It increases rather slowly and has

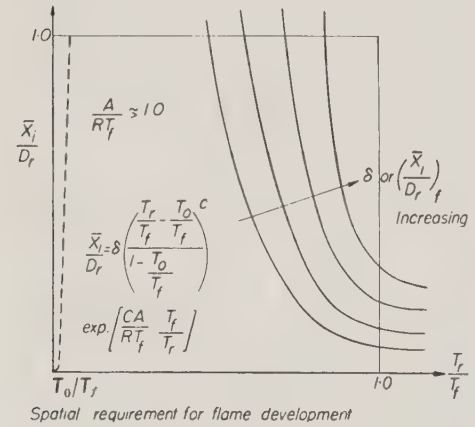

Figure 4. Approximate location of initial local temperature maximum, $\bar{x}_i/D_r$, as a function θ_r for various values of δ, from kinetic requirement. Here c corresponds to n

its largest negative slope, $\partial(\bar{x}_i/D)/\partial\theta_r = -\Lambda$ at $\bar{x}_i/D_r = 0$, $\theta_r = 1$. Since T_0/T_f is usually small, this curve of heat balance is essentially universal for a given value of Λ.

The kinetic equation, 3, provides another set of curves (*Figure 4*). Mathematically, equation 3 gives $\bar{x}_i/D_r = 0$ at $T_r = T_0$ since $\exp[nA/RT_f\theta_r]$ is finite, however large it may be. As soon as $T_r > T_0$, $\bar{x}_i/D_r$ rapidly becomes very large, reaches a maximum and then rapidly decreases and asymptotically approaches zero exponentially as $T_r \to \infty$. The derivation of equation 3 is not valid if T_r is not considerably larger than T_0. That part of the curve near $T_r \cong T_0$ is not sensible physically and should be discarded. Interest is focused only on the region $T_f > T_r \gg T_0$. Denote the value of $\bar{x}_i/D_r$ at $\theta_r = 1$ by $(\bar{x}_i/D_r)_f = \delta \exp[nA/RT_f]$. Then

$$x_i/D_r = (x_i/D_r)_f \exp\left[nA\left(\frac{1}{\theta_r} - 1\right)\Big/ RT_f\right] \quad (6)$$

assuming $(\theta_r - \theta_0)/(1 - \theta_0) \cong$ constant compared to the exponential term, and

$$\frac{\partial}{\partial\theta_r}(x_i/D_r) = -(x_i/D_r)_f \frac{nA}{RT_f}\frac{1}{\theta_r^2} \exp\left[nA\left(\frac{1}{\theta_r} - 1\right)\Big/ RT_f\right] \quad (7)$$

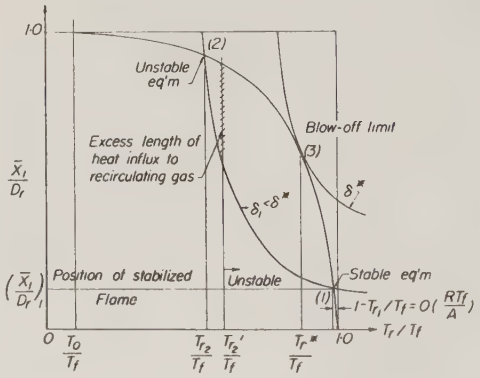

Figure 5. Graphical solution of energy balance and kinetic requirement

The intersections of the two curves representing the two equations 2 and 3 are the possible equilibrium configurations compatible with the fluid mechanical and the chemical kinetic requirements. There may be either 1 or 3 intersections, but the one in the vicinity of $T_r \cong T_0$ is entirely fictitious as previously indicated. If we discount that intersection around $T_r \cong T_0$, the two curves may either intersect at two points, 1 and 2, may be tangent to each other at one point 3 or may not intersect at all. *Figure 5* illustrates the possibilities. The point 3 corresponds to the condition at the 'blow-off' limit which will be discussed later. The case of no intersection corresponds to the conditions that no stabilized flame is possible, that is, the heat balance and the kinetic requirement

cannot be met simultaneously in the steady state.

Only one of the two equilibrium points represents the physically observable configuration that is stable towards small disturbances. At point 2 assume T_r is increased by some external source to a higher value T_r' and maintained until the quasi-steady state value of $\bar{x}_i/D_r$ compatible with equation 3 is reached. This value of $\bar{x}_i/D_r$ is smaller than the original value at point 2. If this T_r' is to be sustained by the heat transfer across the wake boundary a reduction in $\bar{x}_i/D_r$ from point 2 will also be required, but this reduction, required to maintain the heat balance, is less. Thus the excessive decrease of $\bar{x}_i/D_r$ due to too early a development of the flame provides additional area for transfer of excess heat into the re-circulating mass and raises its temperature still further. The result is further reduction of $\bar{x}_i/D_r$ with no possibility of returning to the original point 2. A slight decrease of T_r below the equilibrium value at point 2 results in an excessive increase of $\bar{x}_i/D_r$ as compared with that required kinetically and a corresponding deficit of heat inflow which cools the re-circulating gas further. The system is unstable and will diverge from the equilibrium position 2 once it is disturbed. Similar observations at point 1 where the relative magnitude of the slope $\partial(\bar{x}_i/D_r)/\partial\theta_r$ of the two curves is reversed, shows that the equilibrium point 1 is stable and is therefore the one physically observed. It should be remarked that the quasi-steady argument is not always reliable. The discussion of the physical process accompanying the previous quasi-steady argument, however, appears to be on a sound physical basis. The above conclusion is expected to be confirmed by a more careful stability analysis. The stable equilibrium point corresponds to the one with higher wake temperature T_r and a smaller value of $\bar{x}_i/D_r$ for the initiation of flame.

BLOW-OFF CRITERION AND CORRELATION WITH EXPERIMENT

At the critical condition of blow-off, the two curves on the $\bar{x}_i/D_r$ and θ_r plane must be tangent to each other. Therefore the following two relationships are satisfied at the blow-off limit.

$$(\bar{x}_i^\star/D_r)_1 = (x_i^\star/D_r)_2 \quad ,$$
$$\left[\frac{\partial(\bar{x}_i/D_r)}{\partial\theta_r}\right]_1^\star = \left[\frac{\partial(\bar{x}_i/D_r)}{\partial\theta_r}\right]_2^\star \tag{8}$$

where superscript $\star$ indicates the quantities evaluated at the blow-off limit and subscripts 1 and 2 indicate quantities evaluated with the heat balance equation 2 and the kinetic relationship 3 respectively.

If it is assumed that $\theta_0 \ll 1$, and $(\theta_r^\star)^2 \cong$ const compared to the variation of the exponential term with $(\theta_r^\star - 1)/\theta_r^\star$ then the wake temperature at blow-off is given by

$$1 - \theta_r^\star = \left\{\left(1 + 4(\Lambda - 1)\Big/\frac{nA}{RT_f}\right)^{\frac{1}{2}} - 1\right\}\Big/2(\Lambda - 1) \tag{9}$$

The value of $\bar{x}_i^\star/D_r$ is obtained directly as

$$\bar{x}_i^\star/D_r \cong \Lambda(1 - \theta_r^\star)/\{\Lambda(1 - \theta_r^\star) + 1\} \tag{10}$$

assuming $\theta_r^\star \cong 1$, an approximation that will be shown to be reasonable for $nA/RT_f \gg 1$.

The blow-off conditions (8) may be put in the following form with the same assumptions as used to obtain $\theta_r^\star$

$$\Lambda(1 - \theta_r^\star)/\{\Lambda(1 - \theta_r^\star) + 1\} = \delta \exp\left[nA/RT_f\theta_r^\star\right] \tag{11}$$

where δ is given by equation 5. The value of $\theta_r^\star$ is given by 9. To find an explicit expression of the blow-off velocity $W^\star$ it becomes apparent that we have to make strong assumptions about many physical relationships and constants. Clearly D/D_r, the ratio of the flame-holder dimension to its wake length, must depend upon the Reynolds number $W^\star D/\nu$ of the flow where ν is the kinematic viscosity of the combustible. It also may depend upon many other dimensionless variables, not excluding those pertaining to parameters of chemical kinetic origin. D/l is the ratio of the flame-holder dimension to the effective flat plate length that defines the shear condition on the flame-holder just upstream of the wake. Clearly D/l will depend on the Reynolds number, the flame-holder geometry, etc. Furthermore the magnitude of n, although it is relatively well defined, should be more precisely determined because it enters into the exponents of D, p and T in any stability parameter.

As an approximation consider $(D/D_r)(D/l)^{n-1}$ to be a purely fluid mechanical quantity which may be represented as $\propto (R_e)^q$ where q is some unknown constant. ΔH is the heat of reaction per unit mass of the combustible gas mixture and is approximately the same as $\bar{c}_p(T_f - T_0)$ if some average specific heat $\bar{c}_p$ is taken. Thus

$$\delta = \left[\Theta_2 R_e^q \frac{W\tau}{D}\right]^n \tag{12}$$

Then the equation for the blow-off velocity $W^\star$ may be obtained as

$$W^\star/D^{(1-q)/(1+q)}\nu^{q/(1+q)} = \Theta_3\left[\frac{\Lambda(1 - \theta_r^\star)}{\Lambda(1 - \theta_r^\star) + 1}\right]^{(1/n)\{1/(1+q)\}} \times \left[\frac{1}{\tau}\exp\left\{-\frac{A}{RT_f}\left[1 - \left(1 - \frac{1}{\theta_r^\star}\right)\right]\right\}\right]^{1/(1+q)} \tag{13}$$

The correlation between the blow-off velocity $W^\star$ with the scale of the flame-holder D depends crucially on the value of q which is a constant primarily of fluid mechanical origin through

$$(D/D_r)^{1/n}(D/l)^{(n-1)/n} \propto \left(\frac{W^\star D}{\nu}\right)^q$$

Knowledge of the fluid mechanics of this system is too meagre to enable a guess at the nature of such a relationship and the approximate magnitude of the constant q; but it is clear that q should have different values in different ranges of Reynolds numbers corresponding to laminar or turbulent conditions of the wake. When the Reynolds number is large, say $>10^4$, the wake may be entirely turbulent so that little dependence, if any, of D/D_r on R_e may be expected. On the other hand, for sufficiently small R_e, the wake may be completely laminar, so that D/D_r will decrease with increasing Reynolds number. The Reynolds number dependence of D/l is probably less important since $(n-1)/n$ is relatively small. l is the equivalent plate length defined by the skin friction or the curvature of the velocity profile at the separation point on the flame-holder. Since the bulge forms in the re-circulation zone it is the boundary layer effect on the hot side which is most important. Its effect will, however, be rendered small by the small power $(n-1)/n$. The small effect of boundary layer suction on the cool side alone, as reported by Williams *et al.*[9], partially supports this conclusion.

The blow-off velocity $W^\star$ is now displayed as a function of Λ, $(1-\theta_r^\star)$, q, n and D, ν, T_f, τ, A which are given quantities. To facilitate correlation and further discussion, some order of magnitude considerations will be introduced.

(1) If $4(\Lambda-1)/(nA/RT_f) \gg 1$ (corresponding to laminar flow along *OP* and very turbulent flow along *PS*, see *Figure* 2) then from equation 9

$$\Lambda(1-\theta_r^\star) \gg 1 \text{ and } 1-\theta_r^\star \ll 1 \text{ for } \frac{nA}{RT_f} \gg 1$$

so that $W^\star/D^{(1-q)/(1+q)}\nu^{q/(1+q)}$

$$= \Theta_3\left[\frac{1}{\tau}\exp\left(-\frac{A}{RT_f}\right)\right]^{1/(1+q)} \qquad (14)$$

(2) If $4(\Lambda-1)/(nA/RT_f) \ll 1$ then from equation 9

$$\Lambda(1-\theta_r) \cong \Lambda \Big/ \frac{nA}{RT_f} \text{ and } 1-\theta_r^\star \ll 1 \text{ for } \frac{nA}{RT_f} \gg 1$$

so that $W^\star/D^{(1-q)/(1+q)}\nu^{q/(1+q)}$

$$= \Theta_4\left(\Lambda \Big/ \frac{nA}{RT_f}\right)^{(1/n)\{1/(1+q)\}} \left[\frac{1}{\tau}\exp\left(-\frac{A}{RT_f}\right)\right]^{1/(1+q)} \qquad (15)$$

It is to be noted that as $4(\Lambda-1)/(nA/RT_f)$ increases there is a finite limit for $W^\star$ instead of its being unbounded, as the approximation for small $4(\Lambda-1)/(nA/RT_f)$ indicates. Furthermore, the two formulae for $W^\star/D^{(1-q)/(1+q)}\nu^{q/(1+q)}$ are essentially the same, the dominant term being $\exp(-A/RT_f)$.

A check on the correlation indicated above has been carried out utilizing Haddock's[10] data for cylinders in a gasoline fuel mixture. An activation energy of 40 kcal/mol, as suggested by Avery and Hart[11], was taken. Salé's[12] calculation for hexane was adopted for determining T_f from the equivalence ratio ϕ. One free constant is involved corresponding to the selection of $\Theta_3\tau^{-1/(1+q)}$ so as to fix the level of the blow-off velocity. The other constant q was determined to give a best fit of the data. Its value of 0·3 corresponds to a $W^\star \propto D^{0.54}$ dependence which is quite close to various experimental results. The correlation is shown in *Figure 6*. Its reasonableness gives some support to

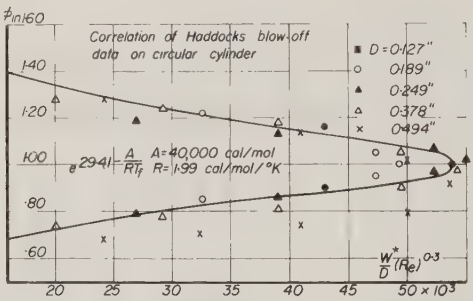

Figure 6. Correlation of Haddock's data with present theory

the present result; but it should be pointed out that the Arrhenius factor plays such an important role as to be primarily responsible for the good correlation.

IMPLICATIONS OF THE ANALYSIS

(1) Zukoski and Marble[5] have advanced the idea of a critical 'ignition delay time' which is roughly the time of contact between the cool combustible and hot wake. This 'delay time', defined as $\tau_{B.O.} = D_r/W^\star$, where D_r is the measured length of the re-circulation zone, was shown by experiment to be only a function of the equivalence ratio, ϕ. Additional experiments also showed that as blow-off was approached the temperature of the re-circulation zone decreased only slightly and furthermore the variation of θ_r *versus* $W^\star/W$ was similar for all types of bluff bodies tested. Both of these experimental results can be inferred from this analysis.

It can be seen that the minimum value of $\theta_r^\star$, from equation 9, is given by $(1-RT_f/nA)$ which occurs at $\Lambda = 1$. Its maximum value is unity. The maximum rate of change of $\theta_r^\star$ with respect to $(\Lambda-1)$ is proportional to $(RT_f/nA)^2$ and also

occurs for $\Lambda = 1$. If RT_f/nA is of order 10^{-1} (a reasonable value) then $\theta_r^\star$ should be rather insensitive to changing conditions (changes in Λ) in conformity with Zukoski and Marble's experimental results.

Zukoski and Marble questioned the validity of any thermal theory for bluff body flame stabilization on the basis of their measurements. However, the presence of an Arrhenius factor in the kinetic expression does indicate the importance of small temperature changes in affecting blow-off. Their observation of a nearly universal relation for θ_r, independent of free stream and bluff body parameters, is supported by this analysis which shows from equation 9 that $1 - \theta_r^\star$ is primarily a function of nA/RT_f if $nA/RT_f \gg 1$. This can be shown explicitly by a close look at $1 - \theta_r^\star$ as given by equation 9. Furthermore, for any θ_r with $\theta_0 \ll 1$ one can solve for θ_r from equation 2 and see that with $x_i/D_r \ll 1$, $\theta_r \cong \Lambda/(\Lambda + x_i/D_r)$ showing little dependence of θ_r on Λ when $\Lambda \gg x_i/D_r$.

The simplest interpretation of the $\tau_{B.O.} = f(\phi)$ result is that the critical $\bar{x}_i$ should equal D_r. That is, Zukoski and Marble look upon the blow-off process as one in which a particle of combustible moves along the dividing streamline (OS), *Figure 2*, with a certain inherent ignition lag depending upon its equivalence ratio. If ignition does not occur by the time it has moved a distance D_r then blow-off will occur. The time $\tau_{B.O.} = D_r/W^\star$ available for ignition must equal the so-called ignition delay time. This time should then be primarily a function of equivalence ratio independent of the properties of the re-circulation zone. From this analysis one does get $\bar{x}_i^\star/D_r \cong 1$ for $4(\Lambda - 1)/(nA/RT_f) \gg 1$, leading to $(1\ \Lambda - \theta_r^\star) \gg 1$. However, as indicated above, $1 - \theta_r^\star$ is a very weak function of Λ for $RT_f/nA \ll 1$, and for experiments within a reasonable Reynolds number range Λ should not vary by orders of magnitude. Therefore $\bar{x}_i^\star/D_r$ should also be virtually constant. Forming the ratio $\tau_{B.O.} = D_r/W^\star \propto \bar{x}_i^\star/W^\star$ it can be seen from equations 14 or 15 that $W^\star \propto D^{(1-q)/(1+q)}$ giving

$$\tau_{B.O.} \propto D_r D^{(q-1)/(1+q)} f(\phi)$$

At large Reynolds numbers D/D_r has little dependence on R_e implying $q = 0$. Thus $\tau_{B.O.}$ would be only a function of equivalence ratio. This shows that even if $D_r/W^\star$ is a function of ϕ only it does not necessarily imply $\bar{x}_i^\star/D_r = 1$. The result is probably not general since other experiments[13] have indicated a variation of $D_r/W^\star$ with Reynolds number.

(2) The physical meaning of $\bar{x}_i^\star$ is essentially the stand-off distance of the flame just before blow-off. This distance is usually small compared to D_r. When $4(\Lambda - 1)/(nA/RT_f) \ll 1$ one gets $\Lambda(1 - \theta_r^\star) \cong \Lambda RT_f/nA \ll 1$ implying $\bar{x}_i^\star/D_r \ll 1$. However, even if $4(\Lambda - 1)/(nA/RT_f) \cong 1$ and $RT_f/nA \cong 10^{-1}$ $\bar{x}_i^\star/D_r \cong 0{\cdot}22$. The percentage change in $\bar{x}_i/D_r$ as blow-off is approached can, however, be quite large, as seen from *Figure 5*, even though visually one sees little movement of the flame as blow-off is approached and achieved.

(3) Fetting, Choudhury and Wilhelm[14] report, in this symposium, on the effect of introducing small quantities of various fuels, inert gas, and oxidizer upstream and downstream of the flame attachment zone on a bluff body. Employing a prime propane–air stream they found that small additions of methane, propane, butane, hydrogen, and oxygen not only shifted the blow-off curve along the axis of free stream equivalence ratio but increased the maximum blow-off velocity. Injection of inert gas, even at substantially higher flow rates compared to fuel and oxidizer injection was found to have little effect on the overall blow-off curve. The equivalence ratio shift is not surprising, being in the direction of fuel lean flames for fuel injection, and in the direction of fuel rich flames for oxygen injection. However, the increase in maximum blow-off velocity does not appear to be explicable on the basis of blow-off mechanisms proposed in the past. The present theory can give a rather straightforward qualitative explanation for most of these events.

For fuel lean flames the re-circulating hot gases in the neighbourhood of the flame attachment zone will contain residual oxygen. Injection of additional fuel directly into these hot gases will raise their temperature slightly, due to partial combustion, and thus accelerate the formation of the initial local temperature maximum. The fundamental result of the flat plate analysis, given by equation 1, which takes the form given by equation 4, is strictly valid for the case of chemical reaction beginning at the point of contact between hot products and cool combustible. Pre-injection of fuel into the hot products can be considered as an upstream shift of the origin of chemical reaction. Thus $\bar{x}_i/D_r$, measured from the point of contact, is decreased for the same δ and θ_r. Assuming the heat balance, equation 2, unchanged one can imagine a flame-holder operating at the blow-off condition, point 3 in *Figure 5*. Injection of fuel will tend to shift the curve for $\delta^\star$ downwards so that the operating conditions are stable for the *same* $\delta^\star$. Therefore, to achieve blow-off $\delta^\star$ must be increased to a new value $\delta^\star_{\text{inj}}$ corresponding to the blow-off velocity with injection. Therefore the maximum blow-off velocity should increase, as observed experimentally. For fuel-rich flames with oxygen injection a parallel argument applies.

The explanation given above implies that direct injection into the re-circulating zone downstream of the flame attachment zone should have a larger

effect on maximum burning velocity than upstream injection ahead of the attachment alone. This inference is borne out in the case of oxygen and hydrogen injection where the experimental maximum blow-off velocity increase was much greater for downstream than upstream injection. However, for hydrocarbon injection the experimental maximum blow-off velocity increases were approximately the same for both upstream and downstream injection, with perhaps some indication of a higher maximum blow-off velocity with downstream injection. Some increase for upstream injection should be expected since the concentration of fuel and subsequent concentration gradients, across the dividing streamline (OP), *Figure 2*, are even greater than the case of stoichiometric fuel/air ratio so that $\bar{x}_i^*/D_r$ will be smaller than in the case of no injection at $\phi = 1$. The negligible sensitivity of maximum blow-off velocity for propane–air flames to the mode of hydrocarbon injection remains to be explained.

(4) The dependence of the blow-off velocity W^* (equations 14, 15) on the temperature and pressure of the incoming combustible appears to be quite complicated. One may ask if the frequency factor $1/\tau$ of the overall kinetic rate expression depends on T and/or p, and how the conductivity ratio Λ depends on T and/or p? There is little that can be said quantitatively, but if there is any dependence on T it is primarily the absolute magnitude of flame temperature T_f that matters. Since T_0/T_f is much less than unity, the percentage variation of T_f as a result of the variation of T_0 is relatively insignificant. Consequently the dependence of the blow-off velocity W^* on the cool gas temperature should be due to the kinematic viscosity coefficient ν and the Arrhenius factor which may be written as

$$\exp(-A/RT_f) \cong \exp(-A/R\Delta T_f)\exp(AT_0/R\Delta T_f^2)$$

$$\text{since } T_0 \ll \Delta T_f$$

where $\Delta T_f = T_f - T_0 = \Delta H/\bar{c}_p$ is essentially a constant for a given combustible mixture. Now $\exp[-AT_0/R\Delta T_f^2]$ is of the order of unity because $A/RT_f \sim \mathrm{O}(10)$, while $T_0/\Delta T_f \sim \mathrm{O}(10^{-1})$ for ordinary chemical fuels burning under laboratory conditions. Therefore if the viscosity coefficient μ is approximately proportional to T^ω, then

$$W^* \propto T_0^{(1+\omega)q/(1+q)} \exp\left[\frac{A}{(1+q)R}\frac{T_0}{\Delta T_f^2}\right] \quad (16)$$

The Arrhenius factor introduces an exponential dependence of W^* on T_0, while the viscosity coefficient gives a power law dependence. For a limited range of T_0 the exponential dependence may be locally represented by some power law to fit the conventional representation of the stability parameter W^*/T_0^β. Since q is a relatively small number and $(1+\omega)/(1+q)$ is roughly unity, the temperature dependence through the kinematic viscosity coefficient may not be too important as compared with that through the kinetic expression. The lack of constancy of the exponent β in the stability parameter, as revealed by different experiments, may be understood through this reasoning as due to $\beta \cong AT_0/(1+q)R\Delta T_f^2$. Thus the present analysis indicates that the temperature dependence of the blow-off velocity on T_0 may be exponential rather than some power of T_0.

The pressure dependence of the blow-off velocity certainly originates partly from the Reynolds number through density. It is not clear whether Λ and/or $1/\tau$ is pressure dependent. Another important source of pressure dependence is through the gross order of the chemical kinetic processes which are inadequately represented in equations 14, 15 primarily because $\bar{x}_i/l$ has been evaluated carefully only for a first order reaction. Attempts at analytically determining $\bar{x}_i$ for chemical reactions different from first order are being carried out. Little can be said from the present blow-off formulation concerning the effect of pressure until the effect of the order of reaction is better understood.

(5) Probably the most important inference to be gleaned from this analysis is the relative importance of the local flame attachment zone as compared with the bulk of the re-circulation zone. For $A/RT_f \gg 1$ it was shown that $\bar{x}_i^*/D_r$ is always quite small and both θ_r^* and θ_r are virtually constant. Therefore, very little happens in the bulk of the re-circulation zone as blow-off is approached and achieved. Fetting, Choudhury, and Wilhelm[14] observed that a streamlined body of moderate length gave the same blow-off results as did a circular cylinder of equal diameter. This indicates that the re-circulation zone may be distorted, within certain limits, and still not radically change flame stabilization properties. Other investigators[13] have also commented on the importance of this local region. The following section will treat this small zone in some detail.

STABILITY ANALYSIS CONSIDERING LOCALIZED STREAMTUBE CONTROL VOLUME

The preceding discussion has demonstrated the possibility of blow-off based upon an overall energy balance for the bluff body wake. It has been seen that as blow-off is approached the wake temperature decreases slightly as $\bar{x}_i/D_r$ increases appreciably, percentage-wise. Nevertheless, for $4(\Lambda - 1)/(nA/RT_f) \ll 1$, $\bar{x}_i^*/D_r \ll 1$. Thus the properties of the bulk of the re-circulation zone do not, to first approximation, vary as blow-off is

approached and achieved. This inference strongly suggests that the local zone in the immediate neighbourhood of initial contact between cool combustible and hot combustion products may be controlling. A closer look at this region leads to still another mechanism for blow-off in which the temperature, where the bulge forms, is the primary variable. This is in contrast to the previous result in which the average temperature of the re-circulation zone as a whole was the primary blow-off variable. The following analysis assumes that a re-circulation zone, at temperature T_r, exists which serves as a continuous energy source for the initial mixing zone. It will be shown that even with T_r held constant, blow-off can occur.

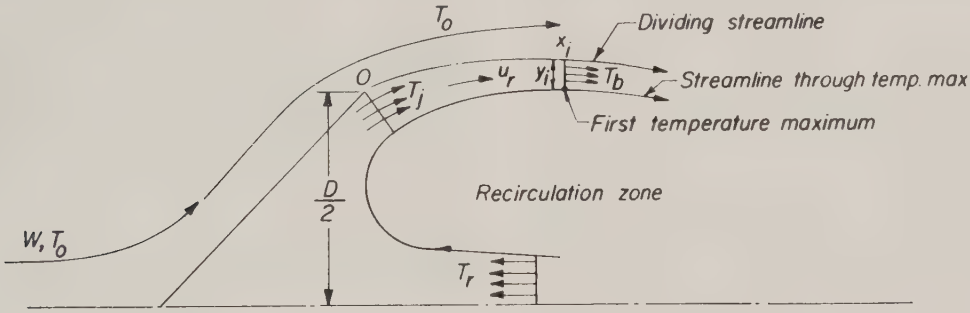

Figure 7. Control volume for localized analysis

The localized control volume is constructed in the following way. Consider the streamtube defined by the separation streamline and the streamline passing through the initial local temperature maximum. Thus the streamtube is within the re-circulation zone, at the boundary between fresh combustible and burned products. The control volume for energy balance includes the portion of this streamtube between the separation point on the bluff body (point O) and the station x_i where the local maximum first appears. *Figure 7* illustrates the model.

An immediate advantage of this localized model is: heat addition due to chemical reaction may be neglected, as only after local temperature maximum has formed does chemical reaction become important. The temperature T_j of mass entering the control volume is somewhat less than T_r because of heat loss to the flame-holder, for example. The connection between T_f, T_r, T_j will not be spelt out, but it can be assumed that T_r has the same dependence on T_f as shown previously for the recirculation zone control volume. The following additional assumptions are adopted: (1) the variation of flow properties across the streamtube is ignored and average values implied; (2) energy entering the control volume across the streamline passing through the initial local temperature maximum is negligible compared to that leaving the control volume across the dividing streamline (*Figure 7*). With these stipulations conservation of energy gives

$$\dot{m}c_p(T_j - T_b) = \alpha x_i[(T_r + T_b)/2 - T_0] \quad (17)$$

for $c_p = \text{const}$. The quantity α is the heat transfer coefficient across the dividing streamline.

The mass flow rate $\dot{m}$ may be estimated by writing

$$\dot{m} = \rho u_r y_i$$

where u_r is the flow velocity in the streamtube, y_i the depth at which the initial temperature maximum appears. Its magnitude is most simply estimated by introducing the concept of a difference time $\bar{t}$ that is assumed equal to the time x_i/u_r. Then

$$y_i \propto \left(\frac{\lambda}{\rho c_p}\bar{t}\right)^{1/2} \cong \left(\frac{\lambda}{\rho c_p}\frac{x_i}{u_r}\right)^{1/2}$$

$\rho = \rho_0 T_0/T_b$, $\mu = \mu_0 T_b/T_0$ (consistent with analysis of reference 7)

The dependence of y_i on T_b can be neglected if $(T_b - T_0)/(T_j - T_0) \cong 1$. Equation 17 then becomes

$$x_i/D \propto \frac{P_r R_e^{t+1}}{N_u^2}\left[\frac{T_0}{T_b}\frac{T_j - T_b}{T_j + T_b - 2T_0}\right]^2 \quad (18)$$

where it has been assumed that $u_r \propto WR_e^t$ $P_r = c_p u/\lambda$, and $N_u = \propto D\lambda$.

For convenience this is finally written as:

$$(x_i/L)_1 = \left[\frac{T_0}{T_b}\frac{T_j - T_b}{T_j + T_b - 2T_0}\right]^2 \quad (19)$$

where

$$L = DP_r R_e^{t+1} K_1/N_u^2$$

K_1 being an arbitrary dimensionless constant.

Equation 19 gives x_i/L as a function of T_b with T_j and T_0 as parameters. For a given T_0, x_i/L is

shown in *Figure 8* for several T_j. It is directly seen from equation 19 that

$$\frac{\partial}{\partial T_b}\left(\frac{x_i}{L}\right)_1 = \begin{cases} 0, & T_b = T_j \\ -\dfrac{T_j + T_0}{T_0(T_j - T_0)} < 0, & T_b = T_0 \end{cases} \tag{20}$$

and that

$$\frac{\partial}{\partial T_j}\left(\frac{x_i}{L}\right)_1 > 0, \quad \frac{\partial^2}{\partial T_b^2}\left(\frac{x_i}{L}\right)_1 > 0 \text{ for } T_0 \ll T_b < T_j$$

The dependence of x_i on several flow properties is known only for mixing in the wake of a flat plate, and is given by equation 2. For this application the hot stream temperature T_{II} is taken as

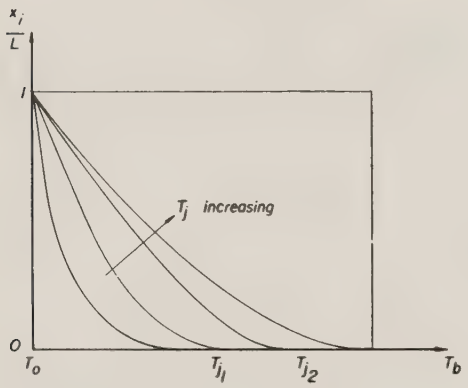

Figure 8. Energy balance for localized streamtube control volume

$(T_j + T_b)/2$ in the heat loss term $(T_{II} - T_I)$, while T_{II} is replaced by T_b in the reaction rate term. Furthermore, the free stream velocity u_I is replaced by u_r and the exponent 3/2 by a non-specified exponent n as done previously.

The replacement of T_{II} by T_b in the reaction rate term is reasonable since chemical reaction is negligible up to the point where the local maximum forms, due to negligible combustible concentration. The replacement of 3/2 by n is a consequence of the unknown fluid dynamical situation in the mixing region behind a bluff body as discussed earlier.

If one lets $l \propto D(R_e)^s$ and assumes $(c_p/\Delta H)[(T_j + T_b)/2 - T_0]$ to be constant since T_j and T_b will be close to the flame temperature, then

$$\left(\frac{x_i}{L}\right)_2 = K_2 \frac{N_u^2}{P_r}(R_e)^q \tau^n \left(\frac{W}{D}\right)^n \exp\frac{nA}{RT_b} \tag{21}$$

where K_2 is an arbitrary dimensionless constant and $q = s - t + n(t - s) - 1$.

These results, embodied in equations 19 and 21, are essentially the same as obtained for the re-circulation zone control volume. At the critical $T_b = T_b^\star$ equation 8 must again be true except for replacement of $\bar{x}_i^\star$ by $x_i^\star$, D_r by L, and θ_r by T_b.

If $T_0 \ll T_b < T_j$ then equation 8 yields

$$-\frac{nA}{R}(T_j^2 - T_b^{\star 2}) \cong T_b^{\star 3} - 2T_jT_b^{\star 2} - T_j^2T_b^\star$$

Further approximation assuming $nA/RT_f \gg 1$ and $T_b^\star = T_j + \varepsilon$ with $\varepsilon \ll T_j$ gives

$$T_b^\star \cong T_j[2(1 - RT_j/2nA)^{1/2} - 1] \tag{22}$$

These approximations are all reasonable, as can be shown numerically. They are not fundamental but merely for the convenience of showing certain results.

Equation 22 gives $T_b^\star$ in terms of T_j. From this, through equation 19, the pre-exponential factor in equation 21 can be evaluated at the critical condition as a function of T_j. A correlation of experimental data is then possible after fixing T_j as essentially the adiabatic flame temperature determined from the equivalence ratio. The correlation would demand

$$\left[\frac{T_0}{T_b^\star}\frac{T_i - T_b^\star}{T_j + T_b^\star - 2T_0}\right]^{2/n} \exp(-A/RT_b^\star) = \left(K_2\frac{N_u^2}{P_r}\right)^{1/n} R_e^{q/n}\frac{W^\star}{D} \tag{23}$$

The variation of the pre-exponential term in equation 23 is small compared with variation of the exponential itself and may be neglected. The variation of N_u may be lumped in with R_e and P_r considered constant. Then it is seen that equation 23 is similar to equation 14 and results in the same correlation as obtained earlier for the re-circulation zone control volume. An estimate of $(x_i/L)^\star$ can also be obtained. For typical values of R, A, and T_j with n of order unity

$$RT_j/2nA \ll 1$$

Therefore, $(1 - RT_j/2nA)^{1/2} \cong 1 = \frac{1}{2}(RT_j/2nA) - \frac{1}{8}(RT_j/2nA)^2 - \ldots$ and from equation 22

$$T_b^\star \cong T_j[1 - RT_j/2nA - \tfrac{1}{4}(RT_j/2nA)^2] \tag{24}$$

If this be substituted into equation 19 assuming $T_0 \ll T_b < T_j$ one gets

$$\left(\frac{x_i}{L}\right)^\star \cong \left(\frac{RT_0}{4nA}\right)^2 \left[\frac{\{1 + \frac{1}{4}(RT_j/2nA)\}/(1 - RT_j/2nA)}{\times \{1 - \frac{1}{2}(RT_j/2nA)\}}\right]^2 \tag{25}$$

It is seen that $(x_i/L)^\star$ is weakly dependent on T_j

but can be shown to increase with increasing T_j. As a further approximation

$$(x_i/L) \cong (RT_0/4nA)^2 \tag{26}$$

Then a correlation would demand

$$R_e^{a/n} \frac{W^\star}{D} = K_3 \exp(-A/RT_b^\star) \tag{27}$$

for a given combustible and fixed initial conditions. This merely supports the neglect of the pre-exponential term in equation 23.

Fetting, Choudhury, and Wilhelm's[14] results, described earlier, are now clearly predicted from equation 27. Injection of combustible material into the streamtube control volume increases $T_b^\star$ thus increasing $W^\star$ for the same re-circulation zone temperature T_r.

This research is part of the work under OOR DA-36, ORD-2183, sponsored by the Office of Ordnance Research, U.S. Army, and was sponsored in part by Project Squid.

REFERENCES

[1] Williams, G. C., Hottel, H. L. and Scurlock, A. C. Flame stabilization and propagation in high velocity gas streams. *Third Symposium (International) on Combustion*, 1949. Baltimore; Williams and Wilkins

[2] Khitrin, L. N. and Goldenberg, S. A. Ignition of gas mixtures. *Sixth Symposium (International) on Combustion*, p. 522. New York; Reinhold

[3] — — The influence of the initial temperature of a combustible mixture and of the ambient pressure on the stabilization limits, *Sixth Symposium (International) on Combustion*, p. 448. New York; Reinhold

[4] Longwell, I. P., Frost, E. E. and Weiss, M. A. *Ind. Eng. Chem.* 45 (1953) 1629

[5] Zukoski, E. E. and Marble, F. E. Experiments concerning the mechanism of flame blow off from bluff bodies. *Proc. Gas Dynamics Symposium on Aerothermochemistry*. 1956. Northwestern University

[6] Marble, F. E. and Adamson, T. C., Jr. Ignition and combustion in a laminar mixing zone. *Jet Propulsion* 24 (1954)

[7] Cheng, S. I. and Kovitz, A. A. Ignition in the laminar wake of a flat plate. *Sixth Symposium (International) on Combustion*, p. 418. 1956. New York; Reinhold

[8] — — Mixing and chemical reaction in the laminar wake of a flat plate. *J. Fluid Mech.* May 1958

[9] Williams, G. C., Woo, P. T. and Shipman, C. W. Boundary layer effects on stability characteristics of bluff-body flame-holders. *Sixth Symposium (International) on Combustion*, p. 427. 1956. New York; Reinhold

[10] Haddock, G. W. *Jet Propulsion Laboratory Report No.* 3–24 1951. California Institute of Technology

[11] Avery, W. H. and Hart, R. W. Combustor performance with instantaneous mixing. *Ind. Eng. Chem.* 45 (1953) 1634

[12] Vichnievsky, R., Salé, B. and Marcadet, J. Combustion temperatures and gas composition. *Jet Propulsion* 25 (1955) 105

[13] Westenberg, A. A., Berl, W. G. and Rice, J. L. Studies of flow and mixing in the recirculation zone of baffle-type flame-holders. *Proc. Gas Dynamics Symposium*, 1955. Northwestern University

[14] Fetting, F., Choudhury, A. P. and Wilhelm, R. H. Turbulent flame blow-off stability effect of auxiliary gas addition into separation zone. This volume, p. 621

94

STUDIES OF EXCHANGE BETWEEN RE-CIRCULATION ZONE BEHIND THE FLAME-HOLDER AND OUTER FLOW

T. A. BOVINA

The stability of the process of combustion behind the flame-holder greatly depends on the amount of heat received by the fresh mixture from the re-circulation zone. It is therefore advisable to begin investigating the flame-holder operation with a study of heat exchange between the zone and the outer flow.

This paper is devoted to a study of the problems of mass exchange behind the flame-holder. It was assumed that the results so obtained might be applied to the problems of heat exchange.

Proceeding from the peculiarities of the stream behind a bluff body, the exchange between the zone and flow has been assumed to take place mainly as a result of turbulent diffusion.

It has further been supposed that the connection between the zone coefficient D_z, the upstream flow diffusion coefficient D_f, flow velocity V_f and the size of the flame-holder d_{fh} is expressed by the following simple relationship

$$\frac{D_z}{V_z} = K_1 \frac{D_f}{V_f} + K_2 d_{fh} \qquad (1)$$

In this case K_1 and K_2 are coefficients of proportionality.

The relation was subsequently checked experimentally.

We did not succeed in finding a way of directly determining the turbulent exchange coefficient for the re-circulation zone; but we deemed it possible to determine it indirectly from the mean time of the presence of gas in the zone behind the flame-holder (residence time).

We determined τ_{r1} the residence time (mean time of exchange) as a ratio of the volume of the zone to that of the gas flowing through this zone per unit of time.

In diffusion exchange

$$\tau_2 = \frac{V_z r_m}{S D_z} \qquad (2)$$

where V_z, S and r_m are the volume, the surface and the mean radius of the zone respectively. The residence time and the dimensions of the zone being known, it is possible to compute from this formula the mean coefficient of diffusion*. To obtain the residence time was of considerable interest by itself. As is well known, this magnitude forms part of some stabilization theories as their basic characteristic (for instance, Dunsky[1] and Longwell[2] theories). The dependence of this magnitude on various factors, such as the velocity and turbulence of the upstream flow, the dimensions of the flame-holder and the composition of the mixture, have not as yet been defined experimentally, and it has been accepted in the above theories on the basis of indirect considerations†.

The general physical considerations in determining τ_r experimentally were as follows. Some foreign admixture easily carried away by the turbulent displacement of the medium, whose presence can be fixed in some way or other, is introduced into the zone behind the flame-holder. After a stationary process between the inflow and the discharge of the admixture has been established, its feeding is abruptly stopped and the change is recorded in its concentration in time, from the equilibrium Co to (practically) nil. It was found that the change in concentration occurs in accordance with the following equation:

$$C = Co\, e^{-\frac{t}{\tau r}} \qquad (3)$$

where Co is the concentration of the admixture at the initial moment, i.e. when its feeding to the zone is stopped, and is the exponent coefficient, i.e. the time during which the concentration of the admixture diminishes e times. In the physical sense and numerically this value is equal

* The value of D_z was taken as mean value within the whole zone; the corresponding coefficient of proportionality in equation 2 was included in the value r_m.

† Quite recently we have learned of the research work carried out by Quick[3], likewise devoted to exchange behind the flame-holder, which outlines the method of determining the residence time for cold flows. The method does not in principle differ from the one expounded in this paper.

The work refers to one value of the residence time, namely in the case of a conical flame-holder, 64 mm in diameter, with the velocity of flow amounting to 3·8 m/sec. The shape of flame-holder and the conditions of its streamline are different from ours.

to the mean time of the presence of gas during the stationary process (residence time). From equation 3 we obtain the magnitude of the residence time.

In practice τ_r was determined in the following way. In experiments with cold flow, tobacco smoke was introduced into the zone behind the flame-holder. The particles of the smoke were capable of reflecting the light which fell on them. In experiments with combustion, an aqueous solution of salt was injected into the zone. The water evaporated in the hot zone, and the vapours of sodium so formed emitted light*.

The light reflected or emitted by the particles was caught by a photomultiplier, and the induced current was amplified and transmitted to an oscillograph for recording. The experiments were conducted in the region of proportional dependence of the emission on the concentration of the particles. According to our theoretical conceptions, the dependence of the current upon time should have been exponential during the inflow of the luminous particles into the zone and during their discharge (*Figure 1a*); but as we

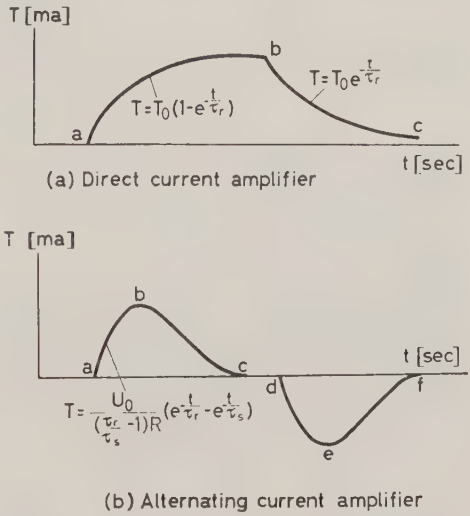

Figure 1. Variation of the power of the current in time during the inflow of luminous particles into the zone and during their discharge

* It was checked by experiment that the amount of injected water and the time of its evaporation had no substantial effect on the thermal conditions of the zone of the emission of sodium vapours.

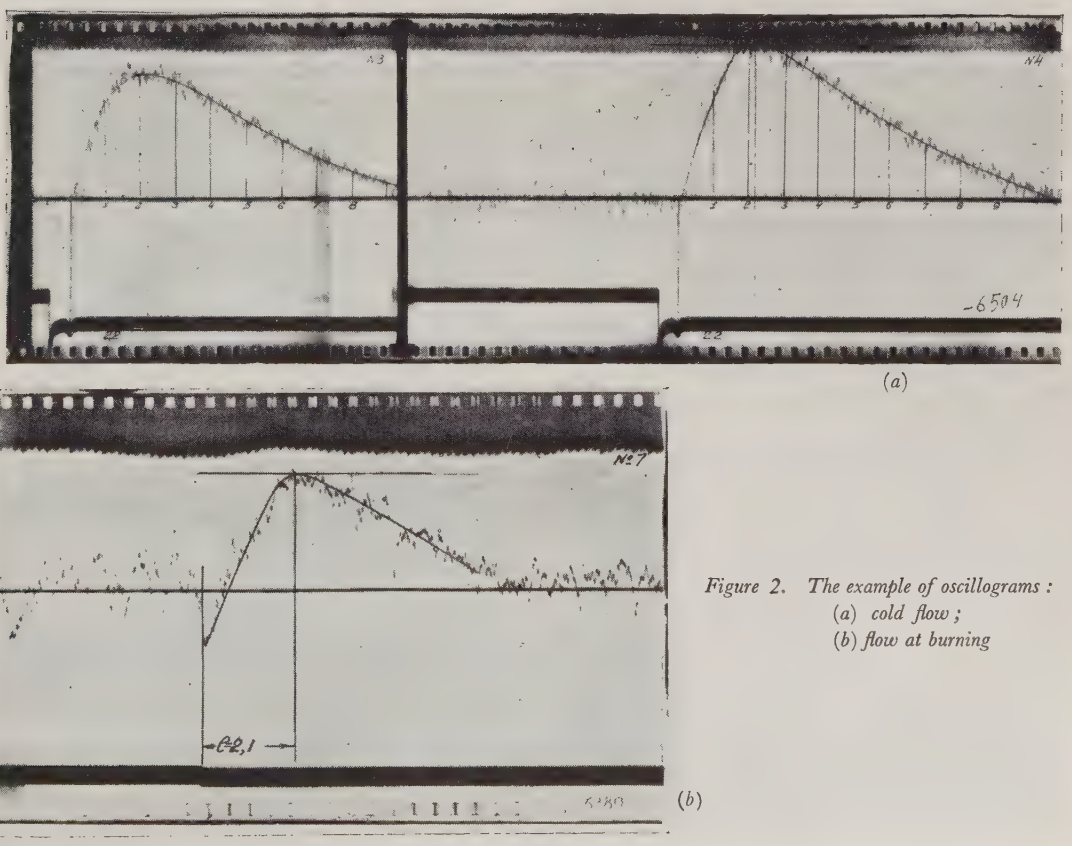

Figure 2. The example of oscillograms :
(a) cold flow ;
(b) flow at burning

employed an alternating current amplifier*, the dependence of the power of the current upon time at the amplifier outlet, i.e. at the oscillograph inlet, should be as follows:

$$I = \frac{V_o}{R}\left(e^{-\frac{t}{\tau_r}} - e^{-\frac{t}{\tau_s}}\right) \cdot \frac{1}{\left(\frac{\tau_r}{\tau_s} - 1\right)} \qquad (4)$$

where V_o is the voltage with I_o; R is the resistance of the loop and the shunts; τ_s is the constant of time of the circuit.

The respective curves appear as shown in *Figure 1b*.

For the sake of conveniently determining τ from the above curves, a connection was derived between the time τ_{max} corresponding to the maximum point of the curve, the constant of time of the circuit, and the residence time

$$\tau_{max} = \frac{ln\tau_s - ln\tau_r}{\frac{1}{\tau_r} - \frac{1}{\tau_s}} \qquad (5)$$

Dependence $\tau_r = f(\tau_{max})$ with $\tau_s = \text{const}$ was plotted as a graph which was used in determining τ_r. A specimen of oscillograms in given in *Figure 2*.

A comparison was made of the rated values of changes in the power of the current (voltage $V_R = I \,.\, R$) in time with the experimental values recorded by the oscillograms (*Figure* 3). The satisfactory coincidence of the experiment with the computations has led to the conclusion that, as a matter of fact, the change in the concentration of luminous particles takes place according to equation 3 and that the formula so

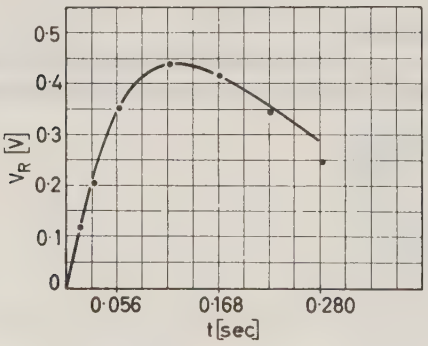

Figure 3. Comparison of the calculated curve $V_R = f(t)$ with the experiment

* The selection of an amplifier operating on alternating current can be accounted for by the fact that it has a number of advantages as compared with a direct current amplifier: the simplicity of design and stability of operation, as well as greater accuracy of determination from the oscillograms.

obtained is suitable for determining τ_r. The accuracy of determining τ_r by the given method was appraised at ± 7–8 per cent.

The experiments were conducted in a rectangular chamber, 90 × 180 mm in size. The V shaped flame-holders, from 20 to 60 mm in size, with the angle of 30 degrees at the apex, were set up at a distance of 250 mm from the end of the chamber (see diagram in *Figure 4*). The velocity

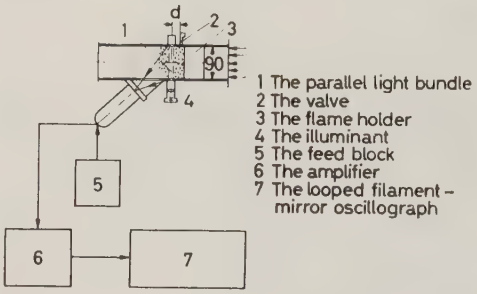

Figure 4. Diagram of the test chamber. Block diagram of the apparatus

of the flow varied from 10 to 70 m/sec in the absence of combustion, and from 60 to 160 m/sec during combustion. The intensity of flow turbulence ranged from 5 to 20 per cent. The equivalence ratio γ varied from 1·25 to 0·69—homogeneous benzene–air mixture was used for the combustion process.

The experiments were analysed statistically—from 10 to 15 photographs were taken at every experiment, and the mean value of τ_r was obtained from the analysis.

According to our knowledge of diffusion exchange, the following relationships between τ_r, size of flame-holder and velocity of flow might be expected. First of all, since r_m and the ratio V_z/S in equation 2 change in proportion to d_{fh} with a change in the size of the flame-holder τ should be proportional to

$$\tau_r \sim \frac{d_{fh}^2}{D_z} \sim \frac{d_{fh}^2}{K_1 + K_2 d_{fh}}$$

where K_1 and K_2 are constants. Or, if K_1 is not to be taken into account, τ_r should change in proportion to d_{fh}.

As is well known, in pipes (R_e — 10^5) the magnitude D_f/V_f remains constant as the velocity of the flow changes (self-preservation turbulence). When, according to reference 1, magnitude D/V (with $d_{fh} = \text{const}$) should likewise remain a constant magnitude

$$\frac{D_z}{V_f} = \frac{V_z r_m}{S \tau_r V_f} = \text{const}$$

As we know, however, that the dimensions of the zone almost do not change with a change in velocity, τ_r should change in reverse proportion to the velocity of the flow.

When a turbulizing grid is installed in the flow, the coefficient of flow diffusion increases, while with an increase in the distance from the grid, turbulence intensity ϵ diminishes and scale l increases. Since, however, the decrease in intensity is in our case more abrupt than the increase in scale, the value $D_f/V_f = \epsilon l$ diminishes as the distance from the grid increases. It may be expected that D_z/V_f will then diminish in a linear sense, while τ_r will increase in the same proportion. *Figure 5* shows, in the case of absence of combustion, the experimental dependence of τ_r upon the size of the flame-holder, the velocity and intensity of turbulence of the upstream flow, as well as changes according to the length of the zone. The graphs show that the results so obtained are in agreement with theoretical premises. In the case of tube ($\sim$ 5 per cent) turbulence, it may be considered that

$$\tau_r \simeq 37 \frac{d_{fh}}{V_f} \text{ [sec]}$$

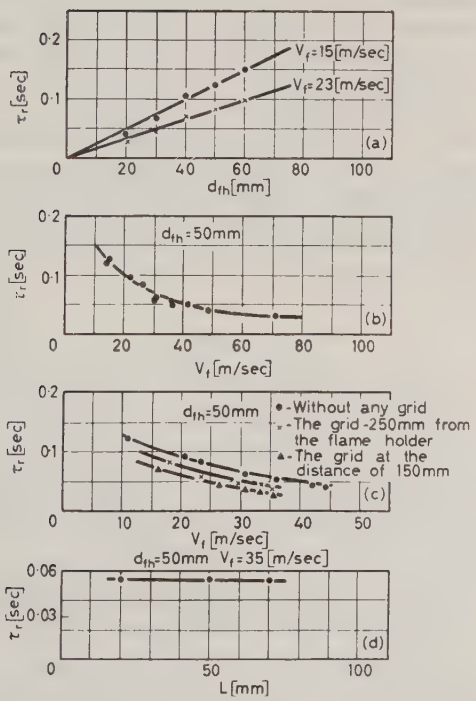

Figure 5. Variation of τ_r with size of (a) flame-holder; (b) flow velocity; (c) turbulence intensity; (d) distance to flame-holder

The values of the mean coefficient of diffusion D of the re-circulation zone were computed by the experimental values of τ_r with various values D_f/V_f of upstream flow as well as with a constant value D_f/V_f and with various sizes of the flame-holders*.

The experimental data were approximated by equation 1 with constants $K_1 = 1$ and $K_2 = 0{\cdot}004$ (*Figure 6*).

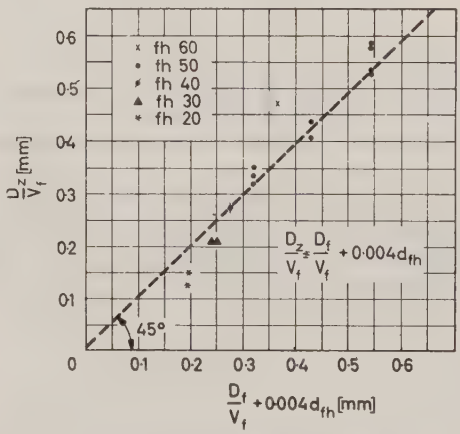

Figure 6. Variation of the diffusion coefficient of the zone (D_z) with the flow parameters (D_f V_f) and the size of the flame-holder (d_{fh})

It can be seen from equation 1 that with

$$d_f \to 0; \quad \frac{D_z}{V_f} \to \frac{D_f}{V_f}$$

We obtained for example value D_z/V_f for the smallest flame-holder $d_f = 20$ mm equal to 0·13 mm, while value D_f/V_f determined directly by the optical diffusion method amounted to 0·12 mm†. The values so obtained seem to testify to the reliability of the computed values of D_z and consequently to the correctness of determining τ_r. This is also borne out by the fact that the values D_z determined indirectly through τ_r approximated the values of diffusion coefficients in the zone of mixing determined directly by means of the optical diffusion method‡.

* In calculating diffusion coefficient the values of r_m, S, V_z for the region bounded by the surface of zero horizontal velocities were used as characteristic values of re-circulation zone (r_m, S, V_z).

† An outline of the optical diffusion method is given in reference 4.

‡ A very thin tube was inserted in the edge of the flame-holder, through which smoke was let through. The approximate value of the diffusion coefficient in the zone of mixing was determined by means of photography and subsequent analysis (assuming the magnitudes of turbulent pulsation as being equal in the direction of the two axes).

The values are given in the following table:

mm	mm	m/sec	*By formula 2*	*By the diffusion method*
50	0·12	44 30 22	0·35 0·33 0·341	0·2 –0·25
	0·25	35·1 29·8 18	0·483 0·444 0·442	0·35–0·4
	0·32	35·1 33 15·7	0·627 0·652 0·584	0·55–0·6

The results of the experiments during combustion are given in *Figure 7*. In the case of tube turbulence during combustion, τ_r may be expressed by the relationship

$$\tau_r \simeq 104 \frac{d_{fh}}{V_f} \text{ [sec]}$$

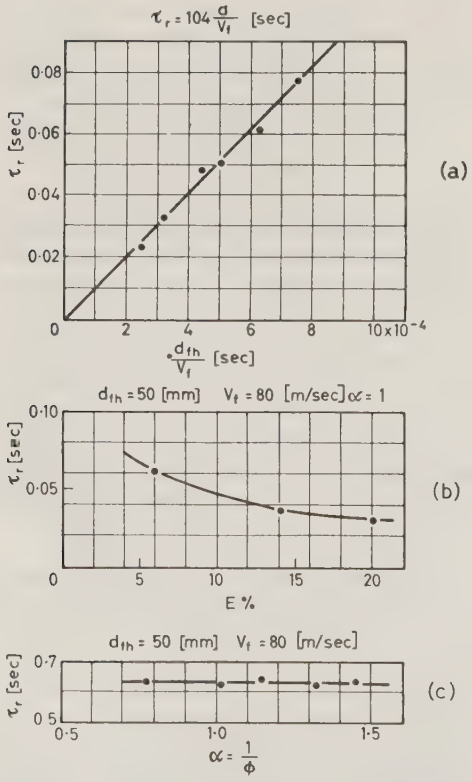

Figure 7. Variation of τ_r with: (a) the ratio of the size of the flame-holder to the flow velocity; (b) the turbulence intensity; and (c) the equivalence ratio

The 3·7 times increase in the residence time during combustion as compared with the case in the absence of combustion is apparently accounted for by a decrease in the general level of turbulence in the zone during combustion, which is indirectly testified by a reduction of the gradient of mean velocities behind the flame-holder. As in the case of cold flows, τ_r diminishes in proportion to the increase in the turbulence of the upstream flow (*Figure 7b*). Within the range of change of equivalence ratio γ from 1·25 to 0·69 (*Figure 7c*), the residence time remains practically constant, which evidently can be explained by the slight change of the diffusion coefficient in the given range of ϕ.

It is to be regretted that it is impossible to make any quantitative appraisals because no data are available concerning the influence of combustion on the characteristics of turbulent motion in the re-circulation zone behind the flame-holder.

CONCLUSIONS

(1) A method of experimentally determining the residence time of gas in the re-circulation zone behind the flame-holder for cold flows and during combustion has been developed.

The method is based on the introduction of luminous particles into the zone and on their photoelectric recording. The determination of the residence time is accurate within ± 7–8 per cent.

(2) Quantitative data of the residence time and the diffusion coefficient on the boundary of the re-circulation zone have been obtained.

(3) The experimental data are qualitatively accounted for by the presence of a turbulent diffusion exchange between the re-circulation zone and the outer flow, and they testify to the possible use of diffusion characteristics in defining the exchange.

BIBLIOGRAPHY

[1] Dunsky, V. F. Investigation of the mechanism of stabilization of flame in the wake behind the bluff body. *M. Sc. Thesis, Central Institute of Aircraft Engine-Building*, 1949

[2] Longwell, D., Frost, E. and Weiss, M. Flame stability in bluff body re-circulation zones. *Industr. Engng. Chem.* 45 No. 8 (1953)

[3] Quick, A. W. Ein Verfahren zur Untersuchung des Austauchvorganges in verwirbelten Stromungen hinter Körpern mit abgelöster Strömung. *Deutsche Versuchsanstalt für Lüftfahrt E.V. Bericht No.* 12

[4] Prudnikov, A. G. Measurements of the turbulence of air flows and flames by the optical-diffusion method. *M. Sc. Thesis, Moscow Physical Technical Institute*, 1956

A THEORETICAL ANALYSIS OF MULTI-STAGE REACTION RATE CONTROLLED SYSTEMS

J. W. HARDCASTLE

INTRODUCTION

The form of the equation for the rate of chemical reaction between two reactants has been known for several years. The practical use of the equation, however, depends on the knowledge of the values of the constants, which have to be determined experimentally.

With the recent work of Longwell and Weiss[1], reliable data applicable to the *iso*octane and air reaction have been obtained, enabling the relevant constants to be determined. These data were used by Herbert[2] to calculate the absolute limits of air loading for a single stage adiabatic and homogeneous reactor to show what margin of improvement might be possible for a practical combustion chamber.

This present work was undertaken to determine whether there are any advantages to be gained by: (1) dividing the reaction zone into two or more stages; and (2) staging the injection of the reactants.

DEVELOPMENT OF THE EQUATIONS

The general equation for reaction rate controlled systems, for mixture strengths weaker than or equal to stoichiometric, may be shown to be:

$$\frac{M_f}{VP^2} = \frac{K}{R^2} \cdot \frac{e^{-E/RT}}{T^{3/2}} \cdot \frac{q(1-\epsilon)(1-\phi\epsilon)}{\epsilon} \left(\frac{1}{\frac{q}{W_f} + \frac{1}{W_o} + \frac{x}{W_n}} \right)^2 \quad (1)$$

The derivation of this equation is given in the appendix.

For a particular value of fuel to oxygen ratio q_j, let

$$K_j = \frac{K}{R^2} \cdot q_j \left(\frac{1}{\frac{q_j}{W_f} + \frac{1}{W_o} + \frac{x}{W_n}} \right)^2 \quad (2)$$

Therefore

$$\frac{M_f}{VP^2} = K_j \cdot \frac{e^{E/RT}}{T^{3/2}} \cdot \frac{(1-\epsilon)(1-\phi_j\epsilon)}{\epsilon} \quad (3)$$

In order to use the above equations it is necessary to know values for the activation energy E, the constant K and the relationship between the consumption efficiency ϵ and the reaction temperature T.

Reference 1 supplies the necessary data for *iso*octane and air mixtures: $E = 42{,}000$ cal/mol, and for an equivalence ratio of 1 and mixture inlet temperature of 400°K, the value of M_f/VP^2 at blow-out is 8·22 lb. *iso*octane/sec ft.^{3} atm^2.

Calculation shows that the R.H.S. of equation 3 has a maximum value when $\epsilon = 0{\cdot}758$, for $\phi = 1$ and $T_i = 400$°K. The corresponding reaction temperature is 2,008°K. Thus the value of K_{st} is found to be $3{\cdot}685 \times 10^{11}$, and by using equation 2 the value of the constant for any mixture strength can be calculated.

This enables the performance of any single stage homogeneous reactor, using *iso*octane and air, to be calculated.

Now consider a system where the products of combustion from a reactor are passed into a second reactor. If stability considerations are fulfilled, then further combustion will take place, giving a final efficiency of, say, ϵ_2.

If the efficiency at the exit of the first reactor is ϵ_1, then the fuel burned will be $\epsilon_1 M_f$. The fuel burned at the exit from the second stage will be $\epsilon_2 M_f$; thus the fuel burned in the second stage $= (\epsilon_2 - \epsilon_1)M_f$. The fuel concentration in the second stage is $(1 - \epsilon_2)$ of the inlet concentration and the oxygen concentration is $(1 - \phi\epsilon_2)$ of the inlet concentration. Thus the equation giving the performance of the second stage is:

$$\frac{M_f}{V_2P^2} = K_j \cdot \frac{e^{-E/RT_2}}{T_2^{3/2}} \cdot \frac{(1-\epsilon_2)(1-\phi_j\epsilon_2)}{\epsilon_2 - \epsilon_1} \quad (4)$$

Similarly, for a third stage:

$$\frac{M_f}{V_3P^2} = K_j \cdot \frac{e^{-E/RT_3}}{T_3^{3/2}} \cdot \frac{(1-\epsilon_3)(1-\phi_j\epsilon_3)}{\epsilon_3 - \epsilon_2} \quad (5)$$

and so on for n stages.

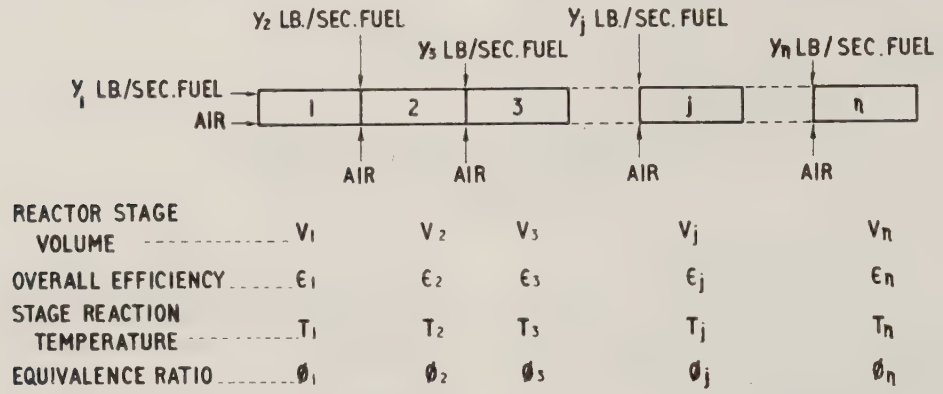

Figure 1. Schematic diagram of a multi-stage homogeneous reactor of n *stages with interstage injection of air and fuel*

The above equations are applicable to systems in which all the fuel and air are admitted to the first stage of the reactor.

For a system in which interstage fuel and/or air are introduced, the equations need to be slightly modified.

Consider a system consisting of n stages in which a total fuel flow of 1 lb./sec is to be burned to an efficiency ϵ_n. The overall equivalence ratio is ϕ_n and the inlet mixture temperature is T_i. The system is shown schematically in *Figure 1.*

In the first stage, a fraction y_1, of the total fuel flow is introduced, together with sufficient air to give an equivalence ratio of ϕ_1. The performance of the stage is given by:

$$\frac{y_1 M_f}{V_1 P^2} = K_1 \cdot e^{\frac{-E/RT_1}{T^{3/2}}} \cdot \frac{(1-\epsilon_1)(1-\phi_1\epsilon_1)}{\epsilon_1} \tag{6}$$

Now $M_f = 1$ lb./sec and $P = 1$ atm, therefore:

$$V_1 = \frac{T_1^{3/2} \cdot e^{E/RT_1} \cdot \epsilon_1 y_1}{K_1 \cdot (1-\epsilon_1)(1-\phi_1\epsilon_1)} \tag{7}$$

where

$$K_1 = \frac{K}{R^2} \cdot q_1 \left(\frac{1}{\frac{q_1}{W_f} + \frac{1}{W_o} + \frac{x}{W_n}} \right)^2 \tag{8}$$

In the second stage a fraction y_2 lb./sec of the total fuel is added to the products of combustion from the first stage together with sufficient air to give an overall equivalence ratio of ϕ_2. The fuel burned in stage 2 is $(y_1 + y_2)\epsilon_2 - y_1\epsilon_1$. Thus the volume of the second stage is given by:

$$V_2 = \frac{T_2^{3/2} \cdot e^{E/RT_2} \cdot [(y_1 + y_2)\,\epsilon_2 - y_1\epsilon_1]}{K_2(1-\epsilon_2)(1-\phi_2\epsilon_2)} \tag{9}$$

For the jth stage, the volume is given by:

$$V_j = \frac{T_j^{3/2} \cdot e^{E/RT_j}}{} \left(\frac{(y_1 + y_2 + \ldots + y_j)\,\epsilon_j - (y_1 + y_2 + \ldots + y_j - 1)\,\epsilon_j - 1}{K_j\,(1-\epsilon_j)\,(1-\phi_j\epsilon_j)} \right) \tag{10}$$

For the nth stage:

$$V_n = \frac{T_n^{3/2} \cdot e^{E/RT_n}}{} \left(\frac{\epsilon_n - (y_1 + y_2 + \ldots + y_n - 1)\,\epsilon_n - 1}{K_n\,(1-\epsilon_n)\,(1-\phi_n\epsilon_n)} \right) \tag{11}$$

Equations 7, 9, 10 and 11 are general expressions and can be applied to any multi-stage homogeneous reactor.

The stability of each stage of a multi-stage reactor must be established for the particular inlet conditions and loading of the stage.

A graph of stage loading against overall efficiency shows that as the loading is increased the efficiency decreases until a maximum loading is reached. Any further increase in loading results in blow-out. The physical interpretation of this process is that for stable combustion the heat released by the reaction must be equal to the heat required to raise the temperature of the incoming reactants to the reaction temperature. When the latter heat quantity exceeds the former, the reaction ceases.

Thus it can be seen that the condition for stability is that the slope of the loading *versus* efficiency curve must be negative.

For any stage (j) the performance curve is given by equation 10.

$$V_j = \frac{T_j^{3/2} \cdot e^{E/TR_j} \cdot \left(\epsilon_j \sum_1^j y - \epsilon_{j-1} \sum_1^{j-1} y \right)}{K_j(1 - \epsilon_j)(1 - \phi_j \epsilon_j)}$$

when the total fuel flow ($\sum_1^n y$) is 1 lb./sec, and the pressure is one atm.

The loading of the stage is proportion to $1/V_j$, so a graph of V_j against $\epsilon_j \sum_1^j y$ (the overall efficiency up to, and including, the jth stage) for the particular value of

$$\epsilon_{j-1} \sum_1^{j-1} y \Big/ \sum_1^j y$$

(the overall efficiency at inlet to the jth stage) will indicate which part of the performance curve will give stable combustion, i.e. where the slope of the curve is positive.

MATHEMATICAL ANALYSIS

Due to the large number of possible variables in the equations, a full analysis of a system with more than two stages is a lengthy and tedious process.

For this reason only a two-stage reactor has been analysed. The analysis was carried out for four different systems, and these are shown schematically in *Figure 2.*

The inlet mixture temperature was taken as 400°K in each case, and by assuming the same rate of fuel supply the systems could be compared on the

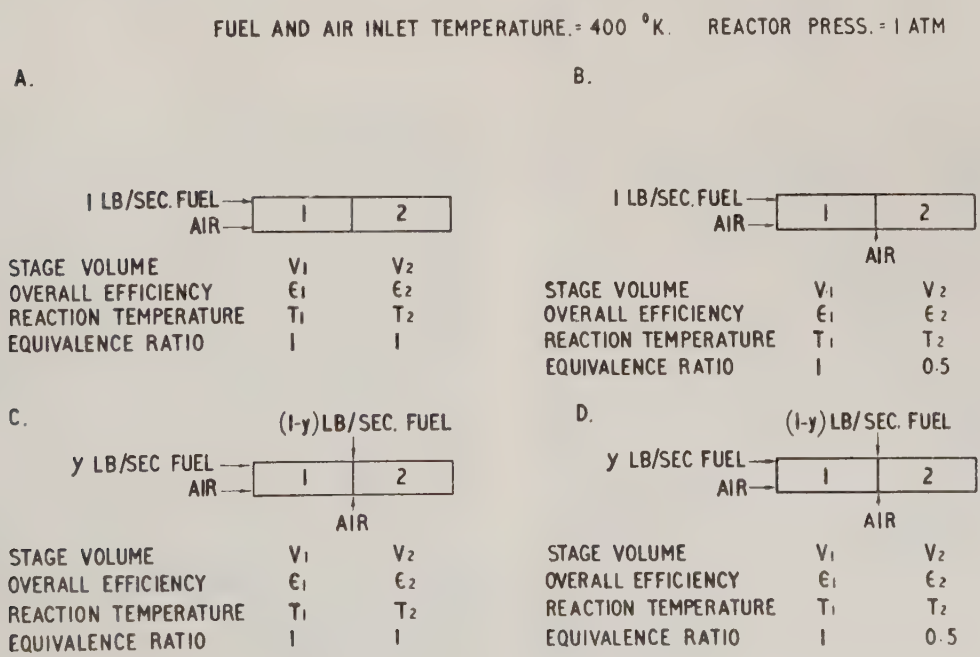

Figure 2. Schematic diagrams of the two-stage homogeneous reactors analysed

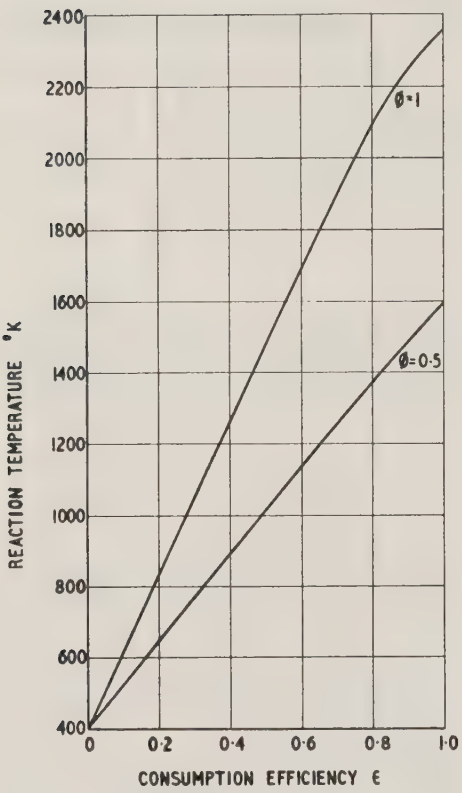

Figure 3. Reaction temperature v. consumption efficiency for iso*octane and air*
$T = 400°K.\ \phi = 1$ and 0·5

CURVE No.	ϵ_1
1	ϵ_2
2	0·758
3	0·80
4	0·90
5	0·95

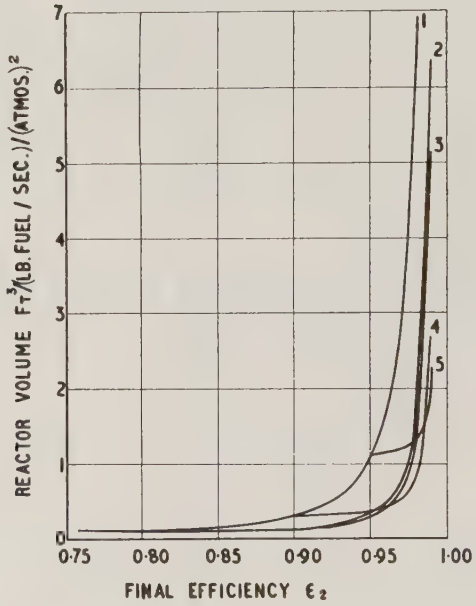

Figure 4. Two-stage combustion of iso*octane and air* $\phi_1 = \phi_2 = 1$. *No interstage addition of fuel* (*see Figure 2a*)

basis of the volume required to give the same outlet efficiency.

The relationship between the reaction temperature and the consumption efficiency for the two mixture strengths of *iso*octane and air considered were taken from reference 1, and are shown in *Figure 3*.

The first system considered was a stoichiometric mixture of *iso*octane and air in which all the fuel was admitted to the first stage of the reactor (*Figure 2a*). The products of combustion were passed to the second stage without any reactant addition. The performance curves for this system are shown in *Figure 4*. Curve No. 1 is a complete performance curve for the first stage from blow-out ($\epsilon = 0{\cdot}758$) to an efficiency of 0·98. The performance curves for the second stage for four values of the first stage efficiency (ϵ_1) are shown. It can be seen that the optimum value of the first stage efficiency depends on the required final efficiency. For example, of the first stage efficiency values chosen, for a final efficiency of 0·99 the optimum value of ϵ_1 is 0·95. For a final efficiency of 0·97, however, the minimum reactor volume is required with a value of $\epsilon_1 = 0{\cdot}90$.

A similar group of performance curves was obtained for the second system analysed (*Figure 2b*). This was a system in which all the fuel was admitted to the first stage with sufficient air to give a mixture of an equivalence ratio of 1 and additional air added between stages to give a second stage mixture of an equivalence ratio of 0·5. The results obtained are given in *Figure 5*. For comparison purposes, the performance curve of a single stage reactor working at an equivalence ratio of 0·5 is also shown.

The curves clearly show the advantage of using stoichiometric mixtures in a reactor. For a multi-stage reactor with the first stage working at an equivalence ratio of 0·5, the minimum stage volume is 7·75 ft.³/(lb.fuel/sec)/atm² giving an outlet efficiency of 0·875. The same efficiency would be obtained in a volume of 0·22 ft.³ with a stoichiometric mixture.

Referring back to *Figure 4*, it becomes apparent that the best method of achieving a given outlet

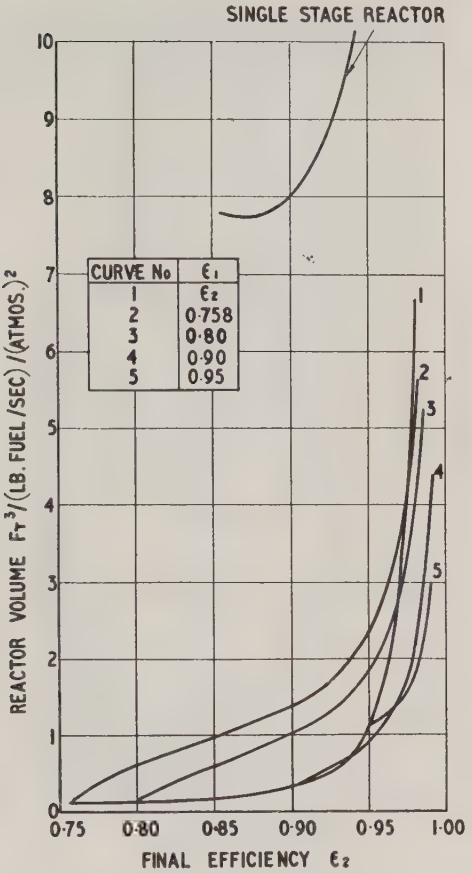

Figure 5. Two-stage combustion of isooctane *and air,* $\phi_1 = 1$, $\phi_2 = 0{\cdot}5$. *No interstage addition of fuel (see Figure 2b)*

efficiency at a final equivalence ratio of 0·5 is to allow all the combustion to take place at an equivalence ratio of 1·0 and then to add dilution air.

The effect of staging the fuel injection is shown in *Figures 6* and *7* for the two systems shown in *Figure 2c* and *d*. Calculations were carried out for a range of first stage and overall efficiencies and the total reactor volume for each condition obtained for varying values of y, the fraction of the total fuel admitted to the first stage. It can be seen from the graphs that the minimum reactor volume, for all the conditions, was obtained when all the fuel was injected into the first reactor stage.

The stability of the stages of the reactors considered can be established by using *Figures 8* and *9*. *Figure 8* shows a series of performance curves for one stage of a reactor working at an equivalence ratio of 1, for varying inlet efficiencies. The curves were based on an original mixture temperature of 400°K. Curves 1 to 5 show a blow-out point, the stable part of the performance curve being for final efficiencies greater than 0·758 to 0·7, depending on the inlet efficiency. Above an inlet efficiency of 0·5 stable combustion is obtained for all loading values. The other part of curve No. 5, which has a positive slope, is also a stable part of the performance curve. The small rise in efficiency associated with this part of the curve, however, limits the usefulness as a practical operating range for a reactor. (N.B. Curves 1 to 4 would have a similar shape to curve No. 5 if the graph was extended to cover the complete range of values of overall efficiency, i.e. from 0 to 1.) *Figure 9* shows a similar series of curves for an equivalence ratio of 0·5.

CONCLUSIONS

(1) Equations have been developed which can be used to evaluate the performance of any multi-stage, homogeneous, adiabatic reactor, providing

CURVE No.	FIRST STAGE EFFICIENCY	OVERALL EFFICIENCY
1	0·758	0·98
2	0·80	0·98
3	0·90	0·98
4	0·90	0·94
5	0·758	0·94
6	0·90	0·90
7	0·758	0·90

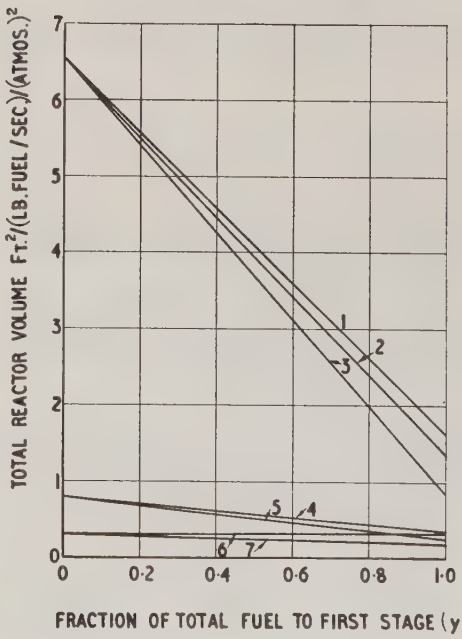

Figure 6. Effect of staged fuel injection on two-stage combustion of isooctane *and air.* $\phi_1 = \phi_2 = 1$ *(see Figure 2c)*

CURVE No.	FIRST STAGE EFFICIENCY	OVERALL EFFICIENCY
1	0·758	0·98
2	0·80	0·98
3	0·90	0·98
4	0·758	0·94
5	0·80	0·94
6	0·90	0·94
7	0·758	0·90
8	0·80	0·90
9	0·90	0·90

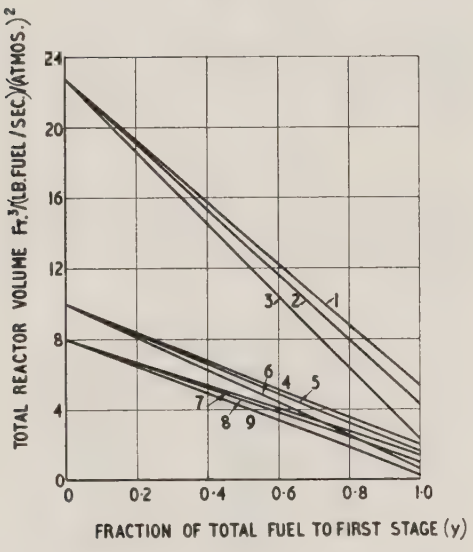

Figure 7. Effect of staged fuel injection on two-stage combustion of isooctane *and air.* $\phi_1 = 1$, $\phi_2 = 0{\cdot}5$ *(see Figure 2d)*

CURVE No.	STAGE INLET EFFICIENCY	STAGE INLET TEMPERATURE °K
1	0	400
2	0·1	625
3	0·2	847
4	0·3	1063
5	0·4	1278
6	0·5	1491
7	0·6	1698
8	0·7	1896
9	0·8	2092
10	0·9	2250

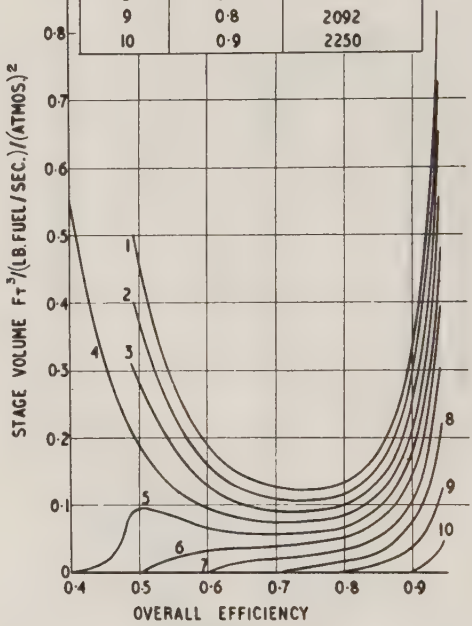

Figure 8. One-stage performance curves for different inlet efficiencies; $\phi = 1$

that the relevant constants for the reactants are known.

(2) Using these equations, an analysis was carried out of four two-stage systems using *iso*-octane and air as reactants.

(3) The analysis showed that there is a considerable advantage to be gained by staging the combustion, particularly where high combustion efficiencies are required.

(4) The minimum reactor volume for a given mixture strength and final combustion efficiency is obtained when all the fuel is admitted to the first stage of a multi-stage reactor, i.e. although it is advantageous to stage the combustion, it is a disadvantage to stage the fuel injection.

(5) For a reactor working at an overall mixture strength weaker than stoichiometric the minimum reactor volume is obtained when all the combustion is completed at an equivalence ratio of one, and dilution air added afterwards.

APPENDIX

Derivation of the reaction rate equation

It is assumed that the velocity of reaction, for a system involving collision between two molecules, is proportional to the number of collisions between the reacting molecules. From kinetic theory it may be shown that the number of collisions (Z_{12}) between unlike molecules is given by:

$$Z_{12} = 2(2\mu)^{\frac{1}{2}}\, n_1\, n_2\, \sigma^2_{12}\, (RT/\mu)^{\frac{1}{2}}$$

where n = number of molecules/unit volume, σ_{12} = effective diameter

$$\left(= \frac{\sigma_1 + \sigma_2}{2} \right)$$

μ = reduced mass $(= m_1 m_2 / m_1 + m_2)$, R = gas constant/molecule, T = absolute temperature.

Since all collisions do not result in reaction it is assumed that only those collisions in which the joint energy of the colliding molecules exceeds a

CURVE No.	1	2	3	4	5	6	7	8	9	10
INLET EFFICIENCY	0	0·1	0·2	0·3	0·4	0·5	0·6	0·7	0·8	0·9
INLET TEMPERATURE °K	400	528	655	782	906	1025	1144	1258	1372	1484

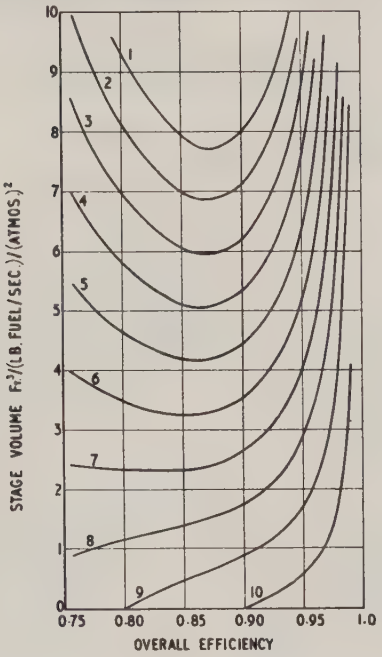

Figure 9. One-stage performance curves for different inlet efficiencies; $\phi = 0{\cdot}5$

certain quantity E give rise to reaction. From kinetic theory, the fraction of molecules which possess an energy greater than E_1 is approximately equal to $e^{-E_1/RT}$. Similarly, the fraction with a minimum energy E_2 is $e^{-E_2/RT}$. The chance that two colliding molecules will have respectively minimum energies E_1 and E_2 is proportional to $e^{-E_1/RT} \times e^{-E_2/RT} = e^{-(E_1+E_2)/RT}$. If $E_1 + E_2 = E$, then the collision efficiency is $e^{-E/RT}$. E is called the activation energy.

At a given temperature, the number of collisions between unlike molecules is proportional to the numbers of the different molecules, $Z_{12} \propto n_1 n_2$, which is thus proportional to the concentration $Z_{12} \propto C_1 C_2$.

Thus the volumetric reaction rate k' is given by: $k' = Z_{12} \cdot e^{-E/RT} = K.C_1.C_2(T)^{\frac{1}{2}}/e^{-E/RT}$, in which K is a constant.

In applying this equation to a particular system, either of the reactants or both together may be used to calculate the amount of reacting material, as only the constant is affected.

In this particular case the equation has been applied to the fuel.

Let x = weight of nitrogen/weight of oxygen = m_n/m_o

q = weight of fuel/weight of oxygen = m_f/m_o

and $\phi = \dfrac{\text{fuel/oxygen ratio}}{\text{stoichiometric fuel/oxygen ratio}} = \dfrac{q}{q_{st}}$

= equivalence ratio

If M_f lb./sec of fuel are supplied to a reactor at an equivalence ratio of less than 1, then defining ϵ as the consumption efficiency, the fuel consumed is ϵM_f. (It is assumed that the reactants are fuel and oxygen only, i.e. the 'inefficiency' is present in the form of original fuel and the fuel which reacts goes completely to carbon dioxide and water.) The total oxygen supplied with the fuel is M_f/q of which $\phi M_f/q$ can be theoretically consumed by the fuel. Thus the actual oxygen consumption is $\epsilon\phi M_f/q$. The inlet concentration of fuel is m_f/V. Thus:

$$\frac{m_f}{V} = \frac{p_f W_f}{RT_i} = \frac{PW_f}{RT_i} \cdot \frac{p_f}{P}$$

$$= \frac{PW_f}{RT_i} \left(\frac{m_f/W_f}{\dfrac{m_f}{W_f} + \dfrac{m_o}{W_o} + \dfrac{m_n}{W_n}} \right)$$

$$= \frac{P}{RT_i} \left(\frac{m_f}{\dfrac{m_f}{W_f} + \dfrac{m_o}{W_o} + \dfrac{m_n}{W_n}} \right)$$

Similarly, the inlet oxygen concentration is:

$$\frac{m_o}{V} = \frac{P}{RT_i} \left(\frac{m_o}{\dfrac{m_f}{W_f} + \dfrac{m_o}{W_o} + \dfrac{m_n}{W_n}} \right)$$

In the reaction rate equation the terms C_1, C_2 and T refer to local conditions in the reactor.

$$\text{Thus } C_o = \frac{P}{RT} \left(\frac{m_o}{\dfrac{m_f}{W_f} + \dfrac{m_o}{W_o} + \dfrac{m_n}{W_n}} \right) (1 - \phi\epsilon)$$

$$\text{and } C = \frac{P}{RT} \left(\frac{m_f}{\dfrac{m_f}{W_f} + \dfrac{m_o}{W_o} + \dfrac{m_n}{W_n}} \right) (1 - \epsilon)$$

$$\text{therefore } \frac{\epsilon M_f}{V} = K \cdot \frac{P^2}{R^2T^2} \frac{m_o\, m_f}{\left(\dfrac{m_f}{W_f} + \dfrac{m_o}{W_o} + \dfrac{m_n}{W_n} \right)^2}$$

$$\cdot (1 - \phi\epsilon) \cdot (1 - \epsilon) \cdot (T)^{\frac{1}{2}} \cdot e^{-E/RT}$$

re-arranging and putting $\frac{m_f}{m_o} = q$

$$\frac{M_f}{VP^2} = \frac{K}{R^2T^{3/2}} \cdot \left(\frac{1}{\frac{q}{W_f} + \frac{1}{W_o} + \frac{x}{W_n}} \right)^2 \cdot q \cdot \frac{(1 - \epsilon)(1 - \phi\epsilon)}{\epsilon} \cdot e^{-E/RT}$$

This is the general equation for reaction rate controlled systems for mixture strengths weaker than or equal to stoichiometric.

The author's thanks are due to Messrs. Armstrong Siddeley Motors Ltd. for permission to publish this paper.

NOMENCLATURE

C	concentration	lb./ft.^{3}
E	activation energy	cal/g/mol
e	base of natural logarithms	
K	rate constant	ft.^{3}/sec/lb. °K$^{1/2}$
M_f	fuel mass flow	lb./sec
m	weight	lb.
n	number of molecules	
p	partial pressure	atm
P	total pressure	atm
q	fuel/oxygen ratio by weight	
R	universal gas constant	1·987 cal/g/mol °K or 1·31 ft.^{3}/atm/lb.mol. °K
T	temperature	°K
V	volume	ft.^{3}
W	molecular weight	
x	nitrogen/oxygen ratio by weight	
y	fraction of total fuel	
Z	collision factor	1/ft.^{3}sec
ϵ	consumption efficiency	
μ	reduced mass	$= \left(\frac{m_1 m_2}{m_1 + m_2}\right)$
σ	collision diameter	
ϕ	equivalence ratio	$= \left(\frac{q}{q_{st}}\right)$

SUFFICES

j	one stage in a multi-stage reactor	
n	number of stages in a reactor	
i	inlet	
st	stoichiometric	
f	fuel	M and W
n	nitrogen	M and W
o	oxygen	M and W

REFERENCES

[1] Longwell, J. P. and Weiss, M. A. High temperature reaction rates in hydrocarbon combustion. *Industr. Eng. Chem.* (*Industr.*) 47 (1955) 1634

[2] Herbert, M. V. Unpublished work at N.G.T.E. (1956)

96

DEVELOPMENT OF A TURBO-JET ALTITUDE WINDMILL RE-LIGHT CORRELATION

H. M. BREWSTER and A. KUSH

INTRODUCTION

One of the major problems still confronting the turbo-jet engine field is to determine the limits within which an engine will successfully and consistently re-light after a flame-out at altitude. Therefore, a large portion of any engine development test programme will consist of determining the altitude windmill re-light characteristics of the engine.

The re-light limits obtained for a given set of external engine conditions; e.g. flight conditions for a standard NACA day or with a given fuel, cannot be easily extrapolated to predict engine re-light behaviour under other circumstances. This can readily be seen from *Figure 1*, which presents the altitude windmill re-light characteristics of a typical turbo-jet engine for three different sets of engine inlet conditions and for two different fuels. For this reason, test programmes must include a number of different fuels and sets of engine windmill conditions for which engine operation is anticipated.

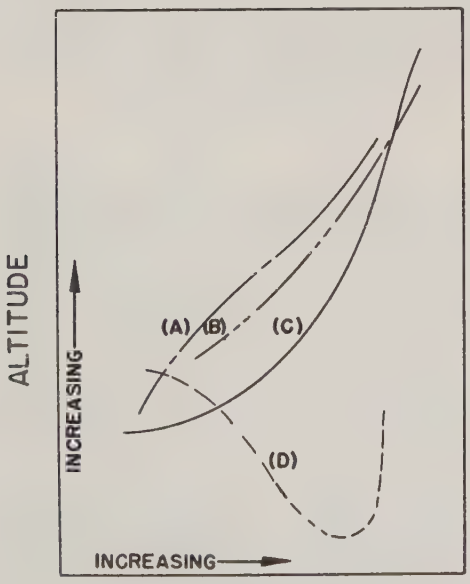

Figure 1. Altitude re-light limits of Engine A. (A) constant engine inlet temperature >0°F, JP–5; (B) standard flight conditions, JP–4; (C) standard flight conditions, JP–5; (D) constant engine inlet temperature <0°F, JP–5

It was felt that the altitude windmill re-light characteristics of an engine could be correlated with the conditions existing within the engine combustor, and that these combustor conditions could then be used to determine re-light capabilities at any desired set of engine windmill conditions.

DEVELOPMENT OF CORRELATION

A successful altitude windmill re-light of a turbo-jet engine depends upon the ignition of the fuel–air mixture present, propagation and stabilization of the flame throughout the combustor, and a subsequent engine acceleration to idle speed. The conditions of the fuel and air present in the combustor during an ignition attempt will therefore determine the success of an attempted windmill re-light. The spark ignition energy of the engine was not considered in the development of the correlation since it is a constant for any engine series.

Combustor fuel considerations

The condition of the fuel in the combustor prior to ignition will depend upon the spray characteristics of the atomizer, the rate of evaporation from the fuel droplets, and the effect of the combustor air flow upon the spray and rate of evaporation.

The spray characteristics of an atomizer can be described by the spray angle and droplet size distribution of the fuel. Droplet size distribution cannot be easily determined[1]. However, Shafer and Bovey[2] have shown that for a given atomizer configuration, the mean droplet diameter of a fuel spraying into stagnant air and the spray angle can be expressed in terms of the physical properties of the fuel.

$$(SC) = f\left[\left(d_f/D_N\right), \left(\alpha\right)\right]$$

$$= f\left[\left(\frac{D_N \Delta P}{\sigma_f}\right), \left(\frac{D_N \rho_f \sigma_f}{\mu_f^2}\right)\right] \quad (1)$$

The term $\frac{D_{N\rho f\sigma f}}{f}$ can be rearranged as follows:

$$\frac{D_{N\rho f\sigma f}}{\mu_f^2} = \left(\frac{D_N V_{f\rho f}}{\mu_f}\right)^2 \left(\frac{\sigma_f}{D_{N\rho f} V_f^2}\right)$$

If we assume that the atomizer nozzle flows full, then $\rho_f V^2{}_a \Delta P_N$ and the spray characteristics of the atomizer can be expressed as

$$(SC) = f\left[\left(\frac{\sigma_f}{D_N \Delta P}\right), \left(\frac{D_N (\Delta P \rho_f)^{\frac{1}{2}}}{\mu_f}\right)\right] \qquad (2)$$

The amount of fuel which will vaporize in the combustor is primarily a function of the partial pressure of the fuel. Frössling[3] has shown this to be true where the combustor inlet air temperature and the fuel temperature are practically the same and well below the average boiling point of the fuel. Such are the conditions in the combustor prior to ignition in an altitude windmill re-light attempt. In addition, the amount evaporated depends upon the velocity of the air and fuel droplets, the combustor static pressure[4] initial fuel droplet size, and other factors shown below.

$$E = f[(D_a), (P_f), (P_b), (V_a), (\rho_a), (\mu_a), (d_f), (M'), (D'), (\mu_{fv}), (V_{fd})] \qquad (3)$$

Restricting the discussion to a given fuel, M' and D' are constants and a dimensional analysis yields

$$E = f\left[\left(\frac{P_f}{P_b}\right), \left(\frac{D_a \rho_a V_a}{\mu_a}\right), \left(\frac{d_f}{D_a}\right), \left(\frac{\mu_{fv}}{\mu_a}\right), \left(\frac{V_{fd}}{V_a}\right)\right] \qquad (4)$$

Over the temperature range encountered in the combustor of a windmilling engine, it was found that (μ_{fv}/μ_a) is practically a constant for M' of the fuel vapour of 150 or less[5]. Recent work[6] also leads to the conclusion that (V_{fd}/V_a) in the re-circulation zone of the combustor will be practically a constant; therefore,

$$E = f\left[\left(\frac{P_f}{P_b}\right), \left(\frac{D_a \rho_a V_a}{\mu_a}\right), \left(\frac{d_f}{D_a}\right)\right] \qquad (5)$$

Since D_a and D_N in equations 2 and 5 are constants for a given engine combustor configuration, a combination of these equations will express the fuel conditions within the combustor during an ignition attempt as

$$(FC) = f[(E), (SC)] = f\left[\left(\frac{P_f}{P_b}\right), \left(\frac{V_a \rho_a}{\mu_a}\right), \left(\frac{(\Delta P \rho_f)^{\frac{1}{2}}}{\mu_f}\right), \left(\frac{\sigma_f}{\Delta P}\right)\right] \qquad (6)$$

In order to maintain the dimensionless characteristics of the parameters of equation 6, and to eliminate the conversion from units in which the various physical fuel properties are usually given, the following parameters were adopted

$$\frac{(\Delta P \rho_f)^{\frac{1}{2}}}{\mu_f} \simeq \frac{[(\Delta P/29{\cdot}92)\ (\rho_f \rho_f')]^{\frac{1}{2}}}{(\mu_f/\mu_f')} = R_{e,}$$

$$\frac{\rho_f}{\Delta P} \simeq \frac{(\sigma_f/\sigma_f')}{(\Delta P/29{\cdot}92)} = W_{e,}$$

ρ_f', μ_f' and σ_f' are values at 60°F for a typical turbo-jet engine fuel. Since the velocity of air in the primary zone of the combustor is difficult to determine, the Reynolds Number, $(V_a \rho_a \mu_a)$, was replaced by the Reynolds Number Index $[R_e I_a = \delta a/(\varphi_a \theta_a)^{\frac{1}{2}}]$. This index refers the Reynolds Number in the combustor to the Reynolds Number which exists at static sea level conditions. Equation 6 can now be written as

$$(FC) = f\left[\left(\frac{P_f}{P_b}\right), \left(R_e I_a\right), \delta a/(\phi_a \theta_a)^{\frac{1}{2}}\right] \left(R_{e,f}\right), \left(W_{e,f}\right]\right) \qquad (7)$$

Flame stabilization requirements

In addition to the requirements necessary to obtain an ignition, conditions must be present within the combustor which will enable a flame to propagate and stabilize. It has been shown that these conditions can be adequately expressed in terms of a combustion parameter[7].

$$(CP) = f\left(\frac{P_b T_a}{V_a}\right) \qquad (8)$$

This parameter can be expressed in terms in which engine windmill data are usually correlated and presented; namely, air flow, compressor pressure ratio, and engine inlet conditions[8].

$$(CP) = f\left[\delta_2 \sqrt{\theta_2} \left(\frac{\delta_2}{W_a \sqrt{\theta_2}}\right) \left(\frac{P_b}{P_2}\right)^2\right] \qquad (9)$$

Thus, the conditions which are present in a combustor of fixed geometry are expressed by equations 7 and 9.

Graphical development of correlation

Sufficient windmill re-light data obtained with the JP–5 from the three windmill test conditions, shown in *Figure 1*, were available to determine the effects of the various combustor parameters of equations 7 and 9. This engine, Engine *A*, contained a canannular type combustor, a high energy spark ignition system, and a downstream injection atomizer system. The engine was

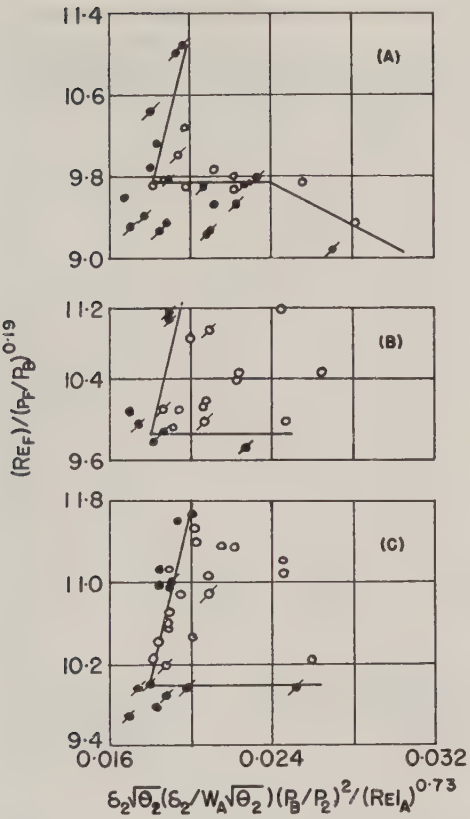

Figure 2. Effect of $(W_{e,f})$ *upon the plots of* $[(R_{e,f})/(P_f/P_b)^{0.19}]$ versus $[(CP)/(R_eI_a)^{0.73}]$. *Engine A. JP-5 fuel.* O *Successful re-light attempt;* ● *unsuccessful re-light attempt;* Ø *repeated attempt*

(*A*) $(W_{e,f}) = 0{\cdot}170$ *to* $0{\cdot}175$
(*B*) $(W_{e,f}) = 0{\cdot}165$ *to* $0{\cdot}170$
(*C*) $(W_{e,f}) = 0{\cdot}160$ *to* $0{\cdot}165$

instrumented to determine engine inlet total and exhaust static pressures (engine ram pressure ratio), combustor static pressure, atomizer pressure drop, engine inlet total temperature, turbine discharge total temperature, combustor inlet total temperature, and fuel temperature in an atomizer. The instrumentation was connected both to direct reading instruments and to a direct recording oscillograph. For a given re-light attempt, engine inlet total and exhaust static pressures, and engine inlet temperature were set to simulate some windmill condition. The ignition system and oscillograph were then energized and fuel flow initiated. A set period of time was allotted for ignition to commence. If the re-light attempt was successful, the data recorded by the oscillograph were read at the point of ignition. If the re-light attempt was not successful (no ignition obtained), the data recorded by the oscillograph were read at the point where the fuel throttle was closed. In a number of instances, ignition was successful but the engine either accelerated very slowly or did not accelerate toward idle speed at all. Observation of the engine disclosed that flames were visible downstream of the engine exhaust nozzle. This type of result (engine hang-up) was considered to be an unsuccessful re-light, and the data recorded by the oscillograph were read at the point of ignition. The probable reasons for engine hang-up will be discussed in a later section of this paper.

The data obtained were then used to calculate the various parameters of equations 7 and 9 for each windmill test condition. A brief description of the analyses conducted to determine their effect follows.

Plots were made of $R_{e,f}$ *versus* (CP) at constant values of $W_{e,f}$ and R_eI_a for several different levels of (P_f/P_b). An envelope for each plot could be estimated, which separated the re-light and no re-light regions. These envelopes were displaced vertically by a function of $(P_f/P_b)^{0.19}$. In a similar manner, the envelopes obtained from plots of $(R_{e,f})/(P_f/P_b)^{0.19}$ *versus* (CP) at constant values of $W_{e,f}$ were displaced horizontally by a function of $(R_eI_a)^{0.73}$. The envelopes then obtained from plots of $(R_{e,f})/(P_f/P_b)^{0.19}$*versus*$(CP)/(R_eI_a)^{0.73}$, examples of which are given in *Figure 2*, were displaced vertically by a function of $(W_{e,f})^{-0.5}$.

The final unique plot of

$$[(R_{e,f})\ (W_{e,f})^{0.5}/(P_f/P_b)^{0.19}]_{\text{JP-5}} \textit{ versus } [(CP)/(R_eI_a)^{0.73}]$$

or for simplicity,

$$(FP)_{\text{JP-5}} \textit{ versus } (AP)$$

presents an envelope, *Figure 3*, within which combustor conditions in terms of the above parameters will lead to a successful altitude windmill re-light.

Altitude windmill re-light data had also been

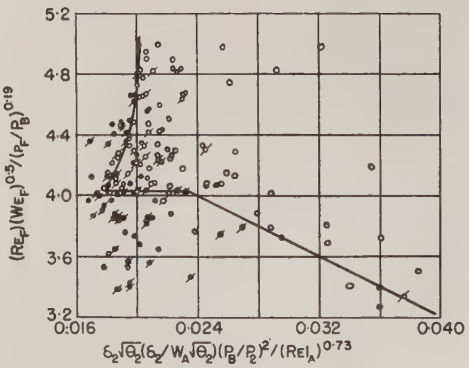

Figure 3. Plot of the altitude windmill re-light correlation relating the fuel and air parameters in the combustor of Engine A. O *Successful re-light attempt;* ● *unsuccessful re-light attempt;* Ø *repeated attempt*

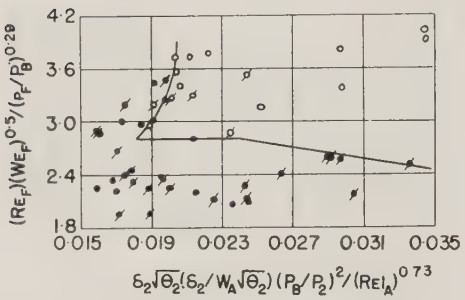

Figure 4. Plot of the altitude windmill re-light correlation relating the fuel and air parameters in the combustor of Engine A for JP–4 fuel. O *Successful re-light attempt;* ● *unsuccessful re-light attempt;* Ø *repeated attempt*

obtained for engine *A* with JP–4 fuel, and the correlation for this fuel was developed in the same manner as described for JP–5 above.

It was determined that the air parameter, (AP), was the same for both fuels, but the fuel parameter for JP–4 was

$$[(R_{e,f})\ (W_{e,f})^{0\cdot5}/(P_f P_b)^{0\cdot29}]_{\text{JP–4}}$$

This correlation is presented in *Figure 4*.

Figures 3 and *4* show that there is a distinct altitude windmill correlation for each of the fuels tested. In order to eliminate this fuel effect, an inspection was made of the parameters involved. The significant fact noted was the difference in the exponents of the (P_f/P_b) terms in $(FP)_{\text{JP–5}}$ and $(FP)_{\text{JP–4}}$. These exponents, which reflect the effect of the fuel vapour pressure, were 0·19 for JP–5 and 0·29 for JP–4.

It is apparent that these exponents must be the same for both fuels if a single generalized correlation is desired. Therefore, the exponent of the partial pressure term was arbitrarily chosen as 0·19. With this selection, JP–5 fuel becomes the base since its fuel parameter remains unchanged. However, the vapour pressure of JP–4 can no longer be used as such in determining its fuel parameter

$$[(R_{e,f})\ (W_{e,f})^{0\cdot5}/(P_{fr}/P_b)^{0\cdot19}] = (FP)_r$$

where P_{fr} is some relative vapour pressure for JP–4. The values of this relative vapour pressure to obtain the same correlation envelope as that for JP–5 were determined by approximation. These approximated relative vapour pressures (P_{fr}) would be of little value unless they could be directly determined from the actual vapour pressure of JP–4 and that of the base fuel, JP–5. Although there is no apparent physical significance of the relative vapour pressure, *Figure 5* represents the relationship of this pressure to temperature, and also provides a simple graphical construction means of determining the relative vapour pressure at any temperature.

Using the relative vapour pressures determined by use of *Figure 5*, a correlation envelope was obtained for JP–4 which was exactly the same as that obtained for JP–5. Therefore, *Figure 3* represents the generalized altitude windmill re-light correlation for Engine *A*.

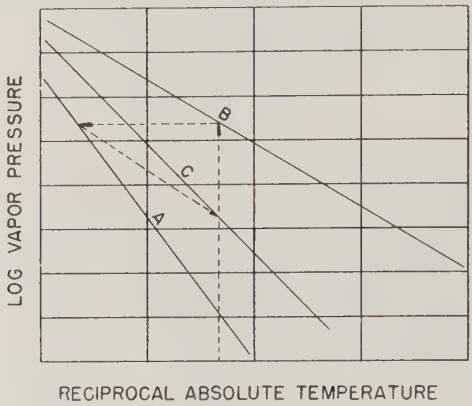

Figure 5. Construction method for obtaining the relative vapour pressure of a fuel. (A) Base fuel, JP–5; (B) JP–4; (C) JP–4 relative to the base fuel

Re-light data were also obtained with JP–5 on a second engine, Engine *B*, containing a combustor whose configuration, atomizer nozzle design, and spark ignition system were quite different from the first engine. Although the effect of the various parameters was the same, *Figure 6*, the region of successful windmill re-light was displaced, indicating the effect of the above-mentioned differences.

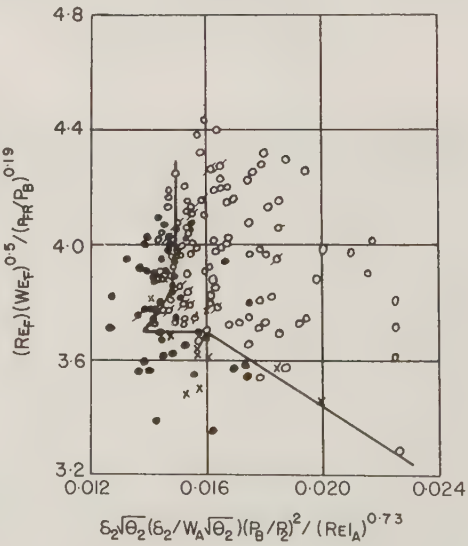

Figure 6. Plot of the generalized altitude windmill re-light correlation relating the fuel and air parameters in the combustor of Engine B. X *Engine hang-up;* O *successful re-light attempt;* ● *unsuccessful re-light attempt;* Ø *repeated attempt*

DISCUSSION

A generalized altitude windmill re-light correlation has been developed. The correlation presents the conditions which must be present in the combustor of a turbo-jet engine, containing a fuel atomizer system, in order to obtain a successful re-light. The correlation expresses these re-light characteristics in terms of engine windmill data readily obtainable in an altitude test facility.

Once the correlation for a given engine has been obtained, it is possible to predict the altitude windmill re-light limits of the engine, e.g. Engine *A*, for any given set of engine windmill conditions. Windmill data correlated in the accepted manner with corrected engine speed can easily be converted into the air parameter. To compute the fuel parameter, the variation of atomizer pressure drop and fuel temperature must be known. The parameters thus obtained for a series of ram pressure ratios at a given altitude are plotted on the correlation plot, and the values at which this windmill data enters or leaves the re-light region is noted. The information thus obtained for a number of altitudes is used to predict the altitude re-light limits of the engine. The predicted altitude re-light limit at standard flight conditions for Engine *A* is compared to data actually obtained in the altitude test facility in *Figure 7*.

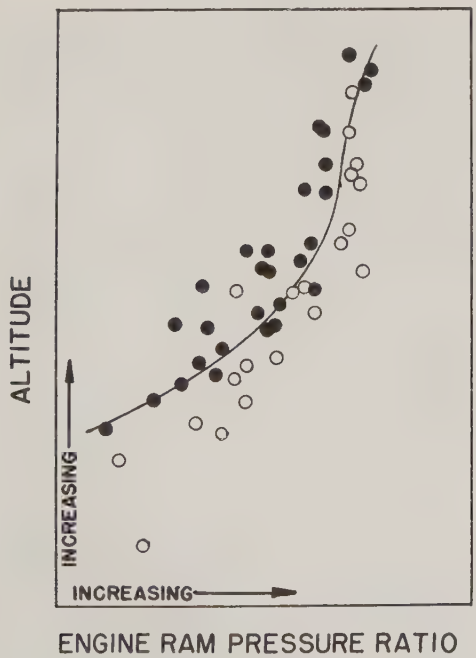

Figure 7. Comparison of the altitude windmill re-light limit for Engine A predicted from the correlation with actual test data. Fuel JP–5. ○ *Successful re-light;* ● *unsuccessful re-light*

During the initial development of the correlation, it would have appeared that the vapour pressure of the fuel could have been neglected. The high energy spark ignition systems currently used provide ignition energies in excess of the minimum required to ignite a vaporized fuel air mixture. A great deal of this energy is therefore available to vaporize the liquid fuel to provide an adequate fuel vapour–air mixture, regardless of the actual fuel volatility. However, the partial pressure of the fuel does affect the flame propagation and flame stabilization processes in the primary zone of the combustor. As the temperature of the fuel entering the combustion chamber increases, the vapour pressure increases approximately as exp $(-1/T°\mathrm{R})$, and a limit is reached where a rich fuel vapour–air mixture will be present. This mixture will inhibit ignition, cause rich blow-out to occur upon ignition, or cause the combustion front to move downstream of the primary zone of the combustor. The latter process can lead to incomplete combustion in the combustor and to flame holding on the turbine nozzles with insufficient energy available to accelerate the engine to idle speed. This latter phenomenon is one reason for the 'engine hang-ups' previously described.

The atomizing characteristics of the fuel, $(R_{e,f})\ (W_{e,f})^{0\cdot5}$, contained in the generalized fuel parameter, improve with increasing fuel temperature. This is important to the success of an attempted altitude windmill re-light. The results presented by many authors[9,10] have shown that ignition, and flame propagation and flame stabilization processes are affected by the spray characteristics. A coarse spray may also lead to incomplete combustion and to flame holding on the turbine nozzles with the end result manifested as an 'engine hang-up'. Too coarse a spray will prevent even the initiation of ignition.

The effect of atomizer fuel temperature upon the generalized fuel parameter of Engine *A* at an air parameter value of 0·022 is shown in Table 1. As fuel temperature is initially increased from −20°F, the rate of increase of $(R_{e,f})\ (W_{e,f})^{0\cdot5}$ is greater than that for $(P_{fr}/P_b)^{0\cdot19}$. At 80°F, the spray characteristics have improved sufficiently for an attempted re-light to be successful. However, as fuel temperature continues to increase, the rate of increase of $(P_{fr}/P_b)^{0\cdot19}$ becomes the controlling factor, and at a fuel temperature of 180°F the fuel parameter falls below the re-light region. This return to the no re-light region is due to a rich fuel vapour–air mixture now present in the combustor. This rich fuel vapour–air mixture is a combination of two effects; first, the vapour pressure of the fuel has increased substantially; second, the continued improvement in the fuel spray characteristics has increased the

TABLE 1

Effect of Fuel Temperature upon the Generalized Fuel Parameter. (Engine *A* at constant windmill condition ($AP = 0{\cdot}022$); fuel, JP–4)

Fuel temperature T°F	*Rate of change of atomizing characteristics* $\frac{\Delta[(R_{e,f})\ (W_{e,f})^{0{\cdot}5}]\ t_2 - t_1}{[(R_{e,f})\ (W_{e,f})^{0{\cdot}5}]\ t_1}$	*Rate of change of partial pressure effect* $\frac{\Delta\ [(P_{fr}/P_b)^{0{\cdot}19}]\ t_2 - t_1}{[(P_{fr}/P_b)^{0{\cdot}19}]\ t_1}$	*Generalized fuel parameter* $(FP)_r$
−20	0·0138	0·0080	3·32
0	0·0106	0·0073	3·57
20	0·0095	0·0067	3·78
40	0·0076	0·0067	3·91
60	0·0070	0·0061	3·98
80	0·0060	0·0056	4·04
100	0·0057	0·0050	4·11
120	0·0049	0·0046	4·14
140	0·0042	0·0049	4·10
160	0·0036	0·0044	4·04
180	0·0031	0·0039	3·97
200	0·0026	0·0032	3·80

$t_2 - t_1 = 10$°F

surface area of the fuel (decrease in individual fuel droplet size) from which vaporization can occur. In this manner, the correlation can be used to study the effect of atomizer fuel temperature upon the altitude re-light limits of an engine.

In general, at a constant engine altitude windmill condition (constant air parameter), a successful re-light will depend upon the fuel spray characteristics at low fuel temperatures and upon the effect of fuel volatility at high fuel temperatures.

The plots of the individual correlations for Engine *A* with JP–5 (*Figure 3*) and JP–4 (*Figure 4*) show that, regardless of the differences in the physical properties of these fuels, there is a single minimum value of air parameter (0·018) below which a successful re-light is not possible. It is possible to obtain a successful ignition, flame propagation, and flame stabilization below this minimum value of air parameter. However, the combustion efficiency is too low and the available energy is not sufficient to accelerate the engine. The lower heat of combustion per unit volume for JP–4 is approximately 93 per cent of that for JP–5. Since fuel flow to the combustor is volumetrically controlled during a re-light attempt, a successful re-light will occur with JP–5 at a given air parameter even if the combustion efficiency is approximately 7 per cent less than with JP–4. Combustion efficiency at constant combustor conditions has been shown to decrease with increase in the mid-boiling point of a fuel[9,10]. It would therefore appear that the greater volumetric heat content of JP–5 is offset by its lower combustion efficiency when compared to JP–4 (mid-boiling point 100°F less than JP–5), and this would give rise to the single minimum value of air parameter for both fuels.

CONCLUSIONS

The altitude windmill re-light correlation provides a unique method of presenting data obtained with varied engine test conditions in terms of engine combustor fuel and air parameters so as to obtain a single boundary between the successful and unsuccessful re-light regions.

The effect of atomizer discharge fuel temperature upon the altitude windmill re-light characteristics of a turbo-jet engine can be determined by means of the correlation. In general, at a constant engine altitude windmill condition, re-light will depend upon the fuel spray characteristics at low fuel temperature, and upon the effect of fuel volatility at high fuel temperatures.

Although the correlation was obtained with a given fuel, it may successfully be used to predict altitude windmill re-light limits of an engine with all current jet engine fuels.

The opinions stated in this article are the private ones of the writers and are not to be construed as official or reflecting the views of the Navy Department or Naval Service at large.

The Bureau of Aeronautics and the Naval Air Turbine Test Station, who supported this research, are thanked for their permission to publish the results. The authors would also like to thank Messrs. W. R. Slivka, M. Savage and M. A. Lott for their critical review of this report.

NOMENCLATURE

Symbol	Definition	Units
D'	Coefficient of diffusivity, fuel vapour-air	ft.²/sec
D_a	Characteristic dimension of the combustor	ft.
D_N	Diameter of fuel atomizer discharge nozzle	ft.
df	Mean diameter of atomizer spray fuel droplets	ft.
M'	Average molecular weight of fuel vapour	lb./mole
P_b	Static pressure in the combustor	"HgA
ΔP	Pressure drop across fuel atomizer	"HgA
P_2	Engine inlet total pressure	"HgA
P_f	Vapour pressure of the fuel at T_f	"HgA
V_a	Air velocity in the primary zone of the combustor	ft./sec
V_f	Fuel velocity in the atomizer nozzle assuming that the nozzle flows full	ft./sec
V_{fd}	Fuel droplet velocity in the primary zone of the combustor	ft./sec
T_a	Combustor inlet total temperature	°R
T_f	Fuel temperature in atomizer nozzle	°R
T_2	Engine inlet total temperature	°R
W_a	Combustor air flow	lb./sec
α	Spray angle of fuel	degrees
δ_a	Ratio of $P_b/29{\cdot}92$	
δ_2	Ratio of $P_2/29{\cdot}92$	
ρ_f	Density of fuel at T_f	lb./ft.³
ρ_a	Density of air at T_a	lb./ft.³
μ_f	Viscosity of fuel at T_f	centipoise
μ_a	Viscosity of air at T_a	centipoise
μ_{fd}	Viscosity of fuel vapour at T_f	centipoise
σ_f	Surface tension of fuel at T_f	dynes/cm
θ_a	Ratio of $T_a/518{\cdot}4$	
θ_2	Ratio of $T_2/518{\cdot}4$	
φ_a	Ratio of μ_a/μ_a at 60°F	

REFERENCES

1 Bevans, R. S. *Conference on Fuel Sprays*, Mar. 30–31, 1949. University of Michigan

2 Shafer, M. R. and Bovey, H. L. *J. Res. nat. Bur. Stand.* 52 (Mar. 1954) 141

3 Frössling, N. *Beitr. Geophys.* 52 Heft 1/2 (1938)

4 Ingebo, R. D. *Nat. Adv. Comm. Aero. Tech. Note 2850* (1953)

5 Maxwell, J. B. *Data Book on Hydrocarbons*, 1950. New York; Van Nostrand

6 Ingebo, R. D. *Nat. Adv. Comm. Aero. Tech. Note 3265* (1954)

7 Childs, J. H. and Graves, C. C. *Sixth International Combustion Symposium.* 1957. New York; Reinhold

8 Wilsted, H. D. and Grey, R. D. *Nat. Adv. Comm. Aero. RM E51B07* (1951)

9 Graves, C. C. and Gerstein, M. *Combustion Researches and Reviews 1955*, 1955. London; Butterworths

10 Hibbard, R. R. and Barnett, H. C. *Selected Combustion Problems—II*, 1956. London; Butterworths

DETERMINATION OF ROCKET MOTOR COMBUSTION PARAMETERS BY MEANS OF A DIVERGING REACTOR

G. S. GILL, E. F. ECKEL, F. A. WILLIAMS and S. S. PENNER

INTRODUCTION AND SUMMARY

The development of high-velocity diverging reactors for the determination of kinetic parameters at elevated temperatures and pressures has been considered by a number of investigators[1,2]. Considerable work has been done on the study of chemical reactions during adiabatic expansion through a de Laval nozzle for the equilibrated reaction products formed after combustion in liquid-fuel rocket engines[1]. Recently a related experimental and analytical procedure has been applied by Wegener to the $2NO_2 \rightleftarrows N_2O_4$ reaction in order to obtain relatively precise kinetic estimates for this chemical transformation[2].

It is the purpose of the present investigations to indicate experimental and analytical procedures which may be used to study kinetic processes, both for heterogeneous and for homogeneous systems, under the conditions actually encountered in rocket engines and for propellant combinations of the type actually used in practical propulsion devices. The experimental studies described in the following section refer to bi-propellant liquid systems. On the other hand, the analytical investigations summarized in the third section (p. 713) include a complete formulation and representative solutions for chemical reactions in a high-velocity gas stream passing through a diverging reactor. A correlation of the experimental results obtained for heterogeneous bi-propellants in terms of a simplified reaction model is described in the last section (p. 722).

It is apparent that full utilization of the results described in the present investigation requires either an experimental programme on pre-mixed gaseous propellants or else a theoretical analysis of heterogeneous combustion in a diverging reactor. Both of these investigations are currently under study. We expect that valuable insight for an efficient formulation of the problem of heterogeneous combustion will be derived from a basic study on spray formation and combustion which is being carried out by F. A. Williams.

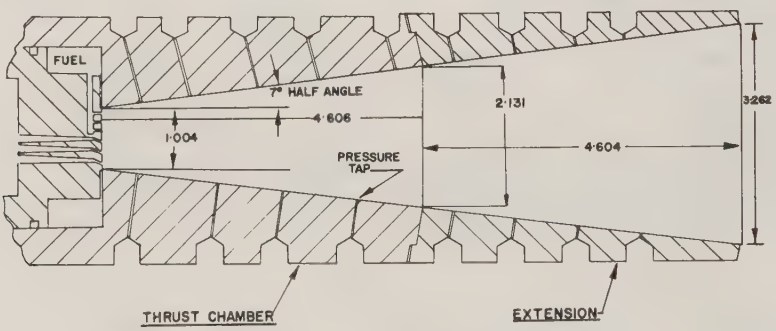

Figure 1. Schematic diagram of a diverging liquid-fuel reactor

EXPERIMENTAL STUDIES

A truncated cone (with a semi-divergence angle of 7°) served as rocket chamber for the initial tests. In order to use this type of engine effectively it is necessary to design an efficient injection system which provides very good mixing at the injector end.

A schematic diagram of the truncated chamber is shown in *Figure 1.* A diagram of the reverse triplet injector using liquid oxygen and jet fuel is shown in *Figure 2.*

In the initial tests, a high heat rejection to the chamber wall and injector face was obtained, which led to distortion of the injector orifices and a high-frequency instability together with losses in pressure and thrust. With improved injector design (see *Figure 2*) a test duration up to 1 second proved to be possible. Pressure profiles and the exhaust flow pattern ('Mach diamonds') were observed as a function of fuel types, injector design

and mixture ratio. A photograph of the exhaust jet is shown in *Figure 3.*

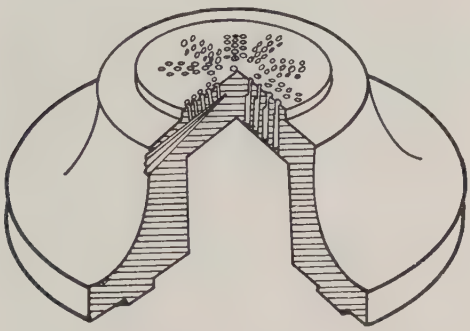

Figure 2. Reverse-triplet injector for use with liquid oxygen and jet fuel (schematic)

Representative experimental results are summarized in Table 1 and will be discussed in greater detail in the last section (p. 722).

formance evaluation for pre-mixed gaseous propellants in a diverging reactor of arbitrary shape. Next representative solutions for simplified models of the flow processes will be described.

Steady, inviscid flow in a channel of variable cross-section with chemical reactions, axial diffusion, and axial heat conduction

The relevant equations are easily derivable from the general set of conservation relations[3,4].

The overall continuity equation is

$$\frac{\mathrm{d}}{\mathrm{d}x}(\rho v A) = 0$$

$$\rho v A \equiv m \tag{1}$$

or

$$\frac{\mathrm{d}\rho}{\rho} + \frac{\mathrm{d}v}{v} + \frac{\mathrm{d}A}{A} = 0$$

Here ρ denotes the density of the fluid mixture, v is the mass-weighted average velocity in the flow $(x-)$ direction, A represents the cross-sectional

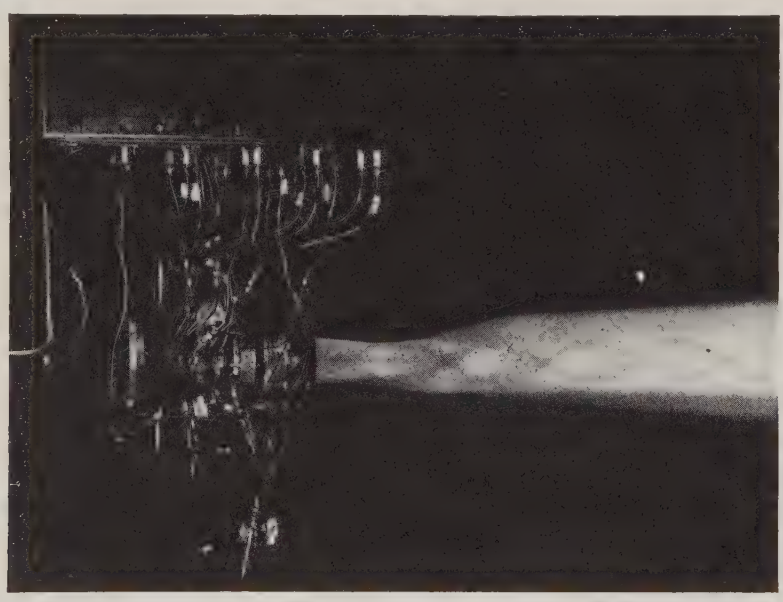

Figure 3. Photograph of the exhaust jet observed for the diverging reactor which shows the Mach diamonds characteristic of supersonic flow

THEORETICAL STUDIES FOR PRE-MIXED GASEOUS PROPELLANTS IN A DIVERGING REACTOR*

In the following paragraphs we present first a complete formulation of the problem of per-

* The discussion in this section is greatly condensed; all intermediate steps in the analysis have been deleted. The interested reader may obtain a more complete description of the theoretical studies by referring to a series of Research Reports published by Rocketdyne during 1957 and 1958.

area of the channel, and m equals the constant mass flow rate. Using a binary mixture approximation, the continuity equation for species K becomes

$$\rho v A \frac{\mathrm{d}Y_{\mathrm{K}}}{\mathrm{d}x} = A w_{\mathrm{K}} + \frac{\mathrm{d}}{\mathrm{d}x}\left[\rho A D_{\mathrm{K}} \left(\frac{\mathrm{d}Y_{\mathrm{K}}}{\mathrm{d}x}\right)\right] \text{ with } K = 1, 2, \ldots, N \tag{2}$$

Here Y_{K} denotes the mass fraction of species K, w_{K} is the mass rate of production of species K per

TABLE 1

Representative Experimental Data Obtained with the Diverging Reactor for LOX–Kerosene Mixtures

F	530 ± 16	456 ± 14	921 ± 18	736 ± 15	816 ± 16
MR	2·27 ± 0·05	2·05 ± 0·04	2·05 ± 0·04	2·17 ± 0·04	2·63 ± 0·05
M_O	1·75 ± 0·03	1·60 ± 0·03	2·79 ± 0·05	2·27 ± 0·05	2·63 ± 0·05
M_F	0·77 ± 0·01	0·78 ± 0·01	1·36 ± 0·03	1·05 ± 0·02	1·00 ± 0·02
M	2·52 ± 0·03	2·38 ± 0·03	4·15 ± 0·08	3·32 ± 0·06	3·63 ± 0·07

Slant distance in.	*Pressure* lb./in.² g				
0·060	340 ± 4	291 ± 4	—	—	—
0·20	335 ± 2	272 ± 2	530 ± 10	452 ± 12	483 ± 13
0·21	290 ± 2	224 ± 2	430 ± 2	375 ± 3	393 ± 3
0·24	284 ± 6	220 ± 5	436 ± 8	372 ± 5	394 ± 5
0·37	236 ± 7	184 ± 5	360 ± 9	310 ± 7	315 ± 7
0·44	187 ± 3	—	307 ± 5	235 ± 3	275 ± 4
0·45	220 ± 2	179 ± 2	332 ± 8	367 ± 10	306 ± 8
0·76	168 ± 1	140 ± 1	264 ± 1	232 ± 2	252 ± 3
1·03	137 ± 10	115 ± 9	220 ± 11	177 ± 2	195 ± 2
1·10	135 ± 1	117 ± 1	215 ± 1	—	—
1·12	130 ± 3	107 ± 2	—	165 ± 4	183 ± 4
1·41	116 ± 2	98·1 ± 2	—	152 ± 10	177 ± 11
1·65	86·0 ± 2	—	—	132 ± 6	159 ± 7
1·88	82·0 ± 3	78·0 ± 3	150 ± 3	116 ± 2	137 ± 13
2·03	—	74·6 ± 3	—	106 ± 0	117 ± 0
2·47	62·0 ± 1	59·0 ± 1	110 ± 1	88·0 ± 2	97·3 ± 2
2·67	—	—	104 ± 2	78·0 ± 1	90·0 ± 1
2·85	50·0 ± 1	47·0 ± 1	92 ± 1	71·9 ± 1	80·0 ± 2
4·01	—	—	—	—	—
4·31	23·5 ± 0·2	22·0 ± 0·2	45·9 ± 1·5	35·4 ± 0·9	38·3 ± 0·9
5·00	16·0 ± 0·7	15·8 ± 0·7	37·0 ± 1·1	26·3 ± 1·2	29·8 ± 1·3
5·87	8·0 ± 0·2	8·1 ± 0·2	23·0 ± 0·2	15·7 ± 0·7	20·4 ± 0·9
6·50	5·1 ± 0·0	5·1 ± 0·0	18·8 ± 0·2	11·9 ± 0·3	15·0 ± 0·3
7·37	2·0 ± 0·0	1·7 ± 0·0	12·2 ± 0·6	7·1 ± 0·0	9·3 ± 0·2
8·00	—	0·0 ± 0·0	9·7 ± 0·5	4·1 ± 0·0	6·6 ± 0·0
8·87	−1·7 ± 0·0	−2·4 ± 0·0	6·2 ± 0·0	1·3 ± 0·0	2·3 ± 0·0
9·18	−3·5 ± 0·0	−3·3 ± 0·0	3·1 ± 0·0	0·0 ± 0·0	1·0 ± 0·0

F = total thrust (lb.)
MR = mass ratio of oxidizer to fuel
M = total mass flow rate (lb./sec)
M_O = oxidizer mass flow rate (lb./sec)
M_F = fuel mass flow rate (lb./sec)

unit volume, and D_K represents an effective diffusion coefficient for species K in the N- component mixture. For the present application the overall momentum equation is

$$v\frac{dv}{dx} = -\frac{1}{\rho}\frac{dp}{dx} \tag{3}$$

Using the approximate relation $h_K = h_K^\circ + \bar{c}_p(T - T^\circ)$ for the specific enthalpy of species K in terms of the standard specific enthalpy of formation h_K° evaluated at T° and the average specific heat $\bar{c}_p$, as well as the expressions $\sum_K Y_K V_K = 0$ (where V_K is the diffusion velocity of species K) and $h = \sum_K Y_K h_K$, it is readily shown that the integrated energy equation becomes

$$\rho v\left[\frac{v^2}{2} + \bar{c}_p(T - T^\circ)\right] + \rho v\sum_K Y_K h_K^\circ - \lambda\frac{dT}{dx} - \rho\sum_K D_K h_K^\circ\frac{dY_K}{dx} = \frac{\text{constant}}{A} \tag{4}$$

The ideal gas equation of state

$$p = \rho R_g T,\ R_g = R/\overline{W},\ \overline{W} = \sum_K X_K W_K \tag{5}$$

will be used with R_g representing the gas constant per unit mass, R the molar gas constant, $\overline{W}$ the

average molecular weight, X_K the mole fraction of species K, and W_K the molecular weight of species K.

For an arbitrary flow problem, involving N distinct chemical species, we have $N + 4$ unknowns, namely, the N mass fractions $Y_K (K = 1, 2 \ldots N)$, p, ρ, T and v. These $N + 4$ unknowns are connected by the $N + 4$ relations specified in equations 1 to 5 for any channel described by $A(x)$. Since $\sum_K Y_K = 1$ only $N + 3$ of the basic equations are independent. For the solution of any given flow problem it is necessary to specify an appropriate number of boundary conditions.

Introduction of the approximation that the Lewis number L_e equals unity, viz., $L_e = \lambda/\rho \bar{c}_p D = 1$ $(D \equiv D_K, K = 1, 2, \ldots, N)$, leads to considerable simplification of the continuity and energy equations. However, we shall not consider here the solution of the resulting Shvab-Zeldovich type problem[5,6].

In the following discussions we introduce two additional simplifying approximations. These are (*a*) neglect of axial diffusion and thermal conduction relative to the large convection terms and (*b*) the use of a single rate-controlling chemical reaction step of the type $n\,Re \rightarrow n\,Pr$ where Re and Pr are symbolic representations for the reactant and product chemical species, respectively, and n defines the order of the chemical transformation. For $n \neq 0$, equations 2 and 4 reduce to

$$\frac{d\varepsilon}{dx} = \frac{nB\,[\exp(-E/RT)]\rho^n(1-\varepsilon)^n}{\rho v W^{n-1}} \tag{2a}$$

and

$$\frac{v^2}{2} + \bar{c}_p T - \varepsilon q = \bar{c}_p T_{st} = \text{constant} \tag{4a}$$

respectively. Here ε is the mass fraction of reaction product; W is the (constant) average molecular weight; E and B denote, respectively, the activation energy and frequency factor for the overall chemical reaction; $q = h^\circ_{Re} - h^\circ_{Pr}$ represents the total heat release per unit mass of products formed; T_{st} identifies the stagnation temperature at the location where $\varepsilon = 0$.

Heat release at sonic plane

Some insight into the performance limits for the flow problem under discussion may be obtained by assuming that all of the heat release occurs in a plane at a specified distance L from the injector end. The injected combustible material first expands subsonically and isentropically in region I for a distance L without heat input (see *Figure 4*). At the plane 1–2 all of the burning takes place and the flow is choked in such a way that a Mach number of unity is reached at station 2. A supersonic isentropic expansion occurs in region II.

For this model equation 2a may be deleted and equation 3 is easily integrated. Algebraic governing equations are therefore obtained. By combining the well known equations for isentropic flow (in regions I and II) and constant-area flow

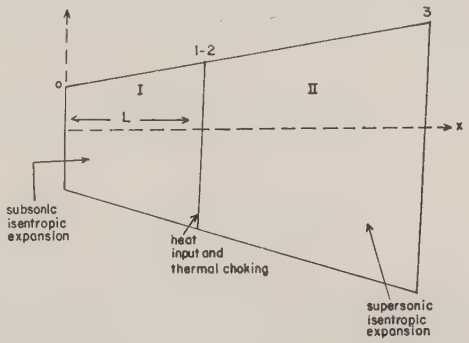

Figure 4. Heat release at the sonic plane in a diverging reactor (schematic)

with heat addition (at the plane 1–2) we obtain the relations

$$\frac{A_1}{A_0} = \frac{M_0}{M_1}\left[\frac{1 + \left(\frac{\gamma_I - 1}{2}\right)M_1^2}{1 + \left(\frac{\gamma_I - 1}{2}\right)M_0^2}\right]^{(\gamma_I+1)/2(\gamma_I-1)} \tag{6}$$

$$\frac{T_{st,1} + (q/\bar{c}_{p,I})}{T_{st,1}} = \frac{1}{M_1^2}\frac{(1 + \bar{\gamma}M_1^2)^2}{1 + \left(\frac{\bar{\gamma} - 1}{2}\right)M_1^2}\frac{1}{2(\bar{\gamma} + 1)} \tag{7}$$

$$\frac{v_3}{v_0} = \frac{1}{M_0 M_1}\frac{1 + \bar{\gamma}M_1^2}{\bar{\gamma} + 1}\left[\frac{1 + \left(\frac{\gamma_I - 1}{2}\right)M_0^2}{1 + \left(\frac{\gamma_I - 1}{2}\right)M_1^2}\right]^{1/2} \times \left[\frac{\left(\frac{\gamma_{II} + 1}{2}\right)M_3^2}{1 + \left(\frac{\gamma_{II} - 1}{2}\right)M_3^2}\right]^{1/2} \tag{8}$$

and

$$\frac{p_3}{p_0} = \left[\frac{1 + \left(\frac{\gamma_I - 1}{2}\right)M_0^2}{1 + \left(\frac{\gamma_I - 1}{2}\right)M_1^2}\right]^{\gamma_I/(\gamma_I-1)}\left(\frac{1 + \bar{\gamma}M_1^2}{\bar{\gamma} + 1}\right) \times \left[\frac{\frac{\gamma_{II} + 1}{2}}{1 + \left(\frac{\gamma_{II} - 1}{2}\right)M_3^2}\right]^{\gamma_{II}/(\gamma_{II}-1)} \tag{9}$$

Here M represents the Mach number, the subscripts 0 and 3 refer to conditions at the injector and exit plane, respectively (see *Figure 4*), γ is the ratio of specific heats, and q equals the amount of heat added at the sonic plane. The average ratio of specific heats between stations 1 and 2 is $\bar{\gamma} \simeq (\gamma_I + \gamma_{II})/2$ (we have chosen $\gamma_I = 1{\cdot}4$ and $\gamma_{II} = 1{\cdot}2$).

the thrust according to equation 8. From equations 7 and 8 it may be seen that increasing q decreases M_1 and increases the thrust. The dependence of v_3 on q is illustrated in *Figure 5* for various values of the exit pressure and fixed inlet conditions. For the subsonic expansion $M_0 \geqslant M_1$; equation 8 thus shows that, for fixed M_1, v_3/v_0 and hence also I_{sp} and thrust are largest when

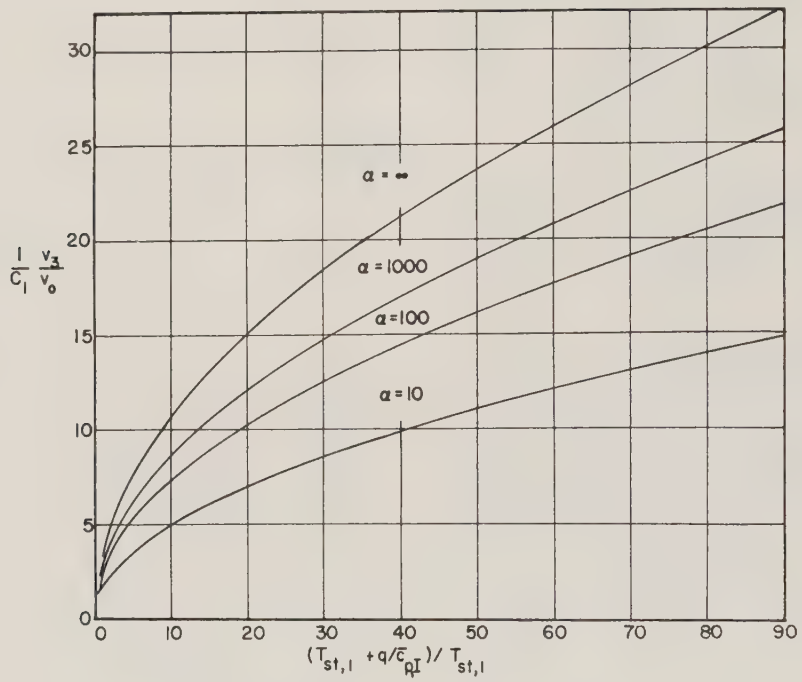

$$C_1 = \frac{1}{M_0}\left[\frac{1 + \frac{\gamma_I - 1}{2} M_0^2}{\frac{\gamma_I + 1}{2}}\right]^{1/2} = \frac{0{\cdot}907}{M_0}(1 + 0{\cdot}2\, M_0^2)^{1/2}$$

$$\alpha = \frac{p_0}{p_3}\left[1 + \frac{\gamma_I - 1}{2} M_0^2\right]^{\gamma_I/(\gamma_I - 1)}\left(\frac{\gamma_{II} + 1}{2}\right)^{\gamma_{II}/(\gamma_{II} - 1)} = 1{\cdot}772\,\frac{p_0}{p_3}(1 + 0{\cdot}2 M_0^2)^{3{\cdot}5}$$

Figure 5. Dependence of exit velocity on heat release at the sonic plane for fixed inlet conditions and various exit pressures

From equation 7 it may be shown that M_1 depends on $T_0 + \frac{1}{2}v_0^2$ and on q. But M_1 determines the area ratio at which the heat input occurs (i.e., L) according to equation 6. Thus there is a (choking) relation between injection conditions, q and L. For given initial conditions, equation 9 determines M_3 in terms of p_3 for fixed q. For specified inlet conditions, v_3/v_0 is a direct measure of thrust (mv_3) and specific impulse ($I_{sp} = v_3/g$, g = gravitational acceleration). Equation 8 therefore shows indirectly the effects of q, p_3, and L on I_{sp}. From equation 9 it is apparent that a decrease in p_3 increases M_3 and, therefore, increases $M_0 = M_1$ which occurs at $L = 0$. In other words, for a given heat of reaction the greatest thrust is obtained when the heat is released at the inlet.

Numerical procedures for performance evaluation

For practical calculations it is usually convenient to select ε and M as independent variables[8]. From equation 4a and the definition $M = v/(\gamma R_g T)^{1/2}$ it is readily shown that

$$T = \frac{h_0 + \varepsilon q}{\bar{c}_p\left[1 + \left(\frac{\gamma - 1}{2}\right) M^2\right]} \qquad (10)$$

where $h_0 = \bar{c}_p T_{st}$ is the specific initial stagnation enthalpy. Similarly,

$$v = \frac{M[(\gamma - 1)(h_0 + \varepsilon q)]^{1/2}}{\left[1 + \left(\frac{\gamma - 1}{2}\right) M^2\right]^{1/2}} \tag{11}$$

$$\rho = \frac{m\left[1 + \left(\frac{\gamma - 1}{2}\right) M^2\right]^{1/2}}{AM[(\gamma - 1)(h_0 + \varepsilon q)]^{1/2}} \tag{12}$$

and

$$p = \frac{m[(\gamma - 1)(h_0 + \varepsilon q)]^{1/2}}{\gamma AM\left[1 + \left(\frac{\gamma - 1}{2}\right) M^2\right]^{1/2}} \tag{13}$$

Equations 10 to 13 relate T, v, ρ, and p to the independent variables ε and M, and to the known constants m, h_0, γ, q and $\bar{c}_p$ as well as to the known function $A(x)$.

A differential equation for the Mach number M is readily obtained by using equations 11 to 13 in equation 3. The result is*

$$\frac{dM^2}{dx} = \frac{M^2\left(1 + \frac{\gamma - 1}{2} M^2\right)}{(1 - M^2)} \times \left[\frac{1 + \gamma M^2}{(h_0 + \varepsilon q)} q \frac{d\varepsilon}{dx} - \frac{2}{A}\frac{dA}{dx}\right] \tag{14}$$

By the use of equations 1, 10, and 12, equation 2a may be written explicitly in the following useful form

$$\frac{d\varepsilon}{dx} = \frac{nB}{W^{n-1}}\left(\frac{m}{A}\right)^{n-1} \frac{(1 - \varepsilon)^n}{M^n} \frac{\left(1 + \frac{\gamma - 1}{2} M^2\right)^{n/2}}{[(\gamma - 1)(h_0 + \varepsilon q)]^{n/2}} \times \exp\left[-\left(\frac{\gamma}{\gamma - 1}\right) \frac{E\left(1 + \frac{\gamma - 1}{2} M^2\right)}{W(h_0 + \varepsilon q)}\right] \tag{15}$$

Because of the non-linearity of equations 14 and 15, exact solutions can be obtained only numerically. A straightforward trial-and-error integration procedure may be developed in which the injector area is fixed and the initial Mach number is varied until an acceptable numerical solution is obtained. While this procedure may be useful for determining the performance of a given motor with specified injection conditions, the method described below is more efficient for obtaining general performance characteristics and design criteria. We eliminate the trial-and-error computation so that each integration yields useful physical results. The (machine) time required for obtaining performance data is thereby greatly reduced.

Reduced variables and basic equations—We introduce the following definitions:

$$\alpha \equiv h_0/q \tag{16}$$

$$\beta \equiv nBm^{n-1}/W^{n-1}[(\gamma - 1)q]^{n/2} \tag{17}$$

$$\theta \equiv \left(\frac{\gamma}{\gamma - 1}\right) \frac{E}{Wq} \tag{18}$$

It is apparent that α is a dimensionless form of the initial stagnation enthalpy, β is a reaction rate constant, and θ represents a dimensionless activation energy. The constant β has the dimensions of a length to the power $2n - 3$ and thus defines a chemical length l for the system through the relation

$$l^{2n-3} = \beta \tag{19}$$

For a representative second-order reaction rate, the length l is of the order of 10^5 cm. A dimensionless physical length ξ may now be defined as $\xi \equiv x/l$; similarly, a dimensionless area $\mathbf{A}(\xi) \equiv A(x)/l^2$ will be used. Equations 14 and 15 may now be written, respectively, as

$$\frac{dM^2}{d\xi} = \frac{M^2\left(1 + \frac{\gamma - 1}{2} M^2\right)}{1 - M^2} \times \left[\left(\frac{1 + \gamma M^2}{\alpha + \varepsilon}\right) \frac{d\varepsilon}{d\xi} - \frac{2}{\mathbf{A}}\frac{d\mathbf{A}}{d\xi}\right] \tag{20}$$

and

$$\frac{d\varepsilon}{d\xi} = \frac{(1 - \varepsilon)^n}{M^n \mathbf{A}^{n-1}} \frac{\left(1 + \frac{\gamma - 1}{2} M^2\right)^{n/2}}{(\alpha + \varepsilon)^{n/2}} \times \exp\left[-\frac{\theta\left(1 + \frac{\gamma - 1}{2} M^2\right)}{\alpha + \varepsilon}\right] \tag{21}$$

Behaviour of basic equations at $M = 1$—Letting the subscript 1 identify conditions at $M = 1$, we find from the condition that $dM^2/d\xi$ is finite at $M = 1$ the relation

$$\mathbf{A}_1^{n-2} \frac{d\mathbf{A}}{d\xi}\bigg|_{\xi=\xi_1} = \left(\frac{\gamma + 1}{2}\right)^{(n+2)/2} \frac{(1 - \varepsilon_1)^n}{(\alpha + \varepsilon_1)^{(n+2)/2}} \times \exp\left[-\left(\frac{\gamma + 1}{2}\right) \frac{\theta}{(\alpha + \varepsilon_1)}\right] \tag{22}$$

* It should be noted that our result differs from that obtained by Chambré and Lin[8], because they omit a term $-dA/A$ on the right-hand side of their equation 12. This error has also been pointed out by B. Jacobsson, *J. aero. Sci.* 14 (1947) 294.

It may also be shown by expanding equations 20 and 21 about the point $M = 1$ that

$$\left.\frac{dM^2}{d\xi}\right|_{\xi=\xi_1} = \frac{1}{\mathbf{A}_1}\left.\frac{d\mathbf{A}}{d\xi}\right|_{\xi=\xi_1}\left\{\frac{(\gamma^2-1)\theta}{4(\alpha+\varepsilon_1)} + \frac{n-\gamma}{2} + \left\{\left[\frac{(\gamma^2-1)\theta}{4(\alpha+\varepsilon_1)}\right]^2 + \frac{(n-\gamma)(\gamma^2-1)\theta}{4(\alpha+\varepsilon_1)} - \frac{(\gamma+1)\theta}{(\alpha+\varepsilon_1)} + \left(\frac{n-\gamma}{2}\right)^2 - \gamma(2-n) + \frac{2n(\alpha+1)}{(1-\varepsilon_1)} + (\gamma+1) \times \mathbf{A}_1\left(\left.\frac{d^2\mathbf{A}}{d\xi^2}\right|_{\xi=\xi_1}\right)\Big/\left(\left.\frac{d\mathbf{A}}{d\xi}\right|_{\xi=\xi_1}\right)^2\right\}^{1/2}\right\} \quad (23)$$

Equation 22 provides a relation between ξ and ε at the sonic plane whereas equation 23 determines the behaviour of the Mach number at this same position.

Method of solution—For efficient numerical calculations we choose the desired values of γ, n, θ, α, and $\mathbf{A}(\xi)$. Next we assume a value for ε_1. The location of the sonic plane, ξ_1, is then determined by equation 22, and $dM^2/d\xi\,|_{\xi=\xi_1}$ and $d\varepsilon/d\xi\,|_{\xi=\xi_1}$ are found from equations 23 and 21, respectively. The positions ξ_+ at $M^2 = 1 + \delta$ and ξ_- at $M^2 = 1 - \delta$ are found from the relations

$$\frac{\delta}{\xi_1 - \xi_-} = \frac{\delta}{\xi_+ - \xi_1} = \left.\frac{dM^2}{d\xi}\right|_{\xi=\xi_1} \quad (24)$$

and then the corresponding values of ε are determined by the analogous relation

$$\frac{\varepsilon_- - \varepsilon_1}{\xi_- - \xi_1} = \frac{\varepsilon_+ - \varepsilon_1}{\xi_+ - \xi_1} = \left.\frac{d\varepsilon}{d\xi}\right|_{\xi=\xi_1} \quad (25)$$

Here δ is, of course, taken to be a small quantity, viz., $\delta \simeq 10^{-3}$. For any assumed value of ε_1 we may thus obtain all properties at $M^2 = 1 + \delta$. A step-wise numerical integration may then be performed. The integration is carried out from $M^2 = 1 - \delta$ until the condition $\varepsilon = 0$ is reached, and from $M^2 = 1 + \delta$ to $\varepsilon \simeq 1$. In this way a physically meaningful solution is obtained without iteration; both the initial Mach number, M_0, and the initial area, A_0, are determined by the choice of ε_1.

Choice of ε_1—The solution considered in the previous sub-section ('Heat release at sonic plane') indicates that ε_1 should be large for best performance. This conclusion is supported by the fact that, for typical values of other parameters, a real solution to equation 23 for $dM^2/d\xi\,|_{\xi=\xi_1}$ exists only when $\varepsilon_1 \geqslant 0{\cdot}2$ for $\theta = 1$ and $\varepsilon_1 \geqslant 0{\cdot}7$ for $\theta = 10$. It is also apparent from equation 23 that the constant of proportionality between $dM^2/d\xi\,|_{\xi=\xi_1}$ and the logarithmic derivative of $\mathbf{A}$ increases from about unity to infinity as ε_1 increases from its minimum value to unity. Reference to equation 22 shows that in the special case $\mathbf{A}^{n-1} \simeq K\xi$, the value of ε_1 is completely determined by K, γ, α, and θ. In general, in order to maintain the sonic plane at a given position (i.e., keep the left-hand side of equation 22 constant) it is seen that we must decrease ε_1 as the initial stagnation temperature (α) is increased. An increase in θ requires a decrease in ε_1; on the other hand, an increase in β tends to increase ε_1 for given $A(x_1)$. Since the heat of reaction appears in the denominator of β, increasing q tends to decrease ε_1.

Methods of obtaining approximate solutions to simplified problems

We shall now consider the case of a second-order reaction ($n = 2$) with zero activation energy ($\theta = 0$). After describing an iterative method for obtaining an approximate solution, we carry out a first iteration and infer some approximate design criteria.

Equations for approximate solution—When $n = 2$ and $\theta = 0$, equations 20 and 21 may be simplified by introducing a new distance variable, η, defined as $d\eta \equiv d\xi/\mathbf{A} = \beta dx/A$. If $d\mathbf{A}/d\xi \equiv \mathbf{A}'(\eta)$, then equations 20 and 21 become, respectively,

$$\frac{dM^2}{d\eta} = \frac{M^2\left(1 + \frac{\gamma-1}{2}M^2\right)}{1 - M^2} \times \left[\frac{(1+\gamma M^2)\left(1+\frac{\gamma-1}{2}M^2\right)}{M^2}\frac{(1-\varepsilon)^2}{(\alpha+\varepsilon)^2} - 2\mathbf{A}'\right] \quad (26)$$

and

$$\frac{d\varepsilon}{d\eta} = \frac{(1-\varepsilon)^2}{(\alpha+\varepsilon)}\frac{\left(1+\frac{\gamma-1}{2}M^2\right)}{M^2} \quad (27)$$

Furthermore, from equations 22 and 23,

$$\frac{1}{A_1}\left.\frac{dA}{d\eta}\right|_{\eta=\eta_1} = \mathbf{A}_1' = \left(\frac{\gamma+1}{2}\right)^2\frac{(1-\varepsilon_1)^2}{(\alpha+\varepsilon_1)^2} \quad (28)$$

and

$$\left.\frac{dM^2}{d\eta}\right|_{\eta=\eta_1} = \mathbf{A}_1'\left[\frac{(2-\gamma)}{2} + \left\{\left(\frac{2-\gamma}{2}\right)^2 + \frac{4(1+\alpha)}{1-\varepsilon_1} + \frac{(\gamma+1)}{(\mathbf{A}_1')^2}\frac{d}{d\eta}\left(\frac{1}{A}\frac{dA}{d\eta}\right)\right|_{\eta=\eta_1}\Bigg\}^{\frac{1}{2}}\right] \quad (29)$$

Equations 26 and 27 with the condition expressed by equation 28 may be solved approximately by either expansion or iteration procedures.

Since an iterative process performed with an integral equation usually converges more rapidly, it is convenient in practice to write the equations in integral form. The integral of equation 26 is

$$-\ln\left[\frac{1}{M^2}\left(\frac{2}{\gamma+1}+\frac{\gamma-1}{\gamma+1}M^2\right)^{(\gamma+1)/(\gamma-1)}\right] = \int_{\eta_1}^{\eta}\frac{(1-\varepsilon)^2}{(\alpha+\varepsilon)^2}\frac{(1+\gamma M^2)\left(1+\frac{\gamma-1}{2}M^2\right)}{M^2} \times d\eta - 2\ln\left(\frac{A}{A_1}\right) \quad (30)$$

whereas equation 27 becomes

$$\left(\frac{1+\alpha}{1-\varepsilon_1}\right)\left(\frac{\varepsilon-\varepsilon_1}{1-\varepsilon}\right)+\ln\left(\frac{1-\varepsilon}{1-\varepsilon_1}\right) = \int_{\eta_1}^{\eta}\frac{1+\frac{\gamma-1}{2}M^2}{M^2}\,d\eta \quad (31)$$

Equations 30 and 31 constitute the desired integral representations.

General method of iterative solution—The iterative solution to equations 30 and 31 may be started by assuming a reasonable function $M^2(\eta)$. This function is to be chosen in such a way that it increases from a value less than unity to a value greater than unity as η goes to infinity. The value of η_1 is determined by setting $M^2(\eta_1) = 1$. Equation 28 may then be used to determine ε_1. The zeroth approximation to $\varepsilon(\eta)$ is obtained by substituting the assumed function $M^2(\eta)$ into the integral in equation 31. Performing the integration and solving the resulting equation for $\varepsilon(\eta)$ yields the desired function. Next these two trial functions $M^2(\eta)$ and $\varepsilon(\eta)$ are substituted into the integral in equation 30. Performing the integration and solving for M^2 yields the first approximation to $M^2(\eta)$. The first approximation to $\varepsilon(\eta)$ may then be obtained by substituting the first approximation for $M^2(\eta)$ into the integral in equation 31. Continuing this process, higher approximations to $M^2(\eta)$ and $\varepsilon(\eta)$ may be obtained which will rapidly converge to the correct solution. The integrals are expected to assume complicated forms and numerical integrations will become necessary. However, for a judicious choice of the initial trial function, accurate values of $M^2(\eta)$ and $\varepsilon(\eta)$ will be obtained in the first iteration.

An approximate iterative solution—In order to carry out the procedure described above, we may assume a zeroth approximation which will yield $\varepsilon(\eta)$ in the form

$$\varepsilon = \frac{\eta-\eta_0}{\eta} \quad (32)$$

This function has the property of increasing monotonically from zero at the injector ($\eta = \eta_0$) to (nearly) unity far downstream. The corresponding zeroth approximation for $M^2(\eta)$ may be obtained by substituting equation 32 into equation 27. We thus find

$$M^2 = \frac{\eta}{\eta\left[\frac{\alpha+1}{\eta_0}-\frac{\gamma-1}{2}\right]-1} \quad (33)$$

The requirement that $\eta = \eta_1$ at $M^2 = 1$ yields the following relation:

$$\eta_1 = \frac{1}{\frac{1+\alpha}{\eta_0}-\frac{\gamma+1}{2}} \quad (34)$$

By substituting these zeroth approximations into equation 30 we obtain, after some manipulations, the first approximation to M^2, viz.,

$$F(M^2) = \frac{1}{M^2}\left(1+\frac{\gamma-1}{2}M^2\right)^{(\gamma+1)/(\gamma-1)} = \left(\frac{A}{A_1}\right)^2\eta\eta_1\frac{\left[\eta\left(\frac{\gamma+1}{2}\eta_1+1\right)-\eta_1\right]^{(\gamma+1)/(\gamma-1)}}{[\eta(\eta_1+1)-\eta_1]^{2\gamma/(\gamma-1)}} \quad (35)$$

A numerical or graphical solution of equation 35 for $M^2(\eta)$ finally yields the desired first approximation. The first approximation to $\varepsilon(\eta)$ may then be obtained by substituting the result into equation 31 and integrating numerically. While equation 34 gives η_0 in terms of η_1, it is necessary to use equation 28 to determine the value of η_1 to be used in equation 35. By substituting equations 32 and 34 into equation 28 we find that

$$\left.\frac{\eta_1^2}{A_1}\frac{dA}{d\eta}\right|_{\eta=\eta_1} = 1 \quad (36)$$

Wedge-like nozzles, $n = 2$, $\theta = 0$

We shall now apply the analysis described in the previous sub-section to wedge-like nozzles in order to obtain performance results and a design criterion.

Design criterion—For the special case in which the nozzle area increases linearly with the physical distance downstream, we may define the constant K^2 as $d\mathbf{A}/d\xi$, whence it follows that $dA/dx = \beta K^2$. Eliminating ξ in terms of η we obtain the results

$$\frac{1}{A}\frac{dA}{d\eta} = K^2 \quad (37)$$

and, in view of equation 36,

$$\eta_1 = \frac{1}{K} \quad (38)$$

The solution to equation 37 is

$$\ln\left(\frac{A}{A_1}\right) = K^2\eta - K \tag{39}$$

which may be substituted into equation 35 to yield an explicit expression for $M^2(\eta)$. From equations 34, 38 and 39 we find

$$\ln\left(\frac{A_0}{A_1}\right) = \frac{K^2\alpha - K\dfrac{\gamma+1}{2}}{K + \dfrac{\gamma+1}{2}} \tag{40}$$

Since A increases linearly with x, equation 40 shows that we must have

$$\frac{\gamma+1}{2\alpha} > K \tag{41}$$

for a solution to be possible. Substituting the physical quantities for K, β, and α (see equations 16 and 17), the inequality 41 becomes

$$\frac{(\gamma+1)^2}{2(\gamma-1)}\frac{q}{h_0}\frac{B}{W^{n-1}}\frac{m}{h_0} > \frac{\mathrm{d}A}{\mathrm{d}x} \tag{42}$$

Equation 42 shows that the heat of reaction and the reaction rate must be sufficiently large, compared with the rate of expansion, for supersonic flow to be possible. The magnitude of the terms in equation 42 is modified somewhat by including first and higher approximations for $\varepsilon(\eta)$. For typical values, the left-hand side of equation 42 is of the order of 10^3 cm, thus indicating that chemical reaction rates will usually be sufficiently rapid to allow extremely large expansion angles.

Performance results—Since η varies over wide limits, whereas ε is always between zero and unity, it is convenient to replace η by ε in order to present the performance results for wedge-like nozzles. Equation 32 may be solved for η as a function of ε. If use is made of equations 28, 36 and 34 to eliminate η_0 and η_1, then the relation

$$\eta = \left(\frac{2}{\gamma+1}\right)\left(\frac{\alpha+\varepsilon_1}{1-\varepsilon}\right) \tag{43}$$

is obtained. From equations 38, 39 and 43 it may be shown that

$$\frac{A}{A_0} = \exp\left[\left(\frac{\gamma+1}{2}\right)\frac{(1-\varepsilon_1)^2}{\alpha+\varepsilon_1}\left(\frac{\varepsilon}{1-\varepsilon}\right)\right] \tag{44}$$

By substituting equations 43 and 44 into equation 35, we obtain the expression

$$F(M^2) = \left(\frac{2}{\gamma+1}\right)(\alpha+\varepsilon_1) \times \exp\left\{(\gamma+1)\frac{(\varepsilon-\varepsilon_1)(1-\varepsilon_1)}{(\alpha+\varepsilon_1)(1-\varepsilon)} + \left(\frac{\gamma+1}{\gamma-1}\right)\ln(\alpha+\varepsilon) - \left(\frac{2\gamma}{\gamma-1}\right)\ln\left[(\varepsilon-\varepsilon_1) + \left(\frac{2}{\gamma+1}\right)(\alpha+\varepsilon_1)\right]\right\} \tag{45}$$

If we denote the right-hand side of equation 45 by $f(\varepsilon)$, then the solution for $M^2(\varepsilon)$ in the first iteration is determined by

$$F(M^2) = f(\varepsilon) \tag{46}$$

The numerical solution has been carried out in the following manner. Values for the parameters γ, α, and ε_1 were selected. In view of equation 28, these parameters define $\mathbf{A}_1$, i.e., a definite value of the ratio of the rate of divergence of the nozzle to the chemical length. Next $F(M^2)$ was computed and plotted as a function of M^2. Finally $f(\varepsilon)$ was calculated and, in view of equation 46, $M^2(\varepsilon)$ was then obtained directly from the graph of $F(M^2)$ *versus* M^2.

Using equations 11 and 13 we may define a dimensionless velocity, V, and a dimensionless pressure, P, by the relations

$$V \equiv \frac{v}{\sqrt{q}} = \left[\frac{M^2(\gamma-1)(\alpha+\varepsilon)}{1+\dfrac{\gamma-1}{2}M^2}\right]^{1/2} \tag{47}$$

and

$$P \equiv \frac{pA_0}{m\sqrt{q}} = \left[\frac{(\gamma-1)(\alpha+\varepsilon)}{\gamma^2M^2\left(\dfrac{A}{A_0}\right)^2\left(1+\dfrac{\gamma-1}{2}M^2\right)}\right]^{1/2} \tag{48}$$

Equations 47 and 48 determine the velocity and pressure as functions of the distance along the nozzle. After having obtained $M^2(\varepsilon)$ according to the procedure described in the preceding paragraph, A/A_0 was computed from equation 44; next P was evaluated according to equation 48 and V was then determined by the use of equation 47.

Calculations have been carried out for $h_0/q = \alpha = 0{\cdot}1$ with ε_1 equal to 0·1, 0·3, 0·5, 0·7 and 0·9. The parameter M^2 is plotted against ε for each value of ε_1 for $\gamma = 1{\cdot}2$ in *Figure 6*. In *Figure 7* plots are shown for P as a function of the dimensionless distance A/A_0 for different values of ε_1 with $\gamma = 1{\cdot}2$. In *Figure 8* the dimensionless velocity V is shown as a function of the dimensionless pressure P for various values of ε_1 with $\gamma = 1{\cdot}2$, while in *Figure 9* the parameter V is plotted against the area ratios A/A_0. Results similar to those shown in *Figures 6* to *9* have been obtained for $\gamma = 1{\cdot}3$.

In order to indicate representative dimensionless values, scales giving the pressure (in atm) as a function of area ratio are shown on the right-hand side of *Figure 7* and scales of the velocity (in ft./sec) are given on the right-hand side of *Figure 9*. The

scale denoted by A corresponds to a heat of reaction $q = 2{,}220$ cal/g while the scale B applies for $q = 555$ cal/g. Both scales A and B have been computed for the mass flow rate per unit injector area, m/A_0, equal to 4·72 lb./in.^{2} sec. It is apparent from equations 47 and 48 that the velocity scale (see *Figure 9*) is independent of the mass flow rate per unit area; on the other hand, the pressure (see *Figure 7*) is directly proportional to m/A_0.

If the reaction rate, nozzle divergence angle, and exit pressure are known, then the specific impulse of an ideally expanded nozzle may be obtained directly from *Figure 8*. The nozzle divergence angle and the reaction rate are first used to compute $\mathbf{A}_1$ and ε_1; P is computed from the exit pressure; P and ε_1 then determine V according to *Figure 8*. The exit velocity may be computed by using the definition of V. The specific impulse is given, as usual, by the ratio of exit velocity to the acceleration of gravity.

Concluding remarks

Our analytical formulations and results should not be applied to bi-propellant liquid-fuel rocket engines since the important assumption that we are dealing with pre-mixed gaseous reactants has

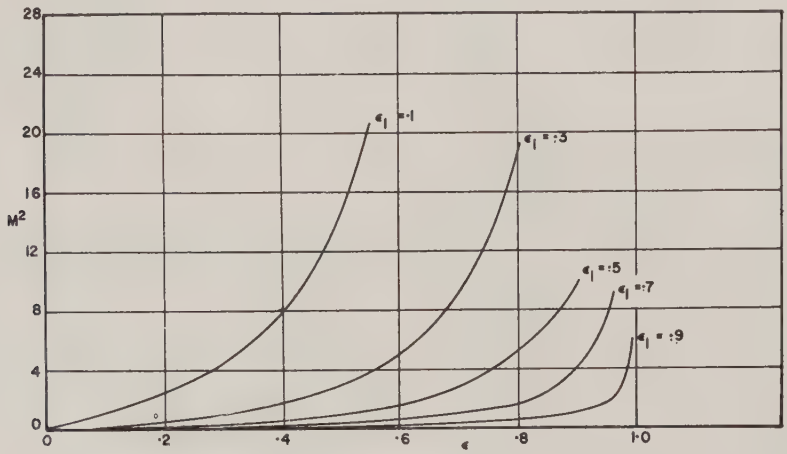

Figure 6. The square of the Mach number M^2 as a function of ε for various values of ε_1 and $\gamma = 1{\cdot}2$

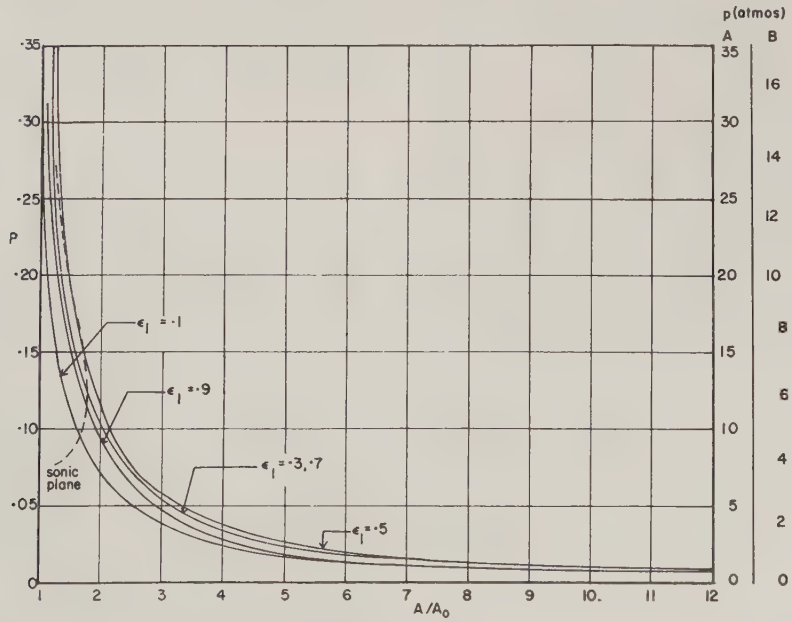

Figure 7. The dimensionless pressure P as a function of the area ratio A/A_0 for various values of ε_1 and $\gamma = 1{\cdot}2$

been used. The experimental data described previously (in pp. 713–722) refer to a heterogeneous bipropellant system. A complete analytical evaluation of a reactor of this type is in progress and will be described in a subsequent publication. The analysis of heterogeneous combustion is not possible at the present time in view of our limited knowledge of spray formation and burning. It is, therefore, interesting to attempt correlation of the experimentally determined pressure profiles in terms of a simplified analytical description which is again strictly applicable only to pre-mixed gaseous reactants. This problem is considered in detail in the following section.

We note that implicit in the plots of results shown in *Figures 6* to *9* is an engine evaluation programme. A comparison between a diverging reactor and a conventional engine, from the point of view of optimizing thrust for a given mass flow rate, is beyond the scope of the present investigations.

CORRELATION OF MEASURED PRESSURE PROFILES IN TERMS OF SECOND-ORDER OVERALL REACTION RATES FOR PRE-MIXED GASEOUS PROPELLANTS

The equation for conservation of momentum may be written in the form

$$\frac{dv}{dx} = -\frac{A}{m}\frac{dp}{dx} \tag{49}$$

It is apparent that measurements of $p(x)$ determine

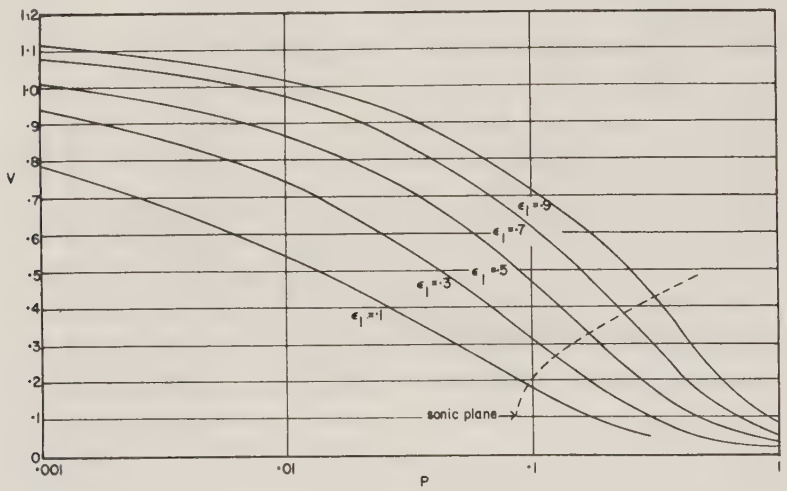

Figure 8. The dimensionless velocity V as a function of the dimensionless pressure P for various values of ϵ_1 and $\gamma = 1{\cdot}2$

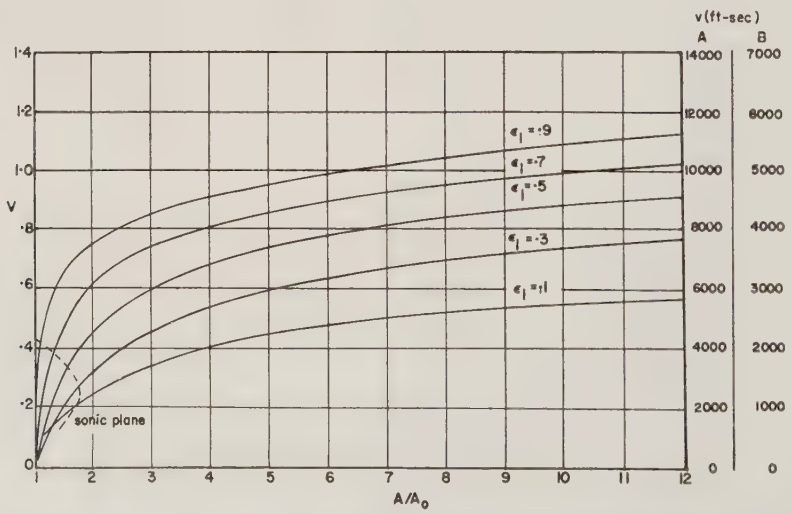

Figure 9. The dimensionless velocity V as a function of the area ratio A/A_0 for various values of ϵ_1 and $\gamma = 1{\cdot}2$

both dv/dx and $v(x)$ for given total mass flow m and specified $A(x)$. From $v(x)$ we may compute

$$\rho(x) = \frac{m}{v(x)A(x)} \tag{50}$$

Next we obtain a first estimate for $T(x)$ through the equation of state by assuming a suitable effective average molecular weight

$$\bar{W}(x) = \sum_{\mathrm{K}} W_{\mathrm{K}} X_{\mathrm{K}}(x) \tag{51}$$

The mole fraction X_{K} is related to the mass fraction Y_{K} through the expression

$$Y_{\mathrm{K}}(x) = \frac{p(x)}{\rho(x)RT(x)} W_{\mathrm{K}} X_{\mathrm{K}}(x) \tag{52}$$

According to the ideal gas law,

$$T(x)^1 = \frac{\bar{W}p(x)}{R\rho(x)} \tag{53}$$

represents a first estimate for the temperature profile if $\bar{W}$ is the effective average molecular weight.

In the absence of axial heat conduction and diffusion, the energy equation may be rewritten as

$$\frac{v^2}{2} = \sum_{\mathrm{K}} (Y_{\mathrm{K},0} - Y_{\mathrm{K}}) h^{\circ}_{\mathrm{K}} - \bar{c}_p(T - T_{st}) \tag{54}$$

if T_{st} is the initial stagnation temperature corresponding to $Y_{\mathrm{K}} = Y_{\mathrm{K},0}$. In equation 54 let $Y_{\mathrm{O}} = Y_{\mathrm{O},0} - Y$, $Y_F = Y_{F,0} - \nu Y$ and $Y_P = 1 - Y_{\mathrm{O}} - Y_F = Y_{P,0} + (1 + \nu)Y$ where Y measures the extent of the overall chemical reaction and ν is the mass of fuel converted for unit mass of oxidizer. Then

$$\sum_{\mathrm{K}} (Y_{\mathrm{K},0} - Y_{\mathrm{K}}) h^{\circ}_{\mathrm{K}} = qY \tag{55}$$

where

$$q = h^{\circ}_{\mathrm{O}} + \nu h^{\circ}_F - (1 + \nu) h^{\circ}_P \tag{56}$$

Equation 54 may be solved for Y with the result

$$Y = \frac{1}{q}\left[\frac{v^2}{2} + \bar{c}_p(T - T_{st})\right] \tag{57}$$

Since the constants $\bar{c}_p$ and q are known for a given chemical system, we may use equation 57 to obtain a first estimate for $Y(x)^{(1)}$ using the known relations for $v(x)$ and $T(x)^{(1)}$. In this manner the measured pressure profile may be correlated with measured composition profiles in first approximation. Better estimates can be derived for both $T(x)$ and $Y(x)$ by a straightforward iteration procedure using equation 52 for the computation of $X_{\mathrm{K}}(x)$ followed by calculation of $\bar{W}(x)^{(1)}$ through equation 51, $T(x)^{(2)}$ through equation 53 which appears in the form

$$T(x)^{(2)} = \frac{\bar{W}(x)^{(1)} p(x)}{R\rho(x)} \tag{58}$$

and finally the evaluation of $Y(x)^{(2)}$ according to equation 57 which becomes now

$$Y(x)^{(2)} = \frac{1}{q}\left\{\frac{v^2}{2} + \bar{c}_p[T^{(2)} - T_{st}]\right\} \tag{59}$$

etc.

If diffusion is neglected, the continuity equations for the separate chemical reactants (fuel and oxidizer) become

$$m\frac{dY}{dx} = AB e^{-E/RT} \rho^2 \frac{(Y_{\mathrm{O},0} - Y)(Y_{F,0} - \nu Y)}{W_F} \tag{60}$$

Since all of the quantities entering into equation 60 are known except for B and E, equation 60 may be used for the computation of effective overall reaction rates utilizing only the measured pressure profile. (Another form of equation 60 is, of course, appropriate if fuel and oxidizer do not enter to the first order into the overall rate equation.)

The preceding analysis justifies the following important conclusions:

(1) From measured pressure profiles for premixed gaseous propellants it is possible (with proper allowance for axial heat conduction and diffusion) to determine effective reaction rates.

(2) For a chemical system with known overall reaction rate it is possible to predict the motor length required for complete burning for specified $A(x)$ and m. This last result can be obtained explicitly by inverting our interpretative procedure.

We have used equations 49 to 60 for interpretation of the experimental data summarized in Table 1. In order to obtain a satisfactory fit to the observed pressure profiles, we find it necessary to assume that both a low-activation energy process (i.e., $E \sim 2$ kcal/mole, diffusion control) and a high-activation energy process (i.e., $E \sim 30$ kcal/mole, chemical control) produce propellant conversion. The diffusion controlled processes are of primary importance near the injector end whereas the chemical processes are rate-controlling further downstream (*cf. Figure 10*). Details concerning interpretation of experimental results will be described in a subsequent publication in which we consider also the influence of heterogeneous burning. A notable feature of our analysis is the observation that the supersonic portion of the flow appears to occur under conditions which do not deviate significantly from an isothermal expansion.

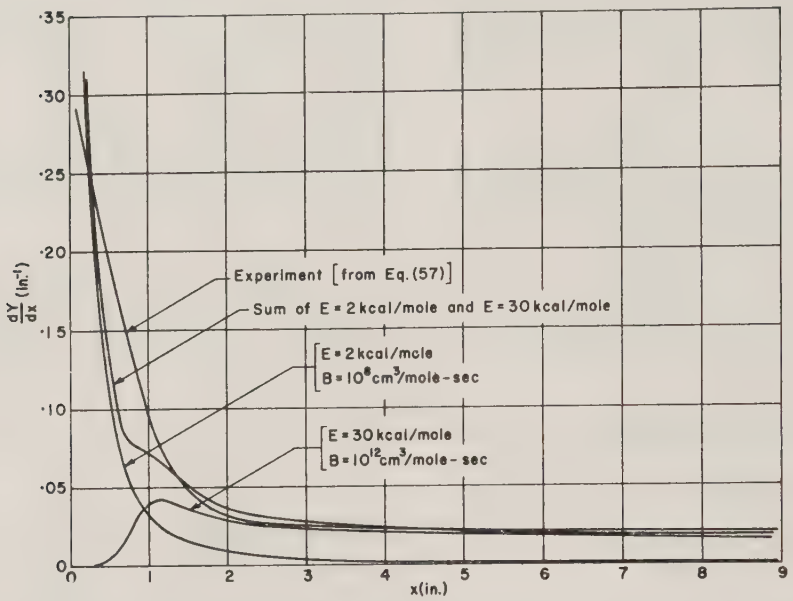

Figure 10. Comparison of the dependence of d*Y*/d*x on x derived from measured pressure profiles with numerical values calculated from equation 60 for various values of E. Note that the frequency factor B occurs as a scale factor and does not influence the* shape *of the* d*Y*/d*x versus x curve*

The experimental work was performed by Rocketdyne, a division of North American Aviation Inc., supported by the United States Air Force.

REFERENCES

[1] Penner, S. S. *Chemistry Problems in Jet Propulsion*, Chap. XXIII. 1957. London; Pergamon Press

[2] Wegener, P. P. *J. aero. Sci.* In press

[3] Penner, S. S. *Chemistry Problems in Jet Propulsion*, Chap. XVIII, 1957. London; Pergamon Press

[4] Hirschfelder, J. O., Curtiss, C. F., Bird, R. B. and Spotz, E. L. *The Molecular Theory of Gases and Liquids*, Chaps. 3, 4, 8 and 9. 1954. New York; Wiley

[5] Zeldovich, Y. B. *Zh. tek. Fiz. Mosk.* 19, No. 10 (1949); translation in *Nat. Adv. Comm. Aero. Tech. Memor.* No. 1296, June 1950

[6] Penner, S. S. and Williams, F. A. *Technical Report No.* 19, *Contract DA* 04-495-*Ord*-446. 1957. Pasadena; California Institute of Technology

[7] Shapiro, A. H. *The Dynamics and Thermodynamics of Compressible Fluid Flow*, Vol. I, Chaps. IV and VII. 1953. New York; Ronald Press

[8] Chambré, P. and Lin, C. C. *J. aero. Sci.* 13 (1946) 537

ADDENDUM

The correlation of experimental data near the injector end has been refined (August, 1958) by using a recently developed theory of spray formation and spray combustion. The effective overall order for the heterogeneous reactions has been found to be close to 2 whereas the mean initial drop diameters required for the correlation of the data turned out to be in the neighbourhood of 10 microns. Details concerning these studies appear in papers by F. A. Williams, *The Apparent Order of Heterogeneous Spray Reactions*, and by G. S. Gill, E. Eckel, F. A. Williams and S. S. Penner, *Heterogeneous Burning in a Diverging Reactor.*

DISCUSSION

MODEL TECHNIQUES
Papers 87, 88, 89

M. W. Thring (*Sheffield*) in opening the discussion said: The use of a relatively enlarged or distorted nozzle to allow for the effect of heating up of a jet of fluid as it is projected into a combustion system is based essentially on two assumptions: first that the angle of spread of the jet is unchanged by the density change, and secondly that the momentum of the jet is conserved to a point where the density has reached nearly the final value. Either of these assumptions may of course be wrong in the open-hearth furnace models, but I am not convinced by the arguments of Hogg, Holden and Siddall that the lack of similarity between the model and the furnace cannot be due to the use of the wrong jet momentum in the model. In our work on jets projected down the axis of a rectangular box we have tended to divide the curve representing the reciprocal of burner fluid concentration (C_b) into two parts. The first part is a straight line through the origin, the slope of which depends purely on the jet momentum or more accurately on the equivalent nozzle diameter —as is shown by the fact that if one plots $1/C_b$ d/L against x/L, where d is the equivalent burner nozzle diameter, L the side of the box, and x the distance from the nozzle, this part of all the curves comes together whatever the jet momentum, provided the flow is fully turbulent. The second part of the curve falls below the continuation of the straight line because of the exhaustion of the amount of air available for mixing, since at infinite distances there is a finite mixing ratio. The shape of this part of the curve therefore depends on the fuel : air ratio supplied to the system. The fact that the curves shown in the paper have three portions rather than the two which we have found is, of course, due to the impact of the jet on the surface.

I therefore tend to attribute the difference in slope in the first part of the authors' curve to the use of an equivalent nozzle diameter or jet momentum which is not appropriate, rather than to a wrong angle of spread, although I admit that the latter would give the same effect. However, I do not think one should postulate this until it is essential.

Turning to the paper by Martin and Webb, I think they have chosen a case on which Spalding's analogue is most likely to succeed. If one were applying the analogue to a pressure jet flame such as in an actual gas turbine combustion chamber, then, to give correct momentum similarity, one should enlarge the diameter of the secondary air jet nozzles on the model by the square root of the ratio of the density of the air going in to that of the flame gases. I am also not fully convinced that this particular analogue is the best method of solving this problem, because I think that a cold aerodynamic model can give the necessary information about the flow pattern and this can then be put into a simple numerical calculation to give the required answer. In particular, the insertion of a tracer at a suitable point downstream, followed by measurements of the resulting concentration of this tracer at the point where the ingoing oil spray is ignited, can give the required information about the stabilization of the flame.

The paper by Lefebvre and Halls provides a very good application of hot model technique with the ingenious idea of replacing the effects of low pressure on the chemistry of the process by the effects of water vapour. The only question I would ask is whether low pressure does not operate by a combination of the physical and chemical processes, each of which requires more room at low pressure. In this case the analogue will not necessarily give the right answer.

As this session relates to model techniques for combustion in practical flowing systems, *Figures 1–4* may be of interest.

E. H. Hubbard (*Sunbury on Thames*): Hogg, Holden and Siddall disagree with Thring on the cause of the discrepancy between the fuel/air mixing as determined in a flame and as observed in an isothermal model of the flame. They suggest that this is due to a change in jet angle as between the two cases, whereas the theory of simple jets suggests that the angle of spread of the jet is constant, and independent of any density or temperature differences between the jet and its surroundings.

It should be emphasized that the discrepancy under discussion, although of fundamental scientific interest, is not a serious handicap to the industrial application of the technique described by the authors for the solution of furnace problems. I feel myself that the gases which issue from the burner nozzle in the flame do have an angle of spread which is the same as that obtained with an isothermal jet, but that the oil droplets do not necessarily have the same angle. *Figure 5* shows the axial air : fuel ratio for 3 oil flames studied by the International Flame Research Foundation.

Figure 1. Models of mixing to indicate flame length in coke oven flues where the similarity criterion must be equality of Reynolds number both at the air and gas inlet, and at the flue, with appropriate geometrical distortion of the former

Figure 2. Model work in which the effect of buoyancy is introduced to model the buoyancy effects on jet flames in furnaces

Figure 3. Flow pattern for oil combustion flames passing down through the brickwork in a rectangular kiln

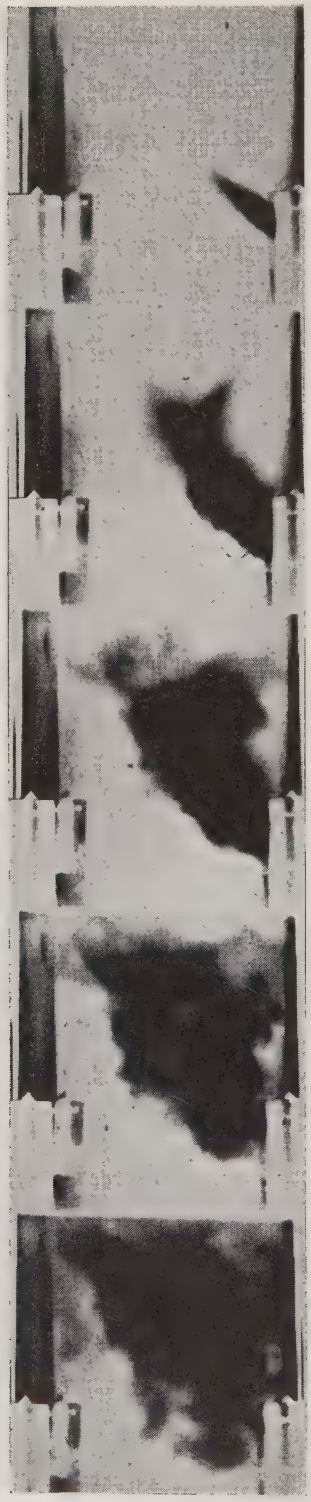

Figure 4. Spread of a pulse indicator through a model of the combustion chamber of a pulverized fuel, corner fired water tube boiler

These experiments are mentioned by the authors. It will be seen that for cases 1 and 3 the same type of differences between hot flame and cold model appears as is mentioned by them. In case 2 the difference is smaller and it is interesting to note that the values for hot flame and isothermal model are almost indistinguishable.

Let us now extrapolate this argument in the other direction to the case where the flame contains a large number of heavy particles as, for

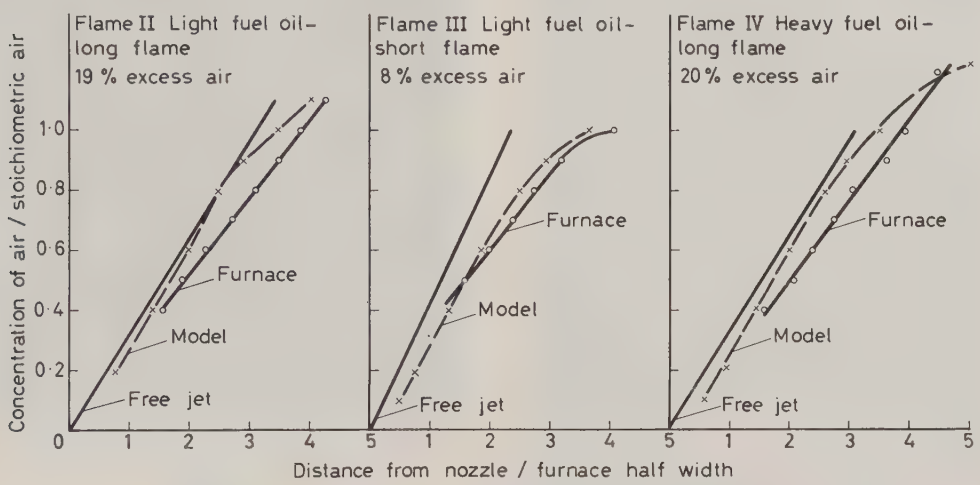
Flame II Light fuel oil-long flame
19 % excess air
Flame III Light fuel oil-short flame
8 % excess air
Flame IV Heavy fuel oil-long flame
20 % excess air
Concentration of air / stoichiometric air
Furnace
Model
Free jet
Distance from nozzle / furnace half width

Figure 5. Comparison of mixing conditions between furnace and cold model

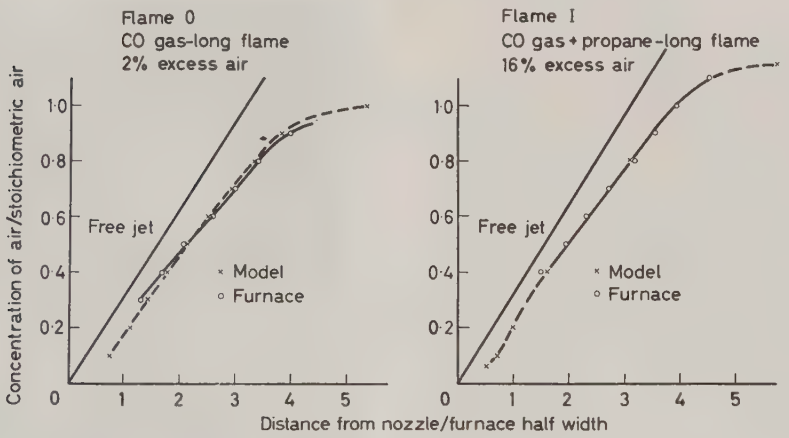

Figure 6. Comparison of mixing conditions between furnace and cold model

that the jet momentum in case 2 was about twice that in cases 1 and 3. In order to increase the momentum of a fluid atomized flame, steam at a higher pressure is used or else more steam is used at the same pressure. It is possible that this may change the degree of atomization of the oil. Quite apart from this it is a well established fact that a high momentum flame contains a smaller number of solid soot particles.

If it be assumed that the presence of particles in the flame is the cause of the discrepancy, then the case of a flame without particles in it should give no such difference. *Figure 6* shows the results for 2 gas flames studied at the same time as the 3 oil flames mentioned above, and here it can be seen

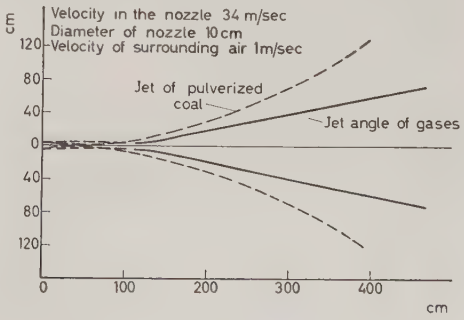

Figure 7. Angle of spread of a jet of pulverized coal compared with that of the air that carries it

example, a flame of pulverized coal. This has been studied for a case with similar aerodynamic geometry and *Figure 7* shows the results. It will be seen that the distribution of the gases, in this case a stream of transport air, is roughly as would be expected from single jet theory; that is after an initial zone the jet spreads with constant angle and the radial distribution is roughly gaussian. A study of the particles in this case is easier than in an oil flame because it is possible to use the ash in the coal as a tracer. Here the distribution of ash is more nearly triangular than gaussian and the angle of spread increases with distance from the burner. The reason for this behaviour of the ash is suspected to be due to a slight turning movement of the jet stream, but it is not relevant to the pressure discussion. What is relevant is the fact that in this case the gases and particles are not following the same path.

The authors have, of course, used a chemical balance on the elements of carbon, oxygen, hydrogen and nitrogen in order to calculate the fuel/air mixing in the flame, as have many other workers in this field. Care must be exercised in interpreting these results, however, if for example one of these elements is present in both the solid and the gaseous phases and these phases are travelling by different paths.

A. E. Clarke (Burnley): The hydraulic flow visualization technique using air as a tracer has been used in the Burnley Laboratories over a number of years and in spite of any theoretical objections that may be raised, such as density changes, the technique has proved invaluable in combustion chamber research and development.

As an example of its recent use, the method has been employed to visualize the degree of mixing in the spherical combustor. Flow patterns obtained from a two-dimensional model confirm that a strong re-circulation was associated with a high maximum heat release rate (as illustrated in *Figures 8–12*). The results also suggest that the spherical combustor is imperfectly stirred and to some degree more heterogeneous than had previously been thought.

C. Holden (Rotherham); After presenting our paper the following comments are made in the light of more recent work.

Recent velocity measurements at 9 ft. from the burner tip showed the diameter of the flame at this section to be 32 in. Assuming that the jet originates from the nozzle, this gives a jet angle of between 16 and 17° which is in accordance with the value given in the paper.

The nozzle of the burner used on the actual furnace had a convergent-divergent profile and the estimated exit velocity of the steam was about 3,000 ft./sec. On the other hand the nozzle used in the model was a simple convergent type giving an exit velocity for the air of a little over 1,500 ft./sec.

Figure 8. Two-dimensional hydraulics flow model. Longwell sphere, 68 holes (42 holes blanked off)

Figure 9. Two-dimensional hydraulics flow model. Cylindrical injector (type 4), 68 holes (42 blanked off)

It has been shown by Anderson and Johns* that, neglecting the effect of the oil droplets, even with the supersonic furnace jet the potential core

* Anderson, A. R. and Johns, D. R. Characteristics of free supersonic jets exhausting into quiescent air. (Work carried out at the U.S. Naval Air Development Centre, Johnsville, Pa.) *Jet Propulsion* 25 (1955).

Figure 10. Two-dimensional hydraulics flow model. Cylindrical injector (type 4), 12 holes (8 blanked off)

Figure 11. Two-dimensional hydraulics flow model. Cylindrical injector (type 4), 3 holes (2 blanked off)

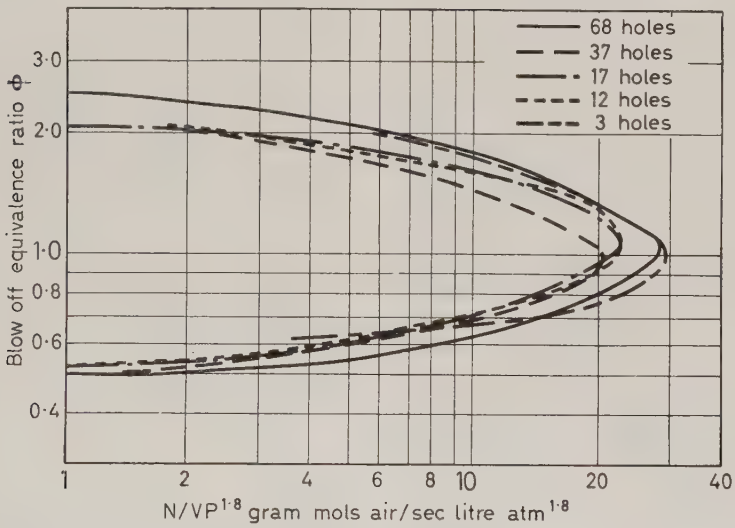

Figure 12. Comparison of blow-off curves for several injectors. Total hole area constant

should not extend more than 15 in. downstream of the outlet: this is in fact almost the same as the equivalent length of the potential core in the model. Also, as can be seen from the graphs in *Figure 7* in our paper, the length of the potential core would have to be about 3 to 4 ft. to explain the difference in axial mixing. This does not seem feasible if we consider the action of the steam alone, but it must be remembered that in the early regions of the jet the oil droplets have an effective entraining power much less than an equivalent mass of gas with the same momentum. This could give rise to the apparent displacement of the origin.

The difference in the velocities of the nozzle fluids in furnace and model will also be important in determining the mass diffusing outwards at each section of the jet. *Figure 12* in our paper compares eddy diffusivities which should, of course, be weighted with velocities for each condition studied. Because of this, the difference in rates of entrainment is even greater than the ratio of the

eddy diffusivities would suggest: also, if velocities are taken into account, it transpires that when working with an air temperature at the nozzle of 0°C and a surrounding temperature of 60°C (condition *c*, *Figure 12*) the decrease in velocity brought about by the cooling of the nozzle fluid more than offsets the decrease in eddy diffusivity, resulting in even faster mixing. This has been substantiated by more recent work on a model at these conditions.

Therefore, we conclude that the time scale in the model must be reduced. This could possibly be achieved by the use of a convergent-divergent nozzle which would increase the velocity or perhaps by distorting the model.

Replying to the remarks of Thring, we have carefully measured the burner thrusts on both model and furnace. On the basis of the similarity criteria put forward by Thring at the Fourth Symposium on Combustion, these were equivalent.

Referring to the point made by Hubbard, I agree that the effect of the oil droplets should not be ignored but unfortunately, as yet, we have no estimation of the magnitude of the effect. What we have found is that for the same nozzle pressure a convergent-divergent nozzle gives a greater thrust, while a simple convergent nozzle gives a greater initial entrainment. We are sure that this is because with a convergent-divergent nozzle the oil droplets are accelerated to a higher velocity and therefore carry a larger share of the momentum than in the case of the simple convergent nozzle.

A. Hogg (Rotherham): In reply to Thring's comment that the difference in entrainment rates between the model and the furnace could be explained by a difference in thrust rather than a difference in jet angle, I should like to emphasize that the evidence supporting our conclusions is threefold. First, as has been shown in equation 15, the regression line which will be obtained if too high a value of thrust was assumed is an approximate straight line, whereas that obtained has a definite curvature (*Figure 8*). Secondly, the predicted angle of the furnace jet when a regression line of the form of equation 19 is assumed is about 16°, which agrees well with both the visual jet angle and the angle which has recently been determined from a velocity traverse of an actual furnace flame. Thirdly, we have used conditions in the model which correspond to those of curve *c* in *Figure 12*, in which the rate of entrainment in the model was greater than that when the conditions were similar to *a*. In this case, the momenta of the two jets were the same and the difference in entrainment rates is explicable using equation 6 weighted with a velocity factor. Thus, although the evidence in each particular case may not be conclusive, taken together the facts substantiate our conclusions that the difference in entrainment rate is not due to a difference in thrust, but is due to a difference in jet angle between furnace and model.

E. E. Zukoski (California): The thermal balance model of flame stabilization, on which the analogue discussed by Martin and Webb is based, is in apparent disagreement with much of the existing experimental data concerning flame stabilization. Hence it would have been more useful if the authors had examined the basis for the analogue rather than its application to a complex burner design.

In addition, the use of the analogue for pre-

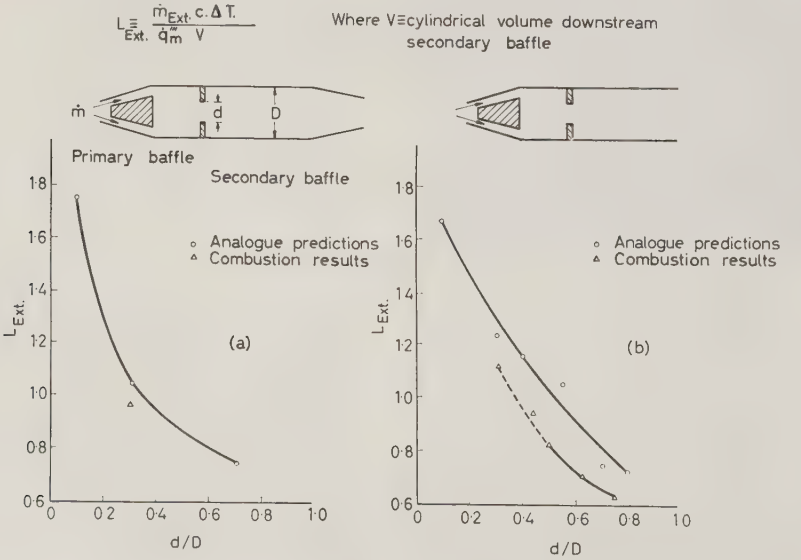

Figure 13

diction of the stability limits of baffle flame-holders is inappropriate even if the assumption is made that the stabilization model is correct. This contention is based on the well established fact that the flow field about a baffle is greatly modified when combustion is initiated. For example, consider the flow about a circular cylinder. For high Reynolds numbers, vortices are shed from the cylinder to form the familiar Kármán vortex street, and the more or less stagnant region just downstream of the cylinder is of the order of one diameter in length. In contrast, when a flame is attached, no vortices are shed and the stagnant zone is as much as ten diameters long. The baffle drag coefficient is changed from about 1·2 for no combustion to 0·75 with combustion. Thus, the change in the general flow pattern is of a gross nature and the change in length of the stagnant region, which is the critical zone for stabilization, is of the order of one magnitude.

These general remarks are directly applicable to the particular burner model discussed by Martin and Webb. The flow without combustion cannot be considered to be even approximately similar to the flow with combustion and, therefore, application of the analogue is not valid even if the suspect stabilization model were correct.

Abdulla El-Bahadli (London): Further work has been carried out on the axi-symmetrical analogue for high intensity combustion chambers built by Joseph Lucas, Ltd., with the view of obtaining a quantitative comparison of its predictions with the results on the 2 in. flame tube quoted by the authors.

The comparison is indicated in *Figure 13 a and b* which are for chambers whose wall geometries differ as shown by the sketches above the respective graphs. At the exit of the chamber in *Figure 13a* there is a cone to limit the entrainment of air from the surroundings which takes place in the chamber in *b*.

The graphs show the effect of changing the geometry of the secondary annular baffle (d/D) on the loading factor at extinction ($L_{\text{ext.}}$). It is seen that the analogue prediction is higher than the flame tube results by up to 26 per cent in the case of the chamber in *Figure 13b* and by about 8 per cent in the case of the chamber in *Figure 13a*, at the available point at $d/D = 0{\cdot}3125$.

Another point to be noted is that for the same d/D, the extinction loading factor for the chamber in *Figure 13a* is mainly lower than for the chamber in *b*. This effect is both predicted by the analogue and suggested by the flame tube results. It may be connected with the failure of both the analogue and the flame tube to accommodate the whole length of the flame behind the secondary baffle.

The predictions of the analogue when $L_{\text{ext.}}$ for the flame tube was calculated using the results of Longwell and Weiss from their spherical reactors, agreed with the combustion chamber results both qualitatively and quantitatively. Further quantitative comparisons are of course needed and present work on the analogue takes note of this need.

A. H. Lefebvre (Derby): The authors have used Spalding's analogue to demonstrate that flame stability improves as the size of baffle is increased. Surely this result could have been predicted from a knowledge of the *modus operandi* of the analogue without recourse to actual experiment?

There are many sound technical reasons why this analogue should not work, and it is hoped that those who advocate its use will soon provide a much more convincing demonstration of its potentialities than is afforded in the experiments reported in this paper.

A. E. Clarke (Burnley): Some of the original testing of the Spalding analogue for a single stream chamber was carried out in the Burnley Laboratories. Originally, the analogue results were in direct variance to the combustion ones: however, later work indicated that the limited range of test conditions had not given a true picture and the more detailed work showed the analogue to be in agreement with the combustion results. Thus, it would appear that qualitatively the analogue will predict relative stability in the one-stream chamber.

The practical difficulties experienced, however, in setting up and operating the analogue has led to the opinion that it would probably be quicker to manufacture the actual combustion chamber and test it than to use this technique.

D. B. Spalding (London): In answer to Thring, I agree that the system considered may be particularly favourable. Tests have shown that predictions for centrally mounted baffles show poorer absolute agreement with real flames, but good qualitative agreement. The analogue programme is designed to establish the area of validity of the method.

In answer to Zukoski, I agree that differences exist between hot and cold flows. This qualitative information was well known before the analogue programme started. The programme is intended to establish the *magnitude* of differences: are they sufficiently small for predictions based on cold models to agree with combustion experiments? Results by Martin and Webb and El-Bahadli suggest an affirmative answer in the case considered.

Answering a question by Weinberg, the analogue is incapable of correctly predicting the propagation of confined turbulent flames, since these are dominated by density differences which are not simulated by the analogue.

J. W. Useller (Cleveland): Lefebvre's study parallels an investigation we conducted at the N.A.C.A. several years ago in which water vapour was introduced into a full-scale turbo-jet engine after-burner.

Our results showed not only a decrease in combustion efficiency and stability limit as the water : air ratio was increased, but also a dependence of this decrease in performance on the equivalence ratio and hence the temperature.

For this reason I would like to suggest that there is an effect on the reaction kinetics of the combustion process, as well as the thermodynamic effect discussed in the paper. This is supported by early work by Lewis and von Elbe that demonstrated an influence of water vapour on the combustion reaction. Therefore, I submit that the proposed analogue may not be entirely suitable for simulation of combustion operation under reduced pressure conditions. Our results were published in *Jet Propulsion* several years ago.

P. Eisenklam (London): Lefebvre and Hall make an important reservation in their conclusions by saying that 'this simulation technique *cannot* be

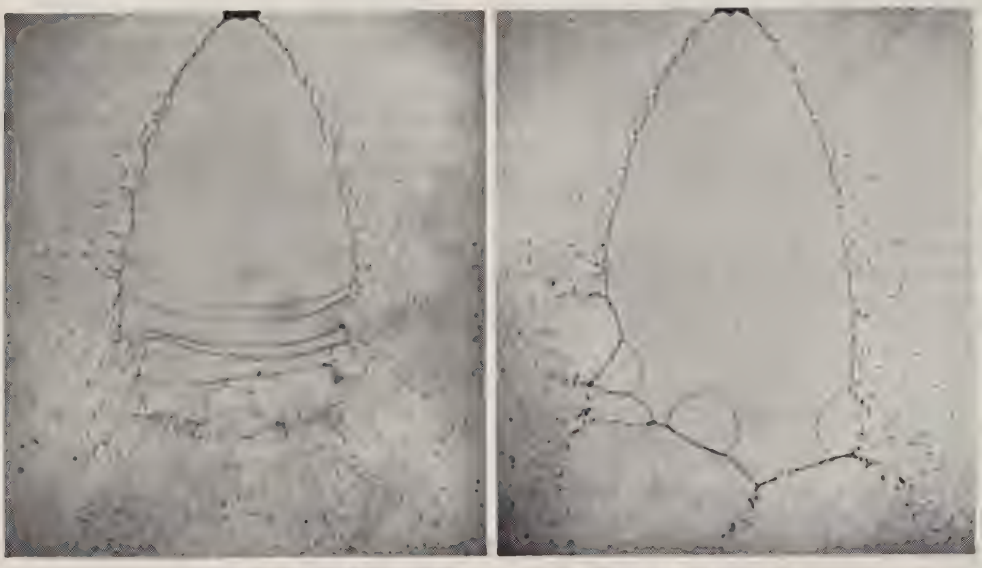

Figure 14. Effect of oxidant pressure on spray formation from atomizer

b

Figure 15. Effect of flame on spray formation from atomizer

applied to systems whose low-pressure performance is limited by mixing or by fuel atomization'.

It is difficult to find a system in practice which is in no way affected both by atomization *and* mixing. Both these factors are considerably influenced by ambient pressure, and this effect cannot be simulated by a reduction in ambient temperature.

The effect of ambient pressure on a spray sheet from an atomizer is shown in *Figure 14*. The sheet *in vacuo* is much thinner at the region of atomization than is the sheet in a standard atmosphere and hence the resulting drop size is different. In fact it is often larger at subatmospheric pressure, i.e. atomization deteriorates*.

The degree of turbulence and re-circulation, which is presumably altered by lowering the ambient pressure in the chamber, also affects fuel atomization. It is in no way a foregone conclusion that increased re-circulation will produce better atomization. *Figure 15* shows three sprays from the same fan-spray nozzle under atmospheric ambient conditions with the flame being brought increasingly nearer to the injection point to give the effect of increased re-circulation. At *a* there is no flame at all, at *b* the flame is well below the area of disintegration and at *c* the flame is attached to the sheet. The disintegration of the sheet in the latter case is seen to have changed considerably.

If simulation methods are employed which do not take account of the aerodynamics as well as the transport properties of the atmosphere in the combustion chamber, it is necessary to show good agreement of the results with actual results at sub-atmospheric ambient pressures. The spark ignition results shown in *Figure 4* of the authors' paper do not provide confirmation, since stability phenomena are much more affected by atomization.

V. Doroshenko (Moscow): Adding water to the fuel line of the gas turbine combustion chamber influences the combustion process in the burning zone in a different manner from changes in air pressure. For this reason the method is not appropriate in gas turbine practice. I think that addition of water is the most suitable method of simulating the pressure effect for the ramjet and after-burning chambers if the inlet air or gas temperatures are sufficiently high.

A. K. Sargent and P. F. Orchard (Bristol): The suggestion of Lefebvre for the use of water injection to simulate low-pressure effects in the testing of gas turbine chambers is a brave attempt to remove the necessity for low-pressure test equipment. We feel, however, that such a technique can only be used, and then with reservations, to yield comparative information between chambers of closely allied geometry, operating with homogeneous pre-mixed fuel and air, and can in no measure be applied in a quantitative manner as suggested in the paper.

As stated by Greenhough and Lefebvre (*Sixth Symposium*, p. 858) the method may generally be applicable to combustion systems where the aerodynamics of the burning zone are not unduly influenced by the fuel injection process. Toone and Arkless (Paper 120) showed that there is a considerable change in the fuel injection process in a typical gas turbine chamber as the pressure changes. Clearly the gas turbine chamber does not meet the necessary requirements for the method to be quantitatively accurate.

One would expect the severity of the combustion problem to be increased with water injection, but it would be very difficult to predict the extent of this increase. In this Symposium, Voevodsky has suggested that water does not only act as a diluent in the hydrocarbon reaction but takes part in the reaction $H_2O + H\dot{O}_2 \rightarrow H_2\dot{O}_2 + OH$. Although this reaction probably does not occur under many conditions it is a possibility at the higher temperature in the flame.

The authors' concentration on the peak of the stability loop is surprising since practical engines have to operate over a range of air : fuel ratios. In the *Third Symposium*, the results of Blanc, Guest, von Elbe and Lewis show that the effects of a diluent on blow-off pressure are not the same for both the peak and the width of an ignition loop.

Estimation of the severity of the combustion is by no means simplified by the work of Toone and Arkless who have measured an activation energy of 13,000 cal/g mol in their typical chamber, as opposed to the Lefebvre assumption of 42,000 cal/g mol. Considerably greater substantiation of the quantitative nature of this work is required than that quoted in the paper where no direct comparison of the effect of pressure and water injection is attempted. Can it be that no such data exist?

Application of the method to the testing of ignition systems of widely differing types is obviously likely to be misleading, due to the model pressures and temperatures being different to the practical conditions and the changes to the heat transfer processes that this difference would produce.

Finally the authors' third conclusion is much too sweeping in our experience and, we would suggest, not in line with general experience, since improvements in performance of existing chambers are usually effected by alterations to admission ports and hence the mixing pattern.

* Fraser, R. P. and Eisenklam, P. Liquid atomization and the drop size in sprays. *Trans. Instn. Chem. Engrs, Lond.* 34 (1956) 294.

A. E. Clarke (Burnley): The method described, in which water injection is used to simulate low pressures, has to some extent been substantiated by work carried out in the Lucas Laboratories, using steam to bring about flame extinction. The same assumptions are made—namely that the steam acts purely as a diluent and slows down the rate of reaction due to the thermal and inerting effects. Using a simple kinetic prediction the amount of water vapour to bring about extinction was very similar to that measured by practical tests on the rig (see *Figure 16*). This was

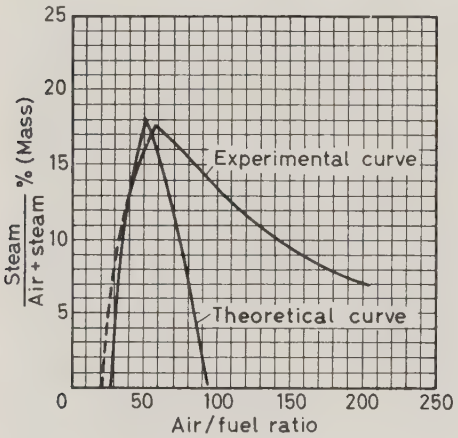

Figure 16. Limiting inlet steam concentrations versus air : fuel ratio

particularly true at rich conditions and at the peak of the extinction loop. On the weak side of the loop there was some divergence which may be attributed to droplet size effects.

A. H. Lefebvre (Derby): Useller's observations that the effect of water in reducing combustion performance appears to increase as the equivalence ratio departs from unity is in agreement with our own experience and is, in fact, predicted by the simple theory we have used. The relationship we quote, namely that the addition of one pound of water for each pound of fuel is equivalent to halving the gas pressure, applies only to stoichiometric mixtures where, in practice, most performance comparisons are made.

In reply to Eisenklam, the only justification we have for neglecting atomization effects is that in all present-day gas turbine systems atomization does not, under normal operating conditions, limit performance.

We would agree with Doroshenko that in testing combustion chambers it is better to inject the water into the air upstream of the chamber rather than to spray it through the atomizer along with the fuel. All our experience has been with the former method.

As Zukoski suggested during the discussion, one can do much useful testing at atmospheric pressure but, if full-scale systems are used, then combustion efficiencies will always be near to 100 per cent. This makes it difficult to detect the influences of changes in design and/or operating conditions on performance.

Sargent and Orchard charge us with 'a brave attempt to eliminate the necessity for low-pressure test equipment'. It is unfortunate if this impression has been given because in the last paragraph of the section entitled 'Application to Combustor Development' it was emphasized that a main object of the technique is *not* to eliminate actual low-pressure testing but to confine it to combustion systems which appear most promising on the basis of tests previously carried out with the water injection technique.

The changes in burning pattern referred to by Toone and Arkless are due not to changes in fuel distribution or mixing pattern, but to the variation of chemical reaction rates with pressure. It is our contention that a similar change in reaction rate can be brought about by varying the quantity of added water instead of the pressure. Of course the presence of water must influence the chemistry of the flame. The whole object of this paper has been to demonstrate that such influences are sufficiently small to be neglected.

It is ironic that we should be criticized for placing too much emphasis on the peaks of stability loops because without this technique it is practically impossible to determine the complete stability loops of most fully developed combustion systems at low pressure. Engineers are only too familiar with stability graphs which have been subjected to considerable artistry in that portion of the loop which is supposed to represent the peak. The water injection technique allows the peaks of ignition and stability loops to be easily and clearly defined and we make no excuse for stressing this important advantage.

It is difficult to understand why the results of Blanc *et al.* in the *Third Symposium* should have been quoted by Sargent and Orchard because in fact these data demonstrate very convincingly how the addition of a diluent can simulate a reduction in pressure both in terms of the peak and width of the stability loops. Presumably confusion arose because these results are plotted on the basis of percentage fuel instead of the more usual fuel : oxygen ratio.

It is suggested that our assumed activation energy of 42,000 cal/g mol is far too high, but this value has been generally used by all workers since Longwell and it is difficult to justify the use of any other. The theoretical relationship we have derived between the quantity of added water and the equivalent fall in pressure is based

on this value of activation energy, and the close agreement between this relationship and that obtained in practice is demonstrated in *Figure 16* of the paper by Greenhough and Lefebvre in the *Sixth Symposium.*

The application of the technique to the development of ignition systems has proved very fruitful indeed as we are sure Sargent and Orchard could themselves testify. Obviously the method cannot be applied blindly to all types of ignition system; for example, it could not be used to compare ignition systems whose electrical discharge characteristics are affected differently by changes in ambient pressure.

Our third conclusion is based on the argument that, at high pressures, chemical reaction rates are so rapid that the rate of combustion is determined solely by the rate at which fuel, air and hot combustion products can be mixed. However, as the pressure is reduced, reaction rates fall rapidly and eventually a pressure is reached below which they control performance. We did not wish to imply that at these conditions any changes in mechanical design would not affect performance because this would have been tantamount to suggesting that combustion performance is independent of combustor design, which is manifestly absurd. Our views on the importance of design are reflected in the emphasis we place on techniques which allow the relative merits of various proposed designs to be quickly and cheaply assessed.

PRACTICAL SYSTEMS

Papers 90, 91, 92, 93, 94, 95, 96, 97

S. L. Bragg (Derby): Clarke, Harrison and Odgers are attempting to fill a long-felt want when they introduce a pressure drop factor into the loading parameter, in order to correlate results with different injectors on their Longwell type 'stirred reactor'. It must, however, be pointed out that acceptance of their parameter,

$$(N/P^{1.8}V)/(\Delta P/P)^{\frac{1}{2}}$$

would invalidate the original correlations of Longwell and Weiss on the basis of

$$(N/P^{1.8}V)$$

alone. Consider, for example, two exactly similar reactors, one double the size of the other: on Longwell's basis the larger one would blow out at eight times the mass flow of the smaller (pressure and mixture ratio being maintained constant) while on the authors' basis, the larger one would *not* blow out at this flow since the value of $(\Delta P/P)^{\frac{1}{2}}$ is doubled. Since the mixing processes should be similar in similar reactors, it is the authors' result that is the doubtful one. A better way of correlating performance with different injector designs, suggested at the Sixth Symposium by Greenhough and Lefebvre, would be to use a factor corresponding to the old 'pressure loss factor' on jet engines, which is independent of mass flow. Since no obvious reference dynamic head is available, I would suggest the use of the constant,

$$D^2(2g\rho\Delta P)^{\frac{1}{2}}/N$$

where D is the reactor diameter. This might still correlate Clarke's results while preserving Longwell's correlation.

I think it is possible to generalize Hardcastle's paper by saying that if the absolute maximum intensity is required, then it pays to run the primary burning zone at the peak heat release rate, which corresponds to a near-stoichiometric mixture ratio and a burnt : unburnt constituents ratio of 85 : 15. In order to achieve high efficiencies, however, in the minimum volume, burning should always be completed in a secondary zone with a progressively weakening mixture, since the extra oxygen available more than compensates for the slight reduction in temperature: this point is not brought out in the paper.

It must also be pointed out that the chamber of limiting intensity is inherently unstable, since the slightest change in operating conditions blows it out. The optimum chamber, then, may be the one in which most of the combustion occurs at high intensity, but in which a small pilot zone of low loading maintains combustion during transient conditions of overload.

The troublesomeness of such transients can be inferred from the paper by Brewster and Cush, although the correlations achieved by these authors are probably peculiar to their own engine system. There would appear to be a very strong case for ensuring, by the use of pilot zones, pyrophoric ignition, oxygen enrichment, or otherwise, that lighting requirements do not provide a serious limit to combustion chamber improvement.

The next three papers all have relevance to the question of flame stabilization behind a bluff body. It now seems generally agreed that the critical region is the mixing zone between the free stream and the re-circulation. The excellent paper by Bovina provides experimental measurements of transfer coefficients in this region: it is very interesting to note that these were considerably reduced when burning was taking place, which suggests that cold flow models may not always accurately mirror hot flow conditions. The apparatus of Jensen and Shipman could, if the pilot zone mixture ratio were adjusted to be the same as that of the main stream, serve as a

model for the elucidation of processes in this vital mixing zone: it seems a pity that the earlier analyses of Spalding and Marble were not applied to the correlation of their results.

Cheng and Kovitz, in their paper, do consider the processes in the critical region to be analogous to the problem of propagation of flame from a hot to a cold stream, but they base their analysis largely on a thermal exchange, balancing a heat loss from the re-circulating zone before the flame is established against a heat gain later. Surely the latter is a very doubtful quantity, and the early heat loss is in fact made up by a corresponding *mass* transfer of fresh combustibles, which later burn to restore the temperature. The authors explain the anomalous results of Fetting, Choudhury and Wilhelm (Paper 86) by assuming the gases injected into the re-circulation to react with the re-circulating stream, and so modify its conditions where it meets the fresh gases: such an explanation could, of course, be fitted into the other theories of flame stabilization and cannot really be used as a justification of the new theory.

Although a fairly full treatment of the theory of the diverging reactor is presented in the paper by Gill, Eckel, Williams and Penner, only the simplified analysis is used for comparison with the practical results. It would appear from *Figure 10* in their paper that reaction in the later stages proceeds as one would expect, but that near the injector, when only a small proportion of propellants has reacted, the reaction rate is faster than would be expected at the corresponding low average temperature. This suggests that the mixture in that region is very inhomogeneous, reaction proceeding briskly in regions of high temperature, into which all the cold fresh propellants have not yet been mixed. It would be interesting to know what actual values of space heat release rates are achieved in this system, for comparison, for example, with those in Clarke's paper.

Finally, Thring's paper emphasizes that, as in rocket engines, chugging in industrial furnaces is avoided by reducing the effective ignition delay time and by stabilizing the flame close to the burner, but how are these desiderata best achieved?

J. W. Hardcastle (Coventry): Bragg's comments concerning conclusion number five were correct. For a given fuel rate, combustion at an equivalence ratio of one does not necessarily give the minimum reactor volume. The optimum equivalence ratio depends on the final efficiency required and will be slightly weaker than stoichiometric for high values of the final efficiency.

In reply to Bragg's further comments, for a *homogeneous* reactor the minimum reactor volume is achieved by introducing all the fuel and sufficient air to give the optimum mixture strength (stoichiometric or slightly weaker) into the first stage.

For a *practical* system, which Bragg chose to consider, the mixture strength which he recommended is possibly correct.

E. E. Zukoski (California): The model of flame stabilization proposed by Cheng and Kovitz suggests that at the stability limits a laminar flame is formed a short distance downstream of the bluff body, in the mixing zone between the cold combustible mixture and the hot re-circulating gas. If the approach stream velocity is increased slightly, the formation of the flame is no longer possible and the flame blows off. Thus the model suggests that the critical region for blow-off is very close to the flame-holder.

This picture can be tested by the elementary process of actually examining flame blow-off from a bluff body by visual observation or by high-speed photography. Both methods clearly demonstrate that the failure of the propagating flame, which is the usual definition of blow-off, occurs at the downstream end of the re-circulation zone and not near the flame-holder. In fact, for either laminar or turbulent flows, the re-circulation zone with flame attached close to the flame-holder can exist as a residual flame, *cf.* Scurlock *et al.* (*Third Symposium (International) on Combustion*), for conditions far outside the usual stability limits.

The blow-off of this residual flame also occurs from the downstream end; thus, as the severity of operating conditions is increased, the residual flame is observed to shorten and, in some very stable cases, blow-off will occur only when the residual flame is reduced to a length of about one flame-holder diameter.

This description of blow-off and of residual flames has been generally accepted since presentation of papers in the *Third Combustion Symposium* and has been substantiated by many detailed experiments since that time.

Hence, it is evident that the model proposed by Cheng and Kovitz is not a correct description of the most gross features of blow-off of propagating flames or of residual flames.

C. W. Shipman (Worcester): It is assumed by Cheng and Kovitz that blow-out occurs because the point of establishment of a self-propagating flame is too far downstream of the point of initial contact between hot, re-circulating gas and the cold, unburned feed, upsetting the balance between the energy lost from the re-circulating gases and the energy supplied by the flame. According to this model, as one approaches the unstable condition from a stable condition the location of the point of ignition should move downstream, and the flame should lift from the flame-holder. High speed schlieren cinemato-

graphy of the blow-out process* has shown that the downstream portions of the flame are extinguished first, this finding being the same for both propagating and residual flames, i.e. the flame blows 'out' and not 'off'.

Two other pieces of experimental evidence may be cited. First, short exposure, high sensitivity schlieren photographs of stable flames* have shown increasing inhomogeniety at the downstream end of the re-circulation zone as the blow-out condition is approached. Secondly Matton† found from measurements of ion concentration in the re-circulation zone that the ion density was low, corresponding to that for burned gases, until the blow-out condition was reached, at which time the concentration rose, indicating the presence of active combustion. Thus, it appears that near the blow-out condition parcels of unburned gas are thrown into the re-circulation zone. Blow-out could be the result of extension of this process, but it does not appear possible to distinguish this from the simple dissipation of the hot gas by turbulent transport because of the interaction between the re-circulation zone and the shear flow at its boundaries.

Thus, while there appears to be general agreement*§ that stabilization is due to transport between hot, burned, re-circulating gas and the cold feed, there seems to be some evidence that in the practical range of operation the blow-out is caused by events taking place downstream of the point at which the propagating flame is established. It is reasonable to expect that the re-circulation in the immediate wake is the source of feed-back required to make these 'downstream' events result in instability. This means that the analytical studies of Cheng and Kovitz‡ and of Marble and Adamson‖ are important for the study of the stability problem but may not be directly related to the blow-out. It is clear that considerably more experimental information on the character of combustion in turbulent shear flow must be accumulated before the problem can be treated more thoroughly.

S. I. Cheng (Princeton): Shipman argues from experiment that the initial cause of blow-out and/or blow-off is the breakdown, due perhaps to turbulence, of the rear portion of the flame and re-circulation zone. That is, the flame seems to disappear with extinction of the downstream portion first. This, he says, contradicts the position held by us, namely, that it is the initial region of mixing between cool combustible and (re-circulating) hot combustion products that is controlling.

(*a*) It must first be emphasized that the present theory is an attempt to describe the series of steady-state configurations that lead to instability. It does not concern itself with the non-steady phenomena at blow-off, as revealed by high speed schlieren cinematography.

(*b*) The condition of the flame near the downstream portion of the wake region could conceivably be independent of the flow situation near the initial mixing region. That is, as the flow proceeds downstream from the 'separation point', the turbulence which develops may break up and 'extinguish' the rear portions of the flame, even though stable, steady-state conditions exist in the initial mixing region.

(*c*) Matton's observation, as quoted by Shipman, does show that the re-circulation zone is affected by the downstream breakup of the flame front. Therefore, as conceded by Shipman, it is possible for the initial mixing zone to be influenced by the downstream turbulence.

(*d*) It seems to us that if blow-off is caused by a large increase in turbulent transport between free stream and re-circulation zone, then as blow-off is approached the temperature of the re-circulating gases should decrease significantly. This, however, is not observed (Zukoski and Marble). On the other hand the present model does demonstrate the existence of instability with very small drop in re-circulation zone temperature and even with constant re-circulation zone temperature.

(*e*) If turbulent transport in the rear of the re-circulation zone is controlling, then small changes in the state of the initial mixing zone should be unimportant. This, however, is contrary to observations by Fetting, Choudhury and Wilhelm, quoted in the paper. They observed marked increases in blow-off velocity with small additions of combustible to the initial mixing zone.

We concede the possibility of events as described in paragraph (*b*) above but maintain that they are not consistent with paragraphs (*d*) and (*e*). Visually, blow-off appears to be a sudden disappearance of flame, at least when no residual flame remains. The present theory predicts that the equilibrium point of ignition is moved significantly downstream percentage-wise but the absolute magnitude of the movement is very small. Therefore, while the downstream dissolution of the flame is easily seen, the change in x_i (defined

* Williams, G. C. and Shipman, C. W. *Fourth Symposium (International) on Combustion*, p. 733. 1953. Baltimore; Williams and Wilkins.

† Matton, G. *Sixth Symposium (International) on Combustion*, p. 770. 1957. New York; Reinhold.

‡ Cheng, S. I. and Kovitz, A. A. *Sixth Symposium (International) on Combustion*, p. 418. 1957. New York; Reinhold.

§ Zukoski, E. E. and Marble, F. E. The role of wake transition in the process of flame stabilization on bluff bodies, in *Combustion Researches and Reviews* (AGARD). 1955. London; Butterworths.

‖ Marble, F. E. and Adamson, T. C. Ignition and combustion in a laminar mixing zone, in *Selected Combustion Problems* (AGARD). 1954. London; Butterworths.

in the paper) may not be observable by ordinary means.

In conclusion, while it is conceded that the present theory may not give sufficient conditions for a stable propagating flame anchored on a bluff body, there is no evidence to suggest that it does not describe necessary conditions for such flame stabilization.

A. A. Putnam (Columbus): High speed photographs of the pulsating flame which occurred in Thring's oil-fired boiler seem to indicate that the pulsation is not the same type as we observed in tests of residential heating units fired with gun-type burners of about one gal/h capacity. Our pulsating flame involved a periodic re-ignition of a combustible mixture by hot non-radiating gases. This could either occur in the low-pressure part of the cycle in the central re-circulation zone around the fuel spray and be followed by a rapid expansion to maximum burning rate in the high-pressure part of the cycle: or in the high-pressure part of the cycle in the annular re-circulating region between the fuel spray and the back wall, followed by a slow expansion, and in some cases extinction, as it was drawn back towards the air inlet and then by a rapid expansion at the correct time, one half cycle later, as it was blasted out into the central region by the pulsating gas flow cycle. Since Thring's type of oscillation, ours, or possibly others, could occur in an oil-fired unit, it is well to generalize his results to some extent.

As an example, we have found that the acceleration term associated with flow through a restriction, which is the second term in equation 1, cannot be neglected for any of our restrictions, as Thring has found he can do in equation 4 for the combustor exit. Undoubtedly because of the difference in method by which the flame-driven oscillation occurs, we do not observe all the results that are listed in the second paragraph. With reference to item 2, a direct contradiction has been observed. With reference to items 3 and 4, if all other factors are held constant, either improvement or worsening of the noise condition may result from the recommended changes.

Our oscillations are definitely acoustic in nature, although components of the system may be treated in many instances by the Helmholtz type analysis. One component of our system, the blast tube, appears to have a natural frequency of an aerodynamic rather than acoustic nature. Predicting a frequency for this component, which includes blockage discs, cylinders and swirl vanes, by standard acoustic computations, gives a highly unsatisfactory result, possibly large by a factor of ten. However, the use of an experimentally determined natural frequency to characterize this component in an acoustic analysis of the remainder of the system works satisfactorily. Thus, even in our system we appear to have one component of the nature that Thring attributes to his entire oscillating system.

A. H. Lefebvre (Derby): It would clearly be of considerable advantage to the combustion engineer if, for any given operating conditions of pressure, inlet temperature and fuel : air ratio, he could express the heat release of his combustors as a percentage of the maximum attainable. In this respect the Burnley experiments are likely to prove more valuable than Longwell's earlier work because they are being carried out at the right order of pressure loss. However, the tentative conclusion that combustion intensity is proportional to $(\Delta P/P)^{0.5}$ should be applied with some reserve. In practical systems the influence of pressure loss on performance is largely dependent on the absolute value of pressure. At very low pressures, say a few lb./in.^{2}, the effect of pressure loss is probably greater than the present authors suggest. As the pressure is increased the influence of specific pressure loss begins to diminish and, eventually, a pressure level is reached beyond which any further increase in pressure loss can actually reduce combustion efficiency. This type of combustion inefficiency is caused by the chilling, through too rapid mixing, of partially burned combustion products in the dilution zone*.

The authors of this paper could perform a useful service by employing their apparatus to determine the influence of inlet air temperature on combustion performance. Bragg† calculated that $M/VP^2 \propto \exp.\ (T/400)$ for an equivalence ratio, ϕ, of 1. Subsequently Lefebvre‡ calculated for kerosine/air mixtures that

$$\frac{M}{VP^2} \propto \exp \frac{T}{b}$$

where $b = 150$ for $\phi = 0{\cdot}5$, $b = 340$ for $\phi = 1{\cdot}0$, and $b = 250$ for $\phi = 1{\cdot}5$.

These results, which show a marked variation of temperature dependence with equivalence ratio, have never been subjected to experimental investigation. The authors' apparatus appears to lend itself ideally to such a purpose.

B. P. Mullins (Pyestock): A consideration of the residence or reaction times in stirred spherical reactors of the type described by Clarke *et al.* indicates that this form of reactor is not strictly chemically limited.

I have computed the mean reaction temperatures corresponding to several equivalence ratios

* Bragg, S. L. and Holliday, J. H. *Selected Combustion Problems* (AGARD). 1955. London; Butterworths.

† Bragg, S. L. Rolls-Royce internal report, July 1953 (unpublished).

‡ Lefebvre, A. H. Rolls-Royce internal report, October 1955 (unpublished).

in the range 0·5 to 0·7 on the basis of 90 per cent combustion efficiency, with combustion loss appearing as carbon monoxide, for most of the fuels mentioned by Longwell*. Then, from the flow data he gave, I have deduced an overall reaction time for the various experimental conditions for each fuel. I have plotted these times on the basis of 'log time *versus* reciprocal absolute temperature' and have compared the resulting curves with the corresponding ignition delay curves obtained with the N.G.T.E. rig†. The results are shown in *Figures 17* and *18* for two of

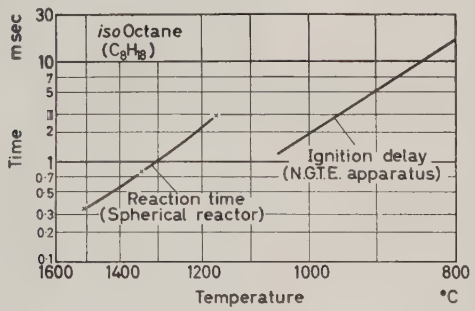

Figure 17

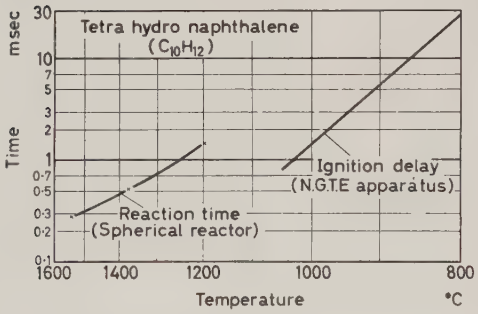

Figure 18

the eight fuels examined, viz. *iso*octane and tetra-hydro-naphthalene. In each illustration the left-hand curve represents the sum of the time to prepare a hot mixture (by the mixing of cold added reactants with existing hot products in the sphere) plus the pre-flame time (i.e. ignition delay) plus the post-flame time (i.e. time to burn-out to 90 per cent combustion efficiency). The right-hand curve in each of the two illustrations represents the pre-flame time (i.e. ignition delay) only†. Essentially similar sets of curves were obtained in the cases of the other six fuels, but space does not permit me to detail all of these here.

In some experiments which I have made with rapid mixing of gaseous fuel in the N.G.T.E. ignition flow rig I found that the burning time (corresponding to the flame length) was no greater than the pre-flame time (ignition delay). This is not surprising when one considers that the post-flame reactions occur at much higher temperature than the pre-flame reactions. It therefore seems probable that the total chemical time for combustion would not exceed twice the value of the ignition delay times plotted in the right-hand curves which, incidentally, were obtained at one atm pressure. The deduction may then be made by general comparison of the left-hand and right-hand curves in *Figures 17* and *18* that the reaction times corresponding to each left-hand curve are not solely chemical in nature but include substantial physical delay times, presumably mixing times. Since the right-hand curves will be higher at low pressures* this would bring the left-hand and right-hand curves more nearly into line, suggesting the expected result that mixing time is less significant in the spherical reactor at low-pressure conditions.

It is not really too surprising that the residence time in the stirred spherical reactor contains an appreciable mixing time, whereas the residence time plotted from the N.G.T.E. apparatus tests does not. For, whereas in the spherical reactor experiment an endeavour is made to submit *all* of the fuel to the same mixing and chemical treatment, in the N.G.T.E. rig, when $\phi < 0{\cdot}5$, only a *small portion* of the added fuel (sufficient to produce a visible flame position) is required to be thoroughly mixed with the airstream, which is a much less arduous requirement. The former apparatus represents an attempt to obtain results of direct relevance to turbo-jet combustion conditions: the latter apparatus represents an attempt to produce fundamental data under conditions resembling those obtaining in turbo-jet combustion systems.

It is evident that more fundamental data on pre-flame and post-flame chemical reaction times are required at high temperatures for various fuel/air mixtures over a range of static pressures and preferably also over a wide range of equivalence ratios embracing the value 1·0. When these data are available comparisons such as the one I have tried to make now will be precise and meaningful rather than merely indicative. I might add, however, that my general conclusion is in accord with the findings of other workers, among whom may be mentioned Avery, Blichner and Hottel, with each of whom I have had fruitful discussions which I gratefully acknowledge.

Olav E. Blichner (Norway): Work which has been carried out under Squid project No. 7036 at the Fuels Research Laboratory of the Chemical Engineering Department, M.I.T., has given results which may have some bearing on the paper by Clarke, Harrison and Odgers.

* Weiss, M. A., Lang, R. J. and Longwell, J. P. *Industr. Eng. Chem.* (*Industr.*) 50 (1958) 257.

† Mullins, B. P. *Fuel* 32 (1953) 363.

* Mullins, B. P. *Fuel* 32 (1953) 343.

Experimental investigations with a 4 in. inner diameter Longwell and Weiss type spherical reactor and with a new type of cylindrical reactor, with Vycor glass windows, showed evidence of fluid dynamic effects on the blow-off point of such reactors.

A pre-mixture of propane and air was introduced through two spherical injectors containing 24 holes of 0·055 in. diam and 80 holes of 0·030 in. diam, respectively. The total area of the holes was the same in both cases, thus securing the same mass flow into the reactor for the same upstream pressure. Running at four different mass flows (approximately 50, 90, 130 and 170 $\times$ 10^{-5} lb. moles/sec) the blow-out point for various fuel : air ratios was approached by lowering the reactor pressure.

For all four mass flows a general trend was apparent. At lean mixture ratios, the 80 hole blow-out curve gave somewhat higher values than the 24 hole one. In the region of equivalence ratios between 0·6 and 0·7 the curves cross, while the values of the 24 hole blow-out curve became higher than those of the 80 hole towards stoichiometric mixture ratios.

The general shape of the 24 hole curves were similar to those of Longwell and Weiss, while the shape of 80 hole curve more resembled the curve of Baker, Hottel and Williams.

It was also observed that different mass flow rates gave different blow-out curves, the trend being the same for both the 24 and the 80 hole injectors. An increase in blow-out value was observed when decreasing the mass flow rate. This was true up to a point, after which the blow-out curve decreased with further decrease in mass flow rate.

Contrary to theory the plot of spatial mass flow rate against reactor pressure, at various fuel : air ratios, gave a linear relationship rather than the expected logarithmic.

Visual observation through windows in a cylindrical reactor, where the jets flowed radially from a central cylinder, gave evidence of the existence of discrete flow zones within the reactor. Observations of both a 4 and a 12 hole injector showed that combustion took place over the surface of the jets which penetrated towards the outer wall. The centre core of the jets, however, seemed to be transparent and caused a darkening of the refactory at the point of impingement, thus strongly indicating the existence of cool, unburnt gases which do not burn until they enter the re-circulation zone.

The cylindrical reactor, using a 12 hole injector, gave a blow-out curve which, for the very lean mixture ratios, was somewhat lower than the Longwell and Weiss one, while it became slightly higher towards stoichiometric fuel : air ratios.

Concluding, it seems that varying the injector hole-size and spatial mass flow rate at a given fuel : air ratio does affect the reaction rate in a stirred reactor; and that there exist, within the reactor, definite flow and combustion patterns which, to a large extent, are determined by the above-mentioned factors.

J. Odgers (Birmingham): With regard to Bragg's comments, the inclusion of the dimensionless term $(\Delta P/P)^{0.5}$ certainly improves the scatter on our own results. It is interesting to examine the original Longwell data, having made an estimate of the pressure loss through the injectors. It will be seen that the points having comparatively low-pressure drops lie on the flat portions of the curve whilst the high-pressure loss points are largely confined to that portion of the curve near to the peak. The result is that correction for pressure loss, as described in the paper, produces a new curve substantially as valid as the original one.

Lefebvre's remarks on the effect of pressure drop at pressures above one atm are most interesting and in view of this I thoroughly endorse the importance of stressing the pressure range. The term $(\Delta P/P)^{0.5}$ must certainly be applied with caution and in order to explore this fact more fully, pressure-loss measurements have now been made across the injector holes, though we have not yet analysed the results.

The time/temperature curve of Mullins is of great interest and I can only suggest that the increase of reaction time over the pre-flame time is due to inhomogeneity in the bomb. This is to some extent supported by the re-circulation pattern exhibited in hydraulic studies of transparent models.

It is unfortunate that Blichner's results were not available before the meeting since they certainly appear to show a pressure-drop influence of some kind and merit much more attention.

PART IX

DETONATION AND ITS INITIATION

98

DETONABILITY AND CHEMICAL KINETICS: PREDICTION OF LIMITS OF DETONABILITY OF HYDROGEN

F. E. BELLES

INTRODUCTION

One of the central problems of research in detonation is to clarify the process of transition from ordinary flame to detonation wave. Thanks to the recent photographic studies of Greifer *et al.*[1] the widely accepted qualitative features of the initiation of a detonation from a flame have been confirmed. A flame, proceeding from the closed end of a tube, sends out a pre-flame shock that heats and compresses the unburned gas. The shock is an essential part of the flow pattern[2]: since the flow must come to rest behind the advancing flame at the closed end of the tube, a shock must exist to push the unburned gas ahead at a velocity just equal and opposite to that of the burned gas. The flame accelerates as it over-runs the shock-treated mixture so that ever stronger compression waves are sent out, as described by Chu[3]. The shock is thereby reinforced. Eventually it becomes strong enough to cause the mixture between flame and shock to auto-ignite locally, further strengthening the shock so that successive auto-ignitions occur closer and closer to it. When auto-ignition occurs at the shock front, the shock is very greatly accelerated, and after one or more such accelerations the detonation wave is born.

Thus, the work of reference 1 showed that the pre-requisite for transition to a detonation is a pre-flame shock strong enough to ignite the mixture almost instantaneously, that is, strong enough to cause the mixture to explode. One therefore sees a qualitative connection between the hydrodynamics and the chemical rates leading to explosion. In order to spell out the connection in a quantitative way, details of the explosion kinetics are required. These are not available for most fuels; for hydrogen, however, the necessary data are known.

It is the purpose of this paper to combine kinetic data with the observed wave behaviour during transition from flame to detonation, and to show how the result leads to predictions of the limits of detonability of hydrogen. The manner in which the predicted limits depend on mixture temperature and pressure, and on the properties of the mixture—that is, on the proportion and specific heat ratio of inert gas—will also be discussed. Comparison will be made with the limited experimental data available.

PREDICTION OF LIMITS OF DETONABILITY

It has already been stated, on the basis of observations[1], that transition to detonation occurs when the pre-flame shock becomes strong enough to cause the mixture to explode. The prediction of limits of detonability will therefore take the following course:

(1) The chemical-kinetics condition for branched-chain explosion of hydrogen will be defined in terms of temperature, pressure and mixture composition.

(2) Standard shock-wave equations will be used to express, for a given mixture, the temperature and pressure of the shocked gas in terms of shock strength (Mach number).

(3) Steps (1) and (2) will be combined so as to express the explosion condition in terms of shock strength and mixture composition. Critical shock strengths for explosion will be found.

(4) It will be found on the basis of conservation of energy that some mixtures, on burning, can support a shock of the critical strength, whereas others cannot. Thus, the limits of detonability will be found.

Chemical kinetics

The following gas-phase kinetics for the oxidation of hydrogen are used (reference 4, p. 9):

$$OH + H_2 \xrightarrow{k_1} H_2O + H \qquad (I)$$

$$H + O_2 \xrightarrow{k_2} OH + O \qquad (II)$$

$$O + H_2 \xrightarrow{k_3} OH + H \qquad (III)$$

$$H + O_2 + X \xrightarrow{k_4} HO_2 + M \qquad (IV)$$

k_1, k_2, k_3 and k_4 being the rate constants of reactions I to IV respectively.

The branched-chain explosion limit condition derived from this set of reactions using the steady-state approximation is (reference 4, p. 10):

$$\frac{2k_2}{k_4[X]} = 1 \qquad (1)$$

In words: Explosion occurs when the rate of the chain-branching reaction II is equal to half the rate of the chain-breaking reaction IV.

Using the rate constants of Lewis and von Elbe (reference 4, p. 59), and expressing the concentration [X] in terms of temperature and pressure by means of the gas law, equation 1 becomes

$$\frac{3{\cdot}11\,Te^{-8550/T}}{f_x P} = 1 \qquad (2)$$

In equation 2, f_x is an effective mole fraction of third bodies for the formation of HO_2 in reaction

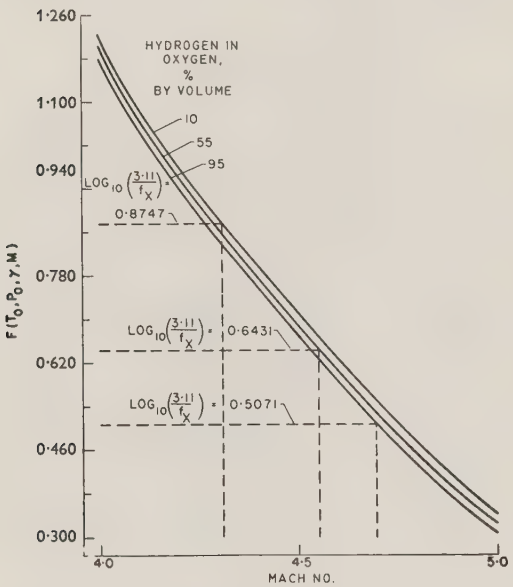

Figure 1. Typical solutions for critical shock Mach numbers. H_2–O_2 *mixtures;* T_0, 300°K; P_0, 1 atm

IV, and is given by the following empirical equation (reference 4, p. 34)

$$f_x = f_{H_2} + 0{\cdot}35f_{O_2} + 0{\cdot}43f_{N_2} + 0{\cdot}20f_{A_r} + 1{\cdot}47f_{CO_2} \qquad (3)$$

The numerical factors in equation 3 express ratios of the rate of reaction IV with various third bodies, to the rate with H_2 as the third body.

In the subsequent development, it is convenient to use equation 2 in the following logarithmic form

$$\frac{3{,}710}{T} - \log_{10}\left(\frac{T}{P}\right) = \log_{10}\left(\frac{3{\cdot}11}{f_x}\right) \qquad (4)$$

If a given hydrogen mixture, having a characteristic value of f_x dependent upon its composition, is raised to a temperature and pressure that satisfy equation 2 (or equation 4), the mixture will explode.

Shock-wave relations

The pressure and temperature behind an incident shock may be calculated from the following equations, given, for example, in reference 5

$$P = \frac{P_0}{\alpha}\left(\frac{M^2}{\beta} - 1\right) \qquad (5)$$

$$T = \frac{T_0\left(\frac{M^2}{\beta} - 1\right)\left(\beta M^2 + \frac{1}{\gamma}\right)}{\alpha^2 \beta M^2} \qquad (6)$$

The quantities α and β are convenient functions of the specific heat ratio, and are defined as $(\gamma + 1)/(\gamma - 1)$ and $(\gamma - 1)/2\gamma$ respectively. Equations 5 and 6 apply to the ideal case in which the specific heat ratio is constant; however, it will be shown that the shock strengths required to cause explosion in hydrogen mixtures are sufficiently low that real-gas effects are not very important.

Explosion condition as function of shock strength

It is clear from equation 2 that, for a given mixture, many combinations of temperature and pressure will satisfy the explosion limit condition: but if we specify the initial temperature and pressure, and if we further specify that temperature and pressure are to be raised by means of a shock wave, then there is only one shock Mach number that will provide the necessary combination of temperature and pressure for explosion. This critical Mach number may be found by combining equations 4, 5, and 6. Solving for $1/T$ and T/P from equations 5 and 6, and substituting in equation 4, one obtains

$$\frac{3{,}710\alpha^2\beta M^2}{T_0\left(\frac{M^2}{\beta} - 1\right)\left(\beta M^2 + \frac{1}{\gamma}\right)} - \log_{10}\left[\frac{T_0\left(\beta M^2 + \frac{1}{\gamma}\right)}{P_0 \alpha \beta M^2}\right]$$

$$= F(T_0, P_0, \gamma, M) = \log_{10}\left(\frac{3{\cdot}11}{f_x}\right) \qquad (7)$$

Critical shock Mach numbers

Equation 7 may be solved graphically; *Figure 1* shows typical plots of the left-hand side of equation 7 against Mach number, for several hydrogen–oxygen mixtures. The values of specific heat ratio were obtained from the following relation

$$\gamma = \frac{\sum_i \frac{f_i \gamma_i}{\gamma_i - 1}}{\sum_i \frac{f_i}{\gamma_i - 1}} \left(\text{since } \gamma = C_p/C_v = \frac{R\gamma/\gamma - 1}{R/\gamma - 1}\right) \qquad (8)$$

where γ is the specific heat ratio, C_p, the molar heat capacity at constant pressure, C_v the molar

heat capacity at constant volume (cal/mole °K), and R is the gas constant (cal/mole °K).

Each mixture has characteristic values of f_x and γ. Therefore, solution of equation 7, for a given initial temperature T_0 and pressure P_0, yields a critical shock Mach number M_c that is just sufficient to cause the mixture to explode. Values of critical shock Mach number M_c for explosion were obtained in the manner shown in *Figure 1* for a range of hydrogen concentrations, expected to cover the detonable range, for hydrogen–oxygen and hydrogen–air mixtures. The results are compiled in Table 1.

TABLE 1

Critical Shock Mach Numbers for Explosion of Hydrogen Mixtures at 300°K

System	H_2 *in mixture*, vol. %	*Critical shock Mach numbers*		
		$P_0 = 1{\cdot}00$ atm	$P_0 = 0{\cdot}75$ atm	$P_0 = 0{\cdot}50$ atm
H_2–O_2	10	4·342	4·202	4·034
	25	4·439	4·295	4·110
	40	4·519	4·375	4·180
	55	4·586	4·441	4·238
	70	4·640	4·495	4·291
	85	4·690	4·543	4·341
	95	4·726	4·576	4·370
H_2–Air	10	4·392	4·247	4·069
	20	4·448	4·304	4·115
	30	4·497	4·353	4·157
	40	4·542	4·397	4·196
	50	4·578	4·433	4·231
	60	4·614	4·469	4·265
	70	4·651	4·504	4·301

Criterion of detonability

Conservation of energy provides the link between the calculated critical shock Mach numbers for explosion, and the prediction of limits of detonability. The pre-flame shock provides a mechanism whereby some of the energy released by combustion is distributed to unburned gas ahead of the flame. Ultimately, this energy is recovered by the burned gas, when the flame consumes the shocked mixture. But if the enthalpy increase in the shocked state corresponding to the critical shock Mach number is greater than the heat of combustion, an impossible situation arises. No transition to detonation could ever occur, even if the tube were indefinitely long. The criterion for the detonability of a mixture is therefore

$$\Delta h_s \leqslant \Delta h_c \tag{9}$$

Δh_s being the enthalpy rise across shock of critical Mach number (cal/g mixture) and Δh_c the heat of combustion (cal/g mixture).

The energy increase of the shocked state is obtained from

$$\Delta h_s = \bar{c}_p(T_t - T_0) \tag{10}$$

where the total temperature T_t is given[6] by

$$T_t = T_0\left(1 + \frac{\gamma - 1}{2}M_c^2\right) \tag{11}$$

Values of $\bar{c}_p$, the average specific heat of mixture at constant pressure (cal/g mixture) for use in equation 10 were taken as

$$m\bar{c}_p = \sum_i f_i \bar{C}_{p_i} \tag{12}$$

where

$$\bar{C}_{p_i} = m_i\bar{c}_{p_i} = \frac{\int_{T_0}^{T_t} C_{p_i}\,\mathrm{d}T}{(T_t - T_0)} \tag{13}$$

$$= A_i + \tfrac{1}{2}B_i(T_0 + T_t) + \tfrac{1}{3}C_i(T_0^2 + T_0T_t + T_t^2)$$

where $\bar{C}_p$ is the average molar heat capacity at constant pressure (cal/mole °K), and m is

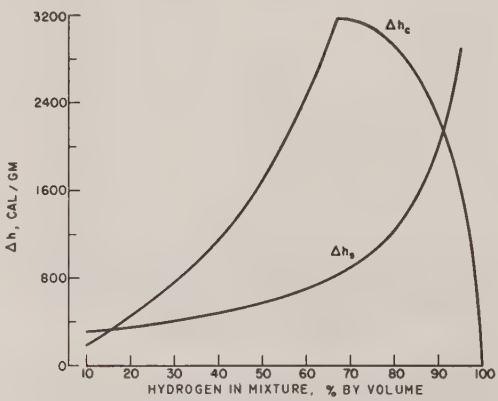

Figure 2. Heat of combustion and enthalpy rise across critical shocks in H_2–O_2 *mixtures.* T_0, 300°K; P_0, 1 atm

the average molecular weight (g/mole). The coefficients A_i, B_i, and C_i were taken from reference 7.

In order to obtain predicted limits of detonability, a graphical method was used. For a series of mixtures of a given type, that is, H_2–O_2 or H_2–air, the curve of Δh_c against per cent H_2 was plotted; this curve has its maximum at stoichiometric. On the same graph, the curve of Δh_s against per cent H_2 was plotted; it rises monotonically, and cuts across the Δh_c curve at two concentrations. The criterion of detonability (equation 9) is satisfied only between these two concentrations; hence, they are the predicted limits of detonability. *Figure 2* is a plot of the sort just described for hydrogen burning in oxygen.

RESULTS

Comparison of predicted and observed limits

Predicted and observed lean and rich limits of detonability are shown in Table 2. Initial mixture conditions were 1 atmosphere pressure and 300°K. The results for hydrogen–oxygen and hydrogen–air are compared with limits reported by Lafitte[8]. Thus, there are four points of comparison. In all cases, the predicted and measured limits agree strikingly well; the largest discrepancy, 2·5 per cent hydrogen, is in the lean limit of hydrogen in air.

Effects of variables on predicted limits

Inert gas—Inert gases affect the predicted limits because of variations in specific heat ratio and in

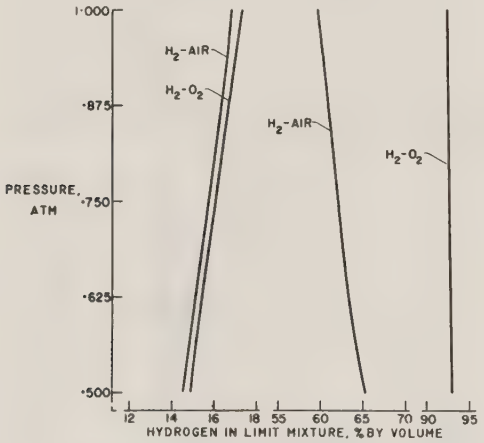

Figure 3. Effect of pressure on predicted limits of detonability. T_0, 300°K

chain-breaking efficiency. The larger the effective γ of the mixture, the larger the value of the left-hand side of equation 7, for a given value of M. Thus, for a given value of f_x, the critical shock Mach number will be lower, and the limits will be wider. Conversely, if the chain-breaking efficiency is large, the right-hand side of equation 7 is small, the critical shock Mach number increases, and the limits narrow. Both effects should contribute to cause narrow limits for mixtures containing carbon dioxide, that is, low γ and large f_x. For argon-containing mixtures, on the other hand, a low lean limit would be predicted, due to changes of γ and f_x in the opposite directions.

It should be noted that inert-gas effects show up chiefly in the predicted lean limits. At concentrations towards the rich limit, the properties of the mixture are largely governed by the high proportion of hydrogen present; and the rich limit is therefore mainly governed by the amount of oxygen available to burn fuel and produce energy for driving the shock wave.

Initial mixture pressure—The explosion condition (equation 7), from which the critical Mach numbers are obtained, may be rearranged as follows

$$\frac{3{,}710\alpha^2\beta M^2}{T_0\left(\frac{M^2}{\beta}-1\right)\left(\beta M^2+\frac{1}{\gamma}\right)}-\log_{10}\left[\frac{T_0\left(\beta M^2+\frac{1}{\gamma}\right)}{\alpha\beta M^2}\right]=\log_{10}\left(\frac{3{\cdot}11}{f_x}\right)-\log_{10}P_0 \qquad (14)$$

It is seen from equation 14 that, at pressures below 1 atmosphere, the right-hand side will increase, and reference to *Figure 1* shows that the critical shock Mach number will decrease. Consequently, the limits of detonability will widen at reduced pressures. The effect is due to the smaller amount of three-body chain breaking (reaction IV) at low pressure. *Figure 3* shows the predicted variation of limits of detonability with pressure for hydrogen burning in oxygen and in air. These results would of course become invalid should the tube be narrow enough and the pressure low enough to make surface reactions important.

Initial mixture temperature—Equation 7, from which M_c is obtained, is a function of T_0 explicitly, and also implicitly through the dependence of γ on temperature. Proper evaluation of the effect of mixture temperature on limits of detonability would have to include the implicit dependence, and this was not done in the present work.

TABLE 2

Predicted and Observed Limits of Detonability o Hydrogen Mixtures at 300°K and 1 atm

System	*Lean limit*, vol. % *hydrogen*	*Rich limit*, vol. % *hydrogen*
H_2–O_2	16·3 (15*)	92·3 (90*)
H_2–Air	15·8 (18·3*)	59·7 (58·9*)

* Observed limits, reported in reference 8.

However, approximate calculations of the temperature effect were made for a limited temperature range, 200 to 400°K. Constant γ of 7/5 and corresponding constant heat capacity of $(7/2)R$ were assumed, so the results apply to H_2–O_2 and H_2–air mixtures. At 300°K, the limits differed by 1 to 3 per cent hydrogen from the more carefully computed values listed in Table 2. Rich and lean limits for both H_2–O_2 and H_2–air, normalized to the data of Table 2 at 300°K, are plotted against mixture temperature in *Figure 4*.

It is seen that the limits are expected to widen as mixture temperature is raised, in a nearly

linear fashion but at a slow rate. The effect is quite similar to that observed for limits of flammability[9].

DISCUSSION

Agreement of predicted and observed limits

From the results of this study, it seems definite that the limits of detonability of hydrogen are well accounted for by the kinetic requirements for explosion. Furthermore, the agreement shown in Table 2 provides quantitative support for our qualitative physical model of the transition from flame to detonation. It may be noted that the steady-state approximation, from which the explosion limit condition (equation 1.) was derived, appears to be valid.

Limits due to decaying detonation waves

There is an aspect of the agreement between predicted and measured limits that deserves comment. In all cases, the experimental limits were determined by starting a detonation in the test mixture, either by means of a detonation in an adjoining stoichiometric H_2–O_2 mixture or by means of a small explosive charge. The behaviour of the resulting wave was then examined. This was done to avoid the very long tubes needed for transition from flame to detonation near the limits. The calculations, on the other hand, are based on the model of a flame transforming to a detonation. Nevertheless, the calculated and observed results agree, though one might reasonably expect that the limits would depend on the intensity of the 'ignition source'. No such dependence is found, because the detonation tube is made as long as practicable, so as to dissipate extra energy from the incident detonation wave before the wave that is to be observed passes the measuring stations. Then, with the excess energy gone, the mixture will support a stable detonation wave, if it is detonable; otherwise, the wave will decay to a flame plus a shock, and since the shock will be too weak to cause immediate auto-ignition, a detonation cannot re-form.

Now, it is well known that a detonation may be described as a shock driven by heat release, and that the reaction occurs very close to the wave, that is, that there is essentially immediate auto-ignition. But we have already found that there is a critical Mach number for auto-ignition at the wave front, so we may state that a detonation wave will not propagate stably unless its Mach number is equal to or greater than the critical Mach number. Another criterion for detonability may therefore be written

$$M_D \geqslant M_c \qquad (15)$$

Equation 15 is completely equivalent to the previous criterion (equation 9) because the energy available to produce the wave of detonation Mach number M_D is the same, for a given mixture, as that available to produce a shock wave of critical Mach number M_c; namely, the heat of combustion Δh_c. Thus, an alternative way to predict the limits of detonability of hydrogen is as follows:

(1) Calculate detonation velocities over range of mixtures expected to include the limit

(2) Divide each velocity by the speed of sound, to transform it to a detonation Mach number M_D

(3) Plot ratios of M_D to M_c against hydrogen concentration.

The mixture for which the ratio becomes equal to unity will be the limit mixture.

This procedure is illustrated in *Figure 5* for the

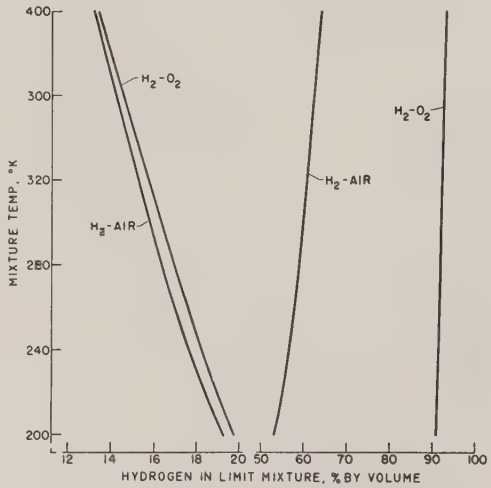

Figure 4. Effect of temperature on predicted limits of detonability. P_0, 1 atm

case of lean hydrogen–air mixtures. Detonation velocities were calculated, neglecting dissociation, by the method and with the thermodynamic data of reference 4. Critical Mach numbers were obtained from a plot of the appropriate values in Table 1. It is seen that the predicted limit is 16·8 volume per cent hydrogen in air, compared to 15·8 per cent by the previous method. The two results may be regarded as the same, the small difference arising from the somewhat different methods of handling the heat capacities in the two cases.

Neglect of dissociation is probably justifiable, because the limits lie at concentrations such that the detonation temperatures are rather low. Nevertheless, some energy is tied up in dissociation and is unavailable for driving the wave; undoubtedly, the most accurate predictions of limits would require use of equation 15, with values of M_D that include effects of dissociation. Such calculations are tedious, and would not change the limits enough to affect the force of the

arguments herein. The essential point is that the same limits occur, whether a flame plus a shock builds up to a detonation, or a detonation dies away to a flame plus a shock.

Application to fuels other than hydrogen

The treatment carried out in this paper is based upon the clean-cut explosion limit condition resulting from the branched-chain nature of the hydrogen–oxygen reaction. A similar treatment could in principle be applied, for example, to moist or hydrogen-containing carbon monoxide; for it, too, burns in a branched-chain mechanism. In short, limits could be calculated for any case in which a branched-chain explosion condition is known.

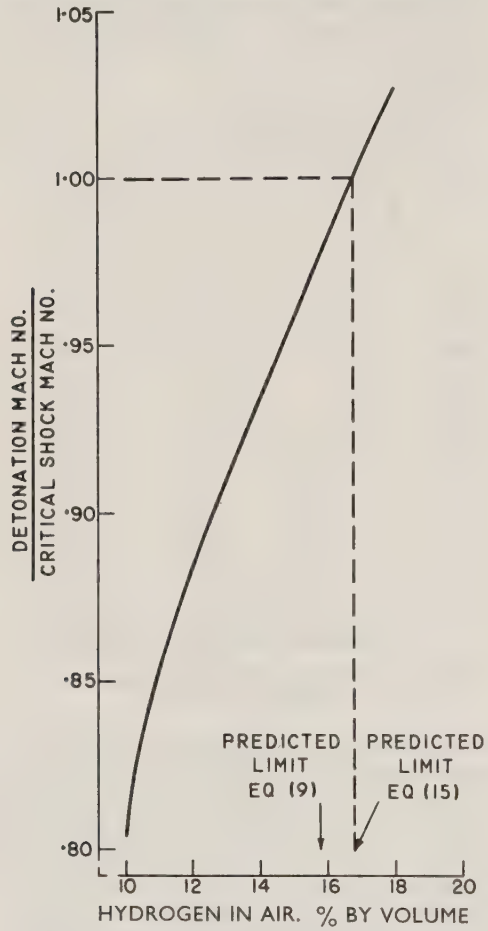

Figure 5. Comparison of detonation Mach number and critical shock Mach number for lean H_2–Air mixtures. T_0, 300°K; P_0, 1 atm

It is not clear whether the work could be extended to fuels for which the kinetics are known, but which do not have an explosion condition, such as the hydrogen–bromine reaction or the ozone decomposition. It would be interesting to attempt this with the aid of an artificial, but reasonable, explosion condition. For example, it might be specified that effectively immediate explosion occurs if the reaction is complete within a time comparable to the passage of a gas parcel through a real shock wave, that is, one which is 100 or so free-paths thick.

There may be a question as to whether all fuels are capable of undergoing a transition from flame to detonation. Since a pre-flame shock both heats and compresses the unburned gas, it will increase the mass burning rate provided the following inequality holds

$$du_m = \left(\frac{\partial u_m}{\partial T}\right)_P dT + \left(\frac{\partial u_m}{\partial P}\right)_T dP > 0 \quad (16)$$

where u_m is the mass burning rate (g/cm² sec).

If the inequality is indeed satisfied, the shock can be continually strengthened. Whether or not it can be strengthened enough to cause immediate auto-ignition depends upon the energy released on combustion; but assuming that this energy release is sufficient, one may inquire whether inequality 16 holds for a variety of fuels.

It is found experimentally that burning velocity depends on mixture temperature and pressure in the following way

$$u_f \propto T_0^a \quad (17)$$

and

$$u_f \propto P_0^b \quad (18)$$

where u_f is the burning velocity (cm/sec).

Using equations 17 and 18, it may be shown that the inequality 16 can be re-stated as follows

$$d \log u_m = [(a - 1)dT + (b + 1)dP] > 0 \quad (19)$$

All data with which the author is familiar indicate that inequality 19 will always be fulfilled: dT and dP are of course positive behind a shock; the temperature exponent, a, is always larger than unity; and while the pressure exponent, b, is often negative, it is never as small as -1.

Consequently, production of a strong shock is possible in all known cases. Since such a shock is required for transition from flame to detonation, it is concluded that detonation can always occur if there is enough energy released in combustion, although a very long run-up distance may be required in some cases.

CONCLUSIONS

The following conclusions were reached:

(1) The limits of detonability of hydrogen arise from the kinetic requirements for explosion. The limits are well predicted with the aid of kinetics obtained from low-temperature explosion-limit studies.

(2) The same limits may be predicted from two different models: a flame plus a shock developing into detonation, or an overdriven detonation decaying into a flame plus a shock.

(3) Critical shock Mach numbers for explosion and, hence, limits of detonability, may be calculated for any fuel for which the kinetics and a branched-chain explosion condition are known. The extent of agreement with observed limits should constitute a check on the validity of the kinetics.

It is a pleasure to acknowledge the help of Diane H. Lucas in making some of the calculations for this paper.

REFERENCES

[1] Greifer, B., Cooper, J. C., Gibson, F. C. and Mason, C. M. Combustion and detonation in gases. *J. appl. Phys.* 28, No. 3 (1957) 289

[2] Courant, R. and Friedrichs, K. O. *Supersonic Flow and Shock Waves*, p. 224. 1947. New York; Interscience

[3] Chu, Boa-Teh. On the generation of pressure waves at a plane flame front. *Fourth Symposium (International) on Combustion*, pp. 603–612. 1953. Baltimore; Williams and Wilkins

[4] Lewis, B. and von Elbe, G. *Combustion, Flames, and Explosions of Gases.* 1951. New York; Academic Press

[5] Glass, I. I., Martin, W. and Patterson, G. N. *A Theoretical and Experimental Study of the Shock Tube. UTIA Rep. No. 2.* Inst. Aerophys. Univ. Toronto (Nov. 1953)

[6] Ames Research Staff. Equations, tables and charts for compressible flow. *Nat. Adv. Comm. Aero. Rep. 1135* (1953) (Supersedes *N.A.C.A. Tech. Note 1428*)

[7] Glasstone, S. *Thermodynamics for Chemists*, p. 503. 1949. New York; Van Nostrand

[8] Laffitte, P. F. Flames of high-speed detonation. *Science of Petroleum, Vol. IV*, pp. 2995–3003. 1938. London; Oxford University Press

[9] Coward, H. F. and Jones, G. W. Limits of flammability of gases and vapors. *U.S. Bur. Min. Bull. 503* (1951)

LIMIT AND SPIN EFFECTS IN HYDROGEN-OXYGEN DETONATIONS

W. E. GORDON, A. J. MOORADIAN and S. A. HARPER

INTRODUCTION

This paper reports work on two rather poorly understood detonation phenomena. One has to do with detonation limits and the other with the intriguing spin phenomenon.

In connection with the problem of limits, Zeldovitch[1] has considered the problem of heat losses and his theoretical deductions probably explain the low-pressure detonation limit in many cases. Brinkley and Richardson[2] showed that when the reaction fails to reach completion in front of the Chapman-Jouguet (C–J) plane, combustion may build up in the expansion wave and lead to an instability. Their theory explains the pulsating detonations sometimes found in near-limit mixtures. Detonation limits probably reflect combined effects of reaction-kinetic behaviour and heat losses. They are therefore of more interest for the light they may shed on reaction mechanisms than for the insight they give into the hydrodynamic aspects of detonation. Knowledge of the limits is, of course, of considerable practical importance for the safety of many industrial processes and for engine combustion.

Published work on detonation limits is not extensive. Wendlandt[3] and Lafitte and Breton[4] studied hydrogen mixtures. Harper and Gordon[5] worked on ozone detonations.

The spin phenomenon has received more experimental attention. The original discovery of spinning detonations by Campbell and Woodhead[6] in 1926 was followed by a series of ingenious experiments by the British scientists[7–10]. A mathematical description of this strange effect was supplied by Fay[11], who identified it as a travelling wave phenomenon and correctly adduced the spin frequency.

LIMIT PHENOMENA

Our apparatus and experimental methods are briefly described in a forthcoming paper[12], and more fully by Mooradian and Gordon[13]. The detonation tube was 12 m long and 20 mm diameter. The front 2 m section contained the driver gas, usually knallgas ($2H_2$-O_2). This initiating mixture was separated from the experimental section by a Cellophane diaphragm. The pressure of the driver gas was usually made higher than that of the experimental mixture in order to overdrive the detonation. We refer to the ratio of the pressure of the driver gas to that of the mixture as the 'initiator ratio'.

We found detonation limits both in pressure and composition. The limit was easily recognized: the over-driven detonation in an above-limit mixture settled to a final steady velocity, but in a below limit mixture it suddenly failed and degenerated into a simple shock, without combustion. The behaviour of some of these near-limit detonations is illustrated in *Figure 1*.

The curves in *Figure 1* show the progress of the detonation or shock wave in terms of the Mach number, i.e. the ratio of the detonation or shock-wave velocity to the sound speed. Typical behaviour is illustrated in *Figure 1a*. In this case, steady detonation is impossible when the initial pressure is below 1·0 atm.

Detonation failure is not essentially altered by increasing the strength of the initiating shock. If the mixture conditions are very close to the limit, however, the detonation may appear to stabilize over a certain distance in the tube; actually, it is in the over-driven state during this time (see, for example, the curve at 0·75 atm in *Figure 1a*). The over-driven detonation settles fairly slowly toward the C–J condition, but if this condition is not stable, it fails before reaching the C–J point. Thus, the period of over-driven detonation may be long or short depending on the distance from the limit boundary. The curves in *Figure 1* may be understood in these terms.

Hydrogen–air mixtures behave in a peculiar way, as illustrated in *Figure 1d*. Here, the progress of the detonation wave has a tendency to oscillate, a property that becomes very pronounced at the limits. Such behaviour is predicted by Brinkley and Richardson[2]: the reaction fails to reach completion in front of the C–J plane; as a result, the wave deteriorates; then, a reaction zone, developing in the expanding part of the wave, moves up to the front and imparts a second acceleration; the phenomenon repeats. The piezoelectric gauge records for these mixtures lend additional support to this explanation. The pressure effects in such cases are discussed by Mooradian and Gordon[13].

Spin is found in high degree in all near-limit

mixtures. The spinning propagation mode seems to be associated only with detonations near the C–J point; it is absent in strongly over-driven detonations but suddenly appears when the over-driven wave settles toward the stable velocity. Spinning occurs even in below-limit mixtures during the short period when the wave is near the C–J velocity. This behaviour is also described[13].

DETONATION LIMITS

The limit boundaries for four different diluent systems are mapped in *Figure 2*. The exact position of the limits is of course slightly uncertain; the triangular points in the lower part of each diagram indicate the two near-limit conditions tested, the upper point being stable and the lower point unstable. The position of the composition limit is likewise experimentally uncertain; it lies between

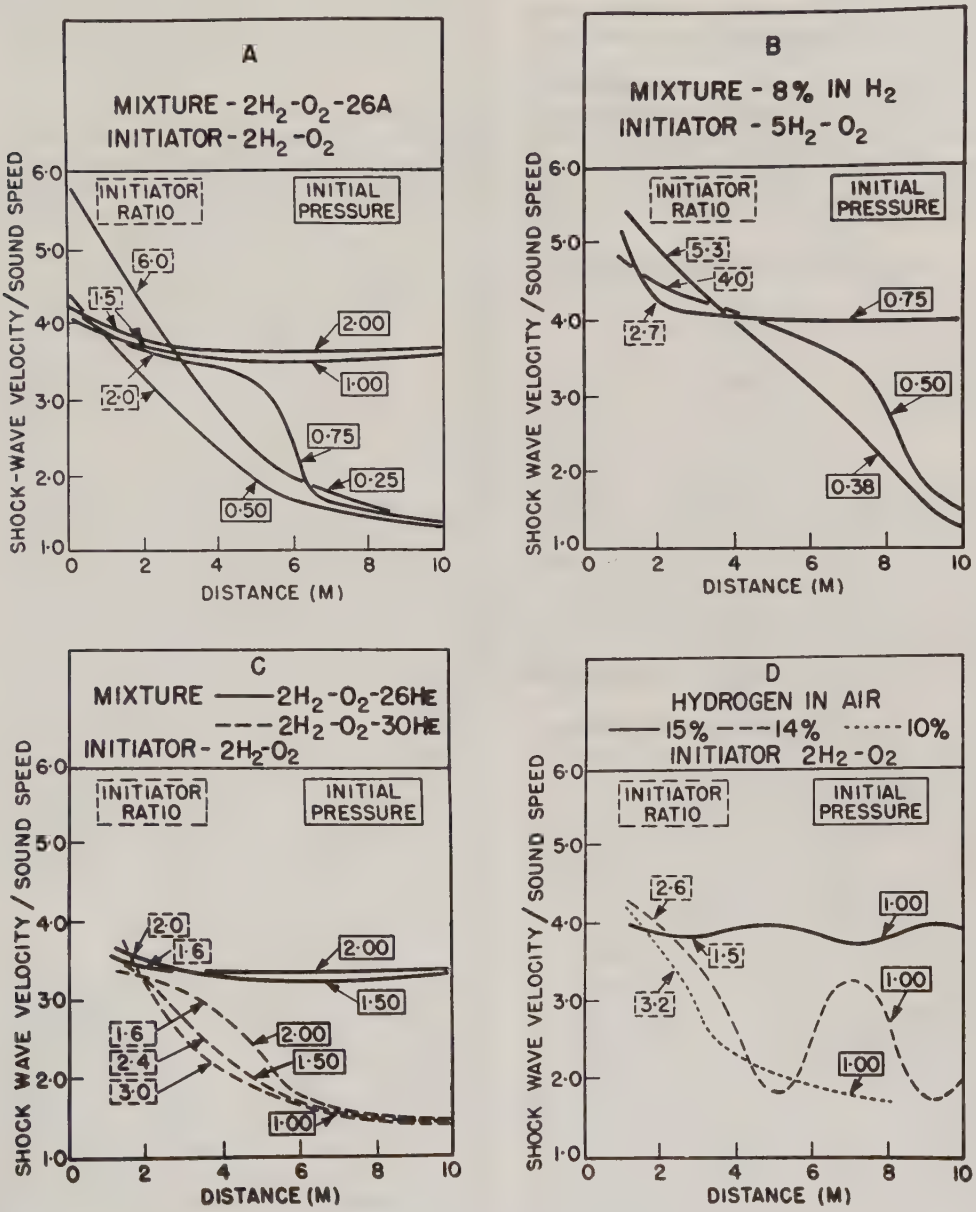

Figure 1. Shock-wave behaviour near the detonation limits

the dashed and the solid line at the left side of the shaded area. The cross-hatched areas indicate the regions in which various spin modes were observed. The spin behaviour is described below.

Effect of water vapour

To our considerable surprise, we discovered that traces of water vapour affect the limits in H_2–air mixtures. Such an effect may also occur with other diluents besides air but we did not investigate it. The role of water vapour was discovered in the following accidental manner: duplicate experiments that were separated by an interval of time were found not to agree; the cause for the discrepancy was traced to the different amounts of water present in gas drawn from a high-pressure hydrogen cylinder on these two occasions, the cylinder pressure in the first instance being about 1,500 lb. in. and in the second about 300 lb. in.^{2}. Since the gas in the cylinder was saturated with water vapour at ambient temperature, the mole-fraction of water was different in the two cases, When experiments were repeated with controlled amounts of water, we found that a 15 per cent H_2–air mixture will support a stable detonation when it has as much as 50 parts per million of water vapour (by mole fraction), but does not detonate stably with 500 parts per million.

We may compare this result with similar phenomena found for the explosion limits described by Lewis and von Elbe[14]. The inhibiting effect of water vapour here has been attributed to the high efficiency of the water molecule as the third body, M, in the chain-breaking reaction, $H + O_2 + M = HO_2 + M$. For example, von Elbe and Lewis[15] calculated from their data on the second explosion limit that a water molecule is 70 times more effective than an argon molecule in this reaction.

Low-pressure limits

Zeldovich[1] has investigated the system of equations that describes a stable detonation wave in which there are heat losses to the tube. He assumes the von Neuman-Zeldovich-Doring detonation model, in which a shock-front is followed by a stationary reaction zone. The reaction time, τ, determines the length of the reaction zone and therefore the amount of heat that is lost to the tube. The heat that is lost results in a drop of the detonation velocity and therefore lowers the temperature at the shock-front by a given amount. Since the shock-front temperature in turn affects the reaction time according to Arrhenius' law, we can represent these effects by a closed system of equations that may or may not have a real solution. In this way Zeldovich finds that detonation should be impossible when the velocity drops by some 10 to 15 per cent below the ideal C–J value. The data given in a forthcoming paper[12] show that in many cases the deviation from theoretical velocity

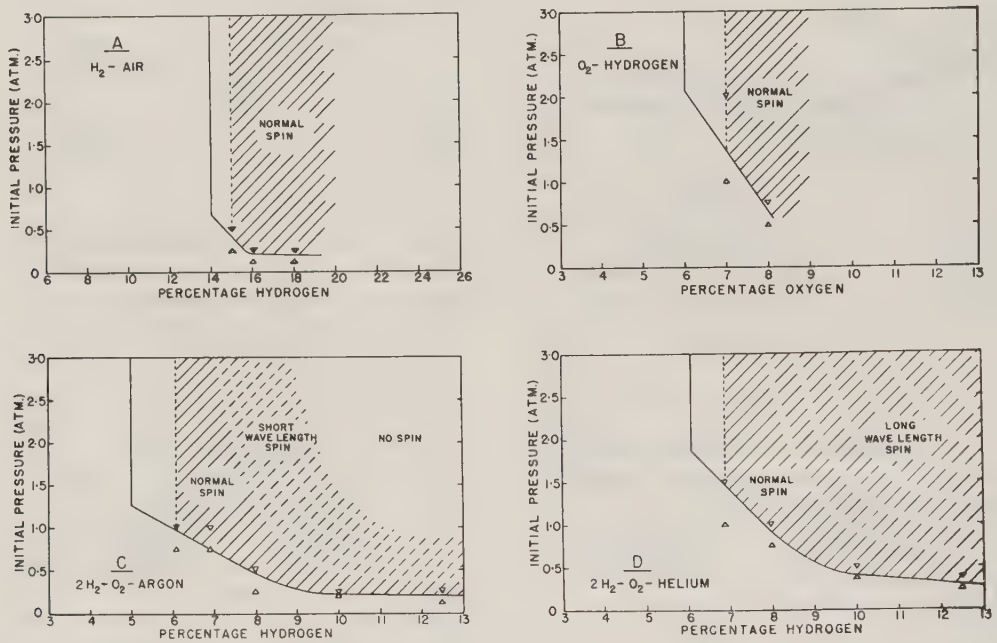

Figure 2. Detonation limits in various hydrogen mixtures

in the neighbourhood of the low-pressure limit does indeed lie in the 10 to 15 per cent range.

Although Zeldovich's theory seems to explain the low-pressure limits, the result must be partly fortuitous because near-limit mixtures always give spinning detonations. The von Neuman model, therefore, scarcely describes actual conditions.

Composition limits

The most interesting feature of the composition-limit data is the very low hydrogen concentration at the limit for helium and argon-diluted mixtures compared to that for an air-diluted mixture. The heat of combustion for limit mixtures containing monatomic diluents is less than half of that for mixtures containing diatomic diluents. Even when we compare the Chapman–Jouguet temperatures, we find them higher for the limit mixtures diluted with a diatomic gas than for those diluted with a monatomic gas. For example, the C–J temperature in 15 per cent H_2–air is 1,999°K, while in the mixture $2H_2$—O_2—30A, it is only 1,711°K.

The important temperature value, however, is not that at the Chapman–Jouguet point where the reaction is over, but that at the shock-front where the reaction begins. The temperature here turns out to be very close to 1,100°K for all composition-limit mixtures. (This is the shock-wave temperature for a wave of Mach number equal to that of the detonation wave. From *Figure 1*, we note that the Mach number lies between 3 and 4 in all the limiting cases.) According to the von Neuman picture, this is the initiating temperature of the chemical reaction. Even in spinning detonations, which we are dealing with here, the reaction must be initiated by shock-wave heating. The explanation for the composition limits, therefore, is probably this: beyond the limit, the shock temperature drops below a point where reaction is sufficiently rapid to sustain detonation.

Since the hydrogen–oxygen reaction is of a chain-branching type, the limit is probably determined by the critical length of the induction period. In a study of the ignition of hydrogen mixtures by heated wires currently being made at Arthur D. Little, Inc., the induction period has been found to range from about 25 milliseconds at 1,000°K to about 4 milliseconds at 1,100°K. Since the effective average gas temperature close to the wire in these experiments is less than the temperature of the wire itself, we may suppose that the induction period is actually in the microsecond range at a temperature of 1,100°K. This result makes our interpretation of the composition limit appear quite reasonable.

The effect of water vapour also shows that the reaction rate dominates the composition-limit phenomenon.

Comparison of detonation and inflammability limits

A comparison of detonation limits with inflammability limits is interesting. von Elbe and Lewis[15] report a lower inflammability limit for hydrogen in air of 4·00 per cent and an upper inflammability limit of hydrogen in oxygen of 93·9 per cent. (The lower limit of hydrogen in oxygen is 4·65 per cent, fairly close to that in air.)

The molal heat of combustion of the upper-limit mixture is therefore about three times that of the lower-limit mixture. The inflammability limit is determined, in general, by both the transport properties—thermal and material diffusion—and the heat value of the gas. The role of diffusion is dominant in hydrogen mixtures.

For carbon monoxide in oxygen, on the other hand, the lower inflammability limit is 15·5 per cent and the upper limit 93·9 per cent. The heat value of these mixtures is almost equal. Transport properties in this case play a minor role because they are not very different for carbon monoxide and oxygen.

In contrast to the inflammability limit, the detonation limit in hydrogen mixtures is dominated entirely by the heat value. The lower detonation limit for hydrogen in air is about 15 per cent and the upper limit for hydrogen in oxygen, about 93·5 per cent. Thus while the upper detonation limit is about the same as the inflammability limit, the lower detonation-limit mixture is almost four times richer than the inflammability limit mixture.

We see from these comparisons that the detonation limits are not dependent on transport properties. This conclusion is entirely consistent with detonation theory which predicates a minor role for transport phenomena in the reaction zone.

Practical detonation hazards

The hazards of accidental detonation are by no means equal for the upper- and lower-limit mixtures. The hydrogen-rich mixture is by far the less dangerous. The reason is that detonation in hydrogen-rich mixtures is very difficult to initiate. The high acoustic velocity in these mixtures tends to prevent build-up of a shock wave from a flame. Detonation in the rich-limit mixture can be produced only by a strong shock wave.

In lean hydrogen-air mixtures, on the other hand, a very weak shock can build up to detonation. This strong tendency for detonation to develop in lean hydrogen–air mixtures is present even for compositions below the detonation limit, as we can see from *Figure 1d*. The contrasting behaviour of lean and rich mixtures is described by Mooradian and Gordon[13].

Not only are hydrogen-rich mixtures difficult to detonate, but they are even relatively difficult to ignite. To illustrate this fact, we may quote values

of the minimum energy for spark ignition of hydrogen–air mixtures at 1 atm from Lewis and von Elbe[14], as follows: 64 per cent hydrogen, 0·65 millijoules; 30 per cent hydrogen, 0·019 millijoules; 10 per cent hydrogen, 0·16 millijoules. This behaviour is a result of the high thermal conductivity of hydrogen.

of the present work we encountered extremely pronounced oscillations. These were experiments on the propagation of a supported shock wave (produced in a shock tube) in a mixture of ozone, oxygen and nitrogen pentoxide. One of us noted a peculiar banded appearance to the pink flame that was produced in a glass tube by this means. It

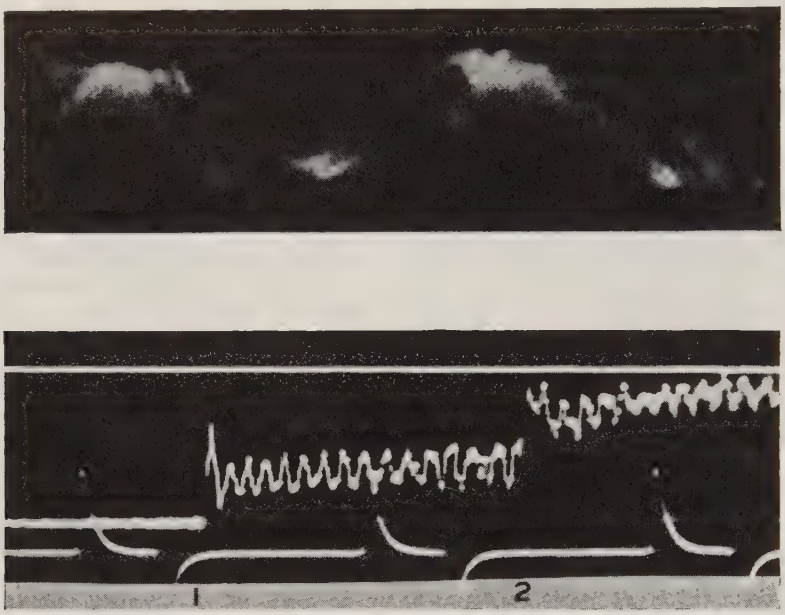

Figure 3. Above: Spinning detonation in a mixture of O_3, N_2O_5 *and* O_2 *at partial pressures of* 18, 9 *and* 5 mm Hg *respectively. Below: Piezoelectric gauge record for the same mixture. The numbers* 1 *and* 2 *mark the beginning of the record on each of the two gauges (slightly retouched for clarity)*

For these reasons, we see that the hazard resulting from small amounts of air leaking or diffusing into hydrogen is much less than that from small quantities of hydrogen diffusing into air.

The composition range of detonable mixtures in a practical situation, that is in cases where detonation has to build up from a flame, would probably be much narrower than that we have given here. The narrowing of the range would occur largely on the hydrogen-rich side. Our limits are the extreme values for the case where the initiating source is strong enough to over-drive the detonation. The limits in a practical situation would have to be determined experimentally.

SPIN

In his first paper on the subject of detonation pressures, Gordon[16] noted that oscillations appeared in the piezoelectric records, especially in dilute mixtures. Much effort was devoted, without success, to eliminating these vibrations. In one case, for example, a section of tube with walls 1·5 in. thick was used. In some early experiments resembled to the naked eye the positive column of a gaseous discharge. A still camera with an open shutter was set up to photograph the phenomenon. The resulting film is shown in *Figure 3*; below it is the pressure record obtained from two piezoelectric gauges placed in the tube at a separation of 105 cm.

Clearly, we had a spinning detonation and the pressure oscillations were associated with it. The quantity obtained by dividing the shock velocity by the oscillation frequency matched almost exactly the pitch of the helical flame path. (The pitch was about 6·2 cm, the shock velocity 950 m/sec, and the vibration frequency 15,000 m/sec.)

The conditions that gave rise to the photograph in *Figure 3* must be considered highly unusual. In fact, we had great difficulty in trying to reproduce them. As a rule there was sufficient luminosity in the wake of the detonation front to fog the whole photograph and to almost obliterate the extra luminosity of the spinning head. In the experiment photographed in *Figure 3*, apparently

only the head itself was luminous. In photographs taken with a rotating-mirror camera, there is less difficulty in detecting the rotating head, but even here, we must suppose that if the luminosity of the head is not great, it may go unnoticed. The piezo-electric gauge, however, provides a sensitive means of detecting spin that is independent of the luminous effects.

The original negative of the photograph in *Figure 3* shows a great deal of structure. The helical path of the spinning detonation is by no means smooth. There appear to be two or three sharp zones of luminosity separated by dark spaces that move in parallel paths. The pressure record reveals the complexity of the phenomenon. There are actually shock fronts far to the rear of the wave front itself. Such behaviour must be expected because of the high pressure gradients in the tube and the well known tendency of compressional waves to become steeper and develop into shocks. Because of this ever-changing pattern of the pressure fluctuations, it is not surprising that spark photographs of the spinning detonation[10] show a very complex structure at the wave front.

Similar pressure oscillations, but of smaller amplitude, were routinely observed in subsequent work with dilute hydrogen mixtures. In fact, they were found in rich mixtures too, although usually with small amplitude. (See *Figure 5* in reference 12.) Spin appeared to be not the exception but the rule.

In an experiment with a carbon monoxide mixture, we identified the frequency of the pressure oscillations with that of the spin found for the same mixture in the photographs of Campbell and Woodhead[6].

In another experiment we placed two pressure gauges on opposite sides of the tube, opposing one another at 180°; the pressure oscillations on the two detectors proved to be in exactly opposite phase, and just cancelled one another.

At about the same time that our work was going on, Fay[17] made a theoretical study of spinning detonation, considering it to be an acoustic vibration or travelling wave. The Rayleigh equations applied by Fay strictly pertain to vibrations of small amplitude. From *Figure 3* we see that the oscillations are far from being infinitesimal. However, the comparisons that Fay makes[11] between his theory and the classical observations of Campbell and the other British workers show remarkable agreement.

In the fundamental mode, or 'normal' spin as we have designated it in *Figure 2*, the vibration has a pitch about equal to three tube diameters. (The factor is not exactly three; it depends on the properties of the detonation product-gases.) The basic property of the spinning wave is the rotational frequency of the high-pressure region at the front. This rotating high-pressure zone persists in the product-gases behind the front with only slightly diminished amplitude. A stationary pressure gauge receives periodic pulses of a frequency comparable with the rotational frequency. Actually, because the high-pressure zone in the wake may not extend behind the front in a straight line parallel to the tube axis, but may be twisted, the frequency recorded on a stationary gauge may not exactly match the rotational frequency.

In *Figure 2* we have applied the term 'wave length' to the quantity obtained by dividing wave velocity by frequency. The ratio of this wave length to the tube diameter for near-limit mixtures was always about three, but in other compositions it was often different, being sometimes smaller ('short' wave length) and sometimes larger ('long' wave length). The short wave length (high frequency) spins are multiple headed[11]. However, we have never observed more than two heads. The long wave length spins that we found in some helium mixtures cannot be correlated at present with Fay's theory.

The remarkable fact is the constancy of spin frequency and amplitude under a given set of conditions. The results of our spin frequency measurements, expressed as a ratio of pitch to tube diameter, are given in Table 1.

For calculating the spinning frequencies in Table 1, we have used the formula given by Fay[17]:

$$\frac{P}{d} = \frac{\pi D_0}{a k_n} \qquad (1)$$

where P is the pitch of the spinning wave, d the tube diameter, D_0 the wave velocity, a the acoustic velocity in the product gases, and k_n the root of the first derivative of a Bessel function. Here n is the number of circumferential crests or spinning 'heads'. The number k_n has the values 1·841 and 3·054 when n is equal to 1 and 2 respectively. The ratio D_0/a is equal to the ratio ϕ of the specific volume in front of the wave to that behind. We have evaluated ϕ for our mixtures[12] and so we use the formula

$$\frac{P}{d} = \frac{\pi}{\phi k_n} \qquad (2)$$

(π is here the universal constant, not the pressure ratio across the wave front).

One notes in Table 1 the abrupt changes in spin mode that occur when the initial pressure is varied, and the progressive shifts of the transition region with composition. The shading in *Figure 2* depicts these regions of various spin types.

With certain exceptions, the results in Table 1 are in fair agreement with Fay's theory. The exceptions are for the stoichiometric mixture and the helium mixtures. The low value of P/d for the

TABLE 1

Comparison of Experimental and Theoretical Spin Frequencies

Mixture	*Initial pressure* (mm Hg)	*Pitch/tube diameter*			*Mixture*	*Initial pressure* (mm Hg)	*Pitch/tube diameter*		
		Obs.	*Obs.* (Ave)	*Theor.* $n = (\ )$			*Obs.*	*Obs.* (Ave)	*Theor.* $n = (\ )$
$2H_2$–O_2	2005	2·55			18% H_2–air	760	2·90		
	1520	2·65				570	3·00		
	760	2·60	2·60	3·14 (1)		380	2·95		
	380	No spin				190	2·70	2·90	2·90 (1)
	190	No spin							
	95	2·10		1·89 (2)	16% H_2–air	1520	3·05		
8% O_2 in H_2	2280	2·85				760	2·95		
	1520	2·85				570	2·95		
	760	2·90				570	3·00		
	570	2·95	2·88	2·87 (1)		570	3·00		
7% O_2 in H_2	2136	2·95				380	2·85		
	1520	2·85	2·90	2·86 (1)		380	2·95	2·96	2·89 (1)
$2H_2$–O_2–13A	2280	No spin			15% H_2–air	1520	2·90		
	1520	No spin				760	2·95		
	760	No spin				570	2·90		
	570	No spin				380	2·90	2·91	2·88 (1)
	380	1·40		1·66 (2)					
	190	2·60		2·74 (1)	$2H_2$–O_2–13He	1900	4·15		
$2H_2$–O_2–17A	2280	No spin				1520	4·60		
	1520	No spin				1140	4·40		
	760	1·65				760	3·80		
	560	1·70				570	3·50	4·08	?
	380	1·50	1·63	1·64 (2)		380	2·65		
	190	2·55		2·71 (1)		285	2·65	2·65	2·74
$2H_2$–O_2–22A	2280	1·65		1·62 (2)					
	1520	Not clear			$2H_2$–O_2–17He	1520	3·70		
	760	2·75				1140	3·45		
	760	2·70				760	3·40	3·52	?
	570	2·65				570	2·65		
	380	2·65	2·68	2·68 (1)		380	2·55		
$2H_2$–O_2–26A	2280	2·80				380	2·50	2·57	2·71 (1)
	1520	2·75							
	760	2·60			$2H_2$–O_2–22He	1520	2·65		
	760	2·55	2·68	2·66 (1)		760	2·60	2·62	2·71 (1)
$2H_2$–O_2–30A	2280	2·85							
	1520	2·60			$2H_2$–O_2–26He	1520	2·65		
	760	2·50	2·65	2·64 (1)		1140	2·65	2·65	2·68 (1)

fundamental mode in knallgas may indicate that the value used for ϕ in equation 2 is too low, that is to say, that the density of the product gases is actually higher than that calculated for the equilibrium C–J point. Such a result would be in accord with the low-pressure value found for this mixture and with other indications discussed in a forthcoming paper[12]. The high P/d values for helium mixtures at high initial pressures cannot be reconciled with Fay's theory even by introducing radial modes[17]. These results are puzzling.

Although the physical characteristics of the spinning detonation now seem fairly well understood, we are far from having a complete theory. We may ask why spin develops only when the detonation is near the Chapman–Jouguet velocity[13]. We may wonder that the manner of initiation is not important. The spinning wave shown in *Figure 3*, for example, was a piston-supported or driven detonation, produced by the expansion of an inert gas behind a bursting diaphragm; it was not started from a deflagration wave. Therefore, spin appears to be a hydrodynamic requirement for the stable propagation of the wave, and not an accidental or minor appurtenance.

Is the spinning wave a completely different regime to that of the normal von Neuman detonation, or can the two regimes be superimposed? Perhaps it is significant that only in mixtures of intermediate composition where there was no spin have we found the 'von Neumann spike' in our pressure records. This was true both for hydrogen–oxygen mixtures and ozone mixtures[5]. It was also observed that the velocity and pressure were closer to the theoretical values in these spin-free mixtures. According to the recent work of Kirkwood and Wood[18,19], the von Neuman detonation model meets with difficulties under certain conditions. Is it possible that a spinning wave always results when a stable von Neuman structure cannot be set up?

This work was done at the University of Missouri under Office of Naval Research Contract, ONR 292-Task Order 1.

REFERENCES

[1] Zeldovich, Y. B. *Theory of Combustion and Detonation of Gases*, 1944. Academy of Sciences of the USSR, Institute of Chemical Physics

[2] Brinkley, S. R. Jun. and Richardson, J. M. *Fourth Symposium (International) on Combustion*, p. 450. 1953. Baltimore; Williams and Wilkins

[3] Wendlandt, R. *Z. phys. Chem.* 110 (1924) 637; 116 (1925) 227

[4] Laffitte, P. and Breton, J. *C. R. Ass. franç. Ar. Sci.* 199 (1934) 146

[5] Harper, S. A. and Gordon, W. E. *International Ozone Conference*, November, 1956. Chicago, Ill. (To be published in *Advances in Chemistry* series)

[6] Campbell, C. and Woodhead, D. W. *J. chem. Soc.* (1926) 3010; (1927) 1572

[7] — and Finch, A. C. *J. chem. Soc.* (1928) 2094

[8] Bone, W. A. and Fraser, R. P. *Phil. Trans. A* 228 (1929) 197

[9] — — *Phil. Trans. A* 230 (1932) 363

[10] — — and Wheeler, W. H. *Phil. Trans. A* 235 (1935) 29

[11] Fay, J. A. *J. chem. Phys.* 20 (1952) 942

[12] Gordon, W. E. and Mooradian, A. J. Data on the effect of initial pressure on detonation velocity and on the pressure in the detonation wave. To be published

[13] Mooradian, A. J. and Gordon, W. E. *J. chem. Phys.* 19 (1951) 1166

[14] Lewis, B. and von Elbe, G. *Combustion, Flames and Explosions of Gases*. 1951. New York; Academic Press

[15] von Elbe, G. and Lewis, B. *J. chem. Phys.* 10 (1942) 366

[16] Gordon, W. E. *Third Symposium on Combustion, Flame and Explosion Phenomena*, p. 579. 1949. Baltimore; Williams and Wilkins

[17] Fay, J. A. *Thesis* 1951. Cornell University

[18] Kirkwood, J. G. and Wood, W. W. *J. chem. Phys.* 22 (1954) 1915

[19] Wood, W. W. and Kirkwood, J. G. *J. chem. Phys.* 25 (1956) 1276

100

CONCERNING SPIN DETONATION

A. S. PREDVODITELEV

Formation of a detonation front in closed vessels is due to accelerated propagation of the flame front acting as a Hugoniot position. This has been experimentally proved by V. A. Popov and G. D. Salamandra. All research work was carried out in the laboratories headed by the author of this paper.

Description of the detonation front formation in closed vessels amounts to solving the equation of the one-dimensional, non-linear wave front on the assumption that the rate at which the chemical reaction proceeds is infinitely great. In fact, under these limitations the method of characteristics permits a single-valued answer adequate to most observations. Discovery of spin detonation suggests that solution of a one-dimensional non-linear wave acoustic equation will not be sufficient for a comprehensive grasp of detonation processes. Spin detonation was observed in cylindrical vessels, and, recently, T. V. Bazhenova and R. I. Soloukhin have observed it in a rectangular vessel. It may be presumed that all cases where spin detonation was observed are connected not with a one-dimensional but with a three-dimensional process. Consequently, it is necessary to solve the non-linear wave acoustic equation without confining the problem to a flat front. Unfortunately so far this problem has not been solved. It has not yet been established to what degree Hugoniot's conditions of compatibility apply to three-dimensional problems. In one-dimensional problems these conditions permitted Hugoniot to completely solve the problem.

Solution of a three-dimensional problem presents very great mathematical difficulties. Therefore, it is desirable to find some roundabout way of solving the problem. This is necessary in order that an experimental researcher might have a clear perspective for staging further experiments. Such an attempt is made in this paper, though the author is far from claiming the complete solution of the problem.

At present we may categorically assert that no shock wave is possible in an undisturbed medium unless there is a flow behind it. The peculiarities of this flow in the case of a flat shock wave are well known. This flow is characterized by a constant velocity and a definite direction. However, it is not the only possible case. We will not contradict the laws of conservation if we distort the flow behind the shock wave in accordance with the geometrical shape of the vessel in which it exists. The hydrodynamics explicity tell us what types of flow can exist in a cylindrical tube.

It is possible that a central nucleus of flows having a constant velocity may be surrounded by turbulent rings, resembling parallel turns of a solenoid. The thickness of this zone has been studied very little. These conditions should attend any flat shock wave appearing in a cylindrical vessel.

Such a wave will never reach the walls, a fact which should be always kept in mind when carrying out experimental study of the wave.

A Poiseuille flow is also possible in a cylindrical tube. However, this flow characterized by parabolic distribution of velocities along the section of the flow is incompatible with simultaneous existence of a flat or slightly distorted shock surface.

A turbulent flow with an almost uniform distribution of mean velocities along the flow section is possible in a cylindrical tube. This flow is based on so-called Prandtl's adjoining layer. It is hard to say how much this flow is compatible with a shock surface. In our personal opinion such flows are incompatible with simultaneous existence of a shock surface. This assertion may, however, be wrong.

Finally a helical flow may exist in a tube. In our opinion such flow is compatible with the simultaneous existence of a shock surface in such a sense that it would be almost adequate for spin detonation. All the above-mentioned flows owe their existence to the tensor of viscous stresses.

The helical motion is characterized by the fact that the vortex axis always coincides with the direction of the motion velocity. Mathematically this condition may be expressed by the relationship of the form

$$\operatorname{curl} \vec{W} = K\vec{W} \qquad (1)$$

The ratio factor is called intensity of turbulent motion. In the general case it may depend on coordinates and time. However, treated in this way, the problem becomes so complicated that so far it has been hardly described at all. We will simplify the problem. Let us confine ourselves to the case where the intensity of the turbulent rotation may be considered to be a constant.

From relation 1

$$\operatorname{div}\operatorname{curl}\vec{W} = K\operatorname{div}\vec{W} = 0$$

Due to this condition the equation of continuity will have the following form:

$$\frac{d\rho}{dt} = \frac{\partial\rho}{\partial t} + (\vec{W}, \operatorname{grad}\rho) = 0$$

and the equation of motion, with due regard for viscosity will have the form

$$\rho - \frac{d\vec{W}}{dt} = -\operatorname{grad} p + \eta\Delta_2\vec{W}$$

For helical motion the second addend of the right-hand side of this equation may be considerably simplified.

Let us write an apparent identity

$$\operatorname{curl}\vec{\omega} = \frac{1}{4}\left[\frac{\partial^2 W_x}{\partial y^2} + \frac{\partial^2 W_x}{\partial z^2} - \frac{\partial}{\partial x}\left(\frac{\partial W_y}{\partial y} + \frac{\partial W_z}{\partial z}\right)\right]$$

However, since the divergence is equal to zero

$$\frac{\partial}{\partial x}\left(\frac{\partial W_y}{\partial y} + \frac{\partial W_z}{\partial z}\right) = -\frac{\partial^2 W_x}{\partial x^2}$$

Therefore, we can write the following equality

$$\operatorname{curl}\vec{\omega} = -\tfrac{1}{4}\Delta_2\vec{W}$$

or considering relation 1

$$K^2\vec{W} = -\tfrac{1}{4}\Delta_2\vec{W}$$

Now the helical motion equation may be written as follows

$$\rho\frac{d\vec{W}}{dt} = -\operatorname{grad} p - 4K^2\eta\vec{W} \qquad (2)$$

This equation was derived on the assumption that viscosity η is independent of coordinates and time.

The following vectorial differential identity is generally known

$$\frac{d\vec{W}}{dt} = \frac{\partial\vec{W}}{\partial t} + \tfrac{1}{2}\operatorname{grad} W^2 + \left[\vec{\omega}, \vec{W}\right]$$

For helical motion the term in square brackets is reduced to zero. Therefore equation 2 may be written

$$\frac{\partial\vec{W}}{\partial t} + \tfrac{1}{2}\operatorname{grad} W^2 + 4K^2\nu\vec{W} = -\frac{1}{\rho}\operatorname{grad} p \qquad (3)$$

where ν denotes kinematic viscosity.

Suppose the flow proceeds with constant enthalpy. Then

$$du + p\,dv + v\,dp = 0$$

Besides, assuming that

$$du + p\,dv = \tfrac{1}{2}\,dW^2$$

then, the flow will be governed by the following equation

$$\rho\frac{\partial\vec{W}}{\partial t} + 4K^2\eta\vec{W} = 0 \qquad (4)$$

Thus, this equation will govern all flows, where apparent motion is transformed into internal energy of the medium and into pressure energy.

Let us resolve vector $\vec{W}$ into two components:

$$\vec{W} = \vec{W}_p + W_i e^{i\omega t} = \vec{W}_p + \vec{W}_s \qquad (5)$$

Suppose the first addend depends only on coordinates and is independent of time. The second addend will depend on the time in the above-mentioned manner.

By substituting function 5 in differential equation 4 we will have

$$\rho\omega i\vec{W}_s + 4K^2\eta\left(\vec{W}_p + \vec{W}_s\right) = 0 \qquad (6)$$

For complex value of the flow velocity the intensity of the vortex rotation will also have a complex value.

Let us assume

$$K = K_0 - K_1 i; \quad \vec{W}_s = \vec{W}_0 + i\vec{W}_1$$

By substituting these expressions in formula 6 and separating real and imaginary parts we will have

$$\rho\omega\vec{W}_0 - 8\eta K_0 K_1\left(\vec{W}_p + \vec{W}_0\right) + 4\eta(K_0^2 - K_1^2)\vec{W}_1 = 0$$

$$\rho\omega\vec{W}_1 - 4\eta(K_0^2 - K_1^2)\left(\vec{W}_p - \vec{W}_0\right) - 8\eta K_0 K_1\vec{W}_1 = 0$$

Velocity W_z directed parallel to the tube axis will be called axial or longitudinal velocity. Velocity W_r directed along the radius will be called radial velocity and, finally, velocity W_n directed along the normal to the plane passing through the radius and the axis of the tube will be called rotary velocity.

Let us write two last vectorial equalities for the components of the velocity directed parallel to the tube axis

$$\rho\omega W_{0z} - 8\eta K_0 K_1(W_{pz} + W_{0z}) + 4\eta(K_0^2 - K_1^2)W_{1z} = 0$$

$$\rho_0\omega W_{1z} - 4\eta(K_0^2 - K_1^2)(W_{pz} + W_{0z}) - 8\eta K_0 K_1 W_{1z} = 0$$

Assuming that the real part of the axial velocity on the tube surface is equal to zero, the above equations give

$$\left.\begin{aligned}(\rho\omega - 8\eta K_0 K_1) W'_{1z} &= 0\\ \rho\omega + 8\eta(K_0^2 - K_1^2)\frac{W'_{1z}}{W'_{0z}} &= 0\end{aligned}\right\} \qquad (7)$$

$$W'_{pz} + W'_{0z} = 0$$

Let us assume that velocity component W_{1z} is not equal to zero. Then from the first two simultaneous equations 7 we will have

$$\left.\begin{aligned}\omega &= \frac{8\eta}{\rho} K_0 K_1\\ \omega &= -\frac{8\eta}{\rho}(K_0^2 - K_1^2)\frac{W'_{1z}}{W'_{0z}}\end{aligned}\right\} \qquad (8)$$

whence

$$\frac{W'_{1z}}{W'_{0z}} = -\frac{K_0 K_1}{K_0^2 - K_1^2} \qquad (9)$$

Subscript 1 shows that the ratios are true only for the wall.

Ratio 9, thus derived, shows that value K_1 will not be equal to zero only when imaginary velocity component W_{1z} is other than zero. If it is equal to zero, no periodic component with a rotary frequency ω is possible. The value of this quantity can be found knowing the ratio of velocity components on the tube wall.

Let us try to find the value of K_0. We will designate the vortex components of the real velocity component as follows

$$\omega_r, \omega_n, \omega_z$$

The following equalities are true for helical motion

$$\frac{\omega_r}{W_r} = \frac{\omega_n}{W_n} = \frac{\omega_z}{W_z} = \frac{K_0}{2} \qquad (10)$$

Due to physical considerations the vortex component directed along the radius should be taken to be zero. Consequently, from the above equalities it follows that velocity W_r must be also equal to zero. Now we have

$$K_0 W_n = 2\omega_n$$

$$K_0 W_z = 2\omega_z$$

However vortexes ω_n and ω_z are respectively equal to

$$\omega_z = -\frac{1}{2}\frac{1}{r}\frac{\partial(W_n r)}{\partial r}; \qquad \omega_n = \frac{1}{2}\frac{\partial W_z}{\partial r}$$

Therefore, we have

$$K_0 W_n = \frac{\partial W_z}{\partial r}; \qquad K_0 W_z = -\frac{1}{r}\frac{\partial(W_n r)}{\partial r}$$

Substituting the first of these equations in the second

$$\frac{\partial^2 W_r}{\partial r^2} + \frac{1}{r}\frac{\partial W_z}{\partial r} + K_0^2 W_z = 0$$

The solution of this equation is well known. It leads to zero-order Bessel function of the first kind, viz.

$$W_z = CI_0(K_0 r) \qquad (11)$$

Here C stands for flux velocity on the tube axis.

Inasmuch as velocity W_z on the wall is equal to zero the following equality can be written:

$$I_0 = (K_0 R) = 0$$

The root of this equation is known to be 2·4. Therefore, vortex intensity K_0 will be given by

$$K_0 = \frac{2{\cdot}4}{R} \qquad (12)$$

Knowing formula 11, giving the law of distribution of axial velocity component, we can easily find the rotary component, viz.

$$W_n = \frac{1}{K_0}\frac{\partial W_z}{\partial r} = -CI_1(K_0 r)$$

For $r = 0$ the velocity component directed along the tube axis will be equal to C. Consequently

$$CI_0(0) = C; \quad I_0(0) = 1$$

This condition leads to zero in the same point of the Bessel function of the first kind and the first order, i.e.

$$I_1(0) = 0$$

Thus, the rotary velocity on the tube axis is equal to zero and grows radially in proportion to the value:

$$I_1(K_0 r)$$

From the rate of change of this function we may draw the following conclusion. The central part of the flow rotates about the tube axis almost like a solid body and only when it approaches the walls the rotary velocity begins to decrease and on the wall itself it becomes equal to

$$W_{nk} = 0{\cdot}52C$$

The differential equations of fluid currents in cylindrical coordinates for the helical motion will have the following form

$$\frac{r\,d\varphi}{-CI_1(K_0 r)} = \frac{dz}{CI_0(K_0 r)}; \; dr = 0$$

Whence

$$r = \text{const}; \; Z = -\frac{I_0(K_0 r)}{I_1(K_0 r)} r\varphi + \text{const}$$

The first of these equations shows that all points of the fluid are located on circular cylindrical surfaces of various radii.

Isocurrents or curves of equal velocities located in the plane passing normally through the cylindrical tube will form a family of concentric circles. The following conditions will apply to each circle

$$r = \text{const} \qquad W_n = \text{const} \qquad (13)$$

Therefore the product Wr will be also a constant

$$W_n r = \text{const}$$

This relation shows that any point of the current lines is governed by the law of areas whose constant changes only when passing from one surface of current lines to another, adjacent to the first. A system of helical lines having the same pitch are described on each surface

$$r = \text{const}$$

The pitch of the helical lines varies from the tube walls to its axis, because the following conditions will apply

$$\text{for} \quad r = R; \quad I_0(K_0 r) = 0; \quad I_1(K_0 r) = 0{\cdot}52$$

Consequently, on the tube wall

$$\frac{I_0(K_0 R)}{I_1(K_0 R)} = 0$$

which means that for any value of angle φ coordinate z is equal to zero. On the contrary, the above ratio will become an infinity on the tube axis since the following relations will apply:

$$I_0(K_0 0) = 1; \qquad I_1(K_0 0) = 0$$

Consequently, in this case coordinate z will become infinite for any value of angle φ.

Two important conclusions may be drawn from the above. First, a fluid flow moving on the tube rolls, as it were, along a system of ring chords which lie in the plane perpendicular to the tube axis. Second, the inclination angle of helical lines or pitch of the helix varies from the wall to the tube axis from zero to 90°.

We have described the behaviour of the real velocity component of a pulsating helical flow. As can be seen from the above arguments we would not be able to detect spin detonation in the absence of pulsations. It is only due to pulsations that the spin detonation becomes possible. The real rotary velocity can be resolved into

$$W_n = W_{pn} + W_{0n}$$

Consequently, from relation 13

$$W'_{pn} R + W'_{0n} R = \text{const}$$

$$W'_{0n} R = \text{const}$$

However since rotary velocity component $\overrightarrow{W_0}$ depends on the tube radius, the axial velocity component will also depend on the tube radius, i.e.

$$W'_{0z} R = B = \text{const} \qquad (14)$$

With the help of relations 14 and 12, formulae 8 and 9 can be written as follows

$$\omega = \frac{8\eta}{\rho} \frac{2{\cdot}4}{R} \cdot K_1; \quad \frac{RW'_{1z}}{B} = -\frac{RK_1}{2{\cdot}4\left(1 - \frac{K_1^2}{K_0^2}\right)}$$

Assuming that K_1 is small as compared with K_0, the above equality reduces to

$$K_1 = -\frac{2{\cdot}4 W'_{1z}}{B}$$

The minus sign must be compensated by the sign of velocity W'_{1z} or velocity W'_{0z}. Therefore, it can be included in constant B. Now rotary frequency ω will be finally given by the following expression

$$\omega = \frac{8\eta}{\rho} \frac{2{\cdot}4^2}{R} \frac{W'_{1z}}{B} \qquad (15)$$

Thus, the pulsation frequency will vary inversely as the tube radius, which is actually observed during experiments. To calculate the pitch of the helix as a ratio between the tube diameter and the distance travelled by the particle for a full cycle we will use the following formula

$$\frac{\pi D}{h} = \frac{2\pi R}{\tau W'_{1z}} = \frac{8\eta}{\rho} \frac{2{\cdot}4^2}{B}$$

or

$$\frac{h}{D} = \pi \frac{B\rho}{2{\cdot}4^2 8\eta} = \pi \frac{W'_{0z} R\rho}{2{\cdot}4^2 8\eta} = \pi \frac{R'_e}{8 \cdot 2{\cdot}4^2}$$

where R'_e stands for the Reynolds number divided by the tube radius.

Taking energy as a criterion for determining stability of pulsatory motions and using the method of small oscillations Orr, Hamel and Kármán calculated the critical Reynolds number to be equal to 44·2.

On the basis of this number the value of ratio h/D will be

$$\frac{h}{D} = \pi \frac{44{\cdot}2}{8 \cdot 2{\cdot}4^2} = 3 \qquad (15a)$$

This number has been experimentally obtained first by Campbell and Woodhead and then by Bon and Fraser as far back as 1926.

T. V. Bazhenova and R. I. Soloukhin obtained almost the same number, though they experimented in a rectangular tube. Of course, in accordance with formula 15 this ratio may vary depending on the Reynolds number which most probably may vary within certain limits.

The above complex motion which may be mistakenly considered to be turbulent is easily

reconciled with the existence of detonation surface.

Let V_n represent velocity of medium behind the detonation surface, as calculated on the basis of the laws of conservation. Assume that this velocity makes angle θ with the tube axis. Then, apparently the following equality will apply

$$V_n = CI_0\left(2{\cdot}4\,\frac{r}{R}\right)\cos\theta \qquad (16)$$

whence

$$\cos\theta = \frac{V_n}{CI_0\left(2{\cdot}4\,\frac{r}{R}\right)} \qquad (16a)$$

From the above ratio it follows that under no circumstances can the detonation zone reach the

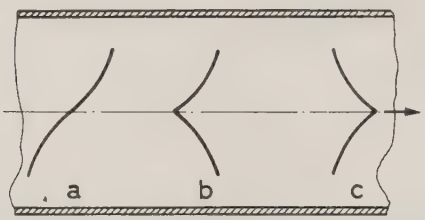

Figure 1

tube walls. It will end where the cosine value equals 1, i.e. where

$$W_n = CI_0\left(2{\cdot}4\,\frac{r}{R}\right)$$

Ratio 16a makes it possible to give a qualitative characteristic of the shape of the detonation front surface. It will be the surface formed by the rotation of the line, shown in *Figure 1a*, about the tube axis.

Condition 16a will be satisfied not only by the above-mentioned surface. It will also be satisfied by the surfaces of rotation formed by the lines shown in *Figure 1b* and *c*. However, these surfaces are highly improbable since they will have a return point on the tube axis whereas the surface corresponding to rotation of the line in *Figure 1a* has a deflection point.

Let us assume that the detonation zone adhering to the tube walls is aglow. This can be achieved by cutting a slot in the wall of a non-transparent tube and studying the phenomenon with the aid of a schlieren apparatus. Let us have a photo plate evenly moving in a plane perpendicular to the slot. This arrangement will make it possible to register the motion of a glowing point in the plane (t, x).

Let us assume that the detonation zone is not moving; its surface lies in the plane perpendicular to the tube axis and rotates with a certain frequency about the tube axis. In this case a vertical line parallel to the time axis will be obtained in the plane (t, x).

Now assume that the plane of the detonation wave is at a certain angle to the tube axis and rotates round the tube with a certain frequency.

In this case a broken line will be obtained in the plane (t, x) [*Figure 2a*].

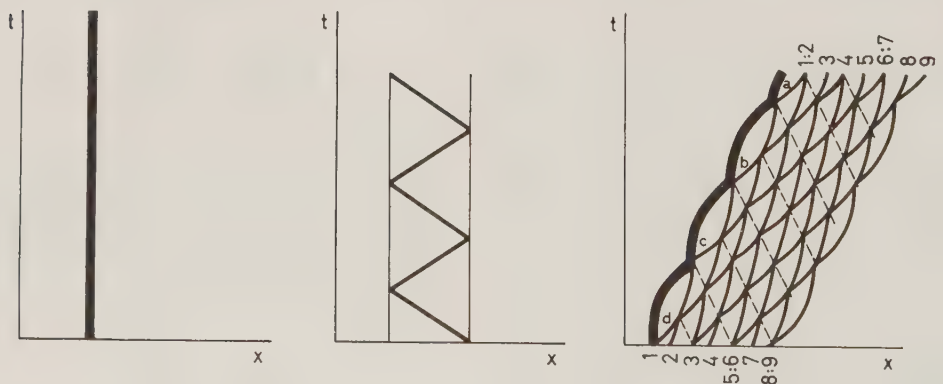

Figure 2

On the tube axis the cosine will be equal to

$$\cos\theta = \frac{V_n}{C}$$

The farther from the cylinder axis the greater the value of the cosine and the smaller the angle. We must give the cosine two values—positive and negative, since a cosine is an even function.

The geometrical break points give two lines parallel to the time axis. The distance between the two lines will depend on the tube diameter and the angle formed by the detonation wave surface with the tube axis. This is shown in *Figure 2b*.

If the detonation wave with an inclined zone begins to move with a certain velocity directed along the tube axis the picture will obviously look as shown in *Figure 2c* (heavy curve).

If an acoustically pulsating helical motion exists behind the detonation zone, a complicated picture will be observed; it will be visible because the central part of the flow rotates almost as a solid body.

Helical lines of hydrodynamic currents will acoustically pulsate and create a number of density variations behind the detonation zone. particles will be shown in the film in the form of high contrast lines. These lines can be traced in *Figure 2c* by proceeding upwards from 'a' to 12, from 'b' to 4, from 'c' to 67, and from 'd' to 9. Lines a4, b3, c2, 1256, 37, 48, etc will move downwards and will not show so distinctly in the photograph. The dotted line appearing in the

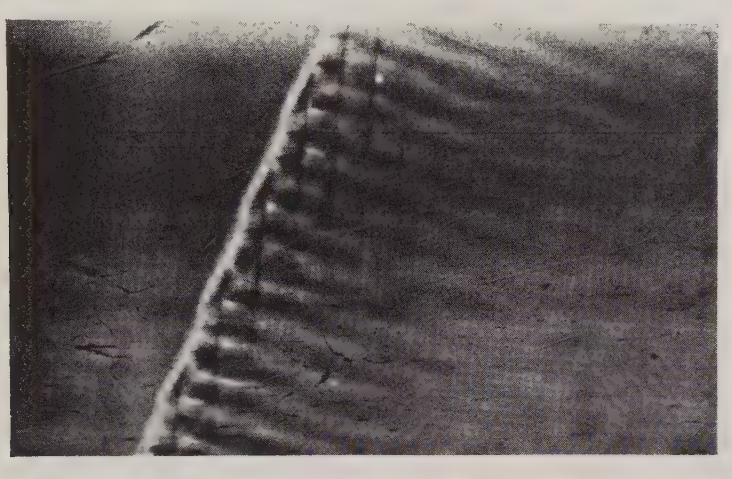

Figure 3

Figure 2c shows one of the possible pictures of density variations moving behind the detonation wave. Line designated '1' shows the motion of one gas particle. At first the particle moves with a slow velocity; then its velocity increases due to rotation (see the film); after that the particle slows down again, etc. The places corresponding to smaller velocities will appear on the film in the form of high contrast spots. Thus, successive motions of gas picture runs through geometrical points where the successively moving particles come into contact. These points should produce especially clear imprints on the film.

This picture is supplemented by the photograph of the spin detonation obtained by T. V. Bazhenova and P. I. Soloukhin. It can easily be seen that the above picture closely resembles the photograph (*Figure 3*).

101

STUDIES IN CONNECTION WITH STABILIZED GASEOUS DETONATION WAVES

J. A. NICHOLLS, E. K. DABORA and R. L. GEALER

INTRODUCTION

Many investigators have been concerned with detonative combustion in the gaseous phase. In general, the agreement between experiment and theory is good wherein the detonation wave is considered as a shock wave followed by combustion. Now practically all of the experimental results, and most of the theoretical predictions, are confined to plane detonation waves moving in a constant area tube; but this is immediately restrictive in that the singular mode of detonation experienced in the stable state is that of the Chapman–Jouguet type. In principle, any degree of strong detonation may be realized provided the proper boundary conditions are imposed[1]. In fact we might even say that weak detonations are possible if we relax the condition that a shock wave must be a part of the structure[1,2] (this is then simply a case of heat addition to a supersonic stream). The reason for the realization of Chapman–Jouguet detonation in tubes is attributed to the trailing rarefaction which reduces the higher downstream pressure necessary to sustain a strong detonation. As is well known, the Chapman–Jouguet detonation wave propagates at the minimum velocity consistent with the conservation laws.

In view of the above considerations it is of fundamental interest to circumvent the limitations here-to-fore imposed and to attempt to attain a standing detonation wave; that is, one that is stationary relative to the tube walls, or laboratory, as the case may be. Achievement of such a wave would conceivably allow experiments on strong detonations as well as those of the Chapman–Jouguet type, much more exhaustive experiments on the structure of the wave leading to information on chemical kinetics, and comparisons between different types of detonation waves. In addition, there is an interest in the use of stabilized detonation waves in a ramjet configuration, which would eliminate the need for subsonic diffusion and essentially reduce the combustion chamber length to zero. Preliminary calculations on this facet reveal that performance comparable with current ramjet practice can be achieved but at appreciably higher flight Mach numbers[3].

A research programme has been under way at the University of Michigan which is explicitly aimed at the achievement of a standing detonation wave. The purpose of this paper is to present the approach used, the experimental technique, and some of the preliminary results obtained.

In order to stabilize a gaseous detonation wave certain dynamic conditions must be met, of course, which are dictated by the detonation characteristics of the fuel-oxidant combination employed. These requirements are considered in detail in reference 4 and will be reviewed only in a cursory fashion here. Mach numbers of detonation differ for various combustible mixtures but all are relatively high (in the hypersonic range). Further, there is a temperature effect (static temperature of the unburned gases) such that the Mach number of detonation varies approximately inversely with the square root of the temperature. The pressure effect is relatively slight although the Mach number can be reduced somewhat for subatmospheric pressures. It is evident, then, that the problem requires that a detonatable mixture be accelerated to a high Mach number with high stagnation temperature and pressure. There must then be some mechanism for generating and stabilizing the detonation. In view of the high stagnation temperatures required, mixing of the fuel and oxidant under stagnation conditions is precluded.

The experimental method adopted at the University of Michigan for achieving the above is described in the following section. This is followed by a presentation of results obtained to date and a discussion of the significance of these results.

EXPERIMENTAL ARRANGEMENT AND TECHNIQUE

As indicated above, the experimental difficulties associated with generating the correct conditions for stabilizing a detonation wave are chiefly attributable to the high Mach numbers of detonation; consequently, it behoves one to select a fuel-oxidant combination which minimizes this problem. Therefore, we have selected hydrogen–air as it has one of the lowest Mach numbers of detonation. The experimental arrangement is

shown in *Figure 1* and is described as follows. High-pressure air is reduced from storage tanks (stored at approximately 2,500 lb./in.^{2}) to about 500 lb./in.^{2} and passed through a pebble type regenerative heat exchanger which has been previously heated to about 2,000°F. There is practically no pressure drop across the heat

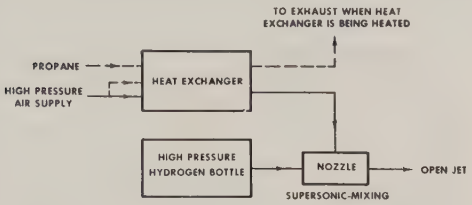

Figure 1. Block diagram of experimental set-up

exchanger and the high-pressure, high-temperature air is introduced to the stagnation chamber of a convergent-divergent, axisymmetric mixing nozzle. Unheated hydrogen is reduced in pressure from a manifold of bottles and introduced at sonic velocity at the throat of the nozzle through a centred coaxial needle. The nozzle and hydrogen injection needle are shown in *Figure 2*. The air and hydrogen mix supersonically in the divergent part of the nozzle. The divergence of the nozzle leads to a pressure and temperature drop during

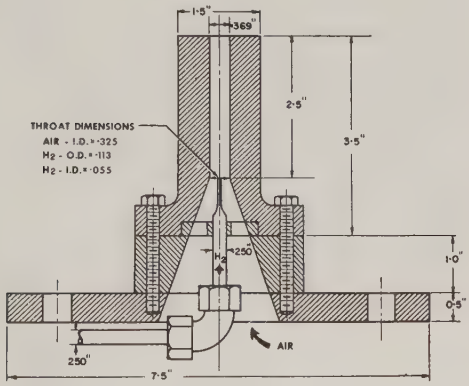

Figure 2. Mixing nozzle

mixing which, along with ignition delays and mixing time requirements, serves to avoid premature combustion. The nozzle is operated in a highly under-expanded state (exit pressure greater than receiver pressure) so that the free axisymmetric jet expands further, thereby dropping the pressure and temperature and increasing the Mach number. The established normal shock wave in the jet serves to ignite the mixture and should, presumably, lead to detonation.

The air heat exchanger mentioned above consists of a steel cylinder 14 ft. long, 2 ft. in diameter, lined with ceramic material, and filled with alumina pebbles. It is heated directly by the combustion products of a propane–air flame and requires 6 to 8 hours of heat-up time. It is designed for pressures up to 1,000 lb./in.^{2} and temperatures up to 2,500°R. Detailed theoretical analyses and experimental evaluations are presented elsewhere[5,6] and will not be repeated here. However, it is pertinent to observe the air delivery temperature as a function of time during a typical experimental run. This is presented in *Figure 3* and reveals relatively constant temperature for a period of over five minutes, which is more than adequate for the experimental requirements.

Earlier considerations of the actual mechanism for stabilizing the detonation wave centred around the idea of expanding the combustible mixture

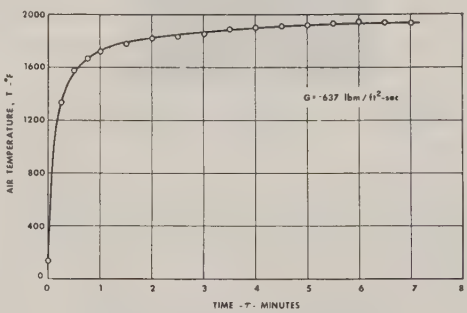

Figure 3. Heat exchanger blow-down performance

to a high Mach number in a two-dimensional nozzle[4]; the wave would then be stabilized on a wedge. This technique has been abandoned for the present in favour of the free jet expansion. It was felt that the possibility of burning in the boundary layer, detonation wave–boundary layer interaction, and detonation waves with extended reaction zones (not to mention materials problems) introduced certain doubts that could be minimized by the following technique. When a free jet leaves an axisymmetric nozzle in a highly under-expanded state, a complex shock structure is observed in the jet[7] which, because of its appearance, is sometimes referred to as a shock bottle. A typical example of this is shown in *Figure 4* (for a more detailed discussion and theory relative to this problem, the reader is referred to reference 8). The flow in the region bounded by the exit plane of the nozzle, the intercepting shock, and the normal shock (Mach disc), is undergoing isentropic expansion so that its Mach number is increasing. All of the flow variables in this region, including concentration, are changing in both the radial and axial directions. For small-scale jets, such as are used in our studies, these changes occur quite rapidly in the flow direction. This region is terminated by the Mach disc which reduces the

flow to subsonic velocity. This pattern is repeated in cyclic fashion until viscous effects take over.

For purposes of this investigation, the gas leaving the nozzle is a non-uniform mixture of hydrogen and air. Under the correct conditions the Mach disc, with the attendant pressure and temperature rise, now serves to ignite the mixture

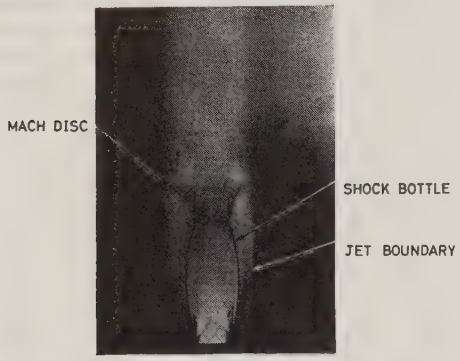

Figure 4. Schlieren photograph of an open jet from an under-expanded nozzle

which could become a standing detonation wave. In the following sections results are presented on initial experiments of this type.

MEASUREMENTS IN UNDER-EXPANDED AXISYMMETRIC JETS

Equipment and procedure for composition and pressure measurements in the cold jet

Hydrogen concentration and pressure distributions were measured in the cold jet by means of a probe mounted on a traversing mechanism which allowed the probe to be positioned at any desired location in the jet. *Figure 5* gives details of the

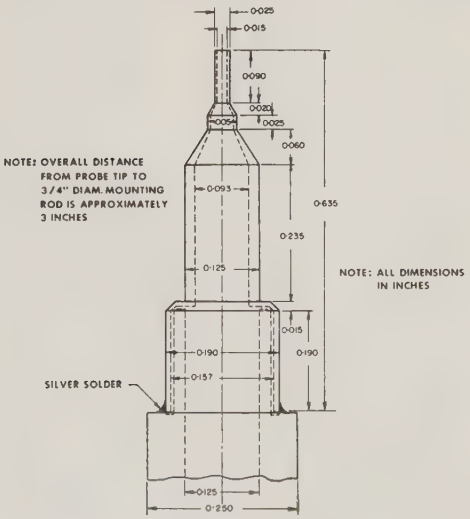

Figure 5. Sampling probe tip

probe tip. A schematic drawing of the sampling equipment is shown in *Figure 6.*

The probe was positioned at the desired radial and axial location. With the needle valve closed the total pressure at that position was read from the pressure gauge and recorded. The sampling bottle was evacuated and the needle valve was then opened to allow the gas entering through the probe tip to slowly fill the sampling bottle to a

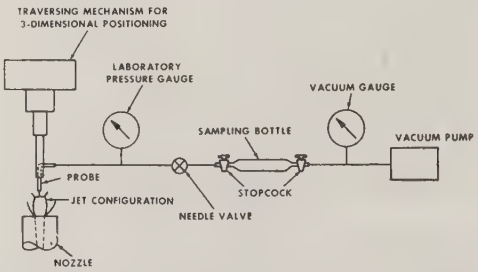

Figure 6. Sampling and pressure measurement flow system

pressure of one atm. The needle valve was closed and the bottle re-evacuated to purge it of any air originally present in the system. The bottle was then re-filled, the stopcocks closed, and the bottle replaced by a fresh bottle for sampling at a new position.

The samples were analysed by absorbing the oxygen from the sample in alkaline pyrogallol solution and measuring the loss in volume at constant pressure. This loss in volume indicated the fraction by volume of oxygen in the sample. Division of this quantity by the fraction of oxygen in air (0·21) yielded the fraction of air in the sample, and subtraction of this quantity from unity yielded the volume fraction of hydrogen.

Results of composition measurements

Radial traverses were made at the nozzle exit and immediately upstream of the Mach disc, for

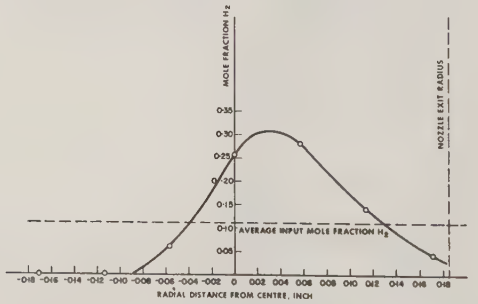

Figure 7. Radial distribution of hydrogen at nozzle exit

flows in which the air mass flow was approximately equal to the design mass flow, but in which the stagnation temperature was room temperature. *Figure 7* shows the volumetric or molar distribution

of hydrogen with radius at the nozzle exit. The maximum does not occur at the jet axis due to misalignment of the hydrogen injection needle; however, this should not affect the qualitative description of the mixing action (a new nozzle is being fabricated which will eliminate this possibility). As expected for incomplete mixing in the nozzle, it is seen that the jet is richer in hydrogen than average at the centre and falls off to zero hydrogen at the jet boundary.

The radial hydrogen distribution at a plane just upstream of the Mach disc is shown in *Figure 8*. It is seen that the concentration of hydrogen is

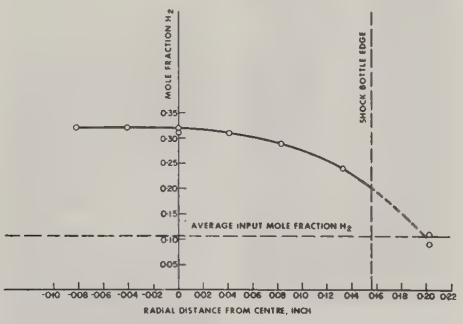

Figure 8. Radial distribution of hydrogen immediately upstream of Mach disc

fairly uniform with radius out to the disc–intercepting shock intersection but that this concentration is 2 to 3 times the average (input) hydrogen concentration. This is explained as follows. Because of the low density within the shock bottle, only a small percentage of the total mass flow passes through the disc. Most of the mass flow passes between the jet boundary and the shock bottle. Consequently, with the outer portion of the jet being very lean in hydrogen (which is reasonable in view of the concentration profile at the exit of the nozzle) it follows that the entire region within the bottle could be richer than average.

These rough measurements qualitatively point out that in order to obtain a given composition at the Mach disc it may be necessary to inject only enough hydrogen to make the average hydrogen concentration as low as one-third of the desired concentration. It would be desirable to investigate this phase of the problem much more thoroughly.

Mach number at Mach disc

As already indicated, total pressure measurements were made at the exit of the nozzle and immediately upstream of the Mach disc. The air mass flow was 0·44 lb./sec, the hydrogen mass flow was 0·0038 lb./sec, and the gas was at atmospheric stagnation temperature. When the air stagnation pressure was 260 lb./in.^{2} abs. the pressure read by a total head tube at the exit of the nozzle averaged 197 lb./in.^{2} abs. and was fairly constant over the nozzle exit diameter. The pressure read by a total head tube immediately upstream of the Mach disc averaged 21 lb./in.^{2} abs. and was fairly constant over the Mach disc diameter. Thus, the Mach numbers at the exit of the nozzle and at the disc were calculated to be 1·92 and 4·66, respectively, assuming a normal shock at the probe followed by isentropic deceleration. A check on the calculation of the disc Mach number was made by assuming the static pressure downstream of the disc to be atmospheric. This is an approximate but reasonable assumption as is indicated in reference 8. With this assumption the ratio of the static pressure downstream of the disc and the stagnation pressure upstream of the disc can be calculated from which a Mach number of 4·98 was obtained. The discrepancy between the two values can be rationalized by the fact that the total pressure probe was actually located at a small but finite distance upstream of the disc, i.e. in a region of lower Mach number than that of the disc, and that the assumption of atmospheric pressure downstream is only approximate.

The main inference made here is that at the conditions listed above, the Mach number at the disc is between 4·50–5·00 which is in the neighbourhood of the detonation wave propagation rate of interest. These results can differ somewhat under elevated temperature conditions; however, the Mach number at the disc can be controlled by variable stagnation pressure. In fact it is interesting that a change in stagnation pressure producing a change in the Mach number at the disc will result in practically no difference in downstream static temperature (for a given stagnation temperature). This should prove to be of great interest in studying ignition by the shock.

EXPERIMENTS ON SHOCK-INDUCED COMBUSTION

In these experiments the desired air flow was established and hydrogen then added until combustion was initiated at the Mach disc. The shock bottle–Mach disc configuration was recorded by schlieren photography on 35 mm ciné film during the operation of the system with air alone, and during the combustion phase. In general, detail in the region downstream of the Mach disc was obliterated with or without combustion. Therefore, when combustion occurred it was not detectable on the schlieren photographs, although the shock-bottle configuration increased in size during the combustion phase; the latter phenomenon may be due only to the introduction of hydrogen, however. In order to compare the relative positions and sizes of the jet configuration and zone of combustion, direct 16 mm ciné

recordings were made of the flame simultaneously with the schlieren recording. A reference object of known dimensions, photographed by both cameras, allowed the determination of absolute distances from the projections of the two ciné recordings.

Figure 9 shows such a pair of photographs magnified to the same scale. The flame shape and position is dotted in on the schlieren photograph. The flow conditions for this particular experiment were as follows:

Air stagnation pressure = 534 lb./in.^{2} abs.	Nozzle exit pressure = 154 lb./in.^{2} abs.
Air stagnation temperature = 2,150°R	Input hydrogen mole fraction = 0·0804 (compared to stoichiometric mole fraction of 0·295)
Air mass flow = 0·464 lb./sec	

Although the average hydrogen volumetric fraction is not stoichiometric the concentration tests made in the cold jet lead one to believe that stoichiometric concentration was possibly approached at the Mach disc. These photographs have recorded combustion following a shock wave. It is seen that there is a small distance between the position of the Mach disc and the initiation of combustion. This distance corresponds to about

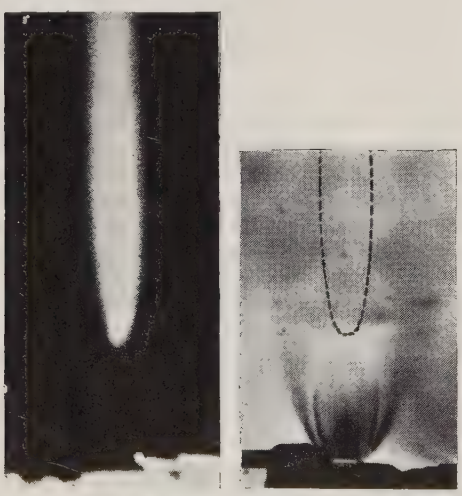

Figure 9. Direct and schlieren photographs of jet during combustion; no apparent burning at nozzle exit

25 μsec and may well represent a chemical time lag between the instant of preparation of the gas for combustion by the shock wave and the time when appreciable chemical reaction can take place.

The results of this experiment present some interesting problems. For one thing, is the stabilized pattern observed (a shock wave followed by combustion but separated by a time lag) to be considered a detonation wave? The situation is somewhat different in this case than that where detonation waves are generated in a tube. In the latter case the propagation of the shock wave is dependent upon the combustion process. In the present case the shock wave is present whether combustion occurs or not. Seemingly, then, the

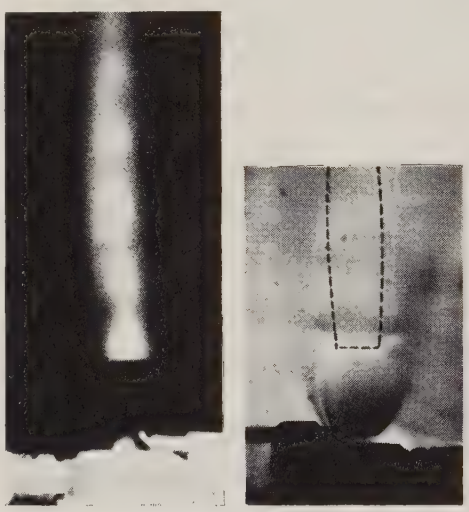

Figure 10. Direct and schlieren photographs of jet during combustion; flame cone at nozzle exit

criterion for establishing identity rests with the consideration as to whether the combustion alters the shock location and hence the free stream Mach number into the disc. Experiments are in progress which are directed towards resolving this question.

It seems reasonable that the distance between the shock wave and combustion zone could be reduced through operation at higher stagnation temperature conditions. This would lead to higher static temperature immediately downstream of the shock wave and the ignition time delay would thus be reduced. It is true that the velocity would be increased but not nearly as much as the time delay would be decreased because of the great difference in temperature dependence. Hence the net effect should be to cause the combustion zone to approach the shock.

Upon achieving merging of the shock wave and combustion it would then be interesting to conduct experiments wherein the stagnation pressure of the jet was reduced; this would lead to lower Mach numbers into the disc. Finally, upon reaching a pressure sufficiently low, the Chapman–Jouguet Mach number of detonation would exceed the incoming Mach number and, it is hypothesized, the wave would move upstream.

Experiments were conducted to test the above concepts. However, the results were inconclusive

because a small zone of burning appeared at the nozzle exit which could not be eliminated. It is felt that this can be attributed to mechanical defects in the nozzle. A sample pair of photographs from this series of experiments is shown in *Figure 10*. The conditions for this experiment were:

Air stagnation pressure = 375 lb./in.^{2} abs.

Nozzle exit pressure = 175 lb./in.^{2} abs.

Air stagnation temperature = 2,110°R

Hydrogen mole fraction = 0·0149

Air mass flow = 0·32 lb./sec

Contrary to the previous experiment it is seen that in this case there is no lag between the shock wave and initiation of incandescence. An explanation for this is that part of the gas was burned in the nozzle, thus increasing the overall stagnation temperature. Upon expansion in the open jet the static temperature decreased sufficiently that the gas was no longer luminous. When this gas passed through the shock wave its static temperature was immediately increased to approximately stagnation temperature; thus, the zone of incandescence was re-established downstream of the Mach disc and appeared to be very flat.

In the above experiment an appreciable increase in nozzle exit pressure (115–175 lb./in.^{2} abs.) was noted at the onset of combustion; also, a temperature increase was detected by a thermocouple immersed in the stream immediately outside the nozzle. Approximate calculations on the above experimentally observed conditions show that the pressure increase can be explained by a relatively small heat addition and that the exit Mach number is approximately one. This indicates that only a small portion of the input hydrogen actually burned in the nozzle. Combustion of the remaining hydrogen undoubtedly occurred downstream of the Mach disc but was photographically undetectable in the wake of the shock incandescence.

DISCUSSION AND CONCLUSIONS

(1) Preliminary experiments on the supersonic mixing of hydrogen and air in a cold jet indicate incomplete mixing within the diverging section of the nozzle and a fairly uniform hydrogen concentration at the Mach disc which is two to three times as great as the average (input) hydrogen concentration. The effect of higher temperatures on the supersonic mixing has not been established and further studies should be made to determine this effect and possibly the effects of other variables such as the gas species, pressure, Mach number, etc.

(2) Cold hydrogen was injected at sonic velocity into a surrounding sonic hot air stream without the occurrence of combustion. The stagnation temperature of the air was 2,150°R and the pressure level at the injection point was 283 lb./in.^{2} abs.

(3) A high stagnation temperature combustible mixture has been accelerated to a high Mach number and ignition has been initiated by a strong normal shock wave in the open jet. The resulting configuration, a shock wave separated by a small distance from the combustion zone, has proved to be extremely stable.

(4) The distance between the shock wave and combustion zone corresponds to an ignition time delay of about 25 μsec. Operation at higher stagnation temperature is expected to decrease this time delay.

(5) Whether the observed stable configuration can appropriately be called a standing detonation wave is open to question. In the sense that a detonation wave is defined as a shock wave followed by combustion, this can properly fit the definition. However, in the case under consideration the shock wave exists whether combustion occurs or not, whereas the combustion maintains the shock wave in tube experiments. It may be necessary to determine the interaction between the shock wave and combustion before further identification can be made.

(6) It is felt that the stabilization of a shock wave–combustion zone in a supersonic jet is a potentially powerful tool in the experimental study of combustion. The steady state flow field will allow more detailed observations as to temperature effects, pressure effects, chemical kinetics, etc.

(7) A logical extension of the work reported herein would be the stabilization of detonation waves on bodies of different shapes for possible application to detonative combustion ramjet engines.

The authors are indebted to R. Dunlap and R. L. Brehm who have actively contributed to the above work and to Professor T. C. Adamson, Jr., for illuminating discussions. Acknowledgment is also extended to other personnel of the Aircraft Propulsion Laboratory who have been of assistance in the experimental work.

This research was supported by the United States Air Force through the Air Force Office of Scientific Research of the Air Research and Development Command, under contract No. AF 18(600)–1199. Reproduction in whole or in part is permitted for any purpose of the United States Government.

REFERENCES

[1] Morrison, R. B. *A Shock Tube Investigation of Detonative Combustion.* 1955. Ann Arbor, Michigan; University of Michigan Press

[2] Reed, S. G., Jr. and Heybey, W. H. Condensation shocks and weak detonations. *Second ONR Symposium on Detonation*, February, 1955

[3] Dunlap, R., Brehm, R. L. and Nicholls, J. A. A preliminary study of the application of steady-state detonative combustion to a reaction engine. *University of Michigan, Engineering Research Institute, 2284–15–T*, September 1957 (also issued as *AFOSR–TN 57—657* and will be published in *Jet Propulsion*)

[4] Rutkowski, J. and Nicholls, J. A. Considerations for the attainment of a standing detonation wave. *Proc. Gas Dynamics Symposium, Northwestern University, 1956* (also issued as *AFOSR–TN 55–216*)

[5] Dabora, E. K. Regenerative heat exchanger with heat-loss consideration. *University of Michigan, Engineering Research Institute, 2284–14–T*, August 1957 (also issued as *AFOSR–TN 57–613* and will be presented at the ASME Semi-Annual Meeting, June 1958, in Detroit, Michigan)

[6] — Moyle, M. P., Phillips, R., Nicholls, J. A. and Jackson, P. L. Description and experimental results of two regenerative heat exchangers. *University of Michigan, Engineering Research Institute, 2284–18–T*, February 1958

[7] Wilcox, D. E., Weir, A., Jr., Nicholls, J. A. and Dunlap, R. Location of Mach discs and diamonds in supersonic jets. *J. aero. Sci.* 24 (1957) 150

[8] Adamson, T. C., Jr. and Nicholls, J. A. On the structure of jets from highly under-expanded nozzles into still air. *University of Michigan, Engineering Research Institute, 2397–5–F*, February 1958

ON AUTOMODELLING PROCESSES IN CHEMICALLY ACTIVE MEDIA

A. S. PREDVODITELEV

INTRODUCTION

A great number of physical phenomena can be divided into two categories, sharply differing from each other from the viewpoint of their mathematical description. One category of phenomena is described by solving one or a set of simultaneous differential equations, with the given initial state of matter and pre-determined conditions on the boundaries of the volume it occupies. To this category also belong all the phenomena which are described by solving boundary problems. There is an equally large group of physical phenomena which by their nature permit one or a set of simultaneous differential equations but for which no boundary conditions can be set, even if the initial state of matter is known. The peculiarities of these phenomena permit their mathematical description on the basis of specific features of differential equations themselves, not on the basis of specific forms of integrals of differential equations. Such phenomena include all automodelling processes, i.e. all processes described by functions which do not contain time in some obvious form. The automodelling factor is especially manifest in coincident processes. In such phenomena these processes are self-coordinated by the time coordinate and we, therefore, cannot use any of the coincident processes as a time-measuring unit.

It is common knowledge that any isolated process occurring within a certain period of time may be employed as the basic principle of design for any time-measuring instrument. For example, the motion of an isothermal surface in space is characteristic of thermal propagation in some medium. This motion may constitute the basic design principle of a thermal clock. Needless to say the above statement implies general possibility and not practicability.

Due to their basic features a large group of phenomena comprising coincident processes cannot be used as a basis of the clock's design as these phenomena are described by functions which are obviously independent of time. In our opinion a special method of description of physical phenomena can be based, in some cases, on the above-mentioned characteristic of coincident processes. The examples analysed below show that this method quickly leads to the desired end and discloses the logical sequence of physical features making up the picture of the phenomenon. Thus the value of this method in this sense alone should attract the attention of scientists and the method itself should be used wherever necessary.

LAWS OF THERMAL PROPAGATION AND RADIATION

As was pointed out above coincident processes always occur in a self-consistent, automodelling manner. Consequently, during thermal propagation in a chemically active medium there must be some isothermal surface travelling in space in accordance with the laws of thermal propagation and the laws of thermal radiation in chemical transformations.

Let formula $f(x_1, x_2, x_3) = S$ represent this surface for each particular moment of time. As the surface travels, the right part of the equation will undergo changes.

The automodelling processes always require a special coordinate ξ which will be determined as follows:

$$\xi = \frac{S}{t}$$

Let us write the equation of thermal conductivity in the form of a linear equation:

$$C_v \rho \frac{\partial T}{\partial t} = K \Delta_2 T \qquad (1)$$

Let us transform the equation relative to the variable ξ. With this aim in view we then perform the following operations:

$$\frac{\partial T}{\partial t} = -\frac{\xi}{t}\frac{\mathrm{d}T}{\mathrm{d}\xi}; \quad \frac{\partial^2 T}{\partial x_i^2} = \frac{\mathrm{d}^2 T}{\mathrm{d}\xi^2} \cdot \frac{1}{t^2}\left(\frac{\partial S}{\partial x_i}\right)^2 + \frac{\mathrm{d}T}{\mathrm{d}\xi}\frac{\partial^2 S}{\partial x_i^2}\frac{1}{t}$$

$$\Delta_2 T = \frac{1}{t}\frac{\mathrm{d}T}{\mathrm{d}\xi}\Delta_2 S + \frac{H^2}{t^2}\frac{\mathrm{d}^2 T}{\mathrm{d}\xi^2}$$

where H expresses the first differential parameter of the surface $f = S$.

Equation 1 can now be written as follows:

$$-t\frac{dT}{d\xi}(K\Delta_2 S + C_v\rho\xi) = KH^2\frac{d^2T}{d\xi^2} \quad (1a)$$

The equation thus obtained will now certainly include time; thus the described phenomenon can be used in the design of the clock.

We assumed that, in accordance with the law given above, heat propagates in a chemically active medium. Let us observe the kinetics of the process by a concentration of some substance. Let y represent the concentration of this substance; then the rate of reaction may be expressed in the following way:

$$\frac{\partial y}{\partial t} = f(y) \quad (2)$$

We have not set a task of analysing one particular case; what we are trying to do is to show, in the clearest manner possible, a general idea which may prove to be quite helpful in many instances.

Let us transform equation 2 relative to the variable ξ. As a result we have:

$$-\frac{\xi}{t}\frac{dy}{d\xi} = f(y) \quad (2a)$$

Since the processes are self-consistent, time t may be subtracted from equation 1a with the aid of equation 2a. Hence:

$$\xi\frac{dy}{d\xi}\frac{dT}{d\xi}\frac{1}{f(y)}(K\Delta_2 S + C_v\rho\xi) = KH^2\frac{d^2T}{d\xi^2} \quad (3)$$

Let us consider the process characterized by plane symmetry, though it is not necessarily so. In this instance the first differential parameter of the surface $f = S$ will turn into a unity and the second into zero.

Bearing this in mind we can write equation 3 as follows:

$$C_v\rho\xi^2\frac{dy}{d\xi}\frac{dT}{d\xi}\cdot\frac{1}{f(y)} = K\frac{d^2T}{d\xi^2} \quad (4)$$

thus we obtain a differential equation which can be applied to coincident processes of substance transformation and to thermal propagation in some medium.

Let us place ourselves at some point in the medium with the instruments to instantaneously measure the temperature and concentration of some chemically active substance. Assuming that as a result of observations we have found:

$$y = \psi(t); \quad T = \phi(t)$$

Substituting time t in these functions by S/ξ, we obtain:

$$y = \psi\left(\frac{S}{\xi}\right); \quad T = \phi\left(\frac{S}{\xi}\right)$$

These functions have the following derivatives:

$$\frac{dy}{d\xi} = -\dot{\psi}_t\frac{S}{\xi^2}; \quad \frac{dT}{d\xi} = -\dot{\phi}_t\frac{S}{\xi^2};$$

$$\frac{d^2T}{d\xi^2} = \dot{\phi}_t\frac{2S}{\xi^3} + \ddot{\phi}_t\frac{S^2}{\xi^4}$$

Since $\dot{\psi}_t$ coincides with the function $f(y)$ we have:

$$\frac{dy}{d\xi}\frac{1}{f(y)} = -\frac{S}{\xi^2}; \quad \frac{\dfrac{d^2T}{d\xi^2}}{\dfrac{dT}{d\xi}} = -\left(\frac{2}{\xi} + \frac{\ddot{\phi}_t}{\dot{\phi}_t}\frac{S}{\xi^2}\right)$$

Now we can write equation 4 as follows:

$$C_v\rho S = K\left(\frac{2}{\xi} + \frac{\ddot{\phi}_t}{\dot{\phi}_t}\frac{S}{\xi^2}\right) \quad (5)$$

We now have the following equation for stabilized coincident processes:

$$(C_v\rho)_0 S_0 = K\frac{2}{g} + \left(\frac{\ddot{\phi}_t}{\dot{\phi}_t}\right)_0\frac{S_0K}{g^2}$$

Here index (0) means that we should take initial state values. Since the process under consideration is stabilized the coordinate ξ must be constant and should coincide with the surface travel velocity limiting the beginning of the process.

For the final state of the medium, i.e. when the chemical transformation is completed, we have the following equation:

$$(C_v\rho)_1 S_1 = K\frac{2}{g} + \left(\frac{\ddot{\phi}_t}{\dot{\phi}_t}\right)\frac{KS_1}{g^2}$$

which will be true only when the second surface limiting the zone of coincident processes is following the first surface with the same velocity.

By subtracting the first of these equations from the second we shall have:

$$\overline{C_v\rho}\delta S + \bar{S}\delta(C_v\rho) = \left(\frac{\overline{\ddot{\phi}_t}}{\dot{\phi}_t}\right)\frac{K}{g^2}\delta S + \frac{K}{g^2}\bar{S}\delta\left(\frac{\ddot{\phi}_t}{\dot{\phi}_t}\right) \quad (6)$$

In this case symbol δ denotes finite differences, and the bar means that the arithmetical mean is taken from the initial and final values of a certain quantity.

Equation 6 thus obtained can be written as follows:

$$\left[\overline{C_v\rho} - \frac{K}{g^2}\frac{\ddot{\phi}_t}{\dot{\phi}_t}\right]\delta S = \left[\left(\delta\frac{\ddot{\phi}_t}{\dot{\phi}_t}\right)\frac{K}{g^2} - \delta(C_v\rho)\right]\bar{S} \quad (6a)$$

but this equation must contain neither variable t nor variable S in obvious form. Therefore the terms within the brackets turn to zero, and this

shows what purpose the following equations should achieve:

$$g^2 = \left(\frac{K}{C_v\rho}\frac{\dot{\phi}_t}{\phi_t}\right)_0 ; \; g^2 = \left(\frac{K}{C_v\rho}\frac{\dot{\phi}_t}{\phi_t}\right)_1 \qquad (7)$$

As soon as the ignition starts the temperature of the medium cannot be considered independent of the concentration of the chemically active substance. Let us express the relationship by:

$$T = \Phi(y)$$

hence:

$$\left.\begin{aligned} \frac{\partial T}{\partial t} &= \frac{\partial \Phi}{\partial y} ; \; \frac{\partial y}{\partial t} = \frac{\partial \Phi}{\partial y} f(y) \\ \frac{\partial^2 T}{\partial t^2} &= \frac{\partial^2 \Phi}{\partial y^2} f^2(y) + \frac{\partial \Phi}{\partial y} f(y) \end{aligned}\right\} \qquad (8)$$

To fix the initial point we will assume that the concentration y of the chemically active agent is equal to zero.

The first of equations 7 can be written as follows:

$$g^2 = \left(\frac{K}{C_v\rho}\right)_0 \left[\frac{\dfrac{\partial^2\Phi(0)}{\partial y^2(0)}}{\dfrac{\partial\Phi(0)}{\partial y}} f(0) + \frac{\partial f(0)}{\partial y}\right] \qquad (9)$$

This is a general formula expressing the velocity of the normal flame front. As can be seen, to calculate the formula it is necessary to know the conditions of ignition and the law of chemical reaction.

It stands to reason that the normal flame front velocity can also be deduced from the second formula 7. For this purpose we will assume that the concentration of chemically active agent in formulae 8 is maximum, this, however, involves considerable difficulties because frontal burning is attended by incomplete combustion.

Let us write formula 9 as follows:

$$g^2 = \left(\frac{K}{C_v\rho}\right)_0 \frac{\ddot{\Phi}_y(0)}{\dot{\Phi}_y(0)} f(0) \left[1 + \frac{\dot{f}_y(0)\dot{\Phi}_y(0)}{f(0)\ddot{\Phi}_y(0)}\right] \qquad (10)$$

By extracting a square root from this expression we shall find:

$$g = \left\{a\frac{\ddot{\Phi}_y(0)}{\dot{\Phi}_y(0)} f(0)\right\}^{\frac{1}{2}} \cdot \left\{1 + \frac{\dot{f}_y(0)\dot{\Phi}_y(0)}{f(0)\ddot{\Phi}_y(0)}\right\}^{\frac{1}{2}} \qquad (10a)$$

where a stands for temperature conductivity of the medium.

If the second addend in the expression (under the second square root) is considered a small value as compared with unity, then formula 10 can be simplified by substituting the second root with its approximate value. We then have:

$$g = \left\{a\frac{\ddot{\Phi}_y(0)}{\dot{\Phi}_y(0)} f(0)\right\}^{\frac{1}{2}} + \frac{a^{\frac{1}{2}}\dot{f}(0)(\dot{\Phi}_y(0))^{\frac{1}{2}}}{2\{f(0) \cdot \ddot{\Phi}_y(0)\}^{\frac{1}{2}}} \qquad (10b)$$

The expression thus obtained proves that we cannot always count on describing the normal front velocity by nominal formulae.

So far we have considered a quiescent medium, but it is not difficult to make the necessary calculations for a moving medium. In this case partial time derivative in the equation of thermal conductivity should be substituted by complete time derivative.

This generalization will bring about a substitution of the variable ξ in equality 3a by the following value:

$$(\xi - W_n) = \mathrm{h}$$

The rate of reaction cannot be expressed by partial derivative either and it should be substituted by a full derivative. This generalization will cause changes in equality 2a; instead of variable ξ it will contain value h.

In the final formula, 4, factor ξ^2 will be substituted by h^2.

Thus, with the front stabilized its propagation velocity will be expressed by the following ratio:

$$\mathrm{h}^2 = \left[a\frac{\ddot{T}_\xi f(y)}{\dot{T}_\xi \dot{y}_\xi}\right]_0 \qquad (11)$$

Index 0 shows that the square bracket refers to the initial point.

FACTORS CONTROLLING THE PROCESS OF COMBUSTION

We shall now try to establish factors controlling the process of combustion of particles in heterogeneous medium.

Let us place the origin of coordinates in the centre of a spherical particle. The equation of thermal conductivity will have to be written in terms of spherical coordinates.

If we transform this equation relative to variable ξ, then in terms of spherical coordinates we shall have:

$$-t\frac{\mathrm{d}T}{\mathrm{d}\xi}\left[K\left(\frac{\partial^2 S}{\partial r^2} + \frac{2}{r}\frac{\partial S}{\partial r}\right) + C_v\rho\xi\right] = K\frac{\mathrm{d}^2 T}{\mathrm{d}\xi^2}$$

After subtracting time with the aid of the equation for chemical reaction rate we get the following equation:

$$\xi\frac{\mathrm{d}y}{\mathrm{d}\xi}\cdot\frac{\mathrm{d}T}{\mathrm{d}\xi}\frac{1}{f(y)}\left[K\left(\frac{\partial^2 S}{\partial r^2} + \frac{2}{r}\frac{\partial S}{\partial r}\right) + C_v\rho\xi\right] = K\frac{\mathrm{d}^2 T}{\mathrm{d}\xi^2} \qquad (12)$$

In the case of spherical symmetry we shall have for the surface $f = S$:

$$(x_1^2 + x_2^2 + x_3^2)^{\frac{1}{2}} = r$$

Consequently the following ratios are true:

$$\frac{\partial^2 S}{\partial r^2} = 0 \; ; \; \frac{\partial S}{\partial r} = 1$$

hence, formula 12 can be written as:

$$\xi \frac{dy}{d\xi} \frac{dT}{d\xi} \frac{1}{f(y)} \left[\frac{2a}{r} + \xi \right] = a \frac{d^2T}{d\xi^2} \qquad (12a)$$

The first addend in the square bracket represents the velocity of travel of an isothermal surface; the second addend expresses the flame front velocity which is constant for the stabilized state in self-consistent processes. To prevent the front against breaking off from the particle it is necessary to have equality of these two values in absolute value and difference in signs. In other words the terms in the square bracket must turn to zero, and it means that the second temperature derivative by variable ξ is equal to zero, i.e. we have:

$$\frac{d^2T}{d\xi^2} = 0$$

We have already seen that during the process of combustion temperature T cannot be considered independent of concentration; therefore we have:

$$\frac{d^2T}{d\xi^2} = \frac{d^2\Phi}{dy^2} \left(\frac{dy}{d\xi} \right)^2 + \frac{d\Phi}{dy} \frac{d^2y}{d\xi^2} \qquad (13)$$

Function $\Phi(y)$, connecting temperature with concentration, must possess the following properties.

Temperature does not depend on concentration when the latter is varied between:

$$0 < y < y_1$$

Temperature equals $\Phi(y)$ when concentration is varied between

$$y_1 < y < \infty$$

We must determine this circumstance by the presence of an inflection point in the function $\Phi(y)$, with the concentration of the chemically active agent equalling y_1. In terms of mathematics it means that to allow the existence of a stabilized process of thermal propagation around a burning particle, the second derivative from the function $\Phi(y)$ must turn to zero. If this condition is superimposed on equality 13 we shall have:

$$\frac{d^2y}{d\xi^2} = 0 \; ; \; \frac{dy}{d\xi} = \text{const} = -B \qquad (14)$$

The expression thus obtained with the aid of equation 2a may be written as follows:

$$\frac{\partial y}{\partial t} = -\frac{\xi^2}{r} \frac{dy}{d\xi} = B \frac{\xi^2}{r} \qquad (14a)$$

Variations in the quantity of substance of the burning particle per time unit may be expressed as follows:

$$\frac{dM}{dt} = 4\pi r^2 \rho \frac{dr}{dt}$$

Variations in the quantity of substance of the new product may be written in the following way:

$$\frac{dM'}{dt} = 4\pi r_1^2 h \frac{\partial y}{\partial t} = 4\pi r_1^2 h B \frac{\xi^2}{r}$$

where r_1 represents the radius of combustion zone beginning, and h combustion zone thickness. Both variations in mass must be equal to each other; hence, we have:

$$4\pi r^2 \rho \frac{dr}{dt} = 4\pi r_1^2 h \frac{B\xi^2}{r}$$

or denoting the surfaces of the spheres by S and S_1 respectively, we have:

$$\frac{dS}{dt} = \frac{8\pi S_1}{S} \cdot \frac{h}{\rho} B\xi^2 = 8\pi \left(1 + \frac{\Delta S}{S} \right) \frac{h}{\rho} B\xi^2 \qquad (15)$$

The formula thus obtained presents considerable interest. Indeed if we consider value $\Delta S = (S_1 - S)$ small as compared with the surface S and the combustion zone thickness constant, then the stabilized combustion process will go on with the rate of variation of the particle surface remaining constant.

The characteristic feature of our line of argument is that we do not analyse in detail the process of changes in the mass of a particle; therefore the above holds good for the combustion process of a liquid drop and its evaporation; for combustion of a metallic part whose surface is liquid during burning; and, finally, for the combustion of a coal particle which is always enveloped with a cloud of after-burning carbon monoxide.

The above law was experimentally found in 1882 by a Russian scientist, Srednevskey, when he was investigating the rate of evaporation of liquid drops. Later it was confirmed by V. A. Fedoseev and D. I. Polestchuk when they were carrying out research work in the field of combustion and evaporation of liquid drops. This law is also applicable to the combustion of sufficiently large coal particles as was proved by research made by V. I. Blinov.

Formula 15 is interesting from another point of view: it shows in what conditions Srednevskey's law becomes invalid.

If the evaporating particle is located in the flow then in equation 12 variable ξ should be substituted by:

$$\xi - W_h = \mathrm{h}$$

Srednevskey's law will hold true in this case under certain circumstances, but first of all the following condition must be kept:

$$a\Delta_2 S + \mathrm{h} = 0; \quad a\Delta_2 S + \xi = W_n \qquad (16)$$

and secondly, we should have an equality of the following kind:

$$\frac{dy}{dt} = \frac{\mathrm{h}}{S} B \qquad (16a)$$

In the case under consideration value S must not be identified with the sphere radius; thus, the Laplace operator and value S in formulae 16 and 16a are left unexpanded. Combustion will take place in the manner illustrated in *Figure 1a*, the dark part of the illustration being the combustion zone. As can be seen, it has the shape of a parachute, and this type of burning we termed parachute combustion.

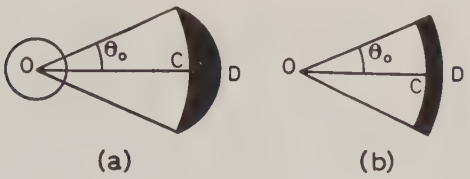

Figure 1

Let us approximate the volume of the darkened area in *Figure 1a* by an equivalent volume in *Figure 1b* for the sake of simplicity of calculations.

Let R_0 represent line OC in *Figure 1b*, and R_1 line OD.

Bearing this in mind we will solve the following integral:

$$\frac{dM'}{dt} = \int_{R_0}^{R_1}\int_{0}^{\theta_0} \frac{\xi \text{h} B}{S} r^2 \sin\theta \, d\theta \, dr \, 2\pi$$

In this, the integral value S in the first approximation may be identified with radius r.

This condition allows us to express the mass of substance burnt per time unit in the darkened spherical depression by the following:

$$\frac{dM'}{dt} = \xi \text{h} B\pi(R_1^2 - R_0^2)(1 - \cos\theta_0)$$

$$= \xi \text{h} B\pi(R_1 - R_0)(R_1 + R_0)(1 - \cos\theta_0)$$

which can be written approximately as:

$$\frac{dM'}{dt} = \xi \text{h} B 2\pi R_0 h(1 - \cos\theta_0)$$

where h represents the average thickness of the spherical depression.

On the other hand the mass of burnt substance per time unit can be written as follows:

$$\frac{d}{dt}\left(\frac{4}{3}\pi r^3 \rho\right) = \frac{\rho r}{2}\frac{dS}{dt} = \frac{dM}{dt}$$

The comparison of the last two equations gives:

$$\frac{dS}{dt} = 4\pi \bar{\xi} \text{h} B \frac{R_0}{\rho} h \frac{1 - \cos\theta_0}{r} \qquad (17)$$

Apparently we should take an angle equal to $(180 - \theta_0)$ for the angle of blow-out.

Some considerable time ago, in the laboratory named after Zhukovskey of the Moscow University, G. I. Lukyanov experimentally proved the relationship between the angle of blow-out and the radius of the streamlined ball for the flow velocity of 10 m/sec. This relationship is illustrated in the following table.

Ball radius (m)	θ_o (deg.)	*Velocity* (m/sec)
0·038	144	10
0·060	151	
0·084	156	
0·120	158	

If, using the table, we draw a chart showing the relationship of the function $(1 - \cos\theta_0)$ to the ball radius, we shall obtain a curve pictured in *Figure 2* which shows that the above relationship is approximated reasonably well by a direct line not passing through the origin of coordinates. The constants of a straight line are connected with flow velocity.

The true relationship of the function $(1 - \cos\theta_0)$ is shown in the same illustration by a dotted line. It stands to reason that in the area of small values of the radius of the streamlined ball in accordance with the curve there is a rectilinear section passing through the origin of coordinates; and it means that the ratio $(1 - \cos\theta_0)/r$ in this area should be regarded as constant.

Since all the values constituting the right part of equation 17 are constant we are justified in drawing the conclusion that the law of Srednevskey to a

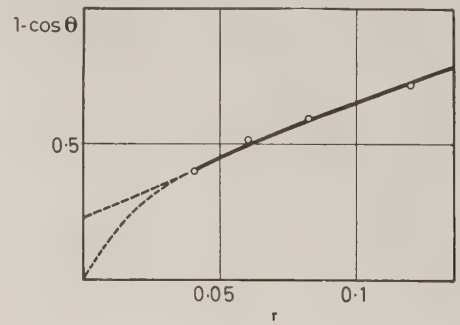

Figure 2

certain degree of precision holds good for the combustion of particles in the flow.

Proceeding from the facts described above we may present the following description of combustion of double-phase mixtures.

As long as the particle is not washed by the flow of oxidant (air) a zone of combustion is formed around it. The inner surface of the zone coincides with the isothermal surface corresponding to ignition point.

The distance at which this surface is located from the evaporation surface of the drop is determined by the equality of the rate of movement of isothermal surface and diffusive isoconcentration surface. Here we are dealing with a specific principle of Guy–Michelson.

If a gas flow is superimposed on this process, the isothermal surface of combustion zone will be distorted according to the laws of thermal propagation in gas flows. With the increase of velocity the combustion zone will break away and will hang over the drop like a parachute. Further increase of velocity will result in incombustibility of the drop. Now if we turn to the system of drops of such density that the drops are small as compared with average distances between them, which is always the case in practice, we can make use of the principle of 'superposition'. We can assert that the combustibility of such a mixture is determined by the limiting values of drop relative velocities at which their parachute combustion is possible.

The turbulization of the flow does not change the description essentially, on the contrary it contributes to the formation of parachute combustion. The presence of pulsating velocities may bring about rather high relative velocities of burning particles.

Careful scrutiny of photographs showing burning turbulent flows may prove that in reality this phenomenon occurs in exactly the same way.

The problem of turbulent combustion of double phase-mixtures in spite of its great practical significance is still far from being thoroughly investigated and understood. It is for these reasons that we deemed it necessary to put forward our views on the problem, particularly as the questions raised in this article have not been discussed in respective scientific publications. Apart from this, the views present a certain interest because on their basis one may come to a simple method of calculation of combustion of liquid fuel in modern jet engines.

THEORETICAL EXAMINATION OF VIBRATORY MOVEMENT OF THE FLAME FRONT IN CLOSED VESSELS

A. S. PREDVODITELEV

DISTORTION OF THE FRONT BY ACOUSTIC WAVES

Interesting phenomena of an oscillatory nature in long open tubes and closed tubes have already been described by Mallard and Le Chatelier.

Figure 1 shows a typical picture of the flame front moving in a closed tube if the combustible mixture is ignited at one end. In this case the front was moving horizontally. However, the picture will not be altered if it is caused to move upwards or downwards. The examination of a series of flash photographs shows that at first the front moves in the usual way and has a semi-spherical shape; then it is gradually flattened and at a certain moment is bent in the centre opposite to the direction of its movement. Then the bend is increased and the flame front assumes the shape of a sharp cone, and as the flame front approaches the ends of the tube it gets into the zone of strong oscillations which blow it off and give it an uncertain shape.

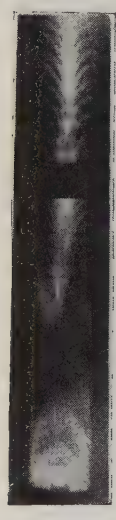

Figure 1

The above phenomenon occurs when the flame formation is accompanied by an acoustic wave process. The latter is brought about by the expansion of the gas where the combustible mixture has already responded. Since the expansion of combustion products is not uniform, the flame front does not move uniformly either. On the whole, this phenomenon resembles the variable motion of a piston. This motion will always result in the oscillations of a gas column.

The description of the above phenomenon should be based on the non-linear equation of acoustics which, for the one-dimensional case, will read as follows:

$$\frac{\partial^2 u}{\partial t^2} = \phi\left(\frac{\partial u}{\partial x}\right) \cdot \frac{\partial^2 u}{\partial x^2}\,;\ \frac{\partial u}{\partial x} = Z \qquad (1)$$

For the sake of simplicity physical analysis may be confined to the one-dimensional case which is quite in keeping with the phenomena taking place in tubes.

Equation 1 results from hydrodynamic equations, no account being taken of viscosity forces, but these forces always play a certain part.

In a paper in 1948 Eckert demonstrated that in addition to equation 1, a circulatory motion is brought about by viscosity no matter how little it may be. If we let R represent circulation expressed by the formula:

$$R = [\text{grad } \vec{W}]$$

an additional equation will be operative in the acoustic field of the medium, given by:

$$\frac{\partial R_1}{\partial t} - \nu_0 \Delta_2 R_1 = \frac{b\nu_0}{\rho_0^2}\left[\text{grad } \rho_1 \text{ grad } \frac{\partial \rho_1}{\partial t}\right] \qquad (2)$$

In this equation circulation R_1 relates to velocity in the first approximation.

Equation 2 existing along with equation 1 is easily solved for the tube in case the sound beam is constant in intensity. Let y represent the relationship of the sound beam radius τ_1 to the tube radius τ_0. The relationship of the distance τ between some point and the tube axis to the tube radius will be designated as x. As Eckert has demonstrated, in this case equation 2 will be solved as follows for constant sound beam intensity:

For $y \leqslant x \leqslant 1$ we shall have:

$$W = -\frac{K p_0^2 \tau_1^2}{2}\left[\left(1 - \tfrac{1}{2}y^2\right)(1 - x^2) + \log x\right]$$

For $0 \leqslant x \leqslant y$ we shall have:

$$W = \frac{K p_0^2 \tau_1^2}{2}\left[\frac{1}{2}\left(1 - \frac{x}{y}\right) - \left(1 - \tfrac{1}{2}y^2\right)(1 - x^2) - \log y\right] \qquad (3)$$

Here p_0^2 represents sound beam intensity, and K the quantity given by

$$K = \frac{b\omega}{2\rho^2 c^4} \qquad (3a)$$

In the latter expression ω stands for the sound beam oscillation frequency multiplied by 2π. The symbol b denotes an expression given by:

$$b = 2 + \frac{\eta_2^1}{\eta_1}$$

The latter item of this expression is the relationship of volumetric viscosity to tangential viscosity.

For gases Stokes' hypothesis is approximately realized. Therefore the relationship between volumetric and tangential viscosity may be assumed to equal $-\frac{2}{3}$. In this case quantity b will be expressed as follows:

$$b = 2 - \frac{2}{3} = \frac{4}{3}$$

In the common case the solution of Eckert's equation shows that the acoustic flux is a vortex originating at the boundaries of the sound beam. As all vortexes, it spreads from its origin closely following the laws of heat propagation.

If the acoustic field of the medium contained in a cylindrical vessel has constant intensity along the section of the tube and fills its entire section, it may be easily seen that the velocity of the flux, determined by formulae 3, becomes zero. When the sound field does not fill the cylinder section, the flux flows along its axis from the sound source

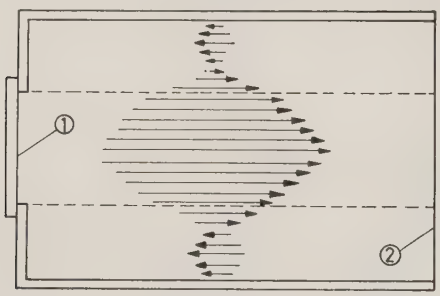

Figure 2. (1) Source of sound; (2) diaphragm. Arrows show theoretically calculated distribution of velocities in the central section of the cylinder. The sound beam has a circular section

and returns along the walls. *Figure 2* shows the distribution of velocities along the tube section with the magnitude and direction of velocity shown by vectors.

It is difficult to assume that the surface of the flame front in the tube should set up an acoustic field which would be constant all along the section of the tube. It is most likely that the sound intensity has a constant value in the central section of the tube and falls sharply off at the walls. In view of this fact the distribution of the acoustic flux along the section of the tube is probably always the same as shown in *Figure 2.*

When the flame front moves across this velocity field, set up by sound oscillations, the following picture should be observed: at the walls of the tube the front propagation velocity and the flux velocity have the same direction; hence, their velocities will be added up. The flame front will be moving faster. At the centre of the tube the flux velocity will be directed opposite to the flame front as the acoustic wave reflected from the tube end will run counter. As a result, the front velocity will fall off and at a certain place in the tube it will be reversed as shown in *Figure 1.*

SPECTRAL CHARACTERISTICS OF VIBRATING FRONT

Apart from the above phenomenon, another one is observed in closed vessels. If the movement of the flame front is photographed on a moving film, an interesting picture will be observed: the front will vibrate at a frequency increasing with acceleration. *Figure 3* shows a typical picture of such a movement of the front. The photograph is part of V. A. Popov's investigation made at the Molecular Physics Laboratory of the Moscow University.

Figure 3

From the viewpoint of the theory of finite amplitude acoustic waves it is easy to describe this phenomenon quantitatively. The following important circumstances should be noted. The experiment does not determine frequency directly; it determines the wavelength by measuring the distances between relative maximums. Hence, the following formula should be used to find the frequency:

$$\nu = \frac{g}{\lambda}$$

where g denotes the finite amplitude sound velocity and λ the wavelength. However, sound velocity depends on the amplitude value and may, therefore, considerably change in magnitude. It may be stated with reasonable assurance that finite-amplitude waves arise in quick-burning mixtures. The setting up of vibration when the mixture is ignited in a closed vessel may be visualized as follows:

At the moment of ignition sound turbulence is formed in the vessel; its main cycle depends on the geometry of the vessel, thus the flame front will begin to vibrate like a movable diaphragm. For the sake of simplicity let us assume that the oscillation cycle of such a quasi-diaphragm remains constant. It is only the velocity of the sound wave that changes, depending on the amplitude and on the thermodynamic condition of the mixture contained in a closed cylindrical vessel; further, we shall see that this assumption is based on experiment.

Let us formulate the following law of sound turbulence:

$$W = a \cos \omega t$$

Here ω is determined depending on the geometry of the vessel. As to the turbulence amplitude, it will depend on the conditions of ignition and the nature of the explosive mixture. With the turbulence at the base of the gas column conforming to the above law, the formula for expansion will be expressed, according to the theory of finite-amplitude oscillations, as follows:

$$Z = \left(1 + \frac{\gamma - 1}{2c} a \cos \omega t\right)^{-\frac{2}{\gamma - 1}} - 1 \quad (4)$$

The above formula may be easily deduced. It may be also found in Hugoniot papers. In this formula c stands for small-amplitude sound velocity, and γ for the c_p/c_v ratio. The velocity of sound wave propagation will be given by:

$$g = c\left[1 + \frac{\gamma - 1}{2c} a \cos \omega t\right]^{\frac{\gamma + 1}{\gamma - 1}} \quad (5)$$

For amplitudes not very large this formula may be written approximately as follows:

$$g = c\left[1 + \frac{\gamma - 1}{2c} a \cos \omega t\right]$$

The main oscillation cycle will be designated as T. Then, for the wavelength being measured, we shall have the following expression:

$$\lambda = gT = \lambda_0\left[1 + \frac{\gamma + 1}{2c} a \cos \omega t\right]$$

Here λ_0 is given by:

$$\lambda_0 = cT$$

Hence, the vibration frequency may be calculated according to the formula:

$$\nu = \nu_0 \frac{1}{\left[1 + \frac{\gamma + 1}{2c} a \cos \omega t\right]} \quad (6)$$

It may be seen from the formula thus obtained that maximum frequency, with a positive cosine, will correspond to such moment t when the product ωt becomes $\pi/2$. Let us measure the distance in fraction of the tube length as V. A. Popov did in his experiments. Then we shall establish the following identity:

$$\omega t = \frac{2\pi t}{T} = \frac{2\pi x}{n}$$

In V. A. Popov's experiments maximum frequency corresponded to distance x equal to 0·9. Then we shall have:

$$\frac{2\pi \cdot 0{\cdot}9}{n} = \frac{\pi}{2}; \; n = 3{\cdot}6$$

Now formula 6 may be re-written as follows:

$$\nu = \nu_0 \frac{1}{\left[1 + \frac{\gamma + 1}{2c} a \cos \frac{\pi x}{1{\cdot}8}\right]} \quad (6a)$$

Maximum frequency in some of V. A. Popov's experiments amounted to 390 c/s. Therefore the last formula may be re-written as follows:

$$\nu = \frac{390}{\left[1 + \frac{\gamma + 1}{2c} a \cos \frac{\pi x}{1{\cdot}8}\right]} \quad (7)$$

In the formula thus obtained the amplitude may be excluded and initial frequency ν, corresponding to coordinate $x = 0$, introduced. Then formula 7 will be expressed as follows:

$$\nu = \frac{390}{\left[1 + \left(\frac{390}{\nu_1} - 1\right) \cos \frac{\pi x}{1{\cdot}8}\right]} \quad (7a)$$

Let us apply the formula thus obtained to the interpretation of V. A. Popov's experiments. For this purpose we shall equalize frequency ν_1 to 170 c/s. Then formula 7a will have the following expression:

$$\nu = \frac{390}{\left[1 + 1{\cdot}29 \cos \frac{\pi x}{1{\cdot}8}\right]} \quad (8)$$

The following table contains the data obtained by V. A. Popov for a certain group of experiments, and calculated according to formula 8:

X	0·0	0·1	0·2	0·3	0·4	0·5	0·6	0·7	0·8	0·9
ν exper.	—	168	170	174	185	205	234	282	345	385
ν calc.	170	171	176	183	196	213	237	272	317	390

As may be seen from the table, the formula we have obtained covers very well the results of the experiments. Some doubts may arise, however, as to the initial and maximum frequencies which at a first glance may seem to be so selected as to make formula 6 fit the experiment. Those doubts will be dispelled if we take into account the following considerations.

According to V. A. Popov's data, sound velocity in a gas, not yet burnt, amounts to 328 m/sec. Then, with the tube 0·91 m long, such as was used in V. A. Popov's experiments, the initial frequency, corresponding to the fundamental frequency of the gas column, will constitute:

$$\nu = \frac{328}{2 \times 0{\cdot}91} = 180 \text{ c/s}$$

For coordination with the experiment we have equalized the initial frequency to 170 c/s. It may be seen that the resultant divergence is within the experimental error since for precise coincidence sound velocity should be set at 310 m/sec and not at 328 m/sec. Such a divergence could take place in V. A. Popov's experiments, thus, the first doubt is disposed of.

Maximum frequency depends on the initial amplitude and on sound velocity at a certain point. Consequently it depends on the conditions of the experiment. In V. A. Popov's experiments the sound oscillation amplitude was not controlled and therefore cannot be pre-determined directly by the conditions of the experiment. However, there are indirect considerations which may help to substantiate its value in V. A. Popov's most interesting observations.

It is quite possible that at the initial moment the speed of turbulent particles W is close to the sound velocity. If this is assumed, maximum frequency may be calculated. In fact, from formula 6a it appears:

$$\frac{v_0}{v_1} - 1 = \frac{\gamma + 1}{2c} a = \frac{\gamma + 1}{2} \text{ or } v_0 = \frac{3 + \gamma}{2} v_1$$

For initial gases the value γ may be assumed to be equal to 1·43.

Then we shall have:

$$v_0 = 2{\cdot}265 \times 170 = 385$$

Thus maximum frequency finds its justification as well.

As to the location of maximum frequency along the length of the tube, it arises just where the sound wave front will be within a quarter-cycle of the fundamental oscillation. Indeed, we have already established the identity:

$$\frac{2\pi t}{T} = \frac{2\pi x}{n}$$

According to the above assertion it follows that:

$$\frac{2\pi}{4} = \frac{2\pi x_0}{n}\ ;\ x_0 = \frac{n}{4}$$

but the value of x_0 equals:

$$\frac{gT}{4L} = x_0 = \frac{n}{4}$$

or

$$gT = nL;\quad g = nLv_1$$

but, on the other hand, for the moment t equal to a quarter-cycle for velocity g we shall have:

$$g = c$$

In other words it is equal to sound velocity at the point the maximum frequency refers to. The numerical expression of this value will be the following in the example under consideration:

$$C = 3{\cdot}6 \times 0{\cdot}91 \times 170 = 557 \text{ m/sec}$$

That means that the gas mixture combustion raises the temperature within a quarter-cycle so that the sound velocity increases 1·7 times its initial value. The figure thus obtained is beyond any doubt and appears plausible since gas pressure in a closed tube may increase almost twice during this time. This is evidenced by a number of direct experiments.

In conclusion, it should be pointed out that the above argument clearly shows the physical condition of the gas mixture if it is caused to burn.

Some of V. A. Popov's experiments that we have used to substantiate our theoretical argument were made with the use of carbon monoxide–oxygen mixtures.

104

DETONATION VELOCITIES IN LIQUID FUEL VAPOURS WITH AIR OR OXYGEN AT 100°C AND ATMOSPHERIC PRESSURE

R. P. FRASER

INTRODUCTION

The velocity of detonation in tubes is not altered by small additions of anti-knocks such as lead tetra-ethyl[1-3]. On the other hand, it has been shown[4] that the preliminary chemical pre-sensitization of the mixture before detonation is established can be altered by the presence of anti-knock compounds, and thus the length of run to detonation in tubes can be altered.

It has also been found[5] in mixtures of pentane with oxygen near the spontaneous ignition temperature that the pre-detonation run diminishes considerably when the mixture is ignited immediately after the appearance of the cool flame; but if ignition is delayed long enough after the cool flame there is a degeneration of the detonating properties of the mixture.

It would appear that the abrupt increase in the auto-acceleration of the reaction in the pre-detonation period, when ignition follows immediately after the appearance of the cool flame, must be attributed to the formation of the maximum concentration of peroxides during this stage, and the disappearance of detonation when ignition occurs after a long period following the cool flame must be due to a reduction in the peroxide concentration and to the dilution of the mixture by products of intermediate oxidation.

The difference between the conditions in tubes and in engines is that in the latter pre-oxidation processes occur at high temperature and pressure. In engines these findings are reflected in the propensity of the fuel to 'knock' as defined by the octane number of the fuel. When detonation is established in gases in a smooth tube which are not pre-sensitized (namely at atmospheric pressure and temperature) the velocity will be determined largely by the heat content of the mixture and the chemical kinetics of combustion.

In some modern combustion engine test equipments using wind tunnels and ducts the possibility of vapour/air mixtures reaching a dangerously high concentration is not so remote and the possible speed of detonation in non-pre-sensitized liquid fuel/air mixtures at atmospheric pressure is of interest.

EXPERIMENTAL

For the measurement of detonation velocities in vapour/air and vapour/oxygen mixtures it was necessary to maintain both the stored vapour mixture and the explosion tube and connecting pipes at a temperature higher than ambient, and it was found most convenient to operate the apparatus at 100°C.

APPARATUS AND PROCEDURE

The vapour mixture was stored in a mercury gas-holder placed within an insulated steam cabinet and maintained at slightly above 100°C. The mixture from the gas-holder passed through the necessary feed valves through flexible tubing within the steam jacketing into the explosion tube, so that at all times the mixture was at or slightly above 100°C.

The appropriate quantity of liquid to be vaporized was weighed accurately and placed in the pipette (*P*) (*Figure 1*) in an oil bath and a

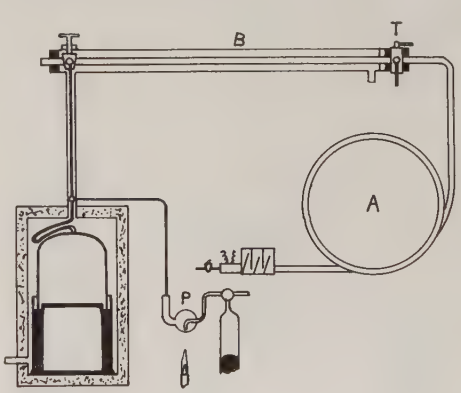

Figure 1

measured volume of oxygen or air was immediately passed over the hot liquid directly into the gas-holder at such a speed that evaporation from the pipette was complete before the oxygen flow ceased.

The method employed to initiate detonation was to fire into the mixture the detonation wave of a

mixture of butane and oxygen, having a similar speed of detonation; thus, in all cases, the detonation was initiated spontaneously. It had previously been found that if the initiating wave had too high or too low a speed of detonation, immediate detonation of the experimental mixture did not occur.

The explosion tube was arranged in two sections. The first section *A* (*Figure 1*) consisted of a firing piece and detonation box and a 7 m run of 12·5 mm bore metal tube connected to one side of a special tap *T*. The second section *B* consisted of a 1·5 m long glass tube of 13 mm bore surrounded by a glass steam jacket. In some cases the steam jacket contained two parallel tubes and the detonation wave was returned and passed through the jacket a second time.

With the explosion tap *T* shut, both sides of the explosion tube were evacuated and section *A* was filled in all cases with a 3·25 per cent butane/oxygen mixture having a speed of detonation of 1,750 m/sec. The explosion section was filled with the vapour mixture to be measured. To ensure proper conjunction of the two mixtures at the tap *T* the cylindrical cavity of the tap was evacuated and also filled with the same butane/oxygen mixture. Before opening the tap and firing the mixtures, each side was brought to atmospheric pressure by taps at the ignition and exhaust ends. The detonation velocity was measured by streak photography in a rotating mirror camera using a 5 in. wide film. To ensure the maximum accuracy of measurement, the equivalent film speed was adjusted so that an image angle of approximately 45 degrees was obtained in the photograph.

Detonation velocities of octane and benzene with oxygen at 100 °C

The detonation limits and velocities of these two fuels are compared in *Figure 2* and Table 1. With octane, the limit speed observed was 1,660

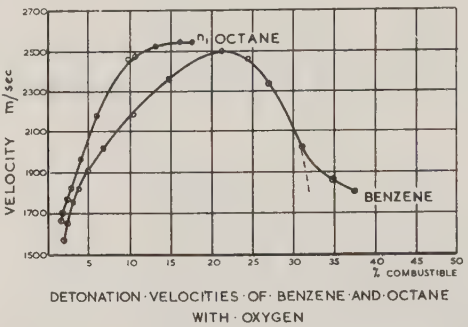

DETONATION VELOCITIES OF BENZENE AND OCTANE WITH OXYGEN

Figure 2

m/sec at 1·55 per cent and the maximum speed of 2,540 m/sec was obtained with the saturation mixture of 17·5 per cent at 100 °C. This mixture also being the higher limit no drop in speed at the upper limit is observed. With benzene the lower limit speed is 1,570 m/sec at 2 per cent and the velocity rises at first rapidly with increased concentration and then more slowly up to a maximum rate of 2,510 m/sec at 21·3 per cent. At the upper limit the fall in speed occurs less rapidly than is usual with other hydrocarbons, the detonation limit occurring at 37·5 per cent.

As with other hydrocarbons the maximum detonation speed mixtures are those containing combustible well in excess of theoretical proportions. Table 1 shows the comparative average

TABLE 1

Octane			*Benzene*		
%	*Spin frequency per sec*	*Average detonation velocity* m/sec	%	*Spin frequency per sec*	*Average detonation velocity* m/sec
1·55	47,000	1,660	2·0	45,000	1,575
1·73	48,000	1,760	2·4	48,800	1,650
1·9	50,000	1,720	3·0	97,000	1,760
2·15		1,765	3·9	185,000	1,825
2·58		1,820	5·0		1,910
3·8		1,960	6·8		2,020
5·7		2,175	10·5		2,190
9·6		2,460	15·0		2,360
10.6		2,470	21·3		2,510
13·0		2,520	24·5		2,470
16·0		2,540	26·9	365,000	2,340
17·3		2,540	31·2	56,000	2,030
			34·8	91,000	1,870
				45,500	
			37·5	Just fails to detonate	

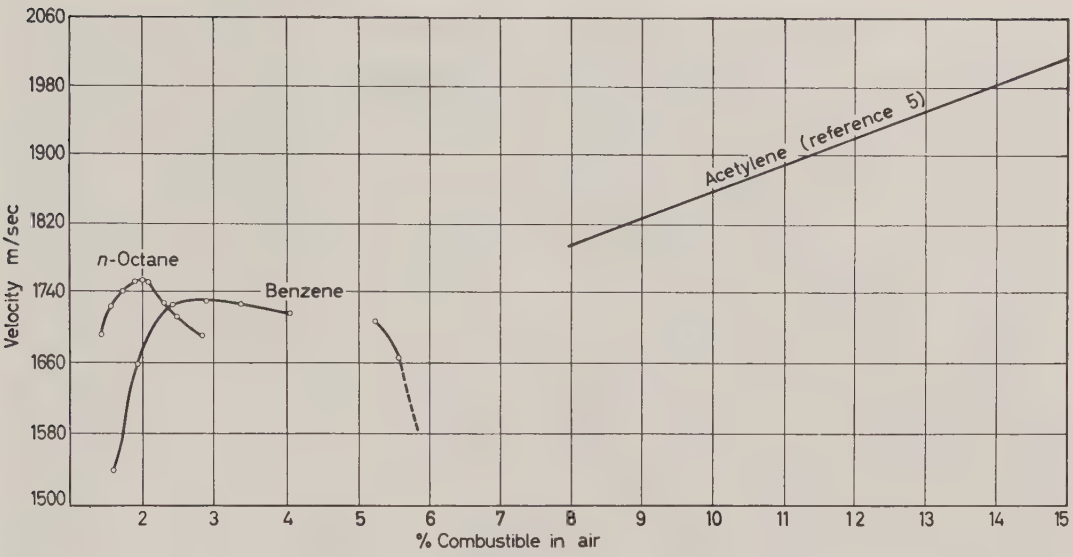

Figure 3

detonation velocities for octane and benzene together with the spin frequencies measured on the photographs (*Figure 4*). It is observed that the

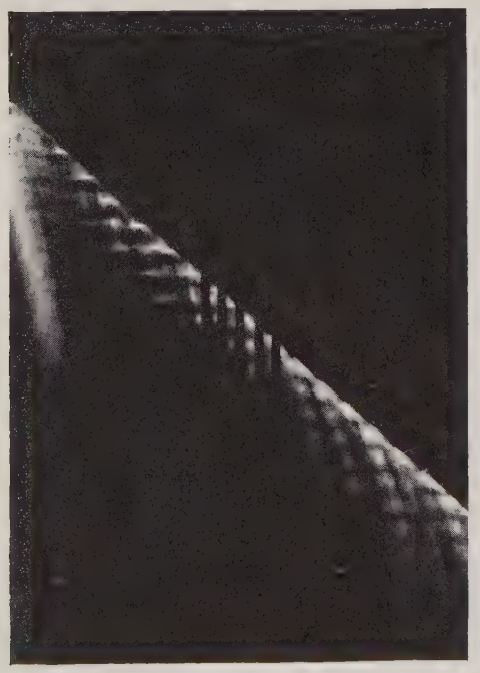

Figure 4

limit frequencies are similar, and are also similar to other gases in this diameter tube. With benzene, spin frequencies increase as the velocities increase, although between 5 and 25 per cent the frequency could not be counted, due, it is thought, to lack of optical definition. At 26·9 per cent a frequency of 365,000 was observed, falling again to the limit frequency with the velocity of detonation.

Detonation velocities of octane, benzene, ethyl alcohol, with air at 100°C

The procedure with these mixtures was the same as with the oxygen mixtures previously described. In each case detonation was initiated by the passage into the mixture of the detonation wave in a 3·25 per cent butane/oxygen mixture.

With octane/air, detonation was propagated

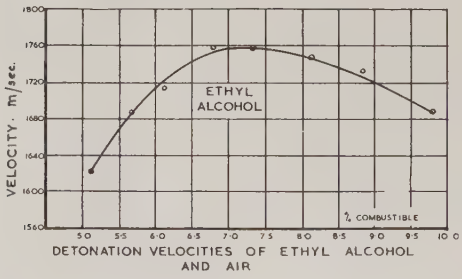

Figure 5

continuously in all mixtures between 1·45 and 2·85 per cent (*Figure 3*), with ethyl alcohol between 5·1 and 9·8 per cent (*Figure 5*) and with benzene between 1·6 and 5·55 per cent (*Figure 3*). With benzene no detonation could be initiated by the means employed between about 4·1 and 5·25 per cent although a number of attempts were

TABLE 2

Octane				*Benzene*				*Ethyl alcohol*				*Petrol*		
Per cent	*lb./air / lb./fuel*	*Average velocity m/sec*	*Spin freq. per sec*	*Per cent*	*lb./air / lb./fuel*	*Average velocity m/sec*	*Spin freq. per sec*	*Per cent*	*lb./air / lb./fuel*	*Average velocity m/sec*	*Spin freq. per sec*	*lb./air / lb./fuel*	*Average velocity m/sec*	*Spin freq. per sec*
1·45	17·0	1,690	47,000	1·63	22·4	1,540	42,000	5·1	11·87	1,625	45,000	6·35 to	9·1 Transient only	
1·58	15·6	1,725	48,000	1·95	18·7	1,660	44,500	5·67	10·5	1,690	47,500	9·6	1,725	48,000
1·75	14·0	1,740	48,500	2·34	15·5	1,730	46,000	6·12	9·72	1,715	48,000	10·4	1,755	49,500
1·90	12·9	1,750	48,000	2·82	12·8	1,730	47,000	6·8	8·67	1,760	49,500	11·5	1,755	48,500
2·1	11·65	1,755	49,000	3·38	10·6	1,730	44,000	7·35	7·98	1,760	49,000	12·5	1,752	48,500
2·28	10·7	1,725	49,500	4·05	8·8	1,720	47,000	8·16	7·11	1,750	49,000	13·9	1,747	48,000
2·5	9·75	1,710	49,000	No detonation between 4·1 and 5%				8·85	6·52	1,735	49,500	14·8	1,720	46,500
2·85	8·53	1,690	48,000	5·25	6·7	1,710		9·8	5·78	1,690	48,500	16·7	1,675	46,000
				5·55	6·3	1,670	47,500					17·9	Transient	

made at each of the following percentages: 4·15, 4·5, 4·85 and 5·0. Between 5·25 and 5·55 per cent detonation was easily established by the butane/oxygen wave. Between 5·55 and 6·3 per cent transient detonation was induced, the wave travelling the benzene mixture for various distances up to about ½ m.

The detonation velocities of all mixtures of octane, ethyl alcohol and benzene were found to lie between 1,540 and 1,760 m/sec (Table 2). It is found that the whole range of velocities for benzene/air are lower than those of either octane or alcohol. The spin frequencies for all air mixtures of octane and alcohol lie between 45,000 and 49,500 per sec in a 13 mm bore tube. With benzene, frequencies are somewhat lower, between 42,000 and 47,500.

It would be expected that as the detonation velocities of such different vapours as benzene, alcohol and octane are very similar, velocities with mixed hydrocarbon such as petrol should all be nearly the same, and this is found to be so. *Figure 6* shows a comparison between all four fuels

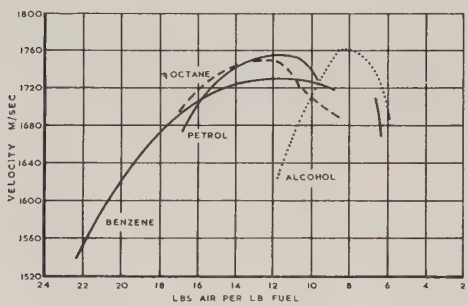

Figure 6

plotted against air/fuel ratio. It will be seen that the curves for octane and petrol are very similar. Benzene has a wider range but lower speeds. Although the velocities of each fuel are very similar, the most striking differences are the slope of the alcohol curve and the discontinuity in the benzene curve.

DISCUSSION

It has been observed that with each hydrocarbon there is a deposition of carbon throughout nearly the whole detonating range. For example: above 5 per cent butane/oxygen and even with 3·25 per cent butane/air carbon is deposited. A carbon film near the lower limit may, however, only become noticeable after several detonations in the same tube. It is thought that the reduction in the available heat due to loss of carbon is responsible for the change in the slope of the benzene/oxygen curve above 5 per cent. The relative suddenness of the alteration in slope would appear to indicate that either a particular partial pressure of hydrocarbon must be reached before appreciable breakdown occurs, or that a definite concentration of carbon must exist before aggregation takes place and the carbon is lost to the combustion.

The shape of the benzene curve near the higher limit is also of interest. From the curve's general outline it would be anticipated by comparison with those of other hydrocarbons that the higher limit of detonation should be reached at about 31–32 per cent whereas detonation is obtained up to 37 per cent. The change of slope near the higher limit seems to indicate that the increased concentration of benzene is not acting as a diluent and it would appear that such additional heat is being derived from the breakdown of the benzene molecule.

The heavy carbon formation obtained in the tube is evidence of this. The photographs also show the presence of large quantities of carbon in the flame. However, the amount of heat liberated on the breakdown of the benzene molecule is relatively small (20 kg cal per g mole), compared with the heat of combustion (771 kg cal mole). An alternative explanation might be suggested.

It is significant that although carbon in small quantities is always deposited from the detonation reaction throughout the whole range above 5 per cent benzene and a heavy deposition of carbon might be expected after 25 per cent benzene, carbon does not appear in quantity until 31·5 per cent is reached. Since carbon does not appear in quantity at 25 per cent it seems reasonable to assume that some or all the C_6H_6 molecules break down. If the break down was to acetylene heat would be lost to the reaction at a rate of 55 kg cal per g mole with a consequent possible slowing down of the combustion. At higher concentrations of benzene any acetylene may be decomposed when heat will be returned to maintain the wave at higher concentrations of combustible.

It would be anticipated that the same factors which produce both the sudden change of slope at the lower limit with benzene/oxygen, and the elongation of the benzene graph at the upper limit, are responsible for the peculiarities observable in the benzene/air curve. If no carbon deposition occurred in the air detonations it would be anticipated that the maximum velocities would be higher, whereas between 2·4 and 4 per cent the velocities are almost the same. This sudden alteration in slope may also be attributed to the lost carbon, although in the air curves the change of slope is very abrupt and occurs at a lower

percentage than in the oxygen case. It is possible that the break in this curve is due to similar effects, as mentioned for the oxygen curve.

My indebtedness to my past colleague, Dr. W. H. Wheeler, for his help in the earlier experiments represented in this paper is gratefully acknowledged.

REFERENCES

[1] Dickson, H. *Trans. Faraday Soc.* 22 (1926) 372
[2] Egerton, A. C. and Gates, S. F. *Proc. Roy. Soc.* 114 (1927) 137
[3] Lafeatte, P. and du Manois, P. *Trans. Faraday Soc.* CR186 (1928) 146
[4] Shtsholkin, A. and Sokolik, A. *Acta Physica Chem. USSR* 7 (1937) 4
[5] Bresquer, R. *et al. Acta Physica Chem. USSR* 7 (1937) 5

THE GENERALIZED HUGONIOT ADIABATIC CURVE

YA. K. TROSHIN

INTRODUCTION

The Hugoniot curve *LGABJM* (*Figure 1*) is known to be divided by secants 1*B* and 1*A* into a detonation section (*BJM*) and a deflagration section (*AGL*). The *AB* branch has no physical sense, since its points would represent a process with imaginary velocity. Point *J* corresponds to steady detonation developing with minimum thermodynamic velocity. As has been shown by Zeldovitch[1] the *BJ* branch represents not fully compressed detonation waves, possible only on artificial ignition of the gas in the tube (for instance on spark ignition), conducted with velocities greater than the thermodynamic detonation velocity. On ignition with a shock wave this branch would be energetically forbidden, since the states of the straight line *MZ*, through which the shock compressed gas would pass, correspond

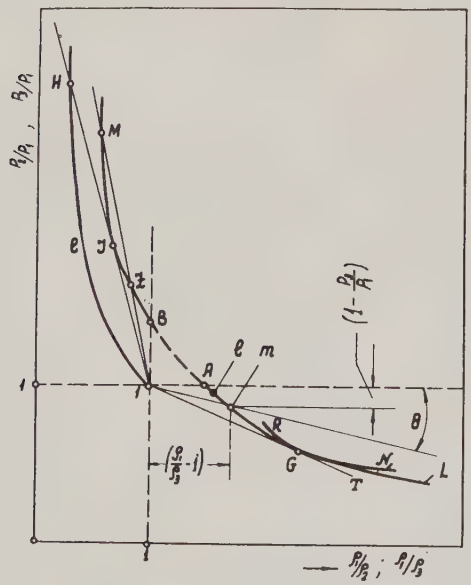

Figure 1. Hugoniot curve

to higher thermal effects of the combustion reaction than those of the given Hugoniot adiabatic curve. The *JM* branch corresponds to overcompressed detonation waves, observed for instance on transfer of detonation from the broad tube into a narrow one, or immediately after transition of combustion to detonation. The *AGL* branch is divided by the tangent (1*GT*) into parts corresponding to weak (*AG*) and strong (*GL*) deflagrations. Points lying on the *GL* branch do not correspond to real combustion regimes, since similarly to *BJ* they would require more energy than that released in the course of the reaction. Although the *AG* branch is quite possible energetically there is a widespread opinion[2-4] that of a series of weak deflagrations only the deflagration at nearly constant pressure, that is normal combustion with velocity u_n (a point on *AG* slightly below point *A*), is of any physical significance.

It will be shown on base of the works on turbulent combustion[5,6] that the *AG* branch corresponds to real regimes of combustion in tubes, the combustion velocity varying from u_n up to the maximum combustion velocity at fully developed deflagration (point *G*).

The same limits of combustion velocity are observed under conditions of unsteady double discontinuity, when the shock wave precedes the flame front with a velocity exceeding that of the flame. However these combustion regimes cannot be represented by points of the Hugoniot curve. The states of gas within unsteady double discontinuities are described by curves plotted from the generalized Hugoniot curve[7] and also analysed here.

Analysis, on the basis of the generalized Hugoniot adiabatic curve, of schlieren photographs of the accelerated flame given in this paper will help to elucidate the mechanism of flame acceleration and of the transition of slow flame to detonation. Let us begin by detailed discussion of deflagration regimes.

REGIMES OF DEFLAGRATION

(Propagation of thermal discontinuities in tubes)

The suggestions of Lewis and von Elbe, and also of Courant and Friedrichs, implying that only that part of curve *AG* which is near to *A* has a physical sense, would be correct if the chemical reaction proceeded steadily in an absolutely flat normal flame front perpendicular to the tube axis. We

are indebted to Shchelkin and Damköhler for their substantiation of the possibility of burning a combustible mixture in a broad zone of turbulent combustion. It is precisely this that enables us now to show that the entire branch of weak deflagrations *AG* has a very definite physical meaning and describes the real regimes of combustion processes in tubes.

Let us, for instance, imagine combustion regimes as shown in *Figure 2*. Here the structure

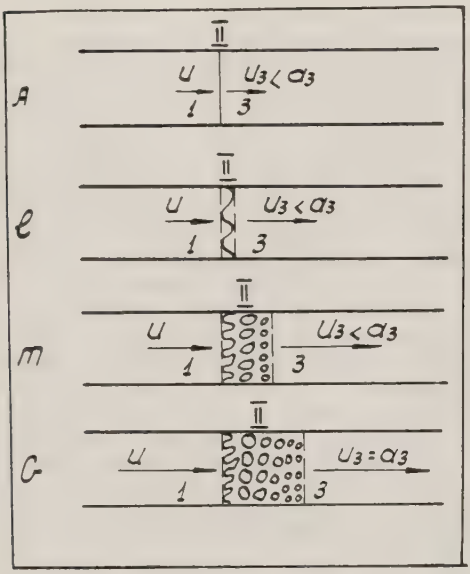

Figure 2. Deflagration regime

of the zone of turbulent flame is depicted, as is conventionally being done now, according to the Shchelkin scheme. It is limited by control planes and is taken as the overall region of the thermal discontinuity, that is as the discontinuity area. It is assumed that this zone is stabilized in a tube of constant cross-section. The initial gas, that is a homogeneous combustible mixture of a given state (p_1, ρ_1) is admitted into the quiescent combustion zone II with a velocity u. The reaction products move out of this zone at a speed of u_3 into region 3 (p_3, ρ_3). It is further assumed that the gas flow in regions 1 and 3 is steady and one-dimensional. In these regions the gas is ideal and has a constant heat capacity. All sorts of losses due to friction, heat loss to the walls, etc., are ignored. The combustion regimes are accomplished by means of successive increase of the overall flame area S in zone II. The combustion heat of unit mass Q and the relation of specific heat capacity $k = (C_p/C_v)$ are given. On these assumptions, the conservation of mass, momentum and energy principles applied to the case of the gas transition from state 1 to state 3 across the region of thermal discontinuity II, leads to the equation for the Michelson straight line:

$$p_3 = p_1 - \rho_1 u(u_3 - u) \tag{1}$$

$$\frac{u}{(p_1/\rho_1)^{\frac{1}{2}}} = \left(\frac{1 - p_3/p_1}{\rho_1/\rho_3 - 1}\right)^{\frac{1}{2}} = (\tau g \theta)^{\frac{1}{2}} \tag{2}$$

and the equation for the Hugoniot deflagration curve

$$\frac{p_3}{p_1} = \frac{\kappa - \rho_1/\rho_3 + \dfrac{2Q}{p_1/\rho_1}}{\kappa\, \rho_1/\rho_3 - 1}\ ;\ \left(\kappa = \frac{k+1}{k-1}\right) \tag{3}$$

The conservation of matter principle permits to relate gas velocities in regions 1 and 3:

$$u_3 = u\,\frac{\rho_1}{\rho_3} \tag{4}$$

$$M_3 = \frac{u_3}{a_3} = \left(\frac{\tau g \theta}{k} \cdot \frac{(\rho_1/\rho_3)}{(p_3/p_1)}\right)^{\frac{1}{2}} \tag{5}$$

As can be seen from equation 1 combustion regimes may be accomplished only when p_3 is less than p_1 by the value of the change in the momentum of the gas that has passed across the region of thermal discontinuity.

Requirements imposed by equation 1 may be satisfied by creating certain conditions of outflow of the reaction products. For example, let the state of the initial gas satisfy normal atmospheric conditions. Let a barometric chamber be connected to the right-hand end of the tube and the reaction products be drawn off continuously. Let the pressure in the chamber be maintained constant for the given combustion regime and its value be in accordance with equation 1. A combustion regime in which the flame area is exactly equal to the cross-section of the tube F (*Figure 2A*) corresponds to normal combustion ($u = u_n$). This regime may be depicted on the *AG* curve in the vicinity of and slightly lower than point *A*, whilst at the limit ($u_n \to 0$) it will be represented by the *A* point itself. On increase of the overall flame area $S > F$ (*Figure 2,l* and *m*), the initial gas blast rate will be $u = u_n\,(S/F)$ and the rate of flow of the reaction products u_3 will rise, while the pressure p_3 will fall off. These combustion regimes correspond to not fully developed deflagrations (points *l* and *m* on the *AG* curve). On further increase of the flame area, the rate of flow of the reaction products attains the local sonic velocity (*Figure 2G*) and the regime of fully developed deflagration (point *G* on the *AGL* curve) sets in.

As can be seen from 3 and 2 and *Figure 1*, the first intersection of the definite Michelson straight line with the Hugoniot deflagration curve allows

us to select from all the possible final states of the gas, represented by the AG branch, a state corresponding to a definite combustion regime with a definite rate of admittance of the initial gas into combustion zone II, the tangent of the slope angle (θ) of the Michelson straight line, for example of the 1–m line, being characteristic of the magnitude of this velocity. The condition of the simultaneous contact of the Michelson straight line ($1GT$) on the deflagration Hugoniot branch (AGL) and the Poisson adiabatic curve (RGN), both passing through point G, gives the equation:

$$\frac{u}{(p_1/\rho_1)^{\frac{1}{2}}} = \left(\frac{k^2-1}{2}\cdot\frac{Q}{p_1/\rho_1}+k\right)^{\frac{1}{2}} - \left(\frac{k^2-1}{2}\cdot\frac{Q}{p_1/\rho_1}\right)^{\frac{1}{2}} \quad (6)$$

The gas rate at the entrance to the combustion zone with a fully developed deflagration can be readily determined from this equation. The following relations are valid for gas density and pressure in the region 3 with fully developed deflagration:

$$\frac{\rho_1}{\rho_3} = \frac{k\left(1+\dfrac{u^2}{p_1/\rho_1}\right)}{(k+1)\dfrac{u^2}{p_1/\rho_1}} \quad (7)$$

$$\frac{p_3}{p_1} = \frac{1+\dfrac{u^2}{p_1/\rho_1}}{k+1} \quad (8)$$

It will be pointed out that at deflagration regimes the Michelson straight line rather characterizes physically consecutive mean gas states at the width of the turbulent flame zone. In each intermediate cross-section of this zone a part of the gas has not reacted at all, whilst the other part has reacted completely. The local states of both these parts (composition, temperature, density) greatly differ. Common are the pressure, which is practically uniform in the given cross-section of the zone, and the mean values of the composition, temperature and density of the gas, which vary from one cross-section to another. For example, by tracing the Michelson line 1–m from point 1 to point m (*Figure 1*) we seem to follow the course of combustion in zone II (*Figure 2-m*). A point on the straight line 1–m lying close to point 1 corresponds to the very beginning of the zone (in the region near the left control surface). Here the percentage of the burned gas is close to zero. Somewhere in the intermediate cross-section of zone II, situated between the control areas, some 50 per cent have been burned out, while at the very end of the combustion zone, close to the right-hand control area, corresponding to a point on the straight line 1–m close to point m, the percentage of burned gas is close to 100. Summing up, it can be seen that under given definite boundary conditions it is possible to effect deflagration regimes for any values of velocity u, from u_n (the straight line 1–A being nearly an isobar) to the maximum velocity u, which corresponds to the thermal crisis (tangent $1GT$). (The problem of a broad deflagration front stability ought to be considered separately.)

The deflagration regimes shown in *Figure 2* can also be effected when the pressure in region 1 (p_1) is much greater than atmospheric pressure, for example under conditions when the outflow of the reaction products from region 3 into the atmosphere is choked, the pressure p_3 being again maintained constant for a given combustion regime and precisely such as it should be according to equation 1. Under real conditions, for example in chambers of liquid-fuel rocket engines, the part of choke is fulfilled by the narrowing (subsonic) part of the supersonic Laval nozzle (*Figure 3*).

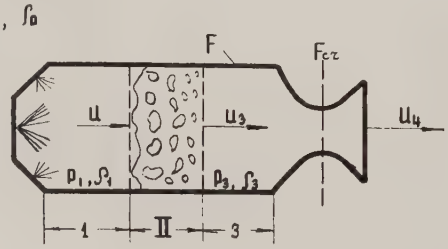

Figure 3. The regime of incompletely developed deflagration in a liquid fuel propellant combustion chamber

Let us assume that the above idealized case is completely retained here; this implies the condition of steady gas flow not only across regions 1 and 3, but also through the additionally connected Laval nozzle. The dependence of the nozzle tapering F/F_{cr} upon the number M_3 is known to be expressed by the following equation:

$$\frac{F}{F_{cr}} = \frac{\left(1+\dfrac{k-1}{2}\cdot M_3^2\right)^{\frac{k+1}{2(k-1)}}}{M_3\left(\dfrac{k+1}{2}\right)^{\frac{k+1}{2(k-1)}}} \quad (9)$$

A comparison of 9 and 5 reveals profound relationship between the position of the point on the deflagration branch corresponding to the given combustion region in the engine chamber and the degree of the nozzle tapering. Indeed, M_3 is related through 5 with the position of the point on the deflagration branch corresponding to a definite combustion regime in the engine chamber, and through 9 with the degree of narrowing of the nozzle. Thus it appears that points lying on the

deflagration branch describe reaction product states for a series of combustion regimes of a whole set of combustion chambers (with constant values K, Q, p_1, ρ_1, F) differing in the magnitude of the critical cross-section of the exit supersonic Laval nozzle (F_{cr}). The lower lies the point on the branch, the more developed is the deflagration and the less needs be the narrowing of the channel required to raise the rate of the flow of reaction products to a sonic, and in the widening part of the nozzle, to a supersonic velocity. In the case of a fully developed deflagration, the rate of reaction products flow in region 3 is equal to the local sonic velocity ($M_3 = 1$), narrowing of the channel not being required, and we have a semi-thermal nozzle with a maximum forced combustion regime. Finally, as has been shown by Zeldovitch[9] deflagration regimes described by the AG branch may theoretically be accomplished even in the case when the combustible gas in the initial state 1 (p_1, ρ_1), corresponding for example to normal atmospheric conditions, remains quiescent in the tube, while combustion zone II propagates as a whole over the particles of the unburnt gas with a velocity u. Such combustion regimes can be effected if pressure p_3 in the same region 3 is maintained constant by means of a barometric chamber and lower than p_1 (at the given combustion regime, that is at a given $S/F = \text{const}$). This pressure p_3 corresponds to velocity $u = u_n . S/F$ (*Figure 4*).

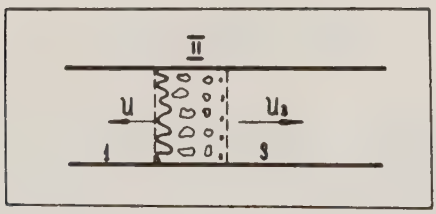

Figure 4. Propagation of deflagration regime in the tube

UNSTEADY PROPAGATION OF FLAME IN TUBES

Irrespective of the variety of conditions under which the combustion process proceeds, the direct transition of gas across zone II is always a deflagration regime. However, in some cases the combustible gas passes from state 1 into end-products 3 directly across zone II (*Figure 4*), and sometimes when the conditions of the thermal discontinuity zone cease to obey the conservation of matter principle, a shock wave is formed in front of the combustion zone due to disintegration of thermal discontinuity.

Returning to the deflagration regime shown in *Figure 4*, let us assume that for some reason or other the flame area has increased, while the pressure in region 3 has remained constant. Lower values of p_3, that is more developed deflagration, should correspond to more expanded flame area S and greater velocity u. Let the conditions of the right side end of the tube be such that p_3 remains constant. Obviously for more developed deflagration to occur under such conditions without deviating from law 1 the pressure in front of the combustion zone II should increase. This condition can only be satisfied by the shock wave, which is now being 'radiated' by combustion zone II. Let the flame area S in an infinitely long tube be constant. Then under the idealized conditions given above after time $\tau = h/D$ has elapsed from the establishment of the shock wave I the velocities of the latter of the zone II and of the gas in regions 2 and 3 will be similar to those given in *Figure 5a*. The same is observed on propagation of flame from the opened (*Figure 5b*) and from the closed (*Figure 5c*) tube end. For all combustion regimes given schematically in *Figure 5*, the shock wave occurs as a necessary condition of the deflagration regime and leads to the regime of propagation of the unsteady double discontinuity, i.e. to the shock wave and to flame moving along the shock-compressed gas in the same direction, but with a velocity lower than that of the shock wave. The latter moves relative to the tube walls and to quiescent gas with velocity D, while zone II moves relative to the shock-compressed

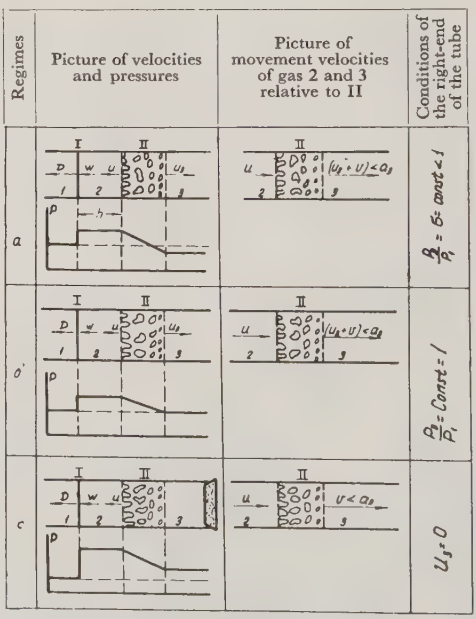

Figure 5. Pre-critical regimes of unsteady double discontinuity distribution under different boundary conditions

gas 2 with a velocity u, and relative to the wall of the tube with a velocity

$$v = u + w \tag{10}$$

where w is the velocity of the shock-compressed gas 2.

In contrast to the steady double discontinuity that occurs during detonation, the characteristic feature of the unsteady double discontinuity ($D > v$) is that at equal periods of time the mass of the shock-compressed gas is greater than the mass of the gas burnt out in combustion zone II, i.e. there is accumulation of gas in zone 2. It is clear that the ordinary Hugoniot adiabatic curve is not capable of describing the propagation of such a double discontinuity, it describes only particular cases of direct transition of a gas from state 1 to state 3, for example deflagration regimes corresponding to the AG branch, or the steady double discontinuity, that is detonation (point J). Taking into consideration that the diverging complex of I and II exists a certain finite time, the transfer of gas across the shock front and across combustion zone II can be followed successively. In the first case at a given shock wave amplitude $\mu = p_2/p_1$ the density and velocity of the shock-compressed gas 2, and also the velocity of the shock wave as such are given by:

$$\phi = \frac{\rho_2}{\rho_1} = \frac{\kappa\mu + 1}{\kappa + \mu} \tag{11}$$

$$\frac{w}{(p_1/\rho_1)^{\frac{1}{2}}} = (\mu - 1)\left(\frac{2}{(k-1) + (k+1)\mu}\right)^{\frac{1}{2}} \tag{12}$$

$$\frac{D\,w}{p_1/\rho_1} = \mu - 1 \tag{13}$$

In the second case we obtain the following equation for the Hugoniot deflagration branch:

$$\frac{p_3}{p_2} = \frac{\kappa - \frac{\rho_2}{\rho_3} + \frac{2Q}{p_2/\rho_2}}{\kappa\,\rho_2/\rho_3 - 1} \tag{14}$$

Equations 14 and 11 can be rewritten as a generalized Hugoniot equation for the gas state within non-stationary double discontinuities

$$\frac{p_3}{p_1} = \frac{\mu\left[\kappa - \frac{\rho_1}{\rho_3}\left(\frac{\kappa\mu+1}{\kappa+\mu}\right) + \frac{2Q}{p_1/\rho_1}\left(\frac{\kappa\mu+1}{\kappa+\mu}\right)\frac{1}{\mu}\right]}{\kappa\,\frac{\rho_1}{\rho_3}\left(\frac{\kappa\mu+1}{\kappa+\mu}\right) - 1} \tag{15}$$

where the variable p_3/p_1 is a function of the argument ρ_1/ρ_3 depending in turn on another variable—parameter μ. This fixed parameter corresponds to a definite flame propagation regime, established for instance by increasing the flame area in zone II. Having established the relationship between ρ_1/ρ_3 and μ and using this equation it becomes possible to describe any given regime of flame propagation, and at the same time to determine all velocities characteristic of this regime and the gas states in regions 2 and 3.

Under any boundary conditions the picture of velocities and of the gas state on propagation of flame in tubes depends essentially on whether the gas transfer across zone II, for a given regime of flame propagation, is a fully developed deflagration (critical regime) or not (pre-critical regime). In the first case zone II moves relative to the reaction products with the local sound velocity, whilst in the second case the velocity is subsonic.

Plots described by equation 15 are given schematically in *Figure 6*. Curve ACJ corresponds to regimes of flame propagation from the

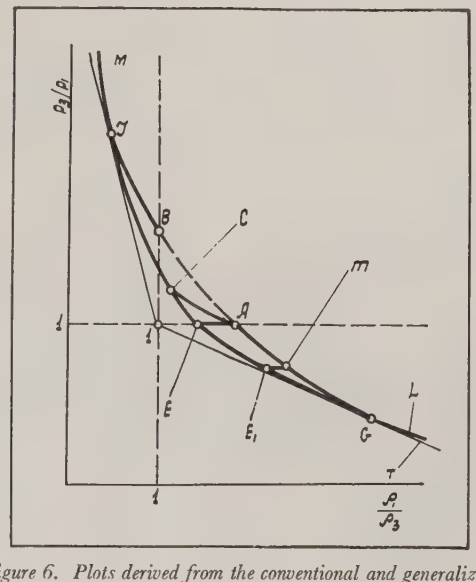

Figure 6. Plots derived from the conventional and generalized Hugoniot curves

closed end of the tube; AC to pre-critical and CJ to critical regimes. Curve $AECJ$ corresponds to flame propagation from the opened end of the tube; branch AE to pre-critical, ECJ to critical regimes. Curve mE_1ECJ corresponds to unsteady regimes of flame propagation, starting with weak deflagration, denoted by point m. The mE_1 branch corresponds to pre-critical regimes, and E_1ECJ to critical ones. In case unsteady regimes of flame propagation start with fully developed deflagration (denoted by point G) pre-critical regimes will be absent and the whole branch GE_1ECJ will correspond to critical regimes.

Let us consider in detail the regimes described by branches of these curves.

Closed tube—On propagation of flame from the

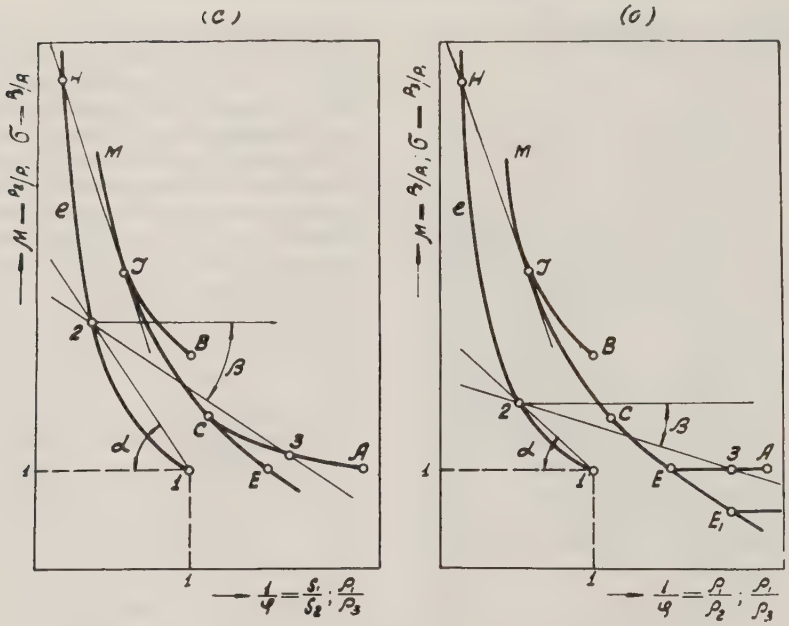

Figure 7. Plotting of the curves derived from the generalized Hugoniot curve

closed end of the tube (*Figure 5c*) the reaction products are quiescent ($u_3 = 0$), if zone II moves relative to gas 3 with a velocity smaller than the local speed of sound ($v < a_3$). Gas states for such pre-critical regimes in zone 3 will be described by points on the *AC* curve (*Figures 6* and *7c*). Point 2 on the adiabatic shock curve 12*eH* corresponds to the state of the shock compressed gas and the velocity of the shock wave is determined by the slope angle (α) of the Michelson straight line 1–2. The relationship between ρ_1/ρ_3 and fixed μ is given by

$$\rho_1/\rho_3 = \phi\,(1 - w/v) \tag{16}$$

$$\frac{1}{k-1}\,v^2 + v\left[\frac{Q}{w} - w\left(\frac{k}{k-1} - \frac{3}{2}\right)\right]$$

$$-\left(\frac{k}{k-1}\cdot\frac{p_1\mu}{\rho_1\phi} + Q + \frac{w^2}{2}\right) = 0 \tag{17}$$

The ordinate of point 3 on the *AC* curve p_3/p_1 can be then estimated from 15 and u from the following equation for the Michelson straight line 2–3:

$$\frac{u}{(p_2/\rho_2)^{\frac{1}{2}}}\quad (\mu\phi)^{\frac{1}{2}} = \left(\frac{\mu\left(1 - \dfrac{p_3}{p_2}\right)}{(\rho_2/\rho_3 - 1)/\phi}\right)^{\frac{1}{2}}$$

$$= \frac{u}{(p_1/\rho_1)^{\frac{1}{2}}}\quad \phi = \left(\frac{\mu - \dfrac{p_3}{p_1}}{\rho_1/\rho_3 - \dfrac{1}{\phi}}\right)^{\frac{1}{2}} = (\tan\beta)^{\frac{1}{2}} \tag{18}$$

The tangent of the slope angle β of this straight line is characteristic of the flame velocity u estimated with respect to substance particles. The lower is μ the lower are α and β and the lower fall the points of the intercept of this straight line with curve *AC*. At the limit (at $\mu = 1$) $p_3/p_1 \to 1$, $u \to 0$, point 3 approaches point *A*. (In reality of course $\mu > 1$ always since $u \to u_n > 0$.) Inversely, the higher is μ (with increase of μ point 2 is shifted up the curve *leH*), the higher are α, β, p_3/p_1, u, w, v and point 3 is shifted in the direction of *C*.

Critical regime sets in when the velocity of zone II movement relative to gas 3 attains the local velocity of sound ($v = a_3$). The value of μ corresponding to transition to critical regimes, is given by

$$\mu = \frac{1}{2}\left[2 + (k-1)\,\frac{Q}{p_1/\rho_1}\right]$$

$$+ \left\{\left[\frac{1}{2}\left(2 + (k-1)\,\frac{Q}{p_1/\rho_1}\right)\right]^2\right.$$

$$\left. + \frac{1}{k+1}\left[\frac{Q}{p_1/\rho_1}\,(k^2-1) + (k+1)\right]\right\}^{\frac{1}{2}} \tag{19}$$

At this μ value the Michelson straight line 2–3 is coming into contact with curve GE_1EJC in point *C*. With further increase of μ (point 2 approaches point *H*) the contact point is shifted up curve *CJ*, approaching point *J*, for which precisely $\alpha = \beta$.

It should be borne in mind that points on the *CJ* branch are describing gas states only immedi-

ately after zone II, since the pressure beyond this zone at $v > a_3$ has no time to become uniform over the whole 3 region.

Opened tube—In this case (*Figure 5-o*) the reaction products flowing out into the atmosphere are moving relative to the tube walls in the direction of its opened end with a velocity u_3, and zone II in the opposite direction with a velocity v, so that the relative velocity of zone II with respect to gas 3 is $u_3 + v$. As long as $(u_3 + v) < a_3$ pressure in the whole region 3 remains equal to atmospheric pressure, since the sound wave, though shifted to the right side by reaction products, will always attain zone II. States of 3 for such pre-critical regimes will be described by points on the straight line *AE* (*Figures 6* and *7o*) parallel to the density axis. Here velocities D and u are determined by tangents of the slope angle (α and β) of Michelson straight lines 1–2 and 2–3 respectively, and 2–3 will accordingly intercept *AE* and the nearer to point *A* the lower is μ.

At the limit (at $\mu \to 1$): $u \to 0$; $\rho_1/\rho_3 \to (\rho_1/\rho_3)_A$. Since $\sigma = p_3/p_1 = \text{const} = 1$, the relationship of ρ_1/ρ_3 to μ is obtained directly from 15. u value is obtained from 18, v from 10 and the value for u_3 is

$$u_3 + v = \frac{\rho_1}{\rho_3}\,\phi \tag{20}$$

The higher is μ the nearer to point E shifts the point of interception of straight lines 2–3 and *AE*. Finally at $u_3 + v = a_3$ the critical regime is attained and the secant 2–3 changes in point E into a tangent with respect to curve GE_1ECJ. The value for this change is obtained from equation

$$\begin{aligned}\mu^3 - \mu^2 &\left[2\sigma - \kappa - \frac{2Q}{p_1/\rho_1}\right] \\ &- \mu\left\{\frac{2Q}{p_1/\rho_1}\left[\sigma\,(k+1) - \frac{1}{\kappa}\right]\right. \\ &\left. + \sigma\left[\frac{k+3}{k-1} - (k-1)\right] + \sigma^2\,(k-1)\right\} \\ &- \sigma\left[\frac{2Q}{p_1/\rho_1}(k-1) - \kappa\,k\right] - \sigma^2\,(k+1) = 0\end{aligned} \tag{21}$$

On increase of μ the contact point is shifted up the curve *EC* (here gas 3 and zone II are still moving in opposite directions). On further increase of μ critical regimes are similar to those for closed tubes.

Rarefication at the tube end—Propagation of flame under these conditions differs from that for the open tube only in the pressure value at the right end of the tube (*Figure 5a*), which remains constant for all pre-critical regimes of the region 3 ($p_3/p_1 = \sigma = \text{const} < 1$). The relationship of ρ_1/ρ_3 to μ for a given σ is obtained from 15, values u, v and u_3 are estimated from 18, 10 and 20 respectively. Gas 3 states are expressed by points on the straight lines mE_1 (*Figure 6*). Similar to *Figure 7o* the Michelson straight line intercepts mE_1 and the lower is μ the nearer to point m falls the intercept. At the limit (at $\mu \to 1$): $u = u_m$; $\rho_1/\rho_3 \to (\rho_1/\rho_3)_m$. The critical regime is attained if $u_3 + v = a_3$ and the secant 2–3 changes in point E_1 into a tangent with respect to curve GE_1ECJ at μ obtained from equation 21.

Immediately after attainment of critical regimes the transfer of shock-compressed gas 2 across zone II will represent, under any conditions at the right end of the tube, a fully developed deflagration regime. Consequently relations 6, 7 and 8 can be made use of if values $p_1\mu$ and $\rho_1\phi$ are substituted for p_1 and ρ_1 respectively. Since the μ value is always fixed, u and also the state of gas 3 (ρ_1/ρ_3, p_3/p_1) can be estimated from these relations. The value v is obtained from 10. If the state of gas immediately after zone II is described by points of section GE_1EC it means that the reaction products and the shock-compressed gas are moving in opposite directions, and if by points of the *CJ* branch then the direction is the same. Consequently the velocity of gas 3 with respect to gas 2 will be

$$u_{3-2} = w + u_3 = \left(\frac{2Q}{\kappa}\right)^{\frac{1}{2}} \tag{22}$$

$$u_{3-2} = w - u_3 = \left(\frac{2Q}{\kappa}\right)^{\frac{1}{2}} \tag{23}$$

u_3 can be obtained from these relations.

APPLICATION TO THE PROBLEM OF TRANSITION FROM SLOW COMBUSTION TO DETONATION

Curves plotted from the generalized Hugoniot equation would contribute to our knowledge on the very complicated process of flame acceleration and on transition from slow combustion to detonation. Indeed, already the existence of branches *ACJ* and *AECJ* allows us to eliminate formal difficulties connected with determination of the nature of this process in tubes, these difficulties being connected with the fact that the Hugoniot curve represents only detonation or normal combustion, but no intermediate regimes.

Analysis of these curves shows that transition from slow combustion to detonation, occurring through intermediate combustion regimes, is possible only with successive acceleration of flame with respect to gas. This is the answer to the main question of the discussion[8–11], whether the velocity of flame u (with respect to gas) would increase, as the velocity of flame v (with respect to the tube walls) is increasing. Analysis of the plots shows that the suggestions of Zeldovitch and Shchelkin on successive increase of flame velocity with respect

to gas are, contrary to Sokolik[8,10], in full agreement with the basic conservation principles. Zeldovitch fully accepts Shchelkin's concept on combustion acceleration being due to the gas flow originating ahead of the flame front. However, differences arise in determining the exact mechanism of the effect of the gas flow upon the flame front. Shchelkin suggests that this mechanism is connected with turbulent motion of gas ahead of the flame front leading to successive increase of the combustion area.

According to Zeldovitch there is a field of non-uniform distribution of unburnt gas flow velocities ahead of the flame front, owing to which the line of the combustion front is expanded. Computation of gas states by means of the generalized Hugoniot curve and analysis of schlieren photographs of flame acceleration in the tube allow us to solve also this problem.

Let us assume in rough approximation that for a short period of time continuously accelerated flame propagates in the tube with a constant velocity v. We can then estimate u, and also the gas state in region 2. Consequently it becomes possible to obtain the value for normal flame velocity under conditions ahead of the combustion zone u'_n and the value

$$u_t + u_p = u - u'_n \qquad (24)$$

where u_t and u_p are fractions of relative flame velocity with respect to substance particles, accounted for by the increase of combustion area due to gas 2 turbulence, and to increase of macro-surfaces of flame by virtue of the velocities profile of unburnt gas 2[5,12,1,13]. u_t and u_p can be estimated separately by analysis of schlieren photographs, such as those given in *Figures 8–10* for accelerated flame in a mixture 2·5 H_2 + 0·4 O_2 + 0·75 air, in a smooth closed tube with a rectangular cross-section 21 × 21 mm. This can be confirmed by calculated and experimental evidence for $v \sim 830$ m/sec, $u \sim 163$ m/sec, $u_t \sim 97$ m/sec, $u_p \sim 56$ m/sec, $u'_n \sim 10$ m/sec, $u_n \sim 5{\cdot}5$ m/sec. As can be seen u_t plays a leading and u_p a subordinate part. Prior to the establishment of detonation the flame front often acquires the form of a cone, its apex being turned towards the reaction products (*Figure 10*). This is apparently due to conditions of flame propagation being for some reasons or other more favourable at the

Figure 8. Schlieren photograph of flame acceleration in a tube

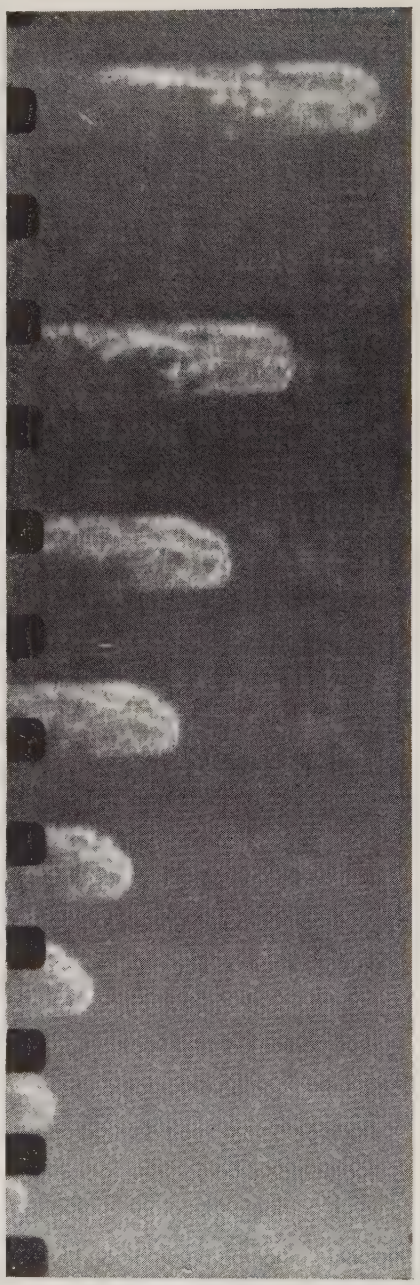

Figure 9. Schlieren photographs of flame acceleration in a tube

Figure 10. Schlieren photographs of the accelerating flame front prior to establishment of detonation in a tube

walls than in the middle of the flow. It can be conceived that the turbulence, due to a greater roughness of metal walls as compared to lateral glass walls, has no time to attain the middle of the flow in the region between the shock wave and the combustion zone II, as a result of which u_t is lower in the middle than at the walls.

The important part played by expansion of the flame area of zone II in attainment of high v values can be illustrated by calculating the regimes of flame propagation from the opened (o) to the closed (c) end of the tube (*Figure 11*). The dependence of S/F on v is given for different combustible mixtures. It appears that maximum expansion of the flame area in zone II is required for the initial combustion stages, when v rises from small values up to $v \sim 250$ m/sec (o regimes) $v \sim 500$ m/sec (c regimes).

As can be seen from the illustrations and Table 1 mixtures with low values of Q and u_n require considerable expansion of the combustion area, whilst for combustible mixtures with high heat capacity and with high u_n the required combustion area expansion is not so important.

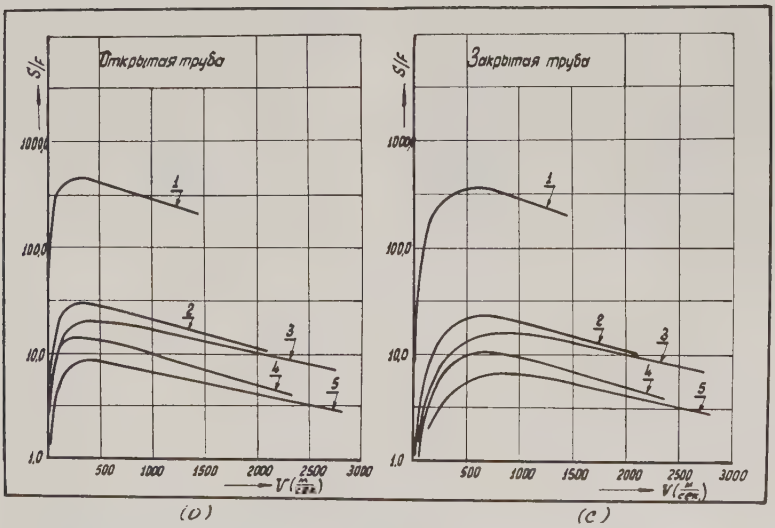

Figure 11. Dependence of S/F on v for different combustible mixtures on propagation of flame from the opened (o) and from the closed (c) end of the tubes

This accounts for difficult transition from slow combustion to detonation in certain cases, and for relatively ready transition in other cases.

TABLE 1

Maximum Combustion Area Expansion Required at Propagation of the Flame Front from the Opened (*o*) to the Closed (*c*) End of the Tube

No. of curve	*Mixture*	*Regime*	$(S/F)_{max}$
1	6·3% CH_4 + 93·7% air	o	422
		c	344
2	H_2 + 1·5 air	o	28·7
		c	22·7
3	2·5 H_2 + 0·4 O_2 + 0·75 air	o	20
		c	16
4	CH_4 + 2 O_2	o	14
		c	10
5	2 H_2 + O_2	o	8·7
		c	6·5

CONCLUSIONS

It has been shown that all points on the weak deflagration branch of the Hugoniot curve correspond to real regimes of gas combustion under different conditions of reaction product outflow.

Gas states within unsteady double discontinuities are represented on the P–V plot by points of the curves derived from the generalized Hugoniot equation. These curves start from points on the weak deflagration branch, pass under the conventional Hugoniot curve (its imaginary and energetically forbidden branch for partly compressed detonation) and end at the Jouguet point on the detonation branch.

Plots obtained from the generalized Hugoniot curve seem to confirm that the transition from slow combustion to detonation, occurring through unsteady double discontinuities, is possible only on successive relative acceleration of the flame with respect to gas.

Calculation of gas states from the generalized Hugoniot curve and analysis of schlieren photographs show that flame acceleration with respect to gas is accounted for mainly by development of the flame area due to turbulence of the unburnt gas.

The author wishes to thank Professor K. I. Shchelkin for the valuable comments and interest in this work.

REFERENCES

[1] Zeldovitch, Ya. B. and Kompaneiets, A. S. *The theory of detonation* (Russian) M. 1955

[2] Lewis, B. and Elbe, G. von. *Combustion, Flames and Explosions of Gases*, p. 246. 1938. New York; Academic Press

[3] — — *Combustion, Flames and Explosions of Gases*, p. 597. 1951. New York; Academic Press

[4] Courant, R. and Friedrichs, K. O. *Supersonic Flow and Shock Waves*, pp. 231, 234. 1948

[5] Shchelkin, K. I. *Doklady Akadem. Nauk SSSR* 23 (1939) 636
— *Zhurn. Techn. Phys.* (Russian) 13 (1943) 520

[6] Damköhler, G. *Zeit. für Elektrochem.* 46 (1940) 601

[7] Troshin, Ya. K. *Izv. AN SSSR, Otd. Techn. Nauk* 1 (1956) 80

[8] Sokolik, A. S. *Zhur. Exp. Theor. Phys.* (Russian) 21 (1951) 1146

[9] Zeldovitch, Ya. B. *Zhur. Exp. Theor. Phys.* (Russian) 21 (1951) 1172

[10] Sokolik, A. S. *Zhur. Exp. Theor.* 21 (1951) 1176

[11] Shchelkin, K. I. *Zhur. Exp. Theor. Phys.* 24 (1953) 586

[12] — *Rapid Combustion and Spin Detonation of Gases.* 1949. M. Voenizdat

[13] Zeldovitch, Ya. K. *Zhur. Techn. Phys.* (Russian) 17 (1947) 3

ON THE PRE-DETONATION PERIOD OF FLAME PROPAGATION

V. A. POPOV

INTRODUCTION

The present paper is concerned with the attempt to determine certain regularities preceding the formation of a detonation wave without going into the details of the flame propagation instrument.

The treatment of experimental results is based on the analytical apparatus of the well known method of characteristics which is used for the solution of problems bound with the one-dimensional non-stable motion.

The conformity of the obtained experimental material and the deduction of the theory makes it possible to draw a conclusion on the cause of the flame vibration in the pre-detonation period.

It is shown that these vibrations may be explained by the interaction of the flame front with the forming shock wave which is proved by the motion of the flame in the initial stage of propagation.

THEORETICAL BASIS

The mechanism of flame propagation in the pre-detonation section (the section from the point of the first flame deceleration to the point of the detonation wave formation[1]) is to a considerable extent open to discussion.

Numerous works demonstrate the particular role of the discontinuous processes accompanying explosive chemical reactions. Hence the study of the explosion formation conditions becomes particularly important[2]. It is known that between strong perturbations and usual sound perturbation there is a considerable difference. Contrary to sound perturbations which are subject to linear differential equations, the propagation of strong perturbations is described by non-linear differential equations, in consequence the laws of superposition, reflection and refraction are incorrect, and furthermore new phenomena occur in particular 'shock waves'.

At the shock wave front the substance is subject to sudden changes in its velocity, pressure and temperature. The initial discontinuity between the two regions of different pressure, density and flow velocity will propagate in the form of a shock wave with a supersonic velocity in relation to a non-perturbated medium.

The mathematical difficulties bound with the solution of general differential equations of conservation at present cannot be overcome.

However, in many cases it is possible to adhere to simplifications reducing the number of independent variables only to two (one-dimensional non-stable motion, stable double-dimensional motion, etc.).

In such cases the problem is brought to a system of quasilinear equations expressed by first order partial derivatives for the functions of two independent variables. If the equations are of a hyperbolic type, quite an accurate mathematical solution may be developed for such a system, and the main role in it belongs to the concept of characteristics.

Examining the motion of a compressible liquid in a cylindrical pipe on the assumption that there will be no losses of heat and forces, depending on its viscosity, the equation of motion and of discontinuity for one-dimensional cases can be written as follows:

$$\frac{\partial u}{\partial t} + u\frac{\partial u}{\partial x} + \frac{1}{\rho}\frac{\partial \rho}{\partial x} = 0 \qquad (1)$$

$$\frac{\partial \rho}{\partial t} + u\frac{\partial \rho}{\partial x} + \rho\frac{\partial u}{\partial x} = 0 \qquad (2)$$

where u—velocity of the point x at the moment of time t, p—the pressure, and ρ—the density of the medium.

The integrals of this system of equations in diverse boundary conditions have the discontinuity of derivatives of different orders. If in this system the equation of energy conservation has the form of the Poisson adiabate

$$p\rho^{-\gamma} = \text{const} \qquad (3)$$

it is not difficult to define the equations of characteristics describing the discontinuities of the second order derivatives, which are propagated in the gaseous media with the following velocity

$$\frac{dx}{dt} = u \pm a \qquad (4)$$

where $a = (\gamma p/\rho)^{1/2}$, the sound velocity.

The relation between the flow velocity u and

the sound velocity a in any point of the medium corresponding to the characteristic, is defined by the following equations

$$da \pm \frac{\gamma - 1}{2} du = 0 \qquad (5)$$

The last equations constitute the base of the graphic method of computation[3], where the parameters of the process are located on the (x, t) and (a, u) planes.

Equation 4 corresponds to the projections of characteristics on the (x, t) plane, while equation 5 corresponds to the projections of the same characteristics on the (a, u) plane.

Every point on the first plane has a corresponding one on the second, so that when certain initial and boundary conditions are being set, the parameters of the medium can be determined at any point and at any moment. The family of characteristics being in the (a, u) plane has the form of direct lines and the graphical computation is significantly simplified.

COMPUTATION

Let us assume that the chemical reaction in a gaseous medium proceeds in a sufficiently narrow zone of the flame front in comparison with the length of the pipe. Let us suppose as well that from the very outset of the process of propagation the effect of the flame on the medium lying in front of it is similar to the effect of a solid piston. It is evident that such an assumption is true only for the initial moments of propagation, when it can be assumed that the gas mass in front of the flame is constant. For the present instance all the regularities of propagation of sound waves generated by the moving pistons will take place in the case of the flame propagation in the pipe.

Detailed grapho-analytical methods of calculations of an easy detonating stoichiometric mixture of hydrogen and oxygen and of a hardly detonating stoichiometric mixture of carbon monoxide and oxygen is stated below.

The mixture has been exploded in a closed pipe, 1,525 mm in length and 20 mm in diameter. The process of flame propagation was analysed on a moving film (*Figure 1*).

The density of the fresh mixture and the sound velocity in it under the experimental conditions were $\rho_0 = 0{\cdot}532$ kg/m^3 and $a_0 = 512$ m/sec respectively.

Figure 2 represents the dependence of the flame front path on the time in non-dimensional values $X = x/L$ and $Z = (a_0/L)t$ where x is a current coordinate of the flame front, L the pipe length, and t time.

Figure 3 represents the dependence of the flame propagation rate on the time t, which is obtained by graphical differentiation of the curve from *Figure 2*.

The computation was made by means of a technical method mentioned by Haller[3]. Introducing non-dimensional parameters $A = a/a_0$,

Figure 1. Photo of the flame motion by means of a moving film, $2H_2 + O_2$

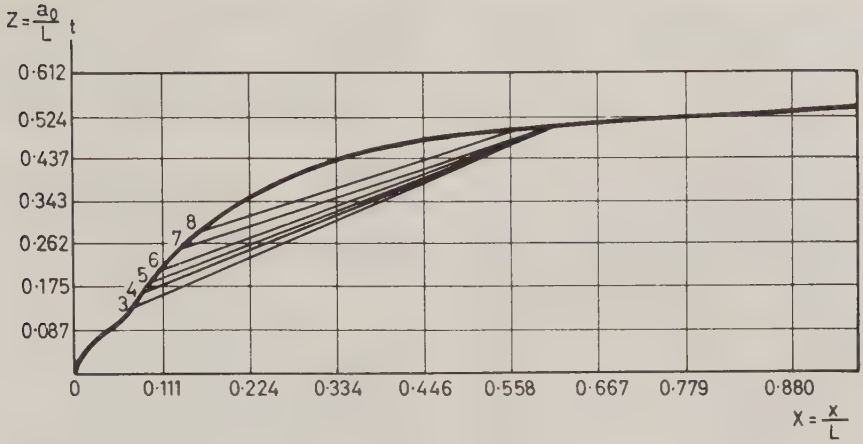

Figure 2. Dependence of the flame path on time in non-dimensional coordinates

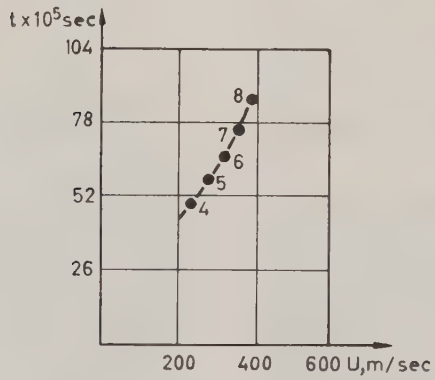

Figure 3. Dependence of the front flame velocity on time, $2H_2 + O_2$

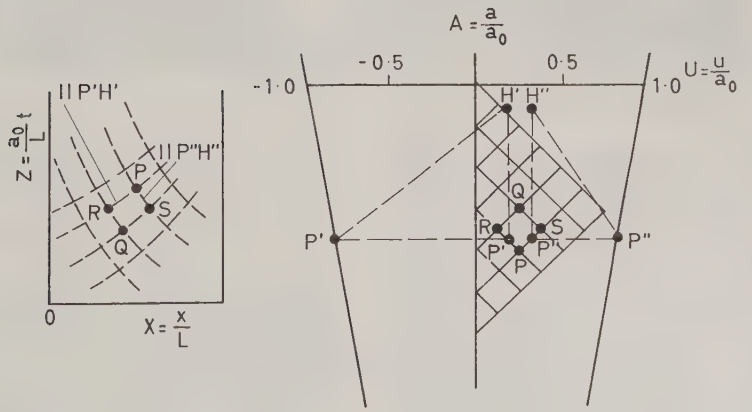

Figure 4. Graphical representation of the method of finding characteristics by Haller

$U = u/a_0$, X and Z, equations 4 and 5 can be rewritten in the following manner

$$\left.\begin{aligned} \frac{dX}{dZ} &= U \pm A \\ \Delta U &= \mp \frac{2}{\gamma - 1} \Delta A \end{aligned}\right\} \qquad (6)$$

Plotting the diagram on the (A, U) plane it is convenient to take the scale for A $2/(\gamma - 1)$ times greater than for U. In this case the projections of the characteristics in this plane will form a net of direct lines at an angle of 45° to the axes of coordinate (*Figure 4*).

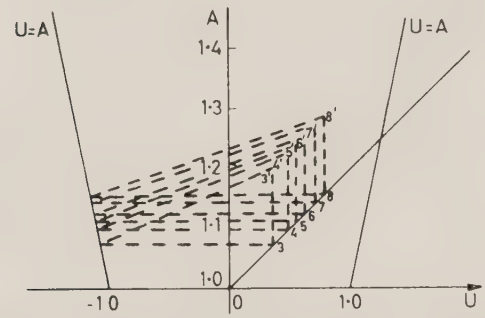

Figure 5. Determination of flame propagation characteristics in the $2H_2 + O_2$ *mixture*

If the coordinates of any points R and S in the (X, Z) and (A, U) planes are known, it is not difficult to determine the parameters, corresponding to the intersection of P and Q characteristics. The coordinates of these points are defined as the coordinates of the intersections of direct lines, which are drawn through R and S at an angle of 45° to the coordinate axes. Tracing in the plane (A, U) direct lines, corresponding to equations $U = +A$ and $U = -A$, finding the points P' and P'' lying in the middle of sections PR and PS and tracing from these points equal sections $P'H'$ and $P''H''$ parallel to the A axis, the unknown slope of characteristics may be found in the (X, Z) plane. The size of sections $P'H'$ and $P''H''$ are equal to $(Z_m U_m)/X_m$, where X_m, Z_m and U_m are the consequent scales of the non-dimensional values. All the constructions which are necessary for the tracing of characteristics in the (X, Z) planes are given in *Figure 5*.

The value of the sections 3–3′, 4–4′ etc. are equal in our case to

$$\frac{Z_m U_m}{X_m} = \frac{114{\cdot}4 \times 40}{180} = 25{\cdot}4$$

All the numerical data obtained during the analysis of the flame front motion in a stoichiometric mixture of hydrogen and oxygen are summarized in Table 1.

TABLE 1

Point	t 10^5 sec	x mm	u m/sec	$X = x/L$	$U = a/a_0$	$Z = a_0 t/L$
3	41·6	110	195	0·072	0·373	0·140
4	50·7	127	260	0·083	0·498	0·171
5	55·8	144	290	0·094	0·565	0·188
6	63·6	163	330	0·108	0·633	0·214
7	76·7	212	375	0·139	0·718	0·258
8	85·7	250	410	0·164	0·785	0·289

Characteristics are plotted for six points, taken from different parts of the curve. It is possible to be convinced of the fact that the characteristics drawn from the points lying between points 3 and 7 intersect simultaneously at the point of the detonation wave formation.

The characteristics of the points lying out of this section do not accumulate themselves in a shock wave of a final amplitude and their effect on the flame front in this case is negligible.

The attempt to interpret from the same positions the photographs of the flame motion in mixtures where the faculty of detonation is much weaker than that of the hydrogen–oxygen mixtures seems as well to be of utmost interest.

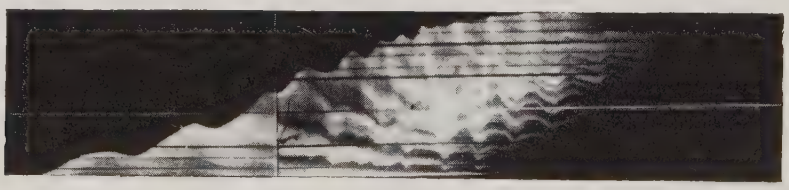

Figure 6. Photograph of the flame motion $(2CO + O_2)$ *taken from a moving film*

As an example let us give a computation of the front motion in a stoichiometric mixture of carbon monoxide and oxygen (*Figure 6*). The lighter part of the picture corresponds to the region of combustion products, and the darker one to the region of the fresh explosive mixture.

The flame front is the boundary between these two regions. As it was pointed out above, the flame front is identified in computations with a

solid wall of a piston, which is being displaced by the law of propagation of the flame front.

The motion of the combustion product in accordance with the fluctuating character of the

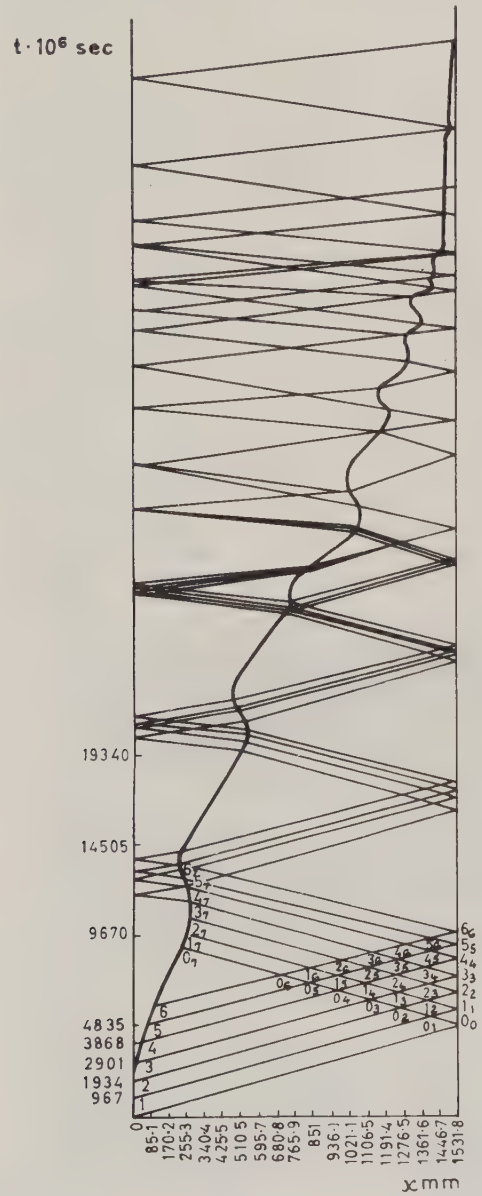

Figure 7. Disposition of characteristics of the flame propagation in the $2CO + O_2$ *mixture*

front displacement is perfectly seen on the photograph. In the subsequent period these smooth movements of combustion products give place to more and more sharp ones. As it will be shown further the motion of combustion products is initiated by their interaction with the shock wave front being formed by many sound waves. Sharp changes of the direction in the motion of combustion products in the subsequent moments are initiated by the action of the previously formed shock wave.

In this case the problem is complicated by the fact that the sound waves, resulting from the motion of the flame front, do not have the time to intersect before reaching the opposite end of the pipe. Being reflected from the end of this pipe the sound waves propagate conversely in the direction of the flame.

It is necessary to notice that the velocity of such a wave will not be constant, its value will depend on the state of the medium at the moment of the passage of sound perturbations through it. It is evident that the velocity of the reflected wave must decrease, because it passes through a medium having a velocity directed conversely to the propagation of this wave. This change in the velocity, as was shown by calculations, is insignificant; however, it was taken into account in the graphical construction. Being reflected from the end of the pipe, the sound waves, interacting with the flame which moves in the same direction, restrict its motion. It is possible that this interaction may reach such a considerable value that the flame will move back to the place of its origin.

Contrary to the previous case the computation of this photograph is carried out not only by a graphical method, but by a grapho-analytical method which in the main differs in no way from the first one. The scale factor (*Figure 7*) is equal to $k = 85/(967 \cdot 10^{-6}) = 88$ m/sec, the velocity of the sound in the fresh gas a_0 is 326 m/sec.

It is evident that in the plane (x, t) the slope of the characteristics $0\text{–}0_0$ from the point *0* is determined by the velocity of the sound in a non-turbulent gas which is equal as it was stated above to 326 m/sec. The tangent of the slope of this characteristic in this case is equal to $k = 326/88 = 3{\cdot}71$.

The inclination of the characteristic $1\text{–}0_1$ from point *1* is defined by constructing it in the plane (u, a), where u is the flow velocity of the media, and a is the velocity of the sound (*Figures 8* and *9*).

Theoretically the velocity of sound perturbation at moments of time *1*, *2*, *3*, *4*, *5*, *6*, marked in plane (x, t) by corresponding points, are defined in plane (u, a) by the characteristic *0–6* at an angle of 45° to the axes u and a. This angle of inclination is determined by the choice of the scale for the $[2/(\gamma - 1)]a$ axis, where γ is the ratio of specific heats of a fresh gas.

The velocities of the sound perturbations, arising from these points, are defined as ordinates of corresponding points in *Figure 8*. The determination of the flame front velocity is analogous to that

used in the previous case (see *Figure 9*). Sound velocities corresponding to point *2* are evaluated by the ordinate axis of point *2*, its abscissa in plane (u, a) being equal to 8 m/sec.

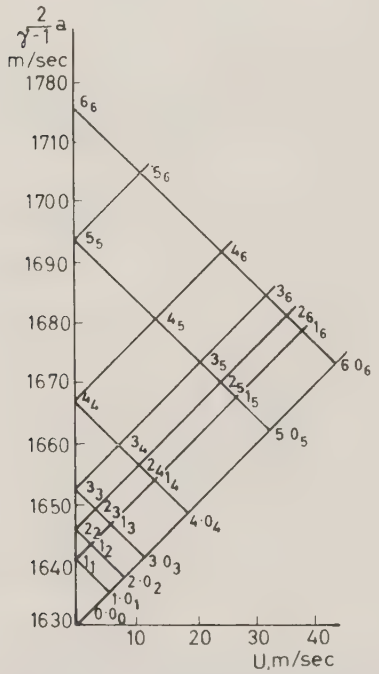

Figure 8. Construction in the (u, a) plane

Analogous computations are fulfilled for all the other points. It is evident that sound perturbations arising from points *1*, *2*, *3*, *4*, *5* and *6* will propagate with constant velocities only up to the

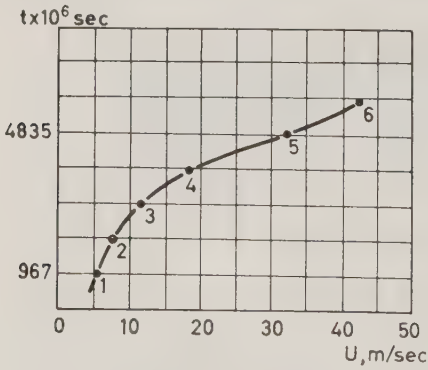

Figure 9. Dependence of the flame front velocity on time in the $2CO + O_2$ *mixture*

moments, marked in plane (x, t) by points 0_1, 0_2, 0_3, 0_4, 0_5 and 0_6 since at the moment 0_1 the perturbation arising from point *1* meets with the perturbation, arising from point *0*, reflected at point 0_0 from the opposite side of the pipe. The 0_0–0_1 characteristic is traced at the same angle as

TABLE 2

Point	u m/sec	$(2/\gamma - 1)a$ m/sec	a m/sec	K $X = Kt = (u \pm a/k)t$
1	2	3	4	5
0	0	1630	326	3·71
1	5·5	1635·5	327·1	3·77
2	8	1638	327·6	3·81
3	11·25	1641·25	328·25	3·86
4	18·5	1648·5	329·7	3·96
5	32	1662·0	332·4	4·13
6	43	1673	334·5	4·29
0_0–0_1	0	1630	326·0	−3·71
0_1–0_2	5·5	1635·5	327·1	−3·65
0_2–0_3	8	1638	327·6	−3·63
0_3–0_4	11·25	1641·25	328·25	−3·60
0_4–0_5	18·25	1648·5	329·7	−3·53
0_1–1_1	0	1641	328·2	3·71
1_1–1_2	0	1641	328·2	−3·71
0_2–1_2	2·5	1643·5	328·6	3·76
1_1–1_3	2·5	1643·5	328·6	−3·71
0_3–1_3	6·25	1647·25	329·5	3·81
1_3–1_4	6·25	1647·25	329·5	−3·69
0_4–1_4	13	1654	330·8	3·91
1_4–1_5	13	1654	330·8	−3·61
1_2–2_2	0	1646·5	329·3	3·74
2_2–2_3	0	1646·5	329·3	−3·74
1_3–2_3	3·25	1649·25	329·8	3·79
2_3–2_4	3·25	1649·25	329·8	−3·72
1_4–2_4	10·5	1656·5	331·3	3·89
2_4–2_5	10·5	1656·5	331·3	−3·66
2_2–3_3	0	1652·5	333·3	3·76
3_3–3_4	0	1652·5	333·3	−3·76
2_4–3_4	7	1660	332	3·86
3_4–3_5	7	1660	332	−3·78
3_4–4_4	0	1667	333·4	3·79
4_4–4_5	0	1667	333·4	−3·79
4_5–5_5	0	1694	338·8	−3·85
5_5–5_6	0	1694	338·8	−3·85
0_5–0_6	32·2	1662	332·5	−3·42
0_6–0_7	43·5	1673	335·1	−3·31
0_5–1_5	26·5	1667·5	333·5	−4·09
1_5–1_6	26·5	1667·5	333·5	−3·49
1_5–2_5	23·5	1670	334	4·06
2_5–2_6	23·5	1670	334	−3·53
2_5–3_5	20·5	1673·5	334·7	4·04
3_5–3_6	20·5	1673·5	334·7	−3·57
3_5–4_5	13·5	1680·5	336·1	3·98
4_5–4_6	13·5	1680·5	336·1	−3·67
0_6–1_6	37·5	1678·5	335·7	4·25
1_6–1_7	37·5	1678·5	335·7	−3·39
1_6–2_6	35	1681	336·2	4·22
2_6–2_7	35	1681	336·2	−3·42
2_6–3_6	32	1684	336·8	4·19
3_6–3_7	32	1684	336·8	−3·47
3_6–4_6	24·5	1691·5	338·3	4·13
4_6–4_7	24·5	1691·5	338·3	−3·57
4_6–5_6	11	1705	351	4·12
5_6–5_7	11	1705	351	−3·87
5_6–6_6	0	1716	353·2	4·02
6_6–6_7	0	1716	353·2	−4·02

the 0–0_0 characteristic which is quite natural, since it is a sound perturbation. The slope of the 0_1–0_2, 0_2–0_3, 0_3–0_4 and other characteristics is determined by the sound velocities corresponding to points 0_1, 0_2, 0_3, etc. and are equal to sound velocities in points *1, 2, 3,* etc.

The sound velocity corresponding to 0_1–1_1 characteristic is determined by the intersection of the 0_1–1_1 characteristic in the plane (u, a), traced at an angle $\pi/2$ to the *0–6* characteristic up to the intersection with the axis $[2/(\gamma - 1)]a$. In this case the ordinate is equal to 1,641 m/sec, and corresponds to the sound velocity equal to 328·2 m/sec (see Table 2).

The 1_1–1_2 characteristic in the plane (x, t) is traced at the same angle for the reason set forth above. The inclination of the 0_2–1_2 characteristic may be determined by the coordinates of the 1_2 point of characteristics' intersection, traced from the points 1_1 and 0_2 in the plane (u, a). In this case this ordinate was equal to 1,643 m/sec corresponding to the sound velocity equal to 328·6 m/sec; the abscissa is equal to 2·5 m/sec. The tangent of the slope angle is $K = (u + a)/k = (2{\cdot}5 + 328{\cdot}6)/88 = 3{\cdot}77$. When the velocity u of the medium and that of the sound a are in one direction, the value of K is obtained by their sum; in other cases it is obtained by their difference. All the rest of the points in *Figure 7* are obtained by analogous computations. The data presented in the computation of this photograph are summarized in Table 2, where the values of the third column are defined from the graph in the plane (u, a).

The values of K are given in the last column, they are equal to the tangent of the inclination angle in a given scale of characteristics in the plane (x, t).

In the table the computing data are given only up to the moment when the sound perturbations attain the end of the tube, near which combustion took place.

The wave computation data in the following moments of time are not presented in this table.

Analysing the results of such an investigation it is easy to see that the beam of sound waves gradually narrows and as it does so its intersection with the flame becomes more sharply defined.

It was assumed in the presented computation that the sound wave velocity after its passage through the flame front changed according to the following relation

$$a_h = a_c \left(\frac{\gamma_h}{\gamma_c} \frac{T_h}{T_c} \frac{\mu_c}{\mu_h} \right)^{1/2}$$

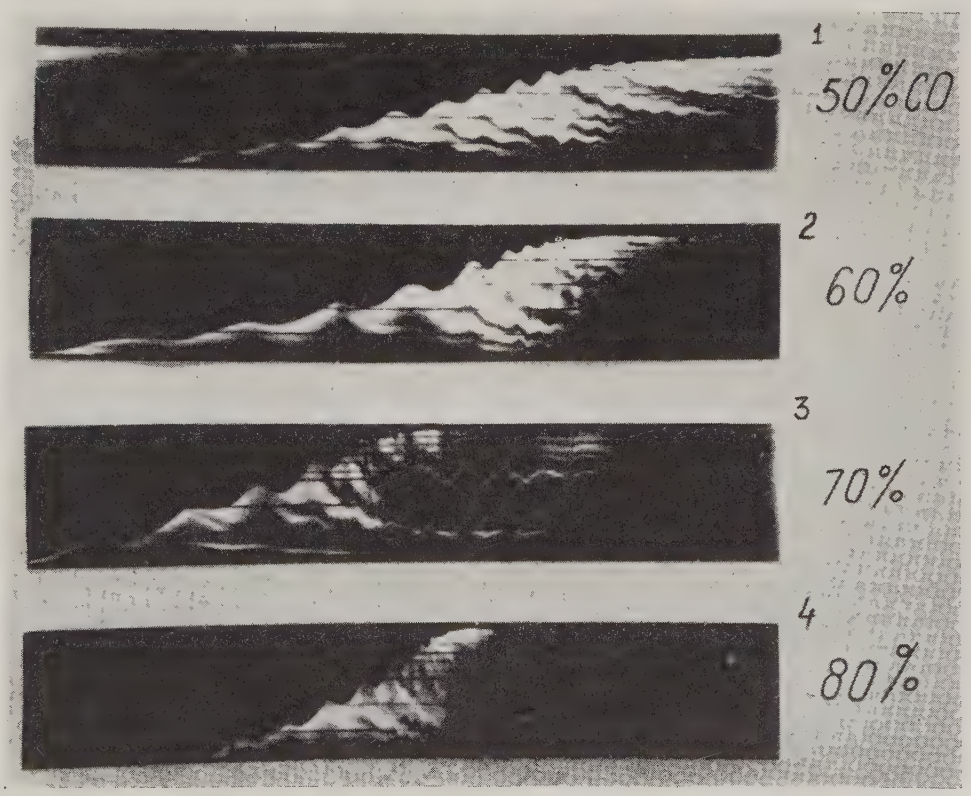

Figure 10. The flame front motion, taken from a moving film, for CO–O_2 *mixtures of different concentrations*

where a_h and a_c are the sound velocities in hot (reaction products) and cold gases, respectively; γ_h and γ_c are the corresponding values of the specific heat relation; T_h and T_c are the corresponding values of temperature; and μ_h and μ_c are the corresponding values of molecular weights.

It is evident that as the flame propagates the reaction products must cool down and as a result will cause a change of sound velocity in hot gas. The computation makes it evident that the temperature changes are so insignificant that the change of sound velocity is not to be taken into account.

After the passage through the flame front the sound waves reflect from the wall a second time and again pass through the flame front. In this case the flame motion does not slow down, but accelerates. In due course the beam of sound waves narrows more and more and this process must last until the formation of a wave with a final amplitude. In this case as it is seen from the photograph, the interaction of the shock wave with the flame front will be more sharply defined.

In the given computation the effect of sound waves reflected from the flame front was neglected. However, for the purpose of giving a complete explanation of the peculiarities shown in the photograph it was necessary to assume that during the interaction of the beam of sound waves with a third 'hump' of the flame front a reflection of the latter takes place, it being necessary to presume that the angle of incidence of the wave is equal to the angle of reflection. This presumption is quite logical, so far as the sound perturbations are defined by linear differential equations with the resulting consequences (principle of superposition, etc.).

Figure 10 shows photographs of flame propagation in oxygen mixtures of different carbon monoxide concentrations (from 50 per cent to 80 per cent CO). Computations similar to those given above were found to be in fair agreement with these experimental data.

CONCLUSION

In conclusion it may be asserted that the character of the flame front motion at the initial section of its propagation can determine the peculiarities of flame propagation in the pre-detonation period.

I am grateful to Professors A. S. Predvoditelev and L. N. Khitrin for their part in the discussions.

REFERENCES

[1] Popov, V. A. *Izvest. Akad. Nauk S.S.S.R., Otdel tekh. Nauk*, No. 3 (1956)
[2] Hugoniot. *J. Éc. polyt., Paris* 57 (1887); 58 (1889)
[3] Haller. *Rev. tech. Sulzer*, No. 1 (1945)

107

ON THE TRANSITION FROM DEFLAGRATION TO DETONATION

S. R. BRINKLEY, Jr. and B. LEWIS

We are concerned with the transition of a deflagration wave (combustion wave), propagating in an explosive gas mixture at a rate of a few m per sec, to a detonation wave, propagating at a rate of a few km per sec. For a background to the discussion of this process it is useful first to consider the flows associated with the idealized cases consisting of one-dimensional deflagration or detonation waves propagating at constant velocity into an explosive gas mixture and supported by a piston moving with constant velocity.

It can be shown[1] that there corresponds a weak deflagration to every piston velocity less than some particular critical velocity. For a given piston velocity the deflagration velocity is explicitly determined by the transport properties (for heat conduction and diffusion) of the unburnt medium ahead of the wave as well as by the state of turbulence in the approach flow to the deflagration wave. The critical piston velocity is that velocity that will support a Chapman-Jouguet deflagration. A deflagration wave is subsonic with respect to both burnt and unburnt material, and the particles are accelerated in passing through the flame front. Boundary conditions are maintained on the piston by means of a simple compression wave that propagates ahead of the deflagration. The complete flow thus consists of a pre-compression wave which imparts a particle velocity in the direction of propagation of the compression wave to the particles of the unburnt material, initially at rest. In passing through the deflagration wave the particles are brought to rest if the piston velocity is zero or in general are decelerated to the piston velocity. The Chapman-Jouguet deflagration is sonic with respect to the burnt material.

It is to be noted that the reference state for the Hugoniot curve for deflagration is the pre-compressed unburnt material.

Similarly, it can be shown[1] that there corresponds a strong detonation to every piston velocity greater than some particular critical velocity. This critical value is that velocity that will support a uniform state behind a Chapman-Jouguet velocity. A detonation wave is supersonic with respect to the unburnt material and subsonic with respect to the burnt material. For piston velocities that are lower than the critical one, the Chapman-Jouguet detonation is connected to the piston by a centred rarefaction wave.

It is to be noted that the reference state for the Hugoniot curve for detonation waves is unburnt material that has not been affected by any signal, such as a compression wave, from the reaction zone.

A detonation wave can be considered to consist of a shock wave followed by a deflagration wave, both propagating with the same velocity. It has been shown[1] that the Chapman-Jouguet detonation is identical with the Chapman-Jouguet deflagration when viewed from a reference state consisting of the pre-compressed unburnt medium instead of the medium in advance of the compression wave, and conversely that the Chapman-Jouguet deflagration when viewed from a reference state in advance of the pre-compression wave instead of the pre-compressed unburnt material is identical with the Chapman-Jouguet detonation.

Thus, one can visualize a continuous transition from deflagration to detonation with increasing piston velocities, the transition occurring for the critical velocity that will support a Chapman-Jouguet deflagration. The inverse transition, for decreasing piston velocities, from detonation to deflagration does not occur, since a Chapman-Jouguet detonation can be connected to a piston whose velocity is less than the critical (or zero) by a centred rarefaction wave.

Before considering the case in which a flame, ignited at one end of a closed cylindrical container, accelerates without a supporting piston and undergoes a transition to a detonation wave, it is necessary to mention some of the properties of flames in order to elucidate the mechanism whereby a flame can be self-accelerating and to discuss some recent experimental studies of the transition.

PROPAGATION OF FLAMES

If the flow through the reaction zone is laminar, the flame consists of a reaction zone for which, in the one-dimensional case, the fraction of energy released at any instant is constant across a cross-section. The burning velocity of such a laminar flame S_L is a characteristic property of the fuel-oxidant system, dependent on temperature, pressure, and composition of the unburnt material, but independent of the characteristics of the approach flow and of burner geometry.

This quantity is a monotone increasing function of temperature. Measurements for several hydrocarbon–air systems have shown that the laminar

burning velocity is approximately proportional to the square of the absolute temperature for these systems over temperature ranges of several hundred degrees above ordinary room temperature. It can be anticipated on theoretical grounds that a stronger dependence on temperature will obtain at higher ambient temperatures and it appears probable that an exponential dependence on temperature would provide a more appropriate law. Lewis[2] has correlated measurements of the pressure dependence of the laminar burning velocity for a number of different fuel-oxidant systems. The results suggest that, at least to a good approximation, the laminar burning velocity at any pressure can be represented as a function of the pressure and the burning velocity at a reference pressure without explicit dependence upon the composition of the fuel-oxidant system. It is to be noted that the effect of an increase of pressure is to increase the laminar burning velocity for mixtures whose burning velocity is greater than about 100 cm/sec and to decrease the laminar burning velocity for mixtures whose burning velocity is less than about 50 cm/sec.

Karlovitz[3] has developed a model of the turbulent combustion wave and describes its structure as consisting of randomly fluctuating wrinkled combustion waves within the volume occupied by the visible turbulent flame brush. The combustion waves are considered to be identical with the normal laminar wave except to the extent that the transport properties of the medium are modified by fine scale turbulence at high turbulence intensity. The increased velocity of the turbulent flame is attributed to the increased area of the combustion wave due to its wrinkled character. The theory based on this model permits a calculation of the turbulent burning velocity if the intensity of turbulence and the laminar burning velocity are given. Karlovitz[3] has also suggested that the turbulent flame is itself a strong source of turbulence, and that such flame generated turbulence must be added to that of the approach flow and that generated by the flow associated with the flame.

An additional very important effect of high intensity turbulence on flame propagation remains to be considered. We have noted that the laminar burning velocity increases rapidly with the temperature of the unburned gas. This property follows from the fact that it is necessary to heat the unburnt medium by the transport of energy from the zone of rapid reaction to a temperature where the reaction rate becomes sufficiently great to maintain the flame. This pre-heating occurs in a preparatory zone. For higher temperatures of the approach flow, less heat is required to raise the temperature to the critical value, resulting in an increase in the laminar burning velocity. The laminar burning velocity tends toward infinity as the approach flow temperature approaches the critical temperature. In a strongly turbulent flame, the wrinkling may become so strong that the average distance between combustion waves becomes comparable to the thickness of the preparatory zone. As a result, the combustion waves are propagating in a preheated medium and the laminar burning velocity may substantially exceed its normal value. In extreme cases, it may reach very high values.

A limiting condition for the propagation at finite velocities of the turbulent flame consists of the flame for which the unburnt mixture contained in the flame brush is pre-heated by the close proximity of the combustion waves to the critical temperature. At this limit, the unburnt mixture contained in the flame brush will react almost instantaneously resulting in combustion that is effectively at constant volume. In this event, a substantial amount of energy is discontinuously liberated accompanied by the generation of strong discontinuous pressure waves. The flame brush will momentarily be reduced in thickness to a nearly plane combustion wave which subsequently will rapidly develop into a turbulent flame brush. A series of such pressure pulses may thus be intermittently produced. Karlovitz[4] has recently employed his model of turbulent combustion for a more detailed description of this limiting condition.

EXPERIMENTAL STUDIES OF THE TRANSITION TO DETONATION

Beginning with the classical work of Berthelot, a number of investigators have studied the transition of a combustion wave to a detonation wave. Their work is summarized in the standard treatises of combustion. Although largely qualitative in nature, the classical work of Berthelot permits the following generalizations as to the nature of the transition:

(*a*) A combustion wave propagating from an open towards a closed end of a cylindrical container filled with an explosive mixture rapidly attains a steady velocity and does not accelerate to a detonation wave.

(*b*) A combustion wave propagating from a closed end of a cylindrical container filled with an explosive mixture whose normal burning velocity is sufficiently high accelerates continuously, whether the opposite end of the container is open or closed. If the container is sufficiently large, such a flame will accelerate to a detonation wave. The length of travel before the formation of a detonation wave is shorter in a closed than in an open container.

(*c*) The details of the transition are strongly influenced by the geometrical configuration of the confining vessel in-so-far as the configuration

affects the reflection of pressure waves generated by the ignition source or by the combustion wave. It has been observed, for example, that the transition to detonation may occur under favourable circumstances at the instant of interaction with the combustion of a pressure wave originating with the ignition source and reflected from a wall of the container.

These experiments have all dealt with initially quiescent gases. They confirm the vital role played by the pre-compression wave, since this wave is not present in the open-ended cylinder with ignition at the open end. The fact that a deflagration wave requires a longer run to accelerate to detonation in a cylinder whose downstream end is open (or in a very long closed cylinder) than in a short cylinder whose downstream end is closed indicates that the reflection of the pre-compression wave at the downstream end and its subsequent interaction with the deflagration wave may be an important part of the mechanism whereby the deflagration wave accelerates.

Shuey[5] has studied the detonation of acetylene in long tubes of diameters between $\frac{1}{4}$ in. and $4\frac{1}{2}$ in. and at several pressures. Ignition was accomplished by means of a squib. In all cases a detonation wave was formed after the deflagration wave has travelled a distance of about 60 tube diameters in the initially quiescent gas. When obstructions were placed in the tube near the ignition source, the distance travelled by the deflagration wave before transition to detonation —a distance that we will term the *run* of the deflagration—was abruptly reduced by a factor of about 12.

In the case of a smooth pipe, turbulence is generated by friction at the wall of the gases set in motion by the deflagration wave. In a manner that is entirely analogous with the ordinary case of pipe flow, this turbulent zone widens until, after a distance of flame travel that is proportional to the pipe diameter, fully developed turbulent flow over the entire cross-section of the pipe would result. At some point in this process the intensity of turbulence is sufficient so that the flame becomes markedly turbulent and the intensity of turbulence thenceforth rapidly increases, as described above, due to turbulence generated by the turbulent flame. In the case of a pipe with obstructions at the ignition end, turbulence is generated at once throughout the cross-section by a mechanism that does not depend on friction at the walls and the strongly turbulent flame is established immediately. We can infer that turbulence is being slowly generated by wall friction during the major portion of the run of 60 diameters in the smooth pipe and that the final rapid acceleration to detonation occurs in a small fraction of the total run. These experiments emphasize the fundamental role played by turbulence in the mechanism of the flame acceleration.

Shchelkin[6] has studied the pre-detonation regime in tubes roughed by the insertion of wire spirals, with results qualitatively in agreement with those of Shuey.

Schlieren photographs of deflagration waves obtained by Greifer[7] for mixtures of hydrogen and moist carbon monoxide with oxygen, contained in a long tube of rectangular cross-section, show cusps occurring within the turbulent flame brush immediately prior to the transition to detonation. These cusps result from discontinuous pressure pulses, generated intermittently within the deflagration wave, and propagate forwards in the direction of flame propagation and backwards into the burnt gases. The propagation velocity of the deflagration wave was increased as each of these pressure pulses overtook the deflagration front. The transition of the deflagration wave to detonation appears to coincide with the generation of one of these pressure pulses.

The intermittent pressure pulses are to be attributed to the almost instantaneous reaction of the unburnt mixture contained in the flame brush as the result of extreme wrinkling of the flame front in a highly turbulent flame as described in the preceding section.

A study confirming the importance of these intermittently generated pressure pulses has been carried out at the University of Toledo by Turin and Huebler[8]. These authors show that a pressure pulse was generated in the flame front after the deflagration wave had travelled about one-sixth the length of the tube, propagating in both directions. The forward moving pulse coalesced with the deflagration wave resulting in its substantial acceleration. The backward moving wave was reflected from the rear wall of the tube and subsequently overtook the deflagration wave, a detonation wave being formed at the instant of interaction of the reflected pressure wave with the deflagration wave. In these experiments only a single pressure pulse was observed, although it is possible that earlier ones would have been noted with pressure gauges of greater resolution. These experiments confirm the interpretation given to Greifer's experiments, and they serve to point out that the reflection of the pressure pulses may play a decisive role under favourable conditions of configuration of the container.

It has frequently been observed that the destructive effects of gaseous detonations occurring in closed containers may be substantially greater than can be accounted for by parameters of the detonation wave computed by the hydrodynamic theory from the ambient conditions obtaining before ignition. We have mentioned that the deflagration wave, prior to the establishment of

detonation, results in compression and heating of the unburnt gas ahead of the deflagration wave by means of the associated pre-compression wave. Thus, the detonation wave, when established, is moving through a pre-compressed and pre-heated medium with the result that its peak pressure may be much greater than would be expected from consideration of the conditions prior to ignition.

The Toledo experiments illustrate this point in a most convincing manner. At the instant of establishment of the detonation wave, the pre-compression shock has a pressure of about five times the initial ambient pressure. As a result, the detonation wave has a peak pressure of approximately five times its normal value. In these experiments the length of the tube was sufficient so that the detonation wave overtook the front of the pre-compression shock before reaching the end of the tube. At this instant, when the detonation wave reached material that had not been reached by the pre-compression wave, its peak pressure dropped to the normal value.

Additional experimental evidence bearing on this effect is provided by Shuey's experiments. In the smooth pipe with a run of about 60 diameters, the detonation wave was of sufficient amplitude to shatter the tube. However, when initial turbulence resulted in a much more rapid acceleration the ensuing detonation wave was contained by the tube.

It can be noted that the most destructive detonation wave will result in a given container if the detonation wave is not formed until almost all of the explosive gas has been consumed by the deflagration wave.

TRANSITION FROM DEFLAGRATION TO DETONATION

We can now describe in greater detail the process by which a deflagration wave accelerates to form a detonation wave. If the velocity of the deflagration wave is not constant but increasing, the pre-compression wave is not a constant shock but a shock of increasing amplitude. The flow in the pre-compressed unburnt medium is thus not a constant flow. A uniform state of rest does not then exist behind the deflagration wave but instead the deflagration wave is connected to the rear wall of the container by a centred rarefaction wave. The flow associated with an accelerating deflagration wave thus differs quantitatively from that associated with a constant deflagration supported by a piston but retains qualitatively the main features of the simpler flow.

For mixtures with a normal burning velocity such that the net effect of the rise in temperature and the rise in pressure resulting from the pre-compression shock is to increase the burning velocity, it is evident that a deflagration wave of constant velocity cannot exist in the absence of a flame-holder in a container closed at the ignition end. This follows from the fact that the pre-compression shock raises the temperature and pressure of the unburnt medium and, hence, increases the burning velocity which in turn increases the amplitude of the pre-compression shock and further raises the temperature of the unburnt gas. It is convenient to describe this mechanism as the 'differential acceleration' of the flame. In comparison to other effects causing the acceleration of the flame, it is a relatively weak mechanism, and it appears to be controlling during the early stages of the acceleration of initially quiescent mixtures where it may trigger the formation of a turbulent flame.

If the container is closed at both ends and relatively short in length, the pre-compression shock is reflected from the downstream end and the reflected wave subsequently interacts with the deflagration wave. Reflection increases the amplitude of the pre-compression shock markedly, the ratio of the pressures of the incident and reflected waves being two in the limit of acoustic waves and increasing rapidly as the amplitude of the incident wave increases to a limiting value (of eight for $\gamma = 1{\cdot}4$). When the reflected wave interacts with the deflagration wave, the velocity of the deflagration wave is abruptly increased owing to the increased pressure and temperature of the medium into which it is propagating. A new pre-compression wave is simultaneously propagated into the unburnt gas, and this wave has a higher amplitude than the one that preceded it because of the increased velocity of the deflagration wave. This sequence of events, which may be repeated a number of times during the acceleration of the deflagration wave, constitutes a powerful mechanism for the acceleration of the flame and is the explanation of the fact that the run for an initially quiescent mixture is markedly shorter in a container that is closed at its downstream end than one whose downstream end is open. Because the effect of reflected waves on the acceleration of the flame is much more effective than the differential acceleration, it appears that a good approximation for the analysis of this process would consist in the assumption of constant flame speed during the interval between interactions. If the burning velocity can be expressed as a function of temperature and pressure, a straightforward analysis of this process for a given container would consist of piece-wise solution of the algebraic equations governing the constant deflagration and shock waves and of the algebraic equations governing the interaction of the shock wave with the wall and with the deflagration wave. Sokolik[9] attributes the entire pre-detonation acceleration to a mechanism of this nature, a view that has been criticized by Zeldovich[9]

who emphasized the role played by turbulence. Oppenheim and Stern[10] have recently applied this mechanism to a detailed analysis for a particular system. Inclusion of the differential acceleration between interactions would complicate the analysis, but it could be carried out, at least in principle, by employing the method of characteristics to determine the complete flow in detail in regions without discontinuities, together with the above-mentioned algebraic relations for the shock and deflagration wave discontinuities.

It can be inferred that such an analysis of the acceleration of a deflagration wave in a short closed cylindrical container, filled with an initially quiescent explosive mixture, would show that the acceleration is at first comparatively small and the major portion of the run of the deflagration wave would take place at comparatively low velocities. It is also apparent that the acceleration is very rapid towards the end of the run. Although it will be pointed out that the final stages of the run are not at present susceptible to exact analysis even in principle, the fact that these stages occur in a small part of the total run would seem to make possible for this case an estimate of the length of the run of acceptable accuracy for engineering purposes.

Shchelkin[11,12] has applied his theory of the turbulent flame to develop a quantitative theory of the pre-detonation acceleration resulting from the generation of turbulence. He does not, however, recognize the importance of the pressure pulses generated intermittently by the turbulent flame brush.

We have pointed out in our discussion of turbulent flame propagation that the propagation of highly turbulent flames is accompanied by the intermittent generation of pressure pulses due to the almost instantaneous reaction of the unburnt gas contained in the turbulent flame brush, and we have cited recent experiments indicating the importance of these pulses to the acceleration mechanism of the deflagration wave during the final stages of the run. Under these conditions of turbulence, the effective flame speed can no longer be represented as a function of the state of the unburnt gas and the conditions resulting in the formation of the pressure pulses cannot be predicted in the present state of turbulent flame theory. For this reason the analysis that has been suggested will not be applicable with any precision to this portion of the run. It follows that the analysis could not be employed in a conservative estimate of the run of the deflagration wave, since the effect of the pressure pulses is to accelerate the deflagration wave and thus to shorten the run.

We now consider briefly the case in which a closed cylindrical container is filled with an explosive gas mixture in a manner such that a high intensity of turbulence is generated in the gas mixture. Under these conditions a highly turbulent flame is established immediately upon ignition. It can be inferred that acceleration of the flame is rapid from its onset with the early production of pressure pulses. The run is, therefore, short and it is not amenable to theoretical analysis.

Finally, we wish to comment on the role played by the deflagration wave on the ultimate destructive effects of the detonation wave if the latter is established in a closed container. During the run of the deflagration wave the pressure and temperature of the unburnt gas are raised by the pre-compression wave generated by the deflagration. This pre-compression is the greater the longer the run of the deflagration wave. When the detonation wave is established, it propagates into a medium of pressure that is greater than the initial pressure prior to ignition with the result that the amplitude of the detonation wave may be very significantly greater than would be the case if the detonation wave were established immediately upon ignition. It is evident that the detonation wave of maximum amplitude forms when the deflagration consumes nearly all of the explosive gas mixture with which the container was initially filled prior to initiation of the detonation wave, thus resulting in maximum pre-compression of the unburnt gas. These considerations can be employed to calculate in a simple manner an upper limit to the detonation pressure. Such a limiting pressure can be employed in conservative design calculations.

REFERENCES

[1] Courant, R. and Friedrichs, K. O. *Supersonic Flow and Shock Waves*, pp. 204–34. 1948. New York; Interscience

[2] Lewis, B. *Selected Combustion Problems*, p. 176. 1954. London; Butterworths

[3] Karlovitz, B. *Selected Combustion Problems*, p. 176. 1954. London; Butterworths

[4] — This volume, paper 83

[5] Shuey, H. M. (Rohm & Haas Co.) private communication

[6] Shchelkin, K. I. *J. Tech. Phys. U.S.S.R.* 17 (1947) 613

[7] Greifer, B. *et al. Proc. Second ONR Conference on Detonation*, p. 163. 1955. Office of Naval Research, Washington

[8] Turin, J. J. and Huebler, J. Unpublished American Gas Association reports

[9] Sokolik, K. S. and Zeldovich, Va. B. *J. Exp. and Theor. Phys. U.S.S.R.* 21 (1951) 1164

[10] Oppenheim, A. K. and Stern, R. A. This volume, paper 110

[11] Shchelkin, K. I. *J. Exp. and Theor. Phys. U.S.S.R.* 24 (1953) 589

[12] — *J. Exp. and Theor. Phys. U.S.S.R.* 29 (1955) 221

SOME OBSERVATIONS ON THE PROBLEM OF TRANSITION BETWEEN DEFLAGRATION AND DETONATION

G. K. ADAMS and D. C. PACK

INTRODUCTION

Since 1945 it has been commonly accepted that the steady state detonation wave can be described by the Zeldovich–Döring–von Neumann model of a shock wave followed by a deflagration, the former initiating the latter through the rise in temperature and pressure across the shock discontinuity. This model has been criticized on the grounds that the predicted pressure 'spike' between the shock and deflagration is not observed, but no more satisfactory alternative has been proposed. Paterson[1], and more recently Hirschfelder and Curtiss[2], have made calculations on the structure of the coupled system of waves in a one-dimensional steady system which suggest that the model is correct when regarded as a limiting case.

Much of what has been written about the transition from deflagration to detonation is based upon this model through the concept that deflagration produces compression waves and that these in turn initiate chemical reaction ahead of the deflagration; but no adequate statement of either the flow dynamics or of the chemical kinetics has yet been made. Chu[3] has discussed the generation of weak compression waves at flame fronts, and some of the consequences which can accelerate the burning; Oppenheim[4] has considered the conditions in the vicinity of the Chapman–Jouguet detonation velocity; but we have not found a clear discussion of how the compression and the flame, or chemical reaction, interact to cause the velocity of propagation to increase from metres to thousands of metres per second.

We have thought it useful to start our discussion by finding the solution of the following problem: what is the state of flow set up by a wave of chemical reaction moving with a given velocity down a tube? To simplify the problem we consider an ideal gas system with constant adiabatic exponent. We take as our initial condition a semi-infinite column of inflammable gas closed at one end and at rest. The chemical reaction releases a quantity of chemical energy, q calories per g, and is supposed to start to move along the column from the closed end, with a speed W referred to sound speed in the stationary, unreacted gas (a_o cm/sec).

A SIMPLE MODEL OF DEFLAGRATION IN A TUBE

The flow state set up for small values of W is well known; the reacted gas in contact with the closed end is stationary and, since the release of energy causes an expansion, the unreacted gas ahead of the reaction wave or flame is caused to move in the same direction as the flame by a compression wave travelling at a velocity greater than W. However, no calculations covering large ranges of W appear to have been made.

Since the state is one of steady flow in each of the three regions in the tube (*Figure 1*), results can be obtained relatively simply by solving simultaneously the conservation equations for the flame and for the compression wave which is, in fact, a shock wave propagating with speed U.

The equations are best solved in terms of particle velocities and sound speeds. In the following text these are referred to the sound speed a_o in the unreacted, stationary gas. Denoting the conditions ahead of the shock, between the shock and flame, and behind the flame by the suffixes o, u, b respectively we may write for the shock:

Conservation of mass:

$$\rho_o U = \rho_u (U - u_u) \tag{1}$$

Conservation of momentum:

$$p_u - p_o = a_o^2 \rho_o U u_u \tag{2}$$

Conservation of energy:

$$(U - u_u)^2 + \frac{2}{\gamma - 1} a_u^2 = U^2 + \frac{2}{\gamma - 1} \tag{3}$$

From these equations we have for the ratio of densities across the shock wave

$$\frac{\rho_u}{\rho_o} = \frac{(\gamma - 1) + (\gamma + 1)(p_u/p_o)}{(\gamma + 1) + (\gamma - 1)(p_u/p_o)} \tag{4}$$

The conservation equations for the flame front give

$$\rho_u (W - u_u) = \rho_b (W - u_b) \tag{5}$$

$$p_u - p_b = a_o^2 \rho_b (W - u_b)(u_u - u_b) \tag{6}$$

and

$$(W-u_b)^2+\frac{2}{\gamma-1}a_b^2 = \frac{2q}{a_o^2}+(W-u_u)^2+\frac{2}{\gamma-1}a_u^2 \quad (7)$$

where we have not, for the moment, assumed that the gas behind the flame is at rest, since we shall later require the equations in the above more general form. The quantity q is the (supposed constant) heat energy per unit mass released on burning of the gas.

Elimination of a_b between equations 7 and 6′ leads to the equation

$$a_u^2=\frac{\gamma-1}{2}(W-u_u)\left(\frac{2q}{a_o^2(u_u-u_b)}+u_u+\frac{2W}{\gamma-1}-\frac{\gamma+1}{\gamma-1}u_b\right) \quad (10)$$

Equations 8, 9 and 10 give three equations relating the five unknowns u_b, a_u, u_u, W and U. If any two of these should be prescribed, the values of the other three may therefore be determined.

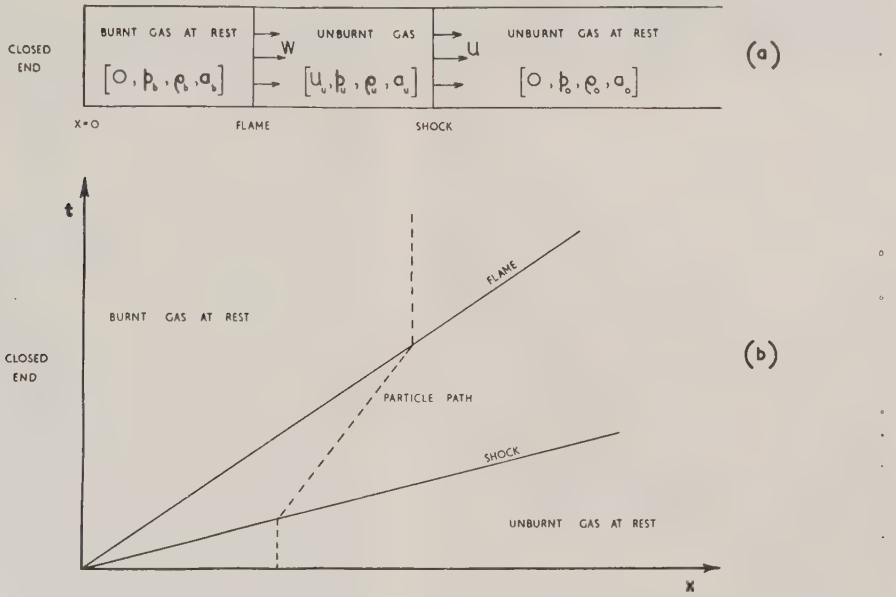

Figure 1. Simple model of low speed deflagration in a tube with a closed end

The densities and pressures may be eliminated by using the relation $a^2=\left(\frac{\gamma p}{\rho}\right)\Big/a_o^2$ for the square of the non-dimensional speed of sound a. Thus, we replace equations 2 and 6 by

$$\frac{a_u^2U}{U-u_u}-1=\gamma Uu_u \quad (2')$$

and

$$\frac{a_u^2(W-u_b)}{W-u_u}-a_b^2=\gamma(W-u_b)(u_u-u_b) \quad (6')$$

From equations 2′ and 3 we derive the relation

$$u_u=\frac{2}{\gamma+1}\left(U-\frac{1}{U}\right) \quad (8)$$

and from equation 2′,

$$(\gamma+1)^2a_u^2=(\overline{\gamma-1}U^2+2)\{2\gamma U^2-(\gamma-1)\}/U^2 \quad (9)$$

For the *closed tube*, $u_b=0$. The equations may then be examined graphically in a simple manner by plotting u_u, a_u^2 as functions of U by means of equations 8 and 9 and then calculating W from equation 10. *Figure 2* shows the results in the form of a plot of u_u, U, a_u^2, a_b^2, p_u and p_b against W, for a reaction with energy release 1,400 cal/g in a medium with $\gamma=1{\cdot}4$. For the purpose of the calculations we put $p_o=1$ atmosphere and $\rho_o=1$ g/litre. The graphs cover a range of values of W from 0 to 10. The significance of this range is made clear if we note that the steady state detonation velocity is 9·0 on this scale and that experimentally determined laminar flame velocities (relative to unburnt gas) fall in the range 0·01 to 0·05.

The main feature of the flow is that the shock wave always travels faster than the flame, even when the latter is moving at a speed faster than that of the steady detonation wave. When $W=4{\cdot}3$, the speed of the flame is equal to the

speed of sound in the burnt gases; since these gases are at rest in the closed tube, this implies that the speed of the flame is sonic relative to these gases. The conditions at this flame speed may be expressed in analytical form by putting $W = a_b$ in the preceding equations. Then, after some little algebra we obtain

$$u_u = \left(\frac{2(\gamma - 1)}{\gamma + 1}\frac{q}{a_o^2}\right)^{\frac{1}{2}} \qquad (11)$$

which gives*

$$U - \frac{1}{U} = \left(\frac{\gamma^2 - 1}{2}\frac{q}{a_o^2}\right)^{\frac{1}{2}} \qquad (12)$$

For $\gamma = 1{\cdot}4$, $q = 1{,}400$ cal/g, $p_o = 1$ atm $= 10^6$ dynes/cm^2, $\rho_o = 1$ g/litre, this gives U

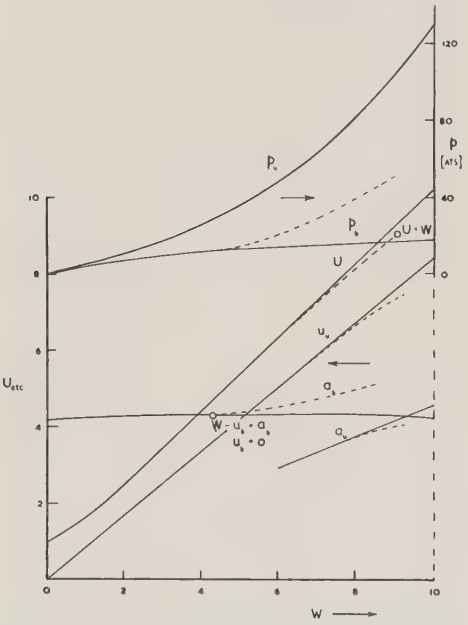

Figure 2. Shock and flame parameters as functions of flame speed in a tube with closed end (dashed curves = $W - u_b = a_b$)

$= 4{\cdot}67$, $u_u = 3{\cdot}73$, $p_u = 25{\cdot}9$ atm, $p_b = 11{\cdot}2$ atm, $a_u = 2{\cdot}3$, $a_b = W = 4{\cdot}3$. The flame speed relative to the unburnt gas, $W - u_u$, is 0·5, i.e. from ten to fifty times the normal laminar flame speeds.

We see that the pressure conditions set up by a flame resemble those for steady detonation in that, associated with the flame, there is always a shock wave and that, relative to the unreacted gas at rest, the pressure is increased in front of the reaction front before falling across it to a value which is greater than the initial pressure.

* If $U^{-1} \ll 1$,

$W : u_u : U = \{(3\gamma^2 + 1)^{\frac{1}{2}} - (\gamma - 1)\} : 2 : (\gamma + 1)$

under condition $W = a_b$.

However, contrary to what has sometimes been assumed, the attainment of sonic speed of the reaction front with respect to the products does not lead to the steady detonation state.

CHAPMAN–JOUGUET DEFLAGRATIONS

The states reached for values of W exceeding the product sound speed correspond to what Courant and Friedrichs[5] term 'strong deflagrations', preceded by a shock wave of higher velocity. They have advanced arguments, based on the structure of the reaction zone, which exclude strong deflagrations as physically possible solutions. Hirschfelder and Curtiss[2] have shown that solutions of the differential equations for the one-dimensional steady state problem are only physically satisfactory when the flame speed is equal to or less than sound speed in the burnt gases. (It does not appear possible to use a more general thermodynamic argument against strong deflagrations. At first sight they might seem to be excluded by the consideration that the entropy change across the reaction wave is a maximum for a sonic (Chapman–Jouguet) deflagration but this is true only for waves in which the unreacted state is specified and the state of the products allowed to vary.) The arguments excluding strong deflagrations are essentially that, as the reaction proceeds, the system must pass through a plane at which reaction is complete and at which the pressure, specific volume and particle velocity correspond to those for a sonic deflagration. In the system we are considering this corresponds to a finite product particle velocity u_b of the same sign as the flame speed W, i.e. moving away from the closed end. The flame speed W is then equal to the sum of this particle velocity and the sound speed. We shall proceed now to discuss the passage of a flame in this condition down a tube closed at one end. The particle velocity behind the reaction front has to be brought to zero at the closed end by a rarefaction wave, centred at the closed end, and travelling behind the reaction front into the burnt gas (*Figure 3*). On such a wave, for an ideal polytropic gas, $u - 2a/(\gamma - 1) =$ constant. Since the speed of this wave cannot exceed the local sound speed, it cannot overtake the reaction front moving at sound speed relative to the gas immediately behind it. (The reverse consideration excludes solutions for $W - u_b < a_b$ with positive values of u_b.)

We impose the condition that

$$W - u_b = a_b \qquad (13)$$

for sonic speed of the flame relative to the burnt gases. When we use the equations in the general form given above, which allows for possible

motion of the burnt gases, and write $W - u_u = z$, we are led to the equations

$$a_b - z = u_u - u_b = + \left(\frac{2q\ (\gamma - 1)}{a_o^2\ (\gamma + 1)}\right)^{\frac{1}{2}} \quad (14)$$

the positive sign corresponding to the fact that $u_u > u_b$, and

$$a_u^2 = z^2 + z\left(\frac{2q(\gamma^2 - 1)}{a_o^2}\right)^{\frac{1}{2}} \quad (15)$$

obtained by insertion of equation 14 in 6′.

Hence we find that

$$z = \left(\frac{(\gamma^2 - 1)q}{2a_o^2} + a_u^2\right)^{\frac{1}{2}} - \left(\frac{(\gamma^2 - 1)q}{2a_o^2}\right)^{\frac{1}{2}} \quad (16)$$

with local sonic speed. The value of U is 9·07 for the conditions in the gases used in the earlier calculations—a value consistent with the idea that the situation here considered corresponds, in fact, to the steady detonation state. For the previously quoted conditions in the unburnt gas ahead of the leading shock wave this yields a detonation speed of 3,400 m/sec.

In this steady detonation state, a_b $(\doteq \frac{1}{2}\gamma u_u)$ $= 5{\cdot}3$. We see that, if the flame speed relative to the products, $W - u_b$, is limited to the sound speed in the products, a relatively small increase in $W - u_b$ over the value required to reach sonic speed with $u_b = 0$ will increase W to the steady detonation speed where the reaction wave and

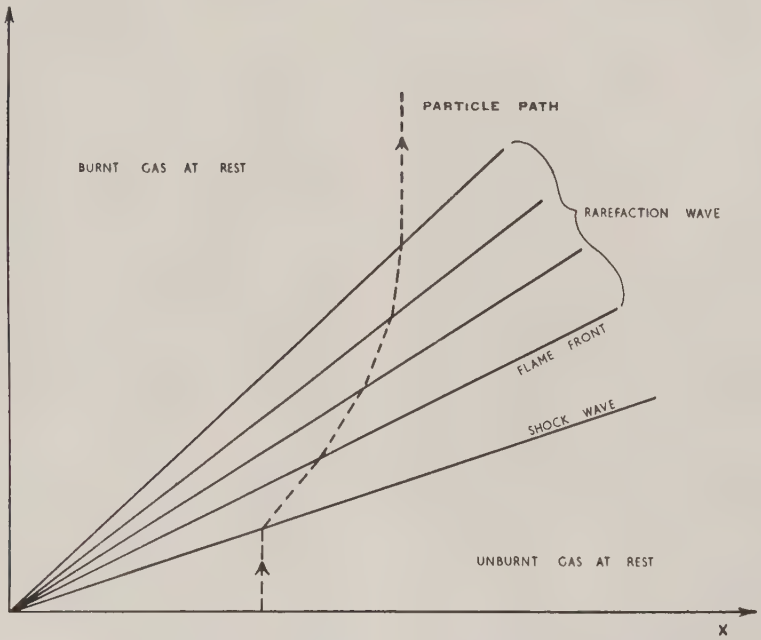

Figure 3. Wave diagram of Chapman–Jouguet deflagration in a closed tube

By virtue of equations 8 and 9, which are independent of u_b, this yields a relationship between W and U. This is Oppenheim's Q-locus, giving the possible flame states with relative sonic speed and a preceding shock wave. It is immediately obvious from equation 16 that W increases monotonically with U. The speed of the flame relative to the burnt gases, a_b, has the same property.

When $W = U$, so that a steady state is reached, we have

$$\frac{\gamma + 1}{2}\, u_u = U - \frac{1}{U} = 2\left(\frac{(\gamma^2 - 1)q}{2a_o^2}\right)^{\frac{1}{2}} \quad (17)$$

The particle velocity ahead of the flame front is seen to be exactly twice what it was when we took the burnt gas to be at rest behind a flame moving the shock front travel at equal velocities (as $W - u_b$ goes from 4·3 to 5·3, W goes from 4·3 to 9·1). (The pressure and temperature in the products increase rapidly, and owing to the net increase in gas density the mass rate of burning increases approximately threefold.)

In the case of an open-ended tube sonic deflagration conditions are reached at a lower value of $W - u_b$ than for the tube with a closed end. (The value depends upon the exit condition.)

The stages in the development of the steady detonation in a tube with an open end with pressure p_o, when ignition is started at the open end, are as follows:

(i) The gas flows at pressure p_o out of the open end with subsonic speed, the relative flame speed also being subsonic.

(ii) The relative flame speed becomes sonic, but $|u_b| < a_b$.

(iii) The flame speed increases, but $W - u_b = a_b$ (Chapman–Jouguet deflagrations); the increasing pressure behind the flame brings a rarefaction wave into being, this reducing the pressure to p_o by speeding up the gas. This regime ends when the velocity at exit is locally sonic (i.e. $|u_{\text{exit}}| = (a_b)_{\text{exit}}$ with pressure p_o).

(iv) Further increases in flame speed lead to further increases of pressure behind the flame. Expansion of the burnt gases leads to sonic speed at the open end, but with pressure in excess of p_o. The gases then issue from the open end as a supersonic jet, expanding to pressure p_o downstream of the end of the tube.

Since, for a tube with an open end, $z \ll a_b$ at the onset of the sonic condition, equation 14 shows that the appropriate value of $W - u_b$ is given approximately by the right-hand side of this equation. Thus even in an open-ended tube the flame speed need be increased only by a factor γ to change from the onset of sonic deflagration to steady detonation.

It appears that in order to explain the transition from combustion to detonation we must show first how the speed of the flame can be accelerated to the state in which it is moving with sonic speed relative to the burnt gas at rest, and then how it can be further accelerated to the steady detonation state, on the basis that relative sonic speed is maintained.

The idea that a deflagration passes into a steady detonation through the Chapman–Jouguet states was developed by Oppenheim, but he supposed that changes occur such that the flame catches up its accompanying shock wave. This cannot be the case; a deflagration wave can at best achieve the speed of its accompanying shock wave, and when this happens the detonation wave is set up.

BUILD-UP OF THE DETONATION STATE

So far we have not considered how the flame speed $W - u_b$ is determined, but have assumed that we may give it any value in order to examine the consequences. If we ignite a combustible gas in a closed tube, the initial speed will be the laminar flame speed, determined by the transport and reaction rate parameters under the conditions at the reaction front. This is small compared with the flame speeds we have considered. As the unreacted gas is set in motion and because of the influence of the walls, first a laminar and then a turbulent boundary layer will be set up. Both of these will increase the apparent flame speed, the first by increasing the area of the flame surface and the second by increasing both the area of the flame surface and the transport properties within the reaction zone. Now the analysis of the effect of an increase in flame speed is quite complicated, but if we consider the simple model of *Figure 1* and consider that the flame speed is given a finite increment at some instant of time, the effect is that shock waves are propagated from the plane front both forwards into the unburnt gas in motion and backwards into the burnt gas at rest (see *Figure 4a*). A contact discontinuity will appear in the burnt gas, across which pressure and velocity will require to be matched. The rearward moving shock wave will be reflected on arrival at the closed end and will cause a further pressure rise in the burnt gas and a further increase in the speed of the flame relative to the tube when it overtakes the flame. The overall effect of the shock waves produced will be to raise the temperature and pressure of the burnt and unburnt gas. It may be assumed that the changes in flame temperature and pressure due to an increase in flame speed from physical causes will themselves modify the speed due to their influence on the chemical reaction rate in the flame. The effect of pressure on flame speed is uncertain in general but is small. Flame temperature has a larger effect and an increase will almost always increase the flame speed, but the change in flame temperature is small until sonic deflagration states are reached because an increase in the enthalpy of the unburnt gases is almost wholly absorbed by the increase in translational energy change across the flame surface.

It would clearly be extremely difficult to treat the situation quantitatively, but it is not so difficult to see how in closed tubes the apparent flame speed may reach, as experimental observation shows, values many times greater than the initial laminar value. This enhancement also occurs in open-ended tubes although to a lesser degree. The dominant factor is usually the increase in flame area by large-scale turbulence or entrainment of unreacted gas behind the reaction front. With a fast burning system it is not difficult to enhance the flame speed by the factor of ten to twenty required to reach sonic speed relative to the products. After that, as we have shown, relatively small increases in flame speed are required to reach the detonation state. Apart from this, another factor may intervene. The existence of steady state flame propagation depends upon the fact that at normal initial temperatures the finite chemical reaction rate ahead of the flame is very small and the resulting energy release is cancelled out by the loss of thermal energy to the surroundings. For any given tube diameter there will be a critical ignition temperature at which, after a (theoretically) infinite time, ignition will occur at the centre of the tube. At a still higher temperature such that the reaction rate is about four times

greater, ignition will occur over the whole cross-section after a time interval:

$$t_u \approx \frac{c}{qk} \frac{RT_u^2}{E} \exp(E/RT_u) \qquad (18)$$

$k \exp(-E/RT_u)$ being the specific reaction rate at T_u. Thus the assumed steady state between the shock and the flame cannot exceed t_u in duration. It follows that there can never be a distance greater than $(U - u_u)t_u$ between the flame and the shock wave ahead of it. When this distance separates the two, the flame speed may be supposed to jump to U and the situation envisaged

FINAL DETONATION STATE

The situation is one which can clearly be imagined as a repeated sequence of events, and the transition from combustion to detonation which may occur in any real system of flame propagation as a result of the generation of heat ahead of it, a problem involving non-steady states, can be transformed into a series of steady states, approaching the detonation speed asymptotically from below. In the first part of the acceleration of the flame, there is little mean forward movement behind the flame. When the apparent flame speed increases beyond sonic speed, however, the burnt gas behind it

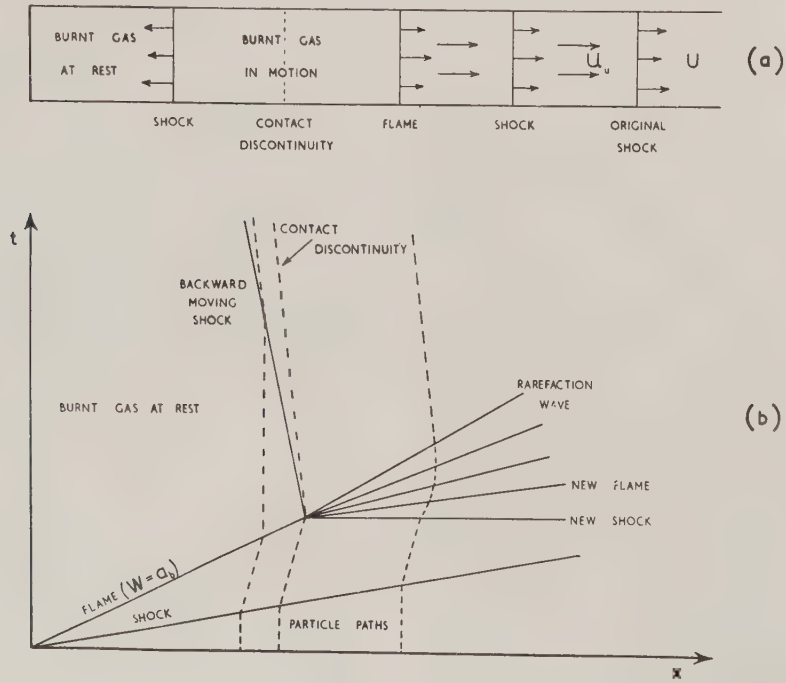

Figure 4. (a) The wave system set up by an increase in flame speed before the Chapman–Jouguet states are reached. (b) Wave diagram illustrating the effect of an increase in flame speed from the onset of Chapman–Jouguet conditions

in *Figure 4* will occur. The behaviour of the rearward moving shock wave has already been briefly remarked upon. The forward moving shock wave will overtake the original shock wave. This leads to a new (single) forward moving shock wave at an enhanced speed intermediate between the speeds of the coalescing shock waves. A weak rarefaction wave is reflected back towards the flame*.

follows at such a speed that the relative velocity of the flame remains sonic. The change from positive velocity of the burnt products to zero speed at the closed end of the tube takes place through an expansion wave, as illustrated in *Figures 3* and *4b*. Further acceleration of the flame produces a higher speed behind the flame and this leads to the rearward propagation of a shock wave which in turn modifies the expansion wave. At each state, however, since $W = u_b + a_b$, the first wavelet in the expansion coincides with the flame front.

* The reflection of a rarefaction wave, which will cool to some extent the previously heated gas, leads one to see the possibility of gas more recently heated by the enhanced shock wave burning before gas which was heated by it at an earlier stage. This seems to supply a mechanism for pre-ignition ahead of the flame. It has, however, been demonstrated experimentally that transition to detonation can take place without the occurrence of pre-ignitions, and pre-ignitions are in no way essential to the theory of detonation developed in this paper.

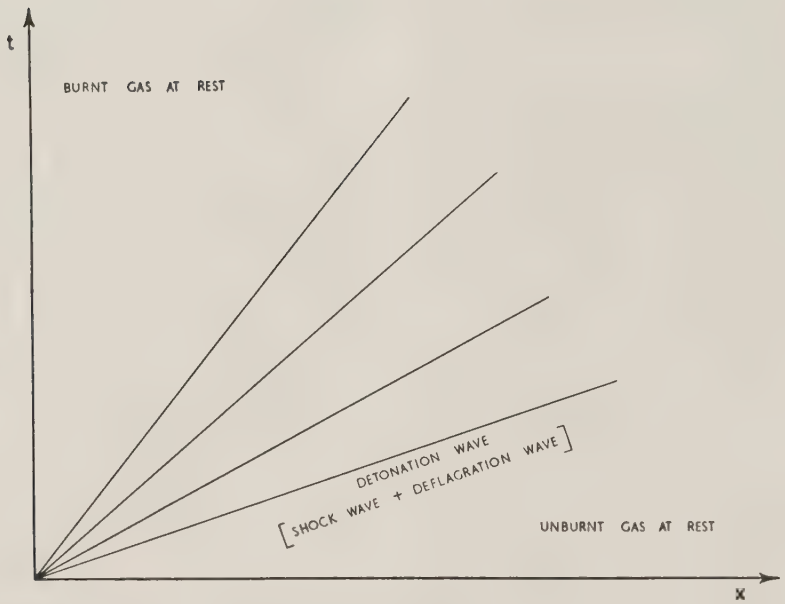

Figure 5a. Steady detonation state set up instantaneously at time $t = 0$. (After Courant and Friedrichs[5])

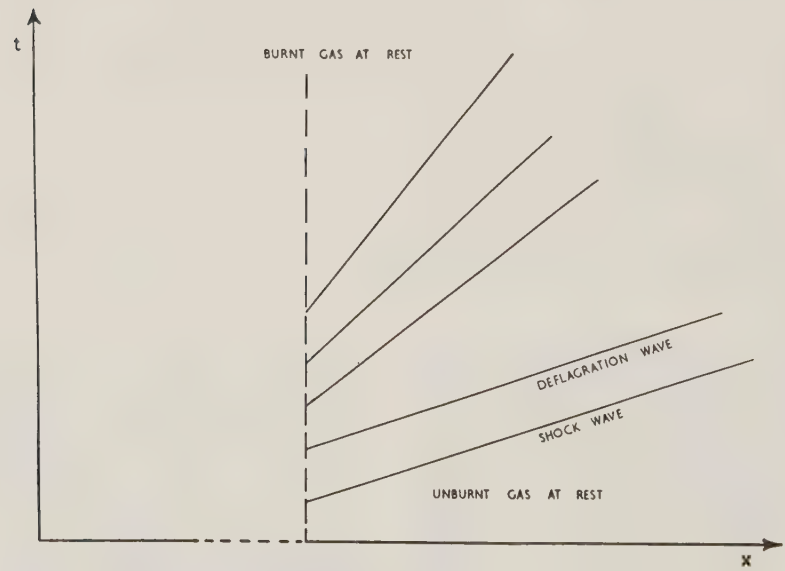

Figure 5b. Final steady detonation state resulting from accelerations of the flame under Chapman–Jouguet conditions

Now the well-known sketch of the steady detonation state given by Courant and Friedrichs (*Figure 5a*) corresponds to a detonation wave set up instantaneously at $t = 0$; it consists of a shock wave followed by a point-centred expansion wave bringing the burnt gas to rest. The steady state envisaged here would correspond to *Figure 5b*, in which both the detonation wave and the expansion wave have been 'opened out', on account of the finite time required to bring about the final state. (The distance between the shock wave and the deflagration wave in *Figure 5b* is

$$\frac{\gamma - 1}{\gamma + 1} Dt_u$$

This is of order 0·5 mm for a gas and 7 mm for a liquid if $t_u = 10^{-6}$ sec.)

To sum up, we have shown that although, in conventional treatments of detonation and deflagration states, these are represented in terms of Hugoniot curves as widely separated states reached by compression or expansion from a common initial state, they are related by a continuous set of solutions of the flow problem corresponding to experimentally realizable situations. In this way one is able to see how, given some mechanism for increasing the flame speed to the required value, transition from deflagration to detonation will take place. Two mechanisms for the increase in flame speed have been discussed.

APPLICATION TO LIQUID EXPLOSIVES

The analysis of the second and third sections may be generalized to the case of liquid explosives by supposing that liquid is converted by the flame into gas in which the ratio of specific heats is μ. At the high pressures involved under detonation conditions we shall suppose that the equation of state of the liquid may be written as $p = K\rho^\gamma$, and that it will be sufficient to use the approximations for a very strong shock wave corresponding to $p_u \gg p_o$. These are

$$\left.\begin{aligned} u_u &= 2U/(\gamma + 1) \\ p_u &= 2\rho_o U^2/(\gamma + 1) \\ a_u^2 &= 2\gamma(\gamma - 1)U^2/(\gamma + 1)^2 \\ \text{and} \qquad \rho_u &= (\gamma + 1)\rho_o/(\gamma - 1) \end{aligned}\right\} \qquad (19)$$

Without going into all the algebra we may say that sonic speed of the flame relative to the burnt gas at rest is reached when the shock wave is travelling ahead at the (actual) speed

$$a_o U = \tfrac{1}{2}\{(\mu - 1)(\gamma + 1)q\}^{\frac{1}{2}}$$

The corresponding speed of the unburnt liquid ahead of the flame is

$$a_o u_u = \{2(\mu - 1)q/(\gamma + 1)\}^{\frac{1}{2}}$$

For the higher flame speeds, when the restriction to sonic speed relative to the burnt explosive is applied, we obtain

$$\begin{aligned} z = W - u_u = (1/\sqrt{2})[&\{(\mu^2 - 1)(q/a_o^2) \\ &+ (\mu - 1)(\gamma + \mu)a_u^2/\gamma(\gamma - 1)\}^{\frac{1}{2}} \\ &-\{(\mu^2-1)(q/a_o^2)+(\mu+1)(\mu-\gamma)a_u^2/\gamma(\gamma-1)\}^{\frac{1}{2}}] \end{aligned} \qquad (20)$$

The steady state detonation corresponds to $W = U$ and on solution of equation 20 subject to equation 19 we obtain for the detonation speeds

$$a_o W = \sqrt{2q(\mu^2 - 1)}$$

with

$$a_o u_u = \frac{2}{\gamma + 1}(2q(\mu^2 - 1))^{\frac{1}{2}} \qquad (21)$$

The result, equation 21, suggests that the speed is practically independent of the assumptions made about the unburnt liquid, depending only upon the heat release per unit mass and the adiabatic index of the product gases. If we put $\gamma = 7$ and $\mu = 3$ (plausible figures for strong shocks in liquids and for gaseous products of liquid explosive respectively) we find that the order of magnitude of the speed of the wave is 9,500 m/sec and the detonation pressure is between 200,000 and 250,000 atmospheres. (When $\gamma = 7$ and $\mu = 3$, there is no loss of pressure across the flame front in the detonation state. There is therefore no 'spike'. The case is a limiting one.) Sonic speed is reached first when $a_b = 0{\cdot}46D$ and $U = 0{\cdot}71D$, where D is the detonation speed; in the steady detonation state the speed of the flame relative to consumed explosive rises to $0{\cdot}75D$. In this case, therefore, the rise in the relative flame speed is almost exactly equal to that of the actual flame speed between the first achievement of sonic speed and the attainment of the detonation state, in marked contrast with the result obtained for gases.

REFERENCES

[1] Paterson, S. *Fifth Symposium (International) on Combustion*, p. 672. 1954. New York; Reinhold

[2] Hirschfelder, J. O. and Curtiss, C. F. *University of Wisconsin, Report on Contract Nord 15884 No. C.M.911*, 1957

[3] Chu, B-T. *Fourth Symposium (International) on Combustion*, p. 603. 1952. Baltimore; Williams and Wilkins

[4] Oppenheim, A. K. *Fourth Symposium (International) on Combustion*, p. 471. 1952. Baltimore; Williams and Wilkins

[5] Courant, R. and Friedrichs, K. O. *Supersonic Flow and Shock Waves*. 1948. New York; Academic Press

DEFLAGRATION TO DETONATION TRANSITION

M. A. COOK, D. H. PACK and W. A. GEY

INTRODUCTION

The transition from deflagration to detonation is a phenomenon of considerable importance in many practical applications of explosives. Its avoidance in propellants is a paramount problem in rocketry as in all types of secondary high explosives involved in fires. Its promotion is a problem of considerable importance in primary high explosives and detonators. Of major interest, therefore, is the theoretical and experimental elucidation of this phenomenon. Only recently has this problem received the consideration it deserves through a concentration and systematic attack on the problem by many laboratories. The approach used by ERG, University of Utah, has been by means of high-speed streak and microsecond, colour, framing photography in gaseous, liquid and solid explosives. In condensed explosives the deflagration stage has for the most part been initiated by the so-called shock-pass-heat-filter (or SPHF) method suggested by a theoretical study by this group of the mechanisms of initiation and propagation of detonation[1]. The SPHF method consists simply of the use of a solid, non-porous plate between a donor high explosive charge, e.g. Composition B, and the test (or receptor) charge. This plate acts as a shock pass and a heat filter to destroy completely the detonation wave and cause the reaction in the receptor to commence either as a deflagration or not at all depending on the thickness S_1 of the SPHF plate. By working within the sensitiveness limit S_1^*, or the maximum plate thickness for which it is possible for the transition to occur, it is possible to study in considerable detail the deflagration to detonation transition, especially by the microsecond colour photography, using auxiliary (front- and back-) lighting techniques, in transparent liquids. Comparisons of the phenomena observed in liquids with the deflagration to detonation transition in gaseous explosives, together with the less easily observed phenomena associated with this transition in solid explosives seem to show that the transition involves essentially the same mechanism in gaseous, liquid and solid explosives.

In this article are summarized the experimental results and interpretations obtained at ERG, the most significant of which are the microsecond photographic results in which the colour observable is shown to be of great importance in defining the various stages of the transition and the actual reaction zone in the pre-detonation, transient detonation and steady detonation regimes. The direct observation of the predicted heat pulse or flash across is believed to constitute a major 'break through' regarding the mechanisms of detonation.

GASEOUS EXPLOSIVES

Figure 1 shows a streak camera record of ignition and the deflagration to detonation transition in the gaseous mixture H_2–O_2 at the mol ratio $H_2/O_2 = 4$ and an initial pressure p_1 of 100 lb./in.^{2} abs. using a 1 in. inside diameter steel shot tube with a 25 cm long, 0·3 cm wide viewing window along the side of the tube. In this case the stable detonation of velocity D = 4,650 m/sec was created 410 μsec after and 21·8 cm from the point of initiation by the spark discharge from a 1 μF condenser at 4,400 V. Simultaneously with the formation of the detonation wave a 'retonation' wave was formed which moved back towards the point of initiation at a velocity of 1,790 m/sec. However, about 58 μsec before this normal, high-order detonation was created, and at a position 10·4 cm from the point of the spark discharge, low-order reactive waves each of velocity about 1,100 to 1,200 m/sec formed and propagated in opposite directions, i.e. both forwards and backwards from the surface of initiation. These low-order reactive waves, moreover, were formed in a region already traversed about 60 μsec earlier by a low intensity, accelerating flame also recorded on the streak camera trace. The low-order forward (reactive) wave, which one may perhaps choose to call a low-order detonation wave, may be seen accelerating in the forward direction, but the reverse or retonation wave that formed simultaneously was apparently approximately stable in velocity in the reverse direction. As the low-order forward wave approached the initial flame front, it accelerated at increased rate and intensity, until at a point about 2 cm behind the precursor flame its velocity was even greater than the stable detonation occurring beyond this initial, much less intense flame front.

Other shock wave phenomena originating on the opposite side of the viewing window were also recorded on this trace, the spark discharge being effected at one end of the viewing window in a tube extending a considerable distance on either side.

COMPOSITION B

In gases the deflagration to detonation transition occurs over a rather broad time-distance profile following simple spark ignition. This is not, however, the case in condensed explosives; either

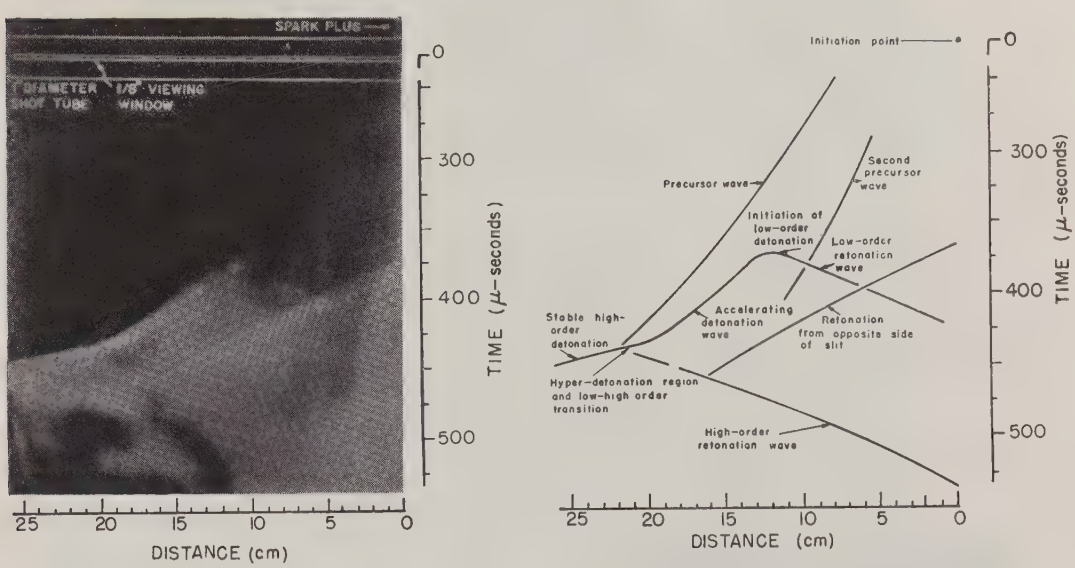

Figure 1. Deflagration to detonation transition in H_2-O_2 *mixture at mol ratio* $H_2/O_2 = 4$ *and* $p_1 = 100$ lb./in^2 abs.

Indeed, the secondary shock that was observed to pass across the field of view from the right may apparently be attributed to exactly the same phenomena recorded across the viewing window on the left, namely an initial low-order detonation, one branch (the retonation part) of which propagated back towards and then beyond the point of initiation, and the true 'retonation' wave from the high-order detonation created also to the right of the point of flame initiation.

Of particular interest in *Figure 1* is the fact that the high-order detonation wave formed actually about 2 cm behind the precursor, luminous front of the disturbance, and propagated through this front at a velocity in excess of the normal detonation velocity. This has been referred to as the hyper-detonation region in the diagram of events shown also in *Figure 1*. The initiation of detonation behind a precursor wave, and an initial hypervelocity region seems to us to be a rather general condition in the deflagration to detonation transition not only in gaseous but also in condensed explosives, as will be seen later. (This phenomenon is not, however, the flash across phenomenon observed in liquid explosives, the corresponding phenomenon in gases being spread out over a much broader space-time profile than in liquid explosives.)

they detonate in simple spark or flame ignition in extremely short times over very small distances, as in primary explosives, or only under very specific and difficult-to-reproduce conditions, as in secondary explosives. It is for this reason that the SPHF method used in conjunction with high-speed photographic techniques is so unique and valuable, i.e. by this method the phenomenon turns out to be easily promoted, quite reproducible, and readily observed.

The composition B receptor charges used in this investigation were cylinders of 5 cm diameter (d) with lengths (L) varied as desired. The glass SPHF sensitiveness limit, $S_1^\star$, of 5 cm composition B using the 5 cm (d) composition B donor charge was $S_1^\star \doteq 8{\cdot}6$ cm, and for the 3 cm (d) donor charge it was $S_1^\star \doteq 4$ cm (see Table 1). It was predicted that $S_1^\star$ should vary approximately as the effective diameter d' ($\doteq d - 0{\cdot}6$ cm). The above results are roughly in accord with this prediction.

At $S_1 \leqslant S_1^\star$ the region where the deflagration to detonation transition occurred was at a distance S_2 from the SPHF plate which distance increased uniformly with the plate thickness S_1 as shown in *Figure 2*. Definitions of the apparent and actual initiation time delays are given graphically in *Figure 3*. Most of the data used in constructing

Figure 2 were obtained by the streak camera method. In taking most of these pictures Dl neutral density filters were placed over the image of the donor and receptor at the camera slit to

between emergence of the shock from the glass plate and initiation of detonation increased linearly with S_2 in composition B (*Figure 2*). This indicates that the detonation wave formed either

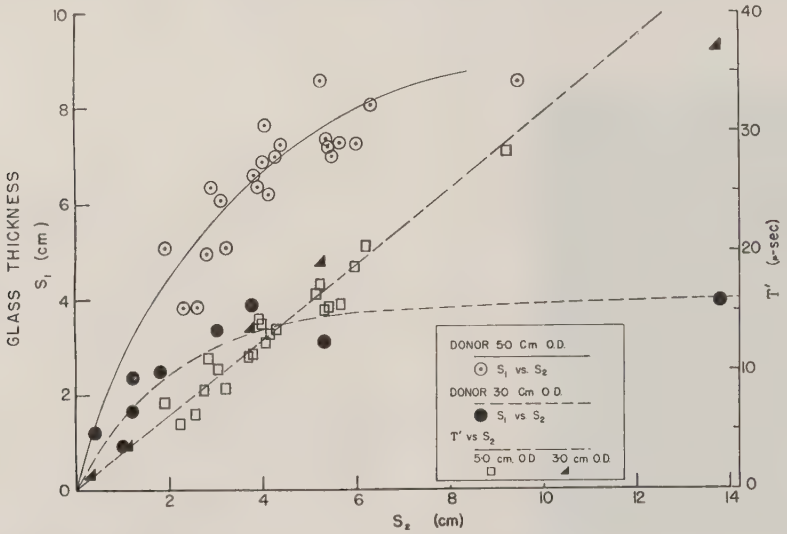

Figure 2. S_2 versus S_1 *and* S_2 versus τ' *for* 5·0 cm *receptor charges, and* 5·0 cm *and* 3·0 cm *donor charges of composition B*

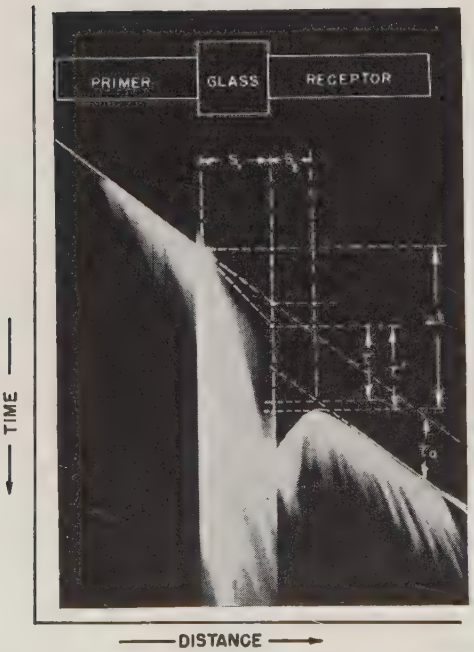

Figure 3. Typical streak camera trace with definitions of S_1, S_2 and delay times

reduce the intensity of light from the charges when the camera aperture was set to show the details of the shock through the glass.

It is particularly noteworthy that the time τ' at the shock front or at a fixed distance behind the front of the shock. The shock, prior to the formation of detonation, apparently travels as a relatively non-reactive, supported shock into composition B at a constant speed of about 2·8 to 3 mm/μsec over the distance S_2 and then suddenly

TABLE 1

Sensitiveness Limit for Initiation of Detonation Through Glass Plates for Some Liquid Explosives and Composition B (Donor—Composition B)

Receptor		*Donor*	
Explosive	*Diameter* cm	*Diameter* cm	S_1^* cm
Composition B	5·0	5·0	7·3–8·7
Composition B	5·0	3·0	4†
D.13	7·5 sq.	3·0	1·24–1·42
D.13	4·7	2·5	1·0†
D.10	7·5 sq.	3·0	1·45†
NM	7·5 sq.	3·0	0·72–0·79
NM/EDA 97.3/2.7	7·5 sq.	3·0	1·27
NM/NC* 90.8/9.2	7·5 sq.	3·0	0·86

* Nitrocotton. † Approximate only.

Figure 4. Framing camera sequence showing SPHF *initiation and propagation both forwards and backwards for* 5·0 (*d*) *composition B* (*donor and receptor*) *at* S_1 = 6·17 cm (2·08 μsec/frame)

becomes a high-order detonation at the distance S_2 from the SPHF plate. We may infer, however, from results of observations of the same phenomenon in the liquid explosives discussed below, that the reaction wave that initiates detonation formed the SPHF method was first pointed out by Cosner and Sewell[2], although it was evident in early streak camera traces by the SPHF method obtained by ERG, University of Utah[3]. It will be the subject of a forthcoming publication by Cook,

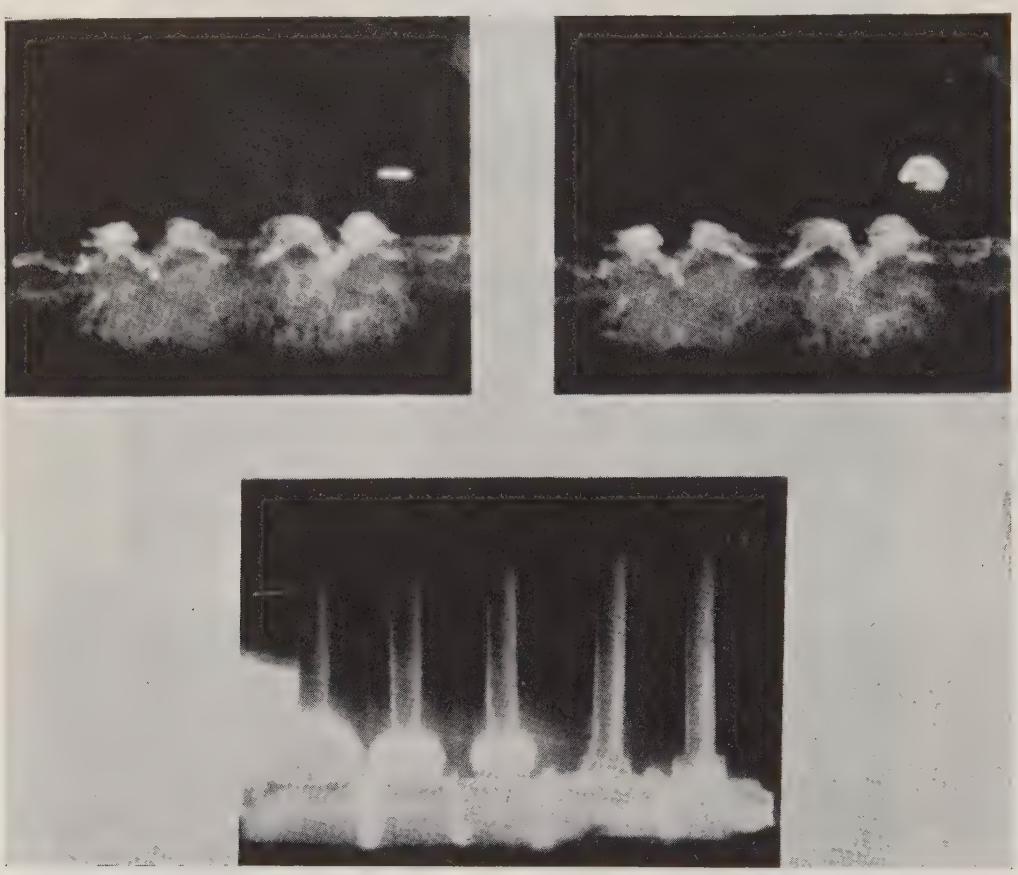

Figure 5. (*Top*) *Frames* 22 *and* 23 *of sequence showing* SPHF *initiation of detonation in* 5·0 cm (*d*) *composition B at* S_1 = 3·92 cm *and* S_2 = 13·8 cm (2·08 μsec/frame). (*Bottom*) *Frames showing* SPHF *initiation of detonation in* 5·0 cm (*d*) *composition B for* S_1 (*left to right*) = 0·78, 1·65, 2·47, 3·37, *and* 4·15 cm, *and* 3·0 cm (*d*) *composition B donor*

initially and had its chief energy support in the reacting explosive right at the SPHF plate-receptor charge interface, and that the initiation wave once formed flashes forwards from this point at a velocity far in excess of the non-reactive shock velocity initiating detonation at S_2 at the instant that it overtook or collided with the non-reactive shock. (See particularly observations with nitromethane (NM) of the flash-across effect and the development of the detonation in Dithekite 13 discussed under the headings Nitromethane and Dithekite.)

As shown in *Figure 3*, the detonation wave that formed in composition B at the distance S_2 from the SPHF plate propagated both forwards and backwards from the plane or surface of initiation. The phenomenon of backward propagation in Cosner, Gey and Pack. The phenomenon of interruption of detonation by SPHF glass and steel plates was first described by Cook, Keyes and Filler[1]. From results of McVey and Boyle[4] the forward detonation wave apparently begins at a velocity about 160 m/sec higher than normal indicating that initiation may occur somewhat behind the shock front, similar to the situation in gases (see *Figure 1*), and that the detonation must therefore first propagate in the compression region of a precursor shock.

Caschia and Whitbread[5], and Lampson and Eichelberger[6], using charges of about 2·0 cm square cross-section did not observe backward propagation. This appears to be due simply to the fact that the critical diameter for backward

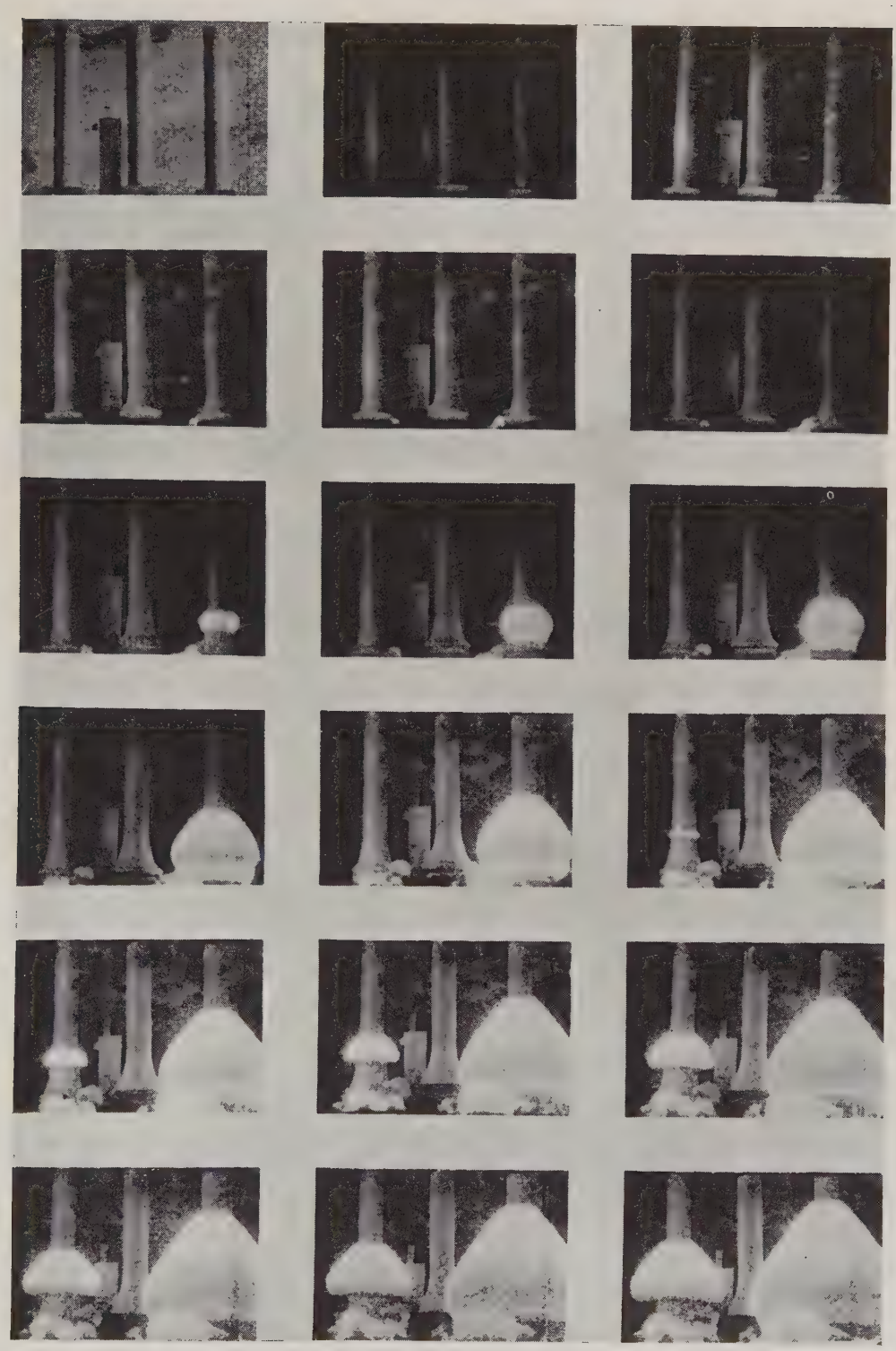

Figure 6. Framing camera sequence of SPHF *initiation of detonation at* $S_1 = 8{\cdot}03$ cm (*right—both forward and reverse*), $S_1 = 8{\cdot}12$ cm (*left—reverse wave failure*) *and* $S_1 = 8{\cdot}15$ cm (*middle—no detonation during observation*). (*Taken at* 2·08 μsec/frame)

propagation in Composition B is greater than 2 cm but less than 5 cm although this critical diameter evidently depends to some extent on S_1.

The backward propagation of detonation in the SPHF plate method is strikingly illustrated by the framing camera sequence (original in colour) shown in *Figure 4* for SPHF-glass-plate initiation of composition B using $S_1 = 6{\cdot}1$ cm and the 5 cm (d) donor. *Figure 5* (top) shows two frames (frame 22 and 23 of a 23-frame sequence, original in colour) in which $S_1 = 3{\cdot}9$ cm, the donor was 3 cm (d), S_2 was found to be 13·8 cm and $\tau = 37$ μsec. The charge was 15 cm long, and the air shock at the end of this charge was already evident on the second (and last) frame after initiation of detonation.

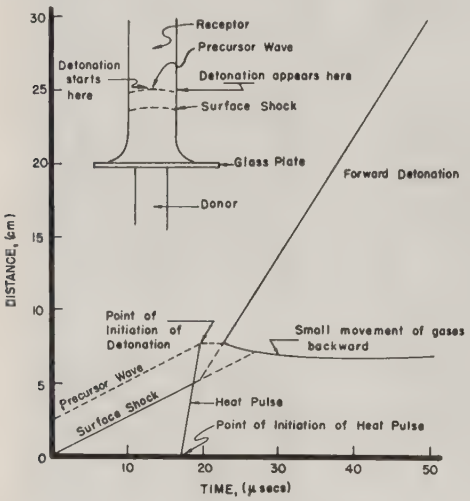

Figure 7. Plot of inert shock, gas and detonation front velocities along cylindrical axis versus *time for* SPHF *initiation of composition B using* 5·0 cm (d) *donor*

Note that backward propagation seems to be in the process of forming, but unfortunately the sequence ran out before the reverse wave had definitely formed. The bottom photograph in *Figure 5* shows initiation in several charges at $S_1 \ll S_1^{\star}$, and therefore at small S_2 values.

Failure of the backward propagation in the 5 cm composition B receptors in the SPHF method has been observed only in the one case shown in *Figure 6*. Results in this case also illustrate the sensitivity of the SPHF method to the plate thickness S_1. Here the SPHF plates were 8·03, 8·12 and 8·15 cm for the left, right, and middle charges, respectively. The left charge detonated both forwards and backwards starting at $S_2 = 4{\cdot}6$ cm, the right one detonated only forwards beginning at $S_2 = 8{\cdot}3$ cm, while the centre charge failed to detonate within the time of observation which was 45 μsec although $S_1 < S_1^{\star}$ in this case also.

When the distance of travel of the shock, the forward, and the rearward detonation fronts were plotted against time, it was observed that the extension of the resulting three lines did not intersect at a common point but formed instead a triangle. The data for one shot are plotted in *Figure 7*, and a possible explanation of the phenomenon indicated by the dotted lines on the figure and by the insert figure. This was accomplished by drawing a constant distance line (representing the interior conditions) from the intersection of the backward gas front and the forward detonation front to a time corresponding to the intersection of the surface shock front and the forward detonation front, and thence a line (representing the precursor wave) drawn parallel to the surface shock front. This concept is consistent with the evidence of a precursor wave[4]. The line representing the travel of the heat pulse is in this case assumed, on the basis of results observed in liquids, to be the cause of the deflagration to detonation transition.

DITHEKITE-13

Dithekite-13 (D.13) is a 'Sprengel'-type liquid explosive comprising a solution of 24·4 per cent mononitrobenzene (MNB), 62·6 per cent nitric acid, and 13 per cent water. It is comparatively easy to handle in tests of the type discussed here because it is mixed just prior to firing. Being clear and of a light straw colour it is excellent for colour photographic observation. Its sensitiveness limit $S_1^{\star}$ with a glass SPHF plate and the 3 cm (d) composition B donor was $1{\cdot}24 < S_1^{\star} < 1{\cdot}42$ cm. Using a 2·5 cm (d) donor instead of a 3·0 cm, $S_1^{\star}$ appeared to be about 1·0 cm, although it was not accurately determined for a 2·5 cm donor. This result was determined in 7·5 cm French square glass tubes cut from 32 oz. French square bottles. Some measurements were made in standard Pyrex (cylindrical) glass tubes of diameter 4·7 cm and other tubes of different shapes. While there appeared to be no appreciable receptor diameter effect on $S_1^{\star}$ in the sizes studied, there was evidence for a small but definite temperature effect. The temperature coefficient of $S_1^{\star}$ has not yet been determined quantitatively.

Figure 8 shows a framing camera sequence taken at 2 μsec/frame of two simultaneous SPHF initiations of detonation in D.13 using glass plates of $S_1 = 1{\cdot}06$ cm (left) and $S_1 = 1{\cdot}14$ cm (right) and the 3 cm (d) composition B donor. The first three frames show spherically expanding, only slightly discoloured, waves moving into the liquid with excellent synchronization of events in each (separately initiated) charge. On frame 4 one may observe a darkening region commencing in each of the liquid charges right at the SPHF plate and rapidly overtaking the front of the non-reactive initial disturbance. (This is the flash-across phenomenon discussed more fully below.) In

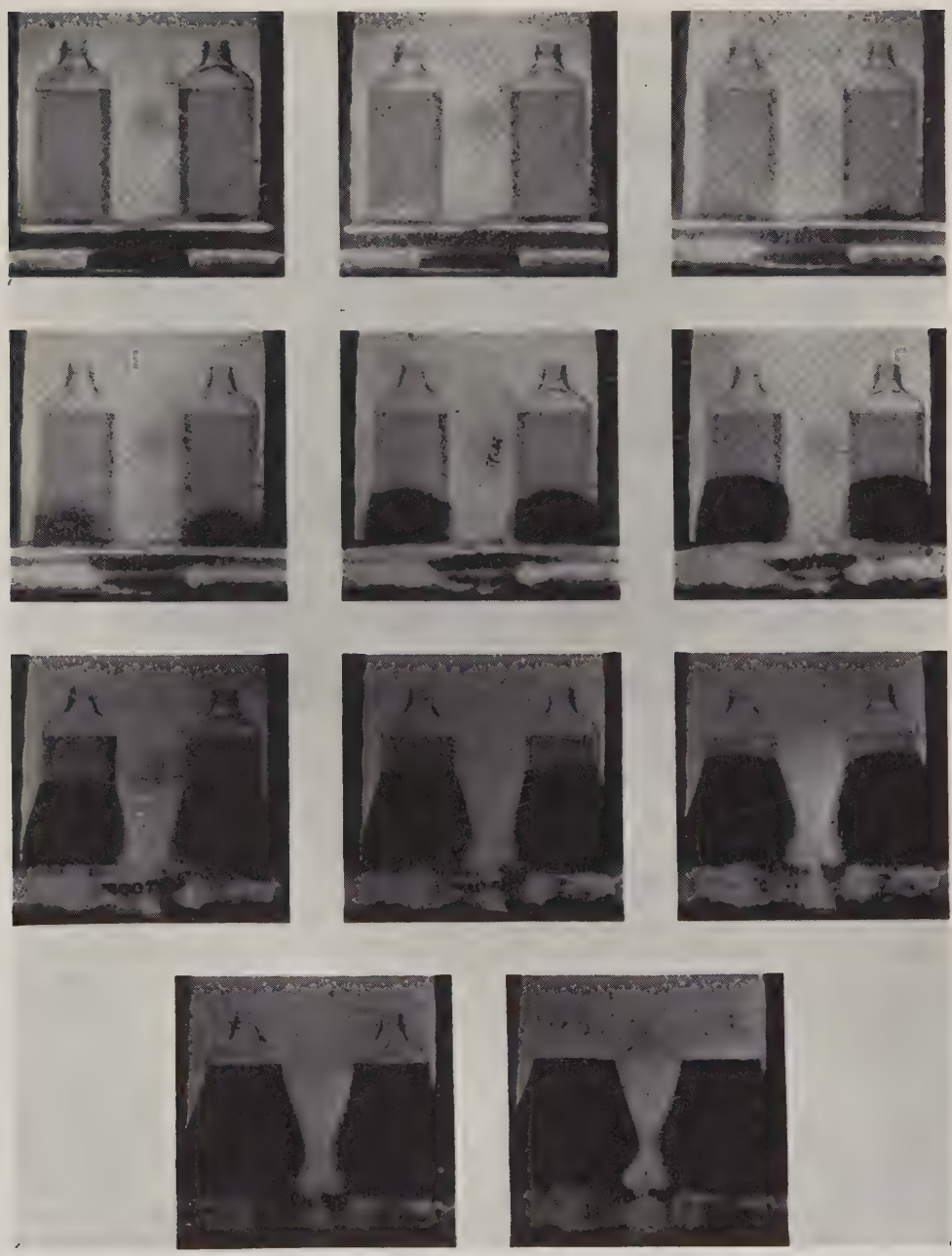

Figure 8. Framing camera sequence of transition from deflagration to detonation by SPHF *method, and reaction zone and plasma in* D.13 (2·08 μsec/frame)

frame 5 this dark region, which corresponds actually to the generation of products of reaction, has become darker and has approached, within about 2 cm, the luminous front in which the fraction N of explosive that has reacted is as yet small. In frame 6 the whole region between the front of the disturbance and the SPHF plate has become appreciably further darkened by products of reaction and at this point detonation is apparently just forming. On frame 7 the dark zone has overtaken within about 1 cm the front of the initial disturbances and detonation has completely formed. It then propagates in the next 8 μsec to the top of the liquid, apparently with a steady front comprising a precursor zone (not easily seen in this case owing to poor contrast) followed by an increasingly darkening zone apparently of steady state length.

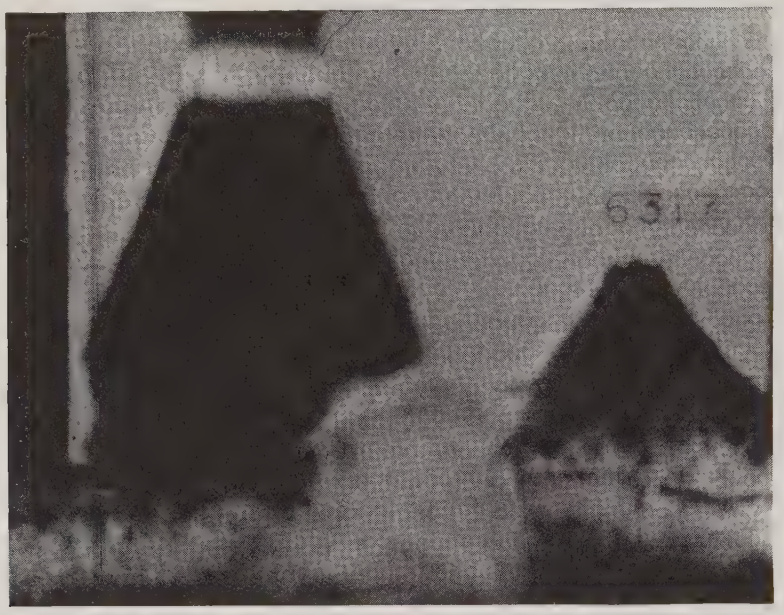

Figure 9. Light from backward detonation of composition B detonated in glass tube is masked by shattering of glass (left). When $L < S_2$ no plasma was produced in composition B (right)

That the steady state detonation zone is of appreciable thickness even between its front and the initial appreciable darkening zone (which itself is not the end of the reaction zone) is strikingly illustrated in frame 11 of this sequence. Here the front of the detonation has just reached the surface of the liquid, as shown by the appearance of the plasma created when the reactive wave reaches the surface[7], while the major darkening region is still more than a centimetre below the surface. There is some framing smear in this case which tends, in view of the high luminosity of the plasma, to exaggerate the length of the precursor zone. The actual distance between the wave front and the beginning of the dark zone was found by careful analysis to be 0·6 cm. This was determined by taking a series of framing camera pictures at different speeds and measuring the apparent length of this zone for each speed. Since the smear varies inversely as mirror speed one computes the actual zone length from the equation

$$x(N') = x'(N') + a/\dot{\theta}$$

where $x(N')$ is the actual length of the zone wherein the definite fractions N' of reaction has occurred (N' being a particular level of darkening), $x'(N')$ is the apparent zone length to fraction N' and $a/\dot{\theta}$ is the smear length, a being a constant and $\dot{\theta}$ the mirror angular velocity. It was estimated from densitometer measurements that the actual reaction zone length a_0 is about twice the value of the initial non-darkened zone, i.e. $a_0 \sim 1{\cdot}2$ cm.

The nature of the SPHF initiation of D.13 appears superficially to be fundamentally different to that of composition B. Detailed study of the process, however, shows that this is not the case but that the SPHF initiation is actually identical in its essential features in the two explosives. On frame 8, *Figure 8*, for example, one will note that the contour shows a rounding at about 3 cm above the SPHF plate. Hence, S_2 was evidently about 3 cm in this case. The only reason that one does

not observe the backward propagation in this case is that the breaking of the glass tube and the dark products of reaction mask it. This is shown by the left-hand side of *Figure 9* which shows the SPHF initiation of composition B in a glass tube. Assuming that the actual distance S_2 is that indicated by the contour, it is evident that the region of transition to detonation, or at least the region of maximum pressure at the instant of transition to detonation, is somewhat behind the front of the disturbance at this instant. This is consistent with the observation of McVey and Boyle that the initial detonation wave in SPHF initiation has a higher than normal velocity[4]. The photograph on the right in *Figure 9* shows a case where $L < S_2$ and $S_1 < S_1^\star$. Note that in this case no plasma appears (because no detonation occurred) even though the charge would have detonated had its length L been greater than S_2. This is a remarkable result which bears on the source of the plasma. It will not, however, be discussed here. A striking factor in the transition from deflagration to detonation in D.13 was the fact that, for the completely non-reactive shock, backlighting gave a clear and distinct outline of the shock wave. But in every case, whenever the transition to detonation occurred, this shock wave had always been completely obliterated before detonation occurred. This is shown in *Figure 10* for D.13 in which a non-reactive shock emerging from an SPHF plate at $S_1 = 1{\cdot}33$ cm ($S_1 > S_1^\star$) is compared with the reactive one ($S_1 = 0{\cdot}8$ cm $< S_1^\star$) several microseconds before the transition to detonation occurred. A comparable situation discussed below was observed in nitromethane.

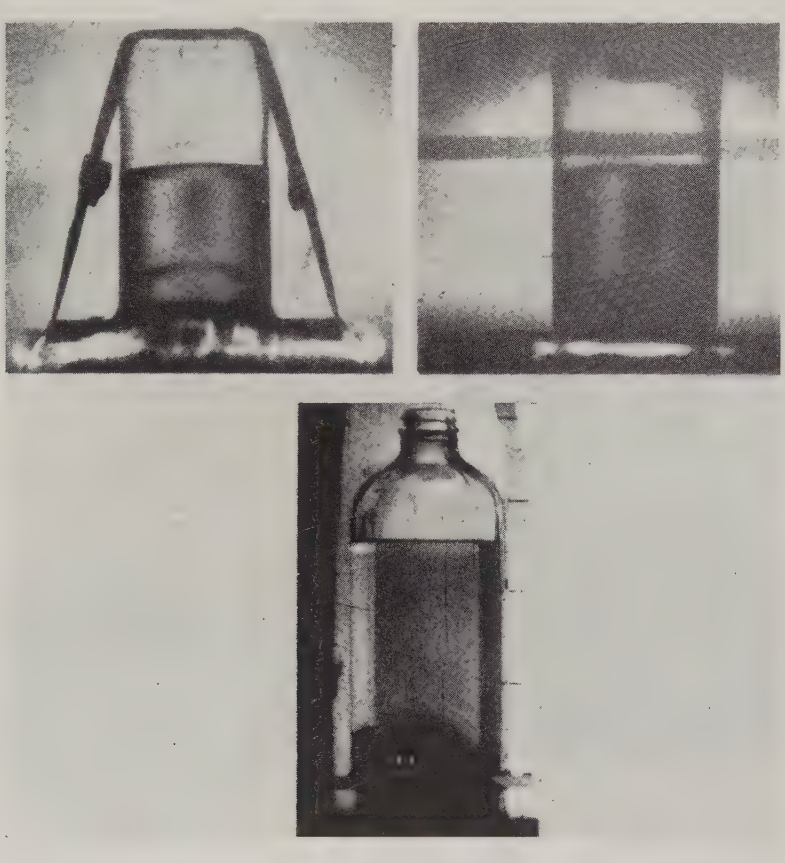

Figure 10. Non-reactive wave (left) versus *reactive wave (right) in the no detonation and pre-detonation region, respectively, and influence of glass beads (bottom) in* D.13 *using* SPHF *method*

Another interesting and important fact bearing directly on the mechanism of initiation of detonation is that D.13 showed a marked increase in $S_1^\star$ when 3 mesh (standard Tyler) glass beads were placed in the liquid. The actual value of $S_1^\star$ for D.13 with the glass beads has not yet been determined, but the value of S_1 at which detonations were still observed was three times greater than $S_1^\star$ in the absence of the glass beads. Moreover, in framing camera sequences in D.13 containing the glass beads one could observe 'hot spots'

between the glass beads (*Figure 10*). These 'hot spots' were clearly the seat of considerable intensification of the pre-detonation reaction.

Figure 11 is a striking streak camera trace of the

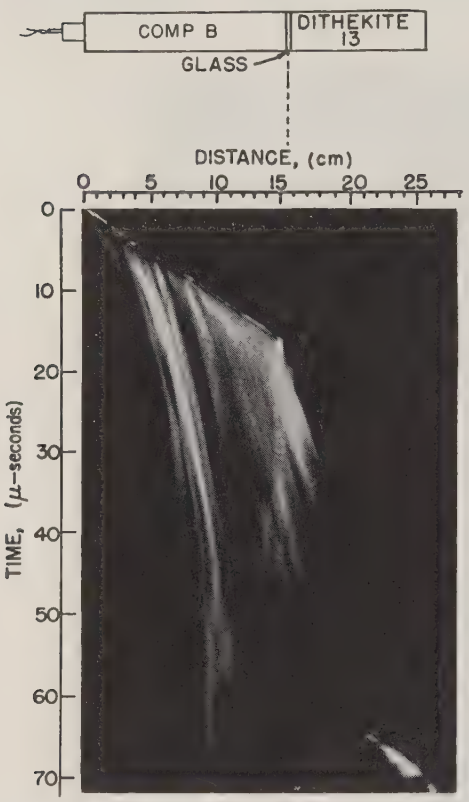

Figure 11. Streak camera trace showing extremely long delay (49 μsec) *in the deflagration to detonation transition* (2·5 cm *composition B donor*, $S_1 = 0{\cdot}99$ cm)

SPHF initiation of D.13 right at the sensitiveness limit showing a phenomenal delaying action of the SPHF plate. In this example the donor was 2·5 cm (*d*) composition B at $S_1 = 1{\cdot}0$ cm and $S_2 = 4{\cdot}1$ cm. The time τ' was 49 μsec.

NITROMETHANE (NM)

The sensitiveness limit $S_1^\star$ for NM using the 3 cm (*d*) composition B donor with receptor tubes comparable in size to those mentioned above for D.13 was $0{\cdot}72 < S_1^\star < 0{\cdot}79$ cm. $S_1^\star$ for NM was increased to nearly double ($1{\cdot}27 \pm 0{\cdot}05$ cm) by adding 2·8 per cent ethylenediamine (EDA).

NM and EDA sensitized NM proved very valuable for studying the chemical reaction zone in the transition to detonation owing to a precursor reddish region in the reaction zone caused apparently by formation of NO_2 in the initial stage of reaction, possibly by thermal cracking of NM. The same coloration was observed, for example, when a saturated ammonium nitrate solution was strongly shocked with the 3 cm (*d*) composition B through a thin SPHF plate.

NM showed a remarkable effect that is highly significant respecting the source of the disturbance that creates detonation and its relation to the shock wave. When S_1 was just slightly greater than $S_1^\star$ there appeared, after the shock had passed into the liquid, the red spot with its greatest intensity at a point directly in contact with the SPHF plate on the central axis of the receptor charge. The intensity of this spot decreased radially outwards towards the then well-defined shock front, finally disappearing about 10 μsec after it formed. This red spot due evidently to NO_2 showed that the chemical reaction built up most rapidly right on the surface of the SPHF plate in contact with the receptor charge as one would naturally expect.

Figure 12 shows frames 15 and 20 of a 23-frame sequence in NM initiated with a 3 cm (*d*) composition B donor charge in the SPHF method through 0·73 cm of glass, i.e. at the narrow edge of the sensitiveness limit. Note that in frame 15 the shock front and a dark front are both quite distinct and unconnected. But in frame 20 the dark front has developed spurs that radiate forwards and terminate in a shock front. In this case the length L was less than $S_2^\star$ (corresponding to $S_1^\star$) and thus prevented observation of a possible deflagration to detonation transition; but it is possible, particularly since $S_1 \doteq S_1^\star$ in this case that it would have occurred in a longer charge. In several experiments shock waves were made to collide from either end of a column of NM using composition B donors and plates of $S_1 > S_1^\star$, in an effort to cause detonation by the colliding shocks, either one of which was too low in intensity to cause detonation in the normal manner described above. None of these produced detonation within the observation time of 50 μsec. However, in one of these attempts in which in this case $S_1 < S_1^\star$ a phenomenal flash-across was observed.

HEAT PULSE IN NM

Figure 13 shows this remarkable effect in the initiation of detonation in NM. Here frames 7 to 12, inclusive, of a sequence taken (original in colour) at 2 μsec/frame show two 5 cm (*d*) composition B donor charges hitting (not quite simultaneously) SPHF plates of thickness 0·54 cm (left) and 0·60 cm (right) on opposite sides of a charge of NM of rectangular cross-section. The shock waves may be seen to enter the charge first at the left on frame 7 and then at the right on frame 8. The two waves are intense enough (since S_1 was considerably less than $S_1^\star$) to initiate nearly immediately the characteristic reddish precursor

reaction of NM, and the waves that may be seen on frames 7 and 9, inclusive, were coloured with the reaction. On frame 9 the two waves from the opposite sides had collided and developed a luminous region at the interface of the collision. It was expected that this intense collision might initiate detonation instantaneously. However, the collision luminosity had completely disappeared on the next frame without any initiation of detonation occurring.

A remarkable new phenomenon, however, took place on frame 9 that was completely unrelated to the colliding shocks. Almost simultaneous with the collision of the waves a bluish-white 'hot spot' could be seen to have developed on the centre of the left SPHF plate. On frame 10 this 'hot spot' and another one that developed subsequently on the opposite SPHF plate had both flashed across the charge and met at the collision interface, and on frame 12 this high luminosity zone had spread across the whole charge. From the framing sequence it could be ascertained that the speed of propagation of the flash-across phenomenon was in excess of 10 mm/μsec. In order to determine the speed of the flash-across phenomenon accurately the shot was repeated and recorded by the streak camera using colour film since we realized that without colour film this phenomenon might easily be missed. Since time resolution may be made much greater on the streak camera it was decided that the effect would probably be observed better with even thinner SPHF plates, and therefore this shot was made with both SPHF plates of 0·31 cm thickness. The trace shown in *Figure 14* (original in colour) verified completely the conclusions reached by the study of the framing camera

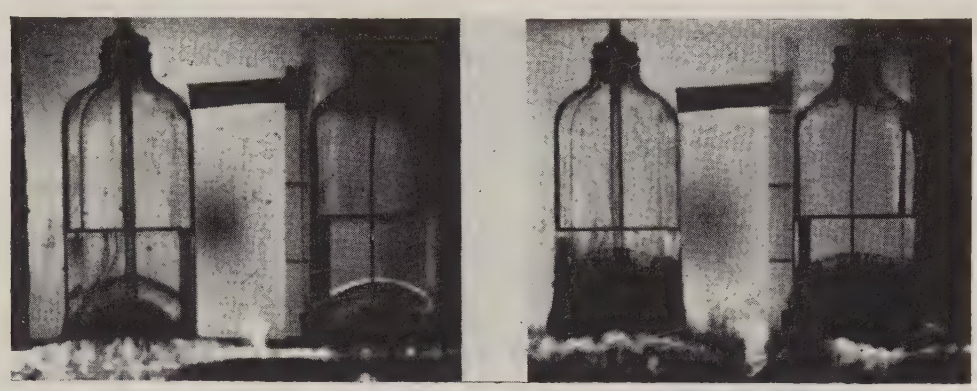

Figure 12. Frames 15 *and* 20 *of a* 23*-frame sequence of the shock and reaction waves in* NM *at* $S_1 \doteq S_1^*$

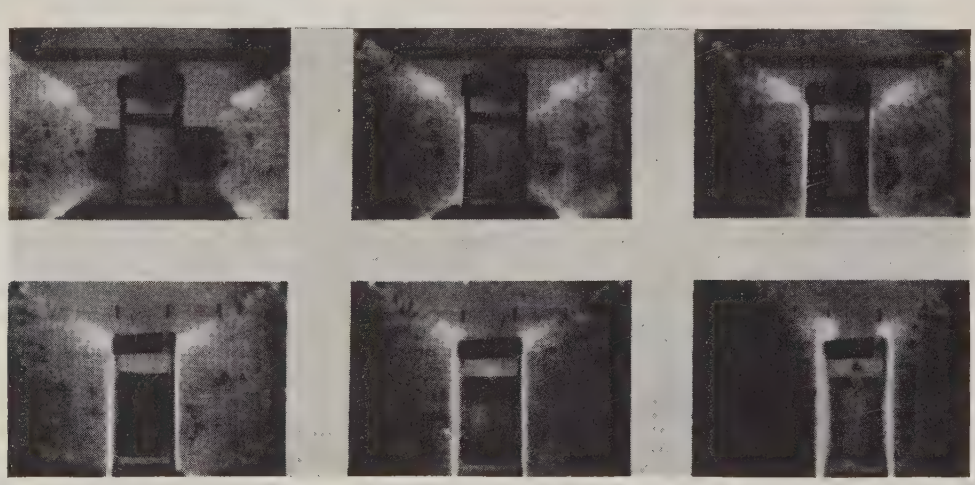

Figure 13. Frames 7–12, *inclusive, of a* 23*-frame sequence of the* SPHF *initiation of* NM *with composition B showing the flash-across phenomenon*

sequence of this phenomenon (*Figure 13*). The initial shocks in this case were strong, overdriven, precursor reaction shocks from the donor charge.

In the streak camera trace, 8·5 μsec after each initial wave entered NM the 'hot spot' appeared at the surface of each plate and flashed to the centre of the charge each at the phenomenal speed of 35 mm/μsec. This is the predicted heat pulse of Cook, Keyes and Filler.

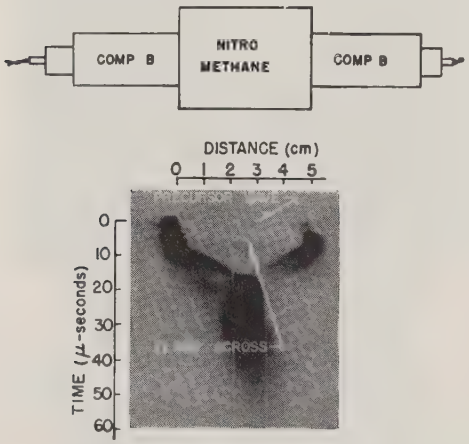

Figure 14. Streak camera trace (original in colour) of heat pulse in the deflagration to detonation transition in NM

If one required that the speed of such hypervelocity events as the flash-across phenomena shown in *Figures 8, 13,* and *14* are too high to allow any appreciable contribution to the events from heat transfer by conduction and/or radiation, one would be faced with a serious dilemma. For example, when the intense shock wave emerging from the SPHF plate passes into the liquid explosive it immediately initiates the endothermic or only weakly exothermic precursor reaction characterized by the reddish colour zone. The reaction then continues and after a time $\tau(S)$ reaches, by exponential temperature build-up by exothermic reaction, the luminous stage in which the colour is bluish-white. In order to explain the high (let us first assume only apparent propagation) rate of the flash-across one would then have to assume in an adiabatic model that $\tau(S)$ decreases linearly with the distance S from the plate in such a way that each element of the liquid arrives correspondingly later at the critical temperature to produce the luminosity at a time such as to give merely the impression of a propagating flash-across phenomenon of velocity 35 mm/μsec. If, for example, one were to assume

$$\tau(S) = \tau_0 - a'S$$

($\tau(S)$ is the time lag to reach the luminous stage for any element of fluid at a distance S from the plate, τ_0 is the time lag to this stage at the SPHF plate, and a' is a positive constant experimentally of magnitude about 1·7 μsec/cm) one would observe, without anything but a temperature characteristic actually propagating, a flash-across having a (apparent) velocity of the magnitude observed. The difficulty imposed by the adiabatic hypothesis is how to explain the linear decrease of $\tau(S)$ with distance, i.e.

$$\mathrm{d}\tau(S)/\mathrm{d}S = -a'$$

One would expect, in an adiabatic model, particularly since the initial wave has in this case effectively a constant velocity, that the time τ for an element of the fluid to reach the temperature corresponding to the bluish-white zone would increase with distance S from the plate owing to a steadily decreasing wave intensity with distance. It therefore appears impossible to explain the flash-across phenomenon by an adiabatic model.

There appears, therefore, to be preponderant evidence that heat transfer is not a negligible factor in detonation, and we therefore consider a non-adiabatic explanation of the flash-across phenomenon. Apparently when the temperature reaches a certain critical level there is a sudden increase in thermal conductivity caused apparently by the temperature reaching a critical ionization threshold. For instance, it has been shown[7] that ionization occurs in various solid explosives in practically every product formed in detonation at the instant it is formed and that the free electron concentration in a detonation reaction zone is therefore very high. Re-combination rates are, of course, high in the detonation of condensed explosives, and ionization thus disappears rapidly and is practically completely absent immediately behind the C–J plane. In fact, as shown by Cook, Keyes and Lee this may be used to measure rather precisely the length of the reaction zone. This effect is apparently responsible for the finite width of the plasma seen in various high-speed colour photographs from the ERG laboratory, and it is remarkable that this plasma has approximately the same width (corrected for speed) as the reaction zone in the explosive. Now below the critical temperature T_c the chemical reaction initiated by the shock wave across the SPHF plate is essentially adiabatic, and the temperature increase in time may then be computed simply by integration of the heat balance equation (for no heat transfer), namely

$$C\,\mathrm{d}T/\mathrm{d}t = Q(N)\,.\,k'\,.f(N)$$

where C is the heat capacity, T the absolute temperature, t the time, $Q(N)$ the heat of reaction, k' the specific rate constant and $f(N)$ the order-of-reaction function. Note that $k'(= k'(T))$ is exponential in T. Therefore, the reaction rate,

and thus also the temperature, build up exponentially in time. But when T reaches the critical level T_c a thermal breakdown (or sharp increase in conductivity) presumably takes place, and one must then modify the heat balance equation to allow for heat conduction. In other words, when the temperature reaches the critical one T_c a much sharper thermal gradient suddenly develops and heat transfer becomes appreciable. The heat balance equation must then be modified as follows:

$$-\rho^{-1}\kappa \, \mathrm{d}T/\mathrm{d}S + C \, \mathrm{d}T/\mathrm{d}t = Q(N) \, . \, k' \, . f(N)$$

where the first term accounting for the thermal conduction becomes of appreciable magnitude, κ being the thermal conductivity, $\mathrm{d}T/\mathrm{d}S$ the temperature gradient, and ρ the density. This explanation of the flash-across is illustrated qualitatively in *Figure 15* for the cases shown in

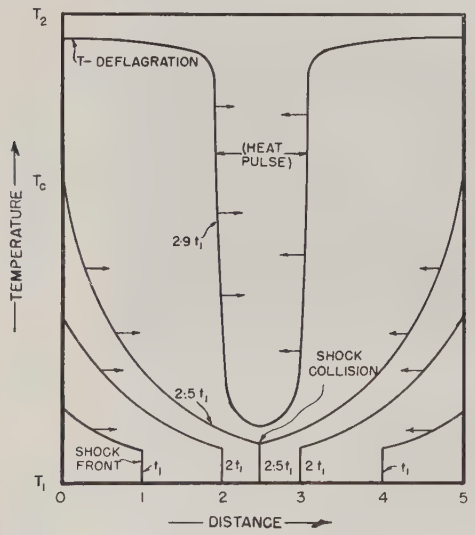

Figure 15. Qualitative theoretical temperature-distance-time profiles in experiments shown in Figures 13 and 14

Figures 13 and *14*. The development of the heat pulse is evidently, therefore, essential for the normal propagation of detonation[1]. Indeed the evidence presented in *Figures 13* and *14* is strong support for the existence of this heat pulse. Moreover, it provides a simple unambiguous explanation for the observed increase of S_2 with S_1 in solid and liquid detonating explosives initiated by the SPHF method.

REACTION ZONE LENGTH IN NM

Results of measurements of the reaction zone length in NM by the microsecond colour framing camera method are of considerable interest. *Figure 16* shows frames 3, 4, 5, 6 and 7 of shots of NM in 7·5 cm French square bottles taken at a speed of 1·4 μsec/frame, and *Figure 17* shows frames 17, 18, 19, 20 and 21 of another shot of NM in a 7·4 cm square cross-section Cellophane tube (0·001 in. thickness) taken at 1 μsec/frame. In *Figure 17* a failure in a simultaneous shot of NM in a French square bottle is also shown. In the failure case $S_1 > S_1^{\star}$, and one is thus able to see clearly the non-reactive shock. In the detonation case (right-hand side) the precursor (reddish) reaction zone is visible for 1·5 μsec. Correcting for smear from results obtained at other speeds one finds that the reddish part only of the reaction zone in NM is 1·2 cm long. Hence, the reaction zone length a_0 of NM is clearly greater, apparently about twice as great, i.e. $a_0 \sim 2{\cdot}4$ cm for this short charge. This result is in sharp contradiction to the result obtained by Cotter[8] for NM who claimed a reaction time in NM less than 0·02 μsec. The explanation of the discrepancy between our results and those of Cotter is easily found. Cotter assumed that the end of the reaction zone was the point of maximum luminosity. Actually, this is really only the beginning, not the end, of the chemical reaction zone. The reddish precursor reaction is not luminous and is made visible only by auxiliary lighting. Luminosity sometimes appears when auxiliary lighting is used at the front, the disturbance being due to refraction effects. Apparently, Cotter was observing only light from the extreme front of this shock, and most of the time only the deflagration stage in the SPHF initiation of detonation. Thus, in this case the colour photographic method makes the situation regarding the reaction zone completely obvious and shows that the assumption that the reaction zone is the zone of zero to maximum luminosity is erroneous.

PRESSURE–DISTANCE RELATIONS IN REACTION ZONE

One may use the blast contour observed in the high speed framing or the high speed streak photographic method to determine the pressure–distance contour in the reaction zone at the periphery of these liquid explosives. Even a casual examination of these contours shows that the peak pressure does not occur at the shock front! In D.13 an initial result showed the pressure to rise slowly over the first 0·7 microseconds to a constant region (apparently the C–J value) for the next microsecond, then to fall to about 5 per cent of the peak pressure in the next microsecond, and finally (following a slight pressure surge up to 15 per cent of the peak pressure) to effectively zero pressure at 8 μsec. These results (which are, of course, complicated by edge effects since they were taken from the contour) thus indicate actually the reverse of a pressure 'spike' in the reaction zone of liquid explosives. This same result is, moreover,

indicated, we believe, by the results of Kistiakowsky and Kydd[9] for gases. This is shown by the following arguments:

Through X-ray absorption measurements in gaseous explosives at pressures between 10 and 100 mm Hg Kistiakowsky and Kydd (K–K) showed that σ_f, the ratio of the density of the wave front to that in the undisturbed explosive, was 3·6 (±15 per cent in 46 examples). Good agreement with theory was found for σ_2, the ratio of the C–J density to the density in the undisturbed explosive, namely, about 1·8. The Zeldovich–Döring–von Neumann (Z–D–N) theory [10–12] required, according to K–K, values of $\sigma_f = 5{\cdot}3$.

Another discrepancy between observations and the Z–D–N theory pointed out by K–K was their failure to observe the induction zone required by the low initial temperature of the Z–D–N model.

The equation of state applicable in gaseous detonation is $p = \rho nRT$. In connection with the pressure-spike theory we are here interested in the ratio

$$P_f = p_f/p_2 = \sigma_f\sigma_2^{-1}(nT)_f/(nT)_2$$

the subscript f designating the shock front and the subscript 2 the 'C–J plane'. According to the measurements of K–K, $\sigma_f\sigma_2^{-1} \doteq 2$. In the Z–D–N theory $\sigma_f \doteq 5{\cdot}3$. The temperature at the front

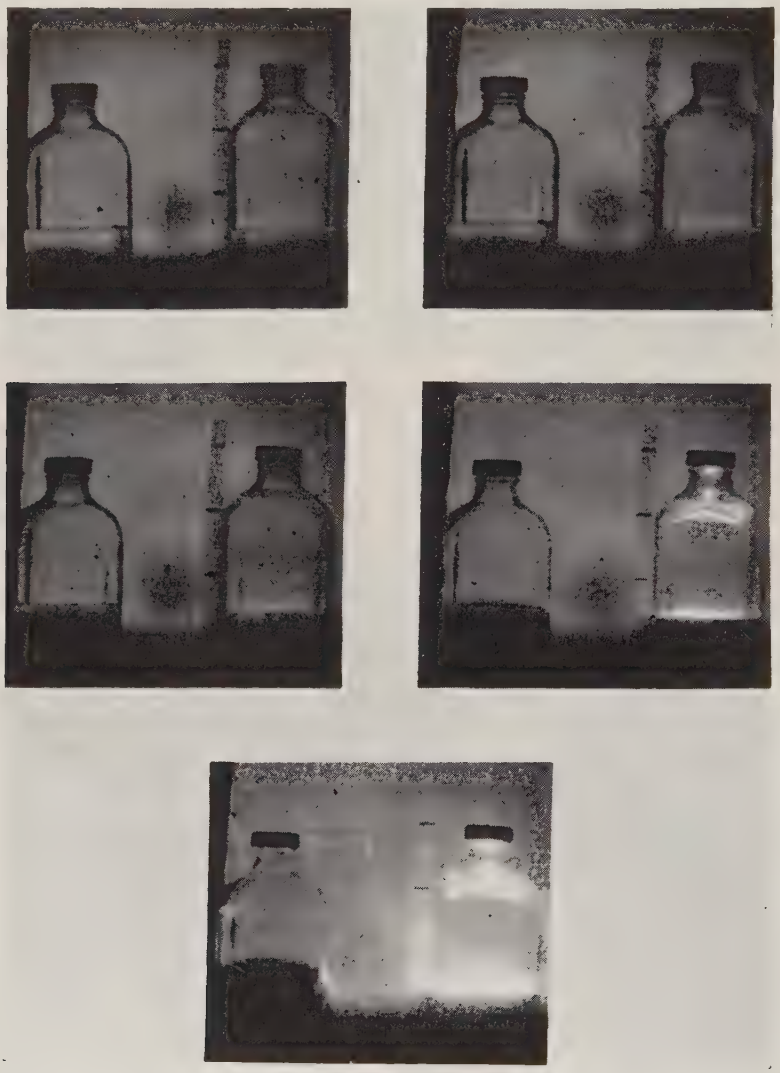

Figure 16. Reaction zone in NM *emerging from surface of liquid in French square bottles (left in propane atmosphere and right in argon atmosphere).* (1·39 μsec/frame)

of the wave in the Z–D–N theory is only about half the final C–J temperature; it is given in this theory by

$$T_f \doteq (P_f^2 \varphi + \bar{C}_{vf} T_1)/\bar{C}_{vf}$$

where φ is the Hugoniot energy at the C–J plane

Z–D–N model, K–K's actual results require $P_f < 0{\cdot}5$, and instead of decreasing with distance behind the shock front P actually increases from the wave front through the reaction zone to the C–J plane. This discrepancy between observations and the Z–D–N model seems, in view of the

Figure 17. Non-reactive shock in a 7·5 cm *French square bottle of* NM *(left) and detonation wave in* 3 in. *(square) Cellophane tube of* NM *emerging from surface in air* (1·04 μsec/frame)

or $1/2(p_2 + p_1)(v_1 - v_2)$, v being the specific volume, and $\bar{C}_{vf}$ the average heat capacity between T_1 and T_f. If one makes use of K–K's measured result, $\sigma_f \sigma_2^{-1} = 2$ and the above equation with the appropriate thermochemistry to compute P_f and T_f in a self-consistent solution, T_f turns out to be less than 700°K and P_f much lower than unity. Instead of the required $P_f = 2$ of the fundamental foundation of the Z–D–N theory, to require heat conduction in the reaction zone. Indeed, in order to account even for a pressure-flat reaction zone, to say nothing of a pressure-spike type zone, K–K's density measurements require that more than 0·6 of the heat in the wave front of the low pressure, gaseous explosives must be heat conducted into the wave front, less than

half of the required heat being attributable to the Hugoniot heat $P^2\varphi$.

If one modifies the Z–D–N model to include appreciable heat conduction the necessity disappears for a 'spike' or at least a 'spike' of the magnitude heretofore considered necessary in the Z–D–N theory. Furthermore, heat conduction, if it is of the magnitude that the above considerations suggest, would also remove the necessity for an induction zone in the Z–D–N model and bring the theory into agreement with observation in this regard also.

Cook, Keyes and Filler[1] proposed in view of K–K's measurements and other observations the adoption of a Z–D–N model modified simply to allow for appreciable heat conduction (the heat pulse) in the reaction zone, the existence of which seems now to have been demonstrated experimentally by the results summarized in this paper.

SUMMARY AND CONCLUSIONS

Transitions from deflagration to detonation observed in gaseous, liquid and solid explosives are described and the transition shown to involve essentially the same phenomena in all three types. Streak photography and microsecond, framing, colour photography were used to study these transition phenomena in H_2–O_2, the liquids Dithekite (nitric acid-nitrobenzene-water) and nitromethane, and in the solid composition B. In initiating each of the condensed explosives, a shock wave from a composition B donor charge was passed into the test (receptor) charge through a glass (called SPHF) plate initiating always a pre-detonation or deflagration reaction in the test charge. Transition from deflagration to detonation was observed to occur usually at some distance S_2 from the glass plate. S_2 increased with S_1 up to the sensitiveness limit $S_1^\star$. For S_1 slightly greater than $S_1^\star$ the shock wave and a reactive zone were usually clearly distinguishable, while for $S_1 < S_1^\star$ the sharp shock discontinuity, evident when $S_1 > S_1^\star$, could not be observed but seemed instead to have been erased or spread out evidently by heat radiated from the pre-detonation reaction. This was especially striking in NM; owing to the initial formation of NO_2 at S_1 just slightly greater than $S_1^\star$ a bright orange-red reaction spot appeared adjacent to the SPHF plate and persisted several microseconds but did not spread much from this point. A flash-across (the predicted heat pulse) of velocity about five times the detonation velocity was observed when $S_1 < S_1^\star$ just prior to the initiation of detonation in NM and Dithekite beginning in the region where only the reaction spot developed when $S_1 > S_1^\star$.

REFERENCES

[1] Cook, M. A., Keyes, R. T. and Filler, A. S. *Trans. Faraday Soc.* 52 (1955) 369; *J. chem. Phys.* 23 (1955) 409

[2] Cosner L. and Sewell, R. W. *Initiation of Explosives Through Metal Barriers*, Paper presented at Symposium on Detonation Wave Shaping, Jet Propulsion Laboratory, Pasadena, California June 5–7, 1956

[3] Cook, M. A. *Time Lag in Propagation of Detonation Through Air, Steel, and Glass*, T.R. XXXI, Contract N7-onr-45107, Explosives Research Group, University of Utah. March 15, 1954

[4] McVey, R. and Boyle, V. M. *Sympathetic Detonation in Composition B Induced by Air Shock from Pentolite and from Composition B.* Memorandum Report No. 1048, Ballistic Research Laboratories, Aberdeen Proving Grounds, Maryland, November 1956

[5] Caschia, G. P. and Whitbread, E. G. *Initiation of Explosives by Shock.* Paper No. 20, Royal Society Symposium on the Initiation and Growth of Explosion in Solids, May 30, 1957

[6] Lampson, C. W. and Eichelberger, R. J. *Initiation of Solid Explosives by Shock Waves and by Impact.* Paper No. 21, Royal Society Symposium on the Initiation and Growth of Explosion in Solids, May 30, 1957

[7] Cook, M. A., Keyes, R. T. and Lee, L. *Measurements of Ionization and Electron Densities in the Detonation Wave in Solid Explosives*, T.R. No. 1, Contract No. AF-18(603)-100, ERG, University of Utah, September 15, 1956

[8] Cotter, T. P. *The Structure of Detonation in Some Liquid Explosives.* Thesis, Cornell University, September 1953

[9] Kistiakowsky, G. B. and Kydd, P. H. *J. chem. Phys.* 25 (1956) 824

[10] Zeldovich, Y. B. *J. exp. Theor. Phys.* 10 (1940) 542

[11] von Neumann, J. *OSRD* 549 (1942)

[12] Döring, W. *Ann. Phys., LP*3 43 (1943) 421

110

ON THE DEVELOPMENT OF GASEOUS DETONATION—ANALYSIS OF WAVE PHENOMENA

A. K. OPPENHEIM and R. A. STERN

PROBLEM

Statement

The purpose of this paper is to present a method of analysis for the evaluation of the consequences of wave propagation and interaction phenomena which are observed during the transition from deflagration to detonation in a constant area duct. The main form of experimental observation available as a basis for such an analysis—and the only one used for this illustration—is the record of shock front and flame traces in the time-distance domain, i.e. the world lines of the waves. The best data of this character were obtained photographically by the use of schlieren optics with a rotating-drum camera. The experimental record selected as a basis for our analysis was presented by Schmidt, Steinicke and Neubert[1,2].

Experimental observations

Figure 1 is a re-plot of Figure 50 of reference 1. It describes the authors' interpretation of their photographic records of the development of detonation in a mixture of 8 per cent propane with 49·7 per cent oxygen and 42·3 per cent nitrogen. The mixture was contained in a 24 × 24 mm cross-section tube approximately 1 m long, ignited at the closed end. The world lines of the waves were recorded after the flame had traversed about 30 cm of the tube's length, and approximately 1·4 msec after the initiation of combustion. The record contains the trace of the flame and of three shock fronts, propagating at velocities of 457, 636 and 875 m per sec, respectively. It appears that when the third shock coalesces with the flame front, a detonation wave originates propagating at a velocity of 2,150 m/s, and, at the same time, a retonation wave starts in the opposite direction with a velocity of 1,050 m/s. The remaining thin lines on *Figure 1* are the results of the present analysis. Indicated there also is an estimate of the flame trace from the initiation of combustion to the instant reported by Schmidt, *et al.*

Thermochemical data

Other data needed for a specific formulation of the problem were deduced from the given composition of the reactive mixture. For this purpose the properties of detonation were first established, on the basis of information published by Weir and Morrison[19], for an equivalent propane–oxygen mixture, and then corrections were made to account for the effects due to the presence of nitrogen in the reactant mixture. The reactant mixture is treated as a perfect gas, and the product as another perfect gas. The specific heat ratios

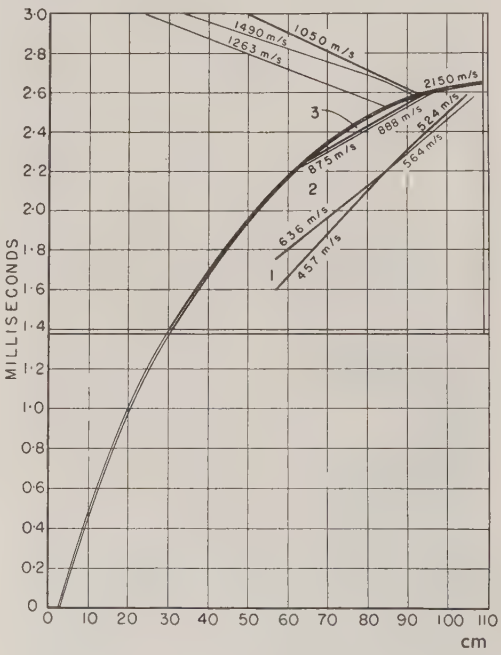

Figure 1. World lines of the development of detonation

of the two gases and the 'effective' heat of reaction are then evaluated so as to match the two boundary conditions of the process: the state attained by constant pressure deflagration and that of the Chapman–Jouguet detonation. The results are summarized in Table 1.

ANALYSIS

Basic principles

The purpose of the analysis is to deduce from the recorded wave world lines the information on the

thermodynamic state of the substance and its motion over the whole space-time domain of the process in order to gain an insight into its dynamic and kinetic characteristics. This, in effect, involves the transformation from the Eulerian system of observation to the Langrangian system of chemical reaction. The problem is reduced to two dimensions by assuming that all the parameters describing the conditions at a given instant in a given section of the reactor tube are only functions of a single space coordinate. This means that the flow is treated essentially as unidimensional and the effects associated with the curvatures of the wave fronts are neglected. Furthermore, the only

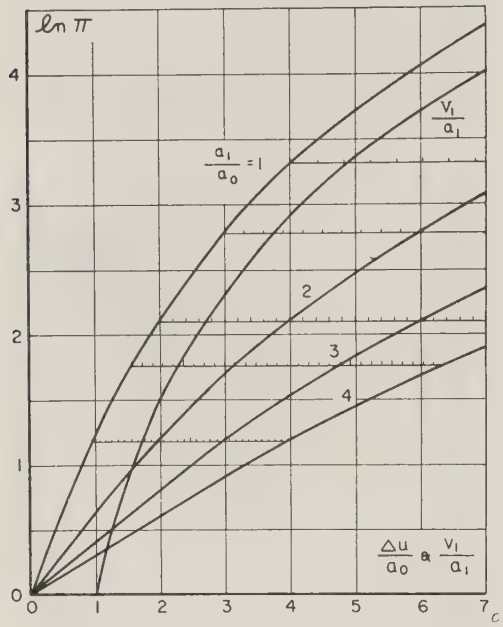

Figure 2. Shock polars in the π-u plane ($k = 4/3$)

changes of state admitted in the analysis are those brought about by the wave action. The wave fronts are considered as plain discontinuities in the flow field, that is, surfaces across which finite changes occur without variation in cross-section area. Notable exception in this respect is the rarefaction fan, which is treated as a zone of continuous isentropic expansion characterized by the condition of a Riemann invariant.

Thus, in the analysis all considerations associated with the structure of wave processes, such as the induction and relaxation phenomena, are neglected in favour of their dynamic effects. The study can be best described as one admitting only consideration 'in the large' and yielding essentially a step-wise description of a process which in reality has a somewhat more continuous character. The step-wise description, however, is well justified in the case at hand by the optically recorded steepness in density gradients of the experimentally observed wave fronts. In other words, the analysis is an extension of the method of characteristics to the consideration of finite discontinuities in the flow field. In recognizing only finite discontinuities it neglects, in essence, the effects of diffusion, viscosity and conductivity, which in reality tend only to make the transitions more gradual than implied by such a treatment. These effects can be later included by using the results of the present solution 'in the large' as boundary conditions for regimes which are then resolved 'in the small'.

In recognizing only processes brought about by wave action, the analysis resembles the conventional gas dynamic treatment of unsteady flow phenomena as propounded by Sauer[3], Schultz–Grunow[4], de Haller[5], Jenny[6], and described in the texts of Courant and Friedrichs[7], Shapiro[8], Oswatitsch[9] and Rudinger[10].

Method of analysis

For the present purpose the graphical method, based on the use of the so-called polar curves in the pressure-velocity and local velocity of sound-particle velocity hodograph planes, has been modified and extended.

The modification consists of the use of the logarithm of pressure ratio (or of local velocity of sound ratio) as the ordinate instead of the conventional linear scale. In spite of its apparent triviality, the result of such a modification is quite significant in that it imparts to the hodograph plane a complete vectorial character, with logarithm of the pressure ratio (or of local velocity of sound ratio) appearing as a real component of the vector representing the change of state. Thus, each subsequent state is obtained as a sum of vectors representing the changes brought about by discontinuities forming the initial boundaries of its regime in the space-time domain. It is of interest to note also that since the entropy change is a weighted sum of the logarithms of pressure and velocity of sound ratios, the logarithmic coordinates are essentially components of an overall entropy change ($\Delta s/R$)-particle velocity (u/a_0) hodograph.

The extension of the method is associated with the fact that whereas the conventional treatment applies principally to unreactive wave processes, the present treats the flame as a deflagration, that is, a discontinuity, associated with a finite pressure change.

The analysis, in effect, admits only the existence of three types of elementary wave processes: the shock, the rarefaction, and the deflagration. They are described in the following section.

WAVE PROCESSES

Shock

Figures 2 and *3* represent the shock polars in the π-u and the α-u planes, respectively. They are plotted to scale for a perfect gas with $k = 4/3$. The equations of the shock polars are:

$$\frac{\Delta u}{a_0} = \frac{2}{k+1}\frac{a_1}{a_0}\frac{(V_1/a_1)^2 - 1}{(V_1/a_1)} \tag{1}$$

$$\pi = 1 + \frac{2k}{k+1}[(V_1/a_1)^2 - 1] \tag{2}$$

$$\alpha^2 = 1 + \frac{2(k-1)}{(k+1)^2}\frac{k(V_1/a_1)^2 + 1}{(V_1/a_1)^2}[(V_1/a_1)^2 - 1] \tag{3}$$

They relate $\Delta u/a_0$, π and α, with a_1/a_0 and V_1/a_1 as parameters.

The polar curve represents the velocity hodograph, that is, the locus of end-points of vectors having state 0,0 as common origin, whose one component is the non-dimensional particle velocity change, $\Delta u/a_0$, and the other component is the

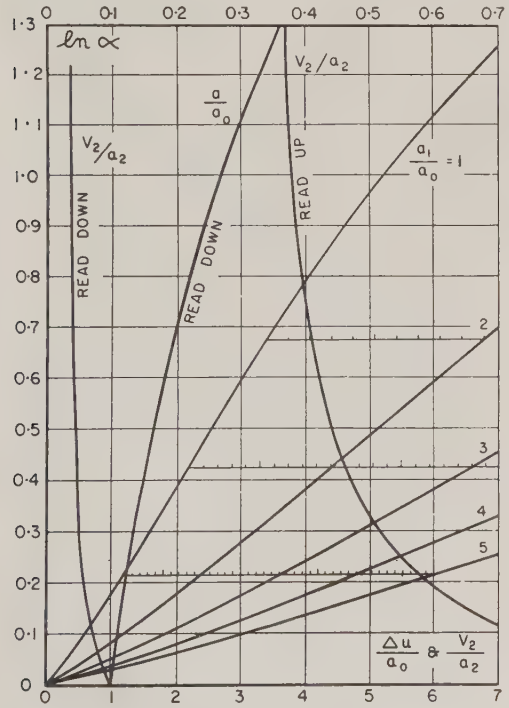

Figure 3. Shock polars in the α-u plane ($k = 4/3$)

logarithm of pressure ratio, $\ln \pi$ (or of local velocity of sound ratio, $\ln \alpha$) brought about by a plane, normal wave of a given kind, in this case a shock. Under these circumstances the polar is a function only of the local velocity of sound of the medium into which the wave propagates. Consequently, each curve of the families represented in *Figures 2* and *3* corresponds to a given value of the non-dimensional velocity of sound of the medium into which the shock propagates, a_1/a_0. Shown plotted are the polars for integral values of this parameter from 1 to 4 with scales for interpolation provided. In addition, *Figure 2* shows the ratio of wave velocity to the local velocity of sound, V_1/a_1 (the local Mach number of the wave front).

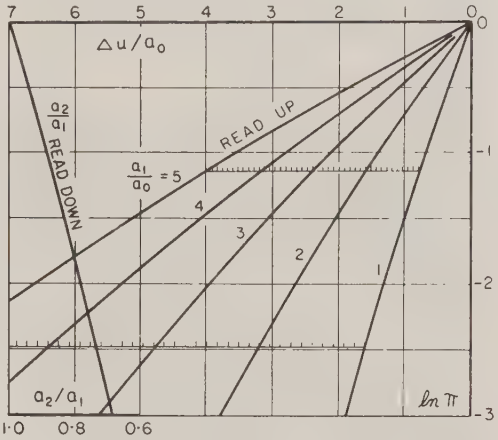

Figure 4. Rarefaction polars in the π-u plane ($k = 4/3$)

while *Figure 3* contains a plot of the ratio of relative particle velocity behind the shock to the local velocity of sound, V_2/a_2.

Rarefaction

Figures 4 and *5* represent the rarefaction polars in the π-u and α-u planes, respectively. They are

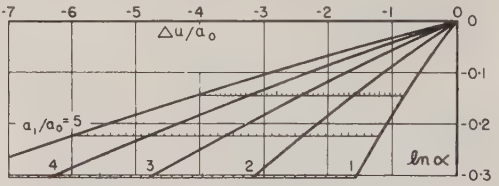

Figure 5. Rarefaction polars in the α-u plane ($k = 4/3$)

drawn to the same scale as the shock polars for a perfect gas with $k = 4/3$, and as the shock polars, they refer to the wave moving to the right. The equations of the rarefaction polars are:

$$\frac{\Delta u}{a_0} = \frac{2}{k-1}\frac{a_1}{a_0}\left[\pi^{\frac{k-1}{2k}} - 1\right] \tag{4}$$

$$\alpha = \pi^{\frac{k-1}{2k}} \tag{5}$$

They relate $\Delta u/a_0$, π and α, with a_1/a_0 as a parameter. As in the case of shock polars, each curve of the family corresponds to a constant value of

the non-dimensional local velocity of sound of the medium into which the rarefaction propagates, a_1/a_0, with interpolation scales provided. The rarefaction wave appears in the space-time domain as a fan whose leading edge propagates into the medium at a velocity equal to the local velocity of sound of the medium, leaving the substance behind the trailing edge with the local velocity of sound corresponding to the state of this substance. The additional curve in *Figure 4* gives the ratio of these local sound velocities, a_2/a_1.

Deflagration

Figures 6 and *7* represent the deflagration polars in the π-u and α-u planes, respectively. They are plotted for reactant mixture considered as a perfect gas with $k_1 = 4/3$ and products considered as a perfect gas with $k_2 = 1{\cdot}3$, while the non-dimensional heat of reaction $Q = 25$. (As shown in Table 1, these values correspond to the case at hand.) The equations of the deflagration polars are:

$$\left(\frac{\Delta u}{a_0}\right)^2 + \frac{2}{k_2+1}\left[(V_1/a_0) - \frac{k_2}{k_1}\left(\frac{a_1}{a_0}\right)^2 (a_0/V_1)\right]\frac{\Delta u}{a_0} + \left[2\frac{k_2-1}{k_2+1}Q - 2\frac{k_1-k_2}{k_2+1}\frac{1}{k_1}\frac{1}{k_1-1}\left(\frac{a_1}{a_0}\right)^2\right] = 0 \quad (6)$$

$$\pi = 1 - k_1(V_1/a_0)\left(\frac{a_0}{a_1}\right)^2\left(\frac{\Delta u}{a_0}\right) \quad (7)$$

$$\alpha^2\left[\frac{k_2+1}{2k_2(k_2-1)} + \frac{1}{2k_2\pi}\right] = \left[\frac{k_1+1}{2k_1(k_1-1)} + \frac{\pi}{2k_1}\right] + \frac{Q}{(a_1/a_0)^2} \quad (8)$$

They relate u/a_0, π and α with V_1/a_0, a_1/a_0, and Q as parameters.

As in previous cases, the deflagration polars are plotted for waves moving to the right. On the left-hand side of *Figure 6* are the non-dimensional wave velocities, V_1/a_0. The deflagration polars and the wave velocity curves are terminated by the locus of the Chapman–Jôuguet deflagrations, that is, deflagrations which move with respect to products at velocities equal to local velocities of sound. The thin lines extending beyond the locus of the Chapman–Jouguet deflagrations represent conditions corresponding to the so-called strong deflagrations—a consequence of the Hugoniot curve theory, having no real physical meaning. The deflagration polars in the α-u plane are drawn in a similar manner, but with lines corresponding to strong deflagrations omitted. Shown in addition are the non-dimensional propagation velocity of the Chapman–Jouguet deflagration Vk_1/a_0 and its ratio to the local velocity of sound immediately in front, Vk_1/a_1.

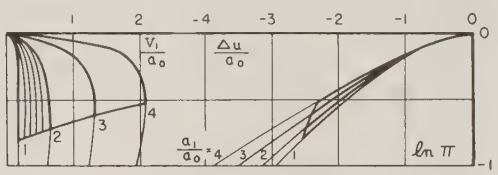

Figure 6. Deflagration polars in the π-u plane ($k_1 = 4/3$; $k_2 = 1{\cdot}3$; $Q = 25$)

The changes of state brought about by a Chapman–Jouguet deflagration are, in our circumstances, functions only of the non-dimensional local velocity of sound[11], a_1/a_0. This feature is reflected in *Figure 8* representing all the parameters

TABLE 1

Thermochemical Data of the Problem

Reactant mixture

Composition per cent: $8C_3H_8$–$50O_2$–$42N_2$
Initial state: 300°K, 1 atm
Average specific heat ratio: 1·37

*Detonation of equivalent propane–oxygen mixture**

Equilibrium temperature: 3,800°K
Composition of products, mols/mol C_3H_8: $2{\cdot}84H_2O$ $-1{\cdot}70CO-1{\cdot}34OH-1{\cdot}65O_2-1{\cdot}29CO_2-0{\cdot}72O-0{\cdot}46H-0{\cdot}31H_2 = 10{\cdot}3$ mols product/mol C_3H_8
Enthalpy†: 380 kcal/mol C_3H_8
Average specific heat ratio: 1·26
Mach No.: 7·4
Heat of reaction‡: $Q = 46{\cdot}3$, $q = 270$ kcal/mol C_3H_8

Detonation of reactant mixture

Adiabatic flame temperature for constant-pressure combustion: 2,090°K
Temperature of the Chapman–Jouguet detonation state: 2,970°K
Composition of products, mols/mol C_3H_8§: $2{\cdot}84H_20-1{\cdot}70CO-1{\cdot}34OH-1{\cdot}30O_2-1{\cdot}29CO_2-0{\cdot}72O-0{\cdot}46H-0{\cdot}31H_2-4{\cdot}9N_2-0{\cdot}70NO = 15{\cdot}6$ mols product/mol C_3H_8
Enthalpy: 550 kcal/mol C_3H_8
Average specific heat ratio: 1·27
Heat of reaction†: $Q = 26{\cdot}3$, $q = 254$ kcal/mol C_3H_8
Mach No.‡: 5·7

* Obtained from reference 19 for equivalent composition, mols: $1C_3H_8 + 6{\cdot}25O_2(k = 1{\cdot}35)$.

† According to reference 20.

‡ Using reference 13.

§ With equilibrium constants from reference 20.

of the Chapman–Jouguet deflagration corresponding to $k_1 = 4/3$, $k_2 = 1{\cdot}3$, and $Q = 25$. They represent the following equations:

$$\left(\frac{\Delta u}{a_0}\right)^2 - \frac{2}{k_2 + 1}\left[(k_2 - 1)Q - \frac{k_1 - k_2}{k_1 - 1}\frac{1}{k_1}\left(\frac{a_1}{a_0}\right)^2\right] = 0 \qquad (9)$$

$$\left(\frac{\Delta u}{a_0}\right)^2 - \left(\frac{a_1}{a_0}\right)^2 \frac{(1-\pi)^2}{\pi k_1(k_2+1) - k_1} = 0 \qquad (10)$$

$$(V_{K_1}/a_0)^2 + (V_{K_1}/a_0)\frac{\Delta u}{a_0}(1 + k_2) - \frac{k_2}{k_1}\left(\frac{a_1}{a_0}\right)^2 = 0 \qquad (11)$$

$$(V_{K_1}/a_0) - \frac{\Delta u}{a_0} = \alpha\frac{a_1}{a_0} \qquad (12)$$

Detonation

The idealized model of detonation is a composite wave consisting of a shock followed immediately by a Chapman–Jouguet deflagration. The state

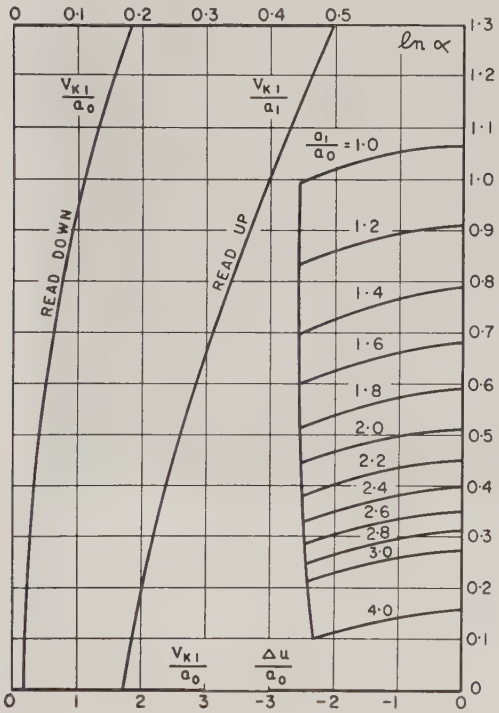

Figure 7. Deflagration polars in the α-u plane ($k_1 = 4/3$; $k_2 = 1{\cdot}3$; $Q = 25$)

behind such a wave propagating into the undisturbed reactant mixture is denoted by symbol J; the corresponding state behind the shock is denoted by symbol N, reflecting the current practice of referring to it as the von Neumann spike. In reality, the von Neumann spike is rounded off by the action of diffusion, viscosity and heat conductivity[12]. This, however, does not detract from the physical significance of state N, which represents actual conditions attained behind the shock when the deflagration lags behind by a distance larger than the shock's relaxation thickness[13]. States J and N can be obtained

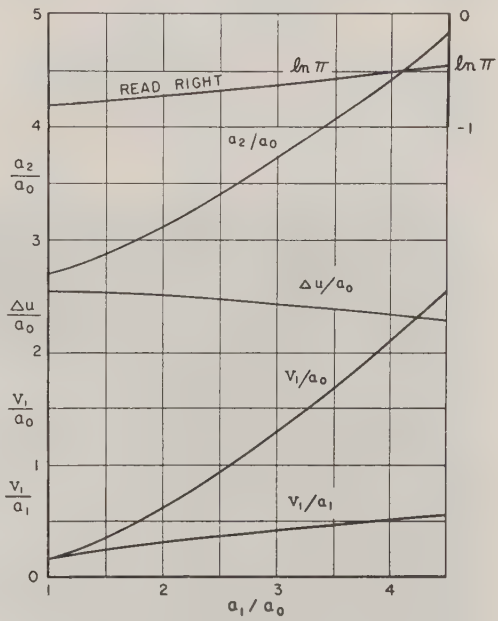

Figure 8. Parameters of the Chapman–Jouguet deflagration ($k_1 = 4/3$; $k_2 = 1{\cdot}3$; $Q = 25$)

graphically from the condition that the velocity of propagation of deflagration into the medium immediately ahead of state J must be equal to the velocity of the shock front relative to the medium behind it, i.e.

$$\frac{V_{K_1}}{a_1} = \frac{V_{S_2}}{a_2} \qquad (13)$$

The locus of the left-hand side is plotted in *Figure 7*, and of the right-hand side, in *Figure 3*. With the use of these curves, states J and N are found first on the α-u hodograph plane (*Figure 11*). This in effect yields the solution of the equation

$$\frac{\frac{2}{k_1 - 1} + 2Q + M_J^2}{\left[\frac{1}{k_1} + M_J^2\right]^2} M_J^2 + \frac{1}{\frac{1}{k_2^2} - 1} = 0 \qquad (14)$$

where $M_J = V_{J_1}/a_1$.

In a similar manner one can determine the corresponding states for detonations propagating into other regimes in the space-time domain. For this purpose the axis of abscissa of *Figure 3* is placed with respect to the α-u hodograph, *Figure 11*, so that it passes through a point representing the state into which the detonation propagates, with

the two axes of ordinates coincident, while the V_{J_1}/a_1 locus remains fixed on the α-u hodograph plane. The ordinate of the state representing the appropriate von Neumann peak is determined by the intersection of the V_2/a_2 locus of *Figure 3* with the locus of V_{J_1}/a_1 as before.

SOLUTION

The solution in the space-time domain is represented by *Figure 12*. The original flame trace is indicated there by a double broken curve. The straight, thick double lines fitted to the curve are the postulated approximations of the present analysis. Thus in effect the original world line of the flame front is represented by four straight-line segments. The shock fronts are denoted by straight continuous lines, the contact surfaces by double thin lines, and the edges of the rarefaction fans are indicated by the chain-dotted lines. The section of the diagram below 1·4 msec is drawn with thin lines since it is not based on experimental evidence—the observed world lines starting from approximately 1·4 msec. Such an extrapolation is needed, however, to set up the initial conditions for the analysis.

Numbering scheme

Each regime in the space-time domain is denoted by a number which indicates its thermodynamic state; the same number refers also to the wave process which created the state. The state behind a shock (as well as the shock itself) propagated into the reactant mixture is denoted by a single digit 1 to 9. The state behind a flame following a single-digit shock has number 1 in front of the shock symbol. Thus state 11 is behind the flame 11 following shock 1. Reflection from the closed end of the tube increases the first digit of the number denoting the wave by 1; 201 is the state behind the reflected shock propagating into 101, etc. Shocks resulting from the merging of two shocks are denoted by the numbers of both shocks with an intervening dot: shocks 2 and 1 merge to form shock and state 1·2, which of course propagates into the same state 0 as shock 1.

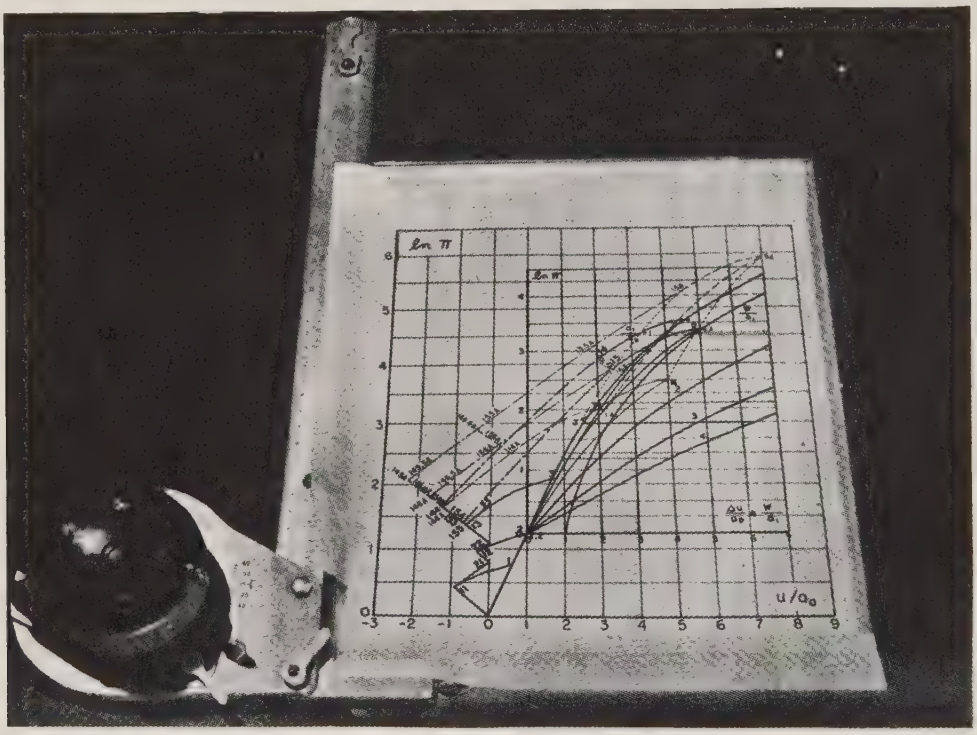

Figure 9. Illustration of the 'two-dimensional slide rule' procedure

Procedure

The solution is obtained by piecing together the hodograph process in the π-u plane using in effect a two-dimensional slide rule procedure. *Figure 10* was in fact obtained by practically utilizing this feature. In order to expedite the construction, a rectangle the size of the elementary polar diagrams, *Figures 2–7*, was cut out in a drafting board, a frosted glass placed in it and illumination provided from underneath. The procedure is demonstrated in *Figure 9*. The π-u hodograph was drawn on tracing paper taped to the cross rules of a drafting machine. The required locus of states at a given step was then obtained

by superimposing the tracing on the proper elementary polar diagram. *Figure 9* illustrates how state 3 of the solution, *Figure 10*, was obtained with the use of *Figure 2* by tracing from it shock polar 2–3 for $a_1/a_0 = 1{\cdot}174$.

The utility of the π-u plane is a direct consequence of the fact that each wave interaction is governed by the dynamic compatibility condition, that is, the condition that any new domain bounded by waves resulting from the interaction must contain particles which are all at the same pressure and move with the same velocity irrespective of their previous history (i.e. irrespectively through which boundary they get into the domain in question). Since such a condition does not apply to any other thermodynamic parameter, each interaction generates in principle a contact surface, that is a surface dividing two different

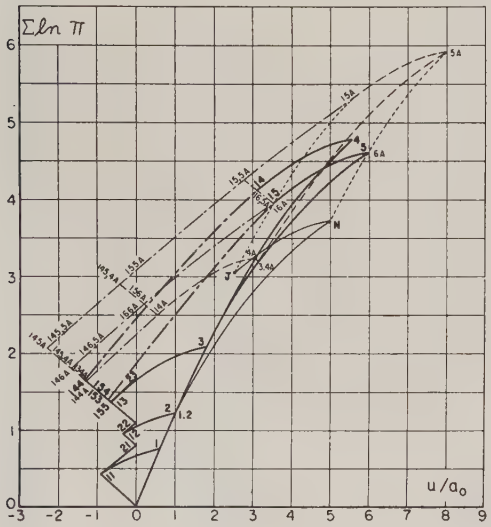

Figure 10. Hodograph of the process in the π-u plane

states within the same domain, which is, of course, parallel to the particle velocity. In other words, the salient feature of the π-u hodograph plane is the property that the domain resulting from any wave interaction is represented there, and only there, by a single point, in spite of the fact that it may represent two states separated by a contact surface. The solution is then constructed graphically on the π-u plane by determining for each wave interaction a point of intersection of the polars for the particular type of waves which bound the domain in question.

Simultaneously with the π-u hodograph, an α-u hodograph is constructed following a similar graphical procedure with the use, of course, of the α-u polars. Unlike the π-u plane, the states on the two sides of the contact surface are here represented by two points, having the same value of abscissa since they correspond to the same particle velocity. In fact, the solution for any given intersection in the α-u plane is obtained after the

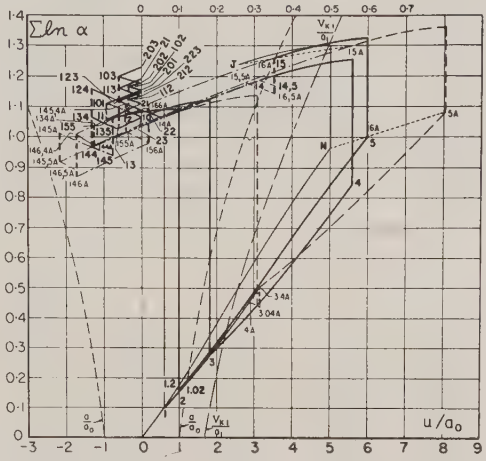

Figure 11. Hodograph of the process in the α-u plane

abscissa has been determined in the π-u plane. Note, for instance, in *Figure 11*, points 11 and 101, points 21 and 201, and points 102, 112, and 12, etc.

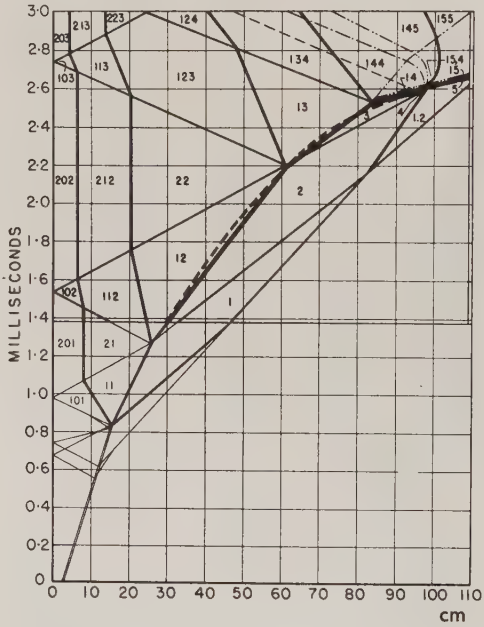

Figure 12. Solution in the space-time domain

Results

The results are represented by *Figures 10, 11* and *12*, and listed in Tables 2 and 3. They were obtained as follows.

State 1 immediately behind a shock of known velocity propagating into a known medium at a given state is fully determined as a point on the

shock polar corresponding to $a_1/a_0 = 1$, *Figure 10*. The polar representing the shock propagating into the products at their initial state, 10, attained by constant pressure combustion, is defined by their non-dimensional velocity of sound $a_1/a_0 = 2{\cdot}90$, and by their thermodynamic properties, which for the present purpose are summarized by the value of $k = 1{\cdot}3$. State 11 is then determined by the intersection of this polar with the deflagration polar corresponding to $a_1/a_0 = 1{\cdot}105$ originating from state 1. On the π-u plane point 11 represents also state 101. Shock 101 is reflected from the closed end to produce state 21, such that particle velocity is 0. This state is given therefore by the intersection with abscissa $u/a_0 = 0$ of an appropriate shock polar originating from state 11. With point 21 thus determined point 12 is found in the same manner as point 11, etc.

It was found that state 13 already represents a Chapman–Jouguet deflagration. Its propagation velocity is lower than that of shock 3. According to the Q-curve theory[12], this will always be the

TABLE 2

State Parameters

State	$\Sigma \ln \pi$	V_1/a_1	$\Sigma \ln \alpha$	a/a_0	u/a_0	V_1/a_0	W/a_0	u m/s	W m/s
0	0	0	0	1	0	0	0	0	0
10	0	0	1·065	2·90	0	0	0	0	0
1	0·756	1·410	0·095	1·100	0·601	1·410	1·410	195	457
11	0·416	0·172	1·055	2·88	− 0·919	0·190	0·791	− 298	256
101	0·416	− 1·22	1·115	3·048	− 0·919	− 3·54	− 3·54	− 298	− 1,148
21	0·790	1·190	1·099	3·010	0	3·740	2·82	0	914
201	0·790	1·190	1·159	3·185	0	3·740	2·82	0	914
2	1·220	1·232	0·1535	1·166	1·001	1·362	1·963	324	636
1·02	1·220	0	0·1535	1·166	1·001	0	1·001	324	
1·2	1·220	1·740	0·165	1·179	1·00	1·740	1·740	324	564
12	0·940	0·170	1·073	2·93	− 0·35	0·200	1·200	− 113	389
112	0·940	− 1·08	1·176	3·063	− 0·35	− 3·42	− 3·42	− 113	− 1,110
102	0·940	− 1·08	1·176	3·241	− 0·35	− 3·42	− 3·42	− 113	− 1,110
22	1·08	1·07	1·089	2·978	0	3·13	2·78	0	900
212	1·08	1·07	1·193	3·113	0	3·28	2·93	0	950
202	1·08	1·07	1·193	3·294	0	3·43	3·08	0	1,000
3	2·083	1·482	0·266	1·306	1·807	1·738	2·739	585	888
13	1·343	0·205	1·025	2·79	− 0·660	0·27	2·077	− 214	671
123	1·343	− 1·16	1·128	3·097	− 0·660	− 3·43	− 3·43	− 214	− 1,110
113	1·343	− 1·16	1·232	3·237	− 0·660	− 3·61	− 3·61	− 214	− 1,170
103	1·343	− 1·16	1·232	3·425	− 0·660	− 3·76	− 3·76	− 214	− 1,220
203	1·68	1·16	1·271	3·561	0	3·85	3·19	0	1,035
213	1·68	1·16	1·271	3·366	0	3·70	3·04	0	985
223	1·68	1·16	1·167	3·223	0	3·54	2·88	0	933
4	4·78	3·61	0·796	2·22	5·60	4·76	6·57	1,815	2,130
14	4·12	0·25	1·185	3·29	3·13	0·82	6·42	1,015	2,080
144	1·655	$\begin{cases} H1{\cdot}00 \\ T1{\cdot}00 \end{cases}$	0·966	2·63	− 1·31	$\begin{cases} H3{\cdot}29 \\ T2{\cdot}63 \end{cases}$	$\begin{cases} 6{\cdot}42 \\ 1{\cdot}32 \end{cases}$	− 425	$\begin{cases} 2{,}080 \\ 428 \end{cases}$
134	1·655	− 1·16	1·064	2·901	− 1·31	− 3·24	− 3·90	− 425	− 1,263
124	1·655	− 1·16	1·167	3·220	− 1·31	− 3·54	− 4·20	− 424	− 1,360
5	4·62	5·10	0·961	2·612	6·00	6·06	7·06	1,945	2,285
15	3·95	0·301	1·26	3·53	3·53	1·06	7·06	1,143	2,285
15,4	3·95	$\begin{cases} H - 1{\cdot}00 \\ T - 1{\cdot}00 \end{cases}$	1·17	3·22	3·53	$\begin{cases} H - 3{\cdot}29 \\ T - 3{\cdot}22 \end{cases}$	$\begin{cases} - 0{\cdot}16 \\ 0{\cdot}31 \end{cases}$	1,143	$\begin{cases} - 52 \\ 100 \end{cases}$
155	1·39	$\begin{cases} H \quad 1{\cdot}00 \\ T \quad 1{\cdot}00 \end{cases}$	1·065	2·90	− 0·73	$\begin{cases} H \quad 3{\cdot}53 \\ T \quad 2{\cdot}90 \end{cases}$	$\begin{cases} 7{\cdot}06 \\ 2{\cdot}17 \end{cases}$	− 236	$\begin{cases} 2{,}285 \\ 704 \end{cases}$
145	1·39	$\begin{cases} H - 1{\cdot}00 \\ T - 1{\cdot}00 \end{cases}$	0·936	2·55	− 0·73	$\begin{cases} H - 2{\cdot}63 \\ T - 2{\cdot}55 \end{cases}$	$\begin{cases} - 3{\cdot}94 \\ - 3{\cdot}28 \end{cases}$	− 236	$\begin{cases} - 1{,}277 \\ - 1{,}063 \end{cases}$
135	1·39	$\begin{cases} H - 1{\cdot}00 \\ T - 1{\cdot}00 \end{cases}$	1·033	2·81	− 0 73	$\begin{cases} H - 2{\cdot}90 \\ T - 2{\cdot}81 \end{cases}$	$\begin{cases} - 4{\cdot}21 \\ - 3{\cdot}54 \end{cases}$	− 236	$\begin{cases} - 1{,}363 \\ - 1{,}148 \end{cases}$

H refers to head of rarefaction fan or its leading edge. *T* refers to tail of rarefaction fan or its trailing edge.

case until the shock exceeds the strength corresponding to the Chapman–Jouguet detonation propagating into the undisturbed reactant mixture.

This can also be ascertained by following the graphical procedure described in the previous section, since, as a consequence of the geometric character of the two curves, V_{J_1}/a_1 (*Figure 7*), and V_2/a_2 (*Figure 3*), all the other detonation states are discrepancy is smaller than the accuracy with which the photographic record can be interpreted.

The problem which arises now is how shock 3 followed by deflagration 13 can eventually produce detonation 5–15.

Since, according to the experimental evidence, *Figure 1*, this happens long before the shock resulting from the reflection of shock 123 can reach

TABLE 3

State Parameters—Alternative Version

State	$\Sigma \ln \pi$	V_1/a_1	$\Sigma \ln \alpha$	a/a_0	u/a_0	V_1/a_0	W/a_0	u m/s	W m/s
4*A*	3·233	1·69	0·433	1·542	3·057	2·23	4·037	990	1,308
14*A*	2·478	0·242	1·065	2·90	0·517	0·37	3·43	167	1,110
144*A*	1·610	*H* 1·00 *T* 1·00	0·965	2·63	− 1·31	*H* 2·90 *T* 2·63	3·43 1·30	− 425	*H* 1,110 *T* 421
134*A*	1·610	− 1·13	1·065	2·878	− 1·31	− 3·15	− 3·81	− 425	− 1,235
3·4*A*	3·17	2·52	0·490	1·632	3·12	2·96	3·52	1,010	1,140
3·04*A*	3·17	*H* − 1·00 *T* − 1·00	0·401	1·497	3·12	*H* − 1·53 *T* − 1·50	1·53 1·62	1,010	496 525
5*A*	5·92	3·74	1·078	2·937	8·03	6·14	9·28	2,600	3,010
15*A*	5·30	0·420	1·30	3·67	5·56	1·25	9·28	1,800	3,010
15,5*A*	4·25	*H* 1·00 *T* 1·00	1·18	3·26	2·78	*H* 3·67 *T* 3·26	9·23 6·04	900	2,990 1,955
155*A*	2·89	*H* 1·00 *T* 1·00	1·02	2·77	− 0·42	*H* 3·26 *T* 2·77	6·04 2·35	− 136	1,955 760
145,4*A*	2·89	− 1·20	1·114	3·046	− 0·42	− 3·48	− 2·96	− 140	− 960
145,5*A*	2·07	*H* 1·00 *T* 1·00	0·914	2·50	− 2·28	*H* 2·77 *T* 2·50	2·35 0·22	− 700	760 71
145*A*	2·07	1·24	1·02	2·77	− 2·28	− 3·27	− 4·60	− 700	− 1,490
6*A*	4·62	5·10	0·964	2·618	6·00	6·06	7·06	1,945	2,285
16*A*	3·95	0·390	1·26	3·53	3·53	1·06	7·06	1,143	2,285
16,5*A*	3·95	*H* − 1·00 *T* − 1·00	1·143	3·14	3·55	*H* − 3·26 *T* − 3·14	0·48 0·41	1,150	156 133
166*A*	2·64	*H* 1·00 *T* 1·00	1·11	3·03	0·20	*H* 3·53 *T* 3·03	7·06 3·23	65	2,285 1,050
156*A*	2·64	*H* − 1·00 *T* − 1·00	0·975	2·66	0·20	*H* − 2·77 *T* − 2·66	− 3·19 − 2·46	65	− 1,035 − 797
146*A*	1·80	*H* 1·00 *T* 1·00	0·875	2·41	− 1·72	*H* 2·66 *T* 2·41	2·86 0·69	− 557	926 224
146,5*A*	1·80	*H* − 1·00 *T* − 1·00	0·847	2·43	− 1·72	*H* − 2·50 *T* − 2·43	− 4·78 − 4·15	− 557	− 1,550 − 1,345
146,4*A*	1·80	*H* − 1·00 *T* − 1·00	0·986	2·68	− 1·72	*H* − 2·75 *T* − 2·68	− 5·03 − 4·40	− 557	− 1,630 − 1,420

H refers to head of rarefaction fan or its leading edge. *T* refers to tail of rarefaction fan or its trailing edge.

above and to the right of states *J* and *N* on both the π-u and the α-u plane. The loci of these states are shown in *Figures 10* and *11* as small broken curves extending from points *J* and *N*.

According to the interpretation of Schmidt, *et al.*[1,2], a detonation was observed to move at a velocity of 2,150 m/s into state 1·2, that is the regime behind the shock resulting from the merging of shocks 1 and 2. The corresponding von Neumann spike and Chapman–Jouguet state are denoted by numbers 5 and 15, respectively. According to our analysis, this detonation propagates at a velocity of 2,285 m/s. The the deflagration, some other mechanism than that which produced states 12 and 13 must now be postulated. In the absence of other evidence we can only surmise that deflagration 13 accelerates for some similar reason to that which caused the original acceleration producing deflagration 11. In order to make the interpretation as simple as possible, it is furthermore postulated that the next deflagration should be such that a rarefaction fan propagating into the state produced by the deflagration would leave behind particles having pressure and velocity of state 15. This, in fact, involves the generation of a shock of minimum

strength which would make the transition from 3–13 to 5–15 dynamically compatible. This condition, then, determines states 4 and 14, and gives rise to states 134 behind a shock moving into state 13, and state 144 behind a rarefaction fan moving into state 14. On the π-u hodograph plane the latter two states are represented by a single point marked in *Figure 10* by number 144.

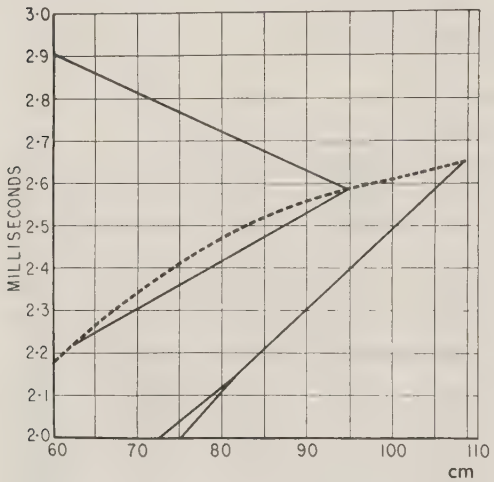

Figure 13. Wave-world lines for alternative solution

Shock 134 represents the well-known retonation wave which is brought about, as the present analysis demonstrates quite clearly, by the dynamic compatibility condition. As a result of our postulate that a shock of minimum strength should do the trick, the world line of retonation shock 134 has a velocity of 1,263 m/s instead of the observed velocity of 1,050 m/s. In order to have the detonation set up at the same point as that indicated by Schmidt, *et al.*, the point where retonation shock 134, deflagration 14, and shock 4 originate is determined so that shock 4 passes through the point of intersection of shock 3 and the contact surface bounding regime 1·2. At this point conditions beyond those of the corresponding Chapman–Jouguet state are obtained (*Figure 4*, reference 11), and the deflagration catches up with the resulting shock. It is then that the dynamic boundary conditions permit the reaction zone of the deflagration to penetrate into the collision zone of the shock. As a result the deflagration becomes weak and is overtaken by the rarefaction fan which follows it, until state 15 is established. The weakening of deflagration 14 gives rise to a rarefaction fan moving to the left, which leaves behind state 15,4 at the same pressure and particle velocity as state 15, and in fact, represented by point 15 on the π-u hodograph, *Figure 10*.

So ends the story according to the simplest interpretation of the observations of Schmidt, *et al.* If the tube were longer, then state J would eventually be established after detonation 5–15 catches up with the shock 1·2. The detailed mechanism of transition from 15 to J, although in principle the same, is somewhat different than that from 14 to 15. It is, however, identical to the transition from 15A to 16A, the states obtained as a result of an alternative solution which is described in the next section.

ALTERNATIVE SOLUTION

The largest discrepancy between the result of the first solution and the original interpretation of Schmidt, *et al.*, is in the position and slope of the retonation wave. From the analysis its velocity appears to be 1,263 m/s while Schmidt, *et al.*, report 1,050 m/s. In an effort to improve the agreement, an alternative solution has been worked out. It is obtained principally by approximating the world line of the flame behind shock 3 with one step more than the first solution.

Up to shock 3 the two solutions are identical. *Figure 13* shows the segment of the space-time domain, from 2 msec onwards and beyond the first 60 cm of the reactor tube, which forms the subject for the alternative solution. *Figure 14*

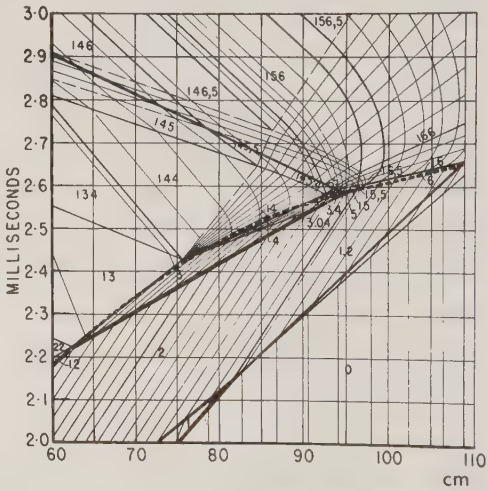

Figure 14. Alternative solution superimposed on the original wave-world lines

shows the alternative solution superimposed on the original world lines. As appears there, the retonation wave this time is much closer to the one observed by Schmidt, *et al.* The step associated with the generation of the retonation wave was in fact determined by requiring it to start with the same velocity as that of the original interpretation. It is later, however, deflected by interaction with rarefaction fan following deflagration 14.

Figure 15 represents the alternative solution in the space-time domain. The corresponding solution in the π-u and α-u hodograph planes is indicated by thin lines with state points denoted by numbers followed by letter *A*.

Since 13 is already a Chapman–Jouguet deflagration, state 14*A* is also a Chapman–Jouguet deflagration, and, as a result of the requirement of dynamic compatibility with state 13, it is followed by a rarefaction fan producing state 144 (determined as the point of intersection of the polar in the π-u plane, *Figure 10*, with shock polar plotted from state 13). This determines also state 134 as indicated in the α-u hodograph, *Figure 11*.

For the next step, in contrast to the previous solution based on the introduction of the weakest shock immediately prior to the establishment of detonation, the onset of the strongest possible shock is now postulated. This is a detonation propagating in this case into state 3·4, which is produced by the shock resulting from merging of shocks 4 and 3. The π-u hodograph, *Figure 10*, demonstrates the consequence of the postulate, that is, how accordingly states 5*A*, 15*A*, 145*A*, and 145,5*A* are determined.

All the states of the alternative solution described so far were obtained as a result of a number of trials, this being in effect a graphical trial and error solution satisfying the condition that shock 145*A* propagating into state 144*A* has a world line with a slope of — 1,050 m/s. The world lines of deflagration are then fitted in the space-time domain for best agreement with the observed flame trace, as illustrated in *Figure 14*.

The only problem remaining now is the transition from state 15*A* to 16*A*, the latter being identical with state 15 of the previous solution. State 6*A*, identical with state 5 of the previous solution, is obtained as representing the von Neumann spike of detonation propagating into state 1·2. As before, when the wave train 5*A*–15*A* crosses the contact surface bounding domain 1·2, the reaction zone of deflagration tends to penetrate into the collision zone of the shock. At the same time, the Chapman–Jouguet deflagration 15*A* becomes a weak deflagration, permitting the rarefaction fan to penetrate into it from behind. The process of the weakening of the shock-deflagration ensemble continues until the ray of the deflagration fan carrying state 15,5*A* is reached. At this point, the rarefaction fan moving to the left produces from it state 16,5*A* which, as shown in *Figure 10*, has pressure and particle velocity identical with those of state 16*A*. The remaining states shown in *Figures 10*, *11* and *15* are then determined in the routine manner, as resulting from the interaction of rarefaction fans and the retonation shock behind the detonation.

CONCLUSIONS

The solution provides a complete description of the thermodynamic and dynamic aspects of the transition from deflagration to detonation derived from experimentally observed wave-world lines.

Consider at first information provided by the particle paths shown as thin lines in *Figure 15*. They were spaced initially at equal intervals in the undisturbed regime *O*, and, consequently, they provide an illustration of stream-tubes corresponding to equal masses of the substance in the space-time domain. Thus, *Figure 15* illustrates dramatically the results of the shock action in pushing forward the reactants in front of the accelerating flame front. It is of interest to note

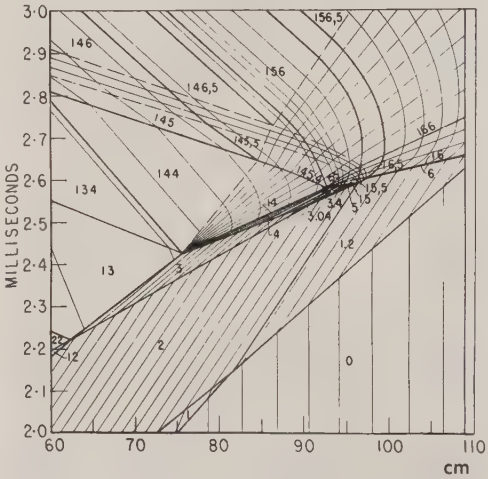

Figure 15. Alternative solution in the space-time domain

how little mass actually passes through the deflagration front. The bulk of the reactants pass through detonations 5*A*–15*A* and 6*A*–16*A*. In fact, the particle paths become there so close to each other that only every third one was plotted.

Most significant is the information obtained on the thermodynamic states of the medium into which the combustion front propagates, the changes of state brought about by its action, and the velocities of the front with respect to the reactant mixture immediately in front. Thus a transition can now be made from the Eulerian system of observation to the Lagrangian system of the process.

As a result, *Figure 16* is obtained, describing the relationship between the reaction rate expressed in g mols of propane per cm^2 of front area per sec as a function of pressure and the adiabatic temperature attained by the reaction. In order to permit deduction on the overall kinetic character of the process, the coordinates of *Figure 16* are: logarithm of the rate, reciprocal of the temperature, and logarithm of the pressure.

Diamonds refer to Chapman-Jouguet deflagrations, and triangles to weak deflagrations. Small inverted triangles correspond to numbers in circles, denoting states into which wave trains propagate, each consisting of a shock followed by a Chapman–Jouguet deflagration. Starting from these are the corresponding loci of states attained

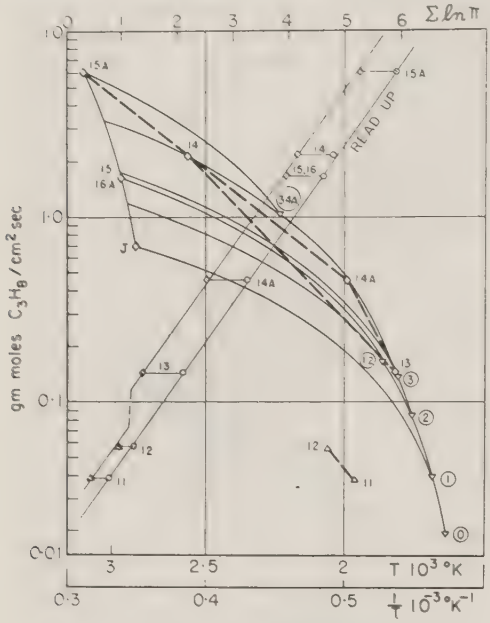

Figure 16. Process parameters

immediately behind such wave trains. They are terminated by the loci of states behind detonations.

Pressure dependence

As far as pressure dependence is concerned, it appears surprisingly simple, the rate being directly proportional to the pressure of the reactant mixture. This seems to indicate a net reaction of first order. Since the current objective is only to illustrate the kind of results obtainable from the analysis, dwelling too much on such a conclusion does not seem justified at this stage, and we prefer to leave this point without further comment.

Temperature dependence

By postulating that one state is transformed into the subsequent one with the same kinetics, the plot of *Figure 16* can be used to determine the average thickness of the reaction zone and the energy of activation for the overall Arrhenius type rate equation. The subsequent states are connected in *Figure 16* by broken lines, and the results are summarized in Table 4. The ratio of the ordinate of *Figure 16* and the steric factor for the reaction is the thickness of the reaction zone.

For any given transition from one state to the subsequent one, it can be either postulated that: (*a*) the slope of the straight line connecting the two points determines the energy of activation, while the intersect with the axis of ordinates divided by the appropriate steric factor determines the corresponding average thickness of the reaction zone, or that (*b*) the transition is associated with a change in the thickness of the reaction zone, while the slope of the straight line connecting the two points bears no relation with the energy of activation.

There seems little doubt, for instance, that the transition from 15*A* to 16*A* or from 14 to 15 is associated with the reaction zone becoming thinner, while the transition from 12 (which is a weak deflagration) to 13 (which is already the Chapman–Jouguet deflagration) is associated with the reaction zone becoming thicker.

Activation energy

A significant result of the analysis is the order of magnitude of the evaluated activation energies. They range from 30 to 66 kcal per mol C_3H_8, in good agreement with values reported in the literature. Fenn and Calcote[14] showed that such activation energies can be calculated from theoretical

TABLE 4
Kinetic Parameters

Transition				$A\delta$	E
From		*To*			
State	*Rate* g mol C_3H_8 / cm² sec	*State*	*Rate* g mol C_3H_8 / cm² sec	g mol C_3H_8 / cm² sec	kcal / g mol C_3H_8
11	0·0383	12	0·0564	$9{\cdot}7 \times 10^2$	39·7
13	0·144	14*A*	0·449	$2{\cdot}4 \times 10^3$	66·3
13	0·144	14	2·14	$8{\cdot}0 \times 10^6$	36·2
14	2·14	15*A*	6·20	$9{\cdot}2 \times 10^2$	30·5
14*A*	0·45	15*A*	6·20	$9{\cdot}2 \times 10^2$	30·5

Tanford–Pease and Zeldovich–Frank-Kamenetskii–Semenov equations, while Penner and Crowe[15] obtained the value of 53 kcal for activation energy for stoichiometric propane–oxygen flame by using the von Kàrmàn eigenvalue thermal theory of laminar flame propagation to rationalize the experimental data of Dugger and Graab (NACA RME 52J24, 1953). Similar values were also obtained from extrapolation[16] of experimental data on propane oxidation obtained by Newitt and Schmidt[17], and by Pease[18].

It appears, therefore, that the development of detonation does not involve anomalous chemical kinetics, and that the process is controlled principally by gas-dynamic wave-phenomena.

Closure

The analysis demonstrates how information on reaction kinetics can be obtained from the dynamic analysis of the observed world lines of waves in the space-time domain. The present solution is offered only as an illustration of the method of analysis and the type of information obtainable. In the case at hand, it seems indeed surprising that so much information was obtained in spite of the far-reaching idealizations on which the analysis was based. It should be noted, however, that for any given case a good deal of simplifying assumptions could be eliminated by a more realistic description of the thermodynamic properties of the substance.

The authors wish to express their thanks to the student members of the Detonation Research team, and especially to Arnold J. Laderman, M.S., and Captain Harold V. Wright, USAF, M.S., for the help they received in the preparation of this publication.

This research was supported by the United States Air Force through the Air Force office of Scientific Research of the Air Research and Development Command, under Contract No. AF49(638)–166. Reproduction in whole or in part is permitted for any purpose of the United States Government.

NOMENCLATURE

a	local velocity of sound defined as $\{(k-1)h\}^{\frac{1}{2}}$
A	steric factor
E	energy of activation
h	specific enthalpy
J	the Chapman–Jouguet detonation
k	average specific heat ratio assumed equal to isentropic exponent
K	the Chapman–Jouguet deflagration
m	molar mass
M	Mach number
N	the von Neumann spike
p	pressure
q	heat of reaction
Q	q/a_0^2 = non-dimensional heat of reaction
R	perfect gas constant
s	specific entropy
T	temperature
u	particle velocity
V	absolute magnitude of relative velocity between particle and wave front
W	$V_1 + u_1$ wave velocity
α	a_2/a_1
δ	average thickness of the reaction zone
π	p_2/p_1

Subscripts

0	denotes the reference state
1	denotes the state immediately before a wave process
2	denotes the state immediately behind a wave process
J	denotes the Chapman–Jouguet detonation
K	denotes the Chapman–Jouguet deflagration
S	denotes shock

REFERENCES

[1] Schmidt, E., Steinicke, H. and Neubert, U. Flame and schlieren photographs of combustion waves in tubes, *Fourth Symposium (International) on Combustion*, pp. 658–666. 1953. Baltimore; Williams and Wilkins

[2] — — — Flame and schlieren photographs of the combustion of gas–air mixtures in tubes, *VDI-Forschungsheft* 431, Ed. B., Vol. 17, p. 31. 1951. Düsseldorf; Deutscher Ingenieur-Verlag

[3] Sauer, R. Charakteristikenverfahren für die Eindimensionale Instationare Gasstromung. *Ingenieur Archiv.* 13 (1942) 79

[4] Schultz-Grunow, F. Nicht-Stationare Eindimensionale Gasbewegung. *Forschungen auf dem Gebiete des Ingenieurs-Wesens* 13 (1942) 125

[5] Haller, P. de. Ueber eine Graphische Methode in der Gasdynamik. *Technisches Rundschau Sulzer* No. 1 (1945) 6–24

[6] Jenny, E. *Berechnungen und Modellversuche über Druckwellen Grosser Amplituden in Auspuffleitungen.* 1949. Basle; E.T.H. Promotionsarbeit, Ameba-Druck; *Brown-Boveri Review* 37, 11 (1950) 447

[7] Courant, R. and Friedrichs, K. O. *Supersonic Flows and Shock Waves*, p. 464. 1948. New York; Interscience

[8] Shapiro, A. H. *The Dynamics and Thermodynamics of Compressible Fluid Flow.* 1954. New York; Ronald Press (especially Part VII, Vol. 2)

[9] Oswatitsch, K. *Gas Dynamics*, 1st ed., 1956. New York; Academic Press (especially pp. 85–176)

[10] Rudinger, G. *Wave Diagrams for Nonsteady Flow in Ducts.* 1955. Toronto, New York, London; van Nostrand

[11] Schultz-Grunow, F. Zur Behandlung Nichtstationarer Verdichtungsstosse und Detonationswellen, *Zeitschrift für Angewandte Mathematik und Mechanik*, 24, Nos. 5–6 (1944) 284

[12] Hirschfelder, J. O., Curtiss, C. F. and Bird, R. B. *Molecular Theory of Gases and Liquids.* 1954. New York; Wiley: London; Chapman & Hall (especially pp. 807–815)

[13] Oppenheim, A. K. Gasdynamic analysis of the development of gaseous detonation and its hydraulic analogy, *Fourth Symposium (International) on Combustion*, pp. 471–480. 1953. Baltimore; Williams and Wilkins

[14] Fenn, J. B. and Calcote, H. F. Activation energies in high-temperature combustion, *Fourth Symposium (International) on Combustion*, pp. 231–239. 1953. Baltimore; Williams and Wilkins

[15] Penner, S. S. and Crowe, T. H. Correlation of laminar flame velocities for hydrocarbon–oxygen–inert gas mixtures. *Proc. Gas Dynamics Symposium on Aerothermochemistry*, pp. 113–131. 1955. Evanston, Illinois; Northwestern University

[16] Jost, W. *Explosion and Combustion Processes in Gases* (Translation by H. O. Croft), pp. 436–437. 1946. New York; McGraw-Hill

[17] Newitt, D. M. and Schmidt, W. G. The oxidation of propane, Part II, The products of the slow oxidation at high pressures. *J. chem. Soc.* 2 (1937) 1665. Part III. The kinetics of the oxidation, *J. chem. Soc.* 2 (1937) 1669

[18] Pease, R. N. The negative temperature coefficient in the rate of propane oxidation. *J. Amer. chem. Soc.* 60 (1938) 2244

[19] Weir, A. Jr. and Morrison, R. B. Equilibrium temperatures and compositions behind a detonation wave. *Industr. Engng. Chem. (Industr.)* 46 (1954) 1056

[20] Rossini, F. D., *et al. Selected Values of Physical and Thermodynamic Properties of Hydrocarbons and Related Compounds, American Petroleum Institute Research Project* 44. 1953. Pittsburgh; Carnegie Press

111

FORMATION OF DETONATION WAVE DURING COMBUSTION OF GAS IN COMBUSTION TUBE

G. D. SALAMANDRA, T. V. BAZHENOVA and I. M. NABOKO

INTRODUCTION

From the moment of its discovery the phenomenon of detonation has been an object of extensive research.

Though a great amount of theoretical and experimental work has been done in connection with the problem of flame propagation during detonation, no clear knowledge has been obtained either of the reasons causing progressive acceleration of the flame which results in transition from slow combustion to detonation or on the nature of this transition itself.

Since transition from laminar combustion to detonation is connected with a basic reshaping of the gas flow and of the reaction transfer, a detailed examination of all stages of pre-detonation combustion with due regard for hydrodynamic and chemical factors affecting this process will be of definite interest. It should be determined, among other things, what role is played in the detonation by the shock waves which appear before the flame front. Depending on its intensity, the shock wave appearing before the flame front may cause additional ignition of the gas in the place where it appeared, far from the flame front, or start a flow of hot unburned gas before the flame front, and steady acceleration of the flame, which eventually leads to the appearance of the detonation wave.

It should be noted that in most investigations devoted to the problem of transition from slow combustion to detonation the process was photographed by the direct method, i.e. photographs were taken of the mixture glow. However, direct photographs may give only a limited knowledge of the processes involved in formation of a detonation wave, since an important part is played in these processes by shock waves which appear before the flame front and which possess no self-glow. To examine the variation of the flame front during transition from slow combustion to detonation in every minute detail the moving image photographs of the process should be supplemented with flash schlieren photographs of various phases of the process. To obtain distinct photographs high-speed processes should be photographed with very small exposures. One of the methods to obtain small exposures is to use impulse light sources. A simple and compact design of a high-frequency flash discharge tube is suggested in this paper.

IMPULSE LIGHT SOURCE GIVING REPEATED FLASHES

Described below is the design of collapsible flash discharge tubes employing ceramic capacitors made of calcium titanate, which we used in photographing the process of gas combustion. Such tubes make it possible to take photographs at a rate of 100,000–150,000 shots per second with exposures not exceeding 5×10^{-7} sec. Tubes are intended for schlieren photography; the tube eyes have been designed as 'linear' and 'point' light sources.

The general view of the 'linear' light source is given in *Figure 1*. The discharge takes place between tungsten electrode 9 and brass plate 10, placed between two porcelain cheeks 11, which limit the spark gap. Contact ring 14 connects the tungsten electrode with the outer plate of capacitor 4. The brass plate is connected with the inner plate of the capacitor by springs 5 attached to Plexiglass plug 6. On the rear wall of tube jacket 3 is mounted cock 1 for pumping the air out of the tube and filling the tube with hydrogen in which the discharge takes place. A removable front wall 8 is held to the tube jacket by bolts 7. Packing is ensured by rubber gasket 13. High voltage fed to the tube is applied to terminals 2 and 12.

Figure 2 shows the supply circuit of the impulse light source.

EXPLOSION CHAMBERS AND EXPERIMENTAL PROCEDURE

Transition from slow combustion to detonation was investigated in closed round-section chambers having a diameter of 42 mm and square-section chamber sized 36·5 mm × 36·5 mm.

The chambers consisted of four blocks having the same cross-section area. One of the blocks was provided with glass windows for photographing the process. The length of the visible part of the chamber was 200 mm. By shifting the block with the glass windows the process could be photographed in any part of the chamber. The end

faces of the chamber were closed by caps; on one of the caps was mounted a spark plug, and the other cap carried a valve used for pumping out the air and filling the chamber with mixture. Hydrogen–oxygen mixtures were used as combustible mixtures, first, because the combustion of such mixtures proceeds at such a high rate that the shock wave and the detonation wave are formed at a relatively small distance from the beginning of the combustion chamber, and secondly, areas, are indicated by dark blotches against light background.

The photograph shows that during initial moments after the mixture was ignited, the front flame spreads at an accelerated rate. A series of disturbances which move in front of the flame run up to each other and are aggregated into a shock wave. The shock wave, thus formed, moves at a velocity of 700 m/sec but it gradually slows down as it spreads in the chamber.

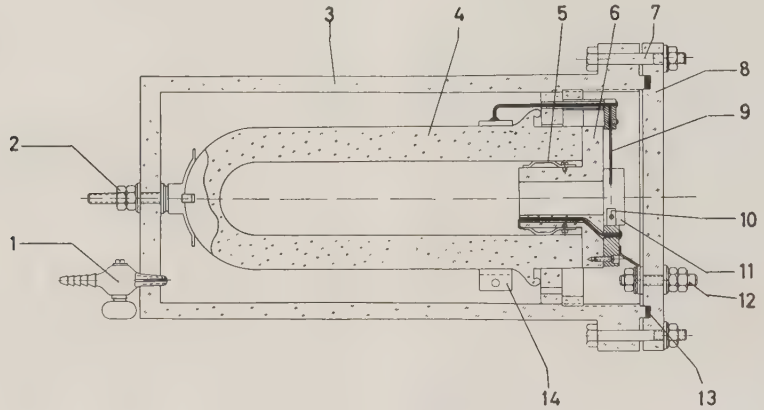

Figure 1. Diagram of 'linear' light source

because hydrogen–oxygen combustion produces light of low actinic value, which facilitates taking high-quality photographs by the schlieren method.

The process was photographed by the schlieren method on film placed on the inside of an evenly rotating drum.

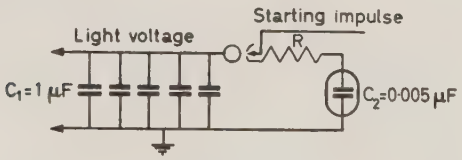

Figure 2. Key diagram showing supply circuit of impulse light source

EXAMINATION OF EXPERIMENTAL RESULTS

Figure 3 is a photograph showing the process of combustion of a stoichiometric hydrogen–oxygen mixture in a two-metre round-section chamber; the photograph was obtained by the moving image method. The flame spreads horizontally from left to right while the film moves upwards.

The scale marks are shown in the photographs in the form of two black lines running parallel to the time axis. The process was photographed with a 'double knife', therefore, all optic non-uniformities, both rarefaction and compression

The first stage of the flame propagation, which is characterized by an accelerated rate of the flame movement, is followed by a slowing down of the flame and then by further acceleration, accompanied by the appearance of new optical non-uniformities after the flame front. Clearly visible before the flame front is a series of disturbances which causes a number of shock waves to form at a relatively small distance from the flame front.

Interaction of the flame with the shock waves forming before that of the flame front during the pre-detonation period of its propagation results in transition from slow combustion to detonation.

It should be noted that contrary to general opinion formation of a shock wave before the flame front does not immediately bring about transition from slow combustion to detonation. The detonation wave is formed at a much later stage; its appearance is due to interaction of the flame with the shock waves which are formed before the flame front during the pre-detonation period of the flame propagation.

After these general remarks on the nature of the process as a whole we will pass to a more detailed examination of each stage of the process.

Initial stage of flame propagation

The qualitative explanation of the flame behaviour during the initial stage of its propagation immediately after the mixture is ignited

near the closed end of the chamber, is as follows. During slow combustion, a small pressure drop in the reaction zone is accompanied by a considerable increase in the specific volume of the combustion products as compared with the specific

Figure 3. Moving image photographs showing combustion of stoichiometric mixture of hydrogen with oxygen in round-section chamber

volume of the combustible mixture prior to combustion. The expansion of the combustion products results in the appearance of a fresh gas flow before the flame front. The problem of gas movement before the flame front during this period may be roughly represented as the problem of gas movement in front of the piston moving inside the tube according to the law which governs actual propagation of the flame. A series of moving image photographs (*Figure 4*) of the combustion process shows that during this period the shape of the flame front practically does not change. A slight expansion of the front boundary can be seen in the photographs; this is due to the increased surface of the flame front owing to the appearance of cells which become clearly visible if the sensitivity of the schlieren apparatus is increased (see *Figure 5*).

Figure 4. Initial stage of flame propagation during combustion of mixture in square-section chamber

Slowing-down stage

As the flame propagates and the volume of the burned mixture expands, the expansion ratio of the reaction products decreases and the flame propagates at a lower rate.

Finally, there comes a moment when the pressure after the front becomes lower than the pressure before the front. This causes the formation of a new flow in the direction opposite to that

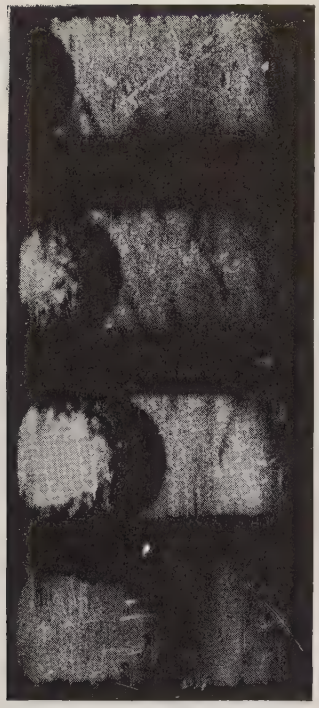

Figure 5. Cell structure of flame front

Figure 6. Flame front during slowing-down stage

Figure 7. Propagation of flame in medium 'prepared' by shock waves

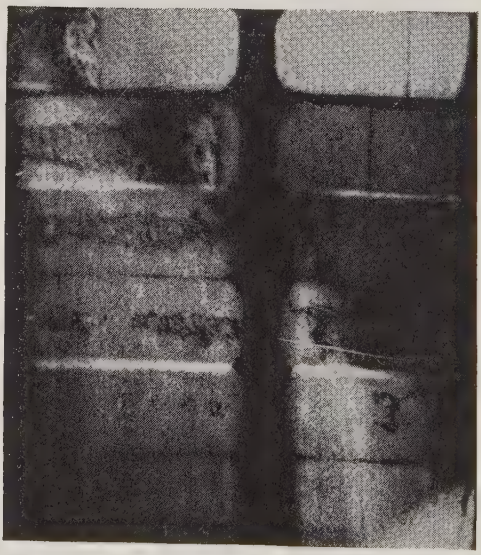

Figure 8. Flame propagation in pre-detonation period

of the flame propagation. Flash photographs of the combustion process at this stage support this theory.

The meniscus-shaped flame front becomes tulip-shaped (see *Figure 6* which shows the flame front during slowing-down stage). Total surface of flame front increases, and flame velocity rises.

New acceleration of flame propagation

An increase in the flame surface is shown by splitting of the flame image on a photosensitive film. At this stage the flame assumes a characteristic shape, which is asymmetrical relative to the tube axis (see *Figure 7*).

The upper part of the flame front is bent forward in the direction of the flame propagation. Such bending of the flame may be explained as follows. At each given moment the combustion zone separates fresh mixture having greater density from the lighter products of combustion. The heavier fresh mixture strives to spread in the lower part of the chamber while the lighter combustion products strive to rise to its upper part. The convection currents due to the force of gravity accelerate propagation of the flame in the upper part of the chamber and slow it down in the lower part.

At this stage a great number of disturbances appear before the accelerating flame front and form shock waves immediately before the flame front. The flame travels in the mixture 'disturbed' by the shock waves. The velocity of the shock waves characterizes their intensity and the condition of the gas in front of the flame. Our calculations show that shock waves formed at later stages and travelling with greater velocities cause gas flows with ever-increasing velocities to appear before the flame front.

Thus, the shock wave which has the velocity of 720 m/sec is followed by the gas flow which has a velocity of about 270 m/sec; the velocity of the gas flow following the third wave is already as high as 300 m/sec and the flow following the fourth wave has a velocity of 560 m/sec. As more and more shock waves are formed before the flame front, not only the velocity of the gas flow in which the flame travels but also the temperature of the gas before the flame front increases. If the temperature of unburnt gas following the first shock wave was 95°C, it was as high as 110°C after the third wave and 180°C after the fourth wave.

From the above analysis of the process it follows that this stage of the process is characterized not only by accelerated rate of the flame propagation but also by accelerated movement of the flame relative to the fresh gas. This is apparently due to the heating of the mixture by the shock waves.

At moments preceding the detonation, a gas flow having a temperature close to the temperature of its ignition is formed before the flame front.

Propagation of flame during pre-detonation period

Figure 8 shows the combustion of the stoichiometric hydrogen–oxygen mixture during the stage immediately preceding transition from slow combustion to detonation.

During this stage of the combustion process the effect on the flame front of the shock waves forming before it is especially pronounced.

The shock wave and the flame front become, as it were, a single complex travelling at the same speed. This complex, however, is not of a stable nature: the shape of the flame front shows slight variation from photograph to photograph.

The flame front is followed by a long comet-like tail; it is possible that the tail is where after-combustion takes place; the accelerated rate at which the flame propagates with the surface of the flame front diminishing may be attributed to forced combustion due to pre-heating of the mixture by shock waves.

CONCLUSIONS

A detonation wave is formed in a long tube as a result of interaction between the flame front and a series of shock waves appearing before the flame front during the pre-detonation period.

In the course of the pre-detonation period the flame front shape undergoes the following changes.

At the beginning of the flame propagation immediately after the ignition, the flame front near the closed end of the chamber has a meniscus-like shape which hardly changes throughout the initial stage of the flame propagation.

During the slowing-down stage the flame front assumes a characteristic tulip-like shape which indicates the presence of a gas flow directed opposite to the flame front.

During the stage following the slowing-down, flame propagation is characterized by considerable increase in the flame surface which results in accelerated propagation of the flame.

A series of shock waves appearing before the flame front causes formation of an ever-accelerating gas flow before the flame front and heats the fresh gas.

During the stage immediately preceding transition from slow combustion to detonation the surface of the flame front diminishes. The flame front is followed by a long comet-like tail where after-combustion takes place.

At this stage of the flame propagation the shock waves appearing before the flame front produce an especially strong influence on the flame front. The shock wave and the flame front form a single complex travelling at the same speed.

This research has been carried out under the guidance of Professor A. S. Predvoditelev in the Combustion Physics Laboratory, Institute of Energetics, the U.S.S.R. Academy of Sciences.

112

THE FORMATION AND STRUCTURE OF GASEOUS DETONATION WAVES

F. J. MARTIN and D. R. WHITE

INTRODUCTION

The work to be described in this paper has been carried out in two quite different pieces of apparatus, using different techniques and different gases. To avoid confusion under these circumstances, it appears best to present the paper in two parts. The first deals primarily with streak camera observations of the mechanics of the formation of detonation waves in acetylene–oxygen mixtures in smooth walled tubes. The second deals primarily with interferometric observations of the structure of detonation waves in hydrogen–oxygen and the flow field just prior to formation of detonation in hydrogen–air.

THE FORMATION OF GASEOUS DETONATION

According to the generally accepted model for a steady detonation wave in an explosive gas mixture, the reactant mixture is compressed and heated by a shock wave to a condition such that rapid chemical reaction (auto-ignition) occurs with a very short induction period. The minimum velocity at which a steady plane detonation wave will propagate is around 1,200–1,500 m/sec for most mixtures, i.e. the minimum shock Mach number is in the range 3 or 4. The question of interest at present is 'How does such a strong shock required for propagation of the detonation develop from an ordinary flame which propagates with a velocity of only 1 to 10 m/sec relative to the gases immediately ahead of it?'

This question has been considered by many investigators[1–6] and there is general agreement about the overall nature of the process. Consider an explosive gas mixture contained in a tube closed at both ends and long compared to the distance of flame travel prior to formation of the detonation wave. Let the mixture be ignited by a weak spark. A flame will start to propagate down the tube. The hot products, having a specific volume of the order of 5–15 times that of the unburned mixture, act as a hot-gas piston and through generation of compression waves impart a velocity down the tube to the unburned gases ahead of the flame. These compression waves travelling into the unburned mixture[7,8] will, under suitable conditions, produce a shock wave travelling ahead of the flame. However, with weak initiation this shock is not ordinarily strong enough to produce a detonation immediately. Further flame acceleration must occur to strengthen the shock (or shocks) if detonation is to develop.

There have been at least two mechanisms proposed for the further flame acceleration. Zeldovich[3] has proposed that due to friction at the walls the unburned gas close to the walls is slowed down with consequent increase in velocity at the centre. The flame propagating into this non-uniform velocity distribution experiences an increase in flame area. Hence further acceleration of the hot-gas piston occurs; and, in turn, the non-uniform velocity distribution becomes more pronounced. The flame acceleration arising in this manner from increasing flame area may finally produce pressure waves strong enough to induce detonation.

The second proposed mechanism[5] attributes the flame acceleration to the development of turbulence in the moving unburned mixture ahead of the flame.

In the present investigation flame velocities and configurations have been observed photographically in the pre-detonation region to further elucidate the mechanism of flame acceleration.

Experimental

Gases were taken directly from commercial cylinders, metered through calibrated sonic-flow orifices, and mixed in a flowing system. The mixture was allowed to flow into the evacuated detonation tube to the desired pressure. Most of the work has been done with 50/50 acetylene–oxygen mixtures at 50 mm of mercury.

The detonation tube was a 2·4 m length of 5 cm i.d. Pyrex pipe, closed at the downstream end with either a Cellophane diaphragm or a 2·4 m length of stainless steel pipe, 5 cm i.d. Observation slits (2 mm), either paraxial or transverse, were formed on the tube with black masking tape. Direct and schlieren photography with a rotating mirror camera were employed. Stereo pictures

by direct photography were also taken when the transverse slit was used.

The mixture was ignited by discharging a 20 μF capacitor charged to 190 volts through a 2D21 thyratron into the primary of a pulse transformer. The secondary was connected to the spark electrode in the end-plate of the detonation tube.

The experimental equipment and techniques are described in a paper to be published shortly.

Results and discussion

For equimolar C_2H_2/O_2 mixtures at 50 mm pressure the flame starts out as a smooth dome and accelerates smoothly to a velocity of about 800 m/sec within a distance of 30 cm or so (*Figure 1a*). When the flame has travelled about 10 cm, a shock about 2 or 3 cm ahead of the flame becomes visible in the schlieren pictures (*Figure 1b*). The flame, preceded by the shock, proceeds at a nearly constant velocity of 800 m/sec for another 50 or 60 cm (*Figure 1a*). The shock travels slightly faster than the flame in this region so that the distance between the two gradually increases (*Figure 1c*). In this region the flame remains a centre-leading dome although bumps do appear in it (*Figure 2b and c*). These are not believed to play an important part in the formation of detonation under our conditions.

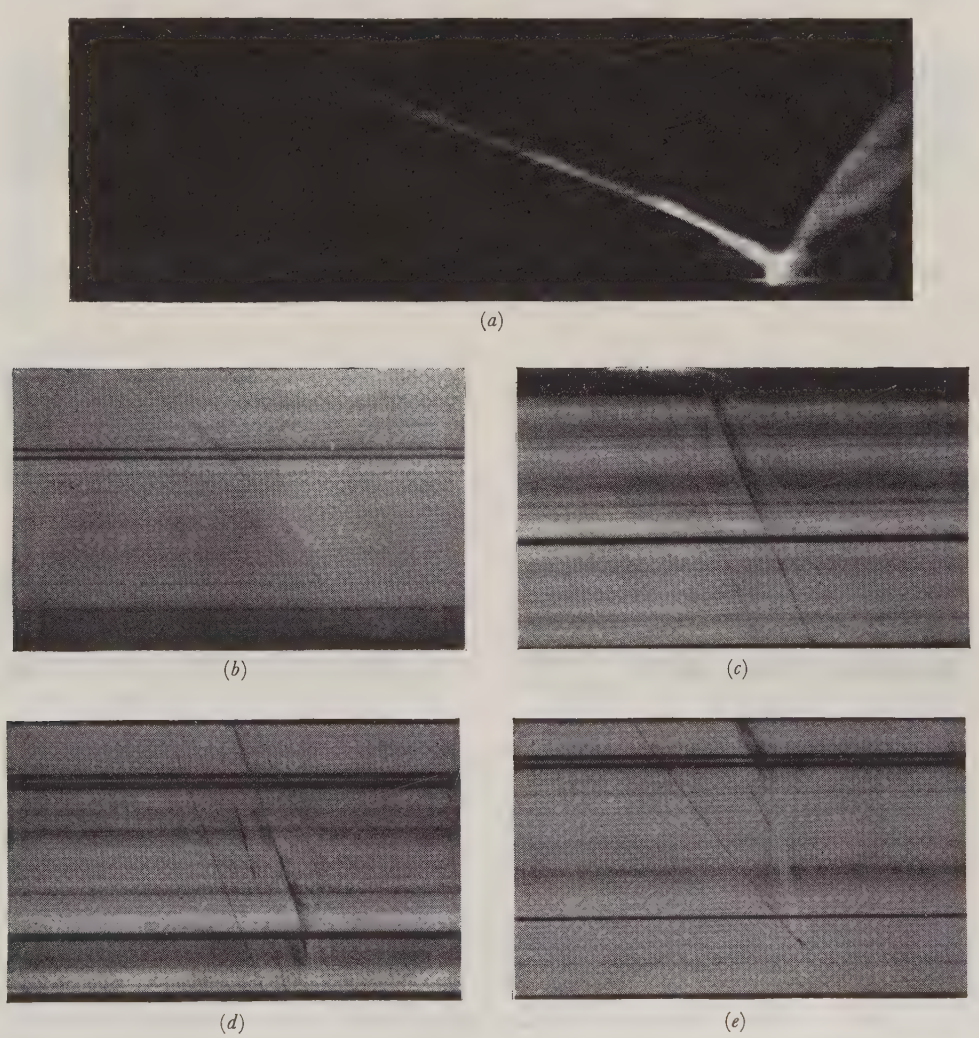

Figure 1. (*a*) *Direct rate photograph, ignition at upper left, distance increases downward and time to the right, marker tapes at* 20 cm *intervals;* (*b*) *schlieren rate picture, double marker tape at* 10 cm, *lower tape at* 20 cm *from spark, upper trace is flame and lower is the shock formed ahead;* (*c*) *schlieren rate picture, marker tapes at* 68·5 *and* 78·5 cm *from spark;* (*d*) *and* (*e*) *schlieren rate pictures, double tapes at* 97 cm, *single tape* 107·2 cm *from spark, two visible shocks ahead of flame, detonation formed at lower edge of picture in* (*d*) *and at double tape in* (*e*)

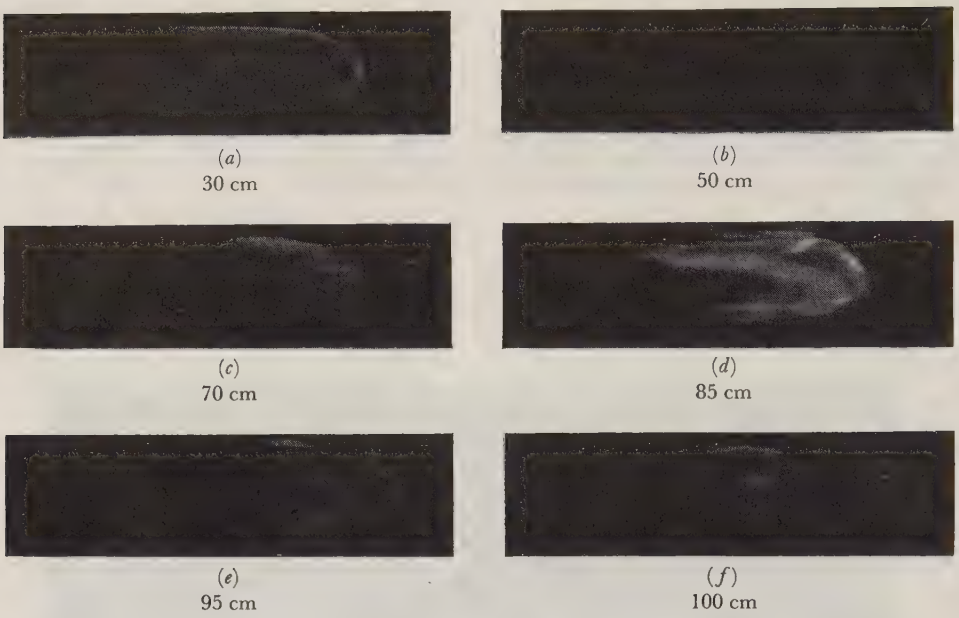

Figure 2. Flame configurations at specified distances from spark end. To convert the horizontal distance scale to that for the vertical direction (approximately), multiply the horizontal distances by 0·64

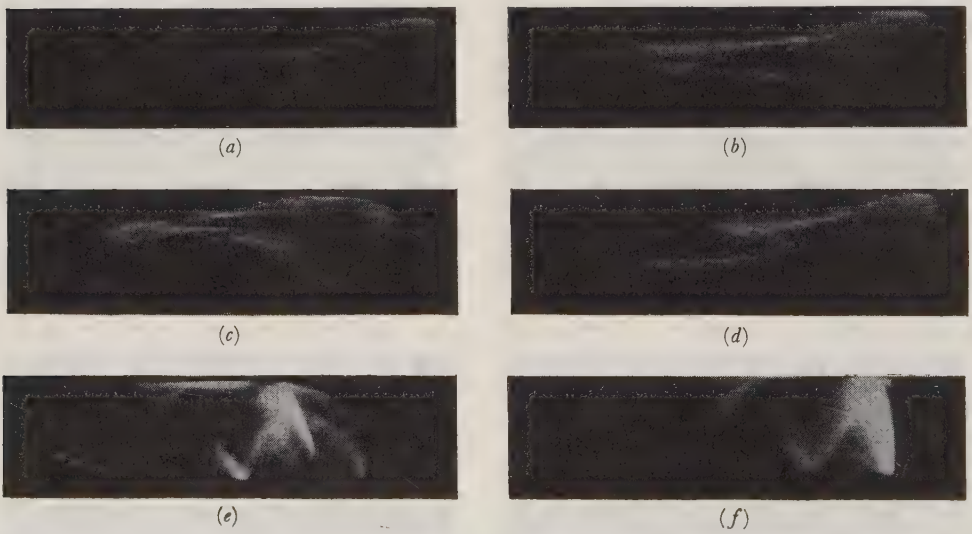

Figure 3. Flame and detonation configurations at 105 cm *from spark end. To convert the horizontal distance scale to that for the vertical direction (approximately), multiply the horizontal distances (1) at the leading edge of the flames by* 1·0, *(2) at the trailing edges by* 0·64, *and (3) for the luminous detonation waves in Figure 3(e) and (f) by* 2·4

At a distance of about 80–90 cm from the spark, the flame configuration undergoes a marked change, the flame accelerates, and after further travel of about 20 cm the detonation wave is formed at or slightly behind the leading edge of the flame. During the final flame acceleration one or more tongues of flame advance ahead along the wall. Very often the flame becomes scoop-shaped as shown in *Figure 3*. The increase in flame area results in acceleration of the flame and generation of compression waves which travel outward from it. The conditions for establishing a detonation wave at the flame front are thus achieved (*Figure 4*).

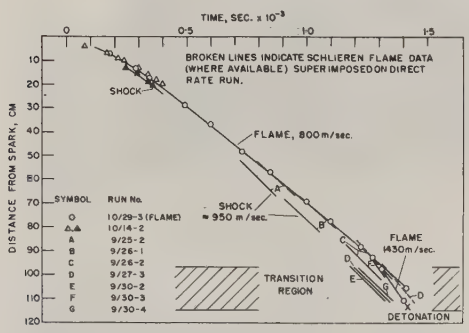

Figure 4. Schlieren data superimposed on direct rate run

If one assumes laminar flow throughout, it appears quite possible to explain the steady flame velocity of 800 m/sec and the dome-shaped flame following Zeldovich[3], that is, the hot-gas piston model.

In an attempt to explain the change in flame configuration and the accompanying flame acceleration, the velocity and state properties of the unburned mixture between the flame and the shock front have been calculated. (It has been assumed that this is a region of uniform temperature and pressure.) A summary of these data is given at the end of the paper.

The slug of gas between the flame and the shock has been suddenly accelerated by the shock to a velocity of 730 m/sec with respect to the tube, i.e. to a Mach number of 1·6. Under these conditions a boundary layer will develop at the walls. Flow within this boundary layer will first be laminar; but when a critical Reynolds number based upon the distance traversed by a mass element behind the shock[9] is exceeded, the boundary layer flow will become turbulent. The transition from laminar to turbulent boundary layer flow is not understood in detail[10]. However, turbulence seems to originate at random in spots from which it spreads with a velocity of the order of 0·1–0·2 that of the spot itself. Transition Reynolds numbers ranging from $0{\cdot}5 \times 10^6$ to 28×10^6 are reported for the supersonic flow of air over flat plates and in tubes. Thus our observed Reynolds number of $\approx 10^7$ at the flame for the slug between the flame and the preceding shock is well above the range within which transition from laminar to turbulent boundary layer flow may be anticipated.

The change in flame configuration from a centre-leading dome to an asymmetric scoop appears to result from the formation of a region of turbulent boundary-layer flow ahead of the flame through which the flame propagates at a rate higher than in the laminar flow regions. The flame area is thereby increased and results in the flame acceleration and formation of the detonation wave.

Thus both turbulence and flame configuration contribute in rather specific ways to the transition from slow burning to detonation under the present conditions.

The behaviour when other gas mixtures are ignited under exactly the same conditions may be quite different. Two such cases will be mentioned briefly.

No detonation is formed with stoichiometric H_2/O_2 at 50 mm. The flame accelerates smoothly to 200 m/sec within 20 cm (*Figure 5*). Thereafter

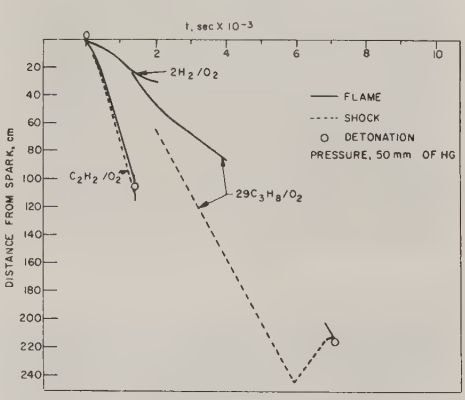

Figure 5. Summarized rate data. The absolute time values are not significant. They have been chosen to give smooth curves when data from separate runs are plotted together

the flame slows down and proceeds down the tube in an oscillatory manner. This first deceleration must result from the formation of a rarefaction wave in the burnt gases which overtakes the flame.

There is insufficient time for a compression wave to travel down the tube and back to cause such a retardation of the flame. Presumably the rarefaction arises from condensation of water at the walls.

With a 2/7 C_3H_8/O_2 mixture the detonation is formed only after the shock preceding the flame has been reflected from the downstream end of the tube and has travelled back up the tube to

meet the flame. The compression waves immediately ahead of the flame actually reverse the direction of the reflected shock (*Figure 6*). This phenomenon has been reported by Payman and Titman[2] for ethylene–oxygen mixtures at atmospheric pressure. The detonation forms at the flame front just after it meets the reflected shock. The detonation travels on through the twice-shocked mixture and frequently shatters the tube in this region.

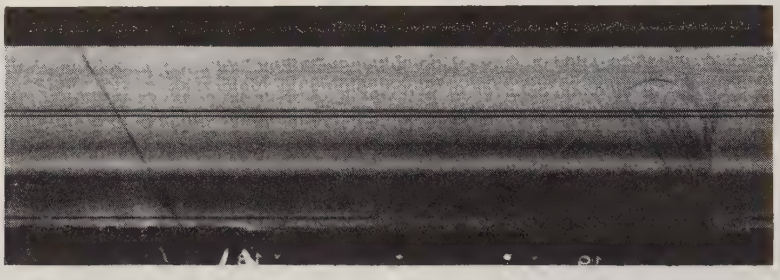

Figure 6. Reflected shock-flame interaction in propane–oxygen. The direction of the reflected shock is reversed by compression waves sent out ahead from the flame

STRUCTURE OF GASEOUS DETONATION

Interferometry has come into common usage for determination of the density distribution in transient flows such as exist in a shock tube. This section of the paper reports early results obtained by the second author (DRW) from a continuing study of low pressure gaseous detonation utilizing interferometry and other shock tube techniques.

The basis for interferometry

The observed quantity in an interferogram is the fringe shift, which is directly related to the change in refractive index of the gas integrated across the test section. From this the change in density may be determined if the specific refractivity is known, as it customarily is. However, when new species are introduced for which the specific refractivity is not known, then the density may not be evaluated quantitatively. Such is the case for flows involving dissociation, ionization, or chemical reaction[11]. Determination of the refractivity of dissociated species and of radicals is a complex problem and will not be discussed here. Generally, however, except in the case of the appearance of an appreciable electron concentration, the change in refractive index and hence the fringe shift remains approximately proportional to the change in density although the constant of proportionality may not be known precisely.

Experimental apparatus

These experiments were conducted in a shock tube designed for research on high temperature gases[12]. The driver section of the shock tube is 11·4 cm i.d., 2 m long, and contains nine spark plugs distributed along its length and connected to fire simultaneously. A transition section at the diaphragm location connects to the driven section which is 13 m long and of 8·2 cm square cross section. A series of detection stations typically 83 cm apart monitor the progress of the wave down the tube.

The window section was, for these experiments, located about 7·6 m from transition section. A Mach–Zehnder interferometer with 22·8 cm optics and a 0·1 μsec spark light source were used to obtain in general three interferograms on each experiment. These are monochromatic ($\lambda = 4{,}122$ Å) and white light interferograms taken with a beam normal to the tube, and an 'offset' monochromatic interferogram taken with a beam passing through the test section at a small angle ($\sim 3{\cdot}3°$) to the tube axis.

Formation of detonation in hydrogen–air

The first reaction following ignition of a combustible mixture near the closed end of a tube sends out compression waves, as does the continuing and accelerating reaction. The pressure profile observed along the tube at any instant must steepen with time as these waves overtake one another to form a shock wave. It is improbable that the first shock wave would form at the location of the first compression sent out after ignition. The transition from deflagration to detonation might then be expected to include the situation where a shock wave not as yet followed immediately by reaction would be travelling in a medium already processed by earlier isentropic unsteady compression waves.

This was the situation observed in experiments with 29 per cent hydrogen–air. The shock tube was used with no diaphragm, and the gases were metered simultaneously through critical flow orifices and flowed through a common 60 cm length of tubing before entering the initially evacuated tube. Velocity measurements showed that the shock wave was accelerating. Pressure

and heat transfer gauges in the tube wall near the test section showed a disturbance of increasing magnitude preceding the discontinuous increase in gauge output resulting from the shock wave.

The interferograms obtained verify this picture both graphically and, where chemical reaction has not begun, quantitatively. To determine the pressure, temperature, and velocity from the observed density, the thermodynamic history of the gas must be known. In the region ahead of the shock wave the flow variables are calculated with the assumption that the observed density increase is caused by an unsteady isentropic compression wave propagating in the same direction as the shock wave. The shock strength is obtained directly from the measured density ratio across the shock, and then the flow variables behind the shock are calculated. This was done for several records similar to *Figure 7a* and *b*. In each of these the flow ahead of the shock was high subsonic with a local Mach number of about 0·8, or a velocity of about 350 m/sec. To demonstrate this flow preceding the shock more graphically, a 0·63 × 2·5 × 8·2 cm block was cemented across the floor of the tube between the windows. Pictures such as *Figure 7c* were obtained. The acceleration of

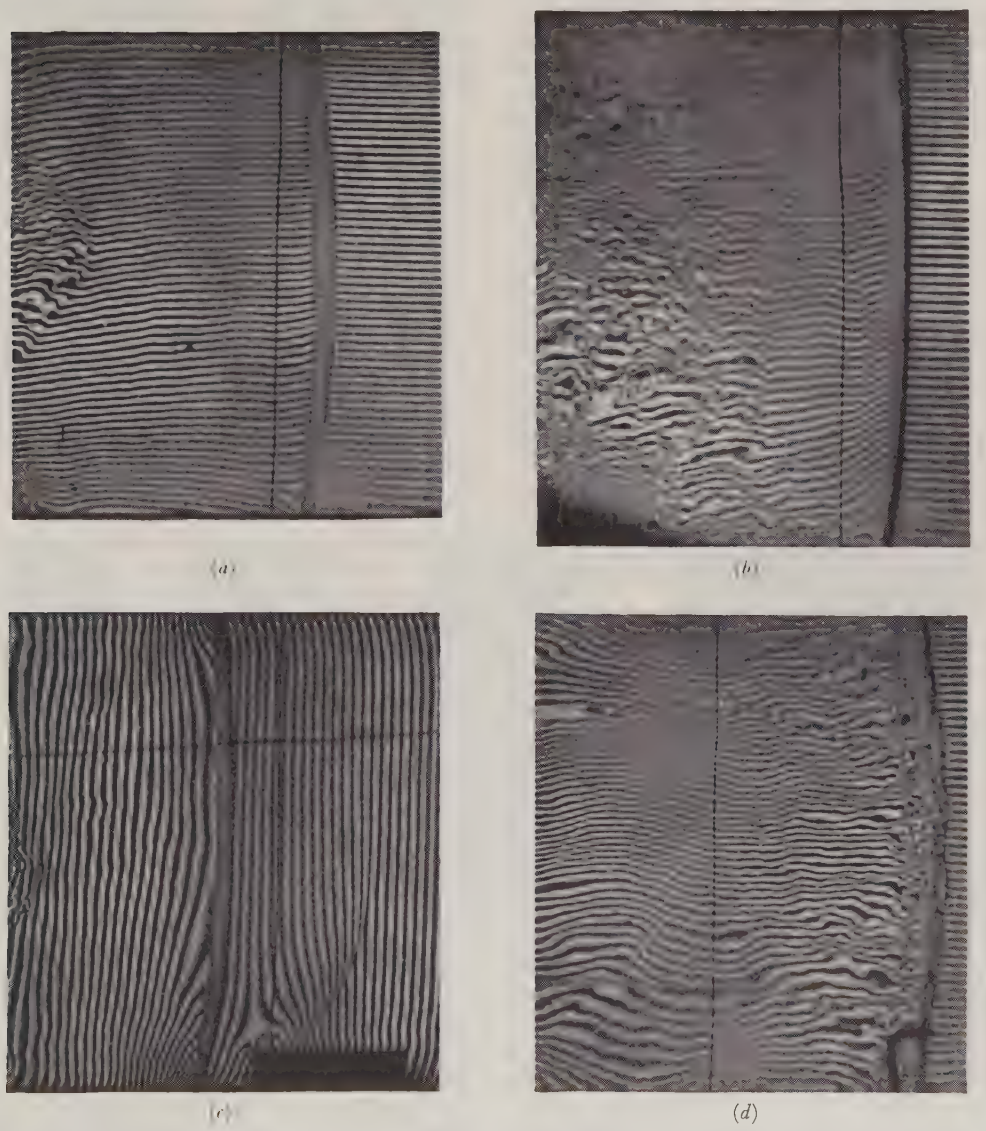

Figure 7. (*a*), (*b*), (*c*) *Shock front in hydrogen–air not as yet overtaken by flame front;* (*d*) *detonation wave; propagation is to the right. A density increase moves the interference fringes downward of* (*c*) *to the left. The full* 8·2 cm *height of the shock tube is seen in the interferogram. Initial pressures were approximately* 80 mm Hg

the flow preceding the shock around the corner of the block nearest the shock produces a typical low density region, and the resulting locally supersonic flow decelerates again through the weak upstream-facing shock wave which extends into the flow from the corner of the block. The curvature of the fringes at the top and bottom wall is due to the boundary layer ahead of the shock.

In *Figure 7c*, the pressures and temperatures before and behind the shock are computed from the measured densities and are respectively 0·33 atm, 408°K and 4·1 atm, 1,250°K. Initial pressure was 0·107 atm. The state of the gas behind the foot of the shock, however, is different from that in the centre of the tube because of the boundary layer ahead of the shock. We assume the limiting condition near the wall for the gas ahead of the shock is that it has the temperature and velocity of the wall. Using the measured shock velocity, the limiting state near the wall for the gas behind the shock is calculated to be 8·2 atm, 1,560°K, a more extreme condition than that in the centre of the tube.

This shock-boundary layer interaction might then cause auto-ignition at the wall even with an arbitrarily smooth wall, and therewith provide another mechanism by which the reaction could overtake the shock during the formation of detonation. In confirmation of this possibility, pictures such as *Figure 7b* show a flame front propagating inwards towards the centre of the tube from the foot of the shock.

In *Figure 7d*, the reaction has overtaken the shock and characteristically the front has lost its smooth appearance and is acquiring an irregular structure. This detonation is still travelling in a moving medium.

Structure of detonation in hydrogen–oxygen

Low pressure hydrogen–oxygen detonations have been observed interferometrically for several methods of initiation and for two mixture ratios, $2H_2 + O_2$ and $3H_2 + O_2$. The first series of experiments[13] was done with $2H_2 + O_2$ under conditions of mixing and initiation similar to those for hydrogen–air. In other experiments two pressure vessels were charged with hydrogen and oxygen in the desired proportions and set aside, the 2:1 mixture for three months, the 3:1 for one month. Before using, a small sample was analysed on the mass spectrometer and shown to have the desired mixture ratio. Both methods of mixing gave equivalent results.

Different modes of initiation were also utilized. A diaphragm was used in the shock tube, and the driver chamber was charged with $2H_2 + O_2 +$ 9He which was then ignited to rupture the diaphragm. For some experiments, designated shock initiation, the driver chamber length was reduced to about 8 cm to minimize overdriving, and charging pressures in the driver from 1 to 3 atm were used. For some experiments with $3H_2 + O_2$, designated strong shock initiation, the full driver volume was used with a charging pressure of 6·8 atm. The stronger modes of initiation reduced the minimum pressure at which detonation could be observed at the window section.

All these detonation pictures show a nonplanar detonation front, one which possesses many irregularities and convolutions whose scale generally increases with decreasing pressure. The interference patterns through the reaction zone have a 'turbulent' appearance and are characteristically different from the smoothly varying fringe shifts observed in a one-dimensional dissociation or ionization relaxation[11] process.

A number of interferograms taken under various conditions are shown in *Figure 8* and the experimental conditions are summarized in Table 1.

TABLE 1

Conditions for Experiments of *Figure 8*

	Mixture	*Pressure* (mm Hg)	*Initiation*	*Mach No.*	*Exp. No.*
a	$2H_2 + O_2$	151	spark	5·1	603
b, c	$3H_2 + O_2$	100	shock	5·00	1,011
d	$2H_2 + O_2$	76	spark	5·0 ± 0·3	822
e	$2H_2 + O_2$	65	spark	4·5 ± 0·3	595
f	$3H_2 + O_2$	30	shock	4·50	1,022
g, h, i	$3H_2 + O_2$	20	shock	2·2	1,031
j	$3H_2 + O_2$	20	strong shock	4·9	1,034
k	$3H_2 + O_2$	37	strong shock	5·4	1,035
l	$3H_2 + O_2$	80	spark	5·4	1,038

Fluctuations in the detonation velocity increased at the lower pressures, and the value given was measured at the window section. Sound velocities used were 536 m/sec for the 2:1 mixture and 602 m/sec for the 3:1 mixture.

The scale of the disturbance becomes small but remains clearly visible at the higher pressures as in *Figure 8a*. Note the vertical variations in the spacing of the horizontal fringes behind the reaction zone, indicating trails of varying density, in *a*, *b*, *d*, and *k*. Pictures *d* and *e* are the most nearly plane records obtained in these pressure ranges—others were much less well defined. The pressure of *f* was the lowest which would propagate a detonation with shock initiation. The structure suggests a relation to spin phenomena. At a lower pressure in the same mixture, the same initiation resulted in the shock wave of *g*, *h*, and *i*, which is used to illustrate the three types of interferograms. The shock width in *i* is due to the angle of the offset light beam. This same offset beam was used for *j* and *k* to show more clearly the wave structure, in these cases of overdriven detonation, and the apparent width is correspondingly increased.

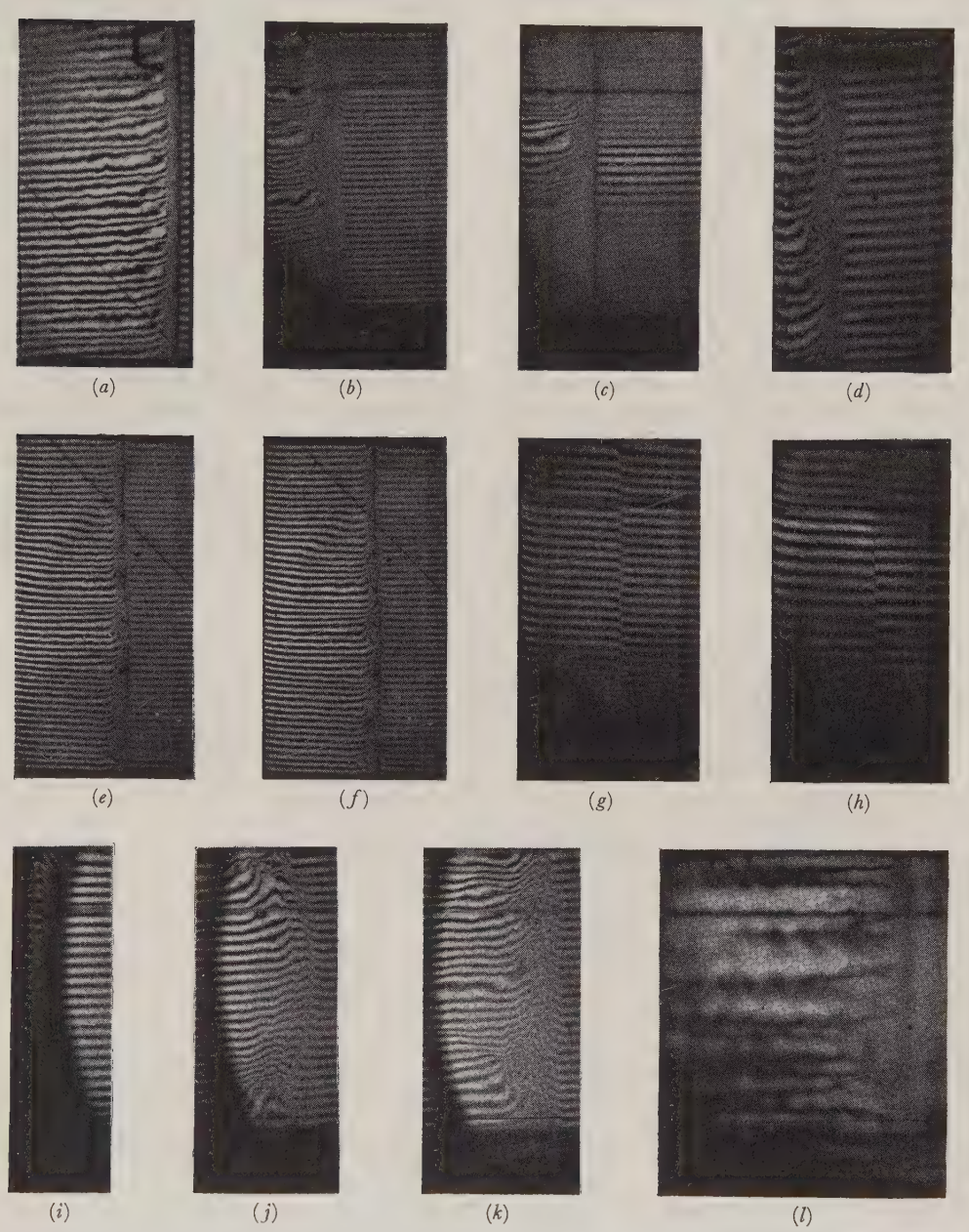

Figure 8. Interferograms of detonation fronts and of a shock front ((g), (h), (i)) in hydrogen–oxygen. Propagation is to the right. A density increase moves the fringes upward. The full 8·2 cm *height of the shock tube is seen. Examples of white light interferograms are (c) and (g), and (i), (j), and (k) are offset monochromatic interferograms: (l) is a contour or 'infinite fringe' interferogram*

The picture of *l* is a 'single fringe' interferogram where each fringe in the flow field is a contour of constant density. The density trails are seen to possess a structure with a periodicity of about three or four reaction zone thicknesses.

Several factors operate which would tend to maintain an oscillatory motion of the shock front. The thickness of the reaction zone introduces some lag between the time at which an element of the shock front has a maximum velocity and the time at which stronger pressure waves produced by the resultant faster reaction are felt at the shock front. Consequently for some frequency of oscillation, the driving force at the shock will be proportional to the displacement of the shock element ahead of the mean position of the front, a phase relation which will oppose the tendency of the shock front to become plane. Furthermore as this shock element oscillates, at a time when it is lagging but overtaking the mean position of the front, it will be a concave and collapsing section of the shock front. At this time, when its velocity exceeds the mean velocity of the front, the density and temperature behind the shock front and consequently the rate of release of energy will exceed the mean value. In addition the presence of sonic velocity at the C–J plane tends to isolate the shock front from overtaking compression or expansion waves, minimizing the damping action which contributes to the stability of a plane shock front.

The period of the unstable oscillation and hence the magnitude of the departures from planarity would according to these considerations increase with the reaction zone thickness and hence become greater at the lower pressures. This is observed. The assumption that the periodicity observed in the density trails of *Figure 8l* results from an oscillation in the strength of the front gives a period for this oscillation of about 4 μsec, in rough agreement with the sum of the transit time of material from the shock to the C–J plane, and the propagation time for sound waves forward to the shock. It has also been observed that when the transverse scale of the disturbance approaches the tube dimensions, reaction cannot be maintained and the wave will not propagate as a detonation.

Summary of Data for C_2H_2/O_2 System

Initial mixture: 50/50 C_2H_2/O_2 at 50 mm of Hg and 300°K

Notation:
- a = sound velocity
- M = Mach No.
- γ = mean heat capacity ratio, C_p/C_v
- V = velocity with respect to tube
- d = tube diameter (5 cm)
- x = distance measured along tube
- b = distance between flame and shock
- t = time measured from passage of shock
- p = pressure (abs)
- T = temperature (abs)
- η = viscosity
- ρ = density

Subscripts:
- s = shock
- f = flame
- 1 = undisturbed region ahead of shock
- 2 = region between the flame and the preceding shock (assumed to be homogeneous except for boundary layer)
- 3 = burned gases

Data: Shock velocity, $V_s = 950$ m/sec; $V_1 = 0$.
The mean value of γ across the shock is taken as the mean of values for C_2H_2 and O_2 at 500°K, i.e. 1·26
The viscosity, η_2, is taken as the mean of values for C_2H_2 and O_2 at 600°K and 1 atm, i.e. 260×10^{-6} poises

Calculated values: $\rho_1 = 7{\cdot}75 \times 10^{-5}$ g/cm^3; $a_1 = 332$ m/sec; $M_s = 2{\cdot}86$; $\frac{p_2}{p_1} = 9{\cdot}01$; $\frac{T_2}{T_1} = 2{\cdot}01$; $\frac{\rho_2}{\rho_1} = 4{\cdot}48$;
$V_2 = 732$ m/sec; $a_2 = 458$ m/sec; $M_2 = 1{\cdot}60$; $\rho_2 = 34{\cdot}7 \times 10^{-5}$ g/cm^3
Mach No. of steady detonation at 2,950 m/sec = 8·9
Reynolds No. of the flow in region 2 based upon the tube diameter,

$$R_{ed} = \frac{dV_2\rho_2}{\eta_2} = 4{\cdot}9 \times 10^5$$

The Reynolds No. defined by Mirels[9] based upon the characteristic length V_2t_f, where t_f is time interval between passage of shock and arrival of flame at a given mass element is

$$R_{ex} = \frac{(V_2t_f)V_2\rho_2}{\eta_2} = \left(\frac{V_2}{V_f - V_2}\right)\frac{bV_2\rho_2}{\eta_2}$$

For our experiments $\frac{V_2}{V_f - V_2} \approx 10$ and $b \approx 2d$. Hence $R_{ex} \approx 20\, R_{ed} \approx 10^7$

CONCLUSIONS

The shock-boundary layer interaction occurring during the transition from deflagration to detonation can cause auto-ignition behind the shock to occur preferentially at the wall even for smooth walls.

A low pressure hydrogen–air or hydrogen–oxygen detonation has an irregular front, plane only on the average, and the departures from planarity increase with the reaction zone thickness. The coupling between the shock front and the reaction zone appears to result in a characteristic instability of a detonation front.

The interferometer is a valuable tool for detonation research.

REFERENCES

[1] Bone, W. A., Fraser, R. P. and Wheeler, W. H. *Phil. Trans. A* 235 (1936) 29

[2] Payman, W. and Titman, H. *Proc. Roy. Soc. A* 152 (1935) 418

[3] Zeldovich, Y. B. Theory of combustion and detonation of gases (translation). *Air Material Command Tech. Rep. No. F–TS–1226–1A (GDAM A9–T–45)*

[4] Kistiakowsky, G. B. *Industr. Engng Chem. (Industr.)* 43 (1951) 2794

[5] Shchelkin, K. I. *J. exp. theor. Phys.* 24 (1953) 589

[6] Oppenheim, A. K. *Fourth Symposium (International) on Combustion*, p. 471. 1953. Baltimore; Williams and Wilkins

[7] Chu, Boa-Teh. *Fourth Symposium (International) on Combustion*, p. 77. 1953. Baltimore; Williams and Wilkins

[8] — *Nat. Adv. Comm. Aero. Tech. Note 3683* (1956)

[9] Mirels, H. *Nat. Adv. Comm. Aero. Tech. Note 3401* (1955)

[10] Dryden, H. L. Transition from laminar to turbulent flow at subsonic and supersonic speeds. *Proceedings of the Conference on High-speed Aeronautics*. 1955. Brooklyn, N.Y.; Polytechnic Institute of Brooklyn

[11] Alpher, R. A. and White, D. R. Refractive index of dissociated and/or ionized gases. *Report No. 58–RL–2079*, General Electric Research Laboratory, Schenectady, N.Y. (1958)

[12] — — *J. fluid Mech.* 3 (1958) 457

[13] White, D. R. *Abstract F5.* Nov. 1957 meeting of Fluid Dyn. Div. Amer. Phys. Soc., Lehigh University

113

GAS IGNITION BEHIND THE SHOCK WAVE

T. V. BAZHENOVA and R. I. SOLOUKHIN

INTRODUCTION

Ignition of gas mixtures by means of shock waves has been studied in a number of experimental research laboratories [1–3]. The methods employed were either the schlieren photography or pressure registration by means of piezo gauges. In these experiments the main features of the phenomena accompanying the ignition of gas behind the shock wave have been determined (ignition delay, initiation of detonation followed by periodic pressure fluctuations). It is interesting to make a detailed analysis of the sequence of these phenomena and, among other things, to find out how the ignition of gas in the flow behind the shock wave is initiated and how the transition to detonation proceeds. In this connection the Combustion Physics Laboratory of the Institute of Energetics of the U.S.S.R. Academy of Sciences has carried out a number of experiments on the ignition of combustible gases in a shock tube. Experiments were also carried out to study the gas ignition behind the impinging shock wave and its interaction with the angular step.

DESCRIPTION OF THE DEVICE

To carry out the experiments a shock tube with a square cross-section of 40 × 40 mm was employed. The total length of the tube is 3·5 m with a 2 m interval between the high pressure block and the point of observation. A section of the tube 200 mm long, with glass side walls, was under observation. The shape and the size of the tube cross-section remained unchanged.

Density disturbances were registered by means of a schlieren apparatus IAB–451 on rotating films. The linear speed of the films varied from 30 m/sec to 120 m/sec.

A flash discharge tube with a flash duration of about 2·5 msec served as the source of light.

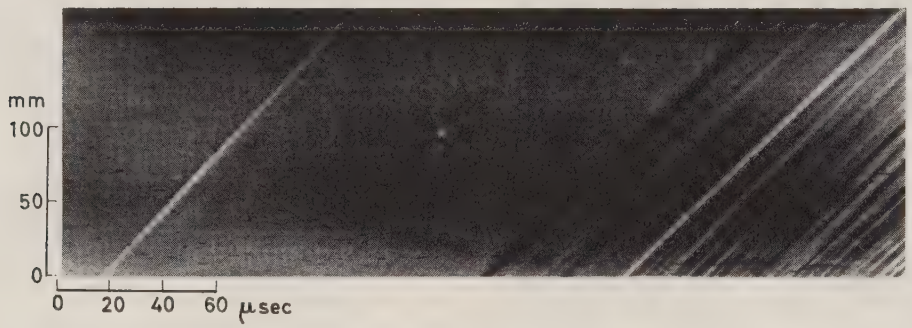

Figure 1. Moving image photographs of the flow established in the shock tube, $M_1 = 5{\cdot}9$

Along with the schlieren photography the pressure process was registered by an impulse piezo gauge made of a ceramic pile of barium titanate with a zinc branch rod, and wax sound insulation from the chamber walls.

The sensitive surface of the gauge formed part of the shock tube wall; and the signal was registered by means of an impulse oscillograph IO-IIIV.

Figure 1 shows typical moving image photographs of a current, initiated after breaking the diaphragm in the shock tube. The photograph was taken at a distance of 2 m from the diaphragm, with air at a pressure of 0·01 kg/cm^2 in the low pressure chamber.

Figure 2 shows the oscillogram of pressure in inert gas. As is shown in the photograph, throughout the whole space the contact surface including the pressure varies insignificantly. The illustrations show the resolving power of the registering apparatus.

It is pointed out that the final length of the sensitive surface of the pressure gauge (diameter 12 mm) considerably limited time resolution of the

processes since these processes undergo considerable changes in the course of less than 5 μsec. The value of pressure registered during this interval was averaged.

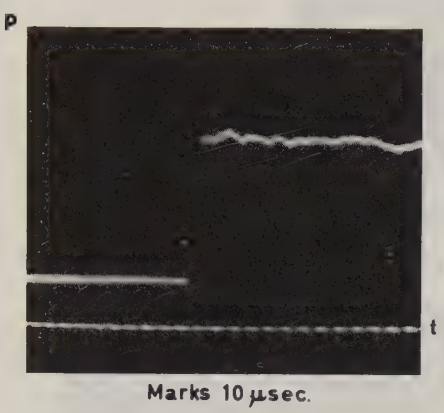

Figure 2. Oscillogram of pressure behind the shock in inert gas

According to our observations, the breaking of the diaphragm and a local temperature rise accompanying it did not lead to ignition of the mixture. This process with relatively weak waves took place much later than the moment of breaking the diaphragm, and developed in the end area of the heated gas. This area was usually located near the hot gas boundary, but in some cases the gas ignited at a great distance from the gas particles which had participated in the diaphragm rupture, thus the main experiments on ignition were carried out without a buffer section between the diaphragm and the mixture under test.

DEVELOPMENT OF THE IGNITION PROCESS OF GAS MIXTURES BEHIND THE SHOCK WAVE IN A CHANNEL HAVING A PERMANENT CROSS-SECTION

Figures 3 to *5* show photographs of three experiments carried out under similar conditions. The section of observation was preceded by a 2 m section filled with a mixture of one part (vol) of

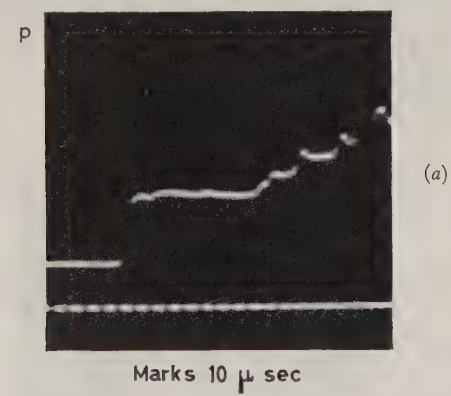

(*a*)

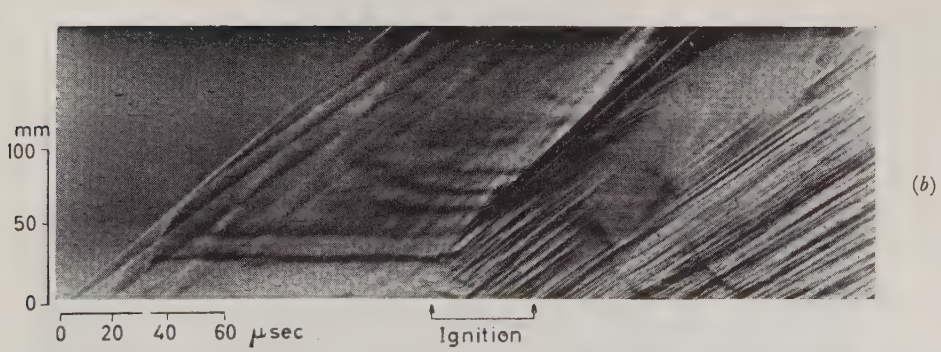

(*b*)

Figure 3. Ignition initiation behind the shock wave in a mixture of natural gas and oxygen

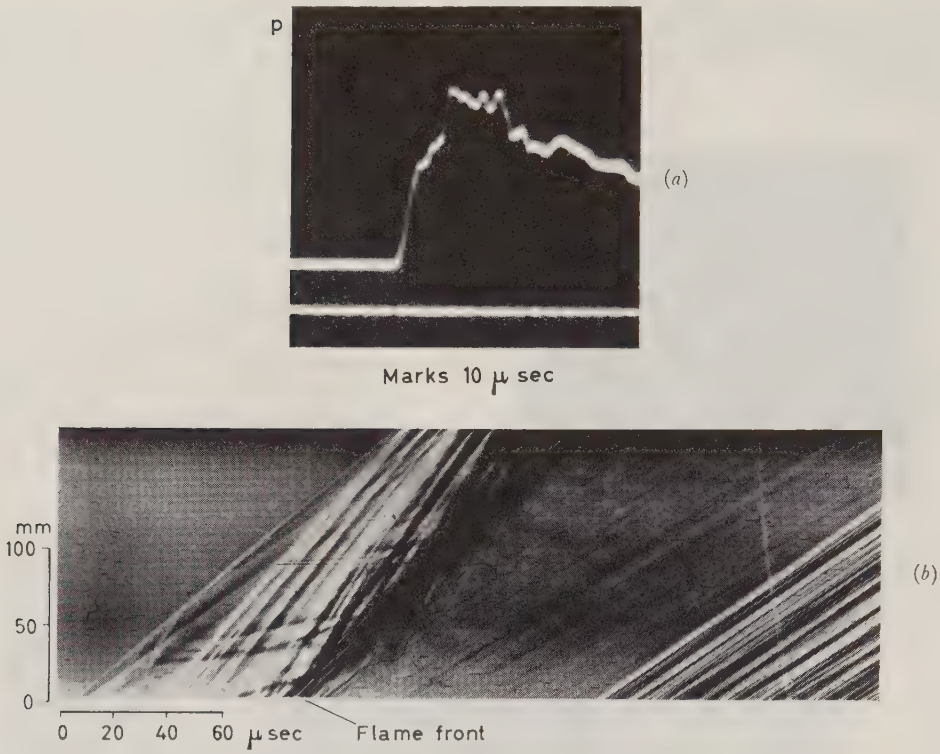

Figure 4. Flame front propagation in the gas behind the shock wave

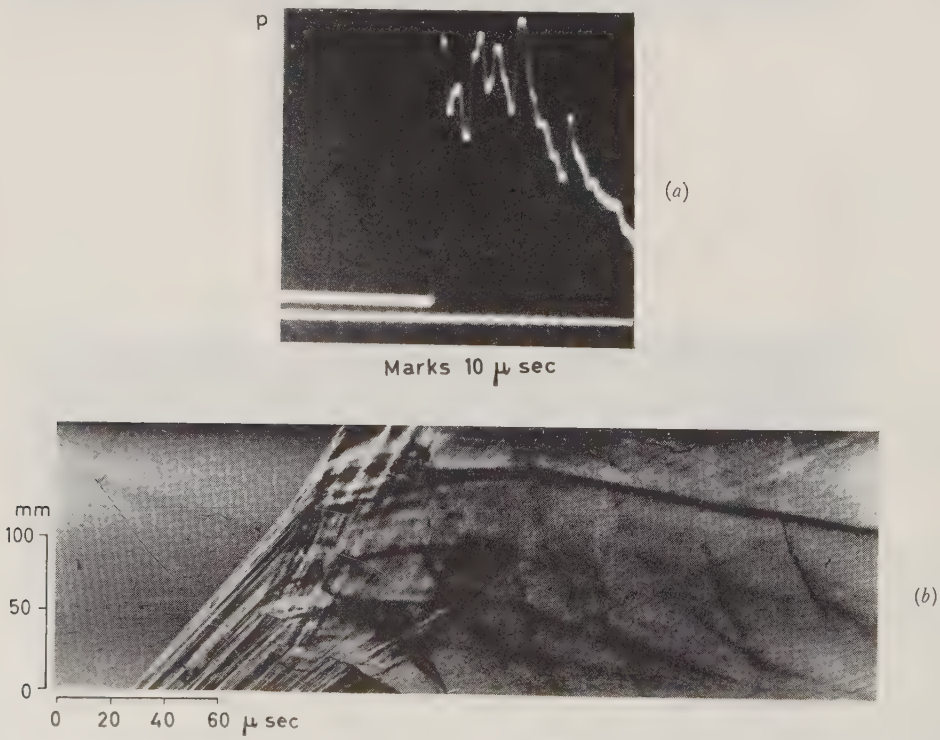

Figure 5. Formation of detonation wave in a mixture of natural gas and oxygen

natural gas and two parts of oxygen at a pressure of 0·06 kg/cm². The cellophane diaphragm was broken by hydrogen at a pressure of about 10 kg/cm².

Because of the inevitable deviations, caused mainly by instability in the diaphragm rupture, the resultant shock waves differed from each other in intensity. As a result of this, different phases of the ignition process were reproduced on the photographs. Shock waves of a smaller intensity compared with the waves shown in *Figures 3* to *5* did not cause ignition while the pressure, measured by a piezo gauge in the front of these waves, was equal to the pressure, calculated on an assumption of a complete absence of chemical reactions. The density field behind the wave was uniform up to the contact surface.

Figure 3a shows the initiation and progress of the gas ignition, also that in this case the gas ignition occurs with considerable delay (induction).

After breaking the diaphragm a flow, identical to the flow in inert gas, is initiated in the gas mixture. The shock wave is followed by a heated gas area of uniform density. In this case the pressure, measured by the oscillogram (to the right of the photograph) throughout this area behind the front, appears to be equal to the pressure behind the shock wave, which has been calculated by the shock wave speed on the assumption of a complete absence of chemical reaction. The relationship of the wave speed to the speed of the undisturbed gas sound is $M_I = 4{\cdot}2$, which corresponds to a temperature of 1,300°K behind the front.

Examining the gas layers adjoining the contact surface it is possible to observe a density change which may be regarded as the beginning of gas combustion. The points of ignition noticeable by the aroused density disturbances, spring up immediately in the end area of the gas and spread together with the gas. The location of these points of combustion is shown by an arrow but the schlieren photographs do not make it possible to determine the location on the tube section. Perhaps they initially spring up in the gas layer adjoining the walls.

Figure 6 shows several flash photographs. It is not difficult to see why the process is initiated in this way if we presume the existence of a final period of the mixture ignition induction. As a matter of fact, at high temperatures the layers of gas adjoining the contact surface are long-lived, it is in this area, therefore, that the combustion process can develop.

Thus, after the 'latent' combustion phase, or the mixture pre-ignition phase, a regular combustion process is initiated. The points of ignition, springing up in the final gas volume, soon establish a boundary between burnt and unburnt gas, that is a flame front. The trace of the established flame front is also marked in the photograph by an arrow. The area of burnt gas of a uniform density can be seen between the flame front and the contact surface.

Figure 6. Moving image photographs of the initial phase of ignition behind the shock wave. Photographs were taken at a rate of 40,000 shots per sec

The established flame front propagates in relation to the gas particles behind the shock wave at a subsonic speed. The relative speed of the flame front propagation in the first photograph is 345 m/sec. As a result of the pressure exerted by the cold gas, the gas is burnt under conditions similar to the conditions of combustion in a constant volume. As a result a zone of burned gas having an increased pressure is formed near the contact surface. The resultant compression not only delays the cold gas movement behind the contact surface but also spreads after the shock wave, overtaking the flame front whose speed is subsonic.

These compression waves can be seen in *Figure 3a*, but they are more clearly visible in *Figure 4*. The compression waves propagation results in an additional temperature rise of the mixture before the flame front, which in its turn leads to an increased speed of the front. In *Figure 4* the flame-front speed in relation to the gas particles in front of the flame reaches 420 m/sec.

Adding to the shock wave, the compression waves considerably increase its speed. In *Figure 4* the shock wave speed corresponds to $M_I = 5{\cdot}5$,

and the temperature behind its front reaches about 1,990°K. The pressure gauge registers the corresponding increase behind the shock wave front (see oscillogram in *Figure 4*). In this case the schlieren photographs and the pressure readings show that the area between the shock wave and the flame front ceases to be uniform because of the compression waves spreading from the combustion area.

Under conditions of such a non-uniform and additionally heated area between the shock wave and the flame front, the final phase of the ignition process sets in—explosion. This phase is well illustrated in *Figure 5*. Since the reaction in the above mentioned area proceeds explosively the shock wave is sharply accelerated, immediately approaching the detonation speed. In this case a compression wave, usually called a retonation wave, spreads backwards through combustion products.

The pressure oscillogram shows that the final gas pressure in this phase of the process is several times more than the gas pressure behind the shock wave causing ignition.

In some cases the detonation front may be formed at a considerable distance from the front of the shock wave causing ignition. For example, *Figure 7* shows ignition of a mixture of 50 per cent of hydrogen and 50 per cent of air at the initial pressure of 0·1 kg/cm² at a distance of 2 m from the diaphragm.

The illustration shows that the mixture density begins to change at several points in the flow field behind the initiating shock wave ($M_1 = 3{\cdot}82$, $T_2 = 1{,}040°K$), and the width of these points slowly increases as they propagate behind the shock wave with the gas.

At a certain stage of this process a sharp increase in the expansion rate of one of the points takes place, and a detonation wave is immediately formed, which spreads in both directions at the same speed. One of these detonation fronts will afterwards catch up with the shock wave front and merge with it.

Thus, merging of the flame front with the ignition shock wave is not a necessary condition of the detonation wave formation.

IGNITION OF GAS MIXTURES WITH GAS FLOW DELAYED IN THE ANGULAR STEP AREA

It is well known that if the intensity of a shock wave formed in gas capable of reactions is not sufficient to cause gas ignition behind the shock, the reaction may be initiated by a temperature rise caused by partial delay of the gas flow due to some obstacle behind the shock.

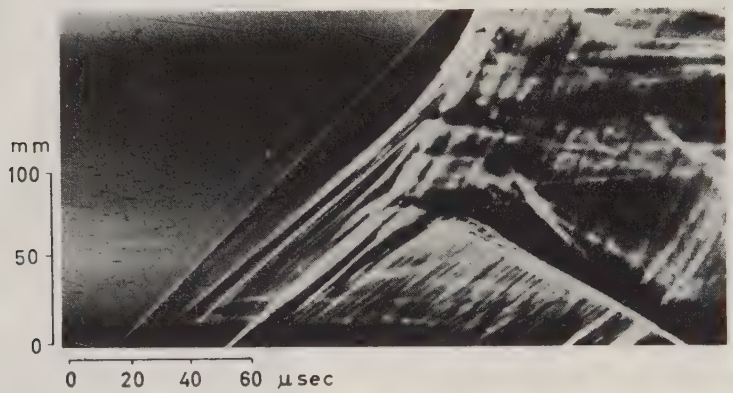

Figure 7. Formation of a detonation wave in hydrogen–air mixture in the shock tube

The shock wave propagating in the tube forms a boundary separating the motionless gas from the gas that has already been put in motion; therefore it is interesting to analyse the phenomena accompanying the gas current in the area of the contracting angular step and to compare the inert gas current with the current of gas capable of ignition.

Figure 8 shows a series of flash photographs and the moving image of the air current formed by the shock wave interacting with the angular step. In the first the shock wave, moving from left to right, is located at some distance from the angular step having an angle of 40°. Density variations characterizing the supersonic flow are seen behind the shock. In the second the shock directly approaches the beginning of the channel contraction, but there are no changes in the gas flow as yet. No. 3 shows the flow turn near the step with new shocks of density springing up and a light area of rarefaction on the second bend of the channel profile. It is clear that the shock continues to spread along the narrow part of the channel. From the next it is possible to conclude that the shock, resulting from the shock wave being reflected from the step, moves towards the gas flow and the

(*a*)

(*b*)

Figure 8. Interaction of the shock front with the angular step in air

Figure 9. Gas ignition in the angular step region with a noticeable delay

(*a*)

(*b*)

Figure 10. Gas ignition in the angular step region with a little delay

Figure 11. Interaction of the detonation wave with the angular step

rarefaction region extends (the rarefaction region boundary is reflected from the upper wall of the channel); then the nature of the flow is changed by the cold turbulized gas coming into view.

In *Figure 8b* the inert gas flow process in the area of the channel angular contraction is shown. The horizontal slit was located along the centre of the chamber. In the step region a reflected wave is seen, propagating up the flow. A complex group of shocks and contact surfaces are spreading in the narrow part of the channel.

Figure 9 shows a series of flash photographs and moving image of the combustible gas mixture flow in a channel with a concave angular step. In this experiment the intensity of the impinging shock wave was not sufficient to ignite gas in the flow behind the shock ($T = 680°K$). When the shock approaches the angular step a flow, identical to the above mentioned flow initiated at the turn of the flow in inert gas, is developed. In the shock, formed at the base of the step, an additional sharp temperature rise of the gas, already heated by the initial shock wave, is effected. Section 4 of *Figure 9a* shows that in the flow behind the second shock, ignition accompanied by bright gas glow is initiated.

The ignition occurs in the delayed heated flow not at the moment of the sharp temperature rise after the shock but after a period of time, probably corresponding to the induction period of the given mixture in conditions, corresponding to the state of the gas behind the shock. The ignition front propagates up and down the flow at a constant speed approximating the speed of detonation.

The moving image of the process (*Figure 9b*) makes it possible to follow more closely the development of the process in time. The initial phases of the flow reconstruction at the entrance to the contracting part of the channel proceed in the same way as in inert gas (*Figure 8b*). In 50 μsec in the area behind the reflected shock it is possible to see the formation of two diverging fronts, which are reproduced on the flash photographs by gas glow.

Figure 10 shows interaction of the step with an impinging wave of greater intensity ($T_2 = 790°K$). As is seen from the photograph, by the moment of the interaction density non-uniformities occur in the gas behind the shock. We identify these non-uniformities with ignition points (*Figure 10a*). In this case the detonation wave is formed immediately at the shock occurring near the step. At the same time the gas begins to glow (*Figure 10b*).

Further increase in the impinging shock wave intensity results in the detonation being formed before interaction with the step. Our experiments have shown that in conditions of the shock tube a spin detonation is constantly initiated. Interaction of such a wave with the angular step is shown in *Figure 11*. The spin structure is retained during the transition to the narrow section of the tube, and a reflected shock wave is formed in the reaction products in the same way as in inert gas.

Some estimates giving the conditions under which various gas mixtures are ignited in the shock tube are given in Table 1.

This work has been carried out in the Combustion Physics Laboratory, Institute of Energetics, Academy of Sciences of the U.S.S.R., under the guidance of Professor A. S. Predvoditelev.

REFERENCES

[1]Mooradian, A. J. and Gordon, W. E. *J. chem. Phys.* 19 (1951) 1166

[2]Berets, Greene, E. and Kistiaksky, G. B. *J. Amer. chem. Soc.* 72 (1950) 3

[3]Shepherd, W. *Third Symposium on Combustion, Flame and Explosion Phenomena.* 1949. Baltimore; Williams and Wilkins

TABLE 1

No.	*Composition of mixture*	*Initial pressure,* kg/cm²	*Pressure behind the wave,* kg/cm²	*Temperature behind the wave,* °K	*Relay,* μsec	*Conditions of observation*
1	Natural gas $+2O_2$	0·06	1·2	1,300	1,200	passing wave
2	$H_2 + O_2$	0·12	1·32	820	700	
3	$H_2 + O_2$	0·1	1·5	970	450	
4	air $+ H_2$	0·1	1·65	1,040	1,100	
5	$4H_2 + O_2$	0·09	0·96	790	1,000	
6	$4H_2 + O_2$	0·09	0·74	680	50	at the step
7	$4H_2 + O_2$	0·09	0·96	790	0	

DISCUSSION

PROPERTIES OF DETONATION WAVES

Papers 98, 99, 100, 101, 102, 103, 104

A. R. Ubbelohde (*London*) opening the discussion said: As is well known, formal hydrodynamic theories of detonation deal merely with overall quantities, such as the energy released in the chemical reactions taking place, the equations of state, and so forth. To obtain real insight into the process of detonation in physicochemical systems it is necessary to work under conditions where the hydrodynamic parameters no longer completely determine the progress of the detonation wave. This is what makes studies of the marginal conditions for detonation, such as are presented in the papers before the meeting, so full of exciting possibilities of studying physicochemical mechanisms of energy release under unusual conditions.

Because these conditions are unusual, it is however necessary to interpret the results with caution. I will mention three points by way of illustration.

(1) When theoretical calculations have been completed that are in satisfactory agreement with the findings, these calculations should always be extended to test how sensitive the agreement is to the values assumed for various kinetic parameters. For example, some quantities such as the detonation velocity are comparatively insensitive to the precise reaction equations assumed, so that 'good agreement' for this particular property of the detonation wave does not provide a very searching test of the mechanisms assumed. It would be useful to know how sensitive the calculations of Gordon, Mooradian and Harper, and of Belles, are to deliberate variations in the quantities assumed to arrive at the results.

(2) Characteristic time intervals in detonation and near-detonation phenomena may become comparable with characteristic times for phenomena such as the transfer of internal energy. This raises the very important problem, particularly for polyatomic molecules containing several atoms, of the proper value of the ratio of specific heats to use in calculating various steps in the process. Again, when the collision frequency becomes comparable with the reciprocal of characteristic times for other transient processes, at low pressures, the use of conventional differential equations for kinetics needs careful examination.

(3) When the reaction products of detonation include solids, such as solid carbon, or solid oxides of boron, aluminium and so on, the time required for complete crystallization and for the full lattice energy of these solids to become available for the hydrodynamic propagation may introduce important restrictions on certain possibilities. These again should become apparent in studies of marginal detonation, or in the transition from deflagration to detonation as described by Fraser.

Finally, it does seem that techniques for establishing stationary detonation waves, as described in a tentative way by Nicholls, Dabora and Gealer, hold out most exciting possibilities for studying transient processes in the mechanisms of energy release in marginal detonation. It is to be hoped that this aspect of such studies will show much progress before the next Symposium.

J. A. Fay (*Massachusetts*): What is the criterion of spin? There appears to be some confusion between authors and it is necessary to re-appraise the method of determining spin. The fluctuating pressure of standing waves might give rise to maxima and thus give the alternating effect associated with spin.

T. Urbanski (*Warsaw*): Referring to the most interesting papers on spin detonation, I would like to draw your attention to my own work on a similar subject referred however to detonation of solid explosives.

The first paper in question was published in 1926 and 1927 (*Roczniki Chem.* and *Z. f. ges. Schiess- u. Sprengstoffwesen* respectively). Photographs of detonating explosives enclosed in glass tubes were taken, and the shape of lights and shadows suggested existence of a spiral way of propagation of detonation. With the help of high-speed photography (*Roczniki Chem.* 1932) I succeeded in obtaining photographs of duration of *ca.* 0·1 msec (*Roczniki Chem.* 1934) and I was able to confirm my former statement. The phenomenon is, however, limited to composite explosives containing ammonium nitrate with TNT and other ingredients, generally speaking to coal-mine explosives. It was never noticed in the case of pure compounds such as TNT, picric acid and gun cotton.

The spin frequency was of the order of 50,000 per sec in 20–30 mm glass tubes.

R. P. Fraser (*London*): In relation to my own paper, and in answer to Fay, I think we can now say that 'spin' occurs in the detonations of all gaseous mixtures in tubes with air or oxygen. The frequency of spin, as observed by the undulations in streak photographs, increases with increasing detonation velocity as you move away from the limits; but, in many fast-burning oxygen mixtures

the effect can no longer be oberved because, I suspect, the resolving power of the moving film camera is not great enough.

It is also now clear that in the same size tube the spin frequency does not increase progressively with the speed of the detonation front but in definite steps, so that it jumps in multiples of the frequency at the limit of detonation. For example: in my paper, Table 1, with benzene vapour in oxygen and a 13 mm bore tube the frequency varies from 45,000 at the lower or higher limit to 4 times this at 3·9 per cent, and 8 times this frequency at 26·9 per cent.

It also is sometimes evident from the photographs that the spin frequency can quite suddenly double itself. I think it is clear that where these high spin frequencies are evident, more than one head of detonation or node is travelling in the tube. In cylindrical tubes, certainly, the evidence of spin can be demonstrated by the cutting of a helix on the silvered inner surface of a tube. At the lower limit of detonation with all gases and vapours so far investigated the helical velocity varies only between 2,300 and 2,600 msec and the ratio helical velocity/forward velocity between 1·45 and 1·52. This must mean that the spiral path followed by the nodes of detonation always have the same pitch; that is to say, that the spiral path makes a constant angle with the generating lines of the cylinder. This angle is $47 \pm 1°$ for all gases with air or oxygen in any diameter tube.

D. Altman (California): The simple formula describing the limits of detonability in the paper is purely thermodynamic in origin. There is a class of condensed explosives which, although they yield a high energy of combustion, are not known to detonate because of a low rate of heat release. Ubbelohde in opening the discussion has mentioned the significance of the kinetic phenomena in describing detonation processes. Have you given any consideration to modifying the simple expression in your paper to account for the combustion efficiency in relation to the detonation life-time so that your expression could be generalized? This combustion efficiency, which would multiply the heat of combustion, would of course contain all of the consequences of burning rate kinetics and side-wise or expansion losses. This factor, however, could probably be simplified to contain the governing influences of the losses and be used to appreciably extend the utility of your simple expression.

H. G. Wagner (Göttingen): The use of HO_2 in kinetics is rather shaky. I would like to point out the discrepancy between observed and calculated critical shock strengths for lean hydrogen mixtures.

F. E. Belles (Ohio): In answer to Altman's question as to whether this treatment could be applied to slower reactions for which kinetics are available, I would first attempt, for the case of a simple unbranched chain reaction, the ozone decomposition. It would be necessary to assume some arbitrary required degree of completion of the reaction within some reasonable time, say that corresponding to the transit time through a real shock wave. It would also be necessary to test the sensitivity of the predicted limit of detonability to these assumptions. If the result were not sensitive, and agreed with the known lower limit of detonability of ozone in oxygen, it might then be safe to proceed to other more complicated systems.

In reply to Wagner's comments: (*a*) Perhaps the best justification for using HO_2 formation as the chain-breaking reaction is that it works. Possibly it works by withdrawing H atoms from the reaction long enough to decouple the shock and the reaction zone. In any event, as Ubbelohde pointed out, the sensitivity of the results to the assumed kinetics should be tested. (*b*) As to the discrepancy between observed and calculated critical shock strengths for explosion of hydrogen mixtures, it could as easily be due to the difficulty of such measurements as to faulty kinetics. Experimentally it is very hard to make certain that the event occurs instantaneously, i.e. with zero time lag between the heating of the gas and its ignition, and that extraneous factors are not affecting the result.

R. P. Fraser (London): Has the author tried to establish the detonation, or supposed detonation, inside the nozzle by over-expanding in the divergence? If this was done in a two-dimensional nozzle, i.e. a slot nozzle, the conditions of association of the combustion wave and shock could be better observed by schlieren photography. I also think the combustion wave may attach itself to the walls.

A. L. Thompson (Montreal): Can you be sure that the air stream is free of dust particles from the ceramic heat exchanger which, if present, might influence the reaction?

W. H. Avery (Silver Spring, Md.): Would Nicholls please present the temperature, pressure and Mach number profiles along the axis? Can the ignition delays noted be related to those measured or extrapolated for this mixture by other methods?

J. A. Nicholls (Michigan): Thompson has inquired as to the possibility of dust being entrained in the jet from the heat exchanger. While this is certainly possible to some extent, we feel confident that it is not unduly influencing our results. Our experimental procedure consists of a few minutes' run at first with air only to stabilize the delivery temperature of the heat exchanger. Hence our test gas does not include the first slug of air to pass through the heated exchanger.

Further, preliminary results on the ignition time delay of hydrogen–air mixtures are close to those reported by Steinberg at the Fifth Symposium for hydrogen–oxygen.

The question has been raised as to the pressure and temperature distribution along the axis of the jet. We can think of the zone bounded by the intercepting shocks and the Mach disc as a zone of approximately isentropic expansion. Thus the pressure and temperature drop and the Mach number increases as we approach the normal shock wave. At this point the pressure and temperature discontinuously increase and the Mach number decreases. Downstream the temperature probably remains sensibly constant until close to the zone of luminosity whereupon it increases rapidly. As for the pressure and Mach number distribution downstream of the shock it is unknown at this time although the pressure cannot be too far from ambient. Experiments are underway to attempt to determine the shape of the stream tube in the zone of chemical reaction.

It should be noted that when combustion is first initiated downstream of the shock, the shock is driven upstream and the resultant configuration is then very stable. Hence there is definitely a coupling between the combustion and shock wave.

TRANSITION TO DETONATION

Papers 105, 106, 107, 108, 109, 110, 111, 112, 113

R. P. Fraser (*London*) (*the chairman*) said: In my view, despite much work, there is still no full explanation of the birth of the primary shock wave which occurs in explosions in tubes. Earlier workers in this field have shown that the origin of the discontinuity producing the shock wave is in the region of flame distortion after the first flame arrest.

A. K. Oppenheim (*California*) opening the discussion said: The organizers scheduled the discussions on detonation for the first day undoubtedly in order to start the Symposium with a bang. Having learnt about the intricacies of the steady-state phenomena at the first session, we are now concerned with the unsteady processes leading to their establishment. At the round-table discussion on future problems which was held at the last Combustion Symposium under the chairmanship of Walter T. Olson, the conclusion was reached that one of the most important unsolved problems in combustion is the transition from flame burning to detonation. The excellent crop of contributions presented here today bears out the fact that the challenge of this conclusion did not go unheeded.

It appears in fact that the problem was tackled by a large number of workers all over the world. Especially noteworthy is this respect are four papers from the U.S.S.R. where the problem was studied over the last decade by Y. B. Zeldovich, K. I. Shchelkin, A. S. Sokolik, and many others. There are two analytical and two experimental papers in this group. Particularly impressive are the photographic records presented in the latter two, and I would like to take this opportunity to congratulate our Russian colleagues for the excellence of their contributions towards the solution of our problem.

There is no need to elaborate upon the difficulties of the problem which, besides its transient and, of course, non-equilibrium character, is dependent as much upon chemical-kinetic as on fluid-dynamic phenomena. In order to make the formulation comprehensible a number of idealizations must be introduced; in particular the motion must be unidimensionalized and simple equilibrium relations assessed. Under such circumstances the description of the process brings out the importance of the wave interaction phenomena —the main subject of all the experimental observations and the analytical studies presented at this session. Unfortunately, at the same time some of the most fundamental effects promoting the development of the process, notably those of turbulence, cannot be adequately described.

As a result of this meeting it appears that our understanding of the transition to detonation has been well enhanced. We have gained more insight into the details of the processes accompanying the development of detonation than we have ever had before. The analysis of experimental observations and their rationalization has been fundamentally improved, but our knowledge is by no means yet at a predictive stage, that is at a level where, having been given the initial conditions, we would be able to predict how the process develops from there on.

Sir Alfred C. Egerton (*London*): In 1924 I had the problem to find out what the effect of anti-knocks was on detonation, so we started by trying to get a detonation set up in gaseous mixtures at a definite position in a tube and then to see whether that position was altered by the presence of the anti-knock. We found that if the back end of the tube was closed and the tubes were uniform that we could get the detonation to occur at a place within less than 1 cm and that lead ethyl rendered it earlier rather than later. During that investigation it became clear that the 'fuzz' which Dixon had put down to photographic halation was not so, but that the detonation wave was set up ahead of the combustion front (which Bone and Fraser's work showed even more clearly), and I was very interested in Oppenheim's *Figure 12*, which seems to represent very closely the behaviour at the seat of detonation. I think that the addition of substances to gaseous mixtures (with modern

techniques of observation) might provide more information about the chemical processes taking place when the change-over occurs.

G. J. Minkoff (London): Fraser's remarks give me an opportunity for drawing attention to a simple geometrical factor which is often overlooked in discussions of the mechanism of the acceleration of a flame travelling within a tube: this applies only to ignition (by spark or hot wire) within a tube, but not to ignition by the application of a flame to an open end of a wide tube. The flame we have in mind* is spherical, and travels at a steady rate until the walls are reached. The ensuing change of flame front into a cylindrical one is illustrated by Ellis' photos (which are reproduced*), and the flame front can be simply shown to cover, in unit time, a distance l which is proportional to the cube of the time. According to Chu† the acceleration of the discontinuity is associated with a pressure wave; the latter can eventually build up to a shock wave. If the latter is caught up by the flame, and interaction can take place, then detonation will eventually ensue, but with a slow flame combustion will eventually only occur at a cross-section of the tube, and will slow down to the normal speed of propagation. These differences are illustrated in the paper with flames of methane (fast) and of carbon monoxide (slow).

S. J. Jacobs (White Oak, Md.): I would like to mention some work by J. Majowicz and S. J. Jacobs on transition from shock to detonation, discussed at the Lehigh meeting of the Fluid Dynamics Division (*Amer. Phys. Soc.*, 1957). Our work used a wedge of explosive initiated by a plane shock. To a great extent the method eliminated all boundary effects except for a rarefaction at the explosive gap interface. We think our work shows that heating by compression will account for initiation of explosives by a strong shock in solids. There is no evidence that heat transfer from the donor explosive occurs to any extent or is necessary to explain initiation by shocks. We do think that the temperature is inhomogeneously distributed in a cast or pressed solid, however. Our results show the time to transition from shock to detonation decreases with increase of shock strength, as might be expected. Typical values of initiation time is of the order of 0·2 to 0·5 μsec for measured transmitted pressures in the range 125 to 75 kilobars. In some cases shocks grow smoothly to the detonation velocity; in others overshoot is observed which then recedes to normal detonation. The observations are fully in agreement with observations on shock initiation of gases as discussed by Oppenheim and previously observed by several authors. Our results qualitatively appear as in *Figure 1.*

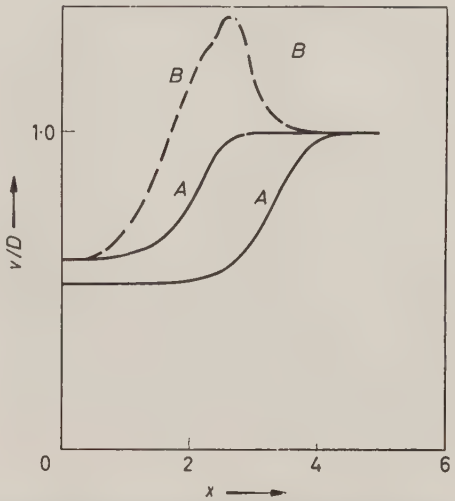

Figure 1. Shock transition to detonation. A, slope of shock curve for a cast explosive (98 per cent *of max. density); B, slope observed for a pressed explosive* (90 per cent *crystal density). v = shock velocity; D = normal detonation velocity*

A. R. Ubbelohde (London): In studying the transition from deflagration to detonation, in gaseous or in condensed systems, the role of the boundary walls of the system can introduce complications which it would be desirable, if possible, to eliminate by suitable experimental devices. For example, in a combustion proceeding in a cylindrical tube, the reflection of pressure waves from the walls can lead to subsequent focusing further along the tube, to a degree which may in fact determine the onset of real detonation. It should not be experimentally impracticable to devise containing walls of such low impedance to shock waves that any reflection is minimized. For example, in gaseous systems, containing tubes of extremely low density per unit area can be devised, by maintaining a balancing pressure of inert gas outside such containers. With solids or liquids inert condensed matter can be provided around the column of explosive material, so as to minimize any reflection of shock waves at the boundaries, with subsequent focusing. Though I do not personally suppose that all transitions from deflagration to detonation involve such reflection and focusing effects, nevertheless it may prove highly desirable to eliminate their influence in studying the transition.

H. M. Cassel (Pittsburgh): Regarding the paper by Martin and White, and the remarks of Minkoff,

* Everett, A. J. and Minkoff, G. J. *Fuel* 33 (1954) 184.

† Chu, Boa-Teh. *Fourth Symposium (International) on Combustion*, p. 603. 1953. Baltimore; Williams and Wilkins.

I would like to report results of a few experiments on accelerated flame propagation through an 8 per cent methane–air mixture in a glass tube of 1 in. inner diameter which had been carried out at the Bureau of Mines during the first quarter of 1957, as a study of pre-detonation phenomena.

The flames were ignited in the centre of a 6 ft. tube, open at both ends. The flame speed was measured on rotating film by the conventional method at 8·5, 13, and 18 cm from the spark plug. To obtain information about the flame shape, moving image pictures were taken with the same camera, turned 90°. Thus it was found that the initially spherical flame, after expanding to the wall, forms an elongated thimble with an approximately half spherical cap and a slightly tapered cylindrical mantle whose area increases as the flame accelerates from 16 to 25 m/sec. With closed end ignition the flame develops a convex cellular structure before the tip caves inward, the part near the wall apparently travelling ahead of the centre (*Figure 2*).

effective flame area, and u the particle velocity of unburned gas.

As u increases, skin-frictional heating may enhance preferential ignition near the wall as shown by our photo as well as those in the paper by Martin and White taken at higher u values by the same method. It should be emphasized, that with this method the time of exposure is longer than with the Schmidt camera.

D. J. Rasbash (Boreham Wood): Experiments had been carried out on explosions in ducts which fully confirmed the view of Brinkley that turbulence generated in the unburned gas plays a vital part in the acceleration of a flame along a duct. For a number of ducts a quantitative relationship had been found between the rate of combustion of the explosive mixture in the duct and the Reynolds number in the unburned gas moving in front of the flame. The combustion rate increased with Reynolds number over the whole range tested ($R_e = 10^4$–10^6). It should be possible to extend this quantitative relationship, using perhaps

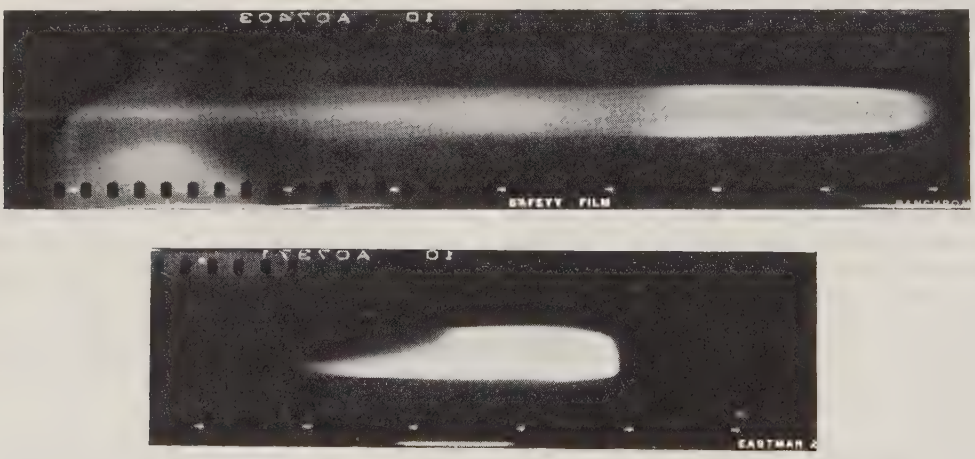

Figure 2. Flame shape at 18 cm *distance, and* 25 m/sec *velocity. Notice the far extending* (*ca.* 3 msec) *after-glow which escapes the short exposure Schmidt camera*

The simple method of high-speed photography here applied reveals about the same detail as the much more elaborate Schmidt camera used by Sir Alfred Egerton and Lefebvre*. Hence it appears that the D–D-transition mechanism proposed by Zeldovich deserves more serious consideration. Accordingly the flame speed, F, is related to the average burning velocity, S, by the equation

$$aF = au + AS$$

where a is the cross-section of the tube, A the

a more general parameter for turbulence than the Reynolds number. This would allow the acceleration of a flame to be calculated and an approach to be made to estimating the possibility of an explosion developing to detonation in duct systems of various kinds. However, it is necessary in making quantitative calculations to make allowance for two factors which do not seem to have been mentioned. The first is the cooling of the burned gases behind the flame and the second is the inertia of the unburned gases ahead of the flame. Both of these will have the effect of reducing the velocity of the unburned gas and therefore will reduce the level of turbulence in this gas.

* Egerton, Sir A. C. and Lefebvre, A. H. *Proc. Roy. Soc. A* 223 (1954) 206.

PART X

SPECIAL FUELS

SOME COMBUSTION PROBLEMS OF HIGH-ENERGY FUELS FOR AIRCRAFT

W. T. OLSON and P. C. SETZE

INTRODUCTION

Research on high-energy fuels for jet-propelled aircraft has been stimulated by the desire to increase aircraft range or other flight performance features. For example, boron, boron hydrides, and certain boron–carbon–hydrogen compounds offer increases in aircraft range. Magnesium and aluminium, on the other hand, can produce higher thrust in an air stream of given mass flow than can hydrocarbons. These fuels are sufficiently dissimilar to conventional fuels in availability, physical properties, combustion characteristics, and exhaust products that new problems in almost all aspects of their use are encountered.

The intention of this paper is to discuss the relations of the basic combustion properties of some high-energy fuels to the problems of applying these fuels in flight propulsion systems. Specifically, this paper reviews thermodynamic performance, combustion limits and efficiency, and oxide deposition. Thus, the paper does not examine all ramifications of high-energy fuels by any means.

Illustrative material is largely drawn from experiments at the NACA Lewis laboratory, although a number of other laboratories have also engaged in research on high-energy fuels[1].

FUEL SELECTION

So-called high-energy fuels are selected because they surpass conventional hydrocarbon fuels on one or more of the following thermodynamic criterions: heat of combustion per pound of fuel, heat of combustion per cubic foot of fuel, or heat of combustion per pound of air. Table 1 lists most of the materials of interest.

TABLE 1

Heating Values of Various Substances

Fuel	*Melting point* °F	*Boiling point* °F	*Specific gravity*	*Heat of combustion**		
				B.Th.U./lb.	B.Th.U./ft.^{3}	B.Th.U./lb. air
Acetylene	− 115·2	− 118·5	0·621 (− 119°F)	20,740	804,000	1,567
Aluminium	1,220	3,735	2·70	13,320	2,246,000	3,475
Beryllium	2,336	5,013	1·816	26,950	3,055,000	3,525
Boron	4,172	4,622	2·32	25,500	3,680,000	2,665
Boron carbide (B_4C)	4,442	> 6,332	2·54	25,200†	3,996,000†	2,526
Carbon	> 6,332	7,592	2·26	14,100	1,991,000	1,229
Decaborane	210	415	0·78 (212°F)	28,300	1,379,000	2,786
Diborane	− 266	− 134·5	0·447 (− 134·5°F)	31,330	872,000	2,100
1-Ethylnaphthalene	5	486	1·008	17,020	1,074,800	1,289
Hydrogen	− 434·8	− 423	0·0708 (− 423°F)	51,660	228,000	1,510
Jet Fuel (JP–4)	< − 76	135–484	0·777	18,620	900,000	1,263
Lithium	366·8	2,502	0·53	18,450	610,500	3,714
Magnesium	1,202	2,025	1·74	10,810	1,174,000	3,813
Pentaborane	− 52·4	136·4	0·63	29,130	1,142,000	2,220
Silicon	2,588	4,712	2·4	13,176	1,974,000	2,681
Titanium	3,272	> 5,432	4·50	8,192	2,301,000	2,845
ZIP	—	—	—	25,000–27,000	—	—

* Condensed phases of oxides at approximately room temperature, except $H_2O(g)$ and $CO_2(g)$.

† Nat. Bur. Stds; Selected Values of Chemical Thermodynamic Properties.

Heat of combustion per pound is the most important thermodynamic property to speed, altitude, and flight range. For a given fuel, maximum range will occur at particular values of speed and altitude; only by going to a fuel with a higher heat of combustion can range, speed, and altitude be increased simultaneously beyond this point.

As the Breguet range equation shows, the ultimate distance an air-borne vehicle will fly is directly proportional to fuel heating value.

$$\text{Range} = h_c \eta \frac{L}{D} \ln \frac{W_{\text{initial}}}{W_{\text{final}}} \qquad (1)$$

where h_c is the heat of combustion of fuel, η is the overall engine efficiency, L/D is the lift to drag ratio, and W is the weight.

The increased importance of fuel heating value at long range is apparent from calculations of the gross weights of hypothetical aircraft to carry a given useful load, for example, 45,000 pounds. The assumptions for this tabulation were that weights of aircraft structure and engines were a fixed fraction of aircraft gross weights and that other terms in the range equation were constant. This treatment oversimplifies the aircraft and engine business, but it shows the main trends (Table 2).

TABLE 2

Range miles	*Gross weight*, lb.	
	JP–4; 18,600 B.Th.U./lb.	*High-energy fuel,* 26,000 B.Th.U./lb.
2,000	112,000	101,000
6,000	450,000	212,000
7,000	990,000	279,000
8,000	—	392,000

Note that the two aircraft are nearly the same weight for 2,000 miles range, but that the hydrocarbon fuelled aircraft 'grows' at a much greater rate than the high-energy fuelled counterpart, other things being equal.

If hydrogen is eliminated from further consideration because it is a low density gas, and if beryllium is eliminated as unavailable, then only a few materials offer increased heat of combustion on a weight basis, notably boron and some boron compounds rich in hydrogen. The U.S. Navy and Air Force have sponsored research towards a suitable high-energy fuel based on boron, carbon, and hydrogen, Project ZIP.

High heat of combustion per unit volume is desirable in order to reduce the size and weight of the structure. The heating value on a volume basis is usually of secondary importance to heating value on a weight basis, however. The drag induced by lifting fuel weight can be expected to be much more important than wave and friction drag due to fuel volume.

Heat of combustion per pound of air is only a crude estimate of the thrust that can be obtained with various fuels. Actually, the specific heats, physical states, heats of phase changes, and the dissociation energies of the combustion products must be considered in any calculation of combustion temperature, thrust, or specific fuel consumption, particularly at high combustion temperatures.

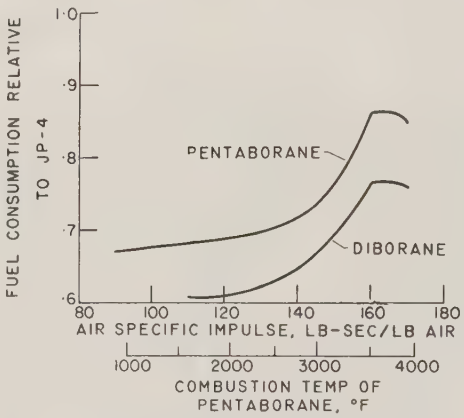

Figure 1. Fuel consumption of diborane and pentaborane relative to JP–4

For example, the improved specific fuel consumption possible with diborane or pentaborane is not simply an inverse ratio of heating values to that of hydrocarbon jet fuel. This effect is illustrated in *Figure 1*, which shows the fuel consumption of diborane and pentaborane relative to JP–4 against air specific impulse. The combustion temperature of pentaborane, which is very close to the combustion temperature of diborane for the same value of air specific impulse, is also shown in *Figure 1*. If combustion temperatures of boron fuels are increased beyond about 3,000°F, considerable heat goes to vaporizing boric oxide. The loss of this heat from the kinetic energy of the exhaust stream is reflected in the specific fuel consumption realized.

Figure 2 presents air-specific impulse across different fuel–air ratios for several fuels (reference 2, with revisions). Air-specific impulse is indicative of thrust that can be obtained with a particular fuel. It is the total momentum (pressure times area plus mean flow times velocity) per unit of mass flow with the exhaust stream at a Mach number of 1·0. Fuel specific impulse is the quotient of air-specific impulse and fuel–air ratio.

Several materials offer significant thrust increases over hydrocarbons, as noted in Table 3 for stoichiometric fuel–air ratios from *Figure 2*.

Magnesium and aluminium are notable in this regard, although this thrust gain would be at the expense of specific-fuel consumption, because their heat of combustion per unit weight is lower than that of jet fuel.

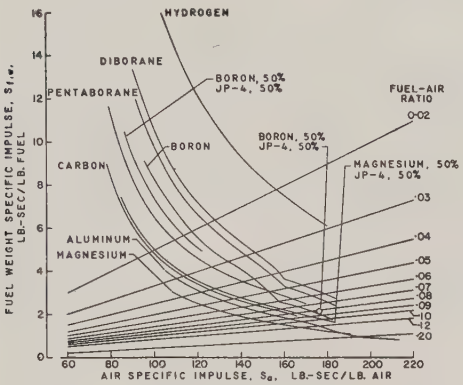

Figure 2. Variation of fuel weight specific impulse with air specific impulse for several fuels. Combustor inlet-air temperature, 560°R; *inlet-air pressure*, 2 atm

TABLE 3

Fuel	*Combustion temperature* °R	*Air-specific impulse* lb.-sec/lb. air
Magnesium	6,200	220 (est)
Aluminium	6,160	213
50% Magnesium in JP–4	4,750	184
Pentaborane	4,850	184
Diborane	4,750	184
Boron	5,100	182
50% Boron in JP–4	4,650	176
JP–4	4,180	170

Research towards application in jet engines has been undertaken on aluminium, magnesium, boron, and boron compounds. The combustion aspects of this research are further reviewed here.

COMBUSTION LIMITS AND EFFICIENCY

Liquid fuels

The discussion of liquid high-energy fuels will be limited to diborane (B_2H_6) and pentaborane (B_5H_9) because they belong to a family of chemical compounds that show the greatest promise as aircraft fuels.

Flammability limits and spontaneous ignition—The range of pressures and equivalence ratios (actual fuel–air ratio divided by stoichiometric fuel–air ratio) over which the combustion of diborane and pentaborane with air can be supported is shown in *Figure 3*. The flammability limits of hydrogen and JP–4 jet fuel are shown for comparison purposes. The lean limit for both diborane and pentaborane occurs at an equivalence ratio of about 0·1 at 1 atmosphere pressure; this value is about the same as for hydrogen. The lean limit for JP–4 occurs at an equivalence ratio of 0·4, about four times higher than for diborane and pentaborane. The rich limit for diborane occurs at an equivalence ratio of about 60 which is about eight times richer than the value for hydrogen, and about fifteen times richer than for JP–4. No rich limit for pentaborane has ever been established because spontaneous combustion of the fuel–air mixture always occurs when attempting to obtain a rich mixture.

In general, mixtures of diborane in dry air do not ignite spontaneously at room temperatures. Pentaborane spontaneously ignites at concentrations above some lean limit, for example, 14 volume per cent in a 6 cm sphere[3]. Exception to both of these statements have been noted, however. Pentaborane must be diluted with large quantities of nitrogen to suppress spontaneous combustion with air[4] at room temperature.

The wide flammability limits and high reactivity of the boron hydrides indicate that they can be burned efficiently over a much wider range of conditions than can hydrocarbon fuels. This is an important aspect of increasing the operational altitude and speed of aircraft.

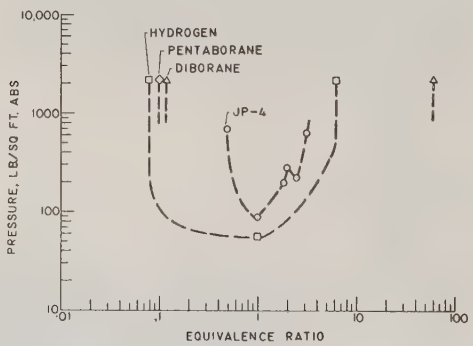

Figure 3. Flammability limits of diborane and pentaborane

Flame speed of diborane and pentaborane—The flame speed of diborane–air mixtures over a range of equivalence ratios from 0·6 to 2·2 have been determined experimentally[5]. The diborane–air flame was stabilized on the end of a quartz tube 0·4 mm in diameter. The flame flashed up the tube if a larger diameter was used. Because of the small tube size errors in diborane–air flame speed of as much as 30 per cent are possible.

The flame speed of pentaborane–air mixtures over a range of equivalence ratios from 0·2 to 1·6 have also been determined experimentally[6].

These flame speed measurements are presented in *Figure 4*; the flame speed of hydrogen–air and propane–air mixtures (using the same technique as the pentaborane–air determination[6]) are shown for comparison. Pentaborane–air mixtures have a peak flame speed of about 550 cm/sec at an

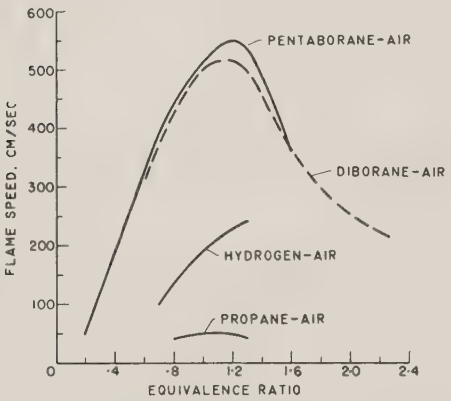

Figure 4. Flame speed of diborane and pentaborane

equivalence ratio of about 1·2. The peak flame speed of diborane–air mixtures is about 515 cm/sec and occurs at an equivalence ratio of 1·07. The flame speeds of pentaborane–air and diborane–air are a little more than twice the peak flame speed of hydrogen–air, and a little more than ten times the peak flame speed of propane–air. Table 4 compares the flame speed of pentaborane–air with hydrogen–air and with propane–air at the same flame temperatures.

TABLE 4

Mixture	*Temperature* °K	*Equivalence ratio*	*Flame speed* cm/sec
Hydrogen–air	2,290	1·4	250
Pentaborane–air	2,290	0·67	370
Propane–air	2,605	1·3	45
Pentaborane–air	2,605	0·925	490

These comparisons again point out the high reactivity of the boron hydrides.

Blow-out velocity—Data on the blow-out velocities of several solutions of pentaborane in JP–4 have been obtained[7]. The apparatus used in this investigation is illustrated in *Figure 5*. These blow-out velocity data were compared with the blow-out velocities of propylene oxide and JP–4 as determined in the same apparatus. In determining the blow-out velocity the atomizing airflow and fuel flow were held constant. The secondary airflow was initially at a low value so that ignition of the fuel–air mixture occurred. The secondary airflow was then gradually increased until flame failure occurred. The results of this investigation are presented in *Figure 6* as blow-out velocity plotted against equivalence ratio. The tests were conducted with four concentrations of pentaborane in JP–4; 3, 10, 20, and 40 per cent pentaborane by weight.

Increasing the pentaborane concentration increases the blow-out velocity considerably. Extrapolation of the 40 per cent pentaborane curve to an equivalence ratio of 0·7 shows a blow-out velocity of slightly more than 120 ft./sec; at the same equivalence ratio the blow-out velocity of JP–4 is about 30 ft./sec and the blow-out velocity

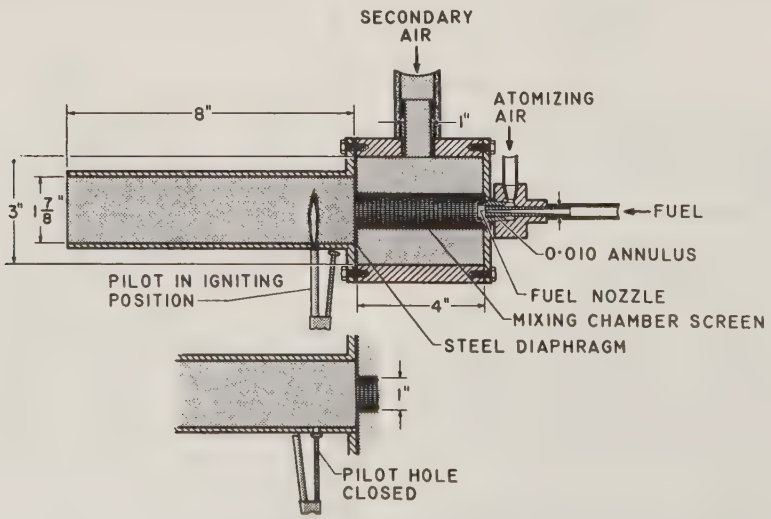

Figure 5. Blow-out velocity apparatus

of propylene oxide 84 ft./sec. The blow-out velocity of 100 per cent pentaborane was not established because of the airflow limitations of the apparatus, however it was estimated to be at least ten times higher than the 40 per cent solution tested. The blow-out velocity of 100 per cent diborane is greater than 500 ft./sec[8] (the limit of the apparatus).

Combustion efficiency—Because of their very high flame speeds, diborane and pentaborane should be expected to produce high combustion efficiencies in turbojets, afterburners, and ramjets, even at operating conditions where hydrocarbon fuels cannot burn.

For example, systematic studies were conducted in a typical turbojet combustor to determine possible relations between combustor performance and fuel properties[9]. Combustion limits and combustion efficiency as a function of fuel–air ratio were determined for several inlet-air velocities at different combinations of inlet-air

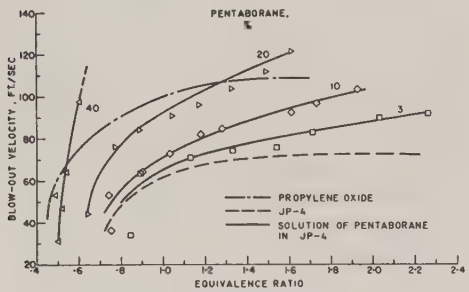

Figure 6. Blow-out velocities of four pentaborane–JP-4 fuel blends

pressure and temperature. Some variations in fuel injector were included in the case of gaseous fuels.

No single fuel property or combination of properties completely correlated all of the data over the entire operating range. A reasonable correlation of the combustion efficiency data was obtained with maximum flame speed for the majority of the fuels and operating conditions, however. An example for one operating condition is shown in *Figure 7*.

Similarly, combustion efficiency was measured for several pure fuels and fuel blends in a simple ramjet type combustor[10]. Homogeneous fuel–air mixtures were admitted to a 5 in. diameter burner spanned by a single, 1½ in.-wide *V* gutter of 45° included angle. Burner length was 36 in. Measurements were made at operating conditions where flame did not spread to the walls and combustion efficiencies were in the 20 to 80 per cent range. The data showed a nearly direct dependence of combustion efficiency on flame speed at different operating conditions, for example, *Figure 8*.

Although diborane and pentaborane were not used in the experiments of *Figures 7* and *8*, the experience with them in other combustors is that they are indeed remarkably easy to burn in typical

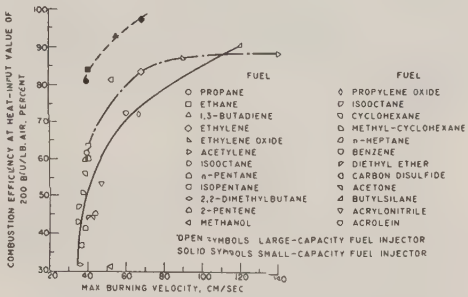

Figure 7. Variation of combustion efficiency with maximum burning velocity for gaseous and liquid fuels. Inlet-air total pressure, 14·3 in. *mercury abs.; inlet-air temperature,* 200°F*; inlet-air reference velocity,* 170 ft./sec

turbojet and ramjet combustor conditions. In conventional turbojets, combustion efficiencies of pentaborane were of the order of 98 per cent for most conditions.

Among the principles of good practice for ramjet combustor design are fine atomization of fuel and rapid and extensive mixing of fuel with air to avoid pyrolysis of fuel. Pyrolysis products of diborane and pentaborane are notoriously difficult to burn. With these highly reactive fuels, the problems accompanying flashback from the piloting source to the injector can be eliminated

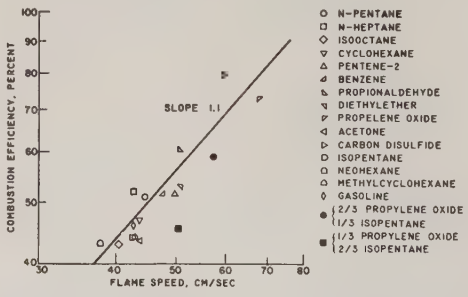

Figure 8. Effect of flame speed on combustion efficiency at an equivalence ratio of 1·0*; inlet-air pressure,* 10 lb./in.² abs. *temperature,* 655°R*; velocity,* 275 ft./sec

for all conditions only by injection at or near the pilot. The familiar problem of properly mixing fuel in the combustion airstream is illustrated in *Figure 9* for pentaborane burning in a 9·75 in. ramjet. When configuration *A* of *Figure 10* was run at equivalence ratios above 0·4, excessive fuel

impinged on the combustor wall. Configuration *B*, on the other hand, with more and larger fuel orifices, did not adequately atomize the fuel at equivalence ratios below 0·5. Low efficiencies near stoichiometric mixtures are probably the result of insufficient mixing of fuel and air.

Thus, although reactive boron compounds simplify the design problem of maintaining stable, efficient combustion in jet engines, they do not eliminate it.

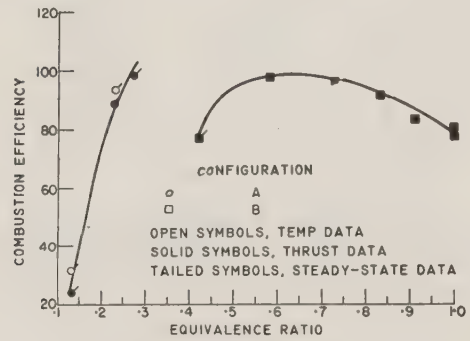

Figure 9. Combustion efficiency of pentaborane in a $9\frac{3}{4}$ *in. diameter ramjet combustor*

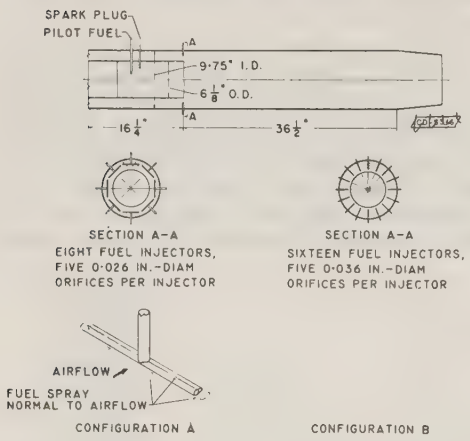

Figure 10. Diagram of ramjet combustor configurations

Solid fuels

Combustion of aluminium, boron, and magnesium has been tried by a number of organizations[1]. Experiments have included solid fuel beds, dusts, wires, metal-impregnated plastic, and suspensions, or slurries, of metal powder in hydrocarbons.

The simplest approach to the problem of storage and handling of solid fuels appeared to be to use them as slurries, high concentration suspensions of metal powders in a liquid hydrocarbon carrier. Experiments were undertaken by NACA from 1950 to 1955 to establish methods of fuel preparation and handling, combustor design principles, and engine performance for slurry fuels[11].

Much information was obtained on fuel preparation and properties. Concentrations of 50 and 60 per cent magnesium or boron, with particle sizes of the order of one or a few microns, were rendered fluid with 1 or 2 per cent of a surface active agent in a hydrocarbon medium such as JP–4. Settling of the metal particles was markedly slowed with 1 per cent or less of a gelling agent, such as aluminium octoate; slurries sufficiently stable for experimental purposes were prepared. Although gelling agents produce high viscosities (5,000 to 20,000 centipoises, Brookfield), at high shear rates viscosity decreases to 1/100 or less of the initial value, and so these slurries can be pumped, flowed, metered, and sprayed in conventional ways.

Burning rates of solid particles—The rate limiting steps in the combustion of magnesium wire[12] and in the combustion of boron dust[13] appear to be heat and mass transfer processes, rather than chemical reaction rates. Thus, general equations for diffusion and heat conduction, as they apply to burning particles, can be set up following the general approach of Spalding[14].

Coffin and Brokaw[15] have developed such equations that yield partial pressures as a function of temperature. Additional calculations produce burning rate. The effects of diffusion and dissociation are treated rigorously; no artificial combustion zones were posited, and chemical equilibrium was assumed to exist throughout the system. The general equations could also be reduced to simplified equations such as those of reference 14. Both detailed and simplified integrations were carried out, and the gross results can be expressed in terms of evaporation constants β and particle lifetimes t_l were calculated for the relations

$$d^2 = d_0^2 - \beta t \tag{2}$$

$$t_l = d_0^2/\beta \tag{3}$$

where d is the diameter at time t and d_0 is the diameter at time $t = 0$.

It was noted that results from the simplified equations agreed well with those from the general equations where compared. Results are abstracted from reference 15 in Table 5.

Note that boron requires nearly ten times as long to burn completely as magnesium, and more than twenty times as long as *iso*octane. These results do not, however, explain fully the difficulty of burning boron particles efficiently in high-speed airstreams, as discussed below. Perhaps the boric oxide near the particle surface becomes momentarily chilled by turbulent gases, coats the particle, and thus prevents further combustion.

TABLE 5

Computed Burning Rates of Various Substances
(Temperature, 300°K; air at 1 atmosphere)

	Burning rate g/cm sec	*Evaporation constant* β, microns^2/sec	*Lifetime of 1-micron particle* t_l, sec
*Iso*octane*	99×10^{-5}	$1{\cdot}11 \times 10^{6}$	$0{\cdot}90 \times 10^{-6}$
Magnesium*	97	0·444	2·25
Boron	13·7	0·0477	21·0
Boron*	14·2	0·0492	20·3
Carbon	13·2	0·053	18·9

* Simplified calculation.

Blow-out velocity. Both boron slurries and magnesium slurries have been evaluated for blow-out velocity in the apparatus depicted in *Figure 5.* Blow-out velocities of 1-micron boron slurries were comparable to those of JP–4 fuel[7] (*Figure 11*); it may be surmised that the boron contributed little or nothing to the flame when near extinction. Magnesium, in contrast, markedly increased the blow-out velocity. Fifteen micron magnesium put the blow-out velocity intermediate to jet fuel and propylene oxide, whose flame speed is 1·8 times jet fuel. Flame with 1-micron particle could

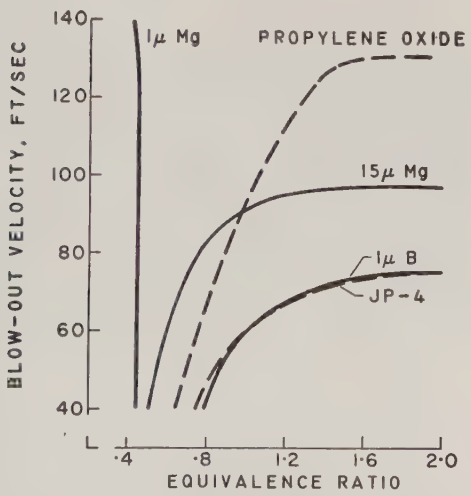

Figure 11. Blow-out velocities of boron and magnesium slurries

not be extinguished within the limits of the apparatus, except by reducing fuel–air ratio to less than 0·4 stoichiometric. In this respect, the 50 per cent, fine-particle, magnesium slurry resembles a 50 per cent solution of pentaborane in JP–4. The high reactivity of magnesium, the high burning rates accompanying small particles, and the high flame temperatures of the system contribute to this remarkably good flame stability.

Combustion efficiency—Experiments to find combustor design principles for boron slurries were conducted in 2, 5, and 16 in. diameter ramjet-type combustion systems. Although heat outputs (B.Th.U./lb. mixture) higher than the theoretical

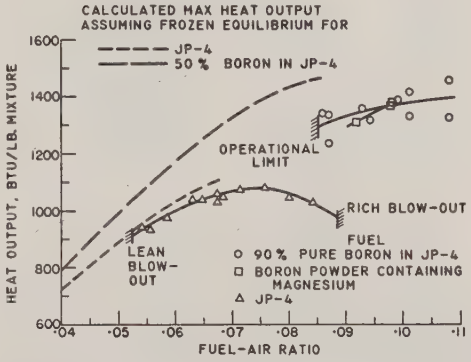

Figure 12. Experimentally determined heat output of boron slurry

for JP–4 fuel were attained with boron fuels at high fuel–air ratios, combustion efficiencies were generally below 85 per cent, and were particularly low at lean fuel–air ratios. For example, *Figure 12* presents results typical of the best design that was tried in the 5 in. combustor[16].

Baffle-type flame-holders performed poorly. Fine atomization was helpful, but fuel composition and combustor lengths from 40 to 100 in. had little influence on combustion efficiency. High local flame temperatures, and circulation of boron fuel into the flame were required for even moderately high efficiencies. The high local temperatures required for good efficiency destroyed combustor parts, however. On the other hand, attempts to keep combustor parts cool lowered efficiency and produced large deposits of boron oxide. In short, satisfactory combustion of boron was not achieved.

The high thrust potential, high fluid density, and high reactivity of magnesium slurry fuel make it suitable for short-range ramjet vehicles. Experiments in connected-pipe tests and in free-jet tests resulted in the design for a small ramjet engine[17] shown in *Figure 13.*

Net thrust coefficient exceeded both the maximum obtained with hydrocarbons (ethylene, in this example), and the maximum theoretically possible with hydrocarbons. Combustion efficiencies were only of the order of 85 per cent, however, and decreased to below 70 per cent at lean conditions.

Subsequently, a series of vehicles with dual 6·5 in. engines were flight tested to Mach numbers

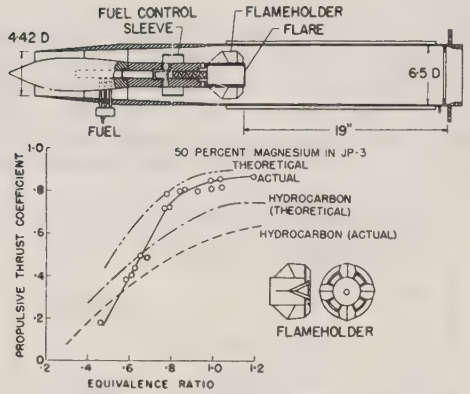

Figure 13. Experimentally determined thrust coefficient of 6·5 in. diameter ramjet with magnesium slurry

as high as 3·84 with magnesium slurry. The purpose of these flights was to procure both aerodynamic and propulsion data.

Combustion of magnesium slurry at afterburner conditions was studied in a 6 in. diameter duct provided with gases from a single turbojet combustor[18] (*Figure 14*). A thrust barrel measured total thrust. The figure shows that magnesium slurry was injected from eight radial stations located exactly at the downstream edge of a single *V* gutter that spanned the test section. JP–3 fuel required injection from a spray bar upstream of the flame-holder to burn; magnesium slurry injected upstream burned out the flame-holder. Some data for this combustor are shown in *Figure 15.* Both higher thrust, predicted thermodynamically, and combustion over a wider range of equivalence ratios were obtained with magnesium slurry than with JP–3. A single, short duration run of magnesium slurry in a full-scale afterburner produced thrust augmentation that checked closely the values from the 6 in. duct experiments.

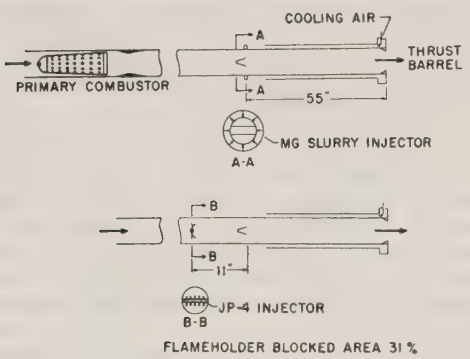

Figure 14. Apparatus used in magnesium slurry afterburner investigation

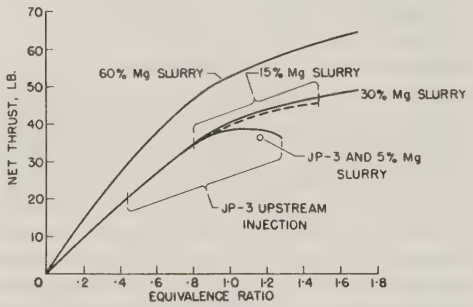

Figure 15. Results of small scale afterburner tests with magnesium slurry

If water injection in the turbojet engine is combined with afterburning, the engine should get the combined thrust augmentation of both systems. However, the experience is that water injection, particularly at high water-flow rates, adversely affects the combustion efficiency in the afterburner when it is burning conventional jet fuels. High water-flow rates may even extinguish the flame. Because of this problem, the effects of water on the combustion of JP–3 and on the combustion of magnesium slurry were determined in the apparatus of *Figure 14*; typical data[19] are given in *Figure 16.* Whereas water injection

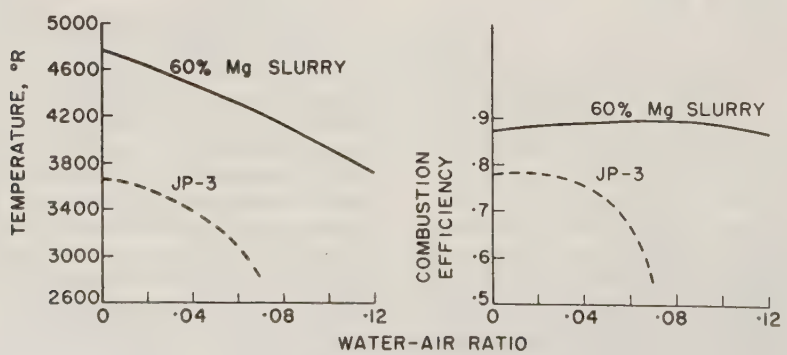

Figure 16. Effect of water injection on the performance of magnesium slurry in a small scale afterburner

rates above 4 per cent of the airflow seriously impaired combustion of JP–3, the combustion efficiency of the magnesium slurry was essentially unaffected at water-flow rates as high as 12 per cent of the airflow.

Research has shown that magnesium burns well, even at conditions where hydrocarbons burn only with difficulty. High thrust has been demonstrated. Fuel preparation and handling remain a problem, heating value is lower than hydrocarbons, and solid magnesium oxide is produced in the exhaust. There does not at present appear to be an application for this fuel that merits accepting its liabilities.

SOLID AND LIQUID COMBUSTION PRODUCTS

The combustion of fuels containing aluminium, boron, or magnesium result in the formation of the metal oxide which is a liquid or solid at most jet engine operating temperatures, as shown in Table 6.

TABLE 6

Element	*Oxide*	*Melting point* °R	*Boiling point* (1 atm) °R
Aluminium	Al_2O_3	4,180	4,550
Boron	B_2O_3	1,300	4,600
Magnesium	MgO	5,530	—

The presence of these solid or liquid combustion products can produce engine performance losses in at least two ways: (1) the oxide collects on critical engine surfaces spoiling the flow of combustion gases and inducing high frictional pressure drops; and (2) the oxide particles in the free stream may be of such a size that they fail to remain in temperature and velocity equilibrium with the gas, and consequently cannot transfer all of their energy to the gas during expansion through the exhaust nozzle.

The problem of oxide collection on critical engine surfaces is not severe when the oxide has an extremely high melting temperature, such as magnesium oxide. The oxides of boron and aluminium, because they are liquid over a portion of the temperature ranges of interest, tend to stick to surfaces, where magnesium oxide, being a solid over the entire temperature range, does not. The same reasoning exists when considering the lack of temperature and velocity equilibrium between the particles and the gas stream. Particles of diameter less than three microns would always remain in equilibrium with the gas, whereas particles of diameter greater than three microns would not. The particles initially formed in the combustion zone are probably submicron in size; however, particles of greater than three micron diameter would result when two or more particles suffer a series of collisions and stick together. Subsequent collisions will produce further growth. This sticking would be expected only with liquid particles, which eliminates magnesium oxide.

Two experimental programmes have been conducted by the NACA to give some insight on the particle size and oxide deposit problem: (1) determination of the formation and growth mechanisms of liquid boric oxide particles formed by the combustion of pentaborane; and (2) determination of the deposition rate of boric oxide particles on a surface.

Formation and growth of boric oxide particles

The particle formation and growth experiment was conducted using pentaborane–air combustion products. The combustion temperatures ranged from 1,200 to 2,300°R and pressures from 1·0 to 1·4 atmospheres. A theoretical analysis of the growth mechanism was conducted so that the experimental data could be extrapolated to conditions other than those tested. The analytical model used was to assume that the boric oxide was formed as a vapour in the primary combustion zone. Rapid addition of secondary air quenches the primary zone to the bulk combustion temperature causing the oxide to condense to particles containing a small number of molecules. These particles collide with one another, each collision resulting in the formation of a larger particle. The results of the analysis show that

$$D_p = \left[20{\cdot}6 \times 10^{-12} C\tau \left(\frac{RT}{\rho} \right)^{\frac{1}{2}} \right]^{2/5} \qquad (4)$$

where D_p is the particle diameter, cm, C is the boric oxide volume concentration, c.c./c.c., τ is the particle residence time, sec, R is the universal gas constant, dyne-cm/mole °K, T is the absolute temperature, °K, and ρ is boric oxide density, g/c.c.

The experimental apparatus (shown in *Figure 17*) consisted of a combustor 4 in. in diameter and 8 ft. long. At some pre-determined distance downstream of the fuel injector a sampling probe removed a portion of the combustion products. Just inside the probe entry liquid nitrogen was injected to quench the combustion products to a temperature well below the freezing point of the boric oxide. The now solid boric oxide particles were removed from the quenched stream with an electrostatic particle precipitator. The particles were analysed for size using electron-photomicrographs. The particle growth time was varied by changing the mass flow (thereby changing the velocity) and by changing the distance from the sampling probe to the fuel injector.

The theoretical equation expressing particle diameter as a function of time predicts that for conventional jet engine operating times, the liquid boric oxide particle diameter would never exceed 0·2 micron. The results of the experi-

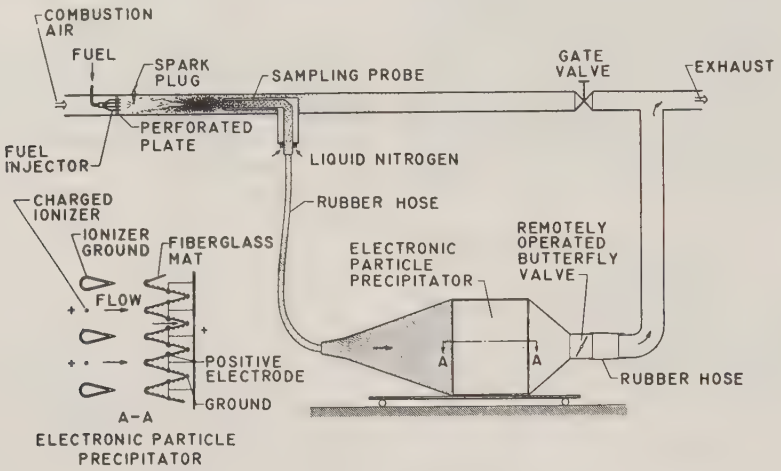

Figure 17. Apparatus used in particle size study

mental programme agreed with the analytical equation within an average deviation of ± 27 per cent. *Figure 18* shows the experimentally measured particle diameter plotted against the theoretical particle diameter (calculated at the experimental

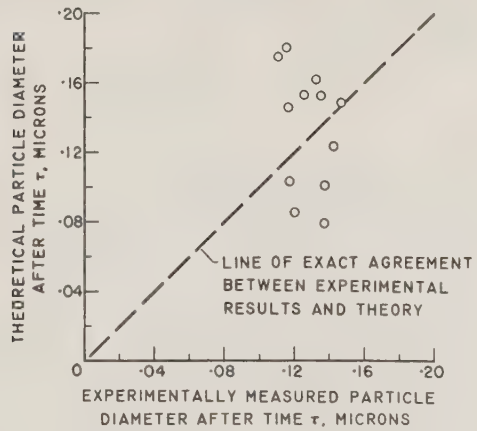

Figure 18. Results of particle size study

conditions using equation 4). If the data points fell on the dotted line exact agreement between theory and experiment would have been obtained.

Deposition rate of boric oxide particles

The deposition rate of boric oxide was measured on a surface immersed in the combustion products from a single turbojet engine combustor burning either pentaborane or trimethylborate–methanol azeotrope, a convenient boric oxide producing fuel. The test conditions covered a range of temperatures from 1,200 to 1,900°R and pressures from 1·0 to 1·5 atmospheres. The deposition rate was measured by running the combustor for some pre-determined length of time, shutting down the apparatus, and weighing the boric oxide deposited on the surface.

An attempt was made to correlate the experimental data with several analytical diffusion models. The best correlation was obtained when the experimental data were fitted to the variables influencing molecular diffusion. This correlation may be expressed as

$$N = 1{\cdot}68\ 10^{-12} n \left(\frac{RT}{\rho D_p^3}\right)^{\frac{1}{2}} \qquad (5)$$

where N is the particle diffusion rate, particles/ft.^{2}-sec and n is the particle volume concentration, particles/ft.^{3} (the remaining symbols and their units are identical with equation 4). An empirically determined constant was used to relate the variables, the resulting average experimental deviation being about ± 15 per cent.

Results of particles size and deposition investigations

From the data obtained from the boric oxide particle size and deposition rate experiments, the following was concluded:

(1) At all conditions of interest in jet engines the liquid boric oxide particles resulting from the combustion of a boron containing fuel are of such a size that they will always be in temperature and velocity equilibrium with the gas stream.

(2) Where conventional flow patterns exist, liquid boric oxide particles deposit on surfaces in a

manner that can be predicted by a molecular diffusion analogy.

The results of the particle size investigation make the calculation of the theoretical performance of boron fuels more reliable because no performance loss due to non-equilibrium between the particles and the gas should exist. The deposition study results make the prediction of deposit accumulations on engine surfaces possible. The prediction of deposition rates might eventually lead to a solution of the problem.

CONCLUSIONS

Based on theoretical performance, a number of substances show promise as fuels for increasing the flight limits of aircraft. Of these substances several have been chosen for research in equipment ranging from bunsen burners to full-scale jet engines; these include slurries of boron or magnesium metal in liquid hydrocarbon and liquid boron hydrides.

High combustion efficiencies with boron slurries were not obtained in practical equipment. Because of the high heats of combustion available in liquid boron compounds, further research on boron slurries has been discontinued.

Slurries of fine magnesium powder in a liquid hydrocarbon have been successfully produced and studied in small-scale and full-scale equipment. Near theoretical performance has been experimentally obtained. The difficulties of producing and handling a slurry of this type are not small, however, and a very special application for this fuel must appear before operational use is justified.

The liquid boron compounds appear to show the greatest promise for operational use in aircraft. Research is proceeding towards development of a fuel with a high heat of combustion that is also reasonably easy to store and handle. Research on combustion and engine problems has proceeded with boron hydrides. Their high reactivity with air makes them easy to burn in jet engine combustors. Not all of the problems are solved, however. The presence of liquid combustion products is a unique and difficult problem. Research is continuing towards a solution of these problems.

REFERENCES

[1] Olson, W. T. and Gibbons, L. C. Status of combustion research on high-energy fuels for ram jets. *Nat. Adv. Comm. Aero. Res. Memor. E51D23* (1951)

[2] Breitweiser, R., Gordon, S. and Gammon, B. Summary report on analytical evaluation of air and fuel specific-impulse characteristics of several nonhydrocarbon jet-engine fuels. *Nat. Adv. Comm. Aero. Res. Memor. E52L08* (1953)

[3] Schalla, R. L. Spontaneous ignition limits of pentaborane. *Nat. Adv. Comm. Aero. Res. Memor. E55B03* (1957)

[4] *Boron Hydrides and Related Compounds*, 2nd ed., May 1954. Callery Chem. Co.

[5] Parker, W. G. and Wolfhard, H. G. Properties of diborane flames. *Fuel* 35 (1956) 323

[6] Berl, W. G., Gayhart, E. L., Maier, E., Olsen, H. L. and Renich, W. T. Determination of burning velocity of pentaborane–oxygen–nitrogen mixtures. *Combustion and Flame* 1 (1957) 420

[7] Cook, P. N., Jr., Lord, A. M. and Kaye, S. Blow-out velocities of various petroleum, slurry, and hydride fuels in a $1\frac{7}{8}$ in. diameter combustor. *Nat. Adv. Comm. Aero. Res. Memor. E54A28* (1954)

[8] Gammon, B. E., Genco, R. S. and Gerstein, M. A preliminary experimental and analytical evaluation of diborane as a ram-jet fuel. *Nat. Adv. Comm. Aero. Res. Memor. E50J04* (1950)

[9] Smith, A. L. and Wear, J. D. Performance of pure fuels in a single J–33 combustor. III—Five hydrocarbon gaseous fuels and one oxygenated-hydrocarbon gaseous fuel. *Nat. Adv. Comm. Aero. Res. Memor. E55K04a* (1956)

[10] Reynolds, T. W. Effect of fuels on combustion efficiency of 5-inch ram-jet-type combustor. *Nat. Adv. Comm. Aero. Res. Memor. E53C20* (1953)

[11] Olson, W. T. and Breitweiser, R. NACA research on slurry fuels through 1954. *Nat. Adv. Comm. Aero. Res. Memor. E55B14* (1955)

[12] Coffin, K. P. Burning times of magnesium ribbons in various atmospheres. *Nat. Adv. Comm. Aero. Tech. Note 3332* (1954)

[13] Combustion of Elemental Boron. *TM 1009, Summary Report June–Oct. 1957.* Nov. 1957. Experiment, Inc.

[14] Spalding, D. B. Combustion of fuel particles. *Fuel* 30 (1951) 121

[15] Coffin, K. P. and Brokaw, R. S. A general system for calculating burning rates of particles and drops and comparison of calculated rates for carbon, boron, magnesium, and isooctane. *Nat. Adv. Comm. Aero. Tech. Note 3929* (1957)

[16] Reynolds, T. W. and Haas, D. P. Performance of slurries of 50 per cent boron in JP–4 fuel in 5-inch ram-jet burner. *Nat. Adv. Comm. Aero. Res. Memor. E54D07* (1954)

[17] Branstetter, J. R., Gibbs, J. B. and Kaufman, B. Magnesium-slurry combustion performance in 6·5-inch-diameter ram-jet engine mounted in connected-pipe facility. *Nat. Adv. Comm. Aero. Res. Memor. E53E27* (1953)

[18] Tower, L. K. and Branstetter, J. R. Combustion performance evaluation of magnesium–hydrocarbon slurry blends in a simulated tail-pipe burner. *Nat. Adv. Comm. Aero. Res. Memor. E51C26* (1951)

[19] — Effect of water vapor on combustion of magnesium–hydrocarbon slurry fuels in small-scale afterburner. *Nat. Adv. Comm. Aero. Res. Memor. E52H25* (1952)

FLAME FRONT STRUCTURES OF LEAN DIBORANE–AIR AND DIBORANE–HYDROCARBON–AIR MIXTURES

P. BREISACHER, D. DEMBROW and W. G. BERL

INTRODUCTION

It is now well known that the chemical reactions in flame fronts are spread out in time and space. For complex fuels and oxidizers a number of stable intermediates appear and disappear in the reaction zone. Significant information about the reaction paths and rates can be obtained from data on local composition and temperature[1]. It is also recognized that the reaction products need by no means come rapidly to thermodynamic equilibrium at the hot boundary of the flame. Several cases of incomplete reaction have been reported, particularly in the system fuel–oxides of nitrogen where appreciable quantities of nitric oxide (NO) may remain in the burned gases in the presence of oxidizable substances[2–6]. A similar observation on carbon-containing fuels indicates that CO is oxidized relatively slowly, in a manner uncoupled from the rate-determining flame reactions[1].

Another case of a flame reaction in several stages has been observed in the system of boron hydride–hydrocarbon–air by Berl and Dembrow[7] and subsequently confirmed by Parker and Wolfhard[8], and by Kurz[9]. In this system two separate and luminous reaction zones are sometimes in evidence. The second reaction zone can be quenched under suitable conditions without markedly affecting the combustion reactions in the first. It was postulated[8] that for systems made up of fuels of widely different reaction rates the more reactive fuel could undergo oxidation before the unreactive fuel which would, in turn, be oxidized at a later stage. Each reaction can be accomplished by a radiation typical of that system. No detailed chemical analysis of the diborane–hydrocarbon–air flames has been undertaken previously to support this hypothesis. The following report summarizes information based on sampling and chemical analysis of the reaction intermediates and products.

APPARATUS AND METHOD

All the analyses were carried out on flames stabilized on an uncooled 1 in. diameter Spalding-type flat flame burner at sub-atmospheric pressure (1/7 atm). Such a burner arrangement is very suitable for sampling experiments since it permits the stabilization of flames over a wide range of compositions and flow rates. As the flame approaches the burner grid heat is removed from the reaction zone thus decreasing the burning velocity and leading to a stable flame position.

The fuels (diborane, methane, propane) were stored in polyethylene balloons for daily use. It was found desirable to surround the diborane balloon with another balloon filled with dry nitrogen to avoid leakage into or out of the diborane container. Bulk storage of diborane was at −40°C to prevent slow thermal decomposition. Flow rates were controlled by needle valves and determined by gas rotameters. The gases were rapidly mixed in a pipe connector and passed into the burner. The entire system is shown schematically in *Figure 1.*

Ignition was accomplished with a Tesla coil discharge from an insulated inlet lead (usually a thermocouple wire) to the grounded burner. Flow rates were adjusted to give a stable flat flame. The exhaust gases were continuously removed by a vacuum pump. The deposition of boric oxide downstream from the burner necessitated frequent cleaning of the system.

Sampling in the gases was done with uncooled stainless steel probes spun down to an inlet diameter of 0·25 mm. Rapid cooling and quenching were obtained by expanding the sampled gases rapidly to low pressure beyond the sample probe inlet. The gas pressure in the sampling bulb was kept below 25 mm to assure sonic flow in the probe tip and rapid expansion beyond. Quartz and glass probes were found unsuitable since under some conditions (high temperature operation) sufficient quantities of boric oxide dissolved in the outer portions of the probe to lead to its destruction on cooling because of differential thermal stresses. Due to rapid plugging it was not possible to sample with probes of very small inlet diameters in those portions of the flame where boric oxide was present.

The sampling technique consisted of the following steps: before sample taking, a counter flow of gas flows through the probe to prevent deposit formation; on sampling, the flow was reversed by connecting to a vacuum reservoir; after sufficient time for sweep-out the gas flow was diverted to an evacuated flask.

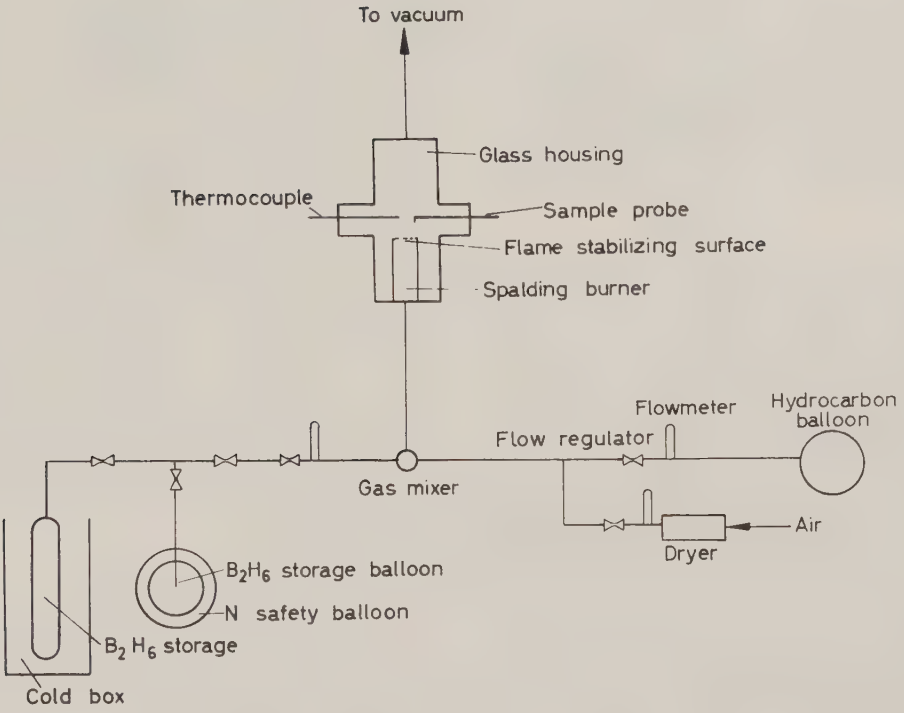

Figure 1. Schematic diagram of burner assembly

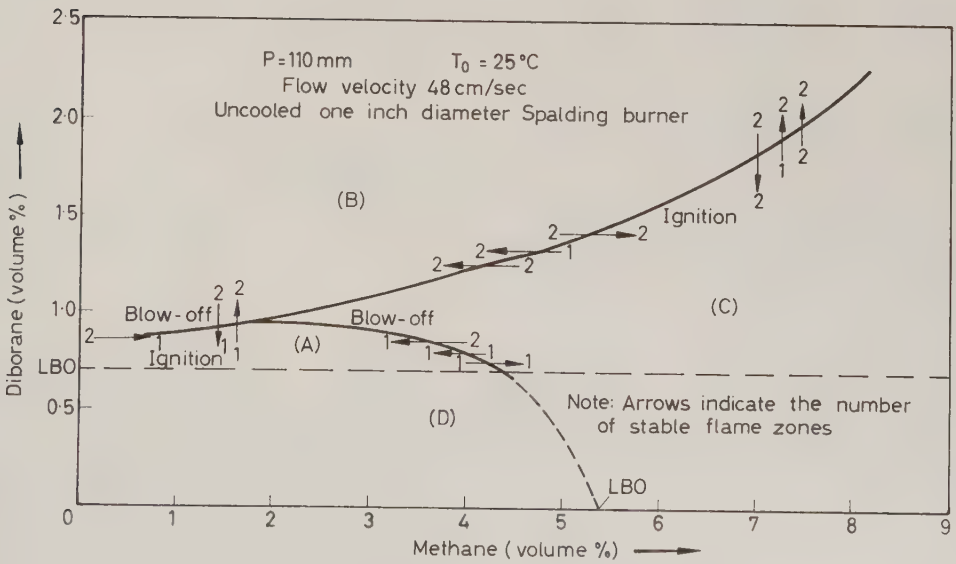

Figure 2. Stability diagram of diborane–methane–air system

The collected gas was compressed into a small volume with mercury and transferred to a gas chromatograph. Known volumes of gas were added to the evacuated inlet system of the chromatograph into which a suitable carrier gas (helium, N_2) was admitted. Permanent gases were identified on a 2 m long molecular sieve column while hydrocarbons were determined on a 4 m tri-*iso*-butylene-firebrick column. Methane experiments were carried out using a mass spectrometer for analysis.

RESULTS

In view of the high burning velocity of diborane, only lean mixtures of diborane–air can be stabilized on the burner. *Figure 2* shows the stability diagram for the diborane–methane–air system at 110 mm Hg and a flow velocity of approximately 48 cm/sec. Diborane–air mixtures below 0·77 per cent B_2H_6 were too lean to stabilize at these flows.

Either one or two reaction zones are stable, depending on mixture composition and ignition means. The first reaction zone involves the oxidation of diborane, but, as shown below, extensive hydrocarbon decomposition occurs in this zone as well. If a second reaction zone is stable further oxidation of the remaining hydrocarbon and products of decomposition occurs there. If the second reaction zone is not stable, a slow oxidation of the products from the first zone occurs in the heated gas.

Figure 2 indicates the mixture regions where one or two reaction zones are stable. In region *A* only one luminous reaction zone is stable. In region *B* two reaction zones are stable, although for lean methane concentrations no emission in the visible spectrum is apparent. Region *C*, on the other hand, can support either one or two reaction zones, depending on the ignition source. Region *D* will not support any diborane flames in the absence of added methane and will not be considered further in this discussion.

Addition of methane to diborane–air mixtures, the composition of which lies between the lean blow-off (LBO) and approximately 0·9 per cent diborane, produces only a single reaction zone and regions *A* and *C* are thus made accessible. For diborane–air mixtures above 0·9 per cent diborane, addition of methane leads to an immediate temperature rise. As the mixture composition enters region *A*, however, a sudden temperature drop occurs and only one reaction zone remains. Additional methane leads to region *C* but not to re-ignition since the temperature rise in the single reaction zone of region *A* is insufficient for the ignition requirements of a second zone. A spark discharge is adequate to bring about this second zone. If the initial diborane–air concentration is above approximately 1·1 per cent diborane, methane addition leads directly to region *C* with two reaction zones.

The arrows and numbers in the stability diagram indicate whether one or two reaction zones are established, as boundary lines are crossed by change of either methane or diborane concentration. All of these transitions have been observed experimentally. The second reaction zone can readily be seen to uncouple when the limiting blow-off concentration is reached. If flame stabilizers are available (wires, for example), the second reaction zone may find a new stable position downstream from the first reaction zone.

The gaseous reaction products were analysed downstream from the diborane–air reaction zone. The results are shown in *Figures 3–6* as a function of distance from the luminous zone for diborane–air, and diborane–air–propane. Temperatures were measured by means of a small (0·003 in.) platinum–platinum/rhodium thermocouple. From the known gas flows, temperature changes and probe positions, an approximate residence time can be obtained for the reactive system beyond the reaction zone.

DISCUSSION

The significant result of the sampling study is the observation that the oxidation of diborane is not complete in the luminous reaction zone, and that in the presence of hydrocarbons the diborane oxidation is accompanied by a considerable decomposition and partial oxidation of the accompanying hydrocarbon. The residence time of the hydrocarbons and their decomposition products in the reaction zone is too short to complete the reaction, which continues to proceed at a much slower rate in the heated gases beyond the luminous zone.

The discussion of the results can be divided into three parts, viz.; (1) the combustion of diborane–air in the absence of hydrocarbons, (2) the combustion of diborane–air in the presence of hydrocarbons, when only one reaction zone is formed, and (3) the combustion of diborane–air and hydrocarbons with the formation of two reaction zones.

Combustion of diborane–air in the absence of hydrocarbons

Hydrogen composition profiles of several diborane–air flames are shown in *Figure 3*. Measured gas temperatures are compared with calculated flame temperatures in *Figure 7*. For the leanest and coolest flames appreciable quantities of hydrogen exist at the downstream edge of the luminous zone (Table 1). This hydrogen is gradually consumed with distance and time and approximately 90 per cent disappears 10 mm beyond the reaction zone. These results indicate that during the diborane oxidation molecular

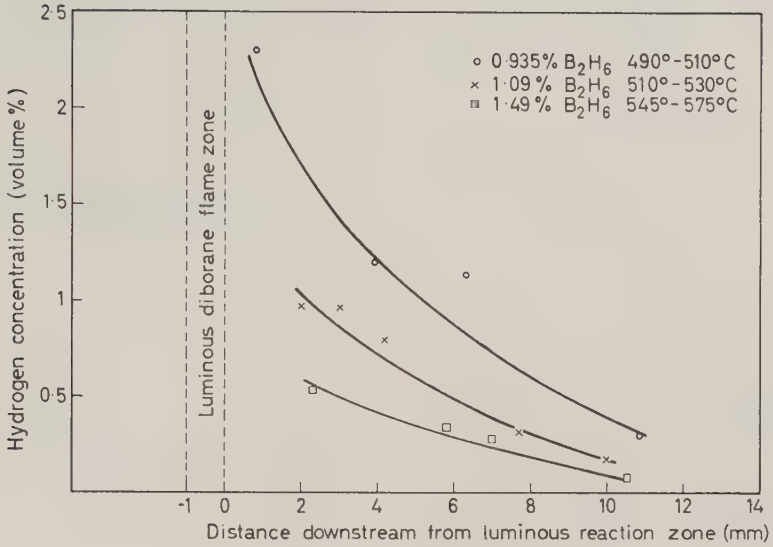
Hydrogen concentration (volume %)
Luminous diborane flame zone
○ 0·935% B_2H_6 490°-510°C
× 1·09 % B_2H_6 510°-530°C
□ 1·49 % B_2H_6 545°-575°C
Distance downstream from luminous reaction zone (mm)

Figure 3. Composition profile of diborane–air flames

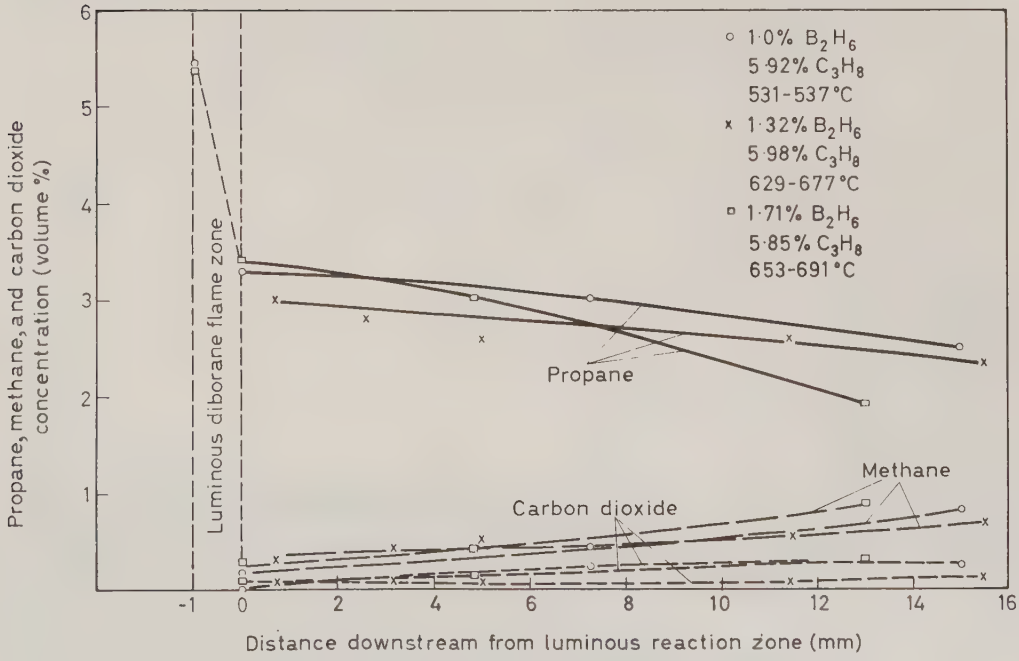

Figure 4. C_3H_8, CH_4 *and* CO_2 *composition profiles of* B_2H_6–*air*–C_3H_8 *flames*

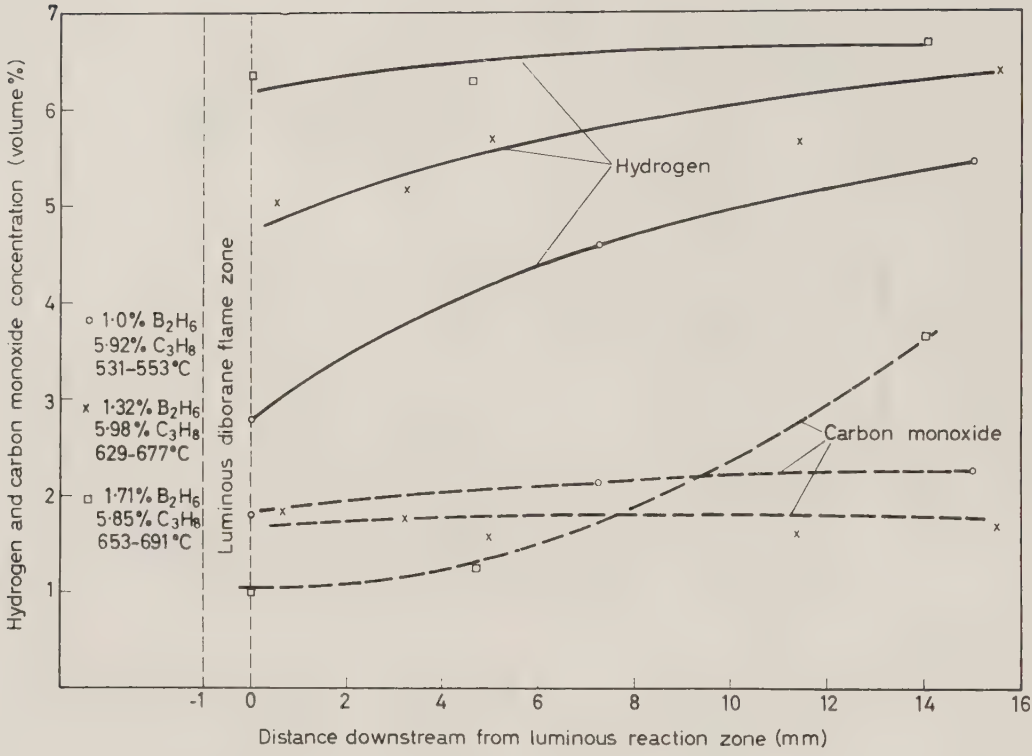

Figure 5. H_2 *and* CO *composition profiles of* B_2H_6*–air–*C_3H_8 *flames*

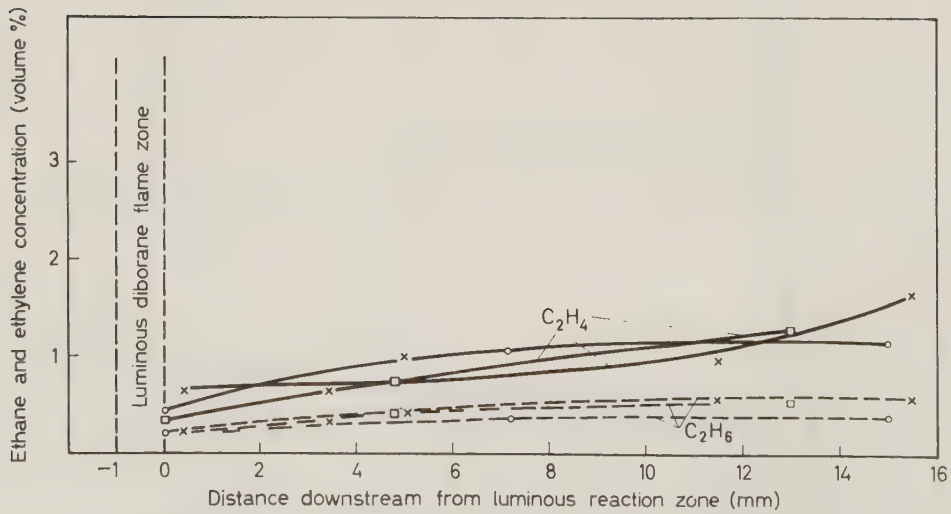

Figure 6. C_2H_6 *and* C_2H_4 *composition profiles of* B_2H_6*–air–*C_3H_8 *flames*

TABLE 1

B_2H_6 *Concentration*	*Fraction of unreacted hydrogen downstream from combustion zone*
0·935	80·3
1·09	29·1
1·49	12·5

hydrogen represents one of the important stable intermediates the subsequent rate of reaction of which is too slow to be completed in the flame zone itself. This oxidation of hydrogen to water is slow and only loosely coupled to the main reactions involved in the diborane oxidation.

It should be noted that in the coolest case investigated about 80 per cent of the hydrogen contained in the fuel is found as molecular hydrogen beyond the luminous reaction zone, thus indicating that any water that may have formed in the flame zone continues to react with diborane or intermediates to form additional hydrogen. This water reactivity distinguishes the combustion of the borohydrides from the combustion of hydrocarbons, of hydrogen and of carbon monoxide in that one of the final products of combustion can rapidly react with the starting material.

Although no detailed information is on hand as yet concerning the structure of the boron hydride–air reaction zone a reaction mechanism along the following lines is suggested:

$$B_2H_6 \rightleftharpoons 2\,BH_3$$
$$BH_3 + O_2 \longrightarrow BH_3OO$$
$$BH_3OO \longrightarrow BH_2O + OH$$
$$BH_2O \longrightarrow BO + H_2$$
$$BO + OH \longrightarrow HBO_2$$

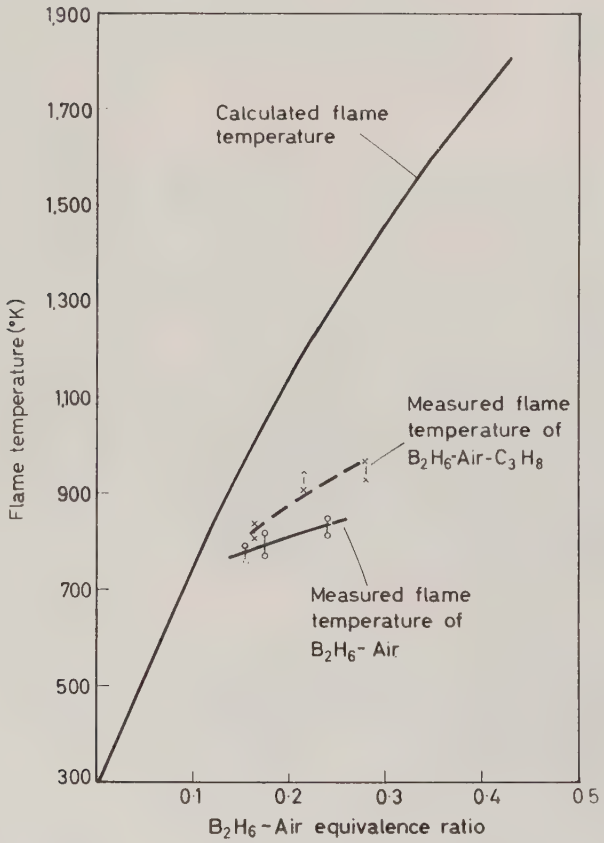

Figure 7. Experimental and calculated flame temperatures ($T_0 = 300°K$)

Spectroscopic evidence exists for the presence of excited BO and BH even at the low temperature of these flames[8,10]. At higher temperatures the gas phase reaction of hydrogen and oxygen becomes increasingly important within the reaction zone.

Rates for the slow oxidation of hydrogen in the nearly isothermal flow behind the flame can be obtained at several temperatures. Distance along the jet can be transformed into time units by assuming that the jet diameter is not changing in the distance of measurement and that gas density can be calculated from the known local composition

and temperature values. The hydrogen oxidation is taking place in an oxygen-rich atmosphere, in which the oxygen concentration changes very little during the course of the reaction. The partial pressures of the reactants are shown in Table 2.

TABLE 2

Mixture Composition in Diborane–Air Flames

B_2H_6 *Concentration*	*Partial pressure* (mm Hg)		
	H_2	O_2	N_2
0·935	3·5	28·0	118
1·09	1·45	26·7	120
1·49	0·84	24·5	119

The rate of hydrogen disappearance is much larger than values reported by Kowalsky[11,12] for the oxidation of hydrogen at comparable pressures in glass vessels. The reaction in the jet is proceeding at pressures which for spherical vessels would be below the first explosion limit. If one assumes that the diffusion distances are very small because of the nearness of boric oxide particle surfaces the explosive regime should occur at higher pressures than in unpacked vessels. The jet is surrounded by the parallel flow of cold air, and no chain initiation is possible from that boundary. However, boric oxide particles (or hydrated products) are intimately dispersed throughout the reacting stream, offering surfaces for chain initiation or breaking.

Combustion of diborane–air in the presence of hydrocarbons

If the mixture ratio of diborane–air is sufficiently low (less than 0·9 per cent B_2H_6), the addition of hydrocarbons in any proportion will not give rise to a second reaction zone in the absence of an external ignition source. The temperature and free radical concentration in and behind the diborane flame are inadequate to supply the ignition requirements for the hydrocarbon or its decomposition products. However, as shown in *Figures 4–6*, extensive cracking and partial oxidation of the hydrocarbon have occurred in the diborane–air reaction zone. This is followed by a slow continued decomposition and partial oxidation at nearly constant temperature. It is evident that the rates of reaction are markedly different in the two zones. The traverse time of the hydrocarbon through the diborane reaction zone cannot be specified with great accuracy since local temperatures and velocities in the flame are not yet available. For a flame thickness of 1 mm the traverse time is less than 3 msec under the flow conditions of these experiments. While 37 per cent of the propane has decomposed in the diborane oxidation zone, the subsequent reaction of an additional 20 per cent of propane requires 16 msec. This indicates that the decomposition of the hydrocarbon is strongly influenced by the reaction processes in the diborane–air flame and, in turn, influences the diborane decomposition.

In the slow subsequent reaction the distribution of products derived from the hydrocarbon does not differ in kind from the products emanating from the diborane flame. One might postulate, therefore, that although the rates are different the principal decomposition path for the hydrocarbon molecule is not markedly different in and beyond the diborane reaction zone. The more rapid rate within the flame, even though the temperatures are lower, must be due to the presence of a considerable number of chain carriers which can not only propagate the diborane flame but initiate thermal cracking and partial oxidation of the hydrocarbon molecule.

A part of the hydrogen appearing beyond the flame is probably coming from the diborane reaction. It is noteworthy that the hydrogen concentration remains high indicating that its rate of formation from the cracking reaction equals the rate of consumption to form water. It is also interesting that no spontaneous ignition of hydrogen is observed even at the highest measured temperature (691°C).

The rate of reaction beyond the diborane flame zone is slow compared to the decomposition in the diborane reaction zone and is made up of a large number of parallel reactions. The oxidation reaction does not go beyond the CO stage. The hydrocarbon interconversion rates appear to be markedly faster than reported by Avery *et al.*[13], in a flow experiment at 526°C.

In the case of propane oxidation the relatively small amounts of C_2H_6 are noteworthy which is in agreement with general thermal cracking experience. The hydrogen mole fraction, though, is greatly in excess of that usually experienced even if one subtracts the diborane contribution which is significant only at lower temperatures. The measured flame temperature of the diborane–hydrocarbon mixtures is always higher than that of an identical diborane–air mixture (*Figure 7*). This indicates that the partial oxidation of the hydrocarbon to CO (and to water) has contributed to the temperature rise in the diborane flame zone.

Combustion of diborane–air and hydrocarbons with the formation of two reaction zones

If the diborane–air temperature rise is sufficiently large, addition of hydrocarbons leads to the establishment of a second reaction zone downstream from the diborane–air zone. The separation from

the diborane zone decreases as the temperature rise in either zone is increased, and an eventual overlapping of the luminous reaction zones is likely. No sampling data are available in the luminous zone or in the in-between non-luminous zone, but it is likely that extensive hydrocarbon decomposition has again taken place in the diborane flame and that the second reaction zone now represents a combustion wave established in the combustion products emanating from the first zone.

Whether the two reaction zones are intimately coupled or not depends on the relative flame speeds of the individual steps. Thus, whenever the flame speed of the hydrocarbon zone (with its composition modified by the reaction in the diborane zone) is equal to or in excess of the diborane flame speed the two zones will be closely coupled and affect one another. In a flat flame burner arrangement both zones will move nearer to the grid where heat rejection to the burner walls increases and a new stable equilibrium position is found.

If the flow speeds and compositions are such that the gas velocity downstream from the diborane zone exceeds the flame speed of the remaining mixture the second zone cannot be maintained and blows off. If wires or grids are present they may act as flame-holders by offering a small re-circulation zone in their wake. In such a case the second flame can be positioned in space at will, although the slow thermal reaction behind the primary reaction zone is still proceeding and will have some effect on the point of stability and the stability requirements.

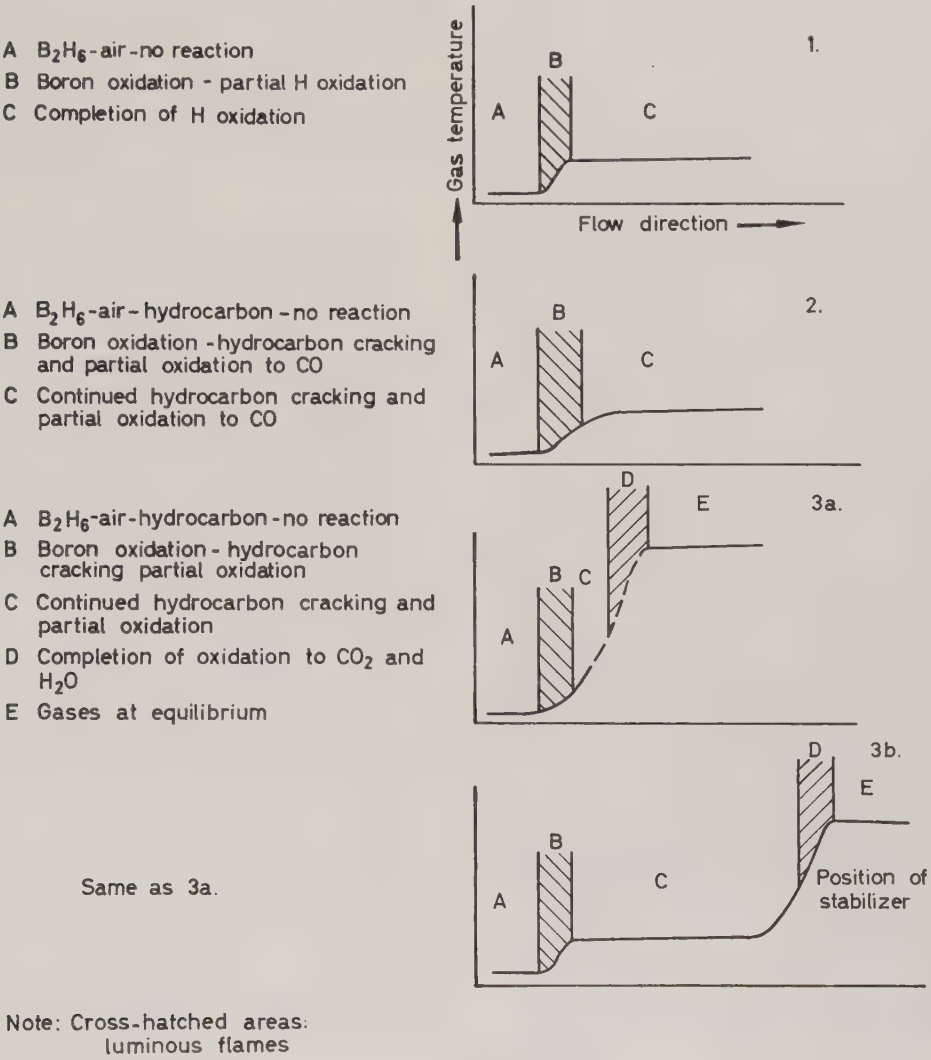

Figure 8. Schematic flame structures

The complex nature of the stability diagram can be accounted for in the following way: As discussed above, extensive decomposition of the hydrocarbon occurs on its travel through the first reaction zone. These products require higher temperatures for ignition than the original hydrocarbon, thus accounting for the rise of the ignition curve with hydrocarbon concentration. On the other hand, the flame speed of the mixture coming from the first reaction zone is a function both of the gas composition and the temperature rise of the first zone. Both parameters change as hydrocarbon and diborane concentrations are altered. Initially, increasing hydrocarbon additions require a higher diborane concentration to stabilize the second reaction zone because of the fact that the temperature in the diborane zone first drops with hydrocarbon addition. At higher hydrocarbon concentrations sufficient heat is released in the diborane zone to reverse this trend. These temperature changes affect the flame speeds of the gases leaving the first zone sufficiently to account for the initial rise and subsequent decline of the blow-off curve for the second reaction zone.

This double reaction zone has been described before in the literature[7,8,9]. Its establishment depends on an adequate initiating agent which may be either the temperature rise in the diborane–air reaction zone or a spark. The latter is needed for ignition if the diborane–air temperature is too low to initiate the second zone. For weak mixtures of hydrocarbons the second reaction zone may not be readily discernible by its luminosity even though temperature rise and composition profiles indicate its existence.

SUMMARY

Three types of flame structures have been identified in the diborane–air–hydrocarbon system (*Figure 8*): (1) Lean diborane–air flames have one luminous reaction zone in which all of the boron is oxidized to boric oxide while the hydrogen is only partially converted to water. The hydrogen oxidation is completed in a diffuse zone downstream from the luminous reaction zone. (2) Addition of hydrocarbons (CH_4, C_3H_8) to lean diborane–air flames leads to considerable cracking and carbon monoxide formation in the luminous diborane oxidation reaction zone. Further cracking and CO formation takes place in a diffuse zone downstream from this reaction zone. (3) For hotter diborane–air mixtures or if an igniting spark is used, a second reaction zone is formed which can couple with the diborane oxidation zone if the flow conditions and hydrocarbon concentrations are suitable. All of the hydrocarbon oxidation reactions are complete downstream from the second reaction zone. The second reaction zone may be lifted away from the diborane zone if the diborane or hydrocarbon concentrations are decreased appropriately.

This work was supported under Contract NOrd. 7386 with the Bureau of Ordnance, U.S. Navy.

REFERENCES

[1] Fristrom, R. M. and Westenberg, A. A. *Combustion and Flame* 1 (1957) 217
[2] Gaydon, A. G. and Wolfhard, H. G. *Flames*, p. 301. 1953. New York; Chapman & Hall
[3] Wharton, W. W., Violett, T. D. and Miller, E. *Sixth Symposium (International) on Combustion.* 1957. New York; Reinhold
[4] Gay, P. and Pratt, M. W. T. *Sixth Symposium (International) on Combustion*, p. 183. 1957. New York; Reinhold
[5] Hall, A. R. and Wolfhard, H. G. *Sixth Symposium (International) on Combustion*, p. 190. New York; Reinhold
[6] Miller, E. and Setzer, H. J. *Sixth Symposium (International) on Combustion*, p. 164. 1957. New York; Reinhold
[7] Berl, W. G. and Dembrow, D. W. *Nature, Lond.* 170 (1952) 367
[8] Parker, W. G. and Wolfhard, H. G. *Fuel* 35 (1956) 323
[9] Kurz, P. F. *Industr. Engng Chem. (Industr.)* 48 (1956) 1863
[10] Berl, W. G., Gayhart, E. L., Olsen, H. L., Broida, H. P. and Shuler, K. E. *J. chem. Phys.* 25 (1956) 797
[11] Kowalsky, A. *Phys. Z., U.S.S.R.* 1 (1932) 595
[12] — *Phys. Z., U.S.S.R.* 4 (1933) 723
[13] Appelby, W. G., Avery, W. H., Meebott, W. K. and Sarton, A. F. *J. Amer. chem. Soc.* 75 (1953) 1809

116

A STUDY OF ALKYLSILANE FLAMES

M. GERSTEIN

INTRODUCTION

For many years attempts have been made to relate the flame properties of hydrocarbons to the chemical reaction processes taking place. The problem is complicated by the fact that flame properties are usually functions of both chemical and physical properties. Hydrocarbons of significantly different flame properties usually also have different flame temperatures and different relative concentrations of combustion products. These differences affect both the rates of chemical processes and the rates of transport of heat and mass. Attempts to minimize these differences by the use of isomeric compounds usually also minimize the difference in flame properties. The low-temperature oxidation of hydrocarbons is also a difficult problem. While large differences exist between the slow oxidation rates of certain isomeric hydrocarbons, attempts to relate these differences to chemical structure are complicated by the fact that the conditions necessary to initiate reaction at one point in the molecule are usually sufficiently severe that the reaction proceeds rapidly through the remainder of the molecule. While primary, secondary and tertiary carbon–hydrogen bonds differ in their ease of attack during oxidation, the differences are not sufficiently great to make it possible to study the individual processes.

Studies of the combustion of alkylsilanes indicate that some of these difficulties may be avoided[1,2]. It was shown[1], for example, that two isomeric alkylsilanes having similar heats of combustion and identical combustion products had considerably different flame velocities. A relationship was indicated[2] between the number of silicon–hydrogen bonds in the fuel molecule and the ease of oxidation under low-temperature conditions. The combustion of alkylsilanes may thus isolate some of the important steps in flame chemistry and ultimately aid in the interpretation of the chemical processes in hydrocarbon flames. This paper is an extension of the studies of alkylsilane flames.

EXPERIMENTAL

The method of preparing the substituted silanes used in this study is described by Tannenbaum *et al.*[3]. They were prepared by reduction of the proper alkylchlorsilane with lithium aluminium hydride in anhydrous ethyl ether or dioxane and purified by distillation. Some of the physical properties of the fuels are listed in Table 1.

The flame velocities were measured by the tube method[4]. After each run with an alkylsilane, a fine deposit of silicon dioxide was left on the tube; this deposit was cleaned out with a glass-wool swab between measurements. To check the effect of the deposit, flame velocities were measured in clean tubes and in tubes coated with varying quantities of silicon dioxide. No effect of the deposit on measured flame velocity could be observed.

TABLE 1

Properties of Some Alkylsilanes

Fuel	*b.p.*[3]* °C	*f.p.*[3] °C	*Heat of comb.*[3] kcal/g	*Max. flame vel.* cm/sec	*Max. expl. temp.*[5] °C
$(CH_3)_4Si$	26·2	$\alpha = -101{\cdot}7$ $\beta = -99{\cdot}5$	10·45	60	450
$(CH_3)_3SiH$	6·7	−135·9	10·34	92	300
$(C_2H_5)_2SiH_2$	56·0	−134·4	10·78	111	255
iso-$C_4H_9SiH_3$	48·6	—	10·94	129	200
n-$C_4H_9SiH_3$	56·4	−138·2	10·93	148	185
CH_3SiH_3	−57·5	−156·8	—	250	126
$CH_2{=}CHSiH_3$	−22·8	$\alpha = -179{\cdot}1$ $\beta = -171{\cdot}6$	10·35	269	90

* Extrapolated

RESULTS AND DISCUSSION

The flame velocities for a series of alkylsilanes are given in Table 1 along with minimum explosion temperatures from Schalla and McDonald[5]. A number of trends are immediately apparent. The maximum flame velocity increases rapidly as the number of silicon-to-hydrogen bonds is increased. Similarly the minimum explosion temperature decreases markedly. The nature of the substituent group is also important. Comparing the four mono substituted silanes in Table 1, the flame velocities vary from 129 cm/sec for the *iso*butylsilane to 269 cm/sec for vinylsilane. A comparison of methylsilane and *n*-butylsilane shows that increasing the length of the carbon chain decreases the flame velocity. Since vinylsilane with two carbon atoms has a higher flame velocity than methylsilane, the reactivity of the substituent is also important. This is further borne out by comparing *n*-butylsilane and *iso*butylsilane. The ratio of the *n*-butylsilane flame velocity to that of *iso*butylsilane is 1 : 15. If the silicon atom were replaced by carbon the ratio of the flame velocities of the analogous hydrocarbons *n*-pentane to *iso*butane would only be 1·05. The effect of hydrocarbon branching is thus more pronounced in the silane derivatives than it is in the analogous hydrocarbon compounds.

Four of the compounds in Table 1 are of particular interest since they are isomers, yet have markedly different flame velocities. These compounds are tetramethylsilane, diethylsilane, *iso*-butylsilane and *n*-butylsilane. In addition to differences in chemical structure, these isomers have slightly different heats of combustion which would lead to slightly different flame temperatures. Diethylsilane which has a heat of combustion about 3·5 per cent greater than that of tetramethylsilane has a flame temperature of 2,278°K only about 1·4 per cent greater than the value of 2,247°K for tetramethylsilane, yet diethylsilane has a flame velocity about 85 per cent greater. If one assumes an activation energy of 40,000 cal/mole, the difference in flame temperature could only account for about 10 per cent of the change in flame velocity. The major portion of the difference in flame velocity must be attributed to differences in reaction rate. It is interesting to note (Table 2) that these compounds have flame temperatures similar to those of the hydrocarbons which would result if the silicon were replaced by carbon, yet in each case the flame velocities are considerably higher for the substituted silane. Again, the effect must be due to differences in reaction rate.

Flame velocity may be considered as a function of reaction rate and transport properties[7] as follows:

$$U_F^2 \alpha (\overline{w})(\alpha^*)$$

TABLE 2

Comparison of Flame Temperatures and Velocities of Alkylsilanes and Hydrocarbons

Compound	*Flame temperature* °K	*Flame velocity* cm/sec
$(CH_3)_4Si$	2,247	60
$(CH_3)_4C$	2,254‡	33†
$(C_2H_5)_2SiH_2$	2,278	111
$(C_2H_5)_2CH_2$	2,249‡	38†
iso-$C_4H_9SiH_3$	(2,290)*	129
iso-$C_4H_9CH_3$	2,253‡	37†
n-$C_4H_9SiH_3$	(2,290)*	148
n-$C_4H_9CH_3$	2,249‡	38†

* Estimated
† Reference 4
‡ Reference 6

where U_F is the flame velocity, $\overline{w}$ is the mean reaction rate and α^* is a thermal diffusivity. For flames of essentially equal flame temperature and identical products of combustion the ratio of the squares of the flame velocities for two compounds should be equal to the ratio of their reaction rates. The results for the four isomeric alkylsilanes are shown in Table 3. Certainly, the differences in

TABLE 3

Relative Reaction Rates of Some Alkylsilanes

Compound	$[U_{Compound}/U_{(CH_3)_4Si}]^2$
$(CH_3)_4Si$	1·00
$(C_2H_5)_2SiH_2$	3·42
iso-$C_4H_9SiH_3$	4·62
n-$C_4H_9SiH_3$	6·09

flame temperature indicated in Table 2 will affect these relative rates, but the general trend will remain unaltered. Assuming any reasonable activation energy, the differences in flame temperature could account for only a small part of the differences in reaction rate. Comparing tetramethylsilane and *n*-butylsilane, their flame temperatures differ by only about 2 per cent while the reaction rates predicted from flame velocities differ by a factor of 6.

Several chemical factors may contribute to the observed differences in reaction rate. The silicon-to-hydrogen bond is more susceptible to oxidation than are the remainder of the bonds in the molecule. This is illustrated by the explosion temperatures which decrease as the number of silicon-to-hydrogen bonds increase; in a similar manner, the

flame velocity increases. Another factor may also be significant. It has been shown for hydrocarbon flames that appreciable decomposition of the original fuel molecule occurs in the early parts of the flame[8]. In general, as the number of substituents increase the thermal stability increases[9] and correspondingly the flame velocity decreases. Both factors may be important in the flame reactions.

As one might expect, blends of an alkylsilane and a hydrocarbon give flame velocities intermediate between the two. The flame velocities of blends of diethylsilane and *n*-pentane are illustrated in *Figure 1*; both fuels have the same

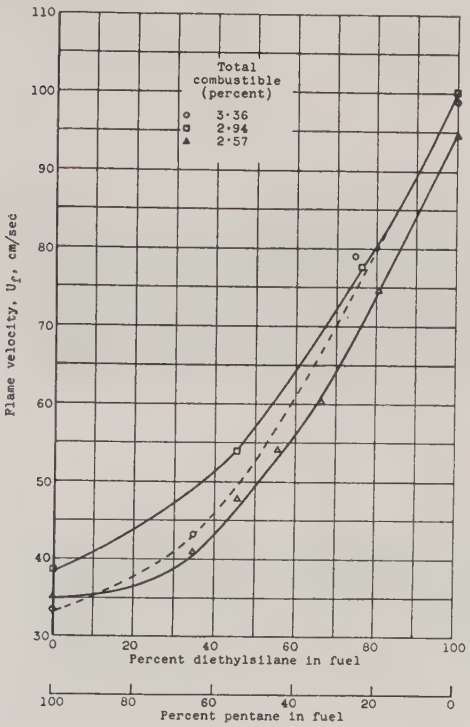

Figure 1. Fundamental flame velocity of diethylsilane–pentane–air mixtures

stoichiometric concentration on a molar basis. It is evident that there is no marked catalytic effect when the alkylsilane is mixed with the hydrocarbon; in fact, the first 20 per cent of diethylsilane increases the flame velocity only about 10 per cent. The flame velocities of the blends are lower than would be predicted from a linear blending relationship and are more closely given by a reciprocal blending relation of the form:

$$U_{F(\text{mix})} = \frac{100}{\frac{n_1}{U_{F_1}} + \frac{n_2}{U_{F_2}}}$$

where n is the molar per cent of the constituent in the mixture.

CONCLUDING REMARKS

Measurements of the flame velocities of some alkylsilane–air mixtures indicate that significant differences in flame velocity occur with changes in chemical structure. Unlike hydrocarbon–air flames, large differences in flame velocity are found for flames of similar flame temperature and identical products of combustion. Since chemical factors appear to have a more pronounced effect on the flame properties of the alkylsilanes than on hydrocarbons, it seems likely that these fuels may prove useful in establishing relationships between chemical structure and flame properties. The similarity of silicon to carbon may also be useful in relating the relationships found for the alkylsilanes to hydrocarbon flames. In order to properly interpret the relationship between the chemical factors and flame velocity for the alkylsilanes it is necessary to obtain more data on the flame properties and on the chemical reactions of these fuels.

REFERENCES

1 Gerstein, M., Wong, E. L. and Levine, O. Flame velocities of four alkylsilanes. *NACA RM E51A08*, 1951

2 Schalla, R. L., McDonald, G. E. and Gerstein, M. Combustion studies of Alkylsilanes. *Fifth Symposium on Combustion (International)*, p. 705. 1955. New York; Reinhold

3 Tannenbaum, S., Kaye, S. and Lewenz, G. F. Synthesis and properties of some alkylsilanes. *J. Amer chem. Soc.* 75 (1953) 3753

4 Gerstein, M., Levine, O. and Wong, E. L. Flame propagation. II. The determination of fundamental burning velocities of hydrocarbons by a revised tube method. *J. Amer. chem. Soc.* 73 (1951) 418

5 Schalla, R. L. and McDonald, G. E. Temperature-composition limits of spontaneous explosion for nine alkylsilanes with air at atmospheric pressure. *NACA TN* 3045, 1955

6 Simon, D. M. Flame propagation. III. Theoretical considerations of the burning velocities of hydrocarbons. *J. Amer. chem. Soc.* 73 (1951) 422

7 Gerstein, M. Review of some recent combustion experiments. *Third AGARD Combustion and Propulsion Colloquium*, Palermo, Sicily, March, 1958

8 Fristrom, R. M. and Westenberg, A. A. Flame zone studies. IV. Microstructure and material transport in a laminar propane-air flame front. *Combustion and Flame* 1 (1957) 217

9 Finholt, A. E., Bond, A. C., Jr., Wilzbach, K. E. and Schlesinger, H. I. The preparation and some properties of hydrides of elements of the fourth group of the periodic system and of their organic derivatives. *J. Amer. chem. Soc.* 69 (1947) 2692

SPONTANEOUS IGNITION PROPERTIES OF METAL ALKYLS

J. MARSEL and L. KRAMER

INTRODUCTION

In addition to being of general interest in the study of combustion mechanisms, the ignition behaviour of the spontaneously flammable metal alkyls is of considerable potential importance from the standpoint of: (1) the use of organometallic compounds as high energy fuels both in air-breathing and rocket engines, and (2) the use of air-hypergoles for slug ignition in ramjet and turbojet engines. Spontaneous ignition data have been obtained for a series of such compounds and fuel blends in both static and flowing systems with air as oxidizer.

Pertinent properties of metal alkyls are given in Table 1. Physical and chemical behaviour as well as special handling and safety techniques for these compounds have been thoroughly discussed in the chemical literature[1,2]. Methods of preparation are fairly simple[2], and the favourable logistics so necessary for large-scale fuel use are present; it has been estimated that production in multi-million lb./yr units would give materials in the general price range of $1 per lb.

STATIC IGNITION

Test apparatus

Static ignition tests were made by injecting fuel into slowly moving dry air at the desired temperature and pressure and photographing the results. The test chamber and accessories are shown in *Figure 1*. It consisted of an 11 in. high section of 10 in. IPS insulated pipe, with flanged cover plate, and 2 × 10 in. Vycor windows at front and back for viewing. Vacuum was maintained by pumping against an adjustable leak rate of dry air into the chamber.

The system was backlighted and timed with a Strobolume lamp furnishing an intense flash of light at 1/48 sec intervals, and photographed by a General Radio Strip Camera with film strip moving continuously past the Vycor window. The appearance of fuel droplets could be photographed during the light flash so that time of injection was known within 0·01 sec. Ignition delay was taken as time of injection to appearance of flame, as indicated on the film. Ignition was additionally checked by photography with a Fastax camera at 2,000 frames/sec.

The system was modified at various times as follows: (*a*) use of spray nozzle for injection, and (*b*) use of refrigerated coils inside the chamber for low temperature ignition (−40 to 20°F).

Experimental results

Figure 2 gives photographs from the strip camera showing several typical ignitions with air at 450°F and 5 in. Hg abs. Film is moving from right to left. *Figure 2a* is boron tripropyl, showing bottom firing after which it strikes back to the point of injection; *2b* is boron triethyl, igniting much closer to the point of injection; and *2c* shows aluminium triethyl igniting with a rapid spread of flame front.

A summary of ignition delays is given in Table 2. It can be seen that aluminium borohydride is the

TABLE 1

Properties of Metal Alkyls

Compound	*Formula*	*B. P.* °C	*Freezing P.* °C	*Density* g/ml
Trimethyl aluminium	$Al(CH_3)_3$	122–125	15·0	0·752 (20°C)
Triethyl aluminium	$Al(C_2H_5)_3$	194–197	−45 to −47	0·836 (20°C)
Triethyl boron	$B(C_2H_5)_3$	95	−92·5	0·688 (25°C)

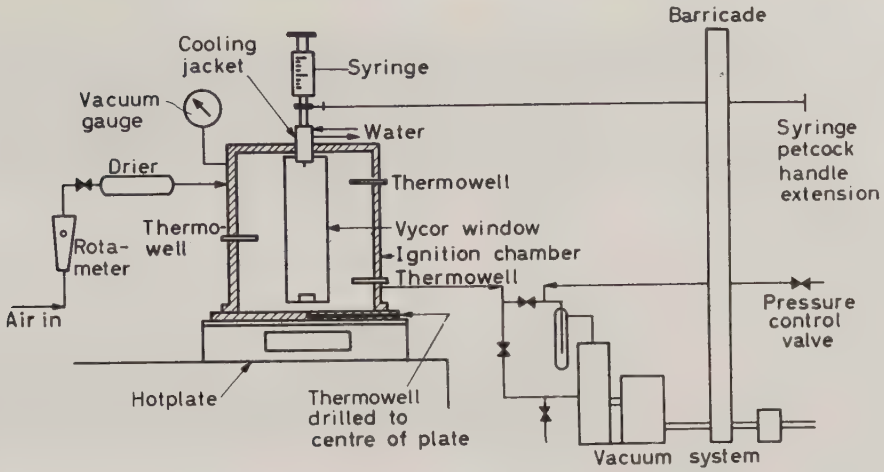

Figure 1. Static test equipment for measuring spontaneous ignition delay

(*a*)

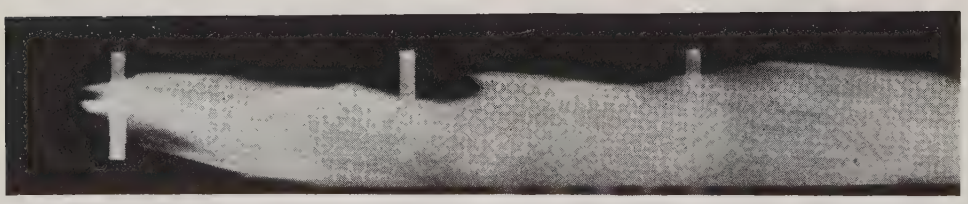

(*b*)

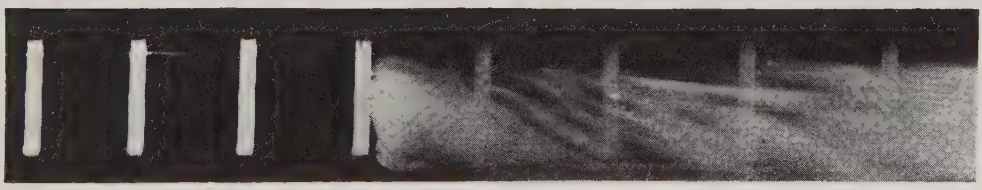

(*c*)

Figure 2. Continuous strip camera film record of ignition. Air is at 450°F *and* 5 in. Hg *abs. Strobolume flash illuminates chamber window every* 1/48 sec (*Read film from left to right*)

TABLE 2

Ignition Delays (Static Chamber) with Air at 450°F and 5 in. Hg. abs.

Fuel	*Ignition delay*, msec
Trimethyl aluminium	12
Triethyl aluminium	40
Aluminium borohydride	<10
Triethyl boron	20
Tripropyl boron	210
Tri*iso*propyl boron	380
Diethyl zinc	no ignition
Triethyl phosphine	310
1-Bromo-1-propyne	2,000

most reactive of the compounds tested, and trimethyl aluminium the most reactive of the metal alkyls.

Other variables

Several other variables affecting ignition were tested. The effect of change in air pressure is shown in Table 3. It is interesting to note that

TABLE 3

Average Values for Ignition Delay of Metal Alkyls at 450°F and Various Pressures

Fuel	*Air pressure*, in. Hg Abs.	*Ignition delay*, msec
Trimethyl aluminium	30	30
	5	12
	2	20
	0·5	20
Triethyl aluminium	5	40
	2	80
Triethyl boron	5	20
	2	50
	0·5	40

although ignition delays are increased at the lower pressures, they are still quite rapid even at 0·5 in.

The effect of JP-5 diluent on ignition delay is noted in Table 4. It is seen that aluminium borohydride is the most effective reagent from a concentration standpoint. Strip camera pictures of the aluminium borohydride ignitions are shown in *Figure 3*. Also to be noted are the rather small concentration limits between ignition and non-ignition.

Dropping the air temperature to 350°F (at 5 in.)

TABLE 4

Ignition Delays of JP-5 Blends at 5 in. Hg and 450°F

Fuel	Per cent JP-5	*Ignition delay* msec
Trimethyl aluminium	48·1	50
Trimethyl aluminium	61·0	460
Trimethyl aluminium	64·3	no ignition
Triethyl boron	48·2	170
Triethyl boron	60·2	200
Triethyl boron	61·5	no ignition
Aluminium borohydride	83·6	10
Aluminium borohydride	91·2	no ignition

had little effect on ignition delay, giving an increase of only 3 msec in the case of trimethyl aluminium. This encouraging fact led to some test work with a refrigerated chamber, which confirmed the low-temperature coefficient of the reaction.

FLOW SYSTEM

Although very good for preliminary screening purposes, the static system has the objection that mixing effects and fuel concentration effects cannot be determined accurately. Accordingly, a flow system which seemed particularly suited for metal alkyl studies was designed and constructed. The very rapid ignition recorded in the static tests precluded investigation of pre-mixed laminar streams of fuel and oxidizer. In addition, since the metal alkyls undergo decomposition and rearrangement at vaporization temperatures, liquid fuel at ambient temperature was used in all runs. In order that mixing of fuel–air be accomplished rapidly, a specially built pneumatic atomizing nozzle was used. This nozzle uses air to shatter a liquid laminar fuel stream; testing indicated that atomization was complete within one msec after fuel–air contact. In the study, variables were air temperature and pressure, equivalence ratio and rate of flow; fuel used was trimethyl aluminium. (A variety of other fuels are in the process of being studied.)

Test apparatus

The system flow diagram is shown in *Figure 4*, and the combustion test chamber in *Figure 5*. The chamber is constructed of Pyrex glass, 11 in. i.d. × 18 in. high. The nozzle is mounted in an aluminium bottom plate. The aluminium top plate is connected to a vacuum manifold which can maintain a chamber pressure ranging from 1 in. Hg abs. to 1 atm.

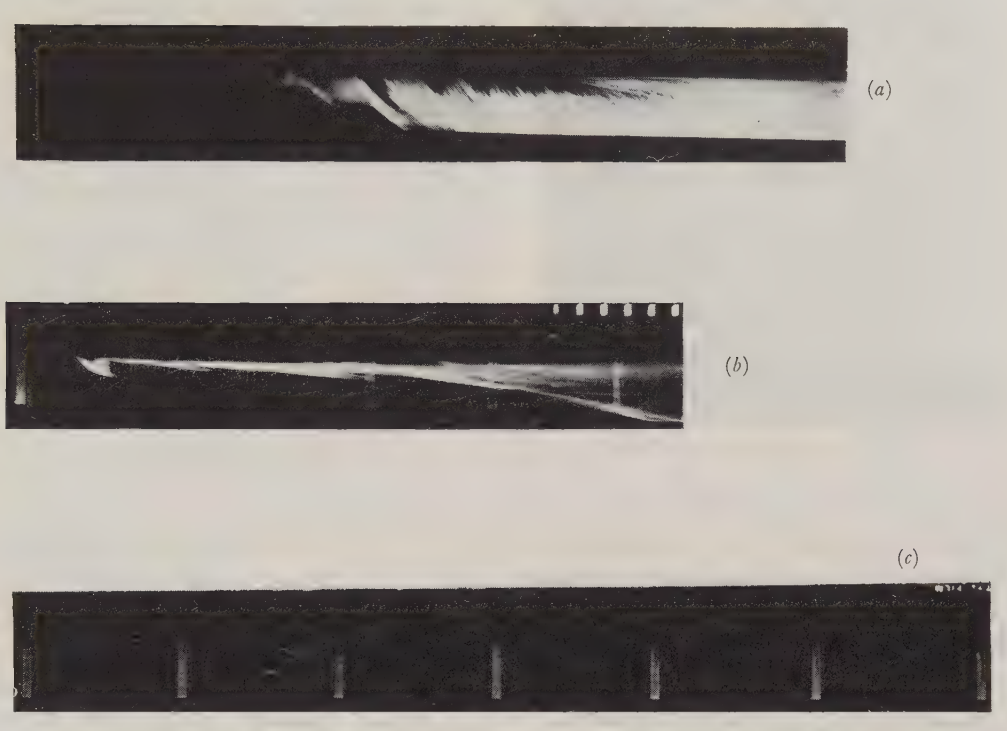

Figure 3. Ignition of solutions of $Al(BH_4)_3$ *and JP-5. (a) shows very rapid ignition of pure* $Al(BH_4)_3$*; (b) is ignition of* 16·4 per cent $Al(BH_4)_3$ *in JP-5, again with rapid but weaker ignition, as indicated by inability to pick up droplets in flame preceding ignition; (c) is* 8·8 per cent $Al(BH_4)_3$ *in JP-5, with some smoking but no ignition*

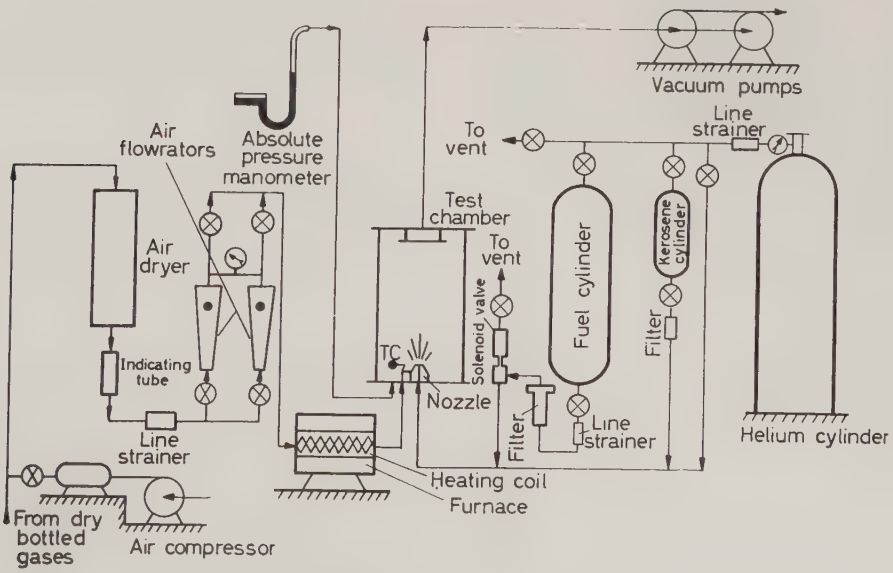

Figure 4. Flow sheet for spontaneous ignition system

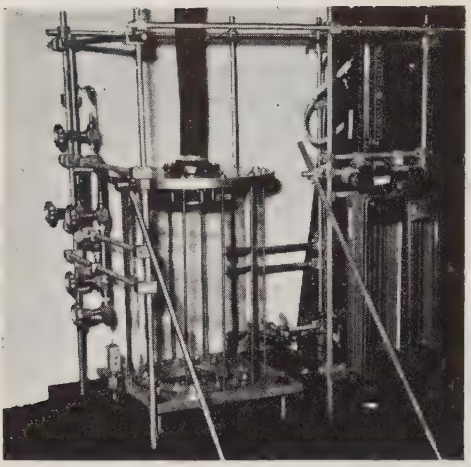

Figure 5. Combustion test chamber

Details of the nozzle are shown in *Figure 6*. Air leaving the nozzle at high velocities (up to Mach 1) shatters the stream of fuel into very fine droplets which appear to be completely dispersed in the gas phase within one in. of the nozzle face. The spray angle is about 14°, and does not appear to be sensitive to variations in air flow rate. Air flow is

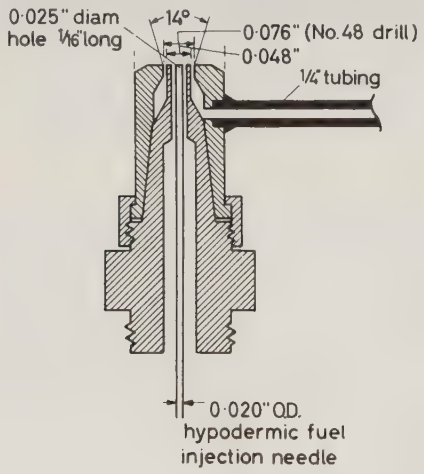

Figure 6. Details of nozzle for atomizing fuel and mixing with oxidant

measured by rotameters. The air is heated by a furnace and the temperature measured just before entering the nozzle.

Liquid fuel at room temperature is admitted to the nozzle through a fuel line made of 0·020 in. o.d. hypodermic tubing. The weight rate of fuel flow through this line is measured as a function of pressure drop through the line; fuel rate is varied by changing the gas pressure (helium) in the fuel cylinder. Calibration checks on needle and line are made prior to every series of runs. Inert gas flows through the needle continuously when fuel is not flowing. Grade F porous stainless steel filters are located prior to the solenoid valve and entrance to the tubing.

The nozzle spray is not directed into the open combustion chamber but into a glass chimney, 0·6 in. i.d. × 6 in. long, located directly on top of the nozzle, as shown in *Figure 7*. This arrangement prevents entrainment of chamber air into the high velocity air stream issuing from the nozzle. Ignition may occur within the chimney or outside; when the latter type of ignition occurs and the flame anchors at the chimney exit, a bunsen type of flame results.

A Fastax camera is used for recording rapid ignition, and a stopwatch for longer delays. Delay

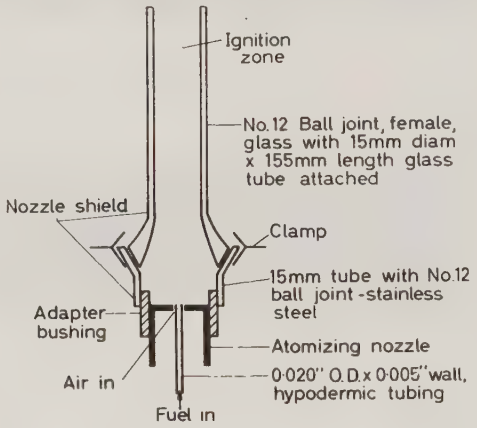

Figure 7. Nozzle chimney, mounted in combustion chamber

is measured as the time interval between appearance of smoke (which occurs immediately upon mixing) and appearance of flame.

Discussion of results

Three types of ignitions were noted: (1) ignition and burning in the chimney, indicating burning velocities greater than gas flow rates; (2) ignition outside the chimney with flame front moving back into the chimney but not to the nozzle; (3) ignition and flame stabilization at the top of the chimney.

Figure 8 shows the results of a series of runs made with trimethyl aluminium and air, plotting ignition delay (τ) against equivalence ratio (ϕ), defined as F/A actual to F/A at stoichiometric. As an example, curve I is for ignition with air at 600°F with the chamber at 10 in. Hg abs. Under these conditions trimethyl aluminium ignited in less than one second inside the chimney (tube) at all values of ϕ greater than 1·4; at values below 1·2, ignition occurred outside the chimney but struck back after a short time. At ϕ values below

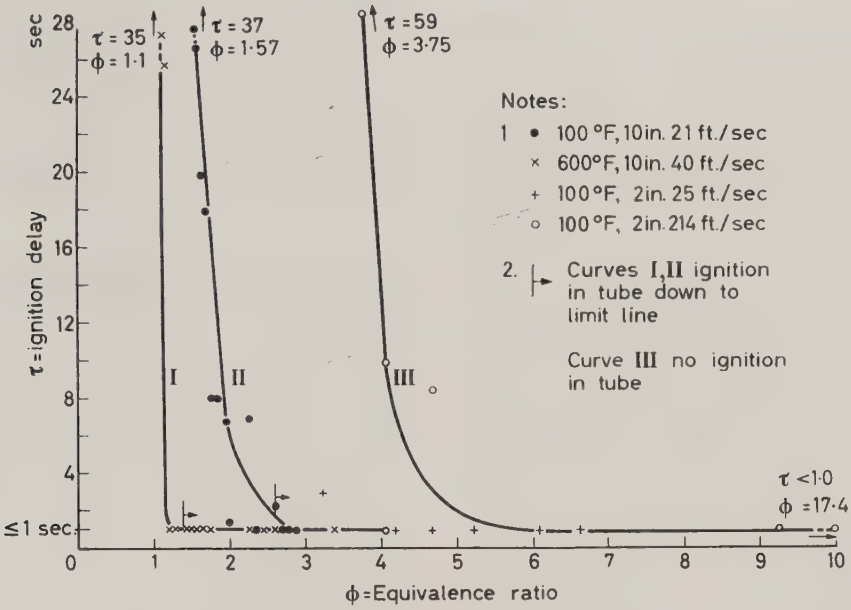

Figure 8. Ignition delays (flow system) with trimethyl aluminium and air

1·1 no further ignition occurred. As regards *Figure 8*, curve IV, representing ignition delays at 2 in. Hg and 600°F, fell almost identically on curve II, and therefore was not represented.

From the data observed to date one may conclude that: (1) F/A ratio has a critical bearing on ignition delay, with high values giving very rapid ignition; (2) the effect of temperature is much more pronounced at lower pressures (except for high values of ϕ): (3) higher pressures give considerably shorter ignition delays.

LOW-TEMPERATURE IGNITION

In low-temperature static chamber testing of the metal alkyls under fuel-rich conditions, it was found that the aluminium compounds (and trimethyl aluminium in particular) showed surprisingly rapid ignition. Dropping the air temperature to −40°F and 2 in. Hg abs. gave delays for TMA in the order of 20–50 msec depending on rate of injection. Certain of these data are summarized in Table 5.

In order to verify this conclusion, a series of flow ignition studies were conducted in 2 and 4 in. glass pipe, with air pre-cooled to −40°F and pressures ranging from 2–10 in. Hg abs. at Mach 0·01. The combustion tube was cooled by a glass jacket through which cold CO_2 was passed. Fuel was injected through a nozzle at 25°C. With fuel-rich systems ignition was of the order of 10–150 msec for trimethyl aluminium. Trimethyl aluminium and triethyl boron were also tested but gave correspondingly greater ignition delays.

Based upon these results, the Wright Aeronautical Division of the Curtiss-Wright Corporation initiated action which resulted in sea level and simulated altitude tests for emergency re-ignition of turbojet engines at the Aircraft Engine Laboratory

TABLE 5

Ignition Delays with Air at −40°F and 2 in. Hg abs. in Flow System

Fuel	*Minimum air velocity*, ft./sec	*Visual observation*	*Photographic observation*
Trimethyl aluminium	11·1	Strong ignition	Less than 20 msec
Triethyl aluminium	10·8	Smoke	Weak ignition after 280 msec
Trimethyl aluminium + 10% JP-5	12·4	Weak ignition	Doesn't show
75 Per cent TMA— 25 Per cent TEA	12·4	Ignition	150 msec

of the Bureau of Aeronautics in Philadelphia. Results of the investigation proved that the discharge of a small quantity (10–15 g) of pyrophoric aluminium alkyl blend into the engine combustion chamber invariably resulted in successful ignition of the engine up to 52,500 ft. conditions (the limit of the facility). Consequently, there is reason to believe that the pyrophoric ignition system can be used successfully at any altitude a jet engine can reach. Some advantages of such a system would be: (1) re-ignition possible at all operating altitudes, (2) shortens starting time cycle; (3) effects substantial equipment and weight savings by eliminating electrical ignition systems; (4) is completely insensitive to shock.

The authors express their appreciation to the Combustion Dynamics Division of the Air Force Office of Scientific Research for their financial support under Contract AF49(638)-173, and the Wright Aeronautical Division of the Curtiss-Wright Corporation for permission to publish certain selected test data.

REFERENCES

[1] KNAP, J. E. *et al. Industr. Engng Chem.* (*Industr.*) 49 (1957) 874

[2] NOBIS, J. F. *Industr. Engng Chem.* (*Industr.*) 49 (1957) 44A

118

THE COMBUSTION OF TITANIUM AND ZIRCONIUM

P. L. HARRISON

The combustion of metals is becoming of increasing importance due to their high heats of oxidation. This can result in high temperatures being produced, and in certain cases the energy release may be very rapid. The rate at which combustion spreads depends upon a number of factors.

One of these is the balance between the rate of heat production and the rate at which it can be removed. This factor is largely dependent upon how finely the metal is divided. A greater division of the metal results in both a higher surface to volume ratio, and hence a higher rate of heat production per unit volume, and a lower cooling rate.

If the surface to volume ratio is very large, the conduction of heat from the combustion zone by the metal is very greatly reduced. Heat loss is then by the relatively slow process of radiation, convection and conduction in a gas, and this leads to neighbouring particles of metal reaching the ignition temperature with great rapidity. If the finely divided powder is loosely packed together, the heat loss by convection is largely eliminated and under such conditions of low heat loss, spontaneous ignition of the metal can occur[1,2].

When solid metal rods are used, conduction by the metal rapidly absorbs large quantities of heat from the burning zone, leaving little heat for raising the temperature of the adjacent metal to the ignition point.

Consequently, as with other combustible substances, when in bulk the metal can be made to burn at a controllable and potentially useful rate, whereas, when finely divided, it will burn with explosive violence.

A study of the combustion of metals is therefore relevant at the present time. On the one hand we have the potential usefulness of these substances when burnt under controlled conditions, as high energy, high temperature-producing, fuels for rocket propulsion. On the other hand, however, we have the hazard they present in the finely divided state—a hazard that is of great importance not only for the industries machining these materials but also for the mining industry, where the combustion of metal wear fragments can be important in the accidental ignition of the explosive gas mixture in the mine[3].

An investigation is being made in this laboratory on the more physical aspects of burning as well as on the rates of heat release.

Apart from the diffusion of oxygen to the surface of the metal an important consideration is the heat of combustion of the metal and whether the metal burns in the solid, liquid or vapour.

Table 1 gives the values for melting and boiling points of four metals and their oxides, together with heats of combustion of the metals.

TABLE 1

	Metals			*Oxides*	
	Melting point °C	*Boiling point* °C	*Heat of combustion* kcal/g	*Melting point* °C	*Boiling point* °C
Al	659	1,800	7·2	2,020	
Mg	651	1,110	6·0	2,800	
Ti	1,730	3,200	4·55	TiO_2 d. 1,640 Ti_2O_3 d. 2,130	—
Zr	1,900	3,000–3,600	2·86	2,600–3,000	4,000?

Other factors that must be considered are the strength and porosity of the oxide, and how tightly it binds on to the parent metal. The properties of the metals and their oxides that are likely to greatly influence the mode of combustion are the melting or boiling points and the stability of the oxide at high temperatures.

EXPERIMENTAL METHOD

The metals were studied in wire form, wire diameters of 1·0 mm and 0·5 mm being used. These wires were supported at the centre of a cylinder and were ignited at one end by passing a high current pulse through a small coil of 0·5 mm diameter titanium wire that was wrapped around the end of the wire. The pulse, obtained by discharging a bank of condensers through the coil, ignited the coil, and this melted and collapsed on to the wire to be studied, thus igniting it. The resulting combustion was followed either by a continuous recording camera or by a ciné camera.

The apparatus is shown in *Figure 1* and consists essentially of a brass cylinder 9 in. in diameter and 15 in. long, closed at both ends by a brass plate, and having a glass window along its length. One of the end plates has two terminals through it so that the igniting current pulse may be fed in.

This cylinder was sufficiently large to ensure that the percentage of oxygen changed by less than 1 per cent during combustion. Experiments were carried out with both vertical and horizontal wires. The wire was supported horizontally on mica knife-edges, as shown, and the field of view was restricted by the adjustable slit. *Figure 1* shows the horizontal set-up. When the vertical set-up was required, the mica supports and adjustable slit were removed. In the vertical

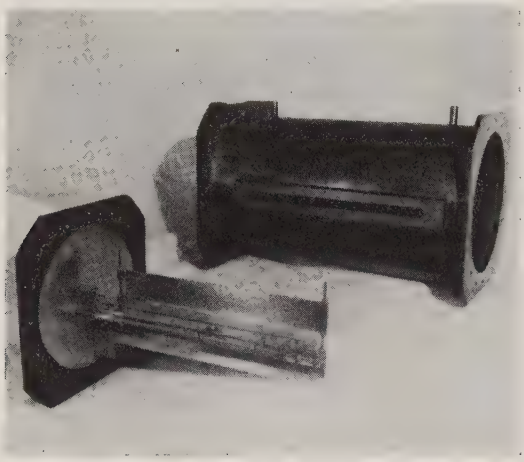

Figure 1

set-up, the wire was supported by clamping at the top and was ignited at the bottom.

In order to fill the chamber with gas of the desired composition it was evacuated and filled with the correct proportions of air and oxygen. All the experiments were done at atmospheric pressure. The velocity of the burning zone along the wire was obtained from the traces produced with the continuous recording camera.

EXPERIMENTAL RESULTS

In the description of the experimental results, the two metals will be dealt with separately.

Burning of titanium wire

Vertical wire—The variation of burning velocity with oxygen percentage for vertical titanium wires is shown in *Figure 2*. It is seen that this velocity increases rapidly with increasing oxygen percentage. With 1 mm diameter wire there is a critical oxygen percentage (51 per cent) below which no burning takes place. Above this percentage, the velocity rises more and more sharply with increasing oxygen percentage up to the upper limit of 100 per cent.

With 0·5 mm diameter titanium wire however this is not the case. First there is no definite cut-off at low percentages. At 40 per cent the combustion often dies out part way along the wire, thus making measurement of velocities difficult. This also occurs above 85 per cent, a fact which will be discussed later. Secondly, the rate of rise of velocity with oxygen percentage shows a marked drop at about 85 per cent.

Figure 2 also shows how the ratio of the velocities for the two wire diameters varies with oxygen percentage. This shows up the marked change of velocity for the thinner wire at 85 per cent.

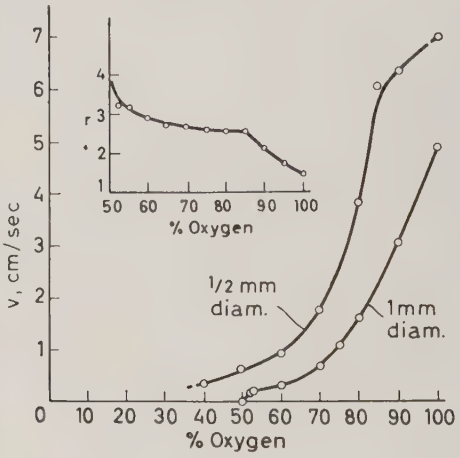

Figure 2

A typical photographic record is shown in *Figure 3*. It is seen that the burning appears to progress discontinuously along the wire, and that

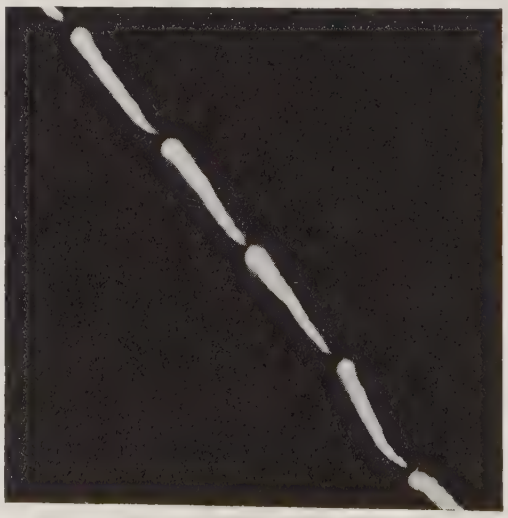

Figure 3

hot material falls from the burning zone at regular intervals along the wire. This was more clearly seen by studying the combustion with a ciné camera.

Figure 4 is a sequence from such a study. It is seen that the burning is associated with a molten globule hanging from the end of the wire. It is this globule that is drawn up in a discontinuous fashion thus producing the jumps in the combustion record. The globule remains stationary in space while the burning front moves along the wire. After this has moved a certain distance, the globule suddenly springs up into a new stationary position and the cycle

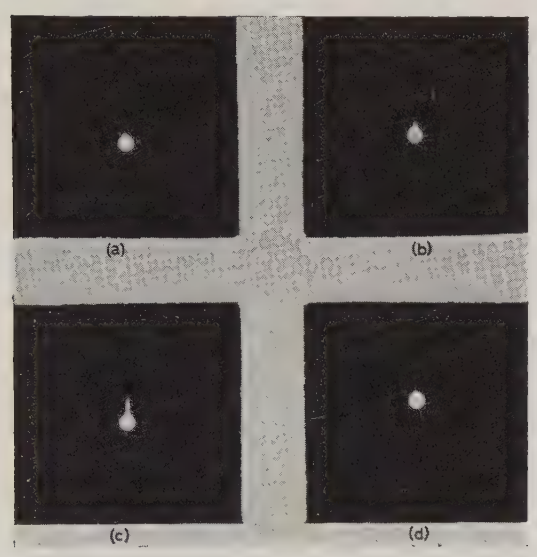

Figure 4

is repeated. Since the globule is constantly increasing in weight there comes a time when it falls off because it has become too heavy to be kept on the wire by surface tension. Since the wire is uniform in diameter and density, and the combustion is in a steady state we would expect such occurrences to be regularly spaced along the wire. *Figure 3* shows that these globules do drop off very regularly.

If this falling of the globule is determined almost entirely by surface tension effects it could be expected that the maximum weight of the droplet would be directly proportional to the diameter of the wire used, and therefore that the distance along the wire between two falls would be inversely proportional to the diameter. The experimental value for the ratio of this distance for the thinner wire to that for the thicker wire equals 2 to within a few per cent, and suggests that surface tension is playing an important part in the combustion.

In the records obtained when the thinner wire is burnt in oxygen percentages in excess of 85, all regularity has gone both in the movement of the globule along the wire and in the rate at which successive globules fall away. In these cases the average rate of falling is very much greater than that for wire of the same diameter at lower percentages.

Horizontal wire—Experiments with horizontal titanium wires of 1·0 mm diameter gave variations of velocity of propagation with percentages that were very similar to those obtained with vertical wires of the same diameter.

The records obtained have precisely the same discontinuous nature, and the studies using the ciné camera with horizontal wires have shown exactly the same globule formation and movement. The mica supports had no effect upon the velocity of burning below 80 per cent oxygen. Above this, each support gave rise to a slight reduction of the velocity. The points for the high percentages were therefore obtained from the records produced by the half of the wire that projected beyond the first support (see *Figure 1*).

Combustion of zirconium

High oxygen percentages—Figure 5 shows the variation of burning velocity with oxygen percentage for vertical wires of zirconium of 0·5 mm diameter. It is seen that the general trend of this

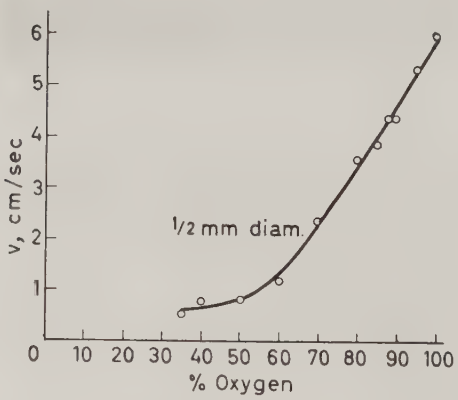

Figure 5

variation is the same as for titanium. A mixture containing 35 per cent oxygen does not represent the lowest limit of combustion. Failure of the ignition wire to burn has not allowed the effect of still lower percentages to be studied.

The mode of burning for the higher percentages is the same as for titanium, namely, the combustion is associated with a molten globule that hangs from the end of the wire. The movement of this globule along the wire is similar to the movement of the globule along the titanium wire.

Low oxygen percentages—At oxygen percentages of 50 or lower the mode of burning is different. The temperature reached is not high enough to melt the bulk of the oxide formed and this

therefore forms a solid sheath over the metal, preventing the formation of a globule. It also hinders the oxygen reaching the surface of the metal, and consequently the combustion of any section of the wire is extinguished before combustion has reached completion. *Figure 6* shows the cross-section of the wire after combustion. The resultant wire is extremely brittle and breaks at the slightest jolt. The oxide layer is comparatively thin; of the order of 0·1 mm for

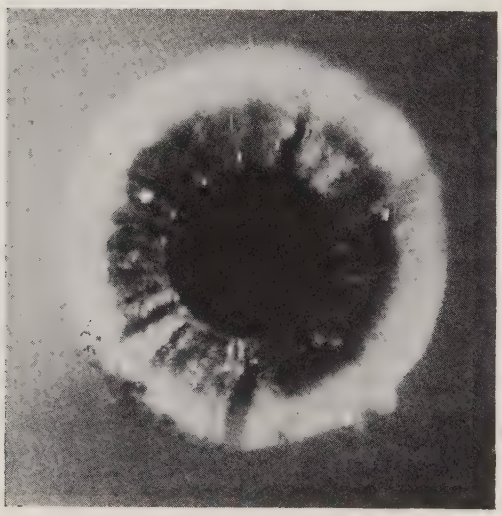

Figure 6

50 per cent and less for the lower percentages. The cavity at the centre is due to shrinkage of the metal on cooling. The metal is obviously very highly stressed during the cooling and solidification and this undoubtedly explains the resulting brittleness.

A further characteristic of this mode of burning is the splitting open of the oxide layer near the end of combustion. This is due to the solidification of the metal.

Experiments with aluminium wires show the cause of the effect. Currents sufficient to melt the aluminium were passed through these wires, the thin tough oxide formed containing the molten metal in the wire form. When the current was switched off, the wire rapidly cooled, and bulges suddenly appeared in the wire, some of them being of sufficient size to split the oxide film open. It was discovered that between these bulges the oxide skin had buckled and collapsed, there being little metal at these points. This was the result of the high surface tension of the molten metal, at temperatures only a little above the melting point, causing the metal to form droplets beneath the oxide skin. The metal bunched itself together at various points along the wire immediately prior to solidifying, and where this was of sufficient magnitude the oxide skin was stretched to breaking point.

With the zirconium wires, the nature of the oxide is such that it stretches very little before it splits, so that there is very little variation of overall diameter of the resulting wire, but the oxide is split open at places along its length. At oxygen percentages only a little below 50 this bursting open is fairly violent and produces a shower of white-hot sparks. At the low percentages however very few sparks are formed and the metal that bursts through forms a collection of small globules in the split. One or two of these globules were found to consist entirely of a very thin hollow shell of oxide.

It should be noted that the division between the mode of burning at the low oxygen percentages and the globule mode in the high percentages is not a sharp one. There is an intermediate zone of percentages where the point of the burning zone travels some distance ahead of the globule. The part of the burning wire that is ahead of the globule commences to form a second globule before the first falls away.

Combustion of metals in bulk

A small furnace was constructed by tying two fire-clay boats together with thick copper wire. This was held horizontal and packed with short lengths of metal wire. A length of 0·5 mm zirconium wire along the centre acted as an ignition wire. A stream of oxygen was passed through the furnace and a high current pulse was switched through the zirconium ignition wire.

With titanium the metal burnt completely. The product of the combustion was a brittle porous bluish-black mass which had a yellow-white coating on the surface. Occasionally intense colours, deep mauves, blues and golden yellows, were formed within this mass. It is not certain whether these were due to lesser oxides of titanium or contamination from the fire-clay troughs. Large quantities of the yellow-white oxide were found deposited at the exhaust end of the furnace which was cooler than the rest.

With zirconium, the oxide formed in the first stages of combustion coated the unburnt metal and extinguished the combustion before much metal had burnt.

Estimate of the temperature

A preliminary investigation of the temperatures reached in metal combustion processes was made in the case of titanium, using this furnace method. A small coil of gold wire was placed in the bottom of the furnace near the oxygen inlet end, and the titanium wire packed in on top of it. The metal was ignited, and when the combustion was complete the furnace was broken open. None

of the gold was found in the original position, but most of it was found deposited at the exhaust end of the furnace, and on the asbestos shield placed nearby, as the grey-violet coloured aurous oxide. The inference is that the gold all boiled away and that the vapour was swept to the exhaust end of the furnace. The boiling point of gold is 2,950°C, and the temperature produced during the combustion must therefore be greater than this.

When a small coil of platinum was placed in a similar place in another furnace, the platinum was found as a spherical lump in the original place. The metal had obviously melted (m.p. 1,769°C)[4] but the temperature had not been above the boiling point of platinum. The boiling point temperature of platinum is in doubt, but it is probable that it is as low as 3,500°C, and so this may be taken as the upper limit of the temperature that can be assigned to the combustion of titanium. These are obviously crude methods of estimating temperatures, and spectroscopic and other methods are being considered.

DISCUSSION

The results of this study show that the combustion of titanium and zirconium takes place at the surface of the molten metal. There is no evidence of substantial vaporization of the metal. The combustion appears confined entirely to the surface of the burning mass and there is no appreciable formation of smoke as there is during the burning of magnesium, which vaporizes prior to burning[5].

Other factors which are shown to be important are the fusibility of the metal oxide and the balance between rate of heat production by oxidation, and rate of heat loss. In metals such as zirconium, where the melting point of the oxide is high, these two factors may interact, so that a slight increase in heat loss over heat production can completely change the mode of combustion. This was found to occur with zirconium wire 0·5 mm in diameter at about 50 per cent oxygen.

Wolfhard and Parker[6] have made measurements of the temperature of oxy-magnesium-powder flames and obtained a value of about 3,000°C. The experiments in this study carried out with the use of gold and platinum wire show that the temperature obtained with burning titanium was of this order. The absence of any appreciable vaporization of the titanium metal shows that the temperature reached in these experiments, during combustion, was below the boiling point of the metal. The majority of references give this as about 3,200°C and this may therefore be taken as the upper limit to the temperature reached. The experiments with zirconium suggest that for conditions that produce a low rate of burning, the temperature is a little lower than the melting point of the oxide which is between 2,600 and 3,000°C. Hence, again, the temperature is of the same order as that found for magnesium by Wolfhard and Parker.

A detailed analytical study of the combustion process is not yet possible, but the following simplified study gives some idea of the results that can be obtained.

We assume that the combustion travels through the wire as a definite flame front with velocity v, and that there is no production of heat ahead of this flame front. A second assumption is that no heat is lost from the surface of the wire ahead of the flame front.

With the x axis along the wire, the heat equation for the wire ahead of the flame front is:

$$k\frac{\partial^2\theta}{\partial x^2} + \rho s v\frac{\partial\theta}{\partial x} = 0$$

where θ is the temperature, k is the thermal conductivity, ρ is the density and s is the specific heat.

The solution of this is

$$(\theta - \theta_a) = (\theta_f - \theta_a)e^{(\rho s v/k)(vt-x)} \qquad (x \geqslant vt)$$

where θ_f is the temperature of the flame front and θ_a is the ambient temperature.

This gives the temperature gradient at the flame front ($x = vt$) as

$$\frac{\partial\theta}{\partial x} = -(\theta_f - \theta_a)\frac{\rho s v}{k}$$

If H is the total heat flowing across the flame front

$$H = -kA\left(\frac{\partial\theta}{\partial x}\right)_{x=vt}$$

which gives an expression for v

$$v = H/A\rho s(\theta_f - \theta_a)$$

where A is the cross-sectional area of the wire.

This analysis is, of course, a very simplified one. In practice there is no definite 'flame' front. Also the burning takes place on the surface only and hence there is conduction into the centre of the wire as well as along it. However, for the globule mode of combustion these differences may not be serious, and this study does give at least qualitative agreement with experimental results.

The temperature gradient at the flame point is given by $\partial\theta/\partial x = -(\theta_f - \theta_a)\rho s v/k$ and is therefore steeper for the higher velocities of propagation. A study of the wire, after combustion had ceased, suggested that this was definitely so. If the combustion is extinguished, conditions are frozen, and the solidified globule is left attached to the unburnt wire. This unburnt wire has an oxide layer of decreasing thickness along

the short section of its length immediately adjacent to the globule. The extent, and variation of thickness with distance from the globule, of this oxide film gives some indication of the temperature gradient occurring at the moment combustion ceased.

At the lower oxygen percentages, corresponding to low velocities, the oxide extends along the wire for a few millimetres. At the high percentages, especially above 85 per cent with 0·5 mm diameter titanium wire, when the highest recorded velocities are obtained, the extent of the oxide is less than 1 mm.

This may provide an explanation of the difficulty experienced in the combustion of 0·5 mm diameter titanium wire at percentages of oxygen greater than 85 per cent. When a globule falls from the end of the wire, the thermal gradient is so steep that only a very little of the metal left is above the ignition temperature. If this portion of the wire is small enough, heat will be conducted away quicker than it is produced and the combustion will die out.

The expression for v makes possible a calculation of the ratio of velocity for two wires of the same material but differing diameter, assuming that $\rho \cdot s$ and $(\theta_f - \theta_a)$ are the same in both cases. With the titanium wire it has been shown that the weight and hence the volume of the globule is proportional to the diameter of the wire. If we assume that the rate of heat production is proportional to the surface area of the globule we have $H \propto a^{2/3}$ and hence $H/A \propto a^{-4/3}$ where a is the radius of the wire. For the two titanium wires used we have $a_1/a_2 = 2$ and this leads to a value for v_2/v_1 of 2·52. Considering the simplified form of the calculations this is in good agreement with the experimentally observed values shown in *Figure 2* in the range 85 to 65 per cent oxygen.

The sudden fall in the ratio of velocities for the two titanium wires at oxygen percentages above 85 can be explained by an increase in the combustion temperature for the thinner wire at these high percentages, since $v \propto 1/(\theta_f - \theta_a)$. Such an increase in temperature explains the much more frequent falls of the globules observed with the thinner wire at these percentages. A higher temperature means a lower surface tension and thus a lower maximum possible weight for the hanging globules. The distance travelled by a globule along the wire before it falls off would therefore be smaller.

This paper has given only a preliminary account of the work now being done on the combustion of titanium and zirconium. Investigations are being extended to other metals, especially those that have oxides with appreciably different properties. A study of the part played by the diffusion of oxygen to the surface and the temperatures obtained is also being undertaken.

I would like to express my thanks to Dr. F. P. Bowden for his interest in this work, and my gratitude to Dr. A. D. Yoffe for his advice and encouragement. I also wish to thank the Safety in Mines Research Board for a grant.

REFERENCES

1 Kopleman, B. and Compton, N. B. *Metal Progr.* 61 (1953) 77
2 Hartmann, I., Nagy, J. and Jacobson, M. *Rep. Invest. U.S. Bur. Min. No. 4835* (1951)
3 Titman, H. *Trans. Instn. Min. Engrs, Lond.* 115 (1955–6) 535
4 Kubaschewski, O. and Hopkins, B. E. *Oxidation of Metals and Alloys.* 1953. London; Butterworths
5 Coffin, K. P. *Nat. adv. Comm. Aero. Tech. Note 3332*
6 Wolfhard, H. G. and Parker, W. G. *Proc. phys. Soc. B* 62 (1949) 523

DISCUSSION

H. P. Broida (*Washington, D.C.*) opening the discussion said: A 'Special Fuels' session sounds as if it would be concerned only with new types of fuels that are, or might be, available for aircraft or rocket use. However, the papers under consideration fit two general categories. First of all there are those papers which are of importance in fundamental questions of combustion—the papers of Gerstein and of Berl *et al.* To some extent the investigation of the burning of titanium and of zirconium by Harrison also belongs to this category.

The others are concerned more directly with practical applications. Olson *et al.* have presented important information in their paper. Marsel and Kramer have shown a practical ignition device for combustion chamber use. The papers discussing diborane flames and on the combustion of titanium and zirconium are also of practical interest but not necessarily of immediate importance.

In reading the paper of Gerstein, I was struck by the implications of his concluding remarks in which he says (on p. 905) that 'Unlike hydrocarbon–air flames, large differences in flame velocity are found for flames of similar flame temperature and identical products of combustion. Since chemical factors appear to have a more pronounced effect on the flame properties of the alkylsilanes than on hydrocarbons, it seems likely that these fuels may prove useful in establishing relationships between chemical structure and flame properties.' In view of such a promising conclusion, I should like to ask Gerstein why it is that so little effort has so far been put into this type of study, considering that some work of this sort started at least as early as 1951?

Berl's paper brings up a similar question. Why are there not more reports at this Symposium of investigations on the combustion of the boron compounds? However, this question ought rightly to be directed to the audience at large, and in fact, might more appropriately be rephrased: Why does this Symposium on combustion put such a large effort into the oxidation of carbon-containing fuels?

In addition to these general questions, I should like to ask Harrison if he would elaborate on a remark in the conclusion of his paper in which he states 'that the combustion of titanium and zirconium takes place at the surface of the molten metal'. Does he consider this to be a gas phase or liquid phase reaction?

One further point of inquiry for Marsel. The possibilities appear great for the use of metal alkyls for combustion chamber ignition. What are some of the difficulties and problems connected with their use?

C. F. Marsel (*New York*), replying to the question 'What are some of the difficulties and problems connected with their use?', asked by Broida in opening the discussion, said: I would like to broaden the context of the question to include the use of the material for the main fuel as well as for auxiliary ignition purposes. This is because the self-igniting properties of the fuels make them of considerable interest for certain practical propulsion systems.

The problems may be subdivided as follows:

Handling—This is not difficult when one becomes accustomed to their special properties: they must be stored under a protective atmosphere of nitrogen; ordinary carbon steel can be used for the construction of containers; organic materials are readily attached, but plastics of the Teflon family are satisfactory.

Thermal stability—This is a more serious problem than with hydrocarbons. There can be considerable pressure build-up in a closed system with storage at elevated temperatures. When subjected to very high heat fluxes, as in regenerative cooling, solid build-up can occur. We are at present studying this problem intensively.

Danger to personnel—Some objections have been raised to the use of these materials for manned vehicles. It is our feeling that this would not be a major problem given the proper type of storage tanks. Naturally this problem would not occur with unmanned missiles.

W. G. Parker (*Birmingham*): Is it feasible to design an aircraft combustor to consume either a hydrocarbon or a boron-type fuel?

W. T. Olson (*Cleveland*): Design features aimed at minimizing boron oxide deposits, such as eliminating or reducing the re-circulation zone in high-speed combustors, for example, would limit the combustor operation on hydrocarbons to low altitude. Such compromises are, however, perfectly feasible.

S. T. Griffiths (*Bletchley*): Broida has suggested further work on alkyl silanes, and this prompts me to draw attention to some work carried out by Wilson and myself which has direct bearing on Gerstein's paper. We have determined the spontaneous ignition temperatures of a number of silanes with alkyl groups ranging from ethyl to

n-amyl, representing the types, R_4Si, R_2SiH, R_2SiH_2 and $RSiH_3$.

The influence of Si-H bonds upon the ease of ignition depends markedly on the length of the alkyl chain; e.g. the effect of Si-H bonding is pronounced in the ethyl series (which accords with Gerstein's findings for the methyl series), whilst with the *n*-amyl series, the influence of Si-H bonding is offset by the ease of oxidation of the alkyl side chain.

I would agree with Gerstein that combustion studies employing alkyl silanes offer an alternative route to methods employing tagged carbon and deuterium atoms used for investigating hydrocarbon/oxidation mechanisms. As an example I would cite results that we have obtained employing isomeric alkyl silanes containing 6 carbon atoms. These results clearly show that the ease of ignition depends markedly upon the position of the silicon atom in the chain. The more symmetrical the molecule is about the silicon atom the greater is the molecule's resistance to oxidation.

A full report of this work appears in *Combustion and Flame* 2 (1958) 244.

P. L. Harrison (Cambridge): In reply to Broida's question, I would first like to draw his attention to work carried out on the combustion of magnesium by K. P. Coffin, and reported by him in the *Fourth (International) Symposium on Combustion.* Coffin concluded from his experimental observations that the magnesium burns in the vapour phase above the surface of the metal, a conclusion that I entirely agree with. A very obvious characteristic of burning magnesium is the formation of large quantities of oxide smoke, and this is undoubtedly due to the formation of the oxide being from the vapour phase reaction between the metal and the oxygen in the atmosphere.

In none of my experiments with titanium and zirconium was there any appreciable formation of oxide smoke. I conclude from this, and from the fact that the photographic images of the burning material are so sharp, that these metals burn in the liquid phase in my experiments

PART XI

INSTRUMENTATION IN COMBUSTION RESEARCH

THE CONTINUOUS FLOW INSTRUMENTAL ANALYSIS OF FLAME GASES

F. H. HOLDERNESS and J. J. MACFARLANE

INTRODUCTION

Chemical analysis of combustion products has been in use for many years as a tool for characterizing combustion systems used in gas turbines.

Such analysis of flame gases is the only means likely to yield information of interest in the design of the primary flame zone. Chemical methods have the particular advantage that they can give quantitative data on combustion behaviour without reference to any of the normal measurements of fuel and air flow, temperature or pressure, and thus without incurring the errors attendant to such measurements. For this reason precise gravimetric analysis of exhaust gases is now an established reference technique for overall combustion efficiency measurement[1].

Analysis of samples from the primary flame zone has played little part in development work on spray type combustion chambers for the gas turbine. This is principally due to the heterogeneous nature of the system and to the steep concentration gradients which occur. To characterize such a system would require sampling at a large number of points, under isokinetic conditions, with the added difficulties imposed by flow reversal and deposition of carbon and cracked products in the probe.

Recent increased interest at N.G.T.E. in pre-vaporized systems, particularly for ramjet pilot chambers, showed a pressing need for the application of rapid analytical methods to primary zone conditions.

The fact that such systems operate with a homogeneous mixture of fuel and air, and are substantially free from carbon formation, removed two of the major sampling difficulties.

OPERATING CONDITIONS

The techniques described below were developed for use with these pre-vaporized systems and the ranges of combustion zone conditions within which measurements were required were thus fairly well defined. Much of the work on ramjet pilot chambers is at simulated altitude conditions and samples must be extracted from zones at pressures down to 0·25 atm absolute. The chambers themselves are small in diameter (2 in.) and operate at high gas velocity. Sampling probes must therefore be designed carefully to minimize distortion of gas flow patterns. It can be assumed that only gas phase components are present under flame zone conditions and no attempt need be made to extract samples isokinetically.

The analytical technique should deal effectively with fuel/air mixtures in the range: equivalence ratio (ϕ) = 2 to ϕ = 0·2. It is however of interest to note that this range might need to be extended at both the weak and the rich ends, and the ways in which this could be achieved are discussed below. Effective measurement of combustion efficiency in the range 0 to 100 per cent is required.

In ramjet research work generally, combustion tests of short duration are common, and although the pilot chambers under consideration here are operated over fairly long periods of time, speed of analysis is regarded as being of prime importance in application of the technique described.

SAMPLING

The sample probes used for the work are of simple design with an aerodynamically faired cooling jacket carrying stainless steel hypodermic gas tubes from two sample ports. The ports are at the ends of a stepped section of the jacket which extends slightly upstream, and the length of which is equal to the radius of the test duct. With this arrangement samples can be taken from any point on a diameter of the duct and in particular from a point very close to the duct wall without interference from the hole through which the probe is introduced. To give strength at high velocity and temperature the probe is supported at both ends, in glands mounted at opposite points on the test duct. This has the further advantage that blockage due to the probe is the same for all stations on the traverse. A typical probe is shown in *Figure 1*.

It is essential to ensure that there is no loss of components by condensation during transfer of sample from sample port to the analysis equipment. This is achieved by chilling the sample in the probe with steam and maintaining the external leads at a temperature of 220°C. It is assumed that this treatment effectively stops the combustion reaction at the sample port. The external leads are of flexible stainless steel tube ($^3/_{16}$ in. bore),

heated electrically by means of glass cloth covered heating tapes, the whole assembly being protected by a Neoprene sheath. This lead is provided in 10 yard lengths, each fitted with leak-proof couplings. In circumstances where access to test rigs is limited, up to 30 yards of lead may be used.

MEASUREMENTS REQUIRED

Complete characterization of the sample could be achieved from measurement of CO_2, CO, H_2, gaseous hydrocarbons and 'fuel' vapour on a dry gas basis, and from these data mixture strength and

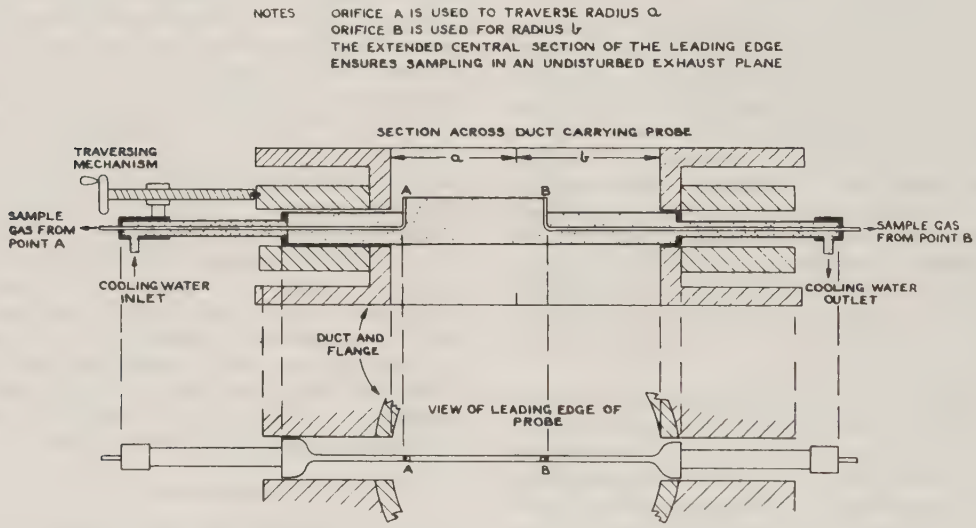

Figure 1. Traversing probe

combustion efficiency could be calculated. The possible presence of large quantities of condensable materials makes it imperative that 'on-the-spot' estimations should be made, and that analyses should be performed on a continuous stream of the sample gas. Unlike all other physical methods of gas analysis, the infra-red gas analyser (I.R.G.A.) can be made to respond specifically to a selected component of a complex gas mixture without resorting to physical separation of the constituents. Of the gases of interest here, CO_2, CO and various individual gaseous hydrocarbons show infra-red absorption and can be measured with I.R.G.A. While hydrogen cannot be measured as such, I.R.G.A. is sensitive to water vapour but the mechanical problems of handling the wet gas make the method less attractive.

Any alternative method for measurement of hydrogen involves some correction for the cross sensitivity of the method to other constituents of the gas. This implies the removal of hydrogen from the gas and the use of this stripped sample in a reference measurement. It has been found that, for the complex mixtures considered here, catalytic combustion in the presence of gaseous hydrocarbons in a continuous flow system cannot be made to give specific removal of hydrogen. Largely for this reason the results of tests with instruments such as the sonic gas analyser have so far been unsatisfactory, a contributory factor being the large inaccuracies always present when attempting to calculate a small quantity from the difference between two large measurements. A further alternative for estimation of hydrogen is by calculation, using analytical data derived from the sample gas after removal of condensable material. The latter must be assumed to be identical with the original fuel used in the test rig. The data required would be: q_{gas} (fuel/air ratio, calculated from CO_2 content measured after complete oxidation of the sample in a furnace); CO_2; CO and gaseous hydrocarbon contents. With sufficient instrumentation to cover the last item (methane and possibly ethane measurements by I.R.G.A.) this technique should give satisfactory results over the entire mixture strength range. No hydrocarbon-sensitive instruments are available at N.G.T.E. and this proposition has not yet been tested.

A simple expedient which can be used to eliminate the necessity for a measurement of hydrogen is to assume that combustion loss due to hydrogen is a constant fraction of the loss due to CO. In a series of experiments where gas composition was checked by detailed laboratory analysis this assumption has been shown to give tolerably small errors, in terms of combustion efficiency, with mixture strengths less than $\phi = 1$. For richer mixtures, a measurement of gaseous

hydrocarbons or an estimation of hydrogen must be undertaken.

'Fuel' vapour concentration can be calculated, by difference, using q_{gas} as defined above, and q_{total}, a similar quantity derived from the gross CO_2 content measured after complete oxidation of the virgin sample in a furnace.

TECHNIQUE CURRENTLY USED

The technique at present in use at N.G.T.E. may be summarized as follows.

Gross CO_2 and hence mixture strength (q_{total}) is measured, after preliminary gasification of the virgin sample over platinum at rig pressure at 1,100°C by one of the following three procedures:

(*a*) By completing oxidation where necessary ($\phi > 1$) over copper oxide at 850°C.

(*b*) By re-processing over platinum at 1,100°C at atmospheric pressure and subsequently measuring the sum of CO_2 and CO concentrations.

(*c*) By re-processing over platinum at 1,100°C with addition of oxygen, the amount added being adjusted to give maximum CO_2 concentration.

It should be noted that the amount of the addition does not need to be measured.

The same arrangements are available for treatment of the sample after condensable material has been removed in a freezing trap at −78°C, and the CO_2 measurement so derived is used to calculate q_{gas}. 'Fuel' vapour concentration may now be calculated by difference from $q_{total} - q_{gas}$.

The net CO_2 and CO contents of the virgin sample are measured directly by I.R.G.A.'s. Condensable material is removed before these measurements are made, merely to avoid contamination of I.R.G.A. cells by condensation. Hydrogen concentration is estimated by calculation assuming gaseous hydrocarbons to be absent.

EQUIPMENT

The equipment used includes two I.R.G.A's, for CO_2 and CO measurements respectively, a furnace system for completion of oxidation, and various ancillary equipment mounted on a control panel. A diagram of the gas flow arrangement is given in *Figure 2*.

The assembled apparatus is unwieldy and for convenience it has been mounted permanently in a small trailer caravan. The heated lead for transfer of sample gas from the probe is inserted through a hole in the wall of the trailer.

Furnace heaters for processing at 1,100°C are low voltage Kanthal elements, mounted in refractory brick, the furnace tubes being of 1 in. diameter Thermal Mullite. The packing of the tubes consists of a nest of lengths of Mullite tubes with a layer of platinum gauze filling each interspace. The outer Mullite tubes are open at one end and drawn down to 0·25 in. bore at the other. The open end is joined, after filling, to a short length of glass tubing by the use of a simple glass-blowing technique. The glass tube is finally drawn down to form an 0·25 in. tubular connection. The furnace tube operating at 850°C is of quartz, protected from the copper oxide gauze packing by a layer of asbestos paper.

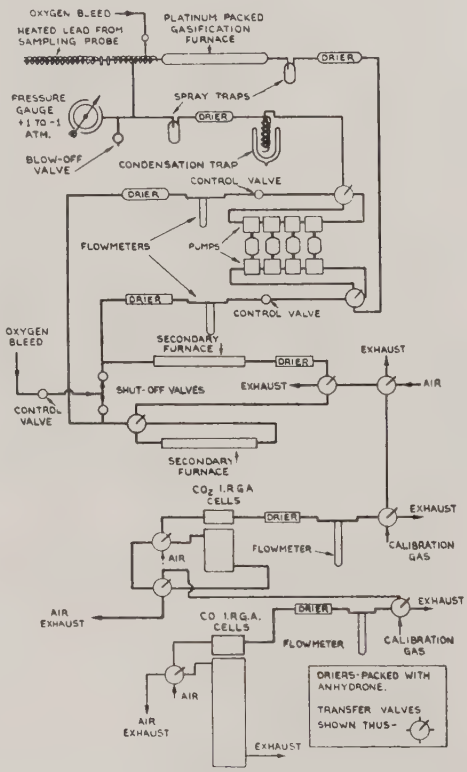

Figure 2. Gas flow diagram

The freezing trap used for removal of condensable components in the sample gas was designed and made at N.G.T.E. to give efficient condensation of kerosine vapour at high flow rates and low absolute pressures, without rapid blockage due to deposition of large masses of ice. The trap consists of a 4 in. length of copper tube (1 in. bore), packed with a graded filter bed in three parts: At inlet a section of 3 mm gauze Lessing rings, next a section of 2 to 3 mm quartz chip and finally a section of 1 to 2 mm quartz chip. The gas flows downwards through this bed after passing through about 8 ft. of $\frac{3}{8}$ in. copper tube formed into a coil. The complete trap is supported in a bath of solid CO_2 (−78°C) in a Dewar flask. Under typical sampling conditions the trap will function satisfactorily for one to two hours before blockage occurs. The trap is cleared by acetone washing followed by air drying and baking at 100°C.

A battery of pumps is provided to induce gas

flow from the sample probe to the measuring equipment. A light diaphragm type of pump marketed by Charles Austin Limited (Type M.U. 19) was chosen for this duty and four of these, connected in cascade, are capable of pumping an adequate supply of sample (50 l./h) from a combustion zone at 0·25 atm pressure. Transfer valves are fitted appropriately so that 1 to 4 pumps may be in operation, or alternatively the pump system may be bypassed altogether. This latter arrangement is for use with test rigs operating at high pressures, when pumping is unnecessary. Provision is also made for connecting the pumps in closed circuit so that they may be started under 'no-load' conditions.

The I.R.G.A.'s installed are 'three-box' models supplied by Sir Howard Grubb, Parsons and Company Limited. Each instrument (about 5 ft. 6 in. tall and 12 in. × 8 in. in cross-section) rests on a foam rubber mat and is bolted to a metal support at a point near the top, using 2 special shock-absorbing bolts fitted with rubber bosses. The construction of the I.R.G.A. is described in detail in reference 2 and its working principle is only briefly indicated here (*Figure 3*). The radiation from a pair of Nernst glowers, chopped at 7 c/s,

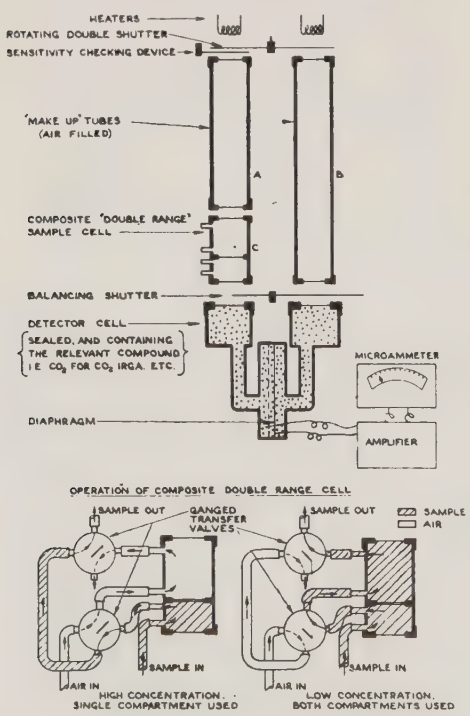

Figure 3. Infra-red gas analyser

passes through two parallel gas cell systems, which may be up to 30 cm long, and is received in a detector cell. The detector cell consists of 2 chambers separated by a flexible metal diaphragm, the chambers containing a suitable partial pressure of the compound to be measured.

The chopped radiation gives alternate heating and cooling of the contained gas, and the resultant oscillation of the diaphragm, which forms one plate of a condenser, produces an a.c. signal which after suitable amplification is rectified and displayed on a d.c. microammeter.

Means are provided for balancing the incident radiation in the two optical paths. The introduction of a sample of gas into a cell in one path causes partial absorption of the incident radiation in this path, the resultant increased amplitude of oscillation of the diaphragm giving an increase in current to the microammeter. Calculation of calibration of the instrument from first principles is complex and empirical calibration with known gas samples is normally used. The sensitivity of the instrument varies for different gases, and for a given gas can be controlled by varying the sample cell length and by adjusting amplifier gain.

In each of the I.R.G.A.'s used in the present application 'dual' cells are fitted, giving a choice of two cell lengths and hence concentration ranges for each instrument. In the CO_2 instrument lengths of 0·5 and 5·0 mm give full scale deflections for a suitable electronic sensitivity setting of about 30·0 and 3·0 per cent CO_2 respectively. In the CO instrument the corresponding lengths are 3 and 30 cm, with full scale deflection for 25·0 and 2·5 per cent CO respectively. When in use, suitable cell lengths may be selected by operation of transfer valves which automatically pass clean air to the unwanted lengths. Each I.R.G.A. is provided with a hand-operated shutter device which can be used for standardizing the instrument. This operates by introducing a length of wire into the 'sample-side' infra-red beam, giving a standard obscuration which simulates a standard absorption. In general the behaviour of this device has been found to be unsatisfactory and the standardization is carried out by introducing a gas of known composition into the sample cell. The composition of the standard binary gas mixture is measured in the laboratory by means of a Rayleigh gas interferometer.

Supplies of clean air are needed for purging I.R.G.A. sample cells when adjusting the instrument zeros, for purging 'unwanted' I.R.G.A. cells and for intermittent regeneration of the copper oxide packing in the 850°C furnace. These supplies are generated by small 'Dymax' type Charles Austen gas pumps, the air being passed through Hopcalite for oxidation of CO, Anhydrone for absorption of water vapour and soda asbestos for absorption of CO_2.

No precise measurements of gas flow rate are needed, as I.R.G.A. calibration is independent of

this factor, flow rate through the apparatus is however controlled at about 30 l./h, and at this value operation of furnaces and freezing traps has been shown to be efficient. Capillary type flow meters made in glass for rough adjustment to this value are mounted on a convenient panel in the trailer.

The 'transfer valves' indicated in *Figures 2* and *3*, and mentioned in the general description above, were designed and made at N.G.T.E. They are of the greased taper plug type, made in metal, the plug being spring-loaded. Each valve has 4 tubular connections and its function could be described as that of a standard 'parallel 2-way tap' with a double inlet.

CRITICAL COMMENTS

Mechanical details

The use of a trailer for mounting the assembled equipment compactly has many advantages. In particular the I.R.G.A.'s are shielded from much of the vibration which is inseparable from ramjet combustion testing. The one major penalty incurred is that sample gas, often at low pressure and loaded with condensable material, must be transferred unchanged from the sampling probe through several yards of heated tubing. The heated leads described above perform reasonably well but a rigorous leak-testing procedure must be adopted. An alternative arrangement would be to mount furnaces and pumps in a small unit which could be sited within a few inches of the probe outlet, the main length of the lead could now be of unheated metal tube in a single piece. If necessary the lead could also be much longer, and the vibration sensitive parts of the apparatus much more remote from the source of the noise.

In normal operation, with test rigs at simulated altitude conditions, a large part of the apparatus is at sub-atmospheric pressure. Since inward leakage of air cannot be tolerated, very careful assembly and maintenance of all connections is essential, and an exhaustive leak testing drill is observed on each occasion when the apparatus is used. No claim is made by the makers of the pumps regarding freedom from leaks, and small leaks are invariably present in new pumps. It has been found that these can be eliminated by simple modifications.

The I.R.G.A.'s used are of the earliest type marketed by Sir Howard Grubb, Parsons and Company Limited and some of the shortcomings discussed below have been minimized in more recent models.

The instruments are extremely sensitive to vibration, both air and ground-borne, and the measures described in the section above do not always provide complete protection in the very high noise levels often encountered.

At high electronic sensitivity, instability of the meter reading is enhanced and for this reason amplifier gain is kept at as low a value as is practicable. A voltage stabilization pack has been fitted to each I.R.G.A., but even so electronic stability and reliability are only fair. The detector cell is sensitive to small variations in ambient temperature, and a thermostatically controlled heater has been fitted to the detector compartment of each instrument. Temperature is maintained at 30°C, a value safely above the maximum ambient temperature likely to be encountered. The 'calibration-wire' as fitted to the instrument was found to be mechanically unreliable and was modified to give a positive and repeatable location of the wire in the optical path. Calibration was first attempted by plotting meter reading against per cent gas composition for a suitable range of sensitivities as indicated by this wire reading. The system was used over a long period, during which it became apparent that there were unexplained variations in the sensitivity represented by a given wire reading. A correction procedure was adopted based on daily checking of the 'wire' sensitivity with a known gas sample. It may be more satisfactory to abandon the 'wire' technique altogether and to adjust the sensitivity at a suitable point on the calibration curve by means of a standard gas mixture, prepared in sufficiently large volume to last for several months. There is a small cross-sensitivity between CO and CO_2 but since both quantities are always displayed it has been a simple matter to apply the relevant corrections. Filter cells fitted in the optical paths of both instruments can however provide a neater solution to this problem. It is only fair to say that the precision required from these instruments in this application is rather higher than that claimed by the makers.

After one or two unpleasant experiences it is worth mentioning here that the neat sample gas taken from combustion zones at $\phi > 1$ even at high efficiency levels can be a highly toxic material. All effluent gas should therefore be piped to the open air.

Sampling and analysis

It has already been pointed out that use of the technique has been limited to pre-mixed systems. The authors have had considerable experience in the design and use of isokinetic sampling probes in the study of exhaust-borne solids. Such a probe can be either a simple cooled tube, flow conditions for which must be established by a separate measurement before sampling, or a more complex and bulky device with means built-in for measurement of internal and external static pressures, so that these can be matched while sampling. In either case it would be necessary to align the sampling

port axis with the local direction of the gas stream. This requirement in a combustion system employing flow reversal implies adjustment of the port to face in any direction while remaining at a given point in space. This is difficult to the point of impossibility.

No fundamental investigation has been made of the efficacy of probe coolants in arresting combustion reactions. It can however be stated that the cooling system used is efficient in keeping the probe metal at a low temperature since no metal oxidation is observed. Catalysis by a hot metal surface, the most likely source of trouble, can therefore be discounted.

The temperature at which it was, in practice, found to be necessary to maintain the sample gas leads is some 50° higher than is indicated by the theoretical deductions given in reference 3.

Side experiments have proved the effectiveness of the platinum-packed furnace at 1,100°C in gasifying fuel/air mixtures up to $\phi = 1{\cdot}5$. Mixtures richer than this tend to deposit carbon. Fixed dilution with air for treatment of mixtures richer than $\phi = 1$ has often been considered. This technique would introduce inaccuracies attendant to the measurement of gas flow rates, and has in fact never been investigated.

Completion of oxidation over copper oxide at 850°C is a satisfactory technique only if carefully handled. Progressive reduction of the oxide must occur in use and frequent regeneration is necessary. Heat released during oxidation of very rich mixtures can cause overheating and the formation of solid reduced plugs.

Thus, summarizing the relative merits of the three alternative procedures listed above for measurement of q_{total}, the following points can be made:

(1) For mixtures weaker than $\phi = 1$ platinum at 1,100°C gives satisfactory complete oxidation.

(2) In the range $\phi = 1$ to $\phi = 1{\cdot}5$, gasification over platinum without oxygen addition is adequate without introduction of the mechanical unreliability of the use of copper oxide. This technique involves measurement of both CO_2 and CO concentrations.

(3) The practical rich limit in (2) above occurs at about $\phi = 1{\cdot}5$ where carbon starts to deposit. With richer mixtures than this, oxygen addition is the only possible technique. The position of the maximum value of CO_2 concentration may be difficult to locate owing to flatness of the characteristic near the peak value. Only limited investigation of this point has been made and further experiments with chart recording are planned. It is conceivable that this technique may prove to be the best one to use at all mixture strengths greater than $\phi = 1$. It is hoped that this investigation will explain the source of occasional negative values of $q_{\text{total}} - q_{\text{gas}}$ which have been observed, and which cannot be accounted for by any detectable mechanical fault, or by random experimental errors.

The condensation trap at −78°C described above has been proved, in the laboratory, to give efficient condensation of hydrocarbons boiling at 120°C and above at all working pressures and flow rates. Where fuel is wholly or partly volatile at −78°C accurate measurement of q_{gas} is impossible. The use of lower temperatures causes partial condensation of CO_2. Net CO_2 and CO measurements can be made in the presence of hydrocarbon vapours with little error due to overlapping infrared absorption, but unknown dilution errors are also introduced under these conditions. Calculation of hydrocarbon vapour concentration would be possible if q_{total}, net CO_2 and CO were known, and if a direct hydrogen measurement were available. It would still be necessary to assume that the hydrocarbon vapour was identical chemically with the original fuel.

Operating time at each sampling station is about 6 min. This is largely dictated by the need for three separate measurements on the single pair of I.R.G.A.'s and the need for checking zero drift. Fuller instrumentation using more recent models, possibly with chart recording, could materially reduce the time. The necessary parallel gas circuits are already existing (*Figure 2*).

CONCLUSIONS

This paper is an attempt to give an unbiased description of the development to date of a very complicated technique. This development is still actively proceeding and it has been shown that many problems remain to be solved. As with most techniques of this kind, development work has been concurrent with the practical use of the equipment and this will continue to be so.

Crown Copyright Reserved

REFERENCES

[1] MACFARLANE, J. J. The application of chemical analysis to the investigation of gas turbine combustion problems. *Proc. XIth International Congress of Pure and Applied Chemistry*, Vol. IV p. 533, 1947

[2] MARTIN, A. E. *The present status of the infra-red gas analyser*. Walkergate, Newcastle-upon-Tyne; Howard Grubb, Parsons and Company Limited

[3] MULLINS, B. P. The vaporization of fuels for gas turbines. Part I—The bubble-points and dew-points of liquid hydrocarbon fuels. *J. Inst. Petroleum*. 32 No. 276 (1946)

THE APPLICATION OF GAS ANALYSIS TO COMBUSTION CHAMBER DEVELOPMENT

B. TOONE and F. ARKLESS

INTRODUCTION

Considerable progress has been made in applying gas analysis techniques to the development of aero gas turbine combustion chambers. Since the combustion of fuel in a combustion chamber is essentially a chemical process, it is of great interest to apply gas analysis techniques to investigate the processes involved.

The methods used have been developed to meet the following requirements: (1) speed of application to test beds spread over a wide area of ground; (2) rapid analyses; and (3) reasonably high degree of accuracy.

Chemical methods of analysis are ruled out by the length of time involved in each analysis and rapid physical methods have therefore been adopted. The speed of application is obtained by using a self-contained mobile laboratory.

Aviation kerosine is a complex mixture of hydrocarbons, but it may be represented by the average molecular formula $C_{12}H_{24}$. The combustion process may then be represented by the following equations:

Primary equations

$$C_{12}H_{24} \rightarrow 12C + 12H_2 \quad (1)$$ Cracking reaction

$$C_{12}H_{24} + 6O_2 \rightarrow 12CO + 12H_2 \quad (2)$$ Partially burnt products

$$C_{12}H_{24} + 18O_2 \rightarrow 12CO_2 + 12H_2 \quad (3)$$ Complete combustion

Secondary equations

$$12C + 12O_2 \rightarrow 12CO_2 \quad (4)$$
$$12CO + 6O_2 \rightarrow 12CO_2 \quad (5)$$
$$12H_2 + 6O_2 \rightarrow 12H_2O \quad (6)$$

} Completely burnt products

Water gas equilibrium

$$CO_2 + H_2 \leftrightarrows CO + H_2O \quad (7)$$

To obtain maximum fuel efficiency from a combustion chamber the combustion products must be carbon dioxide and water only. It is possible that additional side reactions occur, but in the simple scheme considered here these are ignored. The main determinations required are for kerosine, carbon monoxide, carbon dioxide, hydrogen, oxygen and carbon. Water is ignored since its concentration can be calculated, if necessary, from the other primary gaseous constituents.

The combustion chamber considered is of the swirler type with high-pressure fuel spray injection and may be divided into the four main zones shown in *Figure 1*. They are:

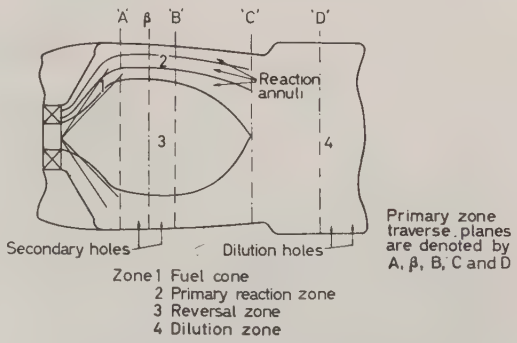

Figure 1. Diagram showing the four zones of combustion rhomba

(1) The fuel cone consisting of high velocity fuel droplets.

(2) A primary reaction zone, in which combustion takes place at fairly high temperatures.

(3) A reversal zone, in which combustion products are re-circulated to mix with incoming combustibles in order to ensure combustion stability.

(4) A dilution zone, in which products from zones 2 and 3 are diluted to give a gas temperature, sufficiently low to ensure a long turbine working life. This temperature is decided by the creep strength of the turbine blade material available and is of the order of 900°C.

The first zone is essentially liquid fuel mixed with a small amount of gas, no investigations into spray structure have so far been made.

In the reaction and the reversal zones, information is required on fuel distribution, gas temperatures, fuel efficiency and oxygen availability. Accuracy here is not so important, nor is it easy to attain since sampling conditions are very difficult.

This type of analysis is described by the term primary zone analysis.

It is important to know the fuel combustion efficiency at the turbine with an accuracy of $\pm$ 0·5 per cent at some engine conditions. This is the main function of exhaust gas analysis, and a high degree of accuracy is required.

INSTRUMENTATION SCHEME

A continuous flow of gas is passed through the instruments, the gas flow circuit being shown in

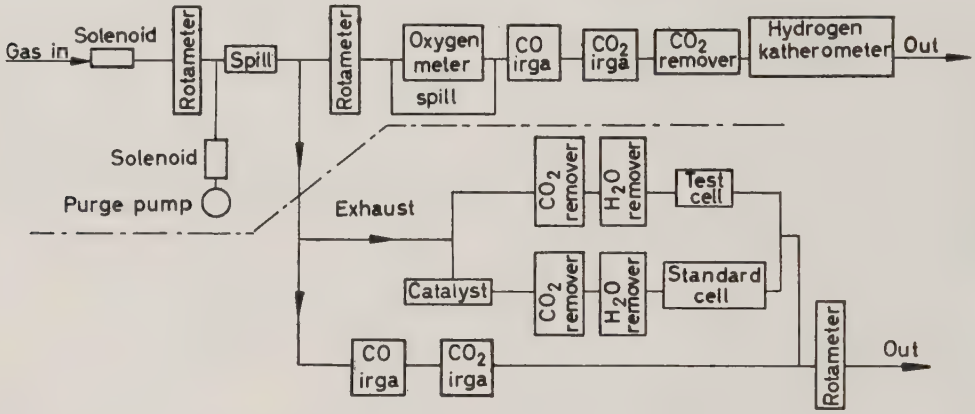

Figure 2. Gas sampling flow through the caravan

Figure 2. Infra-red analysers, working on the absorption bands in the near infra-red between 1·5 and 4·5μ are used to determine the two oxides of carbon. The instruments use the pneumatic condenser detecting cell. It is not proposed to discuss the working principles in detail since these can be obtained from reference 1. There is a small

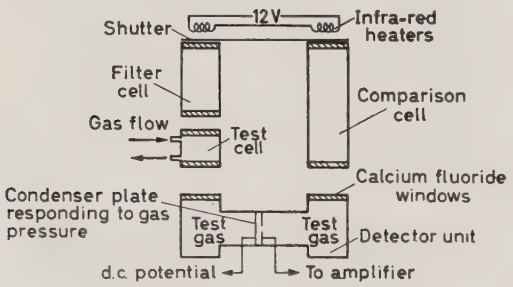

Figure 3. Infra-red analyser radiation bridge

degree of overlap on the absorption bands of CO and CO_2, which can result in some interference on estimations. This can however be avoided by having a filter filled with the interfering gas above the test cell (*Figure 3*). The interfering wavelengths are therefore filtered out and take no part in the radiation balance. Four infra-red analysers are used, two for primary zone CO_2 and CO, and two for exhaust CO_2 and CO. The exhaust instruments are used on various ranges and sensitivities and are calibrated before each test. To improve the accuracy of the exhaust CO_2 determinations a series of split ranges are used namely O — 2, 2 — 4·5, 4·5 — 6·0, 5 — 7·5 per cent v/v. This procedure gives the equivalent of a wide reading scale. On the other hand the primary zone instruments operate on one fixed calibrated scale.

Hydrogen is measured by heat conductivity changes. The detection element is a 0·00125 in. diam nickel wire, running at a temperature of approximately 180°C. The resistance of the detector wire is balanced against a comparison wire by means of a Wheatstone bridge. For primary zone work the comparison wire is run in a cell containing air. Carbon dioxide is the chief interfering gas, and this is removed by a soda lime absorber.

In exhaust gas analysis the amount of hydrogen does not exceed 0·2 per cent and high instrument sensitivity is required. Since the detector relies on changes in heat conductivity, and hence on molecular weight, any changes in gas composition other than hydrogen are likely to interfere with the estimation. Interference by CO_2 is avoided by using a soda lime absorber. As the percentage of CO_2 increases the percentage of O_2 decreases and the resulting change in O_2/N_2 ratio is equivalent to an appreciable amount of hydrogen. To compensate for this change a differential instrument is used in which the gas conductivity of the mixture containing hydrogen is compared with a similar composition with the hydrogen removed. The removal of hydrogen from this comparison cell is effected by a 2 per cent palladium on silica–alumina catalyst, which oxidizes both CO to CO_2 and H_2 to H_2O. The gas flow circuit for this instrument is illustrated in *Figure 2.* The comparison line contains a catalyst followed by magnesium perchlorate and soda lime, to remove water vapour and carbon dioxide respectively.

Magnesium perchlorate and soda lime tubes only are fitted in the test line. Oxidation of hydrogen and carbon monoxide results in a slight difference in oxygen content between the test and comparison cells, for which allowance cannot be made. The error caused by this is only $1\frac{1}{2}$ per cent for 0·3 per cent CO. Using this katharometer it is possible to detect 0·01 per cent v/v of hydrogen with reasonable accuracy.

Unburnt kerosine is determined by oxidizing the combustion gas to give the total carbon dioxide by means of a catalytic furnace. The CO_2 produced by the fuel $(CO_2)_{UF}$ is then obtained from the relationship

$$(CO_2)_{UF} = (CO_2)_T - CO - CO_2 \qquad (8)$$

The catalytic furnace (*Figure 4*) is designed to work under flame-proof conditions. Oxidation is assisted by a catalyst bed of platinum wire and granules of 3 per cent platinum on alumina. To avoid loss of liquid fuel the connecting tube between the furnace and sampling point is kept very short; normally about 2 ft. of high pressure

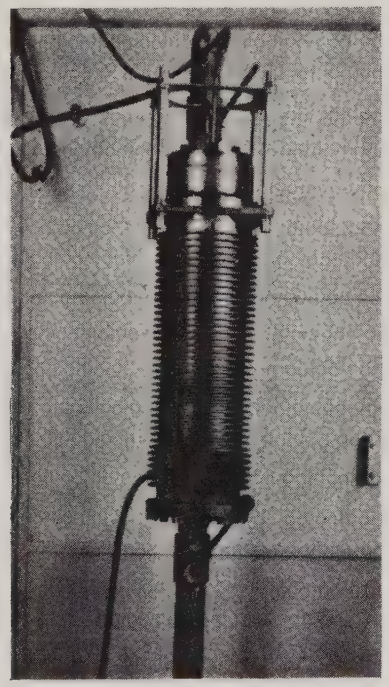

Figure 4. Catalytic furnace for fuel oxidation

Avica braid is used. During primary zone analysis over-rich mixtures are often encountered and it is then necessary to dilute the combustion gases with air before complete oxidation can be achieved. The dilution factor is determined from the ratio of the $(CO_2 + CO)$ concentrations before and after dilution.

Oxygen is the only combustion gas which is paramagnetic. The detector measures a rate of gas flow in the tube *A* towards a magnetic field (*Figure 5*), the magnitude of the flow being related to the oxygen content of the gas. A centre-tapped, heated coil surrounds *A*, and a flow of gas in *A* causes one arm of the coil to be cooled and the other arm to be heated. The resulting resistance changes are measured by a Wheatstone bridge and amplified. Since the paramagnetic force is

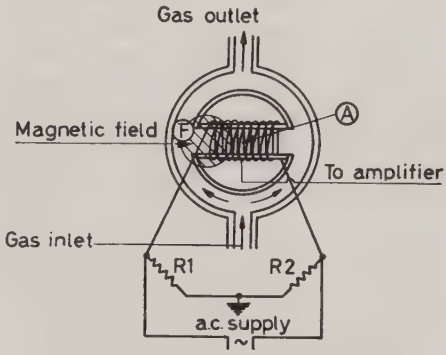

Figure 5. Paramagnetic oxygen meter

dependent on temperature, temperature compensation is provided by a thermistor-controlled feed-back amplifier.

Smoke estimation in exhaust gases is carried out by means of an absorption cell using the near infra-red band of the spectrum. The radiation is measured by an infra-red photocell. To avoid contaminating the absorption cell windows with carbon these analyses are not carried out with a continuous gas flow. The procedure is to pass gas into the cell for 20 sec and then shut off before measuring the decrease in radiation absorbed by the photocell. Standardization is difficult since we have no method of producing standard smoke samples. The standard used is a wire which is passed across the absorption cell, giving a fixed reduction in the radiation passing to the photocell. Unburnt kerosine can interfere with the estimation but down to 90 per cent efficiency the degree of error has been found to be negligible.

INSTRUMENT CALIBRATION

The calibration of instruments is of vital importance, and a system has been devised which enables accurate checks to be made very quickly. Standard gas mixtures of CO_2, CO and H_2 are made up at an initial pressure of 800 lb./in.^{2} abs. Six analyses are carried out using a standard gravimetric technique, to give the accurate compositions.

These standard samples are then used to produce calibration curves. Once the curve has been produced the instruments are calibrated on the top and bottom calibration points only, since it has

been found that curve distortion is negligible. The amount of sample used in a calibration is small, and the average life of the bottles is about nine months. During this period no significant change in analysis has been found.

APPLICATION OF EXHAUST GAS ANALYSIS

One aim of development testing is to raise the combustion efficiency to better than 99 per cent over a wide range of conditions, varying from high altitude cruise, ground level take off, and approach idling. Changes of 0·5 per cent in efficiency are highly relevant. Gas analysis finds its main application in giving accurate estimations of efficiency in the region 90–100 per cent and the

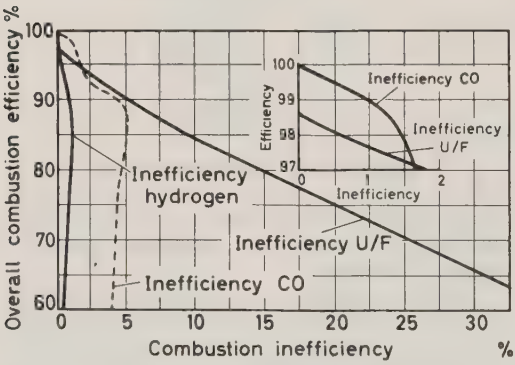

Figure 6. Variation of carbon monoxide, unburnt fuel and hydrogen inefficiency with overall combustion efficiency

following section is concerned with efficiencies of this order.

Combustion efficiency measurements can be carried out by a heat balance experiment.

That is

$$\eta_c = \frac{H_m \times 100}{H_p} \qquad (9)$$

where H_m is actual heat measured/unit time and H_p is potential heat measured/unit time.

Now H_p requires the estimation of air and fuel mass flows, and fuel calorific value. In addition it is common practice in rig testing to simulate the temperature of the compressor delivery air by a pre-heating combustion chamber, and this brings in two more variables, the pre-heat fuel mass flow and the pre-heat efficiency. The value of H_m depends on the mean temperatures at inlet and outlet of the combustion chamber, and the specific heats of the gas products. Of these variables, the air flow and the mean outlet temperature are the most difficult to obtain accurately. The measurement of air flows at high pressures involves the use of an orifice plate or nozzle, working in a strict dimensional set of conditions. It is not easy to measure the air directly by an independent reference, and errors may be of the order of $\pm$ 3 per cent. The outlet gas temperatures may vary about the mean as much as 150–200°C and an extensive traverse is necessary to obtain a mean temperature. It is quite possible to incorrectly sample areas near the outside of the duct and to obtain $\pm$ 5 per cent error in this way.

In addition, thermocouple errors may arise due to radiation and conduction losses at high temperatures and low pressures. Such errors may be reduced by the use of double shielded suction thermocouples, but at the normal altitude test conditions corresponding to 50,000 ft. errors of the order of 1–2 per cent are to be expected: also combustion rigs may suffer heat losses, particularly at low pressure and low air mass flow conditions, which lead to a further 2–3 per cent error, unless the ducts are carefully lagged.

Test results over a period of three years, on various combustion chambers, have shown maximum experimental errors of $\pm$ 8 per cent on combustion efficiencies of the order of 99 per cent, and these errors are due to various combinations of the variables detailed above.

The alternative method of measurement is to use gas analysis to determine the unburnt products in the combustion gas. The essential difference in approach between the two methods lies in the fact that the heat balance method compares two large quantities H_m and H_p to find a small difference, while the gas analysis method measures the small difference directly.

Gas samples are taken from an automatic traversing vane as suggested originally by the N.G.T.E., reference 2. This automatically takes a representative sample from the whole duct area and a gas sample may be obtained in a few seconds. The gas is then passed to the instruments and the amount of unburnt fuel, carbon monoxide, hydrogen and carbon dioxide determined. The total inefficiency η_{ineff} is given by the relationship

$$\eta_{\text{ineff}} = \eta_{\text{ineffCO}} + \eta_{\text{ineffH}} + \text{ineff}UF \qquad (10)$$

It is interesting to look at the way the unburnt constituents vary with the level of efficiency. It has so far been found that between 98·5 and 100 per cent efficiency, carbon monoxide is the cause of inefficiency, while below 98·5 per cent the unburnt fuel inefficiency increases rapidly. Appreciable quantities of hydrogen are rarely found even at low efficiencies. Curves to illustrate these trends are shown in *Figure 6*. To measure inefficiency in the region 98·5–100 per cent, it is sufficient to estimate the carbon monoxide content of the exhaust gas. This covers the essential cruising conditions up to 40,000 ft. Above this altitude, and at idling approach conditions, an assessment of unburnt fuel is necessary.

The accuracy attainable by the gas analysis method must depend on the following factors: (1) the accuracy of analysis of the calibration samples for carbon monoxide; (2) the accuracy of the unburnt kerosine estimation; and (3) the accuracy of the mean sample taken.

Considering first an $\eta = 99$ per cent when unburnt fuel is absent. The analysis of an 0·075 per cent CO sample is only accurate to $\pm$ 5 per cent. However in terms of combustion inefficiency at 0·0167 f.a.r. (fuel air ratio by weight) 0·075 per cent is equivalent to 1·0 per cent inefficiency and this can be measured to perhaps $\pm$ 7 per cent accuracy allowing for 2 per cent instrument error. The efficiency values across the exhaust duct will range from 98·9–99·2 per cent; the sampling error must therefore be negligible. A total inaccuracy of $\pm$ 7 per cent should therefore be attainable. This is equivalent to approximately $\pm$ 0·1 per cent error in η. Thus gas analysis can give an accuracy at 0·0167 f.a.r. of 99 per cent $\pm$ 0·1.

Below 98·5 per cent the accuracy of measurement must decrease. The method used is to oxidize the fuel to carbon dioxide. The carbon dioxide produced must be measured in the presence of large amounts already present, and a differential method is required. Two readings are taken, one for carbon dioxide and one with oxidation products included. The absolute value of the carbon dioxide is not important, so that analytical errors are not relevant. In the region of $\eta = 93$ per cent it is necessary to estimate the equivalent of 4 per cent of fuel inefficiency. At 0·0167 f.a.r. this corresponds to 0·14 per cent of CO_2. Using a range of 2–4 per cent CO_2 over 100 divisions, this is equivalent to seven divisions. It is possible to estimate each reading to $\pm$ 0·25 divisions or $\pm$ 7 per cent which in terms of efficiency is 93 $\pm$ 0·3 per cent. The most important error may arise due to loss of fuel down the sampling line. It has already been pointed out that about 2 ft. of braided hose is used to connect the sampling point to the furnace. A test to investigate fuel losses gave the following mean results, at a mean combustion efficiency of 93·0 per cent.

	$\eta_{\text{ineff}UF}$
1 ft. of line	3·4
6 ft. of line	2·0

If these figures are extrapolated back to zero length of line, assuming the sampling gear corresponds to 1 ft. of extra line, the true unburnt fuel is estimated as 3·9 per cent. Thus a 2 ft. length of hose gives a loss of 0·8 per cent of unburnt fuel inefficiency. The efficiency values across the duct may range from 88–98 per cent so that the sampling accuracy of the automatic sampling gear becomes important. Comparisons made between the sampling gear and a multi-point traverse indicates an accuracy of $\pm$ 0·5 per cent. The accuracy of combustion efficiency figures quoted as 94 per cent is estimated therefore at approximately 94 — 1·6 per cent.

In the foregoing discussion no mention has been made of exhaust smoke. The maximum exhaust smoke so far experienced only contributes approximately 0·3 per cent to the combustion inefficiency. At this level the major effect is the detrimental visual appearance.

PRIMARY ZONE SAMPLING

Extreme difficulty is experienced in carrying out estimations, since large quantities of unburnt fuel and carbon may be encountered, temperatures are often very high and composition contours show sharp gradients. A sampling tube is required which, whilst being robust enough to withstand high velocities, temperatures and pressures, does not cause undue disturbances to the gas flows being traversed.

The materials generally used are stainless steel and nimonic alloys. Since flame temperatures often exceed 1,600°C, sampling tubes must be water cooled; such sampling tubes have been made with diameters as small as $\frac{1}{4}$ in. for use on small combustion chambers. At air pressures below 40 lb./in.^{2} abs. a 60 lb./in.^{2} mains water supply gives an adequate cooling water flow, but at higher air pressures an auxiliary pump is used to give a water pressure of 200 lb./in.^{2}. Most sampling tube failures are not mechanical but are due to blockage by glutinous masses of carbon and unburnt fuel; this occurs rapidly in some cases and makes sampling impossible.

The rates of sampling in primary zone analysis should be isokinetic; that is, the sampling velocity should equal the air-stream velocity or liquid droplets will not be representatively sampled. This is however in most cases not practicable, as flow rates as low as 15 l./h would be required and the time required for a survey prohibitive. During pre-dilution zone analyses sampling rates have been varied from isokinetic in 300 l./h with no excessive deterioration in accuracy.

Further work on sampling errors is however necessary, and for the moment a sampling rate of 300 l./h is used in order to obtain the speed of analysis required.

MEASUREMENT OF PRIMARY ZONE TEMPERATURES

Thermocouples are of limited application in primary zone investigations owing to the radiation losses which take place when measuring very high temperatures. Such losses can be reduced by using multi-shields, but the thermocouple becomes large and presents an appreciable blockage to the combustion gases. In addition the nimonic alloys

would not work at the high temperatures involved, so that platinum–rhodium alloy sheaths would be required, resulting in a very expensive instrument.

Alternatively a choked nozzle could be used in which the value of T is obtained from the $M(T)^{\frac{1}{2}}/AP$. The nozzle is made part of a probe,

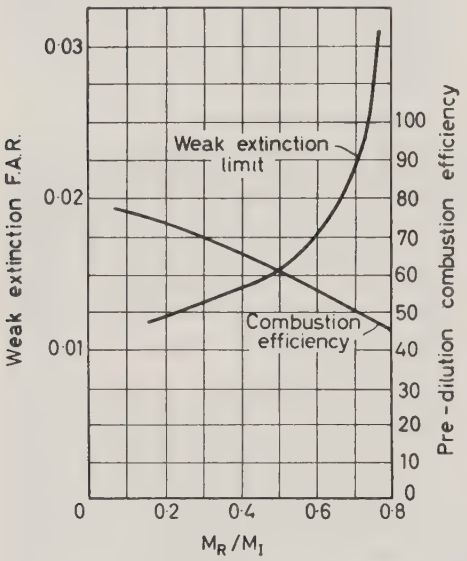

Figure 7. Effect of reversal mass flow on a particular primary zone

and in this case the majority of the probe surface may be water cooled. It is however impossible to prevent some blockage occurring at a sampling tube orifice in the conditions of fuel, carbon and high temperatures existing in a flame. In the case of the choked orifice the slightest reduction in area must effect the calibration, and it is therefore considered that the orifice method must be unreliable.

It is preferred to calculate gas temperatures from gas analysis results. The f.a.r. and η_{ineff} may be calculated from the following expressions in which all concentrations are expressed as per cent v/v.

$$\text{f.a.r.} = \left| \frac{(CO_2)_{UF} + CO + CO_2}{20{\cdot}9 + 0{\cdot}105CO_2 - 0{\cdot}313H_2} \right| \times 0{\cdot}101 \qquad (11)$$

$$\eta_{\text{ineff}} \text{ per cent} = \left| \frac{(CO_2)_{UF} + 0{\cdot}468CO + 0{\cdot}402H_2}{(CO_2)_{UF} + CO + CO_2} \right| \times 100 \qquad (12)$$

An apparent f.a.r. is then calculated from f.a.r. $\times \eta$ and standard heat rise curves are used to compute the gas temperatures. This method of calculation, whilst not strictly correct, gives results within 5 per cent when the inefficiency is due to carbon monoxide. No assessment of accuracy in the presence of unburnt fuel is possible since its physical state and specific heat are not known.

APPLICATIONS OF PRIMARY ZONE ANALYSIS

Reversal zone

The function of the reversal zone is to transport heat and burnt products back through the combustion chamber to mix with the incoming air and fuel. In this way combustion chambers can be made to operate over a wide range of pressures, air mass flows, and f.a.r.'s. The stability of an aircraft combustion chamber is of great importance: it is essential that it should remain burning under rapid acceleration and deceleration conditions, and also be able to suffer the quenching effects of tropical rain and altitude icing conditions.

It seems reasonable to suppose that the maximum amount of heat should be transported back, and it may be concluded from this that a high proportion of incoming air must be reversed. Air

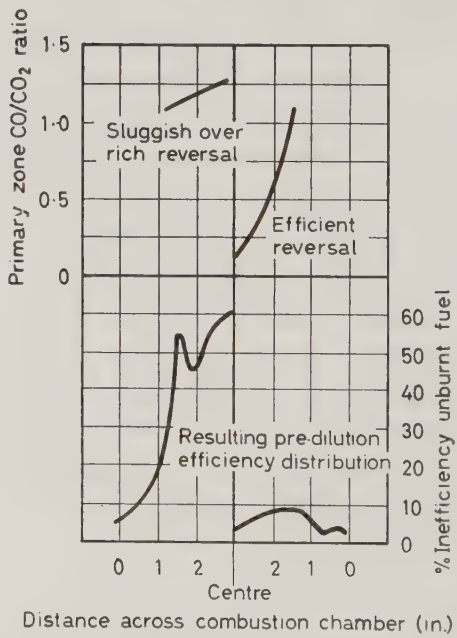

Figure 8. Effect of reversal composition on combustion efficiency

velocity traverses are necessary to determine the reversal quantity. *Figure 7* shows comparisons made between combustion chamber primary zones in which the reversal mass flow is varied.

The reversal flow is plotted as the ratio M_R/M_I, where M_R is cold reversal mass flow and M_I is cold input mass flow.

The figures show clearly that in this case a high reversal mass flow is a disadvantage, since pre-dilution efficiency drops appreciably and the stability of the primary zone also deteriorates. The gas analyses showed that the reversal was becoming weaker as the value of M_R/M_I increased. It is therefore necessary to add also to the criterion of a reversal that it should be efficient and hot. *Figure 8* for instance compares an efficient reversal and a sluggish, over-rich reversal, and it is of interest to note the improved pre-dilution zone efficiencies obtained from the efficient reversal. The reversal richness is plotted here as the ratio $\rho_c = CO/CO_2$. Since the amount of CO increases rapidly in over-rich products, ρ_c is a rapid and convenient way of comparing analysis results.

Since the reversal zone is normally over-rich, little free oxygen is available and the amount of fuel oxidation is considered to be small. The composition is probably controlled by an attempt by the gases to attain the water gas equilibrium

$$CO_2 + H_2 \leftrightarrows CO + H_2O \qquad (7)$$

It is interesting to consider the ratio of carbon monoxide to hydrogen (γ_c). Analytical results generally give values of 1·5 to 2·5.

Theoretical analyses can be obtained from accepted values of k_w where

$$k_w = \frac{|CO|\ |H_2O|}{|CO_2|\ |H_2|} \qquad (13)$$

The results are given in Table 1 and may be compared with typical experimental results in Table 2.

TABLE 1

f.a.r.	% CO_2 *v/v*	% CO	% H_2	% N_2	$\frac{CO}{H_2} = \gamma_c$
0·0675	14·8	—	—	85·2	—
0·075	12·4	3·85	0·8	83·0	4·7
0·0825	10·1	7·3	1·9	81·0	3·8
0·095	7·2	11·8	4·4	76·6	2·7
0·110	5·2	15·6	7·3	71·8	2·1
0·125	3·9	17·8	11·8	66·7	1·5

TABLE 2

% CO_2 *v/v*	% CO	% H_2	$\frac{CO}{H_2} = \gamma_c$
4·5	8·2	5·6	1·5
6·0	9·2	5·2	1·8
11·8	3·2	1·4	2·3
5·5	7·0	4·6	1·5
4·1	5·4	4·0	1·3

Normally the CO values are lower than would be expected and H_2 values higher, which gives low values for γ_c.

If the gas is 'unmixed' as suggested by Hawthorne, Weddell and Hottel[3], a gas sample will consist of gas eddies of various compositions, having different life histories. Considering a simple case of two types of eddy, one having attained sufficient oxygen and the other being oxygen deficient, as follows,

% CO_2	% CO	% H_2	% N_2
14·8	Nil	Nil	85·2
5·2	15·6	7·3	71·8

Gas analysis would record the following mean composition

10·0 7·8 3·6 78·5

The γ_c value of this composition is 2·2 and it corresponds to the type of analysis found in practice. In an 'unmixed' system therefore the values of γ_c will depend on the degree of mixing.

The other reaction of importance occurring in the reversal zone is the pyrolysis of fuel. In the presence of hot reaction products and little oxygen, fuel cracks to carbon and hydrogen. A typical set of carbon concentrations measured across a primary zone is shown in Table 3.

TABLE 3

	Distance across combustion chamber, in.							
	¼	¾	1½	2	2½	3	3½	3¾
Plane A 1¼ in. from burner								
Carbon units	7	130	90	20	30	30	11	8
Plane B 2¼ in. from burner								
Carbon units	8	20	13	4	2	9	8	8
Plane C 4¾ in. from burner—(pre-dilution traverse)								
Carbon units	1·5	2	trace	trace	2	2	3	trace

The unit used is g carbon/l. at s.t.p. × 10^5

In plane *A* the reversal region extends from ¾ to 3 in. and the production of carbon in this region is clearly shown. The ensuing oxidation of carbon is also shown, and in this particular case the carbon concentration after dilution was only 0·4 units.

It is interesting that the present combustion chamber designs have very rich reversals, although the overall primary zone fuel-air ratio is designed to be approximately 0·04. The indications are that attempts to weaken off a reversal results in poor altitude re-lighting and that an over-rich reversal

is required to meet this criterion. The disadvantage of an over-rich reversal is that carbon deposits on burners and combustion chamber walls, and that carbon chilling may occur in the dilution zone, giving a smoky exhaust.

Reaction zone

The primary reaction zone is considered to be an annulus round the reversal zone, see *Figure 1.* The temperature gradients across this zone may

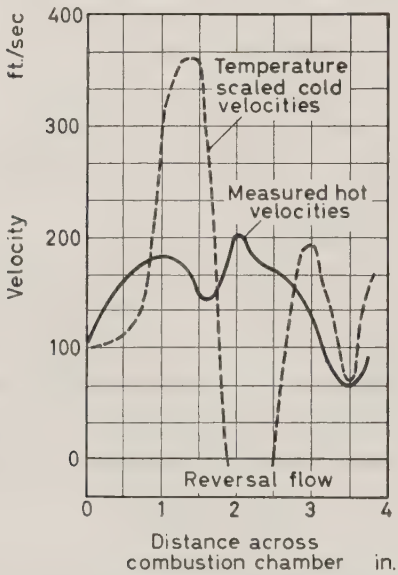

Figure 9. Comparison of pre-dilution zone velocities

be extremely large, since the outside must run cool in order to keep the wall temperatures low, while the inside surface may approach 2,000°C. In order to approach the problem of converting data into reaction rates for fuel, the reaction zone has been divided into three reaction annuli as shown in *Figure 1.* It is then assumed that the main lines of gas flow are confined to the three annuli. The first step is to compute reaction times for each annulus. Cold velocity traverses are carried out at planes *A* and *B* (*Figure 1*) and the figures are temperature scaled to give the hot velocity pattern. This approach assumes that little radial expansion occurs under burning conditions.

Since the length of the reversal is reduced under burning conditions temperature scaling cannot be used in planes *C* and *D*, and attempts have been made to measure hot velocities under these conditions. *Figure 9* compares the hot and cold velocity distributions measured in a pre-dilution plane, and shows the absence of negative hot gas flows.

The hot velocity values can be used to calculate reaction rates for kerosine. Considering the theoretical reaction rate for fuel as being derived from the Arrhenius equation, we can express the rate of fuel reaction per unit volume as follows:

$$\frac{dC_f}{dt} = zC_oC_f \exp |-E/RT| \; T^{-3/2}P^2 \qquad (14)$$

where C_f and C_o are the local concentrations of fuel and oxygen, t is the time available for reaction, z is the collision frequency constant, T and P are the local temperature and pressure, E is the activation energy constant, R is the gas constant.

The validity of this step is discussed briefly in reference 4. Hence

$$\frac{dC_f}{C_f} = zC_o \exp |-E/RT| \; T^{-3/2}P^2dt \qquad (15)$$

Integrating with respect to time

$$\log_e C_f = zC_o \exp |-E/RT| \; T^{-3/2}P^2t + \log_e B \qquad (16)$$

where B is the integration constant.

Thus when $t = O_2, C_f = C_F$ where C_F is the original quantity of fuel. Hence

$$\log_e \frac{C_f}{C_F} = zC_o \exp |-E/RT| \; T^{-3/2}P^2t \qquad (17)$$

or

$$\log_e \eta_{\text{ineff}UF} = kt \qquad (18)$$

where k is defined as the reaction time coefficient.

If values of $\eta_{\text{ineff}UF}$ are plotted against time available for reaction a series of lines can be obtained as shown in *Figure 10.* The slope of these

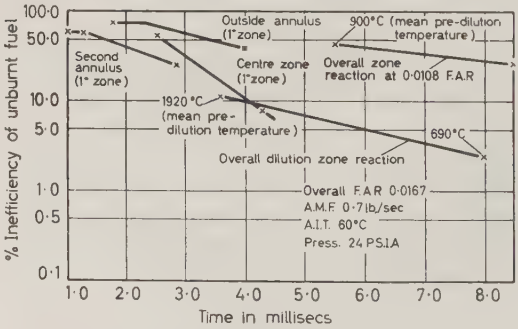

Figure 10. Fuel reaction velocities in primary and dilution zones

lines can then be identified with k the reaction time coefficient. Therefore

$$k = z\,|O_2| \exp |-E/RT| \; T^{-3/2}P^2 \qquad (19)$$

or

$$\log_e \frac{kT^{3/2}}{|O_2|P^2} = -E/RT = \log_e K \qquad (20)$$

where K is the fuel reaction rate coefficient.

If the mean values of T and O_2 are supplied for each zone, values of $\log_e K$ can be plotted

against $1/T$. This procedure has been applied to two combustion chambers and a simple re-heat gutter at different f.a.r.'s and air mass flows. The results of these tests are shown plotted in *Figure 11*. In view of the distances between the sampling planes, the scatter about the mean line is considered to be reasonably good. It is at first sight surprising therefore that the value of E obtained from the slope of the graph is approximately 13,000 cal/g mol, and not 40,000 cal/mol which is generally accepted. It is possible that the concept of temperature may be at fault. Consider an eddy of hot reacting fuel in a matrix of air; the reaction is taking place on the outside surface of the eddy and the temperature would be measured as T_1. If there are two eddies in the same air matrix the reaction rate will be the same on the outside surface of both eddies but the temperature would be measured as $2T_1$. The reaction rate would in this case be independent of temperature, and the value of E would be very low.

It is suggested therefore that the value of E obtained is a result of the heterogeneous mixing conditions and that the temperature dependence of fuel reactions is not as great as would be expected from the activation energy of 40,000 cal/g mol.

The gas traverse plane D (*Figure 1*) is also defined as the pre-dilution traverse. In this plane inefficient products are usually found in one of three possible patterns: (*a*) Unburnt kerosine exists mainly near the wall of the combustion

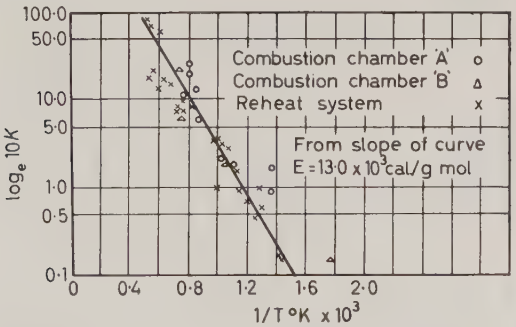

Figure 11. Reaction rate coefficients $v(1/T°K)$

chamber and is typical of fairly low pressure conditions, where fuel reaction rates are low; (*b*) the centre is very rich in unburnt kerosine—this is typical of a sluggish over-rich reversal zone; (*c*) the centre is very rich in carbon monoxide while kerosine is absent—this is typical of high pressure conditions with high fuel reaction rates.

Dilution zone

It was at one time considered that the dilution zone would chill out reactions not complete before dilution; pre-dilution zone analyses have shown that this is a fallacy. At pressures above 30 lb./in.^{2} abs., the rates of reaction in a combustion chamber working at 0·0167 f.a.r. are sufficient to virtually complete the gas reactions in the dilution zone. Inefficiency arises at idling and high altitude cruise conditions which are associated with lower pressures. A typical set of efficiency values is shown in *Figure 12* which relates exhaust combustion efficiency to altitude. Two pre-dilution zone efficiencies are also shown. Approximately 20 per cent of the final combustion

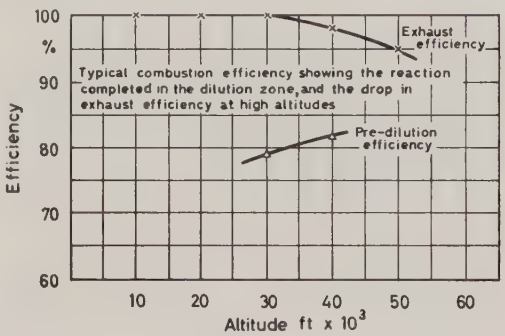

Figure 12

efficiency is gained in the dilution zone; thus the value of the dilution zone as a reaction zone is clearly evident.

CONCLUSION

The results presented show the diversity of data which may be obtained by the application of gas analysis to combustion chambers. Although the time involved in obtaining sufficient results to give a complete picture of a flame is considerable, it is becoming evident that in the long run development time is saved by the improvement in our understanding of the problems involved.

The authors wish to acknowledge permission given by Rolls-Royce Ltd. to publish this paper.

REFERENCES

[1] Martin, A. E. The infra-red gas analyser and what it can do. *Research, Lond.* 6 (1953) 172

[2] Macfarlane, J. J. The application of chemical analysis to the investigation of gas turbine combustion problems. *N.G.T.E. Report No. R.29*; page 4 and Figure 1

[3] Hawthorne, W. R., Weddell, D. S. and Hottel, H. C. Mixing and combustion in turbulent gas jets. *Third Symposium on Combustion Flame and Explosion Phenomena*, p. 266. Baltimore; Williams and Wilkins

[4] Bragg, S. L. and Holliday, J. B. The influence of altitude operating conditions on combustion chamber design. *AGARD Selected Combustion Problems II*, p. 270. 1956. London; Butterworths

APPLICATION OF PHASE-DISCRIMINATION METHOD OF DETECTION TO THE STUDY OF THE SPECTRUM OF THE OH RADICAL IN AN OXY-ACETYLENE FLAME

F. P. DICKEY and J. M. HOFFMAN

As has been pointed out in a recent paper[1], the phase-discrimination method of detection can be useful in conducting certain studies of the infra-red spectra of flames. In that paper it was shown how to apply this method of detection to study the effects of gaseous additives on these spectra. Introducing the additive into an exciting flame periodically, and selectively detecting the periodically interrupted emission due to the additive by means of a phase-sensitive detector, results in the spectrum due to the additive being much stronger than that of the exciting flame.

The phase-discrimination method of detection has been applied to the study of the spectrum of the OH radical in an oxy-acetylene flame. By using this method it is possible to observe the spectrum of the OH radical without the strong background spectrum of water vapour which is also very prominent in the spectrum of the flame. The method makes the identification of the OH lines much easier and more positive. It also makes it possible to observe more of the lines due to OH than could possibly be observed in the spectrum of the flame when it is obtained in the conventional manner.

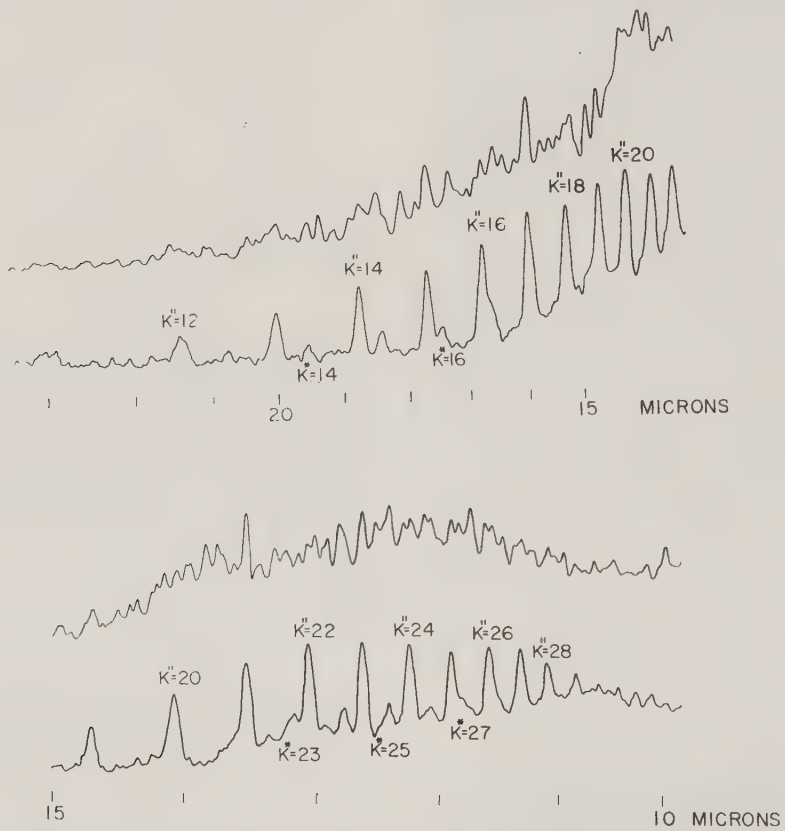

Figure 1. The infra-red spectrum of the oxy-acetylene flame showing the effect of using the phase-discrimination method of detection. Phase-discrimination was used to obtain the lower spectrum of each pair

The results of the study are shown in *Figure 1.*

The spectral range observed extends from 10 to 23 microns. The upper pair of traces were obtained using a KBr prism, and the lower pair were obtained using an NaCl prism. The spectrum shown by the upper curves of each pair is that obtained with the spectrometer in the usual manner. The spectrum shown here agrees with the recent work of Ketelaar, Haas, Hooge and Brockhuijsen[2]. The curves show that it is difficult, and may be impossible, to distinguish the OH lines from the water vapour lines.

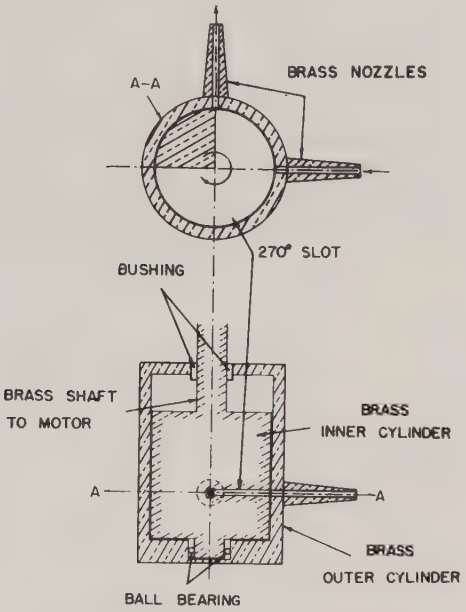

Figure 2. Revolving slot chopper for gases

The lower curve of each spectral region shows the appearance of the oxy-acetylene flame spectrum when the phase-discrimination method of detection is used. The lines due to water vapour have been eliminated while the lines due to OH remain essentially unchanged.

The spectra shown in *Figure 1* were obtained using a Perkin–Elmer Model 12B spectrometer, a Perkin–Elmer Model 107 amplifier, and a Brown Electronik pen recorder. The upper curve for each spectral region was obtained using the spectrometer in the conventional manner. Radiation from the region just above the primary flame was focused on the entrance slit of the spectrometer. The flame was that of a small torch. A mechanical radiation chopper was located just in front of the entrance slit and interrupted the radiation falling on it at a rate of 13 c/s.

There are variations in the spectrum of the oxy-acetylene flame when radiation from different parts of the flame is focused on the entrance slit of the spectrometer. These variations are primarily due to changes in the intensity of the OH lines, and make possible the application of the phase-discrimination method of detection to the study of the OH spectrum of the flame. The OH lines are intense in the region just above the primary flame, and are quite weak in the primary flame itself.

The OH spectrum shown in *Figure 1* was obtained by removing the mechanical radiation chopper from the spectrometer: a mechanical valve was then used to vary the flow rate of the acetylene to the torch at 13 c/s. The flame and optics were adjusted so that during half of each cycle radiation from just above the primary flame fell on the entrance slit of the spectrometer, and during the other half-cycle radiation from the primary flame itself was incident upon the entrance slit. When the valve was properly phased with respect to the mechanical rectifier of the Perkin–Elmer system, the OH spectrum was obtained without the presence of the water vapour lines.

Figure 2 is a drawing of a mechanical valve of the type used in studies involving the phase-discrimination method of detection. This mechanical valve has been called a 'gas chopper'. In obtaining the OH spectrum a double valve was actually used, but a single valve is shown in the illustration because it makes the drawing considerably clearer. The double valve was used because the flow rate of the acetylene was merely varied and not completely interrupted. As is apparent from the drawing the gas flows from the inlet through the slot of the inner rotating cylinder and to the outlet. The 90 degree solid sector keeps both the inlet and the outlet, which are spaced 90 degrees apart, closed during one-quarter of each revolution of the sector; hence, the gas flow is interrupted for half of each revolution. In the case of the double valve, two such paths are placed side by side in the same valve. The separation used is about 1/4 in. The two outlets are connected together at a point just outside the outer hollow cylinder. The solid sectors of each path are so arranged that gas flows through one path for half of each revolution and through the other path for the remainder of the revolution. The flow rates during each half-cycle are then controlled and measured by flow meters located in both of the supply lines to the two inlets of the valve.

Experience gained from the oxy-acetylene flame suggests still another application of the phase-discrimination method of detection to the study of flame spectra in the infra-red. Two different sections of two balanced flames might be viewed alternately and in this way any differences in the spectra from the two regions would be observed while the common characteristics of the spectra would be attenuated. This could be accomplished by a moving mirror system; alternatively, two different sections of the same flame could be viewed.

The OH spectrum in *Figure 1* shows all of the pure rotation lines in the region of 10 to 23 microns. These lines have been identified as the line $K'' = 11$ through $K'' = 29$. The weaker lines in this spectrum are also due to OH. They are the rotation lines of the OH molecule in the first vibration state. A few of these lines have been marked by a $K^{\star}$.

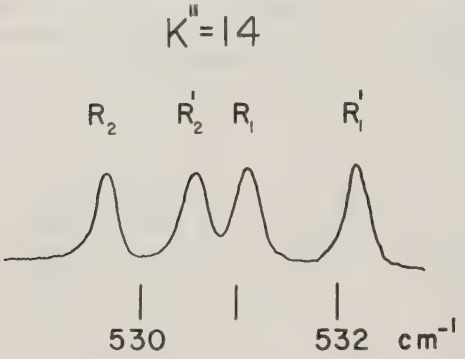

Figure 3. The line $K'' = 14$ when measured using high resolution

A study of the OH spectrum using high resolution has been started. *Figure 3* shows one of the lines, $K'' = 14$, obtained using a prism-grating spectrometer. All of the rotation lines will be observed and their frequencies will be accurately determined. It is interesting to note that each of the lines shown in *Figure 1* actually consists of four lines. The particular line $K'' = 14$ is shown in *Figure 3* because it can be compared with the same line as reported in an article by Madden and Benedict[3]. Their measurements were made in the usual way and there is considerable water vapour background in their spectrum. Our preliminary frequency determinations are in good agreement with those of Madden and Benedict.

The energy level diagram presented in *Figure 4* shows how the lines of $K'' = 14$ occur. In the OH molecule the ground-state levels are $^2\Pi$ states, and the equations for the term values as given by Hill and Van Vleck[4] are:

$$F_1(K) = B_v\{(K+1)^2 - 1 - 1/2[4(K+1)^2 + Y_v(Y_v - 4)]^{1/2}\} - D_vK^2(K+1)^2$$

when $J - 1/2 = K$;

$$F_2(K) = B_v\{K^2 - 1 + 1/2[4K^2 + Y_v(Y_v - 4)]^{1/2}\} - D_vK^2(K+1)^2$$

when $J + 1/2 = K$;

where $Y_v = A_v/B_v$, and A_v is a measure of the strength of coupling between the spin $\boldsymbol{S}$ and the orbital angular momentum $\boldsymbol{\Lambda}$. In the case of OH, A_v is negative indicating that it is an inverted doublet with the $^2\Pi_{3/2}$ state being lower than the $^2\Pi_{1/2}$ state. The Λ doubling may be calculated using the equation given by Van Vleck[5],

$$\nu_\Lambda = -\alpha_p(J+1/2)\left(1 + \frac{2 - Y_v}{\pm X}\right) \mp \frac{4\beta_p}{X}(J - 1/2)(J + 1/2)(J + 3/2)$$

where $X = [4(J+1/2)^2 + Y_v(Y_v - 4)]^{1/2}$, and in the case of OH (inverted doublet) the upper sign goes with the $^2\Pi_{1/2}$ state and the lower sign with the $^2\Pi_{3/2}$ state.

Values for the constants that appear in the previous equations have been given by Dousmanis,

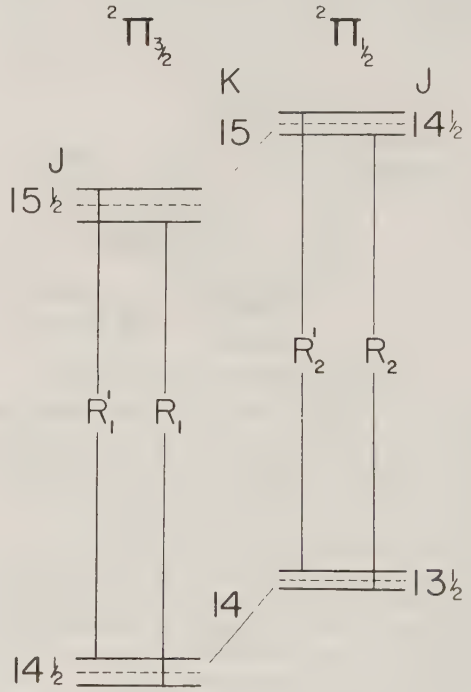

Figure 4. Energy level diagram for the line $K'' = 14$

Sanders and Townes[6]. When these values are substituted into the equations above the following values are calculated for the frequencies of the lines of $K'' = 14$.

Line	*Calc. freq. (OSU)*	*Obs. freq. (Tentative-OSU)*	*Obs. freq. (M. and B.[3])*
R_1'	531·615 cm^{-1}	531·60 cm^{-1}	532·16 cm^{-1}
R_1	530·349	530·53	531·09
R_2'	529·847	530·03	530·56
R_2	528·821	529·16	529·69

Our observed frequencies listed here are tentative, and will no doubt be slightly different when more accurate measurements are made. The relative accuracy of our present measurements is good, as is indicated by the good agreement between the values for splitting when calculated from our observed values and those which result from the measurements of Madden and Benedict. The fact that there is some disagreement with the calculated values means that the values of the molecular constants may have to be changed slightly. Furthermore, it will probably be necessary to take into account higher-order terms than are included in the formulae given here. This will not be known until the high-resolution study is completed.

This work was supported in part through a contract between the Air Force Cambridge Research Center, Air Research and Development Command of the United States Air Force, and The Ohio State University Research Foundation.

REFERENCES

[1] Dickey, F. P., Kopczynski, S. and Bell, G. *J. chem. Phys.* 25 (1956) 180
[2] Ketelaar, J. A., Hass, G., Hooge, F. N. and Brockhuijsen, R. *Physica* 21 (1955) 695
[3] Madden, R. P. and Benedict, W. S. *J. chem. Phys.* 23 (1955) 408
[4] Hill, E. L. and Van Vleck, J. H. *Phys. Rev.* 32 (1928) 250
[5] Van Vleck, J. H. *Phys. Rev.* 33 (1929) 467
[6] Dousmanis, G. C., Sanders, T. M. Jr. and Townes, C. H. *Phys. Rev.* 100 (1955) 1735

MEASUREMENTS OF FLUCTUATING FLAME TEMPERATURE

MASANAGA KUNUGI and HIROSHI JINNO

INTRODUCTION

Performance evaluation and control of industrial furnaces, as well as the fundamental research of the related combustion phenomena, depend considerably upon a knowledge of the steady temperature of the flame in the furnaces. However, the flames used in such a field are commonly turbulent diffusion flames. The main characteristic of turbulent phenomena is their irregular random nature, and an understanding of temperature fluctuations is one of the more important problems.

The authors made an attempt to measure the fluctuating gas temperature in turbulent diffusion flames with bare thermocouples. Shadow and schlieren pictures of the flames were also taken for a better understanding of turbulence.

Shepard and Warshawsky[1] have developed the electrical techniques for time lag compensations of thermocouples used in the temperature measurement of jet engine gas whose velocity with respect to the thermocouple corresponds to a Mach number ranging from 0·1 to 0·9. In our experiments the velocity of flame gases is low with a Mach number of less than 0·1.

EXPERIMENTAL PROCEDURE AND RESULTS

The flames were formed by city gas issuing vertically from circular tubes into stagnant air with various velocities. Two sizes of burner port were used, of 4·8 mm and 6·4 mm inside diameter. The Reynolds number in our experiments has a maximum value of 8,000 in the burner tube.

For dynamic measurement of fluctuating gas temperatures it is desirable to use a thermocouple of sufficiently small size to achieve adequately rapid response. Such small elements, however, have inadequate service life, so that it is necessary to use somewhat larger elements with appreciable lag. For example, the thermocouples used were made by welding platinum and platinum/13 per cent rhodium wires, each 0·06 mm in diameter

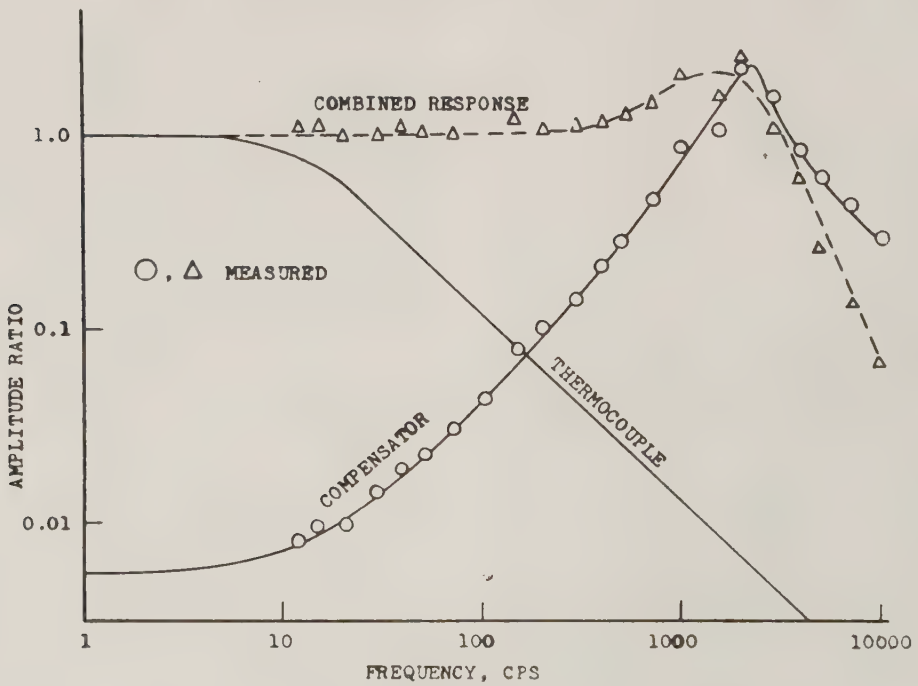

Figure 1. Response of thermocouple with compensator. Time constant of thermocouple is 0·0125 sec

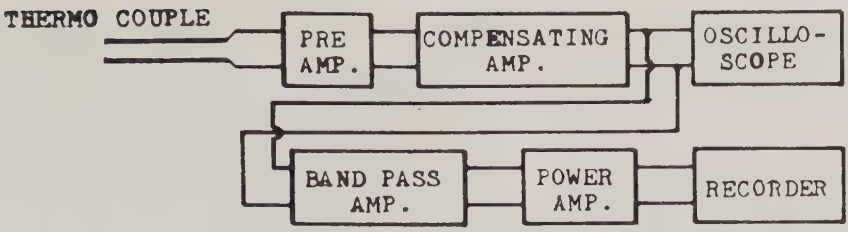

Figure 2. Compensating system for temperature measurements

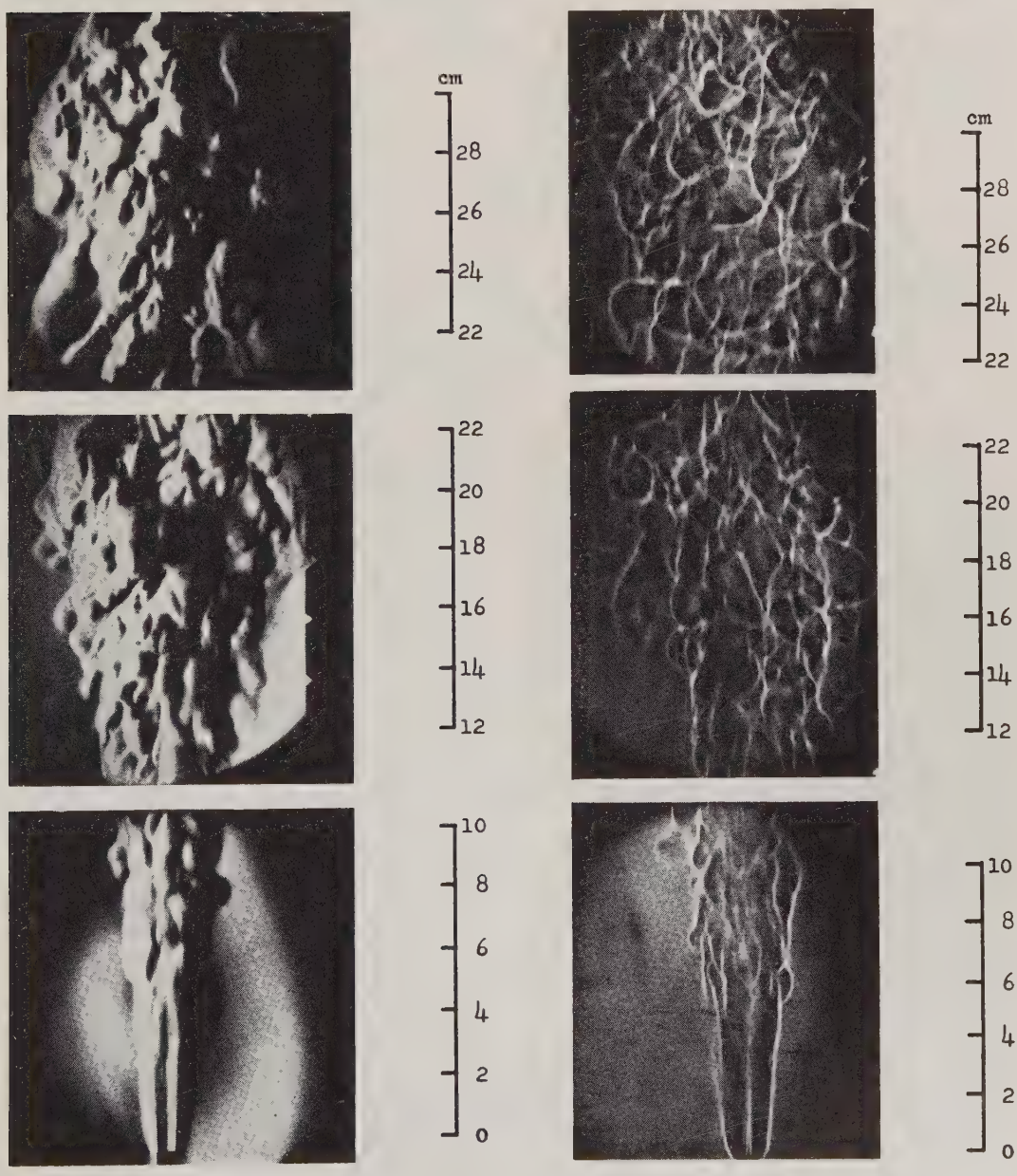

Figure 3. Schlieren (left) and shadow (right) photographs of a turbulent diffusion flame. Burner tube diameter = 4·8 mm, R_e = 5,700, port velocity = 22·8 m/sec

and about 1·5 mm long and attached to 0·5 mm support wire of the same composition.

The bare thermocouple was inserted approximately perpendicular to the gas stream into the flame. With this technique, the flame was not visibly disturbed. The measurements for the aerodynamic conditions in the flame, such as Reynolds number range of 1,500 to 8,000 and Mach number of less than 0·1, were carried out at various points across the flame and at various heights above the burner.

schlieren photographs of the flame is shown in *Figure 3.*

From the pictures it is suggested that in the lower part of the flame the boundary between the unburnt gas and combustion products and the flame envelope are characterized by steep density gradients; and the burning zone lies between these two regions. In the upper part of the flame the appearance is that of irregular turbulence.

For a measurement of the time constant, an alternating electric current was passed through the

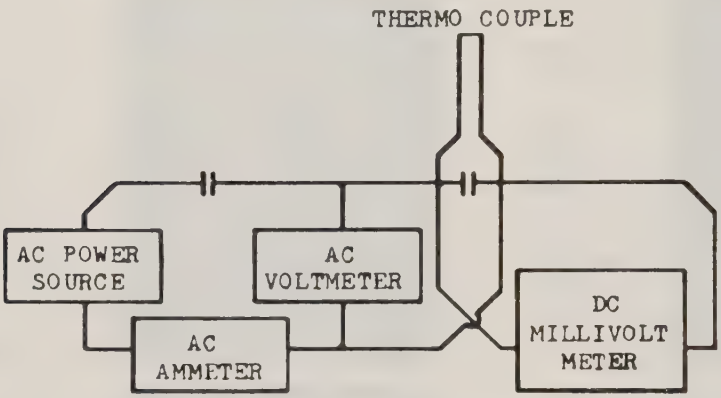

Figure 4. The system for time constant measurement

The compensator for the bar-wire thermocouple used was set and adjusted to match the thermocouple time constant. The value of the thermocouple time constant, however, is a function of the velocity and the density of the gas stream. In practice, therefore, a certain amount of mis-match may exist between the thermocouple time constant and the compensator. The authors corrected experimentally the mis-match under several sets of aerodynamic conditions in the flame as described later.

The typical characteristics of the compensator are shown in *Figure 1* with the frequency response curve predicted from the heat transfer relations for the thermocouple wire of 0·06 mm in diameter in the flame.

From the combined response curve, shown by the dotted line in *Figure 1,* it is seen that the combined response is flat from 10 to about 1,000 cycles per second.

In order to determine also the spectrum of fluctuating temperature, the output from the compensating amplifier was fed into a variable-frequency band pass amplifier.

The complete system, shown schematically in *Figure 2,* consists of the bare thermocouple, pre-amplifier, negative feedback amplifier with compensating network, band pass amplifier, and the cathode ray oscilloscope or recorder.

To visualize the structure of the flame used in our experiment an example of shadow and

thermocouple wire in the flame to heat the junction to about 100°C above the gas temperature. The temperature rise ΔT and the heating current I were measured.[9] The time constant τ is given by $\tau = 1{\cdot}8 \times 10^{-4}(\Delta T/I^2)$. The circuit for this method is presented schematically in *Figure 4.*

The typical time average values of the time constant obtained at various points across a flame and at two heights above the burner are shown in *Figure 5* as a plot of time constants in seconds against radial distance, r mm, from the flame axis.

From the figures it is seen that the value of the time constant in the upper part of the flame is much larger than that in its lower part. This is probably due to the fact that the flame broadens with increasing height and this causes a decrease of the axial velocity of the flame.

The representative fluctuation profiles of gas temperature occurring in turbulent diffusion flames are illustrated in *Figure 6,* in which temperature–frequency relations obtained across the flame are presented.

Figures 6a and *6b* indicate the data measured at two different heights, 6·4 mm and 19·2 mm, of the flame of city gas issuing from a burner port of 6·4 mm in diameter. The Reynolds number is 5,700 in the burner tube. *Figure 6c* refers to the case of the burner port of 4·8 mm diameter.

The vertical axes indicate the amplitude in °C, and the abscissa the frequency in cycles per second. *Tm* and r in the figures represent the

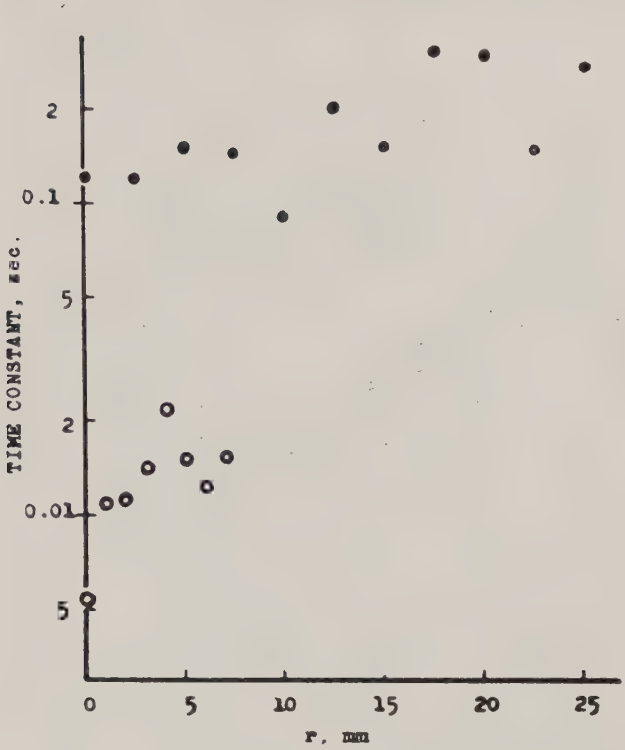

Figure 5. Time constant of thermocouple in the flame city gas leaving a port of 6·4 mm *diameter.* $R_e = 5{,}700$, r = *radial distance in* mm *from flame axis. Symbols* ⊙, ● *indicate the data obtained at different heights* 6·4 *and* 19·2 cm *from the port respectively*

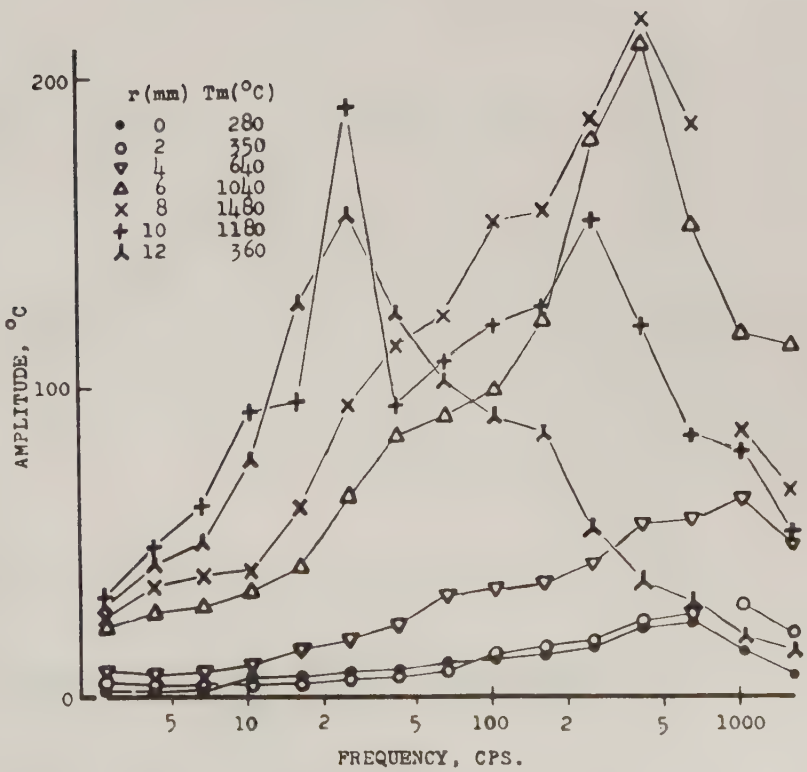

Figure 6a. Fluctuation profiles of gas temperature at height 6·4 cm *of turbulent diffusion flame. Diameter of burner port* = 6·4 mm, *port velocity* = 17·0 m/sec, $R_e = 5{,}700$, r = *radial distance in* mm *from flame axis, Tm = Time-mean temperature in* °C

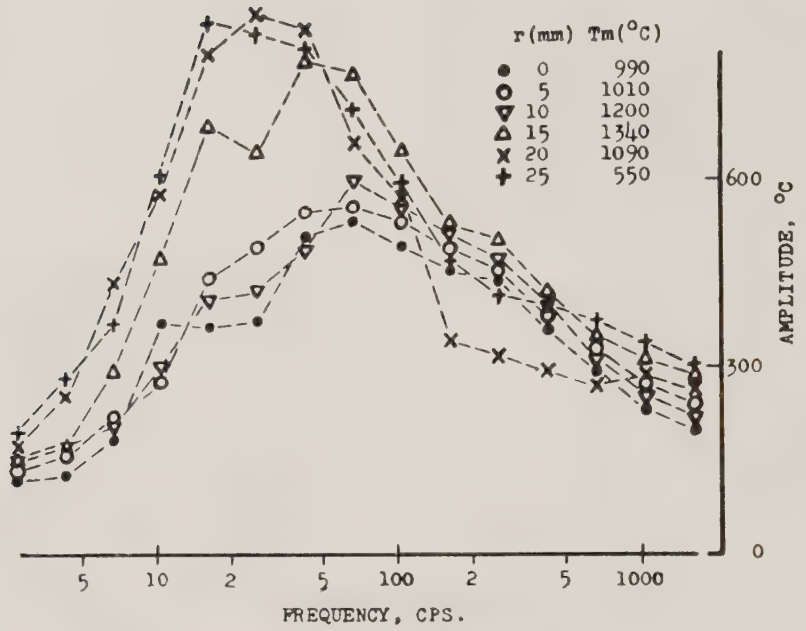

Figure 6b. Fluctuation profiles of gas temperature at height 19·2 cm *of same flame as in Figure 6a*

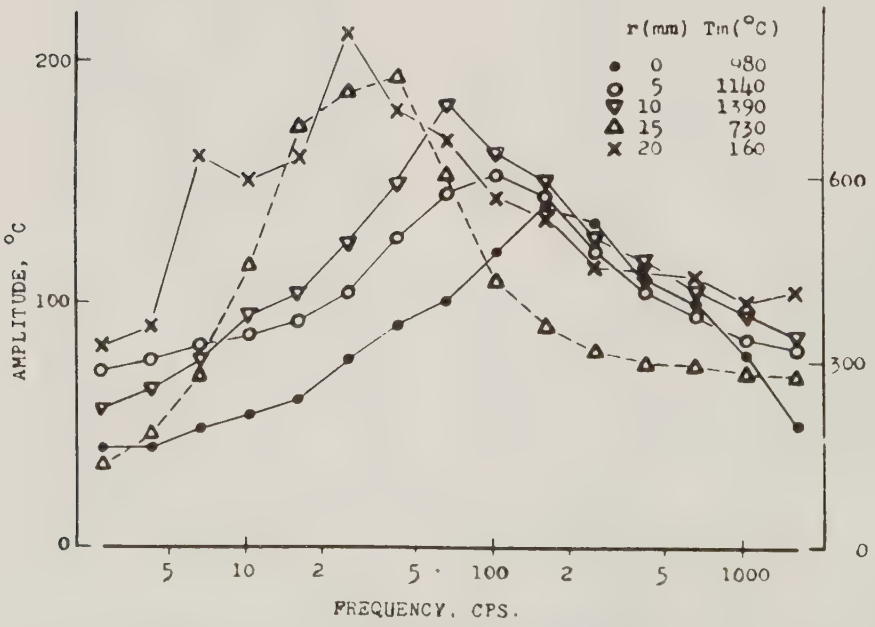

Figure 6c. Fluctuation profiles of gas temperature at height 14·4 cm *of turbulent diffusion flame. Diameter of burner port* 4·8 mm, *port velocity* = 22·8 m/sec, R_e = 5,700

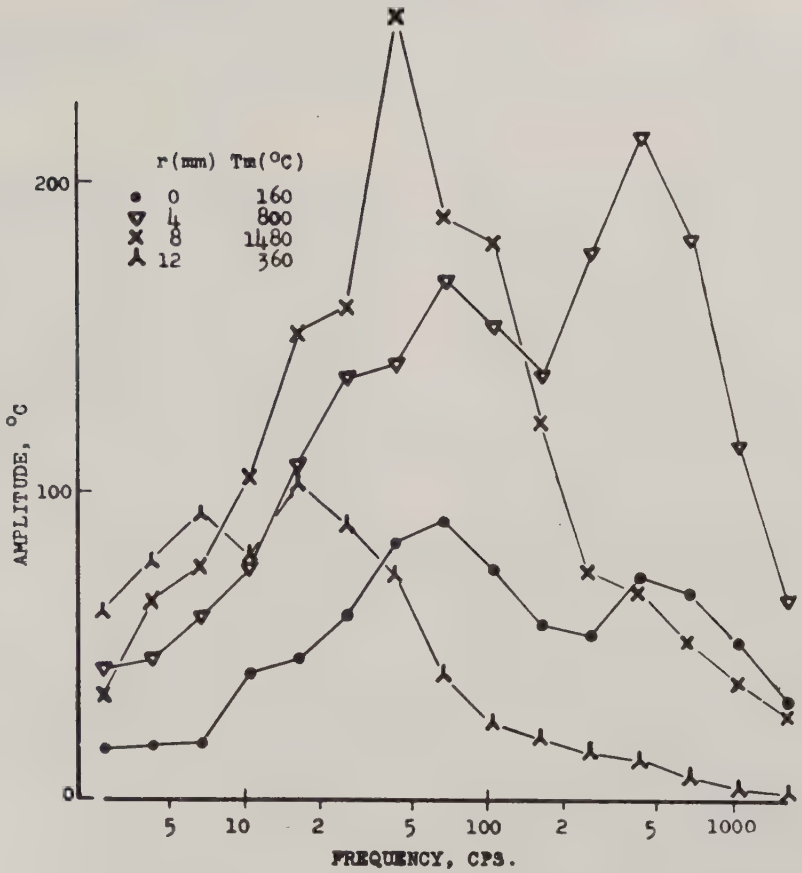

Figure 7a. Temperature fluctuation traverse across laminar flame at height 6·4 mm. *Diameter of burner port* = 6·4 mm, *port velocity* = 8·5 m/sec, R_e = 2,850

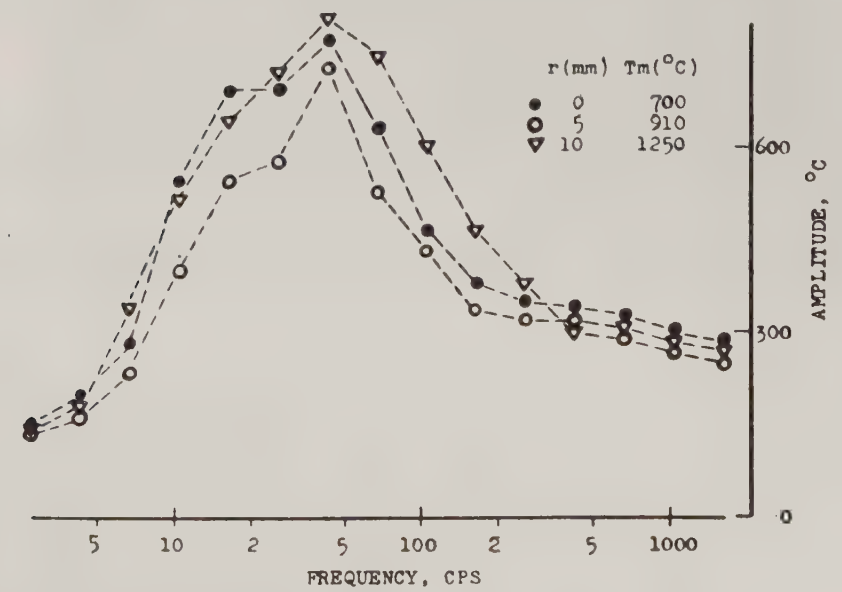

Figure 7b. Temperature fluctuation traverse across same flame as in Figure 7a at height 19·2 cm

time–mean temperature in °C, and the radial distance in mm from the flame axis. In *Figure 6c* the vertical axis on the left refers to the data obtained inside the flame, namely, $r = 0, 5, 10, 20$ mm, and that on the right to the curve shown by the dotted line ($r = 15$ mm).

The curves in *Figure 6a* show that the flame in its lower part is characterized by the three regions having different frequencies of the temperature variations, namely, (1) in the inner jet of unburnt gas (the curves of $r = 0, r = 2$ mm) the amplitude of the temperature is less than 20°C and the typical frequency of the variation seems to be about 1,000 c/s, (2) around the burning zone (the curves of $r = 6$, $r = 8$ mm) the fundamental frequency of the variation is 500 c/s, (3) at the boundary ($r = 10, r = 12$ mm) between the ambient air and the envelope of hot gases the peak in the curves appears at a frequency of approximately 20 c/s.

For the upper portion of the flame *Figure 6b* and *Figure 6c* indicate that the typical temperature fluctuation is represented by two peaks in the curves situated at frequencies of about 20 and 100 c/s, the former occurs at the flame envelope and the latter inside the flame.

In *Figure 7a* and *7b* the results obtained for a laminar flame are shown.

In the lower part of the flame the curves in *Figure 7a* are seen to be fairly similar to that given in *Figure 6a*, except near the flame axis. The upper part of the flame, however, is characterized by the peak of temperature variation at about 50 c/s and its amplitude of 500–600°C, as is evident in *Figure 7b*. The occurrence of such amplitude is probably related to the flickering of the flame caused by the low axial velocity of the flame.

The amplitude of the temperature fluctuation in the flame envelope also seems to be too large. This may be mainly due to the following fact. As is well known, the rate of burning along the diffusion flame depends on the entrainment of air from the surroundings. By analysing the gas composition near the flame envelope, it has been found that the average sample contains substantial amounts of unburned fuel gas and free oxygen[2]. At some time combustion products and fuel gases are transported into the boundary, and at another time the combustion products are replaced by fresh air, so that the large variation of temperature at that portion is to be expected.

CONCLUSION

The fluctuating gas temperature in turbulent and laminar diffusion flames was determined by a bare thermocouple of 0·06 mm diameter combined with compensating networks. From the results obtained it may be concluded that the turbulent diffusion flame is characterized by three typical regions, namely, the inner jet of unburnt gas, the burning zone, and the flame envelope, with the different peaks at frequencies of approximately 20, 100, 500, and 1,000 c/s respectively in temperature–frequency relations.

The difference of the frequency and amplitude of temperature variation in the unburnt gas region between turbulent and laminar flames can be explained by the fact that the unburnt gas stream is affected by the Reynolds number in the burner tube.

In such a flame, fuel and oxygen have to diffuse against the stream of combustion products in order to mix and to react. The air necessary for combustion is drawn in from the surroundings. Accordingly, the characteristics of the temperature fluctuation near the flame envelope may be influenced by the coarseness of turbulent mixing; however, in the burning zone it is believed that the molecular diffusivity and rate of chemical reaction are more effective.

The authors are indebted to Professor I. Sawai for advice with regard to the experimental technique and to Mr. M. Takada for his assistance in carrying out the experiments.

REFERENCES

[1] Shepard, C. E. and Warshawsky, I. *Tech. Note Nat. Adv. Comm. Aero. Wash.* No. 2703 NACA TN2703 (1952); *Instrum. Soc. Amer. Proc.* 7 (1952) 149

[2] Hottel, H. C. and Hawthorne, W. R. *Third Symposium (International) on Combustion*, p. 266. 1949. Baltimore; Williams and Wilkins

SHOCK TUBE STUDIES OF ACETYLENE DECOMPOSITION

W. J. HOOKER

INTRODUCTION

Extensive experimental studies have been conducted on the rate of decomposition of argon–acetylene mixtures by means of shock waves. Activation energies of 26 and 33 kcal/mole, respectively, have been found for the first- and second-order decomposition reactions of acetylene.

EXPERIMENTAL PROCEDURE

The shock tube used for these studies was made of 3 in. seamless steel pipe with a 1·525 m length of high-pressure section and a 1·695 m length of low-pressure section. The entire tube and associated gas-handling systems could be evacuated to a pressure of 0·5 microns with a leak rate of 0·1 microns per minute. The argon–acetylene mixtures used for these experiments were agitated with glass beads in a mixing bottle in order to ensure homogeneous gas compositions. A quantitative infra-red absorption measurement was made prior to each experiment in order to determine the amount of acetylene present in the shock tube.

Figure 1. Photograph of the assembled shock-tube facility with the major parts labelled. A, *Low-pressure end of the shock tube;* B, *Perkin–Elmer infra-red source optics and 13 cycle chopper;* C, *Perkin Elmer infra-red monochromator;* D, *Compartment for indium–antimonide infra-red detector;* E, *Single- and double-path collimating systems;* F, *The* 180 kc *mechanical light chopper;* G, *Carbon arc source;* H, *Condensing optics for monochromator slit;* I, *Shock velocity measuring station*

A well defined curve of temperature *versus* induction time for carbon formation has been established. Analysis of these data suggests that possibly a somewhat better correlation is obtained for decomposition reactions of order $n = 1$ and $n = 1{\cdot}5$ than for $n = 2$. The corresponding activation energies are 10, 13, and 16 kcal/mole for $n = 1$, 1·5 and 2, respectively.

The effects of impurity and diluent gas radiation, as well as molecular and solid particle light scattering, have been shown to have a negligibly small influence on our results.

To obtain nearly isothermal decomposition, the acetylene was diluted with a large excess of argon: 95 per cent of A, 5 per cent of C_2H_2; and 98 per cent of A, 2 per cent of C_2H_2 mixtures were used.

The pressure and temperature of the gases behind the shock wave were calculated from the experimentally measured shock velocities. Shock velocities were determined to within $\pm \frac{1}{2}$ per cent.

A collimating slit system has been used to define within the shock tube two uniform regions. These regions are oriented at right angles to each other in a plane normal to the direction of shock propagation. The spatially resolved volumes extend 1 mm along the axis of the tube, 15 mm normal to the axis of the tube in one direction and 75 mm along the tube diameter. Four sapphire windows are located symmetrically in the wall of the tube at the plane of observation.

A versatile optical system for measuring radiation phenomena behind shock fronts has been constructed (see *Figure 1* for an assembly showing the experimental arrangement). A spherical mirror may be used to image the radiation from one of the regions of observation back on itself, thereby effectively doubling the radiating path. The spectral emission from the single- and double-paths, using a suitable monochromator, may be recorded simultaneously on a single detector. The detector response to the emission from the two radiating paths may be distinguished by passing the emitted radiant energy from one of the paths through a 180 kc mechanical chopper before entering the monochromator. The continuous response of the detector measures the unchopped radiant energy whereas the upper envelope of the alternating signal measures the sum of the chopped and unchopped radiant energies[1,2].

The emitted radiant energies from two (single-) paths at two different wavelengths can also be determined with separate monochromators and detectors.

The mechanical chopper may be utilized also to pass chopped radiant energy from an external light source through one of the regions of observation. In this case, the detector monitoring radiant energy emission from a particular region of observation measures simultaneously emission from the heated gases behind the shock front and the absorption of transmitted radiant energy by these gases.

The amount of radiant energy scattered at right angles to the chopped, transmitted, radiation by the heated gases and solid particles behind the shock front may be measured.

A Perkin–Elmer model 13 infra-red spectrophotometer equipped with a LiF prism was used. An indium–antimonide detector cooled to the temperature of liquid nitrogen was used for spectral measurements in the near infra-red region of the spectrum. Radiation measurements in the visible region of the spectrum were made with a 1P28 photomultiplier detector.

Shock velocity measurements were made by counting the transit time of the shock wave between two fixed stations along the shock tube electronically. Thin film platinum heat gauges[3] at the two stations provided signals indicating the shock arrival. A Berkeley model 7360 Counter displayed the shock passage time.

The signals from the indium–antimonide and photomultiplier detectors were recorded on a Tektronix Model 535 dual-trace oscilloscope.

SIMULTANEOUS ABSORPTION AND EMISSION EXPERIMENTS

Spectrally integrated radiation measurements in the visible region of the spectrum were made of the simultaneous emission and absorption of transmitted radiant energy by the heated gases and solid particles behind the incident shock front. Emission from the acetylene $\sum_u^+ - \sum_g^+$ parallel band at 3,287 cm^{-1} was recorded concurrently.

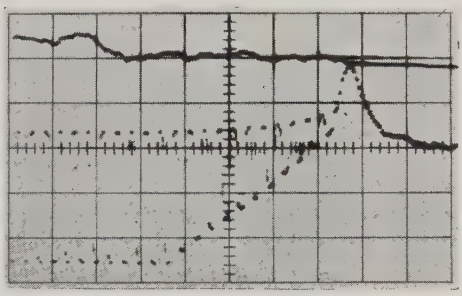

Figure 2. Copy of an oscilloscope record from a simultaneous emission and absorption experiment. The time increases to the right at 20 μsec per major division. The top trace corresponds to acetylene emission at 3,287 cm^{-1}; the intensity increases downwards. The bottom trace shows chopped, transmitted radiation in the visible region of the spectrum with intensity increasing upwards

The oscilloscope records showed an exponential rate of increase of infra-red radiation which reached rapidly a constant value behind the shock wave. There was no measurable decrease in the intensity of the (chopped) radiation from a tungsten light source (approximately 2,500°K colour temperature) until some time after the infra-red radiation had reached its equilibrium value. At this time there was a simultaneous increase in radiation from the heated gases and a decrease in the intensity of the transmitted radiation. *Figure 2* is a copy of an oscillogram for a simultaneous emission and absorption experiment. The incident shock wave arrived at approximately

two divisions from the start of the sweep. The reflected shock wave arrived at approximately 7½ divisions. From these measurements it is clear that the heated gases behind the shock front do not absorb in the visible region of the spectrum until acetylene decomposition occurs. Hence, the absorption is connected with the formation of dissociation products, and not with the thermally excited acetylene[4].

Previous work on carbon formation from acetylene[4,5] has indicated that the spectral distribution of radiation in the visible associated with acetylene decomposition is essentially continous. For this reason, the emission in the visible region of the spectrum will be assumed to be predominantly due to solid carbon particle radiation. The activation energy for carbon formation may then be obtained in a straightforward manner. If we let I_0 equal the integrated intensity of (chopped) radiation incident on the shock tube observation region from the tungsten light source, and if I is the integrated intensity of radiation transmitted through the heated gases and carbon particles behind the shock front, then

$$I = I_0 \exp(-kp_cL) \qquad (1)$$

where k represents the effective absorption coefficient averaged over the visible region of the spectrum in cm^{-1} atm^{-1}, L is the length of a column of carbon particles in cm which are at a pressure of p_c atm.

The time rate of change of carbon particle concentration may then be written as

$$dp_c/dt = [-1/kL]\, d[\ln (I/I_0)]/dt \qquad (2)$$

If the rate of carbon particle formation depends on the acetylene concentration to the order n, then we may assume a rate equation of the form[6]

$$dp_c/dt = \text{constant}\,[\exp(-E/RT)](p_{C_2H_2})^n \qquad (3)$$

where E = activation energy in cal $mole^{-1}$, R = molar gas constant in cal $mole^{-1}$ – $(°K)^{-1}$ and T = temperature in °K. Assuming that k is essentially independent of temperature in the range considered, we may combine equations 2 and 3 to find

$$E = -2{\cdot}303R\, d\log_{10}\{[-1/(p_{C_2H_2})^n][d[\ln (I/I_0)]/dt]\}/d(1/T) \qquad (4)$$

In *Figure 3* we have plotted

$$A_n = -\log_{10}\{[-1/(p_{C_2H_2})^n][d[\ln (I/I_0)]/dt]\}$$

as a function of $(1/T)$ for $n = 1$ and $n = 2$. In this case $d[\ln (I/I_0)]/dt$ is evaluated for the initial increase in absorption, where t has been corrected to particle time behind the incident shock wave. Mixtures of 98 per cent of A, 2 per cent of C_2H_2; and 95 per cent of A, 5 per cent of C_2H_2 were used for these experiments. The total pressure behind the incident shock wave ranged from approximately one to five atmospheres, with a corresponding temperature range of 1,150 to 2,000°K. The points for experiments using 95 per cent of A and 5 per cent of C_2H_2 mixtures have been included by adding a constant factor to the respective ordinates in order to adjust the absolute scales of the two sets of data. It is seen that there is no systematic deviation between the data for the two separate mixtures. The experimental scatter is such as to prevent an unambiguous choice of the order of the decomposition reaction. However, reference to *Figure 3* suggests that the scatter of

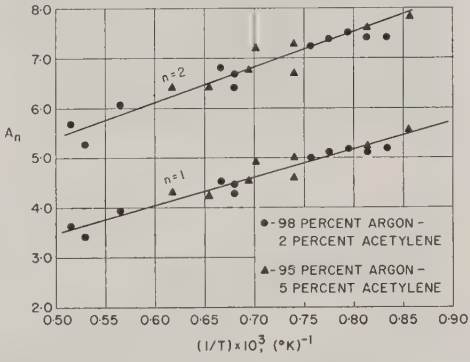

Figure 3. The quantity

$A_n = -\log_{10}\{[-1/(p_{C_2H_2})^n][d[\ln (I/I_0)]/dt]\}$ versus $(1/T)$ *for* $n = 1$ *and* $n = 2$. *The term* $d[\ln (I/I_0)]/dt$ *has been evaluated for the initial absorption*

experimental data in plots of A_n *versus* $(1/T)$ is somewhat smaller for $n = 1$ with $E = 26$ kcal/mole than for $n = 2$ with $E = 33$ kcal/mole.

INDUCTION TIME EXPERIMENTS

Measurements of the induction time for incipient carbon formation from argon–acetylene mixtures were made by recording simultaneously emission from the fundamental vibration-rotation band of acetylene at 3,287 cm^{-1} and the spectrally integrated emission from solid carbon in the visible region of the spectrum. The spectral resolution in the infra-red was approximately 30 cm^{-1}.

The oscillograms showed the familiar rise and levelling off of the infra-red radiation behind the incident shock wave. The level of radiation from the infra-red does not change following the onset of radiation from the visible region of the spectrum. *Figure 4* is a reproduction of an oscilloscope record which illustrates this behaviour. The vertical scale for the signal which is proportional to the visible emission has been increased twentyfold over the corresponding scale in *Figure 2*. This was done to allow a more precise determination of the induction time than was possible with the simultaneous emission and absorption experiments.

The induction time, i.e. the time between the beginning of acetylene radiation (shock arrival) and the onset of visible radiation, is connected in some manner with the time for the molecular vibrations of acetylene to become large enough to induce dissociation. It seems reasonable to assume that an effective activation energy for acetylene

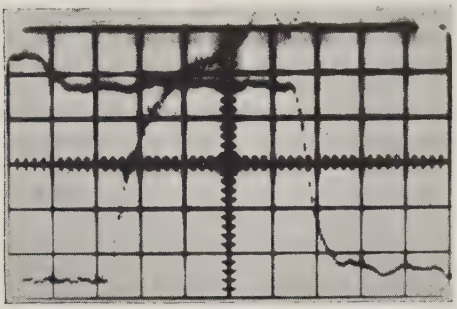

Figure 4. Copy of an oscilloscope record from an induction time experiment. The time increases to the right at 20 μsec per major division. The top trace corresponds to acetylene emission at 3,287 cm^{-1}; the intensity increases downwards. The bottom trace shows carbon radiation in the visible region of the spectrum with intensity increasing upwards

dissociation may be computed from the data. If we assume that at the onset of visible radiation the minimum detectable amount of emission corresponds to equal amounts of carbon being formed for all conditions of temperature and pressure behind the incident shock wave, then we have from equation 3

$$(\Delta p_c)_{\text{initial}} \simeq \text{constant}$$
$$= \text{constant}\,[\exp(-E_D/RT)](p_{C_2H_2})^n \Delta\tau \quad (5)$$

where E_D = activation energy for acetylene dissociation in cal $mole^{-1}$ and $\Delta\tau$ = induction time in microseconds corrected for the difference between laboratory time and particle time behind the incident shock wave. Equation 5 may be solved for the activation energy to give

$$E_D = 2{\cdot}303R\,\mathrm{d}\{\log_{10}[(p_{C_2H_2})^n\Delta\tau]\}/\mathrm{d}(1/T) \quad (6)$$

In *Figure 5* we have plotted

$$B_n = \log_{10}[(p_{C_2H_2})^n\Delta\tau]$$

as a function of $(1/T)$ for $n = 1$, 1·5, and 2. Mixtures of 95 per cent of A and 5 per cent of C_2H_2 were used for these experiments. The ranges of total pressures and temperatures behind the incident shock wave were the same as for the data plotted in *Figure 3*. The activation energies are 10, 13, and 16 kcal/mole for $n = 1$, 1·5, and 2, respectively.

IMPURITY AND INERT GAS RADIATION

Tests were conducted to determine if impurity or inert gas radiation contributed to the measured emission. Pure argon was heated by shock waves to reproduce the conditions of the previous experiments. Spectral measurements in the visible and infra-red regions of the spectrum revealed no detectable radiation.

Further tests were made to determine if molecular or solid particle light scattering aided in the reduction of transmitted radiation intensity in the simultaneous emission and absorption experiments. There was no measurable scattering at right angles to the (chopped) transmitted radiation in the visible region of the spectrum. The tungsten light source and optical geometry for these tests were identical to those for the emission and absorption experiments. However, the sensitivity of the recording circuitry for the photomultiplier measuring scattered light was ten times greater than that of the circuitry for the primary transmitted radiation intensity. Hence, it is felt that light scattering had no influence on measurements from the previous experiments.

Although our experimental results are of a preliminary nature, it is apparent that the facilities and techniques which have been developed will be useful for additional quantitative radiation studies behind shock fronts.

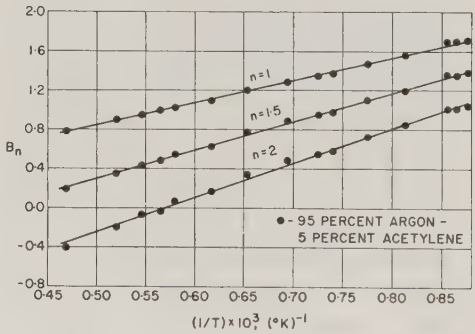

Figure 5. The quantity $B_n = \log_{10}[(p_{C_2H_2})^n\Delta\tau]$ *versus* $(1/T)$ *for* $n = 1$, 1·5 *and* 2

The author is indebted to Dr. S. S. Penner for helpful discussions. The work described in the paper was supported by the U.S. Air Force, Office for Advanced Studies, under Contract AF 18(603)–2.

REFERENCES

[1] Hooker, W., Lapp, M., Weber, D. and Penner, S. S. *J. chem. Phys.* 25 (1956) 1087
[2] Harshbarger, F. *J. chem. Phys.* 24 (1956) 1261
[3] Rabinowicz, J., Jessey, M. E. and Bartsch, C. A. *J. appl. Phys.* 27 (1956) 97
[4] Aten, C. F. and Greene, E. F. *Disc. Faraday Soc.* 22 (1956) 162
[5] Harshbarger, F. *Ph.D. Thesis.* June 1957. California Institute of Technology
[6] Penner, S. S. *Chemical Reactions in Flow Systems*, Chap. 1. 1955. London; Butterworths

COMBUSTION OF *n*-HEPTANE SPRAY IN THE DECOMPOSITION PRODUCTS OF CONCENTRATED HYDROGEN PEROXIDE

J. D. LEWIS and A. C. MERRINGTON

INTRODUCTION

Any understanding of the overall combustion process in liquid propellent rocket engines must be based on a knowledge of injection characteristics and the burning of fuel sprays. Although much attention has been paid to the behaviour of isolated droplets, there is little information available on spray combustion under representative conditions. This has been mainly caused by the complexity of the problem and the formidable experimental difficulties, which are accentuated in the rocket engine where both fuel and oxidizer have to be injected, and combustion temperatures and pressures are high.

This paper describes some experimental techniques that have been developed in conjunction with a practical investigation of the significant phenomena occurring within the combustion chamber of a rocket engine. In order to simplify procedures the experimental programme has been commenced with a study of a single fuel spray burning in a gaseous oxidizing atmosphere at representative pressures. Two specially designed combustion chambers have been used to facilitate gas sampling and direct observation of the flame by means of high-speed photography.

APPARATUS AND PROCEDURE

A fuel-weak mixture ratio (25 : 1 oxidizer to fuel by weight) of *n*-heptane with 85 to 87 per cent concentration hydrogen peroxide has been used throughout these initial tests, the hydrogen peroxide being decomposed catalytically to produce a gaseous oxidizing atmosphere before admission to the combustion chamber. This choice of propellent combination ensured spontaneous ignition of the fuel spray without the need for an igniter, while the average combustion temperature was reduced by the use of a weak mixture ratio. Moreover, the gas analysis by mass spectrometer and the significance of combustion products were simplified by the choice of a hydrocarbon with known properties and composition.

The first combustion chamber with its hydrogen peroxide decomposer unit is shown in *Figure 1.*

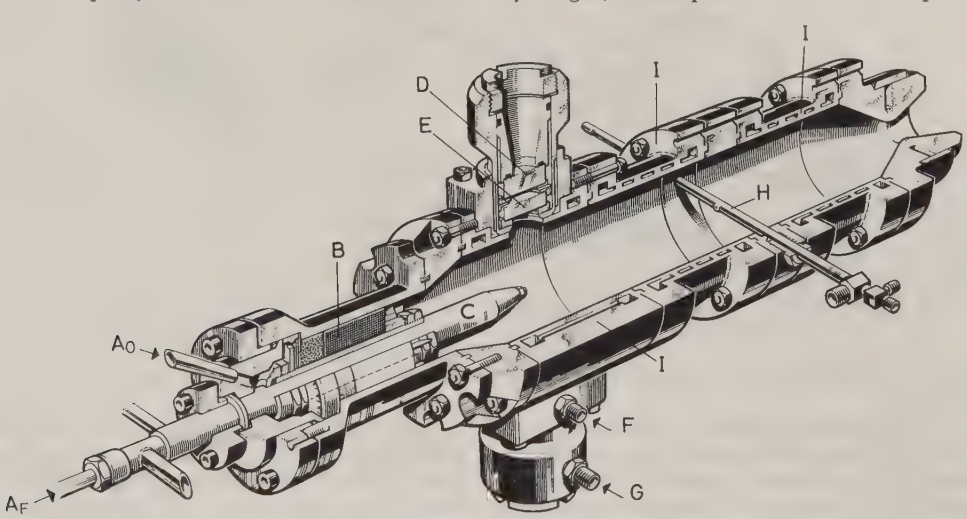

Figure 1. Cylindrical combustion chamber

A_O, oxidizer inlet; A_F, fuel; *B*, decomposer unit; *C*, water-cooled burner; *D*, Perspex window; *E*, quartz window; *F*, water inlet (window coolant); *G*, nitrogen inlet (window purge); *H*, gas sampling probe; *I*, water-cooled chamber sections

This cylindrical chamber consisted of a number of water-cooled sections, each of 3 in. i.d., and a $\frac{5}{8}$ in. diameter exit nozzle. One of the chamber sections was designed to accommodate two small window assemblies which were diametrically opposed, and provision was made for interposing an adaptor ring for a gas sampling probe between any two of the sections. Fuel was injected along the chamber axis through a fan-spray nozzle[1,2] having a flow number of about 0·4. The whole injector assembly was water-cooled to control the fuel temperature, and was inserted along the axis of the hydrogen peroxide decomposer unit in order to preserve symmetrical flow conditions.

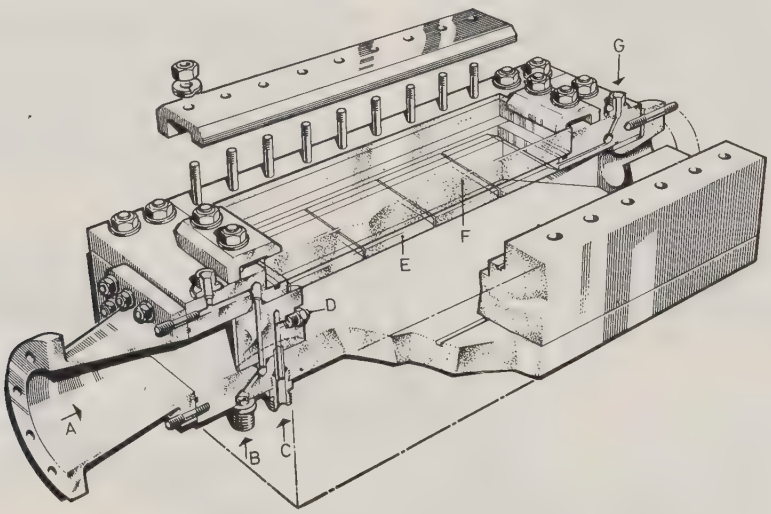

Figure 2. Rectangular combustion chamber

A, oxidizer inlet; *B*, water; *C*, fuel; *D*, fan spray injector, *E*, quartz window; *F*, Perspex window; *G*, nitrogen inlet (window purge)

The second combustion chamber (*Figure 2*) was rectangular in shape, with cross-sectional areas made similar to those of the cylindrical chamber in order to achieve comparable gas velocities, and had a full length observation window. The construction of this window was similar to that of the smaller observation windows used in the cylindrical chamber and comprised a thick Perspex outer pane acting as a stressed member together with inner panes of quartz forming the flame face. Nitrogen was fed through a choked orifice into the interspace between the window panes and was allowed to bleed out into the combustion chamber across the surface of the quartz pane to provide some measure of film cooling. By this means the outer window was protected from the heat of the flame and the thin quartz panes were relieved of the majority of the gas loading. Similar hydrogen peroxide decomposer units and fuel injection nozzles were used in the two combustion chambers. However, in the rectangular chamber the fan-spray nozzle was mounted in a water cooled strut, of streamline section, with the plane of the liquid sheet adjusted to be parallel to the surface of the observation window.

A novel design of water-cooled probe (*Figure 3*) has been used to collect gas samples from various positions in the cylindrical combustion chamber for subsequent analysis by mass spectrometer. The probe design was based on a double sonic orifice system in which the first orifice, located at the sampling point, vented chamber gases to atmosphere through a cooled tube, while the actual gas sample was collected at a pressure of 1–2 mm Hg absolute through an inner probe and second choked orifice situated in the vent pipe a short distance downstream of the first orifice. Advantages claimed for this technique are: (1) rapid quenching of the sample without the need for a diluent; (2) low-pressure sampling to prevent condensation; (3) large samples for gravimetric analysis may be collected simultaneously with the small sample required by the mass spectrometer; and (4) all the low-pressure sample may be transferred to the reservoir of the mass spectrometer, thus avoiding any fractionating effects.

For these initial investigations the sampling probes were fabricated from stainless steel and a water flow rate of approximately 0·09 lb./sec was passed through the 0·25 in. outside diameter cooling jacket. Approximately 0·05 per cent of the total gas flow in the chamber was vented to atmosphere through the 0·013 in. diameter first orifice, whereas the diameter of the second orifice (0·008 in.) was chosen to suit the characteristics of the vacuum pumping system. Downstream of the probe the sampling circuit consisted of a solenoid-operated sampling valve, a small filter

to remove solid particles, the sample bottle with glass shut-off taps, a solenoid-operated isolating valve and the vacuum pump. The two electrically operated valves were necessary in order to minimize the volume of the sampling system and, at the same time, fulfil safety requirements for remote control.

Ciné photographs of flame structure and ignition behaviour were obtained from the rectangular combustion chamber by means of a Fastax high-speed camera operating at 2,000–3,000 frames/sec. In view of the limited running times that were possible with this arrangement, propellent and camera control were effected automatically by the use of process timers; however, a manual over-ride was available in case of emergency. The complete sequence of events was as follows: (1) the camera was started and the oxidizer admission valve opened simultaneously; (2) fuel was admitted to the chamber after an interval of approximately 1·5 sec to allow the camera speed to build up and the operation of the decomposer unit to become stable; (3) after a further 1·5 sec the fuel was switched off and the camera stopped (the camera speed having been adjusted to give a running time of 3·0 sec with a 100 ft. spool of film); and (4) finally, the oxidizer flow was stopped manually after observing the end of visible combustion.

Although the flame in the chamber was self-luminous, additional external lighting was provided to illuminate the fuel spray and to provide an outline of the combustion chamber for location purposes.

Both chambers were operated at an absolute pressure of approximately 17 atmospheres with a total propellent flow rate of 0·7 lb./sec. The propellent flow rates were measured by means of sharp-edged orifices, and the significant variables of pressure and temperature were measured by suitable electrical transducers and recorded photographically on multi-channel recorders during the course of each test.

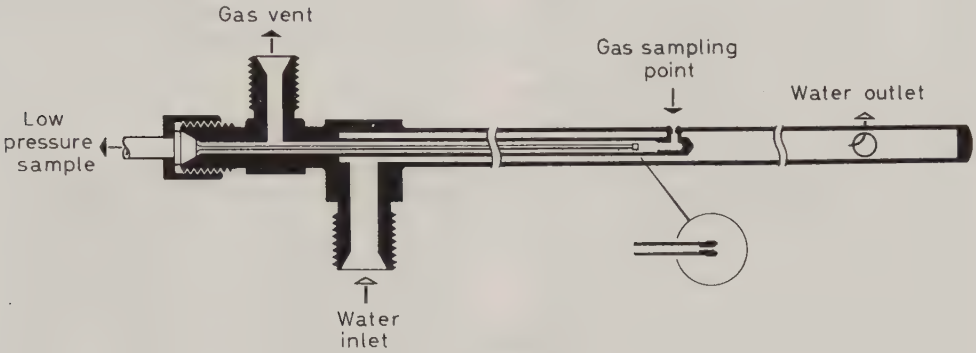

Figure 3. Gas sampling probe

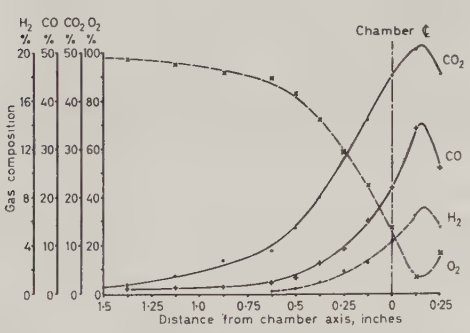

Figure 4. Diametral traverse of circular combustion chamber (sampling probe 5¼ in. from burner perpendicular to plane of liquid sheet)

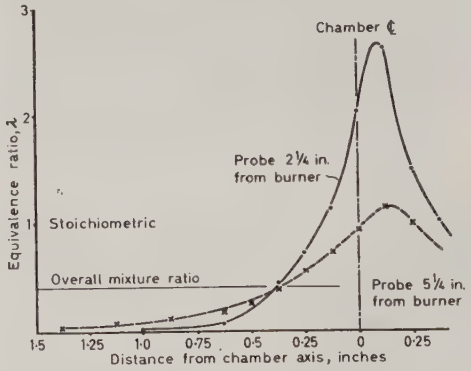

Figure 5. Traverse perpendicular to plane of spray

RESULTS

Some results from gas-sampling investigations in the cylindrical combustion chamber are given in *Figures 4* and *5*. The data for *Figure 4* were obtained from dried gas samples taken along a radial traverse of the combustion chamber, perpendicular to the plane of the liquid sheet, at a position 5·25 in. from the fuel injector. No trace of unburned fuel was found in any of these samples; moreover, if water vapour is assessed from a carbon,

oxygen and hydrogen balance, the gas composition is found to be approximately in chemical equilibrium so that combustion was sensibly complete. It was possible to calculate the local equivalence ratios, λ, from these results (λ is the ratio of the fuel present to that required for stoichiometric combustion) and these are shown in *Figure 5* together with those obtained from a similar traverse 2·25 in. from the fuel injector.

Samples taken 2·25 in. from the fuel injector contained appreciable amounts of unburned heptane, lower hydrocarbons and some combustion products, which indicates that sampling was taking place in the actual reaction zone. Table 1 gives

Stills from typical ciné photographs taken of the rectangular combustion chamber shortly after ignition and during steady running respectively, are given in *Figures 6a* and *b*, which may be compared with spark shadowgraph pictures (*Figures 7a* and *b*) taken during water-flow tests on a similar fan-spray nozzle. *Figure 7a* was taken during the build-up of the spray, and variations resulting from reflected pressure waves in the feed system may be observed; similar irregularities occur in the flame pattern of *Figure 6a*. The more uniform character of the spray during steady flow conditions (*Figure 7b*) is also evident from the flame structure (*Figure 6b*). However, it is of

TABLE 1

Analysis of Sample taken on Chamber Axis 2¼ in. from Fuel Injector
Overall mixture ratio = 25·6 : 1, 87 per cent hydrogen peroxide/*n*-heptane by weight
Chamber pressure = 17·6 atm abs.

Constituent	*Gas composition*			
	Dry sample		*Total sample*	
	% *By volume*	% *By weight*	% *By volume*	% *By weight*
Oxygen (O_2)	34·4	31·8	9·6	13·5
Carbon dioxide (CO_2)	19·3	24·4	5·4	10·4
Carbon monoxide (CO)	18·1	14·6	5·0	6·2
Formaldehyde† (HCOH)	—	—	0·2	0·3
Heptane (C_7H_{16})	4·6	13·2	1·3	5·6
Propylene (C_3H_6)	3·8	4·6	1·1	2·0
Ethylene (C_2H_4)	8·7	7·0	2·4	3·0
Acetylene (C_2H_2)	3·1	2·3	0·9	1·0
Methane (CH_4)	4·4	2·0	1·3	0·9
Hydrogen (H_2)	3·5	0·2	1·0	0·1
Water vapour* (H_2O)	—	—	71·7	57·1

Mean molecular weight = 22·6 Equivalence ratio = 2·04

* Calculated † By volumetric analysis

the detailed results obtained at this plane in the centre of the combustion chamber. The first two columns give the percentage composition by volume and weight derived from the mass spectrometer analysis of a dry sample. The third and fourth columns include water vapour, calculated from a carbon–oxygen–hydrogen balance, together with formaldehyde which was estimated by a volumetric method[3] after passing the vent gases from the sampling probe through a solution of sodium bisulphite. The detection of a number of partial products, especially in samples taken from the main reaction zone, suggested that the sampling technique was reasonably effective in quenching reactions. Furthermore, good reproducibility has been achieved between samples taken from the same point in the combustion chamber on different occasions but under similar running conditions.

interest to note that the flame pictures also reveal the presence of intermittent, rapidly growing, centres of ignition slightly upstream from the main reaction zone.

DISCUSSION AND CONCLUSIONS

These initial investigations have shown that the experimental techniques described in this paper can be applied to the study of combustion processes in the rocket engine and that worth-while results can be expected.

The efficiency of the probe design and sampling methods have been illustrated, although some further advantages may be gained by reducing the overall size of the probe and from more rapid cooling of the collected sample. It has been shown that gas sampling can be used to explore the mixture ratio distribution within the combustion chamber; the technique could, therefore, be used

to determine the effectiveness of injector pattern in a representative size of engine under actual running conditions. A more detailed analysis of the gas sample enables the completeness of combustion at any given plane to be determined; thus it should be possible to evaluate the minimum size of chamber necessary for combustion to reach an acceptable stage. Future developments of sampling and analytical systems will include automatic traversing and positioning of the probe, the collection of samples from pre-determined points during the course of a single traverse and the adaptation of simplified analytical techniques (e.g. infra-red absorption methods) for assessing

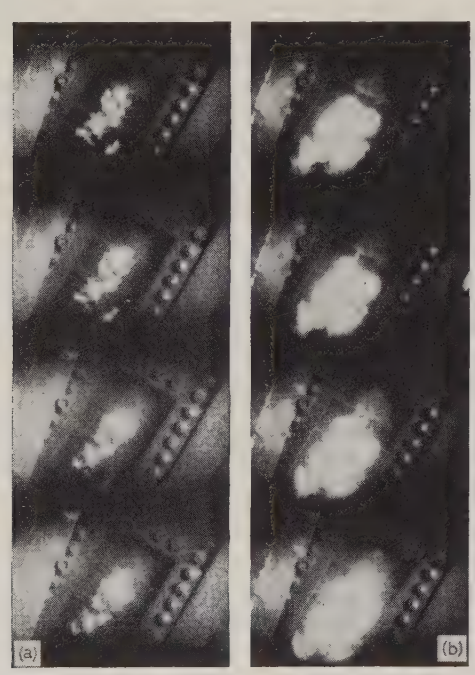

Figure 6. High-speed ciné photographs of flame pattern

mixture ratios when a complete analysis becomes unnecessary.

Photographic studies of flame structure are important means of assessing the behaviour of an injection system under combustion conditions. If these results can be correlated with similar studies and measurements on liquid sprays under simulated experimental conditions it should be possible to assess the significant features of the injection characteristics. It may also be possible to correlate observed variations in the combustion pattern with pressure fluctuations measured at the chamber wall, and thus obtain a guide to the mechanism of combustion instability. A further understanding of this process would be achieved if changes in the flame structure could be related to brief variations in the local gas composition as measured by a 'snap' sampling technique whereby a sample is collected over a period of msec or less.

Although the initial investigations have been carried out under the simplified experimental

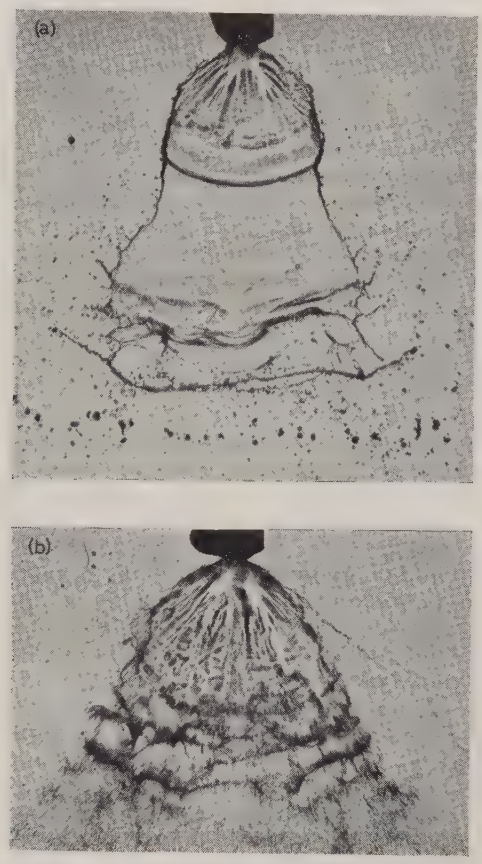

Figure 7. Spark shadowgraph picture of fan spray

conditions of a single fuel spray burning in a gaseous oxidizing atmosphere moving with low velocity, there does not appear to be any fundamental reason why the techniques should not be applied to more complex systems.

Crown Copyright Reserved

The authors wish to acknowledge the assistance given by Dr. G. A. Heath, Mr. J. B. McLean and Miss S. Cato in carrying out the gas analyses referred to in this paper, and by Mr. J. Moloney.

REFERENCES

[1] Fraser, R. P. *Sixth Symposium (International) on Combustion*, p. 687. 1957. New York; Reinhold
[2] — and Eisenklam P. *Trans. Inst. Chem. Eng.* 34, No. 4 (1956) 294
[3] Walker J. F. *Formaldehyde*, p. 374. 1953. New York; Reinhold

DISCUSSION

C. J. Danby (Oxford): Of the papers in this session, three deal with the analysis of combustion products from practical engine combustion chambers. Two of these—those of Holderness and Macfarlane and of Toone and Arkless—describe continuous flow analytical systems employing non-dispersive infra-red gas analysers. These systems are of considerable complexity. On the other hand Lewis and Merrington describe a relatively simple system for the collection of a series of small samples, without condensation or fractionation, for subsequent laboratory analysis by mass-spectrometer or vapour-phase chromatography.

I think it might be useful and interesting if the merits and disadvantages of these two different approaches to this very important analytical problem were discussed.

The very effective phase-discrimination method described by Dickey for the detection of the infra-red spectrum of the OH radical in a flame reminds me that Eltenton in his pioneer work of 20 years ago on the detection of free radicals by mass-spectrometry carried out some experiments with pulsating or oscillating flames. It seems possible that the application of this technique might simplify the interpretation of the mass-spectra of the ions in flames obtained by the methods described by Knewstubb and Sugden in an earlier session.

J. Ogden (Birmingham): Regarding Macfarlane's paper, the only comments I have to offer are: (1) he mentions the use of a $\frac{5}{16}$ in. diameter sampling tube; we at Lucas regularly use $\frac{1}{8}$ in. sampling probes; (2) the quoted error of $\pm$ 5 per cent at efficiencies of $\theta = 20$ per cent seems rather low. I should have thought the error to have been rather more than this under these conditions, due largely to sampling difficulties.

I would disagree with Toone's statement regarding the tendency to approach the water–gas equilibrium at the centre of the re-circulation zone. I would attribute reactions in this zone largely to pyrolysis, the lack of free oxygen preventing any attempts to achieve water–gas equilibrium.

I would like to comment on his statement of low combustion efficiencies measured in the primary zone. Such efficiencies may be due to over-rich conditions and a weaker primary zone would exhibit higher efficiency. These remarks do not imply that a weak primary zone is the hall-mark of a well designed combustion chamber; other factors must be considered.

Finally may I make an appeal for careful consideration to be given to the design of an adequate smoke meter. It has been my experience that optically sensitive smoke meters possess electronic systems that are vibrationally unstable, whilst those meters which are vibrationally stable are optically insensitive.

J. J. Macfarlane (Pyestock): In answer to the point raised by Danby, the apparatus, in spite of its apparent complexity, was designed with the intention of encouraging its use by those unskilled in chemical laboratory techniques. Normal engineering methods and materials are used as far as possible, and it is interesting to note that a young engineer recently started to use the apparatus unaided after a few weeks' supervision. The choice of continuous sampling and analysis, rather than snap sampling with subsequent analysis in the laboratory, is dictated by the nature of the samples and by the need for large numbers of analyses and therefore short working times. The applicability of mass-spectrometric techniques is limited in that they give both too little and too much information. Too little in that the precision is generally low, particularly for one or two important constituents, and too much in that the mass-spectrum of at least one constituent (kerosine) is exceedingly complex. A further good reason for not using one in our present work is that no instrument was available.

In answer to Odgers, I would point out that the sampling probe described is not a simple single-point probe but one fully instrumented for iso-kinetic sampling. The probe diameter ($\frac{5}{16}$ in. o.d.) is thus surprisingly small.

In reply to a question relating to the analysis of gases from a turbulent flame where the gas composition varied with sample flow rate, only becoming constant at sample velocities equal to or greater than the stream velocity, I myself have had no experience of behaviour of this kind in dealing with wholly gaseous products. In view of the small density differences I find it difficult to agree with the questioner in attributing the changes simply to velocity, as if this had been effective, one would have expected a continuous variation in composition in passing through the isokinetic condition. For example, it is known that the apparent concentration of carbon in a gas stream decreases continuously as the sampling velocity increases.

Finally I wish to point out that the statement in the first sentence of our paper applied to combustion development work—not forgetting that spectrographic techniques are also widely used in

fundamental studies of hydrocarbon combustion processes.

B. Toone (Derby): In reply to Danby, the main reasons in favour of a continuous flow analytical system are:

(1) The estimation of total liquid constituents is fairly straightforward by the oxidation method described in our paper. For any method in which the analysis is carried out in the laboratory, a liquid freezing trap is required and such methods are very slow. Approximately 20 analyses per hour can be carried out by the continuous flow method described.

(2) In much of the work carried out at Derby, high-pressure air is used which is in great demand. It is practically impossible to repeat tests if results are incomplete. Using the continuous flow method the results are immediately available and can be assessed as the test proceeds. Any additional analyses or checks may then be carried out at the end of the test.

In reply to Odgers, who queried the statement that the reactants in the re-circulation zone were trying to attain the water–gas equilibrium, we agree that pyrolysis is an important reaction in the zone and this point is made in our paper. In addition, re-circulation zones contain large quantities of CO, CO_2, H_2 and H_2O. We are of the opinion that lack of oxygen does not prevent the gas composition being controlled by the water–gas equilibrium constant. However, as we have pointed out in our paper, the equilibria obtained are not related exactly to the computed temperature, but assuming an 'unmixed' composition, the type of composition achieved in practice can easily be obtained.

With regard to the comment on primary zone efficiencies, it is difficult to generalize on the relationship between the mean f.a.r. in the primary zone and efficiency, since so many factors have to be considered. One of the main functions of our gas analysis equipment is to unravel some of the factors involved.

The problem of smoky combustion has developed in recent years as a result of higher compressor delivery pressures. We have had a prototype optical absorption meter to determine smoke density in use for the last 12 months. It has sufficient sensitivity for the estimation of exhaust gas smoke. Vibrational instability of this type of instrument can usually be eliminated by the use of a good amplifier circuit. The design may not be sufficiently stable for continuous use over a period of time in the way a thermocouple is used, but for comparison of smoke densities over a range of engine rev/min it has proved sufficiently reliable. The speed of determination is excellent, approximately 1 min. being required for checking sensitivity and the actual smoke determination.

F. P. Dickey (Ohio): Since submitting the paper on the application of the phase-discrimination method of detection to the study of the spectrum of the OH radical in an oxy-acetylene flame we have been able to duplicate the results shown in *Figure 1* by using two balanced flames, as suggested in the paper. By the use of a rotating optical system two different sections of the flames are viewed alternately at the chopping frequency of 13 c/s. In one flame a portion of the primary flame is imaged on the slit and with the other flame a region just above the primary flame. This latter position in the flame is much richer in OH radicals.

LIBRARY USE ONLY

QD516
S92
1958